

ISSN 2156-5570(Online)

ISSN 2158-107X(Print)

Editorial Preface

From the Desk of Managing Editor...

It may be difficult to imagine that almost half a century ago we used computers far less sophisticated than current home desktop computers to put a man on the moon. In that 50 year span, the field of computer science has exploded.

Computer science has opened new avenues for thought and experimentation. What began as a way to simplify the calculation process has given birth to technology once only imagined by the human mind. The ability to communicate and share ideas even though collaborators are half a world away and exploration of not just the stars above but the internal workings of the human genome are some of the ways that this field has moved at an exponential pace.

At the International Journal of Advanced Computer Science and Applications it is our mission to provide an outlet for quality research. We want to promote universal access and opportunities for the international scientific community to share and disseminate scientific and technical information.

We believe in spreading knowledge of computer science and its applications to all classes of audiences. That is why we deliver up-to-date, authoritative coverage and offer open access of all our articles. Our archives have served as a place to provoke philosophical, theoretical, and empirical ideas from some of the finest minds in the field.

We utilize the talents and experience of editor and reviewers working at Universities and Institutions from around the world. We would like to express our gratitude to all authors, whose research results have been published in our journal, as well as our referees for their in-depth evaluations. Our high standards are maintained through a double blind review process.

We hope that this edition of IJACSA inspires and entices you to submit your own contributions in upcoming issues. Thank you for sharing wisdom.

Thank you for Sharing Wisdom!

Kohei Arai
Editor-in-Chief
IJACSA
Volume 13 Issue 10 October 2022
ISSN 2156-5570 (Online)
ISSN 2158-107X (Print)

Editorial Board

Editor-in-Chief

Dr. Kohei Arai - Saga University

Domains of Research: Technology Trends, Computer Vision, Decision Making, Information Retrieval, Networking, Simulation

Associate Editors

Alaa Sheta

Southern Connecticut State University

Domain of Research: Artificial Neural Networks, Computer Vision, Image Processing, Neural Networks, Neuro-Fuzzy Systems

Domenico Ciuonzo

University of Naples, Federico II, Italy

Domain of Research: Artificial Intelligence, Communication, Security, Big Data, Cloud Computing, Computer Networks, Internet of Things

Doroła Kaminska

Lodz University of Technology

Domain of Research: Artificial Intelligence, Virtual Reality

Elena Scutelnicu

"Dunarea de Jos" University of Galati

Domain of Research: e-Learning, e-Learning Tools, Simulation

In Soo Lee

Kyungpook National University

Domain of Research: Intelligent Systems, Artificial Neural Networks, Computational Intelligence, Neural Networks, Perception and Learning

Krassen Stefanov

Professor at Sofia University St. Kliment Ohridski

Domain of Research: e-Learning, Agents and Multi-agent Systems, Artificial Intelligence, e-Learning Tools, Educational Systems Design

Renato De Leone

Università di Camerino

Domain of Research: Mathematical Programming, Large-Scale Parallel Optimization, Transportation problems, Classification problems, Linear and Integer Programming

Xiao-Zhi Gao

University of Eastern Finland

Domain of Research: Artificial Intelligence, Genetic Algorithms

CONTENTS

Paper 1: Hand Motion Estimation using Super-Resolution of Multipoint Surface Electromyogram by Deep Learning

Authors: Keigo FUKUSHIMA, Yoshiaki YASUMURA

PAGE 1 – 6

Paper 2: IoT-CID: A Dynamic Detection Technology for Command Injection Vulnerabilities in IoT Devices

Authors: Hao Chen, Jinxin Ma, Baojiang Cui, Junsong Fu

PAGE 7 – 14

Paper 3: English and Romanian Brain-to-Text Brain-Computer Interface Word Prediction System

Authors: Haider Abdullah Ali, Nicolae Goga, Andrei Vasileteanu, Ali M. Muslim, Khalid Abdullah Ali, Marius-Valentin Drăgoi

PAGE 15 – 23

Paper 4: Fine-grained Access Control Method for Blockchain Data Sharing based on Cloud Platform Big Data

Authors: Yu Qiu, Biying Sun, Qian Dang, Chunhui Du, Na Li

PAGE 24 – 31

Paper 5: Smart System for Emergency Traffic Recommendations : Urban Ambulance Mobility

Authors: Ayoub Charef, Zahi Jarir, Mohamed Quafafou

PAGE 32 – 44

Paper 6: A Review of Automatic Question Generation in Teaching Programming

Authors: Jawad Alshboul, Erika Baksa-Varga

PAGE 45 – 51

Paper 7: Application of Stacking Ensemble Machine in Big Data: Analyze the Determinants for Vitalization of the Multicultural Support Center

Authors: RaeHo Lee, Haewon Byeon

PAGE 52 – 57

Paper 8: Research on Precision Marketing based on Big Data Analysis and Machine Learning:Case Study of Morocco

Authors: Nouhaila El Koufi, Abdessamad Belangour, Mounir Sdiq

PAGE 58 – 63

Paper 9: A Sequence-Aware Recommendation Method based on Complex Networks

Authors: Abdullah Alhadlaq, Said Kerrache, Hatim Aboalsamh

PAGE 64 – 72

Paper 10: Mobile Applications for Cybercrime Prevention: A Comprehensive Systematic Review

Authors: Irma Huamanñahui Chipa, Javier Gamboa-Cruzado, Jimmy Ramirez Villacorta

PAGE 73 – 82

Paper 11: Evaluation of the Efficiency of the Optimization Algorithms for Transfer Learning on the Rice Leaf Disease Dataset

Authors: Luyl-Da Quach, Khang Nguyen Quoc, Anh Nguyen Quynh, Hoang Tran Ngoc

PAGE 83 – 91

Paper 12: Associating User's Preference and Satisfaction into Quality of Experience: A Shoulder-surfing Resistant Authentication Scheme by Visual Perception

Authors: Juliana Mohamed, Mohd Farhan Md Fudzee, Sofia Najwa Ramli, Mohd Norasri Ismail, Muhamad Hanif

Jofri

PAGE 92 – 97

Paper 13: Integrating Computer-aided Argument Mapping into EFL Learners' Argumentative Writing: Evidence from Saudi Arabia

Authors: Nuha Abdullah Alsmari

PAGE 98 – 104

Paper 14: An Efficient Computational Method of Motif Finding in the Zika Virus Genome

Authors: Pushpa Susant Mahapatro, Jatinderkumar R. Saini

PAGE 105 – 114

Paper 15: Classification of Agriculture Area based on Superior Commodities in Geographic Information System

Authors: Lilik Sumaryanti, Rosmala Widjastuti, Firman Tempola, Heru Ismanto

PAGE 115 – 121

Paper 16: Analysis of Unsupervised Machine Learning Techniques for an Efficient Customer Segmentation using Clustering Ensemble and Spectral Clustering

Authors: Nouri Hicham, Sabri Karim

PAGE 122 – 130

Paper 17: Complexity of Web-based Application for Research and Community Service in Academic

Authors: Fitriana Fitriana, Sukarni Sukarni, Zulkifli Zulkifli

PAGE 131 – 135

Paper 18: Brain Tumor Detection using Integrated Learning Process Detection (ILPD)

Authors: M. Praveena, M. Kameswara Rao

PAGE 136 – 141

Paper 19: Towards Home-based Therapy: The Development of a Low-cost IoT-based Transcranial Direct Current Stimulation System

Authors: Ahmad O. Alokaily, Ghala Almeteb, Raghad Althabiti, Suhail S. Alshahrani

PAGE 142 – 146

Paper 20: Semi-supervised Text Annotation for Hate Speech Detection using K-Nearest Neighbors and Term Frequency-Inverse Document Frequency

Authors: Nur Heri Cahyana, Shoffan Saifullah, Yuli Fauziah, Agus Sasmito Aribowo, Rafal Drezewski

PAGE 147 – 151

Paper 21: Comparison of Edge Detection Algorithms for Texture Analysis on Copy-Move Forgery Detection Images

Authors: Bashir Idris, Lili N. Abdullah, Alfian Abdul Halim, Mohd Taufik Abdullah Selimun

PAGE 152 – 160

Paper 22: Deep Learning Model for Predicting Consumers' Interests of IoT Recommendation System

Authors: Talal H. Noor, Abdulqader M. Almars, El-Sayed Atlam, Ayman Noor

PAGE 161 – 170

Paper 23: A Machine Learning Model for Personalized Tariff Plan based on Customer's Behavior in the Telecom Industry

Authors: Lewlisa Saha, Hrudaya Kumar Tripathy, Fatma Masmoudi, Tarek Gaber

PAGE 171 – 184

Paper 24: A Systematic Literature Review of Deep Learning-Based Detection and Classification Methods for Bacterial Colonies

Authors: Shimaa A. Nagro

PAGE 185 – 202

Paper 25: Optimization of Multilayer Perceptron Hyperparameter in Classifying Pneumonia Disease Through X-Ray Images with Speeded-Up Robust Features Extraction Method

Authors: Mutammimul Ula, Muhathir, Ilham Sahputra

PAGE 203 – 210

Paper 26: Forecasting Covid-19 Time Series Data using the Long Short-Term Memory (LSTM)

Authors: Harun Mukhtar, Reny Medikawati Taufiq, Ilham Herwinanda, Doni Winarso, Regiolina Hayami

PAGE 211 – 217

Paper 27: Design of a Dense Layered Network Model for Epileptic Seizures Prediction with Feature Representation

Authors: Summia Parveen, S. A. Siva Kumar, P. MohanRaj, Kingsly Jabakumar, R. Senthil Ganesh

PAGE 218 – 223

Paper 28: The Effect of the Aesthetically Mobile Interfaces on Students' Learning Experience for Primary Education

Authors: Nor Fatin Farzana Binti Zainuddin, Zuriana Binti Abu Bakar, Noor Maizura Binti Mohammad, Rosmayati Binti Mohamed

PAGE 224 – 230

Paper 29: Real Time Customer Satisfaction Analysis using Facial Expressions and Headpose Estimation

Authors: Nethravathi P. S, Manjula Sanjay Koti, Taramol. K.G, Soofi Anwar, Gayathri Babu J, Rajermani Thinakaran

PAGE 231 – 238

Paper 30: An Optimized Single Layer Perceptron-based Approach for Cardiotocography Data Classification

Authors: Bader Fahad Alkhamees

PAGE 239 – 245

Paper 31: Observe-Orient-Decide-Act (OODA) for Cyber Security Education

Authors: Dimas Febriyan Priambodo, Yogha Restu Pramadi, Obrina Candra Briliyant, Muhammad Hasbi, Muhammad Adi Yahya

PAGE 246 – 255

Paper 32: Module Partition Method of Embedded Multitasking Software Based on Fuzzy Set Theory

Authors: Yunpeng Gu

PAGE 256 – 265

Paper 33: Comparison of Metaheuristic Techniques for Parcel Delivery Problem: Malaysian Case Study

Authors: Shamine A/P S.Moganathan, Siti Noor Asyikin binti Mohd Razali, Aida Mustapha, Safra Liyana binti Sukiman, Rosshairy Abd Rahman, Muhammad Ammar Shafi

PAGE 266 – 274

Paper 34: An Approach for Optimization of Features using Gorilla Troop Optimizer for Classification of Melanoma

Authors: Anupama Damarla, Sumathi D

PAGE 275 – 286

Paper 35: Review on Multimodal Fusion Techniques for Human Emotion Recognition

Authors: Ruhina Karani, Sharmishta Desai

PAGE 287 – 296

Paper 36: A Comparative Study of Predictions of Students' Performances in Offline and Online Modes using Adaptive Neuro-Fuzzy Inference System

Authors: Sudhindra B. Deshpande, Kiran K.Tangod, Neelkanth V.Karekar, Pandurang S.Upparmani

PAGE 297 – 304

Paper 37: Combining Innovative Technology and Context based Approaches in Teaching Software Engineering

Authors: Shamsul Huda, Sultan Alyahya, Lei Pan, Hmood Al-Dossari

PAGE 305 – 314

Paper 38: Modified Intrusion Detection Tree with Hybrid Deep Learning Framework based Cyber Security Intrusion Detection Model

Authors: Majed Alowaidi

PAGE 315 – 322

Paper 39: Performance Comparison between Meta-classifier Algorithms for Heart Disease Classification

Authors: Nureen Afiqah Mohd Zaini, Mohd Khalid Awang

PAGE 323 – 328

Paper 40: Detection of Severity-based Email SPAM Messages using Adaptive Threshold Driven Clustering

Authors: I V S Venugopal, D Lalitha Bhaskari, M N Seetaramanath

PAGE 329 – 339

Paper 41: Alz-SAENet: A Deep Sparse Autoencoder based Model for Alzheimer's Classification

Authors: G Nagarjuna Reddy, K Nagi Reddy

PAGE 340 – 348

Paper 42: Development of Path Loss Prediction Model using Feature Selection-Machine Learning Approach

Authors: Bengawan Alfaresi, Zainuddin Nawawi, Bhakti Yudho Suprpto

PAGE 349 – 358

Paper 43: Employability Prediction of Information Technology Graduates using Machine Learning Algorithms

Authors: Gehad ElSharkawy, Yehia Helmy, Engy Yehia

PAGE 359 – 367

Paper 44: Otsu's Thresholding for Semi-Automatic Segmentation of Breast Lesions in Digital Mammograms

Authors: Moustapha Mohamed Saleck, M. H. Ould Mohamed Dyla, EL Benany Mohamed Mahmoud, Mohamed Rmili

PAGE 368 – 375

Paper 45: Performance Analysis of Software Test Effort Estimation using Genetic Algorithm and Neural Network

Authors: Vikas Chahar, Pradeep Kumar Bhatia

PAGE 376 – 383

Paper 46: A Computer Vision System for Street Sweeper Robot

Authors: Ouiem Bchir, Sultana Almasoud, Lina Alyahya, Renad Aldhalaan, Lina Alsaeed, Nada Aldalbahi

PAGE 384 – 392

Paper 47: An Experimental Study with Fuzzy-Wuzzy (Partial Ratio) for Identifying the Similarity between English and French Languages for Plagiarism Detection

Authors: Peluru Janardhana Rao, Kunjam Nageswara Rao, Sitaratnam Gokuruboyina

PAGE 393 – 401

Paper 48: Comparing LSTM and CNN Methods in Case Study on Public Discussion about Covid-19 in Twitter

Authors: Fachrul Kurniawan, Yuliana Romadhoni, Laila Zahrona, Jihad Hammad

PAGE 402 – 409

Paper 49: ACT on Monte Carlo FogRA for Time-Critical Applications of IoT

Authors: A. S. Gowri, P. Shanthi Bala, Zion Ramdinthara, T. Siva Kumar

PAGE 410 – 419

Paper 50: Delay-Aware and Profit-Maximizing Task Migration for the Cloudlet Federation

Authors: Hengzhou Ye, Junhao Guo, Xinxiao Li

PAGE 420 – 428

Paper 51: Collaborative Ontology Construction Framework: An Attempt to Rationalize Effective Knowledge Dissemination

Authors: Kaneeka Vidanage, Noor Maizura Mohamad Noor, Rosmayati Mohemad, Zuriana Abu Bakar

PAGE 429 – 435

Paper 52: BiLSTM and Multiple Linear Regression based Sentiment Analysis Model using Polarity and Subjectivity of a Text

Authors: Marouane CHIHAB, Mohamed CHINY, Nabil Mabrouk, Hicham BOUSSATTA, Younes CHIHAB, Moulay Youssef HADI

PAGE 436 – 442

Paper 53: Local Texture Representation for Timber Defect Recognition based on Variation of LBP

Authors: Rahilda Nadhirah Norizzaty Rahiddin, Ummi Raba'ah Hashim, Lizawati Salahuddin, Kasturi Kanchymalay, Aji Prasetya Wibawa, Teo Hong Chun

PAGE 443 – 448

Paper 54: Unethical Internet Behaviour among Students in High Education Institutions: A Systematic Literature Review

Authors: Zakiah Ayop, Aslinda Hassan, Syarulnaziah Anawar, Nur Fadzilah Othman, Rabiah Ahmad, Nor Raihana Mohd Ali, Maslin Masrom

PAGE 449 – 464

Paper 55: Teachers' Attitudes Towards the Use of Augmented Reality Technology in Teaching Arabic in Primary School Malaysia

Authors: Lily Hanefarezan Asbulah, Mus'ab Sahrim, Nor Fatini Aqilah Mohd Soad, Nur Afiqah Athirah Mohd Rushdi, Muhammad Afiq Hilmi Mhd Deris

PAGE 465 – 474

Paper 56: An Algorithm for Shrinking Blood Receptacles using Retinal Internal Pictures for Clinical Characteristics Measurement

Authors: Aws A. Abdulsahib, Moamin A Mahmoud, Sally A. Al-Hasnawi

PAGE 475 – 488

Paper 57: Detection of Cyber-Physical Attacks using Physical Model with Nonparametric EWMA Detector

Authors: Joko Supriyadi, Jazi Eko Istiyanto, Agfianto Eko Putra

PAGE 489 – 496

Paper 58: Performance Evaluation of New Feature based on Ordinal Pattern Analysis for Iris Biometric Recognition

Authors: Sheena S, Sheena Mathew, Bindu M Krishna

PAGE 497 – 506

Paper 59: Mitigation of DDoS Attack in Cloud Computing Domain by Integrating the DCLB Algorithm with Fuzzy Logic

Authors: Amrutha Muralidharan Nair, R Santhosh

PAGE 507 – 516

Paper 60: Federated Learning Approach for Measuring the Response of Brain Tumors to Chemotherapy

Authors: Omneya Atef, Mustafa Abdul Salam, Hisham Abdelsalam

PAGE 517 – 524

Paper 61: A Fake News Detection System based on Combination of Word Embedded Techniques and Hybrid Deep Learning Model

Authors: Mohamed-Amine OUASSIL, Bouchaib CHERRADI, Soufiane HAMIDA, Mouaad ERRAMI, Oussama EL GANNOUR, Abdelhadi RAIHANI

PAGE 525 – 534

Paper 62: Research on Blind Obstacle Ranging based on Improved YOLOv5

Authors: Yongquan Xia, Yiqing Li, Jianhua Dong, Shiyu Ma

PAGE 535 – 542

Paper 63: Classification Method for Power Load Data of New Energy Grid based on Improved OTSU Algorithm

Authors: Xun Ma, Kai Liu, Anlei Liu, Xuchao Jia, Yong Wang

PAGE 543 – 552

Paper 64: Study on the Technical Characteristics of Badminton Players in Different Stages through Video Analysis

Authors: Jin Qiu

PAGE 553 – 558

Paper 65: Deep Architecture based on DenseNet-121 Model for Weather Image Recognition

Authors: Saleh A. Albelwi

PAGE 559 – 565

Paper 66: Research on Improved Shallow Neural Network Big Data Processing Model based on Gaussian Function

Authors: Lifang Fu

PAGE 566 – 573

Paper 67: Conceptual Model of Augmented Reality Mobile Application Design (ARMAD) to Enhance user Experience: An Expert Review

Authors: Nik Azlina Nik Ahmad, Ahmad Iqbal Hakim Suhaimi, Anitawati Mohd Lokman

PAGE 574 – 582

Paper 68: A Novel Prediction Model for Compiler Optimization with Hybrid Meta-Heuristic Optimization Algorithm

Authors: Sandeep U. Kadam, Sagar B. Shinde, Yogesh B. Gurav, Sunil B Dambhare, Chaitali R Shewale

PAGE 583 – 588

Paper 69: A Deep Learning and Machine Learning Approach for Image Classification of Tempered Images in Digital Forensic Analysis

Authors: Praveen Chitti, K. Prabhushetty, Shridhar Allagi

PAGE 589 – 593

Paper 70: Evaluation of Land Use/Land Cover Classification based on Different Bands of Sentinel-2 Satellite Imagery using Neural Networks

Authors: Pallavi M, Thivakaran T K, Chandankeri Ganapathi

PAGE 594 – 601

Paper 71: Exponential Decay Function-Based Time-Aware Recommender System for e-Commerce Applications

Authors: Ayat Yehia Hassan, Etimad Fadel, Nadine Akkari

PAGE 602 – 612

Paper 72: A Comprehensive Assessment Framework for Evaluating Adaptive Security and Privacy Solutions for IoT e-Health Applications

Authors: Waqas Aman, Fatima Najla Mohammed

PAGE 613 – 623

Paper 73: Enhanced Jaya Algorithm for Multi-objective Optimisation Problems

Authors: Rahaini Mohd Said, Roselina Sallehuddin, Nor Haizan Mohd Radzi, Wan Fahmn Faiz Wan Ali

PAGE 624 – 632

Paper 74: Research on the Academic Early Warning Model of Distance Education based on Student Behavior Data in the Context of COVID-19

Authors: Yi Qu, Zhiyuan Sun, Libin Liu

PAGE 633 – 642

Paper 75: Dynamic Polymorphism without Inheritance: Implications for Education

Authors: Ivaylo Donchev, Emilia Todorova

PAGE 643 – 649

Paper 76: Application of Training Load Prediction Model based on Improved BP Neural Network in Sports Training of Athletes

Authors: Lin Liu, Guannan Sheng

PAGE 650 – 657

Paper 77: Analyzing Multi-stage Reverse Osmosis Desalination Using Artificial Intelligence

Authors: Batiseba Tekle, Azmi Alazzam, Abdulwehab Ibrahim, Ghassan Malkawi, Abdulaziz Fares NajiMoqbel, Nissar Qureshi, Ahmed Hamadat, Filomento O. Corona Jr

PAGE 658 – 663

Paper 78: Educational Platform based on Smartphone to Increase Students' Interaction in Classroom

Authors: Mohamed Naser AlSubie, Omar Ben Bahri

PAGE 664 – 668

Paper 79: A Novel Architecture for Community-Sustained Cultural Mapping System

Authors: Chong Eng Tan, Sei Ping Lau, Siew Mooi Wong

PAGE 669 – 674

Paper 80: Research on Personalized Recommendation of High-Quality Academic Resources based on user Portrait

Authors: Jianhui Xu, Mustafa Man, Ily Amalina Ahmad Sabri, Guoyi Li, Chao Yang, Mingxue Jin

PAGE 675 – 683

Paper 81: An Inspection of Learning Management Systems on Persuasiveness of Interfaces and Persuasive Design: A Case in a Higher Learning Institution

Authors: Wan Nooraishya Wan Ahmad, Mohamad Hidir Mhd Salim, Ahmad Rizal Ahmad Rodzuan

PAGE 684 – 692

Paper 82: The Development of an Ontology for Information Retrieval about Ethnic Groups in Chiang Mai Province

Authors: Phichete Julrode, Thepchai Supnithi

PAGE 693 – 698

Paper 83: CoSiT: An Agent-based Tool for Training and Awareness to Fight the Covid-19 Spread

Authors: Henri-Joel Azemena, Franck-Anael K. Mbiaya, Selain K. Kasereka, Ho Tuong Vinh

PAGE 699 – 706

Paper 84: Parallel Hough Transform based on Object Dual and Pypm Library

Authors: Abdoulaye SERE, Moise OUEDRAOGO, Armand Kodjo ATIAMPO

PAGE 707 – 716

Paper 85: Prototyping a Mobile Application for Children with Dyscalculia in Primary Education using Augmented Reality

Authors: Misael Lazo-Amado, Leoncio Cueva-Ruiz, Laberiano Andrade-Arenas

PAGE 717 – 724

Paper 86: Adaptive Lane Keeping Assist for an Autonomous Vehicle based on Steering Fuzzy-PID Control in ROS

Authors: Hoang Tran Ngoc, Luyi-Da Quach

PAGE 725 – 731

Paper 87: Money Laundering Detection using Machine Learning and Deep Learning

Authors: Johrha Alotibi, Badriah Almutanni, Tahani Alsubait, Hosam Alhakami, Abdullah Baz

PAGE 732 – 738

Paper 88: Multi-Channel Speech Enhancement using a Minimum Variance Distortionless Response Beamformer based on Graph Convolutional Network

Authors: Nguyen Huu Binh, Duong Van Hai, Bui Tien Dat, Hoang Ngoc Chau, Nguyen Quoc Cuong

PAGE 739 – 747

Paper 89: Impact of Input Data Structure on Convolutional Neural Network Energy Prediction Model

Authors: Imen Toumia, Ahlem Ben Hassine

PAGE 748 – 757

Paper 90: Decode and Forward Coding Scheme for Cooperative Relay NOMA System with Cylindrical Array Transmitter

Authors: Samuel Tweneboah-Koduah, Emmanuel Ampoma Affum, Kingsford Sarkodie Obeng Kwakye, Owusu Agyeman Antwi

PAGE 758 – 767

Paper 91: A Decision Concept to Support House Hunting

Authors: Tanjim Mahmud, Dilshad Islam, Manoara Begum, Sudhakar Das, Lily Dey, Koushick Barua

PAGE 768 – 774

Paper 92: A Drone System with an Object Identification Algorithm for Tracking Dengue Disease

Authors: Diego Moran-Landa, Maria del Rosario Damian, Pedro Miguel Portillo Mendoza, Carlos Sotomayor-Beltran

PAGE 775 – 781

Paper 93: Analysis of the Intuitive Teleoperated System of the TxRob Multimodal Robot

Authors: Jeyson Carpio A, Samuel Luque C, Juan Chambi C, Jesus Talavera S

PAGE 782 – 788

Paper 94: Exploring Power Advantage of Binary Search: An Experimental Study

Authors: Muhammad Al-Hashimi, Naif Aljabri

PAGE 789 – 795

Paper 95: CertOracle: Enabling Long-term Self-Sovereign Certificates with Blockchain Oracles

Authors: Shaoxi Zou, Fa Jin, Yongdong Wu

PAGE 796 – 804

Paper 96: Evaluation of Online Machine Learning Algorithms for Electricity Theft Detection in Smart Grids

Authors: Ashraf Alkhrshesh, Mutaz A. B. Al-Tarawneh

PAGE 805 – 813

Paper 97: Artificial Intelligence for Automated Plant Species Identification: A Review

Authors: Khaoula Labrighli, Chouaib Moujahdi, Jalal El Oualidi, Laila Rhazi

PAGE 814 – 825

Paper 98: Arduino for Developing Problem-Solving and Computing Competencies in Children

Authors: Cristian Vidal-Silva, Claudia Jimenez-Quintana, Erika Madariaga-Garcia

PAGE 826 – 832

Paper 99: An Integrated Hardware Prototype for Monitoring Gas leaks, Fires, and Remote control via Mobile Application

Authors: Md. Ashiqur Rahman, Humayra Ahmed, Md. Mamun Hossain

PAGE 833 – 840

Paper 100: Performance Evaluation of Raspberry Pi as an IoT Edge Signal Processing Device for a Real-time Flash Flood Forecasting System

Authors: Aslinda Hassan, Haniza Nahar, Wahidah Md Shah, Azlianor Abd-Aziz, Sarah Afiqah Sahiran, Nazrulazhar Bahaman, Mohd Riduan Ahmad, Isredza Rahmi A. Hamid, Muhammad Abu Bakar Sidik

PAGE 841 – 848

Paper 101: Decentralized Payment Aggregator: Hyperledger Fabric

Authors: Md. Al-Amin, Khondoker Shahrina, Rubyet Hossain, Debashish Sarker, Sumya Sultana Meem

PAGE 849 – 857

Paper 102: Efficient HPC and Energy-Aware Proactive Dynamic VM Consolidation in Cloud Computing

Authors: Rukshanda Kamran, Ali A. El-Moursy, Amany Abdelsamea

PAGE 858 – 869

Paper 103: Triple SVM Integrated with Enhanced Random Region Segmentation for Classification of Lung Tumors

Authors: Sukruth Gowda M A, A Jayachandran

PAGE 870 – 877

Paper 104: Optimized Automatic Course Timetabling Service Architecture for Integration with Vendor Management Systems

Authors: Marwah M. Alansari

PAGE 878 – 890

Paper 105: Cryptocurrency Price Prediction using Forecasting and Sentiment Analysis

Authors: Shaimaa Alghamdi, Sara Alqethami, Tahani Alsubait, Hosam Alhakami

PAGE 891 – 900

Paper 106: The Multi-Objective Design of Laminated Structure with Non-Dominated Sorting Genetic Algorithm

Authors: Huiyao Zhang, Yuxiao Wang, Fangmeng Zeng

PAGE 901 – 906

Paper 107: From Monolith to Microservices: A Semi-Automated Approach for Legacy to Modern Architecture Transition using Static Analysis

Authors: Mohd Hafeez Osman, Cheikh Saadbouh, Khaironi Yatim Sharif, Novia Admodisastro, Muhammad Hadri Basri

PAGE 907 – 916

Paper 108: SDN Architecture for Smart Homes Security with Machine Learning and Deep Learning

Authors: Wesam Abdulrhman Alonazi, Hedi HAMD, Nesrine A. Azim, A. A. Abd El-Aziz

PAGE 917 – 927

Paper 109: Skin Melanoma Classification from Dermoscopy Images using ANU-Net Technique

Authors: Vankayalapati Radhika, B. Sai Chandana

PAGE 928 – 938

Paper 110: Method for Determination of Tealeaf Plucking Date with Cumulative Air Temperature: CAT and Photosynthetically Active Radiation: PAR

Authors: Kohei Arai, Yoshiko Hokazono

PAGE 939 – 944

Paper 111: Remote Monitoring Solution for Cardiovascular Diseases based on Internet of Things and PLX-DAQ add-in

Authors: Jeanne Roux NGO BILONG, Yao Gaspard Magnificat BOSSOU, Adam Ismael Paco SIE, Gervais MENDY, Cheikhane SEYED

PAGE 945 – 951

Paper 112: Anomaly Detection in Video Surveillance using SlowFast Resnet-50

Authors: Mahasweta Joshi, Jitendra Chaudhari

PAGE 952 – 956

Paper 113: Address Pattern Recognition Flash Translation Layer for Quadruple-level cell NAND-based Smart Devices

Authors: Se Jin Kwon

PAGE 957 – 960

Paper 114: Hybrid Deep Learning Signature based Correlation Filter for Vehicle Tracking in Presence of Clutters and Occlusion

Authors: Shobha B. S, Deepu. R

PAGE 961 – 969

Paper 115: Improving Slope Stability in Open Cast Mines via Machine Learning based IoT Framework

Authors: Sameer Kumar Das, Subhendu Kumar Pani, Abhaya Kumar Samal, Sasmita Padhy, Sachikanta Dash, Singam Jayanthu

PAGE 970 – 977

Paper 116: Cross-Event User Reaction Prediction on a Social Network Platform

Authors: Pramod Bide, Sudhir Dhage

PAGE 978 – 987

Hand Motion Estimation using Super-Resolution of Multipoint Surface Electromyogram by Deep Learning

Keigo FUKUSHIMA, Yoshiaki YASUMURA
Graduate School of Engineering and Science
Shibaura Institute of Technology
Tokyo, Japan

Abstract—This paper proposes a method for hand motion estimation using super-resolution of multipoint surface electromyogram for prosthetic hands. In general, obtaining more EMGs (ElectroMyoGraphy) improves the accuracy of hand motion estimation, but it is costly and hard to use. Therefore, this method improves the accuracy of hand motion estimation by estimating a large number of EMG signals from a small number of EMG signals using super-resolution. This super-resolution is achieved by learning the relationship between few and many myoelectric signals using a deep neural network. Then, hand motions are estimated from the high-resolution signal using a deep neural network. Experiments using actual EMG signals show that the proposed method improves the accuracy of hand motion estimation.

Keywords—Hand motion estimation; super-resolution; deep neural network; prosthetic hand; electromyography

I. INTRODUCTION

Today, many people utilize prosthetic hands in their daily lives due to accidents or congenital disabilities. Myoelectric prostheses record the electrical signals on the skin surface when muscles are moved, and the prosthetic hand moves based on these signals. This allows for intuitive movement with few restrictions on posture.

As described above, myoelectric prostheses are highly useful, but they have some problems. The prosthetic hand can be manipulated by the wearer's intention, though it is difficult for the wearer to perform all of the activities of daily living. To enable more complex hand motions, the accuracy of electromyographic analysis requires improvement. For this purpose, multipoint surface electromyography is useful [1], [2]. Multipoint surface electromyography is a measurement method of muscle movement using a grid of electrodes on the skin surface. This allows us to measure more detailed temporal and spatial myoelectric information.

Jiangcheng et al. placed 128 electrode channels on the upper arm and classified 27 gestures with 95.3% accuracy [3]. Weijie et al. also showed that a larger number of sensors results in a higher percentage of correct gestures [4]. However, increasing the number of electrodes makes mounting more difficult and electrode costs higher. The number of electrodes needs to be reduced to make it easier to use the prosthetic hand.

In order to operate a prosthetic hand with fewer electrodes, we propose a method to improve prosthetic hand motion by increasing myoelectric data with super-resolution technology. The objective of this study is to accurately estimate hand motion from fewer EMG signals. This method estimates multipoint surface electromyograms from fewer electrodes and operates the prosthetic hand more accurately based on them. For this estimation, a convolutional neural network, which is widely used in image recognition, is used for super-resolution of electromyograms and estimation of hand motions. Super-resolution is a technique to obtain a high-resolution output signal from a low-resolution input signal. This method uses deep learning to learn the relationship between low-resolution and high-resolution signals to create a higher resolution.

II. RELATED WORKS

Since many people use prosthetic hands in their daily lives, many studies have tried to create better prosthetic hands [5]-[9]. A myoelectric prosthetic hand uses the electrical signals generated on the surface of the skin during muscle movement to operate a robotic hand. Myoelectric prosthetics are more useful than other prosthetics, but there are some problems. Myoelectric prosthetics allow some movements, but complex movements are difficult. To enable complex movements, it is necessary to measure many myoelectric signals and estimate movements from these signals.

Hudgins et al. use the multilayer perceptron to identify four forearm movements from myoelectric signals [1]. Ali et al. used a convolutional neural network to identify 10 hand motions from myoelectric signals acquired at 8000 Hz using six-channel electrodes and 0.15 seconds of myoelectric signals as input [2]. This paper shows that with the appropriate hyper parameters and network structure, it is possible to estimate with more than 80% accuracy for all movements. However, the accuracy needs to be further improved for actual use of the prosthetic hand.

Jiangcheng et al. placed 128 electrode channels on the upper arm and classified 27 gestures with 95.3% accuracy [3]. Weijie et al. also showed that the correctness rate of a gesture increases with the number of sensors [4]. Thus, increasing the number of sensors can improve the accuracy of hand motion estimation. However, increasing the number of sensors makes wearing a prosthetic hand more difficult and increases the cost of the

prosthetic hand. For this reason, a method that enables accurate hand motion estimation with fewer sensors is needed.

Therefore, this paper proposes a method that enables accurate hand estimation from fewer sensors. For accurate hand motion estimation, this method uses super-resolution to increase the number of inputs without increasing the number of sensors. This method can be as effective as using many sensors, because super-resolution can generate more input signals from fewer inputs.

III. HAND MOTION ESTIMATION USING SUPER-RESOLUTION

A. Overview

Fig. 1 shows an overview of the proposed method. The inputs are multiple myoelectric signals. These signals are input to a deep neural network for super-resolution, and higher resolution signals are output. This neural network enables super-resolution by learning the relationship between signals at fewer points and those at more points. The super-resolved signals are then input to a deep neural network for hand motion estimation, and the estimation results are output. The estimated result is a class of hand motions.

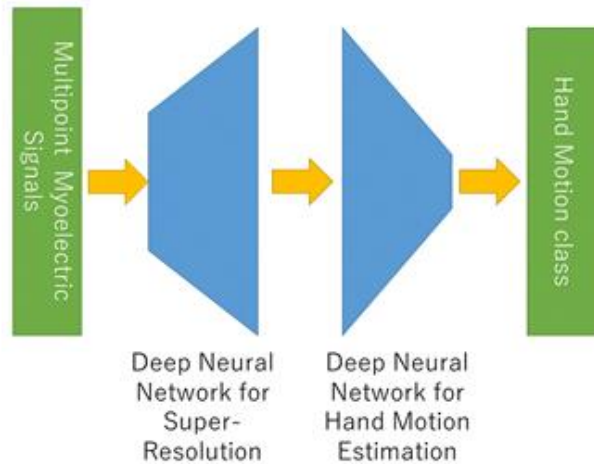


Fig. 1. Overview of the Proposed Method.

B. Super-Resolution for Multiple Myoelectric Signals

Super-resolution has been actively studied in the field of image processing [10]-[15]. Super-resolution in image processing generates a high-resolution image from a low-resolution image. In this study, this technique is used to obtain high-resolution myoelectric signals. Here, super-resolution uses the deep neural network shown in Fig. 2. Input is four-channel 512-sample EMG, output is 16-channel 512-sample EMG. The abbreviations in Fig. 2 mean the following.

- Conv: convolution layer

- PReLU: an activation function called parametric rectified linear unit [16].
- BN: batch normalization.
- Skip connection: a connection between two layers that passes information between them without transformation. Both skipped and un-skipped informations are available.
- Pixel Shuffler: It rearranges each pixel in the input feature map to output a high-resolution feature map [17].
- Residual block: a skip-connected block that learns a residual function by reference to the inputs of the layer, rather than learning a function that is unreferenced.

This neural network is based on SR ResNet [11]. SR ResNet keeps the height and width of the inputs the same size in the middle layer. In contrast, this method compresses the height by a quarter in the middle layer by convolution processing on the input. This is because both the height and width of the input are enlarged when using the Pixel Shuffler. By compressing the input data in advance so that the restored height is the same as the input data, it is possible to achieve more accurate super-resolution than with convolution or pooling processing. In Fig. 2, the output channel rows are replaced. This process is to make it easier to recover the original waveforms by super-resolution processing. The channel sequence is restored before input to the hand motion estimation network.

C. Hand Motion Estimation

Hand motion estimation uses deep neural networks. Fig. 3 shows a deep neural network for the hand motion classification. The input is a 16-channel 512-sample EMG, and the output is a label indicating the gesture. The abbreviations in Fig. 3 are the same as those used in Fig. 2. Max pool means a max pooling layer. Dropout is a method of preventing overfitting by inactivating a certain percentage of nodes while training a neural network [18]. The flatten layer converts the feature map into a one-dimensional vector. The softmax function transforms multiple output values into a sum of 1.0.

The proposed method assumes that hand motions are estimated every 0.25 seconds. A network of electromyograms with four input channels and 512 samples is also created for validation. Côté-Allard et al. [19] performed channel-by-channel convolution for hand motion estimation using multi-channel EMG. This method transforms 16 input channels with 512 sample inputs into 128 channels with a height of 64 and a width of 128 and applies convolution processing. This allows learning of numerical value changes over various times and channels by convolutional processing to achieve high accuracy.

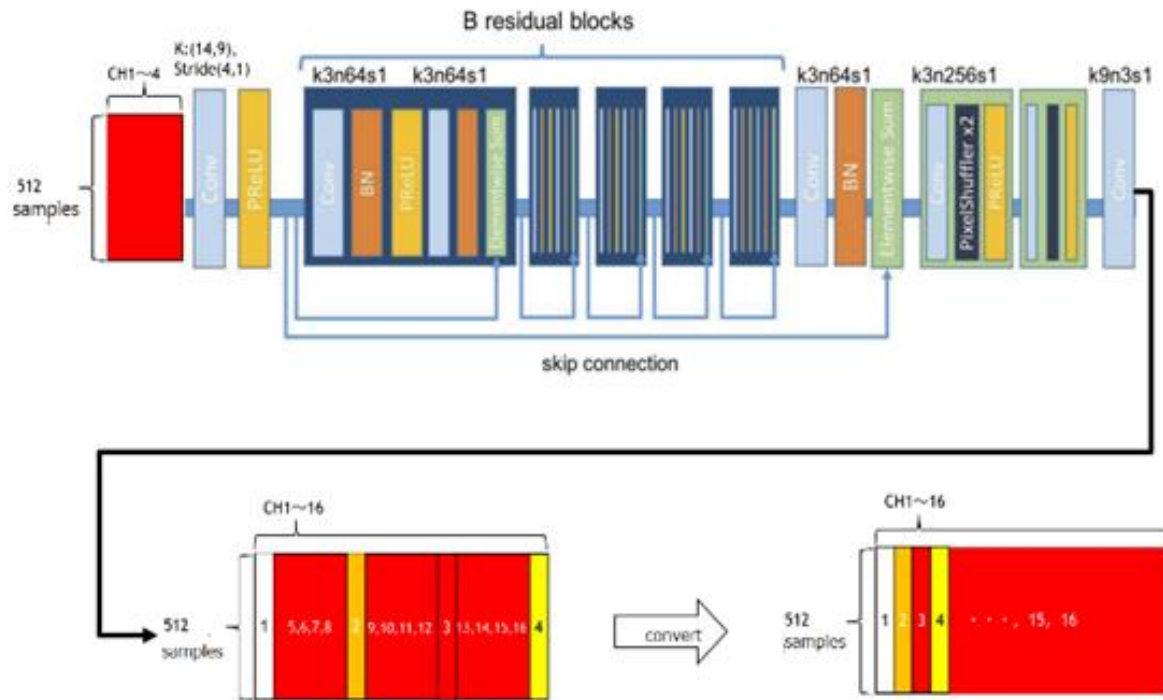


Fig. 2. Deep Neural Network for Super-Resolution.

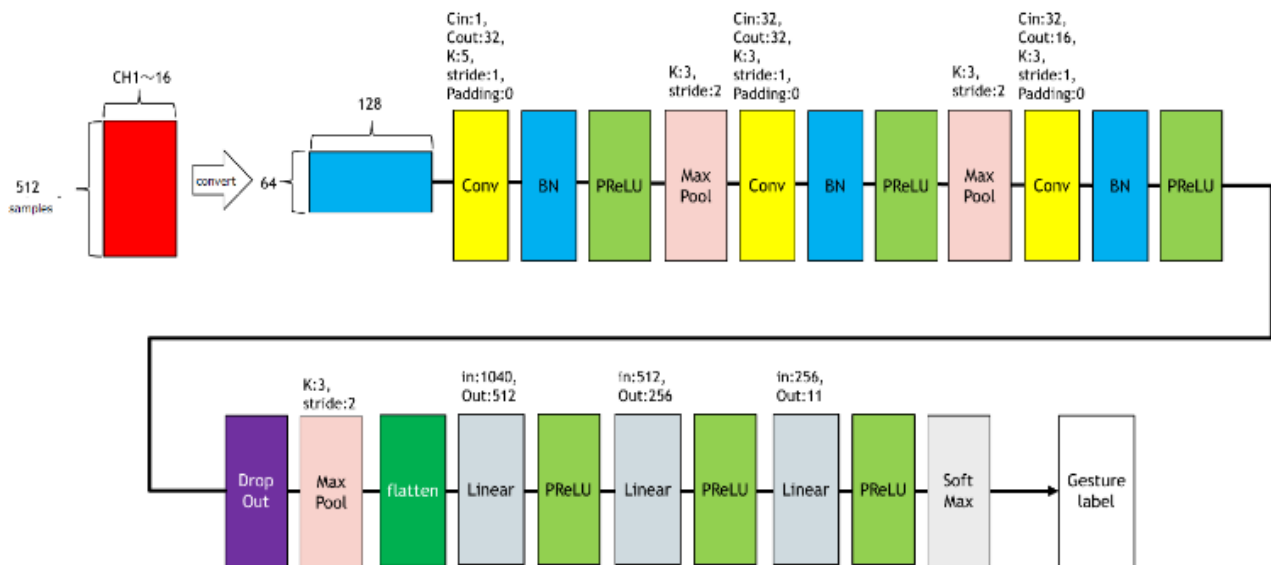


Fig. 3. Deep Neural Network for Hand Motion Estimation.

IV. EXPERIMENTS

This section describes evaluation experiments using actual data to evaluate the effectiveness of the proposed method.

A. Dataset

The dataset in this study was acquired using the following devices. Fig. 4 shows the actual device used for this experiment. This device connects a myoelectric amplifier to a microcontroller board and sends its output to a PC. The electrode is a wet disposable ECG electrode (MSGLT-04). The electrodes were placed as shown in Fig. 5, taking into

consideration the hand motions and the muscle arrangement. The reference electrode was placed at the elbow. The device was used to obtain myoelectric signals at 16 locations. This study uses the gestures in Fig. 6, as in the study by Côté-Allard et al. [19]. Each gesture is performed from a state of relaxation, and the device acquires EMG for 10 seconds during the gesture. The training data is the first nine seconds of data, and the remaining one second of data is used as the test data. To compensate for the small amount of data, the method of Lingfeng et al [20] was used. This produced 197131 training data and 16907 test data.

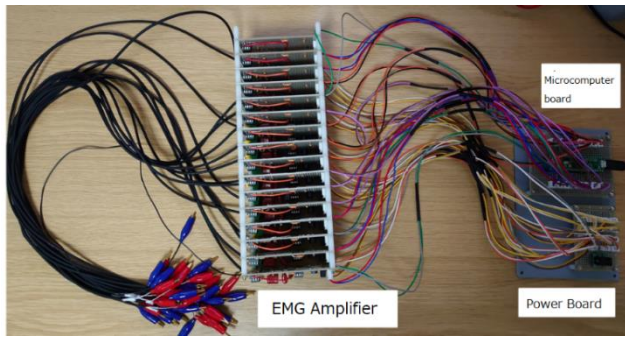


Fig. 4. EMG Measurement Device.

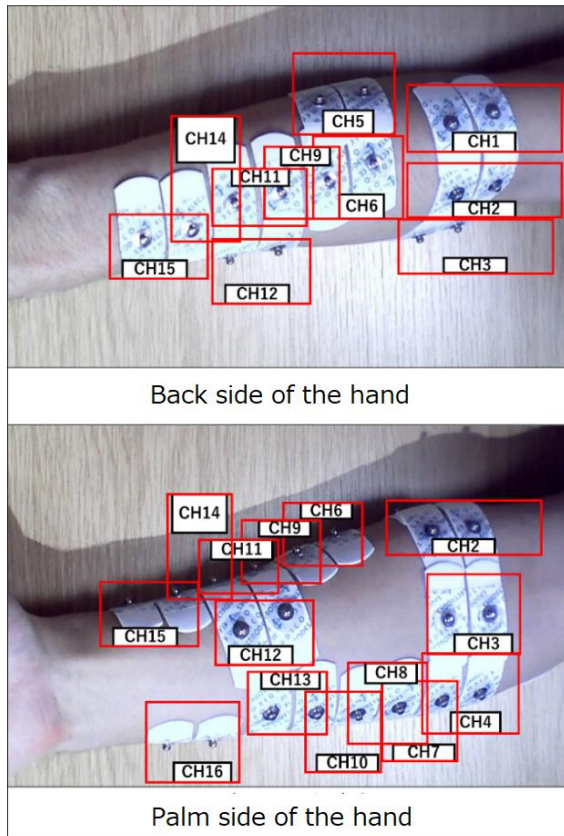


Fig. 5. Electrode Setting.

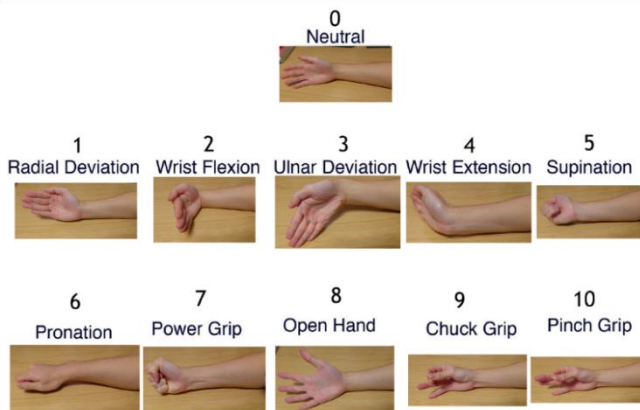


Fig. 6. Gesture Class.

B. Experiment of Super-Resolution

Here, the effect of super-resolution of myoelectric signals is verified using actual data. In this experiment, 4-channel 512-sample, EMG is the input, and the corresponding 16-channel 512-sample EMG is the supervised data. The mean squared error (MSE) was used as the loss function. The MSE is expressed in Equation (1).

$$MSE = \frac{1}{N} \sum_{i=1}^N (y - t)^2 \quad (1)$$

N is the number of samples, and y and t are the output and supervised data, respectively. PSNR, which is also used in general image super-resolution, is used as a measure of the difference between the output and supervised data. PSNR is expressed by Equation (2). The smaller the difference between the output and supervised data, the larger the PSNR. Thus, the larger the PSNR, the better the output.

$$PSNR = 10 \log_{10} \left(\frac{1}{MSE} \right) \quad (2)$$

Using actual data, an effect of super-resolution of myoelectric signals was evaluated in an experiment. Experimental results of super-resolution learning on test data are shown in Fig. 7. Fig. 7 shows the variation of PSNR with the number of epochs. As with deep learning in general, PSNR increases as the epoch increases. This indicates that the accuracy of super-resolution improved without overfitting.

C. Experiment of Hand Motion Estimation

Here we examine the effectiveness of hand motion estimation using super-resolution. In this experiment, a 4-channel input, a 16-channel input, and a 4-channel input increased to 16 channels by super-resolution are compared. Fig. 8 compares the experimental results for each of these inputs. As noted in previous studies, 16 channels performed better than 4 channels on all evaluation items. This means that the accuracy of hand motion estimation is improved when the number of input EMG signals is large. The proposed method using super-resolution achieved better results than the 4-channel method in all evaluation items. This is because the proposed method increases the number of inputs from 4 channels to 16 channels. However, the proposed method was not able to reach 16 channels in all indicators. It is a reasonable result because the proposed method increases the number of channels to 16 with super-resolution, but it is only an estimated value.

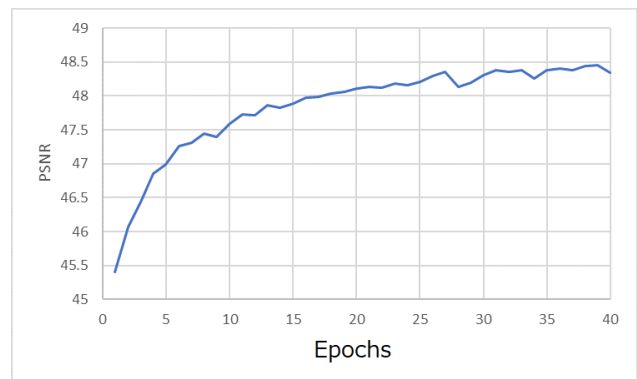


Fig. 7. PSNR for Number of Epochs.

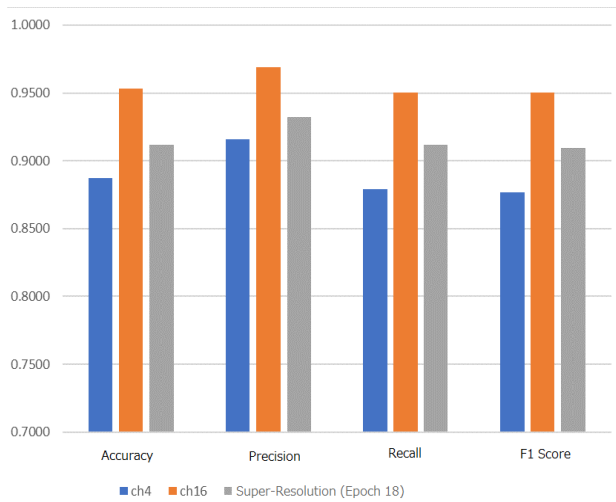


Fig. 8. Results of Hand Motion Estimation.

Based on the above experimental results, the proposed method is able to increase the accuracy of hand motion estimation even though the input is the same as the 4-channel method. This means that the knowledge acquired by the learning of super-resolution increased the accuracy of the estimation. Previous methods have increased accuracy by increasing the number of sensor inputs, however, the proposed method shows that accuracy can be increased without increasing the number of sensors.

Fig. 9 to 11 show the confusion matrices of the 4-channel, 16-channel, and proposed methods, respectively. Fig. 10 shows that the 4-channel input had more misclassifications than the other methods. For example, more of the correct label 8's were estimated as label 9, and more of the correct label 10's were estimated as label 9. The proposed method was able to classify many samples more accurately, although not as accurately as the 16-channel method. Labels 8, 9, and 10 are particularly misclassified, because these motions are close muscular motions.

The time required for hand motion estimation and super-resolution for 16907 EMGs, the test data, was 750 and 398 seconds, respectively. The time per EMG was $(750 + 398) / 16907 \approx 0.0680$ seconds. Since the proposed method is designed to estimate hand motions every 0.25 seconds, the estimation speed is considered fast enough for practical use.

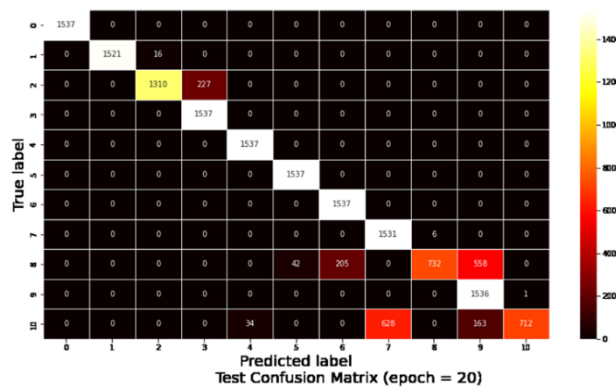


Fig. 9. Confusion Matrix of 4 Channel Input.

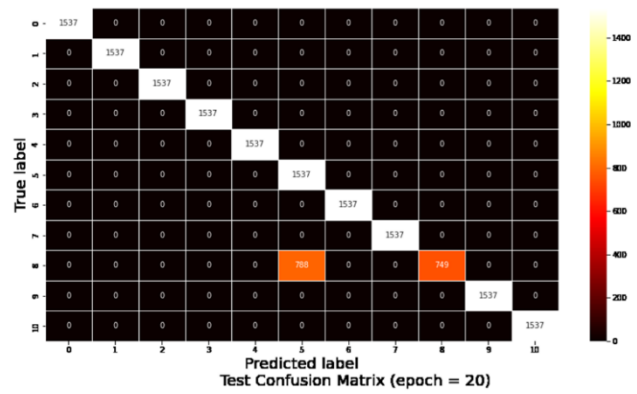


Fig. 10. Confusion Matrix of 16 Channel Input.

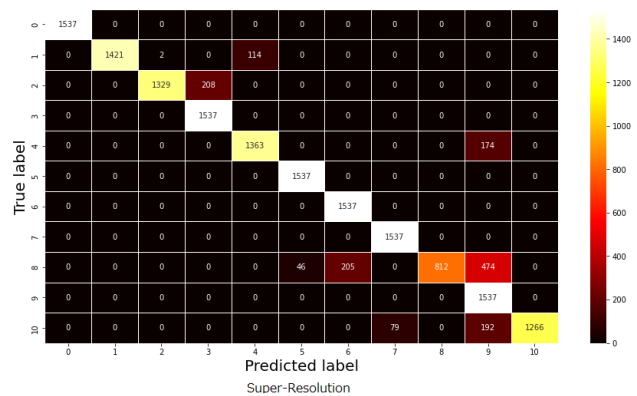


Fig. 11. Confusion Matrix of the Proposed Method.

V. CONCLUSION

In this paper, we proposed a method for estimating hand motions using super-resolution of multi-point surface electromyograms. The method uses a super-resolution network to obtain the relationship between EMGs with a small number of electrodes and those with a larger number of electrodes and estimates unknown high-resolution EMGs from new low-resolution EMGs. By inputting the estimated high-resolution EMG to the hand motion estimation network, hand motion estimation can be performed with fewer electrodes without loss of accuracy.

Hand motion estimation using super-resolution of multi-point surface EMG showed higher performance than hand motion estimation using four channels. This shows that super-resolution of electromyograms is available. This method may be used to reduce the number of electrodes in other EMG techniques as well. The accuracy was lower for gestures with the same moving muscles compared to other gestures. In this paper, the accuracy of super-resolution was evaluated using PSNR, which is used in super-resolution of general images. However, there was no relationship between the PSNR value and the results of hand motion estimation using electromyogram after super-resolution.

A future work is to reduce the number of samples per unit time of the input in super-resolution. Because this method focused on reducing the number of electrodes, the number of samples per unit time of the input was the same as that of the output. If the number of samples per unit time can be reduced,

the devices used for EMG acquisition such as microcontroller and amplifier would become less expensive.

REFERENCES

- [1] HUDGINS, Bernard; PARKER, Philip; SCOTT, Robert N., A new strategy for multifunction myoelectric control. *IEEE transactions on biomedical engineering*, 1993, 40.1: 82-94.
- [2] Ali Raza Asif, et al., Performance evaluation of convolutional neural network for hand gesture recognition using EMG. *Sensors*, 2020, 20.6: 1642.
- [3] Chen, J.; Bi, S.; Zhang, G.; Cao, G. High-Density Surface EMG-Based Gesture Recognition Using a 3D Convolutional Neural Network. *Sensors* 2020, 20, 1201.
- [4] KE, Weijie, et al. Intersected EMG heatmaps and deep learning based gesture recognition. In: *Proceedings of the 2020 12th International Conference on Machine Learning and Computing*. 2020. p. 73-78.
- [5] Lu, H.; Zou, Z.; Wu, X.; Shi, C.; Liu, Y.; Xiao, J. Biomimetic Prosthetic Hand Enabled by Liquid Crystal Elastomer Tendons. *Micromachines* 2021, 12, 736.
- [6] Triwiyanto, T.; Caesarendra, W.; Purnomo, M.H.; Sulowicz, M.; Wisana, I.D.G.H.; Titisari, D.; Lamidi, L.; Rismayani, R. Embedded Machine Learning Using a Multi-Thread Algorithm on a Raspberry Pi Platform to Improve Prosthetic Hand Performance. *Micromachines* 2022, 13, 191.
- [7] L. Vargas, H. Huang, Y. Zhu, D. Kamper and X. Hu, "Resembled Tactile Feedback for Object Recognition Using a Prosthetic Hand," in *IEEE Robotics and Automation Letters*, vol. 7, no. 4, Oct. 2022, pp. 10977-10984.
- [8] Wang, S.; Zheng, J.; Zheng, B.; Jiang, X. Phase-Based Grasp Classification for Prosthetic Hand Control Using sEMG. *Biosensors* 2022, 12, 57.
- [9] L. Vargas, H. Huang, Y. Zhu and X. Hu, Object Recognition via Evoked Sensory Feedback during Control of a Prosthetic Hand, in *IEEE Robotics and Automation Letters*, vol. 7, no. 1, Jan. 2022, pp. 207-214.
- [10] DONG, Chao; LOY, Chen Change; TANG, Xiaou. Accelerating the super-resolution convolutional neural network. In: *European conference on computer vision*. Springer, Cham, 2016. p. 391-407.
- [11] LEDIG, Christian, et al. Photo-realistic single image super-resolution using a generative adversarial network. In: *Proceedings of the IEEE conference on computer vision and pattern recognition*. 2017. p. 4681-4690.
- [12] C. Saharia, J. Ho, W. Chan, T. Salimans, D. J. Fleet and M. Norouzi, "Image Super-Resolution Via Iterative Refinement," in *IEEE Transactions on Pattern Analysis and Machine Intelligence*, 2022doi: 10.1109/TPAMI.2022.3204461.
- [13] Junjun Jiang, Chenyang Wang, Xianming Liu, and Jiayi Ma. 2021. Deep Learning-based Face Super-resolution: A Survey. *ACM Comput. Surv.* 55, 1, Article 13 (January 2023), 36 pages.
- [14] Honggang Chen, Xiaohai He, Linbo Qing, Yuanyuan Wu, Chao Ren, Ray E. Sheriff, Ce Zhu, Real-world single image super-resolution: A brief review, *Information Fusion*, Volume 79, 2022, Pages 124-145.
- [15] Yiqun Mei, Yuchen Fan, Yuqian Zhou; *Proceedings of the IEEE/CVF Conference on Computer Vision and Pattern Recognition (CVPR)*, 2021, pp. 3517-3526.
- [16] HE, Kaiming, et al. Delving deep into rectifiers: Surpassing human-level performance on imagenet classification. In: *Proceedings of the IEEE international conference on computer vision*. 2015. p. 1026-1034.
- [17] SHI, Wenzhe, et al. Real-time single image and video super-resolution using an efficient sub-pixel convolutional neural network. In: *Proceedings of the IEEE conference on computer vision and pattern recognition*. 2016. p. 1874-1883.
- [18] SRIVASTAVA, N.; HINTON, G.; KRIZHEVSKY, A. Dropout: A Simple Way to Prevent Neural Networks from Overfitting. *Journal of Machine Learning Research*. *Journal of Machine Learning Research*, 1929, 1929-1958.
- [19] Côté-Allard, Ulysse, et al. "Interpreting deep learning features for myoelectric control: A comparison with handcrafted features." *Frontiers in bioengineering and biotechnology* 8 (2020): 158.
- [20] Xu, L., Chen, X., Cao, S., Zhang, X., Chen, X., Feasibility study of advanced neural networks applied to sEMG-based force estimation. *Sensors*, 2018, 18(10), 3226.

IoTCID: A Dynamic Detection Technology for Command Injection Vulnerabilities in IoT Devices

Hao Chen¹, Jinxin Ma², Baojiang Cui³, Junsong Fu⁴

School of Cyberspace Security, Beijing University of Posts and Telecommunications, Beijing, China^{1,3,4}
China Information Technology Security Evaluation Center, Beijing, China²

Abstract—The pervasiveness of IoT devices has brought us convenience as well as the risks of security vulnerabilities. However, traditional device vulnerability detection methods cannot efficiently detect command injection vulnerabilities due to heavy execution overheads or false positives and false negatives. Therefore, we propose a novel dynamic detection solution, IoTCID. First, it generates constrained models by parsing the front-end files of the IoT device, and a static binary analysis is performed towards the back-end programs to locate the interface processing function. Then, it utilizes a fuzzing method based on the feedback from Distance Function, which selects high-quality samples through various scheduling strategies. Finally, with the help of the probe code, it compares the parameter of potential risk functions with samples to confirm the command injection vulnerabilities. We implement a prototype of IoTCID and evaluate it on real-world IoT devices from three vendors and confirm six vulnerabilities. It shows that IoTCID are effective in discovering command injection vulnerabilities in IoT devices.

Keywords—Firmware vulnerability mining; command injection; dynamic detection

I. INTRODUCTION

With the development of the Internet and information technologies, IoT devices are extensively used in our life [1], and attacks against IoT devices have been emerged in recent years [2]. The reason is that web interfaces are usually exposed to users to manage the devices, which contain exploitable vulnerabilities.

There are some unique features of the threats caused by vulnerabilities in IoT devices compared to which in PCs or in servers. For example, most existing security mechanism or antivirus products are not available in IoT devices due to the limit of cost and power of IoT devices, which makes it easier to perform further exploits towards certain vulnerabilities [3]. Moreover, one vulnerability may have huge influence on thousands of devices, for the devices from the same vendor usually have similar firmware [4].

Command Injection Vulnerability is one of the most effective and commonest vulnerabilities in IoT devices [14]. Attackers can exploit the target IoT devices through this vulnerability by injecting additional commands into the program. Moreover, the system commands provided by attackers are usually executed with the highest authority in IoT devices.

However, due to the complexity and the specificity of the IoT devices, existing tools cannot effectively detect Command

Injection Vulnerability. For example, Dynamic analysis tools, like fuzzing [5, 7, 9], requires valid communication formats to generate fuzzing samples and can only reach a small portion of all the provided interfaces while static analysis tools, like KARONTE [11] and SaTC [12], cannot efficiently generate interaction paradigms between the front-end files and back-end programs, leading to a lot of false positives which requires further manual check.

Therefore, to ensure the safety and reliability of IoT devices, it is urgent to develop security analysis technology towards IoT devices. In this paper, focusing on Command Injection Vulnerability, we propose a novel dynamic detection technology, IoTCID, to effectively detect command injection vulnerabilities in IoT devices.

Inspired by SaTC [12], in order to generate samples in valid communication formats and to cover interfaces as many as we can, IoTCID first performs a logic analysis to the front-end files which interact with the back-end programs to generate constrained models. It utilizes a novel scheduling strategies based on Distance Function to improve the efficiency of command injection vulnerability detection. We design and implement a prototype of IoTCID and evaluate its efficacy through a set of experiments based on real-world IoT devices and confirm six command injection vulnerabilities. It shows that IoTCID is effective in discovering command injection vulnerabilities in IoT devices.

In summary, our major contributions are as follows:

- 1) We present a dynamic detection technique towards Command Injection Vulnerabilities based on the logic analysis to front-end files and intelligent feedbacks from the back-end programs.
- 2) We design and implement a constrained model generation technique based on the logic analysis to front-end files, providing a valid format for the generation of fuzzing samples.
- 3) We design and implement scheduling strategies based on Distance Function feedback to concentrate resources on the fuzzing samples that may cover risk functions in back-end programs.

The rest of the paper is organized as follows. We first summarize related work in recent years in Section II. We then present an overview of IoTCID, and give a detailed description on design and implementation of each component of IoTCID in Section III. We demonstrate the efficacy of IoTCID through a

set of experiments and present a vulnerability detection case in Section IV. At last, Section V concludes this paper and show the future work of IoTCID.

II. RELATED WORK

In recent security research on IoT devices, fuzzing is the most discussed technique. The general process of fuzzing is to detect the state of the testing program and guide the generation of fuzzing samples with provided feedbacks.

Chen J et al. propose and implement a generation-based firmware fuzzing method, IoTFuzzer[5], which detects vulnerabilities related to memory in IoT devices by analyzing the corresponding Android application. In view of the shortcomings of IoTFuzzer, DIANE[6] proposed a new method for generating fuzzing samples, which is based on the target fuzzing points in the APP that are located before data conversion and after input validation. However, both IoTFuzzer and DIANE conduct black-box fuzzing directly on real devices, limited to providing guidance and feedbacks based on the testing samples.

Zhang Y et al. propose SRFuzzer[7], which mutates the collected network traffic and detects the state of the fuzzing process according to the response-based monitor, routing-based monitor, and signal-based monitor. However, it would be difficult for SRFuzzer to cover the corresponding interface functions without the network traffic in advance.

FirmFuzz[8] runs the target firmware through simulation and collects payloads of different vulnerabilities for fuzzing tests. Zheng Y et al. propose FIRM-AFL[9] to enhance process simulation to fuzz the IoT firmware. However, these methods are all subject to valid inputs.

Although command injection is a common and powerful threat, related detection is less discussed in IoT security research.

Commix[10] is a tool that can automatically detect and exploit command injection vulnerability towards web applications. It sends a data packet attached with a command injection attack vector, and compares the response of the web application with the expected result to determine whether there is a command injection vulnerability. However, Commix needs to collect network traffic in advance, and it makes determine according to the response of the target. When the network delay cannot be guaranteed, there will be a certain false positive, which cannot intuitively reflect the location of the command injection vulnerability.

KARONTE[11], a static analysis framework for embedded firmware, which can detect vulnerabilities caused by its communication by modeling and tracking the interactions between binary programs. However, KARONTE cannot effectively detect command injection vulnerabilities because it does not track the data flow from input entry points to system-like functions. Aiming at the shortcomings of KARONTE, Chen L et al. propose a novel static taint technique, SaTC[12],

to effectively detect security vulnerabilities in web services provided by embedded devices. It mainly locates the communication process between front-end files and back-end programs based on the strings used in the front-end web interface, and applies targeted data flow analysis to accurately detect possible vulnerabilities. However, SaTC uses a clustering algorithm to extract the strings interacting between front-end files and back-end programs, and cannot generate an effective input model for the web interface. Besides, it requires additional manual analysis to confirm the result and eliminate false positives.

In a word, it remains problems in the use of the above detection technologies towards IoT devices. For example, the fuzzing detection technology mainly focuses on memory corruption vulnerabilities, and are subject to the input of valid format while static analysis tools may have low detection efficiency due to excessive analysis. Therefore, aiming at the command injection vulnerability of IoT devices, based on the logic analysis to front-end files and intelligent feedbacks, we propose a dynamic detection model IoTCID, which makes up for the shortcomings of the current command injection detection technology for IoT devices and improves the efficiency and accuracy of command injection vulnerability detection.

III. METHODOLOGY

Generally, IoT devices provide user management interfaces, which are mainly composed of front-end files and back-end programs. Front-end files include HTML, Javascript while back-end programs are generally executable binary files. IoTCID is proposed based on the workflow of the front-end files and back-end programs, as Fig. 1 provides the overview of IoTCID. It first generates constrained models by parsing the front-end files of the IoT device, and then performs binary static analysis on the back-end programs to locate the interface processing function. Then, IoTCID selects high-quality fuzzing samples according to various scheduling strategies based on the feedback from Distance Function. The selected samples are given more mutation time slices and priorities, which makes concentration on the interface process functions that may exist command injection vulnerabilities. Finally, IoTCID confirms the command injection vulnerabilities combined with the fuzzing samples and the parameters of risk functions detected by the probe code.

A. Constrained Model Generation

We propose a technology of constrained model generation based on the logic analysis to front-end files. Through syntax analysis, it generates a corresponding abstract syntax tree according to the front-end file, and extracts the variable reference chains of the abstract syntax tree as well as the variables during the interaction process between the front-end files and the back-end programs. The generated models are used as the format of the fuzzing samples, mainly including the URL, the request type, and the request keywords.

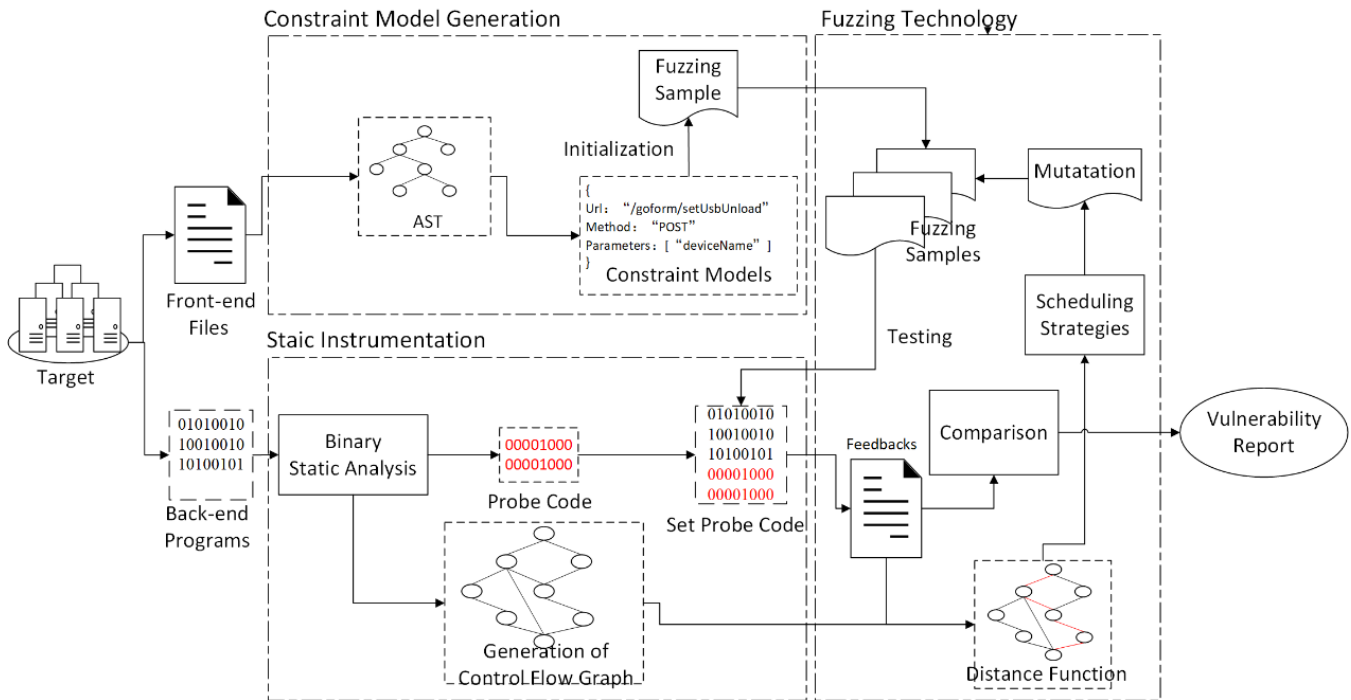


Fig. 1. Structure of IoTCID.

Algorithm 1 shows the analysis process of the function call and variable reference chain of the front-end files, where funcNode is the result of syntax analysis and varName is the parameter of the funcNode. During the analysis, there are two types of function parameters: one of which is directly passed in text value while the other is indirectly passed in variable name. For the direct one, IoTCID uses the regular expression to match and obtain the text value of the parameter. For the indirect one, the text value can be extracted through a recursive method in related function scope.

Algorithm 1: Analysis of Parameters during Interaction

```
Input: funcNode && varNames  
Output: Constrained models  
1. function GET_VALUE(funcNode, varName)  
2.   param ← []  
3.   if varName.type == "Literal" then  
4.     param.append(ANALYSIS(  
5.       funcNode.expression, varName));  
6.   return param  
7.   else  
8.     funcNode = FIND_PARENT(funcNode);  
9.     if funcNode == "" then  
10.      return []  
11.    end if  
12.    GET_VALUE (funcNode, varName);  
13.  end if  
14. end function
```

B. Static Instrumentation

IoTCID obtains the information that may trigger the command injection vulnerability function in the back-end programs through binary static analysis, and sets the probe code to obtain the performing state of the fuzzing samples. We implement a static analysis technique for back-end binary programs. It obtains information about risk functions such as

execve and system which may trigger command injection vulnerabilities. Therefore, we can record the performing paths of fuzzing samples based on binary static instrumentation technology and control flow analysis of the back-end programs.

1) *Acquisition of risk function:* The purpose of acquiring the potential dangerous function is to locate the interface in the back-end programs, which processes the requests from the front-end files according to the URL extracted in Part A, Section III, and construct its control. flow graph. We further obtain the necessary data by analyzing the header of back-end binary programs, the entry point and relevant segments. Finally, we use Capstone [13] to disassemble the code to obtain the information of the target function and related code blocks as well as building a control flow graph.

2) *Generation of probe code:* The probe code collects the performing state of fuzzing samples during the execution process and provides feedbacks to the monitor system. Based on the control flow graph of the risk functions, we set the probe code to provide information feedback of the basic blocks, including the address information and the parameters of the risk functions. The trampoline mechanism is used during the generation of probe code to make association between the set point and the risk functions, and provides the necessary environment preparation for the normal execution of the original program.

C. Fuzzing Technology

We apply distance function to the fuzzing technology to select high-quality fuzzing samples according to various scheduling strategies. While IoTCID is sending fuzzing samples to the back-end program for detecting command injected vulnerability, it selects high-quality one and gives them

more mutation time and priorities based on the result of measuring the feedbacks of fuzzing samples by distance function, which concentrates resources on the fuzzing samples that may cover risk functions in back-end programs, improving the efficiency of command injection vulnerability detection. Finally, combined with the parameters of risk functions and fuzzing samples, IoTCID makes checks on whether there is a suspicious point of command injection vulnerability. Obviously, the distance function and the scheduling strategies are the cores of the fuzzing technology.

1) *Distance function*: The weight of basic blocks, the edge vector of basic blocks and the distance of samples are three components of the distance function. The weight of basic blocks and the edge vector of basic blocks are calculated in the process of binary static analysis while the distance of samples calculation is calculated in the fuzzing process. Table I lists the variables and their meanings of the distance function.

We define the count of successors of Basic Block B which contain the risk functions as the weight of basic block B, as Equation (1) shows.

$$Weight_B = \begin{cases} \text{Sum}(B, \text{Func}), & \text{Func} \notin B \\ W_{Max}, & \text{Func} \in B \end{cases} \quad (1)$$

In Equation (1), $Weight_B$ is the weight of Basic Block B while $\text{Sum}()$ is a function that calculates the count of successors of basic block b which contain risk functions. Moreover, if the risk function is in basic block B, $Weight_B$ is recorded as W_{Max} . After calculating the weight of related basic blocks, we infer the edge from Basic Block A to Basic Block B while Basic Block A is the predecessor of Basic Block B.

$$|Edge_{a,b}| = Weight_b \quad (2)$$

During the process of fuzzing, combined with the probe code we set before, IoTCID obtains the execution path of the fuzzing sample and calculates the function distance according to the control flow graph to evaluate the fuzzing sample with $Score_{test}$.

$$Score_{test} = \frac{\sum |Edge_{a,b}|}{Count_{test}} \quad (3)$$

2) *Scheduling strategy*: Therefore, towards one specific interface, we implement our scheduling strategy according to the distance function. It can be inferred that a fuzzing sample with higher $Score_{test}$ is more likely to trigger the risk functions, so that the mutation resources should be concentrated on these high-quality fuzzing samples, improving the efficiency of command injection vulnerability detection.

Moreover, the following situations should be paid more attention on the basis of experience and practical situations. Details are shown in the control flow graph in Fig. 2.

Case 1. Supposed there is a risk function called in the basic block Target. The execution path of one fuzzing sample shows like Start->Basic Block 1->Basic Block 3->...Target-> End, where there is a loop in the path. Since the fuzzing sample can eventually traverse the basic block Target, we should avoid double counting when calculating $Count_{test}$ and $\sum |Edge_{a,b}|$.

TABLE I. VARIABLES AND MEANINGS IN DISTANCE FUNCTION

Symbol	Name	Meaning
$Weight_B$	The weight of a basic block	The importance of Basic Block B in the control flow
$\overrightarrow{Edge}_{a,b}$	The edge vector of basic blocks	The edge vector from Basic Block A to Basic Block B while Basic Block A is the predecessor of Basic Block B.
$Count_{test}$	The count of edges	The count of edges traversed by the sample before triggering the target basic block
$Score_{test}$	The score of a sample	The count of valid edges traversed by the sample

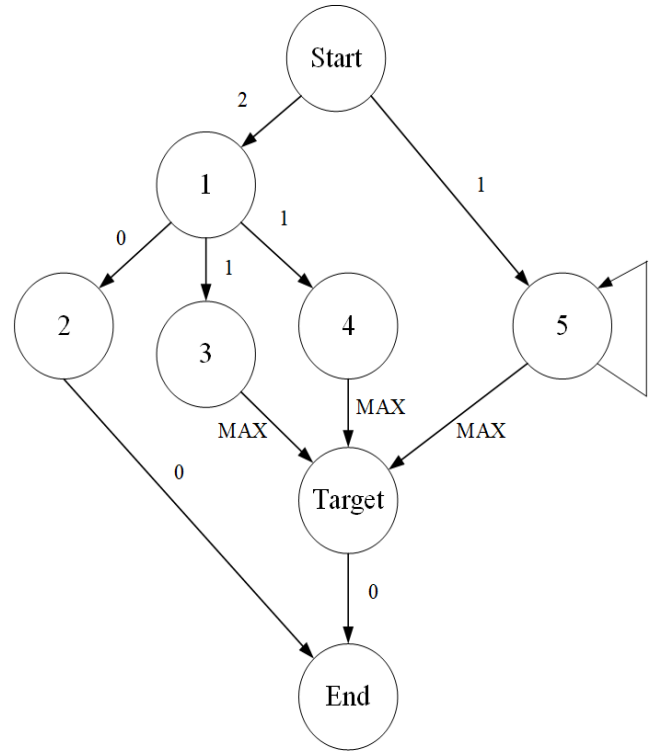


Fig. 2. The Control Flow Graph.

Case 2. Another case is that there are two fuzzing samples respectively travel through basic block 3 and basic block, and both eventually reach the basic block Target. We will find the scores of the two fuzzing samples are the same based on the above theory. However, we find there is a string concatenation functions such as `sprintf` and `strcat`, and the fuzzing sample which reaches basic block 4 should be given a higher priority under this circumstance. The reason is that the cause of command injection vulnerabilities generally originate from the back-end program that concatenates the user's input into a string which further directly works as a parameter of the risk function [14].

Considering the above situations, we propose Algorithm 2 to evaluate the quality of fuzzing samples where `sampleInfo` is the fuzzing samples and `funcGraph` is the control flow graph of function. It first traverses the basic blocks of the interfaces in the back-end program in deep first search (DFS), gathering necessary information, and then calculates $Score_{test}$ of fuzzing samples based on their feedbacks.

Algorithm 2: Assessment of Fuzzing Samples

```
Input: sampleInfo && funcGraph  
Output: Scores of Fuzzing Samples  
1. function ACCESSMENT(sampleInfo, funcGraph)  
2.   infoGraph  $\leftarrow$  DFSTraverse(funcGraph)  
3.   totalEdges  $\leftarrow$  makeEdges(  
     sampleInfo.executionBlocks)  
4.   edgeCount  $\leftarrow$  0  
5.   edgeTotal  $\leftarrow$  0  
6.   for edge in totalEdges do  
7.     if infoGraph.edge. $\overrightarrow{\text{Edge}}$   $\neq$  0 and  
       sampleInfo.edge.flag  $\neq$  1 then  
8.       edgeTotal += infoGraph.edge. $\overrightarrow{\text{Edge}}$ ;  
9.       edgeCount += 1;  
10.      sampleInfo.edge.flag = 1;  
11.     end if  
12.   end for  
13.   if edgeTotal  $\geq$  MAX and  
     IMPORTANT_BLOCKS(  
       sampleInfo.executionBlocks) then  
14.     SET_PRIORITY(sampleInfo)  
15.   end if  
16.   Score  $\leftarrow$  CALCULATE(  
     sampleInfo, edgeTotal, edgeCount)  
17.   return Score  
18. end function
```

Finally, according to $Score_{test}$ of fuzzing samples, we select high-quality fuzzing samples, given higher priority and more mutation time. We further select the samples which have reached the basic block Target and confirm whether there is a command injection vulnerability by comparing its data to the parameter of risk function.

IV. RESULTS AND DISCUSSION

The prototype system of IoTCID consists of three subsystems including the constrained model generation subsystem, the binary static analysis subsystem, and the fuzzing subsystem. The constrained model generation subsystem implemented based on the standard HTML parsing library BeautifulSoup [15] and the standard Javascript parsing library Esprima [16] uses Algorithm 1 to extract the variables during the interaction between front-end files and back-end programs and generate the constrained models of fuzzing samples. The binary static analysis subsystem implemented based on Capstone [13] first obtains the disassembly code of back-end programs, and then establishes the control flow graph as well as sets the probe code using the trampoline mechanism. On the basis of the above two subsystems, the fuzzing subsystem initializes the fuzzing samples by LibFuzzer [17], and performs fuzzing test according to our scheduling strategies.

A. Preparation

We evaluate IoTCID on real-world IoT devices from three vendors, including six routers on two architectures, which are commonly used in our daily life. The target firmware can be obtained from the official website or extracted from the device based on binwalk [18].

In this paper, we design two experiments to prove the efficiency of IoTCID, one of which is the assessment of front-end files analysis while the other is the assessment of fuzzing test. Besides, we compared our tool with SaTC, the state-of-the-art static bug-hunter for IoT devices, which locates the strings

between front-end files and back-end programs based on the interaction and applies data flow analysis to detect vulnerabilities. We perform our experiments on Ubuntu 18.04LTS 64-bit operating system, with Intel Core i5-6300HQ @ 2.30GHz and 16.0 GB RAM.

B. Result and Discussion

Table II lists the result of the instrumentation information of target IoT devices, where T_1 represents the average response time of IoT devices under normal working state while T_2 represents the average response time after the static instrumentation. We get the final result after performing multiple tests to reduce the impact of fluctuations caused by the test environment. It shows that the setting of the probe codes only increases the response time by about 25%, which is an acceptable expense for the next fuzzing test.

Table III lists the analysis result of front-end files towards our target IoT devices. Among them, tURL means the total number of URL interfaces that have data interaction between the front-end files and the back-end programs. eURL means the total number of URL interfaces extracted from the front-end file by the tools. gMod means the total number of the generated constrained models. g% means the accuracy rate of the generated constrained models.

According to Table III, it can be seen according to vURL. We define TP rate (True Positive rate) and FP rate (False Positive rate) for further explanation. The TP rate means the ratio of the correct results to the actual total, which can be inferred by vURL/tURL while the FP rate means the ratio of the incorrect results to the actual total, which can be inferred by (eURL-vURL)/tURL.

As shown in the left side of Fig. 3, it can be found that, except for the X12 series, the TP rates of IoTCID and SaTC are achieving an appreciable rate, which means that both IoTCID and SaTC have correctly extracted most of the URL interfaces provided by the target IoT devices and IoTCID does a better job.

However, the FP rates are various as shown in the right side of Fig. 3. Besides a few identification errors, the main reason of the difference is that IoTCID extracts URLs in the front-end files by analyzing the calling procedures which have data interaction with the back-end programs, while SaTC extracts URLs through regular expressions and clustering algorithms directly, which causes a higher FP rate. For instance, certain URL interfaces that only provide the status of devices should not be presumed to be risks and will not be extracted by IoTCID.

TABLE II. RESULT OF STATIC INSTRUMENTATION

Vendor	Device Series	T1(ms)	T2(ms)
Tenda	AC9	3.87	4.66
	AX12	3.47	4.28
D-Link	D605L	3.94	4.64
	D816	3.81	4.68
L-Blink	X12	4.32	5.53
	X22	4.38	5.49

TABLE III. ANALYSIS RESULT OF FRONT-END FILES

Vendor	Series	tURL	IoTCID				SaTC	
			eURL	vURL	gMod	g%	eURL	vURL
Tenda	AC9	106	94	88	100	87.00	123	86
	AX12	98	102	72	108	87.04	130	71
D-Link	D605L	64	58	53	60	95.00	60	52
	D816	66	57	47	60	91.67	50	40
L-Blink	X12	114	117	101	127	74.80	25	16
	X22	114	117	101	127	74.80	25	16

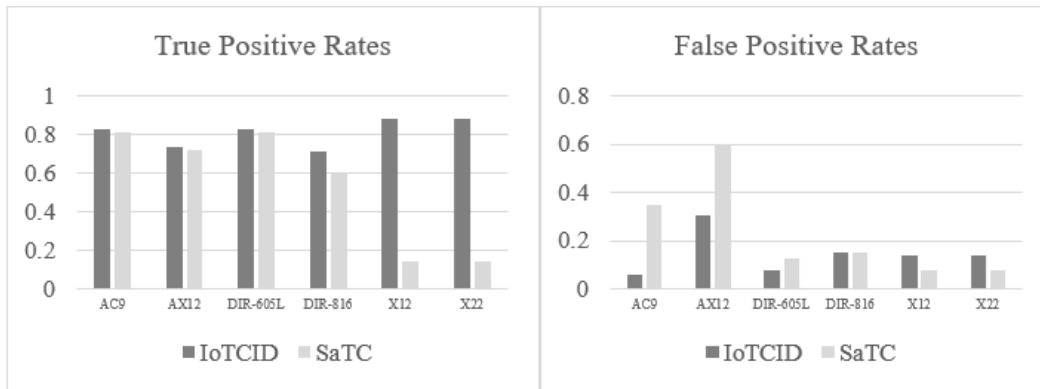


Fig. 3. TP Rates and FP Rates Comparison.

Moreover, IoTCID generates constrained models related to the extracted URLs based on the abstract syntax tree, and has a high accuracy rate in g%. In this experiment, it shows that IoTCID has a better performance in the analysis of the interactions between the front-end files and the back-end programs providing a foundation for the following command injection vulnerability detection.

As Table IV shows, the IoTCID completes all the command injection vulnerability detections towards the target IoT devices and confirms six command injection vulnerabilities, while SaTC only completes a few of them. The reason is that the implementation of SaTC is developed based on angr [19], which is limited in supporting MIPS architecture programs, and prone to cause crash during data flow analysis while IoTCID is designed based on the generation of the constrained models, and confirms whether there is a command injection vulnerability by comparing the fuzzing samples to the feedbacks of the probe code, representing a high degree of support for the detection of multi-architecture programs. Moreover, SaTC only raises alerts after completing the detection and requires further manual analysis to confirm whether the alert is reliable and the command injection vulnerability is controllable, existing certain false positives and costing additional manual analysis time. However, the detection result of IoTCID is based on the feedbacks of the executing program sent by the probe code, so it requires no more manual analysis and the accuracy of the results is guaranteed.

From the above experiments, compared with the existing command injection vulnerability detection tool SaTC towards IoT devices, IoTCID can effectively extract the constrained

models based on the analysis of the interaction between the front-end files and the back-end programs, and improve the accuracy and efficiency of detecting the command injection vulnerabilities through various scheduling strategies.

C. Case Analysis

Taking CVE-2018-14558 as an example, when a user manages an external device, the related front-end file will generate a request (Line 5 in status_usb.js, up side of Fig. 4) combined with the device name and send it to the back-end programs for parsing. The back-end program processes the request through the function "formsetUsbUnload", and generates a string containing the device name as the parameter of the system call. (Line 5 and 6 in httpd, low side of Fig. 4). Because the function "formsetUsbUnload" does not verify the validity of the parameter "deviceName", there exists a typical command injection vulnerability in the function "doSystemCmd", which can be exploited by attackers to execute arbitrary commands.

TABLE IV. RESULT OF VULNERABILITY DETECTION

Vendor	Series	IDs	Time (min)	
			IoTCID	SaTC
Tenda	AC9	CVE-2018-14558	4:40h	-
	AC*	CNNVD-202109-1174	4:26h	3:52h
D-Link	D605L	CVE-2018-20057	3:55h	-
	D816	CVE-2021-39510 CVE-2018-17066	3:31h	-
L-BLink	X*	CNNVD-202011-1320	3:10h	3:40h

```

01.  /*status_usb.js*/
02.  function unlinkUsb() {
03.    var devName = $(this).data("target");
04.
05.    $.GetSetData.setData("goform/setUsbUnload",
06.      "deviceName=" + encodeURIComponent(devName),
07.      unlinkCallback);
08.  }
09.  /*http*/
10.  void formsetUsbUnload(webs_t wp, char_t *path, char_t *query)
11.  {
12.    char *usb_name;
13.    usb_name = websGetVar(wp, "deviceName", byte_520318);
14.    doSystemCmd("cfm post netctrl %dPop=%d,string_info=%s", 51, 3, usb_name);
15.    websWrite(wp, "HTTP/1.0 200 OK\r\n\r\n");
16.    websWrite(wp, "{\r\n\"errorCode\":0\r\n}");
17.    websDone(wp, 200);
18.  }

```

Fig. 4. Interaction between the Front-end Files and the Back-end Programs.

First, IoTCID generates a constrained model by analyzing the interactions between the front-end files and the back-end program, as shown in Fig. 5.

```

{
  Url: "/goform/setUsbUnload"
  Method: "POST"
  Parameters: [ "deviceName" ]
}

```

Fig. 5. A Constrained Model.

```

.txt:004C990C D8 FF BD 27      addiu $sp, -0x28
.txt:004C990C                # End of Function formsetUsbUnload
.txt:004C990C                # -----
.txt:004C9910 24 00 BF AF      sw   $ra, 0x24($sp)
.txt:004C9914 20 00 BE AF      sw   $fp, 0x20($sp)
.txt:004C9918 21 F8 A0 83      move $fp, $sp
.txt:004C9920 28 00 C4 AF      sw   $a0, 0x28($fp)
.txt:004C9924 2C 00 C5 AF      sw   $a1, 0x2C($fp)
.txt:004C9928 30 00 C6 AF      sw   $a2, 0x30($fp)
.txt:004C992C 38 00 C8 AF      la   $a0, _func__12734@plt
.txt:004C9930 28 00 C4 BF      la   $a0, _func__12734@plt
.txt:004C9934 20 00 B2 BF      addiu $a1, $0, (aDevicename_0 - 0x520000) # "deviceName"
.txt:004C9938 54 06 45 24      la   $a0, _func__12734@plt
.txt:004C993C 20 00 B2 BF      addiu $a2, $0, (aCfmPostNetctrl_5 - 0x520000) # "cfm post netctrl %dPop=%d,string_info%
.txt:004C9940 18 03 44 24      addiu $a2, $0, (url_520318 - 0x520000) # "encode"
.txt:004C9944 80 03 B2 BF      la   $a0, websGetVar
.txt:004C9948 21 C8 A0 80      move $t9, $a0
.txt:004C994C 09 F8 20 83      jalr $t9, websSetVar
.txt:004C9950 00 00 00 00      nop
.txt:004C9954 10 00 DC BF      lw   $gp, 0x10($fp)
.txt:004C9958 18 00 C2 BF      sw   $gp, 0x18($fp)
.txt:004C995C 20 88 B2 BF      la   $a0, _func__12734@plt
.txt:004C9960 58 03 44 24      addiu $a0, $0, (aCfmPostNetctrl_5 - 0x520000) # "cfm post netctrl %dPop=%d,string_info%
.txt:004C9964 33 00 85 24      ll   $a1, 0x33
.txt:004C9968 03 00 D6 24      ll   $a2, 0
.txt:004C996C 18 00 C7 BF      la   $a3, 0x18($fp)
.txt:004C9970 18 BF B2 BF      la   $a0, $0, $a3
.txt:004C9974 2C B5 15 08      j    0x504080
.txt:004C9978                # -----
.txt:004C997A                # -----
.txt:004C997C                # -----
.txt:004C997E                # -----
.txt:004C9980                # -----
.txt:004C9982                # -----
.txt:004C9984                # -----
.txt:004C9986                # -----
.txt:004C9988                # -----
.txt:004C998A                # -----
.txt:004C998C                # -----
.txt:004C998E                # -----
.txt:004C9990                # -----
.txt:004C9992                # -----
.txt:004C9994                # -----
.txt:004C9996                # -----
.txt:004C9998                # -----
.txt:004C999A                # -----
.txt:004C999C                # -----
.txt:004C999E                # -----
.txt:004C99A0                # -----
.txt:004C99A2                # -----
.txt:004C99A4                # -----
.txt:004C99A6                # -----
.txt:004C99A8                # -----
.txt:004C99AA                # -----
.txt:004C99AC                # -----
.txt:004C99AE                # -----
.txt:004C99B0                # -----
.txt:004C99B2                # -----
.txt:004C99B4                # -----
.txt:004C99B6                # -----
.txt:004C99B8                # -----
.txt:004C99BA                # -----
.txt:004C99BC                # -----
.txt:004C99BE                # -----
.txt:004C99C0                # -----
.txt:004C99C2                # -----
.txt:004C99C4                # -----
.txt:004C99C6                # -----
.txt:004C99C8                # -----
.txt:004C99CA                # -----
.txt:004C99CC                # -----
.txt:004C99CE                # -----
.txt:004C99D0                # -----
.txt:004C99D2                # -----
.txt:004C99D4                # -----
.txt:004C99D6                # -----
.txt:004C99D8                # -----
.txt:004C99DA                # -----
.txt:004C99DC                # -----
.txt:004C99DE                # -----
.txt:004C99E0                # -----
.txt:004C99E2                # -----
.txt:004C99E4                # -----
.txt:004C99E6                # -----
.txt:004C99E8                # -----
.txt:004C99EA                # -----
.txt:004C99EC                # -----
.txt:004C99EE                # -----
.txt:004C99F0                # -----
.txt:004C99F2                # -----
.txt:004C99F4                # -----
.txt:004C99F6                # -----
.txt:004C99F8                # -----
.txt:004C99FA                # -----
.txt:004C99FC                # -----
.txt:004C99FE                # -----

```

Fig. 6. Probe Code Set.

Then, IoTCID sets up the probe code that records the execution path of the fuzzing samples in the located interface functions and provides with feedbacks by performing binary static analysis on the back-end program, as shown in Fig. 6.

Finally, IoTCID confirms whether there is a command injection vulnerability in the back-end program by comparing the fuzzing samples and the parameters of the risk function, which are provided by the probe code we set before.

V. CONCLUSION

In this paper, we propose and implement a state-of-the-art dynamic detection tool towards command injection vulnerabilities in IoT devices, IoTCID, which generates constrained models based on the logic analysis to front-end files, and selects high-quality fuzzing samples by various scheduling strategies based on the Distance Function. IoTCID has successfully detected seven command injection vulnerabilities in six real-world IoT devices, two of which are previously unknown vulnerabilities and assigned IDs by

CNNVD-202109-1174, CNNVD-202011-1320 after being confirmed by CNNVD.

However, there still remains shortcomings in our tool, such as the limit of the constrained model generation when facing with complex variable references in front-end files and the limit of the throughput of IoTCID for the experiments are currently performing on the devices. Therefore, our future work is as follows:

- 1) Optimization is needed to improve the capability of the constrained model generation in complex variable references in the front-end file.
- 2) Optimization is needed to improve the throughput of IoTCID by building a simulation framework environment.

ACKNOWLEDGMENT

The authors would like to thank the anonymous reviewers for their valuable comments and suggestions. The research was supported by the National Natural Science Foundation of China (Grant No. 61872386, 62001055).

REFERENCES

- [1] State of IoT 2022: Number of connected IoT devices growing 18% to 14.4 billion global. <https://iot-analytics.com/number-connected-iot-devices/>.
- [2] Common IoT Attacks that Compromise Security. <https://socradar.io/common-iot-attacks-that-compromise-security/>.
- [3] Governments Must Promote Network-Level IoT Security at Scale. <https://www.paloaltonetworks.com/blog/2021/12/network-level-iot-security/>.
- [4] Tackle IoT application security threats and vulnerabilities. <https://www.techtarget.com/iotagenda/tip/Tackle-IoT-application-security-threats-and-vulnerabilities>.
- [5] Chen J, Diao W, Zhao Q, et al. IoTfuzzer: Discovering Memory Corruptions in IoT Through App-based Fuzzing[C]//NDSS. 2018.
- [6] Redini N, Continella A, Das D, et al. Diane: Identifying fuzzing triggers in apps to generate under-constrained inputs for iot devices[C]//2021 IEEE Symposium on Security and Privacy (SP). IEEE, 2021: 484-500.
- [7] Zhang Y, Huo W, Jian K, et al. SRFuzzer: an automatic fuzzing framework for physical SOHO router devices to discover multi-type vulnerabilities[C]//Proceedings of the 35th Annual Computer Security Applications Conference. 2019: 544-556.
- [8] Srivastava P, Peng H, Li J, et al. Firmfuzz: Automated iot firmware introspection and analysis[C]//Proceedings of the 2nd International ACM Workshop on Security and Privacy for the Internet-of-Things. 2019: 15-21.
- [9] Zheng Y, Davanian A, Yin H, et al. FIRM-AFL:High-Throughput Greybox Fuzzing of IoT Firmware via Augmented Process Emulation[C]//28th USENIX Security Symposium (USENIX Security 19). 2019: 1099-1114.
- [10] Stasinopoulos A, Ntantogian C, Xenakis C. Commix: Automating evaluation and exploitation of command injection vulnerabilities in web applications[J]. International Journal of Information Security, 2019, 18(1): 49-72.
- [11] Redini N, Machiry A, Wang R, et al. Karonte: Detecting insecure multi-binary interactions in embedded firmware[C]//2020 IEEE Symposium on Security and Privacy (SP). IEEE, 2020: 1544-1561.
- [12] Chen L, Wang Y, Cai Q, et al. Sharing more and checking less: Leveraging common input keywords to detect bugs in embedded systems[C]//30th USENIX Security Symposium (USENIX Security 21). 2021: 303-319.
- [13] Quynh N A. Capstone: Next-gen disassembly framework[J]. Black Hat USA, 2014, 5(2): 3-8.
- [14] Command Injection. https://owasp.org/www-community/attacks/Command_Injection.

- [15] Richardson L. Beautiful soup documentation[J]. Dosegljivo:<https://www.crummy.com/software/BeautifulSoup/bs4/doc/>. [Dostopano: 7. 7. 2018], 2007.
- [16] Hidayat A. Esprima: Ecmascript parsing infrastructure for multipurpose analysis[J]. 2017.
- [17] libFuzzer. <https://lvm.org/docs/LibFuzzer.html>.
- [18] C. Heffner, "Binwalk - firmware analysis tool designed to assist in the analysis, extraction, and reverse engineering of firmware images," <https://github.com/ReFirmLabs/binwalk>, 201 Shoshitaishvili Y, Wang R, Salls C, et al. Sok:(state of) the art of war: Offensive techniques in binary analysis[C]//2016 IEEE Symposium on Security and Privacy (SP). IEEE, 2016: 138-157.

English and Romanian Brain-to-Text Brain-Computer Interface Word Prediction System

Haider Abdullah Ali¹, Nicolae Goga², Andrei Vasilateanu³

Ali M. Muslim⁴, Khalid Abdullah Ali⁵, Marius-Valentin Drăgoi⁶

Faculty of Automatic Control and Computers, University POLITEHNICA of Bucharest, Bucharest, Romania^{1,2}
University of Groningen, Groningen, The Netherlands²

Faculty of Engineering in Foreign languages, University POLITEHNICA of Bucharest, Bucharest, Romania³

Department of Computer Science, Dijlah University College, Baghdad, Iraq⁴

Kurdistan Net Company (O3-Telecom), Erbil, Kurdistan Region, Iraq⁵

Faculty of Industrial Engineering and Robotics, University POLITEHNICA of Bucharest, Bucharest, Romania⁶

Abstract—Brain-Computer Interface (BCI) can recognise the thoughts of a human through various electrophysiological signals. Electrodes (sensors) placed on the scalp are used to detect these signals, or by using electrodes implanted inside the brain. Usually, BCI can detect brain activity through different neuroimage methods, but the most preferred is Electroencephalography (EEG) because it is a non-invasive and non-critical method. BCI systems applications are very helpful in restoring functionalities to people suffering from disabilities due to different reasons. In this study, a novel brain-to-text BCI system is presented to predict the word that the subject is thinking. This brain-to-text can assist mute people or those who cannot communicate with others due to different diseases to restore some of their abilities to interact with the surrounding environment and express themselves. In addition, brain-to-text may be used in different control or entertainment applications. EMOTIV™ Insight headset has been used to collect EEG signals from the subject's brain. Feature extraction of EEG signals for BCI systems is very important to classification performance. Statistical-based feature extraction has been used in this system to extract valuable features to be used for classification. The datasets are sentences involving some commonly used words in English and Romanian languages. The results of the English language elucidated that K-Nearest neighbour (KNN) has a prediction accuracy of 86.7%, 86.1% for Support Vector Machine (SVM), and 79.2% for Linear discriminant analysis (LDA), while the Romanian language has a prediction accuracy of 96.1%, 97.1%, and 94.8% for SVM, LDA, and KNN respectively. This system is a step forward in developing advanced brain-to-text BCI prediction systems.

Keywords—Brain-to-text; Brain-Computer Interface (BCI); Electroencephalography (EEG); Natural Language Processing (NLP); English language; Romanian language

I. INTRODUCTION

Communication between humans and machines is a desired concept for a long time. It was the aim of the Brain-Computer Interface (BCI). BCI can convert phonemes, binary responses, letters, and even words from brain activity [1]. BCIs can help people who have lost their ability to speak or move to restore communication with different body organs. Recently, the main coverage of BCI research is focused on restoring motor skills like, grasping, pointing, typing with a computer cursor [2], or choosing from a list of options. Other

systems may use “steady-state evoked potentials” or “Event-Related Potentials (ERPs)” to spell text out [3]. A BCI system is a collection of hardware devices and software that uses various techniques to record the brain's activity [4]. The data collected through experiments in laboratory conditions give the necessary information about the computation of neural in human beings. The response of neurons may differ between experimental and behaving in natural conditions. Thus, developing powerful decoding algorithms that can deal with the difficulties of naturalistic behaviour is important in developing real-life applications of BCIs [5].

Two approaches to language neural decoding have been used in this field: invasive decoding, based on invasive brain recording methods like Electrocorticography (ECoG); and non-invasive decoding which depends on neuroimaging technologies like EEG. Language decoding from EEG brain activity is significant in developing commonly applicable BCI systems. This technology can help people who are unable to communicate or do daily activities because of severe neuromuscular diseases or disorders. It also offers a great opportunity for neuroscientists to study brain mechanisms or activity [6].

Many years ago, researchers have predicted whether humans and machines can communicate depending on natural speech-related brain activity. In recent years, scientific research has proposed that it is possible to recognise speech from the brain's neural signals like acoustic features or one of some separate words. Expressed words can be decoded from spoken speech through brain waves ECoG recordings [5], EEG recordings, etc.

Feature extraction and classification are important procedures in each BCI model [7]. Features are extracted from a signal obtained from electrodes. Features are distinguished in frequency, time, and spatial domain. Some features of EEG may have great elective power to observe different patterns of EEG. To design and implement a well-trained model, some features with high discriminating ability are required [8].

The performance of the BCI system is mainly relying on the vector's size of the feature, which is acquired from multiple channels. In the classification of the mental tasks, the training samples' availability of features is minimal. Usually,

feature selection is used to improve the classification of mental tasks by eliminating unrelated and unnecessary features [9].

The paper describes a proposed brain-to-text system that is a simple, easy-to-implement, and cost-effective BCI system that aims to help mute or disabled people to communicate with others and electronic devices. The system may also be used for controlling purposes. The system can recognise English and Romanian languages; therefore, it is targeted individuals who can understand these languages. Considering this issue, the next sections practically describe how the brain thoughts can be translated into words starting from the literature review, the method and the techniques used in the study, and the results.

This paper is organised as follows: Section II of this study presents the literature review including background theory and related works. Section III presents the method of the research in detail. Section IV presents results and discussion, and Section V presents the conclusion and future work.

II. LITERATURE REVIEW

A. Background Theory

The brain of humans contains billions of connected neurons. The activity of neurons is varying according to different thoughts, where every thought generates a unique electric brain signal [10]. Brain signals can be detected using different invasive and non-invasive techniques [11]. Non-invasive techniques especially EEG, are widely used in BCI systems due to their ease of use and non-risk since it does not require a surgical invasion [12]. EEG has related to some challenges like low spatial resolution compared to invasive techniques, but it has a good temporal resolution, and may not detect a good signal due to the folding of the cortex or scalp-to-cortex distance [13]. The techniques of signal processing are required to remove the artefacts and noise from the raw EEG signals. This is performed by applying digital filters [4]. In recent years, these challenges have been highly reduced due to the development of hardware and smart software related to BCI research. The EEG signals of brain activity are detected using electrodes that measure the changes in voltage on the scalp [11].

EEG contains important data that will convert into useful information regarding responses to brain stimuli. The type of emotion and the accuracy level of the signal can be identified from the pattern of the brain waveforms. The processing of these signals can allow the control of external devices like the computer cursor, robotic arm, or wheelchairs. It also lets disabled people who have lost their ability to move or talk restore such abilities or express their emotions and thoughts. The signals of the brain can be analysed through three different steps:

- Signal Acquisition.
- Signal processing.
- Controlling.

Pre-processing step is important to convert the raw data into a useful and efficient format [14]. The obtained signal is

processed to eliminate the artefacts, noise, etc. which could improve the resulting signal. The next step is to extract features from the signal, where the feature is a special measure from a part of a signal. In feature extraction, the most important features required for classification will be extracted.

Feature extraction of EEG signals is one of the important aspects related to the system of BCI due to its important task of obtaining the correct performance of the classification stage [15] because of the complex processes inside the brain [8]. EEG signals are non-stationary, while their spectrum varies with time. These signals need different feature extraction techniques [15].

In brain signals decoding, signal processing comprises two important steps: feature extraction and feature classification [16]. The process of EEG feature extraction involving generate discriminative data features from channels that can increase the variance difference among classes [17]. The huge number of input data increases the execution time and complexity of the system. Obtaining informative features will enhance and increase the accuracy of the classification [7].

The algorithms of feature extraction must handle the signal source, which is usually complex and noisy, and detect interesting features [8]. These algorithms are used to detect the features that are strongly connected with the intent of the subject. The optimal feature set is transferred directly to the classification algorithm that associates the feature with a task to be accomplished [17]. The success of the BCI system's classification is associated with the accuracy, efficiency, and proper selection of feature extraction, thus, improving the accuracy and efficiency of the system [18]. Feature extraction depends on temporal-spatial analysis and/or time-frequency. Some of the techniques used are wavelet transform, autoregressive (AR) models, Fourier transforms (FT), and statistical properties of the signal [8].

The next step is to translate the extracted features into commands to control an external device or to do different mental tasks [8].

The final stage is the classification process which may be solved by adaptive algorithms, linear analysis, non-linear analysis, neural networks, fuzzy techniques, etc. [10]. Classification algorithms used in this work are "K-Nearest Neighbour (KNN), Support Vector Machine (SVM), and Linear Discriminant Analyser (LDA)".

B. Related Works

The following related works introduce several solutions to the issue of BCI brain-to-text which introduced some forms of a utility function that deals with text aspects.

Shuxian Zou et al. [6] have proposed two decoding tasks, the first one is a word prediction task given a context and brain image. The second task is to generate a direct text from a given prefix and a brain image. To implement these tasks, they have proposed an approach that uses a powerful pre-trained encoder-decoder model. The model reaches 7.95% and 18.2% top1 accuracy for more than two thousand words of vocabulary on average for all task participants.

Christian Herff et al. [3], have implemented a brain-to-text system that forms single phones using “Automatic Speech Recognition (ASR)” by converting brain signals into the equivalent text representation during speaking. The results reveal that the proposed system can carry out phone error rates below 50% and word error rates as low as 25%.

G. NJayabhavani et al. [19], have proposed a BCI system to improve the typing of messages by building a mechanized system using a speller-based mechanized messenger. The smartphone, which contains a built-in speller application is connected to an EEG headset. They used wireless EEG neuroheadset-based P300 ERP for the realistic execution of the mechanized messenger. The smartphone application will be activated when a user wants to transmit a text. The obtained text is transferred after processing by the smartphone spell checker. The proposed system will let a user to text while performing other activities. In addition, the time required for typing will be much reduced. The accuracy of the system is about 98% in 16 seconds after target selection.

James W. Minett et al. [20], have analysed the performance of the P300 speller for the Chinese language’s text input. Depending on the implemented Row/Column and single character spellers, the performance of six different paradigms has been tested and compared for thirty Chinese readers. The accuracy of a single character speller is 63.3% of subjects have been capable of obtaining 80% or higher accuracy of classification for fifteen trials. Regarding the communication rate, the optimal paradigm is different from the speller of Row/Column in which stimuli are increased by changing the colour of the background. This paradigm attained 14.5 bits per minute communication rate. The input rate of this system is about 1.1 characters per minute which correspond to approximate 11,000 Chinese characters.

Kiran George et al. [21], have presented a design method to input a simple text acronym in a message through mind thoughts and natural facial expressions. They have shown that “commercially-off-the-shelf (COTS)” BCI technology as well as “Emotiv Control Panel Software Suite” can be used to translate mind thoughts and natural facial expressions into actions by pairing 12 of the most used acronyms of text. EMOTIV™ headset was used to capture the user’s Electromyography (EMG) and EEG data, while “Emotiv Control Panel Software” is used to translate the mind’s thoughts and natural facial expressions into their corresponding text acronym.

Aasim Raheel et al. [22], have presented a powerful solution for using the muscular movement of the eye to type textual content. The fast and accurate movement of the eye can be observed using EEG. They have acquired EEG signals for many users to create a content spelling framework that uses the movement of a cursor over letter sets. All analyses were carried out on datasets of many users to set the indicator in three classes using them as an assist sign for content spelling. The system’s accuracy is 70% for the right movement, 80% for the left movement, and 79% for the blink.

The literature review elucidated that the combination of BCI and machines regarding text generation is a modern and promising study direction. It was also noticed that

enhancements are required to improve writing performance while reducing the system’s complexity. In this context, this study proposes a novel system that may fulfil the gap in brain-to-text research. The system is designed to predict words that human thinks and prints them on the screen. This system can predict some common English and Romanian language words. The system can assist mute people or those who lost their ability to speak due to different reasons like genetic factors, encephalitis, brain diseases and strokes, etc. to communicate with others or machines. Most brain-to-text research or projects discussed the English language only, while the proposed system can deal with the Romanian language as well. The strengths and weaknesses of some similar projects have been analysed as shown in Table I.

TABLE I. RELATED WORKS

Related project	Strengths	Weaknesses	What is new in this study
“Towards Brain-to-Text Generation: Neural Decoding with Pre-trained Encoder-Decoder Models” [6]	<ul style="list-style-type: none"> - Predict words and generate text from fMRI images. 	<ul style="list-style-type: none"> - Low accuracy - Not in real-time - One language only 	<ul style="list-style-type: none"> - Good accuracy - Two languages
“Brain-to-text: decoding spoken phrases from phone representations in the brain” [3]	<ul style="list-style-type: none"> - Convert brain activity into a text representation. - Accurate brain signals. 	<ul style="list-style-type: none"> - Clinical risks. ECoG invasive technique has been used. - Decode spoken speech, not thoughts. - One language only 	<ul style="list-style-type: none"> - No risk - Decode thoughts - Two languages
“A speller based mechanized messenger for smart phones using brain mobile interface (BMI)” [19]	<ul style="list-style-type: none"> - Fast - Good accuracy - In real-time 	<ul style="list-style-type: none"> - The user must select a character from a 6x6 matrix - One language only 	<ul style="list-style-type: none"> - Decode thoughts to text directly - Two languages
“An assistive communication brain-computer interface for Chinese text input” [20]	<ul style="list-style-type: none"> - Good accuracy - Deals with different script language 	<ul style="list-style-type: none"> - The user must focus on a character from a 6x6 matrix on a screen - One language only 	<ul style="list-style-type: none"> - Decode thoughts - Two languages
“Automated sensing, interpretation and conversion of facial and mental expressions into text acronyms using brain-computer interface technology” [21]	<ul style="list-style-type: none"> - Decoding mental states and facial expressions. - In real-time 	<ul style="list-style-type: none"> - Decode several expressions only - One language only - A combination of BCI and keyboard was used. 	<ul style="list-style-type: none"> - Decode thoughts as words - Two languages - Keyboard input is not needed
“Real-time text speller based on eye movement classification using wearable EEG sensors” [22]	<ul style="list-style-type: none"> - Good accuracy - In real-time 	<ul style="list-style-type: none"> - Decodes eye movement based on an alphabet grid, not thoughts - One language only 	<ul style="list-style-type: none"> - Decode thoughts - Two languages

III. METHOD

To implement the proposed system, EEG data collected from a subject has been processed, feature extracted, and classified. Python programming language is used to code all the related signal processing operations and training. The training is carried out first using EEG data. EEG data are collected using EMOTIV™ Insight neuroheadset. The training model is saved after feature extraction and data classification. The prediction process is carried out through the training model by making predictions on new data received from the headset. Fig. 1 shows the basic architecture of the brain-to-text BCI system.

A. Signal Acquisition

To detect and collect EEG brain signals from the subject's head, EMOTIV™ Insight non-invasive neuroheadset has been used. Its 5-channel headset EEG system (see Fig. 2) contains semi-dry polymer electrodes designed for various use of BCI systems and research. EMOTIV™ Insight neuroheadset is made of lightweight materials and provides whole-brain sensing with improved advanced electronics to deliver robust and clean signals. This neuroheadset is compatible with computers and mobile devices and can be connected via Bluetooth Low Energy or a 2.4 GHz wireless dongle [23].

B. Data Collection

The data are recorded using EmotivPRO™. The subject whom the data was collected from is a female who is a native Romanian speaker and fluent in English. She is healthy and reported no history of neurological illness. The recorded data are divided into sentences where each sentence contains some common words. Four sentences in English, as well as four sentences in Romanian, were recorded to be trained. The subject is asked to think of some words in the English language (without speaking) separately during each time of the recording process. For example, the sentence “Boy eats home with family” has five words, each word recorded forty times. The recordings are collected using five sensors of the headset AF3, AF4, T7, T8, and Pz where the sampling rate is 128 samples per second for each channel. The recordings have been exported and saved to be used later in training. The INACTIVE case in which the headset is not worn by the subject is also recorded. The BLINK case is also considered and recorded to recognise the blinking status of the subject and to enhance training accuracy. The same procedure is applied for the remaining English sentences and the sentences in the Romanian language like “Eu merg acasa cu familia”.

C. Feature Extraction

After data has been obtained and exported, the next step is to extract features from the collected data. The statistical features like max, min, average, median, and standard deviation are simple, easy to compute, and easy to implement. 25 features have been extracted and used in this BCI system (five features for each channel of the headset).

D. Classification Algorithms

Several machine learning classifiers have been tested in this study, which are SVM, KNN, and LDA. The SVM algorithm is a classifier based on statistical learning theory that is usually used for classification in BCI systems. SVM

identifies the decision boundary between the class samples [24]. The linear SVM kernel function parameter has been chosen for this work due to its high computational speed and capability to deal with multi-class issues [8]. KNN is a supervised learning algorithm which is very easy to implement. It stores all the available cases and new cases have been classified depending on a similarity measure. KNN classifies them according to the featured values' estimation, which can be done by comparing the training data with testing data [10]. The distance weight function KNN parameter has been used in this work. One of the most popular classification algorithms in BCI is LDA [25]–[27]. It classifies a set of observations into predetermined classes. The three algorithms are usually used with BCI and work well with multi-class problems and large databases.

A cross-validation procedure has been applied to evaluate and test the performance of the three algorithms. The best values of cross-validation of the three algorithms and the nearest neighbours value of KNN are practically founded as illustrated in the results section.

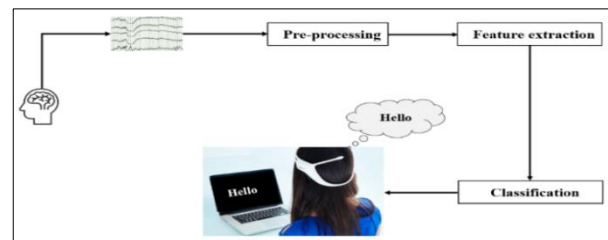


Fig. 1. Brain-to-text System Architecture.

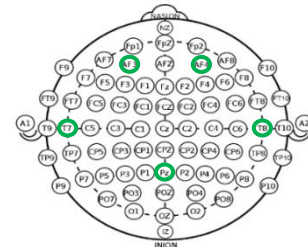


Fig. 2. Emotiv™ Insight Sensors (10-20 System EEG).

```
Begin
Initialise i = 0
#Set root directory of CSV files
For path, subdirectories, files in root:
  Get directoryList
  #Set path
  path_name = path+'/**/*'.csv'
  Read CSV files
  For csvFiles in read_files:
    Extract features from all CSV files of each subdirectory
    Creating DataFrames
    Concatenate DataFrames together
  Endfor
#Update i to get new subdirectory
i=i+1
Endfor
#Divide data into attributes and labels
X = frame.drop('Word', axis=1)
y = frame['Word']
Specify training algorithm
Train the model using cross-validation
#Save the pretrained model
filename = 'final_model.sav'
End
```

Fig. 3. Training Pseudocode.

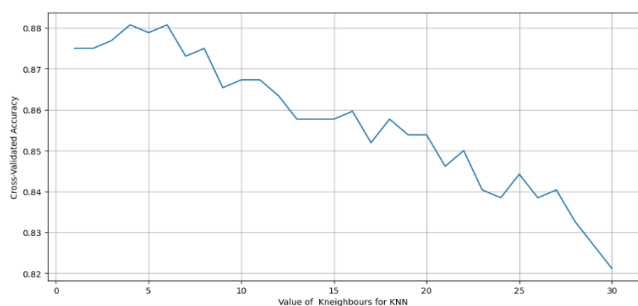
Fig. 3 shows the detailed pseudocode of the training process. As the EEG data are already collected from the subject and saved, the directory of these data must be specified to read the files and extract the feature. After specifying labels and attributes, the training starts using the three classification algorithms mentioned above through the cross-validation method.

IV. RESULTS AND DISCUSSION

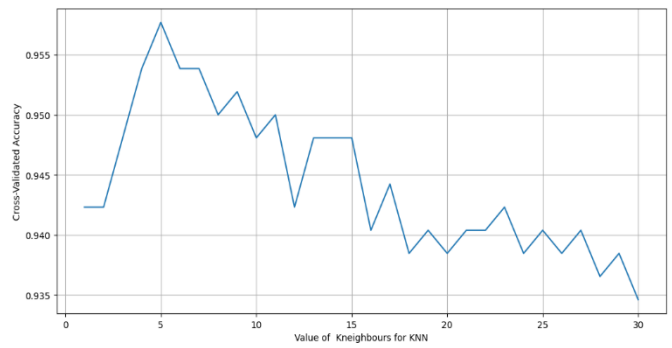
The parameters of the classification algorithms should be tuned to find the optimal hyperparameters. Specifying the optimal hyperparameters would enhance the overall performance and accuracy of the model. The “gridsearch” method has been used to find the optimal hyperparameters efficiently. The training process has done separately for each English and Romanian dataset. Table II shows the optimal hyperparameters and the configuration of each dataset for KNN, SVM, and LDA which have been found practically. The percentage of data used for training and testing can also be found in Table II, which differs according to the language and algorithm used. Fig. 4, 5, 6, and 7 show Hyperparameters graphs of KNN, SVM, and LDA. Fig. 4 elucidates that the effective values of n-neighbours are 6 and 5 for both English and Romanian datasets while the curve start dropping after six leading to low accuracy. As can be shown in Fig. 5, the effective k-fold values could be between 5 and 10 in most figures of English and Romanian datasets, where the accuracy is slightly changed. The prediction accuracy of English words is 86.7% for KNN, 86.1% for SVM, and 79.2% for LDA while the prediction accuracy of Romanian words is 96.1%, 97.1%, and 94.8% for SVM, LDA, and KNN respectively. The confusion matrices of the three algorithms for English and Romanian are shown in Fig. 8 and Fig. 9. The results of Romanian words are more accurate than in English words most probably because the subject is a native Romanian speaker.

TABLE II. KNN, SVM, AND LDA HYPERPARAMETERS SETTINGS

Algorithm	Parameters for the English dataset	Parameters for the Romanian dataset
KNN	Number of neighbours = 6 Weight function = distance Number of kfolds = 8	Number of neighbours = 5 Weight function = distance Number of kfolds = 10
SVM	Kernel type = linear Number of kfolds = 10	Kernel type = linear Number of kfolds = 9
LDA	Slover = svd Number of kfolds = 8	Slover = svd Number of kfolds = 7

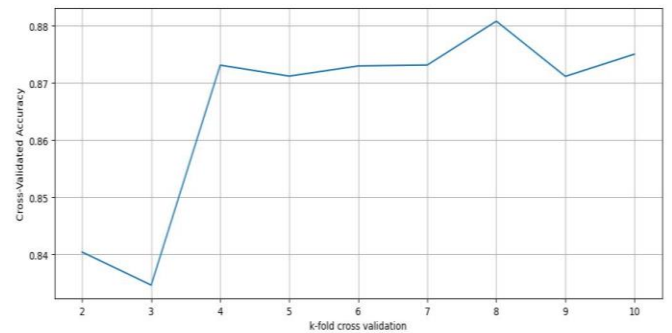


(a)

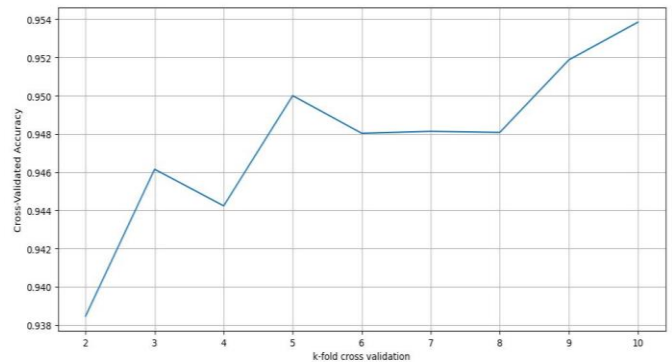


(b)

Fig. 4. (a). Number of k-neighbours of KNN-English., (b). Number of k-neighbours of KNN-Romanian.

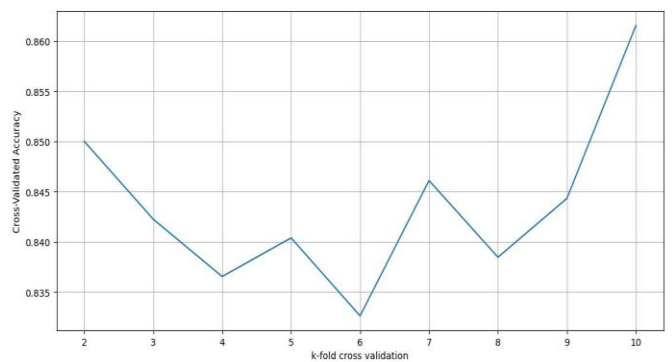


(a)

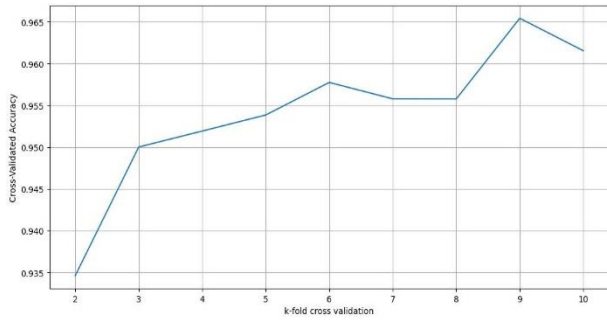


(b)

Fig. 5. (a) Performance of different k-fold of KNN-English. (b). Performance of different k-fold of KNN-Romanian.

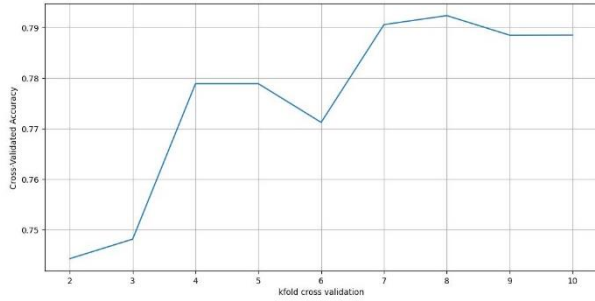


(a)

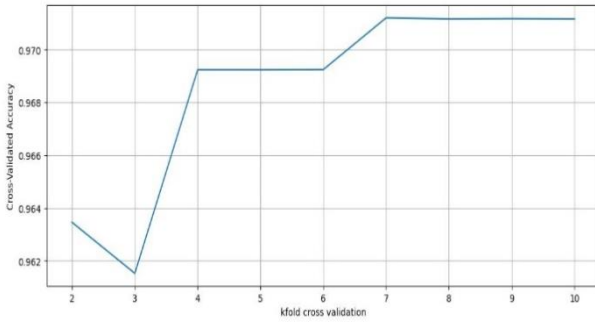


(b)

Fig. 6. (a) Performance of different k-fold of SVM-English. (b) Performance of different k-fold of SVM-Romanian.

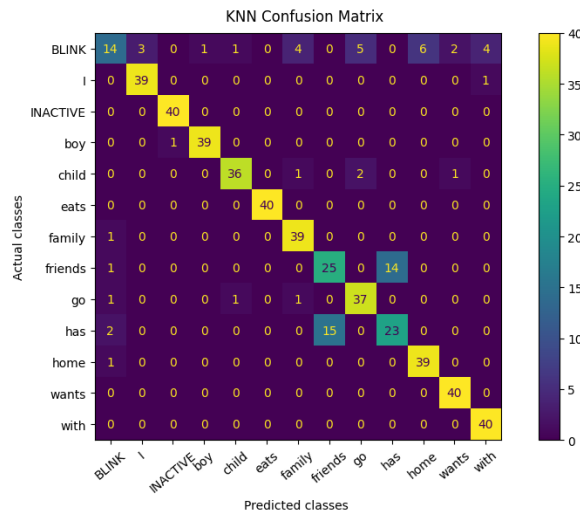


(a)

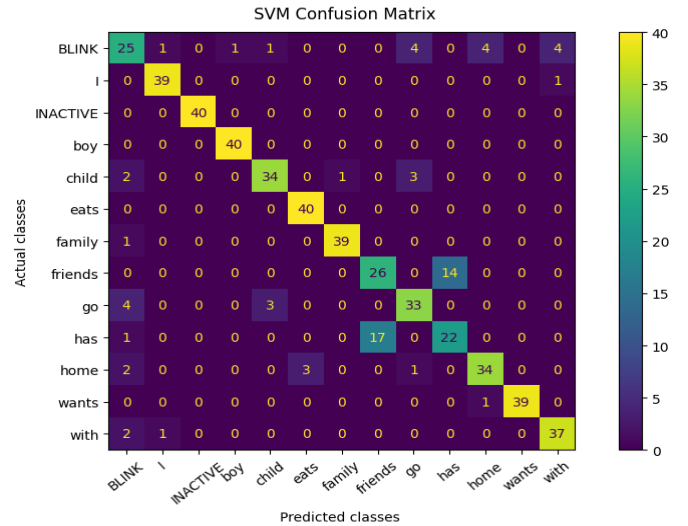


(b)

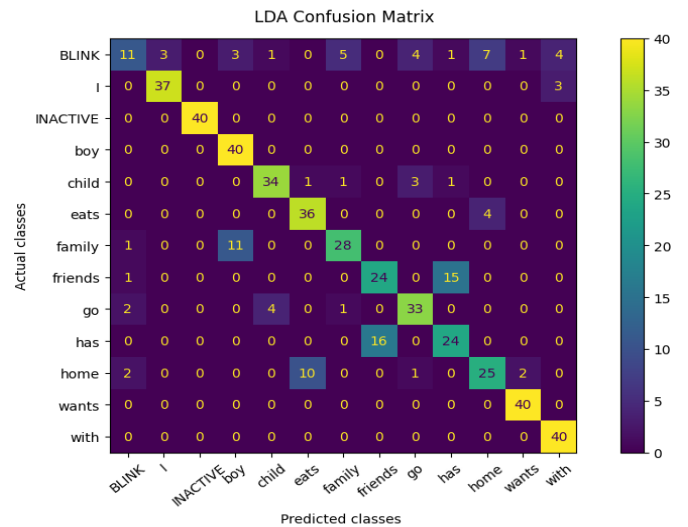
Fig. 7. (a) Performance of different k-fold of LDA-English. (b) Performance of different k-fold of LDA-Romanian.



(a)

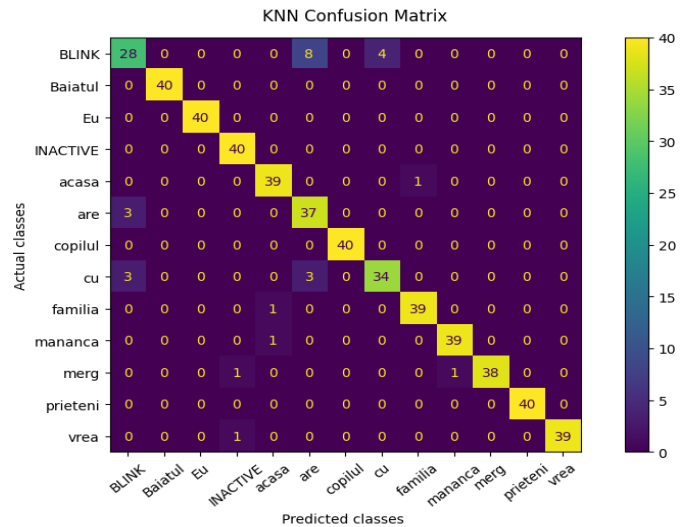


(b)

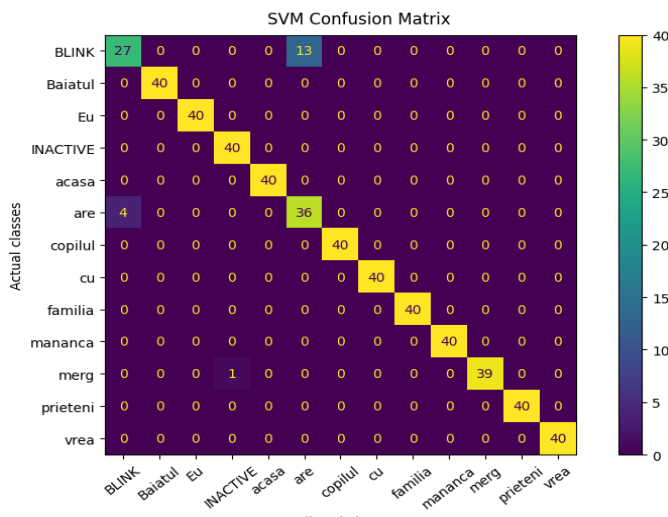


(c)

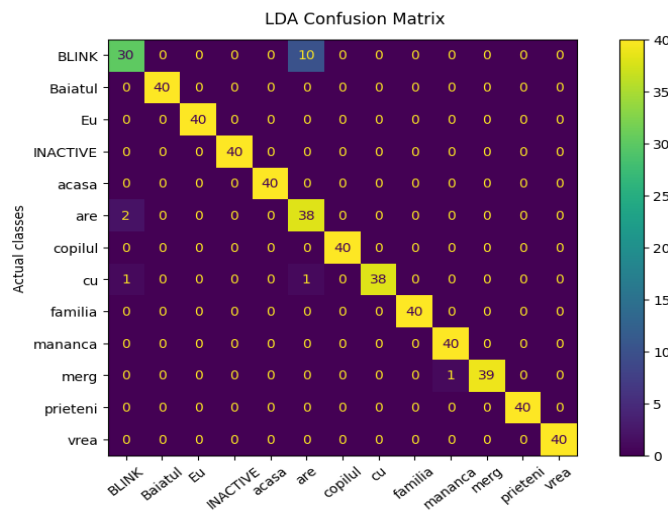
Fig. 8. Confusion Matrix of KNN- English, (b). Confusion Matrix of SVM-English, (c). Confusion Matrix of LDA- English.



(a)



(b)



(c)

Fig. 9. (a). Confusion Matrix of KNN- Romanian, (b). Confusion Matrix of SVM- Romanian, (c). Confusion Matrix of LDA- Romanian.

In Table III and Table IV, True Positive Rate (TPR) or recall computes the ability of the model to detect positive samples which must be close to one for better results, and precision or “positive predictive value” is the ratio of positive samples that are correctly classified to the total number of classified positive samples where precision value must be close to one also for better results. Precision helps to find the machine learning model’s reliability to positively classify the model. It can be noticed from the Tables that the KNN is the best classification algorithm for the English dataset while LDA is the best classification algorithm for the Romanian dataset.

The system testing is conducted using the pre-trained model with real-time EEG data streamed from the subject’s brain through the headset. Fig. 10 shows different execution screenshots for English and Romanian words. The subject was asked to think of the previously trained words where the desired word should be printed on the screen. The BLINK word in the figure refers to blink status when the subject

blinks her eyes, while the red words present a misclassification status. The results may be affected by limitations like the mood of the subject, ability of focusing, or whether is he/she patient. Although some miss classifications occurred during the execution, a limited group of words have been used in this work, and the study is conducted on one person only, the system has successfully decoded thoughts which are a necessary step toward human interaction with computers or the surrounding environment through speech imagery.

TABLE III. PRECISION AND RECALL OF ENGLISH CLASSIFICATION

Classifier Class	KNN		SVM		LDA	
	Precision	Recall	Precision	Recall	Precision	Recall
BLINK	0.7	0.35	0.68	0.62	0.65	0.28
I	0.93	0.97	0.95	0.97	0.93	0.93
INACTIVE	0.98	0.97	1	1	1	1
Boy	0.97	0.97	0.98	1	0.74	1
Child	0.95	0.9	0.89	0.85	0.87	0.85
Eats	1	1	0.93	1	0.77	0.9
Family	0.87	0.97	0.97	0.97	0.8	0.7
Friends	0.62	0.62	0.6	0.65	0.6	0.6
Go	0.84	0.93	0.8	0.82	0.8	0.82
Has	0.62	0.57	0.61	0.55	0.59	0.6
Home	0.87	0.97	0.87	0.85	0.69	0.62
Wants	0.93	1	1	0.97	0.93	1
With	0.89	1	0.88	0.93	0.85	1

TABLE IV. PRECISION AND RECALL OF ROMANIAN CLASSIFICATION

Classifier Class	KNN		SVM		LDA	
	Precision	Recall	Precision	Recall	Precision	Recall
BLINK	0.82	0.7	0.87	0.68	0.91	0.75
baiatul	1	1	1	1	1	1
eu	1	1	1	1	1	1
INACTIVE	0.95	1	0.98	1	1	1
acasa	0.95	0.97	1	1	1	1
are	0.77	0.93	0.73	0.9	0.78	0.95
copilul	1	1	1	1	1	1
cu	0.89	0.85	1	1	1	0.95
familia	0.97	0.97	1	1	1	1
mananca	0.97	0.97	1	1	0.98	1
merg	1	0.95	1	0.97	1	0.97
prieteni	1	1	1	1	1	1
vrea	1	0.97	1	1	1	1

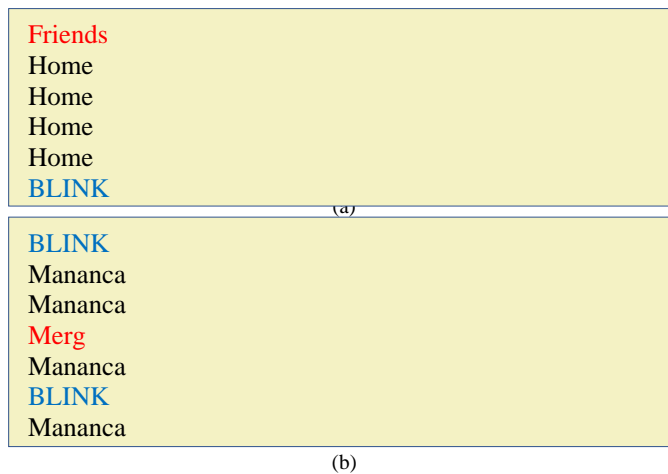


Fig. 10. (a) Real-time Words on Execution Screen-English, (b). Real-time Words on Execution Screen-Romanian.

V. CONCLUSION AND FUTURE WORK

There is always a necessity for a new natural approach to control and communicate with electronic devices and machines than the usual digital input approaches like touchscreens and buttons which may be limited to healthy people more than people with disabilities and diseases. Brain-to-text is a very modern field of research, and more research and gaps can be achieved and fulfilled in this field, especially in the medical domain. In this study, a brain-to-text BCI system is presented to mentally predict the word in English and Romanian languages. The system can help the disabled who cannot write or mute people to communicate with others or machines in writing in real-time. It will translate the neural activity into text using algorithms for feature extraction and classification. The three algorithms used in this system show promising results like high accuracy and prediction speed, especially KNN in English and SVM in Romanian.

In future work, more feature extraction and classification techniques like Fast Fourier Transform (FFT), neural networks, etc. may be used to enhance the accuracy and prediction of the system, considering increasing the collected EEG signals and samples. In addition, more languages like Arabic, which is written from right to left and its script is totally different from Latin script may be involved to target different language speakers.

REFERENCES

- [1] L. Li and S. Negoita, "Brain-to-speech decoding will require linguistic and pragmatic data," *Journal of neural engineering*, vol. 15, no. 6, p. 63001, 2018, doi: 10.1088/1741-2552/aae466.
- [2] F. R. Willett, D. T. Avansino, L. R. Hochberg, J. M. Henderson, and K. V. Shenoy, "High-performance brain-to-text communication via handwriting," *Nature*, vol. 593, no. 7858, pp. 249–254, 2021, doi: 10.1038/s41586-021-03506-2.
- [3] C. Herff et al., "Brain-to-text: decoding spoken phrases from phone representations in the brain," *Frontiers in Neuroscience*, vol. 9, p. 217, 2015, doi: 10.3389/fnins.2015.00217.
- [4] H. A. Ali et al., "EEG-based Brain Computer Interface Prosthetic Hand using Raspberry Pi 4," *International Journal of Advanced Computer Science and Applications*, vol. 12, no. 9, 2021, doi: 10.14569/IJACSA.2021.0120905.

- [5] T. Bhatnagar, "Application of Artificial Intelligence in Developing a Brain to Text System to Help the Disabled," *International Journal for Research in Applied Science & Engineering Technology (IJRASET)*, vol. 6, no. 3, pp. 411–414, 2018, doi: 10.22214/ijraset.2018.3066.
- [6] S. Zou, S. Wang, J. Zhang, and C. Zong, "Towards Brain-to-Text Generation: Neural Decoding with Pre-trained Encoder-Decoder Models," in *NeurIPS 2021 AI for Science Workshop*, 2021, p. 5.
- [7] S. Selim, M. Tantawi, H. Shedeed, and A. Badr, "A comparative analysis of different feature extraction techniques for motor imagery based BCI system," in *Joint European-US Workshop on Applications of Invariance in Computer Vision*, 2020, pp. 740–749.
- [8] V. Rathod, A. Tiwari, and O. Kakde, "Feature Extraction and Classification for Electro-Encephalography Based BCI: A Review," *Helix*, vol. 10, no. 04, pp. 345–349, 2020.
- [9] A. Gupta et al., "On the utility of power spectral techniques with feature selection techniques for effective mental task classification in noninvasive BCI," *IEEE Transactions on Systems, Man, and Cybernetics: Systems*, vol. 51, no. 5, pp. 3080–3092, 2019.
- [10] M. K and M. B. Anandaraju, "A comparative study on feature extraction and classification of mind waves for brain computer interface (BCI)," *International Journal of Engineering & Technology*; Vol 7, No 1.9 (2018): Special Issue 9DO - 10.14419/ijet.v7i1.9.9749, Mar. 2018.
- [11] H. A. Ali, N. Goga, A. Vasilateanu, L. A. Ali, G. S. Abd-almuhsen, and H. K. Naji, "A Quantitative Research to Determine User's Requirements for the Mind-Controlled Prosthesis Arm Intelligent System," in *2021 13th International Conference on Electronics, Computers and Artificial Intelligence (ECAI)*, 2021, pp. 1–8.
- [12] H. A. Ali, N. Goga, C. V. Marian, and L. A. Ali, "An Investigation of Mind-Controlled Prosthetic Arm Intelligent System," in *The 16th International Scientific Conference "eLearning and Software for Education"*, 2020, pp. 17–26.
- [13] S. Saha et al., "Progress in brain computer interface: challenges and opportunities," *Frontiers in Systems Neuroscience*, vol. 15, p. 20, 2021, doi: 10.3389/fnsys.2021.578875.
- [14] A. M. Muslim, S. Mashohor, R. Mahmud, G. Al Gawwam, and M. binti Hanafi, "Automated Feature Extraction for Predicting Multiple Sclerosis Patient Disability using Brain MRI," *International Journal of Advanced Computer Science and Applications*, vol. 13, no. 3, 2022, doi: 10.14569/IJACSA.2022.0130353.
- [15] L. Vega-Escobar, A. E. Castro-Ospina, and L. Duque-Muñoz, "Feature extraction schemes for BCI systems," in *2015 20th symposium on signal processing, images and computer vision (STSIVA)*, 2015, pp. 1–6.
- [16] X. Mao et al., "Progress in EEG-based brain robot interaction systems," *Computational intelligence and neuroscience*, vol. 2017, p. 25, 2017, doi: 10.1155/2017/1742862.
- [17] M. Z. Baig, N. Aslam, and H. P. H. Shum, "Filtering techniques for channel selection in motor imagery EEG applications: a survey," *Artificial intelligence review*, vol. 53, no. 2, pp. 1207–1232, 2020, doi: 10.1007/s10462-019-09694-8.
- [18] K.-S. Hong, M. J. Khan, and M. J. Hong, "Feature extraction and classification methods for hybrid fNIRS-EEG brain-computer interfaces," *Frontiers in human neuroscience*, vol. 12, p. 246, 2018, doi: 10.3389/fnhum.2018.002.
- [19] G. N. Jayabhavani, N. R. Raajan, and J. Abirami, "A speller based mechanized messenger for smart phones using brain mobile interface (BMI)," in *2013 International Conference on Emerging Trends in VLSI, Embedded System, Nano Electronics and Telecommunication System (ICEVENT)*, 2013, pp. 1–5, doi: 10.1109/ICEVENT.2013.6496561.
- [20] J. W. Minett, G. Peng, L. Zhou, H.-Y. Zheng, and W. S.-Y. Wang, "An assistive communication brain-computer interface for Chinese text input," in *2010 4th International Conference on Bioinformatics and Biomedical Engineering*, 2010, pp. 1–4, doi: 10.1109/ICBBE.2010.5515559.
- [21] K. George, A. Iniguez, and H. Donze, "Automated sensing, interpretation and conversion of facial and mental expressions into text acronyms using brain-computer interface technology," in *2014 IEEE International Instrumentation and Measurement Technology Conference (I2MTC) Proceedings*, 2014, pp. 1247–1250, doi: 10.1109/I2MTC.2014.6860944.

- [22] A. Raheel, S. M. Anwar, M. Majid, and B. Khan, "Real time text speller based on eye movement classification using wearable EEG sensors," in 2016 SAI Computing Conference (SAI), 2016, pp. 161–164, doi: 10.1109/SAI.2016.7555977.
- [23] A. A. Haider et al., "EEG-based Brain Computer Interface Prosthetic Hand using Raspberry Pi 4," *International Journal of Advanced Computer Science and Applications*, vol. 12, no. 9, pp. 44–49, 2021, doi: 10.14569/IJACSA.2021.0120905.
- [24] N. E. M. Isa, A. Amir, M. Z. Ilyas, and M. S. Razalli, "Motor imagery classification in Brain computer interface (BCI) based on EEG signal by using machine learning technique," *Bulletin of Electrical Engineering and Informatics*, vol. 8, no. 1, pp. 269–275, 2019, doi: 10.11591/eei.v8i1.1402.
- [25] P. Ghane, N. Zarnaghinaghsh, and U. Braga-Neto, "Comparison of Classification Algorithms Towards Subject-Specific and Subject-Independent BCI," in 2021 9th International Winter Conference on Brain-Computer Interface (BCI), 2021, pp. 1–6.
- [26] Y. Zhang, W. Chen, C.-L. Lin, Z. Pei, J. Chen, and Z. Chen, "Boosting-LDA algorithm with multi-domain feature fusion for motor imagery EEG decoding," *Biomedical Signal Processing and Control*, vol. 70, p. 102983, 2021, doi: <https://doi.org/10.1016/j.bspc.2021.102983>.
- [27] F. Lotte et al., "A review of classification algorithms for EEG-based brain-computer interfaces: a 10 year update," *Journal of neural engineering*, vol. 15, no. 3, p. 31005, 2018.

Fine-grained Access Control Method for Blockchain Data Sharing based on Cloud Platform Big Data

Yu Qiu*, Biying Sun, Qian Dang, Chunhui Du, Na Li
State Grid Gansu Electric Power Company Internet Division, Lanzhou, China

Abstract—Blockchain technology has the advantages of decentralization, de-trust, and non-tampering, which breaks through the limitations of traditional centralized technology, so it has gradually become the key technology of power data security storage and privacy protection. In the existing smart grid framework, the grid operator is a centralized key distribution organization, which is responsible for sending all the secret credentials, so it is easy to have a single point of failure, resulting in a large number of personal information losses. To solve the problems of inflexible access control in smart grid data-sharing framework and considering the limitation of multi-party cooperation among grid operators and efficiency, an attribute-based access control scheme supporting privacy preservation in smart grid is constructed in this paper. A fine-grained access control scheme supporting privacy protection is designed and extended to the smart grid system, which enables the system to achieve fine-grained access control of power data. A decryption test algorithm is added before the decryption algorithm. Finally, through performance analysis and comparison with other schemes, it is verified that the performance of this system is 7% higher than the traditional method, and the storage cost is 9.5% lower, which reflects the superiority of the system. Full optimization of the access policy is achieved. It is proved that the scheme is more efficient to implement the coordination and cooperation of multiple authorized agencies in the system initialization.

Keywords—Power grid data; blockchain technology; data sharing; fine-grained access control; game strategy; ciphertext key

I. INTRODUCTION

With the wide application of big data, fog computing, and Internet of Things technology, more and more applications store a large number of users' private data in the near-end fog node for computing. This solves the problem of insufficient storage space or limited computing resources of most mobile terminals in the current Internet of Things environment. At the same time, with the rise of new network architectures such as SDN, the computing, and storage capabilities of edge network devices and core gateway devices are continuously enhanced [1]. However, because the private data of users can bring commercial value to criminals, Internet of Things devices with weak performance have become the main target of hackers [2]. To prevent the user's data from being stolen, it is necessary to authenticate all unknown devices in the environment through identity authentication and other technical means, and then grant the corresponding device access to data after passing the identity authentication. However, most of the existing identity authentication schemes ignore the user's privacy disclosure in the authentication

process, including the user's functional attributes, real identity privacy and geographical location privacy.

Power data can be used by other organizations outside the grid system, for example, to calculate costs, monitor unexpected behavior, and predict future conditions. However, the power data of a single smart meter contains private information such as household habits, which needs to be protected. Therefore, how to balance the availability and privacy of power data is a problem faced by the smart grid [3]. In addition, RTUs and power consumers want to control access from users. Users want to get different power information depending on their specific tasks. For example, maintainers and system engineers monitor the network, while costing and analysis will be performed by auditors [4]. Therefore, in the smart grid system, it is particularly important to achieve fine-grained access control of power data [5]. However, most of the existing smart grid schemes focus on information aggregation but ignore the privacy protection and access control in the process of power data sharing.

Blockchain technology is a trusted storage network composed of distributed equal nodes, consisting of tamper-proof block data and automatically executable smart contract code, which has the characteristics of tamper-proof, coordination autonomy, high security, and trust of decentralized decision-making [6]. In the research of data sharing mechanisms based on blockchain, Dai Mingjun et al. [7] promoted the storage space of blockchain through distributed storage (DS) based on network coding (NC). Yang Jiachen et al. [8] introduced encryption algorithms to solve the problem of distributed secure storage of big data. Wang Zuan et al. [9] separated the original data storage and data transactions by using a double-chain structure and combined with proxy re-encryption technology to achieve secure and reliable data sharing. In 2016, Alharbi et al. [10] proposed an efficient privacy-preserving identity-based signature (IBS) scheme for smart grid communication. In 2017, a smart grid communication model [11] was proposed by Sedaghat et al., in which the cloud proxy service center, as a trusted third party with powerful computing power, is responsible for partially decrypting the shared ciphertext to reduce the burden of authorized users. In 2019, a privacy-preserving power data aggregation scheme [12] was proposed by Liu et al., but this scheme does not consider the access control of shared data.

This paper aims to design a fine-grained access control scheme supporting privacy preservation in the cloud environment. Firstly, a fine-grained access control scheme for data sharing with a completely hidden access policy is constructed. Then, based on this, extended research on

application scenarios is carried out, and an attribute-based access control scheme supporting privacy preservation in a smart grid is constructed.

The main innovations of this paper are:

- 1) The access policy and attribute set are transformed into vectors, and the access policy is completely hidden.
- 2) An attribute-based access control scheme supporting privacy preservation in a smart grid is constructed. Combine blockchain technology to control data sharing and access.
- 3) The scheme in this paper can realize the independent work of multiple distribution network operators, realize lightweight encryption, and improve decryption efficiency.

Content and structure of this paper are as follows:

- 1) Elaborate the research direction, introduce the research background and content;
- 2) Introduce the theoretical content of the relevant basic content;
- 3) Design the security game strategy of power grid big data access control system;
- 4) Establish a shared data access scheme for power grid block chain;
- 5) Realize the attribute-based access control scheme for the power grid privacy protection;
- 6) Summarize the paper and look forward to the next step.

II. RELATED WORK

A. Access Control Security Model

With the rapid development of the ubiquitous power Internet of Things (IoT), various IoT intelligent terminal devices deployed in the smart grid generate a large amount of data. Although the application of cloud Internet of Things technology has effectively solved the problem of massive data collection, storage and sharing, the smart grid is faced with a huge number of intelligent terminal devices deployed in all aspects of the grid, users with a sharp increase in data and mixed personnel. Therefore, the data privacy security issues that involve posing a serious security threat [13]. These security threats are mainly manifested in:

Data security risk: the combination of smart grid and Internet of Things technology, and the application of various emerging technologies in the smart grid makes the system complexity of the smart grid become higher. The security risk of various types of data is increased [14]. The application of cloud Internet of Things technology effectively realizes the collection, storage, and management of terminal data, but when it interacts with users, business systems, and power grid researchers, the misoperation and illegal access will cause data leakage.

User privacy risk: In the smart grid, while protecting the privacy data of ordinary users, it is also necessary to prevent the leakage of grid system data. Users' personal information and power consumption data belong to users' privacy; and the important operation data of each link of the smart grid system also need to be protected [15]. In the face of distributed attacks by illegal elements, illegal access by malicious users

and illegal operations by staff, the privacy data of power grid users and systems will be threatened.

B. Safety Requirements

According to the security threat analysis of data privacy protection in the smart grid cloud Internet of Things, effective access control methods are adopted to achieve the goal of data privacy security, and the following security requirements are considered:

- 1) **Authentication:** The identity of the user connected to the smart grid control center needs to be authenticated to prevent the user from stealing private data under false names. Data visitors must be authenticated with the control center in both directions [16].
- 2) **Data confidentiality:** When a visitor in the smart grid needs to decrypt and obtain encrypted data, its attribute set needs to meet the access policy requirements defined by the data owner, and unauthorized visitors cannot access user data.
- 3) **Anti-collision attack:** Unauthorized users cannot combine their key information to decrypt the ciphertext through the collusion of multiple users.
- 4) **Forward-backward confidentiality:** The newly authorized visitor cannot decrypt the previous ciphertext data with his own private key; the unauthorized visitor cannot decrypt the decrypted ciphertext data [17].
- 5) **Data integrity:** All kinds of private data must be encrypted before they can be transmitted between entities to avoid illegal tampering, damage and plagiarism during transmission and storage [18].

III. POWER GRID BIG DATA ACCESS CONTROL SYSTEM

The system consists of five main bodies, as shown in Fig. 1.

Grid Operator (GO): As a certification center, the GO is responsible for setting up the smart grid system, distributing GIDs to users, and granting access to users. In addition, GO distributes identity keys for legitimate users.

Multiple Distribution Operators (DGOs): As multiple attribute authorities, each DGO is responsible for establishing its own domain, managing attributes, and distributing attribute keys to users according to the attribute set.

Cloud storage server: It is responsible for storing power data in the form of ciphertext. The cloud storage server does not participate in the access control and data decryption process.

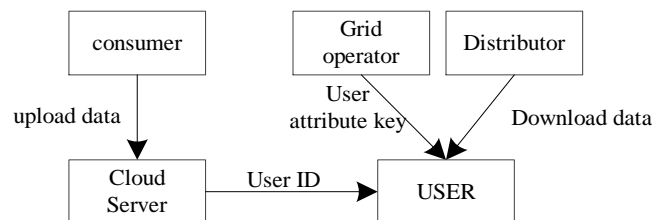


Fig. 1. Access Control System Model of Smart Grid.

Power data owners: Power data owners include RTUs and power consumers. The owner of the power data can define an access policy, use it to encrypt the power data, and upload it to the cloud storage server.

Users: Users may be maintainers, system engineers, researchers, policymakers, and auditors of power systems [19]. After the user downloads the encrypted power data from the cloud storage server, if the user wants to decrypt it, he needs to prove his identity to GO and initiate a key request to DGOs.

A. Fine-grained Shared Security Game Strategy

This section will elaborate the security model of the scheme based on the security game between the attacker A and the simulator B . Among them, the security game will have the following stages:

Initialization: attacker A sends fine-grained authority DGO_k^* to emulator B , and B gets the public parameter pp of the system.

Authority establishment: for each fine-grain authority, that simulator B runs an authority establishment algorithm. The public key PK_k and the private key SK_k are obtained, and then the public key PK_k is published to A [20].

Stage 1: Attacker A submits attribute vector \bar{y} and GID and initiates a user key challenge to impersonator B . Wherein the vector \bar{y} is generated by encoding the attribute set S' randomly selected by A . B runs the user key generation algorithm and replies the corresponding $SK_{k,j}$ and SK_{gid} to A . In phase 1, A may interrogate the key within the PPT.

Challenge: A submits two messages M_0, M_1 of equal length and two policy vectors \bar{x}_0, \bar{x}_1 to B . Wherein, the vectors \bar{x}_0 and \bar{x}_1 are respectively encoded and generated by the access strategies W'_0 and W'_1 selected by A [21]. But it must be satisfy that neither that vector \bar{x}_0 nor the vector \bar{x}_1 is orthogonal \bar{y} , that is, $(\langle \bar{x}_0, \bar{y} \rangle \neq 0) \wedge (\langle \bar{x}_1, \bar{y} \rangle \neq 0)$. Simulator B tosses a coin to generate a random bit $\xi \in \{0,1\}$, and then runs the encryption algorithm to generate the corresponding ciphertext CT_ξ and sends it to attacker A .

Stage 2: As in stage 1, A then makes a user key challenge to B . But must satisfy that vector \bar{x}_0 . Neither \bar{x}_1 nor the vector \bar{y} is orthogonal.

Guess: A guesses ξ and gives ξ' . If $\xi' = \xi$, then A

$$Adv_A = \left| \Pr[\xi' = \xi] - \frac{1}{2} \right|$$

wins and the winning margin is

B. Threshold Access Policy

The key technologies of threshold access policy encoding are divided into the following two parts:

1) The access policy W is transformed into a vector \bar{x} :

First, the power data owner defines an access policy $W = \{t_{1,n_1}, t_{2,n_2}, \dots, t_{j,n_j}\}$, selects t random coefficients $a_i \in \mathbb{Z}_p$, and sets a polynomial $f(x)$ of order $t-1$ as follows:

$$f(x) = a_{t-1}x^{t-1} + \dots + a_1x + a_0 \pmod{p} \quad (1)$$

Then, for each element $t_{i,j}$ in the access policy W , the component elements of the corresponding vector \bar{x} are generated:

$$\begin{cases} x_i = \begin{cases} f(t_{i,j}) & t_{i,j} \in W \\ 0 & t_{i,j} \notin W \end{cases} : \forall i = 1, \dots, L-1 \\ x_L = -f(0) = -a_0 \end{cases} \quad (2)$$

2) Convert the attribute set S_k to a vector \bar{y} :

Let $S = \{v_{1,n_1}, v_{2,n_2}, \dots, v_{j,n_j}\}$ and $U_k = \{w_{1,n_1}, w_{2,n_2}, \dots, w_{j,n_j}\}$ be two attribute sets of the same length, where S represents the attribute set of the user in the system, and U_k represents the attribute set managed by the authority DGO_k . For a corresponding location that is not an attribute managed by U_k , let $w_{i,j} = 0$. Define $S_k = S \cap U_k = \begin{cases} v_{i,j} & v_{i,j} = w_{i,j} \\ 0 & v_{i,j} \neq w_{i,j} \end{cases}$. Then, calculate the value of the Lagrange polynomial $\Delta_{v_{i,j}, S}(x)$ at $x=0$, where $\Delta_{v_{i,j}, S}(x) = \prod_{k \in S, i \neq k} \frac{x - v_{k,j}}{v_{i,j} - v_{k,j}}$. For each element $v_{i,j}$ in the attribute set S_k , a component element of the corresponding vector \bar{y} is generated:

$$\begin{cases} y_i = \begin{cases} \Delta_{v_{i,j}, S}(0) & v_{i,j} \in S_k \\ 0 & v_{i,j} \notin S_k \end{cases} : \forall i = 1, \dots, L-1 \\ y_L = 1 \end{cases} \quad (3)$$

Attention:

$$\langle \bar{x}, \bar{y} \rangle = f(0) \Leftrightarrow t_{i,j} = v_{i,j} (i \geq t) \Leftrightarrow S \perp W \quad (4)$$

The above calculations only appear in the exponential part of the decryption phase.

IV. BLOCKCHAIN SHARED DATA ACCESS SCHEME

$u = \{att_1, \dots, att_L\}$ is defined as the global attribute set of the system and $H: \{0,1\}^\lambda \times Z_p^{l+1} \rightarrow Z_p^{k+1}$ is a collision-resistant hash function. The specific construction of the attribute-based access control scheme supporting privacy protection in the smart grid is as follows:

System initialization: This phase consists of the following two algorithms. GO generates the whole system by running the system establishment algorithm, and DGOs generates its own domain by running the authority establishment algorithm.

GO-Setup: Run the group generator g to generate the bilinear group $(p, g_1, g_2, e, G_1, G_2, G_T)$. GO builds N authorities for the system, respectively: $DGO_1, DGO_2, \dots, DGO_N$, where each DGO_k manages a mutually exclusive set of attributes $U_k = \{Att_1, Att_2, \dots, Att_{n_k}\}$, and $|U_k| = n_k$. Let $\sum_{sign} = (keygen, Sign, Verify)$ be a signature scheme. Select the random matrix $A, B \in Z_p^{(k+1) \times k}$, $P \in Z_p^{(k+1) \times (k+1)}$, calculate $P_1 = g_1^A, P_2 = g_2^B, X = g_1^{P^T A}$, and return the common parameter pp as follows:

$$pp = \{G_1, G_2, G_T, e, p, g_1, g_2, P_1, P_2, X, Verify\} \quad (5)$$

DGOS-Setup: For any authority DGO_k in the system, select two random matrices $U_k, W_k \in Z_p^{(k+1) \times (k+1)}$ and a random vector $\bar{\alpha}_k \in Z_p^{k+1}$, calculate $V_{1,k} = g_1^{U_k^T A}, V_{2,k} = g_1^{W_k^T A}, Y_k = e(g_1, g_2)^{\bar{\alpha}_k^T A}$, and then publish the public key PK_k of DGO_k and keep the private key SK_k .

$$PK_k = \{V_{1,k}, V_{2,k}, Y_k\}, SK_k = \{U_k, W_k, \bar{\alpha}_k\} \quad (6)$$

Authentication and key distribution: When a user joins the system, GO assigns a unique GID to the user. If the user wants to decrypt the ciphertext, first, the user needs to convert the attribute set S into a vector $\bar{y} = \{y_j | j \in [1, L]\}$, the user needs to submit the attribute set S and the attribute vector \bar{y} to request the key from GO. For the legal user who has completed the registration, GO will distribute the identity key

SK_{gid} with the signature to the legal user by running the identity key generation algorithm. Next, the user needs to submit the attribute set S , the attribute vector \bar{y} , and the identity key SK_{gid} with the GO signature to request the attribute key from the DGOs. Each DGO_k then uses Verify to verify the signature. Once the verification is passed, each DGO_k generates attribute keys $SK_{k,j}$ by running the attribute key generation algorithm and sends them to the user. This process involves the following two algorithms:

Identity key generation (GO-KeyGen): For the authentication center GO in the system, randomly select two vectors $\bar{y} \in Z_p^{(k+1)}, \bar{r} \in Z_p^k$ and calculate the user identity key:

$$SK_{gid} = P_2^{\frac{\bar{r}}{u + \bar{y}}} \quad (7)$$

Where, $u = H(GID, \bar{y})$.

Attribute key generation (DGOS-KeyGen): For each authority DGO_k in the system, it is first necessary to convert the attribute set S_k into a vector $\bar{y} = \{y_j | j \in [1, n_k], \sum_{k=1}^N n_k = L\}$, where $S_k = S \cap U_k$, according to Section 4.1.5, and then calculate the user attribute key:

$$SK_{k,j} = g_2^{\bar{\alpha}_k} [(SK_{gid}^T)^{y_j} U_k^T + W_k^T]^T \quad (8)$$

Data release: The power data owner defines an access policy W , and converts it into a vector \bar{x} ; then, the power data M_p is encrypted by the following encryption algorithm, and the ciphertext CT_p is uploaded.

Encrypt: For the power data owner in the system, randomly select two vectors $\bar{s}, \bar{s}^* \in Z_p^k$ and calculate the ciphertext $CT_p = \{C_0, C_1, C_k, C_j^*, C_{k,j}\}$ as follows:

$$\begin{cases} C_0 = M_p \cdot \prod_{k=1}^N Y_k^{\bar{s}} = M_p \cdot e(g_1, g_2)^{\sum_{k=1}^N \bar{\alpha}_k^T \cdot A \bar{s}} \\ C_1 = P_1^{\bar{s}} \\ C_k = V_{2,k}^{\bar{s}} = g_1^{W_k^T A \bar{s}} \\ C_{k,j} = [X^{x_j} \cdot V_{1,k}]^{\bar{s}} = g_1^{(x_j P^T + U_k^T) A \bar{s}} \\ C_j^* = P_1^{\bar{s} \cdot x_j} (k \in [1, N], j \in [1, L]) \end{cases} \quad (9)$$

Data recovery: Any user can access the power data encrypted in the cloud, but only when $S \perp W$, the authorized user can successfully decrypt it. In order to reduce the cost of decryption, the decryption process is divided into two stages: decryption test and complete decryption. The user first runs the test algorithm to verify $S \perp W$ or $S \nabla W$. If $F(W, S) = 1$ is output, the user runs the full decryption algorithm; otherwise, the decryption is terminated. Details are as follows:

Decryption Test Phase: User calculation:

$$F(W, S) = \sum_{j=1}^{l+1} C_j^{*y_j} \quad (10)$$

Attention: $F(W, S) = 1 \Leftrightarrow \sum_{j=1}^L x_j y_j = 0 \Leftrightarrow S \perp W$. If output $F(W, S) = 1$, so, it represents $S \perp W$, then the user will proceed to the next stage for full decryption; otherwise, the user will terminate decryption.

Dec-Phase: Once the above test Phase is passed, it indicates $S \perp W$, and the user has performed the following calculations:

$$C_0 \cdot \frac{e(\prod_{k=1}^N \prod_{j=1}^L C_{k,j}^{y_j} \cdot C_k, SK_{gid})}{e(C_1, \prod_{k=1}^N \prod_{j=1}^L SK_{k,j})} = M_p \quad (11)$$

V. ATTRIBUTE-BASED ACCESS CONTROL SCHEME FOR PRIVACY PROTECTION IN POWER GRID

System initialization Setup1 (PK, MSK):

Enter the security parameters to obtain the public key PK and the master key MSK.

Encrypt (M, PK, W) CT: Input message M, public key PK, and access policy W to get ciphertext CT.

Key GenPK, MSK, S SK: Input public key PK, master key MSK and attribute set S to get user key SK.

Decrypt CT, SK, PK M or: input ciphertext CT, user key SK and public key PK, if $S \nabla W$, output message M; otherwise, the algorithm aborts and outputs.

System Setup (GO-Setup): This phase is executed by GO, which inputs security parameters I^{λ} and obtains system public parameters PP , as well as a pair of signature and authentication keys (Sign, Verify).

DGOS-Setup: This algorithm is executed by DGOs, which inputs the subscript k of DGOk and outputs the public and private keys.

User key generation (KeyGen): includes two stages of identity key generation and attribute key generation, as follows:

1) Identity key generation phase (GO-KeyGen): This phase is executed by GO. Input the global identity GID of the user to get the identity key SK_{gid} of the user.

2) Attribute key generation phase (DGOS-KeyGen): This phase is performed by DGOs, inputting the private key SK_k and the encoding vector \vec{y} of the attribute set S, and then outputting the attribute key $SK_{k,j}$ of the user.

Encrypt: The algorithm is run by the owner of the power data, inputting the public key PK_k , power data M_p , and the encoding vector \vec{x} of the access policy W, and outputting the power data in encrypted form $SK_{k,j}$.

Decrypt: This algorithm includes two phases: decryption test and full decryption, as follows:

1) Decryption Test Phase: Input the power data CT_p in encrypted form and the encoding vector \vec{y} . If $F(W, S) = 1$, proceed to the next phase; otherwise, the algorithm is aborted.

2) Complete Decryption Phase (Dec-Phase): Input the power data CT_p in encrypted form, the encoding vector \vec{y} , the user's attribute key $SK_{k,j}$ and the user's identity key SK_{gid} , and output the power data M_p or \perp .

VI. EXPERIMENTAL ANALYSIS

A. Experimental Platform

The experimental environment builds a micro-cloud environment to simulate the big data service under the cloud platform. The server-side and client-side configurations are shown in Table I.

This paper is based on the Pairwise Cryptography Laboratory (PBC) and uses 160-bit elliptic curve groups over a 512-bit finite field, which are used to calculate the cost of the test operation and the decryption operation.

B. Performance Analysis

In the simulation test, E_{G_1} , E_{G_2} and E_{G_T} respectively represent the time cost of an index operation in G_1 , G_2 and G_T . N_w and N_s represent the number of attributes in the access policy and user attribute set, respectively. The \hat{e} represents the time cost required to compute a bilinear function. The $O(H)$ represents the time required to compute a hash function. The P_i indicates the number of possible values for a multivalued attribute.

1) *Theoretical analysis*: In Table II, this scheme is further compared with scheme [22-25] from four aspects of key generation cost, encryption cost, test cost and decryption cost.

TABLE I. EXPERIMENTAL PLATFORM CONFIGURATION PARAMETERS

Configurations	Type	
	Server side	Client side
CPU	Core(TM) i7-10900k4.6GHz	Core(TM) i5-10400f 4.3GHz
Memory	128G	16G
System	Windows Server LTSC Preview	Windows 11

TABLE II. PERFORMANCE COMPARISON OF SMART GRID ACCESS CONTROL SCHEMES

Plan	Types	Independent authorized agency	Decryption test	Full hiding strategy	IPE	Adaptive safety
[22]	MA-ABE	√	×	×	×	×
[23]	MA-ABE	√	×	×	×	×
[24]	MA-ABE	√	×	×	×	×
[25]	D-MA-ABE	×	×	√	√	√
The plan	MA-ABE	√	√	√	√	√

TABLE III. COMPARISON OF COMPUTATIONAL COMPLEXITY OF SMART GRID ACCESS CONTROL SCHEMES IN DIFFERENT STAGES

Plan	User key generation		Encryption			Decryption test			Fully decrypted		
	E_{G_2}	$O(H)$	e	E_{G_1}	E_{G_T}	e	E_{G_1}	E_{G_T}	e	E_{G_2}	E_{G_T}
[25]	N_s	N_s	1	$1 + N_w$	1	-	-	-	2	2	$2p_i N_s$
The plan	N_s	0	1	$1 + 3N_w$	1	0	$p_i N_s$	0	1	$3p_i N_s$	3

It can be seen from Table III that this scheme is more efficient than the scheme [25] in the key generation and decryption stages because of the calculation of the hash function in the scheme [25].

2) *Simulation test*: The actual performance of the present protocol and the protocol [25] will be tested. The results show that, compared with the scheme [25], the present scheme has obvious advantages in both the key distribution phase and the decryption phase. Fig. 2 shows the comparison of the storage cost of this scheme and the scheme [25] in each stage of the algorithm. In the simulation, the lengths of the elements in the bilinear groups G_1 , G_2 , and G_T are set to 512 bits. Assume that there are 10 authorities in the system, that is, $N=10$, and specify that each authority manages five attributes.

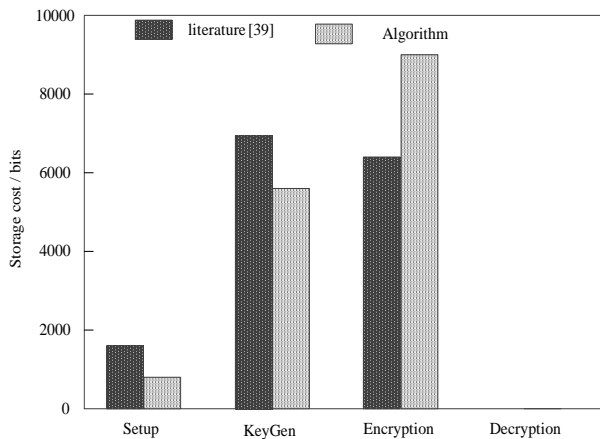


Fig. 2. Storage Cost Comparison.

It can be seen from Fig. 2 that, compared with the scheme [25], the construction of this scheme requires less space to store the public key and the secret key of the user. Fig. 3, Fig. 4 and Fig. 5 respectively show the running time comparison of the user key distribution algorithm, the encryption algorithm and the decryption algorithm in this scheme and the scheme [25].

Fig. 3 shows that the running time of the user key distribution algorithm of the two schemes increases linearly with the number of attribute sets.

As can be seen from Fig. 4, the efficiency of the encryption algorithm in this scheme is obviously low, which is a compromise for security performance.

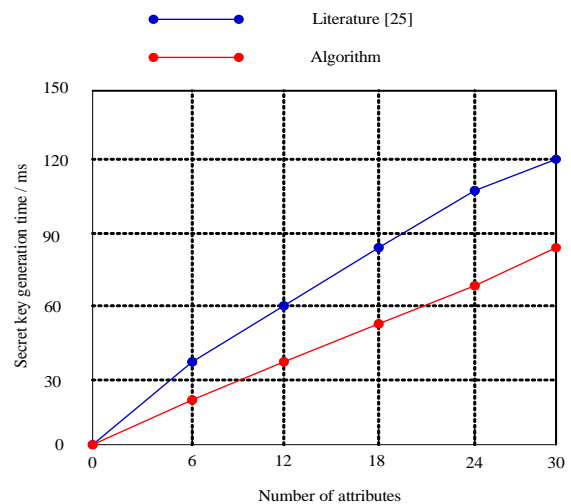


Fig. 3. Comparison of Secret Key Generation Time.

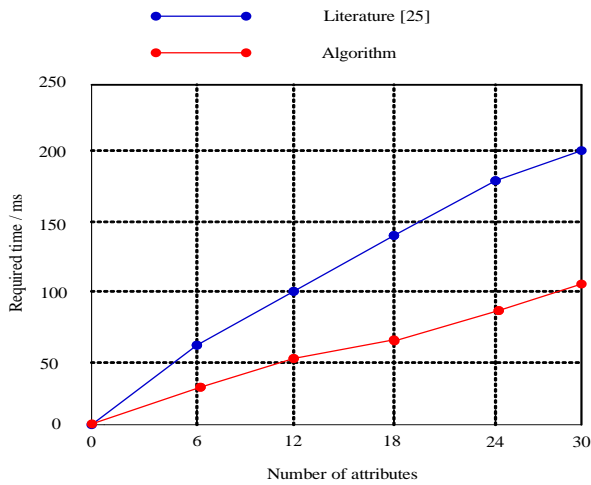


Fig. 4. Time Comparison of Encryption Algorithms.

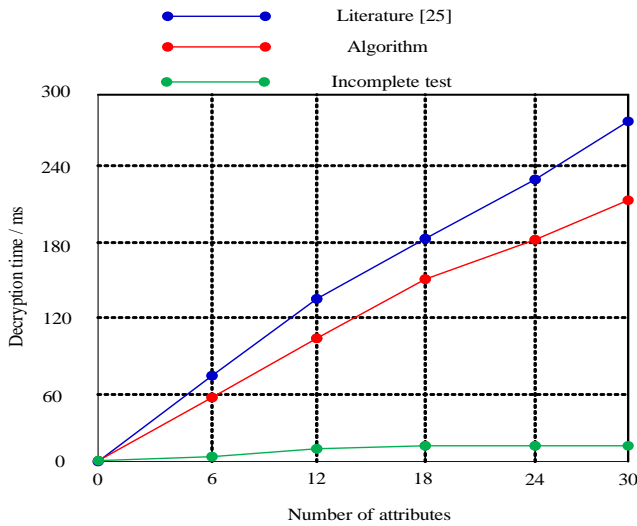


Fig. 5. Time Comparison of Decryption Algorithms.

As shown in Fig. 5, the decryption test algorithm in this scheme takes significantly less time than the full decryption algorithm. If the attribute set of the user does not satisfy the access policy, the scheme only executes the decryption test algorithm and does not need to execute the complete decryption operation. Due to the decryption test operation, the time required for successful decryption of the present scheme is much shorter than that of the scheme [25].

C. Discussion

If the distributions of encryption and decryption are statistically similar, there is no one simulator B that can distinguish the two strategies by any advantage.

Proof: In the challenge phase, simulator B randomly selects A, to satisfy.

Then generate:

$$C_{k,j} = g_1^{(x_{b,j}P^T + U_k^T)(A\bar{s} + b^\perp \hat{s})} = g_1^{x_{b,j}P^T(A\bar{s} + b^\perp \hat{s})} \cdot g_1^{U_k^T(A\bar{s} + b^\perp \hat{s})} \quad (12)$$

Given $g_1^A, g_1^{A\bar{s} + b^\perp \hat{s}}, g_1^{U_k^T A}, g_2^B$, this term $g_1^{U_k^T(A\bar{s} + b^\perp \hat{s})}$ is uniformly distributed in the group. Therefore, there is no adversary that can distinguish strategies $Game_3$ and $Game_4$ with any advantage.

In the strategy $Game_4$, in the opponent's view, the choice of b by the simulator B is statistically independent, and the opponent cannot win the strategy by any advantage.

If the K-Linear assumption holds, the privacy-preserving power data access control scheme is IND-CPA secure.

It is proved that under the k-Linear assumption, based on the proof of the above lemma, the attacker's advantage in winning the real security strategy is negligible. Therefore, the attacker cannot break the scheme in the PPT.

VII. CONCLUSION

In this paper, a fine-grained access control scheme is proposed to support data sharing in the smart grid. The main work includes:

- 1) The decentralized attribute-based encryption scheme is extended to the smart grid system, which is based on a more flexible threshold access structure.
- 2) In order to improve the efficiency, a test phase is added before the data is completely decrypted, which avoids many unnecessary decryption operations.
- 3) Based on the k-Linear assumption, it is proved that the scheme achieves adaptive security.

Performance analysis shows that this scheme has obvious advantages compared with similar schemes.

The content of this paper can protect the privacy information of the trajectory data, and improve the availability of the data. Finally, through the experimental verification, it is proved that the proposed method not only protects the privacy information of trajectory data but also improves the availability of data.

In the next step, when the privacy budget is allocated by the special series method. Although infinitely many points can be protected, if there are too many position points in trajectory data, the smaller the privacy budget allocated to the later position points is, the larger the corresponding added random noise is. Then, the availability of the data will be reduced.

REFERENCES

- [1] Zhang P, Song J. Research progress on performance optimization of blockchain consensus algorithm. Computer Science, 2020, 47(12): 296-303.
- [2] Lu G, Xie L, Li X. A comparative study of blockchain consensus algorithms. Computer Science, 2020, 47(6A): 332-339.
- [3] Bamakana S, Motavali A, Bondarti A. A survey of blockchain consensus algorithms performance evaluation criteria. Expert Systems with Applications, 2020, 154: 1-21.
- [4] W. Sun, L. Wang, P. Wang, and Y. Zhang. Collaborative blockchain for space-air-ground integrated network. IEEE Wireless Communications, 2020, 27(6): 82-89.
- [5] Sel D, Zhang K, Jacobsen H. Towards solving the data availability problem for sharded Ethereum. SERIAL 2018-Proceedings of the 2018

- Workshop on Scalable and Resilient Infrastructures for Distributed Ledgers, 2018, 1: 25-30.
- [6] Liu X, Feng J. Trusted blockchain oracle scheme based on aggregate signature. *Journal of Computer and Communications*, 2021: 95-109.
- [7] Fan H, Liu Y, Zeng Z. Decentralized privacy-preserving data aggregation scheme for smart grid based on blockchain. *Sensors*, 2020, 20(18): 1-14.
- [8] Xue Z, Pan X, Lv Z, et al. Application of blockchain in energy and power business. *Journal of Physics: Conference Conference Series*, 2020, 1626(1): 1-7.
- [9] Zeng Z, Li Y, Cao Y, et al. Blockchain technology for information security of the energy internet: fundamentals, features, strategy and application. *Energies*, 2020, 13(4): 1-24.
- [10] J. Huang, C. Lin, H. Zhou, Z. Xu, and C. Lin. Research on key technologies of deduction of multinational power trading in the context of Global Energy Interconnection. *Global Energy Interconnection*, 2019, 2(6): 560-566.
- [11] Y. Jiang, C. Wang, Y. Wang, and L. Gao. A cross-chain solution to integrating multiple blockchains for IoT data management. *Sensors (Switzerland)*, 2019, 19(9): 1-18.
- [12] G. van Leeuwen, T. AlSkaif, M. Gibescu, and W. van Sark. An integrated blockchain-based energy management platform with bilateral trading for microgrid communities. *Applied Energy*, 2020, 263(1): 114613.
- [13] M. Kim, et al. A secure charging system for electric vehicles based on blockchain. *Sensors (Switzerland)*, 2019, 19(13): 1-22.
- [14] E. Mengelkamp, J. Gärtner, K. Rock. Designing microgrid energy markets A case study: The Brooklyn Microgrid. *Applied Energy*, 2018, 210: 870-880.
- [15] Z. Ji, X. Wang, C. Cai, and H. Sun. Power entity recognition based on bidirectional long short-term memory and conditional random fields. *Global Energy Interconnection*, 2020, 3(2): 186-192.
- [16] T. Alladi, V. Chamola, J. J. P. C. Rodrigues, and S. A. Kozlov. Blockchain in smart grids: A review on different use cases. *Sensors (Switzerland)*, 2019, 19(22): 1-25.
- [17] J. Zhang, et al. Design scheme for fast charging station for electric vehicles with distributed photovoltaic power generation. *Global Energy Interconnection*, 2019, 2(2): 150-159.
- [18] P. Liu, W. Jiang, X. Wang, H. Li, H. Sun. Research and application of artificial intelligence service platform for the power field. *Global Energy Interconnection*, 2020, 3(2): 175-185.
- [19] B. Hong, Q. Li, W. Chen, B. Huang, H. Yan, K. Feng. Supply modes for renewable-based distributed energy systems and their applications: case studies in China. *Global Energy Interconnection*, 2020, 3(3): 259-271.
- [20] N. Saxena, B. J. Choi. Authentication Scheme for Flexible Charging and Discharging of Mobile Vehicles in the V2G Networks. *IEEE Transactions on Information Forensics & Security*, 2017, 11(7): 1438-1452.
- [21] M. S. Rahman, A. Basu, S. Kiyomoto, M. Z. A. Bhuiyan. Privacy-friendly secure bidding for smart grid demand-response. *Information Sciences*, 2017, 379: 229-240.
- [22] K. Xue, Y. Xue, J. Hong, W. Li, H. Yue, D. S. L. Wei, P. Hong. RAAC: Robust and Auditable Access Control With Multiple Attribute Authorities for Public Cloud Storage. *IEEE Transactions on Information Forensics and Security*, 2017, 12(4): 953-967.
- [23] Aitzhan N Z, Svetinovic D. Security and Privacy in Decentralized Energy Trading Through Multi-Signatures, Blockchain and Anonymous Messaging Streams. *IEEE Transactions on Dependable and Secure Computing*, 2018, 15(5): 840-852.
- [24] Fan, T.; He, Q.; Nie, E.; Chen, S. A study of pricing and trading model of Blockchain & Big data-based Energy-Internet electricity. In *Proceedings of the 3rd International Conference on Environmental Science and Material Application (ESMA 2018)*, Chongqing, China, 25 - 26 November 2018: 1 - 12.
- [25] POP, Claudia, et al. Blockchain based decentralized management of demand response programs in smart energy grids. *Sensors*, 2018, 18(1): 162.

Smart System for Emergency Traffic Recommendations: Urban Ambulance Mobility

Ayoub Charef¹, Zahi Jarir², Mohamed Quafafou³

Department of Computer Science, Faculty of Science, Cadi Ayyad University, Marrakech, Morocco^{1,2}

Department of Computer Science, University of Aix-Marseille, Marseille, France³

Abstract—With the increasing evolution of advanced technologies and techniques such as the Internet of Things, Artificial Intelligence and Big Data, the traffic management systems industry has acquired new methodologies for creating advanced and intelligent services and applications for traffic management and safety. The current contribution focuses on the implementation of a path recommendation service for paramedics in emergency situations, which is one of the most critical and complex issues in traffic management for the survival of individuals involved in emergency incidents. This work mainly focused on the response time to life-threatening incidents, which is an indicator for emergency ambulance services and for recommending a fastest ambulance route. To this end, we propose a hybrid approach consisting on a local approach using machine learning techniques to predict the congestion of different sections of a map from an origin to a destination, and a global approach to suggest the fastest path to ambulance drivers in real time as they move in OpenStreetMap.

Keywords—*Recommendation systems; emergency urban traffic; ambulance mobility; emergency navigation services*

I. INTRODUCTION AND MOTIVATION

Nowadays traffic congestion represents a real major issue for all societies and also an inconvenience for the townspeople because of the increase of population and vehicles in an urban zone. The level of these challenges encountered varies from one region to another depending on road infrastructure resources, road safety education, people's behavior [1], etc. Traffic blockage becomes one of the major and most difficult problems in various urban areas according to the negative effects it induces to the various actors of the road: road users, pedestrians, police officers, which in turn result in various social and economic problems according to [2]. Among these effects and by the observation that the frequency of road accidents and their effects are increasing, more and more every day [3]. Therefore, most of the ministries of equipment and transport over the world have invested in road infrastructures by installing the latest generation technologies and solutions to be able to reduce the level of stress and save the lives of citizens. Moreover, the emergency rescue research is receiving more and more attention. The most important factor in an emergency rescue is rescue timeliness, and often makes a difference between life and death [4].

However, finding an effective response to this challenge is considered as complex and tedious research topic in the literature. Despite the advances and published results of scientific contributions on this topic, this challenge remains open. This complexity is compounded when other constraints

or factors must be met, such as the inability to create emergency lanes due to narrow roads, undeveloped urban road infrastructure, etc.

In this paper the proposed approach consists of offering an emergency mobility service with the advantage of continuously recommending to ambulance drivers with the fastest way to reach the destination. The data used comes from road infrastructure sensors, Internet of Things installed in roads, etc. as well as data from previously traveled routes, such as incidents, line changes, travel time, traffic flow, etc. All these data enable us to calculate the speed interval and travel duration for every route taken by an ambulance in response to an emergency. In this contribution, this paper mainly focuses on how to reduce ambulance travel time by addressing the challenges of an efficient ambulance response. To achieve this goal, the proposed approach is twofold: 1) to analyze the mobility of emergency ambulances and identify the main factors preventing their travel, and 2) to model the fastest travel recommendation solution to improve ambulance mobility time by focusing on data collection from roadway infrastructure sensors, archived data on confirmed past travel history.

The remainder of the paper is organized as follows. Section II exposes a related work on path recommendation solutions for Emergency Medical Transportations (EMTs) in emergency states presented in the literature. Section III details the constraints to be considered when proposing an emergency path recommendation solution. Section IV describes the multilayer architecture of the proposed recommendation solution. Section V explains the multi-agents modeling approach, while data and random traffic generation used for an experimentation is exposed in section VI. Section VII presents details of the proposed hybrid approach for predicting the traffic state based on machine learning techniques, and proposing the fastest path to a destination in real-time using Dijkstra algorithm. Finally, Section VIII concludes the paper and presents some future works.

This section starts by exposing some interesting finding published in literature concerning the prediction of travel path for emergency vehicles (EV). Then it focuses on some important machine learning algorithms predicting urban traffic congestion.

II. LITERATURE REVIEW

A. Trajectory Prediction for Emergency Vehicles

Traffic congestion contributes greatly either indirectly or directly to both economic and health losses in countries.

According to [5], other repercussions of traffic jams include prolonged time loss, especially during peak hours, mental stress, traffic accidents, air pollution, noise, and disturbance [6]. Therefore, it is difficult for emergency vehicle services to achieve short response times during interventions without using effective advanced solutions, techniques and technologies. In the literature, several approaches have been proposed to reduce ambulance response time. This delay is mainly due to several traffic lights management, uncontrolled intersections, that creates a crowd of vehicles and thus puts ambulances on hold.

The work presented in [7] suggests a solution to make on the traffic lights for ambulance from the start position to the scene of an incident or where a patient is. However, the proposed solution is very restrictive since signalized intersections could present colossal travel delays. So the most generally taken on procedure for EV prioritization is traffic light need control. In the same context, authors in [8] propose a method of controlling traffic lights and performing the aforementioned task to allow the ambulance to cross all intersections without waiting. However, road signs remain an uncontrollable problem.

Authors in [9] propose an Android application with an Internet of Things (IoT) network model for an EV routing using Fuzzy logic-based data fusion. The data fusion approach calculates the exact congestion for a certain place by taking into account crowd inputs and sensory data. However, the suggested system requires the crowdsourced data to be assessed for trust in order to confirm the identity of the crowdsourced user. Moreover, strong communication protocols are required when using IoT in order to reduce the danger of security threats.

In other work, [10] uses radiofrequency sensors to count vehicles, which are equipped with radio frequency identification tags, to propose a dynamic traffic signal as a solution to avoid ambulance blockage. However, the proposed solution is also very restrictive since vehicles should be equipped with radio frequency identification tags.

The work in [11] proposes a unique decentralized approach to geofencing based on radio frequency and global navigation satellite system that allows emergency service vehicles to pass through intersections with the least amount of delays by giving them the right of way green signal. In the same context [12] proposed a cooperative vehicle-road scheduling method that includes a real-time route planning module and a group traffic signal management module.

The approach presented in [13] provides green indicators to help EV to pass through intersections quickly without stopping, and restores the road network to the normal situation as soon as possible by using linear programming to find the shortest green time in each phase after an EV passes the intersection. However, the proposed contribution does not take into account the dynamics the global traffic state and the impact of a scheduling strategy on the ordinary vehicles.

The authors in [14] propose an algorithm for finding the shortest or fastest path. This algorithm based on Ant Colony Optimization with Fuzzy Logic to deal with local path planning for obstacle avoidance by taking into account wind, flow air,

and dynamic obstacles. However, the weakness of this approach is that the response time of the algorithm is very slow.

In the same context, [15] and [16] proposed an ASNN-FRR (A traffic-aware neural network for fastest route recommendation) model suggesting a fastest route recommendation. This model uses two powerful predictors for $g(\cdot)$ and $h(\cdot)$ functions of A* algorithm respectively, to find fastest path between two points origin-destination (OD) based on travel time estimation. However, the trajectory recommendation is given initially, the problem here is that the authors do not take into account that urban traffic changes over time.

By collecting and analyzing social media data and using new technologies of granular computing that transforms big data collections into granular information, [17] proposes a fastest path optimization model to incorporate the impact of traffic events and generate the optimal routing strategy. However, the obtained results show that the strategy is good for public transport and not for the emergency vehicles.

To help EVs such as ambulance, fire engine, and police vehicles to greatly benefit from accurate path prediction systems, [18] and [19] suggested a ventilation network model to automatically assess and determine potential escape routes. A variant of Dijkstra's algorithm is used to forecast intricate pathways between any two sites across a model. However, the proposed model uses data from the begin and not take in consideration frequent traffic changes.

The proposed approach in [4] offers a data-driven system for precisely predicting the path taken by an ambulance moving with blue lights and sirens in response to an emergency situation. This technique calculates the typical response time of an ambulance to an emergency call using historical data, and then estimates the travel time from these speeds for each route. Finally, it finds the quickest path between any beginning and finishing points using a common graph-theoretic approach based on Hidden Markov model. However, historical data can only be used to make predictions; in contrast, emergency situations need using real-time data.

The work of [20] uses the technique of multiple classifiers with maximum vote to predict the route to the destination with the highest degree of accuracy and select the best path to reach the destination as quickly as possible. Three algorithms—the artificial neural network (ANN), the k-nearest neighbors (KNN), and the support vector machine (SVM) are the foundation of this system. As classifiers, which can't foresee the quickest path between two points. By and by, the real travel season of a similar route can be exceptionally irregular at various times or simultaneously of day on various days, because of the blockages from vehicles.

B. Traffic Congestion Prediction

Several interesting contributions focus on traffic congestion prediction problems to avoid traffic jams and minimize travel time. The objective of this subsection is to present some of them in order to highlight the most used techniques.

Table I shows the comparison of Proposed Approach with Existing works in Literature.

TABLE I. COMPARISON OF PROPOSED APPROACH WITH EXISTING MODELS

Reference	Methodology	Prediction studies	Target domain	Prediction by area	Prediction on intersection	Runtime prediction for EVs	Historical Data /Runtime Data
[20]	ANN And KNN	Machine learning	predict congestion	✓	✗	✓	✓
[21]	Genetic Algorithms	Probabilistic reasoning	analyse short-term congestion.	✓	✗	✗	✓
[22]	Genetic Algorithms	Probabilistic reasoning	predict congestion at desired point.	✗	✓	✗	✗
[24]	particle swarm optimization	Probabilistic reasoning	predict the urban traffic congestion	✓	✗	✗	✗
[25]	KNN, SVM, Hybrid Model	Machine learning	short-term volume prediction	✗	✗	✓	✓
[26]	Extended Kalman filter	Machine learning	Traffic Congestion Estimation	✗	✗	✗	✗
[27]	neural network	Machine learning	predict congestion	✓	✗	✗	✗
[28]	Bayesian network	Probabilistic reasoning	congestion probability	✗	✗	✗	✗
[29]	deep learning	Machine learning	traffic flow	✓	✗	✗	✗
[33]	fuzzy logic inference	Probabilistic reasoning	Traffic Flow Detection	✗	✗	✓	✓
[34]	Evolutionary Crisp Rule Learning	Probabilistic reasoning	predict congestion level	✗	✗	✓	✗
[36]	Fuzzy logic evaluation	Probabilistic reasoning	Traffic pattern determination	✗	✗	✗	✗
[37]	SRHTCP (fuzzy logic)	Machine learning	predict congestion level	✗	✗	✗	✓
[38]	Artificial neural network	Machine learning	T. Congestion state	✗	✗	✓	✓
[39]	Regression model	Machine learning	Traffic congestion score	✗	✗	✗	✗
The Proposed Solution	Sliding Window	Machine learning	predict traffic congestion level	✓	✓	✓	✓

The approach suggested in [21] that the combination of a Genetic Algorithm and the Cross Entropy method for the optimization of a Parallel Hierarchical Fuzzy Rule-Based System would help to develop a synergy between exploration and exploitation to improve the system's parameters.

The authors in [22] designed an approach based on hierarchical fuzzy rule based system and genetic algorithms to build traffic congestion prediction systems from a large number of input data. However, this approach does not take into consideration many parameters that will have to be obtained in real time.

In the same context [23] and [24] estimate and predict traffic congestion in large-scale urban regions using a fuzzy comprehensive evaluation method. This method involved mapping the floating vehicle in sample points using data from its route. However, the authors focus on the traffic prediction on the roads and don't take in account the intersections where the congestion is more interesting to manage.

In the paper [25], a hybrid model of SVM and KNN is proposed as a short-term prediction technique for highway exiting traffic. However, the problem is that the traffic data are not strictly periodic. For example, in the normal day the peak

hours could vary from 4:30pm to 6:00pm, but on weekdays usually happen in afternoon. In the same context, the work presented in [26] consists on creating a multimodal Big data fusion framework for traffic congestion prediction. This work uses a highway traffic dataset to predict traffic travel times using data mining predictive and Extended Kalman filters. However, the weakness of the approach lies in the non-use in the traffic data used of certain important qualified parameters such as time and area.

The works proposed in both [27] and [28] are based on the Bayesian Network analysis approach to model the probabilistic dependency structure between causes of congestion on a particular road segment and analyzing the probability of traffic congestion given various roadway condition scenarios. However, the obtained results show that the both approaches take a lot of time for making prediction, and thereafter cannot be considered as real time solution.

In [29], offers a fusion deep learning model that takes spatial-temporal correlation into account in order to address the issue of predicting urban road traffic flow and increase prediction accuracy.

Referring to the literature, this work can summarize that the challenge of emergency traffic recommender systems is still an open problem and the proposed approaches are not complete to be used in such situations. Firstly, the majority of these evoked contributions attempt to forecast traffic flows for a specific area of the urban road network and are mainly based on the variations of the time series specific to this area. However, they must take into account the entire region, including origin and destination, as a whole. Also, the prediction response must be provided at runtime and continuously. In addition, most traffic jam prediction are for road segments and not for intersections, despite the fact that most of the time traffic jams start from intersections.

This motivates us to propose an emergency traffic recommender system combining optimal path problems and real-time congestion prediction to find the fastest route from an origin to a destination. This system is based on a flexible architecture having the advantage to collect useful information gathered from road infrastructure, traffic tracking, etc., and to process and provide real-time congestion prediction using machine learning algorithms and in particular classification algorithms. The main reason for choosing classification algorithms is that their processing time is lower than deep learning algorithms according to [30], and they also meet the goal of reaching a fastest path.

III. RESEARCH METHODOLOGY

The objective of the current contribution is to propose an emergency traffic recommendation solution having the advantage of proposing fastest routes from an origin to a destination while avoiding as much as possible that ambulances get stuck in traffic jams during their travels. The implementation of such an emergency traffic recommendation system requires massive empirical data to build the most appropriate and fastest path for ambulance drivers. Therefore, this paper proposes a flexible architecture that has the advantage of collecting all the required data from the environment and also of processing them in real time to respond to the travel emergency.

The proposed architecture uses techniques to collect, filter, store and process the data in real-time, and machine learning algorithms to analyze and predict the fastest path in real time throughout the mobility.

To build this architecture, we started by understanding, identifying, and analyzing all parameters involved in the emergency traffic recommendation process before the modeling phase. The necessary parameters we have identified mainly belong to two main categories: static and dynamic parameters. Static parameters refer to data that do not change during the period of travel, such as infrastructure data, traffic signals, road structures, red light scheduling, etc. While the dynamic category focuses on variables whose values change over time, such as traffic trips.

Traffic congestion prediction has two essential steps of forecast model development and data collection. Each step of the process is important and, if performed incorrectly, could have an impact on the results or consequences of the next steps. After data collection, data processing assumes an imperative

part to prepare the training and testing datasets, and help to predict the traffic flow as well as an estimated traffic congestion state. In addition, proposed traffic datasets are divided into two categories: stationary data and probe data. Additional categories for fixed information includes sensor and fixed cameras. Probe data includes data collected from GPS or applications installed on vehicles, traffic parameters we have identified mainly belong to two main categories: static and dynamic parameters. Static parameters refer to data that do not change during the period of travel, such as infrastructure data, traffic signals, road structures, red light scheduling, etc. While the dynamic category focuses on variables whose values change over time, such as traffic trips, data collected by IoT connected objects, or sensors, driver behaviors, traffic flow, etc. Fig. 1 summarizes the components and parameters taken into account by the proposed architecture.

In order to propose a flexible model for emergency traffic services for the case of ambulance mobility, this paper was interested in the use of multi-agent system (MAS). That is more adapted to this case and meets our needs perfectly. Moreover, it has the ability to hold the properties of distributed systems, to meet the required coordination which consists in organizing the cooperation between the connected objects by sharing knowledge and relying on the capabilities and knowledge of each entity, and to adapt to artificial intelligence techniques. For all these reasons, in this paper, we have opted for SARL (Multi-agent programming language of system) as an agent programming language because of its robustness, the multitude of features offered, etc. the proposed architecture is shown in Fig. 2.

The Fig. 3 represent the main layers of the emergency traffic recommender system concern the multi-agent system module, a data management module represented by a NoSQL solution (mongoDB in this work), an extraction and decision module for traffic management, and a mobility services module that represents the interface of the recommendation system offering to the ambulance drivers real-time positioning information, the fastest path between a departure point and destination, etc. This last module interacts with the multi-agent system module, which through the agents, allows to manage each physical object (sensors, IoT, etc.). These agents are permanently connected to the road infrastructure. Based on the information collected from the physical infrastructure, this module is able to compose the required event or task using a coordination process and send it to the navigation services module.

The Traffic Management Extraction and Decision module provides the overall decision on the appropriate measure of mobility, fluidity in the segments and nodes to traverse to reach a destination from an origin. This decision is based on historical urban traffic states, data collected in real time by the multi-agent system. To implement the proposed solution, we propose a hybrid approach: 1) a local approach dedicated to traffic prediction based on a learning algorithm and 2) a global approach to propose the fastest path from an origin to a destination based on the output of the local approach.

The aim of the next section is to detail the proposed MAS module.

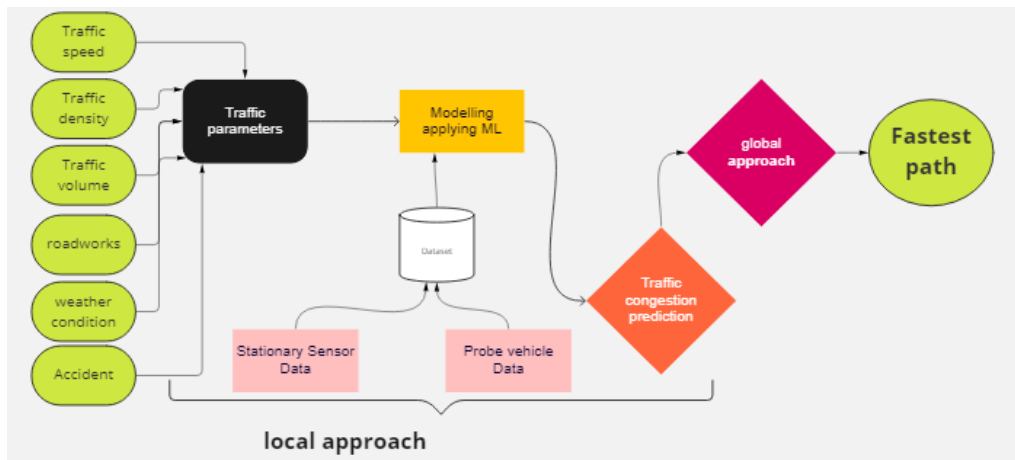


Fig. 1. The Proposed Architecture for Emergency Traffic Recommendation System.

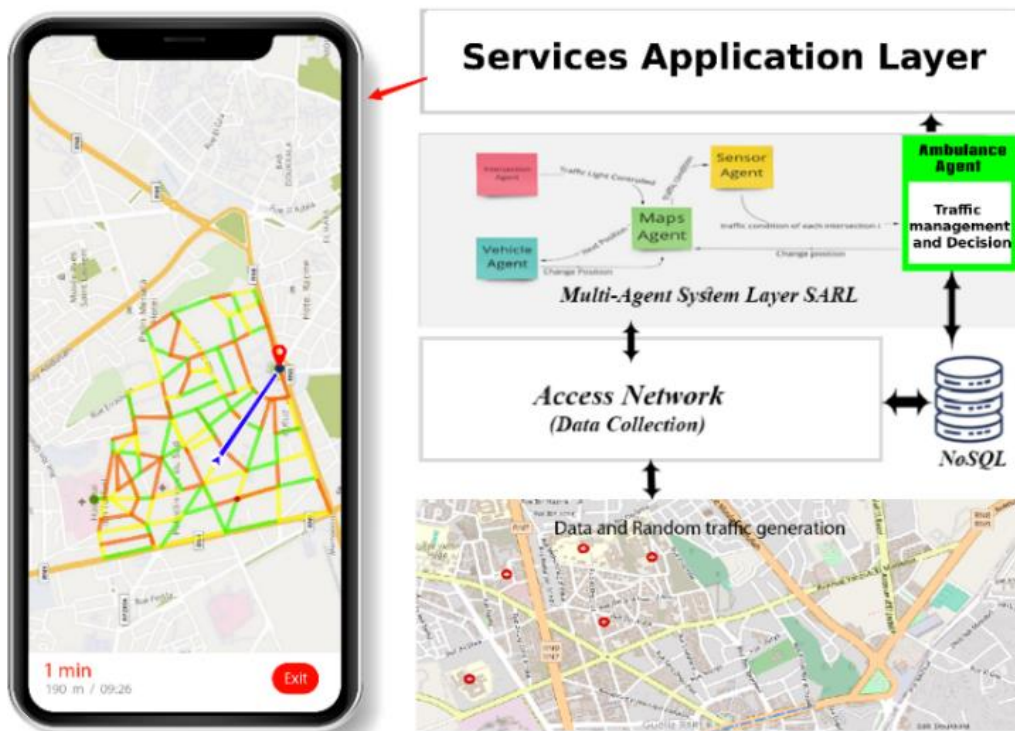


Fig. 2. An Architecture of Multi-Agent with SARL.

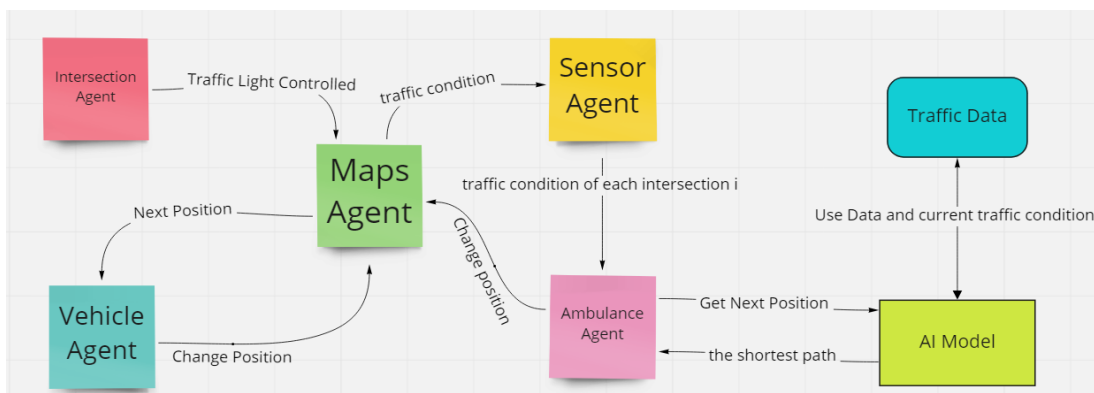


Fig. 3. The Proposed Architecture for Emergency Traffic Recommendation System.

IV. MULTI-AGENT SYSTEM MODELLING

To recommend the shortest time-based path in the case of an emergency from a departure point to an arrival point for an ambulance driver, the proposed approach was interested in the use of multi-agent systems, we have opted for SARL as an agent programming language that provides a set of concepts for the development of holonic systems (agents composed of other agents, with possibly new capacity) and based on events for communication between agents.

The proposed MAS contains five categories of agent:

- The maps agent, which is responsible for the simulation of traffic on the map, the input and the output of the agent vehicle, and also communicates with the other agents, for example giving the current coordinates to the ambulance agent.
- The sensor agent, responsible to collect data for each section on the map. For each section, we have two sensor agents positioned at the entry and exit of the section. The aim of this agent is to calculate the flow and the density of the vehicles on each section.
- The Intersection agent that takes control of the traffic light and priority of an intersection.
- The vehicle agent.
- The ambulance agent which represents the ambulance driver.

Table II summarizes all functions and events used to communicate between agents.

The agent ambulance needs to make a decision at each intersection from the origin to destination. So to choose the right direction it will communicate with the map agent to get its current position after that communicate with all sensor agents in each section of the road from its position to the arrival point to get the traffic condition for each section at instant T and used to predict the traffic condition at T+Δt to find uncongested road segments that will allow it to reach the arrival point.

According to fluid mechanics, the flow rate q is equal to the product of the concentration k and the velocity of the flow v, the average velocity for a traffic flow at time t and point x is defined by the ratio between the flow rate and the density such that:

$$v(x, t) = \frac{q(x,t)}{k(x,t)} \quad (1)$$

Therefore, the proposed methodology was adopted to predict the flow and density of each section on the map and then calculate the average speed as a function of time to cross each different section. The main idea of this study is to identify similar patterns from the historical data of density and flow, and as an input real time data to predict the next state of the Traffic.

TABLE II. AGENT TYPES USED IN PROPOSED MULTI-AGENT SYSTEMS

Agent	Event	Functions
Intersection	TrafficLightEvent: for each ΔT the Intersection agent send the traffic light condition to the maps agent	control the traffic light and priority of intersection
Vehicle	SendPositionEvent: for each ΔT the vehicle agent sends their position to the maps agent: to get permission to move to the next position.	move from intersection to other
Maps	After receiving the request from the vehicle agent to change their position, depending on the capacity of the red light or the priority the agent maps to verify the request, if possible it emits ChangePositionEvent: to give permission to the vehicle agent to change his position. In addition, the maps agent is able to detect every vehicle entering or leaving on section j, and it sends this information to the input sensor agent j and output sensor agent j.	simulation of traffic
Sensor	after receiving the request from the ambulance agent, it uses the information received from the maps agent to calculate the flow and density and send SendEtatTrafficEvent to respond to this request.	calculate traffic flow, density and speed
Ambulance	GetEtatTrafficEvent : send message to Sensor Agent to get (flow and density) of each edges of maps.	is VehicleAgent with some exception (move from an origin to destination, always have a priority in intersection)

V. DATA AND RANDOM TRAFFIC GENERATION

To evaluate the proposed approach and given the lack of empirical data, we were interested in randomly generating data representing vehicles, on road sections and intersections, that move randomly with a constant speed. The main properties of this traffic generation are presented as follows.

- Initialization at t=0: Assign to each intersection a number of vehicles NV.
- For each intersection I at time t with the number of vehicles NVi(t), assign to each exit section of intersection I a random percentage XTi(t) % of NVi(t).
- The exit sections of an intersection I correspond to the entry sections at other intersections J1, J2, ...Jn.
- the following equations are presented by [31].
- The traffic flow is the number N of vehicles passing a period Δt at point x,

$$Q_{\Delta t}(x) = Q(x, t \rightarrow t + \Delta t) = \frac{N}{\Delta t} \quad (2)$$

- The density K is the number M of vehicles between x and $x+\Delta x$ at time t .

$$K_{\Delta x}(t) = K(x \rightarrow x + \Delta x, t) = \frac{M}{\Delta x} \quad (3)$$

- These two equations (1) and (2) allow us to calculate the time needed to go from an intersection I to an intersection J .

An example of traffic visualization after vehicle generation is shown in Fig. 4

A. Data Mining

It incorporates choice interaction as information determination, pre-handling as information cleaning from missing qualities, copies, inconsistencies, and incorrect information, dimensional reduction transformation using 0–1 ranges for normalizing, and choice interaction as information determination. By using the formula below, it is very likely possible to determine data normalization.

$$V^i = \frac{v - \min_a}{\max_a - \min_a} (new_max_a - new_min_a) + new_min_a \quad (4)$$

Where:

- v_i = updated data following normalization.
- V = normal data (without normalization).
- new_max_a = the new maximum value is 1.
- The new min_a variable's maximum value is 0.
- max_a = the column's highest value.
- min_a is the column's lowest value.

B. Algorithm for Congestion Coloring in Sections and Intersections

The upstream and downstream movements of road segments in a road network frequently have an impact on the traffic conditions of those segments. For instance, congestion frequently starts on one or more road segments and expands to other road segments over time. Fig. 5 illustrates congestion by

assigning colors to road segments; the red, yellow, and green lines represent congested, slightly congested, and uncongested road segments, respectively.

To visualize changes in congestion on a map, we propose to color the sections and intersections according to the following two rules:

Rule 1 — CI_j is the maximum capacity of the intersection J , so if the value of $NV_j(t)$ approaches CI_j then it will have congestion. Three classes of congestion are considered by this experiment: Class 0 for $NV_j(t) \leq CI_j/3$ (green coloring), Class 1 for $CI_j/3 < NV_j(t) \leq 2CI_j/3$ (yellow coloring) and Class 2 for $2CI_j/3 < NV_j(t) \leq CI_j$ (red coloring).

Rule 2 — CT_k is the maximum capacity of the section K , so if the value of $XV_k(t)$ approaches CT_k then it will have congestion. Three classes of congestion are considered in this experiment: Class 0 for $NV_k(t) \leq CT_k/3$ (green coloring), Class 1 for $CT_k/3 < NV_k(t) \leq 2CT_k/3$ (yellow coloring) and Class 2 for $2CT_k/3 < NV_k(t) \leq CT_k$ (red coloring).

The idea is to exploit the fact that traffic jams move, dissipate or form from one section to another or from one intersection to another [32]. In order to recognize these congestions and show them on a map, we are interested in the sliding window algorithm to predict the state of a section exiting an intersection I at time t based on the traffic history of the entry sections of the same intersection I at time $t+\Delta t$.

For a more efficient recommendation system, it is mandatory that the prediction time of the traffic parameters is as fast as possible. In other words, the faster path recommendation must be present before the ambulance arrives at the next intersection.

The data of this simulated history is stored in a MongoDB database and comes from the traffic flows (number of cars per two minute) randomly generated on 84 intersections and 300 sections on the map of the city Marrakech in Morocco. These collected data which correspond to about 1000 hours of execution of the traffic generation algorithm generated more than 30000 elements for each section.



Fig. 4. Example of Traffic Generation between Intersections and Sections.

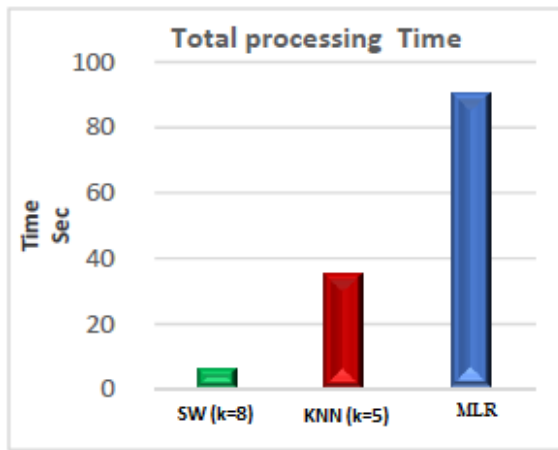


Fig. 5. The Processing Time of SW, KNN and MLR.

VI. PROPOSED METHODOLOGY BASED ON HYBRID APPROACH

Recall that the proposed approach is based on hybrid approach: 1) a local approach dedicated to traffic prediction based on a machine learning algorithm and 2) a global approach to propose the fastest path from an origin to a destination.

A. Local Approach: Traffic State Prediction using Machine Learning

The traffic conditions on the same road throughout time exhibit some degree of regularity and consistency. As a result, future road traffic circumstances can be reliably predicted using an accurate comparison of historical and current road traffic conditions [40] and [41].

To identify the more suitable machine learning model for the proposed local approach, this work presents in the following subsections a comparison between the sliding window model, multivariate linear regression model and K-nearest Neighbor model. So we first construct a representative high-capacity historical database. Next, we define the elements of the model, including the value of K sliding window, Finally, a similar traffic flow matching to the present actual time and the observation data from the history database are retrieved to predict the traffic flow at the next time based on the observed values of the input and the search mechanism.

1) *Sliding window algorithm*: This algorithm has the advantage to mathematically model the aforesaid defined dependencies. Therefore, it is able to make the relationship between the historical data and previous k min data to predict the future traffic conditions [42].

The reason for applying the sliding window matching is that there is always a slight variation in traffic conditions that may depend on the variation of the last few minutes and also a dependence between the traffic conditions that persist in the current day and those of previous days [33] and [35]. Therefore, the previous days of the same time are checked to find similar traffic conditions. The sliding window is a good technique to capture the variation that could correspond to the real time variation.

The algorithm is as follows:

1. The matrix "TC" of the last k min for current day's width size $k \times i$, i is the number of the sections of intersection I.
2. Consider the matrix "PY" of n min data of size n i.
3. From the matrix "PY," create k sliding windows, each of size $n * i$, as $W_1, W_2, W_3,$ and W_{n-k-1} .
4. With the matrix "TC" as $ED_1, ED_2, ED_3, \dots, ED_{n-k-1}$, represent the Euclidean distance of each sliding window.
5. Select matrix W_i as:

$$W = \text{Corresponding Matrix (Min.(ED}_i))$$

$$\forall i \in [1, n-k-1]$$
6.
 - (i) Calculate the variation vector, abbreviated "VC," for the matrix "TC" of dimension $k-1 * 1$.
 - (ii) Calculate the variation vector for matrix "W" with dimension $k-1 * 1$ as "VP" for WC.
 - (iii) $M_c = \text{Mean}(VC)$
 - (iv) $M_p = \text{Mean}(VP)$
 - (v) Estimated Variation "V" = $(M_c + M_p)/2$
 - (vi) To determine the anticipated traffic situation in $t + \Delta t$, add "V" to the existing traffic condition at t.

The performance of the Sliding Window is affected by the chosen number of neighborhoods (the parameter K). Table III shows the method used to determine the K sliding windows (k=8 in this case).

Algorithm.1 Sliding window

Input: hisdata[[]], runtimeData[[]].

Output: pValue : prediction Value.

```

1: min = infinity
2: for i in (0, hisdata.length) do
3:   sum = 0
4:   for j in (0, runtimeData.length) do
5:     for k in (0, runtimeData.length) do      d      Euclidean
        distance
6:       sum = sum + (runtimeData[j][k] - hisdata[j+i][k]) *
          (runtimeData[j][k] - hisdata[j+i][k])
7:     sum = √ sum
8:   end for
9: end for
10: if sum >= min then
11:   min = sum
12:   for k in (0, runtimeData.length) do
13:     pValue ← pValue + hisdata[i+b][hisdata[i].length-1]
          + hisdata[i][hisdata[i].length-1]
14:   end for
15: end if
16: end for
17: return pValue = pValue / runtime.length * 2.

```

The steps to calculate the Longest Substring k sliding windows are explained below:

- Selection of beginning data as the system's basic knowledge base.

- find the k sliding windows.
- The preparation of the training data in the form of the criteria's worth of fresh information about which the status is unknown
- Evaluation of each training set's state in accordance with predetermined rules to provide system knowledge.
- Based on each sample's training data and testing data, a distance calculation is made for each sample. the Euclidian equation:

$$d(x, y) = \sqrt{\sum_i^n (x_i - y_i)^2} \quad (5)$$

- determining the testing data's status based on the average of K samples of training data from sliding windows.

Testing results for training data 70% and testing data 30% the confusion matrix result with sliding window method can be seen in Table III.

TABLE III. SLIDING WINDOW TESTING RESULTS FOR TRAINING DATA 70% AND TESTING DATA 30%

K value	Accuracy	Precision	Recall	Classification Error	Mean squared Error
5	83.85%	83.22%	84.93%	16.15%	0.157
6	84.49%	83.75%	85.60%	15.51%	0.143
7	84.57%	84.30%	86.23%	15.43%	0.115
8	85.98%	85.69%	88.45%	14.02%	0.104
9	84.22%	85.08%	85.45%	14.78%	0.121

2) *Multivariate linear regression*: An effective way of modeling and prediction to investigate the quantitative relationship between the dependent and independent variables is to create a multivariate linear regression model utilizing historical data. Assume that there are m independent variables stated as X_{tj} ($j = 1, \dots, m$), the sample size is n, and the dependent variable is expressed as y_t at t. Then, the multivariate linear regression model can be written as follows.

In case of multivariate linear regression, results are depending on multiple input values. The parameters used in the implementation are: m-row for the number of training elements (the number of vehicles in each section at time t), n-column for the number of features (the number of section and intersection).

Algorithm.2 Multivariate linear regression

Input: data set $D = \{(x_1, y_1), (x_2, y_2) \dots (x_n, y_n)\}$ at t

Output: $\theta = [w_1, w_2, \dots, w_d, b]$

- 1: Define the loss function $J(\theta) = 1/2n \sum^n (\theta^T x_i - y_i)^2$
 - 2: Generating the randomly θ^0
 - 3: **repeat**
 - 4: $\theta^k = \theta^{k-1} - a(\partial J(\theta) / \partial \theta)$ where θ^k is the value of k^{th} iteration and a is the iteration Step.
 - 5: until $J(\theta^{k+1}) - J(\theta^k) < \epsilon$
 - 6: return θ
-

3) *KNN*: K Nearest Neighbor calculation falls under the Supervised Learning class and is utilized for grouping (most usually) and regression. It is a flexible calculation additionally utilized for ascribing missing qualities and resampling datasets. As the name (K Nearest Neighbor) proposes it thinks about K Nearest Neighbors (Data highlights) anticipate the class or continuous value for the new Data point.

KNN is a non-parametric supervised learning technique, that allows to classify the data point to a given category with the help of training set. The parameters used in the implementation are: $K = 5$ (after the test result), the number of vehicles of each intersection and road and the traffic states (0: free-flowing traffic/1: semi-congested/2: congested).

Algorithm.3 KNN

D: the set of learning objects.

$Z(I) = (NV_1, NV_2, \dots, NV_k, t)$ the vector of real-time values, such that NV_{ij} represents the number of vehicles in the input section j of intersection I at time, t) with j belongs to $1 \dots k$

CG is the set of traffic states (0: free-flowing traffic/1: semi-congested/2: congested)

L class used to label the objects:

(CG, the number of vehicles in the exit edge of the intersection I at time $t + \Delta t$)

Input: $Z(I)$

Output: $z = (CG, \text{number of vehicles in the edge}) \in L$, class of z

- 1: **for** object y in D **do**
 - 2: calculate $d(z, y)$, the distance between z and y
 - 3: **end for**
 - 4: select N of D, the set (neighborhood) of the k nearest training objects for z.
 - 5: $cap - max$ is the maximum capacity of the output section of the intersection I
 - 6: returns = $\sum_{y \in N} NV(t) / cap - max$
-

B. *Comparison between Multivariate Linear Regression, KNN and Sliding Window*

Table IV compares the performance values that sliding window, multivariate linear regression, and KNN provide in three separate simulation tests: 70:30, 50:50, and 30:70. When compared to Multivariate Linear Regression and KNN, Sliding Window's performance metrics of accuracy, precision, recall, classification error, and mean squared error yield better results. Accordingly, Sliding Window's prediction is more accurate than both of these methods.

Fig. 5 shows the comparison of the processing time of the three algorithms. The result shows that the processing time of SW, KNN and MLR is 13, 38, 87 seconds respectively.

TABLE IV. COMPARISON ANALYSIS OF SLIDING WINDOW, KNN AND MULTIVARIATE LINEAR REGRESSION

Sim Test	Method	Accuracy	Precision	Recall	Classification Error	Mean Squared Error
70:30	SW	85,98%	85,69%	88,45%	14,02%	0,104
	KNN	84,44%	84,41%	84,2%	15,56%	0,124
	MLR	77,25%	72,08%	83,03%	22,75%	0,345
30:30	SW	87,38%	88,84%	89,30%	12,62%	0,061
	KNN	87,13%	88,44%	88,56%	12,87%	0,083
	MLR	76,57%	72,21%	82,46%	23,43%	0,339
30:70	SW	81,94%	78,05%	86,07%	18,06%	0,179
	KNN	81,30%	76,89%	84,77%	18,70%	0,196
	MLR	56,13%	54,23%	66,89%	43,87%	0,463

C. Global Approach: Prediction based on the Traffic Flow Coefficient

To determine the fastest path between a starting point and all other intersections of a graph (map), we propose as a first contribution to adapt Dijkstra's algorithm to take into account the traffic flow parameter. The value of this parameter is computed according to the real time traffic density, the traffic history, the road condition (public works, ...), etc. This value is also continuously calculated from the data collected at the moment by the road infrastructure sensors in order to find the fastest path from a starting point and to exclude the road with a high degree of congestion. Before presenting the equation (7) used to determine the time needed to cross each road, in [31] present the equations it refers to.

The density K is expressed as the number of vehicles per unit length (veh/km or veh/m).

$$k = \frac{TO}{L+l} \quad (6)$$

where TO is the occupancy rate, L is the length of the assumed vehicles and l is the length of the detection loop, tell that Q is the traffic flow.

$$Q = K \times V \quad (7)$$

Thus, the velocity v is expressed as follows.

$$V = \frac{Q}{TO} \times (L + l) \quad (8)$$

Finally, the travel time Ti for edge i is calculated as follows.

$$Ti = \frac{vi}{Di} \quad (9)$$

The algorithm 2 used follows the following steps:

1. Initialize all roads with a high degree of "infinite" congestion, in other words vehicles cannot move. Moreover, the ambulance is initially at the starting point at time T0.
2. Activate the starting point (algorithm 4 line 4)
3. Calculate the temporary travel time of all intersections adjacent to the current intersection by adding their times (algorithm 4 line 7).
4. If the calculated time of an intersection is less than the current time, update the time and set the current intersection

as the antecedent. This step is also called updating and is the central idea of Dijkstra. (algorithm 4 line 9-19)

5. Set the intersection with the minimum temporary time as active. Mark its travel time as permanent. (algorithm 4 line 10)
6. Repeat steps 3 to 5 until there are no more intersections with a permanent time, whose neighbors still have a temporary travel time.

Algorithm.4 Dijkstra

Input: current-Point: the current ambulance junction, destination, graph of time at T0 d travel time for (each section i and each node j), from the prediction Algorithm.

Output: path[] : the fastest path.

- 1: **while** (current- Point! = destination) **do**
 - 2: min = infinity
 - 3: **for** vertex v in Graph **do**
 - 4: time[v] =infinity // initial travel time from current-Point to vertex v is set to infinity
 - 5: previous[v] =undefined // Previous node in fastest path from current-Point
 - 6: **end for**
 - 7: time[current-Point]=0 // travel time from current-Point to current-Point
 - 8: Q = set // the set of all nodes in Graph
 - 9: **while** sum >= min **do**
 - 10: u = node // node in Q with fastest time[]
 - 11: remove u from Q
 - 12: **for** neighbor v of u **do** //where v has not yet been removed from Q.
 - 13: alt = time[u] + timebetween(u; v)
 - 14: **if** alt < time[v] **then**
 - 15: time[v] = alt
 - 16: previous[v] = u
 - 17: **end if**
 - 18: **end for**
 - 19: **end while**
 - 20: fastest path = previous[] // the ambulance moves to the next point
 - 21: current = Next-Point // from fastest-path
 - 22: Graph =prediction- travel - time(T0 + t) d graph of time at T0+t
 - 23: **end while**
-

VII. EMERGENCY TRAFFIC RECOMMENDER SYSTEM IMPLEMENTATION

To implement the proposed emergency traffic recommender system, this paper opted for the agent-oriented programming language SARL, the DBMS MongoDB, and the JavaScript language to build the emergency navigation service for paramedics based on OpenStreetMap.

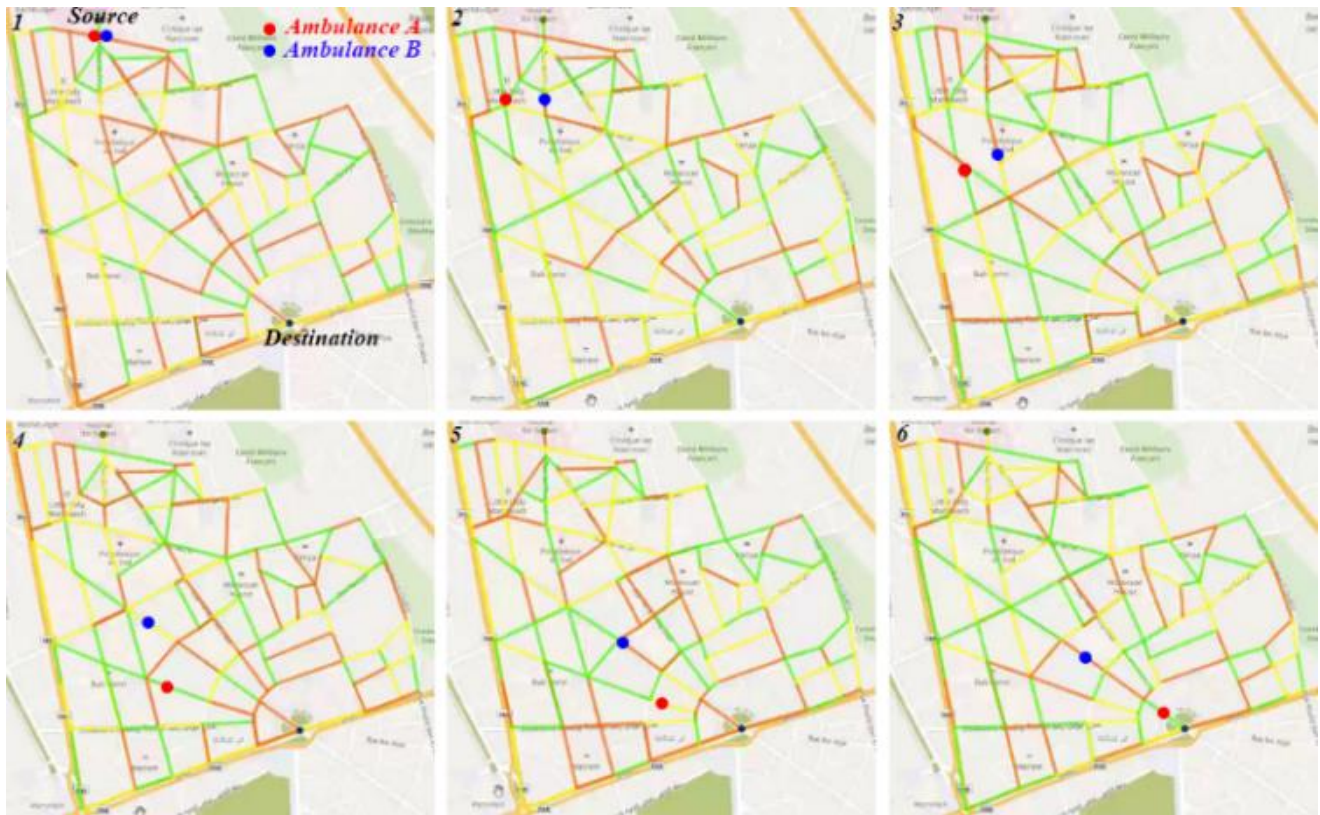


Fig. 6. Update of the Recommended Path to the Destination.

Fig. 6 illustrates the different stages of movement of the two ambulances A, B. The first ambulance A (red dot) uses the proposed recommendation system to avoid congestion, while the second ambulance B (blue dot) uses classical Dijkstra's algorithm to find the fastest path between the starting point and the destination.

TABLE V. COMPARISON BETWEEN THE PERFORMANCES OF THE THREE METHODS ON DIFFERENT TIMES OF THE SIMULATION

simulation time	Method	distance	time of trips	Fastest Path time
2:00 pm	KNN	1.5 km	449 s	449 s
	MLR	1.7 km	483 s	
	SW	1.5 km	449 s	
2:40 pm	KNN	1.7 km	413 s	413 s
	MLR	1.7 km	413 s	
	SW	1.7 km	413 s	
3:00 pm	KNN	1.7 km	285 s	285 s
	MLR	1.7 km	285 s	
	SW	1.7 km	285 s	
3:20 pm	KNN	1.7 km	435 s	419 s
	MLR	1.5 km	428 s	
	SW	1.9 km	419 s	

The Table V compares the performances of congestion prediction that sliding window, multivariate linear regression, and KNN provide in different moments of the simulation. The

result shows that the Sliding Window's prediction is better than both of these methods. Sliding Window has the advantage to make the ambulance avoiding traffic congestion every time, and taking different way to destination by using the fastest way based on the distance and traffic congestion.

Based on the results obtained, we are currently working on improving the proposed equation (8) to include more detailed parameters such as road condition (public works, presence of accidents, ...), type of vehicle crowd, speed of the vehicle crowd, etc.

VIII. CONCLUSIONS

The objective of this contribution is to propose a solution for traffic recommendation in emergency situations in order to avoid ambulances to be stuck in traffic jams at the time of trips and interventions. For this purpose, we proposed an architecture based on machine learning techniques for classification and collection of the required information to predict the fastest path to ambulances. Given the lack of empirical data, this paper proposed a random traffic generation algorithm to experiment with the recommendation solution. Based on the generated dataset, we proposed a hybrid approach composed of a local approach to visualize the state of congestion on the map of the city of Marrakech under OpenStreetMap, and a global approach to suggest the fastest path as the ambulance moves. The local approach relies on the Sliding window technique to predict the congestion of sections in three classes: congested, slightly congested and not congested sections. While the global approach implements the Dijkstra algorithm using the multi-agent system modeling language SARL.

The proposed recommendation solution predicts the fastest path for emergency situation from an origin to a destination. Since these recommendations may or may not be taken into consideration by drivers, we are currently integrating drivers experience interaction with the recommender system to build more efficient emergency traffic recommender system.

REFERENCES

- [1] P. Zhao, Z. Yu, Investigating mobility in rural areas of China: Features, equity, and factors, *Transport Policy* 94 (2020) 66–77.
- [2] L. Changle, Y. Wenwei, M. Guoqiang, X. Zhigang, Congestion Propagation Based Bottleneck Identification in Urban Road Networks, *IEEE TRANSACTIONS ON VEHICULAR TECHNOLOGY*, VOL. 69, NO. 5, MAY 2020.
- [3] H. Hammad, M. Ashraf, F. Abbas, H. Bakhat, A. Qaisrani, M. Mubeen, S. Fahad, M. Awais, Environmental factors affecting the frequency of road traffic accidents: a case study of sub-urban area of Pakistan, 11674–11685 (2019). <https://doi.org/10.1007/s11356-019-04752-8>.
- [4] M. Poulton, A. Noulas, D. Weston., G. Roussos, Modelling metropolitan-area ambulance mobility under blue light conditions. DOI 10.1109/ACCESS.2018.2886852, *IEEE Access*.
- [5] M.S. Ali, M. Adnan, S. Muhammad Noman, B. Fazal Abbas. "Estimation of traffic congestion cost-A case study of a major arterial in karachi," *Procedia Engineering*, vol. 77, pp. 37–44. <https://doi.org/10.1016/j.proeng.2014.07.030>.
- [6] A.M. De Souza, C.A. Brennand, R.S. Yokoyama, E.A. Donato, E.R. Madeira, L.A. Villas, (2017). Traffic management systems: A classification, review, challenges, and future perspectives. *International Journal of Distributed Sensor Networks* 2017, Vol. 13(4).
- [7] M. Weisfeldt, L. Becker, Resuscitation after cardiac arrest: a 3-phase time-sensitive model, *JAMA*, vol. 288, no. 23, pp.3035–3038.
- [8] K. Athavan, G. Balasubramanian, S. Jagadeeshwaran , N. Dinesh, (2012). Automatic ambulance rescue system. *IEEE. second international conference on advanced computing & communication technologies. IEEE Transactions on Vehicula*, Vol. 69, NO. 5.
- [9] V. Servizi, C. Pereira, MK. Anderson, A. Nielsen, Transport behavior-mining from smartphones: a review, *European Transport Research Review; Heidelberg* Vol. 13, N° 1, (Dec 2021). DOI:10.1186/s12544-021-00516-z.
- [10] S. Vasuki, G. Ruthvik, (2015). Automated traffic signal for hassle free movement of ambulance. *IEEE international conference on electrical, computer and communication technologies*. doi: 10.1109/ICECCT.2015.7226114.
- [11] P. Rosayyan, S. Subramaniam, S. Ganesan, Decentralized Emergency Service Vehicle Pre-emption System Using RF Communication and GNSS-Based Geo-Fencing . *IEEE Transactions on Intelligent Transportation Systems*, 1–10. doi:10.1109/its.2020.3007671.
- [12] L. Ding, D. Zhao, Z. Wang, G. Wang, C. Tan, L. Fan, H. Ma, Learning to Help Emergency Vehicles Arrive Faster: A Cooperative Vehicle-Road Scheduling Approach. *arXiv:2202.09773*. <https://doi.org/10.48550/arXiv.2202.09773>.
- [13] L. Zhong, Y. Chen, A Novel Real-Time Traffic Signal Control Strategy for Emergency Vehicles. *IEEE Transactions on Intelligent Transportation Systems*, 19(1), 13–24. doi:10.1109/its.2016.2625324.
- [14] Dimitrios V. Lyridis, An improved ant colony optimization algorithm for unmanned surface vehicle local path planning with multi-modality constraints, 2021, *Ocean Engineering*, Vol: 241, 109890, <https://doi.org/10.1016/j.oceaneng.2021.109890>.
- [15] R. Chen, C. Gotsman, Efficient fastest-path computations for road maps. *Comp. Visual Media* 7, 267–281 (2021). <https://doi.org/10.1007/s41095-021-0211-2>.
- [16] W. Sun, C. Zhu, L. HuiL, ASNN-FRR: A traffic-aware neural network for fastest route recommendation. *Geoinformatica* (2021). <https://doi.org/10.1007/s10707-021-00458-7>.
- [17] Li, X., Zhou, J. & Pedrycz, W. Linking granular computing, big data and decision making: a case study in urban path planning. *Soft Comput* 24, 7435–7450 (2020). <https://doi.org/10.1007/s00500-019-04369-6>.
- [18] C.M. Stewart, S.M. Aminossadati, M.S. Kizil, EMERGENCY EGRESS PATHWAY PREDICTION USING VENTILATION MODELS. *The Australian Mine Ventilation Conference* 2017, No: Stewart_089.
- [19] S. Ye, (2012), A reliability-based approach of fastest routes planning in dynamic traffic network under emergency management situation. *International Journal of Computational Intelligence Systems*, 4(6), 1224–1236. doi:10.1080/18756891.2011.9727871 10.1080/18756891.2011.9727871.
- [20] J. Cyriac, K.S. Vijula Grace, (2020). A New Approach for Accurate Path Prediction Using Multiple Prediction System. <https://doi.org/10.1016/j.matpr.2020.03.599>.
- [21] P. Lopez-Garcia, E. Onieva, E. Osaba, A. D. Masegosa, A. Perallos, (2016) "A hybrid method for short-term traffic Congestion forecasting using genetic algorithms and Cross entropy," *IEEE Transactions on Intelligent Transportation Systems*, vol. 17, no. 2.
- [22] X. Zhang, E. Onieva, A. Perallos, E. Osaba, V. C. S. Lee, (2014) "Hierarchical fuzzy rule-based system optimized with genetic algorithms for short term traffic congestion prediction," *Transportation Research Part C: Emerging Technologies*, vol. 43, pp. 127.
- [23] X. Kong, Z. Xu, G. Shen, J. Wang, Q. Yang, B. Zhang, (2016). "Urban traffic congestion estimation and prediction based on floating car trajectory data," *Future Generation Computer Systems*, vol. 61, pp. 97–107.
- [24] Q. Yang, J. Wang, X. Song, X. Kong, Z. Xu, B. Zhang, (2015) Urban traffic congestion prediction using floating car trajectory data, in *Proceedings of the International Conference on Algorithms and Architectures for Parallel Processing*, pp. 18–30, Springer, Zhangjiajie, China.
- [25] X. Wang, K. An, L. Tang, X. Chen, (2015), "Short term prediction of freeway exiting volume based on SVM and KNN," *International Journal of Transportation Science and Technology*, vol. 4, no. 3, pp. 337–352.
- [26] T. Adetiloye, A. Awasthi, (2019), "Multimodal big data fusion for traffic congestion prediction," *Multimodal Analytics for Next-Generation Big Data Technologies and Applications*, Springer, Berlin, Germany, pp. 319–335.
- [27] X. Liu, Y. Feng, Q. Wang, H. Zhang, X. Wang, (2014), "Prediction of urban road Congestion using a bayesian network approach," *Procedia—Social and Behavioral Sciences*, vol. 138, no. C, pp. 671–678.
- [28] J. Kim, G. Wang, (2016), "Diagnosis and prediction of traffic Congestion on urban road networks using bayesian networks," *«Transportation Research Record: Journal of the Transportation Research Board*, vol. 2595, no. 1, pp. 108–118.
- [29] Y. Zheng, C. Dong, D. Dong, S. Wang, (2021), Traffic Volume Prediction: A Fusion Deep Learning Model Considering Spatial–Temporal Correlation. <https://doi.org/10.3390/su131910595>.
- [30] A. Aslam, E. Curry, Investigating response time and accuracy in online classifier learning for multimedia publish-subscribe systems. *Multimed Tools Appl* 80, 13021–13057 (2021). <https://doi.org/10.1007/s11042-020-10277-x>.
- [31] C. Buisson, (2010), *Lesort J Comprendre le trafic routier. Methods and calculus*. CERTU, 111p, 2010, Coll. References, 978-2-11-098892-8.
- [32] L. Manman, L. Jian, S. Jiahui, T. Qiang, (2019), Day-to-Day Evolution of Traffic Flow with Dynamic Rerouting in Degradable Transport Network. <https://doi.org/10.1155/2019/1524178>.
- [33] C. Wentao, W. Jie, (2019), Research on traffic flow congestion based on Mamdani fuzzy System, <https://doi.org/10.1063/1.5090755>.
- [34] E. Onieva, P. Lopez-Garcia, A.D. Masegosa, E. Osaba, A. Perallos, (2016), A Comparative Study on the Performance of Evolutionary Fuzzy and Crisp Rule Based Classification Methods in Congestion Prediction, <https://doi.org/10.1016/j.trpro.2016.05.368>.
- [35] J. Zaki, A. Ali-Eldin, S. Hussein, S. Saraya, F. Areed, (2019), "Time aware hybrid hidden Markov models for traffic Congestion prediction," *International Journal on Electrical Engineering and Informatics*, vol. 11, no. 1, pp. 1–17.
- [36] J. Wang, Y. Mao, J. Li, Z. Xiong, W. Wang, (2015), Predictability of road traffic and Congestion in urban areas, *PLoS One*, vol. 10, no. 4, Article ID e0121825.

- [37] F. Tseng, J. Hsueh, C. Tseng, Y. Yang, H. Chao, L. Chou, Congestion prediction with big data for real-time highway traffic. 2018, IEEE Access, 1–1. doi:10.1109/access.2018.2873569.
- [38] K. Nadeem, T. Fowdur, (2018), Performance analysis of a real-time adaptive prediction algorithm for traffic congestion, *Journal of Information and Communication Technology*, vol. 17, no. 3, pp. 493–511.
- [39] L. Jiwan, H. Bonghee, L. Kyungmin, J. Yang-Ja, A prediction model of traffic congestion using weather data,” in *Proceedings of the 2015 IEEE International Conference on Data Science and Data Intensive Systems*. Lee, J., Hong, B., Lee, K., & Jang, Y.-J. (2015). A Prediction Model of Traffic Congestion Using Weather Data. 2015 IEEE International Conference on Data Science and Data Intensive Systems. doi:10.1109/dsd.2015.96.
- [40] S. Azimi, R. Delavar, A. Rajabifard, (2017). Multi-agent simulation of allocating and routing ambulances under condition of street blockage after natural disaster. *The International Archives of the Photogrammetry, Remote sensing and spatial Information Sciences*, Volume XLII-4/W4.
- [41] S. Ibri, M. Nourelfath, H. Drias, (2012). A multi-agent approach for integrated emergency vehicle dispatching and covering problem, *engineering applications of artificial intelligence*, Volume 25, Issue 3.
- [42] P. Kapoor, S. Singh Bedi, Weather Forecasting Using Sliding Window Algorithm, Hindawi Publishing Corporation ISRN Signal Processing Volume 2013, Article ID 156540, 5 pages <http://dx.doi.org/10.1155/2013/156540>.

A Review of Automatic Question Generation in Teaching Programming

Jawad Alshboul, Erika Baksa-Varga

University of Miskolc, Faculty of Mechanical Engineering and Informatics, Miskolc, Hungary

Abstract—Computer programming is a complex field that requires rigorous practice in programming code writing and learning skills, which can be one of the critical challenges in learning and teaching programming. The complicated nature of computer programming requires an instructor to manage its learning resources and diligently generate programming-related questions for students that need conceptual programming and procedural programming rules. In this regard, automatic question generation techniques help teachers carefully align their learning objectives with the question designs in terms of relevancy and complexity. This also helps in reducing the costs linked with the manual generation of questions and fulfills the need of supplying new questions through automatic question techniques. This paper presents a theoretical review of automatic question generation (AQG) techniques, particularly related to computer programming languages from the year 2017 till 2022. A total of 18 papers are included in this study. one of the goals is to analyze and compare the state of the field in question generation before COVID-19 and after the COVID-19 period, and to summarize the challenges and future directions in the field. In congruence to previous studies, there is little focus given in the existing literature on generating questions related to learning programming languages through different techniques. Our findings show that there is a need to further enhance experimental studies in implementing automatic question generation especially in the field of programming. Also, there is a need to implement an authoring tool that can demonstrate designing more practical evaluation metrics for students.

Keywords—Question generation; question generation techniques; automatic question generation; teaching programming

I. INTRODUCTION

A. Background

In recent years, a number of researchers have been attracted from different disciplines toward automatic question generation for educational purposes [1] [2] [3]. The researcher in [4] defined question generation as “It is an activity of automatically generating questions for different inputs like raw text through semantic illustration”. The definition shows that the generated question type can differ like being a sentence, a semantic map, or a paragraph. The educational question generation is not a new concept, but it has a long history and can be traced back to the use of logic in questions [2], [4], [5]. Cohen is the pioneer of this research area who initially proposed the content for generating questions through an open formula and used one or more unbound variables [1]. Whilst research on generating questions is carried out for a long time, using techniques for automatic question generation for teaching computer programming has raised interest only recently amongst various

research communities, because it requires inclusion of cognitive science, natural language processing and human interaction with computers. Intelligent Tutoring System (ITS) is the recently proposed computer-based teaching context to help students learn programming languages but to the best of our knowledge, computer-based applications for teaching programming are not widely implemented [2]. With rising novice computer scientists, specific questions are generated which can address knowledge gaps that were often negligible in the manual process of articulating questions [6]. In support of enhancing the metacognitive skills of students, asking students to generate questions can be a constructive process but the use of various metacognitive skills can be time-consuming and needs extended knowledge of various metacognitive strategies.

B. Problem Statement

The success of a rule-based question generation (QG) method depends on the quantity and quality of teachers’ domain knowledge, language knowledge and the amount of time spent on it. On the other hand, data-driven techniques have recently emerged such as deep neural network-based methods that are considered a promising approach for different tasks like recognizing entities, and sentiment categorization. In particular, teaching programming skills to students require extensive motivation which cannot be an easy task from the teachers’ perspective. A key issue is, that students interact with a program that has limited, syntactic and semantic level knowledge of a programming language (for example a compiler or interpreter), while teachers know and therefore can teach also the logic of programming. This requires teachers’ knowledge of how to apply the key concepts of computer programming and teach them to students with appropriate models of Automatic Question Generation (AQG).

The research in [7] provided a question generation method considering a generative encoder-decoder model. The researchers in [5] mentioned that although there are advances made in the neural models for automatic question generation, there is still a gap indicating a comprehensive survey on how different learning paradigms can present improvements in automatic question generation that broadens the input spectrum of instructors for teaching programming. This shows that various studies have been conducted on automatic question generation process for educational purposes, but to the best of our knowledge, there are only a few studies reporting on the state-of-the-art techniques used for automatic question generation in teaching programming languages, especially for the previous six years i.e. 2017 till 2022. Thus, the objective of this study is to review recent studies that provided different

techniques for automatic question generation with reference to various methods required for teaching programming.

This review extends the systematic review previously conducted on automatic question generation by Kurdi et al. [8] that covered literature from 2014 and up to 2019, respectively, by focusing on the domain of computer programming. The extensive amount of research that has been published since Kurdi et al, an extension of these studies is reasonable at this stage as it helps in understanding recent developments in the given field. The present article uses the previous article by Kurdi et al. [8] as a starting point and extending the review in a number of ways like additional review questions and criteria for inclusion/exclusion, which is discussed in the methodology section.

C. Research Questions

The questions that will be addressed in this research comes as follows:

- What are the recent developments made in the techniques for automatic question generation in teaching programming?
- What is the difference in the state of the field focusing on before COVID-19 and after COVID-19 period?
- What can be the future directions based on identified gaps in the field of automatic question generation in teaching programming?

D. Research Objectives

To address research questions the following objectives are considered for this work:

- To review recent literature on the approaches and techniques used for automatic question generation in teaching programming.
- To analyze and compare the state of the field before COVID-19 and after COVID-19 period.
- To provide summary of the challenges and future directions in the field of automatic question generation in teaching programming.

The remaining parts of the paper is structured as follows: Section II represent a literature review which will address previous work on the field. Section III describes the methodology used to conduct this review. Section IV shows the analysis and findings for the papers considered. Section V concludes the paper. Finally, Section IV describes future directions of this work.

II. LITERATURE REVIEW

Manual question creation consumes much time and labor. The concept of question generation was envisioned back in 1960s [4]. It is generally estimated that learning scientists believe that the provision of high-quality learning questions must use the basics of language knowledge and domain knowledge and so approach the activity using “rule-based” technique [9]. The given approach used syntactic changes to transform declarative sentences into questions. For example, multiple choice questions were generated using rules of term

extraction. Next, questions were sometimes generated using over-generate-and-rank manner that helped in ranking questions [7]. The given methods were limited in their wider applications and rules were also based on a few subjects, like English language. They were not easily applied to other domains, since defining rules and procedures needed considerable efforts from expertise. The given methods are also very limited and do not offer high quality questions, thereby limiting the implementation of rule-based generators. However, entering into digital landscape required wider-scale online learning; hence, the demand for automatic question generation is also increased along with massive number of online courses available to learners. In order to address this need, various computational techniques like deep neural network-based state-of-the-art techniques were proposed [7] [6]. Du et al [4] is pioneered in providing encoder-decoder sequence learning that was later on used for automatic question generation. The given model automatically captured question-asking patterns without taking any help from hand-crafted rules, indicating supreme performance over previous rule-based methods. However, it had a major gap identified by scholars that this technique was helpful in collecting data for machine reading comprehension tasks. Notably, such datasets included a very limited number of useful questions for learning, indicating that extended research is needed to offer question generations for complex learning documents to facilitate teachers.

Assessing students’ answers manually is also a time-consuming mission. Depending on the type of the question, this action can also be automatized more or less. Question types of quizzes are generally categorized into two groups: objective questions and subjective questions. Objective means that there is only one correct answer, which can be checked automatically. The objective questions request the learners to select the correct answer from several options or offer a number of words/short sentences as options or to complete a sentence. Multiple-choice, matching, true-false, and fill-in-the-blank are examples of objective questions, and they are considered the most popular ones, since they provide automatic assessment methods due to its their unambiguous, quick and trusted evaluation process. On the other hand, the subjective questions ask for a written answer composed by the learners and such answer might be short or long. A short answer could be up to three sentences while a long answer might be as long as an essay. The subjective questions should have an increased attention by the teachers to assess learner’s deep knowledge and understanding of the topics, similarly to the traditional education system that have been employed for centuries [10].

Most researchers have focused on generating objective-type questions, automatically or semi-automatically, while limited focus has put on subjective question generation because scoring is a difficult challenge in the case of subjective assessment. Comparing the level of difficulty to generate questions and in assessing the learner’s answers, learner's assessment of the textual question types is very easy for close questions and multiple-choice questions, easy for open-close questions, and difficult for subjective questions. Recent advances in deep learning-based natural language processing (NLP) offer promising solutions in answer assessment of objective-type questions [10].

A. Automatic Question Generation Process

In recent years, there has been an emerging interest in AQG from the text, which is explained as an activity to generate a question from a passage and optionally an answer. According to [11], AQG helps in curating question-answer datasets and improves our experience in Artificial Intelligence (AI) systems and helps in designing educational materials. But for this purpose, it is equally important for the questions to be grammatically error-free and answerable. Pertinent approaches emphasize on encoding the whole passage as the relationship is shown between them using complicated operations and then questions are generated in one single passage [12]. However, empirical studies show that if careful analysis is carried out for question generation, there are some approaches that probably miss out one or more of the essential aspects of the questions. For example, as mentioned in Table I, the question is generated by the single-pass baseline model that is grammatically correct but it does not fit to the answer [3].

TABLE I. THE PASSAGES AND THE QUESTIONS GENERATED FROM THEM USING REFNET [8]

<i>Passage 1: Functioned by Napoleon army in 1800, Warsaw was given the authority of the newly established Duchy of Warsaw</i>
<i>Questions: Baseline: What was the governor of the newly established Warsaw?</i> <i>RefNet: Who gave freedom to Warsaw?</i> <i>Reward-RefNet: Whose army was given freedom in 1800?</i>
<i>Passage 2: In order to fix the process of carbon dioxide into the sugar molecules, the enzyme called rubisco is used by chloroplasts.</i>
<i>Questions: Baseline: What is used by chloroplasts?</i> <i>RefNet: What is used by chloroplasts to fix carbon dioxide?</i> <i>Reward RefNet: What is used by chloroplasts to fix carbon dioxide into the sugar molecules?</i>

Table I shows that there is a visible scope of enhancing the general quality of the question generation process in contemporary field of teaching [6]. In the literature, scholars argue that one way is to approach this by constantly re-visiting the passage and then answer them with the goal to refine the preliminary draft by producing a better question in the second stage and then bringing further enhancements in the further stages [1][8]. This can be done using a comparison between human process of generating questions and with the computer-generated models [3]. In the examples above RefNet (Refine Network) was used as the model to evaluate the initial questions generated and then carried out a second test to generate revised questions. The Reward RefNet used explicit reward signals to attain the refined questions with two attributes: fluency and answering. This RefNet is a sequence-to-sequence model that includes two decoders called Initial and Refined decoder. According to [13], the proposed dual model helped generating the final question by revisiting the adequate parts of the input passage and preliminary draft.

B. Automatic Question Generation in Teaching Programming

The Literature exhibited various approaches for automated generation of questions, based on the extraction of featured words given on the topic and established variations on the same question for object-focused programming quizzes. For example, [13] used programming-by-example for code snippets that was a test regulated by synthesis. Recently, the research

article [15] provided facts for generating questions for teaching programming languages. The study reported in [16] found that students are taught by teachers to produce a program but they are not fully sure about the use of their own codes as they failed to grasp basic concepts. But if students are taught using Quality License Scheme (QLS,) it can prompt them to have a deeper level of understanding of given concepts. Schulte's Block Model of Program is another model used by scholars to attain better understanding of programming that needs different levels of knowledge about the program, and its purpose. However, experts argue that such models need knowledge at different levels ranging from individual building blocks to the integration of constructs to complete deficient Research shows that we cannot evaluate how coding process works as it requires skills and debugging process and the aptitude of learners to trace code that helps them write automatically testable code [18]. It is hypothesized that writing codes in a programming language requires preceding abilities of learners to write comparable codes that can be better understood by questions about learner's code (QLCs) approach that helps in learning programming comprehensions. On the other hand, in 2019, scholars of the George Washington University created a software that produced program-tracing questions for introducing programming content to students [12]. But this system also failed as the majority of questions were not applicable due to their complex nature. Later, scholars used Turing test as the tool to determine algorithm-based questions and identify the extent to which they could be helpful for teachers to generate questions that analyze students' learning abilities [14]. But this Turing test also did not pass as it failed to identify the particular issue in the algorithm when generating questions. Later and to extend this work, the researchers in [3] proposed a system called QuizJET, as another tool for generating questions, especially for teaching Java. This QuizJET was based on template-based questions that was linked to different concepts of Java and was actively used for generating quizzes; however, the research conducted in [16] did not find any correlation between the success rates of QuizJET and students' home assignment work, because QuizJET was more focused on understanding programs while home assignments were focused on writing skills of computer programming learners. Despite all these, QuizJET was identified as a valuable source in preparing students for exams.

III. METHODOLOGY

This study uses systematic literature review as the methodological approach to assess and understand the pertinent literature linked with research questions. From a number of approaches available in the literature for systematic review of studies, this study uses the approach provided by the researchers in [16] who provided detailed guidelines for conducting reviews. The methodological review consists of three key stages which in turn included ten sub activities. The details are showcased in Fig. 1. In the preliminary stage, the given questions were addressed; what are the key areas for which question generation is being designed; what are the different techniques and tools used for question generation process in teaching programming; what are the different modes of delivery for the creation of question generation in teaching programming; and how authors validated such techniques.

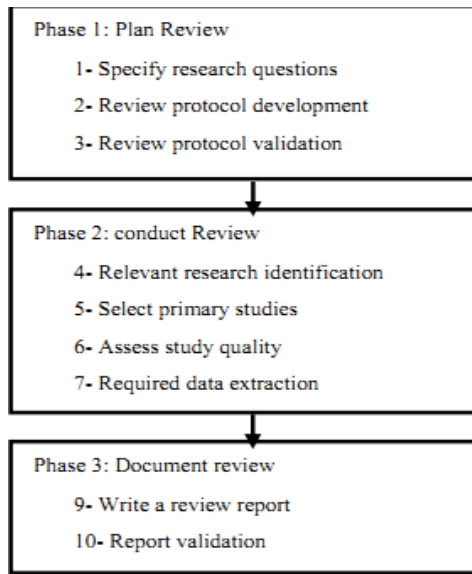


Fig. 1. Phases of Review Adopted from [16].

The questions were generated to complete the preliminary stages and then the sub-activity was carried out by reviewing protocols for the study. The review included determined time span for the published papers, and keywords along with the sources of publications to find most accurate data. The focus of research articles spanned for the last six years i.e. 2017 till 2022 and the sources were obtained from IEEE Xplorer, science direct, Google scholar, and SCOPUS. Table II shows the sources and keywords used to search the materials. Whereas Table III presents the considered papers in each year.

The search process offered a set of total 100 articles and they were then screened on the basis of their titles and abstracts. After filtration, only 18 articles were left that met the inclusion criteria of this study. In order to strengthen the search linked with the articles, backward snowballing provided by [19] was also adopted to identify the most cited articles. This step was ensured to address questions of the study in an effective manner so that no question was left unanswered. The inclusion criteria of this study are based on the research questions of this study and in the end, this study only included those articles that were accurately linked to the research questions of this study.

TABLE II. REVIEW TABLE

Year	Sources	Key words
2017-2022	IEEE Xplorer, Science direct, Google Scholar, SCOPUS	question generation techniques, teaching programming, automatic question generation techniques

TABLE III. YEAR WISE SEARCH RESULTS

Year	Number of papers
2017	4
2018	2
2019	3
2020	3
2021	5
2022	1

IV. RESEARCH ANALYSIS AND DISCUSSION

This study has reviewed a total of 18 papers for AQG in teaching programming in the past six years from 2017 to 2022. Older papers are excluded from the search criteria. Most of them used automated evaluation tools [4][5] [6] [14] [17] or they used automated contexts for programming languages [20] [21] [15]. It was also identified that generating feedback for the questions produced to teach programming languages are equally important. Most of the tools were used to grade student solutions but there were some that offered extended feedback and could be used to support learning process of students.

The study conducted in [21] described the attributes of the tools and identified challenges and some future directions. However, a study by [19] selected some papers and mentioned qualitative elements at the time of evaluating tools for question generation. It was also found that the majority of the studies i.e. 12 out of 18 studies lacked comprehensiveness and the scope of the tools varied immensely. Tools are mostly grouped but there is no such agreement on the naming of different groups. Eight papers discussed technical aspects of teaching tools used for programming languages.

As observed from Table IV, studies [1][3][4][5][14][21] used web-based solution to generate questions for students on the online platform. Whereas some of them proposed a theoretical framework like [7][13] [15][22] and the rest of the studies proposed it as a computer application [12] [16][19] [23] [24]. The main observation on the literature is that most of the applied applications use web-based solution to generate general questions from existing materials using different techniques like Artificial Intelligence, Machine Learning, Deep Learning, and traditional custom-made algorithms.

This review paper is different from other reviews as it focused on the dimensions of generating questions and the feedback in teaching programming tools by closely evaluating the various types of feedback provided on the techniques.

A. Comparison of State-of-the-Field before Covid-19 and after Covid-19

The findings of the study show that teachers require various kinds of tools and techniques when they generate new programming questions. In order to find out the state of the field before COVID-19 and after COVID-19, a review of the techniques used for generating questions by programming teachers shows that varying techniques have been employed to address certain needs of the instructors. The analysis also showed that prior to COVID-19, scholars have been involved in generating questions for teaching programming using Bayesian Network [5], ITSB tool (Delphi IDE) [2], Artificial Neural Network (ANN) based technique [13][17] [9], and ANN combined with Vortex Optimization Algorithm [7]. All these tools were either based on web-based or experimental or theoretical framework that does not exhibit strength of one technique over another technique for generating questions. Some interesting facts were revealed during the analysis. These are the following: 1) after COVID-19, the instructors valued code-writing question generation techniques like Junit that is a web-based tool and used user feedback as a validating tool. 2) Next, ITA [12], JAVA software, C programming for generating

questions, CodeTraining [15], dynamic codes [16] and PQG model [23] were employed by instructors for generating questions that were identified as the key source of positive ratings in the assessment of students during exams. 3) The analysis of articles published after COVID-19, i.e. from 2020 till 2022, valued code-tracing procedures as compared to pre-COVID-19 that seems a major difference between the two periods. 4) Before COVID-19 the focus was on supporting students in learning (finding answers for questions from long texts). Whereas after COVID-19 the focus has shifted to supporting teachers in generating online quizzes and assessing student assignments automatically. This difference also exhibits that the extensibility of tools used for generating

questions got significantly positive ratings from users as compared to pre-COVID-19 tools [23]. This finding is interesting as it identified that the models used after COVID-19 address the needs of particular users and provided only extensible questions to the instructors to be used after edits in practice. On the other hand, the analysis also shows that the automatic question generation process through code-tracing method is very limited and can generate questions when the topic is wide and it is difficult for instructor to cover all ideas when making the questions. One plausible explanation could be, that instructors now anticipate the questions to be more in line with the content they teach in the class.

TABLE IV. ANALYSIS OF ARTICLES

Year of publication	Title of the study	Domain	Aim	Tool for generating questions	Mode of delivery	Validating study
2017	[5]	Computer Science	Teaching programming language	Bayesian Network	Web-based	Experimental
2017	[2]	Computer Science	Teaching programming language	ITSB tool (Delphi IDE)	Web-based	User feedback
2017	[7]	Computer Science	Teaching programming language	Artificial Neural Network based technique & Vortex Optimization Algorithm	Theoretical framework	Experimental
2017	[13]	Computer Science	Teaching programming language	Artificial Neural Network	Theoretical framework	User feedback
2018	[4]	Computer Science	Teaching programming language	Bayesian Network	Web-based	Student feedback
2018	[18]	Computer Science	Teaching programming language	Automatic Item Generation (AIG)	test-item templates	User feedback
2019	[1]	Computer Science	Teaching programming language	ITA	Web-based	Teacher feedback
2019	[23]	Computer Science	Teaching Programming Language	SQL question Generation (DB-Learn)	Computer based application	User feedback
2021	[19]	Computer Science	Teaching programming language and question generation	Question Similarity mechanism.	Application	Teacher feedback and user response
2019	[21]	Computer Science	Teaching programming language	ITA	Web-based	Experimental
2020	[3]	Computer Science	Teaching programming language	JUnit	Web-based	User feedback
2020	[12]	Computer Science	Teaching programming language	ITA	Computer based application	Student performance
2020	[22]	Computer Science	Teaching programming language	AA	Theoretical framework	Teacher feedback
2021	[6]	Computer Science	Teaching programming language	JAVA software	Web-based	Student performance
2021	[14]	Computer Science	Teaching programming language	Java Programming Course	Web-based	Student performance
2021	[15]	Computer Science	Teaching programming language	CodeTraining	Theoretical framework	User feedback
2021	[16]	Computer Science	Teaching programming language	Dynamic codes	Computer based application	Student performance
2022	[24]	Computer Science	Teaching programming language	PQG model	Computer based application	Student performance

B. Techniques of Automatic Question Generation in Teaching Programming

Intelligent Tutoring Systems (ITS) are mainly identified as major systems for teaching programming domain. The analysis of articles showed that there are some general ITS techniques such as the tools that use model tracing for analyzing the process followed by students to solve problems in programming languages. The authors contrasted production rules and buggy rules in [16] while other researchers in [19] used constraint-based modeling techniques that is based on three levels, logical, empirical and data-based constraints. This model has a major limitation for how to conduct loop and eliminate the chances of generating error messages that could affect teachers' ability to generate questions. This study identified theoretical and practical gaps in the literature that could be used as future direction by scholars.

Dynamic code analysis through automated testing is another technique used by [13] as the way to teach programming and then generate questions for analyzing students' abilities and knowledge skills. According to [25], this was identified as the major type of automated testing but it lacked modern techniques necessary for unit testing and property-based testing, mostly executed through pertinent test frameworks like JUnit. In order to address this limitation, the research in [19] used another technique, called basic static analysis and identified the misunderstood concepts and the inadequacy of code structures. However, recently the article [15] also concluded that Program Transformations are another language processing tool that reduces the syntactical complications and help instructors to produce same level of abstraction when designing questions. Notably, all the tools identified during the analysis of articles showed that they fall within two major categories; automated assessment (AA) and intelligent tutoring system (ITS). Automated assessment focused on the use of tools that evaluate students' abilities to solve questions with a feedback report, but ITS helps students to reach solutions with novice feedback that is helpful for teachers to generate questions [17][18].

A recent study conducted by [15] mentioned that previous meta-analysis methods have been used to recognize the factors affecting students' performance but this study is pioneered in evaluating students' computer programming skills through Educational Data mining approaches. The authors stated that there are various categorizations of algorithms for identifying student's performance studying computer programming and the most effective is to use pooled approach to estimate students' performance progress in programming as their educational domain. The authors tried to identify the probable sources of heterogeneity by using subgroup analysis and sensitivity analysis; however, a major gap is identified in defining the sources of variability as authors were unable to establish any in their cases. It is highly likely that the key reason for this colossal heterogeneity was linked with some studies that were obtained from the varying sample sizes; however, it needed further research that could help in adopting different algorithms for assessing student performance.

A study by [16] provided important contribution in generating quizzes for C programming language. The key

contribution of this study is that authors solved the programming questions and generated questions by following an entity discovery approach. It was estimated during the analysis of the question generation process that teachers and students can use them for solving quizzes and attain concepts in a better way. However, this study has a major limitation of practical knowledge related to precision and inclusion of more features like mining answers from the posts and grouping the questions into different levels of their difficulty. On the other hand, an article by [12] generated questions for teaching C programming through JAVA software application that illustrated the likelihood to produce automatic quizzes. It is estimated that if students have acquired knowledge for C programming language, students are able to learn other programming languages in a better way. This paper has a key strength to test the students' knowledge about how to define the C language functions; however, knowledge gap is identified about how students can enhance their aptitude skills for programming in other languages. This restricts the generalizability of the study on learning other programming languages. Although an article by [12] used educational software for studying JAVA language and then assessed their skills towards basics of object-focused programming. The authors provided very important contribution by generating automatic quizzes for JAVA programming through six different types of parametrized questions. This particular technique had major implication in theory as every time the test is conducted to test comprehensive skills of learners, new questions are generated. However, this article did not specify how learners can answer accurate questions based on their programming knowledge. CodeTraining is a very new approach that used an authoring tool for Gamified Programming Learning Environment; however, this particular tool lacks approaches on how teachers can create questions through the integration of different resources [25]. It is also suggested that future scholars can extend knowledge based on Gamification Programming Learning Environment by conducting experimental studies and through the use of an authoring tool that demonstrates how to design questions relevant to the course.

V. CONCLUSION

The objectives of this study are attained by offering a picture of the existing state of teaching programming and the tools used for generating questions. We have discussed the gaps in each article and the limitations of each article that could be used as future research directions. The article also addressed the objective related to comparing state of the field situation in the pre-COVID-19 and during COVID-19 periods. During the review of the studies, various effective methods were identified to that can be helpful in generating questions. A total of 18 papers were analyzed from the year 2017 up to 2022 that were relevant to the given topic of the study. The key techniques included AA and ITS and in particular, Dynamic code analysis, JUnit tests, JAVA programming software, CodeTraining, Program Transformations, PQG model and Educational Data mining approaches. Some gaps are related to the inefficacy linked with the models and the techniques adopted by scholars for generating questions. The inability to properly evaluate students' performance and abilities is related to the quality of the data used for that evaluation. Future studies may seek to

focus on the development of techniques based on key approaches identified in this study to improve the applicability of techniques on a wider scale and in practical context. Furthermore, interested researchers can work on the identified promising research topics in question generation for educational purposes.

VI. FUTURE RESEARCH DIRECTIONS

Based on the literature, the following points represent promising research topics for the interested researchers in question generation for educational purposes:

- Implementing question generation approaches to generate questions on programming languages topics.
- Enhancing experimental reporting, standardizing evaluation metrics, and studying and developing more practical evaluation metrics.
- Extracting informative sentences from existing sentences need to be improved.
- Generating questions from several sentences and summarizing sentences based on their relations need to be explored.

ACKNOWLEDGMENT

The authors gratefully acknowledge the financial assistance from the Institute of Information Science, Faculty of Mechanical Engineering and Informatics, University of Miskolc.

REFERENCES

- [1] A. A. Soofi and M. Uddin, "A Systematic Review of Domains, Techniques, Delivery Modes and Validation Methods for Intelligent Tutoring Systems," *International Journal of Advanced Computer Science and Applications*, vol. 10, no. 3, 2019, doi: 10.14569/IJACSA.2019.0100312.
- [2] C.-P. Wu and S.-L. Wu, "Development of a Web-Based Learning System to Engage Students in Question Generation Activities," *International Journal of Future Computer and Communication*, vol. 6, no. 3, pp. 119–122, Sep. 2017, doi: 10.18178/ijfcc.2017.6.3.502.
- [3] K. Cunningham, R. A. Bejarano, M. Guzdial, and B. Ericson, "‘Im not a computer’: How identity informs value and expectancy during a programming activity," in *14th International Conference of the Learning Sciences*, 2020, pp. 705–708.
- [4] A. L. Santos, "Enhancing Visualizations in Pedagogical Debuggers by Leveraging on Code Analysis," in *Proceedings of the 18th Koli Calling International Conference on Computing Education Research*, Nov. 2018, pp. 1–9, doi: 10.1145/3279720.3279732.
- [5] C. Vieira, A. J. Magana, M. L. Falk, and R. E. Garcia, "Writing In-Code Comments to Self-Explain in Computational Science and Engineering Education," *ACM Transactions on Computing Education*, vol. 17, no. 4, pp. 1–21, Sep. 2017, doi: 10.1145/3058751.
- [6] D. Moonsamy, N. Naicker, T. T., and R. E., "A Meta-analysis of Educational Data Mining for Predicting Students Performance in Programming," *International Journal of Advanced Computer Science and Applications*, vol. 12, no. 2, 2021, doi: 10.14569/IJACSA.2021.0120213.
- [7] E. de Angelis, F. Fioravanti, A. Pettorossi, and M. Proietti, "Semantics-based generation of verification conditions via program specialization," *Sci Comput Program*, vol. 147, pp. 78–108, Nov. 2017, doi: 10.1016/j.scico.2016.11.002.
- [8] G. Kurdi, J. Leo, B. Parsia, U. Sattler, and S. Al-Emari, "A Systematic Review of Automatic Question Generation for Educational Purposes," *Int J Artif Intell Educ*, vol. 30, no. 1, pp. 121–204, Mar. 2020, doi: 10.1007/s40593-019-00186-y.
- [9] H. Keuning, J. Jeuring, and B. Heeren, "A Systematic Literature Review of Automated Feedback Generation for Programming Exercises," *ACM Transactions on Computing Education*, vol. 19, no. 1, pp. 1–43, Jan. 2019, doi: 10.1145/3231711.
- [10] B. Das, M. Majumder, S. Phadikar, and A. A. Sekh, "Automatic question generation and answer assessment: a survey," *Res Pract Technol Enhanc Learn*, vol. 16, no. 1, p. 5, Dec. 2021, doi: 10.1186/s41039-021-00151-1.
- [11] J. Laine, T. Lindqvist, T. Korhonen, and K. Hakkarainen, "Systematic Review of Intelligent Tutoring Systems for Hard Skills Training in Virtual Reality Environments," *International Journal of Technology in Education and Science*, vol. 6, no. 2, pp. 178–203, May 2022, doi: 10.46328/ijtes.348.
- [12] N. A. B. Aziz, "Choosing Appropriate Retrieval based Learning Elements among Students in Java Programming Course," *International Journal of Psychosocial Rehabilitation*, vol. 24, no. 5, pp. 5448–5455, Apr. 2020, doi: 10.37200/IJPR/V24I5/PR2020251.
- [13] L. Zavala and B. Mendoza, "On the Use of Semantic-Based AIG to Automatically Generate Programming Exercises," in *Proceedings of the 49th ACM Technical Symposium on Computer Science Education*, Feb. 2018, pp. 14–19, doi: 10.1145/3159450.3159608.
- [14] R. Garcia, K. Falkner, and R. Vivian, "Instructional Framework for CS1 Question Activities," in *Proceedings of the 2019 ACM Conference on Innovation and Technology in Computer Science Education*, Jul. 2019, pp. 189–195, doi: 10.1145/3304221.3319732.
- [15] R. Rodriguez-Torrealba, E. Garcia-Lopez, and A. Garcia-Cabot, "End-to-End generation of Multiple-Choice questions using Text-to-Text transfer Transformer models," *Expert Syst Appl*, vol. 208, p. 118258, Dec. 2022, doi: 10.1016/j.eswa.2022.118258.
- [16] S. G. Aithal, A. B. Rao, and S. Singh, "Automatic question-answer pairs generation and question similarity mechanism in question answering system," *Applied Intelligence*, vol. 51, no. 11, pp. 8484–8497, Nov. 2021, doi: 10.1007/s10489-021-02348-9.
- [17] R. Layona, B. Yulianto, and Y. Tunardi, "Authoring Tool for Interactive Video Content for Learning Programming," *Procedia Comput Sci*, vol. 116, pp. 37–44, 2017, doi: 10.1016/j.procs.2017.10.006.
- [18] M. Divate and A. Salgaonkar, "Automatic Question Generation Approaches and Evaluation Techniques," *Curr Sci*, vol. 113, no. 09, p. 1683, Nov. 2017, doi: 10.18520/cs/v113/i09/1683-1691.
- [19] S. S. Alanazi, N. Elfadil, M. Jarajreh, and S. Algarni, "Question Answering Systems: A Systematic Literature Review," *International Journal of Advanced Computer Science and Applications*, vol. 12, no. 3, 2021, doi: 10.14569/IJACSA.2021.0120359.
- [20] J. Salac and D. Franklin, "If They Build It, Will They Understand It? Exploring the Relationship between Student Code and Performance," in *Proceedings of the 2020 ACM Conference on Innovation and Technology in Computer Science Education*, Jun. 2020, pp. 473–479, doi: 10.1145/3341525.3387379.
- [21] Ms. R. S. M. Sc. MPhil and Ganesh. K., "Automatic Question Paper Generator System," *International Journal of Trend in Scientific Research and Development*, vol. Volume-3, no. Issue-3, pp. 138–139, Apr. 2019, doi: 10.31142/ijtsrd21646.
- [22] Y. Choi and C. McClenen, "Development of Adaptive Formative Assessment System Using Computerized Adaptive Testing and Dynamic Bayesian Networks," *Applied Sciences*, vol. 10, no. 22, p. 8196, Nov. 2020, doi: 10.3390/app10228196.
- [23] K. Atcharyachanvanich, S. Nalintippayawong, and T. Julavanich, "Reverse SQL Question Generation Algorithm in the DBLearn Adaptive E-Learning System," *IEEE Access*, vol. 7, pp. 54993–55004, 2019, doi: 10.1109/ACCESS.2019.2912522.
- [24] H. Roitman, U. Singer, Y. Eshel, A. Nus, and E. Kiperwasser, "Learning to Diversify for Product Question Generation," Jul. 2022.
- [25] W. He, J. Shi, T. Su, Z. Lu, L. Hao, and Y. Huang, "Automated test generation for IEC 61131-3 ST programs via dynamic symbolic execution," *Sci Comput Program*, vol. 206, p. 102608, Jun. 2021, doi: 10.1016/j.scico.2021.102608.

Application of Stacking Ensemble Machine in Big Data: Analyze the Determinants for Vitalization of the Multicultural Support Center

Raeho Lee¹

Department of Korean Language & Literature
Kangwon National University
Chuncheon, 24341, Republic of Korea

Haewon Byeon^{2*}

Department of Digital Anti-aging Healthcare (BK-21)
Inje University
Gimhae 50834, Republic of Korea

Abstract—For multicultural families to successfully promote social adaptation and achieve desirable social integration, the role of the multicultural family support center (Multi-FSC) is crucial. In addition, it's important to examine the factors that will contribute to the multicultural support center's vitality from the standpoint of the customers. In this study, machine learning models based on a single machine learning model and stacking ensemble using survey data from all multicultural families were used to examine the determinants for the utilization of multicultural family support centers for multicultural families. Additionally, based on the constructed prediction model, this study offered the foundational data for the revitalization of the multicultural support center. In this study, 281,606 adults (19 years or older), 56,273 of whom were married immigrants or naturalized citizens as of 2012, were examined. The stacking ensemble method was employed in this work to forecast the use of multicultural family support centers. In the base stage (model) of this model, logistic regression was employed, along with Classification and Regression Tree (CART), Radial Basis Function Neural Network (RBF-NN), and Random Forest (RF) model. The RBF-NN-Logit reg model had the best prediction performance, according to the study's findings (RMSE = 0.20, Ev = 0.45, and IA = 0.68). The findings of this study suggested that the prediction performance of the stacking ensemble can be improved when creating classification or prediction models using epidemiological data from a community.

Keywords—Stacking ensemble machine; radial basis function neural network; random forest; multicultural family support centers; prediction model

I. INTRODUCTION

In South Korea, the number of married immigrants and foreign workers has increased rapidly since the 1990s. Consequently, South Korea has also transformed into a multicultural society starting in the 21st century. Multicultural Demographic Statistics [1] reported that the number of foreigners residing in South Korea was 1.13 million as of 2011, exceeding 2.3% of the resident registration population in South Korea. Furthermore, multicultural marriages increased by 4.0% (24,721 cases), and the proportion of multicultural marriages in total marriages in South Korea was 10.3%, up 1.1% from 2019 [1]. If current trends continue, the number of married immigrant families will exceed 2 million, accounting for 5% of the total population, by 2050 [2]. In addition, the Ministry of Education, Science and Technology [3] estimated that one out of five

citizens in their 20s will be from multicultural families and one out of three newborns will be born in multicultural families in 2030. South Korean society must prepare for measures to cope with various issues, which may arise during the paradigm shift to multiculturalism (e.g., early adaptation of marriage immigrants to South Korean society), as well as these rapid changes in the demographic structure.

As the number of multicultural families has increased, support for multicultural families has also been diversifying over the past 20 years [4]. Currently, the South Korean government has established and operated multicultural family support centers nationwide as a part of national policy for stably supporting a multicultural society [5]. The multicultural family support center (Multi-FSC) is a central management that has been operated since 2006 for the purpose of helping marriage immigrants to adapt to South Korean society quickly and supporting for stable family life of multicultural families through providing services including family education, counseling, and cultural programs for multicultural families. Twenty-one centers were established in 2006, and the number of centers increased to 201 by 2012, following the passage of the Multicultural Families Support Act (No. 8937) in 2008 [6,7].

In one aspect, as the number of multicultural family support centers was increasing, the necessity of careful management for participants was emphasized in addition to the effectiveness of services [8]. Nevertheless, studies on the Multi-FSC have focused on the results of one region or just analyzed the achievement or satisfaction of multicultural support projects [9, 10, 11, 12].

The role of Multi-FSC is very important for the successful social adaptation support and desirable social integration of multicultural families. In addition, it's important to examine the factors that will contribute to the multicultural support center's vitality from the standpoint of the customers. This study explored the predictors for the use of Multi-FSCs for multicultural families using machine learning models based on a single machine learning model and stacking ensemble using the survey data of all multicultural families. Furthermore, based on the developed prediction model, this study provided foundational data for the revitalization of the multicultural support center.

*Corresponding Author.

II. MATERIALS AND METHODS

A. Source Data

This study analyzed survey data from a national survey of multicultural families (NS-mulfam) that the Ministries of Health, Welfare and Family Affairs, Justice, and Gender Equality jointly conducted in 2017 on multicultural families living in South Korea. The purpose of the NS-nulfam was to create tailored policies by identifying the living circumstances and welfare requirements of multicultural families [13]. The general characteristics of multicultural families, employment, economic status, marriage, health, and medical care were among the survey's questions. The NS-nulfam targeted 154,333 married immigrants for its survey, all of whom were living in South Korea. A survey on married immigrants, a survey on their spouses, and a survey on their kids were all independently conducted as part of this study. The survey subjects were sampled by using the status of foreign residents in 16 cities and provinces in South Korea and the basic status data of multicultural families organized by the Ministry of Public Administration and Security. The survey was carried out from July 20 to October 31, 2017, and a separate sample design was not taken into consideration because this study used a complete enumeration. According to the Multicultural Families Support Act (No. 8937), the multicultural families used in this research were defined as either 1) families made up of marriage immigrants and South Korean citizens who became citizens by birth, acknowledgment, or naturalization, or 2) families made up of foreigners who became citizens of South Korea by acknowledgment or naturalization and South Korean citizens who became citizens by birth, acknowledgment, or naturalization. After removing 1,618 individuals who were under the age of 19 from the study, 281,606 adults (56,273 men and 225,333 females) who were married immigrants or naturalized as of 2012 were examined.

B. Definition of Variables

The outcome (label) was defined as the use experience of a Multi-FSC (not aware of or never used it OR used it before). Features included gender, marital status (single, having a spouse, bereavement / widowed, or divorcement / divorced / separation / separated), highest education level (elementary school or below, junior high school, high school, or college or higher), occupation (regular worker, temporary worker, day-to-day worker, self-employed with employees, self-employed without employees, or unpaid family worker), age (19-29, 30-39, 40-49, 50-, 60-69, or 70 years old or older), family relationship satisfaction (not applicable, satisfactory, not satisfied or dissatisfied, or dissatisfied), relationship satisfaction with a spouse's siblings (not applicable, satisfactory, not satisfied or dissatisfied, or dissatisfied), relationship satisfaction with children (not applicable, satisfactory, not satisfied or dissatisfied, or dissatisfied), life satisfaction (good, moderate, or bad), relationship satisfaction with a spouse's parents (not applicable, satisfactory, not satisfied or dissatisfied, or dissatisfied), heritage // nationality of origin (Chinese, Korean-Chinese, Taiwanese or Hong Kong, Vietnam, Philippines, Japan, Mongolia, Uzbekistan, Russia, Thailand, Cambodia, North America, other southeast Asian countries, Western Europe, or Southern Asia), Korean

citizenship (yes or no), social discrimination experiences (yes or no), and subjective state of health (good, moderate, or bad).

C. Base Model (Single Machine Learner): Classification and Regression Tree (CART)

One of the statistical decision classification methods, CART, uses the Gini Index to quantify impurity [14]. It is a binary split-based technique that only creates two child nodes from a parent node [14]. Advantages of CART include its ability to handle both continuous and categorical data as well as the ease with which its rules may be understood [15]. The likelihood that two randomly selected items from n elements belong to separate groups is known as the Gini coefficient [16]. The classifier and ideal classification that reduce the Gini coefficient the most are chosen as a child node once the algorithm has determined how much the Gini coefficient has decreased.

D. Radial basis Function Neural Network (RBF-NN)

RBF-NN is a data mining modeling technique that finds hidden patterns in data by repeating learning from real data and mimicking the human brain's neural network [17, 18]. It is a nonlinear flexible model used to forecast using data with complicated structures [17,18]. The neural network is a hierarchical algorithm made of several processing components [19]. The relationship between input and output is learned while weights are repeatedly changed using historical input data and corresponding output values [19]. The neural network is made up of an input layer made up of nodes that correspond to input variables and a hidden layer (or layers) made up of numerous hidden nodes. The hidden node uses a nonlinear function to handle the linear combination of variable values given from the input layer and sends it to the output layer or another hidden layer. The coupling function for the hidden layer in this work was RBF-NN, which employs the Radial Basis function. Fig. 1 illustrates the RBF-NN idea.

E. Random Forest (RF)

The RF algorithm randomly selects which decision trees to learn [21]. Multiple bootstrap samples are used in this technique to create a decision tree for each sample, and the results showing the highest frequency among the decision tree results are used to forecast the outcome of a new dataset [22]. In Fig. 2, the RF structure is shown.

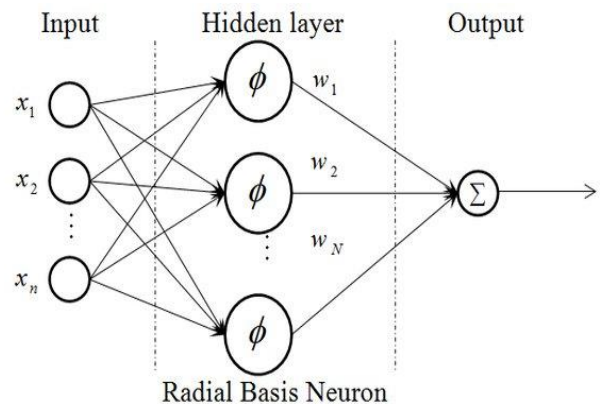


Fig. 1. Structure of the RBF-NN Modeling [20].

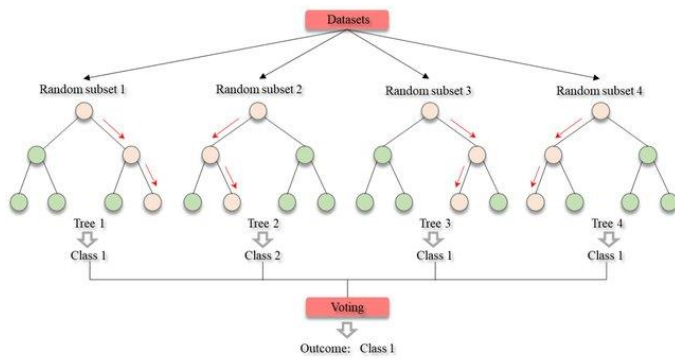


Fig. 2. Structure of the Random Forest Modeling [23].

F. Meta Model (Stacking Ensemble)

The stacking ensemble technique was used in this study to predict the use of Multi-FSCs. In recent years, stacking ensemble outperforms a single machine learning model in terms of generalization and robustness, and it has been used for classification and prediction in a variety of fields [24, 25, 26, 27, 28]. This technique generates a new model by stacking several different models [29]. It improves the final model's performance by combining the strengths of each model and supplementing the weaknesses of each model through two stages (base and meta) [29].

In the base stage (model), this model used RBF-NN, CART, and RF. In the meta stage, the model used the logistic regression algorithm (model). The regression algorithm is the most straightforward way to maximize generality and stability while increasing the reliability of the base model, and it is unlikely to overfit the training data [30]. Due to this, the regression algorithm has been employed in numerous recent publications [30, 31] as the meta model for the stacking ensemble algorithm. For the same reason, the regression algorithm for a meta model was used in this study. Fig. 3 illustrates the final stacking ensemble model's structural layout.

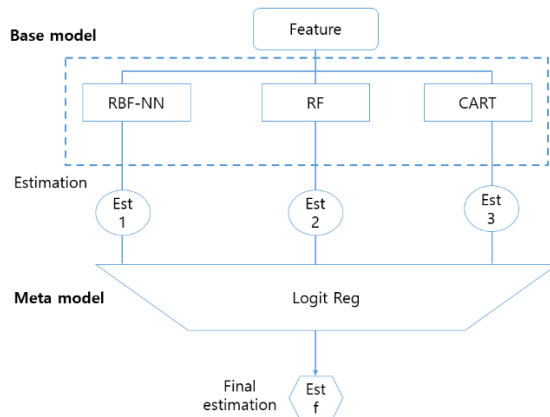


Fig. 3. Structure of the Prediction Model (Stacking Ensemble).

G. Meta Model (Stacking Ensemble)

Through the use of seven-fold cross-validation, each machine learning model was verified. With this approach, ten groups of equal size are randomly selected from the entire sample, and one group is used for validation while the other is

used for learning. Seven times are run through this procedure to ensure that the knowledge is retained. The root-mean-square error (RMSE), error variance (Ev), and index of agreement (IA) were used in this study to assess how well the developed models performed as predictors. A lower RMSE among these indices denotes a prediction model with greater accuracy, whereas a lower Ev denotes a model with greater stability. A model becomes more stable as IA gets closer to 1.

III. RESULTS

A. General Characteristics of Subjects by the Experience of using the Multi-FSC

Table I depicts the general characteristics of the research subject based on their experience with the Multi-FSC. Among the 281,606 subjects, 95,826 subjects (34.0%) had used the Multi-FSC at least once, while 185,780 subjects (66.0%) had not used the Multi-FSC. The results of chi-square test showed that the group with experience of using the Multi-FSC and the group without experience of using the Multi-FSC had significantly ($p < 0.05$) different age, gender, relationship satisfaction with children, the highest level of education, family relationship satisfaction, relationship satisfaction with a spouse's parents, siblings, subjective health status, life satisfaction, occupation, nationality of origin, South Korean citizenship, and social discrimination experience.

TABLE I. GENERAL CHARACTERISTICS ACCORDING TO THE EXPERIENCE OF USING THE USING THE MULTI-FSC, N (%)

Variables	Experience of using the Multi-FSC		p
	Yes (n=95,826)	No (n=185,780)	
Age			<0.001
19-29	42,122 (55.9)	33,258 (44.1)	
30-39	32,219 (37.5)	53,794 (62.5)	
40-49	16,905 (23.8)	54,090 (76.2)	
50-59	3,511 (11.3)	27,586 (88.7)	
60-69	827 (6.6)	11,614 (93.4)	
70+	244 (4.3)	5,438 (95.7)	
Gender			
Male	4,079 (7.2)	52,194 (92.8)	
Female	91,747 (40.7)	133,586 (59.3)	
Marital status			<0.001
Single	481 (5.9)	7,639 (94.1)	
Having a spouse	92,910 (36.4)	162,535 (63.6)	
Bereavement/widowed	872 (16.5)	4,421 (83.5)	
Divorcement/divorced/separation/separated	1,564 (12.3)	11,185 (87.7)	
Residence			<0.001
Urban	61,866 (28.0)	159,150 (72.0)	
Countryside	33,961 (56.0)	26,630 (44.0)	
Level of education			<0.001

Elementary school or below	9,522 (35.4)	17,407 (64.6)	
Junior high school	23,060 (37.1)	39,103 (62.9)	
High school	41,661 (33.1)	84,172 (66.9)	
College or higher	21,583 (32.4)	45,098 (67.6)	
Family relationship satisfaction			<0.001
Good	68,356 (33.5)	135,699 (66.5)	
Moderate	23,033 (37.9)	37,757 (62.1)	
Bad	3,956 (45.8)	4,685 (54.2)	
Relationship satisfaction with a spouse's parent			<0.001
Not applicable	14,336 (22.1)	50,554 (77.9)	
Satisfactory	44,747 (37.4)	74,819 (62.6)	
Not satisfied or dissatisfied	29,032 (39.9)	43,670 (60.1)	
Dissatisfied	7,230 (44.3)	9,098 (55.7)	
Relationship satisfaction with a spouse's siblings			<0.001
Not applicable	4,794 (16.5)	24,236 (83.5)	
Satisfactory	45,496 (34.5)	86,465 (65.5)	
Not satisfied or dissatisfied	36,005 (39.3)	555,691 (60.7)	
Dissatisfied	9,049 (43.5)	11,749 (65.1)	
Relationship satisfaction with children			<0.001
Not applicable	16,878 (19.1)	71,568 (80.9)	
Satisfactory	68,229 (44.3)	85,703 (55.7)	
Not satisfied or dissatisfied	8,851 (32.6)	18,272 (67.4)	
Dissatisfied	1,387 (34.8)	2,598 (65.2)	
Subjective health status			<0.001
Good	64,320 (37.0)	109,636 (63.0)	
Moderate	24,853 (32.2)	52,363 (67.8)	
Bad	6,653 (21.9)	23,781 (78.1)	
Life satisfaction			<0.001
Good	51,458 (35.9)	91,996 (64.1)	
Moderate	37,758 (32.7)	77,859 (67.3)	
Bad	6,611 (29.3)	15,925 (70.7)	
Heritage / nationality of origin			<0.001

Chinese	18,294 (28.6)	45,602 (71.4)	
Korean-Chinese	14,865 (15.6)	80,600 (84.4)	
Taiwanese or Hong Kong	453 (11.3)	3,572 (88.7)	
Japan	6,240 (37.4)	10,431 (62.6)	
Mongolia	1,769 (55.5)	1,420 (44.5)	
Vietnam	32,898 (66.1)	16,900 (33.9)	
Philippines	10,145 (69.3)	4,502 (30.7)	
Thailand	1,930 (57.5)	1,426 (42.5)	
Cambodia	3,805 (73.4)	1,381 (26.6)	
Uzbekistan	1,300 (57.0)	981 (43.0)	
Russia	570 (30.5)	1,299 (69.5)	
North America	466 (4.7)	9,514 (95.3)	
Other southeast Asian countries	832 (35.7)	1,499 (64.3)	
Southern Asia	792 (36.4)	1,384 (63.6)	
Western Europe	111 (4.8)	2,213 (95.2)	
Occupation			<0.001
Regular worker	13,441 (24.6)	41,230 (75.4)	
Temporary worker	16,681 (33.0)	33,880 (67.0)	
Day-to-day worker	7,324 (21.2)	27,158 (78.8)	
Self-employed with employees	401 (9.8)	3,672 (90.2)	
Self-employed without employees	2,365 (24.1)	7,430 (75.9)	
Unpaid family worker	72,410 (56.6)	72,410 (56.6)	
Korean citizenship			<0.001
Yes	35,709 (27.0)	96,491 (73.0)	
No	60,117 (40.2)	89,288 (59.8)	
Social discrimination experiences			0.001
Yes	40,162 (34.4)	76,705 (65.6)	
No	55,665 (33.8)	109,075 (66.2)	

B. A Comparison of the Prediction Performance of Models Anticipating the Utilization of the Multi-FSC

Fig. 4 to 6 depict the prediction performance (RMSE, Ev, and IA respectively) of six machine learning models for forecasting the use of Multi-FSCs. The findings revealed that the RBF-NN-Logit reg model had the best prediction performance (RMSE=0.20, Ev=0.45, and IA=0.68).

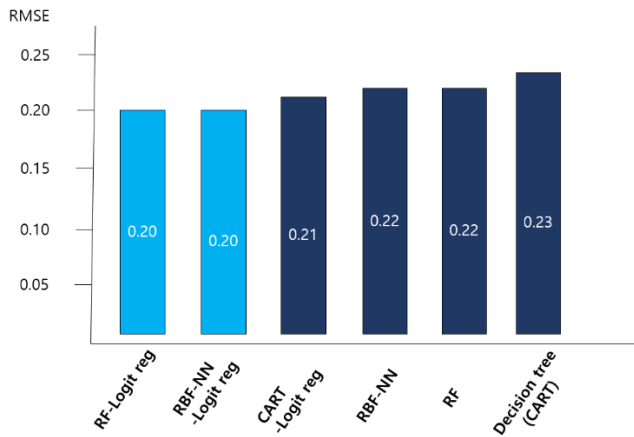


Fig. 4. Models for Machine Learning Compared using the Root-mean-Square Error.

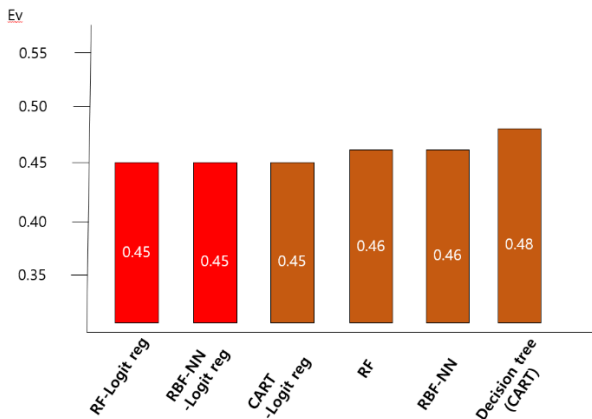


Fig. 5. Models for Machine Learning Compared using Error Variance.

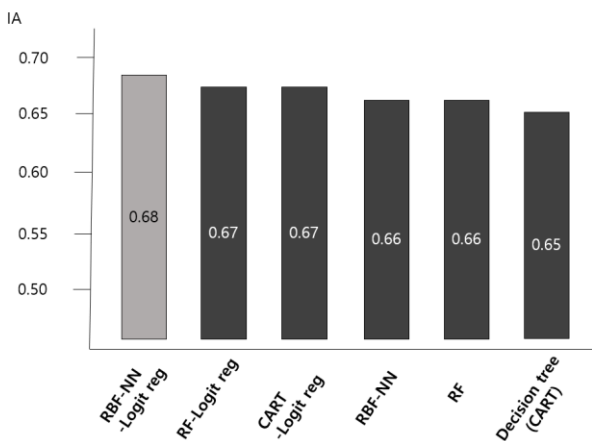


Fig. 6. Models for Machine Learning Compared using Index of Agreement.

C. Predictors for the use of Multi-FSCs in South Korea

The normalized importance of the variables of the RBF-NN-Logit reg model, the final model, is presented in Fig. 7. The results confirmed that gender (100%), relationship satisfaction with children (93%), age (85%), country of origin (69%), relationship satisfaction with a spouse's siblings (61%), and relationship satisfaction with a spouse's parents (57%) were a

significant factor that carried a significant amount of weight in the South Korean experience of using Multi-FSCs. The gender (female) of these was the one that had the greatest impact on the final model.

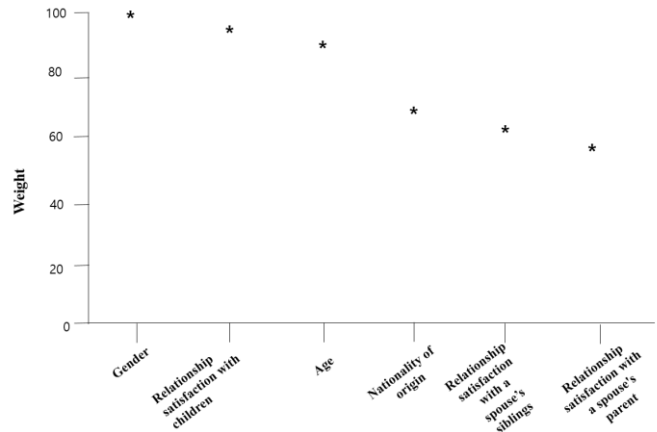


Fig. 7. Variable's Importance for use of Multi-FSCs (only top 6).

IV. CONCLUSIONS

In our study, the RBF-NN-Logitreg model predicted gender, relationship satisfaction with children, age, country of origin, relationship satisfaction with spouse's siblings, and relationship satisfaction with spouse's parents for the application of Multi-FSC. The South Korean government can use these forecast results as policy data to further promote Multi-FSC.

Using six machine learning techniques—three base models and three stacking ensemble models—this study created prediction models for factors linked to the use of the Multi-FSC in South Korea and evaluated the effectiveness of the models. The RBF-NN-Logit reg model based on the stacking ensemble algorithm had the best prediction performance, according to the results. Given that their RMSE was 0.03 less than that of the base models, prediction models based on the stacking ensemble technique in particular demonstrated improved accuracy (single machine learning model). Furthermore, given that their EV was 0.03 higher than the EV of base models, they had better stability. The findings of this study suggested that the prediction performance of the stacking ensemble may be superior to that of the single machine learning model when developing classification or prediction models using epidemiology data from a community.

The stacking ensemble takes longer to run than the single machine learning model because its algorithm is more complex than the base model [32, 33, 34, 35, 36, 37]. Furthermore, depending on the combination of the base model and meta model, it has been reported that it is more likely to cause overfitting than a single machine learning model in some cases [32, 33, 34, 35, 36, 37]. As a result, more research is required to evaluate the prediction performance of the stacking ensemble. Future research is required to investigate the stacking ensemble model with the best performance using more diverse combinations of base models and meta models in order to find a model that can minimize overfitting while maximizing accuracy.

ACKNOWLEDGMENT

This study was supported by 2021 Research Grant from Kangwon National University.

REFERENCES

- [1] Statistics Korea, 2019 Multicultural Demographic Statistics. Statistics Korea, 2021. <http://kostat.go.kr>.
- [2] Ministry of Public Administration and Security, Statistical foreign migrants 2019. Ministry of Public Administration and Security, Seoul, 2019.
- [3] Ministry of Education, Science and Technology, Status of multicultural families and support measures, Ministry of Education. Science and Technology, Seoul, 2018.
- [4] D. H. Lee, A study on multicultural families support act. The Journal of the Korea Contents Association, vol. 19, no. 7, pp. 650-658, 2019.
- [5] Y. J. Oh, Role of multicultural family support center for school adaptation of elementary school children of multicultural families. Cultural Exchange and Multicultural Education, vol. 7, no. 3, pp. 79-99, 2018.
- [6] J. H. Song, and T. Y. Lee, A study on the legislative process of the support for multicultural families act. Social Policy, vol. 39, no.3, pp.151-179, 2012.
- [7] A. Kim, Social exclusion of multicultural families in Korea. Social Sciences, vol. 74, p. 63. 2018. <https://doi.org/10.3390/socsci7040063>
- [8] K. J. Seon, The relationship between job-stress and psychological-exhaustion of counselors at multicultural family support center. Journal of The Korea Society of Computer and Information. vol. 18, no. 7, pp. 157-164, 2013.
- [9] H. A. Lee, Analysis of satisfaction with the fatherhood programs provided in healthy family and multicultural family support center. Korean Family Resource Management Association, vol. 22, no. 3, pp. 61-76, 2018.
- [10] M. K. Park, Y. J. Cha, and H. J. Lee, The effects of using the multicultural family support centers on the bicultural identity of the multicultural youths: focusing on propensity score matching. The Journal of Multicultural Society, vol. 12, no. 3, pp. 107-140, 2019.
- [11] M. Chin, S. Noh, and H. So, Awareness of healthy family support center and multicultural family support center and parenting stress and family healthiness. Journal of Korean Home Management Association, vol. 35, no. 3, pp. 113-126, 2017.
- [12] I. Kwon, B. Lee, and S. Kim, The experience of alienation of marriage migrant women in the healthy family and multicultural family support center. Welfare & Cultural Diversity Studies, vol. 22, no. 2, pp. 41-73, 2020.
- [13] Ministry of Gender Equality & Family, A study on the national survey of multicultural families. Ministry of Gender Equality & Family, Seoul, 2012.
- [14] W. Chen, X. Xie, J. Wang, B. Pradhan, H. Hong, D. T. Bui, Z. Duan, and J. Ma, A comparative study of logistic model tree, random forest, and classification and regression tree models for spatial prediction of landslide susceptibility. Catena, vol. 151, pp. 147-160, 2017.
- [15] H. Byeon, Development of prediction model for endocrine disorders in the Korean elderly using CART algorithm. International Journal of Advanced Computer Science and Applications, vol. 6, no. 9, pp. 125-129, 2015.
- [16] H. Byeon, and R. Lee, Prediction model for the smoking in Korean adolescent using CART algorithm. Information, vol. 17, no. 12A, pp. 6273-6278, 2014.
- [17] F. Bonanno, G. Capizzi, G. Graditi, C. Napoli, and G. M. Tina, A radial basis function neural network based approach for the electrical characteristics estimation of a photovoltaic module. Applied Energy, vol. 97, pp. 956-961, 2012.
- [18] J. D. Wu, and J. C. Liu, A forecasting system for car fuel consumption using a radial basis function neural network. Expert Systems with Applications, vol. 39, no. 2, pp. 1883-1888, 2012.
- [19] A. D. Dongare, R. R. Kharde, and A. D. Kachare, Introduction to artificial neural network. International Journal of Engineering and Innovative Technology, vol. 2, no. 1, pp. 189-194, 2012.
- [20] H. He, Y. Yan, T. Chen, and P. Cheng, Tree height estimation of forest plantation in mountainous terrain from bare-earth points using a DoG-coupled radial basis function neural network. Remote Sensing, vol. 11, no. 11, pp. 1271, 2019.
- [21] M. Belgiu, and L. Drăguț, Random forest in remote sensing: a review of applications and future directions. ISPRS Journal of Photogrammetry and Remote Sensing, vol. 114, pp. 24-31, 2016.
- [22] V. F. Rodriguez-Galiano, B. Ghimire, J. Rogan, M. Chica-Olmo, and J. P. Rigol-Sanchez, An assessment of the effectiveness of a random forest classifier for land-cover classification. ISPRS Journal of Photogrammetry and Remote Sensing, vol. 67, pp. 93-104, 2012.
- [23] J. Yang, J. Gong, W. Tang, Y. Shen, C. Liu, and J. Gao, Delineation of urban growth boundaries using a patch-based cellular automata model under multiple spatial and socio-economic scenarios. Sustainability, vol. 11, no. 21, pp. 6159, 2019.
- [24] S. Cui, Y. Yin, D. Wang, Z. Li, Y. Wang, A stacking-based ensemble learning method for earthquake casualty prediction. Applied Soft Computing, vol. 101, pp. 107038. 2021.
- [25] M. Akour, I. Alsmadi, and I. Alazzam, Software fault proneness prediction: a comparative study between bagging, boosting, and stacking ensemble and base learner methods. International Journal of Data Analysis Techniques and Strategies, vol. 9, no. 1, pp. 1-16, 2017.
- [26] J. Lee, J. Kim, and W. Ko, Day-ahead electric load forecasting for the residential building with a small-size dataset based on a self-organizing map and a stacking ensemble learning method. Applied Sciences, vol. 9, no. 6, pp. 1231, 2019.
- [27] T. P. Williams, and J. Gong, Predicting construction cost overruns using text mining, numerical data and ensemble classifiers. Automation in Construction, vol. 43, pp. 23-29, 2019.
- [28] Y. Xiong, M. Ye, and C. Wu, Cancer classification with a cost-sensitive naive bayes stacking ensemble. Computational and Mathematical Methods in Medicine, vol. 2021, pp. 5556992, 2021.
- [29] G. Wang, J. Hao, J. Ma, and H. Jiang, A comparative assessment of ensemble learning for credit scoring. Expert Systems with Applications, vol. 38, no. 1, pp. 223-230, 2011.
- [30] L. Feng, Y. Li, Y. Wang, and Q. Du, Estimating hourly and continuous ground-level PM2.5 concentrations using an ensemble learning algorithm: the ST-stacking model. Atmospheric Environment, vol. 223, pp. 117242, 2020.
- [31] J. Chen, J. Yin, L. Zang, T. Zhang, and M. Zhao, Stacking machine learning model for estimating hourly PM2.5 in China based on Himawari 8 aerosol optical depth data. Science of The Total Environment, vol. 697, pp. 134021, 2019.
- [32] F. Divina, A. Gilson, F. Gómez-Vela, M. García Torres, and J. F. Torres, Stacking ensemble learning for short-term electricity consumption forecasting. Energies, vol. 11, no. 4, pp. 949, 2018.
- [33] E. Menahem, L. Rokach, and Y. Elovici, Troika—an improved stacking schema for classification tasks. Information Sciences, vol. 179, no. 24, pp. 4097-4122, 2009.
- [34] M. Surdeanu, and C. D. Manning, Ensemble models for dependency parsing: cheap and good?. In Human Language Technologies: The 2010 Annual Conference of the North American Chapter of the Association for Computational Linguistics, pp. 649-652, 2010.
- [35] J. Yan, Y. Qi, and Q. Rao, Detecting malware with an ensemble method based on deep neural network. Security and Communication Networks, vol. 2018, p. 7247095, 2018. <https://doi.org/10.1155/2018/7247095>.
- [36] S. Young, T. Abdou, and A. Bener, Deep super learner: a deep ensemble for classification problems. In Canadian Conference on Artificial Intelligence, pp. 84-95, 2018.
- [37] J. Moon, S. Jung, J. Rew, S. Rho, and E. Hwang, Combination of short-term load forecasting models based on a stacking ensemble approach. Energy and Buildings, vol. 216, pp. 109921, 2020.

Research on Precision Marketing based on Big Data Analysis and Machine Learning: Case Study of Morocco

Nouhaila El Koufi, Abdessamad Belangour, Mounir Sdiq
Laboratory of Information Technology and Modeling (LTIM)
Faculty of Sciences, Ben M'sik, Hassan II University, Casablanca, Morocco

Abstract—With the growth of the Internet industry and the informatization of services, online services and transactions have become the mainstream method used by clients and companies. How to attract potential customers and keep up with the Big Data era are the important challenges and issues for the banking sector. With the development of artificial intelligence and machine learning, it has become possible to identify potential customers and provide personalized recommendations based on transactional data to realize precision marketing in banking. The current study aims to provide a potential customer's prediction algorithm (PCPA) to predict potential clients using big data analysis and machine learning techniques. Our proposed methodology consists of five stages: data preprocessing, feature selection using Grid search algorithm, data splitting into two parts train and test set with the ratio of 80% and 20% respectively, modeling, evaluations of results using confusion matrix. According to the obtained results, the accuracy of the final model is the highest (98.9%). The dataset used in this research about banking customers has been collected from a Moroccan bank. It contains 6000 records, 14 predictor variables, and one outcome variable.

Keywords—Precision marketing; big data analysis; machine learning; potential customers prediction algorithm (PCPA)

I. INTRODUCTION

After entering the 21st century, the world witnessed a rapid growth in internet technology which resulted in the development of online transactions and the change in consumer habits and consumption patterns. The traditional model of bank marketing seriously hinders the development of the bank sector due to the lack of understanding of clients' needs, inability to adapt to the modern market characteristics, and the lack of personalized recommendations for quality customers. However, Big data analysis and machine learning techniques applied in precision marketing will provide ideal results to traditional marketing. Therefore, the banking industries need to change their old marketing model toward a precision marketing model based on big data analysis, artificial intelligence (AI), and modern information technology to realize long-term development.

The advancement of big data technology has also contributed to the acceleration of transformation from traditional banking to modern and digital banking. Meanwhile, machine learning techniques and big data analysis technology play an essential role in the precision marketing of banking

services. Machine learning techniques provide the possibility to extract facts, information, and patterns about customers from the large amount of data gathered in banks [1]. Analyzing and extracting knowledge from such data can provide a decision-making foundation for banking companies.

The marketing strategy is a long-term scheme that principally studied the marketing and market environment to understand market opportunities and meet the customers' needs. It covers everything from the study of the situations confronted by enterprises marketing under current market conditions and competitions, the choice of customers, and the channel of communication between companies and clients. Whereas precision marketing refers to a marketing strategy that has a clear focus, it targets the consumers that have a great willingness to consume. Based on modern information technology, precision marketing precise the position accurately to build personalized communication between enterprises and customers so that companies can realize long-term development and maximize wealth.

Theoretically, precision marketing is a marketing strategy that aims to understand customers well and their actual needs. Practically, based on big data analysis, machine learning techniques, and modern technology, precision marketing can render the prediction reasoning nearest to customers' needs. The principle of precision marketing was first proposed back in 1999 by Lester. In 2004, the 4R rule of precision marketing was declared by Brebach and Zabin. Then, Philip Kotler gave a clear introduction to precision marketing. Jin et al. [2] have stated that companies can achieve high sales performance by adapting precision marketing.

Precision marketing can not only achieve high sales and decrease the purchase cost of customers but also help companies to build a loyal customer base. The modern bank is customer-centric. It focuses on how understanding customers' behaviors to provide clients with accurate and quality services via a digital operation technologies chain. Banks not only need to realize deals with customers but also need to maximize wealth and ensure return rates last long. Thanks to the fast development of information technologies, precision marketing realize the goal of enterprises to understand clients and provide them with the right product at the right time and via appropriate methods. Precision marketing contains four parts: target customer, right message and channel, and a good time.

The main objective of this paper is to propose a new precision marketing model based on big data analysis and machine learning techniques to identify potential customers. The rest of this paper is organized as follows: we review previous related works in the next section. In Section III, we present and discuss the proposed methodology. Section IV is reserved to illustrating and analyzing our simulation results and performance evaluation. Finally, the conclusion of our paper is in Section V.

II. RELATED WORK

A. Literature Review

We present a summary of what has been proposed in precision marketing based on machine learning and big data by renowned researchers. In this subsection, we have reviewed various researches related to our work.

Chiu et al. [3] have proposed an Omni-channel Chatbot that merges IOS, Android, and Web components. Based on convolutional neural networks (CNNs), the proposed chatbot can provide personalized service and precision marketing. In order to show the advantages of the new method, a case study of a shared kitchen is utilized, which can be employed for other consumer applications like personalized services and clothing selection.

Zhang et al. [4] developed a predictive model to forecast high potential luxury car buyers using car owners' and telecom users' data. They combined two machine learning algorithms, logistic regression, and neural network mining. A case study of a traffic management department and telecom operators in a medium-growth city in china is used to demonstrate the efficiency of the new model.

In [5], Xia Liu has compared the CNN model, LSTM model, LSTM attention model, and CNN + LSTM attention. As a result, the performance of the CNN + LSTM attention model and the LSTM attention model is better, with the highest overall accuracy of testing and training. The model is applied to precision marketing for obtaining precision consumer portraits'.

In [6], Xie et al. have used Hamming distance classification algorithm and BP Neural network to classify clients using purchase data to release the purpose of precision marketing. In order to solve the problem of the chosen transportation program, the related decision objectives, and location selection. Xiao et al. [7] built a precision marketing optimization strategy using neural network modeling and the fuzzy method.

In [8], Chong et al. adopted neural networking for consumer product demand prediction. In order to show the advantage of the proposed solution, an electronic data from Amazon.com was used. This data is about promotional marketing information and online reviews.

Tang et al. [9] proposed an advanced K-means clustering algorithm to provide an accurate customer division. Scholars have applied this new method in the precision marketing of ETC credit cards to precisely detect potential ETC users. To build a precision marketing device for forecasting the cumulative number of voice app users for China Mobile communications, Yan et al. [10] adopted ARIMA modeling.

The proposed method gives a reference to understanding its market demand.

The studies in precision marketing based on Big data analysis and machine learning are fewer in the banking field. The related research of machine learning in the banking sector mainly focuses on banking crisis prediction and forecasting customer churn. In [11], Jessica et al. adopted artificial neural network modeling that predicts the short-term financial distress for Spanish banking. A predictive model based on Big data analysis and crisis Index to predict the banking crisis was proposed in [12]. Zizi et al. [13] used logistic regression and neural network modeling based on financial indicators to forecast financial distress in the bank sector.

In this study, we propose a new precision marketing model based on banking big data to forecast potential target customers and realize accurate marketing of bank housing loans. The proposed PCPA algorithm is based on big data and machine learning technology. The process of PCPA consists of five steps: data selection and understanding, data cleaning and filtering, feature selection, data modeling, and results evaluation. After a comparison of various famous machine learning methods [14], we chose XGBoost as the central algorithm of PCPA. Moreover, we have preprocessed the data and extracted the significant features using the Grid search algorithm for well understanding of the data.

III. PROPOSED WORK

A. System Architecture

In this subsection, a pictorial representation of the whole process of PCPA is illustrated in Fig. 1. The process of PCPA consists of six phases: data selection and understanding, data cleaning and filtering, feature selection, splitting the prepared data, modeling, and results evaluation.

B. Description of Proposed Model

1) *Data selection and understanding*: The dataset used in this study is from a Moroccan bank, Attawfiq Micro-Finance. The data consists of 6000 records and 14 variables; it contains demographic information and information about customers' behaviors. The provided data are from 2018 to 2021. For building a suitable predictive model, a selection of important information from data was established using advanced data variance analysis and analyzing attributes correlation (using Correlation matrix).

Each case from the final dataset is represented by thirteen variables used as input to the proposed model and one categorical variable that represents whether the customer has applied for a housing loan (Housing_credit) as output. Table I represents the attributes of the data. We represent the coded of some indicators in Table II.

2) *Data cleaning and filtering*: The data cleaning and filtering stage consists of cleaning the selected data from missing values, outliers, noise, etc. This phase is eliminatory for reducing the dimensions of the dataset and reducing the time of required computation. In order to extract deeper insights, we have considered the data visualization in this methodology.

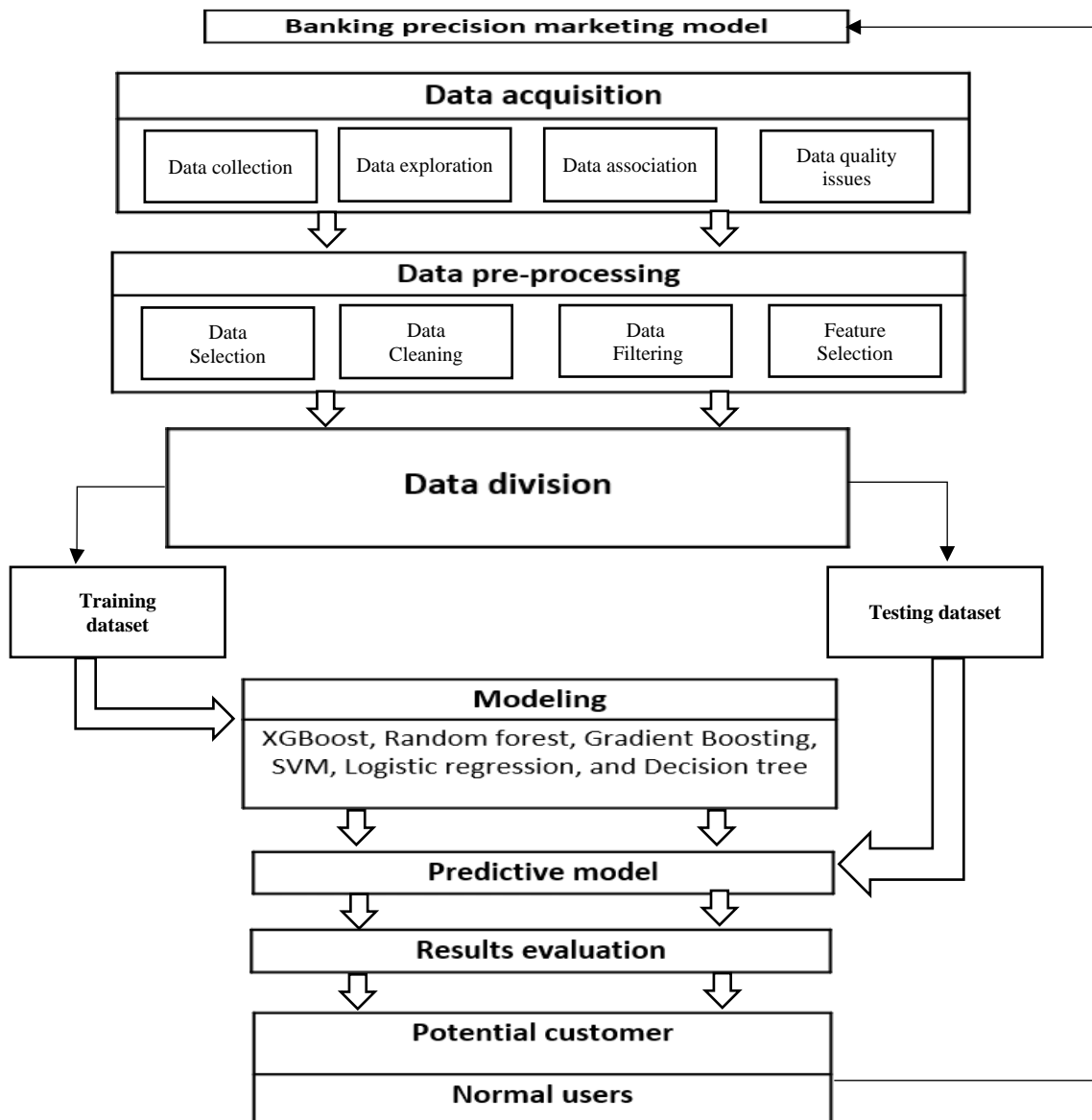


Fig. 1. PCPA Architecture.

3) *Feature selection*: The feature selection stage plays an essential role in extracting the critical features and removing the non-significant attributes from the dataset. Also, it contributes to the improvement of model performance and reduces the time of training and validation. Firstly a uni-variate selection is applied then, Grid search (GS) method is used to choose the optimal parameter.

4) *Modeling*: As we declared above, our proposed PCPA is based on machine learning techniques and big data. In this phase, we have applied five machine learning algorithms, namely, XGBoost, Random forest, Gradient Boosting, SVM, Logistic regression, and Decision tree. Then after comparison of the accuracy and performance of the five models, we choose XGBoost as the central algorithm of PCPA because it illustrates the most excellent accuracy and performance. The results of all the models are presented in Section IV.

5) *Results evaluation*:

a) *Confusion matrix*: In order to evaluate and measure the performance of the predictive models for forecasting the potential customers correctly, we have applied different metrics: namely, precision, recall, accuracy, and F-measure. The calculation of these four measures depends on information extracted using the confusion matrix. After the prediction, the confusion matrix analyzes the value of accurate and wrong predictions. In Table III, the representation of the confusion matrix is presented.

TP: These are the correctly predicted negative values which mean that the value of the actual class is potential, and the value of the predicted class is also potential customers.

TN: These are the correctly predicted negative values which mean that the value of the actual class is non-potential and the value of the predicted class is also non-potential customers.

FP: The number of non-potential customers, but the predictive model has forecasted them incorrectly (as potential).

FN: The number of potential customers, but the predictive model has forecasted them incorrectly (as non-potential).

TABLE I. CONFUSION MATRIX

	Potential	Non-Potential
Potential	TP	FN
Non-Potential	FP	TN

b) Performance indicators

Accuracy: The proportion of the number of all right predictions is known as accuracy. It is calculated by the following formula:

$$Accuracy = \frac{(TP + TN)}{(TP + FP + TN + FN)} \quad (1)$$

Precision: It is the proportion of true positives to all positives. It is calculated by the following formula:

$$Precision = \frac{TP}{TP + FP} \quad (2)$$

Recall: It is used to calculate the real positive rate. It is calculated by the following formula:

$$Recall = \frac{TP}{TP + FN} \quad (3)$$

F1-measure: The weighted harmonic average of precision and recall is called F1-measure.

$$F1 - measure = \frac{(2 \times Precision \times Recall)}{(Precision + Recall)} \quad (4)$$

TABLE II. CHARACTERISTICS OF BANK CUSTOMERS

Attribute	Possible Value	Type
Age	20-60 year	Numerical
Marital status	0-3	Categorical
Income(dh)	1-5	Numerical
Education level	0-6	Categorical
Housing	0-3	Categorical
Family_numbrs	1-6	Numerical
Gender	0-1	Categorical
Experience	0-42	Numerical
Lodgment_situation	0-1	Categorical
Credit Card	0-1	Categorical
ASCC	0-9,30	Numerical
Securities_account	0-1	Categorical
Online_bank_service	0-1	Categorical
Housing_credit	0-1	Categorical

TABLE III. DESIGNATION OF SOME INDICATORS

Attribute	Attribute Value
Marital status	0—Single 1—Married 2—Divorced
Income(dh)	1—[0dh-3000dh] 2—[3001dh-5000dh] 3—[5001dh-8000dh] 4—[8001dh-10000dh] 5—10000dh>
Education level	0—Baccalaureate 1— Baccalaureate+2 2— Baccalaureate+3 3— Baccalaureate+5 4— Baccalaureate+8 5—No diploma
Property_Area	0—Urban 1—Semi-Urban 2—Rural
Gender	0 — Female 1— Male
Lodgment_situation	0 — Personal house 1— Parent house 3— House renter
Credit Card	0 — No 1— Yes
Securities_account	0 — No 1— Yes
Online_bank_service	0 — No 1— Yes
Housing_credit	0 — No 1— Yes

C. PCPA Algorithm

Algorithm 1: Proposed algorithm for Potential Customers prediction

Input: The training dataset consisting of input features such as xi and output label y;

Output: Predicted labels; Potential or not potential

Procedure;

1. **Data selection and understanding;**
2. **Data cleaning and filtering;**
3. **Feature selection using Grid search algorithm;**
4. **Data modeling using XGBoost, Random forest, Gradient Boosting, SVM, Logistic regression, Decision tree;**
5. **Results Evaluation (confusion matrix);**

IV. RESULTS AND DISCUSSION

The PCPA is based on machine learning technology and big data. First, we split the data into two parts train with a proportion of 80% and a test set with a ratio of 20%. We tested the pre-processed data on various famous classification algorithms that we have chosen based on our previous study [14], such as XGBoost, Random forest, Gradient Boosting, SVM, Logistic regression, and Decision tree. Then we compared the performance of the selected machine learning methods based on performance indicators (Accuracy, Precision, Recall, F-measure, and Cross-validation score). We presented the findings in Table IV. According to the comparison of the performance of the six machine learning methods illustrated in Table IV and Fig. 2, the RF and GBDT have the highest accuracy (98, 9%). RF achieved good precision with 93, 6%, Recall of 93,5%, and an F-measure of 93,5%. Another model which illustrates good results is

XGBoost. It reached a good accuracy with 98,1%, F-measure with 90,8%, Cross-validation score of 90,1%, and highest Recall of 95,4%. Also, the SVM gave significant results, registered a good accuracy of 97, 1%, Recall of 88,7%. We can notice that the GBDT shows a better performance amount the other models in terms of Accuracy, Precision, Recall, F-

Measure, and Cross-validation score. It accomplished the highest accuracy compared to other i.e. 98, 9%, precision with 96,3%, F-measure 92,9%, Cross-validation of 94,2% with good Recall 89,7%. Hence Gradient Boosting outperforms the other ML methods used in our work. This is why, we choose Gradient Boosting as the central algorithm of PCPA.

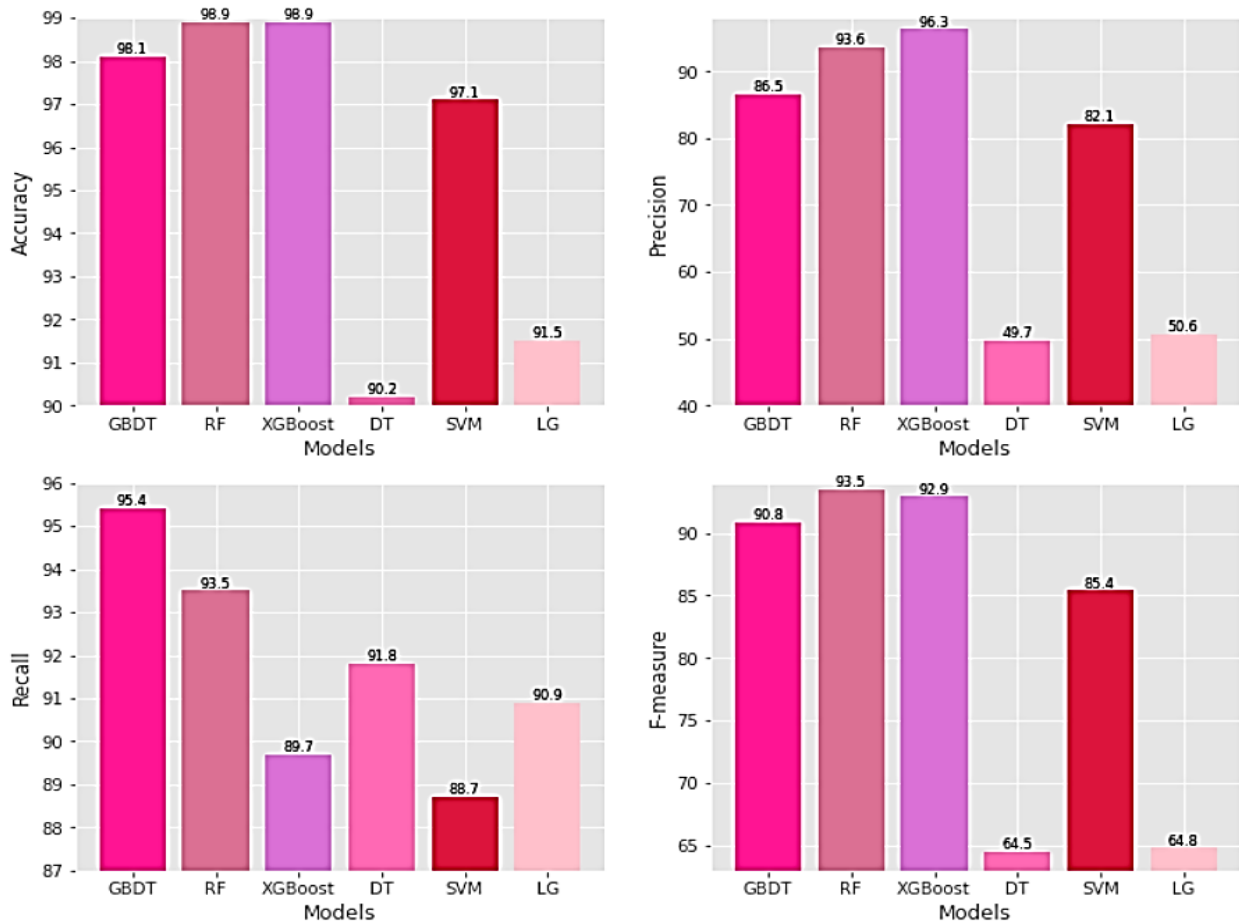


Fig. 2. Evaluation of Models on Performance Indicators (Accuracy, Recall, Precision, F-measure).

TABLE IV. COMPARISON OF MACHINE LEARNING MODELS

Model	Accuracy (%)	Precision (%)	Recall (%)	F-Measure (%)	Cross Validation (%)
XGBOOST	98,1	86,5	95,4	90,8	90,1
RF	98,9	93,6	93,5	93,5	91,8
GBDT	98,9	96,3	89,7	92,9	94,2
DT	90,2	49,7	91,8	64,5	61,2
SVM	97,1	82,1	88,7	85,4	88,1
LG	91,5	50,6	90,9	64,8	65,3

V. CONCLUSION

In this study, we have proposed a PCPA algorithm for precision marketing based on machine learning and Big data analysis. We have used a dataset collected from Moroccan banking. Our model predicts potential housing loan customers from whole banking users. This prediction can help the marketing department to target quality customers at a low cost

and fast time. At the same time, we compared the efficiency of different famous machine learning approaches, which are: XGBoost, Random forest, Gradient Boosting, SVM, Logistic regression, and Decision tree in terms of accuracy, F-measure, recall, precision. The results illustrate that Gradient Boosting achieved better performance amount the other ML methods used in terms of accuracy, F-measure, recall, precision, and cross-validation score. Hence we choose Gradient Boosting as the central algorithm of PCPA.

REFERENCES

- [1] C. X. Yu, Z. X. Min, M. Ying and G. Feng, "Research Progress and Trend of the Machine Learning based on Fusion," International Journal of Advanced Computer Science and Applications(IJACSA), vol. 13, pp. 1-7, July 2022.
- [2] H. Jin, C. Chi and X. Gao, "Strategic Research on Accurate Marketing to Enhance Consumer Experience of Social Media Users," 2nd International Conference on Economic Development and Education Management (ICEDEM 2018), Atlantis Press, vol. 290, pp. 455-458, December 2018.
- [3] M. C. Chiu and K. H. Chuang, "Applying transfer learning to achieve precision marketing in an omni-channel system—a case study of a sharing

- kitchen platform,” International Journal of Production Research, vol. 59, pp. 7594-7609, January 2021.
- [4] H. Zhang, L. Zhang, X. Cheng and W. Chen, “A novel precision marketing model based on telecom big data analysis for luxury cars,” International Symposium on Communications and Information Technologies (ISCIT), IEEE, Qingdao, China, vol. 59, pp. 307-311, November 2016.
- [5] X. Liu, “E-Commerce Precision Marketing Model Based on Convolutional Neural Network,” Scientific Programming, vol. 2022, pp. 1-11, March 2022.
- [6] Y. Xie, X. Liu, Y. Wen and Y. Xiao, “Precision Marketing Based on Hamming Distance Classification Algorithm,” Computer Science and Application, vol. 9, pp. 1403-1406, September 2018.
- [7] K. Xiao and X. Hu, “Study on maritime logistics warehousing center model and precision marketing strategy optimization based on fuzzy method and neural network model,” Polish Maritime Research, vol. 24, pp. 30-38, September 2017.
- [8] X. Tang, C. Cheng and L. Xu, “Research and Application of Precision Marketing Algorithms for ETC Credit Card Based on Telecom Big Data,” Signal and Information Processing, Networking and Computers. Springer, Singapore, vol. 677, pp. 1075-1084, December 2020.
- [9] K. Xiao and X. Hu, “Research and Application of Precision Marketing Algorithms for ETC Credit Card Based on Telecom Big Data Signal and Information Processing, Networking and Computers. Springer, vol. 677, pp. 1075-1084, December 2021.
- [10] B. Yan and Z. Chen, “A prediction approach for precise marketing based on ARIMA-ARCH Model: A case of China Mobile,” Communications in Statistics-Theory and Methods, vol. 47, pp. 4042-4058, January 2018.
- [11] J. Paule-Vianez, M. Gutiérrez-Fernández and J. L. Coca-Pérez, “Prediction of financial distress in the Spanish banking system: An application using artificial neural networks,” Applied Economic Analysis, vol. 28, pp. 69-87, December 2019.
- [12] M. Musdholifah, U. Hartono and Y. Wulandari, “Banking crisis prediction: emerging crisis determinants in Indonesian banks,” International Journal of Economics and Financial, vol. 10, pp. 124, February 2020.
- [13] Y. Zizi, A. Jamali-Alaoui, B. El Goumi, M. Oudgou and A. El Moudden, “An optimal model of financial distress prediction: A comparative study between neural networks and logistic regression,” Risks, vol. 9, pp. 200, November 2021.
- [14] N. El Koufi, A. Belangour, A. El Koufi and M. Sadiq, “A systematic literature review of machine learning techniques applied to precision marketing,” Technical and Physical Problems of Engineering (IJTPE), vol. 14, pp. 104-110, September 2022.

A Sequence-Aware Recommendation Method based on Complex Networks

Abdullah Alhadlaq, Said Kerrache, Hatim Aboalsamh
College of Computer and Information Sciences,
King Saud University, Riyadh 11543,
Saudi Arabia

Abstract—Online stores and service providers rely heavily on recommendation software to guide users through the vast number of available products. Consequently, the field of recommender systems has attracted increased attention from the industry and academia alike, but despite this joint effort, the field still faces several challenges. For instance, most existing work models the recommendation problem as a matrix completion problem to predict the user preference for an item. This abstraction prevents the system from utilizing the rich information from the ordered sequence of user actions logged in online sessions. To address this limitation, researchers have recently developed a promising new breed of algorithms called sequence-aware recommender systems to predict the user's next action by utilizing the time series composed of the sequence of actions in an ongoing user session. This paper proposes a novel sequence-aware recommendation approach based on a complex network generated by the hidden metric space model, which combines node similarity and popularity to generate links. We build a network model from data and then use it to predict the user's subsequent actions. The network model provides an additional information source that improves the recommendations' accuracy. The proposed method is implemented and tested experimentally on a large dataset. The results prove that the proposed approach performs better than state-of-the-art recommendation methods.

Keywords—Sequence-aware recommender systems; complex networks; similarity-popularity

I. INTRODUCTION

A recommendation system (RS) is a software tool that uses various techniques and algorithms to filter the relevant information from the vast amount of information found in an online platform based on multiple factors to provide users with item recommendations that most likely suit their preferences. RSs have been applied in various domains, including travel and hotel industries, online shopping, books, and movie recommendations [1].

Conventionally, the recommendation problem is abstracted as a matrix-completion problem where users correspond to rows, items correspond to columns, and the numerical cell values indicate the user-item ratings. The goal of matrix completion is to predict the ratings of unseen items for a given user based on historical data [2]. Although this abstraction has proved helpful in various ways, it suffers from the limitation of not utilizing the sequence of user interaction logs that are often available in real applications [3]. Moreover, conventional recommendation systems assume user profile availability and long-term historical data. However, such long-term data does not always exist for many reasons, such as the user being new to the system, having opted not to log in, or if the user is

enabling tracking countermeasures [4], [5]. For this, sequence-aware recommendation systems (SARS) have recently been developed to harness the rich information from logged users' interactions with the system. The goal is to derive predictions for subsequent user actions based on the recent series of actions in the ongoing user session, thus, bringing highly relevant and practical computational tasks to real-life applications.

Despite the ongoing efforts to improve SARS, the accuracy of recommendations remains an open challenge. Most of the existing complex models, including deep learning and matrix factorization, are outperformed by straightforward trivial approaches such as the k nearest neighbors' approach [6], [7]. One of the most promising directions to remedy this is using graph (or network) models to generate recommendations. In network-based recommenders, where nodes represent users or items and the weighted links between the nodes represent relevancy, the analysis derived from the graph structure can produce accurate predictions. Many network-based recommendation approaches have been introduced in the literature, including approaches based on real-world networks [8]–[10]. However, most approaches use networks without underlying models or established properties. Using complex network models with well-understood and proven properties can improve the quality of recommendations and constitutes a promising research direction.

Moreover, one of the most relevant recent advances in complex network modeling to the field of sequence-aware recommendation is the development of efficient navigation and routing algorithms [11], [12]. Since the interaction between the user and items in SARS can be seen as navigation in the space of items, this hints at the possibility of using complex network models to guide the recommendation process.

In this paper, we propose a novel sequence-aware recommender system approach that takes advantage of complex network models, primarily the hidden metric space model [13], to generate more accurate recommendations. The hidden metric space model is a complex network model that suggests the existence of a hidden metric space underlying any observed complex network. The distance between the nodes abstracts their similarities, whereas their degrees represent popularity [12]. Our method utilizes the rich navigation information within the large logs of sequentially ordered actions to improve recommendation accuracy. Moreover, introducing predefined model characteristics as an additional source of information enriches the model to overcome the limitations of data sparsity and limited coverage. Additionally, constructing graph models to guide the recommendations resembles a neighborhood struc-

ture that is intuitive and easy to understand and allows efficient recommendation queries. Another advantage of using graphs is the ability to interpret and visualize the recommendations, which is often a limitation in other complex methods. Finally, the resulting algorithm is trained and tested on a large public dataset and evaluated using standard performance measures to compare its performance to state-of-art methods.

The remainder of this paper is organized as follows. Section II covers background and related work. Section III describes the details of the proposed method. Section IV presents the experimental setup and performance evaluation results. Finally, Section V summarizes the work and presents future research directions.

II. BACKGROUND AND RELATED WORK

In this section, we briefly introduce recommender systems, particularly sequence-aware recommender systems, followed by an overview of the complex networks and the hidden metric space model.

A. Sequence-Aware Recommender Systems

The goal of sequence-aware recommender systems is to predict the evolution of the user's current session. They achieve this goal by predicting the user's next action using extracted features from historical sessions' logs tracked by the application [4]. Fig. 1 shows a schematic illustration of the recommendation process under the sequence-aware setting. The recommender system's input takes the form of an ordered set of users' logged actions (sessions). These actions consist of various user interactions towards an item, such as 'clicks', 'views', or 'purchases', or actions towards the application, such as 'searches' or 'applies filters'. The computational task of sequence-aware recommenders is mainly to process the input to build a model that attempts to identify recurring patterns

in the sequences of actions. For example, this pattern may reflect the co-occurrence of actions or their sequential ordering. Finally, the system's output is the predictions for the user's next action (or set of actions) derived from the identified pattern based on the current user session.

Although the output from traditional RS and SARS aims at the same goal: to provide an item recommendation for the users, their settings and characteristics are distinct in several ways. First, the standard input for traditional RS takes the form of user, item, and rating tuples without any information about the user's behavior or interactions with the items or the application. In contrast, the primary input for SARS is the rich sequential session data. Moreover, a standard RS takes the form of a matrix-completion problem, as illustrated in Fig. 2, in which the task is to fill the predicted ratings given by users to items based solely on the long-term observed user behavior and preferences. This formulation, however, can not accommodate the sequential input representation [2].

The problem of sequence-aware recommendation has been increasingly attracting researchers. Early research efforts proposed oversimplified model-free attempts to provide recommendations driven by data pattern mining and association rules techniques. However, since the 2010s, machine learning and time-series techniques have shifted the algorithmic approaches towards adopting more sophisticated models to tackle the problem [14]. Models such as Markov chain models [15], [16], graph-based models [17]–[19], factorization-based models [20], recurrent neural networks [21]–[23] and attention mechanisms [24] contributed to improving sequence-aware recommendation systems [6].

Several graph-based approaches for sequence-aware recommenders exist in the literature that extends the work proposed for traditional recommender systems. In these methods, the graph is often modeled as a bipartite graph having items and

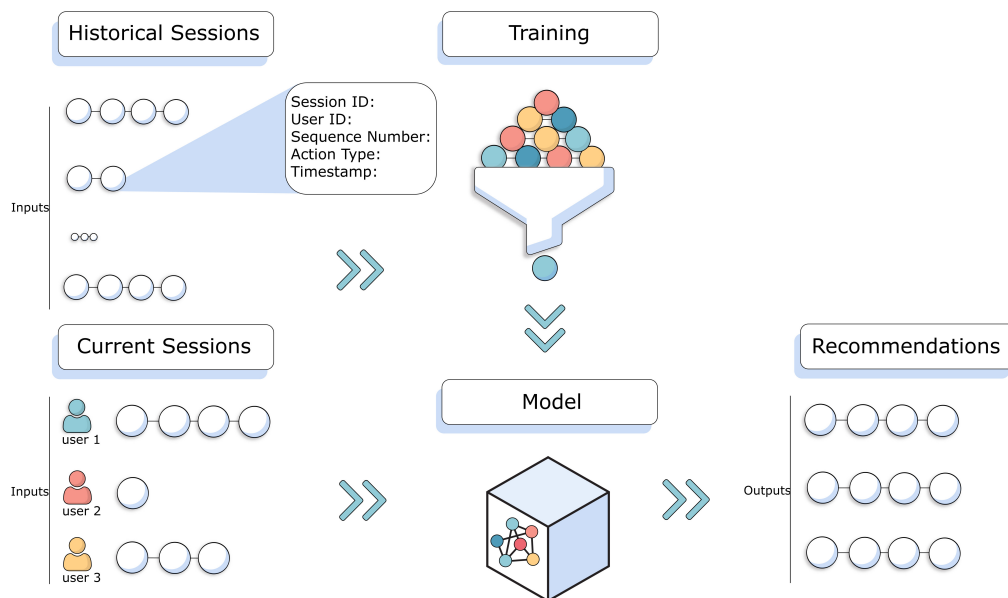


Fig. 1. A High-Level Representation of Sequence-Aware Recommender Systems Process.

	Item 1	Item 2	Item 3	Item 4
User 1				
User 2				
User 3				
User 4				

Fig. 2. Representation of the User-Item Matrix in Traditional Recommender Systems. The Goal of the Recommender is to Complete this Matrix.

users on separate sides. However, this poses a limitation as these approaches fail to exploit the rich information in sessions. To overcome this issue, authors in [17] proposed the session-based temporal graph (STG) method that incorporates temporal dynamics and short- and long-term preferences. The STG graph is represented as a two-sided bipartite graph (tripartite), with one side of the graph connecting users with items they have interacted with before (i.e., long-term interactions) and the other side connecting the current user session with session items (i.e., short-term interactions). The graph is then traversed to recommend items via random walk.

Similarly, the Geographical-Temporal influences Aware Graph (GTAG) method [18] uses a tripartite graph representation. However, GTAG incorporates geographical location to enhance the point of interest recommendations and traverse the resulting graph model in a breadth-first propagation manner. Both methods, however, as in all multipartite graphs models, which do not allow edges between nodes on the same side, fail to exploit information on any independent side, for example, item-to-item data. Additionally, both methods construct a simple graph without an underlying model. Conversely, the proposed method in this article relies on constructing a graph with an underlying model and established properties to guide the recommendations.

In recent years, researchers have attempted to achieve accurate recommendations by providing explicit interpretations of the challenges and tasks in the SARS and then attempting to tackle the identified challenges by designing appropriate algorithms. Quadrana et al. [3] suggest that the main tasks of sequence-aware recommender systems are adopting the recommendation context, such as the current weather or the current user location, detecting the shared and individual trends, identifying the repeated patterns in user behavior, and finally identifying the order constraints of the sequence in the session. Jannach et al. [25] state the price discounts and current offers on items as a success factor for SARS and emphasize the impact of the user's short-term intentions rather than only long-

term ones. Wang et al. [14] further focus on understanding the inner interactions within the session and the interactions between the sessions as the two key challenges to reducing the complexity of the SARS structure.

B. Complex Networks and Hidden Metric Space Model

Complex networks refer to a class of graphs that exhibit nontrivial topological features that can be observed in real-life networked systems. Those features are not observable in simple graphs such as regular and purely random graphs but in networks resulting from complex natural phenomena such as social, biological, technological, and physical systems [26]. For example, when modeling a real-life social network, where the nodes represent the people and the edges between the nodes represent the relationships between them, the resulting graph possesses a complex network structure. Its topology reveals some fundamental complex network properties and characteristics [27], such as the small-world [28] and the scale-free properties. Scale-free networks gained significant interest within the network science community upon the publication of the Barabási and Albert model [29]. The latter generates scale-free networks with short paths and highly connected nodes as hubs and is considered one of the earliest models to capture real-life natural network properties [30].

Efforts to design network models that capture more faithfully the properties of real-life networks have continued after the work of Barabási and Albert model [29]. The hidden metric space model [13] suggests the existence of a hidden metric space underlying any scale-free complex network and contains all the nodes of the observed network. The nodes are positioned and linked in the hidden metric space based on their similarity and popularity. The distance between nodes abstracts the nodes' similarities, and their degrees reflect their popularity. Thus, the shorter the distance between nodes in the hidden metric space and the more popular they are, the higher probability of them connecting in the observed network.

One of the successful applications of the hidden metric space model is its capacity to guide the routing function in networks by greedily moving toward the node nearest to the target [31]. Unlike many complex network models, such as the small-world model or Barabási and Albert model, the hidden metric space model generates an embedding of the network, which provides a useful representation of the items for downstream applications. Furthermore, the model not only aims at capturing the network's structural properties but also describes how these properties are connected with essential functionalities. In [32], the authors propose a recommendation method for predicting user-item ratings using a hidden metric space model based on popularity and similarity. By using this complex network model, the approach is able to outperform existing methods in term of prediction accuracy. The successful use of the model in the traditional recommendation setting as demonstrated in [32] and various other domains, including developing efficient information routing algorithms [11], network modeling [12], information routing and signaling [31], link prediction [33]–[35] hints at the possibility of applying it to guide the recommendation in a SARS settings.

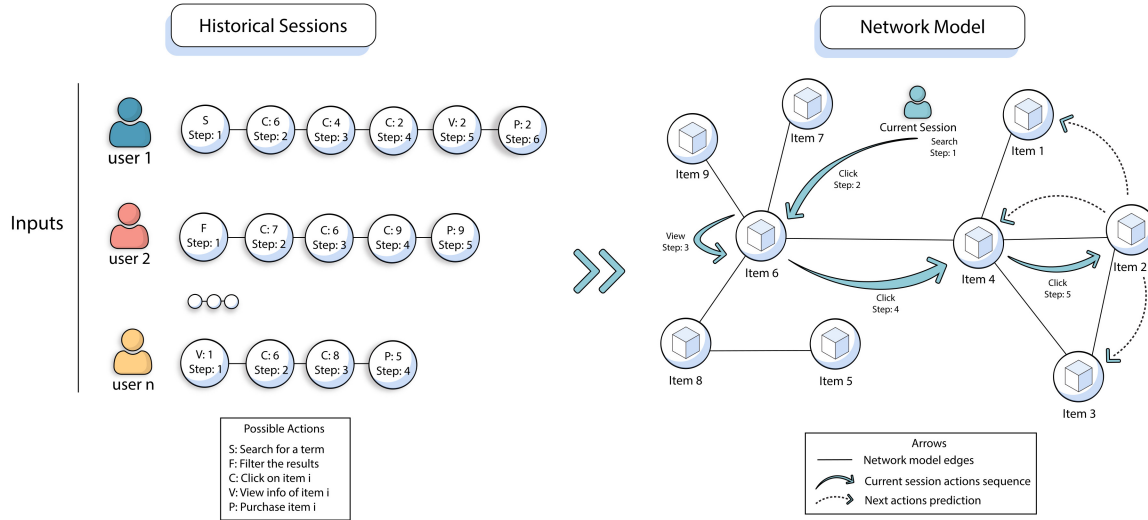


Fig. 3. Illustration of the Proposed Approach. Items are Modeled as Nodes in a Complex Network and are Connected based on Similarity and Popularity.

III. PROPOSED METHOD

In this paper, we propose a sequence-aware recommendation method based on complex networks where items are modeled as a graph embedded in D -dimensional space with a scale-free network structure controlled by an underlying hidden metric space. Since the goal of a SARS is to predict the next click the user will perform in a session, the problem is defined as the task of ranking the most probable next item. The output of the recommender is an ordered list of items $r \in R^*$ for each session s , where R^* is a subset of the group of all possible items permutations, and each predicted ordered list of recommendations r consists of i items of length between 0 and t . First, each item in the system i is assigned a point x^i in a D -dimensional Euclidean space:

$$x^i = (x_1^i, x_2^i, \dots, x_D^i)^T, i = 1, \dots, n, \quad (1)$$

where n denotes the number of items. The position of the items reflects their description or features. Hence, each dimension represents a latent feature or a combination of features relevant to the item. The probability p_{ij} of connection between two items nodes i and j is based on two factors, their similarity reflected by their distance and popularity (or degree) as derived from the hidden metric model:

$$p_{ij} = \left(1 + \frac{d^2(x^i, x^j)}{\kappa_i \kappa_j}\right)^{-\alpha}, \quad (2)$$

where κ_i and κ_j denotes the hidden degree (popularity) of items i and j , respectively, and $d^2(x^i, x^j)$ is the squared distance between them. The parameter $\alpha > 1$ controls the weights given to distance and popularity.

According to Eq. (2), the connection probability between nodes in the generated network increases when popularity increases and decreases with the squared hidden distance (dissimilarity) increase. The reason behind this choice is that generated network will have three characteristics observed in real-life complex networks. First, a pair of popular nodes will

have a higher probability of being connected even if they are far away from each other or dissimilar. A pair of nodes with moderate average popularity will be connected if the distance is moderate, and a pair of nodes with low popularity on average will get connected if the distance is short.

As illustrated in Fig. 3, items are embedded in a D -dimensional space, where the distance between them encodes their similarity, which, combined with item popularity, results in a network model. The model can be used to compute the probability of a pair of nodes being connected and predict the next clicked item in a sequence. We need to calculate the item's popularity and similarity to construct the model. The node's degree represents its popularity and can therefore be directly calculated from the number of clicks or interactions the item has in historical sessions. Next, we assign each node a position in D -dimensional space to calculate the distances. Since we cannot readily obtain the positions of the nodes, we infer them from the history of interactive sessions. We first estimate the link probabilities directly from historical data and then use them to infer the items' positions. There are arguably many ways to estimate connection probabilities. However, the method we adopt in this work is to assume that the connection probability is proportional to the number of items co-occurrence in sessions calculated by the cosine similarity as follows:

$$p_{ij} \propto sim(i, j) = \frac{\sum_{s \in S} i_s j_s}{\sqrt{\sum_{s \in S} i_s^2} \sqrt{\sum_{s \in S} j_s^2}}, \quad (3)$$

where i_s is set to 1 if item i is present in session s and 0 otherwise. From that, we obtain the set P of all connections probabilities p_{ij} such that $p_{ij} > 0$. It is now possible to deduce the distance d_{ij}^2 in Eq. (2) as follows:

$$d_{ij}^2 = \kappa_i \kappa_j \left(p_{ij}^{-1/\alpha} - 1\right). \quad (4)$$

Hence, the problem of estimating the items' positions is reduced to finding coordinates x^i , such that the resulting Euclidean distances are as close as possible to the distances prescribed by Eq. (4). This problem falls into the category of nonlinear optimization problems that can be solved by minimizing an objective function that measures the difference between the computed and observed distances:

$$\sum_{p_{ij} \in P} \left(\|x^i - x^j\|_2^2 - d_{ij}^2 \right)^2, \quad (5)$$

where $\|\cdot\|_2$ stands for the L_2 norm. In order to avoid overfitting, a regularization term is added, resulting in the following objective function:

$$f(x^1, \dots, x^n) = \sum_{p_{ij} \in P} \left(\|x^i - x^j\|_2^2 - d_{ij}^2 \right)^2 + \lambda \sum_{i=1}^n \|x^i\|_2^2. \quad (6)$$

Since this objective function is not convex, only local minima can be computed. Several algorithms for local optimization exist to solve this minimization problem, and most of them require computing the gradient of the objective function:

$$\frac{\partial f}{\partial x^i} = \sum_{p_{ij}, p_{ji} \in P} 4(x^i - x^j) \left(\|x^i - x^j\|_2^2 - d_{ij}^2 \right) + 2\lambda x^i. \quad (7)$$

The proposed method's objective is to predict a list of items ordered by the likelihood that the user will click next in the active session. Once we have the item embeddings, we can use different techniques to capture the user's short-term interest in the current session to predict the next item. We propose to use the K nearest neighbors technique, where distance is measured in terms of connection probability. Thus, the method recommends the items with the highest connection probability to the most popular item the user interacted with in the active session. In other words, the method generates a list of t items ordered decreasingly by the probability of connection to the most popular item in the active session as calculated by Eq. (2).

IV. EXPERIMENTAL EVALUATION

This section presents the experimental framework used to evaluate the proposed method's performance. First, we present the experimental setup and describe the dataset, the dataset preparation techniques, the competing methods, the evaluation metrics, the training method, and the parameter tuning technique. Finally, we compare the overall performance results against competing methods.

A. Dataset Description

The dataset used in this paper is the Trivago dataset [36], [37] presented in the 2019 RecSys challenge obtainable online from a publicly available data source (<https://recsys2019data.trivago.com>). The dataset contains sequences of various users actions on the Trivago hotels booking website. It contains

981,655 users, 927,142 hotels, and 1,202,064 sessions containing a total of 19,715,327 user actions.

The dataset is pre-split into 80%-20% splits for train and test sets, respectively. The splits were used as they are in this experiment. We cleaned the dataset by removing sessions that do not lead to a hotel booking. Each session in the test set ends with a hidden hotel booking action and a list of a maximum of 25 hotels in the impressions list, and the goal is to reorder the list of impressions in decreasing order by the likelihood of user clicks.

B. Evaluation Criteria

The proposed approach is evaluated using the test set by applying standard metrics for the sequence-aware recommender systems evaluation. There are different evaluation techniques and accuracy measures for sequence-aware recommender methods in the literature. However, since the output of a sequence-aware recommender system typically takes the form of ordered lists, it is applicable to use standard information retrieval accuracy metrics [6] such as mean reciprocal rank (MRR) and mean average precision (MAP).

The MRR measures the place of the correct item in the predicted list. Given a test set S^{Test} containing previously unseen sessions, the MRR is defined as:

$$MRR = \frac{1}{|S^{Test}|} \sum_{s \in S^{Test}} \frac{1}{Rank_s} \quad (8)$$

where $Rank_s$ is the place of the correct item in session s . From Eq. (8), we can see that, at most, the MRR reaches 1 if the algorithm consistently predicts the item correctly by placing it first in the list and reaches $1/t$, where t is the length of the recommended list when the recommender consistently predicts the item the last in the list. On the other hand, the MAP evaluates the predicted list up to a specific cut-off point N . MAP@ N does not consider the order of the list. However, it checks if the correct item is present within the first N items in the list.

$$MAP@N = \frac{1}{|S^{Test}|} \sum_{s \in S^{Test}} \frac{Top(s, N)}{N} \quad (9)$$

where $Top(s, N)$ is a function that returns 1 if the correct item for session s is in the top N items in the predicted list and returns 0 otherwise. In this experiment, we use the following values for N : 1, 3, 5, and 10.

C. Implementation

The experimental framework, competing methods, data preprocessing, and experimental evaluation are implemented using python with standard numerical and data manipulation libraries.

Several specialized software libraries can be used to solve the optimization problem, which is the most crucial step in our proposed method. Interior Point OPTimizer (IPOPT) [38] is a stable and well-tested advanced nonlinear programming (NLP) solver based on an interior-point filter with a line-search algorithm for large-scale nonlinear optimization. Efficient and effective linear solvers are required by IPOPT and are essential

for solving the optimization problem. Therefore, The solver MA57, part of the HSL package [39], was used in the experiment.

IPOPT NLP solver requires, at each iteration, essential information about the optimization problem in order to solve and proceed iteratively toward the solution. At each step, the following information is required, given the current values of the unknowns:

- The objective function as defined in Eq. (6).
- The gradient of the objective function (vector of first derivatives with respect to all unknowns) as defined in Eq. (7).
- The Hessian of the objective function (matrix of all second derivatives). This matrix is very large. However, the library offers the possibility of approximating the Hessian numerically. This option has been used in order to avoid large memory consumption.

D. Competing Methods

To assess the effectiveness of the proposed method, we compare it with a set of commonly used baselines and state-of-the-art methods:

- Random: Even though this is not a recommendation method, it provides insight into the lowest acceptable value that other methods must achieve on this dataset.
- Items Popularity (I-POP): A naive baseline predictor that consistently recommends a list of the most popular items in the training set without considering user actions or similarities. Regardless of its simplicity, it often provides a stable baseline in sequence-aware recommender systems.
- Items Click-out Popularity (IC-POP): Similar to I-POP, however, only clicked-out items are considered when determining the item's popularity.
- Items Metadata K -Nearest Neighbors (IM-KNN): An implementation of a content-based filtering method that predicts the current user's next action based on the k -most similar neighbors to the previously clicked item. The similarity between the items is determined by the cosine similarity of the item's metadata.
- Items Co-occurrence K -Nearest Neighbors (IC-KNN): An implementation of an item-based collaborative filtering method that predicts the current user's next action based on the k -most similar neighbors to the previously clicked item. The similarity between the items is determined by the number of co-occurrence between them in sessions, calculated by cosine similarity.
- Logistic Regression (LR) [36]: A method that predicts whether the item is clicked-out or not (i.e., binary classification). The method requires the extraction of specific features. We adopted the same problem formalization and feature selection as in [36].

TABLE I. PERFORMANCE RESULTS OBTAINED ON THE TRIVAGO DATASET

Method	MRR	MAP@1	MAP@3	MAP@5	MAP@10
Random	0.177	0.054	0.051	0.049	0.047
I-POP	0.262	0.116	0.091	0.078	0.061
IC-POP	0.288	0.137	0.103	0.086	0.065
IM-KNN	0.613	0.526	0.210	0.139	0.081
IC-KNN	0.620	0.523	0.215	0.145	0.084
LR	0.641	0.537	0.228	0.151	0.086
MLP	0.631	0.520	0.227	0.150	0.086
Proposed	0.644	0.540	0.230	0.153	0.087

- MLP Regressor (MLP): Multilayer perceptron is a neural network model that trains using backpropagation with no activation function in the output layer. We used the same features as in the LR model.

E. Parameters Settings and Tuning

For the proposed method, several adjustable parameters require tuning. The number of dimensions D , the regularization coefficient λ , and the constant α . In this experiment, we used grid search to determine those parameters. The number of dimensions D is tried with $\{5, 10, 20\}$. The regularization λ is selected from the set $\{0.1, 0.01\}$. Finally, the constant α is chosen from $\{1, 2, 3\}$.

An important issue when fitting our model to data is the initialization step. Since the objective function is non-convex, only local minima can be found, and consequently, the initial values of the unknowns significantly affect the quality of the solution. In particular, initialization with the same values, such as setting all coordinates to 0, causes the gradient in Eq. (7) to vanish, and the optimizer stops immediately. Hence, a random initialization is essential to avoid the trivial solution where all items are assigned the same position.

F. Experimental Results

Table I summarizes the results in terms of MRR and MAP. The results are also displayed in Fig. 4 for the case baseline methods and Fig. 5 for state-of-the-art methods. The results show that the proposed method produces better scores than other competing methods under all considered metrics.

As expected, popularity-based methods (I-POP and IC-POP) score weak results as they rely solely on an item's popularity and ignore the user features. In other words, those methods are expected not to achieve well as they do not produce personalized recommendations.

Interestingly, the proposed method performed better not only against KNN-based methods (IM-KNN and IC-KNN), which rely on similarity measures without requiring feature extractions, but also against feature-based methods (MLP and LR), which require considerable effort in the feature engineering process. This is particularly important given that the Trivago dataset is rich in information, which may not be true for all datasets.

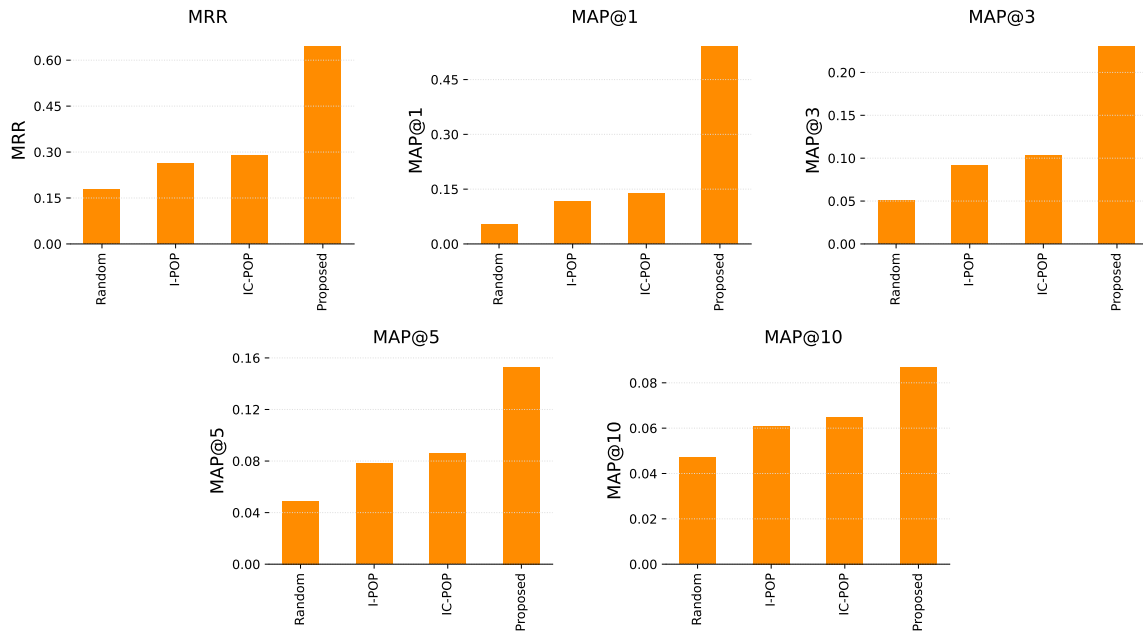


Fig. 4. Comparison of the Performance of the Proposed Approach against Baseline Methods on the Trivago Dataset.

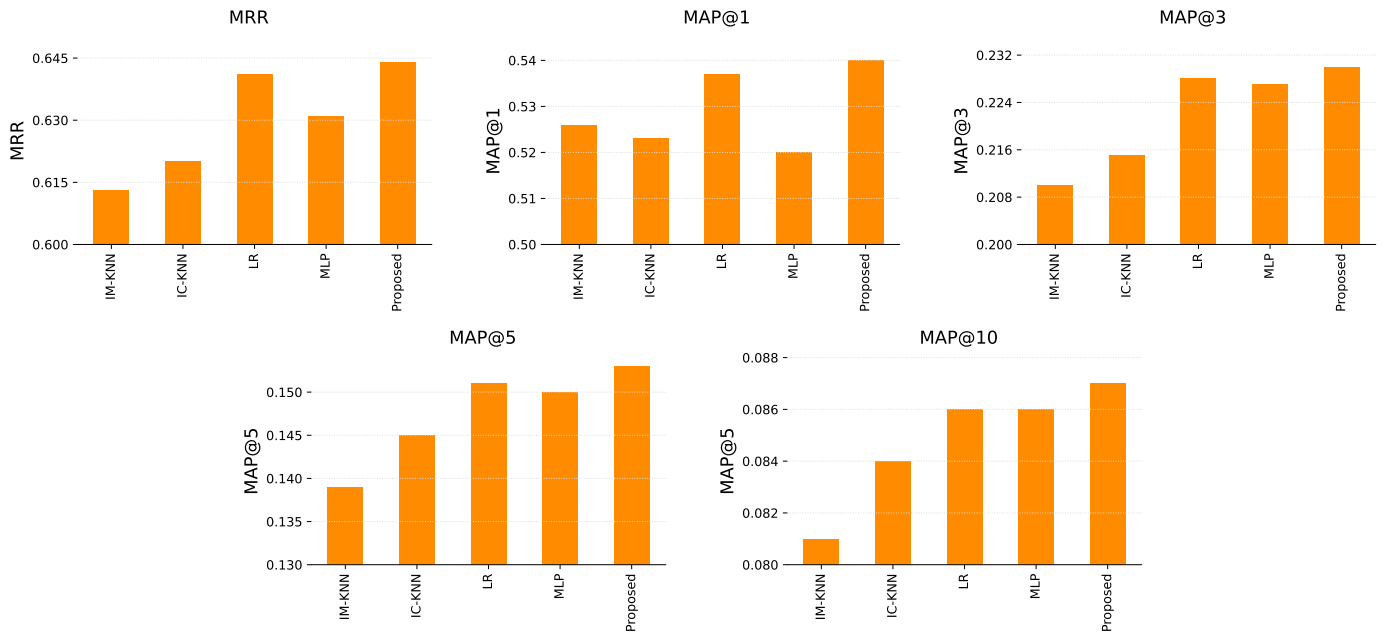


Fig. 5. Comparison of the Performance of the Proposed Approach against State-of-the-Art Methods on the Trivago Dataset.

Since the proposed approach does not involve the additional semantic information available in Trivago datasets, we expect it to perform very well on datasets with limited information (similar to KNN-based approaches) while providing better results.

V. CONCLUSION AND FUTURE WORK

This paper demonstrates the potential of using complex networks with underlying similarity-popularity models for a sequence-aware recommendation system. The experimen-

tal results show that the proposed method performs better than state-of-the-art methods in terms of MRR and MAP. Furthermore, the proposed method does not rely on feature extraction, making it suitable for generalizing datasets with limited information while providing better results.

In future work, we propose testing the method on other datasets from various domains to confirm its generalization capacity. Moreover, additional similarity-popularity models other than the hidden metric space model can be explored. Such models range from basic similarity-popularity dot-product to

more recent and sophisticated models found in the literature. In this work, once the items are embedded, we use the k -nearest neighbors technique to capture the user's current session and predict the next item. However, it is possible to use more advanced techniques such as deep neural networks, namely the LSTM or GRU variants of recurrent neural networks, by feeding the network the user's current sequence of actions and item embeddings as input and then training it to predict the next item.

ACKNOWLEDGMENT

This research work is supported by the Research Center, CCIS, King Saud University, Riyadh, Saudi Arabia.

REFERENCES

- [1] J. Bobadilla, F. Ortega, A. Hernando, and A. Gutiérrez, "Recommender systems survey," *Knowledge-Based Systems*, vol. 46, pp. 109–132, 2013.
- [2] D. Jannach, P. Resnick, A. Tuzhilin, and M. Zanker, "Recommender systems—beyond matrix completion," *Communications of the ACM*, vol. 59, no. 11, pp. 94–102, 2016.
- [3] M. Quadrana, P. Cremonesi, and D. Jannach, "Sequence-aware recommender systems," *ACM Computing Surveys (CSUR)*, vol. 51, no. 4, pp. 1–36, 2018.
- [4] D. Jannach, "Keynote: Session-based recommendation—challenges and recent advances," in *Joint German/Austrian Conference on Artificial Intelligence (Künstliche Intelligenz)*. Springer, 2018, pp. 3–7.
- [5] H. Fang, G. Guo, D. Zhang, and Y. Shu, "Deep learning-based sequential recommender systems: Concepts, algorithms, and evaluations," in *International Conference on Web Engineering*. Springer, 2019, pp. 574–577.
- [6] M. Ludewig and D. Jannach, "Evaluation of session-based recommendation algorithms," *User Modeling and User-Adapted Interaction*, vol. 28, no. 4, pp. 331–390, 2018.
- [7] S. Latifi, N. Mauro, and D. Jannach, "Session-aware recommendation: A surprising quest for the state-of-the-art," *Information Sciences*, vol. 573, pp. 291–315, 2021.
- [8] Z. Huang, D. D. Zeng, and H. Chen, "Analyzing consumer-product graphs: Empirical findings and applications in recommender systems," *Management science*, vol. 53, no. 7, pp. 1146–1164, 2007.
- [9] T. Zhou, J. Ren, M. c. v. Medo, and Y.-C. Zhang, "Bipartite network projection and personal recommendation," *Phys. Rev. E*, vol. 76, p. 046115, Oct 2007.
- [10] M. Zanin, P. Cano, J. M. Buldú, and O. Celma, "Complex networks in recommendation systems," in *Proceedings of the 2Nd WSEAS International Conference on Computer Engineering and Applications*, ser. CEA'08. Stevens Point, Wisconsin, USA: World Scientific and Engineering Academy and Society (WSEAS), 2008, pp. 120–124.
- [11] M. Boguná, F. Papadopoulos, and D. Krioukov, "Sustaining the internet with hyperbolic mapping," *Nature communications*, vol. 1, p. 62, 2010.
- [12] M. Boguna, I. Bonamassa, M. De Domenico, S. Havlin, D. Krioukov, and M. Serrano, "Network geometry," *Nature Reviews Physics*, vol. 3, no. 2, pp. 114–135, 2021.
- [13] M. A. Serrano, D. Krioukov, and M. Boguná, "Self-similarity of complex networks and hidden metric spaces," *Physical review letters*, vol. 100, no. 7, p. 078701, 2008.
- [14] S. Wang, L. Cao, Y. Wang, Q. Z. Sheng, M. A. Orgun, and D. Lian, "A survey on session-based recommender systems," *ACM Computing Surveys (CSUR)*, vol. 54, no. 7, pp. 1–38, 2021.
- [15] S. Rendle, C. Freudenthaler, and L. Schmidt-Thieme, "Factorizing personalized markov chains for next-basket recommendation," in *Proceedings of the 19th international conference on World wide web*, 2010, pp. 811–820.
- [16] R. He and J. McAuley, "Fusing similarity models with markov chains for sparse sequential recommendation," in *2016 IEEE 16th International Conference on Data Mining (ICDM)*. IEEE, 2016, pp. 191–200.
- [17] L. Xiang, Q. Yuan, S. Zhao, L. Chen, X. Zhang, Q. Yang, and J. Sun, "Temporal recommendation on graphs via long-and short-term preference fusion," in *Proceedings of the 16th ACM SIGKDD international conference on Knowledge discovery and data mining*, 2010, pp. 723–732.
- [18] Q. Yuan, G. Cong, and A. Sun, "Graph-based point-of-interest recommendation with geographical and temporal influences," in *Proceedings of the 23rd ACM international conference on conference on information and knowledge management*, 2014, pp. 659–668.
- [19] C. Li, L. Hu, C. Shi, G. Song, and Y. Lu, "Sequence-aware heterogeneous graph neural collaborative filtering," in *Proceedings of the 2021 SIAM International Conference on Data Mining (SDM)*. SIAM, 2021, pp. 64–72.
- [20] S. Kabbur, X. Ning, and G. Karypis, "Fism: factored item similarity models for top-n recommender systems," in *Proceedings of the 19th ACM SIGKDD international conference on Knowledge discovery and data mining*, 2013, pp. 659–667.
- [21] D. Jannach and M. Ludewig, "When recurrent neural networks meet the neighborhood for session-based recommendation," in *Proceedings of the Eleventh ACM Conference on Recommender Systems*, 2017, pp. 306–310.
- [22] B. Hidasi, A. Karatzoglou, L. Baltrunas, and D. Tikk, "Session-based recommendations with recurrent neural networks," *arXiv preprint arXiv:1511.06939*, 2015.
- [23] Y. K. Tan, X. Xu, and Y. Liu, "Improved recurrent neural networks for session-based recommendations," in *Proceedings of the 1st workshop on deep learning for recommender systems*, 2016, pp. 17–22.
- [24] C. Xu, J. Feng, P. Zhao, F. Zhuang, D. Wang, Y. Liu, and V. S. Sheng, "Long-and short-term self-attention network for sequential recommendation," *Neurocomputing*, vol. 423, pp. 580–589, 2021.
- [25] D. Jannach, M. Ludewig, and L. Lerche, "Session-based item recommendation in e-commerce: on short-term intents, reminders, trends and discounts," *User Modeling and User-Adapted Interaction*, vol. 27, no. 3, pp. 351–392, 2017.
- [26] X. F. Wang and G. Chen, "Complex networks: small-world, scale-free and beyond," *IEEE Circuits and Systems Magazine*, vol. 3, no. 1, pp. 6–20, 2003.
- [27] W. Yuan, D. Guan, Y.-K. Lee, S. Lee, and S. J. Hur, "Improved trust-aware recommender system using small-worldness of trust networks," *Knowledge-Based Systems*, 2010.
- [28] D. J. Watts and S. H. Strogatz, "Collective dynamics of 'small-world' networks," *Nature*, vol. 393, no. 6684, p. 440, 1998.
- [29] A.-L. Barabási, R. Albert, and H. Jeong, "Scale-free characteristics of random networks: the topology of the world-wide web," *Physica A: Statistical Mechanics and its Applications*, vol. 281, no. 1-4, pp. 69–77, 2000.
- [30] A.-L. Barabási, "Scale-free networks: a decade and beyond," *Science*, vol. 325, no. 5939, pp. 412–413, 2009.
- [31] M. Boguná, D. Krioukov, and K. C. Claffy, "Navigability of complex networks," *Nature Physics*, vol. 5, no. 1, p. 74, 2009.
- [32] A. Alhadlaq, S. Kerrache, and H. Aboalsamh, "A recommendation approach based on similarity-popularity models of complex networks," 2022.
- [33] F. Papadopoulos, C. Psomas, and D. Krioukov, "Network mapping by replaying hyperbolic growth," *IEEE/ACM Transactions on Networking*, vol. 23, no. 1, pp. 198–211, 2014.
- [34] R. Alharbi, H. Benhidour, S. Kerrache, and K. Riyadh, "Scalable link prediction in complex networks using a type of geodesic distance," 2016.
- [35] S. Kerrache, R. Alharbi, and H. Benhidour, "A scalable similarity-popularity link prediction method," *Scientific reports*, vol. 10, no. 1, pp. 1–14, 2020.
- [36] J. Adamczak, Y. Deldjoo, F. B. Moghaddam, P. Knees, G.-P. Leyson, and P. Monreal, "Session-based hotel recommendations dataset: As part of the acm recommender system challenge 2019," *ACM Transactions on Intelligent Systems and Technology (TIST)*, vol. 12, no. 1, pp. 1–20, 2020.
- [37] P. Knees, Y. Deldjoo, F. B. Moghaddam, J. Adamczak, G.-P. Leyson, and P. Monreal, "Recsys challenge 2019: Session-based hotel recom-

- mendations,” in *Proceedings of the 13th ACM Conference on Recommender Systems*, 2019, pp. 570–571.
- [38] A. Wächter and L. T. Biegler, “On the implementation of an interior-point filter line-search algorithm for large-scale nonlinear programming,” *Mathematical Programming*, vol. 106, no. 1, pp. 25–57, 2006.
- [39] HSL, “collection of Fortran codes for large-scale scientific computation,” <http://www.hsl.rl.ac.uk/ipopt>, [Online; accessed 10-10-2022].

Mobile Applications for Cybercrime Prevention: A Comprehensive Systematic Review

Irma Huamanñahui Chipa¹, Javier Gamboa-Cruzado², Jimmy Ramirez Villacorta³
Facultad de Ingeniería de Sistemas, Universidad Nacional Mayor de San Marcos, Lima, Perú^{1,2}
Facultad de Ingeniería de Sistemas e Informática, Universidad Nacional de la Amazonía Peruana, Iquitos, Perú³

Abstract—Now-a-days, cybercrime, cyberattacks, cyber security, phishing and malware are taking a more notorious role in people's daily lives, not only at the international level. The great technological leaps brought with them new modalities of cybercrime, the number of victims of cybercriminals has increased considerably. The objective of this study is to determine the state of the art about Mobile Applications and their impact on Computer Crime Prevention. Therefore, it has become necessary to know what preventive measures are being taken, such as techniques for detecting computer crimes, their modalities and their classification. To close this knowledge gap, a systematic literature review (SLR), a methodology proposed by Kitchenham & Charters, was proposed to obtain the detection techniques and classification of computer crimes based on the review of 68 papers published between the years 2017 and 2022. Likewise, different tables and graphs of the selected studies are provided, which offer additional information such as the most used keywords per paper, biometric networks, among others.

Keywords—Computer crimes; cyberattacks; cyber security; mobile apps; phishing; machine learning; malware; systematic literature review

I. INTRODUCTION

Due to the Covid-19 pandemic, the use of Information and Communication Technologies (ICT) has taken an enormous leap forward, especially in the less developed countries of Latin America. In the labor field, many continue to opt for teleworking, online sales have increased notoriously, in the same way computer crimes in all its forms have also been increasing. A computer crime is a crime committed through the use of electronic tools and methods, against people or organizations [1, 6]. It should also be noted that computer crimes have a tendency to become a long-term factor in the political and economic process, due to the lack of great success in counteracting them [4]. There are several types of cybercrime, for which various criteria must be used to classify them [2]. There are two categories of computer crimes: those that are computer or cell phone assisted, such as child pornography, fraud, money laundering and cyberstalking, while computer crimes that are computer-centric include hacking, phishing and website defacement [6]. As well as there are computer crimes there are also techniques to counter various computer crimes; such as Machine Learning, Data mining, Neural network, Firewall, etc. [2, 6, 8, 27,68].

Being clear about the types of cybercrime and possible techniques to counteract them, would be of great help if these in turn are disseminated to users, so that they can avoid becoming victims of cybercriminals. In 2017 cybercrime costs

amounted to approximately \$600 billion in the United States, by 2019 they increased by 118% in the first half of the year leading to huge losses and financial implications, and by 2020 the statistics increased from 71% in mobile malware and 689% in PowerShell malware [1].

Therefore, it is important to determine the types of computer crimes and techniques that help to counteract them and above all to have a dissemination plan to all users of mobile applications, who day by day perform different operations online, or simply use their cell phones to enter their social networks. There are different studies in which they apply other technologies and tools such as Machine Learning to prevent computer crimes [2, 6, 8, 27,68], as well as they also use artificial intelligence to be able to counteract computer crimes [70, 71].

Given this worrying reality, i.e., the lack of knowledge of the advances and achievements of experimental research worldwide and its impact on the prevention of computer crimes in the countless articles published, and the limited dissemination of systematic review articles on the subject will allow the international research community to close these technological and scientific gaps.

In the present study, the aim is to conduct a comprehensive systematic review of research regarding mobile applications that help prevent computer crimes. Few studies involving both variables were found, but studies found on other tools and technologies that help to counteract computer crimes are also shown.

The structure of the document is organized as follows. Section II presents the Background of the study. The research methodology is presented in Section III. Section IV presents the research results and discussions. Section V presents the conclusions and future studies. Finally, Section VI presents the acknowledgements.

II. BACKGROUND AND RELATED WORKS

In this study, no SLR has been found that is focused on presenting how mobile applications can improve the prevention of computer crimes, however, some papers have been found that partially provide answers to the problem of computer crimes, not necessarily using mobile applications, but other technologies and some potential methods and techniques to detect computer crime threats.

The authors Al-Khater, Al-Ma'adeed, Ahmed, Sadiq & Khan [6] conducted a comprehensive literature review on

computer crime detection techniques, for this purpose they first made a classification of the types of computer crimes, then they presented the computer crime detection techniques using Statistical methods, Machine Learning, Neural Networks, Deep Learning, Fuzzy Logic Neural Network, Data Mining and other techniques. They managed to make a broad classification of computer crimes, they also analyzed numerous studies regarding the detection rates achieved and some limitations, advantages and disadvantages of each technique.

Wiafe, Nti, Nyarko, Assyne & Gulliver [70], conducted an SLR with 131 papers, which were analyzed using quantitative and qualitative methods, to minimize the knowledge gap regarding artificial intelligence methods to combat computer crimes. The study was focused on intrusion prevention and detection systems, where it was determined that the most used technique was support vector machines.

Author Jeong [71] also conducted a literature review on security threats and crimes related to Artificial Intelligence. His paper defines the term Artificial Intelligence crime and classifies it into 2 categories: Artificial Intelligence as a crime tool and Artificial Intelligence as a target crime, inspired by a taxonomy of cybercrime: Computer as a crime tool and Computer as a crime tool. Through the proposed taxonomy, foreseeable Artificial Intelligence crimes are systematically studied and related, forensic techniques are also addressed.

Weichbroth & Łysik [72], performed a RSL on a set of keywords, aiming to identify and analyze existing threats and best practices in mobile security. To obtain the results, 167 users were evaluated; the results show a high awareness of threats and their countermeasures in the mobile application domain. While recognizing the risks associated with physical and social factors, the majority of respondents stated the use of integrated methods to mitigate the negative impact of malware and social engineering scams.

Liu, Xu, Zhang, & Sun [73] conducted a systematic literature review, where they suggest that machine learning is an effective and promising way to detect Android malware. This paper presents a comprehensive survey of Machine Learning-based Android malware detection approaches, they also present the background of Android applications including Android system architecture, security mechanisms, and Android malware classification with the aim to help scholars get a complete picture of Machine Learning-based Android malware detection.

The RSL provides a comprehensive review of new threats and techniques to be able to counter cybercrime, given the new juncture of the Covid-19 pandemic, there have been huge leaps in the use of ICT and thus new cybercrime threats have also been generated. To process the information extracted from the papers, the artificial intelligence tool (RAj) developed by the author Dr. Javier Gamboa Cruzado has been used.

III. METHODOLOGY

The review method used is based on the fundamentals and guidelines of Kitchenham & Charters [69]. The method allows the formulation of research questions, objectives, search

sources and their respective strategies, also allows the selection of studies by exclusion criteria, achieving the identification of studies, also applying quality criteria, data extraction and finally the synthesis of findings. It can be seen in Fig. 1.

A. Research Problems and Objectives

In the SLR conducted, the formulation of the research questions made it possible to formulate the search strategies necessary to achieve a good extraction and analysis of the data. It also made it possible to identify the research objectives, as shown in Table I.

B. Search Sources and Search Strategies

The libraries used to perform the research searches are: Web of Science, Scopus, ProQuest, ScienceDirect, ACM Digital Library, Wiley Online Library and Taylor & Francis Online.

The search strategy included keywords relevant to the research. As shown in Table II.

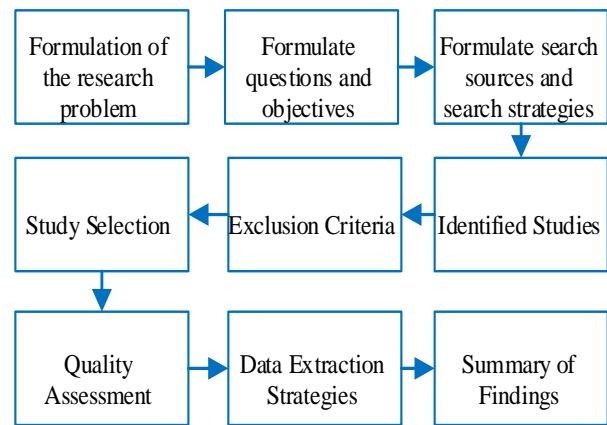


Fig. 1. Stages of Systematic Literature Review.

TABLE I. RESEARCH QUESTIONS AND OBJECTIVES

Research Question	Objective
RQ1: What are the most commonly used techniques in Computer Crime Prevention investigations?	To know the techniques of Computer Crime Prevention.
RQ2: What are the most used Keywords in Mobile Application research and Cybercrime prevention?	Determine the most used keywords in the papers on Mobile Applications and Cybercrime prevention.
RQ3: What are the most cited papers, by country, number of citations and by source in research on mobile applications and cybercrime prevention?	Identify the most cited papers by country, number of citations and sources in research on mobile applications and cybercrime prevention.
RQ4: What are the types of computer crimes in the investigations reviewed?	To know the classification of computer crimes in the investigations reviewed.
RQ5: Which Authors are Co-Occurring in Research on Mobile Applications and Cybercrime Prevention?	Determine the authors who frequently co-occur in research on mobile applications and cybercrime prevention.

TABLE II. SEARCH DESCRIPTORS AND THEIR SYNONYMS

Descriptor	Type of Variable
Mobile Applications/ Applications	Independent Variable
Computer Crime Prevention/ Computer Crimes	Dependent Variable

The search equations were used according to the selected sources, as shown in Table III.

TABLE III. SOURCES AND SEARCH EQUATIONS

Source	Search Equations
Web of Science	(ALL=((“mobile apps”) OR apps AND (“prevention from cybercrime”) OR cybercrime))
Scopus	(ALL (“mobile apps”) OR ALL (apps) AND ALL (“prevention from cybercrime”) OR ALL (cybercrime))
ProQuest	(“mobile apps”) OR apps AND (“prevention from cybercrime”) OR cybercrime
ScienceDirect	((“mobile apps” OR apps) AND (“prevention from cybercrime” OR cybercrime))
ACM Digital Library	[[All: “mobile apps”] OR [All: apps]] AND [[All: “prevention from cybercrime”] OR [All: cybercrime]]
Wiley Online Library	(“mobile apps” OR apps) AND (“prevention from cybercrime” OR cybercrime)
Taylor & Francis Online	[[All: “mobile apps”] OR [All: apps]] AND [[All: “prevention from cybercrime”] OR [All: cybercrime]]

C. Identified Studies

The search yielded 561,055 papers, see Fig. 2.

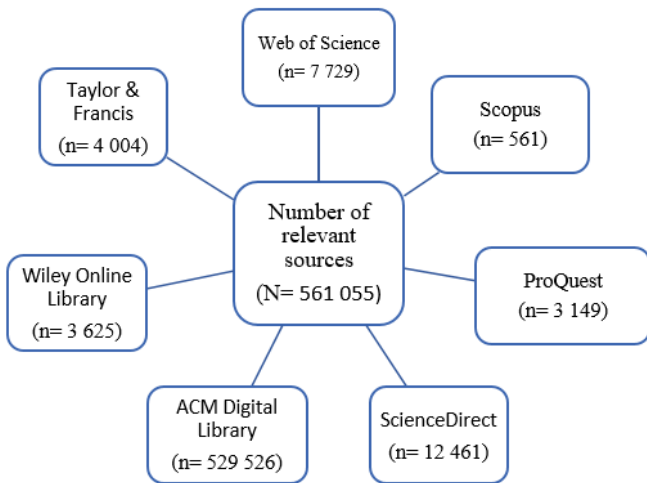


Fig. 2. Number of Studies Identified.

D. Exclusion Criteria

Six exclusion criteria (EC) were applied in order to obtain papers with more relevance to the present investigation. The EC were as follows:

- CE1: The papers are older than five years.
- CE2: The papers are not written in English.
- SG3: The full text of the paper is not available.
- SG4: The papers were not published in Conferences or peer-reviewed Journals.

SD5: The titles and keywords of the papers are not very appropriate

SD6: The proposed solution does not apply to the prevention of cybercrime.

E. Study Selection

To select the most relevant studies, exclusion criteria were applied to ensure that the papers selected were relevant to the research. Quality criteria were then applied to ensure that the papers selected provided solutions and answers to the research questions. See Fig. 3.

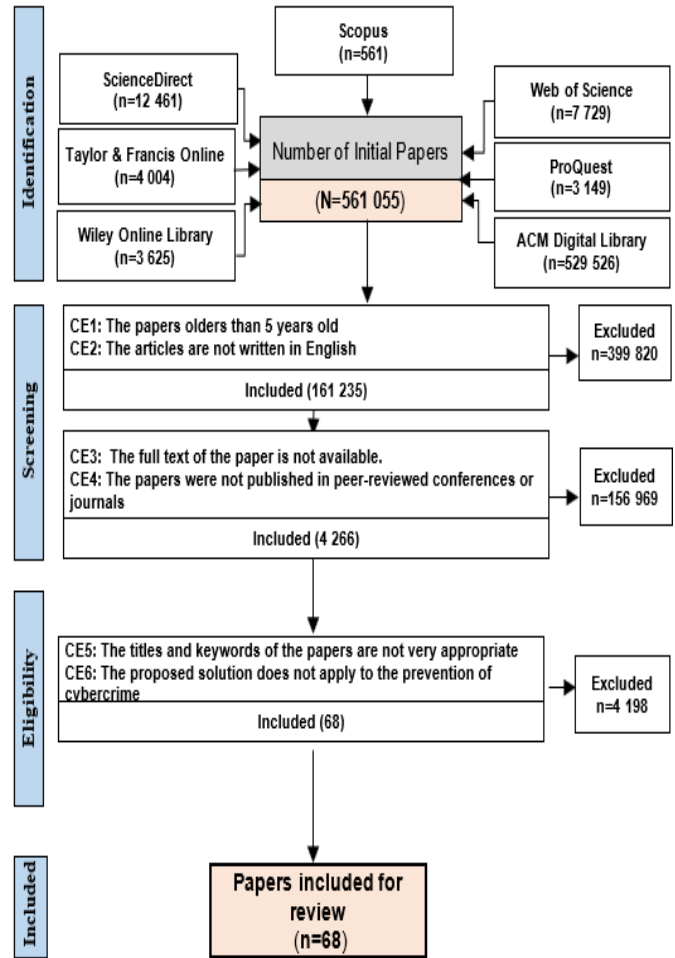


Fig. 3. PRISMA Flowchart.

F. Quality Assessment

As a final step for the selection of the papers, four quality criteria (QA) were applied, with the aim of selecting papers that are of quality for the literature review. Quality criteria used:

- QA1. Is the purpose of the research clearly explained?
- QA2. Is the research methodology clearly explained?
- QA3. Is the specific subject area used clearly defined?
- QA4. Are the results of the experiments performed clearly identified and reported?

These rules were applied to identify the final list of research papers reviewed. After the evaluation of the 4 QAs to the 68 papers, it was determined that all of them had met the quality criteria.

G. Data Extraction Strategy

Once the final list of papers was obtained, the necessary information was extracted to support and answer the research questions.

The information extracted from the papers were the following: Article ID, title of the paper, URL, source, Country, Number of pages, language, type of publication, authors, affiliation, number of citations, abstract, keywords, sample size.

The Mendeley tool was used to manage the papers, as shown in Fig. 4.

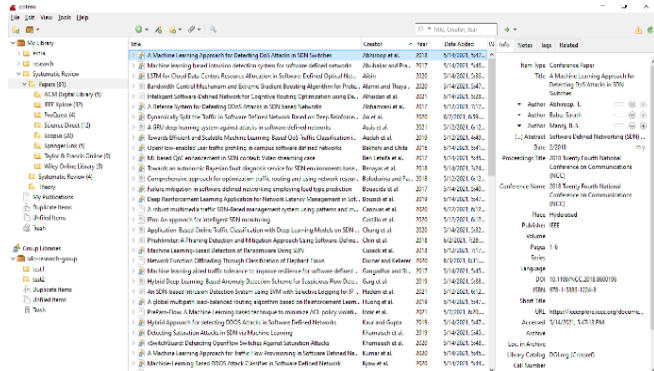


Fig. 4. Document Management with Mendeley.

H. Summary of Findings

The data extracted to answer the research questions were tabulated as quantitative data where an in-depth analysis of the data was performed in order to answer each research question, also allowing statistical comparisons between all findings per research question.

IV. RESULTS AND DISCUSSION

A. General Description of the Studies

The 68 papers selected were processed and the necessary information was extracted. Table IV shows the two types of publications used in the reviewed research: 66 were published in Journals and 2 in Conferences.

The authors Meneses, Silva & Colaço [74], also considered two types of publications for their research: Journal with 29% and Conference with 71%.

Other authors considered more types of publications, for example: Hijji & Alam [75], considered seven types of publications for their research of 52 documents such as: (Journals: 23.1%, Conferences / Workshops: 1.9%, White papers: 17.3%, Report articles: 19.2%, websites: 21.2%, blogs: 13.5% and News report: 3.8%).

Likewise, Cascavilla, Tamburri & Van [76], for their research considered three types of sources: Workshop, Conference and Journal.

TABLE IV. SOURCES AND SEARCH EQUATIONS

Type of Publication	N° Papers
Journal	66
Conference	2
Total	68

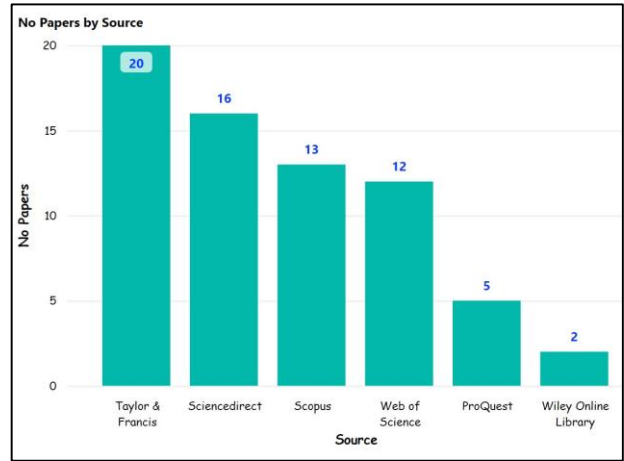


Fig. 5. Papers by Source.

Fig. 5 shows the number of articles selected by type of source, where it can be seen that Taylor & Francis contributed 20 papers, while ScienceDirect contributed 16 papers, followed by Scopus with 13 papers, Web of Science with 12 papers, ProQuest with 5 papers and Wiley Online Library with 2 papers.

For the present study, seven types of important sources were initially considered, but after applying the exclusion criteria, six types of sources were left.

Other authors such as Meneses, Silva & Colaço [74] considered five types of sources to search for the papers of their research on the detection of new fraudulent intelligences: ACM, Engineering Village, IEEE, Scopus and Web of Science.

Fig. 6 shows the 68 papers selected for SLR grouped by country. It can be seen that United Kingdom is the country that publishes the most papers, with 19 papers representing 20.88%, followed by US with 13 papers representing 14.29%.

For the authors Tandon, Kaur, Mäntymäki & Dhir [77], the country that contributed most to their research was the USA with 135 papers followed by the United Kingdom with 82 papers.

For Sonkor, & García de Soto [78], they classify the reviewed publications by country according to 3 categories: (a) Construction and Cybersecurity (USA with 42%, United Kingdom with 33%, United Arab Emirates with 17% and South Africa with 8%), (b) Construction and OT (The levels of operational technology) (USA with 20%, Germany with 16%, Hong Kong with 8%, Russia with 8% and others with 48%) and (c) OT and cybersecurity (USA with 18%, China with 12%, Singapore with 9%, United Kingdom with 9%,

Australia with 6%, Germany with 6%, Japan with 6% and others with 33%).

B. Answers to Research Questions

RQ1: What are the most commonly used techniques in Cybercrime Prevention investigations?

The results of the literature review found 14 computer crime detection techniques. Which are not necessarily listed in a specific order, the % obtained should be considered to determine which technique is the most applied. Table V shows the computer crime detection techniques.

The most applied techniques are Machine Learning which is found in 19 papers [6], [8], [12], [19], [26], [27], [32], [34], [46], [47], [48], [49], [50], [56], [59], [60], [63], [64] and [68] with 26.4% of the total, likewise Data Mining is found in 12 papers [6], [23], [27], [34], [47], [48], [49], [50], [54], [55], [61] and [68] with 16.7%.

The authors Al-Khater, Al-Ma'adeed, Ahmed, Sadiq & Khan [6], considered in their research that the detection techniques for computer crimes are: Statistical, Machine Learning (which is divided into Neural (Deep Learning and Fuzzy Logic Neural)), Data Mining and other techniques such as Computer Vision Techniques, Biometric Techniques, Cryptography and Forensics tools. Although the authors classified the techniques in 4 groups, there is agreement with the types of techniques mentioned.

With the authors Meneses, Silva & Colaço [74] do not agree with part of their classification of the detection techniques found, such as: Data Mining and Machine Learning.

TABLE V. COMPUTER CRIME DETECTION TECHNIQUES

Detection Techniques	Reference	Qty. (%)
Statistical	[6]	1 (1.4)
Machine Learning	[6] [8] [12] [19] [26] [27] [32] [34] [46] [47] [48] [49] [50] [56] [59] [60] [63] [64][68]	19 (26.4)
Data Mining	[6] [23][27][34][47][48][49][50][54][55] [61][68]	12 (16.7)
Neural network	[6] [26][27][49][50][56][59][68]	8 (11.1)
Deep learning	[6] [27][49][50][59][68]	6 (8.3)
Fuzzy logic neural network	[6]	1 (1.4)
Computer Vision Techniques	[6]	1 (1.4)
Biometric Techniques	[6]	1 (1.4)
Cryptography	[6][11][23][27][38][55][64]	7 (9.7)
Forensics tools	[6][61]	2 (2.8)
Proxies	[34]	1 (1.4)
Firewalls	[2][6][11][23][27][29][38][40][55] [56][62][68]	12 (16.7)
Cyber Liability Insurance	[5]	1 (1.4)

Guo, Cho, Chen, Sengupta, Hong & Mitra [79], considered as data-driven deception detection techniques: data driven, social honeypots, user profile, message content, network structure, early detection, information propagation mitigation and blockchain - based authenticity. Therefore, there is no agreement on any detection technique because the authors more focused on online social deception techniques.

The authors Bangui & Buhnova [80], in their research regarding Machine Learning techniques for intrusion detection, considered the following techniques: Neural networks with 34%, followed by SVM with 20%, Regression techniques with 10%, Learning Automata with 7%, Markov models with 7%, k-means with 7%, Naive Bayes with 7%, Decision Tree with 3%, Random Forest with 3% and K-NN with 3%. There is only agreement on some techniques since the study is more focused on Machine Learning techniques.

Based on the results shown in Table V, it can be inferred that, although the most used techniques are Machine Learning, Data Mining and Neural network, they are applied jointly and with other techniques, such as Deep learning, Fuzzy logic neural network, among others, to obtain better results in Computer Crime Prevention. In this sense, applying these techniques in different organizations and countries, would improve the performance of their computer systems, generating reliability in the organization and reducing maintenance costs.

RQ2: What are the most used Keywords in Mobile Application research and Cybercrime prevention?



Fig. 6. Papers by Country.

According to the results of the literature review, the most used keywords are: cybercrime with 23 repetitions, followed by cybersecurity with 14 repetitions. See Fig. 7 and Fig. 8.

Although the most repeated keywords are Cybercrime and Cybersecurity, it should be emphasized that the word covid-19 conceptually is not related to the research, but as a result of the current situation, it managed to increase computer crimes, and even causing the emergence of new modalities of computer crimes, due to the technological leap worldwide.



Fig. 7. Keywords Most Frequently Repeated in the Papers.

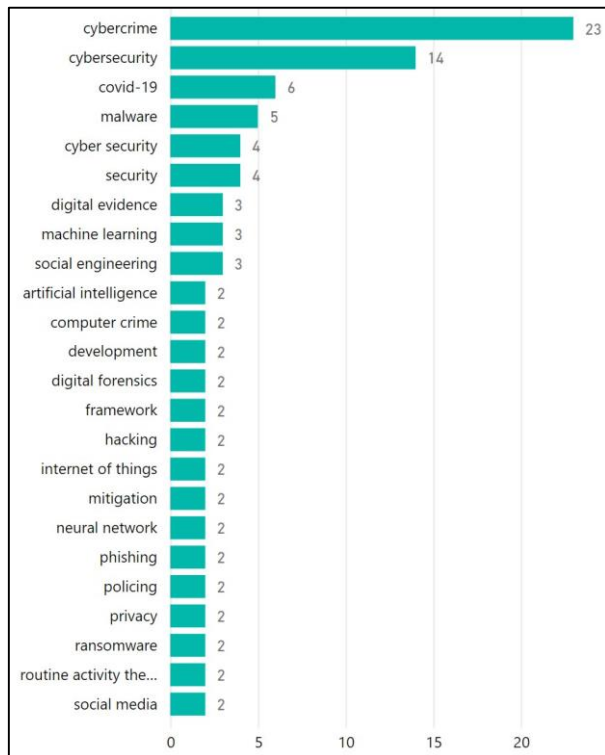


Fig. 8. Number of Keywords in the Papers.

For Tandon, Kaur, Mäntymäki & Dhir [77], in their research regarding the management of computer crimes, considers that the keyword Blockchain is the most used keyword with 311 times in the keywords per author and 138 times per paper. While the research is not closely related to cybercrime it touches on cybercrime issues in parts of the paper.

It can be emphasized that the keywords of this research should be considered in the bibliographic searches regarding Mobile Applications for the prevention of Computer Crimes. They should also be included as keywords in papers produced as a result of experimental research and systematic literature reviews.

RQ3: What are the most cited papers, by country, number of citations and by source in research on mobile applications and cybercrime prevention?

Table VI shows the list of the most cited papers by country, number of citations and source in this study. Of the 68 papers selected for the literature review, the 2 most cited papers are: paper [37] with 67 citations, which was published in ScienceDirect and its author is from United Kingdom, followed by paper [61] with 40 citations which belongs to Web of Science and its author is from Lithuania.

The papers [37, 61], are the most cited, therefore, they are the most relevant of the research. The paper [37] investigated human factors in cyber security, while the paper [61] proposed a tool based on digital evidence object models and habit attribution for computer crime investigation. No other studies with the same research question were found for comparison.

TABLE VI. MOST CITED PAPERS BY COUNTRY AND SOURCE

Ref.	No. Quotations	Country	Source
[37]	67	United Kingdom	ScienceDirect
[61]	40	Lithuania	Web of Science
[57]	39	South Africa	Taylor & Francis
[27]	37	Australia	Scopus
[16]	37	United Kingdom	Taylor & Francis
[25]	34	United Kingdom	Scopus
[44]	29	The Netherlands	Taylor & Francis
[60]	27	Canada	Scopus
[50]	24	Eswatini	ScienceDirect
[45]	24	Japan	Wiley Online L.
[32]	24	United Kingdom	ScienceDirect
[56]	18	United Kingdom	Taylor & Francis
[51]	17	Norway	Taylor & Francis
[42]	17	United Kingdom	Taylor & Francis
[11]	15	The Netherlands	Taylor & Francis
[29]	15	USA	Web of Science
[36]	13	Germany	ProQuest
[64]	11	United Kingdom	Scopus
....		
Total	600		

Based on what has been reported, it can be concluded that it is necessary to review in detail the papers published in the United Kingdom, Lithuania and South Africa in the experimental studies on Mobile Applications for Cybercrime prevention that will be developed in other countries and in the future.

RQ4: What are the types of computer crimes in the investigations reviewed?

The results of the literature review found 23 types of computer crimes. Which are not necessarily listed in a specific order, the % obtained should be considered to determine which computer crime is most committed by computer criminals. Table VII shows a list of the types of computer crimes.

The types of computer crimes most commonly used by criminal offenders are: Malware present in 39 papers: [1] [2] [3] [4] [5] [6] [7] [9] [12] [15] [16] [21] [22] [23] [24] [25] [26] [29] [32] [33] [34] [35] [40] [42] [43][44] [46] [47] [48] [49] [51] [55] [57] [59] [62] [63] [64] [65] and [68] and represents 14.2% of the total papers, followed by Phishing found in 31 papers [1] [2] [6] [7] [9] [14] [15] [16] [21] [22] [23] [24] [25] [26] [27] [34] [37] [39] [41] [42] [43] [44] [48] [50] [55] [56] [57] [60] [62] [64] [64] and [68] with 11.3% of the total.

The authors Hijji & Alam [75] in their classification of techniques used for cyber-attacks during the Covid-19 pandemic indicate that the type of computer crime Phishing is the most used with 35.3%, followed by Spam with 16.3%, and among the most important are Scams with 13.7%, Smishing with 12.4%, Extortion with 2.6%, cyberbullying with 2.0% and cyberstalking with 1.3%. It is agreed that Phishing is one of the most used computer crimes.

An & Kim [34], classified computer crimes differently, separating into 2 groups crime articles for services (Phishing, Brute Force attack, DDoS attack, Spamming) and crime articles for products (Drive-by download, Botnet, Exploit, Ransomware, Rootkit and Trojan) do not agree with some of the mentioned types.

For the authors Iakovakis & Xarhoulacos [81], the types of computer crimes produced during Covid-19, are: Phishing with 59%, Malware - Ransomware with 36%, Malicious Domains with 22% and new falsehoods with 14%. According to the results the study agrees that both Phishing and Malware are the most used computer crimes.

Other authors such as Wiafe, Nti, Nyarko, Assyne & Gulliver [70], considered according to publications per year the following computer crimes: Intrusion, encryption and certification, imaging and captcha, phishing, malware, traffic, DoS and others.

Karie, Kebande & Venter [82], consider that the major motivations for attacks are computer crimes with 81.7%, followed by Cyber Espionage with 12.2%, Cyber Warfare with 4.3% and Hactivism with 1.7%.

TABLE VII. MOST CITED PAPERS BY COUNTRY AND SOURCE

Type of Cybercrime	Reference	Qty. (%)
Cyber Terrorism	[6] [11] [17] [39] [41] [42]	6 (2.2)
Cyber Warfare	[3] [6] [11] [39]	4 (1.5)
Cyber Espionage	[3] [6] [11] [39]	4 (1.5)
Child Pornography	[2] [6] [9] [19] [30] [41] [50]	7 (2.5)
Cyber Bullying	[6] [10] [43]	3 (1.1)
Cyber Extortion	[23] [42]	2 (0.7)
Cyberstalking	[2] [6] [9] [28] [50] [57] [68]	7 (2.5)
Cyber Fraud / Online Fraud	[2] [6] [9] [10] [16] [22] [28] [30] [33] [43] [53] [57] [65]	13 (4.7)
Phishing	[1] [2] [6] [7] [9] [13] [14] [16] [21] [22] [23] [24] [25] [26] [27] [34] [37] [39] [41] [42] [43] [44] [48] [50] [55] [56] [57] [60] [62] [64] [68]	31 (11.3)
Denial of service Attack / DOS	[5] [6] [9] [14] [16] [25] [27] [35] [42] [43] [44] [52] [62]	13 (4.7)
SQL Injection Attack / SQL injection	[5] [6] [7] [27] [66]	5 (1.8)
Malware	[1] [2] [3] [4] [5] [6] [7] [9] [12] [15] [16] [21] [22] [23] [24] [25] [26] [29] [32] [33] [34] [35] [40] [42] [43] [44] [46] [47] [48] [49] [51] [55] [58] [59] [62] [63] [64] [65] [68]	39 (14.2)
Trojans	[6] [9] [15] [24] [34] [57] [59] [64] [68]	9 (3.3)
Identity Theft	[1] [2] [6] [8] [9] [11] [24] [28] [29] [36] [40] [41] [42] [43] [45] [46] [48] [57] [68]	19 (6.9)
Key Logger	[15] [56]	2 (0.7)
Screen Logger	[9]	1 (0.4)
Evil Twin	[9]	1 (0.4)
Botnets	[3] [6] [10] [12] [20] [23] [27] [34] [35] [43] [63][64] [65]	13 (4.7)
Social Engineering	[1] [2] [5] [6] [9] [14] [21] [23] [24] [25] [26] [27] [34] [38] [41] [42] [48] [55] [57] [62] [64] [65] [66]	23 (8.4)
Worms	[3] [6] [9] [27] [56] [57] [59]	7 (2.5)
Ransomware	[1] [5] [14] [15] [20] [21] [23] [24] [25] [27] [29] [31] [32] [34] [35] [38] [41] [43] [47] [48] [51] [55] [57] [59] [60] [64] [67]	27 (9.8)
Hacking	[2] [6] [11] [14] [15] [16] [17] [18] [19] [22] [25] [28] [30] [31] [34] [35] [39] [41] [44] [46] [47] [50] [55] [56] [57] [60] [61] [62] [63] [64]	30 (10.9)
Data breach	[5] [15] [21] [25] [27] [42] [43] [60] [68]	9 (3.3)

Likewise, Guo, Cho, Chen, Sengupta, Hong & Mitra [79], considered according to their classification five groups of computer crimes: False Information (False News, rumors, information manipulation, fake reviews), Luring (Phishing, spamming), Fake Identity (fake profile, compromised account, profile cloning attack), Crowdturfing (Crowdturfing), Human targeted attacks (human trafficking, cyberbullying, cybergrooming and cyberstalking).

On the other hand, Senarak [83] considers as a category of computer crimes to: Hacktivism, Cyber criminality, Cyber espionage, Cyber terrorism and Cyber war.

And the author Jeong [71], in his research regarding security threats, crimes and forensic analysis of artificial intelligence, the most committed computer crime is Advanced Computer as Tool Crime.

The detailed identification of types of cybercrime is expected to further accelerate the development of Mobile Applications that enable the prevention of Cybercrime in all business sectors, leading to the emergence of new businesses based on this technology and a booming economy based on data protection.

RQ5: Which Authors are Co-Occurring in Research on Mobile Applications and Cybercrime Prevention?

According to the literature review, authors E. Rutger Leukfeldt and Steve Van de Weijer present three co-occurrences (weight 3). See Fig. 9.

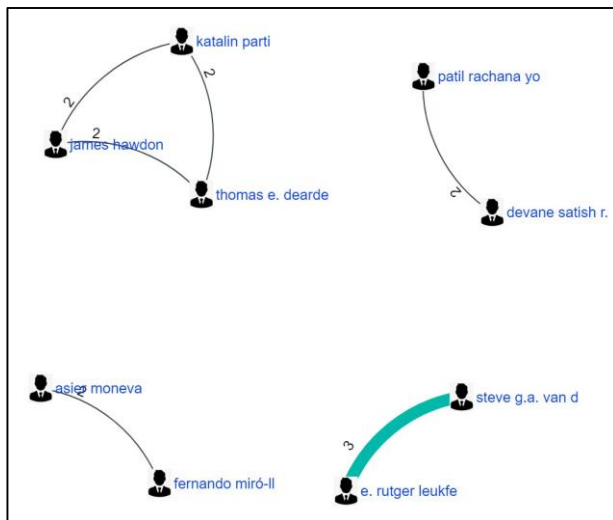


Fig. 9. Co-authorship Bibliometric Network.

While authors E. Rutger Leukfeldt and Steve Van de Weijer are presented together in three papers, it is important to mention that authors James Hawdon, Katalin Parti and Thomas Dearde are presented together in two papers.

For Tandon, Kaur, Mäntymäki & Dhir [77], the author presenting the highest co-occurrence in the selected studies is Wang X. Do not agree with the authors because the research focused more on blockchain.

V. CONCLUSIONS AND FUTURE RESEARCH

This study has managed to identify and analyze which are the most used techniques for the detection of computer crimes, the classification of computer crimes, the most used words in the papers, the most used keywords, the most cited papers and the authors that present cooccurrence in their research based on the research questions posed and analyzed with the systematic literature review between 2017 and 2021 in several databases. The results of the review determine that the most used techniques for the detection of computer crimes are: Statical, Machine Learning, Data Mining, Neural network, Deep learning, Fuzzy logic neural network, Computer Vision Techniques, Biometric Techniques, Cryptography, Forensics tolos, Network Encryption, Proxies, Firewalls and Cyber Liability Insurance. The most used technique is Machine Learning. Likewise, computer crimes were classified as follows: Cyber Terrorism, Cyber Warfare, Cyber Espionage, Child Pornography, Cyber Bullying, Cyber Extortion, Cyber Extortion, Cyberstalking, Cyber Fraud / Online Fraud / Fraud, Cyber Laundering, Phishing, Denial of service Attack, SQL Injection Attack, Malware, Unauthorized System Access, Trojans, Identity Theft, Key Logger, Screen Logger, Evil Twin, Botnets, Social Engineering, Worms, Ransomware, Hacking and Data breach. Few co-authorships were identified among the researchers and very few systematic reviews that made use of bibliometric networks; however, this did not improve the interpretation of the results. Future research should consider a larger number of articles for review and analysis.

REFERENCES

- [1] A. Alzubaidi, "Measuring the level of cyber-security awareness for cybercrime in Saudi Arabia," *Heliyon*, vol. 7, no. 1, 2021, doi: 10.1016/j.heliyon.2021.e06016.
- [2] N. Akdemir and C. J. Lawless, "Exploring the human factor in cyber-enabled and cyber-dependent crime victimisation: a lifestyle routine activities approach," *Internet Res.*, vol. 30, no. 6, pp. 1665–1687, 2020, doi: 10.1108/INTR-10-2019-0400.
- [3] A. Claver, "Governance of cyber warfare in the Netherlands: an exploratory investigation," *Int. J. Intell. Secur. Public Aff.*, vol. 20, no. 2, pp. 155–180, 2018, doi: 10.1080/23800992.2018.1484235.
- [4] R. I. Dremluiga and A. I. Korobeev, "Trends and Methods of Fighting Cybercrime in the Russian Federation in Terms of the Transition to a Digital Economy," vol. 7, pp. 191–200, 2021.
- [5] A. M. Algarni, V. Thayananthan, and Y. K. Malaiya, "Quantitative assessment of cybersecurity risks for mitigating data breaches in business systems," *Appl. Sci.*, vol. 11, no. 8, 2021, doi: 10.3390/app11083678.
- [6] W. A. Al-Khater, S. Al-Maadeed, A. A. Ahmed, A. S. Sadiq, and M. K. Khan, "Comprehensive review of cybercrime detection techniques," *IEEE Access*, vol. 8, pp. 137293–137311, 2020, doi: 10.1109/ACCESS.2020.3011259.
- [7] A. Moneva, E. R. Leukfeldt, S. G. A. Van De Weijer, and F. Miró-Llinares, "Repeat victimization by website defacement: An empirical test of premises from an environmental criminology perspective," *Comput. Human Behav.*, vol. 126, no. September 2020, 2022, doi: 10.1016/j.chb.2021.106984.
- [8] A. Basuchoudhary and N. Searle, "Snatched secrets: Cybercrime and trade secrets modelling a firm's decision to report a theft of trade secrets," *Comput. Secur.*, vol. 87, 2019, doi: 10.1016/j.cose.2019.101591.
- [9] A. Okutan and Y. Çebi, "A Framework for Cyber Crime Investigation," *Procedia Comput. Sci.*, vol. 158, pp. 287–294, Jan. 2019, doi: 10.1016/J.PROCS.2019.09.054.

- [10] Benoît Dupont, "Enhancing the effectiveness of cybercrime prevention through policy monitoring," *J. Crime Justice*, vol. 42, no. 5, pp. 500–515, 2019, doi: 10.1080/0735648X.2019.1691855.Abstract.
- [11] B. van den Berg and E. Keymolten, "Regulating security on the Internet: control versus trust," *Int. Rev. Law, Comput. Technol.*, vol. 31, no. 2, pp. 188–205, 2017, doi: 10.1080/13600869.2017.1298504.
- [12] C. Cilleruelo, Enrique-Larriba, L. De-Marcos, and J. J. Martinez-Herraiz, "Malware Detection Inside App Stores Based on Lifespan Measurements," *IEEE Access*, vol. 9, pp. 119967–119976, 2021, doi: 10.1109/ACCESS.2021.3107903.
- [13] C. Cross, "Dissent as cybercrime: social media, security and development in Tanzania," *J. East. African Stud.*, vol. 15, no. 3, pp. 442–463, 2021, doi: 10.1080/17531055.2021.1952797.
- [14] C. Joyce, F. L. Roman, B. Miller, J. Jeffries, and R. C. Miller, "Emerging Cybersecurity Threats in Radiation Oncology," *Adv. Radiat. Oncol.*, vol. 6, no. 6, p. 100796, 2021, doi: 10.1016/j.adro.2021.100796.
- [15] C. Harfield and J. Schofield, "(Im)material culture: towards an archaeology of cybercrime," *World Archaeol.*, vol. 52, no. 4, pp. 607–618, 2020, doi: 10.1080/00438243.2021.1882333.
- [16] D. Buil-Gil, F. Miró-Llinares, A. Moneva, S. Kemp, and N. Díaz-Castaño, "Cybercrime and shifts in opportunities during COVID-19: a preliminary analysis in the UK," *Eur. Soc.*, vol. 23, no. S1, pp. S47–S59, 2021, doi: 10.1080/14616696.2020.1804973.
- [17] D. Broeders, F. Cristiano, and D. Weggemans, "Too Close for Comfort: Cyber Terrorism and Information Security across National Policies and International Diplomacy," *Stud. Confl. Terror.*, vol. 0, no. 0, pp. 1–28, 2021, doi: 10.1080/1057610X.2021.1928887.
- [18] D. S. W. Wong and S. F. Fung, "Development of the cybercrime rapid identification tool for adolescents," *Int. J. Environ. Res. Public Health*, vol. 17, no. 13, pp. 1–13, 2020, doi: 10.3390/ijerph17134691.
- [19] D. Johnson, E. Faulkner, G. Meredith, and T. J. Wilson, "Police Functional Adaptation to the Digital or Post Digital Age: Discussions with Cybercrime Experts," *J. Crim. Law*, vol. 84, no. 5, pp. 427–450, 2020, doi: 10.1177/0022018320952559.
- [20] D. Anagnostakis, "The European Union-United States cybersecurity relationship: a transatlantic functional cooperation," *J. Cyber Policy*, vol. 6, no. 2, pp. 243–261, 2021, doi: 10.1080/23738871.2021.1916975.
- [21] E. Ventrella, "Privacy in emergency circumstances: data protection and the COVID-19 pandemic," *ERA Forum*, vol. 21, no. 3, pp. 379–393, 2020, doi: 10.1007/s12027-020-00629-3.
- [22] E. R. Leukfeldt and T. J. Holt, "Cybercrime on the menu? Examining cafeteria-style offending among financially motivated cybercriminals," *Comput. Human Behav.*, vol. 126, no. February 2021, p. 106979, 2022, doi: 10.1016/j.chb.2021.106979.
- [23] E. Kalaimannan, S. K. John, T. DuBose, and A. Pinto, "Influences on ransomware's evolution and predictions for the future challenges," *J. Cyber Secur. Technol.*, vol. 1, no. 1, pp. 23–31, 2017, doi: 10.1080/23742917.2016.1252191.
- [24] F. E. Eboibi, "Cybercriminals and Coronavirus cybercrimes in Nigeria, the United States of America and the United Kingdom: cyber hygiene and preventive enforcement measures," *Commonw. Law Bull.*, vol. 47, no. 1, pp. 113–142, 2021, doi: 10.1080/03050718.2020.1834424.
- [25] M. Hijji and G. Alam, "A Multivocal Literature Review on Growing Social Engineering Based Cyber-Attacks/Threats during the COVID-19 Pandemic: Challenges and Prospective Solutions," *IEEE Access*, vol. 9, no. January, pp. 7152–7169, 2021, doi: 10.1109/ACCESS.2020.3048839.
- [26] H. Ahmad and L. Erdodi, "Overview of phishing landscape and homographs in Arabic domain names," *Secur. Priv.*, vol. 4, no. 4, pp. 1–14, 2021, doi: 10.1002/spy2.159.
- [27] I. H. Sarker, A. S. M. Kayes, S. Badsha, H. Alqahtani, P. Watters, and A. Ng, "Cybersecurity data science: an overview from machine learning perspective," *J. Big Data*, vol. 7, no. 1, 2020, doi: 10.1186/s40537-020-00318-5.
- [28] T. E. Dearden, K. Parti, and J. Hawdon, "Institutional Anomie Theory and Cybercrime—Cybercrime and the American Dream, Now Available Online," *J. Contemp. Crim. Justice*, vol. 37, no. 3, pp. 311–332, 2021, doi: 10.1177/10439862211001590.
- [29] J. Hawdon, K. Parti, and T. E. Dearden, "Cybercrime in America amid COVID-19: the Initial Results from a Natural Experiment," *Am. J. Crim. Justice*, vol. 45, no. 4, pp. 546–562, 2020, doi: 10.1007/s12103-020-09534-4.
- [30] J. A. M. Schiks, S. G. A. van de Weijer, and E. R. Leukfeldt, "High tech crime, high intellectual crime? Comparing the intellectual capabilities of cybercriminals, traditional criminals and non-criminals," *Comput. Human Behav.*, vol. 126, no. July 2021, p. 106985, 2022, doi: 10.1016/j.chb.2021.106985.
- [31] J. Burton and C. Lain, "Desecuritising cybersecurity: towards a societal approach," *J. Cyber Policy*, vol. 5, no. 3, pp. 449–470, 2020, doi: 10.1080/23738871.2020.1856903.
- [32] J. S. Atkinson, J. E. Mitchell, M. Rio, and G. Matich, "Your WiFi is leaking: What do your mobile apps gossip about you?," *Futur. Gener. Comput. Syst.*, vol. 80, pp. 546–557, 2018, doi: 10.1016/j.future.2016.05.030.
- [33] J. Herrero, A. Torres, P. Vivas, A. Hidalgo, F. J. Rodríguez, and A. Urueña, "Smartphone addiction and cybercrime victimization in the context of lifestyles routine activities and self-control theories: The user's dual vulnerability model of cybercrime victimization," *Int. J. Environ. Res. Public Health*, vol. 18, no. 7, 2021, doi: 10.3390/ijerph18073763.
- [34] J. An and H. W. Kim, "A Data Analytics Approach to the Cybercrime Underground Economy," *IEEE Access*, vol. 6, pp. 26636–26652, 2018, doi: 10.1109/ACCESS.2018.2831667.
- [35] K. K. e Silva, "Vigilantism and cooperative criminal justice: is there a place for cybersecurity vigilantes in cybercrime fighting?," *Int. Rev. Law, Comput. Technol.*, vol. 32, no. 1, pp. 21–36, 2018, doi: 10.1080/13600869.2018.1418142.
- [36] L. Studen and V. Tiberius, "Social media, quo vadis? Prospective development and implications," *Futur. Internet*, vol. 12, no. 9, 2020, doi: 10.3390/FII12090146.
- [37] L. Hadlington, "Human factors in cybersecurity; examining the link between Internet addiction, impulsivity, attitudes towards cybersecurity, and risky cybersecurity behaviours," *Heliyon*, vol. 3, no. 7, p. e00346, 2017, doi: 10.1016/j.heliyon.2017.e00346.
- [38] L. Y. Connolly and D. S. Wall, "The rise of crypto-ransomware in a changing cybercrime landscape: Taxonomising countermeasures," *Comput. Secur.*, vol. 87, 2019, doi: 10.1016/j.cose.2019.101568.
- [39] L. Maschmeyer, R. J. Deibert, and J. R. Lindsay, "A tale of two cybers - how threat reporting by cybersecurity firms systematically underrepresents threats to civil society," *J. Inf. Technol. Polit.*, vol. 18, no. 1, pp. 1–20, 2021, doi: 10.1080/19331681.2020.1776658.
- [40] M. Solihat and R. V. Wulansari, "Internet of Things Cyber Security in Digital Era," *IOP Conf. Ser. Mater. Sci. Eng.*, vol. 1158, no. 1, p. 012017, 2021, doi: 10.1088/1757-899x/1158/1/012017.
- [41] M. M. Singh and A. A. Bakar, "A systemic cybercrime stakeholders architectural model," *Procedia Comput. Sci.*, vol. 161, pp. 1147–1155, 2019, doi: 10.1016/j.procs.2019.11.227.
- [42] M. Camillo, "Cyber risk and the changing role of insurance," *J. Cyber Policy*, vol. 2, no. 1, pp. 53–63, 2017, doi: 10.1080/23738871.2017.1296878.
- [43] M. Riek and R. Böhme, "The costs of consumer-facing cybercrime: An empirical exploration of measurement issues and estimates†," *J. Cybersecurity*, vol. 4, no. 1, pp. 1–16, 2018, doi: 10.1093/cybsec/tyy004.
- [44] M. Weulen Kranenbarg, T. J. Holt, and J. L. van Gelder, "Offending and Victimization in the Digital Age: Comparing Correlates of Cybercrime and Traditional Offending-Only, Victimization-Only and the Victimization-Offending Overlap," *Deviant Behav.*, vol. 40, no. 1, pp. 40–55, 2019, doi: 10.1080/01639625.2017.1411030.
- [45] M. G. Umlauf and Y. Mochizuki, "Predatory publishing and cybercrime targeting academics," *Int. J. Nurs. Pract.*, vol. 24, pp. 1–7, 2018, doi: 10.1111/ijn.12656.
- [46] M. L. Williams, M. Levi, P. Burnap, and R. V. Gundur, "Under the Corporate Radar: Examining Insider Business Cybercrime Victimization through an Application of Routine Activities Theory," *Deviant Behav.*, vol. 40, no. 9, pp. 1119–1131, 2019, doi: 10.1080/01639625.2018.1461786.

- [47] M. L. Han, B. Il Kwak, and H. K. Kim, "CBR-Based Decision Support Methodology for Cybercrime Investigation: Focused on the Data-Driven Website Defacement Analysis," *Secur. Commun. Networks*, vol. 2019, 2019, doi: 10.1155/2019/1901548.
- [48] M. M. Ahsan Pritom, K. M. Schweitzer, R. M. Bateman, M. Xu, and S. Xu, "Characterizing the Landscape of COVID-19 Themed Cyberattacks and Defenses," *Proc. - 2020 IEEE Int. Conf. Intell. Secur. Informatics, ISI 2020*, no. i, 2020, doi: 10.1109/ISI49825.2020.9280539.
- [49] M. Alazab, "Automated malware detection in mobile app stores based on robust feature generation," *Electron.*, vol. 9, no. 3, 2020, doi: 10.3390/electronics9030435.
- [50] N. M. Karie, V. R. Kebande, and H. S. Venter, "Diverging deep learning cognitive computing techniques into cyber forensics," *Forensic Sci. Int. Synerg.*, vol. 1, pp. 61–67, 2019, doi: 10.1016/j.fsisy.2019.03.006.
- [51] N. N. Schia, "The cyber frontier and digital pitfalls in the Global South," *Third World Q.*, vol. 39, no. 5, pp. 821–837, 2018, doi: 10.1080/01436597.2017.1408403.
- [52] P. R. Yogesh and R. Devane Satish, "Formal Verification of Secure Evidence Collection Protocol using BAN Logic and AVISPA," *Procedia Comput. Sci.*, vol. 167, no. 2019, pp. 1334–1344, 2020, doi: 10.1016/j.procs.2020.03.449.
- [53] P. R. Yogesh and R. Devane Satish, "Backtracking Tool Root-Tracker to Identify True Source of Cyber Crime," *Procedia Comput. Sci.*, vol. 171, no. 2019, pp. 1120–1128, 2020, doi: 10.1016/j.procs.2020.04.120.
- [54] P. Sharma, D. Arora, and T. Sakthivel, "Enhanced Forensic Process for Improving Mobile Cloud Traceability in Cloud-Based Mobile Applications," *Procedia Comput. Sci.*, vol. 167, no. 2019, pp. 907–917, 2020, doi: 10.1016/j.procs.2020.03.390.
- [55] R. A. Ramadan, B. W. Aboshosha, J. S. Alshudukhi, A. J. Alzahrani, A. El-Sayed, and M. M. Dessouky, "Cybersecurity and Countermeasures at the Time of Pandemic," *J. Adv. Transp.*, vol. 2021, no. 2003, 2021, doi: 10.1155/2021/6627264.
- [56] K. M. Rajasekharaiah, C. S. Dule, and E. Sudarshan, "Cyber Security Challenges and its Emerging Trends on Latest Technologies," *IOP Conf. Ser. Mater. Sci. Eng.*, vol. 981, no. 2, 2020, doi: 10.1088/1757-899X/981/2/022062.
- [57] R. Naidoo, "A multi-level influence model of COVID-19 themed cybercrime," *Eur. J. Inf. Syst.*, vol. 29, no. 3, pp. 306–321, 2020, doi: 10.1080/0960085X.2020.1771222.
- [58] R. Collett, "Understanding cybersecurity capacity building and its relationship to norms and confidence building measures," *J. Cyber Policy*, pp. 1–20, 2021, doi: 10.1080/23738871.2021.1948582.
- [59] R. Damaševičius, A. Venčkauskas, J. Toldinas, and Š. Grigaliūnas, "Ensemble - based classification using neural networks and machine learning models for windows pe malware detection," *Electron.*, vol. 10, no. 4, pp. 1–26, 2021, doi: 10.3390/electronics10040485.
- [60] S. Hakak, W. Z. Khan, M. Imran, K. K. R. Choo, and M. Shoaib, "Have You Been a Victim of COVID-19-Related Cyber Incidents? Survey, Taxonomy, and Mitigation Strategies," *IEEE Access*, vol. 8, pp. 124134–124144, 2020, doi: 10.1109/ACCESS.2020.3006172.
- [61] Š. Grigaliūnas and J. Toldinas, "Habits attribution and digital evidence object models based tool for cybercrime investigation," *Balt. J. Mod. Comput.*, vol. 8, no. 2, pp. 275–292, 2020, doi: 10.22364/BJMC.2020.8.2.05.
- [62] S. Horgan, B. Collier, R. Jones, and L. Shepherd, "Re-territorialising the policing of cybercrime in the post-COVID-19 era: towards a new vision of local democratic cyber policing," *J. Crim. Psychol.*, vol. 11, no. 3, pp. 222–239, 2020, doi: 10.1108/JCP-08-2020-0034.
- [63] S. Piasecki, L. Urquhart, and P. D. McAuley, "Defence against the dark artefacts: Smart home cybercrimes and cybersecurity standards," *Comput. Law Secur. Rev.*, vol. 42, p. 105542, 2021, doi: 10.1016/j.clsr.2021.105542.
- [64] S. Broadhead, "The contemporary cybercrime ecosystem: A multi-disciplinary overview of the state of affairs and developments," *Comput. Law Secur. Rev.*, vol. 34, no. 6, pp. 1180–1196, 2018, doi: 10.1016/j.clsr.2018.08.005.
- [65] S. Ambore, C. Richardson, H. Dogan, E. Apeh, and D. Osselton, "A resilient cybersecurity framework for Mobile Financial Services (MFS)," *J. Cyber Secur. Technol.*, vol. 1, no. 3–4, pp. 202–224, 2017, doi: 10.1080/23742917.2017.1386483.
- [66] S. G. A. van de Weijer, T. J. Holt, and E. R. Leukfeldt, "Heterogeneity in trajectories of cybercriminals: A longitudinal analyses of web defacements," *Comput. Hum. Behav. Reports*, vol. 4, no. June, p. 100113, 2021, doi: 10.1016/j.chbr.2021.100113.
- [67] T. Stevens and K. O'brien, "Brexit and cyber security," *RUSI J.*, vol. 164, no. 3, pp. 22–30, 2019, doi: 10.1080/03071847.2019.1643256.
- [68] Y. E. Suzuki and S. A. S. Monroy, "Prevention and mitigation measures against phishing emails: a sequential schema model," *Secur. J.*, no. 0123456789, 2021, doi: 10.1057/s41284-021-00318-x.
- [69] B. A. Kitchenham and S. Charters, "Guidelines for performing Systematic Literature Reviews in Software Engineering. EBSE Technical Report EBSE-2007-01. School of Computer Science and Mathematics, Keele University," no. October 2021, p. 2007, 2007.
- [70] I. Wiafe, F. Nti Koranteng, E. Nyarko Obeng, N. Assyne, A. Wiafe, and S. R. Gulliver, "Artificial Intelligence for Cybersecurity_ A Systematic Mapping of Literature _ Enhanced Reader." .
- [71] D. Jeong, "Artificial intelligence security threat, crime, and forensics: Taxonomy and open issues," *IEEE Access*, vol. 8, pp. 184560–184574, 2020, doi: 10.1109/ACCESS.2020.3029280.
- [72] P. Weichbroth and Ł. Łysik, "Mobile Security: Threats and Best Practices," *Mob. Inf. Syst.*, vol. 2020, 2020, doi: 10.1155/2020/8828078.
- [73] K. Liu, S. Xu, G. Xu, M. Zhang, D. Sun, and H. Liu, "A Review of Android Malware Detection Approaches Based on Machine Learning," *IEEE Access*, vol. 8, pp. 124579–124607, 2020, doi: 10.1109/ACCESS.2020.3006143.
- [74] C. V. Meneses Silva, R. Silva Fontes, and M. Colaço Júnior, "Intelligent Fake News Detection: A Systematic Mapping," *J. Appl. Secur. Res.*, vol. 16, no. 2, pp. 168–189, 2021, doi: 10.1080/19361610.2020.1761224.
- [75] M. Hijji and G. Alam, "A Multivocal Literature Review on Growing Social Engineering Based Cyber-Attacks/Threats during the COVID-19 Pandemic: Challenges and Prospective Solutions," *IEEE Access*, vol. 9, no. January, pp. 7152–7169, 2021, doi: 10.1109/ACCESS.2020.3048839.
- [76] G. Cascavilla, D. A. Tamburri, and W. J. Van Den Heuvel, "Cybercrime threat intelligence: A systematic multi-vocal literature review," *Comput. Secur.*, vol. 105, p. 102258, 2021, doi: 10.1016/j.cose.2021.102258.
- [77] A. Tandon, P. Kaur, M. Mäntymäki, and A. Dhir, "Blockchain applications in management: A bibliometric analysis and literature review," *Technol. Forecast. Soc. Change*, vol. 166, no. October 2020, 2021, doi: 10.1016/j.techfore.2021.120649.
- [78] M. S. Sonkor and B. García de Soto, "Operational Technology on Construction Sites: A Review from the Cybersecurity Perspective," *J. Constr. Eng. Manag.*, vol. 147, no. 12, 2021, doi: 10.1061/(asce)co.1943-7862.0002193.
- [79] Z. Guo, J. H. Cho, I. R. Chen, S. Sengupta, M. Hong, and T. Mitra, "Online Social Deception and Its Countermeasures: A Survey," *IEEE Access*, vol. 9, pp. 1770–1806, 2021, doi: 10.1109/ACCESS.2020.3047337.
- [80] H. Bangui and B. Buhnova, "Recent advances in machine-learning driven intrusion detection in transportation: Survey," *Procedia Comput. Sci.*, vol. 184, no. 2019, pp. 877–886, 2021, doi: 10.1016/j.procs.2021.04.014.
- [81] G. Iakovakis, C. G. Xarhoulacos, K. Giovas, and D. Gritzalis, "Analysis and Classification of Mitigation Tools against Cyberattacks in COVID-19 Era," *Secur. Commun. Networks*, vol. 2021, 2021, doi: 10.1155/2021/3187205.
- [82] N. M. Karie, V. R. Kebande, and H. S. Venter, "Diverging deep learning cognitive computing techniques into cyber forensics," *Forensic Sci. Int. Synerg.*, vol. 1, pp. 61–67, 2019, doi: 10.1016/j.fsisy.2019.03.006.
- [83] C. Senarak, "Port cybersecurity and threat: A structural model for prevention and policy development," *Asian J. Shipp. Logist.*, vol. 37, no. 1, pp. 20–36, 2021, doi: 10.1016/j.ajsl.2020.05.001.

Evaluation of the Efficiency of the Optimization Algorithms for Transfer Learning on the Rice Leaf Disease Dataset

Luyi-Da Quach, Khang Nguyen Quoc, Anh Nguyen Quynh, Hoang Tran Ngoc
FPT University, Cantho city, Vietnam

Abstract—To improve the model's efficiency, people use many different methods, including the Transfer Learning algorithm, to improve the efficiency of recognition and classification of image data. The study was carried out to combine optimization algorithms with the Transfer Learning model with MobileNet, MobileNetV2, InceptionV3, Xception, ResNet50V2, DenseNet201 models. Then, testing on rice disease data set with 13.186 images, background removed. The result obtained with high accuracy is the RMSprop algorithm, with an accuracy of 88% when combined with the Xception model, similar to the F1, Xception model, and ResNet50V2 score of 87% when combined with the Adam algorithm. This shows the effect of gradients on the Transition learning model. Research, evaluate and draw the optimal model to build a website to identify diseases on rice leaves, with the main functions including images and recording of disease identification points for better management purposes on diseased areas of rice.

Keywords—Optimization algorithm; transfer learning; RMSprop; rice leaf disease; Adam

I. INTRODUCTION

Transfer learning is a popular method used for machine learning recognition problems, with the goal of reusing as a starting point for a second task. Therefore, a Transfer learning model is used to learn on a certain source task and pre-trained this model, then it is used for another model so that the new model learns on the target tasks faster. With the use of pre-trained models, Transfer learning models take a big step up from previous models in improving the accuracy of recognition model and classification based on object features.

In practical applications, Transfer learning models are quite commonly used to improve the accuracy of deep learning models. Specifically in this regard, some studies can be mentioned such as: the problem of identifying patients with Parkinson's disease [1], predicting air quality at large time resolution [2], using VGG-16 classifies retinopathy caused by diabetes [3], improving the process of sleep organization method [4], improving ad accuracy by checking clicks [5], improving the accuracy in counting the number of wheat ears [6], improving the accuracy in classifying medicinal leaves [7], classifying diseases in poultry [8], etc. In general, when using a Transfer learning model with different data sets, the accuracy of the model is also significantly improved when the accuracy increases from 5-8%. This makes an important contribution in predicting more accurately in the recognition problem. However, the Transfer learning model also cannot

get high accuracy on a number of different data sets. Therefore, the transfer learning model is interested in order to improve the accuracy of the model.

In improving, the accuracy of the Transfer learning model is also approached in various data problems. In which, there are some applied studies in improving the accuracy of Transfer learning models from input data, or combining algorithms. For the improvement of input data, these studies can be mentioned: A Stacked Denoising Autoencoder [9], Sparse Fingerprinting [10], converting High-Resource to Low-Resource Language [11], time series data augmentation [12], combine images [13], For the algorithm, there are studies such as Vector Segmentation [14], Kidney Segmentation [15], SURF features [16], etc. This shows that improving the accuracy of the Transfer learning model has been extremely attended in recent times, especially in the use of optimization models, in which there are some studies such as: using particle swarm optimization (PSO)[17], heuristic optimization for gesture recognition [18], approaching adaptive fine-tuning for routing through custom or pre-trained layer – called SpotTune [19], using hyper-parameters optimization to identify diseases on maize leaves [20], using Bayesian optimization to create a mixed-signal analog circuit model [21], Adam Deep Learning optimization algorithm for recognizing flower images with background [22],

In general, in the past time, there have been many studies to improve the accuracy of Transfer learning models, but there has been no research to evaluate the accuracy by combining Transfer learning models with optimal algorithms. advantage on the rice leaf disease dataset. The main contribution of the study is the implementation of the tasks below:

- Combining optimization algorithms with Transfer learning models on rice leaf disease dataset has no image background.
- Evaluate the optimal model after testing; aim is checking the appropriateness of the Transfer learning model and the optimization algorithm.

Finally, the study uses the Transfer learning model and the optimal algorithm with the highest accuracy to build a system. This system is used to diagnose rice diseases by imaging.

II. TRANSFER LEARNING MODELS

In this section, the study will present six Transfer learning models used, through the introduction to get an overview of

the model. In recent years, the MobileNet model has had good results for identifying and implementing embedded and mobile systems. There are different versions of this architecture. MobileNet [23], introduced in 2017, used depth integrals and started with two singles global hyper parameters that effectively balance latency and accuracy. MobieNetV2 [24] was introduced two years later with residuals opposite the number of linear bottlenecks between classes. This model takes tight low dimensional space (bottleneck) as input which is then expanded on high dimensional space. With filtered by deep light convolution, then projected back to low dimensional space with linear convolution. MobileNetV3 [25] is the higher generation of Mobilenets which is public at the ICCV conference in 2019, this model is a config for CPUs in mobile phones with the association of hardware-aware network architecture search (NAS), and the NetAdapt algorithm enhanced through novel architecture refinements. There are two sub-models in this model, MobileNetV3-Large and MobileNetV3-Small, with high and low resource-use matching, which helps the model to promote efficiency on hardware effectively. Another model to be introduced is the network model that goes deeper and deeper, which also makes the training process more difficult and degrades the accuracy of the training rapidly. To solve this problem, in 2016, Deep

Residual Learning (ResNet) [26] implemented connection skipping and used batch normalization techniques, using Residual Block to remove the connection layer. This block allows each layer to connect its inputs to its outputs. Families in ResNet include ResNet50, ResNet101, and ResNet152 [27], corresponding to a network of 60 layers, 101 classes, and 152 classes trained on the ImageNet dataset. In 2018, similar to ResNet, the InceptionV3 model [28] is a network trained on the ImageNet dataset. It is introduced as a convolutional neural network model consisting of multiple convolution and maximal steps. DenseNet [29] further modified the model for ResNet, the purpose is that instead of aggregating the output feature maps from all previous layers, it will concatenate all feature maps sequentially instead of summarizing them. Merge output feature maps from all previous layers. DenseNet is used in three variants, DenseNet-121, DenseNet-169, and DenseNet-201. In 2020, EfficientNetB0 [30] was introduced with multiple optimizations when scaling each dimension using a fixed set of scaling factors. This approach surpasses other mod-ern models trained on the ImageNet dataset. In 2017, Xception [31] was introduced as an extension of the Inception architecture, which is intended to replace standard Inceptions with depth-separable aggregates. The architectural models used in this study is shown in Fig. 1.

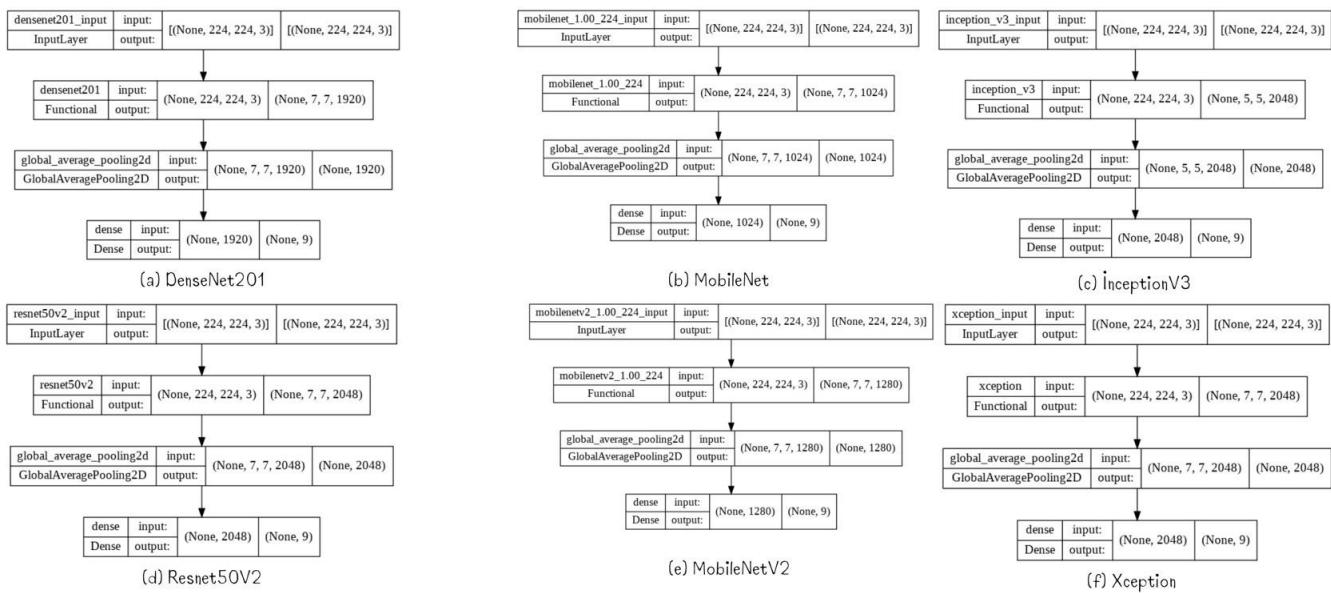


Fig. 1. The Architecture of the Models is used in the Study to Evaluate the Effectiveness of the Optimization Algorithm on Transfer Learning Models.

III. OPTIMIZATION ALGORITHM

In this section, the study will theoretically present some optimization algorithms used in the research. The main purpose helps to correct the learning coefficient to accelerate the training, increase the accuracy with fast convergence on the Transfer learning model.

A. Adaptive Moment Estimation (Adam)

Adam algorithm [32] adjusts the learning rate for each weight of the neural network by calculating the first and second intervals of the slope. This makes the algorithm optimal in using the learning rate selection method based on the particular situation. Adam algorithm uses parameters v_t ,

m_t to estimate of the first moment (the mean) and the second moment (the uncentered variance) of the gradients respectively; β_1, β_2 is speed of movement, g_t is gradient at time t in the formula (1-4) and (5) is the Adam update rule, it is the same as in the RMSprop optimization algorithm.

$$m_t = \beta_1 m_{t-1} + (1 - \beta_1) g_t \quad (1)$$

$$v_t = \beta_2 v_{t-1} + (1 - \beta_2) g_t^2 \quad (2)$$

$$\hat{m}_t = \frac{m_t}{1 - \beta_1^t} \quad (3)$$

$$\hat{v}_t = \frac{v_t}{1 - \beta_2^t} \quad (4)$$

$$W_{t+1} = W_t - \frac{\eta}{\sqrt{v_t + \epsilon}} \cdot \hat{m}_t \quad (5)$$

B. Adaptive Gradient Algorithm (Adagrad)

Adagrad algorithm [33] implements varying the learning rate to reduce gradients in machine learning techniques. The use of learning weights based on previous inputs to automatically adjust the learning rate to the best divisor instead of a single learning rate, which makes Adagrad better than other algorithms. In the formula (6), η is learning rate, ϵ is guaranteed parameter, g_t is gradient at time t , G_t is the diagonal matrix containing the square of the derivative of the parameter vector at t .

$$W_{t+1} = W_t - \frac{\eta}{\sqrt{G_t + \epsilon}} \cdot g_t \quad (6)$$

C. Root Mean Squared Propagation (RMSprop)

For gradient normalization, RMSprop [34] uses the mean square of the gradient. This helps balance the step size – reduce the step for large gradients to avert Exploding Gradient and increase the step for small gradients to sidestep Vanishing Gradient. Formula (7) is used to calculate the running time parameter $E[g^2]_t$, and form aa rules for formula (8).

$$E[g^2]_t = 0.9E[g^2]_{t-1} + 0.1g_t^2 \quad (7)$$

$$W_{t+1} = W_t - \frac{\eta}{\sqrt{E[g^2]_t + \epsilon}} \cdot g_t \quad (8)$$

D. Adaptive Delta (Adadelata)

Adadelata algorithm [35] allows to reduce the learning rate on each dimension of SGD. Adadelata restricts the previously accumulated gradients to a predefined size w , which makes the difference in the algorithm by not having to sum the previously squared gradients together. The sum of the gradients is defined recursively as the descending average of all previous gradients. The only variables that affect the running average $E[t]$ at time step t are the previous average and the current gradient (9). By substituting the descending mean on the previous squared gradients for the diagonal matrix ($G[t]$), in terms of parameter update vector $\Delta\theta_t$ (10).

$$E[g^2]_t = \gamma E[g^2]_{t-1} + (1 - \gamma)g_t^2 \quad (9)$$

$$\Delta\theta_t = - \frac{\eta}{\sqrt{E[g^2]_t + \epsilon}} g_t \quad (10)$$

E. Stochastic Gradient Descent (SGD)

Stochastic is a variant of Gradient Descent [36]. Instead of after each epoch we will update the weight (Weight) once, in each epoch with N data points we will update the weight N times. Therefore, it is usually much faster and can also be used to learn online. SGD performs frequent updates with high variance causing the objective function to fluctuate a lot with the corresponding formula with $x(i)$ and $y(i)$ presented for each training instance.

$$\theta = \theta - \eta \cdot \nabla_{\theta} J(\theta; x^{(i)}; y^{(i)}) \quad (11)$$

IV. METHODOLOGY

A. Data and Data Preparation

With the background dataset provided by the Mekong Delta Rice Institute taken by phone (Samsung SM-N770F)

with image size (1816x4032). We combed and collected additional leaf disease datasets from multiple sources including Kaggle, GitHub, and from previous related studies in Google Scholar¹. This dataset contains fully captured rice leaf images from leaf roll to leaf apex, which increases the accuracy of the model and is accompanied by a more complete assessment (Fig. 2). By collecting progress, our dataset consists of 9839 images of diseased leaves of rice consisting of the eight most common diseases namely Bacteria blight, Brown spot, Hispa, Leaf scald, Leaf blast, Leaf smut, Narrow brown spot, and Tungro with the characteristics shown in Fig. 3. There are 3347 images of Healthy leaves. After gathering data, the original size of images in the dataset has various sizes. Hence, we resize it to a large size (1024 x 1024 pixels) for keeping the quality of the image and having a standard size. Besides, we split this dataset into 3 parts: training, validation, and testing with a ratio is 60:30:10 is shown in the Table I.

Since the data is enough, research used various preprocessing steps like image resizing to 224 x 224 and using the processing function of each Transfer learning model to preprocess images to train. With preprocessing dataset, the image in the dataset transforms into an array of RGB colors. The value of each element in array that was scaled to [0; 1], [-1; 1], or [0; 255] depending on each Transfer learning model is shown in Fig. 4.

B. Evaluation Methods

Accuracy is an instance that is precisely determined from the total number of data sets. In other words, it is the correct predictions made by the model relative to the total predictions. It is given by equation (12)

$$Accuracy = \frac{TP+TN}{Total\ sample} \quad (12)$$

In which, TP (True Positive): Total number of Positive matches. TN (True Negative): Total number of Negative matches.

TABLE I. STATISTICS OF TRAINING, VALIDATION AND TESTING DATASETS FOR EACH TYPE OF RICE LEAF DISEASE

Class	Training	Validation	Test	Total
Bacteria blight	496	248	83	827
Brown spot	1,738	869	290	2,897
Hispa	1,189	594	198	1,981
Leaf blast	1,803	901	301	3,005
Leaf scald	214	107	37	358
Leaf smut	203	102	34	339
Narrow brown spot	211	105	36	352
Tungro	48	24	8	80
Healthy	2,008	1004	335	3,347
Total	7,910	3,954	1,322	13,186

¹ The aggregated dataset is stored at <https://github.com/raianrido/diseases-on-rice-leaf>

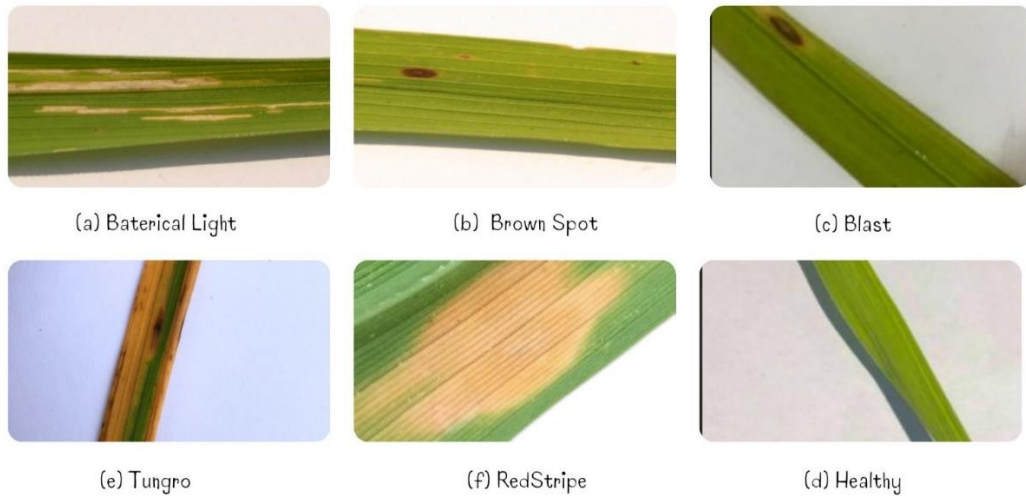


Fig. 2. Images are Collected from the Rice Institute in the Mekong Delta.



Fig. 3. Illustrated Image of Disease Data on Rice Leaf.

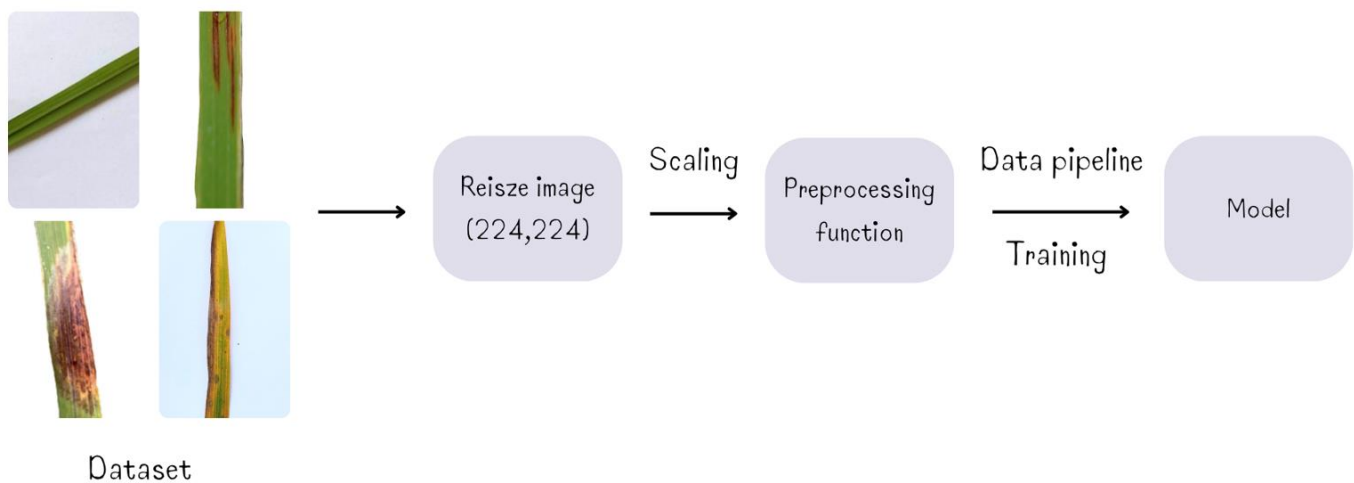


Fig. 4. Data Preparation on Rice Leaf Disease Dataset.

Loss function evaluates the effectiveness of the learning algorithm for the model on the used data set. It produces a non-negative real number representing the distinction between two quantities: a , the predicted label, and y , the correct label. This is a reward-punishment mechanism, the model will have to pay a penalty each time the prediction is wrong and the penalty is proportional to the size of the error. In any supervised math problem, the goal always includes reducing the total penalty payable. In the ideal case $a = y$, the loss function will return a minimum value of 0. Cross-entropy (CE) is considered as a measure of classifier performance (13).

$$CE = -\sum_i^c a_i \log(p_i) \quad (13)$$

In which, c is the number of classes, a_i the actual value, p_i is the predicted value.

The Confusion matrix gives a better view of how the data points are classified as true/false. It is the summary used to evaluate the classification model performance. The number of true and false predictions is summarized by the count values and broken down by class. When trying to increase the accuracy of the model, the recall will decrease and vice versa. The parameter F1-score reconciles the two values above.

$$F_1 - Score = \frac{2}{\frac{1}{Recall} + \frac{1}{Precision}} \quad (14)$$

$$Precision = \frac{TP}{Total\ predicted\ positive} = \frac{TP}{TP+FP} \quad (15)$$

$$Recall = \frac{TP}{Total\ actual\ positive} = \frac{TP}{TP+FN} \quad (16)$$

In which, FP (False Positive) is the total number of cases that predict the observations of the label Negative to Positive, FN (False Negative) is the total number of cases that predict the observations of the label Positive to Negative.

F1-Score is a harmonized average of Precision and Recall. It can have the lowest score of 0 (perfect precision and recall) and the highest of 1. The quality of the model in machine learning or deep learning depends on the value of the F1-Score, F1 is high which demonstrates the model is reasonable. Combining Transfer learning model and optimization algorithm.

In this research, Transfer learning will help resolve the issue by utilizing a previously trained in ImageNet dataset as the base for a new model. Transfer learning allows us to customize an already-trained model for a specific problem. Therefore, we are fine-tuning the last layer of six Transfer learning models for the classification of leaf disease consisting of MobileNet, MobileNetV2, InceptionV3, Xception, Resnet50V2, and DenseNet201. By the base layer of model architecture, whose weights were pre-trained and imagined to be frozen, the default input is 224x224 pixels for each image. Then we add the last layers global_average_pooling2d (None, 512) and Dense (0,9) with the activation 'SoftMax'. Before training, each model compiles one in five optimization algorithms. The proposed work offers deep learning, which

causes an increase in diseases on rice leaf classification efficiency. The research plotted the history of training processing with accuracy in the training dataset and validation dataset to evaluate the difference between each model with optimization. All optimization algorithms have a default value of a parameter such as a learning rate is 0.001. After training progress, we plotted the confusion matrix and classification report on the testing dataset to have a different view of accuracy in each class and model (Fig. 5).

C. Results

The study is tested on the system CPU Intel Xeon X5675 3.07 GHz, RAM 24 Gbytes and graphics devices NVIDIA Quadro K2200. Experimental results on five optimization algorithms combined with six Transfer learning models on the rice leaf disease data set are presented in Table II and Fig. 6. The study evaluates the accuracy with parameters F1-Score and Accuracy. The results obtained are as follows:

- For the F1-Score evaluation, the association of the ResNet50V2 model, Xception, and Adam algorithm at 87% was the model that reached the highest results, and the lowest was 50% when combining the MobileNet model and Adadelta algorithm.
- For accuracy evaluation, the results show that the discrepancy when the highest accuracy is RMSprop algorithm applying to the Xception model is 88%, and the lowest is 49% when incorporating MobileNet and Adadelta.

D. Application System

A website system is built based on the Xception trained model which compiles RMSprop algorithm with 88% accuracy on the test data set (Fig. 7), with main functions including:

Image recognition: When the user uploads an image at the browse button under the title Detect now and clicks submit, the image will be recognized to detect the disease and return the disease name, symptoms, treatment, and prevention measures in both English and Vietnamese.

- Report false identification and contribute to the system: This is a report function button, helping users to contribute images related to the disease when the system recognizes it wrong. Nevertheless, it will be put into the retraining system when passing the check processing by the admin. At that time, the Report screen will be divided into 3 states: pending (waiting for approval), reject (report has been processed and user information reported is not valid (false)), accept (system error, needed repair and optimization).
- Disease area map: When the user uses the system to identify the disease, the system will use the user's location (Google API) to get information and create a map of the disease. Each color of the dot corresponds to a different disease.

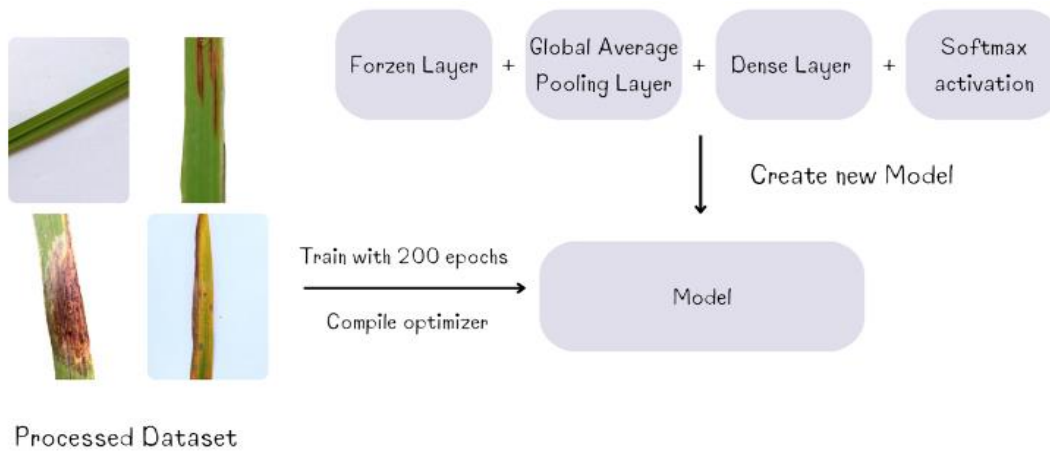


Fig. 5. Illustrating the Combining Transfer Learning Model and Optimization Algorithm.

TABLE II. RESULT TABLE OF COMBINING THE OPTIMAL ALGORITHM WITH THE TRANSFER LEARNING MODEL

Optimization Algorithms	SGD		Adam		Adagrad		Adadelta		RMSprop	
	F1-Score	Accuracy	F1-Score	Accuracy	F1-Score	Accuracy	F1-Score	Accuracy	F1-Score	Accuracy
MobileNet	84%	75%	86%	76%	77%	69%	50%	49%	85%	76%
MobileNetV2	84%	74%	83%	73%	79%	70%	53%	55%	83%	73%
InceptionV3	81%	76%	82%	76%	77%	70%	55%	58%	81%	74%
Xception	84%	76%	87%	80%	76%	67%	52%	55%	81%	88%
ResNet50V2	85%	77%	87%	78%	81%	73%	54%	57%	84%	76%
DenseNet201	80%	71%	80%	69%	77%	69%	85%	77%	80%	69%

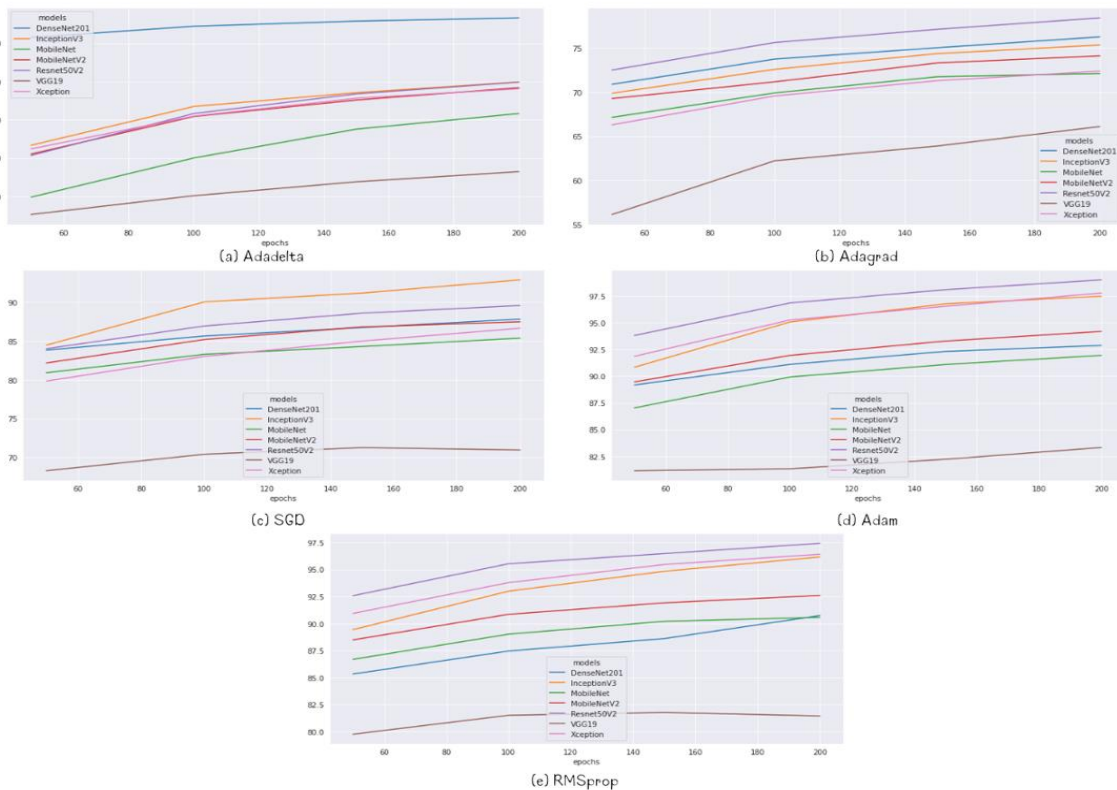
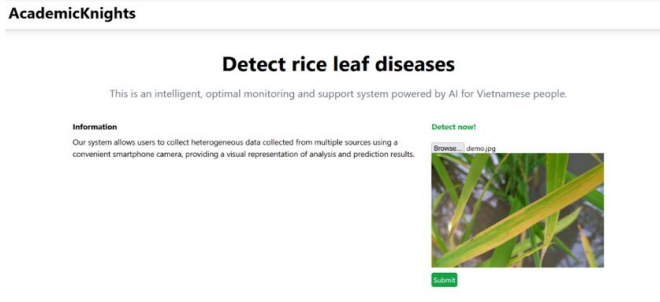


Fig. 6. Compare the Accuracy of Each Algorithm when Combined with Each Transfer Learning Model.

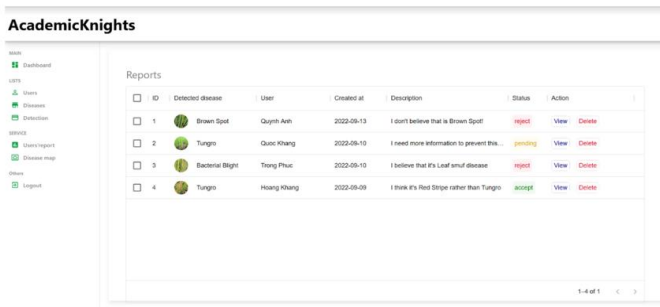
(a) Illustration of disease identification screen



(b) Illustration of disease identification on the leaves



(c) Illustrations of reported images that were wrongly predicted



(d) Illustrate the points on the disease identification

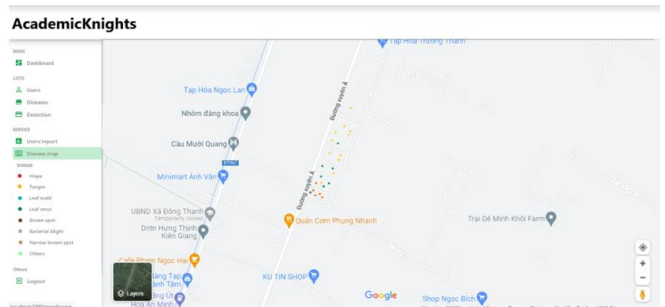


Fig. 7. Illustrate the Website System to Detect Diseases on Rice Leaves.

V. DISCUSSION

Based on test results at Table II and Fig. 6, ResNet50V2 and Xception models combined with Adam algorithm show the efficiency of the algorithm. Analysis of the results shows that Adam algorithm performs better than other algorithms when the accuracy is always high at 87% (F1-Score) and 80% (accuracy). This is because the Adam algorithm further extends stochastic gradient descent to update the network weights during training. The Adam algorithm updates the learning rate for each individual network weight when using a random gradient descent algorithm. Therefore, the optimizers of the Adam algorithm inherit the features of the Adagrad and RMSprop algorithms. In Adam algorithm, instead of adjusting the learning rate based on the first moment (average) but in RMSprop it also uses the second moment of the gradient. In which, the cause comes from the representations of the decay rate β_1 and β_2 of the average of the gradients (17). Regardless, the model that compiles the Adam algorithm is still flawed by incorrectly receiving many images of healthy rice leaves, which figure shows this error.

$$m_t = \beta_1 m_t + (1 - \beta_1) \left[\frac{\delta L}{\delta w_t} \right] v_t = \beta_2 v_{t-1} + (1 - \beta_2) \left[\frac{\delta L}{\delta w_t} \right]^2 \quad (17)$$

However, when evaluating the accuracy of the algorithm, the optimal model RMSprop shows high efficiency when applied on six models tested on research with parameters of accuracy and F1-Score. This is because RMSprop maintains a moving average of the quadratic gradient, while adjusting the updates to the weights by this magnitude.

In the opposite direction, Adadelta shows no efficiency when combined with Transfer learning model. As proof for this, we can see the results of 5/6 models such as MobileNet, MobileNetV2, InceptionV3, Xception and ResNet50V2. But it works well on the DenseNet201 model (Fig. 8 shows diagnostic discrepancies on some data sets). This result is because the Adadelta algorithm does not use a learning rate parameter. Instead, the algorithm uses its own rate of change as a parameter to adjust the learning rate. Adadelta needs to use two state variables to store the quadratic moments of the gradient and of the change in parameters. In addition, Adadelta uses a leak average to store dynamic estimates of the required statistics. As a result, the learning rate has to be changed manually and the learning rate will decline and become smaller at some point. Therefore, after a certain number of iterations, the model will no longer be able to learn new knowledge.

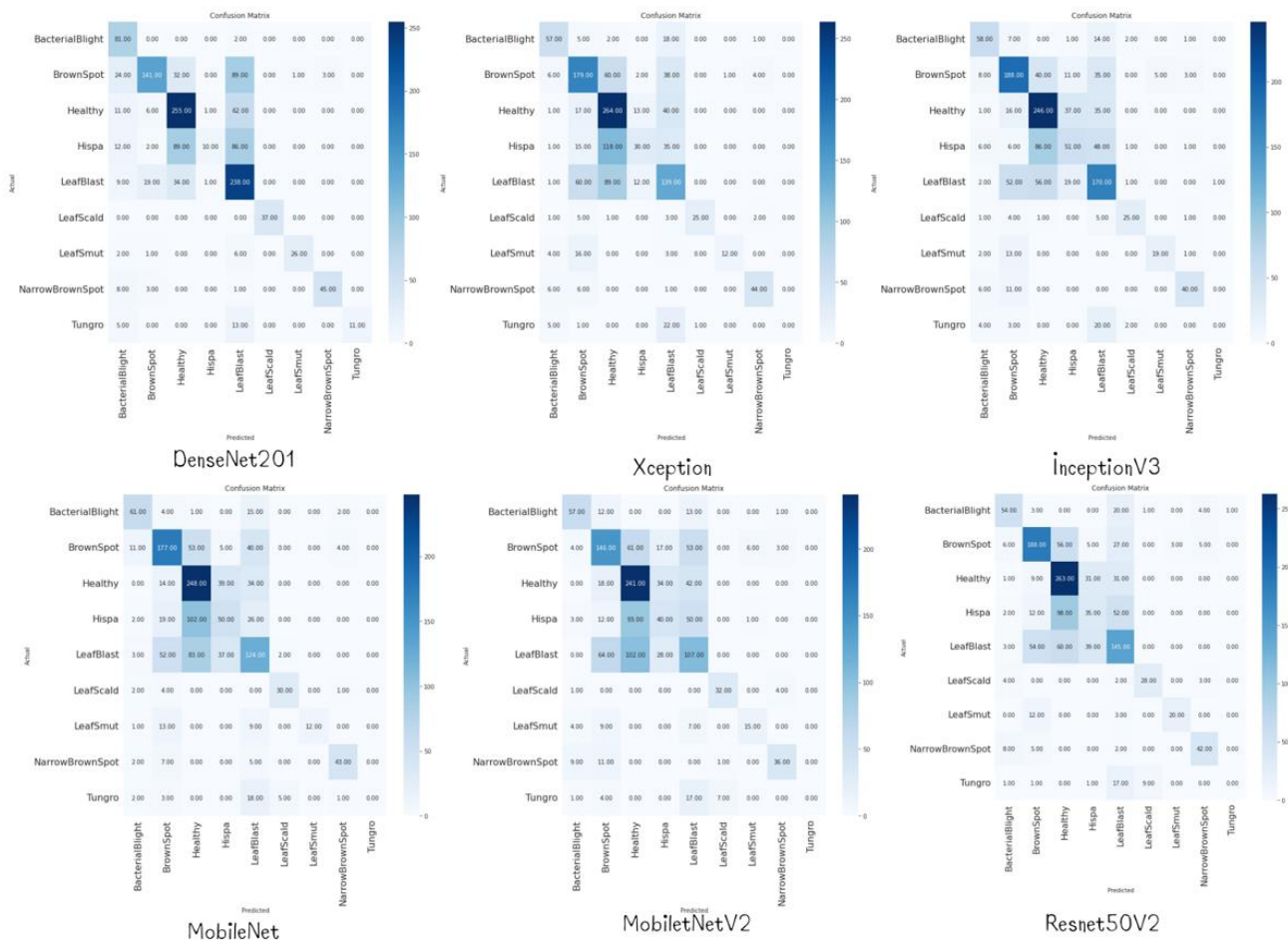


Fig. 8. Confusion Matrix of Adadelta Algorithm with Transfer Learning Models.

VI. CONCLUSIONS

The study proposes that Adam's method is effective when combined with Transfer learning models through gradient expansion to update network parameters and reduce random gradients. This also works for the SGD and RMSprop models. Besides, the low accuracy may come from the influence of input parameters. Although the used image has eliminated the background influence of the image, the resolution parameters cannot be controlled because it is taken from many different sources, in which the data source is generated from study with higher accuracy.

VII. FUTURE WORKS

Based on the research results, it can be seen how effective the optimization algorithms are on different Transfer learning models. However, in this study, we have not gone into detailed evaluation of the combination of models with the optimal algorithm when adjusting the learning rate. Therefore, the study opens up the research and evaluation of the changes of the parameters on the model with the optimization algorithm. Accordingly, the proposal of follow-up studies can more closely evaluate the relationship between the parameters in the optimal model, the influence of the input data set on experiment, and so on. In further research, Transfer Learning

models will be fine tuning with a more complex output structure and compile implementation with more optimization algorithms, increasing the efficiency of the model.

REFERENCES

- [1] J. C. Vásquez-Correa et al., "Transfer learning helps to improve the accuracy to classify patients with different speech disorders in different languages," *Pattern Recognition Letters*, vol. 150, pp. 272–279, Oct. 2021, doi: 10.1016/j.patrec.2021.04.011.
- [2] J. Ma, J. C. P. Cheng, C. Lin, Y. Tan, and J. Zhang, "Improving air quality prediction accuracy at larger temporal resolutions using deep learning and Transfer learning techniques," *Atmospheric Environment*, vol. 214, p. 116885, Oct. 2019, doi: 10.1016/j.atmosenv.2019.116885.
- [3] N. B. Thota and D. Umma Reddy, "Improving the Accuracy of Diabetic Retinopathy Severity Classification with Transfer learning," in *2020 IEEE 63rd International Midwest Symposium on Circuits and Systems (MWSCAS)*, Springfield, MA, USA, Aug. 2020, pp. 1003–1006. doi: 10.1109/MWSCAS48704.2020.9184473.
- [4] H. Phan et al., "Towards More Accurate Automatic Sleep Staging via Deep Transfer learning," *IEEE Trans. Biomed. Eng.*, vol. 68, no. 6, pp. 1787–1798, Jun. 2021, doi: 10.1109/TBME.2020.3020381.
- [5] Y. Su et al., "Improving click-through rate prediction accuracy in online advertising by Transfer learning," in *Proceedings of the International Conference on Web Intelligence*, Leipzig Germany, Aug. 2017, pp. 1018–1025. doi: 10.1145/3106426.3109037.
- [6] J. Ma, Y. Li, H. Liu, Y. Wu, and L. Zhang, "Towards improved accuracy of UAV-based wheat ears counting: A Transfer learning method of the ground-based fully convolutional network," *Expert*

- Systems with Applications, vol. 191, p. 116226, Apr. 2022, doi: 10.1016/j.eswa.2021.116226.
- [7] N. Duong-Trung, L.-D. Quach, and C.-N. Nguyen, "Learning Deep Transferability for Several Agricultural Classification Problems," *ijacsa*, vol. 10, no. 1, 2019, doi: 10.14569/IJACSA.2019.0100107.
- [8] L.-D. Quach, N. Pham-Quoc, D. C. Tran, and Mohd. Fadzil Hassan, "Identification of Chicken Diseases Using VGGNet and ResNet Models," in *Industrial Networks and Intelligent Systems*, vol. 334, N.-S. Vo and V.-P. Hoang, Eds. Cham: Springer International Publishing, 2020, pp. 259–269. doi: 10.1007/978-3-030-63083-6_20.
- [9] C. Kandaswamy, L. M. Silva, L. A. Alexandre, R. Sousa, J. M. Santos, and J. M. de Sa, "Improving Transfer learning accuracy by reusing Stacked Denoising Autoencoders," in *2014 IEEE International Conference on Systems, Man, and Cybernetics (SMC)*, San Diego, CA, USA, Oct. 2014, pp. 1380–1387. doi: 10.1109/SMC.2014.6974107.
- [10] K. Adamkiewicz, P. Koch, B. Morawska, P. Lipiński, K. Lichy, and M. Leplawy, "Improving UWB Indoor Localization Accuracy Using Sparse Fingerprinting and Transfer learning," in *Computational Science – ICCS 2021*, vol. 12747, M. Paszynski, D. Kranzlmüller, V. V. Krzhizhanovskaya, J. J. Dongarra, and P. M. A. Sloot, Eds. Cham: Springer International Publishing, 2021, pp. 291–302. doi: 10.1007/978-3-030-77980-1_23.
- [11] S. Durrani and U. Arshad, "Transfer learning from High-Resource to Low-Resource Language Improves Speech Affect Recognition Classification Accuracy." *arXiv*, Mar. 04, 2021. Accessed: Sep. 16, 2022. [Online]. Available: <http://arxiv.org/abs/2103.11764>.
- [12] K. Bandara, H. Hewamalage, Y.-H. Liu, Y. Kang, and C. Bergmeir, "Improving the accuracy of global forecasting models using time series data augmentation," *Pattern Recognition*, vol. 120, p. 108148, Dec. 2021, doi: 10.1016/j.patcog.2021.108148.
- [13] T. K. Yoo, J. Y. Choi, J. G. Seo, B. Ramasubramanian, S. Selvaperumal, and D. W. Kim, "The possibility of the combination of OCT and fundus images for improving the diagnostic accuracy of deep learning for age-related macular degeneration: a preliminary experiment," *Med Biol Eng Comput*, vol. 57, no. 3, pp. 677–687, Mar. 2019, doi: 10.1007/s11517-018-1915-z.
- [14] V. Gripon, G. B. Hacene, M. Lowe, and F. Vermet, "Improving Accuracy of Nonparametric Transfer learning Via Vector Segmentation," in *2018 IEEE International Conference on Acoustics, Speech and Signal Processing (ICASSP)*, Calgary, AB, Apr. 2018, pp. 2966–2970. doi: 10.1109/ICASSP.2018.8462273.
- [15] J. B. Graham-Knight et al., "Accurate Kidney Segmentation in CT Scans Using Deep Transfer learning," in *Smart Multimedia*, vol. 12015, T. McDaniel, S. Berretti, I. D. D. Curcio, and A. Basu, Eds. Cham: Springer International Publishing, 2020, pp. 147–157. doi: 10.1007/978-3-030-54407-2_13.
- [16] L.-D. Quach, N. P. Quoc, N. H. Thi, D. C. Tran, and M. F. Hassan, "Using SURF to Improve ResNet-50 Model for Poultry Disease Recognition Algorithm," in *2020 International Conference on Computational Intelligence (ICCI)*, Bandar Seri Iskandar, Malaysia, Oct. 2020, pp. 317–321. doi: 10.1109/ICCI51257.2020.9247698.
- [17] B. H. Nguyen, B. Xue, and P. Andraea, "A particle swarm optimization based feature selection approach to Transfer learning in classification," in *Proceedings of the Genetic and Evolutionary Computation Conference*, Kyoto Japan, Jul. 2018, pp. 37–44. doi: 10.1145/3205455.3205540.
- [18] T. Ozcan and A. Basturk, "Transfer learning-based convolutional neural networks with heuristic optimization for hand gesture recognition," *Neural Comput & Applic*, vol. 31, no. 12, pp. 8955–8970, Dec. 2019, doi: 10.1007/s00521-019-04427-y.
- [19] Y. Guo, H. Shi, A. Kumar, K. Grauman, T. Rosing, and R. Feris, "SpotTune: Transfer learning Through Adaptive Fine-Tuning," p. 10.
- [20] M. Subramanian, K. Shanmugavadivel, and P. S. Nandhini, "On fine-tuning deep learning models using Transfer learning and hyper-parameters optimization for disease identification in maize leaves," *Neural Comput & Applic*, vol. 34, no. 16, pp. 13951–13968, Aug. 2022, doi: 10.1007/s00521-022-07246-w.
- [21] J. Liu, M. Hassanpourhadi, Q. Zhang, S. Su, and M. S.-W. Chen, "Transfer learning with bayesian optimization-aided sampling for efficient AMS circuit modeling," in *Proceedings of the 39th International Conference on Computer-Aided Design, Virtual Event USA*, Nov. 2020, pp. 1–9. doi: 10.1145/3400302.3415687.
- [22] J. Feng, Z. Wang, M. Zha, and X. Cao, "Flower Recognition Based on Transfer learning and Adam Deep Learning Optimization Algorithm," in *Proceedings of the 2019 International Conference on Robotics, Intelligent Control and Artificial Intelligence - RICAI 2019*, Shanghai, China, 2019, pp. 598–604. doi: 10.1145/3366194.3366301.
- [23] A. G. Howard et al., "MobileNets: Efficient Convolutional Neural Networks for Mobile Vision Applications." *arXiv*, Apr. 16, 2017. Accessed: Sep. 17, 2022. [Online]. Available: <http://arxiv.org/abs/1704.04861>.
- [24] M. Sandler, A. Howard, M. Zhu, A. Zhmoginov, and L.-C. Chen, "MobileNetV2: Inverted Residuals and Linear Bottlenecks." *arXiv*, Mar. 21, 2019. Accessed: Jun. 27, 2022. [Online]. Available: <http://arxiv.org/abs/1801.04381>
- [25] A. Howard et al., "Searching for MobileNetV3," in *2019 IEEE/CVF International Conference on Computer Vision (ICCV)*, Seoul, Korea (South), Oct. 2019, pp. 1314–1324. doi: 10.1109/ICCV.2019.00140.
- [26] K. He, X. Zhang, S. Ren, and J. Sun, "Deep Residual Learning for Image Recognition," in *2016 IEEE Conference on Computer Vision and Pattern Recognition (CVPR)*, Las Vegas, NV, USA, Jun. 2016, pp. 770–778. doi: 10.1109/CVPR.2016.90.
- [27] O. Russakovsky et al., "ImageNet Large Scale Visual Recognition Challenge," *Int J Comput Vis*, vol. 115, no. 3, pp. 211–252, Dec. 2015, doi: 10.1007/s11263-015-0816-y.
- [28] J. M. Ahn, S. Kim, K.-S. Ahn, S.-H. Cho, K. B. Lee, and U. S. Kim, "A deep learning model for the detection of both advanced and early glaucoma using fundus photography," *PLoS ONE*, vol. 13, no. 11, p. e0207982, Nov. 2018, doi: 10.1371/journal.pone.0207982.
- [29] G. Huang, Z. Liu, L. van der Maaten, and K. Q. Weinberger, "Densely Connected Convolutional Networks." *arXiv*, Jan. 28, 2018. Accessed: Jun. 27, 2022. [Online]. Available: <http://arxiv.org/abs/1608.06993>.
- [30] M. Tan and Q. V. Le, "EfficientNet: Rethinking Model Scaling for Convolutional Neural Networks." *arXiv*, Sep. 11, 2020. Accessed: Jun. 27, 2022. [Online]. Available: <http://arxiv.org/abs/1905.11946>.
- [31] F. Chollet, "Xception: Deep Learning with Depthwise Separable Convolutions," in *2017 IEEE Conference on Computer Vision and Pattern Recognition (CVPR)*, Honolulu, HI, Jul. 2017, pp. 1800–1807. doi: 10.1109/CVPR.2017.195.
- [32] D. P. Kingma and J. Ba, "Adam: A Method for Stochastic Optimization." *arXiv*, Jan. 29, 2017. Accessed: Jul. 05, 2022. [Online]. Available: <http://arxiv.org/abs/1412.6980>.
- [33] J. Duchi, E. Hazan, and Y. Singer, "Adaptive Subgradient Methods for Online Learning and Stochastic Optimization," p. 39.
- [34] F. Zou, L. Shen, Z. Jie, W. Zhang, and W. Liu, "A Sufficient Condition for Convergences of Adam and RMSProp," in *2019 IEEE/CVF Conference on Computer Vision and Pattern Recognition (CVPR)*, Long Beach, CA, USA, Jun. 2019, pp. 11119–11127. doi: 10.1109/CVPR.2019.01138.
- [35] M. D. Zeiler, "ADADELTA: An Adaptive Learning Rate Method," 2012, doi: 10.48550/ARXIV.1212.5701.
- [36] S. Ruder, "An overview of gradient descent optimization algorithms." *arXiv*, Jun. 15, 2017. Accessed: Sep. 17, 2022. [Online]. Available: <http://arxiv.org/abs/1609.04747>.

Associating User's Preference and Satisfaction into Quality of Experience: A Shoulder-surfing Resistant Authentication Scheme by Visual Perception

Juliana Mohamed¹, Muhamad Hanif Jofri⁵
Department of Information Technology
Center for Diploma Studies (CeDS)
Universiti Tun Hussein Onn Malaysia (UTHM)
Johor, Malaysia^{1,5}

Mohd Farhan Md Fudzee², Sofia Najwa Ramli³, Mohd
Norasri Ismail⁴
Faculty of Computer Science and Information Technology
(FSKTM), Universiti Tun Hussein Onn Malaysia (UTHM),
Johor, Malaysia^{2,3,4}

Abstract—Authentication acts as a secured method of usability concepts to certain transactions, especially for online banking transaction. Existing method is lacking in terms of usability, thus, making the goal of usability for authentication activities unsuccessful. A study has discovered some key concepts of usability in terms of Human Computer Interaction (HCI) by comparing two existing models of two different factors: environmental factors and display factors. An algorithm shows the authentication step during the online transaction activity. This paper is to prove that shoulder-surfing resistant authentication scheme that uses visual colour-blind mode-based model meets all the requirements of usability, hence, achieved the goal of usability of authentication. This study will bring forward an algorithm that examined the stated authentication scheme with the two factors, i.e environmental and display, during the authentication activity.

Keywords—Authentication; usability; algorithm; model

I. INTRODUCTION

Online banking application deals with varied issues of authentication, confidentiality, integrity and non-repudiation [1]. A secured application is highly dependent on the procedures of authentication to the online banking transaction. Authentication has been widely studied for its security and trustworthiness [1][2]. A success authentication method makes users satisfy with the services.

There are several methods of authentications that can be studied from [3][4]. These methods are highly related with users' experience and interface [5][6]. Authentication method is applied to most of authentication procedures during login process to any page or application, as well as in online transaction [7][8][9]. However, most of the studies are limited to usability towards users' experience and satisfaction [10][11]. This motivates us to investigate deeply to the authentication purposes and processes.

The objectives of this research are to: 1) identify shoulder surfing attack by utilizing users' visual perception model to the authentication; 2) propose a shoulder-surfing Resistant Authentication Scheme using Visual perception colour blind mode-based model and algorithm by taking into account users' quality of experience (QoE); and 3) analyze the proposed authentication scheme against usability, accessibility performance and shoulder surfing attack to the human computer interaction (HCI). Hence, the research is significant to the authentication step during the online transaction activity due to the shoulder-surfing attack.

This study will examine the usability in terms of human computer interaction (HCI) which is based on human preference and human satisfaction of quality of experience (QoE) [12][13]. This paper will be comparing the two existing authentication model that are based on environmental and display factors, and find the possible limitation of a compatible model of graphical-based authentication to the authentication activities.

II. LITERATURE REVIEW

There are two types of element that can give some impact readability: environmental factors and display factors [14] [15]. Regarding the surrounding environment, the users' reading experience is directly affected by ambient brightness, viewing angle, and distance. From here, the size of the visual image of an item created in the viewers' eyes is influenced by viewing distance. The users' eyesight has a strong correlation with ambient brightness. According to geometrical optics, the viewers' perception of brightness is determined by the viewing angle and distance [16]. In addition, display parameters such as resolution and colour scheme, as well as screen brightness are also among important influencing factors [17].

A. Hybrid Keypad

Human factor is the most crucial part while handling any online activities. Human preference and satisfaction have been widely discussed from the view of usability to the authentication. The existed model of authentication is called the Hybrid keypad [18][19]. The model creates coloured-hybrid-image keypads using superimposition. The keypad is developed automatically by appearing to the screen when user requests the one-time password (OTP). Fig. 1 depicts the existing model.

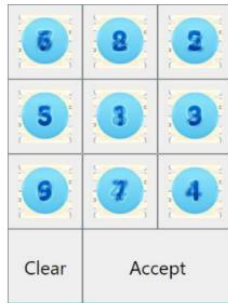


Fig. 1. The Existing Model of Hybrid Keypad.

Fig. 1 shows the illustration of Hybrid keypad. From the perspective of display factors, this model confuses the actual users when they keyed in their OT, due to two or more numbers that are overlapped on the keypad. However, the limitation of this model caused by environment factors is still uncertain, as to whether adding color-complementary components can further diminish the attacker's appearance and counteract the low frequency.

B. HideScreen

A researcher has developed HideScreen, utilizing human vision and optical system features, where users' on-screen information may be hidden from shoulder surfers [20]. That is, when the on-screen information (OSI) was viewed from outside of the specified range, HideScreen discretized the OSI into grid patterns in order to neutralize the low-frequency components, thus allowing the OSI to "blend into" the background. Fig. 2 shows the process of the grid patterns model.

The existing model, however, only allows spatial frequency by focusing on the protection of short texts and complex pictures on the screen, which is shown on soft keypad or keyboard. This limitation focuses solely on display factors. On the other hand, from the perspective of environmental factors, there have been various graphical schemes that are resistant or immune to shoulder-surfing but they have substantial usability problems, where most notably are in terms of time and effort required to log in. This paper will be discussing on the said problems. The comparison of the two factors is depicted in the Table I.

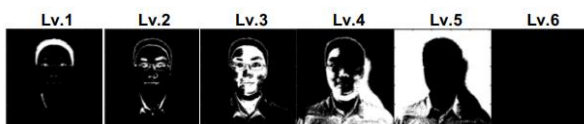


Fig. 2. The Existing Model of Grid Patterns.

TABLE I. COMPARISONS BETWEEN TWO FACTORS

Model	Environment factor	Display factor
Hybrid keypad	Adding colour-complementary components which can further diminish the attacker's appearance, and counteract the low frequency	Confusing to user due to overlapping numbers on the keypad
HideScreen	Substantial usability problems, most notably time and effort required to log in	Allows spatial frequency by focusing on the protection of short texts and complex pictures on the screen shown on soft keypad or keyboard
Shoulder-surfing resistant authentication scheme using visual colour-blind mode-based	Auto glare/auto hide which cannot be seen by shoulder surfer see from their angle	Using four colour-blind charts with eight-numbers combination

III. PROPOSED MODEL AND ALGORITHM

Due to the problems counter from the authentication type, a proposed model has been created to encounter the authentication problem. Shoulder-surfing resistant authentication scheme that uses visual colour-blind mode-based model was proposed to address the problem of shoulder surfing attack, in order to identify any suitable authentication approach, as well as to simulate and analyse the proposed mechanism in terms of usability of HCI. The proposed model was accessible from the smartphone screen with no hybrid keypad provided to the user.

A. Shoulder-surfing Resistant Authentication Scheme using Visual Colour-blind Mode-based Model

The model represents a set of four randomly colour-blind pictures in every session. Each picture contained two-digits number that was as similar as a TAC. Uniquely, the model enabled HideScreen or glare to the process by utilising the complex pixels of complementary Red, Green, Blue (RGB) colours of each picture whenever shoulder surfer sees to the actual user [21][22]. Users can access the proposed model from their smartphone screen. Fig. 3 illustrates the proposed authentication model.

During the transaction, users will request the one-time password (OTP) to the server. Server will react by randomly selecting four charts of colour-blind, with the combination of two number in each chart. Two matching colors were used for each chart to maintain the view of user perception. Next, the server will send the requested OTP to the users. Here, the OTP pictures will enable the auto glare or hide. The users must keyed in the OTP within 60 seconds since it will be automatically nullified after the period of time. The server will compare the keyed-in OTP with the one been sent. If the OTP is a matched, the authentication will be considered as successful, but if it is not, the users were to repeat the procedure. In addition, the proposed model can be used to all types of users including the one with colour vision deficiency.

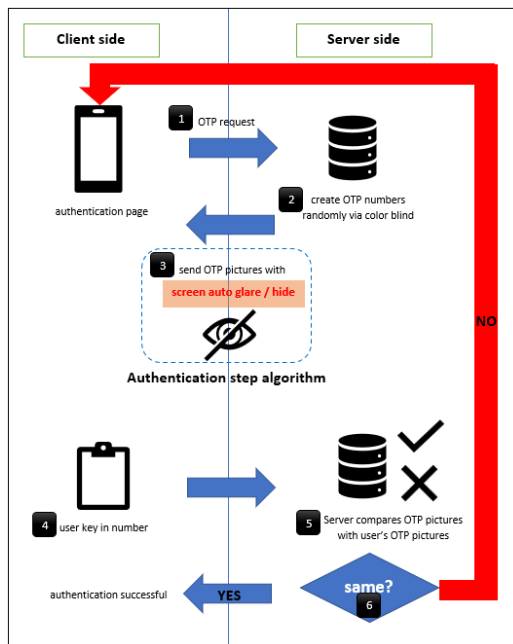


Fig. 3. Shoulder-surfing Resistant Authentication Scheme using Visual Colour-blind Mode-based Model.

B. Shoulder-surfing Resistant Authentication Scheme using Visual Colour-blind Mode-based Algorithm

The algorithm represents the focus area of authentication step during the activity. From Fig. 4, the method started with the number of incoming requests, then sorted out based on their priority and order. Later, the server will load and announce QoE offer upon initiation. This method assumed that the provider's system that handled the incoming requests has access to this data. The number of requests that can be fulfilled within the advertised waiting time can be estimated based on the current server load. Fig. 4 depicted to the authentication step of algorithm.

Algorithm 1: Authentication Step

```

INPUT:  $B, \bar{U}, s, E$ 
OUTPUT: Settlement of ( $S_i$ )
BEGIN
1:  $B \leftarrow t_i \in \bar{U}$ 
2: FOR  $t$  DO
3:    $B \leftarrow \bar{U}, s$  read colour-blind chart
4:   Estimate  $B$  can be served within the  $E$ 
5:   FOR each  $B$  DO
6:     IF  $B$  can be served within the  $E$  THEN
7:       Authentication successful ( $B, S_i$ )
8:     ELSE
9:       Perform 'auto glare/auto hide'
10:      IF request within actual  $E$  THEN
11:        Authentication successful ( $B, S_i$ )
12:      ELSE
13:        Request  $E$  from  $s$ 
14:        Authentication successful ( $B, S_i$ )
15:        accepted by  $s$ 
16:      END IF
17:    END IF
18:  END FOR
19: END FOR
END

```

Fig. 4. Authentication Steps' Algorithm.

The programme will, then, extract the requests, their priorities, and the prospective providers server loads for each job, which was declared as the parameter to the algorithm. The authentication stage will further determine the total requests that can be fulfilled within the advertised E . Line 5 will, lastly, carry out the requests. As a result, the request for these duties will be completed. If this is not the case, the authentication step will request E from the provider in line 9 and conducted the "auto glare" or "auto hide" function. Table II depicted to the abbreviation from Algorithm 1.

TABLE II. LIST OF COMMONLY USED NOTATION

Notation	Description
B	Request
\bar{U}	OTP priority
E	Estimate time
s	Server load
T	Task
t_i	Number of tasks
S_i	Authentication settlement

IV. EXPERIMENTAL SETUP

The study continued with simulation setup by using an application namely 'i-Smart Bank apps' which was developed using Android Studio and the database was supported by Firebase. This experiment was to show the authentication step during online transaction activities.

During the experiment, the users' reading experience was directly impacted by the ambient brightness, viewing angle, and distance. From here, the visual image of an item created in the viewers' eye was influenced by viewing distance. The users' eyesight has a strong correlation with ambient brightness. According to geometrical optics, the viewers' eyes perception of brightness is determined by the viewing angle and distance. Moreover, display parameters, such as resolution and colour scheme and screen brightness, are among important influencing factors.

Fig. 5(a), (b) and (c) illustrate steps involved during the authentication activities when users keyed in the one-time password. During the activity, the users will receive randomly chosen colour-blind chart with numbers to be keyed in. This activity will enable auto glare or auto hide which disallow shoulder-surfer to see what is happening to users' smartphone. Here, viewing angle and distance played an important role in determining whether the authentication will be succeeded or not. In addition, resolution and screen brightness also gave some influence to this activity.

Table III shows the measurement setup for this experiment. The relationship between luminance contrast and screen brightness will be discovered further in the study. These variables were chosen in order to test the algorithm for authentication procedures. The measurement setup testing was used to compare the algorithm step. This setup started with 10% to 100% for QoE of users' satisfaction.

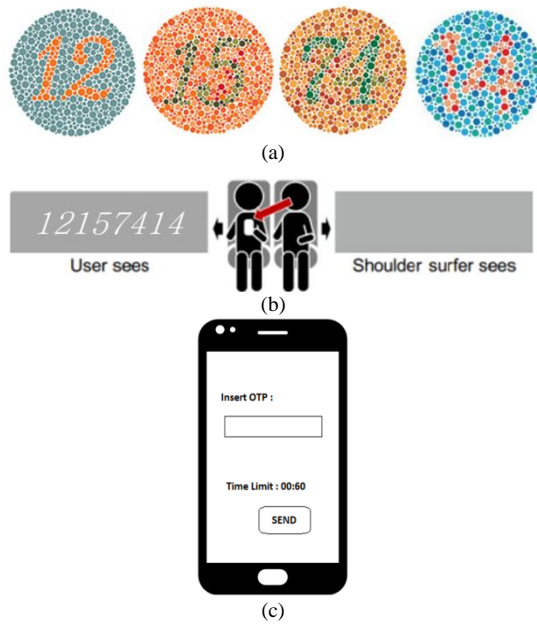


Fig. 5. Simulation Setup, (a) Example of Server Database (b) Example of Shoulder Surfing and the Effect after Applying Hide Screen or Glare (c) Example of a User Interface.

TABLE III. MEASUREMENT SETUP

Display brightness	Contrast luminance
10	0.1
20	0.2
40	0.4
60	0.6
80	0.8
100	1.0

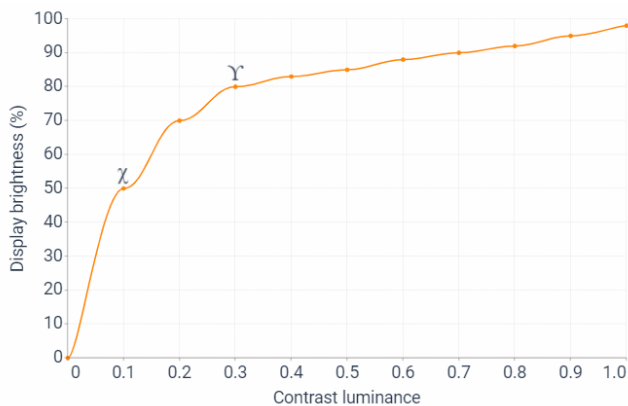


Fig. 6. Influence Trend to Human Vision (Display Brightness to Contrast Luminance).

Fig. 6 shows the contrast influence trend to human vision. From here, users' reading experience was found to be better when the contrast value is γ , with an improvement of 80%; but, when the contrast value is χ , the reading experience was extremely bad, with an improvement of just 50%, substantially impairing reading.

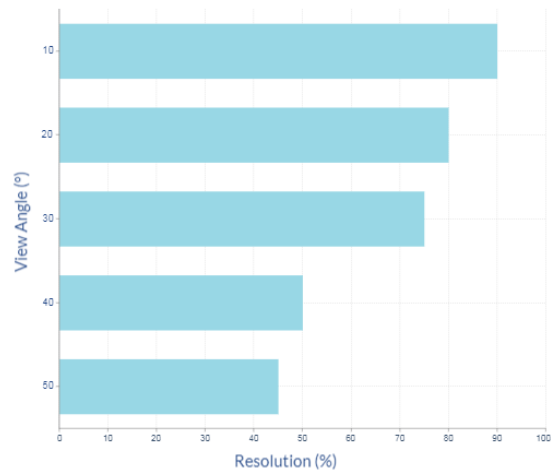


Fig. 7. Some Effect of Viewing Angle to Resolution.

Fig. 7 shows some effect of viewing angle to resolution. Users used i-Smart Bank apps at 10°, 20°, 30°, 40° and 50°, respectively while keeping the viewing distance of 20 cm, ambient brightness, and screen display content remained the same in order to verify the influence of viewing angle on the reading experience. As the viewing angle expanded, the users' relative visual performance fluctuated.

V. RESULTS AND DISCUSSIONS

The proposed model reviewed the experimental result of viewing angle by the shoulder-surfer and the authority users. This study also compares the limitation of existing models based on two factors: environmental factors and display factors. The environmental factor will be investigated based on view angle, meanwhile the display factor will be examined based on resolution of smartphone. The result is shown in the following table.

Table IV shows the test started at 0° of view angle. This experiment continued with another three different types of view angle. Users, as shown in Table II, were asked to hold their smartphone in different view angles. Another shoulder-surfer volunteer were standing at the same distance but with different view angle. This experiment started with some contents were displayed and the shoulder-surfer were asked to read it before the actual users. The test and its results were recorded.

From Fig. 8, the resolution of shoulder-surfer was increased up to 90% at a distance of 20 cm, proving that the experiment had no appreciable effects on users or the regular use. In comparison, the resolution values from shoulder-surfer at 20 cm to 40 cm were barely above the boundary but less than 60%. However, the resolution clearly decreased below the boundary at distances greater than 60 cm. Nevertheless, shoulder-surfers seldom position themselves at an angle less than 40 degrees when standing 20 cm to 40 cm from the screen. In actuality, a shoulder surfers' viewing angle is always wide when the distance between them is modest. As a result, when resolution values from shoulder-surfer dropped as viewing distance increased, their overall reading experiences are still excellent and much exceed the minimal resolution barrier at 50% in the case of real applications.

TABLE IV. EXPERIMENTAL SETUP ENVIRONMENT

View Angle (°)	Distance (cm)	Ambient Brightness
0	20	150
20	40	300
40	60	500
60	80	800

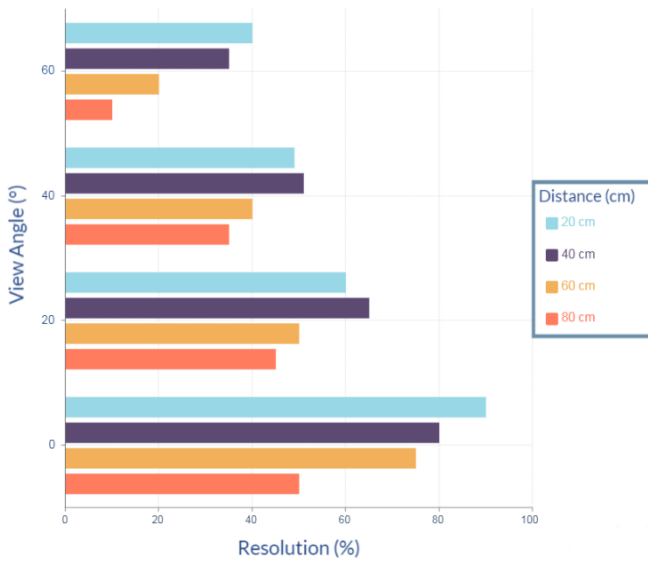


Fig. 8. Experimental Result from Resolution vs. View Angle.

The resolution values from shoulder-surfers at four viewing positions: (20 cm, 40°), (40 cm, 40°), (60 cm, 20°) and (80 cm, 20°) were close to 50% minimum boundary, while the resolution values located outside the four points area were significantly less than 50%. This suggests that a privacy space might be constructed, i.e when actual users are in a secure environment, reading is going well and the resolution value is higher than the required minimum of 50%. The shoulder-surfer will have a terrible reading experience, or may not even be able to read when they were outside of the safety zone. Furthermore, it should be emphasised that this security zone is not a permanent location. A safe zone is established provided that the farthest viewing distance for the user is 50 cm. Depending on the actual users' reading distance, which ranges from 20 cm to 80 cm, the safe zone narrows as the reading distance between the user and the screen decreases. In conclusion, the authentication procedure works well with the proposed model, and meets all requirements based on the key concepts of usability, thus, archive the users' preference and satisfaction to QoE.

VI. CONCLUSION

This study has discovered the key concepts of usability in terms of Human Computer Interaction (HCI) by comparing two existing model models with two factors: environmental factors and display factors. Shoulder-surfing resistant authentication scheme using visual colour-blind mode-based model is proven to meet all the requirements of usability, hence, achieved the goal of usability of authentication. Hopefully, in future, the study will be able to bring forward an

algorithm by investigating the colour scheme, i.e the matching two complementary colours by the two factors of environmental factors and display factors during the authentication activity.

ACKNOWLEDGMENT

This research was supported by Universiti Tun Hussein Onn Malaysia (UTHM) through Tier 1 (H808).

REFERENCES

- [1] Windasari, N. A., Kusumawati, N., Larasati, N., & Amelia, R. P. (2022). Digital-only banking experience: Insights from gen Y and gen Z. *Journal of Innovation & Knowledge*, 7(2), 100170.
- [2] Naem, E. A. A. (2020). *Enhance Graphical Password Authentication using One Time pad* (Doctoral dissertation, Sudan University of Science and Technology).
- [3] Singh, A. K., & Gandhi, G. C. (2020). Computer Architecture: A New Weapon to Secure Web Services From Bots. *International Journal of Smart Security Technologies (IJSST)*, 7(1), 41-48.
- [4] Hamdy, M. (2021). A Comparative Study on Authentication Strategies of Various Online Banking Platforms.
- [5] Zhou, L., Wang, K., Lai, J., & Zhang, D. (2021, November). Behaviors of Unwarranted Password Identification via Shoulder-Surfing during Mobile Authentication. In *2021 IEEE International Conference on Intelligence and Security Informatics (ISI)* (pp. 1-3). IEEE.
- [6] Kakadia, D., & Ramirez-Marquez, J. E. (2020). Quantitative approaches for optimization of user experience based on network resilience for wireless service provider networks. *Reliability Engineering & System Safety*, 193, 106606.
- [7] Kaushik, M., Rawat, A., Sisaudia, V., & Parashar, L. (2022, June). A Novel Graphical Password Scheme to Avoid Shoulder-Surfing Attacks in Android Devices. In *2022 2nd International Conference on Intelligent Technologies (CONIT)* (pp. 1-6). IEEE.
- [8] Zhou, L., Wang, K., Lai, J., & Zhang, D. (2021, November). Behaviors of Unwarranted Password Identification via Shoulder-Surfing during Mobile Authentication. In *2021 IEEE International Conference on Intelligence and Security Informatics (ISI)* (pp. 1-3). IEEE.
- [9] Bošnjak, L., & Brumen, B. (2020). Shoulder surfing experiments: A systematic literature review. *Computers & Security*, 99, 102023.
- [10] Hassan, M. A., & Shukur, Z. (2021, January). A secure multi factor user authentication framework for electronic payment system. In *2021 3rd International Cyber Resilience Conference (CRC)* (pp. 1-6). IEEE.
- [11] Bai, W., Pearson, M., Kelley, P. G., & Mazurek, M. L. (2020, September). Improving non-experts' understanding of end-to-end encryption: An exploratory study. In *2020 IEEE European Symposium on Security and Privacy Workshops (EuroS&PW)* (pp. 210-219). IEEE.
- [12] Kara, P. A., Tamboli, R. R., Shafiee, E., Martini, M. G., Simon, A., & Guindy, M. (2022). Beyond perceptual thresholds and personal preference: towards novel research questions and methodologies of quality of experience studies on light field visualization. *Electronics*, 11(6), 953.
- [13] Fatima, K., Bawany, N. Z., & Bukhari, M. (2020, October). Usability and accessibility evaluation of banking websites. In *2020 International Conference on Advanced Computer Science and Information Systems (ICACSIS)* (pp. 247-256). IEEE.
- [14] Sukaris, S., Renedi, W., Rizqi, M. A., & Pristyadi, B. (2021, February). Usage behavior on digital wallet: perspective of the theory of unification of acceptance and use of technology models. In *Journal of Physics: Conference Series* (Vol. 1764, No. 1, p. 012071). IOP Publishing.
- [15] Băce, Mihai, Alia Saad, Mohamed Khamis, Stefan Schneegass, and Andreas Bulling. "PrivacyScout: Assessing Vulnerability to Shoulder Surfing on Mobile Devices." *Proceedings on Privacy Enhancing Technologies* 1 (2022): 21.
- [16] Chandrakanth, P., Chavan, S., Verghese, S., Gosalia, H., Raman, G. V., Shettigar, C. K., & Narendran, V. (2022). Smartphone Gonioscopy With a Magnifying Intraocular Lens: A Cost-effective Angle Imaging Device. *Journal of Glaucoma*, 31(5), 356-360.

- [17] Elliott, M. A., Nothelfer, C., Xiong, C., & Szafir, D. A. (2020). A design space of vision science methods for visualization research. *IEEE Transactions on Visualization and Computer Graphics*, 27(2), 1117-1127.
- [18] Anthonio, H., & Kam, Y. H. S. (2020, December). A Shoulder-Surfing Resistant Colour Image-based Authentication Method Using Human Vision Perception with Spatial Frequency. In 2020 15th International Conference for Internet Technology and Secured Transactions (ICITST) (pp. 1-5). IEEE.
- [19] Binbeshr, F., Kiah, M. M., Por, L. Y., & Zaidan, A. A. (2021). A systematic review of PIN-entry methods resistant to shoulder-surfing attacks. *computers & security*, 101, 102116.
- [20] Hodes, L. N., & Thomas, K. G. (2021). Smartphone screen time: inaccuracy of self-reports and influence of psychological and contextual factors. *Computers in Human Behavior*, 115, 106616.
- [21] Guido, R. C. (2022). Wavelets behind the scenes: Practical aspects, insights, and perspectives. *Physics Reports*, 985, 1-23.
- [22] Pridmore, R. W. (2021). Complementary colors: A literature review. *Color Research & Application*, 46(2), 482-488.

Integrating Computer-aided Argument Mapping into EFL Learners' Argumentative Writing: Evidence from Saudi Arabia

Nuha Abdullah Alsmari

Department of English, College of Science and Humanities
Prince Sattam bin Abdulaziz University
Alkharj, Saudi Arabia

Abstract—This paper aims to examine the effects of Computer-Aided Argument Mapping (CAAM) on Saudi EFL learners' argumentative writing performance across the development of writing content and coherence and their self-regulated learning skills. A total of 40 second-year university EFL learners were purposively selected as a one-group of pre- and post-test design. Using a mixed-method approach, three research tools were utilized: pre- and post-writing tests, a Self-regulated Learning Scale (SRLS), and semi-structured interviews. Quantitative results demonstrated that EFL learners' argumentative writing performance made noteworthy gains, as manifested by the statistically significant differences between their pre- and post-test scores. Significant positive correlations were also found between the EFL learners' overall argumentative writing performance and the SRL factor subscales, indicating an increase in the self-regulation mechanism relative to planning, self-monitoring, evaluation, effort, and self-efficacy. Qualitative results indicate that the participants have positively embraced the integration of CAAM to improve their writing skills and self-regulation processes. Recommendations for implementing digital mapping to revolutionize EFL learning classrooms in this digital era are provided.

Keywords—Argumentative writing; argument mapping; computer-aided argument mapping; self-regulated learning; Saudi EFL learners

I. INTRODUCTION

There is a consensus that developing effective writing competency is a challenging task, especially among EFL learners [1]. As English is used as the medium of instruction in various academic fields at higher education institutions in Saudi Arabia and numerous other EFL countries, writing has become a necessary prerequisite for foreign language learners to be successful in other fields that demand a written representation of knowledge [2]. In addition, international students are not permitted to enroll in various academic programs unless they fulfill certain requirements; one is attaining a specific level on a standardized English test (e.g., TOEFL, or IELTS). Some academic institutions impose an extra requirement that entails attaining a minimum score on the writing section, thus increasing the need to master advanced L2 writing skills to achieve success in higher education [11].

The complexity of L2 writing is inherent in the development of effective writing ability that comprises knowledge of the content and task, lexical complexity, cohesion, coherence, and fluency of ideas [7], [8]. Writing genres (such as argumentative writing and expository writing) also contribute to the inherent complexity involved in writing compositions due to the special lexicon and syntactical features as well as the structure [8]. These tasks overburden learners' cognitive loads during the learning process, creating a mental block against acquiring new information [15]. One way to support learners in managing their cognitive learning processes is to adopt certain problem-solving solutions, such as generating maps and diagrams [3], [7], [14].

Mapping or diagramming serves as a learning tool that helps facilitate comprehension when there is an abundance of data to process within a short amount of time. It encourages learners to engage in the process of developing ideas and information, as it activates the schemata necessary to organize ideas and content for writing. Learners will gain a full grasp of their thoughts and produce more developed and coherent outputs, thus stimulating their critical thinking, problem-solving [12], and self-regulation abilities [9]. As a result, they will optimize their learning performance and mental capacity. Writing is a complex skill that requires a strategic approach to accelerate EFL learners' control, confidence, and subsequent proficiency [5], [18]. Presumably, if learners are taught to map their ideas, they will be able to plan, monitor, and evaluate their progress [12].

This study was intended to examine the effects of computer-aided argument mapping (CAAM) on Saudi EFL learners' performance in argumentative writing, as well as their self-regulated learning skills.

II. LITERATURE REVIEW

A. Argument Mapping

Argument maps (AMs) are visual aids that facilitate the comprehension and evaluation of arguments [3]. They are organized in text-based, hierarchical representations in which propositions are displayed in color-coded boxes and linked with arrows to indicate the relationships among them [4], [17]. AMs visualize reasoning in a clear and concise fashion by diagramming the inferential construction of an argument [3]. It is a pedagogical tool that increases the opportunity for

comprehensive learning. Recent studies [3], [7], [12] have revealed the instructive benefits of AMs. For example, AMs have been adopted in language teaching methods in general [14], and in EFL writing in particular [7], [12]. According to [7], a well-constructed argument diagram enhances critical thinking skills and writing performance among EFL learners. AM stimulates EFL learners' schemata, which are essential for the development of argumentative writing.

The author [4] evaluated the effects of promoting critical thinking through AM compared to a strategy of generating themes from texts and sorting them hierarchically. Although AM training had no significant impact on students' critical thinking skills, the experimental group exceeded the no-instruction control groups on the evaluation and inductive reasoning tests. That is, after the intervention, EFL learners were able to compose more cohesive and developed writing. The study of [10] has further supported the use of AM for developing second-language learners' composition writing. The author [3] contends that "...the process of making an argument map is advantageous since it encourages students to construct and/or reconstruct their arguments with a level of clarity and thoroughness" (p. 115). Fig. 1 presents the main conventions used in AM.

Fig. 1 illustrates the major themes in an argument map. The primary premise is situated at the top. The arguments for the primary premise are represented by green boxes and connected by arrows to the primary premise. The primary premise in the figure has two arguments, 1A and 1B. Individual premises are placed inside white boxes shaded with green. Each premise is presented separately, with its own justification. Linked premises are grouped to support the conclusion. Additionally, claims with objections are marked in red. Writers designate reasons and objections using words such as "supports" and "opposes," respectively [3].

B. Computer-Aided Argument Mapping (CAAM)

The advent of computer software has accelerated the task of creating user-friendly AMs. While AM can be taught effectively using pen and paper [7], CAAM can facilitate and speed up the mapping process efficiently, as it employs a number of programs specifically developed to enable users to quickly display arguments and reasons using cells and line diagrams [3], [17]. CAAM is an instructional system intended to promote learners' critical thinking by visually representing reasoning for any subject area [9] as well as offering a convenient workspace and a dashboard for building AMs [17]. Users can construct maps by simply inserting text into cells and then moving them to any desired location on the map using various levels of reasoning boxes. These cells can be modified, eliminated, or transferred to a different location. Although CAAM programs do not analyze or check the soundness of arguments, they help learners analyze and evaluate their arguments in a practical, visual, and professional way. According to [3], CAAM encourages students to compose arguments openly and thoroughly.

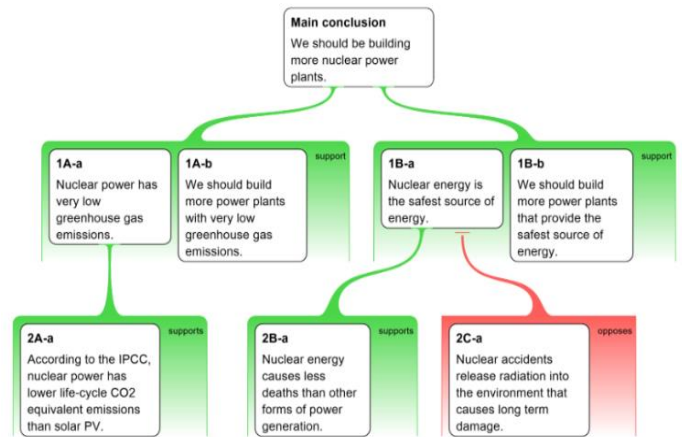


Fig. 1. Argument Mapping Demonstrating the Main Conventions.

CAAM serves as a platform that helps learners form conceptualizations by diagramming and revising reasoning clearly so that knowledge gaps and errors can be identified and reasoning can be reformulated [9], providing a better performance at argument analysis and evaluation. CAAM allows learners to access their previous essays in another panel while simultaneously accomplishing their AM in the panel, as well as helping them to be considerate of cohesion and coherence throughout the mapping process (see Fig. 2). In addition, CAAM offers learners the means for extensive problem-solving and critical thinking practice through activities with varying levels of complexity, which helps them develop these skills [6]. It enables learners to experiment practically with multiple logical structures and move the parts of an argument freely, allowing them to become more aware of the structure of their arguments, which is a prerequisite to critical thinking and self-regulation. Fig. 2 displays an excerpt of a learner's AM conducted via CAAM.

Numerous studies have demonstrated empirical evidence for the efficacy of CAAM in developing students' writing skills [3], [9], [14] and critical thinking skills [3], [12], [17]. The author [17] conducted a study using one-subject CAAM-based interventions during a three-month course and reported that courses teaching AM increased critical thinking performance. The authors [9] examined the effects of implementing CAAM to improve EFL students' self-regulated writing. After completing the self-regulation pretest in writing skills, the respondents were randomly divided into two experimental groups and a control group. The experimental groups who carried out their writing composition via CAAM software during the course of the training outperformed the control group and enhanced the self-regulation of their writing.

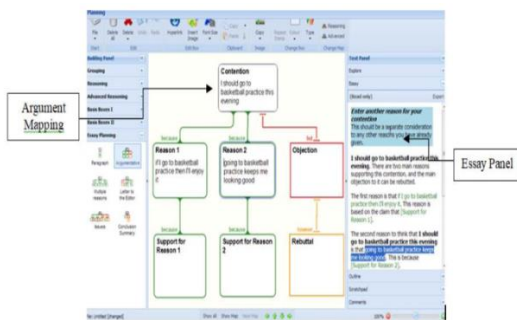


Fig. 2. Example of a Student's Argument Map (AM) Produced in CAAM.

C. Self-Regulated Learning

A number of empirical studies [16], [13], [14], [19] have viewed SRL as a valuable new construct in the field of education. For example, the authors [16] described SRL as an active process in which learners are able to self-regulate by setting goals for their learning, monitor their learning processes, control and regulate their own thinking, and evaluate and reflect on their learning. The author's [19] view asserts that self-regulated learners actively adopt motivational, behavioral, and metacognitive approaches and dynamically engage in their learning processes.

Researchers have further revealed that learner-related factors, such as learning styles, personality traits, self-regulation, beliefs, and motivation, can substantially influence language learning progress [8], [14]. The author [16] argued that learners who self-regulate need to strategically consider how to approach a task, monitor their own progress while performing the task, assess the process and output after completing the task, review what they have accomplished and failed to accomplish, and further develop more strategies to use, which provide them more opportunities to execute tasks the next time. However, apart from understanding what areas to optimize and how to optimize them, self-regulated learners need to be stimulated to progress [19]. The authors [9] claimed that self-regulatory capacity can interact with cognitive factors since, as underscored by [14], learners who self-regulate can set goals, monitor, self-reflect, and assess their progress. The procedures involved in argument mapping are structured by planning and monitoring throughout the task, which helps raise learners' self-reflection and self-evaluation. With reflection and critical thinking, learners can maximize their self-regulated learning potential because they have fully acknowledged their role in the task.

A number of studies have been conducted that relate to teaching and learning EFL writing, such as critical writing using digital diagramming [7], descriptive writing achievement via CAAM [8], and teaching reasoning via CAAM [3]. However, to the researcher's knowledge, no study has focused on the effectiveness of CAAM in developing EFL learners' performance in argumentative writing and promoting SRLs, particularly in the Saudi EFL context. The study is significant because it contributes pertinent information to higher education institutions in EFL contexts. It is hoped that the findings will help EFL teachers gain better knowledge of language learning from the learners' perspectives and provide additional insights into the advantages of teaching English

writing with CAAM, thereby aiding EFL learners' argumentative writing skills and their ability to self-regulate their learning. Accordingly, the current study sought to answer the following research questions:

- 1) How does the CAAM intervention affect Saudi EFL learners' argumentative writing performance and self-regulated learning skills?
- 2) Is there a significant correlation between Saudi EFL learners' performance in argumentative writing composition and their ability to self-regulate their learning after the CAAM intervention?
- 3) How do Saudi EFL learners perceive the CAAM intervention?

III. METHODOLOGY

A. Research Design and Participants

The study employed a mixed-methods approach on a single group of pre- and post-test designs. The quantitative measures were used to explore the extent to which the integration of CAAM affected EFL learners' argumentative writing skills relative to the development of writing content and coherence, and self-regulated learning variables. The qualitative measures served to reveal how respondents perceived the experiment and the advantages relative to their argumentative writing tasks. The intervention was conducted over 11 weeks. The study sample consisted of 40 English majors at Prince Sattam bin Abdulaziz University who enrolled in the Essay Writing 2 course (3 credits), which was intended to promote EFL learners' academic writing and critical thinking.

B. Research Instruments

Data were collected using four instruments: (1) a pre- and post-writing test, (2) a self-regulation learning scale (SRLS), and (3) semi-structured interviews. In the pre- and post-writing tests, the respondents developed an argumentative essay of at least 250 words in one hour. The topic was chosen from a list of the topics typically used for IELTS writing task 2 and aligned with topics they were studying in their Essay Writing 2 course. Prior activities, such as brainstorming, posing questions, and reading text to accelerate learners' schemata, which took an hour, were also performed. The scoring rubric evaluated four components: conclusion, premises, evidence, and counter-arguments. The topics were screened by three English lecturers at the University for their cognitive and cultural appropriateness prior to distribution.

Pre- and post-writing tests were checked for elements such as writing content and coherence, and marks were awarded based on a four-factor rubric including a conclusion, premises, evidence, and counter-arguments. "Conclusion" received 1 mark if the respondent stated the conclusion of the argument properly and zero mark if not. "Premises" received a mark that reflected the number of premises the respondent could give based on the topic. "Counter-arguments" received a mark that reflected the number of counter-arguments the respondent could include. "Evidence" received a mark that reflected the number of premises that were supported by facts. Similarly, under writing coherence, "Logical connections 1" received a

mark that reflected the number of connections between a premise and the conclusion the respondent could make. “Logical connections 2” received a mark that reflected the number of connections between premises. “Signposts” received a mark that reflected the number of signposts that were properly and correctly used, and zero marks were awarded if no signposts were used. One point was rewarded if the signposts were weak, and two points if the signposts were strong. The writing rubric was screened by three English lecturers at the University for its Cognitive Appropriateness prior to use.

The self-regulation learning scale (SRLS) was distributed before and after the intervention to assess self-regulation as a fairly constant trait across various learning settings. The scale was originally devised by [16] and comprised 46 items grouped into six categories: planning (9 items), self-monitoring (8 items), effort (10 items), reflection (5 items), evaluation (8 items), and self-efficacy (10 items). The planning, self-monitoring, effort, and self-efficacy subscales were revised and converted into a five-point Likert scale ranging from (1) strongly agree to (5) strongly disagree, and the reflection subscale ranging from (1) never, (2) rarely, (3) sometimes, (4) very often to (5) always. The subscales’ reliability scores were 0.85, 0.82, 0.84, and 0.80, respectively. A pilot study was conducted to examine the reliability of the survey involving 30 participants from the same population, but who were not part of the study sample. A reliability value of 0.85 was reported.

The semi-structured interviews were carried out at the end of the intervention to gain more information about how often and when the CAAM was used, as well as how this instructional intervention aided EFL learners’ argumentative writing processes across the development of writing content and coherence.

C. Intervention

Using CAAM, participants were trained to analyze and evaluate one or more issues from multiple perspectives and eventually construct their own arguments by writing essays once a week. The intervention consisted of weekly one-hour sessions over an 11-week period and utilized three stages: planning, monitoring, and evaluation; corresponding tasks undertaken at each stage. The first session was the introduction, in which argumentative writing was presented and key concepts of CAAM were demystified, described, and discussed. The three stages were completed within the 2nd to 11th sessions.

During the planning stage, the activities included advanced organization and schema building. The teacher introduced the writing topic to be discussed and asked the participants to brainstorm and share their thoughts with their peers.

During the monitoring stage, learners constructed argument maps and were asked to share them with their peers to refine their ideas prior to writing and solve issues concerning inconsistent premises, inaccurate counter-arguments, and the like. Meanwhile, the researcher provided feedback to those who encountered difficulties during their work.

The evaluation stage was composed of submission, discovery, and reflection parts in which participants composed their essays and sent their argument maps via CAAM software to the researcher. Indirect corrective feedback was also provided to monitor the respondents’ writing processes. When essays were handed back to the respondents, they had the chance to self-reflect and self-evaluate their performance as well as negotiate their written work with peers. Thus, they shared some possible solutions for issues they may encounter in the future. Finally, revising and editing checklists were also provided to help participants revise and edit their writing products.

D. Data Analysis

Quantitative data were statistically analyzed using descriptive and inferential statistics, including means, frequency, and percentage. Paired-sample t-tests were conducted to compare the means of two sets of tests to reveal the effects of the intervention and verify whether there was a significant difference between the pre- and post-test writing tests. The Pearson correlation coefficient was also calculated to examine the relationship between the use of CAAM and respondents’ argumentative writing across the development of writing content and writing coherence, as well as their SRLSs. Qualitative data were analyzed, coded, and interpreted using thematic analysis to capture the respondents’ opinions and understanding of the use of CAAM to process their argument writing. Accordingly, the following themes were identified: theme 1 pertains to the benefits of using CAAM, theme 2 includes quality practice, theme 3 includes learners’ perceptions of CAAM integration, and theme 4 pertains to the enhanced SRL of the respondents.

IV. RESULTS AND DISCUSSION

A. Quantitative Analysis

1) *EFL learners’ argumentative writing performance before and after the CAAM intervention*: Results from the t-test analysis revealed that participants’ argumentative writing differed significantly with respect to the development of content and coherence before and after the CAAM intervention. As shown in Table I, statistical comparisons of the overall mean scores before the intervention ($M = 8.93$, $p < .000$) and after the intervention ($M = 18.36$, $p < .000$) indicate statistically significant differences as manifested by p-values that are less than the 0.05 level of significance. That is, the performance of EFL learners’ argumentative writing with respect to the development of content and coherence improved substantially after the CAAM intervention.

Table II shows the statistical differences in EFL learners’ argumentative writing across the four components constituting the development of writing content (premises, conclusion, evidence, and counter-arguments) on the pre- and post-writing tests. All four components were significantly higher on the post-test scores, as manifested by p-values of less than the 0.05 level of significance. The “counter-argument” part was the most improved element ($M = 5.61$), while the “conclusion” part demonstrated the least improvement ($M = 4.35$).

TABLE I. PAIRED-SAMPLE T-TEST OF EFL LEARNERS' ARGUMENTATIVE WRITING PERFORMANCE ACROSS DEVELOPMENT OF WRITING CONTENT AND COHERENCE BEFORE AND AFTER CAAM INTERVENTION

Components	Pretest		Post-test		t-value	Sig. (2-tailed)
	Mean	Std	Mean	Std		
Development of writing content	6.22	1.22	12.33	1.73	-20.54	0.000
Development of writing coherence	4.11	1.15	8.96	1.11	-17.52	0.000
Overall	10.35	1.79	21.30	2.07	-19.31	0.000

TABLE II. PAIRED-SAMPLE T-TEST OF EFL LEARNERS' ARGUMENTATIVE WRITING PERFORMANCE ACROSS DEVELOPMENT OF WRITING CONTENT IN THE PRE- AND POST-WRITING TEST

Development of writing content	Pretest		Post-test		t-value	Sig. (2-tailed)
	Mean	Std	Mean	Std		
Conclusion	1.44	0.35	4.35	0.60	-6.74	0.000
Premises	1.45	0.39	5.45	0.71	-13.62	0.000
Evidence	1.63	0.30	5.50	0.96	-11.38	0.000
Counter-arguments	1.69	0.31	5.61	0.74	-16.92	0.000
Overall	6.22	1.22	21.30	2.07	-22.66	0.000

Table III provides the statistical differences of EFL learners' argumentative writing in terms of coherence on the pre- and post-tests. This component consists of three elements: (a) Logical connections 1 (referring to logical relations between the premises and the conclusion), (b) Logical connections 2 (referring to logical relations between premises), and (c) Signposts. The three components of argumentative writing differ significantly before and after the strategy intervention, as indicated by p-values of 0.000, which are less than the 0.05 level of significance. The logical connections 1 component was the most improved element (M = 3.01) compared to the pre-test score, whereas the "logical connection 2" component was the least improved (M = 2.87).

TABLE III. PAIRED-SAMPLE T-TEST OF EFL LEARNERS' ARGUMENTATIVE WRITING PERFORMANCE ACROSS WRITING COHERENCE IN THE PRE- AND POST-WRITING TEST

Development of Writing Coherence	Pretest		Post-test		t-value	Sig. (2-tailed)
	Mean	Std	Mean	Std		
Logical connection 1	1.67	0.58	3.01	0.82	-10.23	0.000
Logical connection 2	1.23	0.41	2.87	0.69	-8.31	0.000
Signposts	0.99	0.67	2.0	0.39	-9.11	0.000
Overall	3.89	1.04	7.88	1.11	-17.53	0.000

B. Correlations between EFL Learners' Argumentative Writing Performance and SRL after CAAM Intervention

To confirm whether there were any correlations between EFL learners' argumentative writing performance and SRLs, the Pearson correlation was computed. Table IV indicates that SRLS is significantly correlated with the EFL learners' overall argumentative writing performance ($r = 0.53, p < 0.01$). Specifically, strong positive correlations exist between the EFL learners' overall argumentative writing performance and the planning ($r = 0.65, p < 0.01$), self-monitoring ($r = 0.52, p < 0.01$), evaluation ($r = 0.45, p < 0.01$), effort ($r = 0.71, p < 0.01$), and self-efficacy ($r = 0.55, p < 0.01$) subcategories. There was a moderate positive correlation with the reflection ($r = 0.35, p < 0.01$) subcategory. Overall, using CAAM as an instructional tool to improve argumentative writing influenced EFL learners' SRLs.

TABLE IV. CORRELATIONS BETWEEN THE EFL LEARNERS' ARGUMENTATIVE WRITING PERFORMANCE AND SRLS AFTER CAAM INTERVENTION

	SRLSs	Pearson correlation
Argumentative writing performance	Planning	0.65**
	Self-efficacy	0.55**
	Self-monitoring	0.52**
	Effort	0.71**
	Evaluation	0.45**
	Reflection	0.35**
	Overall	0.53**
** $p < 0.01$		

V. QUALITATIVE ANALYSIS

A. EFL Learners' Perceptions of the CAAM Intervention

Twenty-eight respondents from the study sample participated in the semi-structured interviews. The findings revealed several themes related to EFL learners' perceptions of the benefits of using CAAM to compose their argumentative writing compositions. The sub-themes cover effective visualization of arguments, reducing cognitive overload, assuring quality in practice, and activating SDLs.

When EFL learners were interviewed about the role of CAAM in processing their argumentative writing tasks, they responded that CAAM aided them in forming better visualizations of their arguments. It enabled them to construct their arguments quickly and easily, including evidence, objections, and counter-arguments, using box and line diagrams [3] with the possibility of generating, modifying, or transferring these boxes to a new position as needed. The participants exploited this CAAM feature effectively to regulate their writing performance, as one respondent noted:

I) CAAM helped me identify complex arguments quickly. I can divide them into smaller sections. I can distinguish the support and objections of my arguments as well as my conclusion.

Argumentative writing is often open-textured and sometimes ambiguous [3], thus, distinguishing conclusions, support, and objections requires more time and effort due to the lexical complexity of the text itself. The use of CAAM

helped participants distinguish conclusions and premises, and thereby facilitated a better flow of knowledge in the brain that avoided mental overloading, as one described:

2) CAAM allowed me to map graphically my arguments, and enabled me to interpret them correctly without overloading my mind with a lot of information.

Using CAAM offered ample opportunities for quality practice and online feedback, ensuring that the tasks were enjoyable and effective. Some respondents reported feeling motivated in constructing these activities, as they were directed gradually in using CAAM to map their arguments, which inspired them to successfully write down their arguments into text composition.

3) CAAM helps improve my writing skill because it made me practice purposefully. It also guided me throughout the process by informing us what to do next and what to avoid. I enjoyed the gradual complexity of the tasks in CAAM (R18, 78-81).

CAAM integration not only improved participants' writing output but also enhanced their self-regulation learning skills as they were inclined to plan, self-monitor, reflect on, and evaluate their learning processes. As one participant stated:

4) With CAAM, I can have an overview of my work and monitor by double checking to see if my writing content and conclusions are correct and free of mistakes and contradictions.

The use of CAAM activated brainstorming techniques, which helped participants activate prior knowledge and create new ideas that they may associate with their writing tasks. It also promoted EFL learners' self-monitoring processes by motivating them to double-check their ideas and arguments two or three times, edit their work more closely, or compare it to other arguments as these participants contended:

1) The brainstorming activity triggered my background information and helped me link to the new topic to be developed.

2) I can double-check my arguments by simply moving the elements of an argument with multiple logical structures to another position. Also, group sharing drew my attention to points of misunderstanding or not fully understood. Collaboration gave me inspiration and guidance about my arguments (R6, 98-101).

Some respondents further reported that evaluating their writing performance based on whether the arguments were correct made them more determined to keep writing and to use the right argumentative markers in the future. It also helped them trace their performances.

1) Mapping my arguments helped me examine my performance, whether or not I got the correct arguments and evidences. I also self-evaluate my work after receiving feedback from my peers. If I didn't succeed, I challenge myself to do better in the future.

Collaboration via CAAM further allowed EFL learners to reflect on their contributions, whether they successfully or unsuccessfully grasped the argument, and whether they used effective or ineffective approaches. One participant expressed her opinion regarding this:

1) CAAM gave me the chance to assess the quality of my writing performance. I also consider the views my peers suggested on my text.

VI. CONCLUSION

The study findings revealed that Saudi EFL learners' use of CAAM accelerated their argumentative writing performance with respect to the development of content and coherence. Given the useful features of CAAM, EFL learners' reasoning skills have been enhanced substantially, which is considered a potential factor for successful argumentative writing. CAAM provided them with more enjoyable and productive experiences throughout the entire writing process, down to the final product. It offered not only a stimulating environment for writing but also served as a reliable scaffold for the writing and editing process. Through CAAMs, maps can be constructed easily and edited freely; therefore, learners can engage in many practical exercises, which consequently enable them to engage in self-regulated learning because they are able to practice different argument structures to determine which works best for them. CAAM facilitates the production of coherent paragraph texts since these mappings serve as a support tool to aid EFL learners in their English writing.

Results have also demonstrated a significant correlation between EFL learners' overall writing performance and the implementation of CAAM, as confirmed by the marked improvement in their writing output after the intervention. As for writing content, EFL learners were able to provide various premises to back up their theses and distinguish their argument conclusions as well as present supporting evidence and counter-arguments. They also demonstrated writing coherence by logically connecting their premises with their conclusions, as well as using their linguistic signposts more effectively on the writing post-tests, resulting in more coherent and cohesive essays. The study findings coincide with [8], who reported the effectiveness of implementing CAAM on descriptive and expository writing in an EFL context and found that CAAM improved coherence, cohesion, grammar, and task achievement. This study focused on how EFL learners compose the argumentative content of their writing, emphasizing the conclusion statement and how it can be reinforced with evidence and counter-arguments. It also examined the use of coherence markers to determine whether EFL learners are able to make logical relations between their premises and conclusions as well as between premises.

By using CAAM, learners develop better critical attitudes toward arguments, evaluate arguments better, and become more open-minded in their thinking processes [7]. A learner who is able to think analytically and learn independently is more likely to be purposeful, strategic, and persistent in learning [19]. Results have further revealed that the learners became more aware of their self-regulated learning, as reflected in their inclinations toward planning, self-efficacy,

self-monitoring, effort, and self-evaluation. These results are consistent with [14], who argued that the use of CAAM involves well-planned and well-monitored processes that help raise learners' self-evaluation and self-reflection. Similarly, the authors [7] claimed that if CAAM is often used, learners' critical thinking will be enhanced and self-reflection can be optimized, which may foster learners' SRL because self-regulated learners have acknowledged their role in the task.

Pedagogically speaking, the study findings have implications for EFL materials development, which contributes to learners' improvement of argumentative writing skills and a better comprehension of their self-regulated learning procedures in general and EFL writing in particular. Identifying learners' personality traits and offering them facilities to promote their performance can lead to remarkable accomplishments in EFL instruction. Likewise, the findings provide thoughtful insights into utilizing CAAM within writing courses to revolutionize EFL learning classrooms in this digital era, especially since educators are dealing with tech-savvy learners who often enjoy utilizing technological-based platforms for more effective and meaningful learning. Further research needs to be conducted on the utilization of CAAM in different disciplines to further strengthen the many benefits of CAAM.

REFERENCES

- [1] C. Bailey and P. Bizzaro, "Emancipatory assignments for English language learning: toward deficiency-free writing," in B. Chamcharatsri and A. Lida (Eds.), *International perspectives on creative writing in second language education* (pp. 46–64). Routledge, 2022.
- [2] K. Cho and C. D. Schunn, "Scaffolded writing and rewriting in the discipline: a web-based reciprocal peer review system," *Computers & Education*, vol. 48, no. 3, pp. 409–426, 2007.
- [3] W. M. Davies, A. Barnett, T. van Gelder, "Using computer-aided argument mapping to teach reasoning," in J. A. Blair (Ed.), *Studies in critical thinking 2nd Edition*, (pp. 115–152). Windsor Studies in Argumentation, Windsor, ON, Canada, 2021.
- [4] C. P. Dwyer, M. J. Hogan, and I. Stewart, "The promotion of critical thinking skills through argument mapping," in C. P. Horvart, & J. M. Forte (Eds.), *Critical thinking* (pp. 97–122). Nova Science Publishers, 2011.
- [5] C. Eccius-Wellman and J. Santana, "Variables that influence language proficiency in students from public and private high schools in Mexico," *MEXTESOL Journal*, vol. 44, no. 2, pp. 1–13, 2020.
- [6] M. Eftekhari, E. Sotoudehnama, and S. Marandi, "Computer-aided argument mapping in an EFL setting: does technology precede traditional paper and pencil in developing critical thinking?" *Educational Technology Research and Development*, vol. 64, pp. 339–357, 2016.
- [7] M. Harrell and D. Wetzel, "Improving first-year writing using argument diagramming," in M. Knauff, M. Pauen, N. Sebanz, and I. Wechsmeuth (Eds.), *Proceedings of the 35th Annual Conference of the Cognitive Science Society* (pp. 2488–2493). Cognitive Science Society, 2013.
- [8] Malmir and F. Khosravi, "The effect of argument mapping instruction on L2 writing achievement across writing task and writing components: a case study of Iranian EFL learners," *Applied Research on English Language*, vol. 7, no. 4, pp. 514–538, 2018.
- [9] P. Pahlavani and P. Maftoon, "The impact of using computer-aided argument mapping (CAAM) on the improvement of Iranian EFL learners' writing self-regulation," *The Journal of Teaching Language Skills*, vol. 7, no. 2, pp. 127–152, 2015.
- [10] N. Pinkwart, K. D. Ashley, C. Lynch, and V. Alevan, "Evaluating an intelligent tutoring system for making legal arguments with hypotheticals," *International Journal of Artificial Intelligence in Education*, vol. 19, no. 4, pp. 401–424, 2009.
- [11] J. C. Richards and J. Pun, A typology of English-medium instruction. *RELC Journal*, 2021.
- [12] R. J. Robillos and P. Phantharakphong, "Enhancing EFL learners' argumentative abilities in written composition and critical thinking dispositions through argument mapping within metacognitive approach," *Asian EFL Journal*, vol. 27, no. 3.3, pp. 181–208, 2020.
- [13] R. J. Robillos, "Instruction of metacognitive strategies: its role on EFL learners' listening achievement and awareness of their metacognitive listening strategies and self-regulation," *Asian EFL Journal*, vol. 27, no. 3.2, pp. 442–452, 2020.
- [14] R. J. Robillos, "Learners' writing skill and self-regulation of learning awareness using computer-assisted argument mapping (CAAM)," *Journal of Teaching English with Technology*, vol. 21, no. 4, pp. 76–93, 2021.
- [15] J. Sweller, "Cognitive load theory, learning difficulty, and instructional design," *Learning and Instruction*, vol. 4, pp. 295–312, 1994.
- [16] T. T. Toering, *Self-regulation of learning and the performance level of youth soccer players*, vol.43, no.4, 2021.
- [17] T. van Gelder, Using argument mapping to improve critical thinking skills. In M. Davies and R. Barnett (Eds.), *The Palgrave handbook of critical thinking in higher education* (pp. 183–192). Palgrave MacMillan, 2015.
- [18] J. Zheng, "The metacognitive strategy in English listening comprehension," *Theory and Practice in Language Studies*, vol. 8, no. 2, pp. 226–231, 2018.
- [19] B. J. Zimmerman, Investigating self-regulation and motivation: historical background, methodological development, and future prospect. *American Educational Research Journal*, vol. 45, no. 3, p. 16, 2008.

An Efficient Computational Method of Motif Finding in the Zika Virus Genome

Pushpa Susant Mahapatro¹, Jatinderkumar R. Saini^{2*}

Vidyalankar School of Information Technology, Wadala, Mumbai, India¹

Symbiosis Institute of Computer Studies and Research, Pune, India²

Symbiosis International (Deemed University), Pune, India^{1,2}

Abstract—The Zika virus (ZIKV) outbreak and spread is a global health emergency declared by World Health Organization. ZIKV rapidly spread across the world, causing neurological disorders. It is gaining public and scientific consideration. ZIKV genome biology and molecular structure are better understood with published papers. Genetic regulation is better understood by finding the motif in the DNA Genome sequence. The transcription factor binding sites need to be identified to understand the genetic code. There is diversity in gene expression. Motif-finding methods work towards efficiently identifying the repeated patterns in the genome. ZIKV genome sequence is used in the study. Identifying the motif is still a difficult task. There is a low probability of identifying the binding sites. Finding all possible solutions is challenging as it requires a lot of time and has high space complexity for finding long motifs. The Greedy search technique with pseudocount finds the motif in real-time. The count matrix is computed, and the profile matrix is constructed from the genome of the Zika virus. The calculated consensus string helps in calculating the score of the motif. The Greedy motif search technique is applied in this paper to find the motifs in the Zika virus Genome. This technique is not applied earlier to find the motifs in Zika Virus. The motifs are identified using a Greedy motif search without pseudocount and with pseudocount.

Keywords—Consensus string; genome study; greedy search technique; motif search; pseudocount; regulatory proteins; ZIKV; Zika virus

I. INTRODUCTION

The Zika virus (ZIKV) was first separated from a rhesus macaque in Uganda in 1947. The study of ZIKV was not given importance till 2015. In 2015, Brazil's big epidemic of ZIKV infections was linked to intensification in microcephaly cases. ZIKV can spread sexually and is known to persevere in the male and female reproductive systems. West Nile virus (WNV), Dengue virus (DENV), Yellow fever virus (YFV), and Japanese encephalitis virus (JEV) are included in the family Flaviviridae, genus Flavivirus. These are mosquito-borne pathogens. Zika virus also belongs to the same family of viruses. The ZIKV lifespan has Aedes mosquitoes and monkeys, whereas a broader range of mosquito species transmits WNV.

World Health Organization (WHO) has acknowledged the Zika virus (ZIKV) as a public health crisis worldwide. ZIKV is a flavivirus. It has its place in the family of Flaviviridae. It is spread over several parts of Africa, Southeast Asia, and the Pacific island. In August 2016, the ZIKV outburst in Brazil was the major ever recorded, with a projected 165000 doubted

cases. ZIKV is transmitted through monkeys and the Aedes genus [1]. ZIKV infection causes slight illness, headache, and rash. A recent study suggested that the virus causes neurological disorders such as Guillain-Barre syndrome. ZIKV is transmitted from mother to child and is also transmitted sexually. It has identical symptoms as compared to different arboviral diseases like DENV. Analysis based on symptoms is unpredictable for precise detection. Test center analysis is vital to obtain conclusive results. A suitable choice of molecular analysis is meaningful for routine ZIKV or flavivirus detection. No specific treatment for the infection is available. The course of injection and medicine development is extremely complicated. Anti-ZIKV vaccine development may take several years. Traditional drug development policies make the circumstances worse. Silico methods are helpful in enlightening possible vaccine candidates.

This fast rise of ZIKV cases and its consequence is severe. The disease has provoked the research community to produce interventions to battle Zika disease. The disease mechanism is presently unstated. Reviewing and analyzing ZIKV genome ecology and pathogenesis can provide awareness of ZIKV. microRNAs are also found to play a significant part in virus-related diseases and activation of the phenomenal immune response. Methodical genome-wide study of the ZIKV genome may assist in designing antiviral therapeutics. Zika virus has a 10.7 kb genome of single-stranded RNA. Multiscale examination of the genomic data produced throughout the widespread of infection and available in public databases was combined. The focus of the study was to inspect virus-related appearance at different scales [2] [3].

The research problem was understanding the regulatory mechanism of genes. This involves finding transcription factor binding sites. Identifying regulatory networks is also challenging. The objective of the research was to find the regulatory relations of genes. It is better considered with the identification of motifs. Motifs are known to have complex forms. An essential class of motifs is spaced motifs. It consists of short segments separated by nucleotides of different lengths. Locating motifs is a difficult task. Existing algorithms identify short contiguous motifs. Better algorithms identify spaced motifs with a different number of spaces in between [4]. So, this research is significant as it will help in identifying the spaced motifs with a mutation at one or more places in the genome.

In this Research paper, a literature review is conducted on various studies conducted on the Zika virus. The study is

*Corresponding Author.

conducted on phylogenetic analysis, ZIKV circulation in different countries, RNA-protein interaction, Viral RNA targets, Host cell-binding mechanism of ZIKV, Motif finding and Genetic behaviors of ZIKV, ZIKV infection, and the role of E-protein amino acids and many other aspects of Zika virus. The count matrix and profile matrix is calculated on the dataset of the Zika virus genome with pseudocount. The Greedy motif search method is applied to the dataset, and results are tabulated with and without pseudocount.

II. LITERATURE REVIEW

Zika virus has turned out to be a worldwide health problem as it is linked to potential congenital disabilities. The virus was revealed 70 years ago; still, the genomic construction and genetic variation are not fully known. The genome structure is compared with different other flaviviruses. Structural and functional similarity is found between the various flaviviruses' genome structures. The similarity is found in the conserved terminal structures. So, it is concluded that the Zika virus shares a high constitutional and functional similarity with other viruses of the Flavi family. It is known from the genomic comparison. Also, the prediction of motifs in viral proteins in the Zika virus with other viruses shows similarities. All Zika virus strains in America have similarities with the strains in Asia. Some conserved amino acids differentiate earlier African strains from Asian and American strains. Studies provide clues for different viruses' studies.

The Zika virus spread over more than fifty nations of the world. The evolution and spread are understood by studying the replication in the genome. Zika infection happens when an infected mosquito bites a person. It is also transmitted from one person to another person due to various reasons. ZIKV molecule needs to be studied to understand the infection in detail. It can also help in finding a solution to the problem. The neural progenitor cell growth is affected by ZIKV infection in monkeys [5] [6]. The same things happen in the case of humans. The virus damages the DNA of humans and monkeys. It also initiates DNA damage responses. The DNA damage response is then attenuated. The cycle of the growth of the virus is considered to determine the behavior of the virus during

different times of the day. The virus may behave differently during the day and during the night. A different mutation of the Zika virus is reported in America. These mutations are different from the mutations found in Asia and Africa. The *Aedes Aegypti* mosquito was studied with mutation, and the results were compared with the studies performed without mutation. Fitness is increased for new mutations. It increases the risk of the spread of the virus. Fitness is reduced for original mutations. Zika virus infects the immunocompetent adult. It precipitates and increases brain damage due to antiviral responses. The immune system of mice is studied. The modifications stimulated by the Zika virus were found. A significant decline in micro-organisms like Actinobacteria and Firmicutes phyla was found due to the Zika virus infection. A boost of Spirochaetes and Deferribacteres was prominent in infected mice compared to healthy mice. The modulation caused the enhancement of white blood cells. The Zika virus induced the modulation of microbiota. Birth defects are caused due to utero exposure to the Zika virus. The ill effects of this virus were not prominent in the early stages of birth. The researchers concluded that if they studied the toddlers till twenty-four months, then the effects would be clear. It was concluded that the women who became pregnant during the year 2016 were to be studied. It was the time of the outbreak of the Zika virus in America. The study was conducted on the neurodevelopment stages of toddlers from birth to twenty-four months. The behavior of the child was normal before and after birth. The activities of the body seemed to be reduced as the child started growing. The child started showing the symptoms of birth defects. The connection of birth defects to Zika virus infection was later identified. As such, no vaccine was available for the disease, and treatment of the condition was not possible. People were not aware of such an infection. A vaccine named VacDZ was produced using the dengue vaccine as a reference [7]. The immune responses are seen to the Zika virus. The vaccine seems to be showing positive results in mice infected with the Zika virus. Blood samples were collected from Brazil to study the impact and spread of the virus. The people of Brazil were impacted by three viruses: Zika, chikungunya, and dengue. The situation was challenging to handle and trace the spread of the virus [8]. The review of the literature is presented in Table I.

TABLE I. LITERATURE REVIEW

Sr. No.	Year	Ref.	Topic	Concept/ Theoretical Model	Paradigm/ Method	Context/ Setting/ Sample	Findings	Research Gap
1	2016	[2]	ZIKV circulation in America and phylogenetic analysis	ZIKV is a global public health problem. The genetic alterations and genomic structure are constantly under study.	The comparison of the genome organization of mosquito-borne diseases and the ZIKV genome was made to understand to features of the Zika virus genome. The conserved terminal structure is studied.	The similarity of structural and functional components was found between the Zika virus genome and other viruses. It was clear with sequence comparison and prediction of functional motifs.	American strains of the Zika virus form a unique clade with the Asian lineage. A sequence of preserved amino acids was identified that discriminated the Asian strains from the African strains. Studies provide an overview of the characters of the ZIKV genome.	Critical study to be conducted in the virological and epidemiological domain.
2	2018	[3]	RNA-protein interaction	RNA-protein interactions control	RaPID has usage in different applications.	A new mutant BirA has been introduced to progress the	A direct study of Protein-RNA interaction is enabled	The RNA protein connections can be further studied

			detection in living cells	cellular functionalities and diseases. Proximity-dependent protein labeling is used by RNA-protein interaction detection (RaPID).	It helps in assessing protein binding to mutant RNA motifs in human hereditary illnesses in finding potential post-transcriptional networks in breast cancer.	BirA-labelling component of RaPID.	in living cells. The timescale of interaction is as short as 1 min.	to understand more about cellular functionalities.
3	2018	[5]	small-molecule ligands in Viral RNA targets	Conserved structured motifs are contained in RNA genomes. These are attractive targets for small molecules of viral infection.	Conformational states are affected by ligand binding. These play an important role in the infection process.	HIV and Hepatitis C virus are studied. Inhibition process, RNA functions ligands are focused. The RNA targets in other viral pathogens are also studied.	The structural viral RNA motif is targeted by small molecules called ligands.	Ligand's discovery guides therapeutic opportunities. It guides the participation in key processes of infection as well as high conservation of pathogens.
4	2019	[6]	Host cell-binding mechanism of ZIKV	Two reputed binding mechanisms of inherited and emerging Zika viruses were identified. It features the envelope protein residue ASN154.	ASN 154 was visible to neuronal cells and fibroblasts to classical Zika virus protein and cell communications.	Peptides meaningfully expressed Vero cell contamination by ZIKV strains. A putative binding mechanism of ancestral African ZIKV strains and emergent Western Hemisphere strains is represented.	Western hemisphere strains may additionally be capable of utilizing PS-mediated entry to infect host cells. The region surrounding E protein ASN154 is capable of binding fibroblasts and primary neuronal cells	PS-mediated entry may be a secondary mechanism for infectivity utilized by Western Hemisphere strains.
5	2021	[4]	Motif finding and Genetic behaviors of ZIKV	The genome of ZIKV is used for the study. Circadian behavior and the appearance of genetic factors are considered.	Motif finding is done using a count matrix and profile matrix. The score of the consent string is calculated.	The Brute force method is certain to find the motif, but it will take a huge amount of time. So other techniques are to be used.	The motif finding is done using Greedy search techniques, and results are analyzed.	The score can be enhanced using other techniques, such as Gibbs Sampler.
6	2021	[9]	ZIKV infection and the role of E-protein amino acids	Learning of E-proteins in ZIKV infection, as it is the furthest proteins in the constitution of ZIKV	ZIKV uses covering proteins to bind to cell addition receptors.	Many sites are situated in an unusual position of the protein construction, such as the α -helix in the stem area.	Cover protein amino acids that contribute to the flavi virus initial contamination process are presented.	A detailed study of E-protein assistance can accomplish an efficient antigen strategy.
7	2021	[10]	Dengue virus whole genome of structural landscape	Protein binding domains and secondary structure is to be used for categorization	A prediction score of 85% is to be achieved with a secondary structure. The consensus secondary structure of profiles is computed. For computation, silico models are used.	Viruses of Dengue and Ebola are less structured. Viruses show structural patterns.	A correlation between the number of interaction sites with human proteins and the secondary structure of 89% is achieved in ZIKV.	Further classification of complex viruses to be done using the given approaches
8	2021	[11]	Dependent immune response genes of DENV provoke the countenance of PAF1	To establish infection, DENV disturbance of innate excepted responses is critical. DENV non-structural protein five plays a dominant part in such distress.	PAF1, LEO1, CTR9, and CDC73 are primary members of PAF1C. It helps in the immune reaction. It encourages the appearance of	Knockout of PAF1 enhances the DENV infection. NS5 atomic localization and the C-terminal area of the methyl transferase field are compulsory for its	PAF1C plays a significant role in restricting DENV reproduction.	A study can be performed on PAF1C role in dengue virus replication.

					antiviral, antimicrobial, and inflammatory responses.	communication with PAFIC.		
9	2021	[12]	Viral and molecular factors on ZIKV entry	Flavivirus are arthropod-borne pathogens for a wide range of mortality.	Around seventy viruses are contained in the genus. Different viruses present different clinical presentations even though the genomic and structural similarity is seen.	New methods to control virus infection are searched in order to control the disease.	Different steps present in the arboviruses entry process are attachment, internalization, endosomal escape, and capsid uncoating. Cellular machinery, host factor, and cellular pathways are taken over by events.	These are required as possible approaches for developing broad-spectrum antiviral drugs.
10	2021	[13]	The search for pseudoknots and three-layered associations in the genome of ZIKV RNA	The Flavivirus RNA genome covers a number of functionally significant constructions in 30 untranslated regions.	The genome sequence has diversity, and its identification is difficult. Flavivirus replication is well understood with the prediction of structure and helps in the development of antiviral strategies.	An algorithm is developed for structure design examination in the RNA sequence. Secondary constructions, pseudoknots, and triple base interactions are also identified. The structural descriptor is constructed by means of the data on preserved flavivirus 3'UTR constructions. It enclosed a variety of designs in these motifs.	The construction of a database of flavivirus 3'UTR structures is done. A total of areas identical to the overall design of exoribonuclease Xrn1-resistant RNAs in the rising collection of bug-specific flaviviruses is recognized.	Diagnostics, genotyping, mutational study, and drug design can be done with the record of flavivirus RNA.
11	2022	[14]	The common protein - Binding Motif of ZIKV and Dengue is PEX 19	ZIKV capsid (C) protein regulates peroxisomes. It causes reduced production of interferons as it interacts with protein PEX19	The usage and interaction of C interaction with PEX19 in the Zika virus are studied. The importance and usage of peroxisomes are also studied.	Peroxisomes are required for the replication of DENV. A conserved PEX19 binding motif is used for DENV and Zika virus C binding. This motif commonly occurs in cellular peroxisomal membrane proteins (PMPs).	This paper find identifies and questions how flavivirus C might downregulate peroxisomal abundance	Study to be conducted on the unknown role of peroxisomes in ZIKV.
12	2022	[15]	RNA requisite proteins used for interior Initiation of mRNA conversion	Viruses utilize the host's protein synthesis mechanism for interpreting their mRNAs. Viruses are obligate intracellular parasites.	The virus-related mRNA (vRNA) contends with the host mRNA together with ribosomes, tRNAs, and the eukaryotic translation initiation factor (eIFs) pool.	Viruses targets host eIFs, and RNA essentials reprogram cellular gene expression, guaranteeing the favored transformation of mRNAs.	vRNA IRES facilitated conversion beginning is highlighted. The role of RNA-required proteins (RBPs), other than the established conversion initiation factors, in modifying their movement is also discussed.	Accepting how the PTMs of ITAFs impact viral IRES activity also arises as a striking study domain.
13	2022	[7]	Computational method to cure ZIKV infection by the screening of phytochemicals against NS5	ZIKV study provides stimulation for new and capable anti-ZIKV agents. RNA-dependent RNA polymerase (RdRp) is found to be significant among all. It is considered a valuable drug target.	The cellular dock approach is used to reasonably screen the files of 5000 phytochemicals to find inhibitors against NS5 RdRp.	Polydatin, Dihydrogenistin, Liquiritin, Rhapontin, and Cichoriin were investigated with NS5 RdRp. The replicated complexes showed steadiness.	Natural and low price medicines are to be produced against the Zika virus	The efficiency of can be obtained by further study and research

14	2022	[8]	Tick-Borne Encephalitis Viral disease and the contribution of IFITM Proteins	A study is conducted on the Tick-borne encephalitis virus. The factors that inhibit the multiplication are Interferon-induced transmembrane proteins,	The part of IFITM proteins in the reticence of TBEV infection is studied. IFITM3 plays the important role of including analysis of useful motifs.	The role and additive action of endogenous IFITMs in TBEV dominance is confirmed.	TBEV might, to some extent, run off interferon and IFITM interceded containment throughout high-density co-culture infection.	Cell-to-cell reach may form an approach for viruses to break out from native host defenses.
----	------	-----	--	---	---	---	---	---

From the detailed literature review, it is identified that different categories of algorithms are applied to find the motif in DNA sequence. The limitations found in the previous search are that the Greedy motif search without pseudocount and with pseudocount is not applied to find motifs in the Zika virus [16]. Heuristics algorithms worked for solving combinatorial, but bit did not work for large datasets [17]. The greedy motif search algorithm is proposed to find the motif in RNA sequences [18]. A greedy mixture learning technique is proposed for finding motifs in already known motifs in real proteins by using the PRINTS datasets [19]. Time series-based data of different lengths are aligned and joined using the Greedy search technique [20]. The Greedy search algorithm is used to discover motifs in hm03r, yst04r, and yst08r. The results show that the algorithm is effective in finding motifs in the DNA sequences of hm03r, yst04r, and yst08r [21]. DNA motif discovery is made using the Greedy motif search method over the datasets - GATA1, SOX2, OCT4, STAT3, and KLF1 [22]. So, a research gap is identified that the Greedy search technique for motif finding is not applied to the genome of the Zika virus.

III. MATERIALS AND METHODS

A. Data Collection: Zika virus genome

ZIKV genome structure data from openly existing catalogs are collected and used in this study. The Zika virus genome sequence is available at NCBI [23]. ZikaVirus.fasta is the file name of the dataset. Fasta is a file format; the genome sequence is stored as a nucleotide sequence. The size of the dataset is 10.7 KB.

B. Gene Representations

RNA is formed using DNA. RNA further gets converted into proteins. Four ribonucleotides from the RNA. These four nucleotides are namely Adenine, Cytosine, Guanine, and Uracil. DNA replaces Thymine with Uracil. Amino acid sequences of proteins are formed by RNA transcripts [9]. Proteins regulate the function of the cell. Ori is the replication for the origin of DNA, so DNA replication starts at ori. Ori has some specific properties. Biologists find it difficult to identify the position of replication. Some other complicated tasks happening inside the cell are transcription and transpiration. The transcription process replaces what happens inside the cells. Thymine (T) that occurs in DNA is getting converted into Uracil (U) during the transcription process. The amino acids sequence is formed from RNA. There are a total of twenty different amino acids in RNA [13]. Three different nucleotides form these amino acids, also called 3-mers or codons. Each combination of these 3-mers forms different amino acids following a genetic code. Due to transcription, different genes can form RNA. Different genes may transcribe at different rates. This property is also called gene expression. Due to gene expression, different cell at different parts of the body of any

living being behaves differently. Brain cells behave differently compared to skin cells. They differ in features and functionality. Cells with different variations know how to keep track of time. The variation in cell functionalities is known to occur in people infected with ZIKV. Pro-inflammatory reactions are prominent in women infected with the Zika virus.

IV. COMPUTATION OF MOTIF IN ZIKA VIRUS GENOME

Zika virus genome nucleotide sequence has a length of 10780. The length is calculated using the program. Based on the profile matrix of the Zika virus, the probability of a string can be calculated. The regulatory motif binds to specific short DNA. It regulates the gene. The site of binding is generally the upstream region and is important to identify. A method to identify the motif is useful for gene study.

A. Importance of Motif

Motifs are important to identify and study. Motifs have finite lengths. These are short sequences in DNA. Sequence motifs are used to signify transcription factor binding sites. Transcription regulations are better assumed with motif sequences. Dynamic sites of enzymes and proteins are characterized by motifs. The individual instances of the motif is calculated and scored using the ideal motif. An ideal motif is not known and can only be predicted. To recognize motif, a k-mer string is selected from each string. Based on identical nucleotides, each motif is scored. A list of t strings is created. The length of the string in each list is n. a motif collection is created by selecting k-mer nucleotides from each string. A t X k motif matrix is formed. From the t X k matrix created, the nucleotides are counted and stored in an array. There are four different types of nucleotides, so four rows are created. The first row represents nucleotide A, the second row represents C, the third row represents G, and the fourth row represents T. Now in the matrix, the columns are viewed to find the nucleotide with the highest count. So for that column, the nucleotide with the highest count is represented in the uppercase letter. Different motif matrices for DNA strings if formed using different values of k. The aim is to obtain the most conserved motif matrix. The conserved matrix also means the matrix has more capital letters. The minimum score is to be obtained for the collection of k-mers.

B. Calculating the Count Matrix

A count matrix is formed for the Motifs. It is 4 X k matrix. It is abbreviated as count (Motifs). It is the sum of each nucleotide column-wise. The element (I, j) represents I nucleotide in jth column. The count matrix obtained is further used for the calculation in the next steps [4].

C. Finding the Count Matrix with Pseudocount

Pseudocount is a small number that is added to zeroes. This improves the unfair scoring. This method is named Laplace's Rule of Succession. In motifs, pseudocount method, one or a small number is added to the count matrix. The different matrices are formed for calculations. These are the motif, count, and profile matrices. A count matrix of 4 X k is formed for a given matrix. This count matrix's (I, j) element represents nucleotide I of column j. Pseudocounts one is added to each element of this count matrix.

'A': [46, 38, 40, 42, 43, 37, 34, 47, 46, 51, 42, 42, 43, 47, 39, 46, 47, 37, 40, 50, 39, 43, 41, 46, 37, 40, 43, 42, 41, 31, 37, 41, 37, 45, 41, 47, 37, 46, 41, 49, 38, 47, 42, 42, 48, 41, 45, 52, 39, 48, 42, 47, 30, 50, 42, 52, 40, 41, 40, 47, 34, 51, 53, 37, 51, 41, 46, 59, 48, 51],

'C': [24, 40, 35, 30, 25, 35, 38, 34, 37, 31, 28, 35, 24, 36, 42, 39, 35, 44, 37, 33, 47, 32, 38, 35, 36, 43, 39, 29, 41, 34, 39, 36, 44, 38, 35, 34, 33, 42, 27, 36, 37, 37, 32, 37, 42, 35, 40, 25, 33, 34, 33, 30, 50, 43, 32, 25, 36, 34, 33, 34, 43, 27, 27, 31, 33, 37, 35, 27, 34, 32],

'G': [42, 54, 47, 46, 50, 50, 43, 36, 47, 46, 49, 48, 58, 39, 46, 51, 39, 51, 44, 43, 34, 50, 41, 43, 57, 44, 42, 47, 42, 46, 49, 49, 40, 38, 42, 46, 43, 39, 58, 43, 48, 46, 51, 48, 42, 47, 39, 44, 57, 50, 50, 53, 51, 36, 49, 42, 41, 47, 48, 43, 53, 43, 41, 51, 49, 49, 49, 36, 46, 39],

'T': [46, 26, 36, 40, 40, 36, 43, 41, 28, 30, 39, 33, 33, 36, 31, 22, 37, 26, 37, 32, 38, 33, 38, 34, 28, 31, 34, 40, 34, 47, 33, 32, 37, 37, 40, 31, 45, 31, 32, 30, 35, 28, 33, 31, 26, 35, 34, 37, 29, 26, 33, 28, 27, 29, 35, 39, 41, 36, 37, 34, 28, 37, 37, 39, 25, 31, 28, 36, 30, 36]}}

D. Framing the Profile Matrices with Pseudocount

Finding a perfect motif is a challenging task. It binds the finest to the transcription site. A motif discovery problem is solved by finding the similarity to the ideal motif. A motif similar to an ideal motif is calculated, as an ideal motif is not known. Capital letters are used to denote the most common nucleotide in each column. Motif[i][j] represent the ith row and jth column. If the matrix has more capital letters, it means the matrix is more conserved. The genome of the Zika virus is used to create different motif matrices for different values on k. The count of the small letter is noted. The sum of this count gives the score of the matrix. Then a k-mer is assumed, which will reduce the value of the score. The profile of the motif matrix is calculated. The elements of the count are divided by the number of rows. The sum of any column of the profile matrix is unity. The profile matrix for the Zika virus genome is given below.

'A': [0.29, 0.24, 0.25, 0.27, 0.27, 0.23, 0.22, 0.3, 0.29, 0.32, 0.27, 0.27, 0.27, 0.3, 0.25, 0.29, 0.3, 0.23, 0.25, 0.32, 0.25, 0.27, 0.26, 0.29, 0.23, 0.25, 0.27, 0.27, 0.26, 0.2, 0.23, 0.26, 0.23,

0.28, 0.26, 0.3, 0.23, 0.29, 0.26, 0.31, 0.24, 0.3, 0.27, 0.27, 0.3, 0.26, 0.28, 0.33, 0.25, 0.3, 0.27, 0.3, 0.19, 0.32, 0.27, 0.33, 0.25, 0.26, 0.25, 0.3, 0.22, 0.32, 0.34, 0.23, 0.32, 0.26, 0.29, 0.37, 0.3, 0.32],

'C': [0.15, 0.25, 0.22, 0.19, 0.16, 0.22, 0.24, 0.22, 0.23, 0.2, 0.18, 0.22, 0.15, 0.23, 0.27, 0.25, 0.22, 0.28, 0.23, 0.21, 0.3, 0.2, 0.24, 0.22, 0.23, 0.27, 0.25, 0.18, 0.26, 0.22, 0.25, 0.23, 0.28, 0.24, 0.22, 0.22, 0.21, 0.27, 0.17, 0.23, 0.23, 0.23, 0.2, 0.23, 0.27, 0.22, 0.25, 0.16, 0.21, 0.22, 0.21, 0.19, 0.32, 0.27, 0.2, 0.16, 0.23, 0.22, 0.21, 0.22, 0.27, 0.17, 0.17, 0.2, 0.21, 0.23, 0.22, 0.17, 0.22, 0.2],

'G': [0.27, 0.34, 0.3, 0.29, 0.32, 0.32, 0.27, 0.23, 0.3, 0.29, 0.31, 0.3, 0.37, 0.25, 0.29, 0.32, 0.25, 0.32, 0.28, 0.27, 0.22, 0.32, 0.26, 0.27, 0.36, 0.28, 0.27, 0.3, 0.27, 0.29, 0.31, 0.31, 0.25, 0.24, 0.27, 0.29, 0.27, 0.25, 0.37, 0.27, 0.3, 0.29, 0.32, 0.3, 0.27, 0.3, 0.25, 0.28, 0.36, 0.32, 0.32, 0.34, 0.32, 0.23, 0.31, 0.27, 0.26, 0.3, 0.3, 0.27, 0.34, 0.27, 0.26, 0.32, 0.31, 0.31, 0.31, 0.23, 0.29, 0.25],

'T': [0.29, 0.16, 0.23, 0.25, 0.25, 0.23, 0.27, 0.26, 0.18, 0.19, 0.25, 0.21, 0.21, 0.23, 0.2, 0.14, 0.23, 0.16, 0.23, 0.2, 0.24, 0.21, 0.24, 0.22, 0.18, 0.2, 0.22, 0.25, 0.22, 0.3, 0.21, 0.2, 0.23, 0.23, 0.25, 0.2, 0.28, 0.2, 0.2, 0.19, 0.22, 0.18, 0.21, 0.2, 0.16, 0.22, 0.22, 0.23, 0.18, 0.16, 0.21, 0.18, 0.17, 0.18, 0.22, 0.25, 0.26, 0.23, 0.23, 0.22, 0.18, 0.23, 0.23, 0.25, 0.16, 0.2, 0.18, 0.23, 0.19, 0.23]}}

E. Calculating a Consensus String for the Genome of the Zika Virus and Score

The consensus string of the Zika virus is calculated from the genome and is given below.

AGGGGGGAGAGGGAGGAGGACGAAGGAGGTGGC
AGATAGAGAGGAGAAGGGGGAGAGGGAGAAGAGGA
AA. The score of the consensus string is calculated to be 7444.

V. DISCUSSION OF RESULTS

A. Using Profile Matrix for Calculation

Iterative algorithms use select different alternatives during each iteration. The greedy search technique selects the most attractive alternative in each iteration. The profile matrix of the Zika virus is calculated in the preceding section and is used the same. The likelihood of any string can be intended. The probability of the consensus string is also calculated.

B. The Search of Binding Sites

The Greedy motif algorithm is implemented with pseudocount. The results of the Greedy motif search with pseudocount are summarized in Table II. The table contains values from 3-mer strings to 15-mer strings. The string with one nucleotide and two nucleotides have little significance and are hence ignored.

6	8-mer	508	443	GCTGG', 'AATGATAG', 'GACCCTAA', 'GCAGCTGG', 'GTGGATGG', 'CCGCCTG G', 'GAGGCTGG', 'TTGGCTGG', 'GACCCTGG', 'GGCCCTGG', 'CATGCTGT', 'AAAGCTGA', 'GGGGCTGG', 'GGCCCTGG', 'GTTGCTGT', 'CATGGTGG', 'AAC CCTGG', 'AGGACTGG', 'GTCTCTGG', 'GAGGATGT', 'GATCATTG', 'GAAGCTA T', 'GTGACTGG', 'AAAAGTGG', 'GAGCATGG', 'GAGTCTGT', 'GAAGCTGT', 'GAGAGTGC', 'GAATTGG', 'GTGGCTAG', 'AGGCTGG', 'CTGGCTGG', 'GAG AATGA', 'CAAAGTGG', 'CAACCTAG', 'GAGGCTGA', 'CCAAGTGG', 'GATGATA G', 'CTGGATGG', 'CATTGTGG', 'GAGACTGC', 'ACTGATGG', 'CTACCTGG', 'GAGTGTGG', 'AAGACTTG', 'CAACATGG', 'GTACATGG', 'ACACCTGG', 'GAA GCTGG', 'CATGCTGC', 'GAAGGTGG', 'GAAGAGGG', 'CACGCTGG'] 443
7	9-mer	603	531	'CAGAAGAGA', 'TTGTGGATG', 'TGGGACAGG', 'GGGAGGCTG', 'GGGAAGTTA', 'TGGACAGG', 'TGGAAAGCC', 'GAGAAGAGG', 'TGGTGGAGC', 'TGGCAGAGG', 'TGGAAATATA', 'TGGCGGCTG', 'TGGTGGGGG', 'TGGAAACCC', 'TGGGGGAGG', 'TTGGGGCGC', 'ATGAGGAGG', 'ATGAAGATC', 'TGGAAAGCTA', 'GGGATGTGG', 'AGGAATAGC', 'TGGTTGTGG', 'AAGAAGAGT', 'TTGAAGAGG', 'GAGAGGAGA', 'TGGAAAGGC', 'TGGATGGGG', 'TAGAAGAGA', 'TGGCTGGGA', 'ATGAAGCTC', 'TGGTAAAGG', 'GGGAGCGG', 'TGGAGGCTG', 'TTGCAGAGC', 'TTGATGATA', 'TGGATGGGA', 'AGGACGGGA', 'TGGAGCATC', 'TGGCAGCTC', 'TGGAAAGGG', 'TGGAACAGA', 'GGGAAGACT', 'GGGCTGAGA', 'TAGGTGATG', 'AGCTTGGGG', 'GAGAAGCTG', 'AAGAAGCCA', 'AGGATGGGA', 'TAGAGGAGA', 'TGGAAAGA'] 531
8	10-mer	697	639	C', 'CCGCTTGAAC', 'GGTGTGGCAA', 'GAGATGGTTG', 'GAGGGGGCTG', 'GCT ATGGGTG', 'GGGTGGAGC', 'GAAGTGAAG', 'ATGATGAAA', 'GGTATGGGGG', 'GGGGCGCATG', 'GCTCTGGCAC', 'CGCATTGAAA', 'ACCATGGAAG', 'GATGT GGTGA', 'AGTTTTCAAG', 'GTTGTGAAA', 'GCTAGGCAAA', 'GCAGTGAAG', 'GACAAGGAAA', 'AATTTGAAA', 'GATGGGGAGA', 'GGTGTGAAG', 'CAGGAGG AAG', 'GAGAATGAAG', 'AAAAGGGAAA', 'AAGGGGGAGC', 'GAGATGCAAG', 'G CAACGGATG', 'GATATGGGAA', 'CAACTGGATG', 'GGACGGGAGG', 'GGGATGGAG C', 'AATGTGGCAG', 'GAAAGGGAGA', 'CACATGGAAG', 'AAAAGGGAAG', 'CAT AGGGCAC', 'GGTGTGAAG', 'CTTGGGGAAA', 'GCTGTGCAGC', 'GCCTGTGAGC', 'GAACTGGAGA', 'CATATTGACG', 'GAGTTCCAC'] 639
9	11-mer	806	745	CGGCTGAG', 'TGGTGGGGAT', 'AAACCCTGGAG', 'AGGACTGGTCA', 'TGGAGCG AAAA', 'AGGCCAGTGA', 'AGGATCCGAG', 'AGGACATGGGC', 'GGGATGTGGT ' , 'AAGAGTTTTCA', 'TGGTTGTGGAA', 'AGAAGAGTTCA', 'TGAAGAGGAAA', ' TGGACAAGGAA', 'GGAATTTGGAA', 'TGGATGGGGAG', 'AGGAGGTGGT', 'TGCA GATGACA', 'GGCCCTTGGCA', 'CAGTTATGGAC', 'GGGAGCGGACA', 'TAGAGATG CAA', 'GAGAAAGTGAC', 'AGGTTCTTGA', 'TGGATGGGACA', 'GGGAGGTCCAT', ' , 'GGGAGACTGCT', 'GGGACCTCCGA', 'TGGAAAGGGAG', 'AGGAGAACGC', 'G AAAAAGGGAA', 'AGAACATTA', 'AGGTGATGAAG', 'TACACCTGGAG', 'AGAAG CTGGGA', 'AGGACACTGAG', 'AGGATGGGAAA', 'TGGATCTCCAG', 'CAGAGACTC CA'] 745
10	12-mer	922	846	'GTGGAAGAAGCA', 'TGGAAACCCTGG', 'GGGAGGACTGG', 'CGAAAAGCAACA', 'TAGGAGGCCAGT', 'TTGAAAGGATCC', 'TGGAAAGCTATGA', 'GGGATGTGGTGA', 'AGGAAAAAGTGG', 'TAGGGTGCCAGA', 'TACCAAAGAAGA', 'AGGAAAAAGAGT', 'AGGAAAGAGAGC', 'GGGAAAAAGAGA', 'TGGATGGGGAGA', 'TAGAAGAGATGA', 'GAGGAAGGATGT', 'TGGAGAAAGGGC', 'CTGAAAAAGGGA', 'GGGAGCGGACA', 'TGCAAGACTTGT', 'CAGAGAAAGTGA', 'GTGAAGCCAATT', 'TGGAAACCCTCA', 'AGGACGGGAGGT', 'GGGCGGGATGGA', 'CGCAAATGTGGC', 'TGGAAAGGGAGA', 'GTGGAACAGAGT', 'GGGAAAAAGGGA', 'TAAAAACACAGT', 'GTGAAGAAGGGT', 'CTGGAGTGTGT', 'GGGAAACCAAGC', 'AGGACACTGAGT', 'GGGAAAAGAAGG', 'GTTAGAGGAGA', 'GGAAAGACCAGA'] 846

11	13-mer	1008	945	G', 'TGTATAAAAGTGT', 'ATGGGGGAGGACT', 'TGGAGCGAAAAGC', 'AGGAGGCC AGTGA', 'AGTGAGCACGCGG', 'ATGGAAGCTATGA', 'TGGGATGTGGTGA', 'TGGT CAGCAAAGA', 'ATGAGCATGGTCT', 'ATCAACAAGGTGC', 'TTGAAGAGGAAAA', ' AGGAAAGAGAGCA', 'TGGGAAAAGAGA', 'TTGAACGAGGATC', 'AGAAGAGATGAGT , 'AGGAAGGATGTAT', 'TGGAGAAAAGGCA', 'TGAAAAGGGAAA', 'AGACCAAAG GGGG', 'ATGGAGGCTGAGG', 'AGTGACCAACTGG', 'TTGAATGATATGG', 'AGGAC ACACAAGA', 'AGGTCATTGTGG', 'AGCATCCGGGAGA', 'TGCCCAAATGTGG', 'A TGGAAAGGGAGA', 'TGGAACAGAGTGT', 'TGGGAAAAGGGA', 'TGGGCTGAGAACA' , 'TGGGTGAAGAAGG', 'AGTCAGCCACAGC', 'TGGGAAACCAAGC', 'TGAGCCCCTC AGA', 'TGGGAAAAGAAGG', 'TGGTTAGAGGAGA', 'GGGAAAGACCAGA'] 945
12	14-mer	1113	1046	, 'AGCTCCCAACATGA', 'TGAAGCTATGAGG', 'TCAAAACCTGGGA', 'TTCAGG AAAAAGT', 'AGGGTGCCAGACCC', 'TGTACCAAAGAAGA', 'TGAAGACTGCAGT', 'AGTGGACAAGGAAA', 'TGATGGGAAAAGA', 'TTCTTGAACGAGGA', 'TGAAGGGCT GGGAT', 'TGCTGGCTGGGACA', 'ATGGAGAAAGGGCA', 'AGCTGAAAAGGGA', 'T CGAGACAAGACCA', 'ATGGAGGCTGAGGA', 'TGGTTGCAGAGCAA', 'TGAATGATATG GGA', 'TGGGACAACTGGGA', 'TGCCGCCACCAAGA', 'TGGAGCATCCGGGA', 'TTA TTTCCACAGAA', 'TGGGAGAACTACCT', 'GTGTGGATTGAGGA', 'TGGGAAAAGGGGA A', 'TGAGAACATTAATA', 'TTGGGTGAAGAAGG', 'TGCTGTAAGCACCA', 'AGCTG GAAACCAA', 'AGAGGACACTGAGT', 'ATGGGAAAAGAAGG', 'TGGTTAGAGGAGAC' , 'TGGGAAAGACCAGA'] 1046
13	15-mer	1190	1138	GGATCCGCA', 'CTTTGACGAGAACCA', 'CTGGGATGTGGTGC', 'GGTCAGCAAAGAG TT', 'TAGGGTGCCAGACCC', 'GTTTCATCAACAAGGT', 'AGGAAAAGAGTGGGA', 'C AAGGAAAGAGAGCA', 'ATGGGAAAAGAGAA', 'CTTGAACGAGGATCA', 'GTTGAAGG GCTGGGA', 'CAGGAGGAAGGATGT', 'AATGGAGAAAAGGGCA', 'AGGAAAAGCAGTTAT , 'TTCGAGACAAGACCA', 'TATGGAGGCTGAGGA', 'ATGGCAGTCAGTGGGA', 'TGT GAAGCCAATTGA', 'CTGGGAAGAAGTTC', 'CTTCAACAAGCTCCA', 'GGCGGGATG GAGCA', 'GTGGCAGCTCCTTTA', 'CATGGAAAAGGGAGAA', 'GTGGATTGAGGAGAA', 'TGGGAAAAGGGAA', 'ATTAACAAACAGTC', 'TTGGGTGAAGAAGGG', 'TAGTCA GCCACAGCT', 'CTGGGAAACCAAGCC', 'AGTCAAAAACCCCA', 'ATGGGAAAAGAAG GT', 'GTGGTTAGAGGAGAC', 'TGGGAAAGACCAGAG'] 1138

The results of various k-mers are tabulated. The score of the Greedy motif search without pseudocount is compared with the score of the Greedy motif with pseudocount. The score of the Greedy motif search without pseudocount and with pseudocount is calculated for string of length three to string of length fifteen. It is found that the score is less for calculations with pseudocount so these results are more promising compared to motifs obtained without pseudocount. For 15-mer string, the score is 1190 for the Greedy motif search and 1138 for the Greedy motif search with pseudocount. If the score is low means, the performance of the algorithm is good. For the fifteen nucleotides long string, a score of 1190 is obtained for the Greedy motif search without pseudocount. A score of 1138 is obtained for the Greedy motif search with pseudocount. So, the results have considerably improved by using the Greedy motif search with pseudocount.

VI. CONCLUSION AND FUTURE WORK

The genome of ZIKV is considered for the study. In the case of an infected mother, ZIKV causes neurological disorders in babies. The causes and effects of ZIKV were not identified earlier as the symptoms of the disease are mild headache and fever. Later it was linked to reduced brain activities in babies. The diseases pass from the infected mother to the child. Medicines or vaccines for this infection are not available. This research paper studies the Zika virus genome to get more insight into the molecular structure. For a given profile matrix, the probability of every k-mer string is calculated and tabulated. The score is calculated with the Greedy motif search without

pseudocount and with pseudocount. The results are computed and tabulated. The comparison shows the results are improved with the Greedy motif search with pseudocount. The aim is to reduce the score, and it is obtained with a Greedy motif search with pseudocount. The Greedy motif search for motif finding is applied to PRINTS datasets, hm03r, yst04r, and yst08r, in earlier research. It is also applied to datasets GATA1, SOX2, OCT4, STAT3, and KLF1. It is not applied to the Zika virus to identify the motifs in the Zika virus genome. It is concluded that the Greedy motif search with pseudocount performs better than the Greedy motif search without pseudocount as it gives a score of 1138 over a score of 1190.

REFERENCES

- [1] P. S. Mahapatro and J. R. Saini, "An Innovative Computer Programming based Analysis of Zika Virus for Identification of Genome Replication Location," IEEE Explorer, 2021.
- [2] Q. Ye, Z.-Y. Liu, J.-F. Han, T. Jiang, X.-F. Li and C.-F. Qin, "Genomic characterization and phylogenetic analysis of Zika virus circulating in the Americas," Infection, Genetics and Evolution, vol. 43, no. 43, 2016.
- [3] M. Ramanathan, K. Majzoub, D. Rao, P. Neela, B. Zarnegar, S. Mondal, J. Roth, H. Gai, J. Kovalski, Z. Siphshvili, T. Palmer, J. Carette and P. Khavari, "RN A-protein interaction detection in living cells," Nature Methods, vol. 15, no. 3, 2018.
- [4] P. S. Mahapatro and J. R. Saini, "Genetic Behaviour of Zika Virus and Identification of Motif," International Journal of Advanced Computer Science and Applications, vol. 12, no. 9, 2021.
- [5] T. Hermann, "Viral RNA targets and their small molecule ligands," Topics in Medicinal Chemistry, vol. 27, 2018.

- [6] C. Rieder, J. Rieder, S. Sannajust, D. Goode, R. Geguchadze, R. Relich, D. Molliver, T. King, J. Vaughn and M. May, "A novel mechanism for zika virus host-cell binding," *Viruses*, vol. 11, no. 12, 2019.
- [7] A. Rehman, U. Ashfaq, M. Javed, F. Shahid, F. Noor and S. Aslam, "The Screening of Phytochemicals Against NS5 Polymerase to Treat Zika Virus Infection: Integrated Computational Based Approach," *Combinatorial Chemistry and High Throughput Screening*, vol. 25, no. 4, 2022.
- [8] A. Chmielewska, M. Gómez-Herranz, P. Gach, M. Nekulova, M. Bagnucka, A. Lipińska, M. Rychłowski, W. Hoffmann, E. Król, B. Vojtesek, R. Sloan, K. Bieńkowska-Szewczyk, T. Hupp and K. Ball, "The Role of IFITM Proteins in Tick-Borne Encephalitis Virus Infection," *Journal of Virology*, vol. 96, no. 1, 2022.
- [9] T. Hu, Z. Wu, S. Wu, S. Chen and A. Cheng, "The key amino acids of E protein involved in early flavivirus infection: viral entry," *Virology Journal*, vol. 18, no. 1, 2021.
- [10] R. Delli Ponti and M. Mutwil, "Structural landscape of the complete genomes of dengue virus serotypes and other viral hemorrhagic fevers," *BMC Genomics*, vol. 22, no. 1, 2021.
- [11] M. Petit, M. Kenaston, O. Pham, A. Nagainis, A. Fishburn and P. Shah, "Nuclear dengue virus NS5 antagonizes expression of PAF1-dependent immune response genes," *PLoS Pathogens*, vol. 17, no. 11, 2021.
- [12] C. Cordero-Rivera, L. De Jesús-González, J. Osuna-Ramos, S. Palacios-Rápalo, C. Farfan-Morales, J. Reyes-Ruiz and R. Del Ángel, "The importance of viral and cellular factors on flavivirus entry," *Current Opinion in Virology*, vol. 49, 2021.
- [13] A. Zammit, L. Helwerda, R. Olsthoorn, F. Verbeek and A. Gulyaev, "A database of flavivirus RNA structures with a search algorithm for pseudoknots and triple base interactions," *Bioinformatics*, vol. 37, no. 7, 2021.
- [14] M. Farelo, D. Korrou-Karava, B. K. T. Russell, M. Maringer and P. Mayerhofer, "Dengue and Zika Virus Capsid Proteins Contain a Common PEX19-Binding Motif," *Viruses*, vol. 14, no. 253, 2022.
- [15] B. López-Ulloa, Y. Fuentes, M. S. P. Ortega and M. López-Lastra, "RNA-Binding Proteins as Regulators of Internal Initiation of Viral mRNA Translation," *Viruses*, vol. 14, no. 188, 2022.
- [16] T. Wang and G. D. Stormo, "Combining phylogenetic data with co-regulated genes to identify regulatory motifs," *BIOINFORMATICS*, vol. 19, no. 18, pp. 2369-2380, 2003.
- [17] J. M. C. Garbelini, D. S. Sanches and A. T. R. Pozo, "Expectation Maximization based algorithm applied to DNA sequence motif finder," *IEEE Congress on Evolutionary Computation*, pp. 1-8, 2022.
- [18] J. Gorodkin, L. J. Heyer and G. D. Stormo, "Finding the most significant common sequence and structure motifs in a set of RNA sequences," *Nucleic Acids Research*, vol. 25, no. 18, p. 3724-3732, 1997.
- [19] K. Blekas, D. Fotiadis and A. Likas, "Greedy mixture learning for multiple motif discovery in biological sequences," *BIOINFORMATICS*, vol. 19, no. 5, pp. 607-617, 2003.
- [20] M. Mollah, V. Souza and A. Mueen, "Multi-way Time Series Join on Multi-length Patterns," in *IEEE International Conference on Data Mining*, 2021.
- [21] O. Gokalp, "DNA sequence motif discovery using greedy construction algorithm based techniques," in *5th International Conference on Computer Science and Engineering*, UBMK 2020, 2020.
- [22] C. Saad, L. Noé, H. Richard, J. Leclerc, M.-P. Buisine, H. Touzet and M. Figeac, "DiNAMO: highly sensitive DNA motif discovery in high-throughput sequencing data," *BMC Bioinformatics*, vol. 19, p. 223, 2018.
- [23] National Center for Biotechnology Information, [Online]. Available: <https://www.ncbi.nlm.nih.gov/>. [Accessed 18 Feb 2022].

Classification of Agriculture Area based on Superior Commodities in Geographic Information System

Lilik Sumaryanti¹, Rosmala Widjastuti², Firman Tempola³, Heru Ismanto⁴
Department of Informatic Engineering, Universitas Musamus, Merauke, Indonesia^{1,4}
Department of Agrotechnology, Universitas Musamus, Merauke, Indonesia²
Department of Informatic Engineering, Universitas Khairun, Ternate, Indonesia³

Abstract—Research carries a classification model that combines LQ analysis and hierarchical classification using a single linkage. The classification results are a basis for mapping the potential of agriculture areas based on superior food commodities in Merauke Regency, Indonesia. LQ analysis is used to select food commodities. In contrast, the application of single linkage uses the production of three features, rice, corn, and peanuts, which have an LQ value > 1, to group sub-districts based on agricultural potential. Intelligent mapping is represented by mapping the sub-districts agricultural areas according to the cluster. The classification results show that the first cluster has sixteen sub-district members, the second consists of three sub-districts, and the third cluster consists of one sub-district. Each cluster member has similarities based on the distance measurement with the smallest value using the Euclidean distance. The proposed classification model is a creative idea to map agricultural areas, which can present information on regional potential based on superior food crop commodities.

Keywords—Classification; agriculture; location quotient; single linkage; geographic information system

I. INTRODUCTION

The agricultural sector is an essential source of income in the national economy in Indonesia, as evidenced by its contribution to gross domestic product. The agricultural sector's potential is the basis for developing rural economic activities through business development, namely agribusiness and agro-industry. Merauke is one of the regencies in eastern Indonesia, where most of the population depends on the agricultural sector, especially for rice commodities, and has become a food barn in Papua Province, with rice production in 2022 reaching 354192.32 tons [1]. Agriculture is a sector being the center of attention in efforts to develop and grow the economy that concerns many people's lives, not only the current generation but also the generations to come. Agricultural potential in Merauke Regency for food crops consists of various commodities, namely, rice, corn, green beans, soybeans, peanuts, cassava, and sweet potatoes [2].

The information on agriculture areas in Merauke Regency is presented by survey reports from the Central Statistics Agency or by seeking information directly to visit the place. Making it difficult for those who want to seek information on the agriculture sector's potential, do not support user mobility, and are not efficient in doing so. The agriculture sector's potential has to increase by determining the best commodity of food crops in an area to be used as information for local governments to make programs and policies [3]. The aim of

developing the best commodity is to meet the needs of local consumption in the region and to develop prospects so the production can be exported outside the region. The results of mapping agriculture areas based on superior food crop commodities can be used as a source of information for policymakers, both the government and farmers, to support the sustainability of the livelihoods of people who depend on the agrarian sector to improve their welfare. They can also be used as information for the private sector as potential investors for assisting in finding the potential of agricultural areas based on superior food crop commodities. Building agricultural businesses following strategies maximizes the available and optimally managed agriculture potential. The use of technology with the concept of intelligent agriculture [4] is a significant change in the development of the agriculture sector [5][6]. The applications for agricultural information classification analysis and agriculture production management have been developed [7], such as the classification model used to determine superior food crop clusters [8], The use of machine learning models for crop cultivation prediction [9], allows farmers to assess the cultivated types, monitor plant growth, and choose the correct harvest time [10]. System development using a classification model that combines qualitative and quantitative methods improves the relevance [11], completeness, and accuracy in finding information and increases the utilization of agricultural data information [12].

The proposed classification model for mapping agriculture areas combines two methods, Location Quotient (LQ) and Single Linkage, which aims to determine hierarchically based on regional potential. Using the LQ method to determine the regionally superior food crop commodities in Merauke Regency[13], the classification model produces the best commodity types based on the LQ value > 1. The results are then used as a feature for cluster analysis of agricultural areas using the single linkage method, so the classification accuracy is high. The proposed classification model is generated well with relevant features [14]; the classification model is trained by reducing the number of features that are the results of the LQ method analysis so that the proposed hybrid algorithm can work optimally [15]. Classification of superior food crop commodities provides essential information for mapping agricultural areas. Implementation of Hierarchical classification is widely used for data mining, and the performance of the single linkage method is suitable for handling various types of data [16]. The application of the proposed classification model produces a mapping of agriculture areas in geographic information systems [17]. The

purpose of this research is to map agricultural areas based on potential clusters of superior commodity production areas using a creative classification model that combines LQ analysis with single linkage classification methods. The results of regional mapping are dynamic, so they can be continuously updated according to the production data of food crops.

II. METHOD

The classification model is a combination of LQ and single linkage methods. It aims to group agriculture areas based on superior food crop commodities to present cluster information on the hierarchy and map agriculture areas according to their clusters [18]. Determination of agriculture area clusters using data on the production of food crop commodities in a city and province. The stages of research methods are shown in Fig. 1, explained as follows:

1) Data collection

a) Data on food crop production in Merauke Regency, obtained from reports on agricultural production from the Central Statistics Agency, collected agricultural production data from 2013 to 2022.

b) Collected data on food crop production in Papua Province was based on reports of agriculture production in Papua province sourced from the Central Bureau of Statistics of Papua Province. This data is used as comparison data for the analysis of determining superior food crop commodities in the Merauke Regency.

2) Location Quotient Analysis is a step to analyze by comparing agricultural production data in Merauke Regency with production data in Papua province to determine superior food crop commodities using the LQ method analysis in Merauke Regency.

3) Hierarchical Clustering: the process of determining the clusters of agricultural areas in a hierarchical manner, which forms certain levels such as tree structures because the clustering process is carried out in stages and tiers to determine the potential of agricultural areas by sub-district category.

a) Normalization: the stage for scaling features or data used to determine clusters so that the distance between data is not too conspicuous and can produce valid clustering results.

b) Implementation of Single Linkage and Euclidean Distance: the process of grouping agricultural areas by looking for similarities between two objects /sub-districts with a minimum distance, measuring using Euclidean distance.

c) A *dendrogram* is a stage that shows a visual representation of the steps in cluster analysis that shows how clusters are formed and the value of the distance coefficient at each step.

4) Mapping of agricultural area

a) The district's mapping agriculture areas determine agricultural areas on a map and coordinates points.

b) Determination of the layer structure on the map is a step for following the function of presenting the information [19] for the potential of the agriculture area. In the form of

colored polygons according to the cluster category that has been formed.

The flowchart of the classification model used for mapping agricultural areas based on superior commodities combining LQ and single linkage is shown in Fig. 2.

A. Location Quotient Analysis

Location Quotient (LQ) analysis is a method used to determine regional potential by comparing the role of a sector in a local area to a higher level [20]. The selection of superior food crop commodities can be called a basis if the LQ value is > 1 by analyzing food crop production data in Merauke Regency and Papua Province. LQ value determines superior food crop commodities using the equation [21].

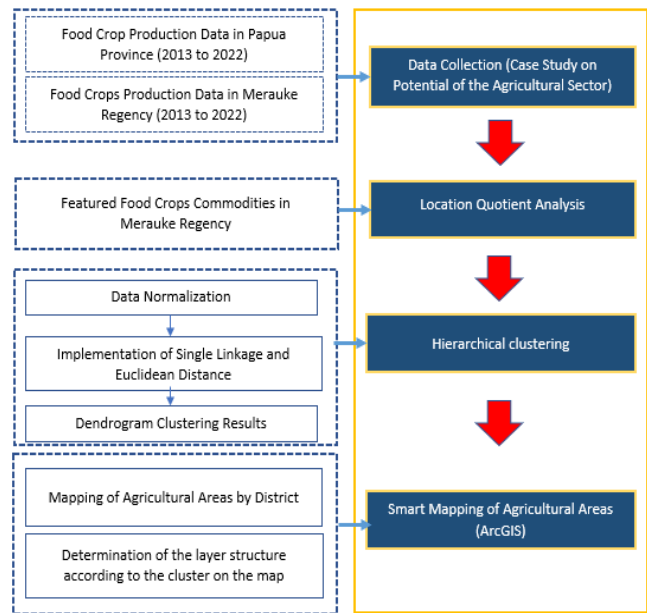


Fig. 1. Research Method Diagram.

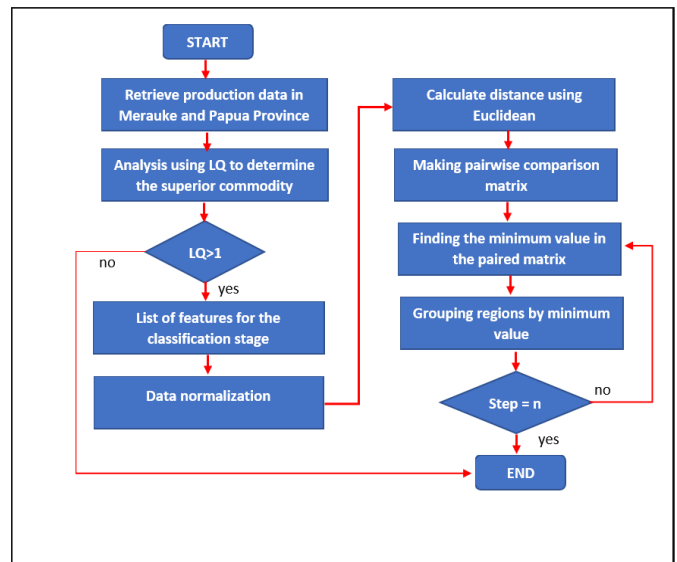


Fig. 2. Flowchart of the Proposed Classification Model.

$$LQ = \frac{\left[\frac{C_i}{\sum_{i=1}^n C_i} \right]}{\frac{D_i}{\sum_{i=1}^n D_i}} \quad (1)$$

The determination of the LQ value depends on the C variable, which is the production of food crop commodities at the city/district level. In contrast, the D variable indicates the province. The criteria for measuring the LQ value to determine the leading food crop commodity are based on the following rules [18]: a) If LQ value >1, indicates that the commodity is a superior food crop, b) If LQ <1 or LQ = 1, it indicates that the food crop commodity is classified as not superior.

B. Hierarchical Clustering using Single Linkage

Cluster analysis is a statistical analysis that aims to group objects based on similar characteristics. These objects will be grouped into one or several groups (clusters) which are identical [13]. The hierarchical method is a cluster analysis that forms certain levels, such as in a tree structure, because the clustering process is carried out in stages and tiers [22].

The results of the hierarchical method analysis can be presented as a dendrogram. The dendrogram is a visual representation of the steps in cluster analysis [23]. It shows how clusters are formed and the value of the distance coefficient at each step [24]. The hierarchical method is divided based on the distance measurement technique between sets used to group objects. Distance measurement in the hierarchical approach includes a single linkage, and the grouping process begins with finding two areas with a minimum distance using the following equation [25].

$$S(v, w) = \min_{ij} \{S(v[i], w[j])\} \quad (2)$$

Measurement of the distance between objects in a single linkage based on the minimum distance, grouped in one cluster using Euclidean Distance based on the following equation [26].

$$d(v, w) = \sqrt{\sum_{i=1}^n (w_i - v_i)^2} \quad (3)$$

Where v, w are two points in Euclidean at n-place, v_i, w_i as vector values indicating the starting point. The use of the hierarchical method with distance measurement techniques provides a solution in its application based on the similarity size to the object's distance [27][28].

III. RESULT AND DISCUSSION

A. Determination of Superior Commodities

The selection of superior food crop commodities is an initial stage of the proposed classification method. Food crop commodities analyzed as superior commodities in Merauke Regency consist of rice, corn, soybeans, peanuts, green beans, sweet potatoes, and cassava. Location quotient analysis compares the yield of food crop production based on commodities in Merauke Regency with regional production in Papua Province. Table 1 shows a recapitulation of data on food crop production in Merauke Regency and Papua Province obtained from survey reports from the Central Statistics Agency

from 2013 to 2022. These data show that rice is a commodity that contributes the most significant production output in Merauke Regency. Determination of superior food crop commodities in Merauke Regency using the LQ method analysis is carried out by comparing the results of food crop production at the Merauke Regency level with production in the Papua province.

Table I shows the LQ calculation results for determining superior commodities based on the rules. If the LQ value >1, then based on the analysis results, it is known that there are three superior food crop commodities in Merauke Regency, namely rice, corn, and peanuts. After analyzing using the LQ method, the next step is classifying agricultural areas based on sub-districts so that regional clusters are formed. Features or data of three types of superior commodities are used as a reference in grouping districts in a set. The analysis of the LQ value uses the recapitulation data of food crop production by applying equation 1, for example:

$$LQ(Rice) = \frac{2520692,44}{2691575,59} / \frac{2670060,14}{6242813,40} = 2,19$$

TABLE I. RESULT OF LQ ANALYSIS

Commodity	Production in Merauke (Ton)	Production in Papua (Ton)	LQ
Rice	2520692,44	2670060,14	2,19
Corn	35007,42	72706,37	1,12
Soya bean	2468,11	29032,61	0,20
Cassava	73755,19	334982,60	0,51
Sweet potato	45862,00	3088929,71	0,03
Peanuts	10063,40	22732,28	1,03
Mung beans	3727,03	24369,69	0,35
Total	2691575,59	6242813,40	

B. Clustering of Agricultural Areas using Single Linkage

The proposed classification model maps agriculture areas with sub-district categories based on superior commodities. Implementation of a single linkage using the production data of these three types of commodities is used to determine regional clusters based on agriculture production survey data from the Central Statistics Agency of Merauke Regency in 2022, shown in Table II. The production of valid sets and normalization of data is carried out using the min-max normalization method. The mapping of agriculture areas in the Merauke Regency consists of twenty sub-districts grouped in clusters of the potential agriculture sector. Applying the single linkage method and calculating the Euclidean distance is used to classify agricultural areas using normalized data. The initial classification step is creating a symmetrical paired matrix by finding the minimum distance between regions to produce regional clusters.

The results of measuring the distance between areas of agriculture potential using the Euclidean distance[26] are shown in Table III. The use of variable D_i is used to represent the name of the agricultural district/area. The results of distance measurements are used to find the minimum value [27] between two districts to apply the classification of agriculture areas using the single linkage method. The smallest distance between two objects at the initial stage of classification is marked with red text in the table. The result of a minimum distance between the D_{13} area representing Naukenjerai and D_{19} representing Elikobel will be grouped into one cluster. For example: $S(v,w)=\min(D_{13},D_{19})=0$.

The next stage is to search for the minimum distance with clusters formed [22] from a combination of D_{13} and D_{19} using equation 2, shown in Table IV. Based on the search results for the minimum value, many regions have the same minimum distance, so at this stage, a merger is carried out between regions in a cluster. If a region has similar features to other regions, it shows a close hierarchical relationship to form a cluster [24], for example: $S(D_{13},D_{19},D_1)=\min(D_{13} \rightarrow D_1, D_{19} \rightarrow D_1) = 0,02$.

The classification step of potential agricultural areas using a single linkage is shown in Table III. The stage of finding the minimum value between the region and the process of grouping regions into specific clusters is repeated continuously until all areas become part of the cluster. The results of the analysis are that three clusters are formed. Each cluster member has similarities based on the distance measurement with the smallest value, represented through superior commodity crop production features.

TABLE II. PRODUCTION OF THREE SUPERIOR COMMODITY IN MERAUKE

ID Distrik	Name of Distric	Production of superior commodity (ton)		
		Rice	Corn	Peanuts
D ₁	Kimaam	2591,60	36,85	0,00
D ₂	Tabonji	591,00	0,00	0,00
D ₃	Waan	109,65	0,00	0,00
D ₄	Ilwayab	18,55	0,00	0,00
D ₅	Okaba	544,05	26,88	0,00
D ₆	Tubang	100,10	0,00	0,00
D ₇	Ngguti	5,75	0,00	0,00
D ₈	Kaptel	16,10	0,00	0,00
D ₉	Kurik	105746,03	712,88	33,00
D ₁₀	Animha	219,01	15,00	0,00
D ₁₁	Malind	50943,60	59,40	70,60
D ₁₂	Merauke	11127,44	60,20	0,00
D ₁₃	Naukenjerai	1727,76	66,72	0,00
D ₁₄	Semangga	62285,81	1238,52	0,00
D ₁₅	Tanah Miring	108983,61	1275,43	59,38
D ₁₆	Jagebob	3615,01	1321,25	713,50
D ₁₇	Sota	22,00	14,30	0,00
D ₁₈	Muting	904,50	78,98	18,70
D ₁₉	Elikobel	2622,50	63,00	0,00
D ₂₀	Ulilin	2018,25	63,00	32,62

TABLE III. COMPARISON MATRIX USING EUCLIDEAN DISTANCE

ID Distric	D ₁	D ₂	D ₃	D ₄	D ₅	D ₆	D ₇	D ₈	D ₉	D ₁₀	D ₁₁	D ₁₂	D ₁₃	D ₁₄	D ₁₅	D ₁₆	D ₁₇	D ₁₈	D ₁₉	D ₂₀
D ₁	0	0,03	0,04	0,04	0,02	0,04	0,04	0,04	1,08	0,03	0,46	0,08	0,02	1,1	1,4	1,39	0,03	0,04	0,02	0,05
D ₂	0,03	0	0,01	0,01	0,02	0,01	0,01	0,01	1,11	0,01	0,48	0,11	0,05	1,1	1,4	1,41	0,01	0,07	0,05	0,07
D ₃	0,04	0,01	0	0,01	0,02	0,01	0,01	0,01	1,11	0,01	0,48	0,11	0,05	1,1	1,4	1,41	0,01	0,07	0,05	0,07
D ₄	0,04	0,01	0,01	0	0,02	0,01	0,01	0,01	1,11	0,01	0,48	0,11	0,05	1,1	1,4	1,41	0,01	0,07	0,05	0,07
D ₅	0,02	0,02	0,02	0,02	0	0,02	0,02	0,02	1,1	0,01	0,48	0,1	0,03	1,1	1,4	1,4	0,01	0,05	0,03	0,06
D ₆	0,04	0,01	0,01	0,01	0,02	0	0,01	0,01	1,11	0,01	0,48	0,11	0,05	1,1	1,4	1,41	0,01	0,07	0,05	0,07
D ₇	0,04	0,01	0,01	0,01	0,02	0,01	0	0,01	1,11	0,01	0,48	0,11	0,05	1,1	1,4	1,41	0,01	0,07	0,05	0,07
D ₈	0,04	0,01	0,01	0,01	0,02	0,01	0,01	0	1,11	0,01	0,48	0,11	0,05	1,1	1,4	1,41	0,01	0,07	0,05	0,07
D ₉	1,08	1,11	1,12	1,12	1,11	1,12	1,12	1,12	0	1,11	0,72	1	1,07	0,6	0,4	1,41	1,11	1,08	1,07	1,07
D ₁₀	0,03	0,02	0,01	0,01	0,01	0,01	0,01	0,01	1,11	0	0,48	0,11	0,04	1,1	1,4	1,41	0,01	0,06	0,04	0,07
D ₁₁	0,46	0,47	0,48	0,48	0,48	0,48	0,48	0,48	0,71	0,48	0	0,38	0,46	0,9	1,1	1,39	0,48	0,47	0,46	0,45
D ₁₂	0,08	0,1	0,11	0,11	0,11	0,11	0,11	0,11	1	0,11	0,38	0	0,08	1	1,3	1,38	0,11	0,1	0,08	0,09
D ₁₃	0,02	0,05	0,05	0,05	0,03	0,05	0,05	0,05	1,07	0,04	0,47	0,08	0	1,1	1,4	1,38	0,04	0,03	0	0,05
D ₁₄	1,06	1,09	1,1	1,1	1,08	1,1	1,1	1,1	0,56	1,09	0,91	1	1,04	0	0,4	1,14	1,09	1,04	1,04	1,05
D ₁₅	1,36	1,39	1,4	1,4	1,38	1,4	1,4	1,4	0,43	1,39	1,07	1,29	1,35	0,4	0	1,34	1,39	1,35	1,35	1,34
D ₁₆	1,39	1,41	1,41	1,41	1,4	1,41	1,41	1,41	1,41	1,41	1,39	1,38	1,38	1,1	1,3	0	1,41	1,35	1,38	1,35
D ₁₇	0,03	0,01	0,01	0,01	0,01	0,01	0,01	0,01	1,11	0,01	0,48	0,11	0,04	1,1	1,4	1,41	0	0,06	0,04	0,07
D ₁₈	0,04	0,07	0,07	0,07	0,05	0,07	0,07	0,07	1,08	0,06	0,47	0,1	0,03	1	1,4	1,35	0,06	0	0,03	0,03
D ₁₉	0,02	0,05	0,05	0,05	0,04	0,05	0,05	0,05	1,07	0,04	0,46	0,08	0,01	1,1	1,4	1,38	0,04	0,03	0	0,05
D ₂₀	0,05	0,07	0,07	0,07	0,06	0,07	0,07	0,07	1,07	0,06	0,45	0,09	0,05	1,05	1,34	1,35	0,07	0,03	0,05	0

TABLE IV. IMLEMENTATION OF SINGLE LINKAGE BASED ON MEASUREMENT OF THE FORMED CLUSTER

ID Distric	D13,D19	D1	D2	D3	D4	D5	D6	D7	D8	D9	D10	D11	D12	D14	D15	D16	D17	D18	D20
D13,D19	0	0,02	0,05	0,05	0,05	0,03	0,05	0,05	0,05	1,07	0,04	0,46	0,08	1,04	1,35	1,38	0,04	0,03	0,05
D1	0,02	0	0,03	0,04	0,04	0,02	0,04	0,04	0,04	1,08	0,03	0,46	0,08	1,06	1,36	1,39	0,03	0,04	0,05
D2	0,05	0,03	0	0,01	0,01	0,02	0,01	0,01	0,01	1,11	0,02	0,47	0,1	1,09	1,39	1,41	0,01	0,07	0,07
D3	0,05	0,04	0,01	0	0,1	0,02	0,01	0,01	0,01	1,12	0,01	0,48	0,11	1,1	1,4	1,41	0,01	0,07	0,07
D4	0,05	0,04	0,01	0,1	0	0,02	0,01	0,01	0,01	1,12	0,01	0,48	0,11	1,1	1,4	1,41	0,01	0,07	0,07
D5	0,03	0,02	0,02	0,02	0,02	0	0,02	0,02	0,02	1,11	0,01	0,48	0,11	1,08	1,38	1,4	0,01	0,05	0,06
D6	0,05	0,04	0,01	0,01	0,01	0,02	0	0,01	0,01	1,12	0,01	0,48	0,11	1,1	1,4	1,41	0,01	0,07	0,07
D7	0,05	0,04	0,01	0,01	0,01	0,02	0,01	0	0	1,12	0,01	0,48	0,11	1,1	1,4	1,41	0,01	0,07	0,07
D8	0,05	0,04	0,01	0,01	0,01	0,02	0,01	0	0	1,12	0,01	0,48	0,11	0,05	1,4	1,41	0,01	0,07	0,07
D9	1,07	1,08	1,11	1,12	1,12	1,11	1,12	1,12	1,12	0	1,11	0,71	1	0,56	0,43	1,41	1,11	1,08	1,07
D10	0,04	0,03	0,02	0,01	0,01	0,01	0,01	0,01	0,01	1,11	0	0,48	0,11	1,09	1,39	1,41	0	0,06	0,06
D11	0,46	0,46	0,47	0,48	0,48	0,48	0,48	0,48	0,48	0,71	0,48	0	0,38	0,91	1,07	1,39	0,48	0,47	0,45
D12	0,08	0,08	0,1	0,11	0,11	0,11	0,11	0,11	0,11	1	0,11	0,38	0	1	1,29	1,38	0,11	0,1	0,09
D14	1,04	1,06	1,09	1,1	1,1	1,08	1,1	1,1	0,05	0,56	1,09	0,91	1	0	0,44	1,14	1,09	1,04	1,05
D15	1,35	1,36	1,39	1,4	1,4	1,38	1,4	1,4	1,4	0,43	1,39	1,07	1,29	0,44	0	1,33	1,39	1,35	1,34
D16	1,38	1,39	1,41	1,41	1,41	1,4	1,41	1,41	1,41	1,41	1,41	1,39	1,38	1,14	1,33	0	1,41	1,35	1,34
D17	0,04	0,03	0,01	0,01	0,01	0,01	0,01	0,01	0,01	1,11	0,01	0,48	0,11	1,09	1,39	1,41	0	0,06	0,07
D18	0,03	0,04	0,07	0,07	0,07	0,05	0,07	0,07	0,07	1,08	0,06	0,47	0,1	1,04	1,35	1,35	0,06	0	0,02
D20	0,05	0,05	0,07	0,07	0,07	0,06	0,07	0,07	0,07	1,07	0,06	0,45	0,09	1,05	1,34	1,34	0,07	0,02	0

C. Classification Result of Agricultural Area

Mapping the potential of agriculture areas by carrying out the intelligent mapping concept is based on the results of regional classification using hierarchical clustering, namely the single linkage method. The implementation proposed a classification model for intelligent mapping by compiling a layer structure that is categorized based on the clusters that have been formed, which consist of three. The layer representation on the map for mapping the potential of agricultural areas is shown through colored polygon images that show the boundaries of agriculture areas based on sub-district categories in Merauke Regency based on their respective clusters.

Fig. 3(a) shows the stages of classifying potential agricultural areas represented in the form of a dendrogram. Sub-districts that have the same color symbol are in one cluster. The first cluster with the blue sign has 16 sub-districts with a low potential for producing only commodities. The second cluster with the red mark has three members, and the third consists of one sub-district.

The area is in one cluster if a sub-district has the same polygon color. The mapping of agriculture areas shown in Fig. 3(b) can represent regions or sub-districts that produce the best production of superior commodities with the following information on the order of clusters:

- 1) Cluster 1 indicates that the area has a low amount of superior commodity production.
- 2) Cluster 2 can be called the central cluster. The sub-districts members of this cluster have a high number of superior commodity productions in the high category, with particular dominance on rice commodities.
- 3) Cluster 3 is the highest level, indicating that cluster members are agricultural areas producing the most increased production of superior commodities with the dominance of two types, corn, and peanuts.

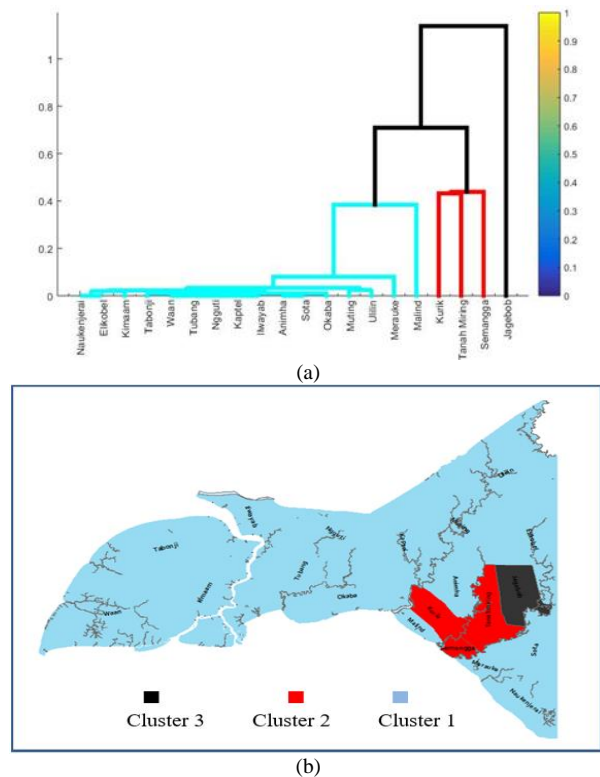


Fig. 3. (a). Dendrogram of Agricultural Area Classification using Single Linkage, (b). Implementation Classification Model for Mapping Agricultural area based on Superior Commodities.

The proposed classification method is the concept of intelligent mapping that helps map agricultural areas that provide information on superior food crop commodities so that it can become data for policymakers. The development of the agriculture industry can increase GDP income from the agriculture sector regionally and nationally, focusing on superior commodities.

IV. CONCLUSION

The classification model combining location quotient analysis and single linkage to group areas based on the agriculture sector's potential showed it could be used as a reference for intelligent mapping in a geographic information system. The classification stage groups sub-districts/regions in a cluster by measuring the minimum distance between two sub-districts that focus on superior commodities that can be used as information for those who need it. The sustainable agriculture industry develops prospects so it can be exported outside the region and improve the welfare of people who depend on the agriculture sector.

The stage of future research is mapping of livestock potential areas that are integrated with agricultural potential by utilizing Global Position System (GPS) technology in geographic information systems, to assist in finding potential land locations for both the agricultural and livestock sectors.

ACKNOWLEDGMENTS

The authors would like to thank the leadership and staff at the Ministry of Education, Culture, Research and Technology. Directorate General of Higher Education, Research and Technology, Republic of Indonesia, who has financed the implementation of this research, based on the research grant contract for fiscal year 2022, number 224/E5/PG.02.00.PT/2022 and also the contract between LPPM Universitas Musamus and researchers 169.3/UN.52.8/LT/2022.

REFERENCES

- [1] Badan Pusat Statistik Provinsi Papua, Provinsi Papua dalam Angka 2022. 2022.
- [2] Badan Pusat Statistik Kabupaten Merauke, Kabupaten Merauke dalam Angka 2022. 2022.
- [3] E. Humaidi, I. Putu Ajie Windu Kertayoga, and Analiasari, "Preparation of a Map of Leading Food Commodities in the Lampung Province Using the Location Quotient (LQ) Method," *IOP Conf. Ser. Earth Environ. Sci.*, vol. 1012, no. 1, 2021, doi: 10.1088/1755-1315/1012/1/012009.
- [4] L. Sumaryanti, L. Lamalewa, and T. Istanto, "Implementation Of Fuzzy Multiple Criteria Decision Making For Recommendation Paddy Fertilizer," *Int. J. Mech. Eng. Technol.*, vol. 10, no. 03, pp. 236–243, 2019, doi: IJMET_10_03_024.
- [5] L. Sumaryanti, T. Istanto, and S. Pare, "Rule Based Method in Expert System for Detection Pests and Diseases of Corn," *J. Phys. Conf. Ser.*, vol. 1569, no. 2, 2020, doi: 10.1088/1742-6596/1569/2/022023.
- [6] M. Altalak, M. Ammad uddin, A. Alajmi, and A. Rizg, "Smart Agriculture Applications Using Deep Learning Technologies: A Survey," *Appl. Sci.*, vol. 12, no. 12, p. 5919, 2022, doi: 10.3390/app12125919.
- [7] S. Gao, "The Application of Information Classification in Agricultural Production Based on Internet of Things and Deep Learning," *IEEE Access*, vol. 10, pp. 22622–22630, 2022, doi: 10.1109/ACCESS.2022.3154607.
- [8] N. Deepa, M. Z. Khan, B. Prabadevi, D. R. P. M. Vincent, P. K. R. Maddikunta, and T. R. Gadekallu, "Multiclass model for agriculture

- development using multivariate statistical method," *IEEE Access*, vol. 8, pp. 183749–183758, 2020, doi: 10.1109/ACCESS.2020.3028595.
- [9] L. Sumaryanti, T. K. Rahayu, A. Prayitno, and Salju, "Comparison study of SMART and AHP method for paddy fertilizer recommendation in decision support system," *IOP Conf. Ser. Earth Environ. Sci.*, vol. 343, no. 1, 2019, doi: 10.1088/1755-1315/343/1/012207.
- [10] S. P. Raja, B. Sawicka, Z. Stamenkovic, and G. Mariammal, "Crop Prediction Based on Characteristics of the Agricultural Environment Using Various Feature Selection Techniques and Classifiers," *IEEE Access*, vol. 10, pp. 23625–23641, 2022, doi: 10.1109/ACCESS.2022.3154350.
- [11] E. Nizeyimana, J. Nsenga, R. Shibusaki, D. Hanyurwimfura, and J. S. Hwang, "Design of Smart IoT Device for Monitoring Short-term Exposure to Air Pollution Peaks," *Int. J. Adv. Comput. Sci. Appl.*, vol. 13, no. 1, pp. 17–24, 2022, doi: 10.14569/IJACSA.2022.0130103.
- [12] H. Yang, T. Wen, X. Yang, and H. Lin, "Deep Learning Agricultural Information Classification Combined With Internet of Things Technology in Agricultural Production and Economic Management," *IEEE Access*, vol. 10, pp. 54713–54719, 2022, doi: 10.1109/access.2022.3176643.
- [13] H. Ismanto, Suharto, Azhari, and L. Arsyad, "Ranking method in group decision support to determine the regional prioritized areas and leading sectors using Garrett score," *Int. J. Adv. Comput. Sci. Appl.*, vol. 9, no. 11, pp. 94–99, 2018, doi: 10.14569/IJACSA.2018.091114.
- [14] F. Kordia and Y. Hossein, "Crop classification based on phenology information by using time series of optical and synthetic-aperture radar images," *Remote Sens. Appl. Soc. Environ.*, vol. 27, no. August 2022, pp. 1–12, 2022, doi: 10.1016/j.rsase.2022.100812.
- [15] F. Ros and S. Guillaume, "A hierarchical clustering algorithm and an improvement of the single linkage criterion to deal with noise," *Expert Syst. Appl.*, vol. 128, no. August 2019, pp. 96–108, 2019, doi: 10.1016/j.eswa.2019.03.031.
- [16] L. Li, J. Cheng, J. Bannister, and X. Mai, "Geographically and temporally weighted co-location quotient: an analysis of spatiotemporal crime patterns in greater Manchester," *Int. J. Geogr. Inf. Sci.*, vol. 36, no. 5, pp. 918–942, 2022, doi: 10.1080/13658816.2022.2029454.
- [17] T. Atmayanti, M. Johari, and A. H. Sukmana, "Location Quotient Analysis in Identifying Leading Sector in East Lombok Regency 2015–2020," *Int. J. Islam. Soc. Sci.*, pp. 28–35, 2021.
- [18] N. Xu, Y. Cheng, and X. Xu, "Using location quotients to determine public-natural space spatial patterns: A Zurich model," *Sustainability*, vol. 10, no. 10, 2018, doi: 10.3390/su10103462.
- [19] A. A. Murad, A. I. Dalhat, and A. A. Naji, "Using geographical information system for mapping public schools distribution in Jeddah City," *Int. J. Adv. Comput. Sci. Appl.*, vol. 11, no. 5, pp. 82–90, 2020, doi: 10.14569/IJACSA.2020.0110513.
- [20] Y. S. Maulana, A. H. Munawar, D. Hadiani, Ratningsih, and T. Wibisono, "Location Quotient Analysis (LQ) in Determining the Excellent Commodity," vol. 27, no. ICOSHEET 2019, pp. 65–68, 2020, doi: 10.2991/ahsr.k.200723.015.
- [21] D. T. Harjanti, M. I. Apriliyana, and A. C. Arini, "Analysis of Regional Leading Sector Through Location Quotient Approach, Shift Share Analysis, and Klassen Typology (Case Study: Sanggau Regency, West Kalimantan Province)," *J. Geogr. Gea*, vol. 21, no. 2, pp. 147–158, 2021, doi: 10.17509/gea.v21i2.38870.
- [22] A. Cena and M. Gagolewski, "Genie OWA: Robustifying hierarchical clustering with OWA-based linkages," *Inf. Sci. (Ny.)*, vol. 520, pp. 324–336, 2020, doi: 10.1016/j.ins.2020.02.025.
- [23] B. Hassan, R. Zineb, L. Amine, and L. Elhoussine, "A Complexity Survey on Density based Spatial Clustering of Applications of Noise Clustering Algorithms," *Int. J. Adv. Comput. Sci. Appl.*, vol. 12, no. 2, pp. 664–670, 2021, doi: 10.14569/IJACSA.2021.0120283.
- [24] F. Schoen and L. Tigli, "Efficient large scale global optimization through clustering-based population methods," *Comput. Oper. Res.*, vol. 127, p. 105165, 2021, doi: 10.1016/j.cor.2020.105165.
- [25] K. K. Mohbey and G. S. Thakur, "An Experimental Survey on Single Linkage Clustering," *Int. J. Comput. Appl.*, vol. 76, no. 17, pp. 6–11, 2013, doi: 10.5120/13337-0327.

- [26] F. Ros and S. Guillaume, "A hierarchical clustering algorithm and an improvement of the single linkage criterion to deal with noise," *Expert Syst. Appl.*, vol. 128, pp. 96–108, 2019, doi: 10.1016/j.eswa.2019.03.031.
- [27] Y. Song, S. Jin, and J. Shen, "A unique property of single-link distance and its application in data clustering," *Data Knowl. Eng.*, vol. 70, no. 11, pp. 984–1003, 2011, doi: 10.1016/j.datak.2011.07.003.
- [28] M. Sammour, Z. A. Othman, Z. Muda, and R. Ibrahim, "An agglomerative hierarchical clustering with association rules for discovering climate change patterns," *Int. J. Adv. Comput. Sci. Appl.*, vol. 10, no. 3, pp. 233–240, 2019, doi: 10.14569/IJACSA.2019.0100330.

Analysis of Unsupervised Machine Learning Techniques for an Efficient Customer Segmentation using Clustering Ensemble and Spectral Clustering

Nouri Hicham, Sabri Karim

Research Laboratory on New Economy and Development (LARNED)
Faculty of Legal Economic and Social Sciences AIN SEBAA, Hassan II University of Casablanca, Morocco

Abstract—Customer segmentation is key to a corporate decision support system. It is an important marketing technique that can target specific client categories. We create a novel consumer segmentation technique based on a clustering ensemble; in this stage, we ensemble four fundamental clustering models: DBSCAN, K-means, Mini Batch K-means, and Mean Shift, to deliver a consistent and high-quality conclusion. Then, we use spectral clustering to integrate numerous clustering findings and increase clustering quality. The new technique is more flexible with client data. Feature engineering cleans, processes, and transforms raw data into features. These traits are then used to form clusters. Adjust Rand Index (ARI), Normalized Mutual Information (NMI), Dunn's Index (DI), and Silhouette Coefficient (SC) were utilized to evaluate our model's performances with individual clustering approaches. The experimental analysis found that our model has the best ARI (70.14%), NMI (71.75), DI (75.15), and SC (72.89%). After retaining these results, we applied our model to an actual dataset obtained from Moroccan citizens via social networks and email boxes between 03/06/2022 and 19/08/2022.

Keywords—Machine learning; customer segmentation; marketing; clustering ensemble; spectral clustering

I. INTRODUCTION

It is possible to win the competition in the market and enhance corporate earnings by better understanding the client's needs. Companies can develop successful marketing strategies if they are aware of the wants and needs of their target audiences. While the requirements and expectations of each customer are unique, many customers share identical or quite similar qualities. Customer segmentation is one method that may be used to put together multiple different consumers who share similar qualities. Improving the quality of the connections with your customers also requires proper consumer segmentation. Marketing intelligence is conducting information analysis to comprehend better a target market and its consumers' demographics [1], [2].

In marketing, it is common for analysts to categorize customers into comparable customer groups to understand better how to advertise to each group of customers. Therefore, segmentation is a collection of approaches that might be useful in categorizing different types of customers. Customers' existing relationships with a company are the primary focus of most direct marketing operations. The more you know about your customer's needs, desires, and

purchasing habits, the easier it is to tailor marketing programs to their needs and desires and how they buy things [3].

Marketers can determine the approach that will be most successful in communicating with each unique consumer by segmenting their customer base. Marketers can zero in on particular demographic, behavioral, and other characteristics of their target audience by conducting in-depth analyses of vast amounts of data about existing and prospective clients [4], [5].

A frequent objective in marketing is to increase the worth of each consumer (revenue and profit). To achieve success in this aspect of the marketing mix, it is vital to understand how a particular marketing action influences customers' behaviour. Regarding customer segmentation, and "action-centric" approach prioritizes the impact that marketing activities will have on a customer's lifetime value (CLV) over the value that marketing activities will have in the short term. This is in contrast to a "short-term value" approach. As a direct result, consumers ought to be divided into distinct categories according to the amount of money they will spend throughout their lifetime [6].

In this paper, we ensemble four basic clustering models (DBSCAN, K-means, MiniBatch K-means, and MeanShift) to develop a novel consumer segmentation strategy based on a clustering ensemble, which yields a more consistent and high-quality result than any of the individual clustering techniques. We then use spectral clustering to combine the findings of different clustering methods to increase the overall quality of our clustering results. After the retention of these results, we applied our model to a real dataset, which was collected from Moroccan residents using a questionnaire sent via social networks and email boxes between 03/06/2022 and 25/07/2022. As for the rest of this paper, it is structured as follows: The literature review is described in Section II, the methodology and proposed model are presented in Section III, the findings are covered in Section IV, as well as the findings, interpretations of the study and directions for future research are presented in Section V.

II. BACKGROUND

Knowing customer behavior in today's highly competitive and ever-changing business environment is crucial. Customers must be categorized according to their demographics and the products they buy. This is an essential component of client

segmentation that enables marketers to target certain target groups more precisely with their promotional, marketing, and product development strategies. The relevance of data-driven marketing, a crucial component in client segmentation, is growing due to the growth of data sources, particularly social networks. Because of their immense size and complexity, modern databases make data-driven marketing and customer segmentation exceedingly challenging in the retail industry. Until recently, traditional cluster analysis approaches were employed on retail databases. Nevertheless, because there are so many different kinds of customers today, statistical clustering algorithms find it harder and harder to evaluate and understand what customers do [7].

In the past five years, due to the recent development of machine learning techniques and data science, many one-of-a-kind algorithms in these two fields have been developed for customer relationship management, specifically for customer segmentation. These algorithms have been developed for customer relationship management (CRM) software [8]. An integrated strategy employing the Apriori algorithm and the CRM method with associated mining is used in customer segmentation [9]. This strategy brings the benefits of both methodologies to bear in solving this challenge. For consumer segmentation, [10] utilized two primary methods: the LRFM (Length, Recency, Frequency, and Monetary) techniques and an extended model known as the LRFM-Average Item (AI) model. Both of these methods utilized LRFM techniques. The authors concluded that adding simple parameters and averages did not improve customer segmentation and did not show a significant change in results. This means that complex parameters are needed for better customer segmentation results.

As demonstrated in [11], an investigation into silent customers was carried out since silent consumers are a category of customers that a company runs the risk of quickly losing. As a result, it is essential to research the characteristics of these clients to arrive at the most appropriate business decisions. This research came up with a K-means method for customer segmentation that focused on silent customers to help the company make more money in the telecom industry.

About the Yunnan Electricity Market, an algorithm for market segmentation was developed in [12] that was primarily concerned with density-based spatial clustering of applications with noise (DBSCAN) and the K-means technique. In [13], the K-means clustering algorithm and the SPSS Software were used to construct a real-time and online system for predicting seasonal sales in annual cycles. This system integrated an important complex feature of temporal spikes in the sales of particular items, making it capable of predicting seasonal sales on annual cycles. The study [14] explains how the technique of unsupervised machine learning can be used to tackle the difficult problem of consumer segmentation by analyzing purchase data from credit cards used by African customers. The objective of [15] customer segmentation with a multi-

layer perceptron (MLP) neural network is to categorize customers into separate groups according to the characteristics of those categories.

Furthermore, in [16], The Mini Batch K-means technique is implemented to group sediment samples. The clustering result will be verified using a set of four typical evaluation indices. Using this approach, simulations show that the Sample network may be divided into three sedimentary clusters: fluvial, marine, and lacustrine. Researchers have found that experimental results on sediment particle size have an accuracy of up to 0.92254367, suggesting that this technique of studying sedimentary environment by grain size works exceptionally well and precisely. On the other hand, in [17], Using the proposed automatic selection of nearest neighbors for density gradients, it is proven to identify the number, position reliably, and form of non-elliptical clusters in multivariate data analysis and picture segmentation using mean shift.

Recent years have seen an increase in ensemble learning (EL), which has emerged as a successful teaching strategy. EL utilizes a meta-classifier to integrate the results of different classification techniques [18]. The complete training set is utilized for training the base classifiers, and the outputs of the base-level model are used as features in the learning process for the meta-classifier. Another thing to add is that EL is superior to other approaches because it combines the most accurate components of numerous machine learning to provide more accurate predictions than any algorithm in the ensemble can produce. This makes EL the method of choice [19].

III. METHODOLOGY

This study offered a new customer segmentation strategy based on the Clustering ensemble technique. DBSCAN, K-means, MiniBatch K-Means, and MeanShift algorithm are used in the suggested method, shown in Fig. 1. The outputs are combined with a consensus function. Stacking ensemble learning allows us to use each model's structural and functional benefits while increasing overall performance. The consensus function and unsupervised machine learning models will be discussed in greater detail in the following paragraphs.

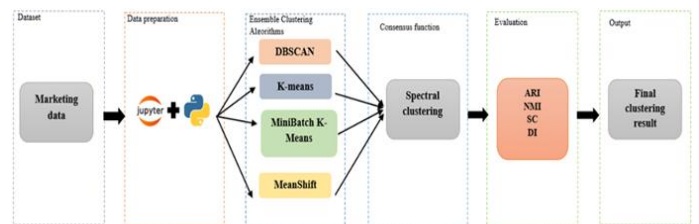


Fig. 1. The Global Architecture.

The general architecture structure is made up of the five fundamental steps listed below:

TABLE I. THE USED DATASET

Variable	Data Type	Range	Description
ID	numerical	Integer	Displays a customer's ID.
Sex	categorical	{0,1}	Customer's gender. 0=male/1=female
Marital status	categorical	{0,1}	Customer's marital status. 0=single/1=non-single
Age	numerical	Integer	The customer's age in years
Education	categorical	{0,1,2,3}	Customer's education. 1=high school, 2=college, 3=graduate
Income	numerical	Real	Customer's self-reported annual US income.
Occupation	categorical	{0,1,2}	Customer's profession. 0=unemployed/1=employee/official/2=management or self-employed
Settlement size	categorical	{0,1,2}	Customer's city size. 0=small/1=midsize/2=big

TABLE II. SOME DESCRIPTIONS OF DATASET

	ID	Sex	Marital status	Age	Education	Income	Occupation	Settlement size
count	35000	35000	35000	35000	35000	35000	35000	35000
mean	1.00	0.457	0.496500	35.909	1.038	120954.419000	0.810500	0.739000
std	5.77e+02	0.4982	0.500113	11.7194	0.599	38108.824679	0.638587	0.812533
min	1.00	00	00	18.00	0.00	35832.00	00	00
25%	1.00	00	00	27.00	1.00	97663.250	00	00
50%	1.00	00	00	33.00	1.00	115548.50	1.00	1.00
75%	1.00	1.00	1.00	42.00	1.00	138072.250	1.00	1.00
max	1.00	1.00	1.00	76.00	3.00	309364.00	2.00	2.00

A. Dataset

The data for this study, which involves 35,000 clients and eight different characteristics, was collected from a supermarket mall. This database includes essential customer information, such as the customer's identification number (Customer ID), annual income, gender, age, and expenditure score. In order to make sense of the marketing team and develop a suitable strategy for the situation, we need to have a solid understanding of these clients, such as who the target customers are. The full dataset description is provided in Table I and II.

1) *Data preparation*: Data selection, preprocessing, and transformation are the three stages of the process that are involved in getting data suitable for an algorithm that does machine learning [20] [21].

2) *Data selection*: At this point, we narrow down all of the data we have access to and are utilizing by selecting a subset of it to work with. Consider the data we already own, the data we do not possess, and the data we can get rid of.

3) *Data preprocessing*: The preprocessing of data is necessary because we frequently receive a large amount of raw data that machine learning algorithms cannot use. It is essential to process the raw data entirely before incorporating it into the various machine learning algorithms. In order to compile our selected data, we first formatted it, then cleaned it, and last, we took some samples from it. The data's poor quality hinders several attempts to process the data.

4) *Data transformation*: Data processing can be transformed through a series of procedures known as "data transformation." Another name for this practice is "feature engineering." The extraction of features from our data is a time-consuming process, but the benefits of machine learning

may be worth the wait. The following are the three most frequent methods in which data is altered:

Depending on the amount being measured, the properties of the pre-processed data may have been given a variety of scales. Each of the characteristics must be the same size.

- **Aggregation**: It is possible that some features can be combined to make a single feature that fits the issue that we are attempting to solve better.
- **Decomposition**: It is possible that intricate elements are easier to understand if they are broken up into chunks. Decomposing the subject into its parts may be helpful. For illustration, a feature that displays the time and date as a long string can be simplified such that it only displays the current hour of the day.

B. Ensemble Clustering Algorithms

The DBSCAN, K-means, MiniBatch K-means, and MeanShift basis clustering algorithms will be the topics of discussion in this article section.

- **DBSCAN**

Density-Based Clustering is a term that refers to different unsupervised learning approaches that identify different clusters in the data. These approaches are premised on the idea that a group in data space is a sector that contains a significant number of points and is partitioned into smaller regions that include a less considerable amount of points [22].

The abbreviation for a technique that uses density-based clustering as its basis is DBSCAN, which stands for Density-Based Spatial Clustering of Applications with Noise. Using large amounts of data with outlying values and noise, clusters of different shapes and sizes can be found [23].

The DBSCAN method makes use of two different parameters, which are as follows [24]:

minPts is the minimum amount of clustered points (also known as a threshold) that are necessary for a region to be considered dense.

Eps() is an abbreviation for the distance measure used to determine which points are located in close proximity to a specific point.

- K-means

Unsupervised machine learning K-means clustering may be used on a dataset to determine the data object groupings within it. There are other alternative data grouping methods, but the k-means clustering method is one of the oldest and simplest to comprehend [25]. The "K-Means algorithm" parameter "k" represents the number of data clusters. We have two ways of picking the right number of clusters: the Elbow method (which graphs random values to achieve the best k value) (see Fig. 5) and the Silhouette score approach (the value which has the greatest score will be considered as the optimal k value) (the value which has the highest score will be taken as the best k value). Using these two, we find the optimum k value is three and train the model using three [26]. According to the Euclidean distance, clustering goals are chosen which reduce the total of squares of all types in a given data set X, which contains n multi-dimensional data points.

$$d = \sum_{k=1}^k \sum_{i=1}^n \Pi(x_i - u_k) \Pi^2$$

K denotes the centers of the first K clusters, u_k is shorthand for the kth cluster center, and x_i is shorthand for the ith data point. The answer to the problem of the centroid u_k can be found as follows:

$$\begin{aligned} \frac{\delta}{\delta u_k} &= \frac{\delta y}{\delta u_k} \sum_{k=1}^k \sum_{i=1}^n (x_i - u_k)^2 \\ &= \sum_{k=1}^k \sum_{i=1}^n \frac{\delta y}{\delta u_k} (x_i - u_k)^2 \\ &= \sum_{i=1}^n 2(x_i - u_k) \end{aligned}$$

Let the second equation be zero. Then $u_k = \frac{1}{n} \sum_{i=1}^n x_i$

- MiniBatch K-means

Clustering on enormous datasets can also be accomplished using the Mini-batch K-means clustering algorithm as an alternative to the K-means technique. It frequently outperforms the standard K-means algorithm when working with big datasets since it does not cycle over the entire dataset. This is because it does not cycle over the entire dataset. It starts by making random data batches to store them in memory. Then, for each loop, it collects a random data batch to update the clusters [27] [29].

The key benefit of mini-batch K-means is that it reduces the processing required to identify clusters. The K-means algorithm may be more to your liking, but when dealing with a big dataset, the mini-batch method is the way to go [28].

- Mean Shift algorithm

The Mean Shift Clustering Algorithm is a technique based on the centroid that is useful in various applications, including unsupervised learning. It is one of the most successful algorithms for a variety of machine learning applications, including clustering, which is one of those applications. Each individual data point is then relocated in the direction of the centroids of the region, which are determined by taking the average of all the other places. A different name for this technique is the mode-seeking algorithm. The benefit of the method is that it disperses groups of objects according to the data without automatically estimating the number of clusters depending on bandwidth. This is an advantage over competing algorithms.

C. Consensus Function

Clustering ensemble (CE) is a method that has emerged as an essential tool for improving the overall quality of clustering solutions. This method merges the multiple clustering results obtained through DBSCAN, K-means, MiniBatch K-means, and MeanShift. This research project describes a novel approach to cluster ensembles predicated on spectral clustering. This function is the first step in the CE algorithm, and it is possible to improve the outcomes of individual clustering algorithms because it is the major step in the algorithm [30] [31]. The final consensus partition is found, which is the result of any CE technique that has been used.

D. Evaluation

Adjust Rand Index (ARI), Normalised Mutual Information (NMI), Dunn's Index (DI), and Silhouette Coefficient (SC) were the performance indicators that we used to compare the results obtained by the proposed method with those obtained by base classifiers (DBSCAN, K-means, MiniBatch K-means, and MeanShift). This allowed us to determine whether or not the method that was proposed was effective. We applied it to the dataset that was described above.

- Adjust Rand Index (ARI)

The adjusted Rand index (ARI) is a measurement that is frequently utilized in the field of cluster analysis to determine the level of agreement that exists between two data partitions. Since the index's inception, there has been a growing amount of interest in investigating cases involving extreme agreement and disagreement under various conditions. This investigation aims to gain a deeper understanding of the index [32], [33].

The following denotes the ARI:

$$ARI = \frac{\sum_{ij} \binom{n_{ij}}{2} - \left[\sum_i \binom{a_i}{2} \sum_j \binom{b_j}{2} \right] / \binom{n}{2}}{1/2 \left[\sum_i \binom{a_i}{2} + \sum_j \binom{b_j}{2} \right] - \left[\sum_i \binom{a_i}{2} \sum_j \binom{b_j}{2} \right] / \binom{n}{2}}$$

Where n_{ji} , a_i and b_j are values from the contingency table.

- Normalised Mutual Information (NMI)

Normalized mutual information, also known as NMI, is a measurement that is frequently utilized to compare different community identification approaches. More recently, the necessity of adjusting information theory-based measures have been advocated because of the so-called selection bias problem. This problem is that these kinds of measures tend to pick clustering solutions that include more communities [34], [35]. The Mutual Information (MI) score is normalized to produce the Normalized Mutual Information (NMI), which scales the results between 0 and 1 (1 perfect correlation).

The following formula shows the NMI:

$$NMI(y, c) = \frac{2 * I(y, c)}{[H(y) + H(c)]}$$

where, 1) y = class names 2) c = group identifiers 3) $H(\cdot)$ = Entropy 4). The formula for the amount of mutual information between y and c is $I(y; c)$.

- Silhouette Coefficient (SC)

A statistic that can be used to evaluate a clustering technique is called the silhouette score. The silhouette score is the sum of two separate scores, referred to as a and b . ‘ a ’ indicates the average range between a sampling site and every other point that is part of the same cluster. [36] In contrast, ‘ b ’ shows the typical mean distance between a sample and all other points that are part of the cluster that is the next closest to it [37]. The following formula is used to determine a sample's score for the silhouette category:

$$s = \frac{b - a}{\max(a, b)}$$

The average of the silhouette scores obtained for each sample constitutes a set's overall silhouette score. The score for the silhouette might range anywhere from -1 to +1. A silhouette score of -1 indicates that the clustering was inaccurate, whereas a score of +1 indicates that the clustering was correct and highly dense. A score of 0 for the silhouette indicates that the groups are overlapping.

- Dunn's Index(DI)

Another statistic might be employed when evaluating clustering techniques, like DI [38]. The formula for calculating DI is dividing the shortest distance between clusters by the most significant size possible. A more significant DI indicates that the clustering is done more effectively. It works under the assumption that more effective clustering results in clusters that are both closely packed and physically distinct from one another [39]. The following formula can be used to determine the value of the Dunn's Index:

$$DI = \frac{\min_{1 \leq i < j \leq n} d(i, j)}{\max_{1 \leq k \leq n} d'(k)}$$

where i, j , and k are indices for groups, d represents the distance between clusters, and d' measures the difference between clusters within the same group.

IV. RESULTS AND DISCUSSIONS

The following information can be found in this section: The research results of our tests assess the effectiveness of the most common diverse analytical and unsupervised techniques and offer a new customer segmentation strategy based on the Clustering ensemble technique. The suggested strategy uses the algorithms DBSCAN, K-means, MiniBatch K-means, and MeanShift.

Before beginning the presentation and discussion of the results obtained, it seems like it would be of some use to us to have a better understanding of the potential connections that exist between the many different variables that are contained within our dataset. The bivariate analysis of the relationships between the various factors is depicted in Fig. 2.

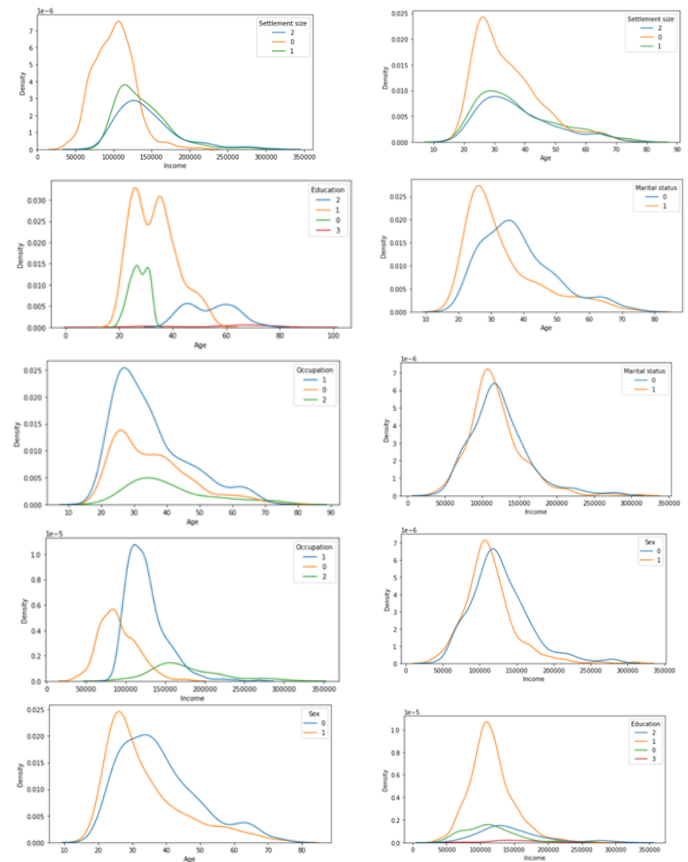


Fig. 2. Bivariate Analysis between the Various Variables.

The analysis of the data reveals several interesting correlations, including the following (Fig. 3):

- 1) People with an occupation of '0' (unemployed) are more likely to reside in smaller cities closer to the customers.
- 2) Married customers are more likely to have post-graduate or high school-level education.
- 3) Married people are more likely to reside in less populous cities.
- 4) A woman on the client list is more likely to be married than a man.

5) Males make up a larger proportion of the customer list than females. On the other hand, the dataset has a disproportionately high number of unemployed women.

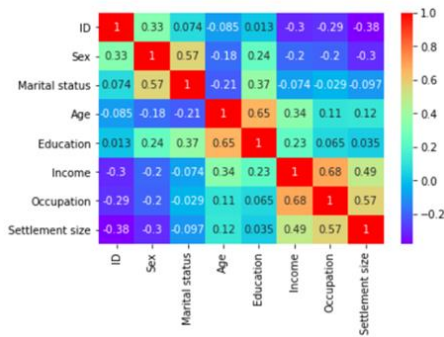


Fig. 3. Correlation between the Various Variables.

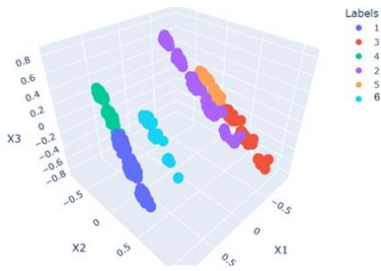


Fig. 4. Clusters Visualization.

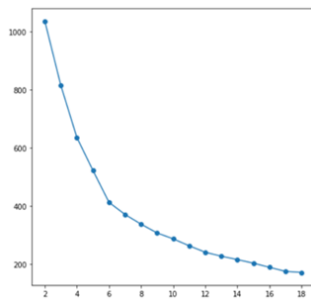


Fig. 5. Elbow Method (k=6).

To begin, we should note that the clusters are incredibly distinct from one another and that the algorithm performs the cluster separation task accurately, given that the clusters' boundaries appear pretty distinct.

In the following, we present the statistical characteristics of the different clusters generated by our model (Fig. 4).

This cluster comprises unemployed, middle-income, single men residing in small cities. As we will see later in the analysis, this also occurs in other clusters. Therefore we conclude that age and education are good cluster separators for clusters 2 and 4 in our dataset.

This cluster consists of married women with a high school diploma or higher and a moderate salary. They are either unemployed or work as employees/officials and reside in small cities. The age falls within the same range as before, so we will disregard it.

Summary statistics of Clusters 1 to 6 are shown below in Tables III to VIII.

TABLE III. SUMMARY STATISTICS OF CLUSTER 1

	count	mean	std	min	25%	50%	75%	max
Sex	9048.0	0.00	0.00	0.0	0.0	0.0	0.0	0.0
Marital status	9048.0	0.00	0.00	0.0	0.0	0.0	0.0	0.0
Age	9048.0	40.00	11.94	20.0	31.0	37.0	47.0	75.0
Education	9048.0	0.82	0.61	0.0	0.0	1.0	1.0	2.0
Income	9048.0	14537.3	3828.6	8239.8	11927.6	13632.3	15975.7	28724.7
Occupation	9048.0	1.26	0.48	0.0	1.0	1.0	2.0	2.0
Settlement size	9048.0	1.52	0.50	0.0	1.0	2.0	2.0	2.0
Labels	517.0	0.00	0.00	0.0	0.0	0.0	0.0	0.0

TABLE IV. SUMMARY STATISTICS OF CLUSTER 2

	count	mean	std	min	25%	50%	75%	max
Sex	5355.0	1.00	0.0	1.0	1.0	1.0	1.0	1.0
Marital status	5355.0	1.00	0.0	1.0	1.0	1.0	1.0	1.0
Age	5355.0	34.28	13.00	18.0	25.0	29.0	40.0	76.0
Education	5355.0	1.33	0.57	1.0	1.0	1.0	2.0	3.0
Income	5355.0	13653.6	3810.3	8880.0	10845.5	12677.8	15510.7	30936.4
Occupation	9048.0	1.26	0.48	0.0	1.0	1.0	2.0	2.0
Settlement size	9048.0	1.26	0.48	0.0	1.0	1.0	2.0	2.0
Labels	5355.0	1.18	0.40	0.0	1.0	1.0	1.0	2.0

TABLE V. SUMMARY STATISTICS OF CLUSTER 3

	count	mean	std	min	25%	50%	75%	max
Sex	5460.0	1.00	0.0	1.0	1.00	1.0	1.00	1.0
Marital status	5460.0	1.00	0.0	1.0	1.00	1.0	1.00	1.0
Age	5460.0	32.41	10.91	18.0	25.00	28.5	36.00	71.0
Education	5460.0	1.21	0.46	1.0	1.00	1.0	1.00	3.0
Income	5460.0	10214.2	2580.1	3583.2	8628.1	10232.3	12045.9	20726.2
Occupation	5460.0	0.42	0.49	0.0	0.00	0.0	1.00	1.0
Settlement size	5460.0	0.01	0.10	0.0	0.00	0.0	0.00	1.0
Labels	5460.0	2.00	0.0	2.0	2.00	2.0	2.00	2.0

Cluster 3 comprises non-single females with at least a high school diploma and a high level of education and income. Large to medium-sized cities are where they reside. This cluster's distribution of Age is also identical; hence this trait does not provide any further information.

If we look at the median Age of the people in clusters 2 and 3, we obtain 28.5 and 29 years, respectively, whereas the median Age of the people in clusters 1 and 4 is significantly older (Clusters 0 and 3 have a median value of 36, while clusters 3 have a median value of 37.). However, the change is not negligible, as we can see from the next cell.

In Table VI, the cluster represented is single men with higher incomes and managerial or self-employed employment. They reside in medium to big urban centers. Education is comparable to cluster one, with the majority holding a high school diploma or less. Ages appear to fall within the same range as cluster one; hence they will not be considered.

Cluster 5 is made up of married or cohabiting men who have completed high school or higher levels of education but have a low to medium income. The vast majority of them hold jobs as employees or officials. It is important to note that this consumer base is equally represented in small, medium, and large cities; hence, we have chosen to ignore that fact in this research. Age suffers from the same issue as the other clusters, which is why it is not taken into consideration.

Cluster 6 is made up of single females of low education. The vast majority of them have completed their high school education, reside in small cities, and are either unemployed or working for someone else.

The performance of this model, which is based on clustering ensemble and spectral clustering, is presented together with its comparison to the performance of other classical models in Table VIII, which allows us to evaluate the effectiveness of our model.

As a result of the findings acquired at the ARI, NMI, SC, and DI levels, respectively, compared to other traditional models, our model demonstrates the highest level of performance across all four evaluation levels.

TABLE VI. SUMMARY STATISTICS OF CLUSTER 4

	count	mean	std	min	25%	50%	75%	max
Sex	4497.0	0.0	0.0	0.0	0.00	0.0	0.00	0.0
Marital status	4497.0	0.0	0.0	0.0	0.00	0.0	0.00	0.0
Age	4497.0	37.56	10.63	21.0	29.75	36.0	42.00	74.0
Education	4497.0	0.73	0.57	0.0	0.00	1.0	1.00	2.0
Income	4497.0	10256.6	2658.4	4368.4	8180.4	10361.8	12039.6	21931.9
Occupation	4497.0	0.36	0.50	0.0	0.00	0.0	1.00	2.0
Settlement size	4497.0	0.06	0.23	0.0	0.00	0.0	0.00	1.0
Labels	4497.0	3.0	0.0	3.0	3.00	3.0	3.00	3.0

TABLE VII. SUMMARY STATISTICS OF CLUSTER 5

	count	mean	std	min	25%	50%	75%	max
Sex	3115.0	0.0	0.0	0.0	0.0	0.0	0.0	0.0
Marital status	3115.0	1.0	0.0	1.0	1.0	1.0	1.0	1.0
Age	3115.0	33.96	10.75	18.0	26.0	31.0	40.0	67.0
Education	3115.0	1.26	0.50	1.0	1.0	1.0	1.0	3.0
Income	3115.0	122976	38529	62263	96769	115369	146519	280570
Occupation	3115.0	0.93	0.63	0.0	1.0	1.0	1.0	2.0
Settlement size	3115.0	0.918288	0.827468	0.0	0.0	1.0	2.0	2.0
Labels	3115.0	4.0	0.0	4.0	4.0	4.0	4.0	4.0

TABLE VIII. SUMMARY STATISTICS OF CLUSTER 6

	count	mean	std	min	25%	50%	75%	max
Sex	7525.0	1.0	0.0	1.0	1.0	1.0	1.0	1.0
Marital status	7525.0	0.0	0.0	0.0	0.0	0.0	0.0	0.0
Age	7525.0	35.14	9.75	19.0	27.0	34.5	41.0	70.0
Education	7525.0	0.93	0.55	0.0	1.0	1.0	1.0	3.0
Income	7525.0	9799.7	2170.2	3676.0	8089.2	10151.1	11326.5	14332.1
Occupation	7525.0	0.37	0.50	0.0	0.0	0.0	1.0	2.0
Settlement size	7525.0	0.07	0.26	0.0	0.0	0.0	0.0	1.0
Labels	7525.0	5.00	0.0	5.0	5.0	5.0	5.0	5.0

Then, we put our model to the test by applying it to an actual database collected from Moroccan residents using a questionnaire sent via social networks and email boxes between the dates of 03/06/2022 and 19/08/2022. This authentic database had 1357 individuals with eight distinguishing traits (the same as the last database). We used the programming language python and its library to manipulate and process the collected data. The results that were obtained are displayed in the figure that follows (Fig. 6).

Comparative analysis of several performance metrics for various models is shown in Table IX.

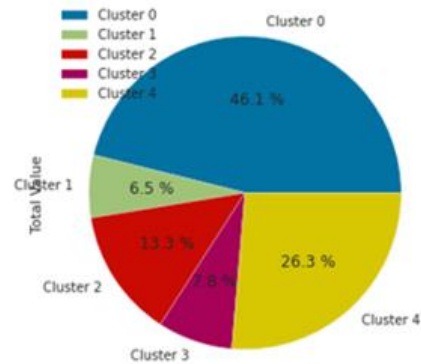


Fig. 6. Percentage of the 5 Clusters.

TABLE IX. COMPARATIVE ANALYSIS OF SEVERAL PERFORMANCE METRICS FOR VARIOUS MODELS

	DBSCAN	K-means	MiniBatch K-means	MeanShift	The proposed model
ARI	0.6953	0.6917	0.6252	0.6164	0.7014
NMI	0.7110	0.7035	0.6937	0.6839	0.7175
SC	0.7215	0.7172	0.6991	0.6927	0.7289
DI	0.7461	0.7201	0.7104	0.7063	0.7515

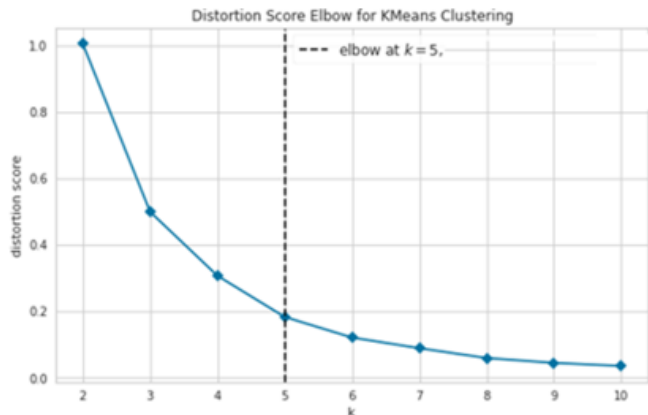


Fig. 7. Elbow Method (k=5).

We can clearly see in Fig. 7 that the elbow method reports five different clusters and that the distribution of these clusters differs from each other; however, cluster 0 has the highest percentage of 46.10%, followed by cluster 4 with a value of 26.30%, while clusters 1, 2 and 3 have a total of 27.60%.

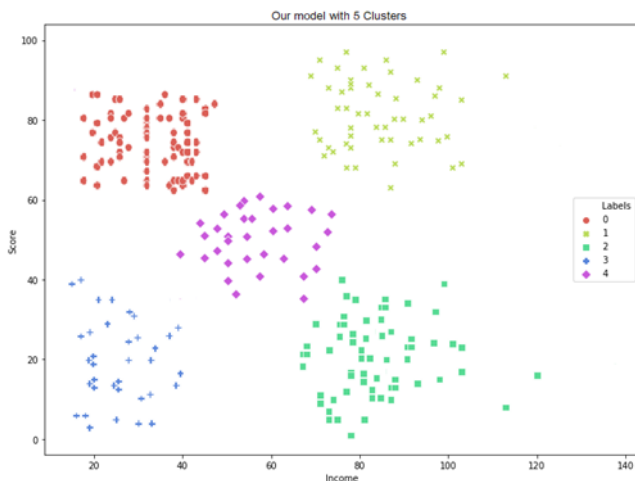


Fig. 8. Presentation of the Clusters According to our Model.

The clusters generated in this real dataset are characterized by the following (Fig. 8):

- Cluster 0 consists of middle-class single men who are highly educated and/or self-employed. We could be inclined to claim they are between twenty and forty years old.

- People in Cluster 1 are evenly split between the sexes; on average are 56 years old and have all earned at least a bachelor's degree.
- Cluster 2 consists of women who are married and have higher incomes, as well as management or self-employed employment. They have education up to a high school diploma and live in medium to large cities.
- Single people of either gender with a middle-class income and education equal to or higher than that of a high school graduate make up cluster 3. They reside in relatively tiny towns and either do not have jobs or work as employees or officials.
- Cluster 4 includes married or cohabiting women who have graduated from high school or above and have a high income. They are either employed or run their businesses. They call somewhat large to sizable cities home.

V. CONCLUSION AND FUTURE DIRECTIONS

This paper proposes a novel clustering ensemble approach; based on a clustering ensemble; in this step, we used four essentials clustering models; DBSCAN, K-means, Mini Batch K-means, and Mean Shift, to provide a superior-conclusion, in terms of consistency and quality, to that produced by the individual clustering algorithms. After that we utilize spectral clustering to merge the multiple clustering results to improve the overall quality of clustering solutions. After the retention of these results, we applied this model to a real dataset, which was collected from Moroccan residents using a questionnaire sent via social networks and email boxes between 03/06/2022 and 19/08/2022. Therefore, the research can involve deep learning models and other performance indicators. The model can also be compared to other datasets.

REFERENCES

- [1] S. Das et J. Nayak, « Customer Segmentation via Data Mining Techniques: State-of-the-Art Review », in Computational Intelligence in Data Mining, Singapore, 2022, p. 489-507.
- [2] X. Xiahou et Y. Harada, « B2C E-Commerce Customer Churn Prediction Based on K-Means and SVM », J. Theor. Appl. Electron. Commer. Res., vol. 17, no 2, p. 458-475, avr. 2022, doi: 10.3390/jtaer17020024.
- [3] C.-L. Wu et N. K. Ma, « The impact of customised mobile marketing on passenger shopping behaviour in the airport terminal », J. Retail. Consum. Serv., vol. 66, p. 102941, mai 2022, doi: 10.1016/j.jretconser.2022.102941.
- [4] A. Griva, « “I can get no e-satisfaction”. What analytics say? Evidence using satisfaction data from e-commerce », J. Retail. Consum. Serv., vol. 66, p. 102954, 2022, doi: https://doi.org/10.1016/j.jretconser.2022.102954.
- [5] H. Jin, « The effect of overspending on tariff choices and customer churn: Evidence from mobile plan choices », J. Retail. Consum. Serv., vol. 66, p. 102914, mai 2022, doi: 10.1016/j.jretconser.2022.102914.
- [6] School of Management, Hospitality and Tourism (ESGHT), Universidade do Algarve, Portugal et al., « Hotel customer segmentation and sentiment analysis through online reviews: An analysis of selected European markets », Tour. Manag. Stud., vol. 18, no 1, p. 29-40, janv. 2022, doi: 10.18089/tms.2022.180103.
- [7] S. P. Nguyen, « Deep customer segmentation with applications to a Vietnamese supermarkets’ data », Soft Comput., vol. 25, no 12, p. 7785-7793, juin 2021, doi: 10.1007/s00500-021-05796-0.

- [8] M. Carnein et H. Trautmann, « Customer Segmentation Based on Transactional Data Using Stream Clustering », in *Advances in Knowledge Discovery and Data Mining*, vol. 11439, Q. Yang, Z.-H. Zhou, Z. Gong, M.-L. Zhang, et S.-J. Huang, Éd. Cham: Springer International Publishing, 2019, p. 280-292. doi: 10.1007/978-3-030-16148-4_22.
- [9] B. Kaur et P. K. Sharma, « Implementation of Customer Segmentation using Integrated Approach », vol. 8, no 6, p. 3, 2019.
- [10] [10] P. P. Pramono, I. Surjandari, et E. Laoh, « Estimating Customer Segmentation based on Customer Lifetime Value Using Two-Stage Clustering Method », in 2019 16th International Conference on Service Systems and Service Management (ICSSSM), Shenzhen, China, juill. 2019, p. 1-5. doi: 10.1109/ICSSSM.2019.8887704.
- [11] Y. Qiu, P. Chen, Z. Lin, Y. Yang, L. Zeng, et Y. Fan, « Clustering Analysis for Silent Telecom Customers Based on K-means++ », in 2020 IEEE 4th Information Technology, Networking, Electronic and Automation Control Conference (ITNEC), 2020, vol. 1, p. 1023-1027. doi: 10.1109/ITNEC48623.2020.9084976.
- [12] X. Wang et al., « Electricity Market Customer Segmentation Based on DBSCAN and k-Means : —A Case on Yunnan Electricity Market », in 2020 Asia Energy and Electrical Engineering Symposium (AEEES), 2020, p. 869-874. doi: 10.1109/AEEES48850.2020.9121413.
- [13] K. R. Kashwan et C. Velu, « Customer Segmentation Using Clustering and Data Mining Techniques », *Int. J. Comput. Theory Eng.*, p. 856-861, 2013.
- [14] E. Umhuza, D. Ntirushwamaboko, J. Awuah, et B. Birir, « Using Unsupervised Machine Learning Techniques for Behavioral-based Credit Card Users Segmentation in Africa », *SAIEE Afr. Res. J.*, vol. 111, no 3, p. 95-101, 2020, doi: 10.23919/SAIEE.2020.9142602.
- [15] Ş. Ozan et L. O. Iheme, « Artificial Neural Networks in Customer Segmentation », in 2019 27th Signal Processing and Communications Applications Conference (SIU), 2019, p. 1-4. doi: 10.1109/SIU.2019.8806558.
- [16] Q. Su, Y. Zhu, Y. Jia, P. Li, F. Hu, et X. Xu, « Sedimentary Environment Analysis by Grain-Size Data Based on Mini Batch K-Means Algorithm », *Geofluids*, vol. 2018, p. 1-11, déc. 2018, doi: 10.1155/2018/8519695.
- [17] T. Duong, G. Beck, H. Azzag, et M. Lebbah, « Nearest neighbour estimators of density derivatives, with application to mean shift clustering », *Pattern Recognit. Lett.*, vol. 80, p. 224-230, sept. 2016, doi: 10.1016/j.patrec.2016.06.021.
- [18] K. Sarkar, « A Stacked Ensemble Approach to Bengali Sentiment Analysis », in *Intelligent Human Computer Interaction*, Cham, 2020, p. 102-111.
- [19] S. Ardabili, A. Mosavi, et A. R. Várkonyi-Kóczy, « Advances in Machine Learning Modeling Reviewing Hybrid and Ensemble Methods », *MATHEMATICS & COMPUTER SCIENCE*, preprint, août 2019. doi: 10.20944/preprints201908.0203.v1.
- [20] L. Berti-Equille, « Learn2Clean: Optimizing the Sequence of Tasks for Web Data Preparation », in *The World Wide Web Conference on - WWW '19*, San Francisco, CA, USA, 2019, p. 2580-2586. doi: 10.1145/3308558.3313602.
- [21] R. Heinrich, « Structured Data Preparation Pipeline for Machine Learning-Applications in Production », p. 6.
- [22] D. Ienco et G. Bordogna, « Fuzzy extensions of the DBScan clustering algorithm », *Soft Comput.*, vol. 22, no 5, p. 1719-1730, mars 2018, doi: 10.1007/s00500-016-2435-0.
- [23] D. Deng, « DBSCAN Clustering Algorithm Based on Density », in 2020 7th International Forum on Electrical Engineering and Automation (IFEEA), Hefei, China, sept. 2020, p. 949-953. doi: 10.1109/IFEEA51475.2020.00199.
- [24] D. Devarapalli, A. S. Virajitha, B. T. Keerthi, et A. P. Devi, « Analysis of RFM Customer Segmentation Using Clustering Algorithms », *Int. J. Mech. Eng.*, vol. 7, no 1, p. 8, 2022.
- [25] K. P. Sinaga et M.-S. Yang, « Unsupervised K-Means Clustering Algorithm », *IEEE Access*, vol. 8, p. 80716-80727, 2020, doi: 10.1109/ACCESS.2020.2988796.
- [26] C. Yuan et H. Yang, « Research on K-Value Selection Method of K-Means Clustering Algorithm », *J*, vol. 2, no 2, p. 226-235, juin 2019, doi: 10.3390/j2020016.
- [27] M. M. Chavan, A. Patil, L. Dalvi, et A. Patil, « Mini Batch K-Means Clustering On Large Dataset », p. 3.
- [28] S. C. Hicks, R. Liu, Y. Ni, E. Purdom, et D. Risso, « mbkmeans: fast clustering for single cell data using mini-batch k-means », p. 29.
- [29] Y. Ren, U. Kamath, C. Domeniconi, et G. Zhang, « Boosted Mean Shift Clustering », in *Machine Learning and Knowledge Discovery in Databases*, vol. 8725, T. Calders, F. Esposito, E. Hüllermeier, et R. Meo, Éd. Berlin, Heidelberg: Springer Berlin Heidelberg, 2014, p. 646-661. doi: 10.1007/978-3-662-44851-9_41.
- [30] D. Tang, J. Man, L. Tang, Y. Feng, et Q. Yang, « WEDMS: An advanced mean shift clustering algorithm for LDos attacks detection », *Ad Hoc Netw.*, vol. 102, p. 102145, mai 2020, doi: 10.1016/j.adhoc.2020.102145.
- [31] N. Nguyen et R. Caruana, « Consensus Clusterings », in *Seventh IEEE International Conference on Data Mining (ICDM 2007)*, Omaha, NE, USA, oct. 2007, p. 607-612. doi: 10.1109/ICDM.2007.73.
- [32] J. E. Chacón et A. I. Rastrojo, « Minimum adjusted Rand index for two clusterings of a given size ». arXiv, 9 décembre 2020. Consulté le: 15 juin 2022. [En ligne]. Disponible sur: <http://arxiv.org/abs/2002.03677>.
- [33] J. M. Santos et M. Embrechts, « On the Use of the Adjusted Rand Index as a Metric for Evaluating Supervised Classification », in *Artificial Neural Networks – ICANN 2009*, vol. 5769, C. Alippi, M. Polycarpou, C. Panayiotou, et G. Ellinas, Éd. Berlin, Heidelberg: Springer Berlin Heidelberg, 2009, p. 175-184. doi: 10.1007/978-3-642-04277-5_18.
- [34] A. Amelio et C. Pizzuti, « Correction for Closeness: Adjusting Normalized Mutual Information Measure for Clustering Comparison: Correction For Closeness: Adjusting NMI », *Comput. Intell.*, vol. 33, no 3, p. 579-601, août 2017, doi: 10.1111/coin.12100.
- [35] S. Romano, J. Bailey, N. X. Vinh, et K. Verspoor, « Standardized Mutual Information for Clustering Comparisons: One Step Further in Adjustment for Chance », p. 9.
- [36] R. Hidayati, A. Zubair, A. H. Pratama, et L. Indana, « Analisis Silhouette Coefficient pada 6 Perhitungan Jarak K-Means Clustering », *Techno.Com*, vol. 20, no 2, p. 186-197, mai 2021, doi: 10.33633/tc.v20i2.4556.
- [37] H. Řezanková, « Different Approaches to the Silhouette Coefficient Calculation in Cluster Evaluation », p. 10, 2018.
- [38] C.-E. Ben Ncir, A. Hamza, et W. Bouaguel, « Parallel and scalable Dunn Index for the validation of big data clusters », *Parallel Comput.*, vol. 102, p. 102751, mai 2021, doi: 10.1016/j.parco.2021.102751.
- [39] S. Mahallati, J. C. Bezdek, D. Kumar, M. R. Popovic, et T. A. Valiante, « Interpreting Cluster Structure in Waveform Data with Visual Assessment and Dunn's Index », in *Frontiers in Computational Intelligence*, vol. 739, S. Mostaghim, A. Nürnberger, et C. Borgelt, Éd. Cham: Springer International Publishing, 2018, p. 73-101. doi: 10.1007/978-3-319-67789-7_6.

Complexity of Web-based Application for Research and Community Service in Academic

Fitriana Fitriana¹, Sukarni Sukarni², Zulkifli Zulkifli³

Midwifery, Faculty of Biomedical Science, Universitas Aisyah Pringsewu, Lampung, Indonesia^{1,2}

Informatics Engineering, Faculty of Informatics & Technology, Universitas Aisyah Pringsewu, Lampung, Indonesia³

Abstract—Research data and community service in academic environment is a very important asset that must be managed properly. They have to be applied synergically in order to obtain as quality standards of higher education. A centralized web-based application designed for research data management and community service have been applied in terms of supporting the managerial of activities. To make the application suitable for users, it is necessary to estimate the size of the software built. This study aimed at measuring the consistency of the apps based on feature point analysis method which is owned by research and community service in Indonesia. Fourteen Modification Complexity Adjustment Factor (MCAF) were used for calculating a program scale with adequate precision. The main cost is determining the quality of application sequentially, which includes measuring the weighted value of feature point components, namely, Crude Function Points (CFPs), calculating the Relative Complexity Adjustment Factor (RCAF), and estimating the Function Point (FP) by using the formula itself. The results depict that the size of application was estimated about 18381 lines using FPA methods and achieved successful estimation with 2.2 percent of deviation.

Keywords—Application complexity; program scale; software size; function point analysis

I. INTRODUCTION

Research data and community service in an academic environment is a very important asset that must be managed properly. Research and community service is an essential factor of higher education in Indonesia. Both have to be applied synergically in order to obtain higher education quality standards. Some institutions have been focused on learning activities only and they neglect research and community service. The quality of their institution is not only seen from their learning quality, but also from the side of their research and community service. 16 of 24 performance indicators of higher education quality standards in Indonesia are determined by research and campus service to the community. These two factors must be considered properly [1]. Higher-education institutions have to pay more attention to the quality of their research and community service. They must be able to present data obtained from the result of their research along with provided contents, processes, assessments, facilities, infrastructure, and funds. If they able to manage all those data, then it can be said that quality of their institution is excellent [2], [3].

Research and community service are generally carried out by lecturers. A source of lecturers' work is not just research, but is a long-term work starting from the implementation of the

research, responsibility and ranging from the baseline to achievement. If management of research data and community service is not running well, so then it will become problematic for lecturers as a researcher.

In order to support this matter, we have developed a centralized web-based application for management of research data and community service which can be used by the academic community such as lecturers and students. The key features of an application consist of a machine login module, a master consumer, a textbook, and journal publishing application. Therefore, the consistency of an application needs to be evaluated in order to determine the status of the product during and after the build. Otherwise, to ensure that the application can run properly, it is necessary to measure the compatibility of the application. Software or application measurement is appraisal method consisting of size, review and adaptation to enhance software development [4]. The tool that is widely used to measure functional size of the software work product is Function Point Analysis (FPA). FPA is the software which is relocated to the production application at project implementation. FPA technique is used to analyze the functionality of the software by using Unadjusted Function Point (UFP) [5]. FPA approach calculates the size of the program in Function Point (FP) units derived from five parameters, namely: Internal Logical File (ILF), External Interface File (EIF), External Input (EI), External Output (EO) and External Inquiries (EQ) which are divided into low, medium or large classes depending on the amount of Record Entity Types (RET), Data Element Form (DET) and File Type Reference (FTR) [6].

The quality of software product is a convenience from the user's point of view that can fulfil many characteristics such as: performance, usability, robustness, and security/safety. Meanwhile a high value of maintainability, availability and reusability were tested for specific quality attribute of software project [7]. Quality software is inseparable from both program code, the suitability of data entered and generated by the software process without errors. Hence, this study aims to estimate the size of web-based application project using FPA method. Subsequently, about 72 features were used to estimate the project size. The estimated size is compared with the actual project size.

II. RELATED WORK

In 2018 [8], the author proposed on designing and implementing a system that makes it convenient for users in analyzing software functionality size based on FP method

referring to IFPUG CPM 4.3.1 standards. The system helps users to perform FP analysis in a faster and easier way without sacrificing accuracy. Whereas, in [9], the author builds the application chat messenger fellow android user through internal operation office. Their result shows that the application can translate automatically into a different language. It also shows the application can achieve the good performance in CPU, RAM, GPU and bandwidth usage.

Furthermore, [10] performs a good estimation of size of a mobile software project using FPA method about 4235 lines. When the estimated size is compared to the actual size, the deviation gained a highly successful estimation by 1.2%. Another study by [11], aims to identify improvements proposed for FPA to make the results generated more accurate. Their paper has presented eleven additional factors for FP analysis and suggested to address FPA as considered as an outdated method given by the great diversity and complexity of currently existing technology scenarios. Bani et. al [12] confirm that Random Forests has a better Confusion Matrix and scored better in both classification accuracy, and precision measures. The results of this work verify the validity of data mining in general and the applied technique in particular for software estimation.

Recently, in [13] it was investigated that the PSO feature selection can increase the accuracy or reduce the RMSE average value to 1552,999. Their result indicates that, compared with the original regression linear model, the accuracy or error rate of software effort estimation has increased by 3.12% by applying PSO feature selection. Also, [14] reviewed the machine learning models have been introduced to handle the flaws of parametric estimation models. These models also complement the modern project development and management.

Commonly, several earlier studies have presented only one type of feature that was used. Therefore, this study uses more features which differ from prior study. We will use the function point analysis method to perform software measurements complexity for research and community service application. Another objective of this research is to measure the consistency of the apps which we hope can provide more understanding about the level of complexity application from user's point of view.

III. RESEARCH METHOD

This research applies a Function Point Analysis (FPA) to measure the complexity of web-based application of research and services community in academic environment. It has been done after making several observations in [14]-[19], in which they also use FPA for measure software complexity.

The proposed stages include: measurement of crude function points (CFP), calculating the relative complexity adjustment factor (RCAF), and measurement function point (FP). The stages of software quality measurement are based on feature point analysis of research and community service application called E-LPPM application which is illustrated in Fig. 1.

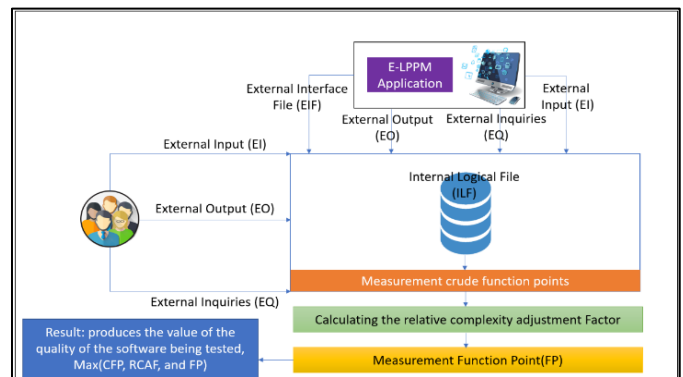


Fig. 1. Stages of Measurement Software.

Calculating the software's quality begins with the determining how to measure the success of software. It has been done with the decipherment of an application into its data and transactional functions. The data functions characterize the functionality afforded to the user by attending to their internal and external requirements in relation to the data, whereas the transactional functions explains the functionality delivered to the user in relation to processing this data by the application.

Second stage is calculating the CFP (Crude Function Points). The number of functional components of the system were first recognized and followed to calculate the complexity of quantization weight of every component including input, output, online queries, logic files, and the external interface.

The next stage is calculating the complexity of transcription factors of RCAF (Relative Complexity Adjustment Factor) for the project. RCAF is to calculate the complexity assessment of software system from several characteristics of subject. Rating scale from 0 to 5 is given to each subject that most affect the development effort required. Lastly, calculating Function Points by the formula:

$$FP = UFP \times VAF \tag{1}$$

The UFP is calculated as the complexities from parameters provided in the question where VAF is Value added Factor $0.65 + (0.01 * TDI)$, where TDI is Total Degree of Influence of the 14 General System Characteristics.

IV. IMPLEMENTATION AND RESULTS

Actual total size of the application which is specified by PHP source code files is 17988 lines in 300 files. Comment line inside the code is also taken in this counting because important comments are the key as the actual code line.

A. Calculating Crude Function Points (CFP)

The number of functional components of the system were first recognized and followed to calculate the complexity of quantization weight of every component.

FP calculation includes five types of software system components following: 1) the number of input applications; 2) the number of output applications; 3) the number of online query applications; 4) the application related to query against the data stored; 5) the number of logical files or tables which are involved; 6) the number of external interfaces. Then given

a weighting factor to every of the above components based on its complexity.

Table I shows the User Function (UF) results for compatibility feature of External Input (EI). There are two modules with low complexity, nine modules with medium complexity, and nine modules with high complexity. The result represents that processes data or control information comes from outside by external applications. As per Table I, this EI is considered as an "Average" complexity EI.

Table II describes Internal Logical File (ILF). There are 11 rows for overall with a low complexity ILF worth 4 points, an average ILF worth 2 points, and a high worth 5 points. ILFs represent data that is stored and maintained within the boundary of the application being counted.

Meanwhile, External Interface File (EIF) listed with their complexity levels is shown in Table III. Low complexity EIF is worth 4 points, an average EIF worth 2 points and high complexity worth 5 points. EIFs represent the data that application used or referenced. This means an EIF is counted for an application in an ILF in another application. As per Table III, EIF is considered as "High".

Using the UF result and complexity of data, UFP value was calculated afterwards and depicted of 276 as shown in Table IV.

TABLE I. THE PERFORMANCE OF MODULES AND COMPLEXITY OF EXTERNAL INPUT (EI)

Module	Complexity
Login System Module	Low
Master User	Low
Upload Textbook Data	Medium
Upload Lecturer Journal Publish Data	Medium
Upload Lecturer Presenter Data	Medium
Upload Main Speaker Data (Keynote / Invited Speech)	Medium
Upload Data Intellectual Property Rights (IPR)	Medium
Upload Data on Grants or Research Funding / External Service Resources Ristekbrin Funds	Medium
Upload Lecturer Output Data	Medium
Upload Lecturer Research Data	Medium
Upload Lecturer Community Service Data	Medium
Input, Update, Delete Textbook Data	High
Upload Lecturer Community Service Data	High
Input, Update, Delete Textbook Data	High
Input Data Publish Lecturer Journal	High
Lecturer Speaker Data Input	High
Input Data Keynote Speaker (Keynote / Invited Speech)	High
Input Data Intellectual Property Rights (IPR)	High
Input Data Grant or Funding Research / Pengabmas External Source Ristekbrin	High
INPUT Data Output Lecturer	High
INPUT Data Advanced Research & Lecturer	High
INPUT Data Pengabmas Lecturer	High

TABLE II. INTERNAL LOGICAL FILE (ILF)

Module	Complexity
Table lppm_user	Low
Table lppm_periode	Low
Table lppm_book	Low
The lppm_patent table	Medium
The lppm_item_pen research table	Low
Table lppm_journal	Medium
Table lppm_luaran	High
Table lppm_author	High
Table lppm_speaker	High
Table lppm_research	High
Table lppm_ext_monev_external	High

TABLE III. EXTERNAL INTERFACE FILE (EIF)

Module	Complexity
Excel Textbook Files	Low
Excel File Publish Lecturer Journal	Low
Excel File Speakers Lecturers	Low
Excel Main Speaker File (Keynote/Invited Speech)	Medium
Excel Intellectual Property (IPR) File	Low
Excel File Grants or Research Funding/External Service Resources Research Funds	Medium
Excel Lecturer Output File	High
Excel Lecturer Research File	High
Excel Lecturer Community Service File	High
Excel Textbook Files	High
Excel File Publish Lecturer Journal	High

After calculating the UFP, then the Relative Complexity Adjustment Factor (RCAF) value was computed and portrayed of 46 as total degree of influence which can be seen in Table V.

Finally, the Function Point (FP) of application was calculated by multiplying the UFP to RCAF as in (2).

$$FP = 276 \times 1.11 = 306.36 \quad (2)$$

To estimate the size of application within source code line, the FP value was multiplied by 60 as reference in the [20] and [21].

$$\text{Size_in_LOC} = 306.36 \times 60 \cong 18381 \quad (3)$$

Size of the project was estimated about 18381 lines using the FPA method. Accomplishment of the project, the actual size was 17988 lines. The estimated size then equaled to the actual size, depicted deviation of around 2.2%. This was considered as successful estimation. Nevertheless, there might be a larger dissimilarity between the estimate and the actual size since acceptable identification of the function type was a tough process.

TABLE IV. CALCULATION OF THE UFP VALUE

Software Parameters	Level of Complexity									Total CF
	Low			Medium			High			
	Count	Weight	Point	Count	Weight	Point	Count	Weight	Point	
	A	B	C=A*B	D	E	F=D*E	G	H	I=G*H	
External Input (EI)	2	5	10	9	6	54	9	2	18	82
External Output (EO)	4	5	20	4	3	12	0	4	0	32
External in Query (EQ)	0	5	0	7	4	28	2	2	4	32
Internal Logic File (ILF)	4	6	24	2	7	14	5	10	50	88
External Interface File (EIF)	3	2	6	3	5	15	3	7	21	42
Unadjusted Function Point (UFP)										276

REFERENCES

- [1] N. Sayidah et al., "Quality and University Governance in Indonesia," *International Journal of Higher Education*, vol. 8, no. 4, 2019, pp. 10–17.
- [2] S. Eliot. "Factors Determining the Quality Management of Higher Education: A Case Study at A Business School in Indonesia. *Jurnal Cakrawala Pendidikan*. 38. 2019, pp. 215-227.
- [3] S. Hidayat, "Peningkatan Mutu Penelitian di Indonesia Dalam Mengatasi Masalah Pendidikan", *Bioilmi*, vol. 4, no. 2, 2018, pp. 34-44.
- [4] John Knight, *Fundamentals of Dependable Computing for Software Engineers*, 1st Edition. CRC Press, 2012.
- [5] D. Longstreet, *Function Points Analysis Training Course*, vol. 2. Longstreet Consult. Inc, 2005.
- [6] C. Angelica et al., "Agile Counting Process of Software Product Maintenance Size: A Statistical Analysis Processo de Contagem de Tamanho Agil de Manutenção de Produto de Software: Uma Análise Estatística". *Espacios*. Vol. 41(32), art.6, 2020.
- [7] I. Charles, and N. I. Caesar. "Quantifying Software Quality in Agile Development Environment". *Software Engineering*. vol. 9, no. 2, 2021, pp. 36-44.
- [8] A. & M. K. Irawati, "Measuring Software Functionality Using Function Point Method Based on Design Documentation," *International Journal of Computer Science Issues*, vol. 9, 2012.
- [9] R. Sanjaya and A. S. Girsang, "Implementation application internal chat messenger using android system," 2017 *International Conference on Applied Computer and Communication Technologies (ComCom)*, 2017, pp. 1-4.
- [10] V. Tunalı, "Software Size Estimation Using Function Point Analysis-A Case Study for a Mobile Application," *Mühendislik ve Teknoloji Sempozyumu*, 2014. pp. 73-76.
- [11] S. and M. A. K. Patwa, "A Study of Function Point Analysis: Some Suggestive Modifications," in *Proceedings of 2nd International Conference on Advanced Computing and Software Engineering (ICACSE) 2019*, 2019, pp. 634–637.
- [12] A. Banimustafa, "Predicting Software Effort Estimation Using Machine Learning Techniques," in *2018 8th International Conference on Computer Science and Information Technology, CSIT 2018*, Oct. 2018, pp. 249–256.
- [13] A. Latif, et al., "Comparative analysis of software effort estimation using data mining technique and feature selection", *JITK*, vol. 6, no. 2, 2021, pp. 167–174.
- [14] R. K. G. Ripu Ranjan Sinha, "Software Effort Estimation Using Machine Learning Techniques," in *Advances in Information Communication Technology and Computing*, 2021, pp. 1-4.
- [15] R. B. H. Eti Kapita, et al., "Analisis kualitas perangkat lunak menggunakan metode function point analysis (study kasus: Transaksi Pembelian di eBay)," *Jurnal Informatika dan Rekayasa Perangkat Lunak*, vol. 1, no. 1, 2019.

TABLE V. CALCULATION OF THE RELATIVE COMPLEXITY ADJUSTMENT FACTOR (RCAF)

System Characteristic	Value
Data Communication	3
Distributed Data Processing	3
Performance	3
Heavily used configuration	3
Transaction rate	4
Online Data Entry	3
End-user efficiency	3
Online Update	3
Complex Process	4
Reusability	3
Installation Ease	3
Operational Ease	3
Multiple Sites	4
Facilitate Change	4
Total Degree of Influence	46

As discussion matters, complexity of the identified function types was a particular matter although International Function Point Users Group (IFPUG) have been provided a broad guideline. Hence, it would be adequate to anticipate a disparity among the estimate and the actual size to a certain point.

V. CONCLUSIONS

In this report, Function Point Analysis software size estimation method was described at some point. The method was used on a web-based application developed by the author, the results were investigated. Applications developed in a web-based are commonly small in size and running properly when compared to regular software tasks like information systems. It is realized that the FPA method yields a perfect estimate for a small-scale web-based application. In extension to function point-based approach, the full data set requires to be prepared for future studies. The observation by end user can be used to make increasingly accurate estimates and classifications of web-based application. Thus, it will be of much support to the researchers' goal in the future for emerging languages and tools of programming tasks.

- [16] B. N. Balaji, et al., "Software cost estimation using function point with non-algorithmic approach," *Global Journal of Computer Science and Technology*, vol. 13, no. 8, 2013, pp. 1-5.
- [17] D. Pratiwi, "Implementation of function point analysis in measuring the volume estimation of software system in object oriented and structural model of academic system," *International Journal of Computer Applications*, vol. 70, no. 10, 2013, pp. 1-4.
- [18] N. Rachmat, "Estimasi ukuran perangkat lunak menggunakan function point analysis-studi kasus aplikasi pengujian dan pembelajaran berbasis web," *Annual Research Seminar*, vol.3, no.1, 2017, pp. 1-5.
- [19] A. Yhurinda, P. Putri, and A. P. Subriadi, "Software Cost Estimation Using Function Point Analysis," *The 4th International Seminar on Science and Technology*, no.1, 2018, pp. 79-83.
- [20] H. Madhav C. and V. Kumar K.S., "A Method for Predicting Software Reliability Using Object-oriented Design Metrics," *2019 International Conference on Intelligent Computing and Control Systems (ICCS)*, 2019, pp. 679-682.
- [21] N. Marcheta, I. Hermadi, and Y. Nurhadryani. "Effort Estimation Modeling of E-Government Application Development Using Function Points Based on TOR and SRS Document. *Journal of Information Technology and Its Utilization*, vol.3, issue 1, 2020, pp. 5-8.

Brain Tumor Detection using Integrated Learning Process Detection (ILPD)

M. Praveena¹

Department of CSE, Koneru Lakshmaiah Education
Foundation, Vaddeswaram, AP, India

M. Kameswara Rao²

Department of ECM, Koneru Lakshmaiah Education
Foundation, Vaddeswaram, AP, India

Abstract—Brain tumor detection becomes more complicated process in medical image processing. Analyzing brain tumors is very difficult task because of the unstructured shape of the tumors. Generally, tumors are of two types such as cancerous and non-cancerous. Cancerous tumors are called malignant and non-cancerous are called benign tumors. Malignant tumors are more complex to the patients if these are not detected in the early stages. Precancerous are the other types of tumors that may become cancerous if the treatment is not taken in the early stages. Machine Learning (ML) approaches are most widely used to detect complex patterns but ML has various disadvantages such as time taking process to detect brain tumors. In this paper, integrated learning process detection (ILPD) is introduced to detect the tumors in the brain and analyzes the shape and size of the tumors, and find the stage of the tumors in the given input image. To increase the tumor detection rate advanced image filters are adopted with Deep Convolutional Neural Networks (D-CNN) to improve the detection rate. A pre-trained model called VGG19 is applied to train the MRI brain images for effective detection of tumors. Two benchmark datasets are collected from Kaggle and BraTS 2019 contains MRI brain scan images. The performance of the proposed approach is analyzed by showing the accuracy, f1-score, sensitivity, dice similarity score and specificity.

Keywords—Machine learning (ML); deep convolutional neural network (D-CNN); brain-tumor-detection; integrated learning process detection (ILPD)

I. INTRODUCTION

A tumor is a type of irregular tissue or cell that didn't have any shape or size [1]. Tumors will grow irregularly and can cause more damage to health if they are not detected in the early stages. These tumors may convert into cancerous or non-cancerous. Generally, the human brain is closed with a strong skull. Skull is a very small area, if it is extended this will become more complicated. Abnormal cells grow more heavily than normal cells and this may transform tumors [2]. It is very tedious to recognize tumors in the brain by using MRI images. This is based on the experience of the doctor and some methods are selected from the treatment of the patient for fast recovery. One of the tough tasks in this context is to detect the particular type of tumor in the early stages; this will help the experts treat the patient accordingly [3]. Hybrid feature extraction is one of the approaches which is used to extract the accurate features that show the huge impact on brain tumor detection [4].

Glioma is one type of brain tumor that shows severe damage to the brain. The properties of glioma are entirely different compared with other types of tumors. This consists of three types of tumors such as whole tumor (WT), tumor core (TC), and enhancing tumor (ET) [5]. Some tumors are very complicated like glioma because to reduce the impact of these tumors surgery is required. Segmentation is one of the most difficult tasks to detect tumors using MRI scan images. In MRI brain image analysis modality gives the unique and key details that belong to every piece of the tumor. The four modalities that are present in the segmentation are T1, T1c, T2, and FLAIR [6]. Multi-atlas segmentation (MAS) is the approach that segments the brain tumor images. To recover the brain image into a normal-looking image the low-rank approach is used. MAS approach is an iterative approach that recovered the image and increases the segmentation accuracy [7]. Brain tumor segmentation has many unsolved issues. Brain tumor segmentation considers every label as one unit [8]. In general, the segmentation of brain images didn't contain the tumor tissue or other anomalies [9]. In brain images, several types of segmented images are present such as gray matter and white matter. Gray matter consists of necrotic cells. White matter consists of militated axons called tracts.

In this paper, Integrated Learning Approach (ILA) is introduced to detect the tumor regions by using advanced filtering techniques and a Deep Convolutional Neural Network (D-CNN).

II. LITERATURE SURVEY

Several authors discussed about the brain tumors detection using MRI images. In this section, various methodologies are discussed about brain tumors detection and also discussed about traditional image processing and DL approaches.

V. Shreyas et al., [10] proposed a novel approach that shows the rapid runtime compared with traditional approaches. The proposed approach Brain Tumor Segmentation (BraTS) achieved better performance by showing a dice score of 83% in the full tumor region, 75% in the core region, and 72% in the intensified tumor region. The proposed BraTS is 18 times faster than the other existing approaches. M. Ali et al., [11] introduced the two new segmentation approaches such as 3D CNN and U-Net are merged to give the better accurate results. The training is given by using the BraTS-19 challenge dataset that gives the segmentation of the brain input images. This system segments the tumor sub-regions that are used to predict the final output.

A. Kumar et al., [12] developed the ML approach to recognize tumor in brain by using the MRI images. This approach uses the Particle Swarm Optimization (PSO) for feature selection and Support Vector Machine (SVM) for classification of tumors. This approach achieved better results in classification of input images.

Zhang, D et al., [13] proposed the unique segmentation approach called a task-structured brain tumor segmentation network (TSBTS net). This approach mainly focused on predicting the tumor regions in the given dataset images. From the modality data the weights are also extracted in this approach. The proposed approach achieved better segmentation performance compared with existing approaches. Zhou C et al., [14] proposed the One-pass Multi-task Network (OM-Net) be used to solve the irrelevant issues in detecting the tumor regions. The OM-Net is the combination of segmentation and DL model that consists of shared parameters and used to learn the merged features. This is also the task specific parameters to learn preferential features. Badrinarayanan V., [15] proposed the novel deep fully segmented approach called as SegNet. SegNet is one of the decoder networks which is mapped with the low-resolution encoder that uses pixel-wise classification. Hu, K. et al., [16] proposed the novel tumor segmentation technique based on a multi-cascaded convolutional neural network (MCCNN) and fully connected conditional random fields (CRFs). This technique is a combination of MCCNN and CRFs. Each feature has its properties to detect the brain. The proposed technique finds the image patches that are extracted from axial, coronal, and sagittal used to train the three segmentation approaches. This will give the final segmented output.

III. ROLE OF DEEP LEARNING (DL)

In recent years, CNN becomes more popular in the classification of images. Pereira S et al., [17] introduced the dynamic partition approach that uses the CNN that has a 3 x 3 core size. This approach will follow the steps such as preprocessing, training, and validation of the dataset. The dataset used to analyze the algorithm is BraTS 2015. Hao et al., [18] proposed the automatic segmentation approach that uses the U-net D-CNN. This is applied to BraTS 2015 dataset. Better segmentation is applied in this to get accurate results. Wang et al., [19] introduced the cataract network. The proposed network follows several steps for tumor segmentation. Secondly, the bounding box is implemented on tumor image, and the segmented region is shown. By using the multi-view fusion techniques the false positives are reduced. Myronenko A [20] introduced the 3D tumor segmentation approach that uses the auto-encoder to redesign the brain tumor images. The dataset is the 2018 BraTS Challenge used for result analysis. Xue F et al., [21] introduced the 3D MRI tumor segmented technique. The input uses the encoder and decoder defines several block sizes and weight loss. The training is also increased in this paper. Zhou X et al., [22] introduced 3D approach for segment the brain tumor images. To achieve high performance the 3D shuffleNetV2 as encoder, and decoder with residual blocks are used. Saman S et al., [23] introduced the active lineation model for the MRI brain tumor images with segmentation. This approach is mainly used to extract the features that belong to tumor parts in MRI. Liu et

al., [24] discussed the DL approach that learns the set of convolution and deep supervision. This technique is replaced with the feature extraction that leans with group convolution. The dataset is collected from BraTS2018 and the proposed technique detects the segmented region of an input image.

M. Rizwan et al., [25] introduced a new approach called Gaussian Convolutional Neural Network (GCNN). CNN applied two benchmark datasets to classify the multiple tumor diseases. This is mainly focused on finding the grades of the tumor. The accuracy of GCNN is 99.8% for one dataset and 97.15% for another dataset. Bhuiyan et al., [26] proposed an automated approach to finding the cancer cells present in the human brain. The proposed approach is combined with several ground-truth-level approaches giving better approaches than existing approaches. Compare with all the existing models, the proposed approach achieved the 98.6% of accuracy. Yazdan SA et al., [27-32] proposed the automated diagnostic approach called as Multi-Scale CNN (MSCNN) to classify [32-36] the brain tumors. Compare with AlexNet and ResNet the proposed MSCNN achieved the accuracy of 91.2%.

IV. VGG 19 FOR MRI BRAIN IMAGES

Visual Geometry Group (VGG) is the CNN architecture which consists of number of layers. Transfer learning is one of the domains that reduce the training set size and computation time when deep learning models are built. This domain helps us to transfer the pre-trained learning to a new model. This is utilized in the segmentation of tumors, classifications of tumor images, etc. The proposed approach is integrated with advanced image filters with VGG-19 and Deep CNN. In this paper, VGG-19 is used as the pre-trained model which contains 19 layers. VGG19 is mainly used to recognize the brain tumors. From the ImageNet database, the training is done with huge number of predefined brain tumors and other types of brain images. Based on this pre-trained model the tumor and non tumor images are classified. The input size of brain images are converted to 224 by 224.

The VGG contains very small convolutional filters. VGG-19 contains 19 convolutional layers and three are fully connected layers (see Fig. 1).

Input: The input brain image size is 224x224. For this tumor detection, the image is cropped to the center of the image for maintaining consistency.

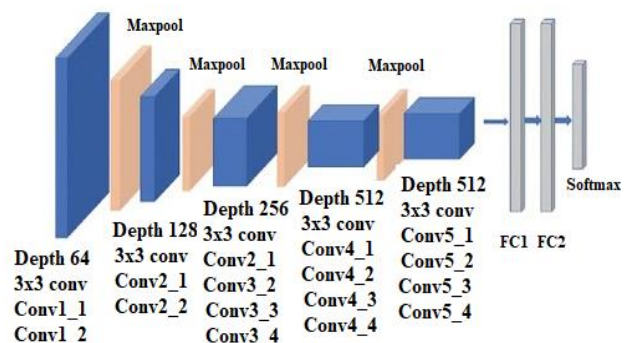


Fig. 1. Shows the Architecture of VGG19 with Total Number of Layers Present in this Process.

Convolutional Layers: This layer contains the minimal responsive field, i.e., 3×3, very small size catches the up/down and left/right. In this scenario, the 1x1 filters also act as the linear transformation of the input. The continuation of this is done by the ReLu function, which reduces the training time by using the AlexNet.

Hidden Layers: These layers used the ReLu in VGG. To reduce the memory consumption and training time ReLu is used by the VGG. This will show the huge impact on overall accuracy.

Fully-Connected Layers: In VGG-19 there are three fully connected layers. Among these, two layers contain 4096 and 3rd contains 1k channels and one for every class.

V. IMAGE FILTERING AND PRE-PROCESSING OF INPUT BRAIN IMAGE

Image filtering is one of the significant tasks that will analyze the specific features of the image. There are various operations that show impact on image filtering such as smoothing and sharpening. The properties of the image filters are represented as:

$$f(a) = \alpha a + \beta \quad (1)$$

The result of the integer is rounded and fixes the range [0, 255]. The color component value (R, G, or B) is represented as x. α is the contrast with the range ($\alpha > 1$ initializes high contrast and $0 < \alpha < 1$ low contrast). To make it easy for making changes in "brightness" and "contrast" the formula is given as:

$$f(x) = \alpha (a - 128) + 128 + b \quad (2)$$

Where b controls brightness.

More complex contrast adjustments can be done using arbitrary "curves" $f: [0, 255] \rightarrow [0, 255]$, which are provided by the user of the image processing software using graphical tools.

By using the linear smoothing layer the quality of the input image is improved as shown in Fig. 2. These are very good filters that can easily remove the noise from the images. By using the weighted sum of the pixels the linear filter is implemented. In every window, this weighted sum is implemented using a convolution mask. A filter that does not have the weighted sum of pixels then is considered non-linear filters.

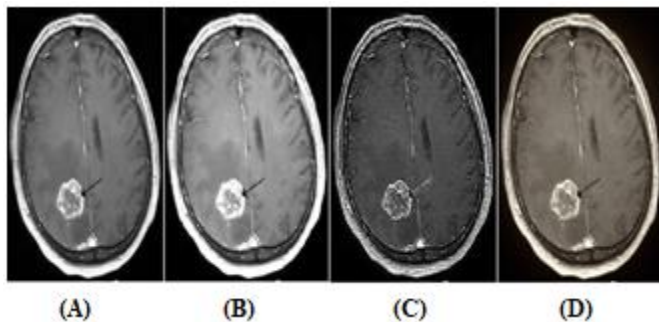


Fig. 2. (A) Input Image, (B) Filtered Image, (C) Sharpen Image and (D) Pre-Processed Image.

A. Mean Filtering

This is one of the better filtering approaches which are used in this paper. By using the local averaging operation (LAP), the filtering approach is implemented. In this context, the pixels are replaced with all the nearest values of the input image.

$$h(a, b) = \frac{1}{M} \sum_{(k,l) \in N} f(k, l) \quad (3)$$

Where 'M' represents the total pixels in the nearest 'N'.

B. Region based Segmentation for Finding the Statistical Information of the Input Image

Region based mathematical model is used to find the statistical information of the image. For example, the region in the image u of the image domain calculates the intensity of the mean of X with u.

$$\mu_u = \frac{1}{|X|} \int_u X(a) da \quad (4)$$

Where $|X| = \int_u da$ (the measure of X, or the variance within X).

$$\sigma_u^2 = \frac{1}{|X|} \int_u (\mu_u - X(a))^2 da \quad (5)$$

Equation 4 and 5 combined to show the hybrid model.

$$u_t + F ||\nabla u|| = 0 \quad (6)$$

Where, $u = u(a, t)$ initializes the level sets of curves of family C (a, t). F is used to combine the equations.

C. Preprocessing

In this step, the input images subtracts the mean " μ " for every sample image " i " and standard deviation (SD) " σ " divides to extract " i_0 " output image as:

$$i_0 = \frac{i - \mu}{\sigma} \quad (7)$$

D. Deep CNN

Deep CNN is focused on finding the important patterns from the MRI dataset. Deep CNN or CNN works better on brain MRI image classification for detecting the tumor or non-tumor images. The D-CNN takes the input image and classifies the image based on specific types such as tumor or abnormality is present or not. This classification of tumor images is based on image resolution. Image resolution mainly considers the height (h), width (w), dimension (d). For this brain image segmentation, two types of images are present such as RGB and grayscale images. RGB image contains 8 x 8 x 3 array of matrix and the grayscale image contains a 6 x 6 x 1 array of the matrix. To segment the image into two parts the threshold-based segmented approach is integrated with the input image. Based on the pixel values the segmentation is done. For every image, the pixel values are different for the tumors and background of the image. The system will set the threshold value. The threshold value is based on pixel values are between low and high. According to this, the classification is done.

E. Non Linearity (ReLU)

Rectified Linear Unit (ReLU): This is utilized to analyze output and shows result as positive or zero. Positive represents the tumor is present and zero represents no tumor. In general, ReLU is very fast and easy to implement on MRI brain images. The output of the ReLU is given below.

$$f(x) = \max(0, x) \quad (8)$$

F. Pooling Layer

This layer mainly reduces the size of the input image without losing any pixels. This layer consists of two pooling hidden layers contains five nodes at each pool and this will help the proposed algorithm to limit the iterations. MRI brain image is reduced by size and extracts only tumor affected image which is most important for classification.

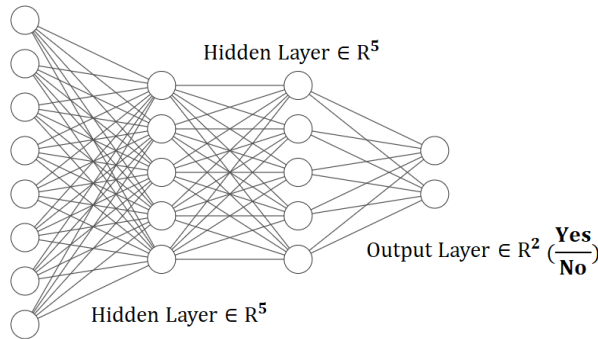


Fig. 3. The Overall Process of MRI Input Image and Output of the Image.

Fig. 3 shows the number of layers that are used to process the MRI input images. The input layer consists of eight nodes and one pooling layer consists of two hidden layers with five nodes each. Finally, the output layer shows the final output of the input image which is tumor present or not.

VI. DATASET DESCRIPTION

Two datasets used for experimental analysis are Brain Tumor Segmentation Challenge (BraTS) 2019 [17] (see Fig. 7 and Fig. 8) and Kaggle dataset (see Fig. 5 and Fig. 6). These datasets contain two folders such as training and testing. BraTS 2019 contains 259 high and low-grade glioma patient samples. From these samples, 125 are unknown status [18]. This dataset contains five types of images namely T1, T1ce, T2, and FLAIR images as shown in the Fig. 4. The dimensions are 240 x 240 x 155 with 1mm³ resolution. The algorithm shows the three-segmented regions such as deep segmented region, normal region, and light segmented region (see Tables I to III).

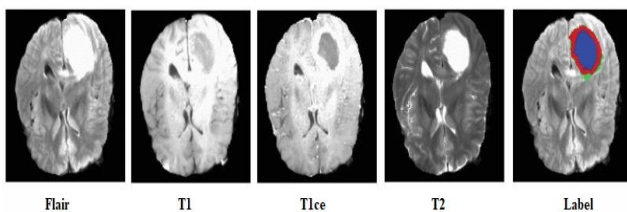


Fig. 4. Types of Images Present in Dataset.

A. Limitations and Challenges

- Finding the accurate location of tumor becomes more challenging task.
- Finding the abnormal cells becomes more complex by using the state-of-art approaches.
- Accurate classification of tumors and cancer cells is detected using MRI scan images.
- Two types of datasets are used to diagnose the MRI scan images.

VII. PERFORMANCE METRICS

The performance of the proposed models is analyzed by using the confusion matrix (CM). This is the advanced representation to predict the accurate prediction of diseases. This presents the actual value and predicted value of the given inputs. To count the overall values the following are the attributes used to find the accurate values.

True Positive (TP)-This initializes the actual value as positive (tumor identified) and the predicted value is also positive (tumor identified).

True Negative (TN)-This initializes the actual value as negative (No tumor) and the predicted value is also negative (No tumor).

False Positive (FP)-This initializes the actual value as positive (tumor identified) and the predicted value is negative (No tumor).

False Negative (FN)-This initializes the actual value as negative (No tumor) and the predicted value is also positive (tumor identified).

Specificity: This parameter mainly detects the total number of TP and FP and this parameter has more potential to predict the background region.

$$\text{Specificity} = \frac{TN}{TN+FP} \quad (9)$$

Sensitivity This parameter mainly detects the total number of TP and FN and this parameter has more potential to predict the segmented region.

$$\text{Sensitivity or Recall} = \frac{TP}{TP+FN} \quad (10)$$

Accuracy is one metric that measures the reliability of the classification result. The formula is give below.

$$\text{Accuracy} = \frac{TP+TN}{TP+FN+FP+TN} \quad (11)$$

Precision: The percentage of quality of predictions is defined as:

$$\text{Precision} = \frac{TP}{TP+FP} \quad (12)$$

TABLE I. TRAINING AND TESTING TIME (SEC) FOR TWO DATASETS

Algorithms	Training Time (Sec)	Testing Time (Sec)
EfficientNetB0 [28]	66.78	69.12
YOLO5 (You Only Look Once) [29]	74.67	75.78
ILPD	49.89	56.89

TABLE II. PERFORMANCE OF EXISTING AND PROPOSED ALGORITHMS APPLIED ON NAVONEEL BRAIN TUMOR IMAGES

Algorithms	Specificity	Sensitivity	Accuracy	Precision
YOLO5 (You Only Look Once) [28]	90.2%	91%	93.1%	91.6%
EfficientNetB0 [29]	99.2%	99.5%	98.8%	99.4%
ILPD	99.45%	99.71%	99.23%	99.6%

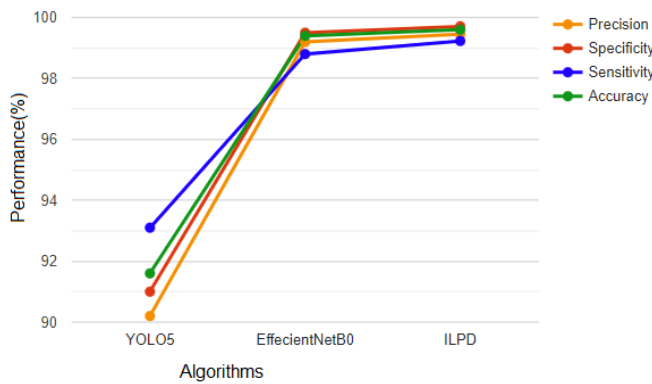


Fig. 5. Line Graph Representation for Kaggle Dataset.

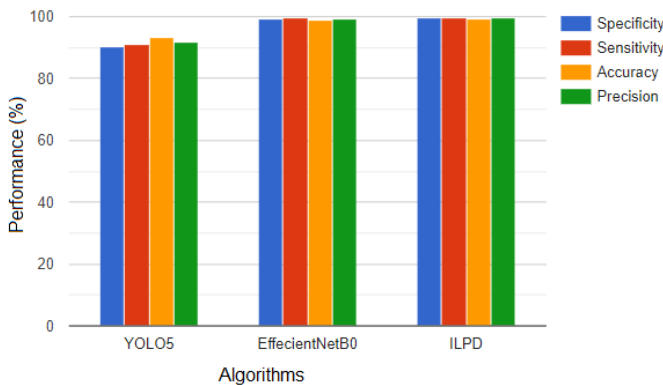


Fig. 6. Bar Graph Representation for Kaggle Dataset.

TABLE III. PERFORMANCE OF EXISTING AND PROPOSED ALGORITHMS APPLIED ON BRA1S 2017 BRAIN TUMOR IMAGES

Algorithms	Specificity	Sensitivity	Accuracy	Precision
YOLO5 (You Only Look Once) [28]	91.2%	92%	92.1%	92.9%
EfficientNetB0 [29]	98.12%	99.1%	98.1%	99.1%
ILPD	99.7%	99.5%	99.9%	99.1%

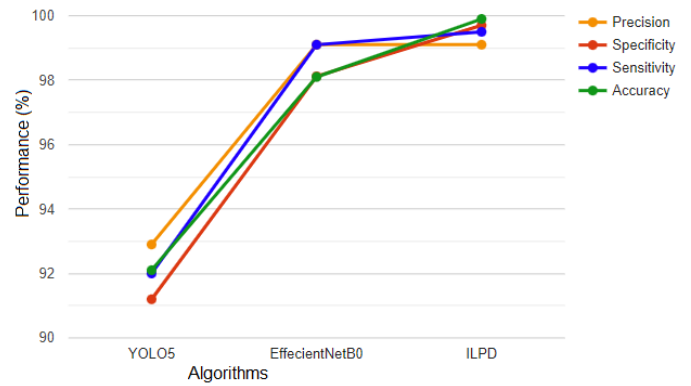


Fig. 7. Line Graph Representation for BraTS Dataset.

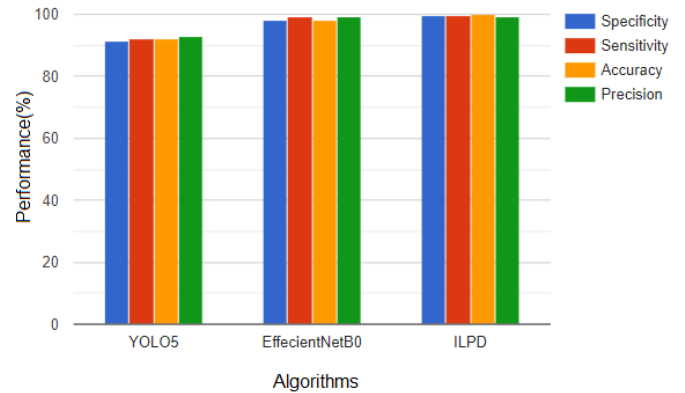


Fig. 8. Bar Graph Representation for BraTS Dataset.

VIII. CONCLUSION

In this paper, the ILPD is the efficient approach for finding tumors in the given MRI images. The MRI image is preprocessed and filtered by utilizing the advanced filtering approach. The classification is mainly focused on detecting the tumors or healthy images by using Integrated Learning Process Detection (ILPD). The final output consists of two neurons that belong to tumor or normal image. Two segmented images are represented by showing red and green color regions. From these images the features are extracted from last convolution layer. The ILPD focused on solving various issues in detecting brain tumors by using the segmentation approach and advanced image filters with the preprocessing method. Advanced image filters eliminate the noise from the MRI images and segment the images and represent the tumors with the green and red colors. Red represents the deep tumors and the green represents the tumors with low density. The performance of the existing and proposed approach shows the results based on the parameters. The ILPD achieved precision (99.67%), dice score (98.87), sensitivity (97.89%), specificity (99.12%), and accuracy (98.45%). The dice score shows the efficiency of the segmented image. In the future, the deeply segmented approach is used to increase the performance in terms of detecting the density of the image.

REFERENCES

- [1] Brain Tumor. Accessed: Apr. 11, 2021. [Online]. Available: <https://www.healthline.com/health/brain-tumor>.

- [2] A. Rehman, M. A. Khan, T. Saba, Z. Mehmood, U. Tariq, and N. Ayesha, "Microscopic brain tumor detection and classification using 3D CNN and feature selection architecture," *Microsc. Res. Technol.*, vol. 84, no. 1, pp. 133–149, 2021.
- [3] Haq EU, Jianjun H, Huarong X, Li K, Weng L. A Hybrid Approach Based on Deep CNN and Machine Learning Classifiers for the Tumor Segmentation and Classification in Brain MRI. *Comput Math Methods Med.* 2022 Aug 5;2022:6446680.
- [4] A. Gumaei, M. M. Hassan, M. R. Hassan, A. Alelaiwi and G. Fortino, "A Hybrid Feature Extraction Method With Regularized Extreme Learning Machine for Brain Tumor Classification," in *IEEE Access*, vol. 7, pp. 36266-36273, 2019, doi: 10.1109/ACCESS.2019.2904145.
- [5] Zhang Yue, Zhong Pinyuan, Jie Dabin, Wu Jiewei, Zeng Shanmei, Chu Jianping, Liu Yilong, Wu Ed X., Tang Xiaoying, "Brain Tumor Segmentation From Multi-Modal MR Images via Ensembling UNets", *Frontiers in Radiology*, Volume-1,2021, DOI:10.3389/fradi.2021.704888.
- [6] Ranjbarzadeh, R., Bagherian Kasgari, A., Jafarzadeh Ghouschi, S. et al. Brain tumor segmentation based on deep learning and an attention mechanism using MRI multi-modalities brain images. *Sci Rep* 11, 10930 (2021). <https://doi.org/10.1038/s41598-021-90428-8>.
- [7] Tang, Z., Ahmad, S., Yap, P. T. & Shen, D. Multi-atlas segmentation of MR tumor brain images using low-rank based image recovery. *IEEE Trans. Med. Imaging* 37(10), 2224–2235. <https://doi.org/10.1109/TMI.2018.2824243> (2018).
- [8] A. de Brebisson, G. Montana, Deep neural networks for anatomical brain segmentation, in: *Proceedings of the IEEE Conference on Computer Vision and Pattern Recognition Workshops*, 2015, pp. 20–28.
- [9] B. Patenaude, S. M. Smith, D. N. Kennedy, M. Jenkinson, A bayesian model of shape and appearance for subcortical brain segmentation, *Neuroimage* 56 (3) (2011) 907–922.
- [10] V. Shreyas and V. Pankajakshan, "A deep learning architecture for brain tumor segmentation in MRI images," 2017 IEEE 19th International Workshop on Multimedia Signal Processing (MMSp), 2017, pp. 1-6, doi: 10.1109/MMSp.2017.8122291.
- [11] M. Ali, S. O. Gilani, A. Waris, K. Zafar and M. Jamil, "Brain Tumour Image Segmentation Using Deep Networks," in *IEEE Access*, vol. 8, pp. 153589-153598, 2020, doi: 10.1109/ACCESS.2020.3018160.
- [12] A. Kumar, A. Ashok and M. A. Ansari, "Brain Tumor Classification Using Hybrid Model Of PSO And SVM Classifier," 2018 International Conference on Advances in Computing, Communication Control and Networking (ICACCCN), 2018, pp. 1022-1026, doi: 10.1109/ICACCCN.2018.8748787.
- [13] Zhang, D. et al. Exploring task structure for brain tumor segmentation from multi-modality MR images. *IEEE Trans. IMAGE Process.* <https://doi.org/10.1109/TIP.2020.3023609> (2020).
- [14] Zhou, C., Ding, C., Wang, X., Lu, Z. & Tao, D. One-pass multi-task networks with cross-task guided attention for brain tumor segmentation. *IEEE Trans. Image Process.* 29, 4516–4529. <https://doi.org/10.1109/TIP.2020.2973510> (2020).
- [15] Badrinarayanan, V., Kendall, A. & Cipolla, R. SegNet: a deep convolutional encoder-decoder architecture for image segmentation. *IEEE Trans. Pattern Anal. Mach. Intell.* 39(12), 2481–2495. <https://doi.org/10.1109/TPAMI.2016.2644615> (2017).
- [16] Hu, K. et al. Brain tumor segmentation using multi-cascaded convolutional neural networks and conditional random field. *IEEE Access* 7, 92615–92629. <https://doi.org/10.1109/ACCESS.2019.2927433> (2019).
- [17] Pereira S, Pinto A, Alves V. Brain tumor segmentation using convolutional neural networks in MRI images. *IEEE Trans Med Imaging.* 2016;35(5):1240–51.
- [18] Hao D, Yang G, Liu F, Mo Y, Guo Y. Automatic brain tumor detection and segmentation using U-Net based fully convolutional networks. In: *Annual conference on medical image understanding and analysis*. Springer, Cham; 2017.
- [19] Wang G, Li W, Ourselin S, Vercauteren T. Automatic brain tumor segmentation using cascaded anisotropic convolutional neural networks. *Comput Vis Pattern Recognit.* 2017;12(5).
- [20] Myronenko A. 3D MRI brain tumor segmentation using autoencoder regularization. Berlin: Springer; 2018.
- [21] Xue F, Nicholas T, Meyer C. Brain tumor segmentation using an ensemble of 3D U-nets and overall survival prediction using radiomic features. *Comput Vis Pattern Recognit.* 2018;279–288.
- [22] Zhou X, Li X, Hu K, Zhang Y, Chen Z, Gao X. ERV-Net: An efficient 3D residual neural network for brain tumor segmentation. *Expert Syst Appl.* 2021;170.
- [23] Saman S, Narayanan S. Active contour model driven by optimized energy functionals for MR brain tumor segmentation with intensity inhomogeneity correction. *Multimedia Tools Appl.* 2021;80(4):21925–54.
- [24] Liu H, Li Q, Wang L. A deep-learning model with learnable group convolution and deep supervision for brain tumor segmentation. *Math Probl Eng.* 2021;3:1–11.
- [25] M. Rizwan, A. Shabbir, A. R. Javed, M. Shabbir, T. Baker and D. Al-Jumeily Obe, "Brain Tumor and Glioma Grade Classification Using Gaussian Convolutional Neural Network," in *IEEE Access*, vol. 10, pp. 29731-29740, 2022.
- [26] Bhuiyan, M.R.; Abdullah, J. Detection on Cell Cancer Using the Deep Transfer Learning and Histogram Based Image Focus Quality Assessment. *Sensors* 2022, 22, 7007.
- [27] Yazdan SA, Ahmad R, Iqbal N, Rizwan A, Khan AN, Kim DH. An Efficient Multi-Scale Convolutional Neural Network Based Multi-Class Brain MRI Classification for SaMD. *Tomography.* 2022 Jul 26;8(4):1905-1927.
- [28] Shelatkar T, Urvashi D, Shorfuzzaman M, Alsufyani A, Lakshmana K. Diagnosis of Brain Tumor Using Light Weight Deep Learning Model with Fine-Tuning Approach. *Comput Math Methods Med.* 2022 Jul 1; 2022:2858845.
- [29] H. A. Shah, F. Saeed, S. Yun, J. -H. Park, A. Paul and J. -M. Kang, "A Robust Approach for Brain Tumor Detection in Magnetic Resonance Images Using Fine tuned EfficientNet," in *IEEE Access*, vol. 10, pp. 65426-65438, 2022.
- [30] C. R. T, G. Sirisha and A. M. Reddy, "Smart Healthcare Analysis and Therapy for Voice Disorder using Cloud and Edge Computing," 2018 4th International Conference on Applied and Theoretical Computing and Communication Technology (iCATccT), Mangalore, India, 2018, pp. 103-106, doi: 10.1109/iCATccT44854. 2018. 90 01280.
- [31] A. M. Reddy, K. SubbaReddy and V. V. Krishna, "Classification of child and adulthood using GLCM based on diagonal LBP," 2015 International Conference on Applied and Theoretical Computing and Communication Technology (iCATccT), Davangere, 2015, pp. 857-861, doi: 10.1109/ICATccT.2015.7457003.
- [32] Ayaluri MR, K. SR, Konda SR, Chidirla SR. 2021. Efficient steganalysis using convolutional auto encoder network to ensure original image quality. *PeerJ Computer Science* 7:e356 <https://doi.org/10.7717/peerj-cs.356>.
- [33] Mallikarjuna A. Reddy, Sudheer K. Reddy, Santhosh C.N. Kumar, Srinivasa K. Reddy, "Leveraging bio-maximum inverse rank method for iris and palm recognition", *International Journal of Biometrics*, 2022 Vol.14 No.3/4, pp.421 - 438, doi: 10.1504/IJBM.2022.10048978.
- [34] A. M. Reddy, V. V. Krishna, L. Sumalatha and S. K. Niranjan, "Facial recognition based on straight angle fuzzy texture unit matrix," 2017 International Conference on Big Data Analytics and Computational Intelligence (ICBDAC), Chirala, 2017, pp. 366-372, doi: 10.1109/ICBDACI.2017. 80 70865.
- [35] Ilaiah Kavati, A. Mallikarjuna Reddy, E. Suresh Babu, K. Sudheer Reddy, Ramalinga Swamy Cheruku, Design of a fingerprint template protection scheme using elliptical structures, *ICT Express*, Volume 7, Issue 4, 2021, Pages 497-500, ISSN 2405-9595, <https://doi.org/10.1016/j.icte.2021.04.001>.
- [36] Sudeepthi Govathoti, A Mallikarjuna Reddy, Deepthi Kamidi, G BalaKrishna, Sri Silpa Padmanabhuni and Pradeepini Gera, "Data Augmentation Techniques on Chilly Plants to Classify Healthy and Bacterial Blight Disease Leaves" *International Journal of Advanced Computer Science and Applications (IJACSA)*, 13(6), 2022. <http://dx.doi.org/10.14569/IJACSA.2022.0130618>.

Towards Home-based Therapy: The Development of a Low-cost IoT-based Transcranial Direct Current Stimulation System

Ahmad O. Alokaily, Ghala Almeteb, Raghad Alhabiti, Suhail S. Alshahrani
Dept. of Biomedical Technology, College of Applied Medical Sciences
King Saud University, Riyadh, Saudi Arabia

Abstract—Transcranial direct current stimulation (tDCS), a neuromodulation technique that is painless and noninvasive, has shown promising results in assisting patients suffering from brain injuries and psychiatric conditions. Recently, there has been an increased interest in home-based therapeutic applications in various areas. This study proposes a low-cost, internet of things (IoT)-based tDCS prototype that provides the basic tDCS features with internet connectivity to enable remote monitoring of the system's usage and adherence. An IoT-enabled microcontroller was programmed with C++ to supply a specific dose of direct current between the anode and cathode electrodes for a predefined duration. Each tDCS session's information was successfully synchronized with an IoT cloud server to be remotely monitored. The accuracy of the resulting stimulation currents was close to the expected values with an acceptable error range. The proposed IoT-based tDCS system has the potential to be used as a telerehabilitation approach to enhance safety and adherence to home-based noninvasive brain stimulation techniques.

Keywords—IoT; Internet of medical things; tDCS; home-based; brain stimulation; cloud

I. INTRODUCTION

Neurostimulation has a long and rich history of gaining scholarly and public interest. The use of electricity in treating medical disorders was well documented in ancient times. The first documented evidence of electrical stimulation dates to ancient Greek, when Plato and Aristotle explained the torpedo fish's potential to generate therapeutic effects through its electric discharges [1, 2]. In the first century AD, Scribonius Largus reported that placing a live torpedo fish over a patient's scalp had curative effects in healing headaches and gout [2, 3]. Moreover, in the late 11th century, Ibn-Sidah suggested that torpedo fish could be used to treat epilepsy by placing them on the patients' foreheads [2, 4]. It is important to note that the electrical energy produced by electric fish is an alternating current. Nevertheless, in the 18th century, Giovanni Aldini was one of the first to use galvanism in medicinal applications, creating direct current stimulation [5, 6]. Since then, transcranial electrical stimulation has progressed from simple galvanic batteries to the most precise and advanced electronic microprocessors [1, 7].

From a biomedical engineering perspective, there are three electrical interactions between tissues and electronic systems. The first type is invasive, in which medical devices are surgically placed into the body to restore function. The second

type is minimally invasive, when medical instruments are temporarily inserted for diagnosis and short-term treatment. The last type involves noninvasive devices used for monitoring, diagnosis, and treatment [8].

Transcranial direct current stimulation (tDCS) is a noninvasive brain stimulation technique that modulates cortical excitability by transmitting a low-intensity direct current to facilitate or inhibit cortical neuronal activities [9]. This approach has been shown to be safe and painless and to induce long-lasting excitability changes [10]. The cortical excitability changes caused by tDCS are presumed to follow the long-term potentiation (LTP) and long-term depression (LTD) neuroplasticity mechanisms [11]. Two standard stimulation montages are used in tDCS protocols. First, the anodal tDCS induces an enhancement in the cortical excitability (i.e., LTP-like effect) by depolarizing the resting membrane potential. Second, the cathodal tDCS induces a reduction in cortical excitability (i.e., LTD-like effect) by hyperpolarizing the resting membrane potential [12, 13].

In the past two decades, many studies have investigated the tDCS effects and their biomarkers in neuropsychiatric, cognitive, and motor disorders. tDCS is a promising and effective therapeutic tool in several conditions such as stroke, Parkinson's disease, Alzheimer's disease, depression, and schizophrenia [14]. For instance, a tDCS study was conducted on 10 clinically depressed patients. Half of them (five patients) received a 1mA anodal stimulation for 20 minutes per day, and the other half underwent sham treatment. The study showed that the tDCS stimulation led to a significant decrease in depression symptoms in the sample group compared with the sham group, suggesting tDCS can be an effective treatment for acute major depression [15]. In addition, tDCS antidepressant effects were shown to last up to 30 days after treatment [16].

It was also reported that almost 30% of patients with schizophrenia suffer from auditory hallucinations that are refractory to medications [14]. For this reason, the treatment of hallucinations in schizophrenia was studied using tDCS. Brunelin et al. [17] investigated the effect of tDCS on 30 patients with schizophrenia randomly assigned to receive an active 2mA tDCS or sham stimulation. A significant decrease in the severity of the hallucinations was observed, suggesting that tDCS could reduce symptoms of hallucinations, and the reduction lasted for up to three months [17]. Moreover, eight sessions of anodal tDCS treatment were applied to 13 patients

diagnosed with Parkinson's disease and compared with a control group of 12 Parkinson's patients who received sham stimulation. Using 2mA for 20 minutes over three weeks led to an enhancement in the anodal tDCS stimulation group's upper extremity bradykinesia and gait [18]. Furthermore, tDCS showed promising results in enhancing cognitive performance in healthy populations [19]. For example, a study aimed to investigate the effect of tDCS on attention demonstrated a significant increase in concentration for a group who underwent 2mA tDCS when compared with those receiving 0.1mA [20].

Certain health-related events such as the global spread of COVID-19 have revealed the necessity of telehealth applications in various areas [21]. Such applications have proven to be a practical and effective approach by facilitating remote access and monitoring of healthcare services and reducing the associated contamination risks during the pandemic [21]. Furthermore, telehealth-based tDCS systems have therapeutic potential as they enable use for severely ill patients, enhance the recruitment rate in clinical studies, and optimize patients' and physicians' schedules [22].

Several investigators have developed a smart tDCS system to facilitate the in-home-based approach of tDCS. For instance, Sourav et al. [23] developed an Android application-controlled tDCS system with an adjustable headset to enhance the user's experience. This system was able to deliver a constant current of 0.1–2.5 mA and can store the session's information on external memory.

Additionally, Charvet et al. [24, 25] implemented supervision protocols of telemonitored tDCS and investigated the feasibility of monitoring and controlling the delivery of home-based tDCS sessions. The stimulation in these studies was applied using the Soterix mini-Clinical Trials tDCS device (Soterix Medical, New York, NY, USA). The tDCS sessions were monitored in real-time via the videoconferencing platform. It was concluded that telemonitored tDCS has a high compliance rate with no observed technical issues.

In this paper, a home-based tDCS device equipped with the internet of things (IoT) and controlled by a microcontroller is proposed. The internet cloud-based storage and monitoring system would be integrated with the traditional tDCS device to help healthcare providers monitor the system remotely. The main objective of the approach is to improve the patients' experience since it is a home-based device, self-administered with minimal training and cost-effective.

The remainder of this paper is organized as follows: Section II describes the main hardware components of the proposed IoT-based tDCS as well as the software structure and interface. Section III discusses the integration and validation of the proposed system. Finally, Section IV concludes the objective of this study and suggests future directions.

II. METHODS

The proposed system consists of electrical hardware, custom-made software, and an IoT platform. The custom-made software controls the stimulation duration and intensity of the pulses, and the IoT platform registers session information on the cloud. The block diagram of the IoT-enabled home-based tDCS system is illustrated in Fig. 1.

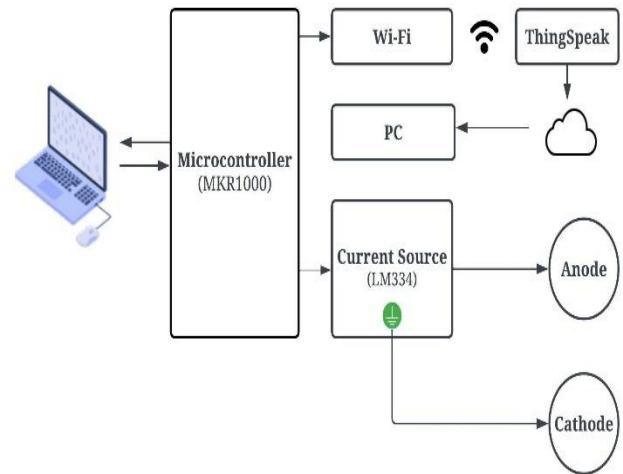


Fig. 1. Block Diagram of the Proposed IoT-based tDCS Device.

A. Hardware

The proposed IoT-based tDCS device consists of the following main hardware components:

- **Computer:** The proposed tDCS must be connected to a personal computer (PC) or notebook to power the system and send the commands to the microcontroller through a simple and user-friendly interface.
- **Microcontroller:** A low-cost consumer-grade microcontroller with internet connectivity (Arduino MKR1000) was used to control and regulate the operation of the proposed IoT-based tDCS system.
- **Current regulators:** Four three-terminal adjustable current sources (LM334-Z; Texas Instruments, USA) that operate with a sense voltage of 64 mV were connected in a parallel configuration to provide 0.5 mA in each loop, with a maximum current of 2 mA when the microcontroller triggered all loops. The LM334-Z was connected to digital pins 2, 3, 4, and 5.
- **tDCS electrodes:** A pair of commercially available tDCS electrodes (anode and cathode) as well as electrode wires, sponges, and an elastic headband for electrode placement (TheBrainDriver, USA) were used in the testing of the current tDCS system.
- **Resistors:** Four sets of resistors with an equivalent resistance of 128 Ω were connected in a parallel configuration to ensure that each loop in the tDCS circuitry provided 0.5 mA.
- **Light-emitting diodes (LEDs):** Four green LEDs were used as visual indicators of the current intensity.

B. Internet of Things (IoT) Platform

The ThingSpeak platform was used in the IoT-based tDCS device because it has the advantage of simplicity. A private channel was set to record, monitor, and retrieve real-time information on the stimulation duration and selected current intensity. The collected data are used for further analyses.

C. Software Architecture

The control and user interaction of the IoT-based tDCS prototype were programmed with an open-access Arduino IDE based on the C++ language. The flowchart of the system is shown in Fig. 2. A custom-made algorithm based on a switch statement to select an option from a set of defined discrete options was uploaded to the microcontroller (Arduino MKR 1000). The discrete options were constructed based on the most commonly used tDCS settings, which depend on the current intensity and stimulation duration. Thus, for this tDCS prototype, four current intensity options (low: 0.5 mA, medium: 1 mA, high: 1.5 mA, and very high: 2 mA) and three stimulation duration options (5, 10, and 20 minutes) were selected, defined, and coded to be received as a serial input entered by the user as illustrated in Table I. Based on the entered session's condition code, the microcontroller would activate all or some of the defined digital pins to supply the required current level for the selected time. Each digital pin (pins 2, 3, 4, and 5) on the microcontroller has a voltage of 3.3V when triggered, which is sufficient to supply 0.5 mA of direct current. Additionally, the operation of the IoT-based tDCS system could be terminated at any time during the session by pressing any keyboard character. Furthermore, data points were uploaded to the ThinkSpeak cloud when the session was started and at the end of each session. The recorded data points report the selected stimulation current intensity and duration of each session.

D. System Testing and Validation

The amount of current produced by the system was continuously measured using a digital multimeter (DMM) for each condition separately and compared with the expected calculated values to ensure an accurate and stable operation of the proposed IoT-based tDCS device. The stimulation duration was also recorded and confirmed with each selected state. Moreover, the real-time data synchronization accuracy between the proposed device and the ThinkSpeak cloud was validated.

TABLE I. THE TDCS STIMULATION SESSION SETTINGS

Current Intensity levels	Session Setting Code (entered by users)	Delivered Current (mA)	Session Duration (min)
Low	L05	0.5	5
	L10		10
	L20		20
Medium	M05	1	5
	M10		10
	M20		20
High	H05	1.5	5
	H10		10
	H20		20
Very High	VH05	2	5
	VH10		10
	VH20		20

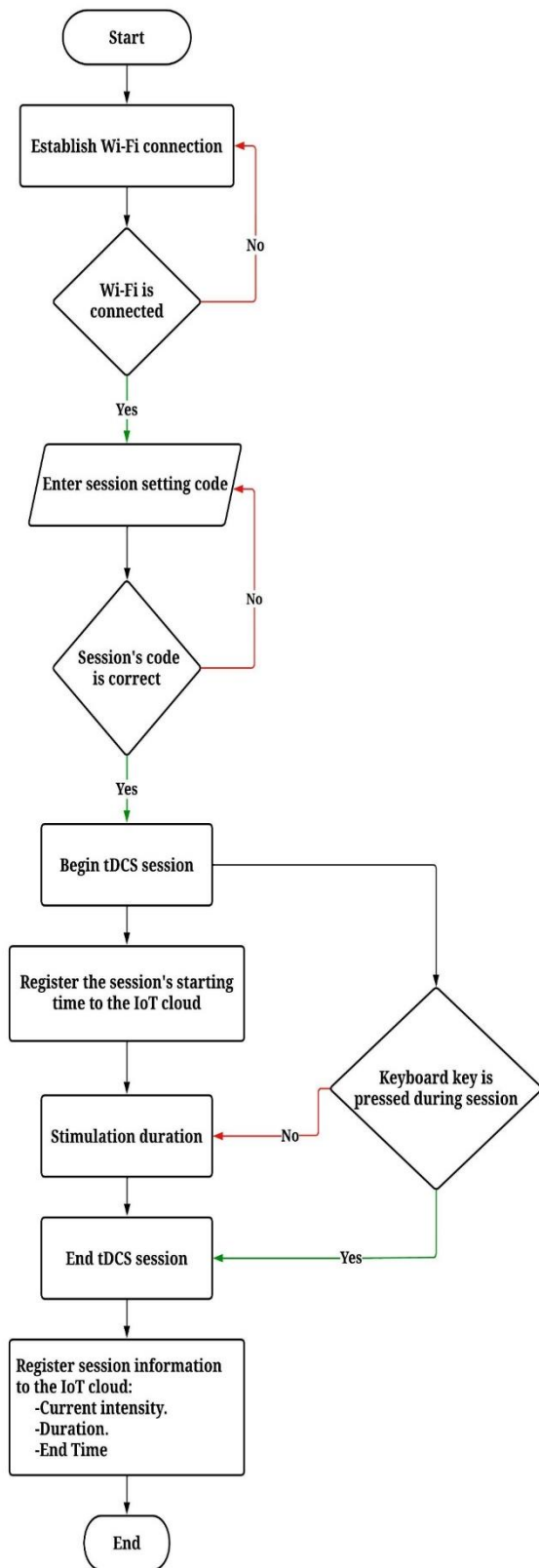


Fig. 2. Flowchart Illustrating the Operation Principle of the Proposed IoT-based tDCS Device.

III. RESULTS AND DISCUSSION

A. System Integration

The IoT-based tDCS system hardware was securely placed in a compact, lightweight box (20 cm x 20cm x 9 cm), as shown in Fig. 3. The LEDs were lit up according to the selected amount of current passing between the anode and cathode.

B. System Validation

The IoT-based current outputs were measured using a DMM (GDM-451, GW Instek) for all current intensity settings and compared with the calculated current output. The measured currents were 0.58, 0.99, 1.6, and 2 mA for the low, medium, high, and very high settings, respectively. Furthermore, the error percentage of the output current intensity ranged from -1% to +16%, as shown in Table II. However, when the selected current was at the higher end of the system output (i.e., high and very high), the output current measured between the anode and cathode showed a minimum to 0% error compared with the expected current intensity. Compared with another study that implemented a mobile-controlled tDCS system [23], our approach has significantly lower error rates.

In addition, all the proposed tDCS current and duration settings were tested, and successful real-time information was uploaded to the private channel on the ThingSpeak platform, as shown in Fig. 4. Two recorded readings were registered on the ThingSpeak private channel as starting and ending points. The starting point was marked at 0, while the ending point was marked at the selected current intensity and duration. This provided the advantage of remote monitoring and registration of the tDCS session data, which can benefit healthcare providers.

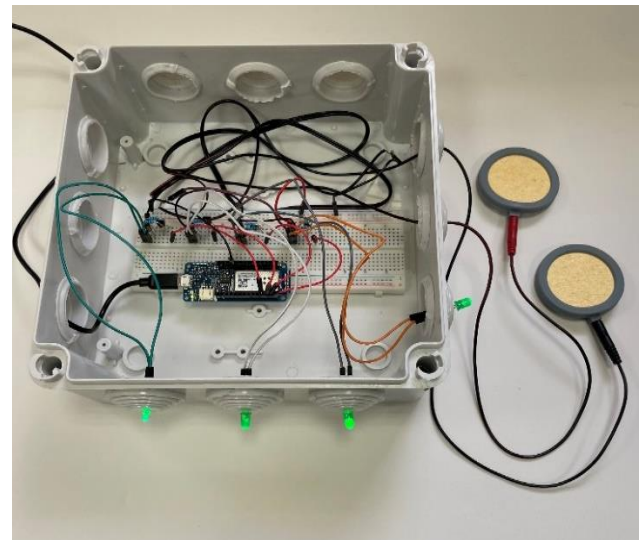


Fig. 3. Photograph of the IoT-based tDCS Device.

TABLE II. THE COMPARISON BETWEEN CALCULATED CURRENT INTENSITY AND MEASURED CURRENT INTENSITY AND THE ERROR PERCENTAGE AT DIFFERENT CURRENT INTENSITY LEVELS

Current Intensity Levels	Calculated Current Intensity (mA)	Measured Current Intensity (mA)	Error (%)
Low	0.50	0.58	+16.00%
Medium	1.00	0.99	-1.00%
High	1.50	1.60	+6.67%
Very High	2.00	2.00	0.00%

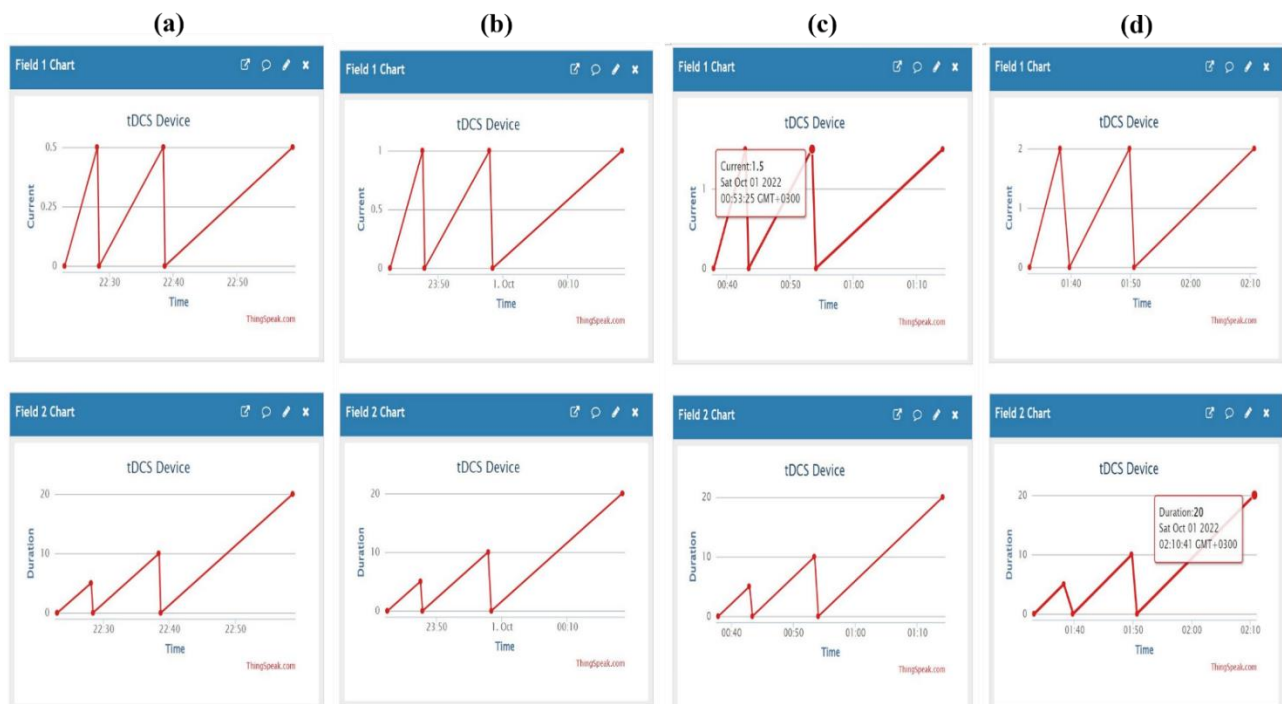


Fig. 4. The Figure Shows a Caption of the ThingSpeak Channel Information: Column (a) Exhibits Trials Taken at L05, L10, and L20 Settings. Column (b) Exhibits Trials Taken at M05, M10, and M20 Settings. Column (c) Exhibits Trials Taken at H05, H10, and H20 Settings. Column (d) Exhibits Trials Taken at VH05, VH10, and VH20 Settings.

Moreover, the proposed IoT-based tDCS system could be configured based on the subject's needs as prescribed by clinicians. Thus, the safety of delivering in-home tDCS sessions will be enhanced by ensuring that users can only apply the recommended current intensity and duration for each session.

IV. CONCLUSION

The present study focused on the feasibility of developing an IoT-based tDCS prototype using low-cost materials and a free-of-charge and accessible IoT platform. The use of IoT in our system could enhance the safety and adherence to home-based noninvasive research and therapy.

Future studies will be conducted to further improve the system's performance. Moreover, upon receiving the internal review board's approval, testing on human subjects will be investigated to evaluate the system's efficacy. Finally, the feasibility of a clinician remotely controlling the tDCS system over the internet will be explored.

REFERENCES

- [1] C. Sarmiento, D. San-Juan, and V. Prasath, "Brief history of transcranial direct current stimulation (tDCS): from electric fishes to microcontrollers," *Psychological medicine*, vol. 46, no. 15, pp. 3259-3261, 2016.
- [2] A. Priori, "Brain polarization in humans: a reappraisal of an old tool for prolonged non-invasive modulation of brain excitability," *Clinical neurophysiology*, vol. 114, no. 4, pp. 589-595, 2003.
- [3] G. Tsoucalas, M. Karamanou, M. Lymperi, V. Gennimata, and G. Androutsos, "The "torpedo" effect in medicine," *International maritime health*, vol. 65, no. 2, pp. 65-67, 2014.
- [4] J. Delbourgo, *A most amazing scene of wonders: electricity and enlightenment in early America*. Harvard University Press, 2006.
- [5] P. B. Fitzgerald, "Transcranial pulsed current stimulation: a new way forward?," vol. 125, ed, 2014, pp. 217-219.
- [6] F. Z. d. S. Arêas, G. P. T. Arêas, and R. Moll Neto, "Giovanni Aldini and his contributions to non-invasive brain stimulation," *Arquivos de Neuro-Psiquiatria*, vol. 78, pp. 733-735, 2020.
- [7] W. Paulus and A. Opitz, "Ohm's law and tDCS over the centuries," *Clinical Neurophysiology: Official Journal of the International Federation of Clinical Neurophysiology*, vol. 124, no. 3, pp. 429-430, 2012.
- [8] F. X. Palermo and J. C. Castel, "Electrical stimulation device and method for the treatment of neurological disorders," ed: Google Patents, 2011.
- [9] A. R. Brunoni et al., "Clinical research with transcranial direct current stimulation (tDCS): challenges and future directions," *Brain stimulation*, vol. 5, no. 3, pp. 175-195, 2012.
- [10] M. A. Nitsche and W. Paulus, "Sustained excitability elevations induced by transcranial DC motor cortex stimulation in humans," *Neurology*, vol. 57, no. 10, pp. 1899-1901, 2001.
- [11] C. J. Stagg, A. Antal, and M. A. Nitsche, "Physiology of transcranial direct current stimulation," *The journal of ECT*, vol. 34, no. 3, pp. 144-152, 2018.
- [12] T. Tanaka, Y. Isomura, K. Kobayashi, T. Hanakawa, S. Tanaka, and M. Honda, "Electrophysiological effects of transcranial direct current stimulation on neural activity in the rat motor cortex," *Frontiers in Neuroscience*, vol. 14, p. 495, 2020.
- [13] J. Green, S. Jang, J. Choi, S. C. Jun, and C. S. Nam, "Transcranial Direct Current Stimulation (tDCS): A Beginner's Guide for Neuroergonomists," in *Neuroergonomics*: Springer, 2020, pp. 77-101.
- [14] S. M. Szymkowicz, M. E. McLaren, U. Suryadevara, and A. J. Woods, "Transcranial direct current stimulation use in the treatment of neuropsychiatric disorders: a brief review," *Psychiatric annals*, vol. 46, no. 11, pp. 642-646, 2016.
- [15] F. Fregni, P. S. Boggio, M. A. Nitsche, M. A. Marcolin, S. P. Rigonatti, and A. Pascual-Leone, "Treatment of major depression with transcranial direct current stimulation," 2006.
- [16] P. S. Boggio et al., "A randomized, double-blind clinical trial on the efficacy of cortical direct current stimulation for the treatment of major depression," *International Journal of Neuropsychopharmacology*, vol. 11, no. 2, pp. 249-254, 2008.
- [17] J. Brunelin et al., "Examining transcranial direct-current stimulation (tDCS) as a treatment for hallucinations in schizophrenia," *American Journal of Psychiatry*, vol. 169, no. 7, pp. 719-724, 2012.
- [18] D. H. Benninger et al., "Transcranial direct current stimulation for the treatment of Parkinson's disease," *Journal of Neurology, Neurosurgery & Psychiatry*, vol. 81, no. 10, pp. 1105-1111, 2010.
- [19] A. Pisoni, G. Mattavelli, C. Papagno, M. Rosanova, A. G. Casali, and L. J. Romero Lauro, "Cognitive enhancement induced by anodal tDCS drives circuit-specific cortical plasticity," *Cerebral Cortex*, vol. 28, no. 4, pp. 1132-1140, 2018.
- [20] B. A. Coffman, M. C. Trumbo, and V. P. Clark, "Enhancement of object detection with transcranial direct current stimulation is associated with increased attention," *BMC neuroscience*, vol. 13, no. 1, pp. 1-8, 2012.
- [21] A. C. Smith et al., "Telehealth for global emergencies: Implications for coronavirus disease 2019 (COVID-19)," *Journal of telemedicine and telecare*, vol. 26, no. 5, pp. 309-313, 2020.
- [22] A. Cucca, K. Sharma, S. Agarwal, A. S. Feigin, and M. C. Biagioni, "Telemonitored tDCS rehabilitation: feasibility, challenges and future perspectives in Parkinson's disease," *Journal of neuroengineering and rehabilitation*, vol. 16, no. 1, pp. 1-10, 2019.
- [23] M. S. U. Sourav, A. Rahman, A. Al Mamun, and F. M. Alamgir, "Standard Transcranial Direct Current Stimulation (tDCS) Model," *International Journal of Computer Networks and Communications Security*, vol. 5, no. 12, pp. 264-270, 2017.
- [24] L. E. Charvet, B. Dobbs, M. T. Shaw, M. Bikson, A. Datta, and L. B. Krupp, "Remotely supervised transcranial direct current stimulation for the treatment of fatigue in multiple sclerosis: results from a randomized, sham-controlled trial," *Multiple Sclerosis Journal*, vol. 24, no. 13, pp. 1760-1769, 2018.
- [25] L. Charvet et al., "Remotely supervised transcranial direct current stimulation increases the benefit of at-home cognitive training in multiple sclerosis," *Neuromodulation: Technology at the Neural Interface*, vol. 21, no. 4, pp. 383-389, 2018.

Semi-supervised Text Annotation for Hate Speech Detection using K-Nearest Neighbors and Term Frequency-Inverse Document Frequency

Nur Heri Cahyana¹, Shoffan Saifullah², Yuli Fauziah³, Agus Sasmito Aribowo⁴, Rafal Drezewski⁵

Department of Informatics, Universitas Pembangunan Nasional Veteran Yogyakarta Yogyakarta, Indonesia^{1,2,3}

Department of Information Systems, Universitas Pembangunan Nasional Veteran Yogyakarta Yogyakarta, Indonesia³

Faculty of Information and Communication Technology, Universiti Teknikal Malaysia Melaka, Malaysia⁴

Institute of Computer Science, AGH University of Science and Technology, Cracow, Poland^{2,5}

Abstract—Sentiment analysis can detect hate speech using the Natural Language Processing (NLP) concept. This process requires annotation of the text in the labeling. However, when carried out by people, this process must use experts in the field of hate speech, so there is no subjectivity. In addition, if processed by humans, it will take a long time and allow errors in the annotation process for extensive data. To solve this problem, we propose an automatic annotation process with the concept of semi-supervised learning using the K-Nearest Neighbor algorithm. This process requires feature extraction of term frequency-inverse document frequency (TF-IDF) to obtain optimal results. KNN and TF-IDF were able to annotate and increase the accuracy of < 2% from the initial iteration of 57.25% to 59.68% in detecting hate speech. This process can annotate the initial dataset of 13169 with the distribution of 80:20 of training and testing data. There are 2370 labeled datasets; for testing, there are 1317 unannotated data; after preprocessing, there are 9482. The final results of the KNN and TF-IDF annotation processes have a length of 11235 for annotated data.

Keywords—Natural language processing; text annotation; semi-supervised learning; TF-IDF; K-NN

I. INTRODUCTION

The concept of text mining in natural language processing is often experienced in the annotation process, including the length of the human annotation process in data labeling. This annotation process also often causes errors due to time pressure and instructions to complete it [1]. In addition, sometimes, they are not trained and skilled in annotating specific fields. Thus, it is necessary to annotate with little knowledge (data labels) from humans semi-automatically, making complete annotations with machine learning.

Text classification also includes processing, which puts documents into predetermined categories [2]. Text classification can be done for solving several cases, such as sentiment analysis [3], emotion analysis [4], and hate speech detection [5], [6].

This study discusses detecting hate speech in the text, especially in text annotation. The discussion starts with determining the hate speech category, then grouping documents into those categories and validating them. The hate speech detection process in documents uses the basic principles of sentiment analysis, starting with document preprocessing,

vectorization, modeling, and validation. There are three models in the classification of sentiment analysis (or hate speech): machine learning, lexicon, and mixed models [7]. The lexicon and mixed models need a hate speech dictionary. This study uses a machine learning approach because the lexicon of hate speech in Indonesian is not widely available. The machine learning approach is divided into three approaches: supervised, unsupervised, and semi-supervised [8]. The unsupervised approach causes hate speech categories not to be directed as needed. It all depends purely on the condition of the document features. However, in supervised and semi-supervised, researchers can direct the categorization of hate speech into two or three categories: very hate speech, low hate speech, and non-hate speech. Based on existing research, annotators generally polarize hate speech into only two categories (hate speech and non-hate speech). Human annotators can assess the presence of hate speech in a document.

The hate speech annotation process is where experts separate or provide information on documents into two categories: groups of documents containing elements of hate (hate speech) and groups of documents that do not contain elements of hate (non-hate speech). This annotation follows the ways of annotating sentiments which are generally in two polarities (positive and negative) as used in [9]–[18]. This annotation process requires an expert (human annotator) who understands the meaning of hate speech and has experience annotating opinion documents.

This study aims to use the model of semi-supervised text annotations automatically by K-Nearest Neighbor. In addition, we have not been able to determine the best vectorizer because, as in [14], we used TF-IDF. This study's results differ from [19] with increased accuracy in the model that produces hate speech annotated datasets.

II. METHOD

A. Similar Research on Semi-supervised Text Annotation

Typically, in semi-supervised text annotations, the annotator uses the sentiment lexicon to annotate the unlabeled data and manually revise the annotated data sample. This approach requires more time to revise the annotations [20]. AraSenCorpus in [20] is a self-learning approach to automate annotations and reduce human effort. AraSenCorpus is a semi-

supervised framework for annotating a sizeable Arabic text corpus using a small subset of manually annotated tweets and extending it from a large set of unlabeled tweets to reduce human effort in annotating. This process uses the FastText neural network and the LSTM [21] deep learning classifier to manually expand the annotated corpus and ensure the quality of the newly created corpus, respectively (Fig. 1).

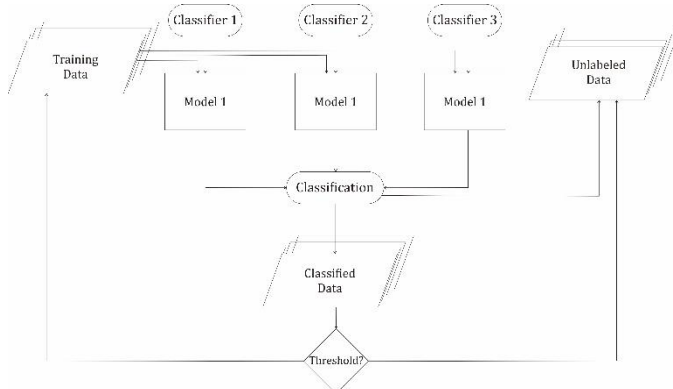


Fig. 1. AraSenCorpus Architecture [20].

This study performs a two-way (positive and negative) and three-way (positive, negative, and neutral) sentiment classification. In the case of two-way classification, AraSenCorpus improved the sentiment classification results from 80.37% to 87.4% using the 2017 SemEval dataset and from 79.77% to 85.2% using the ASTD dataset. The three-way classification gives 69.4% accuracy for the SemEval 2017 dataset, while the best system gives 63.38% using the F1-score and from 64.10% to 68.1% using the ASTD dataset. However, according to our assessment, the classification process is not determined by the type of classifier. Accuracy also depends on the vectorizer used. Another weakness is that if the iteration has been done many times and the classification results are consistently below the threshold, there is no visible solution to whether the dataset will still be included or discarded.

Another semi-supervised annotation study involved two targets: sentiment analysis and emotion analysis on an English textual review of three digital payment applications. The approach used involved supervised and unsupervised machine learning techniques. Data annotation involves three assistants from the field of Psychology. Annotators were recruited to label sentiments and emotions for 3,000 reviews. If the sentiment is neutral, the emotion is labeled neutral and excluded from the emotion analysis because no emotion can be detected from the neutral document. The machine learning algorithms are Support Vector Machine, Random Forest, and Naïve Bayes. Random Forest yielded the best accuracy for sentiment (F1 score = 73.8%; Kappa Cohen = 52.2%) and emotion (F1 score = 58.8%; Kappa Cohen = 44.7%) [22]. The architecture of the model used is shown in Fig. 2. The advantage of the approach used in [22] is that analyzing sentiment and emotion is carried out simultaneously. The downside is that the average accuracy for emotion classification based on Random Forest and SVM is around 61.3% (deficient), even though it uses a quite sophisticated algorithm. Another weakness is in the annotation process step. Sentiment and emotion annotations are carried out simultaneously so that it is prone to ambiguity in labeling

positive sentiments with negative emotions (anger, sadness, fear, disgust) or vice versa. This model also cannot anticipate if the annotation results are low in accuracy as in the AraSenCorpus Architecture (Fig. 2) [20].

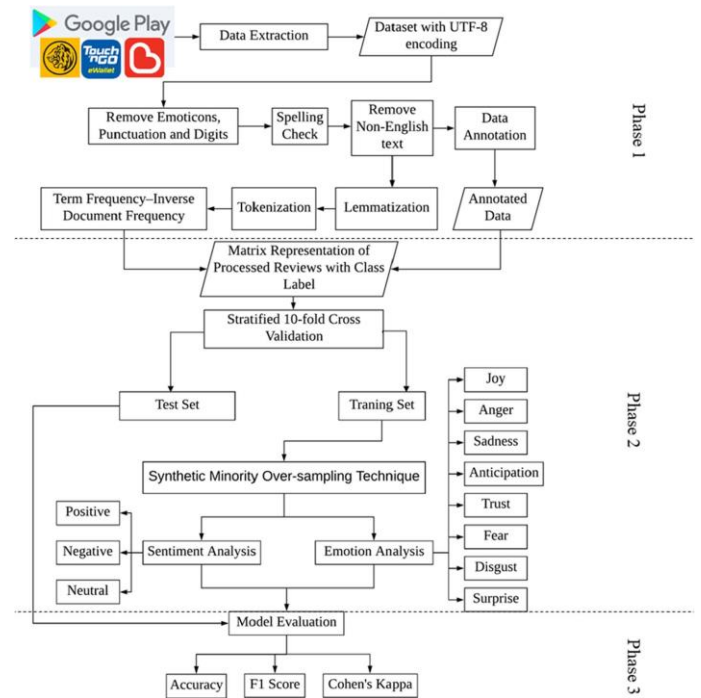


Fig. 2. Semi-Supervised Sentiment-Emotion Architecture [22].

B. Proposed Method

The semi-supervised text annotation method for hate speech that we propose is a new method that has never been used in any research. The semi-supervised text annotation begins with reading 2000 hate-speech training data and 9000 non-annotated testing data. The flow of the semi-supervised text annotation process is shown in Fig. 3.

The semi-supervised hate speech annotation process (Fig. 3) starts from step 1, reading the DT as training data annotated as hate speech (by experts). Step 2 reads unannotated UD data. Step 3 is the text preprocessing of DT and UD. Step 4 is the meta-vectorization process. The meta-vectorization process converts the clean DT and UD datasets into four types of vectors. The first vector is VBoW, created using the Bag-Of-Word method. The second vector is VTFIDF, created using the TF-IDF method [23], [24]. Step 5 is the process of preparing training data. Step 6 is the setup of machine learning algorithms.

The algorithm involved is K-Nearest Neighbor (K-NN). Step 7 is the creation of a meta-learning model. The meta-vector and meta-learning models will produce vectorization and machine-learning approaches. The combination of machine learning will be used for the auto-annotation process. Steps 8 and 9 prepare vector datasets that have not been annotated. In step 10, it will be checked if there is still a dataset that has not been annotated then the process will continue to step 11, namely the process of annotating the dataset. The annotation process is done by predicting labels by the vector and machine

learning combinations. The prediction results are also subject to validation to determine their accuracy—the auto-annotation process results in Step 12 as a meta-labeled dataset. In Step 12, a voting process will be carried out to determine the label for each dataset record. The voting counts used the sample of the voting process for labeling decisions. There are two types of weight: the total W (weight) score of the vectorization-machine-learning model for the hate-speech polarity and the W (weight) score from the vectorized-machine-learning model for the non-hate speech polarity. In Step 13, if the polarity score of hate speech or non-hate speech exceeds the threshold, then the dataset and its annotations will be transferred to data training. If not, it will be re-annotated in the next cycle. In step 14, the data will be looping processed three times for optimization. If it is more than three times, then the rest of the Unlabeled Dataset will go to Step 15, which is manual annotation. The results of manual annotations will be combined with the training data.

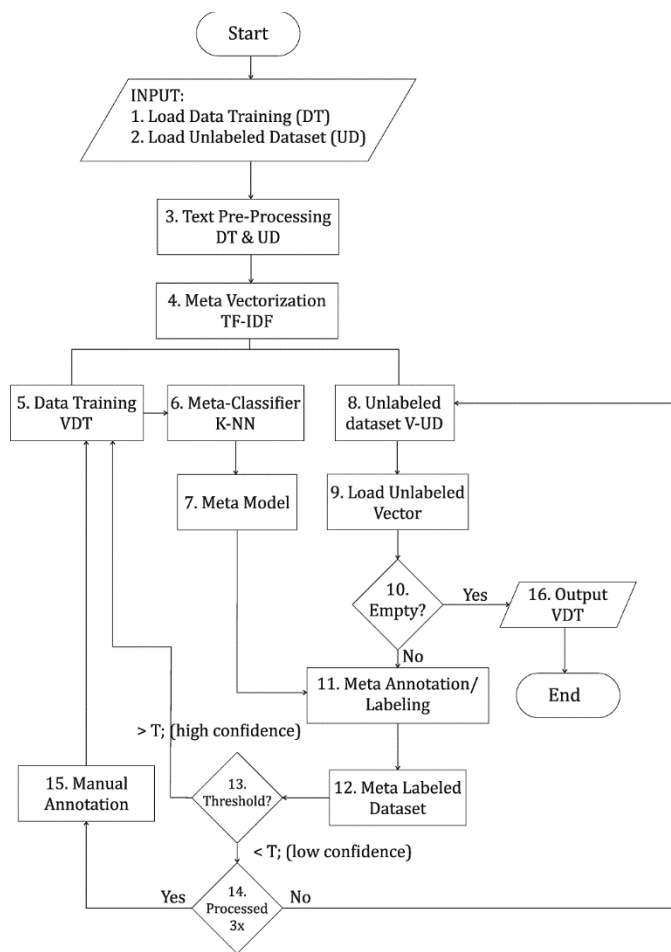


Fig. 3. Semi-Supervised Hate Speech Annotation Model (Proposed).

III. RESULTS AND DISCUSSION

A. Population and Sampling

Based on the monitoring of data sources, it is known that the dataset size is dynamic, meaning that these opinions continue to grow, even though the presidential-vice presidential debate or the Covid-19 pandemic has already occurred. A new video on the official channel also appeared, followed by

viewers' opinions. So this study concludes that the population size is unknown, and it is impossible to download all comments from the YouTube repository. So the research determined that the sampling method used was purposive sampling. This purposive sampling method was chosen for the following reasons:

- 1) Our initial observations found hate speech in YouTube video comments on the topic of the 2019 Indonesian presidential debate and Covid-19. So, the data are suitable for our study.
- 2) The data from YouTube video comments are public and can be downloaded for free

The number of videos related to the presidential debate samples required refers to previous similar studies. In the process of getting the population of comments from videos, this study uses videos that meet the following criteria:

- 1) The data collection stage downloads all comments from the presidential debates one to five, each broadcast in full by two official channels. So this study downloads comments from 10 presidential debate videos and five Covid-19 news.
- 2) The data collection stage also downloads from the official channel comments from videos that do not show the whole presidential debate but are considered necessary to download because of the high number of views, more than 10,000 views, and comments above 1000 comments on exciting topics.

B. Data Annotation

In supervised learning, opinion data must be annotated by experts responsible for labeling hate speech on opinion data. So the data labeling process is the first step of knowledge transfer before categorization is carried out. The level of hate speech used for the labeling process is shown in Table I.

TABLE I. HATE SPEECH LEVELS IN THIS RESEARCH

No	Level	Code	Information
1.	Very Hate	VH	Hate speech that has the potential to cause dangerous social unrest
2.	Hate	H	Hate speech does not have the potential to cause harmful social unrest
3.	Non-Hate	NH	No hate speech

An annotator is an expert with expertise and knowledge following the political realm. Experts know the fields of social humanities and information technology (social media). The method of annotating opinions has also been determined. There are two experts and a team, all of which annotate hate speech, sentiment, and emotion. Steps of the annotation process:

- 1) The first expert will take around 2,000 opinions and then describe Very Hate, Hate or non-Hate.
- 2) The first expert's annotation results will be kept and not given to the second expert. Only comments from the first-choice expert are given to the second expert for hate speech annotation. The second expert does not know the first expert's annotation label. Then proceed with automatic annotation by

algorithms on data sets that experts do not annotate. This method is a semi-supervised text annotation based on meta-learning, which will automatically perform hate speech annotation, as shown in Fig. 4.

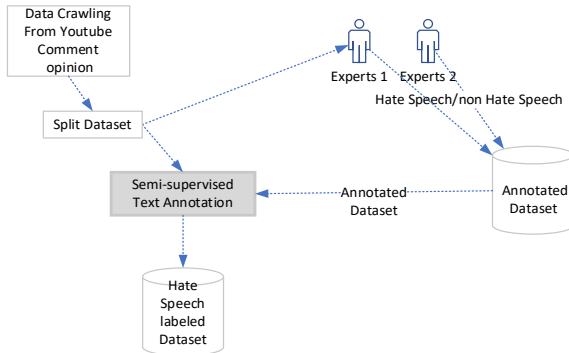


Fig. 4. Hate Speech Levels in this Research.

C. Scenarios and the Results of Text Annotation using K-NN and TF-IDF

This study uses a scenario with the composition of training data, testing data, and threshold: 20%, 80%, and 80%. As for the training data, the initial labeling process was carried out by experts. This annotation process is tested using data, as shown in Table II. In contrast, 80% of data is testing data used to verify the accuracy of the annotation process with a data-limiting threshold of 80%.

TABLE II. SCENARIO

No	Parameters	Value	Information
1.	Threshold	80	Presents
2.	Data training annotated	2370	Length of datasets
3.	Data training un-annotated	9482	Length of datasets
4.	Data testing	1317	Length of datasets
5.	Total of datasets	13169	Length of datasets

The KNN method can perform initial training data with a sample of 20% and has an accuracy of 57.25%. After validating using TF-IDF vectorization, the best iteration is 59.68% so this method can increase the accuracy by 2.43%.

The implementation of KNN and TF-IDF with this scenario resulted in 11,235 annotated data from the total dataset processed after preprocessing of 11,852. So in this process, there are still 617 data that have not been annotated. It happens because the process still has shortcomings from the initial annotation process. In the future, the initial accuracy of the annotation will be improved to optimize the final annotation. In addition, other vectorization and classification methods will also be implemented.

IV. CONCLUSION

The results of the presented research are the KNN and TF-IDF models of speech classifiers with semi-supervised hate speech annotations to detect hate speech on social media with low accuracy. The applied TF-IDF vectorization method increased the accuracy by 2.43%. Thus, future works will

increase by using the percentage variation of data labeling on the initial annotation (5%, 10%, 20%) and threshold (0.6, 0.7, 0.8, and 0.9). Besides, the vectorization will be improved by applying methods such as Bag-Of-Word and Word2Vec. The classification methods will be improved and compared with other methods like Random Forest (RF), Extra Tree (ET), Naïve Bayes (NB), Support Vector Machine (SVM), and Decision Tree (DT).

ACKNOWLEDGMENT

This research was supported by LPPM Universitas Pembangunan Nasional “Veteran” Yogyakarta.

REFERENCES

- [1] K. Miok, G. Pirs, and M. Robnik-Sikonja, “Bayesian Methods for Semi-supervised Text Annotation,” 14th Linguist. Annot. Work., pp. 1–12, 2020, [Online]. Available: <http://arxiv.org/abs/2010.14872>.
- [2] M. Bouazizi and T. Ohtsuki, “Multi-class sentiment analysis on twitter: Classification performance and challenges,” Big Data Min. Anal., vol. 2, no. 3, pp. 181–194, 2019, doi: 10.26599/BDMA.2019.9020002.
- [3] M. Chen, K. Ubul, X. Xu, A. Aysa, and M. Muhammad, “Connecting Text Classification with Image Classification: A New Preprocessing Method for Implicit Sentiment Text Classification,” Sensors, vol. 22, no. 5, p. 1899, Feb. 2022, doi: 10.3390/s22051899.
- [4] M. Z. Asghar et al., “A Deep Neural Network Model for the Detection and Classification of Emotions from Textual Content,” Complexity, vol. 2022, pp. 1–12, Jan. 2022, doi: 10.1155/2022/8221121.
- [5] P. William, R. Gade, R. esh Chaudhari, A. B. Pawar, and M. A. Jawale, “Machine Learning based Automatic Hate Speech Recognition System,” 2022 Int. Conf. Sustain. Comput. Data Commun. Syst., pp. 315–318, Apr. 2022, doi: 10.1109/ICSCDS53736.2022.9760959.
- [6] K. Miok, B. Škrlić, D. Zaharie, and M. Robnik-Šikonja, “To BAN or Not to BAN: Bayesian Attention Networks for Reliable Hate Speech Detection,” Cognit. Comput., vol. 14, no. 1, pp. 353–371, Jan. 2022, doi: 10.1007/s12559-021-09826-9.
- [7] P. Sudhir and V. D. Suresh, “Comparative study of various approaches, applications and classifiers for sentiment analysis,” Glob. Transitions Proc., vol. 2, no. 2, pp. 205–211, 2021, doi: 10.1016/j.gltp.2021.08.004.
- [8] C. R. Aydin and T. Güngör, “Sentiment analysis in Turkish: Supervised, semi-supervised, and unsupervised techniques,” Nat. Lang. Eng., vol. 27, no. 4, pp. 455–483, 2021, doi: 10.1017/S1351324920000200.
- [9] S. Aman and S. Szpakowicz, “Identifying expressions of emotion in text,” Lect. Notes Comput. Sci. (including Subser. Lect. Notes Artif. Intell. Lect. Notes Bioinformatics), vol. 4629 LNAI, no. September 2007, pp. 196–205, 2007, doi: 10.1007/978-3-540-74628-7_27.
- [10] A. Krouska, C. Troussas, and M. Virvou, “The effect of preprocessing techniques on Twitter sentiment analysis,” IISA 2016 - 7th Int. Conf. Information, Intell. Syst. Appl., 2016, doi: 10.1109/IISA.2016.7785373.
- [11] A. M. Ningtyas and G. B. Herwanto, “The Influence of Negation Handling on Sentiment Analysis in Bahasa Indonesia,” Proc. 2018 5th Int. Conf. Data Softw. Eng. ICoDSE 2018, pp. 1–6, 2018, doi: 10.1109/ICODSE.2018.8705802.
- [12] J. Savigny and A. Purwarianti, “Emotion classification on Youtube comments using word embedding,” in International Conference on Advanced Informatics: Concepts, Theory and Applications, 2017, pp. 1–5, doi: 10.1109/ICAICTA.2017.8090986.
- [13] K. Mulcrone, “Detecting Emotion in Text,” 2012.
- [14] W. C. F. Mariel, S. Mariyah, and S. Pramana, “Sentiment analysis: A comparison of deep learning neural network algorithm with SVM and naïve Bayes for Indonesian text,” J. Phys. Conf. Ser., vol. 971, no. 1, 2018, doi: 10.1088/1742-6596/971/1/012049.
- [15] T. Sutabri, A. Suryatno, D. Setiadi, and E. S. Negara, “Improving Naïve Bayes in Sentiment Analysis For Hotel Industry in Indonesia,” in Proceedings of the 3rd International Conference on Informatics and Computing, ICIC 2018, 2018, pp. 1–6, doi: 10.1109/ICIC.2018.8780444.
- [16] M. Lailiyah, S. Sumpeno, and I. K. E. Purnama, “Sentiment analysis of public complaints using lexical resources between Indonesian sentiment

- lexicon and sentiwordnet,” in 2017 International Seminar on Intelligent Technology and Its Application: Strengthening the Link Between University Research and Industry to Support ASEAN Energy Sector, ISITIA 2017 - Proceeding, 2017, vol. 2017-Janua, pp. 307–312, doi: 10.1109/ISITIA.2017.8124100.
- [17] U. Makhmudah, S. Bukhori, J. A. Putra, and B. A. B. Yudha, “Sentiment Analysis of Indonesian Homosexual Tweets Using Support Vector Machine Method,” Proc. - 2019 Int. Conf. Comput. Sci. Inf. Technol. Electr. Eng. ICOMITEE 2019, pp. 183–186, 2019, doi: 10.1109/ICOMITEE.2019.8920940.
- [18] T. F. Abidin, M. Hasanuddin, and V. Mutiawani, “N-grams based features for Indonesian tweets classification problems,” Proc. - 2017 Int. Conf. Electr. Eng. Informatics Adv. Knowledge, Res. Technol. Humanit. ICELTICS 2017, vol. 2018-Janua, no. ICELTICS, pp. 307–310, 2017, doi: 10.1109/ICELTICS.2017.8253287.
- [19] Nurfaizah, T. Hariguna, and Y. I. Romadon, “The accuracy comparison of vector support machine and decision tree methods in sentiment analysis,” J. Phys. Conf. Ser., vol. 1367, no. 1, 2019, doi: 10.1088/1742-6596/1367/1/012025.
- [20] A. Al-Laith, M. Shahbaz, H. F. Alaskar, and A. Rehmat, “AraSenCorpus: A Semi-Supervised Approach for Sentiment Annotation of a Large Arabic Text Corpus,” Appl. Sci., vol. 11, no. 5, pp. 1–19, 2021, doi: 10.3390/app11052434.
- [21] Y. Mao, A. Pranolo, A. P. Wibawa, A. B. Putra Utama, F. A. Dwiyanto, and S. Saifullah, “Selection of Precise Long Short Term Memory (LSTM) Hyperparameters based on Particle Swarm Optimization,” 2022 Int. Conf. Appl. Artif. Intell. Comput., pp. 1114–1121, May 2022, doi: 10.1109/ICAAIC53929.2022.9792708.
- [22] V. Balakrishnan, P. Y. Lok, and H. Abdul Rahim, “A semi-supervised approach in detecting sentiment and emotion based on digital payment reviews,” J. Supercomput., vol. 77, no. 4, pp. 3795–3810, 2021, doi: 10.1007/s11227-020-03412-w.
- [23] Y. Fauziah, S. Saifullah, and A. S. Aribowo, “Design Text Mining for Anxiety Detection using Machine Learning based-on Social Media Data during COVID-19 pandemic,” in Proceeding of LPPM UPN “Veteran” Yogyakarta Conference Series 2020–Engineering and Science Series, 2020, vol. 1, no. 1, pp. 253–261, doi: 10.31098/ess.v1i1.117.
- [24] S. Saifullah, Y. Fauziah, and A. S. Aribowo, “Comparison of Machine Learning for Sentiment Analysis in Detecting Anxiety Based on Social Media Data,” Jan. 2021, [Online]. Available: <http://arxiv.org/abs/2101.06353>.

Comparison of Edge Detection Algorithms for Texture Analysis on Copy-Move Forgery Detection Images

Bashir Idris¹, Lili N. Abdullah², Alfian Abdul Halim³, Mohd Taufik Abdullah Selimun⁴

Multimedia Department, Faculty of Computer Science and Information Technology^{1, 2, 3}
Universiti Putra Malaysia (UPM), Selangor, Malaysia^{1, 2, 3}

Computer Science Department, Faculty of Computer Science and Information Technology⁴
Universiti Putra Malaysia (UPM), Selangor, Malaysia⁴

Abstract—Feature extraction in Copy-Move Forgery Detection (CMFD) is crucial to facilitate image forgery analysis. Edge detection is one of the processes to extract specific information from Copy-Move Forgery (CMF) Images. It sensitizes the amount of information in the image and filters out useless ones while preserving the important structural properties in the image. This paper compares five edge detection methods: Robert, Sobel, Prewitt (first Derivative), Laplacian, and Canny edge detectors (second Derivatives). CMFD evaluation datasets images (MICC-F220) are tested with both methods to facilitate comparison. The edge detection operators were implemented with their respective convolution masks. Robert with a 2x2 mask, The Prewitt and Sobel with a 3x3 mask, while Laplacian and canny used adjustable masks. These masks determine the quality of the detected edges. Edges reflect a great-intensity contrast that is either darker or brighter.

Keywords—Edge detection; first derivative; second derivatives; robert; sobel; prewitt; laplacian; canny edge detector

I. INTRODUCTION

Image forensic analysis requires good-quality images in any orientation to accurately detect the image textural properties. A good quality image can give the best evaluation when investigating a crime scene on any query image. Therefore, the analysis of CMFD detection image texture plays a significant role in image forensics. Edge-based segmentation is one of the methods used to analyze image textures in CMFD.

Segmentation is an essential determinant for image information understanding and retrieval. It is also one of the frequent topics of discussion in the image processing and computer vision community [1]. Theoretically, image segmentation separates digital image data into a set of visually separate and identical regions based on parameters such as pixel intensity, similarity, discontinuity, cluster data, and so on [2]. The primary objective of segmentation is to clearly identify an image object from its background. Researchers have categorized segmentation into different techniques. The author [3] express segmentation as threshold techniques, edge detection techniques, region-based techniques, and connectivity-preserving relaxation methods. In [1] segmentation is seen as threshold-based, regional growth, edge, and segmentation based on clustering and weakly-supervised learning in CNN. In 2022, due to a significant improvement

over the last four decades from the traditional segmentation-based method to advance deep learning algorithms, [2] categorized segmentation algorithms into rule-driven and data-driven methods. Methods for cleaning objects that rely on one or more rules are referred to as rule-driven. Classification methods that learn features from data, such as ANN and DL, are referred to as data-driven. According to [2], several rule-based segmentation methods, such as fuzzy-based image segmentation (FBS), have been abandoned because they do not give satisfactory performance or because their lengthy computation times do not sufficiently substantiate their use. However, the reviewed literature mentioned that thresholding and edge detection methods are the most popular and applicable traditional image segmentation methods. This paper primarily focused on the edge detection-based segmentation method.

Edge detection is a method for recognizing the points or pixels in an image where the luminance varies abruptly or significantly. These points are clustered along segments of lines known as edges. Edge detection seeks to identify and locate image discontinuities. Due to the high frequency of both noise and image, edge identification becomes problematic. This paper discusses the edge detection techniques to address the choice of an edge detection method based on distinctive edge identification, noisy removal, etc.

Filtering is a method of correcting or improving the process of selecting the best keypoints in an image [4]. Edge detectors utilize filters to highlight edges while removing noise in a given image. Smoothing, sharpening, and edge enhancement are some image-filtering activities invoked using filtering methods. These activities are used interchangeably to enhance images for proper image-processing applications [5]. The filters are utilized for locating the sharp, discontinuous edges. These discontinuities cause variations in pixel intensities, which define the object's boundaries [5]. By applying filters to images, salient key points can be efficiently located for object detection.

Edges are of fundamental importance during any image-processing task. The intensity values of pixels that share a neighborhood are compared in detecting edges. The significant changes in the dense regions are located as edges. These dense areas are often difficult to trace due to the presence of noise. The presence of noise in the image affects the detection of the Edges; therefore, noise needs to be cleaned before the detection

of edges [6]. Noise reduction has been a challenge in the edge detection process, attracting the attention of many scholars in different areas of application that use images. Edge detection algorithms have been used for decades and have recently been employed in various domains because of their ability to detect and differentiate good boundaries in images.

Research has been conducted over the past decades to detect abrupt changes in image intensities (edges). Edge detection was employed in glass production for texture analysis [6], Canny Edge Detection Algorithm for Congregating Traffic Information [7], Sobel edge detector for synthetic aperture radar (SAR) detection [8], Laplacian edge detector for bladder cancer diagnosis [9], Kirsch edge detector for sharpening effect in images [10], Sobel edge detector for hardware implementation on the FPGA Nexys 4 DDR Board [11], copy-move forgery detection in digital images [12].

This paper presents an analysis of five types of edge detectors. It examines the edges by applying various edge operators and their respective filters. Five selected images in the MICC-F220 CMFD dataset are tested and compared to each other. This paper presented the related work in Section II; Section III presents the algorithms based on the first derivatives and explains the edge detector operators and their various masks. Section IV presented an algorithm based on the second Derivative, and Section V presented the result of the five operators. Finally, Section VI discussed the result, and the conclusion was depicted in Section VII.

II. RELATED WORK

As shown in Fig. 1, an angle gradient vector indicates the intensity change at that edge pixel. The cycle spot in Fig. 1 is the corresponding gradient vector on one data point or pixel. The intensity changes from 0 to 255 in the gradient direction at that pixel. The gradient's magnitude determines the edge's strength by calculating the gradient in uniform regions; a zero vector is obtained, indicating that there are no edge pixels. In natural images, where there are rarely ideal discontinuities or uniform regions, as seen in Fig. 1, thus, the gradient magnitude is evaluated to determine whether to detect the edge pixels. Edge detection is one of the simplest and oldest image-processing procedures, it is frequently employed in recently advanced edge detection algorithms. Edge detection is a technique for detecting abrupt changes in image intensity. The use of first-order or second-order derivatives can be employed to detect those changes [13]. Edge detection methods were developed in the 1970s using small operators such as Sobel (3x3) to compute an approximation of the image's first Derivative. Edge detection involves the application of different size operators because the change in image intensity depends on the image scale. This variation in intensity can be demonstrated as a peak in Fig. 3, using gradient-based operators (first Derivative) or a sharp zero-crossing on gaussian-based operators (second Derivative), respectively.

The edge detection algorithms are divided into two distinct categories: Gradient-based (first Derivative) and Gaussian-based (second Derivative) [10]. An adaptive mask convolves the input image, resulting in a gradient image with edges recognized via the thresholding technique. To detect edges, the gradient operators (Sobel, Prewitt, and Roberts) examine the

maximum and minimum intensity values. They determine the distribution of intensity values in each pixel's neighborhood to see if it should be categorized as an edge. Sobel, Prewitt, and Roberts operators are time-consuming and cannot be deployed for real-time applications (Bhardwaj & Mittal, 2012). On the other hand, the Laplacian of Gaussian (LoG) is categorized under the Gaussian-based method (second Derivative). Gradient-based operators are filters with various kernel sizes convolved with the original input image to produce the image gradient. Zero-crossing or second-order derivative methods are other names for Gaussian-based approaches. They significantly extract sharp zero-crossing points, and zero-crossing indicates the presence of maxima (an edge) [3]. The Canny operator is well-known for its exceptional performance, as it goes through noise reduction, gradient magnitude calculation as gradient operators, thresholding to maintain firm edges while deleting weak ones, and finally, non-maximum suppression for edge thinning through Hysteresis [8], [10].

Various survey has been conducted to investigate the impact of edge detection in digital images. This can be summarized in Table I.

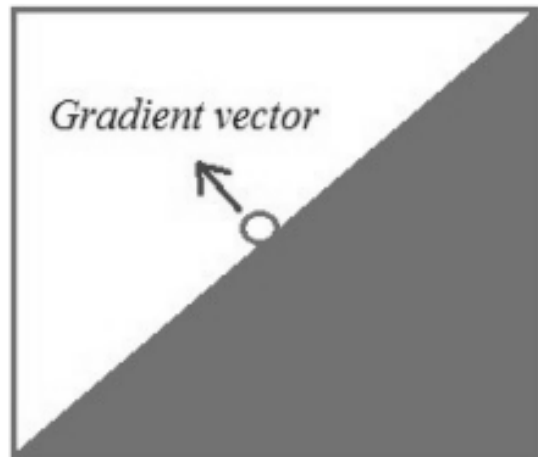


Fig. 1. Gradient Vector with Red Spot Indicating the Location of a Pixel.

TABLE I. RELATED EDGE DETECTION SURVEY

S/N	Year	Author	Description of Survey
1	2022	Kheradmand, & Mehranfar [2]	Edge Segmentation-based techniques
2	2022	Jin et al.[14]	Recent advances in image edge detection
3	2017	Song, & Yan, [1]	Image Segmentation Techniques
4	2015	Öztürk & Akdemir [6]	Edge Detection Algorithms for Glass Production analysis
5	2015	Vikram Mutneja [15]	Methods of Image Edge Detection
6	2015	Li et al. [16]	Visual Feature Detection
7	2013	Lopez-Molina et al. [17]	Quantitative error measures for edge detection
8	2012	Shrivakshan et al. [17]	Color filter technology
9	2011	Papari, & Petkov [18]	Edge and line-oriented contour detection

III. ALGORITHMS BASED ON FIRST DERIVATIVE (GRADIENT-BASED)

The main difference between the algorithms based on the first derivatives is the nature of the mask or filters (known as low pass filters) they applied during the computation of the derivatives. A general flow diagram for computing the First Derivative of an image is presented in Fig. 2.

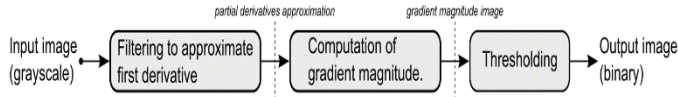


Fig. 2. Block Diagram of the First Derivative Edge Detection Algorithms [13].

The intensity variations in the magnitude and direction of an image f can be calculated using the gradient operator (∇). It is a well-known tool in image processing for calculating image orientations. Let's consider a 1 D image signal to detect an edge.

A. Edge Detection using Gradient Operator based on 1D Image

Consider a 1D image signal with edges in Fig. 3.

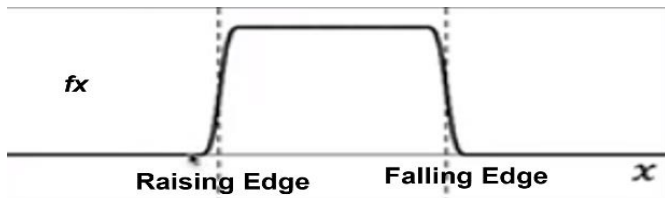


Fig. 3. Image Signal ($f(x)$).

The first Derivative of the image is computed to determine the intensity changes in the above image, $f(x)$. Ideally, the Derivative of a continuous function represents the amount of change in the function [19]. When dealing with edges, those changes are obtained from the function. When the first Derivative of f for x is applied to the image in Fig. 3, it is transformed into the image in Fig. 4. The local extrema indicate the edges in the image. Finding the absolute value of the first Derivative obtained the two peaks (local extrema Fig. 4). The location of the peaks indicates where the edges occur, and the height of the peaks expresses the strength of the edges (local maxima Fig. 4).

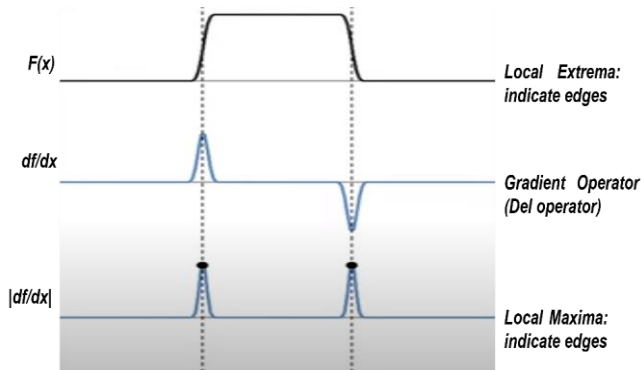


Fig. 4. First Derivative of f with Respect to x .

B. Edge Detection using Gradient Operator based on 2D image

When the above idea is applied to 2 D images, it is referred pure derivatives (partial Derivatives). According to calculus, a partial derivative of a 2D continuous function represents the number of changes along each dimension [19]. The gradient operator (partial Derivative) represents the most rapid change in intensity (see Fig. 5).

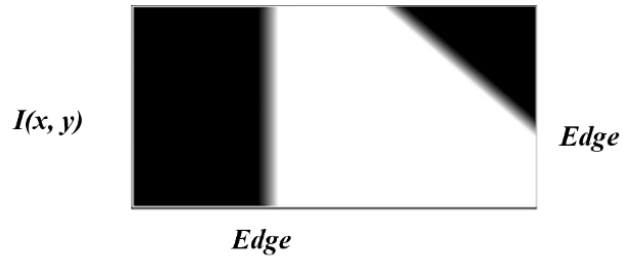


Fig. 5. Edge Detection using 2D Image.

The gradient operator is computed by:

$$\Delta I = \left[\frac{\partial I}{\partial x} + \frac{\partial I}{\partial y} \right] \quad (1)$$

When equation (1) is applied to an image, it produces two numbers; the Derivative of the image (∂I) with respect to x and y . these two numbers (vectors) comprise all information needed to know about the edges. For example:

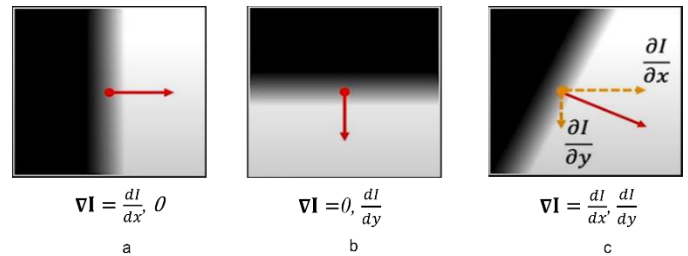


Fig. 6. Gradient Operator when Applied to an Image.

After applying the del operator, (ΔI), Fig. 6 produces two number vectors along each edge. Image (a) is a vertical edge with a non-zero value for the x direction and a zero value for the y component. Image (b) is a horizontal edge, with zero for the x direction and a non-zero value for the y component. Image (c) is a tilted edge and therefore has a non-zero value for both the x and y direction. From these two numbers at each pixel, we can obtain both the edge strength and the edge orientation. The magnitude equals the sum of squares of the two partial derivatives, and their square root equals 1. While the orientation of the edge is measured with respect to the horizontal axis, Eq. 3.

$$\text{Gradient Magnitude } S = \|\nabla I\| = \sqrt{\left(\frac{\partial I}{\partial x} + \frac{\partial I}{\partial y}\right)^2} \quad (2)$$

$$\text{Gradient Orientation } \theta = \tan^{-1} \left(\frac{\frac{\partial I}{\partial x}}{\frac{\partial I}{\partial y}} \right) \quad (3)$$

When Eq. 2 and Eq. 3 are applied to discrete images, we will have a finite difference approximation for the partial Derivative (f) for x and y . To find the difference in the x and y direction, we need at least two pixels in each direction, making four pixels in Fig. 7. Assuming the physical distance between the pixels is epsilon. We obtain a finite difference in the image as in Fig. 7.

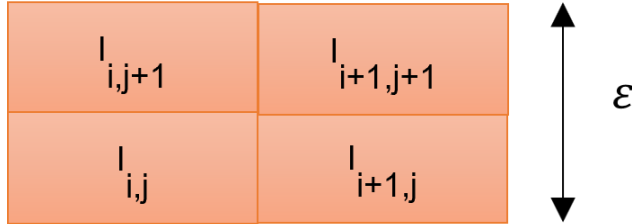


Fig. 7. Four Pixels Images in 1D Image.

$$\frac{dI}{dx} \approx \frac{1}{2\epsilon} ((I_{i+1,j+1} - I_{i,j+1}) + (I_{i+1,j} - I_{i,j})) \quad (4)$$

$$\frac{dI}{dy} \approx \frac{1}{2\epsilon} ((I_{i+1,j+1} - I_{i+1,j}) + (I_{i+1,j} - I_{i,j})) \quad (5)$$

Eq. 4 and Eq. 5 can be applied as a convolution using the filter in Eq. 6 and Eq. 7 to convolve the image for x and y . when this is done, the values obtained are enough to determine the edge magnitude and orientation.

$$\frac{dI}{dx} \sim \frac{1}{2\epsilon} \begin{pmatrix} -1 & 1 \\ -1 & 1 \end{pmatrix} \quad (6)$$

$$\frac{dI}{dy} \sim \frac{1}{2\epsilon} \begin{pmatrix} 1 & 1 \\ -1 & -1 \end{pmatrix} \quad (7)$$

With the gradient approach, a variety of gradient operators have been proposed over the last few decades [6], [20]–[23], which include Robert, Prewitt, Sobel (3x3), and larger Sobel (5x5). The Sobel operator (3x3) has been broadly used across various applications in the literature. The Derivative is found in the diagonal direction to the orthogonal direction of the convolution. The main obstacle of these operators lies mainly between the Robert operator, a small operator, and the larger Sobel. The Robert (2x2) operator with four-pixel values has a perfect localization ability for the edges but is very sensitive to noise because of the fewer pixels to revolve around. Any minor modification with any of those pixels can affect the detection accuracy. Therefore, noise sensitivity does not produce a good edge in a noisy image. On the other hand, the larger Sobel operator (5x5) has very poor localization accuracy. This is because when the operator becomes larger, determining an edge at a particular pixel can be affected by the activities happening in other larger pixels around it, affecting the edge localization. From a practical point of view, getting the orientation and magnitude does not declare an edge to be an edge. It still needs to be localized by thresholding. In this case, two standard thresholds are applied such that for a threshold T , the edge is obtained when Eq. 9 is satisfied:

$$||\nabla I(x,y)|| < T \quad (\text{not an edge}) \quad (8)$$

$$||\nabla I(x,y)|| > T \quad (\text{an edge}) \quad (9)$$

By introducing hysteresis-based thresholding, two thresholds are used (T_0 , T_1) to obtain an edge, Eq. 11 and Eq. 12.

$$||\nabla I(x,y)|| < T_0 \quad (\text{not an edge}) \quad (10)$$

$$||\nabla I(x,y)|| < T_1 \quad (\text{an edge}) \quad (11)$$

$$T_0 \leq ||\nabla I(x,y)|| < T_1 \quad (\text{an edge if the neighboring pixel is an edge}) \quad (12)$$

An edge pixel is defined by two fundamental characteristics: its edge strength, which is equal to the gradient magnitude, and its edge direction, which is equal to the gradient angle. However, for a discrete function, a gradient is not defined; instead, the gradient may be defined as an ideal continuous image, which is inferred using some specific operators. These operators use a pre-determined convolution mask to detect edges.

C. The Roberts Cross Operators

Roberts (1963) introduced the Roberts Cross operator. He clearly and concisely measures a 2-D spatial gradient on an image. As a result, high spatial frequency zones are emphasized, which typically correspond to edges. The operator's input and output are grayscale images in the most common situation. The estimated absolute magnitude of the spatial gradient of the input image at that point is represented by pixel values at each position in the output. Eq. 13 and Eq. 14 are the 2x2 convolution mask that convolves images in x and y directions (G_x , G_y). These masks are made such that G_y is a 90° rotation of G_x [11].

Roberts Operators Masks

$$G_x = \begin{bmatrix} 1 & 0 \\ 0 & -1 \end{bmatrix} \quad (13)$$

$$G_y = \begin{bmatrix} 0 & 1 \\ -1 & 0 \end{bmatrix} \quad (14)$$

Eq. 13 and Eq. 14 can be applied independently to the query image to obtain separate gradient components at each orientation. The absolute value of the combination of the gradient components (G_x , G_y) gives the magnitude at each point in Eq. 16 and the orientation of the gradient in Eq. 17.

$$|G| = \sqrt{G_x^2 + G_y^2} \quad (15)$$

Which can also be computed approximately as:

$$|G| = |G_x| + |G_y| \quad (16)$$

The angle θ of orientation is given by:

$$\theta = \arctan \left(\frac{G_x}{G_y} \right) - \frac{3\pi}{4} \quad (17)$$

D. Sobel Operator

The Sobel operator introduced by [21] indicates a high-frequency spatial region. The Sobel operator is achieved through a 2D image spatial frequency measurement by converting the image into grayscale and computing the absolute approximate gradient magnitude value at each point.

The Sobel operator is convolved using a (3x3) convolution kernel. With one kernel rotated 90 degrees over the other. Eq. 18 and Eq. 19 show the Robert cross operators.

Sobel Operators Masks

$$G_x = \begin{bmatrix} 1 & 0 & -1 \\ 2 & 0 & -2 \\ 1 & 0 & -1 \end{bmatrix} \quad (18)$$

$$G_y = \begin{bmatrix} 1 & 2 & 1 \\ 0 & 0 & 0 \\ -1 & -2 & -1 \end{bmatrix} \quad (19)$$

Sobel kernels can be used to compute separate measurements of the gradient component at each orientation, which are later combined to form the magnitude of the gradient for x and y orientations. The gradient magnitude can be computed using Eq. 20 and Eq. 21, while the orientation is computed using Eq. 22.

$$|G| = \sqrt{G_x^2 + G_y^2} \quad (20)$$

It can further be approximated by:

$$|G| = |G_x| + |G_y| \quad (21)$$

The angle of orientation is given by:

$$\theta = \arctan\left(\frac{G_y}{G_x}\right) \quad (22)$$

One of the problems of Sobel is using a gaussian smooth to reduce noise, which in turn affects the detection of a good edge. Despite this limitation, Sobel exhibits the quality of edge detection applied to solving various computer vision problems [24].

E. Prewitt Operator

The Prewitt operator introduced by [25] has similar properties to that of Sobel, such as convolution kernels. The kernel for the Prewitt operators are shown in Eq. 23 and Eq. 24. When applied to a noiseless and well-contrasted image, it is a computationally less expensive and faster edge detection method (Pujare et al., 2020). It is a gradient-based edge detection operator, and it has gradient features. Compared to the success of edge detection in complex images, the success of the Prewitt operator is greater than Roberts's operator [6]

$$G_x = \begin{bmatrix} 1 & 0 & -1 \\ 1 & 0 & -1 \\ 1 & 0 & -1 \end{bmatrix} \quad (23)$$

$$G_y = \begin{bmatrix} 1 & 1 & 1 \\ 0 & 0 & 0 \\ 1 & -1 & -1 \end{bmatrix} \quad (24)$$

The gradient-based operators can be determined using some pre-determined steps known as algorithms. Algorithm 1 is one

of the general algorithms used for gradient-based edge detection.

Algorithm 1: Gradient-based edge detection algorithm

```

1: Define x and y operators(ox and oy)
2:  $g_x \leftarrow \text{convolve}(\text{img}, o_x)$ 
3:  $g_y \leftarrow \text{convolution}(\text{img}, o_y)$ 
4:  $\text{maxM} \leftarrow 0$ 
5: for pixels |i| in image do
6:    $\text{Mag}|i| \leftarrow \text{Eqn. 17}$ 
7:   if  $\text{Mag}|i| > \text{maxM}$  then
8:      $\text{maxMag} \leftarrow \text{Mag}|i|$ 
9:   end if
10: end for
11: for pixels i in image do
12:   if  $\text{Mag}|i| \geq \text{thresh} \times \text{maxMag}$  then
13:      $\text{detected\_edges}|i| \leftarrow 1$ 
14:   else
15:      $\text{detected\_edges}|i| \leftarrow 0$ 
16:   end if
17: end for
18: return detected_edges

```

IV. ALGORITHMS BASED ON SECOND DERIVATIVES (NON-GRADIENT-BASED)

The methods outlined in the previous discussions merely involve filtering the image with various masks without considering the edges' properties or the image's noise. The second Derivative first dealt with the noise problem before going into edge detection. It is based on the concept introduced by Haralick and Marr and Hildreth Algorithms [26], [27]. This idea brings us to the concept of the Laplacian operator.

A. Laplacian Operator

Pierre-Simon de Laplace first applied the Laplace operator to the study of celestial mechanics or the motion of objects in space, and it is named after him. Since then, the Laplace operator has been used to represent many phenomena, including electric potentials, heat and fluid flow diffusion equations, and quantum physics. It's also been requested in discrete space, where it's been employed in image processing and spectral clustering applications [28].

The intensity variations in the sharp zero-crossing of an image f can be calculated using the Laplacian operator (∇^2). Consider a 1D signal $f(x)$ in Fig. 8. The edge is located at the local extrema, which is the first Derivative of the signal ($\partial f / \partial x$). But in the case of the second Derivative of the image (i.e., the Derivative of an image ($\partial^2 f / \partial^2 x$)). The zero-crossing through each peak of the signal indicates an edge. Peaks are not obtained at the edges, but a strong zeros-crossing indicates an edge (Fig. 8).

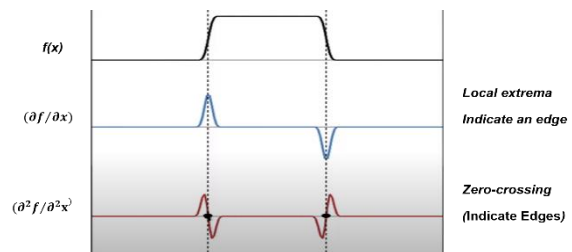


Fig. 8. Second Derivative in 1D Signal.

The zero-crossing is obtained through the Laplacian operator in Eq. 25, known as dell square operator II.

$$\nabla^2 I = \frac{\partial^2 I}{\partial x^2} + \frac{\partial^2 I}{\partial y^2} \quad (\text{D1 square II}) \quad (25)$$

When Eq. 25 is applied to an image, the edges obtained are zero-crossing in the Laplacian of the image. The Laplacian operator does not provide the direction of the edges but a sharp zero-crossing which indicates the location of the edge. In discrete images, the second Derivative is in terms of finite difference (difference of the difference). This difference requires at least three pixels (3x3), known as the 3x3 Laplacian operator. Assuming the physical distance between the pixels is epsilon. We obtain a finite difference using the 3x3 image pixels in Fig. 9.

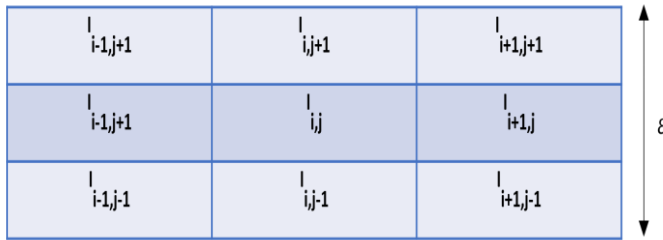


Fig. 9. 3x3 Laplacian Operator.

Fig. 9 is a 3x3 Laplacian operator called the "Del square operator II," where the epsilon (ε) denotes the distance between the pixels. It is referred to as the sum of the second Derivative of the image for x and the second Derivative of the image for y. For example, obtain an output of the Laplacian operator for the center pixel (I_{i,j}) from the above 3x3 operator. Eq. 26 and Eq. 27 are derived.

$$\frac{\partial^2 I}{\partial x^2} \approx \frac{1}{\epsilon^2} (I_{i-1,j} - 2I_{i,j} + I_{i+1,j}) \quad (26)$$

$$\frac{\partial^2 I}{\partial y^2} \approx \frac{1}{\epsilon^2} (I_{i,j-1} - 2I_{i,j} + I_{i,j+1}) \quad (27)$$

$$\nabla^2 I = \frac{\partial^2 I}{\partial x^2} + \frac{\partial^2 I}{\partial y^2} \quad (28)$$

Adding Eq. 26 and Eq. 27 and the Derivative of I with respect to y formulate the convolution mask in Eq. 29:

$$\nabla^2 \approx \frac{1}{\epsilon^2} \begin{bmatrix} 0 & 1 & 0 \\ 1 & -4 & 1 \\ 0 & 1 & 0 \end{bmatrix} \quad (29)$$

The convolution mask in Eq. 29 obtained the second Derivative for x and the second Derivative for y. However, the edge can appear in any orientation. Assuming the edge appears in 450°, the epsilon in that direction (I_{i,j}, I_{i+1,j+1}) is not yet accounted for. This problem is peculiar to a continuous grid. However, the convolution can be modified on a discrete grid to fit all possible orientations in the image. The modified convolution, which is the most applicable Laplacian operator, is obtained in Eq. 30:

$$\nabla^2 \approx \frac{1}{6\epsilon^2} \begin{bmatrix} 1 & 4 & 1 \\ 4 & -20 & 4 \\ 1 & 4 & 1 \end{bmatrix} \quad (30)$$

One of the common algorithms used to implement the Laplacian operator for finding zero-crossing is the Marr-Hildreth algorithm [13]. This method obtains a sharp zero-crossing point by applying a convolution with a gaussian kernel and approximating the Laplacian operator with a 3x3 filter. Presented in Fig. 10 is a general flow diagram for finding zero-crossing, while Algorithm 2 is used for the implementation [13].

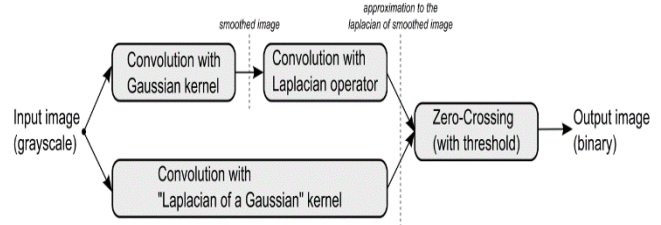


Fig. 10. Marr-Hildreth Algorithm;s Block Diagram for Finding Zero-crossing [13].

Algorithms 2: Marr-Hildreth edge detection algorithm

Input required: input img, sigma value σ, size of kernel k, and threshold for zero-crossing Tzc

```

1:   If kernel size then
2:     Kernel ← compute_kernel k(n,σ)
3:   imggm ← convolve (img, k)
4:   #Define Laplacian operator Laplacian L
5:   imgl ← convolve(imggs, L)
6:   else
7:     log_k ← compute_log_k(n,σ)
8:     imgl ← convolve(imggs, log_k)
9:   end if
10:  maxL ← 0
11:
12:  for pixels i in images imgl do
13:    if imgl [i] > maxl then
14:      maxL ← imgl [i]
15:    end if
16:  end for
17:  for pixels i in images imgl, except borders do
18:    for pair (pts1, pts2) of opposite neighbors
19:      of p in inlap do
20:        if (sign(imgl[pts1]) ≠
21:           sign(imgl[pts2])) and (|imgl[pts1]| > TZC then
22:           detected_edges[i] ← 1
23:         else
24:           detected_edges[i] ← 0
25:         end if
26:       end for
27:     end for
28:   return edges

```

B. Canny Edge Detection

The Canny Edge Detection Algorithm consists of a specific sequence of steps. Smooth the image with a Gaussian filter first. Then, compute the gradient magnitude and orientation by approximating the partial derivatives with finite-difference approximations. The gradient magnitude is then subjected to a non-maximum suppression. Then, the double threshold technique to find and connect edges [20] using Eq. 31.

$$G(x, y) = \frac{1}{2\pi\sigma^2} e^{-\frac{x^2+y^2}{2\sigma^2}} \quad (31)$$

Where x and y distance from the origin to the horizontal and vertical direction, respectively, σ is the Gaussian factor that determines the level of smoothing. The gradient of the smoothed array $G(x,y)$ is employed to generate the x and y Partial Derivatives. After that, the results of x and y partial are added to obtain the normal gradient. Then non-maximum suppression is applied after determining the edge direction through the use of two thresholding in the Hysteresis [15][20].

Non-maximum suppression: Facilitate the detection of thin layered edges that produces smarter edges. The Canny edge detector employs non-maximum suppression to emphasize the local maxima as edges while suppressing all other ones along with the gradient magnitudes.

Other operators employed the use of a single threshold value to remove edges that do not meet the required edge limit. Canny uses Hysteresis with upper and lower threshold values to suppress the edge that falls below the required threshold limit. If the high threshold is $T1$, the low threshold is $T2$, and the gradient magnitude is GM , then $GM < T1$ are dropped, and $GM > T1$ are maintained as the edge. However, an edge that falls between $T1$ and $T2$, is only maintained if it has a pixel value higher than $T2$ [11] and is expressed it as:

$$GM < T1 = \text{drop}$$

$$GM > T1 = \text{maintain}$$

$$\text{If } T2 \leq GM < T1$$

$$GM = \text{edge if Pixel } GM > T2 \forall i \in I(x, y)$$

The canny edge detector has the advantage of intensive noise filtering than other detectors. It has three distinct attributes that differentiate it from the other detectors. Table II shows the advantages and disadvantages of various edge detection methods.

Low error rate: The detected edges are refined not to include non-edges. It also ensures that all occurring edges are not missed. This is achieved by Eq. 32.

$$SNR = \frac{\int_{-w}^w G(-x)f(x)dx}{n_0 \sqrt{\int_{-w}^w f^2(x)dx}} \quad (32)$$

Where f is the filter, G is the edge signal; the denominator is the root-mean-square (RMS) response to noise $n(x)$ only.

Good localization ensures a minimal distance between the actual edge and the detected edge which is expressed in Eq. 33.

$$\text{Localization} = \frac{1}{\sqrt{E[X_0^2]}} = \frac{|\int_{-w}^w G'(-x)f'(x)dx|}{n_0 \sqrt{\int_{-w}^w f'^2(x)dx}} \quad (33)$$

Single response rate: Each detected edge should maintain a single response in the total edges detected. This is implicit in the first criterion but made explicit about eliminating multiple responses. The first two criteria can be minimized by setting the parameter in Eq. 34 [29].

$$f(x) = G(-x) \quad (34)$$

TABLE II. ADVANTAGES AND DISADVANTAGES OF VARIOUS EDGE DETECTION METHODS

Edge detection methods	Advantages	Disadvantages
An algorithm based on the first Derivative (Robert, Prewitt, and Sobel)	Fast and more accessible in computation Edges are detected along with their orientation.	Sensitive to noise. The inaccurate and unreliable edge detection output
An algorithm based on the second Derivative (LoG)	Due to ease in an approximation of gradient magnitude, the cross-operation detection of edges and their orientation is also simple The characteristics of all directions of the image are fixed. A wide testing area around the pixel is possible	The detection of edges and their orientation degrades the magnitude of the edges and increases the noise Malfunctioning at the corners, curves, and where the grey level intensity function varies
Canny Edge Detector	Better detection in noise conditions.	Do not require zero crossing. Difficult to specify a generic threshold value that works well across all images

V. EXPERIMENTAL RESULT AND DISCUSSION

The edge detection methods discussed in the paper are applied to five sample images taken from the MICC-F220 CMFD evaluation dataset. The result of each algorithm is shown in Fig. 11.

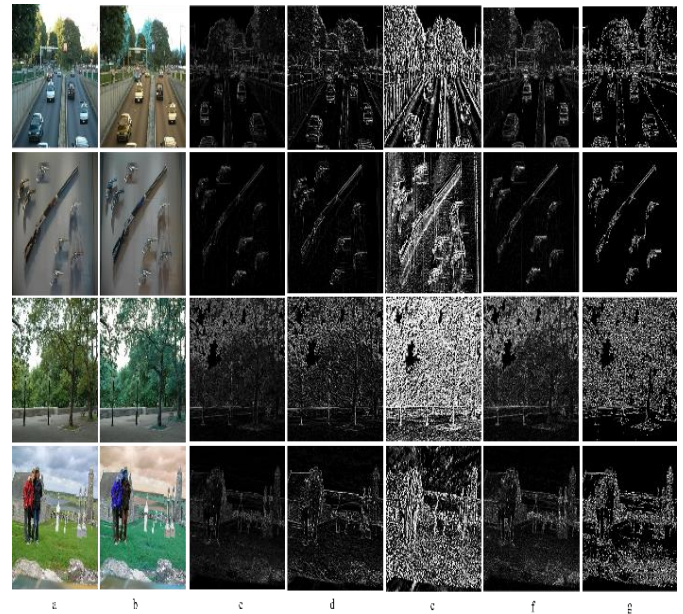


Fig. 11. Comparison of Edge Detection Algorithms using Five Sample Images from MICC-F220 Benchmark Dataset, (a) Original Image (b) Grayscale (c) Robert (d) Prewitt (e) Sobel (f) Laplacian and (g) Canny Edge Detector.

VI. DISCUSSION

Edge detection methods play an important role in object detection. It is used primarily in the pre-processing stage before feature extraction, an essential step in CMFD. Images are converted to grayscale to reduce noise. Edge detection based on first derivatives is generally sensitive to noise and, in most cases, produces unrealistic features.

We have implemented five selected images from MICC-F220 datasets. Roberts, Sobel, Prewitt, Laplacian, and canny edge detectors have been implemented on those images. The result in Fig. 11 shows that the edges in (c, d and e) detected using Robert, Prewitt, and Sobel, are too cluttered and almost lost the important image structures. The image appeared noisy with thick layered unsmoothed edges, mainly the result in (e), the Sobel, the edges appeared two to three times the pixel thickness. Since most of those images appeared to have lost their essential edge information, the results did not show the appropriate edge structure. However, the result can still indicate the geometric parts of the images but does not reveal the thin layer edges, essential for feature extraction in CMFD.

On the other hand, edge detectors based on second derivatives, such as Laplacian and canny edge detectors, use adjustable parameters such as the size of the Gaussian filter and threshold [20]. The edges are smoothly detected on the image, and almost no noise pixels were detected while protecting the important structural properties in the images, as shown in Fig. 11 (f and g). However, the canny method produces smoother and thin edges than the Laplacian. In Fig. 11 (g), we can see a good view of the various image structures. Fewer noise pixels were detected compared to gradient-based edge detectors.

VII. CONCLUSION

This study demonstrates that the Canny approach can produce equally acceptable edges with smooth continuous pixels and thin edges. Unlike the canny method, the Laplacian method also has better edge features compared to Robert, Prewitt, and Sobel method. These methods cannot generate a smooth and thin edge. However, the Laplacian and Canny algorithms are often susceptible to noise pixels. Sometimes it is impossible to filter a noisy image perfectly. Noisy pixels that are not eliminated will affect the outcome of edge detection. Based on our investigation, we have determined that between the Canny and other edge detection algorithms, Canny edge detection provided a superior response for CMFD images in MICC-F220 datasets.

REFERENCES

- [1] Y. Song and H. Yan, "Image Segmentation Techniques Overview," *AMS 2017 - Asia Model. Symp. 2017 11th Int. Conf. Math. Model. Comput. Simul.*, pp. 103–107, 2018, doi: 10.1109/AMS.2017.24.
- [2] N. Kheradmandi and V. Mehranfar, "A critical review and comparative study on image segmentation-based techniques for pavement crack detection," *Constr. Build. Mater.*, vol. 321, no. January, p. 126162, 2022, doi: 10.1016/j.conbuildmat.2021.126162.
- [3] P. Dhankhar and N. Sahu, "A Review and Research of Edge Detection Techniques for Image Segmentation Related papers A Review and Research of Edge Detection Techniques for Image Segmentation," *IJCSMC J.*, vol. 2, no. 7, pp. 86–92, 2013.
- [4] S. Jeyalakshmi and S. Prasanna, "A Review of Edge Detection Techniques for Image Segmentation," *Int. J. Data Min. Tech. Appl.*, vol. 5, no. 2, pp. 140–142, 2016, doi: 10.20894/ijdm.102.005.002.008.
- [5] G. T. Shrivakshan, "A Comparison of various Edge Detection Techniques used in Image Processing," *Int. J. Comput. Sci. Issues*, vol. 9, no. 5, pp. 269–276, 2012.
- [6] Ş. Öztürk and B. Akdemir, "Comparison of Edge Detection Algorithms for Texture Analysis on Glass Production," *Procedia - Soc. Behav. Sci.*, vol. 195, pp. 2675–2682, 2015, doi: 10.1016/j.sbspro.2015.06.477.
- [7] T. Tahmid and E. Hossain, "Density based smart traffic control system using canny edge detection algorithm for congregating traffic information," *3rd Int. Conf. Electr. Inf. Commun. Technol. EICT 2017*, vol. 2018-Janua, no. December, pp. 1–5, 2018, doi: 10.1109/EICT.2017.8275131.
- [8] R. F. Abbas, "A proposed approach to determine the edges in SAR images," *Iraqi J. Sci.*, vol. 61, no. 1, pp. 185–192, 2020, doi: 10.24996/ijcs.2020.61.1.21.
- [9] I. Lorencin, N. Anđelić, J. Španjol, and Z. Car, "Using multi-layer perceptron with Laplacian edge detector for bladder cancer diagnosis," *Artif. Intell. Med.*, vol. 102, no. May 2019, 2020, doi: 10.1016/j.artmed.2019.101746.
- [10] J. S. S. Yin, T. T. Swee, A. Bin Yahya, M. T. F. Thyne, and J. S. Y. Xian, "Mini Kirsch edge detection and its sharpening effect," *Indones. J. Electr. Eng. Informatics*, vol. 9, no. 1, pp. 228–244, 2021, doi: 10.11591/ijeel.v9i1.2597.
- [11] A. Pujare, P. Sawant, H. Sharma, and K. Pichhode, "Hardware Implementation of Sobel Edge Detection Algorithm," *ITM Web Conf.*, vol. 32, p. 03051, 2020, doi: 10.1051/itmconf/20203203051.
- [12] P. Niyishaka and C. Bhagvati, "Copy-move forgery detection using image blobs and BRISK feature," *Multimed. Tools Appl.*, 2020, doi: 10.1007/s11042-020-09225-6.
- [13] H. Spontón and J. Cardelino, "A Review of Classic Edge Detectors," *Image Process. Line*, vol. 5, pp. 90–123, 2015, doi: 10.5201/ipol.2015.35.
- [14] J. Jing, S. Liu, G. Wang, W. Zhang, and C. Sun, "Recent advances on image edge detection: A comprehensive review," *Neurocomputing*, vol. 503, pp. 259–271, 2022, doi: 10.1016/j.neucom.2022.06.083.
- [15] D. Vikram Mutreja, "Methods of Image Edge Detection: A Review," *J. Electr. Electron. Syst.*, vol. 04, no. 02, 2015, doi: 10.4172/2332-0796.1000150.
- [16] Y. Li, S. Wang, Q. Tian, and X. Ding, "A survey of recent advances in visual feature detection," *Neurocomputing*, vol. 149, no. PB, pp. 736–751, 2015, doi: 10.1016/j.neucom.2014.08.003.
- [17] C. Lopez-Molina, B. De Baets, and H. Bustince, "Quantitative error measures for edge detection," *Pattern Recognit.*, vol. 46, no. 4, pp. 1125–1139, 2013, doi: 10.1016/j.patcog.2012.10.027.
- [18] G. Papari and N. Petkov, "Edge and line oriented contour detection: State of the art," *Image Vis. Comput.*, vol. 29, no. 2–3, pp. 79–103, 2011, doi: 10.1016/j.imavis.2010.08.009.
- [19] G. X. Ritter and J. N. Wilson, *Handbook of Computer Vision Algorithms in Image Algebra*. CRC Press, CRC Press LLC, 1996.
- [20] Z. Othman, M. Rafiq, and A. Kadir, "Comparison of Canny and Sobel Edge Detection in MRI Images," pp. 133–136, 2009.
- [21] I. E. Sobel, "Camera Models and Machine Perception," *University Microfilms, Inc., Ann Arbor, Michigan THIS*, 1970.
- [22] N. Nausheen, A. Seal, P. Khanna, and S. Halder, "A FPGA based implementation of Sobel edge detection," *Microprocess. Microsyst.*, vol. 56, no. September 2016, pp. 84–91, 2018, doi: 10.1016/j.micpro.2017.10.011.
- [23] C.-C. Zhang and J.-D. Fang, "Edge Detection Based on Improved Sobel Operator," *Adv. Comput. Sci. Res.*, vol. 52, no. 16, pp. 129–132, 2016, doi: 10.2991/ceis-16.2016.25.
- [24] D. Kim, "Sobel Operator and Canny Edge Detector," pp. 1–10, 2013, [Online]. Available: <http://www.egr.msu.edu/classes/ece480/capstone/fall13/group04/docs/danapp.pdf>.
- [25] J. M. S. Prewitt, *Object enhancement and extraction. Picture processing and Psychopictorics*, 1970.
- [26] R. M. Haralick, *Digital Step Edges from Zero Crossing of Second Directional Derivatives*. Morgan Kaufmann Publishers, Inc., 1987.

- [27] D. Marr and E. Hildreth, "Theory of edge detection," Proc. R. Soc. London - Biol. Sci., vol. 207, no. 1167, pp. 187–217, 1980, doi: 10.1098/rspb.1980.0020.
- [28] P.-S. Laplace, A Philosophical Essay on Probabilities, vol. 2, no. 38. 1903.
- [29] I. E. Igbiosa, "Comparison of Edge Detection Technique in Image Processing Techniques," Int. J. In. f. Technol. Electr. Eng., vol. 2, no. 1, pp. 25–29, 2013.

Deep Learning Model for Predicting Consumers' Interests of IoT Recommendation System

Talal H. Noor¹, Abdulqader M. Almars², El-Sayed Atlam³, Ayman Noor⁴

College of Computer Science and Engineering, Taibah University, Yanbu, Medina, KSA^{1,2,3,4}
Computer science, Tanta University, Egypt³

Abstract—This electronic the Internet of Things (IoT) technology has contributed to several domains such as health, energy, education, transportation, industry, and other domains. However, with the increased number of IoT solutions worldwide, IoT consumers find it difficult to choose the technology that suits their needs. This article describes the design and implementation of an IoT recommendation system based on consumer interests. In particular, the knowledge-based IoT recommendation system exploits a Service Oriented Architecture (SOA) where IoT device and service providers use a registry to advertise their products. Moreover, the proposed model uses a Long Short-term Memory (LSTM) deep learning technique to predict the consumer's interest based on the consumer's data. Then the recommendation system do the mapping between the consumers and the related IoT devices based on the consumer interests. The proposed Knowledge-based IoT recommendation system has been validated using a real-world IoT dataset collected from Twitter Application Programming Interface (API) that include more than 15,791 tweets. Overall the results of our experiment are promising in terms of precision and recall. Furthermore, the proposed model achieved the highest accuracy score compared with other state-of-the-art methods.

Keywords—Internet of things; IoT; knowledge-based; recommendation system; service-oriented architecture; SOA; long short-term memory; LSTM; deep learning

I. INTRODUCTION

The number of Internet of Things (IoT) devices connected to the internet is growing exponentially. According to statistics [1], the number of devices connected to the internet will keep increasing to reach 19.1 billion devices by the year 2025. IoT technology plays a vital role in improving services provided in several domains such as energy, transportation, food production, water supply, health care, education, and other crucial services [2,3,4,5]. IoT Technology has the capability of solving several issues related to smart grids, warming systems, saving water, increasing smart farms, and are considered to be the main part when it comes to smart cars.

With the accelerated growth in the number of connected IoT devices and the targeted services that the IoT devices are designed for, IoT services' consumers face an issue in choosing the appropriate IoT devices and services that suits their needs [6,7,8,9]. Therefore, novel techniques are required to help IoT services' consumers in choosing the suitable IoT devices and services that makes their life easier and their daily activities more efficient. Traditional techniques presented in the literature that involves recommendations from other

consumers or IoT devices and services reputation based on other consumers' ratings might be impractical in this case (i.e., such as collaborative filtering or content-based techniques). For example, let us say consumer x recommended IoT device i to consumer y because it's good in saving energy. However, consumer y misses IoT device t that have more features related to consumer y field which is health (i.e., consumer y is a doctor and more interested in health related gadgets and IoT devices). Knowledge-based techniques can be more beneficial especially when predicting suitable IoT devices and services based on the IoT services' consumers knowledge [10] (i.e., consumer interests are derived from her knowledge).

Consumer interest recognition is becoming an important research problem [11,12]. Consumer interest analysis is the procedure of evaluating, identifying, and understanding the interests, sentiments, qualities, attitudes, and traits of an individual. The consumer interest analysis is beneficial in identifying targeted consumers and improving consumer's service experience. Social media is a good platform for consumer interest analysis where the consumers text, photos, shares, likes, dislikes are used to understand the consumers behavior [13,14,15]. Knowledge-based techniques are used to improve the recommendation process of IoT devices for IoT services' consumers. Hence, this research focuses more on the knowledge of IoT services' consumers by analyzing their tweets from Twitter. Then based on the consumers interests profiling, the knowledge-based recommender system starts the mapping process between the IoT devices registered by IoT device and service providers and the appropriate consumers.

The purpose of this article is to present the design and implementation of a knowledge-based IoT recommendation system architecture to enhance the recommendation of IoT devices and services for users of IoT services. The knowledge-based IoT recommendation system is based on a Service Oriented Architecture (SOA) and a deep learning model to predict the consumer's interest using the consumer's data. The contribution of this work can be outlined as follows:

- 1) A knowledge-based IoT recommendation system based on SOA is designed and implemented to recommend IoT devices and services to consumers.
- 2) This study uses a deep learning model called Long Short-term Memory (LSTM) to classify IoT services' consumers based on their interests.
- 3) The knowledge-based IoT recommendation system is demonstrated using a prototype implementation and experiments using a Twitter API dataset with 15,791 tweets.

The rest of the article is organized as follows: The literature review is discussed in Section II, the design of the knowledge-based recommendation system architecture and the IoT services consumers' interest analysis are presented in Section III, the implementation and experimentation are discussed in Section IV, Section V concludes with some concluding remarks and directions for future work.

II. LITERATURE REVIEW

Several research works have recognized the significance of recommendation systems for IoT environments and discussed different recommendation techniques including: i) content-based, ii) collaborative filtering, iii) knowledge-based, and other techniques [16,17,18,19,20]. Other researchers conducted more specific survey papers on IoT recommendation systems related to the fields of context-aware [21], trust [22], and mobile health (m-health) [23]. Some research works used a content-based technique to recommend IoT devices and services. For example, Frey et al. [24] propose a novel recommendation system that collects IoT related information into inventories from smartphones to facilitate IoT device providers in recommending new personalized IoT devices that are similar to the ones that IoT services consumers are using. In particular, the recommendation system consists of three layers including: i) data gathering from mobile device, ii) building a digital inventory, and iii) creating personalized recommendations. Unlike this research work that neglects the idea of predicting suitable IoT devices and services based on the IoT services' consumers knowledge, a knowledge-based technique is employed when predicting suitable IoT devices and services. In other words, it's more likely that the IoT services' consumers would prefer IoT devices and services that are related to their interest.

Other research works used a collaborative filtering technique to recommend IoT devices and services. For example, Forouzandeh et al. [25] propose an IoT recommendation system based on a collaborative filtering technique. In particular, the system analyzes IoT services consumers' behaviors and uses the Cosine similarity to aggregate the distance between two IoT devices or IoT services consumers. The proposed system architecture consists of three modules including IoT devices, IoT services, and IoT services consumers. Kashaf [26] presents an IoT recommendation system based on a clustering technique that overcomes traditional collaborative filtering techniques that suffer from scalability and sparsity issues. In particular, the study compares the performance of several clustering algorithms including k-means, fuzzy c-mean, single-linkage, and self-organization maps. In the evaluation of these clustering algorithms the authors used several datasets including: i) LDOS-CoMoDa (i.e., movie ratings), ii) InCarMusic (i.e., music ratings), iii) Apps in Frappe' (i.e., apps ratings), iv) POI in STS (i.e., rating of places), v) TripAdvisor (i.e., hotel ratings), vi) apple store ratings (i.e., apps ratings), and vii) drug review (i.e., patent reviews on drugs); where the performance of self-organization maps overcomes the other clustering algorithms. Unlike these research works that use collaborative filtering techniques for recommending IoT devices and services and use datasets that

are not related to IoT devices and services to evaluate their proposed approaches; A real-world IoT dataset collected from Twitter, which included 15,791 tweets, was used to evaluate our proposed approach of analyzing consumers' interests in IoT services.

Some research works used a hybrid technique to recommend IoT devices and services. For example, Bouazza et al. [27] propose an IoT recommendation system based on a hybrid technique (i.e., collaborative filtering and knowledge-based techniques). In particular, the authors propose to use collaborative filtering and ontology to recommend IoT services that suit IoT services consumers' needs. The proposed ontology namely, Social IoT (SIoT) consists of two different ontologies including social network ontology and IoT ontology. The proposed system uses SIoT ontology to identify the relationship between the IoT services consumer, IoT devices and IoT services to aggregate the IoT services consumer preferences. Moreover, the proposed system determine the top N IoT services based on other IoT services consumer ratings. Yao et al. [28] present a novel framework for recommending things of interest in IoT environments. In particular, the proposed framework is based on a probabilistic matrix factorization model. The model uses three different matrices including: i) user-user relationship matrix, ii) the thing-thing correlation matrix, and iii) the user-thing usage matrix. Unlike these research works that uses ontologies to predict the IoT services' consumers prior knowledge about IoT devices and services, our proposed approach complements these research works by using a deep learning model namely, Long Short-term Memory (LSTM), to classify IoT services' consumers based on their interest and recommend the appropriate IoT devices and services accordingly.

Knowledge-based techniques and IoT technology is used in the literature for recommendations for smart city development and education systems. For example, Xin et al. [29] propose a knowledge-based education recommendation system utilizing IoT technology. In particular, the proposed recommendation system uses an ontology of scientific papers in the field of entrepreneurship (i.e., the authors used it as an example of building an ontology for the education system) and factorization matrix to measure the relevance of users' feedback. Bokolo [30] presents a case-based reasoning recommender system for smart city development (i.e., case-based reasoning is considered as a knowledge-based technique). The main notion of the system is to build a case library which represents a prior experience in the development of smart cities and measure the similarity of the current case with the ones stored in the library. Unlike these research works that use knowledge-based techniques and IoT technology for the recommendations of smart city development and education systems, knowledge-based techniques are used in recommending appropriate IoT devices and services.

IoT technology is also utilized in the literature for context-aware recommendation systems. For example, Cha et al. [31] present an IoT platform for real-time context-aware recommendation. In particular, the architecture of the proposed IoT platform uses a geofencing technique to model the user context-aware based on the location, time and

surroundings data collected from IoT users' devices. The proposed IoT platform has been demonstrated using a tourism application. Gyrard and Shetha [32] propose a knowledge-based recommendation system that uses IoT technology for the health-context recommendations. In particular, the proposed system exploits a knowledge repository which consists of linked open datasets and ontologies to recommend alternative medicine for daily discomforts such as fever and headaches. Jabeen et al. [33] present a hybrid-based cardiovascular health recommendation system that uses IoT technology. In particular, the proposed system uses four classifiers including Multi-layer Perceptron (MLP), Support Vector Machines (SVM), Random Forest (RF), and Naive Bayes (NB) for the process of classifying cardiovascular diseases. The classifiers are capable of predicting eight types of cardiovascular diseases (e.g., Hypertension and Acute Coronary Syndrome) using a dataset of cardiovascular diseases. In addition, the proposed system uses collaborative filtering technique for community advice on treatments. Gladence et al. [34] propose a recommendation system for home automation using IoT technology. In particular, the authors use Natural Language Processing (NLP) and voice recognition to help unfortunate people to gain control over IoT devices and the propose system makes recommendations based on the users iterations with the system. Mohamed et al. [35] present a collaborative filtering recommendation system for e-commerce products that uses IoT technology. In particular, the proposed system uses data collected from IoT devices to identify user behavior and other users' feedback on products to make the recommendation of personalized e-commerce products. Unlike these research works that uses IoT technology for recommending products and other context-aware related recommendations such as health related applications, this paper focus on recommending IoT devices and services.

III. KNOWLEDGE-BASED IOT RECOMMENDATION SYSTEM ARCHITECTURE

In this paper, a knowledge-based IoT recommendation system architecture is proposed that uses the Service Oriented Architecture (SOA) to deliver IoT devices and services' recommendations based on IoT services consumers' prior knowledge about IoT devices and services. Fig.1 depicts the architecture of our knowledge-based IoT recommendation system which consists of three different layers including: i) the IoT Device and Service Providers Layer, ii) the Knowledge-based IoT Recommendation Layer, and iii) the IoT Services Consumers Layer.

The IoT Device and Service Providers Layer. This layer consists of several IoT device and service providers where IoT devices are provided through shipping companies to IoT services consumers. IoT services are normally provided through web portals and mobile applications. The IoT device and service providers interact with Knowledge-based IoT Recommendation Layer through the IoT Device and Service Registry where they can advertise their IoT devices and services. In order to register the IoT devices and services, the

providers need to add the IoT device or service ID, description, and choose an IoT category. In this phase of our work, five different categories are identified for IoT devices and services namely Health, Energy, Education, Transportation, and Industry.

The Knowledge-based IoT Recommendation Layer. This layer consists of eight components including: i) IoT Services Consumers Identity Management (IdM), which is responsible for managing the IoT services consumers identities and require IoT services consumers to register their credentials when they attempt to use the recommender system for the first time, ii) IoT Services Consumers Tweets Collector which is responsible for collecting the IoT services consumers tweets from Twitter API (i.e., this component will be elaborated further in Section 3.1) after requesting their permission to gain access to their Twitter account, iii) Term Frequency–Inverse Document Frequency (TF-IDF) Calculator which is responsible for measuring the terms relevance in the IoT services consumers tweets (i.e., which will be explained in detail in Section 3.2.1), iv) IoT Services Consumers' Interests Analysis which is responsible for identifying the IoT services consumers' interests (i.e., prior knowledge about IoT devices and services, more details about the IoT services consumers' interests identification are presented in Section 3.2.2), v) Categorized IoT Services Consumers is responsible for storing the IoT services consumers categories based on the identified interests (i.e., whether the IoT services consumers interested in IoT devices or services related to the health, energy, education, transportation, or industry domain), vi) IoT Device and Service Registry is responsible for managing the IoT devices and services advertisements where IoT device and service providers are required to register their IoT devices and services by adding the IoT device or service ID, description, and choose an IoT category as aforementioned earlier, vii) Recommendation Handler is responsible for handling IoT device and service recommendation requests from IoT services consumers and recommendation feedbacks, and viii) Recommendation Mapper which is responsible for mapping the recommendations based on the IoT services consumers' category (i.e., based on their interests) and the IoT device and service registered in the IoT Device and Services Registry (i.e., this component will be elaborated further in Section 3.2.3).

The IoT Services Consumers Layer. This layer consists of several IoT services consumers who use IoT devices received from IoT device and service providers through shipping companies. IoT services consumers also use IoT services through web portals and mobile applications. The IoT services consumers interact with Knowledge-based IoT Recommendation Layer through the Recommendation Handler where they can request an IoT device and service recommendation and receive the recommendation feedback. In order for the IoT services consumers to start using the recommender system, they are required to register their credentials first through the IoT Services Consumers Identity Management (IdM).

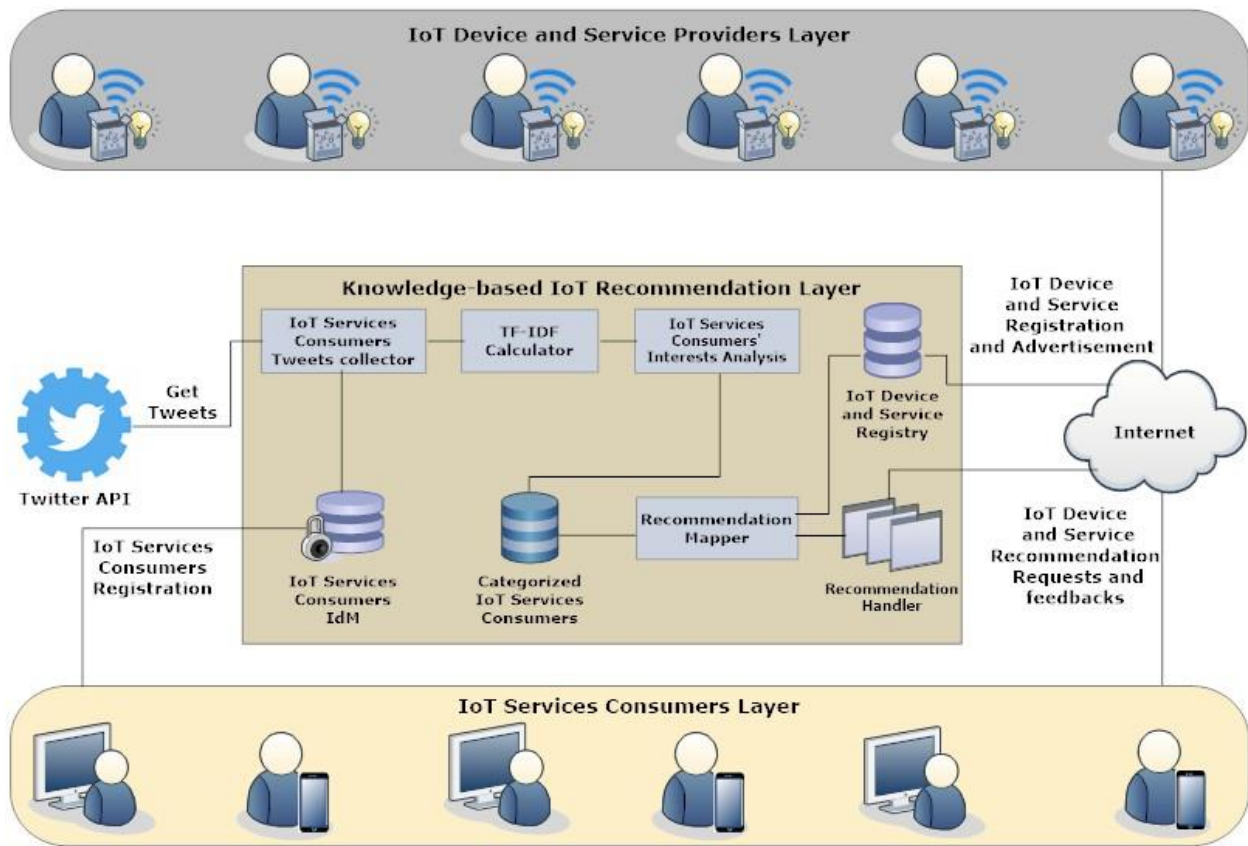


Fig. 1. A Knowledge-based IoT Recommendation System Architecture.

A. IoT Services Consumers' Tweet Collector

The IoT Services Consumers' Tweets Collector is used to get the IoT services consumers tweets based on IoT categories. According to several research works the IoT devices and services are applied in several domains including health, energy, education, transportation, and industry [16,17,18,19,20]. Thus, these application domains were used as categories for IoT service consumers' interests. Then, several keywords are used to retrieve tweets related to each IoT proposed interests' category as shown in Table I (i.e., in Section 4.2, the dataset is described in more detail). Then the IoT services consumers' tweets collector uses these keywords to collect the IoT services consumers tweets from Twitter API.

B. IoT Services Consumers' Interests Analysis

1) *Term Frequency-Inverse Document Frequency (TF-IDF)*: Term frequency and inverse document frequency (TF-IDF) is a statistic metric used in text mining that determines how relevant a term is to a particular IoT services consumers tweet comparing with all IoT services consumers tweets. TF-IDF assigns two scores to each word in an IoT services consumers' tweets: term frequency (TF) and inverse document frequency (IDF). IDF calculates a word's inverse document frequency, whereas TF calculates the number of times a term appears in an IoT services consumers' tweets. In this paper, the TF-IDF is computed for the most frequent K vocabularies for all posts for the purpose of modeling different terms. Each

IoT services consumers tweet has a K-word dictionary reflecting the importance of each term, and the value is 0 if the term does not appear in the IoT services consumers' tweets. A matrix of $K \times N$ can be constructed as the input of LSTM model (see Section 3.2.2) based on the corresponding K-word TF-IDF dictionary. The TF-IDF weight of that sentence is computed by multiplying the two scores [36].

TABLE I. THE IOT PROPOSED INTERESTS' CATEGORIES AND RELEVANT KEYWORDS

IoT	Keywords
Energy	Energy Consumption Energy Conservation Energy Technologies
Health	Health Technologies Wearable Technologies Digital Health Health Informatics
Industry	Industry Technologies Smart Industry Industry Solutions
Transportation	Transportation Solutions Smart Transportation Transportation Technologies
Education	Smart Classrooms Education Technology Education Automation

Where TF-IDF denotes the importance of a phrase in an IoT services consumers' tweet. The higher the TF-IDF weight score, the more significant the term in the IoT services consumers' tweets. The suggested model extracts and models different terms in our dataset using the TF-IDF measure. The following equations (1) and (2) can be used to compute TF and IDF of terms:

$$TF(t) = \frac{\text{Number of times word appear in documents}}{\text{Total number of words in documents}} \quad (1)$$

$$IDF = \log \frac{\text{Total number of documents}}{\text{Frequency of word in all documents}} \quad (2)$$

Here, the TF-IDF value is computed by making a product of the two statistics which means the weight of the words as in Equation (3):

$$TF-IDF(t) = TF(t) * IDF(t) \quad (3)$$

TF-IDF is used in this study because it provides a vector representation of the IoT services consumers tweets. The next step is to analyze the IoT services consumers' interests after computing the TF-IDF for our dataset.

2) *IoT Services consumers' interests classification using LSTM model*: The LSTM model is a powerful deep learning algorithm that produces excellent results and has been applied to several text classification tasks [37, 38, 39, 40]. Our study employs a LSTM model to learn high-level discriminative representations and to identify the IoT services consumers' interests across several categories, including education, energy, health, industry, transportation, and others. Using TF-IDF to extract input representations, the structure of LSTM is expressed in the following manner:

$$i_t = \sigma(W_i \cdot [h_{t-1}, x_t] + b_i) \quad (4)$$

$$f_t = \sigma(W_f \cdot [h_{t-1}, x_t] + b_f) \quad (5)$$

$$o_t = \sigma(W_o \cdot [h_{t-1}, x_t] + b_o) \quad (6)$$

$$c_t = f_t \odot c_{t-1} + i_t \odot \tan h(W_c \cdot [h_{t-1}, x_t] + b_c) \quad (7)$$

$$h_t = o_t \odot \tan h(c_t) \quad (8)$$

i_t , f_t , o_t and c_t are the input gate, forget gate, output gate, and cell input vector respectively. The last hidden state is $h_{[t-1]}$, the current input is x_t , the weighted matrix is W *, and the biases are b *. The σ is a logistic sigmoid function, while the $\tan h$ function is a tangent function. The element-wise product of two vectors is \odot .

Our LSTM model has the following configurations. It uses 2000 epochs and a loss function namely mean squared logarithmic error with adam optimizer. The softmax activation function is used in all the input, hidden and output layers. The total number of tunable parameters used in the proposed model are summarized in Table II.

TABLE II. THE DESCRIPTION OF THE PROPOSED LSTM MODEL

Layer (type)	Output Shape	Param #
Embedding	(None, 25, 50)	1,647,250
Spatial Dropout1d	(None, 25, 50)	0
LSTM	(None, 124)	29,440
Dense	(None, 5)	325
Total params		1,677,015
Trainable params		1,677,015

3) *Recommendation mapper algorithm*: In the knowledge-based IoT recommendation system, we propose that the Recommendation Mapper is responsible for mapping the recommendations based on the IoT services consumers' category $\tau(c)$ and the IoT device (i) or IoT service (i) that has the same IoT device and services category $\tau(i)$ which are registered in the IoT Device and Services Registry R_i . Then the Recommendation Mapper starts the mapping process and updates the recommendation table $\mu(c)$ and present the recommendation m to the IoT services consumers c . Algorithm 1 shows the brief process of the Recommendation Mapper.

Algorithm 1 Recommendation Mapper Algorithm

```
1. Initialization: Compute  $TF - IDF(t) \in C(t)$  if any
2. Prediction: Compute  $i_t, f_t, o_t$ , and  $h_t \in C(t)$  to predict  $\tau(c)$ 
3. Mapping: Check  $R_i$ 
if  $d(i)$  or  $s(i) \in \tau(i) = \tau(c)$  then
    Update  $\mu(c)$ 
else
    Notify  $c$  "There are no recommended IoT devices or services at the
    moment, please try again later."
end if
4. Recommendation: Get  $m \in \mu(c)$ 
for each  $m \in \mu(c)$ 
    Present  $m$  to  $c$ 
end for
```

IV. IMPLEMENTATION AND EXPERIMENTATION

This section describes the knowledge-based IoT recommendation system for evaluating the IoT services consumers' interest classification model collected using Twitter API. Second, we explain the dataset that we have collected using Twitter API to evaluate the IoT services consumers' interest classification model. Finally, the results of the empirical experimentation are discussed to validate the performance of the classification model for IoT services consumers' interests.

A. System Implementation

The implementation of the knowledge-based IoT recommendation system is developed using Flutter 3.0.2 for the mobile application's Graphical User Interfaces (GUIs) to enable IoT device and service registration and advertisement, as well as, IoT device and service recommendation requests and feedbacks. PHP 8.1.7 is used for the mobile application backend. Python 3.10.5 is used for the development of the IoT services consumers' interest classification model in the backend. MySQL 8.0.29 for the development of the database.

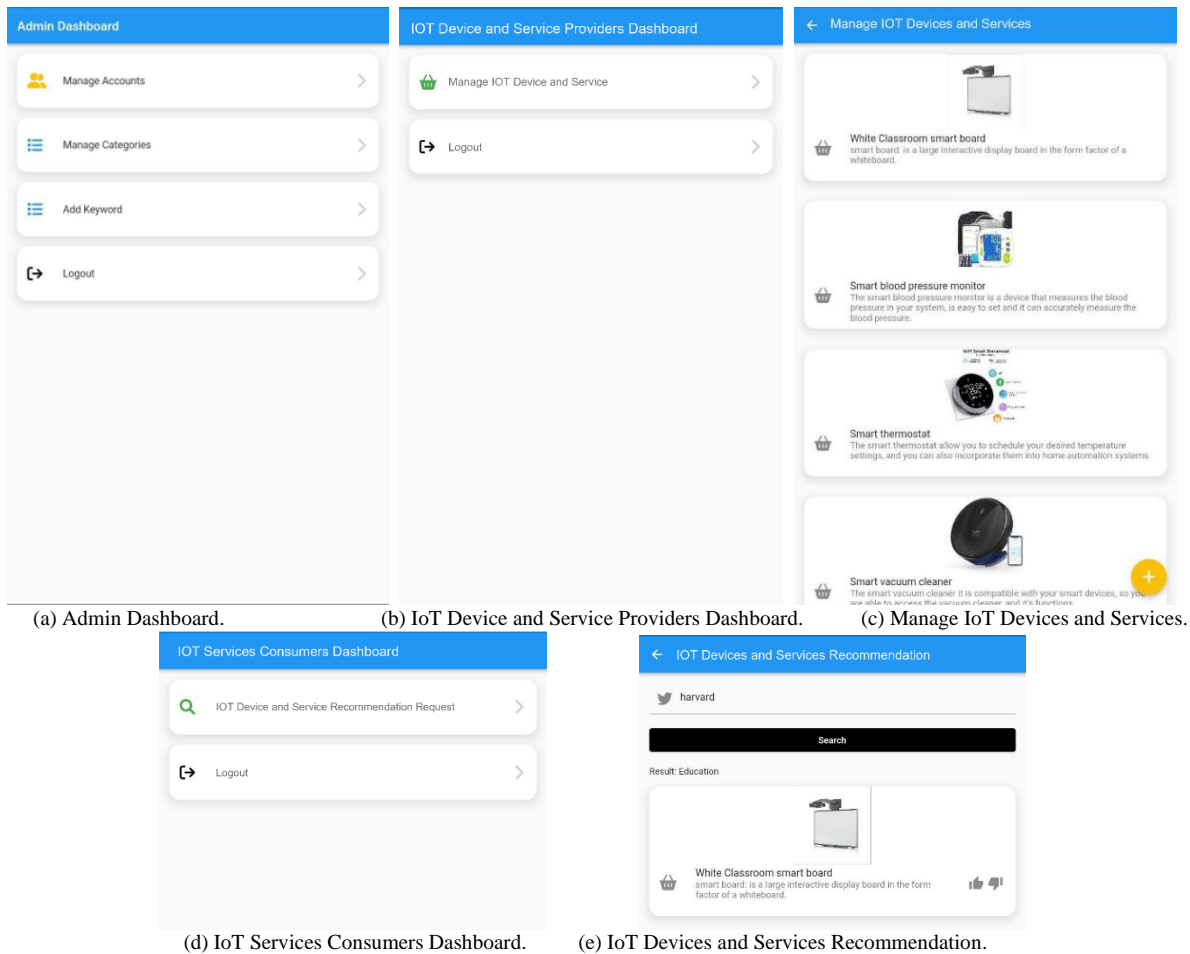


Fig. 2. Knowledge-based IoT Recommendation System's GUIs

The proposed knowledge-based IoT recommendation system uses several GUIs for the Admin, IoT device and service providers, and consumers of IoT services. Fig. 2 illustrates some of the knowledge-based IoT recommendation system GUIs. For example, Fig. 2(a) showcases the admin's dashboard where she can manage the users accounts whether they were IoT device and service providers or IoT services' consumers, manage IoT categories (i.e., as mentioned earlier, the proposed method categorized IoT devices or services into several categories including health, energy, education, transportation, and industry, where the admin can eventually add new categories as required), add keywords related to the IoT categories to enable the IoT services consumers' interests analysis. Fig. 2(b) illustrates the IoT device and service providers dashboard where they can manage their IoT device or service registration and advertisement by adding an ID, name, description, and image for each IoT device or service as shown in Fig. 2(c). Fig. 2(d) showcases the IoT services' consumers' dashboard where they can request IoT device or service recommendation after requesting their permission to gain access to their Twitter account. Fig. 2(e) illustrates the

IoT device and service recommendation to the IoT services' consumers which is based on their interests. Moreover, a like/dislike buttons are added to have some feedback from the IoT services' consumers (i.e., this will help us in calculating the True Positives (TPs), False Positives (FPs), False Negatives (FNs), True Negatives (TNs) later on).

B. Data Description

To evaluate the performance of the IoT services consumers' interest analysis which is the core of the proposed knowledge-based IoT recommendation system, a real-world IoT dataset is collected using Twitter Application Programming Interface (API). The dataset was collected from August 2021 until October 2021. It contains around 15,791 distinct tweets and 11,421 users. Fig. 3 displays the number of tweets for each category. After that the following pre-processing was performed on the dataset: (i) lower casing all words; (ii) filtering out all stop-words non-alphabetic characters; and (iii) removing all words that occurred too rarely in the documents. Finally, the labeling process is conducted to annotate tweets for the classification task using LSTM model.

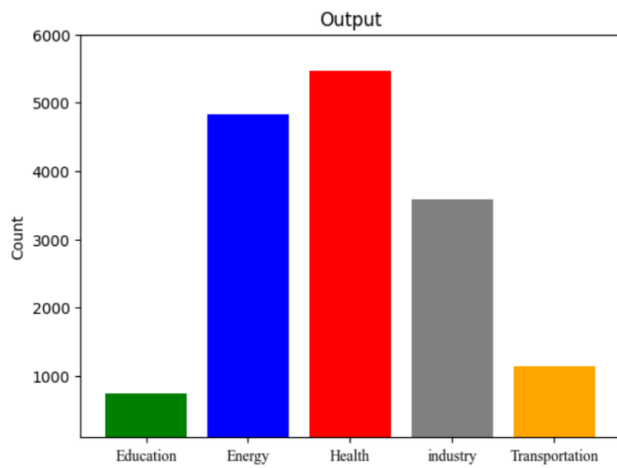


Fig. 3. Data Description.

C. Performance Evaluations

To evaluate the IoT services consumers' classification using LSTM model, we split the dataset into training and testing datasets 70% and 30% respectively. The training dataset includes 12,632 tweets from 7,995 users and the testing dataset includes 3,426 tweets from 3,159 users whereas we divide these users into 5 groups representing the IoT services' consumers interests categories including health, energy, education, transportation, and industry. In the following Section 4.3.1, we describe the evaluation methods used to test our model's performance. We then described the comparison methods in Section 4.3.2. Section 4.4 summarizes the results of our experiments.

1) *Evaluations methods*: Several well-known evaluation metrics [40] are used including accuracy, precision, recall, and F1-score which are calculated based on the numbers of True Positives (TPs) (i.e., the IoT services consumers' interests classification model predicted positive and it is true), False Positives (FPs) (i.e., the IoT services consumers' interests classification model predicted positive and it is false), False Negatives (FNs) (i.e., the IoT services consumers' interests classification model predicted negative and it is false), True Negatives (TNs) (i.e., the IoT services consumers' interests classification model predicted negative and it is true). These evaluation metrics are calculated as follows:

$$Accuracy = \frac{TPs + TNs}{TPs + FPs + TNs + FNs} \quad (9)$$

$$Precision = \frac{TPs}{TPs + FPs} \quad (10)$$

$$Recall = \frac{TPs}{TPs + FNs} \quad (11)$$

$$F1-Score = 2 * \left(\frac{Precision * Recall}{Precision + Recall} \right) \quad (12)$$

2) *Methods for comparison*: The proposed approach was compared with three well-known models:

a) *Naive Bayes (NB)*: is a supervised machine learning method that utilizes Bayes theory to identify consumer attitudes [41, 42].

b) *Support Vector Machine (SVM)*: is a supervised machine learning algorithm that has been used for understanding consumer interests [43,44].

c) *Logistics Regression (LR)*: is another machine learning model that has been used to analyze user interests from Twitter data [45, 46].

d) *Long- Term Short Memory (LSTM)*: A deep learning model that can be used to perform sentiment analysis on social.

Media [36,47,48].

D. Result and Discussion

The empirical experimentation is performed for the IoT services consumers' interests classification model against the five groups of the IoT services' consumers' interests where the precision, recall, and F1-Score is calculated for each category as shown in Fig. 4. The highest result in precision appeared in the health category to reach 0.96 as shown in Fig. 4(c). Fig. 4(c) shows the highest recall score of 0.95. The highest result in F1-score appeared in the education category and energy category and it is recorded at 0.95 and 0.96 respectively.

This study used several methods for conducting a comparative study. The LSTM model is compared with three well-known models: NB, SVM, and LR. These models are evaluated in terms of accuracy. Fig. 5 shows the accuracy results for our model compared with other classifiers. Compared to LSTM, SVM, and LR, Naive Bayes performed the worst with an accuracy score of 0.82. Conversely, LSTM has the highest accuracy score when compared to other methods. The LSTM achieved an accuracy of 0.96. Fig. 6 illustrates the training accuracy and validation accuracy of the proposed model. According to the results, the proposed model can identify consumers' interests from social media effectively, resulting in high accuracy in IoT devices and services recommendations. Fig. 7 illustrates the IoT services consumers' interests classification model confusion matrix. The LSTM model correctly predicted 0.96 tweets, while it mis-predicted 0.4.

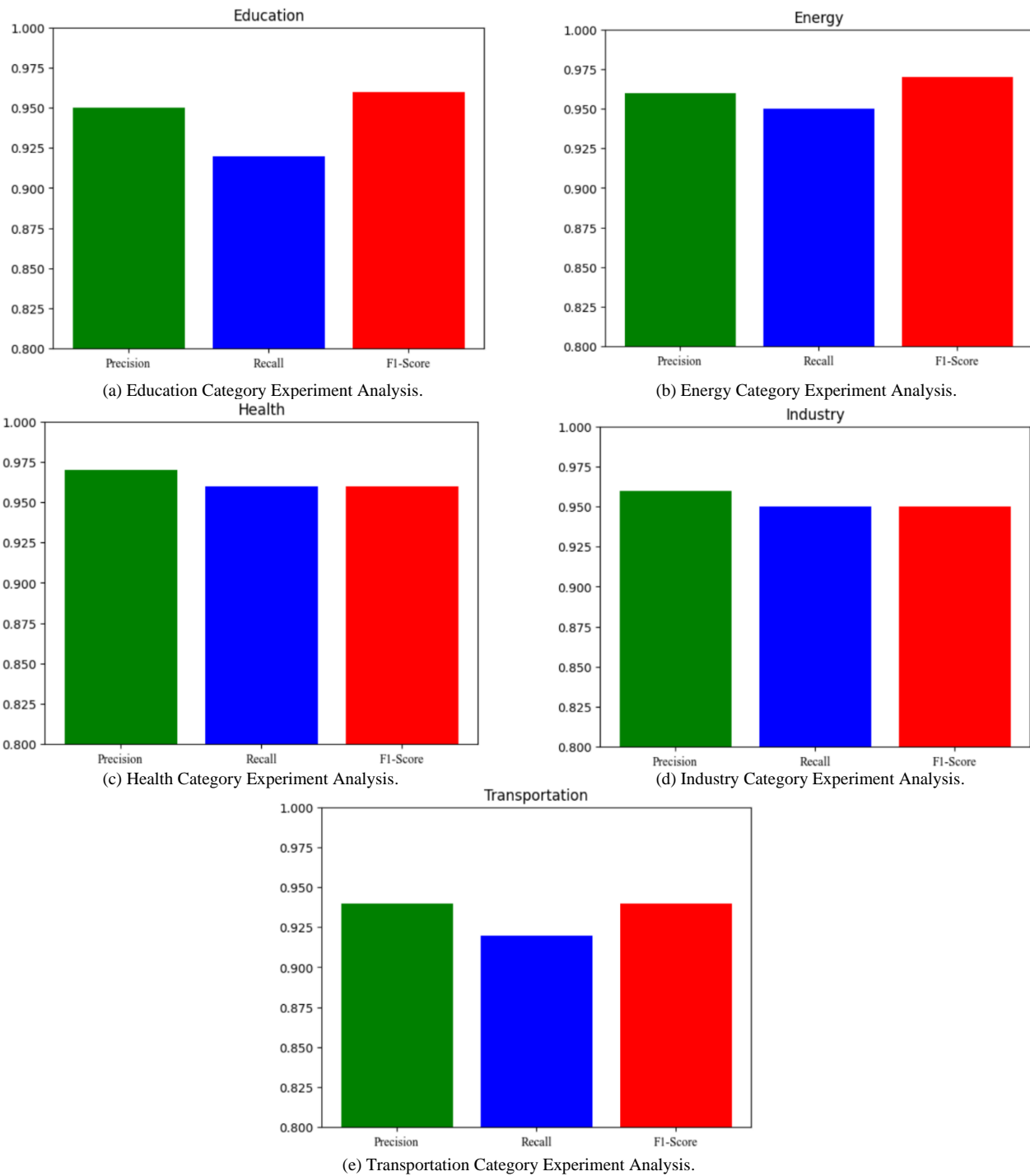


Fig. 4. The IoT Services Consumers' Classification Model Empirical Experimentation Analysis.

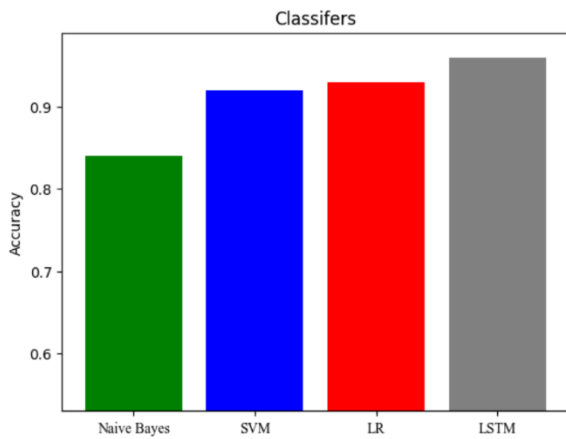


Fig. 5. Accuracy of the Proposed Model Compared to other Classifiers.

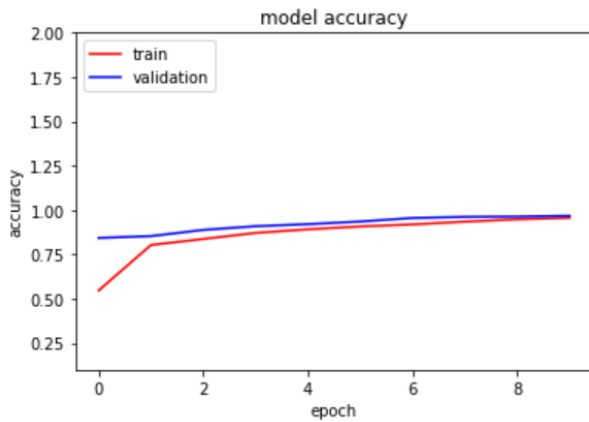


Fig. 6. The Accuracy of the Proposed Model.

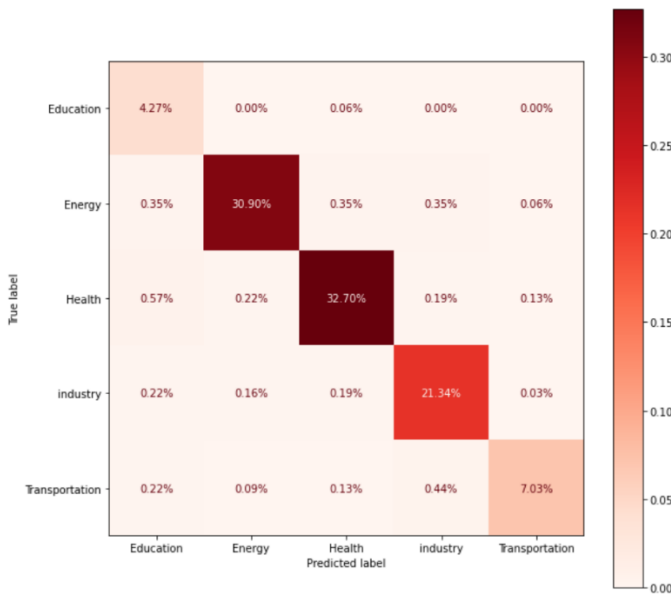


Fig. 7. The IoT Services Consumers' Classification Model Confusion Matrix.

V. CONCLUSION

IoT devices connected to the internet have increased dramatically and played an important role in several domains such as health, energy, education, transportation, industry, and other domains. With this increase, IoT services' consumers find it difficult to choose the suitable IoT devices and services that solve their problems. This paper explores how consumers' knowledge about IoT services can be used to predict suitable devices and services. Therefore, a knowledge-based IoT recommendation system is introduced based on SOA to allow IoT device and service providers to register and advertise their IoT device and services and recommend IoT devices for IoT services consumers based on their interest. In particular, this paper presents an IoT services consumers' interests classification model that uses a deep learning model namely, Long Short-term Memory (LSTM), to classify IoT services' consumers based on their interest. In order to demonstrate the feasibility of our proposed approach, a real-world IoT dataset is collected from Twitter that includes more than 15,791 tweets, a prototype system is implemented, and empirical experiments were conducted. The results of the experiments on the IoT services consumers' interests classification model were promising where the overall average results in accuracy, precision, recall, and F1-score are 0.96, 0.95, 0.96, and 0.95 respectively.

In future work, the IoT recommendation system will be extended to be a hybrid recommendation system, which can be enhanced by collaborative filtering techniques. Furthermore, several IoT categories and languages such as Arabic will also be added to evaluate the accuracy of the proposed model. As part of our recommendation system, videos can also be added to explain how to use IoT devices.

REFERENCES

- [1] L. S. Vailshery, "Number of Internet of Things (IoT) Connected Devices Worldwide from 2019 to 2030," 2022 (accessed June 10, 2022).
- [2] B. Oladayo and Z. Sherali, "Toward Efficient Smartification of the Internet of Things (IoT) Services," *Future Generation Computer Systems*, vol. 92, pp. 663–673, 2019.
- [3] R. R., Batcha, and M. K., Geetha, "A Survey on IOT Based on Renewable Energy for Efficient Energy Conservation Using Machine Learning Approaches," in the 3rd International Conference on Emerging Technologies in Computer Engineering: Machine Learning and Internet of Things (ICETCE), IEEE, pp. 123–128, Jaipur, India, 7–8 February, 2020.
- [4] M. Al-Emran, SI. Malik, MN. Al-Kabi, "A Survey of Internet of Things (IoT) in Education: Opportunities and Challenges," In Aboul Ella H, Roheet B, Nour Eldeen M. K, Mohamed Hamed NT., eds. *Toward Social Internet of Things (SIoT): Enabling Technologies, Architectures and Applications* Springer, pp. 197–209, 2020.
- [5] TH. Noor, "Behavior Analysis-based IoT Services for Crowd Management," *The Computer Journal*, vol. 65, pp. 1-12, 2022.
- [6] S. Hamad, Z. Sheng and W. Zhang, "Realizing an Internet of Secure Things: A Survey on Issues and Enabling Technologies," *IEEE Communications Surveys & Tutorials*, vol. 22, no. 2, pp. 1372–1391, 2020.
- [7] L. Yao, X. Wang, Z. Quan and S. Dustdar, "Recommendations on the Internet of Things: Requirements, Challenges, and Directions," *IEEE Internet Computing*, vol. 23, no. 3, pp. 46–54, 2019.
- [8] TH. Noor, "A Service Classification Model for IoT Services Discovery," *Computing*, vol. 103, no. 11, pp. 2553–2572, 2021.

- [9] TH. Noor, "A Gesture Recognition System for Gesture Control on Internet of Things Services," *Journal of Theoretical & Applied Information Technology*, vol. 96, no. 12, pp. 3886–3895, 2018.
- [10] H. El Bouhissi, M. Ketam and A. Salem, "Towards an Efficient Knowledge-based Recommendation System," in the 2nd International Workshop on Intelligent Information Technologies and Systems of Information Security (IntelITSIS). Central Europe (CEUR) Workshop Proceedings. pp. 38–49, Khmelnytskyi, Ukraine, March 24–26, 2021
- [11] DC. Funder, Persons, "Behaviors and Situations: An Agenda for Personality Psychology in the Postwar Era," *Journal of Research in Personality*, vol. 43, no.2, pp. 120–126, 2009.
- [12] MV. Ferrari, "The Platformisation of Digital Payments: The Fabrication of Consumer Interest in the EU FinTech Agenda," *Computer Law & Security Review*, vol. 45, pp. 105687, 2022.
- [13] N. Ahmad, J. Siddique, "Personality Assessment Using Twitter Tweets," *Procedia Computer Science*, vol. 112, pp. 1964–1973, 2017.
- [14] PH. Arnoux, N. Boyett, J. Mahmud, R. Akkiraju, "Tweets to Know You: A New Model to Predict, Personality with Social Media," in the 11th International AAAI Conference on Web and Social Media (ICWSM). Association for the Advancement of Artificial Intelligence (AAAI), pp. 472–475, Montreal, Quebec, Canada, May 15–18, 2017.
- [15] G. Carducci, G. Rizzo, D. Monti, E. Palumbo, M. Morisio, "Twitpersonality: Computing Personality Traits from Tweets Using Word Embeddings and Supervised Learning," *Information*, vol. 9, no. 127, pp. 1–22, 2018.
- [16] A. Felfernig, SP. Erdeniz, M. Jeran, "Recommendation Technologies for IoT Edge Devices," *Procedia Computer Science*, vol. 110, pp. 504–509, 2017.
- [17] S. Sharma, K. Gupta, D. Gupta, "The Amalgamation of Internet of Things and Recommender Systems," *Journal of Physics: Conference Series*, vol. 1969, no. 1, pp. 012-040, 2021.
- [18] A. Felfernig, S. Polat-Erdeniz, C. Uran, "An Overview of Recommender Systems in the Internet of Things," *Journal of Intelligent Information Systems*, vol. 52, no. 2, pp. 285–309, 2019.
- [19] D. Gupta, "A Comprehensive Study of Recommender Systems for the Internet of Things," *Journal of Physics: Conference Series*, vol. 1969, no.1, pp. 012-045, 2021.
- [20] P. Ahlawat, C. Rana, "A Comprehensive Insight on Machine Learning enabled Internet of Things Recommender Systems (IoTRS)," in the International Conference on Advances in Management Practices (ICAMP 2021). Social Science Research Network (SSRN), pp. 1–12, Delhi, India, December 17–18, 2021
- [21] D. Nawara, R. Kashef, "Context-Aware Recommendation Systems in The IoT Environment (IoT-CARS) - A Comprehensive Overview," *IEEE Access*, vol. 9, pp. 144270-144284, 2021.
- [22] V. Mohammadi, AM. Rahmani, AM, Darwesh, "Trust-based Recommendation Systems in Internet of Things: Systematic Literature Review," *Human-centric Computing and Information Sciences*, vol. 9, no. 1, pp. 1–61, 2019.
- [23] SP. Erdeni, I. Maglogiannis, A. Menychtas, A. Felfernig, "Recommender Systems for IoT Enabled m-Health Applications," in the 14th IFIP International Conference on Artificial Intelligence Applications and Innovations (AIAI). International Federation for Information Processing Working Group (IFIP WG), pp. 227–237, Rhodes, Greece, May 25-27, 2018.
- [24] RM. Frey and R. Xu, "A Novel Recommender System in IoT," in the 5th International Conference on the Internet of Things (IOT 2015). IEEE, pp. 1-2, Seoul, South Korea, October 26-28, 2015.
- [25] S. Forouzandeh, AR. Aghdam, M. Barkhordari "Recommender System for Users of Internet of Things (IOT)," *International Journal of Computer Science and Network Security (IJCSNS)*, vol. 17, no. 8, pp. 46-51, 2017.
- [26] R. Kashef, "Enhancing the Role of Large-Scale Recommendation Systems in the IoT Context," *IEEE Access*, vol. 8, pp. 178248–178257, 2020.
- [27] H. Bouazza, B. Said, FZ. Laallam, "A hybrid IoT Services Recommender System using Social IoT," *Journal of King Saud University-Computer and Information Sciences*, pp.1–13, 2022.
- [28] L.Yao, QZ. Sheng, AH. Ngu, "Things of Interest Recommendation by Leveraging Heterogeneous Relations in the Internet of Things," *ACM Transactions on Internet Technology (TOIT)*, vol. 16, no. 2, pp. 1–25, 2016.
- [29] X. Xin, T. Shi, M. Sohail, "Knowledge-based Intelligent Education Recommendation System with IoT Networks," *Security and Communication Networks 2022*; 2022.
- [30] B. Anthony, "A Case-based Reasoning Recommender System for Sustainable Smart City Development," *AI & SOCIETY*, vol. 36, no. 1, pp. 159–183, 2021.
- [31] S. Cha, MP. Ruiz, M. Wachowicz, LH., I. Maduako, "The Role of an IoT Platform in the Design of Real-time Recommender Systems," in the IEEE 3rd World Forum on Internet of Things (WF-IoT). IEEE, pp. 448–453, Reston, VA, USA, December 12-14, 2016.
- [32] A. Gyrard, A. Sheth, "Towards an IoT Knowledge-based Cross-domain Well-being Recommendation System for Everyday Happiness," *Smart Health*, vol. 15, pp. 1–19, 2020.
- [33] F. Jabeen, M. Maqsood, MA. Ghazanfar, "An IoT Based Efficient Hybrid Recommender System for Cardiovascular Disease," *Peer-to-Peer Networking and Applications*, vol. 12, no.5, pp. 1263–1276, 2019.
- [34] LM. Gladence, VM. Rathna, E. Brumancia, "Recommender System for Home Automation Using IoT and Artificial Intelligence," *Journal of Ambient Intelligence and Humanized Computing*, vol. 11, no. 4, pp. 1–9, 2020.
- [35] S. Mohamed, K. Sethom, AJ. Obaid, "IOT-Based Personalized Products Recommendation System," *Journal of Physics: Conference Series*, vol. 1963, no. 1, pp. 012–088, 2021.
- [36] El-S. Atlam, J. Aoe, "Document Similarity Measurement Using Field Association Term," *Information Processing and Management Journal*, vol. 39, no. 6, pp. 809-824, 2003.
- [37] A. Graves, "Generating sequences with recurrent neural networks," *arXiv preprint arXiv:1308.0850* 2013.
- [38] AM. Almars, M. Almaliki, TH. Noor, MM. Alwateer, E. Atlam, "HANN: Hybrid Attention Neural Network for Detecting Covid-19 Related Rumors," *IEEE Access*, vol. 10, pp. 12334–12344, 2022.
- [39] AM. Almars, "Attention-based Bi-LSTM Model for Arabic Depression Classification," *CMC-COMPUTERS MATERIALS & CONTINUA*, vol. 71, no. 2, pp. 3091–3106, 2022.
- [40] I. Gad, D. Hosahalli, "A Comparative Study of Prediction and Classification Models on NCDC Weather Data", *International Journal of Computers and Applications*, vol. 44, no. 5, pp. 414–425, 2022.
- [41] W. Ahmad, P. Murti, "Naïve Bayes Classifier for Journal Quartile Classification," *International Journal of Recent Contributions from Engineering Science IT*, vol. 7, no. 2, pp. 809-824, 2019.
- [42] H. Chen, X. Zhao, "Improved naive Bayes classification algorithm for traffic risk management," *EURASIP Journal on Advances in Signal Processing*, vol. 2021, no.30, pp. 1-12, 2021.
- [43] D. SrivastavaLekha, B. Bhambhu, "Data classification using support vector machine," *Journal of Theoretical and Applied Information Technology*, vol. 12, no. 1, pp. 1-7, 2010.
- [44] J.Cervantes, U. Lopez, "A comprehensive survey on support vector machine classification: Applications, challenges and trends", *Neurocomputing 2020*; 408: 198-215.
- [45] Q. Abdulqader, "Applying the Binary Logistic Regression Analysis on The Medical Data", *Science Journal of University of Zakho 2017*; 5(4): 330-340.
- [46] M. Sekiya, T. Toshiaki, "Linear Logistic Regression for Estimation of Lower Limb Muscle Activations", *IEEE Transactions on Neural Systems and Rehabilitation Engineering 2019*; 27(3): 523 - 532.
- [47] F. Mohammed, M. Doreswamy, "Parallel Genetic Algorithms for Optimizing the SARIMA Model for Better Forecasting of the NCDC Weather Data", *Alexandria Engineering Journal 2020*; 60: 1299-1316.
- [48] M. Zohair, E. Atlam, "Bidirectional Residual LSTM -based Human Activity Recognition", *Journal of Computer and Information Science 2020*; 13(3): 1-40.

A Machine Learning Model for Personalized Tariff Plan based on Customer's Behavior in the Telecom Industry

Lewlisa Saha¹, Hrudaya Kumar Tripathy², Fatma Masmoudi³, Tarek Gaber⁴

School of Computer Engineering, KIIT, Deemed to be University, Bhubaneswar, India^{1,2}

College of Computer Engineering and Sciences, Prince Sattam Bin Abdulaziz University, Alkharj, 11942, Saudi Arabia³

School of Science, Engineering, and Environment, University of Salford, Manchester, UK⁴

Abstract—In the telecommunication industry, being able to predict customers' behavioral pattern to successfully design and recommend a suitable tariff plan is the ultimate target. The behavioral pattern has a vital connection with the customers' demographic background. Different researches have been done based on hypothesis testing, regression analysis, and conjoint analysis to determine the interdependencies among them and the effects on the customers' behavioral needs. This has presented us with ample scope for research using numerous classification-based techniques. This work proposes a model to predict customer's behavioral pattern by using their demographic data. This model was built after investigating various types of classification-based machine learning techniques including the traditional ones like decision tree, k-nearest neighbor, logistic regression, and artificial neural networks along with some ensemble techniques such as random forest, adaboost, gradient boosting machine, extreme gradient boosting, bagging, and stacking. They are applied to a dataset collected using a questionnaire in India. Among the traditional classifiers, decision tree gave the best result of 81% accuracy and random forest showed the best result among the ensemble learning techniques with an accuracy of 83%. The proposed model has shown a very positive outcome in predicting the customers' behavioral pattern.

Keywords—Customer behavior; data analytics; ensemble learning; machine learning; telecommunication industry

I. INTRODUCTION

Telecommunication industry is one of the world's largest services providing industry and is known for having the highest number of customers. Customers are the most vital entity of any business platform, and the telecom sector is no exception to that. Bringing in new customers, understanding their needs and requirements, dividing the customers into proper groups to be able to offer the right product or service, gain their loyalty and retain them in the long term are the targets of any customer-centric business. As for the telecommunication sector, retaining customers has become a necessity to survive in the competitive market.

In [1], the authors have discussed the framework containing the development over the recent years in the Indian mobile communication sector. Over 23 years, the Indian telecom sector has seen a fundamental shift in communication modes from fixed line to mobile, making India the world's second-largest telephone market. The exponential rise of smart phones and the

Internet in 2013 marked the beginning of the era of convergence of two technologies: mobile and the Internet. In India, mobile penetration (density) has increased from 4% in 1995, when mobile telephony was first introduced, to 88.50% in 2019 (with 1165.46 million subscribers). The low density of mobile telephony in rural India remains an issue. This high mobile density in urban India is owing to higher per capita income, education, and network externality (as compared to rural India), resulting in a single user owning numerous subscriber identity modules (SIM). The Indian population's total teledensity has surged up to 90.1% as of March 2019 [2]. In this paper, authors have given a deep insight into the telecommunication industry and their relationship with their customers and how it has developed over the years. The necessity to maintain existing consumers has grown over time as the number of new entering customers decrease. The urban India had a teledensity of 159.66% in March 2019, while rural India had a teledensity of 57.5%. This demonstrates the significant differences in people's socioeconomic position based on where they live. For example, metro cities like Delhi had a teledensity of 238.57%, Kolkata had a teledensity of 165.51%, and Mumbai had a teledensity of 165.62 %, whereas the states of Bihar had a teledensity of 59.95 %, Assam had a teledensity of 68.81 %, and so on. As a result, the location is crucial in determining the demands and requirements of customers. This latter compels us to go on to the next level in customer relationship management: customer segmentation.

In the telecommunication sector, geographic location, socio-economic background, age group, gender identity, and so on have a profound impact on the selection of tariff plans by their respective customers. A significant variation in the selection of tariff plans can be observed between customers belonging to a metropolitan city to that of a rural area. Hence, this invites scope for better customer segmentation and customization of services. To address this existing generalized tariff system in the Indian telecommunication industry, our work focuses on predicting customer behavioral pattern that would lead to better-personalized tariff plans by designing a flexible tariff plan for the customers in accordance with their needs.

Keeping those aspects in the hindsight, we propose to analyze the customers' demographic data using different classification-based machine learning techniques such as decision tree, logistic regression, k-nearest neighbor, and

artificial neural network among traditional classifiers and random forest, Adaboost, extreme gradient boosting, gradient boosting machine and stacking among ensemble learning techniques. This study is used to train the model into predicting the customers' behavioral pattern in the form of call duration and data consumption. The result of the proposed model is at par with the desired outcome. With a larger amount of data the performance of the model could be improved and could be enhanced significantly.

The rest of the paper is organized as follows: Section II shows the related works in the research area. Section III discusses the machine learning techniques used in the proposed research model. Section III also provides a detailed idea about the dataset used and the methodology followed in the research. The results that are obtained by the research are detailed in Section IV, Section V highlights the discussion of the present work and the whole work has been concluded in Section VI.

II. RELATED WORK

The Telecom sector offers services that broadcast voice, data, sound, text, video, and other signal forms. It also consists of wired and wireless activities. Nowadays, when the Internet is the dominating factor, the telecommunication industry has grown tremendously. In order to meet the increasing demand for data consumption, the telecommunication service industry needs to rise so that it can keep up with the high usage of social media platforms. Over the years, authors across the globe have worked with different datasets belonging to the telecommunication sector spanning various countries. Hence, we try in our work to analyze and assimilate a few of the previous works based on tariff plan design in the telecommunication sector. Authors in (Nkordeh et al., 2017) [3] discussed the growth of GSM in the Nigerian telecommunication industry over the period time of 2001 to 2016. They performed a detailed market analysis of the annual growth based on subscribers, revenue growth, and market penetration and how it caused the loss of subscribers. In (Shao et al., 2017) [4], the authors have performed a study which adopts MTFPI (Malmquist total factor productivity index) and data envelopment analysis to conclude that because of their high acceptance of technology developments, the telecommunication service industries had a higher rate of productivity growth. In [5] the author intended to offer a CRM optimization scheme for the telecommunications industry utilizing business intelligence (BI). In the first phase of their work, they conducted a literature survey for all available assignments in the Scopus and web of science. New concepts were introduced to the current work in its second phase and the third phase, the new approach was implemented by a Brazilian telecommunications operator. Authors in [6] used hypothesis testing to study the impact of business intelligence on CRM from the perspective of the employees of telecommunication companies in Oman. Tong et al. discussed a way of increasing customer loyalty through the use of net promoter data mining (NPS) which depended on information gained on decision tree model and k-means clustering [7]. They attempted to identify the reasons for customer loyalty and conclude the connection between the NPS and the financial performance of the customer groups. Jose et al. sought to determine the important parameters affecting the performance of the telecommunication contact

center which was vital to customer satisfaction [8]. A case study on Big Data Analytics in the incoming and external contact center was undertaken by the authors by using principal component analysis (PCA), factor analysis, regression analysis, and cross-tabulation. Bahri-Ammari and Bilgihan proposed a framework that uses hypotheses testing for examining the relationship between customer satisfaction and loyalty and customer retention [9]. In reconciling customer satisfaction among mobile telecommunication providers, Newton and Ragel reviewed the potential relational linkages concerning customer loyalty with the help of correlation and regression analysis [10]. The authors intended to detect the degree, relationships, and impact of customer satisfaction and reliability. In their article, Belwal and Amireh have been focused on the Omani telecommunications market and have evaluated the service quality of two main Omani telecom companies: Omantel and Ooredoo [11]. This was tested on customer attitudinal loyalty to see how the five SERVQUAL factors influenced it, by using a machine learning technique called structural equation modeling.

In a variety of industries, including telecom, understanding how consumers make tariff decisions is a key issue. Most telecommunication service providers assign customers with a variety of mobile plans from which they can choose one that best suits their monthly needs. As mentioned in [12] due to many service providers, the telecom business has become extremely competitive. Their study proposed an association-based rule mining technique to help telecom operators select optimal recharge combo deals that are appropriate for their clients. In another work, Gerpott and Meinert used hypotheses testing on data obtained from the German subsidiary of a large multinational MNO to analyze the degree of tariff plan misfit depending on the socio-demographic features [13].

Consumer overspending in mobile plan selections may result in higher revenues for telecom service providers. However, it could ultimately lead to less satisfied customers and are thus more prone to churn, which is a major problem for telecom service providers. As a result, enhancing customer happiness by encouraging them to make better choices is a superior long-term approach. Author in [14] studied the impact of launching of JIO on the Indian telecommunication market which led to a one-dimensional design of the tariff plans in the long term and resulted in the need for getting a better understanding of the customers' requirements. Bibim and Ramanathan tried to use conjoint analysis to determine the best combination of data, voice, and SMS for postgraduate and undergraduate students, as well as to investigate how they use it [15]. The suitable effects on customer loyalty and customer relationship management in the Indian telecommunications sector had been shown by [16] with the help of Exploratory Factor Analysis and Regression Analysis.

The most challenging issue is the difficulty to comprehend consumers' tariff options. Although customers aspire to save money by selecting a cost-cutting strategy, they are only partially focused on resolving the issue. As a result, rather than making tariff decisions based on predicted demand, they tend to simplify the process by employing cognitive shortcuts, such as heuristic thinking, which leads to systemic tariff biases. Ignoring how consumers utilize heuristic thinking can lead to

failures in consumer protection and market control policies. The authors in [17] have investigated the quality of decision making in a lab setting where consumers were presented with a limited number of mobile phone plan options. However, they have not dealt with varying degrees of tariff complexity as well as unknown usage. According to Jin et al., the goal of their study has been to check whether consumers employ a specific type of heuristic reasoning, known as salience-based decision making when choosing mobile plans and they preferred the approach of hypotheses testing [18]. Based on market segmentation theory, Shuochen et al. have introduced a matching model that links tariff packages and consumers' usage behavior (e.g., total minutes utilized, data consumption, etc.) [19]. Gerpott and Meinert have looked at the relationship between outgoing mobile voice minutes and monthly mobile internet data traffic in a sample of 11,614 residential postpaid members over 25 months, from October 2011 to October 2013 by using regression analysis [20]. Díaz examined the factors determining customer satisfaction and customer loyalty in the Peruvian mobile market [21]. Multinomial logit and the GSEM estimates have showed, based on a survey of 1259 customers, how customer satisfaction determinants can be assessed when satisfaction has been measured using ordered categorical data.

Ascarza et al. have examined the efficacy of retention campaigns with the help of a large-scale field test where recommendations for plans have been provided to some customers and not others [22]. Lee et al. have used conjoint analysis in their research to study the effects of B2B service introduction in the Korean telecommunication industry [23]. In their research, Garcia-Marioso and Suárez have examined the reasons that motivate consumers to transfer mobile operators by using logit model over data from a longitudinal survey of 4110 Spanish mobile users conducted over the period of 2015 and 2016 [24]. Xu et al. presented a system for predicting customer turnover that employed an ensemble-learning technique, including stacking models and soft voting [25]. Bachan and Gaber performed churn prediction by using decision tree, logistic regression, and support vector machine [26]. Capponi et al. used a formal economic model to investigate the incentives for businesses and to offer tailored pricing plans when customers were on the verge of quitting and their service utilization was heterogeneous [27]. Kim et al. addressed a few of the research gaps such as lack of customer support and subscription work that had been based on the benefits and rewards that result in customer subscription, subscription switching costs, and retention of customer support [28].

After analyzing various previous works, we notice that even though various machine learning techniques, alongside many non-IT-based techniques, have been used time and again by researchers to get a better understanding of the customers. These works have primarily revolved around regression analysis and hypothesis testing. To provide personalized tariff plans, many works have tried to study the customers' behavioral pattern. The authors have mostly concentrated on finding the interrelationship among the constraints by using the correlation coefficient and likelihood ratio to get a better understanding of the customers' behavior. Hence, the objective of our work is to take a different approach where irrespective of the interdependency among the constraints. It is not the focal

point of the work. A step-by-step learning approach has been considered where the pattern of different constraints and how it can impact the main governing aim has been comprehensively analyzed.

III. MATERIALS AND METHODS

Classification falls under the supervised learning category, where the targets are also given access to the input data. Supervised learning is a type of machine learning where the output is predicted by the machines using well-labeled training data that has been used to train the machines. The term "labelled data" refers to input data that has already been assigned the appropriate output. This section accounts for a detailed description about different traditional as well as ensemble learning based classifiers used in the proposed model.

A. Traditional Classifiers

1) *Decision tree*: A decision tree is considered one of the few most generally used grading systems in classifying data or understanding the hidden pattern of a particular data collection. It consists of a group of nodes among which the first node is designated as the root node while the rests are known as internal and leaf nodes. The last layer of the decision tree consists of leaf nodes which usually have a predefined class target value. The primary backbone for building a decision tree is repeatedly dividing the nodes on each level based on the criteria for splitting [29]. This splitting and expanding phases last until a stopping criterion are encountered. The various criteria can be represented as follows numerically,

$$InformationGain(b_i, R) = Entropy(z, R) - \sum_{u_{i,j} \in dom(b_i)} \frac{|σ_{b_i=u_{i,j}R}|}{|R|} \cdot Entropy(z, σ_{b_i=u_{i,j}R}) \quad (1)$$

Where,

$$Entropy(z, R) = \sum_{d_j \in dom(z)} - \frac{|σ_{z=d_jR}|}{|R|} \cdot \log_2 \frac{|σ_{z=d_jR}|}{|R|} \quad (2)$$

$$Gini(z, R) = 1 - \sum_{d_j \in dom(z)} \left(\frac{|σ_{z=d_jR}|}{|R|} \right)^2 \quad (3)$$

Where, R = a training set; b_i = a discrete attribute; z = target attribute; $u_{i,j}$ = values.

2) *K-Nearest Neighbor*: The KNN classifier assesses the similarity between the new system and the training process instances to classify a new process into either normal or intrusive classes. It also uses the class-label of the nearest k classes to predict the new process class. The assumption behind the procedure is that the processes of the same class are grouped into the vector space. The computation of the neighbor elements depends on the value of k which is the number of neighbors to describe the class of the data. The election of the immediate neighbors is done by majority voting. This is a straightforward solution but depends on the value of k . Euclidean distance metric can be used to calculate the distance and the mathematical representation has been shown in equation 4 [30, 31].

$$d(x, y) = \sqrt{(x_1 - y_1)^2 + \dots + (x_n - y_n)^2} \quad (4)$$

3) *Logistic regression*: Logistic regression is a sort of statistical probabilistic model of categorization. It is also used to forecast a category variable that depends on the predictor variables of one or more of them (such as client characteristics). In our problem, it is used after extensive data preprocessing on the original dataset [25]. The logistic regression uses sigmoid function and it will output the probability which will then be mapped to the two or more classes.

$$s(z) = \frac{1}{1+e^{-z}} \quad (5)$$

where, $s(z)$ = output between 0 and 1 (probability estimate); z = input to the function; e = base of natural log.

For multiclass logistic regression, the binary classification is run multiple times, once for each class. Prediction = max (probability of the classes).

4) *Artificial neural network*: The artificial neural network (ANN) is a mathematical representation that is strongly based on the functional and structural aspects of the human nervous system. Each input of a neural network is multiplied by a weight which is then added to the sum of these weighted inputs, and the bias in the layers following the input layer. The network's last layer contains the transfer function, also known as an activation function, which helps in achieving the desired scalar output. The following is the mathematical representation of an artificial neuron:

$$O(t) = f(\sum_{i=1}^n v_i(t) \cdot I_i(t) + c) \quad (6)$$

where; $O(t)$ is the output which is found from the neural network at a given time, f represents the activation or transfer function, c is the bias, $I_i(t)$ and $v_i(t)$ are the inputs and their weights respectively [32].

B. Ensemble Learning

Ensemble learning is a collection of distinct learning machines or classifiers that work together to produce more accurate and reliable results by combining all methods. An inducer, also known as a strong learner in ensemble methods, is a learner that is randomly well correlated with the actual classification of the labeled training set. While a weak learner is related to the true classification to some extent. Boosting, bagging, and random forests are some of the new techniques that have emerged because of the ensemble learning framework. In the training of the base model, parameter values vary as well, allowing different ensemble components to offer their uniqueness to the framework. As a result, ensemble systems are incredibly versatile and efficient in real-world applications, giving them the ability to solve and approach a wide range of problems. In ensemble learning, there are various aggregation strategies; bagging is one of them, and it is employed in prediction models to reduce variance. Other strategies include: stacking which tries to reduce prediction bias, and boosting which aids in the conversion of several weak learners into an aggregated strong model [29,25]. Fig. 1 shows a generalized tree representation of the work behind ensemble learning.

1) *Random forest*: Random forest is an ensemble study that uses more than one decision-making tree for classification and regression. There is some randomness while selecting the subset and characteristics for the nodes of each tree in the random forest classifier. The Gini index is one of the criteria to divide the data into random forest. The random forest is also important for variables, which does not only contribute to the development of a precise model but also contributes to prediction [29,30]. Fig. 2 shows the tree representation of the working behind a random forest ensemble model.

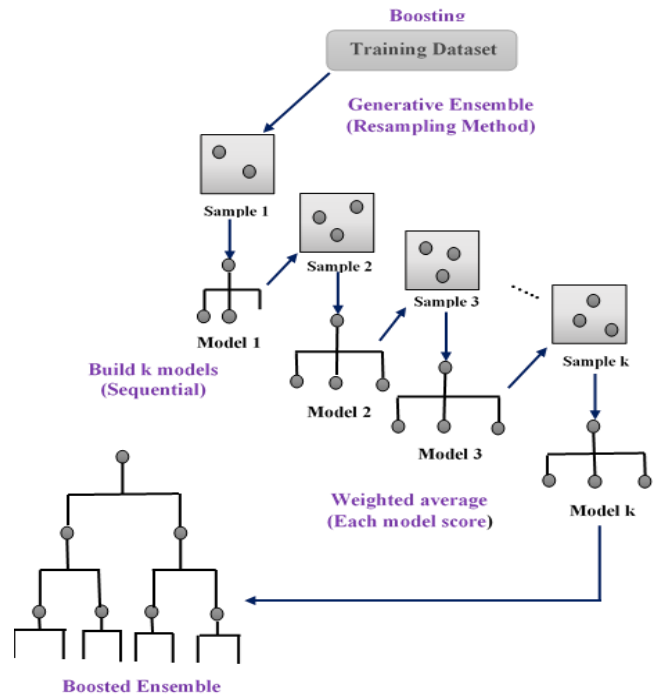


Fig. 1. Tree Representation of Ensemble Learning.

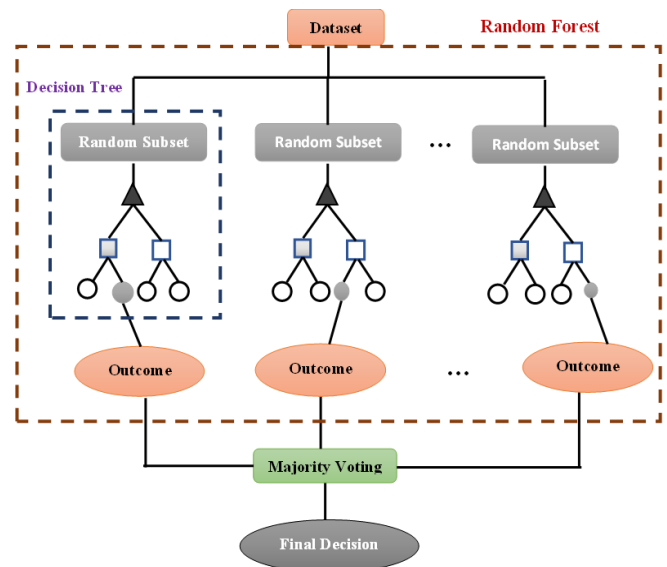


Fig. 2. Tree Representation of Random Forest.

2) *Gradient Boosting Machine (GBM)*: GBM is a frequently used machine learning approach for both regression and classification issues. It is highly effective in solving a wide variety of practical applications. The GBM approach is considered an approach for numerical optimization, which seeks to identify an additive model to minimize loss. The GBM approach builds a new decision tree (i.e., "weak learners") at each step, which will lower loss function most effectively [33, 34, 35].

$$F_M(x) = F_{M-1}(x) + \gamma_M h_M \quad (7)$$

where, M= number of iterations; γ_M = multiplier; $h_M(x)$ = a base learner.

3) *Extreme Gradient Boosting (XGB)*: XGBoost is a regression tree with the same Decision Tree principles. It promotes regression and classification. This approach is an effective and scalable gradient booster (GBM) variation which is frequently used for computer vision, data mining, and other applications. The training is carried out via an "additive strategy": a tree ensemble model utilizes t additive functions to predict the output, given a molecule i using a descriptor x_i vector [36,37]. The mathematical representation of a simplified objective of XGBoost has been shown in equation 7.

$$L^{(t)} = \sum_{i=1}^n \left[g_i f_t(x_i) + \frac{1}{2} h_i f_t^2(x_i) \right] + \Omega(f_t) \quad (8)$$

where, $L^{(t)}$ is the objective function at iteration t and g_i and h_i are the first and second order gradient statistics of the loss function.

4) *AdaBoost*: AdaBoost is the acronym for adaptive boosting. It is a form of classification algorithm model of dichotomy which trains and combines a range of weak classifiers to fulfill the classification criteria of datasets. AdaBoost is adapted to increase the weight of a sample misclassified by the previous weak classifier and to reduce the weight of the correctly classified sample to the following weak learner. AdaBoost's instance categorization can be expressed mathematically as:

$$H(x) = \text{sign}(\sum_{t=1}^T \alpha_t \cdot M_t(x)) \quad (9)$$

where M_t represents the classifiers while α_t is the individual weight of each classifier [38, 39].

5) *Bagging*: Bagging is an ensemble learning approach for improving the accuracy of other learning algorithms' predictions. An ensemble method of learning is a strategy that integrates numerous machine algorithms for the prediction that can be done with better accuracy and stability than with only a single algorithm. Bagging is very effective for decision tree, even though it may be used for various types of classification techniques. Bagging is a technique for combining numerous complex models and then averaging (in regression) or majority voting (in classification) the outputs of the different models of the same kind to create a more powerful prediction model [40, 30].

Input: Data set $D = \{(x_1, y_1), (x_2, y_2), \dots, (x_m, y_m)\}$;
Base learning algorithm L ; Number of base learners T .

Process:

1. **for** $t = 1, \dots, T$:
2. $h_t = L(D, D_{bs}) // D_{bs}$ is the bootstrap distribution
3. **end**

Output: $H(x) = \arg \max_{y \in Y} \sum_{t=1}^T (h_t(x) = y) \quad (10)$

IV. PROPOSED METHODOLOGY

A. Dataset Used

A survey in the form of a questionnaire was used to collect the data from different mobile phone users. It has been prepared after consulting with an Indian telecommunication service provider. It was designed by using google form and has been shared among different Indian telecommunication subscribers through different social media platforms, emails, and messages. The data was collected from the legal users of different Indian service providers in the form of a categorical form dataset. The questionnaire contains multiple-choice questions. The unclean dataset contains 476 user information and 88 attributes. Then, we have proceeded to the preprocessing steps which led to the formation of the final refined dataset containing 476 user information and 16 attributes. Table I shows the attribute list of the cleaned dataset and Table II shows the lists of attributes used to calculate the three target attributes obtained after the preprocessing.

TABLE I. FINAL ATTRIBUTE LIST AND THEIR DESCRIPTION

Attribute Name	Labels Assigned	Label Distribution	Description
Type of service used	<ul style="list-style-type: none"> • Cellular Prepaid • Cellular Post-paid 	418 58	Connection type
Age group	<ul style="list-style-type: none"> • Under 18 • 19 – 25 Years • 26 – 40 Years • 41- 55 Years • 56 and above 	4 347 77 19 29	Customer age group
Gender	<ul style="list-style-type: none"> • Male • Female • Non-Binary • Others 	309 166 0 1	Customer gender identity
Occupational status	<ul style="list-style-type: none"> • Employed • House wife • Business • Student • Retired 	71 17 8 359 21	Customer occupational background
Income group (income per month)	<ul style="list-style-type: none"> • Below Rs. 20,000 • Rs.20,000 – 50,000 	47 64 28 29	Customer monthly income

	<ul style="list-style-type: none"> Rs. 50,000 – 1 Lakh Above Rs. 1 Lakh Dependent 	308	
Education	<ul style="list-style-type: none"> Non-graduate Graduate Post-graduation and above 	300 115 61	Customer educational background
You have been using cellular services for	<ul style="list-style-type: none"> Less than 1 Year 1 to 3 years More than 3 Years 	21 117 338	Duration for which the customer has been using the telecom service
Average expense on cellular services per month will be about	<ul style="list-style-type: none"> Less than Rs. 500 Rs. 500 – 1000 Rs. 1001 – 3000 More than Rs. 3000 	308 141 23 4	Approximate monthly expenditure on monthly recharge
Do you use internet	<ul style="list-style-type: none"> Yes No 	471 5	If the customer uses internet
Preferable medium for messaging:	<ul style="list-style-type: none"> SMS/ Offline messaging Platform Online Messaging Platform 	13 463	Customers' preferred medium of messaging
How frequently do you travel?	<ul style="list-style-type: none"> Once a year Twice a year More than twice 	177 126 173	An approximate number of times the customer travels
Where do you travel the most?	<ul style="list-style-type: none"> Within the country Outside the country 	444 32	Travelling preference
Do you use the same number while travelling?	<ul style="list-style-type: none"> Yes No 	450 26	Preferred number used during travelling
Total time spent on call during weekdays	<ul style="list-style-type: none"> 1 to 3 hours 3 hours to 5 hours 5 hours to 10 hours More than 10 hours 	0 204 144 128	Number of hours spent on call during the weekdays and over the weekend. (Target Data)
Total time spent on call during weekends	<ul style="list-style-type: none"> 1 to 3 hours 3 hours to 5 hours 5 hours to 10 hours More than 10 hours 	0 172 154 150	
Total data consumptions	<ul style="list-style-type: none"> Less than 500 MB 500 MB to 1 GB 1 GB to 3 GB More than 3 GB 	74 66 211 125	Amount of mobile data consumed. (Target Data)

TABLE II. TARGET ATTRIBUTES AND THEIR DETAILS

Target Attributes	Attributes used to obtain the Target Attributes	Description
Total time spent on call during weekdays	Preferable time to connect during the weekdays (Monday- Friday): [Family]	Preferred time of the day to connect over calls during the weekdays. <ul style="list-style-type: none"> Morning (6am – 12 pm) Afternoon (12pm – 5pm) Evening (5pm – 10pm) Night (10pm – 6am)
	Preferable time to connect during the weekdays (Monday- Friday): [Relatives]	
	Preferable time to connect during the weekdays (Monday- Friday): [Friends]	
	Preferable time to connect during the weekdays (Monday- Friday): [Colleague]	
	Preferable time to connect during the weekdays (Monday- Friday): [Others]	
	Time spent for total calls per day during weekdays (Monday- Friday): [Family]	
	Time spent for total calls per day during weekdays (Monday- Friday): [Relatives]	
	Time spent for total calls per day during weekdays (Monday- Friday): [Friends]	
	Time spent for total calls per day during weekdays (Monday- Friday): [Colleague]	
	Time spent for total calls per day during weekdays (Monday- Friday): [Others]	
Total time spent on call during weekends	Preferable time to connect during the weekends (Saturday- Sunday): [Family]	Preferred time of the day to connect over calls during the weekend. <ul style="list-style-type: none"> Morning (6am – 12 pm) Afternoon (12pm – 5pm) Evening (5pm – 10pm) Night (10pm – 6am)
	Preferable time to connect during the weekends (Saturday- Sunday): [Relatives]	
	Preferable time to connect during the weekends (Saturday- Sunday): [Friends]	
	Preferable time to connect during the weekends (Saturday- Sunday): [Colleague]	
	Preferable time to connect during the weekends (Saturday- Sunday): [Others]	
	Time spent for total calls per day during weekends (Saturday- Sunday): [Family]	
	Time spent for total calls per day during weekends (Saturday- Sunday): [Relatives]	
	Time spent for total calls per day during weekends (Saturday- Sunday): [Friends]	
	Time spent for total calls per day during weekends (Saturday- Sunday): [Colleague]	
	Time spent for total calls per day during weekends (Saturday- Sunday): [Others]	

	Time spent for total calls per day during weekends (Saturday- Sunday): [Others]	
Total data consumptions	Usage of internet in hours: [Morning (6am-12pm)]	Number of hours internet is being used. <ul style="list-style-type: none"> • Less than 1 hour • 1 hour to 2 hours • 2 hours to 3 hours • More than 3 hours
	Usage of internet in hours: [Afternoon (12pm- 5pm)]	
	Usage of internet in hours: [Evening (5pm- 10pm)]	
	Usage of internet in hours: [Night (10pm- 6am)]	
	What are you surfing? [Morning (6am-12pm)]	Type of content being used on the internet. <ul style="list-style-type: none"> • Videos • Social Media • Websites • Chats
	What are you surfing? [Afternoon (12pm- 5pm)]	
	What are you surfing? [Evening (5pm- 10pm)]	
	What are you surfing? [Night (10pm- 6am)]	
	What type of websites are you surfing?	<ul style="list-style-type: none"> • Educational • Business • Entertainment
	What do you download from Internet?	<ul style="list-style-type: none"> • Videos • Images • Documents • Mp3 files • Software
What type of calls are you making through Internet?	<ul style="list-style-type: none"> • Video Calls • Voice Calls • None 	
Do you use paid music streaming platform?	<ul style="list-style-type: none"> • Yes • No 	

From Fig. 3, it can be seen that a greater number of weekday calls ranging from three to five hours, and during the weekends a larger number of calls exceeds 10 hours. Our dataset lacks any record which ranges between one to three hours. Fig. 4 shows the count of customers based on their data consumption. As it can be seen in both graphical representations, data imbalance is an issue. However, balancing out the data doesn't have any positive effect on the model outputs. Hence, the step of data balancing was not further considered during the execution of the models.

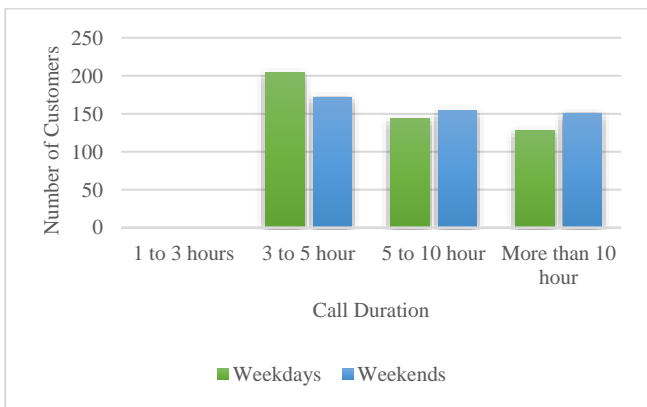


Fig. 3. Count of Customers for Each Call Duration Range during Weekdays and Weekends.

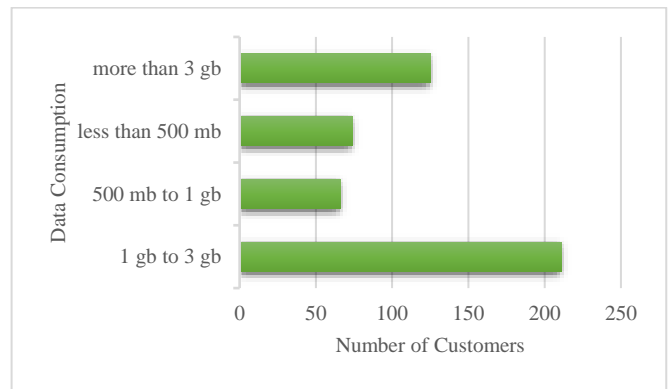


Fig. 4. Count of Customers for Each Data Consumption Range.

B. Proposed Model

The work proposes a research model which predicts customers' behavioral data like call duration and data consumption, by analyzing their demographic data such as age, gender identity, occupation, education and so on. Different constraints have been taken into consideration to design a generalized model that would provide a better prediction. Even though the machine learning techniques that are used here are already existing and well-known, the proposed approach has not been used in the Indian telecommunication sector. Fig. 5 shows the diagrammatic approach toward the research objective in a step-by-step style.

Step 1: Data collection. As discussed in Section 4.1, the data has been collected using a questionnaire through a survey among regular telecom subscribers of the Indian telecom industry. After the data has been collected, it has been divided into two parts: the customer demographic data and customer behavioral data.

Step 2: Data Preprocessing. Since the main target is to predict the customers' call duration and data consumption, the behavioral data obtained are used to calculate target attributes as mentioned in Table II. For calculating the data consumption, depending on the browsing history using Internet, the option is replaced by an Internet data unit such as Streaming Video: 353 Mb/Hour; social media: 20 Mb/Hour; Websites: 25Mb/Hour; Chats (if both Video and Voice calls or just Video call): 100 Mb/Hour; Chat (if just voice call): 60 Mb/Hour. For situations where multiple options are selected by the users, the option having the maximum value is selected. Once the target is calculated, the attributes that are used for the purpose and all the other attributes irrelevant to the study are dropped. On the other hand, the demographic data are only cleaned by removing redundant data and null values. After completing all the preprocessing steps, the data has been encoded using one-hot encoding technique.

Step 3: Training, Testing, and Validation. After the preprocessing has been completed, the data have been encoded by using the one hot encoding technique and partitioned for the training and testing purpose. The split for the training and testing has been 80% and 20% respectively. As discussed in Sections 3.1 and 3.2, multiple ensemble models and traditional classifiers have been used for the prediction purpose. Other than

all the techniques discussed previously, a stacking ensemble model has been used as one of the ensemble techniques for the predictive system which has been shown in Fig. 6. The stacking model consists of two levels. Level 0 comprises four base classifiers: Decision tree (DT), Random Forest (RF), Logistic Regression (LR), k-nearest neighbor (KNN); and level one consists of LR as the meta classifier. A soft voting technique has been used to predict the final output of the stacking ensemble model. Majority voting, plurality voting, and weighted voting can be used for individual classifiers that produce clear class labels, although soft voting is typically preferred for individual classifiers that produce class probability outputs. When all the individual classifiers are treated equally, the simple soft voting approach simply averages all the individual outputs to produce the combined output, but if we combine the individual outputs by using

various weights, a weight specific to each classifier is generated, and the total output for class c_j is,

$$H^j(x) = \sum_{i=1}^T w_i h_i^j(x) \tag{11}$$

where w_i is the weight assigned to the classifier h_i .

Other used ensemble models: Random Forest, AdaBoost, XGB, GBM, and Bagging. Among these models, Random Forest has given the best accuracy of 83%. The traditional classifiers used have been Decision Tree, Logistic regression, k-Nearest Neighbor, and ANN. Table III presents the detailed tuning parameter specifications of different classifiers that are used in the research during the implementation by using Python.

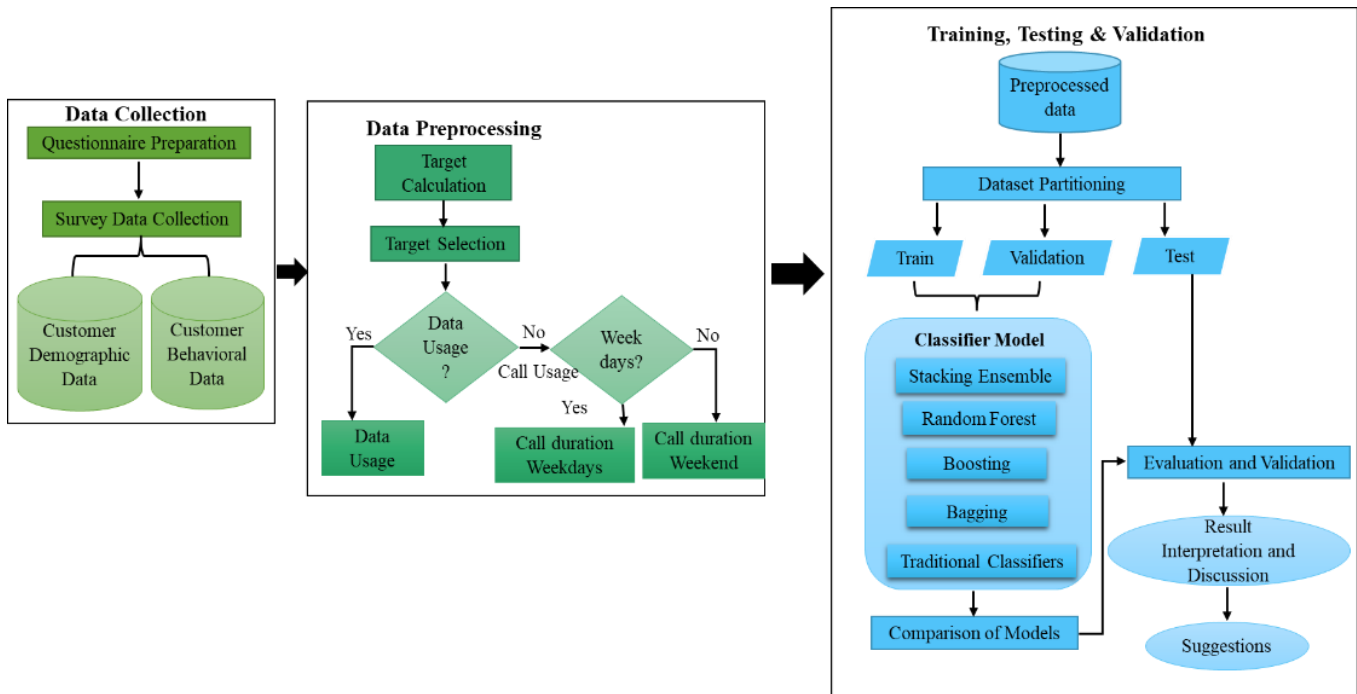


Fig. 5. The Proposed Research Model.

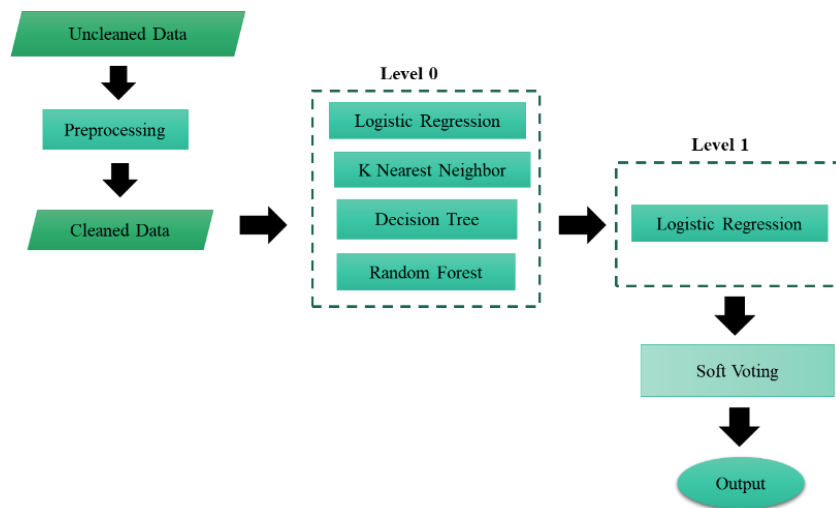


Fig. 6. Schematic Diagram of the Stacking Model.

TABLE III. PARAMETER SPECIFICATIONS

Technique used	Specifications
Random Forest	Criterion =Gini, Max Depth=3, Min Samples Split=5, Estimators=10
AdaBoost	Learning Rate=0.09, Estimators=10
XGM	Booster= Gbtree, Learning Rate=0.1, Max Depth=2, Estimators=20
GBM	Criterion=Friedman Mse, Learning Rate=0.01, Max Depth=3, Min Samples Split=2, Estimators=60
Bagging	Estimators=300, Random State=10
Stacking	Cv=10, Estimators= [Decision Tree Classifier, Random Forest Classifier, Logistic Regression, K Neighbors Classifier], Final Estimator= Logistic Regression
Decision Tree	Max Depth=2, Criterion = Gini, Min Samples Split=2
Logistic Regression	Solver = Liblinear, Max Iter=10000
k-Nearest Neighbor	Metric= Minkowski, Neighbors=38, P=2
Artificial Neural Network	Dense = 32, Activation=Relu Dense = 16, Activation=Relu Dense = 3, Activation=Softmax Optimizers = Adam, Learning Rate=0.001 Loss = Categorical Crossentropy

C. Performance Metrics

In this work, the proposed predictive model for customer behavior has been evaluated by using accuracy, precision, sensitivity, specificity, F1 score, and kappa analysis. The fraction of total samples properly classified by the classifier is called accuracy.

$$Accuracy = \frac{TP+TN}{TP+TN+FP+FN} \quad (12)$$

where TP denotes true positive, FP denotes false positive, TN denotes true negative, and FN denotes false negative. Precision is what percentage of positive forecasts were truly positive.

$$Precision = \frac{TP}{TP+FP} \quad (13)$$

The sensitivity is the fraction of all positive samples that the classifier accurately identified as positive.

$$Sensitivity = \frac{TP}{TP+FN} \quad (14)$$

Specificity is the fraction of all negative samples that have been accurately identified as negative.

$$Specificity = \frac{TN}{TN+FP} \quad (15)$$

F1 score is the combination of precision and sensitivity.

$$F1\ score = 2 \times \frac{Precision \times Sensitivity}{Precision + Sensitivity} \quad (16)$$

For qualitative items, kappa analysis is a statistical measure of inter-rater reliability.

$$k = \frac{p_o - p_e}{1 - p_e} = 1 - \frac{1 - p_o}{1 - p_e} \quad (17)$$

The kappa coefficient varies from 0 to 1 and following statements can be made,

< 0 = agreement equivalent to a chance

0.1 – 0.2 = slight agreement

0.21 – 0.40 = fair agreement

0.41 – 0.60 = moderate agreement

0.61 – 0.80 = substantial agreement

0.81 – 0.99 = almost perfect agreement.

V. RESULTS

In this work, different classification techniques have been applied to the customers' demographic data to predict their behavioral pattern. As discussed in the previous section, the data collected has been preprocessed to calculate the target attributes: total call duration during weekdays, total call duration during the weekend, and total data consumption. After preprocessing, the desired target has been selected for the classification. In this work, few ensemble learning techniques and some traditional classifiers have been applied. K-fold cross validation has been used, as well, to validate the models, where k is been maintained at 10 irrespective of models. As shown in Tables IV and V, random forest has given the best accuracy of 83% among all the techniques applied. Apart from the performance metrics, the reliability of the model has been tested by using kappa analysis. Random Forest has shown the best result among all the classifiers that are applied with a kappa value of 0.74, which comes under the categorization of substantial agreement. When kappa analysis was performed on the ensemble models, except for the bagging technique, all models have given values within the range of 0.61 to 0.88 which signifies substantial agreement. Models that recorded accuracy of over 80% were AdaBoost, XGB, and the stacking ensemble model whose kappa values have been 0.71, 0.71, and 0.69, respectively. Among traditional classifiers, decision tree has given the best result with an accuracy of 81% and 0.71 kappa value. The other traditional classifying techniques with kappa value of substantial agreement are logistic regression and k-nearest neighbor.

Fig. 7-9 show the bar graph plot of the accuracy, specificity, and precision measures of all the classifiers that are used in this work. Fig. 10 shows the obtained F1-scores and sensitivity from all the classifiers. Concerning the specificity, it can be inferred that there is a small number of false negative samples. As kappa values have been calculated for substantiating the reliability of the proposed approach, Fig. 11 presents the bar plot of the accuracy of each classifier, as well as their corresponding kappa values and Fig. 12 shows a bar plot of the kappa values in decreasing order.

TABLE IV. PERFORMANCE OF ENSEMBLE MODELS

Classifiers	Accuracy	Precision	Sensitivity	Specificity	F1-score	Kappa
Random Forest	0.83	0.83	0.83	0.91	0.83	0.74
AdaBoost	0.81	0.82	0.81	0.90	0.81	0.71
XGB	0.81	0.82	0.81	0.90	0.81	0.71
GBM	0.78	0.77	0.78	0.89	0.78	0.66
Bagging	0.73	0.72	0.73	0.88	0.72	0.58
Stacking	0.80	0.80	0.80	0.93	0.79	0.69

TABLE V. PERFORMANCE OF TRADITIONAL CLASSIFIERS

Classifiers	Accuracy	Precision	Sensitivity	Specificity	F1-score	Kappa
Decision Tree	0.81	0.82	0.81	0.90	0.81	0.71
Logistic Regression	0.74	0.74	0.74	0.87	0.74	0.61
k-Nearest Neighbor	0.76	0.76	0.76	0.89	0.76	0.63
Artificial Neural Network	0.72	0.72	0.72	0.86	0.72	0.57

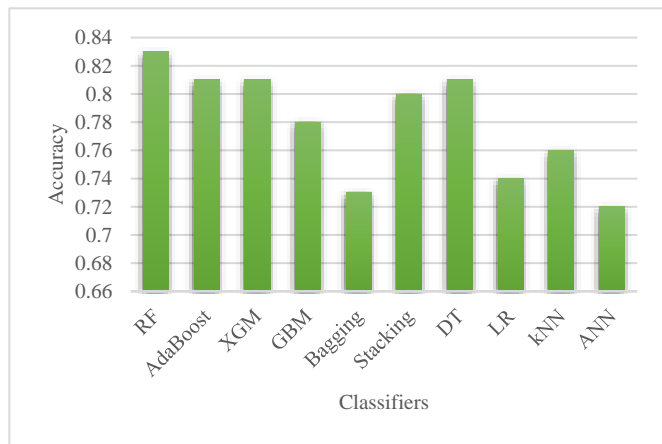


Fig. 7. Accuracy Plot of different Classifiers.

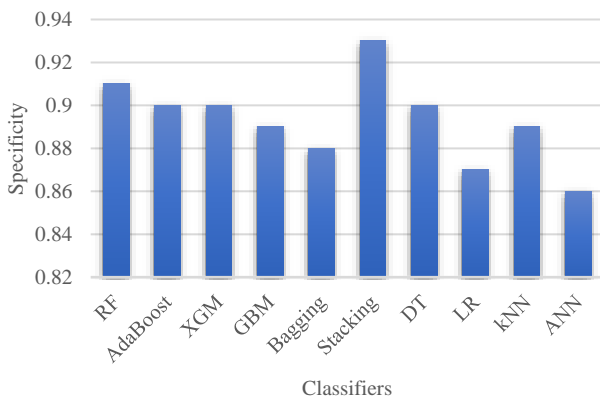


Fig. 8. Specificity Plot of different Classifiers.

Table VI shows some instances of test cases that have been used to test the classification models. It can be seen that test cases 1, 2, and 3 are predicted correctly by using all the classifiers except KNN, which has the least average success rate among all classifiers. Test case 4 is incorrectly predicted by

most of the classifiers other than bagging, stacking, and ANN. Even though the performance accuracies obtained during training of the bagging and ANN models are lower than the other classifiers, yet when applied to certain test cases they have performed better.

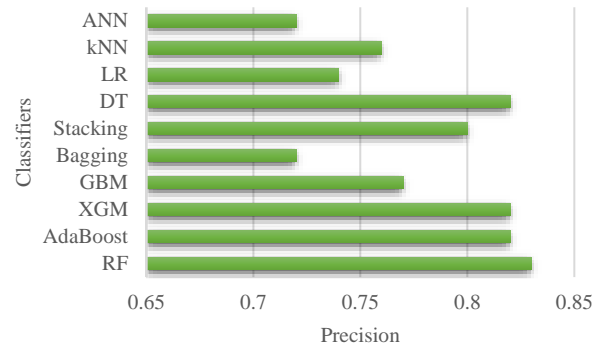


Fig. 9. Precision Plot for different Classifiers.

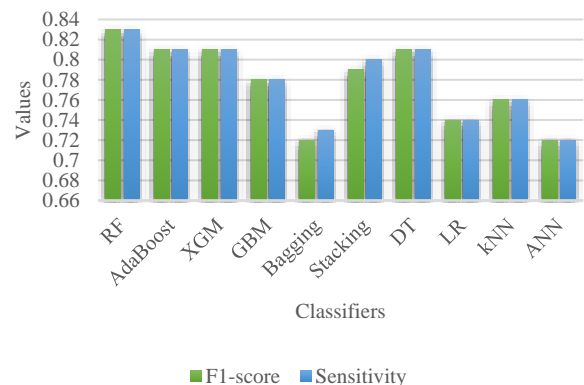


Fig. 10. F1-score and Sensitivity Plot of the Classifiers.

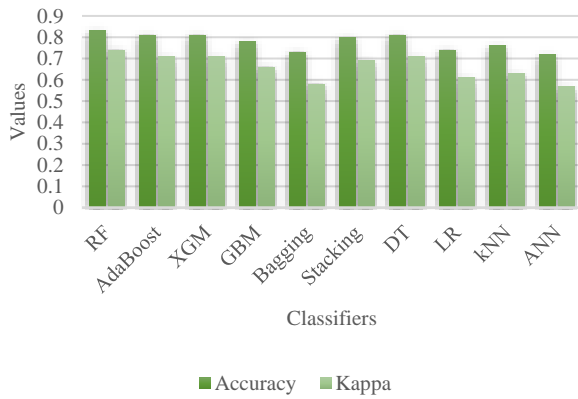


Fig. 11. Accuracy and Kappa Value Plot of the Classifiers.

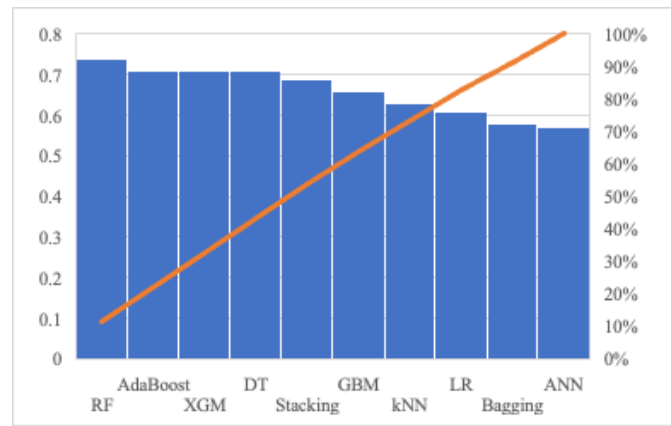


Fig. 12. Kappa Value Plot for Different Classifiers in Decreasing Order.

TABLE VI. DIFFERENT TEST CASE SCENARIOS

Test Case	Actual Class	Predicted Class/ Output									
		RF	AdaBoost	XGM	GBM	Bagging	Stacking	DT	LR	kNN	ANN
1	1	1	1	1	1	1	1	1	1	1	1
2	2	2	2	2	2	2	2	2	2	1	2
3	0	0	0	0	0	0	0	0	0	0	0
4	1	2	2	0	2	1	1	0	1	2	1
5	2	2	2	2	2	2	2	2	1	2	2
Average success rate (%)		80	80	80	80	100	100	80	80	60	100

VI. DISCUSSION

Personalized tariff plans can solve a lot of problems for the Indian telecom industry. The current generalized status of the tariff, plan design has led to a lot of dissatisfaction among the customers. This can be solved by better analyzing the customers' behavioral pattern and how it varies depending on their socio-economic background. To offer a better recommendation to customers, flexible tariff plans need to be designed and hence the requirement for an effective predictive system.

In this work, a predictive system has been designed to be able to predict customers' behaviors: call duration and data consumption. Different classification models have been tested on the data obtained from the customers to get a better prediction of the customers' behavioral pattern. This can help with understanding what kind of tariff plan should be recommended and for which segment of the customers. Every customer's needs vary based on their lifestyle and background. An ideal scenario for the proposed work would be the current situation where students, teachers, and IT sector personnel has been working online which have led to a drastic increase in data consumption among these people. Therefore, the tariff plans that are recommended for these people should include higher data allocation than those who are working offline. Again, the total call duration of females who are housewives and in the age group over 56 is different from those who are working and of

the age group of 26 to 40. Thus, a desperate need for flexible tariff plans. As shown previously, this work is based on customers' age group, gender identity, educational background, occupational status, monthly income, expenditure on mobile plans, and so on to predict their behavioral pattern.

Comparing to different works of literature on customers' behavioral pattern, this work focuses on determining the feasibility and efficiency of using classification techniques on customers' demographic data to detect patterns. According to the results obtained through this work, ensemble learning techniques and ANN can be used to predict the customers' call duration and data consumption with high efficacy. Service providers can use this proposed model to predict the call duration and data consumption which can be used to design more flexible tariff plans catering to the customers' needs in a much more personalized form. This research model can also be used for customer segmentation depending on their socio-economic background, which will make it easier for recommending the right tariff plan. This can also help with customer retention since retaining the right customer is one of the major goals of any telecom service provider. Investing in the right customer can lead to higher profit for the business. As the dataset varies in all the previous works, hence a usual comparative study was not feasible for the proposed work. Therefore, Table VII only highlights the different inferences that are reached for the general goal of tariff plan design.

TABLE VII. HIGHLIGHTS OF DIFFERENT WORKS BASED ON TARIFF PLAN DESIGN

Reference	Techniques Used (IT based)	Dataset used	Performance Metric/ Inference Drawn
Bahri-Ammari and Bilgihan, 2017	Hypothesis Testing	Customer survey data from mobile telecom industry in Tunisia.	Path Coefficients and t-test: 0.815 (5.888)
Newton and Ragel, 2017	Correlation and Regression Analysis.	Customer data in mobile telecommunication industry in Batticalao.	Adjusted R square of Model A= 0.786. Adjusted R square of Model B= 0.804.
Belwal and Amireh, 2018	Partial Least Square based Structural Equation Modelling	Survey data from Omani Telecom industry.	Cronbach's alpha score greater than 0.7 and composite reliability scores 0.70–0.90
Tong et al., 2017	Information Gain on Decision tree Model and k mean Clustering.	Survey data from customers of telecom industry.	Accuracy of 71.24%
Jose et al., 2017	Principle Component Analysis (PCA), Factor Analysis, Regression Analysis and Cross Tabulation.	Data from Telecom contact center.	Sampling adequacy is validated with KMO test score of 0.739.
Gerpott and Meinert, 2017	Hypothesis testing	Data obtained from the German subsidiary of a large multinational MNO.	McFadden's pseudo R2 of 0.085 and coefficient of determination of 0.318.
Bibin and Ramanathan, 2018	Conjoint analysis	Survey data of students.	Result showed that better network and low cost are the main reasons for their choice of service provider.
Dubey and Srivastava, 2016	Exploratory Factor Analysis, Regression Analysis.	Customer Survey data from Indian telecommunication industry.	KMO test score of 0.833.
Jin et al., 2021	Hypothesis testing	Major telecommunication operator in China.	Probability of switching up = 0.002 Probability of switching down = 0.010
Shouchen et al., 2017	Distance method by norm method	Dataset from China telecommunication industry.	The matching result indicates that 302 676 users' current tariff package are not optimized selection and should shift their consumption suit.
Gerpott and Meinert, 2016	Regression analysis	A dataset of residential users of mobile communication services.	63.2% of sampled subscribers share a positive/ complementary relationship between the two services whereas a considerable proportion of 36.8% of subscribers substitutes call minutes by data consumption.
Diaz, 2017	Generalized Structural Equation Modelling (GSEM), Multinomial Logit	Real-life survey data from Peru.	Wald Tests shows that the estimation is statistically significant at 1%.
Lee et al., 2018	Conjoint Analysis	Real life survey data from South Korean Telecom	Conjoint analysis show that free data service provides significantly greater benefits on average than smartphone interphone and Enterprise messenger services do.
García-Mariño and Suárez, 2019	Logit model	Real-life survey data collected by Spanish Markets and Competition Authority.	estimated correlation coefficient 0.043, p value= 0.669
Kim et al., 2019	Statistical Analysis	Real life data from Korean company.	In the model 1, amount of the variance (R2=0.210, p < 0.001). In the model 2, amount of the variance (the increase of R2=5.6%, p < 0.001)
This Work	Random Forest	Survey data collected through questionnaire	Accuracy= 83%, Kappa Value= 0.74.

Most of the existing works implementing machine learning are applied on real-life customer data and the inference drawn from those works also varies based on the techniques and the used dataset. (Tong et al., 2017) have used machine learning technique of decision tree and have achieved an accuracy of 71.24%. Compared to our work, this work has produced higher accuracy. Whereas works like (Bahri-Ammari and Bilgihan, 2017; Newton and Ragel, 2017; Gerpott and Meinert, 2016) have used correlation coefficients to draw the inference for their work. In another study (Maji et al., 2017) have implemented pattern recognition by using rule-mining based apriori algorithm to study their customers. Considering the varying factors in every research study on personalizing tariff plans drawing a comprehensive comparative study seems to be not

feasible. As governing hypotheses of each problem varies greatly among each other, hence drawing a common point of inference is not reasonable enough in this kind of situation.

The major challenge that are faced throughout our work is the data collection. In the telecommunication industry, customer data involves the intricate policies of privacy and security preservation. Therefore, collecting enough data has been a huge challenge. For any data related research, the quality of the data is a major concern. In this work, the data collected from customers directly has been assumed to be accurate and thorough. But the concern regarding the accuracy of the information provided by the customers remains.

Highlights of the contributions of the present work:

- Predicts customers' behavioral pattern by analyzing their demographic data by using classification-based learning methods.
- Helps with customer segmentation which in turn will help recommending the right service to the customers.
- Contributes to designing a personalized tariff plan which will cater to the customers' requirements at a much more reasonable price.

VII. CONCLUSION

Because of the high efficiency of classification-based learning models, the proposed model produced a higher success rate in predicting the customers' behavior. Among traditional classifiers, the decision tree has given the best result with an accuracy of 81% among other techniques. Also, the reliability of the model has been tested using kappa analysis and showed to be higher than all other investigated classifiers with a value of 0.71. While the ensemble classifier, random forest, has given the best accuracy of 83% among other techniques with kappa value of 0.74. Although the proposed work has provided satisfactory results, it has certain limitations. The major shortcoming of the work can be identified as the size of the dataset which has impacted the performance of certain classifiers to a great extent. Therefore, in future, the work can be extended by using a much larger dataset such that inherent patterns can be identified with more precision. Also, a more robust and generalized model could be designed that would work irrespective of the type of dataset.

REFERENCES

- [1] Gupta, R., & Jain, K. (2020). What drives Indian mobile service market: Policies or users?. *Telematics and Informatics*, 50, 101383.
- [2] Saha, L., Tripathy, H. K., Nayak, S. R., Bhoi, A. K., & Barsocchi, P. (2021). Amalgamation of Customer Relationship Management and Data Analytics in Different Business Sectors—A Systematic Literature Review. *Sustainability*, 13(9), 5279.
- [3] Nkordeh, N., Bob-Manuel, I., & Olowononi, F. (2017). The Nigerian telecommunication industry: Analysis of the first fifteen years of the growths and challenges in the GSM market (2001–2016).
- [4] Shao, B. B., Lin, W. T., & Tsai, J. Y. (2017). An empirical study of the telecommunications service industries using productivity decomposition. *IEEE Transactions on Engineering Management*, 64(4), 437-449.
- [5] Valentim, L. C., Quelhas, O. L. G., & Ludolf, N. V. E. (2019). Proposição de sistemática para implantação de Customer Relationship Management apoiado por Business Intelligence a organizações do setor de telecomunicação. *Sistemas & Gestão*, 14(3), 232-244.
- [6] Al-Zadjali, M., & Al-Busaidi, K. A. (2018). Empowering CRM through business intelligence applications: A study in the telecommunications sector. *International Journal of Knowledge Management (IJKM)*, 14(4), 68-87.
- [7] Tong, L., Wang, Y., Wen, F., & Li, X. (2017). The research of customer loyalty improvement in telecom industry based on NPS data mining. *China Communications*, 14(11), 260-268.
- [8] Jose, B., Ramanan, T. R., & Kumar, S. M. (2017, November). Big data provenance and analytics in telecom contact centers. In *TENCON 2017-2017 IEEE Region 10 Conference* (pp. 1573-1578). IEEE.
- [9] Bahri-Ammari, N., & Bilgihan, A. (2017). The effects of distributive, procedural, and interactional justice on customer retention: An empirical investigation in the mobile telecom industry in Tunisia. *Journal of Retailing and Consumer Services*, 37, 89-100.
- [10] Newton, S., & Ragel, V. R. (2017). The effectiveness of relational bonds on customer loyalty mediated with customer satisfaction: telecommunication industry, Batticaloa. *Asian Journal of Economics, Business and Accounting*, 1-11.
- [11] Belwal, R., & Amireh, M. (2018). Service quality and attitudinal loyalty: Consumers' perception of two major telecommunication companies in Oman. *Arab economic and business journal*, 13(2), 197-208.
- [12] Maji, G., Mandal, S., Bhattacharya, S., & Sen, S. (2017, March). Designing combo recharge plans for telecom subscribers using itemset mining technique. In *2017 IEEE International Conference on Industrial Technology (ICIT)* (pp. 1232-1237). IEEE.
- [13] Gerpott, T. J., & Meinert, P. (2017). Choosing a wrong mobile communication price plan: An empirical analysis of predictors of the degree of tariff misfit among flat rate subscribers in Germany. *Telematics and Informatics*, 34(4), 303-313.
- [14] Haq, N. (2017). Impact of Reliance JIO on the Indian telecom industry. *International Journal of Engineering and Management Research (IJEMR)*, 7(3), 259-263.
- [15] Bibin, P. B., & Ramanathan, H. N. (2018). Identifying the Best Mobile Combo Tariff Plan for Professional Students: An Application of Conjoint Analysis. *International Journal of Business Analytics and Intelligence*, 6(2), 36.
- [16] Dubey, A., & Srivastava, A. K. (2016). Impact of service quality on customer loyalty-A study on telecom sector in India. *IOSR Journal of Business and Management (IOSR-JBM)*, 18(2), 45-55.
- [17] Friesen, L., & Earl, P. E. (2015). Multipart tariffs and bounded rationality: An experimental analysis of mobile phone plan choices. *Journal of Economic Behavior & Organization*, 116, 239-253.
- [18] Jin, H., Lu, Z., Huang, L., & Dou, J. (2021). Not too much nor too little: Saliency bias in mobile plan choices. *Telecommunications Policy*, 45(4), 102071.
- [19] Shuochen, X., Lianju, N., & Wenying, Z. (2017). Study of matching model between tariff package and user behavior. *The Journal of China Universities of Posts and Telecommunications*, 24(3), 91-96.
- [20] Gerpott, T. J., & Meinert, P. (2016). The impact of mobile Internet usage on mobile voice calling behavior: A two-level analysis of residential mobile communications customers in Germany. *Telecommunications Policy*, 40(1), 62-76.
- [21] Díaz, G. R. (2017). The influence of satisfaction on customer retention in mobile phone market. *Journal of Retailing and Consumer Services*, 36, 75-85.
- [22] Ascarza, E., Iyengar, R., & Schleicher, M. (2016). The perils of proactive churn prevention using plan recommendations: Evidence from a field experiment. *Journal of Marketing Research*, 53(1), 46-60.
- [23] Lee, H., Choi, H., & Koo, Y. (2018). Lowering customer's switching cost using B2B services for telecommunication companies. *Telematics and Informatics*, 35(7), 2054-2066.
- [24] García-Mariño, B., & Suárez, D. (2019). Switching mobile operators: Evidence about consumers' behavior from a longitudinal survey. *Telecommunications Policy*, 43(5), 426-433.
- [25] Xu, T., Ma, Y., & Kim, K. (2021). Telecom Churn Prediction System Based on Ensemble Learning Using Feature Grouping. *Applied Sciences*, 11(11), 4742.
- [26] Bachan, L., & Gaber, T. (2021, March). Predicting Customer Churn in the Internet Service Provider Industry of Developing Nations: A Single, Explanatory Case Study of Trinidad and Tobago. In *International Conference on Advanced Machine Learning Technologies and Applications* (pp. 835-844). Springer, Cham.
- [27] Capponi, G., Corrocher, N., & Zirulia, L. (2021). Personalized pricing for customer retention: Theory and evidence from mobile communication. *Telecommunications Policy*, 45(1), 102069.
- [28] Kim, M. K., Park, M. C., Lee, D. H., & Park, J. H. (2019). Determinants of subscriptions to communications service bundles and their effects on customer retention in Korea. *Telecommunications Policy*, 43(9), 101792.
- [29] Chakrabarti, S., Swetapadma, A., & Pattanaik, P. K. (2021). A channel independent generalized seizure detection method for pediatric epileptic seizures. *Computer Methods and Programs in Biomedicine*, 209, 106335.

- [30] Alsouda, Y., Pillana, S., & Kurti, A. (2019, May). Iot-based urban noise identification using machine learning: performance of SVM, KNN, bagging, and random forest. In Proceedings of the international conference on omni-layer intelligent systems (pp. 62-67).
- [31] Liao, Y., & Vemuri, V. R. (2002). Use of k-nearest neighbor classifier for intrusion detection. *Computers & security*, 21(5), 439-448.
- [32] Chakrabarti, S., Swetapadma, A., Ranjan, A., & Pattnaik, P. K. (2020). Time domain implementation of pediatric epileptic seizure detection system for enhancing the performance of detection and easy monitoring of pediatric patients. *Biomedical Signal Processing and Control*, 59, 101930.
- [33] Touzani, S., Granderson, J., & Fernandes, S. (2018). Gradient boosting machine for modeling the energy consumption of commercial buildings. *Energy and Buildings*, 158, 1533-1543.
- [34] Drucker, H., Schapire, R., & Simard, P. (1993). Improving performance in neural networks using a boosting algorithm. In *Advances in neural information processing systems* (pp. 42-49).
- [35] Beygelzimer, A., Hazan, E., Kale, S., & Luo, H. (2015). Online gradient boosting. arXiv preprint arXiv:1506.04820.
- [36] Ma, B., Meng, F., Yan, G., Yan, H., Chai, B., & Song, F. (2020). Diagnostic classification of cancers using extreme gradient boosting algorithm and multi-omics data. *Computers in biology and medicine*, 121, 103761.
- [37] Sheridan, R. P., Wang, W. M., Liaw, A., Ma, J., & Gifford, E. M. (2016). Extreme gradient boosting as a method for quantitative structure–activity relationships. *Journal of chemical information and modeling*, 56(12), 2353-2360.
- [38] Wang, F., Jiang, D., Wen, H., & Song, H. (2019). Adaboost-based security level classification of mobile intelligent terminals. *The Journal of Supercomputing*, 75(11), 7460-7478.
- [39] Freund, Y., & Schapire, R. E. (1996, July). Experiments with a new boosting algorithm. In *icml* (Vol. 96, pp. 148-156).
- [40] Sreng, S., Maneerat, N., Hamamoto, K., & Panjaphongse, R. (2018). Automated diabetic retinopathy screening system using hybrid simulated annealing and ensemble bagging classifier. *Applied Sciences*, 8(7), 1198.

A Systematic Literature Review of Deep Learning-Based Detection and Classification Methods for Bacterial Colonies

Shimaa A. Nagro

College of Computing and Informatics, Saudi Electronic University, Riyadh, Saudi Arabia

Abstract—Deep learning is an area of machine learning that has substantial potential in various fields of study such as image processing and computer vision. A large number of studies are published annually on deep learning techniques. The focus of this paper is on bacteria detection, identification, and classification. This paper presents a systematic literature review that synthesizes the evidence related to bacteria colony identification and detection published in the year 2021. The aim is to aggregate, analyse, and summarize the evidence related to deep learning detection, identification, and classification of bacteria and bacteria colonies. The significance is that the review will help experts and technicians to understand how deep learning techniques can apply in this regard and potentially further support more accurate detection of bacteria types. A total of 38 studies are analysed. The majority of the published studies focus on supervised-learning-based convolutional neural networks. Furthermore, a large number of studies make use of laboratory-prepared datasets as compared to open-source and industrial datasets. The results also indicate a lack of tools, which is a barrier in adapting academic research in industrial settings.

Keywords—AI; bacterial-colonies; classification; deep learning; detection; literature review

I. INTRODUCTION

Bacteria are unicellular microorganisms that are present on everything around us. A single drop of sea water contains at least a million cells of bacteria [1]. Knowledge of the bacterial genre is extremely important in microbiology. Accurate and quick recognition of the bacterial genre is crucial in various fields including clinical diagnosis, medicine, water and food industry, etc. [2] [3] [4].

In the traditional identification process, preparing samples requires not only substantial time but also specific equipment and costly chemicals. This step must take place before the identification process can even start. The resultant samples are observed by experts to identify features in traditional laboratory setups. Samples are also compared with standard reference images for accurate identification, which is a tedious and time-consuming task [5].

The most important feature for recognition of bacteria is shape. Bacteria can be classified into numerous categories based on its shape. Some of the prominent shapes include spiral, longitudinal, and cylindrical. Since various types of bacteria share very similar shapes, however, considering shape alone makes differentiation difficult. Therefore, other characteristics such as presence and shape of colonies and morphology are

exploited to correctly recognize bacteria. In short, identifying type of bacteria is arduous even for experienced microbiologists [5].

Image processing and computer vision techniques have revolutionized the approach to bacterial identification with the ability to process and classify large amounts of data. Yet identifying patterns to derive conclusions from complex, dynamic, and heterogeneous data created by computerized techniques is another challenge for scientists. Evolution of machine learning techniques has enabled scientists to classify, predict, and identify patterns from large amounts of data [6]. Deep learning is a subset of machine learning that has shown tremendous success in various fields including identification and classification of bacteria.

Systematic literature reviews (SLRs) aggregate, classify, and analyse state-of-the-art information from existing literature. SLRs are a type of secondary study that collects and summarizes the literature published in a particular area. The studies under review are referred to as primary studies [7].

This paper presents an SLR on deep-learning-based classification and identification of bacterial colonies. This work aggregates, analyses, and summarizes 38 studies related to deep-learning-based bacterial classification. The aim of this study is to benefit new researchers by providing organized insights from the literature. Furthermore, this SLR is also beneficial for practitioners since it highlights the latest tools, techniques, and frameworks in this area. Specifically, this paper provides the following contributions:

- Identification of the deep-learning-based bacterial classification techniques presented in the literature. This paper presents a taxonomy and classifies existing literature according to types of deep learning approach, types of learning, and tools used to perform bacterial colony classification.
- A descriptive analysis of quantitative data and a thematic analysis of qualitative data to provide insights into deep learning approaches and datasets. This paper also presents a comparative analysis to find the similarities and differences in performance evaluation metrics and tools available in existing studies.
- Insights for practitioners into the latest advancements in tools, techniques, and frameworks in the deep-learning-based classification of bacterial colonies.

- Reporting of benchmark datasets and performance evaluation metrics used to measure the performance of deep learning approaches for bacterial colony classification.

The rest of the paper is organized as follows: Section II discusses the background of various deep learning approaches in general. Section III presents the research methodology applied in this study. Section IV presents the results of this study. Finally, Section V presents a discussion followed by the conclusion.

II. BACKGROUND

A. A State-of-the-Art Survey on Deep Learning Theory and Architectures

Deep learning is an advanced subset of machine learning, which is now emerging in numerous traditional and new areas. Deep learning has gained tremendous attention from researchers and practitioners in recent years. In comparison with conventional techniques, deep learning has generated experimental results that show extraordinary success in different fields such as cyber security, natural language processing, image processing, biotechnology, speech recognition and translation, and robotics [8] [9] [10]. In deep learning architecture, there are quite a few intermediary layers between the input and output layers. These intermediary layers allow deep learning models to pick up patterns and perform classifications. Deep learning is a general solution that can apply to almost any field, whether new or old, and has proven successful in solving almost any kind of problem [11].

B. Types of Deep Learning Techniques

Deep learning techniques can be classified into three categories: supervised, unsupervised, and semi-supervised learning techniques.

1) *Supervised deep learning techniques:* Supervised deep learning techniques make use of labelled input and output datasets. Examples of supervised deep learning techniques are Deep Neural Network (DNN), Convolutional Neural Network (CNN), and Recurrent Neural Network (RNN).

2) *Unsupervised deep learning techniques:* In machine learning, unsupervised deep learning techniques make use of unlabelled datasets. Clustering is an example of unsupervised deep learning. In unsupervised deep learning, learning agents identify and study indefinite relationships among input data. It promises to identify extremely intricate and nonlinear models with many free parameters. Deep unsupervised learning makes use of millions of parameters and unlabelled data. Generative Adversarial Network (GAN), Restricted Boltzmann Machine (RBM), and Auto Encoder techniques are used in unsupervised deep learning.

3) *Semi-supervised deep learning techniques:* This type of learning occurs when datasets are not completely labelled. It is a blend of unsupervised and supervised deep learning. First, the role of supervised deep learning is to identify key features from the data for which outputs are known. Then unsupervised deep learning takes place, in which less information about the data is

available, basically no information about the output. This unsupervised deep learning helps in exploiting just input data to identify other features. For instance, in a face recognition problem, supervised learning can identify that eyes are an important feature to differentiate faces from other objects. Then unsupervised learning identifies other new features such as eyebrows and noses and lips as important to identify a face in case eyes are not visible. Thus unsupervised learning improves the overall generalizability of a semi-supervised learning model [12]. Semi-supervised deep learning techniques include Deep Reinforcement Learning (DRL), GAN, and RNN.

Deep Neural Network (DNN): An Artificial Neural Network (ANN) has been mapped on human neurons to solve identification- and classification-related problems. A DNN is an advanced form of ANN that consists of several hidden layers between input and output layers. Each layer contributes to improving classification accuracy. The following sections discuss specialized forms of DNNs. Fig. 1 shows the architecture of a DNN.

Convolutional Neural Network (CNN): CNNs are a type of ANN that support recognition- and classification-related tasks. CNNs are similar to a multi-layered simple neural network, albeit with the difference that unlike in other neural networks, the layers in CNNs are stacked. A CNN works in a similar way to how humans process visuals, with the ability to process multidimensional images [11]. The basic architecture of a CNN consists of a feature extractor and a classifier. This architecture can be further distributed into three type of layers: convolutional, pooling, and fully connected layers. These layers are sandwiched between input and output layers. At the input layer, the input parameters are specified, including height, width, and depth. Odd numbered layers are for pooling, whereas even numbered layers are dedicated for convolution tasks. Convolutional layers extract and create feature maps, which are then processed through an activation function and biased to produce the final output. The function of each odd pooling layer is to reduce the dimensions of the output produced by the former convolution layer. This step is necessary because the exponential increase in dimensions make the dimensions increasingly difficult for the computer to process. Finally, the output produced by pooling and convolutional layers is given as an input to the classification layer, or the fully connected layer [13]. In the classification layer, the features are collected, and activation functions are applied. This layer is computationally expensive, so alternatives such as global and average pooling layers have been reported that reduce parameters, thereby reducing the overall complexity at this layer. Fig. 2 presents architecture of a CNN.

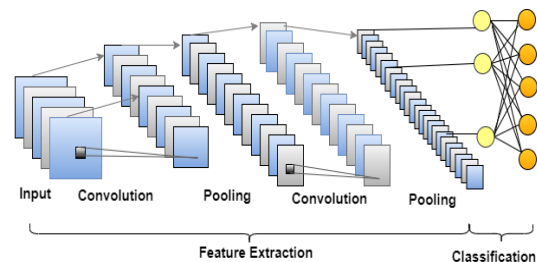


Fig. 1. Deep Neural Network.

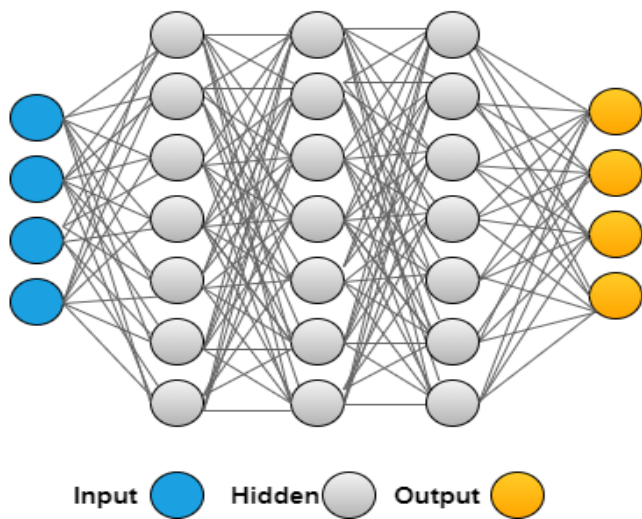


Fig. 2. Convolutional Neural Network.

Recurrent Neural Network (RNN): CNN and conventional neural networks work on fixed sized vectors as input and output, e.g., the images and probability of classes respectively. In contrast, the distinguishing quality of an RNN is that it can handle variably sized vectors. RNNs are iterative in nature, which allows them to pass on information through each iteration. RNNs can be considered as replicas of the same network. They can retain information from the past to interpret, present, and predict the future. For instance, an RNN model can retain information about previous video frames to understand the present and to predict and produce future frames. RNNs have also been used to solve natural language processing [14], text mining, time series, and financial data related problems [6]. The limitation of this neural network is that it faces a ‘vanishing gradient problem’, though this problem has been solved in the literature by the invention of Long Short-Term Memory (LSTM).

Generative Adversarial Network (GAN): A GAN involves unsupervised deep learning where the dataset is not labelled. It uses input data to generate previously unknown patterns and then uses learnt patterns to generate new but similar samples of data. GANs make use of two neural networks, i.e., a generator and a discriminator. These neural networks compete against each other in an adversarial fashion. The generator generates sample data, whereas the discriminator compares the sample with input data and determines whether the generated sample is close enough to be acceptable. The feedback is fed back to the generator, which helps it to perform better. GANs have been used to solve numerous problems in diverse fields. GANs use deep learning methods, which is why they are categorized as both semi-supervised and unsupervised learning. For instance, GANs support image, video, and voice generation. GANs are also being used in game development.

Restricted Boltzmann Machine (RBM): RBM is another example of unsupervised learning. Just like GAN, RBM is also a generative approach that generates samples based on unlabelled input data. An RBM is composed of two layers, i.e., hidden and visible. The standard Boltzmann Machine is known for its slow learning process. The training part in an RBM can be exhibited using a Boltzmann Machine, which is a two-

layered network. It makes use of randomly distributed probability-based binary pixel and feature detectors. The RBM is based on hidden variables and undirected graphs. The stochastic nature of the RBM and its slow training phase makes the overall approach computationally expensive. RBMs can be used to solve classification and dimension reduction problems.

Deep Reinforcement Learning (DRL): This learning approach learns from an unknown environment. DRL is different from other supervised and unsupervised deep learning approaches since these approaches model data while DRL models environments. DRL can be thought of as an approach that suggests actions to be performed based on a given environment. Other deep learning approaches are exploited by DRL to model data based on the environment being modelled. DRL can be applied in numerous fields to determine actions, for instance, in engineering and mathematics. In addition, it can be used for decision making in investment markets.

Deep Auto Encoder (DAE): This approach is categorized as unsupervised deep learning. Auto encoders are used for encoding input data and to learn features from it. DAE consists of two parts: the encoder and decoder. In the encoding part, input data is encoded. In the decoding part, real features are generated. DAE encoders can be thought of as stacked data-driven auto encoders and are famous for solving dimension reduction problems. However, there are a few limitations to DAE approaches. For example, they are highly sensitive to input errors and face the ‘vanishing error’ problem [11].

Transfer Learning (TL): In conventional machine learning practices, a model is designed, created, and trained to produce accurate results. Mostly weights are initialized randomly before the start of a training process. As a result, models learn slowly, adjusting the weights on each iteration to reach a certain level of accuracy. TL is different from the traditional machine learning training process. It makes use of source information to improve the learning rate of a related target model. TL is a process in which pre-trained models are used to initialize the weights of a new model. This process can greatly improve the time required by a target model to reach higher classification accuracy. Performance of TL is dependent upon the DL algorithm being used by the model. Usually the last layer of the pre-trained model is removed, and a fully connected model is attached with the number of classes in the target model. If the target model performs well as compared to a model that learnt from scratch, then this process will be considered as positive TL. However, if the target model does not benefit from pre-trained model and performance is degraded as compared to the model that learnt from scratch, then this will be considered as negative TL [15]. This learning produces the best results when there is a limited amount of training data [13].

III. PROPOSED METHODOLOGY

This study presents an SLR by following the guidelines presented by [16] [17]. These guidelines are well accepted in the software engineering community and have been followed by a number of studies [18] [19]. Fig. 3 shows the review protocol. This review is divided into three phases. The first phase presents the plan. This phase presents the research questions that are formulated based on the objectives of this study. The second phase is divided into three parts: definition

of the search strategy with the help of keywords, formulation of inclusion and exclusion criteria for study selection, and data extraction of selected attributes to answer the research questions. Finally, the data is synthesized. In the third phase, the results are reported by answering each research question. The following sections align with the phases and steps as outlined in Table I.

A. Research Questions

The following research questions align with the objectives of this study.

RQ 1. What is most state of the art in the field of deep-learning-based detection and classification of bacterial colonies?

This question is further sub-divided into the following questions:

RQ 1.1 What are the techniques/deep learning models that have been used in the primary studies?

Motivation: This research question is answered by identifying the deep learning models used in each primary study, for instance, the CNN and RNN. The summarized research methodology of deep learning models presented in primary studies are reported. The reporting covers, for instance, the number of layers and steps used during the pre-processing, training, and testing phases of each study.

RQ 1.2 Which types of learning have been applied?

Motivation: This research question aims to present the types of learning used by the techniques. For instance, supervised learning, unsupervised learning, and semi-supervised learning. This is assessed by mapping each deep learning model on the taxonomy presented in Fig. 4.

TABLE I. STEPS FOLLOWED IN EACH PHASE

Phases	Steps Followed
Planning	Problem Formulation
	Protocol Development
	Research Questions
	Online Digital Library Selection
	Formulation of Query String
	Inclusion and Exclusion Criteria Definition
Conducting Review	Study Selection
	Attribute Identification
	Data Extraction
	Data Analysis
Reporting	Report Results

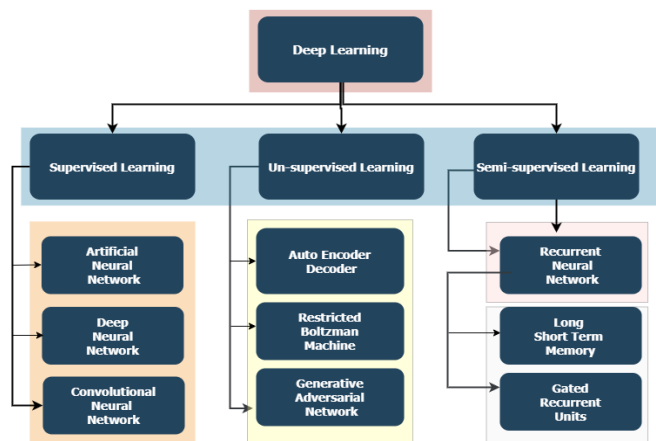


Fig. 4. Taxonomy of Deep Learning Methods.

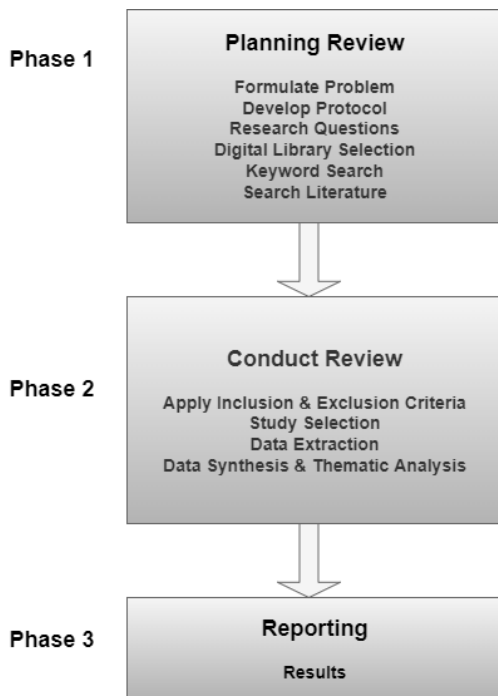


Fig. 3. Review Protocol.

RQ 1.3 What tools are available for deep-learning-based detection and classification of bacterial colonies?

Motivation: Availability of tools is an important concern for practitioners. To answer this research question, we aim to discover and report the tools developed and used by primary studies. The answer to this research question includes a list of tools presented and used in primary studies.

RQ 2. What type of datasets have been used for evaluation in the primary studies related to deep-learning-based detection and classification of bacterial colonies?

Motivation: The answer to this research question involves identifying the name and types of datasets used for the training and testing of deep learning models presented in primary studies. The datasets are categorized into three categories: academic, open-source, and industrial. Datasets constructed in lab environments that are not affiliated with any organization or institute are considered academic. Open-source datasets are those that are publicly available, well known, and used in similar studies. Datasets received from a specific organization that are not publicly available and solely used for the scope of a particular primary study are called industrial datasets. This research question is further divided into the following sub-questions.

RQ 2.1 What are the characteristics of the datasets?

Motivation: This research question aims to identify the characteristics of data, such as type of sample (microscopic images, spectroscopic data, genomic data, etc.); number and size of dataset; and number of classes. The answer to this research question is a comparative analysis presented in a table listing dataset name, number of classes, type, and size.

RQ 2.2 What performance evaluation metrics do the studies use to evaluate the performance of deep-learning-based techniques for the detection and classification of bacterial colonies?

Motivation: This research question aims to investigate the performance of a deep learning model based on its ability to perform the classification accurately. To answer this research question, the evaluation data of each model were extracted for a given dataset. Different studies incorporate different metrics for performance evaluation depending on the dataset and deep learning technique used. Performance metrics can be accuracy (in percentage), Area Under the ROC Curve (AUC), precision, receiver operating curve, F1 score, sensitivity, confusion metrics, etc. The answer to this research question is a comparative analysis presented in a table providing the name of the deep learning model, dataset, and highest accuracy achieved on that dataset.

B. Digital Library Selection

The search was carried out using the large extensive databases shown in Table II. We searched a total of five digital databases: Google Scholar, IEEE Explore, ACM, PubMed, and Springer. We searched on the basis of keywords, titles, abstracts, and (in the case of Google Scholar) full texts to identify the relevant primary studies. These libraries provided almost complete sets of relevant studies. To complete the search process, a manual search was also conducted by looking into relevant journals and identifying articles from references of primary and secondary studies.

TABLE II. DIGITAL LIBRARIES AND URL

Digital Library	Uniform Resource Locator
Google Scholar	https://scholar.google.com
ACM	https://dl.acm.org
IEEE Explorer	https://ieeexplore.ieee.org
PubMed	https://pubmed.ncbi.nlm.nih.gov
Springer	https://springer.com

C. Query String Formulation

By using the keywords identified in Table III, query strings were formulated. Keywords were identified based on the research questions. Synonyms and alternate terms and spellings were used to perform the advanced search. Query strings were used to perform advanced searches on the digital databases. The Boolean operator OR was used for synonyms and alternate keywords, and the operator AND was used for connecting keywords and phrases. Multiple versions of query strings were developed and executed on different databases in order to find as many relevant studies as possible.

TABLE III. QUERY STRING

Digital Library	Key Words Searched
Google Scholar	("Deep Learning" AND Bacteria*) AND (Classification OR Identification) AND Microscope* AND Image
IEEE Explore	("Document Title": Deep Learning) AND ("Document Title": Bacteria Classification)
Springer Link	"Deep Learning" AND Bacteria AND Classification
PubMed	((Deep Learning) AND (Bacteria[Title/Abstract])) AND (Classification[Title/Abstract])
ACM	[Publication Title: deep learning] AND [Abstract: bacteria*] AND [Abstract: classification identification] AND [Publication Date: (01/01/2021 TO 12/31/2021)]

Table III presents the main query strings applied to the digital databases.

D. Inclusion and Exclusion Criteria

An SLR includes and excludes papers from the study pool with the help of well-defined criteria. In order to select relevant papers, a simple yet straight forward inclusion and exclusion criteria was formulated. In the first phase of study selection, studies were selected based on their titles. In the next phase, abstracts of studies were reviewed. Finally, full texts of included studies were reviewed, and any study that was not in alignment with the inclusion criteria was excluded. The inclusion and exclusion criteria are stated below:

1) Inclusion Criteria

IC1: Published in the year 2021

IC2: Written in the English language

IC3: Full text of paper is available

IC4: Peer reviewed

IC5: Discusses deep learning methods to detect and classify bacterial colonies

2) Exclusion Criteria

EC1: Published before 2021

EC2: Written in a language other than English

EC3: A version other than the most recent version (if multiple versions are available)

EC4: Non-peer reviewed (e.g., presentations or books)

EC5: Duplicate article

EC6: Discusses classification of other microorganisms such as viruses and other non-bacterial microorganisms

E. Conducting Systematic Literature Review

This section presents the study selection, data extraction, and synthesis process.

1) *Selection of primary studies:* The search across five online digital libraries retrieved a total of 310 articles. In the first pass, the titles and abstracts of all the articles were

analysed. As a result, 50 articles were selected (IC2, EC2, IC5, and EC6). In the second pass, the duplicate articles (i.e., papers appearing more than once) were removed (EC5). Furthermore, any non-peer reviewed articles such as books, magazines, lecture notes, editorials, and presentations were removed (IC4, EC4). Articles whose full text was unavailable were also excluded (IC3, EC3). A manual search was also conducted by looking into relevant journals and identifying articles from the references of primary and secondary studies. As a result, a total of 38 articles were present in the study pool. Fig. 5 shows the study selection process.

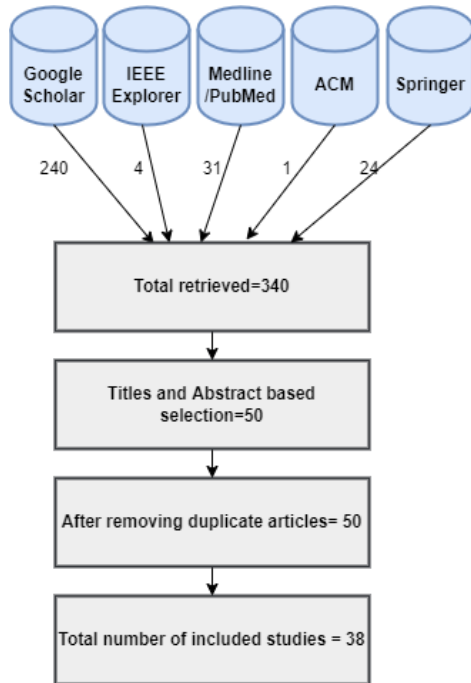


Fig. 5. Study Selection Process.

2) *Data extraction and synthesis:* The selected attributes were extracted from the primary studies and stored in a spreadsheet for analysis. We also extracted the quantitative data, such as number of datasets, size, number of classes, and accuracy, and the qualitative data, such as type of learning, type of dataset, and steps followed to develop the deep learning model. Data synthesis is a technique to summarize reported evidence from included primary studies to answer research questions. Table IV presents the data attributes extracted from each of the primary studies and maps those attributes on each respective research question. To synthesize qualitative data, a descriptive analysis was conducted, and to synthesize quantitative data, a thematic analysis was performed.

IV. RESULTS

This section presents the results and answers the research questions presented in section 3.1.

RQ 1. What is most state of the art in the field of deep-learning-based detection and classification of bacterial colonies?

TABLE IV. DATA ATTRIBUTES' MAPPING ON RESEARCH QUESTIONS

Data Attributes	Possible Values	Research Question
Deep Learning Model	e.g. CNN, RNN, DBN, AE	RQ 1.1
Type of Learning	Supervised Unsupervised Semi-Supervised	RQ 1.2
Tool	Tool Name	RQ 1.3
Tool Language	e.g. MATLAB, Python etc.	RQ 1.3
Tool Availability	Available Not available	RQ 1.3
Name of Dataset	e.g. DIBaS	RQ 2
Dataset Type	Academic Open source Industrial	RQ 2
No. of Classes	e.g. 3, 5	RQ 2.1
Type of data sample	Spectroscopic, microscopic, etc.	RQ 2.1
Highest Accuracy Achieved	Value in percentage	RQ 2.2
Evaluation Metrics	F1 score, precision, sensitivity, etc.	RQ 2.2

To identify what is most state of the art in deep learning approaches used for bacteria classification and identification, the information presented in Table IV was extracted and used to answer all sub questions.

RQ 1.1 What deep learning models/architectures have been used in the primary studies?

The primary studies were classified using thematic analysis, which involves identifying different patterns. A word cloud based on the extracted keywords is presented in Fig. 6. More than 75% of the primary studies are based on different architectures of CNN. Fig. 7 shows the distribution of deep learning architectures. Studies were further classified according to various CNN architectures, for example, ResNet, UNet, SqueezeNet, MobileNet, and InceptionNet. Fig. 8 shows the distribution of architectures within CNNs. A large number of primary studies incorporate ResNet architecture because it can accommodate as many as one thousand layers to achieve greater performance. The following sections discuss the research summaries of the studies categorized in each of these architectures.

1) *CNN-Based architectures:* In [20], the authors identify and classify three types of food-borne bacteria with a cytometric approach on micro-fluidic impedance. The three type of bacteria, namely 'Salmonella Enteritidis', 'Vibrio Parahaemolyticus', and 'Escherichia coli', were classified with the help of a CNN with 100% accuracy. The authors claim that this impedance-based technique can classify unlabelled data. This system can also detect pathogenic bacteria, thus it could be prolific in clinical diagnosis. Regarding the architecture of the CNN, the CNN was composed of one input layer, two convolutional layers, one fully connected layer, and one output layer. The depth of convolution was 8, and Rectified Linear Unit (ReLU) was used as an activation function. The same

In [26], the authors develop a spectra identification technique to identify the bacteria responsible for causing urinary tract infections (UTIs). A CNN was developed to perform the classification of bacterial species and their sensitivity to antibiotics. The proposed CNN model consists of four convolutional and max pooling layers. Two fully connected layers were used for classification. The results indicate that, as compared to traditional UTI bacterial identification techniques, this technique based on surface-enhanced Raman spectroscopy is faster and has an accuracy level of 96%.

In [27], the authors develop a deep learning approach to identify the geometrical characteristics of sulfate-reducing bacteria in order to avoid corrosion. They use a deep CNN model on Scanning Electron Microscopic (SEM) images. A modified watershed algorithm was used for bacterial cell segmentation before counting of the cells and identification of geometric properties such as height and width. The model takes unprocessed SEM images as input and produces geometric properties (height and width) as output. The model uses Deeplabv3+ pre-trained on ResNet50, ResNet18, and MobileNet. The results show that the proposed model can detect individual and clustered bacterial cells effectively in the presence of other objects.

In [28], the authors developed a CNN-based classifier to distinguish between two types of bacteria, i.e., MRSA and MSSA. The proposed CNN is a shallow model that takes 1D spectra as input and extracts feature maps. The model classifies spectra into two classes, so it can be considered as a binary classifier. The results indicate that the proposed approach can identify and distinguish two types of bacteria with an accuracy of 100%. In [29], the authors made use of a CNN-based model called VGG-16 for classification of bacterial colonies. Pre-trained VGG-16 was used with atrous convolution instead of a conventional CNN. The proposed model altered the standard VGG16 model by introducing additional dilated convolutional layers; the rest of its architecture was similar to original VGG-16. The performance of the proposed approach on test data was 94.8%.

In [30], the authors investigate the identification of growth paths of E.coli bacteria on non-transparent metallic mediums. Their aim was to identify multiple stages of bacterial image formation. These steps included identification of base, colony formation, bacterial dispersion, and crystallization. They incorporate a deep CNN model with four convolution layers followed by max pooling layers and a classification layer followed by a SoftMax layer. The authors in [31] attempt to develop a system to automatically calculate the number of bacterial cells in a colony in water samples. A CNN was developed to identify a specific type of bacteria called E-coli. The CNN model comprises six convolutional followed by two fully connected layers. Another deep learning model R-CNN was employed to automatically count the number of bacterial cells in a colony. This model was developed with the help of previously trained ResNet-50, hence use of TL. Classification layers of ResNet were replaced by a layer with nine neurons representing nine classes of R-CNN. The results indicate that the proposed models works significantly well with an accuracy

of 97% in automatic detection and cell counting of E-coli bacteria in colonies.

The authors in [32] use a CNN to detect bacterial cells from three-dimensional (3D) fluorescent microscopic images. The CNN is composed of 11 layers in total, distributed as follows: two convolutional layers followed by max pooling layers and two fully connected dense layers that use SoftMax function. The results indicate that the proposed approach works effectively with an accuracy of 95% and can detect bacterial cells from 3D fluorescent images.

2) *ResNet architecture*: In [33], the authors aim to identify the structural features of the G20 bacteria that are normally present on steel surfaces and cause corrosion. Data samples are SEM images. Mask Region CNN (RCNN) and Deep Convolutional Neural Network (DCNN) were used for segmentation of bacterial instance and identification of grouped bacteria respectively. The authors incorporate a previously developed platform named DeepLABv3+ for implementing deep learning architectures. RCNN is a pre-trained architecture with pre-extracted feature maps of images. Comparison was performed with deductions of experienced human experts. The results indicate that RCNN and DCNN are far faster with an accuracy of 81% as compared to manual and conventional approaches to detect bacteria from biofilms.

In [34], the authors present a CNN-based approach to classify three species of gram-positive bacteria through Whole Slide Images. Data were pre-processed to segment bacteria from background. The segmented bacteria images were then fed to a classifier, which classified them into three classes. Pre-trained ResNet was used to segment the bacteria from the background. The authors conclude that ResNet architecture can be effective in differentiating among three gram-positive bacteria with an accuracy of 81%.

In [35], the authors propose a bacilli detection approach based on deep CNN. Specifically, ResNet, SqueezeNet, and VGG-16 are used for training and testing to identify which models work best in bacilli identification. Use of pre-trained architecture indicates that the models used TL. Bacterial images were segmented from the background using K-means clustering and colouring techniques. Images were resized to 224x224x3 and fed to the model. ReLU and sigmoid activation functions were used between layers. Overall, SqueezeNet outperformed the other CNN models with an accuracy of 97%.

The authors in [36] employed five CNN-based architectures to differentiate between 33 different species of pathogenic microbes. These architectures included ResNet50, Mobile Net, ResNetv2, Inception Net, and DenseNet. All the architectures used TL, i.e., they were pre-trained to reduce the time required to achieve better performance. Fine tuning was used to vary the weights of parameters in deep and shallow layers. Shallow layers identified basic line features whereas deeper layers identified other complex features. The input to the models was a 224x224 image. Stochastic Gradient Approach was used to prevent the technique from getting stuck in local minima. MobileNet performed better than the other architectures with an accuracy of 96.8%.

In [37], the authors developed a tool called Motility-J to identify bacteria and detect surfaces that are covered with pathogenic bacteria. The authors emphasize that pathogenic bacteria develop features such as flagella to move across surfaces in order to survive in a constrained environment. The tedious task of labelling datasets was alleviated by labelling images with a semi-automatic technique. The authors used image segmentation to identify the part of image where bacteria are present from the background image and used that part as input to the model. A number of image processing techniques such as noising and erosion were used to obtain bacteria segments. A number of CNNs were used including ResNet50, ResNet101, FBNet, and EfficientNet B3 with fine tuning and TL. Fine tuning was done such that the last convolutional layer was replaced by a linear layer. All the models were trained using input images.

In [38], the authors differentiate longitudinal bacterial divisions (Fission) from horizontal and other divisions. They make use of a pre-trained CNN called ResNet with TL. Comparison was conducted of a pre-trained model with an un-trained model. The results indicate that classification accuracy for pre-trained ResNet was 99.67%, better than un-trained ResNet.

3) *UNet architecture*: In [39], the authors developed an approach for segmentation and classification of six bacterial species. They employed UNet architecture for segmenting the SEM image into foreground and background images. In the classification part, VGG16 was used to classify bacteria species before counting the number of cells. The authors kept the segmentation and classification independent so that they could learn independently and improve their individual accuracies. The results indicate that the performance of the proposed approach as compared to standard CNN was better with a classification accuracy of 95.8%.

The authors in [40] aim to identify bacteria and other harmful pathogens that contaminate the bloodstream and cause life-threatening health problems. The authors incorporated CNN-based architecture called UNet to identify the presence or absence of bacterial cells in dark field microscopic images. The authors emphasize that UNet architecture works well in image segmentation and object detection. The authors divided the architecture into four models. The first model used the concept of early stopping to prevent over fitting in case the performance on the training set does not increase even after a few iterations. The second model does not apply early stopping. The third model implements a loss function. The results indicate that the proposed UNet third model performed well with an accuracy of 96.6%.

In [41], the authors build on a previously proposed BCM3D approach. BCM3D is a combination of image processing techniques and CNN to detect, count, and segment single cell bacteria from biofilms. BCM3D2.0 addresses the challenge of segmenting bacterial cells from dense biofilms and a low signal-to-background ratio. Fluorescence microscopic images were used to train and test the new approach. The authors processed the images and created two types of transitional images for object localization and boundary detection. The proposed

approach not only creates a 3D outline of an object but also measures its distance from nearby objects. A UNet-based CNN was incorporated with two convolutional layers followed by max pooling and a linear function followed by a classifier. Another CNN was trained to determine the physiological shape of segmented objects. This CNN consisted of three convolutional layers: two average pooling layers followed by a sigmoid layer.

In [42], the authors aim to measure the number and length of bacterial cells and the overall area covered by biofilms. They claim to have solved the object segmentation problem that occurs in closely located or overlapping cells. The authors combined deep-learning-based UNet model with 'region-based ellipse fitting technique' to segment, count, and measure bacterial cell instances from biofilms. UNet architecture is an encoding decoding model where convolution and deconvolution take place on input images. The final output of the model is a logically outlined mask of bacteria cell instance where each pixel is categorized to a particular class. In the second phase, the ellipse technique was applied, in which centroids and distances were calculated and ellipses with similar angles were combined iteratively. This technique performed well with a recall of 93.6%.

4) *SqueezeNet*: The authors in [43] propose 12 CNN-based models to classify bacterial species. The proposed models have minor differences, though all were pre-trained and fine-tuned. An open-source dataset called DIBaS was used to train and test the models. Furthermore, the dataset was augmented to increase its size. Augmentation was done by cropping and zooming in multiple times. A total of 24,073 images (including the originals) were present after the augmentation. Models were trained by resizing the images to 224x224 pixels. Some architectures used in this paper are Efficient-net, SqueezeNet, Mobilenetv2, Mobilenetv3, and ShuffleNet. Almost all the architectures used pre-trained models and fine-tuned them such that the last layer was modified to 32 neurons representing the number of bacterial classes. Fine-tuning also reduced the number of parameters drastically thus enabling the models to consume less resources. Comparison of proposed models was done with other techniques with and without data augmentation. The results indicate that augmentation can have a great impact on performance of a model.

In [35], the authors propose a bacilli detection approach based on deep CNN. Specifically, SqueezeNet, ResNet, and VGG-16 are used for training and testing to identify which models work best in bacilli identification. The open-source dataset ZNSM-iDB, which has 2,000 images, was pre-processed with colouring techniques. Bacterial images were segmented from the background using K-means clustering and colouring techniques. Images were resized to 224x224x3 and fed to the model. ReLU and sigmoid activation functions were used between layers. Overall, SqueezeNet outperformed rest of the CNN models with an accuracy of 97%.

5) *Inception net*: The authors in [44] developed a classifier to identify the presence and absence of filamentous bacteria in waste water. They used pre-trained inception v3, an open-

source CNN-based architecture, to train the classifier into two classes. Inception v3 was developed by Google. It consists of 22 layers and 24 parameters. It has been trained on an image-net dataset, which is well known and large. Using a pre-trained inception net allowed the authors to use it as it was for identifying bacteria in waste water. The results indicate that the Inception v3 classifier was able to identify filamentous bacteria in abundance.

6) *Stacked auto encoder*: In [45], the authors present a DNN-based approach to differentiate between two types of bacteria: MSRA and MSSA. Stacked Auto Encoder is used to perform the training and testing of the unlabelled dataset. The authors highlight that auto encoders are good at learning complex features from unlabelled data. They stack a number of auto encoders such that the first's hidden layer will feed the second's hidden layers followed by SoftMax layers. Comparison of the proposed approach was conducted with six machine learning approaches including K nearest neighbours, Support vector machine, and decision trees. The results indicate that the proposed stacked Auto Encoder accurately detects MSSA and MSRA bacteria with an accuracy of 97.6% and AUC of 0.99.

7) *Recurrent neural network long short-term memory*: in [46], the authors aim to identify bacteria from marine water. A model based on Recurrent Neural Network (RNN) called Long Short-Term Memory (LSTM) was employed to do the task. The results were compared with a simple CNN mode with two convolutional layers and max pooling and a classification layer. The LSTM model consisted of two LSTM layers, each with 64 neurons followed by a classifier with 8 neurons representing eight marine bacterial species. Both models were trained, validated, and tested on the same data so that performances would be comparable. The results indicate that the proposed LSTM method performed better than the conventional CNN with an accuracy of 94%. Furthermore, the LSTM-based model was faster and more accurate.

The authors in [47] investigate the use of LSTM for identification and classification of food-borne bacteria. The authors make use of Hyper Spectral Microscopic Images, which were pre-processed and fed to an LSTM model as well as to three other models: PCA KNN, SCM, and LDA. The results of the LSTM model were compared with those of the three classifiers. The LSTM model is composed of several blocks, a dense layer and a SoftMax layer that contains five neurons representing five classes of bacteria. Three types of Region of Interest (ROI) were utilized to extract features of bacteria: inner cell, outer layer and boundary ROIs. The results indicate that centre ROI is a better feature to consider for bacterial classification. The proposed RNN-based LSTM model performed better than other models with an accuracy of 92.9 %.

RQ 1.2 Which types of learning have been applied?

This research question is answered by mapping each type of deep learning model on the taxonomy proposed in Fig. 3.

In [20], the authors make use of unlabelled impedance data, which means the proposed technique is unsupervised. The

authors in [26] use unlabelled Raman spectroscopy data to identify UTI-causing bacteria. The authors in [28], proposed binary classifiers using unsupervised learning. The classifiers detect two types of bacteria: MSSA and MRSA. The authors in [45] make use of stacked auto encoders for training and testing an unlabelled dataset, so we categorize this study under unsupervised learning models. The authors in [35] perform unsupervised learning as they detect bacilli-shaped bacteria from an open-source dataset of microscopic images. In [48], the authors develop a binary classifier using supervised learning. The proposed classifier classifies bacteria into two classes: harmful and benign bacteria. The authors in [49] propose a graph-based unsupervised technique called M-Lcuts that identifies numerous bacterial clusters in 3D space.

The authors in [47] make use of live spectral analysis to train an RNN-based LSTM model. The authors in [46] propose an RNN-based model called LSTM to identify bacteria from marine water. Since the authors consider the LSTM model semi-supervised, we categorize it under semi-supervised learning.

The authors in [21] collected six types of bacteria through a gram-staining method from a university in Malaysia. The dataset was annotated hence this technique can be classified as supervised learning. In [50], the authors differentiated between three strains of 'Klebsiella pneumonia' by using supervised learning'. The study [22] use a labelled dataset to detect bacterial vaginosis. The authors in [38] and [40] performed supervised learning by manually labelling the dataset into two classes. The authors in [23] performed bacteria sequence classification by using labelled barcode sequences of an open-source dataset. In [51], the authors performed supervised learning as they annotated the dataset into two classes: Escherichia coli and 'Mysococcus Xanthus'. The authors in [39], [27], and [33] used a labelled SEM-based dataset for identifying and classifying bacteria species. In [52], the authors used a labelled dataset to investigate the classification accuracies of some deep learning architectures on three types of bacteria. In [44], the authors used supervised learning and annotated microscopic images obtained from waste water. The authors in [24] used supervised learning for identification of food-borne bacteria, specifically 'Salmonella Typhimurium'. The authors in [53] make use of an annotated dataset of microscopic images to identify bacteria from images. In [25], the authors performed supervised learning as they made use of an annotated dataset composed of microscopic images. The authors in [43] proposed a supervised learning approach for quick identification of bacteria. In [54], the authors propose a supervised learning method to differentiate between different species of gram-positive bacteria through Hyper-spectral Microscopic Images. The authors in [29] performed supervised-learning-based bacterial colony classification by employing TL. The authors in [37], [31], and [41] made use of supervised learning to train models. In [36], the authors propose a fine-tuning-based supervised learning approach for pathogenic bacteria identification. Similarly, the authors in [30], [42], and [32] also made use of supervised learning techniques.

To summarize, 77% of the architectures belong to supervised learning and thus make use of annotated or labelled datasets. Furthermore, 5% of the architectures belong to semi-

supervised learning. The remaining 18% of architectures belong to unsupervised learning. Fig. 9 presents the distribution of deep learning techniques for bacterial classification using three types of learning approaches. Fig. 10 presents the distribution of techniques within unsupervised learning architectures.

RQ 1.3 What tools are available for detection and classification of deep-learning-based detection and classification of bacterial colonies?

Development of tools has important implications for practitioners. Development of automated deep learning tools allows academic research to support practitioners. It also helps novice researchers and beginners to adapt to deep learning methods by overcoming the technology barrier. Table V presents the list of available tools in the field of bacterial detection and classification in deep learning. It also presents their languages, frameworks, and usage information.

Seven deep learning tools are available for detection and classification of bacteria and their colonies. These tools perform various functions and work on different levels. Functions such as image segmentation, de-noising, cell counting, and labelling can be performed. For instance, the authors in [53] develop a tool called eHooke for automatic analysis of images to detect bacteria. In particular, spherical bacteria are targeted. An ANN was used as a deep learning model to detect this bacteria. eHooke was developed in Python. The eHooke tool is available publicly for download. ZeroCostDL4Mic was used in [52]. This tool supports different architectures like U-Net, CARE, pix2pix, StarDist, and SplineDist. Furthermore, the authors in [51] propose Mistic, which is a tool based on CNN and UNet architecture that helps in image segmentation in dense and multi-species environments. Mistic can work on numerous types of images such as two-dimensional (2D) fluorescence, bright field, and phase contrast images, and it does not depend on microscopes. It makes use of Shape Index map (SI), which can be derived from microscopic image data, so diverse types of sample data can be used for bacterial identification. A CNN-based UNet architecture is trained to identify the shapes of bacteria by extracting their features. The general workflow of Mistic is to take input of any type of image, convert that input into SI, and then segment by UNet. Mistic-Pip and Mistic-GUI are available for download. The authors in [37] developed a tool called Motility-J to identify bacteria and detect surfaces covered with pathogenic bacteria. The tedious task of labelling datasets was also improved by labelling images with semi-automatic technique. eHooke, Mistic, and MotilityJ have been used for image segmentation and classification. Interestingly, the majority of the tools have been developed using Python language. Fig. 11 presents the common frameworks reported by primary studies for development of deep learning architectures whereas Fig. 12 presents languages used by primary studies for implanting architectures. The majority of studies have used TensorFlow, PyTorch, and Keras framework and Python for implementing architectures.

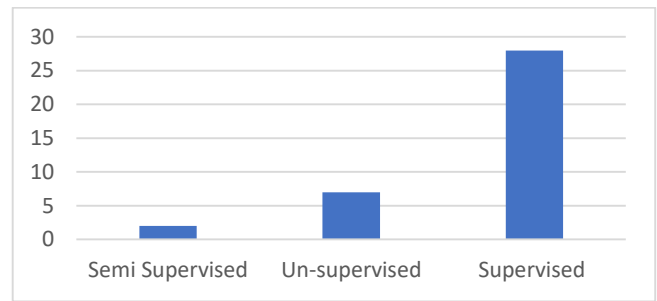


Fig. 9. Distribution of Deep Learning Techniques.

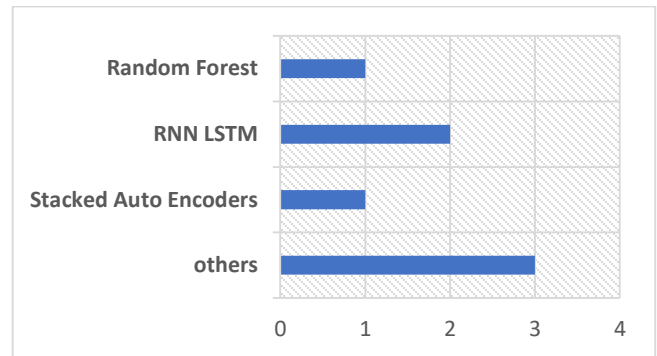


Fig. 10. Unsupervised Learning Architectures.

TABLE V. LIST OF AVAILABLE TOOLS IN BACTERIA DETECTION AND CLASSIFICATION

Ref.	Tool Name	Language	Framework	Usage
[37]	MotilityJ	Java, Python	PyTorch	Classification and segmentation
[31]	Mobile Application GUI	MATLAB	TensorFlow	Bacteria colony quantification
[38]	Anonymous	Python	PyTorch	Classification of longitudinal bacteria division
[51]	Mistic-Pip, Mistic-GUI	Python	TensorFlow	Segmentation in dense colonies
[52]	ZeroCostDL4Mic	Python	Google Colab	Image segmentation, Image de-noising, labelling for rod and spherical shape bacteria
[44]	Automated Microscopic Image Acquisition System	Python	TensorFlow	Obtaining image from waste water
[53]	eHooke	Python	eHooke	Classification, segmentation and quantification of spherical bacteria

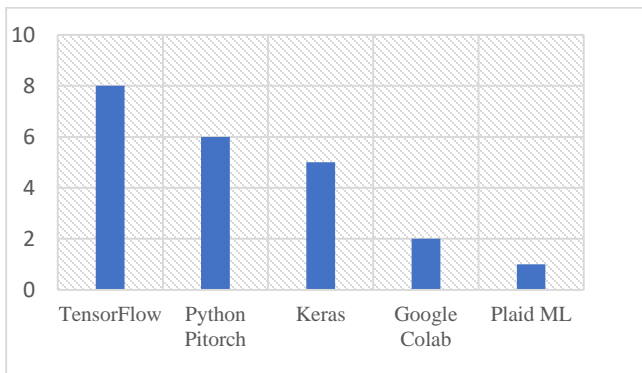


Fig. 11. Frameworks used to Implement Deep Learning Architectures.

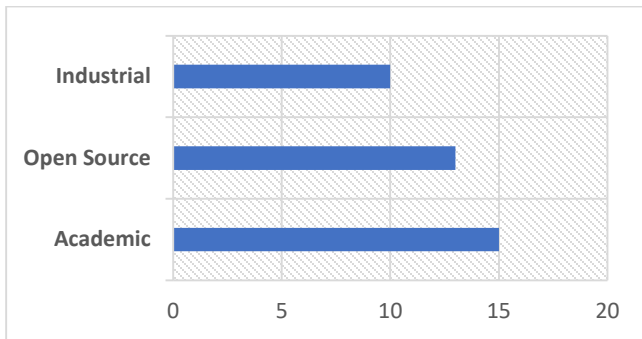


Fig. 12. Languages used to Implement Deep Learning Architectures.

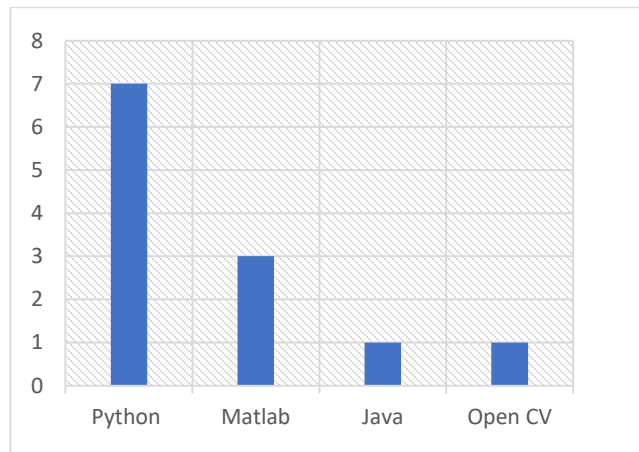


Fig. 13. Types of Datasets.

RQ 2 What type of datasets have been used for evaluation in the primary studies related to deep-learning-based detection and classification of bacterial colonies?

Fig. 13 shows the distribution of type of datasets used by the primary studies. Most of the datasets are academic. Namely, 40% (15) of the primary studies use academic datasets, meaning these datasets were constructed in lab environments and are not associated with any organization or institute. For instance, one study grew bacteria in lab settings under certain temperatures using chemical reagents [33]. Industrial datasets were used in 26% (10) of the primary studies. These datasets come from a specific organization, are not publicly available, and are solely used for the scope of that particular primary study. For instance, one study collected water samples from five domestic waste

water treatment plants in Japan [44]. Since a particular type of waste water treatment plant in Japan was targeted for sample collection, this dataset is categorized as industrial. Finally, open-source datasets were used in 34% (13) of the studies. Open-source datasets are publicly available, well known, and have been used in similar studies. For instance, one study used an open-source database called DIBaS, which is freely available and has been used in other similar studies [25].

The authors in [55] classify bacterial species in the DIBaS dataset. DIBaS is an open-source dataset with 33 classes of bacteria and other microorganisms. This dataset was augmented to increase its size and to avoid over-fitting. Images were resized as 224x224x3. Another open-source dataset of 205 images was incorporated by [48]. In this case, the dataset was divided into different ratios of training and testing data. The open-source dataset DIBaS was also used by [25] for training and testing. The dataset was reduced to 1,669 relevant microscopic images that were resized to 128x128x3. The authors in [35] used the open-source dataset ZNSM-iDB, with 2,000 images pre-processed with colouring techniques. Bacterial images were segmented from the background using K-means clustering and colouring techniques. Images were resized to 224x224x3 and fed to the model. The authors in [29] also used the DIBaS dataset for training, validating, and testing the proposed model. Since the number of relevant images in original dataset was small, data augmentation was used to increase dataset size. Augmentation was done by zooming, flipping, and cropping the original images multiple times. An open-source dataset named ‘‘Bacteria Detection with Dark-field Microscopy’’ (BDDM) used by [40] for training and testing UNet architecture. It contains 366 images of size 128x128, which were manually labelled. The authors in [36] and [43] used DIBaS for training and testing the models. The dataset was augmented to increase its size. Augmentation was done by cropping and zooming in multiple times. A total of 24,073 images (including originals) were present after augmentation. Models were trained by resizing the images to 224x224 pixels. Table VI presents list of open-source datasets in the context of primary studies.

RQ 2.1 What are the characteristics of the datasets?

TABLE VI. OPEN-SOURCE DATASETS REPORTED AND USED IN PRIMARY STUDIES

Dataset	Size	Type	Classes
16SsRNA	393	Gene barcode	3
DIBaS	3000	Microscopic images	33
2DBEST	66	SEM Images	4
BDDM	366	Dark-field Microscopic Images	2
ZNSM-iDB	800	Microscopic Images	2

In [20], the authors detect and classify three types of food-borne bacteria: ‘Salmonella Enteritidis’, ‘Vibrio Parahaemolyticus’, and ‘Escherichia coli’. An academic dataset of 600 microfluidic data was used for training the model. TL is used when there is limited availability of training data. In [21], the authors augmented an industrial dataset with random image transformations such as rotations and reflections in order to reduce the dataset’s bias and increase its size. A total of 44,985

images divided into six classes of bacteria were in the laboratory-provided datasets. Images were resized to 224x224. The authors in [50] used 610 gram-stained microscopic images of dimension 3500x5760. This dataset was provided by a hospital and prepared in a laboratory setting. Three classes were used in the dataset to distinguish between the clones of *Klebsiella pneumoniae*. The authors in [22] obtained three datasets from three different hospitals in China to automatically detect bacterial vaginosis from gram-stained microscopic images. Several data augmentation methods like scale jittering and image flipping were used to reduce sampling bias. A total of 29,095 images were used and divided into three smaller datasets. All images were resized to 1024x768. Since the datasets used by [22] and [50] were provided by hospitals, they are categorized as industrial datasets. Another study used an open-source dataset of 15,090 microscopic images to differentiate longitudinal bacterial divisions (Fission) from horizontal and other divisions [38]. This dataset was also used by [56] and [57]. In these studies, the dataset was manually labelled and divided into two types of classes, 'longitudinal' and 'other', to classify bacterial division. Apart from labelling, a number of pre-processing steps were performed on the open-source dataset, and images were resized to 128x128. The authors in [23] used the open-source dataset 16SrRNA for classifying bacterial sequences into a taxonomy. The authors concluded that performance can be enhanced by increasing the size of dataset, i.e., by including more samples in datasets. The authors in [37] addressed the tedious task of labelling datasets by labelling images with a semi-automatic technique. In this technique, images are segmented to identify the part of the image where bacteria are present from the background image, and that part is used as input for the model. A number of image-processing techniques such as noising and erosion were used to obtain bacteria segments. The dataset was augmented by applying filters, zooming, and flipping to increase its size. Models were trained using input images of two sizes. A total of 2,772 images were used for training and testing; these images are available for download. An industrial dataset of microscopic images was used to train the models. Images were resized to 100x100x3.

Fig. 14 presents the different data samples and their frequencies. Many studies have used microscopic data. Many have also used spectroscopic data samples in their datasets.

In [51], the authors used two academic datasets composed of 695 fluorescence, bright-field, and phase contrast images to train models for bacterial cells detection and classification in complex multi-cellular environments.

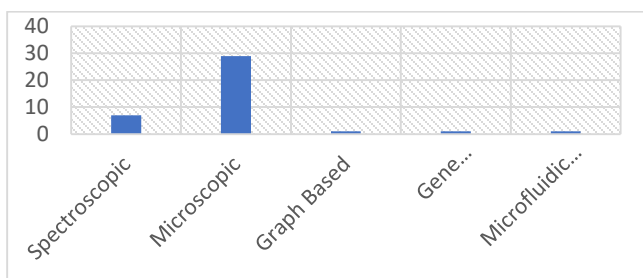


Fig. 14. Types of Data Samples.

In [52], the authors developed different datasets in order to segment three types of bacteria. Since the datasets were developed and labelled in laboratory settings, they are categorized as academic datasets. Datasets contain different types of samples such as bright field, wide field, and fluorescence images. Datasets were augmented to increase the size. These datasets are available for download. The authors in [41] prepared an academic dataset composed of fluorescence microscopic images to train and test deep learning models. The authors processed the images and created two types of transitional images for object localization and boundary detection. The augmented dataset contains 733 images. In [32], the authors detected bacterial cells from the 3D fluorescent microscopic images of an academic dataset. The authors classify the detected cells into two classes: bacteria and non-bacteria. The dataset was prepared by using 3D images of Zebrafish intestine. The image size is 10x30x30. The authors in [24] applied a number of pre-processing steps to their datasets. For instance, a magnetic field was used to convert 3D signals into 2D data. Each 5000x3000 image was divided into one hundred 500x300 images. Two datasets were used for training and verification, including an academic and an open-source dataset named 'VOC 2007'.

The authors in [39] used an academic dataset composed of SEM images. Three datasets created in a laboratory environment were used for training and testing: the first contained two types of bacteria; the second contained two different types of bacteria; and the third contained six types of bacteria, including those present in the first and second dataset. The third dataset was considered challenging because bacteria present in this dataset resemble each other in shape. Images were resized to 400x400 before being fed to UNet architecture. The authors in [58] used an open-source dataset composed of spectral data. This dataset was pre-processed and augmented before it was fed to the deep learning model. In [26], a 3000 Raman spectra from an industrial dataset was used for identification of UTI-causing bacteria. This dataset was divided for training and testing purposes. In [45], the authors used 33,951 unlabelled spectroscopic data from an academic dataset to train and test the model, which was able to differentiate between two types of bacteria: MSRA and MSSA. The authors in [46] also used spectral data from an academic dataset to classify bacteria into eight classes. In [28], an industrial dataset obtained from a hospital was used. This dataset contains 1,000 spectra from 25 different bacterial species. Data were randomly divided for training and testing purposes in 9:1.

The authors in [44] used a pre-trained Inception v3 model to identify the presence and absence of filamentous bacteria in waste water. An industrial dataset of 13,860 images was prepared in a laboratory setting by obtaining waste water samples from eight different waste water plants in Japan. In [31], the authors prepared an extensive dataset by collecting water samples from 1,301 locations. This dataset was pre-processed, and images were resized to 3228x3215.

In [34], pre-processing steps were performed to segment bacteria from the background of Whole Slide Images into three bacterial classes. Three types of industrial datasets were used to train models. A labelled dataset was used for segmentation whereas an unlabelled dataset was fed to the fine-tuned CNN

classifier. An academic dataset was used by [53], where training data comprised of around 11,000 wide-field microscopic images and around 9,000 SIM images. In each case, 10% of the images were set aside randomly and used for a test set.

One study made use of 6,900 SEM images of size 1280x960 as an academic dataset [30]. A sliding window of size 40x40 was used to scan them. In [33], the authors used SEM images as data samples for identification of structural features of G20 bacteria. An academic dataset with 66 images and two classes was divided into validation, testing, and testing data. The authors in [42] used a dataset of 290 SEM images. The data were pre-processed to remove any noise and resized to 512x512. In [27], an open-source dataset called 2DBEST composed of 66 SEM images was used to train the DCNN model. This dataset contains images of size 229x256.

In [54], the authors differentiate between different species of gram-positive bacteria through Hyper-spectral Microscopic Images of an industrial dataset. Bacteria were segmented from a 512x512 image background with the help of a binarization image-processing technique. The authors in [47] made use of a pre-processed industrial dataset of Hyper Spectral Microscopic Images to classify food-borne bacteria into five classes.

RQ 2.2 What performance evaluation metrics do the studies use to evaluate the performance of deep-learning-based techniques for the detection and classification of bacterial colonies?

Performance evaluation of bacteria detection and classification techniques involves well-known evaluation metrics. Metrics such as accuracy, F1 score, precision, and confusion matrix are commonly used to compare the performance of a newly proposed technique with previously available techniques. Apart from these metrics, criteria such as computation complexity, cost, size of dataset, and level of pre-processing activities are also used to evaluate the performance

of deep learning classifiers and extracted features. Deep learning models are inherently complex in nature. For instance, the number of layers in a CNN may increase overall computational cost and complexity.

$$Accuracy = (TP + TN)/(TP + FP + TN + FN) \quad (1)$$

$$Precision = TP/(TP + FP) \quad (2)$$

$$Recall/Sensitivity = TP/(TP + FN) \quad (3)$$

$$Specificity = TN/(TN + FP) \quad (4)$$

$$F1\ Score = (2 * Sensitivity * Precision)/(Sensitivity + Precision) \quad (5)$$

$$Dice\ Index = (2(A \cap B))/(A + B) \quad (6)$$

Equations 1–6 can calculate accuracy, precision, sensitivity, and F1-score. Here ‘TP’ stands for ‘true positive’, or the correct identification of bacteria presence. ‘TN’ stands for ‘true negative’, indicating correct identification of absent bacteria. ‘FP’ represents ‘false positive’, or the false presence of bacteria as absent, whereas ‘FN’ stands for ‘false negative’, or the incorrect identification of absent bacteria as present. Accuracy is the sum of correct identifications (both present and absent) divided by total samples. Precision is the fraction of correctly identified positive instances over all positive instances. Sensitivity is the proportion of correctly identified positive instances out of all positive instances. Specificity is calculated as correctly identified negative instances over all negative instances. The receiver operating curve (ROC) presents the true positive rate against the true negative rate and is also known as the precision-recall rate. F1-score is a statistical measure that is calculated as the geometric mean of specificity and sensitivity. Confusion matrix represents the rate of misclassified bacterial instances. Rows in the confusion matrix represent actual classes while columns represent predicted classes. The evaluation metrics used by the studies included in this review are presented in Table VII.

TABLE VII. EVALUATION METRICS USED IN PRIMARY STUDIES

Reference	Highest Accuracy	Precision	Recall	Sensitivity	Specificity	FP Rate	Confusion Matrix	F1-Score	AUC/ROC
(Zhang et al., 2021b)	100%						✓		
[21]	99.24%				✓	✓	✓		
[50]	65%				✓	✓	✓		
[22]	89.3			✓	✓				✓
[38]	99.6	✓	✓					✓	
[23]	91.7	✓	✓			✓		✓	✓
[51]	76%								
[51]	95.8%		✓						
[52]	98%	✓	✓	✓	✓				
[44]		✓	✓	✓	✓				
[24]	86%	✓							
[33]	81%	✓	✓					✓	
[53]	86%						✓		
[26]	96%						✓		

[40]	96%								
[25]	97%								
[27]	74%								
[45]	97.66%			✓	✓		✓		✓
[28]	100%						✓		
[43]		✓	✓					✓	
[29]	94.8%	✓	✓					✓	
[34]	81%	✓	✓					✓	✓
[35]	97%	✓	✓				✓	✓	
[36]	96.8%						✓		
[48]	95%	✓						✓	
[55]	96.2%	✓		✓	✓		✓	✓	
[47]	92.9%						✓		
[49]	✓							✓	
[46]	94%								
[30]	93%						✓		
[54]	98%			✓	✓				
[41]	90%							✓	
[42]	93%	✓	✓					✓	
[31]	97%	✓		✓			✓	✓	
[32]	95%								
[58]	92%								
[37]	100%	✓	✓					✓	

V. DISCUSSION AND IMPLICATIONS

This secondary study, an SLR, has reviewed a total of 38 primary studies. This section discusses the results and their implications.

Most of the articles reviewed focus on supervised learning techniques. Only a few papers discuss unsupervised learning techniques. More contributions to semi-supervised and unsupervised learning techniques are needed. Overall, 77% of the primary studies focus on supervised learning, 18% focus on unsupervised learning, and only 5% focus on semi-supervised learning techniques. In short, semi-supervised learning is a potential area that can be further explored for bacterial colony detection and classification. This implication is noteworthy for researchers who want to contribute in the area of deep-learning-based identification and classification of bacterial colonies. Within supervised learning, the majority of studies have focused on CNNs and their different architectures. Around 86% of the supervised learning techniques focus on different CNN architectures. ResNet (48%) and UNet (20%) dominate as compared to other CNN architectures such as SqueezeNet and AlexNet. There is a need to investigate the evidence regarding how to select a particular CNN architecture according to type and size of dataset. Such research may enable new researchers and practitioners to select the best deep learning model according to the size and type of their data.

Development of tools plays an important role in applying academic research to industrial practices. Lack of tools can be a great barrier when it comes to adopting academic research into industrial practices. Only a few tools are available publicly. The majority of the primary studies did not develop end-to-end

tools, with some providing only implementation details and others mentioning no implementation details at all. Most deep learning methods are computationally expensive, with optimization demanding an extremely large number of parameters and with memory constraints that necessitate simultaneous use of Graphics processing unit (GPUs). There is a need for stand-alone tools that can operate without technological constraints such as memory and that are accessible even to beginners or practitioners who might not possess technical understanding of architectural details.

Datasets are the fundamental entities that determine performance in deep learning methods. It was observed that 40% percent of the primary studies used academic datasets. Thus most data samples were constructed in laboratory settings. While 34% of the primary studies employed open-source datasets, only 26% used industrial datasets. Datasets created in laboratory settings under specific conditions always have an inherent bias, which is a threat to validity of results. Future research must incorporate more industrial datasets so that academic research can solve real industrial problems. Furthermore, a large number of benchmark open-source datasets must be readily available to researchers so that performance of different methods can become comparable. Hence, creating and updating of open-source datasets also needs researchers' attention.

A number of studies performed data augmentation to increase the size of datasets and reduce the bias of sampling. Images were augmented in a number of ways. For instance, the authors in [22] performed jittering and horizontal and vertical flips. Yet there is little discussion on the cost of augmentation and comparison of performance of deep learning models with

and without augmentation. It would be interesting to conduct such empirical studies and compare the cost and accuracies.

Performance evaluation of the primary studies was conducted using well-known evaluation metrics such as precision, recall, FP rate, AUC/ROC, and F1-score. Accuracy, precision, F1-score, confusion matrix, and recall were most frequently used for performance evaluation.

This study can benefit researchers and practitioners by providing them a bird's eye view as well as an in-depth analysis of existing research in the area of deep-learning-based identification and classification of bacterial colonies. Researchers can benefit from the classification of existing studies on the taxonomy of deep learning models. This study helps to identify where primary studies are lacking so that researchers can target and contribute to those areas. This study also benefits practitioners by outlining recent developments in academic research so that they can adopt those developments in the industry with confidence and evidence.

VI. CONCLUSION AND FUTURE DIRECTIONS

This study analysed 38 articles and identified trends in most commonly used deep learning techniques, commonly used datasets, and availability of tools. The study has presented a taxonomy of deep learning techniques and mapped existing primary studies to identify the gaps in the literature. Furthermore, a thematic and descriptive analysis was conducted on qualitative and quantitative data respectively to answer the research questions and provide insights into deep learning approaches. The study reports on benchmark datasets used by deep learning approaches for bacterial colony classification. This study also presents a comparative analysis to find the similarities and differences in performance evaluation metrics used in primary studies. The results indicate that most of the articles focus on supervised learning techniques. Within supervised learning, the majority of the articles focus on CNN. Only a few used unsupervised learning techniques. Development of tools plays an important role in applying academic research to industrial practices, yet only a limited number of tools are publicly available. The results also indicate that a majority of the primary studies use academic datasets. Furthermore, accuracy, precision, F1-score, confusion matrix, and recall were the most frequently used performance evaluation metrics. This study is beneficial for researchers as it helps to identify areas where they can contribute.

In the future, more contributions towards semi-supervised and unsupervised learning techniques are needed. Future research works must incorporate more industrial datasets so that academic research can solve real industrial problems. Furthermore, there is a need for stand-alone tools that can operate without technological constraints so that beginners and practitioners can use them.

REFERENCES

- [1] Wassenaar TM. Bacteria: the benign, the bad, and the beautiful. John Wiley & Sons; 2011 Nov 3.
- [2] Joy, Chethna, G. Naveen Sundar, and D. Narmadha. "AI Driven Automatic Detection of Bacterial Contamination in Water: A Review." In 2021 5th International Conference on Intelligent Computing and Control Systems (ICICCS), pp. 1281-1285. IEEE, 2021.
- [3] Kc, K., Yin, Z., Wu, M., and Wu, Z.: 'Evaluation of deep learning-based approaches for COVID-19 classification based on chest X-ray images', Signal, Image and Video Processing, 2021, 15, (5), pp. 959-966.
- [4] Du, Y., Han, D., Liu, S., Sun, X., Ning, B., Han, T., Wang, J., and Gao, Z.: 'Raman spectroscopy-based adversarial network combined with SVM for detection of foodborne pathogenic bacteria', Talanta, 2022, 237, pp. 122901.
- [5] Zieliński, B., Plichta, A., Misztal, K., Spurek, P., Brzywczy-Włoch, M., and Ochońska, D.: 'Deep learning approach to bacterial colony classification', PloS one, 2017, 12, (9), pp. e0184554.
- [6] Mahmud, M., Kaiser, M.S., McGinnity, T.M., and Hussain, A.: 'Deep learning in mining biological data', Cognitive Computation, 2021, 13, (1), pp. 1-33.
- [7] Xiao, Y., and Watson, M.: 'Guidance on conducting a systematic literature review', Journal of Planning Education and Research, 2019, 39, (1), pp. 93-112.
- [8] Berman, D.S., Buczak, A.L., Chavis, J.S., and Corbett, C.L.: 'A survey of deep learning methods for cyber security', Information, 2019, 10, (4), pp. 122.
- [9] Shvets, Alexey A., Alexander Rakhlin, Alexandr A. Kalinin, and Vladimir I. Iglovikov. "Automatic instrument segmentation in robot-assisted surgery using deep learning." In 2018 17th IEEE international conference on machine learning and applications (ICMLA), pp. 624-628. IEEE, 2018.
- [10] Young, T., Hazarika, D., Poria, S., and Cambria, E.: 'Recent trends in deep learning based natural language processing', IEEE Computational Intelligence Magazine, 2018, 13, (3), pp. 55-75.
- [11] Alom, M.Z., Taha, T.M., Yakopcic, C., Westberg, S., Sidike, P., Nasrin, M.S., Hasan, M., Van Essen, B.C., Awwal, A.A., and Asari, V.K.: 'A state-of-the-art survey on deep learning theory and architectures', Electronics, 2019, 8, (3), pp. 292.
- [12] Valpola, H.: 'From neural PCA to deep unsupervised learning', in 'Book Advances in independent component analysis and learning machines' (Elsevier, 2015), pp. 143-171.
- [13] Subramanian, N., Elharrouss, O., Al-Maadeed, S., and Chowdhury, M.: 'A review of deep learning-based detection methods for COVID-19', Computers in Biology and Medicine, 2022, pp. 105233.
- [14] Socher, Richard, Cliff C. Lin, Chris Manning, and Andrew Y. Ng. "Parsing natural scenes and natural language with recursive neural networks." In Proceedings of the 28th international conference on machine learning (ICML-11), pp. 129-136. 2011.
- [15] Perkins, D.N., and Salomon, G.: 'Transfer of learning', International Encyclopedia of Education, 1992, 2, pp. 6452-6457.
- [16] Petersen, K., Feldt, R., Mujtaba, S., and Mattsson, M.: 'Systematic mapping studies in software engineering', in Editor (Ed.) (Eds.): 'Book Systematic mapping studies in software engineering' (2008, edn.), pp. 1-10.
- [17] Kitchenham, B., Brereton, O.P., Budgen, D., Turner, M., Bailey, J., and Linkman, S.: 'Systematic literature reviews in software engineering—a systematic literature review', Information and Software Technology, 2009, 51, (1), pp. 7-15.
- [18] Kumar, S., Kar, A.K., and Ilavarasan, P.V.: 'Applications of text mining in services management: A systematic literature review', International Journal of Information Management Data Insights, 2021, 1, (1), pp. 100008.
- [19] Imtiaz, J., Sherin, S., Khan, M.U., and Iqbal, M.Z.: 'A systematic literature review of test breakage prevention and repair techniques', Information and Software Technology, 2019, 113, pp. 1-19.
- [20] Zhang, S., Han, Z., Feng, Z., Sun, M., and Duan, X.: 'Deep learning assisted microfluidic impedance flow cytometry for label-free foodborne bacteria analysis and classification', in Editor (Ed.) (Eds.): 'Book Deep learning assisted microfluidic impedance flow cytometry for label-free foodborne bacteria analysis and classification' (IEEE, 2021, edn.), pp. 7087-7090.
- [21] Akbar, S.A., Ghazali, K.H., Hasan, H., Mohamed, Z., and Aji, W.S.: 'An enhanced classification of bacteria pathogen on microscopy images using deep learning', in Editor (Ed.) (Eds.): 'Book An enhanced classification of bacteria pathogen on microscopy images using deep learning' (IEEE, 2021, edn.), pp. 119-123.

- [22] Wang, Z., Zhang, L., Zhao, M., Wang, Y., Bai, H., Wang, Y., Rui, C., Fan, C., Li, J., and Li, N.: 'Deep neural networks offer morphologic classification and diagnosis of bacterial vaginosis', *Journal of Clinical Microbiology*, 2021, 59, (2), pp. e02236-02220.
- [23] Helaly, M.A., Rady, S., and Aref, M.M.: 'Deep learning for taxonomic classification of biological bacterial sequences': 'Book Machine learning and big data analytics paradigms: Analysis, applications and challenges' (Springer, 2021), pp. 393-413.
- [24] Hu, Q., Wang, S., Duan, H., and Liu, Y.: 'A fluorescent biosensor for sensitive detection of salmonella typhimurium using low-gradient magnetic field and deep learning via faster region-based convolutional neural network', *Biosensors*, 2021, 11, (11), pp. 447.
- [25] Mai, D.-T., and Ishibashi, K.: 'Bacteria shape classification using small-scale depthwise separable CNNs', in Editor (Ed.) (Eds.): 'Book Bacteria shape classification using small-scale depthwise separable CNNs' (IEEE, 2021, edn.), pp. 2940-2943.
- [26] Fu, Q., Zhang, Y., Wang, P., Pi, J., Qiu, X., Guo, Z., Huang, Y., Zhao, Y., Li, S., and Xu, J.: 'Rapid identification of the resistance of urinary tract pathogenic bacteria using deep learning-based spectroscopic analysis', *Analytical and Bioanalytical Chemistry*, 2021, 413, (30), pp. 7401-7410.
- [27] Rahman, M.H., Duckworth, J., Ragi, S., Chundi, P., Gadhamshetty, V.R., and Chilkoor, G.: 'Deep learning approach to extract geometric features of bacterial cells in biofilms': 'Book Advances in data science and information engineering' (Springer, 2021), pp. 359-368.
- [28] Wang, S., Dong, H., Shen, W., Yang, Y., Li, Z., Liu, Y., Wang, C., Gu, B., and Zhang, L.: 'Rapid SERS identification of methicillin-susceptible and methicillin-resistant *Staphylococcus aureus* via aptamer recognition and deep learning', *RSC Advances*, 2021, 11, (55), pp. 34425-34431.
- [29] Patel, S.: 'Bacterial colony classification using atrous convolution with transfer learning', *Annals of the Romanian Society for Cell Biology*, 2021, pp. 1428-1441.
- [30] Wong, P.-C., Fan, T.-E., Lee, Y.-L., Lai, C.-Y., Wu, J.-L., Chang, L.-H., and Su, T.-Y.: 'Detection and identification of the stages of DH5-Alpha *Escherichia coli* biofilm formation on metal by using an artificial intelligence system', *Microscopy and Microanalysis*, 2021, 27, (5), pp. 1218-1225.
- [31] Mohammad Khan, F., Gupta, R., and Sekhri, S.: 'Automated bacteria colony counting on agar plates using machine learning', *Journal of Environmental Engineering*, 2021, 147, (12), pp. 04021066.
- [32] Mhathesh, T., Andrew, J., Martin Sagayam, K., and Henesey, L.: 'A 3D convolutional neural network for bacterial image classification': 'Book Intelligence in big data technologies—Beyond the hype' (Springer, 2021), pp. 419-431.
- [33] Ragi, Shankarachary, Md Hafizur Rahman, Jamison Duckworth, Jawaharraj Kalimuthu, Parvathi Chundi, and Venkataramana Gadhamshetty. "Artificial intelligence-driven image analysis of bacterial cells and biofilms." *IEEE/ACM Transactions on Computational Biology and Bioinformatics* (2021).
- [34] Alhammad, Sarah, Kun Zhao, Anthony Jennings, Peter Hobson, Daniel F. Smith, Brett Baker, Justin Staweno, and Brian C. Lovell. "Efficient DNN-Based Classification of Whole Slide Gram Stain Images for Microbiology." In 2021 Digital Image Computing: Techniques and Applications (DICTA), pp. 01-08. IEEE, 2021.
- [35] Shwetha, V., Keerthana Prasad, Chiranjoy Mukhopadhyay, Barnini Banerjee, and Abir Chakrabarti. "Automatic Detection of Bacilli Bacteria from Ziehl-Neelsen Sputum Smear Images." In 2021 2nd International Conference on Communication, Computing and Industry 4.0 (C2I4), pp. 1-5. IEEE, 2021.
- [36] Jha, Nirajan, and Dibakar Raj Pant. "Stochastic Gradient Descent and Discriminative Fine Tuning on ResNet, DenseNet, Inception-ResNet and MobileNet for the Multi Class Pathogenic Microbes Classification." (2021).
- [37] Casado-Garcia, A., Chichón, G., Domínguez, C., García-Domínguez, M., Heras, J., Ines, A., López, M., Mata, E., Pascual, V., and Saenz, Y.: 'MotilityJ: An open-source tool for the classification and segmentation of bacteria on motility images', *Computers in Biology and Medicine*, 2021, 136, pp. 104673.
- [38] Garcia-Perez, C., Ito, K., Geijo, J., Feldbauer, R., Schreiber, N., and Zu Castell, W.: 'Efficient detection of longitudinal bacteria fission using transfer learning in deep neural networks', *Frontiers in Microbiology*, 2021, 12.
- [39] Kakishita, Y., Ray, A., Hattori, H., Hisada, A., Ominami, Y., Baudoin, J.-P., Khalil, J.Y.B., and Raoult, D.: 'Quantitative analysis system for bacterial cells in SEM image using deep learning', in Editor (Ed.) (Eds.): 'Book Quantitative analysis system for bacterial cells in SEM image using deep learning' (IEEE, 2021, edn.), pp. 01-06.
- [40] Sundar, G.N.: 'Effective deep learning model to identify harmful bacteria in blood samples for healthcare application', *Turkish Journal of Computer and Mathematics Education (TURCOMAT)*, 2021, 12, (6), pp. 3475-3487.
- [41] Zhang, J., Wang, Y., Donarski, E., and Gahlmann, A.: 'BCM3D 2.0: Accurate segmentation of single bacterial cells in dense biofilms using computationally generated intermediate image representations', *bioRxiv*, 2021.
- [42] Abeyathna, Dilanga, Terrance Life, Shailabh Rauniyar, Shankarachary Ragi, Rajesh Sani, and Parvathi Chundi. "Segmentation of Bacterial Cells in Biofilms Using an Overlapped Ellipse Fitting Technique." In 2021 IEEE International Conference on Bioinformatics and Biomedicine (BIBM), pp. 3548-3554. IEEE, 2021.
- [43] García, R.G., Rodríguez, S.J., Martínez, B.B., Gracidas, C.H., and Torres, R.M.: 'Efficient deep learning architectures for fast identification of bacterial strains in resource-constrained devices', *arXiv preprint arXiv:2106.06505*, 2021.
- [44] Satoh, H., Kashimoto, Y., Takahashi, N., and Tsujimura, T.: 'Deep learning-based morphology classification of activated sludge flocs in wastewater treatment plants', *Environmental Science: Water Research & Technology*, 2021, 7, (2), pp. 298-305.
- [45] Ciloglu, F.U., Caliskan, A., Sarıdag, A.M., Kilic, I.H., Tokmakci, M., Kahraman, M., and Aydin, O.: 'Drug-resistant *Staphylococcus aureus* bacteria detection by combining surface-enhanced Raman spectroscopy (SERS) and deep learning techniques', *Scientific Reports*, 2021, 11, (1), pp. 1-12.
- [46] Yu, S., Li, X., Lu, W., Li, H., Fu, Y.V., and Liu, F.: 'Analysis of Raman spectra by using deep learning methods in the identification of marine pathogens', *Analytical Chemistry*, 2021, 93, (32), pp. 11089-11098.
- [47] Kang, R., Park, B., Ouyang, Q., and Ren, N.: 'Rapid identification of foodborne bacteria with hyperspectral microscopic imaging and artificial intelligence classification algorithms', *Food Control*, 2021, 130, pp. 108379.
- [48] Akshay, S. "Classification of Beneficial and non-Beneficial Bacteria using Random Forest Algorithm." In 2021 Third International Conference on Inventive Research in Computing Applications (ICIRCA), pp. 1-9. IEEE, 2021.
- [49] Wang, J., Zhang, M., Zhang, J., Wang, Y., Gahlmann, A., and Acton, S.T.: 'Graph-theoretic post-processing of segmentation with application to dense biofilms', *IEEE Transactions on Image Processing*, 2021, 30, pp. 8580-8594.
- [50] Borowa, Adriana, Dawid Rymarczyk, Dorota Ochońska, Monika Brzywczy-Włoch, and Bartosz Zieliński. "Deep learning classification of bacteria clones explained by persistence homology." In 2021 International Joint Conference on Neural Networks (IJCNN), pp. 1-8. IEEE, 2021.
- [51] Panigrahi, S., Murat, D., Le Gall, A., Martineau, E., Goldlust, K., Fiche, J.-B., Rombouts, S., Nölmann, M., Espinosa, L., and Mignot, T.: 'Mistic, a general deep learning-based method for the high-throughput cell segmentation of complex bacterial communities', *Elife*, 2021, 10, pp. e65151.
- [52] Spahn, C., Laine, R.F., Pereira, P.M., Gómez-de-Mariscal, E., von Chamier, L., Conduit, M., de Pinho, M.G., Jacquemet, G., Holden, S., and Heilemann, M.: 'DeepBacs: Bacterial image analysis using open-source deep learning approaches', *bioRxiv*, 2021.
- [53] Saraiva, B.M., Krippahl, L., Filipe, S.R., Henriques, R., and Pinho, M.G.: 'eHooke: A tool for automated image analysis of spherical bacteria based on cell cycle progression', *Biological imaging*, 2021, 1.
- [54] Liu, K., Ke, Z., Chen, P., Zhu, S., Yin, H., Li, Z., and Chen, Z.: 'Classification of two species of Gram-positive bacteria through hyperspectral microscopy coupled with machine learning', *Biomedical Optics Express*, 2021, 12, (12), pp. 7906-7916.

- [55] Mai, D.-T., and Ishibashi, K.: 'Small-scale depthwise separable convolutional neural networks for bacteria classification', *Electronics*, 2021, 10, (23), pp. 3005.
- [56] Pende, N., Leisch, N., Gruber-Vodicka, H.R., Heindl, N.R., Ott, J., Den Blaauwen, T., and Bulgheresi, S.: 'Size-independent symmetric division in extraordinarily long cells', *Nature Communications*, 2014, 5, (1), pp. 1-10.
- [57] Leisch, N., Pende, N., Weber, P.M., Gruber-Vodicka, H.R., Verheul, J., Vischer, N.O., Abby, S.S., Geier, B., Den Blaauwen, T., and Bulgheresi, S.: 'Asynchronous division by non-ring FtsZ in the gammaproteobacterial symbiont of *Robbea hypermnestra*', *Nature Microbiology*, 2016, 2, (1), pp. 1-5.
- [58] Tafintseva, V., Shapaval, V., Blazhko, U., and Kohler, A.: 'Correcting replicate variation in spectroscopic data by machine learning and model-based pre-processing', *Chemometrics and Intelligent Laboratory Systems*, 2021, 215, pp. 104350.

AUTHORS' PROFILE

Shimaa A. Nagro is an assistant professor of computer science at Saudi Electronic University in the Kingdom of Saudi Arabia. Her research interests include electronic learning, deep learning, and Human-Computer Interaction.

Optimization of Multilayer Perceptron Hyperparameter in Classifying Pneumonia Disease Through X-Ray Images with Speeded-Up Robust Features Extraction Method

Mutammimul Ula¹

Sistem Informasi, Fakultas Teknik
Universitas Malikussaleh
Aceh, Indonesia

Muhathir^{2*}

Teknik Informatika, Fakultas Teknik
Universitas Medan Area
Medan, Indonesia

Ilham Sahputra^{3*}

Sistem Informasi, Fakultas Teknik
Universitas Malikussaleh
Aceh, Indonesia

Abstract—Pneumonia is an illness that affects practically everyone, from children to the elderly. Pneumonia is an infectious disease caused by viruses, bacteria, or fungi that affect the lungs. It is quite difficult to recognize someone who has pneumonia. This is because pneumonia has multiple levels of classification, and so the symptoms experienced may vary. The multilayer perceptron approach will be used in this study to categorize Pneumonia and determine the level of accuracy, which will contribute to scientific development. The Multilayer Perceptron is employed as the classification method with hyperparameter learning rate and momentum, while SURF is used to extract the features in this classification. Based on the experiments that have been carried out, in general, the learning rate value is not very influential in the learning process, both at the momentum values of 0.1, 0.3, 0.5, 0.7, and 0.9. The best desirable accuracy value for momentum 0.1 is at a learning rate of 0.05. The best desirable accuracy value for momentum 0.3 is at a learning rate of 0.09. The most desirable accuracy value for momentum 0.3 is at a learning rate of 0.05 and 0.07. At a learning rate of 0.03 the highest ideal accuracy value is obtained. The best desirable accuracy value for momentum 0.9 is at a learning rate of 0.09. this research should be redone using the number of hidden layers and nodes in each hidden layer. The addition of a hidden layer, as well as variations in the number of nodes in the hidden layer, will affect computation time and yield more optimal accuracy results.

Keywords—Multilayer perceptron; SURF; pneumonia hyperparameter

I. INTRODUCTION

Medical images have an important role in classifying or identifying a disease. One of the most frequently used techniques is X-ray Photo [1] [2] [3]. This technique is used by radiologists to be able to see and find out information about the patient's body condition. In addition, it has advantages, easy to use, and has a high economic value [4] [5]. A chest X-ray is used by radiographs to see the condition of the patient's chest area. The results of this chest x-ray illustrate the condition of the patient's body starting from the chest, lungs, heart, and trachea [6] [7]. Lung infections caused by bacteria, viruses, fungi, or parasites will be marked with a white-gray area. The pattern area makes it easier for doctors to identify the patient's illness, such as pneumonia [8] [9].

*Corresponding Author.

Pneumonia is a type of acute respiratory infection (ARI) at the bottom caused by inflammation of the tissues and air sacs in the lungs by bacteria, viruses, fungi, or parasites. The air sacs are filled with fluid which can cause coughing up phlegm, fever, difficulty breathing, and chills [10] [11]. Pneumonia is an airborne disease. Elderly people aged 65 years and over are a high-risk group for pneumonia. In the elderly the pneumonia rate has a high degree of severity of disease, it can even lead to death [12] [13].

Pneumonia classification using the k-nearest neighbor method with glcm feature extraction is the topic of Wijaya's 2020 study. the findings of his study suggest that cropping an x-ray image of the lungs can improve accuracy. the greatest accuracy per class is 66.20 percent while utilizing gray level co-occurrence (glcm) feature extraction and k-nearest neighbor (knn) classification for k = 5. the maximum level of accuracy is 72.90 percent for the virus lung picture object because the gray level co-occurrence (glcm) does not indicate the proper value, the precision and recall levels tend to have the same value [14].

The CNN model in classifying CT image data sets and determining the probability of COVID-19 infection, according to Xu [15] in his study. In this work, two test models were used: one that ignored the distraction component and another that took into account the distraction effect by adding a noisy-OR bayesian function. the acquisition of classification evaluation with 79.4 % accuracy, 68.9% precision, 76.5 % recall, and 72.5 % f1-score in the initial model. While the acquisition of classification evaluation in the second model had 86.7 % accuracy, 81.3 % precision, 86.7 % recall, and 83.9 % f1-score.

Detection of COVID-19 Infection in Chest X-rays Based Deep Transfer Learning, according to Das [16], explains to circumvent the low sensitivity of RT-PCR, chest X-ray images were employed to detect and diagnose COVID-19 in this study. CT scans were favored over chest X-rays. We chose chest x-ray images since X-ray machines are less expensive than CT scan devices. Furthermore, X-rays emit less ionizing radiation than CT scans. Chest X-ray scans of COVID-19 infected patients show several unique patterns and bilateral alterations, according to the exhaustive review. Manual COVID-19 testing from chest x-ray images, on the other hand, is a difficult task. As a result,

utilizing deep learning-based methodologies, an automatic analysis of chest X-rays was performed in this article. Deep transfer learning methods were capable of training network weights on big datasets as well as fine-tuning the weights of pre-trained networks on small datasets. Using multiple performance metrics like as accuracy, f-measures, sensitivity, specificity, and kappa statistics, extensive comparison analyses have been undertaken to evaluate the performance of the suggested model. The proposed model outperforms competing models, according to comparative analyses. deep understanding Under test conditions, the VGGNet model has an accuracy of 89.30 %, F-measure 90.07 %, sensitivity 91.22 %, specificity 89.12 %, and kappa statistic 90.12 %, while in training conditions it has an accuracy of 90.32 %, F-measure 91.69 %, sensitivity 91.83 %, specificity 90.16 %, and kappa statistic 91.54 %.

Optimizing [46] the hyper-parameters of multi-layer perceptron with greedy search, in experiment using Fashion MNIST and Kuzushiji MNIST datasets, is the topic of Bae's et al [36]. The proposed algorithm shows the similar performance as compared to complete search, which means the proposed algorithm can be a potential alternative to complete search. Experiments used with variations in the learning rate [0.1; 0.05; 0.01; 0.005; 0.001] the most optimal results are at a learning rate of 0.1 and 0.001[36].

Ke [37] in his report 2021 discusses enhancement of multilayer perceptron model training accuracy through the optimization of hyperparameters: a case study of the quality prediction of injection-molded parts. In the experiment the learning rate used [0.1; 0.001; 0.0001; 0.0001; 0.00001] and the activation functions [Sigmoid, Tanh, ReLU, LeakyReLU, ELU] the most optimal accuracy results are at a learning rate of 0.1 both in the activation functions of Sigmoid, Tanh, ReLU, LeakyReLU, and ELU[37].

Kerny et al. [39] research uses deep learning model inception to determine medical conditions. Layer training was done using Adam Optimizer with a learning rate of 0.001 and stochastic gradient descent in batches of 1,000 photos each step. In all categories, training lasts 10,000 steps or 100 epochs.

A wavelet technique was included as a noise remover before the forecasting data was processed using the ANN model, according to Ekonomou [40], who found that while the ANN model produced good results when used to solve forecasting situations, more optimal results were obtained. This model demonstrates that in order to produce more accurate results, ANN still has to be expanded with different combinations and enhancements.

In his manuscript addressing the case of the Power System Topology Observability analysis, Reddy [43] also investigated the enhanced Neural Network Hopfield model; the Power System Topology Observability was then analyzed using the particle swarm optimization technique as a comparative model. According to his research, the improved Hopfield Neural Network model required the least amount of computational time when compared to the particle swarm optimization algorithm, which had a time ratio of 0.2811: 18,592 in seconds. The Hopfield model also required the fewest iterations to produce the best results. When compared to the particle swarm optimization

approach, the upgraded neural network requires less iterations which had an iterations ratio 45:189.

In his research, Alqudah [44] claimed that by integrating the deep learning model as a feature extraction process and machine learning as a classification, the CNN model had been improved from the basic Neural network model. This study examined the accuracy, sensitivity, specification, and precision of the image size input model with variations of 32x32, 64x64, 128,128,256, and achieved the best results at 64x64 image input circumstances with successive values of 80.07, 79.24, 89.55, and 78.80.

The ResNet model was used by Latif [45] in his research on pneumonia detection. The CNN model (9 layers), CNN model (10 layers), CNN model (12 layers), ResNet V1 (3 blocks), and ResNet V2 (12 blocks) were all tested in trials to get the best results. The CNN model's results took less time to accomplish than those of the ResNet model, with training times of 26.72 minutes, 28.10 minutes, 36.18 minutes, 9.09 hours, and 14.58 hours. However, with accuracy scores of 80.88, 81.24, 80.28, 87.67, and 88.67 correspondingly, the ResNet model outperforms CNN.

In the comparison of chest X-rays presenting as pneumonia versus normal, we achieved an accuracy of 92.8%, with a sensitivity of 93.2% and a specificity of 90.1%. The area under the ROC curve for detection of pneumonia from normal was 96.8%. Binary comparison of bacterial and viral pneumonia resulted in a test accuracy of 90.7%, with a sensitivity of 88.6% and a specificity of 90.9%. The area under the ROC curve for distinguishing bacterial and viral pneumonia was 94.0%.[39].

According to earlier studies, multilayer perceptron as a classification approach and speed up robust feature (SURF) as feature extraction have not been identified in X-Ray Image Classification research. The multilayer perceptron classification approach with variations in momentum and learning rates, as well as SURF as its feature extraction model, will be investigated in this study in categorizing pneumonia based on X-Ray pictures.

This work uses SURF as a feature selection and feature extraction model because surf can reduce data loss in the high-quality data extraction process [35]. Feature selection and feature extraction are difficult tasks when getting high-dimensional data [41][42][47].

II. STUDY LITERATURE

A. Pneumonia

Pneumonia is inflammation of the lung parenchyma where the acini are filled with inflammatory fluid with or without infiltration of inflammatory cells into the walls of the alveoli and interstitial spaces characterized by coughing accompanied by rapid breathing and/or shortness of breath in children under five [17]. Pneumonia causes inflammation of the lungs that makes breathing difficult and oxygen intake less. Pneumonia is a disease caused by microorganisms such as pneumococcus, staphylococcus, streptococcus, and viruses whose mode of transmission can be through the medium of air, saliva splashes, direct contact through the mouth, and contact with shared objects [18] [19].

Indonesia as a country located in the tropics has the potential to become an endemic area for infectious diseases which at any time can be a threat to public health. Pneumonia is the second leading cause of death for children under five in Indonesia after diarrhea. The number of pneumonia sufferers in Indonesia in 2013 ranged from 23-27% and deaths from pneumonia were 1.19% [20].

B. Multilayer Perceptron

The Multilayer Perceptron is a variant of the original Perceptron model proposed by Rosenblatt in 1950 [21]. Neural Network Model or Neural Network is a brain computing system. This is because Neural Networks are inspired by the human brain which can provide input, process, and produce output. Neural Network can produce output because it has acquired the knowledge gained through the learning process [22] [23]. Neural Networks here have several functions, such as pattern classification, mapping patterns from input to new at output, storing patterns to be recalled, mapping similar patterns, optimizing problems, and predictions [24] [25].

Neural Network Multilayer Perceptron is a development of Neural Network Perceptron. Developed to cover the weakness of the Neural Network Perceptron, namely performing complex logic operations [26].

The perceptron algorithm, which forms the basis of the Multilayer Perceptron model, was invented by Frank Rosenblatt, funded by the United States Maritime Research Department at the Cornell Aviation Laboratory in 1957.

Multilayer Perceptron is arranged in three levels consisting of one input layer, one or more hidden layers, and one output layer. So that later the process will run from the input layer to the output layer, which there is no repetition. Neural Network architecture like this is called feedforward [27], Fig. 1.

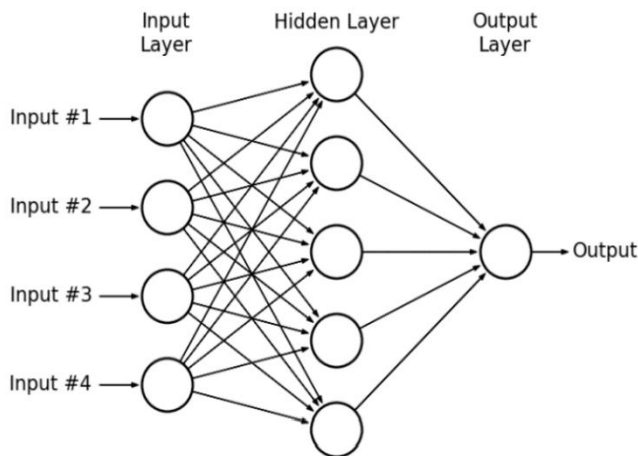


Fig. 1. Research Architecture Multilayer Perceptron.

C. Surf

The Speed Up Robust Feature (SURF) algorithm was first published by researchers from ETH Zurich, Herbert Bay in 2006 [28]. In its development Herbert Bay was assisted by two colleagues, namely Tinne Tuytelaars and Luc Van Gool [29] [30]. The SURF algorithm can detect local features in an image reliably and quickly. This algorithm is inspired by the Scale

Invariant Feature Transform (SIFT), especially at the scale space representation stage. The SURF algorithm uses a combination of an integral image algorithm and blob detection based on the determinants of the Hessian matrix [31].

SURF is a very powerful local feature detector, which can be used in computer vision such as object recognition and 3D reconstruction [32]. One of the advantages of SURF is its processing speed, this is due in part to the use of integral images. The value of this integral image comes from the sum of the grayscale values of the image [33]. SURF is designed to extract the uniqueness and similarity of features from images. The SURF algorithm is divided into several stages, namely interest point detection and feature description [34].

III. RESEARCH METHODS

A. Dataset

The dataset used in this study was taken from the Kaggle dataset source which can be accessed via the following link <https://www.kaggle.com/paultimothymooney/chest-xray-pneumonia>. Consists of 5,863 X-Ray images (Jpeg) and has two categories, namely Pneumonia and Normal.

B. Data Analysis

Biomedical images come in a wide variety of shapes and sizes. Images for a comparable pathological condition could alter significantly from person to person, and even from encounter to encounter. These discrepancies could be due to variances in illumination, marker stains (for pathological investigations), image extraction procedure, image dimension, and so on. Image preprocessing guarantees that all of the photos are in the same format and are free of noise that is irrelevant to the study.

C. Research Architecture

This study's research architecture is based on multiple previous investigations [35][38]. A training model and a test model are included in the created model. (See Fig. 2).

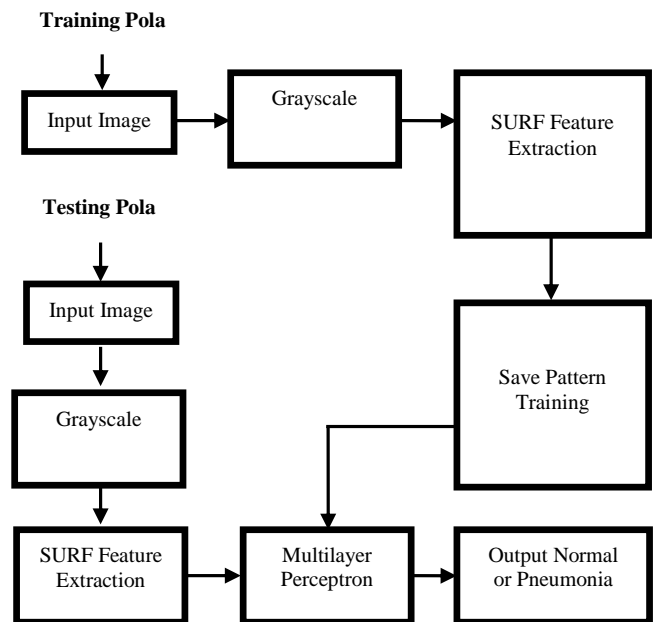


Fig. 2. Research Architecture [35] [38].

Fig. 2 shows the research steps that will be carried out with two processes, the first is the training process, namely the process of extracting data (grayscale to minimize the color space in the image from three color spaces R, G, B into one color space, namely grayscale and extracting by utilizing the SURF feature). and the data is stored as a pattern model that will be used in the testing phase, the second testing process is the process of matching the pattern model that has been trained by utilizing the Multilayer perceptron method as a classification.

IV. RESULTS AND DISCUSSION

A. Pneumonia X-Ray Sample Set

Fig. 3 shows some pneumonia samples and normal x-ray images used in this study Fig. 3.

Sample X-ray Set of Pneumonia is illustrated in Fig. 3.

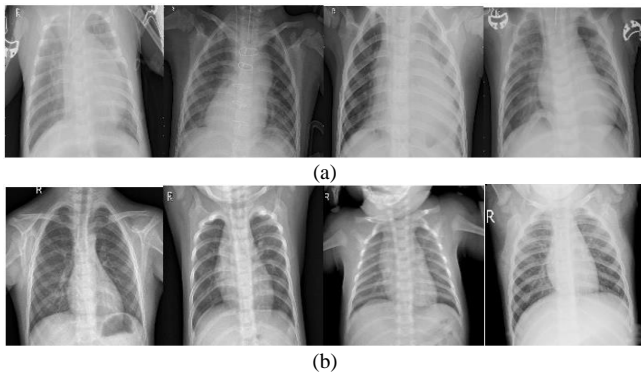


Fig. 3. Sample X-Ray Set (a) Pneumonia, (b) Normal.

B. Surf Detection

The results of feature SURF detection are marked with a circle on the image, Fig. 4 shows the results of feature SURF detection with 100 strongest values on the X-ray Set Pneumonia image.

C. Performance Measure

A confusion matrix was used to describe the performance of a classification model on a test dataset for which the true values were known. It enables the visualization of an algorithm's performance.

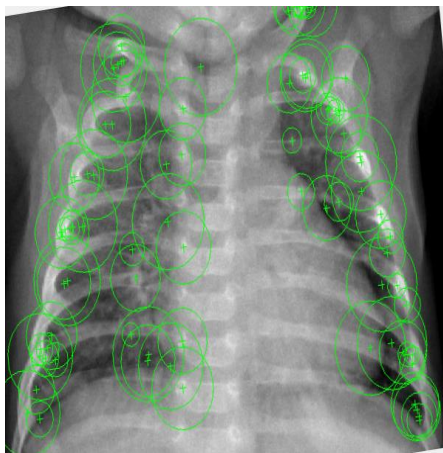


Fig. 4. Surf Detection.

A method's accuracy indicates how accurate the projected values are. Precision refers to the measurement's repeatability, or how many of the forecasts are right. The recall specifies how many right answers are found. The f1-score calculates a balanced average outcome by combining precision and recall. The equations below illustrate how to calculate these values, with TP, TN, FP, and FN standing for true positive, true negative, false positive, and false negative, respectively.

$$\text{Accuracy} = \frac{TP+TN}{TP+FP+TN+FN} \quad (1)$$

$$\text{Precision} = \frac{TP}{TP+FP} \quad (2)$$

$$\text{Recall} = \frac{TP}{TP+FN} \quad (3)$$

$$\text{F1 - Score} = \frac{2 \times \text{Precision} \times \text{Recall}}{\text{Precision} + \text{Recall}} \quad (4)$$

D. Experiment

The classification process using a multilayer perceptron was tested with variations in the learning rate [0.1; 0.3; 0.5; 0.7; 0.9; 0.01; 0.03; 0.05; 0.07; 0.09; 0.001; 0.003; 0.005; 0.007; 0.009; 0.0001; 0.0003; 0.0005; 0.0007; 0.0009;] and momentum variation [0.1; 0.3; 0.5; 0.7; 0.9] to determine the optimal level of accuracy on the multilayer perceptron in classifying Pneumonia with condition 100 epochs. The experimental results are presented in Table I, Table II, Table III, Table IV and Table V.

TABLE I. MULTILAYER PERCEPTRON WITH 0.1 MOMENTUM

Learning Rate	ACCURACY	Precision	Recall	F1-Score
0.1	0.824	0.824	0.824	0.824
0.3	0.822	0.823	0.822	0.822
0.5	0.818	0.819	0.818	0.818
0.7	0.816	0.818	0.816	0.816
0.9	0.813	0.814	0.813	0.812
0.01	0.825	0.826	0.825	0.825
0.03	0.824	0.824	0.824	0.824
0.05	0.827	0.828	0.827	0.827
0.07	0.82	0.82	0.82	0.82
0.09	0.826	0.826	0.826	0.826
0.001	0.819	0.821	0.819	0.819
0.003	0.823	0.824	0.823	0.823
0.005	0.823	0.824	0.823	0.823
0.007	0.823	0.824	0.823	0.823
0.009	0.825	0.826	0.825	0.825
0.0001	0.771	0.805	0.771	0.764
0.0003	0.816	0.821	0.816	0.816
0.0005	0.82	0.822	0.82	0.82
0.0007	0.819	0.821	0.819	0.819
0.0009	0.82	0.821	0.82	0.819

TABLE II. MULTILAYER PERCEPTRON WITH 0.3 MOMENTUM

Learning Rate	ACCURACY	Precision	Recall	F1-Score
0.1	0.828	0.828	0.828	0.828
0.3	0.819	0.82	0.819	0.819
0.5	0.817	0.818	0.817	0.817
0.7	0.812	0.813	0.812	0.812
0.9	0.814	0.816	0.814	0.814
0.01	0.824	0.825	0.824	0.824
0.03	0.827	0.828	0.827	0.827
0.05	0.821	0.821	0.821	0.821
0.07	0.827	0.828	0.827	0.827
0.09	0.828	0.828	0.828	0.828
0.001	0.82	0.821	0.82	0.82
0.003	0.823	0.824	0.823	0.823
0.005	0.823	0.823	0.823	0.823
0.007	0.825	0.826	0.825	0.825
0.009	0.826	0.827	0.826	0.826
0.0001	0.784	0.809	0.784	0.779
0.0003	0.819	0.821	0.819	0.818
0.0005	0.82	0.821	0.82	0.819
0.0007	0.82	0.821	0.82	0.819
0.0009	0.819	0.82	0.819	0.819

TABLE IV. MULTILAYER PERCEPTRON WITH 0.7 MOMENTUM

Learning Rate	ACCURACY	Precision	Recall	F1-Score
0.1	0.824	0.824	0.824	0.824
0.3	0.822	0.823	0.822	0.822
0.5	0.818	0.819	0.818	0.818
0.7	0.812	0.813	0.812	0.812
0.9	0.814	0.816	0.814	0.814
0.01	0.824	0.825	0.824	0.824
0.03	0.827	0.828	0.827	0.827
0.05	0.821	0.821	0.821	0.821
0.07	0.82	0.82	0.82	0.82
0.09	0.826	0.826	0.826	0.826
0.001	0.819	0.821	0.819	0.819
0.003	0.823	0.824	0.823	0.823
0.005	0.823	0.824	0.823	0.823
0.007	0.825	0.826	0.825	0.825
0.009	0.824	0.825	0.824	0.824
0.0001	0.822	0.822	0.822	0.822
0.0003	0.795	0.81	0.795	0.792
0.0005	0.82	0.821	0.82	0.819
0.0007	0.819	0.821	0.819	0.819
0.0009	0.82	0.821	0.82	0.819

TABLE III. MULTILAYER PERCEPTRON WITH 0.5 MOMENTUM

Learning Rate	ACCURACY	Precision	Recall	F1-Score
0.1	0.813	0.813	0.813	0.813
0.3	0.815	0.816	0.815	0.815
0.5	0.81	0.81	0.81	0.81
0.7	0.808	0.809	0.808	0.808
0.9	0.811	0.812	0.811	0.811
0.01	0.821	0.822	0.821	0.821
0.03	0.823	0.824	0.823	0.823
0.05	0.827	0.828	0.827	0.827
0.07	0.827	0.827	0.827	0.827
0.09	0.819	0.819	0.819	0.819
0.001	0.822	0.823	0.822	0.822
0.003	0.823	0.823	0.823	0.823
0.005	0.825	0.826	0.825	0.825
0.007	0.824	0.825	0.824	0.824
0.009	0.822	0.822	0.822	0.822
0.0001	0.795	0.81	0.795	0.792
0.0003	0.82	0.821	0.82	0.819
0.0005	0.82	0.821	0.82	0.819
0.0007	0.819	0.82	0.819	0.819
0.0009	0.821	0.822	0.821	0.821

TABLE V. MULTILAYER PERCEPTRON WITH 0.9 MOMENTUM

Learning Rate	ACCURACY	Precision	Recall	F1-Score
0.1	0.813	0.813	0.813	0.813
0.3	0.822	0.823	0.822	0.822
0.5	0.818	0.819	0.818	0.818
0.7	0.816	0.818	0.816	0.816
0.9	0.811	0.812	0.811	0.811
0.01	0.821	0.822	0.821	0.821
0.03	0.823	0.824	0.823	0.823
0.05	0.827	0.828	0.827	0.827
0.07	0.827	0.827	0.827	0.827
0.09	0.828	0.828	0.828	0.828
0.001	0.82	0.821	0.82	0.82
0.003	0.823	0.824	0.823	0.823
0.005	0.823	0.823	0.823	0.823
0.007	0.824	0.825	0.824	0.824
0.009	0.824	0.825	0.824	0.824
0.0001	0.822	0.822	0.822	0.822
0.0003	0.795	0.81	0.795	0.792
0.0005	0.82	0.821	0.82	0.819
0.0007	0.819	0.82	0.819	0.819
0.0009	0.821	0.822	0.821	0.821

Based on the results of the experiments, the accuracy, precision, recall, and f1-score obtained a relatively stable value, with the lowest accuracy value being 78.4% and the highest accuracy value being 82.8%, the lowest precision value being 80.5% and the highest precision value being 82.8%, the lowest recall value being 78.4% and the highest recall value being 82.8%, the lowest f1-score being 76.4% and the highest f1-score being 82.8%.

Fig. 5 illustrates the entire experiment, from the highest classification report level to the lowest classification report level.

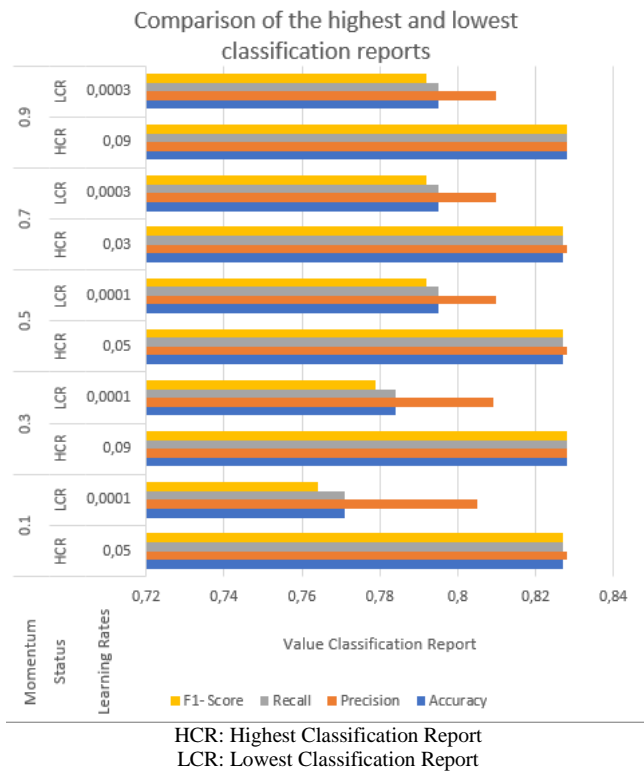


Fig. 5. Comparison of Highest and Lowest Classification Report.

E. Discussion

The highest classification report rate was found at the momentum condition 0.3 and the learning rate 0.09, and at the momentum condition 0.9 and the learning rate 0.09, with 82.8 %, 82.8 % precision, Recall 82.8 %, and f1-score 82.8 %, based on the results of 100 experiments with variations in the momentum value and variations in the learning rate value.

Detection of COVID-19 Infection in Chest X-rays Using Deep Transfer Learning is a previous study. In training conditions, the VGGNet model has an accuracy of 90.32 %, F-measure 90.07 %, sensitivity 91.22 %, specificity 89.12 %, and kappa statistic 90.12 %, while it has an accuracy of 90.32 %, F-measure 91.69 %, sensitivity 91.83 %, specificity 90.16 %, and kappa statistic 90.54 %.

Using the bayesian noise-OR function to account for the effects of interference on the image, previous research discussed the CNN Model in classifying CT image data sets and determining the probability of COVID19. The results of the

classification report 86.7 % accuracy, 81.3 % precision, 86.7 % recall, and 83.9 % f1-score.

Deep learning and the inception have been used in previous research. To learn about medical disorders. The layers are trained using the Adam Optimizer with a learning rate of 0.001 and stochastic gradient descent in batches of 1,000 images each step. In all categories, training lasts 10,000 steps or 100 epochs. In a comparison of pneumonia to normal chest X-rays, we achieved an accuracy of 92.8 %, with a sensitivity of 93.2 % and a specificity of 90.1 %. The area under the ROC curve for pneumonia detection from normal was 96.8%.

The classification of pneumonia is covered by khairina[48]. The successes in this study are with the level of accuracy, precision, recall, and f1-score with values of 0.8067, 0.7948, 0.9237, and 0.8544 in identifying the symptoms of pneumonia by combining the K-Nearest Neighbor method with the Histogram of Oriented Gradient as a feature selection and feature extraction model.

IV. CONCLUSION

Based on the experiments that have been carried out, in general, the learning rate value is not very influential in the learning process, both at the momentum values of 0.1, 0.3, 0.5, 0.7, and 0.9. The best desirable accuracy value for momentum 0.1 is at a learning rate of 0.05. The best desirable accuracy value for momentum 0.3 is at a learning rate of 0.09. The most desirable accuracy value for momentum 0.3 is at a learning rate of 0.05 and 0.07. At a learning rate of 0.03 the highest ideal accuracy value is obtained. The best desirable accuracy value for momentum 0.9 is at a learning rate of 0.09 this research should be redone using the number of hidden layers and nodes in each hidden layer. The addition of a hidden layer, as well as variations in the number of nodes in the hidden layer, will affect computation time and yield more optimal accuracy results.

REFERENCES

- [1] L. Listyalina, "Peningkatan Kualitas Citra Foto Rontgen Sebagai Media Deteksi Kanker Paru," Jurnal Teknologi Informas, Vol. 12, Pp. 110-118, 2017.
- [2] M. Muhathir, S. Theofil Tri Saputra, and A.-K. Al-Khowarizmi, "Analysis K-Nearest Neighbors (KNN) in Identifying Tuberculosis Disease (Tb) By Utilizing Hog Feature Extraction," Al'adzkiya Int. Comput. Sci. Inf. Technol. J., vol. 1, no. 1, pp. 33-38, 2020.
- [3] I. Sirazitdinov, M. Kholiavchenko, T. Mustafaev, Y. Yixuan, R. Kuleev and B. Ibragimov, "Deep Neural Network Ensemble for Pneumonia Localization from A Large-Scale Chest X-Ray Database," Comput. Electrical Eng. Vol. Vol. 78, P. 388-399, 2019.
- [4] K. E. Asnaoui, Y. Chawki and A. Idri, "Automated Methods For Detection And Classification Pneumonia Based On X-Ray Images Using Deep Learning," Electrical Engineering And Systems Science , Pp. 1-28, 2020.
- [5] I. M. D. Maysanjaya, "Klasifikasi Pneumonia Pada Citra X-Rays Paru-Paru Dengan Convolutional Neural Network," Jurnal Nasional Teknik Elektro Dan Teknologi Informasi, Vol. Vol. 9 No. 2, Pp. 190-195, Mei 2020.
- [6] Y. Dong, Y. Pan, J. Zhang and W. Xu, "Learning To Read Chest X-Ray Images From 16000+ Examples Using Cnn,," International Conference On Connected Health: Applications, Systems And Engineering Technologies (Chase), Pp. 51-57, 2017.
- [7] B. Biswas, S. Ghosh, S. Bhattacharyya, J. Platos, V. Snasel and A. Chakrabarti, "Chest X-Ray Enhancement To Interpret Pneumonia Malformation Based On Fuzzy Soft Set And Dempster - Shafer Theory Of Evidence," Appl. Soft Comput. J., Vol. Vol. 86, Pp. 105889,, 2020.

- [8] P. Rajpurkar, K. Z. J. Irvin, H. M. B. Yang, T. Duan, D. Ding, A. Bagul, R. Ball, C. Langlotz, K. Shpanskaya, M. Lungren Dan A. Ng, "Chexnet: Radiologist-Level Pneumonia Detection On Chest X-Rays With Deep Learning," Arxiv Prepr, P. 3–9, 2017.
- [9] Y. Shindo et al., "Risk factors for drug-resistant pathogens in community-acquired and healthcare-associated pneumonia," *Am. J. Respir. Crit. Care Med.*, vol. 188, no. 8, pp. 985–995, 2013, doi: 10.1164/rccm.201301-0079OC.
- [10] M. Mahin, S. Tonmoy, R. Islam, T. Tazin, M. M. Khan, and S. Bourouis, "Prediction of COVID-19 and Pneumonia using Deep Learning," *J. Healthc. Eng.*, vol. 2021, no. may, pp. 1–11, 2021, doi: <https://doi.org/10.1155/2021/3514821>.
- [11] A. Rahmawati, D. Wintana, S. Suhada, Gunawan and H. Sulaiman, "Klasifikasi Naïve Bayes Untukmendiagnosis Penyakit Pneumoniapadaanak Balita(Studi Kasus : Uptd Puskesmas Sukaraja Sukabumi)," *Kumpulan Jurnal Ilmu Komputer*, Vol. 6, No. 3, Pp. 241-253, 2019.
- [12] R. L. Abdjul and S. Herlina, "Asuhan Keperawatan Pada Pasien Dewasa Dengan Pneumonia : Study Kasus," *Indonesian Jurnal Of Health Development*, Vol. Volume 2 Nomor 2, Pp. 102-107, 2020.
- [13] V. H. Mulyani, "Rumah Sehat Dan Imunisasi Dasar Lengkap Sebagai Risiko Penyebab Kejadian Pneumonia Balita Di Kabupaten Jember: Studi Korelasi," *Jurnal Kesehatan Lingkungan*, Vol. 12, No. 1, Pp. 30-38, 2020.
- [14] C. Wijaya, H. Irsyad and W. Widhiarso, "Klasifikasi Pneumonia Menggunakan Metode K-Nearest Neighbor Dengan Ekstraksi Glem," *Jurnal Algoritme*, Vol. 1, No. 1, Pp. 33-44, 2020.
- [15] X. Xu et al., "A Deep Learning System to Screen Novel Coronavirus Disease 2019 Pneumonia," *Engineering*, vol. 6, no. 10, pp. 1122–1129, 2020, doi: 10.1016/j.eng.2020.04.010.
- [16] N. Narayan Das, N. Kumar, M. Kaur, V. Kumar, and D. Singh, "Automated Deep Transfer Learning-Based Approach for Detection of COVID-19 Infection in Chest X-rays," *IRBM*, Jul. 2020, doi: 10.1016/J.IRBM.2020.07.001.
- [17] G. Mackenzie, "The definition and classification of pneumonia," *Pneumonia*, vol. 8, no. 1, pp. 1–5, 2016, doi: 10.1186/s41479-016-0012-z.
- [18] A. J. J. Lister, C. F. Le, E. S. G. Cheah, M. N. M. Desa, D. W. Cleary, and S. C. Clarke, "Serotype distribution of invasive, non-invasive and carried *Streptococcus pneumoniae* in Malaysia: a meta-analysis," *Pneumonia*, vol. 13, no. 1, 2021, doi: 10.1186/s41479-021-00086-7.
- [19] D. Varshni, K. Thakral, L. Agarwal, R. Nijhawan and A. Mittal, "Pneumonia Detection Using Cnn Based Feature Extraction," *Ieee*, Pp. 1-7, 2019.
- [20] R. R. Wahid, S. I. Pradika and F. A. Putra, "Sistem Klasifikasi Pneumonia Menggunakan Deep Convolutional Neural Network Untuk Mengurangi Jumlah Kematian Balita Indonesia," *Jurnal Narodroid*, Vol. Vol. 6 No 1, Pp. 1-7, Jan 2020.
- [21] H. Ramchoun, M. A. J. Idrissi, Y. Ghanou and M. Ettaouil, "Multilayer Perceptron: Architecture Optimization And Training," *International Journal Of Interactive Multimedia And Artificial Intelligence*, Vol. 4, No. 1, Pp. 26-30, 2016.
- [22] A. A. Ewees, M. A. Elaziz, Z. Alameer, H. Ye Dan Z. Jianhua, "Improving Multilayer Perceptron Neural Network Using Chaotic Grasshopper Optimization Algorithm To Forecast Iron Ore Price Volatility," *Elsevier*, Vol. Volume 65, Pp. 1-12, 2019.
- [23] M. Windarti Dan P. T. Prasetyaninrum, "Prediction Analysis Student Graduate Using Multilayer Perceptron," *Atlantis Press Sarl*, Vol. Volume 440, Pp. 53-57, 2019.
- [24] N. D. Girsang and M. Muhathir, "Classification Of Batik Images Using Multilayer Perceptron With Histogram Of Oriented Gradient Feature Extraction," vol. 4, no. February, pp. 197–204, 2021.
- [25] M. H. Santoso, D. A. Larasati, and M. Muhathir, "Wayang Image Classification using MLP Method and GLCM Feature Extraction," *J. Comput. Sci. Inf. Technol. Telecommun. Eng.*, vol. 1, no. 2, pp. 111–119, 2020, doi: 10.30596/jcositte.v1i2.5131.
- [26] F. R. Lima-Junior and L. C. R. Carpinetti, "Predicting Supply Chain Performance Based On Scor@ Metrics And Multilayer Perceptron Neural Networks," *International Journal Of Production Economics*, Vol. 212, Pp. 19-38, 2019.
- [27] N. B. Gaikwad, V. Tiwari, A. Keskar and N. C. Shivaprakash, "Efficient Fpga Implementation Of Multilayer Perceptron For Real-Time Human Activity Classification," *Ieee Access*, Vol. 7, Pp. 26696-26706, 2019.
- [28] M. Muhathir, W. Hidayah, and D. Ifantiska, "Utilization of Support Vector Machine and Speeded up Robust Features Extraction in Classifying Fruit Imagery," *Comput. Eng. Appl.*, vol. 9, no. 3, pp. 183–193, 2020.
- [29] N. A. Arifin, B. Irawan and C. Setianingsih, "Traffic Sign Recognition Application Using Speeded-Up Robust Features (Surf) And Support Vector Machine (Svm) Based On Android," *Ieee Asia Pacific Conference On Wireless And Mobile (Apwimob)*, Pp. 52-58, 2017.
- [30] A. K. A. Hassan, B. S. Mahdi and A. A. Mohammed, "Writer Identification Based Onarabic Handwriting Recognition Byusing Speed Uprobust Feature And K-Nearest Neighbor Classification," *Journal Of University Of Babylonforpure And Applied Sciences*, Vol. 27, No. 1, Pp. 1-10, 2019.
- [31] B. Xie, J. Li and X. Zhao, "Strain Measurement Based On Speeded-Up Robust Feature Algorithm Applied To Microimages From A Smartphone-Based Microscope," *Sensors*, Vol. 20, Pp. 1-16, 2020.
- [32] S. Banerjee, S. K. Chaturvedi and S. P. Tiwari, "Development Of Speed Up Robust Feature Algorithm For Aerial Image Feature Extraction," *Incas Bulletin*, Vol. 11, No. 4, Pp. 49-60, 2019.
- [33] A. K. A. Hassan, B. S. Mahdi and A. A. Mohammed, "Writer Identification Based On Arabic Handwriting Recognition By Using Speed Up Robust Feature And K- Nearest Neighbor Classification," *Journal Of University Of Babylon For Pure And Applied Sciences*, Vol. 27 No. 1, Pp. 1-10, 2019.
- [34] S. A. K. Tareen and Z. Saleem, "A Comparative Analysis Of Sift, Surf, Kaze, Akaze, Orb, And Brisk," *International Conference On Computing, Mathematics And Engineering Technologies – Icomet*, Vol. %1 Dari %2978-1-5386-1370-2, 2018.
- [35] Muhathir, R. A. Rizal, J. S. Sihotang and R. Gultom, "Comparison Of Surf And Hog Extraction In Classifying The Blood Image Of Malaria Parasites Using Svm," *International Conference Of Computer Science And Information Technology (Icosnikom)*, 2019, doi: 10.1109/ICoSNIKOM48755.2019.9111647.
- [36] Bae, M. (2021). Optimizing the Hyper-parameters of Multi-layer Perceptron with Greedy Search. *American Journal of Computer Science and Technology*, 4(4), 90–96. <https://doi.org/10.11648/j.ajcst.2021.0404.11>.
- [37] Ke, K. C., and Huang, M. S. (2021). Enhancement of multilayer perceptron model training accuracy through the optimization of hyperparameters: a case study of the quality prediction of injection-molded parts. *International Journal of Advanced Manufacturing Technology*. <https://doi.org/10.1007/s00170-021-08109-9>.
- [38] Muhathir and Al-Khowarizmi, "Measuring the Accuracy of SVM with Varying Kernel Function for Classification of Indonesian Wayang on Images," in 2020 International Conference on Decision Aid Sciences and Application (DASA), 2020, pp. 1190–1196. doi: 10.1109/DASA51403.2020.9317197.
- [39] D. S. Kermary et al., "Identifying Medical Diagnoses and Treatable Diseases by Image-Based Deep Learning," *Cell*, vol. 172, no. 5, pp. 1122–1131.e9, 2018, doi: 10.1016/j.cell.2018.02.010.
- [40] L. Ekonomou, V. Mladenov and C. Christodolou, "A short-term load forecasting method using artificial neural networks and wavelet analysis," *International Journal of Power Systems*, vol. 1, 2016.
- [41] P. Ray and S. Reddy, "Various dimension reduction techniques for high dimensional data analysis: a review," *Artificial Intelligence Review*, 2021.
- [42] M. Muhathir, R. Muliono, And M. Hafni, "Image Classification Of Autism Spectrum Disorder Children Using Naïve Bayes Method With Hog Feature Extraction," *Journal Of Informatics And Telecommunication Engineering*, Vol. 5, No. 2, Pp. 494–501, Jan. 2022, Doi: 10.31289/Jite.V5i2.6365.
- [43] S. S. Reddy, "Power System Topological Observability Analysis Using Improved Hopfield Neural Network," *Journal of Electrical and Electronics Engineering*, vol. 9, 2016.
- [44] A. M. Alqudah, S. Qazan and I. Masad, "Artificial Intelligence Framework for Efficient Detection and Classification of Pneumonia

- Using Chest Radiography Images," Journal of Medical and Biological Engineering, 2021.
- [45] G. Latif, F. Y. A. Anezi, F. N. Sibai and J. Alghazo, "Lung Opacity Pneumonia Detection with Improved Residual Networks," Journal of Medical and Biological Engineering, 2021.
- [46] B. Umroh, Muhathir, and Darianto, "The Optimum Cutting Condition when High Speed Turning of Aluminum Alloy using Uncoated Carbide," IOP Conf Ser Mater Sci Eng, vol. 505, no. 1, p. 12041, May 2019, doi: 10.1088/1757-899x/505/1/012041.
- [47] R. Muliono, Muhathir, N. Khairina, and M. K. Harahap, "Analysis of Frequent Itemsets Mining Algorithm Againsts Models of Different Datasets," J Phys Conf Ser, vol. 1361, no. 1, p. 12036, Nov. 2019, doi: 10.1088/1742-6596/1361/1/012036.
- [48] N. Khairina, T. T. S. Sibarani, R. Muliono, Z. Sembiring, And M. Muhathir, "Identification Of Pneumonia Using The K-Nearest Neighbors Method Using Hog Fitur Feature Extraction," Journal Of Informatics And Telecommunication Engineering, Vol. 5, No. 2, Pp. 562–568, Jan. 2022, Doi: 10.31289/Jite.V5i2.6216.

Forecasting Covid-19 Time Series Data using the Long Short-Term Memory (LSTM)

Harun Mukhtar¹, Reny Medikawati Taufiq², Ilham Herwinanda³, Doni Winarso⁴, Regiolina Hayami⁵

Informatics engineering department, Faculty of Computer Science, Universitas Muhammadiyah Riau, Pekanbaru, Indonesia^{1, 2, 3, 5}
Information system department, Faculty of Computer Science, Universitas Muhammadiyah Riau, Pekanbaru, Indonesia⁴

Abstract—Confirmed statistical data of Covid-19 cases that have accumulated sourced from (<https://corona.riau.go.id/data-statistik/>) in Riau Province on June 7, 2021, there were 63441 cases, on June 14, 2021, it increased to 65883 cases, on June 21, 2021, it increased to 67910, and on June 28, 2021, it increased to 69830 cases. Since the beginning of this pandemic outbreak, it has been observed that the case data continues to increase every week until this July. This study predicts cases of Covid-19 time series data in Riau Province using the LSTM algorithm, with a dataset of 64 lines. Long-Short Term Memory has the ability to store memory information for patterns in the data for a long time at the same time. Tests predicting historical data for Covid-19 cases in Riau Province resulted in the lowest RMSE value in the training data, which was 8.87, and the test data, which was 13.00, in the death column. The evaluation of the best MAPE value in the training data, which is 0.23%, is in the recovered column, and the evaluation of the best MAPE value in the test data, which is 0.27%, in the positive_number column. In the test to predict the next 30 days using the LSTM model that has been trained, it was found that the performance evaluation of the prediction results for the positive_number column and the death column was very good, the recovery column was categorized as good, the independent_isolation column and the care_rs column were categorized as poor.

Keywords—Time series prediction; forecasting; recurrent neural network; long short-term memory

I. INTRODUCTION

Indonesia is one of the countries hit by the Covid-19 pandemic which continues to increase every day. Covid-19 outbreak due to the coronavirus began to appear in mid-December 2019 in China, precisely in the city of Wuhan, and has spread to several countries worldwide. The World Health Organization (WHO) had declared January 30, 2020, a public health emergency. The Covid-19 pandemic entered Indonesia on March 2, 2020, it is known from existing information that there have been Indonesian citizens who have been infected. The two 64-year-old women, and their 31-year-old daughter were declared positive for Covid-19 after having contact with a Japanese citizen [1], [2].

The Riau Provincial Government made various efforts to suppress the transmission of the coronavirus, namely by providing health protocol directions, including washing hands, maintaining a distance of two meters, avoiding crowds, avoiding touching your face with your hands, and maintaining a healthy diet. This is in the spotlight with the aim of suppressing the addition of new cases and reducing the death rate. Confirmed statistical data for the accumulation of the

Covid-19 cases sourced from (<https://corona.riau.go.id/data-statistik/>), in Riau Province on June 7, 2021, as many as 63441 cases; on June 14, 2021 it increased to 65883 cases, on June 21, 2021 it increased to 67910, on June 28, 2021 it increased to 69830 cases, and so on. Since the beginning of the outbreak of this pandemic outbreak, it has been observed that case data continues to grow every week until this August [3]. Riau Province is one of the areas in Indonesia which is included in the dangerous zone.

A method is needed to estimate the number of Covid-19 cases every day with data in Riau Province. Forecasting is a technique for predicting conditions that will occur in the future based on data from the past. Predicting the Covid-19 phenomenon based on incident data with sequential time series can be done using the Machine Learning approach [4]. The predicted data in this study are classified as time series. Time series data is a series of observed data based on a certain time interval. The time-series approach explains that the model is influenced by data that occurred in the past [5]. This study makes predictions using the Long Short-Term Memory (LSTM) algorithm. LSTM can store memory information for patterns in the data for a long time simultaneously. LSTM is used for data processing, one of which is time-series data, including that carried out in research by [6] using the LSTM machine learning method, to predict the spread of Covid-19 cases in India based on the realization of prevention that have been implemented such as social restrictions and lockdowns. Then research [7] also uses the LSTM architecture, in forecasting time series data in predicting the development of Covid-19 transmission in Canada.

Based on the previous description, this study aims to predict cases of Covid-19 time series data in Riau Province, using the LSTM algorithm, by achieving the maximum level of accuracy and producing the slightest difference in values between the actual data and prediction [8]. The data sample used was obtained from public data which amounted to 64 lines of accumulated data on Covid-19 cases in Riau Province, starting from June 7, 2021, to August 9, 2021. Referring to the reference, the attributes used as input data are positive numbers, self-isolation, hospitalization, recovery, and death.

II. LITERATURE REVIEW

Forecasting is a challenging part of time series data analysis. The dominant factors that affect the performance and accuracy of time series data analysis and the forecasting techniques used are based on the type of data and its context. Several problem domains that have dependent variables such

as seasons, economic shocks, unexpected events, and internal organizational changes that produce data also affect predictions [9]. Another review by the same author points out evaluation, and dynamic modeling is exciting fields of study with a wide variety of packages in business, economics, finance, and computer science. The reason for evaluating the collection time is to look at the observations of the time collection path and build a mode to explain the shape of the information and then predict the value of gathering time density. Due to the importance of time collection forecasting in many branches of implemented science, it is important to build robust modes with the aim of increasing forecasting accuracy [10].

Forecasting techniques are used in various case studies, such as in predicting the future affordability of Covid-2019 throughout countries by utilizing real-time information from the Johns Hopkins dashboard [11]. Indicates the accuracy of the flow of foreign tourist arrivals in the Intelligent Tourism System (ITS), using the Long Short Term Memory Neural Network (LSTM) method [12]. Forecasts the arrival of foreign tourists in the Covid-19 pandemic situation, using the LSTM artificial neural network approach [13]. Conducted a study predicting the value of financial market assets in the future with higher accuracy [14].

LSTM is a variation of RNN and has been proven to carry out proper time collection mastering due to the fact that LSTM can preserve contextual data in addition to conducting primarily based totally on sure time-collection events [15]. LSTM is a form of iterative community which has been tested to be very successful on several problems, given its capacity to differentiate between maximum current and initial instance through assigning extraordinary weights to each at the same time as forgetting reminiscences deemed imprecise to predict subsequent outputs [16]. Siami-Namini *et al.* [10], compared Deep Learning algorithms such as LSTM and traditional algorithms such as ARIMA to estimate time series data. They got the result that LSTM is better than ARIMA. More specifically, the average reduction in the error rate obtained by LSTM is between 84 - 87 percent compared to ARIMA. Dutta *et al.* [17] use machine learning to help doctors verify and predict disease growth shortly. The result of their research is that the combination of machine learning models (CNN-LSTM) outperforms other models.

By evaluating the prediction outcomes of the LSTM and AT-LSTM fashions, it may be visible that the AT-LSTM overall performance is higher due to the fact the smallest MAPE cost is obtained. MAPE is a degree of the predictive accuracy of forecasting strategies in data and is greater persuasive whilst evaluating the overall performance of fashions on one-of-a-kind facts sets, as it is now no longer most effective considering the deviation among the expected cost and the authentic cost; however additionally considers the ratio among them [18].

Comparing the LSTM and BI-LSTM forecasting models, where the BI-LSTM combines the LSTM in the incoming collection school system instead of using a single LSTM and ends up with a decreased RMSE compared to the LSTM version. The BI-LSTM version plays higher than the LSTM

version due to the fact that the BI-LSTM version has backward propagation at every time the school expects data. Therefore, the prediction version proposed using the BI-LSTM can be utilized by the public and companies for forecasting the inventory market [19]. To test the performance of the prediction engine, Root Mean Square Error (RMSE) was used. The error or difference between the objective and the obtained output price is minimized by using the RMSE price. RMSE is the rectangular root of the implication/rectangular implication of all errors. The use of RMSE may be very unusual and lead to first-degree forecasting errors of metrics for the prediction of numerical data [20].

III. RESEARCH METHODOLOGY

The study predicts Covid-19 cases in Riau Province using the Long Short-Term Memory algorithm, carried out with data mining flow steps for forecasting as shown in Fig. 1.

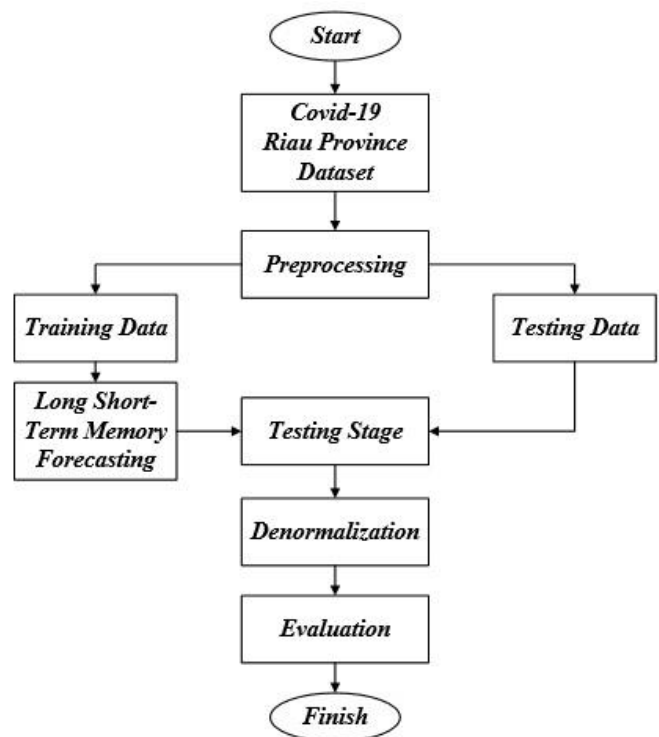


Fig. 1. Forecasting Workflow.

A. Dataset

The dataset being searched comes from public data obtained from the official website <https://corona.riau.go.id/data-statistik/>. This dataset is a time-series data type, containing information on Covid-19 cases in Riau Province, which is visualized in the form of a bar graph. Data collection starts from June 7, 2021, to August 9, 2021. The dataset consists of 64 rows of data manually entered in a Microsoft Excel spreadsheet and saved in .csv file format and named the file dataset_covid19_riau. Table I is a representation of time series data that has been accumulated, from Covid-19 cases that have occurred in Riau Province.

TABLE I. COVID-19 RIAU PROVINCE DATASET

date	total_ positive	self_ isolation	hospital_ care	recover	decease
6/7/2021	63441	4335	867	56546	1693
6/8/2021	63786	4060	837	57183	1706
6/9/2021	64188	3836	806	57827	1719
6/10/2021	64626	3836	762	58297	1731
6/11/2021	65010	3808	715	58744	1743
...
8/5/2021	102926	12365	1392	86375	2794
8/6/2021	105125	13416	1374	87486	2849
8/7/2021	106376	13574	1376	88526	2900
8/8/2021	107532	12783	1356	90466	2927
8/9/2021	108316	12012	1362	91963	2979

B. Preprocessing

This time-series data processing leads to one sample of attribute data as input and output data for the future, and determines how many prediction outputs are generated. Processing of data categorized as numerical data is carried out by normalizing the min-max scale. The min-max normalization preprocessing stage is the stage of changing the value of the actual numeric data (units, tens, hundreds, thousands, and so on) to a scaled value between 0 (as the minimum value) to 1 (as the maximum value) [3]. The data normalization process for all columns is intended as data input into the LSTM forecasting engine, which accepts input values with a distance between 0 to 1. For example, the smallest value in the positive_number column, which is 63441, is changed to 0, then the largest value 108316 is changed to 1. The other data values are converted to decimal numbers between 0 and 1. Table II is the result of normalization data in the positive_number column.

TABLE II. DATA NORMALIZATION RESULTS

date	positive_number	data normalization
6/7/2021	63441	0
6/8/2021	63786	0.007688022
6/9/2021	64188	0.01664624
6/10/2021	64626	0.026406685
6/11/2021	65010	0.034963788
...
8/5/2021	102926	0.879888579
8/6/2021	105125	0.928891365
8/7/2021	106376	0.956768802
8/8/2021	107532	0.982529248
8/9/2021	108316	1

C. Composition of Training Data and Test Data

The dataset is divided into two, namely training data and test data. The proportion of distribution for training data is more than for test data. The training data is intended to build a forecasting learning machine with the Long Short-Term

Memory (LSTM) algorithm, and the test data is intended for testing in predicting Covid-19 cases in Riau Province. The separation process of training data and test data is carried out with a division ratio of 85:15. As much as 85% of the total dataset, namely 54 data lines, starting from June 7, 2021, to July 30, 2021, is used for training data in order to build a forecasting engine with the LSTM algorithm. As much as 15% of the total dataset, which is 10 data lines, starting from July 31, 2021, to August 9, 2021, is used for test data in predicting the next accumulated cases of Covid-19 in Riau Province.

D. Long Short-Term-Memory Forecasting

Build an LSTM forecasting architecture using the python hard module, then import the sequential model, LSTM layer, and dense layer. A sequential model is a model that has one input layer, several hidden layers, and one output layer. By creating a new variable, namely the model, the architecture that is built is composed of one hidden LSTM layer with 50 units of neurons or nerves that function to process input data, which in the LSTM layer also becomes an input layer with shape parameters that have been made in the previous program code. It also uses the sigmoid activation function parameter. Dense layer functions as an output that receives the input information that has been processed in the hidden layer. After that call the compile() function to configure the data training process, with adam optimization and perform a loss percentage calculation with the mean squared error, to review the information on the predicted error rate that is targeted to a minimum. The LSTM forecasting architecture can be seen in Fig. 2.

```
Model: "sequential_17"  
  
Layer (type)                Output Shape                Param #  
-----  
lstm_17 (LSTM)              (None, 50)                 10200  
-----  
dense_16 (Dense)            (None, 1)                  51  
-----  
Total params: 10,251  
Trainable params: 10,251  
Non-trainable params: 0
```

Fig. 2. LSTM Forecasting Architecture.

E. Testing Predictions of Covid-19 Cases in Riau Province

The tests carried out were comparing and calculating the difference between the results of the actual test case data values and the test data values for the predicted accumulated Covid-19 cases. The prediction testing process is carried out with training data that has gone through the training stage. Furthermore, predictions of positive cases of Covid-19 are carried out on training data, starting from June 8, 2021, to July 29, 2021, and test data starting from August 1, 2021, until August 8, 2021.

F. Denormalization of Actual Data and Predicted Data

After the test is complete, the prediction results on the two data are data that are still normalized. The normalized values in the training data, test data, training data prediction results, and test data prediction results are converted into actual values by a denormalization process and then display the overall

results of these actual values. The results of denormalization can be seen in Table III and Table IV.

G. Evaluation of Test Results

In proving the accuracy and performance of the LSTM forecasting engine, it is necessary to calculate the difference between the predicted data value and the actual data value, based on the results of the Covid-19 prediction test in Riau Province. First measured by calculating the level of accuracy using the calculation of Root Mean Square Error (RMSE) to find the smallest error, which can be seen in the following equation (1).

$$RMSE = \sqrt{\frac{\sum_{i=1}^N (y - \hat{y})^2}{N}} \tag{1}$$

Where N is the number of observed data, $y_1, y_2, y_3, \dots, y_n$ is the observed value, while $\hat{y}_1, \hat{y}_2, \hat{y}_3, \dots, \hat{y}_n$ is the predicted value.

The higher the resulting RMSE value, the lower the level of accuracy, and the lower the resulting RMSE value, the higher the level of accuracy [5]. The second measure is the Mean Absolute Percentage Error (MAPE) calculation, to determine LSTM performance evaluation in forecasting (forecasting), which can be seen in the following equation (2).

$$MAPE = \frac{100}{N} \sum_{i=1}^N \frac{|y_i - \hat{y}_i|}{y_i} \tag{2}$$

TABLE III. EXAMPLE OF TRAINING DATA DENORMALIZATION RESULTS

No	Training Data	Practice Prediction Results	Difference
0	63786.0	63429.894531	356.105469
1	64188.0	63789.914062	398.085937
2	64626.0	64209.484375	416.515625
3	65010.0	64666.703125	343.296875
4	65398.0	65067.613281	330.386719
5	65720.0	65472.753906	247.246094
...
47	88019.0	87932.093750	86.906250
48	89115.0	88988.500000	126.500000
49	90582.0	90112.601562	469.398438
50	91857.0	91613.523438	243.476562
51	93913.0	92914.335938	998.664063

TABLE IV. EXAMPLES OF TEST DATA DENORMALIZATION RESULTS

No	Testing Data	Practice Prediction Results	Difference
0	98310.0	98246.726562	63.273438
1	99380.0	99438.843750	-58.843750
2	100623.0	100510.085938	112.914062
3	102086.0	101750.359375	335.640625
4	102926.0	103204.218750	-278.218750
5	105125.0	104035.960938	1089.039062
6	106376.0	106202.570312	173.429688
7	107532.0	107427.906250	104.093750

The use of MAPE in the evaluation of the prediction results can calculate the measurement accuracy of the actual value and the predicted value. MAPE calculates the error from the observation and prediction data, that is expressed in percent value [18]. The MAPE value criteria are shown in Table V.

TABLE V. MAPE QUALITATIVE CRITERIA [21]

MAPE Value	Interpretation
<10%	Evaluation of forecasting model capability is very good
10% - 20%	Evaluation of forecasting model capability is good
20% - 50%	Evaluation of forecasting model capability is sufficient
>50%	Evaluation of forecasting model capability is poor

Evaluation of predictions on statistics of COVID-19 instances is performed in five columns, specifically, positive_number, independent_isolation, hospitalization_rs, recovered, and died. Information on the assessment effects in every column, in predicting the dataset of showed Covid-19 instances that befell in Riau Province, is offered in Table VI.

Fig. 3 shows the positive case prediction test results, the yellow line shows the actual value of the training data, which coincides with the red dotted line, which is the predicted value of the training data, with an evaluation of RMSE 246.92 and MAPE 0.24%. Then the black line shows the actual value of the test data, which coincides with the green dotted line which is the predicted value of the test data, with an evaluation of RMSE 423.85 and MAPE 0.27%.

Fig. 4 shows the results of the self-isolation case prediction test, the yellow line shows the actual value of the training data, which coincides with the red dotted line, which is the predicted value of the training data, with an evaluation of RMSE 236.41 and MAPE 4.39%. Then the black line shows the actual value of the test data, which coincides with the green dotted line which is the predicted value of the test data, with an evaluation of RMSE 815.17 and MAPE 5.36%.

Fig. 5 shows the results of the prediction test for hospitalization cases, the yellow line show the actual value of the training data, which coincides with the red dotted line which is the predicted value of the training data, with an evaluation of RMSE 33.21 and MAPE 3.61%. Then the black line shows the actual value of the test data, which coincides with the green dotted line which is the predicted value of the test data, with an evaluation of RMSE 33.03 and MAPE 2.00%.

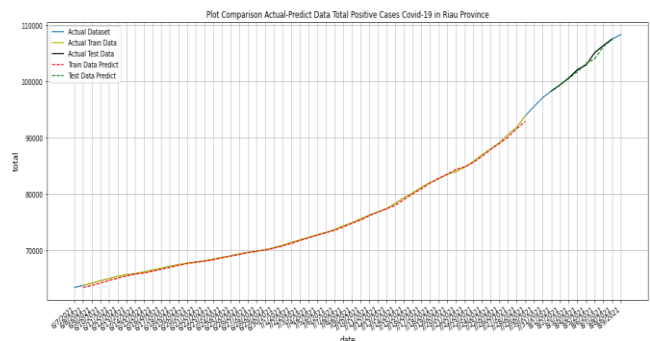


Fig. 3. Prediction Result of Positive Number.

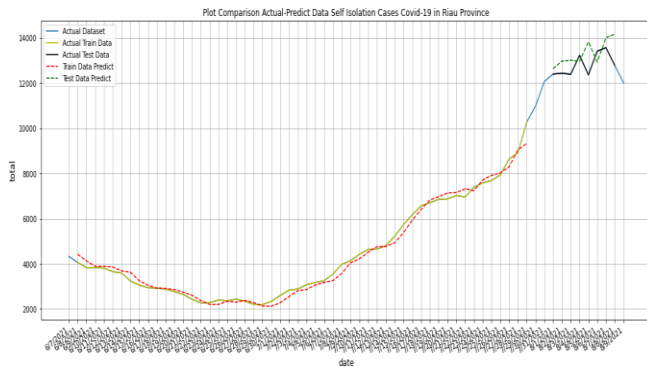


Fig. 4. Prediction Results of Isolation Cases.

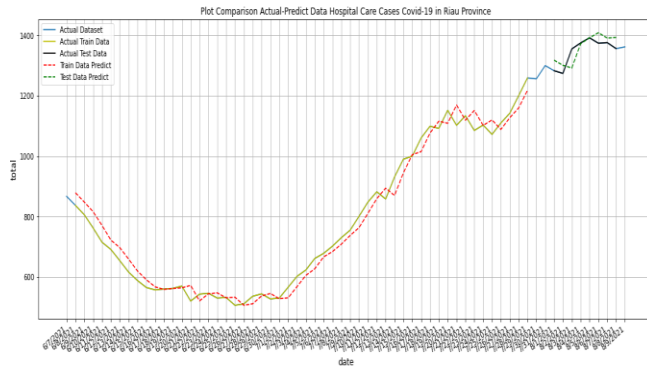


Fig. 5. Prediction Results of Hospitalization Cases.

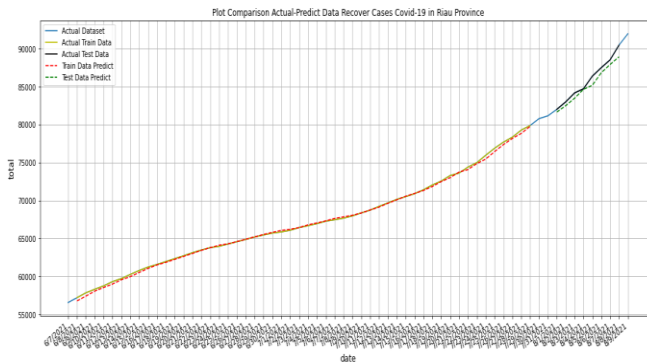


Fig. 6. Prediction Results of Healed Cases.

Fig. 6 shows the results of the prediction test for cured cases, the yellow line, show the actual value of the training data, which coincides with the red dotted line which is the predicted value of the training data, with RMSE 201.34 and MAPE 0.23% evaluation results. Then the black line shows the actual value of the test data, which coincides with the green dotted line which is the predicted value of the test data, with an evaluation of RMSE 827.57 and MAPE 0.81%.

Fig. 7 shows the death case prediction test results, the yellow line, show the actual value of the training data, which coincides with the red dotted line, which is the predicted value of the training data, with an evaluation of RMSE 7.51 and MAPE 0.32%. Then the black line shows the actual value of the test data, which coincides with the green dotted line which is the predicted value of the test data, with an evaluation of RMSE 17.85 and MAPE 0.54%.

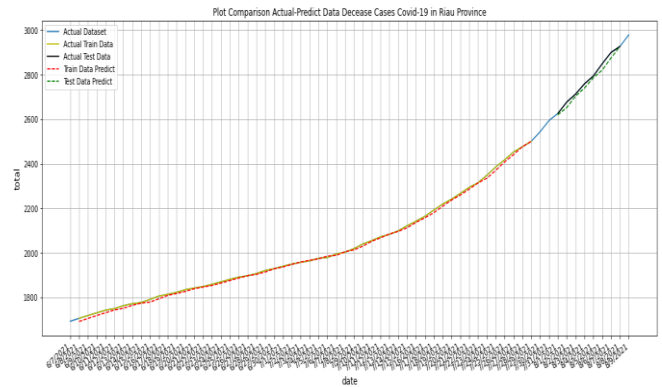


Fig. 7. Prediction Results of Death Cases.

In the graph above, it can be explained that the blue line is the overall data or dataset of Covid-19 cases that have accumulated in Riau Province. The yellow line shows the actual value of the training data, which coincides with the red dotted line which is the predicted value of the training data. Then the black line shows the actual value of the test data, which coincides with the green dotted line which is the predicted value of the test data.

TABLE VI. CONCLUSION OF EVALUATION OF HISTORICAL DATA PREDICTION TEST

No	Column Name	RMSE		MAPE		MAPE Criteria
		Actual & Prediction Training Data	Actual & Prediction Testing Data	Actual & Prediction Training Data	Actual & Prediction Testing Data	
1.	total_positive	246.92	423.85	0.24%	0.27%	Very Good
2.	self_isolation	236.41	815.17	4.39%	5.36%	Very Good
3.	hospital_care	33.21	33.03	3.61%	2.00%	Very Good
4.	recover	201.34	827.57	0.23%	0.81%	Very Good
5.	decease	7.51	17.85	0.32%	0.54%	Very Good

From Table VI, it can be seen that the column that has the lowest evaluation of the RMSE value in the training data is 7.51 and the test data is 17.85 in the death column, meaning that the actual data and the predicted data have the smallest difference in values. Then the evaluation of the best MAPE value in the training data, which is 0.23%, is in the recovered column, and the evaluation of the best MAPE value in the test data, which is 0.27%, in the positive_number column. The MAPE value in the table above is the average MAPE value of all existing data. Overall, the implementation of the Long Short-Term Memory (LSTM) algorithm, in predicting each column of Covid-19 cases in Riau Province, resulted in excellent forecasting machine learning capabilities.

H. Future Covid-19 Predictions

With a dataset of 64 data lines, predictions of Covid-19 cases are made for the next 30 days, using LSTM forecasting. The predicted value data obtained are then combined in tabular form with the initial dataset, and make a line graph comparing the actual data (blue line) and predictive data for 30 days in the future (red line). A composite graph between the initial dataset and the predicted results for each column.

Fig. 8 shows dataset on the number of positive cases with a blue line graph. In this case, where data is showing the number 108316, it is predicted that the number of positive cases in the next 30 days with a red line graph will be an increase which accumulated as many as 14939 cases.

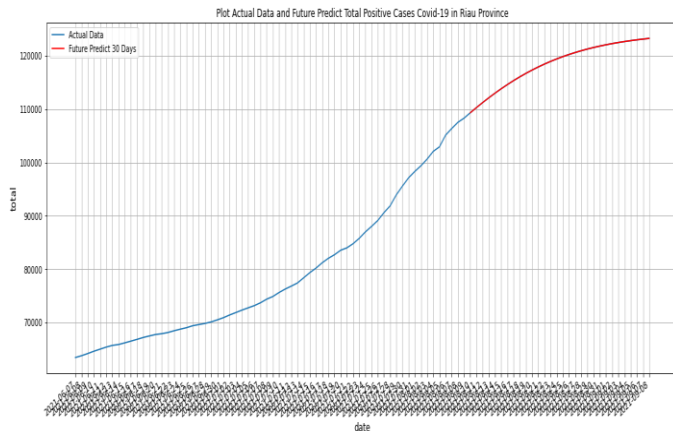


Fig. 8. 30 Days Prediction of Positive Number.

Fig. 9 shows dataset on the number of positive cases with a blue line graph. In this case, where data is showing the number 12012, it is predicted that the number of positive cases in the next 30 days with a red line graph will be an increase which accumulated as many as 11200 cases.

Fig. 10 shows dataset on the number of positive cases with a blue line graph. In this case, where data is showing the number 1362, it is predicted that the number of positive cases in the next 30 days with a red line graph will be an increase which accumulated as many as 336 cases.

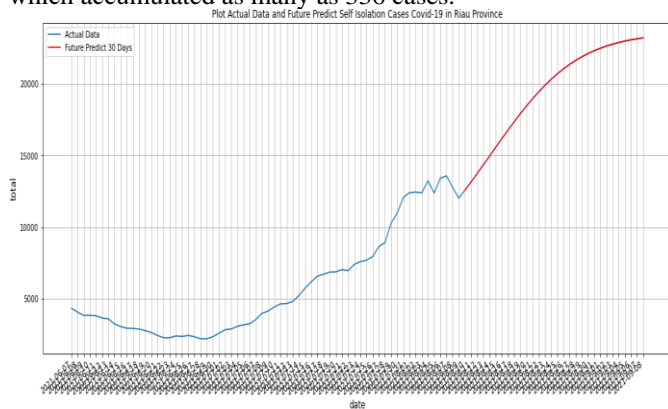


Fig. 9. 30 Days Prediction of Independent Isolation Cases.

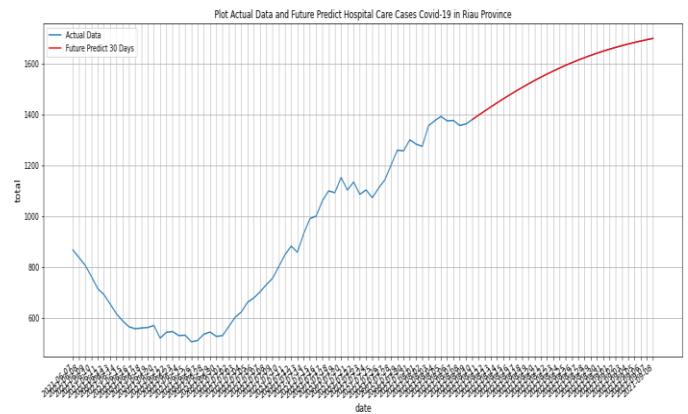


Fig. 10. Prediction of 30 Days of Hospitalization Cases.

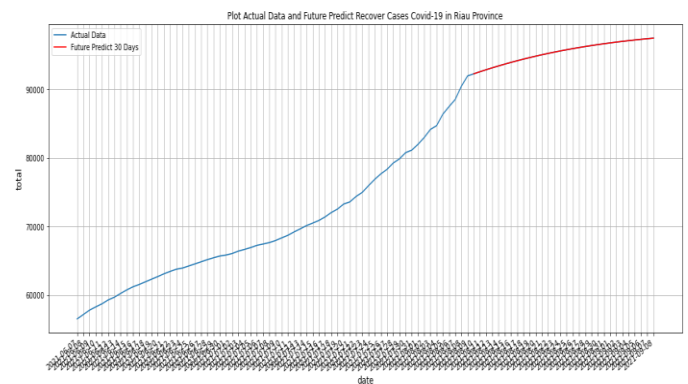


Fig. 11. Prediction of 30 Days of Cure Cases.

Fig. 11 shows dataset on the number of positive cases with a blue line graph. In this case, where data is showing the number 91963, it is predicted that the number of positive cases in the next 30 days with a red line graph will be an increase which accumulated as many as 5512 cases.

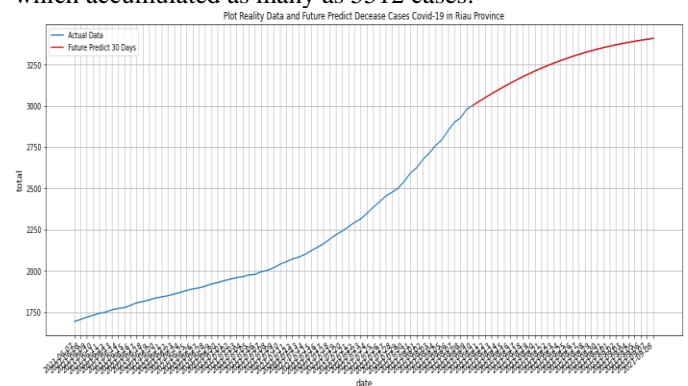


Fig. 12. Prediction of 30 Days of Death Cases.

Fig. 12 shows dataset on the number of positive cases with a blue line graph. In this case, where data is showing the number 2979, it is predicted that the number of positive cases in the next 30 days with a red line graph will be an increase which accumulated as many as 430 cases.

TABLE VII. CONCLUSION OF FUTURE PREDICTION TEST EVALUATION

No	Column Name	RMSE	MAPE	MAPE Criteria
		Reality Data & Future Predict 30 Days	Reality Data & Future Predict 30 Days	
1.	total_positive	1148.67	0.86%	Very Good
2.	self_isolation	13775.46	257.89%	Poor
3.	hospital_care	795.79	107.84%	Poor
4.	recover	13833.96	11.10%	Good
5.	decease	294.68	7.24%	Very Good

Table VII is the evaluation of the LSTM model for testing the prediction results for the next 30 days, with the real data that has been running from the initial data acquisition. The positive_number column obtained an RMSE value of 1148.67 and a MAPE value of 0.86%, then the death column with an RMSE value of 294.68 and a MAPE value of 7.24%. LSTM's prediction performance on the two columns is categorized as very good. The cured column has a good predictive performance with an RMSE value of 13833.96 and a MAPE value of 11.10%. This column of positive_number, recovered, and dead obtains the difference between each value in the data row and the difference in the average value which is not far away. The last two columns, namely isolation_mandiri and care_rs, obtained prediction performance that was categorized as poor because the MAPE value was above 50% and the RMSE value was very far, as seen from the difference in comparison between the real data values and the predicted results.

IV. CONCLUSION

From the results of research on forecasting that have been carried out, several conclusions can be drawn including (1) the application of the Long Short Term-Memory algorithm can be used to predict cases of time series data that have accumulated from Covid-19 in Riau Province which has occurred within a day; (2) prediction testing on a dataset consisting of 64 data lines, produces the lowest RMSE value in the training data, which is 8.87 and the test data, which is 13.00, in the death column. The evaluation of the best MAPE value in the training data, which is 0.23%, is in the recovered column, and the evaluation of the best MAPE value in the test data, which is 0.27%, is in the positive_number column; (3) evaluation of the Long Short Term-Memory algorithm in predicting historical data on Covid-19 cases that have accumulated in Riau Province, resulting in excellent forecasting machine learning capabilities, with the MAPE value criteria below 10% in both training data and test data; in the column of positive_number, independent_isolation, care_rs, recovered, and died; (4) in the test to predict the next 30 days using the LSTM model that has been trained, it was found that the performance evaluation of the prediction results for the positive_number column and the death column was very good, the recovery column was categorized as good, the independent_isolation column and the care_rs column were categorized as poor.

REFERENCES

- [1] Z. E. Rasjid, R. Setiawan, and A. Effendi, "A Comparison: Prediction of Death and Infected COVID-19 Cases in Indonesia Using Time Series Smoothing and LSTM Neural Network," *Procedia Comput. Sci.*, vol. 179, pp. 982–988, 2021.
- [2] F. W. Wibowo and Wihayati, "Prediction Modeling of COVID-19 on Provinces in Indonesia using Long Short-Term Memory Machine Learning," *J. Phys. Conf. Ser.*, pp. 1–12, 2021.
- [3] F. D. Adhinata and D. P. Rakhmadani, "Prediction of Covid-19 Daily Case in Indonesia Using Long Short Term Memory Method," *Teknika*, vol. 10, no. 1, pp. 62–67, 2021.
- [4] S. Elsworth and S. Güttel, "Time Series Forecasting Using LSTM Networks: A Symbolic Approach," pp. 1–12, 2020.
- [5] W. Hastomo, A. S. Bayangkari Karno, N. Kalbuana, A. Meiriki, and Sutarno, "Characteristic Parameters of Epoch Deep Learning to Predict Covid-19 Data in Indonesia," *J. Phys. Conf. Ser.*, vol. 1933, pp. 1–6, 2021.
- [6] A. Tomar and N. Gupta, "Prediction for the spread of COVID-19 in India and effectiveness of preventive measures," *Sci. Total Environ.*, vol. 728, pp. 1–6, 2020.
- [7] V. K. R. Chimmula and L. Zhang, "Time series forecasting of COVID-19 transmission in Canada using LSTM networks," *Chaos, Solitons Fractals J.*, pp. 1–7, 2020.
- [8] N. Yudistira, "COVID-19 Growth Prediction using Multivariate Long Short Term Memory," *IAENG Int. J. Comput. Sci.*, vol. 47, no. 4, pp. 829–837, 2020.
- [9] S. Siami-Namini, N. Tavakoli, and A. S. Namin, "The Performance of LSTM and BiLSTM in Forecasting Time Series," *Proc. - 2019 IEEE Int. Conf. Big Data*, pp. 3285–3292, 2019.
- [10] S. Siami-Namini, N. Tavakoli, and A. Siami Namin, "A Comparison of ARIMA and LSTM in Forecasting Time Series," *Proc. - 17th IEEE Int. Conf. Mach. Learn. Appl.*, pp. 1394–1401, 2019.
- [11] N. S. Pun, S. K. Sonbhadra, and S. Agarwal, "COVID-19 Epidemic Analysis using Machine Learning and Deep Learning Algorithms," *medRxiv*, pp. 1–10, 2020.
- [12] Y. Li and H. Cao, "Prediction for Tourism Flow based on LSTM Neural Network," *Procedia Comput. Sci.*, vol. 129, pp. 277–283, 2018.
- [13] S. Polyzos, A. Samitas, and A. E. Spyridou, "Tourism demand and the COVID-19 pandemic: an LSTM approach," *Tour. Retreat. Res.*, vol. 46, no. 2, pp. 175–187, 2021.
- [14] A. Moghar and M. Hamiche, "Stock Market Prediction Using LSTM Recurrent Neural Network," *Procedia Comput. Sci.*, vol. 170, pp. 1168–1173, 2020.
- [15] Q. Zhuge, L. Xu, and G. Zhang, "LSTM Neural Network with Emotional Analysis for Prediction of Stock Price," *Eng. Lett.*, vol. 25, no. 2, pp. 167–175, 2017.
- [16] D. M. Q. Nelson, A. C. M. Pereira, and R. A. De Oliveira, "Stock Market's Price Movement Prediction With LSTM Neural Networks," *IEEE Trans. Neural Networks*, vol. 21, no. 8, pp. 1378–1378, 2017.
- [17] S. Dutta, S. K. Bandyopadhyay, and T.-H. Kim, "CNN-LSTM Model for Verifying Predictions of Covid-19 Cases," *Asian J. Res. Comput. Sci.*, vol. 5, no. 4, pp. 25–32, 2020.
- [18] X. Zhang, X. Liang, A. Zhiyuli, S. Zhang, R. Xu, and B. Wu, "AT-LSTM: An Attention-based LSTM Model for Financial Time Series Prediction," *IOP Conf. Ser. Mater. Sci. Eng.*, vol. 569, pp. 1–7, 2019.
- [19] M. A. Istiake Sunny, M. M. S. Maywood, and A. G. Alharbi, "Deep Learning-Based Stock Price Prediction Using LSTM and Bi-Directional LSTM Model," *2nd Nov. Intell. Lead. Emerg. Sci. Conf.*, pp. 87–92, 2020.
- [20] R. Murtaza, P. Harshal, and V. Shraddha, "Predicting Stock Prices Using LSTM," *Int. J. Sci. Res.*, vol. 6, no. 4, pp. 1754–1756, 2015.
- [21] E. Vivas, H. Allende-Cid, R. Salas, "A Systematic Review of Statistical and Machine Learning Methods for Electrical Power Forecasting with Reported MAPE Score," *Entropy*, vol. 22, no. 12, pp. 1-24, 2020.

Design of a Dense Layered Network Model for Epileptic Seizures Prediction with Feature Representation

Summia Parveen¹

Assistant Professor, Department of Computer Science and Engineering
Sri Eshwar College of Engineering, Coimbatore, India

S. A. Siva Kumar²

Associate Professor, Department of Electronics and
Communication Engineering
Dr. N. G. P. Institute of Technology, Coimbatore, India

Kingsly Jabakumar⁴

Assistant Professor, Department of Electronics and
Communication Engineering
Christ the King Engineering College, Coimbatore, India

P. MohanRaj³

Assistant Professor, Department of Electronics and
Communication Engineering
Sri Ramakrishna Engineering College, Coimbatore, India

R. Senthil Ganesh⁵

Assistant Professor, Department of Electronics and
Communication Engineering, Sri Krishna College of
Engineering and Technology, Coimbatore, India

Abstract—Epilepsy is a neurological disorder that influences about 60 million people all over the world. With this, about 30% of the people cannot be cured with surgery or medications. The seizure prediction in the earlier stage helps in disease prevention using therapeutic interventions. Certain studies have sensed that abnormal brain activity is observed before the initiation of seizure which is medically termed as a pre-ictal state. Various investigators intend to predict the baseline for curing the pre-ictal seizure stage; however, an effectual prediction model with higher specificity and sensitivity is still a challenging task. This work concentrates on modelling an efficient dense layered network model (DLNM) for seizure prediction using deep learning (DL) approach. The anticipated framework is composed of pre-processing, feature representation and classification with support vector based layered model (dense layered model). The anticipated model is tested for roughly about 24 subjects from CHBMIT dataset which outcomes in attaining an average accuracy of 96% respectively. The purpose of the research is to make earlier seizure prediction to reduce the mortality rate and the severity of the disease to help the human community suffering from the disease.

Keywords—Epilepsy seizure; pre-ictal state; deep learning; feature representation; vector model

I. INTRODUCTION

A patient affected continuous seizures due to Epilepsy, a neurological order. This disease is afflicted on more than 1% of the world population. Medicines or surgical therapy were given to the patients afflicted by this disease [1]. In more than 40% cases, seizures cannot be manipulated with the recent models which consist of surgical procedures [2]. Hence, it is immensely vital that seizures can be treated with the help of medication by anticipating the consequent seizures before they arise. To sense brain activity, EEG signals are monitored [3].

Denoting EEG electrodes on the tissue termed intracranial EEG signals recorded these signals. The advancements in electrical signals of the internal brain are noticed by EEG recording and it is termed as scalp EEG or electrodes implantations of internal brain.

These states consist of preictal state, i.e. 30 minutes a seizure takes place. Then, Ictal state, i.e. the seizures' starting and ending are the same period and finally, post-ictal state, i.e. period after the seizure occurs [4]. The initial state gives knowledge about the starting of a seizure, which is beneficial for us; as it is the period before the seizure happens. Identifying preictal state can assist in eliminating seizures with treatment. Multiple EEG signal generation channels for interictal, preictal, and ictal states are exhibited sequentially [5]. There is a contradiction among these two states based on amplitude and frequency. It substantially enlarges in the preictal state on the contrary to interictal state. This case instigates predicting epileptic seizures successfully by categorizing interictal and preictal signals.

After digitization with a sampling rate from 200Hz to 5000Hz, EEG signals are captured with headsets and processed. These signals are clarified during the seizure onset by a neurologist on the particular software [6]. Before preictal seizure onset, the individuals' state is examined for 30 to 90 minutes. It is the next state of post-ictal state and ends before preictal state. However, interictal is the normal brain state. The aim is to accomplish preictal and interictal state classification, as mentioned previously [7]. Numerous researchers have suggested ML and DL approaches for seizures prediction. Pre-processing, features extraction and classification are included in this method. Pre-processing is terminated in the initial step to detach noise and accelerate

SNR. EEG signal filtering in the time domain with notch and bandpass Butterworth filters are added as common pre-processing methods. When enforced on EEG signals, the spatial and optimized pattern filter renders superior SNR. To preprocess EEG signals, EMD is beneficial. We can increase the SNR as it affords intrinsic mode and preserves low-frequency components. To make the proper victual in CNN, Wavelet and Fourier transform is also utilized [8]. Features are removed, and relevant features are preferred after noise removal, which affords high interclass and intra-class variance. For forecasting epileptic seizures, researchers have removed handcrafted features in both temporal and spectral features. The first four statistical moments are embraced in temporal features, PSD and spectral moments are embraced as special features [9]. After the progression of DL approaches, automatic feature extraction with CNN has also been utilized by many researchers and these features are removed based on class information. After feature selection with the CNN model, classification is executed. Various investigators utilized SVM, RF, K-NN, NB and MLP for classifications. In some cases, CNN, LSTM and RNN can also be utilized for classification, which included in deep learning classifiers [10]. However, there are some flaws over the existing models. The major limitation is the lack of prediction rather than classification. Earlier prediction helps to reduce the mortality rate and proper decision can be done to help the patients to get rid of the disease. This research focuses on modelling a dense layered network for epileptic seizure prediction and evaluates various metrics like sensitivity and specificity. The dense network model alleviates the vanishing-gradient problem, strengthen feature propagation, encourage feature reuse, and substantially reduce the number of parameters. The purpose of the research is to make earlier seizure prediction to reduce the mortality rate and the severity of the disease to help the human community suffering from the disease. The major contributions of the proposed model are:

- 1) Initially, an online available dataset known as CHBMIT is considered to perform the analysis for epileptic seizure prediction;
- 2) Fourier transform is applied for performing feature representation to enhance the quality of prediction;
- 3) Finally, a dense layered network model is proposed to perform the prediction process. The significance of the model is achieved with metrics like accuracy.

The work is provided as: Section II provides a comprehensive analysis on various prevailing approaches. The methodology is elaborated in Section III and the numerical results are discussed in Section IV. The summary is discussed in Section V.

II. RELATED WORKS

EEG signal-processing features extraction and classification are associated with seizure prediction systems. Various ML and DL approaches are proposed by many researchers for forecasting epileptic seizures, manipulating scalp EEG signals and enrol EEG signals with electrodes placed on the patient's scalp. Many researchers in recent years have proposed prediction methods [11]. Three common steps

are embraced by all these methods, which comprise EEG signal pre-processing, extracting features from EEG signals and classification between preictal and interictal states.

During EEG signals acquisition, noise is attached, which deals with the SNR of EEG signals, consequently in poor categorization among preictal and interictal states. Various kinds of noise affect EEG signals embracing power line of 50 to 60 HZ baseline noise because of intervention of numerous electrodes and noise annex because of the electrical activity embracing eye movement and heart pulse [12]. Hence, to multiply SNR for progressive outcomes, it is excessively linked to discharge noise as pre-processing step to enlarge SNR, different pre-processing techniques are scheduled by researchers [13]. To eliminate noise, low/high pass filtering is used by author [14]. Using scalp EEG signals for seizure prediction, numerous pre-processing approaches are utilized by researchers [15]. For noise removal, Zandietal, Feietal and Myersetal have utilized Bandpass filtering. To preprocess the dataset in the frequency domain, the author has enforced FFT [16]. In pre-processing of EEG signals, Truongetal has practised short-time Fourier transform. Cause of non-stationary EEG signals, STEFT has been suggested for pre-processing. For pre-processing the signals, both EMD and WT are utilized by [17]. Based on frequency components, EMD separates signals into intrinsic mode functions. Wavelet transforms for pre-processing, Khan et al., have enforced. Using spatial and adaptive filtering, local decomposition and other methods helps in noise extraction from EEG signals [18].

Features are detached after EEG signals pre-processing to classify various seizure states. Utilizing deep learning methods, features can be divided into two ways: extracting handcrafted features is the first, and automated feature extraction is another. Handcrafted features embrace uni- and multivariate features in both the frequency and time domains. Statistical moments define variance, entropy, skewness and kurtosis, entropy, PCA and Lyapunov exponent are embraced in temporal features [19]. Spectral moments and PSD are embraced in special features. Handicraft features have been divided into various seizure prediction methods in recent days, where researchers are embraced zero-crossing intervals, BoW, spectral features in the frequency domain, spatial pattern filtering and for automated feature extraction, some studies have utilized convolutional neural networks [20] – [22]. CNN separating features separate features keeping the target classes beneath consideration with high inter –lasso's variance with the support of CNN in this method. On scalp EEG signals, feature extraction techniques in state-of-the-art seizure prediction methods [23].

Classification between preictal and interictal states is done once the features have been separated from EEG signals. For categorizing EEG signals with seizure prediction, both ML and DL approaches are utilized by researchers. Nearest neighbour, Naive Bayes, support vector machine, Gaussian mixture model, DT, and RT are added to machine learning classification methods. The deep CNN, RNN, and LSTM units are embraced in deep learning classifiers. Variation mixture models are utilized in recent studies. An extreme learning machine and certain threshold to differentiate among interictal

and precital classes are utilized for classification and are tried quietly as a classifier support vector machine by [24]. For various seizures classification, convolutional neural networks are also utilized. Currently, researches utilized classification techniques are shown in [25]. The limitations in automatic detection of interictal spikes and epileptic seizures are preferred using the deep learning approach. The major research gap is the lack of accurate prediction of the disease and the computational complexity encountered during the prediction process. Based on these issues, the proposed model intends to reduce the complexity in the prediction process and enhance the accuracy.

III. METHODOLOGY

We used the CHBMIT dataset, freely available to the public, to apply our suggested methodology. It is a collection of 24 frontal ECG signals from patients aged 2 to 22. The section that follows gives a thorough summary of this database.

A. Dataset

A patient's EEG signals may be captured using electrodes placed on the forehead (scalp electrode) or by transplanting the electrical stimulation in the brain parenchyma (EEG signals). We utilized a publicly accessible collection of head EEG signals from CHBMIT (ECG recordings) from the pediatric subjects with intractable seizures. This dataset was compiled via a partnership between Children's Hospital Cambridge and Harvard and is freely accessible on Pysionet.org. It contains 22 participants, all humans, comprising 17 and 05, female and male, respectively ranging in age from 1.5 years to 19 years for females and 3 years to 22 years for males. Twenty-three microphones positioned on the scalps of people living with Epilepsy helped capture the dataset. All EDF files were turned to .mat documents using the MATLAB 'edfread' program. The sampling rate for the data was 256 Hz. MATLAB 2020a plays a substantial role in pre-processing and classification approach as the simulation environment is ease of use, it helps to make prediction faster. That participant's material has been separated into numerous files with an hour-long recording. The Preictal state in this country occurs before the onset of the ictal stage. The database is described in full in Table I.

B. Prediction Model

A strategy for predicting seizures begins a few seconds well before the commencement of the seizure, is described here. The suggested method's flowchart is shown in Fig. 1 and Fig. 2. We utilized the publicly available CHBMIT electroencephalographic dataset, which includes 24 people and signals collected with 23 wires and digitized at 256 Hz. The data source is freely accessible for download. "edfread" converts these outputs to mat files. Whitehead wide bandwidth removes background noise from EEG data. After noise reduction, STFT is done to boost the noise ratio and translate signals to the frequency domain. It is possible to extract several individually created univariate and multivariate characteristics in both the time and frequency domains [26]. These traits are not, however, retrieved based on the classification method to which they belong. So we used DNN to extract characteristics. As they are retrieved with the aid of

class information taken into account, these characteristics provide superior covariance variance [27]. Following DNN feature extraction, fully linked layers are swapped out for SVM. DNN extracts features whereas SVM classifies interictal & preictal segments. STFT, DNN, and SVM are briefly explained in the following subgroups.

C. Fourier-based Feature Analysis

Short-Time Fourier Transform (STFT) converts the time to frequency domain. Due to non-stationary characteristic of EEG data, STFT produces superior pretreatment results since it catches variations in the signals that last for a brief period. On an equally spaced interval of 30 seconds, we used STFT.

TABLE I. DATASET DESCRIPTION

Type	Scalp EEG
Subject	22
Male	5
Female	17
Channel	23
Sampling rate	256
Total seizures	198
Recordings	644

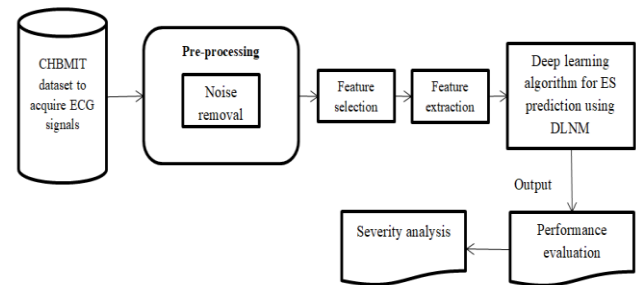


Fig. 1. Block Diagram of Proposed Model.

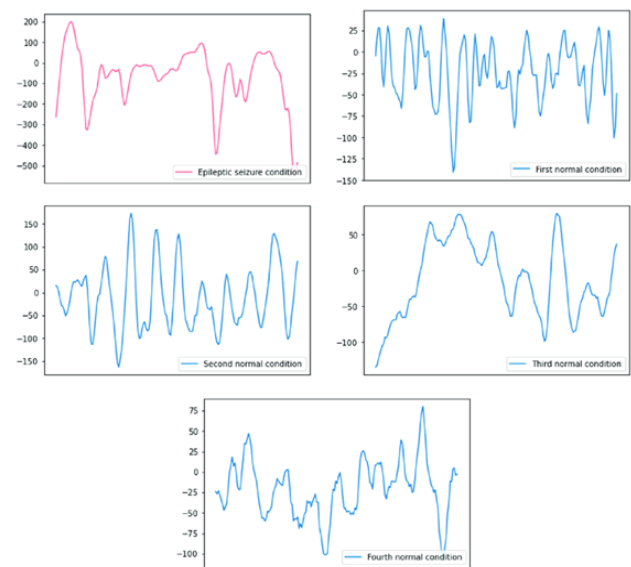


Fig. 2. Epileptic Seizure Dataset based Sample Waveforms.

D. Dense Layered Network Model (DLNM)

This architecture is provided to make the prediction process based on the dataset class labels. The model includes three sections: input, feature representation and output layer for classification purpose. The extracted features are provided as the input to the input layer. The feature representation section helps in extracting the most influencing feature that shows major impact in triggering the disease as in Fig. 3. Finally, the output layer is to extract the outcome. DLNM is frequently employed for input and time-varying series categorization and semantic segmentation [28]. It has many layers: compression, pools, and conventional neural network-based final layers for identification. Eq. (1) & (2) display the DNN updated weights.

$$\Delta W_l(t + 1) = -\frac{x\lambda}{r} W_l - \frac{x}{n} \left(\frac{\partial C}{\partial W_l} \right) + m\Delta W_l(t) \quad (1)$$

$$\Delta B_l(t + 1) = -\frac{x}{n} \left(\frac{\partial C}{\partial B_l} \right) + m\Delta B_l(t) \quad (2)$$

Here, W stands for weighting, l for layers, and B for bias, while $x, n, m,$ and t are regularisation parameters. The artificial neuron, which may be a gaussian, softmax, or linear transfer unit, comes after compression. Eq. (3), (4) & (5) present exponential, softmax and linear transfer unit model parameters.

$$y = \frac{1}{1+e^{-x}} \quad (3)$$

$$\sigma(z) = \frac{e^z}{\sum_{j=1}^k e^{z_j}} \quad (4)$$

$$f(x) = \max(0, x) \quad (5)$$

The mathematical notation used in this section is shown in Table II. The layer used to decrease the number of features is called the pooling layer. The two most popular pooling techniques are maximum and average. In this suggested technique, 16 filters (5*5) were used in the convolutional layer (CL), batch normalization with 0.4 dispersion, 32 filters (3*3) is utilized in the second CL, batch normalization, and 64 filters of 3*3 is the third layer. In all layers, an improved activation function non-linear unit is employed. After each convolution operation, batch normalization and convolutional with 2*2 are used. Well, after the third layer, some characteristics combine both classes. Fig. 2 depicts the DLNM used in our suggested strategy for image retrieval. In the suggested method, learnable CNN settings are 32576.

E. Support Vectors for Classification

After extracting DLNM characteristics, we utilized SVM to classify interictal and nine-month states. Linear and non-linear SVMs are the two main categories inside which SVMs may be separated. We can discover support vectors and build a maximum margin using slope and intercept if we have feature space variables. They are known as linear SVMs. We cannot know when to use a linear barrier since data cannot be linear. SVM maps data into higher dimensional space. As a result, making it is simple to separate the data. The use of kernel functions accomplishes it. The recurrent neural network, linear, and gaussian hemispheres are a few of the

often used kernels. This study uses linear SVM to categorize preictal and nine-month states.

TABLE II. DLNM NOTATION

Symbol	Explanation
$\Delta W(t + 1)$	Revised weight
$\Delta B(t + 1)$	Revised bias
L	Layer number
Λ	Regularized parameter
Y	Activation function (sigmoid)
$\sigma(z)$	Activation function (softmax)
$f(x)$	ReLU

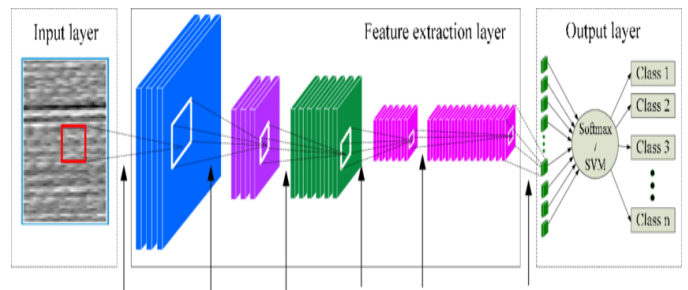


Fig. 3. Proposed DLNM.

IV. RESULTS AND DISCUSSION

We used our suggested technique on 24 CHBMIT scalp EEG dataset individuals to classify interictal and preictal states and predict epileptic episodes. Our average sensibility is 93%, and our specificity is 91%. The strategy we suggest has a 21-minute average anticipation time. The results of our suggested technique are compared to cutting-edge seizure prediction systems. It has been shown that our suggested strategy for anticipating grand mal seizures outperforms prevailing techniques based on specificity and sensitiveness. Preictal class is a college career according to our definition. Hence a 100 % detection rate with few FPR is crucial. These ROC curves assess the effectiveness of approaches by plotting sensibility against a false positive rate. A method's performance is deemed satisfactory if positive result alarms do not rise as sensitivity increases. In terms of attaining real positive rates with few false reports, it is evident that our suggested strategy works better. As a result, it can be said that the suggested strategy accurately predicts seizures in people with Epilepsy. Here, single input is given and multiple class labels based classified outcomes of extracted as output. The outputs are related to the dataset class labels.

The extracted features are provided as the input to the DLNM. The features are identified to enhance the quality of prediction. The effectiveness of the systems is determined by comparing the classification choices made by the classification to the manual choices made with each session through one or more new born EEG specialists. The classifier's conclusion is captured by the binary classification, which has four types: true positives (TP), epochs properly identified as seizures; false positives (FP), epochs wrongly

tagged as seizures; true negatives (TN), successfully identified non-seizure epochs; and false negatives (FN).

Accuracy (Acc): It is the number of occurrences accurately identified. The formulae given below are to determine accuracy:

$$Accuracy = \frac{TP+TN}{(TP+FN+TN+FP)} \quad (6)$$

Precision (Pn): It is calculated as the ratio of accurately forecasted to total positive observations.

$$Precision = \frac{TP}{TP+FP} \quad (7)$$

Recall (Rc): The percentage of total useful content that the good stuff identifies is known as recall.

$$Recall = \frac{TP}{TP+FN} \quad (8)$$

Sensitivity (Sn): Sensitivity is the only positive metric considering all situations.

$$Sensitivity = \frac{TP}{TP+FN} * 100 \quad (9)$$

Specificity (Sp): It measures the number of correctly detected true negatives and is computed as follows:

$$Specificity = \frac{TN}{TN+FP} * 100 \quad (10)$$

F-measure: It is a harmonic average of memory and accuracy. The highest possible F grade is 1, which denotes faultless accuracy and recall.

$$F - measure = \frac{2*recall*precision}{recall+precision} \quad (11)$$

Table III depicts the comparison of the anticipated DLNM with other approaches for error computation, i.e. MAE and RMSE along with execution time. The MAE value DLNM model is 3.2 which is lesser than SVM, RF, k-NN, NB and MLP (see Table III) and the RMSE of the anticipated DLNM is 11.2 which is lesser than SVM, RF, k-NN, NB and MLP. The execution time of DLNM is 0.02 seconds lesser than SVM, RF, k-NN, NB and MLP (see Fig. 4 and Fig. 5).



Fig. 4. Confusion Matrix.

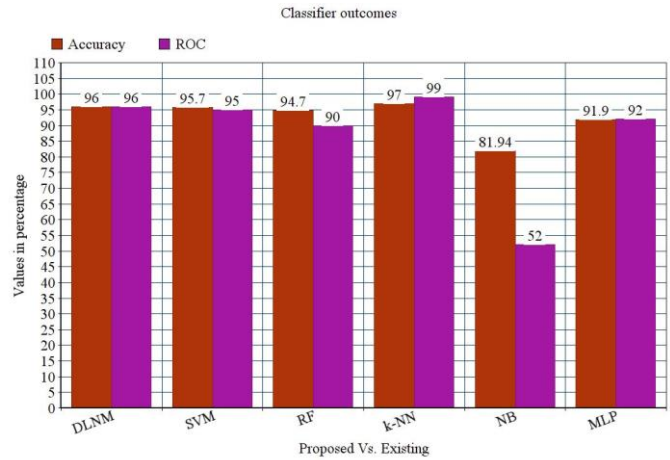


Fig. 5. Accuracy and ROC Comparison.

TABLE III. CLASSIFIER OUTCOMES

Method	Accuracy (%)	ROC	MAE	RMSE	Time (s)
DLNM	96	96	3.2	11.2	0.02
SVM	95.6	95	4.2	20.6	0.30
RF	94.7	90	5.4	22.6	10.36
k-NN	97.0	99	6.67	15.27	17.04
NB	81.9	52	29.64	38.84	3.68
MLP	91.9	92	12.8	25.5	22.05

Table III depicts the comparison of the anticipated DLNM model with various prevailing approaches like SVM, RF, k-NN, NB and MLP. DLNM's accuracy is 96% which is 0.4%, 1.3%, 14.1% and 4.1% higher than SVM, RF, NB and MLP and 1% lesser than k-NN. The recall of the anticipated model is 92% which is 7%, 3%, 5%, 6% and 8% higher than other approaches. DLNM's F-measure is 92% which is 7%, 3%, 5%, 7% and 8% superior to others. The DLNM precision is 92% which is 7%, 3%, 5%, 6% and 8% superior to others (see Fig. 6 and Fig. 7). Based on these analyses, it is proven that the anticipated DLNM model works well compared to other approaches in terms of performance indices.

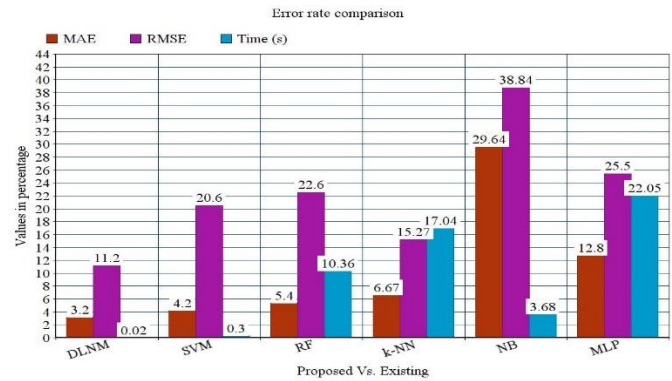


Fig. 6. Error Rate Comparison.

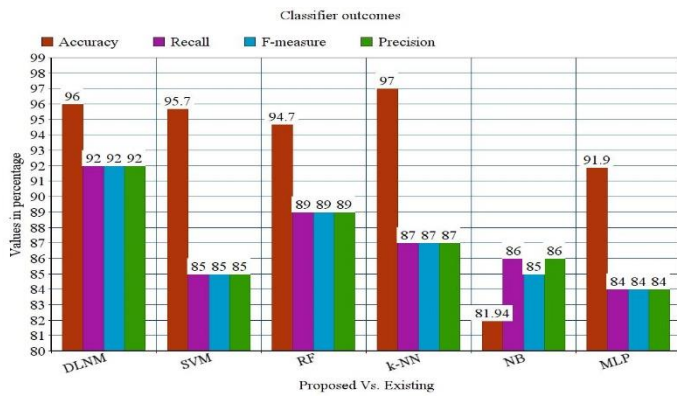


Fig. 7. Performance Metric Outcomes.

V. CONCLUSION

This work has suggested a technique for predicting epileptic seizures with DL. Individuals with Epilepsy may lead risk-free life when an adequate event prognosis is achieved. The suggested approach combines morphological operations with DLNM and identification using a DL classifier to outperform existing approaches with prediction accuracy. The novelty of identified with the DLNM model is its ability to encourage feature reuse, reduced number of parameters and stronger feature propagation which enhances the prediction outcome. Nevertheless, there is still space for development in several areas if filtering is improved in the future to improve the signal-to-noise ratio. Deep learning algorithms for feature extraction and classifying need several parameters. Future studies may thus be done to lower the number of factors. The suggested approach offers patient-specific seizure prediction, similar to other cutting-edge approaches. Continued studies on non-patient individual epileptic seizure prediction systems are necessary.

VI. FUTURE RESEARCH

In the future, this work is extended with multi-modal analysis and the hybrid learning approach is adopted for performing the prediction. The quality of prediction has to be improved further to make faster prediction outcomes.

REFERENCES

[1] M. Sazgar, M. G. Young, "Seizures and Epilepsy," in: Absolute Epilepsy and EEG rotation review, Springer, New York, 2019, pp. 9–46.
[2] R. S. Fisher, "The new classification of seizures by the international league against epilepsy," *Curr. Neurol. Neurosci. Rep.*, vol. 17, no. 6, pp. 48, 2017.
[3] A. A. Aljumah, M. G. Ahamad, M. K. Siddiqui, "Application of data mining: diabetes health care in young and old patients," *J King Saud Univ Comput Inform Sci.*, vol. 25, no. 2, pp.127–136, 2013.
[4] G. A. Singh, P. K. Gupta, "Performance analysis of various machine learning-based approaches for detecting and classifying lung cancer in humans," *Neural Comput. Appl.*, vol. 31, no. 10, pp. 6863–6877, 2019.
[5] Y. Paul, "Various epileptic seizure detection techniques using biomedical signals: a review," *Brain Inform.*, vol. 5, no. 2, pp. 6, 2018.
[6] P. Boonyakitanton, A. Lek-uthai, K. Chomtho, J. Songsiri, "A review of feature extraction and performance evaluation in epileptic seizure detection using EEG," *Biomed. Signal Process. Control*, vol. 57, pp. 101702, 2020.
[7] A. van Westrhenen, T. De Cooman, R. H. Lazeron, S. Van Huffel, R. D. Thijs, "Ictal autonomic changes as a tool for seizure detection: a systematic review," *Clin. Auton. Res.*, vol. 29, no. 2, pp.161–181, 2019.

[8] A. Sharmila, P. Geethanjali, "A review on the pattern detection methods for epilepsy seizure detection from EEG signals," *Biomed Eng /Biomedizinische Technik*, vol. 64, no. 5, pp. 507–17, 2019.
[9] A. Quintero-Rincón, C. D'Giano, H. Batatia, "Seizure onset detection in EEG signals based on Entropy from generalized gaussian pdf modelling and ensemble bagging classifier," In: *Digital Health Approach for Predictive, Preventive, Personalized and Participatory Medicine*, pp. 1–10. Springer, New York, 2019.
[10] S. Lahmiri, "An accurate system to distinguish between normal and abnormal electroencephalogram records with epileptic seizure-free intervals," *Biomed. Sign. Process. Control*, vol. 40, pp. 312–317, 2018.
[11] C. Donos, M. Dümpelmann, A. Schulze-Bonhage, "Early seizure detection algorithm based on intracranial EEG and random forest classification," *Int. J. Neural Syst.*, vol. 25, no. 05, pp. 1550023, 2015.
[12] H. R. Al Ghayab, S. Li Y, Abdulla, M. Diykh, X. Wan, "Classification of epileptic EEG signals based on simple random sampling and sequential feature selection," *Brain Inform.*, vol.3, no.2, pp.85–91, 2016.
[13] M. N. Adnan, M. Z. Islam, "Forest CERN: A new decision forest building technique," In: *Pacific-Asia Conference on Knowledge Discovery and Data Mining*, pp. 304–315, 2016.
[14] J. R. Quinlan, "C4.5: Programs for machine learning," Morgan Kaufmann Publishers Inc., San Francisco, 1993.
[15] S. Arlot, A. Celisse A, "A survey of cross-validation procedures for model selection," *Statistics surveys*, vol. 4, pp. 40–79, 2010.
[16] M. K. Siddiqui, M. Z. Islam, M. A. Kabir, "A novel quick seizure detection and localization through brain data mining on ECoG dataset," *Neural Computing and Applications*, pp. 1–14, 2018.
[17] H. Lee, S. Kim, "Black-box classifier interpretation using decision tree and fuzzy logic-based classifier implementation," *Int. J. Fuzzy Logic Intell. Syst.*, vol. 16, no. 1, pp. 27–35, 2016.
[18] M. N. Adnan, M. Z. Islam, "Forex++: A new framework for knowledge discovery from decision forests," *Aust. J. Inform. Syst.*, 2017.
[19] Y. Zhang, Y. Zhang, J. Wang, X. Zheng, "Comparison of classification methods on EEG signals based on wavelet packet decomposition," *Neural Comput. Appl.*, vol. 26, no. 5, pp. 1217–1225, 2014.
[20] A. F. Gill, S. A. Fatima, M. U. Akram, S. G. Khawaja, S. E. Awan, "Analysis of EEG signals for detection of epileptic seizure using hybrid feature set," In: *Theory and Applications of Applied Electromagnetics*, pp. 49–57, 2015.
[21] M. P. Orellana, F. Cerqueira, "Personalized epilepsy seizure detection using random forest classification over one-dimension transformed EEG data," *bioRxiv*, pp. 070300, 2016.
[22] A. Yan, W. Zhou, Q. Yuan, S. Yuan, Q. Wu, X. Zhao, J. Wang, "Automatic seizure detection using Stockwell transform and boosting algorithm for long-term EEG," *Epilepsy Behav.*, vol. 45, pp. 8–14, 2015.
[23] P. Sherubha, "Graph Based Event Measurement for Analyzing Distributed Anomalies in Sensor Networks", *Sādhanā(Springer)*, 2020, pp. 45:212.
[24] P. Sherubha, "An Efficient Network Threat Detection and Classification Method using ANP-MVPS Algorithm in Wireless Sensor Networks", *International Journal of Innovative Technology and Exploring Engineering (IJITEE)*, ISSN: 2278-3075, vol. 8, no. 11, September 2019.
[25] P. Sherubha, "An Efficient Intrusion Detection and Authentication Mechanism for Detecting Clone Attack in Wireless Sensor Networks", *Journal of Advanced Research in Dynamical and Control Systems (JARDCS)*, vol. 11, no. 5, pp. 55-68, 2019.
[26] H. U. Amin, A. S. Malik, R. F. Ahmad, N. Badruddin, N. Kamel, H. Hussain, W. T. Chooi, "Feature extraction and classification for EEG signals using wavelet transform and machine learning techniques," *Austr. Phys. Eng. Sci. Med.*, vol. 38, no. 1, pp. 139–149, 2015.
[27] M. Mursalin, Y. Zhang, Y. Chen, N. V. Chawla, "Automated epileptic seizure detection using improved correlation-based feature selection with random forest classifier," *Neurocomputing*, vol. 241, pp. 204–214, 2017.
[28] P. Fergus, A. Hussain, D. Hignett, D. Al-Jumeily, K. Abdel-Aziz, H. Hamdan, "A machine learning system for automated whole-brain seizure detection," *Appl. Comput. Inform.*, vol. 12, no. 1, pp. 70–89, 2016.

The Effect of the Aesthetically Mobile Interfaces on Students' Learning Experience for Primary Education

Nor Fatin Farzana Binti Zainuddin¹, Zuriana Binti Abu Bakar², Noor Maizura Binti Mohammad³, Rosmayati Binti Mohamed⁴

Faculty of Ocean Engineering Technology and Informatics
University Malaysia Terengganu, 21300 Kuala Terengganu, Terengganu

Abstract—Mobile devices such as mobile phones are becoming more important to school students today. This is due to the COVID-19 pandemic, mostly traditional face-to-face learning has shifted to online learning such as learning via a mobile platform. Mobile learning also known as m-learning, is defined as learning in numerous situations through social and content interaction utilizing personal electronic devices. M-learning applications not only need to have efficient functions, but it also has to attract students to learn by providing an attractive interface. An aesthetic of a mobile interface is essential since it could influence the user's learning experiences, but vice versa for non-aesthetic interfaces. User experience (UX) encompasses an extensive range of outcomes of the user-device interaction, including cognitions, attitudes, beliefs, behaviour, behavioural intentions, and affect. However, this study focuses on UX in terms of learnability, satisfaction, and efficiency since most previous studies were not explicitly focused on examining these three (3) UX components. Thus, this study aims to investigate the effect of aesthetically mobile interfaces on the learnability, satisfaction, and efficiency of primary school students, specifically, for *Kelas Al-Quran and Fardu Ain (KAFA)* students. This study found that aesthetically mobile interfaces significantly affected students' learning experiences regarding learnability, satisfaction, and efficiency. In conclusion, the findings of this study could serve as guidelines for future research in the field of mobile interface design.

Keywords—Aesthetic; non-aesthetic; mobile interfaces; primary education

I. INTRODUCTION

The rapid growth of technology is one of the factors that contribute to incorporating education with technology such as learning online using the mobile application. This is further encouraged by the COVID-19 pandemic, in which most traditional face-to-face learning has shifted to online learning such as learning via the mobile platform. Online learning including mobile learning requires an aesthetic interface to attract students to learning and further could assist students to focus and feel less bored when facing mobile devices for a quite long time during online learning. This is due to online learning, students do not have peers that have a physical presence and this environment could make students feel bored and lose focus.

Mobile learning (m-learning) is the use of ubiquitous portable technologies, in conjunction with mobile phone networks and wireless, to enable, enhance, assist, and expand the reach of learning and teaching [1]. In addition, define M-learning as any learning that occurs when the learner is not in a

fixed specified location or uses the learning possibilities afforded by mobile technology [2].

User interface design (UID) is the process of developing interfaces that focus on styling and connectivity. Place the user in control, reducing the user's memory load, and making the interface consistent are three (3) factors for effective user interfaces [3]. The impact of mobile devices today makes creating user interfaces crucial [4]. Designers can use various ideas to create the most efficient design interface for m-learning education that could give a beneficial user experience to learners when using mobile learning devices for learning.

This paper focuses on three (3) user experience components which are learnability, satisfaction, and efficiency. This is because most of the previous studies investigated usability theory including learnability, efficiency, memorability, errors, satisfaction, ease of use, attractiveness, easy access, a user-friendly interface, and others [5][6][7]. On the other hand, in particular, fewer studies focus on learnability, efficiency, and satisfaction [8]. Taken together, this paper focuses on the effects of aesthetically mobile learning interfaces on students' experiences which are learnability, satisfaction, and efficiency.

The paper is organised as follows. The extensive research background is explained in Section II. Next, the methodology adopted for this research is described in Section III, followed by the results and discussion in Section IV, and future works in section V. Finally, conclusion are described in Section VI.

II. RESEARCH BACKGROUND

This part describes the main components of this study which are user interface design and user experience that consists of satisfaction, efficiency, and learnability.

A. User Interface Design

Every technological device lately has an interface through which people can interact with the application [9]. This definition explains how an interface links the user and the content, allowing the content to adapt to the user's needs. Furthermore, the interface design is similar to a quality experience in that cognition, perception, semantics, and ergonomics must be integrated into the design process. Some operations necessitate usability testing to ensure that user interaction is supported [10].

Interface design is a crucial stage in system development because it provides an essential interaction on user experience. In addition, that interface design is linked to interaction design

because both interact to see how interfaces interact and are part of the system development process [11]. As a result, digital information is a critical area for application design interfaces. Designers can employ a variety of approaches to create the most efficient design interface for m-learning education. A graphic designer, a user interface designer, and a programmer typically work together at this stage to create interfaces for mobile applications. Table I summarises research on mobile interface design.

From Table I, it can be seen that most previous studies used various elements in mobile interface design, such as four (4) UID elements, UID patterns, UID framework, called “Mobile Web UI Transformation Framework”, design patterns and others. Although there were many studies that have been done on mobile interface design, however, a few study specifically focused on design principles for designing mobile interfaces such as proximity, balance, proportion, and others. Thus, this study applied nine (9) design principles to design m-learning application interfaces for this study which are balance, proportion, simplicity, alignment, movement, hierarchy, consistency, contrast, and proximity for the m-learning application for this study.

TABLE I. LITERATURE STUDIES ON MOBILE INTERFACES DESIGN

Author(s) name and years	The summary of the studies
Kalimullah and Sushmitha (2017)[12]	There are four (4) UID elements: mobile design guidelines, Unitarian Universalist principles, mobile health guidelines, and inclusive design guidelines.
Punchoojit and Hongwarittorn (2017)[13]	The design applied UID patterns: customization/personalisation, screen design, layout, learning potential, feedback, user control, navigation/orientation, help/support, error, interactivity, time required engagement, and readability.
Oyibo et al. (2018)[14]	Find out how the Canadian and Nigerian cultures perceive various mobile UID, which differ in terms of colours, images and layouts. The design applied a UID framework, called “Mobile Web UI Transformation Framework” or, simply, “Action-Artifact (A2) Framework”, to systematically modify the UI design of four hypothetical webpages adapted from existing websites in the market.
Braham et al., (2019)[15]	Examines user interfaces design pattern structures to support the adaptive mobile application that enable a more versatile and powerful organization of mobile interface emens, as well as their adaption to context changes and user requirements in specific scenario.
Bunian et al., (2021)[16]	Introduces visual search framework, that takes as input a UI image (wireframe, high-fidelity) and retrieves visually similar design examples.
Grandi et al., (2021)[17]	Utilizing Virtual Reality (VR) to simulate Augmented Reality (AR), that can design and evaluate the benefits of idealized User Interfaces
Börsting et al., (2022)[18]	Formulated several principles and patterns to simplify User Interfaces design for Augmented Reality (AR) applications

B. User Experience and Mobile Design

The goal of designing user experience is to train the next generation of user experience and interactive system designers [19]. There is already much interest in creating appealing, user-friendly m-learning applications to increase end-user adoption. Table II contains some guidelines for designing user interfaces for mobile applications. These guidelines are based on user interface design criteria and sub-criteria [20] and focus on the interface design of children’s mobile educational applications: cognitive load, graphical design, learning potential, readability, engagement, learnability, and satisfaction [21].

TABLE II. USER EXPERIENCE GUIDELINES OF MOBILE DESIGN

User experience elements	Sub criteria	Guidelines
Cognitive Load	Content/ concept	<ul style="list-style-type: none"> i. Use appropriate language ii. Use appropriate content
Graphical Design (Efficiency)	<ul style="list-style-type: none"> i. Aesthetic ii. Size/Font style iii. Colours iv. Icons v. Menu vi. Buttons 	<ul style="list-style-type: none"> i. Attractive, simple and organised, the design ii. Use proper size and font style iii. Use bright colours for children iv. Icons with the information have to be relevant v. Provide a proper touch for the screen menu vi. Provide colourful and animated buttons
Learning Potential	<ul style="list-style-type: none"> i. Ease to learn ii. Education value iii. Suitability 	<ul style="list-style-type: none"> i. Ease of learning ii. Suitable for educational content iii. Suitable for all users and controlling learners.
Readability	No sub-criteria	<ul style="list-style-type: none"> i. Readability ease ii. Provide appropriate text, size and spacing.
Engagement	Motivation to learn	<ul style="list-style-type: none"> i. Endorse commitments ii. Provide interesting rewards.
Satisfaction	No sub-criteria	<ul style="list-style-type: none"> i. Flexibility and efficiency of use ii. Aesthetic and minimalist design
Navigation/Orientation (Learnability)	<ul style="list-style-type: none"> i. Easy to navigate ii. Start screen / Main menu iii. Hierarchal menus iv. Scrolling 	<ul style="list-style-type: none"> i. Facilitate orientation ii. Navigation facility iii. Clear and consistent navigation iv. Give clear buttons for navigation i. Provide the main navigation menu ii. Straightforward main menu or start page link i. Hierarchal menu for easy navigation i. Scrolling may be problematic for children to scroll and view when much information is present.

The user experience and sub-criteria of mobile design illustrated in Table II demonstrate that many essential criteria, such as efficiency, satisfaction, learnability, and others, could be considered when designing interfaces.

TABLE III. LITERATURE STUDIES OF USER EXPERIENCES IN MOBILE LEARNING

Author(s) name and year	The use of user experience
Ismail et al. (2010)[10]	Examine learners' students' perceptions of the satisfaction experience using Mobile learning in School of Distance Education, University Sains Malaysia (USM).
Ali et al. (2014)[7]	Investigate two (2) models, which are Model A and Model B, on mobile learning smartphone applications from the user's perspective regarding ease of use, user satisfaction, attractiveness, and learnability.
Popovic et al. (2016)[6]	The development of electronic learning is based on efficient delivery of services by using a Learning Management System (LMS) to provide all the necessary study materials, easy access, and a user-friendly interface.
Joo et al. (2016)[4]	Analyze the relationships among factors predicting online university students' ease of use, perceived usefulness, expectation-confirmation, satisfaction, continuance intention and actual usage of m-LMS.
Kumar and Chand (2019)[5]	Categorised these user experience factors into 15 major factors; attitude, intention, ease of use, enjoyment, learner interest, prior experience, usefulness, learnability, anxiety, personal, technological, social, financial, pedagogical, and readiness.

A gap in the literature refers to a user experience research problem that has not been resolved in the study area. Previous studies have found a few gaps in the literature that can be filled. According to Table III, previous research has made less attempt to specifically focus on learnability, efficiency, and satisfaction. As a result, this study will focus on learnability, efficiency, and satisfaction as user experience criteria that must be investigated. The following sub-sections will explain satisfaction, efficiency and learnability.

1) *Satisfaction*: Satisfaction is defined as the absence of discomfort and positive feelings about using a product, and it is determined by the content, user guide, and beauty application interfaces [22]. While, satisfaction is the user's level of enjoyment as a result of interacting with the social networking application in a limited context of use in terms of learning the application, using the application, conducting a specific task, finding the attributes, knowledge navigation, trying to recover from error, and completing a task anywhere and at any time [23]. Furthermore, satisfaction is defined as a pleasant feeling experienced when receiving something desired or when performing an action desired, as well as the act of fulfilling (achieving) a need or wish [24]. Satisfaction is challenging to quantify because numerous factors influence it. Many businesses use usability testing to determine customer satisfaction or ask customers to complete a survey. Satisfaction is also linked to end-user confidence, which is especially important in health care due to the need for accurate information. As a result, a health care mobile application must

be developed with caution, especially the graphical user interface elements that directly affect the user's ease of use [25].

2) *Efficiency*: According to definition of efficiency, efficiency in user's completing the task in a given context of use is expressed in actions per second [23]. Efficiency is also defined as the number of resources used to achieve users' objectives with precision and completeness [20]. Furthermore, the less time spent regulating access permissions, the more time there is to capitalise on the value of those sources.

3) *Learnability*: Some researchers said that there is little agreement on how learnability should be defined [26]. Previously, user interfaces necessitated training and new learnability techniques that allowed users to become proficient with a little trial and error quickly. The term learnability refers to how easy a product is to comprehend. Numerous authors have defined learnability, further discussing a definition applied to various forms of learning, both initial and long-term [27]. A system's learnability also implies that it should be simple to learn so the user can begin working with it quickly [22].

III. METHODOLOGY

This part describes the research methodology used to conduct the research that contributed to the findings in this study. The Cronbach alpha is explained, including the One-way repeated measures (ANOVA). The interfaces are designed using a variety of design principles which are used stimuli of this study.

A. Stimuli

This study considers three (3) pages of learning, including Homepage, Introduction page, and Learning page. Overall, there are 15 mobile interfaces that applied nine (9) design principles: balance, proportion, simplicity, alignment, movement, hierarchy, consistency, contrast, and proximity. Each interface applied three (3) combinations of design principles. Table IV, Table V and Table VI illustrate three (3) design principles for the Homepage, Introduction page, and Learning page, respectively.

TABLE IV. COMBINATION OF DESIGN PRINCIPLES FOR HOMEPAGE

Interfaces	Design principle
1	Balance, Proportion, Simplicity
2	Alignment, Movement, Hierarchy
3	Balance, Consistency, Simplicity
4	Balance, Proportion, Alignment
5	Balance, Consistency, Contrast

TABLE V. COMBINATION OF DESIGN PRINCIPLES FOR INTRODUCTION PAGE

Interfaces	Design principle
6	Balance, Proportion, Simplicity
7	Balance, Contrast, Simplicity
8	Balance, Proportion, Simplicity
9	Balance, Alignment, Proximity
10	Balance, Proportion, Contrast

TABLE VI. COMBINATION OF DESIGN PRINCIPLES FOR LEARNING PAGE

Interfaces	Design principle
11	Proportion, Contrast, Consistency
12	Contrast, Proximity, Proportion
13	Balance, Consistency, Simplicity
14	Balance, Alignment, Proximity
15	Balance, Proximity, Contrast

This study was implemented for Kelas Al-Quran and Fardhu Ain (KAFA) students. KAFA is an additional subject for primary schools' students from Year 1 to Year 5 that consists of Jawi, Ibadat, Aqidah, Bahasa Arab, Adab, Penghayatan Cara Hidup Islam, Sirah dan Al-Quran. In year 5, at the end of the KAFA learning, students have to sit for an assessment test called Ujian Penilaian Kelas Kafa (UPKK). However, during the COVID-19 pandemic, KAFA class was also executed online like the other common subjects. Therefore, the KAFA subject needs to transform from a conventional learning approach to online learning, such as learning using a mobile platform. Therefore, this study will focus on the KAFA subject as content materials for this study.

B. Development of KAFA M-Learning

This prototype was created with NetBeans IDE 8.0, which supports language on development for the Java SE 87 specification and JDK 1.8 language features. It also includes a WebLogic server that supports Apache Tomcat. In contrast, a database is a collection of structured data that uses numbers as the primary key in a data relationship and uses the concept of normalisation to detail the data it requires. A database is a collection of data used by a company-owned application system and managed by a database management system [28]. Fig. 1, Fig. 2 and Fig. 3 show KAFA M-learning application interfaces for the homepage, introduction page and learning page.

C. Data Collection

KAFA M-learning application was developed for implementation of this study. The participants were required to use two (2) sets of interfaces, namely Apple and Pineapple, representing aesthetic and non-aesthetic interfaces. The participants were not informed that the Apple interface represents aesthetic interfaces and vice versa to avoid influencing them when answering questionnaires for user experience elements. In addition, the prototype and questionnaire used Bahasa Melayu because Bahasa Melayu is the national language and the main spoken language in Malay. Thus, it may affect the questionnaire feedback if using the English language.

This study involved 40 participants from primary school students. The range of the participants' ages was from 9 to 12 years. This range of participants was chosen because they were involved in KAFA class. The participants consisted of 25 females and 15 males.

Then, participants are required to answer the questionnaire to investigate the effect of aesthetic (Apple) and non-aesthetic (Pineapple) interfaces on students' experiences which are learnability, satisfaction and efficiency. The questionnaire consists of 15 questions for both interfaces. Furthermore, five

(5) questions are allocated for each user experience component. Questions 1 to 5 are learnability questions, Questions 6 to 10 are satisfaction questions, and questions 11 to 15 are efficiency questions. The questionnaire scale ranges from 1 = lowest to 5 = highest.

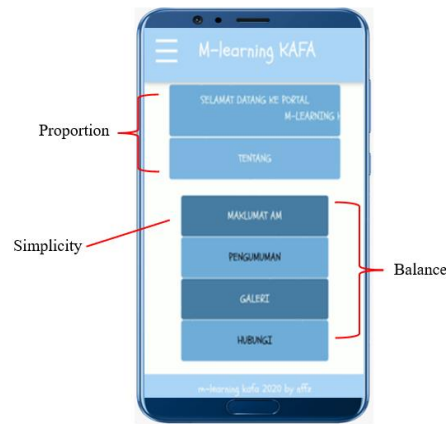


Fig. 1. KAFA M-learning Application Interfaces for Homepage.



Fig. 2. KAFA M-learning Application Interfaces for Learning Page.

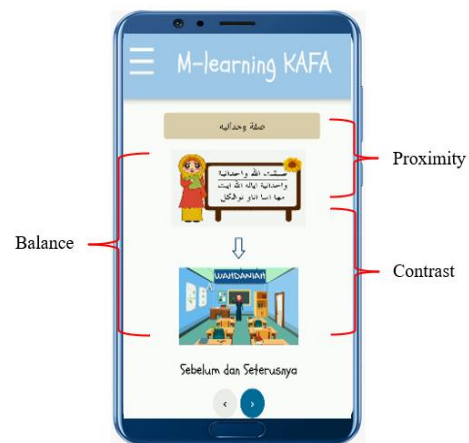


Fig. 3. KAFA M-learning Application Interfaces for Introduction Page.

D. Data Analysis

Two (2) types of analysis are involved in this study which are preliminary analysis and main analysis. The Cronbach’s Alpha reliability, skewness, and kurtosis measurements were conducted for preliminary analysis. Further, the main analysis is conducted using the One-way repeated measures ANOVA test. ANOVA test has been done using Statistical Package for the Social Sciences (SPSS) 27.0. ANOVA (also known as a within-subjects ANOVA) is applied in this study to determine whether three (3) or more groups are different, where the participants are the same in each group. This study used the same group of primary school students for three (3) different user experience questionnaires: learnability, satisfaction, and efficiency.

IV. RESULTS AND DISCUSSIONS

The findings of this study are divided into two (2) categories, which are as follows:

- Preliminary results of aesthetics interfaces and non-aesthetics interfaces.
- Main results of the effect of aesthetics interfaces and non-aesthetics interfaces.

A. Preliminary Results

This section explains the preliminary results for aesthetic and non-aesthetic interfaces regarding user experience components such as learnability, satisfaction, and efficiency. Cronbach’s Alpha reliability values for aesthetic and non-aesthetic interfaces are 0.654 and 0.651, respectively, as shown in Table VII. From Table VII, it is found that, the aesthetic and non-aesthetic interface scales have acceptable internal consistency reliability, as measured by Cronbach’s Alpha greater than 0.6 [29].

Skewness and kurtosis normality tests were performed on user experience components: learnability, satisfaction, and efficiency for both aesthetic and non-aesthetic interfaces. The skewness and kurtosis normality test results for both types of interfaces are shown in Tables VIII and IX.

The skewness values of aesthetic interfaces are shown in Table VIII, which are learnability is -0.298, satisfaction is -0.782, and efficiency is -0.755.

The skewness values of non-aesthetic interfaces are shown in Table IX, which are learnability is -0.450, satisfaction is -0.917, and efficiency is -0.659.

According to the skewness results in Tables VIII and IX, aesthetic and non-aesthetic interfaces are considered an acceptable skewness value for a normally distributed set of test scores because it is very close to zero and is most likely just a chance fluctuation from zero [30]. Kurtosis values in Tables VIII and IX revealed that aesthetic and non-aesthetic interfaces are considered acceptable kurtosis values for a mesokurtic (ordinarily high) distribution because it is close to zero [30].

As a result, skewness and kurtosis for both aesthetic and non-aesthetic interfaces follow a normal distribution. Thus, the parametric test, one-way repeated measures (ANOVA), is suggested as an analytical approach in the main study.

TABLE VII. CRONBACH’S ALPHA RELIABILITY RESULTS FOR AESTHETIC AND NON-AESTHETIC INTERFACES

Aesthetic interfaces	Cronbach’s alpha values	
	Statistic	No. of items
	0.654	15
Non-Aesthetic interfaces	0.651	15

TABLE VIII. SKEWNESS AND KURTOSIS NORMALITY RESULTS OF AESTHETIC INTERFACES

User experience	Skewness		Kurtosis	
	Statistic	Std. Error	Statistic	Std. Error
Learnability	-0.298	0.374	-0.726	0.733
Satisfaction	-0.782	0.374	-0.275	0.733
Efficiency	-0.755	0.374	-0.427	0.733

TABLE IX. SKEWNESS AND KURTOSIS NORMALITY RESULTS OF NON-AESTHETIC INTERFACES

User experience	Skewness		Kurtosis	
	Statistic	Std. Error	Statistic	Std. Error
Learnability	-0.450	0.374	0.022	0.733
Satisfaction	-0.917	0.374	-0.016	0.733
Efficiency	-0.659	0.374	-0.475	0.733

B. Main Result: Effect of Aesthetic and Non-aesthetic Interfaces on user Experiences

The repeated one-way measurements: The ANOVA test was used to assess the effect of aesthetic interfaces on user experience, specifically learnability, satisfaction, and efficiency. The multivariate effects of user experience components for aesthetic interfaces are shown in Table X.

Table X depicts there were significant effects on:

- 1) Learnability, Wilks’ lambda = 0.486, F(4, 36), p < 0.0005, multivariate partial eta squared = 0.514.
- 2) Satisfaction, Wilks’ lambda = 0.187, F(4, 36), p < 0.0005, multivariate partial eta squared = 0.813.
- 3) Efficiency, Wilks’ lambda = 0.265, F(4, 36), p < 0.0005, multivariate partial eta squared = 0.735.

TABLE X. SIGNIFICANT MULTIVARIATE EFFECTS ON AESTHETIC INTERFACES

User experience components	Learnability	Satisfaction	Efficiency
Wilks' lambda	0.486	0.187	0.265
F	9.509 ^b	39.029 ^b	24.961 ^b
Hypothesis df	4.000	4.000	4.000
Error df	36.000	36.000	36.000
Sig.	.000	.000	.000
Partial Eta Squared	0.514	0.813	0.735

TABLE XI. SIGNIFICANT MULTIVARIATE EFFECTS ON NON-AESTHETIC INTERFACES

User experience components	Learnability	Satisfaction	Efficiency
Wilks' lambda	0.371	0.216	0.299
F	15.244 ^a	32.596 ^b	21.120 ^b
Hypothesis df	4.000	4.000	4.000
Error df	36.000	36.000	36.000
Sig.	.000	.000	.000
Partial Eta Squared	0.629	0.784	0.701

Table XI depicts there were significant effects on:

- 1) Learnability, Wilks' lambda = 0.371, F(4, 36), p < 0.005, multivariate partial eta squared = 0.629.
- 2) Satisfaction, Wilks' lambda = 0.216, F(4, 36), p < 0.005, multivariate partial eta squared = 0.784.
- 3) Efficiency, Wilks' lambda = 0.299, F(4, 36), p < 0.005, multivariate partial eta squared = 0.701.

The summary results of the significant effect of aesthetic and non-aesthetic interfaces on user experiences are shown in Table XI. It was found that, the p-value of aesthetic and non-aesthetic interfaces is less than 0.05, indicating a statistically significant effect [30] for the learnability, satisfaction and efficiency value for Wilks' Lambda are 0.371, 0.216, 0.299, with probability value of 0.000 (which really means p < 0.005). Therefore, both aesthetic and non-aesthetic interfaces significantly impact students' learnability, satisfaction, and efficiency.

The findings indicate that the effects of aesthetic and non-aesthetic interfaces on primary school students when using KAFA M-learning application interfaces support the hypothesis that aesthetic and non-aesthetic interfaces of mobile interfaces, have a significant impact on students' learnability, satisfaction, and efficiency. Although all multivariate tests yield the same result, Wilks' Lambda is the most frequently reported statistic. The effect is statistically significant if the Wilks' Lambda value is p < 0.0005. This study concludes that the effects of aesthetic and non-aesthetic interfaces are significant because the p-value is less than 0.005. This evidence supports the hypothesis that the similarity of aesthetic interfaces influences the primary student participants' perceptions [30].

V. CONCLUSION

As a conclusion, the primary goal of this study is to investigate the impact of aesthetic and non-aesthetic interfaces on students' experiences of learnability, satisfaction, and efficiency. The survey was carried out with the participation of 40 primary school students. The study findings revealed that aesthetic and non-aesthetic interfaces significantly impact students' learnability, satisfaction, and efficiency.

This study also could help user interface designers by providing guidelines for designing M-learning interfaces that could create better learning experiences for primary school students in terms of learnability, efficiency, and satisfaction. This user experience is essential because M-learning applications need to have efficient functions, but it also needs

to attract students to learn by providing an attractive interface. Therefore, the UI designer can use these guidelines in the future to design an aesthetic interface for mobile learning applications.

VI. FUTURE WORKS

It is recommended that further research might explore Analysis of covariance (ANCOVA) for data analysis. This is because ANCOVA has several techniques and models for better solutions. The formulas will help to find the results easily [31]. Besides that in other areas such as business, management, and others, user interface design also can use ANCOVA technique.

ACKNOWLEDGMENT

This research is supported by a grant from the Fundamental Research Grant Scheme (FRGS) and the Ministry of Higher Education (MOHE), reference code FRGS/1/2-18/ICT04/UMT/03/1.

REFERENCES

- [1] Hashemi, M., Azizinezhad, M., Najafi, V., & Nesari, A. J. (2011). What is mobile learning? Challenges and capabilities. *Procedia - Social and Behavioral Sciences*, 30, 2477–2481. <https://doi.org/10.1016/j.sbspro.2011.10.483>.
- [2] Pilar, Rodríguez-Arancón; Jorge, Arús; Cristina, Calle (2013). The Use of Current Mobile Learning Applications in EFL. *Procedia - Social and Behavioral Sciences*, 103(), 1189–1196. doi:10.1016/j.sbspro.2013.10.446.
- [3] Foster, E. C. (2021). User Interface Design. *Software Engineering*, 237–254. <https://doi.org/10.1201/9780367746025-17>.
- [4] Zen, M. and Vanderdonckt, J. (2014) Towards an Evaluation of Graphical User Interfaces Aesthetics Based on Metrics. In *IEEE 8th Int. Conf. Research Challenges in Information Science, RCIS 2014, Marrakech, Morocco, May 28–30, 2014*. pp. 1–12.
- [5] Joo, Y. J., Kim, N., & Kim, N. H. (2016). Factors predicting online university students' use of a mobile learning management system (m-LMS). *Educational Technology Research and Development*, 64(4), 611–630. <https://doi.org/10.1007/s11423-016-9436-7>.
- [6] Kumar, B. A., & Chand, S. S. (2019). Mobile learning adoption: A systematic review. *Education and Information Technologies*, 24(1), 471–487. <https://doi.org/10.1007/s10639-018-9783-6>.
- [7] Popovic, O., Markovic, D. S., & Popovic, R. (2016). MTester - Mobile learning system. *Computer Applications in Engineering Education*, 24(3), 412–420. <https://doi.org/10.1002/cae.21719>.
- [8] Ali, A., Alrasheedi, M., Ouda, A., & Capretz, L. F. (2014). A Study of The Interface Usability Issues of Mobile Learning Applications for Smart Phones from the User's Perspective. *International Journal on Integrating Technology in Education*, 3(4), 1–16. doi:10.5121/ijite.2014.3401.
- [9] Harrison, R., Flood, D., & Duce, D. (2013). Usability of mobile applications: literature review and rationale for a new usability model. *Journal of Interaction Science*. <https://doi.org/10.1186/2194-0827-1-1>.
- [10] Ismail, N. A., Ahmad, F., Kamaruddin, N. A., & Ibrahim, R. (2016). A Review on Usability Issues in Mobile Applications. *IOSR Journal of Mobile Computing & Application*, 3(3), 47–52. <https://doi.org/10.9790/0050-03034752>.
- [11] Lund, L. (2015). Aesthetics in User Interface Design: The Influence on Users' Preference, Decoding and Learning. In *Blekinge Institute of Technology, Faculty of Computing, Department of Technology and Aesthetics*.
- [12] Kalimullah, K., & Sushmitha, D. (2017). Influence of Design Elements in Mobile Applications on User Experience of Elderly People. *Procedia Computer Science*, 113, 352–359. <https://doi.org/10.1016/j.procs.2017.08.344>.
- [13] Punchoojit, L., & Hongwarittorn, N. (2017). Usability Studies on Mobile User Interface Design Patterns: A Systematic Literature Review. *Advances in Human-Computer Interaction*, 2017. <https://doi.org/10.1155/2017/6787504>.

- [14] Oyibo, K., Adaji, I., & Vassileva, J. (2018). The influence of internet experience on the judgment of mobile web design. Proceedings of the 32nd International BCS Human Computer Interaction Conference, HCI 2018, April 2021. <https://doi.org/10.14236/ewic/HCI2018.16>.
- [15] Braham, A., Buendía, F., Khemaja, M., & Gargouri, F. (2019). Generation of adaptive mobile applications based on design patterns for user interfaces. Multidisciplinary Digital Publishing Institute Proceedings, 31(1), 19.
- [16] Bunian, S., Li, K., Jemmali, C., Harteveld, C., Fu, Y., & Seif El-Nasr, M. S. (2021, May). Vins: Visual search for mobile user interface design. In Proceedings of the 2021 CHI Conference on Human Factors in Computing Systems (pp. 1-14).
- [17] Grandi, J. G., Cao, Z., Ogren, M., & Kopper, R. (2021, March). Design and Simulation of Next-Generation Augmented Reality User Interfaces in Virtual Reality. In 2021 IEEE Conference on Virtual Reality and 3D User Interfaces Abstracts and Workshops (VRW) (pp. 23-29). IEEE.
- [18] Börsting, I., Karabulut, C., Fischer, B., & Gruhn, V. (2022). Design Patterns for Mobile Augmented Reality User Interfaces—An Incremental Review. *Information*, 13(4), 159.
- [19] Benyon, D. (2019). *Designing user experience*. Pearson UK.
- [20] Henderson, A. (2002). *Interaction design: beyond human-computer interaction*. Ubiquity. <https://doi.org/10.1145/512526.51252>.
- [21] Nielsen, J. (1993). *Iterative User-Interface Design*. Computer. <https://doi.org/10.1109/2.241424>.
- [22] Mkpojiogu, E. O. C., Hussain, A., & Hassan, F. (2018). A systematic review of usability quality attributes for the evaluation of mobile learning applications for children. AIP Conference Proceedings, 2016. <https://doi.org/10.1063/1.5055494>.
- [23] Alnanih, Reem; Ormandjieva, Olga; Radhakrishnan, T. (2013). [IEEE 2013 Joint Conference of the 23rd International Workshop on Software Measurement and the 8th International Conference on Software Process and Product Measurement (IWSM-MENSURA) - Ankara, Turkey (2013.10.23-2013.10.26)] 2013 Joint Conference of the 23rd International Workshop on Software Measurement and the 8th International Conference on Software Process and Product Measurement - A New Quality-in-Use Model for Mobile User Interfaces. , (), 165–170. doi: <https://doi.org/10.1109/IWSM-Mensura.2013.32>.
- [24] Cambridge University Press (2022). *English Dictionary: Satisfaction*. Retrieved from <https://dictionary.cambridge.org/dictionary/english/satisfaction>.
- [25] Thinnukool, O., & Kongchouy, N. (2017). The user's satisfaction of graphic user interfaces in designing for health care mobile application. *Journal of Telecommunication, Electronic and Computer Engineering*, 9(1–5), 11–15.
- [26] Lee, S., & Sah, Y. J. (2020). Development of an Approach to Measuring Learnability Based on NGOMSL from Perspectives of Extended Learnability. *International Journal of Human-Computer Interaction*, 36(2), 199–209. <https://doi.org/10.1080/10447318.2019.1625569>.
- [27] Dix, A., & Abowd, G. (2014). *Human-Computer Interaction Human-Computer Interaction*. May.
- [28] Teorey, T. J., Lightstone, S. S., Nadeau, T., & Jagadish, H. V. (2011). *Database modeling and design: logical design*. Elsevier.
- [29] Van Griethuijsen, R.A.L.F., van Eijck, M.W., Haste, H. et al. Global Patterns in Students' Views of Science and Interest in Science. *Res Sci Educ* 45, 581–603 (2015). <https://doi.org/10.1007/s11165-014-9438-6>.
- [30] Pallant, J. (2011). *Statistic material for English International Learners (EIL) SPSS Survival Manual A Step by Step Guide to Data (Issue 2)*.
- [31] Langel, R. a. (1982). *Understanding Analysis of Covariance (Ancova)*. 9, 250–253. [http://oak.ucc.nau.edu/rh232/courses/EPS625/Handouts/ANCOVA/Understanding ANCOVA.pdf](http://oak.ucc.nau.edu/rh232/courses/EPS625/Handouts/ANCOVA/Understanding%20ANCOVA.pdf).

Real Time Customer Satisfaction Analysis using Facial Expressions and Headpose Estimation

Nethravathi P. S¹

Faculty, Institute of Engineering & Technology, Srinivas University, Mangalore, India

Manjula Sanjay Koti²

Faculty, Dept. of MCA, Dayananda Sagar Academy of Technology & Management, Karnataka, India

Taramol. K.G³

Faculty, School of Business, Manipal Academy of Higher Education, Dubai International Academic City, Dubai

Soofi Anwar⁴

Faculty of Business with Accounting, University of Stirling, Al Dhait South, Ras Al Khaimah, United Arab Emirates

Gayathri Babu J⁵

Faculty, Department of Business Administration, Shree Devi Institute of Technology, Mangalore, India

Rajermani Thinakaran⁶

Faculty of Data Science and Information Technology, INTI International University, Nilai, Negeri Sembilan, Malaysia

Abstract—One of the most exciting, innovative, and promising topics in marketing research is the quantification of customer interest. This work focuses on interest detection and provides a deep learning-based system that monitors client behaviour. By assessing head position, the recommended method assesses customer attentiveness. Customers whose heads are directed toward the promotion or the item of curiosity are identified by the system, which analyses facial expressions and records client interest. An exclusive method is recommended to recognize frontal face postures first, then splits facial components that are critical for detecting facial expressions into iconized face pictures. Mainly consumer interest monitoring will be executed. Finally, the raw facial images are combined with the iconized face image's confidence ratings to estimate facial emotions. This technique combines local part-based characteristics through holistic face data for precise facial emotion identification. The new method provides the dimension of required marketing and product findings indicate that the suggested architecture has the potential to be implemented because it is efficient and operates in real time.

Keywords—Customer monitoring; convolutional neural network; facial expression recognition; facial analysis; head pose estimations component; CNN Model; object localization; face boosting

I. INTRODUCTION

The usual way is for a salesperson to study client behavior during the shopping phase or advertisement watching and then recall customer interest. However, every salesperson needs special talents for this job, and each spectator may interpret consumer behavior differently. In this aspect, only a few extraordinarily tactful and competent salespeople can have good salesperson-customer interactions [1]. According to [2], subjective emotional perception-based approaches may not always represent the human emotional state appropriately. On the other hand, automatic measurements provide a more exact and dependable result. As a result, developing non-invasive,

objective, and quantifiable measures for tracking client interest is crucial.

Human choices can be analyzed in various ways such as brain images [3]; an electroencephalogram also known as EEG [4], [5]; eye tracking [6], [7]; heart rate registration [8]; and other approaches have been a recent topic in the existing literature. Customer behavior classification [9 - 11] and customer face analysis studies have also been used in several studies [12], [13].

Estimating a client's visual focus of attention is one approach of evaluating their interest. Head posture is quantified in research on visual center of attention [14 - 16]. Recognizing consumer sentiments for advertising purposes is also a difficult and quickly growing academic area [17]. The intuitive decision-making process is substantially influenced by one's mood [17]. People who are in a good mood assume that everything is well and that they are safe in their surroundings. When they're in a poor mood, though, they believe things aren't going well and that an incident is approaching, and needing their attention [18]. Marketers must consider their customers' emotions and moods [19]. Knowing mental status of the buyer helps marketer in creating good business [19]. According to [20], annoyance, anxiety, sorrow, and disgust are all bad feelings, but happiness is a good emotion. Because it's difficult to discriminate between good and negative emotions, surprise isn't mentioned. According to [21], happy clients are positive, confident, passionate, stimulated, and thrilled.

The goal of this study is to develop a deep learning-based method for tracking client interest that relies on head-pose alignment and facial expression identification. The recommended method identifies the visual center of attention by first recognizing the human face and then analyzing the head posture orientation because the camera is an important item, the frontal faces suggest the visual center of focus. If the observed face is concentrated on the advertisement or product of interest, the algorithm begins to recognize the facial expression.

Customers' facial expressions are captured by the equipment over a period of time that may be assessed by specialists. Based on the gathered facial expressions, the system decides if the customer is in a good or poor mood. Based on the gathered data the system concludes he/she is in good or poor mood. The image can be captured by the camera and used to estimate face expression detection. As a result, determining client interest may be done non-invasively, quantitatively, and at a minimal cost. The suggested approach might be beneficial for identifying marketing campaigns and other corporate initiatives that clients would be interested in. Salespeople can also make changes to their marketing materials based on client feedback. This software could also help salespeople respond more effectively to customer emotions, leading to higher satisfaction.

The suggested study's main contributions can be stated in four points:

- 1) A system is proposed for measuring customer interest that is non-invasive, objective, and quantifiable.
- 2) Because the proposed system does not have the feature to save customer facial photos, personal privacy is protected. The system processes current client photos and does not require them to be saved for later processing. If there is a need to keep track of a customer's facial expressions, de-identified iconized face photos can be saved. Face expression data is included in iconized face photos while maintaining personal privacy.
- 3) A three-cascade Convolutional Neural Network (CNN) model is proposed which performs multiple tasks. In the third part CNN combines raw face images with iconized image confidence values. Part-based information is included in the confidence values of iconized images, whereas holistic details are included in raw face images. Improved facial expression detection is possible thanks to the combination of part-based and holistic data.
- 4) The system recognises and localises the face components that are crucial for facial expression detection in the facial component segmentation step, resulting in an ionised image. The CNN permits directed training at the facial emotion recognition stage by compelling earlier layers of the architecture to learn to identify and locate the essential face components using the confidence values of that ionized picture as input.

Consumer interest monitoring using CNN is performed for all mentioned three steps. Detecting frontal faces, classifying facial expressions, head posture estimation and facial expression detection are performed.

The next parts, which are organized as follows, give further information. The literature evaluation of current state-of-the-art methods that are relevant to the proposed methodology is summarized in Section II. Section III delves into the suggested technique, while Section IV covers the results, analysis, arguments, and inferences, while Section V wraps up the paper by summarizing some of the work's future directions.

II. LITERATURE SURVEY

Several publications in the literature describe how to use images or videos to solve real-world problems. For video processing, speed is critical, and many frameworks are being

developed to improve it [22 - 24]. Real-world challenges include object identification [25], text detection [26], [27], facial expression recognition [28], head position estimation [15], and so on. This section looks into the work's two key components: facial expression recognition and head posture estimation.

A. Facial Expression Recognition

Avatar animation [29]; smart environments [30 - 33]; robotics [34]; medical [35]; traffic [36], [37]; and human-computer interaction [38 - 44] are some of the applications of automated facial expression recognition. Ekman and Friesen's six universal facial expressions, namely disgust, happiness, fear, wrath, sadness, and surprise, were commonly utilised in automated facial expression detection experiments in their early research [45].

Geometric and appearance-based algorithms for facial expression recognition have been identified [46]. The features derived from positional correlations between facial components focus on geometric-based approaches [46]. Appearance-based features determine face texture [47 - 49]. Histogram of oriented gradients (HOG) [50], principal component analysis (PCA) [51], local binary pattern (LBP) operator [52], and other appearance-based methods have been used for facial emotion identification.

In the field of face expression analysis, the use of machine learning approaches specifically the deep learning is a recent trend. To extract just particular properties for expressions and examine the six essential expressions, Lopes et al. [53] used a CNN network with picture pre-processing techniques such as image rotation, face cropping, and intensity normalization. Pitaloka et al. [54] analyzed six essential sentences using a CNN. They used many data normalization techniques, scaling, face detection, cropping, and resizing algorithms. Matsugu et al. [55] recommended that CNNs be used to give a rule-based technique for detecting smiles and faces.

B. Head Pose Estimation

Visual surveillance [56], [57]; driver attention [58], [59]; the visual focus of attention [15], [60]; and robotics [61] have all been investigated using head posture estimation appearance-based, model-based, manifold embedding, and nonlinear regression techniques are used to create head position prediction systems [62]. Appearance-based strategies compare a new head picture to a set of head posture templates to determine which viewpoint is the most related Appearance-based approaches have the drawback of only being able to predict discrete posture locations [63].

Furthermore, certain templates [63] necessitate long picture comparisons. In model-based strategies, geometric information or facial landmark locations are employed to estimate head position [63]. The amount and quality of geometric signals produced from the image determine the accuracy of model-based techniques. In manifold embedding techniques like PCA [63], dimensionality reduction strategies are used. [64] Estimated head location by projecting images into a PCA subspace and comparing the results to a collection of embedded templates. The problem with manifold embedding is that it can be modified by factors other than location and identity, such as lighting [63]. A labelled training set is used in nonlinear

regression algorithms to construct a nonlinear mapping from pictures to postures [62]. According to [62], a dataset with consistency is required to train the parameters a nonlinear regression.

CNNs [62] are a nonlinear regression technique. CNNs give better accuracy in performance for difficult head pose orientations. In [65] described a CNN technique for estimating head posture. Three CNNs make up their network, each of which corresponds to one of three head posture types: yaw, pitch, or roll. To estimate head posture, [66] used a combination of regression models and CNN-based classification. [67] estimated head posture and located landmarks using local and global data collected from a CNN. For head posture estimation, [62] employed CNN and adaptive gradient methods. The literature shows that none of the existing methods used a cascade of the best deep learning architecture in each element and explored how it works. As we already cited, there is substantial evidence that the use of cascaded CNNs has the potential to provide the most optimized and robust results. Hence, in this study, we proposed a three-cascaded CNN architecture to analyze customer satisfaction in real-time.

III. METHODOLOGY

Each face picture is trimmed using the Viola and Jones Algorithm [68] to eliminate background information and leave just expression and head pose-specific data. The proposed technique makes use of the Viola and Jones algorithm, which allows for quick feature evaluations while also reducing the complexity of feature detection for each frame [68]. When this coordinate is included, as shown in (1), the integral image at the point x, y comprises the total of the pixels above and to the left of x, y [68].

$$jj(x, y) = \sum_{x' \leq x, y' \leq y} j(x', y') \quad (1)$$

A raw picture is $j(x,y)$, while an integral image is $jj(x,y)$. The integral image may be computed in one pass over the raw picture using (2) and (3) [68]. Where $a(x, y)$ stands for the cumulative row total, $a(x, -1)$ stands for zero, and $jj(-1, y)$ stands for zero.

$$a(x, y) = a(x, y-1) + j(x, y) \quad (2)$$

$$jj(x, y) = jj(x-1, y) + a(x, y) \quad (3)$$

The recommended system's initial stage determines if the client is looking at the correct advertisement or product. The suggested approach that classifies a head in frontal versus non-frontal profile can use the coarsest level head position estimation. Non-frontal faces are ignored when frontal faces are provided to CNN-2 for facial component segmentation. At 00, 450, 900, 1300, and 1800, the CNN-1 has been taught to estimate head position (Fig. 1).



Fig. 1. Sample Image Snapshots with Different Head Pose Positions.

CNN 1: To modify the backbone network design for the pose estimation issue, we use differentiable neural architecture search (NAS). Differentiable Neural Architecture Search is what we employ (NAS). NAS is formulated as a nested optimization problem. Fig. 2 shows the complete information, including the Differentiable neural architecture search, efficient backbone, efficient head, and Cost optimization.

CNN 2: Faces such as the mouth, eye, and brow areas are separated from the rest of the image by the CNN-2. Face component segmentation is a binary classification problem using the face component and the backdrop. The original raw images and corresponding training masks are partitioned into 16 * 16 non-overlapping blocks before moving to the training step. The majority class is assigned to blocks that contain more than 80% of the face component or backdrop pixels. The remaining mixed-class blocks are omitted during training. According to our tests, the threshold value of 80% was calculated. Fig. 3 depicts the image's construction block steps. Two channels are the output of the fully connected layer, one of which provides confidence values for facial components and the other of which contains confidence values for the backdrop. The higher component confidence value in the fully linked layer creates iconized facial images. Additionally, two channels' confidence values are passed to the CNN-3's input for guided image training and more powerful face expression identification. A movable window is used for testing, as stated in [69].

Stage	Output size	Layer	
		Small	Large
Input	256 × 256	—	
Conv3 × 3	128 × 128	[32, s2]	
SepDepth3 × 3	128 × 128	[16, s1]	[24, s1]
NAS Stage1	64 × 64	[24, s2] [24, s1] × 3	[32, s2] [32, s1] × 5
NAS Stage2	32 × 32	[32, s2] [32, s1] × 5	[64, s2] [64, s1] × 7
NAS Stage3	16 × 16	[64, s2] [64, s1] × 9	[96, s2] [96, s1] × 9
NAS Stage4	16 × 16	[96, s1] × 8	[160, s2] × 10
TransConv	32 × 32	[64, s2]	
TransConv	64 × 64	[32, s2]	

Fig. 2. Neural Architecture Search Architecture.

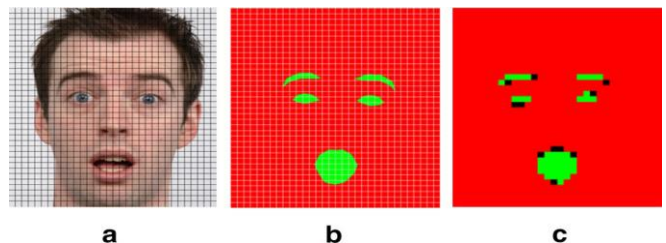


Fig. 3. Sample Image which Shows the Non Overlapping Parts. Black is the Ignored Part, Green is the Facial Component and Red is the Background in the Image C which Shows the Built and Labeled Part. Ground Truth is B and A is the Sample Divided Input Image.

CNN 3: The standard Xception model inspired this architecture. SeparableConv is the modified depthwise separable convolution, as shown in Fig. 4. SeparableConvs are considered as Inception Modules and used throughout the deep learning architecture, as can be established. All flows have residual (or shortcut/skip) connections, which ResNet first proposed.

The proposed method for consumer interest monitoring uses CNNs to complete the three learning steps. The method begins with CNN-1 detecting frontal faces. The frontal pictures are then

split using CNN-2 in order to maintain facial components such as critical and important trains of facial expression. Finally, CNN-3 uses CNN-2's fully connected layer confidence values together with raw facial photos to classify facial expressions. The proposed CNN design is shown in Fig. 5.

Fig. 5. Sample Image which shows the non-overlapping parts. Black is the ignored part, Green is the facial component and red is the background in the image C which shows the built and labeled part. Ground truth is B and A is the sample divided input image.

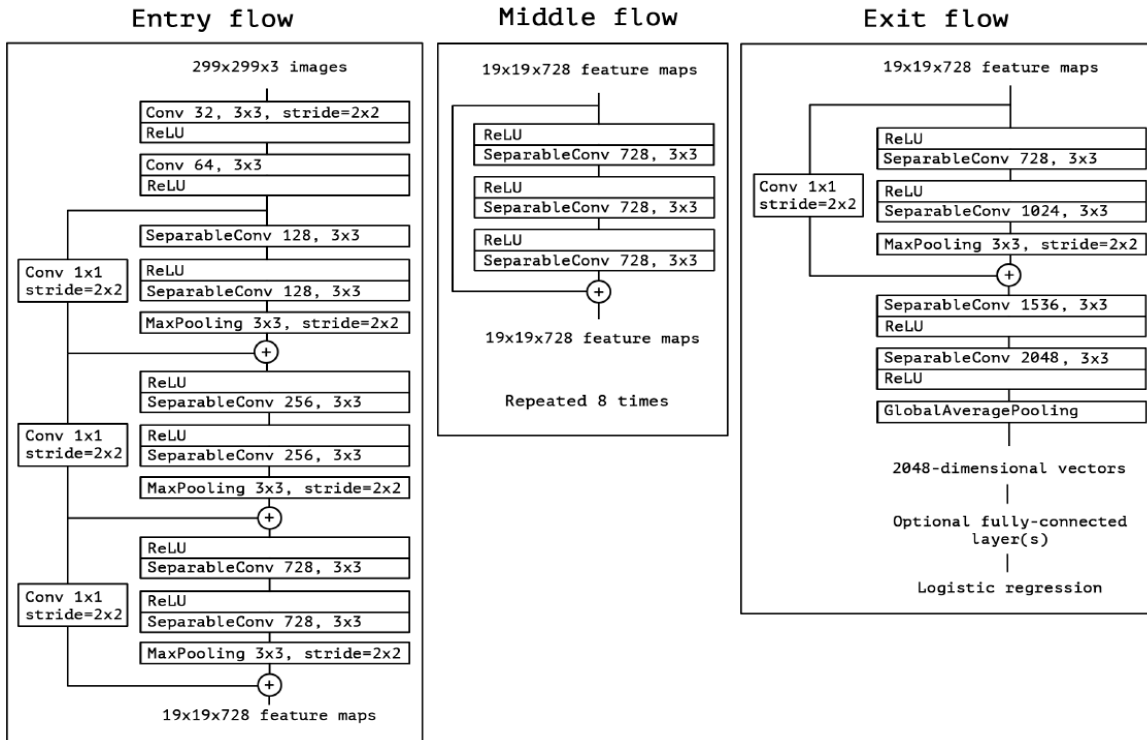


Fig. 4. Standard Exception Architecture.

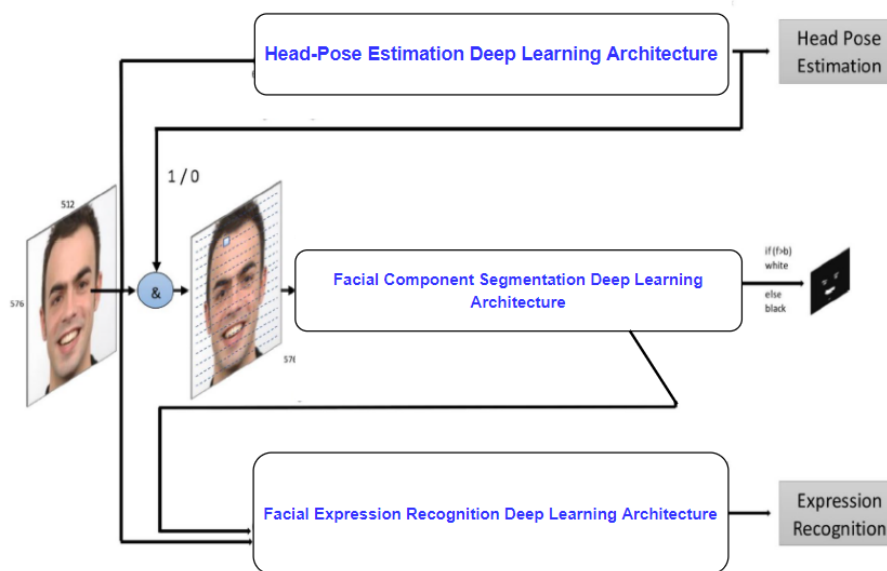


Fig. 5. Complete Work Flow of the Proposed Architecture.

IV. RESULTS AND ANALYSIS

The proposed deep learning architecture was built using the Keras library with Tensor Flow as the back-end. The Radboud Face Database (RaFD) was used to train and test the network [70].

In this work, 8040 photographs were utilised to estimate head posture, while 1206 frontal images were used to detect face expressions from RaFD (for angry, pleased, disgust, surprise, sad, and fear). The training and testing sets for head posture estimation and facial expression detection were divided into two equal halves. There are no photographs in the testing and training sets that belong to the same person. Raw facial images were used to train the algorithm in the head posture assessment phase. Although the suggested approach can distinguish between frontal and non-frontal profile head positions, it was trained to recognise five separate yaw movement angles. Table I shows the head posture estimate confusion matrix for RaFD.

Using the Karolinska Directed Emotional Face (KDEF) database, the proposed technique was also evaluated [71]. KDEF is ideal for evaluating proposed system performance since it incorporates both head posture angle and facial expression labels of the face photos. KDEF consists of 4900 pictures taken from five different angles and with seven different face expressions. 4900 shots were utilised to estimate head position, while 840 frontal images were used to recognise facial expressions. Because of the small number of images in these collections, they were divided into two groups for training (90%) and testing (10%). Table II shows the KDEF's head posture estimate confusion matrix.

Each picture was clipped to contain facial areas of the brows, eyes, and mouth in order to build learning masks for the face element segmentation approach. The Face++ toolbox (Face++ 2017) was then used to detect critical facial points. On a human face, the toolkit can recognise 83 important regions. Training masks were made at 45 key locations. Each essential point was connected to make a polygon. These polygons were used to create training masks. After that, the pictures were thresholded to create a final training set. Fig. 6 depicts the producing process. The system was trained on a 5-channel input for facial emotion recognition (comprising a 3-channel raw facial picture and 2-channel ionized face confidence values).

The system was trained on a 5-channel input for facial emotion recognition (comprising a 3-channel raw facial picture and 2-channel iconized face confidence values). Table III shows the RaFD confusion matrix for emotion recognition. When the confusion matrix is used to recalculate the accuracy of positive and negative expressions, positive expression (happy) has a 95.11 percent accuracy, while negative expression (anger, disgust, fear, and sadness) has a 92.88 percent accuracy. Table IV also includes the KDEF confusion matrix for face expression recognition.

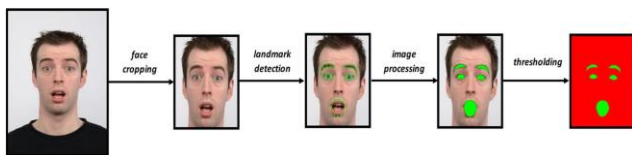


Fig. 6. Sample Image form the Database with Generating Flow.

TABLE I. HEAD POSE ESTIMATION ON RAFD: CONFUSION MATRIX

Actual	Predicted (in %)				
	0	45	90	135	180
0	98.66	1.34	0	0	0
45	0	99.11	0.89	0	0
90	0	0	100	0	0
135	0	0.82	0	99.18	0
180	0	0	0	0	100
Average:	99.43				

TABLE II. HEAD POSE ESTIMATION ON KDEF: CONFUSION MATRIX

Actual	Predicted (in %)				
	0	45	90	135	180
0	99.02	0.98	0	0	0
45	0	100	0	0	0
90	0	0	100	0	0
135	0	0	0	100	0
180	0	0	0	0.84	99.16
Average:	99.64				

TABLE III. CLASSIFICATION CONFUSION MATRIX ON KDEF DATABASE: EMOTION RECOGNITION (%)

Actual\Predicted	Anger	Disgust	Fear	Happy	Sad	Surprised
Anger	95.92	1.11	0	0	2.97	0
Disgust	2.01	95.66	0	0	0	2.33
Fear	0	0	88.23	0	10.00	1.77
Happy	0	3.11	0	95.11	1.78	0
Sad	3.85	4.55	0	0	92.34	0
Surprised	0	0	0	0.77	0	99.23

TABLE IV. CLASSIFICATION CONFUSION MATRIX ON KDEF DATABASE: FACIAL EXPRESSIONS (%)

Actual\Predicted	Anger	Disgust	Fear	Happy	Sad	Surprised
Anger	89.12	3.14	0	0	7.74	0
Disgust	0	91.66	0	0	8.34	0
Fear	0	0	84.23	0	11.23	4.54
Happy	0	0	0	98.11	0.34	1.55
Sad	5.66	0	0	0	94.34	0
Surprised	0	0	0	1.77	0	98.23

Because the RaFD database contains strange expressions, our system may experience certain mistakes. Fig. 7 depicts a visual representation of some of our mistake instances. The proposed system's performance was compared to that of previous face emotion recognition studies. The comparison's findings are shown in Table V. The results of facial expression recognition utilising 3-channel raw image, 1-channel iconized image, and 5-channel composite image for RaFD are shown in

the table below. Table VI illustrates the execution times for three different types of CNNs, as well as the overall execution time, with estimated values for one picture. The segmentation procedure takes up a significant amount of time.

The proposed pipeline is intended for photos with a resolution of 576 * 512 pixels and discrete facial components. CNN-1 and CNN-3 use 64x64 images as inputs, while CNN-2 uses 576x512 images. As a result, it takes longer for CNN-2 to process the input pictures. Performance declines by 13% if the segmentation phase is bypassed in order to save time (85.12 percent for raw input image data vs. 95.11 percent for the data from the five channel).

The details of hyperparameters and their values are Threshold 0.005, Learning rate 0.10, Input channels 3 5 5, regularization strength of 0.0005 and the Batch-size 3. The train and test of the aligned face are regular and saturated well, but the unaligned looks are quite different. But they still saturate at the same number of epochs, but the variations can be observed in Fig. 8.

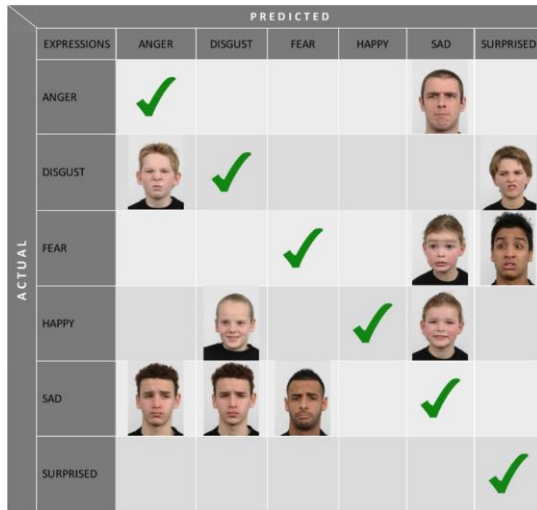


Fig. 7. Misclassification of Results and its Visualizations.

TABLE V. FACIAL EMOTION RECOGNITION OF PROPOSED METHOD WITH OTHER STUDIES ON RAFD / KDEF DATABASES

Methods	Database	Accuracy (in %)
HoG + NNE [1]	RaFD	93.75
Surf Boosting [64]	RaFD	90.64
Gabor F. + GLCM [36]	RaFD	88.41
LSiBP + SVM[68]	KDEF	84.07
HoG + AdaBoost [38]	KDEF	87.20

TABLE VI. EXECUTION TIME FOR CNN STRUCTURES

CNN Structures	Task	45	90	135	Time
1	Estimation of Head Pose				~0.02
2	Segmentation of Facial Component				~0.13
3	Recognition of Facial Expression				~0.80
0.31 Sec. is the total execution time for one image					

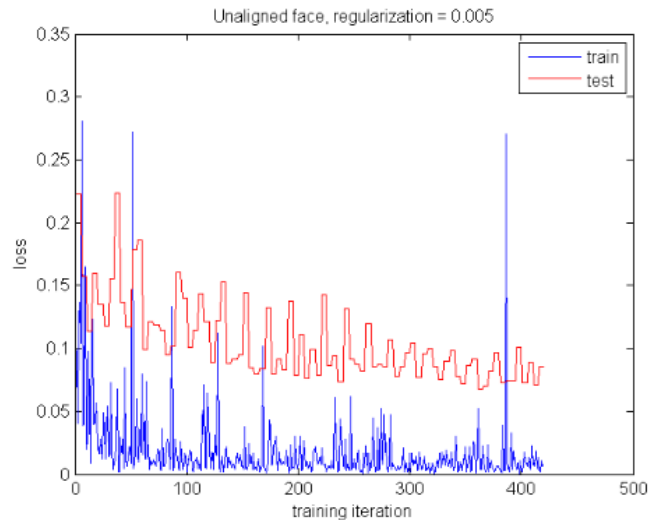


Fig. 8. Train and Test Curves of Unaligned Face Images.

V. CONCLUSION AND FUTUTRE DIRECTIONS

A unique deep learning system for automatic head posture estimation and face emotion identification is proposed. The proposed method started with developing a noninvasive, quantifiable approach for tracking client interest. The suggested system is made up of three CNN structures in a cascade. The first CNN's task is to estimate head posture. Face segmentation was taught to the second CNN structure. Face recognition and classification were encoded into the third CNN. The latter two steps (CNN-2 and CNN-3) allow for guided picture classification and the integration of part-based and holistic data. The RaFD dataset demonstrated that head posture estimation was 99.43 percent accurate and face expression detection was 93.20 percent accurate in experimental tests. The average accuracy of positive and negative emotions is 93.99.

The proposed approach can aid in the measurement of relevant marketing and product likability as well as the quantification of the client interest. It can also be used to identify sales-boosting company initiatives. According to customer feedback, marketing efforts can alter their methods. Future direction includes the temporal analysis of the data and the optimization space used in the architecture. Track human faces and use object localization so that the system can watch and index an individual's facial expressions over time. Exploring the proposed architecture with people of different regions and cultural background and testing it on various other domains.

REFERENCES

- [1] Ozdemir, M. A., Elagoz, B., Alaybeyoglu, A., Sadighzadeh, R., & Akan, A. (2019, October). Real time emotion recognition from facial expressions using CNN architecture. In *2019 medical technologies congress (tiptekno)* (pp. 1-4). IEEE.
- [2] Missaglia, A. L., Oppo, A., Mauri, M., Ghiringhelli, B., Ciceri, A., & Russo, V. (2017). The impact of emotions on recall: An empirical study on social ads. *Journal of Consumer Behaviour*, 16(5), 424-433.
- [3] Dockès, J., Poldrack, R. A., Primet, R., Gözükan, H., Yarkoni, T., Suchanek, F., ... & Varoquaux, G. (2020). NeuroQuery, comprehensive meta-analysis of human brain mapping. *Elife*, 9, e53385.
- [4] Craik, A., He, Y., & Contreras-Vidal, J. L. (2019). Deep learning for electroencephalogram (EEG) classification tasks: a review. *Journal of neural engineering*, 16(3), 031001.

- [5] Cook, I.A., Warren, C., Pajot, S.K., Schairer, D. and Leuchter, A.F., 2011. Regional brain activation with advertising images. *Journal of Neuroscience, Psychology, and Economics*, 4(3), p.147.
- [6] Wedel, M. and Pieters, R., 2000. Eye fixations on advertisements and memory for brands: A model and findings. *Marketing science*, 19(4), pp.297-312.
- [7] Ungureanu, F., Lupu, R.G., Cadar, A. and Prodan, A., 2017, October. Neuromarketing and visual attention study using eye tracking techniques. In 2017 21st international conference on system theory, control and computing (ICSTCC) (pp. 553-557). IEEE.
- [8] Micu, A.C. and Plummer, J.T., 2010. Measurable emotions: How television ads really work: Patterns of reactions to commercials can demonstrate advertising effectiveness. *Journal of Advertising Research*, 50(2), pp.137-153.
- [9] Popa, M., Rothkrantz, L., Yang, Z., Wiggers, P., Braspenning, R. and Shan, C., 2010, October. Analysis of shopping behavior based on surveillance system. In 2010 IEEE International Conference on Systems, Man and Cybernetics (pp. 2512-2519). IEEE.
- [10] Liu, J., Gu, Y., & Kamijo, S. (2017). Customer behavior classification using surveillance camera for marketing. *Multimedia Tools and Applications*, 76(5), 6595-6622.
- [11] Liu, J., Gu, Y. and Kamijo, S., 2018. Integral customer pose estimation using body orientation and visibility mask. *Multimedia Tools and Applications*, 77(19), pp.26107-26134.
- [12] Kasiran Z, Yahya S (2007) Facial expression as an implicit customers' feedback and the challenges. In: *Computer graphics, imaging and visualisation*, IEEE, pp 377-381
- [13] Teixeira, T., Wedel, M. and Pieters, R., 2012. Emotion-induced engagement in internet video advertisements. *Journal of marketing research*, 49(2), pp.144-159.
- [14] Ba, S. O., & Odobez, J. M. (2010). Multiperson visual focus of attention from head pose and meeting contextual cues. *IEEE Transactions on Pattern Analysis and Machine Intelligence*, 33(1), 101-116.
- [15] Riener, A. and Sippl, A., 2014. Head-pose-based attention recognition on large public displays. *IEEE computer graphics and applications*, 34(1), pp.32-41.
- [16] Sheikhi, S. and Odobez, J.M., 2015. Combining dynamic head pose-gaze mapping with the robot conversational state for attention recognition in human-robot interactions. *Pattern Recognition Letters*, 66, pp.81-90.
- [17] Karu-Salo, I., 2013. The effect of universal emotions on customer behaviour. *Estonian Business School*, pp.1-72.
- [18] Kahneman D. *Thinking, fast and slow*. Macmillan; 2011 Oct 25.
- [19] Sangeeta, S., 2013. Module-6 Consumer Behavior. Vinod Gupta School of Management, Indian Institute of Technology: India. Article. Available on: <http://nptel.ac.in/courses/110105029/pdf>, 20, pp.6-23.
- [20] Ekman P, Friesen WV (1975) *Unmasking the face: a guide to recognising emotions from facial clues*. Consulting Psychologists Press, New Jersey (Prentice Hall [Palo Alto, CA]).
- [21] Laros, F.J. and Steenkamp, J.B.E., 2005. Emotions in consumer behavior: a hierarchical approach. *Journal of business Research*, 58(10), pp.1437-1445.
- [22] Yan, C., Zhang, Y., Xu, J., Dai, F., Li, L., Dai, Q. and Wu, F., 2014. A highly parallel framework for HEVC coding unit partitioning tree decision on many-core processors. *IEEE Signal Processing Letters*, 21(5), pp.573-576.
- [23] Yan, C., Zhang, Y., Xu, J., Dai, F., Zhang, J., Dai, Q. and Wu, F., 2014. Efficient parallel framework for HEVC motion estimation on many-core processors. *IEEE Transactions on Circuits and Systems for Video Technology*, 24(12), pp.2077-2089.
- [24] Bayrakdar, S., Akgün, D. and Yücedağ, İ., 2017. An accelerated approach for facial expression analysis on video files. *Pamukkale University Journal of Engineering Sciences*, 23(5), pp.602-613.
- [25] Yan, C., Li, L., Zhang, C., Liu, B., Zhang, Y. and Dai, Q., 2019. Cross-modality bridging and knowledge transferring for image understanding. *IEEE Transactions on Multimedia*, 21(10), pp.2675-2685.
- [26] Yan, C., Xie, H., Chen, J., Zha, Z., Hao, X., Zhang, Y. and Dai, Q., 2018. A fast uyghur text detector for complex background images. *IEEE Transactions on Multimedia*, 20(12), pp.3389-3398.
- [27] Yan, C., Xie, H., Liu, S., Yin, J., Zhang, Y. and Dai, Q., 2017. Effective Uyghur language text detection in complex background images for traffic prompt identification. *IEEE transactions on intelligent transportation systems*, 19(1), pp.220-229.
- [28] Oztel, I., Yolcu, G., Öz, C., Kazan, S. and Bunyak, F., 2018. iFER: facial expression recognition using automatically selected geometric eye and eyebrow features. *Journal of Electronic Imaging*, 27(2), p.023003.
- [29] Zalewski, L. and Gong, S., 2005, June. 2d statistical models of facial expressions for realistic 3d avatar animation. In 2005 IEEE Computer Society Conference on Computer Vision and Pattern Recognition (CVPR'05) (Vol. 2, pp. 217-222). IEEE.
- [30] Kim, J. B., Hwang, Y., Bang, W. C., Lee, H., Kim, J. D., & Kim, C. (2013, January). Real-time realistic 3D facial expression cloning for smart TV. In 2013 IEEE International Conference on Consumer Electronics (ICCE) (pp. 240-241). IEEE.
- [31] Takahashi, M., Clippingdale, S., Naemura, M. and Shibata, M., 2015. Estimation of viewers' ratings of TV programs based on behaviors in home environments. *Multimedia Tools and Applications*, 74(19), pp.8669-8684.
- [32] Teyeb, I., Jemai, O., Zaied, M., & Amar, C. B. (2015, December). Vigilance measurement system through analysis of visual and emotional driver's signs using wavelet networks. In 2015 15th International Conference on Intelligent Systems Design and Applications (ISDA) (pp. 140-147). IEEE.
- [33] Lozano-Monator, E., López, M. T., Vigo-Bustos, F., & Fernández-Caballero, A. (2017). Facial expression recognition in ageing adults: from lab to ambient assisted living. *Journal of Ambient Intelligence and Humanized Computing*, 8(4), 567-578.
- [34] De Carolis, B., Ferilli, S., & Palestra, G. (2017). Simulating empathic behavior in a social assistive robot. *Multimedia Tools and Applications*, 76(4), 5073-5094.
- [35] Yolcu, G., Oztel, I., Kazan, S., Oz, C., Palaniappan, K., Lever, T. E., & Bunyak, F. (2017, November). Deep learning-based facial expression recognition for monitoring neurological disorders. In 2017 IEEE International Conference on Bioinformatics and Biomedicine (BIBM) (pp. 1652-1657). IEEE.
- [36] Shaykha, I., Menkara, A., Nahas, M., & Ghantous, M. (2015, September). FEER: Non-intrusive facial expression and emotional recognition for driver's vigilance monitoring. In 2015 57th International Symposium ELMAR (ELMAR) (pp. 233-237). IEEE.
- [37] Zhang, Y., & Hua, C. (2015). Driver fatigue recognition based on facial expression analysis using local binary patterns. *Optik*, 126(23), 4501-4505.
- [38] Terzis, V., Moridis, C. N., & Economides, A. A. (2013). Measuring instant emotions based on facial expressions during computer-based assessment. *Personal and ubiquitous computing*, 17(1), 43-52.
- [39] Zhao, Y., Wang, X., Goubran, M., Whalen, T., & Petriu, E. M. (2013). Human emotion and cognition recognition from body language of the head using soft computing techniques. *Journal of Ambient Intelligence and Humanized Computing*, 4(1), 121-140.
- [40] Niforatos, E., & Karapanos, E. (2015). EmoSnaps: a mobile application for emotion recall from facial expressions. *Personal and Ubiquitous Computing*, 19(2), 425-444.
- [41] Baldassarri, S., Hupont, I., Abadía, D., & Cerezo, E. (2015). Affective-aware tutoring platform for interactive digital television. *Multimedia Tools and Applications*, 74(9), 3183-3206.
- [42] Benmohamed, A., Neji, M., Ramdani, M., Wali, A., & Alimi, A. M. (2015). Feast: face and emotion analysis system for smart tablets. *Multimedia Tools and Applications*, 74(21), 9297-9322.
- [43] Arigbabu, O. A., Mahmood, S., Ahmad, S. M. S., & Arigbabu, A. A. (2016). Smile detection using hybrid face representation. *Journal of Ambient Intelligence and Humanized Computing*, 7(3), 415-426.
- [44] Samara, A., Galway, L., Bond, R., & Wang, H. (2019). Affective state detection via facial expression analysis within a human-computer interaction context. *Journal of Ambient Intelligence and Humanized Computing*, 10(6), 2175-2184.
- [45] Ekman, P., & Friesen, W. V. (1971). Constants across cultures in the face and emotion. *Journal of personality and social psychology*, 17(2), 124.

- [46] Pons, G., & Masip, D. (2017). Supervised committee of convolutional neural networks in automated facial expression analysis. *IEEE Transactions on Affective Computing*, 9(3), 343-350.
- [47] Lee, C. C., Shih, C. Y., Lai, W. P., & Lin, P. C. (2012). An improved boosting algorithm and its application to facial emotion recognition. *Journal of Ambient Intelligence and Humanized Computing*, 3(1), 11-17.
- [48] Ghimire, D., & Lee, J. (2013). Geometric feature-based facial expression recognition in image sequences using multi-class adaboost and support vector machines. *Sensors*, 13(6), 7714-7734.
- [49] Perumal Ramalingam, S., & Chandra Mouli, P. V. S. S. R. (2018). Modified dimensionality reduced local directional pattern for facial analysis. *Journal of Ambient Intelligence and Humanized Computing*, 9(3), 725-737.
- [50] Ghimire, D., & Lee, J. (2012). Histogram of orientation gradient feature-based facial expression classification using bagging with extreme learning machine. *Advanced Science Letters*, 17(1), 156-161.
- [51] Sobia, M. C., Brindha, V., & Abudhahir, A. (2014, February). Facial expression recognition using PCA based interface for wheelchair. In 2014 International Conference on Electronics and Communication Systems (ICECS) (pp. 1-6). IEEE.
- [52] Zhao, G., & Pietikainen, M. (2007). Dynamic texture recognition using local binary patterns with an application to facial expressions. *IEEE transactions on pattern analysis and machine intelligence*, 29(6), 915-928.
- [53] Lopes, A. T., De Aguiar, E., De Souza, A. F., & Oliveira-Santos, T. (2017). Facial expression recognition with convolutional neural networks: coping with few data and the training sample order. *Pattern recognition*, 61, 610-628.
- [54] Pitaloka, D. A., Wulandari, A., Basaruddin, T., & Liliana, D. Y. (2017). Enhancing CNN with preprocessing stage in automatic emotion recognition. *Procedia computer science*, 116, 523-529.
- [55] Matsugu, M., Mori, K., Mitari, Y., & Kaneda, Y. (2003). Subject independent facial expression recognition with robust face detection using a convolutional neural network. *Neural Networks*, 16(5-6), 555-559.
- [56] Chen, C., & Odobez, J. M. (2012, June). We are not contortionists: Coupled adaptive learning for head and body orientation estimation in surveillance video. In 2012 IEEE Conference on Computer Vision and Pattern Recognition (pp. 1544-1551). IEEE.
- [57] Kang, S. K., Chung, K. Y., & Lee, J. H. (2014). Development of head detection and tracking systems for visual surveillance. *Personal and ubiquitous computing*, 18(3), 515-522.
- [58] Murphy-Chutorian, E., Doshi, A., & Trivedi, M. M. (2007, September). Head pose estimation for driver assistance systems: A robust algorithm and experimental evaluation. In 2007 IEEE intelligent transportation systems conference (pp. 709-714). IEEE.
- [59] Alioua, N., Amine, A., Rogozan, A., Bensrhair, A., & Rziza, M. (2016). Driver head pose estimation using efficient descriptor fusion. *EURASIP Journal on Image and Video Processing*, 2016(1), 1-14.
- [60] Ba, S. O., & Odobez, J. M. (2008). Recognizing visual focus of attention from head pose in natural meetings. *IEEE Transactions on Systems, Man, and Cybernetics, Part B (Cybernetics)*, 39(1), 16-33.
- [61] Gaschler, A., Jentzsch, S., Giuliani, M., Huth, K., de Ruiter, J., & Knoll, A. (2012, October). Social behavior recognition using body posture and head pose for human-robot interaction. In 2012 IEEE/RSJ International Conference on Intelligent Robots and Systems (pp. 2128-2133). IEEE.
- [62] Patacchiola, M., & Cangelosi, A. (2017). Head pose estimation in the wild using convolutional neural networks and adaptive gradient methods. *Pattern Recognition*, 71, 132-143.
- [63] Murphy-Chutorian, E., & Trivedi, M. M. (2008). Head pose estimation in computer vision: A survey. *IEEE transactions on pattern analysis and machine intelligence*, 31(4), 607-626.
- [64] McKenna, S. J., & Gong, S. (1998). Real-time face pose estimation. *Real-Time Imaging*, 4(5), 333-347.
- [65] Tran BH, Kim Y-G (2017) Deep head pose estimation for faces in the wild and its transfer learning. In: Seventh international conference on information science and technology (ICIST). IEEE, pp 187-193.
- [66] Mukherjee, S. S., & Robertson, N. M. (2015). Deep head pose: Gaze-direction estimation in multimodal video. *IEEE Transactions on Multimedia*, 17(11), 2094-2107.
- [67] Xu, X., & Kakadiaris, I. A. (2017, May). Joint head pose estimation and face alignment framework using global and local CNN features. In 2017 12th IEEE International Conference on Automatic Face & Gesture Recognition (FG 2017) (pp. 642-649). IEEE.
- [68] Viola, P., & Jones, M. J. (2004). Robust real-time face detection. *International journal of computer vision*, 57(2), 137-154.
- [69] Long, J., Shelhamer, E., & Darrell, T. (2015). Fully convolutional networks for semantic segmentation. In *Proceedings of the IEEE conference on computer vision and pattern recognition* (pp. 3431-3440).
- [70] Langner, O., Dotsch, R., Bijlstra, G., Wigboldus, D. H., Hawk, S. T., & Van Knippenberg, A. D. (2010). Presentation and validation of the Radboud Faces Database. *Cognition and emotion*, 24(8), 1377-1388.
- [71] Lundqvist, D., Flykt, A., & Öhman, A. (1998). Karolinska directed emotional faces. *Cognition and Emotion*.

An Optimized Single Layer Perceptron-based Approach for Cardiotocography Data Classification

Bader Fahad Alkhamees

Department of Information Systems, College of Computer and Information Sciences
King Saud University, Riyadh 11543, Saudi Arabia

Abstract—Uterine Contractions (UC) and Fetal Heart Rate (FHR) are the most common techniques for evaluating fetal and maternal assessment during pregnancy and detecting the changes in fetal oxygenation occurred throughout labor. By monitoring the Cardiotocography (CTG) patterns, doctors can measure fetus state, accelerations, heart rate, and uterine contractions. Several computational and machine learning (ML) methods have been done on CTG recordings to improve the effectiveness of fetus analysis and aid the doctors to understand the variations in their interpretation. However, getting an optimal solution and best accuracy remains an important concern. Among the various ML approaches, artificial neural network (ANN)-based approach has achieved a high performance in several applications. In this paper, an optimized Single Layer Perceptron (SLP)-based approach is proposed to classify the CTG data accurately and predict the fetal state. The approach is able to exploit the advantages of SLP model and optimize the learning rate using a grid search method in which we can arrive at the best accuracy and converge to a local minima. The approach is evaluated on CTG dataset of University of California, Irvine (UCI). The optimized SLP model is trained and tested on the dataset using a 10-fold cross-validation technique to classify the CTG patterns as normal, suspect or pathologic. The experimental results show that the proposed approach achieved 99.20% accuracy compared with the state-of-the-art models.

Keywords—Cardiotocography; machine learning; artificial neural network (ANN); learning rate; grid search; 10-fold cross-validation

I. INTRODUCTION

Nowadays, development and research have been taking place in the healthcare area, and they will continue to expand the analysis by gathering all relevant data from different devices or methods in medical domains, such as medicine, biotechnology, and biomedical [1, 2]. Electronic Fetal Monitoring (EFM) is one of the common methods used to assess fetal well-being during labor [3, 4]. During labor, the fetus is relatively inaccessible as a result, the clinician evaluations depend just on the available and indirect fetal condition measures [5]. The EFM is the most effective method in assessing the fetal status. Also, it is safety through recording maternal Uterine Pressure (UP) and FHR during labor and delivery, that is, the Cardiotocography (CTG) procedure [6]. In addition, nowadays (over 90%) of the labors are electronically monitored by using sensors in order to measure and record UC and FHR [4]. The EFM is commonly used to assess fetal well-being through labor [4]. In the past, before using the EFM the fetal heart rate was measured through the fetal stethoscope [4]. There was a disadvantage of using the stethoscope because it

was not able to detect the FHR subtle changes [6]. On the other hand, the EFM is able to overcome this problem by giving the continuous monitoring of the fetus during pregnancy and labor. The EFM has other effective roles. It is able to give minute-by-minute information on the fetus status. Also, it can note the historical information on fetal status accurately and give insight into the stresses on the fetus. The EFM consists of the Cardiotocography which is continuous recording of the fetal heart rate and the (ST) which is used to analyze the fetal electrocardiogram (FEKG) [5, 7].

The CTG is the check-up that is generally done during the last three months of pregnancy. This test is for checking the heartbeats of the baby if it has a regular rate and changeability [8]. In general, the baby's heart rate is 110 to 160 beats for each minute [9]. The Cardiotocography expression composed of: (cardio-) which means the fetal heartbeat, (-toco-) which means Uterine contractions and (-graphy) which means recording [9]. EFM enables us to detect the “at risk fetus” early for medical intervention where the delay or failure in detection of abnormal fetus in the CTG recordings can lead to fetal death or injury; which may be a brain injury [10]. In addition, some reviews on birth-related brain injury cases noted that nearly (50%) of brain-injuries refer to preventable medical errors especially the wrong FHR signal analysis [10]. For example, the recognition of the acceleration and deceleration samples in FHR signal is a fateful matter. Because it is important for the detecting of fetal intrauterine distress where there is any delay or failure in their recognition may cause a fetal injury [10].

More than half of these deaths are the result of improper diagnoses made based on FHR pattern recordings and treatments given to the fetus [11, 12]. Despite its practicality, CTG monitoring may not always be effective, especially in low-risk pregnancies. If fetal pain is incorrectly assessed, it could lead to ineffective treatments, and if fetal well-being is improperly investigated, it could leave out necessary treatments [11]. Difficulties in the interpretation of CTG records require methods for computer-assisted analysis where the computer analysis of classifying the FHR and Uterine Contraction (UC) is generally more accurate than human analysis. Classifying the fetal heart rate and fetal state from CTG patterns using computational methods will provide more accurate and less confused medical intervention decisions which provided in the appropriate time is a very important decision in the fetal life where any fault or delay could lead to fetal death or injury [10].

Using effective machine learning (ML) classification methods for classifying the CTG patterns may increase

significantly the performance of predicting the fetal state [13]. Moreover, selecting the appropriate values for the parameters of ML methods is considered as one of the factors that effect on the success of ML-based applications on the various medical data samples [13, 14]. Where, if these parameters have inappropriate values then the classification process will be more difficult during training to get optimal or near optimal solutions. The optimization of ML parameters is the process of choosing the most appropriate values on the data in order to increase the accuracy and performance of ML methods [15].

Among the different ML methods, artificial neural network (ANN) has a high capability to model the relationships between output and input data points, which are complex like data of medical field. However, optimizing Single Layer Perceptron (SLP) parameters is also critical to get a high accuracy output of the medical applications. This paper tries to reduce the risk of misclassification and its negative impact by exploiting the advantages of SLP model and learning rate optimization to arrive at the best accuracy and converge to a local minima.

This study intends to design an optimized SLP-based approach for classifying the CTG data accurately and predicting the fetal state. The developed approach selects the best value for learning rate hyper-parameter and converge to a local minima. The main contributions of this research work are itemised in the following lines.

- An accurate approach using optimized SLP model and a grid search algorithm is proposed to classify the CTG patterns as normal, suspect or pathologic.
- By using the grid search algorithm, an optimal or near-optimal value of learning rate is selected to improve learning process of SLP model, arriving at the best accuracy and converge to a local minima.
- The optimized SLP model is trained and tested on the dataset using a 10-fold cross-validation technique to achieve the diversity in learning the SLP model.
- The performance of the optimized SLP model is evaluated and compared with the recent work on the same CTG dataset.

The rest of the paper is structured as follows: Section II provides the related work of the proposed approach. Section III gives an explanation about the materials and methods of the research study. Section IV describes the experimental results with discussion and outcomes. Finally, Section V summarizes the conclusions and future work.

II. RELATED WORK

There are a number of studies and methods that have been presented by many researchers and professionals on medical data and healthcare [16]. Data mining and machine learning techniques are one of these methods, which are applied in different stages of medical applications, including data collection, storage allocation, analytics, pre-processing, and classification or predication [17]. However, the focus of this section aims to evaluate the various classification approaches and methods used on the Cardiotocography (CTG) data

patterns. According to Grivell et al. [11], the evaluation of CTG patterns is an important diagnostic procedure, used to measure the maternity during pregnancy and detect the fetal heart rate.

Using ML, e-health software, and traditional pregnancy tests, Akbulut et al. [18] created a framework for prediction in e-health applications that can assist doctors and pregnant women in identifying congenital abnormalities. In order to process the clinical data and maternal predicting for fetal anomalies, nine binary-classification models that have been trained on 96 pregnant women in the clinical datasets were compared for performance. Decision forest models have the highest forecasting accuracy, at 89.5%, during development tests.

Huang [19] used three different machine learning techniques to analyze the CTG data in order to predict fetal distress. Employing statistical features taken from empirical mode decomposition was suggested by Krupa et al. [20]. (EMD). The sub-band decomposition's extracted features were categorized as either normal or risky. For the test data, they achieved an accuracy of 86%. Another study described a two-step analysis of fetal heart rate data that enables accurate risk prediction. Support Vector Machines (SVM), fuzzy, and multilayer perceptron are used to classify the FHR signals. Sundar et al. [21] implemented a new model that classifies the CTG data using ANN. The F-score and Recall were used to evaluate the performance. They also suggested the use of k-means clustering for CTG classification. Moreover, Ocak and Ertunc [22] used adaptive neuro-fuzzy inference systems (ANFIS) for classifying CTG data patterns. Genetic Algorithm (GA) and SVM methods have been implemented for CTG classification by Ocak [23].

In 2019, Potharaju et al. [24] examined the CTG classification using J48, Ridor, Jrip, NBStar, Kstar, and IBk. They used the SMOTE technique to balance the dataset after realizing the CTG data was inherently unbalanced. Their experimental findings show that a balanced dataset performs classification more effectively than one that is unbalanced. After choosing the top six features, they also experimented with three feature selection techniques to assess the effectiveness.

An associative classification (CBA) model has been put forth by Piri and Mohapatra [25] for the analysis of Cardiotocographic fetal evaluation. When choosing a smaller data set with the most crucial features, they also considered the significance of each feature. Zhang and Zhao's [26] developed a decision-support system for clinical fetal risk diagnosis using a cutting-edge machine learning method through pertinent features, which are extracted from the CTG recordings. Therefore, this research showed that hybrid AdaBoost and PCA were effective for classifying the CTG results and determining the fetal status. AUC, sensitivity, and specificity are just a few of the performance classification criteria that have been adopted.

Rough Neural Network has been proposed by the authors in [27] as one of the most popular data mining methods for categorizing medical data in the classification of Cardiotocography data. They timed the classification process

and measured the accuracy outcomes. The WEKA tool uses a variety of algorithms, including neural networks, decision tables, bagging, and the nearest neighbor, among others, to analyze Cardiotocographic data. In a study, Hoodbhoy et al. [28] evaluated the efficiency of using CTG data to identify high-risk fetuses using ML techniques. They developed the prediction task using XGBoost to obtain the fetal outcome specified in the classification model.

Recently, Yan and Han [29] proposed a Cost-Sensitive Stacked Generalization (CSSG) approach for re-sampling based on two layers analytics model to sample the distribution of imbalanced class in the dataset. With 17 imbalanced public data sets, the results indicated that their method performed better in classification than other ensembles and single algorithms. Brown and Mues [30] have set themselves the task of analyzing various approaches used to analyze credit score data that is unbalanced. As there are typically many more defaulted loans than there are non-defaulting observations in a portfolio, imbalanced data sets frequently occur in a loan scoring environment. The appropriateness of predictions for loan default is examined by random forests, gradient boosting, and SVM, in addition to the use of conventional classification methods such as neural networks, logistic regression, and decision making trees.

Some under-sampling methods have been studied, for example, Shang [31] in his paper introduced two kinds of sampling methods for missing data in the networks. These two methods are uniform and non-uniform random sampling. In uniform random sampling, a fraction of data sample (q) is arranged uniformly at a random manner in the dataset. This kind of sampling is commonly used in some other work of different applications. In non-uniform random sampling, the data sample is generated by selecting the nearest neighbors data of a seed point, then, its second nearest neighbors data and so on until a fraction of data sample ($1 - q$) in the entire dataset are selected.

Additionally, a popular SMOTE algorithm for cardiovascular data are examined by Rahman and Davis [32]. They also recommended a modified under-sampling technique using clusters that can produce high-quality training samples for classifier design while also balancing the data. Yen and Lee [33] utilized clusters-based under-sampling approach to choose representative data for examining the under-sampling impact on the distribution of unbalanced classes, with the goal of improving the classification accuracy for minority classes. The experimental results of the approach showed that the cluster-based approach outperformed the other under-sampling methods used in earlier studies.

To address imbalanced and limited CTG data, Piri and Mohapatra [34] have proposed a different number of re-sampling methods and two ensemble models to balance the training samples and improve the classification task. They applied several ML models such as Support vector machine (SVM), Random Forest (RF), Decision Tree (DT) K-Nearest Neighbors (KNN), Logistic Regression (LR), and Gaussian Naive Bayes (GNB). They achieved a 95% classification accuracy using RF model on the balanced dataset. From the previous studies and related work, still there is a need to

optimize the learning process and improve the accuracy of CTG data classification. In this work, an optimized SLP-based approach is proposed to classify accurately the CTG data as normal, suspect or pathologic for predicting the fetal state.

III. MATERIALS AND METHODS

This section explains the materials and methods of the research study. It describes the dataset used for obtaining the experimental result and gives an explanation about the methods of the proposed approach. In the following subsections, the dataset, methods, and the approach will be given in more detail.

A. CTG Dataset

In this proposed work, the CTG dataset obtained from the UCI repository [35] is chosen for conducting the experiment of the study. It is prepared for CTG trace analysis and the discovery of fundamental attributes. The dataset contains two attributes (FHR pattern and fetal state) represent the target labels and 21 distinguished features (LB-FHR; AC; FM; UC; etc.). Because the target attribute of the study includes the normal, suspect, and pathological classes, the Fetal state attribute is used as class label to solve a three-class problem and determine the fetal health-state using the other attributes; and the FHR pattern class label is removed from the dataset. According to the fetal state target class, the number of instances in the dataset is distributed into three groups: 1655 instances for normal class, 295 instances for suspect class, and 176 instances for pathological class. The distribution of instances for the three target classes is presented in Fig. 1.

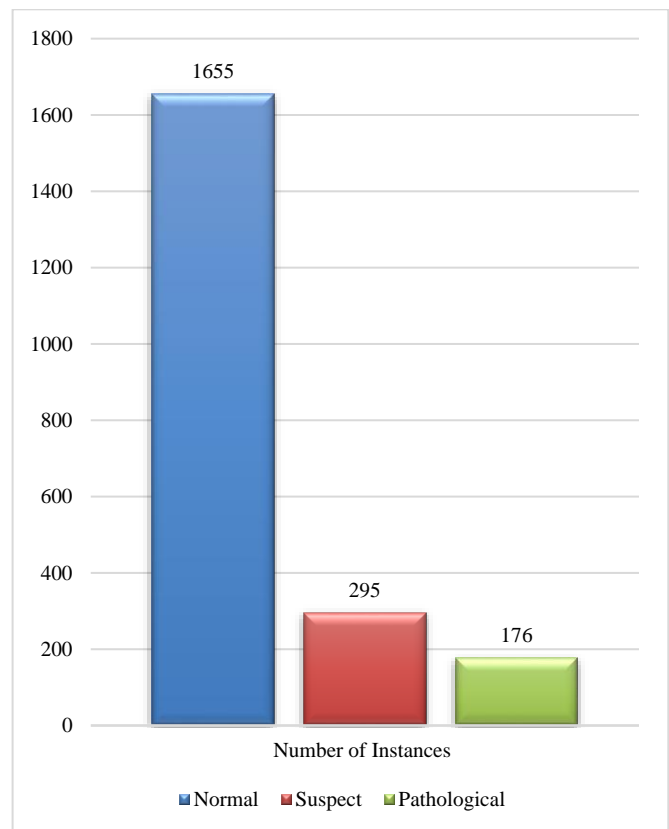


Fig. 1. The Distribution of Instances for the Three Target Classes.

TABLE I. THE ATTRIBUTES INFORMATION OF THE CTG DATASET

No.	Attribute	Description
1	LB-FHR	The baseline (beats per minute)
3	FM	The number of fetal movements for each second
2	AC	The number of accelerations for each second
5	DL	The number of light decelerations for each second
4	UC	The number of uterine contractions for each second
6	DS	The number of severe decelerations for each second
8	ASTV	The percentage of time with abnormal short term variability
7	DP	The number of prolonged decelerations for each second
9	MSTV	The mean value of short term variability
11	MLTV	The mean value of long term variability
10	ALTV	The percentage of time with abnormal long term variability
12	Width	The width of FHR histogram
14	Max	The maximum of FHR histogram
13	Min	The minimum of FHR histogram
15	Nmax	The number of histogram peaks
17	Mode	The histogram mode
16	Nzeros	The number of histogram zeros
18	Mean	The histogram mean
20	Variance	The histogram variance
19	Median	The histogram median
21	Tendency	The histogram tendency
22	CLASS	The FHR pattern class code (1 to 10)
23	NSP	The fetal state class code (N = Normal; S = Suspect; P = Pathologic)

The information of the attributes is given in Table I. As shown in Fig. 1, the number of instance for each class shows that the CTG dataset is imbalanced. Therefore, it is important to build a robust ML method to improve the performance in present of the imbalanced class problem.

B. Single-Layer Perceptron (SLP)

Single-layer perceptron (SLP) is the first and most fundamental model of ANN. The feed-forward neural network is another name for it [36]. The threshold transfer between the nodes serves as the foundation for the SLP's operation. This is the most basic type of ANN used to solve machine learning problems with linear cases. It is a straightforward neural network with only one layer is known as a single layer perceptron [37]. There are only two layers for input and output in the single layer perceptron (See Fig. 2). The name single layer perceptron refers to the fact that it only has one layer. As opposed to a multilayer perceptron, it lacks hidden layers.

The single layer perceptron computation is the sum of the input vectors multiplied by the corresponding vector weight. The input to an activation function will be the value displayed as the output. Four components make up the perceptron: the input values or one input layer, the weights and biases, the network sum, and the activation function as seen in Fig. 3.

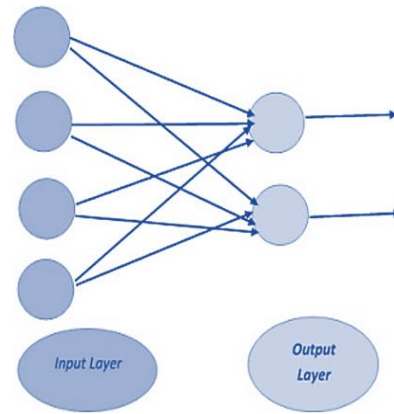


Fig. 2. Two Layers for Input and Output in the Single Layer Perceptron Classes.

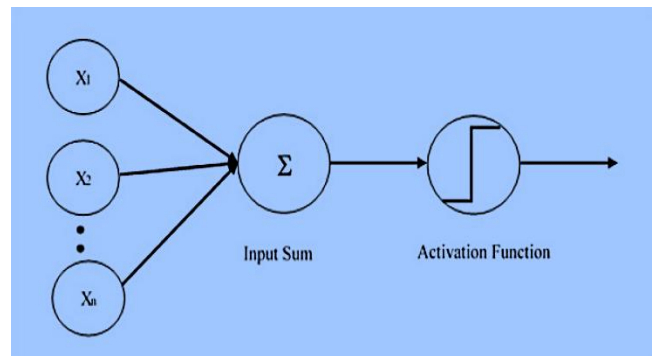


Fig. 3. The Components of Single Layer Perceptron.

C. Grid Search Technique

A grid search or a parameter sweep, it is just a search process through a manually specified subset of the hyper-parameter space of a learning algorithm [38]. It is considered a traditional method of performing hyper-parameter optimization. A performance metric, typically determined by cross-validation on the training set or evaluation on a hold-out validation set that can guide the grid search technique. Before using grid search, it may be necessary to manually set bounds and discretize certain parameters because the parameter space of a machine learning may include real-valued or unbounded value spaces [39].

For instance, a typical classifier with a kernel function, which has a regularization constant C and a kernel hyperparameter γ . They can be tuned for good performance on unseen data. Since both parameters are continuous, one chooses a limited number of "reasonable" values for each in order to perform a grid search, such as:

$$C \in \{10, 100, 1000\}$$

$$\gamma \in \{0.1, 0.2, 0.5, 1.0\}$$

Then, using each pair (C, γ) in the Cartesian product of these two sets, grid search trains the classifier. The performance of the classifier is then assessed using a held-out validation set (or by internal cross-validation on the training set, in which case multiple classifiers are trained per pair). The settings that received the highest score during the validation process are finally returned by the grid search algorithm. The

hyper-parameter settings are typically evaluated independently of one another, allowing the grid search method to operate in parallel [39].

D. Proposed Approach

The proposed approach aims to build an effective and robust SLP classification model that archives a high accuracy for classifying the CTG patterns and predicting the fetal state. It contains two main phases presented in Fig. 4. The approach exploits the advantages of SLP model and optimizes the learning rate using a grid search method in which we can arrive at the best accuracy and converge to a local minima.

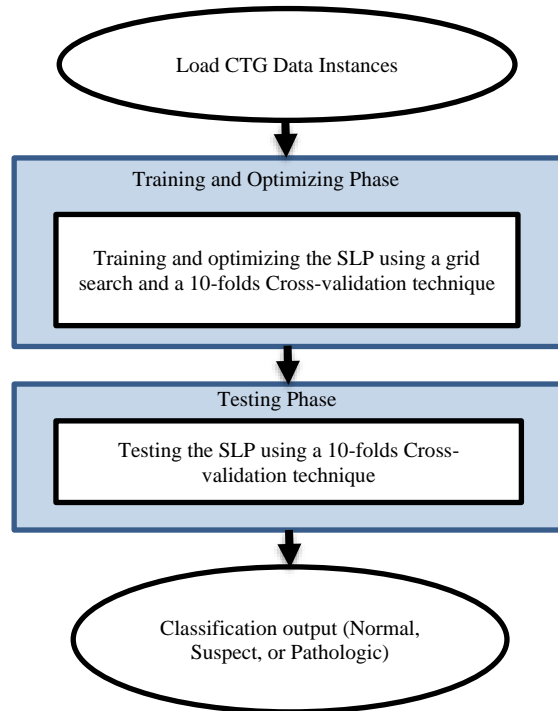


Fig. 4. Flowchart of Proposed Approach.

1) *Training and optimizing phase*: This subsection explains the training and optimizing phase of the SLP model. The training process is conducted on the CTG dataset using a 10-folds cross-validation technique. In this technique, the dataset is divided into ten subsets and the SLP model is trained using nine out of ten subsets for ten times. The remaining set each time is used in the validation process. The output of this phase is the best model from the ten trained SLP models. Then, the classification result is evaluated through the best model on the whole dataset in the testing phase. The optimizing process of the SLP model is performed to determine the optimal value of the learning rate during the training step by the grid method algorithm. The grid search method selects a set of possible values for the learning rate and evaluates the result for each value.

2) *Testing phase*: After dividing the dataset to ten subsets and training the SLP model on nine subsets, the remaining subset from the ten subsets is used for testing the trained SLP model. This procedure is repeated for ten times until all ten subsets are involved in the validation process of the trained

models. The classification result is obtained by testing the dataset on the best model of trained in the training and optimizing phase for getting the final result of the approach. The classification test result is measured using a number of evaluation metrics such as accuracy, F1-score, precision, and recall, which will be described in the experimental results section.

IV. EXPERIMENTAL RESULTS AND DISCUSSIONS

In this section, the performance of proposed approach is analyzed using a 10-fold cross-validation technique to classify the fetal state from CTG data instances. The experimental results are performed on a laptop with the Intel Core i7, 2.50 GHz CPU, 16GB RAM and Windows 10. The proposed approach is implemented using a WEKA data mining tool. A number of evaluation metrics such as precision, recall, F-score, and accuracy are computed from the classification outputs. These metrics are computed using the following equations:

$$Precision = \frac{TP}{(TP+FP)} \quad (1)$$

$$Recall = \frac{TP}{(TP+FN)} \quad (2)$$

$$F1-score = 2 * \left(\frac{Precision * Recall}{Precision + Recall} \right) \quad (3)$$

$$Accuracy = \frac{(TP+TN)}{(TP+FP+TN+FN)} \quad (4)$$

Where FN, FP, TN, and TP are the false negative, false positive, true negative, and true positive instances, respectively. The confusion matrix for the classification task is also used. To measure the confusion matrix, FN, FP, TN, and TP are required.

The evaluation results of the approach are also compared with the various recent existing methods and approaches designed for CTG fetal state classification. The experimental parameters of the SLP model are established in Table II.

The values of the model's parameters in Table II are selected experimentally where the learning rate is chosen to be optimized using a grid search method with 10-fold cross-validation technique. The grid search method starts the searching operation among a set of possible values, which are 0.0005, 0.001, 0.005, 0.01, 0.1, 0.15, 0.2, 0.25, and 0.3. Then, the model is trained at each value of these possible learning rate values. The best value of learning rate hyper-parameter is 0.1. Fig. 5 shows the results of accuracy at these different values of learning rate.

TABLE II. EXPERIMENTAL PARAMETERS OF PROPOSED APPROACH SLP MODEL

Parameter	Value
Hidden nodes	19
Momentum	0.2
Batch Size	100
Learning Rate	0.1
Number of Epochs	500

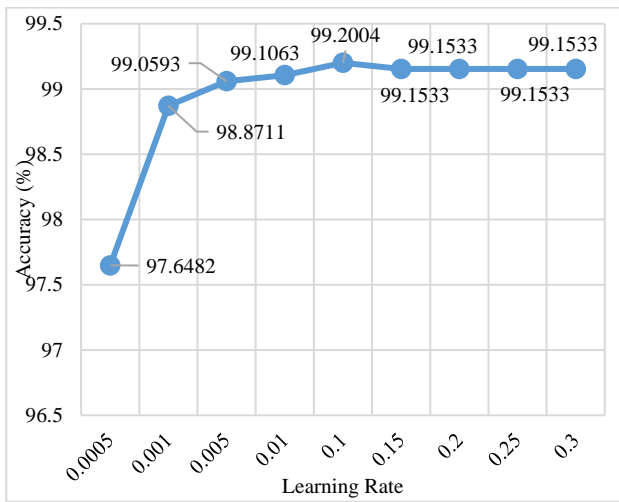


Fig. 5. Accuracies of SLP Model at different Learning Rate.

Also, Fig. 6 demonstrates the classification confusion matrix of optimized SLP model. We can see that 1649 from 1655 normal instances are classified correctly as normal class and 285 of 295 suspect instances are classified correctly as suspect class, as well as 175 of 176 pathologic instances are classified correctly as pathologic class. These classification results confirm the ability of SLP model to classify the CTG patterns in accurate manner.

		Actual Classes		
		Normal	Suspect	Pathologic
Predicted Classes	Normal	1649	6	0
	Suspect	9	285	1
	Pathologic	0	1	175

Fig. 6. Confusion Matrix of SLP Model Test Classification.

According the result of confusion matrix in Fig. 6, Table III displays the results of other evaluation metrics. It shows that the model achieves 99.2% of accuracy and 0.992 for weighted average F1-score, recall, and precision metrics.

To highlight the performance of the proposed approach, the accuracy result obtained on the dataset is compared with the other models proposed in the recent current study [34] for classifying CTG data into normal, suspect, and pathologic classes. The visualization of this comparative analysis is presented in Fig. 7.

TABLE III. RESULTS OF EVALUATION METRICS FOR SLP MODEL

Class Name	Precision	Recall	F-score
Normal	0.995	0.996	0.995
Suspect	0.976	0.966	0.971
Pathologic	0.994	0.994	0.994
Weighted Avg.	0.992	0.992	0.992
Accuracy	99.2004%		

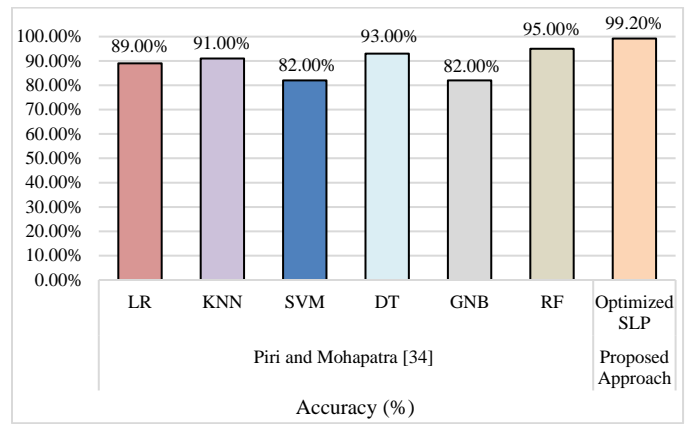


Fig. 7. Comparison Results of Accuracy for Developed SLP Model and other Models in the State-of-the Art.

From the comparison analysis, we can see that among the different models in [34], the DT and RF have the best accuracy results, which are 93% and 95%, respectively. However, the optimized SLP model has the highest accuracy (99.2%) compared with DT and RF.

V. CONCLUSIONS AND FUTURE WORK

Fetal state detection from the CTG data using classification methods has become an important task for developing various medical applications. In this paper, an optimized SLP-based approach is introduced for improving CTG data classification and analysis. The approach is able to select an optimal learning rate value of SLP model and make the learning process converge to a local minima, achieving a best accuracy result. The experimental results of the research are conducted on CTG dataset and by using a number of evaluation metrics, such as accuracy, F1-score, precision, and recall. The optimized SLP model is trained and tested on the dataset using a 10-fold cross-validation technique to generalize the training phase of developed model. The obtained results on the test process revealed that the optimized SLP model has the highest accuracy result (99.2%) compared with the models used in the recent study of related work. According to the accuracy results of the state-of-the-art models, the accuracy of optimized SLP model is increased by 4.2%. Therefore, the SLP has the ability to classify the CTG patterns in an accurate manner. In future work, a combination of different methods and deep learning models will be explored to classify the CTG data and detect fetal heart state.

ACKNOWLEDGMENT

“This research was supported by the Researchers Supporting Project number (RSP2022R493), King Saud University, Riyadh, Saudi Arabia.”

REFERENCES

- [1] P. R. Williamson, D. G. Altman, J. M. Blazeby, M. Clarke, D. Devane et al., "Developing core outcome sets for clinical trials: Issues to consider," *Trials*, vol. 13, no. 1, pp. 1-8, 2012.
- [2] G. Acampora, D. J. Cook, P. Rashidi and A. V. Vasilakos, "A survey on ambient intelligence in healthcare," *Proceedings of the IEEE*, vol. 101, no. 12, pp. 2470-2494, 2013.

- [3] C. Edwin and S. Arulkumarn, "Electronic fetal heart rate monitoring in current and future practice," *Journal Obstet Gynecol India*, vol. 58, no. 2, pp. 121-130, 2008.
- [4] A. Sweha, T. W. Hacker and J. Nuovo, "Interpretation of the electronic fetal heart rate during labor," *American family physician*, vol. 59, no. 9, p. 2487, 1999.
- [5] Z. Alfirevic, D. Devane and G. M. Gyte, "Continuous cardiotocography (ctg) as a form of electronic fetal monitoring (efm) for fetal assessment during labour," *Cochrane database of systematic reviews*, no. 5, 2013.
- [6] Y. Oyelese, M. Chavez and A. M. Vintzileos, "Assessment of fetal well-being: Fetal heart rate monitoring and the fetal biophysical profile," in *Clinical maternal-fetal medicine online*: CRC Press, 2021, pp. 67.1-67.17.
- [7] I. Amer-Wählin and K. Maršál, "St analysis of fetal electrocardiography in labor," in *Seminars in Fetal and Neonatal Medicine*, 2011, vol. 16, no. 1, pp. 29-35: Elsevier.
- [8] P. Gupta, A. Saxena, T. Garg, A. Khatri and R. Mittal, "A prototype for realtime monitoring of fetal health using a pressure sensitive material and sensor based belt," in *2018 International Conference on Advances in Computing, Communication Control and Networking (ICACCCN)*, 2018, pp. 935-940: IEEE.
- [9] A. Martin, "Fetal heart rate during labour: Definitions and interpretation," *Journal de gynécologie, obstétrique et biologie de la reproduction*, vol. 37, pp. S34-45, 2008.
- [10] L. A. Cibils, "Clinical significance of fetal heart rate patterns during labor: Ii. Late decelerations," *American Journal of Obstetrics Gynecology*, vol. 123, no. 5, pp. 473-492, 1975.
- [11] R. M. Grivell, Z. Alfirevic, G. M. Gyte and D. Devane, "Antenatal cardiotocography for fetal assessment," *Cochrane database of systematic reviews*, no. 9, 2015.
- [12] M. Cesarelli, M. Romano and P. Bifulco, "Comparison of short term variability indexes in cardiotocographic foetal monitoring," *Computers in biology medicine*, vol. 39, no. 2, pp. 106-118, 2009.
- [13] Y. Lu, Y. Gao, Y. Xie and S. He, "Computerised interpretation systems for cardiotocography for both home and hospital uses," in *2018 IEEE 31st International Symposium on Computer-Based Medical Systems (CBMS)*, 2018, pp. 422-427: IEEE.
- [14] A. Çetin, "Use of three-tier classification system during intrapartum electronic fetal heart rate monitoring," *Basic Clinical Sciences*, vol. 1, no. 4, pp. 71-76, 2010.
- [15] L. Yang and A. Shami, "On hyperparameter optimization of machine learning algorithms: Theory and practice," *Neurocomputing*, vol. 415, pp. 295-316, 2020.
- [16] J. Benneyan, R. Lloyd and P. Plsek, "Statistical process control as a tool for research and healthcare improvement," *BMJ Quality Safety*, vol. 12, no. 6, pp. 458-464, 2003.
- [17] I. Yoo, P. Alafaireet, M. Marinov, K. Pena-Hernandez, R. Gopidi et al., "Data mining in healthcare and biomedicine: A survey of the literature," *Journal of medical systems*, vol. 36, no. 4, pp. 2431-2448, 2012.
- [18] A. Akbulut, E. Ertugrul and V. Topcu, "Fetal health status prediction based on maternal clinical history using machine learning techniques," *Computer methods programs in biomedicine*, vol. 163, pp. 87-100, 2018.
- [19] M.-L. Huang and Y.-Y. Hsu, "Fetal distress prediction using discriminant analysis, decision tree, and artificial neural network," 2012.
- [20] N. Krupa, M. A. MA, E. Zahedi, S. Ahmed and F. M. Hassan, "Antepartum fetal heart rate feature extraction and classification using empirical mode decomposition and support vector machine," *Biomedical engineering online*, vol. 10, no. 1, pp. 1-15, 2011.
- [21] C. Sundar, M. Chitradevi and G. Geetharamani, "An analysis on the performance of k-means clustering algorithm for cardiotocogram data clustering," *International Journal Computer Science Application*, vol. 2, no. 5, pp. 11-20, 2012.
- [22] H. Ocak and H. M. Ertunc, "Prediction of fetal state from the cardiotocogram recordings using adaptive neuro-fuzzy inference systems," *Neural Computing Applications*, vol. 23, no. 6, pp. 1583-1589, 2013.
- [23] H. Ocak, "A medical decision support system based on support vector machines and the genetic algorithm for the evaluation of fetal well-being," *Journal of medical systems*, vol. 37, no. 2, pp. 1-9, 2013.
- [24] S. P. Potharaju, M. Sreedevi, V. K. Ande and R. K. Tirandasu, "Data mining approach for accelerating the classification accuracy of cardiotocography," *Clinical Epidemiology Global Health*, vol. 7, no. 2, pp. 160-164, 2019.
- [25] J. Piri and P. Mohapatra, "Exploring fetal health status using an association based classification approach," in *2019 International Conference on Information Technology (ICT)*, 2019, pp. 166-171: IEEE.
- [26] Y. Zhang and Z. Zhao, "Fetal state assessment based on cardiotocography parameters using pca and adaboost," in *2017 10th international congress on image and signal processing, BioMedical engineering and informatics (CISP-BMEI)*, 2017, pp. 1-6: IEEE.
- [27] B. Amin, M. Gamal, A. Salama, I. El-Henawy and K. Mahfouz, "Classifying cardiotocography data based on rough neural network," *International Journal of Advanced Computer Science Applications*, vol. 10, no. 8, 2019.
- [28] Z. Hoodbhoy, M. Noman, A. Shafique, A. Nasim, D. Chowdhury et al., "Use of machine learning algorithms for prediction of fetal risk using cardiotocographic data," *International Journal of Applied Basic Medical Research*, vol. 9, no. 4, p. 226, 2019.
- [29] J. Yan and S. Han, "Classifying imbalanced data sets by a novel re-sample and cost-sensitive stacked generalization method," *Mathematical Problems in Engineering*, vol. 2018, 2018.
- [30] I. Brown and C. Mues, "An experimental comparison of classification algorithms for imbalanced credit scoring data sets," *Expert Systems with Applications*, vol. 39, no. 3, pp. 3446-3453, 2012.
- [31] Y. Shang, "Subgraph robustness of complex networks under attacks," *IEEE Transactions on Systems, Man, Cybernetics: Systems*, vol. 49, no. 4, pp. 821-832, 2017.
- [32] M. M. Rahman and D. N. Davis, "Addressing the class imbalance problem in medical datasets," *International Journal of Machine Learning Computing*, vol. 3, no. 2, p. 224, 2013.
- [33] S.-J. Yen and Y.-S. Lee, "Cluster-based under-sampling approaches for imbalanced data distributions," *Expert Systems with Applications*, vol. 36, no. 3, pp. 5718-5727, 2009.
- [34] J. Piri and P. Mohapatra, "Imbalanced cardiotocography data classification using re-sampling techniques," in *Proceedings of international conference on machine intelligence and data science applications*, 2021, pp. 681-692: Springer.
- [35] K. Bache and M. J. U. h. a. i. u. e. m. Lichman, "Uci machine learning repository. University of california, irvine, school of information and computer sciences (2013)," pp. 0162-8828, 2019.
- [36] G. P. Zhang, "Neural networks for classification: A survey," *IEEE Transactions on Systems, Man, Cybernetics, Part C*, vol. 30, no. 4, pp. 451-462, 2000.
- [37] X. Zhang, X. Chen, J. Wang, Z. Zhan and J. Li, "Verifiable privacy-preserving single-layer perceptron training scheme in cloud computing," *Soft Computing*, vol. 22, no. 23, pp. 7719-7732, 2018.
- [38] L. Zahedi, F. G. Mohammadi, S. Rezapour, M. W. Ohland and M. H. Amini, "Search algorithms for automated hyper-parameter tuning," *arXiv preprint arXiv:14677*, 2021.
- [39] J. Bergstra, R. Bardenet, Y. Bengio and B. Kégl, "Algorithms for hyper-parameter optimization," *Advances in neural information processing systems*, vol. 24, 2011.

Observe-Orient-Decide-Act (OODA) for Cyber Security Education

Dimas Febriyan Priambodo¹, Yogha Restu Pramadi²
Obrina Candra Briliyant³, Muhammad Hasbi⁴, Muhammad Adi Yahya⁵
Cyber Security Departement, Cyber and Crypto Politechnic, Bogor, Indonesia^{1,2,3,5}
Informatic Departement, STMIK Sinar Nusantara, Surakarta, Indonesia⁴

Abstract—A cyber range is a term to define an isolated simulation environment that can be used for cybersecurity training. As a training tool, the cyber range has a crucial role in improving the competence of its users. Isolated environmental conditions allow users to increase competence through cybersecurity training based on predetermined scenarios. There is no standard for scenario in training, most of them using common case. In this research, the cyber range is built based on the cyber range taxonomy and uses the observe-orient-decide-act (OODA) loop that has been proven for military education. The OODA loop is implemented and helps guiding each step of the attack and its handling in the built scenario. The scenario chosen is a case of data theft since data theft incidents have often occurred so that it is easier for user to understand. OODA loop for cyber range meets 16 of the 17 characteristics in the cyber range taxonomy. The final cyber range acceptance rate was 81.82%. The results of this acceptance give confidence that this new method can be used as an alternative to learning cybersecurity.

Keywords—Cyber security; cybersecurity education; cyber range; OODA loop; play-role scenario

I. INTRODUCTION

There are no renowned holistic Security Operating Center standards or industry specific guidelines [1]. It has deep impact for cyber range especially for education. Lack of standardization leads to the need for solutions.

In cyber security education, one of the factors that support the success of implementing a cybersecurity curriculum [2] is the availability of isolated laboratories for learning [2]. Most isolated laboratories that are specifically used for cybersecurity learning are scenario-based. Scenarios are prepared using field experience.

From this, a big problem arises, there is no standardization in real world of SOC, so how to transfer experience in education especially in scenario for cyber range.

Observe-Orient-Decide-Act (OODA) loop is a well-known analytical framework for decision-making developed by John Boyd [3]. The method has been used in the military world long time ago and has been proven to provide experience and improvement for military students. This is inspiring to be applied in cyber security learning as well as being a standard and measuring its suitability in meeting the need for cyber security learning tools. In bigger scenario SOC is giving many

open problems described in Vielbert's paper [4]. The problem can be minimized by proper cyber security laboratories.

Several methods of building cyber ranges have been carried out previously, as summarized in the research of [5], [6], and [7] to overcome similar problems. The data presented by [6] shows that the most commonly used experimental method is the simulation method due to its ease of use.

A cyber range with data exfiltration attack simulation is built in this research that simulates a real attack case. The built cyber range is expected to be used as a learning tool to understand cyber-attacks better and apply the framework of thinking according to the OODA loop in further learning. The final results of the research were then validated with the user acceptance test (UAT) to find out whether the system built could meet the needs of cyber security learning.

II. RELATED WORKS

A. ISMS Role in The Improvement of Digital Forensics Related Process in SOC's

This research [8] presents similar solution for better SOC with Plan, Do, Check, Act. The purpose of this research is to provide an Information Security Management System solution that complies with ISO 27001:2013. Focus in digital forensic and not for education purpose.

B. Design and Implementation of a Research and Education Cybersecurity Operations Center

This paper [9] show common SOC and tools inside it. This research also builds simulation with honeypot and dashboard and also implementing OODA loop in concept of SOC not in scenario build.

C. Design and Implementation of a Research and Education Cybersecurity Operations Center

This research [10] present Action Observe Hypothesis method to build SOC. Using Questionnaire for post task, same method with user acceptance test in this research. This research focus in recap many SOCs and implemented with multi honeypot for implementation.

Novelty in this paper is the use of multiple Intrusion Detection System (IDS) with agent based and rule based also Elasticsearch, Logstash and Kibana (ELK) for dashboard. OODA loop implemented inside scenario build and detail

inside it to provide experience for student. This research is also suitable for Covid-19 learning situation which implement VPN for student and lecture for remote education and proofed with User Acceptance Test for validation with curriculum.

III. RESEARCH METHODOLOGY

The research design refers to knowledge embodied in development, techniques, methods, models, and theory development to map out how to produce artifacts or products that meet predetermined functional requirement [11]. In this study, the research design used was Design Science Research (DSR) as seen in Fig. 1. DSR was chosen since it has the principle of “learning through development (making artifacts),” which is appropriate when applied to this research. DSR is a method of determining and conducting research with the ultimate goal of an artifact of recommendations. DSR can also be defined as a method oriented to solving specific problems to get the right solution even though the solution is not optimal.

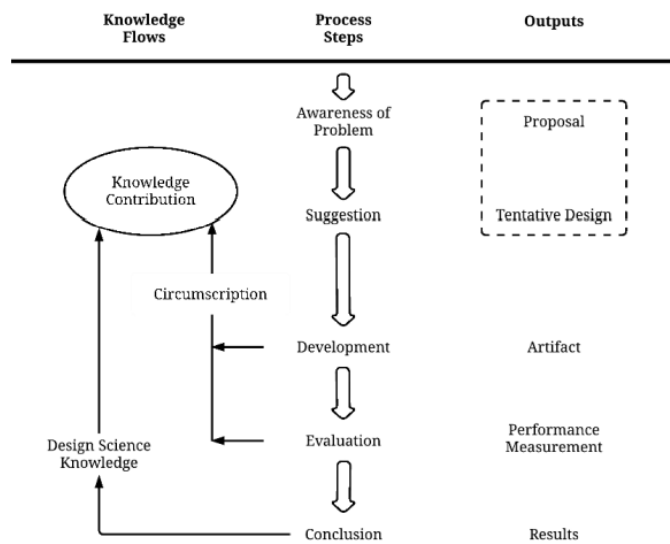


Fig. 1. DSR Process Model Cycle.

Fig. 1 shows the relationship of each process, the flow of knowledge, and the output of the DSR, which is called the DSR cycle.

A. Awareness of Problem

Researchers identify problems that will be raised for research or problem formulation [11]. Sources of problems can be obtained from various existing sources. The problem identification process can be carried out in various ways such as literature study, practice, and discussion or interview. Once identified, the problem must also be defined. The problem definition process be done through a literature study to state that the problem has not been resolved and the solutions offered will contribute academically. In addition, problem definition also includes determining the scope of the problem to be solved using available resources.

B. Suggestion

The suggestion stage contains suggestions or solutions offered by researchers to overcome the problems that have been defined at the awareness of problem stage. These

solutions can be generated based on existing research or through the thoughts and creativity of researchers in solving problems using appropriate research methods. The solution can be a new idea or combine an existing solution with something different. The result of this stage is a tentative design that describes the solution to the problems in the previous stage.

The pattern chosen to be used in the suggestion stage is modeling existing solutions and combining partial solutions. The existing solution modeling pattern is a design used to model solutions that have been used to overcome similar problems [11]. The results of the solution modeling are then developed and adapted to be a solution to the current research problems. The pattern of combining partial solution is a pattern that is used to take some concepts, ideas, or solutions from related references that can support the construction of solutions from the research conducted [11].

C. Development

The development stage is the stage to implement or develop a tentative design that has been made at the suggestion stage. The pattern used in the development stage is the same as the suggestion stage, namely modeling existing solutions and combining partial solutions. The explanation of the two patterns is also the same as the one at the suggestion stage. In addition, the solutions developed at the development stage are also prepared based on the tentative designs that have been made at the suggestion stage. In the development stage of this research, the cyber range is built based on the cyber range taxonomy from the research of Yamin et al. [7], attack simulation laboratory of Mahardhika research [12], and the benefits of building cyber ranges from the research of Leitner et al. [13] through a pattern of combining partial solutions while still considering the tentative designs that have been made. The combined results of the research of Yamin et al. [7] and Mahardhika [12] is used to compile a needs analysis in the design and construction of cyber ranges. In addition, the research of Grant et al. [14] also Debatty dan Mees [15] is used to create solution modeling in the form of scenarios and topology of the cyber range environment through the existing solution modeling pattern.

D. Evaluation

The results of the artifact implementation at the development stage are then evaluated at this stage based on predetermined functional specifications. The process carried out at the evaluation stage is to determine how well the performance of the artifact is based on the empirical method used. This stage is an opportunity to make improvements to the artifact based on the experience gained during the previous stage. This is also called the circumscription of the DSR cycle. The pattern used in the evaluation stage is demonstration. After the development stage is complete, the cyber range will be demonstrated. For validation a number of Cyber and Crypto Politechnic cadets will be asked to run the scenario that has been built according to the steps stated in the user manual for the attack simulation laboratory. After running the scenario, cadets will be asked to fill out a UAT questionnaire. UAT is needed to find out whether the cadets are able to apply the OODA loops framework during running APT attack scenarios. In addition, UAT is also used to measure whether the attack

simulation laboratory built has met the learning needs of the Cyber and Crypto Politechnic and can increase cyber situation awareness among Cyber and Crypto Politechnic cadets. Validation is done with UAT. The results of filling out the UAT questionnaire were then analyzed using a Likert measurement scale.

E. Conclusion

This is the last stage of the research cycle in DSR. The result of this stage is the solutions delivering that answer the formulation of the problem in research. In addition, the results obtained at the evaluation stage will also be presented at the conclusion stage. The process carried out at the conclusion stage is symbolized by a small arrow outwards in the DSR cycle. The purpose of the arrow is that the results of the research must be communicated or published so that they can contribute to science in the related field [16].

IV. IMPLEMENTATION

A. Design of Cyber Range

Cyber range design is done through a literature study of solutions and related research. The literature study was conducted on the research of Grant et al.[14], Debatty and Mees [15] to produce a cyber range design in the form of a tentative network infrastructure design from the cyber range and analysis of cyber range needs.

B. Tentative Design

Based on the literature study conducted on the research of Grant et al.[14], the network security infrastructure in an organization generally consists of a firewall, DMZ, servers, and workstations located in the Intranet. In addition, there is also an IDS located in the DMZ. Placing the IDS on the DMZ allows the IDS to monitor network traffic between the Intranet to the Internet, between the DMZ to the Internet and between machines within the DMZ. Network security infrastructure in organizations from the research results of Grant et al. [14] is in Fig. 2.

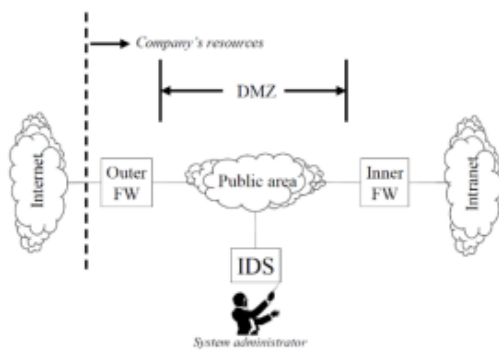


Fig. 2. Network Security Infrastructure in Organizations.

In addition to this research, a literature study was also conducted on the research of [15]. From the research of [15], obtained infrastructure for simulation of a small organization network consisting of firewall, DMZ, honeypot, vulnerable web server, internal workstation, Security Onion server for monitoring, and traffic generator. Virtual workstations are also provided for users connected to the internal network. The

design of the organization's network simulation infrastructure can be seen in Fig. 3.

From the results of a literature study conducted on [12], obtained information that the attack laboratory topology can be built on the CAN topology provided that it has two main components, network infrastructure as the target of attack and APT group [17] infrastructure. Topology design of attack simulation laboratory in [12] research can be seen in Fig. 4.

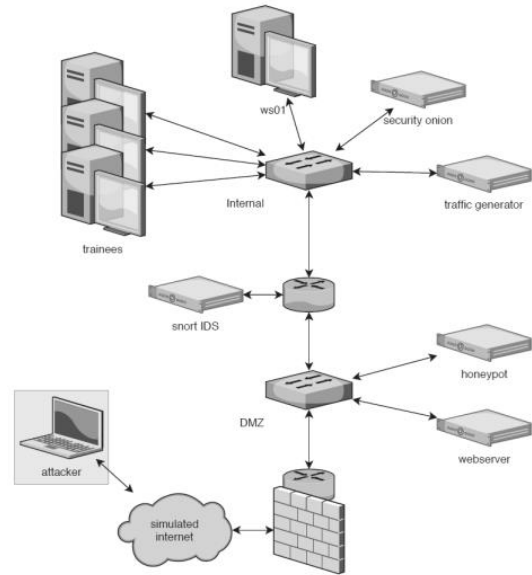


Fig. 3. Organizational Network Simulation Infrastructure.

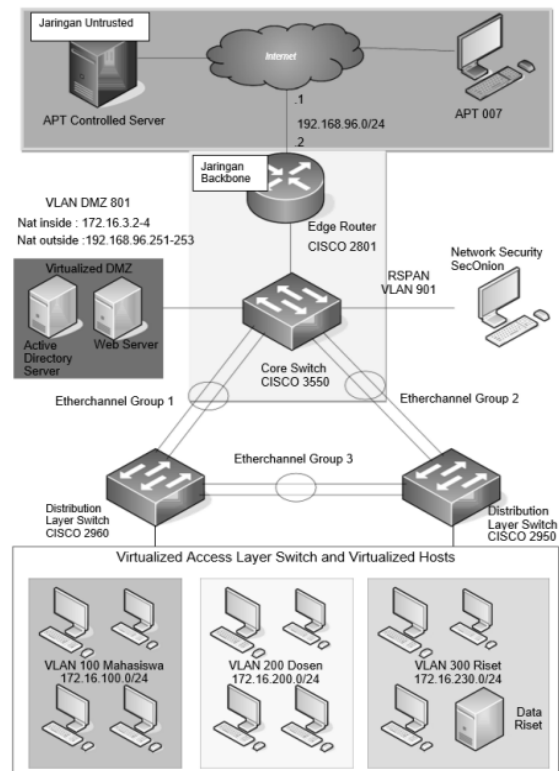


Fig. 4. Attack Simulation Laboratory Topology[12].

By utilizing the results of the literature study from previous research, a tentative design was designed as the final result of the suggestion stage in the DSR cycle as well as an initial design in the development of cyber range infrastructure. The design results of the cyber range design that have been made can be seen in Fig. 5.

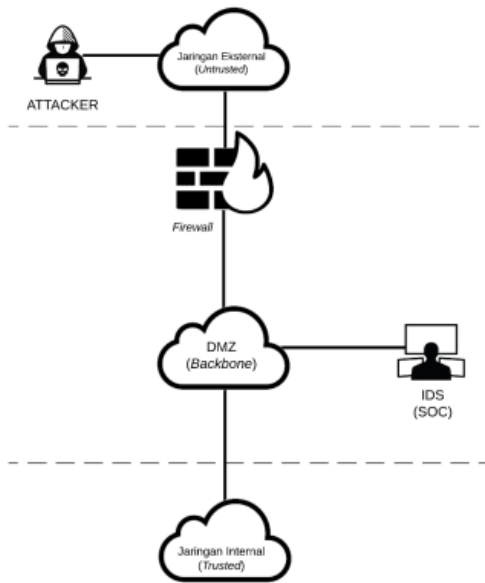


Fig. 5. Cyber Range Tentative Design.

The tentative design of cyber range divides the network into, external network (untrusted) in Table III, DMZ, backbone network, and internal network (trusted), all part was built in hardware listed in Table I and virtual machine listed in Table II. On the external network, there is an attacker's infrastructure consisting of various tools or virtual machines that aim to steal data from the internal (trusted) network seen in Table IV. Meanwhile, on the backbone and DMZ networks shown in Table V and Table VI, there is a main infrastructure to connect every device in the cyber range, firewalls, and IDSs that monitor activities in the internal network and the DMZ. On the internal network, there is an infrastructure of the target that is vulnerable to attacks from external networks seen in Fig. 6

TABLE I. CYBER RANGE HARDWARE

No	Hardware	Qty	role	Spesification
1	Cisco Catalyst 3650	1	Router and Switch	24X10/100/1000 Ethernet and 4X 1G uplink port
2	Supermicro Racksverer	1	pfsense	4X intel Xeon @2,13 GHz RAM 8GB HDD 1TB NIC 2 ethernet port
3	Server	1	Network Security Monitoring	6X intel Xeon @3,07 GHz RAM 32 GB HDD 1TB NIC 4 ethernet port
4	HPE Proliant DL20 Gen 10	2	Attacker VM, DMZ, Target VM	8X intel Xeon @3,5 GHz RAM 16 GB HDD 1TB NIC 2 ethernet port

TABLE II. CYBER RANGE VIRTUAL MACHINE

No	VM ID	role	Spesification
1	101	Attacker	OS Kali Linux CPU 2 Core RAM 4 GB HDD 100 GB
2	201	Domain Controler & Mail Server	OS Zentyal CPU 4 Core RAM 8 GB HDD 250 GB
3	301	Web Server	OS Ubuntu Server CPU 2 Core RAM 2 GB HDD 250 GB
4	410	Target	OS Windows 10 CPU 2 Core RAM 3 GB HDD 50 GB
5	510	Target	OS Windows 10 CPU 2 Core RAM 3 GB HDD 50 GB
6	610	Target	OS Windows 10 CPU 2 Core RAM 3 GB HDD 50 GB

TABLE III. UNTRUSTED NETWORK INFRASTRUCTURE

No	tools	Label	Subnet	IP (VPN)
1	Virtual Host (kali linux)	Caldera 101	192.168.41.0/24	192.168.170.2/24

TABLE IV. TRUSTED NETWORK INFRASTRUCTURE

No	tools	Label	VLAN	IP/Subnet
1	Virtual Switch	Keuangan & SDM	110	192.168.110.1/24
2	Virtual Switch	Produksi & Pemasaran	120	192.168.120.1/24
3	Virtual Switch	Operational Technology	130	192.168.130.1/24
4	Virtual Switch	Client 410	110	192.168.110.0/24
5	Virtual Switch	Client 510	120	192.168.120.0/24
6	Virtual Switch	Client 610	130	192.168.130.0/24
7	Virtual Switch	Security Onion	10	192.168.10.10/24

TABLE V. BACKBONE INFRASTRUCTURE

Tools	Interface	IP	node
pfsense (firewall)	em0 (LAN)	192.168.2.1/24	Core switch
	em1 (WAN)	192.168.41.222/24	LAN PoltekSSN
	VLAN 10	192.168.10.1/24	
	VLAN 110	192.168.100.1/24	
	VLAN 120	192.168.120.1/24	
	VLAN 130	192.168.130.1/24	
	Gigabyte Ethernet 1/0/21		PVE1
	Gigabyte Ethernet 1/0/22		PVE2
	Gigabyte Ethernet 1/0/23	Monitor Interface	SOC
Gigabyte Ethernet 1/0/24	192.168.2.2/24	pfsense (firewall)	

TABLE VI. DEMILITARIZED ZONE (DMZ) INFRASTRUCTURE

No	Tools	VLAN	IP
1	Virtual Active Directory Server & Virtual Mail Server	800	192.168.3.2/29
2	Virtual Web Server		192..168.3.3/29

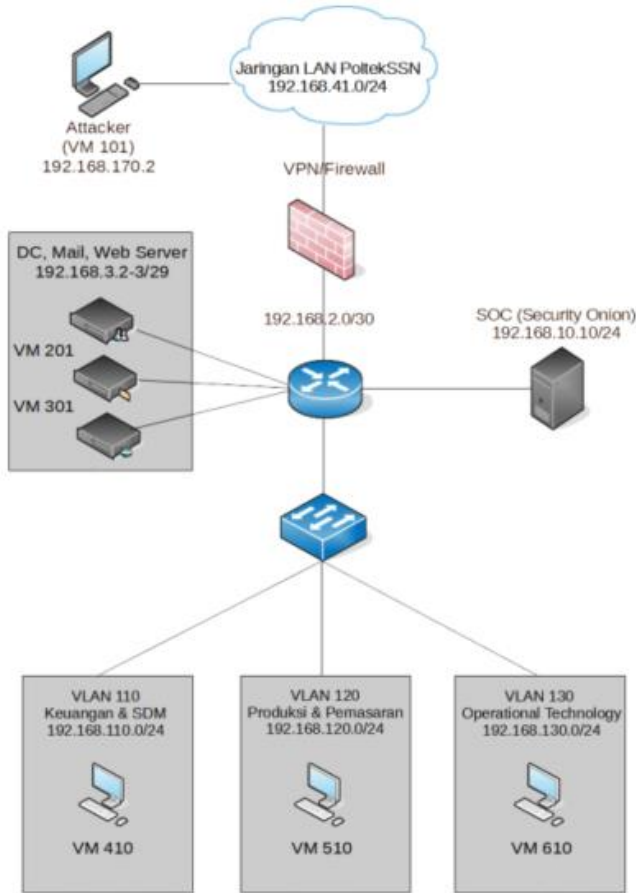


Fig. 6. Cyber Range Design.

C. Needs Analysis

Based on a survey conducted in the research of Yamin et al.[7], a system can be classified as a cyber range if it fulfills part or all of the components of the cyber range taxonomy. In the construction of cyber ranges in this study, the cyber range taxonomy is used as the basis for compiling a needs analysis of the built cyber ranges. The complete components of the cyber range taxonomy can be seen in Fig. 7.

D. Scenario

The scenario explains the objectives of the cyber range development, the environment in the form of the infrastructure used, the storyline behind the operation of the cyber range, the scenario application domain, and various tools used in the construction of the cyber range. Scenarios built-in cyber range is based on OODA loops. Every step taken by the attacker and the defender is arranged based on each stage in the OODA loop, which includes observing, orienting, deciding, and acting.

In the attack simulation scenario, initially cyber range users perform the task of the Red Team or Red APT group to attack

with the aim of stealing data. After the attack was carried out, the students carried out the task of the blue team as SOC to monitor the attacks that occurred and take action against these attacks. The stages of the data exfiltration as resesarch by F Ullah [18] carried out by Red APT based on the OODA loop are as follows:

1) *Observe*: Red APT collects information through various sources related to target. From the results of the information collected, Red APT found several names of employees from target along with their email addresses. The names include Joko Nugroho (jnugroho@cybergym.local), Aurora Rahayu (arahayu@cybergym.local), and Caraka Kurniawan (ckurniawan@cybergym.local). This information is found on the website page of example target as shown in Fig. 8.

2) *Orient*: Red APT plans to exploit the weaknesses of the employee's nature to gain access to the target system. Red APT plans to make job offers with salaries and facilities that are more attractive than those offered by target to these employees via email.

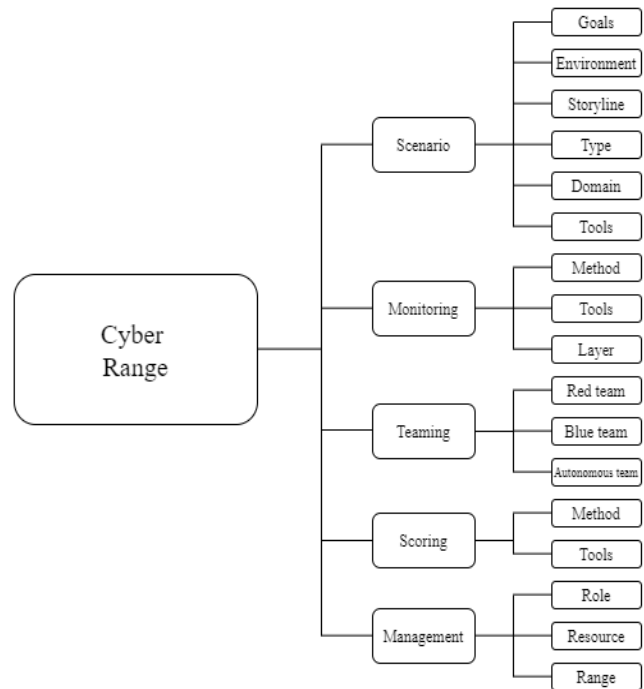


Fig. 7. Cyber Range Taxonomy

Pengalaman Kerja di PT TRINAKLIR

Joko Nugroho (jnugroho@cybergym.local), Aurora Rahayu (jnurroho@cybergym.local), Caraka Kurniawan (ckurniawan@cybergym.local)

We have created a fictional band website. Lorem ipsum dolor sit amet, consectetur adipiscing elit, sed do eiusmod tempor incididunt ut labore et dolore magna aliqua. Ut enim ad minim veniam, quis nostrud exercitation ullamco laboris nisi ut aliquip ex ea commodo consequat. Duis aute irure dolor in reprehenderit in voluptate velit esse cillum dolore eu fugiat nulla pariatur. Excepteur sint occaecat cupidatat non proident, sunt in culpa qui officia deserunt mollit anim id est laborum consectetur adipiscing elit, sed do eiusmod tempor incididunt ut labore et dolore magna aliqua. Ut enim ad minim veniam, quis nostrud exercitation ullamco laboris nisi ut aliquip ex ea commodo consequat. We have created a fictional band website. Lorem ipsum dolor sit amet, consectetur adipiscing elit, sed do eiusmod tempor incididunt ut labore et dolore magna aliqua. Ut enim ad minim veniam, quis nostrud exercitation ullamco laboris nisi ut aliquip ex ea commodo consequat. Duis aute irure dolor in reprehenderit in voluptate velit esse cillum dolore eu fugiat

Fig. 8. Example Target Website for Observing

3) *Decide*: Red APT creates a payload in the form of an executable file that contains an access trojan command. The payload contains the command to execute the CALDERA agent. Payload is disguised by giving a file icon in the form of a job offer poster and providing a file name with the suffix.jpg. Windows operating system by default does not display the extension of a file, so naming a file with a .jpg ending will give the target the illusion that the received file is an image file.

4) *Act*: Red APT sends the payload accompanied by an attractive offer sentence using an email address with the name of the Company's HRD. The payload is sent to the email addresses of the three employees of target and hopes that there are employees who are interested and open the payload file. Fig. 9 shows the view of the email containing the payload received by the target.

Open the payload file and ignore the UAC notification on the computer gave an effect to automatically install trojan. After the payload installation process is complete, a backdoor is created so that Red APT has access to the victim's computer to steal database files on the target computer in SQL format. Agent implemented show in caldera dashboard seen in Fig. 10. The file theft was carried out using data exfiltration and data staging techniques using CALDERA. Fig. 11 shows the techniques used by Red APT to carry out data theft.

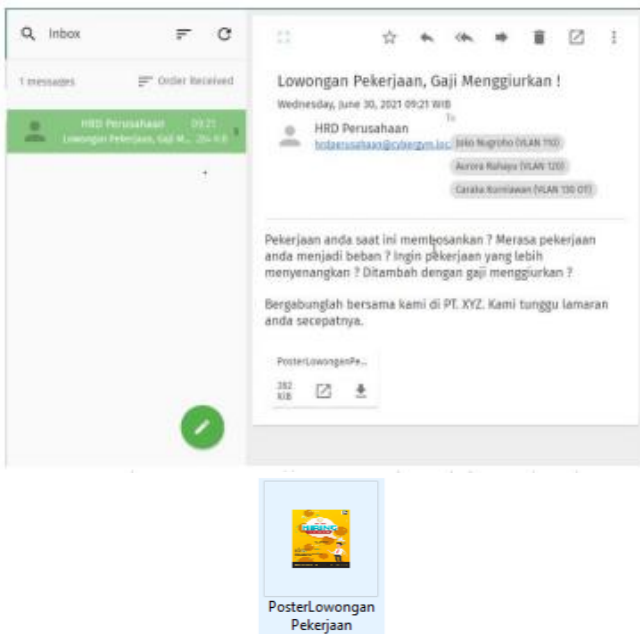


Fig. 9. Email Contains Payload.

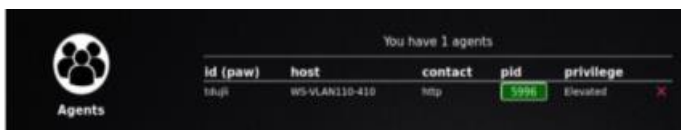


Fig. 10. Caldera Dashboard.

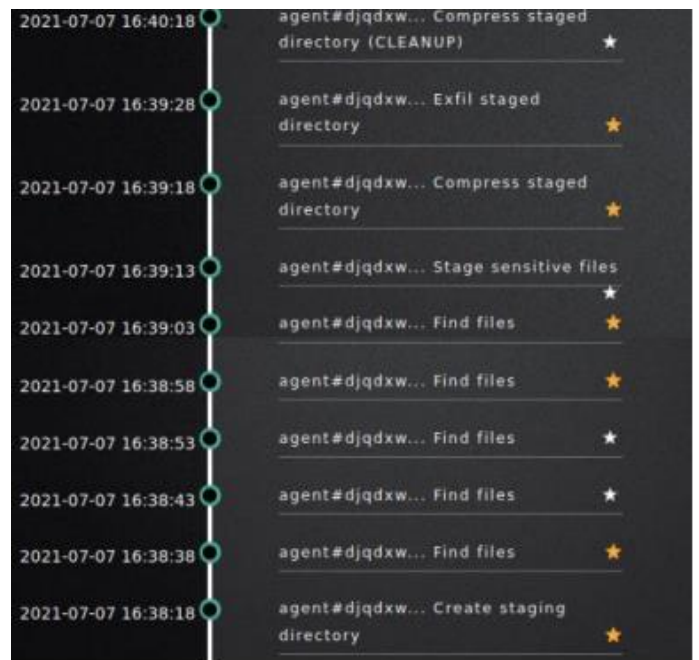


Fig. 11. Red APT Data Theft Techniques.

5) *Observe*: The OODA loop is an iteration, so after the goal of the attack, data theft is achieved, Red APT will return to the observe stage with the knowledge that has been obtained from the previous OODA iteration. In the next iteration, Red APT can explore the system to find data, information, or other vulnerabilities that can be exploited.

In future research RED team can be improved [19] by implementing automated system as Applebaum's research. Meanwhile, the OODA loop carried out by SOC defender to detect anomalies and APT. APT has been studied in [20] and [21] research. OODA loop for blue team or defender in research scenario is as follows:

1) *Observe*: SOC target or defender team checks the results of network monitoring through Security Onion to find and collect network data. Security onion is agent based for cyber-attack defense [22]. The network monitor display on Security Onion can be seen in Fig. 12.

2) *Orient*: Filter and check for alerts detected by Security Onion. From these alerts, SOC performs an analysis to find suspicious activity. At this stage, the SOC can download the .pcap file to facilitate the analysis process. Based on the results of the analysis, it was found that there is HTTP access to an unknown IP address. Fig. 13 shows an HTTP access alert from a 192.168.110.2 (VM 410) to 192.168.170.2 (VM 101).

After further inspection with PCAP file, it was suspected that there was the theft of files from one computer because there was a file that was compressed in the .zip format as shown in Fig. 14. This allegation was also strengthened by evidence in the form of an email sent to several employees of PT TRINAKLIR containing a payload.

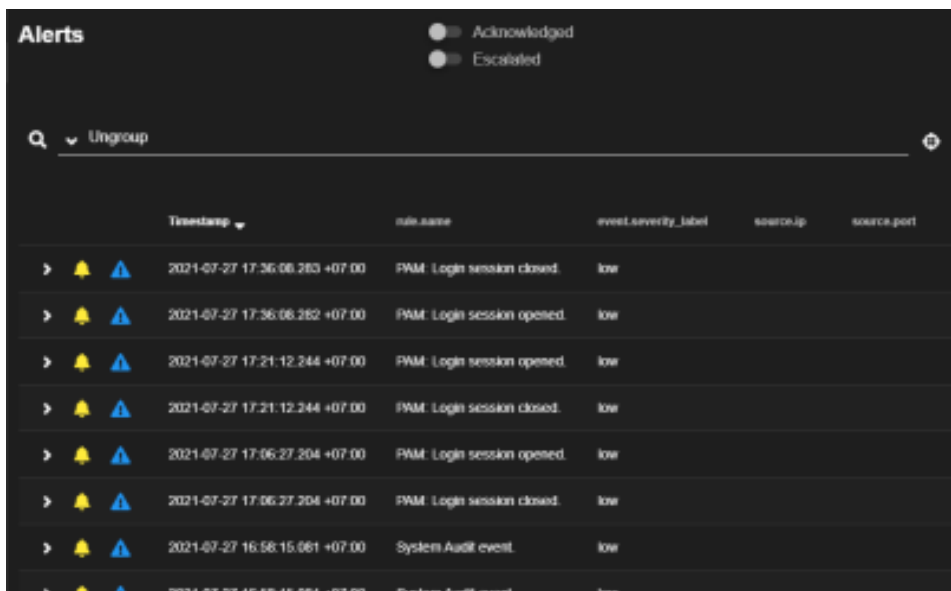


Fig. 12. Network Monitor Display on Security Onion.



Fig. 13. HTTP Access Alert Detail.



Fig. 14. Compressed File Delivery.

3) *Decide*: SOC determines solutions or steps that need to be taken to deal with attacks that occur and prevent similar

incidents. These solutions can be in the form of creating incident tickets, forensic analysis of the victim's computer, blocking IP addresses from attackers, as well as cyber security awareness education to employees. However, in this scenario, the actions taken are limited to only generating tickets with TheHive escalated case from alert seen in Fig. 15 for the incidents that occur.

4) *Act*: Case from Fig. 15 can be more explored for detail. In simulating real SOC that has some tier, the case in TheHive is built for the task of assigning work to other SOC members as shown in Fig. 16.

5) *Observe*: The OODA loop is an iterative process, so that after the previous incident has been successfully handled, the SOC returns to monitor the network to maintain the security of target's network [23].

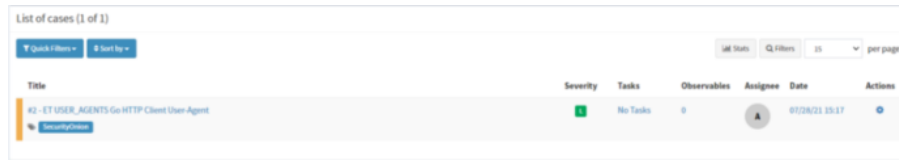


Fig. 15. Ticket Registered.

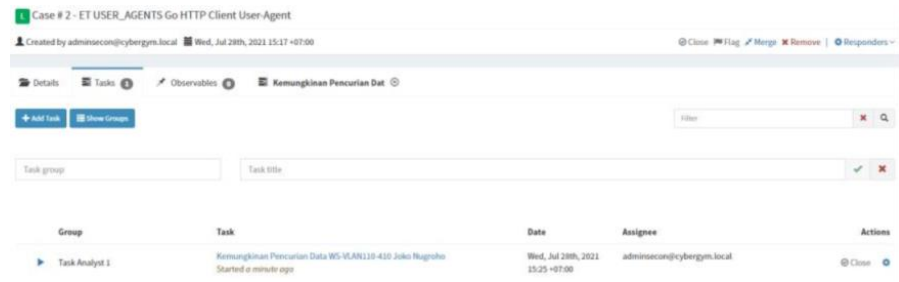


Fig. 16. Task Generated.

E. UAT Questionnaire

Evaluation of research results in the form of the cyber range is also carried out through UAT testing with respondent, 11 cybersecurity lecture (all population of cybersecurity engineering programme). Making instruments in the questionnaire aims to determine whether the features of the cyber range have met the cyber range taxonomy and can meet the needs of cyber security learning tools. The results of filling out the questionnaire were then analyzed using a Likert scale. The Likert scale is a measurement scale that aims to measure respondents' opinions on research results from very positive to very negative and in the form of words [24][25][26]. Table VII is list of questionnaire in this research.

TABLE VII. USER ACCEPTANCE TEST QUESTIONNAIRE

No	Statement	SS	S	R	TS	STS
1	The operation of the cyber range is easy for first-time users to learn					
2	The steps in the attack simulation scenario at the cyber range are in accordance with the OODA loop so that it is easy to understand and execute.					
3	Cyber range can meet cyber security learning					
4	Cyber range provides an isolated environment to execute simulated attack scenarios.					
5	All the tools in the cyber range work well.					
6	The monitoring system on the cyber range is running well.					
7	Cyber range can help cadets understand the role of the red team and blue team.					
8	The scoring method (assessment of attack simulation results) on the cyber range is running well.					
9	Cyber range management or management can be done easily					

F. UAT Questionnaire Analysis

The results of the UAT response data were then analyzed to measure the respondent's level of agreement with each statement in the UAT questionnaire using the following equation:

$$\frac{\sum(a \times b)}{c \times d} \tag{1}$$

a = total number of respondents who chose the b answer

b = score of the answer choices

c = respondent total

d = highest score

Furthermore, the results of the previous calculations are summed and recalculated to determine the level of acceptance of the cyber range that was built as a whole using the following equation:

$$\frac{\sum wx}{x \times y \times z} \times 100\% \tag{2}$$

w = total score of respondent's choice

x = total statement

y = total answer

z = highest score

Where w is score total of respondent's choice, x is total statement, y is total respondent, z is highest score.

V. RESULT AND DISCUSSION

A. Result of Reaching the Needs

The cyber range that has been built is then evaluated to find out the results of meeting the needs of the cyber range against the needs analysis that has been compiled based on the cyber range taxonomy. Based on the results of fulfilling the needs, cyber range meets 16 of 17 seen in Table VIII. Characteristics that are not fulfilled is special tools for scoring. In this cyber range, scoring is done by checking the success of the attack stages as well as ticketing with the help of Security Onion

monitoring tools, CALDERA attack automation tools and TheHive ticketing tools. The overall cyber range acceptance rate with formula 2 is 81.82%.

TABLE VIII. FULFILLMENT NEEDS RESULT

No	Req	Characteristics of Taxonomy	Fulfilled
1	Cyber range has a clear scenario development goal, namely simulating data theft attacks.	Scenario (Goals)	Yes
2	Cyber range provides an isolated environment to execute simulated attack scenarios in physical, virtual, or hybrid forms consisting of the target and attacker infrastructure.	Scenario (Environment)	Yes
3	Cyber range provides the storyline of the scenario to provide an overview of how the scenario execution process.	Scenario (Storyline)	Yes
4	Cyber range provides a static or dynamic scenario.	Scenario (Type)	Yes
5	The scenario in the cyber range is applied to a particular domain.	Scenario (Domain)	Yes
6	Cyber range can use a variety of tools to build or run a scenario.	Scenario (Tools)	Yes
7	Cyber range provides a particular method for monitoring the simulation of attacks carried out.	Monitoring (Method)	Yes
8	Cyber range provides special tools for monitoring systems.	Monitoring (Tools)	Yes
9	The monitoring system in cyber range works at the TCP/IP layer.	Monitoring (Layer)	Yes
10	Cyber range provides a red team role.	Teaming (Red team)	Yes
11	Cyber range provides a blue team role.	Teaming (Blue team)	Yes
12	Cyber range provides the role of an autonomous team.	Teaming (Autonomous team)	Yes
13	Cyber range provides a specific scoring method.	Scoring (Method)	Yes
14	Cyber range provides special tools for scoring.	Scoring (Tools)	No
15	Cyber range provides role management features.	Management (Role)	Yes
16	Cyber range provides computing resource management features	Management (Resource)	Yes
17	Cyber range provides range management features.	Management (Range)	Yes

B. UAT Questionnaire

Table IX is compilation of UAT result. Analysis results of the UAT response data with formula 1 is 405 in the Agree area seen in Fig. 17.

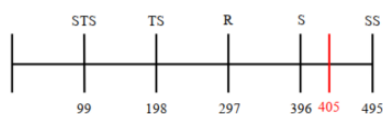


Fig. 17. Questionnaire Result.

TABLE IX. USER ACCEPTANCE TEST RESULT

respondent	P1	P2	P3	P4	P5	P6	P7	P8	P9
1	3	4	5	4	4	4	5	3	4
2	4	4	5	5	4	4	5	4	4
3	2	4	5	5	4	4	5	2	4
4	4	4	5	5	4	5	5	5	4
5	3	4	5	4	4	4	4	3	3
6	2	4	5	5	3	3	4	4	3
7	4	4	5	5	4	4	5	4	4
8	4	4	4	4	4	4	4	4	2
9	4	4	4	4	4	4	4	4	3
10	4	5	5	5	5	4	5	4	4
11	4	4	4	5	4	4	5	4	4
Total	38	45	52	51	44	44	51	41	39
Percentage	69,09	81,81	94,55	92,73	80,00	80,00	92,73	74,55	70,91

VI. CONCLUSION

Based on meeting the needs, the cyber range meets 16 of the 17 characteristics in the cyber range taxonomy. Based on the results of the UAT questionnaire, a score of 405 was obtained in the Agree area, and the overall cyber range acceptance rate was 81.82%. This result also states that Observe-Orient-Decide-Act (OODA) for Cyber Security Education can be implemented globally.

VII. FUTURE WORKS

The scenario contained in the cyber range is only a simulation of data theft attacks. It is necessary to build a simulation with other cases to meet the learning needs of a more complete range of cybersecurity. The CALDERA agent tool can only run on Windows operating systems. It is necessary to add other similar tools so that attack simulations can be carried out on other operating systems. System performance from cyber reach has not been tested through stress tests or measured by certain methods. Cyber range performance testing and scenario and tool enhancement can be used as further research.

REFERENCES

- [1] I. Bica and R. Reyhanitabar, "Preface," Lect. Notes Comput. Sci. (including Subser. Lect. Notes Artif. Intell. Lect. Notes Bioinformatics), vol. 10006 LNCS, p. V, 2016, doi: 10.1007/978-3-319-47238-6.
- [2] S. Azadegan and M. O'Leary, "An undergraduate Cyber Operations curriculum in the making: A 10+ year report," IEEE Int. Conf. Intell. Secur. Informatics Cybersecurity Big Data, ISI, pp. 251-254, doi: 10.1109/ISL2016.7745484.
- [3] F. P. B. Osinga, Science, Strategy and War, 1st ed. Ney York: Routledge, 2007.
- [4] M. Vielberth, F. Bohm, I. Fichtinger, and G. Pernul, "Security Operations Center: A Systematic Study and Open Challenges," IEEE Access, vol. 8, doi: 10.1109/ACCESS.2020.3045514.
- [5] N. Chouliaras, G. Kittes, I. Kantzavelou, L. Maglaras, G. Pantziou, and M. A. Ferrag, "Cyber ranges and testbeds for education, training, and research," Appl. Sci., vol. 11, no. 4, pp. 1-23, doi: 10.3390/app11041809.

- [6] E. Ukwandu et al., "A review of cyber-ranges and test-beds: Current and future trends," *Sensors (Switzerland)*, vol. 20, no. 24, pp. 1–36, 2020, doi: 10.3390/s20247148.
- [7] M. M. Yamin, B. Katt, and V. Gkioulos, "Cyber ranges and security testbeds: Scenarios, functions, tools and architecture," *Comput. Secur.*, vol. 88, p. 101636, 2020, doi: 10.1016/j.cose.2019.101636.
- [8] M. H. Khyavi, "ISMS role in the improvement of digital forensics related process in SOC's," *Cryptogr. Secur.*, 2020.
- [9] C. DeCusatis, R. Cannistra, A. Labouseur, and M. Johnson, *Design and implementation of a research and education cybersecurity operations center*. Springer International Publishing, 2019.
- [10] C. Zhong, A. Alnusair, B. Sayger, A. Troxell, and J. Yao, "AOH-Map: A Mind Mapping System for Supporting Collaborative Cyber Security Analysis," *Proc. - 2019 IEEE Conf. Cogn. Comput. Asp. Situat. Manag. CogSIMA 2019*, pp. 74–80, 2019, doi: 10.1109/COGSIMA.2019.8724159.
- [11] V. K. R. Baskerville "Foreword From Vaishnavi and (W. K., *Design Science Research Methods and Patterns: Innovating Information and Communication Technology*, 2nd ed. New York: CRC Press.
- [12] S. Mahardhika, "Analisis Pemodelan Serangan Advanced Persistent Threat dengan Menggunakan Diamond Model of Intrusion Analysis dan Kill Chain." Sekolah Tinggi Sandi Negara.
- [13] M. Leitner, "AIT Cyber Range: Flexible Cyber Security Environment for Exercises, Training and Research," *ACM Int. Conf. Proceeding Ser.*, doi: 10.1145/3424954.3424959.
- [14] T. J. Grant, H. S. Venter, and J. H. P. Eloff, "Simulating adversarial interactions between intruders and system administrators using OODA-RR," *ACM Int. Conf. Proceeding Ser.*, vol. 226, pp. 46–55, 2007, doi: 10.1145/1292491.1292497.
- [15] T. Debatty and W. Mees, "Building a Cyber Range for training CyberDefense Situation Awareness," *2019 Int. Conf. Mil. Commun. Inf. Syst. ICMCIS 2019*, pp. 1–6, 2019, doi: 10.1109/ICMCIS.2019.8842802.
- [16] V. K. R. B. "Foreword F. Vaishnavi and (W. K., *Design Science Research Methods and Patterns: Innovating Information and Communication Technology*, 2nd ed. New York: CRC Press.
- [17] F. Extension and P. R. Brandao, "Advanced Persistent Threats (APT)-Attribution-MICTIC," *J. Comput. Sci.*, vol. 17, no. 5, pp. 470–479, 2021, doi: 10.3844/jcssp.2021.470.479.
- [18] F. Ullah, M. Edwards, R. Ramdhany, R. Chitchyan, M. A. Babar, and A. Rashid, "Data exfiltration: A review of external attack vectors and countermeasures," *J. Netw. Comput. Appl.*, vol. 101, pp. 18–54, doi: 10.1016/j.jnca.2017.10.016.
- [19] A. Applebaum, D. Miller, B. Strom, C. Korban, and R. Wolf, "Intelligent, automated red team emulation," *ACM Int. Conf. Proceeding Ser.*, vol. 5-9-Decemb, pp. 363–373, doi: 10.1145/2991079.2991111.
- [20] M. B. Khan, "Advanced Persistent Threat: Detection and Defence," arXiv, 2020.
- [21] J. H. Joloudari, M. Haderbadi, A. Mashmool, M. Ghasemigol, S. S. Band, and A. Mosavi, "Early detection of the advanced persistent threat attack using performance analysis of deep learning," *IEEE Access*, vol. 8, pp. 186125–186137, 2020, doi: 10.1109/ACCESS.2020.3029202.
- [22] J. D. Yoo, "Cyber attack and defense emulation agents," *Appl. Sci.*, vol. 10, no. 6, pp. 1–20, doi: 10.3390/app10062140.
- [23] J. Silvander and L. Angelin, "Introducing intents to the OODA-loop," *Procedia Comput. Sci.*, vol. 159, pp. 878–883, doi: 10.1016/j.procs.2019.09.247.
- [24] A. Joshi, S. Kale, S. Chandel, and D. Pal, "Likert Scale: Explored and Explained," *Br. J. Appl. Sci. Technol.*, vol. 7, no. 4, pp. 396–403, 2015, doi: 10.9734/bjast/2015/14975.
- [25] B. P. Subedi, "Using Likert Type Data in Social Science Research: Confusion, Issues and Challenges," *Int. J. Contemp. Appl. Sci.*, vol. 3, no. 2, pp. 2308–1365, 2016.
- [26] James T Croasmun and Lee Ostrom, "Using Likert-type scales in the social sciences," *J. Adult Educ.*, vol. 40, no. 1, pp. 19–22, 2011.

Module Partition Method of Embedded Multitasking Software Based on Fuzzy Set Theory

Embedded Multitasking Software

Yunpeng Gu¹

Yangzhou Polytechnic Institute
Art Design College, Yangzhou, 225107, China

Abstract—In order to improve the reliability of embedded multitask software, a module partition method based on fuzzy set theory is proposed to solve the problem of large number of software failures and high frequency of failures. Firstly, the characteristics of embedded multitask software are analyzed, and the constraint parameter distribution model is constructed. Then the reliability parameter analysis model of embedded multitask software is constructed, and the multilevel fuzzy metric structure combined with quantitative recursive analysis method is used to complete the division of embedded multitask software modules. The simulation results show that the accuracy of the proposed method exceeds 99% after the number of iterations exceeds 50. The experimental results show that the method has high reliability, high precision and high practicability.

Keywords—Multitasking; embedded; modular; fuzzy set theory

I. INTRODUCTION

In the running of embedded software, the efficiency of information processing can be improved by dividing modules under multi-tasks [1, 2]. However, this method is easy to lead to software function conflicts, which will lead to software failures, and software reliability cannot be guaranteed, affecting the user experience. In the process of using embedded multitask software, the application direction of software can be combined to divide the modules, so as to improve the reliability of software application [3]. At present, some scholars have made relevant research on this. Some scholars proposed a software module division method based on the combination of genetic algorithm and particle swarm optimization, established a mathematical model of the division problem, used genetic algorithm to find a feasible solution, and used particle swarm optimization to find the optimal scheme [4]. Other scholars proposed to maintain the independence of modules by scheduling model partition [5]. However, this method does not consider the reliability of software module partition, so this paper proposes an embedded multi-task software module partition method based on fuzzy set theory. This method can improve the reliability of software module division on the basis of maintaining module independence, thereby reducing the probability of software failure and improving the customer experience. Embedded multitasking software reliability test is based on the reliability of embedded multi-tasking constraint parameter analysis

software. The embedded multitasking software reliability parameters analysis model established the embedded multitasking software module which is divided by the intelligent analysis method and embedded multitasking software module partition method based on fuzzy set theory is put forward [6]. Firstly, the constraint parameters of embedded multi-task software module partition are analyzed, and then the software compatibility and human-computer interactions are tested by using multi-layer index parameter constraint control method. Combined with the software reliability constraint index, the software reliability automatic test is realized. Finally, the simulation results show that this method is effective in improving the partition ability of embedded multitask software modules. The proposed method can effectively divide embedded multitask software modules, improve the reliability of software, and provide new ideas and ways for software improvement in the current market.

II. RELIABILITY CONSTRAINT INDEX AND FEATURE ANALYSIS OF EMBEDDED MULTITASKING SOFTWARE

A. Reliability Constraint Index of Embedded Multitasking Software

In order to realize the partition of embedded multitask software modules, it is necessary to analyze the application characteristics of embedded multitask software modules. Based on the attribute, portability and importance of embedded multitask software, reliability constraint index analysis method is used to analyze the application of the software. The software reliability analysis mainly has four dimensions, namely, reliability measurement parameters, reliability parameter system, reliability measurement indicators and reliability indicator system. Among them, reliability measurement parameter refers to the mathematical attribute of quantitative description of reliability. Reliability parameter system is a set of software reliability parameters. Reliability metrics refer to the required value of a software reliability parameter. The reliability index system is the required value of all reliability parameters of a certain software. Analyze the characteristics of software module with product application. The product adaptability index distribution of embedded multitasking software is shown in Fig. 1.

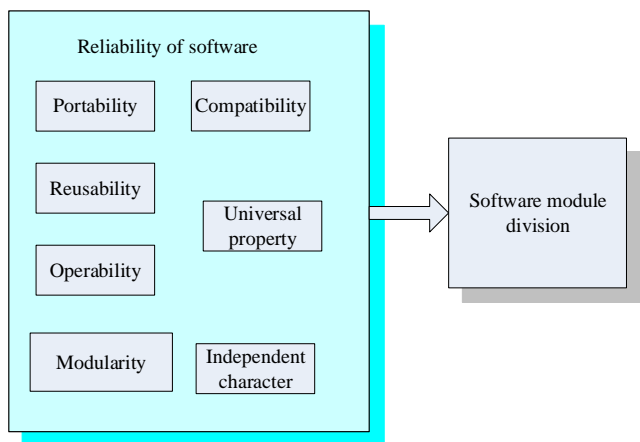


Fig. 1. Product Adaptability Index of Embedded Multitasking Software.

According to Fig. 1, the embedded multitask software modules are divided according to their quality. In combination with the operability of software applications, the adaptive feature detection model of embedded multitask software is established. In addition, the distributed algorithm [7] is used to establish the partition model of embedded multitask software modules, which improves the universality of embedded multitask software. A software quality measure is carried out by adopting a quantitative analysis method of software reliability. The reliability test of the software is mainly divided into the structural test and the object-oriented test. The complexity and the reliability distribution of the software are combined, and the embedded multi-task software module is divided into two levels. According to the above analysis, the parameter system of the secondary constraint index of the software reliability is established as shown in Fig. 2.

According to the reliability constraint parameter system of embedded multitask software shown in Fig. 2, the reliability of embedded multitask software is tested and evaluated by structure-oriented method.

The reliability of embedded multitask software refers to the probability that the software will not cause system failure within the specified time under the specified environment. Software reliability is one of the important indexes to measure software quality. It is not only related to software errors, but also related to system input and system use. Generally

speaking, the more software failures occur or the shorter event interval, the lower software reliability.

Embedded multitask software reliability test is to ensure and verify the reliability of the software. It is a kind of random test. Its main feature is to test software according to the way users actually use software. Generally, embedded multitask software reliability test is divided into software reliability growth test and software reliability verification test. If there is no requirement of reliability index and the current reliability level needs to be evaluated, there are also embedded multitask software reliability bottom test. The reliability test of embedded multitask software is different from the general software test (such as unit test, integration test, function test, performance test, boundary test, etc.) in terms of test purpose, test method, test object, etc. The comparison between embedded multitask software reliability verification test and general software test is shown in Table I.

In Fig. 2, t_1 ~ t_4 refer to reliability, failure probability, mean time before failure and mean time between failures respectively; wherein, reliability refers to the probability of success of software to complete specified functions under specified conditions and within specified time. Failure probability refers to the probability of losing normal operation and specified functions under specified conditions and within specified time. Average time before failure refers to the mean value from the current time to the next failure time. Mean time between failures refers to the mean time interval between two successive failures. The reliability test of embedded multitask software generally uses black box test, because it is a use-oriented test, it does not need to understand the structure of the program and how to realize it. The main flow of software reliability test is shown in Fig. 3.

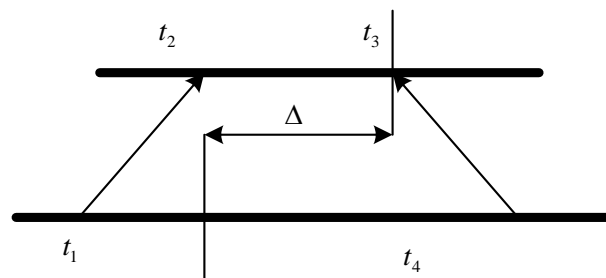


Fig. 2. Software Reliability Two-level Constraint Index Parameter System.

TABLE I. COMPARISON BETWEEN RELIABILITY VERIFICATION TEST AND GENERAL TEST OF EMBEDDED MULTITASK SOFTWARE

Item compared	Software reliability verification test	General software testing
Test purpose	Quantitative estimation of reliability level of software products	Discovery of software errors
Tester	The user usually takes part in the test	It is usually measured by the developer
Testing stage	Software acceptance phase	Trial software development stage
Test method	Random test based on software operation profile.	Testing based on requirements / structure
Test object	The final form of software products	Intermediate form of software products
Test feature	Do not eliminate software defects	Modify software errors and constantly improve software quality

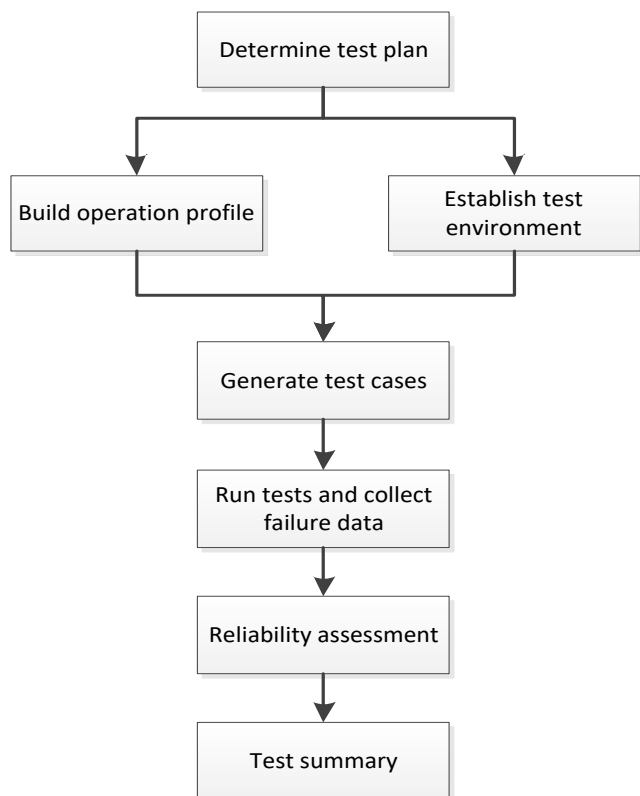


Fig. 3. Reliability Testing Process of Embedded Multitask Software.

The main idea of embedded multitask software reliability test is to test the software at random according to the statistical rules of users' actual use. At present, the use of software is usually modelled in the form of operation profile. The construction of operation section can be refined layer by layer from top to bottom. The development process of the operation profile is shown in Fig. 4.

1) The customer profile consists of independent customer type series.

Customer type is one or more customers in the group who use the system in a similar way. These customers are significantly different from other customers in the way of using the software.

The probability of occurrence needs to be determined for each customer type in the customer profile. In the case of single software customer, there is no need to establish customer profile.

2) User profile is a set of user groups and their probability of occurrence, which is usually based on the customer profile.

3) System mode profile is a set of system mode and its corresponding probability of occurrence. System patterns can be derived from software requirements or usage analysis.

4) The function profile is to decompose the functions required by the system in the system mode and determine the probability of each function.

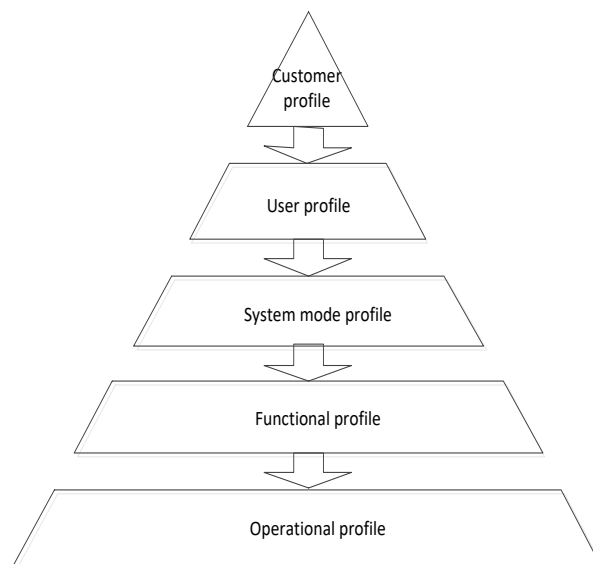


Fig. 4. Operation Profile Development Process.

The construction of function profile usually needs to get the function list according to the software development task or the software requirements document, and then combine with various situations of the operating environment, and assign the probability of occurrence for each function.

5) Operation profile is a set of operations and their probability of occurrence. The main step to determine operation profile is to list operations and determine the probability of occurrence of each operation. A function can be mapped to one or more operations, and a group of functions can also be re merged into a group of different operations, so the list of operations can be obtained according to the function profile.

The embedded multitask software reliability test environment refers to the software and hardware environment that provides test input and collects test output for the tested software. For the reliability test of real-time embedded software, we can use the test environment of full digital simulation technology, hardware in the loop simulation platform and system joint test. In order to get the real reliability test results, the reliability test should be carried out in the real environment. But in many cases, it is unrealistic to test the software reliability in real environment, so the software reliability test usually uses the semi physical simulation environment. Generally, the test environment of semi physical simulation (or full digital simulation) has the following requirements:

1) The operations involved in the operation profile can be performed in the test environment.

2) Meet the real-time requirements of the test excitation, that is, the excitation input meets the requirements of the input interface, data format and input timing of the real cross-linking environment, and the input logic of the real cross-linking environment is the same.

3) Be able to collect test result data for software reliability test analysis.

The failure data of embedded multitask software is the basis of software reliability test and evaluation. In the process of reliability test execution, it is necessary to record the actual results of each test case as required, and judge whether the use case passes according to the expected test results of each use case and the pass criteria of the use case. If not, record it. The problems found in the reliability test of embedded multitask software should be analyzed and dealt with according to the types of problems. The software problems caused by the defects of the tested embedded multitask software itself should be included in the failure of the tested software. The software problems caused by the improper design of the test environment, test methods and test cases other than the tested software should not be included in the failure of the software. In addition, the category and severity level of each embedded multitasking software problem should be described. The categories of software problems include design problems, document problems, program problems and other problems. The severity level of the problems can be described by level 4.

Reliability verification test is a kind of statistical test, which should be selected in the test planning stage. When choosing the statistical test plan, many factors should be considered, such as the type of verification index, the quality requirements of software, the maximum test time, the maximum failure number, the test cost, the trade-off between cost and time. For the verification test of product reliability using success rate, the verification test scheme of success rate is usually used. The specified success rate is the probability that a product will complete the required function or that the product will succeed in the test under the specified conditions. The observed success rate can be defined as the ratio of the number of products that have not failed to the total number of test products at the end of the test or the ratio of the number of successful tests to the total number of tests. The main parameters of the success rate verification test scheme are:

R : Success rate;

R_0 : Acceptable success rate;

R_1 : Unacceptable success rate;

d : Identification ratio of success rate $(1-R_1)/(1-R_0)$;

n : Receive the required number of fixed tests;

r : Accumulated failure number;

r_{RE} : Rejection failure number;

α : Manufacturer's risk, i.e. rejection probability when $R-R_0$;

β : User risk, i.e. the probability of reception when $R-R_1$.

The verification test scheme of success rate includes the truncated sequential statistical scheme and the fixed number test statistical scheme. The schematic diagram of the truncated sequential statistical scheme is shown in Fig. 5.

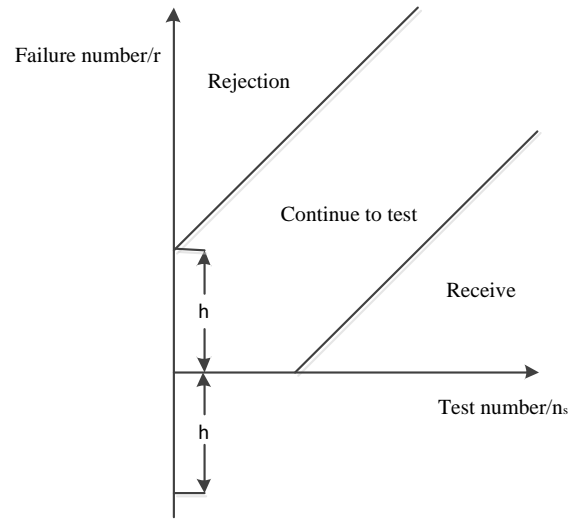


Fig. 5. Schematic Diagram of Truncated Sequential Statistical Scheme.

When $r \leq s \cdot n_s - h$, receive;

When $r \geq s \cdot n_s + h$, rejection;

When $s \cdot n_s - h \leq r \leq s \cdot n_s + h$, continue the test.

Sequential test to cut off line, acceptance or rejection criteria.

When $n_s = n_t$, when $r < r_t$, receive;

When $r > r_t$, reject;

Among them, n_s is the number of tests accumulated in the sequential test scheme, s is the slope of the receiving and rejection lines, h is the intercept of the receiving and rejection lines on the vertical line, n_t is the number of truncated tests, and r_t is the number of truncated failures.

Given R_0 , d , α , β , the test number n required for receiving the judgment and the failure number r_{RE} required for making the rejection judgment can be obtained by looking up the table. The comparison between the two schemes is shown in Table II.

TABLE II. COMPARISON OF TWO STATISTICAL SCHEMES

Comparison items	Advantage	shortcoming
Truncated sequential Statistical scheme	1. The minimum number of average tests and failures required for judgment; 2. It has a certain maximum value in cumulative test number and cumulative failure number.	1. The number of failures and the cost of tested products vary greatly; 2. The maximum number of accumulated tests and failures may exceed the equivalent number of accumulated tests and failures.
Fixed number test Statistical scheme	1. The change range of failure number and cost of tested products is small; 2. The maximum number of cumulative tests is less than that of similar truncated sequential tests.	1. The average failure number and test number are large; 2. In order to make a judgment, the products with good quality and bad quality shall experience the most cumulative tests or failures.

The embedded multitask software reliability testing technology is applied to a configuration item software of an airborne weapon product. Firstly, according to the requirement documents and the actual operation of the embedded multitask software, the operation profile covering the whole working process of the software is constructed. Extract specific system execution task scenarios, design test cases for each scenario respectively, and describe the test cases in detail. Object oriented reliability testing method. The calculation formula of software package constraint index is as follows:

$$MHF = \frac{\sum_{i=1}^{TC} \sum_{m=1}^{M_d(C_i)} (1-V(M_{mi}))}{\sum_{i=1}^{TC} M_d(C_i)} \quad (1)$$

$$V(M_{mi}) = \frac{\sum_{j=1}^{TC} is_visible(M_{mi}, C_j)}{TC - 1} \quad (2)$$

$$is_visible(M_{mi}, C_j) = \begin{cases} 1, & \text{if } \begin{cases} j \neq i, \\ C_j \text{ may call } M_{mi} \end{cases} \\ 0, & \text{otherwise} \end{cases} \quad (3)$$

In the formula, TC is the total number of attributes distributed by embedded multitasking software, and $M_d(C_i)$ represents the number of categories in reliability attribute category C_i .

The regression analysis of embedded multitasking software reliability measurement is carried out by using the method of multi-factor metrology [8]. Combined with the method of bottom design and top-level encapsulation, the product quality of embedded multitasking software is evaluated. Multi factor measurement is a method of measuring multiple evaluation units by using multiple indicators. Its basic idea is to convert multiple indicators into an indicator with comprehensive evaluation ability, so as to reduce calculation complexity and improve calculation efficiency and accuracy. Based on the above, the ambiguity constraint parameters of embedded multitasking software module division are obtained.

$$AHF = \frac{\sum_{i=1}^{TC} \sum_{m=1}^{A_d(C_i)} (1-V(A_{mi}))}{\sum_{i=1}^{TC} A_d(C_i)} \quad (4)$$

$$V(A_{mi}) = \frac{\sum_{j=1}^{TC} is_visible(A_{mi}, C_j)}{TC - 1} \quad (5)$$

$$is_visible(M_{mi}, C_j) = \begin{cases} 1, & \text{if } \begin{cases} j \neq i, \\ C_j \text{ may call } A_{mi} \end{cases} \\ 0, & \text{otherwise} \end{cases} \quad (6)$$

In the formula, the $A_d(C_i)$ is the number of the attributes of the C_i , the constraint index parameter model divided by the embedded multi-task software module is constructed according to the analysis, and the indexes such as the correctness, the reliability, the operation efficiency, the integrity and the usability of the software are determined, and a constraint parameter index distribution model for dividing the embedded multi-task software modules is constructed [9, 10, 11].

B. Reliability Feature Analysis of Embedded Multitasking Software

Let the reliability measurement domain of embedded multitask software be U , and U can be expressed by exact numerical value. Linear programming technology is used to analyze the reliability characteristics of embedded multitasking software, and the next year planning analysis is carried out combined with the inheritance of software reliability. The reliability characteristic analysis model of embedded software is established, and the output: $SC_i(Ex_i, En_i, He_i)$, $I = 1, 2, 3, \dots, n$. The formula for calculating the reliability feature distribution of embedded multitasking software is as follows:

$$MHF = \frac{\sum_{i=1}^{TC} M_i(C_i)}{\sum_{i=1}^{TC} M_a(C_i)} \quad (7)$$

$$M_a(C_i) = M_d(C_i) + M_i(C_i) \quad (8)$$

Wherein, $M_i(C_i)$ is the reliability test factor of $C_i(i = 1, 2, \dots, n)$ class, and the reliability design of embedded multitask software is carried out with the method of fuzzy clustering analysis. The calibration model characteristics of embedded multitasking software reliability measurement are expressed as $U \rightarrow [0, 1], \forall x \in U, x \rightarrow SC(x)$. The reliability feature analysis of embedded software is carried out by using the method of multimodal data fusion feature analysis, and the comprehensive measurement model of software is described as follows:

$$AIF = \frac{\sum_{i=1}^{TC} A_i(C_i)}{\sum_{i=1}^{TC} A_a(C_i)} \quad (9)$$

$$A_a(C_i) = A_d(C_i) + A_i(C_i) \quad (10)$$

In the formula, the software reliability attribute class function is $A_i(C_i)$, and the quantitative characteristic formula of reliability test with property class $C_i (i=1,2,\dots,n)$ is the number of attributes whose $En_i = (Ex_i - Ex_{i-1})/3$ $A_d(C_i)$ is $C_i (i=1,2,\dots,n)$. Based on the analysis, the constraint parameter distribution model of embedded multitask software module partition is constructed, the ambiguity factor of embedded multitask scheduling and module segmentation is established, and the embedded multitasking software module is divided into embedded multitasking software modules combined with fuzzy dynamic testing method [12].

III. OPTIMAL DESIGN OF EMBEDDED MULTITASK SOFTWARE MODULE PARTITION METHOD

A. Embedded Multi-task Scheduling and Module Segmentation and Ambiguity Analysis

On the basis of constructing the constraint parameter distribution model of embedded multitasking software module partition, the optimal design of embedded multitasking software module partition is carried out. In this paper, an embedded multitasking software module partition method based on fuzzy set theory is proposed [13]. Fuzzy set theory regards the object to be investigated and the fuzzy concept reflecting it as a certain fuzzy set, establishes an appropriate membership function, and analyzes the fuzzy object through the relevant operations and transformations of the fuzzy set. Based on fuzzy mathematics, fuzzy set theory studies the imprecise phenomena. The module partition of embedded multitask software is an imprecise problem, so the research is based on fuzzy set theory. Factor of embedded multi-task scheduling and module segmentation is established, and the compatibility and human-computer interactions of the software are measured by the method of multi-layer index parameter constraint control. The formula for calculating the coupling factor of embedded multi-task software module is as follows:

$$COF = \frac{\sum_{i=1}^{TC} \left(\sum_{j=1}^{TC} is_client(C_i, C_j) \right)}{TC^2 - TC} \quad (11)$$

$$is_client(C_c, C_s) = \begin{cases} 1 & \text{iff } C_c \Rightarrow C_s \wedge C_c \neq C_s \\ 0 & \text{otherwise} \end{cases} \quad (12)$$

In the formula, $TC^2 - TC$ is the maximum degree of coupling of the reliability distribution of embedded multi-task software. The multi-level fuzzy metric structure model of the embedded multi-task software module is established, and the

method for combining the multi-state factor (POF) is adopted to obtain the multi-dimensional combined test index distribution set of the software to be as follows:

$$POF = \frac{\sum_{i=1}^{TC} M_o(C_i)}{\sum_{i=1}^{TC} [M_n(C_i) \times DC(C_i)]} \quad (13)$$

$$M_d(C_i) = M_n(C_i) + M_o(C_i) \quad (14)$$

The embedded multi-task software reliability measurement model is composed of five states, namely $\lambda = (X, O, A, B, \pi)$, where $X = \{x_i, i=1,2,3,\dots,N\}$ is the fuzzy coupling state factor in the embedded multi-task software reliability measurement model, and the $O = \{o_j, j=1,2,3,\dots,M\}$. O is an embedded multi-task software safety evaluation model observation state, $C_i (i=1,2,\dots,n)$ represents the reliability test set of embedded multi-task software, which is defined as follows:

$$\begin{aligned} \max F(X) &= (F_1(X), F_2(X), \dots, F_n(X)) \\ \text{s.t. } g_j(X) &\leq 0 \quad (j=1,2,\dots,p) \\ h_k(X) &= 0 \quad (k=1,2,\dots,p) \end{aligned} \quad (15)$$

According to the above analysis, the multi-level fuzzy measurement structure model of embedded multitask software module partition is established, and the parameter indexes such as serviceability, compatibility and portability of embedded software are analyzed by combining reliability merging and comprehensive measurement method, so as to improve the ability of embedded multitask scheduling and module segmentation and reliability measurement [14].

B. Embedded Multitasking Software Module Partition and Optimization Measurement

Based on the above contents, the multi-level fuzzy measurement structure model of embedded multitask software module is studied and constructed, and the number of embedded multitask software is set. However, the software module division based on this method has the problem of weak correlation between embedded multitask software. [15]. In order to solve this problem, a method is proposed to optimize the resource allocation of embedded multitask software by using association combination detection, and build an embedded multitask optimal scheduling and adaptive control model. The fuzzy membership function of embedded multi-task software is described as:

$$\begin{cases} L = \{L_1, L_2, \dots, L_q\} \\ R = \{R_1, R_2, \dots, R_p\} \end{cases} \quad (16)$$

In the above formula, V_k represents the nonlinear dynamic measurement function of software reliability. For the k software reliability attribute feature set, set up the security reliability measurement feature distribution set of embedded multitask software, map the reliability linear programming

feature set L_k of embedded multitask software to the target test set R_l by spatial programming method, and calculate the nonlinear feature quantity of software reliability measurement, which is described as follows:

$$G_{EV,q \times p} = \begin{pmatrix} G_{EV,11} & \dots & G_{EV,1p} \\ \dots & \dots & \dots \\ G_{EV,q1} & \dots & G_{EV,qp} \end{pmatrix} \quad (17)$$

Based on the comprehensive measurement model, the quantitative feature distribution set of embedded multitasking software module partition is obtained, and the principal component feature quantity of embedded multitasking software module partition is represented by $SC (Ex, En, He)$. According to the above analysis, the statistical analysis model of embedded multitasking software module partition is constructed, and the statistical feature distribution matrix is obtained as follows:

$$L = \begin{pmatrix} l_{11} & l_{12} & \dots & l_{kp} \\ l_{21} & l_{22} & \dots & l_{2p} \\ \dots & \dots & \dots & \dots \\ l_{q1} & l_{q2} & \dots & l_{qp} \end{pmatrix} \quad (18)$$

The embedded multitasking software module is divided by quantitative recurrent analysis, and the optimized test set function is obtained as follows:

$$V = \begin{pmatrix} v_{11} & v_{12} & \dots & v_{kp} \\ v_{21} & v_{22} & \dots & v_{2p} \\ \dots & \dots & \dots & \dots \\ v_{q1} & v_{q2} & \dots & v_{qp} \end{pmatrix} \quad (19)$$

Based on the above contents, the division of embedded multi task software modules is realized on the basis of ensuring the independence and stability of software modules. [16, 17, 18, 19].

IV. SIMULATION EXPERIMENT AND RESULT ANALYSIS

In order to verify the application performance of the method in the implementation of the embedded multi-task software module division, the simulation test is carried out. The reliability test environment of embedded multitask software is built by the general system test platform Geste. Among them, the general embedded software simulation test platform consists of three test hosts, two test targets, related I/O and signal conversion devices. All devices in the platform are connected by Ethernet, and the two test target computers communicate with each other in real time through the memory reflective real-time optical fiber network [20, 21]. Position diagram is shown in Fig. 6.

Software reliability can be tested by using the following definitions: the probability that software will not cause system failure under specified conditions and within specified time. This probability is a function of system input and system use, as well as a function of defects in software. The system input will determine whether existing defects will be encountered. The probability that the software will not cause system failure within the specified time, that is, the success rate of the software. Therefore, the success rate is used to verify the fixed number test statistical scheme. After analysis, it is determined that $\alpha = 10\%$, $\beta = 10\%$, $R_0 = 0.9701$, $R_1 = 0.91$.

$$\text{Identification ratio } D = (1-r_1) / (1-r_0) = 3.01$$

According to $\alpha = 10\%$, $\beta = 10\%$, $R_0 = 0.9701$, $d = 3.01$, the values of parameter n and RRE are obtained by looking up the table: $n = 101$, $RRE = 6$.

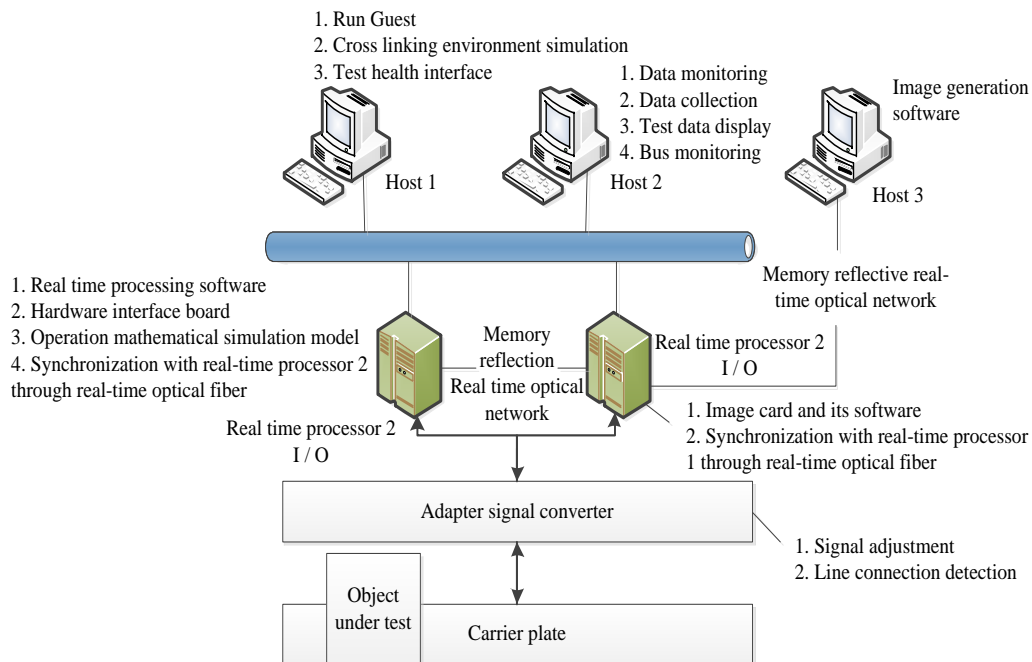


Fig. 6. General System Test Platform Geste Structure Diagram.

Therefore, 101 reliability test cases need to be designed for execution. If the number of software failures is less than or equal to six during the test, the software will be accepted, otherwise it will be rejected [22].

In the software reliability test, there are four failures, less than the maximum number of software failures, which meet the requirements of reliability test program. And the embedded multi-task software module is divided and analyzed in combination with the Matlab and the C ++, the distribution area of the parameter sampling of the embedded multi-task software reliability constraint index parameter is set to [0, 0.6] [0.6, 0.8] [0.8,1], and the distribution of test indicators at all levels is shown in Table III.

By comparing the reliability verification test of embedded multitask software with the general software test, the main process of software reliability test is designed. According to the embedded multitask software, the reliability software and hardware environment of test input and test output are provided [23]. According to the requirements document and the actual operation of the embedded multitask software, the operation section covering the whole working process of the software is constructed, and the specific system execution task scenarios are extracted. Test cases are designed for each scenario respectively, and the test cases are described in detail. The calculation formula of software package constraint index is listed, and the fuzzy constraint parameters of embedded multitask software module division are obtained [24, 25, 26, 27]. Then the fuzzy analysis of embedded multitask scheduling and module division is carried out, the embedded multitask software module is established, and the multi-level fuzzy measurement structure model is divided [28]. According to the test results of the above index parameters, the embedded multitasking software modules are divided, and the reliability test output of each software system is shown in Fig. 7.

TABLE III. DISTRIBUTION OF TEST INDICATORS AT ALL LEVELS OF EMBEDDED SOFTWARE

Primary test index	Weight	II. Test index	Test data
SC1	0.36	INDEX11	0.325
		INDEX12	0.156
		INDEX13	0.446
		INDEX14	0.332
		INDEX15	0.563
		INDEX16	0.532
		INDEX17	0.426
SC2	0.67	INDEX18	0.675
		INDEX21	0.532
		INDEX22	0.436
SC3	0.32	INDEX23	0.547
		INDEX31	0.437
		INDEX32	0.225
		INDEX33	0.853
		INDEX34	0.326
SC4	0.56	INDEX35	0.485
		INDEX36	0.325
		INDEX41	0.567

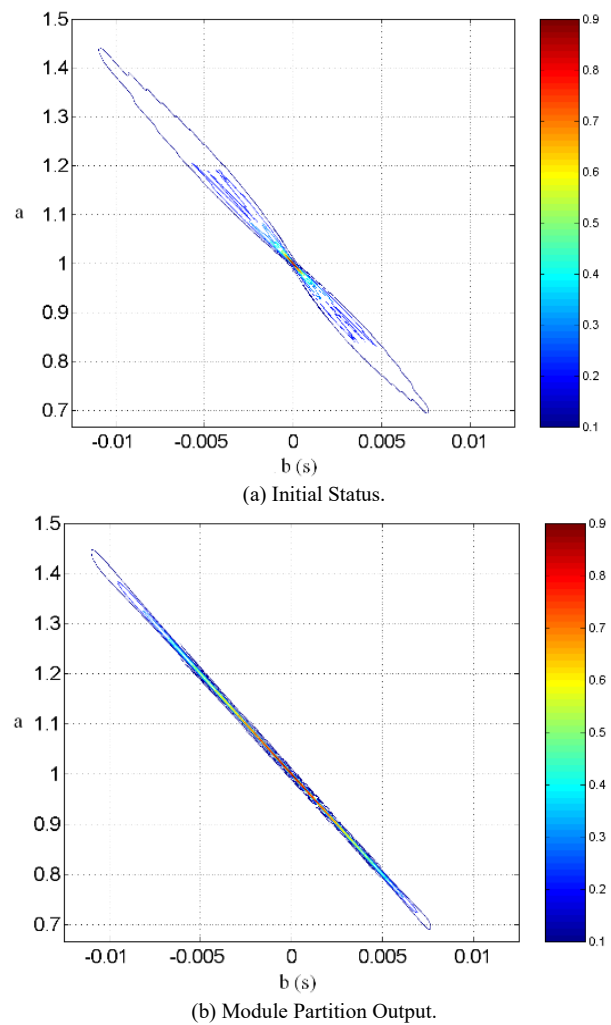


Fig. 7. Reliability Test Output of Software System.

Analysis of Fig. 3 shows that using this method can effectively achieve the embedded multi-task software module division, compare the reliability of the software, get the comparison results as shown in Fig. 8 [29].

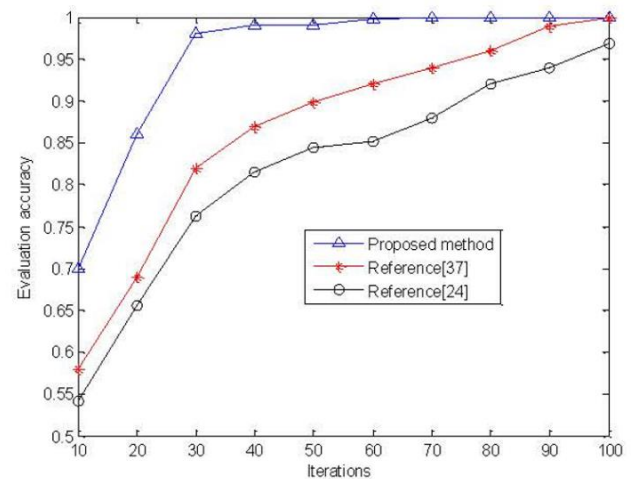


Fig. 8. Reliability Comparison Results for the Software.

In order to understand more clearly and accurately the comparison results of simulation experiments on the reliability of embedded multitask software in this paper, 10 iterations are taken and detailed data comparison is conducted according to Fig. 8 [30, 31, 32, 33]. The comparison data is shown in Table IV [34, 35, 36].

TABLE IV. RELIABILITY COMPARISON DATA OF EMBEDDED MULTITASK SOFTWARE

iterations	Proposed method Evaluation accuracy	Reference [37] Evaluation accuracy	Reference [24] Evaluation accuracy
10	0.7	0.58	0.54
20	0.86	0.82	0.65
30	0.98	0.86	0.76
40	0.99	0.88	0.81
50	0.99	0.90	0.83
60	1	0.92	0.84
70	1	0.93	0.86
80	1	0.95	0.92
90	1	0.97	0.93
100	1	1	0.96

According to Table IV and Fig. 8, when the number of iterations is 10, the accuracy of Proposed method is 0.12 higher than Reference [37], and 0.16 higher than Reference [24]; When the number of iterations is 20, the accuracy of Proposed method is 0.04 higher than Reference [37], and 0.21 higher than Reference [24]; When the number of iterations is 30, the accuracy of Proposed method is 0.12 higher than Reference [37], and 0.22 higher than Reference [24]; When the number of iterations is 40, the accuracy of Proposed method is 0.11 higher than Reference [37], and 0.18 higher than Reference [24]; When the number of iterations is 50, the accuracy of Proposed method is 0.09 higher than Reference [37], and 0.16 higher than Reference [24]; When the number of iterations is 60, the accuracy of Proposed method is 0.08 higher than Reference [37], and 0.16 higher than Reference [24]; When the number of iterations is 70, the accuracy of Proposed method is 0.07 higher than Reference [37], and 0.14 higher than Reference [24]; When the number of iterations is 80, the accuracy of Proposed method is 0.05 higher than Reference [37], and 0.08 higher than Reference [24]; When the number of iterations is 90, the accuracy of Proposed method is 0.03 higher than Reference [37], and 0.07 higher than Reference [24]; When the number of iterations is 100, the accuracy of Proposed method is the same as Reference [37], 0.04 higher than Reference [24]; It can be seen that this method improves the reliability of the software through the division of embedded multitask software modules [37, 38, 39].

V. CONCLUSIONS

The reliability parameter analysis model of embedded multitask software is established, and the embedded multitasking software module is divided by intelligent analysis method. The embedded multitasking software module partition method based on fuzzy set theory is proposed to

construct the constraint parameter distribution model of embedded multitasking software module partition according to the correctness, reliability, running efficiency, integrity and availability of the software. The ambiguity factor of embedded multi-task scheduling and module segmentation is established, the compatibility and human-computer interactions of software are measured by multi-layer index parameter constraint control, the multi-level fuzzy metric structure model of embedded multi-task software module partition is established, and the embedded multi-task software module is divided by quantitative recurrent analysis. It is found that the embedded multitasking software module can be divided effectively by using this method, and the reliability of the software can be improved.

VI. DISCUSSION

In order to solve the problem that the current software module partition method of embedded multitask software is easy to cause software failures and affect user experience, a module partition method of embedded multitask software based on fuzzy set theory is proposed. The basic process of the method is as follows: firstly, the characteristics of embedded multitask software are analyzed, the constraint parameter distribution model is constructed, and the interaction measurement is carried out by combining multitask scheduling and ambiguity segmentation. Then the reliability parameter analysis model of embedded multitask software is constructed, and the multilevel fuzzy metric structure combined with quantitative recursive analysis method is used to complete the division of embedded multitask software modules. In order to verify the application performance of this method in the implementation of embedded multitask software module partition, simulation tests are carried out. The results show that the accuracy of the proposed method is significantly higher than that of the other two methods when the number of iterations is the same. This is because the research builds the optimal scheduling and adaptive control model of embedded multitask software based on fuzzy membership function, which makes embedded multitask software have strong correlation, thus optimizing the reasonable allocation of resources of embedded multitask software. It can be seen that this method improves the reliability of the software through the division of embedded multi task software modules

REFERENCES

- [1] Ma, X.T., Luo, J.Q. & Wu, S.L. 2015. Joint sorting and location method using TDOA and multi-parameter of multi-station. *Journal of National University of Defense Technology* 37(6): 78-83.
- [2] Rodriguez, A. & Laio, A. 2014. Clustering by fast search and find of density peaks. *Science* 344(6191): 1492.
- [3] Zhou, S.B. & Xu, W.X. 2018. A novel clustering algorithm based on relative density and decision graph. *Control and Decision* 33(11): 1921-1930.
- [4] Ma, R.F., Yang, L. & Lei, L.F. 2017. Study on cross-platform modularizing embedded multi-task software framework. *Fire Control Radar Technology* 46(04): 46-50.
- [5] Liu, Y.C., Zhang, H.X. & Huang, H. 2017. Embedded software framework based on Module-MSG. *Computer Engineering and Design* 38(7): 1798-1802.
- [6] Yan, D.L., Zheng, Y., Wang, W.Y. & Chen, Q.J. 2021. Modeling and dynamic analyses of the bulb turbine blade with crack fault. *Applied Mathematical Modelling* 89: 731-751.
- [7] Li, B.F., Tang, Y.D. & Han, Z. 2017. A geometric structure preserving

- nonnegative matrix factorization for data representation. *Information and Control* 46(1): 53-59+64.
- [8] Wu, Y., Shen, B. & Ling, H. 2014. Visual tracking via online nonnegative matrix factorization. *IEEE Transactions on Circuits and Systems for Video Technology* 24(3): 374-383.
- [9] Hu, L.R., Wu, J.G. & Wang, L. 2013. Application and method for linear projective non-negative matrix factorization. *Computer Science* 40(10): 269-273.
- [10] Huang, X.J., You, R.Y. & Zhou, C.J. 2013. Study on optical properties of equivalent film constructed of metal nanoparticle arrays. *Journal of Optoelectronics-Laser* 24(7): 1434-1438.
- [11] Ye, M., Qian, Y. & Zhou, J. 2015. Multitask sparse nonnegative matrix factorization for joint spectral-spatial hyperspectral imagery denoising. *IEEE Transactions on Geoscience and Remote Sensing* 53(5): 2621-2639.
- [12] Zheng, Y.Z. & You, R.Y. 2013. Study on segmented correlation in EEG based on principal component analysis. *Chinese Journal of Biomedical Engineering* 22(3): 93-97.
- [13] Sahu, P.K., Manna, K., Shah, N. & Chattopadhyay, S. 2014. Extending Kernighan-Lin partitioning heuristic for application mapping onto Network-on-Chip. *Journal of Systems Architecture* 60(7): 562-578.
- [14] Komai, Y., Nguyen, D.H., Hara, T. & Nishio, S. 2014. KNN search utilizing index of the minimum road travel time in time-dependent road networks. In: *Proceedings of the 2014 IEEE 33rd International Symposium on Reliable Distributed Systems Workshops. Piscataway, NJ: IEEE* 1: 131-137.
- [15] Ke, S.N., Gong, J. Li, S.N., Zhu, Q., Liu, X.T. & Zhang, Y.T. 2014. A hybrid spatio-temporal data indexing method for trajectory databases. *Sensors* 14(7): 12990-13005.
- [16] Ana Carolina, S.M.C., Bertrand, M. & Adiel Teixeira, D.A. 2015. Fuzzy flow sort: An integration of the flow sort method and fuzzy set theory for decision making on the basis of inaccurate quantitative data. *Information Sciences* 293(15): 115-124.
- [17] Fan, X.M., Song, L.X. & Ji, D.B. 2017. Research on mechanism of algal blooms based on the critical depth theory. *Environmental Science & Technology* 35(7): 77-81.
- [18] Ma, C.L., Shan, H. & Ma, T. 2016. Improved density peaks based clustering algorithm with strategy choosing cluster center automatically. *Computer Science* 43(7): 255-258.
- [19] Pei, D. & Li, L. 2019. Simulation research on security defense of electronic document information transmission. *Computer Simulation* 36(2): 146-149+175.
- [20] Bhavani, R.R. & Jiji, G.W. 2018. Image registration for varicose ulcer classification using KNN classifier. *International Journal of Computers and Applications* 40(2): 88-97.
- [21] Hifi, A.M. 2018. A hybrid reactive search for solving the max-min knapsack problem with multi-scenarios. *International Journal of Computers and Applications* 40(1): 1-13.
- [22] Yang, Z.F., Xu, P., Wei, W.F., Gao, G.Q., Zhou, N. & Wu, G.N. 2020. Influence of the crosswind on the pantograph arcing dynamics. *IEEE Transactions on Plasma Science* 48(8): 2822-2830.
- [23] Wang, B., Zou, F.C., Cheng, J. & Zhong, S.M. 2017. Fault detection filter design for continuous-time nonlinear Markovian jump systems with mode-dependent delay and time-varying transition probabilities. *Advances in Difference Equations* 2017(1): 1-23.
- [24] Citi, H.G. 2019. Important notes for a fuzzy boundary value problem. *Applied Mathematics and Nonlinear Sciences* 4(2): 305-314.
- [25] Wu, J.H., Zhang, L., Yin, S.F., Wang, H.D., Wang, G.L. & Yuan, J.X. 2018. Differential diagnosis model of hypocellular myelodysplastic syndrome and aplastic anemia based on the medical big data platform. *Complexity* (16): 1-12.
- [26] Xiong, Z.G., Wu, Y., Ye, C.H., Zhang, X.M. & Xu, F. 2019. Color image chaos encryption algorithm combining CRC and nine palace Map. *Multimedia Tools and Applications* 22(78): 31035-55.
- [27] Yang, A.M., Li, Y.F., Kong, F.B., Wang, G.Q. & Chen, E.H. 2018. Security control redundancy allocation technology and security keys based on internet of things. *IEEE ACCESS* 6: 50187-96.
- [28] Sarac, Y. & Sener, S.S. 2019. Identification of the initial temperature from the given temperature data at the left end of a rod. *Applied Mathematics and Nonlinear Sciences* 4(2): 469-474.
- [29] Shi, K.B., Tang, Y.Y., Liu, X.Z. & Zhong, S.M. 2017. Secondary delay-partition approach on robust performance analysis for uncertain time-varying Lurie nonlinear control system. *Optimal Control Applications and Methods* 38(6): 1208-1226.
- [30] Song, J.C.; Zhong, Q.; Wang, W.Z. & Su, C.H. 2020. FPDP: Flexible privacy-preserving data publishing scheme for smart agriculture. *IEEE Sensors Journal* (99): 1-1.
- [31] Shi, K.B., Tang, Y.Y., Liu, X.Z. & Zhong, S.M. 2017. Non-fragile sampled-data robust synchronization of uncertain delayed chaotic Lurie systems with randomly occurring controller gain fluctuation. *ISA Transactions* 66: 185-199.
- [32] Wang, P.; Chen, C.M.; Kumari, S., Shojafar, M. & Liu, Y. 2020. HDMA: Hybrid D2D message authentication scheme for 5G-enabled VANETs. *IEEE transactions on intelligent transportation systems* 1-10.
- [33] Wang, X., Liu, Y. & Choo, K.R. 2020. Fault tolerant multi-subset aggregation scheme for smart grid. *IEEE Transactions on Industrial Informatics* 1-1.
- [34] Chen, H., Fang, L., Fan, D.L. Huang, W.J., Huang, J.M., Cao, C.H., Yang, L., He, Y.B. & Zeng, L. 2019. Particle swarm optimization algorithm with mutation operator for particle filter noise reduction in mechanical fault diagnosis. *International Journal of Pattern Recognition and Artificial Intelligence* 34(3): 2058012.
- [35] Li, X., Zhu, Y. & Wang, J. 2019. Highly efficient privacy preserving location-based services with enhanced one-round blind filter. *IEEE Transactions on Emerging Topics in Computing* (99): 1-1.
- [36] Xue, Q., Zhu, Y. & Wang, J. 2019. Joint distribution estimation and naive bayes classification under local differential privacy. *IEEE Transactions on Emerging Topics in Computing* (99): 1-1.
- [37] Chen, H.X., Huang, L., Yang, L., Chen, Y.T. & Huang, J.M. 2020. Model-based method with nonlinear ultrasonic system identification for mechanical structural health assessment. *Trans Emerging Tel Tech* 31(5): e3955.
- [38] Qu, S., Zhao, L. & Xiong, Z. 2020. Cross-layer congestion control of wireless sensor networks based on fuzzy sliding mode control. *Neural Computing and Applications* 32(7): 13505-13520.
- [39] Zhu, Q. 2020. Research on road traffic situation awareness system based on image big data. *IEEE Intelligent Systems* 35(1): 18-26.

Comparison of Metaheuristic Techniques for Parcel Delivery Problem: Malaysian Case Study

Shamine A/P S.Moganathan¹, Siti Noor Asyikin binti Mohd Razali², Aida Mustapha³
Department of Mathematics and Statistics
Faculty of Applied Sciences and Technology, Universiti Tun Hussein Onn Malaysia
Pagoh Education Hub, 84600 Pagoh, Johor, Malaysia

Safra Liyana binti Sukiman⁴
Centre for Language Studies, Universiti Tun Hussein Onn Malaysia, 86400 Parit Raja, Batu Pahat, Johor, Malaysia

Rosshairy Abd Rahman⁵
School of Quantitative Sciences
Universiti Utara Malaysia
06010 Sintok, Kedah Malaysia

Muhammad Ammar Shafi⁶
Department of Technology and Management
Faculty of Technology Management and Business
Universiti Tun Hussein Onn Malaysia, 86400 Parit Raja, Batu Pahat, Johor, Malaysia

Abstract—Most people preferred e-commerce ensuing the Coronavirus Disease-2019 (COVID-19) outbreak, resulting in delivery companies receiving large quantities of parcels to be delivered to clients. Hurdle emerges when delivery person needs to convey items to a large number of households in a single journey as they never face this situation before. As a result, they seek the quickest way during the trip to reduce delivery costs and time. Since the delivery challenge has been classified as an NP-hard (non-deterministic polynomial-time hard) problem, this study aims to search the shortest distance, including the runtime for the real case study located in Melaka, Malaysia. Hence, two metaheuristic approaches are compared in this study namely, Ant-Colony Optimization (ACO) and Genetic Algorithm (GA). The results show that the GA strategy outperforms the ACO technique in terms of distance, price, and runtime for moderate data sizes that is less than 90 locations.

Keywords—Ant-colony optimization; genetic algorithm; delivery problem; comparison; cost; runtime

I. INTRODUCTION

Ever since the chain of Coronavirus Disease-2019 (COVID-19) infections trend up worldwide, peoples' life has been turned upside down. So, do Malaysians. When the former Prime Minister, Tan Sri Dato' Haji Muhyiddin bin Mohd Yassin imposed national lockdown through Movement Control Order (MCO), Malaysians have slowly avoided brick-and-mortar shopping and shop on e-commerce. Previously, e-commerce was a generic buzzword, however, it has become a norm these days.

COVID-19 has led to a significant spike in e-commerce and rapid digitalization in the midst of weakening economic activity in most countries. For instance, in the 2nd period of 2020, Latin America's marketplace Mercado Libre managed to sell double things per day in comparison to the same period in the previous year. In addition, African e-commerce site, Jumia recorded a spike of 50% revenues over the first half of 2020. Throughout August 2019 and August 2020, China's e-commerce percentage of sales rose from 19.4% to 24.6%. Meanwhile, the online percentage of retail sales in Kazakhstan, grew from 5% in

2019 to 9.4% in 2020. In Thailand, installations of shopping applications surged by 60% within a week in March 2020 [1].

Transport plays an essential role in every supply chain and it has an impact on logistics' efficiency and effectiveness. Transportation, inventory keeping, bureaucracy, custom fees, hazard, as well as handling and packaging costs are among six major logistics cost aspects that should have good pre-planning. Route planning is a critical issue in distribution system, and as such, it has been an important topic in logistics field. By focusing on areas such as enhanced productivity and better vehicle usage, effective routing and scheduling can result big savings. According to [2], the goal of reducing transportation costs is to reduce the number of trips.

This research article presents a case study that utilizes Asymmetric Travelling Salesman Problem (ATSP), in which a delivery service is founded to alleviate the burden of delivering items to customers' doorsteps. As a result, this delivery service will travel and organise their routes carefully to multiple locations in order to meet the needs of their consumers within a designated time frame. The primary goal of this study is to evaluate two metaheuristics approaches, namely ACO and GA, and to compare its efficiency metric of minimizing cost and time. The delivery service drivers have a plethora of options, which will allow them to seek for the shortest distance and lowest cost throughout their excursions.

The entirety throughout this paper is organised as follows: Section II highlights relevant studies on the current challenges and ways to overcome, while Section III describes the methodologies used in the study. Section IV presents the outcomes and the discussions, and Section V finishes the article with future work.

II. LITERATURE REVIEW

A. Logistics in Malaysia

Malaysia reported 37% of growth in e-commerce revenues by 2020. The Department of Statistics Malaysia annotated a rise in 23.1% during the first 9 months of 2021, signalling that

this pattern will remain [3]. A study by [4] indicated that e-commerce has boosted the number of buyers in both established and emerging countries, including Malaysia, Singapore, Thailand, and Pakistan since the outbreak. Most of retailers are changing their brick-and-mortar shop to e-commerce platform, as it can maintain the continuity and longevity of their business during these arduous circumstances.

Fig. 1 illustrated Malaysian’s e-commerce users from 2017 – 2025 in three different categories, namely in the past, present and forecasted data of the upcoming years [5]. The figure demonstrates a significant basis on how intra-logistics have increased during this crisis in Malaysia. This is mostly due to the rise of internet purchases for daily necessities [6].

When consumers are actively purchasing online today, the need for shipments are escalating every day. Thus, an extra demand exists during festive seasons, monthly household demands, and monthly sales organised by e-commerce platforms. The warehouse space in courier companies is quite limited to cater these high parcel volumes, resulting dumping of parcels [7][8]. When there are countless of delayed parcels to be delivered, employees must work overtime. Pos Laju riders, one of the delivery companies in Malaysia, are deemed to work on weekends to avert overburdened goods, and deliver hundreds of items every day [7]. According to the previous study [8], this circumstance is frustrating as poor coordination of logistics providers and courier services has disrupted on other activities in the company.

The following figure indicates the number of domestic courier items delivered by courier service providers in Malaysia from 2016 to 2020 (see Fig. 2) [9]. In 2020, the parcel volume distributed by the courier service providers escalate during the endemic, thus, courier companies need to be well-prepared.

Logistics are in demand ever since the COVID-19 pandemic has started. Almost all countries were having lockdowns. The only way to purchase our daily necessities were through online order and have it delivered to our doorstep. Hence, courier companies play a vital role. Planning of dispatches and navigation of vehicles are critical in supply chain operations since it influence distribution of costs and contentment of customers.

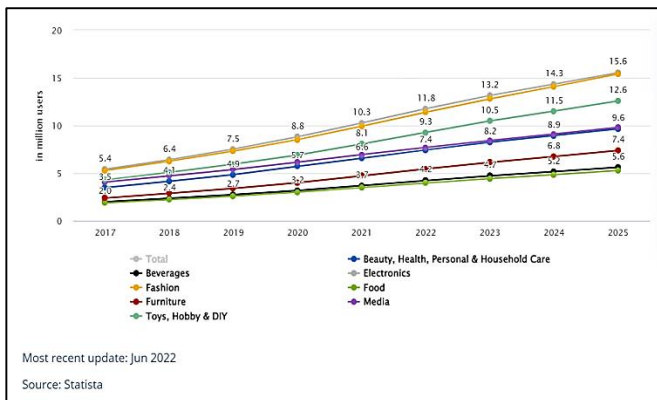


Fig. 1. Malaysian’s e-commerce users from 2017 – 2025 in different Categories [5].

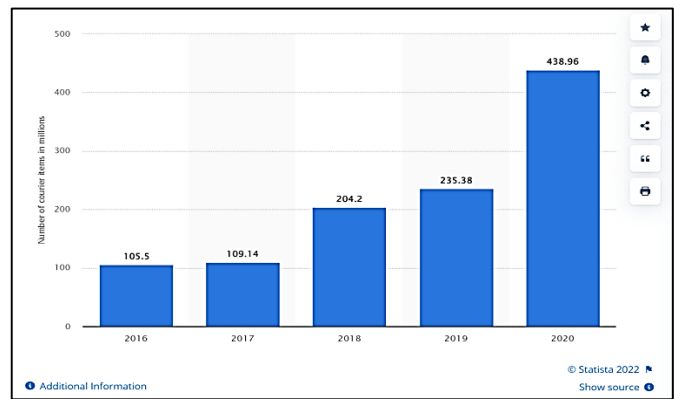


Fig. 2. The Number of Domestic Courier Items Delivered by Courier Service Providers in Malaysia from 2016 to 2020 [9].

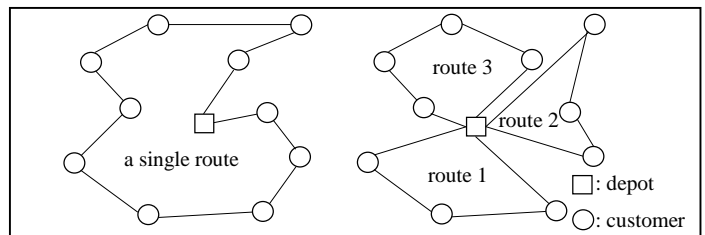


Fig. 3. The Difference between ATSP and VRP [11].

Since the distribution of goods is influenced by various factors such as the requirements of delivery providers, clients, and macro environment, Vehicle Routing Problem (VRP) is one of the most researched subjects in operational research [10]. Thus, logistics providers need to plan well if they want to use VRP or ATSP applications whenever they dispatch customers’ packages. TSP examines a single vehicle visiting numerous customer sites before heading to the depot, and it is aimed that the total journey time or vehicle distance to be as short as possible. VRP is distinct from TSP as it can generate several routes that can travel through all customer locations. The Fig. 3 below shows the difference between ATSP and VRP are shown below [11].

Despite Malaysia's economic development rate is improving, the country's logistical advances remain modest. In order to stay abreast with other South East Asian countries, Malaysia's logistics development was meticulously mapped under the Third Industrial Master Plan (IMP3) in 2006, Unfortunately, Malaysia continues to lag behind neighboring countries such as Singapore, Thailand, and Vietnam in terms of transportation, bureaucracy, and logistics. The problems occur in logistics expansion are insufficient transport infrastructure, underdeveloped transport and logistics services, as well as delayed and costly administrative practices, which contribute to major factors of Malaysia's high logistics costs [12].

B. Algorithms in Logistics Issues

The ATSP is known as a combinatorial optimization problem in operation research and graph theory. It appears in numerous application scenarios, such as cloud computing resource deployment, efficient route search for transport, computational modelling of proteins, semiconductor

manufacturing, X-ray crystallography, school and university scheduling, as well as drone navigation [13]. There is at least one scenario in the ATSP when cost or weight on an arc is not identical in either direction of to or from a node in a travelling graph [14]. ATSP is an efficiency problem that a salesman must solve in order to visit all cities. In an ATSP situation, the distance between cities A and B is not the same as the distance between cities B and A. As a result, the salesman must identify the quickest possible route.

In a study by [15], Farmland Fertility (FF) algorithm is utilized in the experiment to solve the problem. Farming action inspires FF as a metaheuristic. FF assists farmers in obtaining high-quality plant for sale at a premium price. During the process, farmers will typically split their fields into sections by using different materials or treatments depending on the soils. The study develops an agricultural fertility algorithm to tackle ATSP by identifying parameters that influence the outcome [15].

To handle continuous optimization challenges, Social Spider Algorithm (SSA) is proposed based on spiders' information-sharing foraging approach. By retaining SSA's strengths and outstanding performance, [16] propose a novel algorithm called Discrete Social Spider Algorithm (DSSA) to solve discrete optimization problems by making some changes to the computation of Euclidean distance, construction of follow position, movement method, and fitness function. TSPLib benchmark are used to demonstrate DSSA's effectiveness, and the results are compared to six different optimization methods: Improved Bat Algorithm (IBA), GA, an Island-based Distributed Genetic Algorithm (IDGA), Evolutionary Simulated Annealing (ESA), Discrete Imperialist Competitive Algorithm (DICA), and Discrete Firefly Algorithm (DFA). DSSA surpasses other strategies in the simulation data. The experimental results suggest that the DSSA approach is superior than the existing evolutionary algorithms for solving TSP issues and it can be applied to any optimization problems such as routing problems.

ACO is a nature-inspired metaheuristic that is frequently used to develop approximations to overcome optimization problems. Even though ACO is substantially faster than precise approaches, it still can be considered sluggish when it is compared to fundamental problem-specific heuristics. Recent research has demonstrated that algorithm modifications with proper parallel implementation using multi-core CPUs and specialized accelerators can be considered to enhance speed. In this study, [17] offered Focused ACO (FACO), a unique ACO variant. One of the FACO's basic elements is a system for managing large discrepancy between a freshly produced and a previously selected solution. This technique results a more concentrated exploration process, allowing improvements and maintaining performance of existing solution. In addition, it also provides seamless interaction of problem-specific local search. A computational study based on a variety of Traveling Salesman Problem instances reveals that FACO beats state-of-the-art ACOs in tackling big TSP instances.

As for the asymmetric travelling salesman problem, [18] proposed a new GA with optimal recombination and ATSP

adaptive restarts. The crossover operator solves optimal recombination problem (ORP) using a new technique that solves the ATSP on cubic digraphs. Based on Schnabel census estimate, the researchers utilized an adaptive restart rule. A computational experiment on known benchmark examples demonstrates suggested algorithm able to produce results that are comparable to those state-of-the-art ATSP algorithms, confirming that the ORP can be utilized successfully in genetic algorithms. The study also discussed two restarting rules. The first solution employs the conventional restart rule, in which the GA is resumed as soon as the current iteration number equals double the number of iterations when the best incumbent is discovered (denoted GACL). The second strategy is based on the biometrics Schnabel census method that is combined with the maximum likelihood concept. When the population variation becomes low, novel solutions are unlikely to be identified, hence this criterion repeats the process.

Presently, there are lack of research when both methods perform their best at their own way. Hence, in this study, as for GA, it turns out to be the best when the crossover operator is removed, and subsequently the other three mutation operators, flip mutation, swap mutation, and slide mutation were added. Whereas for ACO, the best parameters were studied from various studies, and that parameter values were applied in this study. Therefore, both methods have been compared and evaluated to see which is the best to be applied in this study.

III. METHODOLOGY

In this study, the MATLAB version R2018a software is utilized to compare the effectiveness of the algorithms to some current works. The processor Intel(R) Core (TM) i5-1035G1 CPU @ 1.00GHz has an aspect of Intel Deep Learning Boost technology for speedier artificial intelligence-based computing. Below will further discuss the methods and parameters used in this study.

A. Genetic Algorithm

John Holland is the pioneer to propose GA on computational difficulties of game hypothesis and case recognition. It is based on the fundamental of Darwinian advancement principles of choice, hybridization, and transformation and aims to depict developmental methods [19]. Majority of GA-phrasing comes from the realm of inherited traits [20]. It is claimed to mimic the natural progression of living creatures. Fig. 4 depicts an illustration of a GA [20].

The GA's fundamental structure can be described as follows:

1) *Start*: The process begins when a random pair of chromosomes from all best solution is identified, referred as the population.

2) *Fitness*: The fitness of each chromosome in the population is calculated using the fitness criterion. For an instance, based on a set of 5 genes, each of which would have one of the binary values 0 or 1, one must create a sequence with all 1s. Maximize the amount of 1s as much as possible.

This is an exemplar of an optimization problem. As a result, the fitness function is defined as the number of 1s in the genome. If it has five 1s, it has maximum fitness and solves the problem. If there is no 1s, it has the least fitness [21].

3) *Selection*: Two parent chromosomes are chosen from a population based on their fitness.

4) *Crossover*: Crossover on the specified parent chromosomes result a new offspring set.

5) *Mutation*: If necessary, the newly acquired progeny may also be mutated.

6) *Check*: If the specified criteria are achieved, return the optimal answer and stop.

This study applied the same approach as proposed by [22]. The crossover operator, was not included. According to [22], he does not regard the crossover operator as a necessary component of GA. The author in [22] tested different variants of the GA in terms of diverse crossover and mutation operator combinations in order to solve TSP. The crossover operator was discovered to be catastrophic as it resulted large changes to a given path and unable to impose good solution. As a result, [22] used three distinct mutation operators to generate modifications that were more important in promoting ideal results. Thus, the identical technique as described by Kirk was used in this case study. Fig. 5, Fig. 6, and Fig. 7 show three mutation operators which are elucidated in the following figures [22]:

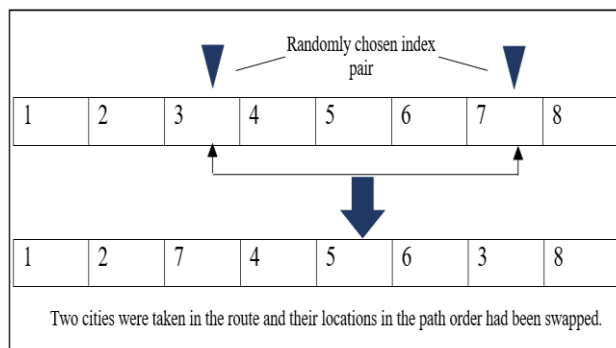


Fig. 6. Swap Mutation [22].

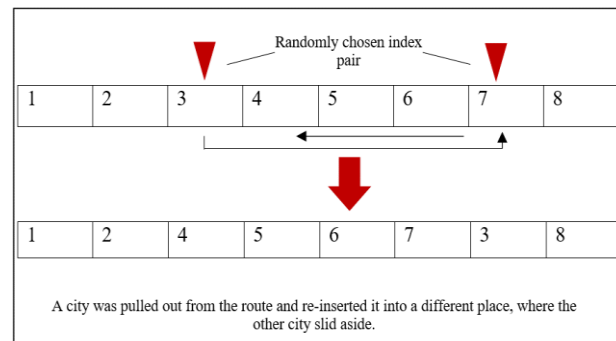


Fig. 7. Slide Mutation [22].

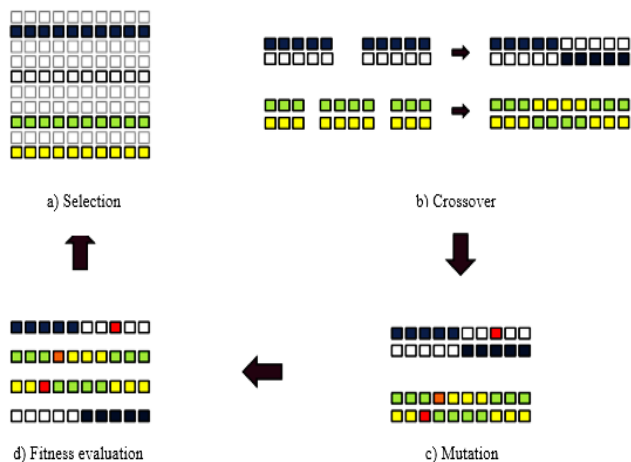


Fig. 4. Illustration of GA [20].

Fig. 8 Depicts the Flowchart of the GA.

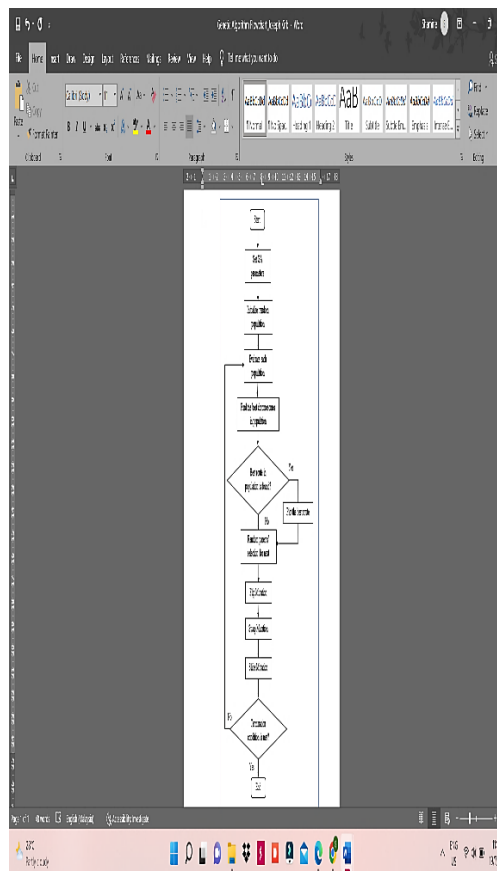


Fig. 8. Flowchart of GA [22].

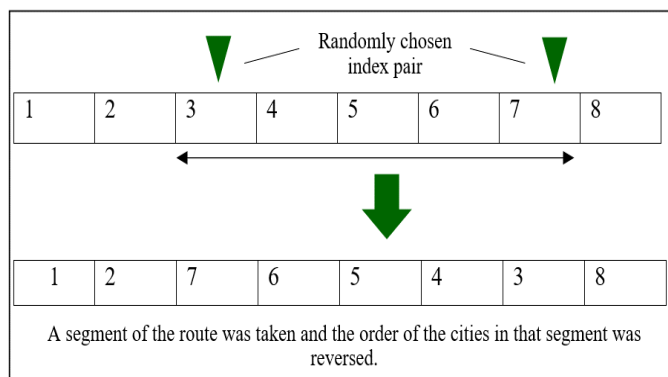


Fig. 5. Flip Mutation [22].

TABLE I. PARAMETER VALUE FOR GA

Parameter	Value
No. of Houses	10, 20, 30, 40, 50, 60, 70, 80, 90, 100
Pop. Size	10
No. of Iteration	1e4
Mutation Probability	$P_m = 1.0$

Table I shows the parameter value of GA that was used in this study. The effect of parameters in both methods play a major role in this study. Among the parameters that are vital in the GA method are population of chromosomes, number of iterations and mutation probability. The population size used is 10. As there were no previous evidence studies on the recommended population size, hence, a simulation of ten-run was done between 10 to 100 population size. It was shown that when population size of 10 was used in the study, the result showed a positive performance. The iteration 1e4, (10000) was used as, right after that, the results occurred are same.

B. Ant-Colony Optimization

The ACO, which is based on ant foraging behavior, was first proposed by [23]. It portrays real-life of ants' behavior to find the short routes between sources of food and their nest, an evolving habit that emerges from an ant's decision to pursue the trail pheromones released by other ants. Fig. 9 shows the basic idea behind an ant colony, with black lines denoting pheromones on every route [24].

Initially, three ants contemplate to travel via the same route to their food. Each ant follows a different course, and one ant moves quicker than the others. This ant will exude a chemical substance (pheromone) while travelling to help other ants to trail and recall their path. The pheromone trail will be stronger on the shorter way than the longer path. Subsequently, the longer road pheromone trail will fade, but the shorter path pheromone trail will become much stronger, resulting the ants to choose the shortest route. Fig. 10 shows the flowchart of ACO algorithm [25].

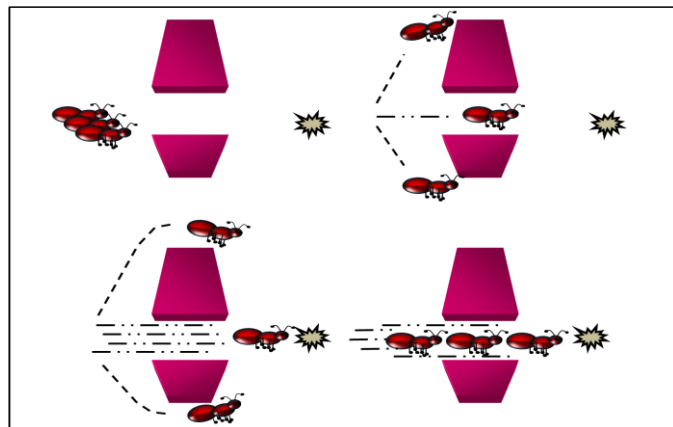


Fig. 9. ACO Behavior at Distinct Time Stamps [24].

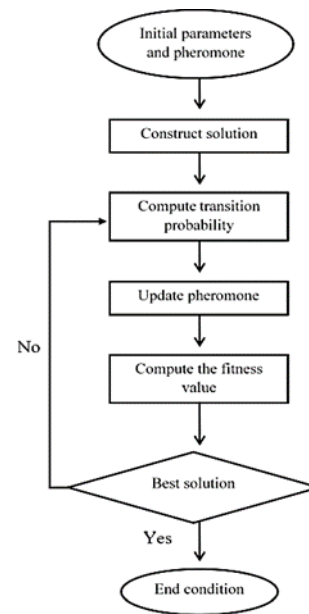


Fig. 10. Flowchart of ACO [25].

TABLE II. PARAMETER VALUE FOR ACO

Parameter	Value
No. of Houses	10, 20, 30, 40, 50, 60, 70, 80, 90, 100
No. of Ants	10
Pheromone Rate (rho)	0.15
No. of Iteration	300

Table II shows the significant parameter values of ACO that was used in this study as it affects the findings. The count of ants in this study is limited to 10. It is because, according to [31], it is suggested to assign the ants within the range of more than 6, but less than 20, for a small or medium scale TSP. Meanwhile, if the number of ants exceeds 16, it will result longer execution time when the complexity of the algorithm increases. Moreover, if the number of the ants is greater than 16, the evaporation rate of pheromone will be quicker resulting an impediment in finding the optimal solution. As a result, the number of ants is set to 10 and the rate of pheromone evaporation is determined to 0.15. This is because if the rate is lesser, there will be more pheromone and higher possibility to get the best findings. The iteration is set to 300 because if it is less, the optimum result cannot be achieved; if it is greater, simply the run time increases with the same outcome.

C. Formulation of Costing in Mathematical Model

The total cost of mathematical model is proposed for this study, as suggested by [26][27]. It has been employed in the pricing calculation after the distance of both approaches are obtained.

Total Cost, Z:

$$Z = \sum_{i=1}^n (LSD \times CS) \tag{1}$$

$$Z = [\sum_{i=1}^n D(L_i, L_j)]CS \tag{2}$$

$$Z = \left[\left[\sqrt{(x_j - x_i)^2 + (y_j - y_i)^2} \right] CS \right] \quad (3)$$

$i, j = \{1, 2, 3, \dots, n\}$

LSD = Length of the shortest path between two locations (D)

D = Distance between L_i and L_j

$L_i = (x_i, y_i)$ initial point (location)

$L_j = (x_j, y_j)$ second point (location)

CS = Cost per 1 kilometer = RM0.80

IV. RESULTS

As a case study, we concentrated on Melaka Tengah district, which is known as one of historical capital in Malaysia. Melaka was discovered in year 1400, with an extent of 314 km². Years after, 3 districts and 29 divisions were identified [28]. Melaka Tengah is also recognised as Malacca's most developing city. The city is divided into residential, industrial, commercial, tourist regions, and administrative areas. According to [29], while the city creates enormous economic gains, it also has a variety of socio environmental implications due to poor transportation. Hence, it is chosen as a research topic for this study. Fig. 11 depicts a map of the Melaka Tengah District [30].

Oh My Foot Delivery is a new delivery firm that is established in this area, and its delivering statistics are used in this study. As a young company, currently there is only one branch located in Melaka Tengah's district. Since the company's position is strategic and there are few residential areas nearby, it has attracted the locals' attention for its delivery service. The company begins to grow when more consumers from further away requested its delivery services. As a result, this study is implemented in order to determine the ideal delivery route. Fig. 12 depicts the MATLAB result's that resembles Google Map.

As demonstrated in Fig. 12, the MATLAB findings are similar to Google Maps; hence the recommended routes from Fig. 13 to Fig. 32 are feasible. The yellow dot on Google Maps indicates both starting and ending point for the journey. Conversely, the red dots indicate the sites in which the deliver must travel in order to deliver packages to clients.

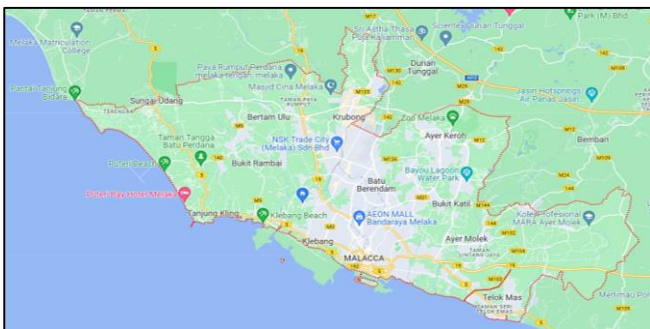


Fig. 11. Map of the Melaka Tengah District [30].

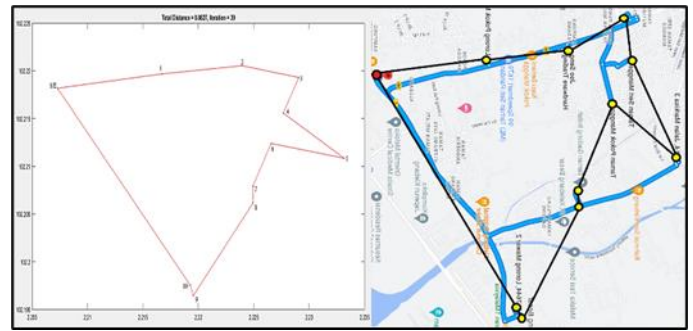
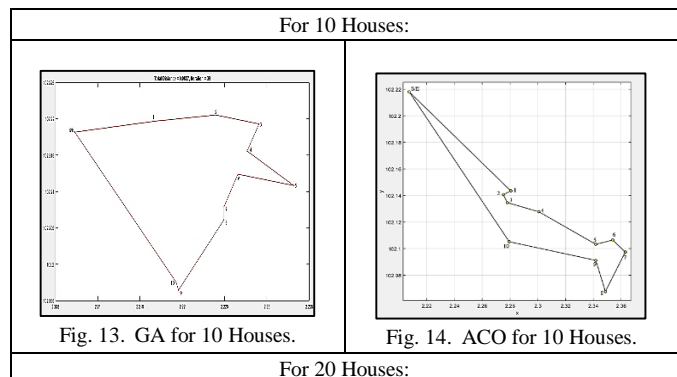
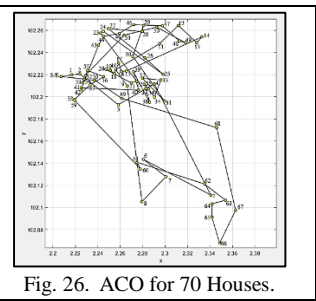
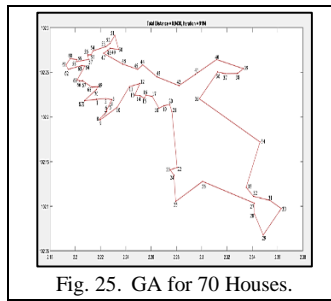
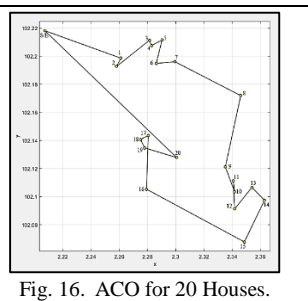
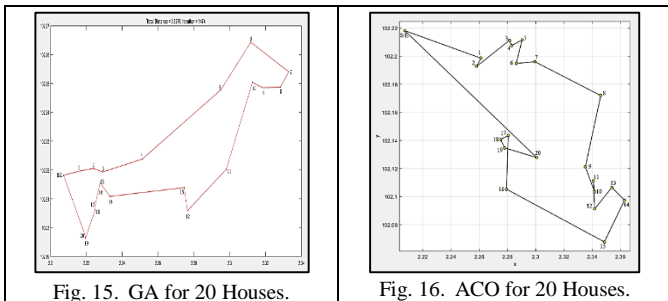


Fig. 12. The MATLAB Result's that Resembles Google Map.

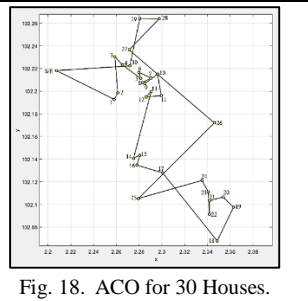
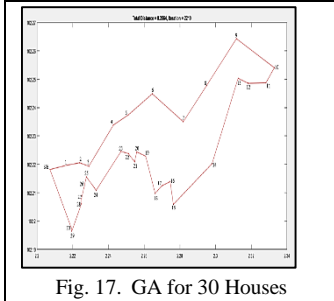
Fig. 13 to Fig. 32 show the simulated results of both GA and ACO methods where each location has been identified from its starting/ending location (S/E) until 10th, 20th, 30th, 40th, 50th, 60th, 70th, 80th, 90th, and 100th location simultaneously with its explanation. the starting and ending points are ensured in the same area (S/E). These roads are listed up to 10, 20, 30, 40, 50, 60, 70, 80, 90, and 100 houses based on insights of few riders who routinely deliver 100 sites in a trip since the pandemic. At times, these riders need to cover ten areas per trip. As a result, from the data provided by the delivery firm, a total of 10, 20, 30, 40, 50, 60, 70, 80, 90, and 100 houses are selected for this case study.

The findings of 10 houses, 20 houses, 30 houses, 40 houses, 50 houses, 60 houses, 70 houses, and 80 houses reveal that GA depicts better way than ACO due to significant reasons. When 90 and 100 points of data are assigned to test, it is discovered that the distance and cost of the ACO approach is lesser than GA. This is due to the fact when the ants choose their path, they are likely to follow the trail indicated by the preceding ant who left a strong pheromone intensity. These ants will choose a path with high probability value that has higher pheromone concentration as it will proceed to the closest desired node. Nodes with low probability values are rejected because they are too far away from the ideal node. As a result of this mechanism, the number of possible paths from one generation to the next grows rapidly, causing ACO to converge faster than GA.

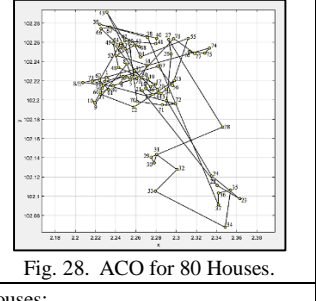
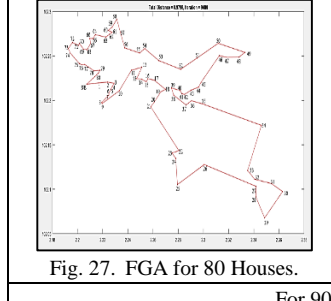




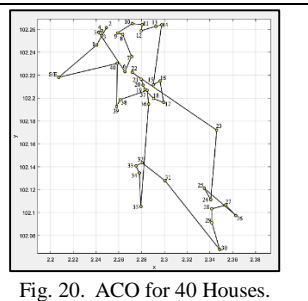
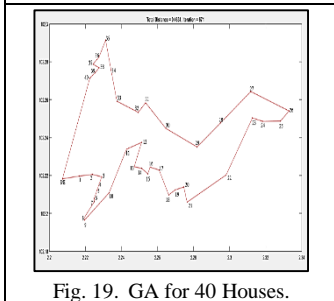
For 30 Houses:



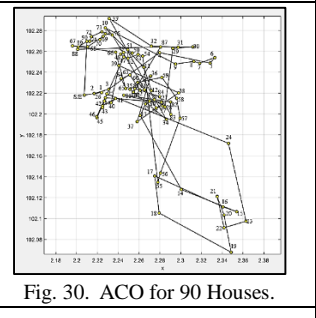
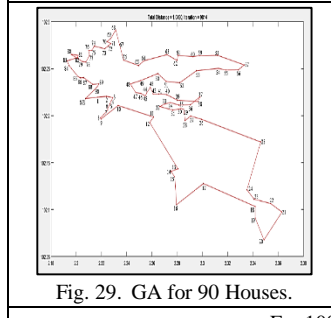
For 80 Houses:



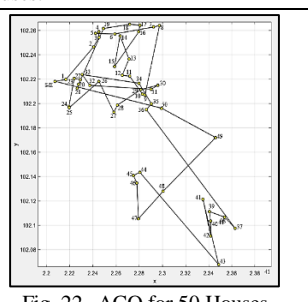
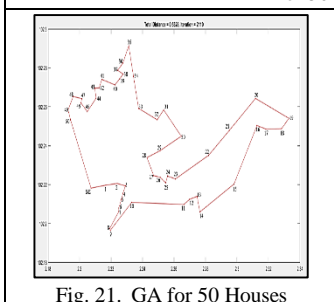
For 40 Houses:



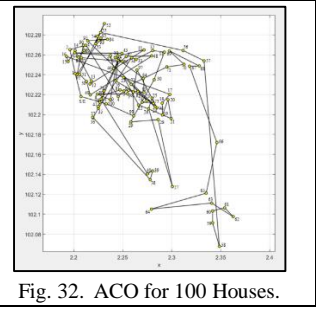
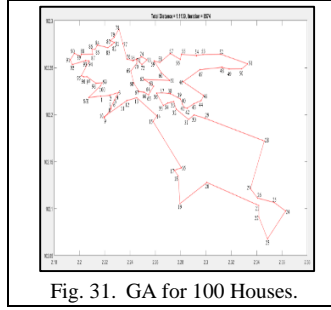
For 90 Houses:



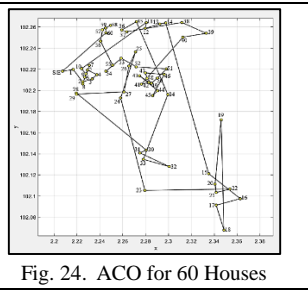
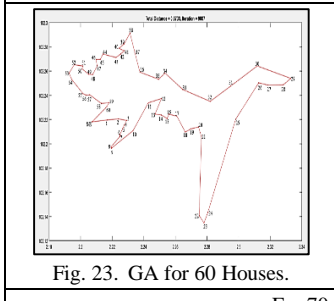
For 50 Houses:



For 100 Houses:



For 60 Houses:



For 70 Houses:

Despite the fact that the ACO's parameters are set at its best according to previous study, there are various reasons why the GA technique is the best solution, including the fact that the run time for all 10, 20, 30, 40, 50, 60, 70, 80, 90, and 100 houses is significantly lesser than the ACO. The crossover probability, P_c , is set to 0 as the deciding factor. Although crossover probability has several effects on the GA studies, it tends to be disastrous because the crossover has significant impact on the given route due to the random changes made in it which will result in longer execution time. As a result, when the chromosome population is set to 50, the crossover probability parameter, $P_c = 0$, the mutation probability, $P_m = 1.0$, and the three mutation operators are utilized, the execution time of the GA is lower than the ACO. Flip mutation, swap mutation, and slide mutation are treated as three mutation operators in the study.

The delivery firm, Oh My Foot Delivery now can use the route proposed by GA method in this study. It is because, previously the delivers need to plan their location from one place to another by calculating it one by one. So, some locations that need to be visited has been missed and the delivers need to go the locations back and forth. However, although the distance has been calculated, but the outcome routes depend on the list the deliver enters. This results in high cost that the firm need to spend as more distances need to be travelled by the delivers.

The algorithms under consideration (the GA and the ACO) are employed to identify the shortest path within the range of scenarios of 10, 20, 30, 40, 50, 60, 70, 80, 90, and 100 home counts. The findings of both methods are compared. Fig. 33 reveals that least distance can be obtained when GA is used as the ACO trend in the distance graph increased compared to the GA trend. Hence, delivery service can save more money on their fuel as well.

TABLE III. COMPARISON OF GA AND ACO

No. of Houses	GA			ACO		
	Dist. (KM)	Cost (RM)	Run Time (s)	Dist. (KM)	Cost (RM)	Run Time (s)
10	20.6	16.48	4.13	92	73.6	15.74
20	83.5	66.8	5.483	141.7	113.36	16.752
30	103.2	82.56	6.185	176.8	141.44	16.857
40	127.7	102.16	6.337	190.05	152.04	17.552
50	139.25	111.4	6.995	207.25	165.8	18.163
60	182.45	145.96	7.418	266.35	213.08	18.496
70	269.55	215.64	7.47	285.35	228.28	20.461
80	302.75	242.2	8.322	316.95	253.56	21.256
90	335.15	268.12	8.955	327.5	262	22.269
100	346.9	277.52	9.242	342.1	273.68	21.364

Table III shows the result of this study that has been summarized, following by graphs in Fig. 32, Fig. 33, and Fig. 34.

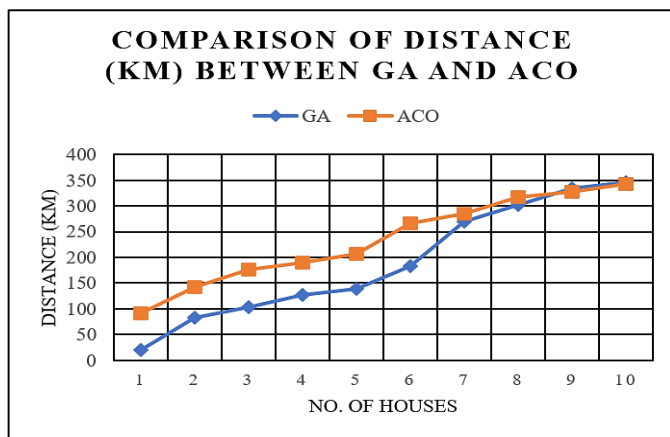


Fig. 33. Comparison of Distance (KM).

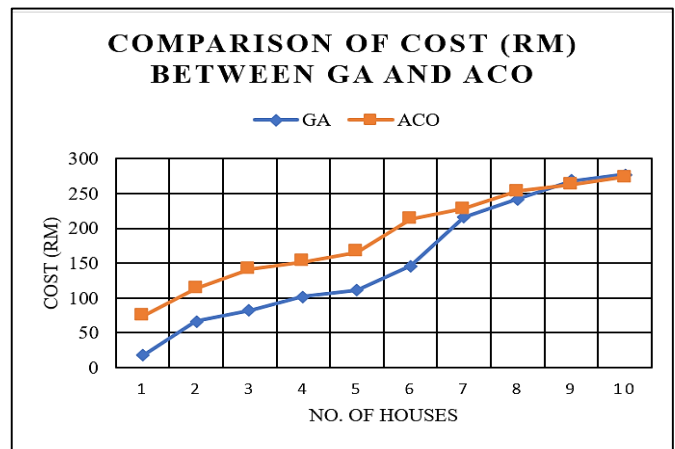


Fig. 34. Comparison of Cost (RM).

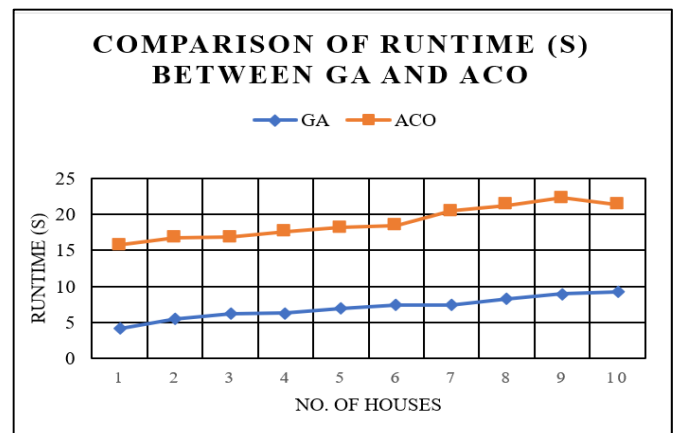


Fig. 35. Comparison of Runtime (s).

Furthermore, when the GA is applied, the graph in Fig. 34 demonstrates the lowest delivery cost which the company has to bear first, then it will be covered by the customers' delivery charge. Thus, it will be beneficial during this pandemic as both parties can save their money and profit from their delivery service. Nevertheless, when 90 and 100 dwellings are specified, the ACO algorithm scored averagely in respect of distance and cost when it is contrasted with the GA technique.

Nevertheless, the GA has yielded to be the most effective method in terms of its runtime under all conditions. It is corroborated through the graph in Fig. 35, which demonstrates a considerable difference in runtime between the GA technique and the ACO technique. From here, we can see that the objectives of this study which is to evaluate ACO and GA, and to compare their performance in terms of minimizing cost and time has been achieved. As a result, it is proven that the GA outperforms the ACO algorithm as it gives the least cost as it proposed the shortest route and minimal running time.

V. CONCLUSION

This research aims to evaluate two metaheuristics strategies to reduce the exact distance of one trip during delivery. The appraisal methodologies used are the GA and ACO, with distance and cost of delivery as significant presenting pointers. When the GA calculation is assigned to

10, 20, 30, 40, 50, 60, 70, and 80 houses, the most minimal distances and lowest expenses are obtained, according to the exhibition correlation. Thus, when it is compared to the ACO method, the GA outperforms in terms of distances, cost, and runtime. It is also acknowledged that the ACO algorithm performs moderately in terms of distances and prices for 90 and 100 houses. Since both methods are the finest in its individual investigations, both methods and its best parameters are compared. As a result, the objective of this study is achieved.

As a recommendation of future work in this research area, the best methodology that is chosen which is GA can be used in other applications of TSP. Those applications that can be taken into account are scheduling, planning, and manufacturing of microchips. It is because, as the crossover operator has been removed from GA in this study, and it shows a positive effect in terms of runtime, it will be intriguing to know what would be the outcome of the method on other applications.

ACKNOWLEDGMENT

Communication of this research is made possible through monetary assistance by Universiti Tun Hussein Onn Malaysia and the UTHM Publisher's Office via Publication Fund E15216, TIER 1 Grant (Q162) and also GPPS Grant (H633).

REFERENCES

- [1] UNCTAD. 2022. How COVID-19 triggered the digital and e-commerce turning point. [online] [Accessed 25 July 2022].
- [2] Ongcunaru, W., Ongkunaruk, P., & Janssens, G. K. (2021). Genetic algorithm for a delivery problem with mixed time windows. *Computers & Industrial Engineering*, 159, 107478.
- [3] V. (2022, June 10). Malaysia E-Commerce Digital Trends in 2022 and the Role of Logistics. Retrieved July 25, 2022.
- [4] Bhatti, A., Akram, H., Basit, H. M., Khan, A. U., Raza, S. M., & Naqvi, M. B. (2020). E-commerce trends during COVID-19 Pandemic. *International Journal of Future Generation Communication and Networking*, 13(2), 1449-1452.
- [5] Statista. 2022. eCommerce - Malaysia | Statista Market Forecast. [online] [Accessed 25 July 2022].
- [6] Gohain, M. (2021). IMPACT OF COVID-19 ON MALAYSIAN E-COMMERCE. *International Journal on Recent Trends in Business and Tourism (IJRTBT)*, 5(4), 8-10.
- [7] Kee, D. M. H., Nasser, S. N. A., Sany, N. S. M., Azhar, T. I., Roslan, Z. H., & Amlı, N. A. (2021). The strategy, impact, and challenges faced by Pos Malaysia Berhad during the COVID-19 crisis. *Journal of the Community Development in Asia (JCDA)*, 4(2), 13-25.
- [8] Mazlan, M. (2021). Challenge E-Commerce to the logistics courier services provider during MCO in Malaysia. *IOSR Journal of Business and Management*, 23(2), 59-62.
- [9] Müller, J., 2022. Malaysia: domestic courier items delivered 2020 | Statista. [online] Statista. [Accessed 27 July 2022].
- [10] Konstantakopoulos, G. D., Gayialis, S. P., & Kechagias, E. P. (2022). Vehicle routing problem and related algorithms for logistics distribution: A literature review and classification. *Operational research*, 22(3), 2033-2062.
- [11] Herdianti, W., Gunawan, A. A., & Komsiyah, S. (2021). Distribution cost optimization using pigeon inspired optimization method with reverse learning mechanism. *Procedia Computer Science*, 179, 920-929.
- [12] Free Essays - PhDessay.com. 2022. Issues and Challenges of Logistics in Malaysia: a Perspective - PHDEssay.com. [online] [Accessed 27 July 2022].
- [13] Huerta, I. I., Neira, D. A., Ortega, D. A., Varas, V., Godoy, J., & Asín-Achá, R. (2022). Improving the state-of-the-art in the Traveling Salesman Problem: An Anytime Automatic Algorithm Selection. *Expert Systems with Applications*, 187, 115948.
- [14] Boryczka, U., & Szwarz, K. (2019). An effective hybrid harmony search for the asymmetric travelling salesman problem. *Engineering Optimization*.
- [15] Grahadian, K., & Sandy, I. A. (2021). A New Metaheuristic Farmland Fertility Algorithm to Solve Asymmetric Travelling Salesman Problem. *International Journal of Engineering Technology and Natural Sciences*, 3(1), 9-15.
- [16] BAŞ, E., & ÜLKER, E. (2021). Discrete social spider algorithm for the travelling salesman problem. *Artificial Intelligence Review*, 54(2), 1063-1085.
- [17] Skinderowicz, R. (2022). Improving Ant Colony Optimization efficiency for solving large TSP instances. *Applied Soft Computing*, 120, 108653.
- [18] Eremeev, A., & Kovalenko, Y. (2021, July). Optimal recombination and adaptive restarts improve GA performance on the asymmetric TSP. In *Proceedings of the Genetic and Evolutionary Computation Conference Companion* (pp. 29-30).
- [19] Saravana, S., & Arulsevi, S. (2021, June). A Fuzzy-GA Based controlling System for Wireless sensor networks. In *I3CAC 2021: Proceedings of the First International Conference on Computing, Communication and Control System, I3CAC 2021, 7-8 June 2021, Bharath University, Chennai, India* (p. 189). European Alliance for Innovation.
- [20] Schroeders, U., Wilhelm, O. and Olaru, G. (2016) 'Meta-heuristics in short scale construction: ANT colony optimization and genetic algorithm', *PLoS One*, Vol. 11, No. 11, DOI:e0167110.
- [21] Mallawaarachchi, V., 2022. How to define a Fitness Function in a Genetic Algorithm?. [online] Medium. [Accessed 27 July 2022].
- [22] Kirk, J. (2021) 'Multiple traveling salesmen problem - genetic algorithm', *MATLAB Central File Exchange* [online] (accessed 30 May 2021).
- [23] Qi, A., Zhao, D., Yu, F., Heidari, A. A., Wu, Z., Cai, Z., ... & Chen, M. (2022). Directional mutation and crossover boosted ant colony optimization with application to COVID-19 X-ray image segmentation. *Computers in biology and medicine*, 148, 105810.
- [24] Almaalei, N. N. H., & Razali, S. N. A. M. (2019). Review of ACO algorithm on network and scheduling problem. *Compusoft*, 8(7), 3250-3260.
- [25] Yoo, K.S. and Han, S.Y. (2013) 'A modified ant colony optimization algorithm for dynamic topology optimization', *Computers and Structures*, Vol. 123, pp.68-78.
- [26] Almaalei, N. N., & Razali, S. N. A. M., Abdulwahab, A. N. M., and Alduais, M. (2018) 'An efficient algorithm to improve oil - gas pipelines path', *International Journal of Engineering and Technology*, Vol. 7, No. 4, pp.5412-5418.
- [27] Almaalei, N. N., & Razali, S. N. A. M. (2019). Performance Evaluation of Different Short Path Algorithms to Improve Oil-Gas Pipelines. *International Journal of Advanced Computer Science and Applications*, 10(11), (pp. 62-67).
- [28] D., 2022. PEJABAT DAERAH DAN TANAH MELAKA TENGAH : Profil Daerah. [online] PEJABAT DAERAH DAN TANAH MELAKA TENGAH : Profil Daerah. [Accessed 27 July 2022].
- [29] Loo, H.S., Chew, B.C. and Hamid S.R. (2018) 'Exploring the factors and strategies in implementation of sustainable land transport system in Ayer Keroh, Melaka', *Journal of Advanced Manufacturing Technology*, Vol. 12, No. 1, pp.159-174.
- [30] Google.com. 2022. Central Mekala District, Malacca [online] [Accessed 27 July 2022].
- [31] Alobaedy, M. M., Khalaf, A. A., & Muraina, I. D. (2017, May). Analysis of the number of ants in ant colony system algorithm. In *2017 5th International Conference on Information and Communication Technology (ICoICT)* (pp. 1-5). IEEE

An Approach for Optimization of Features using Gorilla Troop Optimizer for Classification of Melanoma

Anupama Damarla*, Dr Sumathi D

SCOPE, VIT-AP University, Vijayawada, Andhra Pradesh, India

Abstract—The diagnosis and categorization of skin cancer, as well as the difference in skin textures and injuries, is a tough undertaking. Manually detecting skin lesions from dermoscopy images seems to be a difficult and cumbersome challenge. Recent advancements in the internet of things (IoT) and artificial intelligence for clinical applications have shown significant increase in precision and processing time. A lot of attention is given to deep learning models because they are effective at identifying cancer cells. The diagnosis and accuracy levels can be greatly increased by categorizing benign and malignant dermoscopy images. This work suggests an automated classification system based on a deep convolutional neural network (DCNN) in order to precisely perform multi-classification. The DCNN's structure was thoughtfully created by arranging a number of layers that are in charge of uniquely extracting different features from skin lesions. In this paper, we proposed a deep learning approach to tackle the three main tasks-deep extraction of features (task1) using transfer learning, selection of features (task2)-using metaheuristic algorithms such as Particle Swarm Optimization (PSO), Ant Colony Optimization (ACO), and Gorilla Troop Optimization (GTO) as a feature selector, the extensive feature set is optimized, and the amount of features is reduced to within the range, and a two-level classification (task3) was proposed that are emerging in the field of skin lesion image processing. On the HAM10000 dataset, the proposed deep learning frameworks were assessed. The accuracy achieved on the dataset is 93.58 percent. The proposed method outperforms state-of-the-art (SOTA) techniques in terms of accuracy. The suggested technique is however highly scalable.

Keywords—Skin cancer; image enhancement; deep learning; evolutionary algorithms; Particle Swarm Optimization; Ant Colony Optimization; Gorilla Troop Optimization

I. INTRODUCTION

Epidermis cancer is an invasive disease produced by aberrant melanocyte cell development on the body that tends to reproduce and propagate through lymph nodes, destroying healthy tissue [1]. The ozone layer, that provides protection against UV rays [2] which is depleting causes an increase in skin cancer. On the skin's surface, damaged cells create a lesion that can either be benign or malignant. Melanoma is considered the deadliest form of skin cancer worldwide which emerged as a common disease with highest mortality [3]. Also, it is classified as cancer since it is more hazardous and life-threatening. Melanoma starts in the melanocyte cells, which seem to be brown or black in color and mimic a lesion [4]. Approximately 2500 females and 4700 males have

expired due to melanoma in 2019 [5]. Males have a higher likelihood of developing melanoma than females, according to statistics shown in Fig. 1 [6]. However, precise, reliable early detection is very important as discovered lesions have a 90.0 per cent survival rate [7].

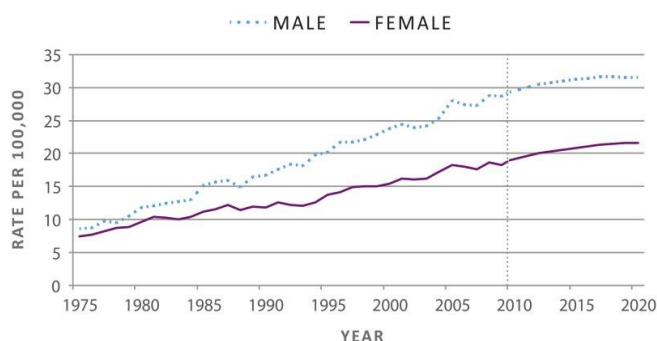


Fig. 1. Age- Adjusted Melanoma Incidence Rates from 1975-2020 [6].

II. RELATED WORK

Although the various table text styles are provided. The formatter will need to create these components, incorporating the applicable criteria that follow.

Skin cancer detection is challenging due to the diversity in skin textures and injuries. Dermatologists therefore employ dermoscopy, a non-invasive tool, to identify skin irregularities at an initial level [8]. The foremost move in dermoscopy was applying the gel for the diseased region. After that, a magnifying tool is used to obtain a magnified image. This magnified image allows you to see the structure of the lesion region more clearly. The dermatologist's experience determines the accuracy of the detection [9]. According to a survey, the detection precision of a dermatologist might range from 75 per cent to 84 per cent [10]. Contrarily, manual dermoscopy diagnosis requires a lot of time and has a significant chance of error, including for dermatology with experience [11]. As a result, studies developed a number of computer-aided diagnostic (CAD) systems using deep CNN features [12].

The acquisition of a three primary stages of a CAD system is a skin imaging dataset, feature extraction and selection, and classification [13]. Data on skin cancer are unreliable and conventional methods are parameterized and require standard normal training data. Each lesion has a unique pattern and therefore these treatments are ineffective. Dermatologists can

*Corresponding Author.

accurately identify malignancies with the help of deep learning methods for classifying skin. In comparison to classic feature extraction strategies, the use of epidermis lesion with deep features identification and classification has become increasingly important in recent years [14]. Deep characteristics, which were used to categorize data, are generated from the completely connected layers of a CNN model. Unlike traditional methods like hue, texture and contour, deep features encompass both local and global information about a picture. The convolutional layer extracts local information such as edge, pixel which differs immediately with adjacent pixels of an image; whereas the 1D layers (global average pooling and fully connected) gather global information such as shape descriptors, contour representations [15]. In traditional techniques, geometric information such as Histogram of Gradients, color and textures (Local Binary Patterns) are extracted independently [16].

Even though deep learning algorithms are extremely adept at processing complicated data, skin categorization remains a difficult task for several reasons:

1) As demonstrated in Fig. 2, the distribution of skin lesion classes in the current dataset is unbalanced, with more than 60% of the photos belonging to the NV: "Melanocytic nevus" class and some classes being extremely rare (less than 2%). The lesion images are classified into seven categories as shown in Table I, with number of lesions.

2) Hairlines, water bubbles, ruler marks, etc. are all examples of noisy artefacts in lesions shown in Fig. 3.

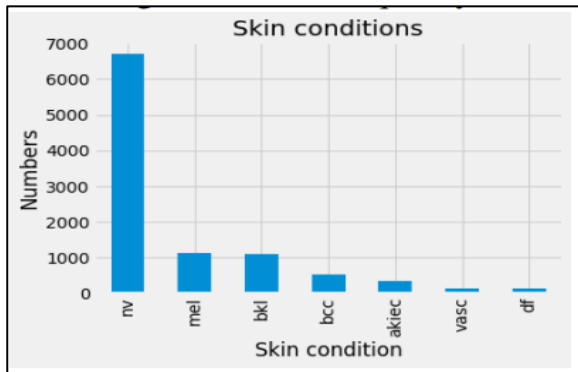


Fig. 2. Class Imbalance [52].

TABLE I. SKIN LESIONS AND INSTANCES COUNT IN HAM10K DATASET [38]

Skin Type	Instances Count
Actinic Keratosis (Akc)	326
Basal Cell Carcinoma (Bcc)	514
Dermatofibroma (Df)	116
Melanoma (Ml)	1114
Nevus (Nv)	6704
Pigmented Benign Keratosis (Bkl)	1098
Vascular Lesions (Vsc)	143
Total	10015

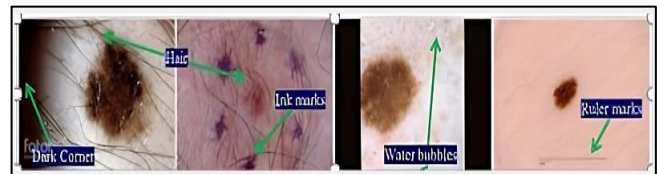


Fig. 3. A Typical Pictorial Presentation of the Skin Images in ISIC 2017 Test Dataset [17].

3) Lacerations are hard to differentiate due to significant intra class variances and inter class commonalities in terms on color, size, site and appearance.

Furthermore, there have been a few obstacles in the development of classification systems and they are provided as given below:

- Initially, there is a discrepancy in the data and there aren't many images with labels.
- Lesser complicated & lighter network designs.
- When techniques are used to categorize skin cancers that are uncommon in the training sample, a misdiagnosis is frequently the outcome.
- Millions of pixel high-resolution images frequently require extensive computing and extra training.
- The different circumstances will cause different noises to be produced (such as different imaging devices, backgrounds).

While prominent pre-trained deep learning networks are trained on diverse datasets, such as ImageNet, they are not used for skin cancer concerns in general [53]. A method for picking the best subset of features based on shape and color to build better and final categorization is required. As a result, the proposed approach shown in Fig. 4 intends to create, implements, and estimate a highly efficient deep learning-based system for malignant vs. benign categorization.

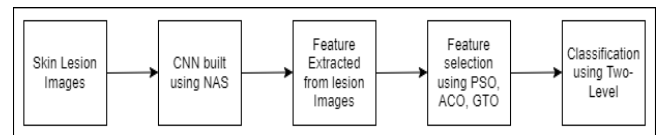


Fig. 4. Flow Structure of Whole Network.

The following is a breakdown of the remaining sections: Section II discusses the research on Neural Architecture Search and optimizers. A public dataset is used in proposed work for skin cancer detection is presented in Section III. In Section IV, a proposed method that explains the CNN, feature selection with three optimization approaches for efficiency with classification in detailed is explained. The results and discussions implemented on the dataset as well as outcomes analysis with other optimizers are seen in Section V, and finally, in Section VI, conclusions are formed.

III. LITERATURE SURVEY

Several methodologies and procedures have been developed for categorization of skin lesions [8]. Zafar et al [18] proposed two pre-trained CNNs U-Net and ResNet called

Res-UNet for segmenting lesion boundaries and significantly improve the classification accuracy. Computer vision-based machine learning approaches were used in the developed methodologies. Machine-learning algorithms made use of supervised learning and deep learning techniques for the accurate identification, segmentation, and classification of epidermis tumors [19]. Aziz et al. [20] used deep features from a pre-trained AlexNet network, which were then classified using SVM. Their method yielded good results in terms of lesion categorization. Ren et al. [21] presented a fusion mechanism [22]. J. Zhang et al. [23] suggested a CNN for epidermis categorization that consisted of several attentions residual learning (ARL) units succeeded by global average pooling and classification layers. Yu et al. [24] developed a CNN-based design that was pre-trained on several picture resolutions. It developed a fully convolutional residual network (CRN) for segmentation and deep residual network (DRN) for classification. Majtner et al. [25] used a used local binary pattern features and hand-crafted Rsurf features for melanoma recognition system. Ahonen et al [26] uses LBP texture features for efficient facial recognition. A new method to analyze the data which were then segmented zone wise and classified using a Support Vector Machine (SVM) [27] algorithm is proposed. On the HAM10000 dataset, Sivasai et al. [32] proposed a DCNN for lesion classification based on MobileNetV2 and Long Short-Term Memory (LSTM). MobileNetV2 outperformed existing CNN models in several ways, which include reduced computational cost, tinier network size, and interoperability with smart devices. Wannipa et al [43] presented a light weight deep CNN called MobileNet for classification of skin lesions. Ahmed et al [44] presented an ensemble CNN model that combines ResNet 50 and InceptionV3 architectures to classify the seven different skin lesion types. The below Table II provides the comparative analysis.

Prior to the attention in deep learning, research on neural architecture search had been undertaken. Three factors characterize each NAS framework: search space, search strategy and performance evaluation technique [28]. NAS was created to find and develop the model that perfectly suits the dataset in use. As a result, the NAS model has a minimal set of parameters but good performance. Models suited for both small and large datasets can be found using NAS [30]. The Global search space and the Cell search space are two types of search spaces. The network-based technique investigates the entire system, whereas the cell-based approach identifies only the cells, which were subsequently stacked to address a task [29]. The count of cells in the stack is determined by the work at hand. Melanoma detection and classification using dermoscopic images, researchers used a deep learning [31] approach. Deep feature extraction was done with a deep residual network, and image encoding was done. To detect and categorize melanoma using discriminating dermoscopy images, SVM classification with chi-square was used. On the difficult ISBI 2016 dataset, the provided technique performed admirably.

Feature selection (FS) is gaining popularity which is a technique for minimizing the dimensionality of data. It reduces data intricacy by deleting superfluous contents that is

critical. This method minimizes the model's complex nature by including only the most relevant features, making it easier to interpret. By filtering out redundant data, FS approaches reduce the dimensionality of network data. As a consequence, FS is a crucial component of data preparation in medical analysis since it impacts accuracy results. Any feature selection problem could be roughly described as an optimization problem. Several Feature selection methods elicited from metaheuristics (MH) methodologies were recently been implemented. Numerous search techniques mainly inspired by nature and mimicking principles of biology, physics, ethology, or swarm intelligence, have been effectively included in metaheuristic algorithms [34]. Those were split into two categories: standard solution-based approaches and population-based approaches. Population-based algorithms have better ability than single solution-based algorithms [35]. The population-based algorithms are categorized into multiple categories: (1) Particle Swarm Intelligence algorithms (SIs), (2) Evolutionary Algorithms (EAs), (3) Natural Phenomenon algorithms (NP). Grasshopper Optimization Algorithm (GOA), Whale Optimization Algorithm (WOA), Elephant Herding Optimization (EHO), Harris Hawks Optimization (HHO), and Moth-flame Optimization (MFO) are some well-known metaheuristic algorithms [36]. The study indicates that population-based algorithms are well suited to solving real-world problems, despite the need for more objective functions [37].

TABLE II. SUMMARY OF LITERATURE REVIEW

Paper ID	Dataset	Model	Accu %	Limitations
[18]	ISIC 2017, PH2	Res-UNet	77.2, 85.4	Need augmentation to prevent overfitting
[19]	ISIC 2017, ISIC 2016	ResNet50, ResNet101	80.6, 91.8, 89.1, 86.8	Dilated convolution, Group Normalization
[20]	-	AlexNet, ResNet18	93.3, 93.8	-
[21]	ISIC 2017	DenseApp	76.9	Model is complex
[22]	ISIC 2017, PH2	MB-DCNN	80.4, 89.4	Improve task Performance simultaneously
[23]	ISIC 2017	ARL-CNN50, ResNet50	91.8, 90.5	Unsupervised Attention learning
[24]	ISBI 2016	FCRN	85.5	Prob graphical models
[25]	-	Rsurf, LBP	80.2	-
[32]	HAM10K	MobileNetV2, LSTM	85	Feature extraction based on biomarkers
[43]	HAM10K	MobileNet	-	-
[44]	-	ResNet-IncepV3	89.9	-

TABLE III. DATASET, METHODS, ACCURACIES AND CLASSES FOR SKIN CANCER

Author	Model	Accuracy %	Classes
Achim et al(2019)	CNN with XGBoost	82.95	5
Pratik et al(2019)	CNN	82	7
Duyen et al(2020)	ResNet50	93	7
Deif et al(2020)	InceptionV3	89.81	2
Shahin et al(2021)	DCNN	91.93	2
Hatice et al(2022)	Insinet	94	2
Mahbubur et al(2022)	DiffusionFiltering	91.65	2

The procedures outlined above follow certain automated lesion classification techniques. The Deep learning models have higher feature extraction accuracy than pre-trained models, and then applying nature-inspired metaheuristic algorithms as a new feature selection model, a latest method for binary-to-multi classification based on deep learning are the top-performing steps. The aim of maximization of accuracy degree of any subset is shown in Table III. The large number of features produces biased findings since data patterns of training set are not uniquely identifiable in testing data. The drawbacks of metaheuristic techniques get struck with the local optima rather than the global optima.

A. Research Gap

Earlier works have been focused on various features such as shape, texture and color either by fusion or through many other techniques. Hence, the focus of this work is on performing the detection of asymmetric borders along with contrast enhancement. Therefore, this motivated us to do this work.

B. Motivation

- The deep neural network has witnessed growth to the next generation by introducing the concept of optimized network. This idea was materialized through the concept of NasNet.
- The predominant factor is to determine a model that would be robust and intractable to seize the global solutions in this complex problem.
- Color channeling embedded with dimension has been given more attention.
- Combining these techniques will achieve high performance.

The solution strategy that does not meet the same efficiency to solve all the problems motivated to propose this method.

IV. METHODOLOGY

The proposed method for skin cancer detection, which is provided in this part, used deep learning and nature inspired algorithms as a feature selection models that aims to improve the performance and the efficiency on selected features. Fig. 5 depicts the architecture of the suggested technique. This method has five main layers: Image acquiring and preprocessing; Extraction of features using NasNet Large;

optimizing the features using PSO, ACO, and GTO; finally, a Two-level classification.

C. Dataset

The dermoscopic method has improved the accuracy of skin cancer diagnosis. With the help of this invasive skin imaging technique, skin lesions can be captured and the clarity of the spots is improved. In this section, the most used dataset named HAM10000 Dataset is utilized to carry out the experimental process, in this area of research. It was investigated in the HAM10000 dataset that samples belonging to minor classes can be detected by popular CNN models.

HAM10000 Dataset: The HAM10k "Human Against Machine with 10,000 Training Images" collection is most famous publicly accessible dataset, containing 10k raw dermoscopic images primarily utilized to detect pigmented epidermis Laceration. Fig. 6 depicts several types of skin cancer. Due to the low inter-class and significant intra-class variance difficulties as shown in Fig. 7 the classification of these skin types is difficult.

The dataset was split into three sections: training, validation, and test. The training set received 70 per cent of the total samples, the validation set received 10 per cent, and the test set received the remaining 20 per cent as shown in Table IV. To provide the network enough training, the percentage of samples within the train set was maintained at a higher level. The network's performance was tracked using validation data to fine-tune the settings. Finally, the network's performance was assessed using the test data.

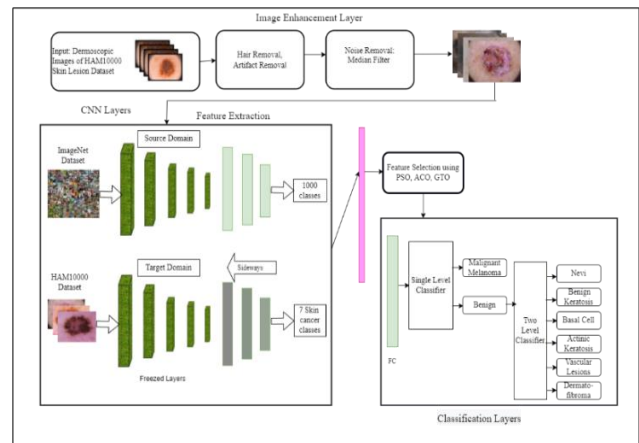


Fig. 5. Skin Lesion Classification using Two-Level Classifiers.

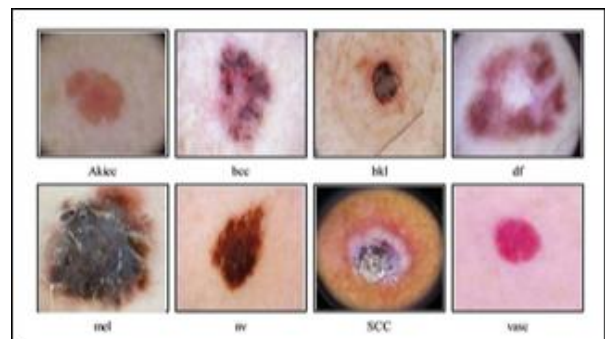


Fig. 6. Sample Skin Lesion types of HAM10000 Dataset [33].

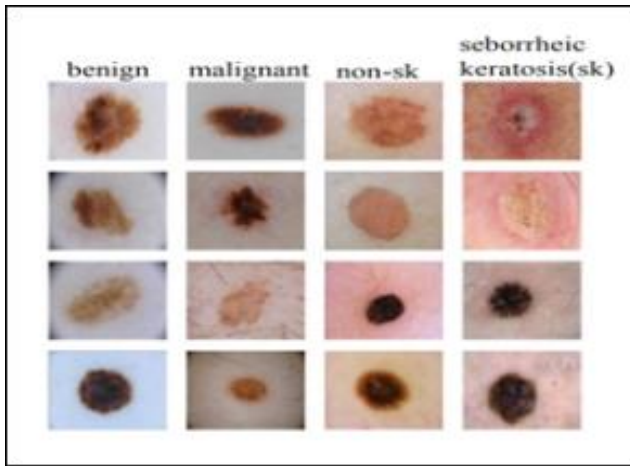


Fig. 7. Skin Lesion Images with Low Inter-class and Significant Large Intra-class Variance [54].

TABLE IV. THE HAM10000 DATASET PROPORTIONS AMONG TRAIN, VALIDATION, AND TEST [39]

Category	Train Samples	Validation Samples	Test Samples	Total Samples
Malignant	3181	454	909	4544
Benign	3830	547	1094	5471
Total	7011	1001	2003	10015

D. Image Enhancement

During the acquisition, coding, transmission, and processing of digital images, noise is constantly present. Noise in an image is defined as an abrupt change in pixel values. Removing noise from digital images is exceedingly difficult without prior knowledge of filtering processes. Image data filtering is a standard step in almost all image processing systems. Filters are used to accomplish this. They reduce noise from the image while retaining their characteristics. The type of data and the filter's behavior determine which filters are used. Various preprocessing filtering techniques, such as mean, median, wiener, and nonlocal means filters, are used to enhance the acquired images.

The initial step in any type of medical image processing is to perform enhancement that aims to improve the quality of the original images and make the subsequent stages of operations easier. Reflections, hair follicles, epidermis lines, air bubbles, and shadows are all common artefacts in skin photographs that affect the image segmentation stage. Intensity correction, color space transformation, artefact removal, and contrast adjustment are some of the approaches that have been introduced for image enhancement. The median filter shown in (1) is a simple way to improve the quality of photographs by eliminating artefacts.

$$y[m, n] = \text{median}(x[i, j], (i, j) \in w) \quad (1)$$

where w describes the weight of neighbors and $[m, n]$ is the median point in the image.

Median filtering is a nonlinear method for image smoothing as shown in Fig. 9. This filter can be used to

smooth skin lesion photos and remove artefacts while maintaining the lesion boundaries. The median filter mask size should really be proportional to the main image to achieve operative smoothing. The pattern of neighbors is used as the 2D window which slides pixel by pixel over the image. They extend border values outside with values at boundary. The median of all image pixels within the window will be used to replace the central pixel. The filter's principal operation is arranging all the pixel values from the window into ascending order and replacing the considered pixel with the middle pixel value. (If the neighborhood has an even pixel count, the average of two middle pixel values is used.) The pseudocode is given below:

```

for (p1=0; p1<n; p1++)
    for (p2=0; p2<n; p2++)
        if(I[p1] < I[p2])
            {
                w=I[p1]
                I[p1] = I[p2]
                I[p2] = w
            }
    
```

Moreover, the filter that has been adopted in this work may be used to smooth pictures, softening large frequency distortions like as noise, additional lines, and hair while preserving crucial information like type, texture, configuration, color and location about the lesions. In contrast to linear filters, which maintains the original image with no edge blurring? Fig. 9 depicts the results.

E. NasNet Large Features Extraction

With the help of the challenging image database ImageNet [37], a deep Neural Architecture Search (NAS) [36] model has been implemented on more than a millions of images. The NasNet Large requires images with an input size of 150 by 150. The Recurrent Neural Network (RNN) in NAS generates a child network with a distinct structure. The holdout method is used to train the child networks to ensure accurateness. To improve the network's architecture, the controller is updated by combining the accuracy of the child connections. Fig 8 depicts the controller structure. The controller delivers hyper parameters as tokens for forecasting feed-forward neural networks with convolutional layers. When the layer exceeds a certain value i.e. 6 normal cells, the architecture generation process is paused. Each prediction is made by a Softmax classifier, and the outcome is fed into the next phase. During the models fine-tuning procedure, it initially discards the models the last three layers and adds a new layer depending on the count of dataset classes. Transfer learning is applied to refine the model after the fine-tuning phase. Several key parameters were selected during the training process, such as the learning rate of 0.001, epochs of 20, minimum batch size of 64, and SGD for learning. Following the fine-tuning of a network on epidermis datasets, features from the average pool layer were collected and used for subsequent process, including feature selection.

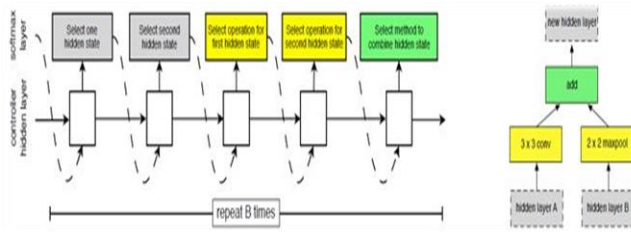


Fig. 8. Controller Architecture Model [45].

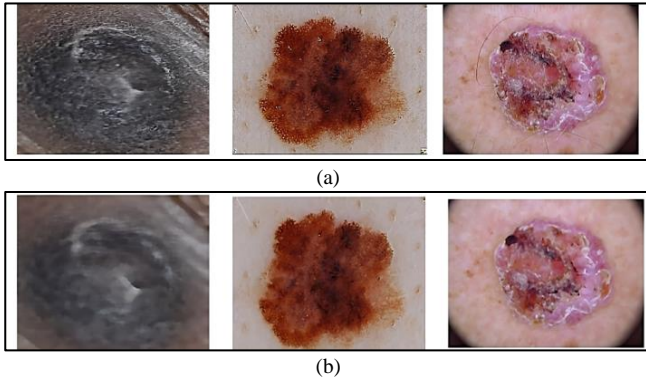


Fig. 9. (a) Original Dermoscopic Images, (b) Images after Pre-processing.

F. Feature Extraction using Color Space

As it is known that melanoma is typically brown, black, or tan in color, although it can also be red or pink as shown in Fig. 10. The feature extraction method focuses on obtaining information from color space. It is normalized from RGB color space using RGB_r where Red_r , $Green_r$, and $Blue_r$ are normalized color channels translated from RGB color space. The value of intensities in each pixel is represented by i and j and the dimension of skin images is stated with $M \times N$. There are now three color channels as shown in (2,3,4):

$$Red_r = Red_r(i, j) \quad (2)$$

$$Green_r = Red_r(i, j) - Green_r(i, j) \quad (3)$$

$$Blue_r = Red_r(i, j) - Blue_r(i, j) \quad (4)$$



Fig. 10. Appearance and Location of Melanoma.

G. Metaheuristic Approaches for Feature Selection

Certain metaheuristic approaches are nature-inspired and are commonly utilized in machine learning for selecting features or optimization. Numerous metaheuristic algorithms are not biologically inspired. Fong et al. [46] selected features from five datasets from the UCI repository using the

Correlation based FS, PSO and Accelerated PSO techniques. When compared to all features, Decision Tree, Naive-Bayes, SVM, and ANN classifiers have a 12.7 per cent, 1.93 per cent, 2.11 per cent, and 0.3 per cent difference in classification accuracy when just 64 per cent, 26 per cent, 26 per cent, and 64 per cent of the entire features are used. Seijas et al [47] classified the MNIST handwriting dataset with SVM Classifier using 3 metaheuristic approaches: Binary Fish School Search (BFSS), Advanced Binary Ant Colony Optimization, and Binary Particle Swarm Optimization. BFSS, ABACO, and BPSO achieve 93.36 per cent, 90.15 per cent, and 92.08 per cent classification accuracy using just 41 per cent, 22.4 per cent, and 27 per cent of the overall characteristics, respectively. Yeh and Chan [48] retrieved 277 characteristics from the MIAS database using 70 benign, 55 malignant, and 69 normal mammograms. For feature selection, they used the Genetic Algorithm (GA), ACO, SA and PSO. PSO discovered a classification accuracy of 96.9 per cent using only 189 features. Naeini et al. [49] worked on two datasets of high-resolution satellite images captured by the WorldView-2 sensors. From satellite images, a total of 173 characteristics are extracted. Particle Swarm Optimization (PSO), Genetic Algorithm (GA), Artificial-Bee-Colony (ABC), and Honey-Bee-Mating (HBM) algorithms pick Object Based Features (OBF). Their research has revealed that PSO is an inexpensive method for recognizing various entities such as trees, buildings, and roadways. Ighazran et al [50] evaluated sentiment analysis using a metaheuristic feature selection. In certain studies, multiple metaheuristic algorithms are coupled to create an advanced hybrid approach that may operate significantly better in feature selection. Arora et al [51] combined the Grey-Wolf and Crow search algorithms to create an approach. They used a total of more than 20 standard benchmark unimodal, multimodal, and fixed-dimensional multimodal mathematical functions and 21 datasets to evaluate the results of the novel hybrid approach with ten popular MH techniques for selecting of features.

1) *Contributions on this work:* The selection of the optimal features is a critical step that improves classification accuracy rate while decreasing computing time. Three metaheuristic algorithms, Particle Swarm Optimization (PSO), Ant Colony Optimization (ACO), and Gorilla Troop Optimizer (GTO), are employed in this work to determine an optimum collection of features. GTO chooses an optimum feature set from among these methods to deliver the best classification accuracy of 93.58 per cent. It was discovered that color features are best for classifying skin lesions stated from section 3.4. Higher accuracy is attained in this work using less than 0.4 per cent of all the characteristics selected by the aforementioned optimizations.

H. Metaheuristic Algorithms

The "curse of dimensionality" refers to the challenge of using a larger collection of features, which can create noise and impede system performance. Reasons for selecting a more limited set of features quicker training, reduced difficulty of the model, and improved model precision, among other criteria like computation time, storage, etc. There are several feature selection techniques like feature ranking, feature

transformation, feature subset selection but the proposed study performs feature optimization and for this, three metaheuristic methods are used in this suggested study. These algorithms are all from the nature-inspired category. PSO, ACO and GTO are all population-based algorithms inspired by nature. To select the best technique, we used metaheuristic techniques from several types of algorithms.

1) *Particle Swarm Optimization (PSO)*: PSO emerges for an optimal outcome iteratively by conducting simultaneous searches on a population of solution candidates known as "particles" whose current particle in the search space reflects a candidate's solution [57]. PSO iteratively seeks the best outcome by travelling every particle in a manner that is a summation of the feature vector together across their individual instantaneous velocity, local best position location, and global best position location. Each particle has a social learning rate as well as an individual best-position learning rate. Every iteration, starting with a random value, the location of each particle is altered. The position of each particle is determined with the own individual best position (PBes) (as determined from the fitness function) as well as the best position of all particles in the population (GBes). Using these data, (5) and (6) are used to modify the particle's position (P) and velocity (V):

$$P(t_i + 1) = -P(t_i) + V(t_i + 1) \quad (5)$$

where

$$V(t_i + 1) = V(t_i) + a_{i1} \cdot ra_{i1} \cdot (PBes(t_i) - P(t_i)) + a_{i2} \cdot ra_{i2} \cdot (GBes(t_i) - P(t_i)) \quad (6)$$

The random number's values ra_{i1} and ra_{i2} ranges between 0 & 1 and a_{i1} , a_{i2} are the learning rates displayed in tabular column 2. The particle's inertia value determines how much of its previous velocity is added to its current velocity. The initial inertia of the particle is its initial inertia. The change in inertia is provided by the inertia damping rate. PSO can be utilized to choose n_s features out of a maximum of n_T features. Once particles are allowed to move in n_T -dimensional space, the features corresponding to the n_s lowest components of the instantaneous position can be recognized as extracted features. It should be emphasized that the search space's axes correspond to the features, and that the selection of an axis is determined by the readings of the position vector along that axis.

2) *Ant Colony Optimization (ACO)*: To determine the shortest path from their location to the food supply and the vice versa, ants search using a metaheuristic algorithm called ACO [55] [56]. An ant will leave a trail of a specific chemical pheromone on its way of travel when it leaves its nest in search of food. The strength of the pheromone trail left by an ant's predecessor can also be determined. The term "stigmergy" refers to an indirect communication technique that chooses the quickest route from the nest location to the food location. Each way has a starting pheromone deposit level and pheromone evaporation rate. ACO can be employed to choose a series of vertices from a plot where the contours

are adaptively balanced by a property called pheromone strength. This property makes sure that an edge that is traversed more often is given more weight. A sequence is produced by the ant's movement. An ant i will select node j at a node with a probability proportional to the strength of the pheromone along the path $i-j$ as shown in (7):

$$p_{ij} = \frac{\tau_{ij}^\alpha}{\sum_j \tau_{ij}^\alpha} \quad (7)$$

where, T_{ij} = pheromone level of a contour i, j and α is a constant known as ant pheromone exponential weight. The pheromone updates with (8)

$$T_{ij} = (1 - \rho) T_{ij} + \Delta T_{ij} \quad (8)$$

where, ρ = evaporation rate & ΔT_{ij} = deposition in the edge is illustrated in (9):

$$\Delta T_{ij} = \sum_k \frac{1}{L_k} \quad (9)$$

Here L_k signifies the value of the k th path that moves along the edges i, j . From a total of n_T features, n_s features are chosen using ACO. Also every features can be thought of as a node in a plot, with initial n_s nodes of the ACO series identifying the selected feature. The final set of features chosen is the one with the lowest cost (error of classification) shown in Fig. 12.

3) *Gorilla Troop Optimizer (GTO)*: The GTO is simple to operate and has a limited number of parameters that must be configured. There are three phases for exploration and two for exploitation. Compared to cutting-edge algorithms, GTO's key benefit is that it quickly discovers the best answer. Gorillas are symbolized as X in this algorithm, while silverbacks were being symbolized as GX.

a) *Exploration Phase*: The exploration stage is primarily used to conduct a global search of space. In GTO [41], every member can be a solution, and at each step of the optimization process, the best solution can be named the silverback gorilla. The following strategies were employed:

- 1) Transitioning to an anonymized region which searches the entire sample space.
- 2) Reducing the search area in order to strike a balance among both exploitation and exploration.
- 3) Ultimately, growing the GTO's capability to examine the region by moving forward towards a known region.

It is numerically expressed in (10,11,12,13,14,15) as:

$$GX(t_i+1)_i = \begin{cases} (tp - bp) \times r_1 + bp, r < p, \\ (r_2 - C) \times X_r(t) + L_g \times H, r \geq 0.5, \\ X(t) - L_g \times (L_g \times (X(t) - GX_r(t)) + r_3 \times (X(t) - GX_r(t))), r < 0.5. \end{cases} \quad (10)$$

$$C = F_i \times \left(1 - \frac{t}{Max_t}\right) \quad (11)$$

$$F_i = \cos(2 \times r_4) + 1 \quad (12)$$

$$L_g = C \times 1 \quad (13)$$

$$H = Z_g \times X(t) \quad (14)$$

$$Z_g = [-C, C] \quad (15)$$

where tp = top position

bp =bottom position of the variable,

$X(t)$ = present position of gorilla

GX_r = Single gorilla group of a particular region

$GX(t_i + 1)$ = the candidate level of gorilla in the t+1 iteration.

p = Migration parameters oscillates [0,1]

$r_1, r_2, r_3, r_4, rand, l$ = random values ranging from [0,1]

X_r = Single candidate gorilla

t_i = Current Iteration

Max_t = Total number of Iterations

L_g = used to calculate silverback gorilla

Z_g = Random number ranging from [-C, C]

The fitness value of each GX solution was determined by the algorithm in the conclusion from the exploration phase, and if $GX(t_i) < X(t)$, the $X(t)$ solution is swapped out for the $GX(t_i)$ solution.

b) *Exploitation Phase*: Two approaches are employed at this point. First is Continue to track the silverback and second is compete for adult female gorillas. The approaches are chosen based on a comparison between C ((11)) and W . (initial values).

Stage 1: If $C \geq W$, the silverback gorilla will choose the below (16,17) for survival.

$$GX(t_i + 1) = L_g \times M \times (X(t) - X_{silverback}) + X(t) \quad (16)$$

$$M = \left(\left| \left(\frac{1}{N} \right) \sum_{i=1}^N GX_i(t) \right|^g \right)^{(1/g)}, \quad g = 2^l, \quad (17)$$

where, $X(t)$ = gorilla position

$X_{silverback}$ = Silverback gorilla position

$GX(t_i)$ = Candidate solution at iteration t

N = Number of gorillas

Stage 2: If $C < W$, compute the (18, 19, 20, 21) i.e., competing for female mating.

$$GX(t_i) = X_{silverback} - (X_{silverback} \times Q - X(t) \times Q) \times A \quad (18)$$

$$\text{Where, } Q = 2 \times r_5 - 1 \quad (19)$$

$$A = \beta \times E, \quad (20)$$

$$E = \{N_1 rand \geq 0.5 \quad N_2 frand < 0.5\} \quad (21)$$

r_5 = random value [0,1]

The amount of variables generated by the GTO algorithm equals the amount of features in the dataset. All variables have a range of [0, 1] with 1 representing that the applicable

attribute is a classification selection candidate. The algorithm then computes every gorilla's fitness as shown in (22).

$$Fitness_i = \alpha \times (1 - C_i) + (1 - \alpha) \times \frac{|BX_i|}{D} \quad (22)$$

$$BX_{ij} = 1 \text{ if } X_{ij} > 0.50$$

where X_{ij} is the dimension value for search agent i at dimension j and α falls within the [0,1] range, and C_i stands for the measured accuracy. D is the dimension of the input train dataset. The finest solution will be the one with the lowest fitness value. Following that, the agents will be modified utilizing the GTO algorithm stages. The updating stage was repeated until the terminal state was reached. Finally, the GTO method produces the optimal solution that includes the feature set, which is then utilized as the following step in reducing the testing dataset by deleting non-relevant characteristics. The objective value of GX is assessed at the conclusion of the exploitation stage, and if it is less than $X(t)$, $GX(t_i)$ replaces $X(t)$ as the best solution (silverback). The accuracy is shown in Fig. 10. The resultant features are finally classified using a two-level classifier.

The parameters for these approaches are the same as those described in Table V.

TABLE V. DIFFERENT METAHEURISTIC ALGORITHM PARAMETERS

Algorithms	Parameters Settings	Values
General Settings	Population Size(N) Max num of Iterations (M) Considered Strategy	20 50(Max) Features
PSO	Acceleration Coefficients (C_1) (C_2) Inertia Weight (W) Num of Iterations	[0.5:2.5] [0.5:2.5] [0.2:0.9] 30
GTO	Beta(β) w p	3 0.8 0.03
ACO	Starting Ant Pheromone Pheromone-exponential-wt Ant Pheromone evaporation Num of Iterations Population Size(number of Ant)	1 1 0.05 30 5

I. Two-Level Classification

For more accurate results, the final characteristics are classified using two-level classification. Given an image $I = \{I_i\}_{i=1}^N$, where $I_i \in [0, 255]^3$ corresponds to one of the seven types of lesion types, the deep neural model performs a series of operations to determine the type of an image $I \in \{1, \dots, 7\}$. A function can be used to express these operations as shown in (23).

$$F(I, W_m) = \underset{M}{\operatorname{argmax}} y_M \quad (23)$$

where W_m is the specifications of the train neural model & y_m are the type probabilities generated by the model.

The presence of unbalanced classes in the dataset is one of the issues that arise during the training stage of any classification model. To assess and handle these scenarios, duo distinct prediction approaches for the deep learning models are proposed:

1) *Single level classifier*: Transfer learning is used to tune the weights of a neural model. This method assigns the input image to one of the two categories. In this case, the impact of unbalanced classes can be significant, necessitating the use of a preprocessing stage to optimize performance. The single level classifier's operation is as follows in (24):

$$F^P(I, W^P) = \operatorname{argmax} y_M, M \in \{1,2\} \quad (24)$$

where W^P indicates the specifications of the refined network for the two categories of epidermis lesions.

2) *Two-level classifier*: Two neural models are combined in this technique to create a two-level classifier. While the second level categorizes the other multiple classes, the first level has been trained to differentiate between the malignant melanoma class and the others. as shown in (25,26):

$$F_{c_1}(I, W_{c_1}) = \operatorname{argmax} \{y, y'\} \quad (25)$$

$$F_{c_2}(I, W_{c_2}) = \operatorname{argmax} y_M, M \in \{2, \dots, 7\} \quad (26)$$

where the refined model for two and six subclasses, respectively, is represented by W_{c_1} . The initial neuron model is transformed into a specialized model that serves as a classification model for the malignant melanoma class, which includes the binary classification on the dataset's images. Only if $F_{c_1}(I, W_{c_1})$ fails to produce the melanoma class is the second classifier used.

V. RESULTS AND DISCUSSIONS

This section compares the proposed optimization method to other metaheuristic feature selection algorithms in order to assess its effectiveness in identifying the best subset of features, such as the original PSO from Fig. 11, ACO from Fig. 12 and GTO shown from Fig. 13. All of these techniques are used on the HAM10000 dataset.

A. Experiments Configuration

It is described how the experiments were set up for this study in Table VI:

TABLE VI. CONFIGURATION DETAILS

Configurations	Specification
Input Image Size	(150x150x3)
MHFS Optimizers	PSO, ACO, GTO
Dataset Split ratio	70-10-20(Tr-V-Ts)
Population Size	30
Epochs Count	50(Max)
Activation Function	Softmax
Pretrained Model	ResNet, Inception, VGG16
Losses Range	Categorical Crossentropy
Parameters optimizer Range	RMSprop, Adam, SGD
Dropout Count	[0:0.6]
Batch Size Range	[4:30]
Technologies	Tensorflow, Keras, Numpy, OpenCV, Matplotlib
Scripting Language	Python
Work Environment	Google Colab with GPU

B. Performance Evaluation

The performance of proposed model was analyzed with the standard classification measures: Accuracy, Precision, Recall (28) and F-measure. It is well known that recall equals the ratio of relevant instances retrieved over the total number of relevant examples, precision equals the proportion of relevant instances among the retrieved instances, and accuracy equals the proportion of genuine detentions from (27, 29). By considering both precision and recall, the F-measure from (30) offers a good overall evaluation of the effectiveness of a particular approach. All metrics are ranked from [0 to 1], with 1 being the best. Below Table VII shows original deep features, Table VIII describes features from PSO, Table IX describes features from ACO, and Table X describes features from GTO extracted from metaheuristic algorithms.

Each metric is formulated as follows:

$$\text{Accuracy} = \frac{TP+TN}{TP+FP+FN+TN} \quad (27)$$

$$\text{Recall (Sensitivity)} = \frac{TP}{TP+FN} \quad (28)$$

$$\text{Precision} = \frac{TP}{TP+FP} \quad (29)$$

$$\text{F-Measure} = 2 \cdot \frac{\text{Precision} \cdot \text{Recall}}{\text{Precision} + \text{Recall}} \quad (30)$$

This work yielded the following results for the suggested framework:

TABLE VII. CLASSIFICATION ACCURACY USING ORIGINALLY EXTRACTED FEATURES FOR HAM10000

Classifier	Accuracy	Recall	Precision	F-Measure
Single-Level	0.85	0.82	0.86	0.84
Two-Level	0.83	0.81	0.89	0.85

The result analysis using various metaheuristic techniques is depicted below.

TABLE VIII. CLASSIFICATION ACCURACY BASED ON PSO SELECTED FEATURES APPROACH

Classifier	Accuracy	Recall	Precision	F-Measure
Single-Level	0.85	0.83	0.87	0.8
Two-Level	0.93	0.85	0.89	0.87

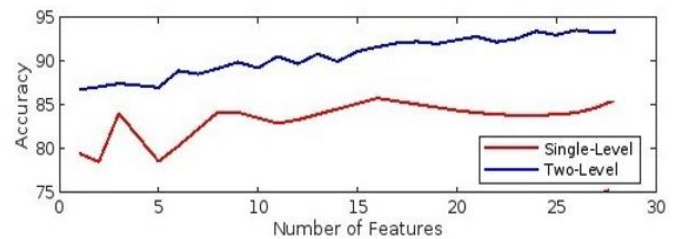


Fig. 11. PSO Selected Features vs. Accuracy.

TABLE IX. CLASSIFICATION ACCURACY BASED ON ACO SELECTED FEATURES APPROACH

Classifier	Accuracy	Recall	Precision	F-Measure
Single-Level	0.76	0.74	0.80	0.77
Two-Level	0.84	0.80	0.90	0.84

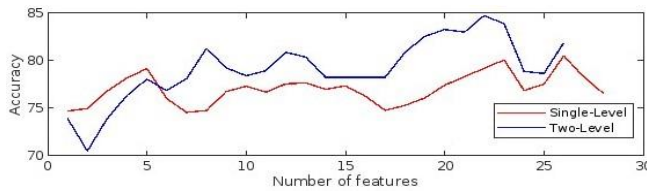


Fig. 12. ACO Selected Features vs. Accuracy.

TABLE X. CLASSIFICATION ACCURACY BASED ON GTO SELECTED FEATURES APPROACH

Classifier	Accuracy	Recall	Precision	F-Measure
Single-Level	0.89	0.84	0.90	0.87
Two-Level	0.93	0.83	0.89	0.86

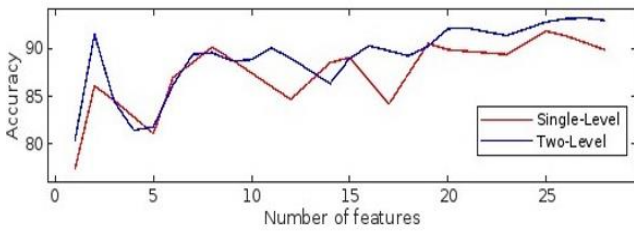


Fig. 13. GTO Selected Features vs. Accuracy.

1) *Result comparison:* The comparative assessment among various similar works using the HAM10000 dataset is shown in Table XI and Fig. 14. In comparison to other related works, the proposed work performs significantly better in terms of classification accuracy with the fewest features.

TABLE XI. COMPARISON ANALYSIS WITH OTHER STATE-OF-ART METHODS USING HAM10000 DATASET

Paper Id	Methodology	Accuracy %
[38]	PCA	89.8
[39]	Bayesian deep learning	83.59
[40]	Transfer learning	85.0
[41]	CNN	80.0
[42]	Application based CNN	78.0
[43]	MobileNet	83.2
[44]	ResNet50+InceptionV3	89.9
Proposed Work	NasNet Large	93.58

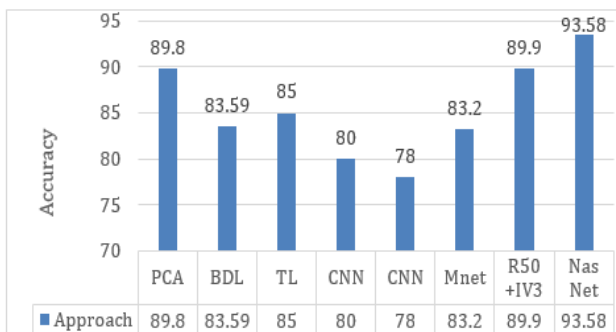


Fig. 14. Comparison of Various Deep Learning Approaches of Accuracy on HAM10000 Dataset.

VI. CONCLUSION

The rising cost of epidermis cancer therapy throws life tough for survivors and their families. Early identification of melanoma skin cancer is critical to curing the condition. In this paper, we proposed two approaches based on domain adaptation for computer-aided diagnosis of skin cancers. We attempted to categorize the other five forms of skin illnesses in addition to the typical non-melanoma and melanoma groups. The NAS strategy and the tools offered were designed to help optimize the model and, as a result, improve research findings. Using the HAM10000 dataset, two alternative recommended models were used: a single level and a two level, the first of which clears in distinguishing between melanoma and non-melanoma images and the second with classifying benign lesions. In this study, the GTO algorithm for selecting features outperforms the PSO and ACO feature selection algorithms. The goal of this study was to provide a feature selection (FS) strategy by increasing the performance of the Gorilla Troops Optimizer (GTO). GTO feature selection algorithm selects set of optimized feature to provide deliver classification accuracy of 89.89 and 93.58. The limitation of the proposed model was computational time. Though the NasNet itself takes time to generate the desired model, feature optimization is additionally added. The aim was met due to finite computational resources within a reasonable period which is a desirable in the field of medical imaging. It is not possible to declare that the most ideal architecture was discovered, but the best-known architecture was attained.

Funding Statement: The authors received no specific funding for this study.

Conflict of Interest: The authors declare that they have no conflicts of interest.

Availability of data and material (data transparency): The data are publicly available at <https://challenge.isic-archive.com/data/>

REFERENCES

- Leiter, U.; Eigentler, T.; Garbe, C. "Epidemiology of skin cancer. In Sunlight, Vitamin D and Skin Cancer"; Springer: Berlin/Heidelberg, Germany, pp. 120–140,2014.
- Dong, Y.; Wang, L.; Cheng, S.; Li, Y. "FAC-Net: Feedback Attention Network Based on Context Encoder Network for Skin Lesion Segmentation". Sensors 21, 5172,2021.
- Dildar M, Akram S, Irfan M, Khan HU, Ramzan M, Mahmood AR, Alsaiani SA, Saeed AH, Alraddadi MO, Mahnashi MH. Skin cancer detection: a review using deep learning techniques. International journal of environmental research and public health. 2021 Jan;18(10):5479.
- Akram, T.; Sharif, M.; Saba, T.; Javed, K.; Lali, I.U.; Tanik, U.J.; Rehman, A. Construction of saliency map and hybrid set of features for efficient segmentation and classification of skin lesion. Microsc. Res. Tech. 82, 741–763,2019.
- Singer S, Tkachenko E, Hartman RI, Mostaghimi A. Gender identity and lifetime prevalence of skin cancer in the United States. JAMA dermatology Apr 1;156(4):458-60, 2020.
- Alom MZ, Aspiras T, Taha TM, Asari VK. Skin cancer segmentation and classification with NABLA-N and inception recurrent residual convolutional networks. arXiv preprint arXiv:1904.11126. 2019 Apr 25.
- Ge Z, Demyanov S, Chakravorty R, Bowling A, Garnavi R. Skin disease recognition using deep saliency features and multimodal learning of dermoscopy and clinical images. InInternational Conference on Medical Image Computing and Computer-Assisted Intervention Sep 10 (pp. 250-258). Springer, Cham,2017.

- [8] Gouabou, A.F.; Damoiseaux, J.-L.; Monnier, J.; Iguernaissi, R.; Moudafi, A.; Merad, D. Ensemble Method of Convolutional Neural Networks with Directed Acyclic Graph Using Dermoscopic Images: Melanoma Detection Application. *Sensors* 21, 3999, 2021.
- [9] Bafounta, M.-L.; Beauchet, A.; Aegerter, P.; Saiag, P. Is dermoscopy (epiluminescence microscopy) useful for the diagnosis of melanoma: Results of a meta-analysis using techniques adapted to the evaluation of diagnostic tests. *Arch. Dermatol* 137, 1343–1350, 2001.
- [10] Argenziano, G.; Soyer, H.P.; Chimenti, S.; Talamini, R.; Corona, R.; Sera, F.; Binder, M.; Cerroni, L.; De Rosa, G.; Ferrara, G.; et al. Dermoscopy of pigmented skin lesions: Results of a consensus meeting via the Internet. *J. Am. Acad. Dermatol* 48, 679–693, 2003.
- [11] Sharif, M.; Akram, T.; Kadry, S.; Hsu, C.-H. A two-stream deep neural network-based intelligent system for complex skin cancer types classification. *Int. J. Intell. Syst.* 2021.
- [12] Alhaisoni, M.; Tariq, U.; Hussain, N.; Majid, A.; Damaševićius, R.; Maskeliūnas, R. COVID-19 Case Recognition from Chest CT Images by Deep Learning, Entropy-Controlled Firefly Optimization, and Parallel Feature Fusion. *Sensors* 21, 7286, 2021.
- [13] Khan, M.A.; Muhammad, K.; Sharif, M.; Akram, T.; Kadry, S. Intelligent fusion-assisted skin lesion localization and classification for smart healthcare. *Neural Comput. Appl* 1–16, 2021.
- [14] Dey, S.; Roychoudhury, R.; Malakar, S.; Sarkar, R. An optimized fuzzy ensemble of convolutional neural networks for detecting tuberculosis from Chest X-ray images. *Appl. Soft Comput.* 114, 108094, 2021.
- [15] Khamparia, A.; Singh, P.K.; Rani, P.; Samanta, D.; Khanna, A.; Bhushan, B. An internet of health things-driven deep learning framework for detection and classification of skin cancer using transfer learning. *Trans. Emerg. Telecommun. Technol.* 32, e3963, 2020.
- [16] Akram, T.; Sharif, M.; Shahzad, A.; Aurangzeb, K.; Alhussein, M.; Haider, S.I.; Altamrah, A. An implementation of normal distribution-based segmentation and entropy-controlled features selection for skin lesion detection and classification. *BMC Cancer* 18, 638, 2018.
- [17] Codella, Noel CF, et al. "Skin lesion analysis toward melanoma detection: A challenge at the 2017 international symposium on biomedical imaging (isbi), hosted by the international skin imaging collaboration (isic)." 2018 IEEE 15th international symposium on biomedical imaging (ISBI 2018). IEEE, 2018.
- [18] Zafar, K.; Gilani, S.O.; Waris, A.; Ahmed, A.; Jamil, M.; Khan, M.N.; Sohail Kashif, A. Skin Lesion Segmentation from Dermoscopic Images Using Convolutional Neural Network. *Sensors* 2020, 20, 1601.
- [19] Song, L.; Lin, J.P.; Wang, Z.J.; Wang, H. An End-to-End Multi-Task Deep Learning Framework for Skin Lesion Analysis. *IEEE J. Biomed. Health Inform.* 24, 2912–2921, 2020.
- [20] Aziz, S.; Bilal, M.; Khan, M.U.; Amjad, F. Deep Learning-based Automatic Morphological Classification of Leukocytes Using Blood Smears. In *Proceedings of the 2020 International Conference on Electrical, Communication, and Computer Engineering (ICECCE)*, Istanbul, Turkey, 14–15 April pp. 1–5, 2020.
- [21] Ren, Y.; Yu, L.; Tian, S.; Cheng, J.; Guo, Z.; Zhang, Y. Serial attention network for skin lesion segmentation. *J. Ambient. Intell. Humaniz. Comput.* 1–12, 2021.
- [22] Xie, Y.; Zhang, J.; Xia, Y.; Shen, C. A Mutual Bootstrapping Model for Automated Skin Lesion Segmentation and Classification. *IEEE Trans. Med. Imaging* 39, 2482–2493, 2020.
- [23] Zhang, J.; Xie, Y.; Xia, Y.; Shen, C. Attention residual learning for skin lesion classification. *IEEE Trans. Med. Imaging* 38, 2092–2103, 2019.
- [24] Yu L, Chen H, Dou Q, Qin J, Heng P-A. Automated melanoma recognition in dermoscopy images via very deep residual networks. *IEEE Trans Med Imaging* 36(4):994–1004, 2016.
- [25] Majtner T, Yildirim-Yayilgan S, Hardeberg JY. Combining deep learning and hand-crafted features for skin lesion classification. In: 2016 Sixth international conference on image processing theory, tools and applications. IEEE, p. 1–6, 2016.
- [26] Ahonen T, Hadid A, Pietikainen M. Face description with local binary patterns: Application to face recognition. *IEEE Trans Pattern Anal Mach Intell* 28(12):2037–41, 2006.
- [27] Arivuselvam B. Skin Cancer Detection and Classification Using Svm Classifier. *Turkish Journal of Computer and Mathematics Education (TURCOMAT)*. 2021 Jun 4;12(13):1863-71.
- [28] T. Elsken, J. H. Metzen, and F. Hutter. "Neural architecture search: A survey," *J. Mach. Learn. Res.*, vol. 20, pp. 55:1-55:21, Mar. 2019.
- [29] B. Zoph, V. Vasudevan, J. Shlens, and Q. V. Le, "Learning transferable architectures for scalable image recognition," in *Proc. IEEE/CVF Conf. Comput. Vis. Pattern Recognit.*, Salt Lake City, UT, USA, Jun pp. 8697–8710, 2018.
- [30] Termritthikun C, Jamtsho Y, Ieamsaard J, Muneesawang P, Lee I. EEEA-Net: An Early Exit Evolutionary Neural Architecture Search. *Engineering Applications of Artificial Intelligence*. Sep 1; 104:104397, 2021.
- [31] Yu, Z.; Jiang, X.; Zhou, F.; Qin, J.; Ni, D.; Chen, S.; Lei, B.; Wang, T. Melanoma Recognition in Dermoscopy Images via Aggregated Deep Convolutional Features. *IEEE Trans. Biomed. Eng.* 66, 1006–1016, 2018.
- [32] Srinivasu, P.N.; SivaSai, J.G.; Ijaz, M.F.; Bhoi, A.K.; Kim, W.; Kang, J.J. Classification of skin disease using deep learning neural networks with MobileNet V2 and LSTM. *Sensors* 21, 2852, 2021.
- [33] Khan MA, Akram T, Sharif M, Kadry S, Nam Y. Computer decision support system for skin cancer localization and classification (2021).
- [34] E.H. Houssein, M.R. Saad, F.A. Hashim, H. Shaban, M. Hassaballah, Lévy Flight distribution: A new metaheuristic algorithm for solving engineering optimization problems, *Eng. Appl. Artif. Intell.* 94 (2020) 103731.
- [35] I.Boussaid, J. Lepagnot, P. Siarry, A survey on optimization metaheuristics, *Inform. Sci.* 237 82–117, (2013).
- [36] Hashim FA, Houssein EH, Hussain K, Mabrouk MS, Al-Atabany W. Honey Badger Algorithm: New metaheuristic algorithm for solving optimization problems. *Mathematics and Computers in Simulation*. Feb 1; 192:84-110, 2022.
- [37] F. Hashim, M.S. Mabrouk, W. Al-Atabany, Gwomf: Grey wolf optimization for motif finding, in 2017 13th International Computer Engineering Conference (ICENCO), IEEE, pp. 141–146, 2017.
- [38] Khan MA, Javed MY, Sharif M, Saba T, Rehman A (2019) Multi-model deep neural network based features extraction and optimal selection approach for skin lesion classification. In: 2019 international conference on computer and information sciences (ICCIS). IEEE, pp 1–7.
- [39] Mobiny A, Singh A, Van Nguyen H Risk-aware machine learning classifier for skin lesion diagnosis. *J Clin Med* 8(8):1241, (2019).
- [40] Moldovan D Transfer learning based method for two-step skin cancer images classification. In: 2019 E-health and bioengineering conference (EHB), pp 1–4, (2019).
- [41] Nugroho AA, Slamet I, Sugiyanto Skins cancer identification system of HAMI0000 skin cancer dataset using convolutional neural network. *AIP Conf Proc* 2202(1):020039, (2019).
- [42] Pai K, Giridharan A Convolutional neural networks for classifying skin lesions. In: TENCON 2019—2019 IEEE region 10 conference (TENCON). IEEE, pp 1794–1796, (2019).
- [43] Sae-Lim W, Wettayaprasit W, Aiyarak P (2019) Convolutional neural networks using MobileNet for skin lesion classification. In: 16th international joint conference on computer science and software engineering (JCSSE), pp 242–247, 2019.
- [44] Shahin AH, Kamal A, Elattar MA Deep ensemble learning for skin lesion classification from dermoscopic images. In: 2018 9th Cairo international biomedical engineering conference (CIBEC). IEEE, pp 150–153, (2018).
- [45] Tsang, S. H. Review: Nasnet-neural architecture search network (image classification), 2020.
- [46] Fong, S., Wong, R., & Vasilakos, A. V. Accelerated PSO Swarm Search Feature Selection for Data Stream Mining Big Data. *IEEE Transactions on Services Computing*, 9(1), 33–45. doi:10.1109/TSC.2015.2439695, (2016).
- [47] Seijas, L.M. Metaheuristics for feature selection in handwritten digit recognition. 2015 Latin America Congress on Computational Intelligence (LA-CCI), 1-6. doi: 10.1109/LA-CCI.2015.7435975, (2015).

- [48] Yeh, J., & Chan, S. Population-based metaheuristic approaches for feature selection on mammograms. 2017 IEEE International Conference on Agents (ICA), 140-144. doi:10.1109/AGENTS.2017.8015321, (2017).
- [49] Naeini, A. A., Babadi, M., Mirzadeh, S. M. J., & Amini, S. Particle Swarm Optimization for Object-Based Feature Selection of VHSR Satellite Images. *IEEE Geoscience and Remote Sensing Letters*, 15(3), 379–383. doi:10.1109/LGRS.2017.2789194, (2018).
- [50] Ighazran, H., Alaoui, L., & Boujiha, T. Metaheuristic and Evolutionary Methods for Feature Selection in Sentiment Analysis (a Comparative Study). *International Symposium on Advanced Electrical and Communication Technologies (ISAECT)*, 1-6, doi:10.1109/ISAECT.2018.8618799, (2018).
- [51] Arora, S., Singh, H., Sharma, M., Sharma, S., & Anand, P. A New Hybrid Algorithm based on Grey Wolf Optimization and Crow Search Algorithm for unconstrained function optimization and feature selection. *IEEE*. doi:10.1109/ACCESS.2019.2897325, (2019).
- [52] Kondaveeti HK, Edupuganti P. Skin cancer classification using transfer learning. In 2020 IEEE International Conference on Advent Trends in Multidisciplinary Research and Innovation (ICATMRI) 2020 Dec 30 (pp. 1-4). *IEEE*.
- [53] B. Zoph, V. Vasudevan, J. Shlens and Q. V. Le, "Learning Transferable Architectures for Scalable Image Recognition," 2018 IEEE/CVF Conference on Computer Vision and Pattern Recognition, pp. 8697-8710, doi: 10.1109/CVPR.2018.00907, 2018.
- [54] Shi X, Dou Q, Xue C, Qin J, Chen H, Heng PA. An active learning approach for reducing annotation cost in skin lesion analysis. In *International Workshop on Machine Learning in Medical Imaging Oct 13* (pp. 628-636). Springer, Cham, 2019.
- [55] Mukherjee S, Adhikari A, Roy M. Melanoma Detection from Lesion Images Using Optimized Features Selected by Metaheuristic Algorithms. *International Journal of Healthcare Information Systems and Informatics (IJHISI)*. 2021 Oct 1;16(4):1-22.
- [56] Aurora, S., Begoña, A., & Carmen, S. Pattern Analysis in Dermoscopic Images. In J. Scharcanski (Ed.), *Computer Vision Techniques for the Diagnosis of Skin Cancer*. Series in Bioengineering. doi:10.1007/978-3-642-39608-3_2, (2014).
- [57] Mukherjee S, Adhikari A, Roy M. Malignant melanoma detection using multi-layer perceptron with optimized network parameter selection by pso. In *Contemporary advances in innovative and applicable information technology 2019* (pp. 101-109). Springer, Singapore.

Review on Multimodal Fusion Techniques for Human Emotion Recognition

Ruhina Karani¹

Research Scholar, School of Computer Engineering and
Technology, MITWPU, Pune, India

Dr. Sharmishta Desai²

Associate Professor, School of Computer Engineering and
Technology, MITWPU, Pune, India

Abstract—Emotions play an essential role in human life for planning and decision making. Emotion identification and recognition is a widely explored field in the area of artificial intelligence and affective computing as a means of empathizing with humans and thereby improving human machine interaction. Though audio visual cues are vital for recognizing human emotions, they are sometimes insufficient in identifying emotions of people who are good at hiding emotions or people suffering from Alexithymia. Considering other dimensions like Electroencephalogram (EEG) or text, along with audio visual cues can aid in improving the results in such situations. Taking advantage of the complementarity of multiple modalities normally helps capture emotions more accurately compared to single modality. However, to achieve precise and accurate results, correct fusion of these multimodal signals is solicited. This study provides a detailed review of different multimodal fusion techniques that can be used for emotion recognition. This paper proposes in-depth study of feature-level fusion, decision-level fusion and hybrid fusion techniques for identifying human emotions based on multimodal inputs and compare the results. The study concentrates on three different modalities i.e., facial images, audio and text for experimentation; at least one of which differs in temporal characteristics. The result suggests that hybrid fusion works best in combining multiple modalities which differ in time synchronicity.

Keywords—Feature-level fusion; decision-level fusion; hybrid fusion; artificial intelligence; EEG

I. INTRODUCTION

Recently, emotion recognition has been explored extensively in the areas of artificial intelligence, affective computing and human computer interaction. Emotion is a psychological events generated by a person's tendency toward need, which can be broadly classified into Physiological arousal and subjective experience [1, 2]. Physiological arousal refers to the physiological responses of the human body, which can be measured by electrical signals like electrocardiogram (ECG) and electroencephalogram (EEG), whereas subjective experience is a phenomenon, which relates to individual's feelings about different emotional states. It is expressed through facial expression, audio, gestures, etc. [1, 3, 4].

Audio visual features are generally treated as vital cues for emotion recognition, but they are prone to deception, if performed deliberately. Physiological signals, on the other hand, cannot be deceived easily as they are based on internal physiological responses. Combining physiological responses

with subjective experiences leads to more accurate emotion recognition.

Although emotion recognition can be achieved through a uni-modal approach, it may not work well for certain conditions of subjective experience where the people are excellent at hiding their emotions or the input data is very noisy. Also cross culture approaches for expressiveness act as barriers to identifying emotions correctly. Multimodal approach, on the contrary, can achieve significant accuracy by combining inputs from multiple modalities [5]. However, to get precise and accurate results, correct fusion of these multimodal signals is required.

A major concern for fusing multiple modalities is deciding the level at which multimodal fusion should occur and how to achieve the fusion [6, 7]. Since different modalities differ significantly in temporal characteristics, synchronization among them plays an important role in multimodal fusion [7]. Multimodal fusion techniques are broadly classified into decision-level fusion, feature-level fusion and hybrid fusion. Decision-level fusion and feature-level fusion are the most regularly used techniques for multimodal fusion in emotion recognition.

The existing literature on review of fusing multiple modalities is either based on signals which are synchronous in time or same type of signals (e.g. Fusion of different 2D images). B. Huang et al. proposed a review of medical image fusion techniques for Computed Tomography Scan (CT), Magnetic Resonance Imaging (MRI), Positron Emission Tomography (PET) and Single-photon Emission Computed Tomography (SPECT) images which describes spatial domain fusion and transform domain fusion [8]. Chen Xiao Yu et al. published a trend of machine learning based on fusion which focused on Ensemble Learning, Transfer Learning and Federated Learning for technology and data fusion [9].

This paper reviews different multimodal fusion techniques for decision level, feature level and hybrid fusion which can be used for human emotion recognition. The study also provides comparative analysis of these techniques. The proposed work focuses on the modalities which are synchronous as well as asynchronous in time to achieve emotion recognition. For experimentation, inputs from multiple modalities like facial images, audio and text are considered.

The paper is organized as follows: Section II describes decision-level fusion and the various techniques used to

achieve it for emotion recognition. Section III is devoted to discussing feature-level fusion and the various techniques used for achieving feature-level fusion. In Section IV, Hybrid approach for multimodal fusion is discussed in detail. Section V provides experimental analysis of different fusion methods. Section VI focuses on the discussion on analyzing and comparing different fusion methods. Section VII concludes the paper.

II. DECISION-LEVEL MULTIMODAL FUSION

Since emotion recognition works with multiple modalities, which differ from each other in various aspects, at times it becomes challenging to extract features from different and coupled modalities. Also, changes in the time synchrony of different modalities affect the dimensions which are used for emotion recognition [10]. To deal with this issue, decision-level multimodal fusion takes each modality independently for classification.

Decision-Level fusion technique first classifies the data of each modality individually and the result is combined at a later stage to achieve fusion. This fusion technique is also called late fusion as combining results occurs at a very late stage after classification. Fig. 1 shows a general framework of decision-level multimodal fusion considering audio, visual, text and EEG input for emotion recognition.

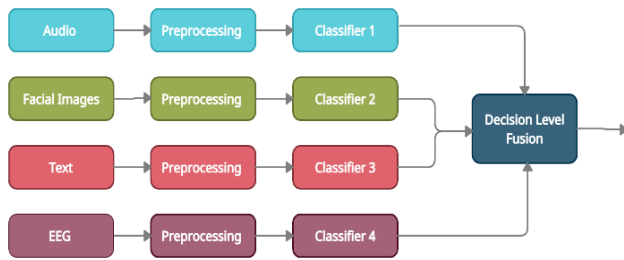


Fig. 1. General Framework of Decision-Level Fusion for Emotion Recognition.

There are various techniques of decision-level fusion that have been experimented with by researchers. This section presents each of these techniques.

A. Support Vector Regression

Support vector regression (SVR) works on the principles of the support vector machine (SVM). The ideology behind SVR is to find the best fit line suitable for the problem at hand. The best fit line in SVR is the hyperplane that contains the maximum number of points. It uses a margin of tolerance in approximation to the SVM. SVR maps to high dimensionality to estimate a function while offering nonlinear complexity [11].

In many studies, researchers have used SVR with the RBF kernel for decision-level fusion of emotion recognition [10, 12]. Haiyang Su et al. used bidirectional long short-term memory for classifying emotions individually from audio, facial images and text along with RBF kernel SVR to achieve significant improvement in classification accuracy [10]. Mihalis A. Nicolaou et al. compared the performance of bidirectional LSTM-NN and SVR on audio, facial expression and shoulder features for predicting spontaneous effect [13].

SVR can compensate for redundant information, which makes SVR suitable for decision-level fusion required for emotion recognition but it does not perform well when the number of feature extracted are more than training samples.

B. Blending Algorithms

Blending algorithm is a technique of ensemble machine learning that uses a metaclassifier to combine the outputs of different machine learning models.

A blending algorithm works in two layers. The first layer uses a traditional approach for training, where multiple basic classifiers are trained on the inputs from different modalities. The second layer is used for combining the outputs of the basic classifiers used in level 1. The outputs of each classifier are combined to form a new training set, which acts as an input to a higher level classifier called metaclassifier. The metaclassifier can use the ensemble learning techniques of bagging, boosting and stacking for combining the results based on the weight, bias and variances of base classifiers [14]. The role of level 1 basic classifiers is to classify the multimodal data, whereas the level 2 classifier is responsible for combining the outputs of base classifiers. Blending algorithms are found to have a better performance in the prediction.

Man Hao et al. used Convolution Neural network and support vector machine as base classifiers for speech and facial images along with the blending algorithm of metaclassifier to achieve multimodal emotion recognition and achieved 81.36% accuracy [14]. Lee et al. used ensemble learning on multimodal acoustic, lexical and discourse features using three classifiers to find negative emotions in spoken dialog [15]. Blending algorithm can be used as a decision-level fusion technique for emotion recognition owing to its improved performance for multimodal inputs. Blending algorithm is stable and less noisy.

C. Brain Emotion Learning Models

The brain emotional learning (BEL) system takes inspiration from the biological amygdala-orbitofrontal model to emulate the high speed of the emotional learning mechanism used by the human brain [16]. The BEL model comprises four main components. Amygdala, Orbitofrontal cortex (OFC), the Thalamus and Sensory cortex. After receiving input signals in the form of emotional stimuli from the Sensory cortex & Thalamus and a reward signals from the external environment, amygdala interacts with the OFC. The OFC evaluates the response of the amygdala based on the input received from the Sensory cortex, which leads to the prevention of improper learning connections. In a nutshell, the Sensory cortex integrates the features extracted from different unimodal inputs and the amygdala and OFC works to form a decision after interacting with the memory [17, 18].

BEL models require rewards extracted from input data and are derived from monotonic reinforcement learning. BEL-based networks are efficient in predicting peak points [19]. This method can be used as a stacking ensemble method in multimodal decision fusion techniques [17]. Zeinab Farhoudi et al. used BEL as a decision-level fusion technique for multimodal audio visual features to achieve a significant

accuracy of 73.9% for emotion recognition [17]. BEL model has good decision-making capability due to its cognitive-based structure. Due to this, Brain Emotional Learning can be used at decision-level fusion for multimodal emotion recognition.

D. Decision Tree based Approach

A decision tree is a non-parametric supervised learning method whose internal nodes represent test and leaf nodes represent classes. Filtering is applied through the nodes to achieve the required output. A decision tree tries learning decision rules from the given input data features.

Yucel Cimtay et al. used a decision tree for fusing multimodal inputs from facial expressions, galvanic skin response (GSR) and electroencephalogram (EEG) to detect emotions where the authors emphasized more on the probability vector received from facial images-based classifier. The condition of the decision tree was set to check whether this probability vector goes below a certain threshold. The research proposes using other modalities only if the specified conditions hold true [20].

Heysem Kaya et al. used a random forest decision tree based model on audio, facial and scenic inputs extracted from videos CVs to achieve decision fusion to estimate a suitable interview variable [21].

Decision trees are suitable for decision-level fusion because of their capability of learning rules according to the requirement. The predictions made by each classifier used for unimodal inputs can be combined based on the specific conditions provided at each node by using decision trees. But, decision trees are unstable data structures and they are prone to inaccuracy.

E. Rule based Approach

Rule-based classifiers are types of classifiers that make the class decision using various “if-else” rules. These classifiers are used to generate a descriptive model as the rules are easily interpretable. The “if” condition is called the antecedent and the predicted class is called the consequent in rule-based classification.

Subhasmita Sahoo and A. Routray has used a rule-based approach for emotion recognition using multimodal audio and video inputs. The rules were set to give high priority to the result of the facial image classifier and low priority to the audio classifier. The results of the audio classifier were acceptable only if there was confusion in the results of the image based classifier [22].

Rule-based classification is a way to achieve decision-level fusion as they have the advantage of fuse the multimodal signal classifier’s output as per the conditions specified in the antecedent.

F. Dempster-Shafer Theory

The Dempster-Shafer (D-S) theory of evidence originated by Dempster [23], and formalized mathematically by Shafer [24]. D-S theory was developed as reasoning and modeling framework with epistemological uncertainty. This framework can be used to integrate multiple sources of evidence and to

agree to a combined degree of belief for different predictions. Compared to the Bayesian model, the D-S theory is an extensive approach to address uncertainty and imprecision [25]. Due to its ability to efficiently handle the uncertainty and inconsistency of multimodal data, D-S theory is widely used in data fusion, fault detection and pattern recognition [26].

The D-S theory is drawn on the concepts of allocating suitable beliefs and probabilities to hypotheses, applying the D-S rule for fusing independent inputs from different sources and arriving at the final decision of the optimal hypothesis in a workable and reasonable manner [25]. Decision-Level fusion make use D-S evidence theory to combine the outputs of each classifier used for multimodal inputs.

Xiao-Dan Zhang used D-S theory for fusing multi-modal text and image inputs after applying KNN and SVM classifiers individually on unimodal input to improve the classification results [27]. Nazmuzzaman Khan et al. claimed that D-S theory has limitations in terms of handling conflicting data. Therefore, they used an improved version of D-S theory using a distance function and evidence-weighted penalty for combining results of different sensors to achieve improved object detection [26]. S. Nemati used D-S theory for decision-level fusion in her approach of hybrid fusion for emotion recognition. The author had applied D-S theory on audio, video and textual multimodal inputs to achieve improved emotion recognition [28]. Yu-Ting Liu et al. used Weighted Fuzzy Dempster-Shafer Framework that can adjust weights of evidence, which is inconsistent for integrating the outputs of EEG and eye movement’s classifiers [25].

G. Decision Template Algorithm

The decision template (DT) algorithm is a simple and efficient fusion algorithm, which uses the average of decision profiles of each classifier used for training multimodal data inputs. These averages are treated as decision templates for each class. Assessing the resemblance between the decision profile and different decision templates helps provide accurate class prediction. Though the algorithm is used widely for decision fusion, it has limitations as it uses average decision profiles and does not emphasize differences in the performance of classifiers [29]. Reza Ebrahimpour et al. used a decision template algorithm for decision-level fusion of different classifiers for handwritten digit recognition [30]. Due to the limitations of the decision template algorithm, Aizhong Mi et al. proposed an improved weighted decision template algorithm that calculates the classifier’s performance using a statistical vector and allocates appropriate weights to each classifier according to the reliability of their outputs. The authors applied this improved approach to the cataract recognition system and received improved results compared to the decision template algorithm [29].

III. FEATURE-LEVEL MULTIMODAL FUSION

Feature-level fusion is a technique, which combines the features from different layers or branches. When applied to multimodal inputs, the feature-level fusion method combines the features extracted from each modality individually using different feature fusion techniques before giving it to a classifier for classification. It is considered a ubiquitous part

of several modern network architectures. Generally, feature-level fusion is implemented using the concatenation operation, but that might not be the best choice for achieving good results.

Fig. 2 depicts a general framework for feature-level multimodal fusion considering four different modalities like facial images, audio, text and EEG for emotion recognition.

Feature-level fusion works with the idea of extracting the most discriminating features from the extracted features and removing redundant information [31, 32]. It works with the conjecture of strict time synchronicity between different modalities and performs distinctively in cases where the modalities differ considerably in temporal characteristics [31, 33]. Fusion at the feature level works best for closely connected and synchronized modalities [31].

If feature-level fusion has to be used for multimodal approaches where individual modalities differ in time synchrony, the relationship between the different feature spaces needs to be explored and the features need to be made compatible [31].

Various techniques for feature-level fusion have been explored by the researchers. This section presents those techniques in detail.

A. Eigen Matrix for Fusion

The German word Eigen means characteristics. The terms Eigenvalues and Eigenvectors in computation deal with determining the characteristics of a matrix. Eigenvalues and eigenvectors are used in various applications, which include Principal Component Analysis, Spectral Clustering, and detection techniques in Computer Vision, etc. Some researchers found its use in feature-level fusion of multimodal inputs, where the individual features are extracted from each modality and serialized to form an Eigen matrix. This Eigen matrix is then normalized to get the fusion Eigen matrix [30]. The formula for Eigen matrix (E) calculation is specified in equation (1).

$$E_j^{(i)} = \frac{(e_j^{(i)} - \mu_j)}{\max e_j^{(i)} - \min e_j^{(i)}} \quad (1)$$

Where $e_j^{(i)}$ represents the j^{th} eigenvalue of i samples, μ_j represents the mean value of the j^{th} feature, and the denominator represents the range of j features.

Jian Che et al. used an Eigen matrix for multimodal feature fusion of longitudinal tear detection of a conveyor belt where the input modalities were images and sound [34]. The authors claimed to have improved accuracy due to multimodal fusion. However, the Eigen matrix technique for feature-level fusion relies on the mean and eigenvalues of each modality to achieve fusion. Therefore, this technique may not be able to use the entire range of diversity for each modality.

B. Canonical Correlation Analysis

Canonical Correlation Analysis (CCA) is a method for analyzing the relationship between two multivariate sets of vectors [28, 35]. CCA is considered as an effective tool in analysis that has an ability to increase statistical power compared to univariate methods due to the use of second-order statistics [28].

CCA has an application in multimodal fusion [35]. It worked to find sets of changed variables having the maximum correlation between the two modalities [28]. CCA, when used for multimodal inputs, take linear combinations of $X1W1$ and $X1W1$ that maximizes the pairwise correlations of two multimodal datasets where $X1$ & $X2$ are two multimodal datasets and $W1$ & $W2$ are canonical coefficient vectors [28].

Shahla Nemati used CCA for feature-level fusion to detect multimodal emotion recognition using audio and visual modalities [28]. The features of individual modalities are first extracted using different feature extraction methods before giving it to CCA for feature-level fusion.

CCA as a method for feature-level fusion uses the concept of maximizing the pairwise correlation between the two modalities. Therefore, applying CCA on more than two modalities will require fusion at multiple levels.

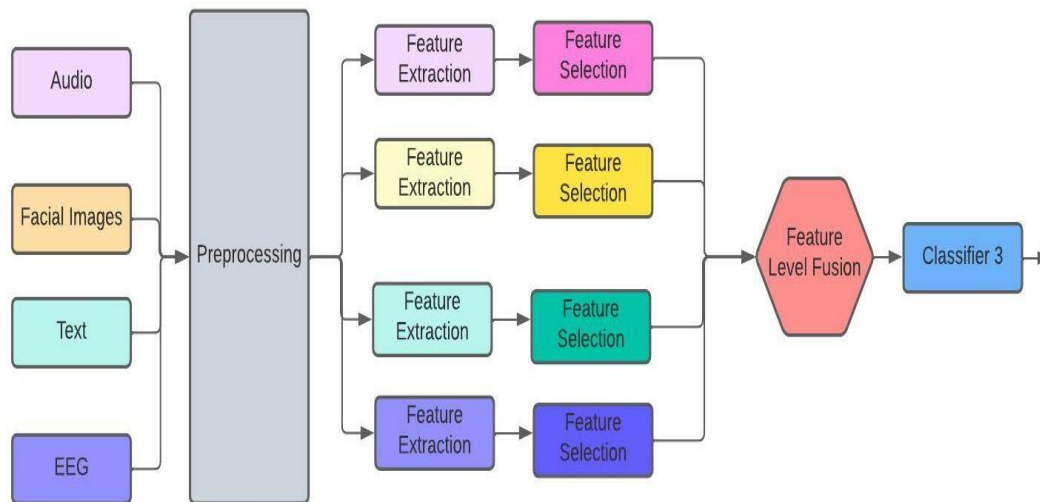


Fig. 2. General Framework for Feature-Level Fusion for Emotion Recognition.

C. Mixture of Brain Emotional Learning Model

The mixture of brain emotional learning models (MoBEL) combines the features of Mixture of Experts neural network (MoE) and Brain Emotional Learning (BEL) model. The BEL model has a good capability of decision-making due to its cognitive-based structure and the MoE model is based on working of the associative cortex of the brain, which has the capacity to integrate information from multiple sources [17, 18]. The presence of the associative cortex improves the brain's capacity of perception of the environment [36]. Therefore, MoE has the capacity to perform better in pattern recognition.

The MoBEL model structure uses the BEL model for expert and gating networks and trains all parts of the network jointly using back-propagation. MoBEL can be used as a fusion network to integrate multimodal features. The MoBEL model is more efficient in terms of processing speed, memory consumption, and neuron numbers than the MOE [17].

Zeinab Farhoudi et al. used MoBEL as a feature-level fusion technique for multimodal audio visual features to achieve a significant accuracy of 81.7% for emotion recognition [17].

D. Merging Features at Hidden Layer

This strategy works with the approach of inserting features of different time durations into different hidden layers of a training network [35]. This technique, though unexplored much, can tackle the problem arising due to asynchronous multimodal features. It also helps resolve the time compatibility issues of different multimodal features.

Given a network having multiple hidden layers and multimodal inputs with different time durations, short - duration features like audio are given as input to the first hidden layer. The output of the first hidden layer is combined with longer time features like visual features and given as input to the second hidden layer. The output of the second layer is then combined with longer duration features from the remaining modalities and given as the input to the third hidden layer. The process is repeated until the features are provided to the network [35].

Shizhe Chen et al. considered this approach for feature-level fusion in emotion recognition using three modalities: audio, images and EEG, wherein the authors used RNN-LSTM network for recognizing and fusing the features [35].

Though this approach can tackle the problems of asynchronous multimodal features, it depends upon the network used for training. Also, for modalities having similar duration, deciding the hidden layer at which these features need to be fused becomes an issue.

E. Concatenation

Concatenation generally uses consolidated dimensions to achieve fusion [37]. The concatenation formula is shown in equation 2.

$$Y = x_1 \cup x_2 \cup x_3 \dots \dots \cup x_k \quad (2)$$

where x_k is a set of output feature maps for the k^{th} layer and Y represents the fusion of all features.

The main goal of concatenation is to enrich the diversity of features for better recognition ability [36]. Sanghyun lee et al. used a concatenation method in a process of multimodal feature fusion for emotion recognition based on audio, visual and textual features for emotion recognition.

Schoneveld et al. used a concatenation method for multimodal feature-level fusion for emotion recognition based on audio visual modalities [38]. The authors also claimed to have improved fusion accuracy by adding hadamard product to concatenation in attention-based approach for emotion recognition [39].

It is the most popular method for feature-level fusion. But it might not be the best choice for multimodal inputs that differ in dimensions.

IV. HYBRID MULTIMODAL FUSION

Feature-level fusion methods require synchronization between different modalities, but it is possible to produce results even when the data from one of the modality is missing. Decision-level fusion, on the other hand, does not require synchrony between different modalities, but its capabilities cannot be exploited fully even if the data from a single modality is missing.

The hybrid fusion method tries achieving the advantages of both feature level and decision-level fusion methods by combining these approaches. The hybrid fusion approach applies feature-level fusion on some synchronous modalities and combines the result of with the remaining asynchronous modalities using decision-level fusion.

The hybrid approach works well for multimodal inputs, where some inputs assume time synchrony and some others are asynchronous in time. Fig. 3 shows the general framework of hybrid multimodal fusion for emotion recognition fusion considering four different modalities like facial images, audio, text and EEG.

Shahla Nemati used a hybrid approach for multimodal emotion recognition based on three modalities viz. audio, visual, and users' comments. The author used feature-level fusion for audio and visual features since they were synchronized. The result is then fed to a classifier for classification. A separate classifier was used for user comments because of its asynchronous nature. In the next step, decision-level fusion was used to fuse the outputs of both classifiers [28].

Zhen-zhong Lan et al. used a hybrid model for multimedia event detection based on visual, audio and textual data. The authors used five classifiers for training based on five features and feature combinations, where feature fusion was performed to combine features and the result of each classifier was combined using decision-level fusion [40].

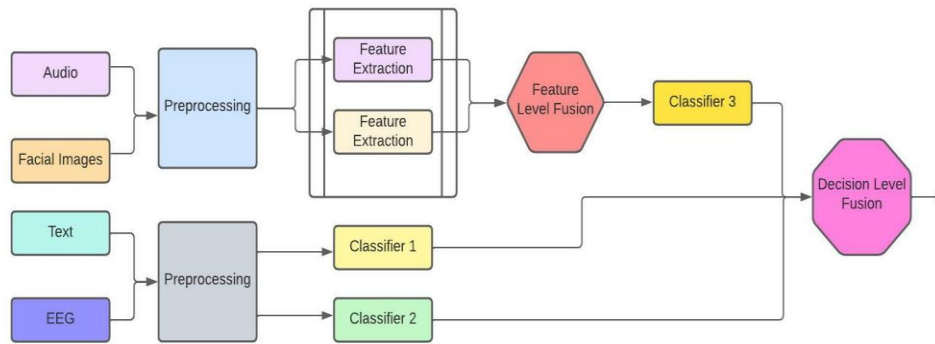


Fig. 3. General Framework for Hybrid Fusion to Emotion Recognition.

Fig. 4 depicts graphical representation of summary of different fusion methods described in review of literature.

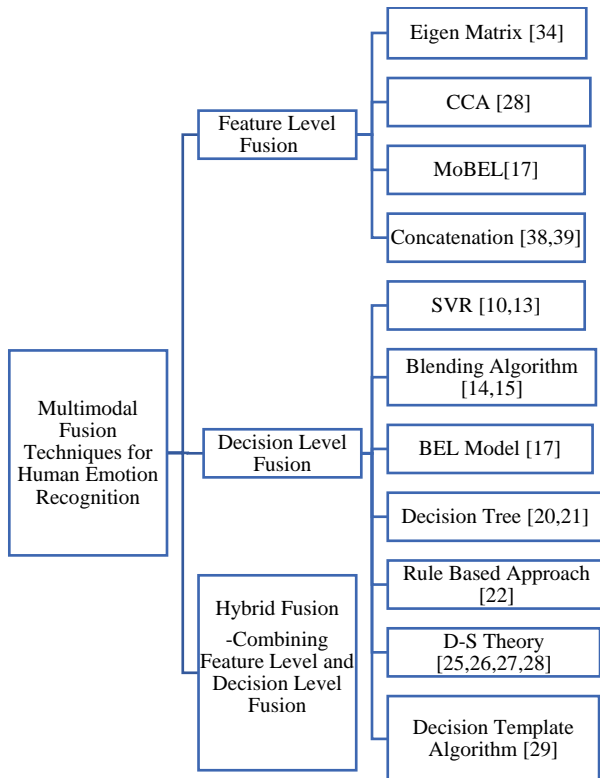


Fig. 4. Summary Diagram of Review of Literature Describing Various Fusion Methods.

V. EXPERIMENTAL ANALYSIS

To analyze the effectiveness of decision level, feature level and hybrid fusion methods in emotion recognition, we focused on facial expression, audio and text as multimodal inputs. We have used RAVDESS dataset [41] for audio data, FER 2013 dataset curated by Pierre Luc Carrier and Aaron Courville [42] for facial images and EMOTION dataset [43] for textual data for the purpose of experimentation. The RAVDESS dataset contains 1440 sample recordings from 24 actors (12 female, 12 male), in a neutral North American accent showing 8 emotions namely calm, happy, sad, angry, fearful, surprise, and disgust [41].

The FER-2013 dataset curated by Pierre Luc Carrier and Aaron Courville contains 28,709 training examples of 48x48 pixel grayscale facial images depicting seven emotions namely angry, Disgust, Fear, Happy, Sad, Surprise and Neutral [42]. The EMOTION dataset contains Twitter messages in English having six basic emotions: anger, fear, joy, love, sadness, and surprise [43].

In order to analyze, we clustered these emotions into three categories i.e. positive, negative and neutral. Since the modalities used for experimentation were not following time synchrony, feature level fusion of text with other two modalities was impractical. For decision level fusion, we have used pre-trained models of CNN by FER and Wav2Vec.

2.0 for classifying facial expressions and audio each providing the accuracy of 59 % and 82.23% respectively and pre-trained BERT model for classifying textual data providing accuracy of 93.8%. The output of each classifier is fused using max voting ensemble algorithm. The decision level fusion is tested on annotated samples of CMU-MOSI dataset which provided accuracy of 59.09 %.

For hybrid fusion, feature level fusion is applied on features extracted from facial images and audio by concatenating them before applying random forest for classification. Feature level fusion provided accuracy of 86.6%. Textual data is classified using Pre-trained BERT model providing accuracy of 77%. The output of feature level fusion is combined with text classifier using max voting ensemble algorithm of decision level fusion. The feature level fusion is tested on annotated samples of CMU-MOSI dataset which provided accuracy of 66.67 %.

Table I describes performance analysis of individual classifier for facial images, audio and text each, feature level fusion of facial images and audio and decision level and hybrid fusion in terms of accuracy.

Fig. 5(a) shows graphical representation for the accuracy comparison of decision level and hybrid model. The decision level fusion is providing the accuracy of 59.09 % whereas feature level fusion gives the accuracy of 66.67% on annotated samples of CMU-MOSI dataset. Fig. 5(b) depicts the individual accuracy graph of facial images, text and audio respectively which provide the accuracy of 59%, 93.8% and 82.23% using CNN and BERT models. The last bar in the figure shows accuracy of 86.6% for feature level fusion of facial images and audio input.

TABLE I. PERFORMANCE ANALYSIS OF DECISION LEVEL AND HYBRID FUSION

Accuracy	Facial Images	Audio	Text
Individual Classification	0.59 (Using CNN)	0.8223 (Using CNN)	0.938 (Using BERT)
Feature Level Fusion	0.866 (Using concatenation & Random Forest)		
Decision Level Fusion	0.5909 (Using blending algorithm)		
Hybrid Fusion	0.6667 (Using concatenation & blending algorithm)		

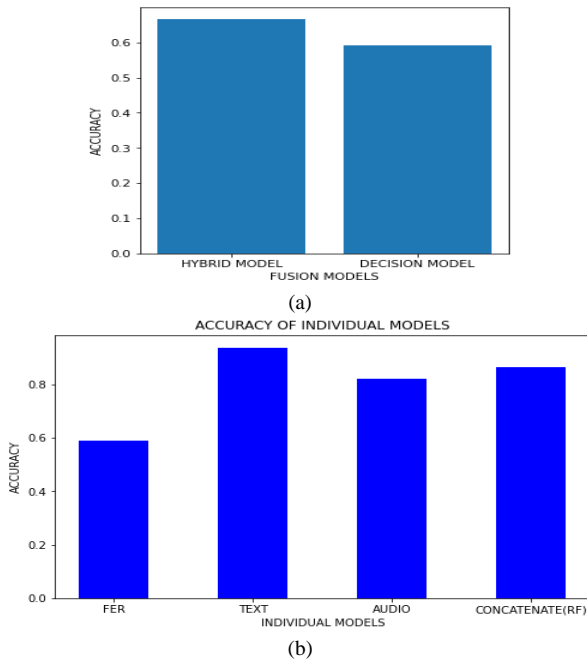


Fig. 5. (a) Accuracy Comparison Bar Graph of Hybrid and Decision Level Fusion, (b) Accuracy Graph of Individual Models and Feature Level Fusion Model of Audio and Facial Images.

VI. DISCUSSIONS

Emotions can be classified based on the discrete theory of emotions, where the emotions are categorized into discrete classes like anger, disgust, fear, joy, sadness and surprise, or based on dimensional emotional models where emotions are classified as a two valence-arousal models or three-dimensional valence-arousal-dominance models. Facial expression - based emotions are generally classified using discrete theory whereas EEG-based emotions use dimensional models for classification. Table II summarizes different multimodal fusion approaches adopted by researchers for emotion recognition.

Although a uni-modal approach can identify emotions to a certain extent, the accuracy of emotion recognition increases with the multimodal approach. While using a multimodal approach for emotion recognition, the main hurdle lies in fusing multiple modalities that differ significantly in temporal characteristics. The feature-based fusion approach is suitable for the inputs, which are synchronous in time.

Hence, this approach may not work well for emotion recognition based on multiple modalities that differ in temporal characteristics. The Eigen matrix technique for feature-level fusion relies on the mean and eigenvalues of each modality to achieve fusion. Therefore, this technique may not be able to use the entire range of diversity for each modality. Moreover, the Eigen matrix needs to be a square matrix, which further puts restrictions on the choice of features to be considered for fusion. CCA as a method for feature-level fusion uses the concept of maximizing the pairwise correlation between the two modalities. But, a traditional CCA can handle only two modalities at a time. Therefore, applying CCA on more than two modalities will require fusion at multiple levels. MoBEL model, when used for feature-level fusion, requires less processing speed, memory consumption, and neuron numbers. Since the MoBEL model is based on brain emotional learning, to exploit it fully, expertise on cognitive-based abilities of the brain is needed. Merging the features at the hidden layer works with the concept of merging the features at different hidden layers according to the duration of features to achieve feature-level fusion. Though this approach can tackle the problems of asynchronous multimodal features, it depends upon the network used for training. Also, for modalities having similar duration, deciding the hidden layer at which these features need to be fused becomes an issue. Concatenation is the most commonly used method for feature-level fusion, but it might not be the best choice for multimodal inputs that differ in dimensions.

Decision-level fusion, on the other hand, does not require synchrony between different modalities. SVR as a method of decision-level fusion can compensate for redundant information, but it underperforms when the number of features exceeds the number of training samples. A blending algorithm works well as a decision-level fusion technique for emotion recognition owing to its improved performance for multimodal inputs. Blending model when used for decision-level fusion is stable and less noisy, but this technique has high time and space complexity. Brain emotional learning can be used at decision-level fusion owing to its good decision-making capabilities. In spite of this, expertise in cognitive-based abilities of the brain is needed to exploit this technique.

Decision trees are considered for decision-level fusion because of their capability of learning rules according to the requirement. But, decision trees are unstable data structures and they are prone to inaccuracy. Rule - based classification is a way to achieve decision-level fusion as they have the advantage of fusing the multimodal signal classifier's output as per the conditions specified in the antecedent. Nonetheless, this requires a deep understanding of the domain for deciding the conditions and demands a lot of manual work. The D-S theory is widely explored for decision-level fusion. It is based on the concepts of allocating appropriate beliefs and probabilities to hypotheses, applying the D-S rule for fusing independent items from different sources and arriving at the final decision of the optimal hypothesis in a workable and reasonable manner.

TABLE II. MULTI-PERSPECTIVE SUMMARIZATION OF MULTIMODAL FUSION METHODS

Paper	Modalities	Task	Dataset	Model	Fusion Method	Fusion Technique	Results
H. Su et al. [10]	Audio, Video and Text	Multi-level segmented decision-level fusion emotion recognition	AVEC2017	BLSTM	Decision Level	SVR	Improved CCC performance of 0.685 on arousal
Nicolaou et al. [13]	Audio and Video	Fusion of audio cues, facial expression and shoulder gesture for continuous emotion prediction	SAL	BLSTM-NN	Decision Level, Feature Level and Output Associative	SVR	Obtained COR as 0.796 & 0.642 and RMSE as 0.15& 0.21 for valence and arousal respectively
Man Hao et al. [14]	Audio and Video	Audio visual Emotion Recognition Framework	eNTERFACE	SVM and CNN	Decision Level	Blending Ensemble	Improved recognition SI accuracy of 81.36% and SD Accuracy of 78.42%
Zeinab Farhoudi and Saeed Setayeshi [17]	Audio and Video	Audio-visual Emotion recognition with the MoBEL fusion network	eNterface'05	CNN and RNN	Decision Level and Feature Level	BEL and MoBEL	Improved audio visual emotion recognition accuracy of 81.7%
Y. Cimtay et al. [20]	Facial expression GSR and EEG	Hybrid multimodal emotion recognition	LUMED-2 and DEAP	CNN	Decision Level	Decision Tree	Obtained maximum one-subject-out accuracy of 91.5% and mean accuracy of 53.8%
S. Sahoo and A. Routray [22]	Audio and Video	Audio visual Emotion Recognition	eNTERFACE'05	HMM and SVM	Decision Level	Rule Based	Obtained average recognition accuracy of 76% for males candidates and 86% for female candidates for subject-dependent cases
S. Nemati [28]	Audio, video and text	Emotion Recognition using audio, video and users' comments	DEAP	SVM and Naïve Bayes	Hybrid	CCA and D-S theory	Obtained 0.85% and 76% of accuracy and f1-measure respectively for Emotion Recognition
Liam Schoneveld et al. [39]	Audio and Video	Emotion recognition using recent advances in deep learning	RECOLA, AffectNet and Google FEC	MTCNN, VGG, LSTM	Feature Level	Concatenation	Obtained CCC of 0.740 for valence and 0.719 for arousal in RECOLA

Although it works well for non-conflicting data, it may lead to inaccuracy for data that are conflicting in nature. The decision template algorithm is also widely used for decision fusion, but it has limitations as it uses average decision profiles and does not emphasize differences in the performance of classifiers. The hybrid fusion method achieves the advantages of both feature level and decision-level fusion methods by combining these approaches. Feature-level fusion methods require synchronization between different modalities, but it is possible to produce results even when the data from one of the modality is missing. Decision-level fusion, on the other hand, does not require synchrony between different modalities, but its capabilities cannot be exploited fully even if the data from a single modality is missing.

The hybrid approach overcomes the limitations of feature and decision level based approaches by applying feature-level fusion on the synchronous modalities and combining the results of with the remaining asynchronous modalities using decision-level fusion.

Results of experimental analysis on audio, facial images and text for emotion recognition show that feature level fusion of text with other two modalities was impractical since the modalities differ in temporal characteristics. Decision-level fusion works well for fusing the modalities differing in time

synchronicity. However, Hybrid fusion works best for emotion recognition using multiple modalities which differ in time synchronicity providing the accuracy of 66.67%. These results can further be improved by taking large data samples for testing.

VII. CONCLUSION

This paper discussed different multimodal fusion techniques for human emotion recognition. The study proposed a review of different state of art techniques for decision level, feature level and hybrid fusion to achieve multimodal emotion recognition.

The paper concentrated on using facial images, audio and text as multimodal inputs for emotion recognition. Experimental analysis of fusion methods was conducted which claimed that decision-level fusion and feature level fusion can be performed when inputs of different modalities are synchronous in time. However, when the inputs are not synchronous in time, suitable choices are decision level fusion and hybrid fusion. Hybrid fusion using concatenation and blending algorithm worked best improving accuracy by 7.6 % compared to decision level fusion. The study however had a limited test dataset. The accuracy results can be further improved if large number of annotated data samples are used for testing.

The review suggested that D-S theory is the most aggressively used method for decision-level fusion followed by rule-based and decision tree methods. Brain emotional learning is the latest approach used but it requires expertise in cognitive-based abilities of the brain. However, the blending algorithm works well for emotion recognition owing to its improved performance for multimodal inputs. For feature-level fusion, the most commonly used method is concatenation. CCA and Eigen matrix methods are also used in many applications for feature level fusion. The state of the art literature for feature fusion uses brain emotional learning but it requires expertise in cognitive-based abilities of the brain. Hybrid method is not explored much in literature. However, from experimental analysis it can be deduced that hybrid approach works best in fusing multiple modalities which differ in time synchrony. This provides a direction for the researchers to explore hybrid fusion approach on multimodal inputs.

The experimental analysis performed in this paper is based on audio, text and image inputs for emotion recognition. As a part of future work, audio-visual and physiological signals like EEG can be used to analyze different fusion techniques. Also, this paper used concatenation and meta classifier technique to evaluate effect of feature level, decision level and hybrid fusion. However, as a part of future work, there is a scope for applying different techniques of feature and decision level fusion discussed in the literature review in order to evaluate their effect on decision level, feature level and hybrid fusion.

REFERENCES

- [1] J. Wang and M. Wang, "Review of the emotional feature extraction and classification using EEG signals," *Cogn. Robot.*, vol. 1, pp. 29-40, ISSN 2667-2413, 2021, doi:10.1016/j.cogr.2021.04.001.
- [2] I. B. Mauss and M. D. Robinson, "Measures of emotion: A review.," *Cogn. Emot.*, vol. 23, no. 2, pp. 209-237, 2009, doi:10.1080/02699930802204677.
- [3] P. Chavan and S. Desai, "A Review on BCI Emotions Classification for EEG Signals Using Deep Learning" ,IOS press journal, *Advances in Parallel Computing*, doi:10.3233/APC210241.
- [4] M. Agrawal et al., "Models for hand gesture recognition using deep learning," 5th International Conference on Computing Communication and Automation (ICCCA), vol. 2020. IEEE, 2020, pp. 589-594, doi:10.1109/ICCCA49541.2020.9250846.
- [5] D. Agarwal and S. Desai, "Multimodal techniques for emotion recognition," International Conference on Computational Intelligence and Computing Applications (ICCICA), vol. 2021, 2021, pp. 1-6, doi:10.1109/ICCICA52458.2021.9697294.
- [6] H. Gunes and M. Pantic, "Automatic, dimensional and continuous emotion recognition," *Int. J. Synth. Emot.*, vol. 1, no. 1, pp. 68-99, 2010, doi:10.4018/jse.2010101605.
- [7] S. Chen and Q. Jin, "Multi-modal dimensional emotion recognition using recurrent neural networks," *Proc. 5th International Workshop on Audio/Visual Emotion Challenge*. New York, NY, USA: Association for Computing Machinery, 2015, pp. 49-56, doi:10.1145/2808196.2811638.
- [8] B. Huang et al., "A review of multimodal medical image fusion techniques," *Comp. Math. Methods Med.*, vol. 2020, p. 2020, article ID 8279342, 16, 2020. doi:10.1155/2020/8279342.
- [9] Chen Xiao Yu et al., "Research Progress and Trend of the Machine Learning based on Fusion," *Int. J. Adv. Comput. Sci. Appl.(IJACSA)*, vol. 13, no. 7, 2022. doi:10.14569/IJACSA.2022.0130701.
- [10] H. Su et al., "An improved multimodal dimension emotion recognition based on different fusion methods," 15th IEEE International Conference on Signal Processing (ICSP), vol. 2020, 2020, pp. 257-261, doi:10.1109/ICSP48669.2020.9321008.
- [11] K. S. Ni and T. Q. Nguyen, "Image superresolution using support vector regression" in *IEEE Trans. Image Process.*, vol. 16, no. 6, pp. 1596-1610, Jun. 2007, doi:10.1109/TIP.2007.896644.
- [12] J. Huang et al., "Continuous multimodal emotion prediction based on long short term memory recurrent neural network" in *Proc. 7th Annual Workshop on Audio/Visual Emotion Challenge (AVEC '17)*. New York, NY, USA: Association for Computing Machinery, 2017, pp. 11-18. doi:10.1145/3133944.3133946.
- [13] M. A. Nicolau et al., "Continuous prediction of spontaneous affect from multiple cues and modalities in valence-arousal space" in *IEEE Trans. Affect. Comput.*, vol. 2, no. 2, pp. 92-105, Apr.-Jun. 2011, doi:10.1109/T-AFFC.2011.9.
- [14] M. Hao et al., "Visual-audio emotion recognition based on multi-task and ensemble learning with multiple features.," *Neurocomputing*, vol. 391, pp. 42-51, ISSN 0925-2312, 2020, doi:10.1016/j.neucom.2020.01.048. Available at: <https://www.sciencedirect.com/science/article/pii/S0925231220300990>.
- [15] C. M. Lee and S. S. Narayanan, "Toward detecting emotions in spoken dialogs" in *IEEE Trans. Speech Aud. Process.*, vol. 13, no. 2, pp. 293-303, Mar. 2005, doi:10.1109/TSA.2004.838534.
- [16] F. Wubing et al., "An improved fuzzy brain emotional learning model network controller for humanoid robots.," *Front. Neurobotics*, vol. 13, 2, 2019, ISSN=1662-5218, doi:10.3389/fnbot.2019.00002.
- [17] Z. Farhoudi and S. Setayeshi, "Fusion of deep learning features with mixture of brain emotional learning for audio-visual emotion recognition," *Speech Commun.*, vol. 127, pp. 92-103, ISSN 0167-6393, 2021, doi:10.1016/j.specom.2020.12.001.
- [18] S. I. Rusu and P. C. M. A. " Learning, memory and consolidation mechanisms for behavioral control in hierarchically organized corticobasal ganglia systems.," *Hippocampus*, vol. 30, no. 1, pp. 73-98, 2020 Jan.. doi:10.1002/hipo.23167.
- [19] E. Lotfi and M. Akbarzadeh-T, " Supervised Brain Emotional Learning" *The*, vol. 2012, pp. 1-6, 2012 International Joint Conference on Neural Networks (IJCNN), doi:10.1109/IJCNN.2012.6252391.
- [20] Y. Cimtay et al., "Cross-subject multimodal emotion recognition based on hybrid fusion" in *IEEE Access*, vol. 8, pp. 168865-168878, 2020, doi:10.1109/ACCESS.2020.3023871.
- [21] H. Kaya et al., "Multi-modal score fusion and decision trees for explainable automatic job candidate screening from video CVs," *IEEE Conference on Computer Vision and Pattern Recognition Workshops (CVPRW)*, vol. 2017, 2017, pp. 1651-1659, doi:10.1109/CVPRW.2017.210.
- [22] S. Sahoo and A. Routray, "Emotion recognition from audio-visual data using rule based decision level fusion," vol. 2016, pp. 7-12, 2016 IEEE Students' Technology Symposium (TechSym), doi:10.1109/TechSym.2016.7872646.
- [23] A. P. Dempster, "Upper and lower probabilities induced by a multivalued mapping," *Ann. Math. Statist.*, vol. 38, no. 2, pp. 325-339, 1967, doi:10.1214/aoms/1177698950.
- [24] G. Shafer, *A Mathematical Theory of Evidence*. Princeton, NJ, USA: Princeton Univ. Press, 1976.
- [25] Y.-T. Liu et al., "Weighted fuzzy Dempster-Shafer framework for multimodal information integration" in *IEEE Trans. Fuzzy Syst.*, vol. 26, no. 1, pp. 338-352, Feb. 2018, doi:10.1109/TFUZZ.2017.2659764.
- [26] N. Khan and S. Anwar, "Improved Dempster-Shafer sensor fusion using distance function and evidence weighted penalty: Application in object detection" in *Proc. 16th International Conference on Informatics in Control, Automation and Robotics*, vol. 1: ICINCO, ISBN 978-989-758-380-3, 2019, pp. 664-671. doi:10.5220/0007917106640671.
- [27] X.-D. Zhang, "Study on Feature Layer fusion Classification Model on Text/Image Information," *Phys. Procedia*, vol. 33, pp. 1050-1053, ISSN 1875-3892, 2012, doi:10.1016/j.phpro.2012.05.172..
- [28] S. Nemati, "Canonical correlation analysis for data fusion in multimodal emotion recognition," 9th International Symposium on Telecommunications (IST), vol. 2018, 2018, pp. 676-681, doi:10.1109/ISTEL.2018.8661140.
- [29] A. Mi et al., "A Multiple Classifier Fusion Algorithm Using Weighted Decision Templates," *Sci. Program.*, vol. 2016, pp. 1-10, 2016, doi:10.1155/2016/3943859.

- [30] R. Ebrahimpour and S. Hamed, Hand Written Digit Recognition by Multiple Classifier Fusion Based on Decision Templates Approach, 2009. doi:10.5281/zenodo.1069935.
- [31] H. Gunes and M. Piccardi, "Automatic temporal segment detection and affect recognition from face and body display," *IEEE Trans. Syst. Man Cybern. B Cybern.*, vol. 39, no. 1, pp. 64-84, 2009, doi:10.1109/TSMCB.2008.927269.
- [32] C. Kamlaskar and A. Abhyankar, "Feature level fusion framework for multimodal biometric system based on CCA with SVM classifier and cosine similarity measure," *Aust. J. Electr. Electron. Eng.*, 1-14, 2022, doi:10.1080/1448837X.2022.2129147.
- [33] A. Corradini et al., "Multimodal input fusion in human computer interaction on the example of the on-going nice project" in *Proc. NATO-ASI Conference Data Fus, Situation Monit. Incident Detect. Alert Resp. Manag.*, pp. 223-234, 2003.
- [34] J. Che et al., "Longitudinal tear detection method of conveyor belt based on audio-visual fusion," *Measurement*, vol. 176, p. 109152, ISSN 0263-2241, 2021, doi:10.1016/j.measurement.2021.109152.
- [35] N. M. Correa et al., "Canonical correlation analysis for data fusion and group inferences: Examining applications of medical imaging data," *IEEE Signal Process. Mag.*, vol. 27, no. 4, pp. 39-50, 2010, doi:10.1109/MSP.2010.936725.
- [36] B. E. Stein et al., "The neural basis of multisensory integration in the midbrain: Its organization and maturation," *Hear. Res.*, vol. 258, no. 1-2, 4-15, 2009, doi:10.1016/j.heares.2009.03.012.
- [37] C. Ma et al., "Multi-layers feature fusion of convolutional neural network for scene classification of remote sensing" in *IEEE Access*, vol. 7, pp. 121685-121694, 2019, doi:10.1109/ACCESS.2019.2936215.
- [38] L. Schoneveld et al., "Leveraging recent advances in deep learning for audio-Visual emotion recognition," *Pattern Recognit. Lett.*, vol. 146, pp. 1-7, ISSN 0167-8655, 2021, doi:10.1016/j.patrec.2021.03.007.
- [39] S. Lee et al., "Multimodal emotion recognition fusion analysis adapting BERT with heterogeneous feature unification" in *IEEE Access*, vol. 9, pp. 94557-94572, 2021, doi:10.1109/ACCESS.2021.3092735.
- [40] Z. Lan et al., "Multimedia classification and event detection using double fusion," *Multimed. Tools Appl.*, vol. 71, no. 1, 333-347, 2014 doi:10.1007/s11042-013-1391-2.
- [41] S. R. Livingstone and F. A. Russo, "The Ryerson Audio-Visual Database of Emotional Speech and Song (RAVDESS): A dynamic, multimodal set of facial and vocal expressions in North American English," *PLoS ONE*, vol. 13, no. 5, p. e0196391, 2018. doi:10.1371/journal.pone.0196391.
- [42] I. J. Goodfellow et al., "Challenges in representation learning: A report on three machine learning contests" in *Lect. Notes Comput. Sci.. ICONIP 2013*, vol. 8228, M. Lee, A. Hirose, Z. G. Hou and R. M. Kil, Eds. Neural Information Processing. Berlin, Heidelberg: Springer, 2013. doi:10.1007/978-3-642-42051-1_16.
- [43] E. Saravia et al., "CARER: Contextualized affect representations for emotion recognition" in *Proc. 2018 Conference on Empirical Methods in Natural Language Processing*. Brussels, Belgium: Association for Computational Linguistics, 2018, pp. 3687-3697, doi:10.18653/v1/D18-1404.

A Comparative Study of Predictions of Students' Performances in Offline and Online Modes using Adaptive Neuro-Fuzzy Inference System

Sudhindra B. Deshpande, Kiran K. Tangod, Neelkanth V. Karekar, Pandurang S. Upparmani
Department of Information Science and Engineering, KLS, Gogte Institute of Technology
Belagavi-06, Karnataka, India

Abstract—Predicting a student's performance can help educational institutions to support the students in improving their academic performance and providing high-quality education. Creating a model that accurately predicts a student's performance is not only difficult but challenging. Before the pandemic situation students were more accustomed to offline i.e., physical mode of learning. As covid-19 took over the world the offline mode of education was totally disturbed. This situation resulted into the new beginning towards online mode of teaching over the Internet. In this article, these two modes are analysed and compared with reference to students' academic performances. The article models a predicting academic performance of students before covid i.e., physical mode and during Covid i.e., online mode, to help the students to improve their performances. The proposed model works in two steps. First, two sets of students' previous semester end results (SEE) i.e., after offline mode and after online mode, are collected and pre-processed using normalizing the performances in order to improving the efficiency and accuracy. Secondly, Adaptive Neuro-Fuzzy Inference System (ANFIS) is applied to predict the academic result performances in both learning modes. Three membership functions gaussian (Gausmf), triangular (Trimf) and gaussian-bell (Gbellmf) of ANFIS are used to generate the fuzzy rules for the prediction process proposed in this paper.

Keywords—ANFIS; fuzzy systems; online learning; e-learning; classroom learning; fuzzy rules; predictions; adaptive neuro-fuzzy inference system; education technology; distance education

I. INTRODUCTION

The Internet has made "Education" as the most exciting domains available in today's society, especially with the interconnectivity of smart and portable devices. Distance and e-Learning has grown in popularity as computer technology has advanced, networks have improved, and smartphones have become more accessible. Technology has transformed general classroom learning into e-Learning by lowering teaching costs and increasing learning efficiency while overcoming space and time constraints. A typical teaching-learning process takes place in a classroom, where a teacher uses lectures, whiteboards, slide projectors, and group discussions to communicate knowledge. To improve their learning skills, students take notes, write tests and assignments, and express doubts and questions. Students must also take tests and assessments on paper and teachers assess performance and knowledge of students in terms of marks. A variety of technological media, smart mobile devices and wireless communication have revolutionized the education system [1].

The e-Learning may happen through a variety of processes and applications such as computer-based training, digital collaborations, web-based training, and virtual classrooms [2].

Whether it is classroom learning or e-learning, one very important aspect is performance evaluation of students. Educational institutes are attempting to include student performance prediction into their educational procedures in order to help the students to improve themselves. Traditional learning modes can be enhanced to online modes by increasing portability and accessibility of mobile networks. Mobile devices can make it possible to capture the user-created content and also can serve as a powerful data collection tool [3]. Gayeski, D., & Russell, J. D. [4] have proposed that evaluations can be done in several ways. The teacher needs to make evaluations to advise students to make decisions and to write recommendations to potential employers. Data mining and machine learning techniques have been in use in HEIs to guide and improve their students' performance by using and exploring the data available in the education domain [5] [6] [7].

Artificial neural networks, Bayesian classifiers, and support vector machine algorithms are some of the techniques used to classify data [8]. Various techniques including classification, clustering, visualization, and regression have been utilized to extract hidden information from educational databases [9]. Classification is a technique for assigning data values to predetermined classes with the goal of predicting the target class for each data value [10][11].

Education data mining peruses extensive educational datasets for important data that can be analyzed deeper. Many educational activities, such as learners' performance prediction, will be supported by the smeared data, allowing teachers to identify potential knowledge about students [12][13]. The Neuro-fuzzy inference system (NFIS) has been effectively implemented in a variety of applications, including control and classification [14]. NFIS is a machine learning tool that integrates fuzzy logic reasoning with the learning capabilities of neural networks, thereby addressing the drawbacks of both neural networks and fuzzy systems when used separately [15]. A tutoring system based on Fuzzy rules [16] which implements a Fuzzy Logic inference engine that can manage different learning activities of students. A tutoring system that uses Fuzzy Logic is demonstrated to monitor the cognitive capability of each student [17].

In this article, ANFIS is applied to evaluate students' academic performance in order to assist them in improving their grades both in online and offline modes. The suggested ANFIS-based solution intelligently mixes fuzzy logic's capability reasoning with neural networks' learning abilities. The use of ANFIS for reliable student performance prediction in online and offline mode, is one of the paper's primary contributions.

II. LITERATURE WORK

A rule mining approach is introduced for evaluating student performance based on the Association Rules [18]. To collect crucial information for the student performance evaluation, Association Rules were used to examine the student dataset. Various data mining techniques are employed to predict student performance. They discovered that the neural network technique outperformed the other data mining strategies, with a prediction accuracy of 74.8% for student performance [19]. Abu Naser et al. used the Artificial Neural Network (ANN) model to predict the performance of Engineering faculty students [20]. They used the students' course scores, number of passed credits, and cumulative grade point average as factors to evaluate the student performance, and the ANN model correctly predicted the performance of students with an accuracy of 80%. A Neuro-Fuzzy learner model was proposed to analyze errors of high school learners' by collecting data using course-related simulation tools namely vectors in mathematics and physics. The system was tested using simulated learner data with different categories of knowledge level. These learners' behaviors correspond to fuzzy values [21]. A model of feed-forward Neural Networks was also trained for error classification purposes. Barber and Sharkey employed the logistic regression method for predicting student performance based on data collected from available students' information, financial data, and learning management systems [22].

A Fuzzy learner model was discussed for student evaluation during learning activities. The procedure is to imitate a human teacher in the classroom. Fuzzy Logic is proposed to track interaction between the tutor and the students and to handle inaccurate information using the ability of Fuzzy Logic [23]. This leads to more accurate answers by students to improve the learning environment.

Xenos, M. [24] has proposed a model of the Bayesian Network to support educational tutors in making decisions under uncertain conditions. The system is implemented with 800 learners studying an informatics course. The system is designed to model learner behavior to predict the success of decision-making by tutors. Fadi R.S [25] has discussed the early stages of data mining in academics and highlighted the potential of data mining in e-Learning and suggested various data mining tools that can be beneficial for e-Learning.

III. MOTIVATION

As the Covid-19 pandemic has affected the activities of higher education institutions (HEI) to promote the protection of teachers, staff, and students during the public health emergency. Institutions had to cancel all face-to-face lectures, including labs and other learning experiences, and determined that teachers would completely convert their courses to emergency online learning, and reduced contacts to prevent the

spread of Virus. So, to strengthen the learning community in this pandemic situation online learning has been promoted. But for the first-time online learning mode is actively used in the education. A comparative analysis is required between online and physical modes of teaching to find out how the student community is adjusting to the online mode of teaching and whether it is successful and helpful even after the Covid pandemic.

IV. THE PROPOSED METHODOLOGY

The proposed methodology is split into four steps. First step deals with data collection and processing; in second part, students' results in the classroom mode are analyzed using ANFIS; in third part, students' results in the online mode are analyzed using ANFIS; lastly, both modes are compared for their performances to evaluate which of the teaching mode is effective in producing good results. Fig. 1 depicts the proposed methodology applied. An Adaptive Neuro-Fuzzy Inference System [26][27] is a sort of artificial neural system that depends on the Takagi– Sugeno fuzzy inference system. It incorporates both neural systems and fuzzy rationale standards; it can catch the advantages of both in a solitary structure. Its inference system compares to an arrangement of fuzzy IF-THEN rules that have learning ability to surmised nonlinear fignctions.

A. Data Collection and Processing

The dataset used consists of 210 samples for Information science students consisting of students' scores in four core subjects and two laboratories ranging from 0 to 100. There are two sets of datasets which are collected. One set belongs to the 1st, 3rd and 5th semester students' semester end examination (SEE) results obtained through classroom learning mode and before the pandemic. Second set consists of SEE results of same students but studied in 2nd, 4th and 6th semester during the pandemic through online mode learning. The preparation of the dataset is the initial stage in the proposed approach. This stage could be crucial for reducing error throughout the learning process and obtaining more precise inputs. Equation (1) is used to normalize datasets using sample mean μ and standard deviation σ .

$$X_i = \frac{x_i - \mu}{\sigma} \quad (1)$$

B. ANFIS Architecture

“Takagi– Sugeno fuzzy inference framework” is used in ANFIS architecture which is an adaptive system that utilizes a directed learning algorithm. Fig. 2 demonstrates the architecture of ANFIS that consists of two sources of information “x” and “y”, and one yield or output “f”.

Takagi–Surgeon model follows the two variants of IF-THEN, are

$$\text{RULE 1} = \text{If 'x' is A1 and 'y' is B1 Then } f_1 = p_1x + q_1y + r_1$$

$$\text{RULE 2} = \text{If 'x' is A2 and 'y' is B2 Then } f_2 = p_2x + q_2y + r_2$$

where A1, A2, and B1, B2 are the membership elements of each info ‘x’ and ‘y’, while p1, q1, r1 and p2, q2, r2 are linear parameters to a limited extent Then (subsequent part) of Takagi– Sugeno fuzzy inference model.

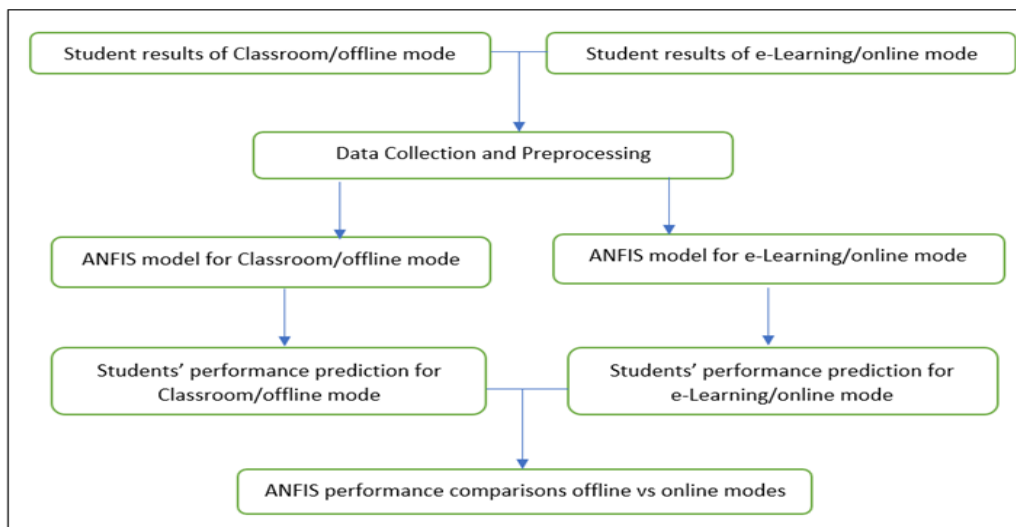


Fig. 1. Proposed Methodology of the Work Carried Out.

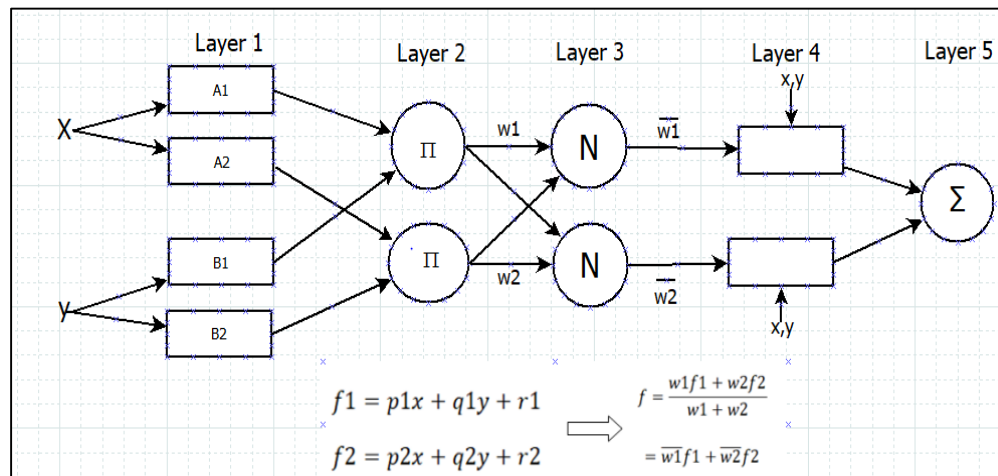


Fig. 2. ANFIS Architecture.

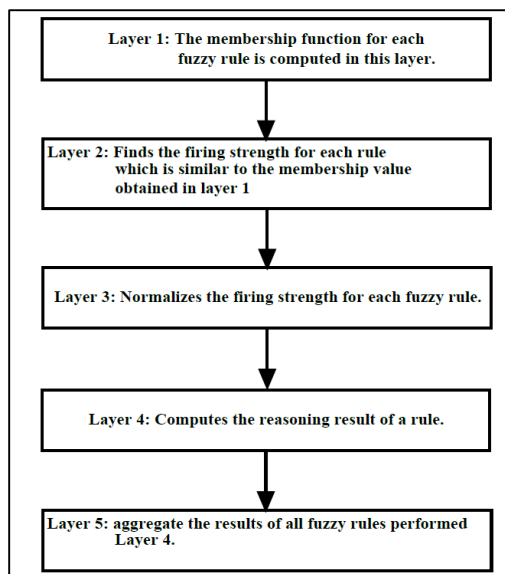


Fig. 3. ANFIS Layers and Functions.

Fig. 3 shows the functions of five layers of ANFIS. The first layer and fourth layer consist of adaptive nodes, while the remaining layers consist of fixed nodes. ANFIS tool in MATLAB provides a Grid partitioning algorithm. The algorithm generates a single-output Sugeno-type FIS by using grid partitioning on the data. `genfis1` generates a Sugeno-type FIS structure used as initial conditions (initialization of the membership function parameters) for ANFIS training. It generates input membership functions by uniformly partitioning the input variable ranges, and creates a single-output Sugeno fuzzy system. The fuzzy rule base contains one rule for each input membership function combination.

The membership function is a curve that defines how each point in the input space is mapped to a membership value (or degree of membership) between 0 and 1. They characterize fuzziness as whether the elements in fuzzy sets are discrete or continuous. The membership functions “`trimf`”, “`gaussmf`” and “`bellmf`” - are explained:

“Triangular function: defined by a lower limit a , an upper limit b , and a value m , where $a < m < b$, as given by equation (2).

$$\mu_A(X) = \begin{cases} 0 & x < a \\ \frac{x-a}{m-a} & a \leq x < m \\ \frac{b-x}{b-m} & m \leq x < b \\ 0 & x \geq b \end{cases} \quad (2)$$

Gaussian function: defined by a central value m and a standard deviation k > 0 as given by the equation (3).

$$\mu_A(X) = e^{-\frac{(x-m)^2}{2k^2}} \quad (3)$$

“The generalized bell function: gbellmf depends on three parameters a, b, and c given by the equation (IV) where the parameter b is usually positive and the parameter c locates the center of the curve.”

$$f(x; a, b, c) = \frac{1}{1 + \left| \frac{x-c}{a} \right|^{2b}} \quad (4)$$

The datasets are partitioned into 70 :30 i.e., 70% training data and 30% testing data. For both models of ANFIS, scores of six subjects are considered as input variables and SGPA as output variable. Three membership functions, gaussian (Gaussmf), triangular (Trimf) and gaussian-bell (Gbellmf) of ANFIS are used to generate the fuzzy rules for both the models.

C. Performance Evaluation

The Root Mean Square Error is a metric for determining the accuracy of a student's performance prediction by comparing the actual observed data values to the ones predicted by the model. The formula in equation (5) is used to calculate the RMSE:

$$RMSE = \sqrt{\frac{\sum_{i=1}^n (X_{obs,i} - X_{model,i})^2}{n}} \quad (5)$$

V. RESULTS AND DISCUSSIONS

Two ANFIS models using three mfs are built for the experimentation; one for classroom/offline mode of learning and second is for online mode of learning. The training data subset is used to train the ANFIS models, while the test data subset is employed to assess the trained ANFIS models' prediction accuracy. Student scores from the previous semester are taken as inputs to the ANFIS models in order to forecast student performances. The testing RMSE values for different epoch numbers will be used to designate the best ANFIS model in both learning modes. By varying the number of training epoch from 50 to 900, the performance of the three ANFIS models based on three types of membership functions (GaussMF, TriMF, and GbellMF) is examined.

A. ANFIS for Classroom / Offline Mode

Table I displays the training and testing RMSEs for offline mode learning approach for the three types of mfs.

Fig. 4 depicts RMSE values of training and testing against the number of epochs for all the three membership functions; and trimf behaviour is found to be worst as the testing RMSE is very high with 0.877 against a very low training error of 0.025. gaussmf performs good in comparison to gbellmf and trimf with 0.334 testing RMSE.

TABLE I. TRAINING AND TESTING RMSES OF GAUSSMF, GBELLMF AND TRIME WITH DIFFERENT EPOCHS FOR OFFLINE MODE

MFs	GaussMF		GbellMF		TriMF	
	Trainin g error	Testin g error	Trainin g error	Testin g error	Trainin g error	Testin g error
50	0.73	0.792	0.78	0.898	0.037	0.987
100	0.659	0.669	0.756	0.87	0.035	0.978
150	0.61	0.77	0.698	0.866	0.035	0.971
200	0.598	0.7	0.645	0.767	0.029	0.899
250	0.245	0.566	0.388	0.689	0.02	0.859
300	0.179	0.456	0.356	0.78	0.021	0.855
350	0.171	0.423	0.355	0.789	0.028	0.889
400	0.169	0.389	0.289	0.677	0.029	0.89
450	0.168	0.389	0.219	0.654	0.032	0.929
500	0.169	0.378	0.17	0.644	0.027	0.877
600	0.168	0.378	0.169	0.655	0.027	0.876
700	0.168	0.345	0.17	0.64	0.025	0.875
800	0.168	0.336	0.17	0.64	0.027	0.875
900	0.168	0.334	0.171	0.639	0.025	0.877

Fig. 5(a) depicts the RMSE values of training for all the three-membership function. It can be observed that at 400 epoch iterations, training RMSE of gaussmf almost reaches a stable value. At 500 epoch iterations, training RMSE of gbellmf and trimf reach stable values. Further increase in the number of epochs may not yield any significant results in predictions causing overfitting of the models. Fig. 5(b) depicts that testing RMSE values of gaussmf is less than the gbellmf and trimf, meaning ANFIS-gaussmf model with least testing RMSE value of 0.334 predicts accurately. And trimf with 0.877 testing RMSE performs the worst in predictions.

A. ANFIS for Online/e-Learning Mode

Table II displays the training and testing RMSEs for online mode learning approach for the three types of mfs of ANFIS.

Fig. 6 depicts MSE values of training and testing against the number of epochs for all the three membership functions for online mode of learning; and trimf behaviour is found to be worst as the testing RMSE is very high with 0.878 against a very low training error of 0.057. It can be observed that gaussmf and gbellmf both perform very well with 0.284 and 0.289 testing RMSEs respectively. ANFIS-gaussmf and ANFIS-gbellmf, both models perform very similar to each other in predicting the performances of students studied through online mode.

Fig. 7(a) depicts the RMSE values of training for all the three-membership function. It can be observed that at 500 epoch iterations, training RMSE of all the three mfs reach stable values. Further increase in the number of epochs may not yield any significant results in predictions causing overfitting of the models. Fig. 7(b) depicts that testing RMSE values of gaussmf and gbellmf are almost same and are very low compared trimf, meaning ANFIS-gaussmf model and ANFIS -gbellmf model predict accurately. And trimf with 0.878 testing RMSE performs the worst in predictions.

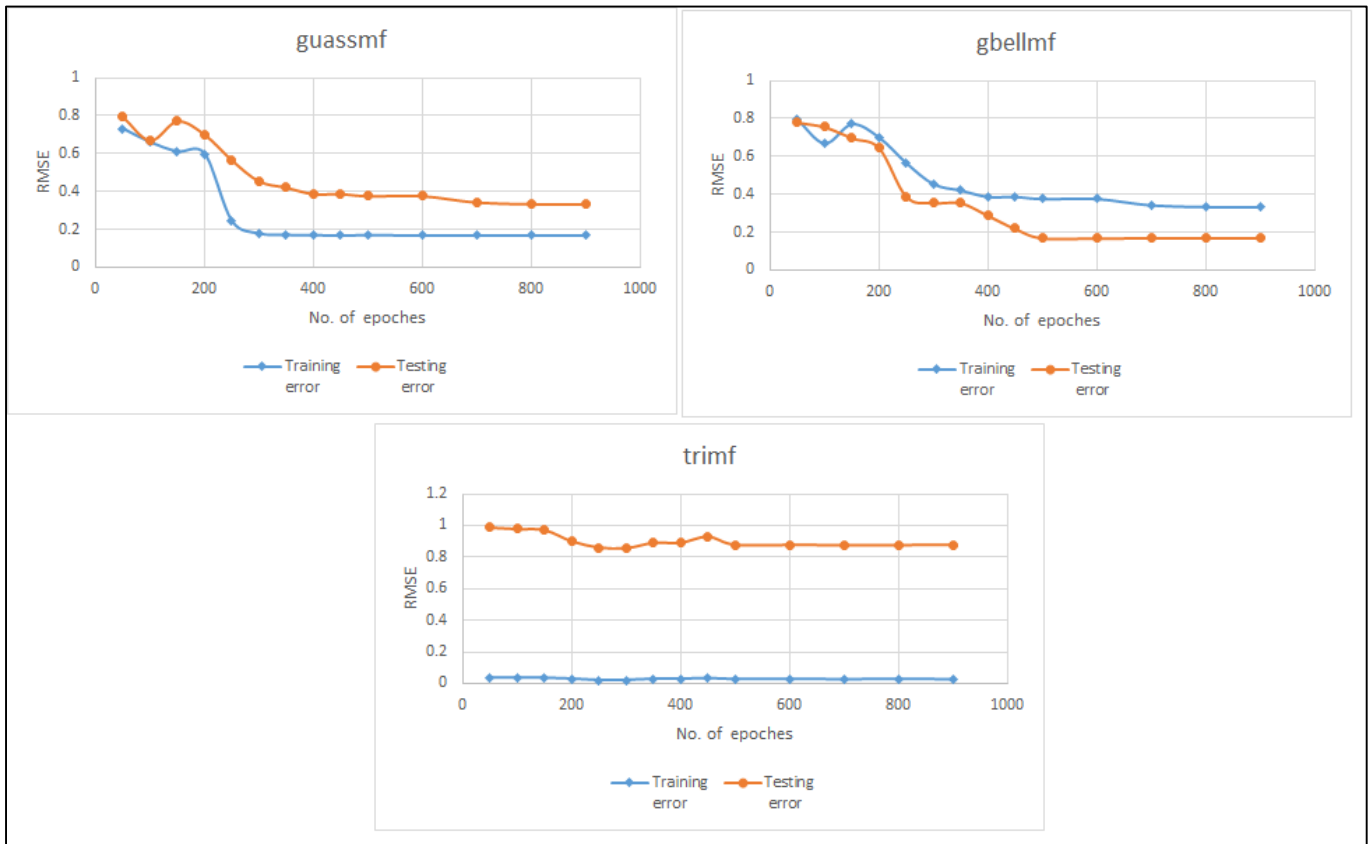


Fig. 4. Training and Testing RMSEs vs the Number of Epochs (a) Guassmf (b) Gbellmf (c) Trimf, for Offline Mode Predictions.

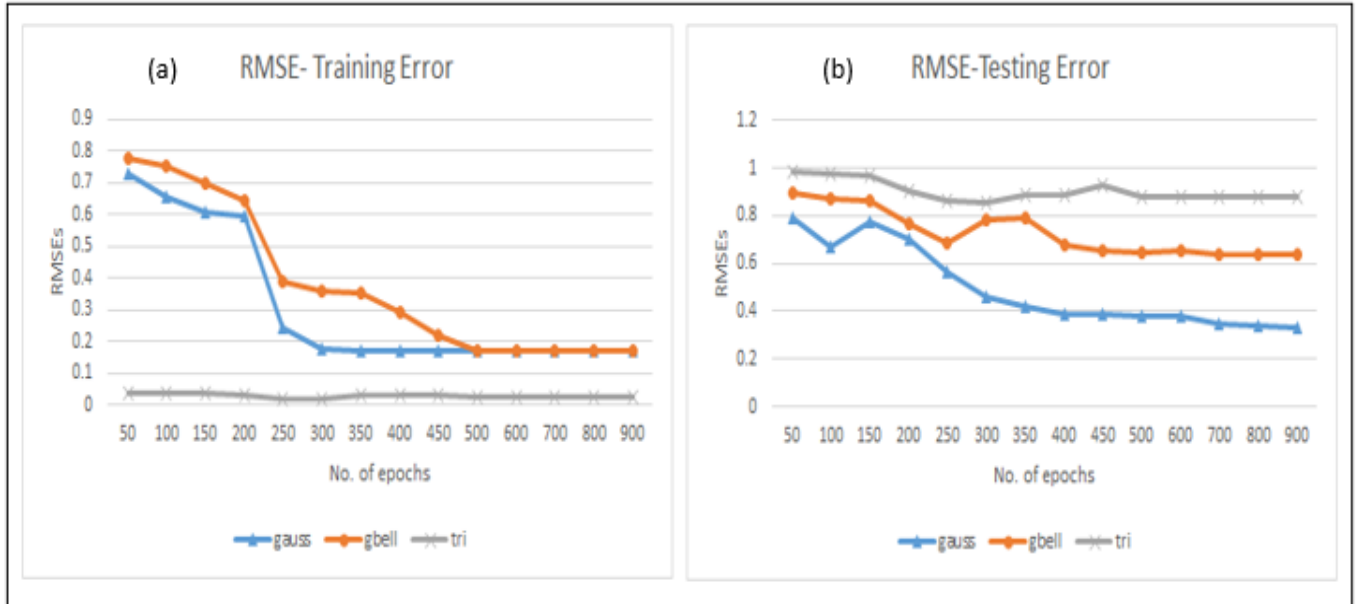


Fig. 5. Training RMSEs of 3 Mfs and Testing RMSEs of 3 Mfs for Offline Mode Predictions.

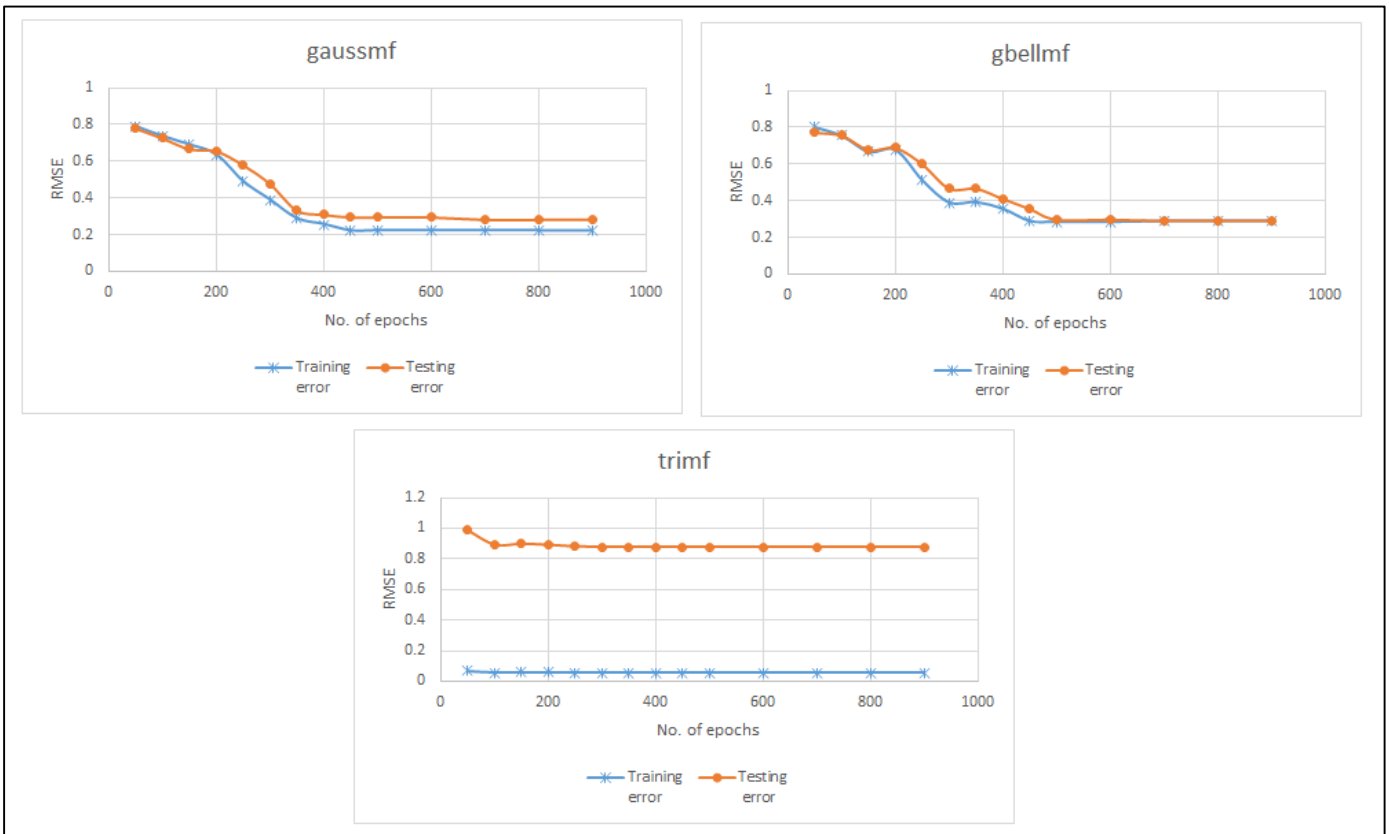


Fig. 6. Training and Testing RMSEs vs the Number of Epochs (a) Guassmf (b) Gbellmf (c) Trimf, for Online Mode Predictions.

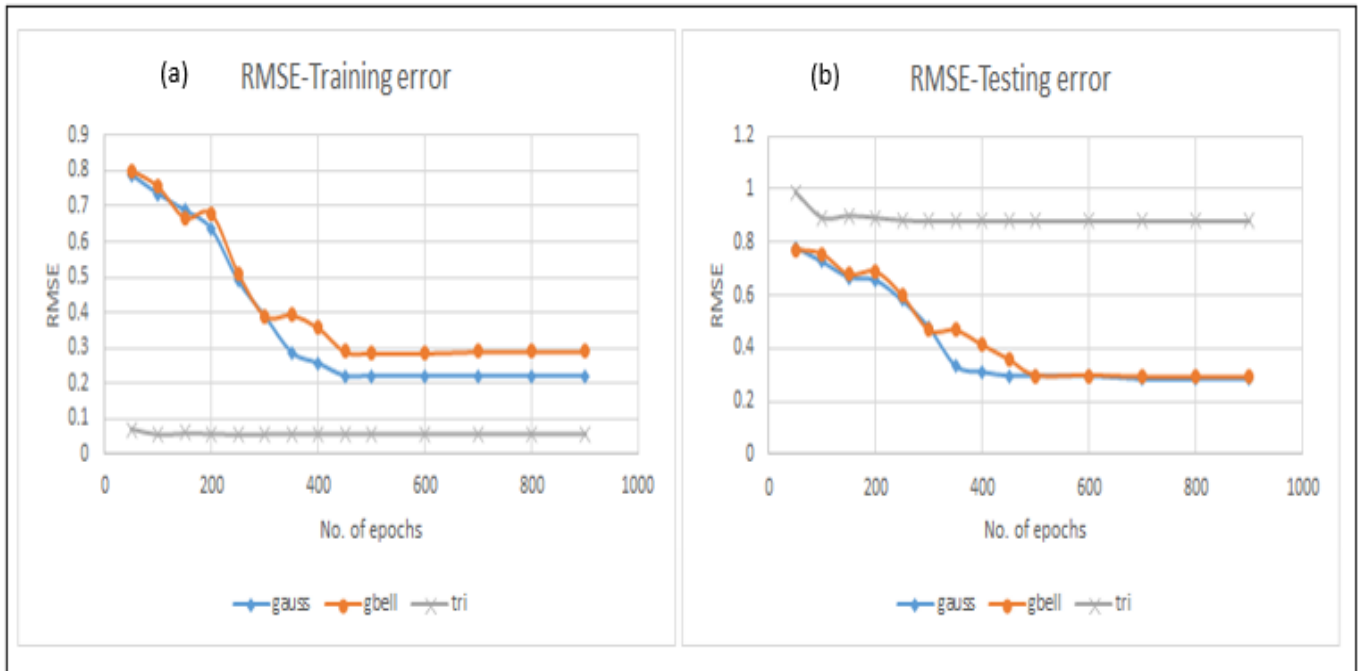


Fig. 7. Training RMSEs of 3 Mfs and Testing RMSEs of 3 Mfs for Online Mode Predictions.

TABLE II. TRAINING AND TESTING RMSES OF GAUSSMF, GBELLMF AND TRIMF WITH DIFFERENT EPOCHS FOR ONLINE MODE

MFs	GaussMF		GbellMF		TriMF	
	Trainin g error	Testin g error	Trainin g error	Testin g error	Trainin g error	Testin g error
50	0.789	0.779	0.801	0.773	0.0697	0.989
100	0.735	0.725	0.755	0.756	0.056	0.892
150	0.689	0.667	0.667	0.678	0.059	0.899
200	0.635	0.655	0.678	0.689	0.058	0.891
250	0.489	0.58	0.511	0.599	0.056	0.881
300	0.389	0.478	0.39	0.467	0.057	0.878
350	0.287	0.334	0.392	0.467	0.057	0.878
400	0.256	0.311	0.356	0.411	0.057	0.878
450	0.221	0.297	0.289	0.356	0.057	0.878
500	0.221	0.297	0.284	0.297	0.057	0.878
600	0.221	0.297	0.284	0.297	0.057	0.878
700	0.221	0.284	0.289	0.291	0.057	0.878
800	0.221	0.284	0.289	0.291	0.057	0.878
900	0.22	0.284	0.289	0.291	0.057	0.878

B. Comparison of Offline and Online ANFIS Models

Table III depicts training and testing RMSE of all three ANFIS mfs for epoch 900 for offline and online learning modes referring to the Tables.

TABLE III. RMSE COMPARISONS OF 3 MFS FOR OFFLINE AND ONLINE MODES

Learning Modes	MFs	GaussMF		GbellMF		TriMF	
	No. of Epochs	Train ing error	Test ing error	Train ing error	Test ing error	Train ing error	Test ing error
	offline mode	900	0.168	0.334	0.171	0.639	0.025
online mode	900	0.22	0.284	0.289	0.291	0.057	0.878

Training and testing RMSE for ANFIS-gaussmf are 0.22 and 0.284; and training and testing RMSE for ANFIS-gbellmf are 0.289 and 0.291. These gaussmf and gbellmf RMSE values of online learning mode show that training and testing RMSEs are almost same without a large variation. And offline mode’s ANFIS-gaussmf testing RMSE (0.334) is larger than the online mode’s testing RMSE ANFIS-gaussmf (0.284); means predicting the performances of student results in online mode is superior and accurate compared to offline predictions.

VI. CONCLUSION

Before the Covid-19 students used to learn engineering subjects through physical i.e., classroom or offline mode by attending classes. At the end of semester students are assessed to check their performances by writing semester end examinations (SEE). As Covid-19 pandemic begun, these offline classes were totally suspended and e-Learning or online

mode of learning using Internet and mobile devices took over the education in a different direction. Online mode in the education domain has initiated a new paradigm shift. So, the students learned through online mode during the pandemic and also SEE were conducted after the semester end. So, there is a need to analyse and predict which mode of education (online or offline) impacted the student’s learning process and improve the learning curve by increasing the performances. This article illustrated the ANFIS approach to model and predict the students’ performances obtained through both modes of learning. Firstly, ANFIS for offline mode was built and found that ANFIS-gaussmf predictions are better. Secondly, ANFIS for online mode was built and found that ANFIS-gaussmf and gbellmf, both predicted the same and well performed. In both, ANFIS-trimf performed very worst. Finally, ANFIS-online mode performed very well compared to ANFIS-offline mode i.e., predicting the performances of student results in online mode is superior and accurate compared to offline predictions.

REFERENCES

- [1] Sterbini, A., & Temperini, M. (2012). Correcting open-answer questionnaires through a Bayesian-network model of peer-based assessment. 2012 International Conference on Information Technology Based Higher Education and Training (ITHET). <https://doi.org/10.1109/ithet.2012.6246059>.
- [2] Smadi, M., Wesiak, G., Guetl, C., & Holzinger, A. (2012). Assessment for/as Learning: Integrated Automatic Assessment in Complex Learning Resources for Self-Directed Learning. 2012 Sixth International Conference on Complex, Intelligent, and Software Intensive Systems. <https://doi.org/10.1109/cisis.2012.210>.
- [3] Cherry, S. M. (2003). The wireless last mile. *IEEE Spectrum*, 40(9), 18–22. <https://doi.org/10.1109/mspec.2003.1228003>.
- [4] Gayeski, D., & Russell, J. D. (2003). Learning unplugged: Using mobile technologies for organizational training and performance improvement. *Performance Improvement*, 42(9), 41–43. <https://doi.org/10.1002/pfi.4930420910>.
- [5] Romero, C., & Ventura, S. (2010). Educational Data Mining: A Review of the State of the Art. *IEEE Transactions on Systems, Man, and Cybernetics, Part c (Applications and Reviews)*, 40(6), 601–618. <https://doi.org/10.1109/tsmcc.2010.2053532>.
- [6] Baker, R. S., & Inventado, P. S. (2014). Educational Data Mining and Learning Analytics. *Learning Analytics*, 61–75. https://doi.org/10.1007/978-1-4614-3305-7_4.
- [7] Chamizo-Gonzalez, Julian, Elisa Isabel Cano-Montero, Elena Urquía-Grande, and Clara Isabel Muñoz-Colomina. Educational data mining for improving learning outcomes in teaching accounting within higher education. *International Journal of Information and Learning Technology*, 32(5), 272–285. <https://doi.org/10.1108/ijilt-08-2015-0020> Chamizo-Gonzalez, J., Cano-Montero, E. I., Urquía-Grande, E., & Muñoz-Colomina, C. I. (2015).
- [8] Sharma, A., Kumar, R., Varadwaj, P. K., Ahmad, A., & Ashraf, G. M. (2011). A comparative study of support vector machine, artificial neural network and Bayesian classifier for mutagenicity prediction. *Interdisciplinary Sciences: Computational Life Sciences*, 3(3), 232–239. <https://doi.org/10.1007/s12539-011-0102-9>.
- [9] Huang, S., & Fang, N. (2013). Predicting student academic performance in an engineering dynamics course: A comparison of four types of predictive mathematical models. *Computers & Education*, 61, 133–145. <https://doi.org/10.1016/j.compedu.2012.08.015>.
- [10] Bhardwaj, B. K., & Pal, S. (2011). [Review of Data mining: a prediction for performance improvement using classification]. *International Journal of Computer Science and Information Security*, 9(4), 1–5.
- [11] Nghe, N. T., Janecek, P., & Haddawy, P. (2007). Review of A comparative analysis of techniques for predicting academic performance]. *Proceedings of the 37th ASEE/IEEE Frontiers in Education Conference (FIE '07)*, T2-G7.

- [12] Yukselturk, E., Ozekes, S., & Türel, Y. K. (2014). Predicting Dropout Student: An Application of Data Mining Methods in an Online Education Program. *European Journal of Open, Distance and E-Learning*, 17(1), 118–133. <https://doi.org/10.2478/eurodl-2014-0008>.
- [13] Jang, J.-S. .R. (1993). ANFIS: adaptive-network-based fuzzy inference system. *IEEE Transactions on Systems, Man, and Cybernetics*, 23(3), 665–685. <https://doi.org/10.1109/21.256541>.
- [14] Dick, S. (2002). A review of: “Neuro-Fuzzy Pattern Recognition Methods in Soft Computing” Sankar K. Pal and Sushmita Mitra John Wiley & Sons, New York, 1999, 375 pp., ISBN 0-471-34844-9. *IIE Transactions*, 34(6), 585–587. <https://doi.org/10.1080/07408170208936921>.
- [15] Singh, R., Kainthola, A., & Singh, T. N. (2012). Estimation of elastic constant of rocks using an ANFIS approach. *Applied Soft Computing*, 12(1), 40–45. <https://doi.org/10.1016/j.asoc.2011.09.010>.
- [16] Kai Warendorf. (1997). (Su Jen Tsao1997., Ed.; pp. 113–146). *J. Artif. Intell. Educ.*
- [17] Di Lascio, L., Gisolfi, A., & Loia, V. (1998). Uncertainty processing in user-modelling activity. *Information Sciences*, 106(1-2), 25–47. [https://doi.org/10.1016/s0020-0255\(97\)10009-3](https://doi.org/10.1016/s0020-0255(97)10009-3).
- [18] P. Ajith, B. Tejaswi, & M.S.S.Sai. (2013). Review of Rule Mining Framework for Students Performance Evaluation. *International Journal of Soft Computing and Engineering (IJSCE)*, 2(6), 201–206. Retrieved from <https://www.ijscce.org/wp-content/uploads/papers/v2i6/F1157112612.pdf>
- [19] Jai Ruby, & K David. (2014). Review of Predicting the Performance of Students in Higher Education Using Data Mining Classification Algorithms-A Case Study. *International Journal for Research in Applied Science & Engineering Technology*, 2(9), 173–180.
- [20] Naser, S. A., Zaqout, I., Ghosh, M. A., Atallah, R., & Alajrami, E. (2015). Predicting Student Performance Using Artificial Neural Network: in the Faculty of Engineering and Information Technology. *International Journal of Hybrid Information Technology*, 8(2), 221–228. <https://doi.org/10.14257/ijhit.2015.8.2.20>.
- [21] Stathacopoulou, R., Grigoriadou, M., Magoulas, G. D., & Mitropoulos, D. (2003). A Neuro-fuzzy Approach in Student Modeling. *User Modeling 2003*, 337–341. https://doi.org/10.1007/3-540-44963-9_46.
- [22] Barber, R., & Sharkey, M. (2012). Course correction. *Proceedings of the 2nd International Conference on Learning Analytics and Knowledge - LAK '12*. <https://doi.org/10.1145/2330601.2330664>.
- [23] Hawkes, L. W., & Derry, S. J. (1996). Advances in local student modeling using informal fuzzy reasoning. *International Journal of Human-Computer Studies*, 45(6), 697–722. <https://doi.org/10.1006/ijhc.1996.0075>.
- [24] Xenos, M. (2004). Prediction and assessment of student behaviour in open and distance education in computers using Bayesian networks. *Computers & Education*, 43(4), 345–359. <https://doi.org/10.1016/j.compedu.2003.09.005>.
- [25] Fadi R.S (2012). Data Mining in M-Learning Domain. *Trends in Innovative Computing- Information Retrieval and Data Mining*, 57-60. <http://www.mirlabs.net/ict12/download/Paper11.pdf>.
- [26] Srdjan Jovic, Jasmina Smigic Miladinovic, Radmila Micic, Sanja Markovic, Goran Rakic (2019). Analysing of exchange rate and gross domestic product (GDP) by adaptive neuro fuzzy inference system (ANFIS). (2019). *Physica A: Statistical Mechanics and Its Applications*, 513, 333–338. <https://doi.org/10.1016/j.physa.2018.09.009>.
- [27] Suparta, W., & Alhasa, K. M. (2015). Adaptive Neuro-Fuzzy Interference System. *SpringerBriefs in Meteorology*, 5–18. https://doi.org/10.1007/978-3-319-28437-8_2.

Combining Innovative Technology and Context based Approaches in Teaching Software Engineering

Shamsul Huda¹, Sultan Alyahya^{2*}, Lei Pan³, Hmood Al-Dossari⁴

School of IT, Deakin University, Melbourne VIC 3125, Australia^{1,3}
Information Systems Department, King Saud University, Riyadh 11451, Saudi Arabia^{2,4}

Abstract—Sustainability in learning is very essential for a sustainable future which largely depends on education. Sustainable learning requires learners to increase and rebuild base-knowledge as the circumstances change and get more complex. This becomes very obvious particularly for information technology (IT) discipline where technology is rapidly changing and practice getting more complicated. Sustainability enables students to use their learning from formal education into practice, provide hands on experience (HOE) and help them rebuild their knowledge base in complex situations. This is also essential to achieve a high graduate outcome rate (GOR) which helps the education sector to become sustainable. In the existing policies and frameworks, institutions are moving towards more off-campus learning and less face-to-face learning. As a result, a downward trend is experienced in students' engagement across IT discipline. This affects students' ability in achieving HOE and appears to be one of the reasons of low GOR which poses a threat to the sustainability in the education sector for both stakeholder and learners' perspectives. This paper presents a combined approach of context-based teaching with incorporation of innovative technology to engage students and achieve a better HOE towards sustainability in learning. The proposed approach was adopted in a software engineering course taught at School of IT at Deakin University, Australia. Students were provided context-based teaching material and industry standard software engineering tools for practice to achieve HOE. Students evaluation and assessment results reports that proposed approach was significantly impacted positively to engage the students in classes towards improved sustainable learning.

Keywords—Sustainable learning and education; context-based teaching; work integrated learning; hands on experience; graduate outcome rate; positive attitude and engagement

I. INTRODUCTION

Sustainability in our future [41] and societies is not easily achievable unless our learning and education sector is sustainable [34], [35], [39]. Therefore sustainability in learning [40] has drawn much attention from many education providers, researchers and stakeholders of sustainable development programs [34], [35], [39]. If education itself is not sustainable then achieving the factors for sustainable development and global citizenship programs is hard to be successful [34], [35]. Sustainable learning is not only limited to the retaining the knowledge [35]. But it is more towards the rebuilding of knowledge and skill-base dynamically as the circumstances change and get more complicated [35], [5]. IT discipline and related industries are facing massive technological evolution [30]. Therefore, sustainable learning is getting more essential component for IT discipline [6].

Sustainable learning requires learners to be proactively engaged in learning from past and present following a constructivist approach that enable them to relearn the knowledge, achieve more HOE and then take the new knowledge into practice for an ever-changing technological discipline [37]. From the stakeholders and business perspective, large-scale investments are also required in the education sectors for sustainability [34]. Therefore, existing policies and educational frameworks are moving towards more on extended off-campus learning and less face-to-face learning. Following the emergence of the pandemic, many institutions are also interrupted from their usual face-to-face learning and are forced to go off-campus/on-line learning [39]. It has been observed a downward tendency in students' proactive engagement which affects achieving HOE and thereby sustainability in learning.

In the information technology discipline, HOE have been explored in many studies [1], [2]. Patricia et al [1] found that more participation on hands on activities help students to achieve higher scores in a standard science-achievement test. Atanas Serbezov [2] et al. showed that students in this discipline need to understand the fundamental working principles of the field instruments' and how these can be integrated into an overall industrial systems in engineering. Literature studies [1],[2] indicate that the main objective of the universities is to provide education to the students in the fundamental areas of the engineering discipline. At the same time, universities need to extend the educational activities to make the educational programs more market oriented and relevant to the corresponding industry trend. Atanas Serbezov [2] et al. found a total of 10% increase in GOR in their quantitative study across few years while they included industry engagement as part of their learning activities.

Sustainable learning in IT discipline requires effective practice in classes to improve HOE by providing students with a real life experience aligned to the theoretical lecture classes. Therefore, many education providers are investigating and testing different ways of teaching methods including located mode practical classes, simulated laboratories, remote laboratories [3], [4] and combination of those [5], [6]. The purpose of these innovative teaching approaches is to engage students and provide HOE which make them ready for the job market after their graduation. In the IT discipline, many software/tools for practical classes are collected from open source or organized from different sources which generally are behind from the dynamic industry market [5]. In many evaluation frameworks [5], with these tools and software

*Corresponding Author.

support for achieving the learning outcome, due to the frequency of practical classes, volume of submissions and complexity of the evaluating the assessments many practical classes are not well assessed. Students are often assessed based only on their summative assessment tasks or based on a combination of assignments and practical assessment tasks with practical assessment tasks have less fraction of total assessment marks of the subject. Therefore, students' participation has been declining in the practical classes in IT discipline across different institutions. This is a concern considering student engagement that results a cohort of technology graduates with inadequate domain knowledge which is a primary obstacle in the pathway of sustainable learning. In achieving successful learning outcome and relearn through deconstruction and reconstruction, student's attitude, motivation and engagement are important [10], [9] which are the key factors for sustainable learning. Therefore many innovative teaching approaches including context-based teaching methods, inquiry-based teaching methods and incorporation of innovation technologies in engineering and IT teaching have been adopted [11], [12]. In [13], Bennett et al. have completed a systematic review and have found that context-based teaching and incorporation of innovation technologies in teaching that worked effectively in developing positive attitude in students' learning activities.

Context-based approaches improve the learning materials and curriculum, then uses different context and applications of the theories in learning activities. Students learn how their learning outcomes can be applied in real life. Many researchers [14], [15], [16] have found that context-based approaches are useful and change students' attitude positively in achieving learning outcomes. However, context-based approaches may vary from discipline to discipline and within a particular discipline the approaches may vary over time. For example, innovation in technology for IT is very fast. This fact significantly affects the industrial market and also changes the job criteria for the graduate. Students need to be able to have a certain level of early experiences which should be achieved through their education in order to get into the job market. To achieve the learning outcomes and be up to date with the fast technological evolution, several factors need to be considered. Approaches to increase the positive attitude in learning activities and engage students into the activities is a possible direction of improvement in achieving hands on experience.

It also has been observed that applications of innovative technologies [17], [18] in teaching approaches including computer simulation, multimedia applications, online assessment process and visualization techniques have led to more positive attitude which motive students to engage and provide them enjoyment during their learning session. For ITE discipline, the use of IT tools and techniques is obvious and most of the intuitions are applying these in their teaching activities. For IT students, these approaches appear to be standard practices and may not be much motivating factor. A more motivating approach will be an approach that can give students hands on experiences (HOE) in the engineering methods and techniques, tools software in IT which will be beneficial immediately after their graduation. In this research, a combination of the above two approaches will be used which

combines context-based and incorporation of innovative technology in order to engage students, relearn knowledge from past and achieve better hands on experiences (HOE). The procedure will incorporate commercially popular tools/software in the learning activities for students' engagement and will provide related learning resources. Improvement of learning material will be done progressively and its practice will be completed in practical classes.

The rest of the paper is presented as following. Section II discusses the related work. Section III discusses proposed methodology (Materials and methods), data analysis and performance measures. Section IV presents the result of this study and last section discusses the conclusions of this study.

II. RELATED WORK

A. Sustainable Learning and Education (SLE) in the Current Literature

To achieve sustainability from stakeholder perspective, educational institutions are moving towards more off-campus education [33]. Therefore sustainability in learning and education is a rapidly growing research area. Jay Hays, Hayo Reinders [34] proposed a detailed curriculum for SLE and identified the expected learning outcome. They also made a conclusion on the principles of sustainable learning. Mina Chiba [34] presented a detailed review of effective teaching methods for sustainable development and global citizenship. Asmat Ara Shaikh, Anuj Kumar et.al, [36] investigated application of artificial intelligence (AI) and its sustainable impact on online learning for off-campus classes. They find that AI is useful in automated identification of gap in learning. Fatma [37] proposed a discriminant analysis technique to predict teachers view towards sustainable education. Fatma [37] concluded that criteria for curricula evaluation and students centered teaching are the key factors that identify teachers' dispositions for sustainable education. O. Polyakova and R. Galstyan-Sargsyan [38] studied tele-collaboration based sustainable education systems. They find that plurilingual competence can be developed in tele-collaboration which helps sustainable university training. Alvyra Galkiene' et al [39] has investigated modeling of the sustainable educational on a group of vulnerable learners and they find that innovative technologies such as digital tools have a positive impact on vulnerable students for sustainable education. Existing literature has a gap to understand how a better HOE can be achieved towards sustainable learning. The problem of achieving high HOE gets more complicated for off-campus students. Many research studies and practices in engineering have been accomplished to address this issue. Considering the importance of HOE in higher education, many teaching approaches have been studied in different literature [1]-[10], [11]-[16], [19] including remotely operated laboratory for off-campus students, simulated laboratory for off-campus and on-campus students, and students' placement and work integrated learning.

B. Remotely Operated Laboratory for off-campus Students

Mihaela M. Albu et al. [3]-[4] have shown a remote operation of power engineering instruments can be used for off-campus students. In these cases [3]-[4] the authors find

that if machines constraints are properly implemented such that students cannot do any mistake beyond the normal operating conditions, then the experimental environment can be set up successfully. However, this study has shown that the approach has limitations where students cannot have full experiences of field experiences in using the power instruments for abnormal situations. In a real life situation, power instruments can go to abnormal condition frequently.

C. Simulated Laboratory for off-campus and on-campus Students

In contrast to remote operated laboratory, simulated laboratory and simulations tools are very common approaches in IT and Engineering discipline. A simulated laboratory is an experimental environment which uses internet, information technology tools [5]-[6], programs and multimedia and networking facilities to simulate a real experimental environment. These approaches are used particularly in Engineering and IT discipline where instruments are very expensive or experiential processes are risky. For example, in IT discipline, conducting experiments for different types of targeted attack on a computer or a network, testing firewall vulnerabilities and cyber warfare in real environment is highly risky. Most classroom experiments use simulated network environment or a combination of simulated and real environment. Simulated tools are beneficial for off-campus education as well. A review [5] shows that simulations tools have many limitations. Many simulation tools [5] cannot facilitate performance analysis, available only for limited protocol, not fault-tolerant, inadequate Graphical User Interface (GUI) and have limited documentation which makes them difficult for off-campus education. A comprehensive study by Muhammad Azizur Rahman [5] on network simulation tools shows that these tools often can reach incorrect implementation solution due to lack of generalization and rigor. To overcome these and in order to provide HOE, a combination of real and simulation environment can be provided. Sushil K. Sharma et al [6] presented a case study on information security education hands on approach at Ball State University, USA for three courses where every course had 20-25 students. It is seen in this study [6] that students were highly engaged in the courses and participation in practical classes was maximum compared to other courses. This kind of real experimental environment provides students HOE and are fruitful for students' engagement as students enjoy the classes and get excited which they cannot do using simulation tools at their home environment. However authors [6] did not mention about any result whether this approach was considered for off-campus students. Literature studies [5]-[6] show that one of the difficulties for many IT courses in IT discipline is many experiments require real environment including security and hardware related subjects which are difficult to offer for the off-campus students due to inability to support for practical classes.

D. Students' Placement and Work Integrated Learning

Students' placement and work integrated learning are also used to provide students with a real life experiences achieve HOE in engineering and IT discipline in many institutions. Work integrated learning (WIL) extends the formal university

studies with a placement in work place before they graduate. WIL can be organized at the end of program or every year or in any particular course. Particularly in engineering and medical discipline [7]-[8] this is compulsory in most of the institution's undergraduate programs. Statistical analysis and research [7]-[8] show that the approaches have been able to fill the gap of students' understanding about the theory and its application in practical work.

E. Gamification Approach of Engaging Students and HOE

In many research studies [26]-[28] gamification has been used for educational process which was successful in engaging students that improved students' motivation towards learning and assessment activities. Gamification process in teaching is defined as the transference of game design in teaching activities to increase students' motivation in learning [28]. Often this process allows students to achieve an instant reward based on their progress in the classroom tasks [26]. In [28], the authors accomplished a study based on gamification with cohort of 97 students which demonstrated a positive impact on students' attitude and achievement. Li Ding, Chan Min Kim et al [29] used a gamification approach in online discussion forum and developed a tool named 'gEchoLu' to investigate the effect of specific game in the tool for engagement. Flipping the class model is a popular approach of engaging students in learning activities. Jingying Wang et al. [25] used a combination of flipping model and innovative technology to engage students. They find that the combined method was successful in knowledge construction and improved the transfer of new knowledge. Curtis R. Henrie, Lisa R. Halverson, Charles R. Graham [30] provides a detailed review on student engagement using innovative technology. In this review [30], they mentioned the limitations and strengths of technology mediated teaching. They [30] find that evaluation of technology-mediated teaching can provide meaningful student engagement data. In [30], it is observed that quantitative observational measures are effective at the activity level which disrupts comparatively less to the students in learning during data collection but expensive.

F. Campus-Class-Technology (CCT) Theory in Engagement

CCT theory was proposed by Selim Gunuc [31] who explained the relationship between technology and student engagement. CCT theory describes that the value given by the student in their university life is one of the important factors for which students have the sense of belonging to a university. Then CCT theory continues a cyclic path which states that academic achievement have influence on the value for which students have the sense of belonging to a university. CCT theory [31] shows that technology is the prime factor which contribute to the student engagement. In [32] Selim Gunuc tested CCT theory with path analysis which was conducted on 332 teachers and students. It was observed that value of belonging positively impacted emotional engagement which predicted behavioral and cognitive engagement. It shows that the use of technology in class was an important factor in student engagement. Although different approaches have been adopted to engage students. In the literature, student engagement in the context of HOE was not revealed much. Therefore, achieving HOE for students still is a crucial research problem for institutions due to the dynamic job

market, changes in technologies and cost due to organize the tools/equipment for engaging students. Therefore, it is important to investigate more on student engagement and achieving HOE.

III. MATERIALS AND METHODS

Research [11]-[13] shows that students' positive attitude and engagement affect largely not only in achieving HOE but also in accomplishing other theoretical learning activities. Therefore engagement has been active research keywords in teaching and learning domain for long time. Many approaches have been proposed including active learning [22], context-based teaching method, inquiry-based teaching method [11]-[13], flipped classroom [20], incorporation of innovation technologies in science teaching have been proposed. Flipped class room allows the students to complete their homework in lecture class time and traditional class activities are accomplished at home [20]. In this case, students watch the lecture video, read the lecture notes and additional reading at home. This is a new instructional model and it is observed that this model helps students to be engaged in the class, particularly for lecture classes. A review of different flipped models has been presented in [21]. However, if there is a downward tendency in attendance in practical classes in the current setup, then flipped model may not be a good choice. In contrast, context-based teaching approaches introduces attractive learning materials in which learning activities are designed based on the application of the theories [14]-[16] with varying context and real life examples. Several research studies [17]-[18] show use of innovative technology including visualization, simulation model of real environment, has also been useful for positive attitude of students towards learning activities. Earlier studies [13]-[16] on students' attitude shows that context-based teaching method and incorporation of innovation technologies in engineering teaching have been effective to gain positive attitude of students towards learning activities. This draws an attention for current studies to focus on these methods [14]-[16] since HOE is more related to context-based approach where learning context varies as technology changes. In addition, inclusion of innovative technology [17]-[18], [30]-[32] can attract students' attitude which can be made available in the practical classes. Based on the literature review, a hybrid model has been proposed that combines the context-based teaching and incorporation of innovative technology. In this context, the proposed approach resembles the active learning approaches [22] in the practical classes where students accomplish meaningful real-life learning activities and can think about what they are doing. However, proposed approach not only considers the meaningful activities, but also considers innovative learning tools to engage students and at the end of practical learning sessions may provide higher level of HOE.

A. Research Design and Procedure

The proposed methodology incorporates attractive industry-aware content and tools/ software which will cover both traditional theories and industry practices in the lecture content of the course. Then those lecture contents are made related to context-oriented practical classes where students will have the activities related to contemporary industry

practices. The assessments will also include the tasks based on the weekly practical classes. The procedure will incorporate innovative commercial software/tools in the learning activities for practical classes and will be made available for off-campus students. Context-based learning material will be delivered progressively on a weekly basis in both lecture and practical classes.

B. Case Study and Data Analysis

The proposed methodology considers the "Software engineering" course as a testbed as the target discipline is engineering and IT. As part of the process, new context-based learning materials have been introduced from the beginning of the trimester in the lecture class in every week. The topics have been selected through the literature study and industry practices, based on author's own industry experiences and through the consultation with industry experts. The industry consultation has been performed with a renowned software modeling expert in Sparx systems, Australia [24]. Participants are post-graduate students.

C. Design of Lecture-practical Content and Assessment Tasks

Summative assessment task is considered for main evaluation of students' engagement and achievement of HOE. The course has two assignments and final examination. During each week, there is an ungraded formative assessment task. For comparison of the proposed methodology, the assessment tasks have been designed such that main objective of the tasks remain same as the previous year. However, the approach of solving the assessment tasks should be based on the new industry practices and context-based teaching. In every lecture, new contents have been added which are practiced in the industry. A typical assessment task is to prepare an analysis and design report to improve an existing web application by identifying new services (epics) where services should include dynamic content update, functional processing, and navigation and over all presentation of the existing web site. The whole analysis process should include modern agile scrum approaches, target is to prepare different artifacts such as personas, a product story map backlog, use UML profile [24] to prepare content and process class models, navigational and functional models and sprint backlog for the proposed services. An example of context-based material is given below: Students need to develop a process class model from the user-interaction scenario of a web application. Students need to keep in mind that the model should be useable later stage in the navigation design and implementation of the application.

1) *Engagement fact in the lecture material:* How to integrate processes in the navigation when any user interaction requires the system to response to the users and; the processes should be visible or system's internal processes. This integration requires students to think and find the processes by investigating the user interaction scenario for the web application. In every lecture, a number of context-based facts were included in order to engage the students. For example, for the above topic, students were shown an example piece of code where the processes from their process model could be used and the way practically it is done using a real

programming environment. In this case, it has been shown to the students the relationship between a Java Server Programming (JSP) technique [42] and Java Bean (JB) instantiation [42] of process classes with their design process classes. These techniques (JSP and JB) [42] are very popular in the current industry practices and students will achieve industry standard HOE through the learning process.

2) *Context-based and innovative industry practice/ activities in the practical classes:* In practical classes students had to use the most popular industry standard software engineering tool “Enterprise Architect (EA)” [24] to design the above models. For example, to relate the theory of lecture with practical, in the practical class, it also has been demonstrated how the code is generated from their design and relationship between design and generated code. That will give them ability to maintain the design and code in future.

3) *Design of assessment task:* Assessment tasks were assigned group wise and were designed so that students must follow the industry standard tool using EA. An assignment group consists of two students. In the first assignment, students have been advised to use supplied commercial

software engineering tool. In the second assignment, it was mandatory to use the provided tool (EA) [24]. In addition to this, the second assignment includes more tasks related to industry practices such as development of Unified Modeling Language (UML) profile [43] and use of the UML profile [43] in their design, development and integration of the data model in the navigational and functional design for a selected web application. An example in the assignment was related to the lecture content where students were asked to develop the analysis and design model of a web application. Students will complete different analyses including content, interaction, functional, configuration and relationship-navigation as part of the requirement analysis. Then students need to prepare different design models including content, navigation, functional, architecture, component and web application extension UML (WAE) model [44]. A part of the assignment task was to prepare the conventional analysis and design models and then integrate this with UML profiling [43]. A part of a sample design task is presented in Fig. 1, Fig. 2 and Fig. 3.

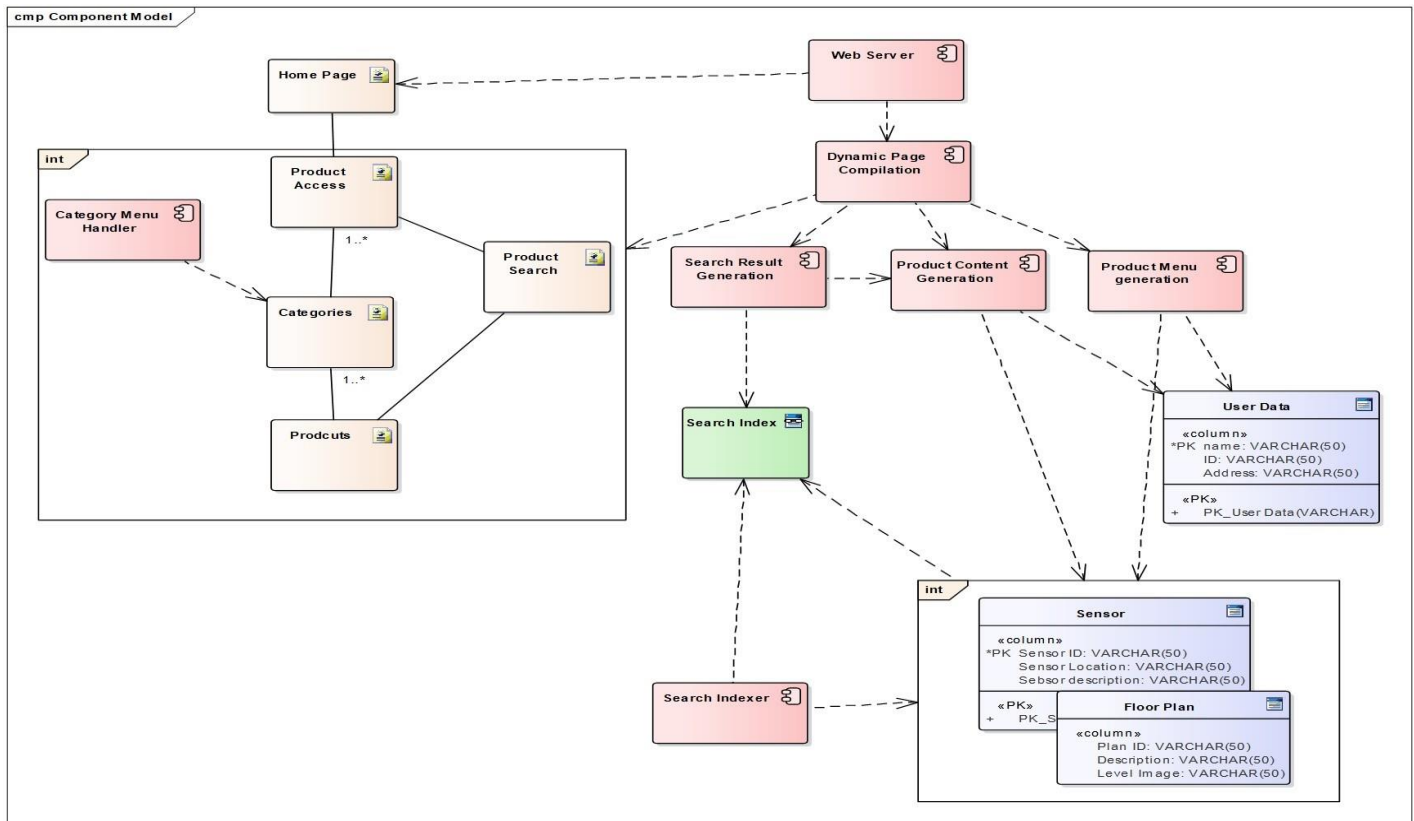


Fig. 1. A Functional Architecture of a Safe Home Web Application. The Design has been Redeveloped using EA following the Source[23].

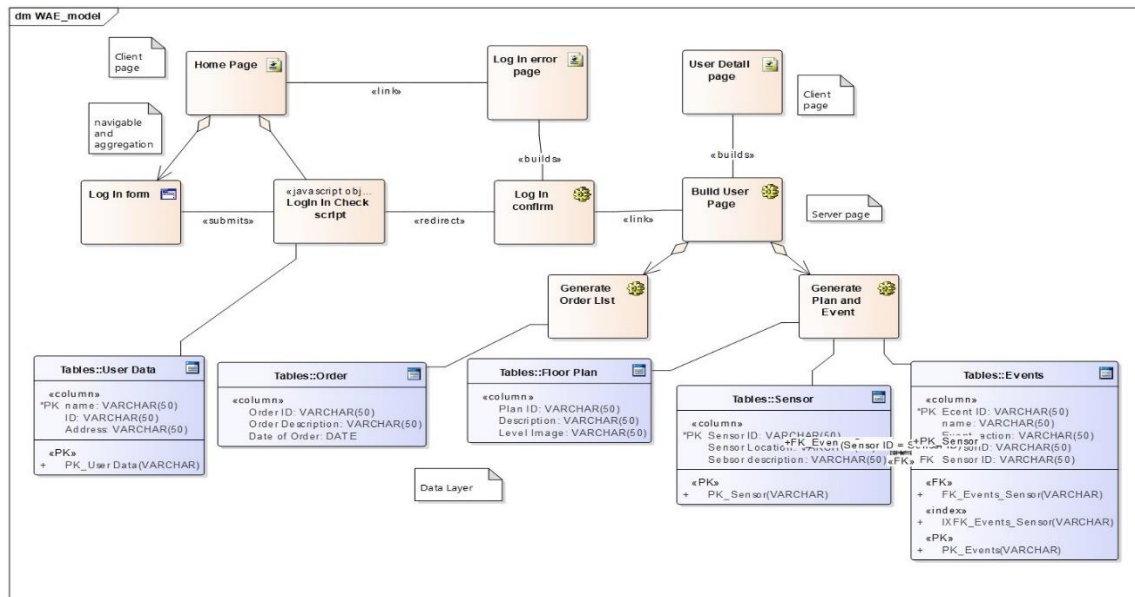


Fig. 2. A WAE Model of a Safe Home Web Application. The Design has been redeveloped by using EA According to [23].

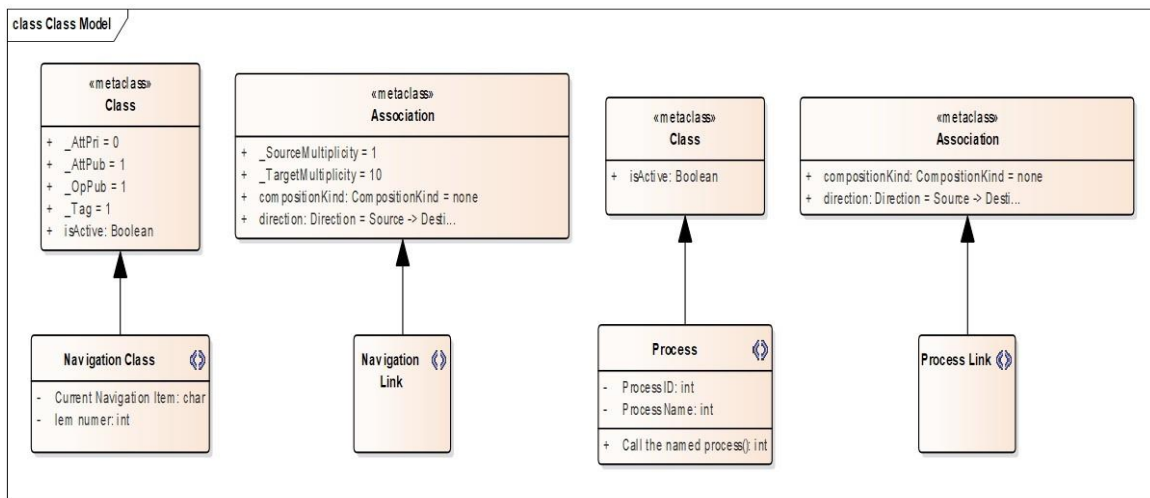


Fig. 3. A Part of a Typical UML that Student will Practice and Integrate in different Levels of their Web Application Analysis and Design.

IV. RESULTS AND DISCUSSION

A. Performance Measures

1) *Students' engagement*: An anonymous survey was conducted at week-6 of 11 week trimester and continued its participation till the end of trimester using CloudDeakin system which is an online teaching and learning system used by Deakin University. Different questions have been presented by asking whether the students were attracted and influenced in the practical and lecture classes through the delivery and teaching material. Students have also been asked whether they think the content will be helpful for them in finding a job. A sample question on assessing students' engagement has been presented as below: "Have these industry related activities using EA attracted and engaged you in the course?" Student's

answer should be in four categories "High", "Medium", "Low" and "Not at all".

2) *Importance of face to face contact*: To justify the significance of face to face contact, survey questions were introduced whether students feel comfortable with face to face teaching in practical class. A sample question is presented here: "Do you think it would be difficult if you don't come in practical class to learn the techniques of EA? (What is the level of difficulty?)" The answer should be: "Very difficult", "Difficult", "Easy" and "Very easy".

3) *Learning achievement*: This has been measured through the achieved marks of two assignments by the students and compared with earlier offer of the course.

The survey results are automatically stored in the CloudDeakin and statistical analysis has been shown in the below Tables I to Table VII.

TABLE I. QUESTIONS RELATED TO THE MEASURE MENTIONED IN ITEM-1: UML PROFILE HAS BEEN PRESENTED IN THE MATERIAL. DO YOU THINK THAT IT WILL HELP YOU LATER?

Answer	Number of Participants	Percentage
True	19	95%
false	1	5%

TABLE II. QUESTIONS RELATED TO THE MEASURE MENTIONED IN ITEM-1: UML PROFILE IS EXTENSIVELY USED IN INDUSTRIES AND ORGANIZATIONS. DO YOU THINK IT CAN BE AN ADDITIONAL INDUSTRY SKILL THAT YOU LEARNT FROM THIS COURSE?

Answer	Number of Participants	Percentage
True	19	95%
false	1	5%

TABLE III. QUESTIONS RELATED TO THE MEASURE MENTIONED IN ITEM-1: IN THIS COURSE, ENTERPRISE ARCHITECT (EA) HAS BEEN INTRODUCED FIRST TIME. MANY NEW AND INDUSTRY STANDARD OBJECT ORIENTED DESIGN TECHNIQUE USING EA HAS BEEN ADDED AND DELIVERED. HAVE THESE INDUSTRY RELATED ACTIVITIES USING EA ATTRACTED AND ENGAGED YOU IN THE COURSE?

Answer	Number of Participants	Percentage
High	8	40%
Medium	11	55%
Low	0	0%
Not at all	1	5%

TABLE IV. QUESTIONS RELATED TO THE MEASURE MENTIONED IN ITEM-1: HOW DID YOU ENJOY THE DEMONSTRATION OF PRACTICAL TASKS INCLUDING THE VIDEO AND IN CLASS DEMONSTRATION?

Answer	Number of Participants	Percentage
Very well	11	55%
Well	6	30%
Less	3	15%

TABLE V. QUESTIONS RELATED TO THE MEASURE MENTIONED IN ITEM-1: ARE YOU ENJOYING THIS COURSE SO FAR?

Answer	Number of Participants	Percentage
Very well	6	30%
Well	11	55%
Medium	1	5%
Not much	2	10%

TABLE VI. QUESTIONS RELATED TO THE MEASURE MENTIONED IN ITEM-2: DO YOU THINK IT WOULD BE DIFFICULT IF YOU DON'T COME IN PRACTICAL CLASS TO LEARN THE TECHNIQUES OF EA? (WHAT IS THE LEVEL OF DIFFICULTY?)

Answer	Number of Participants	Percentage
Very difficult	7	35%
Difficult	13	65%
Easy	0	0%
Very easy	0	0%

TABLE VII. QUESTIONS RELATED TO THE MEASURE MENTIONED IN ITEM-2: IF THIS COURSE IS OFFERED IN FULL ONLINE MODE IN WHICH THERE WILL BE NO PRACTICAL CLASS IN CAMPUS, DO YOU THINK IT WILL BE DIFFICULT FOR YOU? (WHAT IS THE LEVEL DIFFICULTY). GIVEN THAT SAME/CURRENT MATERIALS ARE PROVIDED BY ONLINE ONLY. (WHAT IS THE LEVEL OF DIFFICULTY?)

Answer	Number of Participants	Percentage
Very difficult	4	20%
Difficult	11	55%
Medium	5	25%
Easy	0	0%

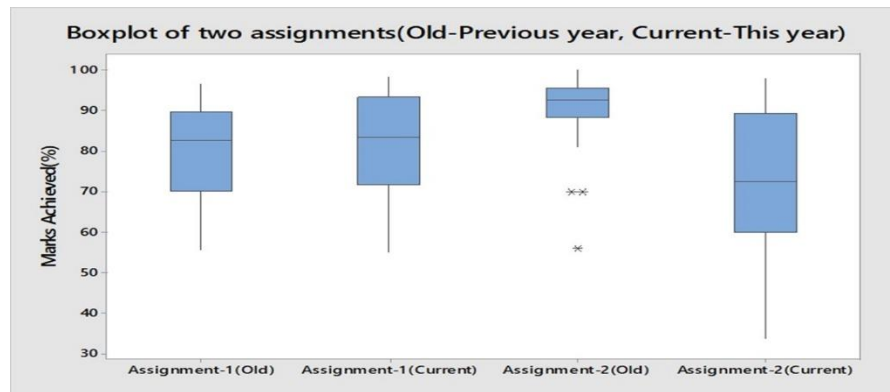


Fig. 4. Boxplot Comparison of Two Assessments' Results for this Year and Previous Year.

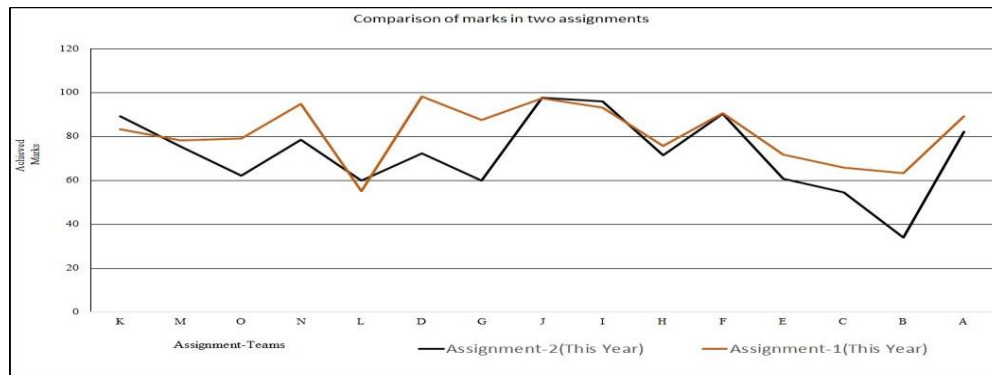


Fig. 5. Group Wise Marks for Two Assignments in this Year.

The survey results clearly show that the proposed approach has been able to engage students with a positive response rate equal to 95% for measure-1 metric within the participants. In the questions measure-2 survey results show that most of the students will face difficulties if they don't attend the practical class and fully online mode of the delivery will also be difficult for the students. To compare the performance of proposed approach for the measure-3, previous year's assessment results of the same course have been compared with this year's results. The students' personal information has been de-identified for both cases and then statistical analysis has been prepared which is presented in Fig. 4. It is observed in the results in Fig. 4 that there is a consistent distribution of marks in first and third quartile of this year's marks. In previous year, the boxplot for assignment-2 has very less gap between upper and lower extreme points with several outliers. In previous year, lower extreme of assignment-2 is also almost equal to the upper extreme point of assignment-2. This clearly shows an unbalanced distribution between the achievements. In contrast, this year boxplots of two assignments have similar patterns and wider extreme points. This shows a consistency and progressive achievement.

Fig. 5 shows that the group-wise marks follow approximately similar pattern across all the group. While in assignment-2, achieved scores are lower than assignment-1, it still follows similar pattern. The reason of lower score in assignment-2 could be explained as the increased difficulty in assessment task-2 compared to assignment-1.

V. CONCLUSIONS

High graduate outcome rate (GOR) is one of the key objectives for a sustainable education system. Achieving a good GOR every year and continually outperform is not so easy. One of the key strategies in this pathway is to achieve sustainability in the learning itself. Equipping the learners with the environment and ways of deconstruction and reconstruction for relearning from past are the key factors to achieve high standard hands on experience (HOE) and thereby sustainability for learning. Among many hurdles to achieve the HOE, one of the most important challenges is to keep students proactively engaged in learning in a blended learning model with off-campus students. In this study, a combination of teaching strategies has been proposed including the context-based teaching and incorporation of innovative technologies to achieve sustainability in the learning and education (SLE). A case study is accomplished where software engineering course was considered as a test bed to justify the performance of proposed approach. In the proposed approach, particularly, high standard industry focused teaching material and commercially popular software engineering tools have been introduced to keep the students engaged and being tuned in the course, thereby achieve more sustainability in learning. The statistical analysis of the results of the case study proves the significance of the proposed approach. However, there are limitations in the proposed approach which can be expanded in a future work. 100% engagement was not possible which can be achieved by applying minor assessment on a weekly basis or a milestone task-based minor assessment in the course and then comparing the learning outcome with the proposed

approach in this study. Other strategies such as a combination of flipped classroom model and innovative tools can also be investigated.

REFERENCES

- [1] P. M. Stohr-Hunt. An analysis of frequency of hands-on experience and science achievement. *JOURNAL OF RESEARCH IN SCIENCE TEACHING* 1996, 10 33, 101–109).
- [2] A. Serbezov and D. Cummings. University-industry co-operation to promote industrial relevance in the field instrumentation component of control education. *IFAC-PapersOnLine* 2016, 49, 309–313.
- [3] G. Mihaela M. Albu, Keith E. Holbert and V. Trusca. Embedding remote experimentation in power engineering education. *IEEE TRANSACTIONS ON POWER SYSTEMS* 2004, 19.
- [4] F. M. M. Albu, A. Ferrero and S. Salicone. Remote calibration using mobile, multi-agent technology.in *Proc. IEEE Instrumentation, Measurement and Technology*, 2003, (21–23).
- [5] F. Z. W. Muhammad Azizur Rahman, Algirdas Paktas. Network modelling and simulation tools. *Simulation Modelling Practice and Theory*, 2009, 17, 1011–1031.
- [6] S. K. Sharma and J. Sefchek, Teaching information systems security courses: A hands-on approach, *Computers and security* 2007, 26,290–299.
- [7] D. Ionescu, The importance of working integrated learning and relevant laboratory experiments in engineering teaching. *Procedia - Social and Behavioral Sciences* 2015, 174,2825 —2830.
- [8] C. A. Mather, A. McKay, and P. Allen, Clinical supervisors' perspectives on delivering work integrated learning: A survey study. *Nurse Education Today* 2015, 35,625–631.
- [9] C. S. Osborne, J., Attitudes towards science: A review of the literature and its implications *International Journal of Science Education* 2003, 25, 1049– 1079.
- [10] D. Fortus, Attending to affect, *Journal of Research in Science Teaching* 2014, 51,821–835.
- [11] D. Klahr and M. Nigam, The equivalence of learning paths in early science instruction effects of direct instruction and discovery learning. *Psychological Science* 2004, 15,661–667.
- [12] S. Hidi and K. A. Renninger, The four-phase model of interest development. *Educational Psychologis* 2006, 2,111–127.
- [13] L. F. Bennett, J. and S. Hogarth, Bringing science to life: A synthesis of the research evidence on the effects of context-based and sts approaches to science teaching. *Science Education* 2007, 91, 347–370.
- [14] J. K. Gilbert, On the nature of context in chemical education. *International journal of science education* 2006, 28,957–976.
- [15] J. E. Halat, E. and N. Aydin, Reform-based curriculum and motivation in geometry. *Journal of mathematics* 2008, 4, 285–292.
- [16] D. Chalmers, Progress and challenges to the recognition and reward of the scholarship of teaching in higher education. *Higher Education Research and Development* 2011, 30, 25–28.
- [17] Patrice Potvin, Abdelkrim Hasni. Interest, motivation and attitude towards science and technology at k-12 levels: A systematic review of 12 years of educational research. *Studies in Science Education* 2014, ,85–129.
- [18] K. Trigwell and S. Shale, Student learning and the scholarship of university teaching. *Studies in Higher Education* 2004, 29, 523–536.
- [19] Shasmul Huda, Student's engagement in achieving hands-on-experience. submitted to the unit EEE733, Assignment-1, Trimester- 2, School of Education, Deakin University, Dec 2016.
- [20] Emily Rose, Ilene Claudius, Ramin Tabatabai, Liza Kearn, Solomon Behar, Paul Jhun. The Flipped Classroom in Emergency Medicine Using Online Videos with Interpolated Questions. *The Journal of Emergency Medicine* 2016, 51,284–291.
- [21] Veronica P.S. Njie-Carr, Emilie Ludeman, Mei Ching Lee, Dzifa Dordunoo, Nina M. Trocky, Louise S. Jenkins. An Integrative Review of Flipped Classroom Teaching Models in Nursing Education. *Journal of Professional Nursing* 2016.
- [22] Roehl, A, Reddy, S. L., Shannon, G. The flipped classroom: an opportunity to engage millennial students through active learning strategies. *Journal of Family Consumer Sciences* 2013 , 105.
- [23] R. S. Pressman and D. Lowe *Web Engineering, A Practitioner's Approach*, McGraw-Hill: USA, 2009; Chapter-1.
- [24] Sparx systems, Enterprise Architect Success Stories, Available online: <http://sparxsystems.com/> (accessed on 11/11/2021).
- [25] Jingying Wang,Min Jou, et.al. An investigation on teaching performances of model-based flipping classroom for physics supported by modern teaching technologies. *Computers in Human Behavior* 2018, 84,36–48.
- [26] Crystal Han-Huei Tsay,Alexander Kofinas, Jing Luo. Enhancing student learning experience with technology-mediated gamification: An empirical study. *Computers and Education* 2018, 121,1–17.
- [27] Luma da Rocha Seixas, Alex Sandro Gomes, Ivanildo José de Melo Filhoa. Effectiveness of gamification in the engagement of students. *Computers in Human Behavior* 2016, 58, 48–63.
- [28] Ibrahim Yildirim. The effects of gamification-based teaching practices on student achievement and students' attitudes toward lessons. *The Internet and Higher Education* 2017, n33 ,86–92.
- [29] Li Ding, Chan Min Kim, Michael Orey. Studies of student engagement in gamified online discussions. *Computers and Education* 2017, 115,126–142.
- [30] Curtis R.Henrie, Lisa R.Halverson, Charles R.Graham. Measuring student engagement in technology-mediated learning: A review. *Computersand Education* 2015, 90, 36–53.
- [31] Gunuc, S., Kuzu, A. Factors influencing student engagement and the role of technology in student engagement in higher education: Campus-class technology theory. *The Turkish Online Journal of Qualitative Inquiry* 2014, 5, 86–113.
- [32] Selim Gunuc, Abdullah Kuzu. Confirmation of Campus-Class-Technology Model in student engagement: A path analysis. *Computers in Human Behavior* 2015, 48, 114–125.
- [33] E. A. Beckmann, P. Kilby, On-line . Off-campus but in the Flow: Learning from Peers in Development Studies. *Australasian Journal of Peer Learning* 2008, 1,61–69.
- [34] Mina Chiba, Manca Sustarsic et al. Investigating effective teaching and learning for sustainable development and global citizenship: Implications from a systematic review of the literature. *International Journal of Educational Development* 2021, 81,1–16.
- [35] Jay Hays, Hayo Reinders. Sustainable learning and education: A curriculum for the future, *International Review of Education* 2020, 66,29–52.
- [36] Asmat Ara Shaikh, Anuj Kumar et.al. The Role of Machine Learning and Artificial Intelligence for making a Digital Classroom and its sustainable Impact on Education during Covid-19. *Materials Today: Proceedings* 2022, Article in Press, .
- [37] Fatma Köybas,I S,Emi'n. Examining Teachers' Disposition Towards Sustainable Education Through Discriminant Analysis. *Research in Pedagogy* 2020, 10, 229–247.
- [38] O. Polyakova, R. Galstyan-Sargsyan, Sustainable Higher Education via Telecollaboration: Improving Plurilingual and Pluricultural Competence. *ISSN 1991-9468 (Print) 2021, 25, 2308–1058.*<http://edumag.mrsu.ru>, DOI: 10.15507/1991-9468.105.025.202104.544- 561.
- [39] Alvyra Galkiene', Ona Monkeviciene', Lina Kaminskiene' et.al. Modeling the Sustainable Educational Process for Pupils from Vulnerable Groups in Critical Situations: COVID-19 Context in Lithuania, Latvia, and Estonia. *Sustainability* 2022, 14,1748–1748.
- [40] Agne Paulauskaite-Taraseviciene, Ingrida Lagzdinyte-Budnike, Lina Gaiziuniene et.al. Assessing Education for Sustainable Development in Engineering Study Programs: A Case of AI Ecosystem Creation, *Sustainability* 2022, 14, 1748.
- [41] Hasbullah Ashari, Iffat Abbas, Asmat-Nizam Abdul-Talib et.al. Entrepreneurship and Sustainable Development Goals: A Multigroup Analysis of the Moderating Effects of Entrepreneurship Education on Entrepreneurial Intention. *Sustainability* 2022, 14, 431–431.

- [42] Oracle, The Java EE 5 Tutorial, Available online: <https://docs.oracle.com/javaee/5/tutorial/doc/bnajo.html> (accessed on 11/11/2021).
- [43] Sparx systems, UML Profiles, Available online: https://sparxsystems.com/resources/developers/uml_profiles.html (accessed on 11/11/2021).
- [44] Cortés, Humberto Navarro, Antonio. Enterprise WAE: A Lightweight UML Extension for the Characterization of the Presentation Tier of Enterprise Applications with MDD-Based Mockup Generation. *International Journal of Software Engineering and Knowledge Engineering* 2017, 27, 1291–1331.

Modified Intrusion Detection Tree with Hybrid Deep Learning Framework based Cyber Security Intrusion Detection Model

Majed Alowaidi

Department of Information Technology, College of Computer and Information Sciences
Majmaah University, Majmaah, 11952, Saudi Arabia

Abstract—In modern era, the most pressing issue facing modern society is protection against cyberattacks on networks. The frequency of cyber-attacks in the present world makes the problem of providing feasible security to the computer system from potential risks important and crucial. Network security cannot be effectively monitored and protected without the use of intrusion detection systems (IDSs). DLTs (Deep learning methods) and MLTs (machine learning techniques) are being employed in information security domains for effectively building IDSs. These IDSs are capable of automatically and timely identifying harmful attacks. IntruDTree (Intrusion Detection Tree), a security model based on MLTs that detects attacks effectively, is shown in the existing research effort. This model, however, suffers from an overfitting problem, which occurs when the learning method perfectly matches the training data but fails to generalize to new data. To address the issue, this study introduces the MIntruDTree-HDL (Modified IntruDTree with Hybrid Deep Learning) framework, which improves the performance and prediction of the IDSs. The MIntruDTree-HDL framework predicts and classifies harmful cyber assaults in the network using an M-IntruDtree (Modified IDS Tree) with CRNNs (convolution recurrent neural networks). To rank the key characteristics, first create a modified tree-based generalized IDSs M-IntruDTree. CNNs (convolution neural networks) then use convolution to collect local information, while the RNNs (recurrent neural networks) capture temporal features to increase IDS performance and prediction. This model is not only accurate in predicting unknown test scenarios, but it also results in reduced computational costs due to its dimensionality reductions. The efficacy of the suggested MIntruDTree-HDL schemes was benchmarked on cybersecurity datasets in terms of precisions, recalls, fscores, accuracies, and ROC. The simulation results show that the proposed MIntruDTree-HDL outperforms current IDS approaches, with a high rate of malicious attack detection accuracy.

Keywords—Cybersecurity; IntruDTree model; convolution recurrent neural network (CRNN); MIntruDTree-HDL; deep learning

I. INTRODUCTION

The Internet is increasing being intertwined with social lives and revolutionising the way people learn or work, but is also getting exposed to serious security lapses [1] and identifying serious and new threats is a critical issue that must be addressed immediately. Cybersecurity is term used to represent technologies and processes designed to protect computers, networks, programmes from unknown attacks or

unauthorised accesses or alterations or destructions of data. The term information security is also used interchangeably with cybersecurity where the former recognizes human functions in security processes while the latter adds extra dimensions in focusing on possible targets [2]. However, since, it focuses on ethical components of society it has important ramifications. Techniques need to protect data in all forms including its processing, transmissions physical/virtual storages in information technologies by setting up higher security levels achieved in adopting professional measures associated with security [3]. Cybersecurity is thus prevention measures from unwanted accesses, usage, disclosures, or modifications of data using computer systems or networks.

Network security systems [4] are made up of two parts namely security systems and computers where Firewalls, antivirus software, and IDSs are all included in the overall picture. External and internal invasions are examples of security breaches. IDSs aid in the detection, determination, and identification of any illegal system activities executed by attackers [5]. Because of their ability to identify zero-day threats, they are enticing. Another benefit is that typical activity profiles can be customized based on the characteristics of systems or applications or networks which makes it difficult for attackers to execute operations unnoticed [6]. Additionally, the data that anomaly-based approaches identify (new assaults) may be leveraged to develop abuse detection signatures. Because previously undiscovered system actions might be classified as anomalies, the fundamental downside of these techniques is their generation of higher false alarms [7]. AIDSs (Anomaly based IDSs), on the other hand, evaluates network activities for trends, automatically construct data-driven models that profile usual behaviours and detect deviations in case of irregularities. The primary advantage of AIDSs over signature based IDSs are their ability to trace previously undisclosed vulnerabilities or cyber-threats [8]. However, treating previously undetected system actions as anomalies may also produce higher false alarms where MLTs can be employed to handle these issues.

Traditional MLTs fall into shallow learning groups as they do not adequately address attack classifications in real world network applications as they concentrate lesser on feature engineering or feature selections. Multi-classification attack detection tasks become less accurate as dataset sizes grow [9]. As a result, DLTs have lately been proposed as a way to improve the intelligence of IDSs, despite the lack of research

to compare such MLTs to publically available datasets [10]. These issues were the base motivation for this work which proposes a hybrid IDSs based on CNNs with evaluations of its efficacy [11].

The remainder of the research is structured as follows: The second section examines some of the most modern strategies for identifying cyber threats. The proposed technique is presented in Section III. Section IV summarises the findings and discusses them. The limitations are highlighted in Section V. The conclusion and future efforts are discussed in Section VI.

II. RELATED WORK

IDSs generally identify malicious activities on networks while monitoring them for analyzing or discovering security risks. Several cybersecurity studies have been conducted with the aim of identifying or preventing cyber-attacks or security breaches. This section details about studies related to strategies for avoiding cyber-attacks.

Martnez Torres et al. [12] pioneered the use of MLTs in cybersecurity, defining several kinds of models based on (1) structures (network based/non-network based), (2) learning methods (supervised/unsupervised), and (3) complexities. Their descriptions were useful for further researchers on usage of MLTs in cybersecurity. Yin et al [13] proposed DLTs for IDSs where RNNs were used. The scheme called RNN-IDS showed that it was suited for building highly accurate classifications were in experimental results, and that their performances in binary/multi-class classifications surpassed performances of traditional MLTs. Kim et al. [14] also suggested DLT based IDSs which was tested on KDD Cup 1999 datasets. The scheme used LSTMs (Long Short Term Memories) with RNNs to learn. The study's results confirmed the success of DLT based IDSs in detecting malicious activities on networks. Al-Qatf et al [15] suggested IDSs based on STL (self-taught learning) frameworks and successful DLTs where the study's suggested method learnt features and reduced dimensionalities for minimizing training/testing execution times while enhancing prediction accuracies of assaults by SVMs (support vector machines). The study's suggested STL-IDSs technique improvised network IDSs while also introducing novel IDSs.

Khan et al. [16] proposed a pattern recognition technique for anticipating Denial of service (DoS) assaults with a higher prediction level. The method through DoS attacks is detected. DoS attacks are extremely serious assault that puts an organization's IT resources at risk by flooding them with fake messages or numerous requests from unauthorised users. Lekha et al [17] offered a broad overview of DMTs (Data Mining techniques) and cyber crimes in banking applications. According to the study, K-Means clustering, Influenced Association Classifiers, and J48 Prediction Trees combinations enabled complete, integrated, and precise cyber crime predictions in the banking sector. Law enforcements need to be strong to combat and prevent terrorism. Mitchell et al [18] developed probabilistic models based on stochastic Petri nets to identify behaviour of malicious nodes in CPSs (cyber physical systems) and IDRSs (intrusion detection and response systems) and thus respond to these real time

malicious events. Three different mechanisms for time-based IDSs were presented by Zimmer et al [19] where execution of illegitimate instructions in real-time CPSs were specifically identified using static timing analyses. Li et al [20] used CNNs with gated recurrent units for their suggested novel IDSs based on DLTs for industrial CPSs. The study used integrated learning in their architecture by allowing multiple industrial CPSs to work together and thus develop comprehensive new models of IDSs. Dutta et al. [21] established robust anomaly detections using semi-supervised MLTs that traced real time assaults. The proposed scheme applied DNNs (deep neural networks) using reconstruction errors for its detections. Their tests on the SWaT dataset show its efficacy by achieving AUC value of 0.9275 and better than other known anomaly detection algorithms. Sarker et al [22] introduced IntruDTree (Intrusion Detection Tree) security model based on MLTs that first examined the importance of security factors before constructing trees from fundamental features for generalizing IDSs. To evaluate performances of their resultant security models, the study compared findings of IntruDTrees with many classical MLTs including NBs (Naive Bayes), LRs (Logistic regressions), SVMs and KNNs (k-nearest neighbours).

IntruDTree did a reasonable job of detecting attempts at intrusion; but, it had issues with overfitting while it was learning, and it was unable to generalize what it had learnt so that it could apply it to new data. As a consequence of this, the goal of this effort is to improve classifier performances while at the same time recognizing cyber intrusions in real time. It increases the learning rates of IDSs, which in turn leads to an effective improvement in the performances and predictions of the system.

III. PROPOSED METHODOLOGY

MIIntruDTree-HDL framework is suggested in this research work for predicting and classifying harmful cyberattacks in networks. The ranking of important features are done by constructing trees in IntruDTree framework. The performances of predictions are enhanced by CNN's convolutions which gather local information, while RNNs acquire temporal aspects. On the completion of the tree from training data, tests are used to validate the suggested framework. The proposed framework reduces computational complexities by reducing feature dimensionalities resulting in minimizing over fits of data and thus lays the base for improved prediction accuracies of unknown test cases. The contributions of this study can be summarized as:

- IDSs based on MLTs are presented emphasizing the importance of high dimensional security features.
- Proposing IntruDTree framework for ranking of security features based on their importance and subsequently uses them to build generalized trees encompassing chosen features.
- Increasing predictive performances of IDSs by using CNNs for collect local information and RNNs for capturing temporal features.
- Testing the IntruDTree framework for evaluating its performances.

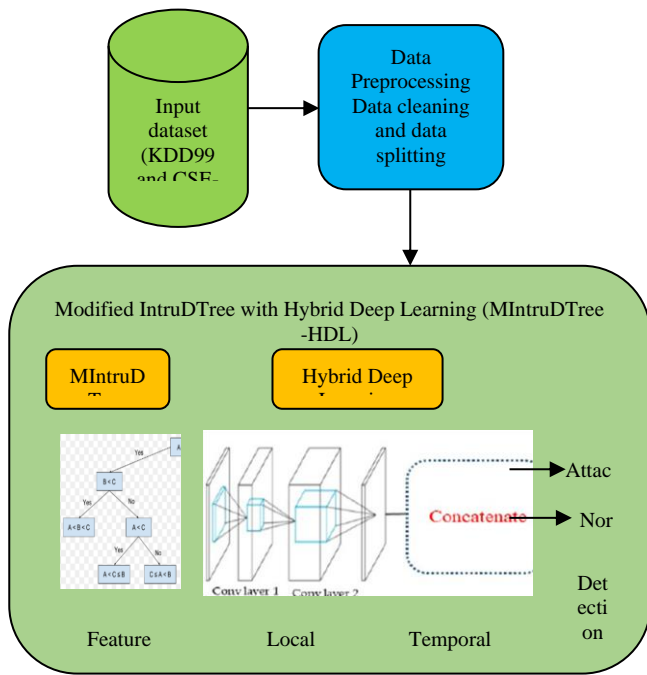


Fig. 1. The Suggested Methodology of this Research Work.

The experiment results of the suggested IntruDTree framework shows that it outperforms prior schemes in its detection previously unseen test cases of cyber intrusions. Fig. 1 depicts the suggested methodology.

A. Materials and Methods

The suggested IntruDTree framework is presented where security datasets are processed using a multitude of steps. Raw data is pre-processed, feature’s relevance are assessed and ranked for building generalized trees. The stages of the proposed methodology are detailed below in this section.

B. Exploring Security Dataset

Security datasets contain collections of data records which include many securities related information that can be used for constructing data-driven IDSs for cyber security. Understanding raw cybersecurity data and security event patterns are critical for detecting malicious irregularities or behaviors [22]. This work used intrusion detection dataset from Kaggle (largest machine learning and data science community) with two types of classes namely normal and anomalous. The dataset had 41 features with 3 qualitative features (protocol type, service, f delay). The other features were quantitative. The dataset’s security aspects are listed in Table I. The dataset had 25,000 examples obtained from simulated military network intrusion settings where US Air Force local area networks were modelled including TCP/IP dumps of data from networks. Networks were in parallel to cyber environments and subjected to a wide range of cyber-attacks or anomalies.

Encoding of features: As previously detailed, dataset had both numeric and notional values of security issues. Though most features were numerically valued, nominally values also existed (protocol type, service, f delay along with classes [anomaly, normal]). All nominal values were translated into

vectors for fitting them into MLTs where "Label Encoding" was used though most studies had used "One Hot Encoding". The values of tcp, udp, icmp, udp, icmp were label encoded for converting them into vectors.

TABLE I. FEATURES AND THEIR DATA TYPES

Feature name	Value Type	Feature Name	Value Type
dst_host_srv_count	Integer	Same_srv_rate	Float
flag	Nominal	dst_host_same_srv_rate	Float
srv_error_rate	Float	dst_host_srv_error_rate	Float
protocol_type	Float	count	Integer
dst_host_same_src_port_rate	Nominal	logged_in	Integer
error_rate	Float	dst_host_srv_diff_host_rate	Float
dst_host_srv_err_rate	Float	src_bytes	Integer
srv_error_rate	Float	service	Nominal
dst_host_count	Float	dst_host_error_rate	Float
srv_count	Integer	dst_host_diff_srv_rate	Float
error_rate	Integer	wrpmg_fragment	Integer
srvidf_host_rate	Float	num_compromised	Integer
hot	Integer	dst_bytes	Integer
duration	Integer	diff_srv_rate	Float
root_shell	Integer	is_guest_login	Integer
urgent	Integer	land	Integer
su_attempted	Integer	num_failed_logins	Integer
num_file_creation	Integer	num_root	Integer
num_access_files	Integer	num_shells	Integer
is_host_login	Integer	num_outbound_cmds	Integer

Table I displays unique data distributions of outlined security methods. This work prepared raw datasets from above-mentioned features for its proposed IDSs based on DLTs. Processes and ranks of security features were based on and targeted DLT requirements and data patterns were constructed for ensuring anomalies and intrusions could be traced by intelligent cyber security services.

C. Preparation of Data from Raw Security Data: Data Preparations Include Encoding Feature and Scaling them According to Parameters of Intrusion Datasets

Feature scaling: Data normalizations are also called feature scaling in data pre-processing. Security feature may have a range of values and need to be scaled or normalized to acceptable ranges. This study used Standard Scaler to equalize security characteristics with mean values of 0 and standard deviations of 1. Subsequently, these normalized values were further analyzed while building the security model.

D. Determining Feature Importance and Ranking

On completion of investigations and preparations, relevance scores of security features were obtained and ranked based on their importance and to choose critical features for future processing. Their values varied between 0 and 1 where

0 indicates that the model's output has no relation to the feature, whereas a value of 1 shows that the model's output has a direct relationship with the feature. Thus, the "purity" of attributes were determined. Gini Indices are well-known measures for assessing node's impurity in statistics and data mining that generally judge frequency of random elements. It is the probability of mistakenly categorizing a randomly selected element in a security dataset based on class distribution of the dataset. In binary splits, Gini Indices of nodes n can be expressed as

$$I_{G(n)} = 1 - \sum_{i=1}^c p_i^2 \quad (1)$$

$$\Delta I_{G(n_p)} = I_{G(n_p)} - p_l I_{G(n_l)} - p_r I_{G(n_r)} \quad (2)$$

where p_i is the likelihood of elements being categorized as belonging to certain security classes and p_l and p_r are percentages of examples in nodes n_p allocated to child nodes n_l and n_r , respectively. Hence, Gini impurity equations determine feature's decreases of impurity. Greater ability of attributes to eliminate impurities improves its significance. Security features are sorted based on their computed importance and after evaluating the features, this work selects top n security features based on their relevance score values in order to develop effective tree-based security models by employing the n features selected.

E. Design of M-IntruDTree (Modified IntruDTree)

The chosen security characteristics are used to build trees for taking decisions by the intelligent data-driven IDS. In this model, all features of the dataset are not chosen instead only security features are chosen based on their relevance scores and ranks. A root is formed first, followed by the construction of connected branches of the tree in which the training dataset is divided into smaller sub-groups. This model properly matches the training data, however fails on generalizations of test data. Models memorizing training data noises tend to miss important patterns as over fits occur. DTs (Decision Trees) perform well on training data, but fail on unknown test data and hence to effectively over the issue of over fits, this study uses I-RLRs (Inductive Rule Learning Rates). Gini Indices are used to identify root node attribute in each level and gradually the tree is built with lower Gini values resulting in adding required counts of branches encompassing internal/leaf nodes with corresponding arcs or connecting edges. Labels on internal nodes are based on defined or selected security criteria while node's leaves are labelled with security features which can be one of the two: anomaly or normal. Fig. 2 displays multi-level trees with terminals or node's leaves with defined labels. This work's IntruDTree concentrates on achieving two main objectives which are reducing dimensionality of features based on their evaluated ranks or relevance and generating multiple-level trees from chosen critical features. Fig. 3 displays IntruDtree's considered IDS features like f latency, services, durations, and logged in.

- I-RERs (Inductive Re-substitution Error Rate): The fundamental idea underlying I-RERs is that instead of writing complete concept descriptions first and then trimming them, individual phrases are cut as soon as they are written which ensures the algorithm can eliminate training instances like trimming even before

learning subsequent phrases and preventing these examples from influencing success of learning clauses. Algorithm 1 depicts pseudo-code of this approach. Traditionally current collection of training examples is separated into growths (generally 2/3) and pruned (typically 1/3). However, due to the growth of collections, only one line is learned. In greedy approaches, literals from phrases are removed till deletions which can diminish validity of sentences are maintained on pruning sets. These sets are then used to derive clauses where prediction accuracy of trimmed clauses fall below empty clauses (i.e., clause with body fail), clauses are removed from concept descriptions, and I-RERs return learnt clauses. As a result, accuracy of trimmed phrases on pruning sets also serve as stopping criteria. The asymptotic complexity of I-RERs is $O(n \log^2 n)$, where n is the size of the training set. The cost of adding one clause in RERs is $O(n \log n)$, since the cost of picking sentences is $\Theta(\log n)$ literals. As a consequence, $O(n)$ instances are tested against fixed sets of criteria. I-RERs consider cutting every literal in phrases. Resulting in evaluating $(\log n)$ literals on (n) samples in pruning sets at most $O(\log n)$ times until the last phrase is discovered. hence, eliminating one clause costs $O(n \log^2 n)$. If I-RERs finish with identified constant sizes, the overall cost is also $O(n \log^2 n)$ which is far less expensive than creating over fits determined by $(n^2 \log n)$ under the same assumptions. For efficiency of computing costs, nodes must contain few values.

- $R(t)$, re-substitution error rates at nodes (t) and done only once.
- $R(Tt)$, re-substitution error rates at branch emerging from nodes (t) can be modified since Tt varies on pruning.
- $|Tt|$, leaf node counts on branches from nodes (t) and may change on pruning.

To calculate re-substitution error rates $R(t)$, data points in each class that arrive at node t are divided by the data point counts in each class that arrive at node t . Assuming the fraction of points in classes are utilized to build class priors, then $R(t)$ can be computed. After pruning, both re-substitution error rates of branches coming out of node t and the leaf nodes counts on the branch coming out of node t fluctuate. These variables will need to be adjusted because the leaf nodes counts would have dropped after pruning. To be more specific, all values for branch's ancestor nodes must be changed where $R(Tt)$ and $|Tt|$ may be computed using a recursive process.

Counts of leaf nodes in branches of nodes (t) are determined using bottom up sweeps of constructed trees. These leaf nodes counts are equal to the sum of counts of leaf nodes on the right child nodes and counts of leaf nodes on the left child nodes. The leaf node counts for child nodes are determined before determining the counts of parent nodes in bottom up sweep operations. The values of $R(Tt)$ are also equal to the sum of two child node values of (t) . These three values are the base for determining ratio $g(t)$ and identifying

weakest connections. The new is the comparable ratio at the weakest connection α which guarantees that sequences of α are obtained in pruning are strictly increasing. When there are many weakest links, for example, if $g_k(t_k) = g_k((t')_k)$, then define:

$$T_{(k+1)} = T_k - T_{(t_k)} - T_{((t')_k)} \quad (3)$$

Branch nodes can be nested or share nodes where pruning procedure resulting in sequence of nested sub-trees can be:

$$T1 > T2 > T3 > \dots > t1 \quad (4)$$

Algorithm 1 describes the general procedure for constructing an IntruDTree. Given a training intrusion dataset, $DS = \{X_1, X_2, \dots, X_m\}$, where m denotes the amount of the data. n -dimensional characteristics are used to represent each instance. The training data is also divided into various cyber-attack classes. CA stands for fnormal and anomaly. An IntruDTree, a rule-based classification tree connected with DS , is the result. Fig. 2 depicts single feature's rules, when flag's value is RSTR, it implies anomalous. Multi-aspect rules for flag values can be SF implies ftb service and duration value of four implies anomalous. By traversing the resulting IntruDTree, multiple rules for security can be retrieved based on which the final outcome would result in normal or abnormal.

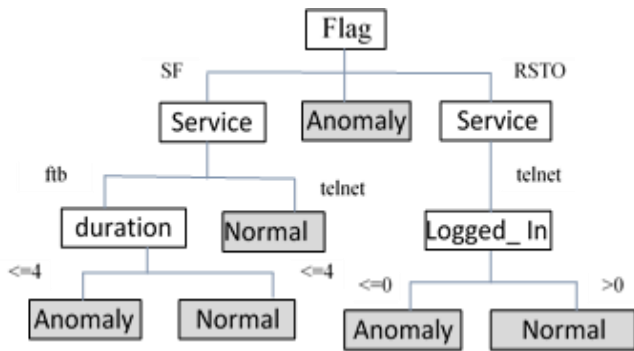


Fig. 2. M-IntruDTree Built from Features.

F. Hybrid Deep Learning Model

With a data processing architecture, hybrid deep learning focuses on tackling actual ID challenges. By combining a CNN and an RNN model, hybrid deep learning reduces these issues [23]. The main structure of the HDL that occurs here is the source of the experiment. Fig. 1 shows the suggested model in further detail. A CNN contains two main components, according to the HDL: (i) a feature extractor; and (ii) a classifier. Convolution and pooling layers are the two layers that make up the feature extractor. The feature map, which is the extracted result, is used as the input to the classification's second component. In this method, CNN gains a thorough understanding of the local characteristics. However, it has a flaw in that it ignores the temporal relationship between significant traits. After the CNN layers, recurrent layers were added to capture both spatial and temporal data more effectively. This method effectively handled the disappearing and inflating gradient difficulties, enhancing the capacity to record and learn from variable extent sequences and spatial and temporal correlations. In the

HDL model, CNNs are hybridized as RNNs, and inputs are initially processed by CNNs, after which the outputs are relayed via recurrent layers to form sequences at time steps, allowing capture of both spatial and temporal characteristics. As with AIDS, the bulk of traffic is categorized based on its behavior, which should not be biased or conflicting with the IP address, hence the IP address characteristics were also eliminated. Training sets were utilized for training while validation sets were used for fast prototype evaluations while training and testing sets evaluated the final model. Moreover, it was noticed that the dataset had too many instances of typical network's traffic, which can impact classifications the model.

Algorithm 1. Pseudocode of MIntruDTree

Data: Dataset: $D = X_1, X_2, \dots, X_m$ // Occurrences of X_i have features and CIs (cyber Intrusions) class information

Result: MIntruDTree

```

1 Procedure MIntruDTree (D, features_list, CIs);
2 //generate feature significance scores
3  $imp\_score \leftarrow compute\_score\ features\_list$ 
4 //Choose significant features
5  $imp\_features\_list \leftarrow ChosenFeatures(\ features\_list, imp\_score, n)$ 
6 TreeGens(D,  $imp\_features\_list$ , CIs)
7  $N \leftarrow createNodes()$  //create tree's root node
8 if all instances in D belong to the same class of CIs then
9 return N as leaf node labelled with class CI.
10 end
11 if  $imp\_features\_list$  is null then
12 return N as leaf node labeled with majority class of D; // majority votes
13 end
14 identify features with highest precedence feature  $F_{split}$  for dividing and assigning  $F_{split}$  to node N.
15 for each feature's value  $val \in F_{split}$  do
16 create subset  $D_{sub}$  of D with val.
17 if  $D_{sub} \neq \emptyset$  then
18 attach node returned by TreeGens( $D_{sub}$ , { $imp\_features\_list - F_{split}$ }, CIs)) to node N;
19 end
20 // Inductive re-substitution error rates
21 calculate  $R(Tt)$  and  $|Tt|$ 
22 modify nested subtrees  $T1 > T2 > T3 > \dots > t1$ 
23 attach leaves labeled with majority class of D to node N;
24 end
25 return N

```

IV. RESULTS AND DISCUSSION

The experimental outcomes of this work are briefly discussed and reported in this section. First, we'll set up our tests to assess the suggested MIntruDTree-HDL cyber security model, and then we'll talk about the outcomes. This project uses the KDD99 and CSE-CIC-DS2018 datasets and is written in Java. These datasets are chosen based on a range of characteristics, including the amount of samples, attributes, and classifications. To compute various performance measures, TPs (true positives), FPs (false positives), TNs (true negatives), and FNs (false negatives) are measured. Precision, defined as the proportion of relevant retrieved instances, was the original performance metric. The second performance

parameter was recall, which was defined as the percentage of relevant instances. Despite their usually contradicting character, the assessments of accuracy and recall are both critical in evaluating the efficiency of a prediction approach. As a result, these two measures may be combined with equal weights to form the F-measure, which is a single metric. The last performance criterion was the accuracy measure, which was defined as the fraction of correctly predicted occurrences compared to all anticipated instances.

Precisions are defined as proportions of accurately identified positive observations against all predicted positive observations.

$$\text{Precision} = \text{TP}/(\text{TP}+\text{FP}) \tag{5}$$

The ratio of accurately detected positive observations to total observations are termed recalls.

$$\text{Recall} = \text{TP}/(\text{TP}+\text{FN}) \tag{6}$$

F-measures can be defined as weighted averages of Precisions and Recalls and hence they consider FPs and FNs.

$$\text{F1 Score} = 2 * (\text{Recall} * \text{Precision}) / (\text{Recall} + \text{Precision}) \tag{7}$$

Accuracies are computed in terms of positives and negatives as shown below:

$$\text{Accuracy} = (\text{TP}+\text{TN})/(\text{TP}+\text{TN}+\text{FP}+\text{FN}) \tag{8}$$

This work selected features that satisfies threshold values of $t = 0.02$ which resulted in the selection of 14 features based on importance scores of Table II.

Fig. 3 illustrates precision comparison values between the proposed and existing method for detecting the cyber-attacks. Therefore, the results verify that the ranking the features using M-IntruDTree can be effective in extracting the given data. Thus the proposed model has the number of useful features does not affect the performance of the jointly learnt features transformation very much. From the given two dataset, KDD99 has high detection rate than the other CSE-CIC-DS dataset.

TABLE II. KDD99 DATASET'S TOP RANKED FEATURES WITH THEIR IMPORTANCE SCORES

Ranking	Security Feature Name	Importance Score
01	src_bytes	0.258093
02	dst_bytes	0.129825
03	flag	0.073396
04	dst_host_same_srv_rate	0.059504
05	dst_host_srv_count	0.053630
06	dst_host_diff_srv_rate	0.046281
07	diff_srv_rate	0.041144
08	count	0.040548
09	same_srv_rate	0.036620
10	protocol_type	0.31650
11	dst_host_same_src_port_rate	0.025566
12	service	0.023904
13	serror_rate	0.023188
14	logged_in	0.020901

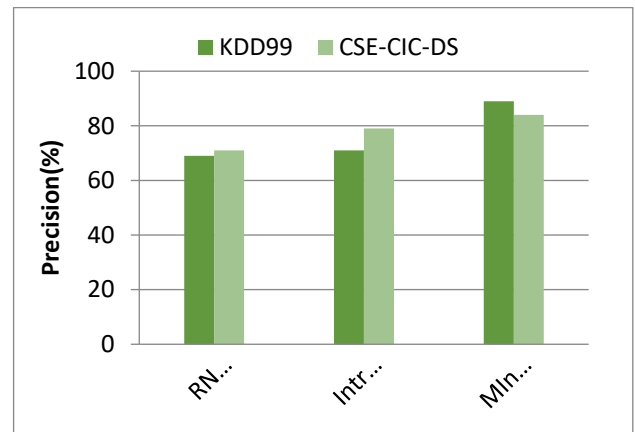


Fig. 3. Precision Comparison Results between the Proposed and Existing Method for Detecting the Cyber.

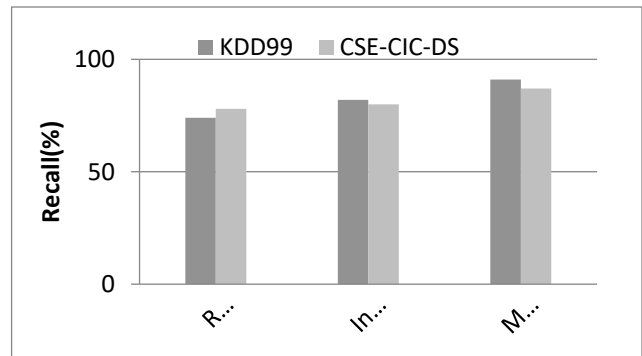


Fig. 4. Comparative Recall Values of the Proposed and Existing Methods for Detecting Cyber Attacks.

Fig. 4 illustrates recall comparisons between the proposed and existing method for detecting the cyber-attacks. Thus the results show that the proposed method gives the high recall results of 91% whereas the existing technique has less recall results such as IntraDTree method metric has 82%, and the RNN-IDSs method metric has 74% for KDD99 data. On the other hand, proposed method gives the high recall results of 87% whereas the existing technique has less recall results such as IntraDTree method metric has 80%, and the RNN-IDSs method metric has 78% for CSE-CIC-DS. Fig. 5 depicts F-measure comparative values of the proposed and existing methods for identifying cyber assaults.

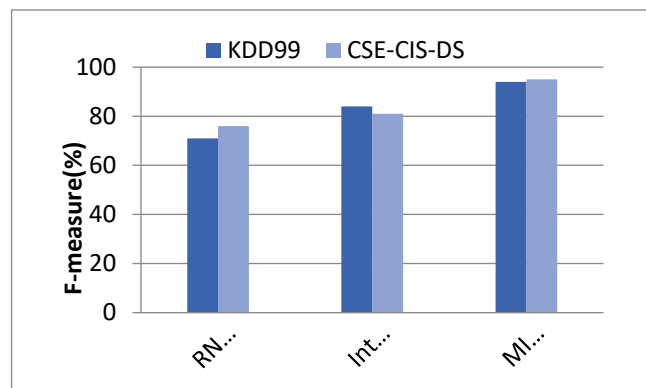


Fig. 5. F-measure Comparative Values of the Proposed and Existing Methods for Identifying Cyber Assaults.

The findings show that the suggested MIntruDTree outperforms existing attack detection strategies in terms of F-measure values.

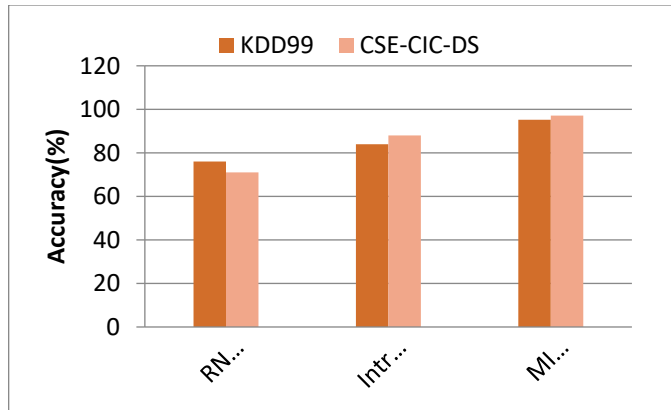


Fig. 6. Comparative Accuracies of Proposed and Existing Methods in Detecting Cyber Attacks.

Fig. 6 depicts the accuracy comparison findings between the proposed and current methods for detecting cyber assaults. In addition, the suggested method's average accuracy of classification rates (in per cent) is shown in comparison to other approaches employing IntruDTree and RNN-IDSs across ten separate runs. As the results show, the suggested technique has greater detection accuracies than previous methods in most circumstances. Furthermore, the rank of feature extraction algorithms is presented based on the detection accuracy attained for a specific dataset. The findings show that the suggested MIntruDTree-HDL approach ranked top when compared to other methods.

V. LIMITATIONS

IDSs also have certain limitations hence this work integrates two techniques for overcoming shortcomings of IDSs where the suggested method benefits by taking advantage of the used approaches. The MIntruDTree-HDL framework is presented to improve learning rates of IDSs and thus effectively enhance its performances and predictions.

VI. CONCLUSION

A modified IDSs tree (MIntruDTree) and a Hybrid Deep Learning (HDL) security model are discussed in this work where important security factors were first prioritized, and subsequently tree-based generalized IDSs were created based on the essential characteristics that were chosen. This was done to ensure that the security model was effective in terms of prediction accuracy for unknown test conditions, as well as efficient by reducing the computational cost of generating the future MIntruDTree-like model by processing fewer features. Following the CNN layers, we added recurrent layers to better capture both spatial and temporal data. We hoped to overcome the vanishing and growing gradient problems with our strategy, improving the ability to collect spatial and temporal correlations and learn effectively from them. The primary motivation for developing IDSs based on DLT categorization. The suggested IDSs aid in the reduction of computing complexity and improve the accuracy and DRs of IDSs. Known classification metrics were used to evaluate both

traditional MLTs and DLTs (DRs, Accuracies, Precisions, Recalls, and F1-scores). The results of the simulations reveal that the proposed MIntruDTree with HDL may successfully calcify harmful attack events. In the KDD99 dataset, the total accuracy of normal and other forms of assaults is approximately 95.24 per cent, while in the CSE-CIC-IDS2018 data, it's around 97.12 per cent. On the basis of the results of the simulation, we can conclude that it is possible to develop an effective security solution against harmful attacks by utilizing a MIntruDTree-based hybrid distributed ledger technology (DLT). This methodology is improved further to include additional deep learning methods and a feature extraction strategy if there are different identification problems in actual datasets currently being used. This is done in preparation for the possibility that these problems may exist.

ACKNOWLEDGMENT

Dr Majed Alowaidi would like to thank the Deanship of Scientific Research at Majmaah University for supporting this work under Project No. R-2022-284.

REFERENCES

- [1] Kott, A. (2014). Towards fundamental science of cyber security. In Network science and cybersecurity (pp. 1-13). Springer, New York, NY.
- [2] Berman, D. S., Buczak, A. L., Chavis, J. S., & Corbett, C. L. (2019). A survey of deep learning methods for cyber security. *Information*, 10(4), 122.
- [3] Lee, W., Stolfo, S. J., & Mok, K. W. (2000). Adaptive intrusion detection: A data mining approach. *Artificial Intelligence Review*, 14(6), 533-567.
- [4] Abou Messaad, M., Jerad, C., & Sikora, A. AI Approaches for IoT Security Analysis. *Intelligent Systems, Technologies and Applications: Proceedings of Sixth ISTA 2020*, India, 1353, 47.
- [5] Buczak, A. L., & Guven, E. (2015). A survey of data mining and machine learning methods for cyber security intrusion detection. *IEEE Communications surveys & tutorials*, 18(2), 1153-1176.
- [6] Chander, B., & Kumaravelan, G. (2021). Cyber security with AI—Part I. In *The "Essence" of network security: An end-to-end panorama* (pp. 147-171). Springer, Singapore.
- [7] Thakur, K., Qiu, M., Gai, K., & Ali, M. L. (2015, November). An investigation on cyber security threats and security models. In *2015 IEEE 2nd international conference on cyber security and cloud computing* (pp. 307-311). IEEE.
- [8] Kantarcioglu, M., & Xi, B. (2016, October). Adversarial data mining: Big data meets cyber security. In *Proceedings of the 2016 ACM SIGSAC conference on computer and communications security* (pp. 1866-1867).
- [9] Singhal, A. (2007). *Data warehousing and data mining techniques for cyber security* (Vol. 31). Springer Science & Business Media.
- [10] Mitchell, R., & Chen, I. R. (2014). A survey of intrusion detection techniques for cyber-physical systems. *ACM Computing Surveys (CSUR)*, 46(4), 1-29.
- [11] Handa, A., Sharma, A., & Shukla, S. K. (2019). Machine learning in cybersecurity: A review. *Wiley Interdisciplinary Reviews: Data Mining and Knowledge Discovery*, 9(4), e1306.
- [12] Martínez Torres, J., Iglesias Comesaña, C., & García-Nieto, P. J. (2019). Machine learning techniques applied to cybersecurity. *International Journal of Machine Learning and Cybernetics*, 10(10), 2823-2836.
- [13] Yin, C., Zhu, Y., Fei, J., & He, X. (2017). A deep learning approach for intrusion detection using recurrent neural networks. *Ieee Access*, 5, 21954-21961.
- [14] Kim, J., Kim, J., Thu, H. L. T., & Kim, H. (2016, February). Long short term memory recurrent neural network classifier for intrusion detection.

- In 2016 international conference on platform technology and service (PlatCon) (pp. 1-5). IEEE.
- [15] Al-Qatf, M., Lasheng, Y., Al-Habib, M., & Al-Sabahi, K. (2018). Deep learning approach combining sparse autoencoder with SVM for network intrusion detection. *Ieee Access*, 6, 52843-52856.
- [16] Khan, M. A., Pradhan, S. K., & Fatima, H. (2017, March). Applying data mining techniques in cyber crimes. In 2017 2nd International Conference on Anti-Cyber Crimes (ICACC) (pp. 213-216). IEEE.
- [17] Lekha, K. C., & Prakasam, S. (2017, August). Data mining techniques in detecting and predicting cyber crimes in banking sector. In 2017 International Conference on Energy, Communication, Data Analytics and Soft Computing (ICECDS) (pp. 1639-1643). IEEE.
- [18] Mitchell, R., & Chen, R. (2013). Effect of intrusion detection and response on reliability of cyber physical systems. *IEEE Transactions on Reliability*, 62(1), 199-210.
- [19] Zimmer, C., Bhat, B., Mueller, F., & Mohan, S. (2010, April). Time-based intrusion detection in cyber-physical systems. In Proceedings of the 1st ACM/IEEE International Conference on Cyber-Physical Systems (pp. 109-118).
- [20] Li, B., Wu, Y., Song, J., Lu, R., Li, T., & Zhao, L. (2020). DeepFed: Federated deep learning for intrusion detection in industrial cyber-physical systems. *IEEE Transactions on Industrial Informatics*, 17(8), 5615-5624.
- [21] Dutta, A. K., Negi, R., & Shukla, S. K. (2021, July). Robust multivariate anomaly-based intrusion detection system for cyber-physical systems. In International Symposium on Cyber Security Cryptography and Machine Learning (pp. 86-93). Springer, Cham.
- [22] Sarker, I. H., Abushark, Y. B., Alsolami, F., & Khan, A. I. (2020). Intrudtree: a machine learning based cyber security intrusion detection model. *Symmetry*, 12(5), 754.
- [23] Abroyan, N. (2017, August). Convolution and recurrent neural networks for real-time data classification. In 2017 Seventh International Conference on Innovative Computing Technology (INTECH) (pp. 42-45). IEEE.

Performance Comparison between Meta-classifier Algorithms for Heart Disease Classification

Nureen Afifah Mohd Zaini, Mohd Khalid Awang

Faculty of Informatics and Computing, Universiti Sultan Zainal Abidin, 22000 Tembil, Terengganu, Malaysia

Abstract—The rise in heart disease among the general population is alarming. This is because cardiovascular disease is the leading cause of death, and several studies have been conducted to assist cardiologists in identifying the primary cause of heart disease. The classification accuracy of single classifiers utilised in most recent studies to predict heart disease is quite low. The accuracy of classification can be enhanced by integrating the output of multiple classifiers in an ensemble technique. Even though they can deliver the best classification accuracy, the existing ensemble approaches that integrate all classifiers are quite resource-intensive. This study thus proposes a stacking ensemble that selects the optimal subset of classifiers to produce meta-classifiers. In addition, the research compares the effectiveness of several meta-classifiers to further enhance classification. There are ten types of algorithms, including logistic regression (LR), support vector classifier (SVC), random forest (RF), extra tree classifier (ETC), naïve bayes (NB), extreme gradient boosting (XGB), decision tree (DT), k-nearest neighbor (KNN), multilayer perceptron (MLP), and stochastic gradient descent (SGD) are used as a base classifier. The construction of the meta-classifier utilised three different algorithms consisting of LR, MLP, and SVC. The prediction results from the base classifier are then used as input for the stacking ensemble. The study demonstrates that using a stacking ensemble performs better than any other single algorithm in the base classifier. The meta-classifier of logistic regression yielded 90.16% results which is better than any base classifiers. In conclusion, we could assume that the ensemble stacking approach can be considered an additional means of achieving better accuracy and has improved the performance of the classification.

Keywords—Heart disease prediction; ensemble stacking; multi classifier

I. INTRODUCTION

According to research published by the World Health Organization (WHO), heart disease has been one of the leading causes of death worldwide. It is estimated to have reached 17.5 million in 2012, 17.9 million in 2016, and 22.2 million by 2030 [1]. Heart disease is very dangerous as it can be a silent killer to a patient. The individual must be alert to the main symptom of heart disease. The usual symptoms of heart disease risk factors include tobacco use, alcohol consumption, physical activity, fruit and vegetable consumption, hypertension, and obesity [2]. Providing high-quality care at affordable rates is a significant problem for the healthcare industry, and accurate diagnoses are the hallmarks of high-quality care [3]. Data mining is an interdisciplinary subject of computer science and statistic whose overall objective is to extract information from a dataset and transform the data into a usable structure [3], [4].

Using magnetic resonance imaging (MRI) and CT angiography to diagnose heart disease is highly complex. The equipment is bulky and prohibitively expensive for most individuals [5]. This research proposes a technique that can reduce the time and effort required for a specialist to diagnose cardiac problems in patients. The study of how to build compelling multi-classifier ensembles has been one of the most studied, and in most cases, ensemble techniques perform better than single classifiers [6]. The approach presented in this paper uses the stacking ensemble method to enhance the accuracy of heart disease prediction. This method is used to improve the overall accuracy of predictions, as the combination of models provides a collaboratively general solid model [7].

The single classifier approach is used most of the time in heart disease prediction research. The accuracy of classification may be improved by combining the results of many different classifiers using a method known as ensemble classification. Despite having the best classification accuracy, current ensemble approaches that include all classifiers are very resource-intensive. In order to create meta-classifiers, the stacking ensemble utilized in this study finds the best subset of classifiers. The study also looks at how effective various meta-classifiers are in improving classification.

Section II of this paper presents a review of related literature. Section III covers the research methodology that intricates the details of datasets and machine learning techniques. The overall results of the experiment are then presented in Section IV. Finally, a conclusion is presented in Section V.

II. LITERATURE REVIEW

A. Data Mining

Data mining is a cognitive method that identifies hidden approach patterns in massive datasets [8]. The effectiveness of data mining depends heavily on the method employed, and the feature is chosen since there are duplications and inconsistencies in healthcare industry medical datasets [9]. Data mining can be applied to improve disease risk assessment, intervention design, and monitoring of chronic conditions [10]. Hence, a reduction in patient admissions and insurance claims is possible.

Data mining is seen as critical yet challenging work that must be completed precisely and efficiently, especially in the healthcare environment. Comparison of different types of classification in machine learning has the potential to provide

high classification accuracy. Prediction accuracy may vary depending on the learning technique used [11].

The classification, which is one type of data mining activity, is crucial since it has the ability to classify such as identify the two categories whether the patient diagnoses with heart disease or non-heart disease. Several usual symptoms can be linked to detect heart disease, but not all are accurate. On the other hand, machine learning, a subset of artificial intelligence, is widely used in renowned research and can be utilised in the healthcare industry to overcome this issue. In return, it can help an expert to detect the disease and suggest an appropriate action to be taken.

B. Ensemble Method

A single classifier, such as Neural Network or Decision Tree, has been widely used in heart disease classification, but the performance of such algorithms is still lacking and need to be improved. Meanwhile, compared to a single classifier, the accuracy of ensemble methods such as stacking is significantly greater. Ensemble method approaches frequently increase predictive performance and this is due to various factors. Overfitting avoidance, computational advantage, and representation are the main factors why the ensemble method is able to improve predictive performance [12], [13]. To distinguish the main factors of the ensemble method, the following description provides examples of both:

1) Overfitting avoidance: Overfitting happens when the classifiers are tightly matched to the training data and thus lose the capacity to generalise to the test data. As a result, the performance of classification in the test set is inferior to the training set [14].

2) Computational advantage: Individual learners who undertake local searches may become mired in local optimality. By merging several learners, the ensemble method reduces the likelihood of achieving a local minimum [12].

3) Class imbalance: When there is a class imbalance in training data, learners will often overclassify the majority group because of its higher prior probability. Consequently, occurrences belonging to the minority group are more frequently misclassified than instances belonging to the majority group [15].

4) Curse of dimensionality: For high-dimension datasets, dimensionality reduction is performed prior to applying the algorithm in order to minimise the impacts of the curse of dimensionality. The more features of the dataset, the more challenges are produced for the algorithm used [16].

This study purposely proves the concept of learning and making decisions is not new to humans. As a human, we employ this concept on a regular basis to make significant decisions, such as seeking advice from multiple experts or consulting with multiple physicians before undergoing major medical treatment [17].

C. Ensemble Stacking

Boosting, bagging, and stacking are the three most prominent ensemble learning approaches in machine learning. Ensemble techniques have been utilised in the current study to

improve heart disease prediction classification accuracy. When weak learners are combined with meta-learners in tandem, a more accurate prediction can be made.

Stacking often accounts for a variety of weak learners [18]. Stacking architecture improves the accuracy of classification over a single classifier as it uses various ways to solve classification problems [19]. Stacking is a learning strategy that uses a meta-classifier to integrate the results of numerous basic classifiers learnt on the same dataset. Each algorithm has its own set of benefits and drawbacks. By merging the classifiers, the outcome may be enhanced.

D. Classification Algorithm in Data Mining

There are two main data mining approaches which are descriptive and predictive. These approaches uncover a hidden pattern in the vast data [20]. Classification can be categorised as supervised machine learning, in which we must train the data. Functional representations include decision trees, logistic regression, naïve bayes, extreme gradient boosting, k-nearest neighbor, extra tree classifier, multilayer perceptron, stochastic gradient classifier, random forest, and support vector machine.

A health management system is often used inside the healthcare setting to keep track of the large amounts of data pertaining to patients and the treatment they get. Such knowledge is useful, particularly if we put it to use in real-world situations. The majority of the medical database consists of discrete data. Thus, making decisions based on discrete facts becomes complex and difficult. Machine Learning which is a subset of data mining, handles large scale well-formatted datasets efficiently [21].

Numerous strategies for predicting heart disease are proposed, each of which employs a unique set of techniques and algorithms. Gaining great service at an affordable price remains the prime and challenging problem for healthcare organisations [22]. This study aims to help the specialist in the detection of heart disease in patients in the early stages.

E. Data Mining in Heart Disease Prediction

The use of data mining is an effort to meet the urgent need to extract relevant knowledge buried in clinical data, specifically to design a solution capable of predicting the presence or absence of heart disease using data mining [23]. In predicting heart disease, several data mining techniques such as regression, clustering, association rule, and classification algorithms consists of naïve bayes, decision tree, random forest, and k-nearest neighbor to categorise various heart disease [24].

According to [25], accuracy and receiver operating characteristics (ROC) are compared. The researcher obtained 303 records with 14 sets of variables and divided the data into training and testing. ROC plot is the most used for evaluating classifier performance. It is based on specificity and sensitivity, which are specificity measures of the negative part, and sensitivity is based on the positive part. Four machine learning algorithms, consisting of logistic regression, random forest, stochastic gradient boosting and support vector machine, are tested for this research. As a result, a comparison between the accuracy and ROC of the model prediction shows

that logistic regression is the highest prediction, with an accuracy of 87.00%.

The research by [26] used Gini index and prediction models. Neural network and Gini index are tested, and the results performed that Gini index results with the most remarkable precision. A decision tree is used to predict the accuracy and sensitivity of coronary illness. Voting methods are known to produce a more precise decision tree. The decision tree makes up of these critical elements, which are the decision hub and edge or branch. The decision hub determines the test features, while the edge or chapter compares to one of the possible quality esteems and denotes one of the property findings. The class to which the question belongs is contained in a leaf, also known as an answer hub.

The author of the study [27] compared the classifier using principal component analysis (PCA) and without PCA. The authors experimented with five types of algorithms for the research. Decision tree, logistic regression, support vector machine, multilayer perceptron, and naïve bayes are tested. Logistic regression achieved the highest with 86.00% without PCA, and random forest achieved the highest with a PCA of 84.00% accuracy. The following areas of interest have seen the most application of PCA, such as classification, data clustering, and dimension reduction.

The study by [28] used a dataset from UCI and proposed four classifiers for the research. Naïve bayes, decision trees, support vector machines, and k-nearest neighbour are tested. According to the researcher, naïve bayes achieves the highest accuracy with 88.67%. Naïve bayes is a straightforward algorithm to implement. Besides, this algorithm also can be categorised as space efficient and fast to train. The author claims that knowledge discovery is essential to handling a large dataset for the identification of heart disease. Managing a massive dataset for heart disease detection and finding the relevant information to forecast a heart attack in its early stages based on patient indicators is challenging.

In 2020, [29] analysed the detection of heart disease using these six algorithms: artificial neural network (ANN), logistic regression, k-nearest neighbour, support vector machine, decision tree, and naïve bayes. The researchers also stated the standard state-of-the-art features selection algorithms consisting of Relief, MRMR, LASSO, and Local-learning-based-features selection (LLBFS) are used to select the features. The researcher also proposes fast conditional mutual information (FCMIM) features selection algorithms for feature selection. LOSO technique (Leave-one-subject-out) cross-validation is applied to select the best hyper-parameter for the best model selection. The best accuracy achieved is SVM with the proposed feature selection algorithm (FCMIM) of 92.37%, which is very good compared to the previously proposed method.

Based on the above discussion, there are two approaches to heart disease prediction: single classifier and meta-classifier. Most of the heart disease prediction research uses the single classifier approach. Existing ensemble methods that incorporate all classifiers are highly resource-intensive, notwithstanding their ability to provide the highest classification accuracy. This paper thus presents a stacking

ensemble that picks the optimum subset of classifiers in order to generate meta-classifiers. In addition, the study examines the efficacy of many meta-classifiers to improve classification. The following section will describe our proposed stacking ensemble in detail.

III. METHODOLOGY

This study is based on the UCI dataset of people with cardiac disease. There are 303 records and 13 attributes in total, which are divided into training and test sets [33]. Table I explains the dataset features for the heart-disease patients.

TABLE I. DESCRIPTION OF ATTRIBUTES DATASET FEATURES

No	Feature Name	Type of data	Data Description
1	X ₁ = age	Numeric	The age of the patients
2	X ₂ =sex	Nominal	Female, male
3	X ₃ = cp	Nominal	Chest pain type Value 0 = Typical angina Value 1 = Atypical angina Value 2 = non-anginal pain Value 3 = asymptomatic
4	X ₄ = trestbps	Numeric	Resting blood pressure
5	X ₅ =Chol	Numeric	Serum cholesterol
6	X ₆ = Fbs	Nominal	Fasting blood sugar
7	X ₇ =restecg	Nominal	Resting electrocardiographic
8	X ₈ =thalach	Numeric	Max heart rate
9	X ₉ = exang	Nominal	Exercise-induced angina
10	X ₁₀ =oldpeak	Nominal	ST depression induced by exercise relative to the rest
11	X ₁₁ =Slope	Nominal	The slope of peak exercise
12	X ₁₂ =Ca	Nominal	Number of major vessels
13	X ₁₃ = Thal	Nominal	The heart status
14	Y = Target	Nominal	Diagnosis of heart disease

A. Proposed Stacking Ensemble

Fig. 1 is a framework on how our proposed meta-classifier is designed, and Table I explains the details of the dataset. The goal of the research is to choose the optimal subset of base classifiers for creating the meta-classifier. Further, the best combination of base classifiers and meta-classifiers is determined by comparing several meta-classifier learning algorithms. The proposed stacking model is described in more detail below:

- 1) Split the data into training and test set.
- 2) Develop base classifiers based on ten different learning algorithms.
 - a) Train and test the base classifiers.
 - b) Rank the base classifiers based on the accuracy of prediction performance.
- 3) Develop meta-classifier based on three different learning algorithms.
 - a) Select the optimum number of base classifiers (2, 4, 5, 7 and 10).
 - b) Test the performance of the meta-classifiers.

4) The final model of ensemble stacking is obtained from the combination of the optimum subset of base classifiers and the meta-classifier algorithm.

From the UCI dataset, 13 attributes and ten base classifiers are utilised, as shown in Fig. 1. The output from the level-1 base classifiers is then applied to the level-2 meta-classifier and followed by the selection of optimal subset of base classifiers. Finally the model is evaluated using three distinct meta-classifiers learning algorithms.

B. Level-1 base Classifiers Construction

The base model classifier is stimulated by certain training data and generates different predictions. The main stage of developing the ensemble technique is to populate the database with a group of base classifiers. As a result, each of the base models will produce its own set of predictions. Base classifiers for this research are created using ten different learning algorithms. Listed below are the selected algorithms:

- 1) $C_1 = \text{LogisticRegression}()$
- 2) $C_2 = \text{KNeighborsClassifier}()$
- 3) $C_3 = \text{DecisionTreeClassifier}()$
- 4) $C_4 = \text{RandomForestClassifier}()$
- 5) $C_5 = \text{GaussianNB}()$
- 6) $C_6 = \text{XGBoostClassifier}()$
- 7) $C_7 = \text{SVC}()$
- 8) $C_8 = \text{MLPClassifier}()$
- 9) $C_9 = \text{SGDClassifier}()$
- 10) $C_{10} = \text{ExtraTreesClassifier}()$

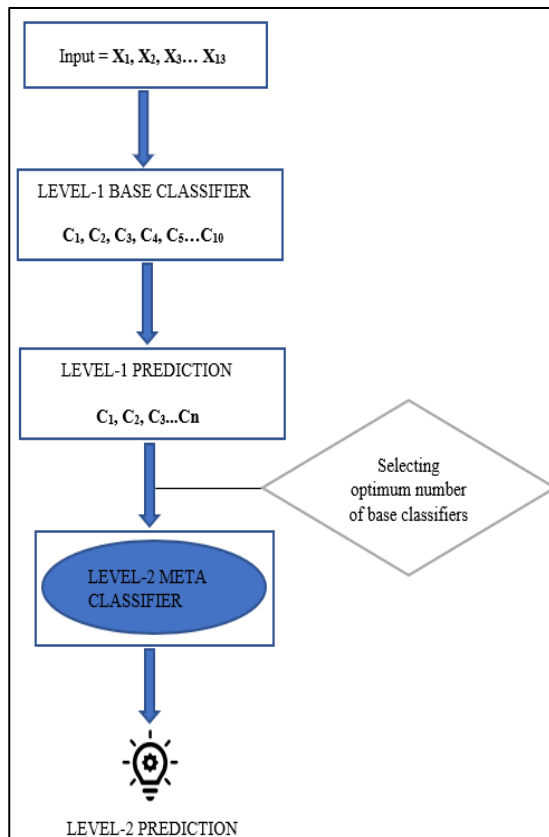


Fig. 1. Proposed Ensemble Stacking for Heart Disease Classification.

C. Level-2 Meta-classifiers Construction

Results obtained from the base classifier are then tested for the ensemble stacking method. Three different learning algorithms are tested with different subset of base classifiers. Meta-learning encompasses a wide range of activities, such as observing the performance of different machine learning models about learning tasks, learning from metadata, and performing a faster learning process for new tasks. A few learning algorithms' classification performances will be evaluated to select optimal meta-model classification. The selected learning algorithms are described below:

- 1) Meta-Classifer using Logistic Regression ()
- 2) Meta-Classifer using Support Vector Machine ()
- 3) Meta-Classifer using Multi-Layer Perceptron ()

Based on their performance, the study has ranked the base classifiers. Five alternative subsets, including 2, 4, 5, 7, and 10 classifiers, were examined using various combinations of the base classifiers. The subset of 5 classifiers is selected as input to the meta-classifier based on the experiments since it outperforms other combinations. There are three types of learning algorithms considered in this study. First, the meta-model is based on Logistic Regression. The second is based on a Support Vector Machine classifier, and the third is based on a Multilayer Perceptron. The performance of each learning algorithm is compared using performance measurements, as discussed in the next section.

D. Performance Measurement

Performance measurement is crucial to data mining evaluation. Several indicators, including accuracy, precision, recall, and F1-score, are used to evaluate the prediction rate and determine the validity of the models [30]. In this research, accuracy is chosen compared to the area under the curve (AUC) because of the percentage obtained. Precision is an upbeat class in which the model is predicted correctly or correctly outputs supplied by the model. The following formula can be used to compute as below [31]:

$$\text{Precision} = \text{TP} / (\text{TP} + \text{FP}) \quad (1)$$

Recall must be high as possible and can be concluded as how the model is predicted correctly. Below is how it can be computed [31]:

$$\text{Recall} = \text{TP} / (\text{TP} + \text{FN}) \quad (2)$$

A model with low precision, high recall, or high precision, low recall is hard to compare. To solve the problem, F-score can be used. This score allows for assessing both recall and precision simultaneously. The following formula can be used to compute [32]:

$$\text{F-Measure} = 2 * \text{Recall} * \text{Precision} / (\text{Recall} + \text{Precision}) \quad (3)$$

IV. RESULTS AND DISCUSSION

The accuracy of heart disease classification will be discussed in this chapter and the findings of a series of experiments undertaken to validate the classification accuracy performance. The outcomes of this study are compared and analysed depending on the algorithm used to test the performance of the proposed strategy.

The performance measures include receiver operating characteristic area under the curve (ROC AUC), precision, recall, and F1 measure. Table II shows the classification's average performance based on precision, accuracy, recall, AUC, and F1 measure.

Table II shows the experimented results for base classifiers based on the accuracy, precision, recall, and F1-score. We have tested and compared ten base models' classifiers, logistic regression, random forest, k-nearest neighbour, decision tree, naïve bayes, support vector machine, extreme gradient boosting, multilayer perceptron, stochastic gradient descent, and extra tree classifier. The best model is MLP, with an accuracy of 88.52%, precision of 86.48%, recall of 94.11%, F1-score of 90.14%, and AUC of 87.79%. While when compared with the decision tree, the accuracy achieved is 72.13%, which is the lowest amongst others, with the precision of 79.31%, recall of 67.64%, F1-score of 73.01%, and AUC of 72.71%.

Table III shows that logistic regression, support vector classifier and multilayer perceptron are chosen as the meta-classifiers. These three meta-classifiers are then experimented with using the subset of base-classifiers. The combination of the base classifier is in the group of two, four, five, seven, and ten classifiers. The formation of the subset is based on the accuracy performance of each of the base classifiers. The base classifiers are ranked according to their prediction performance. Logistic regression is recorded as the best algorithm, tested on a subset of five base classifiers with an accuracy of 90.16%. SVC and MLP achieved 83.60% and 88.52% using the five classifiers.

TABLE II. DETAILS OF PERFORMANCE MEASURE OF THE CLASSIFICATION FOR THE BASE MODEL

Base Model	Accuracy	Precision	Recall	F1-score	AUC
Logistic Regression	85.24%	83.78%	91.17%	87.32%	84.47%
Random Forest	83.60%	85.29%	85.29%	85.29%	83.38%
KNN	81.96%	82.85%	85.29%	84.05%	81.53%
Decision Tree	72.13%	79.31%	67.64%	73.01%	72.71%
Naïve Bayes	85.24%	83.78%	91.17%	87.32%	84.47%
SVC	86.88%	84.21%	94.11%	88.88%	85.94%
XGB	85.24%	85.71%	88.23%	86.95%	84.85%
MLP	88.52%	86.48%	94.11%	90.14%	87.79%
SGD Classifier	83.60%	80.00%	94.11%	86.48%	82.24%
Extra Tree Classifier	86.88%	88.23%	88.23%	88.23%	86.71%

TABLE III. SUMMARY OF META-MODEL ACCURACY USING A DIFFERENT SUBSET OF CLASSIFIERS

Meta-Model Classifiers	Subset of 2	Subset of 4	Subset of 5	Subset of 7	Subset of 10
Logistic Regression	86.88%	88.52%	90.16%	86.88%	83.60%
SVC	86.88%	85.24%	83.60%	83.60%	83.60%
MLP	86.88%	88.52%	88.52%	86.88%	86.88%

Based on the experiment, the subset of two base classifiers, LR, SVC, and MLP achieved the same accuracy of 86.88%. LR and MLP resulted in the same accuracy of 88.52% using a subset of four classifiers, and SVC achieved 85.24%. For a subset of seven classifiers, again, LR and MLP achieved the same accuracy of 86.88%, and SVC achieved 83.60% of accuracy. This experiment also experimented using a subset of ten classifiers. The accuracy achieved for LR and SVC is 83.60%, and MLP attained an accuracy of 86.88%.

As a result, the ensemble technique showed that the best accuracy was achieved utilising a subset of five classifiers using logistic regression as meta-model classifiers. The presumption is accurate when comparing LR to SVC and MLP. This study shows that both the utilisation of large subsets and a limited number of subsets is undesirable. According to the experiments, it's crucial to identify the best subset of base classifiers before building the meta-classifiers in ensemble stacking since doing so could enhance classification performance while also making efficient use of the available resources.

V. CONCLUSION

In conclusion, many people might prevent chronic heart disease attacks with early detection of heart disease. Most research uses a single classifier for prediction, yet the outcome is still unsatisfactory. While compared to utilising a single base classifier, the accuracy performance of heart disease in this research has improved when employing the meta-classifier, such as stacking for the ensemble technique.

Meta-classifier of the Logistic Regression algorithm and a combination of five subsets of base classifiers has achieved the highest accuracy compared to others, with 90.16% accuracy. The subset of base classifiers consists of support vector machine (SVM), multilayer perceptron (MLP), extra tree classifier (ETC), naïve bayes (NB) and extreme gradient boosting (XGB). This study can be proposed to the specialist for the future improvement of heart disease prediction and can be used for medical purposes. The use of ensemble methods such as stacking can enhance the prediction of accuracy.

REFERENCES

- [1] G. İ. Bayram Şahin, "Risk factors of deaths related to cardiovascular diseases in World Health Organization (WHO) member countries," *Heal. Soc. Care*, vol. 30, no. 1, pp. 73–80, 2020.

- [2] Y. Ruan et al., "Cardiovascular disease (CVD) and associated risk factors among older adults in six low-and middle-income countries: results from SAGE Wave 1," *BMC Public Health*, vol. 18, no. 778, pp. 1–13, 2018.
- [3] S. Anitha and N. Sridevi, "HEART DISEASE PREDICTION USING DATA MINING TECHNIQUES," *J. Anal. Comput.*, vol. 13, no. 2, 2019.
- [4] M. Mohamad, M. Y. M. Saman, and N. A. Hamid, "Complexity Approximation of Classification Task for Large Dataset Ensemble Artificial Neural Networks," *Lect. Notes Electr. Eng.*, vol. 520, no. April, pp. 195–202, 2019.
- [5] R. Hasan, S. Ahmed, and A. Afridi, "Heart Sound Analysis for Detection of Cardiovascular Diseases (CVDs) Through Segmentation," *Int. J. Sci. Eng. Res.*, vol. 11, no. Jun 2020, pp. 1–6, 2021.
- [6] T. G. Dietterich, "Ensemble methods in machine learning," *Lect. Notes Comput. Sci.*, vol. 1857, pp. 1–15, 2000.
- [7] R. Atallah and A. Al-Mousa, "Heart Disease Detection Using Machine Learning Majority Voting Ensemble Method," 2019 2nd Int. Conf. New Trends Comput. Sci. ICTCS 2019 - Proc., pp. 1–6, 2019.
- [8] M. Tarawneh and O. Embarak, *Hybrid Approach for Heart Disease Prediction Using Data Mining Techniques*, vol. 29. Springer International Publishing, 2019.
- [9] M. S. Amin, Y. K. Chiam, and K. D. Varathan, "Identification of significant features and data mining techniques in predicting heart disease," *Telemat. Informatics*, vol. 36, pp. 82–93, 2019.
- [10] P. Perner, "Advances in Data Mining Applications," *Lect. Notes Eng. Comput. Sci.*, vol. 5, no. 3, pp. 1–6, 2018.
- [11] A. K. Dwivedi, "Performance evaluation of different machine learning techniques for prediction of heart disease," *Neural Comput. Appl.*, vol. 29, no. 10, pp. 685–693, 2018.
- [12] O. Sagi and L. Rokach, "Ensemble learning: A survey," *Wiley Interdiscip. Rev. Data Min. Knowl. Discov.*, vol. 8, no. 4, pp. 1–18, 2018.
- [13] S. Hisham, M. Makhtar, and A. A. Aziz, "Combining Multiple Classifiers using Ensemble Method for Anomaly Detection in Blockchain Networks: A Comprehensive Review," *Int. J. Adv. Comput. Sci. Appl.*, vol. 13, no. 8, pp. 404–422, 2022.
- [14] M. S. Santos, J. P. Soares, P. H. Abreu, H. Araujo, and J. Santos, "Cross-validation for imbalanced datasets: Avoiding overoptimistic and overfitting approaches [Research Frontier]," *IEEE Comput. Intell. Mag.*, vol. 13, no. 4, pp. 59–76, 2018.
- [15] J. M. Johnson and T. M. Khoshgoftaar, "Survey on deep learning with class imbalance," *J. Big Data*, vol. 6, no. 1, 2019.
- [16] V. Kirankumar, S. Ramasubbareddy, G. Kannayaram, and K. N. Kumar, "Classification of heart disease using support vector machine," *J. Comput. Theor. Nanosci.*, vol. 16, no. 5–6, pp. 2623–2627, 2019.
- [17] K. Raza, *Improving the prediction accuracy of heart disease with ensemble learning and majority voting rule*. Elsevier Inc., 2019.
- [18] M. K. Awang, M. Makhtar, N. Udin, and N. F. Mansor, "Improving Customer Churn Classification with Ensemble Stacking Method," *Int. J. Adv. Comput. Sci. Appl.*, vol. 12, no. 11, pp. 277–285, 2021.
- [19] A. El Sheikh, N. Mahmoud, and A. Keshk, "Heart Disease Classification Based on Hybrid Ensemble Stacking Technique," *IJCI. Int. J. Comput. Inf.*, vol. 8, no. 2, pp. 1–8, 2021.
- [20] S. Umadevi and K. S. J. Marseline, "A survey on data mining classification algorithms," *Proc. IEEE Int. Conf. Signal Process. Commun. ICSPC 2017*, vol. 2018-Janua, no. July, pp. 264–268, 2018.
- [21] I. G. J. Sree, D. Prasanna, B. Y. Rachana, and N. J. Basha, "Performance Analysis of Heart Disease Diagnosis Using Machine," *IJCST*, vol. 9, no. 5, pp. 1–6, 2021.
- [22] A. N. Repaka, S. D. Ravikanti, and R. G. Franklin, "Design and implementing heart disease prediction using naive Bayesian," *Proc. Int. Conf. Trends Electron. Informatics, ICOEI 2019*, vol. 2019-April, no. Icoei, pp. 292–297, 2019.
- [23] M. Bárbara, M., Ferreira, D., Cristiana, N., António, A., & José, "Data Mining for Cardiovascular Disease Prediction," *J. Med. Syst.*, vol. 1, no. 45, pp. 1–8, 2021.
- [24] S. Guruprasad, V. L. Mathias, and W. Dcunha, "Heart Disease Prediction Using Machine Learning Techniques," 2021 5th Int. Conf. Electr. Electron. Commun. Comput. Technol. Optim. Tech. ICEECCOT 2021 - Proc., vol. 1, no. 6, pp. 762–766, 2021.
- [25] N. B. Muppalaneni, M. Ma, and S. Gurumoorthy, *Soft Computing and Medical Bioinformatics*. Springer Singapore, 2019.
- [26] K. Mathan, P. M. Kumar, P. Panchatcharam, G. Manogaran, and R. Varadharajan, "A novel Gini index decision tree data mining method with neural network classifiers for prediction of heart disease," *Des. Autom. Embed. Syst.*, vol. 22, no. 3, pp. 225–242, Sep. 2018.
- [27] C. S. Wu, M. Badshah, and V. Bhagwat, "Heart disease prediction using data mining techniques," in *ACM International Conference Proceeding Series*, 2019, pp. 7–11.
- [28] S. Nayak, M. K. Gourisaria, M. Pandey, and S. S. Rautaray, "Prediction of heart disease by mining frequent items and classification techniques," 2019 Int. Conf. Intell. Comput. Control Syst. ICCS 2019, no. Iccs, pp. 607–611, 2019.
- [29] J. P. Li, A. U. Haq, S. U. Din, J. Khan, A. Khan, and A. Saboor, "Heart Disease Identification Method Using Machine Learning Classification in E-Healthcare," *IEEE Access*, vol. 8, no. M1, pp. 107562–107582, 2020.
- [30] S. Guruprasad, V. L. Mathias, and W. Dcunha, "Heart Disease Prediction Using Machine Learning Techniques," in 2021 5th International Conference on Electrical, Electronics, Communication, Computer Technologies and Optimization Techniques, ICEECCOT 2021 - Proceedings, 2021, vol. 1, pp. 762–766.
- [31] E. Nikoogar, "Hybrid Ensemble Framework for Heart Disease Detection and Prediction," *IJACSA*, vol. 9, no. 5, pp. 243–248, 2018.
- [32] H. Khair and N. M. Dasari, "Exploring Machine Learning Techniques for Coronary Heart Disease Prediction," *Int. J. Adv. Comput. Sci. Appl.*, vol. 12, no. 5, pp. 28–36, 2021.
- [33] D. Newman D, S. Hettich, C. Blake and C. Merz, "UCI Repository of machine learning databases." <http://www.ics.uci.edu/~mllearn/MLRepository.html>, 2021.

Detection of Severity-based Email SPAM Messages using Adaptive Threshold Driven Clustering

I V S Venugopal¹, D Lalitha Bhaskari², M N Seetaramanath³

Department of IT, G V P College of Engineering (A), Andhra Pradesh, 530048, India^{1,3}

Department of CS&SE, AUCE (A), Andhra Pradesh, Visakhapatnam, India²

Abstract—The classification of emails is one crucial part of the email filtering process, as emails have become one of the key methods of communication. The process for identifying safe or unsafe emails is complex due to the diversified use of the language. Nonetheless, most of the parallel research outcomes have demonstrated significant benchmarks in identifying email spam. However, the standard processes can only identify the emails as spam or ham. Henceforth, a detailed classification of the emails has not been achieved. Thus, this work proposes a novel method for the identification of the emails into various classes using the proposed deep clustering process with the help of the ranking of words into severity. The proposed work demonstrates nearly 99.4% accuracy in detecting and classifying the emails into a total of five classes.

Keywords—BoW collection; web crawler; email text extraction; subsetting method; email class detection; ranking method

I. INTRODUCTION

The increase of email communication and people getting higher focus on the email-based communications have opened the door for hackers to target more and more people to be trapped using spam emails.

Email spam prevention remains a difficulty due to attackers using novel ways that evade current spam filters, as noted by H. V. Bathala et al. [1]. An email filter that can detect zero-day attacks is essential. The standard approach offers a method that not only examines the email's body content but also the phishing URLs and spam pictures attached to it. Machine Learning techniques are used to categorise the emails, and a systematic procedure is provided to detect spams. The existing machine learning models are selected using the lazyPredict library. When tested with standard data sets, these smart filters are effective at detecting spam and guarding against zero-day threats. For URL phishing detection, the Stacking classifier performs better with an accuracy of 0.97. In contrast, the perceptron classifier, which has an accuracy of 0.97, is the best at spotting spam email. Other algorithms' results are also included.

M. Hina and colleagues [2] stress the relevance of the detection procedure in their study since email has been used for a long time as a safe and trustworthy method for communication. Email's importance has grown because of the proliferation of quick and secure communication methods. Email management has become more difficult due to the tremendous growth of email data. Until now, emails have been categorised and sorted by sender, size, and date of origin. But there is a need to identify and categorise emails based on their

content. There have been a variety of methods used in the past to classify emails as either spam or non-spam based on their content. A multi-label email categorization system is proposed in the standard approach. Forensic studies of huge email data have been suggested to use an efficient categorization system (e.g., a disc image of an email server). An investigator using this technique would have an advantage when looking into crimes using email. It was shown that Logistic Regression outperforms Naive Bayes, Stochastic Gradient Descent, Random Forest and Support Vector Machines in a comparison of machine learning algorithms. Using benchmark data sets, logistic regression was shown to be the most accurate, with a 91.9 percent accuracy rate for bi-gram features. The similar recommendations can also be observed in the work by Naser et al. [21].

M. K. Islam et al. [3] have shown that email communication is crucial in many aspects of daily life, notably in the workplace. Spam email filtering is critical, especially considering its pervasiveness. Sending massive amounts of undesired communications through electronic means known as spam email, or junk email, constitutes this kind of spam. Due to hazardous frauds or malware hosting sites or viruses attached to the message, most spam emails are not only bothersome but also destructive. In standard measures, the researchers have uncovered the characteristics that set spam apart from other types of email. Including the pooled dataset, the researchers have used four machine learning models and two deep learning models. In addition, the researchers have searched the spam email collection for crucial terms that appear regularly. The researchers have may use this information to identify spam emails for the safety of the employees and the community.

However, the standard mechanism for detection of the spam emails is highly influenced by the use or choice of languages. Hence, many of the standard emails with valid text and information are also often marked as spams causing confusions. Thus, this work decides to solve this problem with deeper classification of the email using proposed machine learning method.

II. FOUNDATIONAL STRATEGY FOR EMAIL CLASSIFICATION

After setting the context in the previous section of this work, in this section of the work, the foundational strategy for email classification is discussed.

Assuming that the total text or the collection of the email texts is $LT[]$ and each email set is $T[]$. Thus, for n number of emails in the total collection can be formulated as,

$$LT[] = \langle T[0], T[1], T[2], \dots, T[n] \rangle \quad (1)$$

Further, each and every email corpus is collection of sender details, receiver details, subject and the actual email text. This can be formulated as,

$$T[] = \langle \text{Sender}, \text{Receiver}, \text{Subject}, \text{Text} \rangle \quad (2)$$

Furthermore, the set of words, which will decide the nature of the email, or popularly called bag or words, denoted as $BOW[]$, also must be populated. Assuming the number of elements in $BOW[]$ are m and each word is denoted as W_x , thus, this can be formulated as,

$$BOW[] = \langle W_1, W_2, \dots, W_m \rangle \quad (3)$$

As per the foundational strategy, the frequency of any word from the $BOW[]$ set must be cross checked in the email text and the frequency of the word must be recorded. This can be formulated as,

$$Fq\{W_x\} = \frac{\phi\{W_x \prec T[i]\{Text\}\}}{\phi\{T[i]\}} \quad (4)$$

Where, W_x is the frequency calculated using the function $Fq\{\}$ and ϕ is the function for extracting the count of the searching word.

Furthermore, the same frequency of the word, $Fq\{W'_x\}$, must be identified in all the text available in the dataset, that is, $LT[]$.

This can be formulated as,

$$Fq\{W'_x\} = \frac{\phi\{W_x \prec LT[]\{T[i].Text\}\}}{\phi\{LT[]\}} \quad (5)$$

During the final phase of the analysis, the document frequency is found to be higher than the dataset word frequency, then the email can be identified as spam or in case the document level frequency is less, then the email can be marked as ham. As, formulated below,

$$T[i]\{True | False\} : Fq\{W_x\} > Fq\{W'_x\} \quad (6)$$

Thus, this is the foundational process for identification of spam or ham in the email corpuses.

This understanding of the foundational method will help in critically analyzing the recent research outcomes in the next section.

III. PARALLEL RECENT RESEARCH OUTCOMES

After having the foundational understanding of the traditional methods for detection of the spams, in this section of the work, the parallel recent research outcomes are discussed.

Spam, according to a study by C. Bansal et al. [4], is the most talked about topic on the Internet today. When you transmit spam, it's simple for spammers to do so. Thousands of spam emails flood inboxes. Files, contacts, and other sensitive information are stolen from the devices by spammers. Even with the most cutting-edge equipment, it's still challenging. Here, the researchers have used a computerised neural network to demonstrate how the researchers have may invert the frequency of Term Frequency documents (TFIDF). The confusion matrix, accuracy, and precision are used to compare the outcomes. The researchers have noticed a propensity to utilise Kaggle data sets with a lower mix of spammy emails and actual emails to evaluate the applicability of ANN. TFIDF-based TFIDF ANN yields a positive return of 97.58%, according to the outputs.

Email communication has become one of the most cost-effective and efficient methods for official and corporate users because of the widespread availability of internet connections. Every day, hundreds of millions of spam emails are sent and received. Spam detection is necessary to safeguard the privacy of people or organisations. Handling large datasets in machine learning is time- and space-consuming in Spam detection. Features must be selected to exclude those that aren't significant to reduce the time and space complexity. The suggested aim in this work is to reduce the time complexity, the space complexity, and the accuracy of the feature selection approach. Both global and local optimization strategies are used in the proposed feature selection method, which combines the chi2 select best method with the Tree-based feature selection method. Four distinct classifiers are put to the test in a series of experiments. According to the results of S. Sharma et al. [5], the suggested concept performs well on precision, memory, and accuracy efficiency tests.

According to A. Karim et al. [6], an intelligent and automated anti-spam framework is required due to the explosive proliferation of spam email and the inherent destructive dynamic inside such assaults on a variety of social, personal, and commercial activities. A growing number of attacks, including virus propagation and identity theft, as well as sensitive data theft, monetary and reputational harm, are taking place. There are now several solutions that don't take into consideration the wide variety of features available in email. Artificial Intelligence, particularly unsupervised machine learning, is preferred approach. Unsupervised learning is being investigated in this study to see whether it can be used to group spam and ham emails. The researchers have wanted to create an unsupervised framework that relies only on unsupervised methods and a clustering strategy that use various techniques, principally the email body and the subject header, to do this. An entirely new binary dataset of 22,000 spam and ham emails was used for the clustering (reduced from eleven to ten after the feature reduction). In this research, seven of the ten features were developed specifically to reflect important analytical email properties from several angles. With five algorithms tested, OPTICS provided the best clustering with a 0.26 percent greater average effectiveness than DBSCAN, its closest competitor. OPTICS and DBSCAN had a combined accuracy of 75.76 percent on average.

Spam e-mail has several detrimental effects, including increased communications overload and cybercrime, as shown by the study of S. A. A. Ghaleb et al. [7]. Spam email has become a key weapon for assaults such as cross-site scripting, malware infection, phishing, and cross-site request forgery, etc., which is the most dangerous feature of spam email. The effectiveness of earlier methods of discovery has been weakened by adaptive unsolicited spam. Using a series of six distinct forms of the extended Grasshopper Optimization Algorithm (EGOAs), this study presents a novel Spam Detection System (SDS) architecture, which is studied and integrated with a Multilayer Perceptron (MLP) for advanced spam email detection. Neural Network (NN) models are created as a result of combining MLP and EGOAs in this context (EGOAMLPs). In this study, EGOAs are used to train the MLP to distinguish between spam and non-spam emails. SpamBase, SpamAssassin, and the UK-2011 Webspam benchmark datasets are used to test these models. A kind of spam email is shown to be useful in identifying the models' efficacy. A comparison of the accuracy, detection rate, and false alarm rate for the EGOAs-trained MLP model indicated that it outperformed the other optimization strategies in this study.

For business reasons, email is the most common way of official communication. Despite the popularity of alternative forms of communication, email continues to grow in popularity. Automated email management is critical in today's world, as the number of emails continues to rise. More than half of all emails are considered spam. This proves that spams are a waste of time and resources for email users, since they provide no relevant information. Understanding the various spam email categorization strategies and their mechanisms is essential for spammers to carry out their illicit actions through spam emails. The study primarily focuses on the machine learning methods used to classify spam. The research also includes a complete evaluation and analysis of research done on various machine learning methods and email properties utilised in various Machine Learning methodologies. Future scholars may find it interesting to know about the issues that M. RAZA et al. [8] describe in their work on spam categorization.

Every day, new technologies and tools are created and made available to the public. Every day, new software and websites are being developed because of technological advancements. As the quantity of software products grows, so does the number of people who use them. As R. Al-Haddad et al. [9] point out, hackers and bad persons will take advantage of this opportunity to commit fraud, hack, or fool, particularly naive users. Email has long been the preferred method of communication in a variety of settings, including academia, business, and the arts. Because so many businesses depend on email to communicate with consumers and with other businesses, fraudsters and phishers devote more time and resources to sending fraudulent emails. As spam and scam emails grow increasingly common, hackers are constantly tweaking their emails to make them seem more authentic. In this study, four machine learning algorithms are used to distinguish between real and fraudulent emails. The studies make use of classifiers such as Decision Tree, Random Forest,

Nave Bayes, and Support Vector Machine. A fresh collection of 11926 emails, 5183 of which are classified as spam and the remainder as regular (ham) emails, is used to test these classification techniques. The findings reveal that SVM performs best when the attained accuracy is more than 98%.

Many organisations and people have found it more convenient to communicate through e-mail. Spammers use this technique to send unsolicited emails to make money, as shown by the study of S. Gibson et al. [10]. Machine learning algorithms that are improved using bio-inspired methodologies will be shown in this article to identify spam emails. A literature study is conducted to investigate the most effective strategies for analysing various datasets to get high-quality findings. On seven separate email datasets, along with feature extraction and pre-processing, substantial research was done to develop machine learning models utilising Nave Bayes, Support Vector Machine, Random Forest, Decision Tree and Multi-Layer Perceptron. Particle Swarm Optimization (PSO) and Genetic Algorithm (GA) were used to improve the classifiers' performance. Overall, Naive Bayes plus Genetic Algorithm outperformed all other methods. Various machine learning and bio-inspired models are also compared to determine which is the most appropriate model.

I. Saha et al. [11] recently shown that under the COVID-19 pandemic, individuals are obliged to adopt a 'work from home' strategy. Nowadays, the Internet serves as an excellent medium for social contact. People's utter reliance on digital platforms puts them up to scammers. It is illegal to employ phishing to get the login credentials of other people on websites like online banking, internet business, e-commerce and even online classrooms and digital markets. Phishers create bogus websites that seem just like the real thing and then send out spam emails to entice unsuspecting victims. When a spam recipient clicks on a link to one of the bogus websites, the phishing scammers steal the user's login credentials. Researchers have developed a wide range of techniques, including blacklists, whitelists, and antivirus software, to identify phishing websites. Defending against cyberattacks is a never-ending challenge for attackers. Phishing websites may now be detected using a data-driven methodology that employs deep learning. Phishing websites are predicted using a feed-forward neural network known as a multilayer perceptron. The data was gathered from Kaggle and consists of 10,000 websites worth of data. There is a total of 10 of them. Accuracy rates for training and testing of the proposed model are 95 percent and 93 percent, respectively.

The rapid rise in the number of internet users has resulted in an increase in email spam, as N. Kumar et al. [12] report. Illegal and unethical practises, such as phishing and fraud, are taking advantage of them. Sending spam emails with dangerous links is a certain way to bring down your system and get your data. Spammers may easily set up a bogus profile and email account, and they target those who aren't aware of the scams. There is a pressing need to identify spam mails that are fraudulent, and this project will do so using machine learning techniques. The work will discuss machine learning algorithms and apply each algorithm to data sets, and then the best algorithm for email spam detection with the best precision and accuracy will be selected.

Spam emails are becoming more widely used in criminal operations such as identity theft, virus propagation, financial loss, and harm to a company's image, among other things, as their effectiveness and diversity expand. These unlawful activities put the privacy of countless individuals and organisations at risk. Numerous studies have attempted to resolve the problem, but none have been successful. The researchers have felt an intelligent and automated approach is the best strategy for dealing with the problems at hand. There have been just a few research on the use of entirely unsupervised frameworks and algorithms to solve the challenge to far. The researchers have plan to provide an anti-spam framework that depends entirely on unsupervised techniques using a multi-algorithm clustering approach to study and examine the possibilities. The first component of the system is examined in detail in this article, focusing on the domain and header information provided in email headers. In this work, a new way of feature reduction employing an ensemble of 'unsupervised' feature selection algorithms was also explored. It was necessary to employ a dataset of 100,000 unique spam and junk email records as the data source. The following are some of the most important findings: 1) Of the six clustering algorithms employed, Spectral and K-means performed well, but OPTICS predicted the best clustering with an average of 3.5% greater efficiency than Spectral and K-means, which were confirmed by a variety of validation techniques. Second, the performance of BIRCH, HDBSCAN, and K-modes was insufficient. As shown in the work of A. Karim et al. [13], the suggested feature reduction framework fulfilled its target with great confidence, and the average balanced accuracy for the optimal three techniques is 94.91 percent.

Phishing e-mails, commonly known as spam, including spear phishing or spam-borne malware have become an increasingly significant issue in recent years, prompting the development of effective, intelligent anti-spam email filters, according to A. Karim et al. [14]. For the identification of clever spam emails, the researchers have thought this survey study on artificial intelligence and machine learning may assist design effective countermeasures. Four components of the email's structure that may be exploited for intelligent analysis were explored in the work: There are MTAs (Mail Transfer Agents) in the heads of emails that offer information about the email's origin, destination, and the number of reroutes it has made along the way. In the SMTP Envelope, the originating source and destination domains and users' identifications are included. (C) The first component of SMTP Data, which includes information such as the sender, recipient, date, and topic. (D) The email body and any attachments are included in this section of the SMTP data. Publications describing each approach were selected, reviewed, and summarised based on the number of relevant papers. The work reveals interesting results, difficulties, and research issues. Research on theoretical and empirical aspects of intelligent spam email identification is now possible thanks to this extensive survey.

There is a lot of evidence, according to M. Gupta et al. [15], that the usage of Short Message Service (SMS) on mobile phones has expanded to such an extent that the devices

are occasionally inundated with spam SMS. Additionally, spam communications might cause a user to lose confidential information. Spam emails may be effectively filtered using a variety of content-based machine learning algorithms. Text messages may be classified as either spam or ham based on certain stylistic characteristics. Text message spam detection may be considerably affected by the inclusion of well-known terms, phrases, and acronyms. Based on their accuracy, precision, recall, and CAP Curve, the study compares several classification approaches on various datasets gathered from prior research. Traditional machine learning approaches have been compared to deep learning methods.

Email is the most favoured means of transferring information over the Internet. Detecting spam is one of the most daunting tasks for email users. Detection and filtering methods may help with this. Support Vector Machine (SVM) methods may play a critical role in spam identification. Using the KFCM technique, the researchers have suggested the usage of a weighted SVM for spam detection. Various classes have different weights, which is reflected in the weight variables. The increase in weight value reduces the amount of email that is incorrectly classified. In accordance with Vishagini et al., the researchers have assessed the effect of spam detection using SVM, WSVM with KPCM, and WSVM with KFCM. [16].

Hacking and malicious email communications are becoming more severe security issues, according to S. Chawathe et al. [17]. Detection of malicious email by automated or semi-automatic means is a critical weapon in the fight against such email threats. For this aim, the work reports use fuzzy rules to categorise email. Using a real dataset, researchers test the performance of a classifier based on fuzzy rules against that of classifiers using crisp rules and decision trees. The usability and editability of the classifiers generated by these approaches are also examined.

If you've ever received an e-mail that you didn't want, you've received spam. Spam email filters are becoming more and more necessary for email users because of the ever-increasing number of spam emails they must deal with. With ever-increasing email volumes, spam classifiers are becoming more ill-equipped to manage them and to identify and detect new spam emails with high performance. It's difficult to classify spam because of the large number of characteristics. An essential part of keyword content categorization is selecting features that are among the most common and successful approaches for reducing feature complexity. As a result, any unnecessary or redundant features that would slow down the system will be removed. Meta-heuristic optimization is the process of selecting the best answer from a set of feasible alternatives while keeping in mind the study's primary goal: performance. Other issues include a lack of clarity in regard to the impact of optimization feature selection on prior work's prominent classifier algorithms, such as K-nearest Neighbor, Naive Bayesian, and Support Vector Machine. So, the goal of this study is to increase feature selection accuracy by using a hybrid Water Cycle and Simulated Annealing approach to optimise findings and assess the suggested Spam Detection method. For this study, the researchers followed a five-step approach to conducting their research. The suggested

spam categorization was put to the test using cross-validation on seven different datasets. Meta-heuristic water cycle feature selection (WCFS) was used as a feature selection method in conjunction with Simulated Annealing, as shown by the findings. The hybridization interleaved hybridization surpassed other feature selection algorithms, such as Harmony Search, Genetic Algorithm, and Particle Swarm, with an accuracy of 96.3 percent. On the other hand, the SVM outperformed other classifier algorithms with an f-measurement of 96.3 percent. As indicated by G. Al-Rawashdeh et al. [18], the number of features using interleaved water cycles and Simulated Annealing has lowered by more than half.

In both personal and professional settings, email is a go-to method for exchanging information. Even though electronic communications, mobile apps, and social networks have become more common, e-mails have remained a vital form of communication. There are several reasons why automated email management is necessary, including spam classification, phishing classification, and multifilter categorization, among others, as the number of vital e-mails grows. All articles on email classification from 2006 to 2016 were analysed using the methodological decision analysis in five areas, including e-mail classification application areas, data sets used for each area of classification, feature space used for each application area, and e-mail classification techniques and performance measures [19].

According to research by W. Z. Khan et al. [20], the issue of email spam has expanded dramatically in the last several years. It's not only a hassle for users; individuals who fall prey to scammers and other assaults suffer as well. Due to the increasing complexity of email spamming methods, which are moving from classic spamming (direct spamming) to more scalable, elusive, and indirect botnets for spreading email spam messages, spamming tactics are becoming more and more complicated. Spamming botnets employ a variety of sources and architectures to churn out enormous amounts of spam through email. There are thorough chronicles of spambots, which meticulously document the sequence of events and significant developments in these spambot networks' evolution. It also seeks to provide a complete review of the various email spamming botnet detection strategies that have been presented in the literature. According to both their nature and technique of detection, as well as a thorough comparison between their strengths and weaknesses, the researchers have sought to classify them. In addition, the researchers have provided an in-depth look at the effectiveness of various methods. Finally, the researchers have look at the future trends and problems in identifying email spamming botnets.

Clearly the global increase of the attacks as showcased in the work by Naser et al. [22] is demanding this research.

Henceforth, in the next section of the work, the persistent bottlenecks of the parallel research outcomes are formulated.

IV. PROBLEM FORMULATION

After realizing the recent improvements over the standard methods for identification of the email types and classifying

the emails into spam or ham emails, in this section of the work, the persistent research problems are identified and discussed in this section of the work.

Firstly, the during the classification of the emails, the emails are either classified as ham, that is safe email or spam, that is unsafe emails. However, the resent research outcomes demonstrate that, identification of the email sub classifications are also important for deploying the current email filters.

According to the Eq. 6, the emails are only been classified as spam or ham. Thus, this problem must be addressed.

Secondly, considering the time complexity of the process, the deployment of such email filtering frameworks is highly complex.

Assuming that the total time complexity of the existing process is T. This can be formulated in the light of Eq. 1 and 3 as,

$$T = n.n * m.m \quad (7)$$

Thus, this can be re-written as,

$$T = n^2 * m^2 \quad (8)$$

Assuming that, $n \approx m$, T can be considered to be as,

$$T(n) = O(n^4) \quad (9)$$

Clearly, this is significantly high and for a large BOW[] set, the complexity can be astronomical.

Hence, this problem must also be solved.

The solutions to these two problems are proposed in the next section of this work.

V. PROPOSED SOLUTION: MATHEMATICAL MODELS

After the detailed analysis of the parallel recent research progress and analysis of the persistent problems in the research, in this section, the proposed strategy is furnished using the mathematical models.

In the light of the Eq. 3, the BOW[] set is expected to contain multiple words, which are expected to contain all the words pertaining towards the suspected emails. It is convenient to convert the BOW[] set into a ranked sets, where the words are ranked in highest to lowest in terms of more risky to less risky. Thus, this can be formulated as:

$$R - BOW[] = \{BOW[], R[]\} \quad (1)$$

Where R[] is the associated rank set and R-BOW[] is the total set with words and the associated ranks.

Further, the threshold for each word in the BOW[] set must be calculated and the rank associated set, R-TH[x] must be formulated as:

$$R - TH[x] = \{Fq(W_x), R[X]\} \quad (11)$$

And,

$$R - TH[x] = \frac{\phi\{W_x \prec T[i]\{Text\}\}}{\phi\{T[i]\}}$$

Again, the global ranks, $RG-TH[x]$ for each word must be calculated for the total dataset as:

$$RG-TH[x] = \{Fq(W'_x), R[X]\} \\ = \frac{\phi\{W_x \prec LT[]\{T[i].Text\}\}}{\phi\{LT[]\}} \quad (12)$$

Finally, the emails must be classified in terms of various classes as,

$$T[i]\{class\} : R-TH[] :: RG-TH[] \quad (13)$$

Henceforth, it is natural to realize that, due to inclusion of the ranks for detecting the class of the email, the proposed method does not only reduce the time complexity to $O(n^2)$, rather also provides deeper classifications of the emails.

Further, based on the proposed mathematical models, in the next section of the work, the proposed algorithm is furnished.

VI. PROPOSED ALGORITHMS

After the detailed analysis of the proposed strategy in the previous section of this work, in this section the proposed algorithms are furnished.

Firstly, the BoW Collection Process using Web Crawler algorithms is furnished.

Algorithm - I: BoW Collection Process using Web Crawler (BCP-WC) Algorithm

Input:

U[] as set of URLs for crawling

Output:

BOW[] set as Bag or Words

Process:

- Step - 1. For each element in the U[] list as U[i]
- Extract the list of words from the U[i] as W[j]
 - If W[j] is noted as negative word
 - Then, BOW[k]=W[j]
 - Else, Continue
- Step - 2. Return BOW[]
-

Even the most powerful search engines are only able to cover a small amount of the Internet's publicly accessible content. An investigation in 2009 found that even the most well-known search engines only index 40 to 70 percent of the searchable Web. A 1999 research by Steve Lawrence and Lee Giles found that no search engine had indexed more than 16% of the Internet at the time. Considering that a crawler gets just a small portion of the web pages, it's critical that the sites it downloads include the most relevant content.

Web pages must be prioritised based on a metric of importance. A page's significance can be gauged by a variety of factors, including the quality of its content, the number of links pointing to it, and even the URL itself (the latter is the case of vertical search engines restricted to a single top-level

domain, or search engines restricted to a fixed Web site). As the whole set of Web sites cannot be known during crawling, creating an effective selection policy is made more complex.

Crawling scheduling policies were initially studied by Junghoo Cho and colleagues. They used a 180,000-page crawl from the stanford.edu domain and a variety of crawling algorithms to generate their data. To see which measures ranked highest in terms of breadth, backlink count, and partial PageRank, researchers used a variety of techniques. According to one of the findings, the best technique for crawlers looking to download pages with high Pagerank early in the crawling process is the partial Pagerank strategy. However, these findings only apply to a single field of study. Cho also completed a PhD in web crawling at Stanford University.

Secondly, the Email Text Extraction using Subsetting Method algorithm is furnished.

Algorithm - II: Email Text Extraction using Subsetting Method (ETE-SM) Algorithm

Input:

LT[] set as collection of emails

Output:

T[] set as collection of texts from all emails

Process:

- Step - 1. For each element in the LT[] set as LT[i]
- Separate LT[i] into subsets using tags
 - If LT[i].tag == body
 - Then, T[j] = LT[i].Text
- Step - 2. Return T[]
-

Spammer infections may have a feature that looks for email addresses on the computer's hard drive and/or network connections. These scanners unearth email addresses that have never been made public online or in Whois. Mail traffic destined for other computers on the shared network segment can be intercepted by a hacked machine on that segment. The spammer receives the harvested addresses back through the virus-created bot-net. Additionally, the addresses may be supplemented with additional data and then cross-referenced in order to obtain financial and personal information about the individuals.

As part of the "e-pending" method of direct-marketing database appending, email addresses are added. Prospect lists are typically obtained by direct marketers from a variety of sources, including subscriptions to magazines and customer lists. Direct marketers can send targeted spam email by scanning the Internet and other resources for email addresses that match the names and street addresses in their database. As with most spammer "targeting," this is not exact; consumers have claimed, for example, receiving requests to mortgage their property at a specific street location — with the address plainly being a business address containing mail stop and office number. Users have experienced similar experiences.

Thirdly, the Email Class Detection using Ranking Method algorithm is furnished.

Algorithm - III: Email Class Detection using Ranking Method (ECD-RM) Algorithm

Input:

BOW[] set as Bag or Words

T[][] set as collection of texts from all emails

Output:

Class of Email as {SPAM - Chain Letters, SPAM - Ads, SPAM - Spoofing, SPAM - Malware, Very positive}

Process:

- Step - 1. For each text in the list BOW[] as BOW[i]
- I. Build the ranking set as R-BOW[i] using Eq. 10
 - II. Calculate the word threshold as R-TH[i] using Eq. 11
 - III. Calculate the global threshold as RG-TH[i] using Eq. 12
- Step - 2. For each word in the email list as T[n][m]
- I. Calculate the word ranks of T[n][m] using Eq. 13
 - II. If T[n][m].Rank == top 40%
 - III. Then, mark T[n][m] as SPAM - Chain Letters
 - IV. If T[n][m].Rank == top 30%
 - V. Then, mark T[n][m] as SPAM - Ads
 - VI. If T[n][m].Rank == top 20%
 - VII. Then, mark T[n][m] as SPAM - Spoofing
 - VIII. If T[n][m].Rank == top 10%
 - IX. Then, mark T[n][m] as SPAM - Malware
 - X. If T[n][m].Rank == top 90%
 - XI. Then, mark T[n][m] as Very positive
- Step - 3. Return class of email
-

For the purpose of sending their messages, spammers may commit fraud. These "disposable" accounts are typically created by spammers using fake names, addresses, phone numbers and other contact details. To pay for these accounts, they frequently make use of stolen or fake credit card numbers. As the host ISPs uncover and shut down each account, they can rapidly move on to the next.

They may go to tremendous efforts in order to hide the origin of their message. Large corporations may outsource the transmission of their messages to another firm in order to deflect criticism or email blocking to a third party. Others use email faking techniques (much easier than IP address spoofing). Because the email protocol (SMTP) does not require any authentication by default, spammers can send messages that appear to come from any email address they want to use. This can be avoided by requiring the usage of SMTP-AUTH, which allows the specific account from which an email originates to be positively identified.

Due to the fact that receiving mail servers record genuine connections from the final mail server, it is impossible for a sender to spoof email delivery chains (the 'Received' header). Spammers use forged delivery headers to fool legitimate servers into believing that an email has already passed through several of their own.

For legitimate email users, spoofing can have catastrophic implications. In addition to clogging up their email inboxes with "undeliverable" emails and loads of spam, they can be incorrectly classified as a spammer. As a result, they may receive a barrage of angry emails from spam victims, as well as the threat of having their Internet service terminated for spamming.

Further, in the next section, the obtained results from the algorithms are furnished.

VII. RESULTS AND DISCUSSIONS

The obtained results from the proposed algorithms are highly satisfactory and are discussed in this section of the work.

Firstly, the dataset analysis is furnished here (Table I).

TABLE I. DATASET CHARACTERISTICS

Parameter	Value
Number of Samples	1929
Spam Emails	1543
HAM Emails	386
Minimum Length of Email Text	111
Mean Length of Email Text	231
Maximum Length of Email Text	334
Missing Words	22279
Unique Words	325287

It is natural to realize that the dataset demonstrates highly unique characteristics to be considered for testing on the proposed algorithms.

The results are also visualized graphically here (Fig. 1).

Secondly, as proposed in the mathematical models and during the algorithm design, the work summarizes the email in terms of overall scores. The details of the assumption of the scores and correlated email classes are furnished here (Table II).

Thirdly, the email classification results are showcased (Table III). The actual tests were carried out on a total of 1923 itemsets, however in this literature only 20 samples are furnished.

The obtained results are also visualized graphically here (Fig. 2).

Further, based on the ranking and matching of the email contents with various classes, the emails are finally classified in five pre-defined classes (Table IV).

Further, the results are visualized graphically here (Fig. 3).

Fourthly, the time complexity analysis of the proposed algorithms is furnished here (Table V).

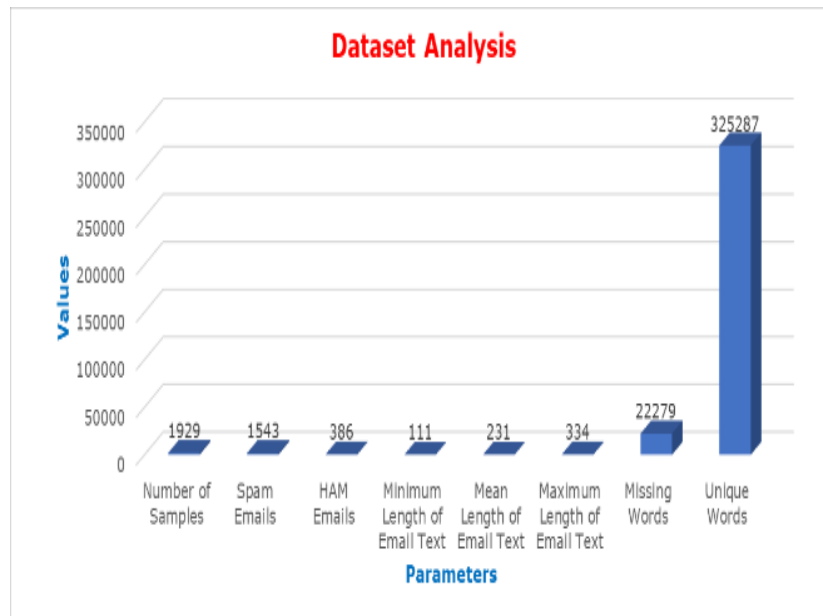


Fig. 1. Dataset Analysis.

TABLE II. EMAIL CLASS AND RANKING MAPPING

Over All Rank	Email Class
0	SPAM - Malware
1	SPAM - Spoofing
2	SPAM - Chain Letters
3	SPAM - Ads
4	Very positive

TABLE III. EMAIL CLASSIFICATION RESULTS

Email Seq. #	No. of Words	Strong - HAM	HAM	Neutral	SPAM	Strong - SPAM
1	37968	0%	17%	82%	1%	0%
2	1420	2%	48%	45%	5%	1%
3	4333	19%	78%	2%	0%	0%
4	2513	1%	7%	69%	21%	2%
5	2264	1%	12%	65%	20%	2%
6	278	5%	72%	21%	1%	0%
7	8207	3%	14%	43%	34%	5%
8	3361	1%	9%	79%	10%	1%
9	1617	21%	66%	12%	1%	0%
10	1184	1%	8%	78%	13%	1%
11	564	1%	17%	75%	6%	1%
12	1150	1%	6%	57%	33%	3%
13	1080	0%	7%	80%	12%	1%
14	6190	0%	1%	10%	81%	8%
15	492	8%	88%	4%	0%	0%
16	784	7%	83%	9%	0%	0%
17	907	8%	80%	8%	3%	1%
18	5153	0%	7%	90%	3%	0%
19	766	1%	6%	27%	58%	8%
20	463	4%	69%	26%	0%	0%

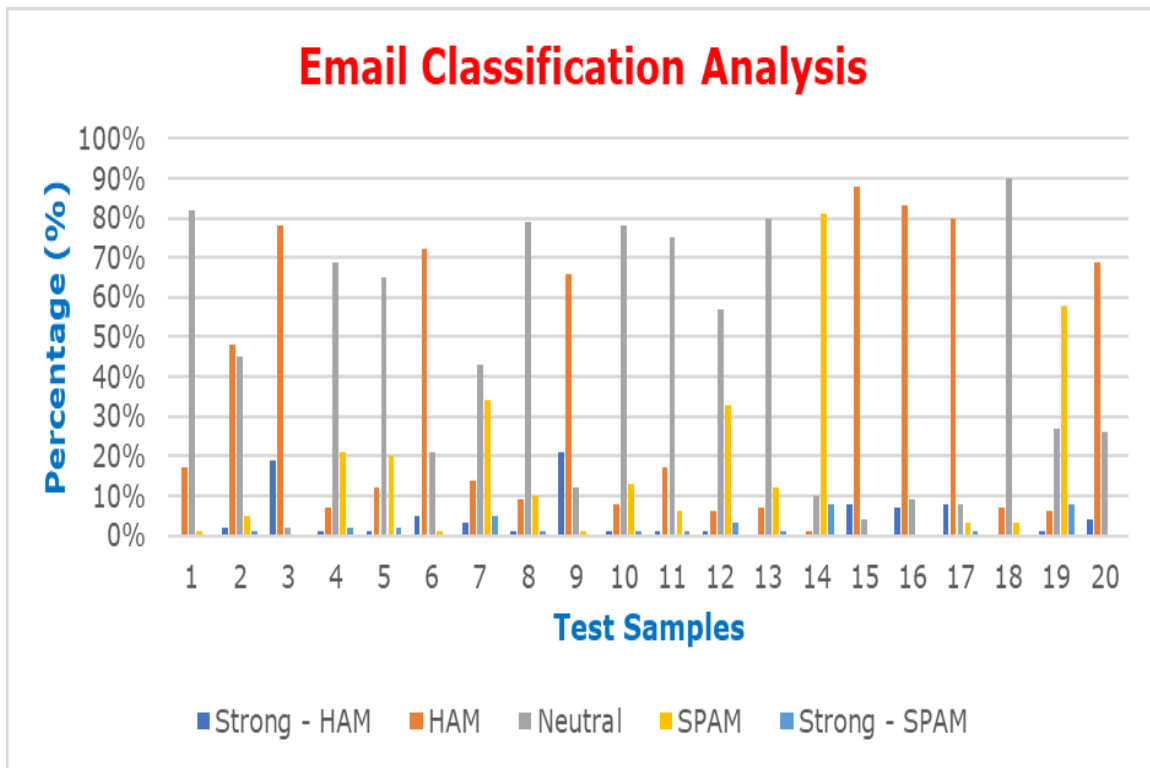


Fig. 2. Email Classification Analysis

TABLE IV. EMAIL FINAL CLASSIFICATION RESULTS

Email Seq. #	Email Score	Detected Email Type
1	2	SPAM - Chain Letters
2	3	SPAM - Ads
3	3	SPAM - Ads
4	2	SPAM - Chain Letters
5	2	SPAM - Chain Letters
6	3	SPAM - Ads
7	2	SPAM - Chain Letters
8	2	SPAM - Chain Letters
9	3	SPAM - Ads
10	2	SPAM - Chain Letters
11	2	SPAM - Chain Letters
12	2	SPAM - Chain Letters
13	2	SPAM - Chain Letters
14	1	SPAM - Spoofing
15	3	SPAM - Ads
16	3	SPAM - Ads
17	3	SPAM - Ads
18	2	SPAM - Chain Letters
19	1	SPAM - Spoofing
20	3	SPAM - Ads

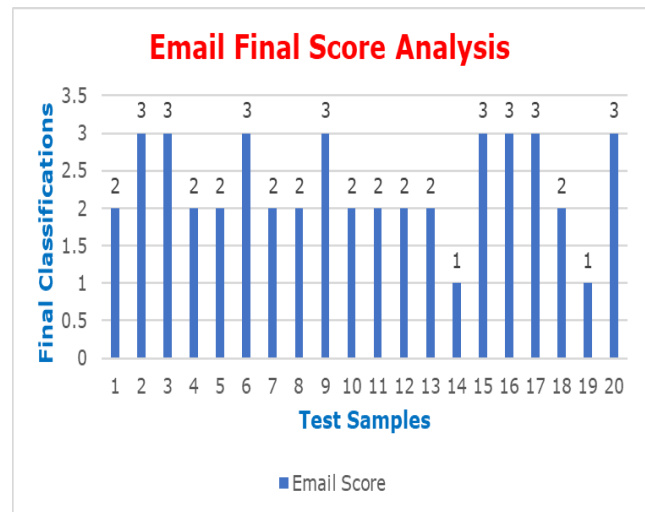


Fig. 3. Email Final Classification Analysis.

It is significant to observe that the time taken to process the complete email and further classify these emails are significantly low. The results are also visualized graphically here (Fig. 4).

Finally, the accuracy analysis results are furnished here (Table VI).

The mean accuracy of proposed system is nearly 99.42%.

Henceforth, in the next section of this work, the proposed strategy is compared with other parallel research outcomes.

TABLE V. EMAIL CLASSIFICATION TIME COMPLEXITY

Email Seq. #	Detected Email Type	No. of Words	Time (ns)
1	SPAM - Chain Letters	37968	164.4
2	SPAM - Ads	1420	6.1
3	SPAM - Ads	4333	18.8
4	SPAM - Chain Letters	2513	10.9
5	SPAM - Chain Letters	2264	9.8
6	SPAM - Ads	278	1.2
7	SPAM - Chain Letters	8207	35.5
8	SPAM - Chain Letters	3361	14.6
9	SPAM - Ads	1617	7.0
10	SPAM - Chain Letters	1184	5.1
11	SPAM - Chain Letters	564	2.4
12	SPAM - Chain Letters	1150	5.0
13	SPAM - Chain Letters	1080	4.7
14	SPAM - Spoofing	6190	26.8
15	SPAM - Ads	492	2.1
16	SPAM - Ads	784	3.4
17	SPAM - Ads	907	3.9
18	SPAM - Chain Letters	5153	22.3
19	SPAM - Spoofing	766	3.3
20	SPAM - Ads	463	2.0

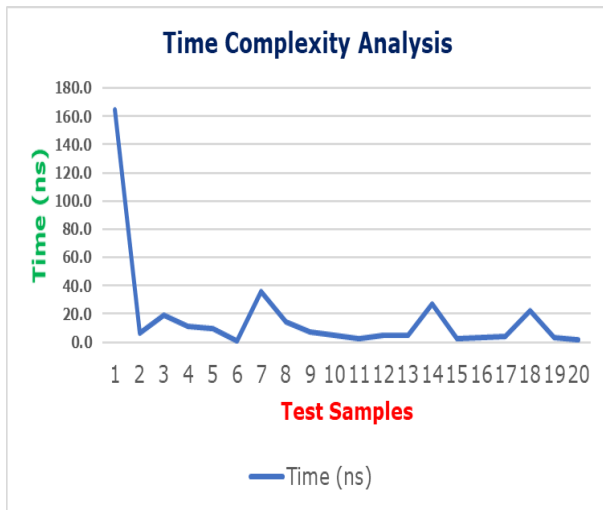


Fig. 4. Email Classification Time Complexity.

TABLE VI. ACCURACY ANALYSIS

Trial Seq #	Number of Samples	Accuracy (%)
1	412	98.943
2	425	99.224
3	468	99.637
4	488	99.997
5	136	99.344

VIII. COMPARATIVE ANALYSIS

In order to achieve the understanding, that the proposed system can outperform the other parallel research outcomes, it is important that the proposed system performances are compared with the parallel research results. Henceforth, the comparative analysis reports are furnished here (Table VII).

TABLE VII. COMPARATIVE ANALYSIS

Author & Year	Proposed Method	Model Complexity	Accuracy (%)
H. V. Bathala et al. [1], 2021	Filtering	$O(n^4)$	96.23
M. Hina et al. [2], 2021	Classification	$O(n^4)$	97.12
M. K. Islam et al. [3], 2021	Word Extraction	$O(n^4)$	97.68
C. Bansal et al. [4], 2021	Hybrid	$O(n^4)$	97.58
S. Sharma et al. [5], 2021	Hybrid	$O(n^4)$	98.32
Proposed Method, 2022	Classification, Ranking, Word Extraction and Deep Clstering	$O(n^2)$	99.42

Further, in the next section of the work, the research conclusion is presented.

IX. RESEARCH CONCLUSION

It's important to categorise emails because they've become one of the most common methods of communication. Because of the wide variety of ways people speak, determining whether an email is safe or not is a difficult task. There have been significant benchmarks established in email spam detection in most of the parallel studies, however. Even so, the standard spam-detection mechanism is heavily influenced by the languages used or chosen. As a result, many standard emails with legitimate text and information are incorrectly labelled as spam. In this way, the proposed machine learning method is used to solve the problem of email classification at a deeper level. Emails can only be categorised as spam or ham by the standard processes. As a result, a precise classification of the emails has thus far failed. As a result, this work proposes a novel method for classifying emails based on their severity using the proposed deep clustering process. With a 99.4 percent accuracy rate, the proposed work can detect and classify emails into a total of five categories.

REFERENCES

- [1] H. V. Bathala, P. V. N. P. Srihitha, S. G. R. Dodla and A. Pasala, "Zero-Day attack prevention Email Filter using Advanced Machine Learning," 2021 5th Conference on Information and Communication Technology (CICT), Kurnool, India, 2021, pp. 1-6.
- [2] M. Hina, M. Ali, A. R. Javed, G. Srivastava, T. R. Gadekallu and Z. Jalil, "Email Classification and Forensics Analysis using Machine Learning," 2021 IEEE SmartWorld, Ubiquitous Intelligence & Computing, Advanced & Trusted Computing, Scalable Computing & Communications, Internet of People and Smart City Innovation (SmartWorld/SCALCOM/UIC/ATC/IOP/SCI), Atlanta, GA, USA, 2021, pp. 630-635.

- [3] M. K. Islam, M. A. Amin, M. R. Islam, M. N. I. Mahub, M. I. H. Showrov and C. Kaushal, "Spam-Detection with Comparative Analysis and Spamming Words Extractions," 2021 9th International Conference on Reliability, Infocom Technologies and Optimization (Trends and Future Directions) (ICRITO), Noida, India, 2021, pp. 1-9.
- [4] C. Bansal and B. Sidhu, "Machine Learning based Hybrid Approach for Email Spam Detection," 2021 9th International Conference on Reliability, Infocom Technologies and Optimization (Trends and Future Directions) (ICRITO), Noida, India, 2021, pp. 1-4.
- [5] S. Sharma and C. Azad, "A hybrid approach for feature selection based on global and local optimization for email spam detection," 2021 12th International Conference on Computing Communication and Networking Technologies (ICCCNT), Kharagpur, India, 2021, pp. 1-6.
- [6] A. Karim, S. Azam, B. Shanmugam and K. Kannoorpatti, "An Unsupervised Approach for Content-Based Clustering of Emails Into Spam and Ham Through Multiangular Feature Formulation," in IEEE Access, vol. 9, pp. 135186-135209, 2021.
- [7] S. A. A. Ghaleb, M. Mohamad, S. A. Fadzli and W. A. H. M. Ghanem, "Training Neural Networks by Enhance Grasshopper Optimization Algorithm for Spam Detection System," in IEEE Access, vol. 9, pp. 116768-116813, 2021.
- [8] M. RAZA, N. D. Jayasinghe and M. M. A. Muslam, "A Comprehensive Review on Email Spam Classification using Machine Learning Algorithms," 2021 International Conference on Information Networking (ICOIN), Jeju Island, Korea (South), 2021, pp. 327-332.
- [9] R. Al-Haddad, F. Sahwan, A. Aboalmakarem, G. Latif and Y. M. Alufaisan, "Email text analysis for fraud detection through machine learning techniques," 3rd Smart Cities Symposium (SCS 2020), Online Conference, 2020, pp. 613-616.
- [10] S. Gibson, B. Issac, L. Zhang and S. M. Jacob, "Detecting Spam Email With Machine Learning Optimized With Bio-Inspired Metaheuristic Algorithms," in IEEE Access, vol. 8, pp. 187914-187932, 2020.
- [11] I. Saha, D. Sarma, R. J. Chakma, M. N. Alam, A. Sultana and S. Hossain, "Phishing Attacks Detection using Deep Learning Approach," 2020 Third International Conference on Smart Systems and Inventive Technology (ICSSIT), Tirunelveli, India, 2020, pp. 1180-1185.
- [12] N. Kumar, S. Sonowal and Nishant, "Email Spam Detection Using Machine Learning Algorithms," 2020 Second International Conference on Inventive Research in Computing Applications (ICIRCA), Coimbatore, India, 2020, pp. 108-113.
- [13] A. Karim, S. Azam, B. Shanmugam and K. Kannoorpatti, "Efficient Clustering of Emails Into Spam and Ham: The Foundational Study of a Comprehensive Unsupervised Framework," in IEEE Access, vol. 8, pp. 154759-154788, 2020.
- [14] A. Karim, S. Azam, B. Shanmugam, K. Kannoorpatti and M. Alazab, "A Comprehensive Survey for Intelligent Spam Email Detection," in IEEE Access, vol. 7, pp. 168261-168295, 2019.
- [15] M. Gupta, A. Bakliwal, S. Agarwal and P. Mehndiratta, "A Comparative Study of Spam SMS Detection Using Machine Learning Classifiers," 2018 Eleventh International Conference on Contemporary Computing (IC3), Noida, India, 2018, pp. 1-7.
- [16] V. Vishagini and A. K. Rajan, "An Improved Spam Detection Method with Weighted Support Vector Machine," 2018 International Conference on Data Science and Engineering (ICDSE), Kochi, India, 2018, pp. 1-5.
- [17] S. Chawathe, "Improving Email Security with Fuzzy Rules," 2018 17th IEEE International Conference On Trust, Security And Privacy In Computing And Communications/ 12th IEEE International Conference On Big Data Science And Engineering (TrustCom/BigDataSE), New York, NY, USA, 2018, pp. 1864-1869.
- [18] G. Al-Rawashdeh, R. Mamat and N. Hafhizah Binti Abd Rahim, "Hybrid Water Cycle Optimization Algorithm With Simulated Annealing for Spam E-mail Detection," in IEEE Access, vol. 7, pp. 143721-143734, 2019.
- [19] G. Mujtaba, L. Shuib, R. G. Raj, N. Majeed and M. A. Al-Garadi, "Email Classification Research Trends: Review and Open Issues," in IEEE Access, vol. 5, pp. 9044-9064, 2017.
- [20] W. Z. Khan, M. K. Khan, F. T. Bin Muhaya, M. Y. Aalsalem and H. Chao, "A Comprehensive Study of Email Spam Botnet Detection," in IEEE Communications Surveys & Tutorials, vol. 17, no. 4, pp. 2271-2295, Fourthquarter 2015.
- [21] A. N. Jaber, L. Fritsch and H. Haugerud, "Improving Phishing Detection with the Grey Wolf Optimizer," 2022 International Conference on Electronics, Information, and Communication (ICEIC), 2022, pp. 1-6, doi: 10.1109/ICEIC54506.2022.9748592.
- [22] A. N. Jaber and L. Fritsch, "COVID-19 and Global Increases in Cybersecurity Attacks: Review of Possible Adverse Artificial Intelligence Attacks," 2021 25th International Computer Science and Engineering Conference (ICSEC), 2021, pp. 434-442, doi: 10.1109/ICSEC53205.2021.9684603.

Alz-SAENet: A Deep Sparse Autoencoder based Model for Alzheimer's Classification

G Nagarjuna Reddy¹
Research Scholar
JNT University
Ananthapuramu, India

K Nagi Reddy²
Professor, Dept. of ECE
N.B.K.R.I.S.T
Vidyanagar, India

Abstract—Precise identification of Alzheimer's Disease (AD) is vital in health care, especially at an early stage, since recognizing the likelihood of incidence and progression allows patients to adopt preventive measures before irreparable brain damage occurs. Magnetic Resonance Imaging is an effective and common clinical strategy to diagnose AD due to its structural details. We built an advanced deep sparse autoencoder-based architecture, named Alz-SAENet for the identification of diseased from typical control subjects using MRI volumes. We focused on a novel optimal feature extraction procedure using the combination of a 3D Convolutional Neural Network (CNN) and deep sparse autoencoder (SAE). Optimal features derived from the bottleneck layer of the hyper-tuned SAE network are subsequently passed via a deep neural network (DNN). This approach results in the improved four-way categorization of AD-prone 3D MRI brain images that prove the capability of this network in AD prognosis to adopt preventive measures. This model is further evaluated using ADNI and Kaggle data and achieved 98.9% and 98.215% accuracy and showed a tremendous response in distinguishing the MRI volumes that are in a transitional phase of AD.

Keywords—Alzheimer's disease; MRI; CNN; sparse autoencoder; DNN; mild cognitive impairment

I. INTRODUCTION

Alzheimer's Disease (AD) is the most predominantly reported dementia observed in elder people more than 60 years old. Late-onset effects of AD are most often seen in the mid-60s, whereas early-onset effects appear between the 30s and the mid-60s. Because of the world's aging population, it is anticipated that around 640 million individuals will be impacted by AD by the year 2050. Each year, more than 10 million fresh dementia cases are diagnosed worldwide, implying one fresh patient for every 3.2 seconds [1]. This situation leads to imposing significant impact on patients' and caretakers' daily living routines, physical and emotional states, and the economy. Early diagnosis is the only solution to find suitable medication that prevents additional damage to the cognitive ability of a patient.

Both the Mini Mental State Examination (MMSE) and the Clinical Dementia Rating (CDR) parameters are commonly used to estimate the severity of AD. Magnetic Resonance Images (MRI) are shown to be the most effective imaging biomarker [2, 3] in clinical assessment for analysing and getting a conclusion about the stage of dementia due to their ability in reflecting the structural details of human brain. In

practise, several computer-aided diagnostic tools that employ machine learning methodologies [4, 5, 6, and 7] such as Support Vector Machine (SVM), K-Nearest Neighbor (KNN), and ensemble methods [8], are suggested, developed and widely implemented using MRI to assist the medical practitioners community.

Due to the rapid advancement of Artificial Intelligence algorithms in diagnosis procedures, the deep learning techniques have been able to categorise, extract high level features, and will also aid in the right diagnosis of AD patients in short span of time. The potential for gratifying feedback from using deep learning algorithms in medical imaging prompted several investigators to emphasize the approach when tackling research difficulties and concerns [9, 10, and 11]. Convolutional Neural Network (CNN) [35] changed the complete picture of pattern recognition especially in AD diagnosis [12] with their capability in extraction of latent features from various objects by fine tuning its hyper parameters using optimizers. Sparse autoencoder (SAE), another architecture of deep learning model has shown exceptional performance in a wide range of unsupervised applications due to their ability in utilizing the sparsity in information bottleneck [13, 14, 15, and 16]. It excels in learning useful feature representations in very complex and large datasets, making it a possible solution to handle the difficulties of AD prediction.

In this research paper, a 3-stage neural network model that combines 3D CNN, SAE, and Deep Neural Network (DNN) is presented. Before feeding MRI volumes into this network, the first MRI volumes are pre-processed and converted into 2D slices in a series. In this research work, only 40 medial slices covering the hippocampal portion were considered so that MRI volume consists of AD symptoms. After pre-processing, convolutional layers in CNN are trained to extract the latent features from MRI data. SAE in the next stage reduces the feature dimension so that only dominant features are incorporated into DNN [17] in the third stage to classify the subjects into AD subcategories namely AD, low and stable Mild Cognitive Impairment (ls-MCI), progressive Mild Cognitive Impairment (p-MCI), and Cognitive Normal (CN). In contrast to earlier approaches, the proposed Alz-SAENet exhibits good accuracy, and fast convergence by leveraging the convolutional layer's potential in CNN and the SAE sparsity.

The key contributions of this work are:

- Alz-SAENet is developed for robust 4-way classification for AD diagnosis.
- For early diagnosis, this model can be utilized since classifying MCI stages were more concentrated.

The rest of this research article is organized as follows: literature is studied and challenges were drawn in Section II. Datasets and design of Alz-SAENet are discussed systematically in Section III. Experimental remarks and discussions are provided and Section IV. Finally, Section V summarized the work and future enhancement of this work.

II. LITERATURE REVIEW

A. Related Works

Jha et al. [18] developed a deep architecture that comprises SAE, scale conjugate gradient, stacked autoencoders, and finally one SoftMax layer for effective classification of AD subjects. When compared to other renowned investigations, this approach demonstrated a significant improvement in diagnosis, yielding an adequate and reliable accuracy of 91.6%.

Jabason et al. [19] described a novel technique to handle the missing data patterns in Alzheimer's diagnostic methods by leveraging the benefits of sparse autoencoder. It is a stacked sparse autoencoder that assign the missing data patterns with values and to select the discriminative features for supporting 3-way Alzheimer's disease diagnosis. The proposed model has attained 95.90% diagnostic accuracy over ADNI dataset by imputing the missing data patterns.

Soliman et al. [20] proposed an enhanced sparse autoencoder base CNN for 3-way Alzheimer's prediction. The authors tuned the hyperparameters of CNN and SAE thoroughly using the Adam optimizer and obtained 87.8% diagnostic accuracy over ADNI datasets. This diagnostic accuracy is attained not only due to the structure of the network and also with the pre-processing phase. Further improvement of diagnostic accuracy is a bit challenging matter.

Venugopalan et al. [21] implemented a deep learning (DL) model for analyzing multimodal data for the 3-way classification of AD. They used Stacked Denoising Autoencoders (SDAE) for feature extraction from multimodal data that comprise both clinical and genetic data and 3D-CNNs are employed for the categorization of MR volumetric data. This model outperformed almost all shallow architectures in terms of key evaluation metrics.

Zhu et al. [22] presented a sparse regression approach that utilizes a novel feature selection algorithm that considers task-wise relations amongst the clinical labels and neuroimaging features and 'self-representation' relations. Authors performed both binary and multiclass classification and this procedure outstripped all the conventional methods by improving the accuracy by an average of 4.5%.

Yagis et al. [23] focused on the end-to-end development of an AD detection technique that integrates supervised prediction with unsupervised representation using convolutional autoencoders. To capture hidden representations

in structural MRI slices, a 2D convolutional autoencoder is built. Testing the network over OASIS repository data, it is revealed that their model beats several competing classifiers with 74.66% accuracy when employing a single slice.

Lin et al. [24] employed CNN to extract discriminative features from MRI volumetric image data. The authors concentrated on some specific subjects in the transition period from MCI to AD. They attained 79.9% accuracy with their model by a solid balance between specificity and sensitivity.

Basheera et al. [25] demonstrated an innovative method to extract the grey matter from the brain voxels, and CNN is employed for AD classification. The authors resliced 18,017 voxels from 1820 MRI volumes that were retrieved from the ADNI repository. With the support of their enhanced Independent Component Analysis (ICA), they extracted hidden structural features from pre-processed voxels. With this hybrid method, authors achieved 90.47% accuracy in the 3-way classification of AD, MCI, and CN subjects. Slow convergence and moderate diagnostic accuracy are challenges here.

Akramifard et al. [26] designed and developed a hybrid method that combines Autoencoder and SVM for Alzheimer's diagnosis using multimodal datasets including MMSE, MRI, PET, CSF, and personal information. An autoencoder is designed to inputting the missing data. PCA is employed for reducing data dimension. Finally, the SVM algorithm is utilized for classification. During the evaluation, their algorithm yielded 95.57% accuracy for multimodal data whereas for only MRI it produced 84.46% diagnostic accuracy. Although the algorithm performance is superior, processing such limited datasets in all phases is a challenging task.

Almughim et al. [27] developed ASD-SAENet, a deep sparse network for distinguishing autism spectrum disorder (ASD) patients from typical control subjects. The authors proposed and implemented an SAE, that proposed an optimized feature extraction procedure for Autism patients' classification. These features are subsequently loaded into a DNN for accurate classification of ASD-prone fMRI brain voxels. Based on both the restored data error and the classifier error, this model is trained to extract optimal hidden details. The model is evaluated over 1,035 Autism Brain Imaging Data Exchange (ABIDE) datasets, and 17 research centers and achieved 70.8% accuracy and 79.1% specificity.

B. Review

Detailed literature analysis is tabulated in Table I. Although the existing literature has many advantages, they are suffering from certain issues viz. number of AD stages, convergence, feature selection, overfitting, and hyperparameters tuning. These challenges to be addressed with productive outcomes by developing a novel network. From overall existing works, it is very clear that 3D CNN will holistically extract MRI latent features and converge quickly. The feature vector obtained from CNN would have huge redundant details that may not affect the classifier overall performance. In second stage, the sparsity of SAE aids in the mapping of low-level features from high-dimensional features while preventing overfitting due to its sample size. Finally, a

DNN is employed for the classification of subjects into four AD categories viz. CN, ls-MCI, p-MCI, and AD. With the

hyperparameters tuning, SAE can avoid overfitting by minimizing its cost function and with quick convergence.

TABLE I. LITERATURE DEEP ANALYSIS

Authors	Data	Methodology	Features	Challenges
Jha et al. [18]	OASIS	SAE	Diagnostic accuracy is obtained as 91.6% over very small datasets.	Diagnostic accuracy is low.
Jabason et al. [19]	ADNI	SAE	Imputation of missing data patterns is employed. 3-way classification is performed.	Accuracy is moderate. Early diagnosis is not precise.
Soliman et al. [20]	ADNI	SAE+CNN	Differentiates healthy controls from AD subjects. 3-way classification is performed.	Suffers from classifying MCI subjects. Less accuracy 87.8%.
Venugopalan et al. [21]	ADNI	3D CNN+ stacked DAE	3-way classification is performed. Multimodal data is used as biomarker for training.	Suffers from limited dataset sizes. Takes long running time. Early diagnosis is a bit tough.
Almuqhim et al. [27]	ADNI	SAE+DNN	Authors designed a network named ASD-SAENet to diagnose Autism Spectrum Disorder. Evaluated their model on ABIDE dataset and 70.8% accuracy is achieved.	Very low accuracy i.e. 70.8%. Features were not extracted separately in this network.
Basheera et al. [25]	ADNI	CNN+ICA	An enhanced Independent Component Analysis is employed for segmentation. For classification, CNN is utilised.	Multiclass classification accuracy is 90.47%. Diagnostic accuracy is moderate. Converging slowly.
Zhu et al. [22]	ADNI	SVM	A novel feature selection approach is employed using task specific relations. Binary and Multiclass classification is performed.	Deep learning could be used to improve the analysis. Diagnostic Accuracy is less.
Yagis et al. [23]	OASIS	2D CAE	Integrated supervised prediction with unsupervised representations using CAE. Single slice of MRI is used in diagnosis.	3D volumetric latent features were not extracted. Diagnostic accuracy is also less i.e 74.66%.
Akramifard et al. [26]	ADNI	CNN+SAE	2D CNN and 3D CNN both were employed. 3-way classification with 89.47% accuracy is obtained.	Tuned hyper-parameters could further enhance these findings.
Dongren et al [8]	ADNI	Ensemble methods	Authors presented a hierarchical grouping process in feature selection method. Binary and 4-way classification both were performed.	Deep learning architectures may improve accuracy further. Diagnostic accuracy is very poor i.e., 54.375%.
Vu et al [32]	ADNI	CNN+SAE	A novel classification model is presented in a multimodality fusion of MRI and PET. 91.14% accuracy is obtained using MRI-PET.	Instead of random, authors could select a specific patch. Overall, system converge very slowly.
Yang et al.	OASIS	SVM+ICA	Machine learning is employed so it is compulsory to specify ROI. 3-way AD diagnosis is employed.	classification accuracy is still not optimal due to various factors. Age and gender are not considered.
Lin et al. [24]	ADNI	CNN	This model is centric about MCI to AD conversion subjects. This approach achieved an accuracy of 79.9%.	AD progression was not analyzed. Diagnostic accuracy is moderate.

III. NETWORK DESIGN AND DEVELOPMENT

This research work seeks to properly diagnose AD stages while using less processing power and storage space. To achieve these goals, 3D CNN along with SAE is presented for obtaining high-level dominant features related to multi-class AD from MRI neuroimage intensities. As shown in Fig. 1, unprocessed MRI volumes are thoroughly scaled, resized, and segmented properly before being directed into the hyperparameters tuned CNN followed by SAE to extract latent features. The low dimensional features from the bottleneck layer of SAE are subsequently loaded into a deep neural network (DNN) which results in the enhanced diagnosis of brain voxels more prone to AD.

A. Dataset

From the ADNI repository, 1120 unprocessed MRI volumes of 460 people of various ages and genders were obtained. We employed 1.5-Tesla, T1-weighted, MRI volumes from the patient community [28] that included patients

ranging in age from 55 to 70 and of different genders. The configuration of the MRI dataset utilized to implement this research is displayed in Table II. In the entire dataset, 351 CN, 230 ls-MCI, 234 p-MCI, and 305 AD subject volumes were meticulously gathered to orient the study effort toward the AD prognosis. Furthermore, 6400 samples of MRI slices were retrieved from the Kaggle repository and utilized for evaluating the proposed network. In all 6400 samples, 3200 CN subjects, 2240 ls-MCI subjects, 896 p-MCI subjects, and 64 AD subjects MRI slices are selected to validate the network capability in classifying the MCI subcategories.

TABLE II. ADNI DATASET CONFIGURATION [28]

Parameters	CN	p-MCI	ls-MCI	AD
Age	55	60	58	62
Gender	60% male	40% male	50% male	30% male
MMSE	29	24	26	21
CDR	0	0.5	0.3	0.5-1

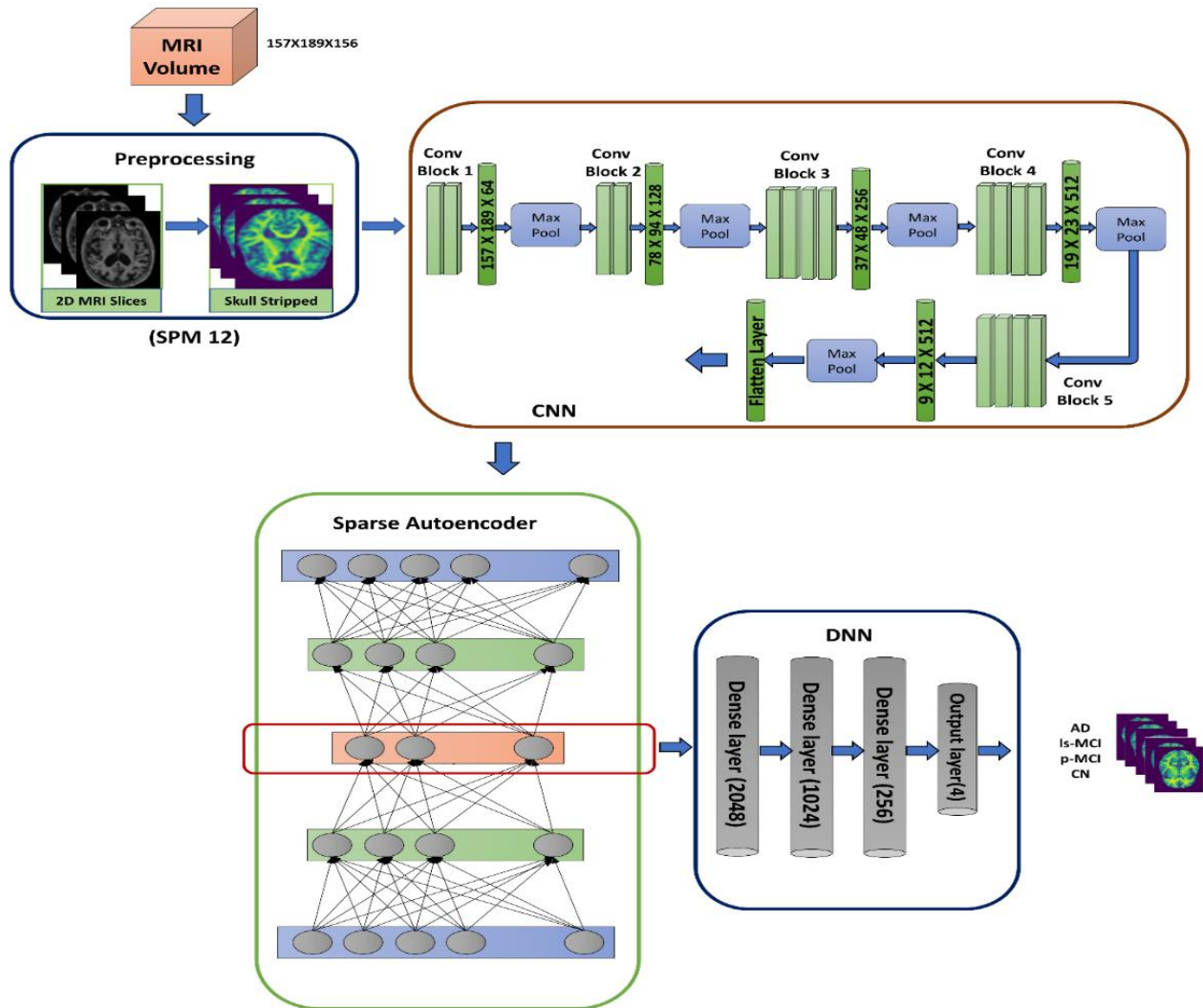


Fig. 1. Alz-SAENet Architecture.

B. Preprocessing

Generally, the raw MRI data are stored in NifTi (.nii) format after retrieving from the ADNI repository. These NifTi files were further pre-processed utilizing the provision of the SPM12 package [29] installed under default settings. This stage pipeline is very much responsible for the removal of non-brain tissues and registering it into Montreal Neurological Institute (MNI) space. After pre-processing, the registered volumes are smoothed and scaled such that all volumes are

with the same dimension of $157 \times 189 \times 156$ and sliced to generate $1.5 \times 1.5 \times 1.5 \text{mm}^3$ voxels. Further, the MRI volumetric data is normalized voxel by voxel such that all intensities in the voxel fall in the 0 to 1 range for additional processing by retaining the disease features. For this investigation, only 40 medial MRI slices were considered such that they replicate AD progression clearly via hippocampal lesions to enable the network to distinguish the AD subjects. Sagittal plane views of pre-processed MRI volume for a sample are shown in Fig. 2.

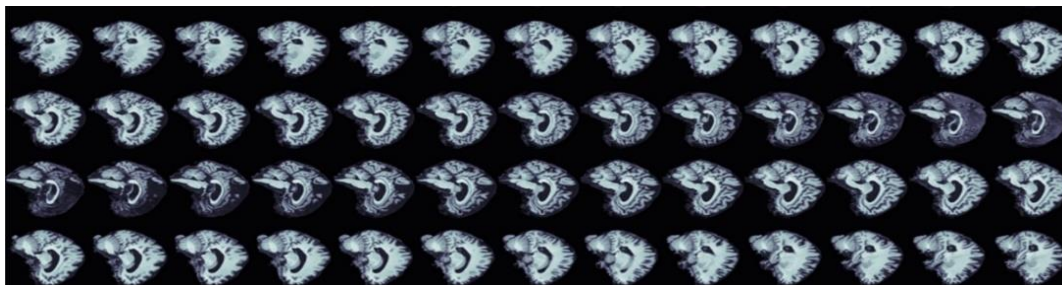


Fig. 2. Pre-processed Medial Sagittal Planes of Brain MRI.

C. 3D CNN

Generally, CNN models consist of convolutional layers, batch normalization layers, pooling layers, and fully connected layers in sequential and backpropagation algorithm is used to learn latent features from MRI slices. Advanced architectures follow more complicated topologies for extracting features in complex applications where highly correlated data is present. In this work, we focused on a sequential model inspired by VGG 19 architecture [30], i.e., one popular version of Visual Geometric Group. VGG19 is a deep CNN that has been trained on millions of images with complex classification tasks.

This architecture consists of five blocks, amongst the very first two blocks comprise two convolutional layers preceded by a pooling layer each, and the last three blocks have four convolutional layers preceded by a pooling layer with a filter size of 2x2x2. In this method, all pretrained layers are frozen, and the output of the last convolution block is considered a discriminative feature of the MRI volume. This feature map is flattened using a flattening layer before being sent to a sparse encoder. All layers, dimensions, and several parameters for training the VGG19 network employed in this work for one MRI slice were tabulated in Table III.

D. Sparse Autoencoder

A sparse autoencoder [31, 32] is merely an autoencoder with a sparsity penalty as a training benchmark. This autoencoder is used to draw more valuable insights from MRI with reasonable dimensionality. In addition, the bias applied at the encoder and decoder forces the AE to restore the input more accurately by avoiding overfitting.

Let s_i is the i^{th} input among the given training samples (s_1, s_2, \dots, s_N). Then, the designed SAE is accomplished to restore the input s_i maximum similar to the estimated function $h_{w,b}(x^i)$. The cost function of SAE consists of three very important factors, viz., Mean squared error (MSE), Weight Decay (WD) and Sparsity [33]. The mean squared error for all N training samples and weight decay is mathematically expressed as in eq. (1) and eq. (2).

$$MSE = \frac{1}{N} \sum_{i=1}^N \frac{1}{2} \|h_{w,b}(x^i) - y^i\|^2 \quad (1)$$

$$WD = \frac{\lambda}{2} \sum_{l=1}^{n_l-1} \sum_{i=1}^{s_l} \sum_{j=1}^{s_{l+1}} (w_{ji}^l)^2 \quad (2)$$

This weight decay eq. (2) helps to avoid overfitting. Overfitting may result from a small value of λ , whereas underfitting may result from a big value of λ . To choose lambda for the term's best match, we, therefore, carried out a number of empirical studies.

TABLE III. LAYERS AND FEATURE MAPS OF 3D CNN

Block	Layer	Dimension	Parameters
	Input	[(None, 157, 189, 3)]	0
1	conv1 (Conv)	(None, 157, 189, 64)	1792
	conv2 (Conv)	(None, 157, 189, 64)	36928
	pool (MaxPooling)	(None, 78, 94, 64)	0
2	conv1 (Conv)	(None, 78, 94, 128)	73856
	conv2 (Conv)	(None, 78, 94, 128)	147584
	pool (MaxPooling)	(None, 39, 47, 128)	0
3	conv1 (Conv)	(None, 39, 47, 256)	295168
	conv2 (Conv)	(None, 39, 47, 256)	590080
	conv3 (Conv)	(None, 39, 47, 256)	590080
	conv4 (Conv)	(None, 39, 47, 256)	590080
	pool (MaxPooling)	(None, 19, 23, 256)	0
4	conv1 (Conv)	(None, 19, 23, 512)	1180160
	conv2 (Conv)	(None, 19, 23, 512)	2359808
	conv3 (Conv)	(None, 19, 23, 512)	2359808
	conv4 (Conv)	(None, 19, 23, 512)	2359808
	pool (MaxPooling)	(None, 9, 11, 512)	0
5	conv1 (Conv)	(None, 9, 11, 1024)	2359808
	conv2 (Conv)	(None, 9, 11, 1024)	2359808
	conv3 (Conv)	(None, 9, 11, 1024)	2359808
	conv4 (Conv)	(None, 9, 11, 1024)	2359808
	pool(MaxPooling)	(None, 4, 5, 1024)	0

Sparsity is the last term of the cost function that help to avoid overfitting by generating the activation for hidden neurons of the SAE to avoid overfitting. The eq. (3) is the average activated value of hidden layer, where ‘a’ is the ReLU activation function.

$$\hat{p}_j = \frac{1}{N} \sum_{i=1}^N [a_j^2(x^i)] \quad (3)$$

The sparsity is calculated so that $\hat{p}_j=p$ constraint is satisfied, where p is the sparsity parameter. The deviation of \hat{p}_j from p help the network to activate and deactivate neurons in the hidden layer. KL divergence is used to define the parameter as in eq. (4).

$$\sum_{j=1}^{s_l} KL(p||\hat{p}_j) = \sum_{j=1}^{s_l} [p \log\left(\frac{p}{\hat{p}_j}\right) + (1-p) \log\left(\frac{1-p}{1-\hat{p}_j}\right)] \quad (4)$$

By combining the three terms, the cost function of the SAE J_{SAE} is defined as shown in eq. (5).

$$J_{SAE} = \frac{1}{N} \sum_{i=1}^N \frac{1}{2} \|h_{w,b}(x^i) - y^i\|^2 + \frac{\lambda}{2} \sum_{l=1}^{n_l-1} \sum_{i=1}^{s_l} \sum_{j=1}^{s_{l+1}} (w_{ji}^l)^2 + \beta \sum_{j=1}^{s_l} KL(p||\hat{p}_j) \quad (5)$$

Here β is the sparse penalty.

The primary goal of the Sparse Autoencoder [34] in this investigation is to reduce the dimensionality of 55,296 features obtained from 3D CNN. The SAE bottleneck layer provides more dominant insights, i.e., features that can be employed in classification. The bottleneck layer size is 2048 hidden units. Output from bottleneck generally has very limited number of features i.e. 2048 elements in the vector. These features are subsequently passed through DNN in final stage for classification purpose.

E. DNN

DNN is an artificial neural network with several hidden layers for solving complex classification problems. All these layers are dense, and the role of DNN here is in the final phase for classifying the latent features obtained from SAE. This DNN comprises two hidden layers, one input and output layer, with sizes 2048, 1024, 256, and 4, respectively. A SoftMax layer is generally employed as an output layer to estimate the incoming feature vector’s four possible classes, i.e., CN, p-MCI, ls-MCI, and AD. A dropout layer is also used between two dense layers to avoid overfitting. Finally, cross-entropy is used for determining the classifier cost function, and the weight decay term is added.

IV. RESULTS AND INVESTIGATIONS

Concurrent training of the SAE and the DNN improved feature extraction while optimizing the classifier’s decision. The training was completed in 50 epochs with 16 batch size.

Sparse penalty, weight decay and sparsity parameter p were initialized 2, 0.0001, and 0.05, respectively. In last 20 epochs, DNN was fine-tuned, and parameters updated to minimize the cost function while the SAE parameters were frozen.

All the experimentations described in this paper were carried out in the Google Colab platform using python scripting with the support of 1X Tesla K80 GPU. To run our deep learning network, the Tensorflow Keras library is employed. To demonstrate the generalizability of the network in AD diagnosis, Alz-SAENet is examined by applying ADNI dataset and the Kaggle dataset in two scenarios.

In the first scenario, the proposed Alz-SAENet architecture is trained over 80% of the whole 1120 MRI volumes of the ADNI dataset that consists of MRI volumes with uniform dimensions of 157*189*156. After rigorous training, the network is tested using the remaining MRI volumes among the dataset acquired. The test results were assessed in terms of diagnostic accuracy, network sensitivity, precision, specificity, Negative Predictive Value (NPV), False Positive Rate (FPR), F1-Score, False Negative Rate (FNR), False Discovery Rate (FDR), and Mathew Correlation Coefficient (MCC). All these parameters are evaluated and listed in Table IV. AD vs CN classification over the ADNI dataset is 99.54% accurate and 100% sensitive, and produce MCC is 89.93%. p-MCI vs ls-MCI classification that facilitates early diagnosis of AD yields 98.56% accuracy, 100% sensitivity and 96.64% MCC. p-MCI vs AD classification is 97.90% accurate, 100% sensitive and 92.10% correlated data. CN vs ls-MCI classification that facilitates early diagnosis of AD yields 97.71% accuracy, 98.15% sensitivity and 95.24% MCC. However, Multiclass diagnosis produced 98.9% accuracy, 97.5% sensitivity and 94.25% MCC. These results demonstrate that Alz-SAENet has significantly classified AD stages, especially for the transitional period between ls-MCI and p-MCI, with an accuracy of 98.56%. The graphical representation is also depicted in Fig. 3.

In the second scenario, the proposed model was evaluated using another repository, i.e. Kaggle, to prove the generalization ability of this network over the unseen data during training. 6400 sample MRI medial slices belonging to four AD classes were acquired from the repository and evaluated in this model. Unlike in the first scenario, the evaluation metrics accuracy, precision, sensitivity, and F1-Score were only obtained and tabulated in Table V. The bar chart for these evaluation metrics is also shown in Fig. 4. AD vs CN classification yields 98.62% accuracy, 92% sensitivity and 98% precision. p-MCI vs ls-MCI diagnosis also attained 98.37% accuracy, 97% sensitivity, and 98% precision. This network produced 98.215% accuracy, 92.25% sensitivity, and 82.25% precision in multiclass classification.

TABLE IV. ALZ-SAENET PERFORMANCE OVER ADNI DATASET

Classification	Accuracy	F1-Score	Sensitivity	Specificity	Precision	NPV	MCC
AD vs CN	0.9954	0.8966	1	0.9953	0.8125	1	0.8993
p-MCI vs ls-MCI	0.9856	0.9761	1	0.9797	0.9534	1	0.9664
p-MCI vs AD	0.9790	0.9450	1	0.9821	0.9452	1	0.9210
ls-MCI vs CN	0.9771	0.9807	0.9815	0.9707	0.9799	0.9729	0.9524
Multiclass	0.989		0.975		0.915		0.9425

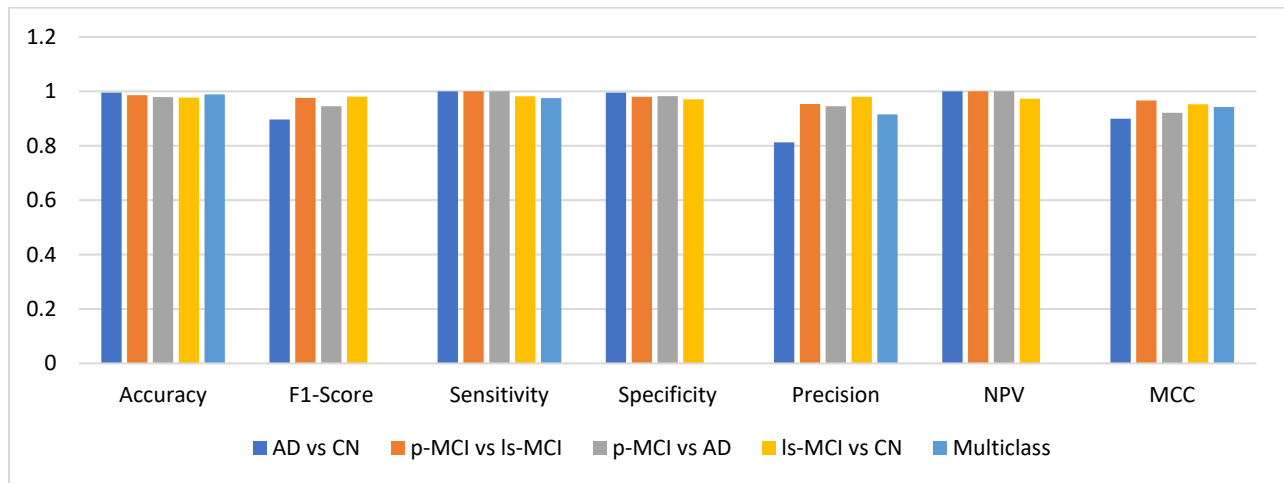


Fig. 3. Graphical Presentation of Alz-SAENet Performance over ADNI Data.

TABLE V. ALZ-SAENET PERFORMANCE OVER KAGGLE DATASET

Classification	Accuracy	F1-Score	Sensitivity	Precision
AD vs CN	0.9862	0.95	0.92	0.98
p-MCI vs ls-MCI	0.9837	0.98	0.97	0.98
p-MCI vs AD	0.9759	0.98	0.97	0.98
ls-MCI vs CN	0.9828	0.49	0.81	0.35
Multiclass	0.98215	0.85	0.9225	0.8225

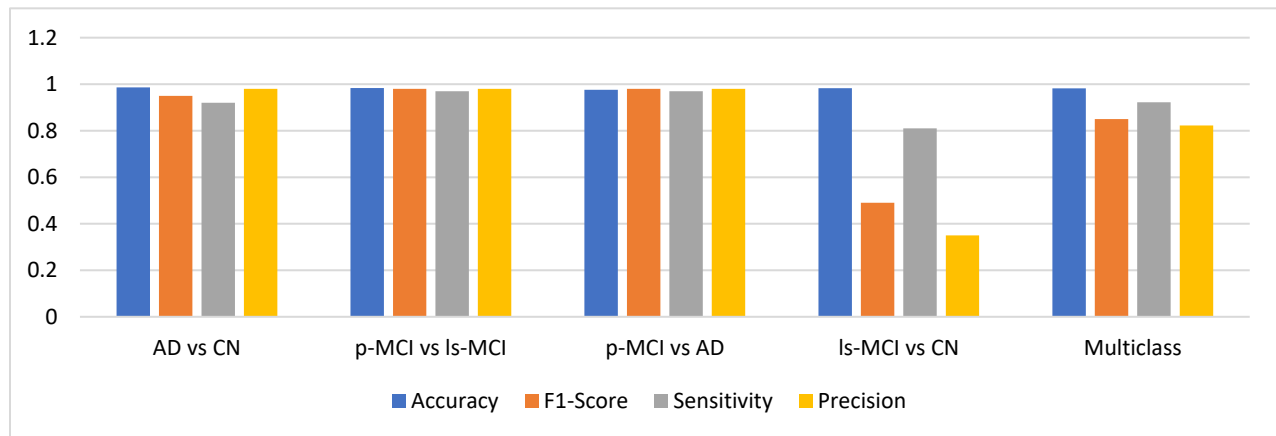


Fig. 4. Graphical view of Alz-SAENet Performance over Kaggle Data.

The results obtained in second scenario reveal that the network has shown good generalizability among the datasets which never seen during training. The model did not overfit due to the unbalanced datasets appeared in training process. This was happened because the SAE hyperparameters are tuned systematically so that its cost function gets minimized as the weight updation is in progress. With this support, the network can reliable outcomes even in non-supportive environments.

Attained results demonstrate that the proposed model, i.e., Alz-SAENet has greater generalizability in classifying the unseen data during the training process. The deep learning techniques from literature [9], [20], [25], and [26] are suffered

from different challenges in terms of convergence speed, overfitting, and hyperparameters tuning to obtain optimal performance from their networks. The results of Alz-SAENet have revealed that it has attained almost all those objectives by leveraging the benefits of Sparse autoencoder by minimizing the cost function.

The proposed model exhibited very poor performance over ADNI data in attaining precision, f1-score, and MCC for classifying AD and CN subjects. When applied to Kaggle data, it has not produced inadequate performance in terms of f1-score, sensitivity, precision, etc. for ls-MCI vs CN classification.

TABLE VI. COMPARISON OF ALZ-SAENET WITH LITERATURE REPORTED

Author	Modality	Datasets	Classifier	Subjects	Classification Metrics		
					Accuracy (%)	Precision (%)	Recall (%)
Soliman et al. [20]	MRI	ADNI	SAE+CNN	Multiclass	87.8	91%	88%
Akramifard et al. [26]	MRI	ADNI	Autoencoder + PCA + SVM	AD vs MCI MCI vs CN AD vs CN	66.84 66.97 84.46	-	48.70 78.94 81.87
Basheera et al. [25]	MRI	ADNI	CNN+ICA	Multiclass AD vs MCI MCI vs CN AD vs CN	86.7 96.2 98.0 100	89.6 93.0 96.0 100	86.61 100 100 100
Alz-SAENet	MRI	ADNI, Kaggle	3D CNN+SAE +DNN	AD vs CN CN vs ls-MCI AD vs p-MCI ls-MCI vs p-MCI Multiclass	99.54 97.71 97.90 98.56 98.90	81.25 97.99 94.52 95.34 91.5	100 98.15 100 100 97.5

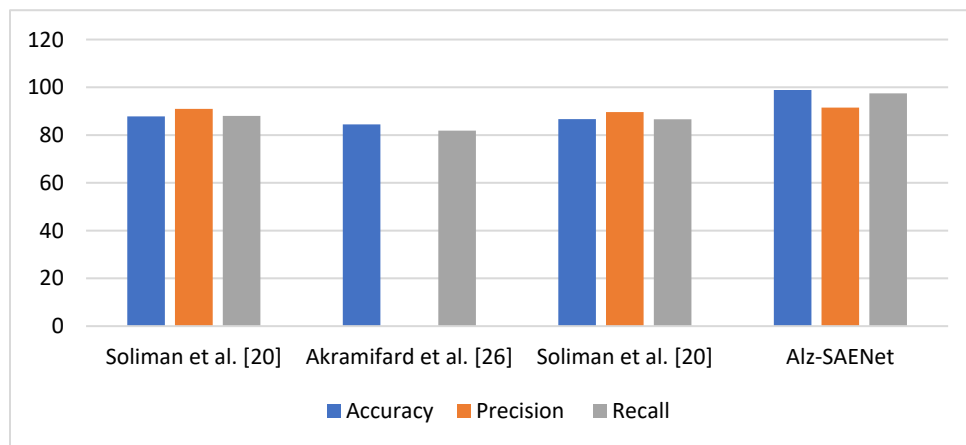


Fig. 5. Comparison of Alz-SAENet with Literature Reported.

The outcomes of the Alz-SAENet, i.e. integrated version of 3D CNN, SAE, and DNN illustrate that the performance of AD diagnosis is enhanced with the support of features that has learned and fine-tuning of hyperparameters of SAE during training. The model performs well on the test data, which is an important indicator of its generalizability, given that the model has never seen the data before. In addition, the proposed approach is also compared with recent literature in deep learning domain on ADNI data. This comparison is evidently shown in Table VI, and the proposed network outperformed all those methods focused by the literature deep analysis in Section II in terms of key parameters accuracy, precision, recall, etc. The same comparison is also depicted in Fig. 5.

V. CONCLUSION

In this paper, we built a novel deep sparse autoencoder-based learning model named Alz-SAENet for classifying brain MRI volumes that exhibit severe AD symptoms to cognitive normal. This network utilized 3D CNN, SAE, and DNN components that assisted in understanding the neurobiological foundations of the AD brain in a better way. 3D CNN extracted 55,296 latent features from MRI volume. These features were flattened and their dimension was reduced through SAE via bottleneck layer and fed to DNN for classifying them into four stages of AD. During testing, this

network gave an accuracy of 98.9% over the ADNI dataset and 98.215% over the Kaggle data. These results demonstrated that Alz-SAENet outscored all the state-of-the-art approaches that worked on AD classification. In the future, we test the architecture over real-world data along with metadata to improve the generalizability, efficiency, and efficacy of early diagnosis of AD. Furthermore, the results obtained for ls-MCI and CN classification over the Kaggle dataset are needed to be enhanced.

REFERENCES

- [1] Gauthier S, Rosa-Neto P, Morais JA, & Webster C. 2021. World Alzheimer Report 2021: Journey through the diagnosis of dementia. London, England: Alzheimer's Disease International.
- [2] Johnson KA, Fox NC, Sperling RA, Klunk WE. Brain imaging in Alzheimer disease. Cold Spring Harb Perspect Med. 2012 Apr;2(4):a006213. doi: 10.1101/cshperspect.a006213. PMID: 22474610; PMCID: PMC3312396.
- [3] Saad, S.H.S., Alashwah, M.M.A., Alsafa, A.A. et al. The role of brain structural magnetic resonance imaging in the assessment of hippocampal subfields in Alzheimer's disease. Egypt J Radiol Nucl Med 51, 53 (2020). <https://doi.org/10.1186/s43055-020-00164-8>.
- [4] Vichianin Y, Khummongkol A, Chiewvit P, Raksthaput A, Chaichanettee S, Aonkaew N, Senanarong V. Accuracy of Support-Vector Machines for Diagnosis of Alzheimer's Disease, Using Volume of Brain Obtained by Structural MRI at Siriraj Hospital. Front Neurol. 2021 May 10;12:640696. doi: 10.3389/fneur.2021.640696. PMID: 34040575; PMCID: PMC8141708.

- [5] B. Rabeh, F. Benzarti and H. Amiri, "Diagnosis of Alzheimer Diseases in Early Step Using SVM (Support Vector Machine)," 2016 13th International Conference on Computer Graphics, Imaging and Visualization (CGiV), 2016, pp. 364-367, doi: 10.1109/CGiV.2016.76.
- [6] S. Aruchamy, V. Mounya and A. Verma, "Alzheimer's Disease Classification in Brain MRI using Modified kNN Algorithm," 2020 IEEE International Symposium on Sustainable Energy, Signal Processing and Cyber Security (iSSSC), 2020, pp. 1-6, doi: 10.1109/iSSSC50941.2020.9358867.
- [7] Reddy, G & K, Nagireddy. (2021). A Robust Machine Learning Approach for Multiclass Alzheimer's Disease Detection using 3D Brain Magnetic Resonance Images. Journal of Engineering Research. 10.36909/jer.10511.
- [8] Yao, Dongren; Calhoun, Vince D.; Fu, Zening; Du, Yuhui; Sui, Jing (2018). An Ensemble Learning System for a 4-Way Classification of Alzheimer's Disease and Mild Cognitive Impairment. Journal of Neuroscience Methods, (), S0165027018300797-. doi:10.1016/j.jneumeth.2018.03.008.
- [9] Jo T, Nho K, Saykin AJ. Deep Learning in Alzheimer's Disease: Diagnostic Classification and Prognostic Prediction Using Neuroimaging Data. Front Aging Neurosci. 2019 Aug 20;11:220. doi: 10.3389/fnagi.2019.00220. PMID: 31481890; PMCID: PMC6710444.
- [10] S. Al-Shoukry, T. H. Rassem and N. M. Makbol, "Alzheimer's Diseases Detection by Using Deep Learning Algorithms: A Mini-Review," in IEEE Access, vol. 8, pp. 77131-77141, 2020, doi: 10.1109/ACCESS.2020.2989396.
- [11] S. Gao and D. Lima, A review of the application of deep learning in the detection of Alzheimer's disease, International Journal of Cognitive Computing in Engineering (2022) 1-8.
- [12] P. Rath, P. K. Mallick, R. Siddavatam, and G. S. Chae, "An empirical development of hyper-tuned CNN using spotted hyena optimizer for bio-medical image classification," Journal of Natural Science, Biology and Medicine, vol. 12, no. 3, 2021.
- [13] Alkabawi, Elham M.; Hilal, Allaa R.; Basir, Otman A. (2017). [IEEE 2017 IEEE International Conference on Systems, Man and Cybernetics (SMC) - Banff, AB (2017.10.5-2017.10.8)] 2017 IEEE International Conference on Systems, Man, and Cybernetics (SMC) - Feature abstraction for early detection of multi-type of dementia with sparse auto-encoder., (), 3471-3476. doi:10.1109/smc.2017.8123168.
- [14] H. B. Baydargil, J. -S. Park and D. -Y. Kang, "Classification of Alzheimer's Disease Using Stacked Sparse Convolutional Autoencoder," 2019 19th International Conference on Control, Automation and Systems (ICCAS), 2019, pp. 891-895, doi: 10.23919/ICCAS47443.2019.8971696.
- [15] Liu, J., Wu, G., Luo, Y., Qiu, S., Yang, S., Li, W., & Bi, Y. (2020). EEG-Based Emotion Classification Using a Deep Neural Network and Sparse Autoencoder. Frontiers in Systems Neuroscience, 14. https://doi.org/10.3389/fnsys.2020.00043.
- [16] An, N., Ding, H., Yang, J., Au, R., and Ang, T. F. A., "Deep ensemble learning for Alzheimers disease classification", <i>arXiv e-prints</i>, 2019.
- [17] Gouse, Mohammed. (2021). Deep Neural Network Concepts for Classification using Convolutional Neural Network: A Systematic Review and Evaluation. Technium Romanian Journal of Applied Sciences and Technology. 3. 58-70. 10.47577/technium.v3i8.4554.
- [18] Jha, Debesh & Kwon, Goo-Rak. (2017). Alzheimer's Disease Detection Using Sparse Autoencoder, Scale Conjugate Gradient and Softmax Output Layer with Fine Tuning. 7. 13-17. 10.18178/ijmlc.2017.7.1.612.
- [19] E. Jabason, M. O. Ahmad and M. N. S. Swamy, "Missing Structural and Clinical Features Imputation for Semi-supervised Alzheimer's Disease Classification using Stacked Sparse Autoencoder," 2018 IEEE Biomedical Circuits and Systems Conference (BioCAS), 2018, pp. 1-4, doi: 10.1109/BIOCAS.2018.8584844.
- [20] Soliman, Sarah & El-Dahshan, El-Sayed & Salem, Abdel-Badeeh. (2021). Diagnosis of Alzheimer's Disease by Three-Dimensional Convolutional Neural Network Using Unsupervised Feature Learning Method. International Journal of Intelligent Computing and Information Sciences. 1-15. 10.21608/ijicis.2021.80596.1103.
- [21] Venugopalan, J., Tong, L., Hassanzadeh, H.R. et al. Multimodal deep learning models for early detection of Alzheimer's disease stage. Sci Rep 11, 3254 (2021). https://doi.org/10.1038/s41598-020-74399-w.
- [22] Zhu X, Suk HI, Lee SW, Shen D. Discriminative self-representation sparse regression for neuroimaging-based alzheimer's disease diagnosis. Brain Imaging Behav. 2019 Feb;13(1):27-40. doi: 10.1007/s11682-017-9731-x. PMID: 28624881; PMCID: PMC5811409.
- [23] E. Yagis, A. G. S. de Herrera and L. Citi, "Convolutional Autoencoder based Deep Learning Approach for Alzheimer's Disease Diagnosis using Brain MRI," 2021 IEEE 34th International Symposium on Computer-Based Medical Systems (CBMS), 2021, pp. 486-491, doi: 10.1109/CBMS52027.2021.00097.
- [24] Lin W, Tong T, Gao Q, Guo D, Du X, Yang Y, Guo G, Xiao M, Du M, Qu X and The Alzheimer's Disease Neuroimaging Initiative (2018) Convolutional Neural Networks-Based MRI Image Analysis for the Alzheimer's Disease Prediction From Mild Cognitive Impairment. Front. Neurosci. 12:777. doi: 10.3389/fnins.2018.0077.
- [25] Basheera, Shaik & Ram, M. (2020). A novel CNN Based Alzheimer's Disease Classification using Hybrid Enhanced ICA Segmented Gray Matter of MRI. Computerized Medical Imaging and Graphics. 81. 101713. 10.1016/j.compmedimag.2020.101713.
- [26] Akramifard H, Balafar MA, Razavi SN, Ramli AR. Early Detection of Alzheimer's Disease Based on Clinical Trials, Three-Dimensional Imaging Data, and Personal Information Using Autoencoders. J Med Signals Sens. 2021 May 24;11(2):120-130. doi: 10.4103/jmss.JMSS_11_20. PMID: 34268100; PMCID: PMC8253314.
- [27] Almuqhim F and Saeed F (2021) ASD-SAENet: A Sparse Autoencoder, and Deep-Neural Network Model for Detecting Autism Spectrum Disorder (ASD) Using fMRI Data. Front. Comput. Neurosci. 15:654315. doi: 10.3389/fncom.2021.654315.
- [28] G. N. Reddy and K. N. Reddy, "Boosting based Deep hybrid Framework for Alzheimer's Disease classification using 3D MRI," 2022 6th International Conference on Devices, Circuits and Systems (ICDCS), 2022, pp. 100-106, doi: 10.1109/ICDCS54290.2022.9780736.
- [29] Ashburner, John & Barnes, Gareth & Chen, Chun-Chuan & Daunizeau, Jean & Flandin, Guillaume & Friston, Karl & Gitelman, Darren & Glauche, Volkmar & Henson, Rik & Hutton, Chloe & Jafarian, Amirhossein & Kiebel, Stefan & Kilner, James & Litvak, Vladimir & Mattout, Jérémie & Moran, Rosalyn & Penny, Will & Phillips, Christophe & Razi, Adeel & Zeidman, Peter. (2021). SPM12 Manual.
- [30] Bhatele K. R, Bhaduria S. S. Classification of Neurodegenerative Diseases Based on VGG 19 Deep Transfer Learning Architecture: A Deep Learning Approach. Biosc.Biotech.Res.Comm. 2020;13(4).
- [31] Mahmoud A., Karamti H. and Alrowais F. (2020). An Effective Sparse Autoencoders based Deep Learning Framework for fMRI Scans Classification. In Proceedings of the 22nd International Conference on Enterprise Information Systems - Volume 1: ICEIS, ISBN 978-989-758-423-7, pages 540-547. DOI: 10.5220/0009397605400547.
- [32] T. Vu, H. Yang, V. Nguyen, A. Oh and M. Kim, "Multimodal learning using convolution neural network and Sparse Autoencoder," in 2017 IEEE International Conference on Big Data and Smart Computing (BigComp), Jeju, 2017 pp. 309-312. doi: 10.1109/BIGCOMP.2017.7881683.
- [33] Antelmi, L., Ayache, N., Robert, P. & Lorenzi, M.. (2019). Sparse Multi-Channel Variational Autoencoder for the Joint Analysis of Heterogeneous Data., Proceedings of the 36th International Conference on Machine Learning in Proceedings of Machine Learning Research, 97:302-311.
- [34] P. Bhatkoti and M. Paul, "Early diagnosis of Alzheimer's disease: A multi-class deep learning framework with modified k-sparse autoencoder classification," 2016 International Conference on Image and Vision Computing New Zealand (IVCNZ), 2016, pp. 1-5, doi: 10.1109/IVCNZ.2016.7804459.
- [35] Gurukumar Lokku, G Harinatha Reddy, M N Giri Prasad, Optimized Scale-Invariant Feature Transform with Local Tri-directional Patterns for Facial Expression Recognition with Deep Learning Model, The Computer Journal, Volume 65, Issue 9, September 2022, Pages 2506-2527, https://doi.org/10.1093/comjnl/bxab088.

Development of Path Loss Prediction Model using Feature Selection-Machine Learning Approach

Improvement of Path Loss Prediction Accuracy in Mixed Land-water Case

Bengawan Alfaresi¹, Zainuddin Nawawi^{2*}, Bhakti Yudho Suprpto³

Doctoral Students of Electrical Engineering, Universitas Sriwijaya, Palembang, Indonesia¹

Electrical Engineering, Universitas Muhammadiyah Palembang, Palembang, Indonesia¹

Electrical Engineering, Universitas Sriwijaya, Palembang, Indonesia^{2,3}

Abstract—Wireless network planning requires accurate coverage predictions to get good quality. The path loss accurate model requires a flexible model for each area including land and water. The purpose of this research is to develop a Cost-Hatta model that can be applied to the mixed land-water area. The approach used of this research is the three methods of feature selection of machine learning. The first stage of the research was the collection of field data. The measurement data included system, weather, and geographical parameters. The next stage was feature selection to obtain the best composition of features for the development of the model. The feature selection methods used were Univariate FS, Genetic Algorithm (GA), and Particle Swarm Optimization (PSO). After obtaining the best features from each method, the next stage was to form a model using four machine learning algorithms, namely Random Forest Regression (RF), Deep Neural Network (DNN), K-Nearest Neighbor Regression (KNN), and Support Vector Regression (SVR). The results of the improvements to the path loss prediction model were tested using the evaluation parameters of Root Mean Square Error (RMSE), Mean Square Error (MSE), and Mean Absolute Percentage Error (MAPE). The results of the testing showed that the improved Cost-Hatta model using the proposed Univariate-RF combination produced a very small RMSE value of 1.52. This indicates that the proposed model framework is highly suitable to be used in a mixed land-water area.

Keywords—Path loss; feature selection; machine learning; mixed land-water; Cost-Hatta

I. INTRODUCTION

Path loss prediction is of great importance in the planning and optimization of coverage in wireless networks [1]. Path loss is used to predict the strength of the signal received by the user. The accuracy of path loss prediction plays an important role in determining the quality of a network design [2]. The complexity of environmental characteristics influences the level of complexity in the prediction of received signal strength. In the propagation process, electromagnetic waves undergo a number of treatments caused by various environmental and weather factors that are present around the propagation media. Some of the nearby objects can affect the treatment of electromagnetic wave propagation [3]. The electromagnetic wave treatments that occur include diffraction, refraction, and reflection [4], [5]. These treatments cause fluctuations in the signal power of the receiver due to a weakening in the power of the electromagnetic signal. This signal attenuation is the result of power loss that arises during

the electromagnetic wave propagation process in wireless networks. Electromagnetic wave propagation is extremely important in wireless communication systems [6].

Indonesia is an archipelago and has at least 5,590 main rivers and 65,017 tributaries spread across several islands in Indonesia, where the main rivers, watersheds (DAS) in Indonesia reach 1,512,466 square kilometers. People who live in watersheds use water transportation in carrying out the economic activities. The current problem is that there is no path loss prediction model that can be used for water areas, thus, current modeling is not accurate if it is used to plan networks in water areas, especially for areas that are passed by water transportation. Therefore it needs predictive modeling of path loss that can be flexibly used in land and water areas.

Research on the modeling of path loss prediction continues to be carried out to obtain high accuracy predictions in various area conditions. A number of researchers have studied path loss prediction in various kinds of conditions using different variables. Future challenges include the development of high speed wireless telecommunication technology with low latency. Accurate path loss prediction has a strong impact on good quality, low latency, and high throughput.

Conventional prediction models developed in the past include empirical and deterministic modeling. Empirical modeling is based on measurements and direct observation in the field. Empirical models provide a statistical picture of the connection between the dependent variables of path loss and a number of measured parameters, specifically frequency, transmitter height, receiver height, and distance between transmitter and receiver [7]. Empirical models are quick and easy to be implemented but have a low level of accuracy, which presents a challenge in empirical model development. Empirical models include Okumura-Hatta, Cost231-Hatta, the ECC model and the Ericsson model [8], [9]. Empirical modeling is the most frequently used type of modeling in planning and optimization systems of wireless networks of telecommunication vendors.

Machine learning is a method of learning about a data set which is used to create a model that can perform a particular task [7]. Machine learning carries out a study of data by learning with the use of algorithms and statistics. Machine learning can be divided into three types, namely supervised learning, unsupervised learning, and reinforcement learning.

*Corresponding Author.

The algorithm of supervised learning can be further divided into two types, namely regression and classification. Based on the research data that exists, the modeling used in path loss prediction falls into the category of supervised learning regression. Regression is characterized by input and output data types in the form of numeric data. Examples of regression types include Support Vector Regression (SVR), Random Forest (RF), Artificial Neural Network (ANN), and K-Nearest Neighbor (KNN). The advantage of machine learning is its high level of accuracy compared with empirical methods [10].

II. RELATED WORK

The focus of the following literature review is the various types of research field, feature variables, and feature selection methods used in the development of path loss prediction models. A number of researchers have developed path loss prediction models using machine learning in various kinds of area condition. These include a study by [11] on indoor building types using an Artificial Neural Network (ANN) model. The research of [12] and [13] also studies path loss prediction with several machine learning models in suburban areas, while [14], [6], and [15] investigate different area types, namely rural, suburban, and urban. Various other research has been developed in different places with a special measuring field, such as the research of [16] which focuses on a vegetation area, and [17], which focuses on the study of path loss prediction in the indoor area of an aircraft cabin. Other studies, such as those by [18], [19], and [20], use an unmanned aerial vehicle (UAV), while the research of [21] focuses on a mixed city-river area. Only a small number of studies have been carried out on path loss prediction in a mixed city-river area. This indicates that there is still room for development of research on path loss prediction in a mixed city-river area.

The types and numbers of input features used in the development of path loss prediction models are highly varied. Research in [22], [23] uses a single input feature, namely distance between the transmitter (TX) and receiver (RX). In addition to using the TX-RX distance feature, the research of [1] includes the feature of frequency as an additional input feature, while [7] also uses two features, with the addition of onboard GPS sensors. The study by [24] uses the feature of TX-RX distance and adds the features of PCC downlink throughput and PDCP downlink throughput as parameters of the input feature. User position based on longitude and latitude is also used as an input parameter, amongst others in the research of [17], to study the indoor area of an aircraft cabin. Longitude and latitude are also used in the research of [11] and [25] to study an outdoor location. In addition to using system parameters, some studies also use environmental parameters as input features. The research of [26], [15] uses the environmental parameters of humidity, temperature, and dew point as input feature parameters. In order to obtain results with a maximum degree of accuracy, some studies use a more complex combination of parameters in accordance with the focus of the characteristics of the research field. The research of [27], [28] uses six input parameters such as longitude, latitude, elevation, altitude, clutter height, and TX-RX distance. This shows that the types and numbers of

features can still be developed to match the specific object of the research field.

From the point of view of feature selection process, it is evident that feature selection is still rarely used in most studies. This is because the number of features used in the modeling is relatively small so there is no need to use a feature selection method. In the research of [12], PCA is used to reduce the number of data features and to simplify appropriate modeling. In addition, some research recommends Opportunities for Further Research that are related to types and development of feature selection methods. The research of [7] recommends the use of a feature selection method for further research on path loss prediction, while [16] also recommends further research on the development of feature selection methods. The purpose of including feature selection is to minimize the possibility of eliminating features that are important and relevant to the prediction model.

Main contribution of this research are proposes development of a path loss prediction model for a land-river area by varying the input parameters derived from system parameters and environmental parameters. The second contribution of this research are this model research combine an empirical model with a machine learning model by using three method features selection approach, namely Univariate, GA and PSO combined with the use of four Machine learning models namely Random Forest (RF), Support Vector Regression (SVR), K-Nearest Neighbor (KNN), and Deep Neural Network (DNN) where from the literature study has never been done before.

III. MATERIAL AND METHOD

This section is divided into a number of stages: measurement, data processing, delta path loss empirical model calculation, feature selection, and modeling.

Fig. 1 shows the stages carried out in this study starting from the measurement stage then the data processing stage, followed by the best feature selection stage using three approaches methods namely Univariate, GA and PSO. The data with the best features are processed and modeled using four types of machine learning models, namely Random Forest (RF), Support Vector Regression (SVR), KNN Regressor and Deep Neural Network (DNN). The four models produced will be evaluated and obtained as the best model based on the level accuracy of RMSE.

A. Measurement Location

The collection of the research data was carried out in the city of Palembang, Indonesia, which is located at 2°59'27.99"S 104°45'24.24"E. The city of Palembang covers an area of 400.61 km², with an average altitude of 8 meters above sea level. Measurements were taken at Ultra High Frequency (UHF) on a 4G LTE 1800 MHz and 2100 MHz network. The data consisted of a number of input features which were divided into two groups, namely system parameters and environmental parameters.

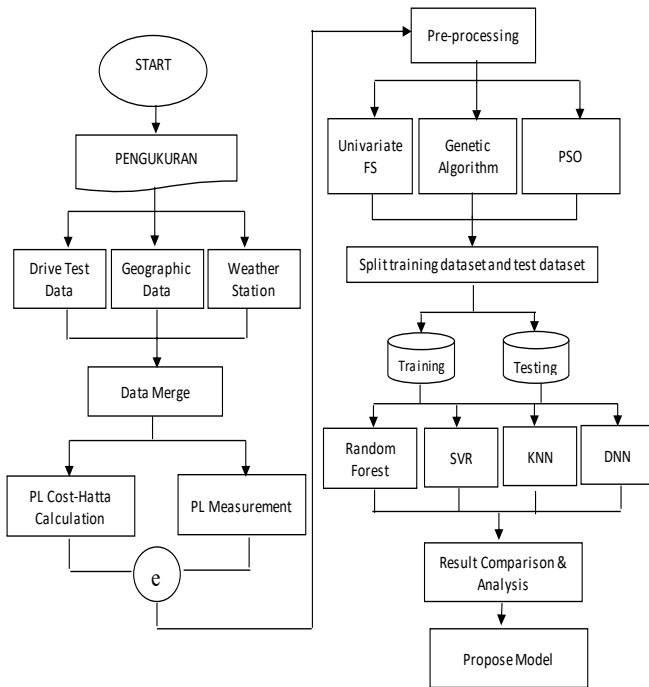


Fig. 1. Research Flow Chart Process.

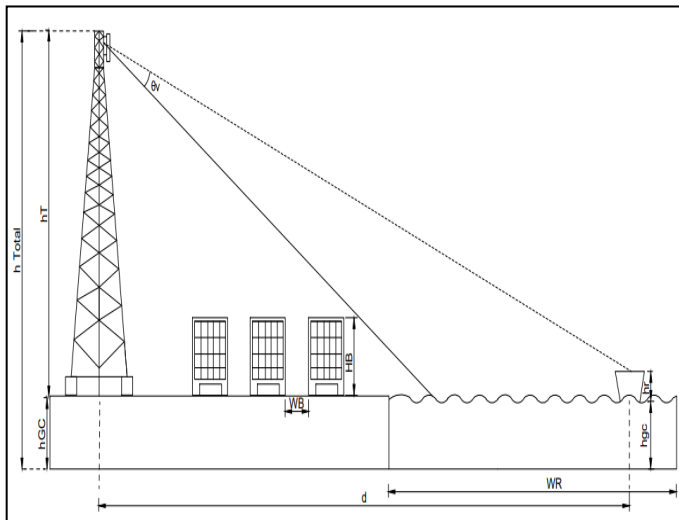


Fig. 2. Measurement Methodology.

Fig. 2 shows the data collection methods for several system parameters such as TX-RX distance, frequency, transmitter height, receiver height, river width, distance between buildings, building height, difference between TX-RX height, distance between transmitter and river border, distance between ship users and river border. The environmental parameters consisted of two segments, namely geographical parameters and weather parameters. The geographical parameters used in this research were slope contour and building density, while the four weather parameters were barometric pressure, temperature, humidity, and dew point.

The data collection was conducted using three measurement methods to obtain the various input and output parameters. A war driving measurement method was used to obtain values of path loss and system parameters. Fig. 3 shows the route taken at the measurement of path loss along the river with a distance of 13 km. The tools used for the war driving measurements were GPS and Dongle which were attached to a laptop. The war driving measurements used two handsets Samsung S5 as receiver, both of which were connected to the laptop. The handsets were locked at the two 4G LTE frequencies. The war driving methodology was used in dedicated conditions or conditions where the handsets were in active (download) mode. At the same time, the weather station tools located at Sriwijaya University took measurements of the weather parameters throughout the data collection. The geographical parameters were obtained based on the geographical maps which were processed using QGIS.



Fig. 3. Selected Route and Building Map on Google Earth for Data Collection.

B. Data Processing

The data processing stage began with the preparation of data from the results of the measurements collected in each of the measurement stages to obtain a number of variables that could be used to create a framework for a model of path loss prediction. The data preparation stage started by processing the data. The results of the war driving measurements in the form of logfiles were treated with time based binning (in seconds) and exported in the form of excel files. The parameter used as path loss value was PUCCH Path Loss. The data of the users' location with the longitude and latitude positions of the data collection were also obtained from this data processing stage. The vertical angle, horizontal angle, and TX-RX distance parameters were calculated based on the angle and position of the BTS transmitter in relation to the user. The distances between the transmitter and river border, and user and river border were calculated based on the straight line intersection of the signal transmission and the river border, which was processed using QGIS.

The geographical parameters of slope contour, building density and distance between buildings were processed using Arcgis. The slope contour was obtained by determining the

difference between the elevation height at the transmitter point and the elevation height at four other points, specifically, 0.25%, 0.5%, and 0.75% of the TX-RX distance, and the difference between the elevation height of the transmitter point (TX) and the elevation height of the receiver point (RX). The average of these values was calculated to find the slope contour value. The building density was found by calculating the number of buildings that were crossed on a straight line between TX-RX, using the intersection on Arcgis. Fig. 4 show a building map was obtained from google earth and converted with Arcgis to find the building points. The distances between buildings were found by calculating the distance between TX-river border (on land) divided by the area of buildings crossed using the intersection on QGIS.



Fig. 4. Building Distribution Map using Arcgis.

Measurements were taken at the weather station to collect weather data about barometric pressure, temperature, humidity, and dew point, which were used as input parameters. The data from the results of the measurements in these three stages were combined to obtain a number of input and output variables.

C. Model Cost-Hatta

The next stage was to find the delta value of the difference between path loss from the result of the measurements and path loss from the result of empirical calculations. The empirical model used in this research was the Cost231-Hatta model. This Cost-Hatta model is a combination of the Cost-231 model and the Hatta model. It can be used to calculate a number of factors, including TX-RX distance, frequency, transmitter height, and receiver height. The Cost-Hatta model is suitable for use in urban areas with a frequency range between 500 MHz – 2000 MHz [29][30]. The formula of the

Cost-Hatta model is shown below:

$$Lu \text{ (dB)} = 46.3 + 33.9 \times \log(f) - 13.82 \times \log(h_{te}) - a(h_{re}) + (44.9 - 6.55 \times \log(h_{te})) \times \log(d) + CM \quad (1)$$

For urban area:

$$a(h_{re}) = 3.2 \times ((\log(11.75 \times h_{re}))^2) - 4.97 \quad (2)$$

For Sub Urban dan Rural:

$$a(h_{re}) = (1.1 \times \log(f) - 0.7) \times h_{re} - (1.56 \times \log(f) - 0.8) \quad (3)$$

CM: 0 dB for medium size towns and suburban areas

CM: 3 dB for downtown areas

Where f is frequency (MHz); h_{te} is height of BTS transmitter antenna (m); h_{re} is height of receiver antenna (m); d is distance between transmitter-receiver (m). The result of the delta calculation of the the difference in path loss was used as an output variable in the modeling.

D. Feature Selection Dan Modelling

The next stage was the process of selecting the features that would be used in the process of developing the model. Feature selection is an important stage in machine learning modelling [31]. This research used three models of feature selection, namely Univariate Feature Selection, Genetic Algorithm, and Particle Swarm Optimization (PSO). The features selected from the three methods were then tested and compared using machine learning.

The Univariate method is a filter method. This kind of method makes an evaluation of every feature in relation to the output variables, then ranks the input features to determine the best features. The Univariate method uses the application of statistical calculations to assign the ranking of each feature. The main criteria used in the Univariate method for the selection of variables are statistical ranking technique and ranking order. After obtaining the ranking results, the next step in this research was to evaluate the number of best features based on the highest ranking, using the “MLPRegressor” model. The python script used was SelectKBest.

The next feature selection method used was Genetic Algorithm. The way this method works is to look for the most suitable composition of features, with the aim of achieving the best prediction accuracy. The Genetic Algorithm method is a search technique based on principles that arise as a result of the inspiration of genetic and evolutionary mechanisms found in a natural system and population of living organisms [32]. In a Genetic Algorithm, every individual in the population represents a candidate solution to the designated problem. The Genetic Algorithm changes a population of individuals by using several genetic functions such as selection, crossover, and mutation [33][34]. Genetic Algorithm is a wrapper method which evaluates every composition of parameter features using machine learning performance as the criteria of evaluation. The genetic algorithm approach is acceptable for various types of solving solutions such as optimization and calls for scheduling[35].

PSO is based on the idea of the social and cooperative behavior of various species to fulfil their food needs, in this case existing in a multidimensional search space [36][37]. The PSO algorithm consists of a number of main parameters that are used by particles to determine the direction and steps that are then used to determine subsequent movement, in P_{best} and G_{best} [36][38]. The position of every particle represents a solution that has a particular fitness value. Particles have their own memory in which they store their best position, referred

to as personal best or $Pbest$ [39]. These particles are evaluated in terms of a particular optimization function to identify their compatibility value and ability to hold the best solution. Every particle determines its next position in the search space based on the function of velocity, which calculates the best position of a particle and the best particle position in a population ($Gbest$). These particles will move at each iteration to a different position until they reach an optimal position [40].

After obtaining the best feature composition, the next step of the research was the modeling phase with machine learning. This research used four machine learning algorithms in the modeling process, namely Multi-Layer Perceptron (MLP), Random Forest, Support Vector Regression (SVR), and K-Nearest Neighbor. In the modeling stage, the prediction model was developed by studying how closely the data of the selected input features correlated with the results of the measurement output data.

E. Evaluation and Deployment

The final step was to evaluate the results of the machine learning modeling using an evaluation matrix. This evaluation parameter was used to observe the best accuracy level of the various machine learning models that had been developed. The path loss prediction model is a regression model in which the performance level of the model is calculated by comparing the prediction value with the actual value. The evaluation matrix used in this research included 3 parameters, namely RMSE, MSE, and MAPERMSE is the root of the Mean Square Error which is the evaluation parameter of the regression case.

$$RMSE = \sqrt{\frac{1}{N} \sum_{j=1}^n (y_j - \hat{y}_j)^2} \tag{4}$$

MAE is the average of absolute value of the difference between the actual value and the predicted value. MAE measures the average error between predictions and actual values.

$$MAE = \frac{1}{N} \sum_{j=1}^n |y_j - \hat{y}_j| \tag{5}$$

MAPE (Mean absolute Percentage Error) is the average value of the percentage error error between the actual value and the predicted value.

$$MAPE = \frac{1}{N} \sum_{j=1}^n \left(\frac{y_j - \hat{y}_j}{y_j} \right) \times 100\% \tag{6}$$

y_j is the measured path loss, \hat{y}_j is the predicted path loss, and N is the number of samples.

IV. RESULT AND DISCUSSION

The preliminary data in this research included a total of 18 candidate variables that consisted of system parameters and environmental parameters. The environmental parameters were divided into two segments, namely geographical parameters and weather parameters. In The first step was to make calculations using the Cost-Hatta model, which is an empirical model. Only four parameter variables were used in this model, namely distance, frequency, height of TX and height of RX. These data were used to determine the value of calculated path loss and to find the delta value of the

difference between the measured path loss and calculated path loss.

The next step was to analyze the selection of the best variables from the 18 candidate variables using the stage of feature selection, as shown in Table I.

TABLE I. CANDIDATE VARIABLE

Variable Name	Variable Description	Level
Distance	Distance between transmitter (TX) and receiver (RX)	meters
Frequency	Frequency used in signal transmission	MHz
Height TX	Transmitter antenna height + altitude location	meters
Height RX	Receiver antenna height + altitude location	meters
Vertical angle	The angle difference between the vertical direction of the antenna and the vertical direction of the receiver	degree
Horizontal angle	The angle difference between the horizontal azimuth of the antenna and the horizontal direction of the receiver	degree
Width of River	River Width	meters
Height of Building	Surrounding building height	meters
Distance between Building	Distance between surrounding buildings	meters
Distance_TX to Border (Land)	Distance between transmitter (TX) and river border / distance on land	meters
Distance Border to User (Water)	The distance between the river border and the user / distance on the waters	meters
Delta Height of TX-RX	The difference between the height of the transmitting antenna and the receiving antenna	meters
Slope Contour	The angle between the horizontal plane and the direction of the contour of the ground	degree
Building Density	The building density between tranceiver and receiver	-
Barometric Pressure	Barometric pressure at the time of measurement	hPa
Temperature	Air temperature at the time of measurement	°C
Humidity	Air humidity at the time of measurement	%
Dew Point	Dew Point Value at the time of measurement	°C

A. Result of Empirical Model by using Cost-Hatta

In the preliminary stage, the path loss value was calculated using the Cost-Hatta empirical model. In the existing models, the Okumura-Hatta models are divided according to type of area, whether urban, suburban, or rural. The results of the Cost-Hatta model calculations were compared with the path loss value from the results of the measurements collected in order to obtain the evaluation parameter value.

TABLE II. EVALUATION PERFORMANCE OF COST-HATTA MODEL

Model	Area	Evaluation		
		RMSE	MAE	MAPE
Cost-Hatta	Urban	31.643	27.114	18.554
	Sub-Urban	25.832	21.319	15.375
	Rural	25.832	21.319	15.375

Table II shows that the Cost-Hatta calculation of urban area had an RMSE value of 27.114 while the suburban/rural

area calculation had an RMSE value of 21.319. This result shows that the calculation model with Cost-Hatta in a suburban area had a higher level of accuracy than the calculation value in an urban area. This indicates that the measurement value in a mixed land-water area was more compatible with the calculation in a suburban area. However, the RMSE value still showed an inadequate level of accuracy because it exceeded the limit of an RMSE value, which should be less than 10. Therefore, there is a need to improve the model of the Cost-Hatta formula by modeling path loss error using machine learning. Path loss error is the difference between the path loss result from the Cost-Hatta calculation and the path loss value from the measurement result. The path loss error value obtained was used as an output variable in the process of prediction improvement.

B. Results of Feature Selection Process

The first step in the process of developing the path loss prediction model was the feature selection process. The feature selection process used three methods to obtain the best composition of features. The composition of features produced by these three methods is as follows:

1) *Univariate feature selection:* The Univariate method was used to select the features with the highest level of correlation. The type of score function used was Mutual Information Regression. The next step was to provide alternative feature combinations based on the different degrees of correlation. The first feature selection method is by using Univariate FS. The score function used is mutual info regression. Univariate feature selection works by selecting the best features based on univariate statistical tests.

Fig. 5 shows that based on metode Univariate FS, frequency has the highest ranking. This indicates that the frequency value had the strongest correlation with the path loss variable, followed by TX-RX distance, border to user distance (water), and distance between buildings (m). This research shows that frequency and distance variables, including TX-RX distance, border to user distance (water), and distance between buildings, play an extremely important role in path loss prediction. The features with the weakest correlation were the parameters of RX vertical angle from TX main beam and building height. The RX vertical angle from main beam variable did not have a significant effect because the measurements were carried out in the NLOS area, so there were many measurement factors that influenced this parameter, such as blockage from buildings and other nearby objects. The building height parameter also had no significant influence because the collection of building data only took into account the height of buildings in the area of the user location point but did not take into account all the buildings between the BTS transmitter location and the receiver location.

Some of these candidate features were modeled simply and evaluated using a machine learning classifier in the form of Random Forest Regression. Table III shows that the best feature combination was achieved by combining the best 17 features, with an RMSE value of 3.07. The combination of these 17 features eliminated the variable with the lowest correlation level to output, which was the RX vertical angle from main beam variable.

TABLE III. CANDIDATE VARIABLE OF UNIVARIATE FEATURE SELECTION

Number of Variables	MAE	MSE	RMSE
1	10.59	171.99	13.11
2	9.13	138.71	11.78
3	9.11	137.15	11.71
4	9.11	140.95	11.87
5	6.68	94.48	9.72
6	6.87	97.13	9.86
7	6.71	93.52	9.67
8	6.74	95.75	9.79
9	6.68	91.89	9.59
10	6.87	98.30	9.91
11	6.53	89.96	9.48
12	6.34	85.27	9.23
13	6.58	88.15	9.39
14	6.62	91.12	9.55
15	6.66	92.65	9.63
16	2.30	10.89	3.30
17	2.18	9.41	3.07
18	2.25	10.38	3.22

2) *Genetic algorithm feature selection:* The Genetic Algorithm feature searches for the best feature composition by performing an evaluation of every feature combination using a classifier with machine learning. The classifier used in this

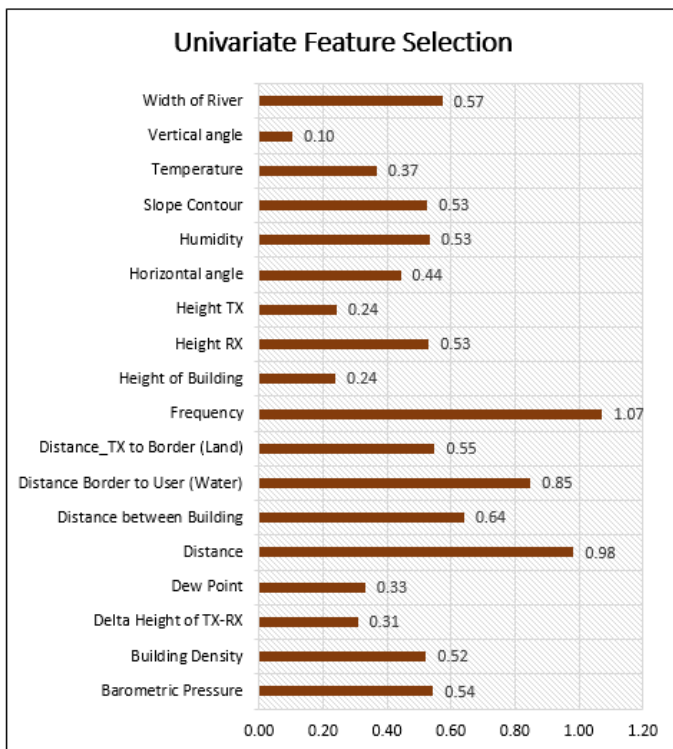


Fig. 5. Value of Mutual Information Univariate for Path Loss Prediction.

research was Random Forest Regression. This research searched for the best composition by altering the values of the parameter settings on the Genetic Algorithm. The population values were changed between 20, 50, and 80. The crossover % values were changed between 0.5, 0.7, and 0.9, and the mutation % values were varied between 0.3, 0.5, and 0.7.

TABLE IV. CANDIDATE VARIABLE OF GENETIC ALGORITHM

Max Iteration	Population	%Crossover	%Mutation	Selected Variable	RMSE
20	20	0.5	0.3	[3,6,8,13,15,16,18]	9.870
20	20	0.7	0.3	[2,3,4,8,9,10,11,17]	7.990
20	20	0.9	0.3	[3,4,5,7,10,13,4,16,18]	11.345
20	20	0.5	0.5	[1,2,3,6,7,8,9,15,16]	8.234
20	20	0.7	0.5	[2,3,4,5,8,10,11,4,17,18]	7.651
20	20	0.9	0.5	[2,3,4,5,7,8,9,10,11,13,15,17,18]	8.382
20	20	0.5	0.7	[2,3,4,6,7,8,9,4,15,16,17]	7.936
20	20	0.7	0.7	[2,3,4,5,7,8,10,12,4,16,17]	7.643
20	20	0.9	0.7	[1,3,4,5,6,9,13,4,15,16,18]	9.037
20	50	0.5	0.3	[3,4,5,8,9,11]	14.477
20	50	0.7	0.3	[2,3,4,5,6,11,12,13,15,16,17]	8.857
20	50	0.9	0.3	[2,3,4,5,9,10,11,15,18]	7.603
20	50	0.5	0.5	[3,5,9,12,13,4,17,18]	10.948
20	50	0.7	0.5	[3,4,5,6,8,9,10,18]	9.988
20	50	0.9	0.5	[1,2,3,6,8,9,10,11,13,15,16,18]	8.183
20	50	0.5	0.7	[2,5,8,9,11,4,16,17]	11.978
20	50	0.7	0.7	[2,3,5,8,9,10,12,15]	8.050
20	50	0.9	0.7	[1,2,3,6,10,13,4,15,16,17,18]	8.298
20	80	0.5	0.3	[3,5,6,8,9,10,12,13,16,17,18]	10.012
20	80	0.7	0.3	[1,2,3,5,6,7,10,11,12,4,15,17,18]	8.058
20	80	0.9	0.3	[3,5,8,10,11,12,13,18]	8.549
20	80	0.5	0.5	[2,3,4,10,11,12,13,4,15,16]	8.167
20	80	0.7	0.5	[2,3,4,6,8,12,13,15,18]	8.399
20	80	0.9	0.5	[1,2,4,5,6,10,11,12,13,4,15]	7.966
20	80	0.5	0.7	[1,2,3,9,10,11,13,17,18]	8.190
20	80	0.7	0.7	[1,3,6,8,9,11,15,16]	8.316
20	80	0.9	0.7	[1,2,3,4,7,12,4,15,16]	7.864

Table IV shows that the best composition of variables achieved was using the variable numbers [2, 3, 4, 5, 9, 10, 11, 15, 18]. These variables are frequency, TX height, RX height, RX vertical angle from TX main beam, distance between buildings, barometric pressure, temperature, slope contour, and border to user distance (water). The parameters selected in the Genetic Algorithm showed quite a marked difference with the Univariate FS. The RX vertical angle from TX main beam and distance between buildings, which had a low correlation with output, were included in the selected parameter composition, as was the TX-RX distance parameter. This was because the GA method did not take into consideration the correlation level between the input and output variables but performed a combination search with the mutation and crossover between the variables.

3) Particle Swarm Optimization (PSO) feature selection: PSO is also a wrapper method, which searches for the best

composition by evaluating every possibility for each candidate combination using machine learning, searching for the best accuracy based on the results of the evaluation. This research carried out a number of trials by altering the values of the PSO parameter settings. Particle number, weighting, and C1/C2 values were changed to obtain the best accuracy value from the selected variables. The number of particles was varied with the values of 40, 70, and 100, while the W and C1/C2 values were varied with the values of 0.2, 0.5, and 0.8.

TABLE V. CANDIDATE VARIABLE OF PARTICLE SWARM OPTIMIZATION

Max Iteration	Particle	W	C1/C2	Selected Variable	Score Error
100	40	0.2	0.2	[1,2,3,4,5,6,8,9,10,11,12,13,4,16,17]	2.433
100	40	0.5	0.2	[2,3,5,6,7,8,11,13,4,15,16,17,18]	2.423
100	40	0.8	0.2	[1,2,3,4,6,7,8,9,12,13,4,15,16,17,18]	2.415
100	40	0.2	0.5	[2,3,4,5,6,7,8,12,13,4,16,17,18]	2.421
100	40	0.5	0.5	[1,2,3,5,6,7,9,10,4,15,16,17,18]	2.419
100	40	0.8	0.5	[1,2,3,4,5,6,7,8,9,10,12,13,16,17,18]	2.416
100	40	0.2	0.8	[2,3,4,5,6,9,10,12,13,4,15,16,17,18]	2.417
100	40	0.5	0.8	[2,3,5,6,7,8,9,10,11,12,13,15,16,17,18]	2.415
100	40	0.8	0.8	[2,3,4,6,7,9,10,11,12,13,4,15,16,17,18]	2.411
100	70	0.2	0.2	[2,3,6,7,8,9,10,11,13,4,15,16,17,18]	2.425
100	70	0.5	0.2	[1,2,3,4,6,7,9,11,12,13,15,16,17,18]	2.419
100	70	0.8	0.2	[2,3,4,6,7,9,11,12,13,4,15,16,17,18]	2.414
100	70	0.2	0.5	[1,2,3,4,5,6,7,8,11,12,13,4,15,16,17,18]	2.419
100	70	0.5	0.5	[2,3,4,5,6,8,9,10,12,13,16,17,18]	2.419
100	70	0.8	0.5	[2,3,4,5,6,7,8,9,10,11,12,13,4,15,16,17,18]	2.411
100	70	0.2	0.8	[1,2,3,4,6,7,8,9,12,13,4,15,16,17,18]	2.415
100	70	0.5	0.8	[2,3,4,5,6,7,8,9,10,11,12,13,4,16,17,18]	2.411
100	70	0.8	0.8	[2,3,4,6,7,9,10,11,12,13,4,15,16,17,18]	2.411
100	100	0.2	0.2	[1,2,3,6,7,9,11,12,4,15,16,17,18]	2.428
100	100	0.5	0.2	[2,3,4,5,6,9,12,13,4,15,16,17,18]	2.420
100	100	0.8	0.2	[1,2,3,5,6,7,8,9,10,12,13,4,15,16,17,18]	2.413
100	100	0.2	0.5	[1,2,3,4,6,7,9,4,15,16,17,18]	2.423
100	100	0.5	0.5	[1,2,3,4,5,6,7,8,9,11,12,13,4,16,17,18]	2.414
100	100	0.8	0.5	[1,2,3,4,6,7,8,9,10,11,13,4,15,16,17,18]	2.417
100	100	0.2	0.8	[2,3,4,5,6,9,10,12,13,4,15,16,17,18]	2.417
100	100	0.5	0.8	[1,2,3,4,5,6,7,8,9,10,11,12,13,4,15,16,17,18]	2.411
100	100	0.8	0.8	[2,3,4,5,6,7,8,9,11,12,13,4,15,16,17,18]	2.413

Table V shows that the best composition of variables was the composition of variables [2, 3, 4, 6, 7, 9, 10, 11, 12, 13,

14, 15, 16, 17, 18]. The variables eliminated from the selected variables were TX-RX distance, RX vertical angle to mainbeam, and building height. This was the same as the Univariate results, where the parameters of RX vertical angle to mainbeam and building height, which had a low correlation, were not included in the selected variables. However, what was significantly different was the parameter of TX-RX distance, which had a sufficiently high level of correlation but was not included in the selected variables in PSO. As in the case of GA, PSO did not take into account the level of correlation between the input and output variables, but carried out a combination search with a particular method. In PSO, the search uses a swarm technique, which is a search based on the history of the best values, whether Pbest or Gbest.

C. Machine Learning Evaluation

In this research, four machine learning models were used to improve path loss prediction. The results of the evaluation parameters using four machine learning model are presented.

Table VI shows the evaluation of combination parameters to the feature selection methods with machine learning models. These results indicate that the best feature selection in DNN modeling is the Univariate method with an RMSE value of 4.49. These results are also shown in the KNN Regressor and Random Forest modeling where the smallest RMSE value uses the Univariate feature selection method where the RMSE values are 3.75 and 1.52 respectively, while the feature selection method using the GA method has the lowest accuracy rate for the use of the three types of algorithms. The SVR modeling shows different results, namely the best feature selection using GA, while the selection feature with the largest RMSE uses Univariate.

Table VII shows the best combination of feature selection methodology and machine learning. In the improvement of the Cost-Hatta model using Univariate-Random Forest, it has the smallest level of accuracy, namely the RMSE value of 1.52, MAE of 1.09 and MAPE of 14.08. The second accuracy value is model improvement using Univariate-KNN with a RMSE value of 3.75, an MAE value of 2.76 and a MAPE value of 35.75. On the third device, using univariate-DNN with an RMSE value of 4.49, an MAE value of 3.31 and a MAPE value of 308.8. While the worst value of accuracy improvement is by using GA-SVR. The value of the level of accuracy in the model is RMSE of 17.09, MAE value of 13.9 and MAPE value of 592.29.

The results of the Cost-Hatta model improvement using a machine learning approach can be seen in Fig. 6. The graph shows that the increasing accuracy using univariate-RF was the highest in RMSE accuracy, which is around 94.12%, followed by Univariate-KNN Regression and Univariate-DNN where the increase values are 85.48% and 82.67%, respectively. The lowest RMSE accuracy increase value is in the GA-SVR combination, with an accuracy increase of 33.84% from the Cost-Hatta RMSE value of 25,832 to 1.52.

TABLE VI. EVALUATION PERFORMANCE OF FEATURE SELECTION – MACHINE LEARNING MODEL

Model	FS	RMSE	MAE	MAPE
DNN	GA	5.58	4.15	720.57
	PSO	5.18	3.86	705.96
	Univariate	4.49	3.31	308.80
KNN Regressor	GA	4.61	3.24	148.09
	PSO	3.88	2.80	89.56
	Univariate	3.75	2.76	35.75
Random Forest Regressor	GA	1.76	1.22	105.79
	PSO	1.58	1.12	36.54
	Univariate	1.52	1.09	14.08
SV Regressor	GA	17.09	13.90	592.29
	PSO	18.08	14.65	634.28
	Univariate	18.21	14.74	252.81

TABLE VII. COMPARISON OF COST-HATTA MODEL WITH MACHINE LEARNING MODIFICATION MODEL

Model	Evaluation		
	RMSE	MAE	MAPE
Cost-Hatta	25.832	21.319	15.375
Cost-Hatta - Univ-DNN	4.49	3.31	308.8
Cost-Hatta-Univ-KNN	3.75	2.76	35.75
Cost-Hatta-Univ-RF	1.52	1.09	14.08
Cost-Hatta-GA-SVR	17.09	13.9	592.29

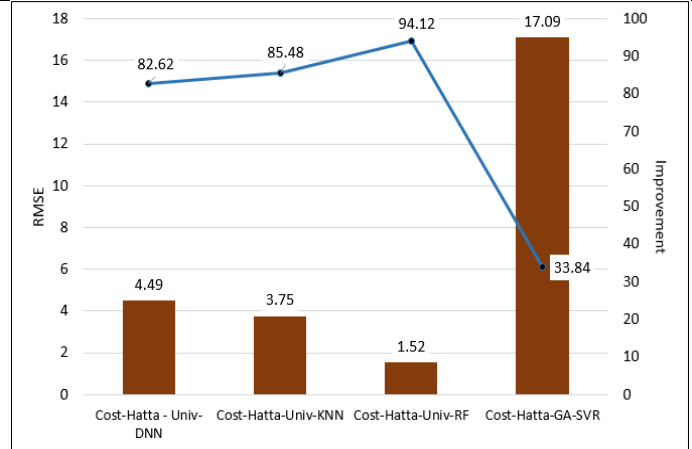


Fig. 6. Improvement Percentage of Machine Learning Model Approachment.

V. CONCLUSIONS

The determination of the features in the modeling will determine the accuracy of the path loss prediction. The condition of different signal propagation area causes the complexity of the various parameters needed in predicting path loss modeling, especially in mixed land-water areas. System parameters and environmental parameters have an influence on the path loss value. The feature selection method approach is needed to choose the best combination of

parameters in the construction of the prediction model. Improvements to the Cost-Hatta model with the feature-selection and machine learning approach resulted in a significant improvement in accuracy. The combination of the Univariate-RF model is the best combination with an increase in accuracy of 94.12% from the previous RMSE Cost-Hatta value. This indicates that the proposed model framework is highly suitable to be used in a mixed land-water area.

VI. FUTURE WORK

In the next research, some suggestion to increase path loss prediction accuracy especially in mixed land water area:

1) Hyper-parameter optimization of machine learning models can be carried out. Metaheuristic methods such as Genetic Algorithm and Particle Swarm Optimization can be used in determining the composition of hyper-parameters to get the best accuracy value.

2) Expand measurement data to get a more varied sample value, especially for weather parameters.

ACKNOWLEDGMENT

The first author is a doctoral student at the Faculty of Engineering Science, Universitas Sriwijaya. The authors would like to thank Universitas Sriwijaya for their support in carrying out this research.

REFERENCES

- [1] Park, D. K. Tettey, and H.-S. Jo, "Artificial Neural Network Modeling for Path Loss Prediction in Urban Environments," *J. LATEX CL FILES*, vol. 14, no. 8, pp. 9–13, 2019, [Online]. Available: <http://arxiv.org/abs/1904.02383>.
- [2] B. Alfaresi, T. Barlian, F. Ardianto, and M. Hurairah, "Path Loss Propagation Evaluation and Modelling based ECC-Model in Lowland Area on 1800 MHz Frequency," *J. Robot. Control*, vol. 1, no. 5, pp. 167–172, 2020, doi: 10.18196/jrc.1534.
- [3] I. Oluwafemi and O. Femi-Jemilohun, "Suburban area path loss propagation prediction and optimization at 900 and 1800 MHz," *J. Eng. Appl. Sci.*, vol. 13, no. 9, pp. 2521–2529, 2018, [Online]. Available: <https://www.scopus.com/inward/record.uri?partnerID=HzOxMe3b&scp=85049520402&origin=inward>.
- [4] A. O. A, T. O. A, M. O. S, and A. J. A, "Experimental Study of Variation of Path Loss with Respect to Heights at GSM Frequency Band," *Int. J. Sci. Res. Sci. Eng. Technol.*, vol. 3, no. 3, pp. 347–351, 2016.
- [5] Alor MO, "Efficient Pathloss Model for determining Mobile Radio Link Design," *Int. J. Sci. Res. Sci. Eng. Technol.*, vol. 3, no. 3, pp. 270–276, 2015.
- [6] M. Ayadi, A. Ben Zineb, and S. Tabbane, "A UHF Path Loss Model Using Learning Machine for Heterogeneous Networks," *IEEE Trans. Antennas Propag.*, vol. 65, no. 7, pp. 3675–3683, 2017, doi: 10.1109/TAP.2017.2705112.
- [7] Y. Zhang, J. Wen, G. Yang, Z. He, and J. Wang, "Path loss prediction based on machine learning: Principle, method, and data expansion," *Appl. Sci.*, vol. 9, no. 9, 2019, doi: 10.3390/app9091908.
- [8] D. A. V. Sreevardhan Cheerla, K. Sindhuja, Ch. Indra Kiran, "Analysis of different path loss models in urban suburban and rural environment," *Int. J. Emerg. Trends Eng. Res.*, vol. 8, no. 7, pp. 2972–2976, 2020, doi: 10.30534/ijeter/2020/14872020.
- [9] O. Shoewu, L. A. Akinyemi, and L. Oborkhale, "Modelling Path Loss in Mobile Communication 4G Network System for Dryland and Wetland Terrains," in *Southern Africa Telecommunication Networks and Applications Conference (SATNAC)*, 2019, pp. 44–49.
- [10] J. Isabona and V. M. Srivastava, "Hybrid neural network approach for predicting signal propagation loss in urban microcells," *IEEE Reg. 10 Humanit. Technol. Conf. 2016, R10-HTC 2016 - Proc.*, 2017, doi: 10.1109/R10-HTC.2016.7906853.
- [11] K. Saito, Y. Jin, C. Kang, J. Takada, and J.-S. Leu, "Two-step path loss prediction by artificial neural network for wireless service area planning," *IEICE Commun. Express*, vol. 8, no. 12, pp. 611–616, 2019, doi: 10.1587/comex.2019gc10038.
- [12] H. S. Jo, C. Park, E. Lee, H. K. Choi, and J. Park, "Path loss prediction based on machine learning techniques: Principal component analysis, artificial neural network and gaussian process," *Sensors (Switzerland)*, vol. 20, no. 7, pp. 1–23, 2020, doi: 10.3390/s20071927.
- [13] B. J. Cavalcanti, G. A. Cavalcante, L. M. De Mendonça, G. M. Cantanhede, M. M. M. De Oliveira, and A. G. D'Assunção, "A hybrid path loss prediction model based on artificial neural networks using empirical models for LTE and LTE-A at 800 MHz and 2600 MHz," *J. Microwaves, Optoelectron. Electromagn. Appl.*, vol. 16, no. 3, pp. 708–722, 2017, doi: 10.1590/2179-10742017v16i3925.
- [14] L. Wu et al., "Artificial Neural Network Based Path Loss Prediction for Wireless Communication Network," *IEEE Access*, vol. 8, pp. 199523–199538, 2020, doi: 10.1109/access.2020.3035209.
- [15] J. E. Ofure, O. D. Oyedum, M. O. Ajewole, and A. M. Aibinu, "Comparative analysis of basic models and artificial neural network based model for path loss prediction," *Prog. Electromagn. Res. M*, vol. 61, no. October, pp. 133–146, 2017, doi: 10.2528/PIERM17060601.
- [16] C. Oroza et al., "A Machine-Learning Based Connectivity Model for Deployments To cite this version: A Machine-Learning Based Connectivity Model for Complex Terrain Large-Scale Low-Power Wireless Deployments," *IEEE Trans. Cogn. Commun. Netw.*, vol. 3, no. 4, pp. 576–584, 2017, doi: 10.1109/TCCN.2017.2741468.
- [17] J. Wen, Y. Zhang, G. Yang, Z. He, and W. Zhang, "Path Loss Prediction Based on Machine Learning Methods for Aircraft Cabin Environments," *IEEE Access*, vol. 7, pp. 159251–159261, 2019, doi: 10.1109/ACCESS.2019.2950634.
- [18] S. Duangsuwan, "Comparison of path loss prediction models for UAV and IoT air-to-ground communication system in rural precision farming environment," *J. Commun.*, vol. 16, no. 2, pp. 60–66, 2021, doi: 10.12720/jcm.16.2.60-66.
- [19] G. Yang, Y. Zhang, Z. He, J. Wen, Z. Ji, and Y. Li, "Machine-learning-based prediction methods for path loss and delay spread in air-to-ground millimetre-wave channels," *IET Microwaves, Antennas Propag.*, vol. 13, no. 8, pp. 1113–1121, 2019, doi: 10.1049/iet-map.2018.6187.
- [20] Y. Zhang, J. Wen, G. Yang, Z. He, and X. Luo, "Air-to-Air Path Loss Prediction Based on Machine Learning Methods in Urban Environments," *Wirel. Commun. Mob. Comput.*, vol. 2018, 2018, doi: 10.1155/2018/8489326.
- [21] ALLAN DOS S. BRAGA et al., "Radio Propagation Models Based on Machine Learning Using Geometric Parameters for a Mixed City-River Path," *IEEE Access*, vol. 8, pp. 146395–146407, 2020, doi: 10.1109/ACCESS.2020.3012661.
- [22] T. Zhang, S. Liu, W. Xiang, L. Xu, K. Qin, and X. Yan, "A real-time channel prediction model based on neural networks for dedicated short-range communications," *Sensors (Switzerland)*, vol. 19, no. 16, 2019, doi: 10.3390/s19163541.
- [23] S. I. Popoola, S. Misra, and A. A. Atayero, "Outdoor Path Loss Predictions Based on Extreme Learning Machine," *Wirel. Pers. Commun.*, vol. 99, no. 1, pp. 441–460, 2017, doi: 10.1007/s11277-017-5119-x.
- [24] S. Ojo, "Radial basis function neural network path loss prediction model for LTE networks in multitransmitter signal propagation environments," *Int. J. Commun. Syst.*, vol. 34, no. 3, 2021, doi: 10.1002/dac.4680.
- [25] A. Tahat, T. Edwan, H. Al-Sawwaf, J. Al-Baw, and M. Amayreh, "Simplistic Machine Learning-Based Air-to-Ground Path Loss Modeling in an Urban Environment," *2020 5th Int. Conf. Fog Mob. Edge Comput. FMEC 2020*, pp. 158–163, 2020, doi: 10.1109/FMEC49853.2020.9144965.
- [26] E. J. Ofure, O. D. Oyedum, M. O. Ajewole, and A. M. Aibinu, "Artificial Neural Network model for the determination of GSM Rxlevel from atmospheric parameters," *Eng. Sci. Technol. an Int. J.*, vol. 20, no. 2, pp. 795–804, 2016, doi: 10.1016/j.jestch.2016.11.002.

- [27] S. I. Popoola, E. Adetiba, A. A. Atayero, N. Faruk, and C. T. Calafate, "Optimal model for path loss predictions using feed-forward neural networks," *Cogent Eng.*, vol. 5, no. 1, 2018, doi: 10.1080/23311916.2018.1444345.
- [28] H. Singh, S. Gupta, C. Dhawan, and A. Mishra, "Path Loss Prediction in Smart Campus Environment: Machine Learning-based Approaches," *IEEE Veh. Technol. Conf.*, vol. 2020-May, 2020, doi: 10.1109/VTC2020-Spring48590.2020.9129444.
- [29] C. Emeruwa and P. Iwuji, "Determination Of A Pathloss Model For Long Term Evolution (Lte) In Yenagoa," *Int. J. Eng. Sci.*, vol. 7, no. 10, pp. 38–44, 2018, doi: 10.9790/1813-0710033844.
- [30] E. R. Abboud, "Propagation Model For the 900 MHz Almadar Aljadid Mobile Network at Tripoli Area Using Linear Regression Method," in *The Proceedings of Second International Conference on Electrical and Electronics Engineering, Clean Energy and Green Computing*, 2015, pp. 5–11.
- [31] A. Sanmorino, Ermatita, Samsuryadi, and D. P. Rini, "Building Research Productivity Framework in Higher Education Institution," *Int. J. Adv. Comput. Sci. Appl.*, vol. 12, no. 6, pp. 184–191, 2021, doi: 10.14569/IJACSA.2021.0120620.
- [32] A. Bhuvaneshwari, "Path loss model optimization using stochastic hybrid genetic algorithm," *Int. J. Eng. Technol.*, vol. 7, no. 4, pp. 464–469, 2018, [Online]. Available: <https://www.scopus.com/inward/record.uri?partnerID=HzOxMe3b&scp=85082355283&origin=inward>.
- [33] F. Moslehi and A. Haeri, "A novel hybrid wrapper-filter approach based on genetic algorithm, particle swarm optimization for feature subset selection," *J. Ambient Intell. Humaniz. Comput.*, vol. 11, no. 3, pp. 1105–1127, 2020, doi: 10.1007/s12652-019-01364-5.
- [34] Y. C. Hsieh, P. J. Lee, and P. S. You, "Immune-based evolutionary algorithm for determining the optimal sequence of multiple disinfection operations," *Sci. Iran.*, vol. 26, no. 2 C, pp. 959–974, 2019, doi: 10.24200/sci.2018.20324.
- [35] A. Brezilianu, L. Fira, and M. Fira, "A genetic algorithm approach for scheduling of resources in well-services companies," *Int. J. Adv. Res. Artif. Intell.*, vol. 1, no. 5, pp. 1–6, 2012, doi: 10.14569/ijarai.2012.010501.
- [36] S. Rukhaiyar, M. N. Alam, and N. K. Samadhiya, "A PSO-ANN hybrid model for predicting factor of safety of slope," *Int. J. Geotech. Eng.*, vol. 12, no. 6, pp. 556–566, 2018, doi: 10.1080/19386362.2017.1305652.
- [37] B. A. A. Yousef, H. Rezk, M. A. Abdelkareem, A. G. Olabi, and A. M. Nassef, "Fuzzy modeling and particle swarm optimization for determining the optimal operating parameters to enhance the bio-methanol production from sugar cane bagasse," *Int. J. Energy Res.*, vol. 44, no. 11, pp. 8964–8973, 2020, doi: 10.1002/er.5605.
- [38] S. Karkheiran, A. Kabiri-Samani, M. Zekri, and H. M. Azamathulla, "Scour at bridge piers in uniform and armored beds under steady and unsteady flow conditions using ANN-APSO and ANN-GA algorithms," *ISH J. Hydraul. Eng.*, vol. 00, no. 00, pp. 1–9, 2019, doi: 10.1080/09715010.2019.1617796.
- [39] T. Si and R. Dutta, "Partial Opposition-Based Particle Swarm Optimizer in Artificial Neural Network Training for Medical Data Classification," vol. 18, no. 5, 2019.
- [40] M. Khari, D. Jahed Armaghani, and A. Dehghanbanadaki, "Prediction of Lateral Deflection of Small-Scale Piles Using Hybrid PSO-ANN Model," *Arab. J. Sci. Eng.*, vol. 45, no. 5, pp. 3499–3509, 2020, doi: 10.1007/s13369-019-04134-9.

Employability Prediction of Information Technology Graduates using Machine Learning Algorithms

Gehad ElSharkawy, Yehia Helmy, Engy Yehia

Dept. Business Information Systems

Faculty of Commerce and Business Administration, Helwan University, Cairo, Egypt

Abstract—The ability to predict graduates' employability to match labor market demands is crucial for any educational institution aiming to enhance students' performance and learning process as graduates' employability is the metric of success for any higher education institution (HEI). Especially information technology (IT) graduates, due to the evolving demand for IT professionals increased in the current era. Job mismatch and unemployment remain major challenges and issues for educational institutions due to the various factors that influence graduates' employability to match labor market needs. Therefore, this paper aims to introduce a predictive model using machine learning (ML) algorithms to predict information technology graduates' employability to match the labor market demands. Five machine learning classification algorithms were applied named Decision tree (DT), Gaussian Naïve Bayes (Gaussian NB), Logistic Regression (LR), Random Forest (RF), and Support Vector Machine (SVM). The dataset used in this study is collected based on a survey given to IT graduates and employers. The performance of the study is evaluated in terms of accuracy, precision, recall, and f1 score. The results showed that DT achieved the highest accuracy, and the second highest accuracy was achieved by LR and SVM.

Keywords—Machine learning; IT graduates; higher education; employability; labor market

I. INTRODUCTION

Due to the dynamically changing job market and the rapid advancements in technology. The growing demand for Information Technology (IT) professionals is one of the highest demands all over the world [1]. Human capital is one of the most important economic assets of production and is considered the main pillar for raising the standard of living and developing human resources on which countries depend in strategic planning to achieve sustainable development, as human capital represents the workforce that engages in all service, production, and consumer activities in society. As a result, higher education institutions (HEIs) produce an increasing number of graduates each year. The mismatch between the higher education outputs and the labor market demands is considered one of the major threats to economic growth which causes high unemployment rate and misplacement problems among higher education graduates in Egypt. The mismatch is due to poor collaboration between the labor market and HEIs. This lack of communication results in the wrong kind of workforce, thus errors in its production are costly [2]–[4]. Thereby, to avoid this mismatch, the HEIs have to ensure the graduates' employability.

Machine learning (ML) techniques can be used to predict the employability signals of IT graduates and identify the most significant factors affecting their employability as early as possible so appropriate actions can be taken to enhance their employability in order to equip them with the appropriate knowledge and skills before they enter the dynamic job market.

There is increasing interest in applying machine learning in higher education, according to certain prior studies to predict the graduates' employability but still, the use of automated machine learning to predict students' employability in its initial stage, ML is a subset of artificial intelligence (AI) in which computers analyze large datasets to learn patterns that will make predictions for new data, in contrast to traditional computer methodologies. In traditional reasoning, algorithms are a set of explicitly defined instructions that computers use to describe or solve problems [5], [6]. As a result, in the hiring process, graduates with experience are in high demand due to high productivity and low training cost than those who did not have any experience. HEIs must undergo frequent evaluations to provide future IT graduates with the demanded skills as it is considered the main factor to produce this workforce [7].

The earlier studies have shown a great interest in examining the mismatch between HEIs output and labor market demands. By applying different ML algorithms. However, these studies focused on one or a few features only. As a result, the two main research questions of this study are:

RQ1) What are the most significant features that affect graduates' competitive advantage to match labor market demands?

RQ2) what are the best machine learning algorithms for employability prediction of IT graduates?

The objective of this study is to develop a prediction ML model for graduates' employability status (predict whether the IT graduate is most likely to be qualified or not qualified to match labor market demands), and for better utilization of the collected dataset which can greatly help understand the extent to which IT graduates were prepared for the highly technical IT careers to enter the workforce.

The findings of this study will help:

- Reduce the gap between labor market demands and HEIs.

- Improve the IT graduates' qualifications to match labor market demands.
- Provide valuable insights for guiding HEIs to make better long-term plans for producing graduates who are knowledgeable and skilled through prediction of their employability status.
- Contribute significantly to the placement process for employers.
- Decrease the high unemployment rate of IT graduates.

The rest of this paper is organized as follows: Section II presents various relevant works in the field of employability prediction. Section III describes the proposed methodology in detail. Section IV shows the results of the used algorithms and the discussion of the analysis of the used features. Section V presents the conclusions of this study with some limitations and improvements.

II. RELATED WORK

In recent years, many researchers attempted to use machine learning in higher education to enhance graduate's features and curricula to support employability [8]. To discuss the contribution of ML in continuous quality improvement. We focused on some of the previous works that used different machine learning techniques such as Artificial Neural Network (ANN), Decision Tree (DT), K-Nearest Neighbor (KNN), Gaussian Naïve Bayes (Gaussian NB), Logistic Regression (LR), Neural Network (NN), Random Forest (RF), Naïve Bayes (NB) and Support Vector Machine (SVM).

In [9], the author predicted which students are most likely to get work after graduation by using data analytics and machine learning techniques such as SVM, LR, ANN, DT, and discriminant analysis. Also, the features used are hard skills, demographics features, extra/co-curricular activities, and internships the data were obtained from student surveys and institutional databases. The SVM classification algorithm achieved an accuracy of 87.26%.

The authors in [10] aimed to identify the most significant factors affecting graduate employability by using three classification algorithms DT, ANN, and SVM. The features used in this research are hard skills, soft skills, demographic features, extra/co-curricular activities, university features, and internships the research data were collected from institutional databases. The SVM algorithm shows 66.096% accuracy.

A web-based application is developed by [11] through applied machine learning algorithms DT, NB, and NN to predict the sustainability of IT students' skills for recruitment mainly hard skills and soft skills, the collected data were from student and recruiter surveys, the NB achieved the highest

accuracy of 69%. In another research [12], supervised machine learning techniques such as LR, DT, RF, KNN, and SVM were used to predict high school students' employability for part-time jobs with local businesses the hard skills, demographic features, and extra/co-curricular activities features were used and collected from student surveys. The LR algorithm achieved an accuracy of 93%.

The authors in [13] analyzed the data from education institutions to predict the students' employability and determine the factors affecting their employability by using hard skills, soft skills, demographic features, extra/co-curricular activities, and university features then applied four ML algorithms which are DT, Gaussian NB, SVM, and KNN. The results achieved an accuracy of 98% by DT and SVM.

Furthermore, a student employability prediction system was developed by [14] using SVM, DT, RF, KNN, and LR algorithms to predict the students' employability, Institutional databases were obtained, and the hard skills, soft skills, and demographic features were used. The results of this research achieved an accuracy of 91% by the SVM algorithm. In [14], the authors identified the most predictive attributes through hard skills, soft skills, and demographic features to determine why students are most likely to get employed using graduates surveys and institutional databases, the applied and compared three methods are SVM, RF, and DT. The SVM achieved the highest accuracy of 91.22%.

The authors in [15] investigated the impact of various institution features on graduate employability using the hyperbox-based machine learning model which achieved 78% accuracy. A hybrid model was proposed by [16] for student employability prediction through a deep belief network and Softmax regression (DBN-SR) the dataset obtained from student surveys and the hard skills, soft skills, demographic features, and university features were used as the adopted features the results achieved high accuracy with 98%.

In [17] predicted the students' employability based on technical skills the institution databases were collected and the following algorithms were applied SVM, LR, DT, RF, AdaBoost, and NB, the highest accuracy achieved is 70% by the RF algorithm. Finally, the authors in [18] developed a model using various machine learning methods DT, RF, NN, and Gaussian NB to forecast candidate hiring by employing different statistical measures on feature selection such as hard skills, demographic features, and professional experience, the highest accuracy was achieved by Gaussian NB with 99%. Table I depicts and summarizes the relevant studies according to their adopted features, dataset sources, ML models, output features, and accuracy of the best-adapted model to answer RQ1.

TABLE I. COMPARISON OF RELATED STUDIES

Reference	Year	Adopted features categories	Dataset sources	ML model	Output features	Accuracy
Hugo [9]	2018	Hard skills Demographics features Extra/co-curricular activities Internship	Student surveys and Institution databases.	-SVM -ANN -LR -Discriminant analysis -DT	Employability: {Employed, Not Employed}	SVM 87.26%
Othman et al. [10]	2018	Hard skills Soft skills Demographic features Extra/co-curricular activities University features Internship	Institutional databases	-DT -ANN -SVM	Employability: {Employed, Not employed}	SVM 66.0967%
Alghamlas and Alabduljabbar [11]	2018	Hard skills Soft skills.	Student surveys and Recruiter surveys.	-DT -NB -NN	Matching to industry-required skills	Naïve Bayes 69%
Dubey and Mani [12]	2019	Hard skill Demographic features Extra/co-curricular activities.	Student surveys.	-LR -DT -RF -KNN -SVM	Hiring: {Hired, Not hired}	LR 93%
Kumar and Babu [13]	2019	Hard skills Soft skills Demographic features Extra/co-curricular activities University features.	Student surveys.	-DT -Gaussian NB -SVM -KNN.	Getting a job: {Yes, no}	DT & SVM 98%
Casuat [21]	2020	Hard skills Soft skills Demographic features	Institution databases.	-DT -RF -SVM -KNN -LR	Employability: {Employed, Less Employed}	SVM 91%
Casuat & Festijo [14]	2020	Hard skills Soft skills Demographic features.	Graduate surveys and Institution databases	-SVM -RF -DT	Employability: {Employed, Less Employed}	SVM 91.22%
Aviso et al.[15]	2020	University features.	Institution databases.	Rule-based Hyperbox model.	Employability: {Yes, no}	78%
Bai and Hira [16]	2021	Hard skills Soft skills Demographic features University features.	Student surveys.	-Softmax regression.	Employability: {Employed, Unemployed}	98%
Laddha et al. [17]	2021	Hard skills.	Institution databases.	-SVM -LR -DT -RF -AdaBoost -NB.	Placement: {Placed, Not placed}	RF 70%
Reddy et al. [18]	2021	Hard skills Demographic features Professional experience.	Employee surveys.	-DT -RF -NN -Gaussian NB.	Recruitment: {Join, Not join}	Gaussian NB 99%

III. METHODOLOGY

In this section, we will discuss the methodology of our study, the machine learning algorithms applied, and the evaluation metrics used in this study. Fig. 1 highlights the research methodology: i) Data collection; ii) applying data preprocessing; iii) Splitting the dataset into two sets, a train set to train the model and a test set to evaluate the model; iv) building our model by applying five ML classification algorithms; v) evaluating the model; vi) outcome the proposed model to predict the qualified IT graduate to meet labor market demands. To answer RQ1: What are the most significant features that affect graduates' competitive advantage to match labor market demands? we followed the methodology steps as shown below.

A. Data Source

The dataset used in this research was obtained based on a survey given to IT graduates and employers in Egypt. We created an online survey with pertinent questions and then distribute it to IT graduates including (Computers & Artificial intelligence, Business information systems, Software Engineering, and Management information systems) and several IT companies from different sectors to get the desired findings. A brief description of each feature selected, and its value is described in Table II. We classified them into four categories (Trainings, Soft skills, Hard skills, and In-demand skills) each category has the most-related features, and the values (0,1) of the first three categories indicated that "0" means the graduate does not been trained or given a specific course during their study years in the college. While "1" means the graduate has been trained or given a specific course in those skills. In the fourth category, the value (0-7) means how many courses or trainings the graduate received from those fields to be qualified for the industry requirements.

B. Data Preprocessing

Data preparation is a critical stage while creating a machine learning model as it is difficult for a machine to read

the raw datasets to produce the expected results [19]. So, data preprocessing make data suitable for a machine learning model. First, we eliminate noise, missing values and make the data consistent. Then, we apply feature selection to identify the relevant features to allow classifiers to reach the optimal performance which has a greater impact on IT graduates' employability to match the labor market demands. Finally, we Split the dataset into two sets (80%) for training to train the model and (20%) for testing to test the accuracy of the model and enhance the performance of our machine learning models.

C. Prediction Models

Five different binary classification algorithms are used to predict the IT graduates' employability using the collected dataset. Because it categorizes new observations into one of two classes. The binary class in our dataset has two values (0) for a not qualified graduate that does not match labor market demands, and (1) for a qualified graduate. The number of records used in this study is 296. We used the following libraries Scikit Learn, Pandas, NumPy, Matplotlib, and Seaborn of the Python programming language. The five classification algorithms are:

Decision Tree Algorithm: is a supervised learning technique equivalent to a series of IF-THEN statements built a structure of branches and nodes based on the evidence obtained for each feature during the method learning process [10]. DT algorithm generates decision trees from training data to solve classification and regression problems. In our proposed model, the Gini method was used to create split points by finding a decision rule that produces the greatest decrease in impurity at a node.

$$G(t)=1-\sum_{i=1}^c p_i^2 \quad (1)$$

where $G(t)$ is the Gini impurity at node t and p_i is the proportion of observations of class c at node t . Recursively, this decision-making process is carried out until all leaf nodes are pure or a certain cutoff is achieved.

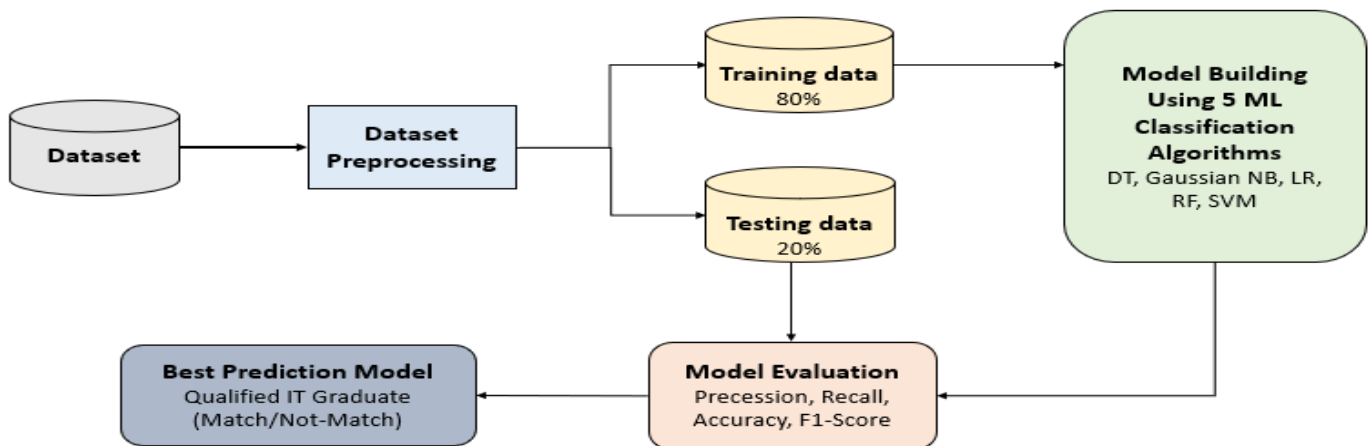


Fig. 1. The Research Methodology.

TABLE II. DESCRIPTION OF DATA FEATURES

Category	Feature	Values	Description
Trainings	Internship	(0,1)	A professional learning experience that provides meaningful work experience related to a student's field of study or career interest for a limited period of time.
	Summer training		A period spent in a reputable company to gain relevant skills and experience in a particular field is usually conducted during July and August of each year.
	Workshops		A period of discussion in which people work on a particular subject by discussing it or doing activities relating to it.
	Co-curricular activities		The activities and learning experiences that take place in the university along with the academic curriculum by students to enhance their skills.
Soft skills	Problem-solving	(0,1)	The act of defining a problem; finding the cause of the problem; identifying, prioritizing, and selecting alternatives for a solution; and implementing a solution.
	Creative thinking		The ability to generate new solutions to problems.
	Time management		The process of planning and organizing how much time to spend on specific activities.
	English proficiency		The ability to use and understand spoken and written English.
Hard skills	Data security	(0,1)	The practice of protecting digital information.
	Network security		The practice of protecting networks and data.
In-demand skills	Data Analytics	(0-7)	The student's knowledge and experience gained in those fields are based on their years of studies at the university through curricula and practical applications of them.
	Artificial Intelligence (AI)		
	Internet of Things (IoT)		
	Machine Learning (ML)		
	Cybersecurity		
	Data Science		
	Cloud Computing		

Gaussian Naïve Bayes (Gaussian NB) algorithm: is a variant of Naive Bayes it is a probabilistic machine learning algorithm used for many classification functions and is based on the Bayes theorem and has a strong assumption that predictors should be independent of each other [13]. The likelihood of the features in our proposed model is assumed to be Gaussian:

$$P(x_i|y) = \frac{1}{\sqrt{2\pi\sigma_y^2}} \exp\left(-\frac{(x_i - \mu_y)^2}{2\sigma_y^2}\right) \quad (2)$$

Where the parameters σ_y and μ_y are estimated using maximum likelihood.

1) *Random forest algorithm*: is a supervised learning algorithm. It can be used both for classification and regression. This model first generates a forest of random trees. The aim of voting to merge random trees in a forest is to eliminate the most predicted tree. If a dataset contains x features, it first chooses a random feature known as y . The algorithm then attempts to merge trees based on the expected outcome and voting procedure [20]. We used the Gini method as mentioned in (1).

2) *Logistic Regression (LR) algorithm*: A LR uses regression analysis, in this method a class variable that is binary classified is required for the logistic regression model [17]. Similarly, the target column named the employability class in this dataset holds two types of binary numbers "0" for a not-qualified IT graduate who has no chance of being employable to meet labor market demands, and "1" for the IT graduate who has been predicted to be qualified and match

labor market requirements. In our proposed model, a linear model is included in a logistic function as follows:

$$P(y_i=1|X) = \frac{1}{1+e^{-(\beta_0+\beta_1x)}} \quad (3)$$

where $P(y_i = 1 | X)$ is the probability of the i th observation's target value, y_i , being class 1, X is the training data, β_0 and β_1 are the parameters to be learned, and e is Euler's number. The logistic function's goal is to interpret its output as a probability by limiting its value to a range between 0 and 1.

3) *Support Vector Machine algorithm (SVM)*: in SVM the classes in the dataset should be pre-defined in this model. It works by using predefined classes to classify the objects in the given dataset. It categorizes transactions by allocating one or more classes in order to increase performance accuracy [21]. We used the linear SVC (Linear Support Vector Classification).

D. Model Evaluation

To evaluate the model effectiveness, a confusion matrix with true positive (TP), false positive (FP), true negative (TN), and false negative (FN) for predicted data is formed. The performance of the study is measured with respect to the accuracy, precision, recall, and F1 score. A brief description of each is described below:

Accuracy: It is a common metric for evaluating classifier performance. It computes the ratio of correctly classified instances to the total number of instances [8]. Its formula is as follows:

$$\text{Accuracy} = \frac{TP+TN}{TP+FP+TN+FN} \quad (4)$$

Precision: is the ratio of true positive instances divided by the total number of instances predicted as positive [22].

$$\text{Precision} = \frac{TP}{TP+FP} \quad (5)$$

Recall: is given as the ratio of relevant instances that are retrieved [22].

$$\text{Recall} = \frac{TP}{TP+FN} \quad (6)$$

F1 score: it is the combination of both precision and recall used to get the average value of them [20].

$$\text{F1 score} = 2 * \frac{\text{precision} * \text{recall}}{\text{precision} + \text{recall}} \quad (7)$$

IV. RESULTS AND DISCUSSION

After data pre-processing, according to the methodology used, out of the total 296 graduates collected, 80% of the data was used as a training dataset, and 20% was kept as a test dataset. The findings related to this study are presented as follows. Fig. 2 shows the correlation matrix for the used features.

The distribution of the employability class (qualified and not qualified) graduates used in this study is illustrated in Fig. 3 the value 0 represents the number of not qualified graduates while 1 represents the number of qualified graduates. From the figure, it may be shown that most involved samples are “not qualified” graduates (82%) than the “qualified” graduates (18%).

In Fig. 4, we present the participants’ distribution in terms of the features that represent the trainings taken during the graduates’ years of study. According to the internship, a total of 11 participants were trained and qualified. Furthermore, 15 participants referred to this training although they were not qualified. A total of 12 participants were trained and qualified because of the summer training. Moreover, the 105 participants referred to this training even though they were not qualified. According to the co-curricular activities, a total of 41 participants were trained and qualified. Whereas 168 participants referred to this training given the fact that they were not qualified. Lastly, 37 people were trained and qualified during the workshops. And 82 participants referred to this training despite the reality that they were not qualified.

Fig. 5 illustrates the participants’ distribution in terms of the features that represent the soft skills the graduates have

been trained or during their years of study. As stated by the problem-solving skills a total of 39 participants were trained and qualified. As well as a number of 110 participants referred to this skill although they were not qualified. Referring to creative thinking skills, a total of 33 participants were trained and qualified. Also, a number of 74 participants referred to this skill although they were not qualified. Based on time management skills, a total of 37 participants were trained and qualified. Moreover, a number of 107 participants referred to this skill although they were not qualified. According to English proficiency skills, a total of 43 participants were trained and qualified. In addition, a number of 102 participants referred to this skill although they were not qualified.

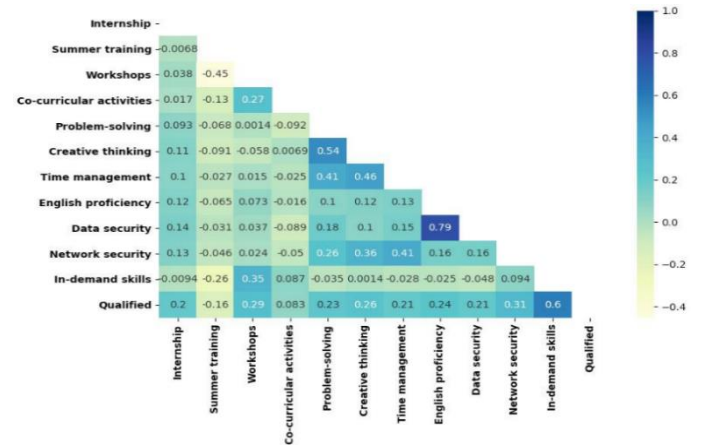


Fig. 2. Correlation Matrix of Selected Features.

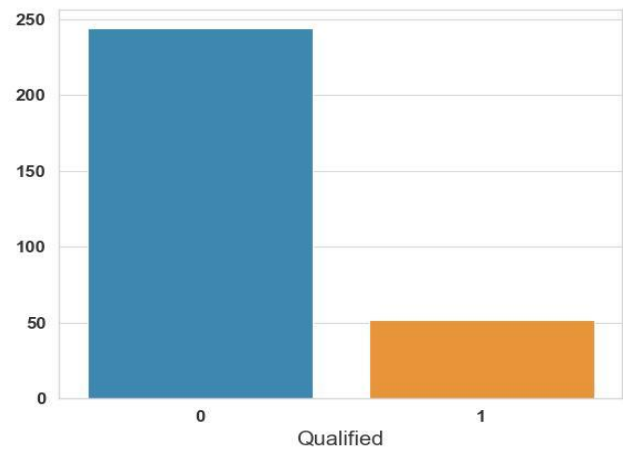


Fig. 3. Count of Employability Class (Qualified/Not Qualified).

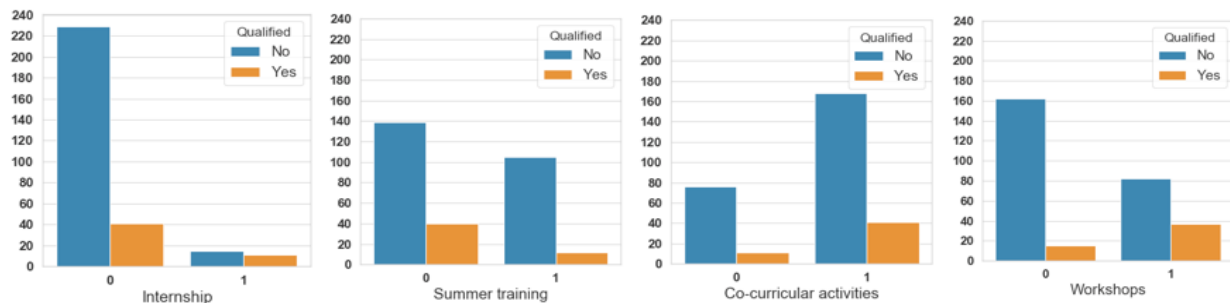


Fig. 4. Respondents' Distribution in Terms of Trainings.

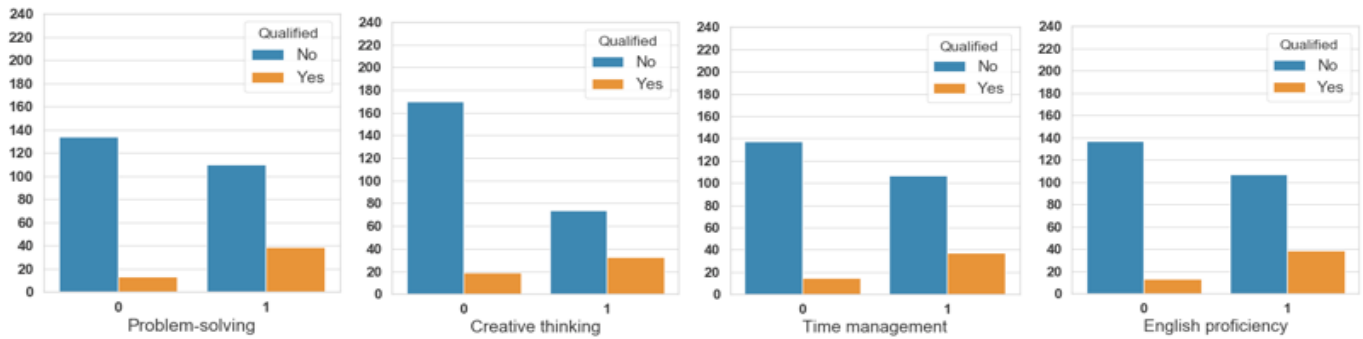


Fig. 5. Respondents' Distribution in Terms of Soft Skills.

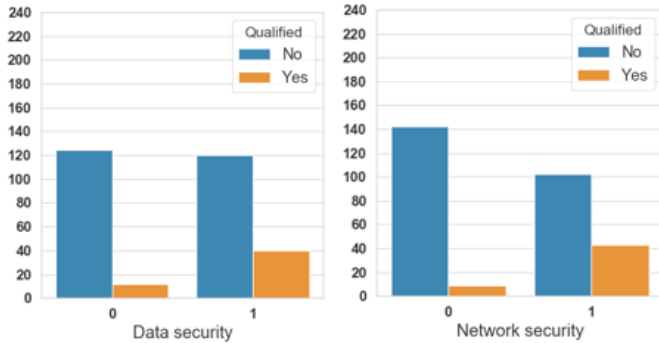


Fig. 6. Respondents' Distribution in Terms of Hard Skills.

Fig. 6 depicts the participants' distribution in terms of the features that represent the hard skills the graduates have been trained on during their years of study. According to the data security skills, a total of 39 participants were trained and qualified. Furthermore, a number of 107 participants referred to this skill although they were not qualified. A total of 40 participants were trained and qualified in network security skills, whereas a number of 120 participants referred to this skill although they were not qualified.

Fig. 7 demonstrates the participants' distribution in terms of the features that represent the in-demand skills required by the industry from the employers' perspectives of the graduates who have been trained on or given a specific course during their years of study. The 0 value means a total of 2 participants did not take any of those skills and were qualified to match labor market requirements whereas 114 participants did not take any of them and found themselves not qualified to be employable. Based on value 7, a total of 7 participants took the seven demanded skills, and they were qualified. Therefore, there are no participants who took those seven skills who were not qualified.

We applied five machine learning classification algorithms for predicting IT graduates' employability. The confusion matrix for each model is illustrated in Table III. Fig. 8 shows the outcome prediction.

Table III reveals that the DT model predicts the highest number of true positives (52 out of 59 test samples) among the five models. Furthermore, LR and SVM models predict the highest number of true negatives (13 among 59 test samples). The lowest number of false positives (0 out of 59 samples) is achieved by DT, RF, and SVM, respectively. The DT,

Gaussian NB, and LR obtained the lowest number of false negatives (0 among 59).

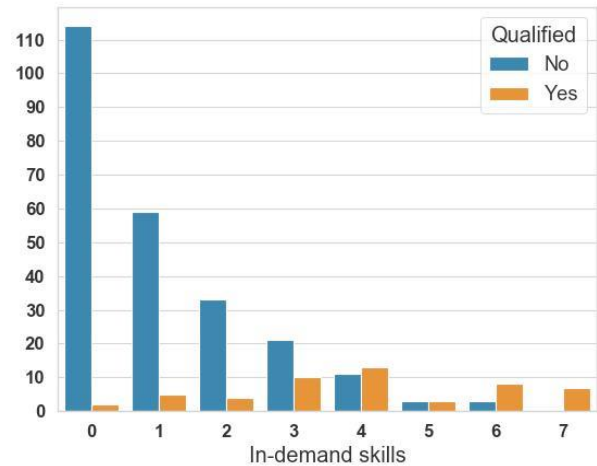


Fig. 7. Respondents' Distribution in Terms of in-demand Skills.

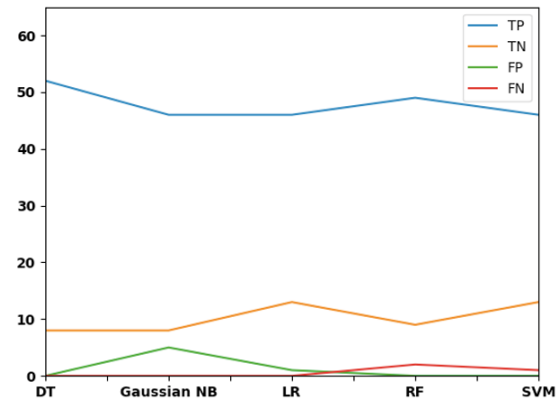


Fig. 8. Confusion Matrix for the Five Machine Learning Models.

TABLE III. CONFUSION MATRIX FOR THE MACHINE LEARNING CLASSIFICATION MODELS

	DT	Gaussian NB	LR	RF	SVM
TP	52	46	46	49	46
TN	8	9	13	9	13
FP	0	5	1	0	0
FN	0	0	0	2	1

The model performance for the employability target class in the form of a confusion matrix is presented in Table IV. In this table, the Match Class “1” means the graduates have chances of being employable and matching the labor market demands. On the other side, Not Match Class “0” denotes the graduates having no chance of being employable, the values of the row illustrating the prediction computed for both classes. As a result, the class precision, recall, and f1 score values are computed and displayed in the table. The class recall and precision values can be used to determine the classifier's overall accuracy. According to the table values, the DT classifier has the highest precision and recall, while the Gaussian NB classifier has the lowest.

The performance of the study was evaluated in terms of accuracy, precision, recall, and F1 score. The calculated performance measures are shown in Fig. 9 and Table V.

RQ2: what are the best machine learning algorithms for employability prediction of IT graduates?

Fig. 9 and Table V indicate that DT outperformed all other machine learning algorithms with a maximum accuracy of 100%, while LR and SVM achieved the second highest accuracy of 98%. DT outperformed by precision, recall, and F1 score of 100%. The second highest F1 score is achieved by LR and SVM at 98%. The second highest precision is achieved by SVM, and the second highest recall is achieved by LR. Most of the techniques have an F1 score higher than 93%, which is comparatively better.

TABLE IV. EVALUATION OF EMPLOYABILITY CLASS (QUALIFIED / NOT QUALIFIED)

Decision Tree Algorithm			
	Precision	Recall	F1 score
Match (1)	1	1	1
Not Match (0)	1	1	1
Gaussian Naive Bayes Algorithm			
	Precision	Recall	F1 score
Match (1)	0.64	1	0.78
Not Match (0)	1	0.9	0.95
Logistic Regression Algorithm			
	Precision	Recall	F1 score
Match (1)	0.93	1	0.96
Not Match (0)	1	0.98	0.99
Random Forest Algorithm			
	Precision	Recall	F1 score
Match (1)	1	0.82	0.9
Not Match (0)	0.96	1	0.98
Support Vector Machine Algorithm			
	Precision	Recall	F1 score
Match (1)	1	0.93	0.96
Not Match (0)	0.98	1	0.99

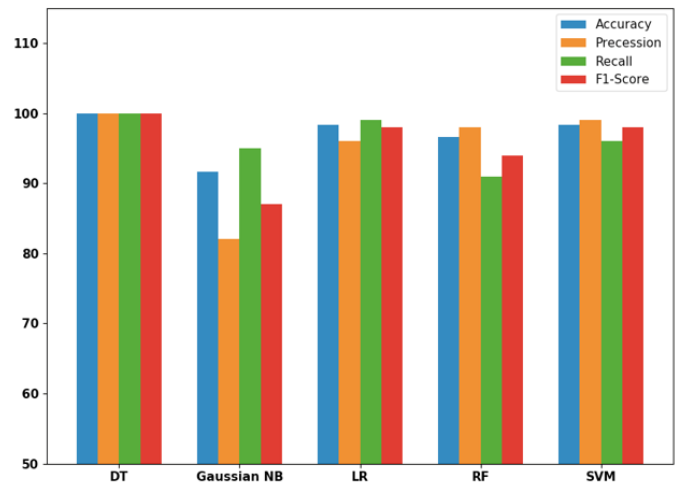


Fig. 9. Performance Measurement using Five Machine Learning Algorithms.

TABLE V. PERFORMANCE EVALUATION OF THE FIVE MACHINE LEARNING ALGORITHMS

	DT	Gaussian NB	LR	RF	SVM
Accuracy	1	0.92	0.98	0.97	0.98
Precision	1	0.82	0.96	0.98	0.99
Recall	1	0.95	0.99	0.91	0.96
F1 score	1	0.87	0.98	0.94	0.98

V. CONCLUSION

The number of information technology graduates produced by higher education institutions has been increasing every year. To overcome their unemployment situation and the mismatch between HEIs outputs and the labor market demands, there is a need for a model that can predict IT graduates' employability to match labor market requirements using machine learning techniques. Therefore, this paper proposed, discussed, and implemented five machine learning classification algorithms namely DT, Gaussian NB, LR, RF, and SVM.

This study achieved high accuracy than earlier works. The highest accuracy is achieved by DT with 100% and the second highest accuracy is achieved by LR and SVM with 98%, whereas the lowest accuracy with 92% achieved by Gaussian NB. The small size of the dataset is the main limitation of this study. From the study, we can conclude that machine learning techniques can predict IT graduates' employability with high accuracy.

The proposed model can be useful and helpful for higher education institutions to make better long-term plans for producing graduates who are knowledgeable, skilled, and fulfill the labor market needs. The findings of the features analysis indicated that moderating the curriculum to include the demanded skills required by industry and improving the teaching and learning methods by offering more training that would produce quality graduates in the following years. Also, the proposed model will be helpful for employers to contribute significantly to the placement process.

For further research, the size of the used dataset can be expanded, and various ML algorithms can be used to get better performance.

REFERENCES

- [1] H. B. Kenayathulla, N. A. Ahmad, and A. R. Idris, "Gaps between competence and importance of employability skills: evidence from Malaysia," *Higher Education Evaluation and Development*, vol. 13, no. 2, pp. 97–112, 2019. doi: 10.1108/heed-08-2019-0039.
- [2] F. Biagi, J. Castaño Muñoz, and G. Di Pietro, "Mismatch Between Demand and Supply Among Higher Education Graduates in the EU," *JRC Tech. Rep.*, pp. 1–21, 2020, doi: 10.2760/003134.
- [3] R. Assaad, C. Krafft, and D. Salehi-Isfahani, "Does the type of higher education affect labor market outcomes? Evidence from Egypt and Jordan," *High. Educ.*, vol. 75, no. 6, pp. 945–995, Jun. 2018, doi: 10.1007/s10734-017-0179-0.
- [4] M. I. Hossain, K. S. A. Yagamaran, T. Afrin, N. Limon, M. Nasiruzzaman, and A. M. Karim, "Factors Influencing Unemployment among Fresh Graduates: A Case Study in Klang Valley, Malaysia," *Int. J. Acad. Res. Bus. Soc. Sci.*, vol. 8, no. 9, Oct. 2018, doi: 10.6007/IJARBS/v8-i9/4859.
- [5] H. Pallathadka et al., "Materials Today : Proceedings Investigating the impact of artificial intelligence in education sector by predicting student performance," *Mater. Today Proc.*, vol. 51, pp. 2264–2267, 2022, doi: 10.1016/j.matpr.2021.11.395.
- [6] H. Zeineddine, U. Braendle, and A. Farah, "Enhancing prediction of student success: Automated machine learning approach," *Comput. Electr. Eng.*, vol. 89, 2021, doi: 10.1016/j.compeleceng.2020.106903.
- [7] M. E. Oswald-Egg and U. Renold, "No experience, no employment: The effect of vocational education and training work experience on labour market outcomes after higher education," *Econ. Educ. Rev.*, vol. 80, 2021, doi: 10.1016/j.econedurev.2020.102065.
- [8] O. Saidani, L. J. Menzli, A. Ksibi, N. Alturki, and A. S. Alluhaidan, "Predicting Student Employability Through the Internship Context Using Gradient Boosting Models," *IEEE Access*, vol. 10, pp. 46472–46489, 2022, doi: 10.1109/ACCESS.2022.3170421.
- [9] L. S. Hugo, "Predicting Employment Through Machine Learning." <https://www.naceweb.org/career-development/trends-and-predictions/predicting-employment-through-machine-learning/> (accessed Oct. 18, 2022).
- [10] Z. Othman, S. W. Shan, I. Yusoff, and C. P. Kee, "Classification Techniques for Predicting Graduate Employability," *Int. J. Adv. Sci. Eng. Inf. Technol.*, vol. 8, no. 4–2, p. 1712, Sep. 2018, doi: 10.18517/ijaseit.8.4-2.6832.
- [11] M. Alghamlas and R. Alabduljabbar, "Predicting the Suitability of IT Students' Skills for the Recruitment in Saudi Labor Market," in 2019 2nd International Conference on Computer Applications & Information Security (ICCAIS), May 2019, pp. 1–5. doi: 10.1109/CAIS.2019.8769577.
- [12] A. Dubey and M. Mani, "Using Machine Learning to Predict High School Student Employability – A Case Study," in 2019 IEEE International Conference on Data Science and Advanced Analytics (DSAA), Oct. 2019, pp. 604–605. doi: 10.1109/DSAA.2019.00078.
- [13] M. S. Kumar and G. P. Babu, "Comparative Study of Various Supervised Machine Learning Algorithms for an Early Effective Prediction of the Employability of Students," *J. Eng. Sci.*, vol. 10, no. 10, pp. 240–251, 2019.
- [14] C. D. Casuat and E. D. Festijo, "Identifying the Most Predictive Attributes among Employability Signals of Undergraduate Students," *Proc. - 2020 16th IEEE Int. Colloq. Signal Process. its Appl. CSPA 2020*, no. May, pp. 203–206, 2020, doi: 10.1109/CSPA48992.2020.9068681.
- [15] K. B. Aviso, J. I. B. Janairo, R. I. G. Lucas, M. A. B. Promentilla, D. E. C. Yu, and R. R. Tan, "Predicting higher education outcomes with hyperbox machine learning: what factors influence graduate employability?," *Chem. Eng. Trans.*, vol. 81, no. 2019, pp. 679–684, 2020, doi: 10.3303/CET2081114.
- [16] A. Bai and S. Hira, "An intelligent hybrid deep belief network model for predicting students employability," *Soft Comput.*, vol. 25, no. 14, pp. 9241–9254, Jul. 2021, doi: 10.1007/s00500-021-05850-x.
- [17] M. D. Laddha, V. T. Lokare, A. W. Kiwelekar, and L. D. Netak, "Performance Analysis of the Impact of Technical Skills on Employability," *Int. J. Performability Eng.*, vol. 17, no. 4, p. 371, 2021, doi: 10.23940/ijpe.21.04.p5.371378.
- [18] D. Jagan Mohan Reddy, S. Regella, and S. R. Seelam, "Recruitment Prediction using Machine Learning," in 2020 5th International Conference on Computing, Communication and Security (ICCS), Oct. 2020, pp. 1–4. doi: 10.1109/ICCS49678.2020.9276955.
- [19] S. R. Rahman, M. A. Islam, P. P. Akash, M. Parvin, N. N. Moon, and F. N. Nur, "Effects of co-curricular activities on student's academic performance by machine learning," *Curr. Res. Behav. Sci.*, vol. 2, no. May, p. 100057, 2021, doi: 10.1016/j.crbeha.2021.100057.
- [20] A. Alhassan, B. Zafar, and A. Mueen, "Predict Students' Academic Performance based on their Assessment Grades and Online Activity Data," *Int. J. Adv. Comput. Sci. Appl.*, vol. 11, no. 4, 2020, doi: 10.14569/IJACSA.2020.0110425.
- [21] C. D. Casuat, "Predicting Students' Employability using Support Vector Machine: A SMOTE-Optimized Machine Learning System," *Int. J. Emerg. Trends Eng. Res.*, vol. 8, no. 5, pp. 2101–2106, May 2020, doi: 10.30534/ijeter/2020/102852020.
- [22] P. Thakar, P. Dr., and D. Manisha, "Role of Secondary Attributes to Boost the Prediction Accuracy of Students' Employability Via Data Mining," *Int. J. Adv. Comput. Sci. Appl.*, vol. 6, no. 11, 2015, doi: 10.14569/IJACSA.2015.061112.

Otsu's Thresholding for Semi-Automatic Segmentation of Breast Lesions in Digital Mammograms

Moustapha Mohamed Saleck¹

LAROSERI Laboratory, Computer Sciences Department
Faculty of Sciences, University of Chouaib Doukkali
EL Jadida, Morocco

M. H. Ould Mohamed Dyla²

Computer Sciences Department
IUP, University of Nouakchott
Nouakchott, Mauritania

EL Benany Mohamed Mahmoud³

Department of Mathematics and Computer Science
FST, University of Nouakchott
Nouakchott, Mauritania

Mohamed Rmili⁴

Computer Sciences Department
Faculty of Sciences, University of Chouaib Doukkali
EL Jadida, Morocco

Abstract—In Maghreb countries, breast cancer considered one of the leading causes of mortality between females. A screening mammogram is a method of taking low energy level x-ray images of the human breast to identify the early symptoms of breast cancer. The shape and contour of the lesion in digitized mammograms are two effective features that allow the radiologists to distinguish between benign and malignant tumors. We propose in this paper a new approach based on Otsu's thresholding method for semi-automatic extraction of lesion boundaries from mammogram images. This approach attempts to find the best threshold value where the weighted variance between the lesion and normal tissue pixels is the least. In the first step, the median filter is used for removing noise within the region of interest (ROI). In the second step, a global threshold decrement was started in order to get the proper range of pixels in which the breast lesion could be segmented by Otsu's thresholding method with high accuracy. The technique of mathematical morphology, especially opening operation is used in this work for removing small objects from the ROI while preserving the shape and size of larger objects that represent the tumors. We evaluated our proposal using 21 images obtained from Mini-MIAS database. Experimental results show that our proposal achieves better results than many previously explored methods.

Keywords—Tumor detection; lesion segmentation; mammogram images; Otsu's thresholding

I. INTRODUCTION

According to the statistics published in 2020 by World Health Organization (WHO) [1] Breast cancer is classified as one of the most common cancer and a leading cause of deaths among women worldwide. The study given by WHO show that 2.3 million women about the world were subjected to diagnosis of breast cancer in 2020, and almost 29.1% of this rate died out (685 000 deaths globally). Mortality rates for breast cancer are increasing at fast and no way to treat this disease yet except early detection that can help in increasing the survival rate. Different modalities of medical imaging

have been used as screening tools for detecting and diagnosis of breast cancer, such as mammography, ultrasound, magnetic resonance imaging (MRI), nuclear medicine imaging, optical imaging, and breast microwave imaging [2]. Mammography is considered as one of the most commonly used tests for detecting breast cancer at early stages [3], it can often help find breast cancer early and reveal different abnormalities before any symptoms appear. The shape and contour of mass represent one of the most important information in analyze of mammograms. Breast mass segmentation has a key role in determining the nature of lesion since the mass having regular shapes have a high probability of being benign and the mass having irregular shapes have a high probability of being malignant. There are many challenges to detect mass contour in mammograms due to several factor including: normal breast tissues seemed to be similar to lesions, low contrast, fuzzy nature of the boundaries, complicated structured background.

In the present study, we introduce a new approach for breast masses segmentation in mammographic images, in this approach we apply Otsu's method in appropriate range of pixels limited by the maximum value of intensity and an optimal threshold where the output of Ostu is made up of two clusters one of them represents the lesion with high contour accuracy. Our proposal is titled semiautomatic because the regions of interest (ROI) are selected manually by expert breast radiologist.

The scheme proposed in this study combines the median filter, Otsu's thresholding and mathematical morphology (opening operation). The remainder of this paper is organized as follows: Section II presents related state-of-the-art works; Section III presents the proposed exploration scheme of breast lesion boundaries from digital mammograms. Section IV shows the experimental results. In Section V we discuss about the results. Finally, the conclusions of this work are presented in Section VI.

II. RELATED WORK

The success of lesion contour detection is directly associated with the choice of the measures and methods. Various approaches have been proposed in the literature for mass segmentation in mammographic images. N.Soliman et al. [4] developed a framework for processing of mammogram images, in their work the authors have used 2D median filter to remove digitization noise from images and morphological operations to remove artifacts, they have used also a fuzzy enhancement technique for contrast enhancement and Otsu's multiple thresholding method for mammogram segmentation. Wessam M. Salama et al. [5] proposed a new framework for breast cancer image segmentation and classification. InceptionV3, DenseNet121, ResNet50, VGG16 and MobileNetV2 models are utilized to classify Mammographic Image, then the modified segmentation of the U-Net model is used for the segmentation process. V. Punithavathi et al. [6] proposed an approach based on Optimized Kernel Fuzzy Clustering Algorithm (OKFCA) to determine the cancer portions in mammogram images, After applying the Hybrid Denoising Filter (HDF) Algorithm in preprocessing, the proposed OKFCA is carried out to find out the cancer segment of mammogram image. J. Anitha et al. [7] presented a new approach based on the global adaptive thresholding to locate the suspicious regions in mammogram images. This optimal global threshold (Dual Stage Adaptive Thresholding (DuSAT)) is selected adaptively by maximizing between-class standard deviation, calculated from the gray level of the preprocessed image through the histogram peak analysis (HPA) of the entire image. Damian Valdés-Santiago et al [8] proposed two algorithms for mass boundaries extraction from mammogram images : a lesion segmentation approach based on a Fuzzy C-means modification using image histogram, and a selection criteria to choose candidate lesions that will serve as input to a classifier based on a binary decision tree. H Azary et al. [9] proposed a semi-supervised technique for mass segmentation in mammogram images in which the authors extracted the pixel information such as : the static, gray level run length matrix features and Fisher discriminant analysis (FDA) to use it in the process of classification. After that, they used a co-training algorithm based on support vector machine and Bayes classifiers for tumor segmentation. In [10] Mohammed Y. Kamil et al. applied two algorithms of the clustering approach were applied to three images from Mini-MIAS Database for determining the boundaries of the tumor. the first is the K-means method and the second is the C-means method, in addition, the lazy snapping algorithm is applied to improve the performance of segmentation of suspect area. The results showed that the second algorithm of clustering is better than the first algorithm in terms of accuracy. In [11] M. Ramli et al. suggested a hybrid method of tumor boundary detection in mammogram images. After noise suppression by using median filter method, the Contrast-Limited Adaptive Histogram Equalization (CLAHE) technique have used for image contrast enhancement. in the first stage of segmentation, the watershed transform technique is applied to extract the original region of interest (ROI), and then, the authors employed the region growing algorithm in determining the tumor's boundaries. R. S. C. Boss, et al. [12] extracted 14 Haralick texture features from mammogram

image using GrayLevel Co-occurrence Matrix (GLCM) for different angles with distance $d = 1$. Fuzzy c-means and K-means algorithms are used to classify texture features in order to segment the region of interests (ROI) for further classification. T.Sadad et al. [13] employed the cascading of Fuzzy C-Means (FCM), morphological operations and region-growing (RG) method for extracting the tumor located in mammograms, the Local Binary Pattern Gray-Level Co-occurrence Matrix (LBP-GLCM) and Local Phase Quantization (LPQ) are also been used for feature extraction. S. S. Ittannavar et al. [14] developed a new multiobjective optimization technique for breast lesions segmentation in mammogram images. The developed model contains three phases: image collection from Digital Database for Screening Mammography (DDSM) and Mammographic Image Analysis Society (MIAS), image enhancing using Contrast-Limited Adaptive Histogram Equalization (CLAHE) techniques, and finally electromagnetism-like (EML) optimization technique is used to detect noncancer and cancer portions on mammograms. In [15] S.H Suradi et al. used Fuzzy Anisotropic Diffusion Histogram Equalization Contrast Adaptive Limited to enhance the breast lesions by reducing the image noise. Then, a Multilevel Otsu Thresholding is applied to detect breast lesions using the e region of interest tool at different intensity levels. T.L.V.N.Swetha et al. [16] developed an approach based on tow combined methods for tumor edges detection, the first is Hybrid image segmentation based on fast sweeping algorithm and dual front evolution with laplacian or gradient, the second is Otsu's thresholding with 10 threshold levels. A.K.Khan et al. [17] proposed an approach based on improved Otsu method and discrete wavelet transform (DWT) for breast lesion detection in mammograms, in their work the adaptive median filtering and adaptive histogram equalization were used in preprocessing step. In [18] M.M.Saleck et al. developed a semi-automatic segmentation of breast masses on mammogram images using the algorithm of Fuzzy C-Means where the number of clusters is known in advance without estimation, the authors play on the set of pixels that subject to clustering by decrement global threshold to obtain the best results of segmentation. The major disadvantage of this approach is the long execution time that it takes, the present work overcome this drawback by providing another approach based on Otsu's thresholding with less execution time.

III. MATERIALS AND METHODS

In this part of paper, we explain the techniques that were used in this study for the detection of lesions boundaries on a mammogram. The methodology comprises the following stages: Image preprocessing. Starts the process of decrement a global threshold and applying Otsu method in each step of decrement operation on the set of selected pixels (input_pixels) that exist between the maximum intensity value and the global threshold. Identify the best value of global threshold for determining the optimal segmentation by applying morphological opening to suppress undesirable objects.

Fig. 1 shows a schematic diagram of the proposed method.

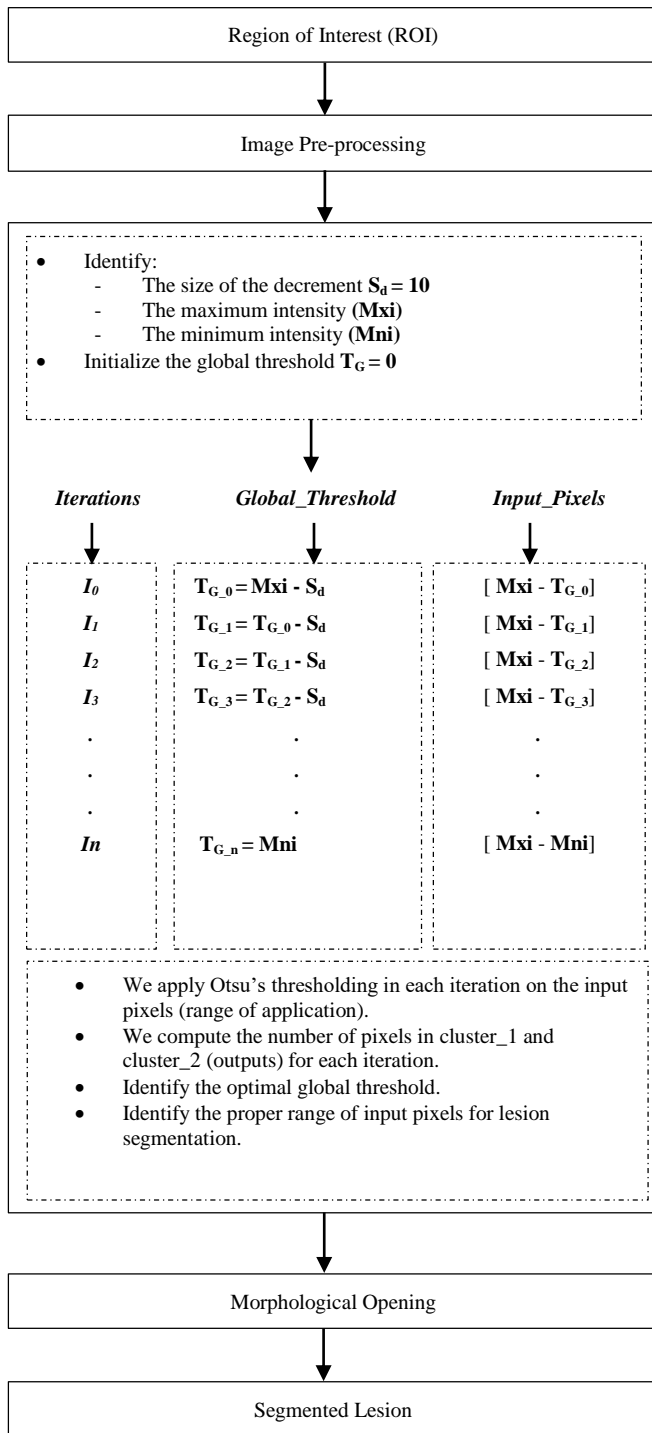


Fig. 1. Block Diagram of the Proposed Method.

A. Region of Intersect Selection

The breast mammography images used to test our proposed methods were extracted from the Mammographic Image Analysis Mini-Mammographic Database (Mini-MIAS) [19]. The dataset includes 322 digital mammograms, the size of each mammogram from the database was reduced to become 1024×1024 , with 8-bits grey scale level and a spatial resolution of 200-micron pixel edge. The ground truth (GT) of these mammograms have been manually extracted by a

radiologist and all abnormalities have been identified and classified. The Region of Interest (ROI) represent the place where abnormalities are identified. In this paper, we use the region of interest with a size of 174×174 pixels, the value 174 is chosen in consultation with the radiologist because it is the radius of the largest mass present in the database [20].

B. Image Pre-processing

Preprocessing steps are very necessary and should be applied before any image-processing technique to ensure a high level of accuracy without any influences from background [21]. Digital mammograms are medical images that are difficult to be interpreted due to the dynamics of intensity and noise appears in images provided by different patients. The basic enhancement required in digital mammograms is denoising [22]. A median filter is a nonlinear filtering technique, it is very effective at removing impulse noise, pepper noise and Gaussian noise. Its strength lies in its ability to keep the sharpness of the image at the time of enhancement. Potency of median filter depends on the size of window [23]. In this work, we applied a median filter with a simple sliding-window of size 3×3 in order to provide smart result in proposed algorithms.

C. Morphological Operations

Morphological Operations is the set of image processing operations that follows the goal of eliminating all the imperfections and maintaining image structure. These techniques include opening operation which is a process that applies erosion on an input image and then dilates the eroded image using the same kernel in both operations. The morphological opening could be used for removing small objects and thin lines in the segmentation results. In this work, we apply morphological opening to retain only the biggest region that represents the tumor with accuracy.

D. Breast Mass Segmentation by Otsu's Thresholding

Otsu's segmentation is a non-parametric and unsupervised technique proposed by Nobuyuki Otsu [24]. It is an automatic threshold selection method that maximizes the between-class variance in order to segment the image into classes using optimum threshold values. To threshold a given image presented in L gray levels, $[0, 1, 2, \dots, L - 1]$ into two classes C_1 and C_2 , we select a threshold k , $0 < k < L - 1$. Where the range $[0, k]$ represent the intensity of pixels for the first class (C_1), while the second class (C_2) is presented by the pixels that have intensity values within the range $[k + 1, L - 1]$.

$P_1(k)$, represent the probability that a pixel is assigned to first class (C_1).

$$P_1(k) = \sum_{i=0}^k P_i \quad (1)$$

$P_2(k)$, represent the probability that a pixel is assigned to second class (C_2).

$$P_2(k) = \sum_{i=k+1}^{L-1} P_i \quad (2)$$

The mean intensity values of classes C_1 and C_2 are defined as:

$$m_1(k) = \sum_{i=0}^k \frac{i P_i}{P_1(k)} \quad (3)$$

$$m_2(k) = \sum_{i=k+1}^{L-1} \frac{i P_i}{P_2(k)} \quad (4)$$

Otsu method tries to minimize the weighted within-class variance defined as:

$$\sigma_\omega^2(k) = m_1(k)\sigma_1^2(k) + m_2(k)\sigma_2^2(k) \quad (5)$$

The variances for classes C_1 and C_2 are defined as:

$$\sigma_1^2(k) = \sum_{i=0}^k [i - m_1(k)]^2 \frac{i P_i}{P_1(k)} \quad (6)$$

$$\sigma_2^2(k) = \sum_{i=k+1}^{L-1} [i - m_2(k)]^2 \frac{i P_i}{P_2(k)} \quad (7)$$

It's difficult to extract the boundaries of masses from mammogram images by using the classic Otsu thresholding technique only except in rare cases, due to the low difference between normal and abnormal tissue in mammograms. Fig. 2 shows the result of segmentation by using the classic Otsu thresholding.

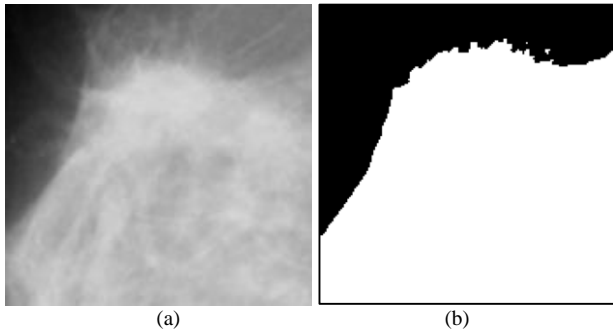


Fig. 2. Lesion Segmentation using Classic Otsu's Thresholding: (a) Original Image (mdb_95 from MIAS). (b) Result of Segmentation (mdb_95).

The fuzzy nature of the mammographic images and the low contrast due to masses obscuration by tissue overlap make the automatic process of lesion boundaries extraction very difficult. To overcome this limitation, we propose in this paper a new approach based on Otsu thresholding where the sets of pixels that will subject to clustering by Otsu thresholding are limited by two parameters:

- The first limit (upper limit) of the range of pixels is the maximum value of intensity, because the suspicious lesions in mammogram image having a high-intensity values compared to other regions.
- The second limit (lower limit) of the range is a global threshold, where all pixels in the ROI with intensities below this threshold value are turned off (will not be subject to process of thresholding by Otsu method).

To threshold a given set of pixels within the range $[Mxi - T_G]$ into clusters C_1 and C_2 by Otsu's thresholding where:

- Mxi is the maximum of intensity in the ROI.
- T_G is a global threshold.

We select a threshold k , $T_G < K < L - 1$, where:

- $[T_G, K]$ represent the intensity of pixels for the first cluster C_1 .
- $[K + 1, Mxi - 1]$ represent the intensity of pixels for the second cluster C_2 .
- $P_1(k)$, represent the probability that a pixel is assigned to first class (C_1).

$$P_1(k) = \sum_{i=T_G}^k P_i \quad (8)$$

- $P_2(k)$, represent the probability that a pixel is assigned to second class (C_2).

$$P_2(k) = \sum_{i=k+1}^{Mxi-1} P_i \quad (9)$$

- The mean intensity values of C_1 and C_2 are defined as:

$$m_1(k) = \sum_{i=T_G}^k \frac{i P_i}{P_1(k)} \quad (10)$$

$$m_2(k) = \sum_{i=k+1}^{Mxi-1} \frac{i P_i}{P_2(k)} \quad (11)$$

- The variances for classes C_1 and C_2 are defined as:

$$\sigma_1^2(k) = \sum_{i=T_G}^k [i - m_1(k)]^2 \frac{i P_i}{P_1(k)} \quad (12)$$

$$\sigma_2^2(k) = \sum_{i=k+1}^{Mxi-1} [i - m_2(k)]^2 \frac{i P_i}{P_2(k)} \quad (13)$$

Run through the full range of k values $[T_G - Mxi]$ and pick the value that minimizes $\sigma_\omega^2(k)$ defined in eq. (5).

In this approach, we start the decrement of the global threshold (T_G) from the maximum intensity (Mxi) in ROI until the minimum value of intensity (Mni) in ROI with a step size $S_d = 10$. Choosing a small decrement step size leads to very slow execution time, however, takes a large decrement step value effects on the segmentation accuracy. To balance between these two points and after many tests, we have deduced that $S_d = 10$ is the optimal value of the decrement step.

Fig. 3 shows the original images from MIAS. Fig. 4 represents the application of the proposed Otsu method on different sets of pixels where each one of these sets exists within a range limited by the maximum intensity and global threshold.

The optimal global threshold (the second limit of the range of input-pixels) is getting by tracking the changes in the number of pixels that belong to each output-cluster during the process of increase in the set of pixels that subject to clustering by Otsu's thresholding. Tables I and II shows the evolution in the number of pixels that belongs to cluster_1 and cluster_2 at each iteration t_i , also the different values of global thresholds and Otsu thresholds for mdb_10 and mdb_134.

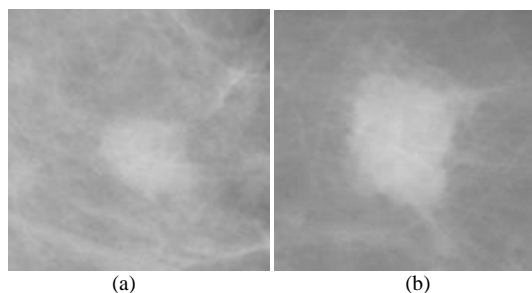


Fig. 3. Original Images: (a) mdb_10 from MIAS (Max Intensity = 206, Min Intensity = 118). (b) mdb_134 from MIAS (Max Intensity = 208, Min Intensity = 119).

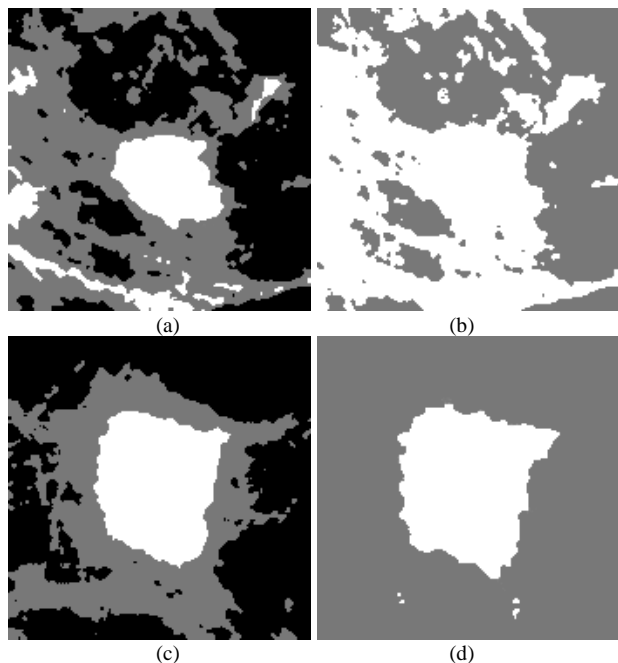


Fig. 4. Application of the Proposed Otsu Method in different Ranges of Pixels. (a) (b): mdb_10 from MIAS. (c) (d): mdb_134 from MIAS. White: Cluster_1. Dark Gray: Cluster_2. Black: Outside the Range (Not Subject to otsu thresholding).

The evolution curves in the following figures (Fig. 5 and Fig. 6) illustrates the changes in the number of pixels of clusters that happen at each iteration t_i .

TABLE I. EVOLUTION OF THE NUMBER OF PIXELS IN CLUSTER 1 AND CLUSTER 2 FOR IMAGE MDB 10 FROM MIAS

Image: mdb_10 from MIAS Database				
The maximum value of intensity (Mxi) = 206				
The minimum value of intensity (Mni) = 118				
Range of pixels	Number of pixels in cluster_1	Number of pixels in cluster_2	Global threshold (T_G)	Otsu threshold
t_1 : [206 - 196]	176	448	196	200
t_2 : [206 - 186]	883	1124	186	194
t_3 : [206 - 176]	1685	4320	176	188
t_4 : [206 - 166]	3875	13288	166	180
t_5 : [206 - 156]	6637	19369	156	177

t_6 : [206 - 146]	6805	22768	146	176
t_7 : [206 - 136]	11734	18119	136	170
t_8 : [206 - 126]	15834	14359	126	167
t_9 : [206 - 118]	15834	14442	118	167

TABLE II. EVOLUTION OF THE NUMBER OF PIXELS IN CLUSTER 1 AND CLUSTER 2 FOR IMAGE MDB 134 FROM MIAS

Image: mdb_134 from MIAS Database				
The maximum value of intensity (Mxi) = 208				
The minimum value of intensity (Mni) = 119				
Range of pixels	Number of pixels in cluster_1	Number of pixels in cluster_2	Global threshold (T_G)	Otsu threshold
t_1 : [208 - 199]	270	554	198	202
t_2 : [208 - 188]	1379	1777	188	196
t_3 : [208 - 178]	2324	2043	178	192
t_4 : [208 - 168]	3441	2068	168	186
t_5 : [208 - 158]	4146	3661	158	180
t_6 : [208 - 148]	4918	10438	148	173
t_7 : [208 - 138]	5361	21398	138	169
t_8 : [208 - 128]	5753	24266	128	166
t_9 : [208 - 119]	6060	24216	119	164

Nbr of pixels

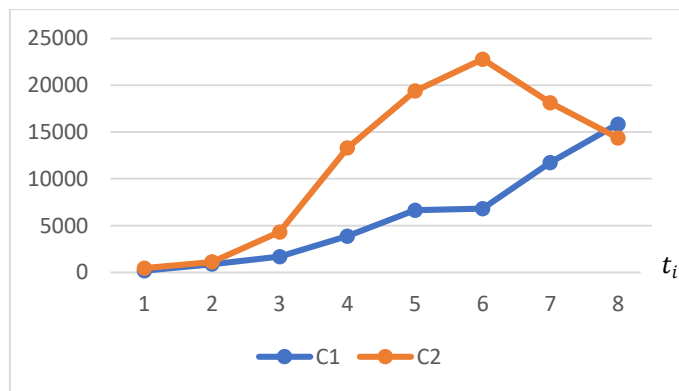


Fig. 5. Evolution of Cluster 1 and Cluster 2 for mdb 10.

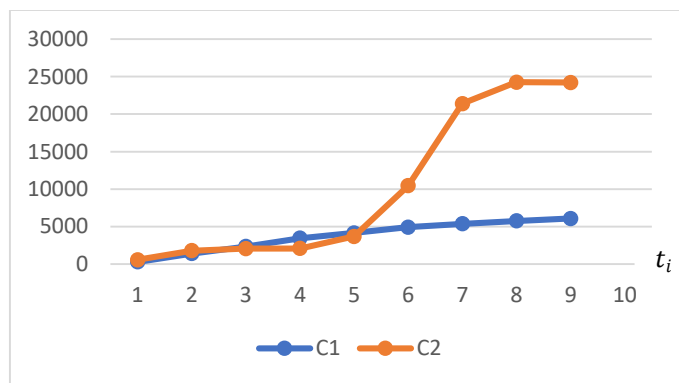


Fig. 6. Evolution of Cluster 1 and Cluster 2 for mdb 134.

After tracing the evolutionary changes in the number of pixels for both clusters (C1 and C2) on 22 images tested in this study, we can distinguish two different sorts of results:

- The first one represents the majority of the cases; this one is characterized by an increase in the number of pixels of cluster 1 and cluster 2 followed by an abrupt decrease in cluster 2. The optimal global threshold for this kind of case is the value that happens an abrupt decrease in cluster 2. Ex: Fig. 5 (mdb 10) the best value of the global threshold is $T_G = 146$ at iteration $t=6$, therefore, the appropriate range of pixels that allow us to get two clusters where the cluster 1 represent the lesion with accuracy in this example is [206 - 146].
- The second is characterized by an increase continues in cluster 2, those cases are rare. The optimal global threshold for this kind is the minimum value of intensity (Mni) in the region of interest (ROI). Ex: Fig. 6 (mdb 134) the best value of the global threshold is the minimum intensity $T_G = 119$.

After finding the suitable range of pixels that can generate high accuracy of lesion boundaries after applying the proposed Otsu method, we apply morphological operations to remove all defects and preserve the region having the highest intensity in cluster 1 that represents the lesion.

IV. EXPERIMENTAL RESULTS

In this section, we present the experimental results for breast mass segmentation in mammogram images using the proposed method. A testing data set of 21 images taken from mini-MIAS database of mammograms were used in this study to test and evaluate the performance of the proposed approach. Three experienced radiologists have intervened for delineating manually the lesions margins. The obtained results in Fig. 7 shows that lesion border extracted by the proposed algorithm approximately follows the lesion contour marked by the radiologists.

To evaluate the efficiency of the proposed algorithm, four performance evaluation metrics were adopted in this paper, such as: overlap, sensitivity, specificity and accuracy [25].

$$\text{Accuracy} = \frac{TP+TN}{TP+TN+FP+FN} \times 100 \quad (14)$$

$$\text{Overlap} = \frac{TP}{TP+FP+FN} \times 100 \quad (15)$$

$$\text{Sensitivity} = \frac{TP}{TP+FN} \times 100 \quad (16)$$

$$\text{Specificity} = \frac{TN}{FP+FN} \times 100 \quad (17)$$

Table III displays the results of metrics of lesion segmentation obtained for measurement the performance of the proposed approach. Table IV presents the comparison with other techniques.

The proposed method is implemented on Python 3.9.5, Pycharm community edition 2021.2.2. The computer used in this work is Dell PC with Processor Intel(R) Core (TM) i5-5300U CPU 2.30GHz (4 CPUs), and 8G Ram.

The average processing time required for completing the process of segmentation using the proposed algorithm is 1.91 s, the runtime time for this approach is less 2 times than the segmentation of breast lesions using Fuzzy c-means algorithm proposed in [18] (Fig. 8).

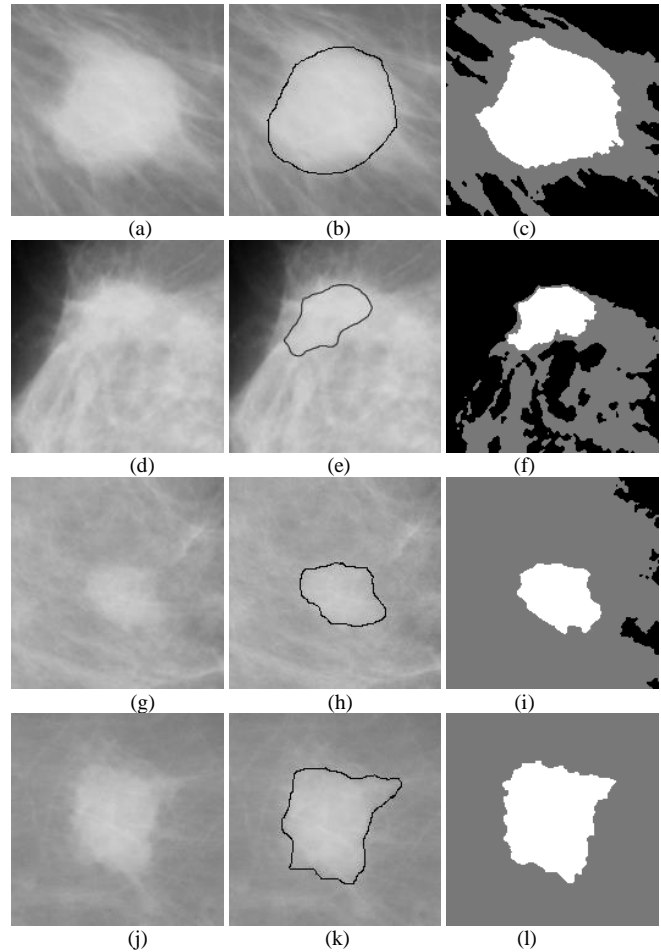


Fig. 7. (a)(d)(g)(j) The Original Mammograms. (b)(e)(h)(k) Lesions Outlines Marked by Radiologist. (c)(f)(i)(l) Lesions Extracted by the Proposed Algorithm.

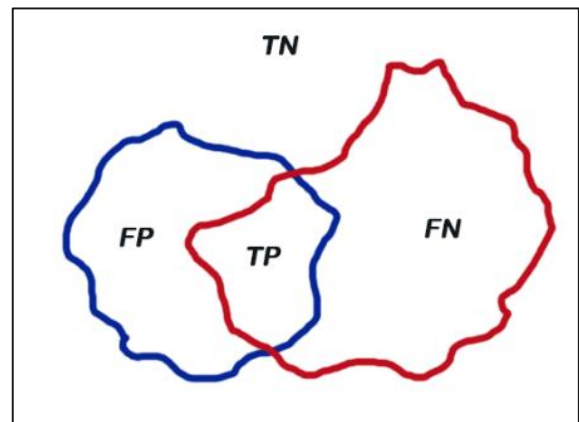


Fig. 8. The Red Contour: Lesion Outlined by a Radiologist. The Blue Contour: Lesion Outlined by a System. TP: True Positives. TN: True Negatives. FP: False Positives. FN: False Negatives.

TABLE III. PERFORMANCE RESULTS OF SEGMENTATION

Number of lesions	21 images from mini-MIAS			
	Accuracy	Overlap	Sensitivity	Specificity
22	95.06 %	80.92 %	97.16 %	73.41 %

TABLE IV. COMPARISON WITH OTHER TECHNIQUES

Methods	Overlap	Accuracy	Sensitivity	Specificity
Proposed method	80.92 %	95.06 %	96.16 %	73.41 %
Watershed and region growing : [26]	80.3 %	91.5 %	91 %	94.35 %
Fuzzy c-means and K-means : [10]	--	91.18 %	--	--
Deep learning : [27]	--	98 %	--	--
Region growing : [28]	79 %	91 %	83 %	97 %

V. DISCUSSION

This study presents a new approach for extracting masses from ROI of digital mammogram images, aiming to assist the radiologist in the identification of the lesion. This approach is based on increasing the set of pixels that subject to clustering by decrement a global thresholding. This processing allows to test the different values of global thresholds in order to obtain the best value. The aim is to select as input the meaningful pixels that can produce in output a clearly delineated lesion after applying Otsu thresholding and morphological operations. In comparing the results of segmentation for mdb_95 from Mini-MIAS database using classic Otsu thresholding illustrated in Fig. 2 and the results of segmentation for the same image showed in Fig. 7(f), we can deduce the efficiency of the proposed method. The strength of this method lies in its ability to eliminate the set of pixels that can have negative effects on the process of segmentation by choosing a suitable global threshold. The run-time of the proposed algorithm is considerably less than the execution time for the proposed method in [18]. This speed of execution compared to fuzzy c-means is due to the simplicity of the Otsu method in terms of algorithm complexity.

VI. CONCLUSION

Breast cancer is the most common type of cancer among women around the world and is the second leading of death after prostate and lung cancer. We aim behind our researches, to develop new methods for helping the radiologists in diagnostic of breast cancer. In this study, we propose a new approach for breast lesion boundary segmentation for a given region of interest (ROI) in mammographic images. The proposed algorithm is an extended version of classical Otsu's technique with additional capability to dynamically change the number of input-pixels that subject to thresholding in order to get the proper set of pixels which can produce as output a segmented lesion with high accuracy. The results obtained in this work show the proposed algorithm outperforms many other methods of breast masses segmentation in performance and that it is faster than the fuzzy c-means technique.

REFERENCES

- [1] S. R. et al Sung H, Ferlay J, "No TitleGlobal cancer statistics 2020: GLOBOCAN estimates of incidence and mortality worldwide for 36 cancers in 185 countries," CA Cancer J Clin, vol. 71, pp. 209–249, 2021, doi: <https://doi.org/10.3322/CAAC.21660>.
- [2] S. Iranmakani et al., "A review of various modalities in breast imaging: technical aspects and clinical outcomes," Egypt. J. Radiol. Nucl. Med., vol. 51, no. 1, 2020, doi: 10.1186/s43055-020-00175-5.
- [3] H. G. Welch, P. C. Prorok, A. J. O'Malley, and B. S. Kramer, "Breast-cancer tumor size, overdiagnosis, and mammography screening effectiveness," N. Engl. J. Med., vol. 375, no. 15, pp. 1438–1447, 2016.
- [4] N. F. Soliman, N. S. Ali, M. I. Aly, A. D. Algarni, and W. El-shafai, "An Efficient Breast Cancer Detection Framework for Medical Diagnosis Applications An Efficient Breast Cancer Detection Framework for Medical," no. September 2021, 2022, doi: 10.32604/cmc.2022.017001.
- [5] W. M. Salama and M. H. Aly, "Deep learning in mammography images segmentation and classification: Automated CNN approach," Alexandria Eng. J., vol. 60, no. 5, pp. 4701–4709, 2021, doi: 10.1016/j.aej.2021.03.048.
- [6] V. Punithavathi and D. Devakumari, "Materials Today : Proceedings A new proposal for the segmentation of breast lesion in mammogram images using optimized kernel fuzzy clustering algorithm," Mater. Today Proc., no. xxxx, 2021, doi: 10.1016/j.matpr.2020.11.931.
- [7] J. Anitha, J. D. Peter, and S. I. A. Pandian, "A dual stage adaptive thresholding (DuSAT) for automatic mass detection in mammograms," Comput. Methods Programs Biomed., vol. 138, pp. 93–104, 2017.
- [8] D. Vald and A. Le, "Mammographic Mass Segmentation Using Fuzzy C – means and Decision Trees," pp. 1–10, 2018.
- [9] O. Article, "A Semi - Supervised Method for Tumor Segmentation in Mammogram Images," 2020, doi: 10.4103/jmss.JMSS.
- [10] M. Y. Kamil, "Mammography Images Segmentation via Fuzzy C-mean and K-mean," vol. 12, no. 1, pp. 22–29, 2019, doi: 10.22266/ijies2019.0228.03.
- [11] M. Rmili, A. El Moutaouakkil, and M. M. Saleck, "Hybrid Mammogram Segmentation Using Watershed and Region Growing," in Advances in Information, Communication and Cybersecurity, 2022, pp. 23–32.
- [12] R. S. C. Boss, K. Thangavel, and D. A. P. Daniel, "Mammogram image segmentation using fuzzy clustering," Int. Conf. Pattern Recognition, Informatics Med. Eng. PRIME 2012, no. March, pp. 290–295, 2012, doi: 10.1109/ICPRIME.2012.6208360.
- [13] T. Sadad, A. Munir, T. Saba, and A. Hussain, "SC," J. Comput. Sci., 2018, doi: 10.1016/j.jocs.2018.09.015.
- [14] S. S. Ittannavar and R. H. Havaladar, "Segmentation of Breast Masses in Mammogram Image Using Multilevel Multiobjective Electromagnetism-Like Optimization Algorithm," Biomed Res. Int., vol. 2022, p. 8576768, 2022, doi: 10.1155/2022/8576768.
- [15] S. H. Suradi, K. A. Abdullah, and N. A. M. Isa, "Breast Lesions Detection Using FADHECAL and Multilevel Otsu Thresholding Segmentation in Digital Mammograms BT - CMBEBIH 2021," 2021, pp. 751–759.
- [16] T. L. V. N. Swetha and C. H. H. Bindu, "Detection of Breast cancer with Hybrid image segmentation and Otsu's thresholding," 2015 Int. Conf. Comput. Netw. Commun. CoCoNet 2015, no. 2008, pp. 565–570, 2016, doi: 10.1109/CoCoNet.2015.7411244.
- [17] A. K. Khan, "Wavelet Based Automatic Lesion Detection Using Improved OTSU Method," vol. 2, pp. 119–127, 2014.
- [18] M. M. Saleck, A. El Moutaouakkil, M. Moucouf, M. Bouchaib, H. Samira, and J. Zineb, "Breast mass segmentation using a semi-automatic procedure based on Fuzzy C-Means clustering," Telkomnika (Telecommunication Comput. Electron. Control., 2018, doi: 10.12928/TELKOMNIKA.v16i2.6193.
- [19] J. Suckling et al., "The Mammographic Image Analysis Society digital mammogram database," 1994.
- [20] K. Vaidehi and T. S. Subashini, "Automatic characterization of benign and malignant masses in mammography," Procedia Comput. Sci., vol.

- 46, no. Ict 2014, pp. 1762–1769, 2015, doi: 10.1016/j.procs.2015.02.128.
- [21] M. Sundaram, K. Ramar, N. Arumugam, and G. Prabin, “Histogram based contrast enhancement for mammogram images,” in 2011 International Conference on Signal Processing, Communication, Computing and Networking Technologies, 2011, pp. 842–846, doi: 10.1109/ICSCCN.2011.6024667.
- [22] A. Makandar and B. Halalli, “Breast Cancer Image Enhancement using Median Filter and CLAHE,” *Int. J. Sci. Eng. Res.*, vol. 6, no. 4, pp. 462–465, 2015, [Online]. Available: <http://www.ijser.org>.
- [23] R. E. W. Rafael C. Gonzalez, *Digital Image Processing*, Third edit. 2007.
- [24] N. Otsu, “A threshold selection method from gray-level histograms,” *IEEE Trans. Syst. Man. Cybern.*, vol. 9, no. 1, pp. 62–66, 1979.
- [25] K. Byrd, J. Zeng, and M. Chouikha, “Performance assessment of mammography image segmentation algorithms,” *Proc. - Appl. Imag. Pattern Recognit. Work.*, vol. 2005, pp. 152–157, 2005, doi: 10.1109/AIPR.2005.39.
- [26] M. Rmili, A. El Moutaouakkil, and M. M. Saleck, “Hybrid Mammogram Segmentation Using Watershed and Region Growing BT - Advances in Information, Communication and Cybersecurity,” 2022, pp. 23–32.
- [27] S. Li, M. Dong, G. Du, and X. Mu, “Attention Dense-U-Net for Automatic Breast Mass Segmentation in Digital Mammogram,” *IEEE Access*, vol. 7, pp. 59037–59047, 2019, doi: 10.1109/ACCESS.2019.2914873.
- [28] M. Rmili, A. El Moutaouakkil, M. M. Saleck, M. Bouchaib, F. Adnani, and E. M. E. Aroussi, “A new approach to the detection of mammogram boundary,” *Int. J. Electr. Comput. Eng.*, vol. 8, no. 5, pp. 3587–3593, 2018, doi: 10.11591/ijece.v8i5.pp3587-3593.

Performance Analysis of Software Test Effort Estimation using Genetic Algorithm and Neural Network

Vikas Chahar, Prof. Pradeep Kumar Bhatia
G. J. University of Science and Technology, Hisar, Haryana, India

Abstract—In present scenario, the software companies are frequently involving software test effort estimation to allocate the resources efficiently during the software development process. Different machine learning models are developed to estimate the total effort that would be required before the software product could be delivered. These computational models are used to use the past data to estimate the efforts. In the current studies, test effort estimation for software is predicted using the Genetic algorithm and Neural Network. The attributes are selected using the Genetic algorithm and similarity measure between the attribute values has been computed using the Cosine Similarity measure. The simulation experiments were done using the PROMISE and Kaggle repository and implementation was done using the MATLAB software. The performance metrics namely, precision, recall, and accuracy are computed to evaluate against the existing techniques. The accuracy of the proposed model is 91.3% and results are improved by 8.9% in comparison to existing technique and comparison has been made for superiority to predict the test effort for software development.

Keywords—Test effort estimation; software testing; machine learning; computational intelligence; neural network

I. INTRODUCTION

The success of a software project mainly depends on the determination of effort for software development [1]. The cost of the software can be computed by determining the efforts for the development of software. Software engineering is the study of techniques, quantifiable approach, software maintenance, and quantifiable approach during the development phase: application of engineering for software testing. The software testing plays a very significant role and accounts almost 50% for the total development in effort estimation.

Software testing allows the evaluation of attributes or system capability in determining the requirements to meet the desired results [2]. Software testing is mainly categorized as static and dynamic testing. In the former testing phase, testing has been done without executing the project and it is related to prevention of defects [3]. The documentation estimation is cheap and code assessment is provided in addition. Moreover, it also includes checklist, estimation of variety of errors, operated in the initial phase, and completion of 100% coverage of statement within less time. In the later testing phase, dynamic testing is very expensive, testing has been done during the execution of the project and it is related to fixing the defects [4]. The bugs estimation and assessment of bottleneck is provided whenever this phase is operated later or in the last phase of the

project. Moreover, it also includes test cases, fixing the variety of errors, and completion of 50% coverage of statement. The primary motive of testing the software is to eliminate the bugs and improve the software security and other aspects such as performance, user satisfaction level, and experience. Furthermore, test effort estimation is necessary for the test process and plays a crucial role in the operation of software development life cycle. Software effort estimation allows the organization to provide or allocate the necessary resources accordingly. The best testing deal not only improves the overall quality but also enhances the customer satisfaction level. In a competitive market, there is a need to determine the highly reliable software effort estimates. In the software project development phase, the accurate estimation allows the success of the project [5]. Further, the cost of the software is estimated using the software effort required for the development of the software. In the literature, there were large number of techniques proposed to predict the software effort accurately. The estimation of software effort is helpful for the allocation of resources in a proper manner. The estimation of software effort in terms of month and day per person, duration of the project is very difficult to predict the project cost. It is crucial to negotiate with the customer by estimating the cost and effort in an accurate manner.

A. Computational Intelligence Techniques for Software Effort Estimation

Inaccurate prediction of software effort and cost usually results in huge financial loss and even in the failure of the project. However, there are number of techniques developed in the past such as expert judgement, machine learning techniques, fuzzy technique, and regression analysis [6]–[8] to minimize the instances of inaccurate prediction. Most of these techniques were based on the algorithmic models such as COCOMO and analogy-based estimation of effort techniques. The analogy techniques generally include the use of different characteristics such as size, interfaces, and effort of new project is estimated by determining the details of project of similar type. Furthermore, there are different techniques designed for different datasets as no single technique is applicable for all the datasets. In this process, programming language, development technique, programmer experience, tools etc. play a significant role in governing the software effort estimate. For instance, soft computing models are used to deal with computational problems and metaheuristic techniques are used to resolve the complex optimization issues [9], [10]. The evolution of neural network, fuzzy logic, support vector machine, optimization

technique, machine learning, chaotic theory, etc. fall under the category of computational intelligence models as shown in Fig. 1 [11].

Computational techniques proved fruitful results in predicting the attributes of software quality. In the past year, the computational models were developed and applied in software engineering to solve the different problems such as determining the prediction of change in software, prediction of stakeholder satisfaction, and estimation of reliability for component-based software projects. The estimation of test effort is generally performed by using the templates of Work Breakdown Structure (WBS) that fragments the project into sub-tasks. The analysis of each task during the testing phase allows the determination of defects and underlying errors. The project requirements are designed, and testing phase has been analyzed thoroughly to avoid any defect. This required a detailed overview of the project prototype and analyzing each task by coordinating with the stakeholders. This generally takes around 1.5-2 weeks to perform test effort estimation. However, employing the machine learning techniques for effort estimation eases the process in a fast manner and it is generally computed by determining the overall time to the total inputs given for the completion of the project. The proposed technique introduces the novel method by integrating the machine learning with genetic algorithm for the effort estimation of software testing. The contributions of the proposed work are summarized as follows: -

- Machine learning techniques are integrated for estimation of software effort.
- A novel combination of Genetic algorithm with Machine Learning is used to predict the software effort.
- Two datasets are employed to evaluate the computational strengths of the designed work.

The rest of the paper is organized as Section II that illustrates the related work, Section III that describes the research methodology including the different datasets and discusses the technique used for software test effort estimation. Section IV illustrates the results and finally concluded in Section V.

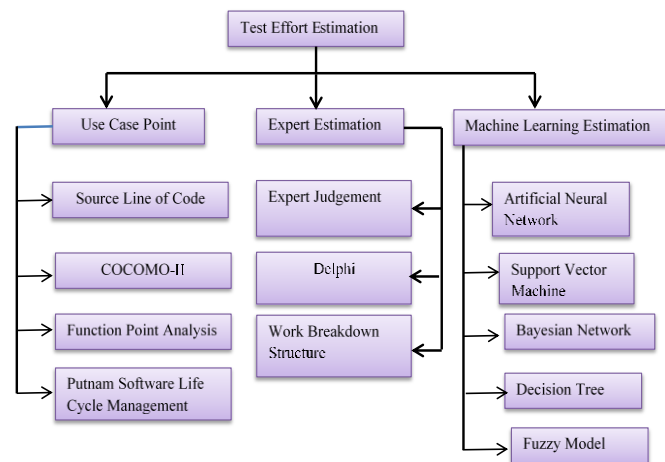


Fig. 1. Test Effort Estimation Models.

II. RELATED WORK

The estimation of effort involved in the software development is a crucial activity for monitoring the project cost, time, and quality as well as for the software development life cycle. As a result, proper estimating was crucial to the success of projects and to lowering risks. Software effort estimation has drawn a lot of research interest recently and has become a problem for the software industry. Many academics and industry professionals have suggested statistical and machine learning-based approaches for estimating software effort over the past 20 years.

Saljoughinejad and Khatibi, 2018 had taken advantage of three metaheuristic techniques to enhance the effort accuracy estimations associated with the COCOMO model. The concept of metaheuristics mainly focused on the detailed analysis of the involved cost drivers involved in the effort estimation. The study had reflected that the integration of techniques such as PSO, Invasive Weed Optimization and GA had significantly improved the accuracy measures associated with estimations. However, despite of better performance, the work was unable to meet the desired level due to instability issues [12].

Nassif et al. 2019 compared the three different fuzzy models to estimate the software effort. The authors designed the models and conduct the regression analysis to evaluate the performance of the proposed system. The evaluation of the proposed regression fuzzy logic was measured by measuring the criteria such as standardized accuracy, effect size, and relative error. The authors used the ISBSG dataset, and it was estimated that different projects have similar size with better productivity ratio. The mean for effort dataset 1 was 883.5 and effort dataset 4 was 706 with a standard deviation of about 1194 with a skewness of about 5.8. Further, Scott Knott test was performed to determine the validity and best performance achieved using the Suzzeno fuzzy model [7].

Ghatasheh et al. 2019, evolutionary algorithms called the Firefly Algorithm was presented for optimising the parameters of three COCOMO-based models. The authors used the NASA dataset in which 30% data was tested and 60% data was trained to acquire the adequate objectives. The proposed model and two additional models that was suggested in the literature as expansions of the fundamental COCOMO model. The evaluation results using the Firefly algorithm show better accuracy. The limitation of the study was instability issues, prediction model; dataset type was affected by size [13].

Chhabra and Singh 2020 had proposed integration of non-algorithmic modelling for software effort estimation based on soft computing approaches. In the process, they had integrated genetic algorithm followed by fuzzy logic and utilized the COCOMO dataset for the evaluation of the designed work architecture. It has been observed that due to improved selection owing to the GA fitness function a 25% reduction has been observed in Mean Magnitude of Relative Error. This high improvement was mainly due to increased stability of GA in optimizing the fuzzy model that improved the overall prediction accuracy for the effort estimation [14].

Öztürk et al. 2021, a feed forward DNN algorithm (FFDNN) was put forth in this article. Finding hyperparameter was done using a binary-search-based technique in the algorithm. In the experiment using two performance parameters, FFDNN performs better than five comparative algorithms. The study's findings indicate that: 1) Using conventional techniques like grid and random search significantly lengthens tuning time. Instead, sophisticated parameter search techniques that was compatible with the structure of regression methods should be developed; 2) SEE performance was improved when the associated hyperparameter search technique was designed in accordance with the key principles of selected deep learning approach; and 3) Deep learning models outperform tree-based regression techniques like CART DE8 in terms of CPU time. The drawback of the study was that tuning time need to plan along with pruning of network [11].

Karimi and Gandomani 2021 This research introduces a new fuzzy inference technique and the differential evolution (DE) algorithm. To estimate software development labor, more precisely, this approach is capable of providing a more accurate estimate for software projects than earlier efforts using the COCOMO model. The suggested approach outperformed existing optimization algorithms derived from genetic, stochastic, conceptual, and Neuro-fuzzy technique, and could increase accuracy using the proposed technique up to 7%. The limitation of the study was assessment criteria and convergence rate, still a challenge for the accurate software effort estimation [15].

Zakaria et al. 2021 had integrated PSO as a swarm intelligence technique to optimize the existing COCOMO II. The optimized set was then fed to different machine learning techniques to evaluate their strength for the prediction of effort using NASA dataset. The machine learning techniques integrated were, Linear Regression (LR), SVM and Random Forest (RF). The simulation analysis had shown that SVM had outperformed the other machine learning techniques in terms of MMRE, accuracy and p-value computed for each of the implemented combination [16].

López-Martín 2022 proposed software testing effort estimation using the machine learning models. The authors investigate the effort of software testing using the datasets stored in the repository. The project selection was entirely based on the rating of data quality, development type, platform, programming language, sizing method, and level of resources for projects. Further, the authors investigate the performance of five machine learning models for software effort estimation using the COCOMO model. The prediction accuracy was computed for different ML techniques such as Neural Network, Decision Tree, Genetic algorithm, SVM and Case based reasoning. The limitation of the study was that software effort estimation depends upon the certain factors such as quality expectations, developer experience, tools and many other that are not sufficient to consider for accurate prediction of software effort estimation [6].

III. RESEARCH METHODOLOGY

The proposed methodology is divided into two parts in which first part Implementation using the Genetic algorithm has

been done and Machine Learning model such as Neural Network toolbox in MATLAB was used for the classification of test effort estimation. The dataset used in this study for implementation are illustrated in the later sections.

A. Dataset

There are several free datasets that were used in the literature such as Kaggle, COCOMO NASA-I, COCOMO NASA-II, Kaggle, and PROMISE [17], [18]. Out of these, Kaggle and Promise datasets have been used in this study. These are further divided into five datasets namely KC1, PC3, PC4, MW1, and CM1 that support these datasets [19]. The PROMISE repository was used to extract the attributes. The dataset is an open source data set and is freely available online [20]. The dataset contains the attributes that are extracted after the operations performed through Object Oriented Programming Architecture (OOPA). As for example, RELY is an attribute that illustrates the reliability of a software and in the similar fashion, RES represents the reusability of the software component. Based on these attribute values, the overall computation effort is also provided. The dataset does not have independent attribute as they have been computed via OOPA. The data retrieval was estimated using the KC1 classes and further defect was analyzed. This study incorporates the Kaggle and PROMISE database datasets that includes different attributes such as KC1, CM1, MW1, PC3, and PC4. The datasets was stored and further assisted for implementation in the MATLAB software. Although, Kaggle and Promise data repository includes the different data, but extraction of relevant data is particularly important before the implementation. Therefore, Cosine similarity technique was applied to extract the data as per requirement for test effort estimation during the software development life cycle.

B. Genetic Algorithm for the Selection of Relevant Attributes

In this study, the relevant attributes have been selected using the Genetic Algorithm which is a heuristic technique employed to avoid the challenges of modelling and optimization techniques. The main features of the GA are to utilize the features of crossover operator and execute the operations to obtain the candidate solutions. The operation steps are graphically illustrated using Fig. 2. The Genetic Algorithm has been applied by considering the following steps: -

- 1) *Start*: The random population is generated considering the n-chromosomes for best solution of the problem. The random population is generated which is of n chromosomes.
- 2) *Fitness*: The fitness function $f(a)$ is evaluated that corresponds to the chromosome (a) in the generated population.
- 3) *New Population*: The new population is initialized by repeating the following steps until the optimal solution is attained.

- *Selection*: The selection has been done by considering the fitness function of two chromosomes and then higher fitness leads to the selection of chromosomes with more possibility.
- *Crossover*: When the probability of crossover crosses then new offspring attained. If there is no crossover, then offspring is a duplicate of parent.

- Mutation: The mutation probability is attained when the new offspring mutates at each position in the population.
 - Accepting: The new offspring has been placed with respect to new population.
- 4) *Replace*: The generated population is utilized considering the aim to execute the new solution.
- 5) *Test*: The best solution has been returned after the current population attained.
- 6) *Loop*: Return to second step.

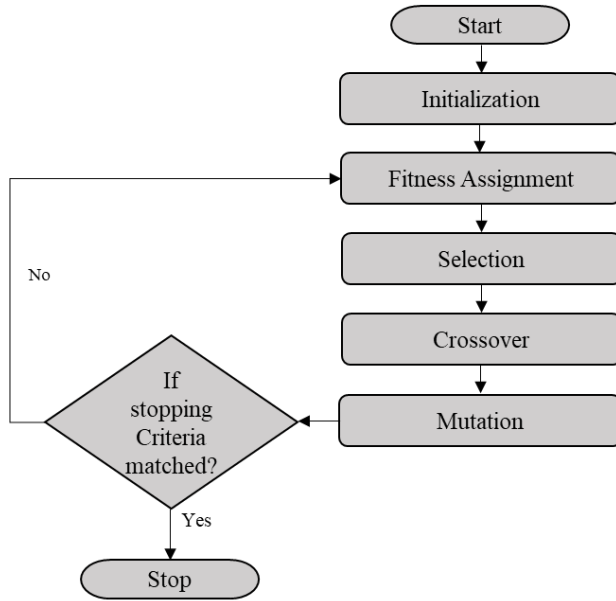


Fig. 2. Operation of GA.

After the operation of GA, further cosine similarity technique has been applied for the selection of similar attributes.

C. Cosine Similarity

Cosine similarity is a technique in which similarity of two documents computed to determine the correlation between the vectors. The information is represented in the vector form that makes the process easier to eliminate the irrelevant data. Furthermore, the angle between the vectors is determined as the cosine angles between the attributes. Cosine similarity is one of the most important similarity measures used for different applications such as clustering, effort estimation, etc. and also used to retrieve essential information. The cosine similarity between two attribute vectors \vec{V}_m and \vec{V}_n is given by;

$$\text{CosSim}(\vec{V}_m \text{ and } \vec{V}_n) = \frac{\vec{V}_m \cdot \vec{V}_n}{|\vec{V}_m| \times |\vec{V}_n|} \quad (1)$$

Here, \vec{V}_m and \vec{V}_n are the n number of dimensional vectors in each term set of $V = \{V_1, V_2, V_3 \dots \dots \dots V_n\}$. Every dimension in the term set includes weight, which is positive, and therefore, the cosine similarity is positive and can be bounded between $\{0,1\}$.

A significant feature of cosine similarity is that it is the independent of its attribute for different set efforts in days or months. For example, integrating two effort values of different days require to obtain a novel attribute value, the cosine similarity between Att' and Att is 1, which indicates that the test effort attributes can be considered identical and can be stored for further processing.

ALGORITHM 2: Cosine Similarity for effort estimation

Input: $data_{files}$

Output: $Cosine\ Similarity_{dataset}$

1. Function: $Cosine\ Similarity_{dataset} = FunctionCosine\ Similarity_{dataset}(data_{records})$
2. // $Cosine\ Similarity_{dataset_relation} = []$;/
3. // $Sim_{count} = 0$; // $identifiedrelationsCount$ / $Similarity\ Index\ calculation\ using\ empty\ array$
4. For $s = 0$ to $data_{records}.count / Totalno.\ of\ data_{records}$
5. $Present_{dataset} = data_{record}(s)$;
6. For $z = 1$ to $totaldata_{records}.count // Nextseries$
7. $P = |Cosine\ Similarity_{dataset}(Present_{catalogue}) - \cos(data_{records}(z))|$;
8. $Cosine\ Similarity_{dataset}[Relation_{count}, 0] = present_catalogue$;
9. $Cosine\ Similarity_{dataset}[Relation_{count}, 1] = data_{records}(z)$;
10. $Cos_{catalogue_relation}[Dataset_{count}, 2] = P$; The similarity value
11. $Simulation_{count} = Sim_{count} + 1$; Count is incremented
12. Endfor;
13. Endfor;
14. Endfunction;

After the extraction of data for software test effort estimation, the data is processed to select the attribute values using the Genetic Algorithm and classification was done later using the Neural Network.

D. Effort Estimation using the Computational Intelligence Models

After the extraction of similar attributes, Neural Network has been applied that contain processing elements that are connected using some weights. It attempts to depict the biological nervous system as per both architectures including information processing logics. This network needs to train first by applying an appropriate learning algorithm for the prediction of weights which are interconnected. After training of weight test signals are classified. The neural network's class used basically for task of classification is called the multilayer perceptron network. The ordinal measures of Neural Networks are as follows (Table I).

TABLE I. ORDINAL MEASURES OF NEURAL NETWORKS

Propagation Architecture	Software test effort estimation
Neuron Count	5-25
Nature of propagation	Progressive
Propagation behaviour model	Levenberg
Root node validation	Mean Squared Error (MSE)
Validation parameters	a) Total number of epochs b) Gradient c) Count of fails in the validation
Cross validation	Linear Regression
Regression equation	$z = ax + b$ (eq hh) Where x is a multi-objective fitness function defined by sigmoid function of neural networks

The neural network propagation is designed using Neural Network toolbox of MATLAB and it is a propagation-based model and hence the number of hidden layers has been varied to check the performance of the network.

ALGORITHM 6: Test effort estimation using the Neural Network (NN)

Input: Optimized feature (T)

Output: Test Effort Estimation Results

1) **Initialization of NN parameters**

$E \rightarrow$ Simulation or Epochs for NN

$N \rightarrow$ Neurons Count

Performance Measure \rightarrow Accuracy, Precision, Recall, and F-measure

Techniques \rightarrow Levenberg Marquardt

Data Division \rightarrow Random

2) **For I = 1 \rightarrow T**

3) **If (T matches with 1st feature category)**

4) Group (1) = Features of training data according to the 1st category

5) **Else if (T matches with 2nd feature category)**

6) Group (2) = Features of training data according to the 2nd category

7) **Else**

8) Group (3) = Extra properties of training data

9) **End-if**

10) **End-for**

11) Initialize the NN using Training data and Group

12) Net = patternet (T, Group, N)

13) Set the training parameters and train the system

14) Net = Train (Net, Training data, Group)

Testing Phase:

15) Current Data = Feature of current efforts in dataset

16) Output = simulate (Net, Current Data)

17) **If Output is valid**

18) **Test Effort Estimation \rightarrow Accurate**

19) **Else**

20) **Test Effort Estimation \rightarrow Inaccurate**

21) **End-if**

22) **Return:** Prediction as an output

Since the NN architecture used multiple hidden layers, therefore the input data is filtered many times and hence chances of providing better results are increased. In this research, the performance of NN is examined and cross-validation outcomes are evaluated.

IV. RESULTS AND DISCUSSION

The performance is evaluated by dividing the total dataset using the separation mechanism of training dataset to testing dataset ratio.

A. Statistical Analysis

The results have been computed using the 70:30, 80:20, and 90:10 ratio analysis. The results obtained using the implemented methodology in which four different performance metrics has been computed as illustrated below: -

$$Precision = \frac{True_{positive\ rate}}{True_{positive\ rate} + False_{positive\ rate}}$$

$$Recall = \frac{True_{positive\ rate}}{True_{positive\ rate} + False_{negative\ rate}}$$

$$F - measure = 2 * \frac{Precision * Recall}{Precision + Recall}$$

$$Accuracy = \frac{True_{positive} + True_{negative}}{True_{positive} + True_{negative} + False_{positive} + False_{negative}}$$

The evaluation has been done to determine the superiority of the proposed approach and labelled dataset has been used which is pre-defined and specific to determine the required outcomes.

Table II shows the Recall, Precision, F-measure, and Accuracy computed using the 70:30 dataset distribution ratio. It is generalized that with increase in the number of projects the recall of the proposed model also gets improved. The proposed model shows a recall of about 0.90% for 80 projects. It is seen that Precision and Recall show 0.9% and 0.91% respectively for 20 projects and 0.90% and 90% for F-measure and Accuracy respectively using the GA and NN. The proposed results for 70:30 analyses are robust and improvised using the Genetic Algorithm in conjunction with NN.

Table III shows the analysis of performance metric computed using the 80:20 ratios. It is generalized that with increase in the number of projects the performance of the proposed model also gets enhanced. The proposed model shows a recall of about 0.93 for 300 projects and F-measure of about 0.92. It is seen that average Precision and Recall show 0.9% and 0.91% respectively and 0.91% and 91% for F-measure and Accuracy respectively using the GA and NN. The proposed

results for 80:20 analyses are robust and improvised using the Genetic Algorithm in conjunction with NN.

TABLE II. PERFORMANCE METRIC OF THE PROPOSED TECHNIQUE USING THE 70:30 RATIO ANALYSIS

Total Number of Projects	Recall	Precision	F-measure	Accuracy
10	0.852212	0.896543345	0.873815768	88.73637
20	0.8604666	0.897088945	0.878396221	88.9276
30	0.8687212	0.897634545	0.882941232	89.11883
40	0.8769758	0.898180145	0.887451329	89.31007
50	0.8852304	0.898725745	0.891927027	89.5013
60	0.893485	0.899271345	0.896368834	89.69253
70	0.9017396	0.899816945	0.900777247	89.88376
80	0.9099942	0.900362545	0.905152751	90.075
90	0.9182488	0.900908145	0.909495825	90.26623
100	0.9195034	0.901453745	0.910389117	90.45746
200	0.920758	0.907999345	0.914334166	90.64869
300	0.9220126	0.914544945	0.91826359	90.83992
400	0.9232672	0.921090545	0.922177588	91.03116
500	0.9245218	0.927636145	0.926076354	91.22239
700	0.9257764	0.934181745	0.92996008	91.41362
1000	0.927031	0.940727345	0.933828955	91.60485

TABLE III. PERFORMANCE METRIC OF THE PROPOSED TECHNIQUE USING THE 80:20 RATIO ANALYSIS

Total Number of Projects	Recall Proposed	Precision Proposed	F-measure	Accuracy
10	0.862212	0.899543	0.880482	88.93637
20	0.870467	0.900089	0.88503	89.1276
30	0.878721	0.900635	0.889543	89.31883
40	0.886976	0.90118	0.894022	89.51007
50	0.89523	0.901726	0.898466	89.7013
60	0.903485	0.902271	0.902878	89.89253
70	0.91174	0.902817	0.907256	90.08376
80	0.919994	0.903363	0.911603	90.275
90	0.928249	0.903908	0.915917	90.46623
100	0.929503	0.904454	0.916807	90.65746

200	0.930758	0.910999	0.920773	90.84869
300	0.932013	0.917545	0.924722	91.03992
400	0.933267	0.924091	0.928656	91.23116
500	0.934522	0.930636	0.932575	91.42239
700	0.935776	0.937182	0.936479	91.61362
1000	0.937031	0.943727	0.940367	91.80485

TABLE IV. PERFORMANCE METRIC OF THE PROPOSED TECHNIQUE USING THE 90:10 RATIO ANALYSIS

Number of Projects	Recall Proposed	Precision Proposed	F-measure	Accuracy
10	0.875412	0.909543	0.892151	89.93637
20	0.883667	0.910089	0.896683	90.1276
30	0.891921	0.910635	0.901181	90.31883
40	0.900176	0.91118	0.905645	90.51007
50	0.90843	0.911726	0.910075	90.7013
60	0.916685	0.912271	0.914473	90.89253
70	0.92494	0.912817	0.918838	91.08376
80	0.933194	0.913363	0.923172	91.275
90	0.941449	0.913908	0.927474	91.46623
100	0.942703	0.914454	0.928364	91.65746
200	0.943958	0.920999	0.932337	91.84869
300	0.945213	0.927545	0.936295	92.03992
400	0.946467	0.934091	0.940238	92.23116
500	0.947722	0.940636	0.944166	92.42239
700	0.948976	0.947182	0.948078	92.61362
1000	0.950231	0.953727	0.951976	92.80485

Table IV shows the analysis of performance metric computed using the 90:10 ratio. It is generalized that with increase in the number of projects the performance of the proposed model also gets improved. The proposed model shows a recall of about 0.94 for 300 projects precision is 0.92 with F-measure of about 0.94. It is seen that average Precision and Recall show 0.92% and 0.91% respectively and 0.91% and 91.3% for F-measure and Accuracy respectively using the GA and NN. The proposed results for 90:10 analysis are robust and improvised using the Genetic Algorithm in conjunction with NN.

Table V shows the comparison of recall analysis with the existing techniques. It is seen that recall for Attri et al. 2019 and without GA show 0.81 and 0.77 respectively for 20 projects. The proposed model exhibited a recall of 0.94 when analysed for 200 projects. Similarly, recall for 1000 projects increases to 0.95 and using Attri et al. work and GA is 0.93 and 0.82 respectively. The overall recall using the proposed approach is 0.92 and 0.86 using the Attri et al. 2019. Thus, the proposed outperformed the existing techniques due to the use of Genetic algorithm and Neural Network.

TABLE V. COMPARATIVE ANALYSIS OF RECALL AGAINST ATTRI ET AL. WORK

Number of Projects	Recall Proposed	Recall Without GA	Recall Attri et al. 2019
10	0.875412	0.77543345	0.81661566
20	0.8836666	0.77597905	0.81902469
30	0.8919212	0.77652465	0.82130693
40	0.9001758	0.78707025	0.82374494
50	0.9084304	0.78761585	0.82596965
60	0.916685	0.78816145	0.82841232
70	0.9249396	0.78870705	0.83274246
80	0.9331942	0.78925265	0.83457478
90	0.9414488	0.78979825	0.83755162
100	0.9427034	0.79034385	0.86264824
200	0.943958	0.79688945	0.88751949
300	0.9452126	0.80343505	0.90388464
400	0.9464672	0.80998065	0.91401356
500	0.9477218	0.81652625	0.92611913
700	0.9489764	0.82307185	0.92945552
1000	0.950231	0.82961745	0.93788335

TABLE VI. COMPARATIVE ANALYSIS OF PRECISION AGAINST ATTRI ET AL. WORK

Number of Projects	Precision Proposed	Precision without GA	Precision Attri et al. 2019
10	0.909543	0.824474	0.8453636
20	0.910089	0.8320093	0.8518202
30	0.910635	0.8395446	0.8582768
40	0.91118	0.8470799	0.8647334
50	0.911726	0.8546152	0.87119
60	0.912271	0.8621505	0.8776466
70	0.912817	0.8696858	0.8841032
80	0.913363	0.8772211	0.8905598
90	0.913908	0.8847564	0.8970164
100	0.914454	0.8922917	0.897473
200	0.920999	0.892827	0.9039296
300	0.927545	0.9003623	0.9103862
400	0.934091	0.9078976	0.9168428
500	0.940636	0.9154329	0.9232994
700	0.947182	0.9229682	0.929756
1000	0.953727	0.9305035	0.9362126

Table VI shows the comparison of precision analysis with the existing techniques. The precision for Attri et al. 2019 and without GA 0.86 and 0.84 for 40 projects. Similarly, precision for 1000 projects the recall value increases to 0.95 for proposed work and Atri et al. work and GA is 0.93. The overall precision using the proposed estimation model is 0.92 and using Attri et al. is 0.89. Thus, an improved performance is exhibited by the proposed work using Genetic algorithm and Neural Network.

TABLE VII. COMPARATIVE ANALYSIS OF F-MEASURE AGAINST ATTRI ET AL. WORK

Number of Projects	F-measure Proposed	F-measure without GA	F-measure Attri et al. 2019
10	0.892151182	0.799202127	0.830740998
20	0.896683196	0.80301799	0.835100588
30	0.901180958	0.806805868	0.839384987
40	0.905644474	0.815973231	0.843741665
50	0.910075216	0.819748813	0.847977383
60	0.914472674	0.823497386	0.852319047
70	0.918838317	0.827219343	0.857654582
80	0.923172111	0.830915072	0.861658862
90	0.927473993	0.834584952	0.866264719
100	0.928363848	0.838229357	0.879716109
200	0.932337179	0.842134687	0.895649385
300	0.936295462	0.84914163	0.907123771
400	0.940238375	0.856148552	0.915425994
500	0.944165606	0.863155454	0.924707115
700	0.948078351	0.870162335	0.929605736
1000	0.95197579	0.877169198	0.93704723

Table VII shows the comparison of F-measure analysis with the existing techniques. The analysis results show that there is an increase in F-measure with increase in project count. It is seen that F-measure for Attri et al. 2019 and without GA is 0.87 and 0.83 for 100 projects. Further, it is observed that the F-measure for 1000 projects shows a rise and increases to 0.95 and Attri et al. and GA is 0.87. The overall average F-measure using the proposed approach is 0.92 and 0.88 using the Attri et al. 2019 which shows that the proposed work outperformed the Attri et al work.

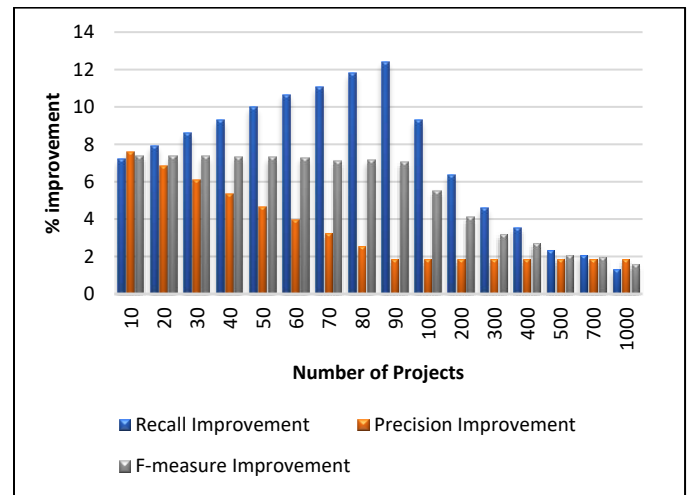


Fig. 3. Improvement Analysis of the Proposed Work over Attri et al. Work.

The observed performance in terms of precision, recall and f-measure values of both proposed and the existing work of Attri et al. are further analyzed to identify the extent of improvement exhibited by the proposed work. The individual % improvement for each of the parameters is individually computed and plotted in Fig. 3 for graphical illustration. It is concluded that despite of the variable % improvement observed

in each of the case, the overall analysis depicts the outperformance of the proposed work.

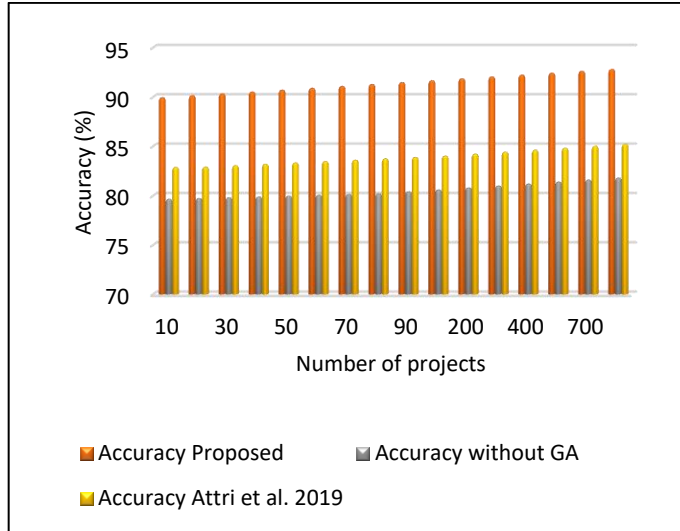


Fig. 4. Comparative Analysis for Accuracy.

Fig. 4 shows the comparison analysis for Accuracy analysis using the proposed and existing techniques. The analysis results show that there is an increase in Accuracy with increase in project count. It is seen that average Accuracy for Attri et al. 2019 and without GA is 84% and 81%. However, the proposed model shows Accuracy of about 91.3. The proposed technique has been improved by 8.9% in comparison to without GA and Attri et al. 2019. Thus, the proposed outperforms the existing work due to the integration of Genetic algorithm and Neural Network.

V. CONCLUSION

In the present work, machine learning based algorithms such as Neural Network, Genetic Algorithm and their attributes selection have been analyzed for the prediction of software effort. Software testing allows the evaluation of attributes or system capability in determining the requirements to meet the desired results. The primary motive of testing the software is to eliminate the bugs and improve the software security and other aspects such as performance, user satisfaction level, and experience. The study is based on the development of computational intelligence models to deal with the different complex problems. The implementation using the PROMISE and Kaggle dataset has been done and machine learning models such as Genetic algorithm and Neural Network used for implementation. The results of the proposed technique are promising. The accuracy of the proposed model is 91.3% and results are improved by 8.9% in comparison to existing technique. In future, an attempt has been made to improve the accuracy using the other computational techniques such as Fuzzy logic.

REFERENCES

- [1] A. Saeed, W. H. Butt, F. Kazmi, and M. Arif, "Survey of software development effort estimation techniques," in Proceedings of the 2018 7th International Conference on software and computer applications, 2018, pp. 82–86.
- [2] V. K. Attri and J. Singh Bal, "An Advanced Mechanism for Software Size Estimation Using Combinational Artificial Intelligence," *Int. J. Intell. Eng. Syst.*, vol. 12, no. 4, 2019, doi: 10.22266/ijies2019.0831.24.
- [3] W. Rhmann et al., "Survey on software defect prediction techniques," *Int. J. Appl. Sci. Eng.*, vol. 17, no. 4, pp. 331–344, 2019.
- [4] C. L. Prabha and N. Shivakumar, "Software defect prediction using machine learning techniques," in 2020 4th International Conference on Trends in Electronics and Informatics (ICOEI)(48184), 2020, pp. 728–733.
- [5] Y. Mahmood, N. Kama, A. Azmi, A. S. Khan, and M. Ali, "Software effort estimation accuracy prediction of machine learning techniques: A systematic performance evaluation," *Softw. Pract. Exp.*, vol. 52, no. 1, pp. 39–65, 2022.
- [6] C. López-Martín, "Machine learning techniques for software testing effort prediction," *Softw. Qual. J.*, vol. 30, no. 1, pp. 65–100, 2022.
- [7] A. B. Nassif, M. Azzeh, A. Idri, and A. Abran, "Software development effort estimation using regression fuzzy models," *Comput. Intell. Neurosci.*, vol. 2019, 2019, doi: 10.1155/2019/8367214.
- [8] A. Banimustafa, "Predicting Software Effort Estimation Using Machine Learning Techniques," 2018 8th Int. Conf. Comput. Sci. Inf. Technol. CSIT 2018, pp. 249–256, Oct. 2018, doi: 10.1109/CSIT.2018.8486222.
- [9] K. Dutta, V. Gupta, and V. S. Dave, "Analysis and comparison of neural network models for software development effort estimation," in Research Anthology on Agile Software, Software Development, and Testing, IGI Global, 2022, pp. 165–193.
- [10] W. Rhmann, B. Pandey, and G. A. Ansari, "Software effort estimation using ensemble of hybrid search-based algorithms based on metaheuristic algorithms," *Innov. Syst. Softw. Eng.*, vol. 18, no. 2, pp. 309–319, 2022.
- [11] M. M. Öztürk, "A tuned feed-forward deep neural network algorithm for effort estimation," *J. Exp. & Theor. Artif. Intell.*, vol. 34, no. 2, pp. 235–259, 2022.
- [12] R. Saljoughinejad and V. Khatibi, "A new optimized hybrid model based on COCOMO to increase the accuracy of software cost estimation," *J. Adv. Comput. Eng. Technol.*, vol. 4, no. 1, pp. 27–40, 2018.
- [13] N. Ghatasheh, H. Faris, I. Aljarah, and R. M. H. Al-Sayyed, "Optimizing software effort estimation models using firefly algorithm," *arXiv Prepr. arXiv1903.02079*, 2019.
- [14] S. Chhabra and H. Singh, "Optimizing design parameters of fuzzy model based COCOMO using genetic algorithms," *Int. J. Inf. Technol.*, vol. 12, no. 4, pp. 1259–1269, 2020.
- [15] A. Karimi and T. J. Gandomani, "Software development effort estimation modeling using a combination of fuzzy-neural network and differential evolution algorithm," *Int. J. Electr. Comput. Eng.*, vol. 11, no. 1, p. 707, 2021.
- [16] N. A. Zakaria, A. R. Ismail, N. Z. Abidin, N. H. M. Khalid, and A. Y. Ali, "Optimization of COCOMO Model using Particle Swarm Optimization," *Int. J. Adv. Intell. Informatics*, vol. 7, no. 2, pp. 177–187, 2021.
- [17] "Software Quality Attributes Dataset | Kaggle." <https://www.kaggle.com/datasets/sayedmohsin/sqa-dataset> (accessed Aug. 09, 2022).
- [18] A. Kaushik and N. Singal, "A hybrid model of wavelet neural network and metaheuristic algorithm for software development effort estimation," *Int. J. Inf. Technol.*, pp. 1–10, 2019.
- [19] P. Singal, A. C. Kumari, and P. Sharma, "Estimation of software development effort: A Differential Evolution Approach," *Procedia Comput. Sci.*, vol. 167, pp. 2643–2652, 2020.
- [20] "PROMISE DATASETS ENGINEERING REPOSITORY." <http://promise.site.uottawa.ca/SERepository/datasets-page.html> (accessed Oct. 21, 2022).

A Computer Vision System for Street Sweeper Robot

Ouiem Bchir, Sultana Almasoud, Lina Alyahya, Renad Aldhalaan, Lina Alsaeed, Nada Aldalbahi

Department of Computer Science, College of Computer and Information Sciences
King Saud University, Riyadh, Saudi Arabia

Abstract—With the spread of Covid-19, more people wear personal protective equipment such as gloves and masks. However, they are littering them all over streets, parking lots and parks. This impacts the environment and damages especially the marine ecosystem. Thus, this waste should not be discarded in the environment. Moreover, it should not be recycled with other plastic materials. Actually, they have to be separated from regular trash collection. Furthermore, littering gloves and masks yields more workload for street cleaners and presents potential harm for them. In this paper, we design a computer vision system for a street sweeper robot that picks up the masks and gloves and disposes them safely in garbage containers. This system relies on Deep Learning techniques for object recognition. In particular, three Deep Learning models will be investigated. They are: You Only Look Once (YOLO) model, Faster Region based Convolutional Neural Network (Faster R-CNN) and DeepLab v3+. The experiment results showed that YOLO is the most suitable approach to design the proposed system. Thus, the performance of the proposed system is 0.94 as F1 measure, 0.79 as IoU, 0.94 as mAP, and 0.41 s as Time to process one image.

Keywords—Covid-19; street sweeper robot; personal protective equipment (PPE); computer vision; deep learning

I. INTRODUCTION

In 2019, the Covid-19 pandemic started. It began to spread widely in early 2020, and was classified pandemic by the World Health Organization on March 11, 2020 when the number of infected cases reached 118,319 cases [1]. Since the infection may be spread by a person's sneezing, coughing, spitting and breathing, most countries' governments have imposed wearing face masks in public places and gatherings. In addition, supermarkets impose the use of gloves as well. This led to a significant increase in the use of face masks and gloves. As a consequence, globally, people are using and disposing of approximately 129 billion face masks and 65 billion gloves every single month during Covid-19 pandemic [2]. Unfortunately, many people are throwing these masks and gloves everywhere such as streets, parking lots, gardens and sidewalks. As a result, they will end up in the ocean through sewer systems creating a new form of pollution. In fact, they will shatter into micro plastics and will be contaminated by dangerous chemicals. Moreover, littering gloves and masks lead to a heavier workload for street cleaners. Furthermore, masks and gloves waste are dangerous for the cleaners' health since they are potentially infected. The same problem encountered by street waste workers, is also faced by recycling waste workers. In addition, Personal Protective Equipment (PPE) cannot be sorted with other material in the recycling centers [3]. In fact, they are thin and easily broken and can block and break down the sorting machine. Therefore, PPE waste materials have to be placed in separate sealed bags or

safely tight garbage containers. Nowadays, it is common to incorporate specialized robots to support workers. These machines lessen the workload since they are able to perform repetitive and simple tasks efficiently. In particular, a street sweeper robot would alleviate the burden of the waste and recycling workers by picking gloves and masks and storing them in sealed containers. In order to make the robots intelligent and aware of their surrounding environment, integrating sensors with robotics is needed. Specifically, computer vision systems that capture images of the scene surrounding the robot and recognize their content, provide the robot with useful information and an understanding of the scene. In particular, the computer vision system of the street sweeper robot would localize masks and gloves. Typically, suitable visual descriptors should be extracted from the captured images in order to segment the image into several objects. Then, another set of features is extracted from each object in order to recognize it using a classifier. Nevertheless, choosing the suitable feature for the segmentation and the recognition task is not straightforward. In fact, it is one of the main difficulties faced by computer vision systems. Recently, the use of Deep Learning (DL) models alleviated this problem by learning suitable features while training the model. The main goal of this paper is to design and implement a computer vision system for a street sweeper robot that recognizes masks and gloves. This system relies on Deep Learning techniques to recognize objects based on their visual properties. For this purpose, we intend to compare three approaches: You Only Look Once (YOLO) model [4], Faster-Region based Convolutional Neural Network (Faster R-CNN) [5], and DeepLab v3+ [6].

II. BACKGROUND

Object recognition is a field of computer vision which localize and categorize objects in images or video frames. It has been employed in many applications such as tumor recognition in medical images [7], face recognition [8], robot navigation [9], self-driving vehicles [10], etc. Generally, object recognition approaches can be either based on conventional machine learning and image processing techniques or based on Deep Learning approaches. In conventional approaches, a selected set of visual descriptors is extracted from the image for the purpose of segmenting the image into meaningful parts. Then, from the object of interest, another selected feature is extracted and conveyed to a classifier to decide on the class of the object.

Alternatively, object recognition Deep Learning approaches are based on CNN. In fact, they use the conventional layers to 1) automatically learn and extract suitable visual descriptors, and to 2) learn the location of the object. Region Conventional

Neural Networks (R-CNN) models are a well-known family for object recognition. It includes R-CNN [11], Fast R-CNN [12], and Faster R-CNN [5]. Each one of these approaches is an improvement of the previous one. R-CNN is based on a region proposal algorithm called "Selective search". It selects 2000 regions from the image. From each region, visual descriptors are automatically extracted using convolutional layers. Finally, each region is classified using one versus all SVM [13] classifier. In order to enhance the time complexity of the model, Fast R-CNN is proposed. Instead of extracting the visual descriptors from the 2000 regions, visual descriptors are extracted from the whole image first. Then, a Region of Interest (ROI) pooling layer is used to pool the visual descriptors of the region of interest from the final feature map. A SoftMax layer finally classifies this region. An extension to R-CNN [11] and Fast R-CNN [12] is Faster R-CNN [5]. It replaces the "Selective search" algorithm by a Region Proposal Network (RPN). In fact, instead of unnecessarily extracting a fixed number of regions that can be empty or include only a part of the object, Faster R-CNN [5] learns the location of the region to be proposed through the use of a small CNN called RPN. These region-based approaches provide two outputs. These are the bounding boxes coordinate that fits the object of Interest and the class of the object.

Instead of using a region proposal module, Single Shot Detectors (SSDs), use a set of predefined anchor points. From each anchor point, a predefined number of bounding boxes are defined. Then, these models learn if the bounding box contains an object or not, predict the offset of the box so it fits tightly the object, and compute the class probability of each object. Finally, the potential recognized objects are pruned to avoid duplicated recognition. There are various SSDs approaches. They differ in the way of defining the anchors. The most well-known SSD model is YOLO [4].

Another way of semantically understanding the scene is through semantic segmentation. The latter is inextricably related to object recognition. However, it differs in that it does not predict the class and the bounding box of the object, but it learns the pixels that form the object [14]. In fact, semantic segmentation entails assigning a semantic category to each pixel in the input picture.

Recent advances in the field of Deep Learning boosted the semantic segmentation research [15]. In fact, the automatic learning of the features through the convolution layers has improved the performance of semantic segmentation approaches. Nevertheless, CNN cannot be used as it is for semantic segmentation. In fact, max pooling and striding that are suitable for feature reduction, induce low feature resolution [16]. Moreover, since objects may be represented with different scales, standard CNN models need to be trained with different scales of the same object [17]. Furthermore, CNN models discard the location information [18]. Therefore, specific Deep Learning architectures for semantic segmentation have been proposed in the literature. Among these approaches, DeepLab v3+ [6] is a well-known Deep Learning approach for semantic segmentation which has been proven to be effective in many applications [19].

III. RELATED WORKS

Due to the Covid-19 pandemic and the need to check if people are wearing the required personal protective equipment (PPE), several masks and gloves recognition systems based on Deep Learning have been reported in the literature [20] [21] [22] [23] [24]. However, no existing work addressed the problem of recognizing masks and gloves thrown in the street. Alternatively, two works based on Deep Learning tackled the problem of recognizing different types of wastes littered in the street [25] [26].

A. Detection of Masks and Gloves Worn by People

The authors in [20] used two Deep Learning models, YOLO (You Only Look Once) [4] and Single-Shot multibox Detector (SSD) MobileNet [27], for the detection and proper wearing of face masks and gloves. First, the model splits the input image into an $S \times S$ grid. After that, the grid containing the center of the ground truth bounding box of an object is activated for the detection. Finally, each grid is responsible for predicting the confidence scores of a number of bounding boxes. The MobileNet architecture has been used as a feature extractor in the SSD MobileNet based approach after combining normal convolution and depthwise convolution. The proposed recognition system considers five categories. Namely, it recognizes if the people are wearing masks, not wearing masks, wearing gloves, not wearing gloves, and if they are not properly wearing the masks. The two Deep Learning models were investigated using a dataset containing 8250 photos collected from the internet. The experimental result showed that the proposed system reached an accuracy of 90.6% when using YOLO [4], and an accuracy of 85.5% when using SSD MobileNet [28].

Similarly, the approach in [21] used two Deep Learning models ResNet-50 [29] and YOLOv2 [30]. Nevertheless, they first used ResNet-50 to extract the visual feature. Then, they used YOLOv2 to recognize facial masks. For the assessment of the proposed approach, two medical face masks datasets, Medical Masks dataset (MMD) [31] and Face Mask dataset (FMD) [32] were merged into a single dataset. These datasets have been augmented before being fed to Resnet-50. It achieved a precision of 81%.

The authors in [22] proposed a Deep Learning approach in order to recognize whether or not people are wearing PPE. More specifically, they adopted the YOLOv4 [33] model. The model has backbone, neck and head parts. In the backbone part, CSPDarknet53 is used as a feature extractor model. In the neck section, Spatial Pyramid Pooling (SPP) and Path Aggregation Network (PAN) are employed. Modified PAN has been used for instance segmentation. For the modification of PAN, they used the concatenation operation instead of the addition operation. The SPP is used to perform max pooling over a feature map. The head part was kept the same as it was in YOLOv3. Four categories have been considered which are, wearing a mask, not wearing a mask, wearing a face shield, and wearing gloves. The authors put together a dataset that includes both collected and captured photos. They collected their own dataset to assess the performance of the system. They obtained a precision of 78% and a recall of 80%.

The study in [23] proposed a mask and face recognition system based on YOLOv3 [34]. First, the videos are recorded using digital cameras. After being processed, they are conveyed to YOLOv3. The latter detects faces and masks. The proposed system was trained on a set of 6,000 photos containing surgical masks which are selected from the MAFA dataset [35]. The experimental results showed that the proposed system achieved an accuracy of 84% in recognizing masks and an accuracy of 96% in recognizing faces. The authors in [24] adopted the VGG-16 [36] Deep Learning model to determine whether or not a person is wearing a facemask and checks if the people in a region are observing physical distance. The model is trained using collected data containing 20,000 images. The input image's height and width are set to 224 pixels. Moreover, data augmentation is employed by applying rotation, rescaling, shifting, and zooming operations. It achieved an accuracy of 97%.

B. General Waste Littered in the Street

The authors in [25] proposed a computer vision system for waste littering quantification. The proposed system is based on a Deep Learning model to localize and classify different types of wastes. They employ the OverFeat-GoogLeNet [37] Deep Learning model. It is an adaptation of the OverFeat model [38] which uses GoogLeNet [39] model as backbone deep network model. The authors collected their own dataset using a high-resolution camera placed on the top of a vehicle to take pictures of wastes on the streets and sidewalks. The performance of the system on the 18,676 collected images is 77.35% for the precision and 60% for the recall. Alternatively, the authors in [26] proposed a robot system that is able to pick up garbage from the grass independently. The computer vision part of the robot aims at recognizing general waste using ResNet-34 [29] and SegNet [40] Deep Learning models. The input image is first segmented using SegNet. The latter is a Deep Learning model designed for segmentation. It is based on a decoder-encoder model where the input image is first down-sampled to learn the visual descriptor, then the obtained visual descriptor is up-sampled to recover the input image resolution. After that, the segmented objects are conveyed to ResNet [29] in order to categorize the waste. In fact, the system considers six categories. Specifically, five classes are used for the waste and one class for non-waste. The system is trained on 40k training pictures and tested on 7k testing pictures. Moreover, they collected 750 more pictures representing non-waste for testing. Experiments have shown that the accuracy of littered waste recognition reached up to 95%.

IV. SYSTEM FOR STREET SWEEPER ROBOT

In order to design a computer vision system that recognizes masks and gloves, we intend to compare the performance of the three approaches: YOLO [4], Faster R-CNN [5], and DeepLab v3+ [6]. First, we need to train the three considered models. In order to train the YOLO [4] model, we feed its input with images representing littered gloves and masks. The labels of these images are also provided to the recognition system to ensure the training. The labels consist of the corresponding categories of the considered objects (gloves and masks), and their surrounding boxes' information, namely, the upper left corner coordinates, the width and height of the box. Similarly,

Faster R-CNN [5] is trained in the same way since it uses the same type of labels. Alternatively, DeepLab v3+ [6] employs a different type of labels. In fact, since it is a segmentation approach, the label of each pixel should be provided. More specifically, the captured images with littered masks and gloves are conveyed to the input of DeepLab v3+ [6]. Moreover, their corresponding masks images are provided to the networks. They consist of the same image where the pixels corresponding to each object are manually colored with a different color.

Using YOLO [4], the masks and gloves will be recognized and localized. The obtained results will be assessed to measure the performance of the YOLO [4] based system in terms of the Average Precision per class, Mean Average Precision, IoU, F1 measure and Time to process one image. Similarly, the same procedure will be used for the Faster R-CNN [5] based system. And for the DeepLab v3+ [6] based system, the obtained results will be assessed in terms of the IoU, F1 measure and Time to process one image. In fact, AP and mAP are not defined in the case of semantic segmentation.

When the performances of the three systems are computed, we compare between them in order to conclude on the best system to be considered. We should mention we prioritize the recognition performance over the time one. However, in case the recognition performance is similar or slightly different, we select the faster model. The selected approach among the three considered ones will be adopted as illustrated in Fig. 1.

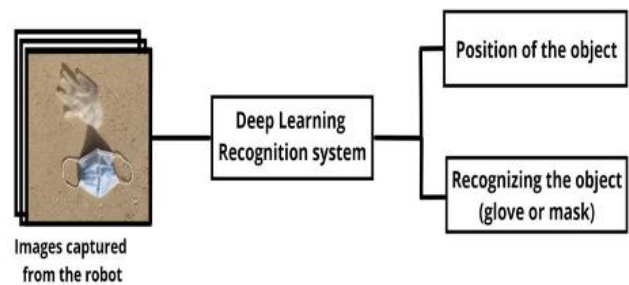


Fig. 1. Proposed System Architecture.

V. EXPERIMENTS

A dataset of 1500 images containing masks and/or gloves is collected. They are captured using a digital camera and have a size of 224 X 224 pixels. Different backgrounds such as grass, stones, and Asphalt concrete with various angles for shooting and different lighting are considered. Moreover, the masks and gloves in the collected dataset differ in terms of number, color, material, and design. Furthermore, these masks and gloves can be twisted, knotted, or choppy. Two Ground Truth labels are considered. The first one consists of labelling the pixels which belong to the gloves, the masks, and to the background. More specifically, for each image in the dataset, the pixels corresponding to the gloves are colored with green, those corresponding to the masks are colored with blue, and all remaining pixels are colored in black. The coloration is done manually. This first type of Ground Truth will be used with DeepLab v3+ [6] which requires pixel wise labelling. Fig. 2 shows a sample image and the corresponding pixel wise labelling as required by DeepLab v3+ [6].

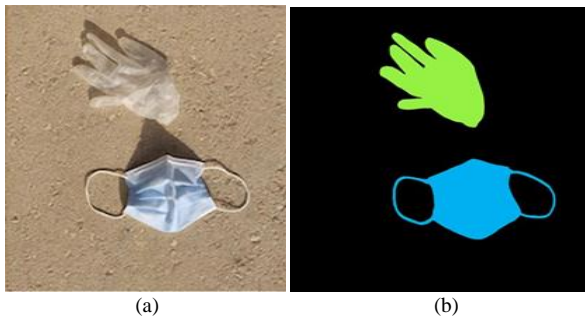


Fig. 2. Sample Pixel Wise Labelled Image. (a) The Sample Image, (b) The Corresponding Ground Truth Required by DeepLab v3+.

Alternatively, for YOLO [4] and Faster R-CNN [5] a different type of Ground Truth labelling is required. In fact, these two approaches, require the bounding boxes coordinates of each object of interest and its corresponding class (mask or glove) with respect to each considered image. The coordinates of the bounding box consist of the upper left coordinates, the width and the height of the rectangle surrounding tightly the object. Fig. 3 depicts sample images and the corresponding bounding boxes of the object of interest.

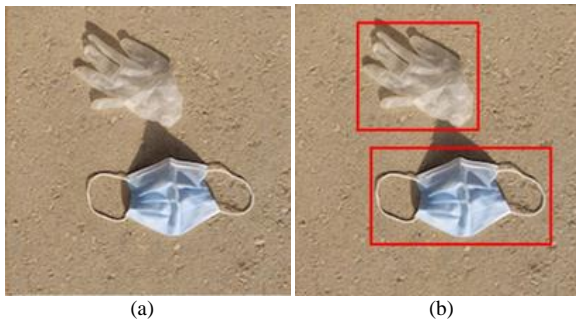


Fig. 3. Sample Labelled Image with Bounding Boxes. (a) The Sample Image, (b) The Corresponding Bounding Boxes Required by YOLO and Faster R-CNN.

A. Experiment 1

This experiment aims at assessing the performance of YOLOv4 [33] to recognize masks and gloves. For this purpose, we want to figure out the best hyper-parameter configuration for YOLOv4 [33]. As such, YOLOv4 model was trained using different values of the learning rate, the momentum and the number of batches. The learning rate is the most crucial hyper-parameter. In fact, a too small value may result in a long training process, whereas a too large value may result in overshooting the global minimum. Table I shows the five considered configurations. In order to determine the best model, the performance results on the validation set of each configuration are reported. They are the IoU, F1 measure, AP, mAP, and Time to process one image.

Fig. 4 shows the performance measures of YOLOv4 [33] model. As shown in Fig. 4, the best performance is obtained when using configuration 3, and the worst performance is obtained when using configuration 4. In fact, the learning rate in configuration 3 is set to 0.001 while the learning rate in configuration 4 is set to 0.1. Thus, the learning rate of 0.1 yielded the overshoot of the optimal model. Moreover, when the number of batches is large, the performance is better. This

due to the fact that the prediction error used to update the weights is computed using a larger number of images at each batch. The obtained results are 0.95 as F1 measure, 0.8072 as IoU, and 0.963632 as mAP using the considered configuration. We should note that configuration 4 performed better in terms of the time to process one image. However, we prioritize the recognition performance over the time one. Moreover, the difference is not significant, we prioritize the recognition performance. Using configuration 3, the results of the validation, and testing are reported in Table II. As shown, there is no significant performance drop when using the test set. Therefore, we can assume that the learned model is not over-fitted.

In order to illustrate the result obtained by the YOLOv4 [33] model, three sample results are depicted in Fig. 5. In Fig. 5(a), Fig. 5(c), and Fig. 5(e), the images fed to the YOLO model are displayed. Moreover, in Fig. 5(b), Fig. 5(d), and Fig. 5(f), the obtained results are shown. More specifically, the bounding box surrounding the object of interest along with the confidence score are displayed. As shown, even if the gloves or masks are folded, or overlap with another object, YOLOv4 [33] model is able to recognize them with a high confidence score.

TABLE I. YOLOV4 [33] HYPER-PARAMETER CONFIGURATIONS

	Learning rate	Momentum	Number of batches
Configuration 1	0.001	0.949	64
Configuration 2	0.01	0.95	128
Configuration 3	0.001	0.949	256
Configuration 4	0.1	0.99	128
Configuration 5	0.001	0.949	8

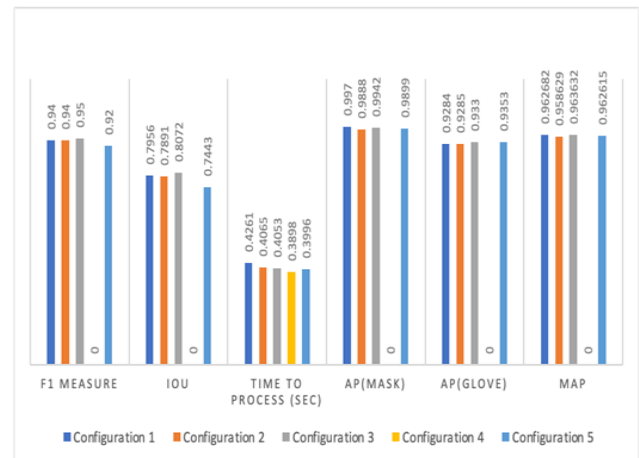


Fig. 4. YOLOv4 [33] Performance Results.

TABLE II. PERFORMANCE OF YOLOV4 [33] MODEL ON THE VALIDATION AND TEST DATASETS

	F1 Measure	IoU	Time to process (in sec)	AP (Mask)	AP (Glove)	mAP
Validation Set	0.95	0.81	0.41	0.99	0.93	0.96
Test Set	0.94	0.79	0.41	0.98	0.90	0.94

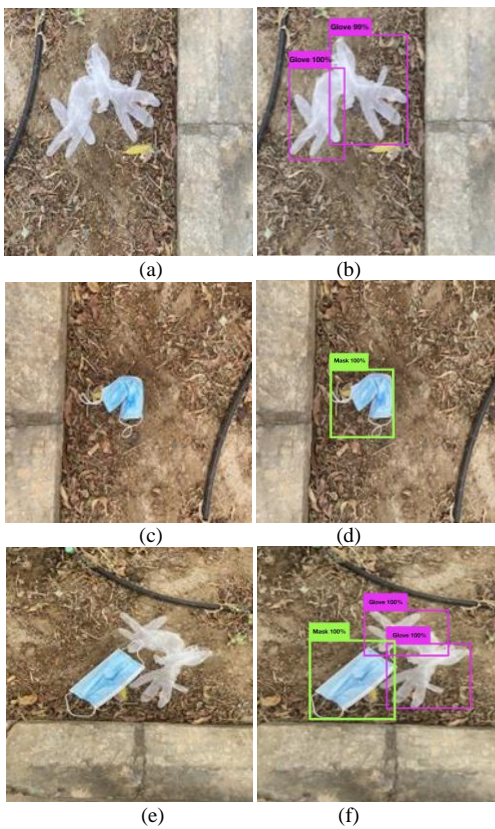


Fig. 5. Three Sample Results Illustrating the Result Obtained when using YOLOv4 [33] Model. (a) Sample Image 1, (b) The Output of Sample Image 1, (c) Sample Image 2, (d) The Output of Sample Image 2, (e) Sample Image 3, (f) The Output of Sample Image 3.

B. Experiment 2

In this experiment, we evaluate the performance of Faster R-CNN [5]. In this regard, the hyper-parameters are tuned using the validation set. Table III shows the five considered configurations.

Fig. 6 shows the performance measures of Faster R-CNN [5] on the validation set with respect to each considered configuration. As shown in Fig. 6, the best result is obtained using configuration 3. Specifically, the hyper-parameters are set to 0.0001 for the learning rate, 0.96 for the momentum and 690 for the number of batches. We should mention that configuration 5 gave slightly better AP with respect to the Mask class, but not with respect to the Glove class. However, in terms of mAP configuration 3 is better. The corresponding performance results are 0.5665 as F1 measure, 0.7337 as IoU, and 0.4350 as mAP. Table IV reports Faster R-CNN performance on both the validation and test sets. As shown, the performance of the test set is not significantly worse than the performance of the validation set, and thus the overfitting assumption is discarded.

Fig. 7 displays three sample results of the Faster R-CNN model. The images conveyed to Faster R-CNN model are displayed in the Fig. 7(a), Fig. 7(c), and Fig. 7(e), respectively. The corresponding output results are shown in Fig. 7(b), Fig. 7(d), and Fig. 7(f), respectively. As shown in Fig. 7, the bounding box surrounding the object of interest along with the

confidence score are depicted. We can notice that Faster R-CNN is able to recognize the withdrawn gloves and masks. Nevertheless, for some cases such the illustrative example displayed in Fig. 7(d), the confidence score is not high. This can be due to the fact the mask is folded.

C. Experiment 3

In order to detect masks and gloves using semantic segmentation, we tuned the hyper-parameters for DeepLab v3+ [6]. In this regard, we trained DeepLab v3+ [6] using ResNet-50 [29] as backbone. Then, using the validation set, we evaluated the model with respect to five considered configurations. In particular, the learning rate, momentum and number of batches were tuned. These five configurations are reported in Table V.

TABLE III. FASTER R-CNN [5] HYPER-PARAMETER CONFIGURATIONS

	Learning rate	Momentum	Number of batches
Configuration 1	0.001	0.96	690
Configuration 2	0.001	0.94	690
Configuration 3	0.0001	0.96	690
Configuration 4	0.00001	0.96	690
Configuration 5	0.0001	0.94	690

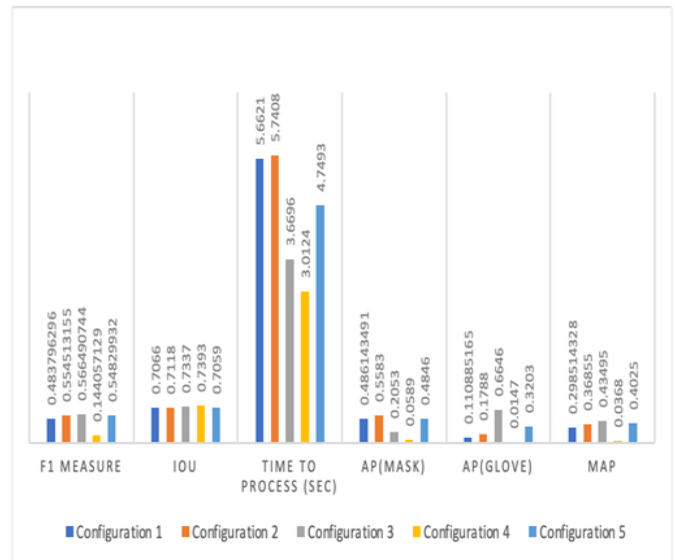


Fig. 6. Faster R-CNN [5] Performance Results.

TABLE IV. PERFORMANCE OF FASTER R-CNN [5] MODEL ON THE VALIDATION AND TEST DATASETS

	F1 Measure	IoU	Time to process (in sec)	AP (Mask)	AP (Glove)	mAP
Validation Set	0.57	0.73	3.67	0.21	0.66	0.43
Test Set	0.50	0.74	3.69	0.21	0.45	0.33

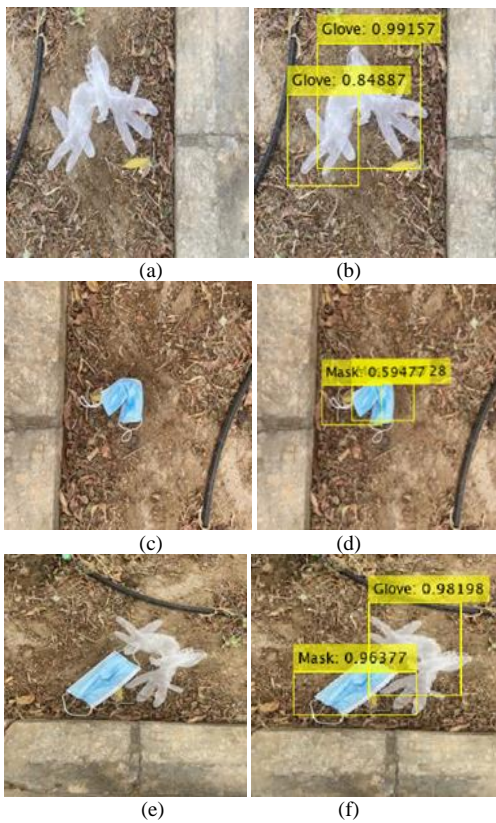


Fig. 7. Three Sample Results Illustrating the Result Obtained using Faster R-CNN Model. (a) Sample Image 1, (b) The Output of Sample Image 1, (c) Sample Image 2, (d) The Output of Sample Image 2, (e) Sample Image 3, (f) The Output of Sample Image 3.

TABLE V. DEEPLAB V3+ [6] HYPER-PARAMETER CONFIGURATIONS

	Learning rate	Momentum	Number of batches
Configuration 1	0.001	0.95	690
Configuration 2	0.01	0.97	690
Configuration 3	0.1	0.99	345
Configuration 4	0.001	0.96	171
Configuration 5	0.001	0.99	690

Fig. 8 displays the performance measures of the system when using DeepLab v3+ [6] semantic segmentation approach with ResNet-50 [29] as backbone. We should notice that contrary to the previous two experiments, only F1 measure, IoU and Time to process are considered. In fact, Average precision performance measure is not defined for segmentation approaches. As shown in Fig. 8, using configuration 1, a learning rate of 0.001, momentum of 0.95 and number of batches of 690, yielded the best performance result with an IoU of 0.9762, and F1 measure of 0.98. In fact, configuration 1 is characterized by a small learning rate avoiding missing the global minimum of the error rate, a large batch size enhancing the error computation, and a relatively smaller momentum (percentage of previous iteration gradients to be considered). Alternatively, a large learning rate of 0.1 (configuration 3) gave the worst result. This can be explained by an under-fitting situation where the model fails to find the global minimum and converges early since the learning step is too large.

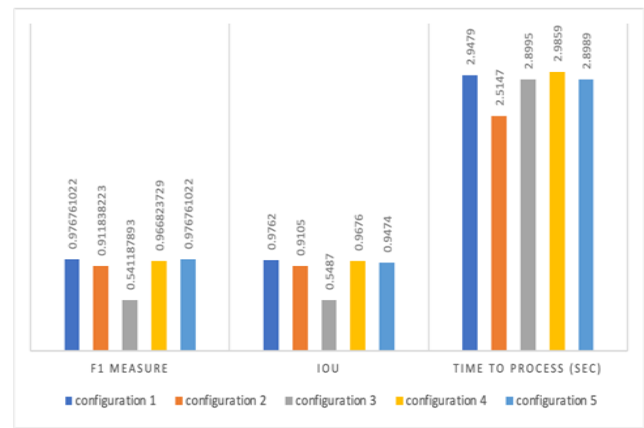


Fig. 8. DeepLab v3+ [6] Performance Results.

Using configuration 1, we evaluated the performance of DeepLab v3+ on the test images. Table VI depicts the performance results of both the validation and the test sets. As reported, there is no drop in the performance when using the test set compared with the performance of the validation set. Therefore, we can conclude that the learned model is not over-fitted.

TABLE VI. PERFORMANCE OF DEEPLAB V3+ [6] MODEL ON THE VALIDATION AND TEST DATASETS

	F1 Measure	IoU	Time to process (in sec)
Validation Set	0.98	0.98	2.95
Test Set	0.99	0.98	3.01

Fig. 9 displays three sample results of DeepLab v3+ model. The input images are shown in Fig. 9(a), Fig. 9(c), and Fig. 9(e), while the corresponding segmented images are depicted in Fig. 9(b), Fig. 9(d), and Fig. 9(f), respectively. In the segmented images, the pixels recognized as masks by DeepLab v3+ are colored in blue, those recognized as gloves with green, and all remaining pixels belonging to the background in black. We can notice that DeepLab v3+ is able to recognize the pixels belonging to withdrawn gloves and masks in different backgrounds, and for various colors of the gloves and the masks.

D. Discussion

Fig. 10 compares the performances of YOLOv4 [33] and Faster R-CNN [5] in terms of AP and mAP. We should notice that AP and mAP aren't defined for semantic segmentation approaches such as DeepLabv3+ [6]. As shown Fig. 10, YOLOv4 outperforms Faster R-CNN in recognizing both gloves and masks. This is also confirmed by the mAP. In fact, it is higher for YOLOv4 than Faster R-CNN. This can be explained by the fact that YOLO uses a single end-to-end network while Faster R-CNN uses two networks. Therefore, this can reduce the error. Moreover, Faster R-CNN is a region based approach where the classification is performed on the selected region only; whereas YOLO employs the whole image to predict the location and class of the object of interest. Thus, YOLO accesses more contextual information and predicts less false positives of the background. Furthermore, since YOLO has one object rule that makes it predict a single object per cell, it encourages the spatial diversity of the detected objects.

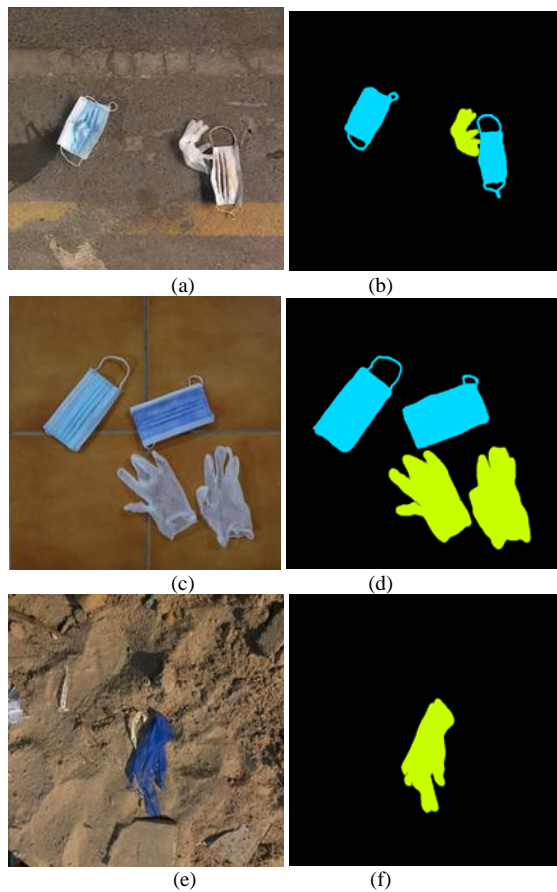


Fig. 9. Three Sample Results Illustrating the Result Obtained when using DeepLab v3+ Model. (a) Sample Image 1, (b) The Output of Sample Image 1, (c) Sample Image 2, (d) The Output of Sample Image 2, (e) Sample Image 3, (f) The Output of Sample Image 3.

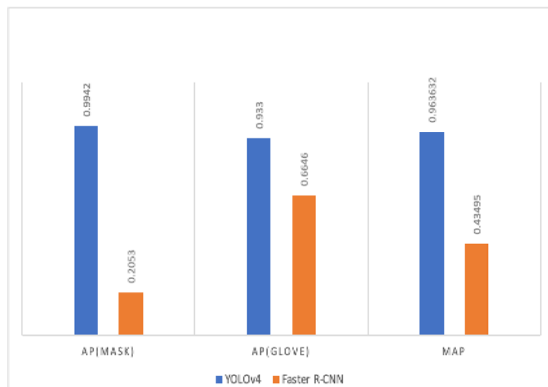


Fig. 10. Performance Comparison of YOLOv4[33], and Faster R-CNN [5] in Terms of AP, and mAP.

Fig. 11 compares the performance of YOLOv4 [33], Faster R-CNN [5], and DeepLab v3+ [6] in terms of F1 measure, IoU, and Time to process one image. As depicted, DeepLab v3+ is better in localizing masks and gloves with an IoU equal to 0.98, compared to an IoU equal to 0.81 for YOLOv4, and 0.73 for Faster R-CNN. This is an expected result since semantic segmentation is a more powerful approach for localizing the object of interest since it works at the pixel level, and not the bounding box like YOLOv4 and Faster R-CNN. Moreover,

DeepLab v3+ is slightly outperforming YOLOv4 and Faster R-CNN according to the F1 measure which combines both the localization and the classification performances of the object of interest. Nevertheless, in terms of processing time, YOLOv4 highly outperforms the other approaches with a time to process one image equal 0.41 s against 3.7 s for Faster R-CNN and 2.95 s for DeepLab v3+. Since the F1 measure difference between YOLOv4 and DeepLab v3+ is not significant while the difference in terms of processing time is large in favor of DeepLab v3+, we choose the YOLOv4 model to design the proposed approach.

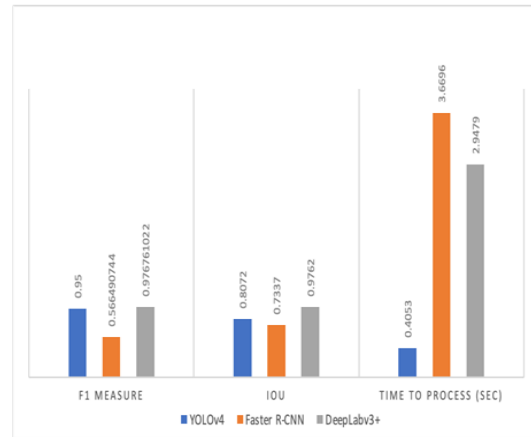


Fig. 11. Performance Comparison of YOLOv4, Faster R-CNN, and DeepLab v3+ in Terms of F1 Measure, IoU, and Time to Process One Image.

In attempt to further enhance the performance of the selected model (YOLOv4), we employed data augmentation. In other words, additional images are considered to train the model. These images are obtained by modifying existing images using rotation, cropping, blurring and adding brightness. The augmented dataset consists of 2073 images, Fig. 12 shows sample images from the augmented dataset. Table VII depicts the performance of YOLOv4 when using data augmentation and without using it. We noticed that using the augmented dataset shows a slight improvement to the results in terms of F1 measure, IoU, AP, mAP.

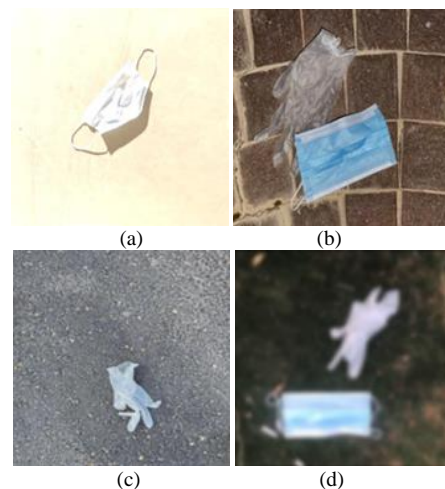


Fig. 12. Sample Images Obtained after the Data Augmentation. (a) Brightened Image, (b) Rotated Image, (c) Cropped Image, and (d) Blurred Image.

TABLE VII. PERFORMANCE COMPARISON OF YOLOV4 [33] WHEN USING DATA AUGMENTATION AND WITHOUT USING IT

	F1 Measure	IoU	Time to process (in sec)	AP (Mask)	AP (Glove)	mAP
Test results with augmented data	0.95	0.81	0.49	0.99	0.94	0.97
Test results without augmented data	0.94	0.79	0.41	0.982	0.901	0.94

E. Conclusion and Future Works

In this paper, we propose to design and implement a computer vision system of a street sweeper robot that recognizes masks and gloves for the purpose of picking them and disposing them in securely tight garbage bags. The proposed system is based on a Deep Learning object recognition approach.

After investigating the related works and studying the related background, we proposed an effective approach to automatically recognize facial masks and gloves which have been littered in the environment. For these purposes, three Deep Learning approaches are compared. These are YOLO, Faster R-CNN and DeepLab v3+. YOLOv4 is selected as the most suitable model for detecting littered gloves and masks. As future works, we propose to investigate emerging deep learning recognition and semantic segmentation approaches. In fact, pattern recognition field is an active field of research with continuous advancement.

REFERENCES

- [1] "Coronavirus Disease 2019 (COVID-19) Situation Report -51 SITUATION INNUMBERS Total and New Cases in Last 24 Hours, Mar. 2020." Who.int. https://www.who.int/docs/default-source/coronavirus/situation-reports/20200311-sitrep-51-covid-19.pdf?sfvrsn=1ba62e57_10 (accessed Sep. 5, 2021).
- [2] S. Hirsh. "Every Month, 200 Billion Face Masks and Gloves Are Going Into the Environment." GreenMatters.com. <https://www.greenmatters.com/p/face-masks-gloves-littercoronavirus> (accessed Sep. 5, 2021).
- [3] S. Waldek. "How to Properly Dispose of PPE." HouseBeautiful.com. <https://www.housebeautiful.com/lifestyle/a33576781/how-to-dispose-ppemasksglovesrecyclable/> (accessed Sep. 12, 2021).
- [4] J. Redmon. "YOLO: Real-Time Object Detection." Pjreddie.com. <https://pjreddie.com/darknet/yolov1/> (accessed Sep. 12, 2021).
- [5] S. Ren, K. He, R. Girshick and J. Sun, "Faster R-CNN: Towards Real-Time Object Detection with Region Proposal Networks," IEEE Transactions on Pattern Analysis and Machine Intelligence, vol. 39, no. 6, pp. 1137-1149, Jun. 2017, doi:10.1109/TPAMI.2016.2577031.
- [6] L. Chen, G. Papandreou, F. Schroff and H. Adam, "Rethinking Atrous Convolution for Semantic Image Segmentation," presented at arXiv, 2021.
- [7] E. Mohd. Azhari, M. Mudzakkir Mohd. Hatta, Z. Zaw Htike and S. Lei Win, "Tumor Detection in Medical Imaging: a Survey," International Journal of Advanced Information Technology (IJAIT), vol. 4, no. 1, pp. 21-30, Feb. 2014, doi: 10.5121/ijait.2014.4103.
- [8] J. Weng and W. Hwang, "Toward automation of learning: the state self-organization problem for a face recognizer," in Proceedings Third IEEE International Conference on Automatic Face and Gesture Recognition, Nara, Japan, Apr. 14-16, 1998, pp. 384-389, doi: 10.1109/AFGR.1998.670979.
- [9] W. Gueaieb and M. S. Miah, "An Intelligent Mobile Robot Navigation Technique Using RFID Technology," in IEEE Transactions on Instrumentation and Measurement, vol. 57, no.9, pp. 1908-1917, Sep. 2008, doi: 10.1109/TIM.2008.919902.
- [10] A. Uçar, Y. Demir and C. Güzelış, "Object recognition and detection with deep learning for autonomous driving applications," in SIMULATION, vol. 93, no. 9, pp. 759-769, Jun. 2017. doi: 10.1177/0037549717709932.
- [11] R. Girshick, J. Donahue, T. Darrell and J. Malik, "Rich Feature Hierarchies for Accurate Object Detection and Semantic Segmentation," in 2014 IEEE Conference on Computer Vision and Pattern Recognition, Columbus, OH, USA, Jun. 23-28, 2014, pp. 580- 587, doi: 10.1109/CVPR.2014.81.
- [12] R. Girshick, "Fast R-CNN," in 2015 IEEE International Conference on Computer Vision (ICCV), Santiago, Chile, Dec. 7-13, 2015, pp. 1440-1448, doi: 10.1109/ICCV.2015.169.
- [13] Yi Liu and Y. F. Zheng, "One-against-all multi-class SVM classification using reliability measures," Proceedings. 2005 IEEE International Joint Conference on Neural Networks, 2005., Montreal, Que, Jul. 31-4 Aug., 2005, vol. 2, pp. 849-854, doi: 10.1109/IJCNN.2005.1555963.
- [14] J. Shi and L. Zhao, "A Review of Lane Detection Based on Semantic Segmentation", in International Journal of Advanced Network, Monitoring and Controls, vol. 6, no. 3, pp. 1-8, Oct. 2021. [Online]. Available: <http://www.ijanmc.org/Uploads/20213/2021-03-01.pdf>.
- [15] T. Lei, Z. Jiao and A. Nandi. "Recent Advances in Image and Video Semantic Segmentation Using Deep Learning." Frontiers.org. <https://www.frontiersin.org/researchtopics/22286/recent-advances-in-image-andvideosemantic-segmentation-using-deeplearning> (accessed Oct. 30, 2021).
- [16] J. Brownlee. "A Gentle Introduction to Pooling Layers for Convolutional Neural Networks." MachineLearningMastery.com. <https://machinelearningmastery.com/poolinglayers-for-convolutional-neural-networks/> (accessed Oct. 30, 2021).
- [17] N. van Noord and E. Postma, "Learning scale-variant and scale-invariant features for deep image classification," in Pattern Recognition, Zhongshan, China, Jan. 2017, pp. 583- 592.
- [18] M. Ghafoorian et al, "Location Sensitive Deep Convolutional Neural Networks for Segmentation of White Matter Hyperintensities," in Scientific Reports, Jul. 2017, pp. 1– 12.
- [19] L. Chen, G. Papandreou, I. Kokkinos, K. Murphy and A. Yuille, "DeepLab: Semantic Image Segmentation with Deep Convolutional Nets, Atrous Convolution, and Fully Connected CRFs," in IEEE Transactions on Pattern Analysis and Machine Intelligence, United States, June. 2016, pp. 99-113.
- [20] S. Khosravipour, E. Taghvaei, and N. Charkari, "COVID-19 personal protective equipment detection using real-time deep learning methods," in arXiv ,Mar. 2021, pp. 11– 20.
- [21] M. Loey, G. Manogaran, M. H. N. Taha, and N. E. M. Khalifa, "Fighting against covid19: A novel deep learning model based on Yolo-V2 with resnet-50 for medical face mask detection," in Sustainable Cities and Society, Nov. 2020, pp. 1-8.
- [22] A. Protik, A. H. Rafi and S. Siddique, "Real-time Personal Protective Equipment (PPE) Detection Using YOLOv4 and TensorFlow," in 2021 IEEE Region 10 Symposium (TENSYMP), 2021, pp. 1-6, doi: 10.1109/TENSYMP52854.2021.9550808.
- [23] R. Avanzato, F. Beritelli, M. Russo, S. Russo and M. Vaccaro, "YOLOv3-based mask and face recognition algorithm for individual protection applications," in Search.bvsalud.org, 2021, pp. 41-45.
- [24] S. V. Militante and N. V. Dionisio, "Deep Learning Implementation of Facemask and Physical Distancing Detection with Alarm Systems," in 2020 Third International Conferencon Vocational Education and Electrical Engineering (ICVEE), 2020, pp. 1-5, doi: 10.1109/ICVEE50212.2020.9243183.
- [25] M. Saeed, A. Kaenel, A. Droux, F. TiEche, N. Ouerhani, H. Ekenel and J. Thiran, "A Computer Vision System to Localize and Classify Wastes on the Streets," in arXiv , 2017, pp 195-204.
- [26] J. Bai, S. Lian, Z. Liu, K. Wang and D. Liu, "Deep Learning Based Robot for Automatically Picking Up Garbage on the Grass," in IEEE Transactions on Consumer Electronics, vol. 64, no. 3, pp. 382-389, Aug. 2018, doi: 10.1109/TCE.2018.2859629.
- [27] A. Howard, M. Zhu, B. Chen, D. Kalenichenko, W. Wang, T. Weyand, M. Andreetto, and H. Adam, "Mobilenets: Efficient convolutional neural

- networks for mobile vision applications,” arXiv preprint arXiv:1704.04861, 2017.
- [28] T. Ghosh, L. Li, and J. Chakareski, “Effective Deep Learning for Semantic Segmentation Based Bleeding Zone Detection in Capsule Endoscopy Images,” 2018 25th IEEE International Conference on Image Processing (ICIP), no. September 2019, pp. 3034– 3038, 2018.
- [29] K. He, X. Zhang, S. Ren and J. Sun, "Deep Residual Learning for Image Recognition," In 2016 IEEE Conference on Computer Vision and Pattern Recognition (CVPR), Las Vegas,NV, USA, Jun. 27-30, 2016, pp. 770-778, doi: 10.1109/CVPR.2016.90.
- [30] R.Li and J.Yang, "Improved YOLOv2 Object Detection Model,"2018 6th International Conference on Multimedia Computing and Systems (ICMCS), 2018, pp. 1-6, doi: 10.1109/ICMCS.2018.8525895.
- [31] Medical mask dataset, Humans in the Loop, 2021. [Online]. Available: <https://humansintheloop.org/resources/datasets/medical-mask-dataset/>.
- [32] Face mask detection, Kaggle, May. 2020. [Online]. Available: <https://www.kaggle.com/andrewmvd/face-mask-detection>
- [33] A. Bochkovskiy, C. Wang and H. Liao, "YOLOv4: Optimal Speed and Accuracy of Object Detection," in arXiv.org, Apr. 2020, pp. 1-17.
- [34] H. Gong, H. Li, K. Xu and Y. Zhang, "Object Detection Based on Improved YOLOv3- tiny," in 2019 Chinese Automation Congress (CAC), 2019, pp. 3240-3245, doi: 10.1109/CAC48633.2019.8996750.
- [35] mafa-dataset, Kaggle, 2021.[Online]. Available: <https://www.kaggle.com/revanthrex/mafadataset>.
- [36] K. Simonyan and A. Zisserman, “Very Deep Convolutional Networks for LargeScale Image Recognition,” presented at the 3rd International Conference on Learning Representations, San Diego. USA , Sep. 2014.
- [37] R. Stewart, M. Andriluka and A. Y. Ng, "End-to-End People Detection in Crowded Scenes," in 2016 IEEE Conference on Computer Vision and Pattern Recognition (CVPR), 2016, pp. 2325-2333, doi: 10.1109/CVPR.2016.255.
- [38] P. Sermanet, D. Eigen, X. Zhang, M. Mathieu, R. Fergus, and Y. Lecun, "OverFeat: Integrated Recognition, Localization and Detection using Convolutional Networks," presented at arXiv, 2021.
- [39] C. Szegedy et al, "Going deeper with convolutions," in 2015 IEEE Conference on Computer Vision and Pattern Recognition (CVPR), 2015, pp. 1-9, doi: 10.1109/CVPR.2015.7298594.
- [40] V. Badrinarayanan, A. Kendall and R. Cipolla, "SegNet: A Deep Convolutional EncoderDecoder Architecture for Image Segmentation," in IEEE Transactions on Pattern Analysis and Machine Intelligence, vol. 39, no. 12, pp. 2481-2495, 1 Dec. 2017, doi: 10.1109/TPAMI.2016.2644615.

An Experimental Study with Fuzzy-Wuzzy (Partial Ratio) for Identifying the Similarity between English and French Languages for Plagiarism Detection

Peluru Janardhana Rao¹, Dr. Kunjam Nageswara Rao², Dr. Sitaratnam Gokuruboyina³

Research Scholar, Department of CS&SE, Andhra University College of Engineering, Andhra University, Visakhapatnam, India¹
Professor, Department of CS&SE, Andhra University College of Engineering, Andhra University, Visakhapatnam, India²
Research Scientist, Institute of Bioinformatics and Computational Biology (Recognized as SIRO), Visakhapatnam, India³

Abstract—With the rapid growth of digital libraries and language translation tools, it is easy to translate text documents from one language to other, which results in cross-language plagiarism. It is more challenging to identify plagiarism among documents in different languages. The main aim of this paper is to translate the French documents into English to detect plagiarism and to extract bilingual lexicons. The parallel corpus is used to compare multilingual text, a collection of similar sentences and sentences that complement each other. A comparative study is presented in this paper, the sentences similarity in bilingual content is found out by using the proposed Fuzzy-Wuzzy (Partial Ratio) based string similarity technique and three various techniques like Levenshtein Distance, Spacy and Fuzzy-Wuzzy (Ratio) similarity techniques in the literature. The string similarity method based on Fuzzy-Wuzzy (Partial Ratio) outperforms in terms of accuracy compared to Spacy, and Fuzzy-Wuzzy (Ratio) techniques for identifying language similarity.

Keywords—Plagiarism; natural language processing; string similarity; levenshtein distance; fuzzy-wuzzy

I. INTRODUCTION

The ability of machines to understand the human language carried by Natural Language Processing is a crucial component of Artificial Intelligence. Search engines' arrival leads to several natural language processing advancements to retrieve the text from electronic documents with string comparison. The machines can recognize and extract patterns from text data by applying several text similarity and information retrieval techniques using NLP. Their meaning identified the closeness between two text words by the NLP technique called Text Similarity.

Natural Language Processing (NLP) in Artificial Intelligence is an important field. NLP plays a vital role in the comprehension of human language by computers. NLP uses different text similarity techniques and the combination that enables machines to create and extract patterns from those text data. The proximity of two text pieces is found out using the text similarity method, which is one of the essential NLP methods. Data needs to be translated in a numerical format to carry out machine learning tasks. TF-IDF, Word2vec and Bag of Words are the different word embedding techniques used for text data encoding. The essential steps in the text-similarity are: Text planning, Feature extraction, Vector similarity and Decision function.

A. WordNet

In English, a large database of nouns, adjectives, verbs and adverbs are grouped into a collection of synonyms. WordNet that includes the link between words in over 200 languages is a lexical database. Synonyms are interlinked with lexical and semantic relations. The structure of the WordNet makes it a helpful tool for NLP. Based on their meanings, the words in WordNet are clustered as a thesaurus cursorily resembles them. Words in the network are close to each other as the definitions of words are precisely defined by WordNet. A synonym is a crucial relation in the midst of words in WordNet.

B. NLTK

The nltk.corpus package in python defines a collection of corpus reader classes that are used to access the contents of different set of corpora. A machine that can understand the meaning of a text needs analysis which is the fundamental idea of NLP.

C. Stop Words

The meaningless words that are designed to be ignored by the search engine to increase the database space or the processing time are stop words. nltk.corpus package in python has a list of stop words in 16 various languages.

1) *Research statement*: The content in French language can be converted into English using conversion tools which cannot be identified in plagiarism detection. The main aim of the research is to find out the copying content in a document after translating French document into English.

2) *Research objectives*: To find the accuracy by conducting an experimental study with Fuzzy-Wuzzy (Partial Ratio) for identifying the similarity between languages.

3) *Research significance*: In recent years the attention in copying the content from various sources increased while writing a new document which is an offence. There are so many plagiarism tools available in the market for checking the originality of the content. Although the tools are working efficiently for the originality checking but still there is a problem that if we copy the content from one language and using converter tools, we can convert that content into English. In such cases it is not possible for the tools to identify the

similarity between the sentences exactly leads to a less similarity index.

II. RELATED WORK

To find and compare cross-language articles on a specific subject, a measure of similarity is required. The basis for this estimation could be bilingual dictionaries or digital techniques, for example, latent semantic indexing (LSI) [16]. To find similar Arabic/English documents in two ways, LSI is used [1]. Monolingual: the first way is to translate the English article into Arab and then map it into space in the Arabic language LSI [10]. The second method is cross-lingual. The paper then compares LSI methods on various parallel and analog English-Arabic companies with a dictionary-based approach [8-9, 11, 13-14]. The cross-language LSI framework displays the results.

String similarity search is used in many real-life applications, like data cleaning, spell checking, fuzzy keyword search or DNA sequence comparison. Given a set of large string and a query string, the problem of string similarity search is to discover all strings in the string set that are identical to the query string efficiently [12]. Similarity is defined by using similarities measures like edit distance or Hamming distance. State Set Index (SSI) is presented as an effective solution to this work's search problem. SSI is interpreted as a finite automaton of non-determinism. SSI introduces a modern state labeling method that makes the index extremely space efficient. In addition, space usage by SSI can be traded against search time. On various sets of individual names with up to 170 million strings from a social network, they measured SSI and compared it to other state-of-the-art approaches. They show that SSI is substantially faster in most cases than other methods and needs less index space.

To retrieve math formulae from the text, three separate assessments were analyzed, in specific, Sequence Matcher, string matching algorithms, Levenshtein, and Fuzzy-Wuzzy. There are four types of Fuzzy-Wuzzy, two versions of which are found to be useful for the retrieval of Math formulae. The retrieval time of partial ratio-based Fuzzy-Wuzzy is less than the ratio-based Fuzzy-Wuzzy [2-7, 15]. They found Fuzzy-Wuzzy outperforms than Levenshtein distance and Sequence matcher techniques in terms of retrieval time and accuracy through their observations.

III. PROPOSED TECHNIQUE

In the proposed technique, French and English documents are first loaded and then stop words and special characters are removed from them. The preprocessed documents are then converted into a list of words. French synonyms are found for each word in the French list of words using NLP and then find the corresponding English synonyms for each French word. English synonyms are found for each word in the English list of words using NLP. Now prepare the final lists list1 and list2

which have all the English synonyms of French list and English synonyms of English list. String similarity between both these final lists is computed using Spacy, Levenshtein Distance, Fuzzy-Wuzzy (Ratio) and Fuzzy-Wuzzy (Partial Ratio) techniques by taking a Threshold as shown in Fig. 1. Compare List1 with List2 and remove all the words that have a match in List2. For the leftover words check semantic closeness and if it satisfies the threshold remove the words. Likewise perform for all words until we get final leftover list.

The similarity between documents is identified with the formula:

$$100 - \left(\frac{\text{finalLeftOverEnglishListLength}}{\text{OriginalEnglishLength}} \right) * 100$$

The presented techniques are discussed below.

A. Spacy

The Spacy technique predicts how two objects are identical by comparing the objects. For flagging replicas, the similarity prediction is helpful. Context-Sensitive tensors and Word vectors are the two approaches to find the relation between the terms assisted by Spacy. Two values 0 and 1 are used to define the spectrum of similarities. The value 1 means that the two sentences are identical, and the value 0 means that the sentences are not similar. In certain instances, they still have a high similarity meaning, even though they have no standard terms. One of the essential steps in NLP is text pre-processing to remove high similarity between unmatched sentences.

B. Levenshtein Distance

The fields in which Levenshtein distance is used are computer science, computational linguistics, bioinformatics, molecular biology, and DNA analysis. The similitude between objective string and source string is evaluated by using Levenshtein Distance. In everyday life, the Levenshtein distance is commonly used. In speech recognition and plagiarism detection, Levenshtein distance is primarily used.

C. Fuzzy-Wuzzy

Fuzzy string matching often described as precise string matching to find a string that almost matches a particular pattern. Applications of Fuzzy String Matching include spell checking, detection of text reuse, spam filtering, and matching DNA sequences in the bioinformatics domain. The string similarity is checked by the Fuzzy-Wuzzy library between two terms or phrases and gives a value between 0 and 1. If the ratio is nearer to 1, the terms are well-matched. If the ratio is closer to 0, the terms are unrelated to each other. The two common fuzzy matches supported by Fuzzy-Wuzzy are suitable for finding the languages close to each other. Pure Levenshtein Distance-based matching is used in Fuzzy-Wuzzy (Ratio) technique and in Fuzzy-Wuzzy (Partial Ratio) technique matching is done based on best substrings.

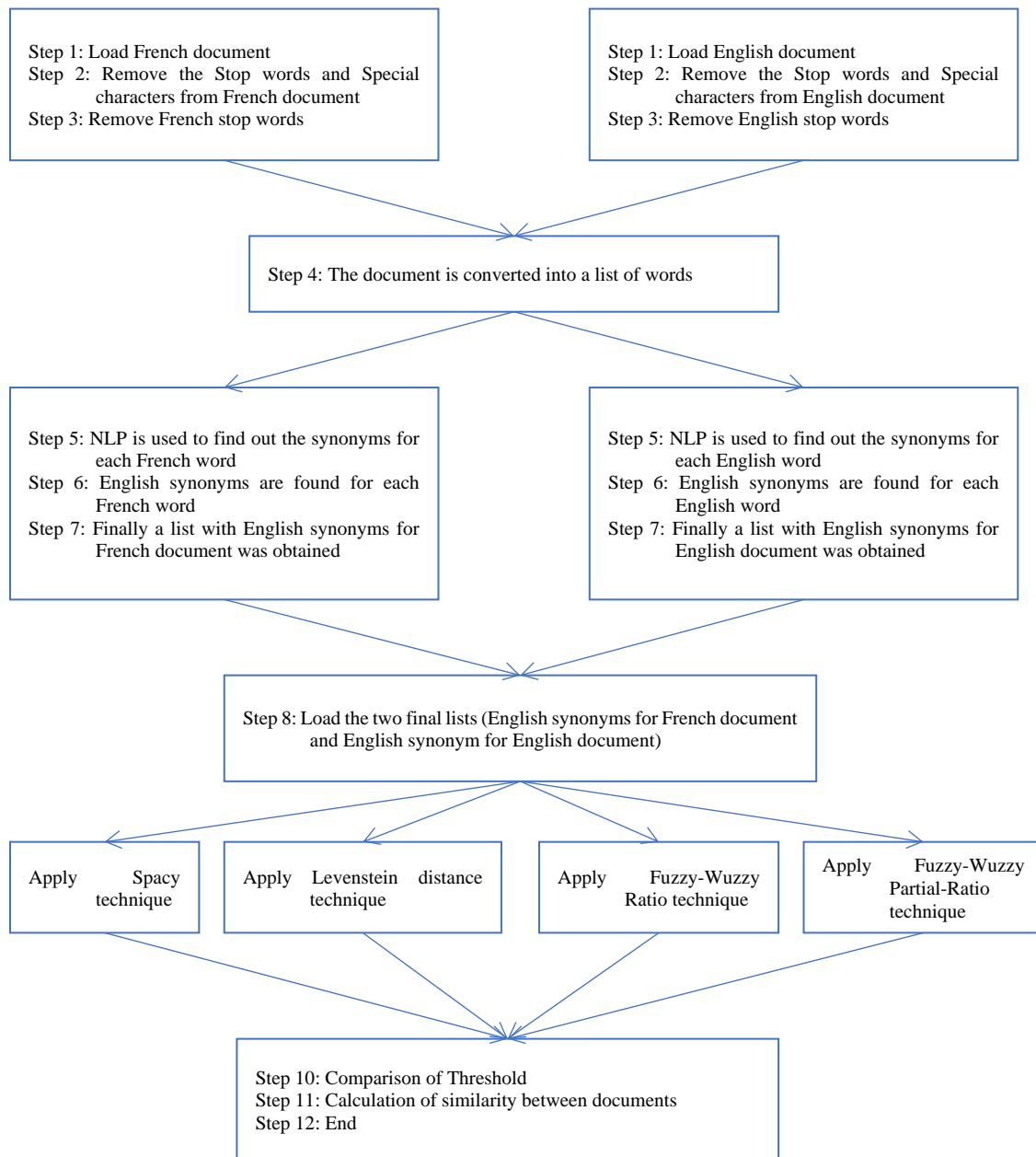


Fig. 1. Flow Diagram of the Presented String Similarity Methods.

IV. RESULTS

The comparison between the proposed and the literature methods is presented in terms of the metric accuracy. The similarity between the languages English and French is calculated by using the accuracy and based on that the presented techniques are compared. The proposed method's competence is presented with three kinds of mappings like one-to-one, one-to-many, and many-to-many between French documents and English documents.

From the results, the results obtainable with proposed Levenshtein Distance is much appropriate for string similarity. The tests carried out on nearly 200 documents; out of the proposed methods Fuzzy-Wuzzy (Partial Ratio) approach listed accuracy values in the range of 99 to 100 percent.

Table I and II represent accuracy with the Spacy, Levenshtein distance, Fuzzy-Wuzzy (Ratio) and Fuzzy-Wuzzy (Partial Ratio) techniques on 16 samples which are one-to-one mappings of French and English documents. In one-to-one mapping, there are four different ways in which the documents are being compared. 1) French Document + English document 2) French document rewrite + English document 3) French document + English document rewrite 4) French document rewrite + English document rewrite. It is observed from the tables that the accuracy ranges from 90.19 to 95.12 for Spacy technique, ranges from 94.63 to 100 for Levenshtein distance, ranges from 82.35 to 97.05 for Fuzzy-Wuzzy (Ratio) technique and ranges from 99.47 to 100 for Fuzzy-Wuzzy (Partial Ratio) technique.

TABLE I. MEASURING ACCURACY IN BETWEEN ENGLISH - FRENCH ONE-TO-ONE DOCUMENTS USING THE PRESENTED TECHNIQUES

Samples	Datasets	Spacy	Levenshtein Distance	Fuzzy- Wuzzy (Ratio)	Fuzzy- Wuzzy (Partial Ratio)
Sample 1	French document + English document	90.76	98.23	94.7	100
	English document + French document re-write	90.87	98.23	94.7	100
	English document re-write + French document	92.88	97.32	88.23	100
	English document re-write+ French document re-write	92.99	97.32	93	100
Sample 2	French document + English document	91.5	98.13	95.79	100
	English document + French document re-write	91.2	98.59	95.32	100
	English document re-write + French document	94.01	98.69	91.17	100
	English document re-write+ French document re-write	93.78	99.13	95.65	100
Sample 3	French document + English document	91.72	99.31	96.9	100
	English document + French document re-write	91.48	99.31	96.56	100
	English document re-write + French document	93.39	98.12	97.05	100
	English document re-write+ French document re-write	93.22	98.12	96.25	100
Sample 4	French document + English document	92.86	96.76	93.23	100
	English document + French document re-write	93.07	96.47	93.23	100
	English document re-write + French document	94.69	98.13	91.17	100
	English document re-write+ French document re-write	94.95	97.86	95.2	100
Sample 5	French document + English document	92.56	96.24	92.22	100
	English document + French document re-write	92.3	94.63	89.81	100
	English document re-write + French document	93.99	97.28	85.29	100
	English document re-write+ French document re-write	93.78	96.79	93.82	100
Sample 6	French document + English document	92.44	97.16	92.3	99.59
	English document + French document re-write	92.94	97.16	91.49	99.59
	English document re-write + French document	93.93	97.31	85.29	99.61
	English document re-write+ French document re-write	94.51	97.31	91.95	99.61

TABLE II. MEASURING ACCURACY IN BETWEEN ENGLISH-FRENCH ONE-TO-ONE DOCUMENTS USING THE PRESENTED TECHNIQUES

Samples	Datasets	Spacy	Levenshtein distance	Fuzzy- Wuzzy (Ratio)	Fuzzy-Wuzzy (Partial Ratio)
Sample 7	French document + English document	91.73	94.8	89.96	100
	English document + French document re-write	91.45	95.15	88.92	100
	English document re-write + French document	93.35	96.01	85.29	100
	English document re-write+ French document re-write	93.15	96.67	92.3	100
Sample8	French document + English document	90.73	97.55	93.7	100
	English document + French document re-write	90.76	97.9	92.65	100
	English document re-write + French document	93.3	98.71	94.11	100
	English document re-write+ French document re-write	93.43	99.03	93.89	100
Sample 9	French document + English document	90.31	96.48	93.54	99.65
	English document + French document re-write	90.46	96.77	92.66	99.65
	English document re-write + French document	93.02	97.13	91.17	99.67
	English document re-write+ French document re-write	93.25	97.65	94.27	99.67
Sample 10	French document + English document	91.51	98.64	94.57	100
	English document + French document re-write	91.53	98.3	94.57	99.7
	English document re-write + French document	93.54	98.77	85.29	100
	English document re-write+ French document re-write	93.49	98.77	95.71	99.47
Sample 11	French document + English document	91.55	97.4	92.5	100
	English document + French document re-write	91.23	96.54	91.93	100
	English document re-write + French document	93.05	97.297	94.11	100

	English document re-write+ French document re-write	92.91	97.29	92.43	100
Sample 12	French document + English document	90.19	96.64	91.76	100
	English document + French document re-write	90.58	96.64	90.54	100
	English document re-write + French document	91.9	97.19	94.11	100
	English document re-write+ French document re-write	92.44	97.47	93.27	100
Sample 13	French document + English document	92.78	98.04	91.53	100
	English document + French document re-write	92.36	98.04	91.2	100
	English document re-write + French document	93.88	96.95	88.23	100
	English document re-write+ French document re-write	93.55	97.25	91.76	100
Sample 14	French document + English document	91.35	96.55	91.95	100
	English document + French document re-write	91.43	96.26	91.37	100
	English document re-write + French document	92.9	96.91	94.11	100
	English document re-write+ French document re-write	93.01	96.63	92.15	100
Sample 15	French document + English document	93.01	100	96.42	100
	English document + French document re-write	93.29	100	93.57	100
	English document re-write + French document	93.84	99.37	82.35	100
	English document re-write+ French document re-write	94.14	98.75	93.75	99.71
Sample 16	French document + English document	93.67	96.27	92.02	100
	English document + French document re-write	93.39	95.74	89.89	100
	English document re-write + French document	95.12	97.56	85.29	100
	English document re-write+ French document re-write	94.87	98.04	93.65	100

TABLE III. MEASURING ACCURACY IN BETWEEN ENGLISH-FRENCH ONE-TO-MANY DOCUMENTS USING THE PRESENTED TECHNIQUES

No of French Samples	No of English Samples	Datasets	Spacy	Levenshtein Distance	Fuzzy- Wuzzy (Ratio)	Fuzzy- Wuzzy (Partial Ratio)
1	1	English document + French document	90.67	98.23	94.71	99.41
1	2		91.13	97.66	89.71	100
1	3		92.28	98.62	92.43	99.65
1	4		92.99	96.76	88.52	100
1	5		92.46	93.02	82.30	99.19
1	1	French document re write + English document	90.87	98.23	94.70	99.41
1	2		91.21	96.72	87.85	100
1	3		92.37	98.62	93.47	99.65
1	4		93.05	96.17	89.70	100
1	5		92.60	93.29	80.96	99.19
1	1	French document + English document re write	92.88	97.32	92.51	99.46
1	2		93.73	98.26	90.43	100
1	3		94.07	97.81	93.75	99.68
1	4		95.00	98.13	89.06	99.73
1	5		94.19	94.81	86.41	99.50
1	1	French document re write + English document re write	92.99	97.32	92.51	100
1	2		93.77	97.39	90.43	99.56
1	3		94.16	97.81	93.75	99.68
1	4		95.09	97.6	89.06	100
1	5		94.31	94.81	86.41	99.75
2	1	English document + French document	90.74	97.64	91.76	100
2	2		91.50	98.13	95.79	100
2	3		92.30	98.28	92.09	99.65
2	4		93.17	96.17	89.70	100
2	5		92.45	93.03	84.18	99.73

2	1	French document re write + English document	90.24	97.64	91.76	100
2	2		91.20	98.59	95.32	100
2	3		91.96	98.62	93.47	99.65
2	4		93.05	96.17	90.0	100
2	5		92.30	92.76	84.45	99.73
2	1	French document + English document re write	92.84	97.32	88.77	100
2	2		94.01	98.69	95.21	100
2	3		94.07	97.5	93.75	99.68
2	4		95.11	97.6	90.93	100
2	5		94.18	94.56	86.41	99.75
2	1	French document re write + English document re write	92.44	97.86	89.93	100
2	2		93.78	99.13	95.62	99.56
2	3		93.73	97.81	95.625	99.68
2	4		94.97	97.6	91.46	100
2	5		94.02	95.06	86.91	99.75
3	1	English document + French document	90.67	98.23	94.71	100
3	2		91.13	97.66	89.71	100
3	3		92.28	98.62	92.43	100
3	4		92.99	96.76	88.52	100
3	5		92.46	93.02	82.30	99.73
3	1	French document re write + English document	90.87	98.23	94.70	100
3	2		91.21	96.72	87.85	100
3	3		92.37	98.62	93.47	100
3	4		93.05	96.17	89.70	100
3	5		92.60	93.29	80.96	99.73
3	1	French document + English document re write	92.88	97.32	92.51	100
3	2		93.73	98.26	90.43	100
3	3		94.07	97.81	93.75	100
3	4		95.00	98.13	89.06	100
3	5		94.19	94.81	86.41	99.75
3	1	French document re write + English document re write	92.99	97.32	92.51	100
3	2		93.77	97.39	90.43	100
3	3		94.16	97.81	93.75	100
3	4		95.09	97.6	89.06	100
3	5		94.31	94.81	86.41	100

TABLE IV. MEASURING ACCURACY IN BETWEEN ENGLISH-FRENCH ONE-TO-MANY DOCUMENTS USING THE PRESENTED TECHNIQUES

No of French Samples	No of English Samples	Datasets	Spacy	Levenshtein Distance	Fuzzy- Wuzzy (Ratio)	Fuzzy- Wuzzy (Partial Ratio)
4	1	English document + French document	90.74	97.64	91.76	97.64
4	2		91.50	98.13	95.79	98.59
4	3		92.30	98.28	92.09	98.96
4	4		93.17	96.17	89.70	99.70
4	5		92.45	93.03	84.18	99.19
4	1	French document re write + English document	90.24	97.64	91.76	97.64
4	2		91.20	98.59	95.32	98.59
4	3		91.96	98.62	93.47	99.31
4	4		93.05	96.17	90.0	99.70
4	5		92.30	92.76	84.45	99.19
4	1		92.84	97.32	88.77	97.86

4	2	French document + English document re write	94.01	98.69	95.21	98.69
4	3		94.07	97.5	93.75	99.37
4	4		95.11	97.6	90.93	99.46
4	5		94.18	94.56	86.41	99.01
4	1	French document re write + English document re write	92.44	97.86	89.93	97.86
4	2		93.78	99.13	95.62	98.69
4	3		93.73	97.81	95.625	99.375
4	4		94.97	97.6	91.46	99.46
4	5		94.02	95.06	86.91	99.01

Table III and IV represent accuracy with the Spacy, Levenshtein distance, Fuzzy-Wuzzy (Ratio) and Fuzzy-Wuzzy (Partial Ratio) techniques for one-to-many mappings of French and English documents. It is observed from the tables that the accuracy ranges from 90.24 to 95.11 for Spacy technique, ranges from 92.76 to 99.13 for Levenshtein distance, ranges from 80.96 to 95.79 for Fuzzy-Wuzzy (Ratio) technique and ranges from 97.64 to 100 for Fuzzy-Wuzzy (Partial Ratio) technique.

TABLE V. COMPARISON OF ACCURACY BETWEEN PRESENTED METHODS FOR ENGLISH-FRENCH MANY-TO-MANY DOCUMENTS WITH FRENCH [1 6] AND DIFFERENT ENGLISH PAIRS

French pair Samples	English pair Samples	Spacy	Levenshtein Distance	Fuzzy-Wuzzy (Ratio)	Fuzzy-Wuzzy (Partial Ratio)
[1 6]	[1 8]	91.4	97.53	92.80	100
[1 6]	[3 10]	90.4	97.50	89.88	100
[1 6]	[2 6]	92.89	95.32	93.41	99.72
[1 6]	[4 7]	92.46	96.39	93.45	100
[1 6]	[3 7]	92.21	97.10	93.01	100
[1 6]	[1 8]	89.54	97.18	90.45	100
[1 6]	[5 9]	90.4	97.50	89.88	100
[1 6]	[4 6]	92.59	95.46	90.78	99.81
[1 6]	[3 9]	91.89	94.02	92.44	100

Table V represents accuracy with the presented techniques for many-to-many mappings of [1, 6] French documents and different English documents. It is observed from the table that the accuracy ranges from 89.54 to 92.89 for Spacy technique, ranges from 94.02 to 97.53 for Levenshtein Distance, ranges from 89.88 to 93.45 for Fuzzy-Wuzzy (Ratio) technique and ranges from 99.72 to 100 for Fuzzy-Wuzzy (Partial Ratio) technique.

Table VI represents accuracy with the presented techniques for many-to-many mappings of [3, 10] French documents and different English documents. It is observed from the table that the accuracy ranges from 89.46 to 98.65 for Spacy technique, ranges from 95.71 to 97.86 for Levenshtein Distance, ranges from 90.45 to 100 for Fuzzy-Wuzzy (Ratio) technique and ranges from 99.25 to 100 for Fuzzy-Wuzzy (Partial Ratio) technique.

Table VII represents accuracy with the presented techniques for many-to-many mappings of [5, 7] French documents and different English documents. It is observed from the table that the accuracy ranges from 89.56 to 94.76 for Spacy technique,

ranges from 96.45 to 98.82 for Levenshtein distance, ranges from 90.66 to 93.47 for Fuzzy-Wuzzy (Ratio) technique and ranges from 99.82 to 100 for Fuzzy-Wuzzy (Partial Ratio) technique.

Table VIII represents the accuracy with the presented techniques for many-to-many mappings of [4, 6] French documents and different English documents. It is observed from the table that the accuracy ranges from 88.94 to 95.05 for Spacy technique, ranges from 95.11 to 98.24 for Levenshtein distance, ranges from 89.20 to 93.56 for Fuzzy-Wuzzy (Ratio) technique and ranges from 99.12 to 100 for Fuzzy-Wuzzy (Partial Ratio) technique.

TABLE VI. COMPARISON OF ACCURACY BETWEEN PRESENTED METHODS FOR ENGLISH-FRENCH MANY-TO-MANY DOCUMENTS WITH FRENCH [3 10] AND DIFFERENT ENGLISH PAIRS

French pair Samples	English pair Samples	Spacy	Levenshtein Distance	Fuzzy-Wuzzy (Ratio)	Fuzzy-Wuzzy (Partial Ratio)
[3 10]	[1 9]	92.71	97.72	93.16	100
[3 10]	[3 6]	90.45	97.63	91.21	99.81
[3 10]	[2 6]	92.55	96.16	92.95	99.77
[3 10]	[4 7]	89.46	97.45	90.45	99.25
[3 10]	[2 8]	92.47	95.86	92.45	99.67
[3 10]	[2 9]	92.71	95.74	93.68	99.64
[3 10]	[5 10]	93.14	95.71	93.66	100
[3 10]	[2 7]	92.48	95.97	92.31	99.64
[3 10]	[2 10]	98.65	97.86	95.66	100

TABLE VII. COMPARISON OF ACCURACY BETWEEN PRESENTED METHODS FOR ENGLISH-FRENCH MANY-TO-MANY DOCUMENTS WITH FRENCH [5 7] AND DIFFERENT ENGLISH PAIRS

French pair Samples	English pair Samples	Spacy	Levenshtein Distance	Fuzzy-Wuzzy (Ratio)	Fuzzy-Wuzzy (Partial Ratio)
[5 7]	[3 9]	92.64	98.60	93.29	99.82
[5 7]	[2 9]	93.11	98.82	93.47	100
[5 7]	[2 8]	92.87	98.66	93.22	100
[5 7]	[1 6]	91.89	97.44	92.59	100
[5 7]	[2 6]	91.94	97.86	92.45	100
[5 7]	[5 7]	90.78	98.45	91.25	100
[5 7]	[5 10]	94.21	96.45	92.78	100
[5 7]	[1 7]	89.56	97.62	90.66	100
[5 7]	[5 9]	94.76	98.55	91.89	99.83

TABLE VIII. COMPARISON OF ACCURACY BETWEEN PRESENTED METHODS FOR ENGLISH-FRENCH MANY-TO-MANY DOCUMENTS WITH FRENCH [4 6] AND DIFFERENT ENGLISH PAIRS

French pair Samples	English pair Samples	Spacy	Levenshtein Distance	Fuzzy-Wuzzy (Ratio)	Fuzzy-Wuzzy (Partial Ratio)
[4 6]	[3 6]	92.89	95.11	93.42	99.24
[4 6]	[3 8]	92.79	96.23	93.29	99.56
[4 6]	[1 7]	93.06	98.12	91.68	100
[4 6]	[4 6]	95.05	97.46	91.02	99.63
[4 6]	[2 8]	92.88	95.54	93.22	99.12
[4 6]	[1 8]	91.64	98.24	91.87	100
[4 6]	[5 10]	90.21	96.77	90.90	99.41
[4 6]	[5 6]	88.94	96.12	89.20	99.39
[4 6]	[2 6]	93.45	96.51	93.56	99.57

TABLE IX. COMPARISON OF ACCURACY BETWEEN PRESENTED METHODS

Technique	One-One Mapping	One-Many Mapping	Many-Many Mapping
Spacy Similarity	90.19-95.12	90.24-95.11	88.94-98.65
Levenshtein Distance	94.63-100	92.76-99.13	95.11-98.82
Fuzzy-Wuzzy (Ratio)	82.35-97.05	80.96-95.79	89.20-95.66
Fuzzy-Wuzzy (Partial-Ratio)	99.47-100	97.64-100	99.12-100

Table IX represents the overall accuracy of the presented techniques with three kinds of mappings like one-one, one-many and many-many between French documents and English documents. Out of all the presented techniques Fuzzy-Wuzzy (Partial Ratio) technique outperformed all the remaining techniques with accuracy ranging from 99.12 to 100.

Table X presents the time taken to find the similarity between languages like English and French. The time calculation was accomplished on various documents of different sizes from 3KB to 50 KB with all the techniques discussed in this article. From the table, it is clear that the Spacy method identifies the similarity between English and French languages in less time than the other techniques in the literature.

Fig. 2 illustrates the data from Table I with eight samples of French and English documents with one-to-one mapping. The graph shows that the string similarity measure values of Spacy and Fuzzy-Wuzzy (Ratio) techniques are less than the Levenshtein Distance and Fuzzy-Wuzzy (Partial Ratio) techniques. It also shows that Fuzzy-Wuzzy (Partial Ratio) technique outperforms the remaining presented techniques.

Fig. 3 illustrates the data from Table III which contains one-to-many mapping of French and English documents. It shows that the accuracy of Fuzzy-Wuzzy (Partial Ratio) technique is more than the accuracy of remaining presented techniques.

TABLE X. TIME REQUIRED TO FIND THE SIMILARITY BETWEEN ENGLISH AND FRENCH DOCUMENTS

Sample Size	Spacy	Levenshtein Distance	Fuzzy-Wuzzy (Ratio)	Fuzzy-Wuzzy (Partial Ratio)
3 KB	5	8	6	5
6 KB	8	14	12	9
9 KB	10	19	14	14
12 KB	13	23	19	18
15 KB	16	28	23	22
18 KB	19	36	27	26
24 KB	26	47	38	37
27 KB	30	52	43	43
30 KB	33	58	47	46
36 KB	38	70	56	55
39 KB	41	75	61	61
42 KB	43	79	67	65
45 KB	46	84	72	71
50 KB	50	92	86	84



Fig. 2. Measuring Accuracy with Fuzzy-Wuzzy, Spacy Similarity and Levenshtein Distance in between French-English One-one Mapping.

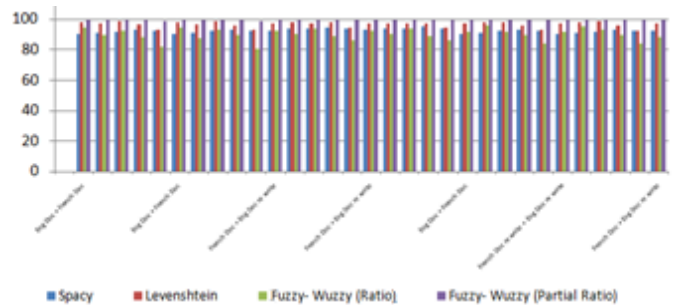


Fig. 3. Measuring Accuracy with Fuzzy-Wuzzy, Spacy Similarity and Levenshtein Distance in between French-English one-many Mapping.

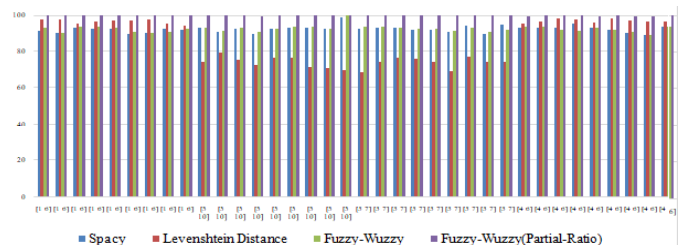


Fig. 4. Measuring Accuracy with Fuzzy-Wuzzy, Spacy Similarity and Levenshtein Distance in between French-English many-many Mapping.

Fig. 4 illustrates the data from Table V to VIII which contains many-to-many mappings of [1, 6], [3, 10], [5, 7] and [4, 6] French Documents and different English documents. It shows that the accuracy of Fuzzy-Wuzzy (Partial Ratio) technique is more than the accuracy of remaining presented techniques.

V. CONCLUSION

In this paper, the cross-language plagiarism detection between French and English documents is discussed. Some string similarity techniques such as Fuzzy-Wuzzy (Ratio), Fuzzy-Wuzzy (Partial Ratio), Spacy similarity, and Levenshtein distance are used to retrieve the similarity of sentences and words in multilingual content. Accuracy is the criterion used in comparing the output of the presented techniques. More methods need to be identified to find a similarity between languages with improved precision. The Fuzzy-Wuzzy (Partial Ratio) accuracy is more significant than Fuzzy-Wuzzy (Ratio), Levenshtein distance, and Spacy similarity, but time required to find the similarity is substantial with Spacy compared to other techniques.

REFERENCES

- [1] D. LANGLOIS, M.Saad, K.SMAILIA, "Alignment of comparable documents: Comparison of similarity measures on French–English–Arabic data", Volume 24, Issue 5September 2018 , pp. 677-694.
- [2] M. Sree Ram Kiran Nag, G. Srinivas, K. Venkata Rao, Sairam Vakkalanka, Nagendram, "Comparative and experimental study in identifying the similarity between languages for plagiarism detection and efficient language translation", Materials Today, Elsevier, PP no 1-8, 2021.
- [3] G.AppaRao, K.VenkataRao, P.V.G.D.Prasad Reddy and T.Lava Kumar, "An Efficient Procedure for Characteristic mining of Mathematical Formulas from Document", International Journal of Engineering Science and Technology (IJEST), Mar 2018, Vol. 10 No.03, pp. 152-157.
- [4] G.AppaRao, G.Srinivas, K.VenkataRao, P.V.G.D.Prasad Reddy, "Characteristic mining of Mathematical Formulas from Document - A Comparative Study on Sequence Matcher and Levenshtein Distance procedure", International Journal of Computer Sciences and Engineering, Apr 2018, Volume-6, Issue-4, pp 400-403.
- [5] G.AppaRao, G.Srinivas, K.VenkataRao, P.V.G.D.Prasad Reddy, "APartial Ratio and ratio Based Fuzzy-Wuzzy Procedure for Characteristic Mining of Mathematical Formulas from Documents", IJSC- ICTACT Journal on Soft Computing, July 2018, Vol 8, Issue 4, pp. 1728-1732.
- [6] K.N.Brahmaji Rao, G.Srinivas, P.V.G.D.Prasad Reddy, "An Experimental Study with Tensor Flow Characteristic mining of Mathematical Formulae from a Document", EAI Endorsed Transactions on Scalable Information Systems, 03 2019 - 06 2019 | Volume 6 | Issue 21 | e6.
- [7] K.N.Brahmaji Rao, G.Srinivas, P.V.G.D.Prasad Reddy, T.surendra, "A Heuristic Ranking of Different Characteristic Mining Based Mathematical Formulae Retrieval Models", Volume-9 Issue-1, October 2019.
- [8] Hieber.F., and Riezler.S "Bag-of-Words Forced Decoding for Cross-Lingual Information Retrieval". In Proceedings of the 2015 Conference of the North American Chapter of the Association for Computational Linguistics: Human Language Technologies, Denver, Colorado, Association for Computational Linguistics, pp. 1172–118.
- [9] Morin.E., Hazem.A., Boudin.F., and Clouet.E.L. 2015, "Lina: Identifying Comparable Documents from Wikipedia". In Proceedings of the 8th Workshop on Building and Using Comparable Corpora (BUCC@ACL/IJCNLP 2015), Beijing, China, Association for Computational Linguistics, pp. 88–91.
- [10] Motaz Saad, David Langlois, Kamel Smaïli, "Extracting Comparable Articles from Wikipedia and Measuring their Comparabilities", Procedia - Social and Behavioral Sciences 95 (2013) 40 – 47.
- [11] Saad.M., Langlois.D., and Smaïli, K. 2014. Cross-lingual semantic similarity measure for comparable articles. In Proceedings of the Advances in Natural Language Processing – 9th International Conference on NLP (PoITAL 2014), Warsaw, Poland, Springer International Publishing, pp. 1-12.
- [12] Dandy Fenz, Dustin Lange, Astrid Rheinländer, Felix Naumann, Ulf Leser. "Chapter 18 Efficient Similarity Search in Very Large String Sets", Springer Science and Business Media LLC, 2012.
- [13] Vulić.I., and Moens.M-F. 2014, "Probabilistic Models of Cross-Lingual Semantic Similarity in Context Based on Latent Cross-Lingual Concepts Induced from Comparable Data". In Proceedings of the 2014 Conference on Empirical Methods in Natural Language Processing (EMNLP 2014), Association for Computational Linguistics (ACL), pp. 349–62.
- [14] Vulić.I., and Moens.M-F. 2015, "Monolingual and Cross-Lingual Information Retrieval Models Based on (Bilingual) Word Embeddings". In Proceedings of the 38th International ACM SIGIR Conference on Research and Development in Information Retrieval, SIGIR '15, New York, NY, USA, Association for Computing Machinery, pp. 363–72.
- [15] K.N.Brahmaji Rao, G.Srinivas, P.V.G.D.Prasad Reddy, B.Tarakeswara Rao "Non-negative Matrix Factorization Procedure for Characteristic Mining of Mathematical Formulae from Documents", Communication Software and Networks, pp: 539-551, Vol-134, Oct 2020.
- [16] Nag, M. S. R. K., Srinivas, G., Rao, K. V., Vakkalanka, S., & Nagendram, S. (2021). Comparative and experimental study in identifying the similarity between languages for plagiarism detection and efficient language translation. Materials Today: Proceedings.

Comparing LSTM and CNN Methods in Case Study on Public Discussion about Covid-19 in Twitter

Fachrul Kurniawan^{1*}, Yuliana Romadhoni², Laila Zahrona³, Jehad Hammad⁴

Department of Informatics Engineering, Universitas Islam Maulana Malik Ibrahim Malang, Malang, Indonesia¹

Department of Informatics Engineering, UIN Maulana Malik Ibrahim Malang^{2,3}

Al-Quds Open University, Bethlehem Branch⁴

Abstract—This study compares two Deep Learning model methods, which include the Long Short-Term Memory (LSTM) method and the Convolution Neural Network (CNN) method. The aim of the comparison is to discover the performance of two different fundamental deep learning approaches which are based on convolutional theory (CNN) and deal with the vanishing gradient problem (LSTM). The purpose of this study is to compare the accuracy of the two methods using a dataset of 4169 obtained by crawling social media using the Twitter API. The Tweets data we've obtained are based on a specific hashtag keyword, namely "covid-19 pandemic". This study attempts to assess the sentiment of all tweets about the Covid-19 viral epidemic to determine whether tweets about Covid-19 contain positive or negative thoughts. Before classification, the Preprocessing and Word Embedding steps are completed, and this study has determined that the epoch used is 20 and the hidden layer is 64. Following the classification process, this study concludes that the two methods are appropriate for classifying public conversation sentences against Covid-19. According to this study, the LSTM method is superior, with an accuracy of 83.3%, a precision of 85.6%, a recall of 90.6%, and an f1-score of 88.5%. While the CNN method achieved an accuracy of 81%, precision of 71.7%, recall of 72%, and f1-score of 72%.

Keywords—COVID-19; LSTM; CNN; sentiment analysis

I. INTRODUCTION

Social media is an online platform through which the community interacts broadly and openly, and it can also be used to disseminate information. Twitter is one of the most popular social networking platforms [1]. With 18.45 million users, Indonesia ranks fifth among countries with the most active engagement on Twitter [2]. The information regarding the Covid-19 pandemic is what is being discussed now.

The Covid-19 pandemic has resulted in the implementation of all regulations and limitations in numerous nations, including Indonesia [3]. As a result, many people express their opinions about Covid-19 on social media; therefore, this discussion or community response can be classified to determine the sentiment of the statement; after determining the classification in the sentence, accuracy calculations can be produced; and the method is required so that classification is carried out structurally.

For measuring categorization accuracy, there are two methods available: Machine Learning [4] and Deep Learning [5]. There are multiple algorithms that can be applied to both models. Deep Learning is a model based on the human brain's

artificial neural network; this model is an implementation of the modern Machine Learning model [6]. Deep Learning is a generic sort of learning that can handle issues in all domains, including categorization [7]; it has been defined as such. The Long Short-Term Memory (LSTM) technique [8] and the Convolution Neural Network (CNN) algorithm [9] can be employed for this categorization within this deep learning system. In the mode of deep learning with several levels (layers), the layers are the input layer, the hidden layer, and the output layer [10]. Before executing calculations using the Deep learning model of conversational sentence categorization. However, the preprocessing procedure must be executed to ensure that the input is first processed using natural language processing (NLP) [11]. NLP is a computerized technology that explains the function of software or hardware that analyzes spoken or written language in a computer system [12]. The primary objective of NLP is to have a computer system that truly understands natural language as closely as possible to humans [13]. In this study, two approaches, LSTM and CNN, will be utilized to compare the accuracy of findings.

Schmid Huber and Hoch Reiter introduced LSTM in 1997 [14]. LSTM is a method derived from the development of the Recurrent Neural Network (RNN) architecture. LSTM handles vanishing gradients by adding a memory cell that can hold information for an extended period [15].

CNN is a multilayer neural network type feed-forward network with two or more deep layers that has good performance in applications involving image data, including computer vision categorization data gathering [16] and NLP [17] with the results obtained being excellent. CNN is not significantly distinct from a typical neural network, which consists of neurons with weight, bias, and activation functions. CNN eliminates the need to do multiple steps on the neural network because it calculates the output using convolution operations on the input layer. Each layer has a distinct filter and mixes the convolution operation's results [18].

In this comparative research of the LSTM and CNN methods on the classification of community dialogues regarding Covid-19 with case studies on Twitter social media. It is intended that the conversations and reactions regarding Covid-19 conducted by the community on social media can be utilized by the Indonesian government to enhance regulations during the pandemic.

*Corresponding Author.

II. RESEARCH METHOD

This study employed an experimental approach, which involved running several tests on the Deep Learning model with the LSTM and CNN techniques considering the following relevant studies.

A. Relevant Studies

In this relevant studies section, it was employed to assemble data pertinent to the study at hand, which will then serve as a basis for further study, comparison, and information gathering. Comparison of relevant studies can be seen in Table I. According to Table I, researchers reviewed five related publications between 2015 and 2021. In comparison to naïve bayes, support vector machines, decision trees, and random forests, the LSTM and Gated Recurrent Units (GRU) methods achieve the highest level of accuracy with a value of 99.9%. LSTM, CNN, and GRU are all neural network examples.

TABLE I. COMPARISON OF RELEVANT STUDIES

Title	Publication Year	Method	Findings
<i>Sentiment Analysis Twitter Bahasa Indonesia Berbasis Word2vec Menggunakan Deep Convolutional Neural Network (Sentiment Analysis Twitter Indonesian Based on Word2vec Using Deep Convolutional Neural Network)</i>	2020 [19]	CNN	In this study, 999 Indonesian tweets were used taken from the social media Twitter. The results of experiments that have been carried out with the Deep Convolutional Neural Network algorithm acquired the highest accuracy value of 76.40%.
<i>Penerapan Convolutional Long Short-Term Memory untuk Klasifikasi Teks Berita Bahasa Indonesia (Application of Convolutional Long Short-Term Memory for Classification of Indonesian News Texts)</i>	2021 [20]	CNN and LSTM	This study aims to analyze the combination of two deep learning methods: CNN and LSTM (C-LSTM). The result of this combination acquired a better performance compared to CNN and LSTM.
<i>Algoritma LSTM-CNN untuk Sentimen Klasifikasi dengan</i>	2021 [21]	LSTM-CNN	Classification using LSTM, LSTM-CNN, CNN-LSTM methods

Title	Publication Year	Method	Findings
<i>Word2vec pada Media Online (LSTM-CNN Algorithm for Sentiment Classification with Word2vec on Online Media)</i>			with the dataset used was Indonesian article title data taken from the Detik Finance website resulting in testing the LSTM, LSTM-CNN, CNN-LSTM methods obtained accuracy results of, 62%, 65% and 74%.
<i>Komparasi Algoritma Machine Learning Dan Deep Learning Untuk Named Entity Recognition: Studi Kasus Data Kebencanaan (Comparison of Machine Learning and Deep Learning Algorithms for Named Entity Recognition: A Case Study of Disaster Data)</i>	2020 [22]	Naive Bayes, Support Vector Machines, Decision Tree, Dan random Forest. LSTM, CNN, GRU.	In this study, the highest accuracy machine learning model was obtained in the random forest method with an accuracy value of 0.98%, in the Deep Learning method there were LSTM and GRU methods with an accuracy value of 0.99%.
<i>A C-LSTM Neural Network for Text Classification</i>	2015 [23]	LSTM, Bi LSTM, C-LSTM	The study stated that by using the combined method of CNN and LSTM to obtain a high accuracy value with an accuracy value of 94.6%

B. Experimental Design

In order to conduct research in a more systematic manner, we designed the experiment as depicted in Fig. 1. From Fig. 1 we compared the LSTM and CNN in general. In the following subsections, the specifics of Fig. 1 will be described.

- Data Crawling

Data crawling is a dataset that refers to conversation sentences originating from Twitter [24] with the hashtag "covid-19 pandemic". Data retrieval method utilizes the mining address provided by the social media platforms mentioned above. The data obtained 9,643 tweets from September 2020 to September 2022, tweet data will be used for two years during the covid-19 pandemic.

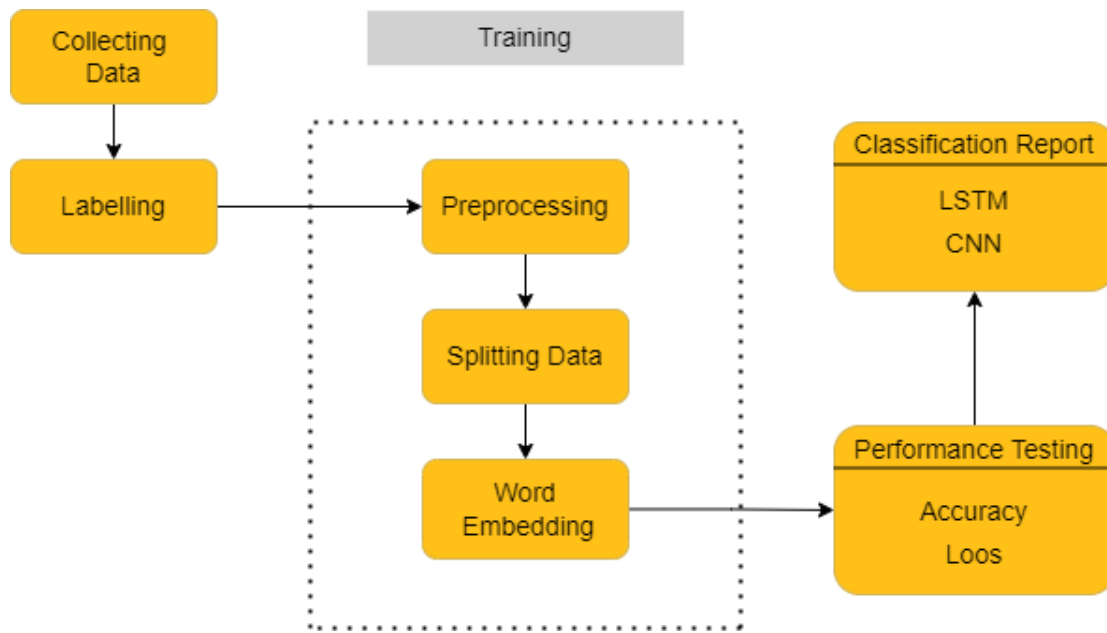


Fig. 1. Experimental Design.

• Data Labelling

In this study, data was labeled manually by language experts who already understand whether a sentence is included in a negative or positive sentence. We give a table (Table II), which contains two columns: tweet and label. The tweet column consists of the tweet status, which is collected from Twitter. The second column is an empty label. The expert should write a specific category of sentiment: negative and positive. Even though the neutral category can improve the overall accuracy, in this research we do not neutral label because it tends to be ambiguity or uncertainty. Uncertainty leads to confusion which may harm the efficiency of the decision [25]. This data labeling was done after crawling the data while the data was still intact therefore sentiment could be identified in the sentence. An example of labeled data can be found in Table II. From Table II, we obtain tweets with labels that have been validated by specialists.

TABLE II. DATA LABELLING

Tweet	Label
Kondisi ekonomi orang tua dan keluarga tengah sulit saat pandemi COVID 19, mahasiswa Unsri menuntut keringanan UKT. https://t.co/WwQ1pDJTrx	Negative
Jumlah kematian Covid-19 pada Juli 2021 merupakan yang tertinggi selama pandemi. https://t.co/Wju16vABcj	Negative
Kerjasama ekonomi Indonesia-Australia ditengah pandemi COVID-19 https://t.co/Zk3DpyiCYi	Positive
Kendati Muhammadiyah telah bekerja luar biasa melawan pandemi Covid-19 dan diapresiasi berbagai pihak, Sekretaris U... https://t.co/e6QIHtoKL9	Positive
Kementerian Kesehatan telah mengeluarkan Surat Edaran nomor HK.02.02/III/15242/2021 tentang Pelaksanaan Vaksinasi C... https://t.co/xc38o9eQgq	Positive

• Text Preprocessing

Text preprocessing is used to improve the model's efficiency and accuracy by reducing unmodeled variations [26]. The selection of appropriate pre-processing methods or a combination of pre-processing methods can affect the performance of the analysis, and improper use of pre-processing techniques can reduce the model's performance [27]. The research underwent four stages during preprocessing, which are as follows:

1) *Cleaning*: Cleaning is a process of removing or eliminating unnecessary words, links, characters, emoticons, and any punctuation which has no relevance to the tweets. Punctuations, for instance (!'#\$%&'[]*+,-./:;<=>?@[^_`{}~), and character symbols or commonly known as emoticons such as 😊 😞 😏 🤔 must be removed. In addition, in this research, the links within the tweet such as [28] mention symbol (@), hashtag (#), retweet symbol (RT), and unnecessary space and enter were removed.

2) *Case folding*: Case Folding is a stage in preprocessing that functions to convert capital letters into lowercase letters.

3) *Tokenizing*: Tokenizing is the process of breaking a document into units of words [8]. This process is used to get a word that will be processed at the next stage.

4) *Stemming*: Stemming is the process of transforming the words contained in the dataset into root words. In Indonesian text, the process of removing affixes in a word. Both affixes at the beginning of words (prefixes), affixes in the middle or insertions (infixes), affixes at the end of sentences (suffixes), or combination affixes from prefixes and suffixes (confixes) were altered. The illustration of stemming preprocessing can be seen in Table III. From table III it is known that there are words that were changed before stemming and already stemming.

TABLE III. STEMMING PREPROCESSING

Tweet	Process
Kerjasama ekonomi Indonesia-Australia ditengah pandemi COVID-19https://t.co/Zk3DpyiCYi	Before Preprocessing
“kerjasama” “ekonomi” “indonesia” “australia” “tengah” “pandemi” “covid”	After Preprocessing

At this stage, it generates a ready-to-use dataset is 2,835 tweets as depicted by the graph in Fig. 2. From Fig. 2 the dataset contains 1,892 tweets of positive sentiment and 943 tweets of negative sentiment.

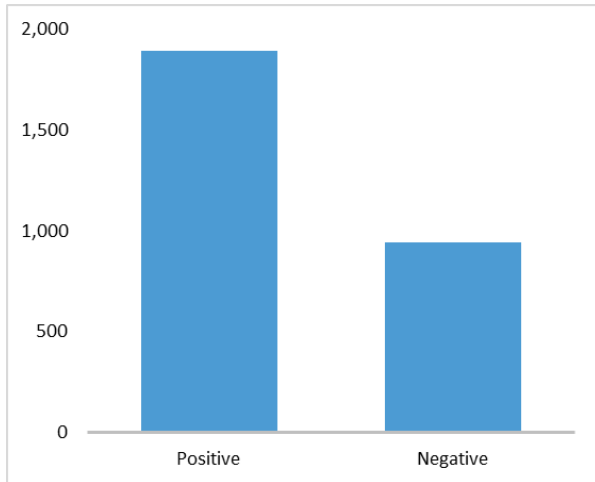


Fig. 2. Dataset Graphic.

- Data Splitting

Splitting data is a type of data sharing that occurs after the data has been processed. Data will split into two or more subsets. Data separation generally divides data into two portions, the first of which is used for test data and the second for training the model. This research divides the data into 80% of the training data and 20% of the testing data.

- Word Embedding

Word embedding is a method of creating a modified vector of word representation types that allows words with similar meanings to have similar representations [29]. In this study, two types of word embedding are used:

1) *Term Frequency-Inverse Document Frequency (TF-IDF)*: This TF-IDF method is an algorithm for merging two methods. Which include the concept of the frequency of occurrence of terms in a document and the inverse frequency containing the word [30]. Term Frequency (*tf*) provides the frequency of a word in each corpus document as in (1). Inverse Data Frequency (*idf*): used to calculate the weight of uncommon terms over the entire corpus of documents. A high *idf* score is assigned to words that appear seldom in the corpus as in (2). Combining these two (*tf* and *idf*) yields the TF-IDF score (*w*) for a word in a corpus document. It is the result of the subsequent in (3). Where $tf_{i,j}$ represents the number of occurrences of *i* in *j*, *j* represents the number of documents containing *i* and *N* represents the total number of documents.

$$tf_{i,j} = \frac{n_{i,j}}{\sum_k n_{i,j}} \quad (1)$$

$$idf(w) = \log \frac{N}{df_t} \quad (2)$$

$$w_{i,j} = tf_{i,j} \times \log \left(\frac{N}{df_i} \right) \quad (3)$$

2) *Embedding Layer*: The embedding layer requires that data first pass through the pre-processing stage, after which the sentence is broken down into word units. The word is then assigned a vector value or weight that is seeded with a small random number [31]. The Embedding Layer is a word embedding method used in the CNN algorithm, the results of which are then processed using the CNN model.

- Classification

1) *LSTM*: By entering input values derived from word weighting or TF-IDF, the LSTM method can classify draft sentences. The LSTM network structure is presented in Fig. 3 [32]. As depicted in Fig. 3, the LSTM algorithm is composed of a neural network and multiple distinct memory blocks called cells. The data gathered by the LSTM method is then stored by the cell, and memory modification is performed by a component known as a gate. In the LSTM algorithm, there are three types of gates: forgate gate, input gate, and output gate.

The initial process of the LSTM in finding the forgate gate was by multiplying the weight with the input value and adding the bias after which the sigmoid activation was carried out with (4).

$$f_1 = \sigma(W_f x_1 + U_f h_{t-1} + b_f) \quad (4)$$

The next step was to store the value of the forgate gate and calculate the input gate and candidate cell state. The input gate and candidate cell state equations are as follows (5) and (6).

$$i_1 = \sigma(W_i x_1 + U_i h_{t-1} + b_i) \quad (5)$$

$$C'_1 = \tanh(W_c x_1 + U_c h_{t-1} + b_c) \quad (6)$$

Then after that, it can compute the value of the cell gates, which was obtained by combining the values of the forgate gate and the input gate. The output gate and hidden layer values could then be obtained in (7) to (9).

$$C_1 = (f_1 * C_{t-1} + i_1 * C'_1) \quad (7)$$

$$o_1 = \sigma(W_o x_1 + U_o h_{t-1} + b_o) \quad (8)$$

$$h_1 = o_1 * \tanh(C_1) \quad (9)$$

In this research, the parameter settings of the LSTM that was utilized included a variety of various hidden layers, specifically 2, 8, 16, 32, and 64, with each layer including a total of 50 neuronal connections. Utilizing a sigmoid activation function, a loss function of the binary crossentropy type, the optimizer adam, a batch size of 32, and an epoch of 20. The employment of a variety of different hidden layer number scenarios has the purpose of determining the influence that the number of hidden layers utilized has on the accuracy as well as the loss that occurs as a result of using those hidden layers.

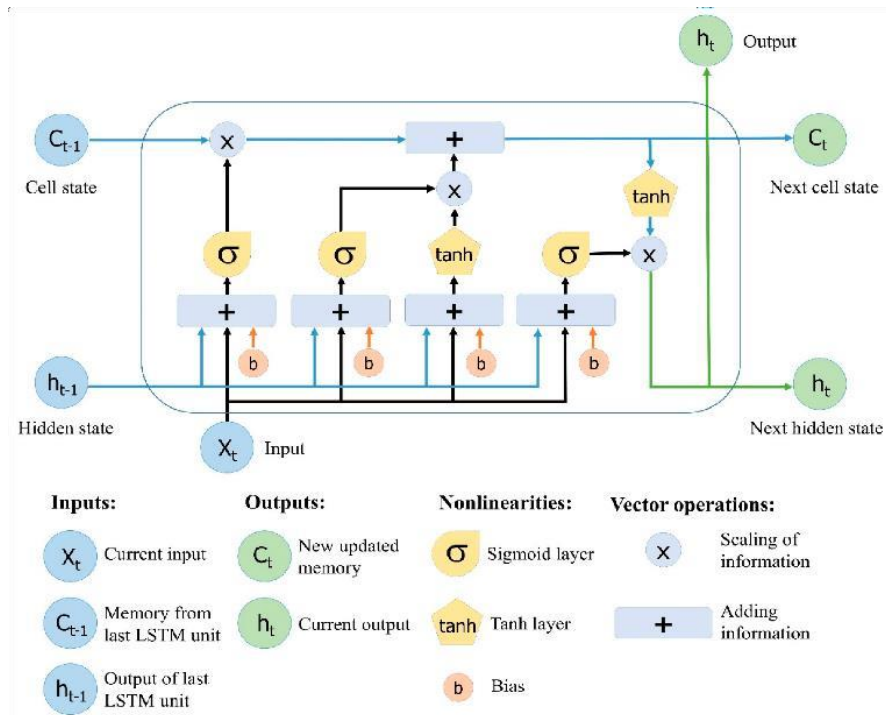


Fig. 3. LSTM Structure.

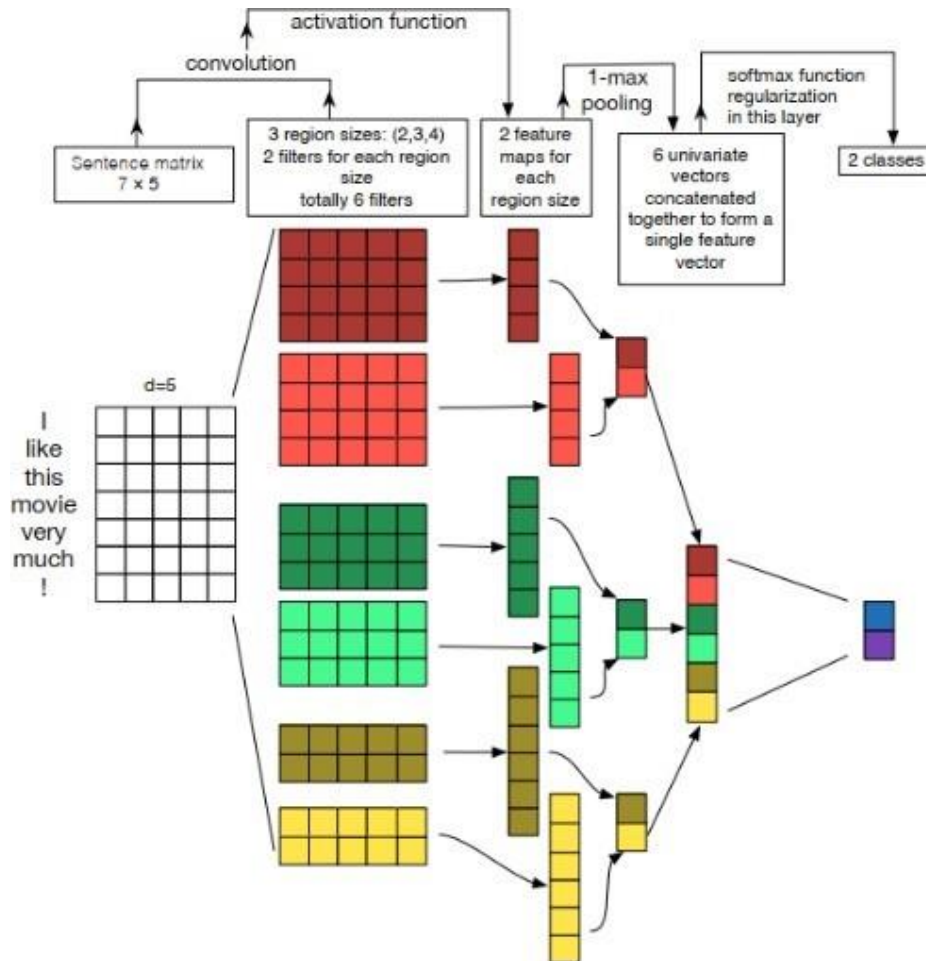


Fig. 4. CNN Model Architecture.

2) *CNN*: The input to a CNN for sentiment analysis tasks is a sentence or document represented as a matrix. The architecture of the CNN for sentiment analysis is depicted in Fig. 4 [33]. Fig. 4 describes the architecture of the CNN that will be used. This particular CNN will have one convolutional layer, and its size will be 2x2, and it will have 100 kernels. After each convolutional layer comes a maxpool layer with a size of 2 x 2, then a fully connected layer with 50 neurons in each hidden layers, and finally, a softmax layer with two neurons to represent the sentiment class comes at the end (Positive and Negative). In addition, the parameter settings used by CNN consist of the use of 20 epochs, the activation function of the Rectified Linear Unit (ReLU), the adam type optimizer, the loss function MSE, and the batch size 32. And there are scenarios using the number of hidden layers consisting of 2, 8, 16, 32, and 64.

Each row in the matrix in the Convolutional Neural Network is a token, usually a word, or it can be a character in the form of a vector that is written into a function in (10).

$$x_1:n = x_1 \oplus x_2 \oplus \dots \oplus n \tag{10}$$

The \oplus operator is a concatenation operator and is used to combine words that have been converted into vectors into a matrix form followed by the activation function of the linear unit rectifier. The feature function is written in (11).

$$c_i = \max(0, w \cdot x_i: i + h_{-1}) \tag{11}$$

Each filter convolutes the sentence matrix $\{x_1:h, 2: h_{+1}, \dots, 1:n\}$ and produces feature-maps with $\epsilon \mathbb{R}^n - h_{+1}$. The feature map function is written in (12).

$$c = [c_1, c_2, \dots, c_n - h_{+1}] \tag{12}$$

Pooling on the feature map is used to continue the training process [34]. MaxPooling is the pooling method used, and it takes the maximum value of $\hat{c} = \max\{c\}$ as a feature based on a filter that aims to get the most important features that represent other features for each feature map. The features derived from the pooling results are employed in the classification process at the fully connected layer.

III. RESULTS AND DISCUSSION

The implementation was carried out by comparing the Long Short-Term Memory (LSTM) and Convolution Neural Network (CNN) methods. With the hidden layer values used for experiments to determine the highest accuracy value in training and the lowest loss value in training, as well as the hidden layer value used for training. It has been determined that (2, 8, 16, 32, and 64). Both methods use an epoch value of 20 in their implementation after determining the hidden layer changes. Table IV and Table V compares the results of the accuracy and loss values in the training that was performed. Table IV shows that the LSTM method generates the highest accuracy value of 99.84% for the hidden layer value of 64 and a loss value of 0.034% for the hidden layer value of 64. The results are presented in the following Fig. 5. It differs from the CNN method, which achieves the highest level of accuracy at the hidden layer value of 64, with an accuracy value of 99.24% and a loss value of 3.95 %. In this instance, the outcome is depicted by the graph in Fig. 6.

TABLE IV. TRAINING ACCURATION

A Number of Hidden Layers	LSTM	CNN
2	99.68%	96.07%
8	99.74%	98.79%
16	99.69%	98.99%
32	99.71%	98.89%
64	99.84%	99.24%

TABLE V. LOSS TRAINING

A Number of Hidden Layers	LSTM	CNN
2	0.096%	13.57%
8	0.062%	5.23%
16	0.066%	2.76%
32	0.054%	5.41%
64	0.034%	3.95%

Fig. 5 is an LSTM graph illustrating the increase in training accuracy. Which indicates that the greater the epoch used, the higher the accuracy value, and if the accuracy value is high, the loss value will decrease. However, this is not always the case, the accuracy value is not always high when the epoch is high, as data and methods also influence the increase in accuracy.

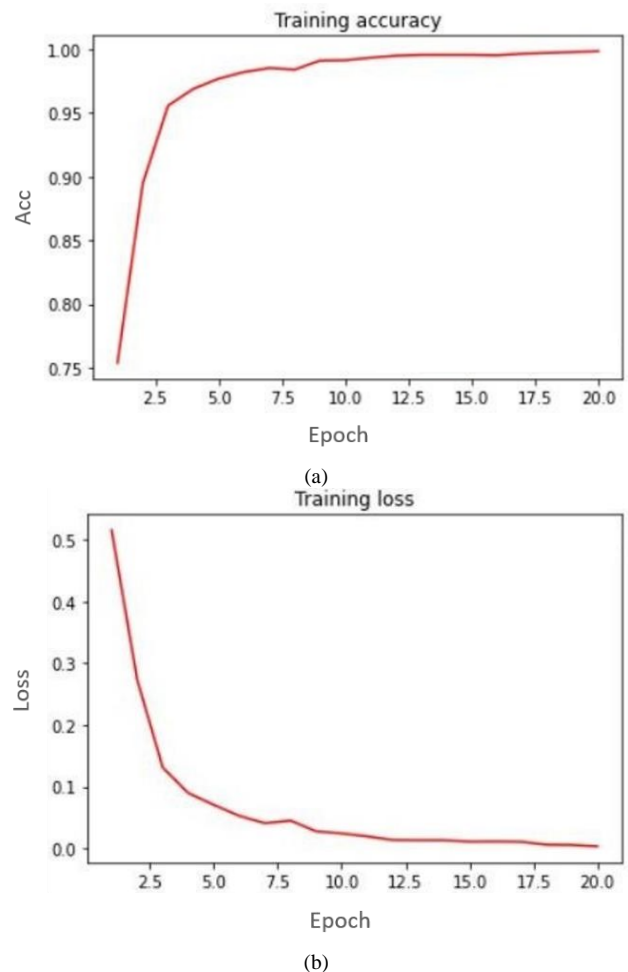


Fig. 5. LSTM Method: (a) Accuracy (b) Loss Graphs.

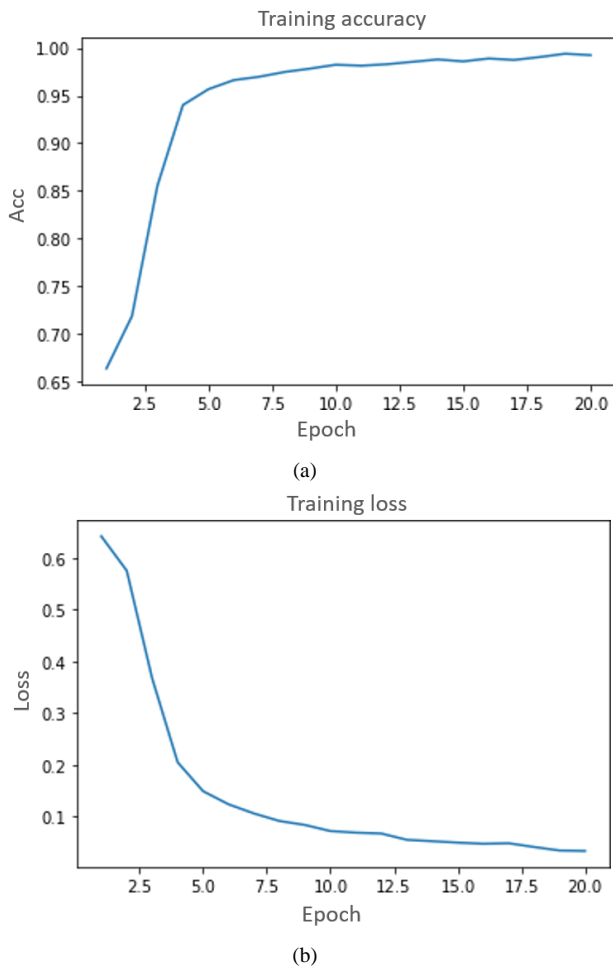


Fig. 6. CNN Method: (a) Accuracy (b) Loss Graphs.

Fig. 6 depicts a graph of the accuracy and loss of the CNN method which demonstrates that as the number of epochs used increases, so does the accuracy of the results. However, a large number of epochs does not guarantee that the accuracy obtained is also large; it is also affected by a number of other factors, such as the number of datasets and methods employed.

The 64th hidden layer will be used in the LSTM and CNN methods for this study. After obtaining the highest accuracy value during training and the lowest loss value during training, the researcher will use a confusion matrix to determine the final accuracy value for both methods. The following is an LSTM confusion matrix as can be seen in Table VI and CNN confusion matrix in Table VII. According to Table VI, the confusion matrix LSTM contains 504 true positive (TP) data, 145 true negative (TN) data, 78 false positive (FP) data, and 52 false negative (FN) data. CNN data from Table VII, TP 203, TN 487, FP 80, and FN 81 for confusion matrix.

TABLE VI. LSTM CONFUSION MATRIX

	Actually Positive	Actually Negative
Predicted Positive	504	78
Predicted Negative	52	145

TABLE VII. CNN CONFUSION MATRIX

	Actually Positive	Actually Negative
Predicted Positive	203	80
Predicted Negative	81	487

After obtaining the table confusion matrix with both methods, the performance values accuracy, precision, recall, and f1-score are reported in Table VIII. It is clear from Table VIII that both LSTM and CNN have good evaluation ratings, which means that they can be utilized for the classification of conversation sentences on Twitter relating to the Covid-19 Pandemic. The accuracy achieved by LSTM is the highest, coming up at 83.30%, whereas CNN only achieves 81.00%. Therefore, one can conclude from this research that the performance of LSTM is superior to that of CNN when it comes to analyzing people's feelings towards the COVID-19 pandemic.

TABLE VIII. VALUES ACCURACY, PRECISION, RECALL AND F1-SCORE

Method	Accuracy (%)	Precision (%)	Recall (%)	F1-Score (%)
LSTM	83.30%	86.50%	90.64%	88.50%
CNN	81.00%	71.73%	71.47%	72.00%

IV. CONCLUSION

A comparison of research that has been done using datasets from social media as many as 2,835 and distribution of data by 80% of training data and 20% of testing data states that the hidden layer and epoch determine the accuracy value, with a hidden layer of 64 and an epoch of 20, the highest training accuracy value is 99.84% and the loss value is 0.034% in the LSTM met. After calculating the accuracy and loss values in training, the LSTM method achieves an accuracy value of 83.30%, precision of 86.50%, recall of 90.64%, and f1-score of 88.50% while the CNN method achieved an accuracy of 81.00%, precision of 71.73%, recall of 71.47%, and f1-score of 72.00%. This states that the LSTM method outperforms CNN in terms of performance measurement, and that both methods can be used to classify conversation sentences about the Covid-19 Pandemic on Twitter.

Many aspects were left for future investigation due to time and computational process. It would be interesting to study the following topic: a) determining whether Twitter is a more dependable source of information than Facebook, WeChat, and Instagram. Nonetheless, it is of the utmost importance to investigate other social media platforms in terms of sentiment analysis to compare. b) This research application is useful for the Coronavirus health issue and can also be adopted as a model for identifying sentiment emotion in future cases of a similar nature.

ACKNOWLEDGMENT

I want to extend a special thank you to my team for this research, which have helped to make this experience motivating to finish all the writing in this paper.

REFERENCES

- [1] A. Arora, S. Bansal, C. Kandpal, R. Aswani, and Y. Dwivedi, "Measuring social media influencer index- insights from facebook, Twitter and Instagram," *J. Retail. Consum. Serv.*, vol. 49, pp. 86–101, Jul. 2019, doi: 10.1016/j.jretconser.2019.03.012.
- [2] T. N. Simanjuntak and S. Pramana, "Sentiment Analysis on Overseas Tweets on the Impact of COVID-19 in Indonesia," *Indones. J. Stat. Its Appl.*, vol. 5, no. 2, pp. 304–313, Jun. 2021, doi: 10.29244/ijsa.v5i2p304-313.
- [3] H. Andriani, S.Si, Apt, M.Sc, Ph.D, "Effectiveness of Large-Scale Social Restrictions (PSBB) toward the New Normal Era during COVID-19 Outbreak: a Mini Policy Review," *J. Indones. Heal. Policy Adm.*, vol. 5, no. 2, May 2020, doi: 10.7454/ihpa.v5i2.4001.
- [4] P. C. Sen, M. Hajra, and M. Ghosh, "Supervised Classification Algorithms in Machine Learning: A Survey and Review," in *Advances in Intelligent Systems and Computing*, 2020, pp. 99–111.
- [5] H. S. Basavegowda and G. Dagnev, "Deep learning approach for microarray cancer data classification," *CAAI Trans. Intell. Technol.*, vol. 5, no. 1, pp. 22–33, Mar. 2020, doi: 10.1049/trit.2019.0028.
- [6] A. Zappone, M. Di Renzo, and M. Debbah, "Wireless Networks Design in the Era of Deep Learning: Model-Based, AI-Based, or Both?," *IEEE Trans. Commun.*, vol. 67, no. 10, pp. 7331–7376, Oct. 2019, doi: 10.1109/TCOMM.2019.2924010.
- [7] A. Aldweesh, A. Derhab, and A. Z. Emam, "Deep learning approaches for anomaly-based intrusion detection systems: A survey, taxonomy, and open issues," *Knowledge-Based Syst.*, vol. 189, p. 105124, Feb. 2020, doi: 10.1016/j.knosys.2019.105124.
- [8] A. Pranolo, Y. Mao, A. P. Wibawa, A. B. P. Utama, and F. A. Dwiyanto, "Robust LSTM With Tuned-PSO and Bifold-Attention Mechanism for Analyzing Multivariate Time-Series," *IEEE Access*, vol. 10, pp. 78423–78434, 2022, doi: 10.1109/ACCESS.2022.3193643.
- [9] A. P. Wibawa, A. B. P. Utama, H. Elmunsyah, U. Pujianto, F. A. Dwiyanto, and L. Hernandez, "Time-series analysis with smoothed Convolutional Neural Network," *J. Big Data*, vol. 9, no. 1, p. 44, Dec. 2022, doi: 10.1186/s40537-022-00599-y.
- [10] S. U. Amin, M. Alsulaiman, G. Muhammad, M. A. Mekhtiche, and M. Shamim Hossain, "Deep Learning for EEG motor imagery classification based on multi-layer CNNs feature fusion," *Futur. Gener. Comput. Syst.*, vol. 101, pp. 542–554, Dec. 2019, doi: 10.1016/j.future.2019.06.027.
- [11] A. Hodorog, I. Petri, and Y. Rezugui, "Machine learning and Natural Language Processing of social media data for event detection in smart cities," *Sustain. Cities Soc.*, vol. 85, p. 104026, Oct. 2022, doi: 10.1016/j.scs.2022.104026.
- [12] S. M. Renz, J. M. Carrington, and T. A. Badger, "Two Strategies for Qualitative Content Analysis: An Intramethod Approach to Triangulation," *Qual. Health Res.*, vol. 28, no. 5, pp. 824–831, Apr. 2018, doi: 10.1177/1049732317753586.
- [13] D. Hussen Maulud, S. R. M. Zeebaree, K. Jacksi, M. A. Mohammed Sadeeq, and K. Hussein Sharif, "State of Art for Semantic Analysis of Natural Language Processing," *Qubahan Acad. J.*, vol. 1, no. 2, Mar. 2021, doi: 10.48161/qaj.v1n2a44.
- [14] M. S. Islam, S. S. Sharmin Mousumi, S. Abujar, and S. A. Hossain, "Sequence-to-sequence Bangla Sentence Generation with LSTM Recurrent Neural Networks," *Procedia Comput. Sci.*, vol. 152, pp. 51–58, 2019, doi: 10.1016/j.procs.2019.05.026.
- [15] A. Nugaliyadde, F. Sohel, K. W. Wong, and H. Xie, "Language Modeling through Long-Term Memory Network," in *2019 International Joint Conference on Neural Networks (IJCNN)*, Jul. 2019, pp. 1–6, doi: 10.1109/IJCNN.2019.8851909.
- [16] E. Setyati, S. Az, S. P. Hudiono, and F. Kurniawan, "CNN based Face Recognition System for Patients with Down and William Syndrome," *Knowl. Eng. Data Sci.*, vol. 4, no. 2, p. 138, Dec. 2021, doi: 10.17977/um018v4i22021p138-144.
- [17] W. Wang and J. Gang, "Application of Convolutional Neural Network in Natural Language Processing," in *2018 International Conference on Information Systems and Computer Aided Education (ICISCAE)*, Jul. 2018, pp. 64–70, doi: 10.1109/ICISCAE.2018.8666928.
- [18] K. Kyeong and H. Kim, "Classification of Mixed-Type Defect Patterns in Wafer Bin Maps Using Convolutional Neural Networks," *IEEE Trans. Semicond. Manuf.*, vol. 31, no. 3, pp. 395–402, Aug. 2018, doi: 10.1109/TSM.2018.2841416.
- [19] H. Juwiantho et al., "Sentiment Analysis Twitter Bahasa Indonesia Berbasis WORD2VEC Menggunakan Deep Convolutional Neural Network," *J. Teknol. Inf. dan Ilmu Komput.*, vol. 7, no. 1, pp. 181–188, 2020, doi: 10.25126/jtiik.202071758.
- [20] Yudi Widhiyasa, Transmissia Semiawan, Ilham Gibran Achmad Mudzakir, and Muhammad Randi Noor, "Penerapan Convolutional Long Short-Term Memory untuk Klasifikasi Teks Berita Bahasa Indonesia," *J. Nas. Tek. Elektro dan Teknol. Inf.*, vol. 10, no. 4, pp. 354–361, Nov. 2021, doi: 10.22146/jnteti.v10i4.2438.
- [21] D. T. Hermanto, A. Setyanto, and E. T. Luthfi, "Algoritma LSTM-CNN untuk Binary Klasifikasi dengan Word2vec pada Media Online," *Creat. Inf. Technol. J.*, vol. 8, no. 1, p. 64, Mar. 2021, doi: 10.24076/citec.2021v8i1.264.
- [22] N. Giarsyani, "Komparasi Algoritma Machine Learning dan Deep Learning untuk Named Entity Recognition: Studi Kasus Data Kebencanaan," *Indones. J. Appl. Informatics*, vol. 4, no. 2, p. 138, 2020, doi: 10.20961/ijai.v4i2.41317.
- [23] C. Zhou, C. Sun, Z. Liu, and F. C. M. Lau, "A C-LSTM Neural Network for Text Classification," *Comput. Lang.*, vol. 1, 2015, [Online]. Available: <http://arxiv.org/abs/1511.08630>.
- [24] D. Assenmacher, L. Clever, L. Frischlich, T. Quandt, H. Trautmann, and C. Grimme, "Demystifying Social Bots: On the Intelligence of Automated Social Media Actors," *Soc. Media + Soc.*, vol. 6, no. 3, p. 205630512093926, Jul. 2020, doi: 10.1177/2056305120939264.
- [25] D. Valle-Cruz, V. Fernandez-Cortez, A. López-Chau, and R. Sandoval-Almazán, "Does Twitter Affect Stock Market Decisions? Financial Sentiment Analysis During Pandemics: A Comparative Study of the H1N1 and the COVID-19 Periods," *Cognit. Comput.*, vol. 14, no. 1, pp. 372–387, Jan. 2022, doi: 10.1007/s12559-021-09819-8.
- [26] J. K. M. Biney, J. R. Blöcher, L. Borůvka, and R. Vašát, "Does the limited use of orthogonal signal correction pre-treatment approach to improve the prediction accuracy of soil organic carbon need attention?," *Geoderma*, vol. 388, p. 114945, Apr. 2021, doi: 10.1016/j.geoderma.2021.114945.
- [27] U. Naseem, I. Razzak, and P. W. Eklund, "A survey of pre-processing techniques to improve short-text quality: a case study on hate speech detection on twitter," *Multimed. Tools Appl.*, vol. 80, no. 28–29, pp. 35239–35266, Nov. 2021, doi: 10.1007/s11042-020-10082-6.
- [28] VIVAcoid, "Polri belum menerbitkan izin rencana PSSI mau menggelar kompetisi Liga 1 musim 2021/22 di tengah pandemi COVID-19," *Twitter*, 2021. <https://twitter.com/i/web/status/1423235846459641860>.
- [29] M. T. Pilehvar and J. Camacho-Collados, "Embeddings in Natural Language Processing: Theory and Advances in Vector Representations of Meaning," *Synth. Lect. Hum. Lang. Technol.*, vol. 13, no. 4, pp. 1–175, Nov. 2020, doi: 10.2200/S01057ED1V01Y202009HLT047.
- [30] N. S. Mohd Nafis and S. Awang, "An Enhanced Hybrid Feature Selection Technique Using Term Frequency-Inverse Document Frequency and Support Vector Machine-Recursive Feature Elimination for Sentiment Classification," *IEEE Access*, vol. 9, pp. 52177–52192, 2021, doi: 10.1109/ACCESS.2021.3069001.
- [31] R. Cai et al., "VIBNN," *ACM SIGPLAN Not.*, vol. 53, no. 2, pp. 476–488, Nov. 2018, doi: 10.1145/3296957.3173212.
- [32] X. H. Le, H. V. Ho, G. Lee, and S. Jung, "Application of Long Short-Term Memory (LSTM) neural network for flood forecasting," *Water (Switzerland)*, vol. 11, no. 7, pp. 1–19, 2019, doi: 10.3390/w11071387.
- [33] W. R. Moskolai, W. Abdou, A. Dipanda, and Kolyang, "Application of Deep Learning Architectures for Satellite Image Time Series Prediction: A Review," *Remote Sens.*, vol. 13, no. 23, p. 4822, Nov. 2021, doi: 10.3390/rs13234822.
- [34] W. Gong, H. Chen, Z. Zhang, M. Zhang, and H. Gao, "A Data-Driven-Based Fault Diagnosis Approach for Electrical Power DC-DC Inverter by Using Modified Convolutional Neural Network With Global Average Pooling and 2-D Feature Image," *IEEE Access*, vol. 8, pp. 73677–73697, 2020, doi: 10.1109/ACCESS.2020.2988323.

ACT on Monte Carlo FogRA for Time-Critical Applications of IoT

A. S. Gowri, P. Shanthi Bala, Zion Ramdinthara, T. Siva Kumar
Department of Computer Science, School of Engineering and Technology
Pondicherry University, Puducherry, India

Abstract—The need for instantaneous processing for Internet of Things (IoT) has led to the notion of fog computing where computation is performed at the proximity of the data source. Though fog computing reduces the latency and bandwidth bottlenecks, the scarcity of fog nodes hampers its efficiency. Also, due to the heterogeneity and stochastic behavior of IoT, traditional resource allocation technique does not suffice the time-sensitiveness of the applications. Therefore, adopting Artificial Intelligence (AI) based Reinforcement Learning approach that has the ability to self-learn and adapt to the dynamic environment is sought. The purpose of the work is to propose an Auto Centric Threshold (ACT) enabled Monte Carlo FogRA system that maximizes the utilization of Fog’s limited resources with minimum termination time for time-critical IoT requests. FogRA is devised as a Reinforcement Learning (RL) problem, that obtains optimal solutions through continuous interaction with the uncertain environment. Experimental results show that the optimal value achieved by the proposed system is increased by 41% more than the baseline adaptive RA model. The efficiency of FogRA is evaluated under different performance metrics.

Keywords—Cloud; edge; fog; Internet of Things (IoT); Reinforcement Learning (RL)

I. INTRODUCTION

The evolution of smart devices has led to the proliferation of the Internet of Things (IoT), thus making the world, a better-connected place for wireless communication and high-speed applications. The “Little Data, Big Stream” notion of IoT is mostly about time-sensitive applications [1]. The number of connected devices per capita is anticipated to be 01 trillion devices by 2025. This massive usage of IoT will generate mobile data services of 150 zettabytes by 2025 which corresponds to 5-7 times of IP traffic today [2]. The immense amount of mobile data can be processed instantaneously, only if the computing facility is available near the data source.

Ultra-low latency, energy efficiency, distributed processing, and storage are a few of the expectations of IoT applications. So far, the cloud was tailored to tackle these demands. But, in reality, the remotely located cloud causes delay and hinders the QoS requirements of the IoT requests [3]. By the time the data from IoT is transmitted to the centralized cloud, the inevitability to act on it might be gone, which cost lives. Disastrous management, Industrial IoT, and real-time aeronautical cum nuclear reactions are some of the time-critical IoT applications where the response delay of even nanoseconds makes a huge difference [4]. Hence, a fog computing paradigm that addresses time-critical applications in its proximity is recommended.

Fog computing is a distributed paradigm where the processing nodes are dispersed geographically near the data source. The proximal distribution of the processing elements promises ultra-low latency for time-critical applications [5]. IoT requires a Resource Allocation (RA) mechanism that prioritizes time-critical tasks over others. Also, a sufficient amount of fog resources may not be available, as and when required. Hence, allocation of compute nodes to the incoming IoT requests, in a resource-constrained fog environment is challenging [6]. The RA mechanism has to adopt an optimal strategy to make a sequence of smart decisions [7]. Although evolutionary algorithms, dynamic programming, and policy gradient are commonly used to derive optimal policy, these techniques require prior knowledge of the model [8]. But, the proposed work FogRA is a sequential decision-making problem in a model-free environment.

The environment involves IoT devices whose behaviour is stochastic and hence the dynamics of the model are not known. In such a case, Reinforcement Learning (RL) is sought to solve the FogRA problem for two reasons. First, RL is a machine learning, trial and error methodology that can self-learn and adapt through continuous interaction in an uncertain environment. Second, by its origin in Markov Decision Process (MDP), RL is a sequential decision theory that generates high-quality decisions in the long term [9].

Monte Carlo (MC), MC-Exploring Starts (MC-ES), and On-Policy Monte Carlo Control (OMC) are variants of RL algorithms that compute optimal policy. They are the straightforward methods that do not bootstrap and eliminate the curse of dimensionality problem [8]. They compute the optimal value by averaging the samples obtained through various iterations and derive the optimal policy from it.

Studies reveal that the existing RA works focused more on the development of frameworks that reduced latency and increased the quality of service [10]. The works carried out using feed-forward NN, MINLP, and other optimization techniques also obtained better outcomes [11]. But these techniques were heuristic-based and time-consuming. Q-learning algorithm of RL was mostly used to devise RA strategy. The combination of RL algorithms with queuing theory and neural networks too proved more efficient but involved cost overhead.

Moreover, the earlier works addressed intra-dependent and parallel tasks, while focus on time-critical applications was hardly found. Further, the earlier RL-based RA works were mostly proactive, in the sense that they depend on history for

prediction and hence mostly model-based [12]. But, the proposed work allocates the fog resources on demand. The reactive technique does not require any dynamics of the model. The availability of the scarce fog resources, and the heterogenous latency requirement of IoT describes the uncertain behavior of the environment. Allocation of fog's limited resources and prioritizing the time-critical requests are highly challenging that need attention. The proposed work is about designing an efficient FogRA system that handles the challenges of model-free stochastic environment at ease.

The proposed work employs ACT enabled MC approach to construct the FogRA system for time-critical IoT applications. The FogRA system involves a smart agent that finds the optimal policy to allocate the fog's limited resources to the time-critical requests. The significance of the work is perceived by its usage in the modern network environment and its potential for the fog computing paradigm. The main contribution of the intended work is summarized as follows:

- A Reinforcement Learning (RL) based FogRA system is developed in which the Fog nodes are used as computing resources, to process incoming requests.
- In the pursuit of maximizing fog utilization, the Fog Controller Agent (FCA) undergoes learning to allocate its resources to time-critical application requests.
- The ACT-enabled FogRA system is proposed using Monte Carlo (MC), MC-Exploring Starts (MC-ES), and On-Policy Monte Carlo Control (OMC).
- The proposed system is compared with an existing Adaptive RA system to evaluate its performance.
- Result demonstrates that the optimal long-term reward achieved by ACT-enabled FogRA is 41% more than the existing RA model.

The rest of the article is structured as follows: Section II discusses the background knowledge that substantiates FogRA as an RL problem. An overview of the RL approach and the formulation of FogRA as an MDP are briefly discussed in this section. The system model of the proposed work is elaborated in Section III. The experimental results are evaluated and analyzed in Section IV, and Section V concludes the paper with prospects for the future.

II. REINFORCEMENT LEARNING BACKGROUND

A. Resource Allocation as RL Problem

As mobile apps go more and more 24/7, online solutions that deliver instantaneous decisions are highly sought. The time-critical IoT requests demand response with almost negligible delay [13]. To achieve delay-less response, fog nodes that reside near the edge devices are used as computing elements. But the distributed nature of fog creates a scarcity of its resources. This makes the allocation of fog resources tedious, hence is considered an essential problem to be dealt with [14]. Due to the limited resources, not all the requests are served in the fog layer. It has to be constantly monitored whether the incoming request is time-critical or not. Prioritizing the time-critical applications to be served in the fog delivers prompt service with negligible and tolerable delay [15].

The FogRA comprises a Fog Controller Agent (FCA) that allocates the available fog resources to the most time-critical tasks. Through continuous interaction with the environment, the agent derives the optimal policy through which it decides whether to allocate the fog resource or not. The problem that involves learning and decision-making as a continuous process is defined as the RL problem [16]. As the allocation of fog resources to IoT requests need constant learning, and decision making, FogRA is considered an RL problem.

RL problem consists of the agent and the environment as the two main components as shown in Fig. 1. An agent is a learner and decision-maker. The environment is the entity with which the agent interacts [17]. Markov Decision Process (MDP) is used to articulate the interaction between the agent and the environment in terms of states, actions, and rewards, MDP is the mathematical framework to define how the environment behaves in response to the agent's action. The Markov process is a memoryless random process [8]. It states that the future is independent of the past given its present. Any environment in which the current state is sufficient to determine the next state, irrespective of its previous states (history) is said to possess the Markov property. Thus, MDP eliminates the need to preserve the value of past states thereby reducing the memory cost considerably.

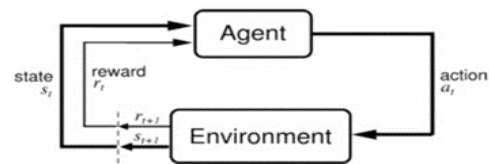


Fig. 1. Agent-Environment Interaction in RL [8].

The agent observes the environment's state ($s_t \in S$) and performs one of the actions ($a_t \in A(s)$) at each time step (t) of the interaction. The agent's activity results in a reward ($r_{t+1} \in R$) and a transition to the following state (s_{t+1}). Hence a sequence of trajectory $s_0, a_0, r_1, s_1, a_1, r_2, s_2, a_2, r_3 \dots \dots \dots$ is observed [18]. The crucial constraint on the agent is that it operates in an uncertain environment.

In most problems, the agent is not guided about the action that it has to carry out, instead, by trial and error, it learns the right action. The agent likely acts differently in a state for the first time, rather than after visiting the same state many times [19]. With experience, the agent learns the consequence of its action on that state. The consequence of an action influences not only the immediate reward but the next state and its subsequent rewards.

RL is a computational approach to designing a goal-directed learning agent that interacts with an uncertain environment [20]. In the Long-term, the agent seeks to maximize the cumulative payoff. At every time step (t), the agent receives a reward in the form of a scalar value which is either positive or negative. A positive value specifies how good the current action is, whereas a negative value indicates the penalty for the wrong action. The sum of the rewards starting from time 't' until the termination time 'T' is defined as returns (G_t). Thus, returns is

the metric that the agent aims to maximize in the long run. The definition of returns varies depending upon whether the task taken into consideration is episodic or continuous.

In Episodic tasks, the interaction between the agent and the environment breaks once the terminal state is reached [8]. The next episode starts in a state independent of the previous one ended. Tasks in episodes of this kind are called episodic tasks. Returns (G_t) for the episodic tasks starting from time 't' is expressed as the sum of undiscounted rewards as shown in equation (1).

$$G_t = r_{t+1} + r_{t+2} + r_{t+2} + r_{t+3} + \dots \dots \dots r_T \quad (1)$$

where r_{t+1} is the reward obtained at time-step (t+1) as an effect of the action (a_t) taken at time-step (t) on the state (s_t). The Time of termination (T), varies from episode to episode. The FogRA problem considered in the work is episodic. Each episode ends when all the fog resources are allocated to the incoming requests. Then the system is reset with the maximum number of fog nodes for the next episode.

On the other hand, for the tasks with continuous states, the interaction between the agent and the environment does not break, but rather continues without any terminal state [8]. Such tasks that do not have an identifiable terminal state are called continuous tasks. The rewards obtained at each time-step of continuous task accumulate to a big value that becomes uncountable. Also, the immediate reward got is more valuable than the one obtained in the future [21]. Hence, the value of the future reward is discounted by a factor of gamma (γ).

The value of gamma ranges from 0 to 1. When $\gamma=0$, the agent is myopic and concerned about maximizing the immediate reward, whereas $\gamma=1$ specifies that the agent gives more importance to the future reward. The literature study shows that values between 0.2 and 0.8 were found to be optimal in many scenarios [15]. Thus, returns (G_t) for the continuous tasks starting from time 't' is expressed as the sum of discounted rewards as shown in equation (2).

$$G_t = r_{t+1} + \gamma^1 r_{t+2} + \gamma^2 r_{t+2} + \gamma^3 r_{t+3} + \dots \dots \dots \quad (2)$$

where G is the reward gained at time-step (t+1) as feedback of the action (a_t) taken at time-step (t) on the state (s_t). The FogRA problem in the work is evaluated as an episodic task, with an initial and terminal state.

The concepts of Value function and Policy play a major role in implementing RL methodology [8]. The value function is the sum of all rewards that are expected in the future from every subsequent state. While the reward signal defines what is beneficial in the immediate sense, the value function signifies what is beneficial in the long run. In short, the reward is the immediate feedback for the current action, whereas the value function is the long-term estimation of rewards [18]. The goal of the agent is to maximize the long-term rewards in the form of the value function. Also, there is no value function without reward. As the iteration proceeds, the actions made by the agent are based on the value function.

The state value function $V(s)$ given by the equation (3), is the expectation of the returns (G_t) at the time 't' from the state s . It is the sum of immediate reward (r_{t+1}) and the discounted

value of the next state $V(s_{t+1})$ estimated iteratively, following the sequence of observation, starting from the state.

$$V(s) = \mathbb{E}[G_t | s_t = s] = \mathbb{E}[r_{t+1} + \gamma V(s_{t+1}) | s_t = s] \quad (3)$$

The value of a state is expressed as a function of expectation because future states are stochastic. Similarly, the action-value function ($Q(s, a)$) given by equation (4), is the expectation on the Returns (G_t) for the action ' a ', taken at time t, in the state ' s '.

$$Q(s, a) = \mathbb{E}[G_t | s_t = s, a_t = a] = \mathbb{E}[r_{t+1} + \gamma Q[s_{t+1}, a_t | s_t = s, a_t = a]] \quad (4)$$

The value obtained by these value functions helps the agent to decide the best action at a particular instant of time. Hence it is essential to know the value of the state and state-action pair. Identifying the best action for a state is termed as policy. Policies are the rules or the strategy the agent adopts to maximize the return in the long run [22]. Policies determine the optimal action that the agent has to adopt to achieve its goal.

The value of a state $V(s)$ following the policy (π) is written as $V_\pi(s)$. Consequently, the value of taking action ' a ' in state ' s ' and following the policy (π) thereafter is denoted as $Q_\pi(s, a)$. The agent looks for a policy that delivers maximum value for the state rather than the highest immediate reward. Unlikely, it is difficult to determine the state value $V(s)$, compared to the reward. Because rewards are the instantaneous feedback from the environment while value functions are long-run values that are estimated iteratively until the value converges with an optimal policy [15]. The value of the state resulting after convergence is the optimal value through which an optimal policy is derived. The agent uses the optimal policy to take the best action thereafter.

The Bellman Optimality equation is one of the methods to find the optimal value function [8]. The optimal value function $V^*(s)$ is one which yields the highest returns compared to all other value functions. $V^*(s)$ is expressed as a value function obtained by taking maximum over the policy (π) as given in the equation (5).

$$V^*(s) = \max_{\pi} V_{\pi}(s) \quad (5)$$

where $V^*(s)$ signifies the maximum quantity of long-term returns that is obtained from the system. Optimal policies also share optimal state-action value pairs $Q^*(s, a)$. The Bellman Optimality equation for Q^* is given by equation (6), which states that the optimal state action-value function is the one that is the maximum of all action functions following the policy π .

$$Q^*(s, a) = \max_{\pi} Q_{\pi}(s, a) \quad (6)$$

The goal of the RL problem is to find the optimal policy that yields the highest returns in the long run. A policy π is better than another policy π' if the value of a state obtained by following policy π is greater than the value of the state obtained by the following policy π' i.e., $V_{\pi}(s) \geq V_{\pi'}(s)$. The optimal policy is derived by taking the maximum over the policy ' π ' under the state ' s ' of the value function as given in equation (7).

$$\pi^* = \operatorname{argmax}_{\pi} V_{\pi}(s), \forall s \quad (7)$$

Computation of optimal policy involves iterative estimation of the value function. RL is a method for the efficient estimation of value functions and optimal policy. As the FogRA problem taken into account is model-free, Monte Carlo (MC), MC Exploring Starts (MC-ES), and On-Policy Monte Carlo Controls methodologies are employed to compute the optimal policy.

B. Monte Carlo Approach

Monte Carlo (MC) is a model-free RL algorithm that learns by averaging the samples drawn from the observation [15]. It learns to derive the policy in an environment where transition probabilities and reward distribution are not known [8]. Hence, the proposed FogRA problem adopts the Monte Carlo method to estimate the optimal policy. An episode is generated starting from an initial state till the terminal state. The trajectory of an episode in the MC algorithm is shown in Fig. 2.

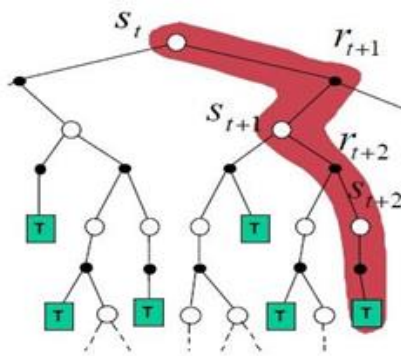


Fig. 2. Back-up Diagram for Monte Carlo Approach [8].

At any instant of time ‘ t ’ the agent observes the state ‘ s_t ’ chooses an action ‘ a_t ’, transits to a new state s_{t+1} , and gains a reward ‘ r_{t+1} ’. Returns G_t is computed for every episode. Then the value of the state $V(s)$ is estimated by averaging the returns. This process is repeated till $V(s)$ converges for all states and thus obtains the optimal value $V^*(s)$ for every state. Then the optimal policy is derived for each state using the equation (7).

Given some experience (samples), FCA estimates the value of states following policy $V_\pi(s)$, for all the non-terminal states s_t that occur in the trajectory. The agent waits until the returns G_t following the visit is known, then use the returns as a target to update $V_\pi(S_t)$ as given in equation (8).

$$V_\pi(S_t) \leftarrow V_\pi(S_t) + \alpha[G_t - V_\pi(S_t)] \quad (8)$$

where G_t , is the actual returns following the time ‘ t ’, and ‘ α ’ is the step size at which the agent learns. Alpha ‘ α ’ is the learning rate hyperparameter. It balances the weight that has been observed in the recent past with the weight of the newly observed target. Equation (8) is also called Exponential Recency Weighted Average (ERWA), which estimates the incremental moving average by giving more weight to the immediate reward [18]. It very much suits a non-stationary environment like FogRA in which the action and the reward undergo continuous learning.

C. Monte Carlo Exploring Starts (MC-ES)

Monte Carlo (MC) estimates the optimal value function $V(s)$ for all states appearing in the episode. It simply looks ahead and chooses the action that leads to the best combination of reward and the next state, which means it does not consider the choice of actions in the state. Another issue is that MC works better when the state space is known in advance. Hence, finding $Q(s, a)$ through MC-ES is the best way, as it considers the choice of actions across all the states and finds the optimal policy by maximizing the action value that produces high returns in the long run [23].

The difference is that the existing adaptive RA model used the MC approach to estimate the value of state ‘ $V(s)$ ’, while the MC-ES uses the state-action value pair ‘ $Q(s, a)$ ’ to improve the policy. The change in the algorithm is that, the returns ‘ G_t ’ is computed as $G_t(s, a)$ rather than $G_t(s)$. Hence, MC-ES evaluates $Q(s, a)$ for all state-action pairs as given in equation (9).

$$Q(s_t, a_t) \leftarrow Q(s_t, a_t) + \alpha[G_t(s, a) - Q(s_t, a_t)] \quad (9)$$

Then the optimal policy $\pi^*(a/s)$ is derived by choosing the action with maximum action value for each state $s_t \in S$ as given by the equation (10).

$$\pi^*(a/s) \leftarrow \operatorname{argmax}_a Q(s, a) \quad (10)$$

D. On Policy Monte Carlo Control (OMC)

The estimation of state-action value function $Q(s, a)$ in MC-ES give rise to two issues. First, it increases the state space from S to $(S \times A)$ leading to memory and time complexity [8]. Secondly, the agent might not be able to explore all state-action pairs, if it acts too greedy towards the policy from the start. Hence, the value of $Q(s, a)$ and the policy obtained through MC-ES, cannot be optimal without a proper balance of exploration and exploitation [23]. Instead, the On-policy Monte Carlo Controls (OMC) estimates the optimal policy through the epsilon (ϵ) greedy approach. The agent picks a random action at epsilon (ϵ) times and acts greedy during the period $(1 - \epsilon)$ times thus balancing the explore-exploit instability [24]. The Epsilon is a value chosen between zero and one by trial and error, and it is problem-dependent.

III. THE PROPOSED WORK

A. System Model

The FogRA system comprises IoT devices and Fog nodes as its core components. The fog nodes reside between the IoT devices and the cloud. These fog nodes are equipped with computing cum network functionality to process incoming requests. FogRA is modeled as an RL problem, where a fog node act as the Fog Controller Agent (FCA). Monitoring the number of fog nodes utilized, observing the time criticality of the incoming request, and then deciding to act accordingly is the prime process of FCA. The fog nodes and the requests from the IoT devices at the edge network make up the environment. The agent-environment interaction of the RL-based FogRA system is portrayed in Fig. 3.

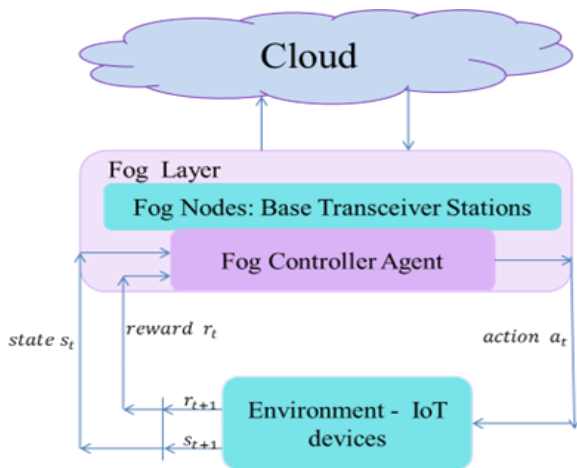


Fig. 3. The FogRA System.

At any instant of time, the time-criticality of the incoming request and the number of utilized fog nodes define the state (s_t). The FCA's decision either to accept the request in fog or decline it forms the action. As a consequence of the action taken, the FCA receives either a positive or negative reward as feedback. The heterogeneity of time-criticality from the IoT and the fog's limited resources make the environment stochastic.

The objective of the ACT-enabled FogRA system is to allocate the fog's limited resources to the time-critical applications within a short time. In the pursuit of the objective, the system maximizes the accepted requests, rewards, and value of state-action pairs which is termed Fog Utilization (U_{Fog}). Fog's limited resource forms the constraint of the resource allocation problem. The objective of the FogRA system is expressed as a multi-objective optimization problem as given in the equation (11).

$$\text{Maximize } U_{Fog} = \sum_{t=0}^T N_{accept} + \sum_{t=0}^T rwd_{accept} + VF_{opt}$$

$$\text{and Minimize } F_{converge} = \sum_{t=0}^T \mathbb{1}_{Time to obtain VF_{opt}}$$

$$\text{s. t. c } \sum_{t=0}^T N_{accept} = N_{max} \quad (11)$$

where, ' T ' is the terminal time-step of each episode. N_{accept} refers to the number of requests accepted by the Fog layer, rwd_{accept} symbolizes the amount of reward received for allocating fog node, VF_{opt} represents the optimal value achieved and N_{max} signifies the number of fog nodes present in the fog layer. $F_{converge}$ refers to the finish time by which all states converge to their optimal value. Hence, the work concentrates on maximizing Fog Utilization and minimizing the convergence time.

FogRA is modeled as MDP to define the mathematical framework of the RL problem. The fog nodes are defined as a set of states in the Markov model, and at each time step, it is in one of the states ($s_0, s_1, s_2, s_3, \dots, \dots, s_n$). At any instant of time $t = 1, 2, \dots, T$, the state is represented by s_t . To achieve the objective, the FCA undergoes learning to choose the best action in a current state.

B. Problem Definition

The Fog Controller Agent (FCA) perceives the state of the environment by constant interaction with it. With the continuous stream of application requests, the FCA takes RA decisions regularly. As the current action taken by the FCA, influences the next state and in turn possibility of future actions and rewards, the FogRA problem is formulated as MDP. The MDP to allocate fog nodes for the time-critical IoT requests is defined as $MDP_{FogRA} = \{S, A, P, R, \gamma\}$ where,

- $S = \{(m, n_t, c_t) / m=10, \text{ and } 0 \leq n \leq N_{max} \text{ and } 1 \leq c \leq C\}$ is the set of possible states of the MDP. At any instant of time, the state of the fog node is expressed as $\{s_0, s_1, s_2, s_3, \dots, \dots, s_t \in S\}$ in which,

$m \in \mathbb{N}$ defines the number of applications considered in the work.

$n_t \in \mathbb{N}$ is the number of fog nodes utilized at any instant of time ' t ' bounded by N_{max} .

$c_t \in \mathbb{N}$ is the time criticality of the incoming request at any instant of time ' t '. It is a random number in the range.

of one and ten with $C = 10$ as the highest priority.

- $A = \{a \in \{\text{'accept'}, \text{'decline'}\}\}$ is the action set where 'accept' denotes allocation of fog node, and 'decline' indicates refusal of fog node.
- $P = S \times A \times S \rightarrow [0,1]$ is the probability of transition $P(s'|s, a)$ to a new state s' from state ' s ' when action ' a ' is taken.
- $R = S \times A \rightarrow \mathbb{N}$ denotes the expected reward when the environment is in state ' s ' and action ' a ' is taken.
- $\gamma \rightarrow 0 < \gamma < 1$ is the discount factor that computes the present value of the expected future reward.

Allocation of fog resources to the IoT application requests depends on the number of available resources and the time criticality of the incoming request. The state of the MDP at any instant of time (t) as defined in equation (12),

$$s_t = m \cdot n_t + c_t \quad (12)$$

where $n_t \in \{0, 1, 2, 3, \dots, \dots, N_{max}\}$ is the number of fog nodes utilized/allocated. The current state is based on the number of utilized fog nodes, and the time-criticality of the successive task. The time criticality of the service request arriving at time ' t ' is denoted by " c_t ". It is obtained based on the latency requirement of the incoming request presented in Table I. " c_t " is calibrated by a ten-point scale ranging between 1 and 10, with 10 being the highest priority. Starting with ten applications (m), the total number of states encountered is $m(N_{max}) + C$. The next state s_{t+1} depends on the current state and the action taken, thereby reflecting the Markov property.

TABLE I. LATENCY TIME-CRITICALITY MAPPING

Applications	Latency Requirement in ms	Time Criticality "c _t "
Tactile Internet	<=5	10
Industrial IoT	6-20	9
Smart Vehicles	21-100	8
Collaborative Research/Educational tools	101-150	7
Audio Conference between Patient-Doctor	151-200	6
Internet Chat	201-250	5
Tele Surgery and Tele Ultra Sonography	251-300	4
Video Conference between Patient-Doctor	301-400	3
Web browsing	401-450	2
Automated Notifications	>=10 secs	1

When the fog node is in one of the possible states $s_t \in S = \{1, 2, 3, \dots, C(N_{max} + 1)\}$, the agent either accepts the incoming task or declines it. Thus, 'A' is the set of actions {accept, decline} where the action 'accept' denotes allocation of a fog resource and 'decline' indicates forwarding the request without allocation of a fog resource. The action chosen is based on the sum of the immediate reward and the value of the possible next state as given in equation (13).

$$action = \begin{cases} \text{accept in fog, if } [rta_{immediate} + \gamma V^*(s_{accept})] > [rtd_{immediate} + \gamma V^*(s_{decline})] \\ \text{decline, otherwise} \end{cases} \quad (13)$$

where the immediate reward is based on the time criticality and intended action as described in the reward system. $rta_{immediate}$ and $rtd_{immediate}$ describes the reward obtained on acceptance and declination respectively. The value of a state denotes the quantity of goodness for the agent to remain in that state. It is determined by its immediate reward and the discounted value of the next possible state. The value of the terminal states is zero.

Similarly, the action from the current state in terms of the state-action pair $Q(s, a)$ is given in equation (14). The choice of the equation for action selection depends on whether the algorithm is MC, MC-ES, or OMC respectively.

$$action = \begin{cases} \text{accept in fog, if } (rta_{immediate} + \gamma Q^*[s, \text{accept}]) > (rtd_{immediate} + \gamma Q^*[s, \text{decline}]) \\ \text{decline, otherwise} \end{cases} \quad (14)$$

An effective reward system influences the learning ability of an agent. With the right reward as the feedback, the FCA learns better and fast. In FogRA the reward is defined as a function of time criticality, priority threshold, and action taken as shown in Table II. Every incoming request is associated with a time-criticality value (c_t) which is appended in an array. Then the median of the array value is computed in every episode to obtain the Priority threshold (pth_t) at the time 't'. Considering the chance of uneven distribution of c_t values, FogRA chooses the median as the measure of central tendency.

TABLE II. REWARD SYSTEM

Action taken	Time-Criticality	Reward
accept	$c_t \geq pth_t$	pth_t
decline	$c_t \geq pth_t$	$-pth_t$
accept	$c_t < pth_t$	$-pth_t/2$
decline	$c_t < pth_t$	$pth_t/2$

At any instant of time, if the time-criticality of the arrived request (c_t) is greater than the priority threshold (pth_t), then the request is considered to be of high priority. Accepting such a request indicates the right action of the agent. Hence, the agent is encouraged with a positive value of the priority threshold as a reward. Declining the high priority request indicates a wrong action, for which the agent is rewarded with a negative value of pth_t . On the other hand, a time-criticality value less than that of the priority threshold indicates the less time-sensitiveness of the incoming request. Accepting the less time-sensitive task is considered a wrong action anyway, hence the agent is rewarded with $(-pth_t/2)$. Otherwise, the agent is rewarded with $(pth_t/2)$ for declining the less time-sensitive request. Thus, the reward obtained at time 't' depends on the priority threshold computed at that time step.

The probability of state transition (P) and reward distribution (R) describes the dynamics of the environment. When the dynamics of the environment are known, the optimal policy is directly obtained through Dynamic Programming (DP) [8]. Also, DP is bound to fixed values of P, R, and policy π . But, the FogRA environment considered in the work is neither stationary nor policy deterministic. With $m(N_{max}) + C$ number of states and 2 actions per state, the problem of computing the transition probability for all states grows exponentially and cumbersome rather than solving the RA problem itself. Hence, Monte Carlo (MC) method that learns the optimal policy without P and R is sought. Hence, the proposed work does not consider the distribution parameters and employs MC to derive the optimal policy.

C. ACT enabled MC for FogRA

Time criticality (c_t) of an incoming request is defined in the range of one to ten, with ten designated as the highest priority. As Fog resources are limited, only those requests whose time criticality value is greater than the priority threshold is given importance to get processed in fog nodes. But, fixing a suitable priority threshold (pth_t) at every time step is not a trivial task in FogRA whose environment is stochastic and non-stationary. An increased pth_t value leads to poor performance of the FCA, in which the number of accepted requests becomes less than the decline. A decrease in the pth_t results in the allocation of fog nodes to non-time-critical applications, which conflicts with the objective of the system. Hence the work suggests Auto Centric Threshold (ACT) that self-generates the threshold at every time step. The incoming time criticality (c_t) is appended in an array. Then, the priority threshold (pth_t) is computed as the median of the time criticality (c_t) values stored in the array at every time step.

Initially, the FogRA system allocates the fog resource with the priority threshold computed at time $t=0$. As the episode proceeds, the FCA learns the best policy in which only those requests with a critical value greater than the recently computed priority threshold are allocated the fog resource. The algorithm to learn the optimal policy by the ACT-enabled MC for the FogRA is given in Algorithm 1.

Algorithm 1: ACT MonteCarlo

```

Initialize  $V(s) = 0 \forall S$ 
Initialize return  $(s)$  // an empty list to save returns of all state in every iteration
1. Read  $N_{max}$  // no-of-fog-nodes
2. For episode count = 1, 2, 3, .....do
3.   While utilized fog node  $\leq N_{max}$ 
4.     Read latency requirement of the incoming request
5.     Obtain the time-criticality " $c_t$ " of the incoming request from Table 1
6.     Obtain the state using equation (12)
7.     Compute the Priority-Threshold ( $pth_t$ )
8.      $rta = \text{get\_reward}(\text{'accept'}, c_t, pth_t)$ 
9.      $rtd = \text{get\_reward}(\text{'decline'}, c_t, pth_t)$ 
10.    Take action on the incoming task based on the equation (13)
11.     $\text{get\_reward}(\text{action}, c_t, pth_t)$ 
12.    Append the reward in the rewards list
13.    increment the utilized_fog_node by one
14.  Compute the returns  $G_t$  for all states appearing in the episode till the terminal state
15.   $V(s) \leftarrow$  incremental average based on the equation (8)
16.  If  $V(s)$  converges for all states then
17.     $V^*(s) \leftarrow V(s)$  for all states
18.    Break
19.  Endif
20. Endfor
21. Use the optimal state value  $V^*(s)$  to update the optimal action in equation (13)

```

The FogRA system is implemented as an episodic task. Once a task arrives, based on its latency requirement, the time-criticality is obtained from the latency time-criticality mapping table. The value of states $V(s)$ is initialized with Zero for all states. Based on equation (13), FCA decides whether to accept the request in the fog or decline it. By continuous interaction with the environment, the FCA updates the state value of all states and derives the optimal policy for every state.

Given the episode, generated by following the policy π (ie., action taken based on equation (13)), the ACT-enabled MC optimal policy algorithm evaluates $V_\pi(S_t)$ for all the non-terminal states S_t occurring in that episode. The returns G_t is computed as the sum of undiscounted rewards starting from the initial state till the terminal state of the episode. The returns of every state are used as the target to update the value of the respective state $V_\pi(S_t)$ as given in equation (8). Episodes are generated as long as the state values converge for all states. Once state value converges, the optimal policy is obtained based on equation (7).

IV. EXPERIMENTAL ANALYSIS AND DISCUSSION

The MDP for FogRA system adopts the definition of state from adaptive resource allocation but differs in certain aspects [15]. First, the proposed work obtains the time-criticality value (c_t) from the Latency Time-criticality mapping Table I, which maps the preference level of the IoT request with its criticality value. Secondly, as the proposed MDP is episodic, the returns are computed with undiscounted rewards. Thirdly, priority threshold is computed by a self-generated Auto Centric Threshold (ACT) method which suits more for the stochastic nature of the IoT environment. Finally, unlike constant value-based rewards, the novel reward system acts in coherence with the priority threshold and provides the best incentive for the agent to learn better and faster.

The experiment is implemented in python Spyder. The simulation was conducted for the latency generated at random. Then the priority level of the request is obtained from the

latency-time criticality mapping Table I. The simulation parameter and their corresponding values are maintained as given in the Table III.

TABLE III. SIMULATION PARAMETERS

Parameter	Description	Values
α	Learning Rate	0.02
pth_t	Priority Threshold	Median of the time-criticality values
ϵ	Probability of Random Action	0.2
γ	Discount Factor	0.6
C	Highest Priority level	10
N_{max}	Max.number of Fog Nodes	15

This section analyses the experimental results obtained through MC, MC-ES, and OMC to evaluate the performance of FCA. The work considers ten IoT applications, hence the value of ' m ' is set to 10 in the work. With the number of fog nodes N_{max} as 15, and the maximum time criticality value C as 10, the MDP leads to $m(N_{max}) + C$ possible states, which are given by $s_t \in S = \{1,2,3, \dots, m(N_{max}) + C\}$. Initially, at the time $t=0$, all fog nodes are available, so the number of occupied fog nodes n_t remains zero in the equation (12) with the possible initial state as $s_0 \in \{1,2,3 \dots C\}$. The MDP terminates at time T when all the fog nodes are occupied, ie., $n_t = N_{max}$ with the possible terminal states as $s_T \in \{CN_{max} + 1, CN_{max} + 2, CN_{max} + 3 \dots \dots C(N_{max} + 1)\}$. Hence, the proposed work is experimented with 160 states, with $\{1, 2, 3, \dots, 10\}$ as one of the possible initial states and $\{151,152,153, \dots, 160\}$ as one of the terminal states.

A. Adaptive MC vs ACT MC

First, the performance of FogRA is evaluated with the adaptive MC and the proposed ACT-based MC model. Fig. 4 reflects the value of a few states estimated by the Adaptive MC algorithm in the earlier work [15]. The adaptive model converges after 10000 episodes resulting in the optimal state value 16. Fig. 5 shows that the ACT-based MC derives an optimal state value of 17.5 which is 9.375 % more than the Adaptive MC. The metrics observed in the implementation of Adaptive and ACT-based MC are tabulated in Table IV.

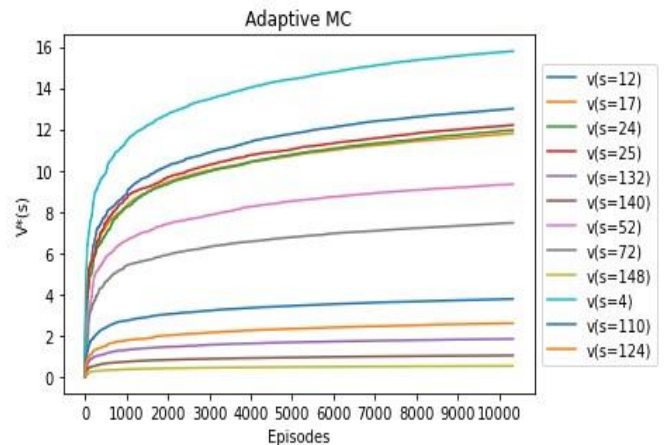


Fig. 4. Optimal State Value in Adaptive RA.

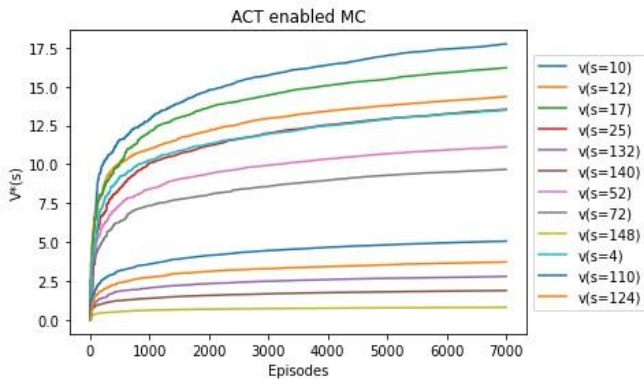


Fig. 5. Optimal State Value with ACT-MC.

The estimation of $V^*(s)$ obtained by the MC algorithm fits more for the model-based MDP. As FogRA is a model-free system, the exploration-oriented ACT MC-ES (Monte Carlo Exploring Starts), is implemented to compare its results with the Adaptive model.

B. Adaptive MC-ES vs ACT MC-ES

The FogRA system is then evaluated in MC-ES for both the Adaptive and ACT model. The ACT-based MC-ES algorithm estimates $Q(s, a)$ rather than $V(s)$. Hence, the state space increases from s to $(s \times a)$, and the action selection depends on equation (14). Fig. 6 and Fig. 7 show the convergence of optimal action-value $Q^*(state, accept)$ and $Q^*(state, decline)$ in Adaptive RA for twelve states chosen at random.

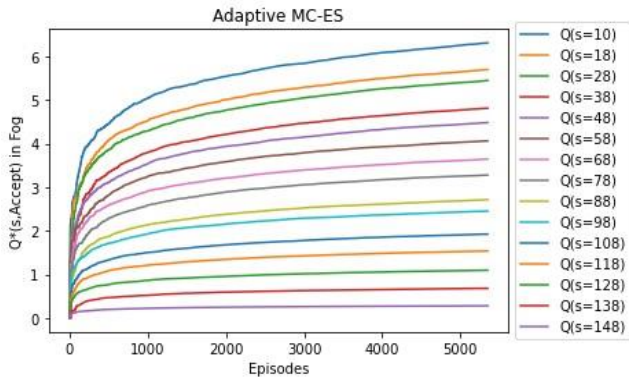


Fig. 6. $Q^*(s, \text{Accept})$ for Adaptive MC-ES.

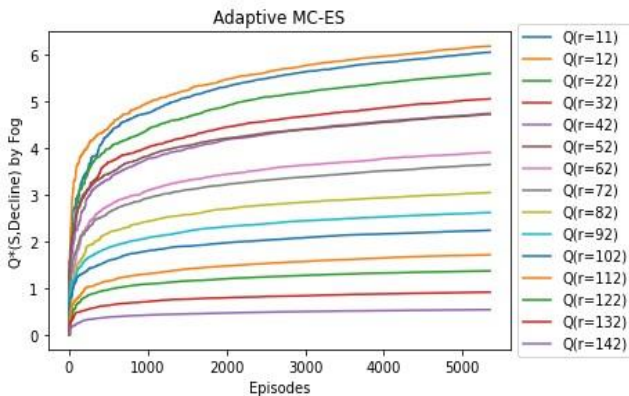


Fig. 7. $Q^*(s, \text{Decline})$ for Adaptive MC-ES.

Unlike the Adaptive approach, the values obtained by ACT-based MC-ES in Fig. 8 and Fig. 9 show improved optimal values comparatively. The estimated $Q^*(s, a)$ value in the Adaptive approach is lesser than the ACT model. The reason behind the poor $Q^*(s, a)$ value is that the Adaptive MC-ES is not able to explore widely in an episodic environment with a limited number of fog nodes.

Table IV shows the improved value from 16 in the MC model to 18.7025 in ACT-based MC-ES. The increase in the percentage of 16.8906% indicates the robustness of the ACT-enabled FogRA over the Adaptive system even in an environment with scarce resources. Still, the improvement is not considered favourable as the action selection process of MC-ES is greedy without enough exploration. Hence, the ACT-based FogRA System is tuned towards a balanced mix of exploration and exploitation in the OMC approach.

C. Adaptive OMC vs ACT OMC

The OMC algorithm estimates the value of state-action pair $Q(s, a)$, but the action based on equation (14) is decided only after a balanced trial of exploration and exploitation. FCA controls the level of exploration and exploitation based on a ϵ -greedy policy and is hence named as On-Policy Monte Carlo Control (OMC). The agent explores such that a random action is picked epsilon times and the greedy action based on equation (14) is picked for the $(1 - \epsilon)$ times. In this case, epsilon (ϵ) is chosen as a small positive number of 0.2 after trial and error. Fig. 10 and Fig. 11 show the convergence of optimal action value $Q^*(state, accept)$ and $Q^*(state, decline)$ for twelve states chosen at random using an Adaptive approach.

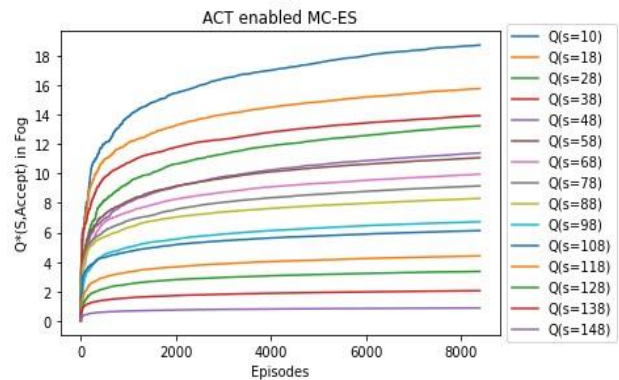


Fig. 8. $Q^*(s, \text{Accept})$ for ACT MC-ES.

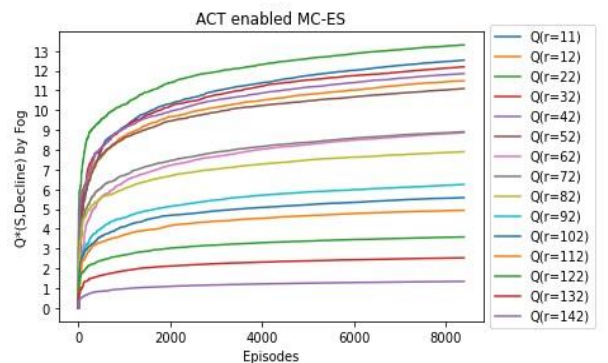


Fig. 9. $Q^*(s, \text{Decline})$ for ACT MC-ES.

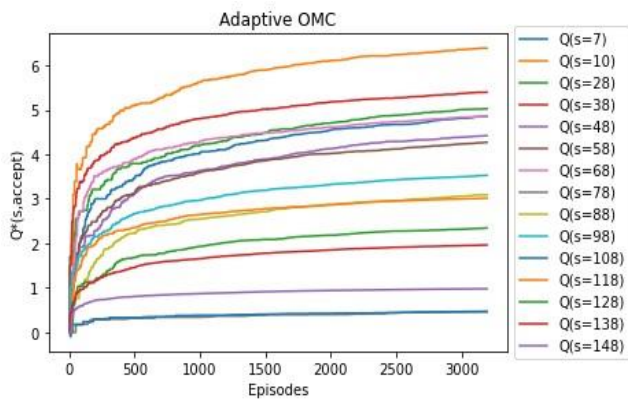


Fig. 10. $Q^*(s, \text{Accept})$ for Adaptive OMC.

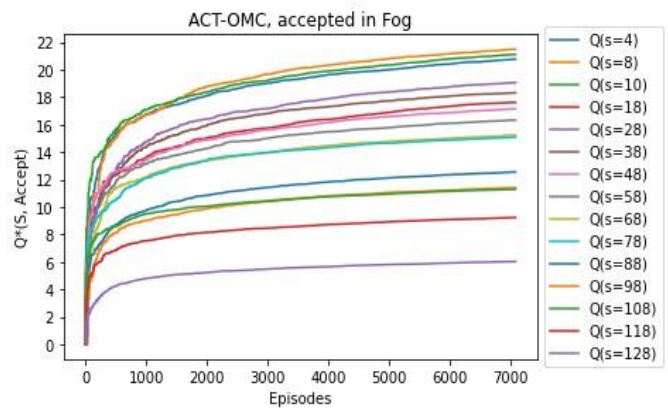


Fig. 12. $Q^*(s, \text{Accept})$ for ACT OMC.

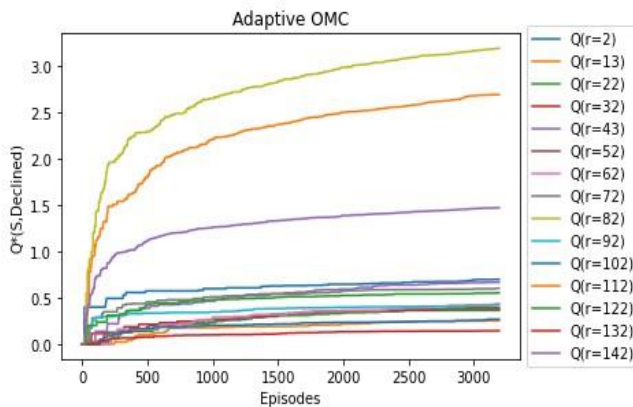


Fig. 11. $Q^*(s, \text{Decline})$ for Adaptive OMC.

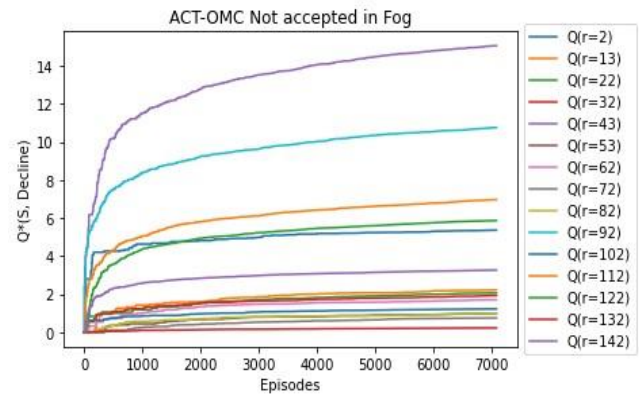


Fig. 13. $Q^*(s, \text{Decline})$ for ACT OMC.

Despite its balanced explore-exploit strategy, the adaptive OMC terminates fast, resulting in minimal $Q^*(s, a)$ value. It expresses the inability of the adaptive system for exploration. Whereas the ACT enabled OMC outperforms its counterpart by improved $Q^*(s, a)$ with minimal termination time in Fig. 12 and Fig. 13. The numerical results obtained during execution are tabulated in Table IV.

The optimal state-action value estimated by ACT-based OMC is increased by 41% more than the Adaptive MC. Thus, the ACT-based OMC surpasses other methods by maximizing long-term returns. The high value of the long-term returns with minimum termination time denotes that the FCA has learned the best policy at a fast rate, thanks to the smart learning ability of the ACT-based On Policy Monte Carlo Control.

TABLE IV. PERFORMANCE EVALUATION

Model	Time in ms	Total no. requests accepted	Total no. requests declined	% requests accepted	% requests declined	Total accepted rewards	Total declined rewards	% accepted rewards	% declined rewards	% penalised episode	% successful episode	V(s), q(s,accept), q(s,decline)
Adaptive MC	43.05	154215	154673	49.92586	50.0741	308412	154673	66.5994	33.4006	0.855948	99.14405	16
ACT MC	27.95	104970	72774	59.05685	40.9432	574736.75	201538.25	74.0378	25.9622	0.01429	99.98571	17.5
Adaptive MC-ES	15.52	81525	80909	50.18962	49.8104	163050	80909	66.835	33.165	0.772769	99.22723	6.5515, 6.64784
ACT MC-ES	23.91	130125	90017	59.10957	40.8904	713079	249600	74.0724	25.9276	0	100	18.7025, 13.1128
Adaptive OMC	8.77	49755	17563	73.9104	26.0896	36531	2692	93.1367	6.86332	4.492011	95.50799	6.38753, 3.5608
ACT OMC	19.19	113745	29342	79.49359	20.5064	305482	10856	96.5682	3.43177	0.316497	99.6835	22.5601, 14.05

V. CONCLUSION AND FUTURE WORKS

In this work, an RL-based ACT-enabled FogRA system is implemented for time-critical applications of IoT. The proposed system instantaneously decides whether to allocate fog resources or not, based on the time-criticality of the incoming request and the availability of fog resources. In the pursuit to derive the optimal policy, the algorithm trains the FCA to learn better decision-making. The RA problem is executed for the incoming requests both on the Adaptive and ACT-enabled FogRA systems. Results show that the ACT-enabled FogRA system prioritizes time-critical applications to allocate fog nodes. Also, utilization of fog resources is maximized in terms of the percentage of requests accepted by fog, rewards obtained and optimal value achieved. The performance assessment of the ACT-enabled FogRA system exhibits an improved optimal state-action value by 41% more than the Adaptive model. In future work, the FogRA system is planned for continuous tasks with the auto-scaling feature of fog resources. Also, it is planned to extend the work as RL enabled Energy Efficient FogRA system that minimizes the energy cost with maximized performance.

REFERENCES

- [1] A. Khanna and S. Kaur, "Internet of Things (IoT), Applications and Challenges: A Comprehensive Review," *Wirel. Pers. Commun.*, vol. 114, no. 2, pp. 1687–1762, Sep. 2020.
- [2] B. Jamil, M. Shojafar, I. Ahmed, A. Ullah, K. Munir, and H. Ijaz, "A job scheduling algorithm for delay and performance optimization in fog computing," *Concurr. Comput. Pract. Exp.*, vol. 32, no. 7, Apr. 2020.
- [3] L. F. Rahman, T. Ozcelebi, and J. Lukkien, "Understanding IoT Systems: A Life Cycle Approach," *Procedia Comput. Sci.*, vol. 130, pp. 1057–1062, 2018.
- [4] M. Mohammed Sadeeq, N. M. Abdulkareem, S. R. M. Zeebaree, D. Mikael Ahmed, A. Saifullah Sami, and R. R. Zebari, "IoT and Cloud Computing Issues, Challenges and Opportunities: A Review," *Qubahan Acad. J.*, vol. 1, no. 2, pp. 1–7, Mar. 2021.
- [5] B. Jamil, M. Shojafar, I. Ahmed, A. Ullah, K. Munir, and H. Ijaz, "A job scheduling algorithm for delay and performance optimization in fog computing," *Concurr. Comput. Pract. Exp.*, vol. 32, no. 7, Apr. 2020.
- [6] F. Murtaza, A. Akhuzada, S. ul Islam, J. Boudjadar, and R. Buyya, "QoS-aware service provisioning in fog computing," *J. Netw. Comput. Appl.*, vol. 165, p. 102674, Sep. 2020.
- [7] R. Mahmud, K. Ramamohanarao, and R. Buyya, "Application Management in Fog Computing Environments: A Taxonomy, Review and Future Directions," *ACM Comput. Surv.*, vol. 53, no. 4, pp. 1–43, Jul. 2021.
- [8] R. S. Sutton and A. G. Barto, *Reinforcement learning: an introduction*. Cambridge, Mass: MIT Press, 1998.
- [9] M. Faraji Mehmandar, S. Jabbehdari, and H. Haj Seyyed Javadi, "A dynamic fog service provisioning approach for IoT applications," *Int. J. Commun. Syst.*, vol. 33, no. 14, p. e4541, Sep. 2020.
- [10] S. Kalantary, J. Akbari Torkestani, and A. Shahidinejad, "Resource discovery in the Internet of Things integrated with fog computing using Markov learning model," *J. Supercomput.*, vol. 77, no. 12, pp. 13806–13827, Dec. 2021.
- [11] M. Salimian, M. Ghobaei-Arani, and A. Shahidinejad, "Toward an autonomic approach for Internet of Things service placement using gray wolf optimization in the fog computing environment," *Softw. Pract. Exp.*, vol. 51, no. 8, pp. 1745–1772, Aug. 2021.
- [12] M. Etemadi, M. Ghobaei-Arani, and A. Shahidinejad, "Resource provisioning for IoT services in the fog computing environment: An autonomic approach," *Comput. Commun.*, vol. 161, pp. 109–131, Sep. 2020.
- [13] A. Mijuskovic, A. Chiumento, R. Bemthuis, A. Aldea, and P. Havinga, "Resource Management Techniques for Cloud/Fog and Edge Computing: An Evaluation Framework and Classification," *Sensors*, vol. 21, no. 5, p. 1832, Mar. 2021.
- [14] O. Fadahunsi and M. Maheswaran, "Locality sensitive request distribution for fog and cloud servers," *Serv. Oriented Comput. Appl.*, vol. 13, no. 2, pp. 127–140, Jun. 2019.
- [15] A. Nassar and Y. Yilmaz, "Reinforcement Learning for Adaptive Resource Allocation in Fog RAN for IoT With Heterogeneous Latency Requirements," *IEEE Access*, vol. 7, pp. 128014–128025, 2019.
- [16] M. K. Pandit, R. N. Mir, and M. A. Chishti, "Adaptive task scheduling in IoT using reinforcement learning," *Int. J. Intell. Comput. Cybern.*, vol. 13, no. 3, pp. 261–282, Jan. 2020.
- [17] F. Bahrpeyma, H. Haghighi, and A. Zakerolhosseini, "An adaptive RL based approach for dynamic resource provisioning in Cloud virtualized data centers," *Computing*, vol. 97, no. 12, pp. 1209–1234, Dec. 2015.
- [18] T. V. Maia, "Reinforcement learning, conditioning, and the brain: Successes and challenges," *Cogn. Affect. Behav. Neurosci.*, vol. 9, no. 4, pp. 343–364, Dec. 2009.
- [19] G. Tesauro, N. K. Jong, R. Das, and M. N. Bennani, "A Hybrid Reinforcement Learning Approach to Autonomic Resource Allocation," in *2006 IEEE International Conference on Autonomic Computing*, Dublin, Ireland, 2006.
- [20] S. Shukla, M. F. Hassan, M. K. Khan, L. T. Jung, and A. Awang, "An analytical model to minimize the latency in healthcare internet-of-things in fog computing environment," *PLOS ONE*, vol. 14, no. 11, p. e0224934, Nov. 2019.
- [21] M. Ghobaei-Arani, S. Jabbehdari, and M. A. Pourmina, "An autonomic resource provisioning approach for service-based cloud applications: A hybrid approach," *Future Gener. Comput. Syst.*, vol. 78, pp. 191–210, Jan. 2018.
- [22] K. Gai and M. Qiu, "Optimal resource allocation using reinforcement learning for IoT content-centric services," *Appl. Soft Comput.*, vol. 70, pp. 12–21, Sep. 2018.
- [23] C. Wang, s. Yuan, k. Shao, and k. Ross, "on the convergence of the monte carlo exploring starts algorithm for reinforcement learning," p. 33, 2022.
- [24] "Miguel Morales - Grokking Deep Reinforcement Learning (2020, Manning Publications) - libgen.li.pdf."

Delay-Aware and Profit-Maximizing Task Migration for the Cloudlet Federation

Hengzhou Ye, Junhao Guo, Xinxiao Li*

Guangxi Key Laboratory of Embedded Technology and Intelligent Systems
Guilin University of Technology, Guilin, China

Abstract—As the result of Open Edge Computing (OEC) project, cloudlet embodies the middle layer of edge computing architecture. Due to the close deployment to the user side, responding to user requests through cloudlet can reduce delay, improve security, and reduce bandwidth occupancy. In order to improve the quality of user experience, more and more cloudlets need to be deployed, which makes the deployment and management costs of Cloudlet service Providers (CLP) significantly increased. Therefore, the cloudlet federation appears as a new paradigm that can reduce the cost of cloudlet deployment and management by sharing cloudlet resources among CLPs. Facing the cloudlet federation scenario, more attention still needs to be paid to the heterogeneity of resource prices, the balance of benefits among CLPs, and the more complex delay computation when exploring task migration strategies. For delay-sensitive and delay-tolerance tasks, a delay-aware and profit-maximizing task migration strategy is proposed considering the relationship between the delay and the quotation of different tasks, as well as the dynamic pricing mechanism when resources are shared among CLPs. Experimental results show that the proposed algorithm outperforms the baseline algorithm in terms of revenue and response delay.

Keywords—Cloudlet federation; task migration; delay-aware; dynamic pricing; profit-maximizing; edge computing

I. INTRODUCTION

With the development of intelligent Mobile Devices (MD), a large number of computation-intensive and delay-sensitive mobile applications keep emerging [1]. To address the resource constraints of mobile devices, tasks are offloaded to remote cloud centers in traditional cloud computing [2][3], but it is followed by the problem of high response delay [4]. This makes it difficult for requirements of delay-sensitive task to be satisfied [5].

To overcome these problems, Mobile Edge Computing (MEC) [6] is proposed and regarded as a promising technology by developing servers at the edge of networks. The proximity of the MEC to the user allows the user to access and use resources with lower response latency. Cloudlets are small cloud at the edge of network and typically deployed in a distributed manner to provide storage and computing resource to MD.

Compared to existing cloud computing, MEC still suffers from constrained resources. A Cloudlet service Provider (CLP) has to deploy more and more proprietary edge devices to meet the needs of its users, resulting in increasing costs to deploy and manage edge devices. Therefore, [7] proposes the edge

federation architecture, which improves the flexibility of resource utilization and reduces the deployment and management costs by seamlessly integrating the edge resources of each CLP. When cloudlets act as edge devices, a cloudlet federation architecture is formed.

Since MD is not uniformly distributed in edge computing systems, some clouds are heavily loaded while others are lightly loaded. Task migration is the principal method used to resolve load imbalance between cloudlets [8-11]. Although many studies have been conducted on cloudlet-based load migration strategies, they have one or more shortcomings: they do not take into account the heterogeneity of resource prices, authentication delays between cloudlet resources of different CLPs, or the impact of service delays on task quotes.

This paper focuses on the task migration problem in the cloudlet federation scenario. Two types of user requests are considered: delay-sensitive and delay-tolerant, and their quotation delay curves are designed respectively. Considering the heterogeneity of resource prices among CLPs, a delay-aware and profit-maximizing task migration strategy is proposed. Our main contributions are as follows:

- For delay-sensitive and delay-tolerant tasks, a delay model and a price model are constructed by taking into account the differences in resource prices of different CLPs.
- A distributed Delay-aware and Profit-maximizing Task Migration (DPTM) algorithm is designed to schedule tasks, which tries to minimize latency and maximize profit.
- A series of experiments are conducted to verify the necessity of considering the cloudlet federation and the advantages of our method in terms of revenue and response delay.

The rest of this article is organized as follows. Section II demonstrates the related work on the task migration in different scenarios. Section III introduces the system model. In Section IV, a task scheduling algorithm considering both profit and delay is proposed. In Section V, we conduct the extensive experiments to evaluate the proposed method and gives the discussion. Finally, Section VI concludes this paper and gives the future works.

*Corresponding Author.

II. RELATED WORK

We review the related works about task migration and schedule in the multi-cloudlet scenario and the edge federation scenario respectively.

A. Task Migration in Multi-cloudlets Scenario

The existing works about task migration in the multi-cloudlets scenarios focus on minimizing delay and energy consumption. The authors in [12] propose an application-aware cloudlet adaption and VM selection framework has been devised for balancing the load in a multi-cloudlet environment. The authors in [13] propose a novel Multi-layer Latency Aware Workload Assignment Strategy (MLAWAS) to allocate the workload of E-Transport applications into optimal computing nodes. In [14] user mobility and task deadline are taken into account when task migration is optimized. Three variants of this problem are analyzed, and a group migration algorithm with known user trajectories is designed. In [15], a heuristic Task Migration Computing Offloading (TMCO) scheme is proposed for the challenges brought by complex network environment and end-user mobility, which can dynamically select the appropriate location to offload tasks for mobile users within the deadline. In [16], for collaborative vehicle edge computing group environment, a computational task migration problem is defined to balance the load and minimize the migration cost, and reinforcement learning algorithm is adopted to solve this problem.

The above researches are based on multi-cloudlet scenarios to optimize the delay and energy consumption of task migrating. However, the traditional multi-cloudlet scenario has the problem of limited resources, and a smaller number of resources are available for task migration. Different from the multi-cloudlet scenario, in the cloudlet federation, the cloudlet resource prices of different CLPs may be different, there are more options for task migration, and the delay computation is more complex.

B. Task Migration in Edge Federation Scenario

Some studies have explored task migration strategies in the context of edge federation or cloudlet federation. The authors in [17] design a task migration strategy for multiple edge servers in mobile networks to minimize the overall service time and develop an intelligent task migration scheme using deep reinforcement learning and Q-learning technology. In [18], the authors propose a latency minimization model to provide higher efficient service provisioning in horizontal edge federation and propose a two-phase iterative approach, which alternately determines optimal task dispatching and computation resource allocation. In order to simultaneously meet the SLA requirements of IoT (Internet of Thing) devices and edge service providers, the authors in [19] design an intelligent request service provisioning system based on reinforcement learning as part of a smart edge orchestrator in the edge federation. Considering the delay and capacity constraints, [20] proposes an optimization model to minimize the total energy cost and the energy efficient offloading ratio of edge nodes.

The above studies either ignore the role of the remote cloud, or do not consider the heterogeneity of resource prices, or do not consider the impact of task delay on user quotation. In our

work, tasks can be migrated to the CLP's own cloudlet, the cloudlet of federate CLP, or the remote cloud. We consider two different types of tasks, time-sensitive and time-tolerance, and consider that their delays have different effects on user quotation. We attempt to optimize the profit and delay of the whole federation.

III. SYSTEM MODEL

In this section, we keep our focus on the cloudlet federation framework, communication and computation models.

A. Cloudlet Federation Framework

Compared with the cloudlet, the cloud usually has sufficient resources and is quite far away from the user. For simplicity, the cloud platform owned by each CLP is not distinguished. Therefore, as shown in Fig. 1, we consider that a cloudlet federation contains a cloud and several CLPs. Each CLP has its own cloudlet servers, and each has a set of users that need to be served. The resource of a cloudlet server is provided in the form of a virtual machine (VM) instance. Let's assume that a VM instance performs only one task at a time.

We assume each CLP has a server as the Federated Cloudlet Manager (FCLM) to provide service and resource interactions. The status of the cloudlet servers is collected by the FCLM, such as available capacity, resource utilization, and cost. Meanwhile, CLPs can communicate with each other through FCLMs and exchange their collected information. When a CLP receives a task from a terminal user, it decides where to offload the task. This could be its own cloudlet, one of the federated cloudlets, or the cloud.

B. Task Requests from Terminal Users

Similar to works in mobile cloud computing [21] and mobile edge computing [22], the quasi-static scenario is considered, where the mobile users remain unchanged during migration. To simplify, we use task or request instead of task request without causing confusion.

Two types of task requests are considered: delay tolerance (DT) and delay sensitive (DS). For a DS task, CLP should minimize its delay while a certain amount of revenue is guaranteed. For a DT task, the priority is profit maximization.

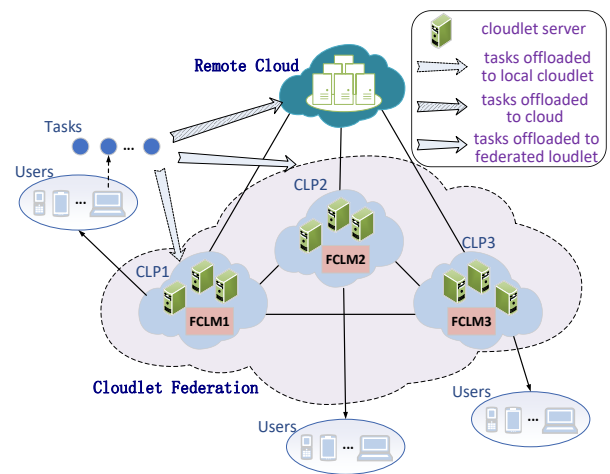


Fig. 1. Cloudlet Federation Architecture.

Regardless of the type of task, we believe that the response delay will affect the user's willingness to pay. In general, the shorter the delay, the higher the user is willing to pay.

A seven-tuple $A = \langle d, req^{ins}, \alpha, t^{ept}, t^{max}, P^{max}, P^{low} \rangle$ is used to describe a task where, d denotes the size of input data, req^{ins} denotes the Million Instructions (MIs) required. α is a 0-1 variable that describes the type of tasks. When α is 0, the type of the task is DT, and when α is 1, the type of the task is DS. We assume a task has an expected delay t^{ept} and a tolerable maximum latency t^{max} . P^{low} and P^{max} represent the minimum and maximum price a user is willing to pay for a task, respectively.

For a DT task, if it can be completed within the expected time, marked as t^{ept} , the user will be satisfied and willing to pay in full, marked as P^{max} . If t^{ept} is exceeded, but the deadline, marked as t^{max} , is not exceeded, the willing fee of the user will gradually decrease, and eventually reach a balance value, marked as P^{low} , between the CLP and the user. Thus, for a DT task, the relationship between the delay t and the user's quotation $Q(t)$ can be shown in (1).

$$Q(t) = \begin{cases} P^{max}, & t < T^{ept} \\ k_{dt} \cdot (T^{max} - t) + P^{low}, & T^{ept} \leq t \leq T^{max} \\ P^{low}, & t > T^{max} \end{cases} \quad (1)$$

Where, k_{dt} is determined by (2).

$$k_{dt} = \frac{P^{max} - P^{min}}{T^{max} - T^{ept}} \quad (2)$$

For DS tasks, users will be willing to pay in full if they can be completed within the expected time. If the delay exceeds the user's expectation, the user's willingness to pay will decrease sharply. If the delay exceeds the deadline, the user will be unwilling to pay, or only willing to pay at a very low price. We chose the latter, meaning that when the deadline is exceeded, the user will be willing to offer only a very low price, which is usually close to or even lower than the CLP cost. We design (3) to describe the relationship between the delay t of a DS task and the user's quotation $Q(t)$.

$$Q(t) = \begin{cases} P^{max}, & t < T^{ept} \\ P^{max}((1 - \alpha(t - T^{ept}))^\beta), & T^{ept} \leq t \leq T^{max} \\ P^{low}, & t > T^{max} \end{cases} \quad (3)$$

Where, α and β are adjustable parameters, and their values should ensure that the curve described by (3) is continuous on the interval $[T^{ept}, T^{max}]$. α indicates the delay sensitivity of the user. The larger the α , the higher is the sensitivity. β reflects the descent gradient of user willingness. The larger the β , the larger is the gradient.

Fig. 2(a) and Fig. 2(b) depict the curves of delay versus quotation for DT and DS tasks, respectively.

C. Delay Model

When the FCLM of a CLP receives a task, the FCLM may schedule it to the local cloudlet, or to the federated cloudlet, or to the cloud. In general, the amount of data output after the task execution is much smaller than the amount of data input before the task execution. Similar to [23] and [24], the transmission time required for the output information of a task to be returned to the user is not considered. Meanwhile, the queuing delay is

negligible when the federated resources are sufficient to handle user tasks.

1) *Local cloudlet*: When a task is scheduled to the local cloudlet, its delay can be divided into two parts. The first part includes transmission delay and propagation delay, denoted as t_{cl}^1 , which can be determined by (4).

$$t_{cl}^1 = \frac{d}{R} + \frac{D_{cl}}{S^P} \quad (4)$$

Where d is the amount of data to be transmitted, R is the data transmission rate, D_{cl} is the distance of the selected local cloudlet from the user, and S^P is the propagation rate. Assume that the value of S^P is the same for all channels and the value of R is the same for all devices.

The second part is the time required for the task execution on the selected cloudlet, denoted as t_{cl}^2 , which is determined by (5).

$$t_{cl}^2 = \frac{req^{ins}}{CPU_{proc} \cdot N_{cpu}} \quad (5)$$

Where req^{ins} is the MIs required to execute the task, CPU_{proc} is the Million Instructions per Second (MIPs) for the CPU provided by the selected cloudlet, and N_{cpu} is the number of CPUs configured by the selected cloudlet.

Thus, the total delay, denoted as t_{cl}^{total} , for a task scheduled to a local cloudlet can be calculated by (6).

$$(6)$$

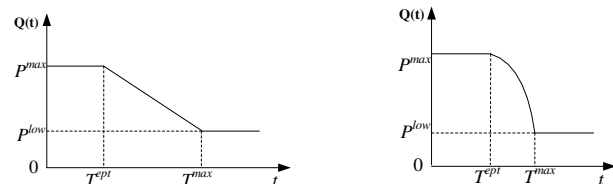
2) *Remote cloud*. When a task is scheduled to the remote cloud, its delay calculation is very similar to that when it is scheduled to a local cloudlet. However, since the user is usually far away from the cloud, the delay of the task will be huge.

The total delay, denoted as t_c^{total} , for a task scheduled to the remote cloud can be calculated by (6).

$$t_c^{total} = t_c^1 + t_c^2 = \frac{d}{R} + \frac{D_c}{S^P} + \frac{req^{ins}}{CPU_{proc} \cdot N_{cpu}} \quad (7)$$

Where, D_c is the distance of the cloud from the user, CPU_{proc} is the MIPs for the CPU provided by the cloud, and N_{cpu} is the number of CPUs configured by the cloud.

3) *Federated cloudlet*. If a task is assigned to the federated cloudlet, its delay includes the following parts: authentication delay between alliances, task offloading delay from user to FCLM, task offloading delay from FCLM to the selected cloudlet, and task execution delay.



(a) For DT task. (b) For DS task.

Fig. 2. Curves of Delay Versus Quotation.

When a task is transferred from the FCLM receiving it to the FCLM of a federation, some authentication information often needs to be exchanged between FCLMs, so as to introduce authentication delay, marked as t_{fed}^1 , which is considered to be a constant.

To avoid CLP user information being detected by the federated CLP, tasks are delivered first to the FCLM that receives them and then to the selected Cloudlet. The delay of offloading the task from the user to the FCLM, denoted as t_{fed}^2 , can be calculated by (8).

$$t_{fed}^2 = \frac{d}{R} + \frac{D_1}{SP} \quad (8)$$

Where D_1 represents the distance between the user and the FCLM associated with it.

The delay of offloading tasks from FCLM to the selected cloudlet is denoted as t_{fed}^3 , which can be calculated by (9).

$$t_{fed}^3 = \frac{d}{R} + \frac{D_2}{SP} \quad (9)$$

Here, D_2 represents the distance between the FCLM associated with the user and the selected cloudlet.

The execution delay of the task, denoted as t_{fed}^4 , can be determined by (10).

$$t_{fed}^4 = \frac{req^{ins}}{CPU_{proc} \cdot N_{cpu}} \quad (10)$$

Where, CPU_{proc} is the MIPS for the CPU provided by the selected cloudlet, and N_{cpu} is the number of CPUs configured by the selected cloudlet. CPU_{proc} and N_{cpu} in (5), (7) and (10) are not symbolically distinguished. In fact, they correspond to different computing resources and take different values.

Thus, the total delay, denoted as t_{fed}^{total} , can be calculated by (11).

$$t_{fed}^{total} = t_{fed}^1 + t_{fed}^2 + t_{fed}^3 + t_{fed}^4 \quad (11)$$

D. CLP Resource Pricing Model

When a CLP needs to rent the cloudlet resources of another CLP, the leasing price of the resources needs to be determined. The consistent pricing strategy is adopted, and the leasing price of resources is considered to be related to the user's quotation, resource cost and resource utilization of CLP.

Assuming that the user quotation of task A is $Quote_A$, the cost of resources needed to execute A is $Cost_A$, and the total cloudlet resources and residual resources owned by some CLP are $Total_{CLP}$ and Res_{CLP} respectively, then the cost of CLP renting the resources required by task A , denoted as $Rent_A^{CLP}$, can be determined by (12).

$$Rent_A^{CLP} = Cost^A + \frac{Total_{CLP} - Res_{CLP}}{Total_{CLP}} (Quote_A - Cost^A) \quad (12)$$

The intuition of (12) is as follows: the rental price of resources should be higher than that of the cost. The net profit between rental price and cost should be positively correlated with the profit of the lease and the resource utilization of the lessor accordingly. The willingness of renting resource is

growth with the user's quoted price, and as the increasing of the resource utilization, the tenant willingness of renting is decreasing.

When a task is executed on the cloud, its profit is the difference between the user's quote and the cost of the cloud resource. When executed on the local cloudlet, its profit is the difference between the user's quote and the local cloudlet resource cost. When executed on the federated cloudlet, its profit is the difference between the user's quote and the rental resource price.

IV. PROPOSED ALGORITHM

Based on the distributed processing idea and greedy strategy, for each CLP, when its FCLM receives a task, we design a Delay-aware and Profit-maximizing Task Migration (DPTM) algorithm to schedule the task. DPTM tries to maximize the profit of CLP while guaranteeing the user delay according to the task type. It first determines the type of tasks. For DS tasks, a scheduling algorithm called Task Migration for DS (TMDS) is proposed. For the DT task, an algorithm called Task Migration for DT (TMDT) is proposed.

A. TMDS Algorithm

For DS task, the goal is to minimize delay on the basis of ensuring profit. For this purpose, locally arrived DS tasks are divided into High Delay Sensitive (HDS) and Low Delay Sensitive (LDS) tasks according to their delay requirements. For a HDS task, local scheduling is preferred. If it cannot be scheduled locally, it is processed as an LDS task. For a LDS task, if the cloud has the highest profit and can guarantee the delay, the cloud is regarded as the best scheduling. Otherwise, on the premise of ensuring profit, the cloudlet with the minimum delay should be sought.

The TMDS algorithm for scheduling DS tasks is shown in Algorithm 1. In Algorithm 1, Avg_k records the average t^{ept} of the last k DS tasks, $t^{ept}(A)$ and $t^{max}(A)$ represent the t^{ept} and t^{max} of task A respectively, $t_{cl}^{total}(VM)$ represents the delay of A when executed on the VM of a cloudlet, $p_{cl}(VM)$ represents the profit when A is executed on the VM of a cloudlet, and $p_c(A)$ represents the profit when A is executed on the cloud. A task is identified as HDS when its t^{ept} is less than Avg_k . In this case, firstly, the VM that can execute A and delay less than $t^{max}(A)$ are searched on the local cloudlet. Otherwise, find all VMs that can execute A with latency less than $t^{max}(A)$ and schedule A to the one with the least latency. If no suitable VM is found after the above two steps, A will be treated as an LDS type.

For a task A identified as a LDS, the latency and profit of A when executed on the cloud are calculated, denoted as $t_c^{total}(A)$ and $p_c(A)$, respectively. If $t_c^{total}(A)$ is less than $t^{max}(A)$ and $p_c(A)$ is greater than 0, the VM with executable A , delay less than $t^{max}(A)$, and profit greater than $p_c(A)$ is sought on the cloudlets of all CLPs. If one or more VMs can be found, the VM with the minimum latency is selected for A . Otherwise, A is scheduled to the cloud.

If $t_c^{total}(A)$ is not less than $t^{max}(A)$ or $p_c(A)$ is not greater than 0, the VM that can execute A and the profit is greater than 0 is searched on the cloudlets of all CLPs, and the one with

minimum delay is the best for A. Otherwise, A will be abandoned.

In Algorithm 1, a maximum of three scheduling attempts is required on each VM for a task. If n is used to represent the number of VMs, the time complexity of algorithm 1 is $O(n)$, that is, algorithm 1 has linear time complexity.

Algorithm 1 TMDS

Input: task A with type of DS
Output: VM is arranged for A
Calculate Avg_k ;
Set $VM_T \langle VM, Time \rangle = \emptyset$;
If ($t^{ept}(A) < Avg_k$) {
 For each VM in local cloudlet {
 Calculate $t_{cl}^{total}(VM)$ using (6);
 If ($t_{cl}^{total}(VM) < t^{max}(A)$)
 add $\langle VM, t_{cl}^{total}(VM) \rangle$ to VM_T ;
 }
 if (VM_T is not null)
 return VM with minimum delay in VM_T ;
}
Calculate $t_c^{total}(A)$ using (7) and $p_c(A)$;
If ($t_c^{total}(A) < t^{max}(A) \&\& p_c(A) > 0$) {
 For each VM in all cloudlets {
 Calculate $t_{cl}^{total}(VM)$ using (6) or (12);
 If ($t_{cl}^{total}(VM) < t^{max}(A) \&\& p_{cl}(VM) > p_c(A)$)
 add $\langle VM, p_{cl}(VM) \rangle$ to VM_T ;
 }
 If (VM_T is not null)
 return VM with minimum delay in VM_T ;
 else
 return VM in cloud;
}
For each VM in all cloudlets {
 Calculate $t_{cl}^{total}(VM)$ using (6) or (12);
 If ($p_{cl}(VM) > 0$)
 add $\langle VM, t_{cl}^{total}(VM) \rangle$ to VM_T ;
}
If (VM_T is not null)
 return VM with minimum delay in VM_T ;
else
 return null;

B. TMDT Algorithm

For the DT task, the goal is to minimize the delay while pursuing the maximum profit. Considering that the delay of a task executed on the local cloudlet is usually less than that on the federated cloudlet or the cloud, in order to save the local cloudlet as much as possible for scheduling DS tasks, DT tasks can only be scheduled to the federated cloudlets with the lower quotation or the cloud. The criterion is profit maximization.

The TMDT algorithm is used to schedule tasks of type DT, as shown in Algorithm 2. For a task A, the profit executed on the cloud, denoted as $p_c(A)$, is firstly calculated. If $p_c(A)$ is greater than 0, the VM that can execute A and have higher profit than $p_c(A)$ is found on all the federated cloudlets, and A is scheduled to the one with the maximum profit. If no such VM can be found, A is scheduled to the cloud. If $p_c(A)$ is not greater than 0, the VM that can execute A and have higher profit than 0 is found on all the federated cloudlets. If such VMs exist, the

one that can make the maximum profit is the best choice. Otherwise, scheduling A is abandoned.

Algorithm 2 traverses all VMs at most two times, so its time complexity is $O(n)$.

Algorithm 2 TMDT

Input: task A with type of DT
Output: VM is arranged for A
Set $VM_P \langle VM, Profit \rangle = \emptyset$;
Calculate $p_c(A)$;
If ($p_c(A) > 0$) {
 For each VM in federated cloudlets
 If ($p_{cl}(VM) > p_c(A)$)
 add $\langle VM, p_{cl}(VM) \rangle$ to VM_P ;
 If (VM_P is not null)
 Return VM with maximum profit in VM_P ;
 Else
 Return VM in cloud;
}
Else {
 For each VM in federated cloudlets
 If ($p_{cl}(VM) > 0$)
 add $\langle VM, p_{cl}(VM) \rangle$ to VM_P ;
 If (VM_P is not null)
 Return VM with maximum profit in VM_P ;
 Else
 Return null;
}

V. RESULTS AND DISCUSSION**A. Simulation Parameters Setting**

We considered the cloudlet federation scenario composed by three individual CLPs and a remote cloud. Each CLP deploys four servers within its managed area as its cloudlet. Each cloudlet server has 20-30 VMs, while the cloud has 2000 VMs. Referring to Amazon, two types of VMs are supported. One with four Virtual CPUs (vCPU) and 16GB of memory, priced at \$0.424, serves DT tasks; the other has two vCPUs and 8GB of memory, priced at \$0.212, serves DS tasks. The processing speed of a vCPU is 20000MIPS. The task type is randomly selected. The influence of distance between servers in a cloudlet is not considered. Other parameters are set as shown in Table I.

B. Comparison with the Baseline Algorithm

In order to verify the effect of the proposed method in terms of time delay and profit, the proposed method is compared and analyzed with DATM and CATM proposed in literature [25]. DATM is a delay-aware task migration algorithm that migrates tasks to the cloudlet that minimizes the latency of task execution. And CATM is a cost-aware task migration algorithm that migrates tasks to the cloudlet that minimizes the cost of task execution. Considering the obvious difference in delay expectation between DS and DT tasks, statistics are carried out for DS and DT tasks respectively when comparing the delay.

Fig. 3 and Fig. 4 compare the average delay of DPTM, DATM and CATM with the number of tasks. Here, Fig. 3 counts all DS tasks, while Fig. 4 counts all DT tasks.

TABLE I. PARAMETER SETTINGS

Parameter	Definition	Value
D_{cl}	Distance of user to local cloudlet	10-50m
D_c	Distance of user to the cloud	1-10km
D_{fctm}	Distance between FCLMs	200-500m
S^p	Propagation speed	3×10^8 m/s
R	Data transmission rate	3Mbps
t^{ept}	Expected delay of DS task	50-100ms
	Expected delay of DT task	200-400ms
req^{ins}	DS task size	1000-2000MI
	DT task size	500-1000MI]
P^{low}	Minimum quotation for DS task	\$2
	Minimum quotation for DT task	\$1
P^{max}	Maximum quotation for DS task	\$3
	Maximum quotation for DT task	\$2
d	Size of input data for task	0.1-2MB
k_{dt}	The parameter in (1)	0.6
β	The parameters in (3)	3

Fig. 3 shows that for DS tasks, DPTM achieves better average delay than DATM, while DATM outperforms CATM. Although DATM is optimized for delay, it does not distinguish between DS and DT tasks. DPTM tries to reserve local cloudlet resources for DS tasks. Therefore, for DS tasks, DPTM obtains a better average delay than DATM.

For the DT task, the results in Fig. 4 show that DPTM achieves better average latency than CATM, but not as good as DATM. DPTM gives priority to DS tasks in terms of latency, thus, for DT tasks, it is not surprising that its average latency is lower than DATM. For CATP, it aims at minimizing task migration cost and does not focus on delay. Although DPTM mainly optimizes the profit for DT tasks, the profit is negatively correlated with the delay, so it optimizes the delay to a certain extent.

Fig. 5 compares the profit with the number of tasks. From Fig. 5, it can be observed that DPTM achieves the best profit, followed by CATM and DATM. The quotation of the task is related to the time delay, while the lease price is related to the resource utilization and the quotation. Therefore, the profit of the task is related to both the time delay and the resource utilization. For CATM, although it aims to minimize the migration cost, the profit decreases due to the high average delay. For DATM, the latency is relatively small, which can increase profits. However, in order to pursue low latency, tasks are preferentially scheduled to the local cloudlet, resulting in high resource utilization of the cloudlet, which pushes up the task quotation and reduces the profit.

In general, DPTM achieves better profit because it treats DT and DS tasks differently and differentiates the relationship between the quotation and the delay of these two types of tasks. For DS tasks, DPTM also achieves better average delay.

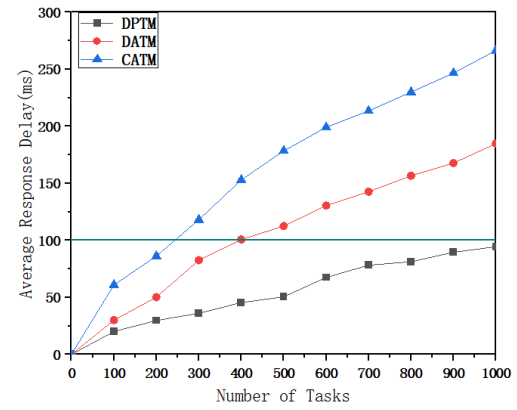


Fig. 3. Average Delay of DS Tasks.

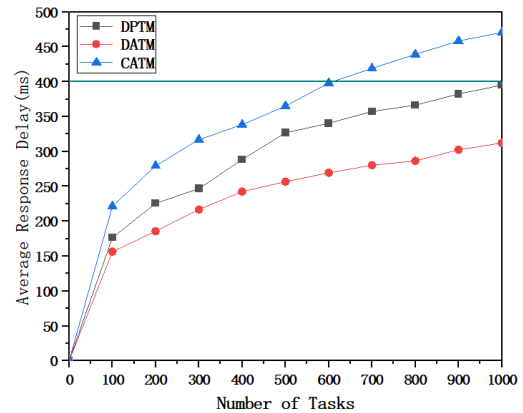


Fig. 4. Average Delay of DT Tasks.

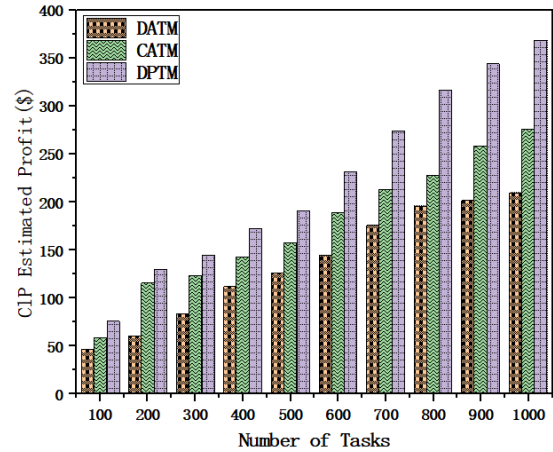


Fig. 5. Average Profit of Tasks.

C. The Necessity of the Federation

To verify the necessity of considering federation, the federation scenario is compared with the non-federation scenario where cloudlet resources cannot be shared between different CLPs.

Fig. 6 compares the average latency of the two scenarios. Where, Fed-DPTM-DS and Fed-DPTM-DT represent the average delay of all DS and DT tasks in the federated scenario, respectively. NonFed-DPTM-DS and NonFed-DPTM-DT indicate the average latency of all DS and DT tasks in the non-

federated scenario, respectively. From Fig. 6, it can be found that the average delay of DS and DT tasks are both significantly reduced when considering federation. This is because in the federation scenario, different CLPs share cloudlet resources, which can reduce the impact of the difference in the number of tasks and the uneven distribution of cloudlet resources among CLPs. For DT tasks, the decrease effect of average delay is more obvious, because DPTM preferentially migrates DT tasks to the federated cloudlet. However, without considering federation, tasks tend to be migrated only to the cloud, resulting in higher latency.

As can be seen from Fig. 7, considering federation can improve profits, and the more tasks there are, the more obvious the improvement effect will be. On the one hand, DPTH is specifically designed for the federation scenario. On the other hand, CLP federation supports cloudlet resources sharing, which reduces the average delay and reduces the probability of tasks being scheduled to the cloud or rejected.

Fig. 8 compares the ratio of the number of rejected tasks to the total number of tasks in the two scenarios. As can be seen from Fig. 8, no matter which scenario, with the increase of the number of tasks, the situation that the task is rejected for scheduling occurs, and the proportion of rejected increases with the increase of the number of tasks. However, compared with the non-federation scenario, the proportion of tasks rejected for scheduling is much lower in the federation scenario.

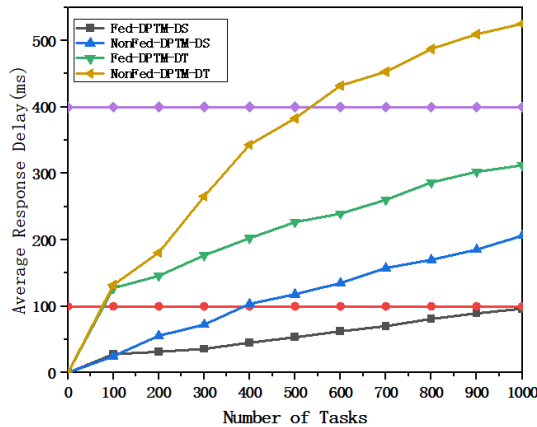


Fig. 6. Profits for the Two Scenarios.

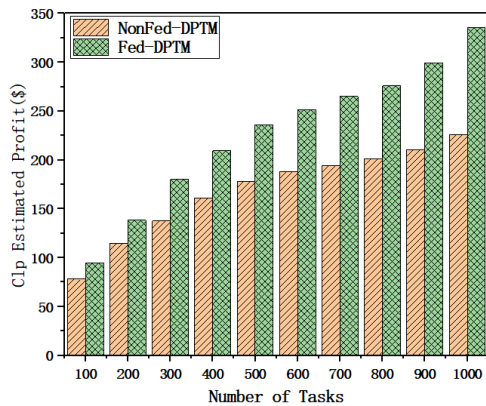


Fig. 7. Average Profit of Tasks.

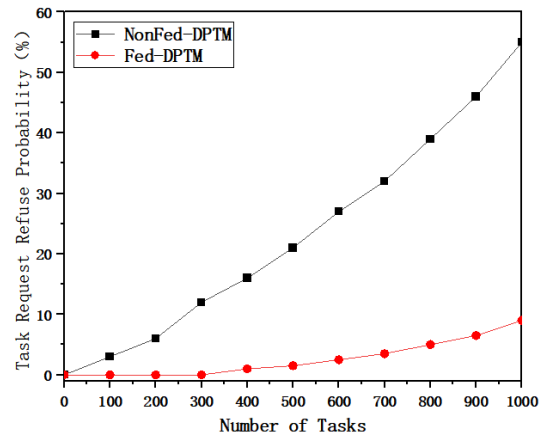


Fig. 8. Refuse Probability of Tasks.

In general, considering the federation scenario, the average delay can be reduced, profits can be increased, and the probability of task rejection can be reduced.

D. Impact of Authentication Delay

During resource sharing, some authentication information may need to be exchanged between CLPs, which may lead to authentication delay. Fig. 9 and Fig. 10 analyze the influence of authentication delay on the average delay of DS and DT tasks, respectively. For DS tasks, the results in Fig. 9 show that when the number of tasks is small (no more than 100), the authentication delay has almost no effect on the average delay, because almost all DS tasks are scheduled to the local cloudlet. However, when the number of tasks is large, the average delay of DS tasks increases with the increase of authentication delay, because more and more tasks have to be scheduled to the federated cloudlet.

As shown in Fig. 10, the average delay of DT tasks increases with the increase of authentication delay, even if the number of tasks is small, because DT tasks are preferentially deployed on the federated cloudlet. Different from DS tasks, authentication delay is not sensitive to the number of DT tasks.

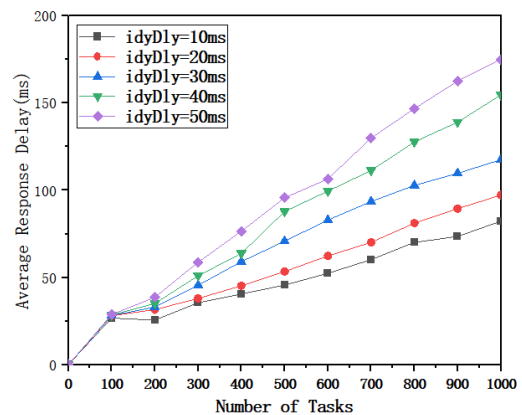


Fig. 9. Impact of Authentication Delay to DS Tasks' Delay.

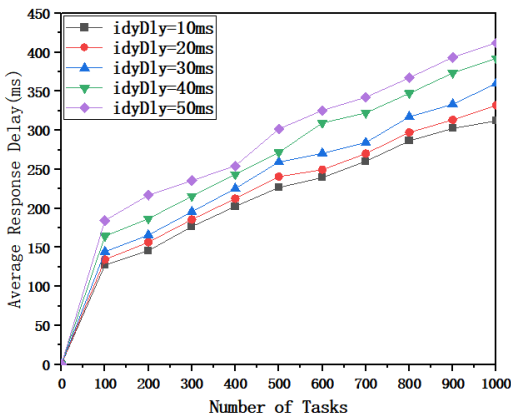


Fig. 10. Impact of Authentication Delay to DT Tasks' Delay.

Fig. 11 analyzes the impact of authentication delay on profit. Fig. 11 shows that the profit decreases as the authentication delay increases. And the longer the delay, the faster the profit decreases. This is because for a DT task, when the delay exceeds the threshold, the quotation is linearly reduced. And for DS tasks, the quotation is exponentially reduced when the delay exceeds the threshold.

In a word, the authentication delay can affect the task delay and profit, so the authentication delay should be minimized.

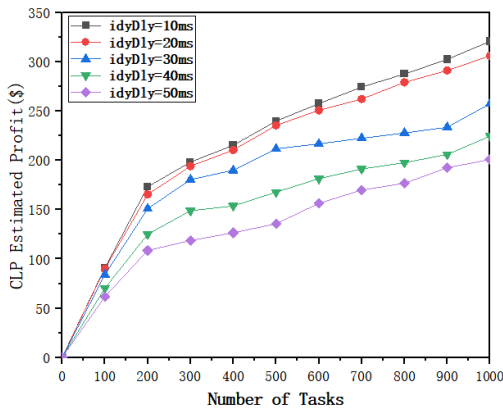


Fig. 11. Impact of Authentication Delay to Profit.

E. Discussion

CLP can share resources with each other in the form of alliances, to solve the problem of resource limitation and the high cost of resource expansion and benefit from the heterogeneity of resource prices provided by different CLPS in alliances. CLP has more options for task migration, resulting in higher benefits. As far as we know, most of the existing studies consider horizontal edge federation or cloud federation, and there are few researches on task migration for the cloudlet federation. Meanwhile, few types of research on task migration for the cloudlet federation combine the powerful computing power of cloud center. For this reason, because of the shortcomings of existing research, this paper considers a cloudlet federation scenario integrating CLP and cloud center computing resources. At the same time, the cost of CLP and task processing delay are considered in the process of task migration, and the authentication delay is considered in the delay calculation.

As shown in Fig. 5 and Fig. 6, the DPTM algorithm proposed in this study balances the needs of users and CLP. The algorithm outperforms the baseline approach in terms of latency and profits of CLP and helps to satisfy more requests. Initially, DPTM divides tasks according to their delay sensitivity. Next, DPTM takes the delay minimization as the optimization goal in the DS task migration and ensures the task delay requirement in the DT task migration. However, the specific calculation process of authentication delay between different CLP resources during task migration and the factors that may affect the authentication delay need to be explored next. At the same time, some users may move during task migration, which is another factor to be considered.

VI. CONCLUSIONS AND FUTURE WORK

Cloudlet federation can effectively reduce the deployment and management cost of cloudlet by sharing resources among CLPs. However, the differences in the number of users and resources among CLPs bring new challenges to task migration. When studying the task migration strategy for the cloudlet federation, two types of tasks, DS and DT, are considered, and the relationship functions between user quotation and delay of these two types of tasks are designed. A task migration algorithm, called DPTM, which takes into account both delay and profit, is proposed. The DPTM algorithm consists of two sub-algorithms: TMDS and TMDT. The former is used to schedule DS tasks with delay as the main optimization objective. The latter is used to schedule DT tasks with profit as the primary optimization objective. Simulation results demonstrate the effectiveness of the proposed method.

In the future, we plan to design a centralized task migration strategy. In addition, the secure access problem when resources are shared between different CLPs is further discussed. Meanwhile, we intend to design a more intelligent task scheduling algorithm based on Artificial Intelligence (AI).

ACKNOWLEDGMENTS

This research was supported by the National Natural Science Foundation of China [grant number 62262011], and the Foundation of Guilin University of Technology [grant number GUTQDJJ2002018].

REFERENCES

- [1] Y. Mao, C. You, J. Zhang, K. Huang, and K. B. Letaief, "A survey on mobile edge computing: The communication perspective," *IEEE Communications Surveys & Tutorials*, vol. 19, no. 4, pp. 2322–2358, August 2017.
- [2] S. Guo, J. Liu, Y. Yang, B. Xiao, and Z. Li, "Energy-efficient dynamic computation offloading and cooperative task scheduling in mobile cloud computing," *IEEE Transactions on Mobile Computing*, vol. 18, no. 3, pp. 319–333, April 2018.
- [3] T. H. Noor, S. Zeadally, A. Alfazi, Z. Quan, "Mobile cloud computing: Challenges and future research directions," *Journal of Network and Computer Applications*, vol. 115, no. 1, pp. 70–85, August 2018.
- [4] M. Chen and V. C. M. Leung, "Reprint of: From cloud-based communications to cognition-based communications: A computing perspective," *Computer Communications*, vol. 131, pp. 77–82, October 2018.
- [5] A. Yousefpour, C. Fung, T. Nguyen, K. Kadiyala, F. Jalali, et al., "All one needs to know about fog computing and related edge computing paradigms: A complete survey," *Journal of Systems Architecture*, vol. 98, pp. 289–330, September 2020.

- [6] K. Gai, M. Qiu, H. Zhao, L. Tao, and Z. Zong, "Dynamic energy-aware cloudlet-based mobile cloud computing model for green computing," *Journal of Network and Computer Applications*, vol. 59, pp. 46–54, January 2016.
- [7] X. Cao, G. tang, D. Guo, Y. Li, and W. Zhang, "Edge federation: towards an integrated service provisioning model," *IEEE/ACM Transactions on Networking*, vol. 28, no. 3, pp. 1116–1129, March 2020.
- [8] R. A. Khan, T. L., and A. Khan, "Cloud Migration: Standards and Regulatory Issues with Their Possible Solutions," *Int. J. Advanced Networking and Applications*, vol. 10, no. 6, pp. 4113–4119, April 2019.
- [9] S. Chen, J. Chen and C. Zhao, "Deep reinforcement learning based cloud-edge collaborative computation offloading mechanism," *Acta Electronica Sinica*, vol. 49, no. 1, pp. 157–166, 2021.
- [10] I. Labriji, F. Meneghello, D. Cecchinato, S. Sesio, E. Perraud, et al., "Mobility aware and dynamic migration of MEC services for the internet of vehicles," *IEEE Transactions on Network and Service Management*, vol. 18, no. 1, pp. 570–584, January 2021.
- [11] H. Yuan, J. Bi, W. Tian, M. Zhou, B. H. Li, and J. Li, "TTSA: An effective scheduling approach for delay bounded tasks in hybrid clouds," *IEEE Transactions on Cybernetics*, vol. 47, no. 11, pp. 3658–3668, July 2016.
- [12] R. Soluma, R. Sasikala, S. Kshira Sager, K. R. Lakshmana, P. Quoc-viet and Dao. Nhu-Ngoc, "CAVMS: Application-Aware Cloudlet Adaption and VM Selection Framework for Multi-cloudlet Environment," *IEEE Systems Journal*, vol. 15, no. 4, pp. 5098–5106, 2021.
- [13] A. Lakhan, M. A. Dootio, T. M. Groenli, A. H. Sodhro and M. S. Khokhar, "Multi-Layer Latency Aware Workload Assignment of E-Transport IoT Applications in Mobile Sensors Cloudlet Cloud Networks," *Electronics*, vol. 10, no. 14, pp. 1719, 2021.
- [14] S. Moon and Y. Lim, "Task migration with partitioning for load balancing in collaborative edge computing," *Applied Sciences-Basel*, vol. 12, no. 3, pp. 1168, 2022.
- [15] B. Qiao, C. Liu, J. Liu, Y. Hu, K. L. Li, and K. Q. Li, "Task migration computation offloading with low delay for mobile edge computing in vehicular networks," *Concurrency and Computation: Practice and Experience*, vol. 34, no. 1, July 2022.
- [16] S. Moon and J. Park, Y. Lim, "Task migration based on reinforcement learning in vehicular edge computing," *Wireless Communications and Mobile Computing*, 2021.
- [17] S. Huang, K. Lin, and C. Hu, "Intelligent task migration with deep Qlearning in multi-access edge computing," *Iet Communications*, vol. 16, no. 11, July 2022.
- [18] C. Liu, F. Tang, Y. Hu, K. L. Li, Z. Tang, and K. Q. Li, "Distributed task migration optimization in MEC by extending multi-agent deep reinforcement learning approach," *IEEE Transactions on Parallel and Distributed Systems*, vol. 32, no. 7, pp. 1603–1614, July 2021.
- [19] M. Z. Nayyer, I. Raza, and S. A. Hussain, "CFRO: Cloudlet federation for resource optimization," *IEEE Access*, vol. 8, pp. 106234–106246, June 2020.
- [20] H. Baghban, C. Huang, and C. H. Hsu, "Resource provisioning towards OPEX optimization in horizontal edge federation," *Computer Communications*, vol. 158, pp. 39–50, May 2020.
- [21] L. Cui, C. X. S. Y, Z. H, X. W and Z. M, "Joint Optimization of Energy Consumption and Latency in Mobile Edge Computing for Internet of Things," *IEEE Internet of Things Journal*, vol. 6, no. 3, pp. 4791–4803, June 2019.
- [22] I. A. Elgendy, W. Zhang, Y. Tian, and K. Li, "Resource allocation and computation offloading with data security for mobile edge computing," *Future Generation Computer Systems*, vol. 100, pp. 531–541, November 2019.
- [23] Y. Wang, M. Sheng, X. Wang, L. Wang, and J. Li, "Mobile-edge computing: Partial computation offloading using dynamic voltage scaling," *IEEE Transactions on Communications*, vol. 64, no. 10, pp. 4268–4282, October 2016.
- [24] X. Chen, Y. Cai, L. Li, M. Zhao, and B. Champagne, "Energy-efficient resource allocation for latency-sensitive mobile edge computing," *IEEE Transactions on Vehicular Technology*, vol. 69, no. 2, pp. 2246–2262, February 2020.
- [25] X. Ma, S. Wang, S. Zhang, P. Yang, C. Lin and X. Shen, "cost-Efficient Resource Provisioning for Dynamic Requests in Cloud Assisted Mobile Edge Computing," *IEEE Transactions on Cloud Computing*, vol. 9, no. 3, pp. 968–980, March 2019.

Collaborative Ontology Construction Framework: An Attempt to Rationalize Effective Knowledge Dissemination

Kaneeka Vidanage¹, Noor Maizura Mohamad Noor², Rosmayati Mohamad³, Zuriana Abu Bakar⁴
Faculty of Ocean Engineering Technology & Informatics, Universiti Malaysia Terengganu^{1, 2, 3, 4}
OREL IT – Research and Development Unit, Sri Lanka¹

Abstract—Ontologies are domain rich conceptualizations, which can be utilized for effective knowledge dissemination strategies. Knowledge dissemination plays a vital role in any industry. In this research, novel framework is designed and experimented for the collaborative ontology construction. With the iterative and incremental involvement of the domain specialists and ontologists rational process has been discussed and planned for the collaborative ontology construction. Additionally, existing shortcomings associated with the current ontology construction methodologies and frameworks also have been rigorously reviewed to identify the shortcomings. Henceforth the responses received from the domain specialists and ontologists, along with the gaps located from the literatures have been utilized as the backbone in designing this novel framework. Designed ontology increments have the potential of effective knowledge distribution once it's coupled with technologies like chatbots. In this research, proposed framework has been deployed in three different domains and three different ontology increments have been created for each domain. Consequently, their efficacy have been tested with the involvement of domain specific stakeholders. Overall results have yielded an 82% of acceptance from the stakeholders.

Keywords—Collaborative; domain-specialists; framework; methodology; ontologies

I. INTRODUCTION

Knowledge is the fuel which drives current economies. Therefore, effective mechanisms on knowledge diffusion are very critical. This research discusses about construction of knowledge enriched ontologies for effective knowledge dissemination. Ontologies are human understandable and machine-readable cognitive conceptualizations associated with a specific domain [1]. Once an ontology is constructed with accurate domain associated conceptualizations, it could be utilized as a centralized resource for effective knowledge dissemination [2]. For an instance, if an ontology is constructed on the domain of COVID-19 pandemic, a chatbot can be coupled with it to ensure engaging knowledge distribution to educate varied populations. Nevertheless, capturing the expert human insights and construction of the ontology can be identified as a challenging yet very critical necessity to be accomplished precisely [3]. Because there are no fully automated mechanisms that exist so far for the ontology construction, hence it's a complex philosophical task, which can only be handled effectively by humans [4].

This research emphasizes on a specialized framework for precise ontology construction amidst collaborative involvements. Because, deriving expert knowledge from humans with multivariate specialties and concisely evolving it to a level of cognitively enriched ontology is not an easy task [3-4]. However, the use case of knowledge distribution via a chatbot becomes operational only if the ontology creation is successful and accurate. Therefore, a systematic approach to efficiently gather knowledge from heterogeneous human experts for the purpose of collaborative ontology development can be characterized as a research gap that needs to be filled.

This research proposes “Collaborativity” framework to fulfill the aforementioned requirement. This novel framework comprises of separately defined dedicated modules to foresee numerous critical aspects associated with collaborative ontology construction. Governing module, operational module, traceability module and opinion aggregation module are such modules residing inside this framework. Those modules collaboratively communicate to streamline the opinion acquisition, process enforcement and decision logging for the enhanced traceability.

Opinion aggregation module utilizes a voting strategy to adequately represent the collaborative participation of all the involved stakeholders. All these strategies will eliminate the black boxes associated with the entire procedure and improve the clarity and the transparency of the entire workflow. Collaborative ontology engineering is the latest trend associated with the ontology construction. Though there are several collaborative ontology construction methodologies available, almost all of them have severe shortcomings. Those aspects will be discussed in detailed during the literature review section. In such setting, this novel framework can be identified as a significant contribution to the domain of collaborative ontology engineering.

II. LITERATURE REVIEW

Ontology construction is a complex process. It's impossible to create an effective ontology from a one shot [5]. This makes, ontology construction procedures iterative and incremental [6]. Another important aspect to consider is the role separation of ontologists and domain specialists. Ontologists are the semantic tech specialists, who create and evolve the ontology as per the specifications and knowledge provided by the domain specialists [7]. Majority of the existing methodologies and

frameworks have not properly distinguished between the roles of ontologists and domain specialists. This leads to operational confusions amidst the ontology construction process. Below Tables 1 to 3 contain a comprehensive review on the deficiencies associated with second, third generation methodologies and frameworks respectively.

As reviewed above, though there are numerous methodologies and frameworks for the ontology construction, almost all of them have multiple weaknesses such as:-

- 1) Ambiguous workflows – This leads to operational glitches of the involved stakeholders.
- 2) Explicit instructions are not provided – Allows excessive freedom to the stakeholders to act as they wish. This tarnishes the process consistency.

3) Role duality issues – Roles of the ontologists and domain specialists are not clearly defined. This leads to lots of operational confusions, during the working of the methodology/framework.

4) Poor logging of the operational decisions. This hinders lateral audits.

5) Absence of a mechanism to handle the collaborative communication flows occur between domain specialists and ontologists.

6) Irrespective of ontology construction being a cognitively enriched mental task; only engineering aspects are considered, ignoring the associated cognitive gravity.

TABLE I. SECOND GENERATION METHODOLOGY REVIEW

Significant second-generation Methodologies	Key deficiencies located on collaborative accomplishments
Methontology [8]	Lack of a clearly defined workflow causes many uncertainties such as; poorly organized activities, and issues with post-audit inspections. Additionally, there is no enough documentation of collaborative decisions made. The responsibilities of the domain experts and ontologists are not regulated.
TOVE [9]	The obligations of the domain specialists and ontologists are not specified. This casts doubt on the parties' ability to maintain interoperability and consensus causing operational glitches
IDEF5 [10]	The procedures for verifying ontology increments are not well-structured. In a group setting, how do you decide whether to move on to the next increment or repeat the same increment again? How does ideology collaboration between domain specialists and ontologists take place? Similarly, there are several process ambiguities.
Enterprise Model [11]	Very abstract and high-level. It is impossible to assess operational success due to a lack of standardized operating procedures (SOPs).
OTKM [12]	Roles of the ontologists and domain specialists are not clearly defined.

TABLE II. THIRD GENERATION METHODOLOGY REVIEW

Significant third-generation methodologies	Key deficiencies located on collaborative accomplishments
Diligent [13]	Users are given an overabundance of control. As a result, the controlled operational flows have been jeopardized.
SMOD [14]	Explicit work procedures are not defined. This allows excessive freedom for the stakeholders, jeopardizing process consistency.
Neon [15]	Many uncertainties, such as poorly coordinated operations and problems with post-audit inspections, are brought on by a lack of a clearly defined workflow. Decisions are not sufficiently documented, as well. There are no rules governing the duties of domain experts and ontologists.
Upon-Lite [16]	Explicit work procedures are not defined. This allows excessive freedom for the stakeholders.
AMOD [17]	The transition process of ontology increments is absent. Several hidden black boxes trigger; great deal of ambiguity.
CO ₄ [18]	Poor processors. The roles of ontologists and domain specialists are not well defined.
(KA) ₂ [19]	Poor processors. The roles of ontologists and domain specialists are not well defined.

TABLE III. FRAMEWORK REVIEW

Framework	Key deficiencies located on collaborative accomplishments
Semiotic [20]	Excessive ambiguity. No structured workflow for transparency and traceability.
RapidOWL [21]	Too lenient, which could jeopardizes the process consistency
Generic Ontology Development Framework [22]	Poor processors. The roles of ontologists and domain specialists are not well defined.
Platform Independent Ontology Development Framework [23]	Explicit work procedures are not defined. This allows excessive freedom for the stakeholders, jeopardizing process consistency.
Industry Relevant Ontology Development Framework [24]	Poor processors. The roles of ontologists and domain specialists are not well defined.
Systemology [25]	Poor processors. The roles of ontologists and domain specialists are not well defined.

The literature review conducted above clearly reveals the shortcomings associated with the existing methodologies and frameworks available for the ontology construction. Therefore, it can be justified as a research gap which requires to be addressed.

III. METHODOLOGY

As the outcome of this research, it suggests a novel framework capable of addressing aforementioned deficiencies. The overall research methodology followed for the construction and evaluation of this framework can be depicted in form of a process diagram as depicted in Fig. 1.

This framework is named as “Collaborativity”, hence its main goal is to collaborate all viewpoints of the stakeholders in a methodical manner and trigger the ontology increment construction. The flow of this framework was developed through several trial-and-error tests with domain specialists, as well as it equips with remedies to the inadequacies found in existing approaches and frameworks discussed in the literature review section.

“Collaborativity” framework comprises of mainly four modules with designated responsibilities. Operational module comprises of a stepwise orchestration on the ontology increment construction. Each important insights generated during the operational module’s steps are logged within the respective tracker sheets structures, belonging into the traceability module. This ensures transparency and assists in latter auditing requirements of the collaborative opinions of the involved stakeholders.

Governing module is mainly responsible for handling the cognitive perspectives and the workflow of the involved stakeholders. As a result of the fact that ontology development is a complicated cognitive process that involves several stakeholders from various domains, a methodical pipeline is required to efficiently handle the collaborative interactions and workflows that occur in the group environment.

The pipeline introduced inside the governing module is defined with the name “Synchronized Action Plan Meet.” This is a time-boxed workflow, governing numerous cognitive and process specific tasks associated with the respective operational module’s phase. This process enforcement has been identified as very vital. Unless it could lead to biases and numerous opinion conflicts among the involved stakeholders. Therefore, governing module plays a vital role in addressing process consistency perspectives. The entire operation inside this framework is governed via pool of ontologists, who are designated with multiple roles as convener, timekeeper and documenter.

Opinion aggregation module is responsible in governing the phase-specific transitions inside the operational module. Fig. 2 depicts the operational workflow of the opinion aggregation module.

Governing module’s “Synchronized Action Plan Meet” process will be applied across all phases of the operational module. Henceforth, all stakeholder’s vote is inquired on the completed phase. If the vote percentage exceed more than 80% of the involved participants, a collaborative decision is taken

for the transition to the next phase of the ontology increment construction. If the majority vote of the stakeholder’s do not exceed 80%, same phases is examined for shortcomings and reiterated with the suggested modifications. This way it ensures, transparency and collaborative participation of the stakeholders for the decisions reached in the forward movement of the ontology increment construction. This idea is enforced by the Power of 80% rule, which is strongly enforced in clinical trials associated with humanoid subjects.

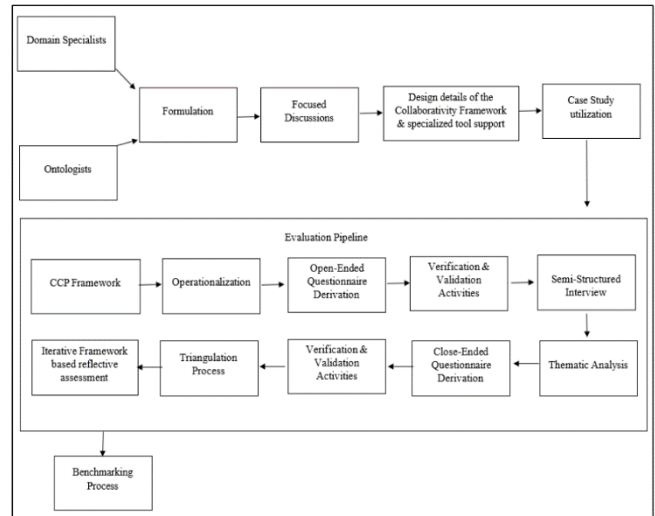


Fig. 1. Research Methodology Flow.

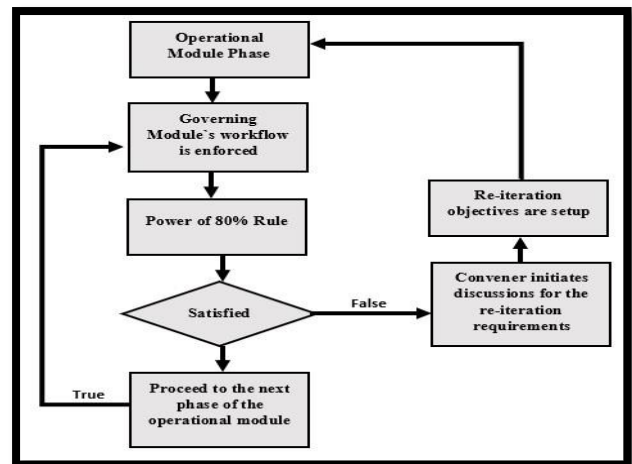


Fig. 2. Opinion Aggregation Module’s Workflow.

Fig. 3 denotes the roles of the governing module, operational module and opinion aggregation modules in conjunction.

Fig. 4 denotes the fixation of all four modules inside the Collaborativity Framework. Fig 4, denotes synchronized action plan meet workflows belonging inside the governing module, mapping between the operational and traceability module as well as the process enforcement of the opinion aggregation module.

It’s significant to emphasize, that each operational module’s step is executed as per the workflow enforced by the governing

module (i.e. synchronized action plan meet phase I and II). Subsequently, transition from one operational module step to the next is controlled by the process enforced via the opinion aggregation module. All collaborative decisions emerged during the stakeholder interactions are logged inside the traceability module's tracker worksheets.

Once the framework's structure is finalized, subsequently, it's decided to apply the framework for three case studies to assess its operational efficacy in order to fulfil this requirement.

COVID-19, Criminal Law and Aquaculture domains were selected. Henceforth, "Collaborativity" framework was applied, and three different ontology increments were created. Henceforth, those were coupled with chatbots and with the involvement of the respective domain specialists' responses derived via the chatbots were reviewed as well as the structures of the constructed ontology increments.

Evaluation pipeline depicted in Fig. 1 was utilized for the assessment of the "Collaborativity Framework." CCP framework [26] and operationalization [27] procedures were utilized in combination to compile applicable sets of questionnaires. Once the basic versions of the questionnaires were compiled, those were validated and verified for their reliability and accuracy.

Henceforth, controlled interview sessions with the respective domain specialists of the three fields were conducted using the compiled questionnaires and responses were recorded.

Consequently, the logged qualitative responses of the stakeholders were reviewed and analyzed using thematic analysis. Outcome of the thematic analysis was utilized to

determine the most significant topics associated with the insights derived from the stakeholder's interviews. Eventually, targeting the significant topics emerged from the qualitative interview responses, series of close ended questions were created again using the CCP and the operationalization procedures [26-27].

Combinations of the quantitative and qualitative questionnaires utilized for the experiment is as depicted in Fig. 5.

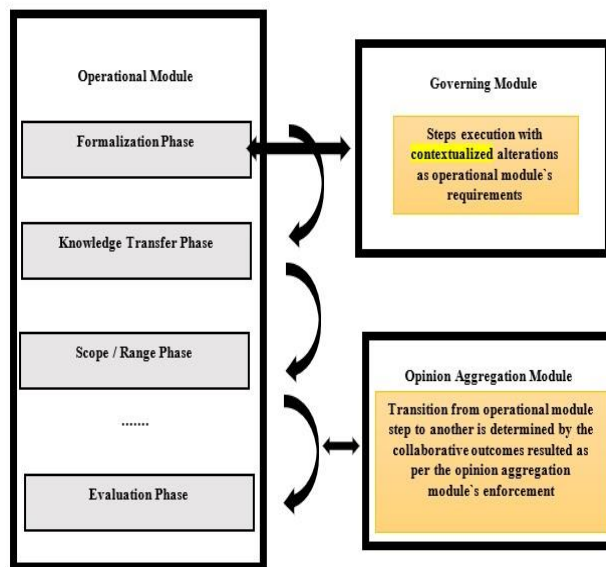


Fig. 3. Combinatory Roles of the Modules.

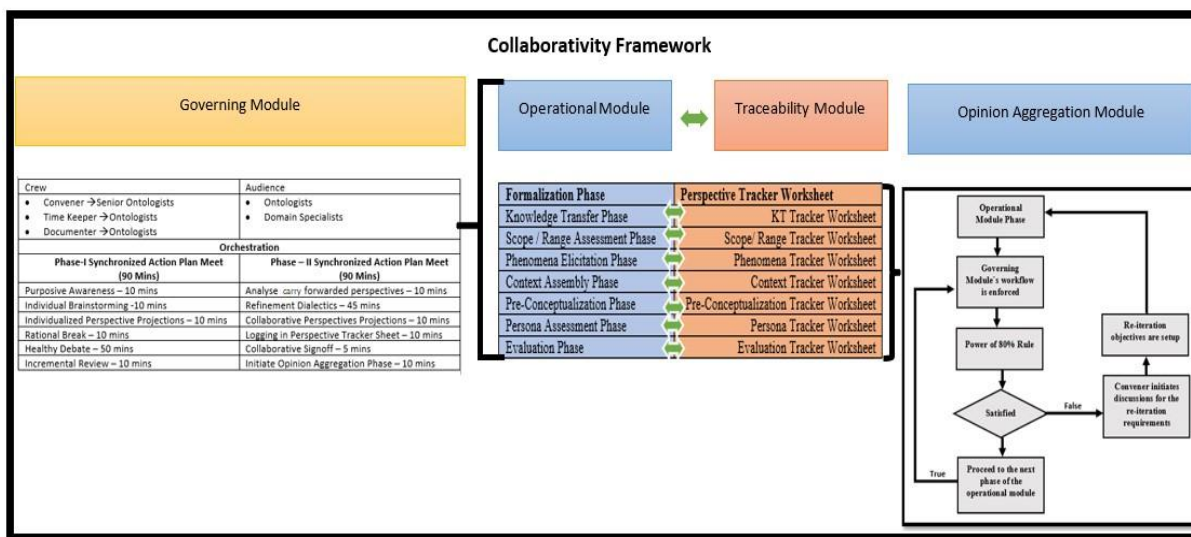


Fig. 4. Collaborativity Framework.

Qualitative Questionnaire	1. What observations have you made about existing frameworks applications on collaborative ontology construction? Please elaborate
	2. What observations have you made about the collaborativity framework's role in collaborative ontology construction? Please elaborate
	3. What do you expect from a novel framework for collaborative ontology construction?
	4. Does this framework ensure collaborative insight? Please explain
	5. Does this framework ensure collaborative consensus? Please explain
	6. Does this framework ensure collaborative goals related to ontology increment construction? Please explain
Quantitative Questionnaire	1. How satisfied are you with the framework's collaborative insight enforcement?
	2. How satisfied are you with the collaborative consensus enforcement of the framework?
	3. How effective are the governing, operational, and opinion aggregation modules in controlling the framework's flow?
	4. How would you rate the overall operation of the framework?
	5. How effective are the "Action plan meets" for communication synchronization and framework's target-oriented execution?
	6. How useful is the Dialectics step for communication synchronization?
	7. How useful is the Opinion assessment heuristic for collaborative communication synchronizations?
	8. How would you rate the overall communication synchronization enforced by this framework?

Fig. 5. Questionnaire Sets.

Reponses for the qualitative questions were retrieved via controlled interview sessions conducted. A special response grid depicted in Fig. 6 was used to record the responses for the quantitative questions.

10	20	30	40	50	60	70	80	90	100
Very poor	Fairly OK-Major revisions			Good & Acceptable- Few minor revisions				Exceptional	

Fig. 6. Quantitative Response Grid.

IV. RESULTS AND DISCUSSION

Significant themes emerged out from the thematic analysis of the interview responses have been logged in Table IV.

Consequently, quantitative close-ended questions were formulated covering the themes emerged from the thematic analysis. Responses of qualitative feedback has been logged in Table V.

Henceforth, Cronbach analysis was performed to assess the reliability of the responses provided and the outcomes for the domains have been logged in the Table VI.

According to Cronbach reliability tests of the user responses, a Cronbach Alpha value ranging in between 0.65 – 0.95 is accepted as a reliable distribution [28]. Therefore, Cronbach reliability test confirms the reliability of the stakeholders` responses yielded, covering all three domains and the ontologists. Table VI denotes the reliability test distribution results.

Additionally, an ANOVA test also has been conducted to reveal the significance of the user responses and to confirm there are no significant statistical anomalies [29]. Table VII denotes the outcomes of the ANOVA test conducted.

As depicted in Table VII, P-value (i.e., 0.23) for the test conducted in greater than the standard alpha value of 0.05 [29]. Hence, it confirms, that the population has responded to the questionnaire without any outliers causing no statistically significant anomalies.

TABLE IV. THEMES REVEALED FROM THE THEMATIC ANALYSIS OF INTERVIEW RESPONSES

Qualitative themes emerged from the controlled interview session conducted on Collaborative Framework	Collaborative Goals
	Transparency of Operations
	Process Enforcement
	User Friendliness

TABLE V. RESPONSE SCORES OF THE CLOSE-ENDED QUESTIONNAIRE

Question Cluster	Domain	Averaged Response Scores
Collaborativity Framework	Law	88%
	COVID-19	85%
	Aquaculture	82%

TABLE VI. CRONBACH ALPHA RELIABILITY TEST SCORES

Domain/Segment	Cronbach Alpha Value
Criminal Law	0.736
COVID-19	0.713
Aquaculture	0.728
Ontologists	0.702

TABLE VII. ANOVA SIGNIFICANCE TEST

ANOVA						
Source of Variation	SS	df	MS	F	P-value	F crit
Between Groups	167.458333		55.8194444	1.5690379	0.22806	3.09839
	3	3	4	3	8	1
Within Groups	711.5	0	35.575			
	878.958333	2				
Total	3	3				

Subsequently, a benchmark test has been conducted to assess the uniqueness associated with the Collaborativity framework. Eight existing and latest methodologies and frameworks have been utilized for this comparative assessment. Results associated with the benchmark test has been logged in the Fig. 7.

Finally, Iterative framework [30] has been utilized to triangulate and amalgamate all the experimental tests conducted against the research's expectation. Iterative Framework is an established research framework utilized to consolidate multiple test experiments against the research's expectations [30]. Table VIII denotes the application of the Iterative Framework for this research study.

Feature Index	Researched Framework: Collaborativity	Existing Methodologies & Frameworks							
		Systemology	Diligent	SMOD	NeOn	U-pon-Lite	AMOD	RapidOWL	Se
1. Layered / Modular Architecture	✓	✗	✗	✗	✗	✓	✓	✓	✓
2. Stakeholder collaboration	✓	✓	✓	✓	✓	✗	✓	✓	✓
3. Ontologists & domain specialists' roles are specifically defined	✓	✗	✗	✓	✗	✓	✓	✗	✓
4. Ontology Increments concept	✓	✗	✓	✓	✗	✓	✓	✓	✓
5. Explicit workflows	✓	✗	✗	✗	✗	✗	✗	✗	✗
6. Holistic instructions	✓	✗	✗	✗	✗	✗	✗	✗	✗
7. Communication management pipeline	✓	✓	✗	✗	✗	✗	✗	✗	✗
8. Collaborative opinion handling	✓	✗	✗	✗	✗	✗	✗	✗	✗
9. Logn of collaborative decisions for latter reference in worksheets structures	✓	✗	✗	✗	✗	✗	✗	✗	✗

Fig. 7. Benchmark Results.

TABLE VIII. APPLICATION OF THE ITERATIVE FRAMEWORK

Iterative Framework's questions		Mapping Evidence
1. What are the data telling me?	•	Four important themes have been yielded from the thematic analysis conducted
	•	Averaged quantitative response score for all three domains: -85%
	•	Averaged Cronbach Alpha Reliability Score: - 0.72
	•	ANOVA Significance Score: -0.23
2. What do you want to know?	•	Overall effectiveness of the newly designed Collaborativity framework for ontology constructions in collaborative atmospheres.
3. Is there a dialectical relationship between 1 & 2	•	Yes. Mapping Evidences of Question 1, reflects the Question 2 , perspectives have been satisfied in a consolidated fashion.

V. CONCLUSION

This research paper discusses about the application of a newly designed framework for effective ontology increment construction on the collaborative group atmospheres. Efficacy of this framework has been tested using case study mechanism. Three independent case studies have been conducted on three different domains. Three separate ontology increments have been compiled and they were tested by the structure and practical applications. For the practical utilization test, the

created ontology increments have been linked with chatbots and validity of the responses provided were assessed by the subject specialists.

COVID-19, ontology increment was tested by general physicians, based on the validity of the responses provided. Criminal Law increment and Aquaculture increment was tested by the respective experts in the fields. Once, these prototypes got evolved to the level of products, they can be effectively utilized to educate and disseminate knowledge on medical students, law students and zoology students. This practical application could immensely reduce the workloads of the university lectures, without penalizing the user experience of the students as well. Currently, the prototype version has yielded up to 82% of user acceptance.

This research contributes a novel ontology construction framework, addressing the deficiencies of the existing methodologies and frameworks. Additionally, its use cases are very valuable to all the fields where knowledge dissemination plays a vital aspect. In future, it's expected to boost the power of this framework via integration computerized tool support as well.

REFERENCES

- Harvey, E. (2016). Sir Tim Berners-Lee on the Future of Ebooks. Book Business Mag.
- Oliveira, D., Sahay, R., & Aquin, M. (2019). Leveraging ontologies for knowledge graph schemas. CEUR Workshop Proceedings.
- Futia, G., Vetro, A., Melandri, A., & de Martin, J. C. (2018). Training neural language models with SPARQL queries for semi-automatic semantic mapping. *Procedia Computer Science*. <https://doi.org/10.1016/j.procs.2018.09.018>.
- Hartig, O., & Pérez, J. (2016). LDQL: A query language for the Web of Linked Data. *Journal of Web Semantics*. <https://doi.org/10.1016/j.websem.2016.10.001>.
- Anutariya, C., & Dangol, R. (2018). VizLOD: Schema Extraction and Visualization of Linked Open Data. *Proceeding of 2018 15th International Joint Conference on Computer Science and Software Engineering, JCSSE 2018*. <https://doi.org/10.1109/JCSSE.2018.8457325>.
- Simperl, E., & Luczak-Rösch, M. (2014). Collaborative ontology engineering: A survey. *Knowledge Engineering Review*. <https://doi.org/10.1017/S0269888913000192>.
- Al-Arfaj, A., & Al-Salman, A. (2015). Ontology Construction from Text: Challenges and Trends. *International Journal of Artificial Intelligence and Expert Systems*.
- Fernandez, M., Gómez-Pérez, A., & Juristo, N. (1997). Methontology: from ontological art towards ontological engineering. *Proceedings of the AAAI97 Spring Symposium Series on Ontological Engineering*.
- Gruninger, M., & Fox, M. S. (1994). The Design and Evaluation of Ontologies for Enterprise Engineering. *Workshop on Implemented Ontologies, European Workshop on Artificial Intelligence, Amsterdam, The Netherlands*.
- Peraketh, Menzel, Mayer, Fillion, F. (1994). *Ontology Capture Method (IDEF5)*.
- Uschold, M., & King, M. (1995). *Towards a Methodology for Building Ontologies. Workshop on Basic Ontological Issues in Knowledge Sharing*.
- Sure, Y., Staab, S., & Studer, R. (2004). On-To-Knowledge Methodology (OTKM). In *Handbook on Ontologies*. https://doi.org/10.1007/978-3-540-24750-0_6.
- Tempich, H. S. Pinto and S. Staab, "Ontology Engineering Revisited: An Iterative Case Study", 3rd European Semantic Web Conference, (ESWC), Research and Applications, Budva, Montenegro, Proceedings, 2006 110, url: https://doi.org/10.1007/11762256_11.

- [14] Peroni, S., Shotton, D., & Vitali, F. (2012). The live OWL documentation environment: A tool for the automatic generation of ontology documentation. Lecture Notes in Computer Science (Including Subseries Lecture Notes in Artificial Intelligence and Lecture Notes in Bioinformatics). https://doi.org/10.1007/978-3-642-33876-2_35.
- [15] Suárez-Figueroa, M. C., Gómez-Pérez, A., & Fernández-López, M. (2015). The NeOn Methodology framework: Ascenario-based methodology for ontology development. Applied Ontology. <https://doi.org/10.3233/AO-150145>.
- [16] De Nicola, A., & Missikoff, M. (2016). A lightweight methodology for rapid ontology engineering. Communications of the ACM. <https://doi.org/10.1145/2818359>.
- [17] Abdelghany, A. S., Darwish, N. R., & Hefni, H. A. (2019). An agile methodology for ontology development. International Journal of Intelligent Engineering and Systems. <https://doi.org/10.22266/IJIES.2019.0430.17>.
- [18] Euzenat, J. (2016). Building consensual knowledge bases: context and architecture. HAL Open Science. <https://hal.archives-ouvertes.fr/hal-01401176/document>.
- [19] RICHARD BENJAMINS, V., FENSEL, D., DECKER, S., & PÉREZ, A. G. (1999). (KA)2: Building ontologies for the internet: a mid-term report. International Journal of Human-Computer Studies, 51(3), 687-712. <https://doi.org/10.1006/ijhc.1999.0275>.
- [20] Toppiano, E., & Roberto, V. (2009). A semiotic framework for ontology development. Proceedings of I-KNOW 2009 - 9th International Conference on Knowledge Management and Knowledge Technologies and Proceedings of I-SEMANTICS 2009 - 5th International Conference on Semantic Systems, May, 738-743.
- [21] Auer, S., Herre, H. (2007). RapidOWL — An Agile Knowledge Engineering Methodology. In: Virbitskaite, I., Voronkov, A. (eds) Perspectives of Systems Informatics. PSI 2006. Lecture Notes in Computer Science, vol 4378. Springer, Berlin, Heidelberg. https://doi.org/10.1007/978-3-540-70881-0_3.
- [22] Rajpathak, D., & Chougule, R. (2011). A generic ontology development framework for data integration and decision support in a distributed environment. International Journal of Computer Integrated Manufacturing. <https://doi.org/10.1080/0951192X.2010.531291>.
- [23] Sanya, I. O., & Shehab, E. M. (2014). An ontology framework for developing platform-independent knowledge-based engineering systems in the aerospace industry. International Journal of Production Research. <https://doi.org/10.1080/00207543.2014.919422>.
- [24] Abdullah, N. S., Sadiq, S., & Indulska, M. (2011). A framework for industry-relevant ontology development. ACIS 2011 Proceedings - 22nd Australasian Conference on Information Systems.
- [25] Rousseau, D., & Billingham, J. (2018). A Systematic Framework for Exploring Worldviews and Its Generalization as a Multi-Purpose Inquiry Framework. Systems, 6(3), 27. <https://doi.org/10.3390/systems6030027>.
- [26] Eslami Andargoli, A., Scheepers, H., Rajendran, D., & Sohal, A. (2017). Health information systems evaluation frameworks: A systematic review. In International Journal of Medical Informatics. <https://doi.org/10.1016/j.ijmedinf.2016.10.008>.
- [27] Dröes, R. M., Chattat, R., Diaz, A., Gove, D., Graff, M., Murphy, K., Verbeek, H., Vernooij-Dassen, M., Clare, L., Johannessen, A., Roes, M., Verhey, F., Charras, K., van Audenhove, C., Casey, D., Evans, S., Fabbo, A., Franco, M., Gerritsen, D., ... Zuidema, S. (2017). Social health and dementia: a European consensus on the operationalization of the concept and directions for research and practice. Aging and Mental Health. <https://doi.org/10.1080/13607863.2016.1254596>.
- [28] Taber, K.S. The Use of Cronbach's Alpha When Developing and Reporting Research Instruments in Science Education. Res Sci Educ 48, 1273-1296 (2018). <https://doi.org/10.1007/s11165-016-9602-2>.
- [29] Campbell, Z., Bray, A., Ritz, A.M., & Groce, A. (2018). Differentially Private ANOVA Testing. 2018 1st International Conference on Data Intelligence and Security (ICDIS), 281-285.
- [30] Srivastava, P., & Hopwood, N. (2009). A Practical Iterative Framework for Qualitative Data Analysis. International Journal of Qualitative Methods. <https://doi.org/10.1177/160940690900800107>.

BiLSTM and Multiple Linear Regression based Sentiment Analysis Model using Polarity and Subjectivity of a Text

Marouane CHIHAB, Mohamed CHINY, Nabil Mabrouk
Hicham BOUSSATTA, Younes CHIHAB, Moulay Youssef HADI

Laboratory of Computer Sciences, faculty of sciences Ibn Tofail University, Kenitra, Morocco

Abstract—Sentiment analysis has become more and more requested by companies to improve their services. However, the main contribution of this paper is to present the results of the study which consists in proposing a combined model of sentiment analysis that is able to find the binary polarity of the analyzed text. The proposed model is based on a Bidirectional-Long Short-Term Memory recurrent neural network and the TextBlob model which computes both the polarity and the subjectivity of the input text. These two models are combined in a classification model that implements each of the Logistic Regression, k-Nearest Neighbors, Random Forest, Support Vector Machine, K-means and Naive Bayes algorithms. The training and test data come from the Twitter Airlines Sentiment data set. Experimental results show that the proposed system gives better performance metrics (accuracy and F1 score) than those found with the BiLSTM and TextBlob models used separately. The obtained results well serve organizations, companies and brands to get useful information that helps them to understand a customer's opinion of a particular product or service.

Keywords—Sentiment analysis; textblob; long short term memory; logistic regression; k-nearest neighbors; random forest; support vector machine; k-means; naive bayes

I. INTRODUCTION

Sentiment analysis is a technique that focuses on the evaluation of emotions, attitudes and opinions. Today, organizations, companies and brands use this technique to obtain useful information that helps them to understand a customer's opinion of a particular product or service. For this purpose, several models of sentiment analysis, which is a field of artificial intelligence, in particular natural language processing, have emerged. In this sense, given the importance of texts coming from Twitter, several studies have been focused on this topic, among these studies, we can cite the analysis of subjectivity [1], the detection of events [2], the evaluation of online reputation [3], the identification of trends on social networks [4]. Sentiments are essentially labeled according to the polarity of the text, i.e., whether the message has a positive, negative or neutral connotation. The determination of polarity can be done at different levels, namely the document [5], the sentence [6], the word [7] or the attribute [8]. In a previous study, Chiny et al. [9] proposed a hybrid sentiment analysis model based on three input models; the LSTM model, the TF-IDF word weighting model and the pre-trained model based on the VADER lexicon. These three models are combined using a classifier that returns the binary

sentiment experienced in the input text. The proposed architecture is characterized by the small amount of data required for training. In addition, the model is characterized by its ability to transfer the knowledge already acquired to process a different dataset than the one that provided the training data. However, in a text, the semantics of a given word does not only depend on the words preceding it, but also on the following words. For this reason, we thought of implementing the BiLSTM model which evolves in both directions rather than the LSTM model which considers the current word and the previous words only as a temporal sequence. Therefore, the aim of this research paper is to propose a hybrid sentiment analysis system by combining two input modules. The first model is based on the use of BiLSTM networks. In the second model, a Textblob sentiment analyser is used to evaluate the subjectivity and polarity of texts. Subjectivity and polarity are features of a linear regression model that returns a single sentiment score. Both models were trained on the US Airlines Sentiments twitter dataset. Each model returns scores of positivity or negativity from the text to be analyzed. Then, these two (input) models are combined into a binary classification model in which the Logistic Regression, k-Nearest Neighbors, Random Forest, Support Vector Machine, K-means and Naive Bayes models are implemented.

After implementing the proposed architecture, we wish to have performance metrics (i.e., accuracy and F1 score) superior to the metrics calculated for the two modules (BiLSTM and TextBlob) separately. The main contribution of this paper is to have a more advantageous performance than the model proposed in the study by Chiny et al. [9]. This improvement will allow organizations, companies and brands to have more relevant and meaningful information that will help them to understand and analyze customer opinions about a product or service provided.

II. RELATED WORK

A. Bidirectional Long Short Term Memory

Processing sequential data and natural language (NLP) leads to several major problems related to the nature of the data. To solve these problems, the authors of [10] used recurrent neural networks (RNN), which are artificial neural networks that use hidden states to model the behavior of dynamic systems.

According to [11], a BiLSTM (Bidirectional Long Short-Term Memory) network is a recurrent neural network that processes data in two different ways. The use of this network is particularly requested in the field of natural language processing. Indeed, the meaning of a word in a sentence may depend on the preceding and following words. Therefore, in this kind of cases, it is desirable to go through the sentence in both directions to get the right meaning. The BiLSTM offers this particularity which makes it different from LSTM networks.

The bi-directional nature of BiLSTM has given it great potential to be at the heart of many works related to natural language processing. For example, Zhou et al. [12] applied a two-way LSTM with 2D max pooling to the Stanford Sentiment Treebank (STS) database; each vector is represented by a 2D matrix. In addition, to find optimal performance, Shen et al. [13] proposed a new design combining the CNN and BiLSTM models. They found that this combination achieved an accuracy of 89.7%. This result is better than that of each of the models individually. In another study, Yoon et al. [14] proposed a CNN-BiLSTM architecture for document-level emotion prediction using multi-channel integration with CNN. The model worked on different datasets and achieved average performance from 51.97% to 70.08%.

Wu Xing et al. [15] used long-term memory (LSTM) to automatically generate poems based on the author's style. In [16], Felix et al. studied bidirectional long-term memory networks (BLSTMs) and i-vectors to model the author's speech. They also used i-vectors to model the longer term acoustic context. Also, in [17], Nowak et al. (2017) compared the LSTM model and the BLSTM model in the emotion classification of Amazon's book review dataset. The results obtained by the authors show that the BLSTM model is more accurate than the LSTM model in this task.

Seneewong Na Ayutthaya and Pasupa (2018) attempted to merge the BLSTM and CNN deep learning models to examine word sequences and discover local text characteristics [18]. The results showed that the combination of deep learning models improved the accuracy of sentiment analysis. Furthermore, deep bi-directional LSTMs (DBLSTMs) have recently been shown to provide performance for solving many problems, such as text analysis. These problems include sentiment classification [19], speech recognition [20], semantic labelling [21] and large-scale acoustic modeling [22]. BLSTM networks have proven useful in discovering character input patterns for processing a wide variety of natural languages.

In the literature, different deep learning algorithms have been applied to process different types of data. The researchers used complex neural networks (CNNs) to process computer vision subjects and analyze text to infer a local structure, while using long-term memory (LSTM) and bidirectional LSTM (BLSTM) for sequential data processing and different language models [23,24,25].

To analyze the sentiment trend of Chinese texts. Gan et al. [26] used a joint multi-channel dilated evolutionary architecture of a convolutional neural network and a

bidirectional long-term memory model (CNN-BiLSTM) with an attention mechanism.

In [27], Wang et al. used a bidirectional short-term memory network enhanced by emotion semantics (BiLSTM) with the multi-headed attention mechanism model (EBIL).

The work of Batbaatar et al. [28] aimed to propose a new neural network architecture, called SENN (Semantic-Emotion Neural Network), which can use both semantic/syntactic and emotional information by adopting pre-trained word representations.

B. Subjectivity and Polarity

Sentiment analysis, also known as opinion research, is aimed at understanding how a reader could interpret a person's subjectivity and translate it into an algorithm capable of performing this task automatically. According to the authors' studies [29, 30], the polarity of a sentiment is a quantified measure on the scale of values corresponding to a positive or negative assessment of emotional significance. From this quantification, we can test the polarity of the subjective text by the classification of sentiment. Indeed, if we have a review about a product, the sentiment analysis system must determine whether the emotion expressed in that review has a positive or negative connotation. In general, the polarity of the text can be positive, negative and sometimes neutral to identify a lack of feeling in a text.

According to [31], studies on polarity analysis are subdivided into two approaches: a lexical approach (also known as a knowledge-based approach) and a machine learning-based approach. The first approach uses dictionaries, such as LIWC (Language Inquiry and Word Count) [32] and Senti Word Net [33]. Generally, a dictionary consists of words and the corresponding classification value. Indeed, in a dictionary, we can find the word "pleasure" with a value +1 which signifies that this word has a positive polarity or, conversely, it can contain the word "hate" with the value -1 representing a negative polarity. According to the authors [32] and [33], adding the values of all the words in the text gives the resulting polarity. The result of the summation (positive or negative) determines the global polarity of the text. On the other hand, the second approach, is based on the use of classification algorithms, such as Naïve Bayes (NB), Maximum entropy (ME) and Support Vector Machines (SVM). These algorithms have been tested by the authors [34, 35, 36, 37] to perform text classification; the obtained results are promising. Polarity determination can be measured at the levels: document [48], sentence [39], word [40] or attribute [41]. The document level treats the whole document as the basic unit. The sentence level draws and determines the sentiment of each sentence in the text. At the word level, each word in the text is analyzed and classified. The attribute level identifies and extracts the attributes of an entity (e.g., product, person, company) in the text and determines the sentiment for each attribute [42].

Subjectivity aims at determining whether a text is subjective (opinion, emotions, evaluations, beliefs or speculations) or simply a fact, while the classification of feelings aims at determining the proper value of this

subjectivity [43]. Subjectivity detection prevents sentiment ranking from considering only texts that are relevant or potentially misleading. In addition, it reduces the size of the set of labels that can be assigned to a text, i.e., it must first be checked whether the text is objective or subjective, and those that are considered as such are subjected to a new classification process that will determine the polarity. In addition, sentiment analysis may involve identifying the target entity, i.e., the subject of the text to which the sentiment is addressed, and identifying the person or organization expressing the opinion [44]. There are texts in which the polarity is not as noticeable, as in mixed experiences, i.e. when there are both positive and negative remarks, which is different from a neutral text that is purely factual.

Among the most commonly used feedback mechanisms in Twitter data analysis is sentiment analysis, which provides insight into the sentiment expressed in messages [45]. This feeling is essentially labelled according to the polarity of the text, i.e. whether the message has a positive, negative or neutral connotation. For companies, this measure provides insight into the public's and market's opinion of themselves.

In [46], the authors found that machine learning techniques applied to sentiment analysis perform better than those obtained by random selection (50%) or by human classification (between 58% and 64%). To generate a classification model, this approach needs a dataset for training.

Pak et al. [47] discuss ways to collect tweets to exploit them in sentiment analysis. They employ a specific lexicon of emotions to reduce the manual tagging of tweets for the classification of feelings. Emotions are classified into two types, happy representing a positive sample and sad for a negative sample.

Among the works that used learning techniques for the classification of feelings, Pang et al. [48] employed Naïve Bayes algorithms, logistic regression and the support vector machine. In this work, the authors used film reviews to classify the polarity of sentiments. But, opinions are considered neutral when there is no opinion in the text or the opinion falls between the two polarities.

III. PROPOSED SENTIMENT ANALYSIS ARCHITECTURE MODEL

The purpose of this research is to propose and test the validity of a new model of sentiment analysis (Fig. 1) composed of two input models. In the first model we used the BiLSTM algorithm, the validation of this model is tested on a corpus of US Airlines twitter sentiments. In the second model, we have exploited the TextBlob sentiment analyzer in the goal to evaluate the subjectivity and polarity of natural language texts. The subjectivity analysis attempts to estimate how subjective or objective the text is, while the polarity analysis determines whether the feeling in the text is positive or negative. The two outputs of the TextBlob model that represent the subjectivity and polarity scores are coupled with a multiple regression model to estimate the weights associated with each of these two features in the category of texts in our

study (short microblogging texts such as those from Twitter). After, the binary sentiment of the input text will be provided by a classifier that uses the scores already calculated by the BiLSTM and TextBlob models.

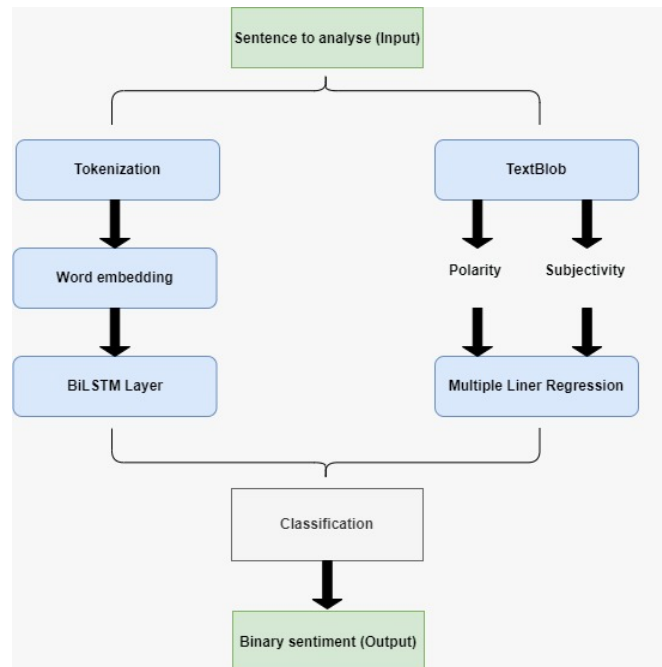


Fig. 1. Proposed BiLSTM and TextBlob based Combined Sentiment Analysis Model.

A. LSTM Bidirectional

The bidirectional LSTM algorithm (BiLSTM) is a recurrent neural network. This algorithm finds its major application in natural language processing. It has the advantage that the input flows in both directions: forward and reverse direction. BiLSTM is a very efficient algorithm for modeling sequential dependencies between words and sentences in both directions of the sequence.

To use the BiLSTM algorithm in the text to be analyzed, we need to do cleaning and filtering, followed by tokenization and then word embedding.

B. TextBlob

The TextBlob sentiment analyzer is a Python library for processing text data. It makes it possible to recognize the subjectivity and polarity expressed in natural language texts. Polarity analysis determines whether a subjective text is positive or negative in a range between [-1, 1], -1 indicating negative feelings and +1 positive feelings.

C. Cleaning and Filtering

To analyze the tweets reliably and correctly by our proposed system, we performed preprocessing on the dataset. The purpose of this preprocessing is to ensure that the tweets will be prepared in a formal language format that will be interpreted by the machine. Subsequently, we chose a dataset of 14,427 unique texts for the training and testing of our model.

D. Tokenisation

Tokenization is a technique used to transform text into single words (unigram) (individual tokens) or combinations of successive words (n-gram). In our model, we have divided the texts into a series of individual tokens in order to use the Glove model. We have defined the sequence length that is equal to the number of time steps for the BiLSTM layer.

E. Word Embedding

Word embedding is a technique based on the linguistic theory founded by Zelling Harris. It is in great demand in the classification of documents [49] because it uses machine learning algorithms to represent textual data (words or sentences of a text) by vectors of real numbers. In our research, this representation facilitates and improves the performance of automatic language processing methods (or Natural Language Processing) and more particularly it simplifies the processing of Sentiment Analysis.

To describe the words of our text by a numerical vector, there are several algorithms including Word2Vec and GloVe. We used the algorithm GloVe (Global Vectors for Word Representation) [50]. This choice is dictated by the nature of our proposed system. We used the calculated 100-dimensional GloVe integrations of 400,000 words.

F. BiLSTMLayer

When defining the BiLSTM layer, we tested several parameters and kept the ones that gave good results. The number of hidden units is set at 256 and the rmsprop optimizer is used, which compares favorably with other adaptive learning algorithms. The Table I summarizes all the hyper parameters of the chosen model.

G. Training and Evaluation of the Model {BiLSTM et TextBlob}

To train and evaluate our proposed system, we chose to use the US Airlines Twitter dataset [51]. This database is exemplary on the binary classification of text. It contains 14449 unique texts. We have selected 7000 reviews in the train and 2000 in the test series of our BiLSTM and TextBlob models.

The TextBlob model allows the calculation of polarity and subjectivity scores separately. We therefore used these two scores as features of a linear regression model to calculate an overall sentiment score. The two input models (BiLSTM, TextBlob) are then combined into a binary classification model.

H. Model de Classification

To improve and increase the performance of predictions on the sentiment conveyed by the input text, we propose a hybrid system consisting of two sentiment analysis models with a classification model. For this, we chose the BiLSTM model in the first place. This model is characterized by its ability to adapt to sequential data processing. In the second step, and to recognize the subjectivity and polarity expressed in the texts, we worked with the TextBlob sentiment analyzer.

TABLE I. HYPER-PARAMETERS OF THE BiLSTM MODEL

Hyper-parameter	value
Bath_size	128
Epochs	2
Outout embedding dimension	100
BiLstm layer internalunits	256
Optimizer	Rmsprop
Loss	Categorical_crossentropy

With this proposal, we aim to have a good accuracy and a good F1 score that will be provided by our system compared to the BiLSM and TextBlob models applied separately on the same data.

To have a general binary prediction (positive or negative) of the sentiment of the input text, the two inputs of our classifier (Fig. 1) are linked directly to the outputs of the BiLSTM and TextBlob models. It should be mentioned that the values of the entries of the classifier are continuous in an interval of [0,1].

We randomly chose 7000 reviews from our dataset. These data are different from the training set and test set data used for the BiLSTM and TextBlob models. To have the predictions calculated by the BiLSTM and TextBlob models, we provided this data as input to our global system. Subsequently, the output of the results are divided into two datasets, 75% for the train set and 25% for the test set of our binary classification model. In this work, we used six classifier algorithms namely: Logistic Regression (LR), k Nearest Neighbors (k-NN), Random Forest (RF), Support Vector Machine (SVM), K-Means and Naive Bayes (NB).

Table II summarizes the chosen hyper parameters that were subsequently applied to our classification models. These hyper parameters are experimentally retained; we have taken those that have given the best possible evaluations for our dataset.

TABLE II. HYPERMETERS APPLIED TO ALGORITHMS IMPLEMENTED IN CLASSIFICATION MODELS

Algorithme	hyperparameter	Value
Logistic Regression	Inverse of regularization	1
K Nearest Neighbors	strength Number of neighbors	13
Random Forest	-Number of in the forest	18
	-Maximum depth of the tree	2
Support vector Machine	Kernel type	rbf
Naïve Bayes	Function	Gaussian
K-Means	n_clusters	3

IV. RESULTS

A. Evaluation of our Proposed Model

To demonstrate the performance improvement brought by the proposed architecture, we trained the whole model with the same set of tests that allowed us to evaluate separately the BiLSTM and TextBlob. Fig. 2 shows the implementation of six different algorithms in the Classifier model.

TABLE III. PERFORMANCE METRICS DISPLAYED BY THE TWO INPUT MODELS ON THE TWITTER US AIRLINES SENTIMENTS

Model	Recal	F1	Accuracy
Bilstm	0.37	0.49	0.85
TextBlob	0.36	0.37	0.87

Table III shows that after training the BiLSTM model, its evaluation on the test data gave an accuracy score of 0.85 and an F1 score of 0.49 and with TextBlob we obtained an accuracy score of 0.87 and an F1 score of 0.34.

Table IV summarizes the performance obtained. These results are obtained after training and evaluating our model which consists of six classification algorithms.

TABLE IV. THE PERFORMANCE MEASURES OF OUR MODULE OBTAINED BY THE IMPLEMENTATION OF THE SIX CLASSIFICATION ALGORITHMS

Algorithme	Recal	F1	Accuracy
Logistic Regression	0.75	0.72	0.89
K Nearest Neighbors	0.80	0.68	0.87
K-Means	0.84	0.73	0.89
Random Forest	0.71	0.71	0.89
Naïve Bayes	0.88	0.64	0.82
Support vector Machine	0.72	0.71	0.89

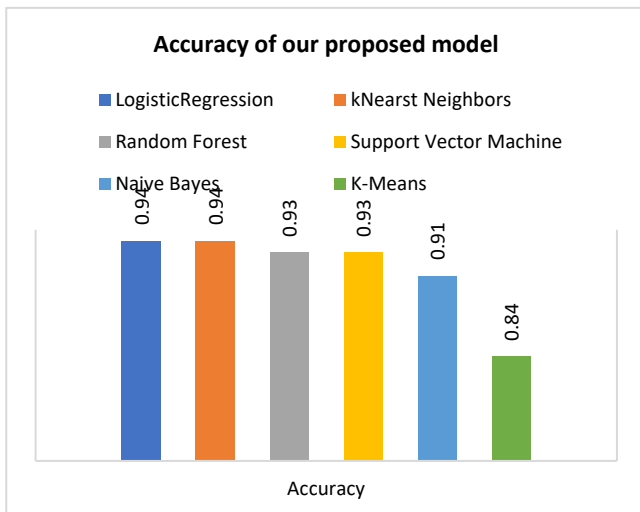


Fig. 2. Accuracy of our Proposed Model.

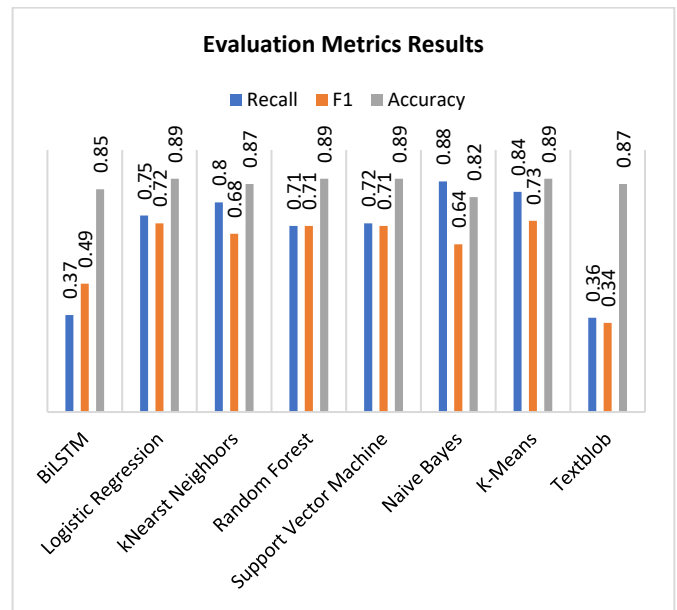


Fig. 3. Evaluation Metrics Results.

Fig. 3 shows the evaluation scores obtained with our model. We obtained six scores which depend on the classification algorithm used. The experimental results showed that the scores of our system are better than those obtained with the two models BiLSTM and TextBlob used separately. We note that the accuracy obtained with the BiLSTM (0.85) and TextBlob (0.87) models perform slightly better than the naive base algorithm (0.82).

Remarkably, it can be seen that the other classifiers Support Vector Mchine, Logistic Regression, Random Forest and K-Means gave a significantly higher accuracy (0.89) compared to the accuracy obtained with the two BiLSTM and TextBlob models. It can also be seen that the logistic regression model also provides a better F1 score (0.72) which is 23% higher than the BiLSTM F1 score (0.49) and 38% higher than the TextBlob F1 score (0.34).

With the exception of the results obtained by the Naive Bayes algorithm, it can be stated that our proposal improves the accuracy and F1 score results provided by the BiLSTM and TextBlob models used individually.

V. DISCUSSION

The experimental results obtained validate the usefulness of our proposed system. They also show the new performances in terms of accuracy and F1 score. Our proposed system, allowed us to have a 4% higher accuracy score and a 24% higher F1 score using the k-Means algorithm. It can be said that the use of BiLSTM and TextBlob input models will be effective in studies interested in sentiment analysis provided that they are hybridized with regression algorithms.

Moreover, most of the proposed models obtained better performances in terms of accuracy and F1 score (K-means, Logistic Regression, svm, Random Forest, K-nn respectively), except for the Naive-Baise model which obtained a slightly lower score in terms of accuracy (0.82) compared to the BiLSTM and Text Blob input models which have an accuracy

score of 0.85 and 0.87 respectively. The main reason could be that the Naive Bayes Classifier algorithm assumes the independence of the variables: This is a strong assumption and is violated in most real cases. Harry Zhang's publication [52] provides an explanation for this counter intuitive performance.

VI. CONCLUSION

Sentiment analysis of tweets remains an important technique to take advantage of the opinions and trends of the public around several events, in order to classify them according to polarity. However, categorizing the polarity of Twitter messages remains a difficult task for a number of reasons, including the speed at which messages are generated, the large number of messages generated on a particular topic, the short duration of those messages, and the familiarity of messages. To overcome these problems, this paper introduced a hybrid sentiment analysis model based on a BiTSM network and TextBlob. The TextBlob model allows the polarity and subjectivity scores to be calculated separately. We therefore used these two scores as features of a linear regression model to calculate an overall sentiment score. The two input models (BiLstm,TextBlob) are then combined into a binary classification model. For the attainment of this, we have implemented the following algorithms: Logistic Regression, k-Nearest Neighbors, Random Forest, Support Vector Machine, K-means and Naive Bayes. Then, both models were trained on a limited amount of data from the twitter US airlines data set.

The results of our experiments showed that the proposed hybrid system shows better performance in terms of accuracy and F1 score, compared to the input models considered in this study (BiLstm and TextBlob). This is mainly due to the different mechanisms implemented in each model. The mutualization of these mechanisms via our hybrid architecture was able to increase the performance demonstrated by the calculated metrics.

It should be noted that due to its bidirectional nature, the implementation of BiLSTM neural networks generates an overhead in terms of computational power and consequently, on the processing time, in this case with respect to long texts. For this reason, we recommend the use of the model proposed in this study to capture feelings in short texts such as tweets.

REFERENCES

- [1] A.Agarwal, B.Xie, I.Vovsha, O.Rambow, R.Passonneau, "Sentiment analysis of Twitter data", Proceedings of the Work shop on Languages in Social Media, 2011, pp.30-38.
- [2] F.Abel, C.Hauff, G.J.Houben, R.Stronkman, K.Tao,"Twitcident: fighting fire with information from social web streams",in:Proceedings of the 21 st International Conference Companion on World Wide Web,2012,pp.305-308.
- [3] M.Yoshida, S.Matsushima, S.Ono, I.Sato, H.Nakagawa, "ITC-UT: tweet categorization by query categorization of on-line reputation management", in: Conference on Multilingual and Multimodal Information Access Evaluation, 2010.
- [4] A. Birmingham, A. Smeaton, "On using Twitter to monitor political sentiment and predict election results", Proceedings of the Sentiment Analysis Where AI Meets Psychology, 2011, pp.2-10.
- [5] A. Yessenalina ,Y.Yue, C. Cardie, "Multi-level structured models for document level sentiment classification ", in: Proceedings of the 2010 Conference on Empirical Methods in Natural Language Processing , Cambridge, MA, 2010, pp.1046-1056.
- [6] T.Wilson , J.Wiebe , P.Hoffmann, "Recognizing contextual polarity in phrase-level sentiment analysis ", in: Proceedings of the Conference on Human Language Technology and Empirical Methods in Natural Language Processing,Vancouver,British Columbia,Canada,2005,pp.347-354.
- [7] A.B.Sayeed, J.Boyd-Graber, B.Rusk, A.Weinberg, "Grammatical structures for word-level sentiment detection ", in: Proceedings of the 2012 Conference of the North American Chapter of the Association for Computational Linguistics: Human Language Technologies, Montreal, Canada, 2012, pp.667-676.
- [8] X.Wang,F.Wei,X.Liu,M.Zhou,M. Zhang, "Topic sentiment analysis in Twitter: a graph-based hashtag sentiment classification approach ", in: Proceedings of the 20 the ACM International Conference on Information and Knowledge Management,Glasgow,Scotland,UK,2011,pp.1031-1040.
- [9] Mohamed Chiny, Marouane Chihab, Omar Bencharef and Younes Chihab, "LSTM, VADER and TF-IDF based Hybrid Sentiment Analysis Model" International Journal of Advanced Computer Science and Applications (IJACSA), 12(7), 2021.http://dx.doi.org/10.14569/IJACSA.2021.0120730.
- [10] M. Schuster, K. Paliwal, "Bidirectional recurrent neural networks ",IEEE Trans. Signal Process,1997, 45,2673-2681.
- [11] P.Zhou, Z. Qi, S. Zheng, J. Xu,H. Bao, B. Xu,"Text classification improved by integrating bidirectional LSTM with two-dimensional max pooling ",arXiv 2016, arXiv:1611.06639.
- [12] Q.Shen, Z. Wang, Y. Sun, "Sentiment analysis of movie reviews based on cnn-blstm", In International Conference on Intelligence Science,Springer: Berlin, Germany, 2017, pp. 164-171.
- [13] J.Yoon, H. Kim, "Multi-Channel Lexicon Integrated CNN-BiLSTM Models for Sentiment Analysis", In Proceedings of the 29th Conference on Computational Linguistics and Speech Processing (ROCLING 2017), Taipei, Taiwan, 27-28 November 2017, pp. 244-253.
- [14] W. Xing , D. Zhikang , Y. Guo , "Fujita H (2019) Hierarchical attention based long short-term memory for Chinese lyric generation ". Appl Intell 49(1):44-52.
- [15] W. Felix, S.Yang , P.Junho , W.Daniel , Z.Puming , "(2019) Deep learning based mandarin accent identification for accent robust ASR",In: INTERSPEECH, pp 510-514.
- [16] J. Nowak, A. Taspinar , R. Scherer , "LSTM Recurrent neural networks for short text and sentiment classification ", In: Proceedings of the international conference on artificial intelligence and soft computing (ICAISC 2017), 11-15 June 2017, Zakopane, Poland.p. 553-562; 2017.
- [17] T. Seneewong Na Ayutthaya ,K Pasupa , "Thai sentiment analysis via bidirectional LSTM-CNN model with embedding vectors and sentic features",In: Proceedings of the 13th International joint symposium on artificial intelligence and natural language processing (ISAI-NLP 2018), 15-17 November 2018, Pattaya,Thailand. p. 84-89; 2018.
- [18] Y.Kim, "Convolutional neural networks for sentence classification ", In: Proceedingsof the 2014 Conference on Empirical Methods in Natural Language Processing,EMNLP 2014, 25-29 October 2014, Doha, Qatar, A meeting of SIGDAT, a Special Interest Group of the ACL, pp. 1746-1751 (2014).
- [19] A.Graves,N. Jaitly, A. Mohamed, "Hybrid speech recognition with deep bidirectional lstm ",In: 2013 IEEE Workshop on Automatic Speech Recognition and Understanding (ASRU), pp. 273-278, December 2013
- [20] H. Sak, A. Senior, F. Beaufays, "Long short-term memory based recurrent neural network architectures for large vocabulary speech recognition",CoRR,abs/1402.1128 (2014).
- [21] J. Zhou, W. Xu, "End-to-end learning of semantic role labeling using recurrent neural networks",In: Proceedings of the 53rd Annual Meeting of the Association for Computational Linguistics, the 7th International Joint Conference on Natural Language Processing of the Asian Federation of Natural Language Processing, ACL 2015, 26-31 July 2015, Beijing, China, vol. 1: Long Papers, pp. 1127-1137 (2015).
- [22] Y. Kim , "Convolutional neural networks for sentence classification ",In: Proceedings of the international conference on empirical methods in natural language processing, (EMNLP 2014), 25-29 October 2014, Doha, Qatar. p. 1746-1751; 2014.

- [23] Y. Wang, M. Huang, X. Zhu, L. Zhao, "Attention-based LSTM for aspect-level sentiment classification", In: Proceedings of the 2016 conference on empirical methods in natural language processing (EMNLP 2016), 1-4 November 2016, Austin, Texas, USA. p.a.606–615; 2016.
- [24] B. Plank, A. Søgaard, Y. Goldberg, "Multilingual part-of-speech tagging with bidirectional long short-term memory models and auxiliary loss", In: Proceedings of the 54th annual meeting of the association for computational linguistics (ACL 2016), 7-12 August 2016, Berlin, Germany. p. 412–418; 2016.
- [25] A. Bakliwal, "Mining sentiments from Tweets", in: Proceedings of the 3rd Workshop in Computational Approaches to Subjectivity and Sentiment Analysis, Jeju, Republic of Korea, 2012, pp.11–18.
- [26] C. Gan, Q. Feng, Z. Zhang, "Scalable multi-channel dilated CNN-BiLSTM model with attention mechanism for Chinese textual sentiment analysis", Future Generation Computer Systems, Volume 118, May 2021.
- [27] S. Wang, Y. Zhu, W. Gao, M. Cao, M. Li, "Emotion-Semantic-Enhanced Bidirectional LSTM with Multi-Head Attention Mechanism for Microblog Sentiment Analysis", Accepted: 20 May 2020; Published: 22 May 2020.
- [28] E. Batbaatar, I. Meijing, K. Ho Ryu, "Semantic-Emotion Neural Network for Emotion Recognition From Text", IEEE, Digital Object Identifier 10.1109/ACCESS.2019.2934529.
- [29] M. Tsytarau, T. Palpanas, "survey on mining subjective data on the web, Ingegneriae Scienza dell' Informazione", University of Trento, Trento, Relatório Técnico DISI-10-045, 2010.
- [30] Y.R.Tausczik, J.W. Pennebaker, "The psychological meaning of words: Liwc and computerized text analysis methods", J.Lang.Social Psychol.29(2010)24–54.
- [31] A.C.E.S. Lima, L.N.Castro, J.M. Corchado, "A polarity analysis framework for Twitter messages, Applied Mathematics and Computation", Volume 270, 2015, Pp 756-767.
- [32] A. Esuli, F. Sebastiani, "Senti Word Net: a publicly available lexical resource for opinion mining", in: Conference on Language Resources and Evaluation, 2006, pp.417–422.
- [33] M. Annett, G. Kondrak, "A comparison of sentiment analysis techniques: polarizing movie blogs", in: Proceedings of the Canadian Society for Computational Studies of Intelligence, 21st Conference on Advances in Artificial Intelligence, 2008, pp.25–35.
- [34] T. Lake, "Twitter Sentiment Analysis, Western Michigan University", Forlient William Fitzgerald, Kalamazoo, MI, 2011.
- [35] A. Birmingham, A. Smeaton, "On using Twitter to monitor political sentiment and predict election results", Proceedings of the Sentiment Analysis Where AI Meets Psychology, 2011, pp.2–10.
- [36] J. Bollen, H. Mao, A. Pepe, "Modeling public mood and demotion: Twitter sentiment and socio-economic phenomena", in: Proceedings of the Fifth International AAAI Conference on Weblogs and Social Media, 2011, pp.450–453.
- [37] A. Yessenalina, Y. Yue, C. Cardie, "Multi-level structured models for document level sentiment classification", in: Proceedings of the 2010 Conference on Empirical Methods in Natural Language Processing, Cambridge, MA, 2010, pp.1046–1056.
- [38] T. Wilson, J. Wiebe, P. Hoffmann, "Recognizing contextual polarity in phrase-level sentiment analysis", in: Proceedings of the Conference on Human Language Technology and Empirical Methods in Natural Language Processing, Vancouver, British Columbia, Canada, 2005, pp.347–354.
- [39] A.B. Sayeed, J. Boyd-Graber, B. Rusk, A. Weinberg, "Grammatical structures for word-level sentiment detection", in: Proceedings of the 2012 Conference of the North American Chapter of the Association for Computational Linguistics: Human Language Technologies, Montreal, Canada, 2012, pp.667–676.
- [40] X. Wang, F. Wei, X. Liu, M. Zhou, M. Zhang, "Topic sentiment analysis in Twitter: a graph-based hashtag sentiment classification approach", in: Proceedings of the 20 ACM International Conference on Information and Knowledge Management, Glasgow, Scotland, UK, 2011, pp.1031–1040.
- [41] A. Kumar, T.M. Sebastian, "Sentiment analysis: a perspective on its past, present and future", Intell. Syst. Appl. 4 (2012) 1–14.
- [42] J. Wiebe, T. Wilson, R. Bruce, M. Bell, M. Martin, "Learning subjective language", Comput. Linguist. 30 (2004) 277–308.
- [43] A. Kumar, T.M. Sebastian, "Machine learning assisted sentiment analysis", in: Proceedings of International Conference on Computer Science & Engineering, 2012, pp.123–130.
- [44] B. Pang, L. Lee, "Opinion mining and sentiment analysis", Found. Trends Inform. Retrieval. 2 (2008) 1–135.
- [45] B. Pang, L. Lee, S. Vaithyanathan, "Thumbs up?: sentiment classification using machine learning techniques", in: Proceedings of the ACL-02 Conference on Empirical Methods in Natural Language Processing, 10, 2002, pp.79–86.
- [46] A. Pak and P. Paroubek, "Twitter as a Corpus for Sentiment Analysis and Opinion Mining", in LREC, 2010, pp. 1320-1326.
- [47] B. Pang, L. Lee, and S. Vaithyanathan, "Thumbs up?: sentiment classification using machine learning techniques", in Proceedings of the ACL-02 conference on Empirical methods in natural language processing, Volume 10, 2002, pp. 79-86.
- [48] F. Sebastiani, "Machine learning in automated text categorization", ACM Computing Surveys, 34, 2002.
- [49] J. Turian, L. Ratinov, Y. Bengio, "Word representations: a simple and general method for semi-supervised learning", In Proceedings of ACL, 2010.
- [50] J. Pennington, R. Socher, D. Christopher, "Manning. GloVe: Global Vectors for Word Representation", Proceedings of the 2014 Conference on Empirical Methods in Natural Language Processing (EMNLP), 2014.
- [51] "Twitter US Airline Sentiment". <https://www.kaggle.com/crowdflower/twitter-airline-sentiment>, February 2015.
- [52] H. Zhang, "The optimality of naive Bayes", Published in FLAIRS Conference, 2004 Cited by 2205 Related articles All 24 versions.

Local Texture Representation for Timber Defect Recognition based on Variation of LBP

Rahillda Nadhirah Norizzaty Rahiddin¹, Umami Raba'ah Hashim²

Lizawati Salahuddin³, Kasturi Kanchymalay⁴, Aji Prasetya Wibawa⁵, Teo Hong Chun⁶

Fakulti Teknologi Maklumat dan Komunikasi, Universiti Teknikal Malaysia Melaka (UTeM), Melaka, Malaysia^{1, 2, 3, 4}

Department of Electrical Engineering, Engineering Faculty, Universitas Negeri Malang, Malang, Indonesia⁵

Department of Information Technology and Communication, Politeknik Mersing, Johor, Malaysia⁶

Abstract—This paper evaluates timber defect classification performance across four various Local Binary Patterns (LBP). The light and heavy timber used in the study are Rubberwood, KSK, Merbau, and Meranti, and eight natural timber defects involved; bark pocket, blue stain, borer holes, brown stain, knot, rot, split, and wane. A series of LBP feature sets were created by employing the Basic LBP, Rotation Invariant LBP, Uniform LBP, and Rotation Invariant Uniform LBP in a phase of feature extraction procedures. Several common classifiers were used to further separate the timber defect classes, which are Artificial Neural Network (ANN), J48 Decision Tree (J48), and K-Nearest Neighbor (KNN). Uniform LBP with ANN classifier provides the best performance at 63.4%, superior to all other LBP types. Features from Merbau provide the greatest F-measure when comparing the performance of the ANN classifier with Uniform LBP across timber fault classes and clean wood, surpassing other feature sets.

Keywords—Automated visual inspection; local binary pattern; timber defect classification; texture feature; feature extraction

I. INTRODUCTION

Malaysia is known for its biological diversity concerning forests and marine environments, making it a megadiverse country. Since 2017, the timber sector has substantially influenced the gross domestic product (GDP). It contributed around RM 759 million to the total foreign investment. It is expected to expand by 65 per cent (RM 491.7 million), augmented by the domestic investment of around RM 267.3 million (35 per cent) annually by 2020 [1]. The amount and distribution of naturally occurring timber flaws have worried timber experts; hence, an appropriate detection method is a crucial examination procedure in the timber industry of Malaysia [2-3].

However, due to its susceptibility and the possibility of human mistakes, manual visual defect evaluation is not only acknowledged as being inaccurate in the timber industry but is also physically demanding. Acute headaches and eye fatigue are connected to strenuous labour [3–5]. The results of the detecting procedure have a significant impact on the quality of timber products [6]. Overlooked or defective products could negatively influence the industry, jeopardizing safety and causing revenue loss due to the inability to address failure or liability claims. As a result, product quality control is critical to prevent manufacturing mistakes and defects before products reach the shipping stage.

The Automated Visual Inspection (AVI) method includes automated image capture, enhancement, segmentation, feature extraction, and categorization. AVI is a completely automated extraction and categorization procedure that would enhance the inspection process and lower labour expenditures [7–9].

This research aims to classify timber faults using a pattern recognition technique contributing to AVI, emphasizing the feature extraction stage. Several studies have used Local Binary Pattern (LBP) to detect timber flaws [10]. LBP can accurately recognize and detect timber defects [11–14]. The technique was considered superior for feature extraction to other techniques based on the research [15].

LBP is still an area of active research in different domains. More recently, extended the methods using LBP to extract features from new finger vein images to improve the recognition performance system [16], spatiotemporal data fusion for producing time-series satellite images for real-world applications [17], and new blood cell classification using a hybrid learning model based on blood cell image identification [18].

Similar work has also been pursued, which utilizes the multiple feature fusion method for video emotion recognition [19]. Each keyframe belonging to real-world video sequences is processed to extract features using Uniform LBP and the scale-invariant feature identification. Conceptually similar work was performed that used LBP for extracting seven types of wheat texture features in East Azerbaijan Province to accelerate the seed supply for cultivation in seed supply centres [20].

The recent literature proposes several techniques related to LBP. Recent work used pseudo-visual search and the histogram of oriented gradients (HOG)–LBP feature fusion for intelligent vehicle detection in severe weather [21]. In addition, to completing local quartet patterns, a new version of LBP plays a crucial role in fabric textile quality-control systems [22]. Moreover, edge-aware filtering and improved LBP (EF-ALBP) is a robust edge extraction method for medical images having redundant noise, blurred details, and low contrast [23].

This study aims to recognize the general challenges concerning the automated visual inspection of timber. The focus was on the feature extraction approach and evaluating the timber defect classification performance across LBP variants. Firstly, we focused on constructing rotation-invariant uniform

feature representation of timber defects based on statistical texture features using a variation of LBP (Rotation Invariant Uniform LBP, Rotation Invariant LBP, Uniform LBP, and Basic LBP). The timber defect images dataset, labelled and validated by industry experts [3], was used here. The dataset represented several species of Malaysian hardwood, namely Rubberwood, KSK, Meranti and Merbau. Sixteen feature sets were produced and tested in the next phase. Subsequently, we evaluated timber defect class discrimination based on sixteen proposed texture feature sets using classification accuracy measures. The performance of the suggested feature set was confirmed by evaluating classification accuracy metrics with the help of common classifiers (ANN, KNN, and J48).

Finally, we compared the performance of the proposed feature sets across timber defects. Due to the superior performance of the ANN classifier in earlier studies compared to other classifiers, we chose to use it. We also used Uniform LBP because of its high classification accuracy than other LBP types. Extensive analysis revealed that all timber species displayed respectable classification accuracy, demonstrating the value of the suggested criteria in class distinction. The discriminating performance of the suggested feature sets across all classes highlighted the possibility of defect detection applications for future research, even though the study focused on identifying defects over clean wood.

II. MATERIALS AND METHODS

A. Approach Overview

This study used the timber defect dataset from the UTeM database [3]. Nine different types of timber defects, including clear wood as shown in Table I, were extracted from 3600 timber defect images (900 samples for each timber species, 100 samples for each timber defect) on several timber species. The dataset for timber defects includes 630 training pictures of clean wood and eight types of natural timber defects. Specimens of light timber, such as Rubberwood, while Meranti, KSK, and Merbau from heavy timbers are from several secondary timber product industries in Melaka, Malaysia, were used to augment the timber defect dataset. Sample collection was limited by the availability of the timber species based on end-products manufactured by the factories commonly used by different timber industries in Malaysia [3].

Ungraded, dressed, dried, and dirt-free sawn timbers used in rough milling were considered for this study. The collected timber samples had a 45-70 mm width, 100-150 mm length, and 18-22 mm thickness. The eight natural timber defects are wane, split, rot, knot, brown stain, borer holes, blue stain and bark pocket. Table II depicts the details of the timber defect image settings used for this research.

Fig. 1 illustrates extracting the statistical texture features based on LBP variants. First, timber defect images were converted to greyscale (tone-independent). Then, (1) is used for parameter setting: radius and the sampling point. All steps are to derive the rotation-invariant uniform formulation based on LBP variations. The LBP was performed by applying pixel labelling using an LBP thresholding formulation. The formulation uses a single parameter setting; sampling point, $sp=8$ and radius, $R=1$. Then, extracting statistical texture

features from an LBP variation for the four timber species. In phase one, sixteen feature sets have been produced and calculated using (1) to (9).

B. Feature Extraction

1) *Basic local binary pattern: basic lbp produces 256 values.* The LBP code for each basic LBP pixel must be determined. The pixel is labelled using decimal numbers by encoding the local structure around each pixel. For example, by deducting the value of the centre pixel, each pixel in a 3×3 neighbourhood is compared to its eight neighbours; if the result is positive, value 1 is used. In contrast, negative results generate 0. The process outputs 8-bit integers by arranging each bit clockwise, starting from the top-left to obtain eight different binary patterns. The mathematical expression of the LBP is specified in (1).

$$LBP_{p,R}(x_c, y_c) = \sum_{i=0}^{p-1} s(g_i - g_c) 2^i \quad (1)$$

TABLE I. TIMBER DEFECT CLASSES [3]









	
Knot	Split
	
Blue Stain	Brown Stain
	
Bark Pocket	Borer holes
	
Rot	Wane

TABLE II. TIMBER DEFECT IMAGE SETTINGS [3]

Sensor used	Optical sensor
Optical imaging device	Area scan cameras
Image setting	1024 by 768 pixels (300dpi) 24-bit depth and 256 intensity levels for the red, green and blue channel
Sub-image setting	60 x 60 pixels

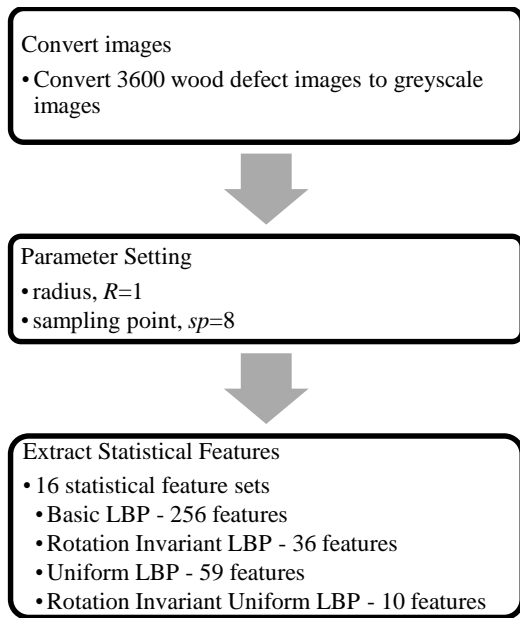


Fig. 1. Process of Extracting Statistical Texture Features based on LBP Variants.

The notation (P, R) designates P sampling points on a circle of radius R; (x_c, y_c) designates the centre of a pixel, g_c represents the grey value of the centre pixel; and g_i ($i=0,1,\dots,P-1$) designates the grey value of the P sampling points next to it. Signed differences $g_i - g_c$ are interpreted as P-bit binary numbers, producing 2^i distinct values. The thresholding function $s(x)$ is defined in (2):

$$s(x) = \begin{cases} 1 & \text{if } x \geq 0 \\ 0 & \text{if } x < 0 \end{cases} \quad (2)$$

2) *Rotation invariant local binary pattern*: Rotation invariant LBP is used to analyze and compute the value of the rotated picture [24]. The g_i grey values along the perimeter of the circle around g_c vary when the image is rotated. The binary pattern rotates in a clockwise direction, resulting in various LBP values. As a result, the lowest value of the binary pattern generated from the direction of maximal rotation is chosen for computation. Similarly, for cluster-like patterns, the rotation invariant LBP with the lowest value of the circular bitwise clockwise direction of the x bit sequence by i steps or the $ROR(x, i)$ can thus be recognize as:

$$LBP_{P,R}^i = \min\{ROR(LBP_{P,R}, i) \mid i = 0, 1, \dots, P - 1\} \quad (3)$$

Rotation invariant LBP can generate 36 different patterns.

3) *Uniform local binary pattern*: Since circular rotation bit patterns with 0-1 or 1-0 transitions are used to determine the LBP uniformity [25], uniformity can be identified from the two transitions comprising a single binary pattern. On the other hand, if the transitions exceed this count, i.e., if the binary pattern comprises more than two transitions, it does not belong to the uniform LBP category. Uniform LBP can be seen in patterns 00000000_2 (0 transition) and 00001000_2 (2

transitions) and each uniform pattern has a separate output label. Transition count calculation can be obtained using (4):

$$U(LBP_{P,R}) = |s(g_{P-1} - g_c) - s(g_0 - g_c)| + \sum_{i=1}^{P-1} |s(g_i - g_c) - s(g_{i-1} - g_c)| \quad (4)$$

There are $P(P - 1) + 3$ different P-bit output labels; eight sampling points produce 59 labels, where 58 are uniform and 1 is non-uniform.

4) *Rotation invariant uniform local binary pattern*: The superscript riu^2 , which donates the maximum uniform value of two, is used by the rotation-invariant uniform patterns, as stated in (5). By definition, $P + 1$ occurs in a circular symmetric neighbour set of P pixels in uniform binary patterns. The above equation determined 27 non-uniform patterns and 9 uniform patterns. The mapping of 8-bit binary numbers from LBP_8 to $LBP_8^{riu^2}$ comprises 10 unique outputs than a 256-element lookup table:

$$LBP_{P,R}^{riu^2} = \begin{cases} \sum_{i=0}^{P-1} s(g_i - g_c) & \text{if } U(LBP_{P,R}) \leq 2 \\ P + 1 & \text{otherwise,} \end{cases} \quad (5)$$

C. Evaluation of Detection Performance

1) *Precision, recall, f-measure, and classification accuracy*: Precision and recall are conventional and appropriate assessment metrics to evaluate the performance of content-based image retrieval. Precision and recall are calculated using positive and negative system replies for every query. [26]. In this study, clear wood images accounted for a significant part of the dataset than timber defect samples. It is typical in the secondary timber industry.

Equation (6) shows precision is the ratio of actual timber defects to the total number of detected ones. Precision, sometimes referred to as positive predictive value, results from the retrieval system's true positive and false positive images. A recall is the ratio of the total number of real defects in the timber to the total number of actual defects in timber, as defined in (7). The recall is a function of the true-positive and false-negative images in the retrieval system [27]. The F-Measure in each class is a composite measure of precision and recall, as shown in (8).

$$\begin{aligned} \text{precision}, P &= \frac{\text{number of true defects}}{\text{number of defects detected}} \\ &= \frac{\text{true defects}}{\text{true defects} + \text{false defects}} \end{aligned} \quad (6)$$

$$\begin{aligned} \text{recall}, R &= \frac{\text{number of true defects}}{\text{number of actual defects}} \\ &= \frac{\text{true defects}}{\text{true defects} + \text{false clear wood}} \end{aligned} \quad (7)$$

$$F - \text{Measure}, F = 2 \frac{PR}{P+R} \quad (8)$$

The experiment aims to improve experiment accuracy, typically measured using classification accuracy [28]. Classification algorithms are assessed using classification accuracy [29], as defined in (9).

$$\text{Classification Accuracy (\%)} = \frac{\text{Number of correct classification}}{\text{Total number of samples}} \cdot 100\% \quad (9)$$

III. RESULTS AND DISCUSSION

A. Classification Performance across LBP Variants

For a more in-depth understanding of the applicability of various characteristics across each LBP variation, the best classification performance is compared to other classifiers for that version. Table III shows the F-measure for each feature set. By integrating precision and recall values, the F-measure benchmark evaluates picture segmentation and classification accuracy. Comparing the ANN classifier to the KNN and J48 classifiers produces good results.

Fig. 2 shows the mean or average percentage classification accuracy of the standard classifier across all LBP variants. Basic LBP has a 48.42% classification accuracy, while Rotation Invariant LBP is 48.7% accurate. Moreover, Uniform LBP has 56.8% accuracy values, while Rotation Invariant Uniform LBP has 52% accuracy values.

B. Classification Performance across Timber Defects

The ANN classifier delivered the best classification performance, as we previously concluded. Performance assessment continues by evaluating the ANN classifier and Uniform LBP across timber defect classes and clear wood. Since Basic, Rotation Invariant, and Rotation Invariant Uniform LBP datasets previously showed low classification performance, we will now look at the classification details of a well-performed Uniform LBP dataset only.

Fig. 3 illustrates the F-measure calculation for timber defect classes. Bark pocket, split, and borer hole classes show the lowest F-measure across all classes, achieving less than 0.63 F-value. Meanwhile, the top three F-measures across timber defect classes are wane, clear wood, and rot. The attributes of the Rubberwood dataset are the most effective in classifying

rot, wane, and brown stain. In contrast, the split was best ranked for the KSK dataset.

TABLE III. CLASSIFIERS COMPARISON WITH F-MEASURE OF LBP VARIANTS

Class	F-measure	Classifier
Basic LBP	0.553	ANN
	0.487	KNN
	0.413	J48
Rotation Invariant LBP	0.515	ANN
	0.502	KNN
	0.444	J48
Uniform LBP	0.634	ANN
	0.629	KNN
	0.441	J48
Rotation Invariant Uniform LBP	0.527	ANN
	0.536	KNN
	0.497	J48

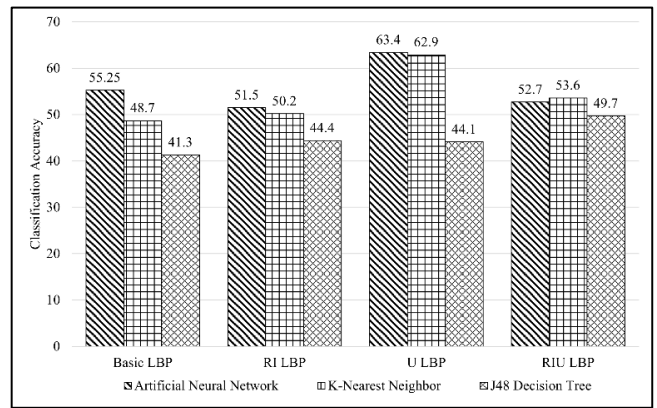
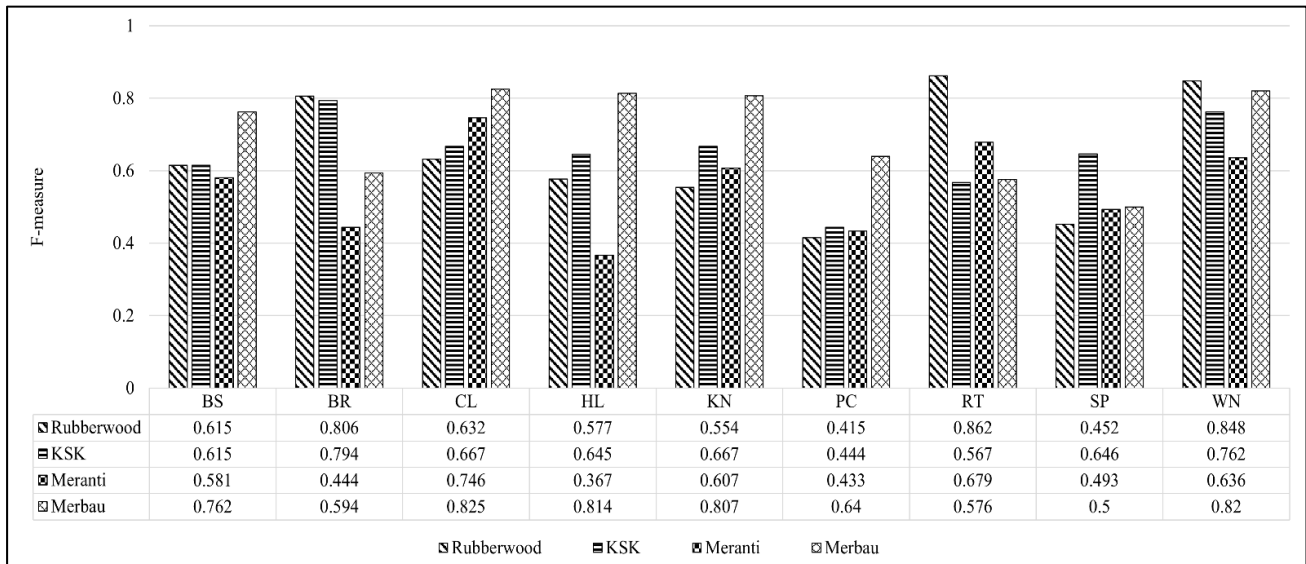


Fig. 2. The Mean or Average Percentage Classification Accuracy of the Standard Classifier Across all LBP Variants (RI LBP = Rotation Invariant LBP, U LBP = Uniform LBP, RIU LBP = Rotation Invariant Uniform LBP).



(BS-Blue Stain, BR-Brown Stain, CL-Clear Wood, HL-Borer Holes, KN-Knot, PC-Bark Pocket, RT-Rot, SP-Split, WN-Wane)

Fig. 3. F-measure for Each Timber Defect Class, Including Clear Wood, Calculated using ANN Classifier and Uniform LBP.

Similarly, the characteristics of Merbau were the best in classifying blue stain, clear wood, borer holes, knot, and bark pocket. Merbau features provide the best F-measure when considering generalised differences among timber defect classes, beating other feature sets.

IV. CONCLUSION

The paper presented the evaluation of timber defect classification performance across LBP variants. The experiment highlights the average percentage classification accuracy for all LBP variants. Comparing all LBP types, uniform LBP with ANN classifier offers the greatest performance at 63.4%. By analyzing the performance of the ANN classifier with Uniform LBP across timber defect classes and clear wood, features from Merbau species give the best F-measure, outperforming other feature sets from other timber species. In line with the findings of this paper, it demonstrates that Merbau-derived traits were most effective for classifying blue stains, clear wood, borer holes, knots, and bark pockets. Moreover, brown stain, split, wane and rot show the lowest F-measure. In this research, statistical texture based on variations of LBP to represent wood surface characteristics was employed. Other texture feature extraction techniques could be explored to further improve the feature representation and for better discrimination capabilities between wood defects and clear wood. Other researchers working on certain timber defect classes focusing on applications will find this discovery useful.

ACKNOWLEDGMENT

This research is supported by Ministry of Higher Education (MOHE), Malaysia through Fundamental Research Grant Scheme (FGRS/1/2022/ICT02/UTEM/02/2) and Universiti Teknikal Malaysia Melaka.

REFERENCES

- [1] MIDA, "Wood-Based and Furniture," Malaysian Investment Development Authority Official Website, 2021. <https://www.mida.gov.my/industries/manufacturing/wood-based-and-furniture/>.
- [2] I. Cetiner, A. A. Var, and H. Cetiner, "Classification of Knot Defect Types Using Wavelets and KNN," *Elektron. ir Elektrotehnika*, vol. 22, no. 6, pp. 67–72, 2016, doi: 10.5755/j01.eie.22.6.17227.
- [3] U. R. Hashim, S. Z. Hashim, and A. K. Muda, "Image Collection for Non-Segmenting Approach of Timber Surface Defect Detection," *Int. J. Adv. Soft Comput. its Appl.*, vol. 7, no. 1, pp. 15–34, 2015.
- [4] R. Qayyum, K. Kamal, T. Zafar, and S. Mathavan, "Wood Defects Classification Using GLCM Based Features And PSO Trained Neural Network," 2016 22nd Int. Conf. Autom. Comput. ICAC 2016 Tackling New Challenges Autom. Comput., pp. 273–277, 2016, doi: 10.1109/ICConAC.2016.7604931.
- [5] U. R. Hashim, S. Z. Hashim, and A. K. Muda, "Automated vision inspection of timber surface defect: A review," *J. Teknol.*, vol. 77, no. 20, pp. 127–135, 2015, doi: 10.11113/jt.v77.6562.
- [6] Y. Zhang, C. Xu, C. Li, H. Yu, and J. Cao, "Wood defect detection method with PCA feature fusion and compressed sensing," *J. For. Res.*, vol. 26, no. 3, pp. 745–751, 2015, doi: 10.1007/s11676-015-0066-4.
- [7] N. D. Abdullah, U. R. Hashim, S. Ahmad, and L. Salahuddin, "Analysis of Texture Features for Wood Defect Classification," *Bull. Electr. Eng. Informatics*, vol. 9, no. 1, pp. 121–128, 2020, doi: 10.11591/eei.v9i1.1553.
- [8] T. H. Chun et al., "Identification of Wood Defect Using Pattern Recognition Technique," *Int. J. Adv. Intell. Informatics*, vol. 7, no. 2, pp. 163–176, 2021, doi: 10.26555/ijain.v7i2.588.
- [9] Y. Zhang, S. Liu, W. Tu, H. Yu, and C. Li, "Using computer vision and compressed sensing for wood plate surface detection," *Opt. Eng.*, vol. 54, no. 10, pp. 103102-1-103102–10, 2015, doi: 10.1117/1.OE.54.10.103102.
- [10] T. Ojala, M. Pietikäinen, and D. Harwood, "Performance evaluation of texture measures with classification based on Kullback discrimination of distributions," *Proc. - Int. Conf. Pattern Recognit.*, vol. 3, pp. 582–585, 1994, doi: 10.1109/ICPR.1994.576366.
- [11] I. M. Khairuddin et al., "Automatic Classification of Wood Texture Using Local Binary Pattern & Fuzzy K-Nearest Neighbor," *Adv. Mater. Res.*, vol. 903, pp. 315–320, 2014, doi: 10.4028/www.scientific.net/AMR.903.315.
- [12] M. Nasirzadeh, A. A. Khazael, and M. Khalid, "Woods Recognition System Based on Local Binary Pattern," *Second Int. Conf. Comput. Intell. Commun. Syst. Networks*, no. 2, pp. 2–7, 2010, doi: 10.1109/CICSyN.2010.27.
- [13] Z. Y. Xiang, Z. Y. Qin, L. Ying, J. L. Quan, and C. Z. Wei, "Identification of Wood Defects Based on LBP Features," in *Chinese Control Conference, CCC, 2016*, pp. 4202–4205, doi: 10.1109/ChiCC.2016.7554010.
- [14] E. A. B. Ibrahim et al., "Evaluation of Texture Feature based on Basic Local Binary Pattern for Wood Defect Classification," *Int. J. Adv. Intell. Informatics*, vol. 7, no. 1, pp. 26–36, 2021, doi: 10.26555/ijain.v7i1.393.
- [15] Prasetiyo, M. Khalid, R. Yusof, and F. Meriaudeau, "A Comparative Study of Feature Extraction Methods for Wood Texture Classification," 2010 Sixth Int. Conf. Signal-Image Technol. Internet Based Syst., pp. 23–29, 2010, doi: 10.1109/SITIS.2010.15.
- [16] H. Ren, L. Sun, J. Guo, C. Han, and Y. Cao, "A high compatibility finger vein image quality assessment system based on deep learning," *Expert Syst. Appl.*, vol. 196, no. January, p. 116603, 2022, doi: 10.1016/j.eswa.2022.116603.
- [17] X. Zhu et al., "A novel framework to assess all-round performances of spatiotemporal fusion models," *Remote Sens. Environ.*, vol. 274, no. March, p. 113002, 2022, doi: 10.1016/j.rse.2022.113002.
- [18] K. A. Davamani, C. R. R. Robin, D. D. Robin, and L. J. Anbarasi, "Adaptive blood cell segmentation and hybrid Learning-based blood cell classification: A Meta-heuristic-based model," *Biomed. Signal Process. Control*, vol. 75, no. October 2021, p. 103570, 2022, doi: 10.1016/j.bspc.2022.103570.
- [19] N. Samadiani et al., "A Multiple Feature Fusion Framework for Video Emotion Recognition in the Wild," *Concurr. Comput. Pract. Exp.*, vol. 34, no. 8, pp. 1–13, 2020, doi: 10.1002/cpe.5764.
- [20] M. Khojastehnazhand and M. Roostaei, "Classification of seven Iranian wheat varieties using texture features," *Expert Syst. Appl.*, vol. 199, no. May 2021, p. 117014, 2022, doi: 10.1016/j.eswa.2022.117014.
- [21] Z. Wang, J. Zhan, C. Duan, X. Guan, and K. Yang, "Vehicle Detection in Severe Weather based on Pseudo-visual Search and HOG-LBP Feature Fusion," *J. Automob. Eng.*, vol. 236, no. 7, pp. 1607–1618, 2021, doi: 10.1177/09544070211036311.
- [22] Z. Pourkaramdel, S. Fekri-Ershad, and L. Nanni, "Fabric defect detection based on completed local quartet patterns and majority decision algorithm," *Expert Syst. Appl.*, vol. 198, no. March, p. 116827, 2022, doi: 10.1016/j.eswa.2022.116827.
- [23] S. Qiao et al., "Edge Extraction Method for Medical Images based on Improved Local Binary Pattern Combined with Edge-aware Filtering," *Biomed. Signal Process. Control*, vol. 74, no. December 2021, p. 103490, 2022, doi: 10.1016/j.bspc.2022.103490.
- [24] M. Pietikäinen, T. Ojala, and Z. Xu, "Rotation-invariant texture classification using feature distributions," *Pattern Recognit.*, vol. 33, no. 1, pp. 43–52, 2000, doi: 10.1016/S0031-3203(99)00032-1.
- [25] T. Ojala, M. Pietikäinen, and T. Mäenpää, "Multiresolution gray-scale and rotation invariant texture classification with local binary patterns," *IEEE Trans. Pattern Anal. Mach. Intell.*, vol. 24, no. 7, pp. 971–987, 2002, doi: 10.1109/TPAMI.2002.1017623.
- [26] M. Verma and B. Raman, "Local neighborhood difference pattern : A new feature descriptor for natural and texture image retrieval," *Multimed. Tools Appl.*, no. May, 2017, doi: 10.1007/s11042-017-4834-3.
- [27] P. Banerjee, A. K. Bhunia, A. Bhattacharyya, P. P. Roy, and S. Murala, "Local Neighborhood Intensity Pattern—A new texture feature descriptor

- for image retrieval,” *Expert Syst. Appl.*, vol. 113, pp. 100–115, 2018, doi: 10.1016/j.eswa.2018.06.044.
- [28] T. Pahlberg, M. Thurley, D. Popovic, and O. Hagman, “Crack detection in oak flooring lamellae using ultrasound-excited thermography,” *Infrared Phys. Technol.*, vol. 88, pp. 57–69, 2017, doi: 10.1016/j.infrared.2017.11.007.
- [29] V. N. T. Le, B. Apopei, and K. Alameh, “Effective plant discrimination based on the combination of Local Binary Pattern operators and multiclass Support Vector Machine methods,” *Inf. Process. Agric.*, vol. 6, no. 1, pp. 116–131, 2019, doi: 10.1016/j.inpa.2018.08.002.

Unethical Internet Behaviour among Students in High Education Institutions: A Systematic Literature Review

Zakiah Ayop¹, Aslinda Hassan², Syarulnaziah Anawar³, Nur Fadzilah Othman⁴, Rabiah Ahmad⁵

Fakulti Teknologi Maklumat dan Komunikasi
Universiti Teknikal Malaysia Melaka, Hang Tuah Jaya
Durian Tunggal, Melaka, 76100, Malaysia

Nor Raihana Mohd Ali⁶, Maslin Masrom⁷

Razak Faculty of Technology and Informatics
Universiti Teknologi Malaysia, Level 7 Menara Razak
Jalan Sultan Yahya Petra, Kuala Lumpur, 54100, Malaysia

Abstract—The modern internet era has several advantages and disadvantages, including the advent of immoral Internet conduct in addition to better, quicker, and increased working capacity in less time. Even though the area of study on unethical Internet activity has advanced, systematic literature reviews from a comprehensive perspective on unethical Internet behaviour among university students are still lacking. As a result, this systematic literature will provide theoretical foundation that address the following research questions: RQ1-How are unethical Internet behaviours among university students classified; RQ2-What are the various theoretical lenses that are used in unethical Internet behaviour research; RQ3-What demographic and risk factors are involved in unethical Internet behaviour research; and RQ4-What are the challenges and research opportunities for unethical Internet behaviour research within university settings? To respond to a formulated set of research questions, a total of 64 publications that were published between 2010 and 2020 underwent a systematic review. The study illustrates how university students' unethical Internet activity is categorised. This study offers a comprehensive grasp of the factors that affect unethical Internet behaviour and an overview of the theories that have been utilised to explain and forecast unethical Internet behaviours in this sector. This study discusses literature gaps for future research to contribute to human ethical behavioural studies.

Keywords—Systematic literature review; unethical Internet behavior; university student; Internet; ethics

I. INTRODUCTION

The academic environment has made extensive use of the Internet as a component of the processes and instruments of learning in both internal and external classroom contexts. However, according to Baum in [1], its usage was motivated by a lack of ethical awareness and education and a lack of regulations governing its use for teaching, learning, and research. Irresponsible exploitation of this essential resource poses a significant threat to the technological community and society. Following the definition set by Jones (1991), ethical behaviours can be defined as legal behaviours that are morally acceptable in the society in which they occur, and unethical behaviours is defined as unlawful actions that are not morally acceptable [2]. Based on definition set by Adenisa in [3], unethical behavior deviates from what is regarded ethically

correct or appropriate for a person, a profession, or an industry. On the other side, ethical action entails doing the right thing, and unethical behavior entails doing the opposite. Ethics in the context of the Internet refers to how people interact with technology and the potential outcomes of those interactions [4]. The Internet can give rise to a plethora of new types of abnormal conduct, some of which are radically new, and others are technologically updated versions of longstanding ethical implications. The Internet Activities Board (IAB) code of ethics is outlined in an RFC document. RFC 1087, Ethics and the Internet, was issued in 1987 to offer a policy for Internet-related ethical behaviour [5]. Based on the IAB, the following actions would constitute unethical behaviour if they were committed intentionally [5]:

- 1) Attempts to access Internet resources without authorization.
- 2) Disrupts the Internet's intended usage.
- 3) Wasting resources (people, capacity, and computers).
- 4) Destroys the integrity of computer-based information by such acts.
- 5) Interferes with consumers' privacy.

Ming et al. (2015) conducted a systematic literature review (SLR) on computer ethical issues. The article presents the review methodology employed, the subject under consideration, and the key findings [6]. The SLR extracted forty studies that focused mainly on software piracy, computer piracy, the PAPA (Privacy, Accuracy, Property, and Accessibility) framework, and other general concerns. The main difference of this SLR is that the SLR conducted by [6] focuses on categories of computer ethics among students and professionals, whereas our SLR concentrate on the categorisation of unethical Internet behaviours in high education settings as well as the demographic and risk factors related to each of the categories.

In 2017, Vossen et al. conducted an SLR to identify descriptors for unprofessional behaviours among medical students. The SLR is intended to investigate, analyse, organize and report the findings of research on the unprofessional behaviour of medical students as observed by stakeholders or acknowledged by students themselves [7]. The literature review focuses on qualitative research to develop themes and

summary descriptors for unprofessional behaviours. On contrary, our SLR focus on unethical behaviour in the cyber environment.

Finally, Costa et al. (2021) did an SLR which focused on the methodology for the scientific production of netiquette research, such as country, date, objectives, methodological design, key factors, sample information, and measurement methods [8]. Their meta-analysis reveals the need to change the theoretical framework and evaluate empirical hypotheses whose samples are supported by participants such as students and others. However, our SLR is centralised on the outcome of unethical Internet behaviour research.

To our best knowledge, not many systematic literature reviews have been conducted on unethical Internet behaviour. This paper presents the results of a systematic literature review (SLR) by categorising the data into a taxonomy that can be used to comprehend the current state of the art of unethical Internet behaviour in higher education. Therefore, the contributions of this SLR are as follows:

- 1) The classification of unethical Internet behaviours. Additionally, based on the literature on unethical Internet behaviours, this review provides an appropriate definition for each category.
- 2) The presentation of theories that have been utilised in previous research on unethical Internet behaviours.
- 3) The identification of demographic and risk factors that are associated with unethical Internet behaviours
- 4) The investigation on the challenges and research opportunities for unethical Internet behaviour in high education settings.

II. REVIEW METHOD

A. Introduction

This section describes the approach for conducting a systematic review of Internet behaviour among Malaysian university students. Literature reviews are a kind of secondary research that helps form primary research results [9], [10] explicit methodology. The Cochrane Collaboration stated that a systematic review attempts to assemble all evidence that meets pre-specified eligibility criteria to address a specific research question [11]. It employs specific, systematic processes that are carefully chosen to avoid bias, resulting in accurate data from which conclusions and judgments may be taken. Kitchenham and Charters (2007) defined a systematic review as a process of discovering, analysing, and interpreting all available studies that are relevant to a specific research question [10].

The review methodology in this paper is based on the standards set by Kitchenham and Charters (2007). According to Kitchenham and Charters (2007), a systematic review of the literature is divided into three phases: planning, conducting, and reporting. The preparation phase of systematic reviews begins with establishing a protocol that will govern the review's conduct. A review protocol details the procedures that will be followed to conduct a systematic review.

A pre-defined protocol is essential to eliminate the risk of researcher bias [3]. The review protocol is based on Khan et al. (2003) five-step process for performing a systematic review, as shown in Fig. 1.

B. Framing Research Questions for the Review

The PICO (population, intervention, control, and outcome) format is a well-known technique for structuring a research question. Petticrew and Roberts (2008); and Kitchenham and Charters (2007) suggest using the PICO format with an additional element: Context. This element refers to the setting in which the intervention is administered or to the participants in the study [10], [12].

Table I shows the research questions' Population, Intervention, Comparison, Outcomes, and Context (PICOC) structure. This systematic literature review included all empirical studies investigating unethical Internet behavior within a higher education setting, regardless of whether the setting has formal or non-formal cyberethics awareness activities. Therefore, this review did not include any specific comparison in the PICOC structure.

In general, the primary purpose of this systematic literature review is to obtain knowledge on the evidence of Internet ethics issues and awareness among university students. Therefore, in order to have this knowledge in the current investigation, the defined the following research questions (RQ):

RQ1 What are the categorizations of unethical Internet behaviour among university students?

RQ2 What are the different theoretical lenses that are used in unethical Internet behaviour research?

RQ3 Which demographic and risk factors are involved in unethical Internet behaviour research?

RQ4 What are the challenges and research opportunities for the unethical Internet behavior research within university setting?

C. Identifying Relevant Works

After identifying the research questions, the subsequent step is to specify the search strategy and search string. The search process's main objective is to discover relevant articles that discuss unethical Internet behaviour in higher education settings. The search strategy included an automated search of digital libraries via a search string constructed from the PICOC structure in Table I.

TABLE I. SUMMARY OF PICOC FOR THIS STUDY

Population	Undergraduate students
Intervention	Awareness in cyberethics
Comparison	None
Outcome	Unethical Internet behaviour
Context	Any empirical studies on unethical Internet behavior within a higher education setting

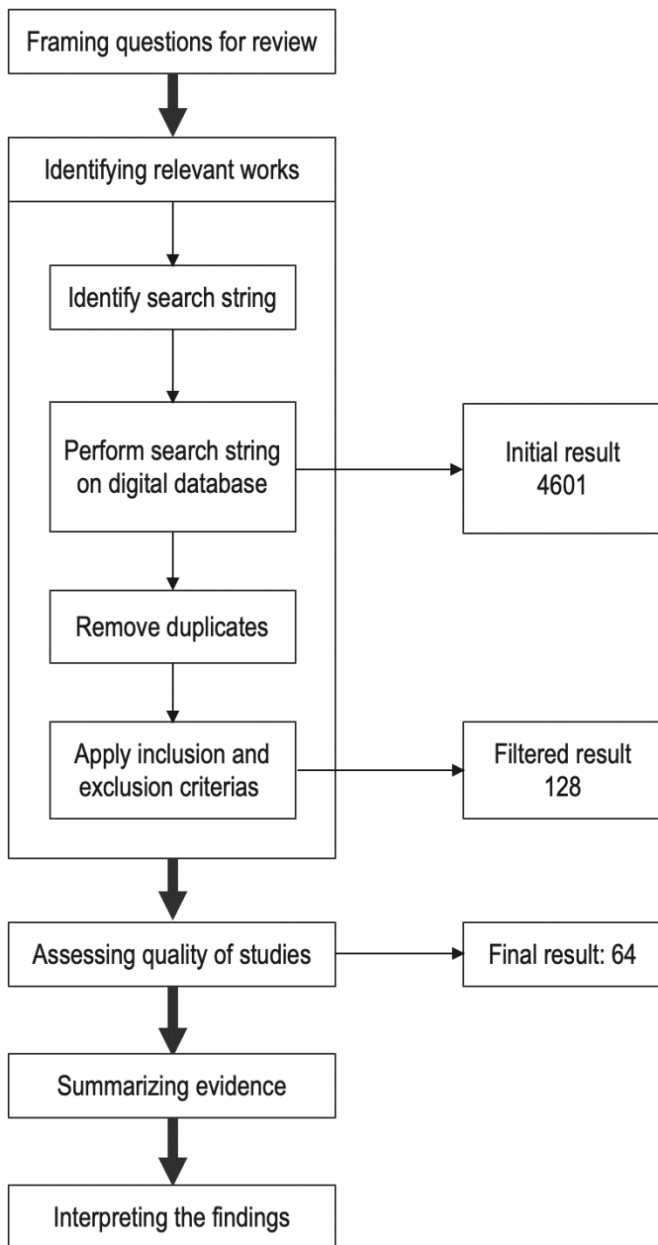


Fig. 1. Systematic Literature Review Methodology for this Study.

1) *Identify search string*: Various keywords have been established with the intent of specifying database search strings and inclusion and exclusion criteria. The search strings were defined by considering the question items' synonyms and other spellings and connecting them with "and" and "or." Following the PICOC structure, the most relevant and applicable terms were selected for the study area. As a result, the following search terms were chosen: "undergraduate", "awareness", "unethical Internet". To examine the inclusion of the review's findings, the outcomes of the initial examination were used as a pilot and passed several phases before specifying the query. Since some of the investigations in the review were not obtained by the first query, the query string was modified and included some more keywords. The

keywords that were added to the search string are as follows: "university student", "university", "Internet ethics", "cyber", "computer", "ethics", "problematic Internet". The whole search phrase used to do the literature search was as follows:

(Undergraduate OR "university student" OR university) AND {[awareness AND (ethic* OR "internet ethics")] OR ("unethical internet" OR "problematic internet" OR "internet ethics")}

2) *Identifying the sources and selection of studies*: The title and abstract of each publication were examined for keywords to get as many relevant articles as feasible. A total of ten digital databases were used in the primary search process: ACM Digital Library, Dimensions, EBSCOhost, Emerald, IEEEExplore, ISI Web of Science, Sage Full Text Collections, Science-Direct, Scopus and SpringerLink.

A systematic literature search was conducted on chosen databases using the search phrase provided above; yielding 4651 studies as a result of the initial search (refer to Table II). In the next step, all remaining articles' inclusion and exclusion criteria were applied before any duplicate papers were removed.

Inclusion criteria:

- Articles from year 2010 - 2020
- Articles must be published in a journal or a conference proceeding
- Articles published must be in university setting
- Articles must be within the area/domain of computer science, engineering, social engineering, social sciences, education, and information science.

Exclusion criteria:

- Articles related to law, policy, and regulations
- Articles related to psychological domain
- Articles related to internet ethics subject and training.

TABLE II. THE RESULTS OF THE SELECTION PROCESS

Online Databases	Initial Results	Selected Studies
ACM Digital Library	452	-
Dimensions.ai	50	20
EBSCOhost	1789	-
Emerald	20	-
IEEEExplore	238	4
ISI Web of Science	42	1
Sage Full Text Collections	22	-
Science-Direct	804	10
Scopus	739	5
SpringerLink	495	24
TOTAL	4651	64

The complete texts and abstracts of the selected articles were evaluated to guarantee that only publications that had been thoroughly investigated were included in the study at the same time. For each selected article, a set of criteria is used to evaluate its quality and determine the relevance of the results and interpretations from the main study. As shown in Fig. 1, the filtered result yielded 128 articles after the initial results were filtered according to inclusion and exclusion criteria, and duplicate articles were removed.

3) Quality Assessment: In accordance with the methodology [10], [13] suggested, this paragraph describes the quality assessment procedure used to determine the quality of each item chosen. The quality of each article included in this research is critical to ensure that high-quality SLR studies on unethical Internet behaviour are made accessible and to avoid bias in terms of the quality of previously published studies. A set of quality checklists is used for each selected article to evaluate its quality. The checklists also determine the relevance of the results and interpretations from the main study. When developing the quality checklist for the review, some of the questions presented in the literature were reused [10], [12], [14].

TABLE III. QUALITY ASSESSMENT CHECKLIST

ASSESSMENT	DETAILS
Was the article refereed?	-
Were the aim of the study clearly stated?	-
Were data collections carried out very well?	Quantitative: The paper explain the questionnaire design procedure (mention the source of existing scale or explaining design procedure for new questionnaire). Qualitative: The paper explain the design of data collection tool (structured/unstructured question for interview or focus group, observation, diary, journal).
	Sampling: The paper mention the number of respondents/participant.
	Duration (Longitudal study/ Qualitative study): The paper mention the recruitment or data collection time frame. For example: 3 weeks, from January to March
Were the approach to and formulation of the analysis well conveyed?	Quantitative: Minimum of descriptive statistics (mean or median) Qualitative: Include participant's quotation or excerpt from data collection tools.
Were the findings credible?	The paper must be methodologically explained.
	The paper must provide assessment validity Quantitative: If the questionnaire is newly developed (not from existing scale), the paper must include validity test (content validity or expert review/construct validity), EFA(Exploratory Factor Analysis), CFA (confirmatory factor analysis) Qualitative: Provide triangulation/expert validation

From the filtered results (refer to Fig. 1, each of these studies was screened according to the quality assessment checklist (refer to Table III). Full articles were utilised when titles and abstracts were insufficient to determine a paper's relevance. The scoring method for the quality assessment was either good, fair, bad, or unknown (i.e. no information was supplied). Anawar oversaw the quality assessment process. Each of the researchers assessed articles from at least two databases. Eventually, 64 articles were chosen as the final study for the systematic survey (refer to Table II).

III. RESULTS AND DISCUSSION

A. Introduction

The search results are generated using the search strings supplied in Section II. The present SLR synthesised a total of 64 main studies (refer to Appendix A: List of the Included Studies). This number was determined following a thorough assessment of the publications included in the current investigation. Notably, the writers focused on research that matched the criteria for inclusion outlined in Section II. The distribution of selected studies according to the digital libraries is shown in Fig. 2. Fig. 3 shows the distribution of all studies from 2010 to 2020.

B. RQ1 - Categorization of Unethical Internet Behavior

For the first research question, the context of the studies specifically focus on certain behaviors was identified in Table IV.

The SLR identified 11 papers studied in cyberbullying, seven articles on cyberslacking, and only one evidence was found in online trolling, catfish, risky online posting and cyber dating abuse.

Cyber slacking is defined as using the Internet and digital technology during scheduled class time for non-class related purposes [15]. Cyber slacking can be divided into in-class (slacking during class) and out-of-class (outside of class) [S1], [16]. From Table IV, seven papers discussed cyberslacking; five studies focus on in-class cyberslacking [S1], [S3], [S5]–[S7] and three studies on out-of-class cyberslacking [S2], [S4], [S7].

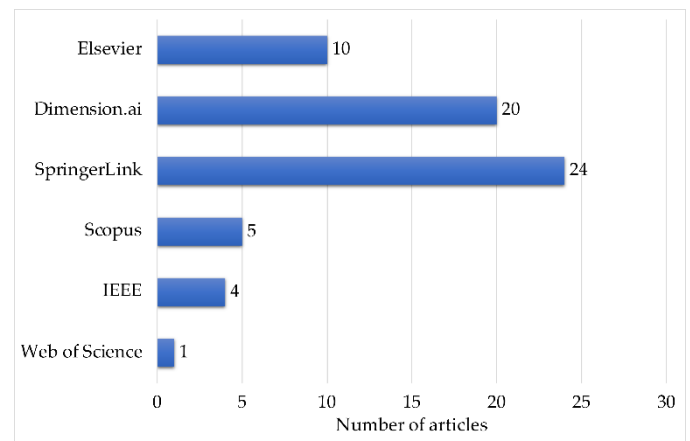


Fig. 2. Number of Publications based on Databases.

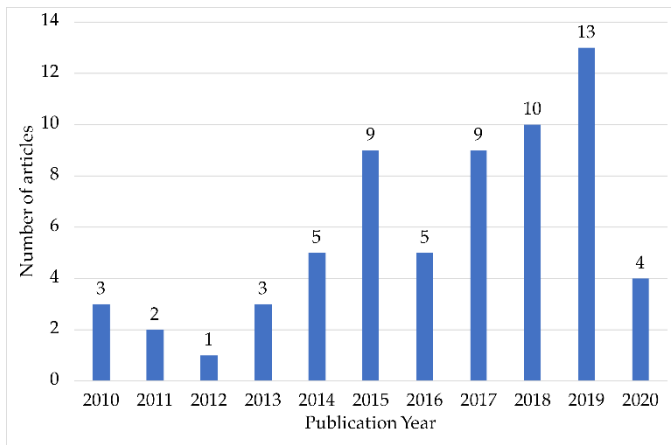


Fig. 3. Distribution of Studies based on Year of Publication.

TABLE IV. TYPE OF UNETHICAL INTERNET BEHAVIOUR STUDIES CONDUCTED FOR STUDENTS IN HIGHER EDUCATION SETTINGS

Unethical Internet Behaviour	Sources	Total Studies
Cyberslacking	[S1], [S2], [S3], [S4], [S5], [S6], [S7]	7
Cyberbullying	[S8], [S9], [S10], [S11], [S12], [S13], [S14], [S15], [S16], [S17], [S18]	11
Risky Online Posting	[S19]	1
Cyber Dating Abuse	[S20]	1
Online Trolling	[S21]	1
Catfish	[S22]	1
Digital Piracy	[S23], [S24], [S25], [S26], [S27], [S28], [S29], [S30], [S31], [S32]	9
Plagiarism	[S27], [S30], [S33], [S34], [S35], [S36], [S37], [S38], [S39], [S40], [S41], [S31], [S32], [S42], [S43], [S44], [S45], [S46], [S47], [S48], [S49], [S50], [S51], [S52], [S53], [S54], [S55]	24
Fabrication	[S37], [S40], [S31], [S42], [S44], [S46], [S56], [S55]	8
Cheating	[S34], [S35], [S37], [S39], [S40], [S31], [S32], [S42], [S57], [S43], [S44], [S46], [S58], [S49], [S51], [S56], [S52], [S59], [S55]	18
Collusion	[S34], [S35], [S39], [S40], [S31], [S42], [S44], [S46], [S49], [S56], [S55]	11
Online Sexual Activity (OSA)	[S60], [S61], [S62], [S63]	4
Online Gambling	[S64]	1

Cyberbullying refers to the use of electronic forms by a group or individuals to act aggressively, repeatedly and over time against a victim(s) who cannot easily defend him or herself or themselves [17] [S10]. Whereas, Charmaraman et al. (2018) defined it as “the use of information and communications technology to intimidate, harass, victimize, or bully an individual or a group of individuals” [18] [S18].

Online trolling is defined as “an action of using Internet by a user using a deceptive identity of sincerely wishing to be part of the group in question, including professing, or conveying pseudo-sincere intentions, but whose real

intention(s) conflict for the purposes of their own amusement” [19] [S21].

Catfish is a malevolent form of online dating deception which involves the creation of a false internet identity to scam, blackmail, or con those they meet in online communities or chat rooms without the intention of meeting in person [S22].

Risky online posting is an activity in which a user discloses inappropriate, personal and unfavourable information by posting personal photos or media clips or sharing personal comments on social media [S19].

Cyber dating abuse is a form of dating violence through technology either by sharing private information on the social media platforms and insulting or threatening using these platforms, but also includes behaviours that intrude on the victim’s privacy or the act of monitoring the victims (e.g. having access to social media or using their partner’s password without permission) [S20].

Trolling, cyberbullying and cyberstalking are similar in the way that the Internet is used to cause harm and distress [S21]. Cyberdating abuse is similar to cyberbullying in that the activities conducted are aggressive and harmful to the victim. Whereas catfish and risky online posting are similar to cyber dating abuse as it involves online relationships. Thus the category cyber abuse is coined from this type of unethical Internet behaviour.

The widespread nature of corruption and financial scandals has directed attention to the ethical decision-making process and the influence of higher education in developing the leaders of tomorrow. Although the university is a place for educators and students to pursue knowledge ethically, academic dishonesty has been widespread in higher education [20]. Kibler (1993) defined academic dishonesty as “forms of cheating and plagiarism that involve students giving or receiving unauthorised assistance in an academic exercise or receiving credit for work that is not their own” [21]. Pavela (1978) identifies four primary types of academic dishonesty behaviour as (i) Cheating: “intentionally using or attempting to use unauthorised materials, information, or study aids in any academic exercise. The term academic exercise includes all forms of work submitted for credit or hours”; (ii) Fabrication: “intentional and unauthorised falsification or invention of any information or citation in an academic exercise”; (iii) Facilitating Academic Dishonesty: “intentionally or knowingly helping or attempting to help another to violate a provision of the institutional code of academic integrity”; and lastly, (iv) Plagiarism: “deliberate adoption or reproduction of ideas or words or statements of another person as one’s own without acknowledgement” [22]. Molnar and Kletke (2012) broadly define cheating as any violation of that definition that goes against a university’s academic integrity policy that includes cheating with or without the use of the Internet, plagiarism and digital piracy [S31]. However, Cho and Hwang (2019) and Molnar (2015) used academic ethics violations and academic dishonesty to refer to plagiarism, cheating and copyright [S32], [S37]. Technology development has facilitated pirating or paying for digital products, making plagiarism interrelated to intellectual property, copyright and authorship [23]. In the context of the

digital era in university, cheating, plagiarism, and digital piracy have been reported as academic dishonesty [24]. Thus, we used academic dishonesty to group these types of unethical behaviours. In this paper, digital piracy is defined as “an unauthorised reproduction, use, or diffusion of a copyrighted digital product” [25]. From the evidence in Table IV, 30 papers have discussed plagiarism which is 24 studies, 18 studies on cheating, eight studies on fabrication, 11 on collusion and nine studies on digital piracy.

Online Sexual Activity (OSA) is defined as “the use of the Internet (via text, audio, video, and graphic files) for any activity that involves human sexuality” [26]. At the same time, Online Gambling refers to “all forms of gambling (including wagering) via the phones and wireless devices” [27]. OSA and online gambling are categorised under Unethical Internet Access as these activities are considered immoral [28] and harmful [29]. The evidence found in the SLR shows four studies in OSA and one study in online gambling (refer to Table IV).

Although cybercrime is part of unethical internet behaviour, no evidence was found in higher education setting. The unethical Internet behaviours presented in Table IV can be categorised into four main categories: cyber abuse, academic dishonesty, unethical website access and cyberslacking, as shown Table V.

Fig. 4 and Fig. 5 present the distribution of the sources for each of unethical Internet behaviours categories. Referring to Fig. 4 and Fig. 5, among the categories, source of evidence from academic dishonesty forms the predominant number of papers accounting for 58 per cent of all 64 papers, followed by cyber abuse produced 23 per cent. Cyberslacking contributed 11 per cent of sources, while the source of evidence from unethical website access constituted 8 per cent.

C. RQ2 - Different Theoretical Lenses that are used in Unethical Internet Behaviour Research

A variety of theories were used to analyse unethical internet behaviour. Researchers have employed integrated theories in certain studies, but in others, they have used a single theory and added new constructs from other models. Table VI shows theories used in unethical internet behaviour research. Different theories were used for each category of unethical internet behaviour research.

Academic dishonesty research is largely influenced by the Theory of Reasoned Action (TRA) and the Theory of Planned Behavior (TPB). TRA and TPB are the most widely accepted academic dishonesty research hypotheses. TRA and TPB have served as a foundation for study in several domains, including the prediction of human behaviour. Specifically, TPB is an expansion of the TRA, which is often used to identify solutions for behavioural change. These hypotheses assert that behavioural purpose is frequently unobservable and the best indication of behaviour as a surrogate for probable behaviour [30], [31]. According to the TPB, academic dishonesty is caused by the opportunity and purpose to engage in dishonest behaviour. Therefore, attempts to prevent academic dishonesty should consider environmental and behavioural factors.

TABLE V. CATEGORISATION OF UNETHICAL INTERNET BEHAVIOURS

Categories	Unethical Internet Behaviours
Cyberslacking (CS) - 7 papers	In-class Cyberslacking
	Out-of-class Cyberslacking
Cyber Abuse (CA) - 15 papers	Cyberbullying
	Risky Online Posting
	Cyber Dating Abuse
	Online Trolling
	Catfish
Academic Dishonesty (AD) - 37 papers	Digital Piracy
	Plagiarism
	Cheating
	Fabrication
	Collusion
Unethical Internet Access (UIA) - 5 papers	Online Sexual Activity
	Online Gambling

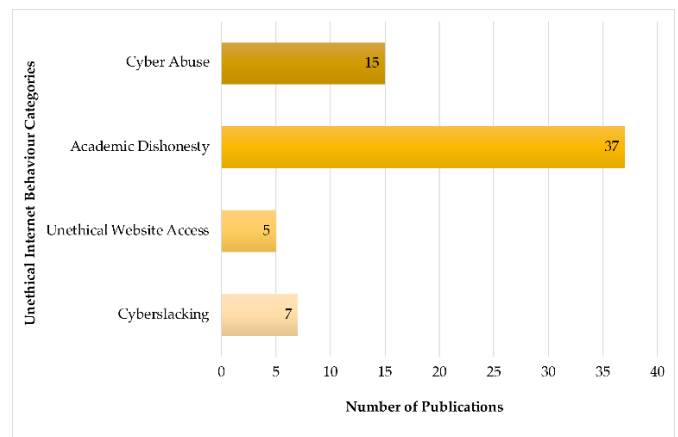


Fig. 4. Distribution of Articles based on Unethical Internet Behaviours Categorization.

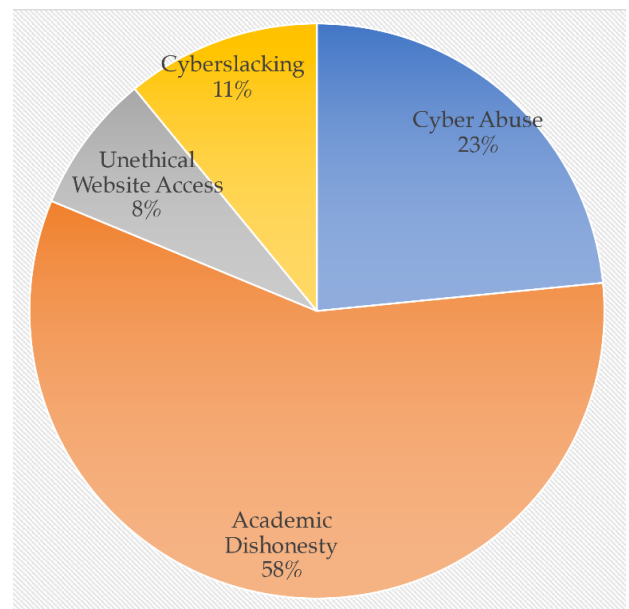


Fig. 5. Distribution Percentage for Unethical Internet Behaviours Categories.

TABLE VI. THEORIES USED IN UNETHICAL INTERNET BEHAVIOUR RESEARCH

No.	Theory	Total Studies	Sources
1.	Theory of Reason Action /Theory of Planned Behaviour	CS (1 paper) AD (19 papers)	[S5] [S23], [S25], [S26], [S27], [S28], [S29], [S33], [S34], [S37], [S38], [S39], [S40], [S32], [S57], [S43], [S46], [S48], [S54], [S55]
2.	User and Gratification	CS (2 papers)	[S2], [S4]
3.	Zimbardo Time Perspective	CS (1 paper)	[S1]
4.	Theories of Meta- Attention	CS (1 paper)	[S7]
5.	Sensation Seeking Theory	UIA (1 paper)	[S61]
6.	Big Five Personality	AD (2 papers) CA (5 papers)	[S41], [S57] [S8], [S11], [S13], [S15], [S21]
7.	Ethical Decision Making	AD (1 paper)	[S25]
8.	Cognitive Moral Development	AD (3 papers)	[S25], [S29], [S38]
9.	Self-Perception Theory	AD (8 papers)	[S26], [S28], [S30], [S38], [S39], [S40], [S51], [S56]
10.	ICT Literacy Self-efficacy	AD (2 papers)	[S36], [S38]
11.	General Aggression Model	CA (10 papers)	[S8], [S9], [S11], [S12], [S13], [S14], [S15], [S20], [S17], [S21]
12.	Lifestyle Exposure Theory	CA (1 papers)	[S13]
13.	Social Media Engagement Theory	CA (1 papers)	[S21]
14.	Attachment Theory	CA (1 papers)	[S22]

Most cyber abuse researchers employed the General Aggregation Model (GAM) in their studies. GAM is a comprehensive and integrated paradigm for studying aggression that considers the role of social, cognitive, psychological, developmental, and biological factors in the emergence of violent behaviour [32]. GAM has been utilised in several abusive behaviour scenarios, including media violence impacts, interpersonal violence, intergroup violence, and pain effects [33]. The dominance of GAM in cyber abuse research on unethical online behaviour is largely because these theories define characteristics associated with cyberbullying, cyber trolling, cyber dating abuse, cyber harassment, and cyber victimisation, all of which are abusive and aggressive behaviours.

User and Gratification Theory (UGT) is frequently discussed in relation to cyberslacking. Blumler and Katz initially presented UGT in order to comprehend why individuals utilise particular sorts of media, what demands they have when utilising them, and what satisfactions they derive from doing so [34]. Individuals employ a particular technology or medium to satisfy their desires or requirements, as determined by UGT. Doty et al. (2020) and Grieve (2017) utilized UGT in their research and discovered that certain factors, such as social connectivity, technological engagement, social interaction, and incentives, led to cyberslacking among students [35], [36].

The Sensation Seeking Theory (SST) was then applied to the category of unethical Internet access. SST is "a characteristic characterised by the pursuit of varied, unique, complicated, and intense feelings and experiences, as well as

the readiness to assume physical, social, legal, and financial risks for such experiences" [37]. Sensation seeking has arisen as an explanation for several behaviours, including sex, computer and video game activity, gambling, and others [38]. Several sensation-seeking variables, including sensitivity to boredom and disinhibition, were discovered to be precursors to online sexual behaviour when this theory was applied to unethical Internet use [39].

According to these findings, several theories dominate the categories of unethical online behaviour. Each category's dominant theory suggests that it is an area that is still in flux. Exploring alternative ideas may yield fresh insights for a deeper comprehension of unethical online behavior research.

D. RQ3 - Demographic and Risk Factors Involved in Unethical Internet behaviour Research

The aim of this section is to present and discuss the demographic and risk factors extracted from the papers listed in Table IV. Demographic factors are used to determine the characteristics of an individual or a population [40]. Among the most often employed demographic characteristics are race, age, income, marital status, and educational attainment [40]. Table VII lists the demographic factors that were investigated in the 64 papers of this literature survey. A risk factor can be defined as a characteristic, condition, or behaviour that makes a person more vulnerable to an event or occurrence [41]. In the context of this survey, risk factor is factors believed to influence the student engagement of unethical internet behaviour in higher education settings. Altogether, 39 factors were identified by a total of 64 studies which investigated how these factors correlated with student engagement of unethical

internet behaviour. Table VIII lists the predictive factors, studies that analyse the factor which gave significant, no significant or mixed effect.

1) *Demographic factors*: According to Table VII, gender and academic performance factors have a profound influence on unethical behaviour in the category of academic dishonesty. From Table VII, 22 studies found that students with high academic achievement exhibit more ethical behaviour than those with low academic performance. Table VII also shows that ten studies reported that gender factor significantly affects AD behaviour.

Among papers that reported gender factor has a significant effect on academic dishonesty in higher education context, [S31], [S40], [S42], reported that male students were more likely than female students to participate in academic dishonesty behaviour. Whereas study in [S58] showed that more female students witnessed cheating in examinations than the male students, and in [S49], more male students admitted to engaging in AD behaviour than female students. A study in [S36] reported that gender does not have a significant effect on AD behaviour; however, students in higher income groups have more tendencies to be involved in AD behaviours.

Among all the demographic factors indicated in Table VII, only the gender factor has a noticeable effect on cyber abuse behaviours. Nine studies [S8], [S9], [S13]-[S16], [S20]-[S22], reported that male students were substantially more likely to engage in cyberbullying than their female counterparts. A study done by [S15] showed that gender was a significant predictor of cyberbullying behaviour, where male students perpetrated cyberbullying more frequently than female students. In the same study, females had higher scores on empathy and more substantial nonverbal skill proficiency. Research in [S16] revealed that males are much more prone to group bullying than females. Research in [S21] and [S22] showed that males were over two times as likely to engage in trolling and catfishing, respectively, than females.

Studies by [S8] and [S9] showed that cyberbullying was more prevalent among those who used the Internet weekly than those who used it less often or moderately. In [S12], the authors studied students' experiences with traditional bullying and cyber-teasing and the role that sociodemographic factors may have in preventing or contributing to these forms of violence. The study also discovered that the majority of cyber-teasing victims also reported being victims of traditional bullying (and vice versa). Traditional bullying victimisation was more prevalent among males than females, and cyberbullying was more prevalent among female students than male students. Students who experienced traditional bullying were more likely to have financial difficulties, family conflicts, and a history of cannabis use.

2) *Risk factors*: Table VIII shows that attitude, intention and controllability were the three most commonly investigated factors in unethical internet behaviour studies. In terms of attitude, 15 articles on academic dishonesty (AD) and one study on cyberslacking (CS) reported that the students' attitudes would influence the student engagement in unethical

Internet behaviour [S5], [S25], [S26], [S28], [S29], [S34], [S38], [S32], [S57], [S43], [S44], [S46], [S48], [S51], [S54], [S55]. At the same time, AD studies by [S27], [S33], [S37], [S39], [S40], reported that attitude has no significant effect. Nine AD studies regarded intention will influence the student engagement in unethical Internet behaviour [S23], [S25], [S27], [S28], [S38], [S48], [S50], [S54], [S55], while two AD studies reported that intention [S40], [S44] has no significant effect on the student engagement. Controllability factors are a group of factors such as Perceived Behavior Control (PBC), self-efficacy, self-control, self-regulation, and self-monitoring. Reportedly, eight AD, one CS, one Cyber abuse (CA) and one unethical internet access (UIA) found that these factors influence the student engagement in unethical Internet behaviour [S5], [S19], [S29], [S39], [S57], [S48], [S50], [S59], [S54], [S55], while Uzun et al. [S38] claimed that self-efficacy has no significant effect.

Concerning self-perception and self-concept factors, six out of 11 studies found that self-perception is an AD factor. Self-perception has significantly influenced student involvement in unethical Internet behaviour [S26], [S28], [S30], [S38], [S39], [S51], and one study by CA found that negative self-concept factor also has a significant influence on student engagement [S14]. However, four AD studies by [S27], [S40], [S48], [S56] claim that self-perception does not have a significant effect.

Behaviour frequency is a group of cyber-bullying, dating abuse, trolling, cyber-victimisation, dating victimisation, or trolling victimisation frequency. Seven out of nine studies in cyber-abuse ascertained that unethical behaviour frequency is a significant factor [S8], [S9], [S11], [S13], [S15], [S20], [S17]. However, two CA studies claim that behaviour frequency is considered as insignificant [S14] [S21].

The nine studies that investigated the effect of characteristics of subject-course produced contradictory findings [S30], [S36], [S31], [S43], [S44], [S47], [S49], [S56], [S52]: six studies reported that the characteristics of subject-course plays essential roles in influencing the student engagement in unethical Internet behaviour. [S36] and [S44] claimed that the characteristics of the subject-course did not influence student involvement. The study by [S56] suggests that different characteristics of subject-course have a different effect on student engagement.

Five AD studies and one CS study out of eight studies analysed that perceived prosecution risk able to influence the student engagement in unethical Internet behaviour [S27], [S40], [S48], [S56], [S52], contrary to the AD studies by [S25] and [S33]. Five AD studies [S29], [S39], [S48], [S54], [S55] and one CS study [S5] out of eight studies reported that norms are a significant factor in student engagement in unethical Internet behaviour. In contrast, the study by [S38] and [S20] of AD and CA respectively claimed that norms are insignificant.

Two studies that investigated the effect of Big Five Personalities on student involvement in unethical Internet behaviours show mixed findings [S41], [S57]. Wilks et al.

[S41] found that conscientiousness and agreeableness behaviours while other factors do not significantly affect student involvement in unethical Internet

TABLE VII. LIST OF DEMOGRAPHIC FACTORS INVESTIGATED IN UNETHICAL INTERNET BEHAVIOUR STUDIES

No.	Demographic Factor	Total Studies	Significant Effect (SE*)	No Significant Effect (NSE)
1.	Age	CS (1 paper) CA (1 paper) AD (13 papers)	[S4] - [S43], [S56], [S58]	- [S8] [S23], [S24], [S34], [S37], [S46], [S48], [S51], [S59], [S54], [S55]
2.	Gender	CS (1 paper) CA (9 papers) AD (30 papers) UIA (3 papers)	[S3] [S8], [S9], [S13], [S14], [S15], [S16], [S20], [S21], [S22] [S35], [S37], [S40], [S31], [S32], [S46], [S47], [S58], [S49], [S51] [S60], [S62], [S63]	- - [S23], [S24], [S30], [S34], [S42], [S43], [S48], [S59], [S54], [S55] -
3.	Ethnic group/Culture	CA (1 paper) AD (6 papers) UIA (1 paper)	[S18] [S25] [S34], [S44] [S64]	- [S42], [S48], [S55] -
4.	Income/Social class	CA (1 paper) AD (7 papers)	[S12] [S36], [S58], [S59]	- [S34], [S37], [S32], [S48]
5.	Education Level	CA (1 paper) AD (10 papers)	[S12] [S53]	- [S24], [S35], [S32], [S47], [S58], [S49], [S51], [S56], [S54]
6.	Marital Status	AD (2 papers)	-	[S24], [S55]
7.	Academic Performance	CA (1 paper) AD (22 papers) UIA (1 paper)	- [S27], [S30], [S34], [S35], [S36], [S37], [S40], [S42], [S44], [S45], [S46], [S47], [S58], [S49], [S50], [S51], [S52], [S53], [S55]	[S11] [S33], [S43], [S56] -
8.	Internet Service Availability	CS (2 paper) AD (5 papers)	[S8], [S9] [S25], [S27], [S36], [S31]	- [S28]
9.	Resources Availability	CS (2 papers) CA (1 paper) UIA (2 papers)	[S8], [S9] [S18] -	- - [S24], [S28]

*SE comprised of Positive Significant Effect and Negative Significant Effect
AD = Academic Dishonesty; CS = Cyberslacking; CA = Cyber Abuse; UIA = Unethical Internet Access

TABLE VIII. LIST OF FACTORS INVESTIGATED IN UNETHICAL INTERNET BEHAVIOUR STUDIES

No.	Factor	Total Studies	Significant Effect (SE*)	No Significant Effect (NSE)	Mixed Effect (ME)
1.	Attitude	CS (1 paper) AD (20 papers)	[S5] [S25], [S26], [S28], [S29], [S34], [S38], [S32], [S57], [S43], [S44], [S46], [S48], [S51], [S54], [S55]	- [S27], [S33], [S37], [S39], [S40]	- -
2.	Intention	AD (11 papers)	[S23], [S25], [S27], [S28], [S38], [S48], [S50], [S54], [S55]	[S31], [S43]	-
3.	Controllability (PBC, Self-efficacy, self-control, self-regulation, self-monitoring)	AD (9 papers) CS (1 paper) CA (1 paper) UIA (1 paper)	[S29], [S39], [S57], [S48], [S50], [S59], [S54], [S55] [S5] [S19] [S63]	[S38] - - -	- - - -
4.	Self-Perception, Self-concept	AD (10 papers) CA (1 paper)	[S26], [S28], [S30], [S38], [S39], [S51] [S14]	[S27], [S40], [S48], [S56] -	- -
5.	Behaviour Frequency	CA (9 papers)	[S8], [S9], [S11], [S13], [S15], [S20], [S17]	[S14], [S21]	-
6.	Characteristics of subject-course	AD (9 papers)	[S30], [S31], [S43], [S47], [S49], [S52]	[S36], [S44]	[S56]
7.	Perceived prosecution risk	AD (7 papers) CS (1 paper)	[S27], [S40], [S48], [S56], [S52] [S5]	[S25], [S33] -	- -
8.	Norms	AD (6 papers) CS (1 paper) CA (1 paper)	[S29], [S39], [S48], [S54], [S55] [S5] [S5]	[S38] - [S20]	- - -

9.	Personalities	AD (2 papers) CA (5 papers)	- -	- -	[S41], [S57] [S8], [S11], [S13], [S15], [S21]
10.	Psychopathology Symptoms	CA (6 papers) UIA (1 paper)	[S9], [S11], [S13], [S17] [S61]	- -	[S8], [S14] -
11.	Experiences	AD (3 papers) CA (4 papers)	[S34], [S44], [S51] [S11], [S12], [S21]	- -	- [S20]
12.	Ethics	AD (6 papers)	[S23], [S32], [S30], [S35], [S37]	[S33]	-
13.	Social Desirability	AD (3 papers) CS (1 paper) UIA (1 paper)	[S33] [S3] [S62]	[S26], [S51] - -	- - -
14.	Morality (moral obligation, moral foundation, moral integrity, moral disengagement, moral justification)	AD (5 papers)	[S29], [S38], [S30]	[S25]	[S49]
15.	Internet usage type	CS (1 paper) CA (4 papers)	- [S10], [S11]	- [S8]	[S2] [S13]
16.	Individual Perceived Pressure	AD (3 papers) UIA (1 paper)	[S43], [S47], [S52] [S61]	- -	- -
17.	Emphasizing-systemizing	CA (3 papers)	[S14]	[S21]	[S9]
18.	Impulsivity	CS (1 paper) CA (2 papers)	- [S14], [S19]	- -	[S6] -
19.	Sensation Seeking	CA (1 paper) UIA (1 paper)	- -	- -	[S9] [S61]
20.	Loneliness	CA (2 papers)	[S8], [S13]	-	-
21.	Perceived benefits	AD (2 papers)	-	[S25], [S42]	-
22.	Idolatory	AD (2 papers)	[S23]	[S25]	-
23.	Music's quality	AD (1 paper)	[S25]	-	-
24.	Novelty seeking	AD (1 paper)	[S25]	-	-
25.	Constructivist Practices in the Learning Environment (CPL)	AD (1 paper)	[S59]	-	-
26.	Time perspective	CS (1 paper)	-	-	[S1]
27.	Escapism	CS (1 paper)	[S5]	-	-
28.	Attention	CS (1 paper)	[S7]	-	-
29.	Interpersonal sensitivity	CA (1 paper)	[S9]	-	-
30.	Psychopathic traits	CA (1 paper)	[S9]	-	-
31.	Disabilities	CA (1 paper)	[S11]	-	-
32.	Attachment	CA (2 papers)	[S22]	[S8]	-
33.	Body Image Dissatisfaction	CA (1 paper)	[S17]	-	-
34.	Anxiety	CA (1 paper)	[S9]	-	-
35.	Self-esteem	CA (1 paper)	[S11]	-	-
36.	Biological clock	CA (1 paper)	-	-	[S15]
37.	Social support	CA (1 paper)	-	[S21]	-
38.	Perceived cost	AD (1 paper)	-	[S23]	-

*SE comprised of Positive Significant Effect and Negative Significant Effect

AD = Academic Dishonesty; CS = Cyberslacking; CA = Cyber Abuse; UIA = Unethical Internet Access effect while others reported a contradictory result. Neuroticism is reported as significant by [S8], [S13], [S15], while other is not.

However, Day et al. [S43] reported that conscientiousness has a positive influence compared to openness, while neuroticism does not significantly affect student engagement in AD. Interestingly, five CA studies show mixed findings [S8], [S11], [S13], [S15], [S21]. All studies found that conscientiousness has a significant effect while openness to experience does not have a significant effect. Only [S8], [S13], [S21], found that agreeableness has a significant effect, while the other find reported that it is not significant. Whereas [S8], [S11], [S15] found that extraversion has a significant

Psychopathology symptoms are a group of factors that include depression, hostility, anxiety, somatization, shyness, and ostracism that were studied in whole or partly. Four CA studies [S9], [S11], [S13], [S17], and one UIA study [S61] found that these factors have a significant effect, while two CA studies [S8], [S14] have a mixed effect.

Experience is factors that involve students' past engagement in unethical behaviour, either as a victim, perpetrator or witness. Students' experience in using tools to conduct the behaviour is also included in this group. Three AD studies [S34], [S44], [S51], and three CA studies [S11], [S12], [S21], found that past experience is a significant factor. Villora et al. [S20] reported that control abuse has a significant effect while direct abuse is not significant showing a mixed effect in this CA study.

Five out of six studies in academic dishonesty investigated that ethics has a significant effect on student engagement in unethical Internet behaviour [S23], [S32], [S30], [S35], [S37], whereas [S33] claimed it is not. Although Akbulut and Dönmez [S26] and Baetz et al. [S51] reported that social desirability does not have a significant effect, however, Riquez et al. [S33], Akbulut et al. [S3] and Rasmussen et al. [S62] refute this finding.

Five studies explored the aspect of morality and provided different effects [S25], [S29], [S30], [S38], [S49]. Most studies yield that morality has a significant effect in influencing student engagement in unethical Internet behaviour [S29], [S38], [S30]. Lin et al. [S25] claimed that morality does not significantly influence student involvement in unethical Internet behaviour. Ampuni et al. [S49] find that a mix of moral integrity and moral disengagement significantly affects student engagement while other aspects do not.

Two out of four CA studies [S10], [S11] reported that internet usage type has a significant effect, while [S8] refuted this claim. Interestingly, one CS study [S2] and one CA study [S13] have a mixed effect. In terms of individual perceived pressure, three AD studies [S43], [S47], [S52], and one UIA study [S61] agreed that it is one of the significant factors that influence student involvement in unethical Internet behaviour. Two studies researched the effect of perceived benefit effectiveness on student behaviour, but reportedly it has no significant effect [S25], [S42].

Empathizing-systemizing is a group of factors such as empathy, cognitive empathy, affective empathy, emotional reactivity and social skills. Cognitive and affective empathy is a significant factor found by [S14] but not by [S8] and [S21]. The only study by [S8] reported that emotional reactivity and social skills significantly affect student behaviour, which has a mixed effect on these factors. Two CA studies agreed that impulsivity has a significant effect on student behaviour [S14], [S19], while one CS study reported a mixed effect [S6]. Attentional impulsiveness is significant, while motor impulsiveness is not.

Regarding sensation-seeking factors, one CA study [S9], and one UIA study [S61] showed mixed effects. A study in [S9] shows that boredom susceptibility, disinhibition, and experience seeking has significant effect while adventure seeking is not. While in [S61], only disinhibition has a significant effect while boredom susceptibility and total sensation seeking have no significant effect.

Another significant factor is loneliness, researched by Kokkinos et al. [S8] and [S13] in CA studies. Other studies, such as Thongmak [S23], reported that idolatry significantly

affects student engagement in unethical Internet behaviour, while Lin et al. [S25] refuted this claim. Attachment is a significant factor by [S22] but not significant in the study by [S8].

Few academic dishonesty studies have investigated novelty seeking, music quality, Constructivist Practices in the Learning Environment (CPL) and perceived cost. Lin et al. [S25] reported that novelty seeking and music quality positively impact the intention of unethical Internet behaviour. A study by Alt [S59] shows that students were less inclined toward academic cheating in constructivist pedagogical practices in the learning environment. Thongmak [S23] reported that perceived cost is not a significant factor in AD studies.

Cyberslacking studies by Rana et al. [S5] and Wu [S7] have investigated that escapism and attention significantly affect cyberslacking behaviour, respectively. On the other hand, Labar et al. [S1] reported factors that have mixed effects on cyberslacking behaviour. The time perspective of past negative and future orientation is significant factors in cyberslacking behaviour. While the time perspective of present fatalistic and present hedonistic are not significant.

On the subject of cyber abuse studies, Kokkinos et al. [S9] claimed that interpersonal sensitivity, psychopathic traits and anxiety determine unethical behaviour. Furthermore, Kowalski et al. [S11] argued that disabilities and self-esteem are also significant factors in the CA study. Additionally, body image dissatisfaction is found to be significant by Balta et al. [S17]. Nevertheless, only social support is found not to be significant by Howard et al. [S21]. Lastly, Kircaburun and Tosunta [S15] showed a mixed effect on biological clock factors: the evening type's chronotype and sleeping quality had a significant effect, while the morning type and the neither morning nor evening type were not significant.

E. RQ4 - Challenges and Research Opportunities for the Unethical Internet Behaviour Research within University Setting

This section aims to address Research Question 4, highlighting some challenges and problems regarding unethical behaviour in a university setting. The presented issues are categorised according to the type of unethical internet behaviour, namely academic dishonesty and cyber abuse, to facilitate the extraction of important challenges that emerged from the reviewed works. Note that this study does not find research area challenges presented by the studies under unethical Internet access and cyberslacking categories. The mapping of challenges in unethical behaviour among university students is summarised in Table IX.

Challenges in addressing academic dishonesty have been discussed in many pieces of literature. Under academic dishonesty, the most widely cited issues are organisational related, followed by awareness problems, cost of software and tools problems, and government enforcement problems. The inflated cost to acquire digital products [S23], [S28], [S30], such as software and digital academic materials, may drive student intention for piracy. Therefore, challenges in keeping these digital products affordable through an effective pricing

model [S23] need to be addressed to reduce digital piracy problems among university students. Additionally, universities must promote awareness of academic integrity among the students and lecturers. On the students' side, there is a lack of

student awareness of digital piracy to be regarded as ethically problematic, as cited in [S26]. Similarly, lecturers lack understanding of what constitutes academically dishonest behaviour [S33], [S35].

TABLE IX. CHALLENGES IN UNETHICAL BEHAVIOUR AMONG UNIVERSITY STUDENTS

Unethical Behaviour	Categories of Challenges	List of Challenges	Total Studies	Sources
Academic Dishonesty	Cost of digital products	1. High costs of digital products that drives piracy behaviour.	2	[S23], [S28]
		2. High costs to manage and update plagiarism checker/detection tools.	1	[S30]
	Awareness	1. Lack of student' s awareness on digital piracy to be regarded as an ethically problematic.	11	[S25], [S26], [S27], [S28], [S30], [S37], [S38], [S41], [S31], [S32], [S57]
		2. Lack of lecturer' s understanding of what constitutes an academically dishonest behaviour.	2	[S33], [S35]
	Organisational	1. Lack of campus Honor Code (acknowledgment by student) as policing initiatives.	3	[S33], [S38], [S54]
		2. Lack of affirmative and systematic punishment	7	[S33], [S31], [S57], [S48], [S52], [S53], [S55]
		3. Lack of anti-plagiarism policy and practice	5	[S33], [S31], [S45], [S56], [S55]
		4. Lack of formalized pedagogy and training that address academic integrity.	13	[S30], [S33], [S37], [S32], [S57], [S43], [S45], [S47], [S48], [S52], [S59], [S54], [S55]
		5. Organizational Culture/ Environmental factors	7	[S28], [S33], [S57], [S43], [S45], [S47], [S55]
	Laws and regulations	1. Lack of law enforcement	1	[S25]
Cyber Abuse	Awareness	1. Lack of awareness among lecturer/ counselor	4	[S8], [S9], [S14], [S19]
		2. Lack of privacy awareness among student	1	[S21]
	Organisational	1. Lack of student support and intervention	6	[S8], [S9], [S11], [S16], [S20], [S22]
		2. Lack of reporting avenue	1	[S8]
		3. Lack of collaboration	2	[S8], [S12]
		4. Lack of formalized pedagogy and awareness program that address cyberabuse.	7	[S8], [S12], [S13], [S14], [S16], [S20], [S17]

There is an abundance of discussion in the literature that cites organisational-related issues in academic dishonesty. The most cited issues are the lack of formalised pedagogy and training that address academic integrity. Authors in [S45] highlighted the importance of the higher learning institution effectively communicating their expectations about learning and integrity to the students. The lack of awareness among students and lecturers regarding academic integrity practice is often attributed to a lack of pedagogical training in teaching academic writing. Ongoing skill development among lecturers in the technical aspect [S45], time management and organisational skill [S57], and academic writing [S45] should be supported by the faculty. The lack of anti-plagiarism policy and practice [S55], [S56], campus "Honor Code" [S33], [S38], [S54], and ineffective punishment [S48], [S52], [S53] challenges must be tackled to reduce breaches of academic integrity. In addition, addressing organisational culture issues [S43], [S57] is especially important to shape and define university's academic integrity's practices. Finally, the lack of law enforcement at the national level [S25] may also contribute to university students' digital plagiarism behaviour.

IV. CONCLUSION

This study provides a systematic literature review of the literature on the current state of unethical Internet behaviour in higher education published in prominent academic journals

from 2010 to 2020. It defines each category based on the research on unethical Internet behaviours; the presentation of theories used in earlier research on unethical Internet behaviour; the discovery of demographic and risk factors linked to unethical Internet behaviour; and finally, the analysis of the issues and research possibilities posed by unethical Internet behaviour in higher education institutions. The findings of this survey from 64 research articles are presented in a taxonomy that can be utilised to comprehend the current state of unethical Internet behaviour in higher education. Regarding the present study's limitations, which occur in research based on a systematic review, there is a possibility of information loss as a result of the searching strategy used in this study. Although the authors strived to create comprehensive keyword and key string listings, it is plausible that some synonyms were overlooked. In constructing the SLR, insufficiency in synthesising keywords and key strings can influence search results. The fact that this analysis is restricted to English language journals and conference publications leaves room for the potential of other pertinent writings that were left out. This limitation may also cause zero evidence of articles discussing cybercrime or hacking, as discussed in RQ1.

Furthermore, this SLR exclude studies on unethical Internet behaviours that are closely related to any type of addiction or disorder that have been defined in The Diagnostic

and Statistical Manual of Mental Disorders, Fifth Edition, Text Revision (DSM-5-TR). The main reason for this exclusion is that the current authors do not have the expertise to analyse such studies. This exclusion may make it more likely that more pertinent articles will be overlooked.

ACKNOWLEDGMENT

This research was supported by the Universiti Teknologi Malaysia (UTM) Collaborative Research Grant National (CRG 47.2) under Grant R.K130000.7356.4B471 and Universiti Teknikal Malaysia Melaka (UTeM) Short Term Grant (PJP) with project number PJP/2019/FTMKCACT/CRG/S01705.

REFERENCES

- [1] J. J. Baum, "CyberEthics: The New Frontier, 2005," *TechTrends: Linking Research and Practice to Improve Learning*, vol. 49, no. 6, pp. 54–56, 2005. [Online]. Available: <https://eric.ed.gov/?id=EJ737703>
- [2] T. M. Jones, "Ethical Decision Making by Individuals in Organizations: An Issue-Contingent Model," *The Academy of Management Review*, vol. 16, no. 2, p. 366, Apr 1991.
- [3] J. O. Adesina, "The Christian Perspective on Worldly Practices in 21st Century Nigeria." *IGI Global*, 2021, pp. 171–184.
- [4] N. S. A. Karim, N. H. A. Zamzuri, and Y. M. Nor, "Exploring the relationship between Internet ethics in university students and the big five model of personality," *Computers & Education*, vol. 53, no. 1, pp. 86–93, Aug 2009.
- [5] Internet Activities Board, "RFC 1087: Ethics and the Internet," 1989. [Online]. Available: <https://www.rfc-editor.org/rfc/rfc1087> <https://tools.ietf.org/html/rfc1087>
- [6] T. M. Ming, M. A. Jabar, F. Sidi, and K. T. Wei, "A systematic literature review of computer ethics issues," *Journal of Theoretical and Applied Information Technology*, vol. 78, no. 3, pp. 360–372, 2015. [Online]. Available: <http://psasir.upm.edu.my/id/eprint/43616/>.
- [7] M. Mak-Van Der Vossen, W. Van Mook, S. Van Der Burgt, J. Kors, J. C. Ket, G. Croiset, and R. Kusurkar, "Descriptors for unprofessional behaviours of medical students: A systematic review and categorisation," *BMC Medical Education*, vol. 17, no. 1, Sep 2017. [Online]. Available: <https://pubmed.ncbi.nlm.nih.gov/28915870/>.
- [8] R. Soler-Costa, P. Lafarga-Ostáriz, M. Mauri-Medrano, and A. J. Moreno- Guerrero, "Netiquette: Ethic, education, and behavior on internet—a systematic literature review," *International Journal of Environmental Research and Public Health*, vol. 18, no. 3, pp. 1–15, Jan 2021. [Online]. Available: <https://www.mdpi.com/1660-4601/18/3/1212/>.
- [9] D. Gough, S. Oliver, and J. Thomas, "Introducing systematic reviews," in *An Introduction to Systematic Reviews*, 2012.
- [10] B. Kitchenham and S. Charters, "Guidelines for performing Systematic Literature reviews in Software Engineering Version 2.3," *Engineering*, vol. 45, no. 4ve, p. 1051, 2007.
- [11] J. P. T. Higgins, S. Green, and (editors), *Cochrane Handbook for Systematic Reviews of Interventions Version 5.1.0 [updated March 2011]*, 2011.
- [12] *Systematic Reviews in the Social Sciences: A Practical Guide*. Blackwell Publishing Ltd, Jan 2008. [Online]. Available: <https://onlinelibrary.wiley.com/doi/book/10.1002/9780470754887>.
- [13] B. Kitchenham, O. Pearl Brereton, D. Budgen, M. Turner, J. Bailey, and S. Linkman, "Systematic literature reviews in software engineering – A systematic literature review," pp. 7–15, Jan 2009.
- [14] N. Salleh, E. Mendes, and J. C. Grundy, "Empirical studies of pair programming for CS/SE teaching in higher education: A systematic literature review," pp. 509–525, 2011.
- [15] A. Taneja, V. Fiore, and B. Fischer, "Cyber-slacking in the classroom: Potential for digital distraction in the new age," *Computers and Education*, vol. 82, pp. 141–151, Mar 2015.
- [16] J. Wu, W. Mei, and J. C. Ugrin, "Student Cyberloafing in and out of the Classroom in China and the Relationship with Student Performance," *Cyberpsychology, Behavior, and Social Networking*, vol. 21, no. 3, pp. 199–204, Mar 2018. [Online]. Available: <https://pubmed.ncbi.nlm.nih.gov/29485288/>.
- [17] P. K. Smith, J. Mahdavi, M. Carvalho, S. Fisher, S. Russell, and N. Tippett, "Cyberbullying: Its nature and impact in secondary school pupils," *Journal of Child Psychology and Psychiatry and Allied Disciplines*, vol. 49, no. 4, pp. 376–385, Apr 2008.
- [18] C. S. Bhat, "Cyber bullying: Overview and strategies for school counsellors, guidance officers, and all school personnel," *Australian Journal of Guidance and Counselling*, vol. 18, no. 1, pp. 53–66, 2008.
- [19] C. Hardaker, "Trolling in asynchronous computer-mediated communication: From user discussions to academic definitions," *Journal of Politeness Research*, vol. 6, no. 2, pp. 215–242, Jul 2010. [Online]. Available: <https://www.degruyter.com/document/doi/10.1515/jplr.2010.011/html>.
- [20] D. L. McCabe and L. K. Trevino, "What We Know About Cheating In College Longitudinal Trends and Recent Developments," *Change: The Magazine of Higher Learning*, vol. 28, no. 1, pp. 28–33, Jan 1996. [Online]. Available: <https://www.tandfonline.com/doi/abs/10.1080/00091383.1996.10544253>
- [21] W. L. Kibler, "Academic Dishonesty: A Student Development Dilemma," *NASPA Journal*, vol. 30, no. 4, pp. 252–67, 1993. [Online]. Available: <https://eric.ed.gov/?id=EJ468340>.
- [22] G. Pavela, "Judicial review of academic decision-making after Horowitz," *School Law Journal*, no. 55(8), pp. 55–75, 1978.
- [23] C. J. Swearingen, "Originality, Authenticity, Imitation, and Plagiarism: Augustine's Chinese Cousins," in *Perspectives on Plagiarism and Intellectual Property in a Postmodern World*, L. Buranen and A. M. Roy, Eds. State University of New York Press, 1999.
- [24] Z. Ercegovac and J. V. Richardson, "Academic Dishonesty, Plagiarism Included, in the Digital Age: A Literature Review," *College & Research Libraries*, vol. 65, no. 4, pp. 301–318, Jul 2004.
- [25] P. Belleflamme and M. Peitz, "Digital Piracy: Theory," in *The Oxford Handbook of the Digital Economy*, M. Peitz and J. Waldfoegel, Eds. Oxford University Press, Aug 2012.
- [26] A. Cooper, E. Griffin-Shelley, D. L. Delmonico, and R. M. Mathy, "Online sexual problems: Assessment and predictive variables," *Sexual Addiction and Compulsivity*, vol. 8, no. 3-4, pp. 267–285, 2001. [Online]. Available: <https://www.tandfonline.com/doi/abs/10.1080/107201601753459964>
- [27] S. Gainsbury, R. Wood, A. Russell, N. Hing, and A. Blaszczynski, "A digital revolution: Comparison of demographic profiles, attitudes and gambling behavior of Internet and non-Internet gamblers," *Computers in Human Behavior*, vol. 28, no. 4, pp. 1388–1398, Jul 2012.
- [28] C. C. MacInnis and G. Hodson, "Surfing for Sexual Sin: Relations Between Religiousness and Viewing Sexual Content Online," *Sexual Addiction and Compulsivity*, vol. 23, no. 2-3, pp. 196–210, Apr 2016. [Online]. Available: <https://www.tandfonline.com/doi/abs/10.1080/10720162.2015.1130000>
- [29] M. Yani-de Soriano, U. Javed, and S. Yousafzai, "Can an Industry Be Socially Responsible If Its Products Harm Consumers? The Case of Online Gambling," *Journal of Business Ethics*, vol. 110, no. 4, pp. 481–497, Oct 2012. [Online]. Available: <https://link.springer.com/article/10.1007/s10551-012-1495-z>
- [30] I. Ajzen, "The theory of planned behavior," *Organizational Behavior and Human Decision Processes*, vol. 50, no. 2, pp. 179–211, Dec 1991.
- [31] M. Fishbein and I. Ajzen, *Belief, attitude, intention, and behavior : an introduction to theory and research*. Reading Mass.: Addison-Wesley Pub. Co., 1975.
- [32] I. Voulgaridou, C. M. Kokkinos, A. Markos, and K. Fanti, "Temporal stability of relational aggression profiles in adolescents," *Journal of School Psychology*, vol. 92, pp. 19–32, Jun 2022.
- [33] J. J. Allen, C. A. Anderson, and B. J. Bushman, "The General Aggression Model," *Current Opinion in Psychology*, vol. 19, pp. 75–80, Feb 2018.
- [34] J. G. Blumler and E. Katz, *The Uses of mass communications: current perspectives on gratifications research*. Sage Publications, 1974.

- [35] D. H. Doty, B. R. Wooldridge, M. Astakhova, M. H. Fagan, M. G. Marinina, M. P. Caldas, and D. Tuñal, "Passion as an excuse to procrastinate: A cross-cultural examination of the relationships between Obsessive Internet passion and procrastination," *Computers in Human Behavior*, vol. 102, pp. 103–111, Jan 2020.
- [36] R. Grieve, "Unpacking the characteristics of Snapchat users: A preliminary investigation and an agenda for future research," *Computers in Human Behavior*, vol. 74, pp. 130–138, Sep 2017.
- [37] M. Zuckerman, *Behavioral expressions and biosocial bases of sensation seeking*. New York: Cambridge University Press, 1994.
- [38] S. S. Lin and C. C. Tsai, "Sensation seeking and internet dependence of Taiwanese high school adolescents," *Computers in Human Behavior*, vol. 18, no. 4, pp. 411–426, Jul 2002.
- [39] R. Velezmore, K. Lacefield, and J.W. Roberti, "Perceived stress, sensation seeking, and college students' abuse of the Internet," *Computers in Human Behavior*, vol. 26, no. 6, pp. 1526–1530, Nov 2010.
- [40] A. Simha and J. B. Cullen, "Academic dishonesty and cheating: Proactive and reactive action implications for faculty and students," in *Handbook of Research on Teaching Ethics in Business and Management Education*. IGI Global, Jan 2011, pp. 473–492. [Online]. Available: <https://www.igi-global.com/chapter/academic-dishonesty-cheating/61824>.
- [41] R. Blasdell, M. Kilburn, L. Krieger-Sample, and R. Oakes, "Violence Against Healthcare Workers," in *Invisible Victims and the Pursuit of Justice*. IGI Global, Jan 2021, pp. 137–170. [Online]. Available: <https://www.igi-global.com/chapter/violence-againstthehealthcare-workers/281354>.
- [S11] R. M. Kowalski, C. A. Morgan, K. Drake-Lavelle, and B. Allison, "Cyberbullying among college students with disabilities," *Computers in Human Behavior*, vol. 57, pp. 416–427, Apr 2016.
- [S12] F. Caravaca Sánchez, M. Falcón Romero, J. Navarro-Zaragoza, A. Luna Ruiz-Cabello, O. Rodrigues Frantzisko, and A. Luna Maldonado, "Prevalence and patterns of traditional bullying victimization and cyber-teasing among college population in Spain," *BMC Public Health*, vol. 16, no. 1, Feb 2016.
- [S13] C. M. Kokkinos and I. Saripanidis, "A lifestyle exposure perspective of victimization through Facebook among university students. Do individual differences matter?" *Computers in Human Behavior*, vol. 74, pp. 235–245, Sep 2017. [Online]. Available: [/record/2017-25545-026](https://doi.org/10.1016/j.chb.2017.05.026)
- [S14] E. İldırım, C. Çalıcı, and B. Erdoğlan, "Psychological Correlates of Cyberbullying and Cyber-Victimization," *The International Journal of Human and Behavioral Science*, vol. 3, no. 2, pp. 7–21, Dec 2017. [Online]. Available: <https://dergipark.org.tr/en/pub/ijhbs/issue/33592/365829>
- [S15] K. Kırcaburun and B. Tosuntaş, "Cyberbullying perpetration among undergraduates: evidence of the roles of chronotype and sleep quality," *Biological Rhythm Research*, vol. 49, no. 2, pp. 247–265, Mar 2018. [Online]. Available: <https://www.tandfonline.com/doi/abs/10.1080/02723646.2017.1352918>
- [S16] R. Randa and B. E. Hayes, "Addressing Onset and Desistance of Bullying Behavior: Surveying Perpetrators," *Violence and Gender*, vol. 5, no. 2, pp. 93–102, Jun 2018. [Online]. Available: [/record/2018-27368-006](https://doi.org/10.1080/10887661.2018.14821492)
- [S17] S. Balta, E. Emirtekin, K. Kırcaburun, and M. D. Griffiths, "The Mediating Role of Depression in the Relationship Between Body Image Dissatisfaction and Cyberbullying Perpetration," *International Journal of Mental Health and Addiction*, vol. 18, no. 6, pp. 1482–1492, Dec 2020. [Online]. Available: <https://link.springer.com/article/10.1007/s11469-019-00151-9>
- [S18] L. Charmaraman, H. B. Chan, S. Chen, A. Richer, and B. Ramanudom, "Asian American social media use: From cyber dependence and cyber harassment to saving face," *Asian American Journal of Psychology*, vol. 9, no. 1, pp. 72–86, Mar 2018. [Online]. Available: [/record/2018-11225-006](https://doi.org/10.1080/10887661.2018.14821492)
- [S19] C. M. White, C. A. Cutello, M. Gummerum, and Y. Hanoch, "A Cross-Cultural Study of Risky Online Self-Presentation," *Cyberpsychology, Behavior, and Social Networking*, vol. 21, no. 1, pp. 25–31, Jan 2018. [Online]. Available: <https://www.liebertpub.com/doi/abs/10.1089/cyber.2016.0660>
- [S20] B. Villora, S. Yubero, and R. Navarro, "Cyber dating abuse and masculine gender norms in a sample of male adults," *Future Internet*, vol. 11, no. 4, p. 84, Mar 2019. [Online]. Available: <https://www.mdpi.com/1999-5903/11/4/84/html>
- [S21] K. Howard, K. H. Zolnieriek, K. Critz, S. Dailey, and N. Ceballos, "An examination of psychosocial factors associated with malicious online trolling behaviors," *Personality and Individual Differences*, vol. 149, pp. 309–314, Oct 2019.
- [S22] M. A. Mosley, M. Lancaster, M. L. Parker, and K. Campbell, "Adult attachment and online dating deception: a theory modernized," *Sexual and Relationship Therapy*, vol. 35, no. 2, pp. 227–243, Apr 2020. [Online]. Available: <https://www.tandfonline.com/doi/abs/10.1080/14681994.2020.1714577>
- [S23] M. Thongmak, "Antecedents and consequences of the intention of young consumers to pirate or buy copyright products," in *IEOM 2015 - 5th International Conference on Industrial Engineering and Operations Management*, Proceeding. Institute of Electrical and Electronics Engineers Inc., Apr 2015.
- [S24] I. K. Mohamud, A. Z. Saidin, and A. M. Zeki, "Attitude towards information property rights among students: The case of International Islamic University Malaysia," in *Proceedings - 2016 4th International Conference on User Science and Engineering, i-USER 2016*. Institute of Electrical and Electronics Engineers Inc., Feb 2017, pp. 145–148.
- [S25] X. Lin, D. Zeng, L. Cheng, and J. Wang, "Study on the influence factors of music piracy in China based on SEM model," in *2015 12th International Conference on Service Systems and Service Management, ICSSSM 2015*. Institute of Electrical and Electronics Engineers Inc., Jul 2015.

APPENDIX A

LIST OF INCLUDED STUDIES

- [S1] A. V. Labar and A. M. Teodorci, "The interplay between time perspective, internet use and smart phone in-class multitasking: A mediation analysis," *Computers in Human Behavior*, vol. 93, pp. 33–39, Apr 2019.
- [S2] D. H. Doty, B. R. Wooldridge, M. Astakhova, M. H. Fagan, M. G. Marinina, M. P. Caldas, and D. Tuñal, "Passion as an excuse to procrastinate: A cross-cultural examination of the relationships between Obsessive Internet passion and procrastination," *Computers in Human Behavior*, vol. 102, pp. 103–111, Jan 2020.
- [S3] Y. Akbulut, O. Dönmez, and Ö. Ö. Dursun, "Cyberloafing and social desirability bias among students and employees," *Computers in Human Behavior*, vol. 72, pp. 87–95, Jul 2017.
- [S4] R. Grieve, "Unpacking the characteristics of Snapchat users: A preliminary investigation and an agenda for future research," *Computers in Human Behavior*, vol. 74, pp. 130–138, Sep 2017.
- [S5] N. P. Rana, E. Slade, S. Kitching, and Y. K. Dwivedi, "The IT way of loafing in class: Extending the theory of planned behavior (TPB) to understand students' cyberslacking intentions," *Computers in Human Behavior*, vol. 101, pp. 114–123, Dec 2019.
- [S6] L. Chen, R. Nath, and Z. Tang, "Understanding the determinants of digital distraction: An automatic thinking behavior perspective," *Computers in Human Behavior*, vol. 104, p. 106195, Mar 2020.
- [S7] J. Y. Wu, "University students' Motivated Attention and use of regulation strategies on social media," *Computers and Education*, vol. 89, pp. 75–90, Nov 2015. [Online]. Available: [/record/2015-49853-007](https://doi.org/10.1016/j.compedu.2015.09.007)
- [S8] C. M. Kokkinos and N. Antoniadou, "Cyber-bullying and cybervictimization among undergraduate student teachers through the lens of the General Aggression Model," *Computers in Human Behavior*, vol. 98, pp. 59–68, Sep 2019.
- [S9] C. M. Kokkinos, N. Antoniadou, and A. Markos, "Cyber-bullying: An investigation of the psychological profile of university student participants," *Journal of Applied Developmental Psychology*, vol. 35, no. 3, pp. 204–214, May 2014.
- [S10] K. Kopecký, "Cyberbullying and Sexting between Children and Adolescents – Comparative Study," *Procedia - Social and Behavioral Sciences*, vol. 149, pp. 467–471, Sep 2014.

- [S26]Y. Akbulut and O. Dönmez, "Predictors of digital piracy among Turkish undergraduate students," *Telematics and Informatics*, vol. 35, no. 5, pp. 1324–1334, Aug 2018.
- [S27]G. Akçayır and M. Akçayır, "Internet Use for Educational Purposes: University Students' Attitudes and Opinions about Copyrights," *Eğitim Teknolojisi Kuram ve Uygulama*, vol. 7, no. 1, pp. 105–105, Jan 2017. [Online]. Available: <https://dergipark.org.tr/en/pub/etku/issue/27428/288490>
- [S28]Y. Akbulut, "Exploration of the antecedents of digital piracy through a structural equation model," *Computers and Education*, vol. 78, pp. 294–305, Sep 2014. [Online]. Available: <https://dl.acm.org/doi/abs/10.1016/j.compedu.2014.06.016>
- [S29]P. Alleyne, S. Soleyn, and T. Harris, "Predicting Accounting Students' Intentions to Engage in Software and Music Piracy," *Journal of Academic Ethics*, vol. 13, no. 4, pp. 291–309, Sep 2015. [Online]. Available: <https://link.springer.com/article/10.1007/s10805-015-9241-7>
- [S30]E. Oh, "Analysis of ethical issues in using information," *Information (Japan)*, vol. 19, no. 8B, pp. 3475–3481, 2016. [Online]. Available: <https://www.proquest.com/openview/7c21ef0f92b345925e22be2d7848f557/1?pqorigsite=gscholarcbl=936334>
- [S31]K. K. Molnar and M. G. Kletke, "Does the Type of Cheating Influence Undergraduate Students' Perceptions of Cheating?" *Journal of Academic Ethics*, vol. 10, no. 3, pp. 201–212, Sep 2012. [Online]. Available: <https://www.infona.pl/resource/bwmeta1.element.springer-0626ad9c-8692-3fad-869e-1d652b8ada90>
- [S32]K. K. Molnar, "Students' Perceptions of Academic Dishonesty: A Nine-Year Study from 2005 to 2013," *Journal of Academic Ethics*, vol. 13, no. 2, pp. 135–150, Jun 2015. [Online]. Available: <https://philpapers.org/rec/MOLSP0>
- [S33]A. Riskey, M. O'Dwyer, and A. Ledwith, "'Thou shalt not plagiarise': From self-reported views to recognition and avoidance of plagiarism," *Assessment and Evaluation in Higher Education*, vol. 38, no. 1, pp. 34–43, Feb 2013. [Online]. Available: <https://www.tandfonline.com/doi/abs/10.1080/02602938.2011.596926>
- [S34]S. K. Taradi, M. Taradi, T. Knežević, and Z. Dogaš, "Students come to medical schools prepared to cheat: A multi-campus investigation," *Journal of Medical Ethics*, vol. 36, no. 11, pp. 666–670, Nov 2010. [Online]. Available: <https://pubmed.ncbi.nlm.nih.gov/20797977/>
- [S35]M. A. Naaj, M. Nachouki, and K. Ammar, "Factors influencing plagiarism and collusion in programming assignments," in 2019 18th International Conference on Information Technology Based Higher Education and Training, ITHET 2019. Institute of Electrical and Electronics Engineers Inc., Sep 2019.
- [S36]J. C. Torres-Diaz, J. M. Duart, and M. Hinojosa-Becerra, "Plagiarism, internet and academic success at the university," *Journal of New Approaches in Educational Research*, vol. 7, no. 2, pp. 98–104, Jul 2018. [Online]. Available: <https://naerjournal.ua.es/article/view/v7n2-4/438>
- [S37]O. H. Cho and K. H. Hwang, "Academic ethical awareness among undergraduate nursing students," *Nursing Ethics*, pp. 833–844, May 2019. [Online]. Available: <https://journals.sagepub.com/doi/abs/10.1177/0969733017727155>
- [S38]A. M. Uzun and S. Kilis, "Investigating antecedents of plagiarism using extended theory of planned behavior," *Computers & Education*, vol. 144, p. 103700, Jan 2020. [Online]. Available: <https://doi.org/10.1016/j.compedu.2019.103700>
- [S39]N. Maloshonok and E. Shmeleva, "Factors Influencing Academic Dishonesty among Undergraduate Students at Russian Universities," *Journal of Academic Ethics*, vol. 17, no. 3, pp. 313–329, Sep 2019.
- [S40]S. C. Yang, F. K. Chiang, and C. L. Huang, "A comparative study of academic dishonesty among university students in Mainland China and Taiwan," *Asia Pacific Education Review*, vol. 18, no. 3, pp. 385–399, Sep 2017. [Online]. Available: <https://link.springer.com/article/10.1007/s12564-017-9497-2>
- [S41]D. C. Wilks, J. N. Cruz, and P. Sousa, "Personality Traits and Plagiarism: an Empirical Study with Portuguese Undergraduate Students," *Journal of Academic Ethics*, vol. 14, no. 3, pp. 231–241, Jun 2016. [Online]. Available: <https://link.springer.com/article/10.1007/s10805-016-9261-y>
- [S42]P. K. Chauhan, E. Wood, T. Plummer, and G. Forsyth, "Peer-Based Interventions on Academic Integrity: Assessing Immediate and Long Term Learning," *Journal of Academic Ethics*, vol. 16, no. 2, pp. 133–149, Jun 2018.
- [S43]C. Freire, "Academic Misconduct Among Portuguese Economics and Business Undergraduate Students- A Comparative Analysis with Other Major Students," *Journal of Academic Ethics*, vol. 12, no. 1, pp. 43–63, Mar 2014. [Online]. Available: <https://link.springer.com/article/10.1007/s10805-013-9199-2>
- [S44]S. Williams, M. Tanner, J. Beard, and J. Chacko, "Academic Misconduct among Business Students: A Comparison of the US and UAE," *Journal of Academic Ethics*, vol. 12, no. 1, pp. 65–73, Mar 2014. [Online]. Available: <https://philpapers.org/rec/WILAMA-4>
- [S45]E. Löfström, E. Huotari, and P. Kupila, "Conceptions of Plagiarism and Problems in Academic Writing in a Changing Landscape of External Regulation," *Journal of Academic Ethics*, vol. 15, no. 3, pp. 277–292, Sep 2017.
- [S46]B. Ives and L. Giukin, "Patterns and Predictors of Academic Dishonesty in Moldovan University Students," *Journal of Academic Ethics*, vol. 18, no. 1, pp. 71–88, Nov 2020. [Online]. Available: <https://link.springer.com/article/10.1007/s10805-019-09347-z>
- [S47]R. Comas-Forgas and J. Sureda-Negre, "Academic Plagiarism: Explanatory Factors from Students' Perspective," *Journal of Academic Ethics*, vol. 8, no. 3, pp. 217–232, Nov 2010. [Online]. Available: <https://link.springer.com/article/10.1007/s10805-010-9121-0>
- [S48]S. K. Camara, S. Eng-Ziskin, L. Wimberley, K. S. Dabbour, and C. M. Lee, "Predicting Students' Intention to Plagiarize: an Ethical Theoretical Framework," *Journal of Academic Ethics*, vol. 15, no. 1, pp. 43–58, Mar 2017.
- [S49]S. Ampuni, N. Kautsari, M. Maharani, S. Kuswardani, and S. B. S. Buwono, "Academic Dishonesty in Indonesian College Students: an Investigation from a Moral Psychology Perspective," *Journal of Academic Ethics*, vol. 18, no. 4, pp. 395–417, Dec 2020.
- [S50]N. Kashian, S. M. Cruz, J. woo Jang, and K. J. Silk, "Evaluation of an Instructional Activity to Reduce Plagiarism in the Communication Classroom," *Journal of Academic Ethics*, vol. 13, no. 3, pp. 239–258, Sep 2015.
- [S51]M. Baetz, L. Zivcakova, E. Wood, A. Nosko, D. De Pasquale, and K. Archer, "Encouraging Active Classroom Discussion of Academic Integrity and Misconduct in Higher Education Business Contexts," *Journal of Academic Ethics*, vol. 9, no. 3, pp. 217–234, Jun 2011. [Online]. Available: <https://link.springer.com/article/10.1007/s10805-011-9141-4>
- [S52]Y. Ma, D. L. McCabe, and R. Liu, "Students' Academic Cheating in Chinese Universities: Prevalence, Influencing Factors, and Proposed Action," *Journal of Academic Ethics*, vol. 11, no. 3, pp. 169–184, Sep 2013. [Online]. Available: <https://www.infona.pl/resource/bwmeta1.element.springerffid0ee4c-47e4-32c7-b612-6fe89fac931f>
- [S53]N. Dalal, "Responding to plagiarism using reflective means," *International Journal for Educational Integrity*, vol. 11, no. 1, pp. 1–12, Jun 2015. [Online]. Available: <https://edintegrity.biomedcentral.com/articles/10.1007/s40979-015-0002-6>
- [S54]G. J. Curtis, E. Cowcher, B. R. Greene, K. Rundle, M. Paull, and M. C. Davis, "Self-Control, Injunctive Norms, and Descriptive Norms Predict Engagement in Plagiarism in a Theory of Planned Behavior Model," *Journal of Academic Ethics*, vol. 16, no. 3, pp. 225–239, Jun 2018. [Online]. Available: <https://link.springer.com/article/10.1007/s10805-018-9309-2>
- [S55]A. M. Imran and M. S. Nordin, "Predicting the Underlying Factors of Academic Dishonesty among Undergraduates in Public Universities: A Path Analysis Approach," *Journal of Academic Ethics*, vol. 11, no. 2, pp. 103–120, Apr 2013. [Online]. Available: <https://link.springer.com/article/10.1007/s10805-013-9183-x>
- [S56]L. Harris, D. Harrison, D. McNally, and C. Ford, "Academic Integrity in an Online Culture: Do McCabe's Findings Hold True for Online, Adult Learners?" *Journal of Academic Ethics*, vol. 18, no. 4, pp. 419–434, Dec 2020.

- [S57]N. E. Day, D. Hudson, P. R. Dobies, and R. Waris, "Student or situation? Personality and classroom context as predictors of attitudes about business school cheating," *Social Psychology of Education*, vol. 14, no. 2, pp. 261–282, Dec 2011. [Online]. Available: <https://link.springer.com/article/10.1007/s11218-010-9145-8>
- [S58]M. Ludlum, L. Hongell, C. Tigerstedt, and J. Teeman, "Academic Ethics: a Pilot Study on the Attitudes of Finnish Students," *Journal of Academic Ethics*, vol. 15, no. 4, pp. 307–320, Dec 2017.
- [S59]D. Alt, "Assessing the Connection between Self-Efficacy for Learning and Justifying Academic Cheating in Higher Education Learning Environments," *Journal of Academic Ethics*, vol. 13, no. 1, pp. 77–90, Feb 2015. [Online]. Available: <https://link.springer.com/article/10.1007/s10805-015-9227-5>
- [S60]F. Tripodi, S. Eleuteri, M. Giuliani, R. Rossi, S. Livi, I. Petruccelli, F. Petruccelli, K. Daneback, and C. Simonelli, "Unusual online sexual interests in heterosexual Swedish and Italian university students," *Sexologies*, vol. 24, no. 4, pp. e84–e93, Oct 2015.
- [S61]R. Velezmoro, K. Lacefield, and J. W. Roberti, "Perceived stress, sensation seeking, and college students' abuse of the Internet," *Computers in Human Behavior*, vol. 26, no. 6, pp. 1526–1530, Nov 2010.
- [S62]K. R. Rasmussen, J. B. Grubbs, K. I. Pargament, and J. J. Exline, "Social Desirability Bias in Pornography-Related Self-Reports: The Role of Religion," *Journal of Sex Research*, vol. 55, no. 3, pp. 381–394, Mar 2018. [Online]. Available: <https://pubmed.ncbi.nlm.nih.gov/29220590/>
- [S63]M. Darvish Molla, M. Shirazi, and Z. Nikmanesh, "The Role of Difficulties in Emotion Regulation and Thought Control Strategies on Pornography Use," *Practice in Clinical Psychology*, vol. 6, no. 2, pp. 119–128, Mar 2018. [Online]. Available: <http://jpcp.uswr.ac.ir/article-1-469-en.html>
- [S64]C. Wong and H. C. Wu, "Gambling behavior of ethnic Chinese and Vietnamese college students in the United States," *International Gambling Studies*, vol. 20, no. 1, pp. 14–36, Jan 2020. [Online]. Available: <https://www.tandfonline.com/doi/abs/10.1080/14459795.2019.1646779>

Teachers' Attitudes Towards the Use of Augmented Reality Technology in Teaching Arabic in Primary School Malaysia

Lily Hanefarezan Asbulah¹, Mus'ab Sahrim², Nor Fatini Aqilah Mohd Soad³
Nur Afiqah Athirah Mohd Rushdi⁴, Muhammad Afiq Hilmi Mhd Deris⁵

Research Centre for Arabic Language and Islamic Civilization, Faculty of Islamic Studies^{1,3,4,5}
Universiti Kebangsaan Malaysia, 43600 Bangi, Malaysia^{1,3,4,5}
Intelligent Cyber- Physical Systems (iCPS), Faculty of Engineering and Built Environment²
Universiti Sains Islam Malaysia, 71800 Nilai, Malaysia²

Abstract—The era of Industrial Revolution 4.0 has brought the debate of teachers' willingness to use information technology in teaching Arabic. Thus, new technologies have emerged with a positive effect on teaching, such as augmented reality technology applied in the education system, especially in teaching. However, there is still limited research with regards to teaching in a foreign language. Therefore, the present study discusses the readiness of teachers from the aspect of knowledge and their attitude towards the use of augmented reality technology in the teaching of Arabic in Malaysia. The study was carried out using quantitative methodology with the use of survey questionnaire that is distributed to 36 Arabic language teachers as respondents. The usage of questionnaires as a research instrument forms the basis for data collection to identify respondents' level of readiness. Afterwards, data analysis was carried out using the Statistical Package for the Social Science version 26 (SPSS). The results of the study show that the level of readiness of the teachers in terms of their attitude towards the use of augmented reality technology in the teaching of Arabic in Malaysia is at a moderate level. Nevertheless, teachers' attitudes and knowledge are still found to be at a low level, especially for veteran teachers who have no experience in information technology to influence their enthusiasm towards the use of technology in their teaching. The implication of the current study is hoped to be useful and beneficial as a guide to stakeholders who are responsible for ensuring the process of teaching and learning Arabic which is based on augmented reality technology can be implemented in a meaningful way, thereby improving the performance of students in mastering the Arabic language.

Keywords—Attitude; teachers; augmented reality; Arabic language; primary school

I. INTRODUCTION

Contemporarily, augmented reality technology has its own advantages and importance in line with the development of various rapidly growing and sophisticated technologies. The augmented reality technology is an application that is often used in developed countries' educational system as a teaching and learning process of the 21st century. With the availability of technology and evidence of its use in most developed countries, it proves that the teaching and learning process in any school or institution in developing countries, especially Malaysia requires an urgent attention in order to keep up with

the current fast changing world order in technological advancement. This is because, the use of technology can apply a culture of innovation among teachers, in addition to encouraging teachers or lecturers to be more creative in teaching which allows teaching and learning to be more interactive that will eventually help raise the quality of education in Malaysia [1].

For a teacher, there are many steps or efforts that need to be known and mastered including knowledge, skills, approaches, attitudes, methods, and the best techniques to make the teaching process interesting. Preliminary research [2] has found that there are a number of learning processes that have the potential to affect the excellence and interest among students during teaching process. Information technology is one that has significant ability to increase student's understanding, thus requires the knowledge and preparation of teachers to make augmented reality technology an educational tool. Active learning is a process that involves the combination of the students and teachers' participation [3]. For example, the teacher provides freedom to the students so that they are able to learn in a more enjoyable atmosphere and this will create interest in the students as well as make the teaching process more effective and fun.

Based on this, the study [4] identified that teaching Arabic is not separated from the influence and role of information technology. This is because research carried out on modules and Arabic language learning techniques have shown the need for the usage of information and communication technology, particularly at primary level. In [5] and [6], there is a common view on the influence of information and communication technology that can attract students to learn Arabic. This statement is also supported by Muhammad Nazir's view in his study which emphasized the function of multimedia Arabic language games which are seen to be able to have a good impact in understanding the Quran [7].

As such, study [8] identified that teachers are the most accurate and responsible individual to implement this transformation in their teaching. This includes integrating technological advances in the teaching of Arabic. Quality teachers have a level of readiness that covers the aspects of knowledge, including attitudes towards the use of technology

and are able to link their knowledge with more effective teaching methods [9]. Next, study [10] found that 21st century education requires teachers to produce students who are creative, critical, and innovative. Therefore, teachers must first be prepared to master and equip themselves with the latest pedagogical knowledge in accordance with the development progress of the Industrial Revolution 4.0 (4IR) so that teaching can be carried out to meet the 21st century learning standards outlined by the Malaysian Ministry of Education while also being able to attract student's interest and motivation in learning, as teacher is the main factor or role model who will contribute to the success of progress in a modern education system on par with other developed countries.

Therefore, the use of augmented reality technology that combines virtual objects into the real world so that users can interact with virtual objects in real time becomes eminent to be applied in the education system of Malaysia, especially in the teaching of Arabic language [11]. The existence of user-friendly augmented reality applications can help teachers integrate virtual and improve the quality of their teaching and learning process to a more realistic experience [12,13]. A study related to the analysis of the use of applications based on augmented reality technology found that in order to make a better learning, student and teachers need a convenient atmosphere in addition to making learning and teaching more interesting to increase students' interest in learning [14]. As can be seen from the development of technology in the national education system, augmented reality technology is a new and sophisticated form of technology that has yet to be fully explored by researchers. Therefore, it is necessary for the current study to focus on the development of augmented reality technology usage in the national education system in line with the 21st century learning standards outlined by the Malaysian Ministry of Education.

II. PROBLEM STATEMENT

Malaysia is now a developing country with an economic condition that is very competitive among developing countries. This has led to the presence of 4IR which emphasizes the construction of virtual reality technology without much use of human energy, which has an impact on various aspects of life. In order to face the challenges of 4IR in the era of national education, especially in the teaching and learning of the Arabic language, it is necessary to get out of the comfort zone.

Arabic language subject requires teaching and learning methods that emphasize practice or practicality based on information technology in line with the development of 4IR. This is due to the fact that Arabic language teachers in primary or secondary schools face problem with students' attitude that are easily bored and then feel that learning Arabic language in the classroom setting is not interesting. This unfavorable condition gets more critical when the conventional way of learning produces many students who are weak in the command of the Arabic language which at later stage causes a decline in Arabic language achievement at the primary and secondary school levels in Malaysia. However, as at current, the national education policy strongly emphasizes the aspect of systematic learning which is expected to change

the direction of learning and teaching in Arabic. Therefore, it is opined that teaching methods that have a combination of practicality and usage of information technology can have a more positive effect in teaching Arabic language [2].

In recent time, teachers' problems in teaching Arabic language are often debated. Many past studies have discussed the issues faced by teachers in delivering Arabic lessons to school students in Malaysia. According to [15], there are various problems faced by Arabic language teachers in Malaysia during lessons' delivery. Among the problems often faced by the teachers are ability, pedagogy, motivation, teaching aids, environment, and lack of exposure related to information technology.

Other researchers found that the level of teachers' readiness for information technology platforms is still at a less than satisfactory level. This has been supported through the study [16] who found that 39 percent of teachers in Malaysian schools have a weak level of knowledge about the use of computers and smartphones in their teaching method and the integration of learning process by using such gadgets. As such, it is opined that more problems will arise if teachers are not interested in mastering knowledge and skills of information technology.

The result of the foregoing shows that there are many studies that have identified problems associated with Arabic language teachers, testing teaching models based on information technology, the methods of teachers who teach Arabic and connection with the use of information technology among others. Nevertheless, the booming era of 4IR also requires and encourages researchers to focus their studies on teaching and learning methods for Arabic subjects that are more practical, such as the use of augmented reality technology as there are still limited researchers in Malaysia compared to other countries. Therefore, the present study aims to identify teachers' readiness from the aspect of attitude towards the use of augmented reality technology in the teaching of Arabic language in Malaysia.

III. AUGMENTED REALITY TECHNOLOGY

A. Concept and Definition

The development of digital technology has led to the dire need of augmented reality technology. According to [17], the concept of augmented reality technology was first introduced by Ivan Sutherland in 1965. However, in the early 1990s, the term augmented reality began to be used by [18], who developed an augmented reality technology system as a tool to train employees at Boeing Corporation USA to understand and operate the wiring of the aircraft.

Thereafter, study [19] introduced the reality-virtuality as a continuum taxonomy that identifies the relationship between the real environment and virtual reality technology or virtual reality. Based on the taxonomy, the virtual environment refers to a virtual reality technology environment that features all objects virtually. Augmented reality technology is located near the real world where it is expanded with virtual objects produced by computers [17].

This technology has the ability to keep users connected to the real world while interacting with virtual and physical objects [20]. Previous researchers stated that augmented reality technology can be defined as a behavior between human and computers, acting as an additional virtual object to the real environment through display of video cameras or other computers gadget in real time [21].

Study [22] stated that augmented reality is a variation of virtual environments or virtual reality environments commonly known as virtual reality. This is a system or application that is able to create a view in the real world by inserting virtual objects produced by computers including objects in 3-dimensional form into the real environment in real time [22].

There are distinct differences between augmented reality technology and virtual reality technology. The later refers to a situation where the goal is to fully immerse the user in a synthetic environment while earlier is a situation where the goal is to complete the user's perception or view of the real world through the addition of virtual objects. The virtual environment completely replaces the real world, while with augmented reality technology users see the real environment, which is the merging of the virtual with the real [17].

Research [23] studied the concept of augmented reality technology and found that there are generally three types of augmented reality methods which are based on marker-based augmented reality technology; (i) Marker-Based Augmented Reality technology, (ii) Markerless Augmented Reality technology, and (iii) GPS Based Tracking. According to [24], marker-based augmented reality technology requires certain markers or labels to register the position of an object that will be displayed in the real environment. Whereas, in the Markerless Augmented Reality method, users do not need to use markers to show digital elements [25]. Also, markerless technology that is growing through android devices can make augmented reality technology more interesting and can be used anytime and anywhere [26].

Nevertheless, the concept of augmented reality technology that uses GPS Based Tracking is the most widely used method nowadays. It is often developed in various mobile phone applications, such as IOS and Android. This technique accesses the GPS and the compass in the mobile device usually takes data from the GPS while the compass shows the desired direction in real time [27].

B. Related Works

Globally, augmented reality technology is used to increase the level of proficiency in Arabic language, especially in Malaysia. A study related to 3D Arabic Augmented Reality (3D BAAR) and focused on the ability to improve Arabic language proficiency among students conducted by [4]. The objective of that research was to test Arabic reading and speaking skills among Year 4 students at a school in the Johor Bahru district through 3D BAAR application that uses augmented reality technology. The results of the study showed a positive effect of the application in improving Arabic reading and speaking skills among the Year 4 students. The majority of students show that they are very satisfied with the

use of applications based on augmented reality technology in their learning. The researchers stated that the students were very interested in the multimedia elements found in the application and displayed through the smartphone screen. Such application allows the students to learn to recognize and pronounce Arabic words with the correct pronunciation. The researchers concluded that the mastery of the Arabic language, such as the ability to speak and read the Arabic language can be improved with the availability of technology based on augmented reality.

Apart from that, the testing of effectiveness of augmented reality applications in basic Arabic language education had been carried out. According to [28], an application has been developed using a Mobile Augmented Reality (MAR) approach specifically for use in teaching basic Arabic language. This application uses the ADDIE (Analyze, Design, Develop, Implement, and Evaluate) technique in terms of design, implementation, testing phase and others. The advantage of the application involves two teaching modules developed by researchers, namely the teaching module and a set of practice questions. The results of the study found that the students showed so much interest in using it, as they stated that the application is interesting, very useful, and easy to use. They are also very satisfied due to the opportunity to learn Arabic words quickly.

Another study by [29] titled "The Application of Augmented Reality Technology in Arabic Language Learning Media: Durus Al-Lughah Volume 1" stated that an application related to augmented reality technology was developed for learning Arabic language at Universitas Darussalam Gontor (UNIDA). The application uses the Android platform and is developed in software, such as Blender 3D, Corel Draw, and Unity 3D. The application is useful for people who use mobile phone with a minimum specification of android version OS 4.0 Jellybean, screen size 4 inches, RAM 512 MB, free memory space (phone memory) with a minimum 200 MB and rear camera 13 MP. The results of the study showed that the application developed is very interesting for learning Durus Al Lughah because it has a very good design, operation, display method, and information structure. However, some aspects still need to be improved from time to time so that the appearance of the application can attract the attention of students to use it in learning Arabic language.

IV. METHODOLOGY

The present study purpose is to determine Malaysian teachers' perspectives and attitude to use augmented reality technology in teaching Arabic language. This study was carried out across 14 states comprising several schools in different locations of Malaysia. The respondents include 36 teachers who are chosen through basic random sampling procedure. The teachers selected to participate in this research are Arabic language teachers who teach at the participating schools.

Additionally, a survey questionnaire containing demographic information and teachers' preparedness was employed in this investigation across several stages. The first stage involves collecting respondents' information by determining variances in respondents' levels of preparation

depending on gender, age, education level, teaching experience, type of option, location of the school where they serve, and experience with various information technologies (IT). The second section is a construct designed to assess teachers' attitudes on the usage of augmented reality technology in the classroom in Malaysia.

Conversely, in order to measure the teachers' attitude in using augmented reality technology, four levels of the Likert scale were employed, namely, 4 (Strongly agree), 3 (Agree), 2 (Disagree), and 1 (Strongly Disagree). A high score will give an impression of a positive level of readiness towards a certain criterion and vice versa. Furthermore, in order to obtain data regarding the constructs found through literature and expert studies, questionnaires were delivered to respondents via Google Forms. Thereafter, the data were then examined using descriptive statistics like frequency, percentage, mean, and standard deviation in the Statistical Package for the Social Sciences (SPSS) version 26 software.

V. ANALYSIS FINDINGS

A. Respondent Demographics

The respondents involved in the present study are Arabic language teachers from schools throughout Malaysia, in which 36 people represent the total number of Arabic language teachers of the population sample. Table I below shows the demographics of the study, which is divided into 7 questions, such as personal background i.e., gender, age, education level, teaching experience, type of option, experience using information technology, and the name of the school where they serve.

Based on Table I, a total of 31 people (86.1%) are female teachers who teach Arabic subjects, and the remaining 5 people (13.9%) are male teachers. The total number of respondents for this study is 36 people. The findings show that from all the respondents of the study, the number of female Arabic teachers from the sample is more than the total number of their male Arabic teachers' counterparts.

In terms of the distribution of respondents age, it can be seen that the largest number of teachers are between the age of 30 to 39 years and between the age of 40 to 49 years, representing 11 people each with a percentage of 30.6%. This is followed by teachers who are within the age of 20 to 29 years, representing a total of 9 people (25.0%), while the least number of teachers are from the age group of 50 to 59 years, representing a total of 5 people (13.9%). This finding explains that the teachers who teach Arabic language subjects in Malaysia are young, in which the majority are between the age of 20 and 39 years with a percentage of 55.6%. This further explains that the strength possessed by Arabic language teachers is from the aspect of human resources, in which the majority of them are adults. This age group teachers are also easier to accept and make changes to their teaching practices. This group is highly motivated and exposed to many of the latest elements in education, especially creative and innovative teaching that are capable of bringing a positive reform to the country's education.

Meanwhile, the demographics of the study sample also show that the majority of teachers who teach Arabic language

have their highest education at the bachelor's degree level, representing a total of 17 people (47.2%). This is followed by the Malaysian Higher Certificate of Religion (STAM) and Malaysian Higher Certificate of Education (STPM), which are 9 people (25%). The total numbers of the Malaysian Certificate of Education (SPM) are as many as 7 people (19.4%). Meanwhile, at the master's degree and Diploma level, there is one person (2.8%) each who has the qualification. Lastly, there seem to be no teachers who teach Arabic language subject with a Doctor of Philosophy (PhD) degree. This confirms the findings of previous studies that stated the number of Arabic language teachers who hold master's and PhD degree are not much in schools compared to teachers who hold bachelor's degree or diploma.

Regarding the aspect of teachers' teaching experience, it was found that respondents who have taught between 5 and 15 years surpass the others with a total of 7 people (47.2%) followed by more than 15 years with a total of 11 people (30.6%). Only 8 people (22.2%) have less than 5 years of teaching experience. This finding explains that the majority of teachers who teach Arabic language in Malaysia have more than 5 years of teaching experience with a percentage of 77.8%. This can be seen that the Arabic language teachers in this study consist of experienced teachers who are able to implement the teaching and learning process effectively.

On the other hand, the majority of respondents are teachers of Al-Quran and Fardhu Ain (KAFA) which represent the type of teacher option that teaches Arabic which are 24 people (66.7%), followed by Islamic Education Teachers (GPI) which are 8 people (22.2%), while only 4 people (11.1%) are Arabic Language Teachers (GBA). This finding shows that there is no religious teacher who teaches Arabic language.

Referring to the aspect of experience using information technology, the majority of respondents have less than 5 years of experience deploying information technology, with a total of 22 people (61.1%) while 14 people (38.9%) have more than 5 years of experience employing information technology. In general, it was found that not all Arabic language teachers are literate in information technology, especially the group of teachers who are categorized as veteran teachers. They struggle to surf the internet and apply various systems and applications that are beginning to be used in the country's education system.

Finally, Table I shows that the majority of respondents serve at Sekolah Kebangsaan Penambang, totalling 13 people (36.1%), followed by respondents from Sekolah Kebangsaan Kedai Buloh 2, which is 5 people (13.9%). Respondents from Sekolah Kebangsaan Che Latif and Sekolah Kebangsaan Pulau Kundor have the same number of 4 people each (11.1%), followed by Sekolah Kebangsaan Pasir Gudang 3 which are 2 people (5.6%). Also, only one respondent (2.8%) is from Sekolah Kebangsaan Bukit Kuchai, including Sekolah Kebangsaan Bandar Seri Alam, Sekolah Kebangsaan Setiawangsa, Sekolah Kebangsaan Convent Jalan Peel, Sekolah Kebangsaan Seafield 3, Sekolah Kebangsaan Taman Desa 2, Sekolah Kebangsaan Salak South and Sekolah Kebangsaan Chicha Menyabong, all represent the least participating respondents.

TABLE I. DEMOGRAPHIC OF RESPONDENTS

Variable	Item	Frequency	Percentage
Gender	Male	5	13.9
	Female	31	86.1
Age	20 to 29 years old	9	25.0
	30 to 39 years old	11	30.6
	40 to 49 years old	11	30.6
	50 to 59 years old	5	13.9
Educational status	SMU/SMA	1	2.8
	SPM	7	19.4
	STAM/STPM	9	25
	Diploma	1	2.8
	Bachelor	17	47.2
	Master	1	2.8
	PHD	0	0
Teaching experience	Less 5 years	8	22.2
	5 to 15 years	17	47.2
	Over 15 years	11	30.6
Option type	Arabic Teacher	4	11.1
	Islamic Education Teacher	8	22.2
	KAFA Teacher	24	66.7
	Dini Teacher	0	0
Experience using Information Technology (IT)	Less 5 years	22	61.1
	Over 5 years	14	38.9
Name of school where you serve	Sk Penambang	13	36.1
	Sk Che Latiff	4	11.1
	Sk Bukit Kuchai	1	2.8
	Sk Kedai Buloh 2	5	13.9
	Sk Pasir Gudang 3	2	5.6
	Sk Bandar Seri Alam	1	2.8
	Sk Setiawangsa	1	2.8
	Sk Pulau Kundor	4	11.1
	Sk Convent Jalan Peel	1	2.8
	Sk Seafield 3	1	2.8
	Sk Taman Desa 2	1	2.8
	Sk Salak South	1	2.8
	Sk Chicha Menyabong	1	2.8

B. Teachers' Attitudes Towards the use of Augmented Reality Technology in Teaching Arabic in Malaysia

This study has used descriptive statistical analysis referred to as descriptive statistics to describe the characteristics of a variable by using indicators of mean, standard deviation, frequency, percentage, and then draw conclusions based on numerical data [30]. For the data obtained from the questionnaire, the present study has used the interpretation value of the mean score level outlined by [31] which is 1.0 to

2.4 indicating a low-level interpretation, while the mean score between 2.5 and 3.4 shows medium level and 3.5 to 5.0 is at a high level.

Table II shows the distribution of frequency, percentage, mean, standard deviation, and mean interpretation based on descending order to identify the level of readiness from the aspect of teachers' attitude towards the use of augmented reality technology in teaching Arabic language subject in Malaysia. The overall mean of all items for teachers' attitudes towards the use of augmented reality technology in teaching

Arabic language subject in Malaysia is 3.36 which is at a simple level of interpretation. This explains that the majority of teachers who teach Arabic language at the school level are at a moderate level in terms of the teacher's attitude towards the use of this technology and they are able to use it effectively in the teaching as well as learning process of Arabic language. This finding shows that all 8 statements presented are at a moderate level of interpretation. The mean range is between 3.28 and 3.44.

Additionally, Table II explains that the two highest mean scores have the same value for the level of readiness from the aspect of teachers' attitudes towards the use of augmented reality technology in the teaching of Arabic in Malaysia, which is a statement that refers to augmented reality technology capable of increasing students' interest in learning the language Arabic (Mean = 3.44, SP = 0.65) and the statement referring to augmented reality technology is able to attract students' attention to focus on a topic being taught (Mean = 3.44, SP = 0.56).

The findings of the study show that 19 teachers (52.8%) strongly agree, 14 teachers (38.9%) agree, and 3 teachers (8%) choose to disagree that augmented reality technology can increase students' interest in learning Arabic language. In addition, a total of 17 teachers (47.2%) strongly agree, 18 teachers (50%) agree and only one teacher (2.8%) chooses to disagree that augmented reality technology is able to attract students' attention to focus on a topic being taught.

Meanwhile, two items in the questions were used to respond to the current study, namely the statement referring to augmented reality technology makes it easier for teachers to deliver teaching information faster and augmented reality technology is very effective in helping to improve the quality of teaching and learning Arabic subjects in Malaysia,

recording the mean score and value of the same standard deviation (Mean = 3.44, SP = 0.56). The two statements also recorded the same frequency and percentage, in which a total of 16 teachers (44.4%) choose strongly agree, 18 teachers (50%) agree and only 2 teachers (5.6%) choose to disagree.

Referring to the statement of augmented reality technology, the percentage of students' proficiency in Arabic language recorded the third lowest mean score (Mean = 3.36, SP = 0.54), showing an increased number with a frequency of agree and strongly agree of 35 people (97.2%), disagree and strongly 1 person disagreed (2.8%). This is followed by the statement that augmented reality technology is a new teaching material around the world of education (Mean = 3.31, SP = 0.62) with a frequency of agree and strongly agree of 33 people (91.7%), disagree and strongly disagree of 3 people (8.3%).

Meanwhile, Table II shows that 2 items out of 8 items related to the level of readiness from the aspect of teachers' attitudes towards the use of augmented reality technology in the teaching of Arabic language in Malaysia, both recorded the same mean score and are the lowest among the statements presented. The statement that refers to augmented reality technology is very suitable to be applied in the teaching of Arabic language in Malaysia (Mean = 3.28, SP = 0.57). A total of 12 teachers (33.3%) chooses strongly agree, 22 teachers (61.1%) agree, and 2 teachers (5.6%) choose to disagree. Meanwhile, for the statement that refers to augmented reality technology is a sophisticated teaching material to be used in Malaysia when teaching Arabic (Min = 3.28, SP = 0.66), the results show a total of 13 teachers (36.1%) strongly agree, 21 teachers (58.3%) agree, and 1 teacher (2.8%) chooses to disagree. However, there is also one teacher (2.8%) who chooses to strongly disagree with the statement.

TABLE II. FREQUENCY, PERCENTAGE, MEAN, STANDARD DEVIATION AND INTERPRETATION OF TEACHERS' ATTITUDES TOWARDS THE USE OF AUGMENTED REALITY TECHNOLOGY IN TEACHING ARABIC LANGUAGE IN MALAYSIA

Statement	Frequency				Mean	SD	Interpretation
	SD	D	A	SA			
Augmented reality technology is able to increase student interest to learn the Arabic language.	0 0%	3 8.3%	14 38.9%	19 52.8%	3.44	0.65	Moderate
Augmented reality technology is capable to draw students' attention to focus on a topic that taught.	0 0%	1 2.8%	18 50%	17 47.2%	3.44	0.56	Moderate
Augmented reality technology make it easier for teachers to deliver teaching information faster.	0 0%	2 5.6%	18 50%	16 44.4%	3.39	0.60	Moderate
Augmented reality technology is very effective to help improve the quality of P&P in Arabic subject in Malaysia	0 0%	2 5.6%	18 50%	16 44.4%	3.39	0.60	Moderate
Augmented reality technology is able to increase the percentage of students' proficiency in Arabic.	0 0%	1 2.8%	21 58.3%	14 38.9%	3.36	0.54	Moderate
Augmented reality technology is a new teaching material in the world of education.	0 0%	3 8.3%	19 52.8%	14 38.9%	3.31	0.62	Moderate
Augmented reality technology is very suitable to be applied in teaching Arabic in Malaysia.	0 0%	2 5.6%	22 61.1%	12 33.3%	3.28	0.57	Moderate
Augmented reality technology is a sophisticated teaching material to use in teaching Arabic language in Malaysia.	1 2.8%	1 2.8%	21 58.3%	13 36.1%	3.28	0.66	Moderate
Overall mean					3.36		Moderate

Overall, the findings explain that teachers who teach Arabic language in Malaysia have a moderate level of attitude towards the use of augmented reality technology. On average, the respondents are positive and open to accepting the use of augmented reality technology in the teaching of Arabic language at school and believe that augmented reality technology is able to enhance the teaching and learning process of Arabic language by combining elements of technology and knowledge. This indirectly means that they will master the creativity of teaching, especially in the aspects of motivation and environment when implementing the teaching process using augmented reality technology.

VI. DISCUSSION

A. *Augmented Reality Technology is a New and Advanced Teaching Material in the World of Education*

According to [32], augmented reality technology is a technology that has been discovered for the past 40 years, which has sophisticated and interesting attributes or characteristics that are able to accommodate deficiencies that are not found in existing teaching media and traditional teaching systems. which has long been practiced in Malaysia. This technology is capable of becoming a new teaching material to be used in the world of education in Malaysia. Augmented reality technology has new and advanced features, such as allowing users to interact in real time with 3D virtual objects as if holding real objects [11,33,34]. It can be said that augmented reality technology is an advanced technology that brings virtual imagination to the real world by mixing the virtual environment with the physical environment instantly [35].

According to the study [36], augmented reality technology can encourage students, especially children to use different and creative new learning approaches. Students can learn independently by using their own style and able to train themselves to act efficiently as well as learn personally. This clearly shows that augmented reality technology is capable of creating new teaching and learning methods that are more interesting, dynamic, interactive, contextual, easy to understand, and be interpreted due to the two-way transfer of information. Therefore, it is not surprising that the finding of this study shows a positive effect on teachers' attitudes towards the use of augmented reality technology in the teaching of Arabic language in Malaysia.

B. *Augmented Reality Technology is Able to Increase Students' Interest in Learning Arabic*

The findings of the study show that the majority of teachers who teach Arabic language have a good opinion that augmented reality technology is effective and able to stimulate interest in learning Arabic language. The effect of using augmented reality technology applications in language learning has also been proven by [37] who used an augmented reality application named Letters Alive! It not only increases the percentage of students' reading proficiency but also in the ability to form sentences correctly. This is in line with the opinion of [38], who stated that the visual effect and user interaction in real time on an object can improve the memory and cognitive process of students in visualization.

Similarly, [39] found that augmented reality technology has advantages, such as being able to attract the attention and stimulate the interest of students, especially children in the learning process because it facilitates the understanding of learning content, maintains long-term memory, and user-friendly. It clearly shows that augmented reality technology provides benefits in the learning of students at the primary level.

Teaching aids used by teachers are referred to as platforms to ease the teachers in providing students clear understanding during teaching. This finding is supported by the study of [40], where the use of teaching aids, such as augmented reality technology has a positive impact in improving students' understanding of a subject.

According to [41], students will increase their interest in learning because of the advantages of augmented reality technology that combines the virtual world with the potential to increase students' imagination in relation to the real world [42]. As such, it is able to mobilize students' creativity in learning, especially in Arabic language. This then allows students' concentration to increase along with their interest in the technology [34].

C. *Augmented Reality Technology is Able to Attract Students' Attention to Focus on a Topic being Taught*

Findings show that the augmented reality technology application is not only able to attract the attention of teachers involved in the study but also prove that the augmented reality technology is able to attract the attention of students to focus on a topic being taught and the students' curiosity in the lessons being studied [11,29]. This statement is supported by the study [33] who found that students, especially children are very interested in using mobile phones in order to learn something new which is often used by them in their daily lives. Therefore, study [33] chose new software which is the use of augmented reality technology in learning words in English where preschool children can use mobile phones in learning as independent learning in line with PAK21.

Study [43] also supported that technology which applies interesting teaching aids and has gamification elements in teaching can increase students' focus and interest. Through this method, the teacher will be able to increase the interest and curiosity of the students towards his/her teaching. This is because, students who get motivation from the teacher will usually be more interested which in turn helps the process of achieving learning objectives.

D. *Augmented Reality Technology makes it Easier for Teachers to Deliver Teaching Information Faster*

The findings of the present study also show that teachers have a positive attitude towards augmented reality technology because not only it helps teachers in carrying out interesting teaching process, but also delivers the teaching information faster [11]. According to [44] augmented reality technology can help teachers to bring learning experiences outside the classroom to students that are previously impossible. Therefore, with augmented reality technology, teaching information can be done quickly. For example, teachers are able to bring the atmosphere of a visit to the zoo without

having to visit the zoo as the augmented reality technology will take the student to a virtual world with the atmosphere of being in the zoo to see animals. Hence, it is proven that using augmented reality technology in learning would help the students to understand something quickly [45,11]. Besides that, the development tools for AR environments have seen significant change over the past ten years, and currently there are many options. However, it is challenging to create an AR educational environment and to develop content in a simple and efficient approach because all these solutions still demand a high level of technical knowledge or a lot of time to generate [50, 51].

E. Augmented Reality Technology is Very Effective in Helping to Improve the Quality of Arabic Subject Teaching and Learning in Malaysia

Findings show that the teachers involved in the present study agree that the use of augmented reality technology is very effective and able to increase the quality of teaching Arabic language. This finding is supported by [24] who stated that most students consider augmented reality technology as an effective learning tool, which can help them understand the concepts learned and ultimately improve the quality of education as well as students' performance. Study [21] stated similar scenario with study [24], arguing that students who use augmented reality technology as a learning aid have shown higher academic performance compared to the use of traditional methods. Furthermore, this believe is supported by the study [25], which described augmented reality technology as interesting and effective to education. It can encourage students to explore learning content from different perspectives. Other than that, study [24] believed that the use of augmented reality technology in the world of education is able to improve the quality of teaching and improve the quality of student learning activities, especially teaching and learning of Arabic language subjects in Malaysia.

Based on a study by [41], the use of augmented reality technology as a teaching method is the latest trend capable of changing the learning landscape from traditional methods to the use of the latest elements, such as animation, simulation, and video. If the use of augmented reality technology is expanded, it will create a fresher, more interactive, and effective teaching as well as learning system. Indirectly, its use can improve the quality of national education [46].

F. Augmented Reality Technology is Able to Increase the Percentage of Students' Proficiency in Arabic

The majority of Arabic language teachers in the present study describe a positive attitude towards the use of augmented reality technology because they believe the technology can improve students' Arabic language. This believe is supported by the study [34] which stated that augmented reality technology can also be used to help visualize abstract concepts to understand the structure of a teaching model that can improve students' understanding of lessons. Also, study [47] stated that augmented reality technology creates an immersive experience by expanding the virtual environment so that students can visualize the content of learning, gain a better understanding, and view on a specific learning topic or subject.

According to [48], the use of technology-based teaching aids will produce students who behave positively, such as studying diligently and making efforts by showing a deep interest in mastering Arabic language subjects. This will be a platform for students' excellent mastery of the subject. A positive attitude will produce encouraging results for their performance.

G. Augmented Reality Technology is Very Suitable to be Applied in Teaching Arabic Language in Malaysia

Findings show that the teachers involved in the present study agree that augmented reality technology is very suitable to be applied in Malaysian education. This is supported by study [33], who stated that augmented reality technology is suitable for preschool children in learning English words. Having the technology according to that study would enable preschool children to learn new words in English through practicing self-learning without the guidance of a preschool teacher.

Similarly, study [49] stated that augmented reality technology is suitable for practice in coloring activities. This is because augmented reality technology can increase the level of creative thinking among preschool children. Preschool teachers in Malaysia can refer to the teaching and learning plan developed to plan coloring activities with the help of augmented reality technology. Augmented reality technology application software developers can also build applications with special features to develop creative thinking among preschoolers.

VII. CONCLUSION

Overall, the present study shows that Arabic teachers' level of readiness from the aspect of attitude towards the use of augmented reality technology in teaching Arabic language in primary school in Malaysia is at a moderate level. However, if there is a low and negative attitude as well as knowledge of teachers, especially for veteran teachers who have no experience in information technology. This will affect their enthusiasm and willingness to practice the method of using augmented reality technology in teaching in the era of the technology, thereby undermining the effectiveness of the technology in the Malaysian education system.

Therefore, the drafters of the Arabic language curriculum at primary and secondary school level under the supervision of the Malaysian Ministry of Education are expected to be able to use the findings of the current study as a guide in designing the use of augmented reality technology in the teaching of Arabic language curriculum. This is because the implementation of augmented reality technology usage in education system requires readiness from all involved parties while considering various aspects. Apart from that, it also requires commitment from the authority in providing training, seminars, and workshops to ensure that the vision and mission of national education is achieved. Besides that, the present study would be helpful to increase the level of teachers' readiness from the aspect of knowledge and attitude to implement teaching using techniques as well as methods that are effective with the use of technology based in regard to 4IR.

Thus, this study's findings are very significant because they can be used to determine the level of readiness in terms of teacher knowledge of the use of augmented reality technology in teaching Arabic in Malaysia. The Ministry of Education Malaysia, through its division School management, can use this study as a starting point to design and plan programs, trainings, seminars, and other activities for teachers. However, this study has some limitations, one of which is that it only included responses from Arabic language teachers employed by Malaysia's Ministry of Education. Therefore, it is suggested that future research be expanded to include private schools in Malaysia or compared to other countries.

REFERENCES

- [1] Ali, D.F., Yahya, S.S. & Omar, M., Penggunaan Aplikasi Augmented Reality dalam Topik Litar Asas Elektronik The Use of Augmented Reality Application in Basic Electronic Circuit Topic Augmented Reality dalam Pendidikan 3(2), 2020, p. 1–7.
- [2] Muna Hamzan, Penggunaan Teknologi Ict Dalam Pengajaran Bahasa Arab Di Sekolah Menengah Kebangsaan Agama, Tesis Sarjana, 2016, Universiti Teknologi Malaysia: 1–30.
- [3] Ghazali Yusri, Nik Mohd Rahimi, & Parilah M. Shah, Sikap Pelajar Terhadap Pembelajaran Kemahiran Lisan Bahasa Arab di Universiti Teknologi MARA (UiTM), GEMA Online Journal of Language Studies, 10(3), 2010, p. 15–33.
- [4] Kamarul, M., Kamaruddin, A., Zakiah Bardan, S., Fazatul, N., Baharuddin, A., Husna, D.N., Wahid, A., Sk, P., Rinting, M., Kemas, T., Tebrau, P. & Puteri, P.I, 3D Bahasa Arab Augmented Reality (3D Baar) Membantu Meningkatkan Penguasaan Bahasa Arab Pelajar, Innovative Teaching and Learning Journal 2(2), 2019, p. 17–31.
- [5] Aqsha, M., & Shahrudin, H. N., Modul Pengajaran dan Pembelajaran Bahasa Al-Quran Bermultimedia, Penerbit Universiti Kebangsaan Malaysia, 2016.
- [6] Zulkifli, M. S., Jamali, H. N., Iksan, H. H., & Ismail, H. A., Modul Pengajaran dan Pembelajaran Interaktif Bahasa Arab di Pusat Bahasa Arab Selangor (Pbas) Interactive Teaching and Learning Modules in Selangor Arabic Center (Pba), 5, 2018, p. 128–137.
- [7] Mohammed Khalid, M. N., Hamid, H., Khalid, M. F., Abu Hassan, M. A., & Daoh, M., Kefahaman Surah Al- Fatihah Melalui Permainan Bahasa Bermultimedia, Journal Of Education And Social Sciences, 7(1), 2017, p. 316–325.
- [8] Hilmi, A., Mohd Zakaria, Z. & Nur Fuad, A.F., Tahap Pengetahuan Guru Bahasa Arab Dalam Melaksanakan Kelas Berbalik [the Level of Knowledge Arabic Language Teachers in Implementing Flipped Classroom], Muallim Journal of Social Science and Humanities 4(3), 2020, p. 50–67.
- [9] Chong, S. & Cheah, H.M., A values, skills and knowledge framework for initial teacher preparation programmes. Australian Journal of Teacher Education 34(3), 2009, p. 1–17.
- [10] Razak, R.A., Kaur, D., Halili, S.H. & Ramlan, Z., Flipped ESL teacher professional development: Embracing change to remain relevant, Teaching English with Technology 16(3), 2016, p. 85–102.
- [11] Norabeerah, S., Halimah Badioze, Z. & Azlina, A., Pengajaran masa depan menggunakan teknologi Augmented Reality dalam pendidikan Bahasa Melayu: Tahap kesedaran guru, Jurnal Pendidikan Bahasa Melayu 2, 2012, p. 1–10.
- [12] Anealka Aziz Hussin, Education 4.0 Made Simple: Ideas For Teaching. International Journal of Education & Literacy Studies 6(3), 2018, p. 92–98.
- [13] Sarah Alia Mohamed Faisal & Nor Hafizah Adnan, Tahap Kesediaan dan Penerimaan Guru dalam Mempraktikkan Penggunaan Teknologi Digital IR 4.0 Sebagai Bahan Bantu Mengajar dalam Pendidikan Rendah, International Journal of Advanced Research in Islamic Studies and Education, 1(3), 2021, p. 66–80.
- [14] Fuaidah, T., Peningkatan Minat Belajar Siswa melalui Media Augmented Reality pada Mata Pelajaran IPA di Kela VI MI Nurus Syafi'i Gedangan Sidoarjo, Skripsi, Universitas Islam Sunan Ampel Surabaya, 2016.
- [15] Abdul Razif Zaini, Muhammad Redzaudin Ghazali, Mohd Rufian Ismail, Noorshamsinar Zakaria, Hasmadi Hamdan & Mohamad Rushdan Hj. Azizan, Permasalahan dalam Pengajaran Bahasa Arab di Malaysia, Persidangan Antarabangsa Sains Sosial & Kemanusiaan (PASAK), April 2017, p. 1–8.
- [16] Mohd Amin Mohd Noh, Mohd Faez Ilias, Kalthom Husain, Muhammad Syakir Sulaiman & Murihah Abdullah, Inisiatif dan Usaha Guru dalam Meningkatkan Pengetahuan Semasa Penggunaan Bahan Bantu Mengajar, Journal of Social Sciences and Humanities, 2016, p. 133–144.
- [17] Roslinda Ramli, Fitri Nurul' Ain Nordin & Nor Effendy Ahmad Sokri, Teknologi Realiti Luasan: Satu Kajian Lepas, e-Jurnal Penyelidikan dan Inovasi 5(1), 2018, p. 17–27.
- [18] Caudell, T. P. & Mizell, D. W., Augmented Reality: An Application of Heads-Up Display Technology to Manual Manufacturing Processes, Proceedings of Hawaii International Conference on System Sciences, 1992, p. 659–669.
- [19] Milgram P, Takemura, H & Kishino F, Augmented Reality: A Class of Displays On The Reality- Virtual Continuum. Proceeding the SPIE, 1994, p. 282–292.
- [20] Tomi, A. B., & Rambli, D. R. A., An interactive mobile augmented reality magical play- book: Learning number with the thirsty crow. Procedia Computer Science, 25, 2013, p. 123–130.
- [21] Danakorn Nincarean A/L Eh Phon, Mohamad Bilal Ali, & Noor Dayana Abd Halim, Potensi Teknologi Augmented Reality dalam Pembelajaran Sains: Satu Tinjauan Terhadap Penyelidikan Lepas. Second International Seminar on Quality and Affordable Education, 2013, p. 326–336. <http://educ.utm.my/wp-content/uploads/2013/11/461.pdf>konsep.
- [22] Azuma, R.T., A Survey of Augmented Reality, Foundations and Trends in Human-Computer Interactions, 8(2-3), 1997, p. 73–272. <https://doi.org/10.1561/11000000049>
- [23] Pench, Smartphone, Smart Object and Augmented Reality, Oneonta, USA, 2011, p. 136–145.
- [24] Khalid, F. & Wong, S. L., An Emic Perspective on Students' Learning Experiences Using Augmented Reality, Workshop Proceedings of the 25th International Conference on Computers in Education, New Zealand: Asia-Pacific Society for Computers in Education, 2017, p. 161–170.
- [25] Endah Wulansari, O.D., Zaini, T. & Bahri, B., Penerapan Teknologi Augmented Reality Pada Media Pembelajaran, Jurnal Informatika Darmajaya 13(2), 2013, p. 169–179.
- [26] Rizki, Hariadi, Christyowidiasmoro, Markeless Augmented Reality pada perangkat android. Jurnal Teknik Elektro, Fakultas Teknologi Industri, Institut Teknologi Sepuluh Nopember, Surabaya, 2012.
- [27] Farhana Nor Shuhada Muhammad Pozi & Fariza Khalid, Kesan Teknologi Augmented Reality dalam Pendidikan Terhadap Peningkatan Motivasi Pelajar, International Conference on Global Education V "Global Education, Common Wealth, and Cultural Diversity", 2017, p. 1199–1208.
- [28] Hashim, N.C., Majid, N.A.A., Arshad, H., Nizam, S.S.M. & Putra, H.M., Mobile augmented reality application for early Arabic language education-: Arabic, ICIT 2017 - 8th International Conference on Information Technology, Proceedings (May 2018): 761–766.
- [29] Fauzan, A., Muriyatmoko, D. & Nahwa Utama, S., Penerapan Teknologi Augmented Reality Pada Media Pembelajaran Bahasa Arab: Durus Al-Lughah Jilid 1, ELSE (Elementary School Education Journal) 4(1), 2020, p. 63–78.
- [30] Ghazali Darusalam, & Sufean Hussin, Metodologi Penyelidikan Dalam Pendidikan: Amalan dan Analisis Kajian, 2016.
- [31] Oxford, R., Language Learning Strategies: What Every Teacher Should Know, 1990, p.136.
- [32] Norabeerah Saforrudin, Technical Skills in Developing Augmented Reality Application: Teachers' Readiness, Visual Informatics: Sustaining Research and Innovations - Second International Visual Informatics Conference, IVIC 2011, Selangor, Malaysia, November 9–11, 2011, Proceedings, Part II.

- [33] Vargavan, S.N. & Yunus, F., Penggunaan Augmented Reality (Ar) Untuk Meningkatkan Kemahiran Membaca Perkataan Bahasa Inggeris Kanak-Kanak Prasekolah. *International Journal of Education* 3(1), 2021, p. 156–172.
- [34] Ilmawan, Pemanfaatan Augmented Reality Sebagai Media Pembelajaran. *Jurnal Pendidikan Teknologi dan Kejuruan* 13(2), 2016, p. 174–183.
- [35] Jantakoon, T., Wannapiroon, P. & Nilsook, P., Virtual Immersive Learning Environments (VILEs) Based on Digital Storytelling to Enhance Deeper Learning for Undergraduate Students. *Higher Education Studies*, 9(1), 2019, p. 144-150.
- [36] Murhayati, S., Abduh, M.A., Andhi, R.R., Yendra, R., Rahman, M. & Fudholi, A., Educational integration of prayer in Islam using an augmented reality approach, *International Journal of Engineering and Advanced Technology* 8(5), 2019, p. 2085–2087.
- [37] Logical Choice, Case Study: Augmented Reality Captivates and Engages Kindergarten Reading Classrooms. *New Supplemental Curriculum: Letters Alive- Transforms Learning for English Language Learners at California School*, May 2012, <http://ww1.prweb.com/prfiles/2011/01/27/4041334/LettersalivebyLogicalChoice.pdf>
- [38] Arnheim, R., *Visual thinking: Los Angeles, CA: University of California Press*, 1969.
- [39] Badu Ganti, M. Z. & Lubis, M. A., Pendekatan Augmented Reality (AR) dalam Pengajaran dan Pemudahcaraan (PdPc) Bahasa Arab di Malaysia. *The 11th International Workshop and Conference of Asean Studies in Linguistics, Islamic and Arabic Education, Social Sciences and Educational Technology*, 2018, pp. 471-478.
- [40] Tan Choon Keong & Carol Abu, *Pengaplikasian Video Youtube: Bahan Bantu Mengajar (BBM) dalam Proses Pengajaran dan Pembelajaran Mata Pelajaran Sains Sosial, Universiti Malaysia Sabah*, 2013.
- [41] Norsham Ali & Isa Hamzah, Penggunaan Augmented Reality (Ar) Menerusi Teknologi Maklumat Dan Komunikasi Dalam Pembelajaran Bahasa Arab Warga Emas. *International journal of islamic and humanities research (QALAM)* 1(4), 2021, p. 1–11.
- [42] Law, Effie Lai Chong & Heintz, Matthias., *Augmented Reality Applications for K-12 Education: A Systematic Review from the Usability and User Experience Perspective*, *International Journal of Child-Computer Interaction*, 2021, p. 109-123.
- [43] Maimun Aqsha, Wan Nurul Syuhada', I.H, Tahap Pengetahuan Dan Kesiediaan Guru-Guru Pendidikan Islam Sekolah Menengah Di Selangor Terhadap Penggunaan Multimedia Dalam Pengajaran Pendidikan Islam. *ASEAN Comparative Education Research Journal on Islam and Civilization (ACER-J)* 1 Volume 1(1) January 2017, 1-13.
- [44] Donally, J., *Learning Transported: Augmented, Virtual and Mixed Reality for All Classrooms*. Portland, Oregon: International Society for Technology in Education, 2018.
- [45] Huda Wahida, R., Fauziah, B., Harryizman, H., Ali Yusny, D., Haslina, M., & Norida, M. D., Using Augmented Reality for Supporting Learning Human Anatomy in Science Subject for Malaysian Primary School. Paper presented at the Regional Conference on Knowledge Integration in ICT (INTEGRATION2010), Putrajaya, 2010.
- [46] Rohaila Mohamed Rosly & Fariza Khalid., *Gamifikasi: Konsep dan Implikasi dalam Pendidikan*. Gamifikasi: Konsep dan Implikasi dalam Pendidikan, 2017, p. 144-154.
- [47] Ahmad Yusof, Adnan, A.A., Mustafa Kamal, A.H.M., Kamal, N.N. & Ahmad, M.A., Education 4.0 Immersive Learning with Spherical Videos (360°) and Virtual Reality (VR) Experiences, *International Invention, Innovative & Creative (InIIC) Conference (November 2019): 978–967*.
- [48] Azlin Ariffin & Suhaimi Taat, *Penguasaan Bahasa Arab: Hubungannya Dengan Sikap Murid dan Pengajaran Guru*. *Malaysian Journal of Social Sciences and Humanities (MJSSH)* 5(3), 2020, p. 13–23.
- [49] Fadilah Abdul Rauf, T. Wee Hoe., *Potensi Realiti Terimbuh Dalam Aktiviti Mewarna: Satu Kajian Di Sebuah Prasekolah*. *Southeast Asia Early Childhood Journal* 9(2), 2020, p. 1–10.
- [50] Martins, V. F., Gomes, L., & Paiva Guimarães, M. D. (2015, June). Challenges and possibilities of use of augmented reality in education. *In International Conference on Computational Science and Its Applications* (pp. 223-233). Springer, Cham.
- [51] Martin-Gonzalez, A., Chi-Poot, A., & Uc-Cetina, V. (2016). Usability evaluation of an augmented reality system for teaching Euclidean vectors. *Innovations in Education and Teaching International*, 53(6), 627-636.

An Algorithm for Shrinking Blood Receptacles using Retinal Internal Pictures for Clinical Characteristics Measurement

Aws A. Abdulsahib¹, Moamin A Mahmoud^{2*}, Sally A. Al-Hasnawi³

College of Graduate Studies, Universiti Tenaga Nasional, Selangor, Malaysia¹

The Institute of Informatics and Computing in Energy, De-partment of Computing²

College of Computing and informatics, Universiti Tenaga Nasional, Selangor, Malaysia²

BIOCORE Research Group, Faculty of Information & Communication Technology, Al-Farahidi University, Baghdad, Iraq³

Abstract—The manual technique that might use for shrinking vessels blood in the retinal fundus images has significant limitations, such as the high rate of time consumption and the possibility of human error, precisely appear with the sophisticated structure of the blood receptacle and a hung amount of the retinal fundus photograph that needs to be anatomic. Moreover, the automatic proposed algorithm that will utilize shrinking and explore helpful clinical characteristics from retinal fundus photographs in order to lead the eye caregiver to early diagnosis for various retinal disorders and therapy evaluations. A precise, quick, and fully-automatic algorithm for shrinking blood receptacles and clinical characteristics measuring technique for internal retinal pictures is suggested in order to increase the diagnostic accuracy and reduce the ophthalmologist's burden. The proposed algorithm's main pipeline consists of two fundamental stages: picture shrinkage and medical feature elicitation. Many exhaustive practices were conducted to evaluate the efficacy of the sophisticated fully-automated shrinkage system in figuring out retinal blood receptacles using the DRIVE and HRF datasets of exceedingly demanding fundus images. Initially, the accuracy of the created algorithm was tested based on its ability to accurately recognize the retinal structure of blood receptacles. In these attempts, several quantitative performance measures precisely five were computed to validate the efficacy of the exact algorithm, including accuracy (Acc.), sensitivity (Sen.), specificity (Spe.), positive prediction value (PPV), and negative prediction value (NPV). When contrast with modern receptacles shrinking approaches on the DRIVE dataset, the produced results have enormously improved by obtaining accuracy, sensitivity, specificity, positive predictive value, and negative predictive value of 98.78%, 98.32%, 97.23%, and 90. Based on five quantitative performance indicators, the HRF dataset led to the following results: 98.76%, 98.87%, 99.17%, 96.88%, and 100%.

Keywords—Segmentation vessels / shrinking blood receptacles; clinical characteristics measurement; internal pictures for retinal; morphological filtering algorithm

I. INTRODUCTION

Direct ophthalmoscope, or manual examination of the internal photograph by a professional, is being replaced by a computer-attribution diagnosis of retinal internal images. Furthermore, the computer-attribution diagnosis of retinal internal pictures is as accurate as a direct ophthalmoscope and

requires less processing and analysis time. Retinal fundus pictures are commonly used to diagnose many eye-related illnesses that lead to vision loss, for instance, diabetic retinopathy in addition to macular degeneration [1]. The extraction of retinal blood vessels from fundus pictures is one of the essential processes in detecting diabetic retinopathy. Even though numerous segmentation approaches have been proposed, segmentation of the retinal vascular network and picture quality remains difficult. Noise (typically owing to uneven lighting) and narrow vessels are now critical obstacles in retinal vascular segmentation. Additionally, most of the proposed segmentation algorithms optimize the preprocessing and blood receptacle segmentation subjects for each dataset separately. As a result, these algorithms can typically reach a high rate of accuracy for the optimized dataset, but their accuracy will be lowered when applied to different datasets. Although most vessel segmentation methods include pretreatment procedures to improve vessel appearance, other plans skip the preprocessing steps and jump straight to the segmentation stage [2].

Blood receptacle segmentation is an essential required step to do the quantitative investigation of retinal photographs, where a set of critically beneficial clinical features such as the tortuosity, length, density, and thickness, of the blood vessel can be extracted from the segmented vascular tree. Furthermore, the segmented vascular tree has also been used in several medical applications, including retinal image mosaic structure, temporary and/or multi-modal image registration, optic disc identification, biometric identification, and fovea localization. Many segmentation approaches nowadays use machine learning ideas in conjunction with traditional techniques to improve segmentation accuracy by providing a statistical analysis of data to enhance segmentation algorithms [3]. Based on the usage of labeled training data, these machine learning principles can be divided into unsupervised and supervised approaches. In a supervised technique, a human operator labels and select a class for every single pixel in the internal picture, such as vessel and non-vessel. A classifier is trained using the tags supplied to the input. A sequence of characteristics vectors is formed from the data being processed (pixel-wise characteristics in picture segmentation defects). Similar samples are grouped into various classes using predetermined characteristics vectors

*Corresponding Author.

that are distinguished without any labels in an unsupervised technique. This accumulating is dependent on several assumptions about the input dataset structure, namely that there are two kinds of classes of the input dataset with identical characteristics vectors (blood receptacle and not blood receptacle). Depending on the situation, this matching metric might be sophisticated or specified by a basic metric like pixel contrasts [4].

The analysis of the blood receptacle tree in internal images with precision and accuracy can provide several essential aspects for diagnosing various retinal disorders. However, when utilized as the first step which is represented by preprocessing for higher-level picture detection, retinal blood vessel segmentation might significantly impact other applications. For instance, reliable blood vessel tree detection might be employed in recording time series internal images, finding the optical disc or over, recognizing the retinal blood receptacle fiber layer, and biometric identification. There is a substantial amount of work on this topic due to the applications wide range and the fact that shrinkage of retinal blood receptacles is one of the critical jobs in retinal picture processing [5].

To increase diagnosis precision and reduce ophthalmologists' burden, an accurate, quick, and totally automatic blood receptacle shrinking and clinical characteristics measuring algorithm for retinal internal pictures is presented. The proposed algorithm's main pipeline consists of two critical stages: picture segmentation and clinical feature extraction. In the segmentation stage, a fully automated segmentation method called a morphological filtering algorithm addressed by MFA is used to find blood receptacles in retinal photographs.

In the morphological filtering algorithm, an efficient and reliable image pre-processing procedure is applied to preserve the vessel's structure and eliminate the noise level using the Anisotropic Diffusion (AD) filtering and Gaussian filtering, respectively. This is followed by removing all undesired objects (e.g., small vessel segments) in the enhanced image by applying morphological operations. Finally, all the retinal blood vessels are detected by utilizing an efficient edge algorithm based on efficient filter which is an improved Canny edge detector. Finally, the output segmented images produced from the proposed segmentation algorithm is fused to produce the final segmented image. In the post-processing step, a novel blood vessel linking procedure is proposed to correctly join the discontinuous blood vessels produced in the segmented picture resulting from the fusing stage. In the clinical features extraction stage, several helpful clinical characteristics are computed, for instance the tortuosity, thickness, density, and length of the blood vessel, which are efficiently used in the early diagnosis of several cardiovascular and ophthalmologic diseases. In this stage, an efficient and accurate algorithm for computing the blood vessel thickness is proposed. The main contributions list can be summarized as follows:

- An accurate, quick, and fully-automated blood vessels shrinkage and clinical characteristics assessment

algorithm is suggested to improve diagnosis precision and reduce ophthalmologists' burden.

- Fully-automated segmentation algorithm is proposed and named as a morphological filtering algorithm to accurately detect the blood vessels in the retinal images.
- A novel blood vessel linking procedure is proposed to correctly join the discontinuous blood vessels produced in the segmented image resulting from the previous step.
- This research considers as a second stage from our main goal by developing a fully automated and real-time retinal blood vessels hybrid segmentation and clinical features extraction model in fundus images and for the first stage represented by trainable filter algorithm that already completed successfully.[6].
- The rest zone of this study is consist of Section II which presented a related works on Blood receptacles shrinking and medical feature measuring algorithm for internal pictures of the retina Section III outlines the major processes of the proposed morphological filtering algorithm, which consists of three primary stages: image preprocessing, morphological operations, and vessel recognition. Several comprehensive tests were undertaken to evaluate the performance and accuracy of the newly created fully-automated shrinkage system for analyzing retinal blood receptacles through utilizing two difficult internal binary photograph datasets, as described in Section IV in addition to Section V discusses the outcome results and future work as a final topic.

II. RELATED WORK

The shrink in the retinal internal image is considered as a first stage concerned with identifying the several diseases that related to the eyes. In general, blood receptacles look like a structure tree. Morphological characteristics includes width, length plus to branching of the eye, and others play an enormous part in detecting and treating various of eyes diseases, according to work published by [5] Classification of microaneurysms and non-macro aneurysms is a concern using morphological filters algorithm to detect diabetic retinopathy in retinal vessels images by utilizing the evaluation matrix such as accuracy, sensitivity, and specificity. In addition, the study did the experiments using the IDRiD dataset with an average result of 80.85%. Thus, its notice some limitations in their proposed methods summarized by resolution point need to be more enhancement. They have used only one dataset in the whole of the experiments. According to S. Annand et al. [7] they are working on Optic disc analysis in retinal blood vessels in the fundus using contourlet sub-bands, superimposed edges with morphological filling through several kinds of datasets, including DRIVE, STARE, MESSIDOR, etc. E-aphtha, Diaretdb1. Moreover, the utilized dataset highlights the accuracy channel that registers 97.15% output result even though the outcome is high. Still, there are some points it needs to be enhance, such as the datasets that are used with significant numbers of users lead to have the

configuration complexity that might happen between the various datasets and the proposed methods. Another work by [8], the study proposed the domain of Retinal Vessel Segmentation in Diabetic Retinopathy Using a Morphological Top Approach in medical Images by implementing two types of data: HAGIS and HRF, which succeed by achieving 95.12%, 94.37%, respectively. Several disorders may be impacted by a particular segmentation procedure, resulting in limits because there are numerous types of diseases, for instance glaucoma, age macular degeneration, hypertension, that concenter harmful and significantly affect the patient's health.

In [9], the work on the execution analysis of auto-detection of diabetic retinopathy utilizing the proposed operation algorithms with the same concept of evaluation matric but with a deferent dataset named by DIARETDB1 to achieve a 98.68% percentage. At some point, the computational timing is quite long, based on several observations. Another study by [10], its introduced analyses of retinal blood receptacle from eyes scope images through utilize morphological method implemented through DRIVE, HRF dataset to extract the Acc., Sen., and Spe. with the exact result of the accuracy is 0.9541,0.9478 respectively. Therefore, there are some misclassified structures, such as vessels giving poor segmentation output. Also, U. Ozkaya et al. [11] presented the efficiency of retinal blood receptacle shrink utilizing morphological operations using DRIVE dataset to achieve 95.61% with some limitations of the proposed methods that do not diagnose critical diseases such as hypertension and diabetic retinopathy. Charu Bhardwaj et al. [12] focusing on the execution analysis of retinal characteristics for diabetic retinopathy characterization and diagnoses by using DRIVE, STARE to extract the evaluation matric category that is divided into three types starting by accuracy and end with specifically to highlight the accuracy average result 95.50%, 94.80% respectively. However, it needs to be more accurate to positively match the manual segmentation results. In this paper, we emphasize the morphological filter algorithm that was modified using a very powerful and common dataset, DRIVE and HRF, for accurate, quick, and full-automatic blood receptacle shrink and clinical characteristics. A measurement approach for retinal internal pictures is presented to enhance or develop diagnostic quality and reduce ophthalmologists' effort.

III. PROPOSED AUTOMATIC BLOOD VESSELS SEGMENTATION AND CLINICAL FEATURE MEASUREMENT ALGORITHM

The quantitative investigation of retinal images is widely utilized for rapid detection, observation, and treatment assessment of cardiovascular and ophthalmologic diseases, for instance, macular degeneration, eyes diabetes, glaucoma, hypertension, arterio-sclerosis, vein occlusion, and choroidal neovascularization. Among these mentioned diseases, diabetic retinopathy and macular degeneration are considered the two main reasons for blindness. Blood receptacle shrink is an essential stage required for the quantitative investigation of retinal photographs, where a set of critically beneficial medical characteristics for instance the density, tortuosity, length, and thickness, of the blood vessel, can be extracted

from the segmented vascular tree. Furthermore, the segmented vascular tree has also been used in several medical applications, including retinal image mosaic structure, temporary and/or multi-modal image registration, optic disc identification, biometric identification, and fovea localization. Accordingly, it is hypothesized that an autonomous method for segmenting and extracting valuable clinical information from retinal blood vessels will aid ophthalmologists and eye specialists in the early diagnosis of various retinal illnesses and the evaluation of treatment options. Fig. 1 shows the projected blood vessel segmentation and clinical features measurement.

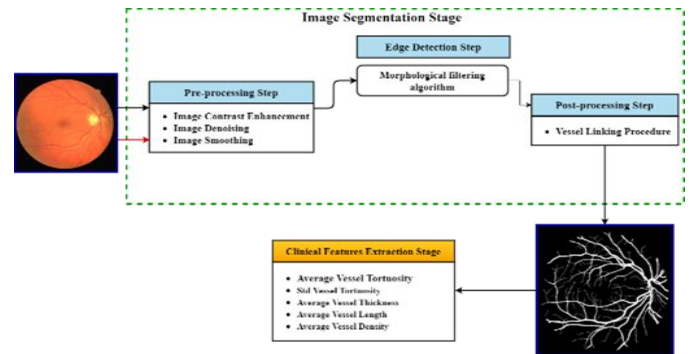


Fig. 1. Diagram of the Proposed Blood Receptacles Shrink and Clinical Features Measurement Algorithm.

A. The Morphological Filter Algorithm

As we presented in Fig. 2 the main steps of the morphological filtering algorithm, which is composed of three main stages, including the image pre-processing stage, the morphological operations stage, and the vessels detection stage. In the image pre-processing step, the AD filtering and Gaussian filtering are applied on top of the extracted green channel of the retinal image to enhance edges' structures and eliminate the noise in the retinal fundus image, respectively. Then, a set of morphological operations are applied on top of the enhanced image produced from the previous stage to discard the background and all the unwanted objects (e.g., small vessel segments). Finally, the retinal blood vessels are detected by utilizing an efficient edge detection algorithm based on edge detector filter addressed by an improved Canny edge detector. The main steps of the selected filter are explained in detail in the next sub-sections.

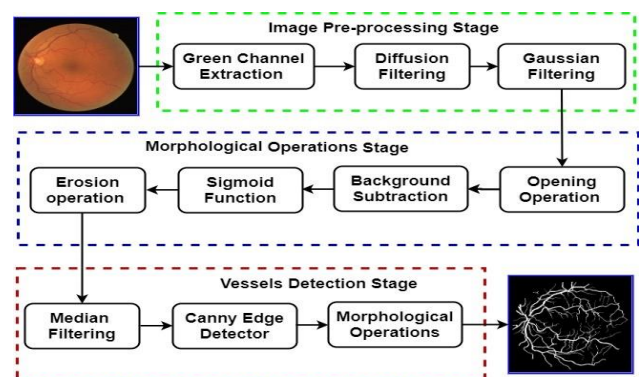


Fig. 2. The Fundamental Stages of the Proposed Morphological Filtering Algorithm for Detecting the Retinal Blood Vessels.

1) *Image pre-processing stage*: In this stage, the crucial aim is to improve the non-uniform illumination, controlling the contrast of the retinal picture and de-creasing the background noise. The main steps of the proposed image pre-processing can be summarized as follows:

a) Extracting the best channel which is the green from the colored retinal internal photograph.

b) Correcting the non-uniform illumination and enhancing the visibility of the edges' tree structures in the retinal internal picture by using AD filter.

c) Applying the 2D Gaussian filter to smooth the retinal image and eliminate the background noise.

Despite of the human observer can efficiently identify the blood vessel structures using the full-color image, however, processing the three channels of the input image can increase the computational complexity of the proposed algorithm where a long time will be required to deliver the final segmented image. Thus, the proposed morphological filtering algorithm starts with extracting the green channel of the input picture because it gives a better distinction between the background layer and the retinal blood receptacle than other channels, as shown in Fig. 3.

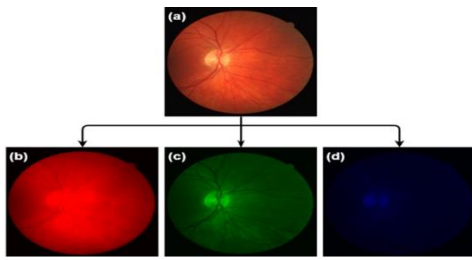


Fig. 3. The Three Channels of the Coloured Retinal Image: (a) Main Picture, (b) Red Conduit Picture, (c) Green Conduit Picture, and (d) Blue Conduit Picture.

In most cases, the retinal images have some background pixels with intensity values similar to the lighter pixels of the retinal blood vessels. These pixels can significantly degrade the outcome of the proposed segmentation algorithm. Therefore, the AD filter [13] was used to the green conduit of the retinal picture after rescaling it to the range of [0, 1], to correct the non-uniform illumination and enhance edges' structures in the retinal picture, as presented in Fig. 3(b). The AD filter can be represented as follows:

$$I_{ij}^{t+1} = I_{ij}^t + \lambda [c_N \cdot \nabla_N I + c_S \cdot \nabla_S I + c_E \cdot \nabla_E I + c_W \cdot \nabla_W I]_{ij}^t \quad (1)$$

Here, I refer to the retinal image, $0 \leq \lambda \leq 1/4$, The (c) parameter represents the conduction coefficients which is updated every iteration as a brightness gradient function, (t) represents the iteration index, and (∇) refers to the nearest neighbour variances in all the directions N, S, E, and W, as bellows:

$$\nabla_N I_{ij} = I_{i-1,j} - I_{ij}$$

$$\nabla_S I_{ij} = I_{i+1,j} - I_{ij}$$

$$\nabla_E I_{ij} = I_{i,j+1} - I_{ij}$$

$$\nabla_W I_{ij} = I_{i,j-1} - I_{ij} \quad (2)$$

In this work, these values of the λ and t parameters are set to 0.20 and 5, respectively. This was followed by applying the 2D Gaussian filter to assure the smoothness in the retinal internal picture in addition to eliminating the background noise, as presented in Fig. 3(c). The 2D Gaussian filter is distinguished by a non-uniform low-pass filter, whose 2D filter coefficients are computed as follows:

$$G(x, y) = \frac{1}{2\pi\sigma^2} e^{-\frac{x^2+y^2}{2\sigma^2}} \quad (3)$$

Here, the (x, y) refers to the filter center, and σ refers to (SD) Standard Deviation of the Gaussian filter.

2) *Morphological operation stage*: Typically, morphological operations can be employed to accurately extract the image's components, which are proven to be extremely helpful for interpreting and representing the different shapes that exist inside the input image rather than pixels' intensities, such as borders, skeletons, and convex hulls [14]. The morphological operations are considered powerful tools that can be efficiently employed in solving several tasks in image processing. Dilation, erosion, opening, closing, bottom-hat, and top-hat transformation are the fundamental morphological operations that can be utilized to segment, manipulate and adjust the objects shown in the input image depending on their structure [15]. In general, these morphological operations were only applied to the binary images, and then they were extended to process the grey-scale images as well. The primary aim of this stage is to define the vessels' structure precisely by eliminating the defects, such as various kinds of noise that can influence the blood vessels' structure and produce more visible structures of the blood vessels. The main stages in the selected morphological operations stage are implemented sequentially as follows:

a) Applying the opening operation with a disk structure element of 3 pixels.

b) A background subtraction procedure was implemented to split the foreground objects from the image's background.

c) A sigmoid function was employed to decrease the effect of the non-uniform illumination of the retinal pictures.

d) Improving the appearance of the retinal blood receptacles by applying the erosion process.

In this stage, two different morphological operations were applied, namely the opening and erosion operations. The morphological operations were further employed in other steps of the proposed blood vessel segmentation algorithm to exclude the unwanted features (e.g., small vessel parts) without changing the main structure of the blood vessel. Usually, the morphological operations take two different parameters, including the picture that needs to be processed. The shape in addition to size of the tree structure element plays a significant role in detecting a feature representation of a given size and shape in the input image. Thus, the size and shape of the structuring element are selected according to the demand and purpose of the adopted application. The erosion

and dilation operations are the essential morphological operations utilized to lessen and boost the objects in the image, respectively. The erosion and dilation operations are defined as follows.

$$f \ominus B = \min_{u,v} (f_{(x+u,y+v)} - B_{(u,v)}) \quad (4)$$

$$f \oplus B = \max_{u,v} (f_{(x-u,y-v)} + B_{(u,v)}) \quad (5)$$

where (f) represents a greyscale image B refers to the structuring element. $f \ominus B$ and $f \oplus B$ represent erosion and dilation, respectively. Morphological opening operation is applied to delete undesired precise structures in the input picture by implementing an erosion procedure followed by a dilation process. In contrast, a morphological closing operation is applied to fill or merge some structures in the input picture by implementing the dilation procedure followed by the erosion process. The morphological opening and closing operations can be defined as follows:

$$foB = (f \ominus B) \oplus B \quad (6)$$

$$f \bullet B = (f \oplus B) \ominus B \quad (7)$$

In this stage, several kinds of experiments were conducted to select the methods of applied in this stage using retinal fundus images with various levels of noise and lighting conditions. The main aim here is to improve the structure of blood vessels without missing essential characteristics in the retinal picture. In the current stage, the opening operation was applied to the enhanced image produced from the prior stage by employing an optic disk element of 3 pixels. Then, a subtraction procedure for the background layer was implemented to split the foreground objects from the image's background and identify the retinal blood vessels accurately. Next, a simple image contrast enhancement process using a sigmoid function [16] is implemented as follows:

$$g(x, y) = \frac{1}{1 + e^{(c \cdot (Th - f(x,y)))}} \quad (8)$$

Where f and g of (x,y) is the input and the enhanced photograph. Herein, the contrast parameter (c) , and the Threshold parameter (Th) , are empirically chosen to be 4 and 0.5, respectively. The main advantage of this step is to decrease the impact of the non-uniform illumination by narrowing in addition to extending the values range of the bright and dark pixels in the retinal photograph, sequentially. Finally, the erosion process was also applied by employing a structural element of 2-pixels to improve the appearance of the retinal blood vessels, as presented in Fig. 3(d). Undesired segments of one-pixel size were excluded.

3) *Vessel's detection stage*: The vessels detection procedure was applied to preserve beneficial structural details of the blood vessels' borders and to carefully discard the unwanted objects. As depicted in Fig. 4, the fundamental steps of the selected vessels detection process might be outlined as follows:

a) Eliminating the noise level produced from the morphological operations stage by applying the median filter.

b) An improved Canny edge detector was employed to accurately identify the blood vessels.

c) A refinement vessel's structure procedure based on applying a set of morphological operations was implemented to maintain the actual thickness of the detected blood vessels and to eliminate unwanted objects in the segmented image.

Initially, the median filter was applied to eliminate the noise produced from the morphological operations stage that can significantly influence the precision of the blood vessels detection in the later steps. The median approach is a non-linear method that is utilized to eliminate the noise from a given image to enhance the outcomes of subsequent processing (e.g., the edge detection process in an image). The median filter is very widely applied in addressing several image processing problems due to its ability in preserving the edges and removing noise. In this work, a media filter of size (5×5) pixels.

The blood vessels were then identified by using an improved Canny edge detector. First, the Gaussian filter was applied to further decrease the noise level in the picture. This was followed by calculating the gradient magnitude along with its vectors for each pixel of the enhanced image. An algorithm of non-maxima suppression was later implemented by utilizing the gradient magnitude and direction to be recognized and assigned as a border pixel by employing the thresholding approach. The main stimulus for applying the improved Canny edges detector is to accomplish some beneficial characteristics, including reducing the possibility of duplicated responses to a singular edge; reducing the likelihood of neglected edges; reducing the distance computed between the pixels of the identified edges and the original edges. These four characteristics might conceder as a critical role in solving the problems of detecting retinal blood receptacles precisely. The main steps of applying the improved Canny edges detector can be summarized as follows:

1) *Smooth Image*: Reducing the noise and smoothing the retinal image by applying the Gaussian filter. Suppose $G(x, y)$ represents the Gaussian filter as revealed in Eq. (9) and $I(x, y)$ represents the retinal image. Then the smoothed image can be obtained by convoluting I with G of (x, y) as follows:

$$S(x, y) = G(x, y) \otimes I(x, y) \quad (9)$$

2) *Gradient Magnitude*: Computing the gradient magnitude of the smoothed image $S(x, y)$ is utilized to compute the variation value of (G_x) and (G_y) , sequentially, same as below:

$$G_x(x, y) \approx [S(x, y + 1) - S(x, y) + S(x + 1, y + 1) - S(x + 1, y)]/2 \quad (10)$$

$$G_y(x, y) \approx [S(x, y) - S(x + 1, y) + S(x, y + 1) - S(x + 1, y + 1)]/2 \quad (11)$$

From Eq. (10) and (11), the gradient magnitude and its direction are computed, respectively, as in Eq. (12) and (13):

$$G(x, y) = \sqrt{G_x^2(x, y) + G_y^2(x, y)} \quad (12)$$

$$\theta(x, y) = \tan^{-1} \left(\frac{G_y^2(x, y)}{G_x^2(x, y)} \right) \quad (13)$$

3) Non-maxima Suppression Algorithm: The computed gradient magnitude usually includes extended ridges nearby the local maximum. Thus, the non-maxima suppression algorithm was applied to thin these extended ridges. A gradient vector (di) composed of four discrete directions (e.g., horizontal, vertical, 45° and - 45°) is computed for each pixel (x, y) of the normal edge. Then the closest direction to $\theta(x, y)$ is defined from these four directions. If the value of gradient magnitude $G(x, y)$ was lower than the vectors (di), then the non-maxima algorithm is equal to zero (suppression); else, $N(x, y) = G(x, y)$.

4) Hysteresis Thresholding Algorithm: This algorithm is applied to detect and connect the pixels of the actual edges.

In most cases, thresholding the input image can produce several false detected edges. To decrease the rate of false detected edges, a thresholding algorithm can be applied using two different threshold values, named the low threshold (TL) and the high threshold (TH). It defines the non-maxima approach NH (x, y) after hysteresis thresholding N (x, y) using the high threshold (TH) and defines the non-maxima approach NL (x, y) after the method of thresholding using the low threshold (TL). Obviously, the NH (x, y) has the stronger edge representations compared with the NL (x, y) which contains the weaker edge representations.

After the improved Canny edge detector has applied, a refinement vessel's structure procedure was implemented to maintain the actual thickness of the detected blood vessels and to eliminate some unwanted objects in the segmented image. This refinement procedure starts by applying the dilation process by employing two line-formed structural elements of three pixels with angles between 90° and 0°, sequentially. Then, the erosion process was implemented by employing a structural element of one pixel to sharpen the edges of the defined blood vessels. Finally, all the objects of an overall area of fewer than 100 pixels were discarded from the final segmented image, as shown in Fig. 4(e).

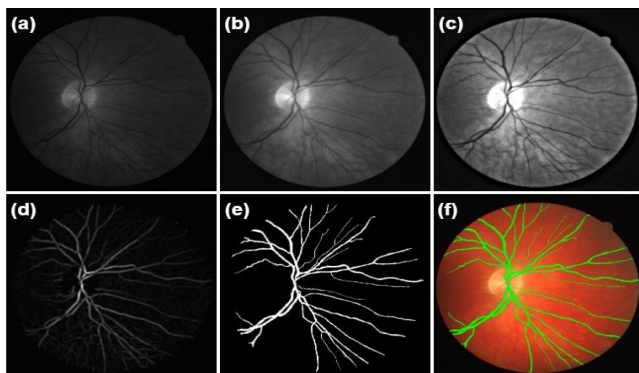


Fig. 4. The Proposed Morphological Filtering Algorithm Outputs: (a) Normalized Green Conduit, (b) AD Output, (c) Gaussian Filtering Output, (d) The Output of the Morphological Operations Stage, (e) The Final Output of the Edge Detection Stage, (f) The Overlapped Automated Segmented Image with the Original Retinal Image.

B. Post-Processing Stage

Once, the segmented retinal image is obtained from the morphological, the output is used to produce the final segmented image. Then, a novel blood vessel linking procedure was proposed to correctly join the discontinuous blood vessels produced in the segmented image resulting from the previous step. These discontinuous blood vessels are presented in the eventual segmented picture due to poor visibility of the specific portions of blood vessels or the noise presented in the retinal image. The accuracy of the extract clinical characteristics, for instance, the thickness, length, density, and tortuosity of the blood vessel can significantly be affected by the appearance of the discontinuous blood vessels. Thus, a new process was selected in this study to correctly join the discontinuous blood vessels in the final segmented photograph. The proposed blood vessel linking procedure was implemented as follows:

1) Producing the skeleton blood vessels structure of the final retinal segmented image, and then identifying the vessels' end-points.

2) Defining a possible highest distance between the endings of each two segments of a disconnected blood vessel. Then a circular-shaped structure element of radius = (highest distance)/2 was placed at the end of each blood vessel. If the ends of the two blood vessels were approaching each other, then the placed structural elements were overlapped, as displayed in Fig. 5(c).

3) Finally, the thinning process was applied to the whole image. Hence, a line of one pixel wide will be left by the thinned structural elements to link the two endings of the vessel. While, the separated ends are recovered to their initial structure, as displayed in Fig. 5(d).

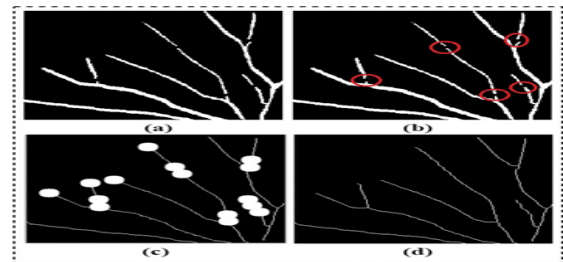


Fig. 5. The Proposed Blood Vessel Linking Procedure: (a) The Segmented Blood Vessel Structures, (b) The Disconnected Blood Vessels Marked in the Red Circles, (c) The Binary Circular-shaped Structural Elements are Drawn at the Ends of each Blood Vessel Segment, and (d) The Resulting Image with Linked Blood Vessels.

C. Clinical Feature Extraction Stage

The abnormalities in the retinal blood vessel structures, including the morphologic modifications in vessel tortuosity, shape, thickness, and length might be connected to the existence of cardiovascular and eye diseases. Therefore, the automatic quantitative analysis process of abnormalities in blood vessel structures can be extremely useful to help ophthalmologists and eye specialists in the early diagnosis of different retinopathies diseases, describe their severity level, and treatment assessments. One of the main aims of this work is to develop an automated morphologic description procedure

to analyze the whole blood vessel network in the retinal image. The clinical features extraction stage computes a set of useful clinical features from the automatically detected retinal blood receptacle in an accurate path. In the current stage, a number of morphological clinical features associated with the healthiness of the retinal blood receptacles are extracted as follows:

1) *Vessel's length*: The length of the retinal blood vessel was computed for each vessel's segment by firstly taking the vessel's skeleton structure, and then the distance between sequential pixels in the blood vessel segment is summed as in Eq. (14).

$$Vessel\ Length = \sum_{i=1}^{N-1} \sqrt{(x_{i-1} - x_i)^2 + (y_{i-1} - y_i)^2} \quad (14)$$

Here, (N) refers to the number of sequential pixels produced from the blood vessel skeleton part, with (x_i, y_i) refers to the pixel's coordinates in the blood vessel part.

2) *Vessel density*: The retinal blood vessels density was calculated by dividing the sum of all the pixels in the blood receptacles by overall area of the whole retinal image as shown in Eq. (15):

$$Vessel\ Density = \frac{\sum The\ vessel\ pixels}{ImageArea\ (mm^2)} \quad (15)$$

3) *Vessel tortuosity*: The tortuosity coefficient of the blood vessel is interpreted as a degree of twists presented in the blood receptacle course, as shown in Fig. 6. Some studies have proved that the vessel tortuosity coefficient can be linked with the average fundus blood pressure, however, no significant increase was observed until the critical blood pressure level is reached [17, 18]. Herein, the mean tortuosity coefficient of the whole retinal blood vessel network was computed. First, the skeleton structure of the blood vessels was produced. This was followed by defining the branch points of the blood vessels to divide the length of Blood Vessel Segment (BVS) into (b) branches as in Eq. (16):

$$BVS = s_1 + s_2 + \dots + s_b \quad (16)$$

Then, the tortuosity coefficient index for the (BVS) was then computed as follows:

$$TC(BVS) = \sum_{n=1}^b \frac{s_{length}(n)}{s_{straight}(n)} \quad (17)$$



Fig. 6. An Example of Severe Retinal Blood Vessel Tortuosity is a Patient with Severe Non-proliferative (NPDR) Disease [19].

where s_{length} refers to the length of the vessel branch, and it was estimated by Eq. (14). $s_{straight}$ is the straight distance between the endings point and was estimated as follows?

$$s_{straight} = \sqrt{(x_N - x_1)^2 + (y_N - y_1)^2} \quad (18)$$

Here, (N) refers to the specific number of essential subjects captured from the sub branch of the blood vessels. While (x, y) refers to the pixel's coordinates in each branch of the blood vessels. Finally, the mean tortuosity coefficient of the entire blood vessels network was acquired by calculating the mean tortuosity values obtained of each blood vessel.

4) *Vessel thickness*: The blood vessel thickness is referred to as the average width of the retinal blood vessels. In this PhD thesis, a new procedure for computing the retinal blood vessel thickness is developed. Fig. 7 presents the outcome results of the enhanced thickness procedure. The primary steps of the developed procedure after identifying each blood vessel were implemented as below:

a) Distance transformation was computed from the photograph of detected retinal blood vessels, where all background pixels in the transformed image become white, while the object pixels become black. This transform calculates the Euclidean distance for each black pixel in the segmented image to the nearest non-zero pixel. In the developed procedure, the distance transform was implemented on the inverse of the binary image of the detected retinal blood vessels. Thus, for each pixel of the detected blood vessel, the Euclidean distance of that specific pixel or subject to the nearest border pixels of the blood vessel was computed.

b) After applying the distance transforms, the blood vessel pixels that have the greatest distance values in the distance transform will be located in the middle of the blood vessel segment. The distance values that represent the halfway edge in between the blood vessel segment were obtained with some leniency of the largest distance values because of the floating-point computation.

c) Eventually, the overall average of accumulated distance values defines the half-width of the blood vessel. Consequently, the blood vessel thickness (width) was measured by multiplying the outcome reached by two.

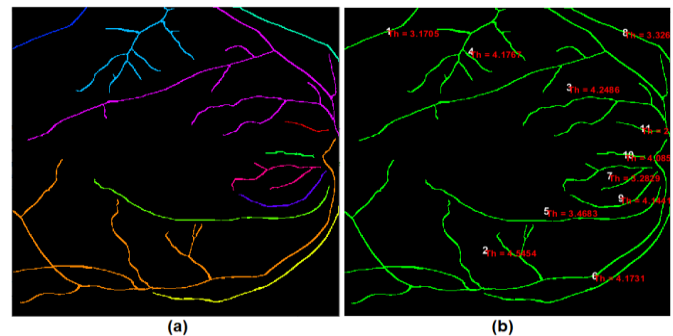


Fig. 7. The Output of the Developed Thickness Procedure: (a) Coloured Labeled Retinal Blood Vessels and (b) Image Map for the Retinal Blood Vessels along with their Indexes and Average Thickness Values.

IV. EXPERIMENTAL RESULT AND DISCUSSION

In the current research, the accuracy of the developed segmentation approach for recognizing retinal blood vessels was tested using two very difficult fundus image datasets, DRIVE [20] and High-Resolution Fundus (HRF) [21]. These datasets were used to test the method.

Firstly, the main details of the applied retinal image datasets in current experiments are present. Secondly, the evaluation procedure of the fully-automated shrinkage algorithm is given along with their combination and compared their performance among (GT) which represents the ground truth pictures. Finally, the execution of the developed algorithms is compared with the modern approaches.

A. Dataset Precise Description

The execution of the selected blood vessel segmentation algorithms has been tested using two established publicly available datasets of retinal fundus images (DRIVE and HRF). These two datasets have gained special popularity due to they provide the associated GT images, in which the blood vessel is manually detected by different expert observers. Thus, they enable the possibility of comparing the results obtained against the provided GT images to check the reliability and quality of the selected algorithm. The main aim of these two datasets is to establish and encourage comparative studies on developing an automated algorithm for retinal blood receptacles in the fundus pictures.

1) *DRIVE dataset [20]*: The DRIVE is consisting of 40 colored retinal pictures split into testing and training sets, each one consisting of 20 pictures. A Mask picture that represents the view field (FOV) of the retina area is supplied for each image together with the corresponding GT image. The blood receptacle in the retinal pictures of the training set was manually segmented by one expert. In this work, the training set was used to figure out the elements of the selected segmentation algorithms. On the other hand, the blood vessels in the testing set images were manually segmented by two other experts. The real execution of the proposed receptacle algorithm was assessed using the testing category. DRIVE database contains retinal images captured from several causes of diabetes up to 400 subjects the record starts with age 25 until 90 years old in the Netherlands. Then, 40 images were randomly chosen, 33 images without diabetic retinopathy registered causes and 7th of the images marked in early diabetic retinopathy. Retinal pictures were captured utilizing a Canon machine with a precise model CR5 non-mydratric 3CCD camera with an angle of 45° as a field of view. All the images were saved in a specific size which is (768 × 584). As an instance of retinal internal photographs from DRIVE dataset responding manually gold standard images are shown in Fig. 8.

2) *HRF dataset [21]*: The HRF dataset has 45 pictures taken by three different groups, such as healthy people, people with diabetic retinopathy, and people with glaucoma.

3) *Each group has 15 pictures* utilizing a mydratric fundus camera with precise model CANON CF-60UVi with

angle 60° as field of view. All the images were saved in JPEG format with 24-bits coloured image. Binary field of view mask pictures of the provided dataset in order to perform the analysis only in the region surrounded by the dark background [see Fig. 9(b)]. In this dataset, the tree of blood vessels was manually traced by several experts in the domain of retinal picture interpretation. For instance, retinal internal pictures from HRF dataset images are shown in Fig. 9.

B. Blood Vessel Segmentation Evaluation

In the binary classification task, every single pixel in the input picture is identified as a blood receptacle by the proposed algorithm. In addition to classified as a blood receptacle in the GT image is computed as a (TP) true positive. Moreover, every single pixel is identified as a blood receptacle in the final segmented picture, yet not in the to the ground truth picture is computed as a (FP) false positive. In the evaluation of the retinal vessel segmentation, the average values of five quantitative performance measures were computed to experiment the quality of the selected algorithms, including the Acc., Sen., Spe., PPV, and NPV. These five quantitative measures are computed as follows:

$$\text{Accuracy (Acc.)} = \frac{TP+TN}{TP+FN+TN+FP} \quad (19)$$

$$\text{Sensitivity (Sen.)} = \frac{TP}{TP+FN} \quad (20)$$

$$\text{Specificity (Spe.)} = \frac{TN}{TN+FP} \quad (21)$$

$$\text{Positive Predictive Value (PPV)} = \frac{TP}{TP+FP} \quad (22)$$

$$\text{Negative Predictive Value (NPV)} = \frac{TN}{TN+FN} \quad (23)$$

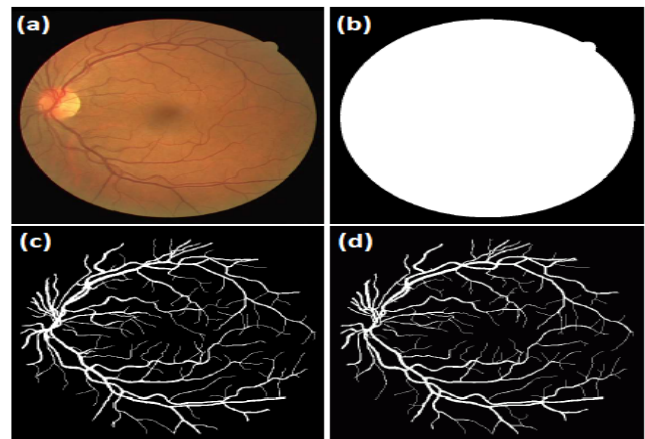


Fig. 8. Image Example from the DRIVE Dataset: (a) The Main Picture, (b) FOV-mask Picture, (c) The Manually Segmented Picture of the First Expert, and (d) Manually Segmented Picture of the Second Expert.



Fig. 9. Image Example from the HRF Dataset: (a) The Main Photograph, (b) FOV-mask Photograph, and (c) The Manually Segmented Photograph of Expert.

Here, the FN, FP, TN, and TP are referring to False Negatives, False Positives, True Negatives, and True Positives sequentially. Acc. measurement is referring to the average of the total amount of correctly identified pixels among to the number of pixels that located in the field of view mask picture. Sen. relates to the selected algorithm’s ability to recognise the blood receptacle pixels accurately. Spe. is the capacity of the suggested method to recognise non-vessel pixels accurately.

The positive prediction value is referring to the pixels’ average correctly classified as vessel pixels. Finally, the negative prediction value is the pixels average to correctly identified as non-blood receptacle pixels (e.g., background).

C. 4.3. Results on Drive Dataset

Firstly, the execution of the selected algorithm for detecting the retinal blood receptacle was checked out based on the DRIVE dataset. Using training group pictures, several executions were done in field to choose the best value for a group of parameters in order to maximize the segmentation quality of the proposed algorithms. For instance, using the proposed morphological filtering algorithm, the (λ) and (t) parameters values are determined to 0.20 and 5, respectively. The 2D Gaussian filter size was set to (7×7) pixels, values of the low threshold (TL) and the high threshold (TH) were set to 25 and 40, respectively. Then, the segmentation accuracy was computed to select the best value of the parameter (t). So, 121 tests were done where the parameter (t) was changed each time by 0.1.

As shown in Fig. 10, the best value of the parameter (t) was set to 0.5. In the evaluation stage, five performance evaluation metrics were computed using the testing images along with the two provided human observers as the GT images.

The adopted five evaluation metrics using the proposed morphological filtering algorithm are shown in Table IV. Using the two provided human observers as the GT images in the DRIVE dataset the proposed morphological filtering algorithm has managed to achieve an overall average Acc. of 98.06%, Sen. of 97.995%, Spe. of 97.775%, PPV of 90.07%, and NPV of 94.725%. Form Table I, although the proposed morphological filtering algorithm has obtained a higher Spe. of 98.32% using the 1st human observer compared to Spe. of 97.23% using the 2nd human observer, better results were obtained using the letter in terms of other evaluation metrics. Then, the proposed blood vessel linking procedure was applied to correctly join the discontinuous blood vessels produced in the segmented retinal image resulting from the previous step. In this work, to validate the advantage of applying the proposed blood vessel linking procedure, the adopted five evaluation metrics were computed with and without the applying the proposed blood vessel linking procedure. An example of the output segmentation results on the DRVIE dataset is shown in Fig. 11.

In this work, On the images that come from DRIVE group dataset, the execution of the suggested algorithms was compared with modern methods for separating blood vessels.

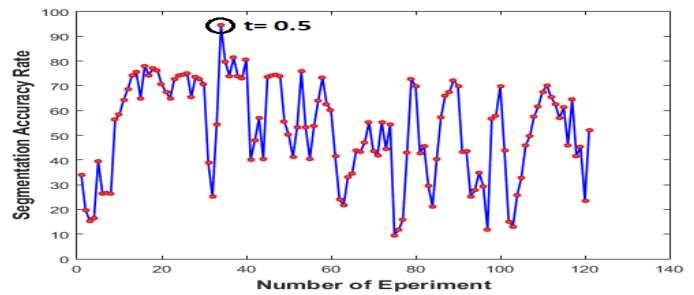


Fig. 10. The Segmentation Accuracy Obtained during 121 Experiments to Fine the Best Value of the Parameter (t) in the using the Proposed Morphological Algorithm.

TABLE I. THE AVERAGE VALUES OF FIVE QUANTITATIVE PERFORMANCE MEASURES USING THE PROPOSED MORPHOLOGICAL FILTERING ALGORITHM ON DRIVE DATASET

Measurements	1st Observer	2nd Observer	Average
Acc.	97.34	98.78	98.06
Sen.	97.67	98.32	97.995
Spe.	98.32	97.23	97.775
PPV	89.92	90.22	90.07
NPV	93.89	95.56	94.725

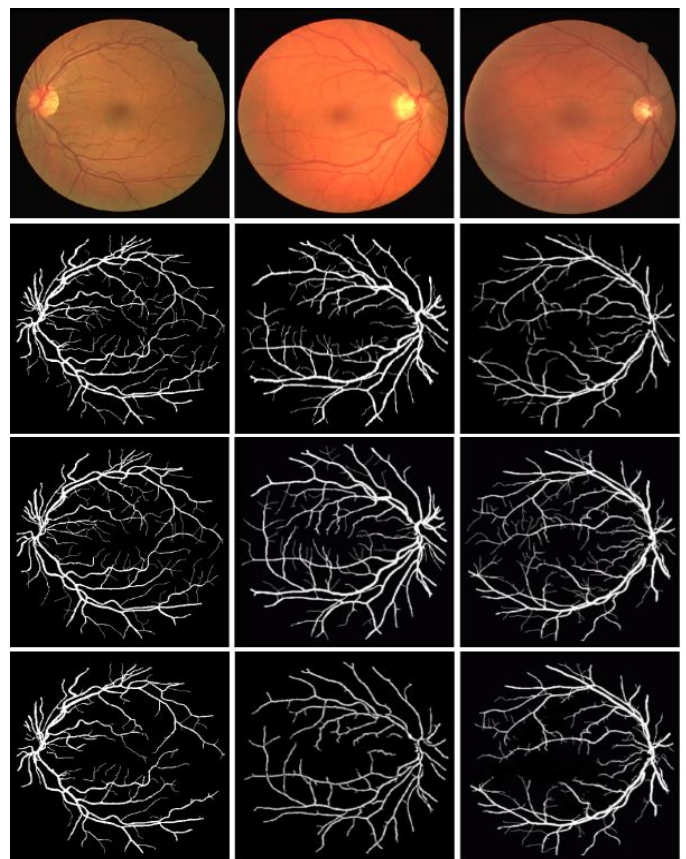


Fig. 11. The Output Segmentation Results in the DRVIE Dataset: The main Picture, The 1st Human Observer Picture, The 2nd Human Observer, and The Output Segmented Picture of the Proposed Morphological Algorithm.

Herein, the results obtained on the 2nd human observer have been considered for comparison purposes. It has been noted that most previously published approaches in the literature are reporting the values of Acc., Sen., and Spe. Thus, the overall average of these three metrics along with the PPV and NPV values have been computed with GT images (2nd human observer) and listed in Table II. Although, Li and his team, [22], Jin, [23], Hassan, [24], Dasgupta and Singh [26], Tamim, [30], and Yang, [28] have achieved a higher Spe. and NPV value compared with the proposed morphological filtering algorithm, they achieved inferior results on the other metrics.

TABLE II. EXECUTION RESULTS OF THE COMPARISON OF THE PROPOSED ALGORITHM WITH THE MODERN VESSEL SEGMENTATION APPROACH ON THE DRIVE DATASET

Approaches	Acc.	Sen.	Spe.	PPV	NPV
Odstrcilik et al. [21]	94.73	78.07	97.12	-	-
Li et al. [22]	95.27	75.69	98.16	-	-
Jin et al. [23]	96.97	78.94	98.70	85.37	-
Hassan et al. [24]	96.25	87.99	97.99	-	-
C. Argyrois [25]	94.79	85.06	95.82	-	-
Dasgupta and Singh [26]	95.33	76.91	98.01	84.98	-
Samuel and Veeramalai [27]	96	82	97	-	-
Yang et al. [28]	95.83	73.93	97.92	77.70	97.53
Kishorea and Ananthamoorthy [29]	94.1	69.9	95.8	85.5	94.8
Tamim et al. [30]	96.07	75.42	98.43	86.34	96.53
Yang et al. [31]	95.22	71.81	97.47	89.23	98.5
Yang et al. [32]	94.21	75.60	96.96	78.54	96.44
Keerthiveena et al. [33]	94.71	92.7	95.6	92.49	95.7
Morphological Filtering Algo.	98.78	98.32	97.23	90.22	95.56

D. 4.4 Result of HRF Dataset

The execution of the selected vessels segmentation algorithm has been assessed using HRF dataset using the same parameters configuration described in Section II.2. Initially, the adopted five evaluation metrics have been calculated to the selected vessel shrink algorithms utilizing the GT pictures provided in the HRF dataset, as shown in Table III. It has been noted that a comparable performance has been achieved with the proposed morphological filtering where a PPV of 96.88% and NPV of 100% have been obtained using the proposed morphological filtering algorithm. An example of the output segmentation results for the HRF dataset group is presented in Fig. 12.

The execution of the selected blood vessel segmentation algorithms has also been compared with the modern approaches to the HRF group, as given in Table IV. It has been observed that some existing approaches have achieved slightly higher segmentation accuracy compared with the proposed algorithms. For instance, Kishorea and Ananthamoorthy [29] have reached an Acc. of 99.6% compared to an Acc. of 98.76% and 98.78 using the proposed morphological filtering algorithm. However, the work presented in [32] has obtained inferior results in terms of other

evaluation metrics, for instance, Sensitivity, Specificity, positive prediction value, and negative predictive value which were compared with the proposed morphological filtering algorithm. On the other hand, Chalakkal et al. [35] have achieved a slightly better Spe. value of 100% compared with a Spe. value of 99.17%, 99.35%, and 99.78%, using the morphological filtering algorithm, respectively. However, they got inferior results on the other evaluation metric (e.g., Acc. and Sen.). Finally, one can see the best Sen. value of 98.87%, 99.12%, and 99.89% has been obtained using the morphological filtering algorithm, respectively, the outcome results compared with the modern approaches to HRF dataset.

TABLE III. EXECUTION COMPARISON OF THE SELECTED ALGORITHMS ON THE HRF DATASET

Measurements	Morphological Filtering Algo.
Acc.	98.76
Sen.	98.87
Spe.	99.17
PPV	96.88
NPV	100

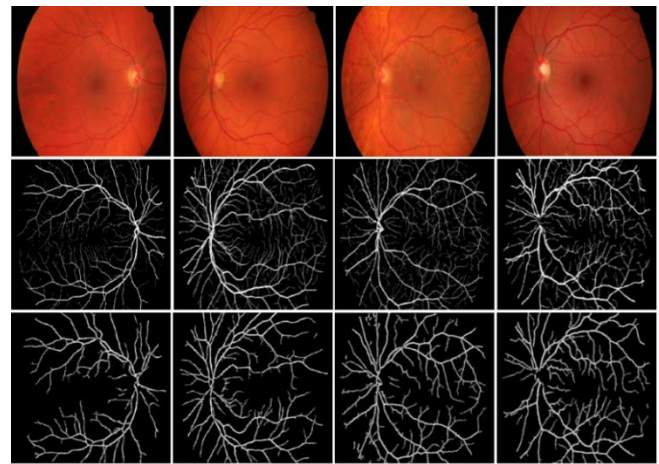


Fig. 12. The Output Segmentation Outcomes on the HRF Group: The main Photograph, The Human Observer Photograph, and The Output Segmented Photograph of the Selected Morphological Filtering.

TABLE IV. EXECUTION COMPARISON OF THE SELECTED ALGORITHMS WITH MODERN BLOOD RECEPTACLE SHRINK APPROACHES ON THE HRF GROUP

Approaches	Acc.	Sen.	Spe.	PPV	NPV
Vostatek [34]	94.3	58.3	97.8	-	-
Kishorea and Ananthamoorthy [29]	99.6	76.52	98.5	87.9	96
Yang [32]	95.17	79.15	96.76	70.79	97.90
Chalakkal [35]	94.4	88.8	100		
Yang [36]	95.49	72.65	97.40	70.03	97.71
Wang [37]	96.54	78.03	98.43	-	-
Khan [38]	95.9	77.2	97.8	-	-
Upadhyay [39]	95.2	75	97.2	72.7	-
Guo and Peng [40]	98.56	80.25	98.54	-	-
Morphological Filtering Algo.	98.76	98.87	99.17	96.88	100

E. 4.5. Clinical Feature Evaluation

In this section, a medical valuation process was conducted to accurately evaluate the efficiency in addition to the reliability of the proposed algorithms in terms of extracting helpful medical features. These clinical features include the tortuosity, length, density, and thickness of the blood vessel, which are efficiently used to detect several ophthalmological diseases. In the conducted experiments, the automated estimations of the four clinical features were calculated by utilizing the definition of the clinical feature on GT pictures in the adopted datasets.

Initially, the automated estimation of the clinical features from the DRIVE dataset using the 1st human observer was computed by the proposed algorithms and directly compared with the reference values generated from the GT images of the 1st human observer. The overall average (AV.), Standard Deviation (STD), Maximum (Max), and Minimum (Min) of each clinical feature on manual in addition to automated generated pictures. Moreover, (Diff) represents the Difference and (Diff %) represents the percentage difference between both of them which are presented in Table V. The overall average of (Diff%) between the manual shrinkage method and automated using the proposed morphological filtering algorithm was less than 19%, 16.5%, 10%, and 18% for the tortuosity, thickness, length, and density, respectively.

TABLE V. EXECUTION COMPARISON WAS CONDUCTED BETWEEN THE MANUAL SHRINKAGE METHOD AND AUTOMATED ESTIMATIONS OF FOUR CLINICAL FEATURES UTILIZING THE 1ST HUMAN OBSERVER OF DRIVE DATASET

	Manual		Morphological Filtering	
	TC	TC	Diff	Diff %
AV.	1.814	1.5015	0.312	18.85
STD	0.8628	0.7877	0.075	9.095
Max	3.78	3.68	0.1	2.680
Min	1.06	1.02	0.04	3.846
	Thick.	Thick.	Diff	Diff %
AV.	3.7735	3.2015	0.572	16.401
STD	0.3722	0.2796	0.092	28.413
Max	4.32	3.72	0.6	14.925
Min	2.98	2.75	0.23	8.02
	NL	NL	Diff	Diff %
AV.	33.447	36.934	-3.48	9.910
STD	4.5592	6.8644	-2.30	40.363
Max	47.48	53.46	-5.98	11.848
Min	28.83	23.89	4.94	18.740
	ND	ND	Diff	Diff %
AV.	0.0129	0.0108	0.002	17.884
STD	0.0103	0.0092	0.001	10.805
Max	0.0343	0.0261	0.008	27.152
Min	0.0025	0.0017	0.0008	38.095

Using the 1st human observer of DRIVE dataset, Pearson correlation plots were also adopted to further confirm the clinical reliability and usefulness of the proposed blood vessel segmentation algorithms as effective tools to provide a precise and automated estimation of the vessel's clinical features. As shown in Fig. 13, the proposed morphological filtering algorithm has managed to achieve (r) representing Pearson's correlation and (p) representing coefficient of: ($r = 0.86, p < 0.0001$) for vessel tortuosity, ($r = 0.86, p < 0.0001$) for vessel thickness, ($r = 0.79, p < 0.0001$) for vessel length, and ($r = 0.91, p < 0.0001$) for vessel density.

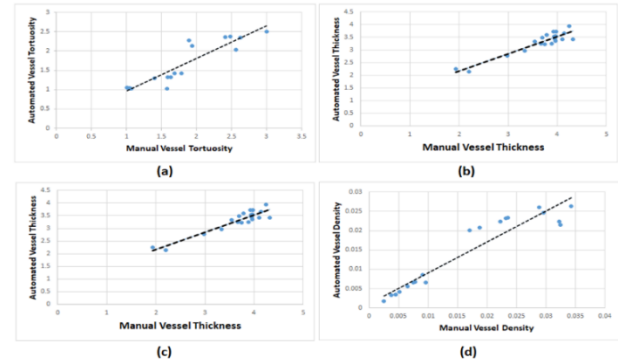


Fig. 13. Correlation Plots between Manual using the 1st Human Observer and Automated Clinical Estimations for the DRIVE Dataset using the Proposed Morphological Filtering Algorithm: (a) Tortuosity, (b) Thickness, (c) Length, and (d) Density. The Same Clinical Evaluation was Carried Out to Get the Automated Estimation of the Clinical Features from the DRIVE Dataset using the 2nd Human Observer.

Fig. 14 and Table VI presents the selected morphological filtering has managed to achieve (R) and (P) with the scale of : ($r = 0.94, p < 0.0001$) for vessel tortuosity, ($r = 0.86, p < 0.0001$) for vessel thickness, ($r = 0.89, p < 0.0001$) for vessel length, and ($r = 0.76, p < 0.0001$) for vessel density.

TABLE VI. EXECUTION COMPARISON WAS CONDUCTED BETWEEN THE MANUAL SHRINKAGE METHOD AND AUTOMATED METHODS OF FOUR CLINICAL FEATURES UTILIZING THE 2ND HUMAN OBSERVER OF DRIVE DATASET

	Manual		Morphological Filtering	
	TC	TC	Diff	Diff %
Average	1.708	1.5015	0.206	12.868
STD	0.903	0.7877	0.116	13.733
Max	4.48	3.68	0.8	19.607
Min	1.01	1.02	-0.01	0.985
	Thick.	Thick.	Diff	Diff %
Average	3.834	3.2015	0.633	17.993
STD	0.378	0.2796	0.099	30.123
Max	4.3	3.72	0.58	14.463
Min	3.12	2.75	0.37	12.606
	NL	NL	Diff	Diff %
Average	33.543	36.934	-3.391	9.622
STD	5.496	6.8644	-1.368	22.145
Max	46.94	53.46	-6.52	12.988
Min	26	23.89	2.11	8.454
	ND	ND	Diff	Diff %
Average	0.013	0.0108	0.0024	20.6010
STD	0.007	0.0092	-0.0017	20.233
Max	0.0344	0.0261	0.0083	27.430
Min	0.0013	0.0017	-0.0004	26.666

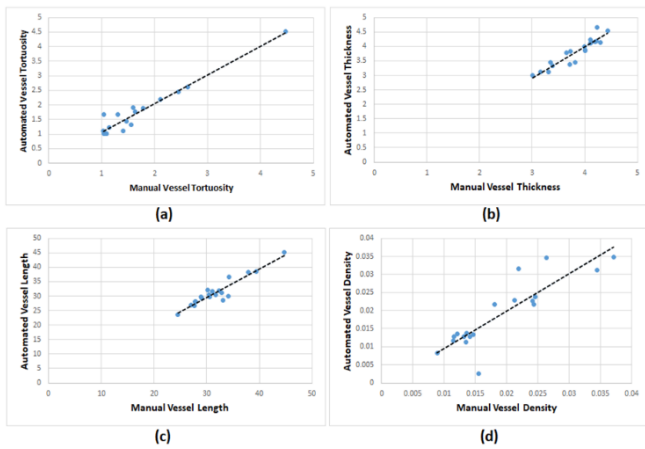


Fig. 14. Correlation Plots between Manual using the 2nd Human Observer and Automated Clinical Estimations for the DRIVE Dataset using the Proposed Morphological Filtering Algorithm: (a) Tortuosity, (b) Thickness, (c) Length, and (d) Density.

TABLE VII. EXECUTION COMPARISON WAS CONDUCTED BETWEEN THE MANUAL SHRINKAGE METHOD AND AUTOMATED METHODS OF FOUR CLINICAL FEATURES UTILIZING HRF DATASET

	Manual	Morphological Filtering		
	TC	TC	Diff	Diff %
Average	1.580	1.5111	0.069	4.485
STD	0.843	0.906	-0.062	7.196
Max	5.38	4.3	1.08	22.314
Min	1.02	1.02	0	0
	Thick.	Thick.	Diff	Diff %
Average	3.834	3.380	0.454	12.584
STD	0.592	0.557	0.034	6.033
Max	5.79	4.98	0.81	15.041
Min	2.67	2.44	0.23	9.001
	NL	NL	Diff	Diff %
Average	28.983	27.949	1.034	3.632
STD	3.673	4.302	-0.628	15.750
Max	38.43	39.73	-1.3	3.326
Min	23.56	20.17	3.39	15.504
	ND	ND	Diff	Diff %
Average	0.0059	0.0054	0.0005	10.087
STD	0.0035	0.0031	0.0003	10.240
Max	0.0189	0.0189	0	0
Min	0.0014	0.0011	0.0002	20.472

The evaluation process is an important task to validate the proposed algorithm and has been used in many studies, such as [29-32]. Further evaluation was performed on HRF Dataset which contains 40 GT images to assess the performance of the selected blood vessel shrinking algorithms. As shown in Table VII, the overall Min, AV, Max, and STD of every clinical feature for the automated and manual pictures were computed along with the Diff and Diff % between them. The average Diff% between manual and automated estimations calculated

using the proposed morphological filtering algorithm was 4.485% v 2.560%, 12.584% v 12.59%, 3.632% v 2.484%, and 10.087% v 5.529% for the tortuosity, thickness, length, and density, respectively. Correlation plots between manual and automated clinical estimations for the HRF dataset using the proposed morphological filtering algorithm are presented in Fig. 15.

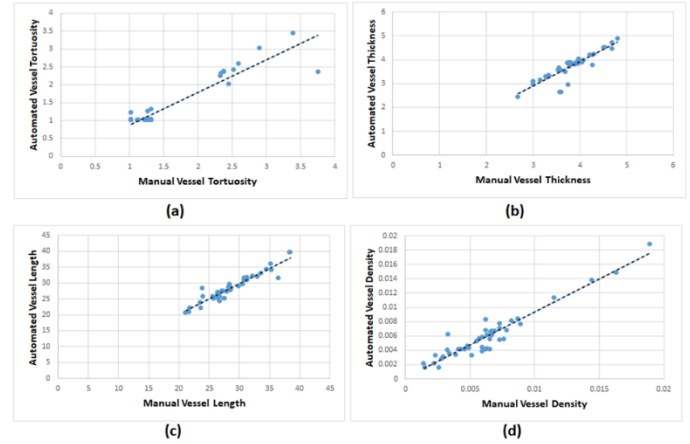


Fig. 15. Correlation Plots between Manual and Automated Clinical Estimations for the HRF Dataset using the Proposed Morphological Filtering Algorithm: (a) Tortuosity, (b) Thickness, (c) Length, and (d) Density.

V. CONCLUSION

In this study, a precise, quick, and fully-automatic blood vessel shrinking in addition to the clinical feature measuring system for retinal fundus images is presented. The proposed morphology has two main steps: separating the blood vessels and pulling out the clinical features. In the blood vessels segmentation stage, a fully-automated segmentation algorithm was proposed and named as a morphological filtering algorithm to classify the blood receptacles in the retinal internal pictures. The algorithm has its own image enhancement procedure which is addressed by pre-processing stage in order to figure out the problems of blurring, variation levels of the light, and poor contrast of the retinal internal picture, plus to promote the early diagnosis of several eye pathologies. Several exhaustive experiments were purely conducted to evaluate the efficacy of the developed fully-automated shrinking algorithm in classified retinal blood receptacles using the DRIVE and HRF datasets of exceedingly demanding fundus images. Initially, the accuracy of the created algorithm was tested based on its ability to accurately recognize retinal blood receptacles. Five quantitative performance measures were computed to validate the efficacy of the selected algorithm, including the accuracy, sensitivity, specificity, positive predictive value, and negative predictive value of 98.78%, 98.32%, 97.23%, 90.22% and 95.56%. According to the HRF dataset results are based on five quantitative performance measures 98.76%, 98.87%, 99.17%, 96.88%, and 100% respectively. Then, the efficiency and reliability of the proposed algorithm in terms of extracting useful and helpful clinical features were also evaluated by conducting a set of extensive experiments. Statistically notable correlations between the manual and automated estimations of the adopted four clinical features have been obtained using the proposed algorithm on both datasets (DRIVE and HRF).

ACKNOWLEDGMENT

This work is sponsored by Universiti Tenaga Nasional (UNITEN) under the Bold Research Grant Scheme No. J510050002 - IC-6 BOLDREFRESH2025.

REFERENCES

- [1] A. A. Abdulsahib1, M. A. Mahmoud, Mazin Abed Mohammed, Hind Hameed Rasheed, S. A. Mostafa4, and M. S. Maashi, Comprehensive Review of Retinal Blood Vessels Segmentation and Classification Techniques Intelligent Solutions for Green Computing in Medical Images, Current Challenges, Open issues, and Knowledge Gaps in Fundus Medical Images. Network Modeling Analysis in Health Informatics and Bioinformatics (2021) 10:20 <https://doi.org/10.1007/s13721-021-00294-7>, vol. springer, 2021.
- [2] S. Lal, S. U. Rehman, J. H. Shah, T. Meraj, H. T. Rauf, R. Damasevicius, et al., Adversarial Attack and Defence through Adversarial Training and Feature Fusion for Diabetic Retinopathy Recognition, Sensors (Basel), vol. 21, Jun 7 2021.
- [3] K. Balasubramanian and N. P. Ananthamoorthy, Robust retinal blood vessel segmentation using convolutional neural network and support vector machine, Journal of Ambient Intelligence and Humanized Computing, vol. 12, pp. 3559-3569, 2019.
- [4] H. Boudegga, Y. Elloumi, M. Akil, M. Hedi Bedoui, R. Kachouri, and A. B. Abdallah, Fast and efficient retinal blood vessel segmentation method based on deep learning network, Comput Med Imaging Graph, vol. 90, p. 101902, Jun 2021.
- [5] O. Ramos-Soto, E. Rodriguez-Esparza, S. E. Balderas-Mata, D. Oliva, A. E. Hassanien, R. K. Meleppat, et al., An efficient retinal blood vessel segmentation in eye fundus images by using optimized top-hat and homomorphic filtering, Comput Methods Programs Biomed, vol. 201, p. 105949, Apr 2021.
- [6] A. A. Abdulsahib, M. A. Mahmoud, H. Aris, S. S. Gunasekaran, and M. A. Mohammed, An Automated Image Segmentation and Useful Feature Extraction Algorithm for Retinal Blood Vessels in Fundus Images," Electronics, vol. 11, p. 1295, 2022.
- [7] M. Z. S. M. L. Jadhav, and V. M. Sardar, "Automated Microaneurysms Detection in Fundus Images for Early Diagnosis of Diabetic Retinopathy, under exclusive license to Springer Nature Singapore Pte Ltd. 2021 V. Bhateja et al. (eds.), Data Engineering and Intelligent Computing, Advances in Intelligent Systems and Computing 1, https://doi.org/10.1007/978-981-16-0171-2_9, 2021.
- [8] S. G. G. S. Anand, Optic disc analysis in retinal fundus using L2 norm of contourlet subbands, superimposed edges, and morphological filling, Springer, vol. 1210: Computer Vision for Clinical Images Published: 24 October 2021, 2021.
- [9] A. S. 2, S. A. 3, P. S. 4, and S. K. B. V, "Retinal Vessel Segmentation Using Morphological Top Hat Approach On Diabetic Retinopathy Images, 978-1-5386-4606-9©2018 IEEE, 2018.
- [10] R. Alaguselvi and K. Murugan, "Performance analysis of automated lesion detection of diabetic retinopathy using morphological operation," Signal, Image and Video Processing, vol. 15, pp. 797-805, 2020.
- [11] J. Dash and N. Bhoi, Detection of retinal blood vessels from ophthalmoscope images using morphological approach," ELCVIA Electronic Letters on Computer Vision and Image Analysis, vol. 16, p. 1, 2017.
- [12] U. Ozkava, S. Ozturk, B. Akdemir, and L. Sevfi, An Efficient Retinal Blood Vessel Segmentation using Morphological Operations, pp. 1-7, 2018.
- [13] S. J. a. M. S. Charu Bhardwaj, "Performance analysis of retinal features for diabetic retinopathy characterisation and diagnosis" Published Online: December 15, 2020pp 253-270, 2020.
- [14] P. P. A. J. MALIK, Scale-Space and Edge Detection Using Anisotropic Diffusion ,IEEE TRANSACTIONS ON PATTERN ANALYSIS AND MACHINE INTELLIGENCE, VOL. 12. NO. 7. JULY 1990, 1990.
- [15] I. D. b and B. C. a. , Buddhajyoti Chattopadhyay a, Enhancing effective depth-of-field by image fusion using mathematical morphology, elsevier, vol. Image and Vision Computing 24 (2006) 1278–1287, 2006.
- [16] F. Susanta Mukhopadhyay and Bhabatosh Chanda, IEEE, Multiscale Morphological Segmentation of Gray-Scale Images, IEEE, vol. TRANSACTIONS ON IMAGE PROCESSING, VOL. 12, NO. 5, MAY 2003.
- [17] A. S. Al-Waisy, R. Qahwaji, S. Ipson, and S. Al-Fahdawi, A multimodal deep learning framework using local feature representations for face recognition, Machine Vision and Applications, vol. 29, pp. 35-54, 2017.
- [18] T. W. J. A. Kylstra I, M.L. Wolbarsht I' 2, M.B. Landers, III 1, and E. Stefansson The relationship between retinal vessel tortuosity, diameter, and transmural pressure, springer, vol. Graefe's Arch Clin Exp Ophthalmol (1986) 224:477-480, 1986, 1986.
- [19] V. M. Martynas Patašius, Arūnas Lukoševičius, Darius Jegelevičius, Model based investigation of retinal vessel tortuosity as a function of blood pressure preliminary results, IEEE, vol. preliminary results Proceedings of the 29th Annual International Conference of the IEEE EMBS Cité Internationale, Lyon, France August 23-26, 2007, 2007.
- [20] V. S. Joshi, Analysis of retinal vessel networks using quantitative descriptors OF VASCULAR MORPHOLOGY, the Biomedical Engineering and Bioengineering Commons, 2012.
- [21] Jan Odstreilik1, Radim Kolar1,2, Attila Budai3, J. H. , J. J. , J. G. , , T. Kubena4, et al., "<Retinal vessel segmentation by improved matched filtering: evaluation on a new high-resolution fundus image data., IET, vol. IET Image Process., pp. 1–11 1 doi: 10.1049/iet-ipr.2012.0455, 2013.
- [22] M. V. L. Li, Y. Nakashima, H. Nagahara, and R. Kawasaki, IterNet: Retinal image segmentation utilizing structural redundancy in vessel networks, Proc. - 2020 IEEE Winter Conf. Appl. Comput. Vision, WACV 2020, pp. 3645–3654, 2020, doi: 10.1109/WACV45572.2020.9093621.
- [23] A. S. A.-W. R. Q. S. I. S. Al-Fahdawi1, A multimodal deep learning framework using local feature representations for face recognition , springer, vol. Machine Vision and Applications DOI 10.1007/s00138-017-0870-2, 2017.
- [24] N. E.-B. G. Hassan, A. E. Hassanien, A. Fahmy, S. Abullahm, and V. Snaesl, Retinal Blood Vessel Segmentation Approach Based on Mathematical Morphology, Procedia Comput. Sci., vol. 65, no. Iccmit, pp. 612–622, 2015, doi: 10.1016/j.procs.2015.09.005., 2015.
- [25] A. C. T. H. Housseem and B. T. F. Cherie, A Multi-scale Tensor Voting Approach for Small Retinal Vessel Segmentation in High Resolution Fundus Images, Comput Med Imaging Graph, 2016. 52: p. 28-43., 2016.
- [26] A. Dasgupta and S. Singh, A fully convolutional neural network based structured prediction approach towards the retinal vessel segmentation, Proc. - Int. Symp. Biomed. Imaging, pp. 248–251, 2017, doi: 10.1109/ISBI.2017.7950512., 2017.
- [27] P. M. Samuel and T. Veeramalai, Multilevel and multiscale deep neural network for retinal blood vessel segmentation, Symmetry (Basel), vol. 11, no. 7, 2019, doi: 10.3390/sym11070946., 2019.
- [28] F. S. Y. Yang, Z. Fu, and R. Fu, Blood vessel segmentation of fundus images via cross-modality dictionary learning," Appl. Opt., vol. 57, no. 25, p. 7287, 2018, doi: 10.1364/ao.57.007287., 2018.
- [29] B. Kishore and N. P. Ananthamoorthy, Glaucoma classification based on intra-class and extra-class discriminative correlation and consensus ensemble classifier, Genomics, vol. 112, no. 5, pp. 3089–3096, 2020, doi: 10.1016/j.ygeno.2020.05.017., 2020.
- [30] M. E. Nasser Tamim, Gamil Abdel Azim and Hamed Nassar, Retinal Blood Vessel Segmentation Using Hybrid Features and Multi-Layer Perceptron Neural Networks, MDPI, vol. Symmetry 2020, 12, 894; doi:10.3390/sym12060894, 2020.
- [31] M. H. J. Yang, J. Fu, C. Lou, and C. Feng, Frangi based multi-scale level sets for retinal vascular segmentation, Comput. Methods Programs Biomed., vol. 197, p. 105752, 2020, doi: 10.1016/j.cmpb.2020.105752., 2020.
- [32] F. S. Y. Yang, Z. Fu, and R. Fu, Discriminative dictionary learning for retinal vessel segmentation using fusion of multiple features, Signal, Image Video Process., vol. 13, no. 8, pp. 1529–1537, 2019, doi: 10.1007/s11760-019-01501-9., 2019.
- [33] S. E. B. Keerthiveena, K. Selvakumar, and T. Yogesh, Computer-aided diagnosis of retinal diseases using multidomain feature fusion, Int. J.

- Imaging Syst. Technol., vol. 30, no. 2, pp. 367–379, 2020, doi: 10.1002/ima.22379., 2020.
- [34] P. Vostatek, Blood Vessel Segmentation in the Analysis of Retinal and Diaphragm Images Blood Vessel Segmentation in the Analysis of Retinal and Diaphragm, 2017.
- [35] W. H. A. R. J. Chalakkal, and S. S. Thulaseedharan, Quality and content analysis of fundus images using deep learning, *Comput. Biol. Med.*, vol. 108, no. March, pp. 317–331, 2019, doi: 10.1016/j.combiomed.2019.03.019., 2019.
- [36] X. Y. Z. Yan, and K. T. Cheng, Joint segment-level and pixel-wise losses for deep learning based retinal vessel segmentation, *IEEE Trans. Biomed. Eng.*, vol. 65, no. 9, pp. 1912–1923, 2018, doi: 10.1109/TBME.2018.2828137.
- [37] A. H. D. Wang, J. Pottenburgh, O. Saeedi, and Y. Tao, Hard Attention Net for Automatic Retinal Vessel Segmentation, *IEEE J. Biomed. Heal. Informatics*, vol. 24, no. 12, pp. 3384–3396, 2020, doi: 10.1109/JBHI.2020.3002985., 2020.
- [38] M. S. S. K. B. Khan, M. Ahmad, and M. Mazzara, A Hybrid Unsupervised Approach for Retinal Vessel Segmentation, *Biomed Res. Int.*, vol. 2020, doi: 10.1155/2020/8365783., 2020.
- [39] M. A. K. Upadhyay, and P. Vashist, Unsupervised multiscale retinal blood vessel segmentation using fundus images, *IET Image Process.*, vol. 14, no. 11, pp. 2616–2625, 2020, doi: 10.1049/iet-ipr.2019.0969., 2020.
- [40] Y. Guo and Y. Peng, BSCN: Bidirectional symmetric cascade network for retinal vessel segmentation, *BMC Med. Imaging*, vol. 20, no. 1, pp. 1–22, 2020, doi: 10.1186/s12880-020-0412-7., 2020.

Detection of Cyber-Physical Attacks using Physical Model with Nonparametric EWMA Detector

Joko Supriyadi, Jazi Eko Istiyanto, Agfianto Eko Putra

Department of Computer Science and Electronics, Universitas Gadjah Mada, Yogyakarta, Indonesia

Abstract—Industrial Control System (ICS) can suffer of cyber-physical attacks resulting in accident, damage, or financial loss. The attacks can be detected in both in physical space or cyberspace of the ICS. The detection in physical space can be based on physical models of the system. To model the physical system this study uses a data-driven modeling approach as an alternative of the analytic one. This study models the system using the dynamic mode decomposition method with control (DMDc) assuming a full state measurement. The attack detector used in some researches with predictive physical models is the cumulative sum (CUSUM), which only applies to normally distribute residual data. To detect any cyber-physical attack, this research uses a nonparametric exponentially weighted moving average (EWMA) detector. This study uses a data set from a testbed of Secure Water Treatment (SWaT). The approach used in this study was successful in detecting 8 out of 10 attacks on the first SWaT subsystem. This study demonstrates that DMDc used in this study results a better goodness of fit and the nonparametric EWMA can be used as an alternative as detector when residual data do not follow a normal distribution.

Keywords—Industrial control systems; cyber-physical attacks; physical model; dynamic mode decomposition method with control (DMDc); nonparametric exponentially weighted moving average (EWMA)

I. INTRODUCTION

Industrial Control System (ICS) is automation system used to control and monitor industrial functionality. It can be found in the industrial sectors and critical infrastructures, such as nuclear and thermal plants, water treatment facilities, power generation, heavy industries, and distribution systems [1].

ICS has four levels to conduct its functionalities [2]. On the field level, it has sensors and actuators. On the control level, it has a programmable logic controller (PLC). It has a human-machine interface (HMI), and on the enterprise level, it has an information technology (IT) system. The second and third levels with their cyber components conduct computation to control physical space. With this trait, ICS is an example of cyber-physical systems.

As a cyber-physical system, ICS carries the risk of cyberattacks aimed to disrupt the physical processes. A cyber-physical attack is an attack via cyberspace that targets the physical system of the ICS. Examples of such attacks are Stuxnet which attacked Iran's uranium enrichment facilities, and Black Energy 3 which struck several power transmission substations in Ukraine [3]. These attacks can have some adverse effects on factory safety or financial loss.

To detect cyber-physical attacks on ICS, researchers develop intrusion detection systems (IDS). There are three IDS categories for ICS [4], protocol analysis-based, traffic mining-based, and control process analysis-based. The former two categories are conducted in cyberspace. The third category is conducted on physical space and includes process data analysis-based, control command analysis-based, and physical model-based techniques [4].

This study is in the field of detection in physical space using a physical model, i.e. the third category in [4]. The work in [5] identify that most of researches in this field do not use input-output approach in modelling physical behavior and most use the simulation data. This research proposes to use dynamic mode decomposition method with control (DMDc) as a system identification with input-output method. It will be applied to a real data from a testbed not at simulation data.

To detect the anomalies, some researches use cumulative sum (CUSUM) that has an assumption that the distribution is normal. In this research we propose to use nonparametric exponentially weighted moving average to cover all distribution condition.

The significant contributions of this work are:

- We anticipate a full state measurement condition of physical systems. To model it, we use DMDc as a kind of a system identification approach.
- We use EWMA detector as an alternative for CUSUM detector to cover a non-normal distribution of residual.

The rest of the paper is organized as follows. In section 2 related works are presented. It posits our research in the field of detection of cyber-physical in physical space of ICS. Section 3 presents the research methods of this study. It covers the DMDc method and EWMA detector. In section 4 the results of the experiment are presented and discussed.

II. RELATED WORKS

According to Urbina *et al.* [5], there are two ways to model physical systems. The first is to develop a physical equation model that connects all the physical parameters to determine the system's dynamics. The second is to create a model based on observation through a technique known as system identification. Most researchers use the first approach, and only a few uses the second.

Researchers in [16] use input-output model developed from physical equation for a water treatment system. Their research leverages connectivity of two subsystems to detect

any cyber physical attack to upstream with behavior of the downstream of the system. Their experiment is launched directly to a real system and their procedure was conducted at the real time.

Our study is focused on the use of system identification and not model the system using physical equation. There are two options in system identification, output only model and input-output model. Researchers in [5] used both approaches to model a physical system. The system is a simulator of frequency control in the power grid. After comparing both models, researchers in [5] concludes that the input-output model has a potential in detection and motivates future researchers to use it to model physical systems. To detect any cyber-physical attacks, there is a need to model the physical model from measurement data in the form of input-output model.

Researchers in [6] used the system identification method to model a physical system with the input-output model. They used a method in a group of subspace models. They used EPANET, a software that can customize a water distribution system simulator as the physical system.

Other researchers [7] conduct modelling with subspace system identification with input-output model with CUSUM detector, bad data detector, and noiseprint. To detect the anomaly, they used CUSUM detector with false positive target around 5%.

Usually, the system identification approach used in [5,9] do not assume that the system being modeled is in full measurement. But nowadays, with the affordability of measurement cost, the system status can be measured in full. Unlike the studies, our study proposes using dynamic mode decomposition with control (DMDc) to model the physical system, assuming a complete system measurement.

The author in [5] used simulations as physical systems to be modeled. But there is a problem with simulations; although the physical model is detailed but the simulation is not in a real situation. Unlike theirs, our study uses a data set from Secure Water Treatment (SWaT), a physical system testbed that mimics a real water treatment system.

Some researchers use the same data set to propose their method to detect cyber-physical attacks. One of them [8] uses a graphical model-based approach that will be compared with our work.

Based on the physical model, cyber-physical attacks can be detected by monitoring an anomaly in the systems. The monitoring systems get inputs from sensors and command controls and then identify any anomalies [6]. Some researchers use CUSUM detector or bad data detector [5, 6, 7, 9, 16]. But the use of both as detector applies only to data with a normal distribution. Because not all conditions meet the normal distribution, our study proposes to use a nonparametric exponentially weighted moving average (EWMA) detector that does not depend on data distribution.

III. RESEARCH METHOD

In this section, we will explain the methods we used in our research. It includes details of DMDc, nonparametric EWMA, and a brief explanation of steps to apply the methods.

A. Physical System Modelling

A discrete state-space model will be used to represent the ICS control system. This model is used because it is generally more compatible with discrete digital controls. For discrete-time systems, the time may be referred as an integer index $k=0, 1, 2, \dots$. In the system, the state as a set of variables from the system can be estimated based on the previous state. Given a linear system has several states, inputs, and output, respectively. The equation of the system can be modeled as shown in (1) and (2).

$$x_{k+1}=Ax_k +Bu_k \quad (1)$$

$$y_{k+1}=Cx_k \quad (2)$$

In (1) and (2), $x_k \in \mathbb{R}^n$ is the state of the system at time k , $u_k \in \mathbb{R}^l$ is the input, and $y_k \in \mathbb{R}^q$ is the output with n , l , and q as number of states, inputs, and outputs respectively. Meanwhile, A is a dynamic matrix, B is the control matrix, and C is the discrete-time sensor matrix. State vector x from the system can be estimated from sensor measurement y . There is a condition called full state measurement if all components of the state vector can be measured.

The system can be modeled with a system identification approach, namely by using measurement data to obtain the desired model. In this study, the dynamic mode decomposition (DMD) method [10] is used, assuming that measurements are made of all states of the system (full-state measurement).

Initially, DMD was developed for systems that do not have input, for example, control input. By taking into account control input, DMD method developed to be DMD with control (DMDc). Both DMD and DMDc methods initially were developed for large dimension systems with a dimension reduction. The next exposition will explain DMDc method based on [10] but without dimension reduction steps.

DMDc analyses the relationship between measurement vectors at $k+1$ (x_{k+1}) with the measurement at k (x_k) and control input at k (u_{k+1}). The three data are assumed to be approximately by linear operators A and B relates as shown in (3).

$$x_{k+1} \approx Ax_k +Bu_k \quad (3)$$

where $x_k \in \mathbb{R}^n$, $u_k \in \mathbb{R}^l$, $A \in \mathbb{R}^{n \times n}$, and $B \in \mathbb{R}^{n \times l}$ with n and l are number of sensors and actuators respectively. DMDc tries to find the solution for operators A and B .

If there are m measurements for n sensors in vector x we can create a matrix X with dimension $n \times m$, $X \in \mathbb{R}^{n \times m}$. We can create matrix Y and Z from matrix X , where Y is matrix X without its first column, while Z is matrix X without its last column. The relationship of matrix Y and Z with matrix A can be described with (4).

$$Y \approx AZ \quad (4)$$

Accordingly, from control vector u , we can create a matrix $\Gamma \in \mathbb{R}^{l \times (m-1)}$ contains the l^{st} data to $m-1^{th}$ data for l actuators. So (4) can be rewritten to be (5).

$$Y \approx AZ + B\Gamma \quad (5)$$

A concatenation method can be used to assign matrix $G = [A \ B]$ and matrix $\Omega = \begin{bmatrix} Z \\ \Gamma \end{bmatrix}$ to solve the (5). Thus, (5) changes to be (6) as follows.

$$Y \approx G\Omega \quad (6)$$

Then Y and Ω is stated as eigen decomposition of the matrix G as shown in (7).

$$G \approx Y\Omega^\dagger \quad (7)$$

Where \dagger means Moore-Penrose pseudoinverse. The accurate and efficient method to find the pseudoinverse is singular value decomposition (SVD), as shown in (8).

$$\Omega = U\Sigma V^* \quad (8)$$

where $U \in \mathbb{R}^{n \times n}$, $\Sigma \in \mathbb{R}^{(n \times m)-1}$ and $V^* \in \mathbb{R}^{(n \times m)-1}$.

Using the SVD of Y , the matrix G can be approximated with (9).

$$G \approx \bar{G} = YV\Sigma^{-1}U^* \quad (9)$$

where \bar{G} is an approximation of the matrix G . From the matrix \bar{G} , the approximation of matrix A and B can be obtained by breaking operator U into two separate components given by (10)

$$[A, B] \approx [\bar{A}, \bar{B}] = [YV\Sigma^{-1}U_1^*, YV\Sigma^{-1}U_2^*] \quad (10)$$

where $U_1 \in \mathbb{R}^{n \times n}$, $U_2 \in \mathbb{R}^{l \times n}$, and $[U^*] = [U_1^* \ U_2^*]$. From (10), the dynamic systems can be constructed to be (11) as follows.

$$x_{k+1} = \bar{A}x_k + \bar{B}u_k \quad (11)$$

Equation (11) is the model we use to mimic the behavior of the physical system.

B. Residual and Non Parametric EWMA

Cyber-physical attacks on industrial control systems have a potential to change sensor readings behavior. Therefore, the difference between the estimates obtained from the model and the sensor readings can be monitored. The behavior of to the difference can be used to indicate if any attack to the system. The difference is called the residual r_k , namely the difference between measurement at k , x_k , and the estimation \hat{x}_k as shown in (12).

$$r_k = x_k - \hat{x}_k \quad (12)$$

The value of estimation \hat{x}_k is determined by (11); thus, (12) can be expressed as (13) as follows.

$$r_k = x_k - (Ax_{k-1} + Bu_{k-1}) \quad (13)$$

The sensors of the system can be more than one, so with $i = \{1, \dots, n\}$, $r_{k,i}$ is residual of sensor i at measurement k . Murguia *et al.* [9] used individual sensor residual to monitor cyber-physical attacks by making them input for CUSUM

detector and bad data detector. The two detectors implicitly assume that the residual follows a normal distribution.

In this study we use a nonparametric Exponentially Weighted Moving Average (EWMA) as the residual does not follow a normal distribution. This approach is generally used to statistically monitor a product's quality or process [11, 12]. The next description will explain the approach as describe in [12].

Given X_k is the individual measurement from the continuously monitored distribution with median θ , SN as statistic sign can be provided by (14).

$$SN_k = \text{sign}(X_k - \theta) \quad (14)$$

where:

$$\text{sign}(x) = \begin{cases} 1 & \text{if } x > 0 \\ 0 & \text{if } x = 0 \\ -1 & \text{if } x < 0 \end{cases} \quad (15)$$

The plotting statistic (Z_k) of the nonparametric EWMA as a sequentially accumulating the sign statistic SN_1, SN_2, SN_3, \dots defined by equation (16).

$$Z_k = \lambda SN_k + (1 - \lambda) Z_{k-1} \quad (16)$$

where λ is a weighting that has a value from 0 to 1, and $Z_0 = 0$.

Two controls can be used for the value of Z , upper control limit (UCL) and lower control limit (LCL), that can reach its steady-state after a long time. They can be determined by using (17).

$$\begin{aligned} UCL &= L \sqrt{\frac{\lambda}{2 - \lambda}} \\ CL &= 0 \\ LCL &= -L \sqrt{\frac{\lambda}{2 - \lambda}} \end{aligned} \quad (17)$$

In (17) CL is the central line valued as 0. The values can be used to determine if the system is under control or not.

The choosing of parameters L and λ is conducted to get the targeted average run length (ARL), namely the number of average measurements before the detector detects an anomaly from a normal condition. Graham [11] has calculated the value of pair parameter L and λ for nonparametric EWMA with the Markov method until $ARL = 500$.

We need to calculate the alarming rate that gives us the number of Z_k values calculated by (16) exceed UCL or LCL for a while. Then we set $Z_k = 0$ if $Z_{k-1} \geq UCL$ or $Z_{k-1} \leq LCL$.

C. Detection Parameter

We assume there is difference behavior between an attack condition with the normal one. In this research we use comparison of false alarm rate (FAR) or false positive rate (FPR) value between both conditions.

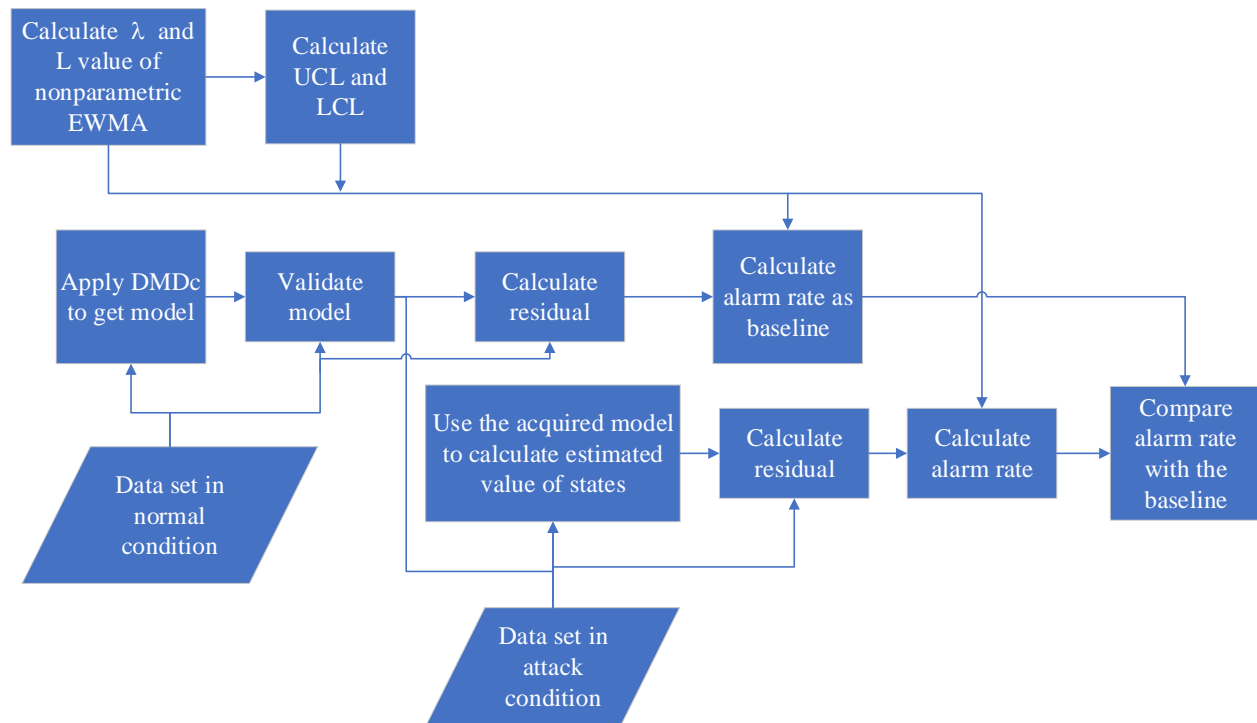


Fig. 1. Flow Chart of Detection System Set up.

The value of FPR is targeted in normal condition and considered as alarm rate of the system or components. Using the value as the baseline we judge a condition is under attack if FPR of a component is significantly more than its normal condition. With its procedure, security operator monitoring the system can detect any potential attack if the alarm rises significantly than the baseline.

D. Research Steps

Before using DMDc to model the physical system, we calculate L and λ values for specified ARL, for example, $ARL=500$ if we expect to get one false alarm per 500 measurements. The values were then used to calculate the value of UCL and LCL.

Parallel with previous steps; the physical system is modeled using DMDc method with the input of the normal condition data. Then the acquired model is validated by calculating its goodness of fit. If the value is satisfying, we calculate residuals as differences between model estimation and measurement. Based on the value of the residual, L , λ , UCL, and LCL, we calculate the value of Z_k . The alarm rate baseline is calculated based on the number of Z_k values that exceed UCL or LCL.

The next step is to use the model to detect cyber-physical attacks. The following procedure will be applied for every attack separately. With the acquired model from the previous steps, residuals' value is obtained by applying DMDc method on the data set in attack condition. Like previous steps in normal conditions, the value of alarm rate can be obtained using a parametric EWMA method.

To judge if the concerned attack is detected, we compare the alarm rate baseline's value of the alarming rate. We believe

that alarm is detected if the alarming rate is ten or more from the baseline. Fig. 1 shows the flowchart of the research steps.

IV. RESULT AND DISCUSSION

In this section, we will discuss our research results based on steps explain in the previous section.

A. Physical Modelling

This study uses the data set collected from a testbed that simulates Secure Water Treatment (SWaT) [13,14]. SWaT is a testbed in a full-scale replica water treatment facility consisting of several subsystem stages. A data set containing network data and process data is generated [13] recorded every second. The data set consists of two parts:

- 1) Data set of the system in a normal state without attack,
- 2) The data set of the system under attack condition.

The SWaT system has six subsystems, as described in [13], from subsystem P1 to P6. For this research, we use the first subsystem, P1 only, namely the subsystem that takes raw water and stores it in a reservoir. This subsystem has several main components [13], namely an MV-101 valve that drains water from the source into the storage tank T.101, whose water level is measured by the sensor LIT-101. Meanwhile, a flow meter FIT-101 is used to measure the source's flow rate into the tank. A pump P-101 is used to drain water from the reservoir to the next subsystem. Also, this subsystem has a pump P-102 as a backup for the pump P-101. Fig. 2 [13] shows the components and piping of the subsystem P-1. Thus, there are two sensors and three actuators in subsystem P1 as shown in Table I.

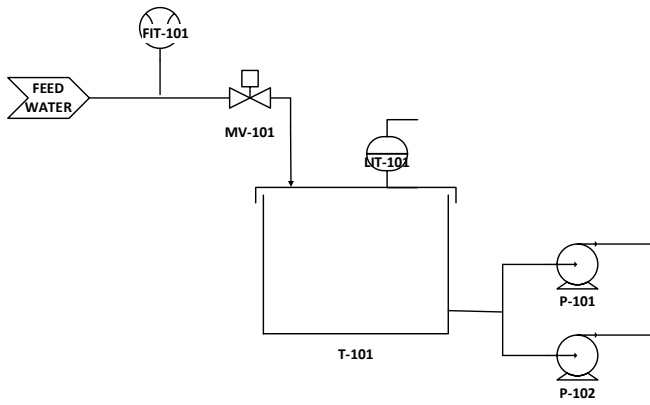


Fig. 2. Subsystem P1 of SWaT [13].

TABLE I. COMPONENTS OF THE SUBSYSTEM P1

Component	Type	Units
Flow rate FIT-101	Sensor	m3/h
Level meter LIT-101	Sensor	mm
Valve MV-101	Actuator	On/off
Pump P-101	Actuator	On/off
Pump P-102	Actuator	On/off

We use DMDc to model the subsystem P1 in the form of the discrete linear model provided by (11). From (11), the vector x contains subsystem P1 as a dynamic variable following the dynamics of water supply and demand for raw water. Thus, the vector x includes the measurement of the LIT-101 sensor. Meanwhile, the vector u in (11) contains the input into the subsystem. Among these inputs is the water supply, whose debit is measured using the FIT-101 sensor. Another information model for subsystem P1 is the pump P-101 pump and its pump P-102 as a backup.

The two pumps are modeled because the two pumps can be turned on alternately. The MV-101 valve is not modeled as it is redundant to the FIT-101. When the MV-101 valve is turned on, water flows with the discharge measured by the FIT-101 sensor. Thus, in (11), subsystem P1 can be modeled in its discrete form with (18).

$$[LIT - 101_{k+1}] = \bar{A} [LIT - 101_k] + \bar{B} \begin{bmatrix} FIT - 101_k \\ P - 101_k \\ P - 102_k \end{bmatrix} \quad (18)$$

In this subsystem modeling, matrix \bar{A} and \bar{B} are matrices that will be sought with the DMDc method by using a dataset in normal conditions without attack as input. Data set for normal conditions without attack contains measurement results of sensors and actuator conditions that are monitored every second. There are 494999 pieces of datum for each sensor and actuator. The first 3.5 hours of data are not used to let the system achieves a steady-state condition. The remainder is divided into two, 70% data for modeling and 30% data for testing.

Start from (5), the matrix Y is obtained as sensor measurement data from the 2nd to m^{th} measurement, the matrix

Z the sensor measurement data from the 1st to $m-1^{th}$ measurement, and the matrix Γ as the actuator data from the 1st to $m-1^{th}$ measurement. Furthermore, by following the procedure as described in (6) to (10), the values of a matrix \bar{A} and \bar{B} in (18) is obtained as follows.

$$\bar{A} = [1.000]$$

$$\bar{B} = [0.195 \quad -0.461 \quad 0.392]$$

With the values of the matrix \bar{A} and \bar{B} , the value of the inflow of water from the source and the water level at $k + 1$ can be estimated based on the measurement value at time k . The comparison of the level value of water in the tank measured by the LIT-101 sensor with the model's estimation results is shown in Fig. 3.

The estimation results are then compared with the actual measurement value to determine the model's level of suitability (goodness of fit) with the measurement results. Based on calculations using data for testing (30% of the overall data), the goodness of fit of the sensor LIT-101 is 99.7%. The value of goodness of fit is better than result in [6] that use another method of system identification. They use simulation data from EPANET, software to simulate a water system. With their method they achieve goodness of fit of 70%.

The value of goodness of fit shows a good agreement between model and measurement. Since the data set to test the model is independent of the training data set, it can be concluded that the model is not overfitted to the training data.

Meanwhile, Fig. 4 shows the error fluctuation in the form of the difference between the measurement results and the model estimation results. The error fluctuation is calculated with (13) as a residual that will be used to monitor the anomalies of subsystem P1.

B. Nonparametric EWMA

The residual as the difference between the estimation results from the model and the measurement at each time k resulted has a non-normal distribution. Therefore, the use of the CUSUM detector cannot be legitimized, and thus the nonparametric EWMA detector as described previously is used in this study.

The EWMA detector has a parameter λ and L as shown in (16) and (17). For this study we choose $ARL_0=500$. For this ARL value we choose a low value of λ ($\lambda=0.01$) to get a smooth change of Z_k sequences. For this value λ , Graham [11] get value of $L = 1.990$ as his calculation with Markov method.

With the value of L and λ , we calculate the control limits for UCL and LCL for a normal condition of their residual value of sensor LIT-101 with (17). The acquired values for UCL and LCL are 0.141067 and -0.141067 respectively.

With the acquired value of the parameters, the value of Z is sequentially calculated by (14). The value of Z_k fluctuates between the value of UCL and LCL as shown in Fig. 5. When it hits one of them the next value will be set to zero and the sequence starts again.

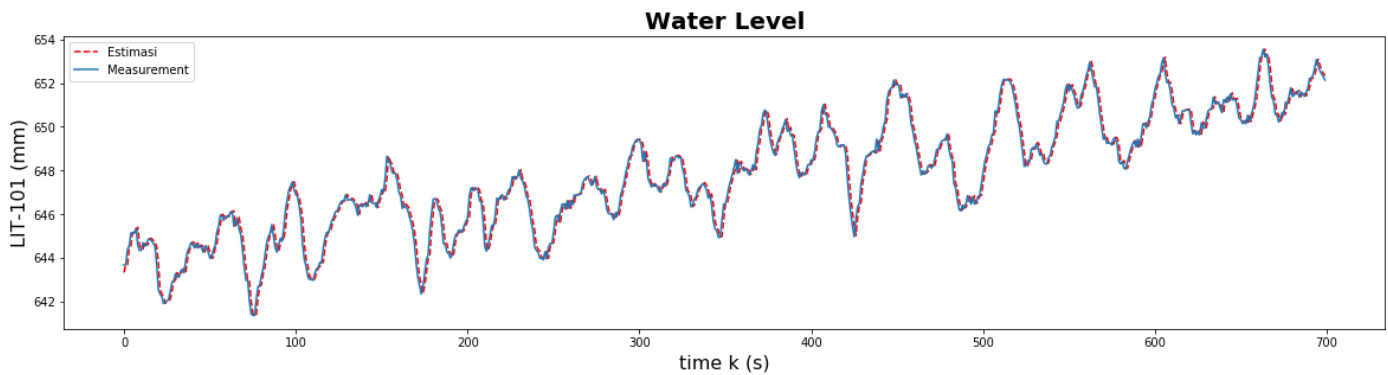


Fig. 3. The Dynamics of the Water Level from Measurement and Estimation.

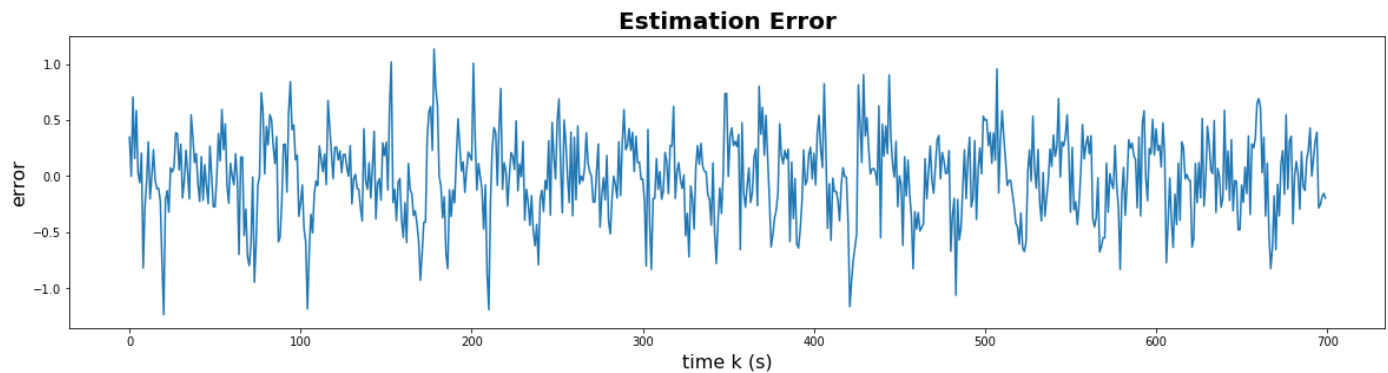


Fig. 4. Error Fluctuation of the Estimation of Water Level.

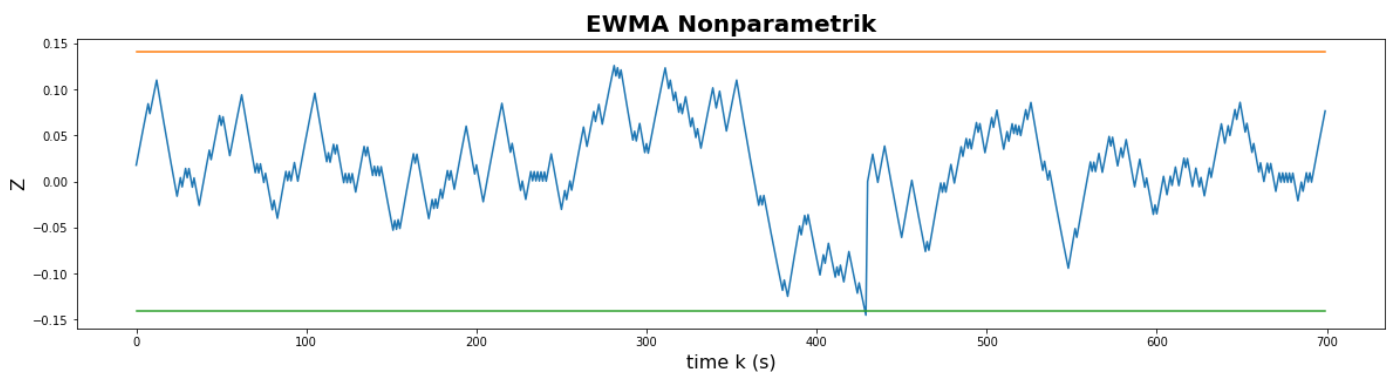


Fig. 5. The Fluctuation of Value Z with UCL and LCL as the Control.

The Z_k value passes UCL and LCL with a ratio of 1 in 489 data (alarm rate equals 0.00204). In other words, about 2.2% deviations from the ARL calculation theoretically using the Markov method of $ARL_0=500$ as the target. From the perspective of detection, the ratio is an expected false alarm rate in a normal condition. We use the value of the ratio as the baseline where the alarm rate of attack conditions will be compared, as we will explain in the next subsection.

The benefit of using nonparametric EWMA than CUSUM as in [5, 6, 9] is there is no need to assume the distribution of residual r as normal. As shown in the next subsection, this approach can be used to detect the cyber-physical attack as other detector.

C. Detection of Cyber-physical Attacks

To test the proposed detection design, we also use data set in [14] that contains sensors and actuators data from the SWAT under attack conditions. The attacks result in the data set use attack and attacker models developed by Adepu and Mathur [15]. The attacker model relates to the attacker's intention with the systems' components, properties, and performance.

The attack model captures the space of potential attacks aimed at achieving a specific set of goals. For example, an attack has a plan to make a tank overflow. The attack needs to consider some points of the system involved, for example, pumps or valves. A suitable procedure to launch the attack consists of identifying the tag in the programmable logic controller (PLC) that should be manipulated and a step to

compromise the link between PLC and supervisory control and data acquisition (SCADA) a step to conduct the manipulation of the tag.

There were 41 attack scenarios launched to the SWaT testbed, but only 36 attacks had physical impacts and were recorded in the data set. From the 36 attacks, there were 10 attacks involving the subsystem P1 in the data set as shown in Table II. All of the attack scenarios were launched to subsystem P1 only, but scenario 26 launched to subsystem P1 together with subsystem P3.

The system model and the nonparametric EWMA detector obtained from the previous section are used to detect cyber-physical attacks based on the data set [12]. The model is used to estimate the LIT-101 sensor reading value at time $k + 1$ with the time k . The estimation result is compared with the sensor reading value, which produces a residual value r_k . Then the residual value is used to detect an attack with an indication if the Z_k value exceeds the UCL or LCL values.

The Z_k value is calculated using (16) and (17) for each attack as described in Table II. As an illustration, Fig. 6 show the behavior of Z_k when subsystem P1 is under attack number 2 condition. Differ from the normal condition as shown in Fig. 5 that show a random behavior, the value of Z_k in attack no 2 as shown in Fig. 6 is systematically pushed to hit its lower threshold LCL. The change of behavior is an indication that the system is not in normal condition and the cyber-physical attack is a probable cause. As explained in the previous subsection, the baseline of false alarm rate (FAR) or False Positive Rate (FPR) for sensor LIT-101 calculated in normal conditions based on the normal condition dataset is 0.0020 (0.2%). To judge if any attacks can be detected, we compare the alarming rate in any attack conditions with the baseline.

TABLE II. DESCRIPTION OF ATTACKS SCENARIO

No.	Attack Number	Description of the attack	Duration (s)
1	1	Open MV-101	940
2	2	Turn on P-102	1407
3	3	Increase LIT-101 by 1 mm per second	383
4	21	Keep MV-101 on continuously; Value of LIT-101 set as 700 mm	701
5	26	P-101 is turned on continuously; a set value of LIT-301 as 801 mm	1445
6	30	Turn P-101 on continuously; Turn MV-101 on continuously; Set value LIT 101 as 700 mmP-101	1171
7	33	Set LIT-101to above H	444
8	34	Turn P-101off	101
9	35	Turn P-101off; keep P-102 off	481
10	36	Set LIT-101 less than LL	474

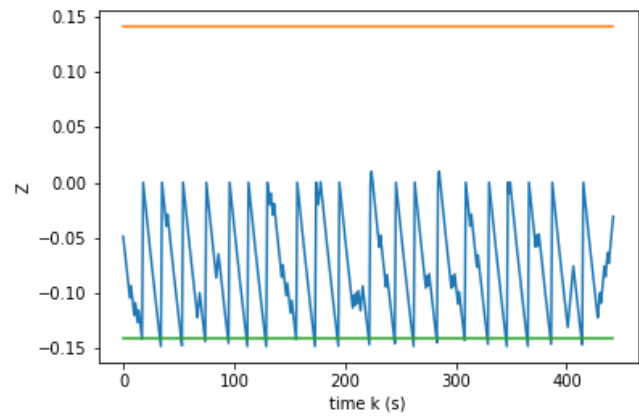


Fig. 6. The Fluctuation of Value Z_k when System is under Attack no.2 Condition.

TABLE III. ALARM RATE FOR ATTACKS INVOLVING SUBSYSTEM P1

No.	Attack Number	Alarm rate (compared to baseline)	Judgment	Detection in [8]
1	1	0.0021 (1.40)	Not detected	Detected
2	2	0.0452 (22.09)	Detected	Detected
3	3	0.0470 (22.99)	Detected	Not detected
4	21	0.0585 (28.62)	Detected	Detected
5	26	0.0505 (24.72)	Detected	Detected
6	30	0.0564 (27.58)	Detected	Detected
7	33	0.0495 (24.24)	Detected	Detected
8	34	0.0297 (14.53)	Detected	Detected
9	35	0.0 (0)	Not detected	Detected
10	36	0.0570 (27.89)	Detected	Detected

We choose if the alarm rate is more than 1 order (multiply by 10) compared to the baseline rate of 0.0020. The choice is based on consideration that person operate and monitor the security system can detect the anomaly in 1 order. Based on this procedure, 8 from 10 attacks can be detected, as shown in Table III. The alarm rates for detected attacks as shown in Table III are 14 to 28 times greater than the baseline of 0.0020.

The results show that our approach can detect all attacks involve sensors as targets (Scenario 3, 21, 26, 30, 33, and 36). This success can be understood because our approach monitors the value of water level. Thus, the discrepancy between sensor reading and model estimation can increase or decrease the Z value systematically.

The other four attacks (scenarios 1, 2, 34, 35) involve actuators only. It is just two (scenarios 2 and 34) of the four attacks that can be detected. Attack scenario 1 opens valve MV-101 when it should be close. The attack cannot be

detected because the level sensor will respond normally with raw water flow. The other three attacks involve one or both pumps. The three attacks cannot be interpreted easily because of a long normal condition pump P-102 as a backup was never turned on.

It is to be noted that the attacks duration is vary from around 1 to 3 times ARL as shown in Table I, except the attack no. 34 is only 100 seconds. Because of the random nature of the residual r , it can be understood that the alarm rate of attack no. 35 is zero. But for the other attacks that our set up can detect them their short durations does not affect the detectability.

As a matter of comparison, Table III contains the research results [8] that used the same SWaT data set but with a different approach. The research uses a novel graphical model-based approach for anomaly detection. From the table, it can be concluded that their system is better than ours to detect attacks on actuators. But their system cannot detect scenario three that ours can detect. The scenario can be under the radar of detection because it increases the reading of the sensor gradually. Based on the consideration our approach has a promising result to be leveraged to detect stealthy attacks.

V. CONCLUSION

In this study, the physical modeling is successfully carried out using the DMDC method with a goodness of fit of 99.7%. It shows that the model has a good agreement with the measurement. The high value of goodness of fit gives the model a potential to be used to detect any anomaly caused by cyber-attack deviating the sensor measurement or actuator signal.

The difference between the model's predictions and the actual sensor measurement results is monitored with a nonparametric EWMA detector to detect anomalies resulting from cyber-physical attacks. From 10 attacks conducted to the subsystem, 8 of them can be detected using method used in this research. Compared with the baseline in normal condition, the alarm rates of detected attacks are 14 to 28 times greater. It shows that this method is successful in detecting most attacks, especially on sensors.

As observed in [5] there is a lack of use of input-output models in security field. Besides that, most of researches in security using physical-model use physical equation and not many researches use data-driven method. The other lack is use of real data or data drawn from testbeds, and mostly use simulation data. Our research fills the lacks by using DMDC as input-output model and it is a kind of system identification using data to model the physical behavior of system. Our research also uses the data collected from a test bed.

When we start our research, we plan to use CUSUM as the detector to detect anomalies as proposed in [5, 6, 9]. But we find that in our research the distribution of residual is not normal. Then the nonparametric EWMA is used to detect the anomalies. This research show that DMDC as a system identification combined with EWMA as detector can be used to detect cyber-physical attacks.

In future, this research can be continued by utilizing the interrelationships between subsystems. In this case, attacks on the upstream subsystems may be detected by the downstream subsystems. With the approach the detection probability may be increased because of the double detection, in the subsystem itself and in its downstream. Differ from [16] we use system identification method with DMDC instead of physical equation.

REFERENCES

- [1] Deval Bhamare , Maede Zolanvari , Aiman Erbad , Raj Jain , Khaled Khan, Nader Meskin , "Cybersecurity for Industrial Control Systems: A Survey", *Computers & Security*, Vol. 89, February 2020.
- [2] M., Krotofil, K., Kursawe, and D. Gollmann, "Securing Industrial Control Systems", in C. Alcaraz, *Security and Privacy Trends in the Industrial Internet of Things*, Springer, Switzerland, pp. 3-27, 2019.
- [3] R. M. Lee, M. J. Assante, T. Conway, "Analysis of the Cyber Attack on the Ukrainian Power Grid", SANS, Washington, DC, 2016.
- [4] Y. Hu, A. Yang, H. Li, Y. Sun, and L. Sun, "A survey of intrusion detection on industrial control systems," *International Journal of Distributed Sensor Networks*, vol. 14, no. 8, 2018.
- [5] D. I., Urbina, J. Giraldo, A. A. Cardenas, J. Valente, M. Faisal, N. O., Tippenhauer, J. Ruths, R. Candell, and H. Sandberg, "Survey and New Directions for Physics-Based Attack Detection in Control Systems", National Institute of Standards and Technology (NIST), US Department of Commerce, 2016.
- [6] C.M. Ahmed, C. Murguia, and J. Ruths, 2017, "Model-based Attack Detection Scheme for Smart Water Distribution Networks", In *Proceedings of the 2017 ACM on Asia Conference on Computer and Communications Security - ASIA CCS '17*, Abu Dhabi, United Arab Emirates, pp. 101–113, 2017.
- [7] Surabhi Athalye, Chuadhry Mujeeb Ahmed, and Jianying Zhou, "A Tale of Two Testbeds: A Comparative Study of Attack Detection Techniques in CPS", In: Rashid, A., Popov, P. (eds) *Critical Information Infrastructures Security, CRITIS 2020*, Lecture Notes in Computer Science, vol 12332.
- [8] Q. Lin, S. Adepu, S. Verwer, and A. Mathur. "TABOR: A Graphical Model-based for Anomaly Detection in Industrial Control Systems", In: *Proceedings of the 2018 Asia Conference on Computer and Communications Security*, Incheon, Republic of Korea, pp. 525-536, 2018.
- [9] C. Murguia and J. Ruths, "Characterization of a CUSUM Model-Based Sensor Attack Detector", In *Proceedings of IEEE 55th Conference on Decision and Control (CDC)*, Las Vegas, USA, pp. 1303–1309, 2016.
- [10] J. L. Proctor, S. L. Brunton, and J. N. Kutz, "Dynamic Mode Decomposition with Control", *SIAM Journal on Applied Dynamic Systems*, Vol. 15, No. 1, pp. 142–161, 2016.
- [11] M. A. Graham, S. Chakraborti, and SW Human, "Nonparametric EWMA Sign Chart for Location Based on Individual Measurements", *Quality Engineering*, Vol. 23, Issue 3, pp 227-241, 2011.
- [12] S. Chakraborti, and M. A. Graham, *Nonparametric Statistical Process Control*, Wiley, New York, NY, 2019.
- [13] K. M. Aung, *Secure Water Treatment Testbed (SWaT): An Overview*, Technical Report, Singapore University of Technology and Design, Singapore, 2015.
- [14] J. Goh, S. Adepu, S., K.N. Junejo, and A. Mathur, "A Dataset to Support Research in the Design of Secure Water Treatment Systems", In *Proceedings of International Conference on Critical Information Infrastructures Security (CRITIS)*, Paris, France, pp. 88- 99, 2016.
- [15] S. Adepu, A. Mathur, "An Investigation into The Response of a Water Treatment System to Cyber-Attacks", In *Proceedings of the 17th IEEE High Assurance Systems Engineering Symposium*, Orlando, FL, USA, pp. 141-148, 2016.
- [16] Qadeer, R., Murguia, C., Ahmed, C. M., and Ruths, J., "Multistage Downstream Attack Detection in a Cyber Physical System", *Cyber ICPS Workshop 2017 in Conjunction with ESORICS 2017*, 14-15 Nopember 2017, 177-185.

Performance Evaluation of New Feature based on Ordinal Pattern Analysis for Iris Biometric Recognition

Sheena S¹, Sheena Mathew²

School of Engineering, Cochin University of Science & Technology, Kochi, Kerala, India

Bindu M Krishna^{3*}

Sophisticated Test and Instrumentation Centre, Cochin University of Science & Technology, Kochi, Kerala, India

Abstract—The Iris recognition technique is currently the most efficient biometric identification system and is a common system on the practical front. Though most of the commercial systems use the patented Daugman's algorithm, which mainly uses wavelet-based features, research is still active in identifying novel features that can provide personal identification. Here the first novel proposal of using ordinal pattern measure based on nonlinear time series analysis is put forth to characterize the unique pattern of the iris of individuals and thereby perform personal identification. Dispersion Entropy is a nonlinear time-series analysis method highly efficient in the characterization of the complexity of any data series with proven effectiveness in the characterization of model system dynamics as well as real-world data series. The results show that dispersion entropy can be used to identify iris images of specific individuals. The efficiency of this method is evaluated by computing correlation and RMSE between dispersion entropy values of normalized iris image rubber sheet data. The experimental results on the popular IRIS database- CASIA v1- demonstrate that the proposed method can effectively perform differential identification of iris images from different individuals. The results specifically indicate that the density of information along the angular direction of iris images which falls along the rows of rubber sheet data. This can be efficiently utilized with the method or ordinal pattern characterization and proves to be having promising potential for being incorporated into biometrics personal identification systems.

Keywords—Dispersion entropy; iris recognition; rubber-sheet data; ordinal patterns; correlation

I. INTRODUCTION

In the past few decades, Iris recognition system has gained the status of the most reliable biometric authentication system. The highly unique pattern for every individual iris has a wealth of texture detail which makes this system extremely outstanding compared to other physiological biometric features like face, palm print, and even fingerprint features. Iris pattern-based Personal Identification system gained popularity because of this texture patterns long-term stability with respect to aging and other physiological changes. Iris is defined as the colored muscular diaphragm located behind the cornea of the eye. It surrounds the pupil sharing a common center with it and controls its size to adjust the amount of light entering through it. It has been scientifically and genetically proven that the microstructure of the iris region of an individual is extremely unique and distinct with respect to

characteristics like shape, size, and shading, thereby sufficient enough to establish a person's identity [1].

Texture analysis in two-dimensional images is generally carried out using methods like Gray Level Co-occurrence matrix and texture entropy [2]. Recently, new approaches based on the quantification of image irregularity using nonlinear measures have proven to be efficient in the characterization of fine details of two-dimensional images [3]. Successful applications of such methods in the characterization and analysis of small fine textural details of images in various technological as well as biomedical fields have been reported in the literature [4]. Efficient characterization of the iris patterns is an ever-demanding research topic due to the fact that its success and failure will lead to extremely sensitive outcomes related to national and international security and related contexts, as well as the reliability of general commercial applications. An application of an efficient nonlinear method of dispersion entropy for iris image characterization and personal identification is proposed in this work. Nonlinear methods-based image processing is a very recent proposal, and only a few reports are available in the literature. These proposals are mainly based on two-dimensional extensions of measures like sample entropy [5], distribution entropy [6], and dispersion entropy [7]. Among these measures, dispersion entropy is focused on overcoming the drawbacks of all its predecessors. It is proven to be extremely efficient in the characterization of one-dimensional as well as multi-dimensional signals, including images [8][9].

Complexity analysis of the dynamical system, as well as real-world systems and signals using the nonlinear time-series analysis method, has gained extreme popularity among the research community and has successfully marked its own place in potential real-world application [10]. The entropy concept can be used to measure the complexity of signals and, thereby, their related system. High complexity is represented using high entropy values, whereas lower entropy values indicate more regularity of a time series [11]. Earlier methods like approximate entropy, sample entropy, permutation entropy, and distribution entropy were reported to be successful in the characterization of the complexity of short time series from various real-world systems [12]. Later research on these measures revealed shortcomings of these measures related to amplitude and noise ratios. Dispersion entropy was later proposed as a fast and powerful approach,

*Corresponding Author.

together with successfully overcoming the drawbacks of the above-mentioned measures. The two-dimensional extension of all these measures, including dispersion entropy, has been reported for the characterization of image texture. When applied to image texture characterization, a high value of entropy indicates that the pixel values have high variance, whereas a low entropy value means the pixel values are relatively uniform. Among these measures, dispersion entropy is proven to be a fast and efficient method for the characterization of both small and large-scale image texture [13].

Considering the efficiency of dispersion entropy of both one and two-dimensional in the characterization of fine-scale irregularities, among all such analysis measures, it is proposed to apply this measure for the characterization of the texture feature of the iris image. Also, the peculiarity in the spread of patterns along the radial directions in iris images is of special concern while applying any measures for iris texture characterization. To the best of the current knowledge, this is the first proposal of applying nonlinear measures of time series analysis for the purpose of feature extraction for iris recognition application since the proposal of using fractal dimension for iris classification. However, it is noteworthy that fractal measures are based on conventional nonlinear time-series analysis methods, which are sensitive to noise and short data length [14].

Taking into consideration this peculiarity of iris images, it is proposed the use of one-dimensional dispersion entropy along the radial as well as angular directions to extract the wealth of information embedded in these images [15]. Further, the efficiency of the proposed method in personal identification is evaluated on the freely available dataset CASIA v1 [16].

The texture information contained in the iris images can be efficiently extracted by using the most appropriate methodology of image characterization. The wealth of information contained in iris texture can be efficiently extracted in the form of entropy values calculated based on dispersion entropy. In general, for image analysis, bi-dimensional extensions of the various ordinal pattern entropy measures are found to be useful, of which two-dimensional dispersion entropy (DispEn_{2D}) is reported to be comparatively more efficient. However, in iris images, local details spread is distributed in the radial direction, which corresponds to the columns of the rubber sheet images [17]. Correspondingly the information density will be higher along the angular directions of the corresponding rows of the normalized rubber sheet images [18]. In the information theory field, image predictability and regularity are evaluated using the recently developed two-dimensional sample entropy (SampEn_{2D}). Though it is efficient in its function, some limitations hold it back. The major limitations: 1) for small images, SampEn_{2D} values are undefined; and 2) for real-world applications, SampEn_{2D} is computationally expensive. These limitations can be overcome by two-dimensional dispersion entropy (DispEn_{2D}) measure.

Section II of this paper elaborates the related works and the materials and methods and database descriptions

illustrated in Section III. It is then presented the novel methodology for iris recognition by using the computation of Non-linear texture feature extraction. Section IV gives an overview of the experimental analysis and the obtained results of this proposed methodology. The conclusion of this methodology is narrated in Section V.

II. RELATED WORKS

Iris pattern-based personal identification was first proposed in 1987 by Flom and Safir, which further gained substantial research interest in the following years [19]. Further, in 1993, Daugman laid a strong foundation for an iris recognition algorithm based on statistical independence evaluated in terms of the phase-dependent feature of the variation in pixel intensity of the iris image. Applying the Gabor filter and Hamming Distance for the integrodifferential operator, a matching parameter was considered the door-opening for the iris recognition process [20]. For feature matching, many researchers have used Hamming Distance, Euclidean Distance, Weighted Euclidean Distance etc. [21]. Daugman's approach is still considered the most common technique applied to several personal identification and authentication systems till date.

The enormous literature on iris recognition systems can generally be classified into three groups based on the following feature identification technique: 1) Phase analysis, 2) Zero crossing, and 3) Texture analysis. The phase analysis approach follows the Daugman's methodology and related modifications, whereas the zero-crossing approach depends on methods like wavelet features [22]. Image texture-based methodology is a relatively recent approach proposed by Li Ma [23]. Further several other methodologies like Gray Level Co-occurrence Matrix (GLCM) [24] include Auto Correlation Function (ACF), Local Binary Pattern [25], Histogram Pattern [26], Haar wavelet [27], Contourlet [28] and Texture code [29] have been identified for iris recognition purpose. To measure the consistency of the iris image of the same eye, two dimensional correlation filters were used by Kumar et.al. [30].

III. MATERIALS AND METHODS

A. Dataset used

The proposed method is evaluated on a publicly available database which is captured with the help of a CASIA close-up iris camera. The database has 108 individuals, with seven images per individual. Out of the seven images of a single person, the first three images are in session 1, and the remaining four are acquired in session 2. A total of 756 images are available. The images are in JPG format.

B. Image Pre-processing

Iris recognition systems mainly involve the following steps: 1) Iris image capturing, 2) Pre-processing, Iris Localization, and Segmentation, followed by 3) feature normalization of the segmented iris region. In the iris localization step, the inner and outer boundaries of the iris portion are identified based on the Hough transform, which involves the Integro-differential operator and is segmented, as shown in Fig. 1(a). Further, the famous Daugman's algorithm is applied to convert the image from a cartesian coordinate

system to a pseudo-polar system. Thus, using the Daugman's algorithm, the circular-shaped Iris region is converted to a rectangular block of a specific size, as shown in Fig. 1(b). For the images investigated here, this Rubber sheet normalization generated images of size 240 x 20 pixels, which hold an immense amount of unique information about each individual [31].

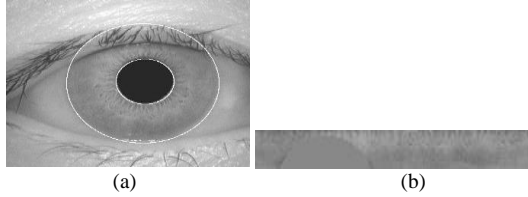


Fig. 1. (a). Segmented Iris, (b). Iris Rubber Sheet Model.

C. Dispersion Entropy

Dispersion entropy is a metric that can be used to evaluate the irregularities of any given time series. The method is economical in terms of computational cost and has proven to be very efficient in characterizing the complexity or orderliness of various real-world time series data [32]. Dispersion entropy is an ordinal pattern-based entropy measure proposed for overcoming the limitations of earlier methods like permutation entropy [33]. Ordinal pattern-based entropic measures are generally evaluated based on the probability distribution of the different possible states of a system estimated from the distribution of its dynamical variables. Sample Entropy can be considered to be the first proposal characterizing uncertainty in system dynamics based on dynamical variables using such probability distribution [34], and has been applied to both signal and image characterization. Though the method was proved to be efficient for such application, in-depth analysis revealed that, certain limitations of Sample Entropy is with respect to signal length. Later research provided better methods like Permutation Entropy which could overcome several limitations of Sample Entropy, but it was again found to fail at certain instances, regarding amplitude differences within a signal [35]. Dispersion Entropy effectively extracts the specific patterns in the ordinal positions of elements in any signal or time series.

For any given time series of 'N' number of elements, $N \times = x_1, x_2, x_3, \dots, x_N$. Multiscale Dispersion Entropy is calculated on coarse-grained versions of the same as follows:

1) The elements x_1 to x_N of the time series are divided into non-overlapping segments of length ' τ '. The average of each segment of length ' τ ' is calculated, thereby generating a coarse-grained version of the same time series. $x_{ki}(\tau) = 1/\tau$. In general, for any time series analysis, a range of scale factors 1 to n are chosen. Thus, for a given time series $X = \{x_1$ to $x_N\}$, 'n' different coarse-grained versions are obtained, corresponding to each of the scale factors 1 to 'n'. Further dispersion entropy is calculated, for each of the coarse-grained time series [36].

2) The element of each of the coarse-grained series is mapped to different classes 'c' using linear or nonlinear mapping approaches. Normal Cumulative Distribution

Function (NCDF) is the most generally used function for this purpose. NCDF generates a new series $y = \{y_1, y_2, \dots, y_N\}$.

3) The new time series y is embedded similar to the approach of Taken's embedding theorem. Thus generating short sequences or embedding vectors Z.

$$z_i^{m,c} = \{z_i^c, z_{i+d}^c, \dots, z_{i+(m-1)d}^c\}$$

Each short sequence is further mapped to a dispersion pattern

$$\pi_{v_0 v_1 \dots v_{m-1}}$$

where

$$z_i^c = v_0, z_{i+d}^c = v_1, \dots, z_{i+(m-1)d}^c = v_{m-1}$$

As every element in any of the coarse-grained series is now represented by integers from 1 to c, according to its class, the number of possible dispersion patterns that can be assigned to each time series $z_i^{m,c}$ is equal to c^m , where 'm' is the number of elements in that coarse-grained series.

4) For each coarse-grained series, the relative frequency of each of the possible dispersion pattern is calculated as follows. $p(\pi_{v_0 v_1 \dots v_{m-1}})$

$$= \frac{\text{Number}\{i | i \leq N - (m-1)d, z_i^{m,c} \text{ has type } \pi_{v_0 v_1 \dots v_{m-1}}\}}{N - (m-1)d}$$

Finally, dispersion entropy for each coarse-grained series is defined according to Shannon's information theorem $DE(x, m, c, d)$.

$$= - \sum_{\pi=1}^{c^m} p(\pi_{v_0 v_1 \dots v_{m-1}}) \cdot \ln(p(\pi_{v_0 v_1 \dots v_{m-1}}))$$

An extension of $DispEn_{1D}$ is then applied, which is named as $DispEn_{2D}$ to verify the effectiveness of this methodology [37]. The result of both $DispEn_{1D}$ and $DispEn_{2D}$ is illustrated in the following section.

D. Iris Feature Extractions

For extracting the texture information, Dispersion Entropy values of order '4' and delay '1' is computed for every row and column of the rubber sheet matrix corresponding to each iris image of the dataset. The dispersion entropy file size of an image is only 12KB. The size of the images in the dataset is in the range of 70KB to 95KB, whereas its Rubber sheet matrix ranges from 33KB to 44KB. Therefore it is recommended to use this dispersion entropy matrix, which can then be modified to make it a code and stored for further iris matching.

For every image of a given subject, the dispersion entropy of order '4' and delay '1' is calculated for the Rubber sheet matrix of images of the size of 20 rows and 240 columns. Considering each of these rows as \emptyset , 1-D series dispersion entropy values computed for every row and column of the Rubber sheet matrix of the image. Thus Dispersion Entropy matrix of rows contains 20 values. Similarly, for columns, each column will be represented by one dispersion entropy value, and hence a total of 240 dispersion entropy values will be obtained for columns also. These values can be stored as

the representational feature for use in further recognition processes.

The efficiency of the DispEn_{2D} is verified with real and synthetic datasets in the following sections. DispEn_{2D} is an extension of DispEn_{1D}.

E. Iris Feature Matching

Further investigation focused on the match between the iris entropy features of different images of the same person as well as the mismatch between different persons. If this entropy value matches the images of the same person and differs widely between the images of two subjects, then it can be used as an identification feature. The feature-matching process is depicted in Fig. 2. This is carried out as follows. For an iris, Rubber sheet of 20 rows and 240 columns, 20 dispersion entropy values for rows and 240 dispersion entropy values for columns were obtained. The correlation between dispersion entropy sets of every image pair is calculated for images of the same person as well as a different person.

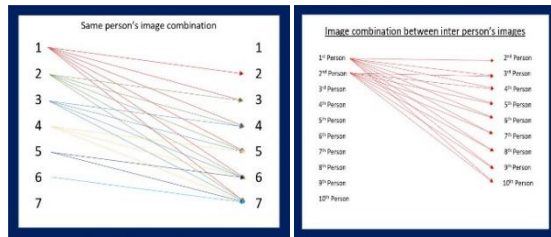


Fig. 2. Feature Matching Process.

In this work, investigation was carried out to find out the effectiveness of this method in the personal identification and classification of iris images. For this purpose, the iris matching between the images of a person and matching between two different persons were evaluated using correlation values between row-wise and column-wise dispersion entropy. From the two separate plots, it is evident that it should be widely different from the same image of a person with another person's image.

Correlation values are calculated between the dispersion entropies of images of the same subjects and that between different subjects to evaluate the efficiency of dispersion entropy in performing personal identification. These values are calculated for every image pair within the seven images of each subject. The average correlation value for all combinations is used as a measure of match between the dispersion entropies of two images of the same eye of a single subject, represented as CORR_{same..}. Similarly, these values are calculated for every image pair among all images between each pair of subject combinations. The average values of these measures are calculated for all image combinations for a given subject for all other subjects in the database represented as CORR_{diff.}. This is performed for the rows and columns separately.

IV. RESULT ANALYSIS AND DISCUSSION

Considering the peculiar nature of pattern spread in iris images, it was hypothesized that one-dimensional dispersion entropy along rows and columns of iris rubber sheets would provide a specific advantage in texture characterization. To

test the hypothesis, investigation was done for verifying the differences in values of these measures for the datasets given in section III. The efficiency of the proposed method of feature representation using investigated in terms of DispEn_{2D} as well as DispEn_{1D} along rows and columns for iris recognition purposes is evaluated separately. Subsets of images from the Kylberg dataset and CASIA v1 are chosen for initial screening of the performance of the two measures in the characterization of general texture images and iris images, as well as in representing the uniqueness of iris patterns of individuals.

Four groups of images, such as blanket1, ceiling1, canvas1, and floor1, were used to analyze the textural information. Four sample images from the Kylberg dataset [38] are shown in Fig. 3, and two images of four different persons taken from CASIA v1 are shown in Fig. 4. Table I below shows the DispEn_{1D} for four scale factor values and DispEn_{2D} values of the four texture image samples. Similarly, Table II and Table III show mean values of the DispEn_{1D} for four scale factor values and DispEn_{2D} values of Iris columns and rows, respectively.

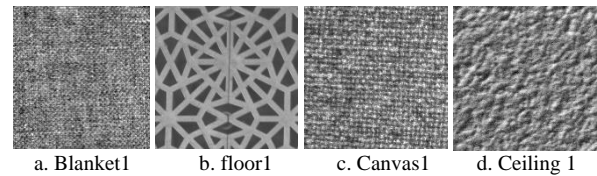


Fig. 3. Sample Set of Images from Kylberg Dataset.

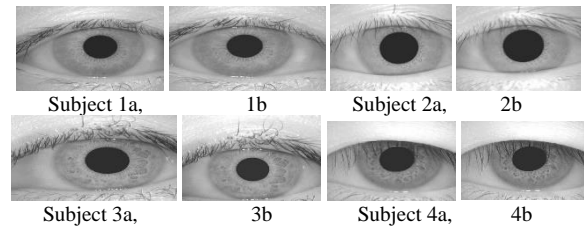


Fig. 4. Sample Images of 4 Different Subjects from CASIA v1 Dataset.

TABLE I. DISPEN_TEXTURE

		Entropy Values		
		DispEn_Column	DispEn_Row	DispEn _{2D}
Blanket 1	Scale1	5.12	5.052	6.735992
	Scale2	5.11	4.836	
	Scale3	4.95	4.686	
	Scale4	4.77	4.537	
Canvas1	Scale1	5.34	5.254	7.262997
	Scale2	5.31	5.273	
	Scale3	5.06	5.049	
	Scale4	4.83	4.825	
Ceiling 1	Scale1	4.88	4.803	6.249361
	Scale2	4.75	4.747	
	Scale3	4.65	4.615	
	Scale4	4.53	4.528	
Floor1	Scale1	2.58	2.543	2.929589
	Scale2	2.87	2.827	
	Scale3	3.06	2.997	
	Scale4	3.20	3.141	

TABLE II. DISPEN_IRIS_COLUMN

	DispEn_Column			
	Scale1	Scale2	Scale3	Scale4
1a	3.059	3.264	3.232	3.214
1b	3.197	3.381	3.365	3.344
2a	2.917	3.148	3.160	3.124
2b	2.897	3.111	3.111	3.104
3a	3.131	3.323	3.324	3.304
3b	2.849	3.009	3.007	3.002
4a	2.714	2.872	2.879	2.884
4b	2.889	3.115	3.113	3.126

TABLE III. DISPEN_IRIS_ROW

	DispEn_Row			
	Scale1	Scale2	Scale3	Scale4
1a	3.680	3.703	3.626	3.567
1b	3.756	3.771	3.663	3.592
2a	3.260	3.351	3.321	3.294
2b	3.163	3.275	3.275	3.243
3a	3.853	3.855	3.754	3.668
3b	3.875	3.891	3.794	3.704
4a	3.571	3.566	3.462	3.388
4b	3.728	3.695	3.572	3.483

Table IV gives the mean correlation and RMSE values between $DispEn_{1D}$ of rows of iris rubber sheets of iris images of every subject in the sample dataset of texture image represented as $DispEn_{1D_Row_{same}}$. Similarly, Table V gives the mean $DispEn_{1D_Row_{diff}}$ values of correlation between rows of iris rubber sheets of every image of each of the subjects with every image of all of the other subjects in the sample data taken from CASIA v1. In the same way, mean correlation and RMSE values between $DispEn_{1D}$ of columns of iris rubber sheets of iris images of the same subject as well as different subjects, are listed in Table VI and Table VII. Table VIII and Table IX show the mean correlation and RMSE values between $DispEn_{2D}$ between the same subject images as well as between images of different subjects represented as $DispEn_{2D_same}$ and $DispEn_{2D_diff}$.

From these values, it can be observed that the correlation values between iris images of the same subject for both rows as well as columns are very high values, all of which fall above 0.95, indicating high similarity, whereas the same values between images of different subjects are all below 0.6. In the case of RMSE, between images of the same subjects are all less than 0.4 and between different subjects is above 0.6. The difference in these values for cases of same subject's images and for images of different subjects is very promising. In the case of $DispEn_{2D}$ the values of correlation and RMSE for images of same subject and those between different subjects in not as widely separated as observed in the case of $DispEn_{1D}$ in both cases of rows and columns. These results indicate the suitability of $DispEn_{1D}$ for personal identification. Further, the efficiency of one-dimensional dispersion entropy for iris biometric identification is explored in the following section, in which its rows and columns features are separately verified.

TABLE IV. ROW_CORRELATION AND ROW_RMSE FOR SAME SUBJECT.

	scale1		Scale2		Scale3		Scale4	
	Corr	Rmse	Corr	RMSE	Corr	RMSE	Corr	RMSE
Sub1	0.99	0.25	0.99	0.21	0.99	0.20	0.98	0.21
Sub2	0.98	0.33	0.97	0.30	0.97	0.25	0.97	0.23
Sub3	0.93	0.39	0.95	0.33	0.95	0.31	0.95	0.29
Sub4	0.96	0.38	0.97	0.31	0.96	0.30	0.96	0.27

TABLE V. ROW_CORRELATION AND ROW_RMSE FOR DIFFERENT SUBJECT

	scale1		Scale2		Scale3		Scale4	
	Corr	Rmse	Corr	Rmse	Corr	Rmse	Corr	Rmse
Sub1	0.9190	0.630	0.928	0.5263	0.93262	0.4565	0.9359	0.40
Sub2	0.9189	0.629	0.9287	0.5252	0.93269	0.4556	0.93592	0.40
Sub3	0.9190	0.629	0.9286	0.5259	0.93265	0.4561	0.93592	0.40
Sub4	0.9191	0.629	0.9287	0.5260	0.93272	0.4563	0.93597	0.40

TABLE VI. COLUMN_CORRELATION AND COLUMN_RMSE FOR SELF MATCH.

	scale1		Scale2		Scale3		Scale4	
	Corr	RMSE	Corr	RMSE	Corr	RMSE	Corr	RMSE
Sub1	0.98	0.29	0.96	0.25	0.64	0.18	0.48	0.08
Sub2	0.99	0.21	0.99	0.17	0.90	0.19	0.36	0.17
Sub3	0.93	0.42	0.86	0.35	0.41	0.29	0.26	0.19
Sub4	0.83	0.19	0.42	0.10	0.29	0.02	1.00	0.00

TABLE VII. COLUMN_CORRELATION AND COLUMN_RMSE FOR DIFFERENT SUBJECT

	scale1		Scale2		Scale3		Scale4	
	Corr	RMSE	Corr	RMSE	Corr	RMSE	Corr	RMSE
Sub1	0.516005	0.641	0.4740	0.373	0.6107	0.133	0.7702	0.053
Sub2	0.516355	0.639	0.4745	0.372	0.6119	0.132	0.7723	0.052
Sub3	0.516314	0.641	0.4743	0.373	0.6115	0.133	0.7724	0.053
Sub4	0.515480	0.643	0.4732	0.375	0.6085	0.134	0.7695	0.053

TABLE VIII. DISPEN_{2D}_SAME FOR IRIS

	Corr	Rmse
Sub 1	0.876	0.348
Sub 2	0.887	0.506
Sub 3	0.762	0.458
Sub 4	0.576	0.247

TABLE IX. DISPEN_{2D}_DIFF FOR IRIS

	Corr	RMSE
Subject 1,3	0.873	0.509
Subject1,5	0.628	0.506
Subject 1,6	-0.445	0.749
Subject 3,5	0.688	0.624
Subject 3,6	-0.377	0.974
Subject 5,6	-0.054	0.608

A. Iris Recognition Analysis using $DispEn_{1D}$

The proposed method of dispersion entropy is applied to iris images of 108 subjects from the CASIA v1 dataset. The dataset contains iris images of 108 subjects; wherein seven images correspond to a single subject. The efficiency of dispersion entropy in characterizing the unique texture of an individual's iris, thereby performing personal identification, is evaluated in terms of correlation, as explained in Section II.

Fig. 5(a-d) depicts the mean values of dispersion entropies of all the images corresponding to each of the subjects along rows, and Fig. 6(a-d) shows the corresponding values for columns. The values of dispersion entropy for the columns fall within the range of 1.8 - 2.8 for scale factor 1 and within the range of 1.5 – 2 for scale factor 2. In the case of rows, the values range between 3 and 4 in both cases of scale factors of 1 and 2. Higher values of dispersion entropy indicate more randomness in pixel intensity values within rows of the Rubber sheet images. It is also noteworthy that in the case of row-wise dispersion entropy, the values are almost in the same range for both instances of scale factors of 1 and 2.

Further investigations on the efficiency of the dispersion entropy feature in characterizing the uniqueness of iris image pattern of an individual and thereby performing personal identification are carried out using a measure of the correlation between different images of the same eye of each of the subjects and between images of eyes of different subjects. Fig. 7(a) to 7(d) show the mean correlation values between row-wise dispersion entropy values of all images of each subject, with its own images represented in green and mean values of correlations between images of each subject with that of all other subjects represented in red. It can be clearly observed that the correlation values between the dispersion entropy of rows of different subjects are lower than between images of the same subject, and these values do not cross over into each other, even in the case of higher scale factors.

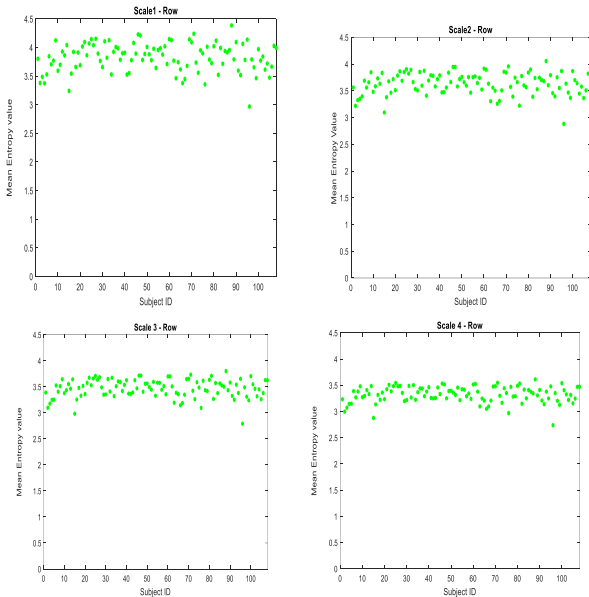


Fig. 5. MVDE Plot, Fig. 5(a) – 5(d). Mean Value Plot for the Row-scale1, Row-scale2, Row-scale3, Row-scale4.

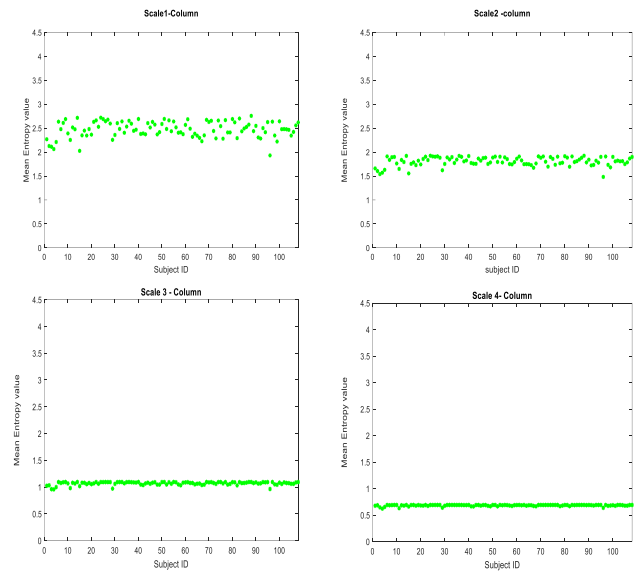
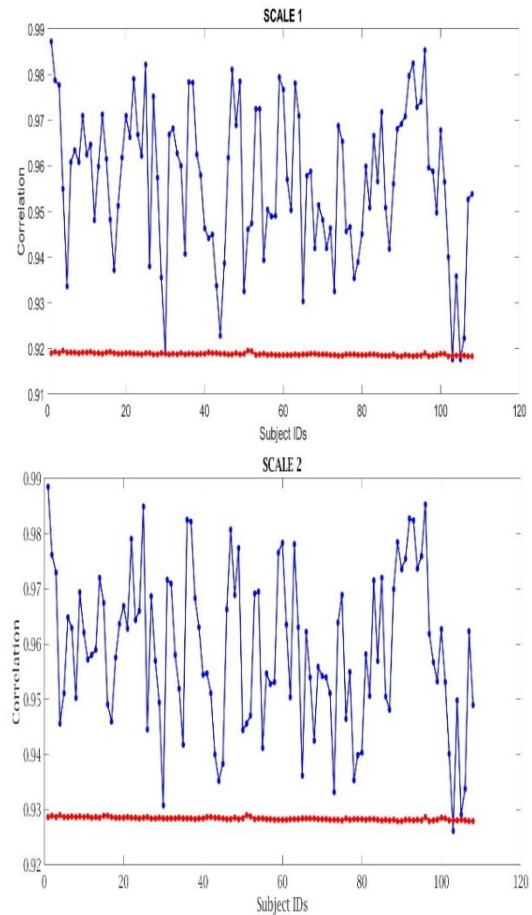


Fig. 6. MVDE Plot, Fig. 6(a) – 6(d). Mean Value Plot for the Column-scale1, Column-scale2, Column-scale3, and Column-scale4.

1) Correlation-row



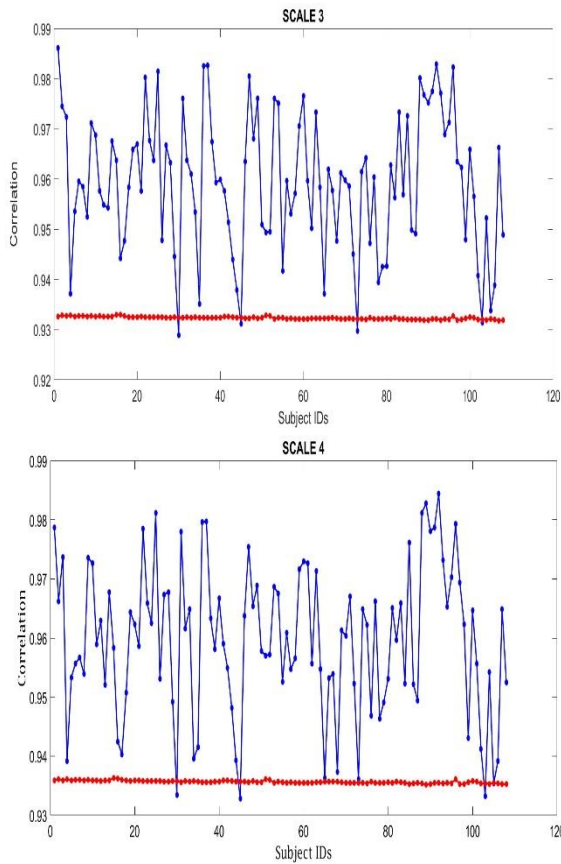


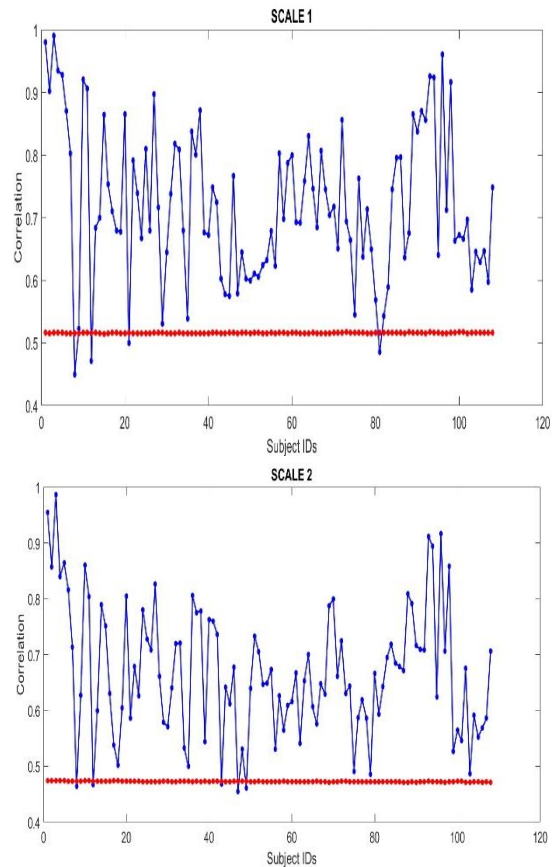
Fig. 7. Correlation Plot for Row Values. 7a. Scatter Plot of Scale 1, 7b. Scatter Plot of Scale 2, 7c: Scatter Plot of Scale 3, 7d. Scatter Plot of Scale 4.

Though it was observed that the dispersion entropy values themselves get reduced with higher scale factors indicating decreased pattern, this however is not drastically hindering the efficiency of this feature in differentiating the images of different subjects. This is especially interesting because the correlation values are around 0.9 for all cases of varying subject correlations, and it is getting slightly increased with an increase in the scale factor. This can be viewed as a consequence of the decrease in dispersion entropy value as a result of the averaging of more and more neighboring pixel intensities with increasing scale factors. In the case of correlation values for the same subject images, the values range between 0.92 – 0.99, indicating very high similarity.

A very encouraging finding in these figures is that the correlation value of the same subject images never crosses below those of different subject values. Though the variation of these values of correlation for the whole dataset of 108 subjects is higher than the variation observed for correlation of different subject images, a majority of these values fall around 0.95 – 0.98. The overall results indicate that the correlation will never be higher than 0.92 or 0.925 for any case of images of different subjects. This is a very strong factor to recommend this feature for the purpose of personal identification, as the chances of wrongly identifying images of different people to be the same are very low.

Fig. 8(a) to 8(d) show the mean correlation values between column-wise dispersion entropy values of all images of each subject, with its own images represented in green and mean values of correlations between images of each subject with that of all other subjects represented in red. The figures indicate that the values of correlation values for images of different subjects fall around the range of 0.5-0.8, which is much low compared to that observed for row-wise dispersion entropy. However, the values of the same subject images show wide variation, with values falling between 0.5 and 1, with a majority of values falling between 0.6 and 0.8. It is noteworthy that though there is not much cross-over of the same subject image correlation into the range of correlation values of different subject images in the cases of scale factors 1 and 2, the different subject image correlation values increase and cross over into the same subject correlation value range in the cases of scale factors of 3 and 4. The better stability of results in the row-wise analysis is in good agreement with the observations and recommendations, which stated that information is more independent along the angular direction [39]. The different rows correspond to different circles, and the pixels along each row represent angular direction. The present results indicate that ordinal pattern-based Dispersion entropy is very efficient in extracting the maximum utility of the statistical independence between the pixel intensity values along the angular direction in each circle.

2) Correlation-column



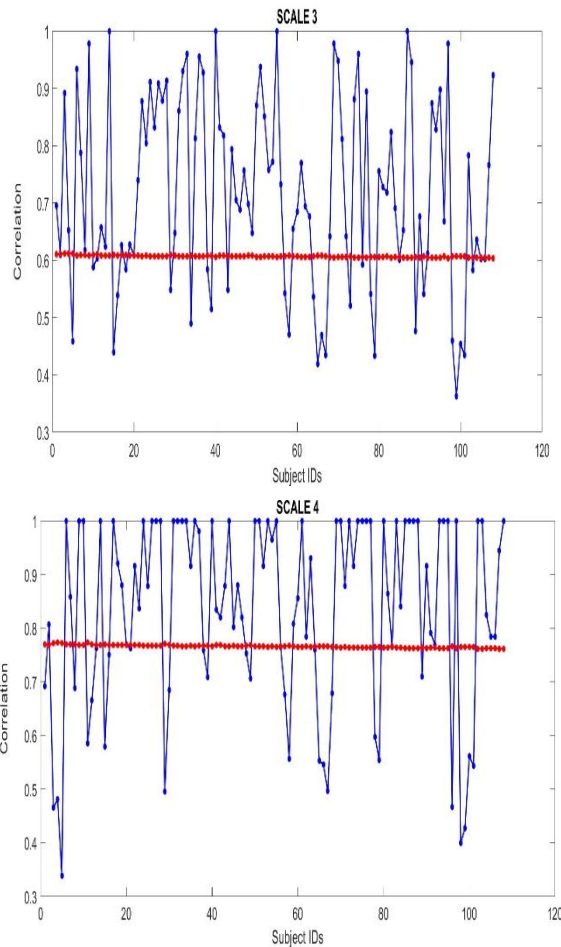


Fig. 8. Correlation Plot for Column Values. 8a. Scatter Plot of Scale 1, 8b. Scatter Plot of Scale 2, 8c. Scatter Plot of Scale 3, 8d. Scatter Plot of Scale 4.

B. Performance Evaluation Measures

The effectiveness of this proposed work is verified using the performance measures such as False Acceptance Rate (FAR), False Rejection Rate (FRR), False Positive Rate (FPR), Specificity, Sensitivity and Equal Error Rate (EER). Following equations are used to formulate the performance evaluation measures

$$\text{False Acceptance Rate (FAR)} = \text{FP} / (\text{FP} + \text{TN})$$

$$\text{False Rejection Rate (FRR)} = \text{FN} / (\text{FN} + \text{TP})$$

$$\text{Equal Error Rate (EER)} = (\text{FAR} + \text{FRR}) / 2$$

$$\text{Precision} = \text{TP} / (\text{TP} + \text{FP})$$

$$\text{Recall} = \text{TP} / (\text{TP} + \text{FN})$$

$$\text{Sensitivity} = \text{TP} / (\text{TP} + \text{FN})$$

$$\text{Specificity} = \text{TN} / (\text{TN} + \text{FP})$$

Where TP and TN represent true positive and true negative, FP and FN represent false positive and false negative. For row values, if the threshold value of scale 1 is set for 0.92 then the FRR is zero, which indicates that no person will be falsely rejected. The threshold can be selected based on the dataset which is used. The Specificity and Sensitivity value shows that this system gives accurate True Negative Rate and True Positive Rate. The results are shown in Table X and Table XI for rows and columns, respectively. By examining the values of the threshold, it can be clearly understood that the row values gives better results than column values. Lower the EER higher the accuracy of the biometric system.

TABLE I. PERFORMANCE EVALUATION OF ROW_DISPEN_{ID}

Threshold	FAR	FRR	FPR	Specificity	Sensitivity	EER
Scale 1	0.92	0.028	0	1	0.972	0.014
	0.919	0.028	0.167	0.166	0.833	0.097
Scale 2	0.93	0.019	0	1	0.981	0.009
	0.9287	0.009	0.103	0.102	0.897	0.056
Scale 3	0.934	0.046	0	1	0.953	0.023
	0.9327	0.037	0.093	0.092	0.907	0.065
Scale 4	0.934	0.056	0	1	0.944	0.028
	0.9327	0.037	0.074	0.074	0.925	0.056

TABLE II. PERFORMANCE EVALUATION OF COLUMN_DISPEN_{ID}

Threshold	FAR	FRR	FPR	Specificity	Sensitivity	EER
Scale 1	0.527	0.044	0	1	0.953	0.022
	0.5167	0.039	0.0833	0.08	0.916	0.061
Scale 2	0.478	0.044	0	1	0.953	0.022
	0.4737	0.049	0.093	0.09	0.907	0.071
Scale 3	0.613	0.239	0	1	0.685	0.120
	0.609	0.248	0.102	0.10	0.898	0.175
Scale 4	0.774	0.25	0	1	0.666	0.125
	0.77	0.25	0.056	0.06	0.944	0.153

V. CONCLUSION

A new method for iris recognition is a nonlinear time series analysis based on Dispersion entropy proposed in this work. Dispersion entropy is estimated based on the complexity of ordinal patterns of elements in a time series. The method is tested on the standard CASIA v1 dataset. The rows and columns of normalized iris images are considered one-dimensional time series, and the corresponding dispersion entropy values are calculated. Correlation between mean dispersion entropy values is calculated to evaluate how efficiently two images of the same subjects can be identified as well as how well two images of different subjects can be differentiated. This is carried out for the dispersion entropy of rows and columns separately. High correlation and values are obtained between different images of the same individual, whereas low correlation values are obtained between images of different subjects. The results of the row-wise analysis demonstrated much higher performance than the column-wise analysis. The results indicate that the dispersion entropy values of one-dimensional series of pixel intensities along rows of normalized iris images are very efficient in characterizing the uniqueness of the iris texture of individuals. The results also point towards the extreme possibility of utilizing the capabilities of nonlinear analysis for iris recognition purposes. These results prove the potential of nonlinear analysis-based texture entropy to be further developed into a tool that can provide a group of features to constitute a feature vector based on ordinal pattern measures of iris image texture for personal identification. This methodology has to be evaluated with other datasets. Also, it is considered the future scope of this work. In addition, similar nonlinear entropy measures can be used to build a feature vector so that the proposed novel approach can be developed.

REFERENCES

- [1] J. Daugman, Biometric Personal Identification System Based on Iris Analysis, United States Patent, no. 5291560, 1994.
- [2] Armi, Laleh, and Shervan Fekri-Ershad. "Texture image analysis and texture classification methods-A review." arXiv preprint arXiv:1904.06554 (2019).
- [3] Ahmadi, Neda, and Gholamreza Akbarizadeh. "Hybrid robust iris recognition approach using iris image pre-processing, two-dimensional gabor features and multi-layer perceptron neural network/PSO." *Iet Biometrics* 7.2 (2018): 153-162.
- [4] Veljko Papic, Jelena Krmar, Texture Entropy-Based Classification for Iris Recognition Systems, *Journal of Circuits, Systems, and Computers*, Vol. 29, No. 4 (2020), World Scientific, DOI: 10.1142/S0218126620500516.
- [5] Silva, Luiz Eduardo Virgili, et al. "Two-dimensional sample entropy: Assessing image texture through irregularity." *Biomedical Physics & Engineering Express* 2.4 (2016): 045002.
- [6] Lee, Dae-Young, and Young-Seok Choi. "Multiscale distribution entropy analysis of heart rate variability using differential inter-beat intervals." *IEEE Access* 8 (2020): 48761-48773.
- [7] M. Rostaghi and H. Azami, "Dispersion Entropy: A Measure for Time-Series Analysis," in *IEEE Signal Processing Letters*, vol. 23, no. 5, pp. 610-614, May 2016, doi: 10.1109/LSP.2016.2542881.
- [8] Ricardo Espinosa, Raquel Bailón, and Pablo Laguna, Two-Dimensional EspEn: A New Approach to Analyze Image Texture by Irregularity, *Entropy* 2021, 23, 1261. <https://doi.org/10.3390/e23101261>.
- [9] Azami, Hamed, et al. "Multiscale fluctuation-based dispersion entropy and its applications to neurological diseases." *IEEE Access* 7 (2019): 68718-68733.
- [10] Rahman, Md Mustafizur, et al. "EEG-based emotion analysis using non-linear features and ensemble learning approaches." *Expert Systems with Applications* 207 (2022): 118025.
- [11] Hamed Azami, Alberto Fernández, et al. Dispersion Entropy for the Analysis of Resting-state MEG Regularity in Alzheimer's Disease. Annual International Conference of the IEEE Engineering in Medicine and Biology Society. IEEE Engineering in Medicine and Biology Society Conference August 2016, DOI: 10.1109/EMBC.2016.7592197.
- [12] Humeau-Heurtier, Anne. "Evaluation of systems' irregularity and complexity: Sample entropy, its derivatives, and their applications across scales and disciplines." *Entropy* 20.10 (2018): 794.
- [13] Azami, Hamed, et al. "Multiscale dispersion entropy for the regional analysis of resting-state magnetoencephalogram complexity in Alzheimer's disease." 2017 39th Annual International Conference of the IEEE Engineering in Medicine and Biology Society (EMBC). IEEE, 2017.
- [14] Li Yu, David Zhang, et al., Coarse iris classification using box-counting to estimate fractal dimensions, *Pattern Recognition* 38 (2005) 1791 – 1798, doi:10.1016/j.patcog.2005.03.015.
- [15] Rostaghi, Mostafa, Mohammad Reza Ashory, and Hamed Azami. "Application of dispersion entropy to status characterization of rotary machines." *Journal of Sound and Vibration* 438 (2019): 291-308.
- [16] "CASIA Iris Image Database, <http://biometrics.idealtest.org/>".
- [17] Azami, Hamed, et al. "Two-dimensional dispersion entropy: An information-theoretic method for irregularity analysis of images." *Signal Processing: Image Communication* 75 (2019): 178-187.
- [18] Ma, L., Tan, T., Wang, Y., Zang, D., Personal identification technique using human iris recognition. *Proceedings of the 25th ICVI, Calgary 2002*, 294-299.
- [19] L. Flom and A. Safir, *Iris Recognition System*, United States Patent, no. 4641394, 1987.
- [20] J. Daugman, Statistical Richness of Visual Phase Information: Update on Recognizing Persons by Iris Patterns, *International Journal of Computer Vision* 45(1), 25–38, 2001.
- [21] R.Ramprasad, C. Rajapriya, S.Senthilvel MCA., Biometric Iris Recognition System Using Edge Detection and Gabor Filter for High Security, *Advances in Computational Sciences and Technology*, ISSN 0973-6107 Volume 12, Number 1 (2019) pp. 7-21.
- [22] Salve, Sushilkumar S. "Iris Recognition Using Wavelet Transform and SVM Based Approach." *Asian Journal For Convergence In Technology (AJCT)* ISSN-2350-1146 (2019).
- [23] Ma, Lin, Kuanquan Wang, and David Zhang. "A universal texture segmentation and representation scheme based on ant colony optimization for iris image processing." *Computers & Mathematics with Applications* 57.11-12 (2009): 1862-1868.
- [24] Asmara, R. A., et al. "Iris feature extraction using Gray Level Co-occurrence Matrix and Gabor Kernel filter its impact on iris Huffman compression image." *Journal of Physics: Conference Series*. Vol. 1402. No. 6. IOP Publishing, 2019.
- [25] Fathy, Waleed S-A., and Hanaa S. Ali. "Entropy with local binary patterns for efficient iris liveness detection." *Wireless Personal Communications* 102.3 (2018): 2331-2344.
- [26] Daugman, John. "New methods in iris recognition." *IEEE Transactions on Systems, Man, and Cybernetics, Part B (Cybernetics)* 37.5 (2007): 1167-1175.
- [27] Podder, Prajoy, M. Rubaiyat Hossain Mondal, and Joarder Kamruzzaman. "Iris feature extraction using three-level Haar wavelet transform and modified local binary pattern." *Applications of Computational Intelligence in Multi-Disciplinary Research*. Academic Press, 2022. 1-15.
- [28] Ezzaki, Ayoub, et al. "Iris recognition algorithm based on Contourlet Transform and Entropy." *ELCVIA: electronic letters on computer vision and image analysis* 19.1 (2020): 53-67.
- [29] Saiyed Umer et al., Texture code matrix-based multi-instance iris recognition, *Pattern Anal Applic* (2016) 19:283–295.

- [30] Rabab M. Ramadan, Iris Compression and Recognition using Spherical Geometry Image, (IJARAI) International Journal of Advanced Research in Artificial Intelligence, Vol. 4, No.6, 2015.
- [31] Li Ma, Yunhong Wang, Tieniu Tan, Iris Recognition Based on Multichannel Gabor Filtering, ACCV2002: The 5th Asian Conference on Computer Vision, 23--25 January 2002, Melbourne, Australia.
- [32] Azami, Hamed, and Javier Escudero. "Amplitude-and fluctuation-based dispersion entropy." *Entropy* 20.3 (2018): 210.
- [33] Bandt, Christoph, and Bernd Pompe. "Permutation entropy: a natural complexity measure for time series." *Physical review letters* 88.17 (2002): 174102.
- [34] Molina-Picó, Antonio, et al. "Comparative study of approximate entropy and sample entropy robustness to spikes." *Artificial intelligence in medicine* 53.2 (2011): 97-106.
- [35] M.Zanin, L, Zunino, O. A. Rosso, and D. Papo, "Permutation entropy and its main biomedical and econophysics applications: A review " *Entropy* vol.14, pp 1553-1577, 2012.
- [36] Ahmed MU, Mandic DP (2012) Multivariate multi-scale entropy analysis. *IEEE Signal Process Lett* 19:91–94.
- [37] Hamed Azami, Luiz Eduardo, Ana Carolina Mieko Omoto, et al. Two-dimensional dispersion entropy: An information-theoretic method for irregularity analysis of images, *Signal Processing: Image Communication* 75(2019) 178-187, ELSEVIER.
- [38] G. Kylberg. The Kylberg Texture Dataset v. 1.0, Centre for Image Analysis, Swedish University of Agricultural Sciences and Uppsala University, External report (Blue series) No. 35.
- [39] Masek, Libor. "Recognition of human iris patterns for biometric identification." PhD diss., Master's thesis, University of Western Australia, 2003.

Mitigation of DDoS Attack in Cloud Computing Domain by Integrating the DCLB Algorithm with Fuzzy Logic

Amrutha Muralidharan Nair¹

Research Scholar

Department of Computer Science Engineering, Karpagam
Academy of Higher Education, Coimbatore, India

Dr. R Santhosh²

Professor

Department of Computer Science Engineering, Karpagam
Academy of Higher Education, Coimbatore, India

Abstract—Cloud computing would be an easy method to obtain services, resources and applications from any location on the internet. In the future of data generation, it is an unavoidable conclusion. Despite its many attractive properties, the cloud is vulnerable to a variety of attacks. One such well-known attack that emphasizes the availability of amenities is the Distributed Denial of Service (DDoS). A DDoS assault overwhelms the server with massive quantities of regular or intermittent traffic. It compromises with the cloud servers' services and makes it harder to reply to legitimate users of the cloud. A monitoring system with correct resource scaling approach should be created to regulate and monitor the DDoS assault. The network is overwhelmed with excessive traffic of significant resource usage requests during the attack, resulting in the denial of needed services to genuine users. In this research, a unique way to the analyze resources used by the cloud users, lowering of the resources consumed is done when the network is overburdened with excessive traffic, and the dynamic cloud load balancing algorithm DCLB (Dynamic Cloud Load Balancing) is used to balance the overhead towards the server. The core premise is to monitor traffic using the fuzzy logic approach, which employs different traffic parameters in conjunction with various built in measured to recognize the DDoS attack traffic in the network. Finally, the proposed method shows a 93% of average detection rate when compared to the existing model. This method is a unique attempt to comprehend the importance of DDoS mitigation techniques as well as good resource management during an attack and analysis of the.

Keywords—DDoS attack; resource scaling; DCLB; fuzzy logic; traffic parameters

I. INTRODUCTION

Cloud computing threats are becoming more prevalent regularly, with attack channels and patterns changing. It provides a wide range of services with considerable benefits for corporate organizations, businesses, and individuals transitioning to this environment. Despite its numerous benefits, security is typically the decisive factor for businesses when determining if cloud infrastructure is the best solution for their users. According to the assault report in [1], the most prominent attack is the DDoS attack among the abundance of attacks affecting the great majority of organizations globally. DDoS attacks have fully-fledged in admiration in recent years because of the simplicity with which they may be deployed. DDoS attacks have increased in recent years because of the

ease with which they may be launched. According to [2], the scale of a DDoS attack, which was just 8 Gbps in 2004, has already surpassed 800 Gbps in 2016. Among the plentiful recent attacks [3], a few significant assaults have expanded a lot of courtesy in the scholarly community [4]. "Lizard Squad attacked", has affected the Microsoft and Sony cloud-based gaming services, knocking them offline on Christmas Day in 2015. "Rackspace", is a cloud service provider, which was affected by a massive distributed denial of service (DDoS) attack against its services.

Another exceptional assault scenario was for the Amazon EC2 cloud servers to be exposed to yet another incredible DDoS attack. These assaults caused major downtime, commercial losses, and other enduring and short-term effects on the victims' businesses. According to "Verisign iDefense Security Intelligence Services" [4], the cloud and SaaS (Software as a Service) industries have been the most targets of DDoS attacks in recent quarters. The contribution to the paper is listed below:

- 1) A thorough understanding of DDoS attacks is offered for the reader to gain correct insight and comprehension.
- 2) A monitoring system to identify DDoS attacks in traffic.
- 3) An effective Load balancing mechanism for smooth conduction of the cloud services.

As a consequence, the DDoS detection and prevention system [5] is an essential element in the overall growth of an organization's statement since it explains the rules and methods for providing security. The academic community has focused on identifying several forms of DDoS attacks in the cloud, such as ICMP, HTTP, and TCP protocol flooding [6]. Our key discovery is associated with resource scaling, which may become less effective if the conflict in the network is developed during the attack. The following is the objective of this research:

- 1) Research the DDoS attack and its impact on the cloud server.
- 2) To create a hybrid approach for mitigating DDoS attacks using DCLB and FUZZY logic.
- 3) To monitor and assess the algorithm's effectiveness in mitigating DDoS attacks.

This paper is mainly focused on the mitigation of DDoS attacks and reducing resources utilization. The framework used for the mitigation process of a DDoS attack contains a monitoring system and a load balancing method.

The research paper is constructed as follows. Section II depicts a study of DDoS attacks and the various methodologies employed. Section III of the study then discusses methodology and terminology. Section IV describes in detail the technique and algorithm used for network monitoring and load balancing. Section V presents the experimental data, and Section VI covers the discussion. Section VII brings the work to a conclusion.

II. RELATED WORK

Wahab et al. [7] developed a two-pronged strategy that enables the hypervisor to create believable confidence in the virtual machine. In this case, the suggested system employs the Game solution guide hypervisor approach to identify the ideal detection as well as load balancing.

Liang et al., [8] provided detailed research on machine learning algorithms utilized for DDoS attack detection. The ML approaches detected the class imbalance problem, but the results reveal that a single method cannot overwhelm the DDoS assault, hence enhancements to the ML-based strategies are necessary.

Kousar et al. [9] presented a novel mechanism by combining the statistics and machine learning models. To identify the DDoS attempt, the work was implemented in the Apache Spark Framework. In addition, the approach detects the attack using the NSL-KDD cup methodology as the benchmark dataset.

Alsirhani et al. [10] proposed a DDoS detection framework based on the "Gradient Boosting Classification Algorithm (GBT)" and the Apache Spark engine. The traffic volume (dataset) and feature space assist in the creation of a depth decision tree to identify the assault.

Cloud-Traceback technology (CTB) was created to detect and also to mitigate the DDoS assaults in cloud computing by identifying the origin of HTTP and XML-based attacks, Chonka et al. [11]. It also introduces the use of backpropagation in conjunction with a cloud defender, which filters out malicious traffic.

Guo et al. [12] suggested a resource allocation approach for cloud data centers called "dynamic resource allocation" to protect the resources against DDoS attacks. This article made use of idle cloud resources and avoided them by employing quick filtering algorithms.

Bikram et al. [13] identify the features of a DDoS assault and propose a system called a "Snort-based Intrusion Detection System (IDS) tool" for DDoS detection. It also describes a system that would alert the network administrator of every attack on any imaginable resource, as well as the sort of attack. It also temporarily suspends the attacker for the network administrator to devise a backup strategy. The proposed method mitigates the impact of DDoS attacks by

detecting them early and altering many parameters that make it simpler to diagnose the problem.

Sathya et al., [14] suggested a new framework entitled "Anti-DDoS" that detects high-rate DDoS assaults. This method uses the "graphical Turing test" and "Authentication model" to prevent the cloud from the attacked. It also uses the count hop filtering technique for detecting the attack, the traffic was controlled using a control list.

Liu et al., [15] proposed a strategy that uses the BIRTH algorithm to detect aberrant traffic flows by employing frequency domain information from the network flow's autocorrelation sequence as a clustering feature.

Sahi et al., [16] demonstrated a methodology for detecting the flooding of DDoS attacks by combining data flow and using a list to blacklist to identify the source IP of attack packets.

Barde et al., [17] A "deception detection" approach were proposed for detecting high-rate DDoS attack traffic in the cloud computing domain.

Navaz et al., [18] provide multi-level detection methodologies for camouflaged small traffic DDoS assaults and employ entropy-based algorithms in combination with anomaly detection systems. The researchers have presented a detection algorithm for flooded DDoS attacks and random DDoS attacks, The method gives acceptable results for DDoS attacks with heavy traffic in a cloud environment, the time required to complete the operation is exceedingly slow. The results in the cloud environment are slower, and the approaches rarely examine the real system that is subjected to a variety of attacks.

Zheng et al., [19] suggested a DDoS attack mitigation architecture that helps to detect and responds to attacks quickly. Furthermore, the author argued that SDN network technology helped in the prevention of DDoS assaults.

Saravanan et al. [20] provided an approach for recognizing and mitigating DDoS attack impact assaults. It employs three screening checks to protect the server against assaults, as well as several limitations to identify the attacks. To repel the attack, it employs two queues.

Scaling the VM's capacity is a critical step in estimating the overall number of requests processed in a particular period. The duration of time necessary to perform the request impacts the number of resources consumed. The scale inside-out strategy enhances capacity while simultaneously scaling internal applications to minimize resource use. Somani et al. [21] pioneered this concept.

This work focuses on DDoS attacks that are primarily aimed at detecting bandwidth and connection flooding. Karan et al., [22] generate a solution by integrating the OpenStack firewall with raw socket programming for monitoring network traffic.

III. DESIGN AND ASSUMPTIONS

In the section, the overall proposed model system design is shown. Each cloud user (CU) will access the cloud resources

effectively. The problem faced by the legitimate user (normal user) is the delay that occurs when the user requests the cloud for particular resources.

As the cloud works on-demand policy [24], the cloud system should be more efficient to provide the resource on time as user requests them. The delay in the network occurs due to some unwanted request that will be placed in the network by the assault(attacker). The attacker floods the network with the unwanted request so that the legitimate user will be halted from the requested resource, such attacks are known as DDoS attack.

So, it is necessary to launch an effective mitigation mechanism to prevent the system from this type of attack. As discussed in the ‘related work’ section, there are a lot of mechanisms to detect the DDoS attack but the challenge faced is to identify the attacker and to make the system work properly by removing the unwanted request and regulating the relationship between the and cloud user (balancing the workload).

As shown in Fig. 1, the overall architecture is divided into two main parts: verification and detection process and service access in cloud computing. In verification and detection process is again subdivided into two, one is VV model (Virtualization & Verification) and the other is LB model (Load Balancing). Each cloud user is owned by a virtual machine to access the cloud resources.

The request will be monitored by the virtualization and verification model (VV model) based on the analysis detect made of the request characteristic; the VV model is consist of 4 phases of the procedure and each phases process help to the DDoS attack. In each phase different value is computed based on the request characteristics. The computed value is compared with some predefined threshold value by using the concept of fuzzy logic [23].

The VV process applies various analyzing strategies to the incoming request such as in & out statistics, checking the protocol, number of requests coming, and packet analysis. The result obtained from the VV model detects the DDoS attack and forwards the results to the LB model.

In the LB model, the request load is balanced by using a dynamic cloud load balancing algorithm (DCLB), it applies a vertical scaling mechanism on resource allocation to mitigate the attack after the detection process. Usually, each cloud user which owns the virtual machine is allocated a sufficient number of resources such as P, D, M, and NT (processor, disk, memory, and network throughput).

The number of connections at a particular time many varies, so the idea is to scale down the resources when the attack is detected in the network. When the attack is detected in the cloud system the resources are minimized and the virtual machine which provides the same request or random request will be halted for some time, so that the legitimate user will be able to access the system efficiently.

A. Notation and Assumptions

Let $CC = \{cc_1, cc_2, \dots, \dots, \dots, cc_n\}$ be the finite set of cloud users in the cloud at a particular time. The cloud user (CC) accesses the cloud through the virtual machines. Each CC is owned by a unique virtual machine $VM_i = \{VM_1, VM_2, \dots, \dots, \dots, VM_n\}$. Each virtual machine VM_i uses some set of resources $\{P_i, D_i, M_i, NT_i\}$ which is represented in vector form.

Along with the cloud user, there is a malicious user known as an attacker which is denoted as AT_i which accesses the cloud as the normal cloud user and captures “n” virtual machine to perform a DDoS attack.

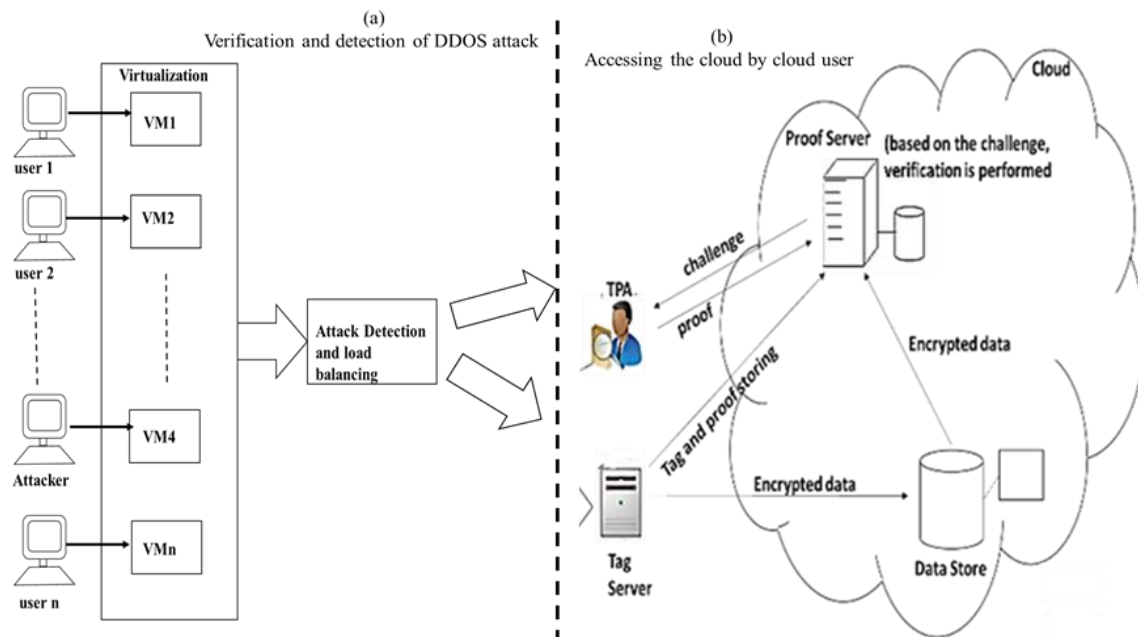


Fig. 1. Overall Proposed System Architecture.

In this proposed system, the request can come from the same source or different sources, so it has been examined that the arrival of several requests from the same source R_{ss} and requests from different resources R_{ds} is less than or equal to the maximum request R_{max} at a particular time.

Also in this system, the number of the incoming packets and the outgoing packet is calculated as n_{rin} and n_{rout} . In the network, there are different protocols from which we can send the request to the cloud such as TCP, UDP, ICMP, etc. In this paradigm, calculating the entropy of protocols that play a substantial role in attack detection, E_p , is critical. In addition, when it comes to protocols, the duration of an IP packet flow is a critical parameter to examine to detect an assault. The flow calculation is denoted as L_{ipflow} in which the average is calculated for all packets from each client virtual machine.

The VV model's output (analysis report) is sent to the LB model, which predicts the manifestation of a DDoS assault, the load balancer checks the result and will reduce the resources allocation by scaling down the Resource Utilization Factor RUF_{nor} to a threshold value which is allocated based on analyzing the intensity of the traffic in the network as RUF_{att} . When RUF_{att} is set instead of releasing the complete resource at a time it will release one by one so that the resource is not affected and legitimate users can also access the resource without any delay.

Virtualization cloud Definition 1: A cloud system consists of a set of cloud users $CC = \{cc_1, cc_2, \dots, \dots, cc_n\}$ owing a set of virtual machines $VM_i = \{VM_1, VM_2, \dots, \dots, VM_n\}$. to access a set of resources, provide by the cloud system.

Each virtual machine owned by the user will have a unique session ID S_{id} , so that it will be easy to identify which the virtual machine is loading the network with heavy traffic. The VV model analysis the traffic and remove the same request coming from the single session of the same virtual machine. Notations used in the proposed system are given below in Table I.

TABLE I. NOTATION USED IN THE PROPOSED SYSTEM

Notation	Description
CC_i	A finite set of cloud users
VM_i	A finite set of Virtual Machine owned by the cloud user
P_i	Processor usage
D_i	Disk usage
M_i	Memory Utilization
NT_i	Network Throughput access
AT_i	Represent the attacker from the set of user
R_{ss}	The request coming from the same source
R_{ds}	The Request coming from a different source
R_{max}	A limited number of requests from the source
n_{rin}	Number of the incoming request
n_{out}	Number of outgoing response
E_p	entropy calculation of different protocol
L_{ipflow}	length of ip packet flow
RUF_{nor}	Normal resource utilization
RUF_{att}	The threshold value is set when an attack occur.
S_{id}	Unique session ID for each user in their owned virtual machine

IV. IMPLEMENTATION OF THE PROPOSED

The overall architecture is of the integrated cloud load balancing algorithm and fuzzy logic (i.e. incorporating different parameters of requests coming from the cloud user) along with the dynamic scaling of resources. The proposed model is divided into two models: VV (Virtualization & Verification) model and LB (Load Balancing) model. These two models are used to spot (detect) and mitigate the attack and help to reduce the access to resources and some other services also.

A. VV Model

In this proposed model, each request coming from the user and the attacker has initially undergone to VV model in which the virtual machine details and request verification is done. The VV model verifies the incoming request that comes from each virtual machine. It also gather the unique session id S_{id} of each request.

The DDoS attack is attained by utilizing a flooding attack in which the request is following the same pattern concerning the protocol also (Fig. 2). The VV model is subdivided into 3 phases: RAI (Request arrival Inspection), PI (Protocol Inspection), and IPI (IP flow inspection).

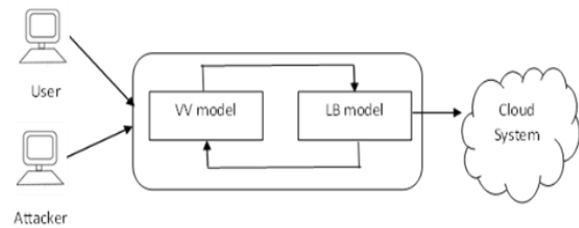


Fig. 2. Overall Implementation Design.

1) RAI: The RAI is the process in which the request arrival is analyzed. Each request comes to the system in the form of a special packet with header fields. The header field help to identify the source and destination address. To identify the chances of a DDoS attack, the source address is considered the critical factor. Here, the packet used is a 32-bit IP packet along with a unique session ID of 4 bits (Fig. 3).

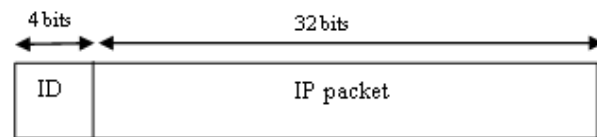


Fig. 3. Packet used for the Accessing the cloud System.

The unique session id is first extracted from each packet. An attack is feasible if the number of requests from the same source consistently exceeds the maximum limit in a certain period. (i.e., $R_{ss} > R_{max}$). If the number of requests comes from a different source at a particular time and exceeds the maximum limit then there is a chance of an attack to occur (i.e., $R_{ds} > R_{max}$). Next, we calculate the ratio of the R_{ss} and R_{ds} which are the main parameter to consider in detecting DDoS attacks. The proportion of incoming and outgoing requests over some timestamp is calculated based on the eq (1),

$$R_{io} = \frac{R_{ss}}{R_{ds}} \quad (1)$$

Usually, the propagation should be constant if the traffic is normal. So here if the R_{io} exceeds the threshold value ($i.e \geq 1$) thus it indicates the event of an attack. It will be balanced if the ratio is less than 1.

2) *PI*: Essentially, if $\langle TCP, UDP, ICMP \rangle \Rightarrow \langle T, U, I \rangle$ packets are employed then, the DDoS attack will be successful [21]. A DDoS attack is indicated by the ratio of these protocols. The formula for calculating the ratio of different methods is displayed in eq (2).

$$R_T, R_U, R_I = \frac{\sum P_T}{\sum Packet_IP}, \frac{\sum P_U}{\sum Packet_IP}, \frac{\sum P_I}{\sum Packet_IP} \quad (2)$$

Then the entropy [25], is calculated for the above-computed value as shown below in eq (3),

$$E_p = \sum^{i \in T, U, I} -P_i \log_2 P_i \quad (3)$$

3) *IPI*: As the arrival and protocol inspection likewise, another significant criterion is the IP Packet flow in the network. Counting the number of packets that fulfill the same criterion yields the average duration of an IP flow. The requirements include the source and destination addresses, as well as the port number and protocol utilized. A packet with the same source and destination might arrive with a different protocol. As a result, the length of the IP flow is computed using Equation (4).

$$L_{ipflow} = avg \left(\frac{\sum ip_packets}{\sum ip_flow} \right) \quad (4)$$

The typical IP flow length is usually between 5 and 10. If the value is close to one, it means an attacking packet was discovered. Here when the attack is detected then the *Attflag* flag is set to one. Which indicates the load balance of the attack occurrences? The entire operation and algorithm utilized for the VV model are detailed below, and a graphical depiction of the method is depicted in Fig. 4.

Algorithm of VV model

Input :

The ip address of the packet,
initial set threshold values

R_{max}

Output:

Attack Detection or accepting the packet

Procedure VV():

1. Retrieve the session id from the request S_{id_i}

Analysis():

i. if $n_{rin} > 100$ then

halt the all the request from the same session ID S_{id_i}

ii. else

1. Compute the R_{ss} and R_{ds}

2. Calculate the ratio of incoming and outgoing packets

3. If $R_{ss} < R_{max}$ && $R_{ds} < R_{max}$ && $R_{io} \leq 1$
goto step 4

4. else

mark the incoming packet as an attack packet set the $att_{flag} = 1$, and move on to the load balancing process.

5. Calculate $R_T, R_U, R_I = \frac{\sum P_T}{\sum Packet_IP}, \frac{\sum P_U}{\sum Packet_IP}, \frac{\sum P_I}{\sum Packet_IP}$

6. Compute the entropy

for ($i \in \langle TCP, UDP, ICMP \rangle$)

$$\{ \quad E_p = \sum -P_i \log_2 P_i \quad \}$$

7. If $E_p \neq 0$ && deviation $(R_T, R_U, R_I)!$ low
goto step 7

8. else

mark the incoming packet as an attack packet set the $att_{flag} = 1$, and move on to the load balancing process.

9. Calculate IP flow average length $L_{ipflow} = avg \left(\frac{\sum ip_packets}{\sum ip_flow} \right)$

10. Calculate the entropy value

for ($i \in \langle TCP, UDP, ICMP \rangle$)

$$\{ \quad E_{ipflow} = \sum -P_i \log_2 P_i \quad \}$$

11. If $5 < L_{ipflow} < 10$ && $2 < E_{ipflow} < 4$

Accept the packet and forward it to the LB module

12. else

mark the incoming packet as an attack packet, set the $att_{flag} = 1$, and move on to the load balancing process.

$$R_{io} = \frac{R_{ss}}{R_{ds}}$$

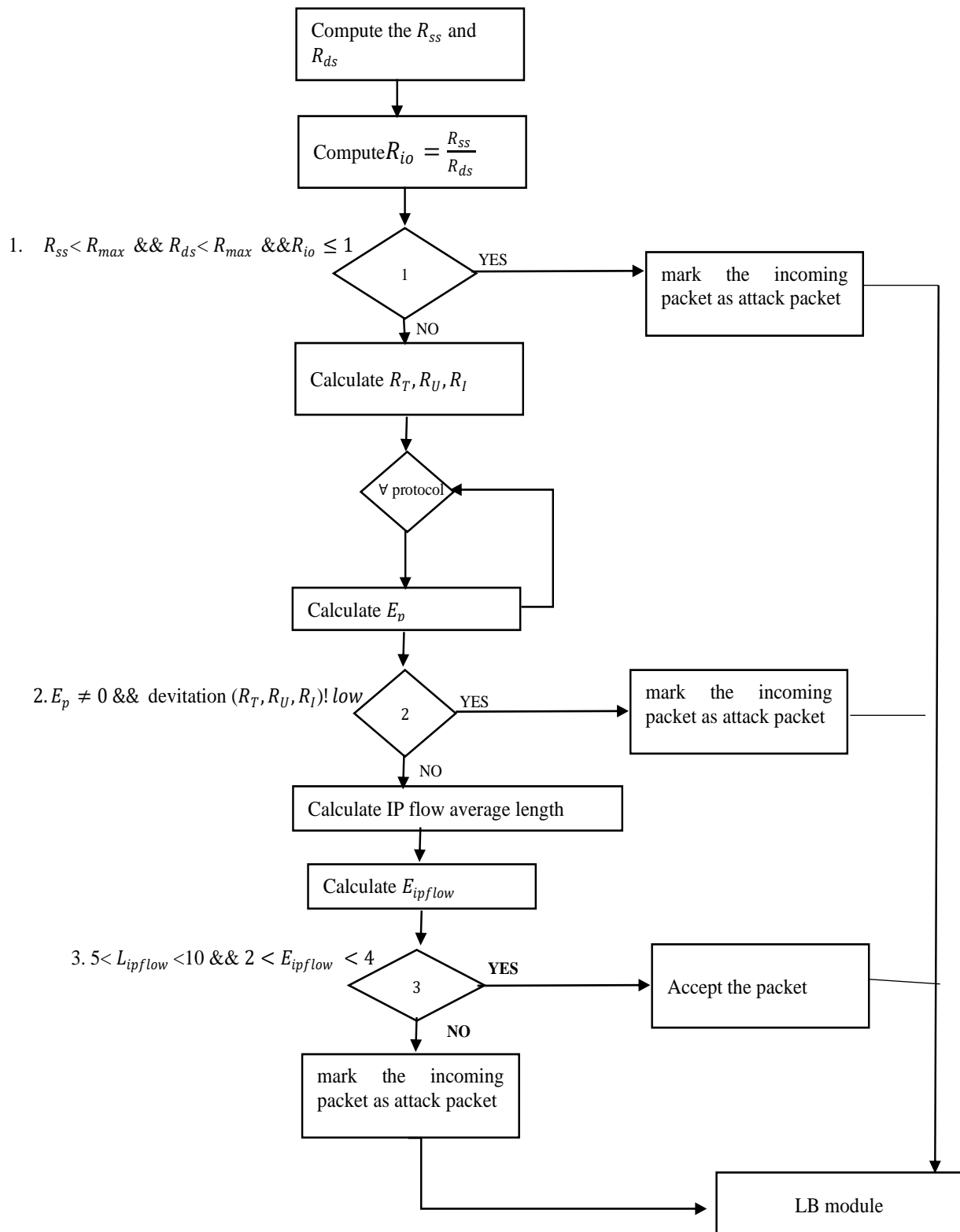


Fig. 4. Flow Chart of VV Model.

B. LB Model

After the VV model, the flow goes to the LB model, in which the resources are balanced based on whether the attack occur or not. The result from the VV model is forwarded to

LB however it is using the MAX-MIN load balancing technique. Initially the services from the cloud will be allocated with favorable resources, if the analysis report shows an occurrence of a DDoS attack, then the MAX-MIN load

balancing is implemented. In these techniques each request will be provided with the initial resources RUF_{nor} as the occurrence of the DDoS attack is detected in the VV model the resource allocation is minimized to RUF_{Att} . RUF_{Att} is a Resource utilization factor that has a threshold value set, when the attack occurred is detected. But here, this proposed system it is dealing with the dynamic nature. The value of RUF_{Att} will varies based on the intensity of the attack, that is, the resources that are suspended will be released one at a time rather than all at once. Minimizing resources during an assault and returning to normal once the attack has ended will boost the virtual machine's capacity. When there is a high volume of traffic, the initial requests are processed, and subsequent requests are retransmitted. This implies that just the index page is displayed to the user, and all subsequent requests are queued or retransmitted. Assaulters who have released a huge volume of traffic will not wait for the provider to respond. As a result, completing the original request may minimize resource use and enhance virtual machine capacity.

Algorithm of LB model

Input :

Analysis report from the VV model
 Att_{flag} value

Output:

Minimize
and maximize the resource usage

Procedure LB():

1. Allocate the resource to the requested services
 - a. Compute $RUF_{nor} = \frac{VM_{CAPACITY}}{n_{maxreq}}$
 - b. Set the resource factor $RF = RUF_{nor}$
2. do
 - a. Call the VV() procedure periodically.
 - b. If $Att_{flag} == 1$
 - i. Compute $RUF_{att} = 1/2(RUF_{nor})$
 - ii. Reduce the $RF = RUF_{att}$
 - c. Else
 - i. Set the resource factor $RF = RUF_{nor}$
3. Continue the process for all requests.

The procedure of LB Model help us to maintain the resources and keep the system throughput same for all the cloud user CU (Fig. 5). The VV model identifies the high-rate traffic, and set the Att_{flag} to 1 other wise the Att_{flag} will be 0 indicate that the traffic is normal.

In the LB model the RUF_{nor} (Resource Utilization Factor) is calculated for the normal traffic of the cloud user CU. This RUF_{nor} will be allocated to the requested user and when the attack is detected, the resource allocated to the CU user will be 50% of RUF_{nor} ($RUF_{att} = 1/2(RUF_{nor})$). So that it helps to maintain the equivalency among the cloud user. All users can access the server and server can process the user request.

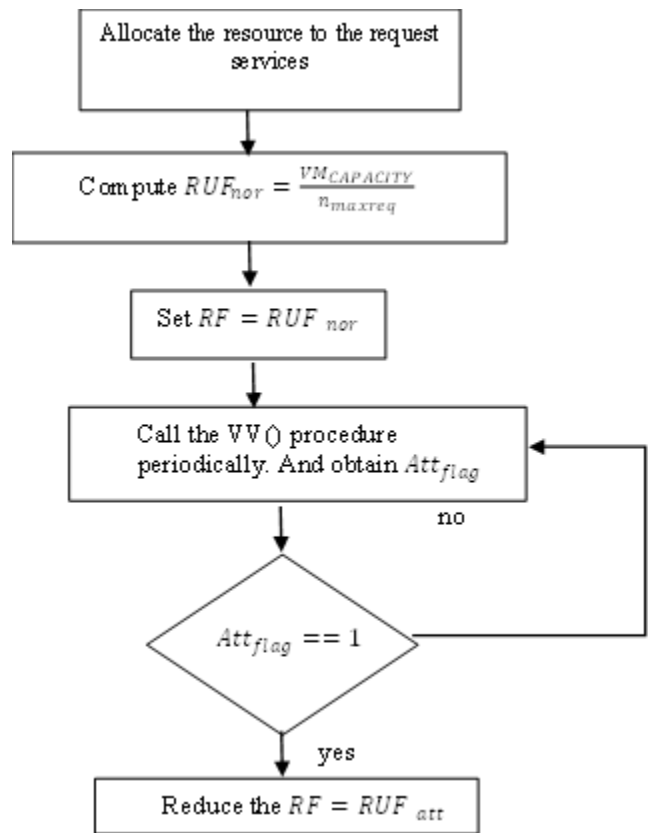


Fig. 5. Working of LB Model.

V. EXPERIMENTAL AND RESULT ANALYSIS

The experiment is carried out by establishing 50 requests to test the availability of cloud service to the requested user even in the event of an attack (including user and attacker requests). At the same timestamp, this request is launched towards the cloud side. The cloud simulator tool is used to mimic the operation of the proposed system and to analyze the system's results. The cloud service taken is the storage of doubled encrypted files and access of the double encrypted file.

A. Computation Cost

The above specified methodology contains operations such as multiplication, division, addition, subtraction and comparison operation with the time t_m, t_d, t_a, t_s and t_c . The time taken for the entropy calculation, IP address comparison etc. as calculated for the two phases: The complexity cost of the VV model when compared with the SIO and ANTI-DDoS model is $2nt_d + (n + 1)t_s + nt_c$ and for the load balancing the cost is $n(t_d + t_c) + \alpha_d$, where α_d is the delay taken to reduce the resource scale from the normal to minimum when attack is detected. The below Table II show the complexity cost of proposed system with the SIO and ANTI-DDoS schemes.

The proposed model is compared with the SIO and ANTIDDOS model, in which the load balancing is the main factor in the above 3 schemes.

TABLE II. COMPUTATIONAL COST

Complexity Cost	Schemes		
	SIO	ANTI-DDOS	Proposed model
Verification Cost	$(n^2 + 1)t_d + 2nt_m$	$n^3t_d + (n + 1)^2t_s + 4nt_c$	$2nt_d + (n + 1)t_s + nt_c$
Load balancing Cost	$nt_d + n^3t_c - (n + 1)^2\alpha_d$	$n(t_d + t_c) + n^2t_s - \alpha_d$	$n(t_d + t_c) + \alpha_d$
Detection cost	$(n + 1)(t_d + n^2t_c)$	$nt_d + n^2t_c$	$(n + 1)t_c$

The load balancing process complexity in SIO model is $nt_d + n^3t_c - (n + 1)^2\alpha_d$ and for ANTIDDOS model is $n(t_d + t_c) + n^2t_s - \alpha_d$, here the complexity is high than the proposed model because in SIO the delay for the resource balancing takes $O(\log n^2 + 1)$ and for the ANTIDDOS model the delay for the resource balancing takes $O(n^2)$. All delay is overwhelm in the proposed model in which the load balancing process complexity is $(t_d + t_c) + \alpha_d$, the delay for the resource balancing is $O(1)$.

Also while comparing the verification cost of SIO and ANNTIDDOS model shows a $O((n + 1)^2)$ and $O((n - 1)^2)$ but the proposed system shows a complexity of $O(2n + 1)$. In the detection process the cost is $O(n + 1)$ for the prosed system which is very less complex that the other two schemes.

B. Result Analysis

It is also seen on the TPA side, where auditing requests are tracked. The cloud server processor is an Intel Xeon CPU with 8GB RAM and a 1TB hard disc. The traffic rate is considered to be between 10 and 500 requests per second and does not exceed 500. To analyze the performance, input files of varied sizes are employed. The system's performance is evaluated using three metrics: attack detection time, Rate of Reporting. The above system is contrasted with the AntiDDoS framework [10] and the Scale in-out model [17]. The experiment was carried out by varying the number of DDoS attacks recorded on the deployed cloud server. The detection rate and false-negative rate for a variety of DDoS assaults were compared for the existing methodologies and the proposed model. Table II displays the results. The system's performance is evaluated by comparing the service provided by the cloud during normal and outage periods. The obtained result is shown below in Table III which is compared with existing methods also.

The above table shows the service time of each request without the resource scale down. When the attack occurred in the system the victim server (cloud server) will process the request, the Table IV shows the proposed model taking less time to process the request than the other two.

Table V shows the service time of each request without the resource scale down. When the attack occurred in the system the victim server (cloud server) will process the request, the Table III shows below describe the proposed model taking less time to process the request than the other two. Tables II and III show that the new system works faster than the previous technique. The average value from each table is calculated and it is observed that the proposed system's average value is less than the earlier methodologies. The proposed approach has a detection rate of 93 percent on

average. As a result, the suggested technique outperforms the other current methods in terms of detection rate. Also, the proposed system service the request at a high rate than the others, the average service time of the request is 41.3s at the normal rate and 76s during the attack period (see Fig. 6 to 8).

TABLE III. PERFORMANCE COMPARISON OF ATTACK DETECTION

Resources request	SIO	ANTI-DDOS	Proposed model
	AD	AD	AD
50KB	39.52	37.12	32.12
100 KB	40.87	37.14	33.11
1 MB	42.3	39.45	33.12
2MB	45.23	42.66	40.06
5MB	49.2	43.23	40.31
10 MB	46.3	45.26	39.26

TABLE IV. PERFORMANCE COMPARISON OF SERVIC TIME BEFORE THE ATTACK

Resources request	Service time Before the attack		
	SIO	ANTI-DDOS	Proposed model
50KB	43.65	33.75	23
100 KB	125.6	41.25	29
1 MB	152.2	45.16	32.13
2MB	187.2	64.14	47.31
5MB	256.7	66.49	49.19
10 MB	358.6	89.69	67.75
Average	158.9	56.7	41.3

TABLE V. PERFORMANCE COMPARISON OF SERVICE TIME AFTER THE ATTACK

Resources request	Service time after the attack		
	SIO	ANTI-DDOS	Proposed model
50KB	42	87	67
100 KB	141	88	69
1 MB	216	85	65
2MB	405	113	80
5MB	634	129	85
10 MB	707	200	90
Average	357.5	117	76

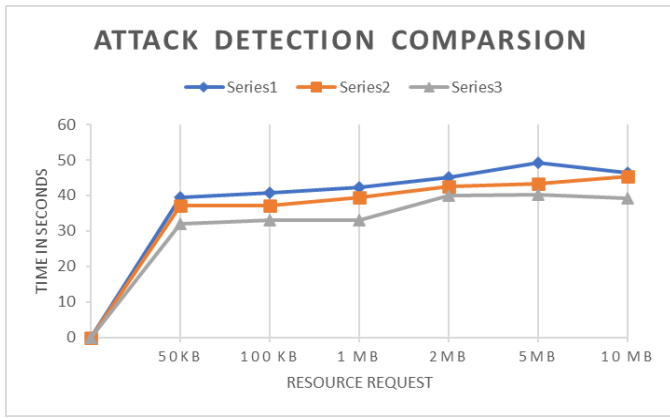


Fig. 6. Performance Comparison of Attack Detection.

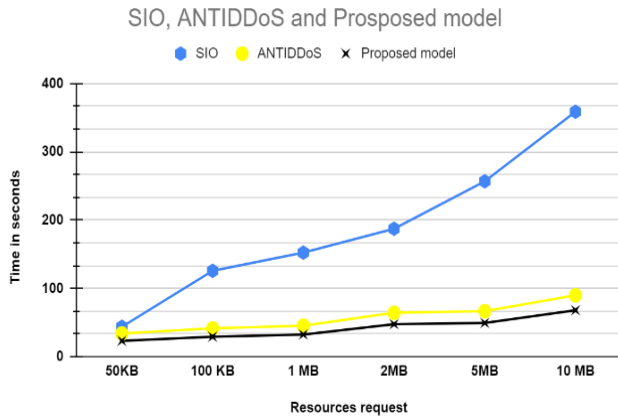


Fig. 7. Performance Comparison of Service time before the Attack.

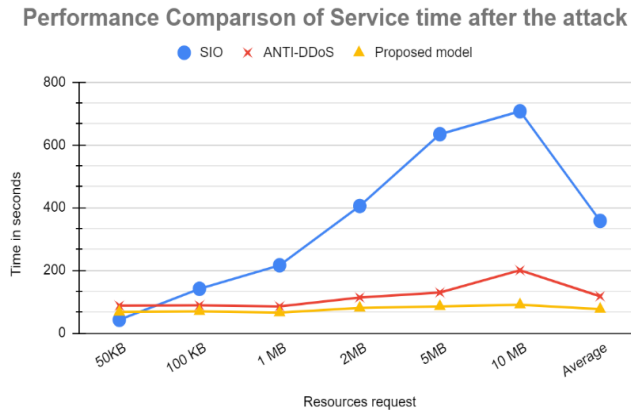


Fig. 8. Performance Comparison of Service Time before the Attack.

VI. DISCUSSION

This paper proposed a new model IDCLB-FL using the integration of Dynamic Load balancing (Min-Max load balancing is used) with Fuzzy Logic. The cloud user CU provide request to the cloud server, the cloud server provide the resources required for the user as their demand. The problem discussed in this paper is the high rate Ddos atack which provide a huge running traffic request along with the legitimate user request. To detect the normal legitimate user

request and unwanted attacker request, a proposed model was designed with 2 phase of detection process. The 2 phase of the model is VV model and LB model, one phase is used to deytected the DDoS traffic and other phases are to balance the load of each request. The feature considered in the VV procedure is:

1) The first feature of In and out requestion ratio is calculated as the R_{ss}, R_{ds}, R_{io} value to compare withe condition $R_{ss} < R_{max} \ \&\& \ R_{ds} < R_{max} \ \&\& \ R_{io} \leq 1$ and based on the analysis, it set the Att_{flag} as 1 or 0.

2) Other feature used in VV procedure is the Entropy calculation of each request based on the protocol used by the traffic request as $E_p \neq 0 \ \&\& \ deviation (R_T, R_U, R_I) \ low$ and based on the analysis, it set the Att_{flag} as 1 or 0.

3) The last feature is IP flow along with the entropy value calculated as, $5 < L_{ipflow} < 10 \ \&\& \ 2 < E_{ipflow} < 4$ and based on the analysis, it set the Att_{flag} as 1 or 0.

4) As the value is of Att_{flag} is set to 1 or 0, the LB model is processed and if Att_{flag} value is 1 then the resource is reduce to be 50% of RUF_{nor} ($RUF_{att} = 1/2(RUF_{nor})$).

5) If Att_{flag} value is 1 then the resource is provided as RUF_{nor} .

C. Limitation of the Proposed Model

The proposed model was test by providing 50 test requests with normal and abnormal traffic pattern. The limitation faced by the system is the time, when detection and verification process take 76s for the 50 requests, but if the number of requests increase the time also increases. Second limitation of the proposed model is that, it is not able to detect the low-rate DDoS attack occurs along with the normal traffic. Third limitation is that, the entropy calculation of each request should lie between the range of 0 and -1, but some time, some normal request also shows the entropy value in this range itself and set the flag as 1 i.e. attack request. So, the proposed model shows a fatal rate of 0.2%.

VII. CONCLUSION AND FUTURE SCOPE

The cloud server's primary priority is protecting the cloud from numerous threats and vulnerabilities. A distributed denial of service attack is the most frequent vulnerability, which prohibits legitimate users from accessing resources. The analytical report received from the preceding experiment demonstrates an effective methodology for mitigating DDoS attacks. This solution provides an efficient framework for verifying each request and securing cloud server services and resources from being manipulated by an attacker. The proposed model is a combination of verification and load balancing, with the concept of fuzzy logic, which helps to detect the attack easily than the others with an average accuracy of 93%. The model effectively removes the high traffic (request) from a single session id and also verifies the other request by some criteria discussed in the implementation session.

The future work will focus on offering an improved method for identifying low-rate DDoS assaults, which are a concern in cloud systems. Also the improved method should reduce the fatal rate from 0.2% to 0%.

REFERENCES

- [1] Arbor Networks, "Worldwide Infrastructure Security Report Volume XI," 2015.
- [2] Arbor Networks Technical Report, "Worldwide Infrastructure Security Report Volume XII," 2016.
- [3] G. Somani, M. S. Gaur, D. Sanghi, M. Conti, and R. Buyya, "DDoS Attacks in Cloud Computing: Issues, Taxonomy, and Future Directions," ACM Computing Surveys, 2015.
- [4] DDoS attacks in Q1 2018, Kaspersky Lab, 2018. [Online]. Available: <https://securelist.com/ddos-report-in-q1-2018/85373/>. [Accessed: 18-Mar.-2019].
- [5] P. Nelson, Cybercriminals Moving into Cloud Big Time, Report Says, <http://www.networkworld.com/article/2900125/malware-cybercrime/criminals-moving-into-cloud-big-time-says-report.html> 2015.
- [6] Tara Seals, DDoS Attacks Spike, Targeting Cloud, <http://www.infosecurity-magazine.com/news/q1-2015-ddos-attacks-spike/> 2015.
- [7] O. A. Wahab, J. Bentahar, H. Otok and A. Mourad, "Optimal Load Distribution for the Detection of VM-Based DDoS Attacks in the Cloud," in IEEE Transactions on Services Computing, vol. 13, no. 1, pp. 114-129, 1 Jan.-Feb. 2020, doi: 10.1109/TSC.2017.2694426.
- [8] X. Liang and T. Znati, "An empirical study of intelligent approaches to DDoS detection in large scale networks," 2019 International Conference on Computing, Networking and Communications (ICNC), 2019, pp. 821-827, doi: 10.1109/ICCNC.2019.8685519.
- [9] H. Kousar, M. M. Mulla, P. Shettar and N. D. G., "DDoS Attack Detection System using Apache Spark," 2021 International Conference on Computer Communication and Informatics (ICCCI), 2021, pp. 1-5, doi: 10.1109/ICCCI50826.2021.9457012.
- [10] A. Alsirhani, S. Sampalli and P. Bodorik, "DDoS Detection System: Utilizing Gradient Boosting Algorithm and Apache Spark," 2018 IEEE Canadian Conference on Electrical & Computer Engineering (CCECE), 2018, pp. 1-6, doi: 10.1109/CCECE.2018.8447671.
- [11] Ashley Chonka, Yang Xiang, Wanlei Zhou, Alessio Bonti, Cloud security defence to protect cloud computing against HTTP-DoS and XML-DoS attacks, Journal of Network and Computer Applications, Volume 34, Issue 4, 2011, Pages 1097-1107.
- [12] S. Yu, Y. Tian, S. Guo and D. O. Wu, "Can We Beat DDoS Attacks in Clouds?," in IEEE Transactions on Parallel and Distributed Systems, vol. 25, no. 9, pp. 2245-2254, Sept. 2014, doi: 10.1109/TPDS.2013.181.
- [13] Bikram Khadka, Chandana Withana, Abeer Alsadoon, Amr Elchouemi, 2015. Distributed Denial of Service attack on Cloud Detection and Prevention. School of Computing and Mathematics, Charles Sturt University, Sydney, Australia Hewlett Packard. International Conference (pp. 1-5). IEEE.,2015.
- [14] A.Saravanan, S.Sathya Bama, Multi-Model Anti-Ddos Framework For Detection And Mitigation Of High Rate Ddos Attacks In The Cloud Environment, International Journal Of Scientific & Technology Research, Volume 9, Issue 03, pp.4503-4511. 2020.
- [15] Liu Z G, Yin X C, Lee H J. A new network flow grouping method for preventing periodic shrew DDoS attacks in cloud computing,18th International Conference on Advanced Communication Technology(ICAICT), 66-69. 2016.
- [16] .Sahi A, Lai D, Li Y.,An efficient DDoS TCP flood attack detection and prevention system in a cloud environment. IEEE Access,6036-6048, 2017.
- [17] Jeyanthi N, Barde U, Sravani M. ,Detection of distributed denial of service attacks in cloud computing by identifying spoofed, International Journal of Communication Networks & Distributed Systems, 262-279. 2013.
- [18] Navaz A S S, Sangeetha V, Prabhadevi C.,Entropy based anomaly detection system to prevent DDoS attacks in cloud, International Journal of Computer Applications, 42-47, . (2013).
- [19] Wang B, Zheng Y, Lou W. ,DDoS attack protection in the era of cloud computing and software-defined networking. Computer Networks, 81(C): 308-319, 2015.
- [20] Saravanan, A., Bama, S.S., Kadry, S. and Ramasamy, L.K., A new framework to alleviate DDoS vulnerabilities in cloud computing. International Journal of Electrical & Computer Engineering (2088-8708), vol.9,2019.
- [21] G. Somani, M. S. Gaur, D. Sanghi, M. Conti and M. Rajarajan, "Scale Inside-Out: Rapid Mitigation of Cloud DDoS Attacks," inIEEE Transactions on Dependable and Secure Computing, vol. 15, no. 6, pp. 959-973, 2017.
- [22] Karan B. Virupakshar, Manjunath Asundi, Kishor Channal, Pooja Shettar, Somashekar Patil, D.G. Narayan," Distributed Denial of Service (DDoS) Attacks Detection System for OpenStack-based Private Cloud", Procedia Computer Science, Volume 167, pp. 2297-2307, 2020.
- [23] Singh, P.K.: Three-way fuzzy concept lattice representation using neutrosophic set. Int. J.Mach. Learn. Cybernet. Vol 8,issue 1, pp. 69–79 ,2017.
- [24] Tasnuva Mahjabin, Yang Xiao, Guang Sun, Wangdong Jiang," A survey of distributed denial-of-service attack, prevention, and mitigation techniques",International Journal of Distributed Sensor Networks,volume 13 ,issue 12,2017.
- [25] Lee, T.-H.; He, J.-D.: Entropy-based profiling of network traffic for detection of security attack. In: TENCON 2009-2009 IEEE Region 10 Conference, pp. 1–5, 2009.

Federated Learning Approach for Measuring the Response of Brain Tumors to Chemotherapy

Omneya Atef¹, Mustafa Abdul Salam², Hisham Abdelsalam³

Faculty of Computers and Information Technology, The Egyptian E-Learning University (EELU), Cairo, Egypt^{1,3}

Faculty of Computers and Artificial Intelligence, Benha University, Benha, Egypt²

Faculty of Computer Studies, Arab open University, Cairo, Egypt²

Faculty of Computers and Artificial Intelligence, Cairo University, Egypt³

Abstract—Brain tumor is a fatal disease and one of the major causes of rising death rates in adults. Predicting methylation of the O6-Methylguanine-DNA Methyltransferase (MGMT) gene status utilizing Magnetic resonance imaging (MRI) imaging is highly important since it is a predictor of brain tumor responses to chemotherapy, which reduces the number of needed surgeries. Deep Learning (DL) approaches became powerful in extracting meaningful relationships and making accurate predictions. DL-based models require a large database and accessing or transferring patient data to train the model. Federated machine learning has recently gained popularity, as it offers practical solutions for data privacy, centralized computation, and high computing power. This study aims to investigate the feasibility of federated learning (FL) by developing a FL-based approach to predict MGMT promoter methylation status using the BraTS2021 dataset for the four sequence types, (Fluid Attenuated Inversion Recovery (FLAIR), T1-weighted (T1w), T1-weighted Gadolinium Post Contrast (T1wCE/T1Gd), and T2-weighted (T2w)) MRI images. The FL model compared to the DL-based and the experimental results show that even with imbalanced and heterogeneous datasets, the FL approach reached the training model to 99.99% of the model quality achieved with centralized data after 300 communication rounds between 10 institutions using OpenFL framework and the improved EfficientNet-B3 neural network architecture.

Keywords—Federated Learning (FL); BraTS2021; Data Privacy; O6-Methylguanine-DNA Methyltransferase (MGMT); OpenFL; EfficientNet-B3; brain tumors; Deep Learning (DL)

I. INTRODUCTION

Brain tumors are a grave problem that threatens human life and leads to death if not diagnosed and treated early. Especially, Glioblastoma (GBM) and astrocytic glioma with molecular features of GBM (WHO Grade 4 astrocytoma). The glioblastoma multiform tumor is a highly malignant brain tumor. Most of these brain tumors occur in adults, and they are characterized by a wide range of symptoms. It has a poor prognosis with a median survival of about ten months in most cases [1]. Recently been discovered that, the presence of a specific genetic sequence in the tumor known as MGMT (o6-methylguanine-DNA methyltransferase) promoter methylation during GBM patient's chemotherapy is a significant and independent predictive factor of favorable survival in glioblastoma patients undergoing the treatment.

MGMT is a protein that repairs damage to the DNA of human body cells. The chemotherapy drugs cause damage to

tumor cells. Thus, the more MGMT protein the tumor produces, the less effective the chemotherapy drug is expected to be, as the protein will repair the damage to the tumor. The detection of MGMT requires the performance of a biopsy (removing tissue from the tumor and analyzing it) and can take several weeks depending on the results and the types of treatments initially implemented, subsequent surgery may be necessary [2]. The development of an efficient method of detection utilizing medical imaging (i.e., MRI, radio genomics) could potentially minimize the number of surgeries.

Deep learning (DL) based applications have shown promising results in this area but to cover all medical questions that can be applied to a vast patient population and ensure high and accurate performance, DL-based applications rely on large, diverse datasets from different health institutions [3]. This is particularly challenging due to the natural sensitivity of healthcare informatics, legal and cultural challenges. Each health institution (e.g., hospital, clinic, lab, etc.) is often resistant to sharing patient data. Moreover, the available data in a single institution is not adequate for the training due to the low incidence rate of brain tumor pathologies and limited patient numbers. These limitations raise the need to seek alternative approaches [4-6].

A recent surge in popularity has been witnessed by federated learning, a paradigm that offers great promise for learning with fragmented, sensitive data. By allowing training a global model through a central server while keeping the data in local institutions where they originated, rather than aggregating data from different places altogether or using the traditional discovery and replication approach, a shared global model can be trained [7-9]. The main idea is moving computations to data, where a globally shared model is brought to where the data is.

II. MOTIVATION AND CONTRIBUTION

In this study, a set of contributions are achieved using the proposed study:

- 1) Development of an improved EfficientNetB3 model relying on the combination of convolution neural network (CNN) and Recurrent neural network (RNN) architectures.
- 2) Four types of Scans are used in this study, while other related work depended on only one or two scans.
- 3) Two approaches are applied based on classical and federated learning.

4) The federated learning showed the ability to deal with data privacy, diversity, real time continuous learning, and hardware efficiency.

III. RELATED WORK

Recently, machine learning and deep learning techniques have been used to predict MGMT status, and it achieved satisfactory results. Korfiatis et al. in 2017 trained three residual deep neural network architectures, ResNet18, ResNet34, and ResNet50 in order to predict MGMT methylation status based on MRI scans with T2 and T1 weighted post-contrast images obtained from Mayo Clinic. [10]. in another work by Yogananda et al., 2021, Based on 3D-Dense-UNets, they developed a T2WI-only network (MGMT-net) to detect MGMT methylation status and segment tumors. Using MRI scans from The Cancer Imaging Archive (TCIA) and The Cancer Genome Atlas (TCGA) datasets [11]. The deep-learning approach developed by Chen et al., 2022 for MGMT promoter methylation using MRI scans of 111 patients was based on ResNet18 with fivefold cross-validation. Four sequences were analyzed for radiomics features for two regions of interest (the whole tumor area and the tumor core area), including T1 weighted images (T1WI), T2 weighted images (T2WI), apparent diffusion coefficient maps (ADC), and T1 contrast-enhanced images (T1CE) [12].

Despite the efficiency of the mentioned works but all of them depended on the classical way of learning, That Lacked patient privacy protection. Even removing metadata such as names or dates of birth is insufficient to protect privacy because it is possible to reconstruct a patient's face from MRI data. This sensitivity of healthcare informatics directed the researchers toward using federated learning in the healthcare applications such as federated medical imaging, federated remote health monitoring, and federated EHRs management applications [13, 14]. Due to the novelty of the approach, there are a few articles on Brain tumor diagnosis using federated learning, and almost all of these articles focus on brain tumor segmentation only.

The first use of federated learning in a multi-institutional collaboration was presented by Sheller et al. in 2019, allowing deep learning modeling without sharing patient data. They used the Brats dataset and achieved 99% of the model performance with a data-sharing model. They compared federated learning with two alternative collaborative learning methods, Cyclic Institutional Incremental Learning (CIIL) and Institutional Incremental Learning (IIL). The comparison shows that these two methods failed to match the performance of federated learning. Even though CIIL may seem like a simpler option, full validation should be carried out periodically, such as at the end of a cycle, which will help in selecting a good model. The validation process would need the same synchronization and aggregation steps as FL and would even add communication costs over FL. in addition, a large number of institutions with small amounts of data do not scale well with IIL and CIIL [15].

Using a deep neural network, Li et al. applied federated learning for the segmentation of brain tumors using the BraTS dataset as a part of the NVIDIA Clara Train SDK. They

studied various practical aspects of the federated model sharing with an emphasis on preserving patient data privacy. While a strong differential privacy guarantee. The experimental results show that the FL training was done at twice the number of epochs in the data centralized training to reach the same result [16].

An FL-based cross-site modeling platform has been proposed by Guo et al. in 2021 for the reconstruction of MRI images collected from a variety of institutions with different scanners and acquisition protocols. The experiments were conducted on a variety of datasets with promising results. Hidden features were aligned with hidden features extracted from various sub-sites [17]. Table I summarizes the effective methods for predicting the MGMT methylation status based on the Classical and the recent federated learning approaches for brain tumor diagnosis.

TABLE I. METHODS FOR BRAIN TUMOR DIAGNOSIS

Related Work	Methods for Brain Tumor			Limitations
	Architecture	Algorithm	Dataset	
Korfiatis et al [10]	DCNN	ResNet18 ResNet34 ResNet50	MRI from Mayo Clinic	Only two type of scans are used, Following classical learning
Yogananda et al [11]	CNN	3D-Dense-UNets,	TCIA and TCGA datasets	Only one type of scans are used, Following classical learning
Chen et al [12]	DCNN	ResNet18	MRI Scans for 111 patients	Following classical learning
Sheller et al [15]	FL , CLL ,IIL	DNN	Different Institutions, collaborated dataset	Brain tumor segmentation model
Li et al [16]	FL	DNN	BraTS 2018	Brain tumor segmentation model
Guo et al [17]	FL	DNN	Multiple Datasets	Model for reconstructing MRI scans

IV. MATERIALS AND METHODS

A. Training Model

The training model is based on an improved EfficientNet-B3 architecture relying on RNN layers. The EfficientNet-B3 was released by Google in 2019. It is a convolutional neural network architecture and scaling technique that uses the compound coefficient technique to uniformly scale depth, width, and resolution in a simple and efficient manner. Which make it is better at analyzing images than the existing Artificial intelligence models such as ResNet, inception and DenseNet [18]. The EfficientNet-B3 is a part of the EfficientNet family, which ranges from B0 to B7. B3 was selected among this family because it offers a good compromise between computational resources and accuracy. The compound scaling method uniformly scales each

dimension with a certain fixed set of scaling coefficients. Instead of randomly scaling up width, depth, or resolution. Equation (1) show how it is achieved mathematically.

Fig. 1 illustrate the architecture of the proposed model. The fully connected features extracted from the EfficientNetB3 are input to a proposed RNN architecture based on a long short term memory (LSTM) layers. The fully connected layer output is input to a sequence input layer, 2 LSTM layers, 2 dropout layers, 1 fully connected layer, and a Softmax layer.

$$S.t. \alpha \cdot \beta^2 \cdot \gamma^2 \approx 2 \quad (1)$$

$$\alpha \geq 1, \beta \geq 1, \gamma \geq 1$$

compound coefficient: ϕ

depth: $d = \alpha^\phi$

width: $w = \beta^\phi$

resolution: $r = \gamma^\phi$

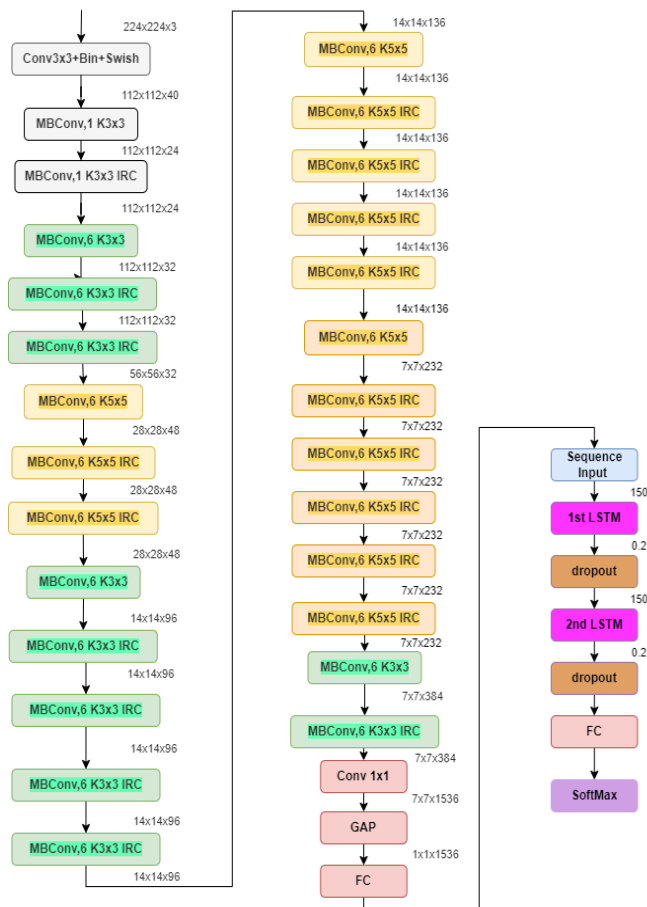


Fig. 1. The Improved EfficientNet-B3 Model Architecture.

The training process carried out on four distinct models based on the scan type FLAIR, T1w, T1wCE, and T2w respectively. Each model calculates a probability that the model belongs to class 0 (no presence of MGMT) or class 1 (present presence of MGMT).

Algorithm 1 shows how the final score per patient is obtained. Although the training model works on each scan

type separately, each scan type has the same pre-processing and training steps. All the resulted predictions are aggregated to finally predict the MGMT value of each patient. The results of the prediction are aggregated together for each patient in order to get the most confident result reached out of all predictions. The aggregation process is applied by obtaining the mean of the four types of scans for each patient individually. Moreover, the maximum and the minimum are also calculated. Then, the difference between the mean and the maximum, and also the variance between the mean and the minimum is compared. Finally, the nearest difference to the mean is the optimal value (maximum or minimum).

Algorithm 1 Predicting MGMT Value

Start

Predicted_MGMT_Value: List

For each scan type ['flair', 't1w', 't1wce', 't2w']:

T_df, V_df, ← training and validation sets data frames

Ts_df ← testing set data frame

T_g, V_g, Ts_g ← Augmentation (T_df, V_df, Ts_df)

Best_model ← train_model (MRI, T_g, V_g, E=20)

Ts_pred ← best_model.Prediction (Ts_g)

Ts_df [Pred_y] ← Ts_pred

M_pred ← Ts_pred.mean ()

Ts_pred_agg ← Aggregate the predictions results on all MRI types for each patient

For each patient_id:

Ts_pred_agg ← Max (Ts_df [Pred_y])

If Max (Ts_df [Pred_y]) – M_pred > M_pred – Min (Ts_df [Pred_y])

Else if Min (Ts_df [Pred_y])

End if

End

Predicted_MGMT_Value ← Ts_pred_agg

End

End

Data augmentation is performed on the images and the type of augmentation applied was based on geometric techniques. The augmentation step aims to balance the number of images in each class before training. The model takes the whole training and validation data (Original and augmented) as an input. The epochs of the model are defined with 20 (E=20), whereas the number of iterations for each epoch is equal to 58. This forms a total of 1160 iterations for the entire model.

B. Federated Learning

To preserve patient data privacy, we need to eliminate the existence of a centralized dataset to prevent data movement and share it with others. On the other hand, the single medical site has its data only, which is a bit amount of data and insufficient to train the model. Federated learning (FL) is a data-private collaborative learning approach that enables multiple health institutions to parallel train a machine learning model at the same time using their own data [19].

The general architecture of federated learning consists of four main components. Fig. 2 illustrates the architecture of the federated learning approach. The training model learned using the local dataset and sends the results to the central server (Aggregator), the server sends these results to the global

model to learn from it. After that, the global model sends back the updated results to all the local models. The whole training process is done through several communication rounds between the aggregator and the collaborators.

- **Aggregator:** is the responsible for the aggregation process, receives updates and results from each local model, and feeds them with the updates.
- **Collaborator(s):** represent the medical institutions.
- **Local Model:** learn from the local data.
- **Global Model:** learn from the local model gradients.

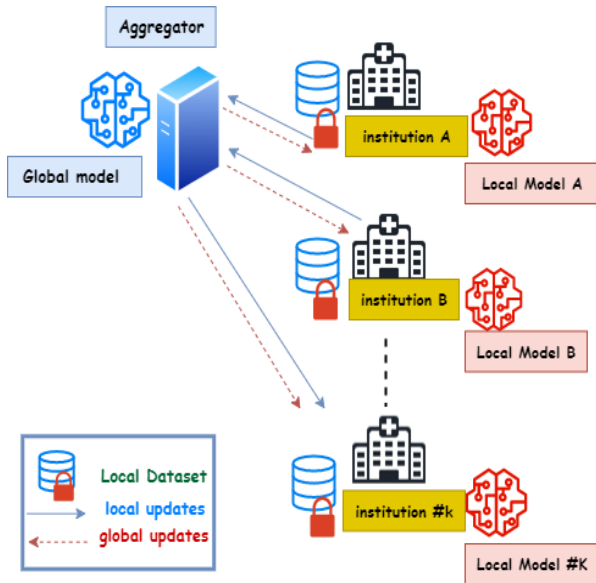


Fig. 2. The Architecture of the Federated Learning Approach – Hospitals Represents the Medical Institution.

In this way, FL enables connecting data from different institutions while not requiring any movement of patient data. Furthermore, FL solves insufficient data volume problem in a single institution.

V. EXPERIMENTAL RESULTS

A. Experimental Setup

1) *BraTS Dataset:* collaboration with the MICCAI Society (the Medical Image Computing and Computer-Assisted Intervention Society), the Radiological Society of North America (RSNA) provided a massive dataset of MRI scans from patients diagnosed with gliomas (BraTS2021) [20]. These scans were obtained from various institutions under standard clinical conditions, and various imaging equipment and protocols were used to produce a heterogeneous image quality reflecting the diverse clinical practices at different institutions. Four different sequence types of images are collected for each patient (Fluid Attenuated Inversion Recovery (FLAIR), T1-weighted (T1w), T1-weighted Gadolinium Post Contrast (T1wCE/T1Gd), and T2-weighted (T2w)). A total of 585 scans were collected for the training set and 87 scans were collected for the testing are sorted by the

patient ID. A binary label is used to describe the methylation status of the MGMT promoter (0: unmethylated, 1: methylated). Fig. 3 shows four types of scans for two patients with various MGMT_value.

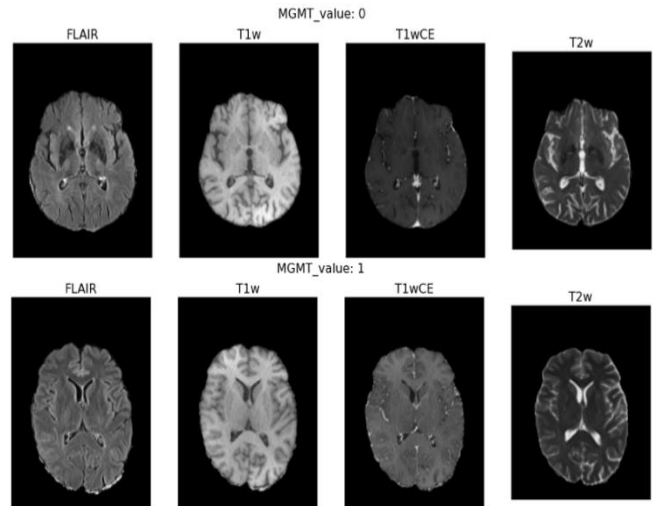


Fig. 3. Sample from the Dataset Includes Two Patients with two different MGMT_Value.

2) *Data Pre-Processing:* This dataset is presented in DICOM (Digital Imaging and Communications in Medicine) format, which is extremely complex and inefficient for image processing and analysis. DICOM has the drawback that a single volume is stored as a series of 2D slices. The FLAIR sequence of patient #00014 is 74 slices as shown in Fig. 4, while the FLAIR sequence of patient #00000 contains 400 slices, making it extremely challenging to analyze.

To facilitate the data handling, the DICOM sequences were converted to the NIfTi (Neuroimaging Informatics Technology Initiative) format.

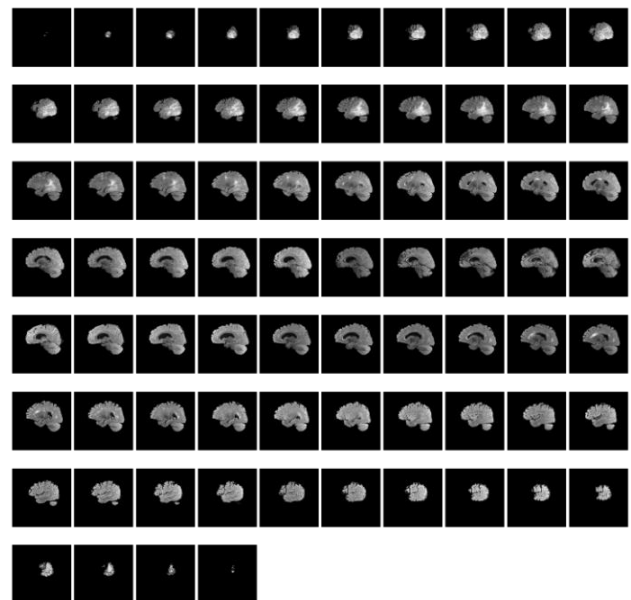


Fig. 4. The FLAIR Sequence of Patient with ID #00014.

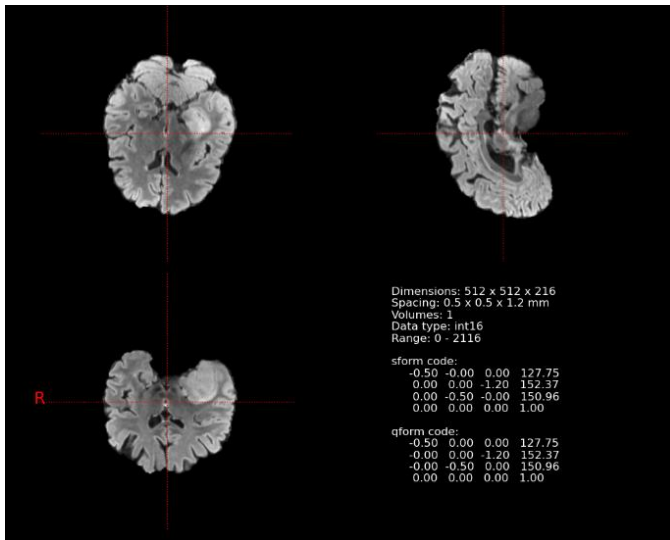


Fig. 5. FLAIR Sequence of Patient 00014 after converting it to the nii Format.

Fig. 5 shows the FLAIR sequence of patient #00014 that was displayed before in Fig. 5 after converting it to NIfTi format. The generated NIfTi file has 512 x 512 x 216 dimensions in x, y, and z. In both x and y dimensions, the spacing between slices is 0.5 mm, and in z dimensions, it is 1.2 mm.

In each NIfTi file, the header file contains sform and qform code matrices, which are always related to the input image. These code matrixes are appropriately remapped when padding, cropping, or applying affine spatial transformations. Whenever the sform is set in processing operations that deal with a single image, it is transformed in the same manner as qform. These matrices displayed in detail with Fig. 6.

Some simple preprocessing transformations applied to the NIfTi files. They normalized, resized and rotated to be easier in loading and processing Fig. 7 displays the nii file for the same patient after applying those preprocessing steps. After resizing the NIfTi files, they have x, y, and z dimensions of 128 x 128 x 64, with a spacing value of 1.0 millimeters between slices. After normalization, the range is reduced from 0-2116 to -1.0-1.0. Furthermore, sform and qform code matrix values have been changed.

3) *Data partitioning*: The host of the provided dataset has confirmed that these three cases have some issues in the training dataset. For the two patients with ID #00109 and #00709, the FLAIR sequences are blank, and for the patient with ID #00123, the TW1 sequence is blank. As a result, 582 patient’s cases were successfully trained. We shared the two training and testing datasets with 10 collaborators, corresponding to the 10 institutions that exist in real life. The resulting patient counts for each of the institutions, which we will refer to as collaborators (C) 1–10 are given randomly with high variations. A local validation set, consisting of 10% of training data of each institution, is also held out as a validation set. The actual numbers of patients at each institution in the training, validation, and testing datasets illustrated in Table II.

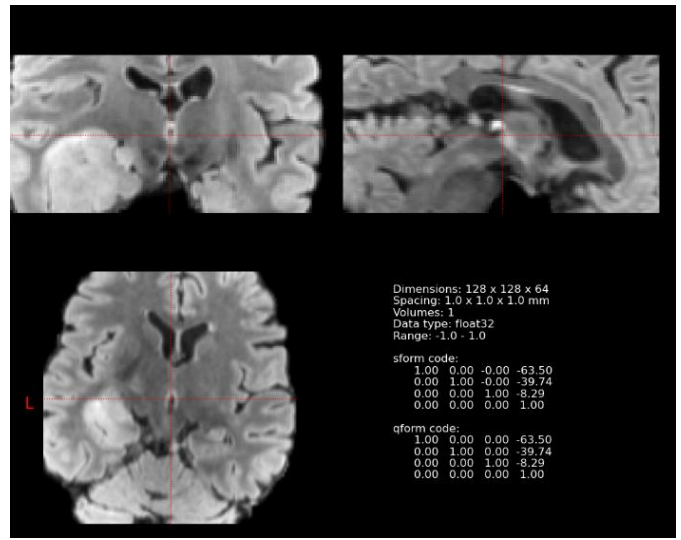


Fig. 6. The FLAIR Sequence of Patient 00014 after the Normalization Process.

TABLE II. PATIENTS DISTRIBUTION FOR EACH COLLABORATOR

Collaborator #Number	Number of Patients		
	Training	Validation	Testing
C1	72	8	10
C2	63	7	9
C3	67	8	9
C4	54	6	8
C5	31	4	8
C6	58	7	8
C7	45	5	9
C8	36	4	8
C9	32	4	8
C10	63	7	10

The data partitioning process followed the Horizontal partitioning (sharding) strategy which partitioned the dataset into multiple different datasets. The partitions all share the same features but have entirely different patients. Similarly, each partition has its own set of data.

4) *Work flow*: Federated Learning projects require a trusted execution environment to support the development process and facilitate the implementation of all necessary features in a secure manner. OpenFL is an open-source Python 3 framework for federated learning developed by Intel Labs in collaboration with the Internet of Things Group. Through a plugin mechanism, ML models and neural network training frameworks such as Tensor Flow and PyTorch can be used to train models. Communication between participants is secured by certificates [21].

OpenFL can be used to establish and run experiments with federations in two different ways: via Director-based workflows and Aggregator-based workflows. Fig. 7 illustrates the Aggregator-based workflow in OpenFL framework, which

is the chosen workflow in the conducted experiment. The federation runs between the aggregator node which owns the learning model and an arbitrary number of collaborators. This workflow is based on creating a workspace at the aggregator node and sending this workspace to each collaborator individually.

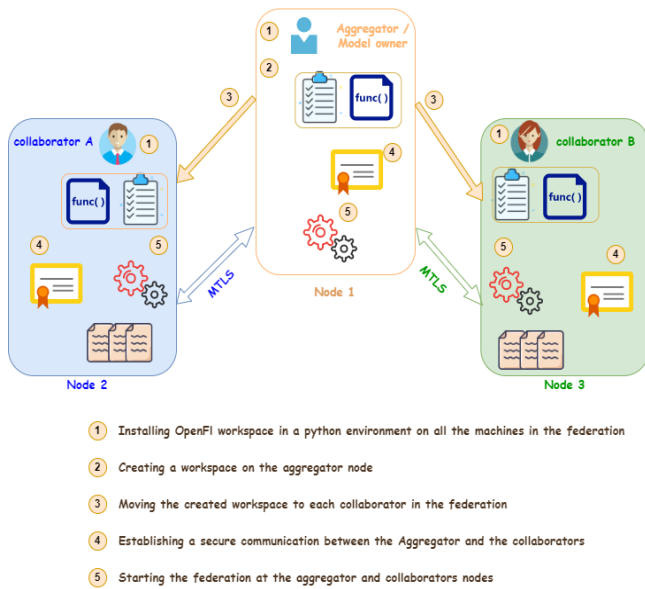


Fig. 7. The Architecture of the Aggregator-based Workflow.

This workspace consists of the plan and the learning model. The plan is a YAML file where the experiment settings are defined and is used to modify the workspace to the needed requirements such as the address of the aggregator, the global model that will be sent to collaborators, the number of federation rounds, and the encryption for network connections. Other parameters describing the model training process can be included as well.

To establish the connection, all participants must provide a valid public key infrastructure certificate signed by a trusted certificate authority (CA). OpenFL uses mutually authenticated transport layer security (TLS) connections. It is possible to create a certificate authority and generate X.509 certificates with OpenFL, but it is intended only for non-production testing. Once the connection is established, the federation starts with the aggregator and the collaborators.

B. Practical Considerations

1) *Training parameters:* Several parameters are adjusted to the EfficientNetB3 architecture to achieve high accuracy performance. The first parameter is the optimizer, and it is selected to be adaptive moment estimation (Adam). The second parameter is the learning rate, and it is set to 0.001. The third parameter is the number of epochs of the model, and it is defined with 20, whereas the number of iterations for each epoch is equal to 58. In order to prevent overfitting, batch normalization is added and a 40% dropout is added before each fully connected layer. A sigmoid activation function is used on the last layer to resolve the two-class classification problem. A binary-crossentropy function is used for the cost

function to solve the two-class classification problem. Also, some parameters are adjusted to the proposed RNN architecture. The number of neurons of each LSTM layer is 150, and the dropout layer has a probability value of 0.2.

2) *Plan parameters:* The experiment conducted with 10 collaborators represent the 10 institutions and lasted for 300 communication rounds to achieve the same results. OpenFL framework supports four aggregation algorithms in this experiment the FedOpt algorithm is used with the Adam optimizer.

C. Experimental Results

We conducted two experiments the first, followed the classical way of learning, the training model use a centralized dataset to predict the MGMT value. In the second, we use the same data set and the same Learning model but with the federated learning approach. The main goal is to show that the developed FL-based model can perform the same as the DL-based model in addition to persevering the patient's privacy, preventing data transferring and aggregation from data owners, and using less computational power, which makes it better for healthcare applications. The two developed model were evaluated according to the performance of the model and the resulting values of the MGMT promoter methylation.

1) *Model performance:* To test the performance of the machine learning model, 10% of the dataset has been allocated for testing the model and it achieved accuracy with a score 96.21% and with 3.783 loss.

The following line charts Fig. 8 illustrate the classical model performance over the twenty epochs for each scan type. a and b represent the training accuracy and Loss of the four scan types and each scan type is colored by a specific color. The first two scan types are colored in yellow and black for Flair and T1w respectively, while the last two scan types are colored in red and blue for T1wce and T2w, respectively. The validation accuracy and loss represented in c and d, respectively.

The Federated learning model was also tested on 10% of the dataset and achieved an accuracy of 96.713% and a loss of 3.287. Fig. 9 shows the performance of the same previous model but as the global model in the FL experiment in terms of training and validation. a and c manifest the validation and training accuracy curve in the yellow and blue colors over 300 rounds and b and c manifest the validation and training loss.

2) *Predicted MGMT_value:* The presence of the MGMT protein is the main desired results of the proposed approach and the most important factor to measure the effectiveness of Federated Learning approach. The results of the two models are shown In Table III and Table IV. Using both federated and classical learning respectively. Each table consists of three columns. The first column represents the records of the patients, while the second column describes the patient ID and it was provided with the dataset, whereas the last column presents the predicted MGMT value. The predicted MGMT value for each patient in the two models are the same, which ensures the efficiencies of the federated

model to work as the classical one and produce the same results.

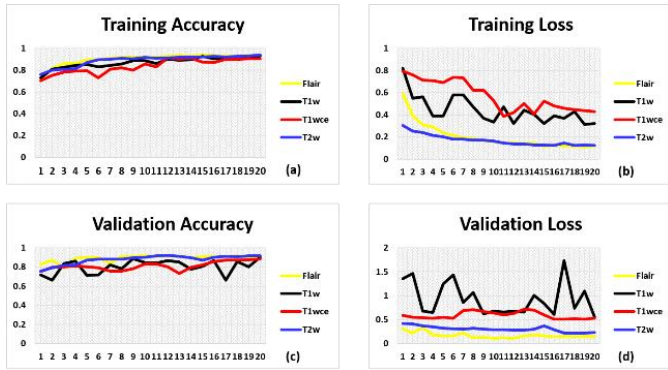


Fig. 8. (a) and (b) Represent the Training Accuracy and Loss for Four Scan Types and (c) and (d) Illustrates the Validation Accuracy and Loss for the Same MRI Scan Types.

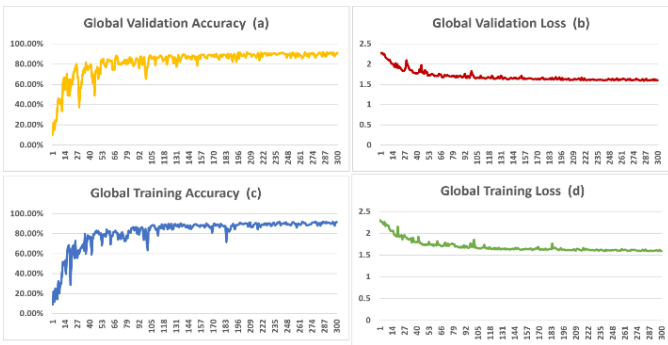


Fig. 9. (a and c) Represent the Global Accuracy Curves on the Training and Validation Data (b and d) Represent the Loss Obtain from the Training and Validation Data.

TABLE III. RESULTS OF THE FEDERATED LEARNING MODEL

Federated Learning Results		
Record	BraTS21ID	MGMT_value
0	1	0.6135
1	13	0.4693
2	15	0.4871
3	27	0.6152
4	37	0.4731
----	-----	-----
80	826	0.5684
81	829	0.5231
82	833	0.4285
83	997	0.5021
84	1006	0.5481

Several trials were applied using different values for the round number. The trials started from 10 rounds till reached 500, and at 300 rounds the performance of the federated and the classical learning was approximately identical. The MGMT values from both models show a 99.99% similarity degree.

TABLE IV. RESULTS OF THE CLASSICAL LEARNING MODEL

Federated Learning Results		
Record	BraTS21ID	MGMT_value
0	1	0.6135
1	13	0.4693
2	15	0.4871
3	27	0.6152
4	37	0.4732
----	-----	-----
80	826	0.5684
81	829	0.5231
82	833	0.4285
83	997	0.5021
84	1006	0.5481

A sample of 87 patients was used in the experiment for testing and obtaining their MGMT values. Fig. 10(a) and (b) visualize the probability distribution of the patients using federated and classical learning respectively. Each class in federated learning is exactly equal in the number of patients to its corresponding class in classical learning.

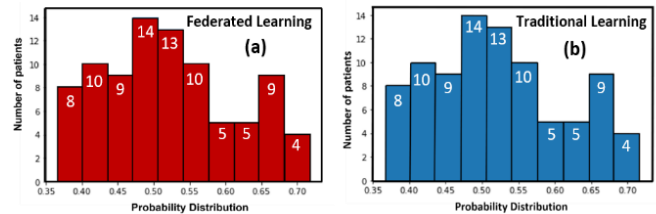


Fig. 10. (a) MGMT Probability Distribution using Federated Learning (b) MGMT Probability Distribution using Classical Learning.

VI. DISCUSSION

The study proposed a methodology based on an improved efficientNetB3 model for the predicating the MGMT promoter methylation of GBM brain tumor with the aim of measuring the response of the tumor to the chemotherapy. At the beginning the data were obtained from the BraTS2021 dataset entirely. The next step is converting the images from the DICOM to NFITI format. The reason for this conversion is to enhance the performance and it can be easy and simple in the processing. Then, the images in the NIFT format are normalized to be ready for feature extraction using the improved efficientNetB3. The features are extracted using the improved efficientNetB3 based on the combination of the CNN and RNN architectures. The entire methodology ran using two different approaches. The first approach is based on classical or conventional learning, while the second approach relies on the federated learning. The illustrated results in Table III, Table IV and Fig. 10, show that the proposed federated model architecture using the OpenFl framework and the BraTS2021 dataset through 300 communication rounds between the aggregator and 10 collaborators managed to surpass the limitation of the classic training model in the following points:

1) *Data privacy*: Each one of the ten collaborators participates in the training process while, keeping its data private, only sharing results and its model gradients.

2) *Data diversity*: Federated learning facilitates training the machine learning model with various and diverse datasets from different institutions, eliminating the need for a centralized data center while making the local data of each collaborator sufficient for the training process as the local training model utilizes its local data and the gradients of the other collaborators.

3) *Real-time continual learning*: Continual learning is done by using client data instead of aggregated data to improve models.

4) *Hardware efficiency*: Since federated learning models operate without a central server, less complex hardware is needed.

VII. CONCLUSION AND FUTURE WORK

Our study explores various practical aspects of the federated model sharing with an emphasis on protecting the privacy of patient data in order to predict the MGMT promoter value of brain tumors. We demonstrate how clinical institutions can train their models without sharing their data by using federated learning. Our FL experiments shows that even with imbalanced datasets, such as the BraTS institutional distribution the FL approach among 10 institutions reached the training model to 99.99% of the model quality achieved with centralized data.

Incorporating such an FL system into a clinical setting for multi-institutional collaboration, which produces computer-aided analytics and assistive diagnostics, is expected to contribute to precision medicine at a catalytic level. Integrating knowledge from another institution into the trained models would be particularly beneficial since patient data wouldn't have to be shared, thereby removing concerns about privacy and data ownership. As a result, the final accuracy achieved a value of 96% on both classical and federated learning. This proves that the federated learning is more efficient in all terms as an environment than the classical learning.

We are striving to improve the performance of the FL model to achieve the results with a smaller number of communication rounds and reduce time consumption in addition to increasing the number of collaborated institutions and exploring different workflows using swarm intelligence.

REFERENCES

- [1] M. L. Goodenberger and R. B. Jenkins, "Genetics of adult glioma," *Cancer Genet.*, vol. 205, no. 12, pp. 613–621, 2012.
- [2] N. Thon, S. Kreth, and F.-W. Kreth, "Personalized treatment strategies in glioblastoma: MGMT promoter methylation status," *Oncol. Targets. Ther.*, vol. 6, pp. 1363–1372, 2013.
- [3] F. Wang, L. P. Casalino, and D. Khullar, "Deep learning in medicine: promise, progress, and challenges," *JAMA Intern. Med.*, vol. 179, no. 3, pp. 293–294, 2019.
- [4] G. Chartrand, P. Cheng, E. Vorontsov, M. Drozdal, S. Turcotte, C. Pal and Samuel Kadoury, "Deep learning: A primer for radiologists," *Radiographics*, vol. 37, no. 7, pp. 2113–2131, 2017.
- [5] J. De Fauw, "Clinically applicable deep learning for diagnosis and referral in retinal disease," *Nat. Med.*, vol. 24, 2018. R. Nicole, "Title of paper with only first word capitalized," *J. Name Stand. Abbrev.*, in press.
- [6] C. Sun, A. Shrivastava, S. Singh, and A. Gupta, "Revisiting unreasonable effectiveness of data in deep learning era," arXiv [cs.CV], 2017.
- [7] N. Rieke, J. Hancox, W. Li, F. Milletari, H. Roth, S. Albarqouni, S. Bakas, M. Galtier, B. Landman, K. Maier-Hein, S. Ourselin, M. Sheller, R. Summers, A. Trask, D. Xu, M. Baust and M. Cardoso, "The future of digital health with federated learning," *NPJ Digit. Med.*, vol. 3, no. 1, p. 119, 2020.
- [8] J. Xu, B. S. Glicksberg, C. Su, P. Walker, J. Bian, and F. Wang, "Federated learning for healthcare informatics," *J. Healthc. Inform. Res.*, vol. 5, no. 1, pp. 1–19, 2021.
- [9] G. Long, T. Shen, Y. Tan, L. Gerrard, A. Clarke, and J. Jiang, "Federated learning for privacy-preserving open innovation future on digital health," in *Humanity Driven AI*, Cham: Springer International Publishing, 2022, pp. 113–133.
- [10] P. Korfiatis, T. L. Kline, D. H. Lachance, I. F. Parney, J. C. Buckner, and B. J. Erickson, "Residual deep convolutional neural network predicts MGMT methylation status," *J. Digit. Imaging*, vol. 30, no. 5, pp. 622–628, 2017.
- [11] C.G.B. Yogananda, a B.R. Shah, a S.S. Nalawade, a G.K. Murugesan, a F.F. Yu, a M.C. Pinho, a B.C. Wagner, a B. Mickey, b T.R. Patel, b Fei, c A.J. Madhuranthakam, a and J.A. Maldjian, "MRI-based deep-learning method for determining glioma MGMT promoter methylation status," *AJNR Am. J. Neuroradiol.*, vol. 42, no. 5, pp. 845–852, 2021.
- [12] S. Chen, Y. Xu, M. Ye, Y. Li, Y. Sun, J. Liang, J. Lu, Z. Wang, Z. Zhu, X. Zhang, and B. Zhang, "Predicting MGMT promoter methylation in diffuse gliomas using deep learning with radiomics," *J. Clin. Med.*, vol. 11, no. 12, p. 3445, 2022.
- [13] D. C. Nguyen, Q. Pham, P. Pathirana and M. Ding, "Federated Learning for smart healthcare: A survey," *ACM Comput. Surv.*, vol. 55, no. 3, pp. 1–37, 2021.
- [14] A. Rauniyar, Desta. Hagos, D. Jha, Jan. Hakegard, U. Bagci, D.B. Rawat and V. Vlassov, "Federated learning for medical applications: A taxonomy, current trends, challenges, and future research directions," arXiv [cs.LG], 2022.
- [15] M. J. Sheller, G. A. Reina, B. Edwards, J. Martin, and S. Bakas, "Multi-institutional deep learning modeling without sharing patient data: A feasibility study on brain tumor segmentation," *Brainlesion*, vol. 11383, pp. 92–104, 2019.
- [16] W. Li, F. Milletari, D. Xu and N. Rieke, "Privacy-preserving federated brain tumour segmentation," arXiv [cs.CV], 2019.
- [17] P. Guo, P. Wang, J. Zhou, S. Jiang, and V. M. Patel, "Multi-institutional collaborations for improving deep learning-based magnetic resonance image reconstruction using federated learning," *Proc. IEEE Comput. Soc. Conf. Comput. Vis. Pattern Recognit.*, vol. 2021, pp. 2423–2432, 2021.
- [18] M. Tan and Q. V. Le, "EfficientNet: Rethinking model scaling for convolutional Neural Networks," arXiv [cs.LG], 2019.
- [19] H. Zhang, J. Bosch, and H. H. Olsson, "Federated learning systems: Architecture alternatives," in *2020 27th Asia-Pacific Software Engineering Conference (APSEC)*, 2020.
- [20] U. Baid, S. Ghodasara, S. Mohan, M. Bilello, E. Calabrese, E. Colak, K. Farahani, J. Kalpathy-Cramer, F.C. Kitamura, S. Pati, L.M. Prevedello, J.D. Rudie, C. Sako, R.T. Shinohara, T. Bergquist, R. Chai, J. Eddy, J. Elliott, W. Reade, T. Schaffter, T. Yu, J. Zheng, BraTS Annotators, C. Davatzikos, J. Mongan, C. Hess, S. Cha, J. Villanueva-Meyer, J. B. Freymann, J. S. Kirby, B. Wiestler, P. Crivellaro, R. R. Colen, A. Kotrotsou, D. Marcus, M. Milchenko, A. Nazeri, H. Shaykh, R. Wiest, A. Jakab, Marc. Weber, A. Mahajan, B. Menze, A. E. Flanders, and S. Bakas, "The RSNA-ASNR-MICCAI BraTS 2021 benchmark on brain tumor segmentation and radiogenomic classification," arXiv [cs.CV], 2021.
- [21] G Anthony Reina, Alexey Gruzdev, Patrick Foley, Olga Perepelkina, Mansi Sharma, Igor Davidyuk, Ilya Trushkin, Maksim Radionov, Aleksandr Mokrov, Dmitry Agapov, Jason Martin, Brandon Edwards, Micah J. Sheller, Sarthak Pati, Prakash Narayana Moorthy, Shih-han Wang, Prashant Shah and Spyridon Bakas, "OpenFL: An open-source framework for Federated Learning," Arxiv.org. [Online]. Available: <https://arxiv.org/pdf/2105.06413.pdf>. [Accessed: 30-Sep-2022].

A Fake News Detection System based on Combination of Word Embedded Techniques and Hybrid Deep Learning Model

Mohamed-Amine OUASSIL¹, Bouchaib CHERRADI², Soufiane HAMIDA³, Mouaad ERRAMI⁴, Oussama EL GANNOUR⁵, Abdelhadi RAIHANI⁶

Electrical Engineering and Intelligent Systems (EEIS) Laboratory, ENSET of Mohammedia
Hassan II University of Casablanca, Mohammedia 28830, Morocco^{1,2,3,4,5,6}
STIE Team, CRMEF Casablanca-Settat, Provincial Section of El Jadida, El Jadida 24000, Morocco²

Abstract—At present, most people prefer using different online sources for reading news. These sources can easily spread fake news for several malicious reasons. Detecting this unreliable news is an important task in the Natural Language Processing (NLP) field. Many governments and technology companies are engaged in this research field to prevent the manipulation of public opinion and spare people and society the huge damage that can result from the spreading of misleading information on online social media. In this paper, we present a new deep learning method to detect fake news based on a combination of different word embedding techniques and a hybrid Convolutional Neural Network (CNN) and Bidirectional Long Short-Term Memory (BILSTM) model. We trained the classification model on the unbiased dataset WELFake. The best method was a combination of a pre-trained Word2Vec CBOW model and a Word2Vec Skip-Word model with a CNN on BILSTM layers, yielding an accuracy of up to 97%.

Keywords—Deep learning (DL); Bidirectional Long Short-Term Memory (BILSTM); Convolutional Neural Network (CNN); Natural Language Processing (NLP); fake news

I. INTRODUCTION

Nowadays, social media has become an integral part of people's lives [1]. It's a fertile ground for connecting people, creating and sharing information, and staying up to date on trending events [2]. However, these advantages, it's become more difficult for many people to find the difference between confirmed facts and low-quality information with purposefully false data, commonly known as fake news [3]. The increased prevalence of fake news is a worrying phenomenon that has the ability to influence individuals' decisions, opinions and that may lead to severe influence on both people and society [4]. Consequently, an increasing number of researchers are focusing their efforts on identifying dubious information and fake news on online social media platforms and trying to develop effective and automatic systems for detecting online fake news using Artificial Intelligence (AI) techniques.

AI techniques have been successfully used in recent years to solve different prediction and classification problems in large range of research fields [5]–[15].

Specifically, the use of either classic machine learning methods or deep learning techniques in the fake news

detection [16] have showed an encouraging results. Traditional machine learning approaches are ineffective for dealing with complicated real-world situations like Natural Language Processing (NLP) tasks and text classification [17], [18]. When compared to Machine Learning (ML) techniques, Deep Learning (DL) has shown significant improvements over time [19]. Furthermore, multiple preprocessing and feature engineering techniques are required for traditional ML algorithms. On the other hand, DL approaches may be able to automatically find useful features in content [20].

In this paper, we present a novel approach to detect fake news based on news content with concatenation of word embedding vectors, and a hybrid approach that combines Convolutional Neural Network (CNN) and Bidirectional Long Short-Term Memory (BILSTM). The main contributions of this study are:

- Proposing a novel CNN-BILSTM hybrid approach and extensive experiments are provided to perform the proposed classifier.
- Using concatenation of word embedding technique Word2Vec (CBOW), Word2Vec (Skip-Gram) and Glove.

The rest of this paper is organized as follows: In Section II some important related works are cited. The mathematical problem formulation and the proposed fake news detection system architecture are described in Section III. The used methods of detection and classification are explained in Section IV. Results and discussion are given in Section V. Finally, Section VI concluded this paper.

II. RELATED WORKS

In recent years, many researchers have attempted to create a system for identifying the fake news [21]–[28]. In [29], the authors achieved an accuracy of 92%. The authors used a Term Frequency and Inverse Document Frequency (TF-IDF) features-based approach to detect fake news, and only machine learning traditional classification techniques. The study compared six different supervised classifiers, K-Nearest Neighbor (KNN), Linear Support Vector Machine (LSVM), Logistic Regression (LR), Decision Tree (DT), Support

Vector Machine (SVM), and Stochastic Gradient Descent (SGD). The SVM classifier achieved the highest accuracy.

To detect emerging rumors of breaking news, the authors in [30] proposed an approach based on word embedding using Word2Vec and trains a recurrent neural network LSTM. The accuracy achieved was 79.5%. However, the model still requires more improvement. In another study [31], the authors proposed a hybrid method based on an LSTM-CNN model for the classification of tweets into rumors and non-rumors (fake vs genuine). The proposed method achieved an accuracy of 82%.

In [32], the authors used a hybrid method that combines BiLSTM with different CNN architectures to detect rumors. They use various pre-trained embedded layers. The best accuracy of the model was 86.12%. The authors of [33] used a hybrid method that combined CNN, LSTM, and BiLSTM to develop different models to detect fake news based on the relationship between article headline and article body. The best accuracy of the proposed models was achieved at 71.2%.

The authors in [34] proposed a novel approach based on word embedding over linguistic features by merging linguistic features with word embedding vectors, then using voting classification approach. The best accuracy achieved was 96.73%. In [35], the authors used linguistic features (stylo-metric, semantic, and syntactic, ...). Moreover, for classification they use voting method based on traditional machine learning algorithms. The best accuracy achieved was 96.36%.

III. PROPOSED FAKE NEWS DETECTION SYSTEM ARCHITECTURE

A. Problem Formulation

In this paper, we introduce the problem of fake news detection as shown in Fig. 1.

Given a news content from a corpus of news titles, the objective is to determine if this text content is a fake news. We can formulate this task like a binary classification problem:

Let $T_i = \{w_1; w_2 \dots w_L\}$ be a sequence of words (tokens) of length L of textual content T_i . Given T_i as an input, the first goal is to represent this sequence of words as a sequence of meaningful vectors $E_{v_i} = \{u_1; u_2 \dots u_L\}$ with $u_i \in \mathbb{R}^D$, the second objective is to train a hybrid CNN-RNN model to classify E_{v_i} as a fake news or real news by giving a label from the set $Y = \{0 : \text{for fake news} ; 1 : \text{for real news}\}$.

B. Proposed Approach

We proposed a four-step framework to detect fake news based on news content. The structure of the proposed system is shown in Fig. 2.

In the first step, we start by applying a series of preprocessing operations on the input data. Among these preprocessing operations, reducing noise, deleting unnecessary repetitions, removing punctuation and alphanumeric characters [36].

Indeed, the preprocessing step is a critical stage in every NLP task. Before we provide the data to the DL model, we

cleaned the raw text by removing punctuation. In this step, we used predefined function in python and regular expression to replace all punctuation with empty string. Moreover, we tried to remove all alphanumeric characters such as hashtags and URLs. For every article, we convert all uppercase characters to lowercase. Finally, we split the cleaned article into vectors of words called tokens.

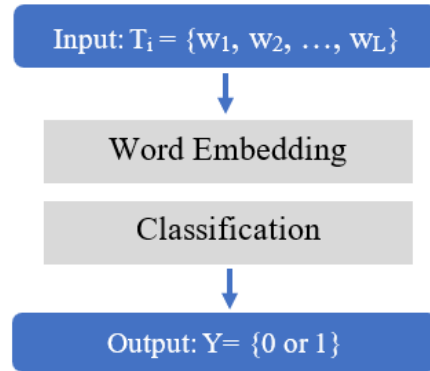


Fig. 1. Formulation of the Proposed Approach of Detection Fake News.

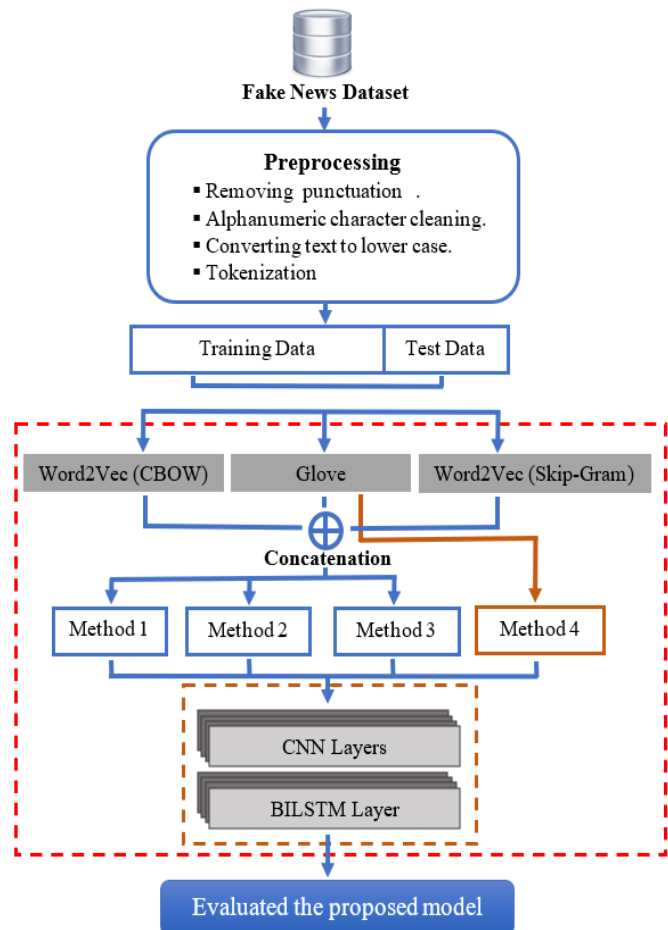


Fig. 2. The Flowchart of the Proposed Approach using CNN-BiLSTM Classifier.

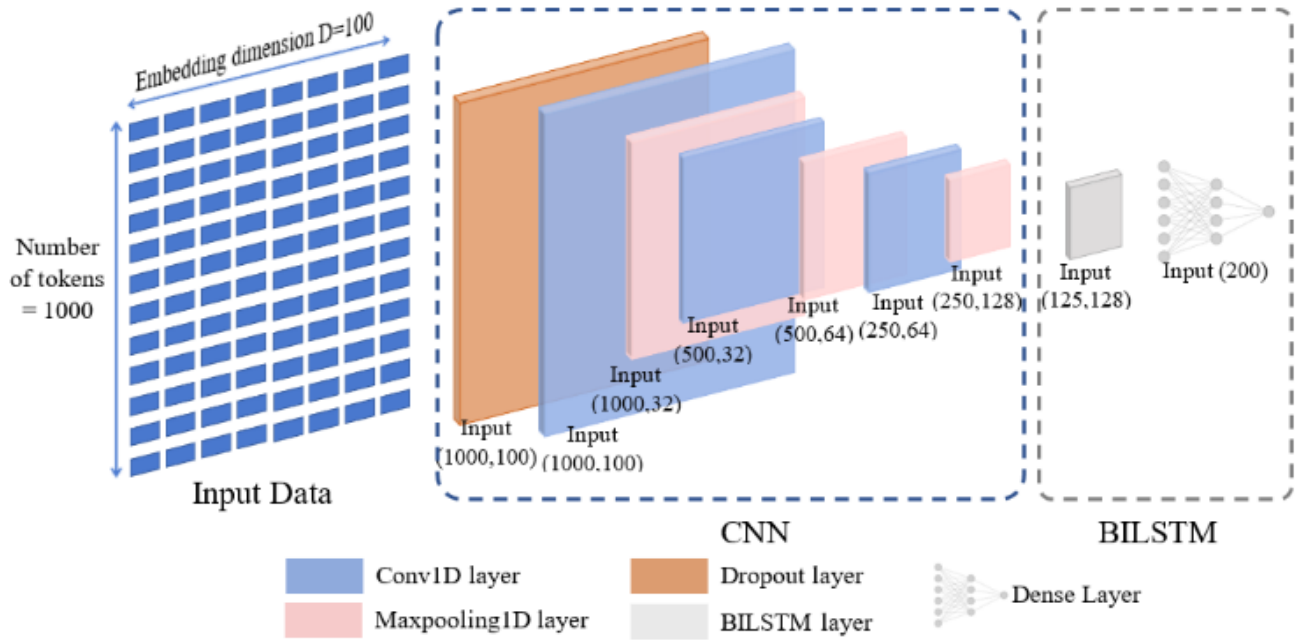


Fig. 3. The Architecture of the Proposed CNN-BILSTM Model

In the next step, the preprocessed input data was converted into word embedding vectors based on the concatenation of two word-embedding techniques. To study the influence of word embedding combination techniques on the proposed model, we proposed four methods to representing words. In method 1, we concatenate the obtained word representation vector using the Word2Vec (CBOW) and the Word2Vec (Skip-Gram) techniques. Method 2 was based on the concatenation of Glove and Word2Vec (Skip-Gram) vectors. In method 3, we concatenate the obtained word representation vector using the Glove and Word2Vec (CBOW) techniques. Method 4 (Baseline) used the Glove word embedding technique. For each method, we provide the obtained vectors to the proposed hybrid CNN-BILSTM network. Then, we conducted four different experiments to study the effect of concatenation. The next step was training the hybrid model. The objective of using CNN layers in this model architecture was to extract fake news features. While, the objective of using BILSTM was to capture the dependencies in the data. The fourth step is to evaluate and compare the application of the four methods on the model.

In Fig. 3, we illustrate CNN-BILSTM architecture used to train the model. From this architecture, we have the convolutional layer that plays a vital role in CNN architecture. It is comprised of a set of convolutional filters [37]. The input data is convolved with these filters to generate the output feature maps [38]. Moreover, the pooling layer is used to sub-sampling and reducing the feature maps dimension with preserving the majority of dominant information. The pooling layer applies statistical methods, such as max pooling, average pooling [39]. The BILSTM Layer. Finally, the Dense Layer consists to connect each unit (neuron) to all neurons of the previous layer and next layer. This layer is activated by an activation function and it is commonly utilized as the CNN classifier [40], [41]. To overcome the overfitting problem, we

used regularization technique based on dropout layers by dropping randomly a number of previous layer outputs during training. This technique is efficient for improving the performance of neural networks especially in vision, speech recognition, document classification tasks [42].

IV. MATERIALS AND METHODS

A. Dataset Description

In this study we use WELFake dataset from [34]. It is one of the largest available datasets that contains 72134 news articles with 37106 fake and 35028 real news. These datasets respect the standards and rules of creating unbiased fake news datasets [43] which in summary are: 1) All articles of dataset should be labeled by experts. 2) Fake news should be collected from different sources. 3) Obtain real news from credible journalism organizations. 4) Collect articles from a variety of news categories in order to create a diverse collection of credible news. The WELFake dataset contains two features (title, content). In addition, all articles are labeled as follow: 0 for fake news and 1 for real news.

As shown in Table I, the dataset was divided into two parts: The training dataset contains 57229 articles, which represents 80% of the global data. Moreover, the testing and validation dataset represent 20% with 14308 articles.

To have a clear view on the dataset, Fig. 4 illustrates the Word Cloud representation for each class.

TABLE I. NUMBER OF USED FAKE AND REAL NEWS ARTICLES

Label	Train	Validation and Test
Real	29207	7302
Fake	28022	7006
Total	57229	14308

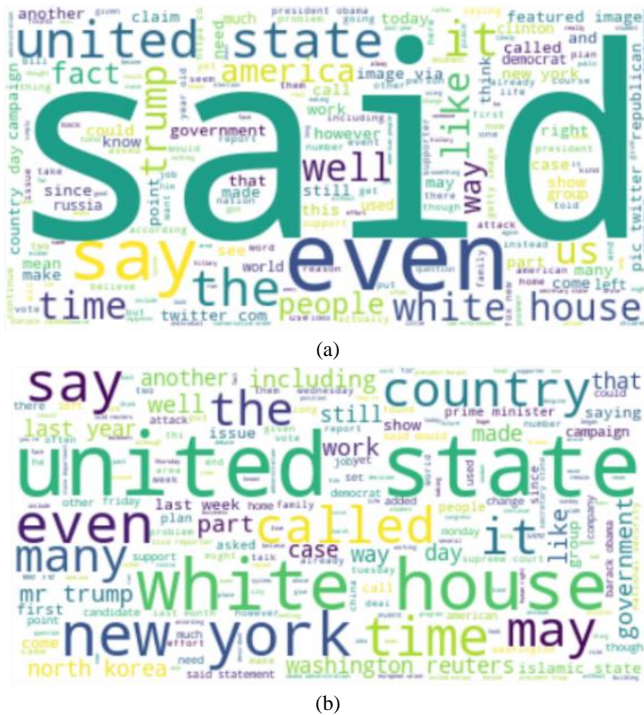


Fig. 4. Word cloud Representations of Dataset: (a) for Real News, (b) for Fake News.

B. Word Representation

Word Embedding (WE) is the representation technique of words that converts words to numerical vectors in \mathbb{R}^D , whose relative similarities correlate with semantic similarity [44]. Several pretrained word-embedding presentations exist for direct use. The most popular word embedding techniques are:

1) *Word2vec*: Word2vec is a well-known word embedding algorithm that has two main variants: Skip-Gram and CBOW, both of them are trained by using a neural prediction-based model [45], Skip-Gram predicts the surrounding words (context-words) from the target word [46]. Given a sequence of training words $w_1, w_2, w_3, \dots, w_L$, Skip-Gram models are trained by maximizing the average log probability:

$$\frac{1}{L} \sum_{t=1}^L \sum_{\substack{j=-c \\ j \neq 0}}^{j=c} \log p(w_{t+j} | w_t) \tag{1}$$

Where c is the size of the training context, and $\{w_{-c}, \dots, w_c\}$ is the word context of the target word w_t . In contrast of Skip-Gram, the objective of Continuous Bag-of-Words Model (CBOW) is to predict a word given its context, CBOW models are trained by maximizing the average log probability:

$$\frac{1}{L} \sum_{t=1}^L \log p(w_t | w_{t-c}, \dots, w_{t-1}, w_{t+1}, \dots, w_{t+c}) \tag{2}$$

2) *Glove*: Glove is a model that produces a word vector space with meaningful substructure, a weighted least squares model trained on global co-occurrence counts of words and therefore making effective use of statistics [47]. The Glove model is trained by minimizing the loss function

$$\sum_{i=1}^L \sum_{j=1}^L f(X_{ij})(v_i^T u_j + b_i + c_j - \log X_{ij})^2 \tag{3}$$

Where $v_i \in \mathbb{R}^D$ is the vector representation of the word w_i , X_{ij} is a weighted count of times word w_j occurs in the context of word w_i , u_j is separate context word vectors, Parameters c_j and b_i represent the bias terms for u_j and v_i , and f is the weighting function defined as follow:

$$f(x) = \min((x/x_{\max})^\alpha; 1) \tag{4}$$

There are different embedding vector sizes with $D=50$, $D=100$, $D=200$, and $D=300$ dimensions. In this paper we choose the pretrained Glove model that trained on one billion words dataset with a dictionary of 400 thousand tokens and $D=50$.

C. Deep Learning Methods

1) *Convolutional neural network*: Convolutional Neural Network (CNN) is a sub-class of deep neural networks. It is particularly used for multimedia content classification tasks such as images and texts, and for time series analysis. One of the main advantages of CNN is recognizing significant features without human intervention [1] that means the ability to solve problems that not contain features which are spatially or temporally dependent. The CNN is inspired from Multi-Layer Perceptron (MLP). Every traditional CNN model includes an input and output layers, and a combination of hidden layers to extract discriminative features [48].

2) *LSTM*: Long short-term memory (LSTM) is an improved version of recurrent layers applied to learn order dependence in time series and sequence data. LSTMs are similar to RNNs, except that the hidden layer is updated using purpose-built memory cells in order to extract dependencies in the data [49]. Fig. 5 illustrates a LSTM memory cell structure.

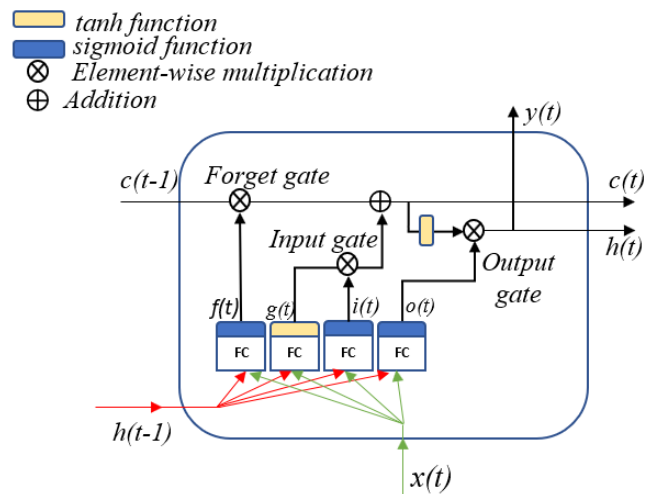


Fig. 5. Single LSTM Memory Cell.

LSTM cell is composed of three gates: input gate, forget gate and output gate. The functions of gates are defined as follow:

$$f_{(t)} = \sigma(W_{x_f}^T x_{(t)} + W_{h_f}^T h_{(t-1)} + b_f) \quad (5)$$

$$i_{(t)} = \sigma(W_{x_i}^T x_{(t)} + W_{h_i}^T h_{(t-1)} + b_i) \quad (6)$$

$$g_{(t)} = \tanh(W_{x_g}^T x_{(t)} + W_{h_g}^T h_{(t-1)} + b_g) \quad (7)$$

$$c_{(t)} = f_{(t)} \otimes c_{(t-1)} + i_{(t)} \otimes g_{(t)} \quad (8)$$

$$y_{(t)} = h_t = o_{(t)} \otimes \tanh(c_{(t)}) \quad (9)$$

$$o_{(t)} = \sigma(W_{x_o}^T x_{(t)} + W_{h_o}^T h_{(t-1)} + b_o) \quad (10)$$

Where, and W_x and W_h are the weight matrices and b is the bias.

3) *BILSTM*: The BILSTM neural network is an advanced version of LSTM. The BILSTM architecture contains LSTM units that function in both directions to integrate left and right context information. Bi-directional network consists of two parallel layers: The forward layer and backward layer extract representation of the left and right context. The outputs of these two layers are then concatenated to produce a complete representation of an element of the input sequence [50]. Fig. 6 illustrates the BILSTM network architecture.

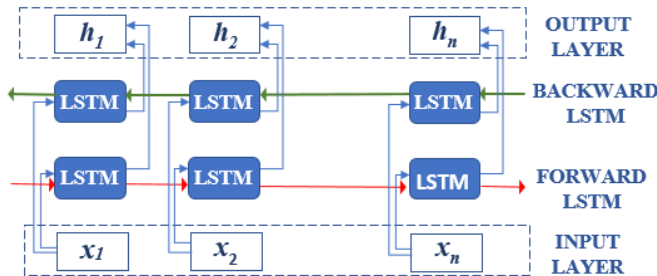


Fig. 6. Simple BILSTM Network Architecture.

V. RESULTS AND DISCUSSION

A. Experimental Setup and Optimal Algorithms Configuration

In this section, we present the experiment and evaluation results on fake news detection. The experimental models are implemented inside an open cloud environment Google Colab

that provides a Tesla K80 GPU with 12GB of GDDR5 VRAM. Python 3.7 and different libraries like TensorFlow and Scikit-learn are used to build the models. In order to find the optimum hyper-parameters of the proposed model, the experiments were conducted with grid search. Table II shows the optimal parameters setting of the model architecture.

B. Evaluation Metrics

We use four metrics to evaluate the results based on the number of True Positives (TP), True Negatives (TN), False Positives (FP) and False Negatives (FN) in the binary classification:

$$\text{Accuracy} = \frac{TP+TN}{TP+FP+TN+FN} \quad (11)$$

$$\text{Recall} = \frac{TP}{TP+FN} \quad (12)$$

$$F_1 \text{ score} = \frac{2 * (\text{precision} * \text{recall})}{\text{precision} + \text{recall}} \quad (13)$$

$$\text{Precision} = \frac{TP}{TP+FP} \quad (14)$$

C. Training Results

Fig. 7 shows the variation of accuracy and loss metrics across epochs. On training, the improvement in term of accuracy and loss of the three models is linear until the 10th epoch. After that, the training performance begins to stabilize and the improvement becomes slow. On the opposite, the validation performance increase with unstable manner.

TABLE II. PARAMETERS SETTINGS OF THE BILSTM-CNN CLASSIFIER

Parameter	Value
Vocabulary size	20 000
Input vector	1000
Word Embedded size	100
Number of convolutional layers	3
Number of filters	128
Filter size	3,5,7
Dropout rate	0,2
Activation function	Sigmoid
Number of epochs	15
Optimization	Adam

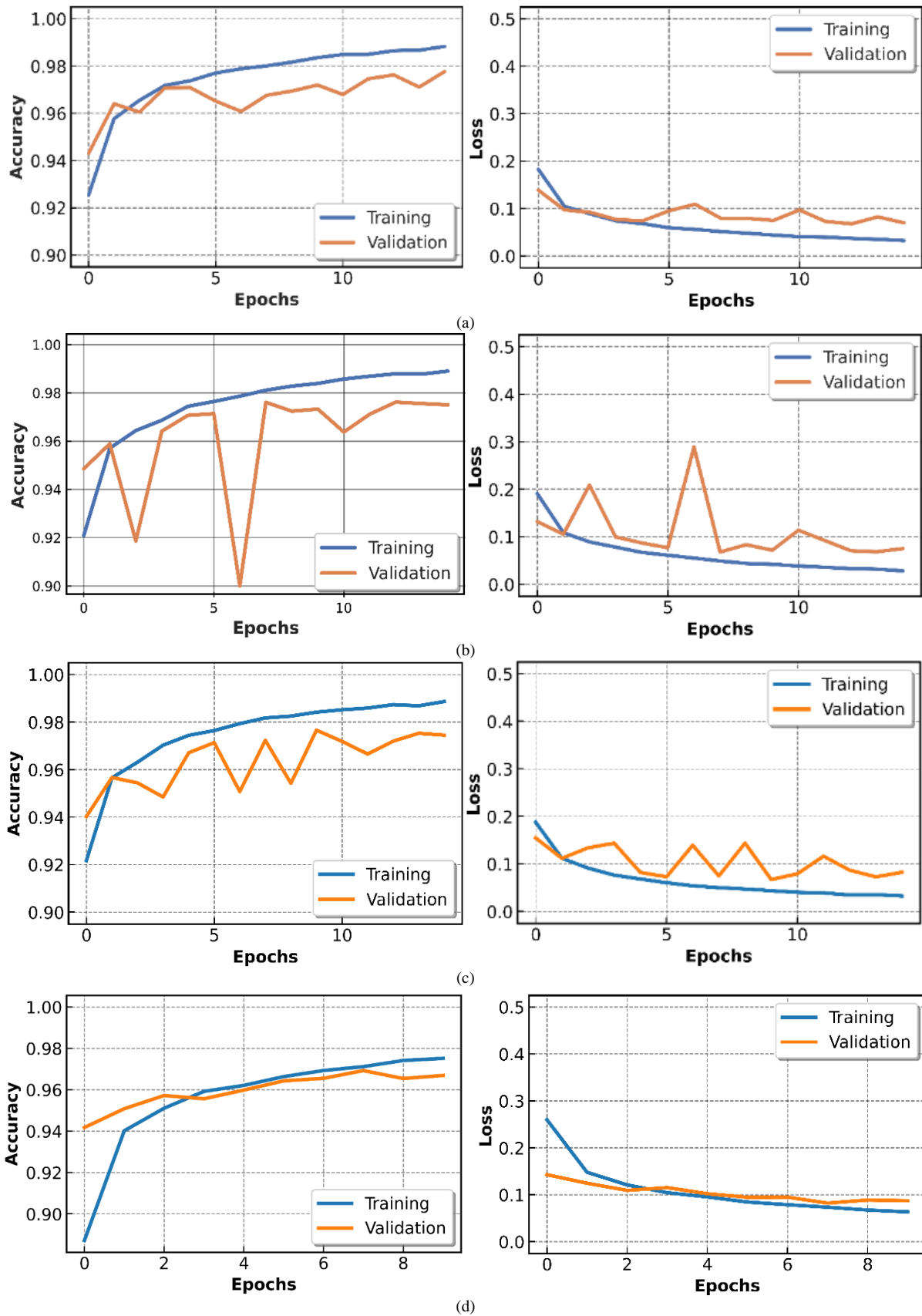


Fig. 7. Accuracy and Loss Curves Obtained by Training and Validating of Proposed Models. (a) Method 1, (b) Method 2, (c) Method 3 and (d) Method 4 (Baseline).

D. Testing Results

Training a CNN models provides a prediction-ready model with the appropriate weights that corresponds to the task being performed. As indicated in Table III, a comparative result in terms of accuracy, recall, F1-score and precision of the model variants. We can clearly observe that the combined word embedded techniques reached an improvement when compared to baseline method.

Among all methods, the method 1 provided the best result in terms of accuracy (97.74%) and precision (97.74%). While, the method 4 based on one-word embedding technique is the lowest in term of accuracy, F1-score and Precision. The method 1 shows better performance in the detection of fake news. The confusion matrix of the proposed model is shown in Fig. 8. We found 3472 news was predicted as fake and was actually fake news. In addition, 66 news was predicted as fake was actually real. On the other hand, 3520 real news were predicted as real and was actually real. Moreover, 96 was predicted as real and was actually fake.

To investigate these findings, a ROC curve illustrating the sensitivity vs specificity (or False Positive Rate versus True Positive Rate) of a diagnostic test might be employed. This shape of the curve enables us to compare several models depending on the value of the AUC variable. This number indicates the total area under the ROC curve between two dimensions. This article depicts the ROC curve for each model considered in this investigation. Fig. 9 depicts a scatterplot of the False Positive Rate (TPR) vs the True Positive Rate (TNR) for the proposed CNN-BILSTM model using word embedding Method 1.

TABLE III. MODELS PERFORMANCE WITH DIFFERENT COMBINATION OF WORD EMBEDDING TECHNIQUES

	Accuracy	Recall	F1-score	Precision
Method 1	97.74%	97.35%	97.75%	98.16%
Method 2	97.71%	98.59%	97.75%	96.93%
Method 3	97.46%	96.99%	97.47%	97.96%
Method 4 (Baseline)	96.56%	97.54%	96.63%	95.74%



Fig. 8. Confusion Matrix for CNN (Method 1).

E. Discussion

In this study, we proposed a hybrid deep learning model to detect fake news based on news content. we used WELFake dataset which is one of the biggest databases accessible and comprises 72134 news, of which 37106 are fraudulent and 35028 are authentic. These datasets adhere to the principles and guidelines of developing impartial fake news. The WELFake dataset includes two characteristics (title, content). Additionally, each article is categorized as follows: zero for false news and one for genuine news. In the first step, we started by applying a series of preprocessing operations on the input data. These operations include reducing noise, deleting unnecessary repetitions, removing punctuation and alphanumeric characters. The preprocessed input data was converted into word embedding vectors based on the concatenation of two word-embedding techniques.

In proposed system architecture, we presented four approaches to represent words in order to examine the effect of word embedding combination strategies on proposed model. In approach 1, the acquired word representation vector is concatenated using Word2Vec (CBOW) and Word2Vec (Skip-Gram). The second method was based on the union of the Glove and Word2Vec (Skip-Gram) vectors. The acquired word representation vector is concatenated using the Glove and Word2Vec (CBOW) approaches in method 3. Method 4 (Baseline) used the Glove approach for word embedding. We submit the acquired vectors for each approach to the suggested hybrid CNN-BILSTM network. For each method, we provided the obtained vectors to the proposed CNN-BILSTM network. The objective of using CNN layers in model architecture was to extract fake news features. Then, we provided the acquired vectors for each approach to the suggested CNN-BILSTM network. The goal of using CNN layers into the model architecture was to extract elements of fake news. The experiments concluded that the combination of two-word embedding vectors offers a benefit and it increases the accuracy of the proposed model when compared to using one-word embedding technique. Table III and Fig. 11 show that the combination of Word2Vec (CBOW) and the Word2Vec (Skip-Gram) gives the best results in term of accuracy and precision when compared to the other possible combinations.

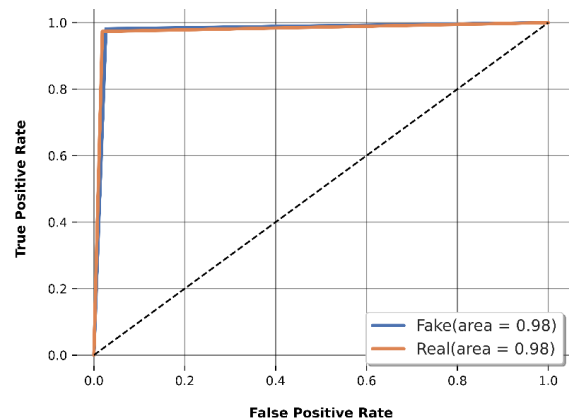


Fig. 9. The ROC Curves of Method 1.

Overall, the results of the experiment indicate that all models attained exceptional precision with a low loss rate. In addition, these findings demonstrate that the incorporation of a hybrid model based on the feature descriptor approach improves prediction performance relative to other models in the literature.

In Table IV, we compare the performance of the proposed model to that of some similar research examined in the present paper.

The Fig. 10 shows the improvement of the proposed method 1 compared to the traditional machine learning methods. The accuracy of the proposed model achieved 97.74%, while DT, RF, LR and SVM achieved a maximum accuracy only up to 93.51%, 94.37%, 95.42% and 97.09%, respectively.

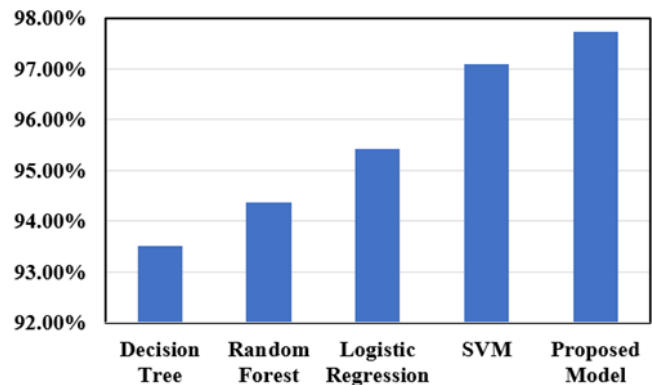


Fig. 10. Accuracy Comparison of Proposed Model with Traditional Machine Learning Algorithms.

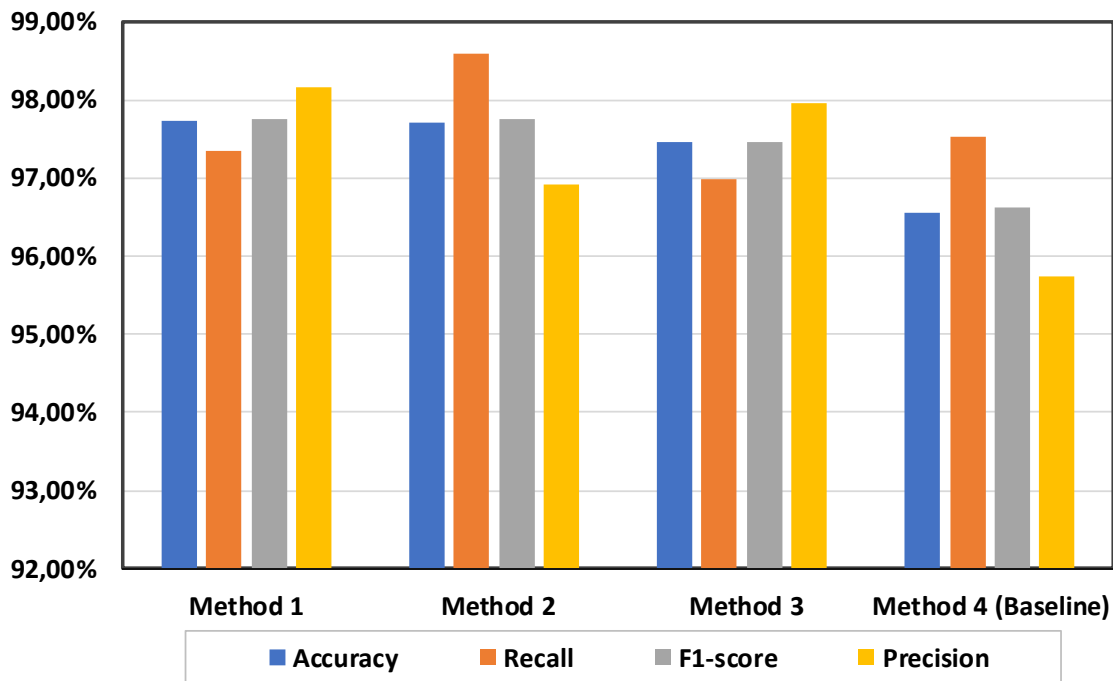


Fig. 11. Summarize of All the Experimental Findings Provided in this Research.

TABLE IV. ACCURACY COMPARISON OF PROPOSED MODEL WITH RELATED WORKS

Authors	Dataset	Feature Representation	Classification Algorithm	Accuracy
[29]	Their own dataset of 25200 articles from Reuters and Kaggle	TF-IDF	KNN, SVM, LR, LSVM, DT	92%
[30]	PHEME	WORD2VEC	LSTM	79.5%
[31]	PHEME	WORD2VEC	Hybrid LSTM-CNN	82%
[32]	PHEME	WORD2VEC-GLOVE-FASTTEXT	Hybrid BILSTM-CNN	86.12%
[33]	FNC-1	GLOVE	Hybrid LSTM/ BILSTM -CNN	71.2%
[35]	ISOT	Linguistic features (stylo-metric, semantic, and syntactic...)	Voting classifier based on traditional machine learning algorithms	96.36%
[34]	WELFake dataset	Combine linguistic feature with Word embedding	Voting classifier based on SVM , DT , NB, Bagging, AdaBoost, KNN	96.73%
Proposed method	WELFake dataset	Combine linguistic feature with Word embedding	CNN-BILSTM	97.74%

VI. CONCLUSION AND PERSPECTIVES

In this paper, we presented a new approach to detect fake news using the unbiased dataset WELFake. The main objective of this research was obtaining a good result and improving the performance of the proposed fake news detection system. In this study. The first task of this approach was representing words to meaningful numerical vectors using combination of different word embedding techniques. The second task was training the proposed hybrid model based on CNN and BILSTM architectures. The obtained results show an improvement in terms of accuracy and precision when compared to traditional machine learning algorithms and related work results. The simple concatenation of the different pre-trained embedding models increases the dimension of embedded vectors. Moreover, that leads to a high computational complexity. To solve this problem in future works, we propose to reduce the dimension of concatenated vectors with preserving characteristics of the original data using features engineering techniques such as features selection and dimensions reduction.

REFERENCES

- [1] J. Gu et al., 'Recent Advances in Convolutional Neural Networks', *Pattern Recognition*, vol. 77, Dec. 2015, doi: 10.1016/j.patcog.2017.10.013.
- [2] K. Shu, A. Sliva, S. Wang, J. Tang, and H. Liu, 'Fake News Detection on Social Media: A Data Mining Perspective', arXiv:1708.01967 [cs], Sep. 2017, Accessed: Apr. 07, 2022. [Online]. Available: <http://arxiv.org/abs/1708.01967>.
- [3] F. B. Gereme and W. Zhu, 'Early Detection of Fake News "Before It Flies High"', in *Proceedings of the 2nd International Conference on Big Data Technologies - ICBTD2019*, Jinan, China, 2019, pp. 142–148. doi: 10.1145/3358528.3358567.
- [4] D. M. J. Lazer et al., 'The science of fake news', *Science*, vol. 359, no. 6380, pp. 1094–1096, Mar. 2018, doi: 10.1126/science.aao2998.
- [5] S. Hamida, B. Cherradi, and H. Ouajji, 'Handwritten Arabic Words Recognition System Based on HOG and Gabor Filter Descriptors', in *2020 1st International Conference on Innovative Research in Applied Science, Engineering and Technology (IRASET)*, Meknes, Morocco, Apr. 2020, pp. 1–4. doi: 10.1109/IRASET48871.2020.9092067.
- [6] O. Terrada, S. Hamida, B. Cherradi, A. Raihani, and O. Bouattane, 'Supervised Machine Learning Based Medical Diagnosis Support System for Prediction of Patients with Heart Disease', *Adv. sci. technol. eng. syst. j.*, vol. 5, no. 5, pp. 269–277, 2020, doi: 10.25046/aj050533.
- [7] H. Moujahid, B. Cherradi, O. E. Gannour, L. Bahatti, O. Terrada, and S. Hamida, 'Convolutional Neural Network Based Classification of Patients with Pneumonia using X-ray Lung Images', *Adv. sci. technol. eng. syst. j.*, vol. 5, no. 5, pp. 167–175, 2020, doi: 10.25046/aj050522.
- [8] O. El Gannour, S. Hamida, B. Cherradi, A. Raihani, and H. Moujahid, 'Performance Evaluation of Transfer Learning Technique for Automatic Detection of Patients with COVID-19 on X-Ray Images', in *2020 IEEE 2nd International Conference on Electronics, Control, Optimization and Computer Science (ICECOCS)*, Kenitra, Morocco, Dec. 2020, pp. 1–6. doi: 10.1109/ICECOCS50124.2020.9314458.
- [9] O. Terrada, A. Raihani, O. Bouattane, and B. Cherradi, 'Fuzzy cardiovascular diagnosis system using clinical data', in *2018 4th International Conference on Optimization and Applications (ICOA)*, Mohammedia, Apr. 2018, pp. 1–4. doi: 10.1109/ICOA.2018.8370549.
- [10] B. Cherradi, O. Terrada, A. Ouhmida, S. Hamida, A. Raihani, and O. Bouattane, 'Computer-Aided Diagnosis System for Early Prediction of Atherosclerosis using Machine Learning and K-fold cross-validation', in *2021 International Congress of Advanced Technology and Engineering (ICOTEN)*, Taiz, Yemen, Jul. 2021, pp. 1–9. doi: 10.1109/ICOTEN52080.2021.9493524.
- [11] S. Laghmati, B. Cherradi, A. Tmiri, O. Daanouni, and S. Hamida, 'Classification of Patients with Breast Cancer using Neighbourhood Component Analysis and Supervised Machine Learning Techniques', in *2020 3rd International Conference on Advanced Communication Technologies and Networking (CommNet)*, Marrakech, Morocco, Sep. 2020, pp. 1–6. doi: 10.1109/CommNet49926.2020.9199633.
- [12] O. Terrada, B. Cherradi, A. Raihani, and O. Bouattane, 'Atherosclerosis disease prediction using Supervised Machine Learning Techniques', in *2020 1st International Conference on Innovative Research in Applied Science, Engineering and Technology (IRASET)*, Meknes, Morocco, Apr. 2020, pp. 1–5. doi: 10.1109/IRASET48871.2020.9092082.
- [13] O. Daanouni, B. Cherradi, and A. Tmiri, 'Predicting diabetes diseases using mixed data and supervised machine learning algorithms', in *Proceedings of the 4th International Conference on Smart City Applications - SCA '19*, Casablanca, Morocco, 2019, pp. 1–6. doi: 10.1145/3368756.3369072.
- [14] O. Terrada, B. Cherradi, S. Hamida, A. Raihani, H. Moujahid, and O. Bouattane, 'Prediction of Patients with Heart Disease using Artificial Neural Network and Adaptive Boosting techniques', in *2020 3rd International Conference on Advanced Communication Technologies and Networking (CommNet)*, Marrakech, Morocco, Sep. 2020, pp. 1–6. doi: 10.1109/CommNet49926.2020.9199620.
- [15] S. Hamida, B. Cherradi, O. Terrada, A. Raihani, H. Ouajji, and S. Laghmati, 'A Novel Feature Extraction System for Cursive Word Vocabulary Recognition using Local Features Descriptors and Gabor Filter', in *2020 3rd International Conference on Advanced Communication Technologies and Networking (CommNet)*, Marrakech, Morocco, Sep. 2020, pp. 1–7. doi: 10.1109/CommNet49926.2020.9199642.
- [16] X. Zhang and A. A. Ghorbani, 'An overview of online fake news: Characterization, detection, and discussion', *Information Processing & Management*, vol. 57, no. 2, p. 102025, Mar. 2020, doi: 10.1016/j.ipm.2019.03.004.
- [17] S. Hamida, B. Cherradi, and H. Ouajji, 'Handwritten Arabic Words Recognition System Based on HOG and Gabor Filter Descriptors', in *2020 1st International Conference on Innovative Research in Applied Science, Engineering and Technology (IRASET)*, Meknes, Morocco, Apr. 2020, pp. 1–4. doi: 10.1109/IRASET48871.2020.9092067.
- [18] S. Hamida, B. Cherradi, O. Terrada, A. Raihani, H. Ouajji, and S. Laghmati, 'A Novel Feature Extraction System for Cursive Word Vocabulary Recognition using Local Features Descriptors and Gabor Filter', in *2020 3rd International Conference on Advanced Communication Technologies and Networking (CommNet)*, Marrakech, Morocco, Sep. 2020, pp. 1–7. doi: 10.1109/CommNet49926.2020.9199642.
- [19] Y. LeCun, Y. Bengio, and G. Hinton, 'Deep learning', *Nature*, vol. 521, no. 7553, pp. 436–444, May 2015, doi: 10.1038/nature14539.
- [20] M. Al-Sarem, A. Alsaedi, F. Saeed, W. Boulila, and O. AmeerBaksh, 'A Novel Hybrid Deep Learning Model for Detecting COVID-19-Related Rumors on Social Media Based on LSTM and Concatenated Parallel CNNs', *Applied Sciences*, vol. 11, no. 17, p. 7940, Aug. 2021, doi: 10.3390/app11177940.
- [21] F. L. Alotaibi and M. M. Alhammad, 'Using a Rule-based Model to Detect Arabic Fake News Propagation during Covid-19', *IJACSA*, vol. 13, no. 1, 2022, doi: 10.14569/IJACSA.2022.0130114.
- [22] Y. Alsaawy, A. Alkhodre, N. M. Bahbouh, A. A. Sen, and A. Nadeem, 'Lightweight Chain for Detection of Rumors and Fake News in Social Media', *IJACSA*, vol. 12, no. 8, 2021, doi: 10.14569/IJACSA.2021.0120860.
- [23] K.-H. Kim and C.-S. Jeong, 'Fake News Detection System using Article Abstraction', in *2019 16th International Joint Conference on Computer Science and Software Engineering (JCSSE)*, Chonburi, Thailand, Jul. 2019, pp. 209–212. doi: 10.1109/JCSSE.2019.8864154.
- [24] X. Cui and Y. Li, 'Fake News Detection in Social Media based on Multi-Modal Multi-Task Learning', *IJACSA*, vol. 13, no. 7, 2022, doi: 10.14569/IJACSA.2022.01307106.
- [25] A. R. Mahlous and A. Al-Laith, 'Fake News Detection in Arabic Tweets during the COVID-19 Pandemic', *IJACSA*, vol. 12, no. 6, 2021, doi: 10.14569/IJACSA.2021.0120691.

- [26] S. Raza and C. Ding, 'Fake news detection based on news content and social contexts: a transformer-based approach', *Int J Data Sci Anal*, vol. 13, no. 4, pp. 335–362, May 2022, doi: 10.1007/s41060-021-00302-z.
- [27] M. Aldwairi and A. Alwahedi, 'Detecting Fake News in Social Media Networks', *Procedia Computer Science*, vol. 141, pp. 215–222, 2018, doi: 10.1016/j.procs.2018.10.171.
- [28] A. Albahr and M. Albahar, 'An Empirical Comparison of Fake News Detection using different Machine Learning Algorithms', *IJACSA*, vol. 11, no. 9, 2020, doi: 10.14569/IJACSA.2020.0110917.
- [29] H. Ahmed, I. Traore, and S. Saad, 'Detection of Online Fake News Using N-Gram Analysis and Machine Learning Techniques', in *Intelligent, Secure, and Dependable Systems in Distributed and Cloud Environments*, vol. 10618, I. Traore, I. Woungang, and A. Awad, Eds. Cham: Springer International Publishing, 2017, pp. 127–138. doi: 10.1007/978-3-319-69155-8_9.
- [30] S. A. Alkhodair, S. H. H. Ding, B. C. M. Fung, and J. Liu, 'Detecting breaking news rumors of emerging topics in social media', *Information Processing & Management*, vol. 57, no. 2, p. 102018, Mar. 2020, doi: 10.1016/j.ipm.2019.02.016.
- [31] O. Ajao, D. Bhowmik, and S. Zargari, 'Fake News Identification on Twitter with Hybrid CNN and RNN Models', 2018, doi: 10.48550/ARXIV.1806.11316.
- [32] M. Z. Asghar, A. Habib, A. Habib, A. Khan, R. Ali, and A. Khattak, 'Exploring deep neural networks for rumor detection', *J Ambient Intell Human Comput*, vol. 12, no. 4, pp. 4315–4333, Apr. 2021, doi: 10.1007/s12652-019-01527-4.
- [33] A. Abedalla, A. Al-Sadi, and M. Abdullah, 'A Closer Look at Fake News Detection: A Deep Learning Perspective', in *Proceedings of the 2019 3rd International Conference on Advances in Artificial Intelligence*, Istanbul Turkey, Oct. 2019, pp. 24–28. doi: 10.1145/3369114.3369149.
- [34] P. K. Verma, P. Agrawal, I. Amorim, and R. Prodan, 'WELFake: Word Embedding Over Linguistic Features for Fake News Detection', *IEEE Trans. Comput. Soc. Syst.*, vol. 8, no. 4, pp. 881–893, Aug. 2021, doi: 10.1109/TCSS.2021.3068519.
- [35] J. F. Ribeiro Bezerra, 'Content-based fake news classification through modified voting ensemble', *Journal of Information and Telecommunication*, vol. 5, no. 4, pp. 499–513, Oct. 2021, doi: 10.1080/24751839.2021.1963912.
- [36] S. Hamida, B. Cherradi, O. El Gannour, O. Terrada, A. Raihani, and H. Ouajji, 'New Database of French Computer Science Words Handwritten Vocabulary', in *2021 International Congress of Advanced Technology and Engineering (ICOTEN)*, Taiz, Yemen, Jul. 2021, pp. 1–5. doi: 10.1109/ICOTEN52080.2021.9493438.
- [37] A. Severyn and A. Moschitti, 'Learning to Rank Short Text Pairs with Convolutional Deep Neural Networks', in *Proceedings of the 38th International ACM SIGIR Conference on Research and Development in Information Retrieval*, Santiago Chile, Aug. 2015, pp. 373–382. doi: 10.1145/2766462.2767738.
- [38] A. Fesseha, S. Xiong, E. D. Emiru, M. Diallo, and A. Dahou, 'Text Classification Based on Convolutional Neural Networks and Word Embedding for Low-Resource Languages: Tigrinya', *Information*, vol. 12, no. 2, p. 52, Jan. 2021, doi: 10.3390/info12020052.
- [39] N. Kalchbrenner, E. Grefenstette, and P. Blunsom, 'I', 2014, doi: 10.48550/ARXIV.1404.2188.
- [40] S. Hamida, B. Cherradi, H. Ouajji, and A. Raihani, 'Convolutional Neural Network Architecture for Offline Handwritten Characters Recognition', in *Innovation in Information Systems and Technologies to Support Learning Research*, vol. 7, M. Serrhini, C. Silva, and S. Aljhdali, Eds. Cham: Springer International Publishing, 2020, pp. 368–377. doi: 10.1007/978-3-030-36778-7_41.
- [41] S. Hamida, B. Cherradi, A. Raihani, and H. Ouajji, 'Performance Evaluation of Machine Learning Algorithms in Handwritten Digits Recognition', in *2019 1st International Conference on Smart Systems and Data Science (ICSSD)*, Rabat, Morocco, Oct. 2019, pp. 1–6. doi: 10.1109/ICSSD47982.2019.9003052.
- [42] N. Srivastava, G. Hinton, A. Krizhevsky, I. Sutskever, and R. Salakhutdinov, 'Dropout: A Simple Way to Prevent Neural Networks from Overfitting', *J. Mach. Learn. Res.*, vol. 15, no. 1, pp. 1929–1958, Jan. 2014.
- [43] G. Gravanis, A. Vakali, K. Diamantaras, and P. Karadais, 'Behind the cues: A benchmarking study for fake news detection', *Expert Systems with Applications*, vol. 128, pp. 201–213, Aug. 2019, doi: 10.1016/j.eswa.2019.03.036.
- [44] A. Mandelbaum and A. Shalev, 'Word Embeddings and Their Use In Sentence Classification Tasks', arXiv:1610.08229 [cs], Oct. 2016, Accessed: Apr. 07, 2022. [Online]. Available: <http://arxiv.org/abs/1610.08229>.
- [45] T. Mikolov, K. Chen, G. Corrado, and J. Dean, 'Efficient Estimation of Word Representations in Vector Space', 2013, doi: 10.48550/ARXIV.1301.3781.
- [46] T. Mikolov, I. Sutskever, K. Chen, G. Corrado, and J. Dean, 'Distributed Representations of Words and Phrases and their Compositionality', 2013, doi: 10.48550/ARXIV.1310.4546.
- [47] J. Pennington, R. Socher, and C. Manning, 'Glove: Global Vectors for Word Representation', in *Proceedings of the 2014 Conference on Empirical Methods in Natural Language Processing (EMNLP)*, Doha, Qatar, 2014, pp. 1532–1543. doi: 10.3115/v1/D14-1162.
- [48] J. Gu et al., 'Recent advances in convolutional neural networks', *Pattern Recognition*, vol. 77, pp. 354–377, May 2018, doi: 10.1016/j.patcog.2017.10.013.
- [49] Z. Huang, W. Xu, and K. Yu, 'Bidirectional LSTM-CRF Models for Sequence Tagging', 2015, doi: 10.48550/ARXIV.1508.01991.
- [50] T. A. Le, M. Y. Arkhipov, and M. S. Burtsev, 'Application of a Hybrid Bi-LSTM-CRF Model to the Task of Russian Named Entity Recognition', in *Artificial Intelligence and Natural Language*, vol. 789, A. Filchenkov, L. Pivovarova, and J. Žizka, Eds. Cham: Springer International Publishing, 2018, pp. 91–103. doi: 10.1007/978-3-319-71746-3_8.

Research on Blind Obstacle Ranging based on Improved YOLOv5

Yongquan Xia¹, Yiqing Li^{2*}, Jianhua Dong³, Shiyu Ma⁴

School of Computer and Communication Engineering, Zhengzhou University of Light Industry, Zhengzhou, Henan, China^{1,2,3}
School of Economics and Management, Beijing Jiaotong University, Beijing, China⁴

Abstract—An improved model based on YOLOv5s is proposed for the problem that the YOLOv5 network model does not have high localization accuracy when detecting and identifying obstacles at different distances and sizes from the blind, which in turn leads to low accuracy in measuring distances. There are two main core ideas: firstly, a feature scale and a corresponding prediction head are added to YOLOv5 to improve the detection accuracy of small objects on blind paths. Secondly, SK attention mechanism is introduced in the feature fusion part. It can adaptively adjust the perceptual field for feature maps of different scales and more accurately extract objects of different distances and sizes on the blind path, which can improve the accuracy of detection and the accuracy of subsequent distance measurement. It was experimentally demonstrated that the improved YOLOv5 model improved the mAP by 6.29% compared to the original YOLOv5 model based on a small difference in time consumption. And for each category of AP values, the improvement ranged from 2.13% to 8.19%, respectively. The average accuracy of the measured distance from the obstacle at 1.5m to 3.5m from the camera is 98.20%. This shows that the improved YOLOv5 algorithm has good real-time performance and accuracy.

Keywords—Binocular ranging; object detection; attention mechanism

I. INTRODUCTION

Blind corridors are one of the main guides for blind people to walk around. However, they are occupied by obstacles in almost every city. This causes inconvenience to the blind. Therefore, accurate identification and distance measurement of obstacles on blind paths is essential for the blind to travel safely.

In life and industrial scenarios, commonly used distance measurement methods include infrared distance measurement, stereo vision distance measurement, laser distance measurement and ultrasonic distance measurement. Among them, stereo vision distance measurement is a technology that allows computers to simulate human visual system to achieve distance measurement. The principle of the traditional stereo vision-based binocular ranging method is to use two cameras to acquire left and right images from the same viewpoint [1]. Then a stereo matching algorithm is used to find out the parallax. Finally, the distance from the target object to the camera is obtained by constructing similar triangles through the camera imaging principle. Stereo matching technology is an important part of binocular distance measurement. Before matching, it first extracts image features.

The mainstream stereo matching algorithms are GC (graph cuts) algorithm based on global feature matching [2], SGBM (semi-global block matching) algorithm based on semi-global feature matching [3], and SIFT(scale-invariant feature transform) algorithm [4], SURF(speeded up robust features) algorithm [5] and ORB(Oriented FAST and Rotated BRIEF) algorithm [6] based on local feature matching, etc. GC, SGBM algorithm can construct parallax images with high accuracy. However, the matching speed is slow, it is difficult to meet the requirements of high real-time, and the parallax image information is relatively simple. SIFT, SURF and ORB are three feature matching algorithms. Generally, feature points are used to match the left and right images from the same viewpoint, and then the distance is calculated according to the disparity of the feature points. The feature points that can be matched together are often those whose gray values change significantly and have similar trends. However, this often leads to the problem of mismatch, and the disadvantage of time-consuming detection of all feature points of the whole map (including uninterested areas).

The matching algorithms introduced above are always unsatisfactory in terms of speed or accuracy. Therefore, this paper uses a deep learning based method to detect the target from the left and right images of the binocular camera, and obtains parallax after getting the position information of the target. Finally, the distance from the target object to the camera is obtained by the binocular ranging principle.

In this research, the purpose is to improve the performance of target detection in blind channel images to solve the above problems. In addition, the speed of detection poses a great challenge to detection algorithm, because blind channel obstacle ranging is often real-time. The You Only Look Once (YOLO) neural network [7] is one-stage target detection algorithm that improves detection speed by making the target classification and localization set a one-level regression problem. YOLOv5 is the fifth version of YOLO, and its target detection performance is better than the first four versions, which is the most widely used version.

Although YOLOv5 can achieve multi-target detection quickly and accurately, it is difficult to apply directly to one specific image for target detection. Therefore, this paper proposes an improved model based on YOLOv5s for the detection and recognition of blind roadway pictures taken by binocular cameras. First of all, for the problem that the depth feature map after YOLOv5 feature fusion causes the loss of small object feature information due to excessive down-sampling, an up-sampling operation is added in the Neck part

*Corresponding Author.

to get a new feature scale for feature fusion with the shallow features of the Backbone network. And a corresponding prediction head is added in the head to improve the detection accuracy of small objects on blind corridors. Secondly, the SK attention mechanism is introduced after the last four feature fusions, which can adaptively adjust the sensing domain for the four different scales of feature maps. Thus, objects of different distances and sizes on the blind path can be extracted more accurately. The accurate recognition of blind obstacle and the accurate measurement of distance are achieved.

Author contributions can be summarized as follows:

- A new feature scale fusion layer is added in YOLOv5, which fuses shallow features in the network to maximize the retention of feature information and avoid the loss of small object features in the deep network.
- The attention mechanism Selective Kernel Networks (SKNet) is added to the feature fusion part in YOLOv5. It can adaptively adjust the perception field for feature maps of different scales, and it has different effects for objects of different distances and sizes on the blind path, so as to extract the target information more accurately.
- Mean Average Precision (mAP) of 0.843 is achieved with the model proposed in this paper on a homemade blind pathway dataset with complex objects. The improved YOLOv 5 model is used to detect and recognize binocular blind road pictures. After obtaining the position information of the same obstacle in the two pictures, the distance of the obstacle is obtained by using the principle of binocular ranging. At the obstacle distance from 1.5 m to 3.5 m from the camera, the average accuracy of measuring distance can reach 98.20%. It's very accurate.

The main part of this paper consists of five parts. Section I is the introduction, which introduces the background and significance of blind distance measurement for obstacle, as well as the research method of this paper and the reasons for adopting this method. Section II is the related work, which introduces the related research about target detection. Section III is the core part of the paper, which introduces the improved model of this paper, and how and why it was improved. In Section IV, the model proposed in the Section III was tested, and the experimental results and analysis were given. Section V is a summary of the overall research methods of this paper and the outlook for the future.

II. RELATED WORK

A. Traditional Object Detection Algorithm

The traditional target detection algorithm [8] can be roughly divided into three steps: region selection, feature extraction and target classification. Region selection refers to first locating the target location. Then the images or image sequences are traversed by sliding windows of different scales and aspect ratios. Finally, all possible positions containing the detected target are framed by an exhaustive strategy. Feature extraction refers to the extraction of visual features of the

target candidate regions. For example, SIFT (Scale Invariant Feature Transformation), HOG (Gradient Direction Histogram) [9], Haar [10] and LBP (Local Binary Pattern) [11] and other feature extraction operators are used for feature extraction. Object classification refers to the classification of the target by using the classifier through the extracted features. The commonly used classifiers are DPM (Deformed Part Model) [12], Adaboost [13], SVM (Support Vector Machine) [14] and so on.

Although traditional object detection methods have achieved certain results in the field of detection, they also have drawbacks. The high time complexity and many redundant windows in the region selection stage by sliding window selection candidate region strategy lead to the performance degradation of subsequent feature extraction and classification. Due to the object's own factors and environmental factors, the manual feature design method is poor in robustness, versatility and detection accuracy [15]. Traditional target detection methods have been difficult to meet people's pursuit of high performance.

B. Deep Learning based Object Detection Algorithms

In 2012, AlexNet [16] based on deep Convolutional Neural Network (CNN) won the ImageNet image recognition competition with a significant advantage. Since then, deep learning has been receiving widespread attention. Object detection is also gradually entered the era of deep learning.

The mainstream object detection algorithms [17] based on deep learning are classified into one-stage object detection algorithms and two-stage object detection algorithms according to whether exist a candidate frame generation stage. The two-stage target detection algorithm first extracts candidate frames for image targets, and then classifies the detection results based on the candidate frames. The representative algorithms have R-CNN [18], Fast R-CNN [19], Faster R-CNN [20] and R-FCN [21], etc. Single-stage target detection algorithms do not generate candidate frames and compute the detection results directly on the image. The classical single-stage target detection algorithms have SSD [22], Retina-Net [23] and YOLO series.

The YOLO algorithm was proposed by Redmon et al. in 2016, and there have been seven generations of iterations so far. YOLOv1 [7] is the first object detection algorithm based on regression analysis. It directly divides the image into regions and predicts the bounding box and probability of each region simultaneously. Its detection speed has been greatly increased. However, the detection accuracy is low, especially for small objects. YOLOv2 [24] built a new backbone network Darknet-19 on top of v1. Darknet-19 has fewer convolution layers, and its performance is higher. YOLOv2 maintains the advantage of fast inference while significantly improving prediction accuracy. However, the backbone network of YOLOv 2 is deeper and the recall rate of small target detection is low. And it is poor for dense group target detection. The underlying network of YOLOv3 [25] is Darknet-53, which borrows the residual structure of ResNet [26] for multiscale prediction. YOLOv3 has obviously improved the overall detection accuracy, detection accuracy for small objects, the inference speed and so on. YOLOv4 [27]

uses CSPDarkNet53 [28] instead of DarkNet53 and SPP+PAN instead of FPN. The computation is further reduced and the detection accuracy is improved. In June 2020, Jocher proposed YOLOv5 [29]. Compared with YOLOv1~YOLOv4, YOLOv5 has small size and short inference time, and is suitable for edge devices with limited computational and storage resources. YOLOv5 contains 4 models, in descending order according to model depth and feature map width, YOLOv5s, YOLOv5m, YOLOv5l, and YOLOv5x. Among them, YOLOv5s was iterated to version 6.1 in March 2022.

III. BLIND OBSTACLE RECOGNITION BASED ON IMPROVED YOLOV5

A. Improved YOLOV5

The network model in this paper is improved based on YOLOv5s version 6.1. The improved part is shown in Fig. 1 at the red box line. Firstly, one up-sampling and one down-sampling operation were added in each Neck part. The up-sampling operation is continued after the second up-sampling to obtain a new feature scale for feature fusion with the shallow features of the Backbone network, and a corresponding prediction head is added to the head. The aim is to improve the detection accuracy of small objects on blind paths. Secondly, the SK attention mechanism is introduced after the last four feature fusions, which can adaptively adjust the perceptual field for the four different scales of feature maps. Thus, the objects of different distances and sizes on the blind corridor can be extracted more accurately.

B. Improved Multi-scale Feature Detection

The YOLOv5 network uses three resolutions of the output feature maps to detect objects of different sizes. When a blind person walks on a blind path, there are inevitably smaller obstacles on the road, so a feature scale to focus on smaller targets and a prediction head accordingly are added, as shown

in the Head section in Fig. 1. After the second up-sampling in the Neck part, the up-sampling operation is continued to obtain a feature map with a resolution of 160×160. This feature map is feature fused with the shallow high-resolution feature layer obtained in the backbone network after the first C3 structure. The obtained high-resolution feature information makes the added prediction head more sensitive to small objects.

Fig. 2 shows the prediction part of the model with four different scales of feature layers, and the grid-based prediction is performed on these four feature layers in turn. The prediction results of each feature layer are the center adjustment parameters t_x and t_y , the width and height adjustment parameters t_w and t_h , and the confidence score of the prior frame, respectively. The center (x, y) and width and height (w, h) of the predicted frame are obtained based on the first four adjustment parameters. Based on the ground truth of the object, the network establishes the loss between the predicted and true values and calculates the loss for each feature layer.

Through the feedback of the loss, the model gradually optimizes the performance and completes the training. The loss of each feature layer is calculated in the same way and is obtained by calculating the sum of the bounding box regression loss, category loss and confidence loss. As shown in (1).

$$\text{Loss} = \lambda_1 L_{cls} + \lambda_2 L_{obj} + \lambda_3 L_{ciou} \quad (1)$$

In equation (1), the rectangular box loss (L_{ciou}) is obtained using CIoU loss [30], and the classification loss (L_{cls}) and confidence loss (L_{obj}) are calculated by BCE (Binary Cross Entropy) loss. λ_1 , λ_2 and λ_3 are balance coefficients.

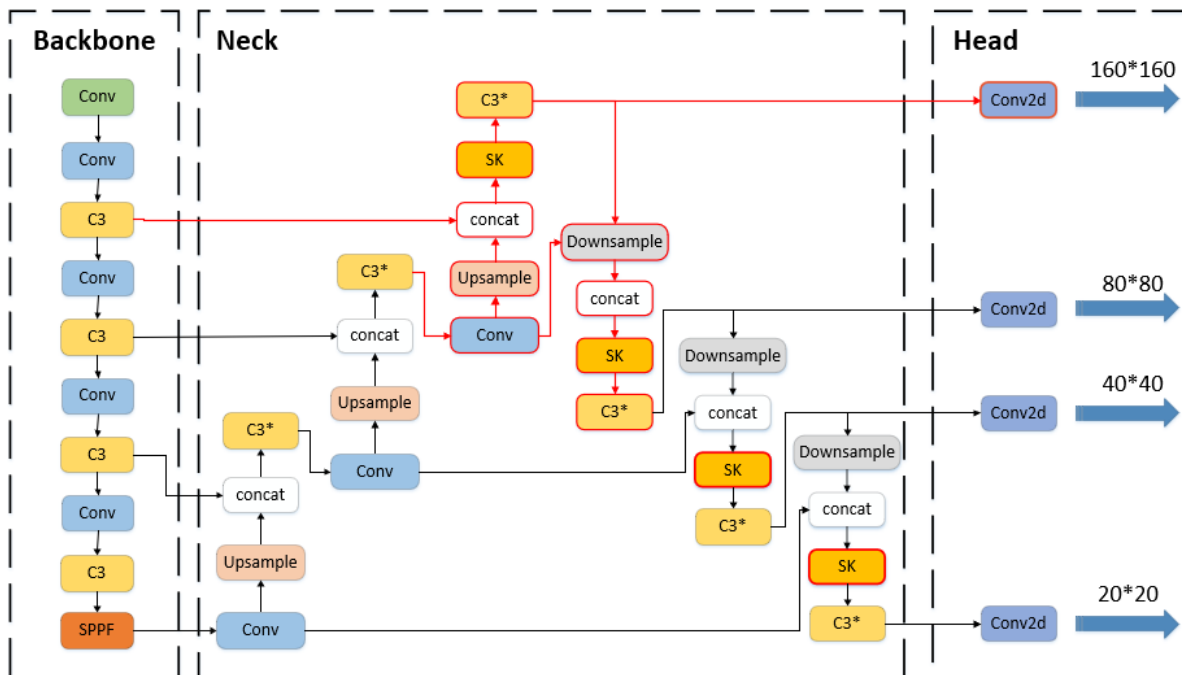


Fig. 1. Improved YOLOv5 Network Model.

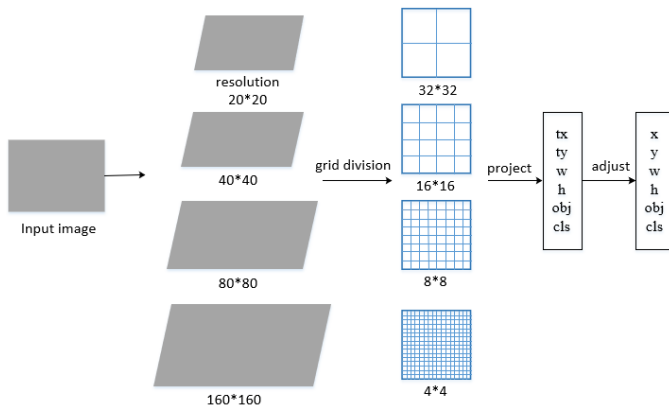


Fig. 2. Improved Model Prediction Section.

C. The SK Attention Mechanism Introduced

The size of the receptive fields of neurons in the visual cortex of the brain is adjusted according to the stimulus when people with normal vision look at objects of different distances and sizes. SKNet (Selective Kernel Networks) [31] is a kind of network with a similar function that adaptively adjusts the size of the receptive fields according to the multi-scales of the input information, so as to extract objects of different sizes and distances more accurately. Since the obstacles on the blind path are different in sizes and the distances, we added the SK attention mechanism to the four feature maps of different resolution sizes obtained after feature fusion in the Neck network. As shown in the Neck part in Fig. 2.

The structure of SKNet is shown in Fig. 3, it is composed of Split, Fuse, and Select. The part of Split obtains two feature maps $U1$ and $U2$ by convolution kernels of 3×3 and 5×5 respectively for the original feature map. Then the feature map U is obtained after the addition operation. The Fuse stage is to calculate each convolutional kernel weight. S is obtained using global average pooling (F_{gp}) for U with dimensionality $C \times 1$, and compact features Z is generated by fully connected layer (F_{fc}) with dimensionality compressed to be $d \times 1$. As in (2-4).

$$F_{gp}(U) = \frac{1}{W \times H} \sum_{i=1}^H \sum_{j=1}^W U(i, j) \quad (2)$$

$$s = F_{gp}(U) \quad (3)$$

$$z = F_{fc}(s) = \delta(BN(Ws)) \quad (4)$$

In (2), W and H are the width and height of the vector U , respectively. i and j are the i -th row and j -th column of U , respectively. In (4), δ is the ReLU activation function and BN denotes the batch normalization operation.

The Select part reclassifies the feature Z into two feature vectors a and b , which are the weights of the two convolution kernels, by a softmax operation (5).

$$a_c = \frac{e^{A_c^z}}{e^{A_c^z} + e^{B_c^z}}, \quad b_c = \frac{e^{B_c^z}}{e^{A_c^z} + e^{B_c^z}} \quad (5)$$

In equation (5), A_c, B_c are the c th row data of A and B . a_c, b_c are the c th elements of a, b respectively.

The final output feature map V is obtained by weighting the previous $U1, U2$ by the two weight matrices a and b . The following (6).

$$V_c = a_c \cdot U1_c + b_c \cdot U2_c, \quad a_c + b_c = 1 \quad (6)$$

where $V = [V1, V2, \dots, VC]$, Vc dimension is $H \times W$. Since the function values of a_c and b_c add up to 1, it is possible to set the weights for the feature maps in the branches.

Since the SKNet attention mechanism uses different convolutional kernel weights for different images, adding the SKNet network to the network to adaptively adjust the perceptual field for our four different resolution feature maps, which will have different effects for objects of different distances and sizes and improve the accuracy of detection.

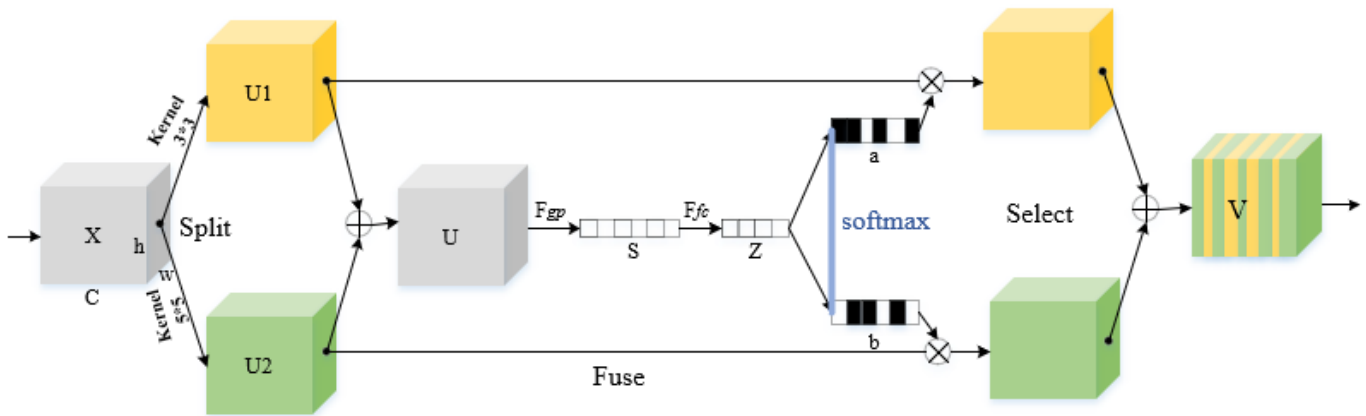


Fig. 3. SKNet Network Structure.

IV. EXPERIMENT AND ANALYSIS

A. Experimental Data

Since there is no authoritative dataset for blind roadway images, this research dataset consists of two main parts. One part is to use some images from The PASCAL Visual Object Classes Challenge 2007/2012 (VOC07+12) dataset, mainly selected images containing people, cats, dogs, and common vehicles. The other part is a manual field photography of the blind road surface and a browser search for keywords such as "blind road occupied" and "blind road obstruction" to get a web page with search results and download images. These two parts were filtered and aggregated to create a total dataset of 1245 images, each with a resolution between 1280×720 and 333×333. Some of the samples are shown in Fig. 4.

The dataset uses the PASCAL VOC format, and the targets in the images are selected by manual annotation of the frames. Eight types of common obstacles were selected as recognition objects, namely, people, bicycles, cars, motorcycles, cats, dogs, fire hydrants, and manhole covers. In addition, the dataset was randomly divided into training set, test set, and validation set according to the ratio of 6:2:2, where there were 747 images in the training set, 253 images in the test set, and 245 images in the validation set.

B. Model Training

Experimental environment configuration: The hardware environment is Intel(R) Core(TM) i7-6500 CPU with 2.50 GHz and 8 GB memory. The software environment is Windows 10 operating system, Python 3.6.15 development language, and PyTorch 1.2.0 deep learning framework.

Training parameters: For model training, the model is initialized using a pre-trained weight file on the COCO dataset, and the model input image size is 640×640. The training period is 100. Batch size is set to 16. The initial learning rate is 0.01. The minimum learning rate is 0.0001. The SGD optimizer is used for optimization. The momentum parameter is 0.937. The decay coefficient of the weights is 0.0005. The learning rate decreases by "cos". And the weights are saved every 10 epochs.

C. Performance Comparison Experiment

The improved network model predicts the images, and the results are shown in Fig. 5 and Fig. 6. Fig. 5 shows the image to be predicted, and Fig. 6 shows the prediction results. From the prediction results, it can be seen that the figure contains some objects that can be basically predicted accurately both in the strong light of day and in the weak light of street light at night. The rectangular box position accurately frames the outer edge of the target. For the partly obscured objects in the target and some small objects at a distance can also be accurately detected.

To validate the performance of the proposed improved YOLOv5 network model, it is evaluated with homemade dataset. Precision, Recall, F1 Score and mean average precision (mAP) are used as evaluation metrics to assess the effectiveness of model training and prediction. The evaluation results are shown in Table I. From Table I, the Recall value, Precision value, and F1 score corresponding to each category

of the improved YOLOv5s network model at Confidence of 0.5 are shown. The performance experiments were also compared with the original YOLOv5s network, the YOLO-FIRI network proposed in literature 32 [32] under homemade dataset. The accuracy and average elapsed time comparison results are shown in Table II.

The mAP values of the three algorithms and the AP values for each category can be seen in Table II. With Recall as the horizontal coordinate and Precision as the vertical coordinate, the curve plotted is the PR curve. The AP value is the area under the PR curve, which represents the average accuracy of a single category. It is used to measure how good the model is on a single category. The mAP is obtained by averaging the AP values of all categories, and is used to measure the goodness of the model in all categories. In terms of accuracy, this paper proposed YOLOv5s model improves the mAP by 6.29% compared to the original YOLOv5 model, and for each category of AP values, the improvement ranges from 2.13% to 8.19%, respectively. Compared to the YOLO-FIRI network, the mAP improved by 2.36%, and the AP values for each category ranged from 1.28% to 4.31%, respectively. This indicates that the improved network has better detection accuracy. The AP values for the three smaller object categories of cats, dogs and fire hydrants are 76.31%, 77.84% and 86.43%, which are 4.11%, 8.19% and 3.96% better than the original YOLOv5s model. This indicates that the improved YOLOv5 network model is more accurate in detecting small objects. In terms of inference time, the average time consumed by the improved model for each image is 12ms, which is not much different from the original YOLOv5s time consumed. Compared to the YOLO-FIRI model, the average elapsed time per image is 2ms faster. This shows that the improved model has a faster inference speed.

AS a whole, the improved YOLOv5s model has better accuracy compared to the original model for a single category versus all categories with comparable time consumption. This shows that the improved algorithm in this paper has good real-time performance and accuracy.

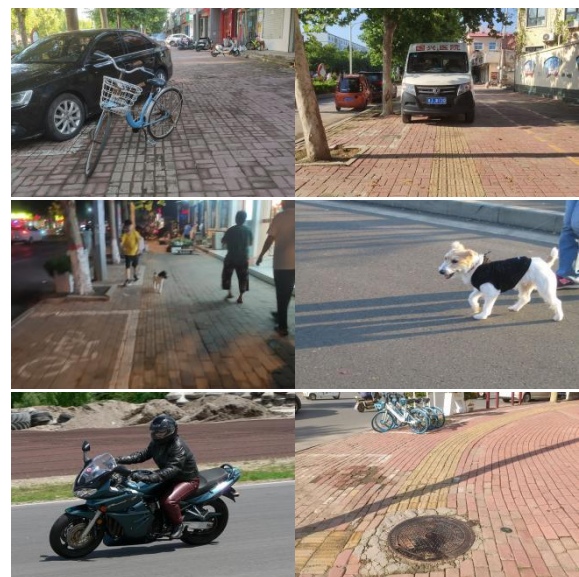


Fig. 4. Partial Sample.

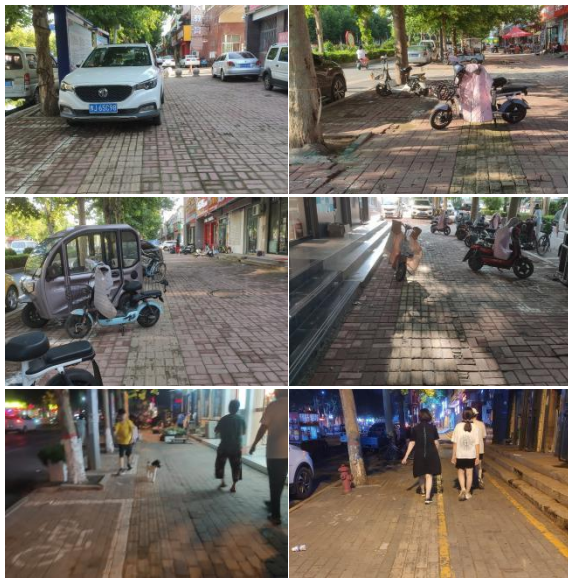


Fig. 5. Image to be Predicted.

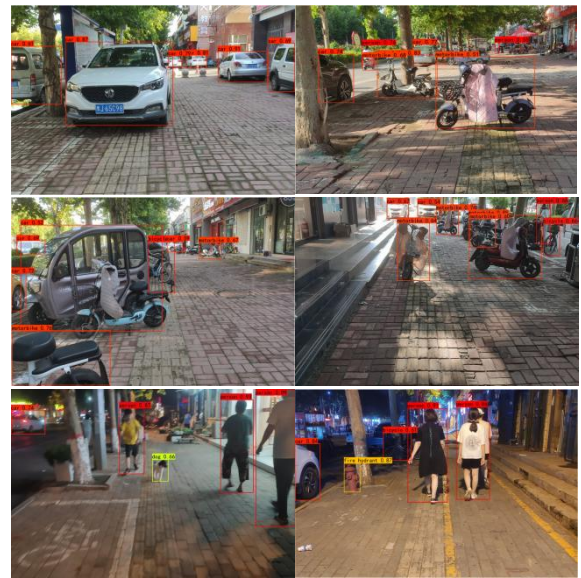


Fig. 6. Predicted Results.

TABLE I. EVALUATION RESULTS

Class	people	cat	dog	bicycle	fire hydrant	motorcycle	car	manhole cover
Precision/%	87.73	85.83	88.74	92.02	86.91	90.37	88.93	87.67
Recall/%	78.94	56.72	54.10	70.14	76.81	70.85	71.86	68.09
F1 Score	83.10	68.30	67.22	79.60	81.55	79.43	79.49	76.65

TABLE II. COMPARISON OF RESULTS

Algorithm	mAP/%	people	cat	dog	bicycle	Fire hydrant	motorcycle	car	Manhole cover	Time/ms
YOLOv5s	78.03	82.56	72.20	69.65	79.89	82.47	84.14	75.89	77.45	10.5
YOLO-FIRI	81.96	85.81	74.15	76.35	86.77	83.78	86.51	81.93	80.38	14
Ours	84.32	89.94	77.84	76.31	88.50	86.43	90.06	83.81	81.66	12

D. Distance Measurement Experiment

To verify the performance of the algorithm in ranging in this paper, this research used binocular cameras to capture pictures of obstacles at 1.5m, 2.0m, 2.5m, 3.0m and 3.5m at the same location. The binocular camera is calibrated with a known focal length of 2.13mm, a baseline length of 60.4mm, and an image element size of 3 μ m.

The prediction was performed after stereo correction of the left and right images at different distances (as shown in Fig. 7). The same nearest obstacle in the two pictures was screened by the center longitudinal coordinates of the outer rectangular box of the obstacle. And then the distance was obtained according to the difference of their center transverse coordinates using the principle of binocular ranging [33], as in (7-8). The experimental results are shown in Table III.

$$Z = \frac{fB}{d} \quad (7)$$

$$d = x_l - x_r = d_x (u_l - u_r) \quad (8)$$

In (8), u_l , u_r are the central pixel horizontal coordinates of the same object rectangular box on the left and right images. d_l , d_r are the central physical horizontal coordinates of the same object rectangular box on the left and right images. d_x is the image element size.



Fig. 7. Graph of Prediction Results for different Distances.

TABLE III. DISTANCE MEASUREMENT RESULTS

Actual distance /m	obstacle on the left/pixel	obstacle on the right /pixel	Parallax /pixel	Measuring distance /m	Accuracy /%
1.5	(475.5,159)	(447.5,158)	28	1.532	97.87
2.0	(542,228)	(521,226)	21	2.042	97.90
2.5	(721,255)	(705,255.5)	16	2.523	99.08
3.0	(790.5,209.5)	(776,208.5)	14.5	2.958	98.60
3.5	(716.5,246)	(704,246)	12.5	3.431	98.03

As can be seen from the data in Table III, the parallax, distance measurement results and accuracy of the nearest obstacle in the figure at a distance of 1.5m to 3.5m from the binocular camera. The measured distances obtained from parallax calculations were 1.532m, 2.042m, 2.523m, 2.958m, and 3.431m at actual distances from 1.5 m to 3.5m, respectively. The accuracy of the measured distance is above 97.87%, and the average accuracy is 98.20%. The accuracy at 2.0m and 2.5m reached 99.08% and 98.60%, respectively. The error was the smallest at the obstacle distance camera at 2.5 m, and the measured distance was the most accurate. This shows that the improved YOLOv5s algorithm has good accuracy and robustness in predicting the recognition of objects at different distances.

V. CONCLUSION

This paper proposes an improved model based on YOLOv5s for blind roadway picture detection. Firstly, a feature scale and corresponding prediction head are added in YOLOv5 to improve the detection accuracy of small objects on blind path. Secondly, SK attention mechanism is introduced in the feature fusion part to adaptively adjust the perceptual field for feature maps of different scales to more accurately extract objects of different distances and sizes on blind path. Finally, the improved network model is used to detect the left and right maps of the binocular camera, and the exact distance of the blind obstacle from the camera is obtained by the binocular ranging principle. The experimental results show that the improved YOLOv5s algorithm can achieve the accurate recognition of blind obstacle and the accurate distance measurement.

In the future, this research will achieve accurate blind path identification. Combining blind path identification with blind obstacle ranging proposed in this paper can form a complete navigation system for the blind. This will be of great help for blind person to travel.

ACKNOWLEDGMENT

This work was supported by the Key Scientific Research Project of Henan Universities. The project is entitled "Research on Stereo Vision Based Ranging Technology for Blind Navigation System". The project number is 22B510018.

REFERENCES

[1] Y. Zheng, P. Liu, L. Qian, S. Qin, X. Liu, Y. Ma, and G. Cheng, "Recognition and Depth Estimation of Ships Based on Binocular Stereo Vision," *Journal of Marine Science and Engineering*, vol. 10, no. 8, pp. 1153, 2022.

[2] Y. Y. Boykov, and M. P. Jolly, "Interactive graph cuts for optimal boundary & region segmentation of objects in ND images," *In*

Proceedings eighth IEEE international conference on computer vision. ICCV 2001 IEEE, vol. 1, pp. 105-112, July 2001.

[3] H. Hirschmuller, "Stereo processing by semiglobal matching and mutual information," *IEEE Transactions on pattern analysis and machine intelligence*, vol. 30, no. 2, pp. 328-341, 2007.

[4] W. Burger, and M. J. Burge, "Scale-invariant feature transform (SIFT)," *In Digital Image Processing Springer*, Cham, pp. 709-763, 2022.

[5] H. Bay, A. Ess, T. Tuytelaars, and L. Van Gool, "Speeded-up robust features (SURF)," *Computer vision and image understanding*, vol. 110, no. 3, pp. 346-359, 2008.

[6] E. Rublee, V. Rabaud, K. Konolige, and G. Bradski, "ORB: An efficient alternative to SIFT or SURF," *In 2011 International conference on computer vision*, pp. 2564-2571, November 2011.

[7] J. Redmon, S. Divvala, R. Girshick and A. Farhadi, "You Only Look Once: Unified, Real-Time Object Detection," *2016 IEEE Conference on Computer Vision and Pattern Recognition (CVPR)*, pp. 779-788, 2016.

[8] W. X. Dong, H. T. Liang, G. Z. Liu, Q. Q. Hu, and X. Yu, "A review of deep convolution applied to target detection algorithms," *Computer Science and Exploration*, vol. 16, no. 5, pp. 1025, 2022.

[9] N. Dalal, and B. Triggs, "Histograms of oriented gradients for human detection," *In 2005 IEEE computer society conference on computer vision and pattern recognition (CVPR'05)*, vol. 1, pp. 886-893, June 2005.

[10] R. Lienhart, and J. Maydt, "An extended set of haar-like features for rapid object detection," *In Proceedings. international conference on image processing*, vol. 1, pp. I-I, September 2002.

[11] T. Ojala, M. Pietikainen, and T. Maenpaa, "Multiresolution gray-scale and rotation invariant texture classification with local binary patterns," *IEEE Transactions on pattern analysis and machine intelligence*, vol. 24, no. 7, pp. 971-987, 2002.

[12] P. F. Felzenszwalb, R. B. Girshick, D. McAllester, and D. Ramanan, "Object detection with discriminatively trained part-based models," *IEEE transactions on pattern analysis and machine intelligence*, vol. 32, no. 9, pp. 1627-1645, 2010.

[13] P. Wang, C. Shen, N. Barnes, and H. Zheng, "Fast and robust object detection using asymmetric totally corrective boosting," *IEEE Transactions on Neural Networks and Learning Systems*, vol. 23, no. 1, pp. 33-46, 2011.

[14] J. L. Balcazar, Y. Dai, and O. Watanabe, "Provably fast training algorithms for support vector machines," *In Proceedings 2001 IEEE International Conference on Data Mining*, pp. 43-50, November 2001.

[15] D. C. Wang, C. S. Bai, and K. J. Wu, "A review of deep learning-based video target detection," *Computer Science and Exploration*, vol 15, no. 9, pp. 1563-1577, 2021.

[16] A. Krizhevsky, I. Sutskever, and G. E. Hinton, "Imagenet classification with deep convolutional neural networks," *Communications of the ACM*, vol. 60, no. 6, pp. 84-90, 2017.

[17] L. P. Fang, H. J. He, and G. M. Zhou, "A review of target detection algorithm research," *Computer Engineering and Applications*, vol. 54, no. 13, pp. 11-18, 2018.

[18] R. Girshick, J. Donahue, T. Darrell, and J. Malik, "Rich feature hierarchies for accurate object detection and semantic segmentation," *I2014 IEEE Conference on Computer Vision and Pattern Recognition*, pp. 580-587, 2014.

[19] R. Girshick, "Fast r-cnn," *2015 IEEE International Conference on Computer Vision (ICCV)*, pp. 1440-1448, 2015.

- [20] S. Ren, K. He, R. Girshick, and J. Sun, "Faster r-cnn: Towards real-time object detection with region proposal networks," *IEEE Transactions on Pattern Analysis and Machine Intelligence*, vol. 39, pp. 1137-1149, 2017.
- [21] J. Dai, Y. Li, K. He, and J. Sun, "R-fcn: Object detection via region-based fully convolutional networks," *Advances in neural information processing systems*, vol. 0, pp. 379-387, 2016.
- [22] W. Liu, D. Anguelov, D. Erhan, C. Szegedy, S. Reed and C. Y. Fu, et al. "SSD: Single shot multibox detector," *In European conference on computer vision*, vol. 9905, pp. 21-37, 2016.
- [23] T. -Y. Lin, P. Goyal, R. Girshick, K. He and P. Dollár, "Focal Loss for Dense Object Detection," *in IEEE Transactions on Pattern Analysis and Machine Intelligence*, vol. 42, no. 2, pp. 318-327, 2020.
- [24] J. Redmon and A. Farhadi, "YOLO9000: Better, Faster, Stronger," *2017 IEEE Conference on Computer Vision and Pattern Recognition (CVPR)*, pp. 6517-6525, 2017.
- [25] J. Redmon, A. Farhadi, "YOLOv3: an incremental improvement," unpublished, 2018.
- [26] K. He, X. Zhang, S. Ren, and J. Sun, "Deep residual learning for image recognition," *In Proceedings of the IEEE conference on computer vision and pattern recognition*, pp. 770-778, 2016.
- [27] A. Bochkovskiy, C Y. Wang, H Y M. Liao, "YOLOv4: optimal speed and accuracy of object detection," unpublished, 2020.
- [28] C. Y. Wang, A. Bochkovskiy, and H. Y. M. Liao, "Scaled-yolov4: Scaling cross stage partial network," *In Proceedings of the IEEE/cvf conference on computer vision and pattern recognition*, pp. 13029-13038, 2021.
- [29] G. Jocher, "YOLOv5[EB/OL]," unpublished, 2021.
- [30] Z. Zheng, P. Wang, W. Liu, J. Li, R. Ye, and D. Ren, "Distance-IoU loss: Faster and better learning for bounding box regression," *In Proceedings of the AAAI conference on artificial intelligence*, vol. 34, no. 07, pp. 12993-13000, April, 2020.
- [31] X. Li, W. Wang, X. Hu and J. Yang, "Selective Kernel Networks," *2019 IEEE/CVF Conference on Computer Vision and Pattern Recognition (CVPR)*, pp. 510-519, 2019.
- [32] S. Li, Y. Li, Y. Li, M. Li and X. Xu, "YOLO-FIRI: Improved YOLOv5 for Infrared Image Object Detection," *in IEEE Access*, vol. 9, pp. 141861-141875, 2021.
- [33] Z. Liu and T. Chen, "Distance Measurement System Based on Binocular Stereo Vision," *2009 International Joint Conference on Artificial Intelligence*, pp. 456-459, 2009.

Classification Method for Power Load Data of New Energy Grid based on Improved OTSU Algorithm

Xun Ma*, Kai Liu, Anlei Liu, Xuchao Jia, Yong Wang

Marketing Service Center, State Grid Hebei Electric Power Co., Ltd., Hebei, China

Abstract—The classification method for power load data of new energy grid based on improved OTSU algorithm is studied to improve the classification accuracy of power load data. According to the idea of two-dimensional visualization of time series, GAF (Geographical Adaptive Fidelity) method is used to transform the current data of power load in new energy grid into two-dimensional image of power load in new energy grid. The intra class dispersion is introduced, and the improved OTSU algorithm is used to segment the foreground and background of the two-dimensional image according to the pixel gray value of the two-dimensional image and the one-dimensional inter class variance corresponding to the pixel neighborhood gray value. The two-dimensional foreground image of power load is taken as the input sample of convolution neural network. The convolution neural network extracts the features of the two-dimensional foreground image of power load through convolution layer. According to the extracted features, the classification results of power load data of new energy grid are output through three steps: nonlinear processing, pooling processing and full connection layer classification. The experimental results show that this method can accurately classify the power load data of new energy grid, and the classification accuracy is higher than 97%.

Keywords—Improved OTSU algorithm; new energy grid; power load; classification method

I. INTRODUCTION

The classification of power load data of new energy grid helps power selling companies accurately grasp the power consumption characteristics of users, introduce a reasonable demand response mechanism and formulate scientific marketing strategies, which is of great significance for peak shaving and valley filling, optimizing power consumption curve, improving power quality and so on [1]. Improving terminal efficiency and guiding users to use electricity reasonably is one of the important contents of power demand side management. To realize this demand side management, it is necessary to timely understand the power consumption of household users and realize the interaction between supply and use. DSM (Demand Side Management) is a means to guide power consumers to adopt a reasonable way of using electricity [2] and achieve energy conservation and emission reduction. Smart grid utilizes advanced technology to dispatch demand side resources and improve the participation rate of power consumers, so as to realize the two-way interaction between information and power. Power consumers can respond to DSM strategy only when they understand their own power consumption mode [3]. For household power users, only electricity meters provide information for both suppliers and users, while the current smart electricity meters only have the

function of time-sharing pricing, which provides limited information. Therefore, in order to enhance the demand response of power users and optimize the power consumption mode [4], it is necessary to effectively monitor the household load and then measure it by classification. The current smart meter has neither time-sharing measurement nor load classification measurement [5], and can not provide power consumption details to power management departments and users, so it is very necessary to classify the power load data of new energy grid.

Image segmentation is an important step in the process of image analysis. Its goal is to divide the regions of interest in the image. Among many image segmentation methods, threshold segmentation technology is a widely used method in image segmentation [6]. Its basic principle is to calculate the segmentation threshold based on the image gray histogram, and then segment the image according to the threshold. OTSU algorithm is a commonly used algorithm in threshold segmentation. It selects the threshold by maximizing the variance between classes [7]. This method has the characteristics of easy to understand principle, considerable segmentation effect and stable algorithm. However, one-dimensional OTSU algorithm can not deal with more complex images. When segmenting images with too small gray difference between the background and the pixels in the target area, false segmentation will occur. Since the OTSU algorithm was proposed, it has attracted widespread attention of researchers. OTSU algorithm mainly lies in its simple principle, efficient calculation, wide application range and good segmentation effect [8]. OTSU algorithm is an image segmentation method without real-time supervision, without parameter regulation and automatic optimization. Based on the one-dimensional histogram, the threshold is selected by maximizing the variance between classes. Although OTSU algorithm has a good segmentation effect, it is prone to false segmentation when the gray value of the image background and the pixel points in the target area are not much different [9]. The segmentation result of one-dimensional OTSU algorithm is not accurate, but it has been reasonably improved in two-dimensional OTSU algorithm. The expression form of two-dimensional OTSU algorithm is good anti-interference ability, but its calculation process is too complex and requires a lot of running time to process it.

A. Related Work

At present, many researchers have studied power load. J. J. Hu et al. applied data mining algorithm to power load forecasting [10], and verified that this method can effectively predict power load through simulation tests; H. Bakhtiari et al.

*Corresponding Author.

Used Markov chain Monte Carlo simulation method [11] to simulate the uncertain random load in the operation of independent microgrid of renewable energy. Although the above two methods can realize the function of power load and uncertain random load prediction, they do not specifically classify the power load of users, so their applicability is poor.

In view of the problems of the above two methods, to further improve the classification accuracy of power load data, the classification method of power load data of new energy grid based on improved OTSU algorithm is studied, and the OTSU algorithm is used to segment the two-dimensional visual image of power load data transformation of new energy grid, so as to obtain the classification results of power load data of new energy grid. The experiment shows that the contribution of this method is that it can accurately classify the power load data of new energy grid, and has high applicability. The specific process schematic diagram of the method used in this paper is shown in Fig. 1.

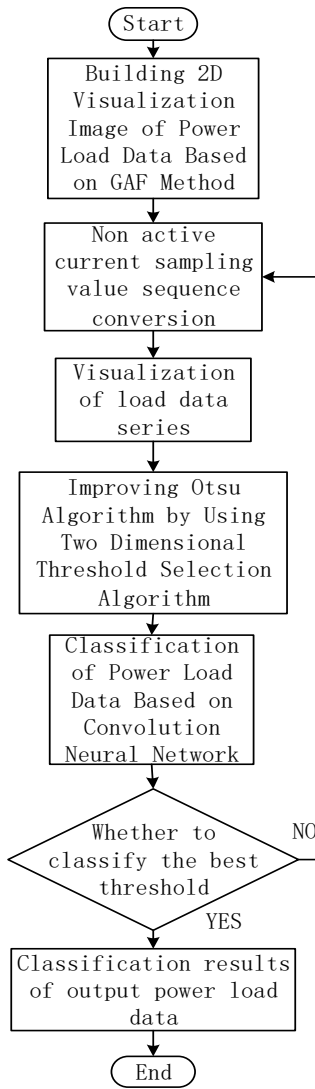


Fig. 1. The Specific Process Schematic Diagram of the Method used in this Paper.

II. MATERIALS AND METHODS

A. Sequence Visualization of Power Load Data of New Energy Grid

The power load data of new energy grid can be visually displayed through the current monitoring data, and the current can be regarded as a one-dimensional sequence related to time in essence. According to the idea of two-dimensional visualization of time series [12], GAF method is introduced into the power consumption field of new energy grid to build a two-dimensional visualization image for the power load data of new

energy grid. Assuming that $X = \{x_1, x_2, \dots, x_n\}$ is a sequence containing n sampling values of non-active components of current, the steps to convert it into a two-dimensional visual GAF diagram of power load of new energy grid are as follows:

1) The elements in X is normalized to the interval $[-1, 1]$, that is:

$$\tilde{x}_i = \frac{(x_i - \max X) + (x_i - \min X)}{\max X - \min X} \quad (1)$$

2) The current sequence after standardization is encoded in polar coordinates, namely:

$$\begin{cases} \Psi_i = \arccos \tilde{x}_i & \tilde{x}_i \in [-1, 1] \\ r = t_i, & t_i - i - 1 \end{cases} \quad (2)$$

Where: \tilde{x}_i is the non-active component of the load current of x_i in new energy grid after standardization; Ψ_i is the arccosine of the encoded sample value; r is the radius after timestamp coding; t_i is the sampling timestamp corresponding to x_i .

Since $\tilde{x}_i \in [-1, 1]$ after standardization, the definition domain of the inverse cosine function is $[-1, 1]$, so $\Psi_i \in [0, \pi]$.

When the current sequence of the power load of the new energy grid is given, each sampling point has and only has a unique mapping result in the polar coordinate system [13], that is, the bijection relationship.

3) After completing the polar coordinate transformation of the current sequence of the standardized new energy grid power load, the GAF method is used to convert the current sequence of the one-dimensional new energy grid power load into an n -order matrix, and the values of the elements in the matrix are mapped to the blue-red color range, making the matrix a two-dimensional image with color and texture distribution [14].

GAF method has two definition methods, namely, Gramian Angular Summation Field (GASF) and Gramian Angular

Difference Field (GADF), and the corresponding matrices A_s and A_D are respectively:

$$A_s = \begin{bmatrix} \cos(2\Psi_1) & \cos(\Psi_1 + \Psi_2) & \cdots & \cos(\Psi_1 + \Psi_n) \\ \cos(\Psi_2 + \Psi_1) & \cos(2\Psi_2) & \cdots & \cos(\Psi_2 + \Psi_n) \\ \vdots & \vdots & \ddots & \vdots \\ \cos(\Psi_n + \Psi_1) & \cos(\Psi_n + \Psi_2) & \cdots & \cos(2\Psi_n) \end{bmatrix} \quad (3)$$

$$A_D = \begin{bmatrix} 0 & \sin(\Psi_1 - \Psi_2) & \cdots & \sin(\Psi_1 - \Psi_n) \\ \sin(\Psi_2 - \Psi_1) & 0 & \cdots & \sin(\Psi_2 - \Psi_n) \\ \vdots & \vdots & \ddots & \vdots \\ \sin(\Psi_n - \Psi_1) & \sin(\Psi_n - \Psi_2) & \cdots & 0 \end{bmatrix} \quad (4)$$

GAF method is evolved from Gram matrix. Polar coordinate system is used to represent time series instead of Cartesian rectangular coordinate system. Trigonometric function is used to refine the implicit current difference information between each two sampling points in the sequence to expand the amount of data, so as to improve the dimension of the sequence. Compared with the one-dimensional sequence of the current of the power load in the new energy grid, the two-dimensional image of the current sequence of the power load in the new energy grid significantly improves the identification of the power load. Polar coordinate coding of current sequence has the following advantages: polar coordinate transformation meets the double shooting condition, and the sampling point of current sequence of each new energy grid load has and only has a unique mapping result in the polar coordinate system, ensuring the uniqueness of the coding process; After the polar coordinate transformation, the time from the upper left corner to the lower right corner of the matrix element increases continuously; Compared with the rectangular coordinate system, the polar coordinate system retains the current magnitude relationship and time information of the new energy grid load between the sampling points. Through the above process, the power load data of new energy grid is transformed into a two-dimensional image of time series.

B. Two-dimensional Image Segmentation of Power Load in New Energy Grid based on Improved OTSU Algorithm

1) Image segmentation method based on OTSU: The gray level $G=1, 2, \dots, L$ of the two-dimensional image of the power load in the new energy grid is set, and f_i is used to represent the total number of pixels contained in the gray level i . The total number of pixels in the two-dimensional image of the power load of the new energy grid is N , $N = f_1 + f_2 + \dots + f_i = \sum_{i=1}^l f_i$. P_i is used to indicate the occurrence frequency of i , a gray-scale pixel, $P_i = f_i / N$, then $P_i > 0$, $\sum_{i=1}^l P_i = 1$. A threshold t is selected to divide all pixels of the two-dimensional image of the power load in the

new energy grid into two parts, C_0 and C_1 , $C_0 = \{1, 2, \dots, t\}$, $C_1 = \{t+1, t+2, \dots, L\}$. The probability distributions of these two types are as follows:

$$\omega_0 = P_r(C_0) = \sum_{i=1}^t P_i = \omega(t) \quad (5)$$

$$\omega_1 = P_r(C_1) = \sum_{i=t+1}^l P_i = 1 - \omega(t) \quad (6)$$

The two types of gray mean values in the two-dimensional image of the power load in the new energy grid are respectively:

$$u_0 = \sum_{i=1}^t i \times P_r(i / C_0) = \sum_{i=1}^t \frac{iP_i}{\omega_0} \quad (7)$$

$$u_1 = \sum_{i=t+1}^l i \times P_r(i / C_1) = \frac{u_r - u(t)}{1 - \omega(t)} \quad (8)$$

$$u_r = u(L) = \sum_{i=1}^l iP_i, \quad u(t) = \sum_{i=1}^t iP_i,$$

Then

$$\omega(t) = \sum_{i=1}^t P_i$$

For any t , the following formula is satisfied:

$$\omega_0 + \omega_1 = 1 \quad (9)$$

$$\omega_0 u_0 + \omega_1 u_1 = u_r \quad (10)$$

The evaluation function is introduced to judge the advantages and disadvantages of the threshold in OTSU algorithm:

$\lambda = \frac{\sigma_B^2}{\sigma_w^2}$, $k = \frac{\sigma_r^2}{\sigma_w^2}$, $\eta = \frac{\sigma_B^2}{\sigma_r^2}$. σ_B^2 , σ_w^2 and σ_r^2 are inter class variance, intra class variance and overall variance respectively. The three decision functions are maximized, and the objective function becomes the selection of the optimal threshold t .

Since $\sigma_r^2 = \sigma_B^2 + \sigma_w^2$, the following relationship is satisfied:

$$k = \frac{1}{1 - \eta} \quad (11)$$

$$\eta = \frac{\lambda}{\lambda + 1} \quad (12)$$

It can be seen from the above formula that the monotonicity of the three decision functions is the same [15]. Since σ_r^2 is a known constant and has nothing to do with the value of t , η

$$\eta(t) = \frac{\sigma_B^2(t)}{\sigma_r^2}, \text{ so } \sigma_B^2$$

is the simplest of the three functions, can be used as a judgment function for the performance of two-dimensional image segmentation of power load in new energy grid:

$$\sigma_B^2(t) = \frac{[u_r \omega(t) - u(t) \omega(t)]^2}{\omega(t)[1 - \omega(t)]} \quad (13)$$

$$u_r = u(L) = \sum_{i=1}^L ip_i, \quad u(t) = \omega(t) = \sum_{i=1}^t ip_i$$

Where,

The optimal threshold t^* of two-dimensional image segmentation of power load in new energy grid is:

$$\sigma_B^2(t^*) = \max_{1 \leq t \leq L} \{\sigma_B^2(t)\} \quad (14)$$

2) *Two-dimensional OTSU algorithm with improved threshold selection algorithm*: Aiming at the high computational complexity of two-dimensional OTSU algorithm, an improved OTSU algorithm is proposed. This algorithm divides the traditional two-dimensional algorithm into two one-dimensional OTSU algorithms: a threshold is obtained from the one-dimensional histogram based on the gray value of the two-dimensional image of the new energy grid's power load, and its purpose is to extract the target; A threshold value [16] is obtained from the one-dimensional histogram based on the neighborhood average gray value of the two-dimensional image of the new energy grid's power load, and its purpose is to filter out noise. The two thresholds obtained by these two one-dimensional OTSU algorithms are used to replace the thresholds of the original two-dimensional OTSU algorithm. This improved algorithm not only considers the gray information of the two-dimensional image of the new energy grid's power load itself, but also considers the information of its neighborhood pixels, so that the algorithm has good denoising ability. From

the frequency f_{ij} of (i, j) in the two-dimensional image histogram of the new energy grid's power load, the frequency

$q_i = \sum_{j=0}^{L-1} f_{ij}$ of the pixel gray value i in the two-dimensional image of the power load of the new energy grid and the

frequency $r_j = \sum_{i=0}^{L-1} P_{ij}$ of the neighborhood gray value j are

derived. By analogy, the probability distribution P_{ij} can be used to obtain the one-dimensional histogram distribution of the pixel

gray value i and the neighborhood gray value j of the two-dimensional image of the new energy grid's power load, and

$$U_i = \sum_{j=0}^{L-1} P_{ij}, \quad V_i = \sum_{i=0}^{L-1} P_{ij}$$

their probabilities are , respectively.,

In two-dimensional OTSU algorithm, edge points and noise points account for a small number [17], that is, the probability corresponding to the noise and edge part can be approximately

$$\sum_{i=s+1}^{L-1} \sum_{j=0}^t P_{ij} = 0, \quad \sum_{i=0}^s \sum_{j=t+1}^{L-1} P_{ij} = 0$$

0, that is, . It can get the

expression of the proportion ω_0 and ω_b of the target and background in the one-dimensional histogram corresponding to the pixel gray value i of the two-dimensional image of the new energy grid's power load as follows:

$$\omega_0 = \sum_{i=0}^s \sum_{j=0}^s P_{ij} + \sum_{i=0}^s \sum_{j=t+1}^{L-1} P_{ij} = \sum_{i=0}^s U_i \quad (15)$$

$$\omega_b = \sum_{i=s+1}^{L-1} U_i \quad (16)$$

The mean vectors corresponding to the two categories are:

$$\mu_{oi} = \sum_{i=0}^s iU_i / \omega_0 \quad (17)$$

$$\mu_{bi} = \sum_{i=s+1}^{L-1} iU_i / \omega_b \quad (18)$$

The overall mean vector of the improved OTSU algorithm is:

$$\mu_i = \sum_{i=0}^{L-1} \sum_{j=0}^{L-1} iP_{ij} = \sum_{i=0}^{L-1} iU_i \quad (19)$$

From the above formulas, it can be deduced that the one-dimensional interclass variance corresponding to the pixel gray value i of the two-dimensional image of the new energy grid's power load is:

$$\sigma_{B_i}(s) = (\omega_0 + \omega_b)(\mu_{oi} - \mu_i)^2 + (\mu_{bi} - \mu_i)^2 \quad (20)$$

Similarly, it can be obtained that the one-dimensional interclass variance corresponding to the neighborhood gray value v of the two-dimensional image of the new energy grid's power load is:

$$\sigma_{B_j}(t) = (\omega_0 + \omega_b)(\mu_{oj} - \mu_j)^2 + (\mu_{bj} - \mu_j)^2 \quad (21)$$

Where: ω_0 and ω_b represent the proportion of target and background respectively, and μ_{oj} , μ_{bj} and μ_j represent the average vector and overall mean vector of the two categories respectively.

According to the principle of one-dimensional Otsu algorithm, the optimal threshold s^* , t^* should meet:

$$\sigma_{B_i}(s^*) = \max_{0 \leq s \leq L-1} \{\sigma_{B_i}(s), \sigma_{B_j}(t^*)\} = \max_{0 \leq t \leq L-1} \{\sigma_{B_j}(t)\} \quad (22)$$

Although the threshold segmentation method for the traditional OTSU algorithm considers the variance between the foreground class and the background class [18], it does not consider the discreteness within the class, so it can not more comprehensively reflect the quality of classification and achieve more accurate segmentation. By introducing the intra class dispersion, the segmentation result of the two-dimensional image of the new energy grid's power load not only achieves the maximum variance between classes, but also better realizes the intra class consistency. The classification discrete measure corresponding to the pixel gray value of the two-dimensional image of the new energy grid's power load is defined as:

$$\tau_{di} = (\omega_0 + \omega_b) \sum_{i=0}^s |\mu_{oi} - iU_i / \omega_0| + \sum_{i=s+1}^{L-1} |\mu_{bi} - iU_i / \omega_b| \quad (23)$$

Based on the above formula, a new threshold recognition function expression is constructed as follows:

$$\xi_i = \omega_0 (1 - \omega_0) \times \sigma_{B_i} / \tau_{di} \quad (24)$$

Similarly, the threshold recognition function ξ_j is also constructed for the one-dimensional histogram composed of the average value of neighborhood gray.

In order to optimize the segmentation effect of two-dimensional image of power load in new energy grid and minimize the dispersion within the class, it is necessary to calculate the maximum value of ξ_i and ξ_j , that is, to calculate the minimum value of τ_{di} and τ_{dj} . In order to quickly and effectively determine the two-dimensional image segmentation threshold of the power load of the new energy grid, the solution of ξ_i and ξ_j is taken as the fitness function, and the genetic algorithm is used to automatically obtain the appropriate threshold vector, so as to realize the two-dimensional threshold segmentation for the two-dimensional image of the power load of the new energy grid.

C. Classification of Power Load Data of New Energy Grid based on Convolutional Neural Network

Compared with the traditional neural network, convolutional neural network has a special structure. The weight structure can reduce the complexity of the classification model and reduce the amount of calculation of the algorithm. Convolutional neural network is often used in image

classification. Images can be directly used as the input of classification model. The extracted three-dimensional feature signals make the classification accuracy of convolutional neural network higher. Convolution neural network is used to classify the load data of new energy grid. Convolution neural network is divided into four parts: convolution, nonlinear processing, pooling and full connection layer classification.

1) *Convolution layer*: In convolution neural network, the main purpose of the first step convolution is to extract its feature matrix from an input image, and extract image features through the graphic signal of the input data, so as to maintain the spatial relationship between pixels. The convolution kernel size $G(s, t)$ used for convolution is $A \times B$, and the weight of convolution kernel function directly affects the effect of the final recognition result. The larger the weight is, the stronger the force is. $C(i, j)$ is the characteristic matrix, which is the convolution matrix obtained by convoluting the two-dimensional image of the power load of the original new energy grid with the convolution kernel G . The operation expression is as follows:

$$\begin{aligned} C(i, j) &= f(x, y) \times G(s, t) \\ &= \sum_{x=1}^a \sum_{y=1}^b G(s, t) \times f(i+x-1, t+y-1) \end{aligned} \quad (25)$$

Where, the value range of s and t is $1 \leq i \leq M - A + 1$, $1 \leq j \leq N - B + 1$.

It is obvious from formula (25) that the convolution neural network algorithm is to use the convolution kernel matrix to filter the original signal image, extract the features of the corresponding positions, and finally obtain a new feature image. One of the most important features of convolution neural network operation is the operation through convolution layer. Multiple convolution checks are used to extract features from the two-dimensional image of power load of new energy grid [19], forming multiple new feature matrices.

It is very important to extract characteristic signals and establish convolution kernel function of characteristic matrix in the convolution process of two-dimensional image of power load in new energy grid. The number of convolution kernels is an important parameter. The extracted number corresponds to the convolution kernel function used in the convolution operation. Different convolution kernel functions are used to convolute the two-dimensional image of the power load of the new energy grid to map different features. The number of convolution kernels corresponds to the number of types of features selected for convolution. The magnitude of the convolution kernel matrix sliding in the image is also an important parameter. When the step is 1, we only move one pixel at a time. When the step is 2, the sliding filter processes two pixels at a time. The larger the step is, the longer the sliding span is, and the smaller the characteristic matrix is generated at the same time. The value of convolution kernel matrix is also

an important parameter. Different convolution kernels map different characteristic matrices. The value in the convolution kernel matrix is needed to control, that is, control the output range of the characteristic matrix.

2) *Nonlinear processing*: After convolution processing of convolution neural network, the second step of nonlinear transformation is required. Its purpose is to process the target in the two-dimensional image of power load of new energy grid by using nonlinear function. The sigmoid function is used for nonlinear processing of the two-dimensional image of the new energy grid's power load, and the expression is as follows:

$$f(x) = \frac{1}{1 + e^{-x}} \quad (26)$$

Nonlinear processing can further purify and sample the data, optimize the data type, and facilitate the subsequent sampling calculation. Nonlinear processing further processes the signal and replaces all negative pixel values to zero during feature mapping. The purpose of nonlinear processing is that most real-world data are not smooth and ideal. It is hoped that through further processing of signal data, convolutional neural network can recognize signals more accurately and reliably.

3) *Pooling processing*: Pooling can also be called subsampling or subsampling. Its purpose is to reduce the dimension of each feature map and retain the most important information. Pool processing can be: maximum value, average value, adjacent and so on. In the process of pooling, a feature window $a \times b$ is defined, and the secondary feature extraction of the first step feature matrix is carried out through the pooling window. Through pooling, we can gradually reduce the size of the input space, make the input dimension smaller and easier to calculate, and retain the important characteristics of the network, so that the small transformation, distortion and translation in the two-dimensional foreground image of the segmented power load of the new energy grid remain unchanged.

4) *Full connection layer classification*: Each pixel of the characteristic matrix in the two-dimensional image of all new energy grid power loads after pooled sampling is arranged in turn to form a feature vector. The feature vector forms a full connection with the output layer as a full connection layer. The full connection layer is the last step of the convolutional neural network, which is used for the output of the whole neural network. In the full connection layer, a classifier is usually trained for the convolutional neural network [20]. Generally speaking, the full connection layer adopts the traditional multi-layer classifier, such as softmax or support vector machine. The purpose of full connection layer is to use the characteristics of data to achieve the classification purpose of input and output through training. The full connection layer is located in the classification link of convolutional neural network structure.

In the process of convolution neural network classifying the power load data of new energy grid, the first step is to select the test set and sample set, and select the foreground image of the two-dimensional image of new energy grid's power load

obtained after segmentation as the input sample of convolution neural network. After determining the test sample and training sample, the classification process is as follows:

1) Initialize the weight matrix and bias parameters of convolutional neural network.

2) Select a sample from the training samples, input the selected samples into the network, and obtain the corresponding actual output value.

3) Calculate the error between actual data input and ideal output.

4) Carry out back propagation and adjust the parameters.

5) Input the remaining training samples into the network in turn until all training samples are input, and complete an iteration.

6) Input the test samples into the trained sample model, and use the classifier to obtain the accuracy of classification.

The convolution neural network is used to classify the segmented two-dimensional image of the power load of the new energy grid, and the classification results of the power load data of the new energy grid are output.

III. RESULTS

In order to verify the classification effectiveness of the classification method for power load data of new energy grid based on the improved OTSU algorithm, the method in this paper is applied to the new energy grid's power consumption management of a power enterprise. The power enterprise uses current sensors to collect the current changes of different smart meters, as shown in Table I.

According to the current changes of smart meters in the new energy grid collected by the current sensor in Table 1, the GAF method is used to build a two-dimensional visual image of the time series of power load data in the new energy grid, as shown in Fig. 2.

According to the experimental results in Fig. 2, the current data related to load data in the new energy grid can be effectively converted into two-dimensional visual images by using the method in this paper, and the two-dimensional visual images can be used to visually display the load changes in the new energy grid. In this paper, the improved OTSU algorithm is used to segment the two-dimensional visual image of time series. The segmentation results of the two-dimensional visual image of the new energy grid's power load data are shown in Fig. 3.

According to the segmentation results of the new energy grid's electricity load image in Fig. 3, the accurate segmentation of the two-dimensional visual image of the new energy grid's electricity load can be achieved by using the method in this paper, and the two-dimensional visual image can be divided into the target foreground area and the background area by image segmentation. The experimental results in Fig. 3 show that the method in this paper has a high image segmentation effect, and the edge of the segmented image is clear, which can effectively display the target information contained in the image.

TABLE I. CURRENT CHANGE ACQUISITION RESULTS

Electric meter account number	58156 /A	84516 /A	89145 /A	68421 /A	68115 /A
10s	1.85	2.16	3.25	1.79	1.94
20s	2.16	2.85	3.46	1.86	1.58
30s	3.28	3.16	2.85	2.35	1.68
40s	2.84	2.75	1.64	1.64	2.34
50s	2.69	3.16	3.69	1.85	2.49
60s	2.75	2.84	2.46	1.54	1.85
70s	3.16	3.64	1.85	1.35	1.95
80s	1.05	3.85	1.62	1.65	2.47
90s	0.95	1.26	1.57	1.05	2.05
100s	3.25	2.64	1.69	2.06	2.13

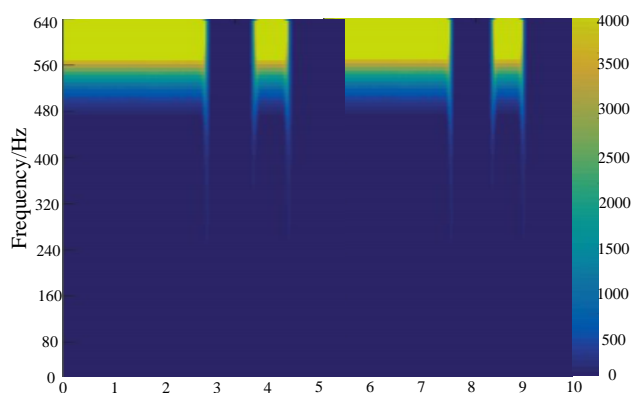


Fig. 2. 2D Visualization of Time Series.



Fig. 3. Image Segmentation Results.

The method in this paper is used to classify the load data managed by a smart meter in the new energy grid to verify the effectiveness of this method. According to the segmented electricity load image of new energy grid, the classification results of electricity load data of new energy grid using this method are shown in Table II.

According to the experimental results in Table II, the improved OTSU algorithm can be used to classify the power load data of new energy grid with high classification accuracy. The experimental results in Table II verify that the method in this paper has high classification effectiveness of power load

data of new energy grid. This method can accurately classify the power load data of the new energy grid, which is helpful for the dispatching management decision-makers of the new energy grid to make the dispatching and management decisions of the new energy grid according to the classification results of the power load data of the new energy grid.

The method in this paper is used to classify the power load data in the new energy grid. The operating power changes of each power load are shown in Table III.

According to the experimental results in Table III, there are obvious differences in the power of different power loads in the new energy grid. The method in this paper can effectively classify the load data of the new energy grid, and accurately analyze the load data of the new energy grid through the power changes of different load types.

Statistics adopts the method in this paper to classify the power load data of new energy grid. For the classification accuracy of different types of load data, the classification performance of this method is verified by the classification accuracy of load data. The statistical results are shown in Fig. 4.

TABLE II. CLASSIFICATION RESULTS OF ELECTRICITY LOAD DATA OF NEW ENERGY GRID

Time	Classification result	Is the classification correct
8:05	Turn on the rice cooker	Yes
8:13	Turn off the rice cooker	Yes
8:25	Turn on the TV	Yes
18:16	Turn on the refrigerator	Yes
18:32	Turn off the tv	Yes
19:25	Turn on the rice cooker	Yes
19:35	Turn off the rice cooker	Yes
19:51	Turn off the refrigerator	Yes
20:18	Turn on energy-saving lamps	Yes
20:23	Turn off the hair dryer	Yes

TABLE III. CHANGES IN OPERATING POWER OF ELECTRICAL LOAD

Electric load type	Max power/W	Minimum power/W	Average power/W
refrigerator	185.6	134.4	148.5
TV set	285.4	234.5	257.6
electric fan	135.5	126.5	129.4
hair dryer	1820.4	1685.4	1710.5
kettle	1864.5	1812.5	1835.7
air conditioner	1358.6	1205.7	1285.4
washing machine	280.6	250.4	265.8
Micro-wave oven	750.4	658.6	716.5
induction cooker	4050.4	3895.8	3925.4
computer	330.5	290.4	315.6

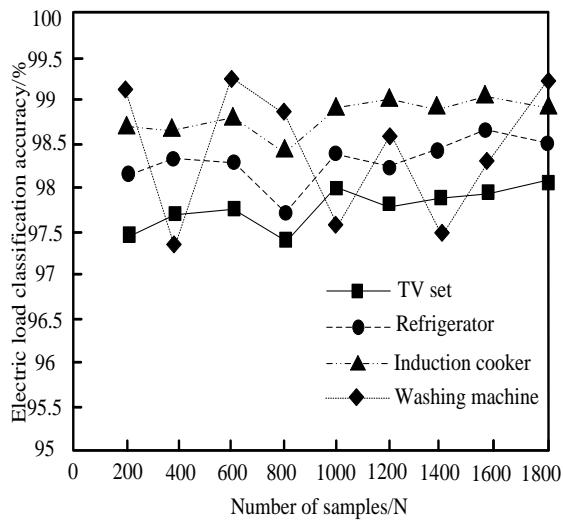


Fig. 4. Load Data Classification Accuracy.

According to the experimental results in Fig. 4, the classification accuracy of different types of power load data using the method in this paper is higher than 97%. The experimental results verify that this method has high classification effectiveness of power load data of new energy grid. For different types of load data, this method can achieve accurate classification. It is verified that the method in this paper has high efficiency of load data classification, and can be applied to the practical application of power load data classification in new energy grid.

The classification calculation time of this method is counted for different types of load data. The statistical results are shown in Fig. 5.

As shown in Fig. 5, the classification time of the present method is less than 50ms, indicating that the method has high load data classification efficiency and is suitable for the practical application of power grid load data classification.

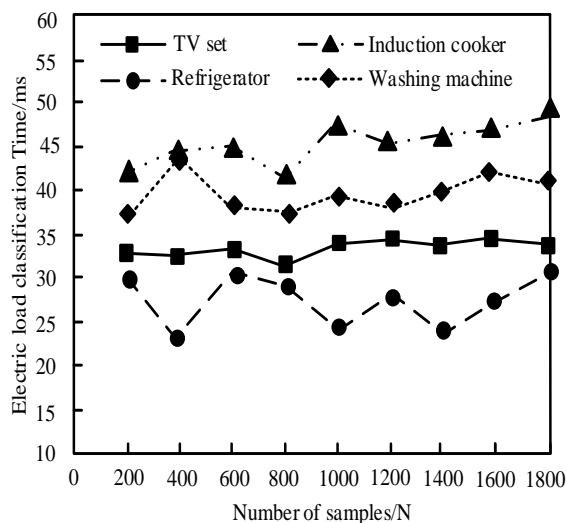


Fig. 5. Classification Time.

IV. DISCUSSION

This paper studies the classification method for power load data of new energy grid based on improved OTSU algorithm, and verifies that this method can accurately classify the data of new energy grid through experiments. The energy problem has always been a problem perplexed by mankind. With the development of the times, the energy crisis and greenhouse effect have become increasingly serious. How to effectively improve energy efficiency and reduce polluting gas emissions has become a high concern and attention of all sectors of society. The new energy grid has become the main trend of the development of the power field. The working state and energy consumption of each power load in the new energy grid can be obtained by classifying the power load data of the new energy grid. According to the comprehensive information such as energy consumption information, time-of-use electricity price and electric energy measurement, effective energy-saving measures can be obtained, reasonable energy-saving plans can be formulated, and targeted power loads can be purchased.

The significance of power load data classification of new energy grid is specifically shown in:

1) In the planning of power system, medium and long-term load forecasting is the basis of power system development planning and fuel planning, while short-term load forecasting is the premise of making daily power generation plan and determining the operation mode of power system. The classification of power load data of new energy grid only through the installation of monitoring equipment at the user's power entrance to understand the power consumption, operation status and operation time of the load, and in-depth understanding of the energy consumption and detailed power consumption information of each load. The fine-grained power consumption information is helpful to obtain the characteristics and power consumption modes of different load types, and more accurately predict the spatial density distribution map of load at various spatial scales and time scales, to improve the accuracy and reliability of load forecasting which greatly improves the scientificity of power system planning and the real-time, safe and economic operation of the power grid.

2) The classification method for power load data of new energy grid can obtain the specific power consumption information of each power load, carefully consider the time-varying characteristics of load operation, provide the possibility for load modeling and dynamic management of load model parameters, improve the operation accuracy of load model in the process of power system simulation, and reduce the economic loss of error caused by load model.

3) The classification of power load data of new energy grid can enable power companies to obtain detailed power consumption information such as the type, working state, power consumption time and energy consumption of different loads, and can help power companies formulate electricity prices and power demand side management more scientifically and provide corresponding incentive policies. At the same time, the working state information of power load can help power companies verify whether users make timely and accurate response to grid

demand according to the relevant demand of power demand side management, such as load shedding during peak hours of grid operation. At the same time, the power supply company can carry out user expansion business according to the power consumption information. For example, the power supply company can formulate a detailed power consumption plan for users and obtain corresponding remuneration.

4) The classification of power load data of new energy grid to obtain the detailed power consumption information of users can greatly improve the visualization of power system, especially for the fault state and abnormal operation state of power grid load, which is conducive to the detection, quasi positioning, self-healing reconstruction and rapid restoration of power supply and other functions of power system distribution network's outage fault.

5) The classification of power load data of new energy grid can obtain the working state, power consumption time and energy consumption of each power load in real time, such as whether the electric kettle is in the heating state, whether the LCD TV is in the working state, and whether the refrigerator is in the fault state.

6) Residential users adjust and optimize their power consumption behavior according to the detailed power consumption information of the power load, so as to achieve the purpose of saving electricity and reducing electricity expenses, such as changing the use time of the power load, avoiding the peak electricity price, or adjusting the operating parameters of the power load, so as to reduce unnecessary power waste.

7) According to the detailed power consumption information, users can quickly and accurately obtain whether the power load is in fault and which equipment is high-efficiency equipment, and use energy-saving power loads as much as possible. For example, if the refrigerator is monitored to be in the operation state of maximum power all the time, rather than the intermittent operation state, the refrigerator is in the fault state; Or if it is judged that the air conditioner consumes too much power, it can be considered to replace the energy-saving air conditioner, which is conducive to saving electricity expenses. At the same time, the detailed electricity consumption information of residents' various loads provides a regulation basis for smart home and household electricity automation.

8) In the research, the challenge encountered in this paper is to use the image segmentation for classification data, which is prone to noise interference and affects the classification accuracy. Therefore, this paper uses the one-dimensional classification threshold to filter out the noise and obtain accurate results.

9) The importance of all quantities in the relationship lies in that this paper uses the average vector and the overall average value corresponding to the gray value of the neighborhood of the new energy grid load two-dimensional image to calculate the one-dimensional inter class variance, find the best gray threshold, and perform more accurate segmentation. By introducing intra class dispersion, the load two-dimensional image segmentation results reach the maximum variance within

the class, and the classification results are optimized; The convolution kernel matrix is used to filter the original signal image, extract image features, and nonlinear process the load two-dimensional image, which improves the accuracy and efficiency of classification.

V. CONCLUSION

With the growing maturity of smart grid and the gradual enhancement of users' awareness of energy conservation, the demand for household electricity transparency on the power demand side is also more urgent. Therefore, in this paper, the classification method for power load data of new energy grid based on the improved OTSU algorithm is studied, to display the collected power load data of new energy grid in the form of two-dimensional images, segment the two-dimensional image of power load data of new energy grid using the improved OTSU algorithm, and use the segmented two-dimensional image to realize the effective classification of new energy grid's power load data. The classification of power load data of new energy grid can optimize the power consumption mode of users and improve the participation of power consumers in demand side management. Due to the limited conditions, the present method has some shortcomings and only study the data classification, and future studies can optimize the user power consumption pattern using the classification results.

VI. FUND

This study did not receive any funding in any form.

VII. CONFLICTS OF INTEREST

The authors declare that they have no competing interests

REFERENCE

- [1] U. K. Kalla, H. Kaushik, B. Singh and S. Kumar. "Adaptive control of voltage source converter based scheme for power quality improved grid-interactive solar pv-battery system." *IEEE Transactions on Industry Applications*, 56(1), 787-799, 2020.
- [2] H. Golmohamadi, "Demand-side management in industrial sector: a review of heavy industries." *Renewable and Sustainable Energy Reviews*, 156(2), 111963, 2022.
- [3] J. Ponoko and J. V. Milanovi, "Multi-objective demand side management at distribution network level in support of transmission network operation." *IEEE Transactions on Power Systems*, 35(3), 1822-1833, 2020.
- [4] L. Fu, B. Liu, K. Meng and Z. Y. Dong, "Optimal restoration of an unbalanced distribution system into multiple microgrids considering three-phase demand-side management." *IEEE Transactions on Power Systems*, PP(99), 1-1, 2020.
- [5] S. Yan, K. Li, F. Wang, X. Ge and S. Chang, "Time-frequency features combination-based household characteristics identification approach using smart meter data." *IEEE Transactions on Industry Applications*, PP(99), 1-1, 2020.
- [6] J. Zhang, Y. Zhou, K. Xia, Y. Jiang and Y. Liu, "A novel automatic image segmentation method for chinese literati paintings using multi-view fuzzy clustering technology." *Multimedia Systems*, 26(1), 37-51, 2020.
- [7] Z. Zhang, C. Luo, H. Wu, Y. Chen, N. Wang and C. Song, "From individual to whole: reducing intra-class variance by feature aggregation." *International Journal of Computer Vision*, 130(3), 800-819, 2022.
- [8] X. Zou, W. Tan, X. Huang, S. Nan, Y. Bai, and X. Fu, "Imaging quality enhancement in binary ghost imaging using the otsu algorithm." *Journal of Optics*, 22(9), 095201 (7pp), 2020.

- [9] A. K. Bhandari, A. Ghosh and I. V. Kumar, "A local contrast fusion based 3d otsu algorithm for multilevel image segmentation." *IEEE/CAA Journal of Automatica Sinica*, 7(01), 203-216, 2020.
- [10] J. J. Hu, H. G. Yang, "Multi-point Power Load Forecasting Method Based on Outlier Data Mining." *Computer Simulation*, 38(12), 66-69+93, 2021.
- [11] H. Bakhtiari, J. Zhong and M. Alvarez, "Predicting the stochastic behavior of uncertainty sources in planning a stand-alone renewable energy-based microgrid using metropolis-coupled markov chain monte carlo simulation." *Applied Energy*, 290(1), 116719, 2021.
- [12] K. C. Kwon, K. H. Kwon, M. U. Erdenebat, Y. L. Piao and N. Kim, "Advanced three-dimensional visualization system for an integral imaging microscope using a fully convolutional depth estimation network." *IEEE Photonics Journal*, PP(99), 1-5, 2020.
- [13] J. R. Huo, "A finite difference method for the allen-cahn equation in polar coordinate system." *Advances in Applied Mathematics*, 10(1), 109-114, 2021.
- [14] R. J. Chu, N. Richard, H. Chatoux, C. Fernandez-Maloigne and J. Y. Hardeberg, "Hyperspectral texture metrology based on joint probability of spectral and spatial distribution." *IEEE Transactions on Image Processing*, PP(99), 1-1, 2021.
- [15] S. Popov, "Conditioned two-dimensional simple random walk: green's function and harmonic measure." *Journal of Theoretical Probability*, 34(1), 418-437, 2021.
- [16] X. Chen and Y. Lu, "Dynamic graph regularization and label relaxation-based sparse matrix regression for two-dimensional feature selection." *IEEE Access*, PP(99), 1-1, 2020.
- [17] D. R. Munirathinam and M. Ranganadhan, "A new improved filter-based feature selection model for high-dimensional data." *The Journal of Supercomputing*, 76(8), 5745-5762, 2020.
- [18] Z. Yang, L. Fan, Y. Yang, Z. Yang, and G. Gui, "Generalized nuclear norm and laplacian scale mixture based low-rank and sparse decomposition for video foreground-background separation." *Signal processing*, 172(Jul.), 107527.1-107527.10, 2020.
- [19] P. Tiede, A. E. Broderick and D. Palumbo, "Variational image feature extraction for the event horizon telescope." *The Astrophysical Journal*, 925(2), 122-131, 2022.
- [20] J. Li, G. Li and H. Fan, "Image reflection removal using end-to-end convolutional neural network." *IET Image Processing*, 14(6), 1047-1058, 2020.

Study on the Technical Characteristics of Badminton Players in Different Stages through Video Analysis

Jin Qiu

Chongqing Institute of Engineering
Chongqing 400900, China

Abstract—Through video analysis, Tai Tzu Ying, an excellent athlete, and badminton player A from Chongqing Institute of Engineering, were studied in this paper. The videos of the two athletes were organized and recorded, and the use of techniques in different stages were compared. The results found that Tai Tzu Ying's serve technique was flexible, with few errors, while Play A's serve technique was single and had many errors; in terms of serve receive, Tai Tzu Ying was more aggressive, mainly using rush shot and spinning net shot, while A mainly used techniques of spinning net shot and lift shot. The comparison of techniques in front, middle and back courts showed that Tai Tzu Ying's playing style was more aggressive, while A's playing style was more conservative. This paper compared the two athletes to understand the technical characteristics of excellent athletes and gave some suggestions for the training of school badminton players.

Keywords—Women's singles; video analysis; athletes; badminton; technical characteristics

I. INTRODUCTION

Badminton is a small-scale ball sport [1]. With the continuous development of sports, badminton has also been widely loved by people [2], continuously popularized [3], and become an important project in the Olympic Games [4]. With the progress and development of the international badminton world, badminton game system has been reformed [5], the badminton technology has also been continuously innovated and changed, the level of athletes has been improved, and the situation of the badminton world has become more complex. With the development of men's technology, women's singles play and technology have also changed, becoming more comprehensive, faster, and more competitive. Research on badminton has also become more extensive and deeper.

Most of the comparisons of technical characteristics of badminton focus on the world's best athletes, and there is a lack of comparisons between excellent athletes and ordinary athletes. The comparison between excellent athletes and ordinary athletes is of great significance to help ordinary athletes better understand the differences between themselves and excellent athletes, learn, and improve. Therefore, in order to further understand the gap between excellent athletes and ordinary athletes, the technical characteristics of excellent athletes and ordinary athletes were studied in this paper. Chinese Taipei player Tai Tzu Ying is ranked No. 1 in the World Badminton Federation and is a very good player with a well-rounded playing style. This paper compared the technical characteristics of Tai Tzu Ying and an average college athlete through video analysis to better understand the gap between them.

II. LITERATURE REVIEW

At present, research on badminton involves sports injuries [6], neurocognition [7], muscle structure [8], and biomechanics [9], but most studies focus on sports training [10], i.e., how to strengthen skill levels. Ardiantoro et al. [11] used the top Indonesian badminton player Jonathan Christie as a model and analyzed the tactical approach of the player using a frequent pattern (FP) growth algorithm to help the coach to improve the performance of the player. Zhou et al. [12] built a model of the score rate and technical movements of badminton in international tournaments with computers based on the probability theory and quantitatively compared the differences in scoring rates in international tournaments, thus providing a basis for improving training. Huang et al. [13] studied the optimization of training patterns for badminton players using the Apriori algorithm, providing a new idea for studying badminton technical movement rules. Pérez-Turpin et al. [14] conducted a study on men's singles and double outdoor badminton matches, recorded 20 men's single matches using a video camera, and compared the use percentage of different techniques using the Dartfish video analysis package.

III. RESEARCH SUBJECTS AND METHODS

A. Research Subjects

Tai Tzu Ying: An excellent female badminton singles player who holds the racket with her right hand and currently ranks No.1 in the world.

Play A: A badminton player from Chongqing Institute of Engineering who holds the racket with her right hand.

B. Research Methodology

1) *Literature method*: We collected and read a large amount of literature on badminton and its technical features through search resources such as the library of Chongqing Engineering College, China National Knowledge Infrastructure (CNKI), Duxiu Academic Web, and Google to understand the current research status and trends.

2) *Video analysis method*: The video data of 20 matches that Tai Tzu Ying participated in between 2016 and 2019 were obtained from the Internet sports video software such as Tencent Sports and Migu Sports, as shown in Fig. 1. The videos of 20 amateur badminton matches that Play A participated in between 2016 and 2019 were obtained from the school for comparison, as shown in Fig. 2. The videos were played by slow playback

and analyzed by pausing frame by frame confirm and record the type of technique and the landing point.

3) *Comparison method:* The excellent athlete Tai Tzu Ying was compared with the ordinary player A to compare the differences in their technical characteristics in different stages, analyze their characteristics in playing style, and provide data support for research.

4) *Data analysis method:* After analyzing the video, the data were organized, processed, and analyzed in Excel to motivate the use of different techniques in front, middle and back courts. The usage rate of every technique was calculated. The graphs were drawn in Excel to present the comparison between Tai Tzu Ying and ordinary athlete A and understand their difference.



Fig. 1. Screenshots of Tai Tzu Ying's Video.



Fig. 2. Screenshots of Play A's Video.

IV. RESEARCH RESULTS

A. Analysis of the Technical Characteristics of Serve and Receive

A successful serve can gain the initiative of a match and put pressure on the opponent. At the same time, a serve can force the opponent to use the technique expected by the server to return the shuttle; therefore, the study of the serve technique is important for the study of points scored and lost. A comparison of the technical characteristics of the two players when serving is shown in Table I and Fig. 3.

It was seen from Table I and Fig. 3 that Tai Tzu Ying mainly used the forehand clear and forehand low serve, with usage rates of 51.2% and 27.1%, and seldom used the flick serve, with the usage rate of around 3%, and the number of serve errors was 87, accounting for 9.2%; player A mainly used the technique of forehand low serve, for 572 times, with the usage rate of 76.9%, about 50% higher than Tai Tzu Ying, and the rest of several techniques were seldom used, with the usage rates below 5%, and she also made many errors, for 103 times, accounting for 13.8%, 4.6% higher than Tai Tzu Ying.

The forehand clear makes the shuttle hang in the air for a long time, which is good for players to adjust position and make

adequate preparation for the next shot, while the forehand low serve can limit the opponent's ability to attack from the back court. In comparison, Tai Tzu Ying's serve was more flexible, with the forehand clear as the main technique, supplemented by the forehand low serve, which is more conducive to mastering the initiative of the match, while Player A's serve was single and had more errors, showing insufficient advantages in serve.

TABLE I. COMPARISON OF TECHNICAL CHARACTERISTICS OF SERVE

Technique	Tai Tzu Ying		Player A	
	Number of uses	Usage rate	Number of uses	Usage rate
Forehand low serve	257	27.1%	572	76.9%
Forehand flick serve	30	3.2%	17	2.3%
Forehand clear	486	51.2%	22	3.0%
Backhand flick serve	32	3.4%	12	1.6%
Backhand net shot	57	6.0%	18	2.4%
Errors	87	9.2%	103	13.8%

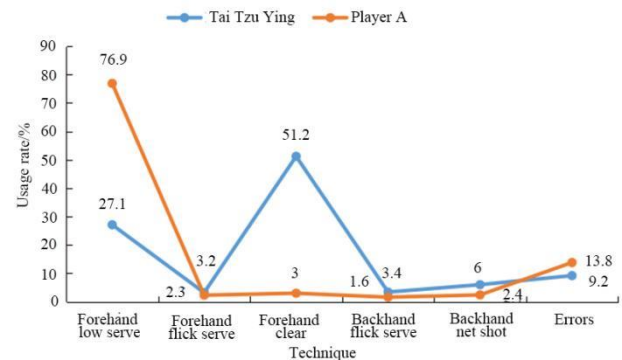


Fig. 3. Comparison of usage Rate between different Serve Techniques.

The comparison of the technical characteristics of serve showed that attention should be paid to the training of students' serve technique to improve the quality of students' forehand serve and students' awareness of serve, and matches could be simulated to strengthen students' anticipation ability to make them fully consider the way of opponent's return and the way of handling the third shot.

A comparison of the technical characteristics of the receiving serve is shown in Table II and Fig. 4.

It was seen from Table II and Fig. 4 that Tai Tzu Ying and player A had a large difference in the technique of returning the front-court serve and had a small difference in the technique of returning the back-court serve. Tai Tzu Ying used push and spinning net shots frequently to return the front-court serve, with usage rates of 45.25 and 33.4%, and mainly used smash to return the back-court serve, with a usage rate of 49.9%, supplemented by clear and lift shot, with usage rates of 28.4% and 21.7%. Player A used net and lift shots to return the front-court serve, with usage rates of 41.4% and 39.4%. The usage rate of push shot of player A was significantly lower than Tai Tzu Ying, and her usage rate of lift shot was significantly higher

than Tai Tzu Ying. The similarity between Tai Tzu Ying and player A was that the usage rate of rush shots was the lowest. In the aspects of returning the back-court serve, player A mainly used the smash and clear techniques, with usage rates of 50.2% and 27.5%, and used the drop shot with the lowest probability, 22.3%.

TABLE II. COMPARISON OF TECHNICAL CHARACTERISTICS OF RECEIVING SERVE

		Tai Tzu Ying		Player A	
		Number of uses	Usage rate	Number of uses	Usage rate
Return of the front-court serve	Push shot	142	45.2%	11	4.4%
	Spinning net shot	105	33.4%	103	41.4%
	Crosscourt shot	47	15.0%	32	12.9%
	Lift shot	13	4.1%	98	39.4%
	Rush shot	7	2.2%	5	2.0%
Return of the back-court serve	Smash	234	49.9%	221	50.2%
	Clear	133	28.4%	121	27.5%
	Drop shot	102	21.7%	98	22.3%



Fig. 4. Comparison of usage Rate between Serve Receive Techniques.

The video analysis found that Tai Tzu Ying changed the route frequently and was offensive when receiving the service, with the main purpose of consuming the opponent’s physical strength. Techniques such as push and spinning net shots are good for limiting the opponent’s attack. Smash is featured by fast attack, tricky landing point, and difficult return. Clear can suppress the opponent at the baseline, which is good for her to seize the initiative. The comparison of the technical characteristics of receiving the serve demonstrated that the player could create good conditions for the subsequent attack by taking the initiative through smash and high shots.

B. Analysis of Technical Characteristics of the Front-court Shot

With the advancement of badminton technology, the net technique has also received more and more attention. Although it is relatively difficult to score through net shots, players can create more opportunities to score through the control of the front court. The comparison of the technical characteristics of the front-court shot is shown in Table III and Fig. 5.

TABLE III. COMPARISON OF TECHNICAL CHARACTERISTICS OF THE FRONT-COURT SHOT

Used technology	Tai Tzu Ying		Player A	
	Number of uses	Usage rate	Number of uses	Usage rate
Lift shot	507	31.7%	464	28.5%
Spinning net shot	453	28.4%	327	20.1%
Push shot	267	16.7%	202	12.4%
Cross-court shot	211	13.2%	315	19.3%
Rush shot	157	9.8%	321	19.7%

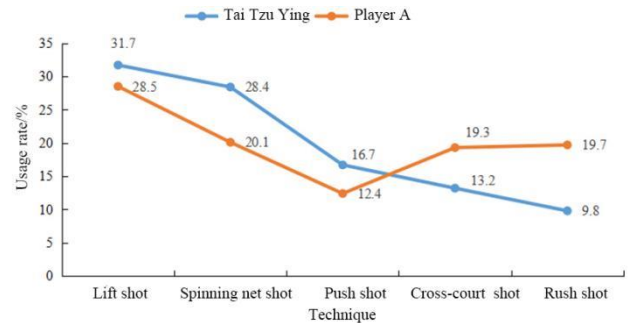


Fig. 5. Comparison of usage Rate between Front-court Shots.

It was seen from Table III and Fig. 5 that Tai Tzu Ying used lift shots most frequently in the front court, with a usage rate of 31.7%, followed by spinning net shots (28.4%). Player A also had a high usage rate of lift shots, but at the same time, the usage rates of other techniques were even, among which the usage rates of cross-court and rush shots were higher than Tai Tzu Ying. The usage rate of cross-court shots of player A was 19.3%, 6.1% higher than Tai Tzu Ying; her usage rate of rush shots was 19.7%, 9.9% higher than Tai Tzu Ying.

Lift shots can mobilize the opponent by opening the distance and running, and spinning net shots can dominate the attack. Tai Tzu Ying forced the opponent to lift the shuttle through net control to increase the chance of attack. Player A opened the distance with the opponent by lift shots and other techniques and also got rid of the opponent’s net control by cross-court and rush shots. The comparison of the technical characteristics of the front-court shots suggested that athletes should strengthen the training of techniques such as lift and net shots and learn to use different techniques to return according to the hitting position, so as to effectively mobilize the opponent.

C. Analysis of Technical Characteristics of the Middle-court Shot

Compared with front-court and back-court shots, the middle-court technique is used relatively less frequently, usually to defend against the attack in passive situations; however, the middle-court technique is also important. Block in the middle court is mainly to return the opponent’s aggressive ball to the opponent’s net. Drive is aggressive and defensive. Lift shots are mainly used for defending. The number of times the technique was used by both players is

shown in Table IV. A comparison of the usage rate is shown in Fig. 6.

It was seen from Table IV and Fig. 6 that Tai Tzu Ying used the technique of block most frequently, 925 times (63.6%), followed by drive (20.2%) and lift (16.2%) when she was in the middle of the court. Player A used blocks most frequently, but the usage rate (58.6%) was 5% lower than Tai Tzu Ying, but its usage rate of lift shots (22.2%) was 6% higher than Tai Tzu Ying.

Both players mainly used the block technique in the middle court, accounting for more than half of all the techniques, but there were still some differences. Tai Tzu Ying was defensive in the middle court, avoiding the opponent's clear by blocks. She also frequently used blocks to get rid of the passive situation. Player A attacked through the combination of block and drive, hindering the opponent's return to gain the initiative. Through the analysis of the excellent player, it was seen that the training of the block technique should be paid attention to in the daily training to avoid being passive in the game.

D. Analysis of the Technical Characteristics of the Back-court Shot

The back court of badminton is the main scoring place. The main techniques used in the back court are clear, drop shot, and smash. Clear is slow and makes the ball hang in the air for a long time, which is helpful to get rid of the passive state and prepare for the next shot. A high shot can also control the opponent in the back court, which can be used to restrain players who are poor in attacking in the back court. Smash is fast and is an effective active scoring technique. A drop shot is a way to mobilize the opponent, which can disrupt the opponent's rhythm and then score on the follow-up smash. The comparison of the technical characteristics of the two players in the back court is shown in Table V and Fig. 7.

TABLE IV. COMPARISON OF THE NUMBER OF TIMES THE MIDDLE-COURT TECHNIQUE WAS USED

Used technology	Tai Tzu Ying	Player A
Block	925	876
Drive	294	286
Lift	235	332

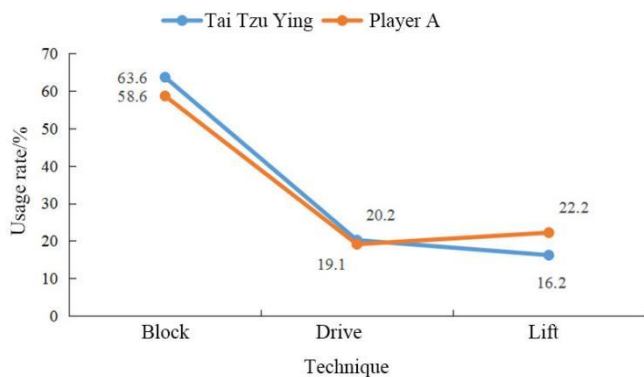


Fig. 6. Comparison of usages Rates of Middle-court Techniques.

TABLE V. COMPARISON OF TECHNICAL CHARACTERISTICS OF THE BACK-COURT SHOT

Used technology		Tai Tzu Ying		Player A	
		Number of uses	Usage rate	Number of uses	Usage rate
Clear	Offensive clear	633	22.78%	721	27.5%
	Defensive clear	253	9.10%	336	12.8%
Drop shot	Slice	698	25.12%	712	27.2%
	Drop spike	305	10.98%	318	12.1%
Smash	Cut smash	78	2.81%	52	2.0%
	Spot smash	231	8.31%	168	6.4%
	Heavy smash	581	20.91%	312	11.9%

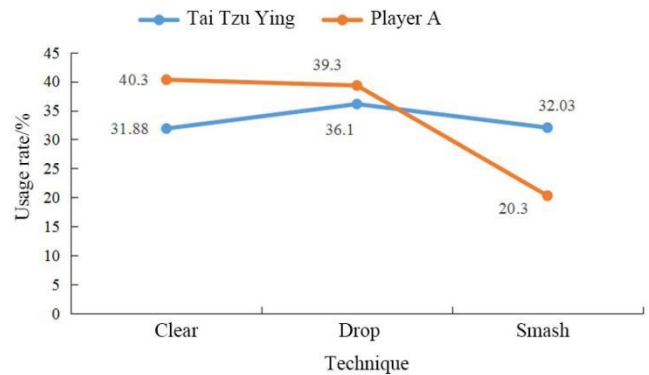


Fig. 7. Comparison of the usage Rate between High Shot, Drop Shot, and Smash.

It was seen from Table V and Fig. 7 that Tai Tzu Ying used the drop shot most frequently in the back court, followed by smash and clear, but the overall differences were not significant, about 30%, indicating that she used the back-court techniques with similar frequencies, while Player A was more likely to use clear and drop shots. The usage rate of clear of player A was 40.3%, close to two fifths; her usage rate of drop was 39.3%, also close to two fifths; her usage rate of smash was 20.3 %, 11.73% lower than Tai Tzu Ying. The difference of the usage rate of smash was the largest difference between Tai Tzu Ying and player A in the usage of back-court techniques.

Offensive clear is more aggressive than defensive clear. Tai Tzu Ying used offensive clear more frequently. Offensive clear is used to speed up the rhythm of the back court to find out the opponent's weakness. Defensive clear is usually used for passive defense. In the use of drop shots, the usage rate of the slice was higher. Tai Tzu Ying consumed the opponent's energy with a lot of slices to make him passively defend in most cases. In the use of smash, Tai Tzu Ying used heavy smash most frequently, which is the most aggressive, followed by spot smash. Overall, Tai Tzu Ying used an aggressive style in the back court. Compared to Tai Tzu Ying, Player A used techniques of drop shots and clears more frequently to mobilize

the opponent; her playing style was defensive and used the technique of smash less frequently. The comparison of the technical characteristics in the back court showed that smash, clear, and drop shots were important techniques, especially clear. To enhance the quality of smash, sports training should strengthen students' strength quality and physical stability.

V. DISCUSSION

With the development of science and technology, video analysis methods have also been well applied in the field of sports. Videos can be processed to find the technical characteristics of athletes to help improve the training efficiency of athletes [15]. Those methods have mature applications in various sports, such as basketball and soccer [16] and have excellent performance in athlete detection and classification, athlete or ball tracking and trajectory prediction, team strategy identification, and sports classification [17].

This paper compared the technical characteristics of two badminton players through the method of video analysis. In the current research on badminton and video analysis, Chen et al. [18] investigated badminton trajectories and stroke types and applied video analysis methods to real-time analysis of badminton matches. Liu et al. [19] designed an end-to-end system for racket motion analysis to improve performance in court identification, 2D trajectory estimation, and hitting recognition. Lin et al. [20] achieved tracking and trajectory prediction of moving objects after segmenting video images. Their method can predict badminton serve trajectories accurately. Ongvises et al. [21] recorded the drop shot in badminton with high-speed video and found that the impact velocity of the racket was proportional to the velocity of the badminton when it left the racket. Most of the comparisons of technical characteristics focus on the comparison between the world's best athletes to provide reference for the development of international competition and to improve the competitive level of the best athletes. There are few analyses between excellent athletes and ordinary athletes; therefore, this paper compared the technical characteristics of Tai Tzu Ying, a world excellent badminton player, with an ordinary college student. The results of the video analysis showed significant differences between the two players in the usage of front-, middle-, and back-court techniques. In general, compared to player A, Tai Tzu Ying has the following technical characteristics.

1) She has a stronger sense of active offense, will fully move the opponent's position, and is good at creating offensive opportunities to score.

2) She has a stronger sense of occupying the net in the front court and is more proactive in receiving and serving to wait for opportunities to attack.

3) She counterattacks in the midfield usually through her defensive skills to turn passive into proactive and realize the integration of attack and defense.

4) She used clear, drop, and smash shots in the back court to disrupt the opponent's judgment and take the initiative.

With the help of video analysis and data analysis, the research results of this paper intuitively show the differences in technical characteristics between the excellent athlete and ordinary athlete, which provides a good reference for better

understanding the advantages of excellent athletes and the shortcomings of ordinary athletes to guide athletes and narrow the gap between ordinary athletes and the world's best athletes. This work contributes to the improvement of the competitive level of badminton players.

VI. CONCLUSION

This paper compared and analyzed the technical characteristics of Tai Tzu Ying and a school badminton player through video analysis. It was found that there were some differences between the two players in the use of different techniques. In general, Tai Tzu Ying used lift shots and spinning net shots frequently in the front court, used block frequently in the middle court, and used drop and smash frequently in the back court, which was more flexible and aggressive. The comparison of the technical characteristics between the two players in this paper provides some suggestions for the training of school badminton players through analyzing the difference between excellent athletes and ordinary athletes in technical characteristics, so that they can learn the characteristics of the excellent athletes to improve their technical level. This paper also verified the reliability of video analysis technology in the sports field. In future research, this method can be applied to other sports to help athletes improve their technical ability more effectively. However, this paper also has some shortcomings. The research sample was relatively single, so the study of technical characteristics was relatively limited. In future research, more in-depth work is needed to further understand the differences between outstanding and ordinary athletes.

REFERENCES

- [1] M. Phomsoupha, and G. Laffaye, "The Science of Badminton: Game Characteristics, Anthropometry, Physiology, Visual Fitness and Biomechanics," *Sports Med.*, vol. 45, pp. 473-495, 2015.
- [2] M. Arora, S. H. Shetty, R. G. Khedekar, and S. Kale, "Over half of badminton players suffer from shoulder pain: Is impingement to blame?," *J. Arthrosc. Joint Surg.*, vol. 2, pp. 33-36, 2015.
- [3] R. Cendra, N. Gazali, and M. R. Dermawan, "The effectiveness of audio visual learning media towards badminton basic technical skills," *J. SPORTIF: J. Penelitian Pembelajaran*, vol. 5, pp. 55, 2019.
- [4] M. Zhang, "Application of data mining technology in badminton spot tactical analysis system," *Agro Food Ind. Hi Tech*, vol. 28, pp. 3398-3401, 2017.
- [5] K. Kishi, Y. Ushiyama, and M. Oba, "A fundamental study for incorporating game rules and developmental processes of techniques of tennis, table tennis, and badminton into beginner coaching:," *Jpn. J. Coach. Stud.*, vol. 31, pp. 67-80, 2017.
- [6] J. Park, Y. H. Lee, I. D. Kong, T. J. Park, J. S. Chang, T. Kim et al., "Ultrasonographic changes of upper extremity tendons in recreational badminton players: the effect of hand dominance and comparison with clinical findings," *Brit. J. Sport. Med.*, vol. 51, pp. 370.1-370, 2017.
- [7] C. H. Wang, C. L. Tsai, K. C. Tu, N. G. Muggleton, C. H. Juan, and W. K. Liang, "Modulation of brain oscillations during fundamental visuospatial processing: A comparison between female collegiate badminton players and sedentary controls," *Psychol. Sport Exerc.*, vol. 16, pp. 121-129, 2015.
- [8] A. M. Nadzalan, N. I. Mohamad, J. Low, and C. Chinnasee, "The Effects of Step Versus Jump Forward Lunge Exercise Training on Muscle Architecture among Recreational Badminton Players," *World Appl. Sci. J.*, vol. 35, pp. 1581-1587, 2017.
- [9] C. H. Cheng, R. W. Chen, L. Y. Chen, X. T. Liu, Y. T. Yin, Y. K. Chen et al., "Biomechanical analysis into the differences between the skilled and non-skilled badminton players performing the overhead stroke," *Physiotherapy*, vol. 101, pp. e233-e233, 2015.

- [10] T. Ozmen, and M. Aydogmus, "Effect of core strength training on dynamic balance and agility in adolescent badminton players - ScienceDirect," *J. Bodyw. Mov. Ther.*, vol. 20, pp. 565-570, 2016.
- [11] L. Ardiantoro, and N. Sunarmi, "Badminton player scouting analysis using Frequent Pattern growth (FP-growth) algorithm," *J. Phys. Conf. Ser.*, vol. 1456, pp. 1-6, 2020.
- [12] C. Zhou, and Y. Jie, "Analysis of Badminton Technical Movement Scoring Rate in International Competitions with the Help of Computer," *J. Phys. Conf. Ser.*, vol. 1992, pp. 022039 (5pp), 2021.
- [13] Q. Huang, and Y. Shi, "Analysis and research on training mode optimization of badminton players based on data mining technology," *Rev. Fac. Ing.*, vol. 32, pp. 294-300, 2017.
- [14] J. A. Pérez-Turpin, C. Elvira, D. Cabello, M. J. Gomis-Gomis, C. Suarez-Llorca, and E. Andreu-Cabrera, "Section III -Sports Training Notational Comparison Analysis of Outdoor Badminton Men's Single and Double Matches," *J. Hum. Kinet.*, vol. 71, pp. 267-273, 2020.
- [15] L. Chen, and W. Wang, "Analysis of technical features in basketball video based on deep learning algorithm," *Image Commun.*, vol. 83, 2020.
- [16] Q. Han, "Research on the Algorithm of Motion Track Recognition in Football Video," *J. Phys. Conf. Ser.*, vol. 1992, pp 1-5, 2021.
- [17] B. T. Naik, M. F. Hashmi, and N. D. Bokde, "A Comprehensive Review of Computer Vision in Sports: Open Issues, Future Trends and Research Directions," 2022.
- [18] B. Chen, and Z. Wang, "A statistical method for analysis of technical data of a badminton match based on 2-D seriate images," *Tsinghua Sci. Technol.*, vol. 12, pp. 594-601, 2007.
- [19] P. Liu, and J. H. Wang, "MonoTrack: Shuttle trajectory reconstruction from monocular badminton video," 2022 IEEE/CVF Conference on Computer Vision and Pattern Recognition Workshops (CVPRW), pp. 3512-3521, 2022.
- [20] Z. Lin, "A prediction method for the service trajectory of badminton moving video based on fuzzy clustering algorithm," *Int. J. Innov. Comput. Appl.*, vol. 12, pp. 216-223, 2021.
- [21] A. Ongvises, and X. Xu, "Shuttlecock Velocity of a Badminton Drop Shot," *Int. School Bangkok J. Sci.*, vol. 7, pp. 1-4, 2013.

Deep Architecture based on DenseNet-121 Model for Weather Image Recognition

Saleh A. Albelwi

Department of Computer Science, Faculty of Computing and Information Technology
Industrial Innovation and Robotics Center, University of Tabuk
Tabuk, Saudi Arabia

Abstract—Weather conditions have a significant effect on humans' daily lives and production, ranging from clothing choices to travel, outdoor sports, and solar energy systems. Recent advances in computer vision based on deep learning methods have shown notable progress in both scene awareness and image processing problems. These results have highlighted network depth as a critical factor, as deeper networks achieve better outcomes. This paper proposes a deep learning model based on DenseNet-121 to effectively recognize weather conditions from images. DenseNet performs significantly better than previous models; it also uses less processing power and memory to further increase its efficiency. Since this field currently lacks adequate labeled images for training in weather image recognition, transfer learning and data augmentation techniques were applied. Using the ImageNet dataset, these techniques fine-tuned pre-trained models to speed up training and achieve better end results. Because DenseNet-121 requires sufficient data and is architecturally complex, the expansion of data via geometric augmentation—such as rotation, translation, flipping, and scaling—was critical in decreasing overfitting and increasing the effectiveness of fine-tuning. These experiments were conducted on the RFS dataset, and the results demonstrate both the efficiency and advantages of the proposed method, which achieved an accuracy rate of 95.9%.

Keywords—Weather recognition; DenseNet-121; deep learning; data augmentation; transfer learning

I. INTRODUCTION

Weather conditions have a significant effect on humans' daily lives and production [1], ranging from clothing choices to travel, outdoor sports, and solar energy systems. The growth of the intelligent transportation field has further prompted the development of a system that can automatically detect weather conditions [2]. Previously, traditional weather classification systems relied on human observation, but these methods are prone to error and are also time consuming. Current weather recognition systems depend on hardware equipment such as sensors [3], but the number of sensors, as well as their upkeep, necessitates both installation and regular maintenance, which can be expensive. This is especially so considering the impact of the weather on the sensors themselves—as the sensors weather various conditions, their accuracy may decrease, which may lead them to report erroneous weather conditions [4].

Recent advances in computer vision have shown notable progress in both scene awareness and image processing problems. One such study utilized multiple techniques to classify, segment, and localize pixels within urban images [5].

Research such as this has led to advances in intelligent vision systems, which can accurately recognize weather conditions using colored images. Due to these advances, as well as the presence of security cameras, computer vision systems are well-suited for automatic weather detection. Machine learning-based methods such as support vector machine (SVM), random forest, k-NN, and neural networks have since been proposed for weather condition recognition. They extract features from images, including saturation, contrast, noise, etc. The drawback is that these systems utilize multifaceted feature engineering as well as manual extraction, both of which increase their complexity and decrease their generalizability [6, 7].

Deep learning models such as AlexNet [8], VGG [9], Inception [10], and ResNet [11] have recently obtained outstanding performances in numerous computer vision applications, including image recognition, object detection, and semantic segmentation [12]. Deep learning models can obtain detailed data from weather images, which makes them more beneficial than classical machine learning methods. This is because deep learning techniques such as convolutional neural networks (CNNs) and ResNet have the capability to extract rich, abstract, and semantic information. For weather recognition in particular, they obtain better information than other techniques. Deep learning is, therefore, a more advanced machine learning method, one that can solve complicated problems that often stump traditional methods [13].

To further improve performance, researchers have constructed deeper and deeper CNNs, as the additional layers improve optimization. For example, AlexNet (the winner of ILSVRC2012) consists of eight layers, including five convolutional layers and three fully connected layers, VGG19 consists of 16 convolutional layers and three fully connected layers. Inception (the winner of ILSVRC2014) is composed of 21 convolutional layers and a single fully connected layer. Though these additional layers improve optimization, they increasingly expose CNNs to the critical issue of vanishing gradients. Several approaches have been proposed to address this, such as ReLU activation [14], batch normalization [15], and powerful weight initialization [13]. A second problem also arose, in that not all deep CNNs could be easily optimized. This has been addressed through two methods: the first is highway networks [16], which allow 2D-CNNs to connect via a memory device, thus training highway networks through gradient descent. The second is ResNets (the winner of ILSVRC2015), which simplified the former technique using a skip connection device, allowing deeper layers to receive data. The latter is

more efficient than the former. DenseNet architecture further improved upon this by connecting all layers with the CNN, thereby improving data flow [17].

This paper proposes a system based on a DenseNet-121 deep learning model to classify weather conditions from images. DenseNet has achieved excellent performance, while also utilizing less memory and processing power than other state-of-the-art techniques. The proposed system can be utilized in the monitoring of traffic conditions, intelligent transit systems, and auxiliary driving features in automobiles, among others. The main advantage of DenseNet-121 is that it addresses vanishing gradients, which has multiple positive effects: one, it lessens the training burden of deep learning models; two, it allows for the reuse of features; and three, it lowers parameter use as compared to other popular deep learning models. The largest challenge in implementing this model was the lack of a labelled training dataset, and so two techniques were implemented: transfer learning and data augmentation. The former uses an ImageNet [18] dataset to pretrain the model, which decreases training time. The latter prevents overfitting, and also improves fine-tuning, by increasing the size of the training set based on image geometric transformations such as rotation, translation, flipping, and scaling. Overall, the proposed system is efficient, effective, and responsive, which allows it to make the best possible decisions even in poor weather conditions. The contributions of this paper are as follows:

- This paper presents a deep learning-based method using DenseNet-121 to effectively classify weather conditions from images in real time. The results have shown importance of model depth, as deeper models offer better results.
- To train the DenseNet-121 model, the proposed model needed large amounts of data. To circumvent the difficulty of obtaining additional weather images, this paper applied transfer learning and geometric image data augmentation techniques to reduce convergence time and increase performance.

The remainder of the paper is organized as follows: Section II provides the recent related works. Section III describes the model in detail. Section IV presents and discusses the experimental results. Finally, the conclusions and future works are presented in Section V.

II. RELATED WORKS

Early weather classification methods often extracted powerful features, a process that needed elaborate, hand-crafted features. Other methods utilized machine learning algorithms for classification, such as support vector machine (SVM), random forest, and K-NN. For example, Roser and Moosmann [6] proposed a method to define regions of interest. They employed a color histogram to extract the feature space, which was then passed into SVM to classify the weather images. The research in [19] concatenated the features extracted from a gradient amplitude histogram, the HSV color space, and road information. The extracted features were then fed into an AdaBoost algorithm to assign the image its weather label. Lagorio et al. [20] designed a statistical model based on a

mixture of Gaussians to identify weather conditions from images. This mixture can identify both spatial and temporal changes, which assists the model in identifying the weather input. The downside of this method is that it cannot capture all weather events; it can only be implemented in particular conditions. Shen and Tan [21] built a weather condition detector, which can identify, for example, cloudy versus sunny weather using light illumination. In general, the methods that utilized hand-crafted weather features did not recognize weather conditions accurately.

Recently, improvements in the fields of deep learning and CNNs have been applied to weather recognition tasks. New research has utilized deep learning algorithms for classifying weather from images. For instance, Xiao et al. [22] presented a MetaCNN for classifying weather phenomena. MetaCNN is a modified version of the VGG16 [9] model. In MetaCNN, the authors replaced the fully connected layers in VGG16 with a single, global, average pooling layer. The final output was a softmax that estimated the probability distribution for each weather class label. The authors introduced a new dataset called the weather phenomenon database (WEAPD) that consists of 6,877 images for 11 different weather classes. Other researchers, such as Huang and Chang [23], employed a self-organizing map (SOM) to automatically classify weather images based on six variables at five different weather stations in Taiwan. Xia et al. [24] modified ResNet-50 to ResNet-15 to classify weather images, where the convolutional layers extracted the weather features that would be fed into the softmax function for classification. Guerra et al. [4] proposed a framework to classify weather as rain, fog, or snow using super-pixel masks that enhanced the input image. Then, the features were extracted using a pre-trained CNN and passed into an SVM for classification. Zhao et al. [1] developed a CNN-RRN model for multi-class weather on a single image, where the CNN was exploited to extract features. Next, the channel-wise attention model chose the most discriminative features; the convolutional LSTM was then used to estimate the weather class label. These deep learning methods of weather recognition are generally superior to traditional methods, but the limitations are as follows: one, these methods utilize large datasets, and two, they require a high-end GPU for training, making them computationally expensive.

Due to the great performance of DenseNet architecture, it has been used in diverse areas, including disease diagnosis, in the detection of Alzheimer's disease using an MRI [25], COVID-19 from chest images [26], and plant diseases [27].

Depth is an important consideration in improving the findings of deep learning models. Because of this, the proposed model is based on DenseNet-121, which has dense connections and thereby increases accuracy. These connections are advantageous because they utilize feature reuse to remain compact; use feed-forward networks; lower the number of parameters needed; increase feature propagation; and encourage feature generation, all of which increase accuracy and speed.

III. PROPOSED MODEL

The workflow of the proposed system is shown in Fig. 1. First, the pretrained DenseNet-121 model was loaded. This

model was trained on ImageNet for weight initialization. The last layer was removed and replaced with a softmax with three neurons, where each neuron predicts the weather condition class (rain, fog, or snow). Then the model was re-trained and fine-tuned with the RFS dataset. In the testing phase, this trained model was efficiently used to estimate weather conditions.

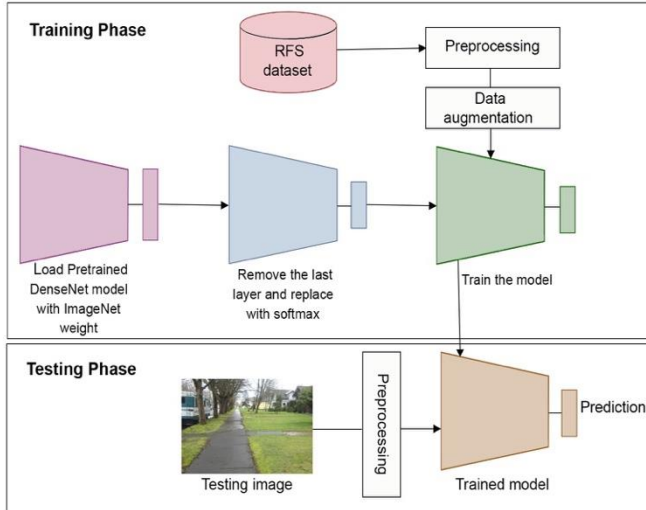


Fig. 1. The Workflow of the Proposed System.

A. Model Architecture

This paper utilized a Dense Convolutional Network (DenseNet) [28] comprised of 121 layers to classify weather images. DenseNet is a special kind of CNN that was originally proposed by Huang et al. It achieved state-of-the-art results on several image classification datasets, such as Cifar-10 and SVHN. In a DenseNet architecture, layers are connected with dense blocks, meaning that each layer utilizes inputs from all previous layers in order to create a feature map that will send data to all of the following layers. Therefore, the l^{th} -layer receives all previous features maps $(x_0, x_1, \dots, x_{l-1})$ as inputs:

$$x_l = H_l([x_0, x_1, \dots, x_{l-1}]) \quad (1)$$

Here, $[x_0, x_1, \dots, x_{l-1}]$ represents the concatenation of all previous feature maps of l^{th} - layer. x_l is the output of the l^{th} layer, and H_l represents l^{th} layer, which is a composition function consisting of three successive operations including batch normalization, a ReLU activation function, and convolution. DenseNet is similar to methods such as ResNet, but the latter combines previous layers with future layers while DenseNet concatenates layers instead. DenseNet approaches the problem of vanishing gradients by reusing features which also reduces the number of parameters. As shown in Fig. 2, DenseNet-121 utilizes four dense blocks. Between each block is a transition layer that utilizes down-sampling on the feature maps to create a 1×1 convolution as well as a 2×2 average pooling layer. The dense blocks comprise multiple convolutional layers, which are connected in series and serve as cross-layer connections between distant layers. To increase non-linearity, DenseNet-121 utilizes a ReLU activation

function to increase non-linearity. The proposed ReLU activation is defined as follows:

$$ReLU(x) = \max(0, x) \quad (2)$$

The last layer is a fully connected layer with a softmax function that predicts the probability of a weather image class.

The softmax is defined by the following equation:

$$sm(z)_i = \frac{e^{z_i}}{\sum_{j=1}^C e^{z_j}} \text{ for } i = 1, \dots, C \quad (3)$$

Here, $z = (z_1, \dots, z_C) \in \mathbb{R}^C$. z is the input vector, and the exponential is implemented for each value z_i . Note that the sum of output vector $sm(z)$ is equal to 1. A summary of the DenseNet-121 model layers is presented in Table I.

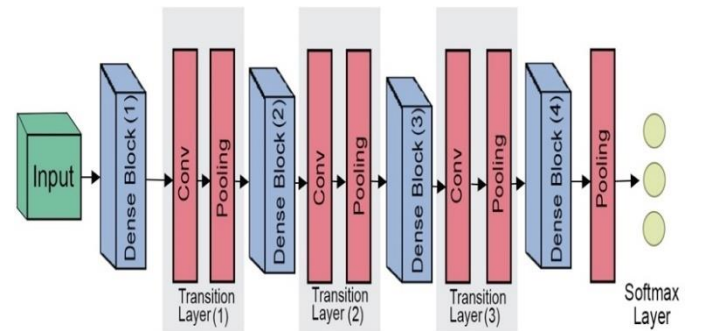


Fig. 2. The DenseNet-121 Architecture, which Consists of Four Dense Block Layers and Three Transition Layers.

TABLE I. LAYERS DETAILS OF DENSENET-121. THE DENSENET-121 HAS 6, 12, 24, 16 LAYERS IN FOUR DENSE BLOCKS

Layers	Output size	DenseNet-121
Convolution	112×112	7×7 conv, stride 2
Pooling	56×56	3×3 max pool, stride 2
Dense Block (1)	56×56	$\begin{bmatrix} 1 \times 1 \text{ conv} \\ 3 \times 3 \text{ conv} \end{bmatrix} \times 6$
Transition layer (1)	56×56	$1 \times 1 \text{ conv}$
	28×28	2×2 average pool, stride 2
Dense Block (2)	28×28	$\begin{bmatrix} 1 \times 1 \text{ conv} \\ 3 \times 3 \text{ conv} \end{bmatrix} \times 12$
Transition layer (2)	28×28	$1 \times 1 \text{ conv}$
	14×14	2×2 average pool, stride 2
Dense Block (3)	14×14	$\begin{bmatrix} 1 \times 1 \text{ conv} \\ 3 \times 3 \text{ conv} \end{bmatrix} \times 24$
Transition layer (3)	14×14	$1 \times 1 \text{ conv}$
	7×7	2×2 average pool, stride 2
Dense Block (4)	7×7	$\begin{bmatrix} 1 \times 1 \text{ conv} \\ 3 \times 3 \text{ conv} \end{bmatrix} \times 16$
Classification layer	1×1	7×7 global average pool
		Softmax layer

B. Transfer Learning

The deep DenseNet-121 model requires a large training set to increase its accuracy rate, but collecting labelled weather images is difficult. Transfer learning (TL) has been proposed as a common technique to address this limitation. The TL strategy pre-trains a model on a large, labelled dataset and then transfers the gained knowledge (learned weights) to other related tasks within the same architecture design. It treats the model as a starting point in the target task's training, which avoids the process of training the model from scratch with random weight initializations. Once TL is complete, the last layer must be altered to the number of required classes and then fine-tuned on the target dataset of interest. Recent research has demonstrated that TL improves performance rates compared to training a model from scratch on a small dataset. In addition, TL enhances generalization, reduces both overfitting training time, and decreases the labeled data required. Recently, TL has been applied widely in computer vision and natural language processing applications [29].

This research used a DenseNet-121 model pre-trained on the ImageNet dataset, which is composed of 1.2 million colored images in 1000 categories; therefore, the initialization of DenseNet-121 weights came from the pre-trained model. The output layer was removed and replaced with another layer containing three neurons, each matching up to a weather class label. A softmax function was applied in the final layer of the proposed model to predict the probability of each class as the output. Finally, the model was trained and fine-tuned across all layers on the RDF weather dataset.

C. Image Data Augmentation

Another way to deal with a limited training set is image data augmentation. This technique alters the images in the existing training set. This leads to an increase in the number of examples, and therefore the diversity, in the training set. Another advantage to data augmentation is the reduction of overfitting. Data augmentation can be divided into two main classes: geometric and color transformations. Geometric augmentation affects only the location of the pixels (e.g., flipping, shifting, cropping, and resizing) as illustrated in Fig. 3. In contrast, color augmentation modifies the values of the image pixels (e.g., blurring and color distortion). Since the color of weather images plays a critical role in recognizing the weather, this paper only applied geometric augmentation to increase the training set while keeping the image pixel values. The geometric augmentation was performed as follows:

- Rotation was performed by rotating the image between 0 and 360 degrees randomly. This research rotated the images randomly in range from 0 to 45.
- Flipping flipped the image across the x and/or y axis.
- Translation moved the image horizontally or vertically (or both). Width translation and height translation were ranges (as a fraction of the total width or height) within which images were randomly translated vertically or horizontally.
- Cropping removed part of the image.
- Scaling increased or decreased the size of the image.



Fig. 3. Different Methods of Data Augmentation Including Rotation, Flipping, Translation, and Cropping and Resizing.

IV. EXPERIMENTAL RESULTS AND DISCUSSION

A. Dataset

In this work, we used the Rain Fog Snow (RFS) weather dataset. This is an open source dataset that was proposed by [2] to support computer vision and deep learning applications in classifying weather via images. The images are collected from different locations with different environmental settings. Each class contains 1100 images. Fig. 4 shows a sample of the RFS dataset for each weather class. This dataset is particularly effective for this research because it contains quality images, various environments, and targeted labels. All images were resized to $224 \times 224 \times 3$ for suitable input into our DenseNet-121 model. We randomly selected 800 images for training and 300 for testing for each class.

B. Pre-processing

Image pre-processing is significant in deep learning models. Min-max normalization is one of the common techniques used to rescale and transform original image pixels into an appropriate size, typically a range between 0 and 1. This removes biases by eliminating differences in magnitude. As a result, this normalization accelerates training and enhances the model's performance. In this paper, we normalized the image pixels in a range from 0 to 1 using the following equation:

$$x' = \frac{x - \min(x)}{\max(x) - \min(x)} \quad (4)$$

where x is the original pixel value, x' is the new value, and $\min(x)$ and $\max(x)$ represent the minimum and maximum pixel values of the image, respectively.

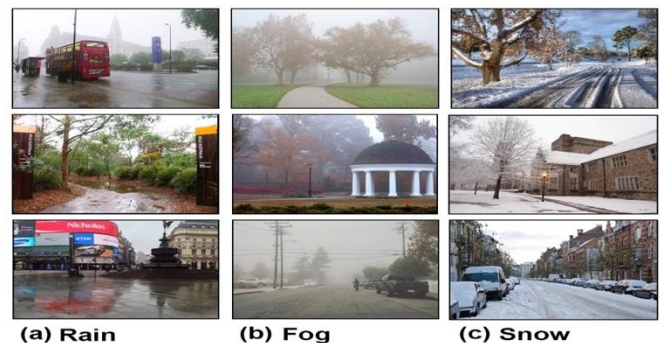


Fig. 4. A Sample of RFS Dataset for each Class. Each Column Represents One Class.

C. Training Setting and Model Implementation

The proposed system was implemented in Python. DenseNet-121, and other deep learning models, were developed using the PyTorch framework. The experiments were then performed using Google Colab Pro to access a faster GPU. Adam [29] optimizer was also used to optimize the weights and biases of the DenseNet-121 with a learning rate of 0.001 and a momentum set to 0.9. The batch size was set to 64 and the number of epochs to 100. The formula for updating weights based on Adam optimizer is defined as follows:

$$\theta_{t+1} = \theta_t + \Delta\theta_t \quad (5)$$

where

$$v_t = \beta_1 * v_{t-1} - (1 - \beta_1) * g_t \quad (6)$$

$$s_t = \beta_2 * s_{t-1} - (1 - \beta_2) * g_t^2 \quad (7)$$

$$\Delta\theta_t = -\lambda \frac{v_t}{\sqrt{s_t + \epsilon}} * g_t \quad (8)$$

Here, λ indicates the initial learning rate, g_t is the gradient with respect to θ_t at time t . v_t represents the first moment estimate, s_t is the second moment, and β_1 and β_2 are hyperparameters. The values of β_1 and β_2 are set to 0.9 and 0.99, respectively. To minimize the loss function, the proposed model utilized a backpropagation algorithm. This research employed categorical cross-entropy as the loss function, defined as follows:

$$\mathcal{L}(\theta) = -\frac{1}{n} \sum_{i=1}^n \sum_{j=1}^C y_{i,j} \log(\hat{y}_{i,j}) \quad (9)$$

where y is the correct output, \hat{y} is the predicted output, n represents the number of training samples, and C is the number of classes ($C = 3$). L_2 regularization was implemented to alleviate overfitting with a weight decay value of 10^{-4} . Data augmentation was implemented using Transforms from the Torchvision library. It contains multiple transforms, which allowed for different types of augmentation on the images. The proposed model was initialized with weights that were pre-trained on ImageNet dataset. Doing this allowed this research to leverage the pretrained model. Then, the model was customized to weather recognition by training and finetuning it on the weather dataset.

D. Results and Discussion

To gauge the efficacy of the proposed system for labelling weather conditions from images using DenseNet-121, the proposed system was compared to deep learning models that obtained state-of-the-art results in a variety of computer vision tasks. These models include AlexNet [8], VGG16 [9], Inception [10], and ResNet-18 [11]. To evaluate the performance of the model, this research used accuracy to measure performance. The accuracy of the testing set was computed as follows:

$$Acc = \frac{\text{Number of correct predictions}}{\text{Total number of testing examples}} \quad (10)$$

To compute this, the proposed DenseNet-121 model was trained on the FRS training set. Once this was completed, this research tested the proposed model and received, as an output, the classification results, which were one of three weather conditions: fog, rain, or snow. The accuracy of this model's

recognition was then tested on over 900 test images. The results are shown in Table II and Fig. 5. The proposed model obtained the best average accuracy 1, with a rate of 95.6%, followed by ResNet-18, AlexNet, VGG16, and Inception, respectively. DenseNet-121 had an accuracy at least 2% higher than the other deep learning models.

The results also show the accuracy of each category for each deep learning model. Among them, the proposed model achieved an accuracy rate on foggy images of 97.55%, 93.55% on rainy images, and 96.98% on snowy images. This means that the proposed DenseNet-121 model achieved superior results on classifying weather conditions from all three image types.

This research also studied the effect of TL for training a model versus training one from scratch with random weights. To do this, this paper evaluated the performance of the proposed DenseNet-121, trained with initial weights set to the pre-trained model from ImageNet dataset, as compared to a second DenseNet-121 model that was trained from scratch with random weights at initialization. Table III displays the results. By utilizing weight initialization, the pre-trained model achieved an accuracy of 95.9% as compared to 91.3% for the model trained from scratch. Performing TL allows the necessary features to be extracted from ImageNet; by doing this, the data is used more efficiently and thereby the proposed model is trained to identify weather conditions more easily. A DenseNet-121 model with random weight initialization obtained accuracy rate of about 59% after the first iteration (see Fig. 6 (a)), while DenseNet-121 based on transfer learning obtained an accuracy rate of 85% after the first iteration. As shown in Fig. 6, the proposed TL model converged in fewer iterations than the model that started with random weights, in respect to loss and accuracy rate. This decreased the computation time.

TABLE II. ACCURACY COMPARISONS OF THE PROPOSED METHOD WITH DIFFERENT DEEP LEARNING MODELS

Model	Foggy (%)	Rainy (%)	Snowy (%)	Avg. Accuracy (%)
VGG16 [9]	93.81	93.54	92.56	93.2
Inception [10]	88.89	89.00	93.40	90.3
AlexNet [8]	92.43	92.64	95.53	93.5
ResNet-18 [11]	92.47	90.79	94.30	93.7
DenseNet-121 (proposed model)	97.55	93.55	96.98	95.9

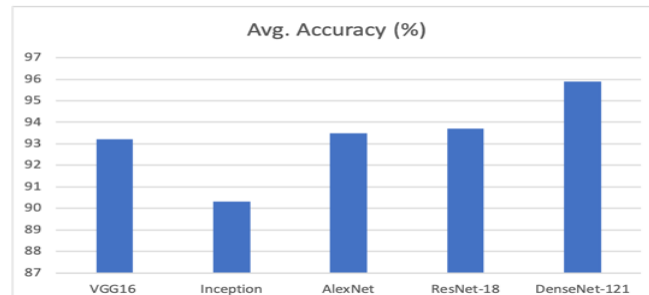


Fig. 5. Comparison of Average Accuracy for different Models.

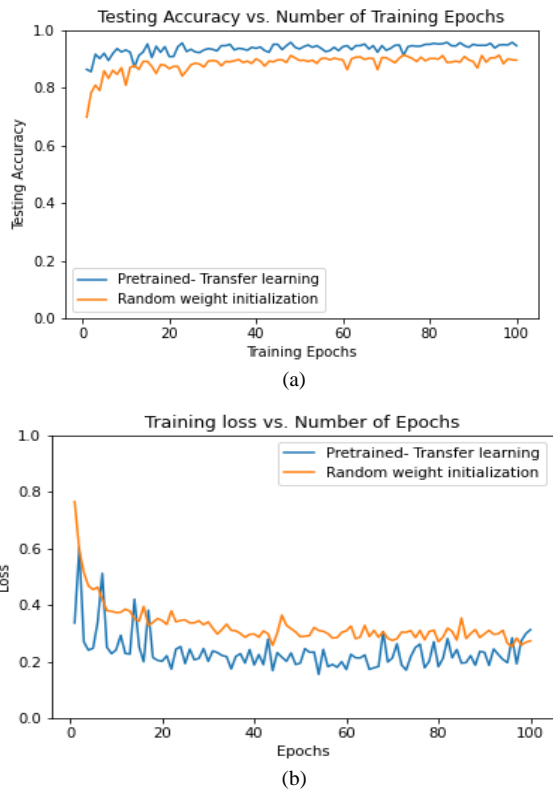


Fig. 6. (a) The Testing Accuracy Achieved from the DenseNet-121 Models Trained from Scratch and with TL. (b) The Loss Values Obtained for the DenseNet-121 Models Trained from Scratch and TL.

TABLE III. COMPARISON OF ACCURACY RATE OF DENSENET-121 BASED ON WEIGHT INITIALIZATION APPROACH

Weight Initialization Approach	Accuracy (%)
Random weight initialization	91.3
Pretained from ImageNet	95.7

Deep learning models require massive amounts of training to achieve high accuracy. The training examples are augmented by rotation, flipping, and shifting, and the accuracy has been, therefore, improved. In addition, pre-training DenseNet-121 with a large dataset such as ImageNet further improved the performance, and the model learned faster than the one trained from scratch. Data augmentation plays a significant role in reducing overfitting in particular when the training set is small.

These results suggest that the performance of the proposed model outperformed previous research and state-of-the-art techniques. Continued hardware and software advances will enable researcher to build deeper neural networks, which have higher representation power than shallower ones. These results demonstrated the importance of network depth, as networks with more layers achieved better outcomes. One of DenseNet's advantages is its increased flow of information and gradients, which improves training time. Each layer can access both the loss function and the original input, creating a deep supervision that trains deep architectures. In addition, feature propagation allows for the repetition, and efficient use, of features. It also reduces the parameters needed and, therefore, reduces the calculations needed, all of which is an advantage because

DenseNet layers are narrow. They may have only 12 filters per layer, and may add only a small set of feature maps to the network's collective knowledge; it is the final classifier that uses all the feature maps to make a decision. This paper's results and analysis show that the proposed model classifies weather conditions accurately by utilizing DenseNet features effectively. Furthermore, the proposed model also works well in real-time environments, which is another advantage.

V. CONCLUSIONS AND FUTURE WORKS

Weather conditions have a significant impact on daily activities. Deep learning models have shown promising results in numerous computer vision and image analysis tasks. Recent research has demonstrated that CNNs can be deeper, and also more accurate and efficient, if there are shorter connections between the inputs and outputs. To test these hypotheses, this paper employed DenseNet-121 to recognize weather conditions from images. The results demonstrated that the proposed system, based on a DenseNet-121 model with transfer learning and data augmentation, maximized the accuracy rate with a small number of training examples. This paper also implemented and evaluated popular deep learning methods for recognizing weather conditions from images.

Future works will focus on simplifying the DenseNet-121 architecture to fit with edge devices while keeping the same performance. In addition, future research should apply self-supervised learning to utilize an unlabelled training set in pre-training, so that the proposed model can learn discriminative features.

REFERENCES

- [1] B. Zhao, X. Li, X. Lu, and Z. Wang, "A CNN-RNN architecture for multi-label weather recognition," *Neurocomputing*, vol. 322, pp. 47-57, 2018.
- [2] K. D. M.-M. McDonald-Maier, J. C. V. G. Guerra, Z. K. Khanam, S. E. Ehsan, and R. S. Stolkin, "Weather Classification: A new multi-class dataset, data augmentation approach and comprehensive evaluations of Convolutional Neural Networks," 2018.
- [3] X. Li, Z. Wang, and X. Lu, "A multi-task framework for weather recognition," in *Proceedings of the 25th ACM international conference on Multimedia*, 2017, pp. 1318-1326.
- [4] J. C. V. Guerra, Z. Khanam, S. Ehsan, R. Stolkin, and K. McDonald-Maier, "Weather Classification: A new multi-class dataset, data augmentation approach and comprehensive evaluations of Convolutional Neural Networks," in *2018 NASA/ESA Conference on Adaptive Hardware and Systems (AHS)*, 2018: IEEE, pp. 305-310.
- [5] M. R. Ibrahim, J. Haworth, and T. Cheng, "WeatherNet: Recognising weather and visual conditions from street-level images using deep residual learning," *ISPRS International Journal of Geo-Information*, vol. 8, no. 12, p. 549, 2019.
- [6] M. Roser and F. Moosmann, "Classification of weather situations on single color images," in *2008 IEEE intelligent vehicles symposium*, 2008: IEEE, pp. 798-803.
- [7] W.-T. Chu, X.-Y. Zheng, and D.-S. Ding, "Camera as weather sensor: Estimating weather information from single images," *Journal of Visual Communication and Image Representation*, vol. 46, pp. 233-249, 2017.
- [8] A. Krizhevsky, I. Sutskever, and G. E. Hinton, "Imagenet classification with deep convolutional neural networks," *Advances in neural information processing systems*, vol. 25, pp. 1097-1105, 2012.
- [9] K. Simonyan and A. Zisserman, "Very deep convolutional networks for large-scale image recognition," *arXiv preprint arXiv:1409.1556*, 2014.
- [10] C. Szegedy et al., "Going deeper with convolutions," in *Proceedings of the IEEE conference on computer vision and pattern recognition*, 2015, pp. 1-9.

- [11] K. He, X. Zhang, S. Ren, and J. Sun, "Deep residual learning for image recognition," in Proceedings of the IEEE conference on computer vision and pattern recognition, 2016, pp. 770-778.
- [12] S. Albelwi, "Survey on Self-Supervised Learning: Auxiliary Pretext Tasks and Contrastive Learning Methods in Imaging," *Entropy*, vol. 24, no. 4, p. 551, 2022.
- [13] K. Zhang, M. Sun, T. X. Han, X. Yuan, L. Guo, and T. Liu, "Residual networks of residual networks: Multilevel residual networks," *IEEE Transactions on Circuits and Systems for Video Technology*, vol. 28, no. 6, pp. 1303-1314, 2017.
- [14] V. Nair and G. E. Hinton, "Rectified linear units improve restricted boltzmann machines," in *Icml*, 2010.
- [15] S. Ioffe and C. Szegedy, "Batch normalization: Accelerating deep network training by reducing internal covariate shift," in International conference on machine learning, 2015: PMLR, pp. 448-456.
- [16] R. K. Srivastava, K. Greff, and J. Schmidhuber, "Highway networks," arXiv preprint arXiv:1505.00387, 2015.
- [17] R. Xian, "Synchronization of Stochastic Memristive Neural Networks with Retarded and Advanced Argument," *Journal of Intelligent Learning Systems and Applications*, vol. 13, no. 1, pp. 1-14, 2021.
- [18] J. Deng, W. Dong, R. Socher, L.-J. Li, K. Li, and L. Fei-Fei, "Imagenet: A large-scale hierarchical image database," in 2009 IEEE conference on computer vision and pattern recognition, 2009: Ieee, pp. 248-255.
- [19] X. Yan, Y. Luo, and X. Zheng, "Weather recognition based on images captured by vision system in vehicle," in International Symposium on Neural Networks, 2009: Springer, pp. 390-398.
- [20] A. Lagorio, E. Grosso, and M. Tistarelli, "Automatic detection of adverse weather conditions in traffic scenes," in 2008 IEEE Fifth International Conference on Advanced Video and Signal Based Surveillance, 2008: IEEE, pp. 273-279.
- [21] L. Shen and P. Tan, "Photometric stereo and weather estimation using internet images," in 2009 IEEE Conference on Computer Vision and Pattern Recognition, 2009: IEEE, pp. 1850-1857.
- [22] H. Xiao, F. Zhang, Z. Shen, K. Wu, and J. Zhang, "Classification of weather phenomenon from images by using deep convolutional neural network," *Earth and Space Science*, vol. 8, no. 5, p. e2020EA001604, 2021.
- [23] A. Huang and F.-J. Chang, "Using a Self-Organizing Map to Explore Local Weather Features for Smart Urban Agriculture in Northern Taiwan," *Water*, vol. 13, no. 23, p. 3457, 2021.
- [24] J. Xia, D. Xuan, L. Tan, and L. Xing, "ResNet15: Weather Recognition on Traffic Road with Deep Convolutional Neural Network," *Advances in Meteorology*, vol. 2020, 2020.
- [25] B. Solano-Rojas, R. Villalón-Fonseca, and G. Marín-Raventós, "Alzheimer's disease early detection using a low cost three-dimensional densenet-121 architecture," in International conference on smart homes and health telematics, 2020: Springer, pp. 3-15.
- [26] L. Sarker, M. M. Islam, T. Hannan, and Z. Ahmed, "COVID-DenseNet: a deep learning architecture to detect COVID-19 from chest radiology images," Preprint, vol. 2020050151, 2020.
- [27] S. Nandhini and K. Ashokkumar, "An automatic plant leaf disease identification using DenseNet-121 architecture with a mutation-based henry gas solubility optimization algorithm," *Neural Computing and Applications*, vol. 34, no. 7, pp. 5513-5534, 2022.
- [28] G. Huang, Z. Liu, L. Van Der Maaten, and K. Q. Weinberger, "Densely connected convolutional networks," in Proceedings of the IEEE conference on computer vision and pattern recognition, 2017, pp. 4700-4708.
- [29] D. P. Kingma and J. Ba, "Adam: A method for stochastic optimization," arXiv preprint arXiv:1412.6980, 2014.

Research on Improved Shallow Neural Network Big Data Processing Model based on Gaussian Function

Lifang Fu

Faculty of Science

Henan University of Animal Husbandry and Economy
Zhengzhou, 450044, China

Abstract—The application of the current new generation communication technology is gradually diversified, and the global Internet users are increasing, leading some large enterprises to increasingly rely on faster and more efficient big data processing technology. In order to solve the shortcomings of the current big data processing algorithms, such as slow computing speed, computing accuracy to be improved, and poor online real-time learning ability, this research combines incremental learning and sliding window ideas to design two improved radial basis function (RBF) neural network algorithms with Gaussian function as the kernel function. The Duffing equation example and the data of "Top 100 single products for Taobao search glasses sales" were used to verify the performance of the design algorithm. The experimental results of Duffing equation example show that when the total sample is 100000, the mean square errors of IOL, SWOL, SVM and ResNet50 algorithms are 1.86e-07, 1.59e-07, 3.37e-07 and 2.67e-07 respectively. The experimental results of the data set of "Top 100 SKUs for Taobao Search Glasses Sales" show that when the number of samples in the test set is 800, the root mean square errors of IOL, SWOL, SVM and ResNet50 algorithms are 0.0060, 0.0056, 0.0069 and 0.0073 respectively. This shows that the RBF online learning algorithm designed in this study, which integrates sliding windows, has a stronger comprehensive ability to process big data, and has certain application value for improving the accuracy of online data based commodity recommendation in e-commerce and other industries.

Keywords—Gaussian function; RBF; big data processing; incremental learning; sliding window

I. INTRODUCTION

With the popularization of cloud computing, the Internet of Things and other technologies, a large number of industries began to explosively appear massive data, and the types of data also increased significantly, which began to show more and more characteristics of big data [1]. However, although the large data set has a large amount of data and low value density, it is still of great analysis and calculation value to discuss it as a whole, and some key information that is conducive to improving the business competitiveness of enterprises or the level of government services can be mined from the huge data [2-3]. However, it puts forward higher requirements for the processing speed and precision of the algorithm. At the same time, under the big data environment, there is another kind of more application demand, that is, the analysis model is updated regularly and in real time according to the updated data, so that the algorithm can meet the requirements of real-time update with the input data [4]. Traditional offline algorithms can not meet the needs of big data application scenarios for data mining,

and the processing accuracy and speed of mainstream online learning algorithms used in the market are still poor. Therefore, it is necessary to design data analysis algorithms that more closely match big data application scenarios, which is also the main motivation for this study. The expected result is that the improved neural network algorithm designed in this research can improve the efficiency and accuracy of big data processing.

II. RELATED WORKS

Experts in the fields of Internet of Things, e-commerce, communication and information have carried out a large number of researches involving various aspects for the rapid analysis and mining of big data. Valerio et al. found that processing online social big data fused with multimedia data sources is highly complex, so the research team evaluated two current state-of-the-art big data processing architectures, namely Lambda and Kappa, the discussion results show that for the investigated problem, Lambda outperforms the Kappa architecture [5]. The Habeeb research team believes that network anomaly detection is the key to Internet security. However, the survey results show that the existing methods for detecting network anomalies are not effective enough. The reason is that the devices connected to the network accumulate a large amount of data, which greatly increases the difficulty of algorithm detection. Therefore, the author first explains the current main methods of real-time big data processing, anomaly detection machine learning algorithms, and then reviews big data processing techniques. Finally, the research challenges of real-time big data processing in anomaly detection are discussed [6]. Zhang et al. proposed a near-computation-enhanced big data processing architecture that can better handle big data and its corresponding applications. The structure consists of near-edge computing and far-edge computing units. Simulation and experimental results show that the task assignment and architecture proposed by the author have certain effectiveness [7]. Lwin designed an extended program toolkit that can assist GIS to process meteorological and geographic big data in view of the weak ability of processing big data in current geographic information systems. The test results show that the toolkit can effectively improve geographic the speed and precision with which information systems process big data [8]. Cigna F et al. found that with the increase of satellite tasks and the increase of task complexity, the big data processing method of communication system is more and more difficult to meet the needs of use, so they designed an improved satellite big data combining deep learning algorithm and online learning idea. The simulation experiment results

show that the model can shorten the time-consuming system processing satellite big data and improve the processing accuracy [9]. Muhammad et al. found that as the amount of data collected during manufacturing increases, monitoring systems are becoming an important factor in management decisions. Therefore, the researchers propose a real-time monitoring system that combines IoT sensors, big data processing, and hybrid predictive models. The results show that IoT-based sensors and the proposed big data processing system are sufficient to effectively monitor the manufacturing process. Furthermore, the proposed hybrid prediction model has better fault prediction accuracy than other models when sensor data is input [10]. Wang et al. believe that with the increasing global requirements for public safety governance, various surveillance sensors installed and used provide a large amount of data for public safety decision makers and managers, and traditional data mining algorithms cannot well summarize these large data. The data value contained in the data, so the author designed a big data mining algorithm that mixes simulated annealing algorithm and RBF neural network. The experimental results show that the algorithm compared with the neural network and machine learning algorithm can better mine the abstract high-dimensional features in the data, and improve the accuracy of the analysis results [11].

To sum up, experts designed a variety of improved algorithms or improved hardware systems to solve the problem of low efficiency of big data processing in communication, industrial production and other fields, and achieved various research results. However, most of the algorithms they designed are complex, difficult to train and time-consuming, and few of them can realize the function of real-time algorithm updating based on new samples. Most importantly, the solutions proposed in these studies are often only for a certain sub field of big data processing, with poor universality. In view of these shortcomings, this research attempts to use a relatively simple RBF neural network to build a processing algorithm for various types of big data in e-commerce, Internet of Things and other industries that can realize online learning.

III. DESIGN OF IMPROVED RBF BIG DATA PROCESSING ALGORITHM BASED ON GAUSSIAN FUNCTION

A. Construction of RBF Algorithm Integrating Gaussian Function and Incremental Learning

After the training data scale increases significantly, the algorithm training time will also increase. If the training time does not change significantly, the computer needs to have stronger computing power [12-13]. In addition, if there are sample types that do not exist before in the increased samples, the algorithm trained to a certain extent cannot adapt to this change well. According to the traditional solution, the model should be retrained at this time. However, the re-learning process needs to retain most of the data left before, which will put forward higher requirements for database data storage [14]. Therefore, the incremental learning method can be used to solve such problems, because the original data is not necessary for the training of the incremental learning algorithm, so that it is less affected by the data size and requires more data storage capacity. It is more suitable for processing continuous large-scale real-time data [15].

The algorithm used in this study is built on the basis of RBF neural network. The RBF neural network is a neural network used to simulate the signal reception and processing between neurons in the human brain, so as to convert the linearly inseparable data in low-latitude space into linearly separable data in high-latitude space, and then cooperate with the combination of data layers to classify and regress the data. The typical structure of the network is shown in Fig. 1.

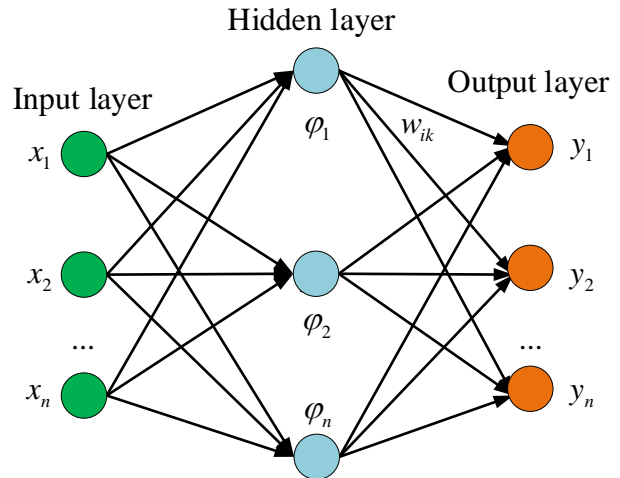


Fig. 1. Typical Structure of RBF Neural Network.

RBF neural network has the advantages of simple structure, fast training speed, good local optimality of algorithm output solution, and high approximation accuracy [16]. The RBF neural network consists of three structures: input layer, hidden layer, and output layer. It is a feedforward neural network and has the performance of approximating complex nonlinear functions. This ability is mainly provided by the hidden layer [17-18]. The hidden layer in the RBF neural network plays a linking role in the whole network. It is not only used to process the input vector using the specified basis function mapping, but also responsible for adjusting the weights to obtain the abstract integrated data of the output.

The following is a detailed discussion of incremental online learning and an analysis of the way it is incorporated into RBF neural networks. When a large data set is given, u one sample is selected as the initial training set, and one sample is added during the incremental learning model construction process L (taking into account the application scenario of this research, the L value is 1), and the online model The input data matrix is constructed recursively, that is, the matrix of the previous stage is the calculation basis of the adjacent matrix, and the algorithm will continue to construct the data matrix until the samples are added, which is the core idea of incremental learning [19]. To achieve incremental learning, the following three conditions need to be met at the same time. First, the model must be able to learn data features that are different from the previous samples. That is to say, if the samples in the input data set (x_j, y_j) have already appeared in the previous model training stage However, when it reappears in the application scene, it will be treated as a new instance of the old class. Finally, when there is a sample in the application scenario that the model has

never seen during training (x_m, y_m) , it will be treated as a new category. Secondly, during incremental learning, only new data and categories that have not appeared in the application scenario are (x_k, y_k) used as training sets [20]. In general, incremental learning mainly has the following three implementations. The first is to filter the most informative samples, the second is to use a combination of multiple trained models to form an integrated model, and the third is to adjust the model indicators and parameters.

It can be seen from the above content that the sample set in incremental learning is in an increasing state, that is, with t the increase of running time, the sample set $\{X_i, Y_i\}_{i=1}^{t-1}$, or $\{(x_i, y_i)\}$ a fixed new $L=1$ sample will be added each time, if $x(t)=[x_1, x_2, \dots, x_t]$, $y(t)=[y_1, y_2, \dots, y_t]^T$, and $x_i \in R^n$, are assumed $y_i \in R$. Then the RBF matrix whose kernel function used in this study is a Gaussian function can be expressed in the form of Equation (1).

$$A = \begin{bmatrix} \phi(\|x_1 - x_1\|) & \phi(\|x_1 - x_2\|) & \dots & \phi(\|x_1 - x_t\|) \\ \phi(\|x_2 - x_1\|) & \phi(\|x_2 - x_2\|) & \dots & \phi(\|x_2 - x_t\|) \\ \dots & \dots & \dots & \dots \\ \phi(\|x_t - x_1\|) & \phi(\|x_t - x_2\|) & \dots & \phi(\|x_t - x_t\|) \end{bmatrix}_{t \times t} \quad (1)$$

where $\phi()$ is the Gaussian kernel function, the radial basis function can be expressed by formula (1),

$$f(x) = \sum_{i=1}^t \beta_i \phi(\|x - x_i\|) \quad (2)$$

However, when using the RBF algorithm based on the Gaussian kernel function to build a big data processing model, it is also necessary to satisfy $f(x_i) = F(x_i)$ or $F = A \cdot \beta$, where A is the radial basis kernel function, $F = [F(1), F(2), \dots, F(t)]^T$, when the function A is a positive definite function or the sample points of formula (2) do not coincide, there is formula (3).

$$\hat{\beta} = A^{-1} \times F \quad (3)$$

It can be seen from formula (3) that $\hat{\beta}$ the inverse function of the radial basis kernel function needs to be calculated first, but when the A dimension is high, the calculation of the inverse matrix consumes a large amount of calculation, so the block matrix technique is used to calculate A^{-1} . It can A_{t+1} be obtained by A_t recursion, and the calculation formula between the two is deduced below. Observing A_{t+1} the A_t elemental composition of and, it is found that the former can be written in the form of formula (4).

$$A_{t+1} = \begin{bmatrix} A_t & H(t) \\ H(t)^T & f(t) \end{bmatrix} \quad (4)$$

In formula (4), $H(t) = [\phi(\|x_{t+1} - x_1\|), \dots, \phi(\|x_{t+1} - x_t\|)]^T$, $f(t) = \phi(\|x_{t+1} - x_{t+1}\|)$. Now define a block matrix

$B = \begin{bmatrix} B_{11} & B_{12} \\ B_{21} & B_{22} \end{bmatrix}$. And when B^{-1} both B_{11}^{-1} exist, there is the relationship of formula (5),

$$B^{-1} = \begin{bmatrix} B_{11}^{-1} & B_{12} \\ 0 & 0 \end{bmatrix} + \begin{bmatrix} B_{11}^{-1} & B_{12} \\ -E & 0 \end{bmatrix} \cdot (B_{22} - B_{21} \cdot B_{11}^{-1} \cdot B_{12})^{-1} \cdot \begin{bmatrix} B_{21} \cdot B_{11}^{-1} - E \end{bmatrix} \quad (5)$$

In Equation (5), B_{11} , B_{12} , are respectively a symmetric matrix and a column vector I , and B_{21} , B_{22} is I^T a non-zero scalar vector q , $A = B_{22} - B_{21} \cdot B_{11}^{-1} \cdot B_{12}$ and if, Equation (5) can be simplified to Equation (6),

$$B^{-1} = \begin{bmatrix} B_{11}^{-1} & 0 \\ 0 & 0 \end{bmatrix} + R \cdot R^T \cdot Z \quad (6)$$

In formula (6) $R = [I^T \cdot B_{11}^{-1} - E]$, $Z = (q - I^T \cdot B_{11}^{-1} \cdot I)^{-1}$, can be obtained by using the block matrix inversion method A_{t+1}^{-1} , see formula (7).

$$A_{t+1}^{-1} = \begin{bmatrix} A_t^{-1} & 0 \\ 0 & 0 \end{bmatrix} + r_1(t+1)r_1(t+1)^T Z_1(t+1) \quad (7)$$

In formula (7) $r_1(t+1) = [H(t)^T \cdot A_t^{-1} \cdot -E]^T$, it can be seen from the $Z_1(t+1) = [f(t) - H(t)^T \cdot A_t^{-1} \cdot H(t)]^{-1}$ observation of formula (7) that it A_{t+1}^{-1} can be obtained by A_t^{-1} calculation, and when it t is small, it A_t^{-1} can be directly obtained. According to the above two points, the large matrix inversion operation process can be effectively avoided, thereby improving the overall calculation efficiency of the algorithm. According to the above design content, an improved RBF neural network algorithm based on the fusion of Gaussian kernel function and incremental learning can be constructed, and the training process is shown in Fig. 2.

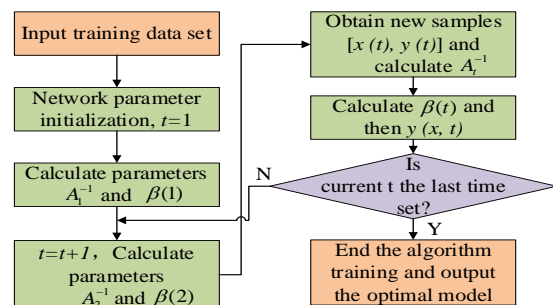


Fig. 2. The Training Flow Chart of the Improved RBF Neural Network Algorithm based on Gaussian Kernel Function and Incremental Learning.

B. Design of Improved RBF Algorithm Combined with Windowed Online Learning Ideas

The improved RBF algorithm based on incremental learning designed in the above content has significant advantages when dealing with static big data, which can simplify the training process and greatly reduce the training time of the algorithm. However, when using this algorithm to deal with another form of big data, that is, dynamic streaming big data that cannot be collected at one time, because dynamic streaming big data is real-time, volatile, bursty, disordered, and infinite. The improved RBF algorithm based on incremental learning previously designed is used to deal with static big data and dynamic big data, and the computing performance is obviously limited, so another processing algorithm needs to be designed for this data form. This research decided to build a windowed learning model by combining radial basis functions and sliding fixed-length windows on the basis of the improved algorithm of incremental learning RBF.

The windowed online learning algorithm is an online learning algorithm based on a sliding window. In this algorithm, new samples can only be added to the window after deleting an old sample, and the total length of the window remains stable. At the same time, in the process of dynamically updating the data set, the data newly added to the algorithm is processed, and the online processing of streaming dynamic big data is realized. Windowed online learning has the following advantages. First, the historical data used by the training algorithm does not need to be stored in a special technology, which can reduce computer memory consumption. Secondly, this type of algorithm can efficiently use the previously trained data while processing the new data, reasonably reduce the processing time of the new data, and reduce the time length of the algorithm. At the same time, in the windowed online learning algorithm, since the training samples are continuously updated and the historical training results are retained to a certain extent, the accuracy of the algorithm can be continuously improved. The last point, which is also the main reason for this research to choose this technology to improve the RBF network, is that the windowed online learning algorithm can update the window by overlapping online, which ensures that no matter how many samples are added, the single training time of the algorithm remains unchanged, so as to improve the training efficiency and effectively solve the processing problem of streaming dynamic big data.

The fixed-length sliding window strategy is adopted here, that is, each time a new sample is input in the algorithm, an old sample will be deleted at the same time, so as to maintain the total number of samples in each training. Assuming that the sample $T = \{x_i, y_i\}_{i=t}^{i=t+m+1}$ will be updated with time t , the sample set can be expressed as $\{x(t), y(t)\}$, x_i , $x(t)$ are the features of the variable sample, t the feature vector of the input sample set at the time, y_i , $y(t)$ respectively represent the label of the variable sample, the input sample set at the t time The label vector, and $x(t) = \{x_t, x_{t+1}, \dots, x_{t+m+1}\}$, $y(t) = \{y_t, y_{t+1}, \dots, y_{t+m+1}\}^T$, $x_t \in R^n$, and $y_t \in R$, m are the window lengths (4 after adjusting the algorithm parameters

many times in this study). t At the moment, the Gaussian kernel function of the RBF radial basis function is in the A_t form of an m order square matrix, and its internal elements can be obtained by analogy with formula (1), which will not be repeated here A_t .

$$A_t = \begin{Bmatrix} h(t) & H(t)^T \\ H(t) & w(t) \end{Bmatrix} \quad (8)$$

Among them $h(t) = \phi(\|x_t - x_t\|)$, $H(t) = [\phi(\|x_{t+1} - x_t\|), \dots, \phi(\|x_{t+m-1} - x_t\|)]^T$, and the $w(t)$ calculation method is shown in formula (9).

$$w(t) = \begin{bmatrix} \phi(\|x_{t+1} - x_{t+1}\|) & \dots & \phi(\|x_{t+1} - x_{t+m-1}\|) \\ \dots & \dots & \dots \\ \phi(\|x_{t+m-1} - x_{t+1}\|) & \dots & \phi(\|x_{t+m-1} - x_{t+m-1}\|) \end{bmatrix}_{(m-1) \times (m-1)} \quad (9)$$

Since $H(t)$, $h(t)$, $w(t)$ represent $m-1$ a column vector of dimensions, a scalar that is not 0, and $m-1$ a square matrix of dimensions, respectively. At the $t+1$ moment, new samples (x_{t+1}, y_{t+1}) are added to the training set, and (x_{t+1}, y_{t+1}) samples are deleted from the training set at the same time, which A_{t+1} can be calculated according to formula (10).

$$A_{t+1} = \begin{bmatrix} w(t) & V(t+1) \\ V(t+1)^T & f(t+1) \end{bmatrix} \quad (10)$$

In formula (10) $V(t+1) = [\phi(\|x_{t+m} - x_{t+1}\|), \dots, \phi(\|x_{t+m} - x_{t+m-1}\|)]^T$, $f(t+1) = \phi(\|x_{t+m} - x_{t+m}\|)$. Therefore, the block matrix calculation method can be used to obtain A_t^{-1} , A_{t+1}^{-1} , and the former calculation method is shown in formula (11)

$$A_t^{-1} = \begin{bmatrix} 0 & 0 \\ 0 & w(t) \end{bmatrix} + R(t) \cdot R(t)^T \cdot Z(t) \quad (11)$$

In formula (11) $R(t) = [H(t) \cdot w(t)^{-1} - E]^T$, $Z(t) = 1 / [h(t) - H(t)^T \cdot w(t)^{-1} \cdot H(t)]$, can be described by formula (12) in the same A_{t+1}^{-1} way.

$$A_{t+1}^{-1} = \begin{bmatrix} w(t)^{-1} & 0 \\ 0 & 0 \end{bmatrix} + R(t+1) \cdot R(t+1)^T \cdot Z(t+1) \quad (12)$$

In formula (12) $R(t+1) = [V(t+1)^T \cdot w(t)^{-1} - E]^T$, $Z(t+1) = 1 / [f(t+1) - V(t+1)^T \cdot w(t)^{-1} \cdot V(t+1)]$. $h(t) \in R$, $H(t) \in R^{m-1}$ is composed of kernel function elements and vectors that delete samples during the sliding window movement, and $f(t+1) \in R$, $V(t+1) \in R^{m-1}$. Observing

formula (12), we can see that if we want to calculate it A_{t+1}^{-1} , we need to find it first $w(t)^{-1}$, and formula (13) can be deduced according to formula (11).

$$A_t^{-1} = \begin{bmatrix} 0 & 0 \\ 0 & w(t)^{-1} \end{bmatrix} + \begin{bmatrix} \frac{1}{Z(t)} & \frac{-H(t)^T w(t)^{-1}}{Z(t)} \\ \frac{-w(t)^{-1} \cdot H(t)}{Z(t)} & \frac{w(t)^{-1} \cdot H(t) \cdot H(t)^T \cdot w(t)^{-1}}{Z(t)} \end{bmatrix} \quad (13)$$

When it A_t^{-1} is known, it can be obtained by its (1,1) position element, and then $\frac{1}{Z(t)}$ the row vector can be obtained Q_1 by using the first row element A_t^{-1} . The calculation method is shown in formula (14).

$$Q_1 = \frac{-H(t)^T w(t)^{-1}}{Z(t)} \quad (14)$$

Then use $w(t)$ the first column vector element to calculate the column vector Q_2 , and the calculation method is shown in formula (15).

$$Q_2 = \frac{-w(t)^{-1} \cdot H(t)}{Z(t)} \quad (15)$$

Finally, combining equations (14) and (15), we can obtain

$$\begin{aligned} Q_3 &= \frac{w(t)^{-1} \cdot H(t) \cdot H(t)^T \cdot w(t)^{-1}}{Z(t)} \\ &= Q_1(t) \cdot Q_2(t) \cdot Z(t) \end{aligned} \quad (16)$$

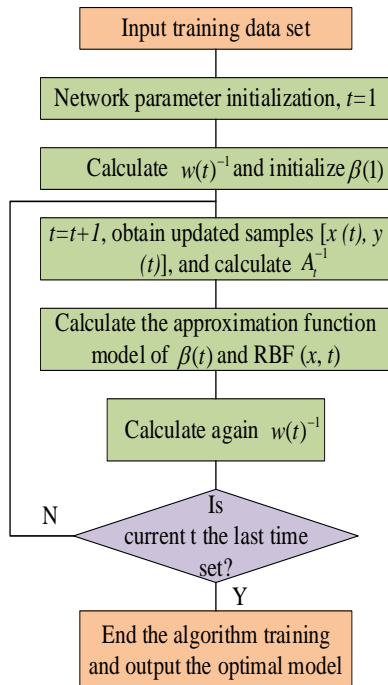


Fig. 3. The Training Flow Chart of the Improved RBF Neural Network Algorithm based on Sliding Window.

From the above content, it can be seen that the $w(t)^{-1}$ numerical value is equivalent to $\phi(t)^{-1}$ the matrix subtraction after removing the first row and the first column $Q_3(t)$, and then combining the formula (10) and formula (12), it can be obtained, that is, the A_{t+1}^{-1} design of the recursive method from A_t^{-1} to to is formed. A_{t+1}^{-1} . So far, the improved RBF online learning neural network algorithm based on sliding window is designed, and its calculation flow is shown in Fig. 3.

IV. IMPROVE THE PERFORMANCE VERIFICATION OF RBF ALGORITHM

A. Algorithm Performance Verification Experimental Design and Data Set Processing

This research plans to design two verification experiments. One is to use the Duffing equation example, which is widely used to verify the training effect of deep learning algorithms, to train and compare the performance of each algorithm. In this study, the parameters in the Duffing equation were set as $p_1 = -1.1$, $p_2 = 0.4$, $\Delta t = 0.01$, $w = 1.7$ and $q = 1.5$, respectively, and the experimental plans of 1000, 3000, 5000, 10000, and 100,000 samples generated by the Duffing equation were set respectively. In order to avoid the influence of errors caused by random factors, each experimental scheme was repeated 10 times. In the experiment, the super parameter acquisition method of each algorithm is to use dichotomy to repeatedly run 10 times within the range of conventional parameter adjustment, and the parameter of the best run result is the final parameter. The second experiment scenario is a typical application scenario of big data mining algorithms, namely the Taobao online store sales forecast experiment. The data in the experiment is the data of “Taobao Search Glasses Sales Top 100 Single Items” provided by a domestic data supplier. The purpose of the experiment is to input this data into the algorithm to predict the sales volume of the glass single product in the store. A total of 5,500 sample data of Taobao e-commerce research and sales TOP100 single products were obtained, which contained a total of 18 variables. Except for the two characteristics of “commercial name” and “credit”, which cannot be numerically processed, the others are numerical characteristics, which are respectively praised. rate, complaint rate only in 30 days, return rate in the past 30 days, sales volume in the past 30 days, original price, discount, postage, sales price, collection volume, days on the shelf, main credit ratio, customer evaluation, seller service points, goods Average refund speed, shipping score, description score. It is necessary to convert the “credit” feature that affects the prediction result in the data set. The value of this feature includes “other”, “blue crown”, “gold crown”, “diamond”, “heart”, and “Tmall”. Each equivalence contains several different secondary classifications. Statistics show that items with different credit ratings correspond to different frequencies of appearance, which means that there is a certain relationship between credit ratings and product sales. Therefore, the credit rating is assigned with reference to Taobao’s credit regulations. The single product credit rating, frequency of occurrence, and numerical ranking results are shown in Table I.

TABLE I. THE STATISTICS OF THE “CREDIT” VARIABLE OF THE TOP100 SINGLE PRODUCT DATA SET OF TAOBAO SEARCH GLASSES SALES

Grade 1 and 2 credit rating	The number of occurrences	Numerical mapping	Grade 1 and 2 credit rating	The number of occurrences	Numerical mapping
Tmall	1125	Twenty-one	1 gold	152	8
1 heart	11	17	2 gold	20	6
2 hearts	15	16	3 gold	33	7
3 hearts	40	18	4 gold	46	9
4 hearts	46	20	1 blue	319	10
5 hearts	45	19	2 blue	289	1
1 drill	144	12	3 blue	346	2
2 drills	168	11	4 blue	184	3
3 drills	249	13	5 blue	122	5
4 drills	417	15	other	5	4
5 drills	272	14	/	/	/

In order to improve the model training effect, the data set also needs to be processed by data dimensionality reduction. In order to compare the performance and application value of the algorithm, this study chose Support Vector Machine (SVM) and ResNet50 to build a comparative analysis model.

B. Analysis of Validation Experiment Results

After the calculation of all experimental schemes under the two experiments is completed, the experimental data are counted. The following first analyzes the performance test experiment based on the Duffing equation example. Under the premise of five sample sizes, the statistical results of the mean square error of each algorithm are shown in Table II.

In order to verify whether there is a significant difference in the calculation results of each algorithm under each total experimental scheme, an F test was performed, and the significance level of the difference was set to 0.05. Note that

IOL and SWOL in Table II represent the improved RBF algorithm based on incremental learning and the modified RBF algorithm incorporating sliding windows designed in this study, respectively. It can be seen from Table II that the root mean square error data P values of the output test set of each group of algorithms under various experimental schemes are all less than the significance level of 0.05, and the difference is considered significant. Specifically, under the experimental schemes of various sample numbers, the mean square error of the SVM model is the largest, followed by the ResNet50 model. The mean square error of the test set of the IOL and SWOL algorithms designed in this research is relatively small, and the mean square error of the SWOL algorithm is relatively small. minimum. For example, when the total sample is 100000, the mean square errors of the IOL, SWOL, SVM, and ResNet50 algorithms are 1.86e-07, 1.59e-07, 3.37e-07, and 2.67e-07, respectively. Then analyze the training time of each algorithm, and the statistical results are shown in Table III.

TABLE II. MEAN SQUARE ERROR STATISTICS OF EACH ALGORITHM ON THE DUFFING EQUATION EXAMPLE SAMPLE TEST SET

Algorithm	Total samples 1000; test set: training set = 300:700	Total samples 3000; test set: training set = 900:2100	Total samples 5000; test set: training set = 1500:3500	Total samples 10000; test set: training set = 3000:7000	Total samples 100000; test set: training set=30000:70000
IOL	3.25e-04	4.36e-06	5.64e-07	3.28e-07	1.86e-07
SWOL	3.06e-04	4.12e-06	5.38e-07	3.02e-07	1.59e-07
SVM	4.57e-04	5.98e-06	6.74e-07	5.35e-07	3.37e-07
ResNet50	3.59e-04	4.41e-06	5.92e-07	4.81e-07	2.67e-07
F value	1.651	1.548	2.154	5.833	9.645
P value	0.034	0.039	0.022	0.007	0.003

TABLE III. STATISTICS ON THE TRAINING TIME OF EACH ALGORITHM ON THE DUFFING EQUATION EXAMPLE SAMPLE (UNIT: SECOND)

Algorithm	Total samples 1000; test set: training set = 300:700	Total samples 3000; test set: training set = 900:2100	Total samples 5000; test set: training set = 1500:3500	Total samples 10000; test set: training set = 3000:7000	Total samples 100000; test set: training set=30000:70000
IOL	3.2	73.8	389.4	3564.4	3.79e+06
SWOL	1.9	30.5	175.2	1442.0	1.48e+06
SVM	5.9	86.2	833.6	7957.9	8.25e+06
ResNet50	4.2	74.2	759.1	6553.1	6.73e+06
F value	1.954	2.694	2.545	2.844	3.177
P value	0.031	0.021	0.020	0.016	0.013

The numbers in the cells of Table III represent the average model training time of the corresponding algorithm under the corresponding experimental scheme. It can be seen from Table III that the P values of the training time data of each group of algorithms under each experimental scheme are all less than the significance level of 0.05, and the difference is considered to be different. significant. Specifically, under the experimental schemes of various sample numbers, the training time of the SVM model is the largest, followed by the ResNet50 model. The training time of the IOL and SWOL algorithms in this study is relatively small, and the training time of the SWOL algorithm is the smallest. For example, when the total number of samples is 100,000, the training time of the IOL, SWOL, SVM, and ResNet50 algorithms are 3.79e+06, 1.48e+06, 8.25e+06, and 6.73e+06, respectively. The following is an analysis of the performance of each algorithm in the second experiment. First, the change of the loss function value of each algorithm during the training process is counted, as shown in Fig. 4.

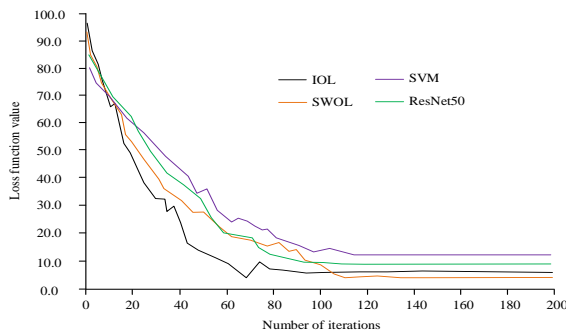


Fig. 4. Changes in the Loss Function Value of Each Algorithm during the Training Process of the e-commerce Dataset.

Observing Fig. 4, it can be seen that with the increase of the number of iterations, the calculation time of each algorithm shows an overall decreasing law, and finally converges. From the point of view of convergence speed, the IOL algorithm has the fastest convergence speed, and the algorithm training is roughly completed around the 85th time, while the SVM algorithm has the slowest convergence speed, which roughly completes the convergence around 117 times. After convergence, the loss function of the SWOL algorithm is the smallest, which is 4.2. The calculation time-consuming situation of various algorithms is counted, as shown in Fig. 5.

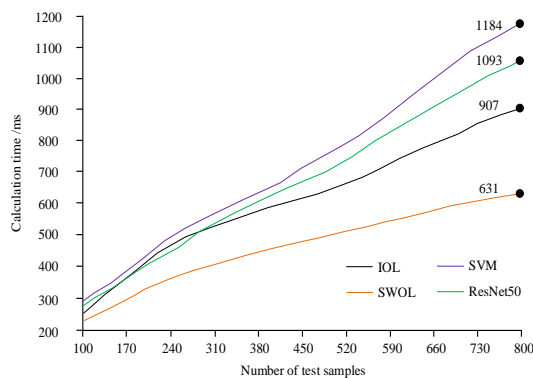


Fig. 5. The Calculation Time Change of Each Algorithm in the e-commerce Data Test Set.

Observing Fig. 5, it can be seen that with the increase of the number of test samples, the time consumption of each algorithm to process the test samples shows an overall increasing trend, but the overall calculation time of the SVM algorithm is the largest, and the overall calculation time of the SWOL algorithm is the smallest. When the number of samples in the test set is 800, the training time of the IOL, SWOL, SVM, and ResNet50 algorithms are 1184ms, 1093ms, 907ms, and 631ms, respectively. The processing performance of the algorithm is analyzed again, and the root mean square error variation of each algorithm on the test set is shown in Fig. 6.

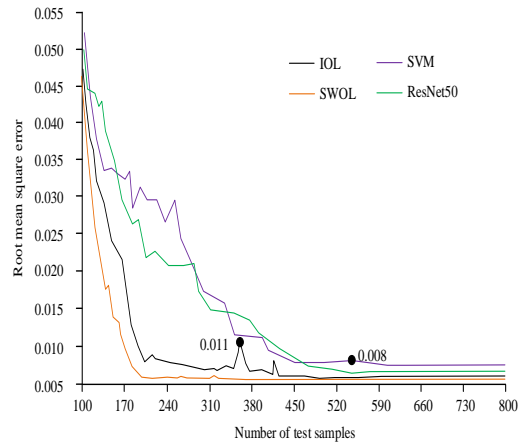


Fig. 6. Variation of the Root Mean Square Error of Each Algorithm in the e-commerce Data Test Set.

Observing Fig. 6, we can see that the root mean square error performance of the IOL and SWOL algorithms designed in this study is better under different test set samples, but the stability of the former is slightly worse than that of the latter, when the number of iterations is about 362 times, the root mean square error of the IOL algorithm has a large rebound. When there are 800 training samples, the root mean square errors of the IOL, SWOL, SVM, and ResNet50 algorithms are 0.0060, 0.0056, 0.0069, and 0.0073, respectively. In order to ensure the reliability of the research results, the change of the mean absolute error of each algorithm on the test set is finally analyzed, as shown in Fig. 7.

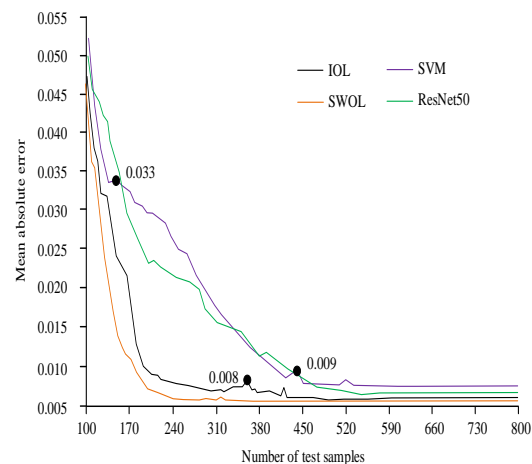


Fig. 7. Absolute Error Variation of Each Algorithm in the e-commerce Data Test Set.

Observing Fig. 7, it can be seen that the overall change of the mean absolute error of each algorithm with the increase of the number of test samples is basically the same as that of the root mean square error, but the variation range of the mean absolute error of each algorithm is reduced, especially the IOL and SWOL algorithms. However, there are still some data rebound phenomena in IOL. For example, when the number of training samples is about 360, the average absolute error of the IOL algorithm briefly rises to 0.008.

Finally, in order to further verify the application effect of the algorithm proposed in this study, 20 online sales store owners were selected from China and invited to use the customer in store consumption prediction system based on this algorithm and other comparison algorithms. The input data of this system are the customer's stay time in the store, the length and content of communication with customer service, the number of page clicks and the number of comparisons of similar products. The mean square error of the prediction results and the satisfaction of the shopkeepers (five point evaluation, the higher the score, the more satisfied) are used as indicators to measure the application effect of the algorithm. Since the data obtained from the experimental results are few and simple, the experimental results are described and analyzed in text. The experimental results show that the mean square error of the prediction results of the customer's in store consumption prediction system based on the IOL, SWOL, SVM and ResNet50 algorithms is 42.7 ¥, 29.6 ¥, 52.3 ¥ and 44.5 ¥ respectively, and the average of the shopkeeper satisfaction scores obtained are 3.85, 4.16, 4.03 and 3.61 respectively. It can be seen that the system designed based on this study has the most accurate consumption prediction and the highest user satisfaction.

V. CONCLUSION

With the increase in the scale of Internet data, the use of big data technology to deal with huge data needs in e-commerce, Internet of Things and other industries is increasing. This research attempts to use the incremental learning idea to construct an improved RBF neural network, and combines the sliding window technology to design another improved RBF neural network. Using a variety of algorithms to predict the results of the Duffing equation example, the results show that when the total sample is 100,000, the mean square errors of the IOL, SWOL, SVM, and ResNet50 algorithms are $1.86e-07$, $1.59e-07$, and $3.37e-07$, respectively. -07 , $2.67e-07$, the training time is $3.79e+06$, $1.48e+06$, $8.25e+06$, $6.73e+06$, respectively. The simulation experiment results of each algorithm in the "Taobao Search Glasses Sales TOP100 Single Product" data set show that when the number of samples in the test set is 800, the training time of the IOL, SWOL, SVM, and ResNet50 algorithms are 1184ms, 1093ms, 907ms, and 907ms, respectively. 631ms, the root mean square error is 0.0060, 0.0056, 0.0069, 0.0073 respectively. The two experimental results show that the two improved RBF algorithms designed in this study have faster training speed and higher data processing accuracy, and the improved RBF algorithm based on sliding window has the fastest speed in processing big data among the comparison algorithms.

REFERENCE

- [1] F. Xu, X. Zhang, X. Song, et al. "Composite control of RBF neural network and PD for nonlinear dynamic plants using U-model," *Journal of Intelligent & Fuzzy Systems*, vol. 35(1), pp.565-575, 2018.
- [2] T. Muling, T. Muqin, Y. Jieming et al. "Optimization of RBF neural network used in state recognition of coal flotation," *Journal of Intelligent & Fuzzy Systems*, vol. 34(2), pp.1193-1204, 2018.
- [3] Y. Li, X. Chu, Z. Fu, et al. "Shelf-life prediction model of postharvest table grape using optimized radial basis function (RBF) neural network," *British Food Journal*, vol. 121(11), pp.2919-2936, 2019.
- [4] Y. Tian, Y.L., He, Q.X. Zhu, "Soft sensor development using improved whale optimization and regularization-based functional link neural network," *Industrial & Engineering Chemistry Research*, vol. 59(43), pp.19361-19369, 2020.
- [5] P. Valerio, P. Antonio, P. Antonio, et al. "Benchmarking big data architectures for social networks data processing using public cloud platforms," *Future Generation Computer Systems*, vol. 89(DEC.), pp.98-109, 2018.
- [6] R. Habeeb, F. Nasaruddin, A. Gani, et al. "Real-time big data processing for anomaly detection: A Survey," *International Journal of Information Management*, vol. 45(4), pp.289-307, 2019.
- [7] L. Zhang, K. Wang, D. Xuan, et al. "Optimal task allocation in near-far computing enhanced C-RAN for wireless Big Data processing," *IEEE Wireless Communications*, vol. 25(1), pp.50-55, 2018.
- [8] K.K. Lwin, Y. Sekimoto, W. Takeuchi, "Development of GIS integrated Big Data research toolbox (BigGIS-RTX) for mobile CDR data processing in disasters management," *Journal of Disaster Research*, vol. 13(2), pp.380-386, 2018.
- [9] F. Cigna, D. Tapete, "Sentinel-1 BigData processing with P-SBAS InSAR in the geohazards exploitation platform: an experiment on coastal land subsidence and landslides in Italy," *Remote Sensing*, vol. 13(5), pp.885 - 910, 2021.
- [10] S. Muhammad, A. Ganjar, F. Norma, et al. "Performance analysis of IoT-based sensor, big data processing, and machine learning model for real-time monitoring system in automotive manufacturing," *Sensors*, vol. 18(9), pp. 2946-2969, 2018.
- [11] L. Wang, Y. Ma, J. Yan, et al. "PipsCloud: high performance cloud computing for remote sensing big data management and processing," *Future Generation Computer Systems*, vol. 78(6), pp.353-368, 2018.
- [12] M. Hai, Y. Zhang, H. Li, "A performance comparison of big data processing platform based on parallel clustering algorithms," *Procedia Computer Science*, vol. 139(10), pp.127-135, 2018.
- [13] J. Neto, A.M. Moreira, G. Vargas-Solar, et al. "A two-level formal model for Big Data processing programs," *Science of Computer Programming*, vol. 215(3), pp.102764-102766, 2022.
- [14] S. Xie, Y. Xie, T. Huang, W. Gui, C. Yang, "Generalized predictive control for industrial processes based on neuron adaptive splitting and merging RBF neural network, *IEEE Transactions on Industrial Electronics*," vol. 66(2), pp.1192-1202, 2018.
- [15] Y. Zhang, X. Hu, Z. Hui, et al. "Parameter interval optimization of the DBD plasma actuator based on orthogonal experiment and RBF neural network approximation model," *Physics of Plasmas*, vol. 28(2), pp.023504- 023505, 2021.
- [16] Y. Yang, X. Lai, T. Luo, et al. "Study on the viscoelastic-viscoplastic model of layered siltstone using creep test and RBF neural network," *Open Geosciences*, vol. 13(1), pp.72-84, 2021.
- [17] N. Shaukat, A. Ali, M.J. Iqbal, et al. "Multi-sensor fusion for underwater vehicle localization by augmentation of RBF neural network and error-state kalman filter," *Sensors*, vol. 21(4), pp.1149 - 1153, 2021.
- [18] Q. Liu, D. Li, S.S. Ge, et al. "Adaptive bias RBF neural network control for a robotic manipulator," *Neurocomputing*, vol.447(4),pp.213-223, 2021.
- [19] Y. Wang, X. Chen, "QSPR model for Caco-2 cell permeability prediction using a combination of HQPSO and dual-RBF neural network," *RSC Advances*, vol. 10(70), pp.42938-42952, 2020.
- [20] A. Sh, A. Hw, T.A. Yang, et al. "Time-delay estimation based computed torque control with robust adaptive RBF neural network compensator for a rehabilitation exoskeleton," *ISA Transactions*, vol. 97(2), pp.171- 181, 2020.

Conceptual Model of Augmented Reality Mobile Application Design (ARMAD) to Enhance user Experience: An Expert Review

Nik Azlina Nik Ahmad¹, Ahmad Iqbal Hakim Suhaimi², Anitawati Mohd Lokman^{3*}

Universiti Kuala Lumpur, Software Engineering Section

Malaysian Institute of Information Technology, Kuala Lumpur, Malaysia¹

Faculty of Computer and Mathematical Sciences, Universiti Teknologi MARA, Shah Alam, Malaysia^{2,3}

Abstract—Rapid technological advancement has altered the demands of user experience (UX) in product design. However, research has shown that there is a gap and paucity of conceptual and practical models in this research field that may serve as guidelines for the design of immersive technologies such as augmented reality (AR) applications. Identifying the variables and components that influence the enhancement of AR design is critical for creating a great UX. The literature indicated that emotion is the primary driver of the UX. Therefore, this study proposed a conceptual design model for AR mobile application that incorporates user interface, interaction, and content design elements while taking their emotions into consideration in order to improve the UX. The focus of this study is to evaluate the proposed conceptual design model of augmented reality mobile application design (ARMAD) through expert reviews. Feedbacks from the expert reviewers are compiled and illustrated in order to refine the initial ARMAD model. The findings showed that majority of the expert reviewers agreed that the conceptual design model is suitable to be used as guideline in designing AR applications that enhances the UX through emotional elicitation. Accordingly, ARMAD model has been refined according to the feedback and suggestions from the expert reviewers. This model will provide researchers and practitioners insight into the essence of AR design that influence the user experience.

Keywords—Augmented reality; conceptual design model; emotional UX; Kansei Engineering; mobile application; user experience

I. INTRODUCTION

Augmented reality (AR) has received increased attention over the last few years and has shaped a new way people interact with technologies. With the advent of smartphones, mobile augmented reality (MAR) has brought new opportunities and experiences, leading to MAR's exponential growth in recent years, with 1.1 billion AR users in 2022 [1]. The report also showed that around 83.1 million individuals will use AR application at least once in a month [1]. The emergence of AR technology has significantly improved the usability and experience of smartphone users. MAR has increased the accessibility to products and services in various sectors including retail [2]–[4], transportation [5]–[7], tourism [8], [9], games [10], [11], health [12], [13], and education [14]–[16].

The advancement in this AR immersive technology has altered the way people interact with devices and information, hence provide new opportunities for investigating how to design in immersive environments. To leverage AR in improving the user experience (UX), the AR application must be meticulously designed to captivate the user's attention and satisfaction. Based on the literatures, there is a clear need for research that considers the user emotions in AR design to enhance UX [17]–[19] since user demand has expanded beyond functionality to also include emotional satisfaction [20]. Similarly, [21] argued that application design should address the whole UX rather than the concept of usability alone. However, the user may experience various design challenges when using such immersive technologies [22], [23]. As AR technology becomes more prevalent, the requirement to grasp the intricacies of MAR interface design to satisfy its users grows [24]. To deliver a positive UX design, designers must address the user challenges by comprehending the factor and components of AR design.

Although the usage of this persuasive technology is on the rise, there is a scarcity of conceptual and practical models to serve as a guide when designing AR applications for UX. Most of the existing models focused only on the AR application development [25], [26], games development [27], [28], or AR for learning [29]. Although there exist models on AR UX, their emphasis has been on overall system development [30] and researching user acceptability on AR applications [31], rather than investigating the relationship between AR design components, emotions, and UX. Therefore, what are the significant components for designing an emotional UX for AR mobile application? This study aims to find out the answer to this question by obtaining and incorporating expert opinions. For that purpose, this study proposed a conceptual model for augmented reality mobile application design (ARMAD) through a combination of user interface (UI), interaction and content design components to better understand the influence of those components on the user's emotional experience. The main concern of the expert validation is to verify the following research questions (RQ):

RQ1) What are the significant components that are required in designing the AR mobile application?

RQ2) Does the design components able to elicit the user's emotion?

*Corresponding Author.

This study employed *Kansei Engineering* (KE) [32]; a widely used method for emotional design research [33]. KE suggested using specimens to identify the relationship between emotion and product design [34]. Therefore, in this study, the specimens were provided to the expert reviewers throughout the validation procedure so that they could experience the AR product samples and evaluate whether the specimens could elicit their emotions. This study is motivated by the advanced technological research and trends in UX and AR. Since the past literatures demonstrated that UX is a phenomenon that contributes to the success of technological products [35]–[37], therefore investigating the potential of emotional UX in the field of AR technology is warranted.

II. RELATED WORKS

A. Emotional user Experience Design

The landscape of UX demand has significantly changed as a result of rapid advancements in information technology. UX is a field in which emotions play a significant role [21], [38]. According to [39], UX design is concerned with the emotional state of the user during, before, and after using a particular technological product. This emotional experience influences the user's proclivity to remain involved with the product in the future. UX design is the practice of designing products with users in mind in order to provide meaningful, relevant, and engaging experiences to the intended users. UX is crucial in technological product design because it has the ability to enhance the user's satisfaction and loyalty [17], [19]. The most crucial factor in deciding how successful a product is how widely it is accepted and adopted by its users [40]. While the user acceptance is often influenced by their user experience, therefore a user's perception and emotions of a product also rely on the quality of their interaction with the product. Unfortunately, the human factor is often disregarded in most product development, as argued by [41], [42]. This is also supported by [43], who advocated for early user involvement in the product design phase. [44] argued that it is extremely important to comprehend how a user feels about the design's aesthetics and other visual elements. In line with this, [19] also argued that incorporating the user's emotions into the design leads in a more satisfying and engaging experience for the user. But how can the user's emotions be incorporated into the product's design? There is a popular method in emotional design research known as *Kansei Engineering* that may address human affect by translating their emotions into design components [34]. KE often entails evaluating product samples or specimens to identify how the design components influence the user's emotional experiences.

B. User Experience in the Augmented Reality Context

AR is a technology that substantially enhances the UX by superimposing audio or visual content [45]–[47]. In another word, AR enables mobile devices to create engaging user experiences by layering digital contents on physical environments [48], [49]. This way, AR application may captivate the user's attention through its immersive environment. It has been argued by [50] that not only it is able to improve the UX, but AR has also elevated the user interface

(UI) to a new level. According to [50], AR is capable of facilitating emotionally engaging experiences. Nevertheless, [51] argued that without careful design, AR application might result in user dissatisfaction and confusion, besides being difficult to comprehend and adapt. As reported by [51], the AR UI that is supplemented with unnecessary information has confused the users and has caused them to have problems to understand the features. This is also supported by [52] who conducted a study on graphical user interface, which found that some of the users have reported funny or negative feelings when using the AR mobile applications, and the design may give users confusion with the unsuitable visual cues displayed on the mobile screen. The limited screen size of a mobile devices also plays a role in triggering user negative emotions, if the screen is cluttered or improperly designed [31], [47]. Hence, [51], [52] has suggested to use proper and only necessary visual design elements in AR design. Therefore, there is a need to explore the possible design components for the AR-based mobile application design that can foster positive emotions and user experience.

Although the literatures asserted that AR mobile applications are capable of delivering a new level of interaction via their virtual UI [47], [50], however there is a lack of models that emphasize on AR mobile application design for the UX. The summary of the existing AR models is presented in Table I.

As depicted in Table I, most of the existing models focused on the overall AR product development [25], [26], [53], [58], user engagement [28], AR learning [29], [55], [56], games development [27], [28], [57], and user acceptance or adoption of the MAR applications [31], [40]. However, none of these models put an emphasis on the AR design components that may elicit a positive emotional UX, thus need further research [59], [60]. Therefore, it is important to have a model that explores the user emotions and investigate how they are influenced by AR design elements in order to design a positive AR user experience.

C. The Importance of Expert Review in Model Development

An expert is someone who can provide a professional and useful opinion based on their knowledge, experience, and reputation in their field of expertise [61]. In research, field experts are the valuable source of information in providing empirical input and judgment in evaluation [62]. Expert opinion is valuable in reviewing a certain model and framework, or when verifying a phrase, method, or approach in research, because in order to acquire relevant and concrete results, a research needs to obtain necessary feedback from the expert knowledge [61]. According to the literature, model validation can be performed by reviewing and enlisting experts in evaluating the suitability and completeness of all variables or components involved, and should be pertinent to the research objective [63]. The procedure of expert review is conducted to ensure that the model is acceptable and that each of its component is pertinent to the research [64]. Therefore, in this study, experts play a significant role in reviewing and verifying the model's suitability for the research at hand.

TABLE I. EXISTING AUGMENTED REALITY APPLICATION MODELS

Source	Model Context	Aspects Discussed	Research Focus
[30]	Conceptual model for AR application design and development for user experience	Design and Implementation of User Experience Model for AR Systems	AR Application development
[26]	Conceptual model for M-learning application development	Enriching learning in architectural classroom with MAR	
[53]	Conceptual model for AR application development (hardware, software) with enjoyable aspect	MAR for cultural heritage towards enjoyable informal learning	
[54]	Conceptual model of MAR for hearing impaired museum visitors' engagement	Design and development of AR application that focus on museum visitor's engagement.	AR user engagement
[40]	Conceptual model for AR adoption	Factors Affecting AR adoption in retail industry	AR acceptance or adoption
[31]	Conceptual Framework for user acceptance	Encourage UX, satisfaction and willingness in E-commerce purchase	
[29]	Conceptual model for AR learning	AR technologies with adaptive learning systems	AR learning
[55]	Conceptual model for designing MAR application to learn basic numbers	AR application development for teaching and learning	
[56]	Conceptual design model for learning	MAR for Geography Fieldwork Learning	
[28]	Conceptual model for user engagement in MAR games	MAR games user engagement	AR Games development
[57]	Conceptual design model for audio-based interaction technique in MAR Games	MAR games	
[27]	Conceptual model for mobile games	MAR games	

III. METHODOLOGY

A. Description of the Proposed Model (ARMAD)

In this section, the proposed model is described in detail. The model is a conceptual design model for AR mobile application. A conceptual design model is a representation of a system that illustrates its components' interdependencies [65]. It serves as a base prior to the product design and requires understanding with design concepts in their entirety [66]. Examining the conceptual design model may provide insight into how well the variables are related in light of the research objective [65]. The purpose of this model is to identify the design components that are able to elicit the user's emotion. As a reflection of the two research questions stated in Section I, the formation of this conceptual design model

attempts to achieve two research objectives; 1) To identify the significant components required in designing an AR mobile application, and 2) To determine whether the design components can evoke the emotions of the user. The expert review procedure was designed to ensure that the ARMAD model was constructed in accordance with the study's objectives. Therefore, the expert review process will focus on these two main concerns of the model.

Generally, the proposed conceptual design model for AR mobile application consists of five main components which are user interface design, interaction design, content design, context of the system, as well as emotion. The method used to construct the ARMAD model is based on [67]. The model is presented in Fig. 1 and each of the model's component is further elaborated below.

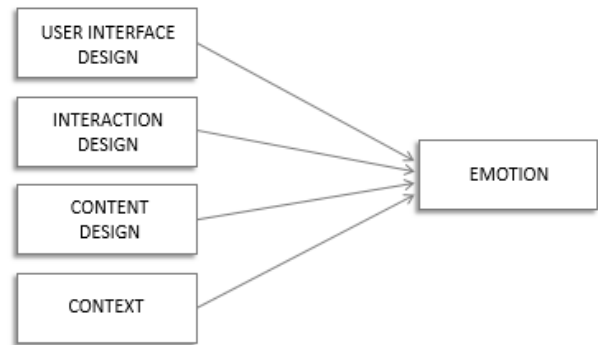


Fig. 1. The Initial Conceptual Model of Augmented Reality Mobile Application Design

The following Table II presents the components of the ARMAD model. Their descriptions are provided in order to explain why each of the components is relevant to this study.

TABLE II. THE MODEL COMPONENTS OF AUGMENTED REALITY MOBILE APPLICATION DESIGN

Components	Description of Significance	Source
User interface	An application's interface is the first station where the user will land on a system. The user interface (UI) will serve as the user's point of contact with the system, allowing them to view, access, or manipulate the information or visual elements on the screen.	[30], [48], [68], [69]
Interaction	To increase individual's involvement with the system so that person in the virtual world may engage naturally and feel in control. By providing users with timely feedback and the means to manipulate the visual elements, the system can provide a realistic simulation to the users.	[21], [30], [70]–[72]
Content	The virtual content is intended to aid users in adapting to their new surroundings and engaging with the system's activities in an immersive environment.	[73]–[76]
Context	The environment in which AR technology being designed will function or be incorporated.	[77]–[79]
Emotion	The perceptions and feelings that develop in the mind of a person as a result of that person's unique set of experiences.	[80]–[82]

B. Procedures for Expert Review

Evaluation strategies based on expert review have proven to be very effective [64]. Therefore, in this study, an expert review procedure was conducted in two main phases to validate the proposed model. As illustrated in Fig. 2, several steps were carried out in order to achieve the review objective; 1) to finalize the list of expert reviewers and 2) to acquire the experts' review findings.

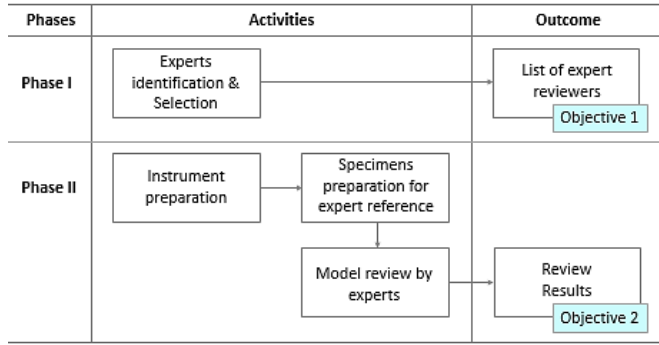


Fig. 2. Phases Involved in Expert Review Procedure

C. Phase I – Experts Identification and Selection

The objective of the first phase is to finalize the list of expert reviewers. According to [63], expert selection is very important in the validation process. This entailed identifying the requirements for expert reviewers, which were set in accordance with the following criteria:

- 1) Possess at least five years of work experience in the relevant fields of this study.
- 2) Have at least practical, teaching, or research experience pertaining to UX design, augmented reality, mobile application design, or Human Computer Interaction (HCI).

All of the selected experts have more than five years of experience in their respective disciplines and have expertise in the relevant domains of UI/UX design, mobile application design, AR, or HCI. According to [83], the ideal number of involvement should be three to five experts in the process of gathering knowledge or making recommendations. Therefore, five experts were chosen to participate in this study and the summary of expert demographics is displayed in Table IV.



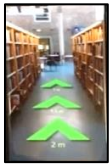

D. Phase II – Instrument and Procedures



The second phase involved model validation by the experts. However, before the validation procedure begins, a set of questionnaire has been prepared as the review instrument. This study employed *Kansei* Engineering (KE) approach to guide the review process due to its applicability in emotional design research. KE procedures entail delivering product specimens for evaluation in order to elicit an emotional response [34]. The specimens are also used to identify whether a particular product design can evoke emotions when using the AR-based products. Therefore, the experts were supplied with six specimens, as depicted in Table III. All specimens are provided in video format with specific links to AR-based products to enhance expert understanding of the relationship between emotions and AR mobile application design. All experts are required to fill out

the questionnaire when evaluating the model, and use the specimens as a reference. The choices of specimens were made based on the relevant market-available products, as suggested by [34]. Since the conceptual design model proposed in this study focused on designing AR mobile application, therefore, the samples of its type were provided as reference to the reviewers, as represented in Table III.

After all the instruments and materials were prepared, the experts were provided with the review form which comprised of five parts: 1) demographic information and research description, 2) consent form, 3) the proposed ARMAD model for their review, 4) list of specimens with working link, and 5) questionnaire. The questionnaire was designed in accordance with the research questions pertaining to why the model was constructed, as stated in Section 1. Since the main concern of the model development was to identify the relevant components for AR mobile application design and to assess if the design components presented in the model are appropriate for emotion elicitation, therefore the questionnaire has been tailored to address these questions. The questionnaire was divided into three sections, which are, 5A) the model's primary components, along with their descriptions, 5B) the relevance of each component to the augmented reality mobile application, 5C) expert's overall opinion which include the model's logical connections and flow, appropriateness of each component, the overall design readability, their agreement with the proposed model, and whether all of the components are suitable for eliciting users' emotions. In addition, they were encouraged to further comment in the provided sections, particularly for the overall opinion part. Since some of the experts are based on international company, therefore the review processes were conducted through email and some through physical meeting. Experts were given two weeks to review the model and complete the questionnaire. In the final step, the review forms were analyzed in order to determine the applicability of the model to be incorporated in the design of AR mobile application that enhances UX via emotions.

TABLE III. LIST OF PROVIDED SPECIMENS FOR EXPERT USE

Specimen UI	Specimen ID & Link	Specimen UI	Specimen ID & Link
	SR001 Specimen Link		SR004 Specimen Link
	SR002 Specimen Link		SR005 Specimen Link

	SR003 Specimen Link		SR006 Specimen Link
---	--	---	--

IV. FINDINGS AND ANALYSIS

A. Expert Review Identification

As previously stated, the purpose of this study is to validate the proposed model through expert review. Following identification process, five experts were selected to participate in this study based on their expertise and specialized knowledge in the fields. This number is adequate according to [83], who suggested that the number of reviewers could range from three to five experts. Table IV displays the demographic information of the experts.

TABLE IV. THE EXPERT DEMOGRAPHICS

Expert	Gender	Field of Expertise	Experience
E1	Male	AR, UI/UX Design, Mobile App Design	9
E2	Male	UX Design	7
E3	Male	AR, UI/UX Design	8
E4	Female	UX Design, HCI	21
E5	Female	AR, HCI	17

B. Analysis of Expert Review

The review results are presented in Table V to Table VII, and in Fig. 3. For part 5A of the questionnaire, all of the experts agreed that the descriptions of the model's components as presented in Table II are correct and should be maintained. While in 5B, the relevance of each component to AR mobile application was rated by the experts, as shown in Table V.

The results of part 5B are depicted in Table V, which indicated that majority of experts are in agreement that the proposed conceptual design model is applicable to the research focus and has pertinent relationship among the components. However, there is an exception for the 'context' component, which according to one of the experts, although relevant to this study, context may not be grouped with other design components. According to the expert, the context however, remains significant in this research to ensure that all design components are designed within a particular system context.

Part 5C sought expert opinions on the model's readability, relationship, and appropriateness, and the findings are shown in Fig. 3. The findings showed that all of the experts agreed that the conceptual design model is readable and understandable, the relationship between each and every component is appropriate and sensible, and the proposed model is practical for the affective design of AR-based mobile applications.

TABLE V. EXPERTS FEEDBACK ON THE RELEVANCE OF EACH MODEL COMPONENT

No.	Proposed Components	(No. of experts = 5)		
		Relevant	Maybe Irrelevant	Not Relevant
1	User Interface Design	5	0	0
2	Interaction Design	5	0	0
3	Content Design	5	0	0
4	Context	4	1	0
5	Emotion	5	0	0

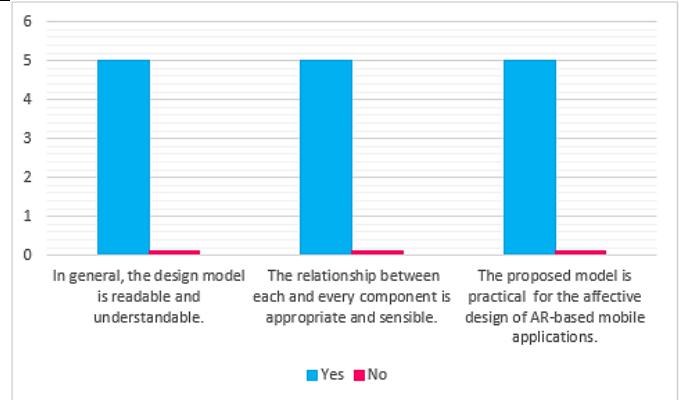


Fig. 3. Expert Opinion on the Model Readability, Relationship, and Appropriateness.

TABLE VI. EXPERTS RESPONSE ON THEIR AGREEMENT WITH THE PROPOSED MODEL

Expert	Summary of Response
E1	Yes, the model is applicable and relevant to various types of AR mobile applications. The model consists of all the important components for augmented reality and has covered the most influential AR parts such as user interface. The UI, as the user's first station, plays a very important role, to allow users interact through it, and to boost user's interest to explore further.
E2	The proposed model meets my agreement. The UX design needs to have sufficient, relevant contents that are customised to particular system context in order for interactions to take place. Since the goal is to enhance the user's experience, this approach is a good fit.
E3	Overall, the model looks good and workable as it emphasis on the UI/UX design. However, I would like to suggest that the context may not be grouped together with other design components, rather, it may stand by itself to support the entire system design in a particular system context.
E4	Yes. The model is well-defined, and its constituent parts are well-suited to the study of emotional design as intended by the researcher.
E5	Agree. Each of the proposed components is vital to the design of a system. The UI, is the core component in system design since it supports communication between user and the system. The interaction component is able to support various kinds of interaction in AR system context, it could be the way the touch the screen to manipulate the digital elements, etc. in addition, the AR system should be supplied with the right contents in order to get the system works. Well, all of the components presented in the model are the essence of a system design. However, since designers have to design AR systems according to a specific AR environment, it is good to consider the inclusion of context as well.

In addition, experts were also asked about the acceptability of the design model. Table VI presents the feedback and comments of experts in response to the question, "Overall, do you agree with the proposed model? Please state reasons for your response". As shown in the table, experts agreed with each component proposed to be associated with any mobile augmented reality application. According to their feedback, the UI, interaction, and content are the essence of AR application design, which should be built within a particular system context or environment, and the user's emotions will play a major role in shaping the user experience.

TABLE VII. EXPERTS FEEDBACK WHETHER THE PROPOSED MODEL COULD ELICIT EMOTION

Expert	Comments
E1	In my view, the user's degree of satisfaction with a product may be impacted by their emotions, at least in part. Designers may achieve user pleasure via thoughtful creation of the UI, interactions, and content. However, for anything to be helpful and satisfying to its intended audience, the design must be appropriate to its context of usage. As demonstrated in specimen 004, design aesthetics have the power to make us feel good.
E2	The UX design cares about the user experience, and it is influenced by the user's emotions. These components appear to meet the design requirements, and as UI/UX designers, we are always thinking about how to improve the user experience and for that reason, we carry out user research on a regular basis.
E3	I've accessed all the specimens supplied to get a feel for the product. Having handled a wide variety of specimens, I've had a wide range of experiences, each of which has influenced my feelings. Some specimens made me feel happy because I found them entertaining, while others made me feel confused.
E4	After reviewing all the specimens, SR006 caught my interest because of its well-designed interface and interactivity it provides. I am very certain that this specimen will be useful for augmented reality type of applications.
E5	The combination of these components is able to stir the user's emotions, and I have personally experienced this after evaluating all of the provided specimens. It is also important that the user interface give clear and concise instructions for user friendliness and understanding.

Table VII presents the experts' response to the question, "Are the components of this conceptual design model (user interface, interaction, content, and context) suitable for eliciting users' emotions?". For this question, experts are required to refer to the provided specimens. The experts found that the specimens have evoked a range of emotions from positive to negative, which led them to agree with the question.

Overall, the findings of the expert review indicated that most of the experts agreed with the proposed conceptual design model with minor modification required, and they considered that the combination of the model's components is capable of eliciting user emotions and is suitable to this research.

C. The Revised Conceptual Design Model

As can be seen in Table V to Table VII and Fig. 3, the majority of experts agreed that the proposed conceptual design model exhibits appropriate components and relationship for the study. However, the goal of this expert review was to obtain complete agreement from all experts in all sections; if

at least one expert disagrees with or is unsure about a model or component, the model should be revised accordingly. Based on the recommendations of the experts, the initial version of the model was refined for better comprehension and to fit the context. The expert E3 has suggested that the 'context' component may not be appropriate to be grouped with other design components since it is not a design component but rather serves to support the design process on a particular system context. Therefore, the expert suggested to remain the context in the model but keeping it separate from other design components. The AR conceptual design model has been revised and redesigned based on the expert's feedback and recommendations. The revised ARMAD model is presented in Fig. 4.

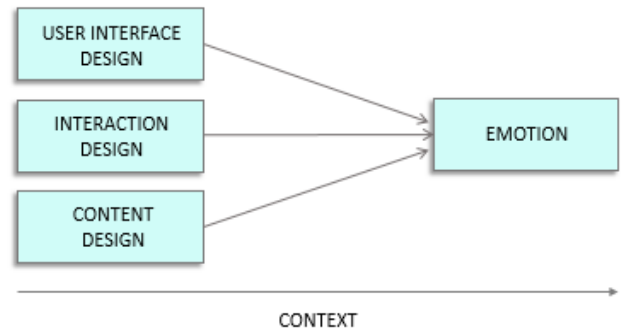


Fig. 4. Augmented Reality Mobile Application Design (ARMAD) Model.

ARMAD model suggested that all the design components; UI, interaction, as well as content should be designed within AR system context in order to make it purposeful. The UI design in this model suggested that the AR mobile application should be designed with interface-environment harmony using suitable visual cues in order to let the user feel presence in the virtual world. In order to enhance positive user experience, the interaction of AR application should be designed with lively interaction that able to provide instantaneous feedback while the users engage with the application. In addition, the design of AR applications needs to take into account the form of virtual content in order to provide insightful information and instructions to users in an immersive environment. The main idea of this model is to understand the influence of the user interface, interaction, as well as content design on the users' emotional experience with augmented reality mobile application.

V. CONCLUSION

Motivated by the advanced technology research and trends in UX and AR, as well as the absence of models in the research area, this study proposed a conceptual model for AR mobile application design (ARMAD) that caters to the users' emotional experiences. The proposed conceptual design model intends to fill the gap of previous AR models that did not address the user emotions in improving the UX. This study sought consultation from experts to validate the initial ARMAD model. In light of this, the expert review methods and procedures involved in this study are outlined in depth. Findings of the expert review are collected and presented in order to improve the ARMAD model. Overall, findings showed that the majority of experts agreed that the conceptual

design model proposed in this study is a useful guide and practical for use in designing the AR mobile application. All of the expert reviewers agreed that the proposed model is suitable for eliciting users' emotions and that the relationship between the model's components are comprehensible, sensible and practical to the research focus. The final step involved refining the model based on reviewers' recommendations. Objectively, this model contributes to defining design elements towards enhancing the emotional UX of AR mobile applications. Understanding user emotions is crucial because it influences the user satisfaction and most importantly, establishes a baseline for designing for a positive UX. This study concludes that the objective of validating the ARMAD model has been met.

The limitation of this research involved the difficulty in obtaining specimens for evaluation since the majority of accessible specimens are in video form. Therefore, only video samples were used as specimens for the reviewer.

Future work should entail creating an AR prototype that incorporates the design components and guidelines proposed in the ARMAD model. Kansei Engineering method may be employed to determine the influence of design elements on user emotions using a self-reporting quantitative approach. The outcomes of the research design may be used to verify the effectiveness of this model.

ACKNOWLEDGMENT

The authors would like to acknowledge the Faculty of Computer and Mathematical Sciences, Universiti Teknologi MARA (UiTM), the Research Initiative Group for Emotion, Kansei and Design Engineering (RIG EKDE), UiTM for all their assistance to the research paper. This work was partially supported under UiTM grant scheme 600-RMC/GPM SS 5/3 (094/2021).

REFERENCES

- [1] T. Alsop, "Global mobile augmented reality (AR) user devices 2019-2024," *Technol. Telecommun. Stat.*, vol. 1, no. 2022, 2022.
- [2] J.-Y. M. Kang, J.-E. Kim, J. Y. Lee, and S. H. Lin, "How mobile augmented reality digitally transforms the retail sector: examining trust in augmented reality apps and online/offline store patronage intention," *J. Fash. Mark. Manag.*, 2022, doi: <https://doi.org/10.1108/JFMM-12-2020-0273>.
- [3] S. R. Nikhashemi, H. H. Knight, K. Nusair, and C. B. Liat, "Augmented reality in smart retailing: A (n) (A) Symmetric Approach to continuous intention to use retail brands' mobile AR apps," *J. Retail. Consum. Serv.*, vol. 60, no. 2021, p. 102464, 2021, doi: <https://doi.org/10.1016/j.jretconser.2021.102464>.
- [4] V. Saprikis, G. Avlogiaris, and A. Katarachia, "Determinants of the Intention to Adopt Mobile Augmented Reality Apps in Shopping Malls among University Students," *J. Theor. Appl. Electron. Commer. Res.*, vol. 16, no. 3, pp. 491–512, 2021, doi: <https://doi.org/10.3390/jtaer16030030>.
- [5] W. Titov, C. Keller, and T. Schlegel, "Augmented Reality Passenger Information on Mobile Public Displays – an Iterative Evaluation Approach," in *International Conference on Human-Computer Interaction. HCII 2021: HCI in Mobility, Transport, and Automotive Systems*, 2021, vol. 12791, pp. 126–143, doi: https://doi.org/10.1007/978-3-030-78358-7_8.
- [6] A. O. Nurminen and K. M. Sirvio, "Bus Stop Spotting: a Field Experiment Comparing 2D Maps, Augmented Reality and 3D Maps," *MobileHCI '21 Proc. 23rd Int. Conf. Mob. Human-Computer Interact.*, no. 37, pp. 1–14, 2021, doi: <https://doi.org/10.1145/3447526.3472051>.
- [7] J. Z. Flores et al., "'ADAPEI-TRANSPORT': A GPS Based Mobile App for Learning Paths and Improving Autonomy for Young Adults Having Intellectual Disabilities to Take Public Transport," in *International Conference on Computers Helping People with Special Needs (ICCHP 2020)*, 2020, vol. 2377, pp. 112–119, doi: https://doi.org/10.1007/978-3-030-58805-2_14.
- [8] E. Ozkul and S. T. Kumlu, "Augmented Reality Applications in Tourism," *Int. J. Contemp. Tour. Res.*, vol. 3, no. 2, pp. 107–122, 2019, doi: [10.30625/ijctr.625192](https://doi.org/10.30625/ijctr.625192).
- [9] T. van Nuenen and C. Scarles, "Advancements in technology and digital media in tourism," *Tour. Stud.*, vol. 21, no. 3, p. 146879762199041, 2021, doi: <https://doi.org/10.1177/1468797621990410>.
- [10] K. M.S.Faqih, "Factors influencing the behavioral intention to adopt a technological innovation from a developing country context: The case of mobile augmented reality games," *Technol. Soc.*, vol. 69, no. 2022, p. 101958, 2022, doi: <https://doi.org/10.1016/j.techsoc.2022.101958>.
- [11] K. Han, K. Park, K.-H. Choi, and J. Lee, "Mobile Augmented Reality Serious Game for Improving Old Adults' Working Memory," *Appl. Sci.*, vol. 11, no. 7, p. 7843, 2021, doi: <https://doi.org/10.3390/app11177843>.
- [12] J. D. Hemanth, U. Kose, O. Deperlioglu, and V. H. C. de Albuquerque, "An augmented reality-supported mobile application for diagnosis of heart diseases," *J. Supercomput.*, vol. 76, no. 2020, pp. 1242–1267, 2020, doi: <https://doi.org/10.1007/s11227-018-2483-6>.
- [13] C. Moro, C. Phelps, P. Redmond, and Z. Stromberga, "HoloLens and mobile augmented reality in medical and health science education: A randomised controlled trial," *Br. J. Educ. Technol.*, vol. 52, no. 2, pp. 680–694, 2020, doi: <https://doi.org/10.1111/bjet.13049>.
- [14] G. Keçeci, P. Yildirim, and F. K. Zengin, "Determining the Effect of Science Teaching Using Mobile Augmented Reality Application on the Secondary School Students' Attitudes of toward Science and Technology and Academic Achievement," *Sci. Educ. Int.*, vol. 32, no. 2, pp. 137–148, 2021.
- [15] M. M. Marques and L. Pombo, "The Impact of Teacher Training Using Mobile Augmented Reality Games on Their Professional Development," *Educ. Sci.*, vol. 11, no. 8, p. 404, 2021, doi: <https://doi.org/10.3390/educsci11080404>.
- [16] C. Papakostas, C. Troussas, A. Krouska, and C. Sgouropoulou, "Exploring Users' Behavioral Intention to Adopt Mobile Augmented Reality in Education through an Extended Technology Acceptance Model," *Int. J. Human-Computer Interact.*, 2022, doi: <https://doi.org/10.1080/10447318.2022.2062551>.
- [17] B. Stangl, D. C. Ukpabi, and S. Park, "Information and Communication Technologies in Tourism 2020," *Inf. Commun. Technol. Tour.* 2020, pp. 181–191, 2020, doi: [10.1007/978-3-030-36737-4_15](https://doi.org/10.1007/978-3-030-36737-4_15).
- [18] A. Dirin and T. H. Laine, "User experience in mobile augmented reality: Emotions, challenges, opportunities and best practices," *Computers*, vol. 7, no. 2, 2018, doi: [10.3390/computers7020033](https://doi.org/10.3390/computers7020033).
- [19] J. Marín-Morales, C. Llinares, J. Guixeres, and M. Alcañiz, "Emotion recognition in immersive virtual reality: From statistics to affective computing," *Sensors (Switzerland)*, vol. 20, no. 18, pp. 1–26, 2020, doi: [10.3390/s20185163](https://doi.org/10.3390/s20185163).
- [20] D. Norman and J. Nielsen, "The Definition of User Experience (UX)," Nielsen Norman Group. World Leaders in Research-Based User Experience, 2017. <https://www.nngroup.com/articles/definition-user-experience/>.
- [21] D. A. Norman, S. Diego, and A. Ortony, "Designers and Users: Two Perspectives on Emotion and Design," *Theor. Pract. Interact. Des.*, no. May, pp. 125–138, 2020, doi: [10.1201/9781482269536-15](https://doi.org/10.1201/9781482269536-15).
- [22] P. Stobiecki, "Augmented reality –challenges and threats," *Ekonom. Probl. Uslug.*, vol. 131, pp. 197–205, 2018, doi: [10.18276/epu.2018.131/2-19](https://doi.org/10.18276/epu.2018.131/2-19).
- [23] D. Marques and R. Costello, "Concerns and Challenges Developing Mobile Augmented Reality Experiences for Museum Exhibitions," *Museum Journal. Wiley Online Libr.*, vol. 61, no. 4, pp. 541–558, 2018, doi: doi.org/10.1111/cura.12279.
- [24] P. J. Van de Broek, C. Onime, J. O. Uhomobhi, and M. Santachiara, "Evolution of User Interface and User Experience in Mobile Augmented and Virtual Reality Applications," *Intech Open*, 2022, doi: [10.5772/intechopen.103166](https://doi.org/10.5772/intechopen.103166).

- [25] E. J. Baker, J. A. Abu Bakar, and A. N. Zulkifli, "A Conceptual Model of Mobile Augmented Reality for Hearing Impaired Museum Visitors' Engagement," *Int. J. Interact. Mob. Technol.*, vol. 14, no. 17, pp. 79–96, 2020, doi: 10.3991/ijim.v14i17.16649.
- [26] S. Hosny, S. Abdel Mohsen, and S. Mansour, "a Conceptual Framework for Enriching Architectural Classroom With Mobile Augmented Reality," *J. Al-Azhar Univ. Eng. Sect.*, vol. 14, no. 50, pp. 158–175, 2019, doi: 10.21608/aej.2019.28486.
- [27] P. A. Rauschnabel, A. Rossmann, and M. C. Tom Dieck, "An adoption framework for mobile augmented reality games: The case of Pokémon Go," *Comput. Human Behav.*, vol. 76, pp. 276–286, 2017, doi: <https://doi.org/10.1016/j.chb.2017.07.030>.
- [28] D. Permadi and A. Rafi, "Developing a conceptual model of user engagement for mobile-based augmented reality games," *J. Teknol.*, vol. 77, no. 29, pp. 9–13, 2015.
- [29] V. V. Osadchyi, H. Y. Chemerys, K. P. Osadcha, V. S. Kruhlyk, S. L. Koniukhov, and A. E. Kiv, "Conceptual model of learning based on the combined capabilities of augmented and virtual reality technologies with adaptive learning systems," *CEUR Workshop Proc.*, vol. 2731, no. November, pp. 328–340, 2020.
- [30] S. Irshad, D. R. A. Rambli, and S. Sulaiman, "Design and implementation of user experience model for augmented reality systems," *ACM Int. Conf. Proceeding Ser.*, no. November, pp. 48–57, 2020, doi: 10.1145/3428690.3429169.
- [31] S. Junsawang and S. Chaveesuk, "User experience of augmented reality to encourage user satisfaction and willingness in e-commerce: A conceptual framework," *Proc. 2019 9th Int. Work. Comput. Sci. Eng. WCSE 2019*, vol. 090, pp. 611–616, 2020, doi: 10.18178/wcse.2019.06.090.
- [32] M. Nagamachi, "Successful Points of Kansei Product," in *7th International Conference on Kansei Engineering and Emotion research 2018 (KEER 2018)*, 2018, pp. 177–187.
- [33] A. M. Lokman, N. N. N. N. Ismail, and A. Hadiana, *Kansei Engineering in Malaysia and Indonesia: A Systematic Literature Review*, vol. 1256 AISC. Springer Singapore, 2020.
- [34] M. Nagamachi and A. M. Lokman, *Innovations of Kansei Engineering*. CRC Press, 2011.
- [35] B. Nyagadza, G. Mazuruse, A. Muposhi, T. Chuchu, T. Makoni, and B. Kusotera, "Emotions' influence on customers' e-banking satisfaction evaluation in e-service failure and e-service recovery circumstances," *Soc. Sci. Humanit. Open*, vol. 6, no. 1, p. 100292, 2022, doi: <https://doi.org/10.1016/j.ssaho.2022.100292>.
- [36] G. C. Guerino and N. M. C. Valentim, "Usability and user experience evaluation of natural user interfaces: a systematic mapping study," *IET Softw.*, vol. 14, no. 5, pp. 451–467, 2020, doi: <https://doi.org/10.1049/iet-sen.2020.0051>.
- [37] J. Sauer, A. Sonderegger, and S. Schmutz, "Usability, user experience and accessibility: towards an integrative model," *Ergonomics*, vol. 63, no. 10, pp. 1207–1220, 2020, doi: 10.1080/00140139.2020.1774080.
- [38] V. Distler, C. Lallemand, and V. Koenig, "How Acceptable Is This? How User Experience Factors Can Broaden our Understanding of The Acceptance of Privacy Trade-offs," *Comput. Human Behav.*, vol. 106, p. 106227, 2020, doi: 10.1016/j.chb.2019.106227.
- [39] D. A. Norman, "Emotion & design," *Interactions*, vol. 9, no. 4, pp. 36–42, 2002, doi: 10.1145/543434.543435.
- [40] S. S. Alam, S. Susmit, C. Y. Lin, M. Masukujjaman, and Y. H. Ho, "Factors affecting augmented reality adoption in the retail industry," *J. Open Innov. Technol. Mark. Complex.*, vol. 7, no. 2, 2021, doi: 10.3390/joitmc7020142.
- [41] A. G. Persada, "Emotional Design on User Experience-based Development System," *Proc. 2018 Int. Conf. Electr. Eng. Comput. Sci. ICECOS 2018*, pp. 225–230, 2019, doi: 10.1109/ICECOS.2018.8605199.
- [42] S. Carthy, K. Cormican, and S. Sampaio, "Knowing me knowing you: Understanding user involvement in the design process," *Procedia Comput. Sci.*, vol. 181, no. 2019, pp. 135–140, 2021, doi: 10.1016/j.procs.2021.01.113.
- [43] B. Fischer, A. Peine, B. Östlund, and P. C. Heyn, "The Importance of User Involvement: A Systematic Review of Involving Older Users in Technology Design," *Gerontologist*, vol. 60, no. 7, pp. E513–E523, 2020, doi: 10.1093/geront/gnz163.
- [44] N. F. Taharim, A. M. Lokman, and W. A. R. W. M. Isa, "Emotion and playful elements in mobile learning," *Int. Conf. Next Gener. Mob. Appl. Serv. Technol.*, pp. 72–76, 2016, doi: 10.1109/NGMAST.2016.23.
- [45] C.-C. Santiago, D. Abad-Vásquez, M. Martic-Nieto, F. Andrés Velásquez-G, J.-L. Pérez-Medina, and S. Luján-Mora, "Towards a New Learning Experience through a Mobile Application with Augmented Reality in Engineering Education," *Appl. Sci.*, vol. 11, no. 11, p. 4921, 2021, doi: doi.org/10.3390/app11114921.
- [46] J. Gäthke, "The impact of augmented reality on overall service satisfaction in elaborate servicescapes," *J. Serv. Manag.*, vol. 31, no. 2, 2020.
- [47] M. Trunfio, M. Della Lucia, S. Campana, and A. Magnelli, "Innovating the cultural heritage museum service model through virtual reality and augmented reality: the effects on the overall visitor experience and satisfaction," *J. Herit. Tour.*, vol. 17, no. 1, pp. 1–19, 2022, doi: 10.1080/1743873X.2020.1850742.
- [48] J. Cao, K.-Y. Lam, L.-H. Lee, X. Liu, P. Hui, and X. Su, "Mobile Augmented Reality: User Interfaces, Frameworks, and Intelligence," no. 111, 2021, [Online]. Available: <http://arxiv.org/abs/2106.08710>.
- [49] K.-H. Chang and T. Seder, "Automotive Augmented Reality: User Experience and Enabling Technology," *Inf. Disp. Front. Technol.*, vol. 38, no. 1, pp. 12–18, 2022, doi: doi.org/10.1002/msid.1272.
- [50] R. Kromhout and L. Calvi, "Augmented Reality as a Mediator for Emotionally Engaging Stories: A case study for AR-based stories related to World War II," *ACM Int. Conf. Proceeding Ser.*, pp. 3–7, 2021, doi: 10.1145/3452853.3452901.
- [51] A. Neb, D. Brandt, R. Awad, S. Heckelsmüller, and T. Bauernhansl, "Usability study of a user-friendly AR assembly assistance," *Procedia CIRP*, vol. 104, pp. 74–79, 2021, doi: 10.1016/j.procir.2021.11.013.
- [52] Y. Jin, M. Ma, and Y. Zhu, "A comparison of natural user interface and graphical user interface for narrative in HMD-based augmented reality," *Multimed. Tools Appl.*, vol. 81, no. 2022, pp. 5795–5826, 2021, doi: <https://doi.org/10.1007/s11042-021-11723-0>.
- [53] U. Chandini Pendi, S. B. Zaibon, and J. A. Abu Bakar, "Conceptual model of mobile augmented reality for cultural heritage site towards enjoyable informal learning aspect," *J. Teknol.*, vol. 77, no. 29, pp. 123–129, 2015, doi: 10.11113/jt.v77.6847.
- [54] E. J. Baker, J. A. Abu Bakar, and A. N. Zulkifli, "A Conceptual Model of Mobile Augmented Reality for Hearing Impaired Museum Visitors' Engagement," *Int. J. Interact. Mob. Technol.*, vol. 14, no. 17, pp. 79–96, 2020, doi: 10.3991/ijim.v14i17.16649.
- [55] S. Nor, W. Shamsuddin, K. Awang, I. Ismail, N. A. Rawi, and M. M. Amin, "A Conceptual Framework for Designing Mobile Augmented Reality in Learning Basic Numbers," *World Appl. Sci. J.*, vol. 35, no. 7, pp. 1048–1053, 2017, doi: 10.5829/idosi.wasj.2017.1048.1053.
- [56] X. Wang, C. P. J. M. Van Elzaker, and M. J. Kraak, "Conceptual design of a mobile application for geography fieldwork learning," *ISPRS Int. J. Geo-Information*, vol. 6, no. 11, p. 355, 2017, doi: <https://doi.org/10.3390/ijgi6110355>.
- [57] M. I. A. M. Filus and D. R. A. Rambli, "A Conceptual Design Framework for Audio Based Interaction Technique in Mobile Augmented Reality Games," *1st Int. Conf. Futur. Trends Comput. Commun. Technol.*, pp. 96–99, 2012.
- [58] S. Irshad, D. R. A. Rambli, and S. Sulaiman, "Design and implementation of user experience model for augmented reality systems," *ACM Int. Conf. Proceeding Ser.*, pp. 48–57, 2020, doi: 10.1145/3428690.3429169.
- [59] S. Stumpp, T. Knopf, and D. Michelis, "User experience design with augmented reality (AR)," *Proc. Eur. Conf. Innov. Entrep. ECIE*, vol. 2, no. December, pp. 1032–1040, 2019, doi: 10.34190/ECIE.19.019.
- [60] V. Krauß, F. Jasche, S. M. Saßmannshausen, T. Ludwig, and A. Boden, "Research and Practice Recommendations for Mixed Reality Design – Different Perspectives from the Community," in *VRST 2021: Virtual Reality Software and Technology*, 2021, pp. 8–10, doi: <https://doi.org/10.1145/3489849.3489876>.

- [61] K. J. Mach, M. D. Mastrandrea, P. T. Freeman, and C. B. Field, "Unleashing expert judgment in assessment," *Glob. Environ. Chang.*, vol. 44, pp. 1–14, 2017.
- [62] D. Veen, D. Stoel, M. Zondervan-wijnenburg, and R. van de Schoot, "Proposal for a five-step method to elicit expert judgment," *J. Front. Psychology*, vol. 8, pp. 1–11, 2017.
- [63] E. Fernández-Gómez, A. Martín-Salvador, T. Luque-Vara, M. A. Sánchez-Ojeda, S. Navarro-Prado, and C. Enrique-Mirón, "Content validation through expert judgement of an instrument on the nutritional knowledge, beliefs, and habits of pregnant women," *Nutrients*, vol. 12, no. 4, 2020, doi: 10.3390/nu12041136.
- [64] S. Abdul Aziz, S. N. Abdul Salam, A. Abdul Mutalin, and S. Ismail, "Validating an integrated multimedia presentation conceptual model through expert reviews," *J. Telecommun. Electron. Comput. Eng.*, vol. 8, no. 8, pp. 161–163, 2016.
- [65] C. Kivunja, "Distinguishing between theory, theoretical framework, and conceptual framework: A systematic review of lessons from the field," *Int. J. High. Educ.*, vol. 7, no. 6, pp. 44–53, 2018, doi: 10.5430/ijhe.v7n6p44.
- [66] A. J. Wodehouse and W. J. Ion, "Information use in conceptual design: Existing taxonomies and new approaches," *Int. J. Des.*, vol. 4, no. 3, pp. 53–65, 2010.
- [67] D. K. Pace, "Ideas about simulation conceptual model development," *Johns Hopkins APL Tech. Dig. (Applied Phys. Lab.)*, vol. 21, no. 3, pp. 327–336, 2000.
- [68] V. Sharma and A. K. Tiwari, "A Study on User Interface and User Experience Designs and its Tools," *World J. Res. Rev.*, vol. 12, no. 6, pp. 41–44, 2021.
- [69] M. A. T. Pratama and A. T. Cahyadi, "Effect of User Interface and User Experience on Application Sales," *IOP Conf. Ser. Mater. Sci. Eng.*, vol. 879, p. 879 012133, 2020.
- [70] A. Berni and Y. Borgianni, "From the definition of user experience to a framework to classify its applications in design," *Proc. Des. Soc.*, vol. 1, no. August, pp. 1627–1636, 2021, doi: 10.1017/pds.2021.424.
- [71] T. Papadopoulos, K. Evangelidis, T. H. Kaskalis, G. Evangelidis, and S. Sylaiou, "Interactions in augmented and mixed reality: An overview," *Appl. Sci.*, vol. 11, no. 18, 2021, doi: 10.3390/app11188752.
- [72] M. Zarour and M. Alharbi, "User experience framework that combines aspects, dimensions, and measurement methods," *Cogent Eng.*, vol. 4, no. 1, 2017, doi: 10.1080/23311916.2017.1421006.
- [73] F. Abdullah, A. Abd. Jamil, and M. R. Abdul Razak, "Discussion of the AR Design Principles for Mobile Augmented Reality Games," *Int. J. Acad. Res. Bus. Soc. Sci.*, vol. 11, no. 8, pp. 375–380, 2021, doi: 10.6007/ijarbs/v11-i8/10738.
- [74] Y. Ghazwani and S. Smith, "Interaction in Augmented Reality: Challenges to Enhance User Experience," *Int. Conf. Virtual Augment. Real. Simulations*, pp. 39–44, 2020.
- [75] S. Liang, "Design principles of augmented reality focusing on the ageing population," *Proc. 30th Int. BCS Hum. Comput. Interact. Conf.*, vol. 30, pp. 1–7, 2016.
- [76] T. Liao, "Future directions for mobile augmented reality research: Understanding relationships between augmented reality users, nonusers, content, devices, and industry," *Mob. Media Commun.*, vol. 7, no. 1, pp. 131–149, 2019, doi: 10.1177/2050157918792438.
- [77] S. Krings, E. Yigitbas, I. Jovanovikj, S. Sauer, and G. Engels, "Development framework for context-aware augmented reality applications," *EICS 2020 - 12th ACM SIG CHI Symp. Eng. Interact. Comput. Syst. Proc.*, 2020, doi: 10.1145/3393672.3398640.
- [78] Y. Sun, Q. Guo, S. Zhao, K. Chandran, and G. Fathima, "Context-Aware Augmented Reality Using Human-Computer Interaction Models," *J. Control Decis. IoT-based Enterp. Manag. Futur. era*, p. 24, 2022, doi: <https://doi.org/10.1080/23307706.2022.2026260>.
- [79] J. Grubert, T. Langlotz, S. Zollmann, and H. Regenbrecht, "Towards pervasive augmented reality: Context-awareness in augmented reality," *IEEE Trans. Vis. Comput. Graph.*, vol. 23, no. 6, pp. 1706–1724, 2017, doi: 10.1109/TVCG.2016.2543720.
- [80] H. Mäkinen, E. Haavisto, S. Havola, and J.-M. Koivisto, "User experiences of virtual reality technologies for healthcare in learning: an integrative review," *Behav. Inf. Technol.*, vol. 41, no. 1, pp. 1–17, 2020, doi: 10.1080/0144929X.2020.1788162.
- [81] M. Minge and M. Thüring, "Hedonic and pragmatic halo effects at early stages of User Experience," *Int. J. Hum. Comput. Stud.*, vol. 109, no. June 2016, pp. 13–25, 2018, doi: 10.1016/j.ijhcs.2017.07.007.
- [82] S. Triberti, A. Chirico, G. La Rocca, and G. Riva, "Developing emotional design: Emotions as cognitive processes and their role in the design of interactive technologies," *Front. Psychol.*, vol. 8, no. OCT, p. 1773, 2017, doi: 10.3389/fpsyg.2017.01773.
- [83] J. Dumas and J. Sorce, "Expert reviews: how many experts is enough?," *Proc. Hum. Factors Ergon. Soc.*, vol. 1, no. October 1995, pp. 228–232, 1995, doi: 10.1177/154193129503900402.

A Novel Prediction Model for Compiler Optimization with Hybrid Meta-Heuristic Optimization Algorithm

Sandeep U. Kadam¹, Sagar B. Shinde², Yogesh B. Gurav³, Sunil B Dambhare⁴, Chaitali R Shewale⁵

Anantrao Pawar College of Engineering and Research, Pune¹

PCET – NMVPM Nutan College of Engineering & Research, Pune²

Zeal College of Engineering & Research, Pune³

D. Y. Patil Institute of Engineering, Management & Research, Pune^{4,5}

Abstract—Compiler designer needs years or sometimes months to construct programs using heuristic optimization rules for a specified compiler. For every novel processor, the modelers require readjusting the heuristics to get the probable performances of processor. The most important purpose of the developed approach is to build a prediction approach with optimization constraints for transforming programs with a lesser training overhead. The problem has occurred in the optimization and it is needed to address it with novel prediction model with derived features & neural network. Here, a novel Compiler Optimization Prediction Model is developed. The features like static and dynamic features as well as improved Relief based features are derived, which are provided as input to Neural Network (NN) scheme, in which the weights are tuned via Honey Badger Adopted BES (HBA-BEO) model. Finally, the NN offers the final predicted output. The analysis outcomes prove the superiority of HBA-BEO model.

Keywords—Compiler; prediction; improved relief; HBA-BEO model; neural network

NOMECLATURE

Abbreviation	Description
ALO	Ant Lion Optimization
AOA	Arithmetic Optimization Algorithm
BES	Bald Eagle Search
BWO	Black Widow Optimization
HBA	Honey Badger Algorithm
HBA-BEO	Honey Badger Adopted BES
LP	Learning Percentage
MSDTM	Multithreaded SPM Data Transfer Model
ML	Machine Learning
NN	Neural Network
SSA	Shark Smell Optimization

I. INTRODUCTION

In response to similar needs in many difficult situations, compiler analysts have devised and implemented a significant variety of optimization compilation option. In reality, it's difficult for the compiler's regular compilation optimization step to adapt to the programme requirements that must be compiled in complex scenarios [6] [7] [8]. On the one hand, compiled programmes have different semantics and compiler aims, making it difficult to achieve the best optimization result using the typical compilation optimization step [9] [10] [11]. If an incorrect optimization pass is utilised, it may have bad consequences for programme performance, among other things [12] [13] [14].

Although these dynamic techniques have been quite effective and appear to be naturally ideal for task-parallel programmes with high input and output flow, they do have significant drawbacks [15] [16]. They can't change settings that have to be resolved at compilation time, such as the layout of data structures in memory, and dynamic monitoring at the library level can't completely rule out future programme behaviour, attempting to prevent some kinds of optimization techniques, and any type of feedback loop will cause some runtime overhead [17] [18]. While the effect can be reduced by proper implementation, simply adding a few more hops and branches to see if any adjustments are needed has a meaningful influence in highly fine-grained circumstances [19] [20] [21] [22]. To address these issues, we present a set of static analyzes that may be used to directly alter a runtime's execution parameters by determining aspects of a task parallel programme [23] [24]. The main problem is compiler optimization and tried to get its solution through A Novel Prediction Model for Compiler Optimization with Hybrid Meta-Heuristic Optimization Algorithm.

The key objectives of this works are:

- To Extracts varied features along with improved relief features from input data.
- To Introduces HBA-BEO model for optimal weight selection in NN.

The paper is arranged as: Section II addresses review. Section III and IV correspond to feature extraction and HBA-BEO based NN for prediction. The Section V and VI describe the results and conclusion.

II. LITERATURE REVIEW

A. Related Works

Jiang *et al.* [1] provided a graph-based compilation optimization pass modelling approach that learned heuristics for programme dependability, as well as a combined programme feature extraction approach. The clang compiler tool was used in this research. For optimization pass election for programme dependability, the model enhanced accuracy rate by 5 percentage points to 11 percentage points. The investigations also showed that the suggested paradigm was quite adaptable.

Nuno et al. [2] presented a new compiler-assisted data streaming mechanism to achieve this goal. It was a substitute to prefetching schemes to conservative code structure; it combined static study and code modification with data stream ability. Memory access were encoded and identified with a particular depiction by means of static study. Then, using a code transformation method, data indexing and addresses computation were separated from computation, resulting in considerable code minimization.

Peter et al. [3] offered a series of new static compiler studies aimed at identifying programme properties that influenced the best settings for a task-parallel runtime environment. The parallel configuration of job spawn, the precision of specific activities, the memory capacity of closures needed for task variables and an estimation of the stack dimension necessary each task were all examples of such aspects. A variety of runtime system settings were then modified at constructing time depending on the outcomes of these investigations.

Xiaohan et al. [4] presented a compiler-directed MSDTM to improve data transmission in a heterogeneous many-core system. Further, compile-time analysis was employed for classification. The recommended MSDTM model reduced appliance implementation time by 5.49 and saves energy by 5.16 based upon test resultants.

Matthew et al. [5] believed that compilers should handle data transfer management, decreasing programmer workload and improving programmes speed and efficiency by lowering the amount of bytes exchanged. We showed that with entire transmit scheduling on accelerated data transfer might eradicate around 99 percent of bytes transferred from accelerator than all data during kernel implementation for all collected data.

III. PROPOSED MODEL WITH IMPROVED FEATURES

A novel compiler prediction model is developed, where features like static and dynamic features and improved Relief features are derived. The derived features are provided as input to NN, in which the weights are tuned via HBA-BEO model. The NN offers the final predicted outcome. Fig. 1 illustrates the picture of deployed scheme.

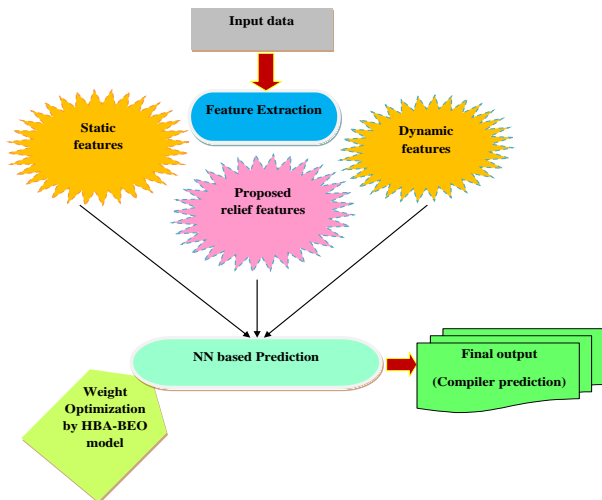


Fig. 1. Developed Compiler Prediction Model.

A. Static Features

The static features [23] extracted in this work are listed in Table I.

TABLE I. STATIC FEATURES

fe_{29}	“Number of basic blocks with phi nodes in the interval [0, 3]
fe_{28}	Number of basic blocks with no phi nodes
fe_{27}	Average of arguments for a phi-node
fe_{26}	Average of number of phi-nodes at the beginning of a basic block
fe_{25}	Average of number of instructions in basic blocks
fe_{24}	Number of instructions in the method
fe_{23}	Number of binary floating point operations in the method
fe_{22}	Number of binary integer operations in the method
fe_{21}	Number of assignment instructions in the method
fe_{20}	Number of conditional branches in the method
fe_{19}	Number of direct calls in the method
fe_{18}	Number of abnormal edges in the control flow graph
fe_{17}	Number of critical edges in the control flow graph
fe_{16}	Number of edges in the control flow graph
fe_{15}	Number of basic blocks with number of instructions greater then 500
fe_{14}	Number of basic blocks with number of instructions in the interval [15, 500]
fe_{13}	Number of basic blocks with number of instructions less than 15
fe_{12}	Number of basic blocks with more than two successors and more than two predecessors
fe_{11}	Number of basic blocks with two successors and two predecessors
fe_{10}	Number of basic blocks with a two predecessors and one successor
fe_{09}	Number of basic blocks with a single predecessor and two successors
fe_{08}	Number of basic blocks with a single predecessor and a single successor
fe_{07}	Number of basic blocks with more than two predecessors
fe_{06}	Number of basic blocks with two predecessors
fe_{05}	Number of basic blocks with a single predecessor
fe_{04}	Number of basic blocks with more than two successors
fe_{03}	Number of basic blocks with two successors
fe_{02}	Number of basic blocks with a single successor
fe_{01}	Number of basic blocks in the method”

B. Dynamic Features

The dynamic features [23] extracted in this work are listed in Table II.

TABLE II. DYNAMIC FEATURES

“Cache line access	CA-CLN, CA-ITV, CA-SHR
Level 1 cache	L1-DCA, L1-DCH, L1-DCM, L1-ICA, L1-ICH, L1-ICM, L1-LDM, L1-STM, L1-TCA, L1-TCM
Level 2 and 3 cache	L2-DCA, L2-DCM, L2-DCR, L2-DCW, L2-ICA, L2-ICH, L2-ICM, L2-LDM, L2-STM, L2-TCH, L2-TCR, L2-TCW, L2/L3-TCA, L2/L3-TCM
Branch related	BR-CN, BR-INS, BR-MSP, BR-NTK, BR-PRC, BR-TKN, BR-UCN
Floating point DP/FP/ SP-OPS	FDV/FML/FP-INS
Interrupt/stall	HW-INT, RES-STL
TLB	TLB-DM, TLB-IM, TLB-SD, TLB-TL
Total cycle/insts.	TOT-CYC, TOT-IIS, TOT-INS
Load/store insts.	LD-INS, SR-INS
SIMD insts.	VEC-DP, VEC-INS, VEC-SP”

C. Improved Relief Features

The Relief feature aids in estimating the superiority of attributes based on how fine their values differentiate among instances, which are nearer to one another. Initially, relief chooses the instances arbitrarily [24]. The arbitrary elected instances are RS_i . The Relief search for its two nearer neighbours: “one from the same class, called nearest hit (NH), and the other from the different class, called nearest miss (NM)”.

The steps of improved relief are:

Algorithm 1
for $i = 1$ to run count m
Automatically evaluate k
Arbitrarily choose RS_i features
Compute hit (NH) and nearest miss (NM)
for $i = 1$ to n do
$we[1] = we[i] - dif(i, RS_i, NH)^2 / m + dif(i, RS_i, NM)^2 / m$
end

As per improved concept, weight $we[i]$ can be computed using tent map. The average of $we[i]$ signifies the harmonic mean.

The extracted features are implied by fe .

IV. HBA-BEO BASED NN FOR PREDICTION

A. Optimized NN

It [16] considers features (fe) as input, as in Eq. (1), wherein nu symbolizes entire feature count.

$$fe = \{fe_1, fe_2, \dots, fe_{nu}\} \quad (1)$$

The NN [16] included “output, hidden and input layers”. The hidden layer $z^{(H)}$ and network outputs \hat{Q}_o are exposed in Eq. (2) and (3). Here, “ $AF \rightarrow$ activation functions, \hat{i} and $j \rightarrow$

neurons of input & hidden layers, $We_{(Bi)}^{(H)} \rightarrow$ bias weight to \hat{i}^{th} hidden neuron, $n_{\hat{i}} \rightarrow$ count of input neurons and $We_{(ji)}^{(H)} \rightarrow$ weight from j^{th} input neuron to \hat{i}^{th} hidden neuron, $\hat{o} \rightarrow$ output neurons, $n_h \rightarrow$ hidden neuron count, $We_{(Bo)}^{(P)} \rightarrow$ output bias weight to \hat{o}^{th} output layer, and $We_{(\hat{i}o)}^{(P)} \rightarrow$ weight from \hat{i}^{th} hidden layer to \hat{o}^{th} output layer”. The error is approximated in Eq. (4), in which, $n_G \rightarrow$ count of output neuron, \hat{P}_o and P_o \rightarrow predicted & actual output. Here, the weights We are optimally chosen via HBA-BEO model. The minimization of Eq. (4) is set as objective in this work.

$$z^{(H)} = AF \left(We_{(Bi)}^{(H)} + \sum_{j=1}^{n_i} We_{(ji)}^{(H)} fe \right) \quad (2)$$

$$\hat{P}_o = AF \left(We_{(Bo)}^{(P)} + \sum_{\hat{i}=1}^{n_h} We_{(\hat{i}o)}^{(P)} z^{(H)} \right) \quad (3)$$

$$er^* = \arg \min_{\{We_{(Bi)}^{(H)}, We_{(ji)}^{(H)}, We_{(Bo)}^{(P)}, We_{(\hat{i}o)}^{(P)}\}} \sum_{i=1}^{n_G} |P_o - \hat{P}_o| \quad (4)$$

The output from NN offers final classified output.

B. Proposed HBA-BEO Algorithm

The developed HBA-BEO is the hybrid conceptual of BES [17] and HBA [18]. It was established that the grouping of two typical optimizations will progress the convergence speed [19] [20] [21] [22].

Selecting stage: This stage decided the optimum region as per the food quantity. As per HBA-BEO, this behaviour is modelled as per HBA update as in Eq. (5), in which Dis_i signifies distance information, $flag \rightarrow$ flag to alter searching direction, ra refers to random constraint, $Y_{prey} \rightarrow$ best position”. As per HBA-BEO, density factor α is computed as in Eq. (6).

$$Y_{new} = Y_{prey} + flag * ra * \alpha * Dis_i \quad (5)$$

$$\alpha = \frac{1.5 * (it_{max} - it + 1)}{it_{max}} \quad (6)$$

Searching stage: This stage is computed in Eq. (7). In Eq. (7), “ Y_{best} refers to elected searching space depending upon best position of eagle, Y_{mean} refers to mean distance amid every positions of bald eagle (population mean), Y_i refers to present position of eagle, ran refers to random constraint produced among [0 - 1], β refers to constant constraint among [0.5, 2], Q refers to constant constraint among 0.5 to 2, and $ran1$ and $ran2$ refers to two arbitrary constraints”. Conventionally,

$r(i)$ is computed as in Eq. (11), however, as per HBA-BEO, $r(i)$ is computed as in Eq. (12), wherein, ran is computed using chaotic cubic map.

$$Y_{new} = Y_i + Z(i) \times (Y_i - Y_{i+1}) + p(i) \times (Y_i - Y_{mean}) \quad (7)$$

$$p(i) = \frac{pr(i)}{\max(|pr|)}, Z(i) = \frac{Zr(i)}{\max(|Zr|)} \quad (8)$$

$$pr(i) = r(i) \times \cos(\theta(i)), Zr(i) = r(i) \times \sin(\theta(i)) \quad (9)$$

$$\theta(i) = \beta \times \pi \times ran1 \quad (10)$$

$$r(i) = \theta(i) + Q \times ran2 \quad (11)$$

$$r(i) = \theta(i) + Q \times ran \quad (12)$$

Swooping stage: This stage is modelled as in Eq. (13).

$$Y_{new} = rand3 \times Y_{best} + pl(i) \times (Y_i - it1 \times Y_{mean}) + Zl(i) \times (Y_i - it2 \times Y_{mean}) \quad (13)$$

$$pl(i) = \frac{pr(i)}{\max(|pr|)}, Zl(i) = \frac{Zr(i)}{\max(|Zr|)} \quad (14)$$

$$pr(i) = r(i) \times \sinh(\theta(i)), Zr(i) = r(i) \times \cosh(\theta(i)) \quad (15)$$

$$\theta(i) = \beta \times \pi \times ran3, r(i) = \theta(i) \quad (16)$$

V. RESULTS AND DISCUSSION

A. Simulation Set Up

The novel prediction model for compiler optimization using NN + HBA-BEO was executed in “Python. Training set: SPEC CPU2006 is developed by the standard performance evaluation organization for the evaluation of general-purpose CPU performance [11]. The input scale of SPEC2006 benchmark can be divided into test, train and reference scale, we use the reference scale to test”. Here, analysis was done for varied metrics like accuracy and varied error metrics like MSE, MSLE and so on. Also, NN+HBA-BEO was proven over NN + BES, NN + HBA, NN + ALO, NN + BWO, NN + AOA and NN + SSA.

B. Performance Analysis

The study on diverse metrics is detailed here. Here, the analysis was done for LPs of 60, 70, 80 and 90 over NN + BES, NN + HBA, NN + ALO, NN + BWO, NN + AOA and NN + SSA models. From Fig. 2, the considered metrics like specificity, sensitivity, accuracy and precision are examined, which were established to be much better over NN + BES, NN + HBA, NN + ALO, NN + BWO, NN + AOA and NN + SSA models. The accuracy of NN + HBA-BEO is high at 90th LP, while precision is high at 80th LP. However, at all LPs, NN + HBA-BEO have established higher outcomes over NN + BES, NN + HBA, NN + ALO, NN + BWO, NN + AOA and NN + SSA models. Thus, NN + HBA-BEO is proven to be enhanced than NN + BES, NN + HBA, NN + ALO, NN + BWO, NN + AOA and NN + SSA models.

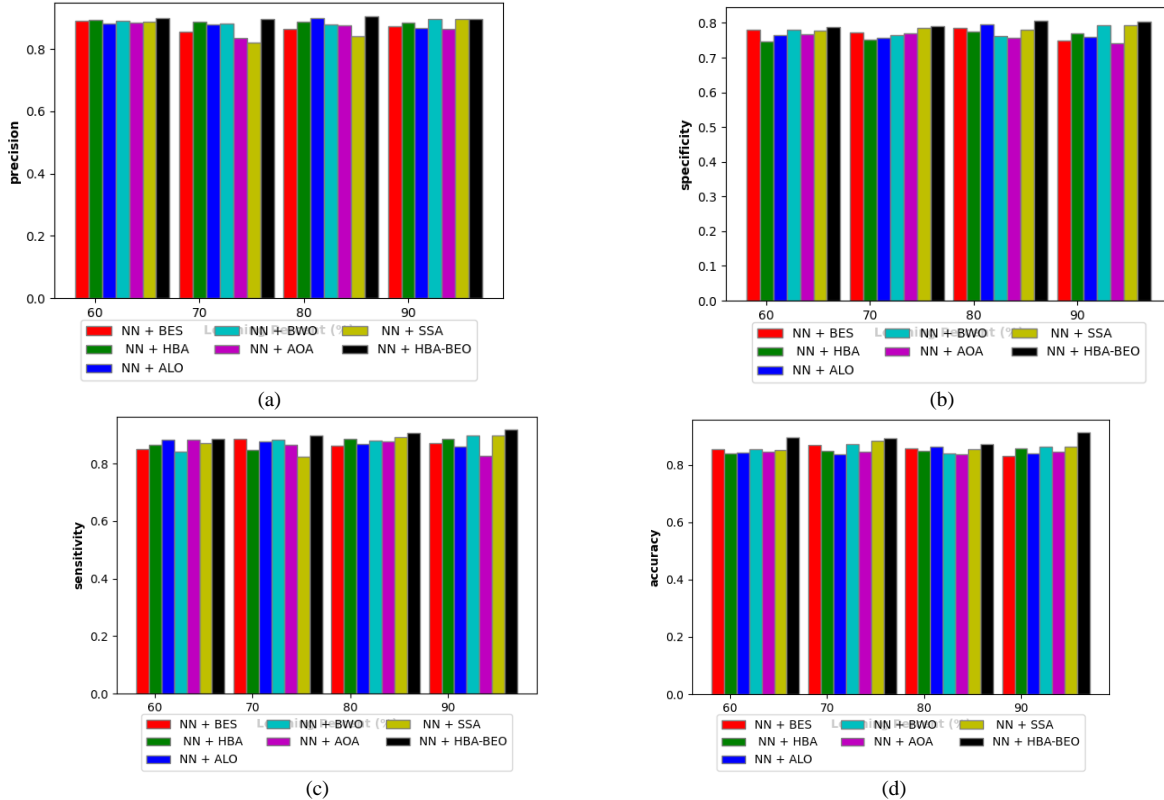


Fig. 2. Analysis on (a) Precision, (b) Specificity, (c) Sensitivity and (d) Accuracy for NN + HBA-BEO over others.

C. Analysis on Error Measures

The performance of adopted NN + HBA-BEO for diverse error (MSE, MSLE, MAE and MAPE) is calculated over conservative NN + BES, NN + HBA, NN + ALO, NN + BWO, NN + AOA and NN + SSA schemes in Fig. 3. The NN + HBA-BEO method is scrutinized for numerous LPs from 60, 70, 80 and 90 over NN + BES, NN + HBA, NN + ALO, NN + BWO, NN + AOA and NN + SSA models. “In statistics, MAE is a measure of errors between paired observations expressing the same phenomenon”. The MAE needs to be less for improved prediction accuracy. As required, the MAE obtained by NN + HBA-BEO is lesser for every LP. The MSLE using NN + HBA-BEO over NN + BES, NN + HBA, NN + ALO, NN + BWO, NN + AOA and NN + SSA is signified in Fig. 3(b). “MSLE can be interpreted as a measure of the ratio between the true and predicted values”. For every LP, the MSLE gained by NN + HBA-BEO is lesser. The assessment of NN + HBA-BEO for MAPE and MSE over MSE, MSLE, MAPE and MAE is signified in Fig. 3(c) and Fig. 3(d). “The MAPE, also known as MAPD, is defined as a measure of prediction accuracy of a forecasting method in statistics”. “In statistics, the MSE or MSD of an estimator measures the average of the squares of the errors, that is, the average squared difference between the estimated values and the actual value”. The MSE and MAPE have to be less for better prediction, which is found to be

accomplished by NN + HBA-BEO for all LPs over NN + BES, NN + HBA, NN + ALO, NN + BWO, NN + AOA and NN + SSA schemes.

D. Study on RMSE

The RMSE values with parameters for each benchmarks in the dataset is exposed in Table III.

TABLE III. RMSE FOR VERIFIED BENCHMARK IN DATASET

Parameters	RMSE
400.perlbench	0.75
401.bzip2	0.661438
403.gcc	0.75
429.mcf	0.75
445.gobmk	0.829156
456.hmmer	0.661438
458.sjeng	0.661438
462.libquantum	0.829156
464.h264ref	0.661438
471.omnetpp	0.707107
473.astar	0.707107
483.xalancbmk	0.661438

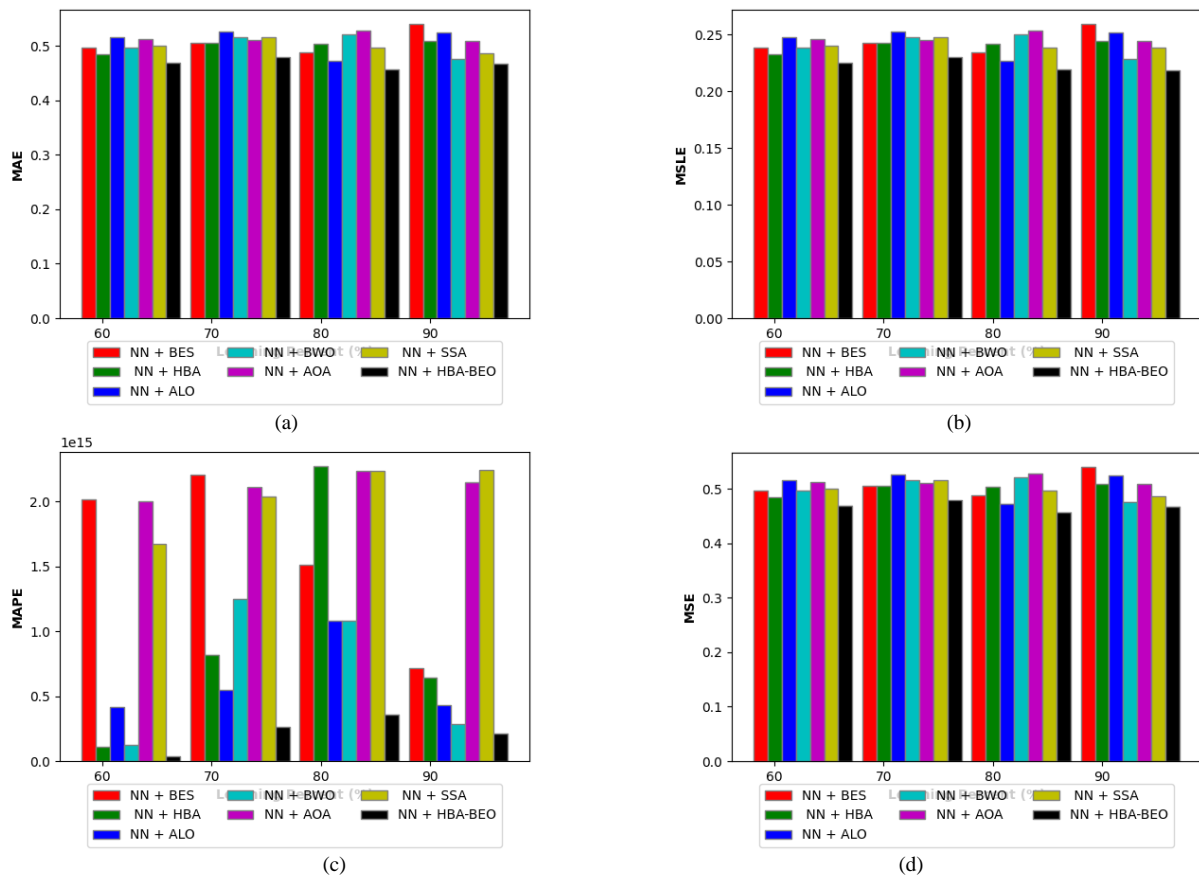


Fig. 3. Attacks Analysis (a) MAE (b) MSLE (c) MAPE and (d) MSE for NN + HBA-BEO Scheme Over Others.

VI. CONCLUSION

This work developed a novel Compiler Optimization Prediction Model. In this research, optimization [25] is the key factor considered and it is achieved through derived features and neural network. The features like static and dynamic features as well as improved Relief based features were extracted. The derived features were given to NN scheme, in which the weights were tuned via NN + HBA-BEO. Finally, the NN offered the final predicted output [26]. Here, the considered metrics like specificity, sensitivity, accuracy and precision were examined, which were established to be much better over BES, HBA, ALO, BWO, AOA and SSA models. The accuracy of NN + HBA-BEO was high at 90th LP, while precision was high at 80th LP. However, at all LPs, NN+HBA-BEO has established higher outcomes over NN + BES, NN + HBA, NN + ALO, NN + BWO, NN + AOA and NN + SSA models.

REFERENCES

- [1] Wu, J. Xu, X. Meng, H. Zhang, Z. Zhang and L. Li, "Compilation Optimization Pass Selection Using Gate Graph Attention Neural Network for Reliability Improvement," in IEEE Access, vol. 8, pp. 150422-150434, 2020, doi: 10.1109/ACCESS.2020.3016758.
- [2] N. Neves, P. Tomás and N. Roma, "Compiler-Assisted Data Streaming for Regular Code Structures," in IEEE Transactions on Computers, vol. 70, no. 3, pp. 483-494, 1 March 2021, doi: 10.1109/TC.2020.2990302.
- [3] Thoman, P., Zangerl, P. & Fahringer, T. Static Compiler Analyses for Application-specific Optimization of Task-Parallel Runtime Systems. J Sign Process Syst 91, 303–320 (2019). <https://doi.org/10.1007/s11265-018-1356-9>.
- [4] Tao, X., Pang, J., Xu, J. et al. Compiler-directed scratchpad memory data transfer optimization for multithreaded applications on a heterogeneous many-core architecture. J Supercomput 77, 14502–14524 (2021). <https://doi.org/10.1007/s11227-021-03853-x>.
- [5] Ashcraft, M.B., Lemon, A., Penry, D.A. et al. Compiler Optimization of Accelerator Data Transfers. Int J Parallel Prog 47, 39–58 (2019). <https://doi.org/10.1007/s10766-017-0549-3>.
- [6] Michael C.Broglioli, "Software and Compiler Optimization for Microcontrollers, Embedded Processors, and DSPs", Software Engineering for Embedded Systems (Second Edition), pp.245-267, 2019.
- [7] A. Serrano-Cases, Y. Morilla, P. Martín-Holgado, S. Cuenca-Asensi and A. Martínez-Álvarez, "Nonintrusive Automatic Compiler-Guided Reliability Improvement of Embedded Applications Under Proton Irradiation," in IEEE Transactions on Nuclear Science, vol. 66, no. 7, pp. 1500-1509, July 2019, doi: 10.1109/TNS.2019.2912323.
- [8] J. Wu, J. Xu, X. Meng, H. Zhang, Z. Zhang and L. Li, "Compilation Optimization Pass Selection Using Gate Graph Attention Neural Network for Reliability Improvement," in IEEE Access, vol. 8, pp. 150422-150434, 2020, doi: 10.1109/ACCESS.2020.3016758.
- [9] Carabaño, J., Westerholm, J. & Sarjakoski, T. A compiler approach to map algebra: automatic parallelization, locality optimization, and GPU acceleration of raster spatial analysis. Geoinformatica 22, 211–235 (2018). <https://doi.org/10.1007/s10707-017-0312-3>.
- [10] A. Serrano-Cases, Y. Morilla, P. Martín-Holgado, S. Cuenca-Asensi and A. Martínez-Álvarez, "Nonintrusive Automatic Compiler-Guided Reliability Improvement of Embedded Applications Under Proton Irradiation," in IEEE Transactions on Nuclear Science, vol. 66, no. 7, pp. 1500-1509, July 2019, doi: 10.1109/TNS.2019.2912323.
- [11] SPEC CPU2006: SPEC CPU2006 benchmark suite. <http://www.spec.org/cpu/>.
- [12] Chetverina, O.A. Alternatives of profile-guided code optimizations for one-stage compilation. Program Comput Soft 42, 34–40 (2016). <https://doi.org/10.1134/S0361768816010035>.
- [13] Beierle, C., Kutsch, S. & Sauerwald, K. Compilation of static and evolving conditional knowledge bases for computing induced nonmonotonic inference relations. Ann Math Artif Intell 87, 5–41 (2019). <https://doi.org/10.1007/s10472-019-09653-7>.
- [14] Goodrich, T.D., Sullivan, B.D. & Humble, T.S. Optimizing adiabatic quantum program compilation using a graph-theoretic framework. Quantum Inf Process 17, 118 (2018). <https://doi.org/10.1007/s1128-018-1863-4>.
- [15] Zhu, D., Yang, Z., Chen, C. et al. Compilation of program-loading spectrum for milling of a motorized spindle based on cutting force model. J Braz. Soc. Mech. Sci. Eng. 41, 187 (2019). <https://doi.org/10.1007/s40430-019-1686-y>.
- [16] Yogeswaran Mohan, Sia Seng Chee, Donica Kan Pei Xin and Lee Poh Foong, "Artificial Neural Network for Classification of Depressive and Normal in EEG", 2016 IEEE EMBS Conference on Biomedical Engineering and Sciences (IECBES), 2016.
- [17] Alsattar, H.A., Zaidan, A.A. & Zaidan, B.B. Novel meta-heuristic bald eagle search optimisation algorithm. Artif Intell Rev 53, 2237–2264 (2020). <https://doi.org/10.1007/s10462-019-09732-5>.
- [18] Fatma A. Hashim, Essam H. Houssein, Kashif Hussain, Mai S. Mabrouk, Walid Al-Atabany, "Honey Badger Algorithm: New metaheuristic algorithm for solving optimization problems", Mathematics and Computers in Simulation, Vol.192, 2022.
- [19] M. Marsaline Beno, Valarmathi I. R, Swamy S. M and B. R. Rajakumar, "Threshold prediction for segmenting tumour from brain MRI scans", International Journal of Imaging Systems and Technology, Vol. 24, No. 2, pp. 129-137, 2014.
- [20] Renjith Thomas and MJS. Rangachar, "Hybrid Optimization based DBN for Face Recognition using Low-Resolution Images", Multimedia Research, Vol.1, No.1, pp.33-43, 2018.
- [21] Devagnanam J, Elango N M, "Optimal Resource Allocation of Cluster using Hybrid Grey Wolf and Cuckoo Search Algorithm in Cloud Computing", Journal of Networking and Communication Systems, Vol.3, No.1, pp.31-40, 2020.
- [22] SK.Mahammad Shareef and Dr.R.Srinivasa Rao, "A Hybrid Learning Algorithm for Optimal Reactive Power Dispatch under Unbalanced Conditions", Journal of Computational Mechanics, Power System and Control, Vol.1, No.1, pp.26-33, 2018.
- [23] Liu, H., Zhao, R., Wang, Q. et al. ALIC: A Low Overhead Compiler Optimization Prediction Model. Wireless Pers Commun 103, 809–829 (2018). <https://doi.org/10.1007/s11277-018-5479-x>. S.Baskar, S. & Lawrence, Dr. L. Arockiam. (2013). C-LAS Relief-An Improved Feature Selection Technique in Data Mining. International Journal of Computer Applications. 83. 33-36. 10.5120/14511-2891.
- [24] A. D. Sutar and S. B. Shinde, "ECU diagnostics validator using CANUSB," 2017 International Conference on Inventive Computing and Informatics (ICICI), 2017, pp. 856-860, doi: 10.1109/ICICI.2017.8365257.
- [25] A. D. Sutar and S. B. Shinde, "ECU Health Monitor Using CANUSB," 2018 Second International Conference on Inventive Communication and Computational Technologies (ICICCT), 2018, pp. 415-419, doi:10.1109/ICICCT.2018.8473000.
- [26] Sagar Shinde, R. Khanna, R. B. Waghulade, "Identification of Handwritten Complex Mathematical Equations", International Journal of Image, Graphics and Signal Processing(IJIGSP), Vol.11, No.6, pp. 45-53, 2019. DOI: 10.5815/ijigsp.2019.06.06.

A Deep Learning and Machine Learning Approach for Image Classification of Tempered Images in Digital Forensic Analysis

Praveen Chitti¹, Dr. K. Prabhushetty², Dr. Shridhar Allagi³

Department of Electronics and Communication Engineering¹

Jain College of Engineering, Visvesvaraya Technological University, Belagavi¹

Department of Electronics and Communication Engineering²

Veerappa Nisty Engineering College, Shorpur

Visvesvaraya Technological University, Belagavi

Department of Computer Science and Engineering, KLE Institute of Technology, Hubballi³

Abstract—Multimedia images are the primary source of communication across social media and other websites. Multimedia security has gained the attention of modern researchers and has posed dynamic challenges such as image forensics, image tampering, and deep fakes. Malicious users tamper with the image embedding noise, leading to misinterpretation of the content. Identifying and authenticating the image by detecting the forgery operations performed on it is essential. In our proposed model, we detect the forged region using the machine learning model SVM in the first iteration and Convolution Neural Network in the second iteration with Discrete Cosine Transform (DCT) for feature extraction. The proposed model is tested with a Corel 10K dataset, and an average accuracy of 98% is obtained for all kinds of image operations, including scaling, rotation, and augmentation.

Keywords—Support Vector Machine (SVM); Discrete Cosine Transform (DCT); Convolution Neural Network (CNN); Image Forensics and Image Forgery

I. INTRODUCTION

With the invention of high-speed networks and advanced storage technologies, the internet used in almost every domain has increased drastically. Significant technological innovations have occupied every area with intelligent technologies and devices. The use of multimedia in social networking and other applications has invited other challenges where intruders modify or forge the data for illicit usage. Digital transformations have opened up a new domain of image forensic analysis. The need for providing authentic documents with integrity is a much-needed research area.

Recent Information and Communication Technology (ICT) has a vast spectrum of applications imbibing from each machine to pools of networks by large organizations. Users over the globe are not limited to work applications but are used for various applications such as personal banking transactions, multimedia data sharing across social media platforms, etc. [1] Larger companies regularly conduct their every transaction and operation across the internet, and more extensive data migrations across the firms occur via the networks comprising lesser secured public internet.

The drastic inventions in the cloud and big data technology solutions have seen exponential usage in social networking and mobile communication applications, leading to more extensive organization information flow operations. This limited the organization's security architecture for handling manipulated and tampered data. The increased activity of users and organizations has led to the misuse of computers and network-related applications ranging from simple password hacks to unauthorized access to servers.

Increased misuse of network and computer-related applications has led to increased research in computer-related investigations. Traditionally auditing the logs was a simple way to trace fraud operations, and the advanced hacking techniques are so powerful that no traces are found in the records. Hence the need for an automated and intelligent way of forensics is necessary. Digital forensics has made advanced developments over the years. The primary reason for the development is intelligence in tools and techniques that use local hardware machines to perform complex auditing tasks more precisely. The difficult task of auditing the logs is automated using machine learning models.

The rapid increase in the digital content comprising images over the internet has challenged the retrieval efficiency of several applications. The content-based image retrieval (CBIR), the effective and modern method for retrieval of images from the web, has addressed the challenge to some extent. CBIR is defined as the operation for retrieving images over the more extensive database in an effective and timely manner using dominant features of stored images such as texture, color, shape, etc. The effectiveness and efficiency of any CBIR model rely entirely on the identified extracted feature subset, as these values are used in the computation of similarity among the stored and retrieved images. Fig. 1 shows the classic examples of image tempering instances.

The primary purpose of the research is to secure the machine learning-based models for forensic analysis in the training and testing phase of the proposed architecture. The primary model experiments with the Support Vector Machine and the transformation functions applied with feature reduction for training the classifier. In the next level, forensic analysis is

performed on the images, which have the specific traces acquired by the operations, such as coding, acquisition, and preprocessing. To enhance the robustness of the model, the Convolution Neural Network (CNN) has been integrated for additional training of the model. CNN is the programming model that aids the machine in learning from the operational data provided. It is a subset of the class for a deep neural network that proactively addresses several image processing operations such as pattern matching and recognition. The model is treated to be complex and interconnected with several neurons in each of the layers.

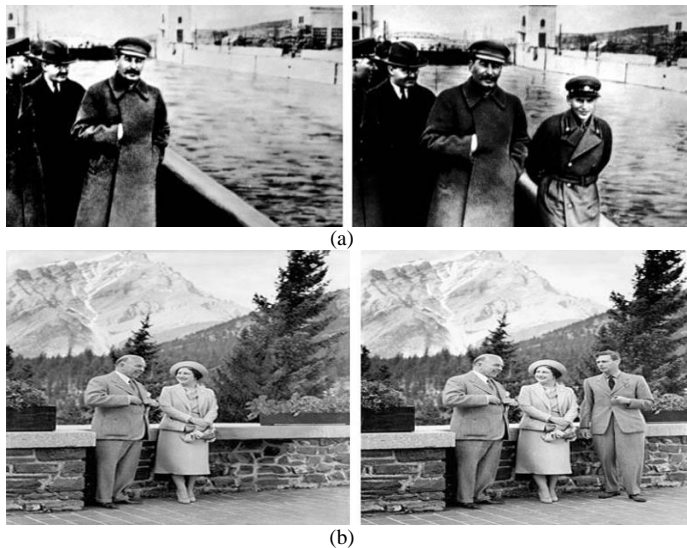


Fig. 1. Image Tempering Throughout the History [Courtesy: <https://twistedstifer.com/2012/02/famously-doctored-photographs/>].

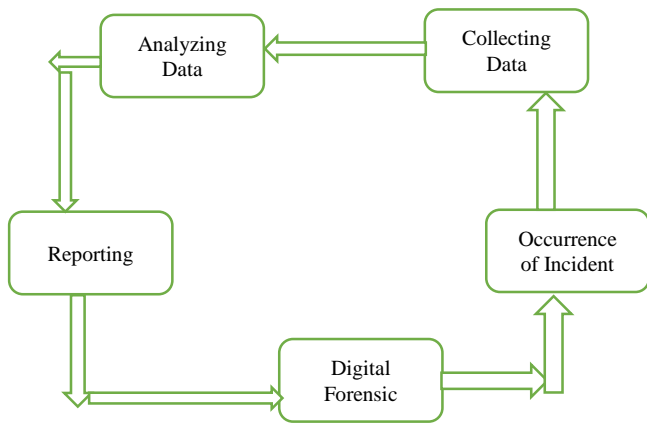


Fig. 2. Dimensions of Digital Forensics.

Fig. 2 provides the dimensions of digital forensics. Digital forensics involves the process of incident occurrence, analyzing collected data, and reporting the traces of anomalies in it.

II. RELATED WORKS

In [2] the work used pre-trained models for the lifecycle of forensic digital imaging tools. The work focused on the detection of a gun in a set of images. The work focused on the four pre-trained models, such as ImageNet-trained models: InceptionV3, Xception, ResNet, and VGG16, on the Adhoc realistic datasets without any of the fine-tuning of the models

used. The results were on par with the realistic determination of guns in the images. The work was limited to a particular class and could be extended with a few more classes to make the model more realistic.

In [3][4] the authors discussed the various needs for using machine learning and deep learning models and their implications. The various experimentations in the article show the augmenting of the performance of traditional models with the integration of machine learning models and the development of the conceptual framework for digital forensics.

The work in [5][6] proposed the support vector machine learning model with DWT and PCA as feature reduction models. The proposed model has experimented with an Adhoc dataset comprising 10000 images, and the proposed work was compared against the decision tree and Bayesian model. The proposed architecture gave the optimized performance of an accuracy of 97% in a limited subset of training images.

In [7] they worked on detecting tampering on the images using the CFA artifacts. The model provided optimal results in the detection of forged region localizations. The model has experimented on the UCID dataset and several images pulled from various social media websites. The model used the scalar-based approach with forensic analysis by machine learning. The experimental results were optimized with this approach and limited to a few classes. The procedure failed when experimented with multi-class label datasets.

The model in [8] addressed image forgery on social media and other prominent websites. The work focused on copy-move forgery detection using block processing and extracted the features transformed from the blocks. The convolutional neural network was for detecting the forgery. The serial pairs of convolutions are used for extracting the features and then enable the classification of images as tampered and originals, including the consideration of transformation operations. For Experimentation, various trigonometric transforms for 1D and 2D are considered. The model gave the optimum accuracy but was limited to the specifically trained dataset and required a robust model to deal with all kinds of images.

The experiments in [9] discussed the significant risks and shortcomings of using CNN models in clinical applications. The research focused on noise discovered in medical images and its impact on deteriorating the model's performance. They proposed a defense mechanism to such noises by incorporating the sparsity of denoising methods performed inherently in the CNN models to enhance the model's accuracy and overall performance. The model gave an accuracy of up to 97%.

The model in [10] discussed the impacts of adversarial perturbations on CNN and its challenges. The model is designed on the new architecture that specifically increases the robustness of the adversarial effects by using feature denoising. The network design consists of blocks that denoise each feature using various nonlocal means and a combination of other filters. The model has experimented on Imagenet, and the model's performance is enhanced by embedding this method in machine learning models.

The work by authors in [11] addressed the problem with the authenticity of the images shared across social media and other

websites. They proposed a digital image forensics model to identify the images' averaging and gaussian filtering. The model first normalized the image and computed the difference in array values for calculating the co-occurrence features. The model achieved higher accuracy for even small-size images with less resolution, but the results were minimal for the higher-size images.

The authors in [12] proposed a model based on the pixel-pair histogram (PPH) and coefficients of an autoregressive moving average model (ARMA). These features are extracted from various directions in an image for computing the median filters. Experimentations were done on multiple single and compound databases, and the model enhanced the accuracies of the models, especially for the JPEG formats and compressed versions of the images.

III. PROPOSED METHODOLOGY

The proposed methodology works in two layers. In the initial phase, the support vector machine is used with the RBF kernel in training the images. In the second layer, CNN is used for training the model for making the classification more robust. Fig. 3 shows the proposed model for forensic image detection.

A. Dataset

To test the proposed model's robustness, experimentations were conducted on a target set of 100000 images. The images span different categories, such as oceans, mountains, fruits, etc. Every image is scaled to 192 X 128. The dataset is spread across 100 categories, composing 100 images in each type. Fig. 4 shows the sample images in the dataset.

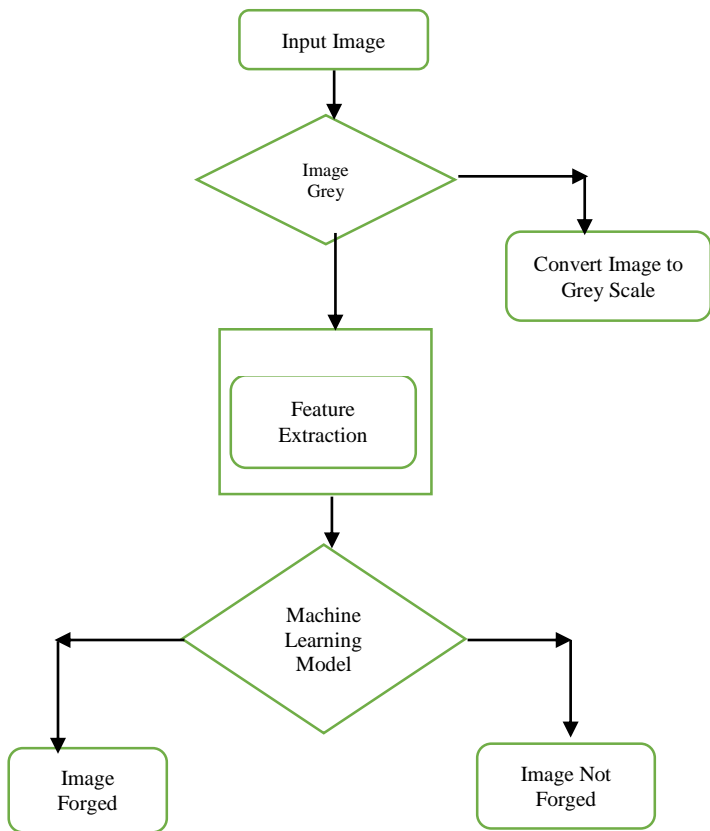


Fig. 3. Proposed Model for Forensic Image Detection.



Fig. 4. Sample Images in the Corel -10K Image Dataset.

Each image has been extracted with 89 features. These features are composed of four sets based on color histogram layout, histogram, co-occurrence, and color moments.

TABLE I. FEATURE SET DESCRIPTION

Feature	Dimensions	Description
Color Histogram	32	HSV is divided into 32 subspaces. 8 for H and 4 for S.
Color Histogram layout	32	Image is divided into four sub-images
Color Moments	9	3 for H, S, and V
Co-occurrence Texture	16	co-occurrence in 4 directions is computed (horizontal, vertical, and two diagonal directions)

B. Feature Extraction and Feature Reduction

Algorithm: Feature Extraction

Input: Image I
 Output: 89 Features i_1, i_2, \dots, i_n
 Step 1: Convert RGB to HSV Image.
 Step 2: Split the input image into H, S, and V sub-image spaces
 Step 3: Canny Operator is used for edge detection and segmentation
 Step 4: Discrete Cosine Transform (DCT) is used for feature extraction
 Step 5: 89 feature sets are extracted from the image

The DCT coefficient entities signify the spatial frequency components in an image, and every pattern of the blocks in an image is augmented with various magnitudes. The extracted features depend on the prominent edge, and the values extracted signify the image's lowest frequencies.

Fig. 5 (a) shows the original image and the extracted features from HSV subspaces in images. Fig. 5 (b) shows the sample extracted feature matrix.

In computing the DCT coefficients matrix, the major component for the spectral coefficients of images represent the lower frequency sections and higher frequency sections with amplitude of areas across the image. Since the most dominating area of interest is around the lower frequency, we discard the values closer to 0. The coefficients of DCT are reduced w.r.t to (1).

$$D_C(u,v,s)=F(u,v) \quad u,v=1,2,3,\dots,s \quad 1 \leq s \leq 8 \dots \quad (1)$$

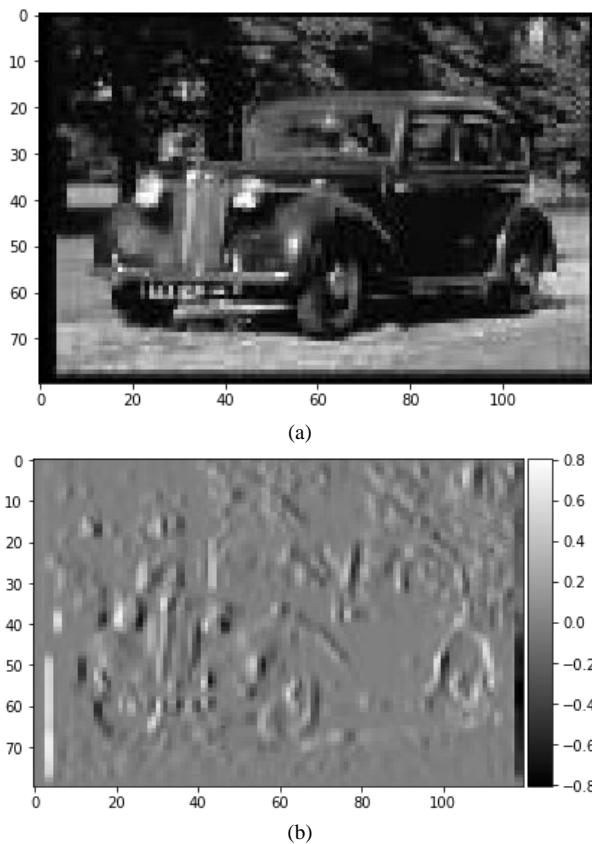


Fig. 5. (a) Original Image. (b) Image Feature Extraction.

Where $F(u,v)$ Represents the DCT coefficients of image block I . $D_C(u,v,s)$ Represent the reduced DCT Coefficient. S represents the reduction scale for the image.

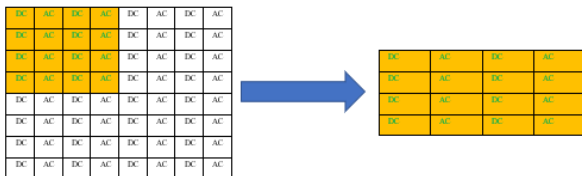


Fig. 6. DCT Reduced Coefficients from 8 X 8 to 4 X 4.

Since the DC coefficients among the adjacent blocks of images are redundant and the AC coefficients are small, these values are ignored. DCT transforms the correlation among the adjacent 8 X 8 blocks of images and is quite dominant. Hence smoothing these edges is necessary. The operation is performed using DCT coefficient values, which will uniformly distribute the frequency across the images. The reduced and smoothed coefficients of DCT are computed as of (2). The sample features extracted using DCT are shown in Fig. 7.

$$D_C = \begin{cases} F(u, v) & (u, v) = 1 \\ F(u, v) + \frac{F(1,1)}{8} & (u, v = 2, \dots, s) \end{cases} \quad (1 < s \leq 8) \quad (2)$$

```
[[0.00841647 0.01402745 0.01683294 ... 0.02244392 0.02972157 0.00841647]
 [0.03112039 0.00841647 0.00841647 ... 0.27485373 0.26081922 0.02972157]
 [0.00841647 0.00841647 0.02719882 ... 0.58496314 0.44741059 0.01683294]
 ...
 [0.00083333 0.00977765 0.00977765 ... 0.3603051 0.34487882 0.04488784]
 [0.00504471 0.01092353 0.0025 ... 0.11630314 0.13617882 0.02524941]
 [0.00452392 0.01320039 0.01794824 ... 0.02244392 0.05497098 0.01963843]]
```

Fig. 7. Feature Matrix using DCT.

IV. MACHINE LEARNING MODELS

In the first phase, the support vector machine with the configuration in Table II is used to train the model. Support Vector Machine (SVM) is majorly used in classification, and recognition tools are embedded to avoid computational complexities. Our work proposes a methodology for detecting the forged image, which might comprise any subpart if the image has been added, removed, or altered. The SVM is used for identifying the similar neighboring regions of an image by matching with other blocks of the image computed. To identify a forged part in an image, the features are extracted w.r.t to HSV, texture, pixel value, and the edges of several regions in an image. The process works in two iterations. In the first iteration, the model is trained with the images without forged parts. The second iteration tests the model with the sample set of images containing the forged part. The SVM model is used to classify the images into two classes: forged or genuine. The model initially identifies the edges and decides the decision boundaries in the training phase. This information will be used for generalizing the images with higher dimensions. A decision space (support vectors) for the set of images is generated using the larger space of trained images which separates the objects belonging to a different class.

All the experiments were conducted on Ubuntu 22.0 LTS 64-bit Operating System with 24GB Ram, intel core i5 @3.40Ghz with python 3.0. The entire dataset was divided in the ratio of 70:30 for the training and testing dataset. In the initial phase, the training is done with a support vector machine with rbf kernel, as mentioned in Table II.

TABLE II. CONFIGURATION OF SVM MODEL

Model	Kernel	γ
Support Vector Machine	rbf	1/n

To make the model more robust, it is trained with the CNN model as specified in Table III in the second phase.

TABLE III. CNN MODEL CONFIGURATION

Image Layer	Filters	Feature map size	Size for filter	Strides	Padding
1 st CNN Layer	664	224*224*64	3*3*3	1	1
2 nd CNN Layer	64	224*224*64	3*3*64	1	1
Max Pooling	1	112*112*64	2*2	2	0

Accuracy: 0.7559631452364789
Precision: 0.7559631452364789
Recall: 0.7559631452364789
Sensitivity: 0.7559631452364789
Specificity: 0.7559631452364789

(a)

Accuracy: 0.9559631452364789
Precision: 0.9559631452364789
Recall: 0.9559631452364789
Sensitivity: 0.9559631452364789
Specificity: 0.9559631452364789

(b)

Fig. 8. (a) Performance Metric of SVM (b) Performance Metric of CNN.

Fig. 8 shows the performance metrics computed for the support vector machine and the CNN. Fig. 9 gives the different forged images detected.

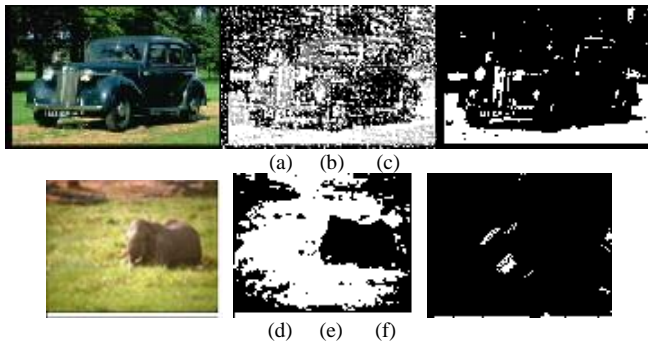


Fig. 9. Results of Proposed Model (a) Input Image (b) Threshold Image (c) Classified as Not Forged (d) Input Image (e) Threshold Image (f) Classified as Forged Image.

V. CONCLUSION

In recent research, many researchers proposed various methods for forgery detection, which can be further categorized into supervised and unsupervised classification models. The two models experimented with, in our work, support vector machine and the convolution neural network have performed well, with an accuracy of 75% and 95%. The CNN model wrongly classified the few forged images to non-forged. These misclassifications were handled correctly in the SVM. Hence the model proposed is trained in two iterations with respect to

SVM and CNN. The combined classifier gave an accuracy of over 98%. The proposed model can be further enhanced with an optimal feature reduction mechanism, and using unsupervised models may augment the model's performance.

REFERENCES

- [1] <https://ciosea.economicstimes.indiatimes.com/blog/how-ai-will-transform-digital-forensics-in-2022-and-beyond/91141155>.
- [2] Del Mar-Raave, J. R., Bahşi, H., Mršić, L., & Hausknecht, K. (2021). A machine learning-based forensic tool for image classification - A design science approach. *Forensic Science International: Digital Investigation*, 38, 301265. <https://doi.org/10.1016/j.fsidi.2021.301265>.
- [3] Qadir, A. M., & Varol, A. (2020, June). The Role of Machine Learning in Digital Forensics. 2020 8th International Symposium on Digital Forensics and Security (ISDFS). <https://doi.org/10.1109/isdfs49300.2020.9116298>.
- [4] Solanke, A. A. (2022, July). Explainable digital forensics AI: Towards mitigating distrust in AI-based digital forensics analysis using interpretable models. *Forensic Science International: Digital Investigation*, 42, 301403. <https://doi.org/10.1016/j.fsidi.2022.301403>.
- [5] Qadir, S., & Noor, B. (2021, May 20). Applications of Machine Learning in Digital Forensics. 2021 International Conference on Digital Futures and Transformative Technologies (ICoDT2). <https://doi.org/10.1109/icodt252288.2021.9441543>.
- [6] Monika, & Passi, A. (2021, August 1). Digital Image Forensic based on Machine Learning approach for Forgery Detection and Localization. *Journal of Physics: Conference Series*, 1950(1), 012035. <https://doi.org/10.1088/1742-6596/1950/1/012035>.
- [7] Singh, G., & Singh, K. (2020, March). Digital image forensic approach based on the second-order statistical analysis of CFA artifacts. *Forensic Science International: Digital Investigation*, 32, 200899. <https://doi.org/10.1016/j.fsidi.2019.200899>.
- [8] Al_Azrak, F. M., Sedik, A., Dessowky, M. I., El Banby, G. M., Khalaf, A. A. M., Elkorany, A. S., & Abd. El-Samie, F. E. (2020, March 2). An efficient method for image forgery detection based on trigonometric transforms and deep learning. *Multimedia Tools and Applications*, 79(25–26), 18221–18243. <https://doi.org/10.1007/s11042-019-08162-3>.
- [9] Robust convolutional neural networks against adversarial attacks on medical images. (2021, December). *Pattern Recognition*, 132, 108923. <https://doi.org/10.1016/j.patcog.2022.108923>.
- [10] Cihang Xie, Yuxin Wu, Laurens van der Maaten, Alan L. Yuille, Kaiming He; Proceedings of the IEEE/CVF Conference on Computer Vision and Pattern Recognition (CVPR), 2019, pp. 501-509.
- [11] Agarwal, S., & Jung, K. H. (2021, January 31). Image Forensics using Optimal Normalization in Challenging Environment. 2021 International Conference on Electronics, Information, and Communication (ICEIC). <https://doi.org/10.1109/iceic51217.2021.9369794>.
- [12] Gao, H. (2020, January 21). Detection of median filtering based on ARMA model and pixel-pair histogram feature of difference image. SpringerLink. Retrieved September 7, 2022, from https://link.springer.com/article/10.1007/s11042-019-08340-3?error=cookies_not_supported&code=4b1663fa-e0a8-49e4-bd2b-bc3865481542.

Evaluation of Land Use/Land Cover Classification based on Different Bands of Sentinel-2 Satellite Imagery using Neural Networks

Mrs. Pallavi M¹

Assistant Professor Dept. of CSE
Presidency University
Bangalore, India

Dr. Thivakaran T K²

Professor Dept. of CSE
Presidency University
Bangalore, India

Dr. Chandankeri Ganapathi³

Associate Professor, Dept. Name of
Civil, Presidency University
Bangalore, India

Abstract—Spatial data analytics is an emerging technology. Artificial neural network techniques play a major role in analysing any critical dataset. Integrating remote sensing data with deep neural networks has led a way to several research problems. This paper aims at producing land use land cover map of Bangalore region, Karnataka, India with various band combinations of sentinel satellite imagery obtained from google earth engine. LULC map classes include water, urban, forest, vegetation and openland. Band combinations of satellite images represent different characteristics of spatial data. Hence, several band combinations are used to build LULC maps. Also, classified maps are generated using different neural networks with pixel-based classification approach. Appropriate performance metrics were identified to evaluate the classification results such as Accuracy, Precision, Recall, F1-score and Confusion Matrix. Among neural networks, Convolutional Neural Network technique outperformed with 98.1 % of accuracy and less error rates in confusion matrix considering RGBNIR (4328) band combination of satellite imagery.

Keywords—Sentinel-2; neural networks; convolutional neural networks; remote sensing data; land use land cover maps

I. INTRODUCTION

Monitoring the Earth's surface has undergone a radical change as a result of advances in satellite remote sensing technology. Sentinel-2 multispectral products, created as a result of the European Space Agency's (ESA) [2] and European Union's (EU) [3] Copernicus Programme, have helped to effectively monitor the Earth's surface [1]. The ESA Sentinel-2 satellite constellation, which includes multispectral scanners on board [35], is the second iteration of the Sentinel satellite programme. Sentinel-2's main goal is to supply high resolution [33] satellite data for observing changes in climate [34], monitoring natural disasters, and tracking changes in land cover and use. It also aims to supplement previous satellite missions like Landsat.

Sentinel level-2A dataset acquired is of one of the metropolitan cities of India i.e., Bangalore which was obtained from Google earth engine. A wide-swath, high-resolution, multi-spectral [2] imaging mission from Europe is called SENTINEL-2. The twin satellites' complete mission specification calls for a high return frequency of five days [33] at

the equator when they are in the same orbit but phased at 180°. With a spatial resolution of four bands at 10 m, six bands at 20 m, and three bands at 60 m, the optical payload on SENTINEL-2 will sample thirteen spectral bands [34]. It is possible to use the 290 km-wide orbital sweep. Based on Level-1C data with atmospheric correction for reflectance from the Bottom of the Atmosphere (BoA), data are used to create the Level-2A product [3]. They are routinely manufactured by ESA as of January 2019, exactly like the level 1C products previously mentioned.

The open access Sen2Cor processor allows users to continue producing their own BoA data from Level 1C. Water vapour map [35], Aerosols optical thickness map and a basic scene classification map [2] are among the extra Sen2Cor algorithm outputs that are included in Level 2A data. Sentinel Satellite Image Time Series (SITS) [3] have recently been productively utilised in the perspective of LULC mapping, illuminating the advantages of having access to such optical and radar SITS in this field. A few noteworthy examples include the creation of country-scale land cover maps using optical Sentinel SITS [4].

The following Table I shows the important features of Sentinel level-2 image.

The ideas of LULC laid the foundation to understand how people interact with the environment [6]. The term "Land Use" describes the purposes for which humans use the land cover, such as anthropogenic activity-induced changes. The term "land cover" describes the natural elements [5] that make up the surface of the Earth, such as agricultural land, aquatic sources, and topsoil. [7].

As deep learning techniques automate feature extraction and classification, it is more suitable and efficient for satellite imagery [8]. Each layer of deep learning model computes new data pattern from previous layers' data understanding of artificial neurons, resulting in order of data generalisations [9]. Convolution [32] and pooling layers [31] are typically followed by a fully connected neural network layer [19] and a suitable activation function [37] in CNNs, finally corresponding LULC class is predicted by softmax function as an output [10].

TABLE I. SENTINEL LEVEL-2 IMAGERY'S CHARACTERISTICS [3]

Spatial Resolution	Band Number	Central Wavelength (nm)	Bandwidth (nm)	Lref (reference radiance) ($W m^{-2} sr^{-1} \mu m^{-1}$)	SNR @ Lref
10m	2	490	65	128	154
	3	560	35	128	168
	4	665	30	108	142
	8	842	115	103	172
20m	5	705	15	74.5	117
	6	740	15	68	89
	7	783	20	67	105
	8b	865	20	52.5	72
	11	1610	90	4	100
	12	2190	180	1.5	100
60m	1	443	20	129	129
	9	945	20	9	114
	10	1375	30	6	50

A. Study Area

The great capital of the Indian Karnataka state, Bangalore [36] is one of the cities with the greatest population growth. The most populated district in the state, accounting for 15.8% of the state's total population, is located in Karnataka's only metropolitan region, which has a total population of 96,21,551 (as of the 2011 census). The district's total area is 2196 sq. km, with 4381 people residing in each sq. km. In terms of both land and population, it is the largest district in the state of Karnataka. The majority of Bangalore's population lives in urban areas, making it the most urbanised district.

Bengaluru as showed in Fig. 1 is located on the Deccan Plateau [28], in the Karnataka state's south eastern part. The Bengaluru district lies between 120 58' to 130 0' North Latitude and 770 37' to 780 18' East Longitude. The district's elevation is typically about 1000m above the mean sea level which bestows it with a healthy climate. The district has four taluks namely Bengaluru North, South, East, and Anekal. The famous IT and BT Electronic City situated in Anekal taluk [36].

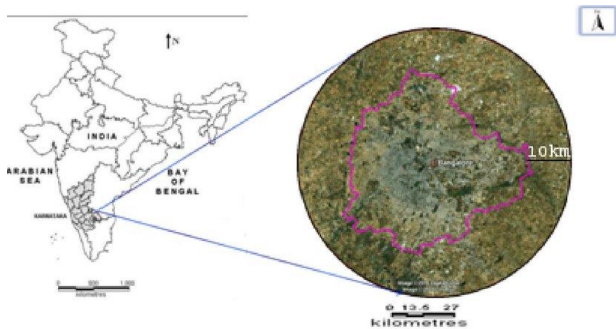


Fig. 1. Bangalore BBMP Limits Study Area [28].

II. RELATED WORK

Sentinel-2 image of Bangalore region was tiled into patches and for the identified land use land cover classes of trained patches, CNN architectures such as DenseNet201, VGG16 and Resnet50 were applied. This yielded better classification results. [27].

Quick Bird datasets of the regions Rome, Las Vegas and Florida were used for the scene classification using Support Vector machine's margin sampling approach and Entropy query by bagging which is a classifier independent method [13]. Kappa index was mainly used along with accuracy to evaluate the pixel based classification in this study.

Four classes (Water, Cropland, Forest and built-up) of LULC generated for the region Mandya, Karnataka using five bands of Sentinel-2A namely SWIT, NIR, Blue, Red and Green with F1-Score of 0.84 using modified Segnet architecture of deep learning [11].

High resolution image datasets of urban areas of China, Italy and Germany were used with Deep Convolutional neural network techniques for the classification of land use and achieved accuracies of about 90% using object-based and pixel-based approaches [12].

Sentinel 2 image bands of 4, 3, 2, 8 were used for the land cover classification of central java region of Indonesia. With the ArcMap tool and supervised classification approach, a very high accuracy of 1 and moderate kappa value of 0.4896 [14] were achieved. Maximum Likelihood classifier used in this research is then assessed by comparing raster values of classified image and actual google earth engine image. For this, acquisition dates of two images are kept same.

Maximum Likelihood Classifier (MLC) and Support Vector Machine (SVM) classifiers of ERDAS imagine tool were applied on Sentinel-2 and Landsat-8 dataset of Istanbul metropolitan city of Turkey's LULC classes [15]. Among these two classifiers, SVM achieved highest accuracy and kappa coefficient of 84.17% and 0.8190 respectively for the sentinel-2 data. Error matrix was calculated against classified random points and reference points of google earth also as an assessment.

Zonguldak, Turkey [16] was considered as the study area in this research. Sentinel -2 MSI and Landsat OLI were used as satellite imageries. MLC was used to generate LULC map. Classification using Sentinel-2 data yielded highest accuracy and kappa coefficient than Landsat-8. Accuracy was assessed with 460 stratified random points.

LULC maps and correlation matrix were generated for the Ahmedabad city of Gujarat state, India from the period 1991 to 2010 so as to know the change of certain land use classes. The main intension of this was to monitor population dynamics, urban expansion. [17].

This study presents application of LULC maps for the prediction of change and spatial distribution for the year 2027 of Ahmedabad city, Gujarat using the integration of cellular automata and artificial neural network model from temporal series of data from 1976 to 2017. [18].

Most of the recent research work focused on the LULC classification of satellite image patches (part of an image) of the interested areas. They were trained and fed to various neural, CNN architectures. But, LULC classification is required for the entire study area to perform change or any other spatial analysis. Only few GIS automated tools could do such classification for the entire study area rather than part of satellite image.

The main objective of this research is to generate optimal [29] land use land cover map using deep neural networks and convolutional neural networks approaches. In addition to this, various combinations of sentinel-2 image were evaluated to know the significance of each band. Finally, proposed model is evaluated using various metrics such as confusion matrix, precision, recall and F1-score. Model is validated with few randomly generated points which are then compared with google earth engine.

III. METHODOLOGY

The Fig. 2 process explains the data preparation before it is fed into the neural network. Firstly, Bangalore data is being extracted from sentinel portal through google earth engine using JavaScript. This requires date and year, proper selection of the region of interest, bands information. For the research we have downloaded, 2019's January till March data and used band combinations such as 843 (NIR, Red and Green), 432 (Red, Green, Blue) [14] and 8432 (NIR, Red, Green, Blue).

There are two important factors to select only Bruhat Bengaluru Mahanagara Palike (BBMP) limits within Bengaluru/Bangalore data. First, is to focus more on the urbanised areas so that change detection of LULC maps would be more interesting for further studies and second, is to reduce the study area image dimension so that computation time can also be lessened greatly. This phase is achieved by clipping only BBMP limits from whole Bangalore data.

As this research is done for medium spatial resolution image of 10m, pixel-based approach is more suitable [30]. Supervised classification approach is considered. For the same, training suites are generated based on the classes (Water, Urban, Forest, Vegetation and Open land). These suites are divided into train and test for the model evaluation. They are normalised within a scale of 255 so as to bring them into uniform range.

A. Neural Networks

The Fig. 3 shows the schematic representation of neural networks made use in the current work.

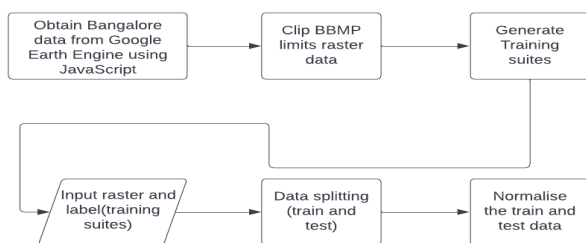


Fig. 2. Data Preparation Process.

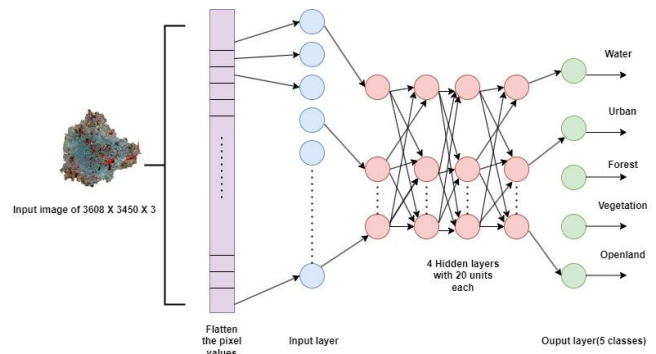


Fig. 3. Proposed Model of Deep Neural Networks.

Deep Neural Networks (DNN) are most efficiently used for multi-class classification [21]. As indicated in the above figure, we have used six layers in our proposed model. Firstly, input image is fed into the network. To ease the task, we have considered 80% of the input image pixels known as trained data out of the entire image. Pixel values are flattened and they are fed as neurons to the input layer. At hidden layer, sum of these inputs along with weights and bias as shown in equation (1) [19] is computed.

Relu activation function is applied to this sum as shown in equation (2) to activate neurons so that vanishing gradient problem could be overcome to some extent [20]. In this case, neuron values less than zero never gets activated. Likewise, process is repeated at next three hidden layers producing 20 units at each layer. Final hidden layer is connected output layer, wherein softmax function as represented in equation (3) finds the final predicted LULC class out of five as mentioned in the above figure.

$$z = \sum_i^n w_i x_i + b \quad (1)$$

here, n is number of input pixels

$$\delta(z) = \frac{1}{1 + e^{-(\sum_i^n w_i x_i + b)}} \quad (2)$$

$$\sigma(z_i) = \frac{e^{z_i}}{\sum_{j=1}^k e^{z_j}} \quad (3)$$

here, k is 5 (number of classes).

Model's hyperparameters include learning rate of 0.001, 100 epochs, batch size of 128. Dropout of 20% and 12 regularisation are considered [38]. We have used keras library to implement this model in python.

B. Convolutional Neural Networks

The Fig. 4. shows the CNN model used in this work.

Convolutional, pooling, and affine layers combine to form Convolutional Neural Networks (CNN). When it comes to visual identification tasks, CNN's perform fantastically and at the cutting edge of technology [22]. CNN's are also used to classify remote sensing images with its extensive features. Here, we have used two layers of convolution and two pooling layers. Basically these layers are used to create feature maps of image size of 1247600 with three channels and 7X7 patch size [9]. Using a filter with a stack of fixed-size kernels (here, 5X5), the feature maps are produced at each layer of convolution and

passed into non-linearity using an activation function. The feature maps are then calculated as the weighted sum of the preceding layer of feature patches (e.g., ReLU) [32]. In this way, they maintain location invariance within the input data array while detecting local correlations (fitted in the kernel size) [37].

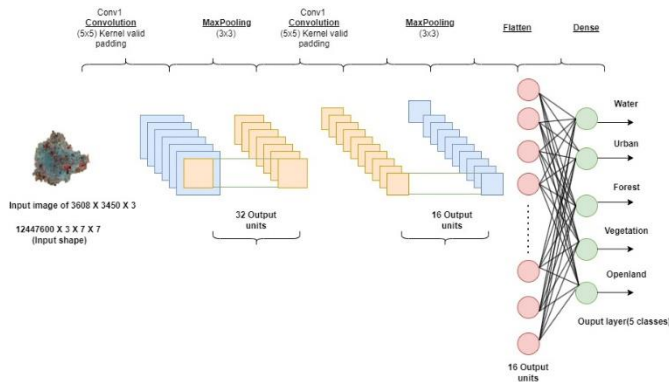


Fig. 4. Proposed Convolutional Neural Network Model.

By computing the maximum or average of nearby units to produce invariance to scaling, minor shifts, and distortions, the pooling layer (3X3) is utilised to minimise the dimension of the resulting feature map. A fully connected neural network and an activation function eventually complete the phases of convolution and pooling layers (32 and 16 units in first and second stage respectively), taking over control of the network's classification phase of five classes as described in the figure by further modeling non-linear relationships [23] of input features.

To train the model and to optimise the input features learnt, we have utilised learning rate of 0.001, epochs of 100, batch size of 128, loss function as Categorical Cross Entropy and Adam as optimiser [38]. The implementation was carried out using Pytorch for its robustness and Speed. Of course, high end system with GPU support was used for the research.

IV. RESULTS AND DISCUSSION

In this section, firstly we have explained the results obtained using neural networks and then convolutional neural networks. For both the methodologies used in this study, BBMP region's sentinel level2 image of the period January to March 2020 data is fed as an input. Corresponding Predicted LULC maps are listed from Fig. 5-10. To create typical LULC map as in Geographical Information Systems (GIS), we have added latitude, longitude, scale bar, text, north arrow [26] to the classified image.

Error matrix is tabulated for all the five LULC classes i.e., Water, Urban, Forest, Vegetation and Openland for both DNN and CNN methods in terms of pixels. To compute this, only test data (20% of 12447600 pixels i.e., 2489520) obtained from the input as depicted in Fig. 2. is considered. Table II to IV and Table V to VII are the error matrices of DNN and CNN respectively.

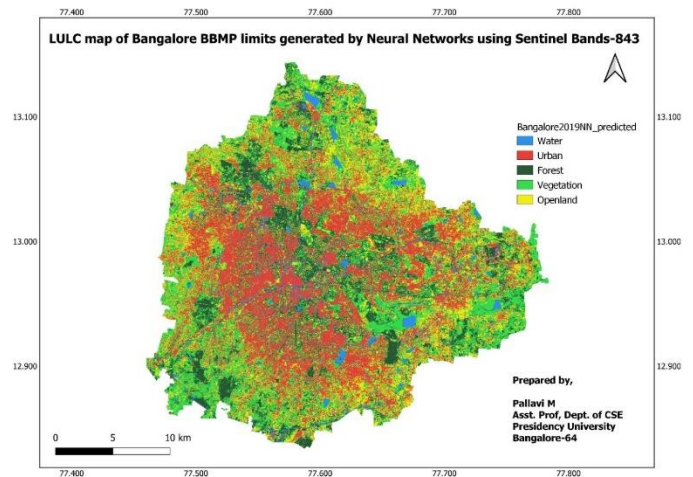


Fig. 5. LULC Classification Map Generated using Deep Neural Networks of the Sentinel Image Band Combination-843.

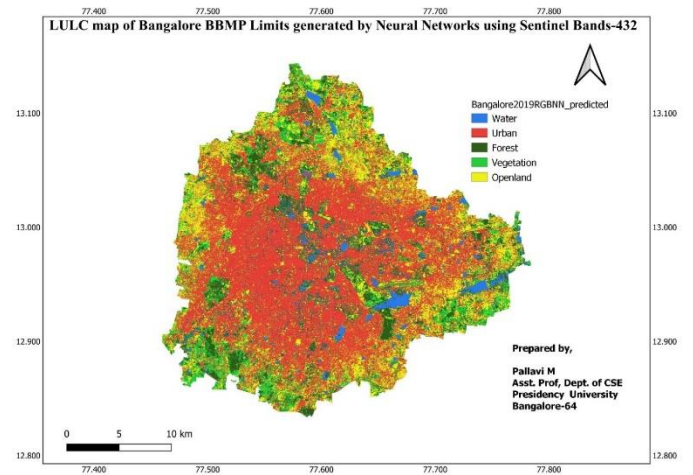


Fig. 6. LULC Classification Map Generated using Deep Neural Networks of the Sentinel Image Band Combination-432.

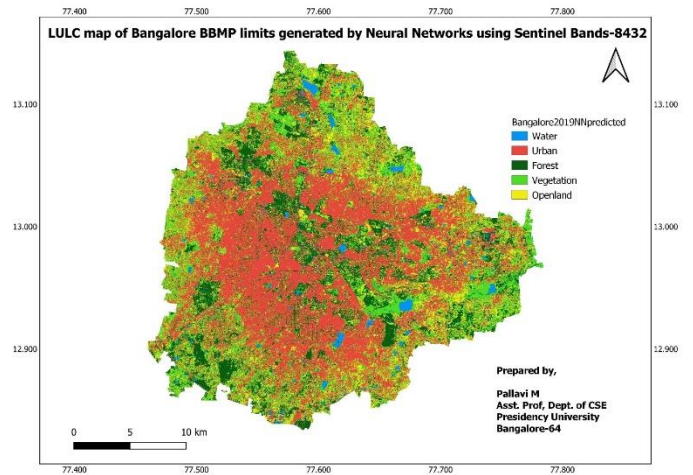


Fig. 7. LULC Classification Map Generated using Deep Neural Networks of the Sentinel Image Band Combination-8432.

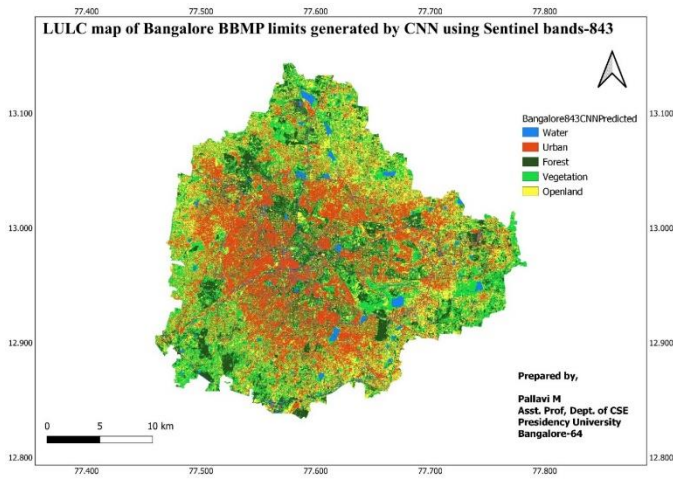


Fig. 8. LULC Classification Map Generated using Convolutional Neural Networks of the Sentinel Image Band Combination-843.

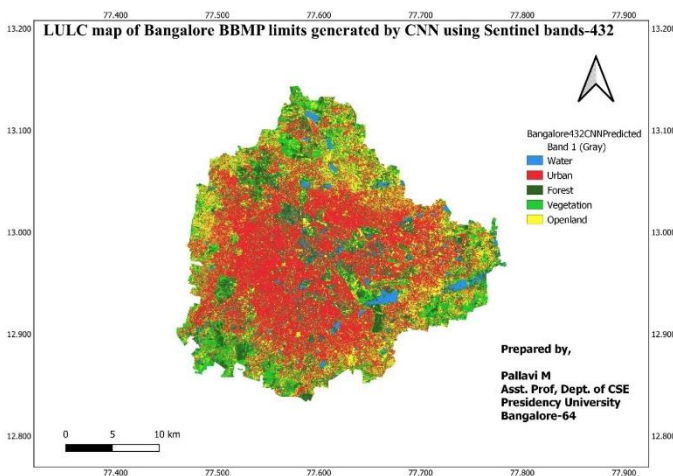


Fig. 9. LULC Classification Map Generated using Convolutional Neural Networks of the Sentinel Image Band Combination-432.

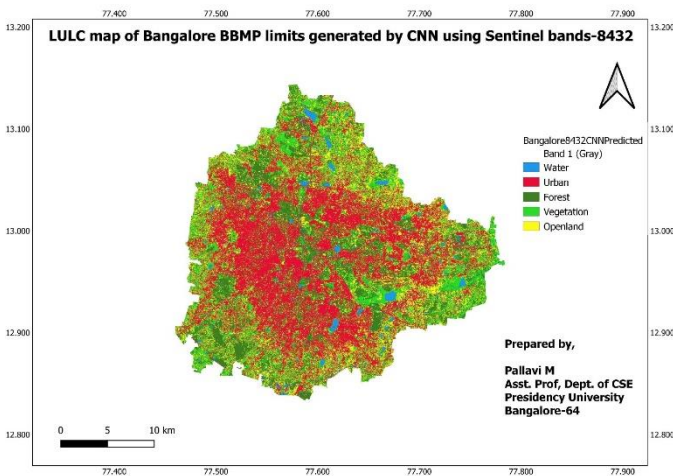


Fig. 10. LULC Classification Map Generated using Convolutional Neural Networks of the Sentinel Image Band Combination-8432.

TABLE II. CONFUSION MATRIX OBTAINED PER CLASS FOR THE TEST DATA USING DEEP NEURAL NETWORKS OF THE SENTINEL IMAGE BAND COMBINATION-843

	Water	Urban	Forest	Vegetation	Openland
Water	62599	517	3208	0	0
Urban	48	413647	729	2111	14688
Forest	2028	0	215668	3064	0
Vegetation	0	304	2419	373329	65736
Open land	0	14248	0	14353	277213

TABLE III. CONFUSION MATRIX OBTAINED PER CLASS FOR THE TEST DATA USING DEEP NEURAL NETWORKS OF THE SENTINEL IMAGE BAND COMBINATION-432

	Water	Urban	Forest	Vegetation	Openland
Water	53054	1271	9012	286	6
Urban	6703	624717	1567	21347	59603
Forest	13225	493	135680	10624	0
Vegetation	41	13464	41	188182	29
Open land	12	42483	0	18721	265349

TABLE IV. CONFUSION MATRIX OBTAINED PER CLASS FOR THE TEST DATA USING DEEP NEURAL NETWORKS OF THE SENTINEL IMAGE BAND COMBINATION-8432

	Water	Urban	Forest	Vegetation	Openland
Water	33210	2062	780	0	0
Urban	975	538202	109	15174	38255
Forest	2768	13	261038	1925	0
Vegetation	0	4306	1926	256390	41863
Open land	1386	14162	8522	31969	210875

TABLE V. CONFUSION MATRIX OBTAINED PER CLASS FOR THE TEST DATA USING CONVOLUTIONAL NEURAL NETWORKS OF THE SENTINEL IMAGE BAND COMBINATION-843

	Water	Urban	Forest	Vegetation	Openland
Water	57826	4237	2610	0	0
Urban	17	417627	2	66	11004
Forest	666	897	207906	12550	0
Vegetation	0	2150	107	373032	17568
Open land	0	7018	0	20414	330205

TABLE VI. CONFUSION MATRIX OBTAINED PER CLASS FOR THE TEST DATA USING CONVOLUTIONAL NEURAL NETWORKS OF THE SENTINEL IMAGE BAND COMBINATION-432

	Water	Urban	Forest	Vegetation	Openland
Water	52002	8033	12427	571	0
Urban	240	624769	3944	30624	22850
Forest	889	8	145358	39	0
Vegetation	1	397	6058	230483	2219
Open land	12	48162	0	21805	255008

TABLE VII. CONFUSION MATRIX OBTAINED PER CLASS FOR THE TEST DATA USING CONVOLUTIONAL NEURAL NETWORKS OF THE SENTINEL IMAGE BAND COMBINATION-8432

	Water	Urban	Forest	Vegetation	Openland
Water	35440	1761	878	0	257
Urban	361	549226	9	6823	2326
Forest	1056	134	259067	5990	6120
Vegetation	0	944	26	301016	3472
Open land	5	9231	95	7331	274330

The equations (4) - (6) are used for model evaluation metrics calculation, where m stands for number of classes (m=5) [24]

$$\text{Accuracy} = \frac{TP_m + TN_m}{TP_m + TN_m + FP_m + FN_m} \quad (4)$$

$$\text{Precision} = \frac{TP_m}{TP_m + FP_m} \quad (5)$$

$$\text{Recall} = \frac{TP_m}{TP_m + FN_m} \quad (6)$$

The Table VIII shows the overall Accuracy, P-Score and R-Score [25] of the DNN model for the test data. Among three different bands used, RGNIR-438 combination yielded the highest score.

The Table IX shows the overall Accuracy, P-Score and R-Score of the CNN model for the test data. Among three different bands used, RGBNIR-4328 combination yielded the highest score.

Fig. 11-16. to depict the Accuracy and loss graph of the DNN model for all the three band combinations used in this study.

TABLE VIII. CLASSIFICATION REPORT OF TEST DATA USING DEEP NEURAL NETWORKS OF VARIOUS SENTINEL BAND COMBINATIONS

Band Combination	Accuracy	P-Score	R-Score
RGNIR-438	95.04	0.950	0.950
RGB-432	92.00	0.920	0.920
RGBNIR-4328	93.32	0.933	0.933

TABLE IX. CLASSIFICATION REPORT OF TEST DATA USING CONVOLUTIONAL NEURAL NETWORKS OF VARIOUS SENTINEL BAND COMBINATIONS

Band Combination	Accuracy	P-Score	R-Score
RGNIR-438	96.8	0.968	0.968
RGB-432	93.6	0.936	0.936
RGBNIR-4328	98.1	0.981	0.981

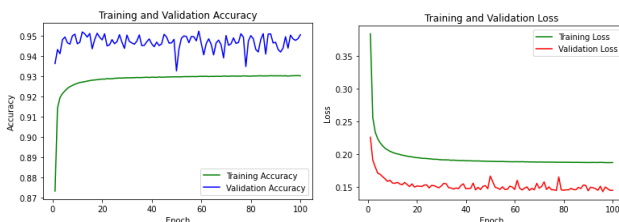


Fig. 11. Graph of Accuracy and Loss of Training and Validation Data using Deep Neural Networks of the Sentinel Image Band Combination-843.

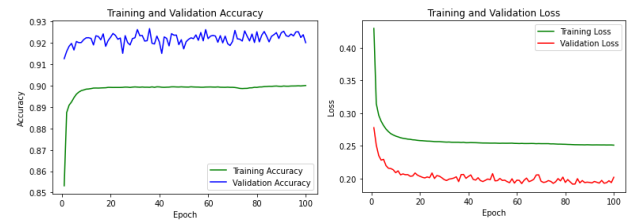


Fig. 12. Graph of Accuracy and Loss of Training and Validation Data using Deep Neural Networks of the Sentinel Image Band Combination-432.

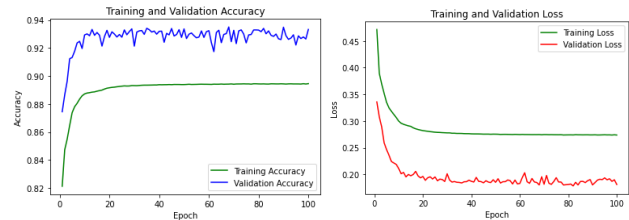


Fig. 13. Graph of Accuracy and Loss of Training and Validation Data using Deep Neural Networks of the Sentinel Image Band Combination-8432.

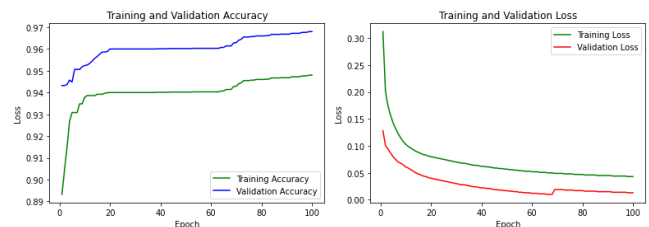


Fig. 14. Graph of Accuracy and Loss of Training and Validation Data using Convolutional Neural Networks of the Sentinel Image Band Combination-843.

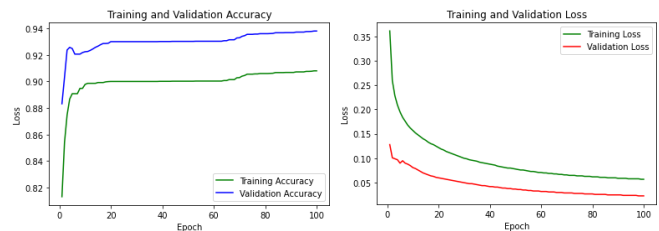


Fig. 15. Graph of Accuracy and Loss of Training and Validation Data using Convolutional Neural Networks of the Sentinel Image Band Combination-432.

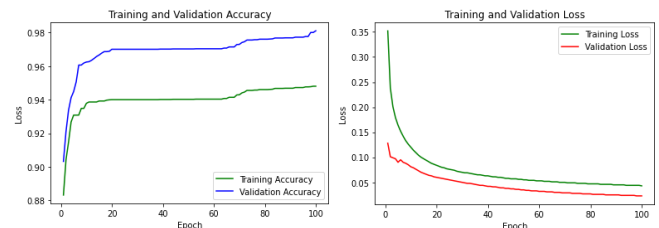


Fig. 16. Graph of Accuracy and Loss of Training and Validation Data using Convolutional Neural Networks of the Sentinel Image Band Combination-8432.

In addition to above results, CNN predicted LULC map of band combination RGBNIR is validated. This was done by generating 50 random points in the predicted image 10 for each class, then it was manually classified using google satellite

imagery. This classification was compared with the predicted image and error matrix for the same is as shown in Table X:

TABLE X. ERROR MATRIX GENERATED AGAINST 10 RANDOM POINTS FOR EACH CLASS WHICH ARE MANUALLY CLASSIFIED WITH GOOGLE SATELLITE IMAGE AGAINST PREDICTED CNN LULC MAP

	Classified (CNN Prediction)	Water	Urban	Forest	Vegetation	Openland	Total
Reference (10 Random points for validation)	Water	10	0	0	0	0	10
	Urban	0	8	0	0	2	10
	Forest	0	0	7	3	0	10
	Vegetation	0	1	2	7	0	10
	Openland	0	1	0	1	8	10

V. CONCLUSION

This study was conducted to examine the LULC maps obtained from neural networks techniques. The main objective was to determine the best suited neural network algorithm and the corresponding band combination with the highest accuracy, precision, recall and less error rate in the confusion matrix. To test all these, we chose Bangalore BBMP limits as the input image to the network and obtained land use and land cover of the typical classes Water, Urban, Forest, Vegetation and Openland. Among CNN and DNN and the sentinel-2 image band combinations RGB, RGBNIR and RGNIR, CNN with RGBNIR outperformed with accuracy 98.1 with less error rates in confusion matrix. Also, LULC map generated by the highest accuracy model (CNN with RGBNIR combination) was assessed with the help of google satellite imagery and confusion matrix was computed where in, error rate was very less.

LULC laid the foundation for further analysis. Mainly, change analysis will be performed and the predictive model would be developed in the upcoming research work mainly applications of LULC.

ACKNOWLEDGMENT

I would like to thank Dean Research and Innovation, Presidency University, Bangalore for providing high end systems to complete the second phase of my research as per the above mentioned results.

Conflicts of interest

The authors have no conflicts of interest to declare

REFERENCES

- [1] Phiri, Darius, Matamyo Simwanda, Serajis Salekin, Vincent R. Nyirenda, Yuji Murayama, and Manjula Ranagalage. "Sentinel-2 data for land cover/use mapping: a review." Remote Sensing 12, no. 14 (2020): 2291.
- [2] Szantoi, Zoltan, and Peter Strobl. "Copernicus Sentinel-2 calibration and validation." European Journal of Remote Sensing 52, no. 1 (2019): 253-255.
- [3] ESA (European Space Agency). 2015a. "Sentinel-2 User Handbook, Issue 1, Rev 2, Revision 2." ESA Standard Document. Accessed July 24 2015, 64 pages.
- [4] Ienco, Dino, Roberto Interdonato, Raffaele Gaetano, and Dinh Ho Tong Minh. "Combining Sentinel-1 and Sentinel-2 Satellite Image Time Series for land cover mapping via a multi-source deep learning

- architecture." ISPRS Journal of Photogrammetry and Remote Sensing 158 (2019): 11-22.
- [5] ED Chaves, Michel, Michelle CA Picoli, and Ieda D. Sanches. "Recent applications of Landsat 8/OLI and Sentinel-2/MSI for land use and land cover mapping: A systematic review." Remote Sensing 12, no. 18 (2020): 3062.
- [6] Gómez, Cristina, Joanne C. White, and Michael A. Wulder. "Optical remotely sensed time series data for land cover classification: A review." ISPRS Journal of Photogrammetry and Remote Sensing 116 (2016): 55-72.
- [7] Lambin, Eric FMDA, Mark DA Rounsevell, and Helmut J. Geist. "Are agricultural land-use models able to predict changes in land-use intensity?." Agriculture, Ecosystems & Environment 82, no. 1-3 (2000): 321-331.
- [8] Vaishnave, M. P., K. Suganya Devi, and P. Srinivasan. "A study on deep learning models for satellite imagery." International Journal of Applied Engineering Research 14, no. 4 (2019): 881-887.
- [9] Vali, Ava, Sara Comai, and Matteo Matteucci. "Deep learning for land use and land cover classification based on hyperspectral and multispectral earth observation data: A review." Remote Sensing 12, no. 15 (2020): 2495.
- [10] LeCun, Yann, Yoshua Bengio, and Geoffrey Hinton. "Deep learning." nature 521, no. 7553 (2015): 436-444.
- [11] Sathyanarayanan, Dinesh, D. V. Anudeep, C. Anjana Keshav Das, Sanat Bhanadarkar, D. Uma, R. Hebbar, and K. Ganesh Raj. "A Multiclass Deep Learning Approach for LULC Classification of Multispectral Satellite Images." In 2020 IEEE India Geoscience and Remote Sensing Symposium (InGARSS), pp. 102-105. IEEE, 2020.
- [12] Zhao, Wenzhi, Shihong Du, and William J. Emery. "Object-based convolutional neural network for high-resolution imagery classification." IEEE Journal of Selected Topics in Applied Earth Observations and Remote Sensing 10, no. 7 (2017): 3386-3396.
- [13] Tuia, Devis, Frédéric Ratle, Fabio Pacifici, Mikhail F. Kanevski, and William J. Emery. "Active learning methods for remote sensing image classification." IEEE Transactions on Geoscience and Remote Sensing 47, no. 7 (2009): 2218-2232.
- [14] Miranda, Eka, Achmad Benny Mutiara, and Wahvu Catur Wibowo. "Classification of land cover from Sentinel-2 imagery using supervised classification technique (preliminary study)." In 2018 International Conference on Information Management and Technology (ICIMTech), pp. 69-74. IEEE, 2018.
- [15] Topaloğlu, Raziye Hale, Elif Sertel, and Nebiye Musaoğlu. "Assessment of Classification Accuracies of Sentinel-2 And Landsat-8 Data for Land Cover/Use Mapping." International archives of the photogrammetry, remote sensing & spatial Information Sciences 41 (2016).
- [16] Sekertekin, A., A. M. Marangoz, and H. Akcin. "Pixel-based classification analysis of land use land cover using Sentinel-2 and Landsat-8 data." Int. Arch. Photogramm. Remote Sens. Spat. Inf. Sci 42 (2017): 91-93.
- [17] Sikarwar, Ankit, and Aparajita Chattopadhyay. "Change in land use-land cover and population dynamics: A town-level Study of Ahmedabad city sub-District of Gujarat." International Journal of Geomatics and Geosciences 7, no. 2 (2016): 225-234.
- [18] Yattoo, Saleem Ahmad, Paulami Sahu, Manik H. Kalubarme, and Bhagirath B. Kansara. "Monitoring land use changes and its future prospects using cellular automata simulation and artificial neural network for Ahmedabad city, India." GeoJournal (2020): 1-22.
- [19] Németh, Gergely Dániel, and Judit Ács. "Hyphenation using deep neural networks." V. Vincze (szerk.) XIV. Magyar Számítógépes Nyelvészeti Konferencia (MSZNY 2018) (2018): 146-158.
- [20] Jin, Jing, Feng, Wei Zhang, Jianan Zhang, Zhihao Zhao, and Qi-Jun Zhang. "Recent advances in deep neural network technique for high-dimensional microwave modeling." In 2020 IEEE MTT-S International Conference on Numerical Electromagnetic and Multiphysics Modeling and Optimization (NEMO), pp. 1-3. IEEE, 2020.
- [21] Tahir, Waleed, Aamir Majeed, and Tauseef Rehman. "Indoor/outdoor image classification using gist image features and neural network classifiers." In 2015 12th International Conference on High-Capacity

- Optical Networks and Enabling/Emerging Technologies (HONET), pp. 1-5. IEEE, 2015.
- [22] Tiwari, Vaibhav, Chandrasen Pandey, Ankita Dwivedi, and Vrinda Yadav. "Image classification using deep neural network." In 2020 2nd International Conference on Advances in Computing, Communication Control and Networking (ICACCCN), pp. 730-733. IEEE, 2020.
- [23] Emmert-Streib, Frank, Zhen Yang, Han Feng, Shailesh Tripathi, and Matthias Dehmer. "An introductory review of deep learning for prediction models with big data." *Frontiers in Artificial Intelligence* 3 (2020): 4.
- [24] Grandini, Margherita, Enrico Bagli, and Giorgio Visani. "Metrics for multi-class classification: an overview." arXiv preprint arXiv:2008.05756 (2020).
- [25] Alejo, Roberto, J. A. Antonio, Rosa Maria Valdovinos, and J. Horacio Pacheco-Sánchez. "Assessments metrics for multi-class imbalance learning: A preliminary study." In *Mexican Conference on Pattern Recognition*, pp. 335-343. Springer, Berlin, Heidelberg, 2013.
- [26] Krygier, John, and Denis Wood. *Making maps: a visual guide to map design for GIS*. Guilford Publications, 2016.
- [27] Pallavi, M., T. K. Thivakaran, and Chandankeri Ganapathi. "A Tile-Based Approach for the LULC Classification of Sentinel Image Using Deep Learning Techniques." In 2022 International Conference for Advancement in Technology (ICONAT), pp. 1-5. IEEE, 2022.
- [28] Setturu, Bharath, Uttam Kumar, and T. V. Ramachandra. "Spatio-Temporal Pattern of Landuse Dynamics for Bangalore, 2010".
- [29] Pallavi M, T. K. Thivakaran, and Chandankeri Ganapathi. "A Land Use Land Cover Map Generation Of Satellite Image Using Deep Learning Techniques." *Indian Journal of Computer Science and Engineering (IJCSE)*, Vol. 13 No. 4 Jul-Aug 2022, DOI: 10.21817/indjese/2022/v13i4/221304027.
- [30] Duro, Dennis C., Steven E. Franklin, and Monique G. Dubé. "A comparison of pixel-based and object-based image analysis with selected machine learning algorithms for the classification of agricultural landscapes using SPOT-5 HRG imagery." *Remote sensing of environment* 118 (2012): 259-272.
- [31] Arora, Divya, Mehak Garg, and Megha Gupta. "Diving deep in deep convolutional neural network." In 2020 2nd International Conference on Advances in Computing, Communication Control and Networking (ICACCCN), pp. 749-751. IEEE, 2020.
- [32] Pomerat, John, Aviv Segev, and Rituparna Datta. "On neural network activation functions and optimizers in relation to polynomial regression." In 2019 IEEE International Conference on Big Data (Big Data), pp. 6183-6185. IEEE, 2019.
- [33] Bousbih, Safa, Mehrez Zribi, Mohammad El Hajj, Nicolas Baghdadi, Zohra Lili Chabaane, Pascal Fanise, and Gilles Boulet. "Sentinel-1 and Sentinel-2 data for soil moisture and irrigation mapping over semi-arid region." In *IGARSS 2019-2019 IEEE International Geoscience and Remote Sensing Symposium*, pp. 7022-7025. IEEE, 2019.
- [34] De Luca, Giandomenico, João MN Silva, Salvatore Di Fazio, and Giuseppe Modica. "Integrated use of Sentinel-1 and Sentinel-2 data and open-source machine learning algorithms for land cover mapping in a Mediterranean region." *European Journal of Remote Sensing* 55, no. 1 (2022): 52-70.
- [35] Traganos, Dimosthenis, and Peter Reinartz. "Mapping Mediterranean seagrasses with Sentinel-2 imagery." *Marine pollution bulletin* 134 (2018): 197-209.
- [36] Dittrich, Christoph. "Bangalore: Globalisation and fragmentation in India's hightech-capital." *Asien* 103, no. 3 (2007): 45-58.
- [37] Ramprasath, Muthukrishnan, M. Vijay Anand, and Shanmugasundaram Hariharan. "Image classification using convolutional neural networks." *International Journal of Pure and Applied Mathematics* 119, no. 17 (2018): 1307-1319.
- [38] Wang, Yifeng, Yang Wang, Hongyi Li, Zhuoxi Cai, Xiaohan Tang, and Yin Yang. "CNN Hyperparameter optimization based on CNN visualization and perception hash algorithm." In 2020 19th International Symposium on Distributed Computing and Applications for Business Engineering and Science (DCABES), pp. 78-82. IEEE, 2020.

Exponential Decay Function-Based Time-Aware Recommender System for e-Commerce Applications

Ayat Yehia Hassan¹, Dr.Etimad Fadel², Dr.Nadine Akkari³
Computer Science, King Abdul-Aziz University, Jeddah, Saudi Arabia^{1,2}
Computer Science, Jeddah International College, Jeddah, Saudi Arabia³

Abstract—Unlike traditional recommendation systems that rely only on the user's preferences, context-aware recommendation systems (CARS) consider the user's contextual information such as (time, weather, and geographical location). These data are used to create more intelligent and effective recommendation systems. Time is one of the most important and influential factors that affect users' preferences and purchasing behavior. Thus, in this paper, time-aware recommendation systems are investigated using two common methods (Bias and Decay) to incorporate the time parameter with three different recommendation algorithms known as Matrix Factorization, K-Nearest Neighbor (KNN), and Sparse Linear Method (SLIM). The performance study is based on an e-commerce database that includes basic user purchasing actions such as add to cart and buy. Results are compared in terms of precision, recall, and Mean Average Precision (MAP) parameters. Results show that Decay-MF and Decay-SLIM outperform the Bias CAMF and CA-SLIM. On the other hand, Decay-KNN reduced the accuracy of the RS compared to the context-unaware KNN.

Keywords—Time-aware recommender system; context-aware recommender system; matrix factorization; K-Nearest Neighbor (KNN); and Sparse Linear Method (SLIM)

I. INTRODUCTION AND BACKGROUND

Recommender systems (RS) are intelligent tools and techniques used to recommend items to a user based on his/her preferences [1]. In Ecommerce Applications, a Recommender system is used to predict the product that a user is most likely to purchase. Companies like Netflix and Amazon use recommender systems to help their users to identify the correct product or movies based on their history[2].

Context-aware recommender systems (CARS) produce more significant recommendations by optimizing preferences to suit the current situation and conditions of the user (e.g., location, time, weather, device, etc.) [15,17]. This method has been proven to be effective in improving the performance of the recommendation system [3]. One of the most important contextual information that has been used in recommender systems is time, especially in the context of e-commerce applications. The winning team of the Netflix Prize competition [5] found that using time context can significantly increase the reliability of the recommendations. As users' preferences change over time, new fashions and interests are constantly emerging [4]. For example: seasonal changes (specific holidays) leading to different shopping patterns. Also, Product popularity are in a constant change. This leads consumers to constantly change their taste. Therefore, it was necessary for the recommendation systems to consider these changes in the

behavior of users. One of the factors that facilitated research on the use of time in recommendation systems is the ease of extracting it, which does not require special devices or effort.

The time Aware Recommender system (TARS) 's primary purpose is to deal with user preferences changes over time [18]. There are two types of user's feedback that can be used with the time: implicit feedback and explicit feedback. In the explicit feedback the system must ask users to provide their ratings for items directly mostly using stars. However, in the implicit feedback approach, the system automatically tracks users' preferences by monitoring the performed actions, such as which item they visited, where they clicked, which items they purchased, or how long they stayed on a web page. In the real word applications, any store can include a time-aware recommender system to work offline without the need to collect new data from users because it can simply use the user's implicit feedback (purchase data) with its timestamp. As it has been proven in this research, choosing the appropriate algorithm to use with the time data will improve the performance of the recommendation system, which will be reflected in the store's revenues. Some research discussed the impact of using time with user's explicit feedback. However, research that consider purchasing information such as [3, 4, 6] did not address the time dimension. Due to the lack of datasets that uses implicit feedback (purchase information) with time factor in the field of e-commerce, the impact of linking these two parameters in the field of e-commerce has not been studied in the literature. Thus, many of the TARS research findings don't apply to e-commerce. As this type of recommender system is concerned with not only the preferences of the user but also with the act of purchasing, which leads to increasing the store's earnings which is the main goal of any business. This work analyzes TARS with purchasing actions on an online shopping domain to achieve the goal of increasing the store revenue by enhancing the accuracy of the top 20 recommended items.

In previous research [51] we incorporated time with the Matrix Factorization (MF) algorithm to improve the recommender system accuracy. In this research, we have used the Decay function method with two other states of art algorithms to compare the results and find out the most appropriate algorithm in the field of e-commerce that can be used with the common actions (add to cart and buy). The work's key contribution is to combine time with RS using two separate methodologies (Bias and Decay) and purchasing actions for online shopping recommendations.

Bias is the first method, which uses time as the third dimension in the (user*item) rating matrix. The Decay function,

on the other hand, generates predicted ratings by combining implicit feedback (add to cart and buy) with temporal dynamics, giving the newly purchased items a higher weight than older ones. Then generating new predicted rates to replace the old rates.

In this research, we evaluated the two techniques using three cutting-edge algorithms: Matrix Factorization (MF) [7], K-Nearest Neighbor (KNN) [8], and Sparse Linear Method (SLIM) [9]. Precision, recall and Mean Average Precision (MAP) were used to evaluate the experimental results.

A. Time-Aware Recommender System Categories

Authors in [19] identified seven methods on how time factor may be used with recommender systems as follow:

- Bias: In this method, the system records the time of the user's rating. Then Time will be added to the collaborative filtering algorithm as the matrix's third dimension. Collaborative filtering will compare users, identify similar users, and then predict user ratings for unrated items.
- Decay: In this method, the system prioritizes new things above those with more recent interactions.
- Micro-profile: The system saves distinct profiles for each user at different times. For example, a user can have two profiles, one for weekends and the other for weekdays.
- Restriction: In this case, the recommender system (RS) matches the user's available time to the time when the item will be used. For example, if the user wants to eat dinner, the algorithm will only suggest restaurants that are open late.
- Time Rating: Time is used to infer user preferences using implicit feedback. For example, the longer a user spends on a product page, the more the consumer likes that product.
- Novelty: The recommendation system defines a limit date and will not recommend any items that are older than this date. For example, on a news website, RS will only recommend news that was published at least one day ago.
- Sequence: The RS tracks items that are consumed one after another or in a certain order. For example, the system will recommend more products that are typically purchased along with the consumed product.

In this paper, we investigated and compare the Bias and Decay categories by incorporating them with RSs Algorithms.

B. Recommender Systems Algorithms

There are three main techniques used in RS: content-based filtering, collaborative filtering, and hybrid filtering. However, our research scope is in Collaborative filtering algorithms (CF) which can be categorized into three main categories: neighborhood-based algorithms such as KNN, latent factor-based algorithms such as MF, and non-neighborhood or latent

factor algorithms such as Sparse Linear Method (SLIM) algorithm [11-14].

• Neighborhood Based Algorithms

The K-Nearest Neighbors (KNN) algorithm depends on finding users who are similar to the current user. The behavior of the current user is thus predicted based on his/her closest neighbors [20]. The interaction matrix serves as the algorithm's initial input. The correlation between users is then used to compute similarity. The cosine similarity is applied and computed in this study as given in equation (1) [8]:

$$sim(u_a, u_b) = \frac{\sum_i r_{u_a,i} r_{u_b,i}}{\sqrt{\sum_i r_{u_a,i}^2 \times \sum_i r_{u_b,i}^2}} \quad (1)$$

Where $sim(u_a, u_b)$ is the correlation between user a and user b and $r_{u_a,i}$ is the rate by the user a for item i. k (number of the nearest neighbors) is a hyper-parameter that must be manually adjusted and cannot be learned by the system. The final step is to use the formula (2)[8] to calculate the rating prediction:

$$P_{u_a,i_x} = r_{u_a}^- + \frac{\sum_{n \in V} (r_{u_n,i_x} - r_{u_n}^-) sim(u_a, u_n)}{\sum_{u_n \in N} |sim(u_a, u_n)|} \quad (2)$$

N is the set of closest neighbors, while $r_{u_n}^-$ is the average rate that one of the users in the N set has provided. P_{u_a,i_x} denotes the predicted rate of user a for item x , r_{u_a,i_x} is the actual rate by user a for item x .

• Matrix factorization Algorithm

Matrix factorization (MF) is a form of latent factors technique used in RSs that uses Collaborative Filtering (CF). MF method begins by randomly initializing two matrices. The first is a (users*factors) matrix, while the second is a (factors*items) matrix. When these two matrices are multiplied together, we get the (users*items) matrix, which is the same size as the Rating Matrix that we're attempting to forecast [21]. The number of latent components we're utilizing to estimate the rating matrix is represented by dimension f (factors). f is usually between 10 and 250.

This method, as stated in equation (3), seeks to fill the matrices P and Q by predicting the ratings in the training set [7].

$$\min \sum_{(u_a,i_x) \in \tau} (r_{u_a,i_x} - P_{u_a,i_x})^2 = \min_{p,q} \sum_{(u_a,i_x) \in \tau} (r_{u_a,i_x} - q_{i_x}^T p_{u_a})^2 + \lambda (\|q_{i_x}\|^2 + \|p_{u_a}\|^2) \quad (3)$$

Where $\lambda (\|q_{i_x}\|^2 + \|p_{u_a}\|^2)$ is a regularization term intended to prevent overfitting. p and q are the two factors matrices.

• Sparse Linear Method (SLIM) Algorithm

Similar to the neighborhood-based approach, the sparse linear method (SLIM) method [9] tries to reduce the error rate by using the loss function rather than similarity to determine the difference between the training set and the test set. Equation (4)[9] illustrates the error function's definition as follows:

$$\min_{w_*} \sum_{(u_a, i_x) \in \tau} (r_{u_a, i_x} - r_{u_a}^T w_{i_x}) + \lambda_1 \|w_{i_x}\|^2 + \lambda_2 \|w_{i_x}\|_1$$
$$s. t \|w_{i_x}\|_1 \geq 0 \quad (4)$$

Where w is the item-item similarity learned by minimizing the error function, w_{i_x} is a column from the w matrix, $r_{u_a}^T$ is the user rate in the training set, r_{u_a, i_x} is the predicted rate for item x , and $\lambda_1 \|w_{i_x}\|^2 + \lambda_2 \|w_{i_x}\|_1$ are regularization terms to prevent overfitting.

C. Evaluation Matrices

There are several measures for defining the quality of the Top-N Recommender system. However, the main three are precision, recall, and MAP [10].

- Precision

The percentage of recommended items in the Top-N set that are relevant is known as precision. For example, if precision at 10 in a top-10 recommended items is 90%. This indicates that 90% of the suggestions are useful to the user. According to [22], precision is calculated as follows:

$$p = \frac{\# \text{ relevant recommended items}}{\# \text{ recommended items}} \quad (5)$$

- Recall

Recall is the percentage of relevant items in the top-N recommended items. For instance, if we measured recall at 10 and discovered that it is 40%. This indicates that the top-N results contain 40% of the entire number of relevant items. The following is the definition of mathematical recall [22]:

$$r = \frac{\# \text{ relevant recommended items}}{\# \text{ all the possible relevant items}} \quad (6)$$

- Mean Average Precision (MAP):

MAP is the mean of average precision, of all users. MAP can be calculated as follows [22]:

$$MAP = \sum_{i=1}^N \frac{P@i}{N} r_i \quad (7)$$

where N is the length of the list of recommended items and $P@i$ is the precision at item i .

The remainder of the paper is structured as follows:

Section II provides a summary of related works. Section III explains Incorporating time context into RS algorithms. The implementation and experiment are found in Section IV. Section V explains the findings and discussion. Finally, in section VI, the conclusion is presented.

II. RELATED WORK

Many scientists investigated how time is used in RS. Some used it with rating prediction recommenders [29,27,30,33], while others used it with Top-N recommendations [25,26,37]. Precision, recall, and MAP may be applied for Top-N recommendations, whereas Mean Absolute Error (MAE) and Root mean squared error (RMSE) can be used for recommendation prediction. We will focus on Top-N recommendations in this study because they are commonly

used in the commercial field, where the purpose of the recommender system is to select a few specific things that are most attractive to the user.

The recommendation process may be carried out in different ways and using a variety of algorithms. Neighborhood-based algorithms and latent factor algorithms are the most popular types of traditional recommender systems. The recommender was applied using Matrix factorization and user-based K-nearest neighbor (KNN) in [23]. They created a simulated rating utilizing the decay function to aggregate implicit feedback datasets with time dynamics. The experimental findings showed that their suggested technique is successful in the multimedia domain for rating prediction and top-N recommendation. The study's [24] objective was to enhance the performance of neighborhood-based recommender systems using the time context with the decay function in addition to ratings. The author [25] employed content-based and collaborative filtering algorithms with pre- and post-filtering that considered the time context. However, they do not provide any experimental tests on a dataset. Researchers in [25] classified the methods of using time context with RSs as decay, restriction, and novelty. Other researchers added the sequence context with the decay function [26].

the research [27] exploited using the time context to enhance the user-based collaborative filtering algorithm and proposed a weight formula to account for changes in the group users' preferences over time. Their technique raises the accuracy of the collaborative filtering (CF) algorithm on a movie dataset. A proactive Context-Aware RS is suggested by [28] for lecturers and scientists who would be providing learning resources for students. In [28], time is employed in the same way as Restriction; the RS seeks to locate learning materials that correspond to the real user's time. [29] suggested a method for predicting user preferences in a recommender system by learning the sequence of purchase history and taking preference changes into account. Using the micro profile technique, they use a Kalman filter to forecast user preference vectors from user characteristics.

Time is widely implemented in the multimedia domain [23, 24, 30-34,52] and learning domain [28, 35-37] [25, 26] according to the literature. However, in the e-commerce field, it is rarely utilized to study purchase data rather than just rating data. We can also see that user preferences fluctuate depending on the season and application domain. As a result, the method for dealing with time in one domain may not apply to another. We used the decay function to apply to the purchase date (add to cart & buying or transactions) in an online shopping system in this study.

Many studies in the literature [24,26,27,30-33,53] used the MovieLens dataset, which contains the rating from the MovieLens website (movielens.org). The ratings are connected to the timestamp. Other research [23, 29] examined the Last.fm dataset, which includes a timestamp and a user's history of listings in addition to the user's properties. The Yelp dataset in [24] only gives a comprehensive perspective of restaurants, including overall user ratings. Finally, the D-Lib Magazine dataset [26] includes articles and numerous shorter items, as

well as digital collections, calls, and notifications from its 265 issues.

According to the literature, most of the datasets used do not include the implicit feedback of purchase data (buy and add-to-cart) linked with time in the e-commerce environment. Table I shows a summary of the related work.

TABLE I. RELATED WORK

REF	Algorithm	Time-aware RS category	Implicit/explicit data	Domain
[23]	KNN MF	Decay	User View history (Implicit)	Music
[24]	KNN	Decay	Rating data (explicit)	- Movies - Business Directory Service
[25]	Hybrid (CF+ Content Based)	- Decay - Restriction - Novelty	Date, Duration, Learning Time (implicit)	Learning
[29]	Kalman filtering - Matrix factorization	Micro-profile	User View history (Implicit)	Music
[38]	CF	Other	-	-
[32]	Matrix-factorization model	Other	Rating data (explicit)	Movies
[30]	Time- and Community-Aware RS	decay	Rating data (explicit)	Movies
[31]	Temporal overlapping community detection method	Other	Rating data (explicit)	Movies
[33]	a novel dynamic recommender system.	Other	Rating data (explicit)	Movies
[36]	knowledge-driven recommender	Restriction	-	Mobile Learning on the Semantic Web
[27]	CF	Decay	Rating data (explicit)	Movie
[28]	Context-aware RS	Restriction	-	Learning
[37]	Hybrid	Sequence	-	Learning environments
[52]	Novel next-item RS	Sequence	Interval and duration (implicit)	Game-playing data
[53]	Hybrid	Other	Rating data (explicit)	Movie

In this research, we have used the Decay function method with three states of art algorithms in the field of e-commerce with two main implicit actions (add to cart and buy). The work's key contribution is to analyze the effect of combining the time context with RSs using two separate methodologies (bias, and decay) and user's implicit feedback for online shopping recommendations.

III. INCORPORATING THE EXPONENTIAL DECAY FUNCTION INTO RECOMMENDER SYSTEM

Our approach consists of three major phases as illustrated in Fig. 1. The first phase is data pre-processing where dataset converted to binary format. The second is the half-life decay function [30,31,33]. Finally, the contextual modeling where

Multidimensional recommender (MD) is generated to produce the Top-N recommended items. the three phases are explained as follows:

A. Pre-Processing Phase

This phase involves converting the dataset in a compact format which includes the interaction condition and its value into a binary format that only uses 0s and 1s as shown in Fig. 2. Converting the event types (add to cart and buy) to numerical numbers is also included in this phase.

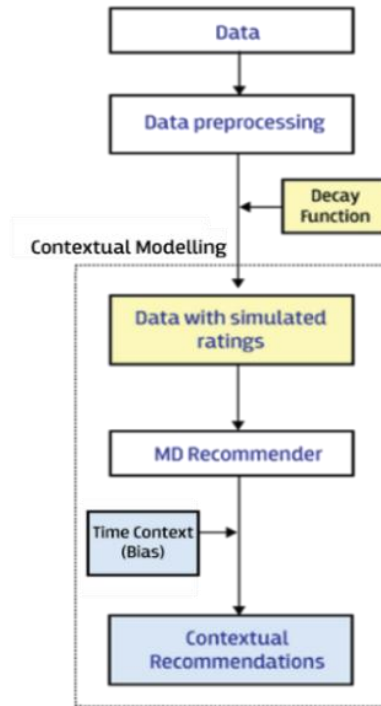


Fig. 1. Incorporating Time Dynamic with Recommender System.

Day of the week	Hour of the day	VisitorID	Event	ItemID
Sun	21	189384	Transaction	299044
Mon	3	287857	Addtocart	5206
Sat	1	158090	Addtocart	10572

Compact Format

Sun	Mon	Tue	Wed	Thru	Fri	Sat	VisitorID	Event	ItemID	1	2	3	...24
1	0	0	0	0	0	0	189384	5	299044	0	0	0	...
0	1	0	0	0	0	0	287857	4	5206	0	0	1	...
0	0	0	0	1	0	0	158090	4	10572	1	0	0	...

Binary Format

Fig. 2. Compact Format to Binary Format.

We assume that user preferences are between one and five, which is the standard scale of user ratings in the literature. The value of purchasing action is set as five in this study as it represents the maximum number of prefaces a user would give to an item. The add-to-cart action is set to four as it represents lower interest than the purchase action.

B. Half-life Decay Function

Generally, Exponential decay is a mathematical term that defines the process of reducing a value with constant percentage rate over time as shown in formula (8), where n represents the decay factor as shown in equation (9) [40].

$$final\ amount = \frac{initial\ amount}{2^n} \quad (8)$$

Where

$$n = (elapsed\ time)/(half\ life) \quad (9)$$

$$half\ life = \frac{\log_2(elapsed\ time)}{\log\left(\frac{initial\ amount}{final\ amount}\right)} \quad (10)$$

In our scenario, we assume that the user's interest in an item decreases over time by a fixed amount of value. We use the elapsed time to determine the half-life in equation (10). The elapsed time is the period between the present date and the time when the user gave an item a rating. The half-life is defined as the number of days required to reduce the weight of a user rate by half. For rating an item, the highest rate is five and the minimum rate is one.

C. Contextual Modeling

In this phase, the filtering according to context is applied as a part of the recommendation algorithms as follows.

- Context-Aware Matrix Factorization (CAMF)

To simulate the interaction between the items and the context, Context-Aware Matrix Factorization (CAMF) adds a factor B, as illustrated in equation (11)[2]:

$$P_{u_a, i_x, c_a} = q_{i_x}^T (p_{u_a} + |N(u_a)|^{-\frac{1}{2}} \sum_{j \in N(u_a)} y_j) + B_{i_x, c_a} \quad (11)$$

These factors B are learned using the error function which can be calculated as shown in equation (12)[2]:

$$\min_{p_*, q_*, y_*, B_*} \sum_{(u_a, i_x, c_a) \in \tau} \left(r_{u_a, i_x, c_a} - q_{i_x}^T \left(p_{u_a} + |N(u_a)|^{-\frac{1}{2}} \sum_{j \in N(u_a)} y_j \right) - B_{i_x, c_a} \right)^2 + \lambda (\|q_{i_x}\|^2 + \|p_{u_a}\|^2 + \sum_{j \in N(u_a)} \|y_j\|^2 + B_{i_x, c_a}^2) \quad (12)$$

where $N(u_a)$ in (11),(12) is the set of items on which the user u_a has given implicit feedback, the vector y_j in (11),(12) represents the value of implicit feedback, and T is the set of all items i that both users U_a and U_b have rated. To avoid overfitting, the regularization term. $\lambda(\|q_{i_x}\|^2 + \|p_{u_a}\|^2)$ is added to the error function.

- Context-Aware Neighborhood Based Algorithm (CA-KNN)

Similar to the Context-Unaware Neighborhood Algorithm, the Context-Aware Neighborhood Algorithm, also known as Differential Context Weighting (DCW) [42], begins by determining the similarity between users. The set T - the set of

all items i that both users u_a and u_b have rated- is used for the summations in the similarity computations. The algorithm then maintains them along with the c_1 and c_2 time contexts where these ratings occurred. Equation (13) shows the incorporation of time in the similarity equation [42]:

$$sim_{ca}(u_a, u_b) = \frac{\sum_{(i, c_1, c_2) \in T} r_{u_a, i, c_1} r_{u_b, i, c_2} J(c_1, c_2, \sigma_1)}{\sqrt{\sum_{(i, c_1, c_2) \in T} r_{u_a, i, c_1}^2 \sum_{(i, c_1, c_2) \in T} r_{u_b, i, c_2}^2 \sum_{(i, c_1, c_2) \in T} J(c_1, c_2, \sigma_1)^2}} \quad (13)$$

Where J is the weighted Jaccard metric which can be computed as given in equation (14)[42] and the set σ contains the weights for each of the potential contexts: [42]:

$$J(c_1, c_2, \sigma) = \frac{\sum_{f \in c_1 \cap c_2} \sigma_f}{\sum_{f \in c_1 \cup c_2} \sigma_f} \quad (14)$$

Finally, the predicted rates can be determined in the same way as the context-unaware method as illustrated in equation (15) [23]:

$$P_{u_a, i_x, c_a} = r_{u_a, c_a}^- + \frac{\sum_{(u_b, c_1) \in V} (r_{u_b, i_x, c_1} J(c_1, c_2, \sigma_2) - r_{u_b, c_a}^-) sim_{ca}(u_a, u_b)}{\sum_{(u_b, c_1) \in V} sim_{ca}(u_a, u_b)} \quad (15)$$

Where (r_{u_b, c_a}^-) is the average user ratings in the active context and the rating r_{u_b, i_x, c_1} is weighted by the Jaccard metric. the context in which the nearest neighbors have rated the item i_x stored in the set V represented by c_1 .

- Context-Aware Sparse Linear Method (CA-SLIM)

Context-Aware Sparse Linear (SLIM) changes the prediction equation based on the context of the rating (c_a) applying equation (16)[41]:

$$P_{u_a, i_x, c_a} = (r_{u_a}^T + d_{c_a}) w_{i_x} \quad (16)$$

In this equation, d_{c_a} is the column in matrix D that contains the rating difference for each item-context interaction, which is referred to as the contextual rating deviations (CRD). The CRDs for all items in the context (c_a) are stored in the vector d_{c_a} . By adding it to the error function, the vectors d_* and the matrix D are learned simultaneously with the matrix W, as illustrated in equation (17)[41]:

$$\min_{w_*, d_*} \sum_{(u_a, i_x, c_a) \in \tau} (r_{u_a, i_x} - (r_{u_a}^T + d_{c_a}) w_{i_x}) + \lambda_1 \|w_{i_x}\|^2 + \lambda_2 \|w_{i_x}\|_1 + \lambda_3 \|d_{c_a}\|^2 + \lambda_4 \|d_{c_a}\|_1 \quad (17)$$

s. t. $|w_{i_x}| \geq 0$

IV. IMPLEMENTATION

The data was taken from a real-world e-commerce website (Gift Shop) and is part of the "Retailrocket" public dataset [39]. A visitor can do three sorts of actions: "view," "add to cart," and "transaction.". interactions are collected over a period of 4.5 months. There are around 8k buy events and approximately 28k add-to-cart events. The day of the week and hour of the day

where the event happened were determined using the user id, item id, and Unix time. For example: “1439694000000, 1, view,100,” means visitorId = 1, clicked the item with id = 100 at 1439694000000 (Unix timestamp). Then, for each of the user's events, we assume a rating value. For example, the transaction event has a value of five and the add-to-cart event has a value of four. We computed the elapsed time for each occurrence. Then we utilized it to calculate a new anticipated rate by giving less weight to the earlier event and finding the half-life value as explained in the previous section.

A. Implementation Tools

The CARSKIT Java Library is used to implement and expand the state-of-art context-aware algorithms. Numerous research [20, 45, 46] have used CARSKIT [44, 47] which is a Java-based open-source package for the context-aware recommendation. As a hardware tool, AZIZ High-Performance Computer (HPC) with 30GB RAM has been used. We modified the CARSKIT code to calculate the precision, recall, and MAP for a different number of recommended items N (from 1 to 20) to be able to track how the algorithms behave as N increases.

B. Algorithm's Hyper-parameters

The parameters applied for each of the recommendation algorithms are shown in Table II. Number of factors parameter is used in MF, If the number of latent variables (number of factors) equals one, we are selecting the most popular things with the most interactions with no regard for personalization. Increasing the number of latent variables (the number of rows or columns associated with a single product or user) would increase personalization, and hence the RS's quality. However, if the number of latent components grows too large, it will generate an overfitting problem, lowering the quality of the recommendations. To avoid the overfitting problem, we'll need some regularization terms which is used to minimize overfitting while increasing the number of latent factors. In MF and SLIM, without a predefined stopping condition, iterative steps will continue forever. A limitation on running time or the number of iterations is often used to interrupt the infinite loop. In KNN which is known as Differential Context Weighting (DCW) [42] the threshold is applied to distinguish between frequent and infrequent variables and Particle Swarm Optimization (PSO) [43] is used to determine how much weight to give to each potential context. PSO iteratively seeks to enhance potential solutions based on a specified quality metric to find the best answer to an issue [16].

Based on the default parameters for CARSKIT [44] and the suitable values for our dataset, we determined the algorithm's hyper-parameter values for our experiment as shown in Table II. We used a factor count of 10 to ensure that we had enough factors to adequately capture the variability in the data, but not too many that the training data would be overfitting. The maximum number of iterations required to obtain an accurate result is 100. Based on the "Retailrocket" dataset, which includes customer data from May 2015 to August 2015, we estimate a half-life of 43 days. The hyper-parameters for the three algorithms (MF, KNN, SLIM) with the three distinct techniques (baseline, bias, and decay) are shown in Table II.

TABLE II. EXPERIMENT CASES AND ASSUMPTIONS

	Algorithms with cases	Hyperparameters	Values
Matrix Factorization	Case#A1: MF (Time un-aware)	Regularization factor	default value
		# of iterations	100
		# of factors	10
	Case#A2: CAMF (Time aware (Bias))	Regularization factor	default value
		# of iterations	100
		# of factors	10
	Case#A3: Decay CAMF (Time aware Decay)	Regularization factor	default value
		# of iterations	100
		# of factors	10
Half-life		43	
Sparse Linear Method	Case#B1: SLIM (Time un-aware)	Regularization factor	default value
		# Of iterations	100
		# Of neighbors	10
	Case#B2: CASLIM (Time aware (Bias))	Regularization factor	default value
		# Of iterations	100
		# Of neighbors	10
	Case#B3: Decay CA-SLIM (Time aware (Decay))	Regularization factor	default value
		# Of iterations	100
		# Of neighbors	10
Nearest Neighbor Algorithm	Case#C1: User-Based KNN (Time un-aware)	# Of neighbors	10
	Case#C2: DCW (Time aware (Bias))	PSO parameters	default value
		Threshold	0,5
	Case#C3: Decay DCW (Time aware (Decay))	PSO parameters	default value
		Threshold	0,5
	Half-life	43	

V. RESULTS

The application of the three RS algorithms Matrix Factorization (MF), K-Nearest Neighbor (KNN), and Sparse Linear Method is examined in this section (SLIM) using two different methods (Bias and Decay) as shown in Table II. The metrics used to analyze the experiment are Precision, Recall, and MAP. N is the number of suggested items, and the metrics are calculated for N=1 to N=20.

A. Case A: Matrix Factorization (MF)

This section uses two methods – Bias (traditional) and Decay- to illustrate the effect of introducing time into the matrix factorization algorithm. The accuracy, recall, and MAP for the MF are shown in Fig. 3, 4, and 5, respectively. The decay technique outperformed the Bias-CAMF and MF in terms of accuracy, recall, and MAP, with a 0.05 percent in precision,

0.45 percent recall, and 0.16 percent MAP as shown in Table III.

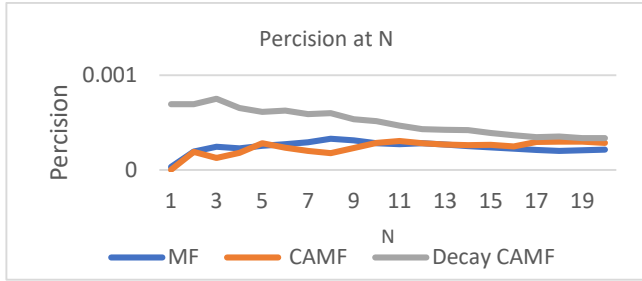


Fig. 3. MF, CAMF, and Decay CAMF Precision.

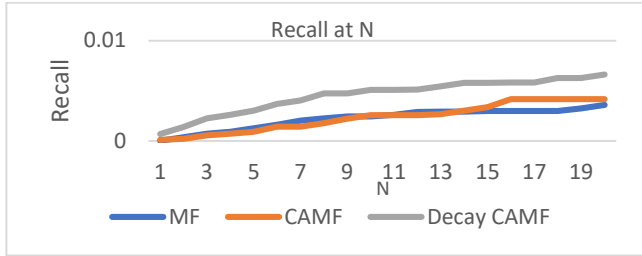


Fig. 4. MF, CAMF, and Decay CAMF Recall.

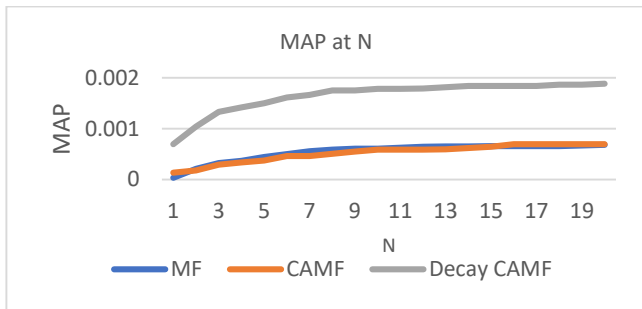


Fig. 5. MF, CAMF, and Decay CAMF MAP.

TABLE III. AVG MF PRECISION, RECALL, AND MAP

	AVG Precision percentage	AVG Recall percentage	AVG MAP percentage
MF	0.020	0.220	0.050
CAMF	0.020	0.240	0.050
Decay & CAMF	0.050	0.450	0.160

B. Case B: Sparse Lanier Method (SLIM)

Using two approaches (Bias and Decay), this section highlights the effect of adding time with the Sparse Lanier Method (SLIM) algorithm. Fig. 6, 7, and 8 depict the SLIM's precision, recall, and MAP, respectively. Table IV shows that the decay technique outperformed the time unaware SLIM and bias CA-SLIM in terms of accuracy, recall, and MAP, with precision, recall, and MAP of 0.22 percent, 1.40 percent, and 0.78 percent, respectively.

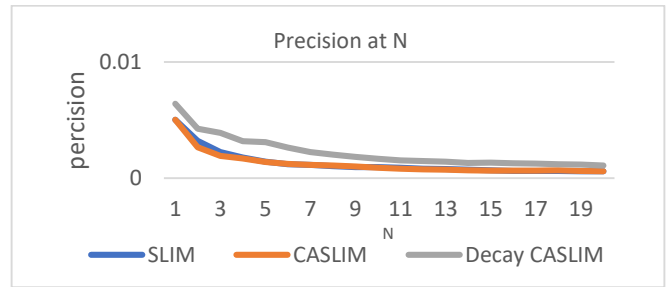


Fig. 6. SLIM, CA-SLIM, and Decay CA-SLIM Precision.

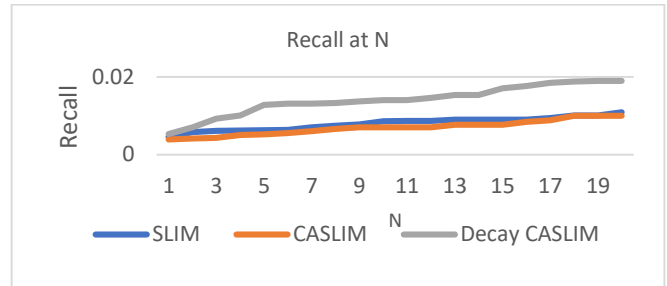


Fig. 7. SLIM, CA-SLIM, and Decay CA-SLIM Recall.

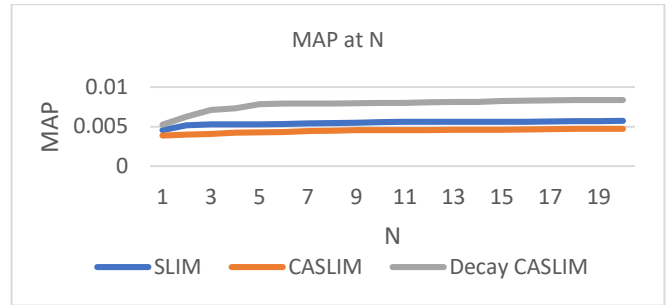


Fig. 8. SLIM, CA-SLIM, and Decay CA-SLIM MAP.

TABLE IV. AVG SLIM PRECISION, RECALL, AND MAP

	AVG Precision Percentage	AVG Recall Percentage	AVG MAP Percentage
SLIM	0.130	0.800	0.550
CA-SLIM	0.130	0.690	0.450
Decay & CA-SLIM	0.220	1.400	0.780

C. Case C: Nearest Neighbor (KNN)

Using two approaches, this section highlights the effect of adding time with the KNN algorithm. Fig. 9, 10, and 11 depict the KNN's precision, recall, and mean absolute deviation, respectively. As shown in Table V, the average results indicate that using the time context in Bias and decay method decreases the efficiency of the RS with Avg precision, recall, and MAP of 0.04%, 0.37%, and 0.10% respectively.

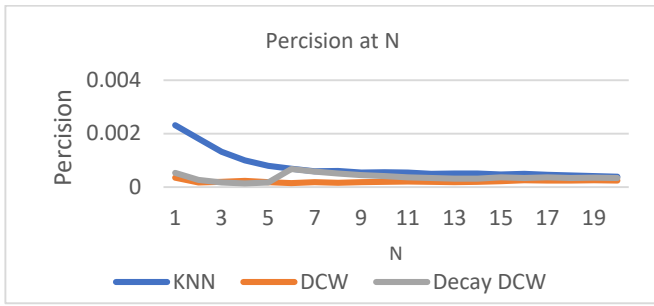


Fig. 9. KNN, DCW, Decay DCW Precision.

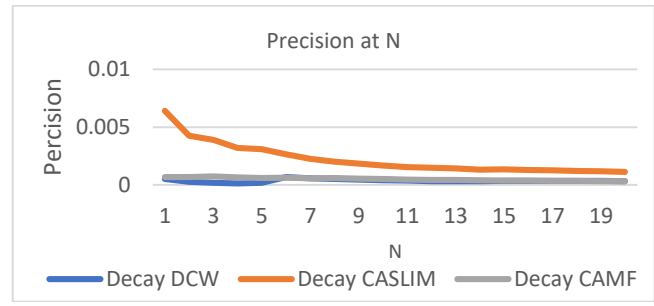


Fig. 12. The Decay Time-Aware Algorithms' Precision.

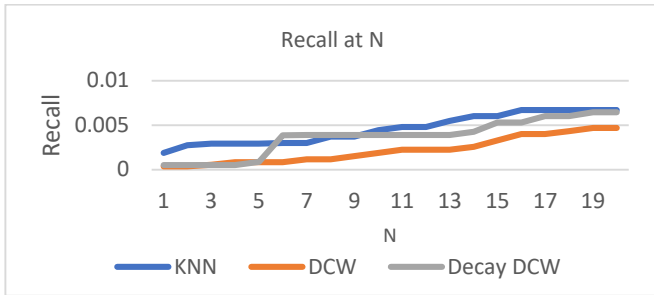


Fig. 10. Fig 1 Recall for KNN, DCW, Decay DCW

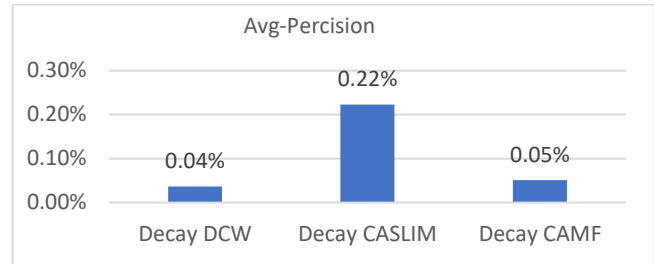


Fig. 13. The Decay Time-Aware Algorithms' Avg- Precision.

As seen in Fig. 14 and 15, Decay CA-SLIM outperformed the other algorithms by a significant margin. With 0.45 percent and 0.37 percent, respectively, while CAMF and DCW have a similar Average-performance.

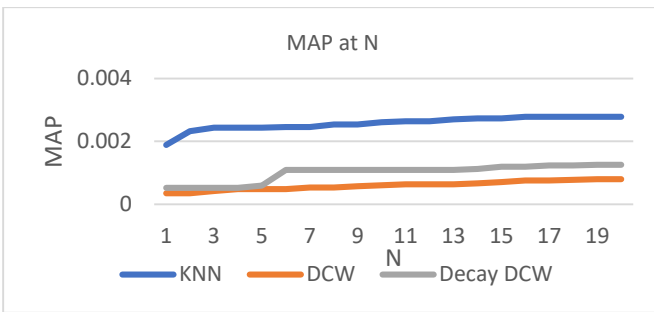


Fig. 11. Fig 2 MAP for KNN, DCW, Decay DCW

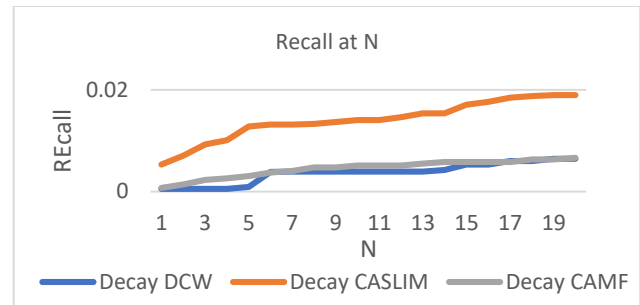


Fig. 14. The Decay Time-Aware Algorithms' Recall.

TABLE V. AVG KNN (RECALL, PRECISION, AND MAP)

	AVG Precision Percentage	AVG Recall Percentage	AVG MAP Percentage
KNN	0.070	0.460	0.260
DCW	0.020	0.220	0.060
Decay DCW	0.040	0.370	0.100

D. Half-Life Decay with All Algorithms (MF, SLIM, KNN) Comparison

The outcomes of three RS techniques (Matrix Factorization (MF), K-Nearest Neighbor (KNN), and Sparse Linear Method (SLIM)) are compared in this section: Fig. 12 and 13 illustrate the accuracy of the three RS methods with The Decay factor. With a significant difference, Decay CA-SLIM outscored the other methods. CAMF and DCW, on the other hand, have approximately similar Average-performances.

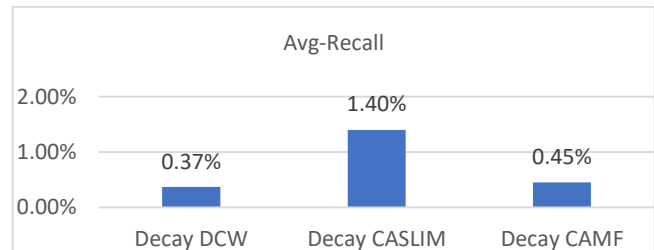


Fig. 15. The Decay Time-Aware Algorithms' Average Recall.

Fig. 16 and 17 depict the MAP for Decay DCW, Decay CAMF, and Decay CA-SLIM, respectively. For the three approaches, the avg-MAP values are 0.1 percent, 0.7 percent, and 0.16 percent, respectively.

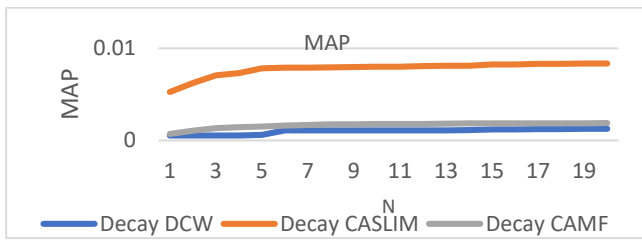


Fig. 16. The Decay Time-Aware Algorithms MAP.

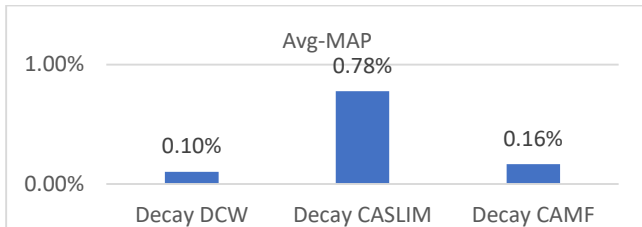


Fig. 17. The Decay Time-Aware Algorithms AVG-MAP.

E. Findings

Based on the experiment results, we conclude that in the e-commerce domain that uses purchasing data, the item-oriented, decay time-aware recommender algorithms outperform baseline context-aware algorithms and context-unaware algorithms. This conclusion is based on the fact that the overall effectiveness improves when time information is used. Furthermore, we arrive at the conclusion that the sparse linear approach, which has proven positive performance for the top-N recommendation in this research may not necessarily transition well to other datasets in the literature.

- The average findings show that the decay technique outperformed the Bias CAMF and time unaware MF, with precision, recall, and MAP of 0.05 percent, 0.45 percent, and 0.16 percent, respectively.
- The decay technique outscored the Bias CA-SLIM and time unaware SLIM approach, with precision, recall, and MAP of 0.22, 1.40, and 0.78, respectively.
- Adding the time context reduces the accuracy of the recommendation process in the KNN technique. In addition to the algorithm's incredibly high running time (weeks to execute one single run), which obstructed us from running all combinations of hyper-parameters.
- Running the KNN and SLIM with no limit on the number of neighbors had to be left out because it took weeks to execute one single run.
- Given that our utilized dataset has a density of = 0.0124 percent. The results suggest that adding decay context-awareness to KNN algorithms reduces the accuracy of the algorithms for all recommendation list lengths N. However, decay context-awareness improves the efficacy of the Sparse Linear Method (SLIM) and Matrix Factorization.
- In the online shopping area, the SLIM method outperforms both the KNN and MF algorithms using the half-life decay function. It also performs well in terms of Top-N recommendations. The increase in

effectiveness was proven to be related to the average number of interactions per item[48].

- In our dataset the number of interactions per user is limited. Therefore, item-oriented algorithms like SLIM perform better than user-oriented algorithms like KNN.
- Because the SLIM method bases its predictions on item similarity coefficients, it works well on our dataset. Due to the data sparsity (limited numbers of interactions per user), some algorithms (e.g., KNN) perform poorly in terms of recommendations accuracy because it depends on the user's similarity.
- Our research results are consistent with the research [9, 49, 50] that reported increases in effectiveness when using SLIM instead of KNN or MF. This is since SLIM is specifically designed for the top-N recommendation task.

Overall, we conclude that, for the datasets with limited numbers of interactions per users the use of item-oriented decay time-aware recommender systems lead to better performance when compared to bias context aware recommender systems and time-unaware recommender systems.

VI. CONCLUSION

This paper used the user implicit feedback (add to cart and buy) associated with time context to improve the RS performance in online shopping systems. Bias and Decay methods were used to incorporate the time data into RSs. The experiment included incorporating time with three state-of-art algorithms (MF, KNN, and SLIM). To compare the performance of the RSs we applied three cases for each algorithm (time unaware RS, Bias time aware RS, and Decay time aware RS). Precision, Recall, and MAP were used to compare the performance between the different algorithms and between the three cases in each algorithm. As a result, Decay-MF and Decay-SLIM outperform the time Bias MF and SLIM. On the other hand, Decay-KNN reduced the accuracy of the RS compared to the context UN-aware KNN. The results that were reached from the study achieved the goal of the research, which is analyzing and finding the most appropriate algorithm in the field of e-commerce to build a time-aware recommendation system using the user's implicit feedback (purchasing data). As a future work, this study might be applied to a larger dataset with all combinations of algorithms' parameters and with unlimited number of neighbors. This study might also be expanded by combining the decay function approach with other RSs algorithms and on different domains datasets.

REFERENCES

- [1] Ricci, F., L. Rokach, and B. Shapira, Recommender systems: introduction and challenges, in Recommender systems handbook. 2015, Springer. p. 1-34.
- [2] Ricci, F., Rokach, L. and Shapira, B, Introduction to recommender systems handbook. In Recommender systems handbook. Springer Boston, MA., 2011: p. (pp. 1-35).
- [3] Schafer, J.B., J.A. Konstan, and J. Riedl, E-commerce recommendation applications. Data mining and knowledge discovery, 2001. 5(1-2): p. 115-153.
- [4] Sarwar, B., et al. Analysis of recommendation algorithms for e-commerce. in Proceedings of the 2nd ACM conference on Electronic commerce. 2000.

- [5] Koren, Y., Bell, R. and Volinsky, C. Matrix factorization techniques for recommender systems. *Computer*, 2009: p. pp.30-37.
- [6] Sarwar, B.M., et al. Recommender systems for large-scale e-commerce: Scalable neighborhood formation using clustering. in *Proceedings of the fifth international conference on computer and information technology*. 2002.
- [7] Paterek., A., Improving regularized singular value decomposition for collaborative filtering, in *In Proceedings of KDD cup and workshop*. 2007. p. 5–8.
- [8] Paul Resnick, N.I., Mitesh Suchak, Peter Bergstrom, and John Grouplens: an open architecture for collaborative filtering of netnews, in *Proceedings of the 1994 ACM conference on Computer supported cooperative In work 1994*, ACM: Riedl. p. 175–186.
- [9] Karypis, X.N.a.G., Slim: Sparse linear methods for top-n recommender systems, in *2011 IEEE 11th International Conference on Data Mining*. 2011, IEEE. p. 497–506.
- [10] Adomavicius, G. and A. Tuzhilin, Toward the next generation of recommender systems: A survey of the state-of-the-art and possible extensions. *IEEE Transactions on Knowledge & Data Engineering*, 2005(6): p. 734-749.
- [11] Burke, R., Hybrid web recommender systems, in *The adaptive web*. 2007, Springer. p. 377-408.
- [12] Kumar, B. and N. Sharma, Approaches, issues and challenges in recommender systems: a systematic review. *Indian J. Sci. Technol*, 2016. 9(47): p. 1-12.
- [13] Mahmood, T.a.R., Improving recommender systems with adaptive conversational strategies, in *In Proceedings of the 20th ACM conference on Hypertext and hypermedia*. 2009. p. (pp. 73-82).
- [14] Ben-Shimon, D., et al., Recommender system from personal social networks, in *Advances in Intelligent Web Mastering*. 2007, Springer. p. 47-55.
- [15] Dey, A.K., Understanding and using context. *Personal and ubiquitous computing*, 2001. 5(1): p. 4-7.
- [16] Schmidt, A., M. Beigl, and H.-W. Gellersen, There is more to context than location. *Computers & Graphics*, 1999. 23(6): p. 893-901.
- [17] Adomavicius, G. and A. Tuzhilin, Context-aware recommender systems, in *Recommender systems handbook*. 2011, Springer. p. 217-253.
- [18] Campos, P.G., F. Díez, and I. Cantador, Time-aware recommender systems: a comprehensive survey and analysis of existing evaluation protocols. *User Modeling and User-Adapted Interaction*, 2014. 24(1-2): p. 67-119.
- [19] De Borba, E.J., I. Gasparini, and D. Lichtnow. Time-aware recommender systems: a systematic mapping. in *International Conference on Human-Computer Interaction*. 2017. Springer.
- [20] van Kortenbof, B.L., Context-Aware Recommender Systems in the E-commerce Domain. 2017.
- [21] Introduction to Latent Matrix Factorization Recommender Systems Available from: towardsdatascience.com.
- [22] Guibing Guo; Jie Zhang; Zhu Sun; and Neil Yorke-Smith. In *Posters*, D., Librec: A java library for recommender systems., in *Late-breaking Results and Workshop Proceedings of the 23rd International Conference on User Modeling, Adaptation and Personalization*. 2015.
- [23] Sánchez-Moreno, D., Y. Zheng, and M.N. Moreno-García. Incorporating time dynamics and implicit feedback into music recommender systems. in *2018 IEEE/WIC/ACM International Conference on Web Intelligence (WI)*. 2018. IEEE.
- [24] de Zwart, T., Time-Aware Neighbourhood-Based Collaborative Filtering. 2018.
- [25] de Borba, E.J., I. Gasparini, and D. Lichtnow. The Use of Time Dimension in Recommender Systems for Learning. in *ICEIS (2)*. 2017.
- [26] Luo, J., et al., A context-aware personalized resource recommendation for pervasive learning. *Cluster Computing*, 2010. 13(2): p. 213-239.
- [27] Karahodza, B., H. Supic, and D. Donko. An Approach to design of time-aware recommender system based on changes in group user's preferences. in *2014 X International Symposium on Telecommunications (BIHTEL)*. 2014. IEEE.
- [28] Gallego, D., et al. A model for generating proactive context-aware recommendations in e-learning systems. in *2012 Frontiers in Education Conference Proceedings*. 2012. IEEE.
- [29] Inuzuka, K., T. Hayashi, and T. Takagi. Recommendation system based on prediction of user preference changes. in *2016 IEEE/WIC/ACM International Conference on Web Intelligence (WI)*. 2016. IEEE.
- [30] Rezaeimehr, F., et al., TCARS: Time-and community-aware recommendation system. *Future Generation Computer Systems*, 2018. 78: p. 419-429.
- [31] Feng, H., et al., Personalized recommendations based on time-weighted overlapping community detection. *Information & Management*, 2015. 52(7): p. 789-800.
- [32] Gueye, M., T. Abdesslem, and H. Naacke, Dynamic recommender system: using cluster-based biases to improve the accuracy of the predictions, in *Advances in Knowledge Discovery and Management*. 2016, Springer. p. 79-104.
- [33] Luo, C., X. Cai, and N. Chowdhury. Self-training temporal dynamic collaborative filtering. in *Pacific-Asia Conference on Knowledge Discovery and Data Mining*. 2014. Springer.
- [34] Chen, J., et al., A Temporal Recommendation Mechanism Based on Signed Network of User Interest Changes. *IEEE Systems Journal*, 2019.
- [35] Arora, R.M.A.T.A., Temporal Recommendations for Discovering Author Interests, in *2019 Twelfth International Conference on Contemporary Computing (IC3) 2019*: Noida, India. p. pp. 1-6.
- [36] Benlamri, R. and X. Zhang, Context-aware recommender for mobile learners. *Human-centric Computing and Information Sciences*, 2014. 4(1): p. 12.
- [37] Chen, W., et al., A hybrid recommendation algorithm adapted in e-learning environments. *World Wide Web*, 2014. 17(2): p. 271-284.
- [38] Wei, S., N. Ye, and Q. Zhang. Time-aware collaborative filtering for recommender systems. in *Chinese Conference on Pattern Recognition*. 2012. Springer.
- [39] Retailrocket recommender system dataset. Available from:<https://www.kaggle.com/retailrocket/ecommerce-dataset>.
- [40] Ludwig-Maximilians, Demonstration of the exponential decay law using beer froth. *EUROPEAN JOURNAL OF PHYSICS*, 2001: p. 21-26.
- [41] Yong Zheng, B.M., and Robin Burke., Cslim: Contextual slim recommendation algorithms, in *Proceedings of the 8th ACM Conference on Recommender Systems*. 2014., ACM. p. 301–304.
- [42] Yong Zheng, R.B., and Bamshad Mobasher, Recommendation with differential context weighting, in *In International Conference on User Modeling, Adaptation, and Personalization*. 2013, Springer. p. pages 152–164.
- [43] Russell, K.J.a.E., Particle swarm optimization, in *1995 IEEE International Conference on Neural Networks*., 1995. p. 1942–1948.
- [44] Yong Zheng, B.M., and Robin Burke. , Carskit: A java-based context-aware recommendation engine. . *IEEE International Conference on Data Mining Workshop (ICDMW)*, 2015: p. 1668–1671.
- [45] Al Jawarneh, I.M., Bellavista, P., Corradi, A., Foschini, L., Montanari, R., Berrocal, J. and Murillo, J.M., A Pre-Filtering Approach for Incorporating Contextual Information Into Deep Learning Based Recommender Systems. *IEEE Computer Society*, 2020: p. 40485-40498.
- [46] Ilarri, S., Trillo-Lado, R. and Hermoso, R., Datasets for context-aware recommender systems: Current context and possible directions, in *2018 IEEE 34th International Conference on Data Engineering Workshops (ICDEW)*. 2018., IEEE. p. 25-28.
- [47] Zheng, Y., A User's Guide to CARSKit. 2015, arXiv preprint
- [48] Pedro G. Campos Soto, . . . Temporal models in recommender systems: An exploratory study on different evaluation dimensions. 2011, Universidad Autónoma de Madrid: Madrid.
- [49] Hoslim, E.C.a.G.K., Higher-order sparse linear method for top-n recommender systems., in *Pacific-Asia Conference on Knowledge Discovery and Data Mining*. 2014, Springer. p. 38–49.
- [50] Karypis., E.C.a.G., Local item-item models for top-n recommendation, in *Proceedings of the 10th ACM Conference on Recommender Systems*. 2016, ACM. p. 67–74.

- [51] A. Hassan, E. Fadel, and N. Akkari, Time-Aware Recommender System For E-Commerce Applications, 2020. p. 534-542.
- [52] Wang, D., Xu, D., Yu, D., & Xu, G. (2021). Time-aware sequence model for next-item recommendation. *Applied Intelligence*, 51(2), 906-920.
- [53] Yang, D., Nie, Z. T., & Yang, F. (2021). Time-aware CF and temporal association rule-based personalized hybrid recommender system. *Journal of Organizational and End User Computing (JOEUC)*, 33(3), 19-34.

A Comprehensive Assessment Framework for Evaluating Adaptive Security and Privacy Solutions for IoT e-Health Applications

Waqas Aman, Fatima Najla Mohammed

Department of Information Systems, College of Economics and Political Science
Sultan Qaboos University, Muscat, Sultanate of Oman

Abstract—There exist numerous adaptive security and privacy (S&P) solutions to manage potential threats at runtime. However, there is a lack of a comprehensive assessment framework that can holistically validate their effectiveness. Existing Adaptive S&P assessment efforts either focus on privacy or security in general, or are focused on specific adaptive S&P attributes, e.g. authentication, and, at certain times, disregards the architecture in which they should be comprehended. In this paper, we propose a holistic assessment framework for evaluating adaptive S&P solutions for IoT e-health. The framework utilizes a proposed classification of essential attributes necessary to be recognized, evaluated, and incorporated for the effectiveness of adaptive S&P solutions for the most common IoT architectures, fog-based and cloud/server-based architectures. As opposed to the existing related work, the classification comprehensively covers all the major classes of essential attributes, such as S&P objectives, contextual factors, adaptation action aptitude, and the system's self-* properties. Using this classification, the framework assists to evaluate the existence of a given attribute with respect to the adaptation process and in the context of the architectural layers. Therefore, it stresses the importance of where an essential attribute should be realized in the adaptation phases and in the architecture for an adaptive S&P solution to be effective. We have also presented a comparison of the proposed assessment framework with existing related frameworks and have shown that it exhibits substantial completeness over the existing works to assess the feasibility of a given adaptive S&P solution.

Keywords—Internet of Things; Adaptive Security; IoT Architecture; e-Health; Effectiveness; Privacy

I. INTRODUCTION

IoT has become an integral part in the automation and extension of various IT-based services. In healthcare, IoT has shown huge potential. Spending on e-health solutions in IoT is expected to stretch 1.1 Trillion dollars by 2025 [1]. IoT in e-health is a developing research area as the world moves towards remote monitoring, real-time and rapid diagnosis and management of illnesses [2]. It is aiding in real-time identification of ailments, attaining more precise health readings, better reach-out to patients in emergencies, and medical care for patients while they are roaming or having mobility difficulties [2]. The range of functionalities provided by IoT in e-health applications has been significantly beneficial and high in demand, especially in the current COVID-19 pandemic situation where hospitals are running at total capacity, requiring more efficient remote healthcare solutions.

Despite the multiple benefits offered by IoT-enabled e-health applications, there is an increasing concern about the potential security and privacy (S&P) threats as it primarily utilizes personal and sensitive information, which can be of considerable value for the attacker, for instance in blackmailing and identity frauds [3],[4]. By nature, IoT devices are dynamic because of the frequent environmental changes, mobility, and their heterogeneous and constantly evolving technology. Such properties can result in a more evolved threat spectrum requiring real-time threats handling. To adapt to such circumstances, many studies have proposed adaptive S&P mechanisms. Adaptive S&P is a system's capability to maintain S&P in the presence of contextual changes [5]. It continuously maintains an optimal S&P level of a managed system through an automated monitor, analyze, and adapt feedback loop, unlike traditional S&P controls such as IDS, anti-malware, firewalls, etc., which have limited protection scope and enforce manual and inflexible threat mitigation strategies [5].

IoT e-health is a critical infrastructure consisting of devices, applications, and individuals that handle sensitive patients' data. Adaptive S&P mechanisms are highly essential, mainly to protect and manage actions, such as access, sharing, and disclosing of the information assets and provide effective S&P within the IoT e-health architecture [6, 7]. Hence, the system needs to be flexible, adaptable, and robust to make real-time S&P decisions based on the requirements of the entities associated with the system [6]. When designing and developing adaptive S&P solutions for IoT e-health, it is vital to consider a set of significant attributes; such as privacy and security objectives, contextual factors, self- properties, adaptation action aptitude and analysis, and adaptation mechanisms to develop a solution that is capable of providing holistic S&P in such dynamic contexts. Moreover, these attributes needs to be realized at particular levels with respect to the different phases in the process and to the underlying architectural needs. If a certain attribute or requirement is improperly enforced in the architectural layers, it may adversely affect the competency of the corresponding adaptation phase. Such misconfiguration may lead to, for instance, scope creep or scope crush of the managed devices, resulting in the adaptive system disorganization and ineptitude.

Regardless of the availability of multiple studies and solutions on adaptive S&P, for instance, [8, 9, 10] emphasize on the need to assess their effectiveness. To validate the efficacy, it is vital to recognize and evaluate the essential factors

necessary for an adaptive S&P solutions and the extent to which they are employed as per adaptation and architectural needs. The existing assessment frameworks focus on a particular set of factors irrespective of the underlying architecture [9,13,14,15] and have a limited scope that only address a part of the problem, [9,13,14,15]. Hence, there is a need of an evaluation framework that can holistically assess the feasibility of a given adaptive S&P mechanism for IoT e-health applications.

In this paper, we present the design of an assessment framework that can guide us to comprehensively assess the feasibility of a potential adaptive S&P solution. It, therefore, also provides a reference model to understand and consider the underlying vital aspects of S&P adaptation. The framework is based on a proposed classification of factors that we have compiled from the existing works. These factors were scattered across the literature under different concerns and with limited scope. We have unified them in a classification of five distinct classes: security objectives, contextual factors, adaptation aptitude, and self-* properties and privacy objectives required for effective S&P adaptation. The proposed framework mainly assesses which factors should be covered, where they should be realized in the adaptation process, i.e., monitoring, analysis, or adaptation, and at which layer of the common IoT e-health architectures, fog or cloud/server, should they be employed. Furthermore, we present a detailed comparison of the proposed framework with the potential equivalent works. We have concluded that our framework provides a more comprehensive platform for assessing a given adaptive S&P solution. The fundamental contribution that our framework dispenses is a set of diverse and inclusive factors required for S&P adaptation and evaluates them in the architecture context is particularly vivid.

II. THE ASSESSMENT FRAMEWORK

In this section, we provide a comprehensive description and illustration of the proposed classification and assessment framework. The classification mainly identifies and groups the key attributes (factors) necessary for a given adaptive S&P system. The assessment framework utilizes this classification by determining their need and purpose based on two key aspects: the overall adaptation process (Monitor, Analyze, and Adapt phases) and the IoT e-health architecture. These two aspects are necessary to be considered because certain attributes necessary for the S&P adaptation needs to be addressed uniquely in various architectures. For instance, for fog-based architectures it is vital to conduct S&P analysis at the gateway than at a centralized server to fulfil the rapid and personalized threat assessment objectives for which fog-based architectures are devised [11], [12]. Moreover, the scope managed by a given gateway in fog-architecture is limited as compared to one managed by a centralized server. This structured approach of the framework design assists in assessing the feasibility of an adaptive S&P solution in its respective architecture.

A. The Proposed Classification

The classification aims to identify and group the fundamental factors necessary for a given adaptive S&P solution. It employs conceptual modeling and provides a basis for comprehending the factors that need to be monitored or

managed, essential to effectively achieve security and privacy objectives, and the ones that may trigger the need of adaptation or may be affected by the adaption processes. Hence, it provides a more comprehensive list of essential factors. The proposed classification, as illustrated in Fig. 1, is developed using the steps followed as:

- Key factors were identified in the current literature on adaptive S&P for IoT e-health.
- Factors that have similar semantic and objective(s) were unified into a common factor. For instance, events per second (eps), productivity, and throughput factors are transformed into a more common and distinct label, throughput.
- To be more comprehensive, certain generic factors are broken down into more detailed and vital factors. For example, QoS is further categorized into response time, latency, and throughput.
- The final list of factors was then grouped into distinct classes. Factors were mapped to the relevant classes based on their overall objectives. Table I provides a brief summary describing each class, listed in Fig. 1, in the context of adaptive S&P solution for IoT e-health

B. The Proposed Assessment Framework

The primary objective of the proposed assessment framework is to holistically assess the feasibility of an adaptive S&P solution for IoT e-health. It considers four essential concepts: The proposed classification, detailed earlier, the adaptation processes, the IoT e-health architecture in which an adaptive S&P is employed, and a Mapping Criteria. A brief description to the later three concepts in the framework are detailed as follows.

1) *The adaptation process:* The adaption process in an adaptive S&P system can be typically divided into three main functionalities or phases [8, 13, 16, 17]: Monitoring, Analysis, and Adaptation. They enable a system to adapt the S&P configurations based on the dynamic changes in the IoT e-health infrastructure in an automated manner. These phases are briefly described as follows:

a) *Monitoring:* The main goal is to observe, gather and transform contextual information. This includes information about the adaptive system itself (internal factors), such as information related to the software and hardware components responsible for the adaptation process. Monitoring also observe external factors such as those related to the monitored devices, users, network and applications. Therefore, it attempts to collect data essential for a context-aware analysis and adaptation [8, 16, 17].

b) *Analysis:* Analysis aims to determine potential threats, assess potential vulnerabilities, and analyze the protection level of security and privacy from the related contextual information gathered during the monitoring phase. Hence, the analysis process involves the intelligence by applying a range of methods needed to investigate, correlate, and analyze the context of the potential threats [8, 16, 17].

TABLE I. A SUMMARY OF THE CLASSIFICATION CLASSES

Factors	Summary
Security Objectives	Include the attributes responsible for ensuring the basic security of the IoT e-health resources covered by the adaptive system, from security threats, e.g., authenticating users based on their biometric information, authorizing users based on their role, e.g., medical staff accessing the staff portal, patients accessing the patient's portal.
Privacy Objectives	Refers to the factors that ensure essential privacy, including access, usage, and collection of the information assets in an IoT e-health environment, e.g., collecting, accessing, and using patient's health records such as x-rays and CT scans.
Contextual Factors	Contextual factors can potentially trigger the need for adaptive S&P. This can include internal factors such as architectural factors and external factors such as user preferences. Hence, in the context of adaptive S&P solution, assessing these attributes is essential mainly to ensure that the adaptive solution can consider contextual aspects to respond to the changing context and respond to S&P threats, thus providing holistic S&P.
Self-*Properties	Self- * Properties are the basis for the adaptive S&P system itself, as they are capabilities responsible for the adaptive nature of such solutions. These properties enable the adaptive solution to adjust its S&P settings in response to a context and adapt and manage the adaptive solution itself in response to S&P threats. For instance, introducing additional encryption mechanisms in response to a low battery event from one sensing device
Adaptation Action Aptitude	A set of factors that may have a negative impact due to the potential adaptation action. For instance, if a low battery occurrence is detected in a monitoring device, the adaptive solution should adjust the encryption mechanisms to ensure trade-offs amongst confidentiality and the availability of the services.

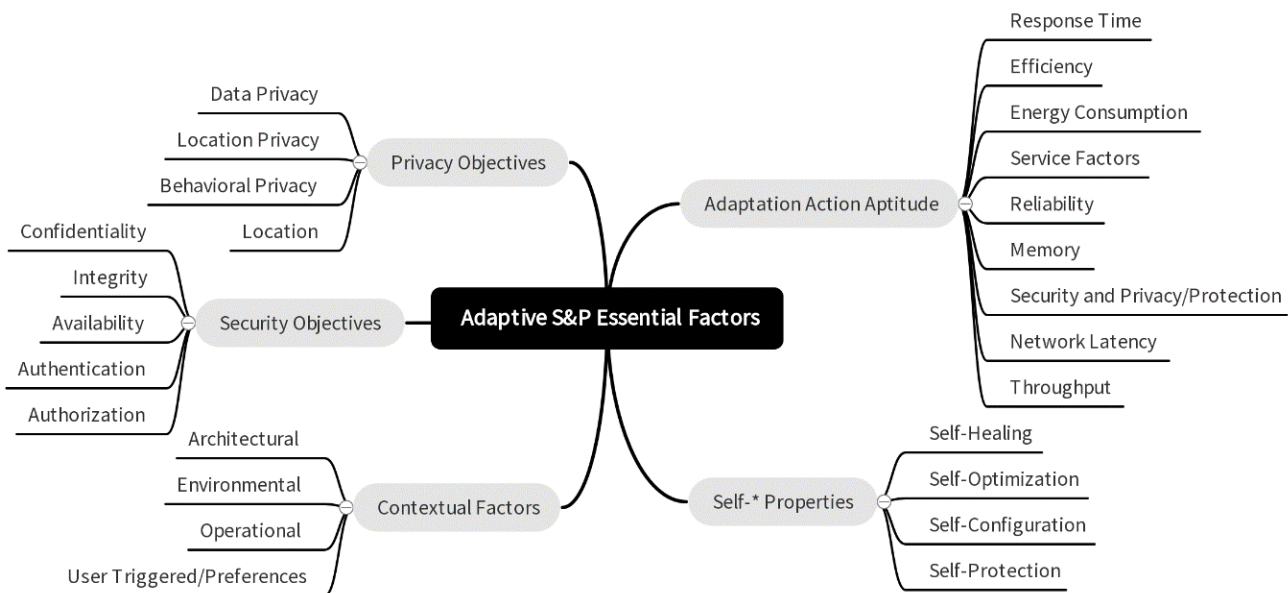


Fig. 1. The Proposed Classification.

c) *Adaptation*: In the adaptation phase, decisions are made to adapt to any given threat situation. The corresponding functionalities identifies a recommended adaptation configuration based on the threat faced and instructs the monitored asset(s) for its adoption. It is recommended that the system is capable of identifying several adaptation actions and select the optimal one [13]. The adaptation process is responsible for the adaptation decision making whereas the actual adaption action is implemented at the monitored object level [8].

2) *IoT eHealth Architecture*: The IoT e-Health architecture specifies the nature of data processing within the overall system [18], [19]. This study considers the two major IoT e-health system architectures, cloud/ server and fog-based system architecture, which are commonly used in the IoT e-Health settings.

a) *Cloud/Server Architecture*: In Cloud/Server architectures, illustrated in Fig. 2, data processing is performed

in a centralized manner, typically using cloud computing or centralized servers controlled by the healthcare service provider [6], [20]. To enforce S&P adaptation in a cloud/server architecture, the monitoring is carried out within the gateway and health systems layer. This includes data collection, filtration, transformation, and further communication, etc., to the upper layers. Device Layer merely act as events generators. However, in certain instances, monitoring is performed at the device layer. For instance, GPS sensors and authentication interfaces can monitor and send out events to the gateway layer, which are further processed by the gateway. In contrast, the analysis and adaptation decision-making is performed at the health systems layer, comprising the cloud/centralized servers [13, 21].

b) *Fog architecture*: Fog architectures, shown in Fig. 3, use the computing resources at the gateway level to carry out the processing of the data gathered from the sensors [22]. The fog nodes, the gateways, perform data normalization, which

consist of storage, computing, and network connectivity, thus enabling them to analyze and make time-sensitive decisions on the time-sensitive data collected [23]. In the context of S&P adaptation, in fog architectures, threat monitoring, analysis, and adaptive decision-making are typically performed at the gateway layer [8, 24]. However, as established earlier, in certain instances, monitoring can also be performed in the device layer. In fog architectures, health-related data collected from the device layer is sent to the cloud. It is part of the primary storage and computing resource, performing data analytics and visualization [23].

3) *The mapping criteria:* The mapping criteria, detailed in Table II, describes information on what and where different attributes should be realized within the different IoT system architectural layers and whether and what adaptation process should be applied on them to enforce effective S&P adaptation. Therefore, it maps a given attribute to the respective architectural layer and adaptation phase based on its requirement in an adaptive S&P solution. Table III – VII illustrate the proposed assessment framework, and shows how the different attributes in the proposed classification have been mapped based on the adaptation process and the IoT e-health architectural layers. For convenience, below we describe how the table structure should be interpreted to comprehend the

architectural and process level requirements of a given attribute:

- The Class and Attributes columns corresponds to the classes and respective factors, as detailed in the proposed classification, which are essential for S&P adaptation.
- The Process column indicate whether or not a given attribute is required be monitored (M), Analyzed (A), or Adapted (Ad). Moreover, it also reflects whether the respective mechanism(s) of the attribute is Utilized (U). An absence of a label indicate that it is not required.
- The System Architecture column, further categorized into Fog and Cloud/Server architecture, indicates where, specifically, in the respective architectures should an attribute is required to be utilized, monitored, analyzed, adapted. For instance, GM depicts that a given attribute needs to be monitored at the Gateway Layer, HU indicates that the mechanism(s) related to the factor should be utilized at the Health System Layer, and GAd shows that the corresponding factor needs to be adapted at the Gateway Layer.

The assessment framework for individual class is illustrated and detailed underneath.

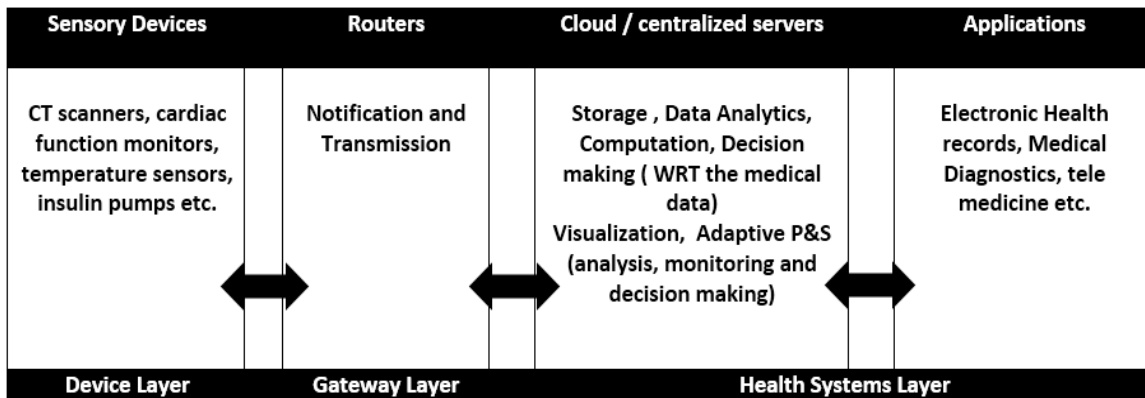


Fig. 2. Figure 2. IoT e-Health Cloud/Server Architecture.

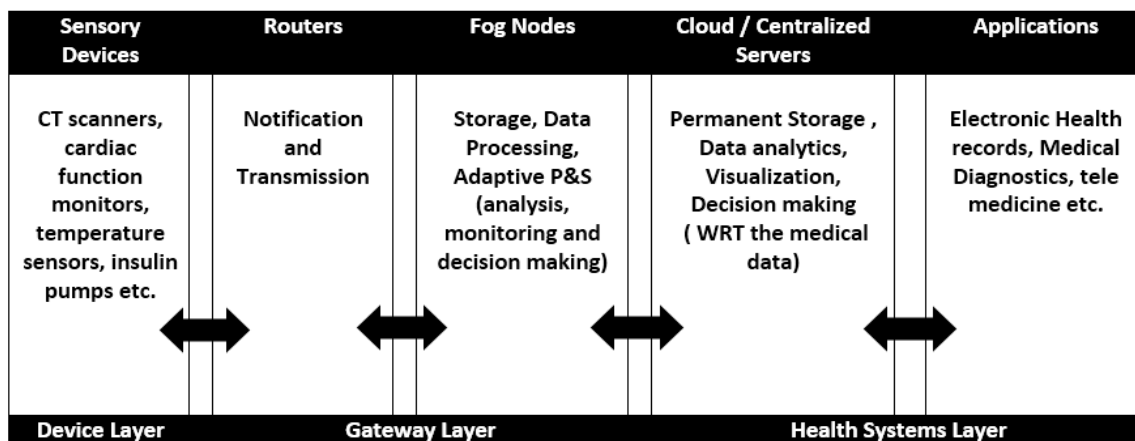


Fig. 3. IoT e-Health Fog Architecture.

TABLE II. THE ASSESSMENT FRAMEWORK'S MAPPING CRITERIA

Criteria #	Criteria for mapping an attribute with the adaptation process
1	Utilized (U): Reflects that the corresponding mechanism or attribute is utilized either as a mechanism to ensure S&P or as a factor/attribute to be evaluated for optimal adaptation decision in the adaptation phase.
2	Monitoring (M): Attributes are mapped to monitoring process when they are required to be <i>observed or monitored</i> for security and privacy threat/risk analysis or when they are utilized in the monitoring process.
3	Analysis (A): Attributes are mapped to the analysis process when they are <i>assessed</i> for the security and privacy threat/risk analysis or when are they utilized in the analysis process.
4	Adaptation (Ad): Attributes are mapped to the adaptation process when they are required to be adapted, evaluated during the adaptation decision, or utilized in the process.
Criteria for mapping an attribute with the adaptation process IoT e-health architecture	
	Attributes are mapped within the fog and cloud/server architecture, with regards to where in the architecture, Device layer (D) , Gateway layer (G) and healthcare service provider controlled layer (H) , Cloud/Central servers, these attributes are required to be (M) , (A) , (Ad) and (U) .

TABLE III. CLASS – SECURITY OBJECTIVES

Class	Attributes	Process	System Architecture				
			Fog Architecture		Cloud/server Architecture		
			Layers				
			D	G	D	G	H
Security Objectives	Confidentiality	M,A,Ad,U	DU	GM,GU GA,GAd	DU	GM,GU	HM,HU, HA,HAd
	Integrity	M,A,Ad,U	DU	GM,GU, GA,GAd	DU	GM,GU	HM,HU, HA,HAd
	Availability	M,A,Ad,U	DM,DU, DA	GM, GU, GA,GAd	DM, DA, DU	GM,GU	HM,HU, HA,HAd
	Authentication	M,A,Ad,U	DM,DU, DA	GM,GU, GA,GAd	DM, DA, DU	GM,GU	HM,HU, HA,HAd
	Authorization	M,A,Ad,U	DU	GM,GU, GA,GAd	DU	GM,GU	HM,HU, HA,HAd

C. Assessing Security Objectives

As highlighted in Table III, mechanisms related to security attributes, e.g. encryption, integrity checks, etc., should be utilized within all the layers to ensure the respective objectives. Authentication, which may consist of a user, API, or service identity confirmation, monitoring and analysis is typically performed at the device level. Similarly, availability, which involves the accessibility and constancy of data, services and devices, are monitored and analyzed at the device layer, particularly when using smart devices. For all other attributes, the gateway layer, within fog architecture, handles all the adaption phases. Availability and Authentication related may be further normalized and correlated for analysis at this layer. In a cloud/server based architecture, the gateway layer mainly serves as an agent to monitor (M) the devices and services under its authorization or scope. Whereas, the health systems layer performs the analysis and adaptation phases for all devices and services. It also handles complex or high level monitoring and analysis of events arriving from potential multiple gateways as well this generated by its native applications or services.

D. Assessing Privacy Objectives

As illustrated in Table IV, similar to the security objectives class, methods or mechanisms related to each highlighted privacy attribute should be utilized within all the layers in both architectures. In a fog-based architecture, the gateway layer is responsible for performing all the adaptation phases for its

underlying devices and services. Location is typically monitored at the device layer, as there can be devices that would require monitor to send out alerts, hence it needs to be monitored at the device layer and further normalized at the gateway. In a cloud/server- based architecture, a particular gateway monitors its respective devices and services. The health systems layer carries out all the adaptation phases for the entire scope including its own hosting services.

E. Assessing Contextual Factors

The Contextual factors focuses on the importance of any internal or external changes that may be experienced at any layer of the architectures. Such changes may trigger the need of S&P adaptation. Therefore, all related factors should be monitored at every layer within both architectures, as reflected in Table V. However, environmental factors, which mainly refer to changes that may occur outside a monitored device, should be monitored at the gateway layer [11, 13, 14, 25, 26, 27, 28]. Users (patient, practitioners, and system admins) should be permitted to change their preferences, and therefore, the corresponding mechanism should be enforced for utilization at all layers. typically monitored at the device layer, as there can be devices that would require monitor to send out alerts, hence it needs to be monitored at the device layer and further normalized at the gateway. In a cloud/server- based architecture, a particular gateway monitors its respective devices and services. The health systems layer carries out all

the adaptation phases for the entire scope including its own hosting services.

F. Assessing Factors Affecting Adaptation Action Aptitude

Adapting any attribute, for example adapting to new confidentiality settings, may have a negative impact on the

system’s performance, usability, or S&P objectives. Therefore, it is essential to evaluate the aptitude of a potential solution to a faced threat in the adaptation phase. Attributes corresponding to this notion are captured in the Adaption Actions Aptitude class. Table VI illustrates the most common and vital attributes that are necessary to be evaluated in the adaptation phase (Ad).

TABLE IV. CLASS – PRIVACY OBJECTIVES

Class	Attributes	Process	System Architecture				
			Fog Architecture		Cloud/server Architecture		
			Layers				
			D	G	D	G	H
Privacy Objectives	Data Privacy	M,A,Ad, U	DU	GM,GU,GA,GAd	DU	GM,GU	HM,HU,HA,HAd
	Communication Privacy	M,A,Ad, U	DU	GM,GU,GA,GAd	DU	GM,GU	HM,HU,HA,HAd
	Behavioral privacy	M,A,Ad, U	DU	GM,GU,GA,GAd	DU	GM,GU	HM,HU,HA,HAd
	Location Privacy	M,A,Ad, U	DM,DU	GM,GU,GA,GAd	DM,DU	GM,GU	HM,HU,HA,HAd

TABLE V. CLASS – CONTEXTUAL FACTORS

Class	Attributes	Process	System Architecture				
			Fog Architecture		Cloud/server Architecture		
			Layers				
			D	G	D	G	H
Contextual Factors	Architectural Factors	M,A,Ad	DM	GM,GA,GAd	DM	GM	HM,HA,HAd
	Environmental Factors	M,A,Ad	-	GM,GA,GAd	-	GM	HM,HA,HAd
	Operational Factors	M,A,Ad	DM	GM,GA,GAd	DM	GM	HM,HA,HAd
	User preferences	M,A,Ad, U	DM, DU	GM,GA,GAd, GU	DM, DU	GM,GU	HM,HU,HA,HAd

TABLE VI. CLASS – ADAPTION ACTION APTITUDE

Class	Attributes	Process	System Architecture				
			Fog Architecture		Cloud/server Architecture		
			Layers				
			D	G	D	G	H
Adaption Actions aptitude	Response Time	Ad	-	GAd	-	-	Had
	Efficiency	Ad	-	GAd	-	-	Had
	Energy Consumption	Ad	-	GAd	-	-	Had
	Service factors	Ad	-	GAd	-	-	Had
	Reliability	Ad	-	GAd	-	-	Had
	Memory	Ad	-	GAd	-	-	Had
	Security & Privacy	Ad	-	GAd	-	-	Had
	Network Latency	Ad	-	GAd	-	-	Had
	Throughput	Ad	-	GAd	-	-	Had

TABLE VII. CLASS – SELF-* PROPERTIES

Class	Attributes	Process	System Architecture				
			Fog Architecture		Cloud/server Architecture		
			Layers				
			D	G	D	G	H
Self-* Properties	Self-Healing	M,A,Ad, U	DM	GM, GU, GA, GAd	DM	GM	HM, HU, HA, HAd
	Self- Configuration	M,A,Ad, U	DM	GM, GU, GA, GAd	DM	GM	HM, HU, HA, HAd
	Self-Optimizing	M,A,Ad, U	DM	GM, GU, GA, GAd	DM	GM	HM, HU, HA, HAd
	Self-Protecting	M,A,Ad, U	DM	GM, GU, GA, GAd	DM	GM	HM, HU, HA, HAd

Since, the adaptation phase is conducted at the gateway in the fog architecture, and at the health system layer in the Cloud/Server architecture, the highlighted attributes should be evaluated at the respective layers. Assessing these attributes enables to determine if the adaptive S&P solution can ensure trade-offs amongst these attributes during adaptation, especially in a critical environment such as e-health, where time-sensitive decisions are made.

G. Assessing the System's Self-* Properties

To ensure self-management, the adaptive system has to enforce the monitor, analyze, and adaptation loop feedback in its own processes. This implies that the system has to manage the respective adaptation phases and corresponding functions on the corresponding devices and layers. As reflected in Table VII, the self-* properties for all components responsible for monitoring, analysis and adaptation should be monitored at their respective layer where they are implemented. However, further monitoring (high level), analysis, and adaptation should be handled by gateway in the fog architecture whereas the hospital system layer in the Cloud/Server architecture will manage the same.

III. RESULTS AND DISCUSSION

This section critically evaluates the proposed classification and existing assessment frameworks that are proposed for the purpose of assessing adaptive S&P solutions for IoT and/or IoT e-health. The main objective of this effort is to compare our proposed framework with the existing frameworks to evaluate their aptitude in addressing the essential attributes for S&P adaptation with respect to the adaptation process and system architecture. The frameworks that are compared here are: MST [9], AFAS [13], SAS [14] and SMAS [15]. Although there are less numbers of models to be considered for comparison, they are the most related and current efforts with our work and the concept at hand. Furthermore, we intend to reflect on the current practices rather to assess a comprehensive list of existing efforts.

A. The Comparison Approach

The comparison of the frameworks has been made using two dimensions; the evaluation criteria and the comparison score. The criteria intend to determine the comprehensiveness and applicability the reviewed models in the context of Adaptive S&P and aims to conclude:

- Whether or not and to what extent do the reviewed frameworks or models cover the phases in the adaptation process?
- Whether an evaluation framework is suitable to assess Adaptive S&P in a particular IoT-eHealth architecture or both fog-based and server/Cloud-based?
- Which required/identified attributes and to which extent are they addressed by a given evaluation framework or model?

The Comparison score illustrated in Table VIII is an analytical indicator of the level of conformance of an evaluation framework with the comparison criteria, after it is validated.

The higher the score is, the better is the evaluation framework. Hence, it enables us to comprehend the comprehensiveness, applicability, and, therefore, the feasibility of the proposed and existing assessment frameworks in assessing adaptive S&P solutions for IoT e-health. The following table describes the criteria on how each aspect of the comparison approach is scored, in order to evaluate each of the candidate frameworks.

B. Analysis of Security Objectives

The major processes; monitoring, analysis and adaptation has been addressed by all the frameworks, however, AFAS, MST and the proposed framework addresses the utilized (U) process as well as illustrated in Fig. 4. AFAS, SAS and SMAS claim to assess all the attributes under security objectives. However, they provide abstract or insufficient information on the architecture and the architectural layers that the framework assesses. Hence it is unclear on how the adaptation requirements are evaluated within the different architectural layers. Whereas MST considers all the adaptation processes, as well as majority of the security objectives, however the framework is only designed to assess cloud/server based architecture's. Hence having a better comprehension of security objectives for Cloud/Server based architectures as opposed to AFAS, SAS and SMAS. Amongst the assessed frameworks, the proposed framework has a better comprehension of the security objectives, as it evaluates these attributes in the context of both, cloud/ server based and fog architectures. Moreover, the assessed frameworks have addressed the majority of the security attributes. However, the authorization attribute is somehow underestimated, which is concerning.

C. Analysis of Privacy Objectives

As illustrated in Fig. 5, SAS and the proposed framework have addressed all the major processes. Additionally, the proposed framework addresses the utilized (U) process as well. None of the frameworks, except from the proposed framework, addresses all the privacy attributes in the context of architecture. SAS highlights the data privacy attribute however, its realization in the context of the architectural aspects is unclear to draw further conclusions. Furthermore, amongst the privacy attributes, data privacy has been mostly addressed in the evaluated frameworks. However, those discussing it only state its importance and consequences and fail to provide details of it, to be addressed at the corresponding architectural layers to ensure effective S&P adaptation.

D. Analysis of Self-* Properties

Similar to the privacy objectives class, the self-*properties classes as shown in Fig. 6 have been widely ignored by majority of the frameworks. The frameworks AFAS and the proposed framework that do consider this class have addressed all the major adaptation processes. Although it claims to assess all the self-*properties attributes, it provides abstract information on the architectural aspects within its assessment.

Hence it is unclear on how the framework assesses the given attributes within the different architectural layers.

Whereas the proposed framework evaluates the self-*properties attributes amongst different architectural layers for both fog and cloud/server based architectures.

TABLE VIII. COMPARISON SCORE DESCRIPTION

Attribute Context	Criteria Description	Score
Adaptation Process (P)	1 point for each process when an attribute is clearly addressed by an identified adaptation process. Note: maximum points for a process conformance of an attribute vary from attribute to attribute. Refer to <i>The Mapping Criteria</i> for the required processes for each attribute under various classes.	1-4
Architectural (A)	All or the majority of the requirements related to a given attribute are addressed at the corresponding layers for both architectures (fog and Cloud/server)	5
	Few of the requirements related to a given attribute are addressed at the corresponding layers for both architectures (Fog and Cloud/ Server)	4
	All or the majority of the requirements related to a given attribute are addressed at the corresponding layers for a single architectures (fog or Cloud/server)	3
	Few of the requirements related to a given attribute are addressed at the corresponding layers for a single architectures (fog or Cloud/Server)	2

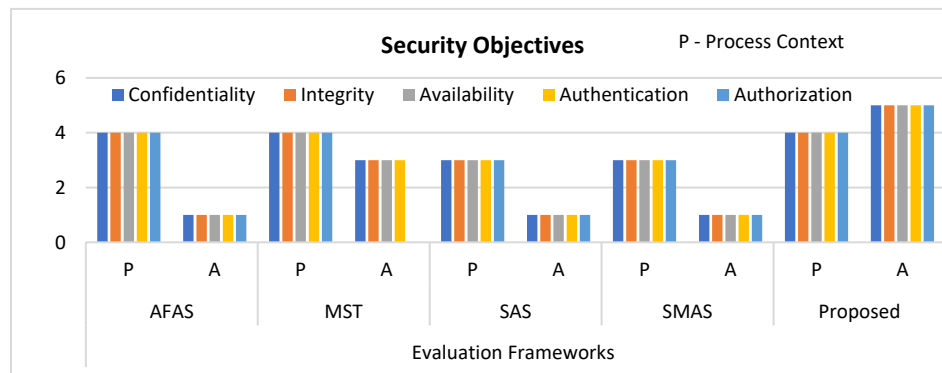


Fig. 4. Comparative Scores of Security Objectives.

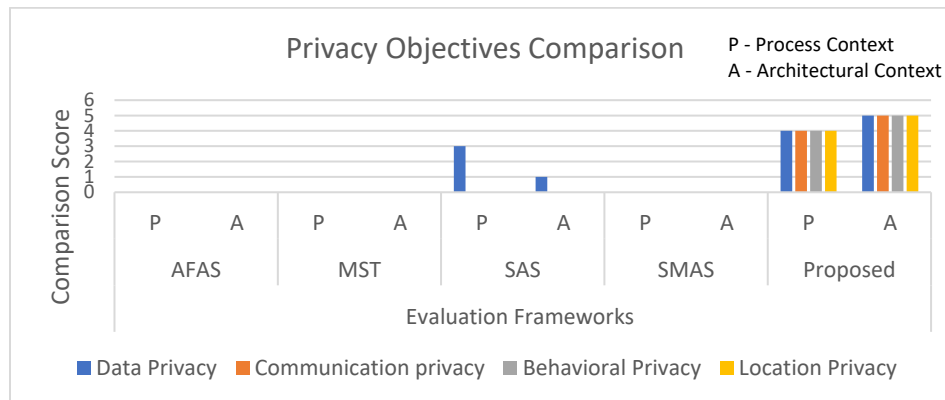


Fig. 5. Privacy Objectives Comparison.

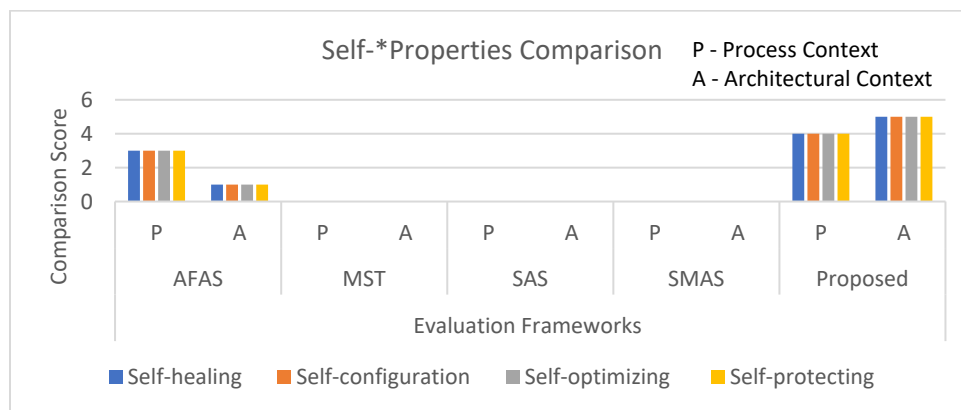


Fig. 6. Self-*Properties Comparison.

E. Analysis of Contextual Factors

The major processes; monitoring, analysis and adaptation have been addressed by all the frameworks as illustrated in Fig. 7. However, the proposed framework addresses the utilized (U) process essential for the user preferences attribute. AFAS and SMAS addresses' majority of the contextual attributes, however the details on the architectural aspects are abstract thus. Hence assessment of these attributes on the architectural layers is indistinct. MST and SAS only consider environmental and operational factors, where MST provides sufficient information on the assessment of these attributes within the layers of cloud/server based architecture. However, SAS provides unclear information on the assessment of these attributes within architectural layers. While the proposed framework considers all the contextual factors within the layers of both architectures.

Amongst the attributes within this class, architectural factors have been ignored by MST and SAS. It is essential to consider architectural factors when assessing adaptive S&P solutions, especially since IoT e-health is a diverse, dynamic,

and mobile architecture where new devices can be added or existing devices can be updated or removed more frequently. Hence, the system should be able to handle such changes [13], [25].

F. Analysis of Adaptation Action Aptitude

As shown in Fig. 8, all the frameworks that consider the adaptation action aptitude attributes consider the main process which is adaptation AD, where these attributes are evaluated. SAS does not consider this class in its evaluation, whereas SMAS only considers Energy consumption, Reliability and S&P attributes but lacks architectural details.

However, AFAS, MST and the proposed framework considers all the attributes under this class. However, in terms of the architectural aspects, the proposed framework assesses these attributes within both architectures, while MST only assess these attributes within cloud/server based architecture, and, AFAS provides abstract information on the assessment of these attributes from an architectural perspective.

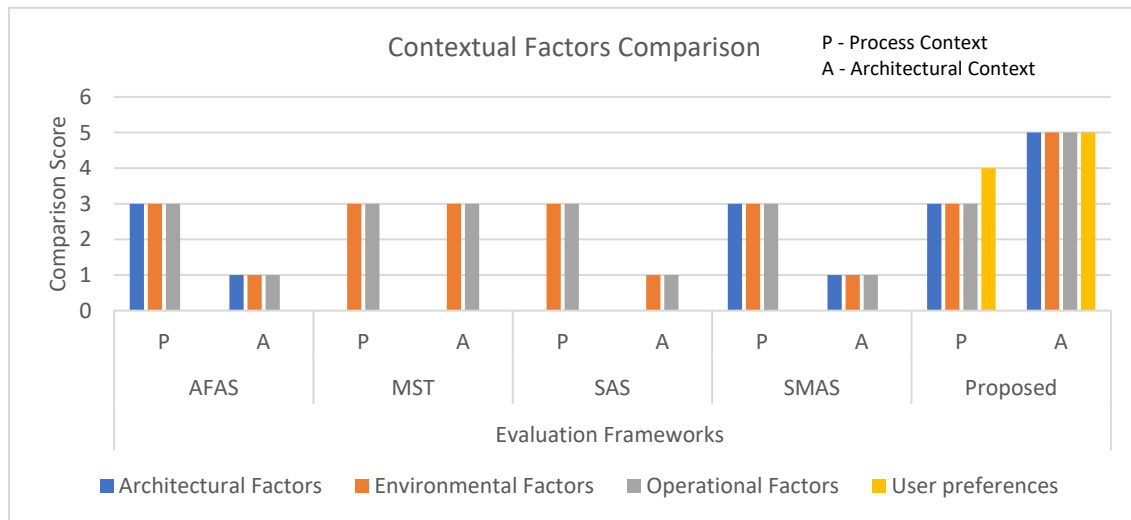


Fig. 7. Contextual Factors Comparison (Note: the Maximum Points for a Process Conformance for Architectural, Environmental and Operational Factors Attributes is 3, Whereas the Process Conformance for user Preferences Attribute is 4).

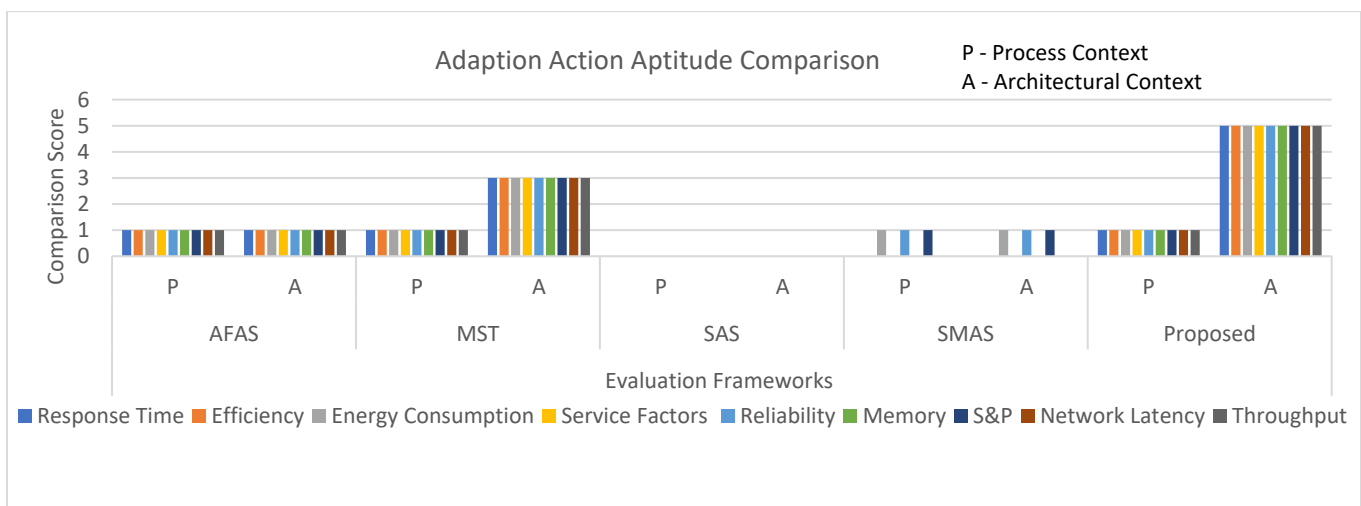


Fig. 8. Adaption Action Aptitude Comparison (Note: The Maximum Points for a Process Conformance for Attributes in this Class is 1).

IV. DISCUSSION ON THE OVERALL COMPARISON

This section highlights the overall outlook of the compared frameworks at the class level. The underneath discussion is based on the observations reflected in Fig. 9, which depicts the maximum points achieved by each compared framework by aggregating their attributes' points in each class, as a result of the above comparison.

It can be observed that although the proposed framework offers a more in-depth view of the security objectives, overall, there seems to be an above average comprehension and consensus on achieving the related attributes. Moreover, except for the proposed framework, all other frameworks have considerably overlooked the privacy aspects. Apparently, privacy objectives are assumed to be enforced with security mechanisms, which should not be exercised as they have different purposes, scopes, and mechanisms. Alongside security objectives, it is vital to address the privacy objectives from different perspectives. The lack of privacy objectives can potentially lead to misuse of patient's sensitive information, such as unauthorized disclosure or usage and even potential identity frauds [3], [4].

Similar to the privacy objectives, the adaptive system's self-* properties are also underestimated. Doing so may lead to the compromise of the system itself. It can be seen that the proposed framework exceptionally stressed on the need of considering the self-* properties. Whereas, AFAS provides fair details of the related properties at the adaptation process level, it lacks to provide enough information on the architectural aspects within its assessment.

MST assesses majority of the attributes for cloud/ server based architectures only. Although AFAS, SMAS, and SAS consider majority of the contextual attributes, these frameworks provide very abstract information on the architectural aspects. It is apparent that the proposed framework fully suffices the adaption action aptitude requirements for both fog and cloud/Server architectures. While, MST assesses all of the attributes for cloud/ server based architecture only. Although AFAS and SMAS consider all the attributes under this class, the frameworks provide unclear information on the architectural requirements.

V. CONCLUSION AND FUTURE PLANS

The proposed framework assists us to recognize, realize, and assess the essential factors for adaptive S&P solutions in the context of the IoT e-health architecture and the adaptation process. It lets us evaluate related solution in a broader spectrum, the overall needs, therefore providing a comprehensive understanding of the overall problem. The comparison made with the existing assessment frameworks reflects that our work introduces considerable improvements by how essentials attributes should be managed in the context of architecture and the adaptation process, which is the key contribution. Most of the frameworks discounted the architectural aspects and their importance, which may negative affect the whole purpose of an adaptive system. Moreover, current assessment frameworks are more focused on a particular set of essential factors or generally highlight them. In contrast, the presented framework provides a holistic set of attributes or requirements that address all the major aspects of an adaptive S&P system and assess them in the context of underlying architecture and the adaptation process. Thus, offers a comprehensive mechanism to assess the feasibility of a given adaptive S&P solution.

Although this study primarily studies e-health as an IoT application, it can be generalized to similar IoT-based architectures. Nevertheless, it needs further investigation to consummate this hypothesis. Furthermore, assessing specific performance and QoS factors of adaptive S&P solutions for IoT e-health from a quantitative perspective could result in a more considerable attempt. In addition, the proposed framework could have added more value if common practices or mechanisms for each attribute were highlighted. This would have offered a sense of trending mechanisms and made the criteria more mature and comprehensive.

In future, we plan to extend this research by addressing the limitation discussed. We plan to study other IoT architectures to investigate if the proposed assessment framework can be utilized or requires further refinements. Moreover, we intend to further improve the proposed assessment framework by investigating the commonly utilized mechanisms for each attribute and analyzing the trends in the mechanisms utilized to make the framework more beneficial and inclusive. Lastly, we intend to work on a more rigor assessment to present a more acceptable capability maturity model.

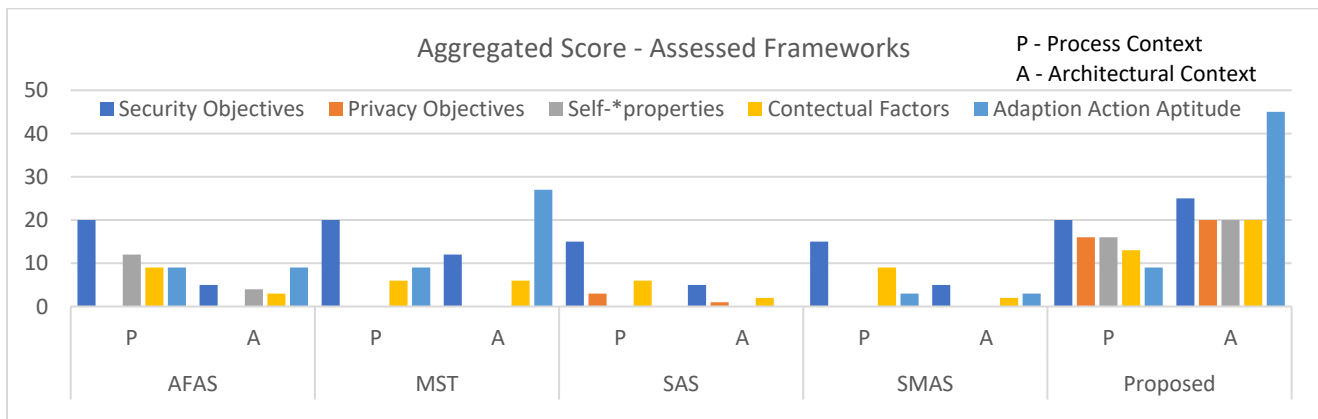


Fig. 9. Aggregated Score of the Compared Assessment Frameworks.

REFERENCES

- [1] Manyika J, Chui M, Bisson P, Woetzel J, Dobbs R, Bughin J et al. *The Internet of Things: Mapping The Value Beyond The Hype*. 24th Ed. New York, NY, USA: McKinsey Global Institute; 2015.
- [2] Malasinghe LP, Ramzan N, Dahal K. Remote patient monitoring: a comprehensive study. *Journal of Ambient Intelligence and Humanized Computing*. 2019 Jan; 10(1):57-76.
- [3] El Emam K. *Guide to the De-Identification of Personal Health Information* [Internet]. 1st Ed. New York, USA: Auerbach Publications; 2013 [cited 12 January 2022]. Available from: <https://bit.ly/3aYSCTy>
- [4] Malin BA, Emam KE, O'Keefe CM. Biomedical data privacy: problems, perspectives, and recent advances. *Journal of the American medical informatics association*. 2013 Jan 1; 20(1):2-6.
- [5] Schaub F, Könings B, Weber M, Kargl F. Towards context adaptive privacy decisions in ubiquitous computing. In *2012 IEEE International Conference on Pervasive Computing and Communications Workshops* 2012 Mar 19 (pp. 407-410). IEEE.
- [6] Boudko S, Abie H. Adaptive cybersecurity framework for healthcare internet of things. In *2019 13th International Symposium on Medical Information and Communication Technology (ISMICT) 2019* May 8 (pp. 1-6). IEEE.
- [7] Yang Y, Zheng X, Guo W, Liu X, Chang V. Privacy-preserving smart IoT-based healthcare big data storage and self-adaptive access control system. *Information Sciences*. 2019 Apr 1;479:567-92.
- [8] Aman W, Kausar F. Towards a Gatewaybased Context-Aware and Self-Adaptive Security Management Model for IoT-Based eHealth Systems. *International Journal of Advanced Computer Science and Applications*. 2019 Jan 1;10(1):280-7.
- [9] Aman W, Snekenes E. Managing security trade-offs in the internet of things using adaptive security. In *2015 10th International Conference for Internet Technology and Secured Transactions (ICITST) 2015* Dec 14 (pp. 362-368). IEEE.
- [10] Gebrie MT, Abie H. Risk-based adaptive authentication for internet of things in smart home eHealth. In *Proceedings of the 11th European Conference on Software Architecture: Companion Proceedings 2017* Sep 11 (pp. 102-108).
- [11] Arfaoui A, Kribeche A, Senouci SM, Hamdi M. Game-based adaptive remote access VPN for IoT: Application to e-Health. In *2018 IEEE Global Communications Conference (GLOBECOM) 2018* Dec 9 (pp. 1-7). IEEE.
- [12] Arfaoui A, ben Letaifa A, Kribeche A, Senouci SM, Hamdi M. A stochastic game for adaptive security in constrained wireless body area networks. In *2018 15th IEEE Annual Consumer Communications & Networking Conference (CCNC) 2018* Jan 12 (pp. 1-7). IEEE.
- [13] Aman W. Assessing the feasibility of adaptive security models for the internet of things. In *International Conference on Human Aspects of Information Security, Privacy, and Trust 2016* Jul 17 (pp. 201-211). Springer, Cham.
- [14] Leister W, Hamdi M, Abie H, Poslad S. An evaluation framework for adaptive security for the IoT in eHealth. *International Journal on Advances*. 2014 Dec 1.
- [15] Savola RM, Abie H. Metrics-driven security objective decomposition for an e-health application with adaptive security management. In *Proceedings of the International Workshop on Adaptive Security 2013* Sep 8 (pp. 1-8).
- [16] Abie H, Savola RM, Bigham J, Dattani I, Rotondi D, Da Bormida G. Self-healing and secure adaptive messaging middleware for business-critical systems. *International Journal on Advances in Security*. 2010;3(1&2).
- [17] Abie H, Balasingham I. Risk-based adaptive security for smart IoT in eHealth. In *Proceedings of the 7th International Conference on Body Area Networks 2012* Feb 24 (pp. 269-275).
- [18] Farahani B, Barzegari M, Aliee FS, Shaik KA. Towards collaborative intelligent IoT eHealth: From device to fog, and cloud. *Microprocessors and Microsystems*. 2020 Feb 1;72:102938.
- [19] Salehie M, Pasquale L, Omoroniyia I, Nuseibeh B. Adaptive security and privacy in smart grids: A software engineering vision. In *2012 First International Workshop on Software Engineering Challenges for the Smart Grid (SE-SmartGrids) 2012* Jun 3 (pp. 46-49). IEEE.
- [20] Gubbi J, Buyya R, Marusic S, Palaniswami M. Internet of Things (IoT): A vision, architectural elements, and future directions. *Future generation computer systems*. 2013 Sep 1;29(7):1645-60.
- [21] Dey S, Sampalli S, Ye Q. A context-adaptive security framework for mobile cloud computing. In *2015 11th International Conference on Mobile Ad-hoc and Sensor Networks (MSN) 2015* Dec 16 (pp. 89-95). IEEE.
- [22] Sethi P, Sarangi SR. Internet of things: architectures, protocols, and applications. *Journal of Electrical and Computer Engineering*. 2017 Jan 26;2017.
- [23] Farahani B, Firouzi F, Chang V, Badaroglu M, Constant N, Mankodiya K. Towards fog-driven IoT eHealth: Promises and challenges of IoT in medicine and healthcare. *Future Generation Computer Systems*. 2018 Jan 1;78:659-76.
- [24] Rahmani AM, Gia TN, Negash B, Anzanpour A, Azimi I, Jiang M, Liljeberg P. Exploiting smart e-Health gateways at the edge of healthcare Internet-of-Things: A fog computing approach. *Future Generation Computer Systems*. 2018 Jan 1;78:641-58.
- [25] Gheisari M, Wang G, Khan WZ, Fernández-Campusano C. A context-aware privacy-preserving method for IoT-based smart city using software defined networking. *Computers & Security*. 2019 Nov 1;87:101470.
- [26] Zemmoudj S, Bermad N, Omar M. CAPM: Context-aware privacy model for IoT-based smart hospitals. In *2019 15th International Wireless Communications & Mobile Computing Conference (IWCMC) 2019* Jun 24 (pp. 1139-1144). IEEE.
- [27] De Matos E, Tiburski RT, Amaral LA, Hessel F. Providing context-aware security for IoT environments through context sharing feature. In *2018 17th IEEE International Conference On Trust, Security And Privacy In Computing And Communications/12th IEEE International Conference On Big Data Science And Engineering (TrustCom/BigDataSE) 2018* Aug 1 (pp. 1711-1715). IEEE.
- [28] Zhu J, Kim KH, Mohapatra P, Congdon P. An adaptive privacy-preserving scheme for location tracking of a mobile user. In *2013 IEEE International Conference on Sensing, Communications and Networking (SECON) 2013* Jun 24 (pp. 140-148). IEEE.

Enhanced Jaya Algorithm for Multi-objective Optimisation Problems

Rahaini Mohd Said¹, Roselina Sallehuddin², Nor Haizan Mohd Radzi³, Wan Fahmn Faiz Wan Ali⁴

Faculty of Computing, Universiti Teknologi Malaysia¹

Faculty of Electrical and Electronic Engineering Technology, Universiti Teknikal Malaysia Melaka¹

Faculty of Computing, Universiti Teknologi Malaysia^{2,3}

Faculty of Mechanical Engineering, Universiti Teknologi Malaysia⁴

Abstract—Evolutionary algorithms are suitable techniques for solving complex problems. Many improvements have been made on the original structure algorithm in order to obtain more desirable solutions. The current study intends to enhance multi-objective performance with benchmark optimisation problems by incorporating the chaotic inertia weight into the current multi-objective Jaya (MOJaya) algorithm. Essentially, Jaya is a recently established population-oriented algorithm. Exploitation proves to be more dominant in MOJaya following its propensity to capture local optima. This research addressed the aforementioned shortcoming by refining the MOJaya algorithm solution to update the equation for exploration-exploitation balance, enhancing divergence, and deterring premature convergence to retain the algorithm fundamentals while simultaneously sustaining its parameter-free component. The recommended chaotic inertia weight-multi-objective Jaya (MOiJaya) algorithm was assessed using well-known ZDT benchmark functions with 30 variables, whereas the convergence matrix (CM) and divergence matrix (DM) analysed the suggested MOiJaya algorithm performances are inspected. As such, this algorithm enhanced the exploration-exploitation balance and substantially prevented premature convergence. Then, the proposed algorithm is compared with a few other algorithms. Based on the comparison, the convergence metric and diversity metric results show that the recommended MOiJaya algorithm potentially resolved multi-objective optimisation problems better than the other algorithms.

Keywords—MOJaya; chaotic inertia weight; ZDT benchmark function; convergence metric; diversity metric

I. INTRODUCTION

As a mathematical instrument that adequately models and solves real-life complexities with multiple objectives and simultaneous enhancement, multi-objective optimisation and its relevant intricacies have garnered much scholarly attention across various disciplines, specifically engineering and sciences. Multiple population-oriented metaheuristic algorithms were recommended for multi-objective problem (MOP) solving. As MOP goals must simultaneously optimise the conflicting nature of multiple objectives given the absence of one distinct alternative to optimise all collaborative counterparts [1], a set of optimal trade-off alternatives (Pareto) was employed as a solution. Thus, a single and optimal solution is non-existent in this regard. Evolutionary algorithms or EAs imply some of the most extensively-utilised algorithms to solve MOPs and numerous issues with competing objectives across industrial, engineering, and research disciplines [2]. Robust optimisation algorithms serve to resolve intricate real-world

MOPs in one run. Relevant research has demonstrated the successful application of multi-objective optimisation, which has extended EAs entailing MOPSO [3], [4], MODE [5], MOACO [6], and MOGA [7] for improved performance in multi-objective optimisation problem solution.

Recent EA developments in the past few decades have rendered the algorithms an efficient means of solving intricate multi-objective evolutionary algorithms (MOEAs). Their competence in simultaneously examining different regions of the Pareto front (PF) and generating a set of Pareto solutions in one run facilitates scholars toward multi-objective and real-life optimisation problems using distinct domains. Nevertheless, the algorithms types rely on algorithm-centric parameter refinements with common controlling parameters. Such specific parameters entail multiple purposes and impact the convergence rates, diversity, efficiency, scalability, exploration, and exploitation within the solution. For example, MOGA constitutes a mutation and crossover operator to attain the exploration and exploitation mechanism. Rao and colleagues established the parameter-free Jaya and MOJaya algorithms in 2016 to address scholars' complexities and control specific parameters for algorithm simulation.

The aforementioned algorithms prove adequate in engineering areas, which entail i) multiple variables and parameters that require observation and ii) control or uncontrol parameters that are deemed challenging to manage without expertise and experience. Specifically, the Jaya algorithm or EA optimisation, which only requires several turning control parameters (population size, number of generations, and design variables), could only alleviate specific complexities. The EAs optimisation has recently solved applications for a single objective, whereas MOJaya resolved multi-objective optimisation problems. The solution consistently shifts towards the most and least optimal solutions that are avoided in simulation under the Jaya algorithm concept. The Update phase serves to modify the solution from earlier generations compared to other algorithms, which require two phases to refine solutions involving teaching-learning optimisation (TLBO), artificial bee colony (ABC), and differential evolution (DE). Intriguingly, the Jaya algorithm optimally manages continuous, discrete, and integer variables [8].

Hence, in this study, the improved MOJaya algorithm is proposed to solve multi-objective optimisation problems, while the properties of MOJaya are preserved. The non-dominated

sorting (NDS) approach with a reference point is used to find dominance relation, where NDS is performed according to the Euclidean distances between each possible solution of the front and reference point. The solution update equation is modified by incorporating the chaotic inertia weight. Finally, the recommended algorithm's performance were tested using ZDT benchmark test problems. The convergence metric and diversity metric evaluate the performance of the recommended algorithms.

The remaining paper is organized as follows: Section II, discusses the improvement Jaya Algorithm and its variations by the previous researcher. Then, the recommended algorithm methodology is presented in Section III. Next, Section IV presents the obtained results and analysis. Finally, the conclusion and future research are presented in Section V.

II. MOJAYA ALGORITHM

Rao's [9] Jaya algorithm is a novel, astute, population-oriented, and parameter-free solution that manages constrained and unconstrained optimisation-related problems. Resultantly, the number of function assessments required to obtain a solution is lesser than that of TLBO. Several limitations have been ascertained despite its consistent attempts to omit the least optimal solutions and iterate the most optimal solution search space. For example, the Jaya algorithm becomes trapped in local optimal solutions where exploitation overrides exploration [10]. The basic Jaya algorithm is updated to relieve researchers (specifically in complex engineering fields) from refining algorithm-centric parameters.

Following past literature, the Jaya algorithm functions to solve multiple real-time and standard benchmark functions with distinct components and variants. This section elaborates on several parameter-free Jaya algorithm variants that were published in relevant research. The MOJaya, a posteriori version of Jaya, was developed in 2017 to solve multi-objective optimisation problems. Although MOJaya algorithm solutions are similarly updated to that of Jaya, MO-Jaya incorporates non-dominated sorting and the crowding distance computing mechanism for successful multi-objective management.

Past scholars demonstrated inconsistent outcomes in terms of multi-objective Jaya algorithm enhancement. Rao and Pawar (2020) recommended a novel and upgraded version (Rao's quasi-oppositional approach) under the Jaya algorithm with multi-objective and quasi-oppositional-oriented-learning techniques to address the diversity in the algorithm searching process. Three multi-objective optimisation case studies involving real-world and intricate engineering optimisation problems were applied with a single-layered microchannel heat sink (SL-MCHS), a double-layered microchannel heat sink (DL-MCHS), and a plate-fin heat sink (PFHS) to examine the recommended algorithm efficiency. The findings derived through the recommended algorithms were compared against those elicited with advanced optimisation algorithms: GA, ABC, DE, PSO, TLBO, MOGA, NSGA-II, real-coded GA (RCGA), direction-based GA, and basic and self-adaptive multi-population (SAMP) Rao algorithms. Essentially, the recommended algorithms proved superior and competitive compared to other optimisation counterparts [11].

The discrete multi-objective Jaya algorithm potentially addresses the flexible job-shop scheduling problem (FJSSP) by regarding the minimisation of makespan and total and critical machine workload as performance measures. Dynamic mutation operator and modified crowding distance measures were proposed to improve search process diversity. In-depth computational experiments were performed by regarding 203 FJSSP instances from past research. A comparison between the recommended algorithm and the weighted sum version demonstrated higher performance than the other approach and other MOEAs. Based on the computational outcomes, the proposed algorithm efficiently obtained diverse and enhanced Pareto-optimal solutions [12].

Rao and Hameer (2019) presented an adaptive multi-team perturbation with multiple teams to navigate the Jaya algorithm and examine its search space. The recommended algorithm was investigated with two multi-objective optimisation case studies of a solar dish Stirling heat engine system and one counterpart of the Stirling heat pump. The suggested algorithm utilised various perturbation equations with dominance principles and the crowding distance estimation approach for simultaneous multiple objective management. As a decision-making approach, the 'technique for order of preference by similarity to ideal solution' was also utilised for optimal solution identification. The computational outcomes elicited by the suggested algorithm proved superior to those attained by other study algorithms [13].

Rao and Saroj (2018) recommended a novel and unique Jaya algorithm for multi-objective design optimisation problem solution. The aforementioned algorithm was applied to resolve the heat exchanger design problem where two conflicting objectives (optimise heat exchangers' total annual cost and effectiveness) were simultaneously regarded. The least optimal Jaya algorithm solutions were substituted with an elitist value at the end of each iteration. As such, local trapping was prevented by arbitrarily selecting duplicate solution parameters. The recommended algorithm also optimally solved the multi-objective heat exchanger design compared to GA and TLBO [14].

The drawbacks inherent in the basic Jaya algorithm were highlighted in past studies. The exploration-exploitation balance implies one of the success criteria for any nature-oriented algorithm. Exploitation depicted a more significant impact than exploration as this algorithm catalyses objective function value towards the most optimal solution space. In this vein, local minima are trapped with less diverse solutions. The Jaya algorithm, which causes premature convergence and impacts solution quality, only upgrades the solution with the most and least optimal solutions from past iterations. Another shortcoming denotes the basic Jaya algorithm weakness regarding information exchange among individuals with no local minima mechanism in the event of a trapped algorithm. Palpably, relevant scholars have strived to integrate multiple methods for the optimal performance of balancing exploration and exploitation capacities and solving multiple real-time and benchmark problems. Exploration-exploitation balance is a pivotal mechanism that efficiently assesses the optimisation algorithm [15]–[17]. The numerous Jaya algorithm refinements

presented in this study primarily emphasised mitigating the basic Jaya algorithm limitations.

However, the results produced inconsistent results while comparing the performance with other results. Hence, the current research strived to (i) employ and assess the proposed techniques for improved MOJaya algorithm performance, (ii) solve multi-objective optimisation problems, and (iii) introduce a chaotic sequence. Inertia chaotic weight was initially adopted in the solution for the updated equation to be elicited from the local optimal solution. Regarding MOJaya, the most optimal solution was derived from the sorted list through non-dominant sorting and a crowding distance mechanism to eliminate the least optimal counterparts, thus leading to local region searches, premature convergence, and lesser diverse solutions.

The previous study observed that researchers are working to improve the MOJaya algorithm's performance. Various techniques are adopted to improve performance and also focus on real-life MOP. The motivation for this paper is as follows. First, the recommended study strategies for the algorithm is presented to improve the exploration of the existing MOJaya algorithm. The recommended algorithm development towards high performance while balancing exploration and exploitation is adopting inertia chaotic weight in the solution for an updated equation provides the best solution for promising and sparse search space regions. Then, the recommended algorithm's performance is evaluated using a two-objective ZDT test performance. Finally, the exiting MOJaya and MOiJaya algorithm with other multi-objective optimization algorithm performance are compared using the convergence and diversity metrics.

III. THE MOIJAYA ALGORITHM

The MOJaya, a posteriori Jaya algorithm version, was employed for stochastically updated Multi-objective optimization problems (MOOP) solutions. The most optimal solution denoted maximum fitness, whereas the worst counterpart implied minimum fitness. The MOJaya algorithm was incorporated into a non-dominant ranking and crowding distance evaluation method to resolve multi-objective algorithm. The MOJaya algorithm pseudo-code is depicted in Algorithm 1.

A. Chaotic Random Inertia Weight Mechanism

The chaos mechanism, a well-established logistic map, was integrated with TLBO and the basic Jaya algorithm for single optimisation. Meanwhile, the chaotic sequence implied two attributes (ergodicity and randomness) that drove the algorithm away from the optimal local solution and enhanced solution quality [18], [19]. The fundamentals of chaotic inertia weight aimed to establish the inertia weight coefficient with chaotic mapping, which is integrate Logistic mapping, the method used in this paper. Inertia weight denotes one of the PSO algorithm parameters that substantially affect global and local searches and PSO algorithm performance through simultaneous particle retention in inertial motion and search space expansion [20]. The chaotic random inertia weight generated as (1) and (2) was incorporated into this study, given its value in demonstrating particle velocity shifts.

Logistic mapping,

$$z = 4 \times z \times (1 - z) \quad (1)$$

Chaotic Inertia weight

$$\varpi = 0.5 \times \text{random}(\) + 0.5 \times z \quad (2)$$

Algorithm 1 : MOJaya algorithm 1

Begin

- Step 1 Initialize the algorithm's control parameters, such as population size (N) and the maximum number of iterations (Gmax). Also initialize the problem-specific parameters such as a number of objectives (M).
- Step 2 Generate the initial solution randomly and evaluate it for each individual. Identify the best and worst solutions.
- Step 3 Find the new solution for all the individuals in a population using the modified solution update equation.
- Step 4 Evaluate the modified solution using Non-dominated sorting with a and ranking method solution using Non-dominated sorting with ranking method.
- Step 5 Combine the new solution with the old one. Sort the combined solution in ascending order. Identify the best and worst from the selected solution to update the solution in the next iteration.
- Step 6 Update the global best solution by comparing the old global best solution with the new best solution.
- Step 7 If the number of iterations reaches the maximum, stop the procedure and report the global best solution; otherwise, repeat the procedure from Step 3.

End

B. Proposed Modification in MOiJaya

The MOJaya algorithm, which entails a non-dominated sorting scheme and crowding distance from the NSGA-II counterpart, is developed to solve the multi-objective optimisation problem by integrating components from current MOEAs. The MOJaya algorithm performs sorting in ascending order by integrating the solutions from present and past iterations. The best solutions for the first N (population size) were selected through the non-dominated ranking scheme from the sorted list. Meanwhile, the most and least optimal solutions were selected from the N (population size) to update the following iteration. The most optimal and random solutions were chosen as the next search direction to explore more space in the early iteration of the algorithm process. The most optimal solution candidate in the algorithm functions to navigate the population towards a better region, whereas a random solution facilitates search space expansion. Searching local region

outcomes results in premature convergence and low diversified solutions as this approach disregards the least optimal solution.

The recommended algorithm and solution update equation was refined by integrating the chaotic sequence to alleviate MOJaya limitations. The random number employed in the MOJaya solution for an updated equation was substituted with a chaotic random inertia weight. The chaotic random inertia weight attributes entailing ergodicity and randomness enabled the algorithm to drive away from the optimal local solution: a regulation to balance the stochastic search and local search probabilities. Additionally, the recommended algorithms were improved in terms of convergence metric and diversity metric. The refined solution for an updated equation is expressed in (3) below:

$$x_{(i+1,j,k)} = x_{(i,j,k)} + \varpi_{(i,j,1)} * \left[x_{(i,j,w)} - |x_{(i,j,k)}| \right] - \varpi_{(i,j,2)} * \left[x_{(i,j,w)} - |x_{(i,j,k)}| \right] \quad (3)$$

The pseudocode for MOiJaya is depicted in Algorithm 2. Fig. 1 illustrates the flowchart parallel to the previously-mentioned refinements.

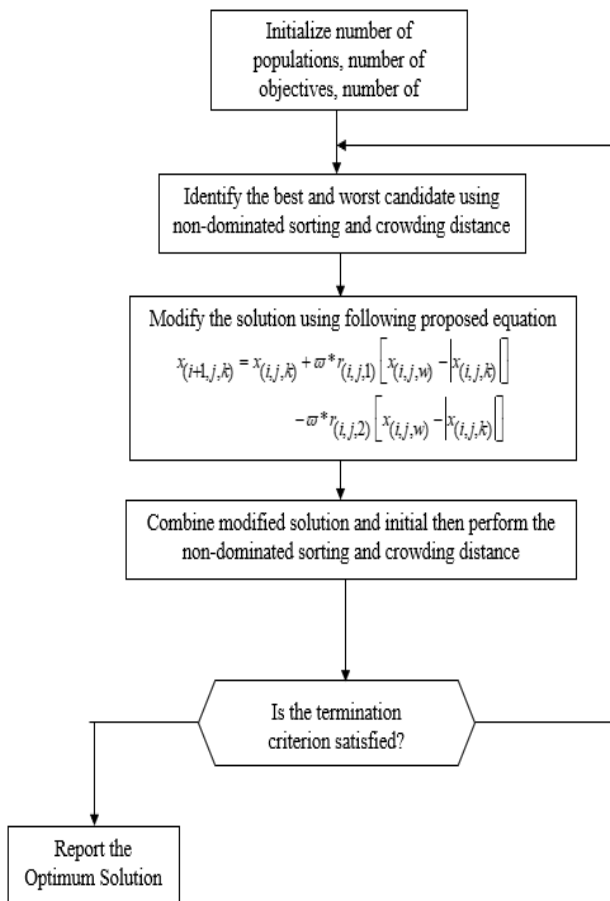


Fig. 1. The Flowchart of MOiJaya Algorithm.

Algorithm 2: MOiJaya algorithm

Begin

Input: Population size N, number of objectives, number of design variables, number of iterations, constrain, and function

Output: Solution f₁ and f₂

1: Initialize population size, initialize the best and worst

2: Generate initial population randomly

For i < var

Generate initial population for variable and objective

End

Find the best and worst candidates using non-dominated sorting and crowding distance

While t < iter.max

Generate new solution using modified solution update equation as equation 3

Evolve

Merge the new and old solution

Perform non-dominated sorting and crowding distance

Select the first N solution

t+1;

End

End

IV. COMPUTATIONAL RESULTS AND ANALYSIS

This section highlights the recommended MOiJaya algorithm assessment. The suggested chaotic-oriented MOJaya algorithm was incorporated into Matlab2020 and examined with ZDT1-ZDT6 for multi-objective benchmark functions using two objectives with 30 variables. The outcomes elicited by the MOiJaya algorithm were compared against those identified in past empirical works with well-known CM and DM. The ZDT functions in PF demonstrated diverse attributes (separable, multimodal, linear, concave, mixed, and biased) that rendered it challenging to solve the problems with MOEAs (Deb et al., 2005). Table I presents the ZDT1-ZDT6 objective test problems.

The suggested MOiJaya algorithm extends to a renowned basic Jaya algorithm that only requires common controlling parameters. The following common controlling parameters are utilised to perform experiments:

Population size : 100

Maximum iteration : 10000

The recommended chaotic-based MOJaya algorithm was compared against SPEA2, NSGA-II, and EDATCMO [21] with two popular MOEA performance metrics (DM and CM) to assess the convergence and diversity solution for Pareto-front.

A. Performance Measures

The common trend in various successful solution methodology development, including MOEAs, involves performance comparison on multiple test problems. Two goals

(discover solutions with close proximity to the Pareto-optimal solutions and alternatives that are distinctly diverse in the elicited non-dominated front) were identified in multi-objective optimisation, unlike the single counterpart. A minimum of two performance metrics proves vital towards the actualization of both multi-objective optimisation goals to ascertain an effective MOEA (Deb, 2001). One performance matrix analyses the progress towards the Pareto-optimal front while the other assesses the solution spread. Three common metrics were employed in this study despite the numerous performance metrics highlighted in past literature, two of which would be implemented for MDEA analysis: CM and DM.

The CM was recommended by [22] to assess the distance between the obtained non-dominated (NF) front and optimal PF. The mathematical equations are expressed as follows (4):

$$d = \min_{j=1} N \sqrt{\sum_{k=1}^M \left(\frac{f_k(i) - f_k(j)}{f_k^{\max} - f_k^{\min}} \right)^2} \quad (4)$$

$$CM = (P(t)) = \frac{\sum_{i=1}^{|F(t)|} d_i}{|F(t)|} \quad (5)$$

Specifically, M denotes the number of objectives, $f_k^{\max} - f_k^{\min}$ imply the maximum and minimum function values of k^{th} and the objective function in the reference set, respectively, and N indicates the reference set size. The minimum value of CM, (5) reflects improved multi-objective optimisation algorithm performance.

The DM was suggested by [22] to assess the extent of solution spread, not unlike DM where optimal algorithms denote lower diversity metrics for evenly-spread solutions on PF. The spread was ascertained by computing each solution gap in PF with the neighbouring solution. The mathematical equation is expressed as follows:

$$DM = \frac{d_f + d_l + \sum_{i=1}^{N-1} d_i - \bar{d}}{d_f + d_l + ((N-1))\bar{d}} \quad (6)$$

Based on the Euclidean distance between the consecutive solutions within the obtained non-dominated set of solutions, \bar{d} denotes the average of all distances, $d_i (i = 1, 2, \dots, N)$ assumes the N solutions in the derived non-dominated set, and d_l reflects the Euclidean distance between extreme and boundary solutions. The $(N-1)$ is utilised as the solution distance that constitutes two solutions.

B. Results on Zdt Test Functions

In this section, five benchmarks are used to test the proposed algorithm and analyzed the obtained results. The five well-known benchmarks of optimization problems have been

listed in Table I. The optimal values of all minimization objective function given in Table I is zero, which is, $f(x_1) = 0$ where x_1 is the optimal solution.

The recommended MOiJaya algorithm was performed 30 times for the chosen test function and corresponding number of objectives. In Table II-VI, we compared the proposed algorithm with the five others algorithm. The purpose of this test is to evaluate the quality of the solutions of purposed algorithm in different benchmarks compared to other algorithms. The mean and standard deviation (sd) values of DM and CM through SPEA2[22], NSGAI [23], FastPGA, and EDATCMO [21], MOJaya, and suggested MOiJaya algorithms on multi-objective benchmark functions ZDT1, ZDT2, ZDT3, ZDT4, and ZDT6. The MOJaya algorithm employs the solution for an updated equation from the basic Jaya counterpart [24]. The common controlling parameters remain the same for both MOJaya and MOiJaya.

C. Results on Zdt Test Functions

In this section, five benchmarks are used to test the proposed algorithm and analyzed the obtained results. The five well-known benchmarks of optimization problems have been listed in Table I. The optimal values of all minimization objective function given in Table I is zero, which is, $f(x_1) = 0$ where x_1 is the optimal solution.

The recommended MOiJaya algorithm was performed 30 times for the chosen test function and corresponding number of objectives. In Table II-VI, we compared the proposed algorithm with the five others algorithm. The purposed of this test is to evaluate the quality of the solutions of purposed algorithm in different benchmarks compared to other algorithms. The mean and standard deviation (sd) values of DM and CM through SPEA2[22], NSGAI [23], FastPGA, and EDATCMO [21], MOJaya, and suggested MOiJaya algorithms on multi-objective benchmark functions ZDT1, ZDT2, ZDT3, ZDT4, and ZDT6. The MOJaya algorithm employs the solution for an updated equation from the basic Jaya counterpart [24]. The common controlling parameters remain the same for both MOJaya and MOiJaya.

In Fig. 2, Pareto optimal for MOiJaya are presented. It is found that the generated Pareto optimal front for MOiJaya quite close to True Pareto front. The convergence metric and divergence metric results for ZDT1 problems in Table II show that MOiJaya has lower values in the metric than all the other algorithms. This shows that MOiJaya is better in diversity and converge than other algorithms.

Fig. 3 shows the Pareto optimal fronts MOiJaya for test problems ZDT2. It is found that from MOiJaya is better in the uniform spread. Though MOiJaya pareto optimal slightly close to True pareto, MOiJaya is better diversity than MOJaya. Table III shows the results of convergence and divergence metric for ZDT2 problems. It is found that MOiJaya is better in diversity than all the other algorithms. From the results, the MOiJaya is worse in convergence metric than SPEA, NSGA-II, FastPGA and EDATCMO but better than MOJaya.

TABLE I. THE ZDT TEST PROBLEMS [22]

Problem	N	Variable bounds	Objective Functions	Optimal Solutions	Comments
ZDT 1	30	[0,1]	$f_1(x) = x_1$ $f_2(x) = g(x) \left[1 - \sqrt{x_1 / g(x)} \right]$ $h(f_1) = 1 + 9 \left(\sum_{i=2}^n x_i \right) (n-1)$	$x_1 \in [0, 1]$ $x_1 = 0$ $i = 2, \dots, n$	Convex
ZDT 2	30	[0,1]	$f_1(x) = x_1$ $f_2(x) = g(x) \left[1 - (x_1/g(x))^2 \right]$ $h(f_1) = 1 + 9 \left(\sum_{i=2}^n x_i \right) (n-1)$	$x_1 \in [0, 1]$ $x_1 = 0$ $i = 2, \dots, n$	nonconvex
ZDT 3	30	[0,1]	$f_1(x) = x_1$ $f_2(x) = g(x) \left[1 - \sqrt{x_1 / g(x)} - \frac{x_1}{g(x)} \sin(10\pi x_1) \right]$ $h(f_1) = 1 + 9 \left(\sum_{i=2}^n x_i \right) (n-1)$	$x_1 \in [0, 1]$ $x_1 = 0$ $i = 2, \dots, n$	Convex Disconnected
ZDT 4	30	[0,1]	$f_1(x) = x_1$ $f_2(x) = g(x) \left[1 - \sqrt{x_1 / g(x)} \right]$ $h(f_1) = 1 + 10(n-1) + \sum_{i=2}^n x_i^2 - 10 \cos(4\pi x_i)$	$x_1 \in [0, 1]$ $x_1 = 0$ $i = 2, \dots, n$	Convex
ZDT 6	30	[0,1]	$f_1(x) = 1 - \exp(-4x_1) \sin^6(6\pi x_1)$ $f_2(x) = g(x) \left[1 - (x_1/g(x))^2 \right]$ $h(f_1) = 1 + 9 \left[\left(\sum_{i=2}^n x_i \right) (n-1) \right]^{0.25}$	$x_1 \in [0, 1]$ $x_1 = 0$ $i = 2, \dots, n$	Nonconvex Nonuniformly spaced

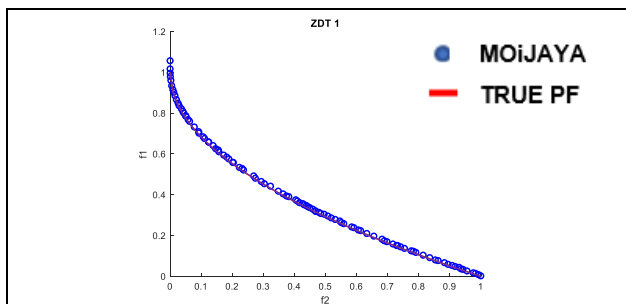


Fig. 2. The Results of Test Problem ZDT1.

TABLE II. COMPARISON OF CM AND DM VALUES OBTAINED WITH ALL ALGORITHMS FOR ZDT1 PROBLEMS

Case	Algorithm	Convergence	Diversity
		(mean±sd)	(mean±sd)
ZDT1	SPEA	0.09462±0.04511	0.42209±0.01012
	NSGA-II	0.10872±0.00362	0.50827±0.02446
	FastPGA	0.09154±0.00621	0.70009±0.01174
	EDATCMO	0.02363±0.00146	0.21738±0.00368
	MOJAYA	0.23346±0.05597	0.02044±0.04281
	MOIJAYA	0.02226±0.00287	0.00168±0.00232

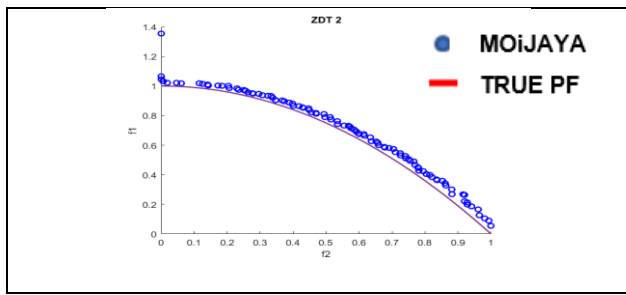


Fig. 3. The Results of Test Problem ZDT2 MOiJaya.

TABLE III. COMPARISON OF CM AND DM VALUES OBTAINED WITH ALL ALGORITHMS ZDT2 PROBLEMS

Case	Algorithm	Convergence	Diversity
		(mean±sd)	(mean±sd)
ZDT2	SPEA	0.08073±0.06101	0.50013±0.01612
	NSGA-II	0.09023±0.00401	0.30163±0.01503
	FastPGA	0.02067±0.00702	0.60034±0.2984
	EDATCMO	0.00821±0.00472	0.20022±0.00863
	MOJAYA	0.26564±0.22560	0.04489±0.02727
	MOiJAYA	0.15267±0.27201	0.03300±0.02923

From the Fig. 4, it is found that the generated Pareto optimal front for MOiJaya quite close to True Pareto front. This is also confirmed with the results of convergence and diversity in Table IV. Comparison with other algorithms shows that MOiJaya outperforms all of them in both metrics.

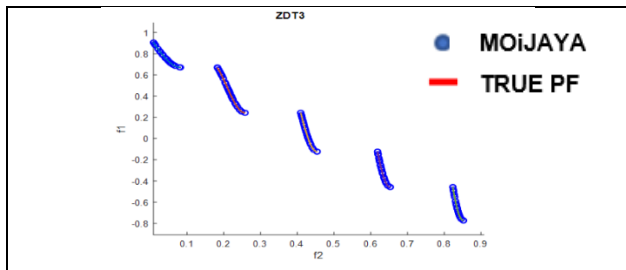


Fig. 4. The Results of Test Problem MOiJaya.

TABLE IV. COMPARISON OF CM AND DM VALUES OBTAINED WITH ALL ALGORITHMS ZDT3 PROBLEMS

Case	Algorithm	Convergence	Diversity
		(mean±sd)	(mean±sd)
ZDT3	SPEA	0.13996±0.07603	0.74932±0.05006
	NSGA-II	0.04208±0.09104	0.85061±0.09025
	FastPGA	0.07024±0.06541	0.85061±0.06453
	EDATCMO	0.02005±0.01843	0.50064±0.06132
	MOJAYA	0.04657±0.00559	0.06691±0.12251
	MOiJAYA	0.03764±0.05113	0.02896±0.00584

It is found in Fig. 5 that MOiJaya is far from True Pareto for this problem. Table V shows the results of convergence and divergence metrics. It is found that MOJaya is better in convergence than all the other algorithm but very close to MOiJaya. But, from the results of diversity, MOiJaya is better than all the other algorithms.

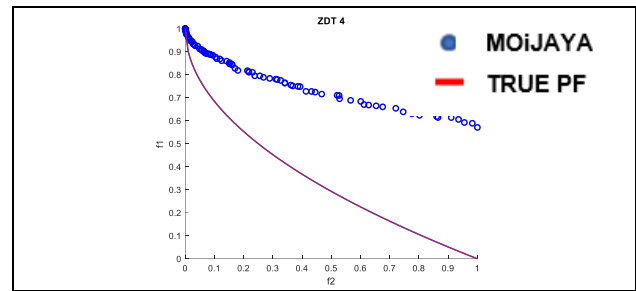


Fig. 5. The Results of Test Problem ZDT4 MOiJaya.

TABLE V. COMPARISON OF CM AND DM VALUES OBTAINED WITH ALL ALGORITHMS ZDT4 PROBLEMS

Case	Algorithm	Convergence	Diversity
		(mean±sd)	(mean±sd)
ZDT4	SPEA	0.62768±0.10676	0.51682±0.07319
	NSGA-II	1.13458±0.90054	0.85454±0.09003
	FastPGA	2.9742±1.94585	0.96856±0.07032
	EDATCMO	0.50547±0.08019	0.96856±0.07032
	MOJAYA	0.21701±0.05162	0.0255±0.06448
	MOiJAYA	0.27136±0.11211	0.01204±0.00448

Test problems ZDT6 Pareto optimal front is presented in Fig. 6, It is found that the generated Pareto optimal front for MOiJaya quite close to True Pareto front. Results in Table VI shows that MOiJaya outperforms all other algorithms in test problem ZDT6 in both metrics.

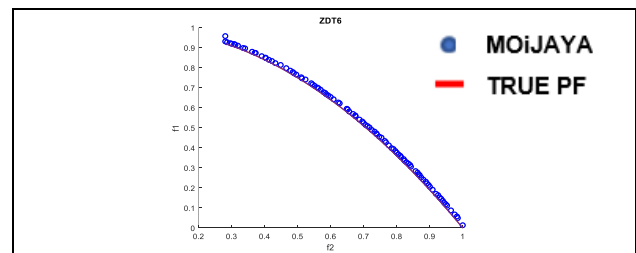


Fig. 6. The Results of Test Problem ZDT6 MOiJaya.

TABLE VI. COMPARISON OF CM AND DM VALUES OBTAINED WITH ALL ALGORITHMS ZDT6 PROBLEMS

Case	Algorithm	Convergence	Diversity
		(mean±sd)	(mean±sd)
ZDT6	SPEA	0.91036±0.09105	0.74532±0.04093
	NSGA-II	0.49311±0.00874	0.63847±0.08006
	FastPGA	0.72347±0.01106	0.84442±0.04034
	EDATCMO	0.10048±0.01002	0.31618±0.01782
	MOJAYA	0.78092±0.47053	0.07634±0.08416
	MOiJAYA	0.07094±0.11630	0.02013±0.02014

In Fig. 2-6, MOiJaya has achieved the two goals of multi-objective optimization: convergence to the true Pareto-front (ZDT 1 and ZDT3) and uniform spread of solution along the front (ZDT1-ZDT6). In all the Tables II-VI, MOiJaya demonstrated better “optimal” values for CM involving ZDT1, ZDT3, and ZDT6 and DM involving all benchmark functions: ZDT1, ZDT2, ZDT3, ZDT4, and ZDT6. Additionally, the results are achieved the following points; in basic MOJaya algorithm, the exploitation is dominate, the recommended algorithm was modified to balance the exploration and exploitation by reducing the dominance of exploitation behavior. Other, using the chaotic inertia weight improve the converge rate and balance the exploration and exploitation. Specifically, the MOiJaya outcomes proved comparable to MOJaya. The MOiJaya curves in all the aforementioned figures were comparable to that of MOJaya regarding convergence and diversity. Conclusively, the performance of MOiJaya in solving multi-objective optimisation problems is deemed encouraging and comparable to other MOEAs.

V. CONCLUSION

The current study introduced an enhanced MOiJaya algorithm to solve multi-objective optimisation problems. Specifically, the proposed method enhanced the current MOJaya algorithm through the chaotic inertia weight-oriented logistic chaotic sequence. The chaotic inertia weight was incorporated into the solution for an updated equation of the current MOJaya to mitigate the dominance of exploitation in this algorithm. The recommended modification also enhanced the multi-objective Jaya algorithm searchability. Chaotic inertia weight was integrated with MOJaya to improve exploration and the exploitation-exploration balance. The proposed MOiJaya approach efficiency was analysed with a benchmark performance ZDT test that was assessed with CM and DM. The recommended algorithm outcomes were compared to the most established findings following past research. Post-comparison, MOiJaya outperformed MOJaya with relatively good performance compared to advanced empirical algorithms. Nevertheless, there is much room for improvement although the suggested MOiJaya algorithm optimised the exploration-exploitation balance. Further research could assess the recommended method with other multi-objective benchmark datasets and real-time multi-objective optimisation problems from various domains.

ACKNOWLEDGMENT

Special appreciation to reviewers for the useful advice and comments. This research was supported by Ministry of Higher Education (MOHE) through Fundamental Research Grant Scheme FRGS/1/2019/ICT02/UTM/02/13 and Research Management Centre (RMC), UTM.

REFERENCES

- [1] L. Fan, T. Yoshino, T. Xu, Y. Lin, and H. Liu, “A Novel Hybrid Algorithm for Solving Multiobjective Optimization Problems with Engineering Applications,” *Math. Probl. Eng.*, vol. 2018, 2018, doi: 10.1155/2018/5316379.
- [2] J. A. Adeyemo and F. A. O. Otieno, “Multi-Objective Differential Evolution Algorithm for Solving Engineering Problems,” *J. Appl. Sci.*, vol. 9, no. 20, pp. 3652–3661, 2009, doi: 10.3923/jas.2009.3652.3661.
- [3] G. C. M. Patel, P. Krishna, P. R. Vundavilli, and M. B. Parappagoudar, “Multi-Objective Optimization of Squeeze Casting Process using Genetic Algorithm and Particle Swarm Optimization,” *Arch. Foundry Eng.*, vol. 16, no. 3, pp. 172–186, 2016, doi: 10.1515/afe-2016-0073.
- [4] G. C. Manjunath Patel, P. Krishna, and M. B. Parappagoudar, “Modelling and multi-objective optimisation of squeeze casting process using regression analysis and genetic algorithm,” *Aust. J. Mech. Eng.*, vol. 14, no. 3, pp. 182–198, 2016, doi: 10.1080/14484846.2015.1093231.
- [5] C. Wang, Y. Fang, and S. Guo, “Multi-objective optimization of a parallel ankle rehabilitation robot using modified differential evolution algorithm,” *Chinese J. Mech. Eng. (English Ed.)*, vol. 28, no. 4, pp. 702–715, 2015, doi: 10.3901/CJME.2015.0416.062.
- [6] S. Rubaice and M. B. Yildirim, “An energy-aware multiobjective ant colony algorithm to minimize total completion time and energy cost on a single-machine preemptive scheduling,” *Comput. Ind. Eng.*, vol. 127, no. January 2017, pp. 240–252, 2019, doi: 10.1016/j.cie.2018.12.020.
- [7] K. Ishfaq et al., “Optimization of WEDM for precise machining of novel developed Al6061-7.5% SiC squeeze-casted composite,” *Int. J. Adv. Manuf. Technol.*, vol. 111, no. 7–8, pp. 2031–2049, 2020, doi: 10.1007/s00170-020-06218-5.
- [8] T. A. Bhilawade, *Advanced Engineering Optimization Through Intelligent Techniques*, vol. 949. Springer Singapore, 2020.
- [9] R. V. Rao, D. P. Rai, J. Ramkumar, and J. Balic, “A new multi-objective Jaya algorithm for optimization of modern machining processes,” *Adv. Prod. Eng. Manag.*, vol. 11, no. 4, pp. 271–286, 2016, doi: 10.14743/apem2016.4.226.
- [10] K. K. Ingle and R. K. Jatoth, “An Efficient JAYA Algorithm with Lévy Flight for Non-linear Channel Equalization,” *Expert Syst. Appl.*, vol. 145, p. 112970, 2020, doi: 10.1016/j.eswa.2019.112970.
- [11] R. V. Rao and R. B. Pawar, “Quasi-oppositional-based Rao algorithms for multi-objective design optimization of selected heat sinks,” *J. Comput. Des. Eng.*, vol. 7, no. 6, pp. 830–863, 2020, doi: 10.1093/jcde/qwaa060.
- [12] R. H. Caldeira and A. Gnanavelbabu, “A Pareto based discrete Jaya algorithm for multi-objective flexible job shop scheduling problem,” *Expert Syst. Appl.*, vol. 170, no. January, p. 114567, 2021, doi: 10.1016/j.eswa.2021.114567.
- [13] R. V. Rao, H. S. Keesari, P. Oclon, and J. Taler, “Improved multi-objective Jaya optimization algorithm for a solar dish Stirling engine,” *J. Renew. Sustain. Energy*, vol. 11, no. 2, 2019, doi: 10.1063/1.5083142.
- [14] R. V. Rao and A. Saroj, “Multi-objective design optimization of heat exchangers using elitist-Jaya algorithm,” *Energy Syst.*, vol. 9, no. 2, pp. 305–341, 2018, doi: 10.1007/s12667-016-0221-9.
- [15] L. Lin and M. Gen, “Auto-tuning strategy for evolutionary algorithms : balancing between exploration and exploitation,” pp. 157–168, 2009, doi: 10.1007/s00500-008-0303-2.
- [16] S. Liu and M. Mernik, “Exploration and Exploitation in Evolutionary Algorithms: A Survey Exploration and Exploitation in Evolutionary Algorithms: A Survey,” no. June, 2013, doi: 10.1145/2480741.2480752.
- [17] E. Alba and B. Dorronsoro, “The Exploration / Exploitation Tradeoff in Dynamic,” vol. 9, no. 2, pp. 126–142, 2005.
- [18] K. Yu, J. J. Liang, B. Y. Qu, X. Chen, and H. Wang, “Parameters identification of photovoltaic models using an improved JAYA optimization algorithm,” *Energy Convers. Manag.*, vol. 150, no. August, pp. 742–753, 2017, doi: 10.1016/j.enconman.2017.08.063.
- [19] R. Venkata Rao and H. S. Keesari, “Improved multi-objective Jaya optimization algorithm for a solar dish Stirling engine,” *Appl. Soft Comput. J.*, vol. 025903, no. November 2018, pp. 800–815, 2019, doi: 10.1063/1.5083142.
- [20] S. Wang, F. Zhou, and F. Wang, “Effect of inertia weight ω on PSO-SA algorithm,” *Int. J. Online Eng.*, vol. 9, no. Specialissue.6, pp. 87–91, 2013, doi: 10.3991/ijoe.v9iS6.2923.
- [21] Y. Gao, L. Peng, F. Li, M. Liu, and X. Hu, “Estimation of Distribution Algorithm with Multivariate T-Copulas for Multi-Objective Optimization,” vol. 2013, no. February, pp. 63–69, 2013, doi: 10.4236/ica.2013.41009.

- [22] K. Deb, A. Member, A. Pratap, S. Agarwal, and T. Meyarivan, "A Fast and Elitist Multiobjective Genetic Algorithm :," vol. 6, no. 2, pp. 182–197, 2002.
- [23] N. K. Madavan, "Multiobjective optimization using a Pareto differential evolution approach," pp. 1145–1150.
- [24] R. V. Rao, *Jaya: An advanced optimization algorithm and its engineering applications*. 2018.

Research on the Academic Early Warning Model of Distance Education based on Student Behavior Data in the Context of COVID-19

Early Warning Model of Distance Education

Yi Qu^{1*}

The Open University of Shaanxi
Sino Swiss School of Tourism and
Hospitality, Xi'an 710119, China

Zhiyuan Sun²

The Open University of Shaanxi
School of Marxism
Xi'an 710119, China

Libin Liu³

The Open University of Shaanxi
School of Basic Subjects
Xi'an 710119, China

Abstract—The COVID-19 epidemic has caused great impact on the entire society, and the spread of novel coronavirus has brought a lot of inconvenience to the education industry. To ensure the sustainability of education, distance education plays a significant role. During the process of distance education, it is necessary to examine the learning situation of students. This study proposes an academic early warning model based on long- and short-term memory (LSTM), which firstly extracts and classifies students' behavior data, and then uses the optimized LSTM to establish an academic early warning model. The precision rate of the optimized LSTM algorithm is 0.929, the recall rate is 0.917 and the F value is 0.923, showing a higher degree of convergence than the basic LSTM algorithm. In the actual case analysis, the accuracy rate of the academic early warning system is 92.5%. The LSTM neural network shows high performance after parameter optimization, and the academic early warning model based on LSTM also has high accuracy in the actual case analysis, which proves the feasibility of the established academic early warning model.

Keywords—COVID-19; Student behavior data; Distance education; Academic early warning model

I. INTRODUCTION

Due to the impact of the COVID-19, teachers' teaching methods and students' learning models in many regions have been transformed into distance education [1]. The online learning mode of distance education involves computer and other technologies. This new teaching mode requires students and teachers to change traditional teaching methods and learning concepts, and adapt to online education and learning mode through new teaching and learning practice approaches [2]. Distance education ensures the continuity of education and provides an effective way for students to learn professional knowledge [3]. Although distance education provides students with a new way of learning, there are obvious problems in online education, which lead to the poor effect of online education. First of all, in online education, students lack the learning atmosphere of offline teaching, and teachers are difficult to manage students' learning behavior, so they generally show a lack of learning initiative. Some research shows that keeping the classroom active during online learning is conducive to improving students' academic performance [4].

In addition, in the survey of distance education for students, it is found that the learning level and self-confidence of students in online education environment are lower than those in offline environment. [5]. This has brought great challenges for students to successfully complete their homework. In order to solve these problems and improve the teaching effect of online teaching, this research uses artificial intelligence technology to establish a learning management system to evaluate students' academic achievements and homework [6]. A reasonable evaluation method can improve students' confidence in learning. An effective evaluation method will strengthen the management effect of teachers on students. The research establishes the academic early warning model of online learning platform using neural network technology, and confirms the validity of the model through experiments. The model can give early warning to students with poor learning conditions with high accuracy. The research is of positive significance to the improvement of academic performance and other comprehensive abilities, and it can help students successfully complete their studies.

II. LITERATURE REVIEW

Early warning systems have been effectively used in medical, ecological and other fields. Ginestra et al. established a sepsis early warning system using machine learning to help nurses and patients predict sepsis symptoms and severe septic shock. Experiments have shown that the early warning system can effectively identify alerts for sepsis symptoms, helping nurses and patients to detect sepsis symptoms in advance [7]. The academic early warning system plays an important role in the analysis of students' learning situation. Through the academic early warning system, the early warning of students' problems in their learning can be realized, and intervention policies and measures can be proposed based on the obtained information and data to help students successfully complete their studies [8]. In the existing literatures, researchers have investigated students' learning motivation and used the learning analysis dashboard to analyze students' learning motivation and academic performance. By taking e students' academic performance as a reference, it is possible to intuitively analyze students' academic performance through the early academic early warning system. However, the early academic warning

*Corresponding Author.

system has a poor degree of automation, cumbersome operation and low accuracy, so it has not been popularized in practical applications [9]. The application of machine learning technology in the early warning system can effectively improve the accuracy of early warning, and realize automatic monitoring and rapid response. Cho optimized and improved the early warning system on the basis of deep learning. The optimized early warning system had a higher accuracy rate and recall rate, which can be used to accurately judge patients' condition [10]. Lin et al. established a bridge scouring early warning system composed of the Internet of things and artificial intelligence. The researchers encapsulated the water level sensor in a stainless-steel ball. The early warning system uses neural networks for deep learning and real-time recording according to the changes of water level [11]. In the application of students' academic early warning system, Rashid et al. used a hybrid system including recurrent neural network and gray wolf optimizer to identify students' weaknesses, predict students' academic performance, and put forward corresponding suggestions. This improved academic early warning system can help teachers to improve the teaching model and improve the learning experience of students at the same time. Although this model has good performance, it is the same as most such systems. It mainly serves offline teaching, and the application effect in online teaching is not good [12]. In general, the academic early warning system has been applied to a certain extent at present, but most of them serve offline, and the accuracy and timeliness need to be improved.

LSTM is a neural network model, which belongs to the field of machine learning. It can effectively save and analyze time series information with strong dependence on time. Among various forecasting models, LSTM-based hybrid models can be used for forecasting foreign exchange fluctuations. Researchers have used LSTM technology to optimize the forecasting model, and the experimental results show that the method combined with LSTM has a high accuracy in foreign exchange volatility forecasting [13]. LSTM combines the convolutional neural network, retains the advantages of the LSTM method itself and time-frequency information, which can be used for the prediction of remaining lifespan and help solve health management problems [14]. In the early warning of industrial systems, Dorgo et al. used LSTM to predict rare operations in chemical technology when processing the information obtained by data mining, and at the same time analyzed time series information to predict the possible consequences of rare operations [15]. Based on its excellent analytical ability, LSTM is also used in the field of education. There are many courses in online education, and the information is miscellaneous. When students face many course data, it is difficult to accurately locate the courses. The researchers proposed a learning framework based on LSTM, and introduced attention mechanism on the basis of LSTM to predict and recommend courses according to students' behavior data [16].

The LSTM neural network retains time-dependent time series information, which can optimize the model in the establishment of early warning models. It is widely used in the establishment of early warning systems in medical, geological, economic and other fields. Students' performance and relevant data in the online learning process show obvious time series

nature, so LSTM network is a more suitable analysis tool. However, after the discussion of literature review, it is found that the application of LSTM in distance education academic early warning model is less. Therefore, this study proposes to use LSTM neural network to analyze students' behavior data, and establishes an academic early warning model for students' learning evaluation in online education.

III. RESEARCH ON THE ACADEMIC EARLY WARNING MODEL OF DISTANCE EDUCATION BASED ON LSTM NEURAL NETWORK

A. Academic Early Warning Model based on LSTM Neural Network

The information is input to the signal X_t in the conventional recurrent neural network and output as h_t , and the input and output of the information are continuously circulated to realize the preservation of the information. However, the recurrent neural network does not have the ability to process long time series. When the distance between the input and the output is large, the output quality of the network will be reduced. LSTM can improve the capacity of the cyclic neural network in time series processing, and store long-term series information by increasing the complexity of the cyclic neural network structure [17]. The standard LSTM consists of three parts: input gate, output gate and forget gate, as shown in Fig. 1.

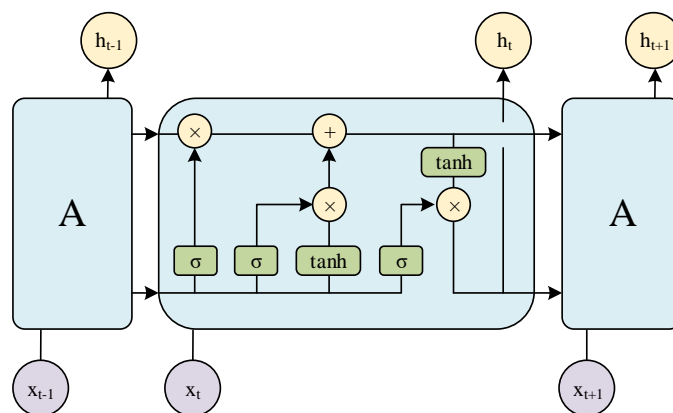


Fig. 1. LSTM Neural Network.

Although LSTM overcomes the gradient loss problem of traditional recurrent neural network, it still faces the problem of gradient decrease when processing longer-period time series [18]. LSTM has a large amount of computation and a deeper network, which takes more time in computation and training [19]. Combining the superiority of LSTM algorithm, this paper presents an academic early warning model of distance education based on student behavior data, and optimizes the method for the problems existing in LSTM. First, collect and clean the relevant distance education data of students, and organize the cleaned data into the format required for input. Second, high-order mapping of data is performed, so that the impact of the experiment on the neatness of the data is reduced. Next, feature extraction is performed according to the data characteristics of students, and classification and training are performed. Then, the long- and short-term neural network input

incentives are optimized, and the results of the optimized network output are cascaded and fused so as to improve the accuracy of the output. Fig. 2 shows the schematic diagram.

To reasonably distribute the attention of administrators to students' studies and facilitate students' self-awareness of their own studies, the academic warnings are divided into green, yellow, orange and red warnings according to the actual situation. Different early warning methods are used for students at different levels in the early warning system, and factors that actually affect learning, such as family circumstances, are fully considered in the early warning process.

B. Research on Feature Extraction and Classification Methods

The deepening of datafication has reformed students' learning methods, and distance education has been widely used in the context of COVID-19. It is necessary to mine data information such as students' achievements in distance education. Based on the distance education network database, the scores of each subject of the students are collected in the cloud. The score table of each student is generated using Excel, and each student is abstracted into a class containing variables such as score information and corresponding credits. See formulas (1) and (2) for the calculation formulas of the average score and the weighted average score of the students' original grades.

$$M = \frac{a_1 + a_2 + a_3 + \dots + a_n}{n} \tag{1}$$

$$B = \frac{a_1m_1 + a_2m_2 + a_3m_3 + \dots + a_nm_n}{m_1 + m_2 + m_3 + \dots + m_n} \tag{2}$$

Where a represents the score of the corresponding subject, the number of subjects is n , and the weight value of the subject

score is m . The variance of the student's grade can be obtained through the above formula, as shown in formula (3).

$$S = \frac{\sum (a_i - M)^2}{n}, i = 0, 1, \dots, n \tag{3}$$

The calculated average scores and weighted average scores of the corresponding subjects of the students are added to the abstract class. The grades and credits corresponding to each subject of the students are saved as float data, and the average scores and weighted average scores are saved as double data. In distance education, in addition to collecting students' subject scores for academic evaluation, students' online course learning information and other information are also collected for academic evaluation. Amplify the corresponding variables in the formed class to generate a 9*N source data matrix. However, information loss is easy to occur during data collection. In this experiment, the RBF kernel function is used to process the data information. In this method, low-dimensional data is mapped to generate high-dimensional data, and high-dimensional vector operations are maintained, so as to solve the problem of accuracy decline caused by missing data. Using data mapping can ignore the problem of linear inseparability, while preserving the integrity of the data. In the source data matrix, the information vector of each row of students is mapped to the high-dimensional space using formula (4) to generate the corresponding vector label.

$$k(a', b') = (\phi(a'), \phi(b')) = e^{-ha^2} \begin{bmatrix} 1 \\ \sqrt{\frac{2h}{1!}} a' \\ \sqrt{\frac{(2h)^2}{2!}} a'^2 \\ \vdots \end{bmatrix} e^{-hb^2} \begin{bmatrix} 1 \\ \sqrt{\frac{2h}{1!}} b' \\ \sqrt{\frac{(2h)^2}{2!}} b'^2 \\ \vdots \end{bmatrix} \tag{4}$$

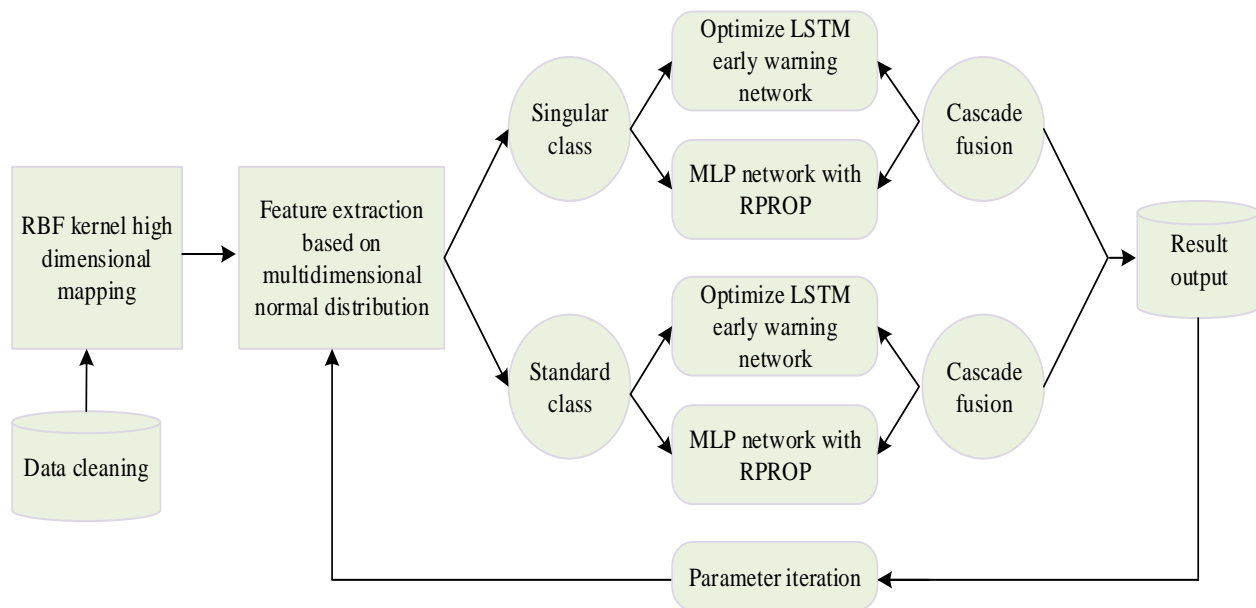


Fig. 2. Early Warning Model based on LSTM.

Where, $a^i = A_i, (i = 1, 2, \dots, n)$ and $b^i = B_i, (i = 1, 2, \dots, n)$ represents the student information vector represented by each row in the source data matrix, and h is a constant value. The representation method of elements in high-dimensional space is shown in formula (5).

$$e_n(a) = \sqrt{\frac{(2\alpha)^2}{n!}} a^n e^{-\alpha a^2}, n = 0, 1, 2 \dots \quad (5)$$

Where, the kernel parameter gamma value of the RBF kernel function is expressed as α . Through function mapping, the vacant data information in the source data matrix can be filled to obtain a full data matrix. In the evaluation of academic tests, the normal distribution can be used to grade the outstanding and backward situations, so as to determine the corresponding number of people, score lines, and winning rates. When the students' grades conform to the normal distribution, the RBF function in formula (6) is used to map the grade information to the high-dimensional space for feature extraction of the multi-dimensional normal distribution, and the students who meet the multi-dimensional normal distribution are divided into standard classes. Students who meet the multidimensional normal distribution are classified as singular.

$$f_a(a_1, \dots, a_k) = \frac{1}{\sqrt{(2\pi)^k |\sum a_i|}} \exp(-\frac{1}{2} (a - \mu)^T \sum a_i (a - \mu)) \quad (6)$$

Where, the mean value is expressed as μ , k is a constant. In the classification based on multi-dimensional normal distribution, data feedback is used to adjust the parameters of multi-dimensional normal distribution, as shown in Fig. 3.

The selection of the threshold in the normal distribution has an important impact on the accuracy of network training results. The optimal solution of the threshold parameter is selected by the parameter iteration method of gradient descent. After repeated attempts of the gradient descent method, the global optimal solution μ of the average threshold can be obtained, which is then normalized by formula (7).

$$X = (Y - \mu) / (Max - Min) \quad (7)$$

Where, Y represents the matrix that needs to be normalized, X represents the matrix obtained after normalization, and Max, Min represent the maximum and minimum vector values of all elements in X , respectively.

C. Research on Early Warning Algorithm based on Improved LSTM

LSTM performs well in processing long time series information. In distance education, the information is recorded as a long time series, which shows a strong dependence on time. The modelling of Multilayer perceptron (MLP) network is easy to realize, and neurons can be constructed according to the actual situation [20]. In this experiment, the MLP network is used to train students' grades. The MLP-based LSTM network uses time to divide the length of information in different dimensions, which reduces the complexity and polymorphism of information on the basis of retaining data features. The other data is back-propagated using the function to increase the speed at which the network operates. At the same time, the LSTM neural network is used to train other data, and the weighting function is introduced to solve the problems of gradient disappearance and gradient explosion. Then, cascade fusion is used to train students' behavioral data to further improve the accuracy of prediction results and solve the problem of academic early warning.

By using multi-dimensional normal distribution to extract the features from student data matrix, two matrices of singular class and standard class can be obtained. The data with high time-series dependence is more sensitive to time. The LSTM with adaptive excitation function is used to train the data with high time-series dependence. The schematic diagram of the neural network unit is shown in Fig. 4. The sum function is introduced into the adaptive excitation function, and the expression of **relu** and **tan** is shown in formula (8).

$$z = \frac{1}{v} \text{relu}(w \frac{x^t}{h^{t-1}}) + \frac{1}{u} \tanh(w \frac{x^t}{h^{t-1}}) \quad (8)$$

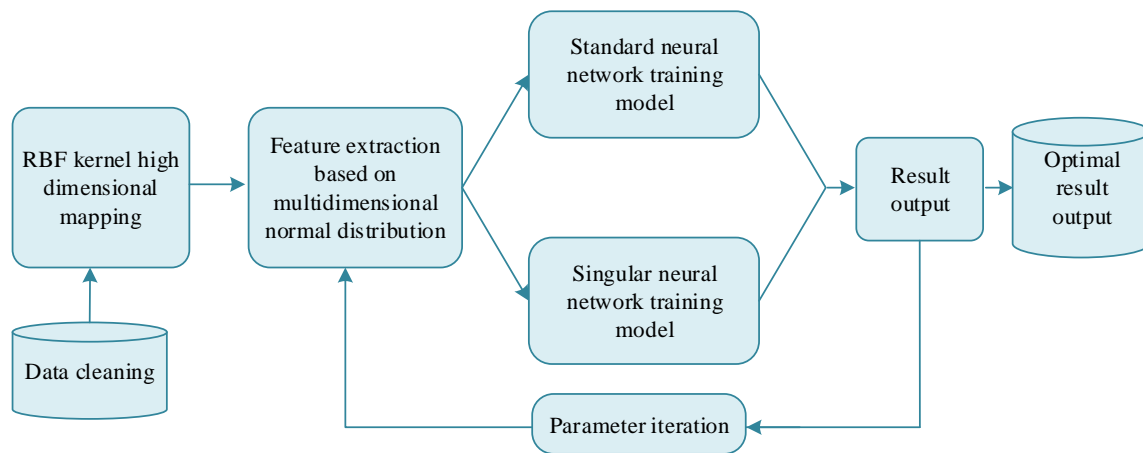


Fig. 3. Feedback-based Parameter Adjustment Process.

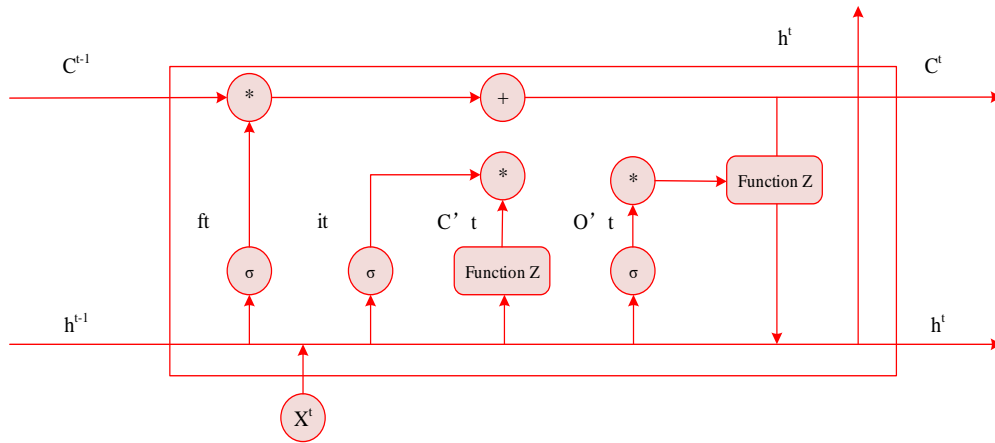


Fig. 4. LSTM Unit with Adaptive Excitation Function.

Where, W represents the function vector, v and u are the weight coefficient, $v+u=1$. The input module of LSTM includes the previous round of information carrier c^{t-1} , the previous round of state quantity output h^{t-1} and the current round of input x^t ; the output module includes the current round of information carrier c^t , the current round of state quantity output h^t and the current round of output y^t . Inputting \tanh function yields a vector z , and then, the state quantity output h^{t-1} of the previous round and the input x^t of the current round are combined into a vector, which is multiplied by W and then by the forgetting gate's matrix weight W^f , the input gate's matrix weight W^i , and the output gate's matrix weight W^o respectively, thus obtaining the output z^f and z^i sum z^o of each door. Thus, the calculation formulas of the current round information carrier, the current round state quantity output and the current round output can be obtained, as shown in formulas (9) to (11).

$$c^t = z^f c^{t-1} + z^i z \quad (9)$$

$$h^t = z^o * \left(\frac{1}{v} \operatorname{relu}\left(w \frac{x^t}{h^{t-1}}\right) + \tanh\left(w \frac{x^t}{h^{t-1}}\right) \right) * c^t \quad (10)$$

$$y^t = \sigma(wh^t) \quad (11)$$

The adaptive excitation function is to obtain the weighted average function after the function is weighted. The adaptive excitation function in formula (12) is used to excite the incoming data in each gate, and the data with high time series dependence is trained. Academic warnings are classified as follow.

$$f(x) = \frac{1}{u} \frac{e^x - e^{-x}}{e^x + e^{-x}} + \frac{1}{v} \max(0, x), u + v = 1 \quad (12)$$

Use formula (8) to iteratively calculate the values of weight coefficients v and u in the adaptive excitation function. When $v=0.643$ and $u=0.357$, the optimal data training results are obtained. RProp is a resilient backpropagation algorithm, and the MLP network with RProp can be used to train data with low time-series dependence such as the scores of various subjects. First, assign an initial value to the weight change and determine its acceleration and deceleration factors. Then, according to the feedback that the error gradient sign change or does not change during the iteration process, the training is decelerated or accelerated respectively to ensure the stable convergence of the system. Finally, backpropagation is performed by combining the sign of the error gradient with the changing step size. When the sign of the error gradient is negative, the weight needs to be appropriately increased to obtain the minimum value, as shown in formula (13).

$$\begin{aligned} \Delta w_{i,j} &= -\eta_{i,j}(t), \text{if } g(y) > 0 \\ \Delta w_{i,j} &= +\eta_{i,j}(t), \text{if } g(y) < 0 \\ \Delta w_{i,j} &= 0, \text{otherwise} \end{aligned} \quad (13)$$

Where, $\eta_{i,j}(t)$ denotes the learning rate of the algorithm. When the directions of the error gradient functions of two adjacent moments are inconsistent, it indicates that the minimum value of the current moment is missed, and the learning rate $\eta_{i,j}(t)$ of the current moment is smaller than the learning rate $\eta_{i,j}(t-1)$ of the previous moment, then multiply $\eta_{i,j}(t-1)$ by η^{up} in the range (0, 1) to obtain the current learning rate. When the directions of the error gradient functions of two adjacent moments are consistent, it indicates that the minimum value of the error function has not been reached. At this time, multiply $\eta_{i,j}(t-1)$ by η^{down} with a range greater than 1 to obtain the current learning rate, as shown in the formula (14).

$$\begin{aligned}\eta_{i,j}(t) &= \eta^{up} \eta_{i,j}(t-1), g(t-1)g(t) > 0 \\ \eta_{i,j}(t) &= \eta^{down} \eta_{i,j}(t-1), g(t-1)g(t) < 0 \\ \eta_{i,j}(t) &= \eta_{i,j}(t-1), otherwise\end{aligned}\quad (14)$$

The neural network system performs classification operations, and then combines the output results and uses formula (15) to fuse the results, so as to present different academic warnings for students.

$$p * a + (1 - p) * b = c \quad (15)$$

Where, P is the weight coefficient, a represents the LSTM prediction result, b represents the MLP prediction result, and the c represents graduation probability.

IV. SIMULATION ANALYSIS OF ACADEMIC EARLY WARNING MODEL BASED ON LSTM

The construction and training of the academic early warning system model of distance education is the key to the development of the system, and the accuracy and running time of the system are affected by the model construction and training results. Determining the number of layers and the number of nodes in the neural network is the main step that affects the construction of the system. In the experiment, the root means square error (RMSE) and the mean absolute error (MAE) are used to verify the number of layers in the neural network. The LSTM-based academic early warning model is repeatedly trained in the training set, and the parameters of the model are continuously adjusted in the process. Fig. 5 shows the training trend of RMSE and MAE values when different models predict time-dependent time series information. The abscissa represents the number of iterations of model training, and LSTM-1 to LSTM-5 represent the number of layers in the neural network, which are 1 to 5, respectively.

In Fig. 5(a), the number of iterations for LSTM-1 and LSTM-2 to start to converge is about 200. The minimum RMSE value of LSTM-1 with 1 neural network layer is 31.84, and the minimum RMSE of LSTM-2 with two neural network layers is 31.84. When the number of layers of the neural network increases to three, the RMSE value decreases more significantly. When the number of iterations is 225, LSTM-3 obtains the lowest RMSE value of 20.17, and the RMSE value remains at this level in subsequent iterations of training. When the number of layers of the neural network increases to four and five layers, the RMSE value has no obvious downward trend. In Fig. 5(b), the change trends of MAE value and RMSE value are consistent. The number of iterations when LSTM-1 and LSTM-2 begin to converge is about 200, the minimum MAE

value of LSTM-1 is 22.91, and the minimum MAE value of LSTM-2 is 18.96. When the number of layers of the neural network increases to three, the downward trend of the MAE value is more significant. When the number of iterations is 225, LSTM-3 obtains the lowest MAE value of 15.17, and the MAE value remains at this level in subsequent iterations of training. When the number of layers of the neural network increases to four and five layers, the MAE value has no obvious downward trend. It can be seen from Fig. 5 that in the training data set, the lowest error values RMSE and MAE are obtained when the number of layers of the LSTM neural network is set to 3 layers. When the number of layers is one or five, underfitting or overfitting may be encountered.

When the LSTM neural network is embedded in the academic early warning model, the embedding size is also one of the important factors affecting the performance of the early warning model. In the experiment, the number of layers of the neural network is set to three, and each neural network layer has different embedding sizes. Fig. 6 shows the training variations of the RMSE and MAE values of the LSTM neural network layers under different embedding sizes. In Fig. 6, LSTM-100 represents a three-layer neural network with an embedding size of 500-250-100, LSTM-150 is 500-300-150, LSTM-200 is 500-350-200, and LSTM-250 is 500-400-250, 500-400-300 for LSTM-300. The number of iterations at which the LSTM-100 and LSTM-150 models start to converge in Fig. 6(a) are 225 and 200, respectively, and the minimum RMSE values are 30.89 and 24.76, respectively. The RMSE value converges faster in the LSTM-200 model, reaching the lowest value of 20.68 after 250 iterations. In LSTM-250 and LSTM-300, there is basically no downward trend of the RMSE value, and the performance of the model is no longer improved. In Fig. 6(b), the MAE value and the RMSE value have the same change trend. The number of iterations at which the LSTM-100 and LSTM-150 models start to converge are 200 and 225, respectively, and the minimum MAE values are 20.03 and 14.98, respectively. The MAE value converges faster in the LSTM-200 model, reaching the lowest value of 13.09 after 200 iterations. When the embedding size increases, there is basically no downward trend of the MAE value. When the LSTM neural network is embedded in the academic early warning model, the size of the embedding size is proportional to the predictive ability of the model. The larger the embedding size, the stronger the data fitting ability. Fig. 6 shows that when the embedding size is 200, the minimum RMSE and MAE are obtained. Combined with the experimental results of the algorithm in different configurations, and considering the complexity and prediction effect, this study selects the embedded size of 200 and the number of neural network layers of three as the default settings for subsequent verification experiments.

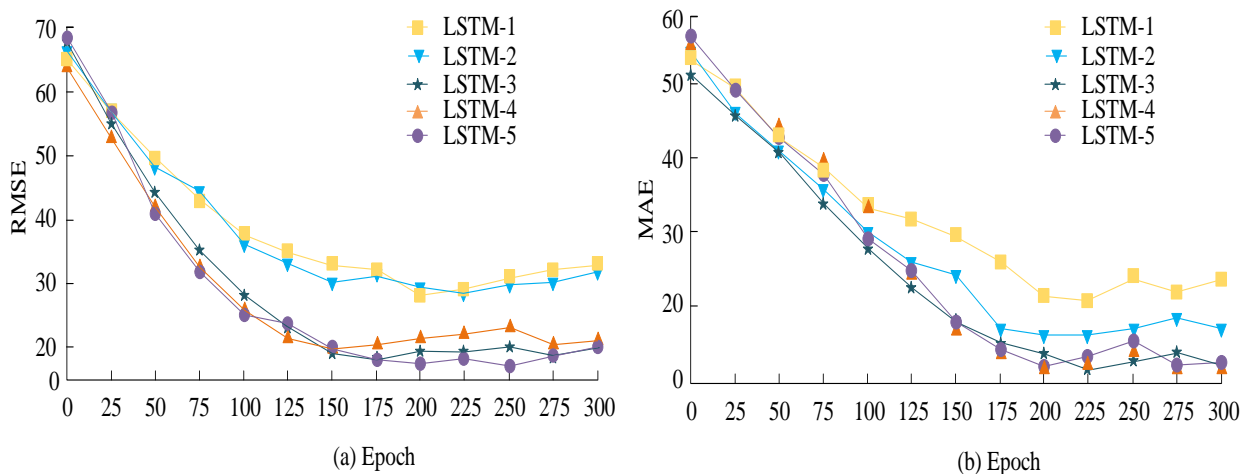


Fig. 5. RMSE and MAE Trends of Graph Neural Network with 1-5 Layers on Training Set.

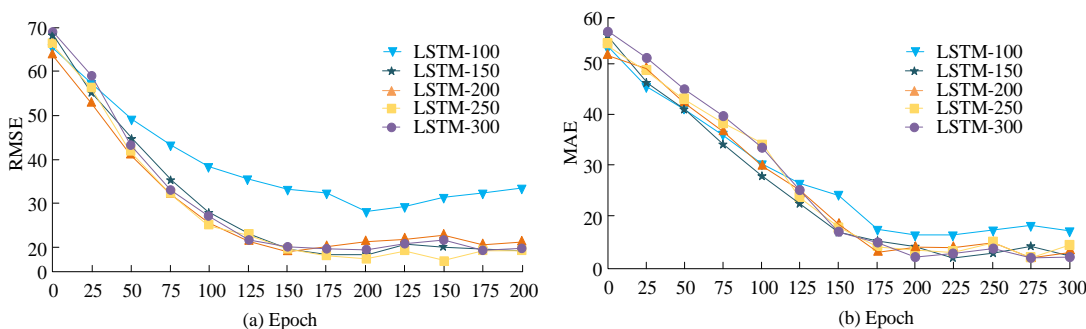


Fig. 6. Change Trends of RMSE and MAE under different Embedding Sizes.

TABLE I. COMPARISON OF EXPERIMENTAL RESULTS OF TIME SERIES STATE PERCEPTION

Algorithm	P	R	F
HC	0.673	0.622	0.646
HN	0.612	0.530	0.568
HM	0.405	0.492	0.444
LC	0.831	0.806	0.818
LN	0.678	0.713	0.695
LM	0.462	0.562	0.507
LSTM	0.886	0.812	0.847
This paper	0.929	0.917	0.923

The basic LSTM algorithm and the optimized LSTM algorithm proposed in this experiment are comparatively analyzed in terms of accuracy (P), recall (R) and the ratio F. Table I shows the experimental results of the HTM algorithm, the basic LSTM algorithm and the optimization algorithm proposed in this experiment in time series state perception. In Table I, H represents the HTM algorithm, L represents the basic LSTM algorithm, and LSTM represents the prediction model based on the basic LSTM algorithm; C represents the system parameter CPU, M represents the system parameter MEM, and N represents the system parameter NET. The sensitivity of the algorithm to abnormal situations can be judged by the accuracy rate, the detection ability of the algorithm to abnormal situations can be judged by the recall rate, and the F value is used to evaluate the overall performance of the algorithm. The

results in Table I show that the accuracy of the optimized LSTM algorithm is 0.929, the recall is 0.917 and the F value is 0.923, which are significantly higher than those of the basic LSTM algorithm. The comparative experimental results show that the accuracy rate of the optimized algorithm is higher, and the probability of false positives of the model is significantly reduced; the recall rate of the optimized algorithm is outstanding, and the probability of false negatives of the model is significantly reduced; the accuracy rate and recall rate of the optimized algorithm are higher, indicating that the overall performance of the optimized algorithm is higher. Based on the experimental parameters set above, the convergence rates of the basic algorithm and the optimized algorithm are compared.

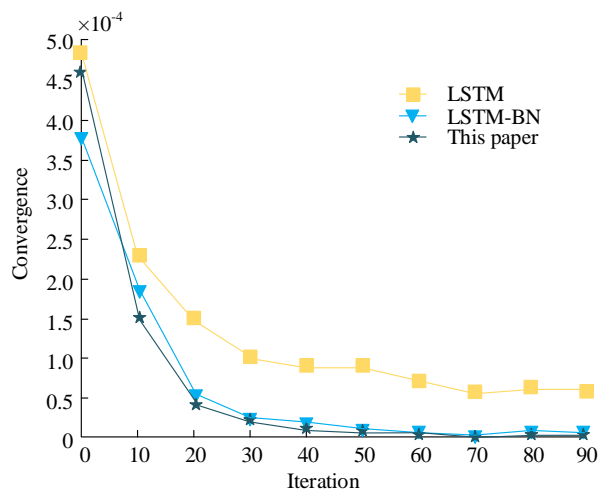


Fig. 7. Comparative Analysis of Convergence Rate.

Whether the model satisfies the convergence condition is mainly judged by comparison with the preset value, judgment of the weight value and the comparison of the maximum number of iterations. The purpose of training the model is to reduce the loss value, and it is necessary to set a threshold in advance to determine whether the training is over. The preset threshold will affect the convergence of the neural network model. When the loss value is less than the preset value, it is considered to end the training. When there is no significant change in the weights between two adjacent iterations, it can be considered that the model has reached a state of convergence with no need to adjust the weights. There are many preset applications for the maximum number of iterations. The iteration period is selected according to the actual situation, and the model is trained to achieve the optimal solution. Fig. 7 shows the comparison results of the convergence rate of the basic method and the optimized method in this experiment. It can be clearly seen that the convergence effect of the optimized method is significantly better than that of the basic method. 80

college students in distance education were randomly selected for the comparative evaluation of the academic early warning system, and the results obtained by the academic early warning prediction model based on the optimized LSTM algorithm were compared with the actual situation.

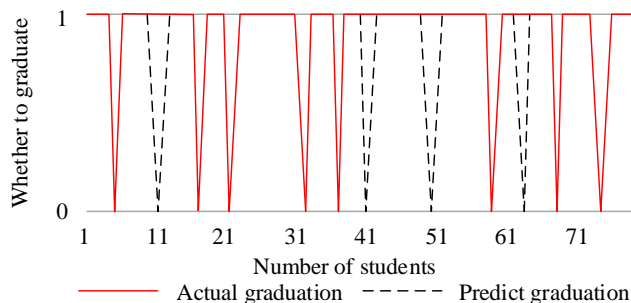


Fig. 8. Comparison of the Actual Results and the Results Predicted by the Academic Early Warning Prediction Model based on Optimized LSTM Algorithm

In Fig. 8, the abscissa represents the number of students, 0 in the ordinate represents ungraduated, and 1 represents graduation. The figure shows that among the 80 college students, six are inconsistent with the actual number of graduates, and the accuracy rate of the academic warning system is 92.5%. In addition, the academic early warning system is used to predict students' enthusiasm for active learning in distance education, and the predicted value is compared with the real situation. Fig. 9 shows the results.

Fig. 9 shows that during distance education, the number of submissions in the academic early warning system is consistent with the actual trend, reflecting that prediction results of learning enthusiasm by the academic early warning system are consistent with the actual situation. The academic early warning system in distance education designed in this experiment has high prediction accuracy and can be applied to students' academic early warning.

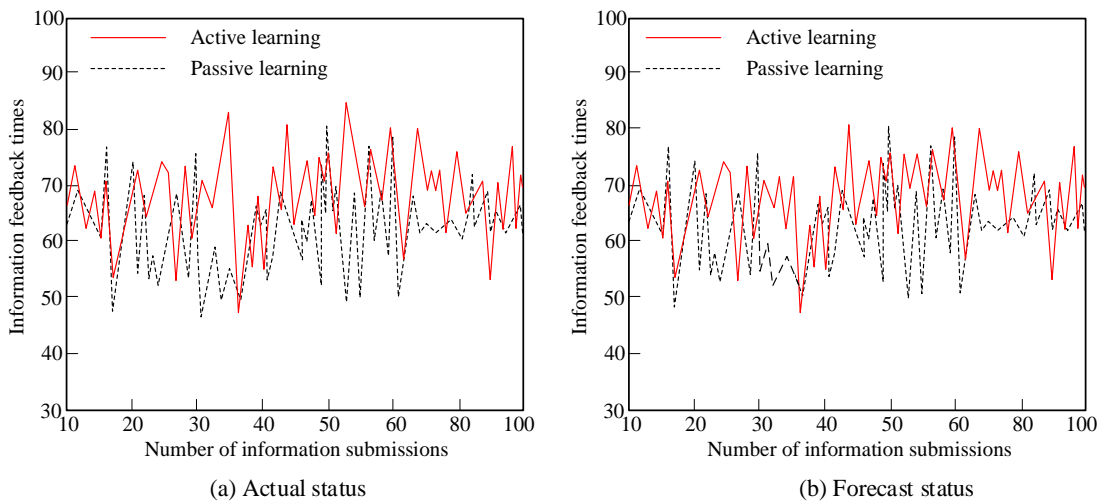


Fig. 9. Interactive Comparison Results of the Two Systems.

V. DISCUSSION

At present, the proportion of middle line education in the whole education industry is gradually increasing. In the online education environment, students' learning behavior is difficult to be monitored. And according to the information in literature [4] and [5], students under online education generally lack initiative and learning self-confidence, and their overall performance is lower than that of offline teaching. The early warning system is mainly a system to detect signs and warn relevant personnel at the early stage of or before the beginning of a negative situation. The quality of current academic early warning systems is uneven. The early warning system in literature [9] has been applied in some colleges and universities, but its operation has a low degree of automation, and its accuracy also has a large room for improvement. The early warning system in [12] and the proposed early warning model both use neural network models, but the performance of the latter is slightly higher than that of the former. In addition, the early warning model in literature [9] and [12] pays more attention to the academic early warning of offline teaching. When the teaching scenario is online, its performance will be further limited. The early-warning model proposed in this study is specially designed for online teaching, which has great application potential in the current social context. From the results of the performance test, the model proposed in this study also has a high degree of early warning accuracy and automation, which can be applied to online teaching scenarios.

VI. CONCLUSION

In the simulation analysis experiment of the academic early warning model based on LSTM, the number of layers of the neural network is set to three and the embedding size is set to 200 through parameter optimization and comprehensive consideration. The accuracy rate of the optimized LSTM algorithm is 0.929, the recall rate is 0.917 and the F value is 0.923, which are significantly higher than those of the basic LSTM algorithm, which has the accuracy rate of 0.886, the recall rate of 0.812 and the F value of 0.847. Comparing the results obtained by the academic early warning prediction model based on the optimized LSTM algorithm with the actual situation, the accuracy of the academic early warning system is 92.5%. To predict the enthusiasm of students for active learning, the number of submissions in the academic early warning system is consistent with the actual trend. The LSTM-based academic early warning model proposed in this experiment has high performance after parameter optimization, and also has high accuracy in actual case analysis, which can be applied to academic early warning in distance education. This research discusses the application of LSTM network in online teaching evaluation, and broadens the application field of LSTM network. At the same time, the research results have brought a practical model to the field of online education, which can improve the teaching effect through accurate and timely warning, and help students learn and teachers teach. However, the running time of the model was not verified, and it was not compared with other existing models in terms of the running time. Therefore, the proposed model may not be the optimal solution in terms of time, and there is still room for further improvement. In the follow-up work, we need to further improve the relevant experimental content.

VII. FINDINGS

The research is supported by: Innovation Team of Digital Communication and Cultural Soft Power (Grant No. TD2021002); Scientific Research Program Funded by Shaanxi Provincial Education Department (Program No. 22JZ0016).

REFERENCES

- [1] K. Cicha, M. Rizun, P. Rutecka, et al. "COVID-19 and Higher Education: First-Year Students' Expectations toward Distance Learning", *Sustainability*, Vol. 13, pp. 1889-1908, 2021. DOI:10.3390/su13041889.
- [2] J. A. Vilchez, J. Kruse, M. Puffer, et al. "Teachers and School Health Leaders' Perspectives on Distance Learning Physical Education During the COVID-19 Pandemic", *Journal of School Health*, vol. 91, pp. 541-549, 2021. DOI: 10.1111/josh.13030.
- [3] V. Domenici, "A Course of History of Chemistry and Chemical Education Completely Delivered in Distance Education Mode during Epidemic COVID-19", *Journal of Chemical Education*, 2020, vol. 97, pp. 2905-2908, 2020. DOI:10.1021/acs.jchemed.0c00739.
- [4] J. E. Baker, "Maintaining an Active Organic Class during the COVID-Induced Online Transition at Two Undergraduate Institutions", *Journal of Chemical Education*, vol. 97, pp. 3235-3239, 2020. DOI:10.1021/acs.jchemed.0c00759.
- [5] J. Wilhelm, S. Mattingly, V. H. Gonzalez, "Perceptions, Satisfaction, and Performance of Undergraduate Students During Covid-19 Emergency Remote Teaching", *Anatomical Sciences Education*, 2021, vol. 15, pp. 42-56, 2021. DOI: 10.1002/asc.2161.
- [6] B. J. Santiago, J. M. O. Ramírez, J. Rodríguez-Reséndiz, et al. "Learning Management System-Based Evaluation to Determine Academic Efficiency Performance", *Sustainability*, vol. 12, pp. 4256-4272, 2020. DOI:10.7763/IJEEEE.2013.V3.233.
- [7] J. C. Ginestra, H. M. Giannini, W. D. Schweickert, et al. "Clinician Perception of a Machine Learning-Based Early Warning System Designed to Predict Severe Sepsis and Septic Shock", *Critical Care Medicine*, vol. 47, pp. 1477-1484, 2019. DOI: 10.1097/CCM.0000000000003803.
- [8] A. S. Sein, M. Daniel, A. Fleming, et al. "Identifying and Supporting Students to Prevent USMLE Step 1 Failures When Testing Follows Clerkships: Insights From 9 Schools", *Academic Medicine*, vol. 95, pp. 1338-1345, 2020. DOI: 10.1097/ACM.0000000000003272.
- [9] S. J. Aguilar, S. A. Karabenick, S. D. Teasley, et al. "Associations between learning analytics dashboard exposure and motivation and self-regulated learning", *Computers & Education*, vol. 162, pp. 104085, 2021. DOI:10.1016/j.compedu.2020.104085.
- [10] K. J. Cho, O. Kwon, J. M. Kwon, et al. "Detecting Patient Deterioration Using Artificial Intelligence in a Rapid Response System", *Critical Care Medicine*, vol. 48, pp. 285-289, 2020. DOI: 10.1097/CCM.0000000000004236.
- [11] Y. B. Lin, F. Z. Lee, K. C. Chang, et al. "The Artificial Intelligence of Things Sensing System of Real-Time Bridge Scour Monitoring for Early Warning during Floods", *Sensors*, 2021, vol. 21, pp. 4942-4959, 2021. DOI: 10.3390/s21144942.
- [12] T. A. Rashid, D. K. Abbas, Y. K. Turel, "A multi hidden recurrent neural network with a modified grey wolf optimizer", *PLoS ONE*, vol. 14, pp. 1-34, 2019. DOI: 10.1371/journal.pone.0213237.
- [13] G. Jung, S. Y. Choi, "Forecasting Foreign Exchange Volatility Using Deep Learning Autoencoder-LSTM Techniques", *Complexity*, vol. 1, pp. 1-16, 2021. DOI:10.1155/2021/6647534.
- [14] M. Meng, M. Zhu. "Deep Convolution-based LSTM Network for Remaining Useful Life Prediction", *IEEE Transactions on Industrial Informatics*, vol. 17, pp. 1658-1667, 2020. DOI:10.1109/TII.2020.2991796.
- [15] G. Dorgo, J. Abonyi, "Learning and predicting operation strategies by sequence mining and deep learning", *Computers & Chemical Engineering*, vol. 128, pp. 174-187, 2019. DOI:10.1016/j.compchemeng.2019.06.006.
- [16] X. Ren, W. Yang, X. Jiang, et al. "A Deep Learning Framework for Multimodal Course Recommendation Based on LSTM+Attention", *Sustainability*, vol. 14, pp. 2907-2920, 2022. DOI:

- <https://doi.org/10.3390/su14052907>.
- [17] D. R. Liu, S. J. Lee, Y. Huang, et al. "Air pollution forecasting based on attention-based LSTM neural network and ensemble learning", *Expert Systems*, vol. 37, pp. 1-16, 2020. DOI:10.1111/exsy.12511.
- [18] O. Jogunola, B. Adebisi, K. V. Hoang, et al. "CBLSTM-AE: A Hybrid Deep Learning Framework for Predicting Energy Consumption", *Energies*, vol. 15, pp. 810-825, 2022. DOI:10.3390/en15030810.
- [19] B. Lagesse, S. Wang, T. V. Larson, et al. "Predicting PM2.5 in Well-Mixed Indoor Air for a Large Office Building Using Regression and Artificial Neural Network Models", *Environmental Science & Technology*, vol. 54, pp. 15320-15328, 2020. DOI:10.1021/acs.est.0c02549.
- [20] K. Y. Almansi, A. Shariff, B. Kalantar, et al. "Performance Evaluation of Hospital Site Suitability Using Multilayer Perceptron (MLP) and Analytical Hierarchy Process (AHP) Models in Malacca, Malaysia", *Sustainability*, vol. 14, pp. 3731-3766, 2022. DOI: 10.3390/su14073731

Dynamic Polymorphism without Inheritance: Implications for Education

Ivaylo Donchev, Emilia Todorova
Department of Information Technologies
St Cyril and St Methodius University of Veliko Tarnovo
Veliko Tarnovo, Bulgaria

Abstract—Polymorphism is a core OO concept. Despite the rich pedagogical experience in teaching it, there are still difficulties in its correct and multifaceted perception by students. In this article, a method about a deeper study of the concept of polymorphism is offered by extending the learning content of the CS2 C++ Programming course with an implementation variant of dynamic polymorphism by type erasure, without using inheritance. The research is based on an inductive approach with a gradual expansion of functionalities when introducing new concepts. The stages of development of such a project and the details of the implementation of each functionality are traced. The results of experimental training showed higher scores of the experimental group in mastering the topics related to polymorphism. Based on these findings, recommendations for the construction of the lecture course and the organization of the laboratory work are suggested.

Keywords—Inheritance; polymorphism; object-oriented; C++; type erasure; pointers; templates; lambda expressions; teaching

I. INTRODUCTION

The study of the concept of polymorphism is widely used in programming courses. Students encounter its forms already in the introductory course and use them successfully, even if they do not perceive them as such at first. This is where function overloading and type casting (coercion polymorphism) come in. Later, parametric polymorphism (templates, generics) is added. However, when one says polymorphism, without specifying what kind, one usually means the inherent OOP inclusion (subtype) polymorphism, implemented through inheritance, virtual methods and dynamic linking (dynamic polymorphism). Subtype polymorphism is a cornerstone of object-oriented programming. By hiding variability in behavior behind a uniform interface, polymorphism decouples clients from providers and thus enables genericity, modularity, and extensibility [1]. This type of polymorphism, together with parametric, forms the more general universal polymorphism category of the popular classification of polymorphism types given in [2], and overloading and coercion form the ad-hoc category.

Bjarne Stroustrup defines polymorphism as “providing a single interface to entities of different types” [3] and distinguishes between dynamic (run-time) polymorphism, implemented through virtual functions through an interface provided by a base class, and static (compile-time) polymorphism through overloaded functions and templates. It is considered useful to differentiate between the two types. The focus is on three matters: time when the selection of the specific

method occurs (run-time or compile-time); different behavior, based on dynamic or static type; means by which it is usually achieved – inheritance in case of dynamic and overloading and templates in case of static.

Virtual functions and inheritance are typical means of achieving dynamic polymorphism, but they have their drawbacks in terms of performance and flexibility. The authors believe that in order to build deep understanding of the concept of dynamic polymorphism, students should have an idea that it can be achieved by other means, such as type erasure. Such an implementation with the currently available capabilities of C++ is cumbersome and error-prone, requires the definition of many types and functions, and provides no distinguishable advantages over inheritance, but has a beneficial impact on developing the programming competencies of computer science students, especially regarding the proper use of pointers.

In this paper, experience of implementing dynamic polymorphism without inheritance is shared (with manual implementation of virtual tables and the implementation of copy and move semantics) within the elective course “Programming in C++” for students majoring in Software Engineering. Their curiosity and previous experience with C# provoked to try to implement a familiar sample project in a new way. The project evolves incrementally with the addition of new functionalities as the relevant concepts are studied. The audience is later expanded to include Computer Science students with no .NET experience in the mandatory C++ Programming course. The difficulties which students encounter are explored and the effect of deeper study of concepts is tracked.

II. METHODOLOGY

A. Motivation

A classic example of inheritance polymorphism that our students have covered in the C# course is the hierarchy shown in Fig. 1. The base class declares a virtual method `Accelerate()`, which the two derived classes override. The classes can be used as follows:

```
Vehicle vehicle = new Car();  
vehicle.Accelerate();  
vehicle = new Truck();  
vehicle.Accelerate();  
List<Vehicle> vehicles = new() {
```

```
new Car(), new Truck(), new Truck(), new Car()
};
foreach (var v in vehicles){
    v.Accelerate();}
```

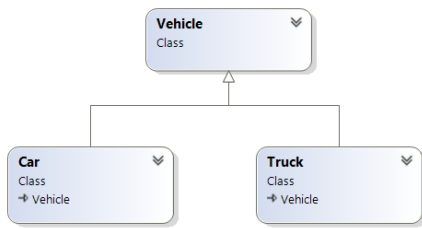


Fig. 1. The Hierarchy that will be Implemented.

With no major changes to the client code, by implementing an interface `IVehicle`, declaring the method `Accelerate()`, the same functionality without inheritance can be obtained. The C++ hierarchy implementation is even shorter – an abstract base class with pure virtual method `Accelerate()`, which is inherited and overridden by the classes `Car` and `Truck`. However, the client code requires use of pointers (dynamic allocation – one of the problems with inheritance), not objects, because abstract class cannot be instantiated:

```
Vehicle *vehicle = new Car{};
vehicle->Accelerate();
delete vehicle;
vehicle = new Truck{};
vehicle->Accelerate();
std::vector<Vehicle*> vehicles{
    new Car{} ,
    new Truck{} ,
    new Truck{} ,
    new Car{}
};
for (auto&& v : vehicles){
    v->Accelerate();
}
```

However, students want to write the code as they are used to with C#:

```
Vehicle v = Car{};
v.accelerate();
v = Truck{};
v.accelerate();
std::vector<Vehicle> vehicles{
    Car{} , Truck{} , Truck{} , Car{} };
for (auto&& v : vehicles) {
    v.accelerate();
}
```

If a default implementation of the method in the class `Vehicle` is added, it is no longer abstract, this code will be

compiled, but there will be not polymorphic behavior – the same method will always be executed – that of the class `Vehicle`. For this code to work correctly, it is needed to implement manually the virtual functions mechanism, which will be done in the following sections.

B. Inheritance Problems

To prove why it is necessary to look for inheritance-free design possibilities, it is needed to look at some of the problems it raises. In his talk at CppCon 2020, Simon Brand summarizes and analyzes five issues related to inheritance [4]:

- Often requires dynamic allocation

This problem is encountered when implementing the hierarchy of Fig. 1. The attempt to store in `vector<Vehicle>` objects of the derived classes `Car` and `Truck` leads to what's called "slicing" – just the inherited from `Vehicle` (base) part of the object are got, and we slice of the dynamic part of the derived object. Usually this is not what is needed. The same is the situation when a function returns an object of the base class by value. To avoid this problem, it is needed to allocate and return a pointer dynamically (in the case of the function), or store a pointer (raw or smart) in a vector:

```
std::vector<std::unique_ptr<Vehicle>> vehicles;
```

- Ownership and nullability considerations

When working with pointers their ownership and validity must always be considered. If `unique_ptr` is used, then the ownership is clear. It is not so clear, however, if a function is returning `unique_ptr`. Questions arise: can it return null? Is it necessary to check? If the function accepts a `unique_ptr` argument, what happens if null is passed? Is that valid? What's the behavior? Too many questions to take care of.

- Intrusive: requires modifying child classes

Supporting inheritance requires modifying child classes.

```
namespace LibOne {
    class Base {
    public:
        virtual void Foo();
    };
}
```

```
namespace LibTwo {
    class Other {
    public:
        virtual void Foo();
    };
}
```

There is a Base class in `LibOne` and then there is some other library `LibTwo` which has an `Other` class. They both have `Foo()` method which returns void and they're virtual. It is not possible to allocate an instance of `LibTwo::Other` and take a pointer to it through a `LibOne::Base`.

```
LibOne::Base* b = new LibTwo::Other{};
```

This will not work because LibTwo::Other does not say it inherits from LibTwo::Other. This can be a problem. Maybe LibTwo::Other cannot be changed like if we could just decorate it to inherit from Base. For example, the code may not be available or there may be other restrictions that prevent from doing so. So, polymorphism with inheritance is intrusive.

- No more value semantics

Again, the question comes to the pointers. If we want value semantics, then something on top must be built. For example, virtual Clone() function which uses the correct dynamic type, dynamically allocate a pointer, and pass it back. That's a way of getting a copy behavior but still it is not the usual C++ value semantics which a lot of code depends on.

- Changes semantics for algorithms and containers

Inheritance changes semantics for algorithms and containers. If a std::sort() is done, maybe sorting on pointers is on, and custom comparator object must be supplied. The same situation is when these things are stored in a std::set. Another situation that must be thought about is that not usual C++ values are used, but it is desirable for most of the C++ development to use value semantics.

C. Implementing Virtual Functions by Hand

The start is with an implementation of the hierarchy of Fig. 1 in the traditional way, by inheritance.

```
class Vehicle {
public:
    virtual ~Vehicle();
    virtual void Accelerate() const = 0;
};
class Car : public Vehicle {
    virtual void Accelerate() const override;
};
class Truck : public Vehicle {
    virtual void Accelerate() const override;
};
```

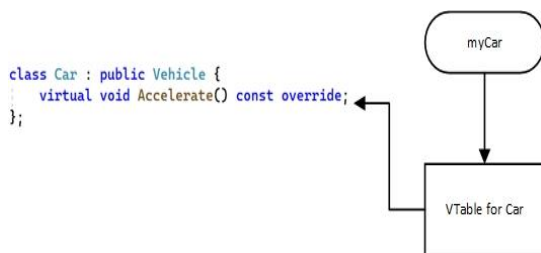


Fig. 2. Situation with an Object of the Car Class.

It is important for students to understand how virtual functions works internally. In Fig. 2 myCar is an object of the Car class. Then it is going to have a pointer to a VTable – a virtual table. This table takes care of how to call virtual functions in a polymorphic object. VTable in turn has a pointer to the Accelerate() function for Car. So, there is a couple of indirections that are gone through when Accelerate() is called. First, the VTable must be grabbed, then the VTable must be

read through to get the Accelerate() function. That can be a performance bottleneck.

The interface to be implemented includes a Vehicle class, which should provide all the necessary functionality for polymorphic behavior. The other two classes Car and Truck just need to have accelerate() functions. These two classes should not inherit Vehicle, but there is a need to support this use case. It should be possible to create a Vehicle from a Car and call accelerate(). The aim is ability to create a Vehicle from a Truck and have it accelerate() and all this should be done without doing any slicing.

```
Vehicle c = Car{};
c.accelerate();
Vehicle t = Truck{};
t.accelerate();
```

To implement the virtual functions manually several steps have to be made:

- Declare virtual table for the abstract interface

First, it is declared what the virtual table layout looks like for Vehicle class.

```
struct VTable {
    void (*accelerate)(void* ptr);
    void (*destruct)(void* ptr);
};
```

VTable has two function pointers – one for accelerate and one for destruct, which will be called by the destructor of the specific object. And since memory within the object will be allocated, it's going to reclaim that memory. The arguments of the two function pointers are void pointers, because in this way the concrete object will be stored internally. Void pointers will be passed, and then the concrete objects are going to cast those pointers internally.

- Define virtual table for a concrete type

```
template<typename T>
VTable vtable_for {
    [](void* p) {
        static_cast<T*>(p)->accelerate(); },
    [](void* p) {
        delete static_cast<T*>(p); }
};
```

This is a variable template (available since C++14). There is an instance of a VTable and it's templated on the concrete type T, i.e., Car or Truck. So, a function which is going to call the correct version of accelerate() is needed, and a function which deletes the object and calls the destructor. Lambdas can be used for this purpose. For a given concrete object the first function pointer is just going to static cast to the concrete type and then call accelerate(). And then the second function is going to static cast and then calls delete. This all works because lambdas which don't capture can decay to function pointers.

- Capture the virtual table pointers on construction

When a Vehicle class is constructed, it is needed to fill in the pointer for the concrete object and pointer to the virtual table. The constructor will be implemented as a template that accepts any type as an argument. In a real situation, of course, it would be good to limit the possible types. Memory will be allocated dynamically for the object received as an argument and a copy of it in p_obj will be saved, and after that a pointer to our virtual table will be taken and stored inside vehicle (in the p_vtable field).

```
class Vehicle {
public:
    void* p_obj;
    VTable const* p_vtable;
    template<typename T>
    Vehicle(T const& obj) :
p_obj(new T(obj)),
p_vtable(&vtable_for<T>)
{}
};
```

It is noted that since there is current access to what type the obj is (Car or Truck), that information is saved for later by grabbing the right VTable pointer and by dynamically allocating a copy of our obj. This technique is called “type erasure”.

- Forward calls through the virtual table

Finally, it is needed to forward the calls through the virtual table.

```
class Vehicle {
    //...
    void accelerate() {
        p_vtable->accelerate(p_obj);
    }
    ~Vehicle() {
        p_vtable->destruct(p_obj);
    }
};
```

Inside the Vehicle class if accelerate() is called, then we indirect through p_vtable and pass it the void pointer. And that is then going to cast inside the function and call the right version. And then similarly for the structure we call destruct().

So now the students have something which works for that use case. It remains to define the classes Car and Truck with the corresponding implementations of the function accelerate().

```
class Car {
public:
    void accelerate() {
        std::cout << "The car accelerates.\n";
    }
};

class Truck {
```

```
public:
    void accelerate() {
        std::cout << "The truck accelerates.\n";
    }
};
```

It is possible to construct car; it is possible to construct vehicle from a car and a truck and make them accelerate and all it works. The goal set at the beginning of the section has been achieved.

D. Adding Copy and Move Semantics

So far, some of the inheritance problems discussed in section B have been solved. There are no more problems with ownership and nullability, because now all memory allocations are handled inside the Vehicle class. There are no pointers externally. We're just dealing with the values. Intrusivity is avoided as well, because now Car and Truck don't inherit from anyone. However, the problem with value semantics remains, because these objects can't be copied or moved, but the VTable can be extended with a copy_() and a move_() function pointers and solve this problem.

```
struct VTable {
    //...
    void* (*copy_)(void* ptr);
    void* (*move_)(void* ptr);
};
```

The first function will allocate a copy, and the second will allocate by moving from the object. This functionality should be implemented by adding two new lambda functions to the variable template vtable_for.

```
template<typename T>
VTable vtable_for {
    //...
    [](void* p) -> void*{
        return new T(*static_cast<T*>(p)); },
    [](void* p) -> void*{
        return new T(std::move(*static_cast<T*>(p))); }
};
```

Now it is only needed in the copy constructor and move constructor of Vehicle to call from the virtual table p_vtable the corresponding functions.

```
Vehicle(Vehicle const& other) :
    p_obj(other.p_vtable->copy_(other.p_obj)),
    p_vtable(other.p_vtable)
{}
Vehicle(Vehicle&& other) noexcept :
    p_obj(other.p_vtable->move_(other.p_obj)),
    p_vtable(other.p_vtable)
{}
```

The same is done for copy assignment and move assignment operators.

```
Vehicle& operator=(Vehicle const& other) {  
    p_obj = other.p_vtable->copy_(other.p_obj);  
    p_vtable = other.p_vtable;  
    return *this;  
}  
Vehicle& operator=(Vehicle&& other) noexcept {  
    p_obj = other.p_vtable->move_(other.p_obj);  
    p_vtable = other.p_vtable;  
    return *this;  
}
```

Now a much more complete interface is created, and a lot of actions can be performed – create vehicle from car and accelerate it; we can reassign it to a truck and make that accelerate. A new vehicle can be created from an old one. All works and there is value semantics even though we're doing dynamic polymorphism. It's just all handled under the covers. Students can even experiment by defining and traversing the vector of cars and trucks because we defined copying and moving.

```
Vehicle v = Car{};  
v.accelerate();  
v = Truck{}; // move assignment!  
v.accelerate();  
Vehicle t{ v }; // copy construction  
t.accelerate();  
std::vector<Vehicle> vehicles {  
    Car{}, Truck{}, Truck{}, Car{} };  
for (auto&& v : vehicles) {  
    v.accelerate();  
}  
t = std::move(v); // move assignment
```

Another inheritance problem is solved. There are already normal copy semantics and container semantics. The problem is that the code written to implement this functionality is too much and must be repeated for each class that needs to be handled dynamically. In addition, it's weird code and it's easy for something to go wrong.

III. IMPLICATIONS FOR EDUCATION

Teachers and students often consider learning programming a difficult pursuit [5]. Inheritance and polymorphism are arguably the most advanced and abstract subjects in object-oriented programming [6]. Their study involves many difficulties, which we will not consider here. The study in [7] identifies as the main cause of most problems the students' inability to understand what is happening with their program in memory, since they cannot build a clear mental model of the program's execution. Therefore, we believe that manually implementing the virtual tables will help overcome these issues. Our experience from the last two academic years shows progress in this direction. Students see that pointers are a very powerful tool and are motivated to study them. They look for literature and consult with the assistants, solve tasks

independently. The result is a deeper understanding of memory management and program execution.

For students who have not studied C++ in the introductory course, after the topics related to the new-to-them syntax in terms of program structure, class definition, object instantiation, and message exchange, one should move on to learning about working with pointers and dynamic memory (something everyone else studied in the introductory C++ course). At an early stage, the topics of implementing the important OOP relations of composition and inheritance, which students know from the introductory course, should also be included. After that comes the time for an in-depth study of polymorphism. For students the goal is to learn to recognize polymorphism and model with it, not just to know its implementation in the specific language.

Dynamic binding and virtual functions should be seen as a mechanism in OOP languages to implement dynamic polymorphism, but not polymorphism to be considered as a consequence of using the mechanism. It is recommended to give a correct classification of the types of polymorphism in lectures in order to clarify the understanding of the concepts and distinguish them from the means of implementation.

A common mistake made by novice programmers is always to try to use the inheritance relationship. Undoubtedly, it is the most important and defining for the paradigm, but its application should not be overexposed in the course. After learning about the disadvantages of inheritance, students themselves will begin to look for alternative designs using other relations. In particular, it provoked interest for generic and functional programming.

Modern programming languages offer concepts from several programming paradigms. It is impossible to learn OOP in isolation from generic, functional, and procedural programming. Therefore, in parallel with OO concepts, other means like templates, lambdas, containers, and algorithms from STL should also go.

An important condition for successful training in OOP is the correct selection of the tasks that are considered in laboratory classes and given for homework. They should be such that polymorphism is a natural part of the solution. Suitable hierarchies to implement (both with and without inheritance) are as follows:

- base class Animal and derived classes Fish, Frog, Bird and polymorphic method Move(),
- base class Pet, derived classes Cat and Dog and polymorphic method MakeNoise(),
- base class Shape, derived Circle, Triangle, Rectangle and polymorphic methods Area() and Circumference(),
- basic class Publication, derived Magazine, Book and polymorphic method Print().

Examples can be both from real life and more abstract. Examples with GUI components can also be used. It is a good idea to add a new class to an already implemented hierarchy, for example adding Motorcycle to Car and Truck. This can be

done as work to do by themselves within the lab exercise or given for homework.

Learning about abstract classes provides a good foundation to demonstrate the full power of polymorphism with perhaps its most typical application – the creation and manipulation of heterogeneous data structures. The vector of Car and Truck objects is such a structure as well. If there is enough time, a manual implementation of a heterogeneous singly linked list or binary tree can also be demonstrated in the training course.

Since the complete implementation of the Vehicle, Car, Truck hierarchy given in this paper covers many topics, it cannot be covered in a single lecture and practiced in a single lab session. It is recommended to teach incrementally, starting with an implementation with inheritance, and going through the type erasure option after discussing pointers, constructors, destructors, type conversion, lambda functions, function templates, variable templates. After the initial version, the project can be extended with an implementation of copy semantics only. This requires first familiarity with operator overloading and copy construction. Move semantics is not required for the classes to work correctly because it can be successfully replaced by copy. But since the choice of the C++ language in most cases is related to the increased requirements for speed and efficiency of code, it is recommended not to neglect it and to give and comment the described implementation of move semantics for the sample hierarchy. When learning the STL library, one can experiment with using different containers of Car and Truck objects and applying algorithms to them.

Since enough empirical data is not collected yet, the classic pedagogical experiment of proving the advantages of extended polymorphism learning is not completed. However, in Table I a comparison of the results for the academic year 2021-2022 is given of the start tests (in the beginning of the course) and the tests conducted immediately after the completion of the section devoted to polymorphism. The experimental group includes the students of the Software Engineering majors, for whom “Programming in C++” is an elective course in the 4th semester (12 people) and the Computer Science major, for whom the course is mandatory, but in the 2nd semester (35 people).

TABLE I. TEST RESULTS

Grade	Bachelor Program					
	SE		CS		Informatics	
	Start level	End level	Start level	End level	Start level	End level
A	25.0%	25.0%	14.3%	20.0%	9.1%	9.1%
B	16.7%	33.3%	22.9%	25.7%	27.3%	27.3%
C	33.3%	25.0%	28.6%	25.7%	18.2%	27.3%
D	16.7%	8.3%	22.9%	22.9%	36.4%	27.3%
F	8.3%	8.3%	11.4%	5.7%	9.1%	9.1%

In order not to distort the results, only data from face-to-face training is used – after the symbolic end of the pandemic. The control group consists of the students of the Informatics major (11 people), who in the 2nd semester are studying a mandatory course OOP in C++. The fact that the experimental

group is heterogeneous is taken into account – for one major, the course is CS1, and for the other, CS2, but with an introductory C# course. Therefore, the first test is slightly different for the Software Engineering major. Language dependent questions are minimized as much as possible. The questions and tasks of the second test are the same for all and entirely related to the correct use of pointers, dynamic memory, and implementation of polymorphism, without specifying in what way.

Another circumstance that prevents accurate interpretation of the data is the small number of students in the control group. The Informatics major is currently the least desired of the three, and it has students ranked second and third preference, which is a demotivating factor.

Nevertheless, both the results of the control tests (Table I) and the direct observations of the students' activity in lectures, laboratory work, project work and homework, indicate that it makes sense to pay more attention to polymorphism in the OOP course. The experimental training conducted helps students to discover the exact relations between objects in the subject area more easily and correctly choose the operations that need to be implemented polymorphically. They are more adept at handling pointers and have a better understanding of the memory model. They recognize the situations in which they need to implement move semantics. They have no problem using lambda expressions in STL algorithms instead of function objects.

At the end of the course, a survey is conducted to determine students' satisfaction with the experiential learning and to specify what they found difficult. The answers are of interest. The question asked to the Software Engineering students was “Why did you choose C++?” (open question). 1/3 of them made such a choice, and 2/3 preferred PHP. Among the answers, it stands out that they read that it is suitable for Video game development, Embedded systems, Compilers and Enterprise software. The syntax of the methods implementing copy and move semantics – copy and move constructors and copy and move assignment operators – is indicated as the most difficult. Students find it difficult to navigate what is what just by the type of parameters. In second place are variable templates, and in third place – the many details of defining lambda expressions. When asked if what they learned about alternative ways of implementing polymorphism was useful, 73% answered yes.

IV. CONCLUSION

In this paper, the need for a more in-depth study of dynamic polymorphism is discussed. Problems associated with its implementation through inheritance and virtual functions are analyzed and a method of training is presented through a step-by-step project development with an alternative to inheritance design based on manual implementation of the functionality achieved with virtual tables. Specific guidelines for organizing training involving this topic are suggested.

As a recommendation to lecturers, it is useful to pay attention to the concept of polymorphism already in the introductory course. Although it is not dynamic there, it is good for students to recognize it early.

REFERENCES

Regarding this implementation of polymorphism with type erasure, the most serious drawback is considered to be that, with the means currently available, it requires writing too much code – a code of high complexity. This is demotivating. Implementation with inheritance is much shorter and straight forward, even more so for students who have studied C#, where alternatives can easily be implemented – implementing interfaces can make it much easier to avoid inheritance. Such an implementation, of course, also has its drawbacks. However, if the proposals made to The C++ Standards Committee to introduce scalable reflection [8] and metaclasses [9] are implemented in the future, the code will be much shorter and clearer, because much of it will be automatically generated and will remain hidden from the client.

In studying the problem, it was found that not many researchers emphasize the weaknesses of inheritance as a tool to achieve polymorphism, and therefore there are not many proposals to overcome these weaknesses. The details in this area are mostly discussed at technical conferences rather than in scientific publications. This, on one hand, limited the possibilities of the research, and on the other, motivated the authors to tackle this problem.

Future work includes monitoring of the development of the language in this direction, although there has been some stagnation in the last 1-2 years. Also, in the future, it is planned to expand the experiment with formal statistical processing of accumulated empirical data.

- [1] Milojković, N., Caracciolo, A., Lungu, M. F., Nierstrasz, O., Röthlisberger, D., Robbes, R., Polymorphism in the spotlight: studying its prevalence in Java and Smalltalk, ICPC '15: Proceedings of the 2015 IEEE 23rd International Conference on Program Comprehension, May 2015, pp. 186–195.
- [2] Cardelli, L., Wegner, P., On understanding types, data abstraction, and polymorphism, ACM Computing Surveys, Volume 17, Issue 4 (December 1985), pp. 471-523.
- [3] Stroustrup, Bj., 2012, Bjarne Stroustrup's C++ glossary, accessed 27 July 2022, <https://www.stroustrup.com/glossary.html#Gpolymorphism>.
- [4] Brand, S., Dynamic polymorphism with metaclasses and code injection, talk at CppCon 2020, September 13-18, online, accessed 29 July 2022, https://www.youtube.com/watch?v=8c6BAQcYF_E.
- [5] Tan, J., Guo, X., Zheng, W., Zhong, Ming., Case-based teaching using the Laboratory Animal System for learning C/C++ programming, Computers & Education, Volume 77, 2014, pp 39-49.
- [6] Liberman, N., Beeri, C., & Kolikant, Y. B. D. (2011). Difficulties in learning inheritance and polymorphism. ACM Transactions on Computing Education, 11(1), pp 1–23, doi:10.1145/1921607.1921611.
- [7] Milne, I., Rowe, G., Difficulties in learning and teaching programming – Views of Students and Tutors. Education and Information Technologies 7, pp. 55–66 (2002). <https://doi.org/10.1023/A:1015362608943>.
- [8] Childers, W., Sutton, A., Vali, F., Vandevoorde, D. (2019), Scalable Reflection in C++, ISO/IEC C++ Standards Committee Papers, JTC1/SC22/WG21, Papers 2019, document P1240R1, mailing2019-10, www.open-std.org/JTC1/SC22/WG21/docs/papers/2019/p1240r1.pdf.
- [9] Sutter, H. (2019), Metaclass functions: Generative C++, ISO/IEC C++ Standards Committee Papers, JTC1/SC22/WG21 - Papers 2019, mailing2019-06, document P0707R4/2019-06-17, <https://www.open-std.org/JTC1/SC22/WG21/docs/papers/2019/p0707r4.pdf>.

Application of Training Load Prediction Model based on Improved BP Neural Network in Sports Training of Athletes

Lin Liu¹

Department of Physical Education
Guilin Medical University, Guilin, 541004, China

Guannan Sheng^{2*}

Faculty of Basic Medical Sciences
Guilin Medical University, Guilin, 541004, China

Abstract—With the enhancement of data mining technology, competitive sports informatization has become an inevitable development trend. It has become a common phenomenon to use data mining technology to help athletes train scientifically, assist coaches in rational decision-making, and improve team competitiveness. In competitive sports, cyclists' adaptation to training has a complex relationship with their physical performance. In order to explore the correlation between data and provide better training data for athletes, this study proposes a load prediction model based on BP neural network (Back propagation, BP). Considering the local convergence and random assignment of traditional BP model, an adaptive genetic algorithm with improved selection operator is used to determine the initial weights and thresholds of BP neural network to improve the accuracy of the prediction model. The experimental results show that the improved adaptive genetic algorithm improves the overall optimization ability of the BP neural network, the improved BP neural network model has good stability in the convergence process, and the algorithm can search for better weight thresholds. Compared with the basic BP neural network prediction model, the accuracy of the optimized prediction model is increased by 11.86%, and the average error value is reduced by 26.21%, which is a guide to improve the training effect of the cycling team's competitive sports.

Keywords—BP neural network; adaptive genetic algorithm; selection operator; training load

I. INTRODUCTION

In competitive sports, effective and scientific training is an important means to improve the performance of athletes. Athletes dedicate most of their professional training to improving fitness, competitiveness and self-confidence [1]. In particular, the physical fitness testing and evaluation of professional athletes, as well as the analysis of physiological and biochemical indicators, are of great significance for understanding the athlete's endurance, current physical fitness, and the scientificity and effectiveness of training interventions [2]. However, the traditional physical fitness index evaluation of athletes is mainly based on manual evaluation, and the accuracy is poor. Data mining is an interdisciplinary technique that can be used to analyze data and gain insights into specific problems [3]. Applying data mining technology to cycling, by analyzing the correlation between a series of physiological and biochemical indicators of cyclists, athletic ability indicators and athletes' training load levels, a cyclist training load prediction

model is established, which not only helps coaches and athletes evaluate them in advance training readiness, while also assisting in training analysis and decision-making [4]. This study uses the information collected by the International Cycling Federation to develop a training load prediction model based on BP neural network. Since the BP neural network is nonlinear and easily trapped in local minima, this study uses an optimized adaptive genetic algorithm to determine the optimal initial weights and thresholds of the BP neural network to solve the problems associated with randomly assigning values [5]. Therefore, it is expected that the rationality of the training plan will be evaluated in advance to prevent adverse consequences for athletes due to unreasonable training plans. The research content can better ensure the safety and effect of athletes' training, and promote the progress of sports evaluation methods.

II. RELATED WORKS

Artificial Neural Network is an intelligent method for processing nonlinear relational data [6]. Due to its good adaptability, good nonlinear mapping and robustness, it is widely used in image processing, image recognition and other fields [7]. The BP network algorithm is simple, easy to implement, small in computation and good in parallelism. It is one of the most widely used and mature neural network algorithms. Because the fastest descending backpropagation method in the BP neural network is to correct the weights based on the negative gradient of the error function, it leads to problems such as low learning efficiency, slow convergence, and easy to fall into local miniaturization. [8]. Scholars at home and abroad have carried out the following researches on the shortcomings of BP neural network; Wu Jie and others. A BP network based on the improved particle swarm optimization algorithm is proposed. By adjusting the adaptability of the learning factor, the convergence speed of the BP neural network and the performance of the global optimal solution are improved. The simulation results show that the improved particle algorithm is better than the standard BP algorithm and particle swarm algorithm [9]. In order to improve the classification accuracy of ECG signals, Wang Li et al. the BP neural network is optimized using an additional momentum adaptive learning rate adjustment algorithm. The simulation results show that the improved BP neural network has better classification and recognition ability, and the accuracy rate of the whole sample classification is 98.4%. The optimization

algorithm has fast convergence speed and high classification accuracy, which is helpful for the detection and diagnosis of heart disease [10]. Zhang D's team proposed that increasing the number of sample locations for training the BP network can improve the accuracy, and as the number of sample locations increases, the rate at which the fitting error decreases will decrease. The simulation results show that increasing the number of sample locations for training the BP neural network can improve the accuracy, and the fitting error decline rate decreases with the increase of the number of sample locations [11]. According to Cy A et al. the problem that BP neural network is easy to fall into the local minimum is solved. The empirical results show that the improved genetic algorithm is better than the traditional genetic algorithm in terms of convergence speed and prediction accuracy [12].

The BP network has in-depth applications in many complex scenarios, and its application in athletes' training provides an important reference for the improvement of athletes' physical and mental fitness. Chen W et al. found that clothing fatigue will affect the effect of sports. At present, there is little research on sports clothing. Therefore, based on the theory of BP and surface electromyography, they predicted the fatigue of athletes and built a prediction model. Finally, the experiment found that the model can provide technical support for athletes' training and development [13]. Zhang Y. et al found that with the arrival of information technology, sports data is becoming more and more important. How to collect human motion data is the key, so based on neural network and density peak clustering algorithm, a motion data model is constructed. After experimental verification, compared with the traditional principal component dimensionality reduction method, the proposed scheme can obtain better feature data, and the effect is better [1, 4]. Li T et al. found that the intelligent sports management system is beneficial to improve the overall training effect of the players, so they built a sports posture recognition model based on BP, and analyzed the motion feature extraction and experimental results. The final experimental results show that this scheme has better performance than other sports management algorithms, providing important data reference for the development of athletes [15].

Based on the above literature research, BP network is competent in many complex environments, and scientific and

effective sports training is the key to ensure the level of sports competition. BP network has outstanding advantages in the field of diagnosis and prediction. Applying it to the field of sports training will provide significant help for effective sports training and promote the development of information technology in the field of sports.

III. CONSTRUCTION OF TRAINING LOAD PREDICTION MODEL BASED ON IMPROVED BP NEURAL NETWORK

A. Design of Training Load Prediction Model based on BP Neural Network

Training is an important daily activity for athletes. Appropriate training can improve their competitive performance, but too much training can lead to injuries, and too little training will not achieve the desired training effect [16]. In this study, a BP network was used to design a training load prediction model for cyclists, which was optimized by an improved adaptive genetic algorithm to evaluate whether the athlete's training plan was reasonable. In cycling training load prediction, the cyclist's load level should be predicted from the athlete's basic physiological and biochemical data, exercise level goals, and exercise content to determine whether the currently planned training load is appropriate. The research required analyzing and processing the data and selecting relevant metrics before building a model to predict the training load of cyclists. The filtered data is divided into a training set and a test set, and the test set data is used to test the accuracy and performance of the full training model in predicting the training load of athletes. For athlete training load prediction, the study selected 25 factors that have an impact on training load based on the recommendations of professional cycling coaches, as shown in Fig. 1.

Exponential differences between the filtered parts of the data, they must be normalized before feeding them into the BP neural network. The core of normalization is to project all data to the same interval after the algorithm has run. The formula for the Min-max normalization process is shown in Equation (1).

$$X = \frac{x_i - x_{\min}}{x_{\max} - x_{\min}} \tag{1}$$




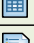




	Height	Weight	Age	Gender		
	Body mass index					
	Functional threshold power					
	Maximum oxygen uptake					
	Average step frequency		Maximum step frequency			
	Average power		Maximum power			
	Leukocyte count	Hemoglobin	Platelet	Red blood cell count	Urea nitrogen	Urine pH
	Creatine kinase	Testosterone	Blood oxygen saturation	Urinary protein	Urobilinogen	Urobilin
	Training items		Training volume			

Fig. 1. Factors Affecting Athletes' Training Load.

In Equation (1), x_i denote the current value of these data, x_{\max} and x_{\min} denote the maximum and minimum values of these data, respectively, which are uniformly distributed in a certain interval after normalization. The number of input and output layers is fixed at one layer, while the hidden layer can have multiple layers. The number of neurons in the input layer is determined by the dimension of the input signal, and the number of neurons in the output layer is defined by the problem to be solved. Function. Through the iterative alternation of these two processes, the connection weights and thresholds of the BP neural network are continuously optimized. Suppose there are m training samples X , x_1, x_2, \dots, x_m , the expected output is t_1, t_2, \dots, t_m , the actual output is y_1, y_2, \dots , There are y_m neurons in the hidden layer. After the activation function is transformed, the expression of the output of the i th neuron in the hidden layer is shown in formula (2).

$$a_i = f(\text{net}_i) = f\left(\sum_{g=1}^n w_{ig} x_g - \theta_i\right) \quad (2)$$

In formula (2), f represents the activation function, represents the neuron in the output layer, represents g the weight factor g from neuron w_{ig} to neuron i , and represents θ_i the threshold of the neuron. The output of neurons in the output layer is shown in formula (3).

$$y_g = f\left(\sum_{r=1}^m a_r w'_{gr} - \theta'_r\right) \quad (3)$$

In formula (3), w'_{gr} is the connection weight between the hidden layer and the output layer, which θ'_r represents the threshold of the neurons in the hidden layer. Let $\text{net}'_g = \sum_{r=1}^m a_r w'_{gr} - \theta'_r$, convert equation (3) to equation (4).

$$y_g = f(\text{net}'_g) \quad (4)$$

The error function is shown in equation (5).

$$E(w, \theta) = \frac{1}{2} \sum_{g=1}^m (t_g - y_g)^2 \quad (5)$$

Equation (6) can be derived from equations (3) and (5).

$$E = \frac{1}{2} \sum_{g=1}^m (t_g - y_g)^2 = \frac{1}{2} \sum_{g=1}^m \left(t_g - f\left(\sum_{r=1}^m a_r w'_{gr} - \theta'_r\right)\right)^2 \quad (6)$$

The output layer is shown in equation (7).

$$\frac{\partial E}{\partial \text{net}'_g} = \frac{\partial E}{\partial y_g} \cdot \frac{\partial y_g}{\partial \text{net}'_g} = \frac{\partial E}{\partial y_g} \cdot f'(\text{net}'_g) \quad (7)$$

The implicit layer is shown in Equation (8).

$$\frac{\partial E}{\partial \text{net}_i} = \frac{\partial E}{\partial a_i} \cdot \frac{\partial a_i}{\partial \text{net}_i} = \frac{\partial E}{\partial a_i} \cdot f'(\text{net}_i) \quad (8)$$

If the error between the desired output and the neural network is too large, gradient descent is used to correct the weights of the layers of the network. The adjustment amount of the weight between the hidden layer and the output layer is $\Delta w'_{gr}$ shown in formula (9).

$$\Delta w'_{gr} = -\eta \frac{\partial E}{\partial w'_{gr}} = -\eta \frac{\partial E}{\partial \text{net}'_g} \cdot \frac{\partial \text{net}'_g}{\partial w'_{gr}} = \eta (t_g - y_g) \cdot f'(\text{net}'_g) \cdot a_r \quad (9)$$

The amount of weight adjustment from the input layer to the hidden layer is Δw_{ig} shown in formula (10).

$$\Delta w_{ig} = -\eta \frac{\partial E}{\partial w_{ig}} = \eta \sum_{g=1}^m (t_g - y_g) f'(\text{net}'_g) w'_{ig} f'(\text{net}_i) x_j \quad (10)$$

Since both the activation functions of the input layer and the output layer use this function, the Sigmoid sum Δw_{ig} transformation is shown in equation (11).

$$\begin{cases} \Delta w_{ij} = \eta \left(\sum_{g=1}^m (t_g - y_g) y_g (1 - y_g) w'_{ig}\right) a_i (1 - a_i) x_j \\ \Delta w'_{gr} = \eta (t_g - y_g) y_g (1 - y_g) a_r \end{cases} \quad (11)$$

In order to build a model for predicting the training load of athletes, it is first necessary to define the structure and covariates of the BP neural network, that is, the number of layers of the BP neural network, the number of neurons, the data set processed, and the selection of initial weights and thresholds.

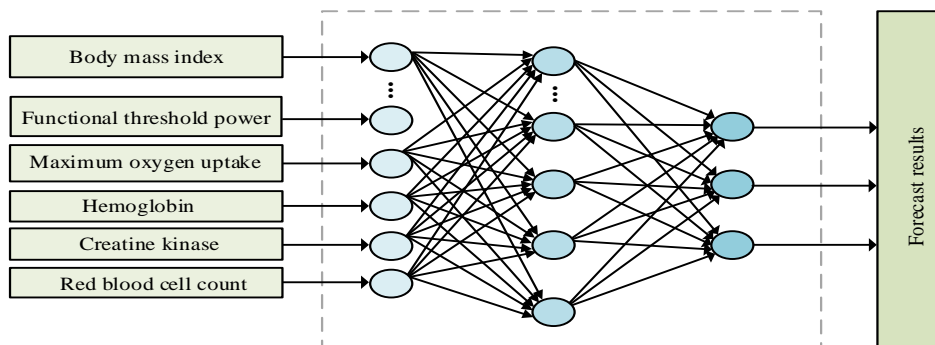


Fig. 2. The Topology of the Network Structure of the Training Load Prediction Model.

In Fig. 2, it can be seen that the structure of the BP neural network consists of an input layer, a hidden layer and an output layer, and the hidden layer can be composed of one or more layers. Since the three-layer BP neural network can approximate any continuous function in the closed interval, the basic three-layer hidden layer is selected as the basis for constructing the network prediction model. In the input layer, the input variables should not be highly correlated, and the input variables should significantly interfere with the output results.

Based on the above analysis of training load intervention factors, a total of 25 related factors were considered as input variables for the study, so the number of neurons in the input layer was set to 25. The prediction purpose of the model is to express the training load level of athletes through the training load results, which can be divided into too little training volume, moderate training volume and too much training volume. Therefore, the number of neurons in the output layer is determined to be three. The number of neurons in the hidden layer can be calculated according to formula (12), and then the optimal number of neurons in the hidden layer is determined by the trial and error method.

$$\begin{cases} n = \sqrt{ml} \\ n = \log_2 m \\ n = \sqrt{m+l} + a \end{cases} \quad (12)$$

In formula (12), n , l and m represent the number of neurons in the hidden layer, the output layer and the input layer, respectively, which a is a constant and its value is in the interval (1,10). Since $l = 3$, $m = 25$, the number of neurons in the hidden layer is in the range of [5, 15] above. Based on this, heuristics are applied to determine the number of neurons in the hidden layer. The number of neurons in the hidden layer is preset to five, and one neuron is added for each experiment. The prediction performance and convergence of the hidden layer with different numbers of neurons are compared in each experiment. The optimal number of neurons in the hidden layer is the final. The trial was determined to be 10.

B. Introducing an Improved Adaptive Genetic Algorithm to Optimize the BP Neural Network

Adaptive genetic algorithm is an improved genetic algorithm, which is characterized by automatically changing the probability of crossover and mutation based on chromosome fitness, reducing the possibility of crossover and mutation of individuals with high fitness, and improving the probability of crossover and mutation of somatic individuals, thereby increasing population diversity and retaining high-value chromosomes [17]. Since BP neural network is nonlinear, model convergence, occurrence of local minima and training time are closely related to the choice of initial weights and thresholds [18]. Initial weights and thresholds are usually randomly generated, and if not chosen properly, the network may not converge or may be constrained by local minima [19]. In order to better solve the random assignment problem of BP neural network, an improved adaptive genetic algorithm is used

to find the optimal initial value and threshold of the network. Real encoding not only eliminates the need for decoding, but also facilitates the computation of genetic operations. Assuming a topological neuron network of 3-2-1, the number of weights and thresholds of the network used in the study is 293. In this neural network, the connection weights between the input and hidden layer neurons are $W_{11}^1, W_{12}^1, W_{21}^1, W_{22}^1, W_{31}^1, \dots$ and W_{32}^1 the connection weights between the hidden layer and output layer neurons are W_{11}^2, W_{21}^2 , between the hidden layer and output layer neurons The thresholds are $\theta_1, \theta_2, \theta_3$. Both connection weights and thresholds are real numbers in the range 0 to 1. By ordering these weights and thresholds in order, $W_{11}^1 W_{12}^1 W_{21}^1 W_{22}^1 W_{31}^1 W_{32}^1 W_{11}^2 W_{21}^2 \theta_1 \theta_2 \theta_3$ real numbers can be encoded, and the resulting real numbers are chromosomes [20]. The BP neural network adjusts the weights and thresholds of the connections with the aim of minimizing the prediction error of the athlete's training load. The adaptive genetic algorithm applied in the study aims to find a set of weights and thresholds that minimize the prediction error, so the fitting function is negatively correlated with the sum of squares of the network output error, that is, the smaller the error, the greater the fit. The calculation of individual fitness is shown in Equation (13).

$$F(x) = \frac{1}{E(x)+1} \quad (13)$$

In formula (13), x represents the current chromosome, which $E(x)$ is the sum of the squared errors of the network output generated by the BP neural network using the current weight-threshold combination represented by the chromosome. For population selection, the roulette method is widely used due to its simplicity and convenience. However, roulette is used to randomly select individuals based on their fitness relative to the ensemble, which may result in individuals with high fitness being ignored. Although the main purpose of the optimization strategy is to select the best individuals from the population, only starting from the best individuals and discarding the individuals with universal fitness will eventually lead to the problem of homogeneous population structure, which is prone to local convergence phenomenon. This study improves the selection operator by introducing an optimal conservation strategy based on a sorted list selection method. The population is first initialized by sorting the individuals in the population from the lowest fitness to the highest fitness and equally dividing the sorted individuals into four parts, as shown in Fig. 3, steps 1-3 for improving the selection operator.

As can be seen from Fig. 3, each segment was selected at a ratio of 0.4, 0.6, 0.8 and 1, resulting in individual numbers of $0.4*5=2$, $0.6*5=3$, $0.8*5=4$ and $1*5=5$. Since six individuals were lost during the selection process, starting from paragraph four, one additional individual was randomly selected at a time, resulting in a final number of six individuals. Insert the selected individual to the end of the individual selected in step 5 to form a new population, steps 4-7 are shown in Fig. 4.

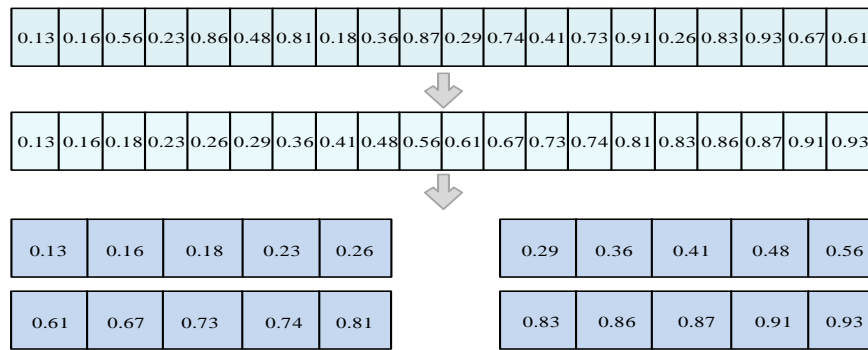


Fig. 3. Introduce the Best Preservation Strategy based on the Sorting List Selection Method to Improve the Selection Operator.

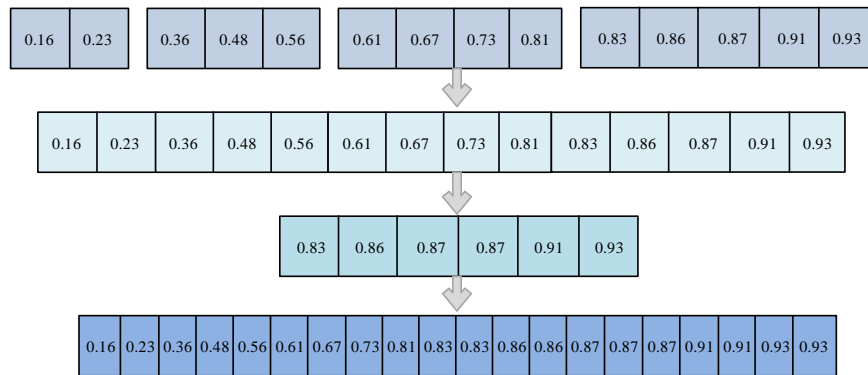


Fig. 4. Introduce the Best Preservation Strategy based on the Sorting List Selection Method to Improve the Selection Operator.

The improved selection operator ensures population diversity by retaining the best individuals and selecting others according to their size. It is also easy to operate because only the fitness is calculated and the best individuals are selected by basic operations like sorting, grouping and insertion. In contrast, the roulette method is computationally intensive because it requires first calculating the fitness of individuals, then calculating the proportion of individual fitness, and then solving for the selection probability. Therefore, improving the selection operator can theoretically improve the selection and convergence ability of the network. New individuals are generated by performing adaptive genetic algorithm operations on crossover and mutation between populations. In order to construct individuals with higher fitness, in the process of crossover mutation operation, the individuals to be processed are selected according to the crossover mutation rate. The crossover rate is ρ_c shown in Equation (14).

$$\rho_c = \begin{cases} \rho_a - \frac{(\rho_a - \rho_b)(f - f_{avg})}{f_{max} - f_{avg}}, & f \geq f_{avg} \\ \rho_a, & f < f_{avg} \end{cases} \quad (14)$$

In equation (14), $\rho_a = 0.9$, $\rho_b = 0.6$. f represents the current individual fitness, f_{max} is the maximum fitness of all individuals in the population, and is f_{avg} the average fitness of

all individuals in the population. The rate of change is ρ_m shown in equation (15).

$$\rho_m = \begin{cases} \rho_i - \frac{(\rho_i - \rho_j)(f_{max} - f)}{f_{max} - f_{avg}}, & f \geq f_{avg} \\ \rho_i, & f < f_{avg} \end{cases} \quad (15)$$

In equation (15), $\rho_i = 0.1$, $\rho_j = 0.001$. IAGABP is an optimized BP neural network algorithm based on an improved adaptive genetic algorithm. It is divided into a genetic algorithm part and a BP neural network part. The specific flowchart of the algorithm is shown in Fig. 5.

As shown in Fig. 5, in the genetic algorithm part, N chromosomes are randomly generated through real-value coding to form the initial population of the algorithm, and the fitness of the entire population is improved through continuous genetic operations until the algorithm terminates in the population after several generations. After the evolution in the BP neural network, the network structure and other parameters are solved first, and the optimal individual in the genetic algorithm is decomposed into a series of initial values and thresholds of the BP neural network. Finally, the network is weighted and thresholded using error backpropagation until the initial error of the network reaches the final state, which constitutes the final model of the BP neural network.

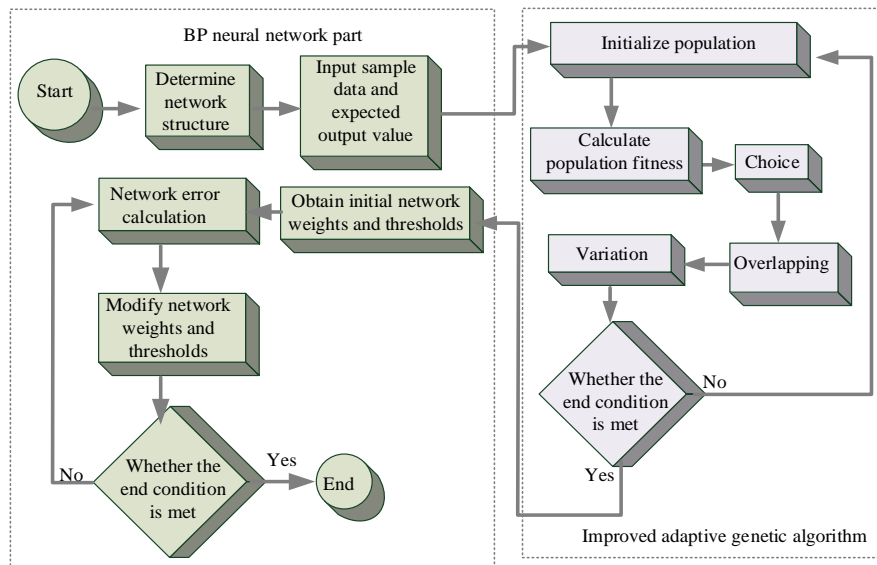


Fig. 5. BP Neural Network based on Improved Adaptive Genetic Algorithm.

IV. FOUR PREDICTION PERFORMANCE TEST OF BP NEURAL NETWORK MODEL BASED ON IMPROVED ADAPTIVE GENETIC ALGORITHM

An improved adaptive genetic algorithm was applied to a BP (Improved Adaptive Genetic Algorithm Back Propagation, IAGABP) neural network to create a predictive model of cyclist training load. The performance of the proposed optimization model is compared with the traditional BP neural network model and the traditional neural network model based on Adaptive Genetic Algorithm Back Propagation (AGABP). The topology of the BP neural network is set to 25-10-3, the target accuracy is 0.001, the maximum number of iterations is 1000, and the learning rate is 0.1. The initial population size of the genetic algorithm is 40, the maximum evolutionary generation is 25, and the prediction results are divided into overtraining, medium training and undertraining. The 5000 pieces of exercise training data recorded are selected as the training sample set, and the other 1985 pieces of training data are used as test samples. The comparison of the error accuracy between the BP neural network model and the IAGABP model is shown in Fig. 6(a), and the comparison of the fitness between the AGABP and IAGABP models is shown in Fig. 6(b).

From Fig. 6(a), it can be seen that the IAGABP model achieves the target accuracy of 0.001 after about 480 iterations, while the BP network model achieves this target accuracy after about 1000 iterations. The IAGABP model exhibits significant advantages and stability in the convergence process. This is because the improved genetic algorithm can obtain better initial weights and thresholds, thereby reducing the time spent by the BP neural network in the process of finding the optimal solution. It can be seen from Figure 6(b) that the fitness of the AGABP model is still unstable after 15 generations of evolution, while the fitness curve of the IAGABP model is gradually stable after 14 generations. The optimal chromosome fitness of the IAGABP model is compared with that of AGABP, improved by 0.24. The results show that the group search performance of the adaptive genetic algorithm can be improved

by improving the selection operator to obtain a better weight threshold.

In deep learning, the loss function curves of the three models trained on the dataset are shown in Fig. 7. The loss function of the AGABP model drops at the fastest speed, and after 20K training steps, its loss function drops rapidly to within 100. The curves of the AGABP model and the IAGABP model are basically the same, and the loss function fluctuates smoothly after 100K steps and remains in the range of 80-100. The loss function of the BP model decreases more slowly, within 120 after 60K steps, and the function value fluctuates between 100 and 110. To sum up, the curve of the IAGABP model is smooth and has good stability and accuracy. The precision-recall curves of the three models are shown in Fig. 8.

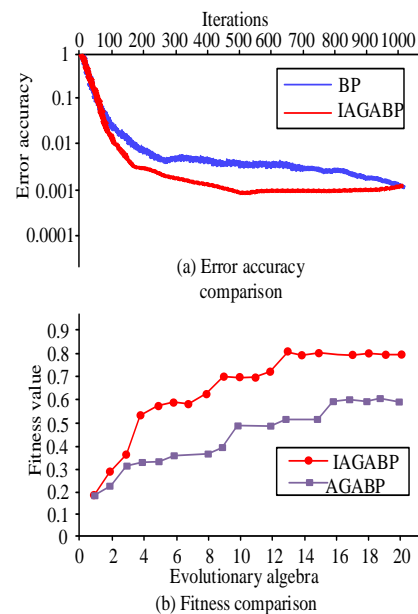


Fig. 6. Performance Test Comparison of Different Models.

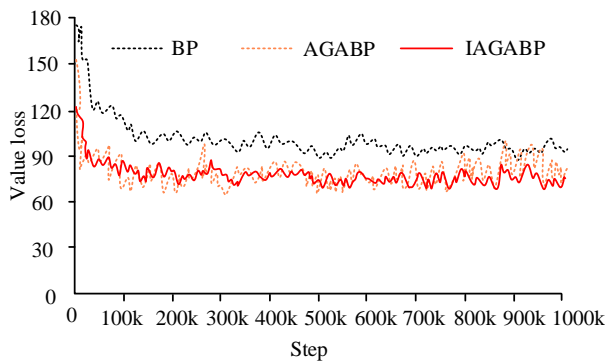


Fig. 7. Loss Functions for Different Models.

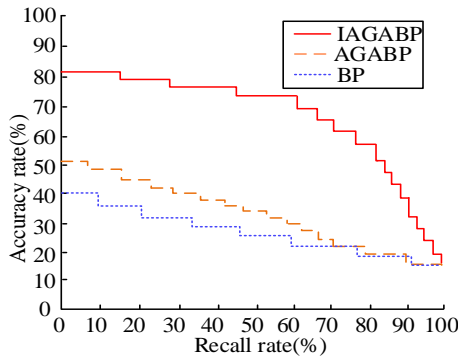


Fig. 8. Precision-Recall Curves for Different Models.

The precision-recall curve can be used to reflect the performance of the model on the task of retrieving similarity. It can be seen from Fig. 8 that the accuracy of the model decreases as the recall rate increases, in which the model IAGABP decreases at the slowest speed in the recall rate interval of 0-70%, and as can be seen from the figure, in this region the precision-recall curve of the model IAGABP is significantly larger than the other two models. This shows that the model IAGABP has the highest accuracy on the similarity search task on the same dataset. The prediction results of the three models based on 2486 test samples are shown in Fig. 9.

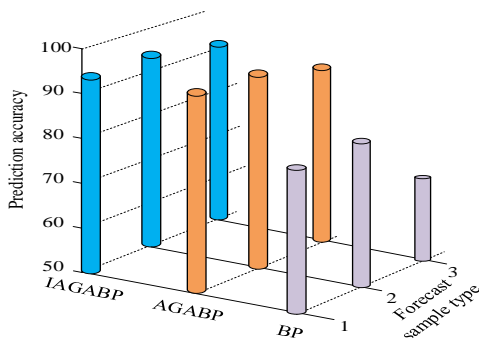


Fig. 9. Prediction Results of the Three Models.

The first type of prediction samples is the accuracy of a small number of trained test samples, the second is the accuracy of a moderately trained test sample, and the third is the accuracy of a large number of trained test samples. From the results in Fig. 9, it can be seen that the AGABP model improves the prediction accuracy by 9.55% compared with the BP neural network model. On the other hand, the IAGABP model with the

improved selection operator is 2.31% more accurate than the AGABP model. This shows that the BP neural network optimized by the improved genetic algorithm is superior to the traditional BP neural network in terms of prediction accuracy and performance, and meets the requirements of athletes' training load prediction.

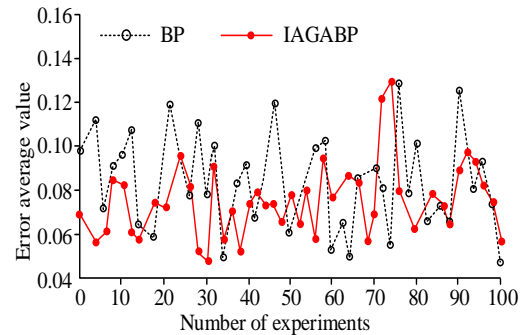


Fig. 10. Average Experimental Error.

In terms of fitting effect and prediction accuracy, the BP neural network based on the improved adaptive genetic algorithm has greatly improved the prediction accuracy. To further evaluate the predictive validity of the model proposed in the study, the study derives the average error of the model using 100 iterations, as shown in Fig. 10. It can be seen that the average error of IAGABP prediction is lower than that of BP neural network which is 0.0867, while the average error of BP neural network is 0.1175.

A comprehensive comparison of the above results shows that the improved IAGABP model has obvious improvements in error accuracy, model accuracy and prediction accuracy compared with the traditional BP model and the AGABP model. Compared with the traditional artificial exercise load index evaluation scheme, its innovation lies in that the IAGABP model is based on more advanced intelligent neural network technology, and performs secondary optimization on the basis of the traditional BP model, avoiding the local convergence of traditional BP and exercise monitoring data. The IAGABP model can realize real-time and effective detection of the physical and mental state data of athletes. At the same time, the relevant monitoring data will be analyzed and diagnosed through the network big data technology to provide athletes with more scientific physical training skills and opinions, avoid physical injuries to athletes, and improve the effect of sports training.

V. CONCLUSION

With the development of big data, many sports are using data mining technology to determine the relationship between athletes' training load and physical fitness, which provides new opportunities for the development of national cycling events. Competitive sports informatization has become an inevitable development trend. Since many factors intervening in the relationship between athletes' training load and physical fitness show nonlinear relationship, this study designed a training load prediction model based on BP neural network as the basic algorithm. In order to further improve the accuracy and convergence of the BP network prediction model, this study

uses the adaptive genetic algorithm to optimize the initial value and threshold of the BP network, and improves the selection operator of the adaptive genetic algorithm. The results show that the BP neural network model based on the improved adaptive genetic algorithm has significant advantages and stability in the convergence process, and the algorithm can search for better weight thresholds. The accuracy rate of athletes' training load prediction is 95.76 %, the average error is 0.0867, which is 11.86% better than the standard BP neural network model, and the average error is 26.21% lower. This meets the requirements of athletes' training load prediction. This study can establish a scientific and reasonable bicycle training load prediction model based on the actual physical condition of non-professional groups, and provide an important reference for scientific sports training. However, there are also shortcomings in the research. Only the indicators of exercise routine training are considered, and the training environment, such as temperature and altitude, is not considered.

REFERENCE

- [1] W. Zhu, H. Wang, X. Zhang, "A collaborative evaluation model for container multimodal transport based on BP neural network", *Neural Computing and Applications*, Vol. 33(2), pp. 1-9, 2021.
- [2] Z. Shen, "Performance analysis of bentonite-pva fiber cement based composites for construction based on BP neural network", *Key Engineering Materials*, vol. 852, pp. 209-219, 2020.
- [3] B. Muñoz-Pardos, S. Sutehall, J. Gellaerts, et al. "Integrating Wearable Sensors into Evaluation of Running Economy and Foot Mechanics in Elite Runners," *Current Sports Medicine Reports*, vol. 17(12):480-488, 2018.
- [4] P. Halén, KM Khan, "Finnish Sports Physiotherapy Conference - Athlete Training and Loading: Helsinki, 7-8 June 2019," *British Journal of Sports Medicine*, vol. 53(3), pp. 137-138, 2019.
- [5] years . Mackendorf , C. M. _ _ Schmid , C.B. Brunckhorst , " CME ECC 65: The Electrocardiogram of Athletes, " *Practice*, Vol. 109(4):253-258. 2020 .
- [6] H. Liu, J. Liu, Y. Wang, et al. "Bridge bellows grouting compaction identification based on BP neural network", *Structure*, Vol. 32(5), pp. 817-826, 2021.
- [7] Q. Lu, R. Yang, M., Zhong, et al. "An Improved Method for Rotating Machinery Fault Diagnosis Using Sensitive Features and rls-BP Neural Networks", *IEEE Transactions on Instrumentation and Measurement*, vol. 69(4), pp. 1585-1593, 2020.
- [8] P. Geng, J. Wang, X. Xu, et al. "Prediction of SOC of power lithium battery based on BP neural network theory based on keras", *International Journal of Core Engineering*, vol. 6(1), pp. 171-181, 2020.
- [9] J. Wu, YM Cheng, C. Liu, et al. "A Modified PSO-Based BP Neural Network for Improving the Current Efficiency of Electrolytic Copper," *Journal of Electrical Engineering and Technology*, vol. 16(3), pp. 1297-1304, 2021.
- [10] Plum. Wang, X. Guo, Y. Hui, "Classification of ECG Signals Based on Improved BP Neural Network", *Electronic Technology Applications*, vol. 45(6), pp. 108-112, 2019.
- [11] D. Zhang, G. Zhang, L. Li, "Calibration of a six-axis parallel manipulator based on BP neural network", *Industrial Robots*, vol. 46(5), pp. 692-698, 2019.
- [12] A. Cy, B. MI, LC Wei, et al. "Improved Adaptive Genetic Algorithm for Vehicle Insurance Fraud Recognition Model Based on BP Neural Network ScienceDirect", *Theoretical Computer Science*, vol. 817, pp. 12-23, 2020.
- [13] Chen W, Li X, Chen X, et al. Research on influence mechanism of running clothing fatigue based on BP neural network. *Journal of Intelligent & Fuzzy Systems*, 2021, 40(4): 7577-7587.
- [14] Zhang Y, Hou X, Xu S. Neural network in sports cluster analysis. *Neural Computing and Applications*, 2022, 34(5): 3301-3309.
- [15] Li T, Sun J, Wang L. An intelligent optimization method of motion management system based on BP neural network[J]. *Neural Computing and Applications*, 2021, 33(2): 707-722.
- [16] Zhang S. Effect of Biological Image Analysis Method Based on Back Propagation Neural Network on Vision Change in Sports Fatigue *Journal of Medical Imaging and Health Informatics*, 2021, 11(4): 1221-1227.
- [17] J. Wallace , E. _ Bedler , T. Covassin , " Assessment and Management of Teaching Trends in Sports-Related Concussions in Athletic Training Programs, " *Journal of Athletic Training Education*, vol. 13(2) , pp. 112-119 , 2018.
- [18] D. Tomchuk, B.E. Anderson, "The Professional Education of Athletic Training Requires Biological Tension," *Journal of Athletic Training Education*, Vol. 16(2), pp. 150-158, 2021.
- [19] K. Sniffen, "Integrating Interprofessional Activities with Physical Therapy and Athletic Training Students in a Shared Professional Curriculum," *International Journal of Health Science Education*, vol. 6(1), pp. 4-4, 2019.
- [20] DH Grove, J. Mansell, "Cultural Competence: Where Are We as Athletic Training Educators?" *Journal of Athletic Training Education*, vol. 15(1), pp. 49-54, 2020.

Analyzing Multi-stage Reverse Osmosis Desalination Using Artificial Intelligence

Batiseba Tekle¹, Azmi Alazzam², Abdulwehab Ibrahim³, Ghassan Malkawi⁴

Abdulaziz Fares NajiMoqbel⁵, Nissar Qureshi⁶, Ahmed Hamadat⁷, Filomento O. Corona Jr.⁸

The Faculty of Computer Information Science, Higher colleges of Technology, Al Ain, United Arab Emirates^{1, 2, 3}

The Faculty of Engineering Technology and Science, Higher colleges of Technology, Al Ain, United Arab Emirates^{4, 5, 6, 8}

Chemistry Department College of Science, United Arab Emirates University, Al Ain, United Arab Emirates⁷

Abstract—Population growth has resulted in a decrease in readily available sources of potable water. Desalination is one of many approaches that has been studied and proposed as a way out of this predicament. In this study, multistage Reverse Osmosis desalination process is used in the model, since it has the potential to achieve a higher purity percentage than the single-stage RO desalination process. Some researchers have studied the distinctive tools of AI, specifically Artificial Neural Network as regression model and the genetic Algorithms as an optimization technique in the process of desalination and water treatments. This paper aims to examine multistage RO desalination by employing various artificial intelligence (AI) techniques, including Artificial Neural Network (ANN) and Support Vector Machine (SVM). Both training methods used for this research come under the category of regression algorithms, which are used to establish a predictive link between variables and labels. The main finding of this study was the noticeable decrease of Mean Square Error (MSE) in second stage when data was trained using the ANN. While on the other hand the MSE increased in second stage when the data was trained using the SVM. It can be concluded that the results of this research indicate that applying ANN and SVM to RO desalination process modelling would yield substantial improvements. Future work will be focusing on predicting and improving the performance of ANN and SVM prediction with other function variables.

Keywords—Artificial intelligence; artificial neural network; desalination; regression; reverse osmosis; support vector machine

I. INTRODUCTION

The problems of water scarcity, which have plagued our world since ancient times, persist today. Clean water is becoming increasingly difficult to come by, and its quality is deteriorating to the point where it is being blamed for the deaths of people in some countries. The demand for and consumption of clean water would rise as a result of the fact that not only humans but also animals and plants require it [1]. The concern is also rising around the world because the current supply of fresh water is insufficient to meet the needs of the global population [2]. We live in a world that is 71% water, with almost 97% of that water held by oceans, yet we have a water shortage [3]. Through a variety of processes that scientists have tried to solve, desalination is one of the most common methods for converting salt water into potable water. Reverse osmosis (RO), which employs a specialized membrane, is a frequently employed desalination method.

Reverse osmosis desalination is a rapidly expanding and popular method used to produce water, and it now accounts for around 70% of the world's water supply.

Reverse Osmosis desalination is a method of separating brackish water from dissolved salts by pumping it under high pressure through a water-permeable membrane. Initially, seawater (brackish water) flows into a primary settling tank. This brackish water is then pumped into the reverse osmosis feed tank. Part of the permeate (clean) water and the strong concentrated brine solution is recycled into the water storage tank with the proper pressure, temperature, and feed [4].

Despite the outstanding performance, the application of RO has some limitations. Those limitations include high pressure required, high cost of membrane replacement, low permeation flux, low membrane durability, high equipment and operating cost that affects the process economically[3]. Therefore, ongoing efforts and studies are needed to be carried out to increase pure water recovery by developing new process configurations that use multi-stage RO and optimization processes (see Fig. 1).

According to studies [5][6] AI has proven to be a versatile tool for learning complex patterns. As explained in that paper, to learn those complex patterns it employs two methods, namely: supervised and unsupervised learning. The supervised learning algorithm is the most commonly used machine learning algorithm, in which a dataset trains an algorithm with known input and responses to make the desired predictions.

This supervised learning algorithm is further classified as Classification and Regression, with Classification being used when categorical response values are separated into specific classes. When you have numerical continuous-response values, you use Regression. According to [7] and [8] research papers, RO dataset responses which had numerical values were implemented, where the Regression algorithm was used for AI techniques. To train the data, they used the Artificial Neural Network (ANN) and the Support Vector Machine (SVM) as Regression algorithms [7]. Both of the techniques were implemented to analyze and compare the performance of the RO desalination process [9].

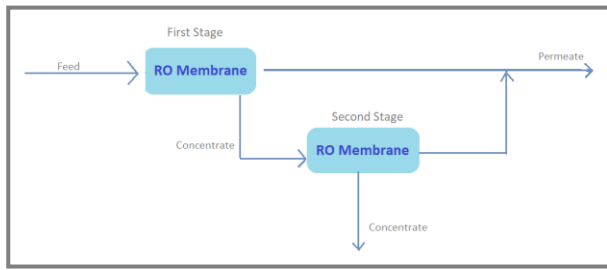


Fig. 1. Multi-Stage RO.

The RO process is used in this paper to convert brackish water to fresh water via a selected membrane. It also investigates how AI can be used to control the factors that contribute to this process. To achieve the best possible result, the various factors that affect these processes were managed using Artificial Intelligence technology.

In this study, a multi-stage RO process is used to achieve permeate water by inhibiting multiple RO membrane stages. This improves water recovery and reduces RO rejection. The concentrate water is collected in a brackish tank obtained from previous cycles, whereas the permeate water is collected in a water storage tank after passing through the multistage membranes.

II. MATERIALS AND METHOD

In this research, a multi-stage RO process is proposed as a means to produce potable water. This research into its acquisition will consist of three stages. First, the study goes over the steps that are taken to collect information for the RO procedure.

For both steps of the RO procedure, the efficacy of data that has been trained using an ANN is discussed. Both sets of simulated data are used to train a Support Vector Machine (SVM) MATLAB will be used by these two AI methods to analyze the water quality that is achieved after several steps have been taken.

A. Acquiring Data from Simulating Reverse Osmosis

Starting with a good simulator, the Reverse Osmosis process is run to get a feel for how it works. The ASPEN Plus platform was suitable for modeling the entire procedure because it provides a realistic insight by allowing the model to be fed brackish water and subsequently yielding clean water.

The information obtained from ASPEN Plus was useful because it mimics the physical RO process, as discussed in the prior study "Using Artificial Intelligence for Reverse Osmosis Desalination." In order to plan for and acquire the data, the actual effect of temperature, pressure, salt concentration, and feed flow rate would be studied and monitored [10].

While holding all other variables constant, a simulation in ASPEN Plus was run to determine the impact of each individual variable on the operation (see Fig. 2). For instance, in Table I, the effect of changing the pressure while holding the other parameters constant was examined in order to better understand the RO.

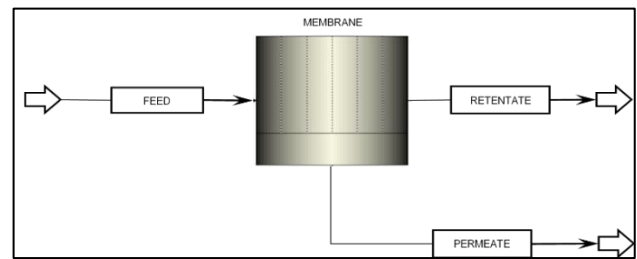


Fig. 2. Schematic Diagram of RO Membrane using ASPEN Plus.

Water flux and salt rejection are both influenced by the pressure that is applied, as shown in Fig.3 and Fig. 4, which depict the performance of stream pressure and the permeate flux, respectively. As can be seen in the graphs, there is a direct correlation between the water flux and the operating pressure. In order to verify the accuracy of the ASPEN Plus experiment and develop an algorithm to aid in the prediction of the parameters in the future, it can be fed into AI training tools. In addition, the AI tools investigate and make predictions about how various elements influence the quality of the membrane's output water (permeate).

A data set of inputs (temperature, pressure, and salt concentration) and outputs (percentage of pure water) is used to train, validate, and test the ANN and SVM tools.

B. Maintaining the Integrity of the Specifications

In this part, an Artificial Intelligence method commonly referred to as an ANN is used to train the data that had been collected so far. An artificial neural network (also known as a neural network) is a type of adaptive system that acquires knowledge through the use of interconnected nodes or neurons arranged in a hierarchical framework similar to the human brain. Because neural networks are data-driven, they can be taught to perform a wide range of tasks, including pattern recognition, data classification, and event prediction [5].

TABLE I. RO MODELLING CONDITION FOR ALTERED PRESSURE

Parameters	Feed Water Temperature, 0C	Flow rate, m3/h	Feed Water Salt Concentration, g/l
	20	8	30

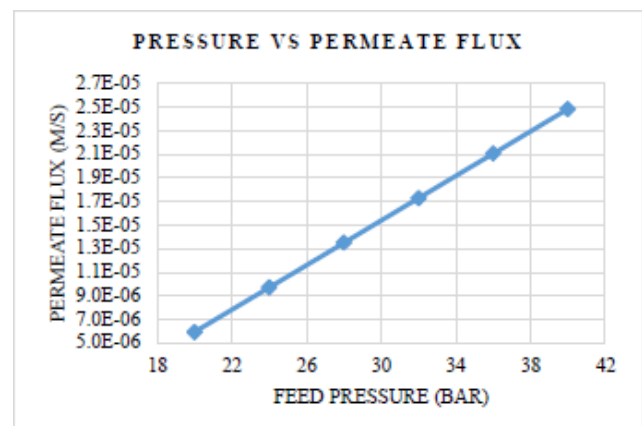


Fig. 3. Effect of Operating Pressure on Water Flux.

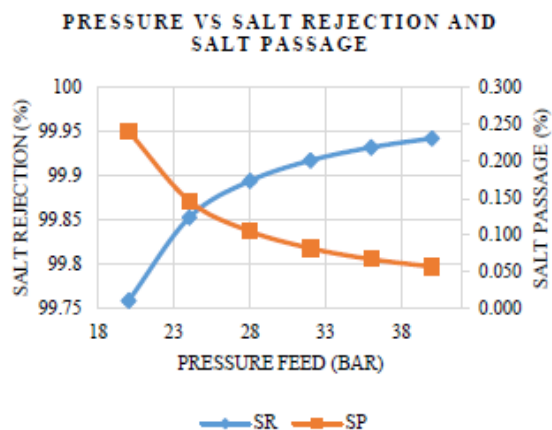


Fig. 4. Effect of Feed Pressure on Salt Rejection and Salt Passage.

In order to better process the input, a neural network can abstract it in layers. Similar to how the human brain learns, it can be trained with lots of examples to recognize patterns in things like speech or images. How its parts are linked together, and how strongly they are linked together (the weights), determine its behavior. During training, these weights are continuously fine-tuned in accordance with some predetermined learning rule until the artificial neural network achieves the desired performance level.

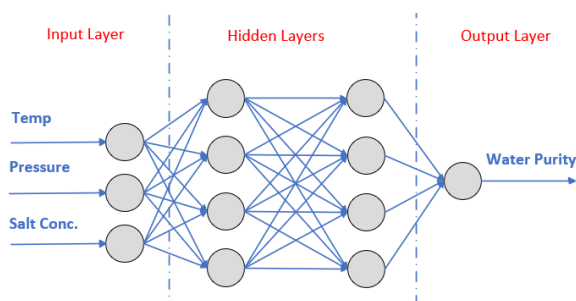


Fig. 5. Architecture of Artificial Neural Network.

The data collected by the ASPEN Plus is used for neural training. The learning technique is then used to train the data in two stages. This promotes to analyze and compare data in order to obtain clean water from the process and predict (Fig. 5).

1) *First stage data training:* In the first phase, the neural network is fed the three variables that together define the RO (see Table II). Those factors are heat, moisture, and saltiness. Training results can be obtained by treating the percentage of pure water as a response and the aforementioned variables as predictors. The initial stage included the implementation of a three-layer hidden layer. 70% was used as the training set, 15% as the validation set, and 15% as the test set. While the Levenberg-Marquardt training algorithm does require more memory than some other methods, it is typically the fastest training algorithm available. The weight and bias values are recalculated using the Levenberg-Marquardt algorithm. (Table III).

2) *Second stage training:* In this project, the Multistage Reverse Osmosis uses a two-stage RO process to obtain clean

water. Following the completion of the first stage RO process, the permeate received is subjected to a second stage RO process (Table IV). This improves clean water recovery while decreasing rejections from the second RO stage (Table V).

C. Training With Support Vector Machine

In this section, the data acquired is going to use SVM to train and predict the purity of water using the RO process. Support Vector Machine (SVM) is one of the supervised learning algorithms that solves regression problems by learning objects and assigning labels.

As it is noted in [1] and [11], SVM's big data environment can be used to help applications with multidomain. Additionally, [12] has been popular as it is simple and flexible to address various classification problems, where SVM specifically affords balanced predictive performance [5]. The objective of this algorithm is to find a plane that maximize the margin between the training data, where to be optimized the hyperplane must yield a maximum margin. According to Fig. 6, the SVM selects the maximum-margin hyperplane which gives the highest accuracy of prediction [13] and [14].

TABLE II. FIRST STAGE TRAINING PROGRESS

Training Progress			
Unit	Initial Value	Stopped Value	Target Value
Epoch	0	40	1000
Elapsed time	-	00:00:3	-
Performance	3.43e+03	13	0
Gradient	5.64e+03	0.601	1e-07
Mu	0.001	1e-06	1e+10
Validation Checks	0	6	6

TABLE III. MODEL SUMMARY AFTER FIRST STAGE RO PROCESS

	Observations	MSE	R
Training	700	13.2622	0.9543
Validation	150	15.6231	0.9468
Test	150	17.2769	0.9498

TABLE IV. SECOND STAGE TRAINING PROGRESS

Training Progress			
Unit	Initial Value	Stopped Value	Target Value
Epoch	0	35	1000
Elapsed time	-	00:00:02	-
Performance	1.34e+03	5.69	0
Gradient	3.56e+03	1.04	1e-07
Mu	0.001	0.01	1e+10
Validation Checks	0	6	6

TABLE V. SECOND STAGE TRAINING RESULT

	Observations	MSE	R
Training	700	5.9063	0.9811
Validation	150	5.8044	0.9778
Test	150	6.0216	0.9808

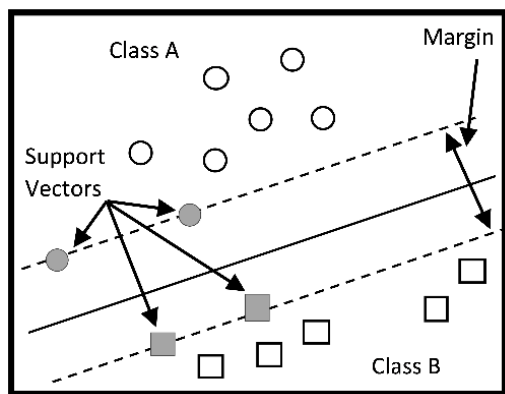


Fig. 6. Hyperplane Margin Selection.

The aim of this research is to predict the purity of water from the three features that determine the RO process. The ‘fittersvm’ function is used to fit an SVM regression model. It is used to cross-validate or train the data set on a low-through moderate dimensional predictor. This function uses kernel function to map predictor data.

The MATLAB R2021b version was used to train the SVR model as it offers a built-in function ‘fittersvm’ to train the given data sets. To get the SVR model, the right input parameters should be provided, such as the training set, kernel function, epsilon, and penalty coefficient. Similarly, the input for this RO desalination process temperature, pressure and salt concentration were given to yield the purity of water in percentage. Using the same ‘fittersvm’ built-function, MATLAB was able to generate the model for the first and second processes. The same data obtained from the ASPEN Plus simulation were used for the training process using the SVM algorithm.

III. RESULT AND DISCUSSION

Two types of Artificial Intelligence techniques were used to analyze the performance of Reverse Osmosis desalination in this research. The ANN and SVM algorithms were used to compare the performance of the desalination process. The aim is to have an efficient prediction learning algorithm from both of the techniques [15]. The results obtained are viewed in two categories for the multistage RO desalination.

A. Analyzing Performance of Multistage RO using ANN

The results from the first stage RO of the variables for temperature, pressure and salt concentration is given in the ASPEN Plus simulation model again for the second RO stage to obtain data on the purity of water in percentage.

This result data is then taken and fed to the neural network software to be trained for prediction. In the second stage of the RO, three layers were implemented for the hidden layer. The data was divided into 70% training data, 15% validation data and 15% test data selected randomly. They were trained in the neural network to give out these results (Table VI).

The graph from Fig. 8 represents the performance of the Mean Square Error (MSE) with respect to each epoch the training of ANN undergoes in the first stage RO process. The MSE is achieved by calculating the mean of the square of the

difference between the actual and the ANN output for all the data points. It can be seen the best validation performance of this RO desalination process was achieved at the 35th epoch(iteration). In the model summary for the first stage (Fig. 7), information about the training algorithm and the result for each data set is presented for the inputs and outputs of the RO desalination process.

The second stage RO dataset of the variables for temperature, pressure and salt concentration is given to the ASPEN Plus simulation model again for the second RO stage to obtain data on the purity of water in percentage.

This result data is then taken and fed to the neural network software to be trained for prediction. In the second stage of the RO, three layers were implemented for the hidden layer. The data was divided into 70% training data, 15% validation data and 15% test data selected randomly. They were trained in the neural network to give out these results. The same Levenberg-Marquardt training algorithm was used in the second stage of training to receive the following results (Table VII).

TABLE VI. MODEL SUMMARY FOR STAGE 1 TRAINING

Model Summary	
Predictors	[Temperature Pressure Salt Concentration]
Responses	[Purity]
Data division	Random
Training Algorithm	Levenberg-Marquardt
Performance	Mean squared error

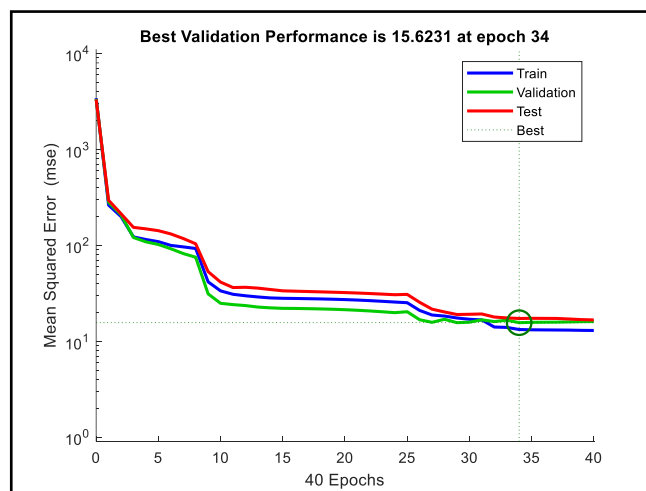


Fig. 7. First Stage Best Validation Performance.

TABLE VII. MODEL SUMMARY FOR STAGE 2 TRAINING

Model Summary	
Predictors	[Temperature2 Pressure2 Salt Concentration2]
Responses	[Purity2]
Data division	Random
Training Algorithm	Levenberg-Marquardt
Performance	Mean squared error

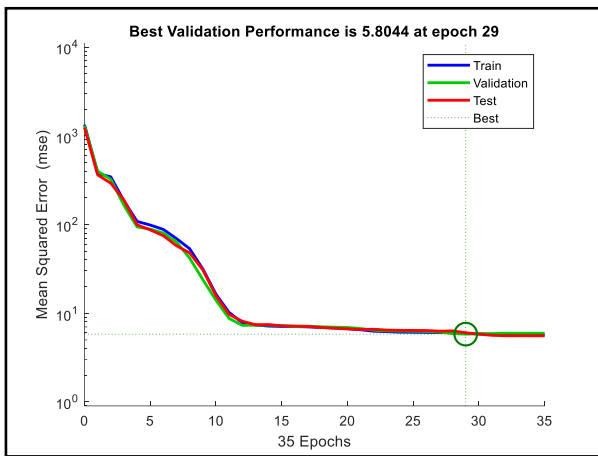


Fig. 8. Second Stage Best Validation Performance.

On the other hand, when referred to Fig. 10, it could be seen a graph plot of MSE vs epochs run to train the second stage RO desalination process using the ANN. As a result, the best validation performance of the second stage training was achieved at 29th epoch which was much better validation performance than the first stage training. The same data division and training algorithm was used to help in comparing both stages of the RO process which can be seen in Fig. 9.

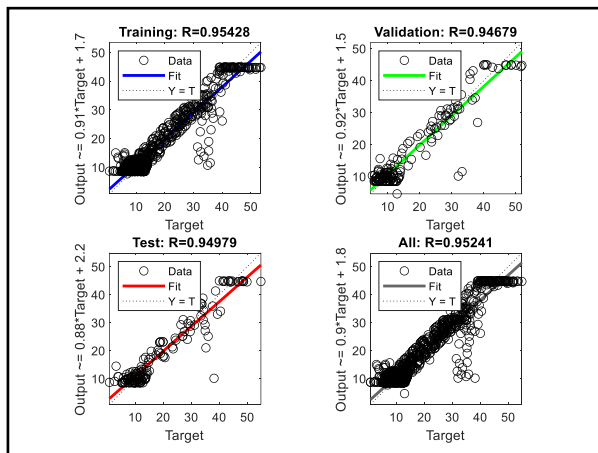


Fig. 9. First Stage RO Training Regression Plot.

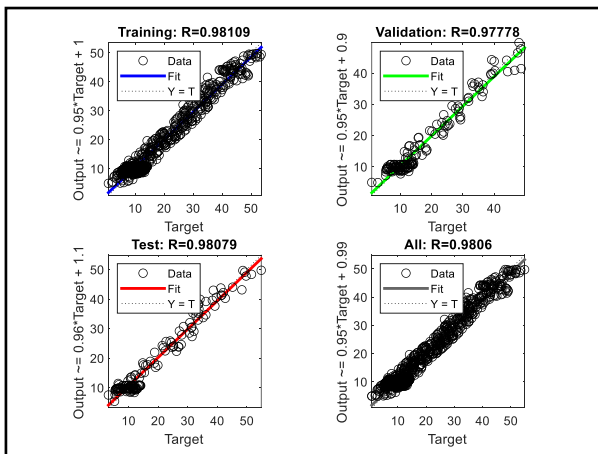


Fig. 10. Second Stage RO Training Regression Plot.

In Fig. 9 and 10, the regression plots can be seen to show the network prediction with respect to responses. Both these graphs test the relation between the actual output with respect to the target for training, validation, and test sets. In these graphs, it can be seen the output (from ANN) is very close to the target (actual purity of water from the process). It can be concluded that the close relationship between ANN output and target can be from the high correlation reflected in the R-value. Moreover, when the graphs are compared for the first stage and second stage, it could be seen that the correlation of the second stage RO process has good performance and would aid better in predicting more accurately.

B. Analyzing Performance of Multistage RO using SVM

The data from the first stage was loaded to MATLAB workspace to go on with the training process. It was trained using a standardized data. This means the software centers and scales each column of predictor data(X) by the weighted column mean and standard deviation. This trains the model by a standardized predictor matrix, while storing the unstandardized data in the model property X. Moreover, the convergence information of the model was set to 'Converged'. When computed the optimizing routine of the Solver was found to be 'SMO' (Sequential Minimal Optimization) and the mean-square error of the model was 0.2630. Each element of the initial estimates of alpha coefficients corresponds to an observation in X. As the Alpha cannot contain any NaNs, it can be observed the model had run properly as it listed all elements (Table VIII).

The data from the second stage RO process was also loaded into MATLAB and trained using the same SVM (Table IX). Temperature, pressure, and salt concentration were all grouped together and trained to produce water purity. This dataset was trained with the 'fitsvm' function and the 'Standardized' model training method [16]. The computed mean square error of the second stage was 1.0451. The resulting epsilon, known as half the width of the epsilon-insensitive band, stores a nonnegative scalar value of 1.2149. Because the Standardize option was set to true during training, the Mu value is also provided, with the length equal to the number of predictors.

TABLE VIII. FIRST STAGE SVM TRAINING

Property	Value
Epsilon	0.9032
Solver	'SMO'
Bias	17.9891
Kernel Parameter	Linear function, scale 1
Alpha	[1;1;0.572330238305089;-0.275138601731484;-0.297191636573605;-1;-1]
Beta	[-0.001485696802116;9.495296357877216;-3.931750668547228]
Mu	[23.555762711655710,23.548202705561412,28.190442046205046]
Sigma	[5.977559943498434,5.982586319655137,5.794770001389037]

TABLE IX. SECOND STAGE SVM TRAINING

Property	Value
Epsilon	1.2149
Solver	'SMO'
Bias	17.74008
Kernel Parameter	Linear function, scale 1
Alpha	105 x 1 double
Beta	[-0.013834278784691; 0.362070130142010;11.741070351439940]
Mu	[24.765164217883978,28.057443299385262,37.792 550502075830]
Sigma	[6.400203608352864,2.922463103239594,5.838943 078299873]

After training the first and second stages of RO desalination with cross-validation SVM, the results for both sets were displayed in Tables VI and VII. When trained with the 'fitsvm' function, the Mean-Squared Error of the loss function was measured for both stages to evaluate the performance of the training. The MSE for the first trained model was 0.2360 and for the second trained model it was 1.0452. This indicates that the output obtained from the first stage of RO desalination training is more similar to the actual output, as it has a lower MSE than the output obtained from the second stage of training. Although the MSE of the second stage was found to be slightly higher, it could be trained to predict the actual water purity when given the correct RO desalination process parameters.

IV. CONCLUSION

This paper used Artificial Neural Network and Support Vector Machine algorithms to train multi-stage Reverse Osmosis desalination data. Both techniques used ASPEN Plus simulation data to predict the entire RO process. ANN trained RO's first and second desalination stages. Training resulted in a high correlation between actual and obtained output and increased water purity.

The trained ANN predicted multistage RO desalination well given the inputs. The SVM can train and predict multistage RO desalination. It used ASPEN Plus simulation data. ANN had a higher classification and prediction rate than SVM despite its shorter execution time. ANN outperformed SVM with multistage RO alignment based on AI function implementations.

This study signifies that the use of Artificial Intelligence techniques could bring ease of processes if implemented well. In this case, the multi-stage RO process was made to be trained both using the ANN and SVM to determine the prediction of water purity. Both techniques would yield an accurate prediction rate based on the data fed previously but exhibit slight differences on their output. This research aimed to study what the differences are amongst both techniques and help determine which to implement on the research. MSE, regression correlation, and other functions can be used to compare the two stages of RO desalination. These findings from training the collected data using ANN and SVM could lead the research to further use other training models on future work to find the best training model that would align with the multi-stage RO process. Future research could focus on predicting multistage RO desalination properties and factors

using ANN and improving SVM prediction performance. Moreover, the exploration and validation of new prediction techniques for different applications could be of great importance for future research.

ACKNOWLEDGMENT

We are appreciative to Higher Colleges of Technology for funding this study and allowing us to use their resources. The funding for this study came from HCT Interdisciplinary Research Grant Fund No.97960.

REFERENCES

- [1] M. Bachar, A. Naddami, A. Fahli, and M. Hilal, "A New Mobile and Hybrid Desalination Unit with Solar Energy and Enhanced Reverse Osmosis," in 2018 6th International Renewable and Sustainable Energy Conference (IRSEC), 2018, pp. 1–5, doi: 10.1109/IRSEC.2018.8702837.
- [2] UNICEF, "WHO (2010) progress on sanitation and drinking water—2010 update," WHO/UNICEF Jt. Monit. Program. Water Supply Sanit. See http://www.wssinfo.org/fileadmin/user_upload/resources/JMP-report-2012-en.pdf (accessed 30/05/2012), 2015.
- [3] M. G. Ahunbay, S. B. Tantekin-Ersolmaz, and W. B. Krantz, "Energy optimization of a multistage reverse osmosis process for seawater desalination," *Desalination*, vol. 429, pp. 1–11, 2018, doi: <https://doi.org/10.1016/j.desal.2017.11.042>.
- [4] Z. Lin, J. Ma, J. Shi, and Y. Liu, "A pilot study of ultrafiltration pretreatment for seawater reverse osmosis desalination in Bohai Bay," in 2011 Second International Conference on Mechanic Automation and Control Engineering, 2011, pp. 33–36, doi: 10.1109/MACE.2011.5986850.
- [5] K. O. Akande, T. O. Owolabi, S. Twaha, and S. O. Olatunji, "Performance comparison of SVM and ANN in predicting compressive strength of concrete," *IOSR J. Comput. Eng.*, vol. 16, no. 5, pp. 88–94, 2014.
- [6] S. Al Aani, T. Bonny, S. W. Hasan, and N. Hilal, "Can machine language and artificial intelligence revolutionize process automation for water treatment and desalination?," *Desalination*, vol. 458, pp. 84–96, 2019.
- [7] R. Moraes, J. F. Valiati, and W. P. G. Neto, "Document-level sentiment classification: An empirical comparison between SVM and ANN," *Expert Syst. Appl.*, vol. 40, no. 2, pp. 621–633, 2013.
- [8] D. A. Pisner and D. M. Schnyer, "Chapter 6 - Support vector machine," A. Mechelli and S. B. T.-M. L. Vieira, Eds. Academic Press, 2020, pp. 101–121.
- [9] G. G. Rajput and B. H. Kaulwar, "A comparative study of artificial neural networks and support vector machines for predicting stock prices in National Stock Exchange of India," in 2019 International Conference on Data Science and Communication (IconDSC), 2019, pp. 1–7.
- [10] N. D. Viet, D. Jang, Y. Yoon, and A. Jang, "Enhancement of membrane system performance using artificial intelligence technologies for sustainable water and wastewater treatment: A critical review," *Crit. Rev. Environ. Sci. Technol.*, pp. 1–31, 2021.
- [11] W. Song, S. Kim, and M. Jae, "New Methodology on Combining Source Term Categories for Multi-Unit Level 3 PRA," *Training*, vol. 78, p. 58.
- [12] S. Suthaharan, "Support Vector Machine BT - Machine Learning Models and Algorithms for Big Data Classification: Thinking with Examples for Effective Learning," S. Suthaharan, Ed. Boston, MA: Springer US, 2016, pp. 207–235.
- [13] W. Noble, "What is a Support Vector Machine?," *Nat. Biotechnol.*, vol. 24, pp. 1565–1567, Jan. 2007, doi: 10.1038/nbt1206-1565.
- [14] W.-H. Chen, S.-H. Hsu, and H.-P. Shen, "Application of SVM and ANN for intrusion detection," *Comput. Oper. Res.*, vol. 32, no. 10, pp. 2617–2634, 2005, doi: <https://doi.org/10.1016/j.cor.2004.03.019>.
- [15] R. Singla, B. Chambayil, A. Khosla, and J. Santosh, "Comparison of SVM and ANN for classification of eye events in EEG," *J. Biomed. Sci. Eng.*, vol. 4, no. 1, p. 62, 2011.
- [16] D. Ni, Z. Xiao, B. Zhong, and X. Feng, "Multiple human-behaviour indicators for predicting lung cancer mortality with support vector machine," *Sci. Rep.*, vol. 8, no. 1, pp. 1–10, 2018.

Educational Platform based on Smartphone to Increase Students' Interaction in Classroom

Mohamed Naser AlSubie¹

Department of Human Studies
Al- Khurmah University College, Taif University
P.O. Box 11099, Taif 21944, Saudi Arabia

Omar Ben Bahri^{2*}

Department of Science and Technology
College of Ranyah, Taif University
P.O. Box 11099, Taif, 21944, Saudi Arabia

Abstract—Current smartphones meet all the criteria for university application. This technology opens the door to develop new techniques to enhance teaching methods. In addition, it presents an interest solution for students' guidance and helping. Thus, the idea of this proposal aims to provide a platform around smart phone based on android to help student and teachers managing their courses. It is based on the Internet of Things to increase digital interaction and improve the teaching process while delivering traditional lectures. The system encompasses three main parts. The first step is carried out for guiding students to find their classroom and teacher's desk. The second part was developed to help teachers to monitor the attendance of students. The third part is dedicated for improving e-learning in classroom by managing the educational process with the purpose of providing the adequate platform for data management. The platform, therefore, succeeded to provide the adequate solution to prevent the misuse of smart phone in classroom, and to enhance the learning methods using smart technologies.

Keywords—Android; classroom; e-learning; data management; IoT; smartphone

I. INTRODUCTION

Today, smartphone immersion phenomenon of almost all students becomes a critical problem from an educational point of view. Obviously, the presence of a mobile phone decreases performance during and negatively affects the ability to concentrate. Unfortunately, smartphone can be a tool for students' distraction. Social Medias are among reasons that cause lack of course follow-up. Gowthami, S., and Kumar, S. V. K, discussed the factors that lead the loss of concentration for students in classroom, such as, the use of smartphone for chatting, playing online and checking e-mails [1]. In addition, Masadeh, T. S. Y, tackled the same problem of students' distraction in classroom by providing the barriers of using smartphones [2]. Furthermore, another research analyzed four hypotheses for the effects of smartphones usage of different cultures including, distraction, addiction, the non-usage of smartphones and the effects of female users [3]. This research conducted to prove the defects of using smartphone in classroom. In addition, Al-Furaih, S. A., & Al-Awidi, H. M. proved the disengagement cause of students when using their smartphones in classroom [4]. Otherwise, a research focused on the use of smartphone even in online courses, proved that students who learn using their smartphone showed a stronger negative effect in academic performance [5].

According to this brief analysis, these factors lead to ensure compliance with the rules and the law. The use of telephones is prohibited in class. It's a way to protect students from loss of concentration due to tablets and phones. Should you or shouldn't you have your cell phone at university? The question, which is a matter of discussion in many universities in the country, leads to a larger problem.

In fact, prohibiting students of using smartphone presents a real challenge. This leads to study the aspects of using smartphones in the classroom, to propose solutions to turn the smartphone into classroom aid. UNESCO in a series of documents on mobile learning paints an excellent portrait of the perceived advantages and disadvantages of using mobile devices in a learning context. Two documents are particularly interesting, namely Policy Guidelines for Mobile Learning [6] and Turning on Mobile Learning in North America: Illustrative Initiatives and Policy Implications [7]. They highlight a number of pedagogical benefits, but also more personal benefits to the use of smartphones in the classroom.

- Possession of a mobile device in the classroom would make it possible to personalize learning by offering the flexibility to pace one's learning and to learn according to one's preferred mode [8].
- Mobile devices in the classroom would facilitate immediate feedback and assessment by leveraging the interactive capabilities of the devices [9].
- Mobile devices would promote productivity and active learning by maximizing the time spent in class and moving away from more passive modes of knowledge transmission [9].

UNESCO also addresses barriers perceived by policy makers and teachers to the use of mobile devices in the classroom for educational purposes [10].

- Issues of behavior and civility are often raised.
- The disruptive and distracting nature of AMCs. For example, a 2013 research report demonstrated that the use of laptops in the classroom can impact concentration and learning both for the student they use it and for the students who are close to the user [11].
- The heterogeneity of mobile devices and the size of screens can be a barrier to their use in class.

*Corresponding Author.

Thus, applications around Smart phone should be developed to prevent its misuse. Incorporating technology into education is a great way to actively engage students, especially as digital media surrounds young people in the 21st century. Interactive white boards or mobile devices can be used to display images and videos, which help students visualize new academic concepts. Learning can become more interactive when technology is used as students can physically engage during lessons and instantly research their ideas, which develops their autonomy.

Therefore, many searches were well developed to include technologies in classroom [12]. These led to prove the reliable ways to use smartphone in classroom preventing its misuse. Here, G. McKinley reviewed the benefits of using smartphone in classroom and how it can be a source of distraction [13]. Therefore, it is pivotal to extract the application of smartphone to be used as learning aid such as, incorporating multitasking by smartphone in order to prevent the blank time [14], accessing supporting information or teaching materials [15].

These projects led to develop application around the smartphone for the real time interaction in classroom, which is the main objective of the proposed idea. It is aimed to turn the smartphone as a learning aid in classroom. The proposed application provided a reliable platform for e-learning improvement. It guides new students to find their classroom or teacher's desk, it helps teachers to monitor attendance of students automatically, it helps students to download daily courses and follow-up from their smartphones and it offers the possibility to perform chatting group for classroom activities.

II. RELATED WORKS

The use of mobile phones in education is both a controversial and fascinating subject. For many, these devices appear as inconvenient objects in the classroom, which disrupt the smooth running and promote the dispersion of the concentration of the students. In addition, there are charters, internal regulations, which explicitly mention the prohibition to bring his telephone in the enclosure of the school establishment, which in the effective uses results in a use outside the courses. This idea is very beneficial during distance learning, which was relied heavily in the period of COVID-19 pandemic. In some reasons, the classroom can be accessed from home relying on interfaces of virtual classroom, including, course materials and homework [9]. In fact, this period proves the efficiency on using technologies in classroom. As cell phones continue to advance in power and functionality and prove their usefulness as an educational tool, the inherent limitations of these technologies should not be ignored. Already not everyone trusts the digital revolution: the supporters of the traditional school and the blackboard are of course opposed to it, but also the defenders of alternative education systems in which the press has often been interested in recent years. More and more voices are raised against these innovations which aim to impose the intensive use of digital technology in schools [16]. Thus, introducing smartphone in classroom is critical, that lead to develop the adequate application and systems around this device. This maintains the advantages of using smartphone in classroom as aid tool. K. Machmud, et al. developed a fruitful method to overcome the

anxiety related to whom learning English as foreign language [17]. In this contest, the use of such application like "Let's talk" can be useful to practice English language [18]. In addition, several applications around smartphone support the theory of using this device in classroom can be beneficial [19] that help to manage course materials. Otherwise, smartphones' applications can be used for attendance monitoring in classroom [20]. In fact, almost applications tackled some aspects of effective uses of smartphone in classroom. This led to develop an application around the smartphone which encompasses the management of attendance, assessments, and course materials management, focusing on students' interaction in classroom using their smart devices.

III. SYSTEM ARCHITECTURE

Fig. 1 presents the entire system's architecture of the proposed application.

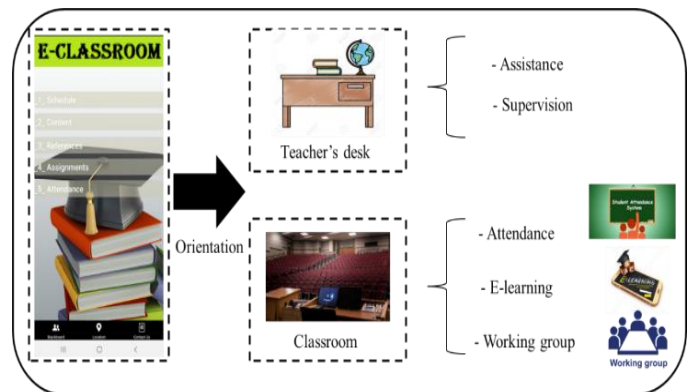


Fig. 1. System Architecture.

The first step is carried out for students' guidance. The student login with his university ID. The application, therefore, moves to the second step by guiding the student to the teacher's desk for assistance or the classroom for attendance. Here, the application provides a new technique to facilitate hand over the assignment. In fact, the Google map was applied to achieve this goal as illustrated in the application interface under the item "location".

The third step will be performed when student find its classroom. It is a great platform to improve techniques of e-learning and attendance monitoring. This technique confirms that the student is part of this course and records the entry time. When the confirmation is done, the application enables student to participate at the course interface which contains the lecture. In addition, it provides the possibility of making discussion groups when assigning activities. Thus, this method offers a new technique to improve e-learning and to use technology to fully engage student physically during the lesson.

IV. METHODOLOGY

In order to ensure the feasibility of the proposed architecture, a multilayer structure was adopted as shown in Fig. 2. The application structure is composed by three layers, including, main, data service and data analysis layers.

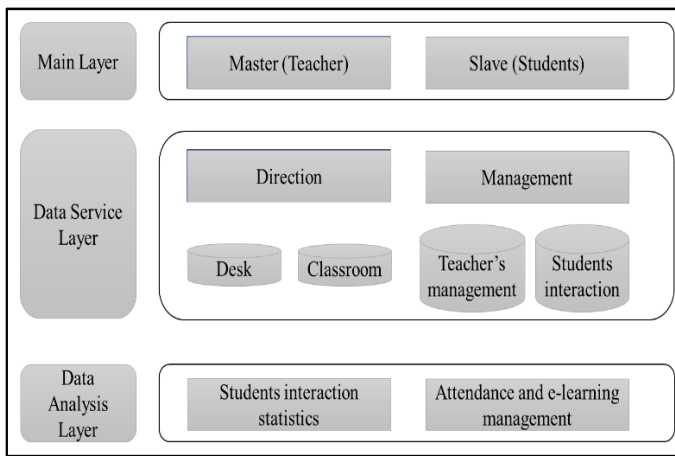


Fig. 2. Multilayer Structure of the Application.



Fig. 3. Application's Interface.

The main layer presents the application's parts, which consists of master-slave architecture; the master (teacher) manages the students' interactions during classroom lesson.

The second layer is composed by the services of the application provided. It is adopted here to aid students for attending their classroom and/or teacher's desk. When student attend his classroom, he will benefit by the system of e-learning maintaining the objective of interaction during the lesson, which will be managed by the teacher.

The last layer ensures the connectivity of the data for analyzing of its statistic.

Based on the smartphone application, this platform encompasses the real-time classroom interaction and evaluation of learning quality. The main parts of the system include teacher data management, student response management, and data statistical analysis, as explained below.

- Teacher data management includes data import, question and exercises management, students' answers, etc.
- Student answer management, including, teacher's exercise answering, submission, results displaying, etc.
- Data analysis including statistical analysis of learning situation, of student attendance, of marks, etc.

V. IMPLEMENTATION AND RESULTS

The platform is implemented based on iBuildApp [21]. The data stored in the server provided by this application. The main interface of the application is presented in Fig. 3. It helps students to attend their classroom. It contains the lessons schedule, the content which will be available upon attending, the course references and assignments that depends on needs.

The application was applied for computer sciences' students of first level. The number of participants reached 25 students. For accessing the platform, students should login with their university ID. Therefore, the teacher can manage attendance easily. In addition, he can hold statistics of students' participations in assignments.

Upon student logs in to the platform, he can upload the content of the course as mentioned in Fig. 4.

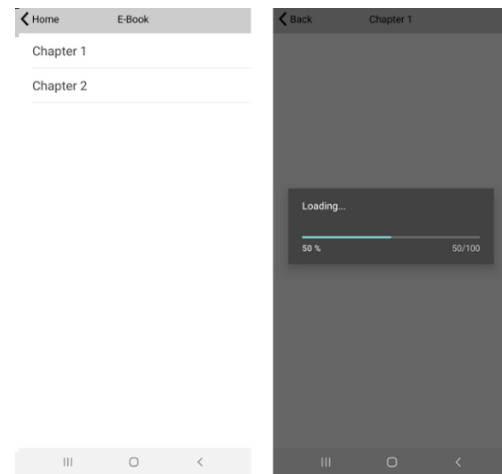


Fig. 4. Course's Content Uploading.

Indeed, the method proposed for accessing the content from the smartphone imposes students to use their devices for learning in classroom. It is proved by the statistics accumulated by the master's platform (Fig. 5).

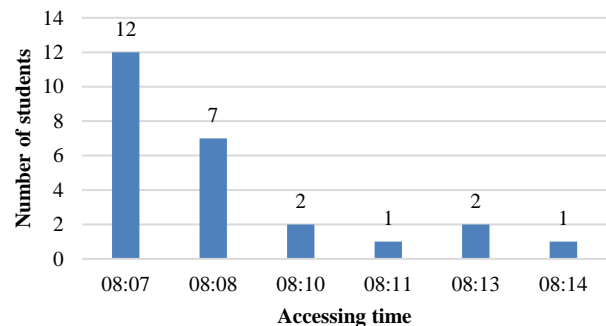


Fig. 5. Content Accessing Time by Students.

The upload of content by students takes about 7 minutes. The time spent is caused by the internet connection for some students. Basically, almost of all students were succeeded to upload the content autonomously. Indeed, the result proves the possibility of transferring the pocket smartphone on classroom aid, without the need of providing training. Otherwise, the master's platform was developed to monitor the participation of students during the lesson, including the online/offline identifications.

In order to fully benefiting the use of smartphone, 8 exercises were conducted for students' evaluation and for applying the teamwork. The exercises were distributed for 8 groups of students. According to Fig. 6, almost all students actively participate in answering assignment. This proves the good effect of students' interaction using this platform. Based on this platform, the student interaction in class was significantly improved. When comparing with the traditional methods, the proposed platform is more efficient.

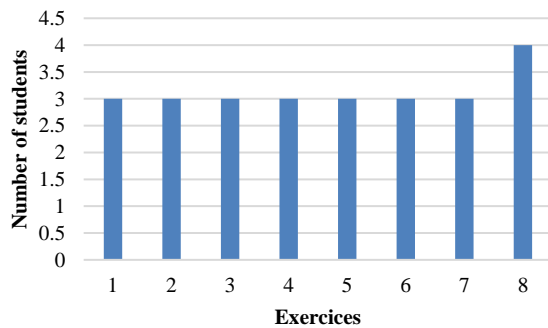


Fig. 6. Groups of Students by Exercises.

To demonstrate the efficiency of the proposed method for teamwork, the master's platform was developed to provide assignments' marks by application. In fact, the instantly evaluation encourages students for interacting. In addition, this method improves the feedback.

VI. DISCUSSIONS

The application was conducted to ensure the adequate evaluation of students preventing the misuse of smartphone in classroom. Thus, the evaluation was performed in three steps: At the beginning, the mid and the end of course.

A. The Evaluation at the Beginning of the Course to

- Become aware of the initial level of the students, so as to adapt their teaching according to their achievements.
- Starting from their devices management to ensure benefiting the platform.
- Engage their interest by asking a cryptic or problematic question.
- Recall, remember, the concepts covered in the previous session.

In fact, smart devices and tablets have invaded markets, homes and even schools, and it has become necessary to take advantage of these modern technologies to benefit the students

in their academic achievement, especially if taking into account the motivation shown by most of them to use their personal devices in the classroom and the long time wasted in front of them. Thus, the quick response of platform accessing by students proves the efficiency of using the proposed application with the targeted users, and to adopt smartphone in classroom. It took all students to get in and start learning about 7 minutes (Fig. 5). In addition, students' enthusiasm for using their devices was noted. It is proven by the participation of students in recalling the main parts of the previous lesson. This ensures that students remain fully focused during the lesson.

B. Mid-Course Assessment for

- Maintain students' attention.
- Make the student active and actor, he participates in his learning for a better appropriation of knowledge.
- Foster discussion and collaboration among groups. They can be asked to think and answer a question.
- Engage all students.

As the students' aspiration to everything technological facilitates the process of their response to the lessons, and then consolidates the educational materials for them in the long run.

In fact, the use of mobile phones in classrooms may result in many problems and inconveniences, especially in light of the predominance of the negative nature of the use of them which is represented in violating the rules of the education system. During the class, isolation from the teacher, sending and receiving messages, exchanging information, and joking with each other, which can lead to a lower level of academic achievement among students. Thus, the master platform was developed to ensure the connection during the lesson. An indicator assigns the log out of student if he opens another application. In addition, the developed platform broadcasts lectures and discussions in a sophisticated way that students can interact with each other and with the teacher. This prevents the misuse of smartphone in classroom, providing the adequate solution to engage students.

C. The Evaluation at the End of the Course for

- Check the students' understanding and be able to readjust their teaching the next session if the concept has not been well understood. It can be a question or an application exercise.
- Promote the recall, and therefore the appropriation, of the main concepts that were discussed during the session.

Regardless of the wide controversy that characterizes mobile education and the differences between academics and those interested in educational affairs around it (mobile education between supporters and opponents), technological development imposes itself on everyone, especially if it is accompanied by great interest and knowledge on the part of the center of the education process, who are the students.

Indeed, the proposed idea succeeded to build a knowledge system, in which the features of the image of mobile learning technology, its environment, characteristics, and benefits

become clear. It is based mainly on telecommunications, so that the learner can freely access educational materials, lectures, and assignments in order to be an active element in the educational process.

Finally, the marks achieved by the students at the end of assignment proved the success of the applied educational process (Fig. 7). It is proved that all students were engaged during the lesson. Reviewing and evaluating the duties and achievements of the students, presenting the results of the assessment and providing feedback to the students, contributed to further enriching the advantages of using the smartphone during the lecture.

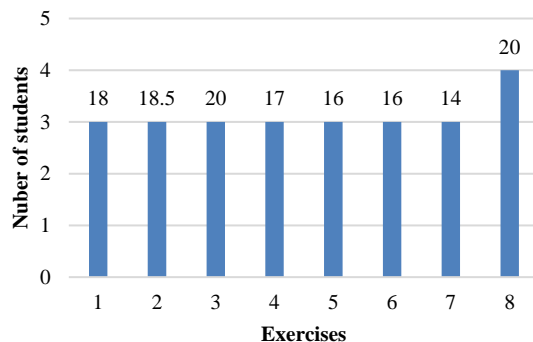


Fig. 7. Assignment's Marks.

VII. CONCLUSION

Smart devices have become necessary to exploit these modern technologies for the benefit of students in their academic achievement, especially if taking into account the motivation factor that most of them show in using their personal devices in the classroom. In fact, the cost of this technology is relatively low; education by mobile phones will not cost students additional financial burdens.

In this paper, a novel technique was applied using this smart device in order to be the main tool of the educational process in classroom. Thus, an application around Android platform was developed to achieve the idea's goal. It provided many layers for teachers to manage their classroom, and the possibility for students to be active element in the educational process.

In addition, the method of assignment answering and evaluating led to the success of adopting smart phone as educational tool in classroom. Adding more activities to the traditional lessons led to the attractiveness of the scientific material and the learning environment.

This platform, therefore, can open the door to develop more applications around smart phones for other courses.

REFERENCES

- [1] S. Gowthami and S. V. K. Kumar, "Impact of smartphone: A pilot study on positive and negative effects," *International Journal of Scientific Engineering and Applied Science (IJSEAS)*, vol. 2, pp. 473-478, 2016.
- [2] T. S. Y. Masadeh, "Smartphone Use In Learning As Perceived By University Undergraduates: Benefits And Barriers," *International Journal of Research-GRANTHAALAYAH*, vol. 9, pp. 56, 2021.
- [3] M. Mahsud, et al., "Addiction to smartphones leading to distraction in the classrooms: Effect of different cultures," *Journal of Statistics and Management Systems*, vol. 24, pp. 741-754, 2021.
- [4] S. A. Al-Furaih and H. M. Al-Awidi, "Fear of missing out (FoMO) among undergraduate students in relation to attention distraction and learning disengagement in lectures," *Education and Information Technologies*, vol. 26, pp. 2355-2373, 2021.
- [5] A. J. Dontre, "The influence of technology on academic distraction: A review," *Human Behavior and Emerging Technologies*, vol. 3, pp. 379-390, 2021.
- [6] M. West and S. Vosloo, "Policy guidelines for mobile learning," UNESCO, 2013. Available online at: <https://unesdoc.unesco.org/ark:/48223/pf0000219641>.
- [7] J. Fritschi and M. A. Wolf, "Turning on mobile learning in North America: illustrative initiatives and policy implications," UNESCO, 2012. Available online at: <https://unesdoc.unesco.org/ark:/48223/pf0000216083>.
- [8] APC Working Group. McGill University. (2010). Guidelines for the Use of Mobile Computing and Communication Devices in Classes at McGill. Available online at: <https://www.mcgill.ca/secretariat/files/secretariat/Mobile-Computing-Commun-devices-MC2-guidelines-11June2010.pdf>.
- [9] Conseil des études de premier cycle. Université de Montréal. (2013). Les technologies en classe : Encadrer leur utilisation pour soutenir l'apprentissage des étudiants. Available online at: http://sse.umontreal.ca/numerique/documentation/EU23_R3.pdf
- [10] F. Sana, T. Weston and N. J. Cepeda, "Laptop multitasking hinders classroom learning for both users and nearby peers," *Computers and Education*, Volume 62, pp. 24-31, 2013.
- [11] M. Green, "Smartphones, distraction narratives, and flexible pedagogies: Students' mobile technology practices in networked writing classrooms," *Computers and Composition*, vol. 52, pp. 91-106, 2019.
- [12] A. Afikah, et al., "Mobile Learning in Science Education to Improve Higher-Order Thinking Skills (HOTS) and Communication Skills: A Systematic Review," *International Journal of Advanced Computer Science and Applications (IJACSA)*, vol. 13, no. 7, pp. 698-704, 2022.
- [13] A. B. Grinols and R. Rajesh, "Multitasking with Smartphones in the College Classroom," *Business and Professional Communication Quarterly*, vol. 77, pp. 89-95, 2014.
- [14] M. Anshari, et al., "Smartphones usage in the classrooms: Learning aid or interference?," *Education and Information technologies*, vol. 22, pp. 3063-3079, 2017.
- [15] J. L. Buck, E. McInnis, and C. Randolph, "The new frontier of education: The impact of smartphone technology in the classroom," *In American Society for Engineering Education*, vol. 1, pp. 1-11, march 2013.
- [16] Y. Park, "A pedagogical framework for mobile learning: Categorization Education Application of Mobile Technologies into for types," *International Review in Open and Distance learning*, vol. 12, pp. 79-102, 2011.
- [17] K. Machmud and R. Abdulah, "Using smartphone-integrated model of teaching to overcome students' speaking anxiety in learning English as a foreign language," *Journal of Arts and Humanities*, vol. 6, pp. 01-11, 2017.
- [18] B. R. Luo, Y. L. Lin, N. S. Chen, and W. C. Fang, "Using smartphone to facilitate English communication and willingness to communicate in a communicative language teaching classroom," *In IEEE 15th International Conference on Advanced Learning Technologies*, pp. 320-322, July 2015.
- [19] S. Kadry and B. Ghazal, "Design and assessment of using smartphone application in the classroom to improve students' learning," 2019.
- [20] S. Anand, K. Bijlani, S. Suresh, and P. Praphul, "Attendance monitoring in classroom using smartphone & Wi-Fi fingerprinting," *In IEEE Eighth International Conference on Technology for Education*, pp. 62-67, December 2016.
- [21] Enterprise Mobile App Store for Apple iOS and Android, iBuildApp. Available online at: <https://ibuildapp.com/>

A Novel Architecture for Community-Sustained Cultural Mapping System

Chong Eng Tan, Sei Ping Lau, Siew Mooi Wong

Faculty of Computer Science and Information Technology
Universiti Malaysia Sarawak (UNIMAS), 94300, Kota Samarahan, Sarawak, Malaysia

Abstract—This paper presents a novel system architecture for implementing a cultural mapping system for the community of Buayan, a remote rural village in Sabah, East Malaysia. By considering various shortcomings of the local environment and the need for a community-sustained system, the cultural mapping system was designed to leverage a new set of architecture to achieve minimal implementation cost and higher reliability to survive the rural environment. The new architecture evolves from previous Telecentres' design and implementation experience that was targeted at larger scale ICT systems. This paper also highlights the critical influence of power provision on the digital system implementation in rural areas, which always incurs a significant amount of the overall implementation cost. An efficient ICT system architecture will significantly reduce the cost of its associated power provision. The implementation of the cultural mapping system using the new ICT architecture at Buayan is also being described.

Keywords—Rural system architecture; telecentre; cultural mapping; sustainability

I. INTRODUCTION

Modern Information and Communication Technology (ICT) advancements have made thousands of online services possible, and the well-established cloud architecture has also enabled more and more highly accessible cloud-based services. The high speed and massive deployment of various means of communication networks, such as optical fibre and mobile cellular data networks, allow access to online systems anywhere and anytime. While the developed world moves rapidly to offer more comprehensive solutions by integrating different services, remote rural places in other parts of the world still struggle with basic amenities and communication access. The development of these remote places can never be treated as equal, as the same online services may not be practical for those living in these areas. The digital divide gap between the rural and urban areas can get more prominent, especially when infrastructure development is driven by commercial entities based on return-on-investment (ROI). The relatively small rural population can be a disadvantage in obtaining the same level of infrastructure development. Due to the different levels of readiness in basic infrastructure, deploying digital systems in remote rural areas would require a more rural-friendly architecture to achieve a more practical and sustainable system implementation in such an environment. In this paper, we describe our work on designing, prototyping, and deploying a custom-made cultural mapping system for the community of Buayan, a remote village in East Malaysia. The village is located at the edge of

mobile network coverage, where the overall network connectivity is relatively poor and slow. On top of that, the relatively inconsistent micro hydropower system used in the village adds a further challenge to deploying service hosting that requires a stable and consistent power source. Hence, we proposed an all-in-one architecture solution inclusive of power, ICT system, and cultural mapping software application that enables the local community to better self-sustain. The proposed architecture is tailored to the Buayan environment and is a smaller-scale version of our previous work on Telecentre design [3]. Apart from enjoying the common benefits of cultural mapping, the Buayan community has another more crucial intention: to inventory the local cultural heritage and community living continuously. These efforts enable the community to better inform the authorities in support of their fight to protect the local heritage and live against the planning of the mega-dam project in the same area. This paper is organised by highlighting the need for cultural mapping in Buayan in Section II, and followed by background on rural ICT system deployments for rural areas in Section III. Section IV summarises the important challenges of ICT system implementation in rural areas that lay the design foundation and consideration for the proposal of the cultural mapping system architecture in Section V. Section VI describes the actual system implementation in Buayan.

II. NEED FOR CULTURAL MAPPING

Cultural mapping is a systematic approach to identifying, recording, classifying, and analysing a community's cultural assets and resources [1]. A software system has been developed to assist with cultural mapping activities for the community of Buayan. Buayan is a remote village in the Ulu Papar region of Sabah in East Malaysia. Although the Dusun people have inhabited the area for at least six generations, the record of their cultural assets and resources has been minimal and incomplete. Access to Buayan requires going through the Crocker Range of a mountain on a bumpy drive. The journey during the monsoon season can be very challenging, even for the most powerful 4-wheel drive vehicles [2]. For the past ten years, the government has had plans to build a hydropower dam that would flood everything, including all cultural heritage within the area. Hence, the villagers have been working hard to convince the government to change the plan for the hydropower dam by justifying to the government agencies the rich heritage and the vast community activities within the sites. The cultural mapping system came in to ease the process of identifying and recording cultural assets of the Buayan community. The cultural mapping system is an

independent system that manages, maintains, and keeps all data locally for the community's sole interest. The community's concern for data privacy is one of the primary considerations of the cultural mapping system design to prevent a third party having ownership or access to the data that might be used against the community itself. As a result, the entire cultural mapping system will be hosted locally within Buayan and accessible only to the Buayan community. In order to achieve such a goal, a robust ICT system architecture must be designed and developed to support the cultural mapping system that is sustainable by the local community in such an environment.

III. BACKGROUND

For the past two decades, the most promising solution towards bridging the digital divide in rural areas has been to erect Telecentres in strategic locations to enable various computer and communication services to serve the surrounding populations. The development of telecentres enables ICT services in the middle of nowhere and acts as a social and economic development centre for the local communities. The complete computer systems, printers, and telephony connected through Very Small Aperture Terminal (VSAT) satellite communication links have made electronic communications such as the Internet and email possible for rural communities. The initial design of telecentres was simply to deploy existing urban computing and communication architecture into rural areas; thus, such deployment is typically very expensive because the telecentre architecture must include a complete power supply infrastructure solely to support the day-to-day operation of the entire telecentre. The eBario Telecentre, deployed in 2002 for the Bario community at the Kelabit Highland in East Malaysia [3], adopted this design. Its power supply infrastructure is a hybrid diesel power generator and a standalone solar power system. The overview of the eBario Telecentre architecture is shown in Fig. 1.

The solar power system was backed by the diesel power generator when it could not provide sufficient power to the

Telecentre. As the cost of diesel and transportation rises year after year, more solar panels and batteries are added to compensate for the reduction in diesel power generators. The battery sub-system of the solar power system has also undergone replacement after five years due to wear and such replacement was very costly. The battery replacement could cost as much as 50% of the entire solar power system implementation due to the conventional solar power system using multiple high-capacity lower voltage modules to form the specific battery bank required by the solar power system. For example, a 24V solar system would require 12 units of 2V battery modules to form a 24V battery bank needed for the 24V solar system. For a 500Ah battery bank, 12 units of 500Ah deep cycle Seal Lead Acid (SLA) are required, and each battery unit can weigh up to 130kg. As a well-known fact, transportation into the rural area is already very costly, and Bario can only be accessed via air during deployment time. Transporting such batteries into Bario requires a Twin-Otter cargo plane into Bario. The biggest drawback of adopting the urban ICT architecture for rural deployment will be the overwhelming requirement for power supply. Table I shows how much the national grid and the standalone solar system cost for the same average daily energy use of 13 kWh.

TABLE I. COMPARISON OF ENERGY COSTING FOR THE SAME AVERAGE DAILY USAGE OF 13KWH BETWEEN THE STANDALONE SOLAR POWER SYSTEM AND THE NATIONAL POWER GRID

Estimated Energy Usage	
Daily usage: 13kWh (six 250W personal computers with eight daily hours of operation) Total usage for ten years: 46,800kWh	
Energy Costing	
Standalone Solar Power System	National Power Grid
First 5 years + initial installation (4kW Solar): RM180k	RM7k (based on RM0.30 per kWh)
Next 5 years (battery replacement): RM50k	RM12k (based on RM0.50 per kWh)
Total expenditure for ten years:	
RM230k	RM19k

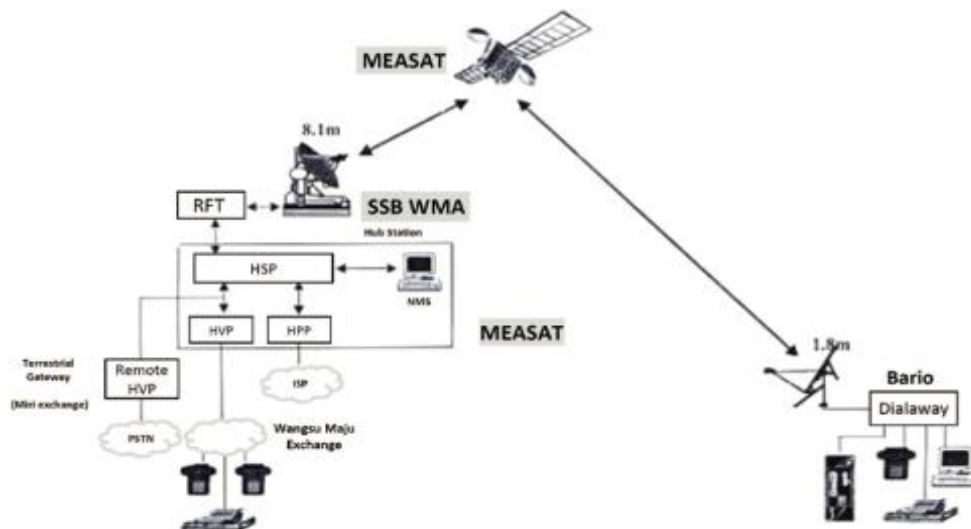


Fig. 1. The eBario Telecentre Architecture [3].

The above comparison shows that the energy cost for 10 years while using the national power grid is less than 10% of the total investment of deploying a standalone solar power system. The rural areas have no access to the national power grid, so the standalone solar system is the only viable power option. Therefore, power provision contributes to a significantly high percentage of the overall ICT implementation cost in rural areas. The overall cost of the solar system is determined largely by its designed power capacity. The higher the power requirements, the more expensive the system is. This includes the higher cost of transporting more solar panels, batteries, and supporting structures into rural areas. Hence, in order to reduce the overall rural ICT deployment cost, a more power-efficient ICT architecture is crucial.

The newer Telecentre model, deployed for rural sites such as Long Lamai, Ba'Kelalan, Buayan, and Larapan in East Malaysia in 2009 [4], has included an upgrade to a more power-efficient computing hardware platform. Instead of adopting conventional desktop computers with energy-hungry cathode-ray tube displays, the new Telecentre model adopted a mixture of energy-efficient desktop computers with liquid crystal displays (LCD) and laptop computers to strike a balance between energy efficiency and hardware cost. Fig. 2 shows the improved eLamai Telecentre computing platform. Portable computers, such as laptops, were still relatively expensive, and mobility of computers was not required by the Telecentres during the time of implementation. With the new computing platform, the average daily energy consumption was a mere 3kWh. This figure shows a significant reduction in energy consumption of about 10kWh per day compared to the previous Telecentre implementation. This reduction would bring down the standalone solar system deployment to as low as RM60k instead of RM230k, as shown in Table II. Hence, the overall maintenance cost could reduce almost three times compared to the previous eBario Telecentre. In the actual eLamai Telecentre implementation, a 4kW solar system was deployed instead of the estimated 3kW system to provide power for other appliances' usage.

TABLE II. COMPARISON OF ESTIMATED OPERATING COST BASED ON THE NEW eLAMAI TELECENTRE'S SOLAR POWER SYSTEM AND THE NATIONAL POWER GRID

Estimated Energy Usage	
Daily usage: 2.88kWh (three 80W desktop computers and three 40W laptop with eight hours daily operation)	
Total usage for 10 years: 46,800kWh	
Energy Costing	
Standalone Solar Power System	National Power Grid
Approximate RM60k	RM4320 (Based on RM0.30 per kWh for first five year, and RM0.50 per kWh for the second five year)

In 2016, a new Telecentre architecture for the Orang Asli Telecentre programme (TPOA) was deployed [5]. The Telecentres consist of a mix of ICT systems with dedicated power supply modules and others that share the centralised

power supply. The introduction of the dedicated power supply module for specific ICT systems, such as local content hosting and critical ICT appliance charging, was to further enhance the reliability of continuous service provision in the rural environment and compensate for the shortcoming of the power-sharing system that could be brought down by overwhelming usage and prolonged bad weather. The overall architecture for the Telecentre model is shown in Fig. 3.

The TPOA Telecentre architecture consists of two solar power systems: one for centralised power provision for non-critical but relatively high power consumption equipment such as VSAT modem/router, management desktop, networked projector, and lighting. Another solar power system is a modular design to support specific and more critical equipment such as content hosting servers, WiFi networks, and charging of tablets. By having a separate power provision architecture, service reliability of critical equipment could be achieved as a centralised power system can be brought down from time to time for many reasons, such as overwhelming usage and bad weather.

Unlike our design, the rural ICT implementations in other parts of the world were primarily focused on implementation strategies and models that did not consider the change in fundamental ICT system architecture that addressed the domestic problems of the rural environment. For example, a software-defined IPv6 network paradigm has been proposed for Nepal [6], but the context of the proposal is very much leveraging on the existing urban network efficiency paradigm for greener ICT. This proposal failed to take the local environment into account in its design considerations.

Most proposed models and strategies rely on existing urban technology building blocks to form solutions for rural implementation. The main research drivers for rural ICT deployment are still in the provision of better quality and cost-effective network accessibility to rural communities. For example, the VillageCell approach [7] focuses on enhancing the current mobile network provision to achieve a better voice call experience that does not address local limitations. In short, the system architecture should adapt to the implementation environment to achieve overall efficiency and minimise over-provision that could cause a hike in overall implementation cost. We are making reference to our previous works on green power architecture considerations for rural computing to customise a novel ICT system architecture for the application of cultural mapping in Buayan. Among the considerations are efficiency of power conversion, storage technology, and microprocessor power mode [8].

IV. CHALLENGES OF ICT SYSTEM IMPLEMENTATION IN THE RURAL

Many factors influence the implementation of ICT systems in the rural environment. Usually, these factors determine the design of the system and also its associated power supply. The following challenges are to be addressed for the specific case of implementing the cultural mapping system for Buayan.

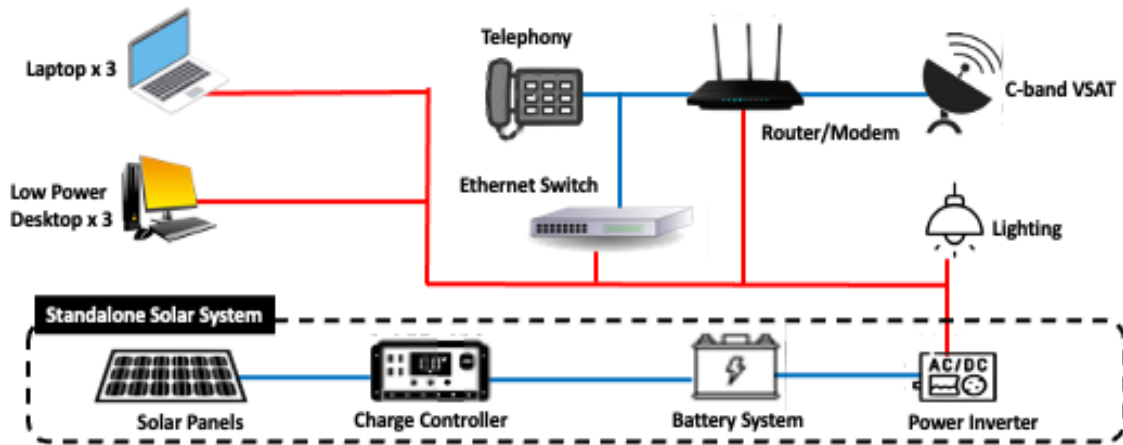


Fig. 2. The eLamai Telecentre Architecture.

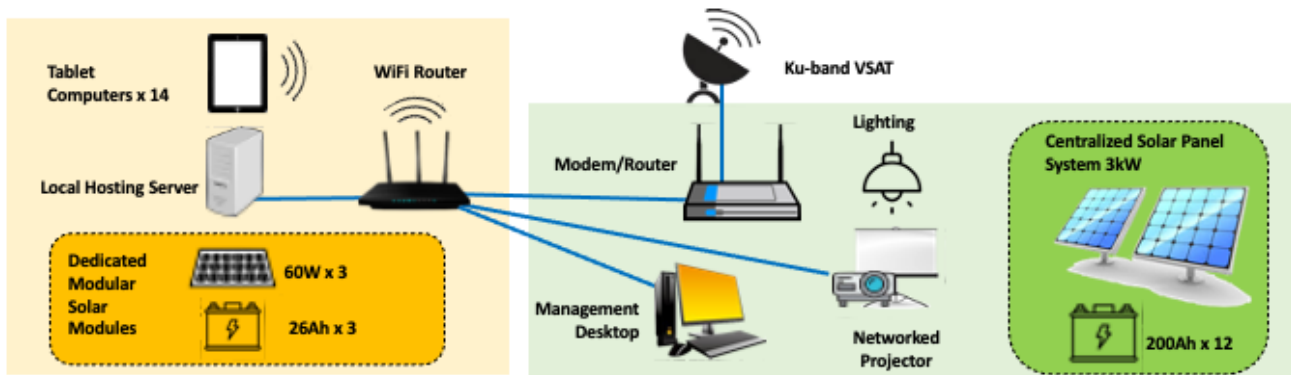


Fig. 3. The TPOA Telecentre Architecture.

A. Reliability and Stability of the Local Electrical Power Supply

The village of Buayan is powered by a community-operated micro hydro system with limited capacity. The operation of the micro hydro system is greatly influenced by the change of seasons: during the drought season, the village will have an intermittent power supply. The intermittent power supply could last for days or weeks if the drought season is prolonged. Such an unreliable and unstable power supply is unsuitable for digital service hosting in the village, as the frequent power cuts could damage the system or corrupt the data. The micro hydropower supply system is community-operated; thus, the community also bears high maintenance costs, resulting in expensive per-kWh charges. Hence, it would be good to have a more reliable power supply module to power the cultural mapping system independently.

B. Difficult Physical Access to the Village

The limited accessibility to the village will lead to higher transportation costs for transporting goods and technical personnel. Hence, the entire digital system and its power supply module should be small enough to be carried easily by the 4-wheel drive vehicle. In such a remote rural area, it can be hard to get technical support for the digital system. Not only does transportation cost more, but it also depends on the weather and the state of the roads.

C. IT Literacy of the Local Community

The adoption of technology in the village is relatively slow due to patchy network connections via the cellular network. Hence, a software system with a steep learning curve is a no-go as any encountered technical problem will render the system useless because no one can resolve the issue. Furthermore, patchy communication access makes providing support over the phone even harder. The community may even have a problem reporting any issues encountered and technical difficulties could take weeks or months to resolve.

V. PROPOSED CULTURAL MAPPING SYSTEM ARCHITECTURE

New system architecture will be proposed that addresses all the shortcomings of the current implementation environment in Buayan. The new system architecture should have the following characteristics:

a) *Highly Efficient in Power Consumption*: The more efficient the system's power consumption, the smaller the power supply system can be used, resulting in a lower cost of maintaining the system and its associated power supply system. Hence, the system design uses an IoT-based CPU with extremely low power consumption (4W to 6W). NAND-based solid state drive storage is adopted for its energy efficiency as well.

b) *Small System Footprint*: The system's footprint should be as small as possible to facilitate transportation into the remote village. With a smaller power requirement, the power supply system can also be made smaller in its physical size. With less than 10W in mind, a renewable energy solar power system has been designed to support the system's operation for 24 hours a day, 7 days a week, and the size of the system is still relatively small for off-road transportation.

c) *Low-Maintenance Software*: Software glitches, such as those in the operating system and the software application for cultural mapping, should be kept to a minimum. A Linux-based command-line interface operating system environment has been used to eliminate graphical user interface-originated problems and to reduce the processing and memory requirements for the system. All services, such as web hosting, database, network sharing, secure socket shell, etc., were executed automatically without user intervention every time the system started. Whenever there is a power cut to the system, the system will be back online automatically once the power is restored.

The cultural mapping system hardware architecture is shown in Fig. 4. The integrated application hosting and the portal system consist of both the IoT computing system with its NAND storage appliance for cultural mapping applications and the solar power controller that provides power to both the IoT system and the external WiFi router that acts as the wireless network interface for user device access, such as an iPad. The renewable solar power system is an appropriate power source owing to the solar power availability in the Buayan region, which has direct normal irradiation of more than 3kWh/m² daily [9]. The proposed solar power system design uses five sets of 30W panels and is configured for a 40Ah lead-acid car battery. The reason for adopting a car battery is that the battery is a consumable item and needs to be replaced every two years. Hence, to enable easy replacement by the community, the battery shall be the type that can be easily found in the nearby town. The solar system-specific battery is relatively more challenging to obtain. The adoption

of the solar power system with charging ports is to create a self-sufficient ecosystem where the same system can also charge the iPad used for accessing the cultural mapping system.

VI. SYSTEM IMPLEMENTATION AT BUAYAN

The system was successfully implemented in one of the households in Buayan in August 2022. Fig. 5 shows the proposed system's implementation, which includes an integrated application hosting and portal system module, a battery bank, and installed solar panels. Fig. 6 shows the community interacting with the cultural mapping system via the iPad.

The deployed system has been observed to be running well 24 hours a day. The solar power supply is consistent, and the hosted cultural mapping service is stable. Local communities have been using the system for cultural inventory every few hours a day. We look forward to further feedback from the users if any new system-related issues are discovered.

VII. CONCLUSION AND FUTURE WORKS

This paper presents the implementation of a new system architecture specifically designed to overcome local limitations to ensure a more reliable, cheaper, and community-maintainable system for the purpose of cultural mapping. The proposed architecture evolved from previous Telecentres design experience to address the community's need for a specific application. By being able to design and implement a system architecture that scales down significantly to minimise power requirements based on its application, the crucial renewable energy solar system design will also be designed into a smaller and portable system, which is critical for rural implementation. The significant costs incurred in digital system implementation in remote rural areas are the provision of power supply and transportation. Although cloud computing might not be suitable based on the patchy and slow network connection in Buayan, remote management will be a good initiative to provide technical support to the Buayan community remotely.

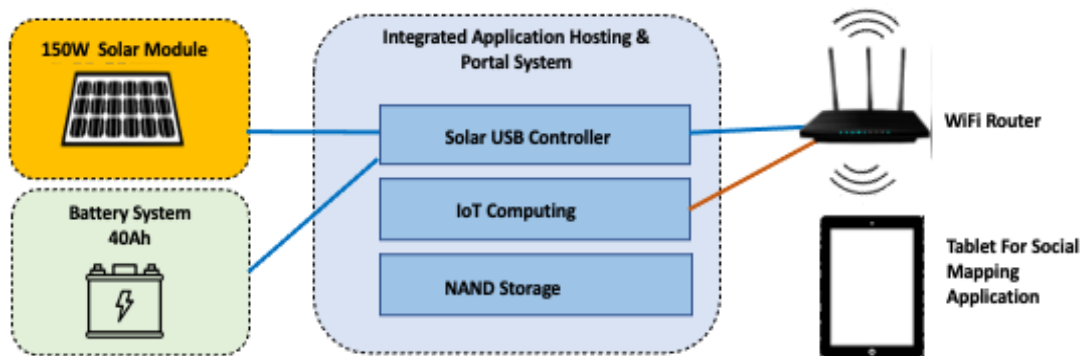


Fig. 4. The Cultural Mapping System Hardware Architecture.

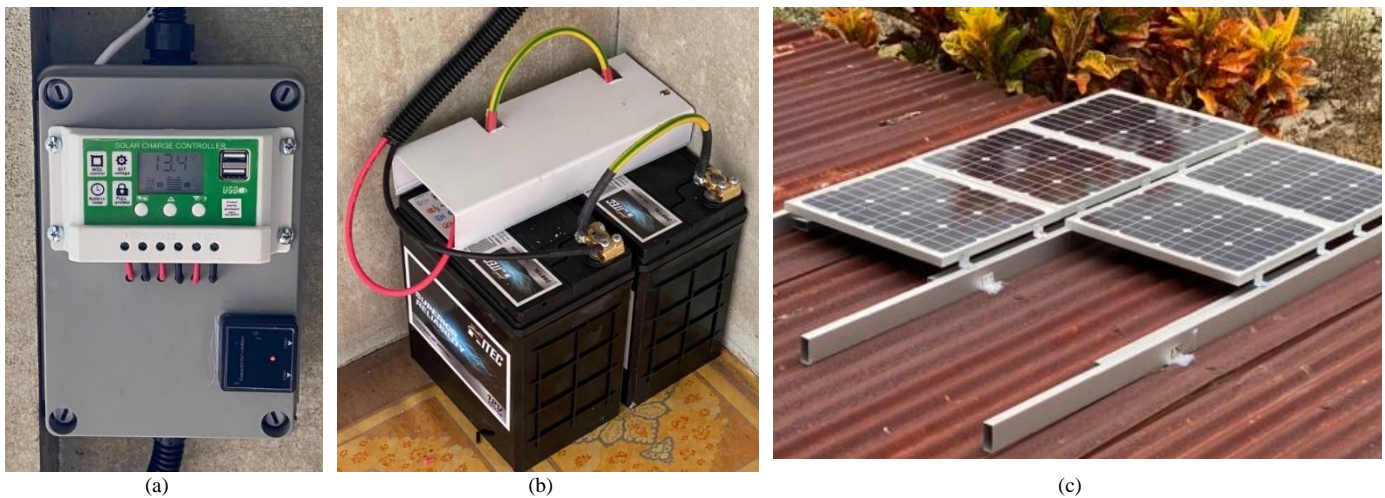


Fig. 5. The Hardware and Software Implementation of the Proposed System at Buayan. (a) The Housing for the Integrated Application Hosting, Portal System Module and Solar Power System with Charging Ports, (b) The Energy Storage System with Two Parallel Connected Car Batteries, and (c) the Five 12V 30W Solar Panels of the System.



Fig. 6. The Community Were Interacting with the Cultural Mapping System via the iPad.

ACKNOWLEDGMENT

This research is fully supported by Universiti Malaysia Sarawak through the Cross Disciplinary Research Grant Scheme F08/CDRG/1825/2019. The authors fully acknowledged the university for the approved fund which makes this research viable and effective.

REFERENCES

- [1] J. Pillai, Cultural mapping: A guide to understanding place, community and continuity, 2nd Editio. Strategic Information and Research Development Centre, 2020.
- [2] L. Powell, "Earth Voices: Kampung Buayan, An Indigenous Micro Hydro Community in Malaysia Borneo," 2019. <https://www.hpnet.org/blog/earth-voices-ft-kampung-buayan-an-indigenous-micro-hydro-community-in-malaysian-borneo>.
- [3] A. W. Yeo, F. S. Hazis, T. Zaman, P. Songan, and K. A. Hamid, "Telecentre Replication Initiative in Borneo Malaysia: The CoERI Experience," *Electron. J. Inf. Syst. Dev. Ctries.*, vol. 50, no. 1, pp. 1–14, Jan. 2012, doi: 10.1002/j.1681-4835.2012.tb00353.x.
- [4] R. Harris, N. A. N. K. Ramaiyer, and J. Tarawe, "The eBario Story: ICTs for Rural Development," in 2018 International Conference on ICT for Rural Development (IC-ICTRuDev), Oct. 2018, pp. 63–68, doi: 10.1109/ICICTR.2018.8706855.
- [5] C. E. Tan, P. Bala, S. Ping, and S. Mooi, "The TPOA Telecentre: A Community Sustainable Telecentre Architecture," *Int. J. Adv. Comput. Sci. Appl.*, vol. 11, no. 8, 2020, doi: 10.14569/IJACSA.2020.0110824.
- [6] B. R. Dawadi, D. B. Rawat, S. R. Joshi, and M. M. Keitsch, "Towards energy efficiency and green network infrastructure deployment in Nepal using software defined IPv6 network paradigm," *Electron. J. Inf. Syst. Dev. Ctries.*, vol. 86, no. 1, Jan. 2020, doi: 10.1002/isd2.12114.
- [7] A. Anand, V. Pejovic, D. L. Johnson, and E. M. Belding, "VillageCell: Cost effective cellular connectivity in rural areas," *ACM Int. Conf. Proceeding Ser.*, pp. 180–189, 2012, doi: 10.1145/2160673.2160698.
- [8] S. G. Yew, C. E. Tan, and R. Thangaveloo, "Green Power architecture considerations for rural computing," in 2011 IEEE 10th Malaysia International Conference on Communications, Oct. 2011, pp. 18–22, doi: 10.1109/MICC.2011.6150292.
- [9] The World Bank, "Solar resource maps of Malaysia," [Online]. Available: <https://solargis.com/maps-and-gis-data/download/malaysia/> [Accessed: 10-Oct-2022].

Research on Personalized Recommendation of High-Quality Academic Resources based on user Portrait

Jianhui Xu¹, Mustafa Man^{2*}, Ily Amalina Ahmad Sabri^{3*}, Guoyi Li⁴, Chao Yang⁵, Mingxue Jin⁶

Faculty of Ocean Engineering Technology and Informatics, Universiti Malaysia Terengganu, Terengganu, Malaysia^{1, 2, 3}

Department of Physical Education, Shenyang Medical College, Shenyang China⁴

Faculty of Ethnic Culture and Vocational Education, Liaoning National Normal College, Shenyang China^{5, 6}

Abstract—With the advent of the era of big data, the phenomenon of information overload is becoming increasingly serious. It is difficult for academic users to obtain the information they want quickly and accurately in the face of massive academic resources. Aiming at the optimization of academic resource recommendation services, this paper constructs a multi-dimensional academic user portrait model and proposes an Academic Resource Recommendation Algorithm Based on user portrait. This paper first, combs the relevant literature and information; Secondly, to obtain the attribute tags of multi-dimensional user portraits, a set of questionnaires are designed to collect the real information of academic users, and the corresponding academic user portrait model is constructed; Then, the collected data is processed through certain rules, and the user is quantitatively modeled based on the data through mathematical means; Finally, through the construction of the completed academic user portrait model, combined with collaborative filtering algorithm, provide personalized academic resource recommendation services for academic users. Through the verification and analysis of simulation experiments, the Academic Resource Recommendation Algorithm Based on the user portrait proposed in this paper plays a great role in expanding users' interest fields and discovering new hobbies across fields and disciplines.

Keywords—Personalized recommendation system; user portrait; academic resources; collaborative filtering

I. INTRODUCTION

Academic users are increasingly finding it difficult to obtain the information they want quickly and accurately in the face of massive academic resources, which often require a lot of time and energy. Therefore, the research of personalized recommendation services for academic resources is particularly important. Personalized recommendation services of academic resources can mine users' potential interests according to the personalized attributes of academic users, to actively recommend the academic resources users need [1]. Therefore, personalized recommendation service of academic resources has greatly improved the shortcomings of traditional retrieval systems, such as redundant information and difficult screening, and can meet various preferences and needs of academic users.

A. The Statement of the Research Problem

At present, most of the recommendation systems in the academic field adopt Content-Based Recommendation methods. The Content-Based Recommendation method focuses on the similarity of content features, which ignores most user preference features, such as the level of academic resources, the

author of academic resources, etc. There are still many common problems in the recommendation of academic resources. For example, the recommendation of multiple types of academic resources, the preferences and needs of users with different identities, etc., resulting in unsatisfactory recommendation results [2].

1) Traditional search engines rely too much on keywords, and do not take into account the retrieval users' own attributes, such as interest preferences, research fields, retrieval purposes and other factors, which do not meet the requirements of personalized recommendation services.

2) The diversity of academic resources in the existing academic recommendation system is low, and it is impossible to recommend interdisciplinary and heuristic resources.

B. Research Objectives

1) To study the existing personalized recommendation algorithms of academic user modeling, academic resource modeling and academic resources.

2) To propose appropriate academic resource recommendation strategies, find the deep connection between user personalization and literature diversity, and recommend users with personalized and diversified recommendation results.

3) Accurately reflect user characteristics, meet users' diverse reading needs, build a multi-dimensional academic user portrait model, and form an Academic Resource Recommendation Algorithm Based on user portrait on the basis of collaborative filtering algorithm.

C. Research Question

There are two important issues that need to be addressed. First, how to calculate the similarity between students through behavioral data, and require that the similarity reflect the interests and learning characteristics of student strengths. Second, after identifying a new sample of near-neighbor students, how to determine the set of recommended courses to be selected based on the near-neighbor students' course selection records [3].

D. Rationale of the Study

In view of the insufficient characteristic information of the current academic resource database, which leads to the incomplete recommendation system, based on the current relatively mature database, this paper uses the literature research method, questionnaire survey method, big data

*Corresponding Author.

analysis and other related research technologies to lay the foundation for the follow-up recommendation system research. At present, the existing recommendation methods are mainly divided into content-based recommendation methods, collaborative filtering-based recommendation methods and hybrid recommendation methods. Based on the previous research, this paper builds a multi-dimensional academic user portrait for academic users, adopts the optimized collaborative filtering recommendation model, and tries to find cross domain academic resources that users are potentially interested in and have certain guiding significance for users [4].

E. Research Gap

From the current status of research, we can see that in recent years, there have been numerous studies on recommendation in education at home and abroad, but most of these studies are on K12 education, i.e., basic education, and fewer studies on learning resource recommendation algorithms for students in higher education. Therefore, it is more difficult to recommend learning resources for students in higher education than for students in basic education. In previous studies on learning resource recommendation, most of them improve the classical collaborative filtering algorithm to achieve the effect of improving the recommendation accuracy, and the user profile is not systematically utilized, which will be affected by factors such as cold start and sparse data matrix, resulting in poor recommendation effect.

To sum up, recommendation system is very crucial to solve the problem of resource overload, which attracts the majority of enterprises and scholars to conduct research. However, the application of recommendation system in the field of online education is not widespread and the recommendation algorithm is not perfect, and there is no integration of user portrait into the process of recommendation algorithm, especially there is no recommendation algorithm of learning resources for college students, and college students, as the backbone of online education, are an important part of online learning users, so it is necessary to realize the recommendation algorithm of learning resources integrating user portrait for college students, and Complete the design and development of the learning resource recommendation platform.

II. LITERATURE REVIEW

Academic resource recommendation service is a relatively mature service in the field of scientific research, and the existing research focuses on different aspects, which cannot meet the diversified needs of users. For example, CiteULiket focuses on maintaining the citation relationship of papers, Google Academic provides a complete paper search function, and Aminer platform uses data mining algorithms and analyzes social networks to provide academic users with not only basic academic resource retrieval services, but also current hot academic topics, visualization of trends in research directions, and deep mining of scholars' social networks and other functions. In order to further improve the academic resource recommendation service. Scholars build recommendation algorithms for academic resources by studying users' academic behaviors to tap users' interests, research directions and other academic preferences. S. Bhaskaran et al. used content filtering algorithms to analyze user behavior, such as citing papers and

displaying ratings, to recommend academic papers of interest to users [5]. M. Venkatesh et al. used machine learning algorithms to construct a user requirements model that can adaptively match user preferences with a target library repository to complete user-oriented personalized recommendations of digital library resources [6].

In recent years, research trends in information behavior models have shown the following four aspects.

First, the research content is further refined, both for a certain type of information behavior and for the characteristics of information behavior models; Second, the research object is further subdivided, the academic user group is divided into multi-level and multi-dimensional, and information behavior models for different subject areas; Third, the factors affecting information behavior are more explored, and efforts are made to explore the micro-level; Fourth, the research methods are diversified, mainly survey and interview methods are used in data collection, supplemented by literature analysis and experimental methods, etc.

In general, the existing domestic and foreign academic resource recommendation systems and recommendation algorithms have met users' personalized needs to a certain extent. However, there are still some problems: firstly, the recommendation algorithms are mostly based on users' academic preferences, which makes the range of academic resources recommended relatively single and the diversity of academic resources low. First, the recommendation algorithms are mostly based on users' academic preferences, which makes the range of academic resources recommendation results relatively single and the diversity of academic resources low, and cannot achieve cross-disciplinary and cross-domain heuristic resources. The recommendation algorithm is mostly based on users' academic preferences. Secondly, in the face of the growth of massive academic resource data, the processing capability and machine learning capability of the system have become the key issues that must be addressed in the future academic resource recommendation system. In the future, the processing capability and machine learning capability of the system become the challenges that must be solved for academic resource recommendation systems.

This section will elaborate and introduce the relevant background knowledge of this research content, including personalized recommendation and user portrait theory and their application in the field of academic resources. Finally, the commonly used evaluation indicators of the recommendation system and the subsequent chapters of this paper are briefly explained, which paves the way for the proof of measuring the scientific effectiveness of this paper.

A. Personalized Recommendation Theory

The purpose of the recommendation system is to use the collected user information and item information to establish user models and item models, and match them according to specific rules. The recommendation algorithm plays a bridge role in this matching rule. Finally, the rules contained in the algorithm are used to filter the calculation results, to find the products that users may be interested in, and recommend them to users. This section selects three types of recommendation

systems related to the research content of this paper for a brief introduction, which are: content-based recommendation system, collaborative filtering-based recommendation system, and hybrid recommendation algorithm.

1) *Content-based recommendation system*: Content based recommendation is also called attribute based on recommendation. In the process of recommendation system, it can be seen that both items and users contain certain attribute information. Because the attribute information of items is relatively static and objective, it is very easy to calculate the correlation between the degrees of similarity. The content-based recommendation algorithm is to discuss whether the actual attributes of the two items to be recommended are similar. As the basis for judging whether to recommend or not, the core task of the algorithm is to calculate the similarity of the attributes of the items as shown in Fig. 1.

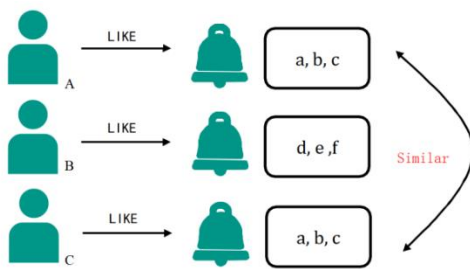


Fig. 1. Content based Recommendation System.

The disadvantages of content-based recommendation are as follows:

- a) Relying on the classification of the objects to be recommended, the quality of recommendation is greatly affected by the nature of the objects to be recommended.
- b) For users, the recommendation process is based on the analysis of existing content, and the recommendation results are difficult to innovate. Therefore, it is difficult to develop new product fields, and the ability to inspire users' interests and hobbies and promote users to contact new things is insufficient.
- c) In front of a new user who has no historical reading record at all, there is no interactive item record, and there is no way to analyze the characteristics of items, so it is impossible to match the content to achieve recommendations, and only provide content to users in a way similar to the "popular list".
- d) It requires a large amount of data of the object to be recommended, takes up large storage and computing space, and increases the cost of recommendation services.

2) *Recommendation system based on collaborative filtering*: In the field of Resource Recommendation Based on collaborative filtering, resources are mainly based on traditional collaborative filtering algorithms. Recommendation work, establish user documents based on the semantic analysis of users' reading literature, find similar user documents and predict users' interests through traditional collaborative filtering methods, and realize personalized recommendation the accuracy of such recommendation algorithms is vulnerable to data sparsity and cold start problems [7]. Therefore, integrate users

according to the types of scoring items and user scoring items, the user similarity is calculated, and the corresponding collaborative filtering algorithm is designed to improve the accuracy of recommendation results [8]. Niu et al. used three different types of information (users, items, user items) to deal with the problem of data sparsity, predicted the item score, and produced high-quality recommendation results [9]. L. Antony Rosewelt et al. proposed to integrate the intimate relationship between friends into the recommendation model to recommend resources for new users under the same interest topic [10].

Collaborative filtering recommendation research has obvious deficiencies in two aspects:

On the one hand, these studies mainly use users' explicit and implicit behavior data to model users' interests, which is prone to the problem of data sparsity; on the other hand, these studies are often based on static scenarios, and it is difficult to cope with the real needs of online mobile recommendation of academic resources under the situation of constantly updating user data and changing user needs.

B. Academic user Portrait

User portraits for academic users are more focused. In order to more accurately recommend academic resources, it is necessary to obtain and describe the characteristics of academic users' interest in academic resources, so as to depict accurate academic user portraits. All the interest characteristics of users can be divided into different types [11]. One classification method is to divide user portraits into explicit features and implicit features according to different acquisition methods. Explicit features refer to a kind of academic user features that can be obtained directly without deep mining, such as name, age, education, major, identity, etc., and also include research directions and research fields independently defined by users. Such features can be collected manually, or automatically retrieved by software on the basis of user consent. The implicit feature is the feature attribute calculated and analyzed after deep mining a series of academic behavior and other information of academic users. Generally, it needs to be collected by software such as web crawlers and obtained by using the relevant algorithms of data mining. Explicit features are simple and fast to obtain, but the level is shallow and the flexibility is not high. Implicit features can mine more interesting features of users, but rely on higher cost calculation, which is a complementary role of explicit features. Users' academic behavior refers to academic related interaction behavior, which can be the retrieval, download, collection, quotation and other behaviors of academic resources. The purpose of analyzing these academic behaviors is to infer users' academic interest tendency, further supplement users' interest characteristics, and improve academic user portraits. The purpose of analyzing these academic behaviors is to infer users' academic interest tendency, further supplement users' interest characteristics, and improve academic user portraits [12].

Before designing an academic resource, recommendation service based on user portrait, it is necessary to establish a multi-dimensional academic user portrait model, which can obtain user attributes in an all-round and multi-level way, accurately reflect user characteristics, and meet users' diverse

reading needs. The multi-dimensional academic user portrait is mainly composed of two parts: dimensional analysis and model construction.

C. Dimension Analysis of Academic User Portrait

The establishment of user portrait dimension is the basis of establishing user portrait model. An ordinary academic user will have a series of information that can affect the acquisition of academic resources, including the most basic attributes of a person, as well as academic preferences fed back from academic behavior. In addition, there are some additional factors that can be defined and distinguished, user information that can optimize the recommendation service of academic resources. This kind of information has obvious personal style, so this paper calls this kind of dimension "academic personality"[13-17].

Accordingly, this paper selects the following three dimensions: basic information, behavioral characteristics and academic personality as the components of the multi-dimensional academic user portrait as shown in Fig. 2.

D. Construction of Multi-dimensional Academic User Portrait Model (MAUPM)

In order to obtain the real data needed in the process of academic user portrait modeling, this paper designs a set of questionnaires for data collection. For the two dimensions of basic information and academic personality, the questionnaire is divided into two parts: The first part mainly adopts the form of multiple-choice questions, including age, gender, education background, major, identity, time engaged in scientific research, research direction and other questions, which are used to collect basic information. In the second part, through the further investigation of users, including the scientific research progress and the proficiency of using the academic resource platform, combined with the identity, professional title, working time and other information obtained in the first part, we can get the users' academic motivation and domain knowledge. For the investigation of cognitive style, the scale test commonly used in the field of psychology is used to set up eight scenarios and let users choose the situation that is consistent with themselves. In order to supplement and verify the authenticity of the results of the scale, the questionnaire also set up a mosaic graphic experiment, which requires users to find the specified simple graphics in a complex graphics. Users who prefer field independent cognitive style can find simple graphics in complex graphics faster [18].

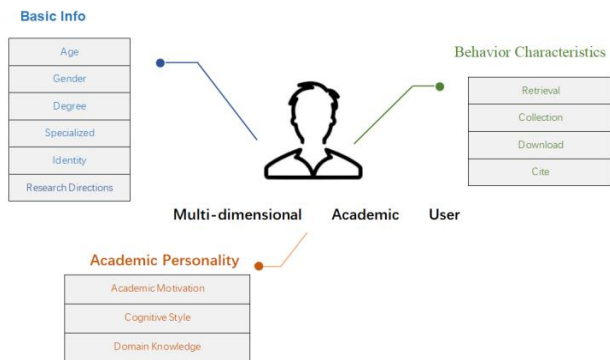


Fig. 2. Multi-dimensional Academic user Portrait Structure.

The results of these questions can finally feedback the "academic personality" of the surveyed users. For the dimension of behavior characteristics, it is obtained by viewing the behavior logs of academic users on the academic resource platform. Based on the collected data, this paper constructs a multi-dimensional academic user portrait model [19].

1) Basic information model: It is divided into six sub dimensions: age, gender, education, major, identity and research direction. In order to simplify the information, the age dimension adopts the form of age group, and the research direction is described by the data filled in by users in the questionnaire. The basic information model is shown in Table I.

TABLE I. BASIC INFORMATION MODEL

Sub Dimension	Value
Age	Under 30 years old, 31-40 years old, 41-50 years old, 51-60 years old, under 60 years old
Sex	Male / Female
Education	Bachelor's degree or below, Bachelor's degree, Master's degree, Doctor's degree or above
Profession	Philosophy, Economics, Law, Pedagogy, Literature, History, Science, Engineering, Agriculture, Medicine
Identity	Students, Teachers
Research Direction	Fill in by yourself, such as "control theory".

Behaviour characteristics are composed of four dimensions: user's retrieval, collection, download and reference.

The values of each dimension are as follows:

- Search dimension: the user's search term K, the time to visit the page t (unit: minutes), and the document name P of the search page.
- Collection dimension: user's collection page document name C.
- Download page: user's download page document name D.
- Citation dimension: user's citation name R.

The behavioural characteristic model is shown in Table II.

TABLE II. BEHAVIORAL CHARACTERISTIC MODEL

Sub Dimension	Value
Retrieval	Search term K
	Access time T
	Search page document name P
Collection	Collection page document name C
Download	Download page document name D
Quote	Reference name R

2) Academic personality model: The three sub dimensions of academic motivation, cognitive style and domain knowledge are described by the data obtained from the questionnaire, in which academic motivation and domain knowledge can be obtained directly from the results checked by users. The academic personality model is shown in Table III.

TABLE III. ACADEMIC PERSONALITY MODEL

Sub Dimension	Value
Academic Motivation	Explicit, Fuzzy
Cognitive Style	Field Independent, Field Dependent
Domain Knowledge	Junior User, Experienced User

In order to accurately judge the cognitive style of academic users, this paper converts some literality in the questionnaire into specific values (scores). Three variables were defined: scale value n , speed value V and cognitive style index s . The n value represents the score of the user in the scale test. The higher the score of each question, the more consistent it is with the described situation, and the user is more inclined to the field independent cognitive style in the situation of this question; The V value represents the user's response in the mosaic graphic experiment. The faster the user completes the mosaic graphic experiment, the more it can reflect the user's field independent cognitive trend; the cognitive style index s reflects the final situation of the user's cognitive style. The higher the s value of the user, the more the user prefers the field independent cognitive style. The lower the S value, the more the user prefers the field dependent cognitive style [20-22]. S value is positively correlated with n value and V value, and the calculation formula of s value is $S = N \times V$.

S is the cognitive style index, n is the score of the scale test questions, and V is the score of the graphic mosaic experiment.

It can be predicted that with the development of new technology, academic personalized recommendation will produce new ideas, models and methods, and the results of recommendation will be more and more satisfactory. In order to solve the problem of information overload, this method will become one of the research contents in the academic field for a long time [23].

III. METHODOLOGY

The portrait constructed above is a three-dimensional map based on semantic information. This chapter will quantify all dimensions in the three-dimensional map, fuse and reconstruct, store each user's information in the form of vectors, and construct a vector-based user portrait. Then, combined with the user based collaborative filtering algorithm, the similarity between vectors is calculated, so as to predict the list of academic resources recommended by users to be recommended [24].

A. User Attribute Vector

This paper divides the academic user portrait into three dimensions: basic attributes, academic personality and behavioral characteristics. Among them, the basic attribute and academic personality are relatively static objective attributes, which can reflect the user's personal attributes over a period of time, and can be clearly expressed through discrete and unique values, for example, the gender can only be "male" or "female". Therefore, in the process of practical application, the basic attributes and academic personality dimensions are combined and deleted to form the user attribute vector. User Info={Age, Gender, Education, Profession, Identity, Motivation, Style} There are two (2) parts deleted: 1. Change the "age" label

to "age range" in order to reduce the number of discrete data and reduce the amount of calculation; 2. The sub dimension of "domain knowledge" is deleted because the domain knowledge level of an academic user has been reflected in the attributes of age, identity, education and major. Deleting this dimension can reduce the workload and avoid defining evaluation indicators, so as to avoid the error loss caused by subjective judgment [25]. According to the multi-dimensional academic user portrait model, the reconstructed and fused user attribute vector and its values are shown in Table IV.

Because the total number of dimensions of user attributes is not large, this paper uses "one-hot" to encode vectors. One hot encoding, alias is an effective bit encoding. The encoding idea is to set n -bit status registers to represent in different states. Each bit register has only "0" and "1" states. No matter how many bits the register has, when representing each state, only one bit is valid, that is, the position representing the state is "1", and the other positions are "0"[26]. For example, if the "age range" attribute has five values, the attribute code form is a Five-Dimensional vector. When the value is "under 30 years old", the attribute code is: age = {1, 0, 0, 0, 0}. When the value is "over 60 years old", the code is: age= {0, 0, 0, 1}.

TABLE IV. USER ATTRIBUTE VECTOR VALUE AND CODING

User Attribute Vector	Value	Code
Age Group	Under 30 years old	{1, 0, 0, 0, 0}
	31-40 years old	{0, 1, 0, 0, 0}
	41-50 years old	{0, 0, 1, 0, 0}
	51-60 years old	{0, 0, 0, 1, 0}
Sex	Male	{1, 0}
	Female	{0, 1}
Education	Below bachelor degree	{1, 0, 0, 0, 0}
	bachelor degree	{0, 1, 0, 0, 0}
	Master degree	{0, 0, 1, 0, 0}
	Doctor degree	{0, 0, 0, 1, 0}
Profession	Philosophy	{1, 0, 0, 0, 0, 0, 0, 0, 0, 0, 0, 0}
	Economics	{0, 1, 0, 0, 0, 0, 0, 0, 0, 0, 0, 0}
	Law	{0, 0, 1, 0, 0, 0, 0, 0, 0, 0, 0, 0}

Identity	Student	{1, 0, 0, 0, 0}
	Assistant	{0, 1, 0, 0, 0}
	Lecturer	{0, 0, 1, 0, 0}
	Associate Professor	{0, 0, 0, 1, 0}
	Professor	{0, 0, 0, 0, 1}
Academic motivation	Explicit Type	{1, 0}
	Fuzzy Type	{0, 1}
Cognitive style	Field Dependence	{1, 0}
	Field Independent Type	{0, 1}

B. Similarity Calculation

The cosine similarity formula is used in this paper, so the similarity formula of user attribute vector is:

$$\text{Sim_Info}(a, b) = \cos(A, B) = \frac{\sum_{i=1}^n A_i B_i}{\sqrt{\sum_{i=1}^n A_i^2} \sqrt{\sum_{i=1}^n B_i^2}} \quad (1)$$

where, a and B are the user attribute vectors of a and B users, and A_i and B_i are the attribute values of each dimension of the two users respectively. The formula of vector similarity in the research field is:

$$\text{Sim_Area}(a, b) = \cos(X, Y) = \frac{N(X) \cap N(Y)}{\sqrt{N(X) \times N(Y)}} \quad (2)$$

$N(X)$ and $N(Y)$ are the number of keywords in the research field vector of users a and B respectively. Suppose that the research field vectors of users a and B are respectively: $\text{User_area_a} = \{\text{User portrait, Recommendation system, Education system}\}$ $\text{User_area_b} = \{\text{User portrait, Marketing, Business Administration}\}$ The denominator is $\sqrt{N(A)} \times \sqrt{N(B)}$ in form according to the similarity formula. [27].

C. Generate Recommendation List

Finally, the user group with high similarity to the users to be recommended is called the "most similar user set", and the academic resources that the "most similar user set" likes but the users to be recommended have not interacted with are recommended to them. Let user A mark the thesis set as P_A , the most similar user set of a as U_A , the recommended thesis set as R , and the thesis set as P . Then user A 's recommended thesis collection is $R_A = \{p \mid p \in P_i, i \in U_A, p \notin P_A\}$.

This recommendation algorithm does not consider the users' scores on the papers, because the collection of papers adopts a single implicit feedback data, and takes the "interaction" between collections, downloads and academic resources as the basis of users' interest [28].

IV. ANALYSIS AND RESULTS

A. Experimental Environment

Experimental Platform: Windows10 64-bit operating system, 11th Gen Intel(R) Core (TM) i7-11800H @ 2.30GHz 2.30 GHz 3.40GHz, 16.0 GB RAM. Tools: Java, Python, SPSS.

B. Data Acquisition and Processing

In order to verify the accuracy of the academic resource's recommendation algorithm proposed in this chapter, 100 users of the questionnaire were selected, and the historical reading list of academic resources was manually collected from them. Each person had a total of five documents, including title, abstract and keyword information. Three of the five papers are used as training sets and two test sets, that is, three papers are the user's "historical reading list" and two papers are the "future real reading list". The questionnaire survey results are obtained from the "questionnaire star" website background management system, stored in SPSS files, and the user attribute vector of each user can be obtained after encoding the data. From the data, the selected 100 users have the same educational background,

major and identity, which provides a practical basis for subsequent recommendations based on collaborative filtering. After grouping and numbering the manually collected user history reading papers, we use python3.0 programming language and TF-IDF algorithm to extract keywords from the title and abstract of the literature. Combined with the keyword information of the literature itself and manual verification, after duplication and error correction, a total of 689 keywords of 350 documents were finally obtained.

1) *Collect questionnaire analysis:* From the questionnaire collected, the proportion of men and women in the surveyed population is 55.48% to 44.52%, about 1:1; Users' majors are mainly engineering, and they are academic users of philosophy, law, pedagogy, science, medicine and management; In terms of academic qualifications, 81.66% are masters, 19.34% are undergraduates, and the user groups are students. The following mainly analyzes the survey results of the third dimension "academic personality" in the user portrait proposed in this paper.

In the survey results of the scientific research stage of this questionnaire, 39.93% of users choose the scientific research preparation stage, 49.72% of users choose the scientific research progress stage, and 10.35% of users choose the scientific research publication stage. It can be seen that academic users will indeed experience different stages of scientific research on the road of scientific research, and they will also have different academic motives in the search process of academic resources. Count the cognitive style index s of the surveyed users and calculate the benchmark value $s = 11.316$, the results show that 55.17% of the academic users participating in the survey have field independent cognitive style, and 44.82% of the users have field dependent cognitive style. For the statistics of domain knowledge level, the information sources include the user's age, education background, professional title, time engaged in scientific research, proficiency in using academic resource platform, etc. In this questionnaire survey, users with bachelor's degrees without exception chose "directly use one or several keywords to search and try to expand the search scope", while nearly half of users with master's degrees chose the same common search methods as users with bachelor's degrees, and 38.46% of users chose "select certain restrictions (phrases, tags, etc.) while using keywords", Another 11.54% of users made the choice of "traversing relevant academic resources with the author or publishing unit and the journal as the search tag". It can be seen that with the gradual accumulation of scientific research experience, academic users' domain knowledge is also expanding, and there are certain differences between primary users and experienced users in the acquisition of academic resources. Therefore, it is essential to integrate the academic experience level of academic users into user portraits. Through the analysis of the questionnaire results, academic users have different academic personalities, and the user portrait integrated into academic personality is more three-dimensional, which can greatly improve the personalization and accuracy of academic resource recommendation services.

C. Implementation of Recommendation Algorithm

The test papers contain the user's real reading list in the future, which can analyze and verify the predicted value and the real value to obtain the accuracy of the recommended algorithm.

Based on the above, the complete recommendation steps for a user to be recommended is shown in Fig. 3.

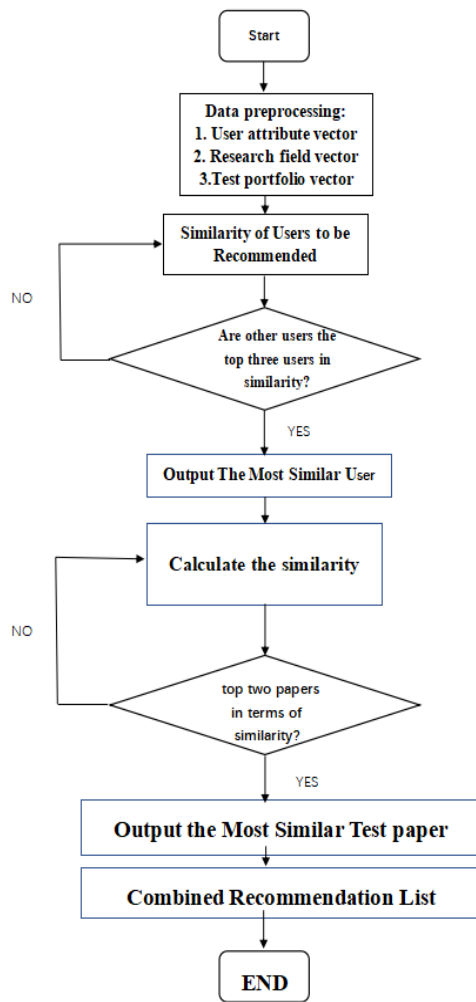


Fig. 3. Algorithm Experiment flow Chart.

V. RESULT AND DISCUSSION

A. Offline Test

Finally, each 100 users will get six recommended papers, and a total of 600 papers will be generated from the recommendation list number the test papers from 1 to 600, and the number of the recommended papers of 100 users and their corresponding test papers, that is, the number of "future real reading list", is shown in Table V.

In this article, "recall rate" and "accuracy rate" will be used as the basis for scoring. Let $R(u)$ represent the user's real reading list in the future, that is, the test paper collection, and $T(u)$ represent the recommendation list finally predicted by the algorithm.

$$\text{Recall} = \frac{\sum_{u \in U} |R(u) \cap T(u)|}{|T(u)|} \quad (3)$$

$$\text{Precision} = \frac{\sum_{u \in U} |R(u) \cap T(u)|}{|R(u)|} \quad (4)$$

TABLE V. COMPARISON BETWEEN RECOMMENDED PAPERS LIST AND REAL READING LIST

No.	Recommended Paper No.	Real reading paper No.	Number of Correct Predictions
1	20,12,3,19,3,15	1 2	0
2	8,6,11,9,3,20	3 4	1
3	9,1,14,13,17,18	5 6	0
4	8,6,9,1,14,13	7 8	1
5	6,5,14,13,17,18	9 10	0
6	8,6,20,12,3,15	11 12	1
7	6,5,9,1,17,18	5,9,17	3
8	8,6,9,1,14,13	6,9,13,14	4
9	6,5,9,1,14,13	1,18	1
10	8,6,9,1,3,20	19 20	1
...

It is calculated that the recall rate of the proposed algorithm in the offline test is 70% and the accuracy rate is 78.7%.

B. User Research Method

This article will pay a return visit to 80 test users. The recommendation list generated by the algorithm is conveyed to the test users to collect their real evaluation. The contents of the return visit and investigation include the following:

1) Satisfaction with the number of papers: Are you satisfied with the number of papers in the recommendation list (Dissatisfied, Generally Satisfied, Relatively Satisfied, Very Satisfied).

2) Thesis title reading interest evaluation: Just observe the title of the paper in the recommendation list. Do you want to click to read it? (No, generally, quiet, very much).

3) Cross domain reading interest evaluation: Have you found any papers that are different from the current research field but still interested in from the list of recommendations? (In conformity, general conformity, relatively conformity, very conformity).

The return visit results are shown in Fig. 4.

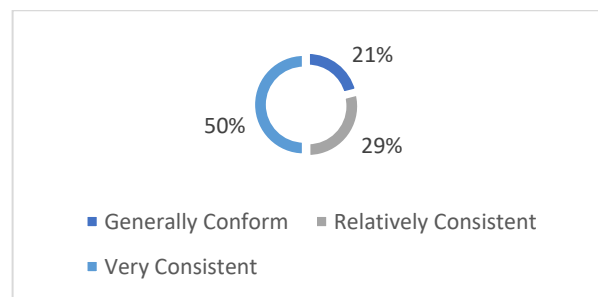


Fig. 4. Satisfaction with the Number of Papers and Reading Interest Evaluation.

The result analysis of the three problems has the following conclusions.

Most of the revisited users are very satisfied with the number of papers in the recommendation list, indicating that the

number of five to six recommended papers can meet the reading needs of ordinary academic users. On the academic resources of retrieval website, the most intuitive part presented to users is the title of the paper. Most revisiting users are satisfied with the recommendation results from the perspective of the title of the paper, of which 84% of the recommended papers are favored by users. 3.53.7% of the revisited users believed that the literature resources in the recommendation list were different from the current research field, but they still had great interest, and 39% of the users were also more willing to read the recommended papers in the interdisciplinary field. It can be seen that the Academic Resource Recommendation Algorithm Based on user portrait proposed in this paper can expand users' research interests, improve users' interdisciplinary and interdisciplinary reading tendency, and help academic users inspire new research directions.

C. Innovation Points

Aiming at the current trend of more and more cross domain cooperation in scientific research, this paper explores the potential interests of users, analyzes the cognitive style trend of users from the perspective of psychology, so as to measure the cross domain academic resource needs of academic users, expand the factors of academic resource recommendation, and further improve the theoretical system of personalized recommendation of academic information resources.

This paper adopts interdisciplinary research, combines computer related technologies such as statistics, psychology, library and information science and data mining, adopts research methods such as questionnaire survey and empirical analysis, and integrates the research ideas of social science into the research of recommendation system, which has strong progressiveness and applicability.

D. Future Work

In the research process, the real user data used are phased static data, and the dynamic time factor is not considered, so the changes of academic users cannot be reflected in the user portrait. In the next work, it can use the existing computer technology to realize the dynamic tracking of user information, which can make up for this shortcoming.

VI. USER INTERFACE OF THE SYSTEM (GUI)

The implementation effect of the academic resource module based on personalized user portrait is shown in Fig 5.-Fig 7.

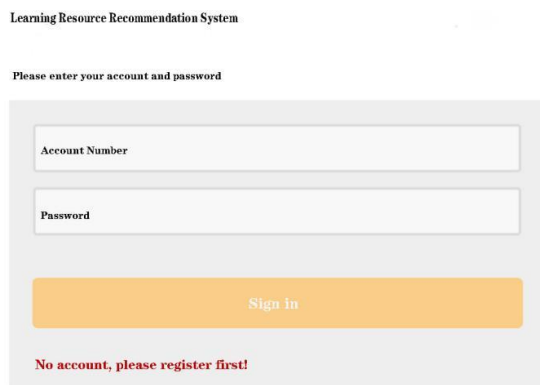


Fig. 5. Learning Resource Recommendation Login Interface.

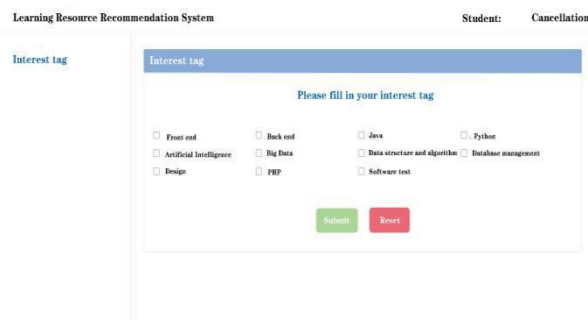


Fig. 6. User Interest Tag Acquisition.

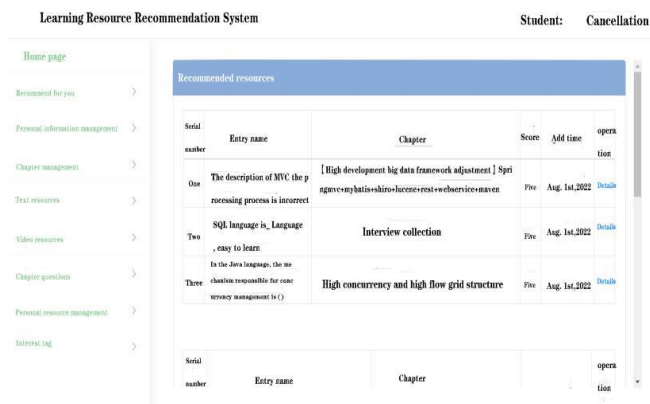


Fig. 7. Personalized Academic Resources Recommendation Display Interface.

VII. CONCLUSION

In recent years, it is more and more difficult for academic users to obtain the information they want quickly and accurately in the face of massive academic resources. Personalized recommendation system can solve this problem. The existing personalized recommendation system improves the shortcomings of the traditional retrieval system, such as information redundancy and difficulty in screening. To a certain extent, it can meet the various preferences and needs of academic users, but it also lacks the deep characterization of users' personal attributes. Therefore, from a new perspective, this paper attempts to mine the attributes of individual users, broaden the dimension of academic user portraits, and enhance the objectivity of academic resource recommendation services. Firstly, this paper studies the relevant knowledge of personalized recommendation system and user portrait theory, focusing on the definition, classification and evaluation indicators of recommendation system, and the construction method of user portrait. Then, in order to integrate the idea of user portrait into the personalized recommendation service of academic resources, based on the construction of a diversified and three-dimensional academic user portrait, the concept of "academic personality" is proposed on the basis of two basic dimensions of users' basic attributes and behavioral characteristics." Academic personality" includes three parts: users' academic motivation, cognitive style and domain knowledge. Through the infiltration of psychological theory, it further complements the portrait dimension of academic users and constructs a multi-dimensional academic user portrait model.

Finally, using the constructed multi-dimensional academic user portrait model, combined with the user based collaborative filtering method, an Academic Resource Recommendation Algorithm Based on user portrait is proposed, which optimizes the existing academic resource recommendation strategies. The experimental results show that the Academic Resource Recommendation Algorithm Based on user portrait proposed in this paper can play a great role in expanding users' interest fields and finding new hobbies across fields and disciplines.

REFERENCES

- [1] Al-Salman, S., & Haider, A. S. Jordanian University Students' Views on Emergency Online Learning during COVID-19. *Online Learning*, 25(1) pp286-302,2021.
- [2] Mabude, C. N., Awoyelu, I. O., Akinyemi, B. O., & Aderounmu, G. A. An integrated approach to research paper and expertise recommendation in academic research. *International Journal of Advanced Computer Science and Applications*, 13(4) doi:https://doi.org/10.14569/IJACSA.2022.0130456,2022.
- [3] Adenariwo, F. K., & Sulyman, A. S. Availability and accessibility of electronic information resources in academic libraries as predictors of academic performance of students. *Library Philosophy and Practice*, 1-10. Retrieved from <https://www.proquest.com/scholarly-journals/availability-accessibility-electronic-information/docview/2705446808/se-2,2022>.
- [4] S. S. Khanal, P. W. C. Prasad, A. Alsadoon, A. Maag, "A systematic review: machine learning based recommendation systems for e-learning," *Education and Information Technologies*, vol. 25 no. 4, pp. 2635-2664, DOI: 10.1007/s10639-019-10063-9, 2020.
- [5] M. Venkatesh, S. Sathyalakshmi, "Smart learning using personalized recommendations in web-based learning systems using artificial bee colony algorithm to improve learning performance," *Electronic Government, an International Journal*, vol. 16 no. 1/2, pp. 101-117, DOI: 10.1504/EG.2020.105253, 2020.
- [6] S. Bhaskaran, R. Marappan, B. Santhi, "Design and analysis of a cluster-based intelligent hybrid recommendation system for e-learning applications," *Mathematics*, vol. 9 no. 2, DOI: 10.3390/math9020197, 2021.
- [7] A. Klačnja-Milićević, M. Ivanović, B. Vesin, Z. Budimac, "Enhancing e-learning systems with personalized recommendation based on collaborative tagging techniques," *Applied Intelligence*, vol. 48 no. 6, pp. 1519-1535, DOI: 10.1007/s10489-017-1051-8, 2020.
- [8] X. Liu, "A collaborative filtering recommendation algorithm based on the influence sets of e-learning group's behavior," *Cluster Computing*, vol. 22 no. S2, pp. 2823-2833, DOI: 10.1007/s10586-017-1560-6, 2020.
- [9] P. Gao, J. Li, S. Liu, "An introduction to key technology in artificial intelligence and big data driven e-learning and e-education," *Mobile Networks and Applications*, vol. 26 no. 5, pp. 2123-2126, DOI: 10.1007/s11036-021-01777-7, 2021.
- [10] L. Antony Rosewelt, R. J. Arokia, "A content recommendation system for effective e-learning using embedded feature selection and fuzzy DT based CNN," *Journal of Intelligent & Fuzzy Systems*, vol. 39 no. 1, pp. 795-808, DOI: 10.3233/JIFS-191721, 2020.
- [11] J. Jeevamol, V. G. Renumol, "An ontology-based hybrid e-learning content recommender system for alleviating the cold-start problem," *Education and Information Technologies*, vol. 26 no. 4, pp. 4993-5022, DOI: 10.1007/s10639-021-10508-0, 2021.
- [12] Y. Han, H. Yao, F. Zhou, "Research on the intelligent ecology of modern vocational education system," *Modern Educational Technology*, vol. 28 no. 1, pp. 114-120, 2020.
- [13] Mabude, C. N., Awoyelu, I. O., Akinyemi, B. O., & Aderounmu, G. A. An integrated approach to research paper and expertise recommendation in academic research. *International Journal of Advanced Computer Science and Applications*, 13(4) doi:https://doi.org/10.14569/IJACSA.2022.0130456,2022.
- [14] H. Chen, C. Yin, R. Li, W. Rong, Z. Xiong, B. David, "Enhanced learning resource recommendation based on online learning style model," *Tsinghua Science and Technology*, vol. 25 no. 3, pp. 348-356, DOI: 10.26599/TST.2019.9010014, 2020.
- [15] S. Wan, Z. Niu, "A hybrid e-learning recommendation approach based on learners influence propagation," *IEEE Transactions on Knowledge and Data Engineering*, vol. 32 no. 5, pp. 827-840, 2020.
- [16] Y. Zhou, C. Huang, Q. Hu, J. Zhu, Y. Tang, "Personalized learning full-path recommendation model based on LSTM neural networks [J]," *Information Sciences*, vol. 444 no. 3, pp. 135-152, DOI: 10.1016/j.ins.2018.02.053, 2020.
- [17] K. Dahdouh, A. Dakkak, L. Oughdir, A. Ibriz, "Large-scale e-learning recommender system based on Spark and Hadoop," *Journal of Big Data*, vol. 6 no. 1, DOI: 10.1186/s40537-019-0169-4, 2021.
- [18] Gray, J. L. Identifying the academic and emotional risk and resource factors of underrepresented students in accelerated coursework (Order No. 28154177). Available from ProQuest Dissertations & Theses Global. (2485082910). Retrieved from <https://www.proquest.com/dissertations-theses/identifying-academic-emotional-risk-resource/docview/2485082910/se-2,2022>.
- [19] M. U. Hulla, M. Hammer, H. Karre, C. Ramsauer, "A case study-based digitalization training for learning factories," *Procedia Manufacturing*, vol. 31, pp. 169-174, DOI: 10.1016/j.promfg.2019.03.027, 2020.
- [20] A. V. Nesterov, "Digitalization of society and the economy: systematization of personal data in information systems," *Scientific and Technical Information Processing*, vol. 47 no. 2, pp. 133-138, DOI: 10.3103/S0147688220020124, 2020.
- [21] T. B. Lalitha, P. S. Sreeja, "Personalised self-directed learning recommendation system [J]," *Procedia Computer Science*, vol. 171, pp. 583-592, DOI: 10.1016/j.procs.2020.04.063, 2020.
- [22] Z. Wei, L. Sun, "How to leverage manufacturing digitalization for green process innovation: an information processing perspective," *Industrial Management and Data Systems*, vol. 121 no. 5, pp. 1026-1044, DOI: 10.1108/IMDS-08-2020-0459, 2021.
- [23] F. Tian, Q. Zheng, K. M. Chao, "Current and future of technologies and services in smart e-learning," *Service Oriented Computing and Applications*, vol. 14 no. 1, DOI: 10.1007/s11761-020-00288-9, 2020.
- [24] H. Ezaldeen, R. Misra, R. Alatrash, R. Priyadarshini, "Semantically enhanced machine learning approach to recommend e-learning content," *International Journal of Electronic Business*, vol. 15 no. 4, pp. 389-413, DOI: 10.1504/IJEB.2020.111095, 2020.
- [25] J. Sun, J. Geng, X. Cheng, M. Zhu, Q. Xu, Y. Liu, "Leveraging personality information to improve community recommendation in e-learning platforms [J]," *British Journal of Educational Technology*, vol. 51 no. 5, pp. 1711-1733, DOI: 10.1111/bjet.13011, 2020.
- [26] D. D. Koffi, N. Ouattara, D. M. Mambe, S. Oumtanga, A. Adje, "Courses recommendation algorithm based on performance prediction in E-learning," *International Journal of Computer Science & Network Security*, vol. 21 no. 2, pp. 148-157, 2021.
- [27] L. Wu, Q. Liu, W. Zhou, G. Mao, J. Huang, H. Huang, "A semantic web-based recommendation framework of educational resources in E-learning," *Technology, Knowledge and Learning*, vol. 25 no. 4, pp. 811-833, DOI: 10.1007/s10758-018-9395-7, 2020.
- [28] X. Jiang, "Computer aided teaching system based on wechat public platform," *Modern Scientific Instruments*, vol. 3, pp. 44-49, 2020.

An Inspection of Learning Management Systems on Persuasiveness of Interfaces and Persuasive Design: A Case in a Higher Learning Institution

Wan Nooraishya Wan Ahmad¹, Mohamad Hidir Mhd Salim², Ahmad Rizal Ahmad Rodzuan³
Faculty of Computing and Informatics, University Malaysia Sabah, Labuan, Malaysia^{1,3}
Institute of IR4.0, Universiti Kebangsaan Malaysia, Selangor, Malaysia²

Abstract—An effective Learning Management System (LMS) is an essential factor that can increase e-learning persuasiveness. One of the components that need to be addressed to design an effective LMS is design interfaces. Instead of developing a new LMS that requires a high cost, evaluating and improving the existing LMS is the best option. Issues like low completion rates and procrastination are common issues related to e-learning usage. These issues can be solved if academic institutions provide a proper LMS for students to change their learning behaviors positively. Many previous studies claimed they managed to implement persuasive technology into e-learning platforms to encourage positive learning behaviors. However, the claims can be questionable if the persuasive e-learning systems are not gone through a proper evaluation phase. This study will use the heuristic evaluation method to assess the persuasiveness level of LMS interfaces. The persuasive Systems Design Model (PSD), on the other hand, is used to evaluate persuasive strategies in LMS. The assessment involves students' perspectives as the primary users to identify potentially behavior change factors, especially on engagement. Thus, the objectives of this study are i) to investigate the persuasiveness of LMS interfaces and ii) to identify persuasive strategies in the LMS design. Apart from that, this study also produces a) recommendations on design examples to increase the persuasiveness of LMS interfaces and b) the mapping of LMS interfaces to PSD framework that can be utilized by higher learning institutions.

Keywords—Learning management system; e-learning; persuasive design; persuasiveness; interface design

I. INTRODUCTION

E-learning or electronic learning is a learning medium which involves processes of delivering learning materials, communicating knowledge, tasks and learning instructions through online mediums [1]. Some examples of the commonly used tools for e-learning include video conferencing solutions, virtual tutoring, and digital libraries [2]. Previous studies reported that the effectiveness of e-learning is high, up to 60% of retaining learning materials compared to a traditional classroom which is up to only 8% to 10% of retention [3]. Because of the potential of e-learning as a platform for future learning, this study focuses on one of the e-learning technologies, which is Learning Management Systems (LMS).

LMS is a platform or medium used to provide learning features such as distributing learning materials and training activities while tracking students' progress [4]. One of the famous examples of LMS is Moodle. An effective LMS can

connect students with instructors outside of traditional classrooms via technology. Other than that, students can also be involved in online discussions through LMS. It even allows asynchronous conversation and facilitates problem-solving to improve the understanding of their enrolled subjects [4]. According to [5], incorporating LMS technology into teaching and learning enhances the accuracy of teaching attempts, student performance, and learning effectiveness. Thus, the LMS interface should be designed by considering students' perspectives as the end-users to prevent students from becoming discontent.

Almost every tertiary education institution worldwide uses LMS in its learning process [6]. Some tertiary education institutions in Malaysia use Moodle as their LMS platform due to its flexibility and versatility in fulfilling learning functions. On the other hand, some institutions develop their own LMS platforms for different reasons, such as cost and other preferences [7]. Despite the benefits that e-learning technologies offer to the learning process, some educational experts argue that there are flaws in e-learning because a significant percentage of students reported dissatisfaction with how technology is used in education [8]. They claimed that the lack of direct interaction between students and teachers is an important issue that needs to be solved to increase the effectiveness of the technology, or else it is worth noting. User acceptability and use are important indicators of the system's success. As a result, student admission must be considered; otherwise, information systems are prone to failure [8]. Persuasive technology is a technology developed that aims at users' behavior change without coercion [9]. A low completion rate due to procrastination is one of the issues related to e-learning that require changing students' behaviors [10]. A previous study claimed they integrated persuasive technology into e-learning platforms to encourage positive learning behaviors [11]. However, the claim can be questionable if the persuasive systems are not going through the proper evaluation phase. Students' evaluation is crucial since they are the primary users of e-learning technology.

This research study used the heuristic of persuasion in interface [12] to assess the persuasiveness of LMS interface and Persuasive Systems Design Model (PSD) [9] to evaluate persuasive strategy in LMS of a higher learning institution. The assessment is made from students' perspective as the primary entity potentially related to behavior changes on engagement. Thus, the objectives of this present study are i) to investigate

the persuasiveness of interface of a learning management system and ii) to identify persuasive strategy in the design of a learning management system. This study contributes to the following: a) recommendation on design examples to increase persuasiveness of LMS interface, and b) the mapping of LMS interface to PSD framework for LMS that can be utilized by higher learning institution particularly to the six most visited interface in the LMS.

The rest of the study is followed by Section II, which provides an outline of the background study and explains past related works. Section III describes the method, materials, and data collection and analysis procedures. Section IV presents two parts of the result and Section V is the discussion to describe the observed scenario. Lastly is the conclusion.

II. BACKGROUND STUDY

A. Persuasion

Persuasion is a form of influence as the technique tries to convince the persuadee of something [9]. There are two forms of persuasion: indirect and direct persuasion [13]. Indirect persuasion is a method that does not make persuasive intent clear. The intent is not expressed clearly without condemning or confronting a person's attitude or endorsing another person who has already accepted the offered message or notion. Direct persuasion is where persuasion has apparent intentions. It provides clear direction to a person with goal setting, including the process and clear instructions to achieve their goal despite their agreement. The LMS is supposed to have direct persuasion because the use of LMS in learning will eventually modify a student's learning habit [14].

Persuasion is the core process of persuasive technologies that modify users' behavior and perceptions through various techniques [15]. Therefore, it has been studied in various domains such as education [14], tourism [16], and health [17]. In addition, the Persuasive Systems Design Model (PSD) [9] has served as the guideline in designing and evaluating persuasive systems. The PSD framework is composed of four types of persuasive design principles: (i) primary task support, (ii) dialogue support, (iii) credibility support, and (iv) social support. The primary task principles are concerned with assisting the user's principal actions and goals. Dialogue support principles relate to human-computer dialogue aid in reaching the system's aim. The credibility support principles address how to design a more credible and convincing system. Finally, the design principles of social support utilize various components of social influence to ensure that the build system inspires the users.

Apart from becoming the core process in persuasive technology, persuasion has become one of the critical user experience attributes in interface design [18]. The potential persuasive impact of these dynamic interfaces is much more significant than a static information display where no interaction is possible. Interface properties are necessary but insufficient to change behaviors and attitudes since change can be constructed by considering user specifications [12]. Although we can enhance efficiency by applying traditional usability techniques, just because people can do something does not guarantee that they will. They must get motivated and

persuaded. A user will become more emotionally involved through repetitive interactions with an interface. Thus, [12] constructed a persuasiveness criteria grid to evaluate the persuasiveness of interfaces. The grid consists of static and dynamic criteria. Static criteria are the features required to start user acceptance and confidence to develop user engagement. The four static components are credibility, privacy, personalization, and attractiveness. Dynamic criteria incorporate substantial temporal factors where the interface elements encourage the user to commit to higher degrees of engagement. The dynamic components comprise solicitation, priming, commitment and ascendancy.

B. Related Works

The two main concerns of persuasiveness studies in human-computer were on persuasive technology [15, 17, 20-23] and interface design [12, 19, 24]. Thus, the focus of persuasiveness is either on a system's perceived persuasiveness [15, 17, 20-22] or the receptiveness of a system's persuasion strategy [12, 19, 23-24]. Persuasiveness or perceived persuasiveness has been defined differently based on the context of the study. The persuasiveness of persuasive technology is defined as persuasive systems' ability to persuade or encourage users to modify their behavior in a good direction [21, 22], while the persuasiveness of interfaces refers to the perceived persuasive design of multimedia interfaces [24].

The following studies explained the previous works related to a system's perceived persuasiveness. Ref [15] concerned about the factors that affect perceived persuasiveness. Survey items were developed based on the construct of PSD framework that measured primary task support, dialogue support, perceived credibility, unobtrusiveness, and design aesthetics. The study conducted on a web-based health program found that the persuasive system categories of the PSD framework affect the perceived persuasiveness of a system. On the other hand, [20] investigated factors influencing the perceived persuasiveness of a web-based health program and whether perceived persuasiveness predicts intention to utilize the intervention and actual system use. The report also indicated that the PSD categories [9] influence perceived persuasiveness and system usage. The study developed survey items to measure perceived persuasiveness and the categories in the PSD framework. After that, the items were used in several studies to assess perceived persuasiveness [21-23]. In addition, [17] adapted the Perceived Persuasiveness Questionnaire [15] to evaluate the perceived persuasiveness of a Nurse Antibiotic Information App (NAIA) using user tests and expert assessments. The expert assessment approach discovered primary task support, credibility, unobtrusiveness, perceived persuasiveness, perceived effort, and perceived effectiveness in the app. A similar outcome was obtained using the user test approach, with good remarks on primary task support, perceived persuasiveness, and unobtrusiveness. Ref [21] studied the impact of perceived persuasiveness of behavior model design on self-efficacy, self-regulation, and result expectancy. The study adopted [20] questionnaire items to measure the perceived persuasiveness of a fitness app. The findings revealed that the perceived persuasiveness of a behavior model design increased users' outcome expectations positively for their engagement in the target exercise behavior.

The study [22] investigated if integrating perceived persuasiveness in the TAM will result in a better model and the moderating effect of culture. According to the findings, individuals in individualist cultures were more likely to recognize the persuasiveness of a fitness app. As a result, incorporating a persuasive construct into the TAM is likely to be relevant compared to collectivist culture. Individualist group involving perceived persuasiveness are more likely to result in long-term persuasive system adoption than the collectivist group with no perceived persuasiveness. The author [23] studied users' susceptibility to the perceived persuasiveness of the fitness app and each persuasive element. The study developed a model to understand better the relationship between perceived UX design traits (such as perceived usefulness, credibility, and aesthetics) and users' susceptibility to persuasive features included in persuasive technologies. Persuasive features from the PSD framework [9], such as Goal setting/Self-Monitoring, Reward, Cooperation, Competition, Social Comparison, and Social Learning, were evaluated, and survey items from [20] were used to assess the fitness app's perceived persuasiveness. According to the findings of the study, perceived usefulness, followed by perceived aesthetics, has the most significant association with users' susceptibility to the persuasive elements.

Meanwhile, the persuasiveness of interfaces lacks attention from HCI researchers except those listed in the first paragraph in Section B. In [19] the authors have developed a set of guidelines to assess the persuasiveness of interfaces. The study examined 15 website and application interfaces to provide a criteria-based approach to classifying and evaluating the persuasive power of interfaces. Eight criteria were established and identified from the 15 interfaces. The criteria were divided into a static and dynamic category; each consisted of four criteria. The static category, which consists of credibility, privacy, personalization, and attractiveness, are related to the content impact to engender user adoption and engagement experience. Static criteria are all the interface elements required to kickstart a process of user engagement. The dynamic category consists of solicitation, priming, commitment and ascendancy. The dynamic criteria serve as an approach to immerse the users in an interactive process that gradually engages them with the interface to motivate users to change their behavior. The criteria for interactive persuasion emphasize the social and emotional aspects of interfaces, complementing the traditional inspection criteria (e.g., clarity, consistency, homogeneity, compatibility, and usability). These criteria involved the temporal aspects of the interface. The study [12] used a set of instructions [20] from an existing e-learning program for self-regulated middle school mathematics learning to conduct a persuasiveness assessment. The findings demonstrated that personalization, attractiveness, solicitation, initiation, and commitment criteria explained the low engagement when using the e-learning program. In addition, the ascendancy criteria were found to be irrelevant for educational interfaces. Credibility and privacy criteria dominated the user engagement with the e-learning program. The author [24] conducted a study based on user time spent to assess the usability and persuasion of social networking mobile

applications such as YouTube and Facebook. The analysis on persuasion reveals that Facebook and YouTube utilize a series of persuasion strategies to engage the user in an engaging cycle and keep them online for a longer time. Using the persuasion criteria [19], the study discovered some criteria emphasize being subtle and obtrusive. The subtle strategies rely on targeted suggestions to distract the user's attention and prompt engagement. In contrast, an obtrusive mechanism, such as a notification system, was used even when the user was not linked to the software.

In summary, health seems to be the domain concern of the previous works investigating persuasive technology's perceived persuasiveness. The persuasiveness of interfaces has been studied diversely, including websites, mobile apps, an e-learning system, and social networking applications. However, this present study focused on the LMS used in a higher learning institution since persuasive learning has become a concern among HCI researchers [14, 25]. Compared to the previous works, this study will conduct an integration study on the persuasiveness of interfaces and persuasion design strategy. Both perspectives are essential in determining user engagement towards using the LMS [14, 25].

III. METHODOLOGY

The methodology approaches in performing the study are described in this section, which includes (a) participant, (b) material, (c) measures and analysis, and (d) procedure. The following are the subsections:

A. Participant

Two experts in Human-Computer Interaction (HCI) and one expert in E-learning were recruited for the evaluation study. They were picked based on their five years of expertise in those research fields, as well as their consistent journal publications in the field. To prevent bias, the hired experts were chosen not among the system's users.

B. Material

SMART2 and SMARTv3 were the two versions of the learning management system from Universiti Malaysia Sabah used as the case study (refer Fig. 1). The SMART2 refers to an older version of the LMS, whilst the SMARTv3 refers to the most recent version. Both system versions have comparable capabilities, although the SMARTv3 has a modest upgrade in the interface design. SMART2 has been used for ten years in UMS before the ICT Department came out with SMARTv3 in the year 2020 on Semester 2. For the last ten years, SMART2 has received complaints from the students and lecturers regarding functionality and interface design. These have made some of the lecturers switch to other platforms for their blended learning.

Six interfaces of both LMS versions were selected based on the frequency of students visiting or using the interface. The interfaces are the homepage before login, course page, assignment view, assignment submit view, forum, and quiz. Fig. 2 illustrates the six selected interfaces of the LMS versions.

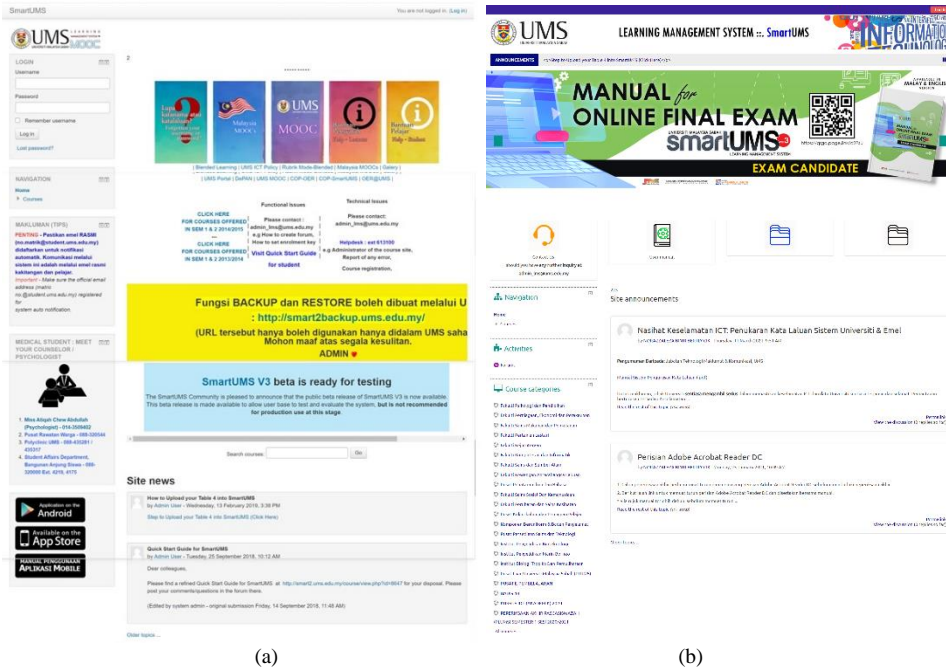


Fig. 1. Learning Management System: (a) SMART2; (b) SMARTv3.

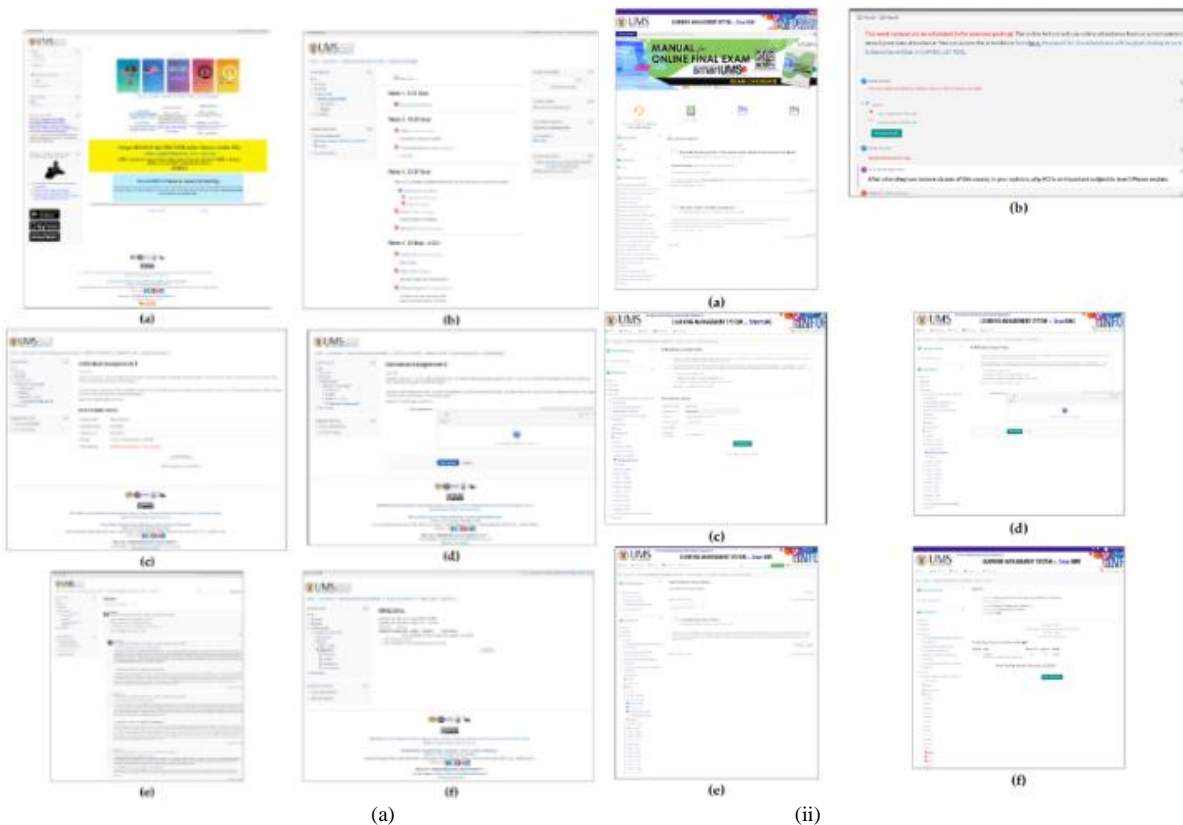


Fig. 2. Interfaces of (i) SMART2; (ii) SMARTv3. The Interfaces are (a) Homepage; (b) Course Page; (c) Assignment View; (d) Assignment Submission; (e) Forum; (f) Quiz.

C. Measures and Analysis

In the evaluation study, a heuristic inspection is performed to assess both persuasiveness of interface and persuasive strategy design to obtain insight from professionals in an

independent walkthrough using established persuasive grid criteria [12] and PSD model [9]. The grid contains eight criteria and 23 sub-criteria. In addition, the experts examined the six selected interfaces of both LMS versions using evaluation

checklists. The checklist required the experts to rate “Yes” and “No” answers, with the “Yes” answer was provided with two options, “Yes Low” and “Yes High” answers. Different from [12], the findings are divided into three types of answer that later grouped as “Satisfied”, “Dissatisfied” and “Unsatisfied”. The responses "yes high" and "yes" were classified as "Satisfied," whereas the response "yes low" was classified as "Unsatisfied." The “Dissatisfied” term came from the response “no” provided by the experts. The term "Unsatisfied" refers to the need for more interface elements relevant to the criterion, whereas "Dissatisfied" refers to the absence of interface components linked to the criteria. The analysis on PSD principles for six screen is classified as “yes” and “no” answers according to the type of LMS and interfaces. The response "yes" indicates that PSD principles were present in the LMS, whereas the answer "no" indicates that PSD principles were not applied in the LMS. Both the heuristic inspections are analyzed using descriptive analysis.

D. Procedure

All three experts were given a printed version of the interfaces so that they may annotate them. Each interface was evaluated according to the qualities of persuasive grid criteria [12] and persuasive strategy design [9]. The experts were also given definitions of the attributes and criteria to use as references. Experts were required to rate each criterion and strategy and make comments or proposals for improving the interface.

IV. RESULTS

This section presented the results on persuasiveness of interface and criteria of persuasive system design.

A. Persuasiveness of Interface

Fig. 3 reported the six screens’ inspections of both systems. The results are illustrated according to the persuasive criteria

and interfaces for each LMS evaluated according to the qualities of persuasive grid criteria [12] and persuasive strategy design [9]. Fig. 4 and Fig. 5 illustrated the compilation of eight persuasiveness criteria for both LMS according to the answers group. The results show that Smart2 and Smartv3 managed to meet the solicitation criteria successfully. The system is expected to create relationship and initiate user action. However, ascendancy, personalization and privacy are found to be the critical persuasive criteria in Smart2. The Smart2 system is also found to lack in providing interfaces that engaged students to commit in the process, the user interface is not aesthetically appealing, and not have enough of elements to instill trust. Due to the lack of commitment criteria, this has resulted in the equal percentage for the initiation criteria in those three types of answers group.

Meanwhile, like Smart2 system, the result shows that Smartv3 system is also lacking in credibility elements that could instill trust apart from just having the university logo and license statement from the authority. The result discovered critical persuasive criteria in the Smartv3’s interface namely attractiveness, personalization, commitment, ascendancy, privacy, and initiation. Although in the context of educational interface, ascendancy is irrelevant [12], the criteria existed in both system in this present study with both systems scored the same percentage in three answers group (satisfied=17%, unsatisfied=22%, dissatisfied=61%). It can be presumed that the compulsory use of LMS in learning has made students develop emotional attachment with both systems through interfaces such as course page, assignment view, assignment submit and forum.

Those four interfaces were successful in instilling a degree of repetition and regularity in students' visits to them, and failing to visit the interfaces will result in students falling behind in their learning.

		INTERFACES ACCORDING LMS TYPE												TOTAL CRITERION PER LMS												
		Homepage		Course page		Assignment view		Assignment submit		Forum		Quiz		SMART2			Smartv3									
		Smart2	Smartv3	Smart2	Smartv3	Smart2	Smartv3	Smart2	Smartv3	Smart2	Smartv3	Smart2	Smartv3	Yes H (+)	Yes	Yes L	No (-)	Yes H (+)	Yes	Yes L	No (-)					
Static criteria	Credibility	Trustworthiness	Yes high	Yes high	Yes low	Yes low	Yes	Yes	Yes low	Yes low	Yes low	Yes low	Yes low	Yes low	Yes low	Yes low	Yes low	Yes low	Yes low	Yes low	Yes low	Yes low	Yes low			
		Expertise	Yes	Yes	Yes low	Yes low	Yes low	Yes low	No	No	Yes low	Yes low	Yes low	Yes low	0	1	4	1	0	1	4	1	4	1		
		Fidelity	Yes low	Yes low	Yes	Yes low	Yes high	Yes high	Yes low	Yes low	Yes low	No	Yes	Yes	1	2	3	0	1	1	3	1	3	1		
		Legitimacy	Yes low	Yes low	Yes low	Yes low	Yes	Yes low	Yes	Yes	Yes	Yes low	Yes	Yes	0	4	2	0	0	2	4	0	2	4	0	
	Privacy	Safeness	Yes	Yes	Yes low	Yes low	Yes low	Yes	Yes low	Yes low	Yes low	Yes low	Yes low	Yes low	0	1	5	0	0	2	4	0	2	4	0	
		Law respect feeling	Yes	Yes	No	No	No	No	No	No	No	No	No	No	0	1	0	5	0	1	0	5	0	1	0	
		Confidentiality	Yes	Yes	Yes low	Yes low	No	No	No	No	No	No	Yes low	Yes low	0	1	2	3	0	1	2	3	0	1	2	3
	Personalisation	Individualization	No	No	Yes	Yes	Yes low	No	Yes low	Yes low	Yes low	Yes	No	No	0	1	3	2	0	2	2	2	2	2	2	
		Group membership	No	No	Yes low	No	No	No	No	No	No	No	No	No	0	0	1	5	0	0	0	6	0	0	6	
	Attractiveness	Emotional attraction	No	No	Yes low	No	No	No	No	No	Yes low	No	No	No	0	0	2	4	0	0	0	6	0	0	6	
Call to action		Yes low	Yes low	Yes	Yes	No	No	Yes low	Yes low	Yes	Yes low	Yes low	Yes low	0	2	3	1	0	1	4	1	1	4	1		
Dynamic criteria	Solicitation	Tunnelling design	No	No	No	No	No	No	No	No	Yes low	No	No	0	0	5	1	0	0	0	6	0	0	6		
		Allusion	Yes	Yes	Yes high	Yes high	Yes	Yes low	No	No	Yes	Yes	Yes	Yes	1	4	0	1	1	3	1	1	1	1		
		Suggestion	Yes low	Yes	Yes high	Yes low	Yes low	Yes low	No	No	No	No	Yes	Yes	1	1	2	2	0	2	2	2	2	2		
	Initiation	Teasing	No	No	Yes	Yes low	No	No	No	No	Yes low	Yes low	Yes	Yes	0	2	1	3	0	1	2	3	0	1	2	3
		Priming	No	No	Yes	Yes low	Yes low	Yes low	No	No	Yes low	No	Yes	Yes	0	2	2	2	0	1	2	3	0	1	2	3
	Commitment	First action guidance	No	No	Yes high	Yes high	No	No	Yes low	Yes low	Yes	Yes	Yes low	Yes low	1	1	2	2	1	1	2	2	1	1	2	2
		Repeated request	Yes low	Yes low	Yes high	Yes high	No	No	No	No	Yes low	Yes low	No	No	1	0	2	3	1	0	2	3	0	2	3	
	Ascendancy	External negative factor avoidance	No	No	Yes	No	No	No	No	No	Yes low	Yes low	No	No	0	1	1	4	0	0	1	5	0	1	5	
		Increased cost	No	No	Yes low	Yes low	No	No	No	No	Yes	Yes	No	No	0	1	1	4	0	1	1	4	0	1	4	
		Prescription of repetition	No	No	No	No	No	No	No	No	Yes low	Yes low	No	No	0	0	1	5	0	1	1	4	0	1	4	
No-limit interaction		No	No	No	No	Yes	Yes low	Yes low	Yes low	Yes	Yes	No	No	0	2	1	3	0	1	2	3	0	1	2	3	
TOTAL INTERFACES PER LMS	Pressure released	No	No	No	No	Yes low	No	Yes low	Yes low	Yes	Yes	No	No	0	1	2	3	0	1	1	4	0	1	4		
	Yes High (+)	1	1	4	3	1	1	0	0	0	0	0	0	0	0	0	0	0	0	0	0	0	0	0		
	Yes (+)	5	6	6	2	4	2	1	7	6	6	6	6	6	6	6	6	6	6	6	6	6	6	6		
	Yes Low	5	4	8	10	6	6	8	8	12	9	6	6	6	6	6	6	6	6	6	6	6	6	6		
No (-)	12	12	5	8	12	14	14	14	4	8	11	11	11	11	11	11	11	11	11	11	11	11	11			

Fig. 3. Results of the Experts Analysis with Eight Persuasive Criteria on Both Smart2 and Smartv3 LMS.

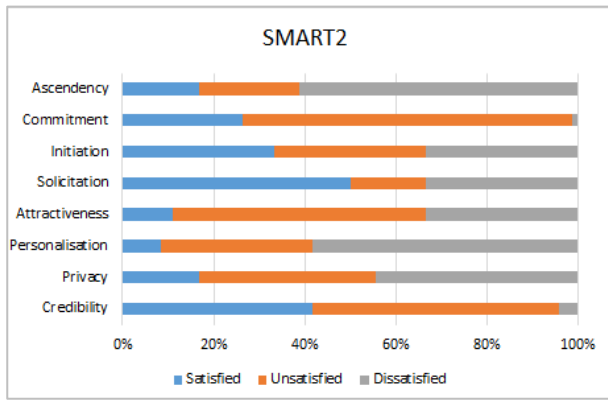


Fig. 4. Compilation of Persuasive Interface Criteria for Smart2.

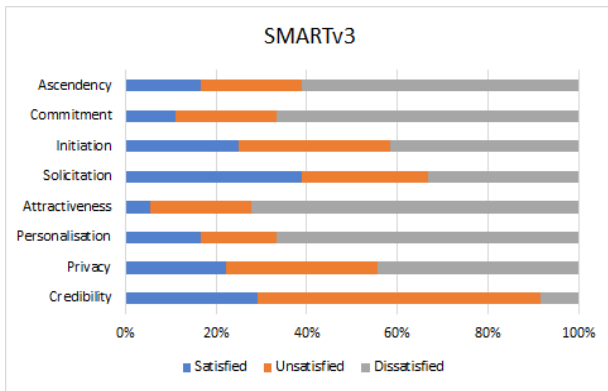


Fig. 5. Compilation of Persuasive Interface Criteria for Smartv3.

Table I outlines some of the critical concerns from both systems that were discovered during the inspection, as well as the corrective suggestions that were made as a result of the findings.

TABLE I. CRITICAL CONCERNS FROM PERSUASIVENESS INSPECTION

Persuasion Interface Criteria	General Comments	Design Examples
Credibility	<ul style="list-style-type: none"> - Improve the surface design of the interface in terms of layout and navigation to increase trustworthiness and legitimacy on user perception towards the system - Allow for various searching approach based on the course code and name, lecturer and course program and faculty 	Use UI elements such as dropdown menu to list the courses users have taken instead of listing everything on the page
Privacy	Make the privacy elements immediately visible to the user without making them to scroll until the end of the page or having them to click on a link.	Use a banner or images that symbolises user's data privacy and security is protected.
Personalisation	<ul style="list-style-type: none"> - Should allow users to tailor the interface according to the their needs to create the sense of belonging. - Lack in mechanism to provide a personalise 	<ul style="list-style-type: none"> - Personalise message that welcome or praise user will attract and engage user to use system.

	message that compliment students progress or achievement - Recommend system to provide a personalised suggestion that can enhanced learning based on student's past activities	-Screen customisation that allow users to change screen display or information layout of their preferences. -Compliment message that show personalise encouragement to students on progression and achievement. -Personalised proposal that reflect from past activities achievement.
Attractiveness	Make use of different color or color themes for emotional design elements such as images, font, icons and emoticons to attract user graphically.	- Using attractive colors or color themes for font and background color. - Pictures, icons, and various emoticons that attract user to initiate actions.
Initiation	Make use of multimedia elements that can persuasively trigger and initiate user to start first action.	- Using blinking graphic to emphasis importance on such links or tasks. - Use motivational element such as reward, badges that encourage user to complete tasks.
Commitment	Improve the interaction by utilising tunnelling approach to make the user involved and engaged with the whole process in order to access the next task and able to invite or remind their coursemates who have not yet completing the task.	-Regularly create tasks to let the user get involved frequently. - Propose a pop-up list to invite or remind other user to complete the next course material.
Ascendancy	<ul style="list-style-type: none"> - Improve UI by applying emotional design elements to create emotional attachment and trigger positive emotion among user. - Should adopt social network design to create immersive interaction and repetative use. 	- Utilise emotional design elements such as images, graphic, animation, video, text, navigation and layout to trigger positive emotion. - User profile page should be design according to social network that allow connection with other user.

B. Persuasive System Design

The result on the inspection of PSD categories is presented in Fig. 6. Finding shows that all four PSD categories; primary task support, dialogue support, system credibility and social support were found in Smartv3, while for Smart2 LMS, social support category were not found from the six screen interfaces, making only three PSD categories namely primary task support, dialogue support, system credibility existed. Both LMSs scored high in implementing system credibility principles, while social support principles were the least PSD implemented.

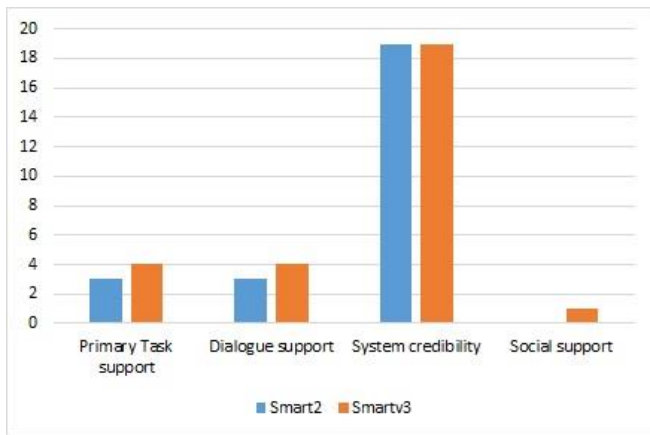


Fig. 6. Summary of PSD in Smart2 and Smartv3.

Fig. 7 illustrated the number of PSD principles implemented in six screen interfaces. It is found that PSD principles were merely implemented in the course page interface compared to others for both LMSs.

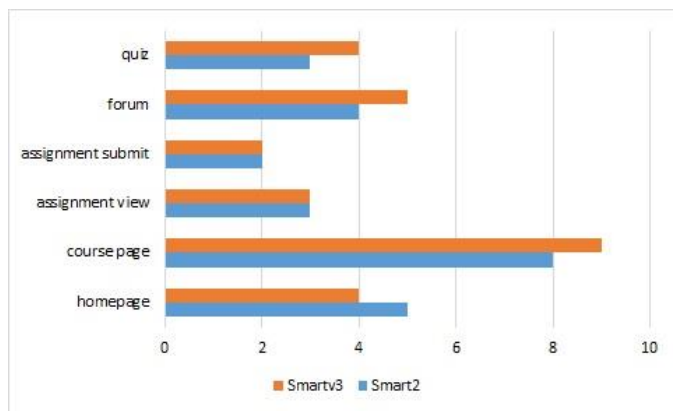


Fig. 7. Numbers of PSD Principles in Smart2 and Smartv3.

A summary of PSD principles found in both systems during the experts' evaluation study is presented in Table II. The findings show that PSD principles are not necessarily implemented in every interface. The implementation of PSD principles depends on the purpose of interface and activities conducted in it. The homepage interface applied system credibility principles in both Smart2 and Smartv3 system according to its function as the introductory interface. The principles are mainly Surface credibility, Real-world feel, Authority, and Third-party endorsement. All four PSD categories were implemented in the course page interface for Smartv3 system, except for Smart2 where none of social support principles is implemented. The course page interface is an instructional component in LMS where it allows for the instructor to create various learning tasks implemented using various forms and deliverables such as animation, games, or video [25]. The interface of assignment view enables student to view and read the assignment provided by the course instructor. The dialogue support and system credibility principles were found in this interface. Those principles are Reminder, Trustworthiness and Surface credibility. The assignment submit's interface consists of two system credibility principles which are Trustworthiness and Surface credibility. Meanwhile,

the forum interface applied PSD principles of primary task support, dialogue support and system credibility, except for Smart2 system where none of primary task support principles are found. The principles consist of Self-monitoring, Liking, Surface Credibility, Real-world feel, and Authority. The same PSD categories were also found in quiz interface where principles of dialogue support and system credibility were implemented in both systems except for Smart2 system only implemented system credibility principles. The applied principles were Reminder, Surface Credibility, and Real-world feel.

TABLE II. PSD PRINCIPLES IN SMART2 AND SMARTV3

Interfaces	PSD Principles		PSD Category
	Smart2	Smartv3	
Homepage	Surface credibility, Real-world feel, Authority, Third-party endorsement	Surface credibility, Real-world feel, Authority, Third-party endorsement	System Credibility
Course page	Reduction, Tailoring, Self-monitoring	Reduction, Tailoring, Self-monitoring	Primary Task Support
	Reminder	Reminder	Dialogue Support
	Trustworthiness, Surface credibility, Real-world feel, Authority	Trustworthiness, Surface credibility, Real-world feel, Authority	System Credibility
	n/a	Social learning	Social support
Assignment view	Reminder	Reminder	Dialogue Support
	Trustworthiness, Surface credibility	Trustworthiness, Surface credibility	System Credibility
Assignment submit	Trustworthiness, Surface credibility	Trustworthiness, Surface credibility	System Credibility
Forum	n/a	Self-monitoring	Primary Task Support
	Liking	Liking	Dialogue Support
	Surface credibility, Real-world feel, Authority	Surface credibility, Real-world feel, Authority	System Credibility
Quiz	n/a	Reminder	Dialogue Support
	Surface credibility, Real-world feel	Surface credibility, Real-world feel	System Credibility

Persuasive design and learning generally have a positive impact to motivate students to learn [25, 26]. The principles of reduction, tailoring and self-monitoring are used in course page to enable course development and implementation. These principles were found to excite students by stimulating intrinsic motivation, assisting students in completing tasks, and encouraging a continuous cycle of online learning [26]. Even though the social learning principle is implemented in both systems, social learning should be the least important concept to adopt in supporting students' learning progress [27] and in promoting student learning engagement [28]. Trustworthiness depicts a reliable system that gives accurate, impartial, and fair information to accomplish the desired behavior [9]. It specifies

an approach for allowing a user to trust the system such as using logo of the organization to show that the system is owned or prepare a list of references or information sources connected to the course material [25]. Generally, the surface credibility is more on the firsthand look of an interface that makes a system looks credible to use. The inspection result shows that all the six-screen managed to portray a surface credibility to its users.

V. DISCUSSION

This study shows that persuasive designs have been implemented in the LMS for higher education. However, the effectiveness of persuasive design principles applied in the interfaces may be argued. Therefore, we mapped a persuasive design framework for LMS that consist of 13 strategies based on the LMS components and activities comprises the four dimensions of PSD. Further reading on the framework can be found in [25]. Table III summarizes the mapping of six screen LMS interfaces with the framework we have previously developed by aligning the interfaces to LMS components and activities.

The study's drawback is limited to one higher learning institution and the five most viewed websites by students. Having two separate versions of an LMS, on the other hand, is sufficient to disclose insights regarding LMS design in a higher learning institution. Nonetheless, future research might be broadened to investigate additional LMS design in different higher education institutions.

TABLE III. MAPPING OF SIX SCREEN INTERFACES WITH PSD FOR LMS

Interfaces	PSD Framework for LMS		
	LMS components	Activities	PSD Principles
Homepage	Administrative	Student enrolment	Praise
	Visual	Interface design	Liking, Trustworthiness, Personalization
Course page	Administrative	Monitor learning progress	Self-monitoring, Reward, Competition, Social comparison
	Instructional	Course development	Tailoring
		Course implementation	Reduction, Self-monitoring
	Support	Tracking learning process	Suggestion, Tunnelling, Self-monitoring
	Visual	Interface design	Liking, Trustworthiness, Personalization
Assignment view	Instructional	Course implementation	Reduction, Self-monitoring
Assignment submit	Instructional	Course implementation	Reduction, Self-monitoring
Forum	Interactive	Communication	Social role, Praise
Quiz	Instructional	Course implementation	Reduction, Self-monitoring
	Interactive	Communication	Social role, Praise

Despite those limitations, this study contributes to the establishment of design recommendations to increase persuasiveness of LMS interfaces in order to ensure that the LMS can capture and engage its users. Furthermore, this study also proposes a framework that can be utilized by higher learning institution, specifically in designing the six most visited interfaces in the LMS by mapping LMS interfaces to PSD.

VI. CONCLUSION

This study examined the persuasiveness of interface and the application of persuasive design in the case of higher learning institution with two versions of learning management system: Smart2 and Smartv3. The results show that both system versions successfully meet the solicitation criteria that managed to establish relationship and prompt user action through its interface design. However, both system versions are lacking in other persuasiveness of interface criteria such as credibility, privacy, personalization, attractiveness, initiation, commitment, and ascendancy. The ascendancy criteria which supposed irrelevant in educational interface happened to be found in both system versions making previous literature and our finding contradict. This study discovered that minimal persuasive design principles have been utilized in LMS for higher education. This has contributed to the development of persuasive LMS framework which can be used as a guideline to design an effective persuasive LMS. In the future, development of a prototype based on the developed framework can be used to assess the framework empirically. The study contributes to the body of knowledge in human-computer interaction in the educational area where the framework can be used to improve the LMS design in encouraging positive learning behavior.

ACKNOWLEDGMENT

This study is part of the research work funded by Universiti Malaysia Sabah under the Grant Scheme Acculturation (SGA) (SGA0017-2019).

REFERENCES

- [1] M. O. Alassafi, "E-learning intention material using TAM: A case study," *Mater Today Proc*, vol. 61, pp. 873–877, Jan. 2022.
- [2] "Five facts on e-learning that can be applied to COVID-19 - Institute for Environment and Human Security." <https://ehs.unu.edu/news/news/five-facts-on-e-learning-that-can-be-applied-to-covid-19.html> (accessed Sep. 26, 2022).
- [3] "The rise of online learning during the COVID-19 pandemic | World Economic Forum." <https://www.weforum.org/agenda/2020/04/coronavirus-education-global-covid19-online-digital-learning/> (accessed Sep. 26, 2022).
- [4] F. Bousbahi and M. S. Alrazgan, "Investigating IT faculty resistance to learning management system adoption using latent variables in an acceptance technology model," *Scientific World Journal*, vol. 2015, 2015.
- [5] H. Fung and A. Yuen, "Factors Affecting Students' and Teachers' Use of LMS – Towards a Holistic Framework," in *international conference on hybrid learning*, 2012, vol. 7411, pp. 306–316.
- [6] N. Phongphaew and A. Jiamsanguanwong, "Usability evaluation on learning management system," in *Advances in Intelligent Systems and Computing*, 2018, vol. 607, pp. 39–48.
- [7] H. Ming Chee, C. Wou Onn, and S. Pei Hwa, "Implementation of LMS among Private Higher Learning Institutions in Malaysia," in *Proceedings of Knowledge Management International Conference*, 2010, pp. 157–163. [Online]. Available: <http://mmlscyber.mmu.edu.my/>.

- [8] Y. H. S. Al-Mamary, "Understanding the use of learning management systems by undergraduate university students using the UTAUT model: Credible evidence from Saudi Arabia," *International Journal of Information Management Data Insights*, vol. 2, no. 2, Nov. 2022.
- [9] H. Oinas-kukkonen and M. Harjumaa, "Communications of the Association for Information Systems Persuasive Systems Design: Key Issues , Process Model , and System Features Persuasive Systems Design : Key Issues , Process Model , and System Features," *Communications of the Association for Information Systems*, vol. 24, no. 28, pp. 485–500, 2009.
- [10] N. Huang, J. Zhang, G. Burtch, X. Li, and P. Chen, "Combating Procrastination on MOOCs via Optimal Calls-to-Action: Evidence from a Field Experiment," *Academy of Management Proceedings*, vol. 2018, no. 1, p. 14171, 2018, doi: 10.5465/ambpp.2018.14171abstract.
- [11] M. H. Mhd Salim, N. M. N. M. Ali, and M. T. M. T. Ijab, "Understanding students' motivation and learning strategies to redesign massive open online courses based on persuasive system development," *International Journal of Advanced Computer Science and Applications*, vol. 10, no. 12, pp. 234–241, 2019.
- [12] E. Brangier, M.C. Desmarais, "Heuristic inspection to assess persuasiveness: A case study of a mathematics e-learning program," in: *International Conference of Design, User Experience, and Usability (DUXU 2014)*. Lecture Notes in Computer Science, vol 8517, A. Marcus, Eds. Springer, Cham. 2014, pp. 425–436.
- [13] T. Aleahmad, A. D. Balakrishnan, J. Wong, S. R. Fussell, and S. Kiesler, "Fishing for sustainability: the effects of indirect and direct persuasion," in *CHI EA '08: CHI '08 Extended Abstracts on Human Factors in Computing Systems*, pp. 3021-3026, April 2008.
- [14] F.A. Orji, J. Vassileva, and J. Greer, "Personalised persuasion for promoting students' engagement and learning," in *Proceedings of the Personalisation in Persuasive Technology Workshop, Persuasive Technology 2018*, Waterloo, ON, Canada, pp.77–87, April 2018.
- [15] T. Lehto, H. Oinas-Kukkonen, Harri, and F. Drozd, "Factors affecting perceived persuasiveness of a behavior change support system", in *Thirty Third International Conference on Information Systems (ICIS 2012) Proceedings*, Orlando, US, pp. 1-15, December 2012.
- [16] N. Ibrahim, M. F. Shiratuddin, K. Wong, "Persuasion techniques for tourism website design," in *The International Conference on E-Technologies and Business on the Web (EBW2013)*, Bangkok, Thailand, pp. 175-180, May 2013.
- [17] N. de Jong, J. Wentzel, S. Kelders, H. Oinas-Kukkonen, J. van Gemert-Pijnen, " "Perceived persuasiveness questionnaire; Evaluation of perceived persuasiveness constructs by combining user tests and expert assessments," in *Proceedings of the Second International Workshop on Behavior Change Support Systems 2014*. A. Öörni, S. Kelders, L. van Gemert-Pijnen, H. Oinas-Kukkonen (Eds.), CEUR-WS.org, Padua, Italy. 2014, pp. 7-15, May 2014.
- [18] L. S. Platt, H. Li, C. E. Bass, and K. Yu, "Validating persuasive experience (PX) theory: Preliminary results of a case study on a corporate wellness program's web-based learning interfaces," in *Proceedings of the 2018 International Symposium on Human Factors and Ergonomics in Health Care*, Boston, Massachusetts, USA pp. 56-63, March 2018.
- [19] A. Nemery, E. Brangier, "Set of guidelines for persuasive interfaces: organization and validation of the criteria," *Journal of Usability Studies*, vol. 9, no. 1, pp 105–128, 2014.
- [20] F. Drozd, T. Lehto, H. Oinas-Kukkonen, "Exploring perceived persuasiveness of a behavior change support system: A structural model," in: *International Conference on Persuasive Technology, PERSUASIVE 2012*. Lecture Notes in Computer Science, vol. 7284, M. Bang, E. L. Ragnemalm (Eds.) Springer, Sweden. 2012, pp. 157-168.
- [21] K. Oyibo, I. Adaji, R. Orji, B. Olabenjo, M. Azizi, J. Vassileva, "Perceived persuasive effect of behavior model design in fitness apps", in *Proceedings of ACM UMAP Conference*, Singapore, July 2018 , pp. 219-228.
- [22] K. Oyibo and J. Vassileva, "HOMEX: Persuasive technology acceptance model and the moderating effect of culture", *Frontiers in Computer Science*, vol. 2, no. 10, pp. 1-17, 2020.
- [23] K. Oyibo, and J. Vassileva, "Relationship between perceived UX design attributes and persuasive features: A case study of fitness application ", *Information*, vol. 12, no. 365, 2021.
- [24] M. Bedjaoui, N. Elouali, and S. M. Benslimane, "User time spent between persuasiveness and usability of social networking mobile applications: A case study of Facebook and YouTube", in *MoMM2018: Proceedings of the 16th International Conference on Advances in Mobile Computing and Multimedia*, Yogyakarta, Indonesia, pp. 15–24, Nov. 2018.
- [25] W. N. Wan Ahmad, A. R. Ahmad Rodzuan, and C. Salimun, "Mapping learning management system features of persuasive design strategies to inform the design of persuasive learning management system", *International Journal of Learning Technology*, vol. 16, no. 3, pp. 246-263, 2021.
- [26] M. M. J. Engelbertink, S. M. Kelders, K. M. Woudt-Mittendorff, and G. J. Westerhof, 2, "Participatory design of persuasive technology in a blended learning course: a qualitative study", *Education and Information Technologies*, vol. 25, pp. 4115–4138, 2020.
- [27] F.A. Orji, K. Oyibo, R. Orji, J. Greer, and J. Vassileva, "Personalisation of persuasive technology in higher education I, in *ACM UMAP 2019 – Proceedings of the 27th ACM Conference on User Modeling, Adaptation and Personalisation*, New York, USA, pp.336–340, June 2019.
- [28] H. H. Selassie, and J. Vassileva, "Susceptibility of graduate assistants to social influence persuasive strategies", in *CRIWG 2017*. Lecture Notes in Computer Science vol. 10391, C. Gutwin, S. Ochoa, J. Vassileva, T. Inoue, Eds. Springer, Cham, 2017, pp.118–131.

The Development of an Ontology for Information Retrieval about Ethnic Groups in Chiang Mai Province

Phichete Julrode¹

Department of Library and Information Science
Faculty of Humanities, Chiang Mai University
Chiang Mai, Thailand

Thepchai Supnithi²

Principal Researcher (LST) Employment
National Electronics and Computer Technology Center
Pathumthani, Thailand

Abstract—This study aims to develop the semantic ontology of information knowledge about ethnic groups by analyzing information from the collection of documentary sources from libraries, research, and the museum for learning about people on the highlands located in Chiang Mai Province. The study is based on the classification theory of ethnic groups in Chiang Mai Province with the intention of establishing the relationship between knowledge structure regarding ethnic groups. The study procedures consist of three stages: 1) Establishing ontology requirements from online data to analyze the data of the keyword from the research database of Chiang Mai University Library's Online Information Resource Database (OPAC) and Ratchamangkhaphisek National Library, Chiang Mai to group the words by studying information resources in Thai language, such as books, textbooks, research papers, theses, research articles, academic articles, and reference books related to ethnic groups. Stage 2) Designing classes, defining main classes, subclasses, hierarchies, and properties in order to establish the relationship of data in each class using the Protégé program. Stage 3) Ontology evaluation, which is divided into two parts: an expert's evaluation of the suitability of the ontology structure using the Inter-Class Relational Accuracy Assessment Scale and an examination of ethnic grouping data. The findings reveal that specifying, definition, scope, and objectives of development are appropriate (average score = 0.97) in three areas: grouping and ordering of classes within the ontology (score value = 0.98), defining affinity names and class properties (score value = 0.96), and suitable overall ontology content (score value = 0.97).

Keywords—Information retrieval; ontology development; ethnic groups; knowledge organization; Chiang Mai

I. INTRODUCTION

The term "Ethnic Group" refers to a group of people who have a long history in Thai society, with different aspects and having their own culture and customs. It is a group in which the population is related to one another, sharing the same racial characteristics, culture, traditions, and language, and is devoted to the conservation, development, and inheritance of ancestral land and ethnic identity from one generation to the next. Ethnicity is the classification of people and their relationships between different groups in society based on cultural differences and inferiority in political power, society, and the economy. However, it may not be a minority that has a smaller population than a society [1], [2], [3]. Formerly, ethnic groups

were diverse and settled in various provinces throughout Thailand [4]. There are currently 67 ethnic groups in 56 provinces with a total population of around 6,100,000 people. Settlements are categorized into four types as follows:

1) The highland ethnic groups, or "hill tribes", consist of 13 groups: Karen, Hmong (Miao), Yao (Mien), Lisu (Lesu), Lahu (Muser), Akha, Lua, Tin, Khmu, Chinese Hor, Tong Su, Kachin, and Palaung (Dara-ang).

2) Ethnic groups that settled on the plains consist of 38 groups, namely Mon, Tai Lue, Tai Song Dam, Tai Yai, Tai Khuen, Tai Yong, Tai Ya, Tai Yuan, Phu Tai, Lao Krang, Lao Ngaew, Lao Ka, Lao Ti, Lao Wiang, Saek, Sere, Prang, Bru (Chao), Song Vo (Tawing), Umpi Kong Kula Chou Oj (Chu Oong), Kui (Suay), Nyah Kur (Chao Bon), Nyaw, Yoy, Khmer Thai, Vietnam (Yuan), Nye Mee Sor (Bizu), Chong, Krachong, Malay, Kaleang, and Lao Song (Tai Dam).

3) Ethnic groups that settled on coastline or "Chao Lay" consist of three groups, including Moken, Moklen, and Urak Lawoi.

4) Ethnic groups that live in the forest consist of two groups: Mlabri (Tong Luang) and Sakai (Mani).

Ethnic groups are people who share a similar way of life, beliefs, culture, customs, and language, as well as a shared history. In addition, each ethnic group organizes its way of life differently. The manner in which each group interacts with each other and their relationships is distinctive [5], [6]. The separation of an ethnic group is essential in a society based on diverse ancestral teaching practices, a group of people with different biological characteristics, histories, and roles in society. Therefore, behavior and beliefs, occurring in human society and referred to as "culture," are different as well. A study of relational ethnography emphasizing ethnic groups as cultural groups that share ancestors or a long history is a study of the organization of social and governance, beliefs, customs and rituals, spoken language, clothes, and so on of each ethnic group. Currently, new generations of ethnic groups are taking a greater role in studying their own ethnic groups, providing them with more opportunities to learn about ethnic cultures [7]. Research information on ethnic groups is abundant and diverse, such as language, culture, literature, history, archeology, pottery, anthropology, folklore, habitation, and way of life,

This research was funded and supported by the Faculty of Humanities, Chiang Mai University. The researcher would like to give special thanks for such support for this research.

which are mostly separated into specific areas. For example, the study of language attitudes of Tai ethnic group toward their own language in the lower northern region and the study of the use of various Tai dialects in the lower northern region. It is a comparison of tendencies and situations in language usage and language attitudes toward their own dialects of Thai people who speak Tai dialect in the lower northern region and a study of the way of life of the Hmong ethnic group in Mae Rim District, Chiang Mai Province [8], [9]. Therefore, searching for relational and related information is limited.

Ontology is a concept applied in knowledge management. It is widely used and studied, and it is able to organize and present knowledge in the form of conceptual groups and interrelationships within the scope of interest [10]. It creates a hierarchical relationship by using the concept of grouping and segmentation [11], [12]. Applying ontology concept to ethnic groups, namely Ethnicity Ontology (EO), was developed as an extension of the Basic Formal Ontology two standard for general reference to ethnographic concepts. It combines semantic datasets from different knowledge sources to compile definitions for interpretation [13]. Gathering data and building relationships in a hierarchical form is often used in the fields of artificial intelligence, semantic web, software engineering, and biomedical informatics [14]. To design and develop ontology for information retrieval of ethnic groups in Chiang Mai, the researcher gathered knowledge of different ethnic groups by having the information integrated according to the concept of ontology, which is a type of knowledge management system that plays an important role in semantic explanations. This is to create a common understanding of a particular field of knowledge using a single concept. This study defined or created a vocabulary system that can be used to illustrate knowledge that represents a comprehensive scope of knowledge. It can be used as a base for semantic searches for the development of knowledge-based systems, as well as a semantic search system for specific information systems related to ethnic knowledge in Chiang Mai province.

II. CONCEPTUAL FRAMEWORK AND METHODOLOGY

A. Objectives

1) Design and develop ontology for information retrieval about ethnic groups in Chiang Mai.

2) Evaluate ontology for information retrieval about ethnic groups in Chiang Mai.

B. Conceptual Framework

The objectives of this study is to design, develop, and evaluate ontology for information retrieval about ethnic groups in Chiang Mai. The researcher conducted the study according to the conceptual framework as shown in Fig. 1.

C. Methodology

1) *Concept and theory*: The development of ontology was based on the basic ontological of knowledge sharing approach [15], which the researcher employed primarily to develop Domain Ontology as the main framework. There are three stages of development as follows.

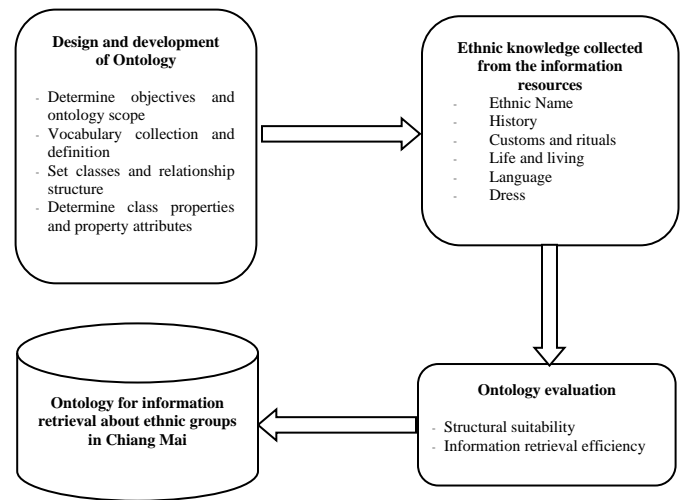


Fig. 1. Conceptual Framework.

a) Determine ontology objectives by studying the ontology requirements from online data to analyze the data of the keyword from the research database of Chiang Mai University Library's Online Information Resource Database (OPAC) and Ratchamangkhaphisek National Library, Chiang Mai for grouping the words.

b) Protégé program was utilized to establish word correlations related to ethnic groups.

c) Ontology evaluation is divided into two parts: the evaluation of the suitability of the ontology structure using the Inter-Class Relational Accuracy Assessment Scale by five experts (two ontology specialists) and an examination of ethnic grouping data (three ontology specialists).

The development process of ontology has applied knowledge engineering theory for developing the ontology to make domain assumptions explicit as a framework [16]. The development process consists of seven stages: 1) determining domain and scope of ontology; 2) lexical clarification; 3) class and class hierarchy establishment; 4) defining relationships; 5) defining properties; 6) defining views on class properties; and 7) creating sample data within that class.

2) Research development process

a) *The development of ontology has three phases*: Phase 1: Determine the objectives and scope and ontology's scope to present a set of terms and concepts related to ethnic groups in Chiang Mai from the online data to analyze the keyword data from the research database from the Online Information Resource Database (OPAC), research database (e-Research), thesis database (e-Thesis), and journal database (e-Journal) of Chiang Mai University Library for 330 items, as well as the National Library of Thailand's Online Information Resource Database (OPAC) for 453 items, for a total of 783. This is to study the term group and apply it suitably for the design and development of ontology, along with the group of obtained words used in interviewing three experts in ethnology to collect information from them. Furthermore, it is to evaluate the correctness of the data obtained from the conceptual and vocabulary analysis processes to classify knowledge

(Knowledge classification approach) of Broughton [12] from the document and systematically prepare it before taking it to the next phase.

Phase 2: From the collection of word groups in phase 1 for developing ontology that consists of vocabulary grouping, setting main classes and subclasses, determining properties and attributes of classes, and creating representative data within classes for defining the vocabulary value and data attributes, the Protégé program was applied to design and develop the ontology, class design, main class and subclass setting, hierarchy, properties, and relationships between classes in a technical connection form.

Phase 3 Ontology evaluation. It is to confirm the academic authenticity of information about ethnic groups in Chiang Mai from experts and use the evaluation results to improve the ontology appropriately. The ontology evaluation is separated into two parts, which are the evaluation of the vocabularies of ethnic groups in Chiang Mai. Then, three ethnic experts would evaluate the structured vocabulary's coherence in the correlation grouping. Additionally, the evaluation of class relationships and class properties would be tested by two experts in ontology, using the accuracy, consistency, and suitability assessment scale of the structure and word relationships by finding the consistency value. To be more accurate and complete, the researcher utilized expert advice to gather, organize, and summarize the results.

b) *Research tool*: Protégé program is a free, open-source knowledge management system program developed by Mark Musen in 1987 and a team at Stanford University [17]. It has established an ontology evaluation approach using the evaluation of Obrst and team [18]. It consists of the evaluation of 1) a process of identifying definitions, scope, and objectives of development; 2) a method of defining a concept or class; 3) a process for defining a class's properties; 4) a process for creating a model or representative data; and 5) applications and development guidelines in the future.

c) *Data analysis*: The researcher analyzed the data by evaluating the Index of Conformity or IOC (Index of item objective congruence) based on advice and suggestions from three experts in ontology and semantic web and two experts in ethnic groups in Chiang Mai, a total of five people. Upon seeking the experts for this study, the researcher required experts who are qualified as academics or researchers in a relevant field with research papers, academic papers, or other works that have been published continuously to date, or who are recognized nationally or internationally, or qualified people with experience doing research or teaching in a related field. The criteria that are acceptable and considered to be consistent or appropriate are a score of 0.5 or higher, whereas a score of less than 0.5 must be improved [19].

III. RESULT AND CONCLUSIONS

The development of ontology for information retrieval about ethnic groups in Chiang Mai aims to design, develop, and evaluate the ontology for information retrieval about ethnic groups in Chiang Mai. The summary of the findings is divided into three parts as follows:

A. Development of a Semantic Ontology of Knowledge about Ethnic Groups in Chiang Mai

The results of the study on ethnic groups in Chiang Mai revealed that the scope of knowledge of ethnic groups in Chiang Mai can be divided into nine groups: 1) ethnic Name; 2) history; 3) customs and rituals; 4) life and living; 5) language; 6) religion and faith; 7) dress; 8) entertainment; and 9) economy and society. The knowledge structure of ethnic groups in Chiang Mai can be divided into nine main classes, 29 subclasses, and 37 subgroups. An example of knowledge structures is shown in Table I.

According to Table I, it shows the main classes and their descriptions of the nine main classes, each with subclasses, subgroups, and properties to describe their relationship to the main class in more detail by dividing 29 subclasses, 37 subgroups, and 37 class properties. An example of the design of ontology can be seen in Table II.

Table II demonstrates the main classes and subclasses, as well as the description of subgroups and their properties, to show the relationship after the design of the ontology and then to establish the relationship with the Protégé program, which illustrates an example of ontology design and shows the relationship between main classes and subclasses as shown in Fig. 2.

TABLE I. CLASS STRUCTURE AND THE DESCRIPTION OF THE MAIN CLASS OF THE ONTOLOGY

Ethnic groups (Ethnic Group: thing) in Chiang Mai who have their own names, customs, religion, dress, etc. can be shown according to the ontology's main classes and subclasses divided by relationships.		
<i>Class no.</i>	<i>Class name</i>	<i>Class description</i>
1.	Ethnic Name	A group of people who are officially named according to documents and research.
2.	History	History, origins, migrations, and settlements of ethnic groups.
3.	Customs and Rituals	The expressions, behaviors, worship, role models, or patterns that most people hold in their ethnic groups serve as a pattern for future generations to follow.
4.	Life and Living	The way of life of people in ethnic groups, such as food, medication, way of life, occupation, animal husbandry, wisdom, utensils, accessories, and social values.
5.	Language	Phonetic characters, words, speech, and symbols are used in place of speech to express one's ethnicity.
6.	Religion and Faith	Forms of belief, faith, religiosity, or cult of belief in regard to many matters in ethnic groups.
7.	Dress	Elements or dress styles of people in ethnic groups.
8.	Entertainment	Grouping together to communicate certain things, emotional expressions, and stories for entertainment and pleasure.
9.	Economy and Society	Earning money, exchange system, economic system of people in ethnic groups that generate income for each other, social organization of people in ethnic groups from the household level to the community level.

TABLE II. AN EXAMPLE OF THE DESIGN OF ONTOLOGY FOR INFORMATION RETRIEVAL ABOUT ETHNIC GROUPS

No .	Main classes	Subclasses	Subgroups	Properties	
1.	Ethnic name	Self-name	Name Meaning	Creating a group name	
		Official name	Official name	Difference	
		Other name	Other name		
2.	History	Origin	Origin	Route of immigration	
		Original settlement	Original settlement		
		Immigration to Thailand	Route		
		Story/myth	myth	Name	Story
				Landmark	Name
Background					
3.	Customs and rituals	Name	Name of ritual		Name
		Time of event	Duration	Duration	
		Purpose	Purpose	Purpose	
		Background/story	Background	Cause	
		Ritual tools	Offerings	Relevance	
			Other tools		
		Method	Method	Procedure	
		Clothing	Clothing	Dress	
Prohibitions /obligations	Prohibitions /obligations	Success			
4.	Life and living	Food	Name	Name	
			Type of food	Type of food	
			Ingredient	Ingredient	
			Seasoning	Seasoning	
			Way of eating	Way of eating	
5.	Language	Spoken language	Speech pattern	Speech pattern	
		Written language	Language family	Language family	
		Letters	Letters origin	Letters origin	
6.	Religion and Faith	Religion	Name	Name	
			Name of sect	Sect	
			Name of cult	cult Beliefs	
7.	Dress	Shirt	Cloth pattern	Background story of cloth pattern	
		Pants			
		Accessories			

		Foot		
			Color tone	Synthetic/natural color
			Material	Material
8.	Entertainment	Place	Gathering center	Appropriateness
		Festival	Festival	Duration
9.	Economy and Society	Economic system	Income	Income
		Financial integration	Income sources	Income sources
		Social dependence	Dependent income	Dependent income

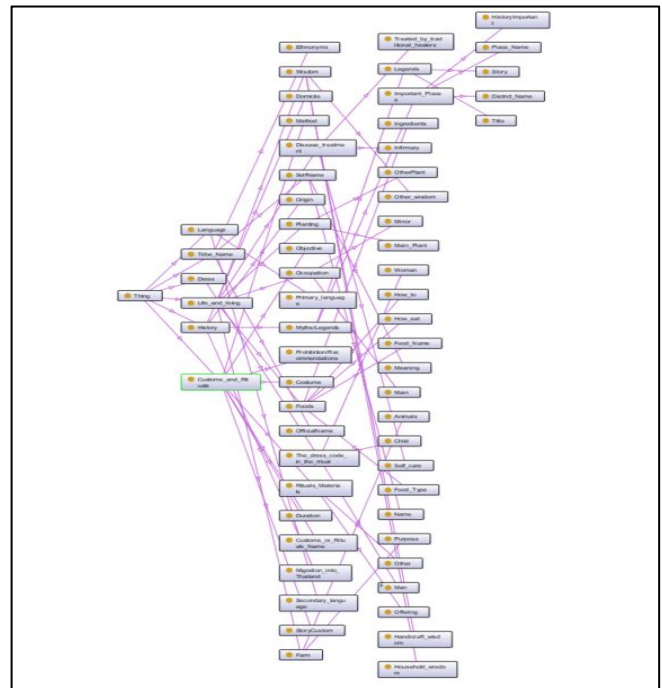


Fig. 2. Relationships between Ontology's Main Classes and Subclasses for Information Retrieval about Ethnic Groups in Chiang Mai.

B. Results of Ontology Evaluation for Information Retrieval about Ethnic Groups in Chiang Mai

Ontology evaluation is divided into two parts, which are the evaluation of the ontology structure by experts and an examination of the data analysis by evaluating the consistency index. The details are as follows:

1) The results of the evaluation of the suitability of the ontology structure for information retrieval about ethnic groups in Chiang Mai by experts found that the suitability of the ontology scored at 0.93. Class grouping, class ordering, class name, property name, the relationship between classes, the name of the relationship between classes, the accuracy and appropriateness of ontology content, and ontology overview were appropriate at 1.00. Followed by ontology class and its properties or attributes, the appropriateness was 0.66, respectively. These results are as shown in Table III.

TABLE III. RESULTS OF ONTOLOGY EVALUATION OF ETHNIC GROUPS

Items	IOC	Results
1. Class grouping within the ontology	1.00	Appropriate
2. Class ordering within the ontology	1.00	Appropriate
3. Ontology classes	0.66	Appropriate
4. Name of classes within the ontology	1.00	Appropriate
5. Properties or attributes of classes	0.66	Appropriate
6. Name of properties	1.00	Appropriate
7. Relationships between classes	1.00	Appropriate
8. Name of the relationships between classes	1.00	Appropriate
9. Accuracy and appropriateness of ontology content	1.00	Appropriate
10. Ontology overview	1.00	Appropriate
Total	0.93	Appropriate

2) The evaluation of data analysis was conducted by determining the Index of Conformity, or IOC (Index of item objective congruence), with an acceptable average score of IOC. If a value is 0.50 or higher, the content is consistent and applicable [20]. The evaluation by two ethnic and cultural experts assessed the analysis of the data by determining the conformity index used to connect and group information of ethnic groups. The overall evaluation results revealed that the ontology structure was consistent and had definition value, scope, and objectives of development. The results were also found to be consistent (score value = 0.89) in three areas: defining relation name and class properties (score value = 0.88), grouping, and ranking of classes within the ontology (score value = 0.90), and the accuracy and appropriateness of the overall ontology content (score value = 0.90), as demonstrated in Table IV.

TABLE IV. RESULTS OF THE ONTOLOGY CONSISTENCY EVALUATION FOR INFORMATION RETRIEVAL ABOUT ETHNIC GROUPS

Items	IOC	Results	
Specifying, definition, scope, and objectives of development are appropriate	1. Name of classes within the ontology	0.95	Consistent
	2. Properties or attributes of classes	0.98	Consistent
	3. Name of properties	0.98	Consistent
	4. Relationships between classes	0.96	Consistent
	5. Name of the relationships between classes	0.98	Consistent
Consistency average	0.97	Consistent	
Class grouping and ordering within the ontology	1. Class grouping within the ontology	0.98	Consistent
	2. Class ordering within the ontology	0.97	Consistent
	3. Ontology classes	0.98	Consistent
Consistency average	0.98	Consistent	
Accuracy and appropriateness of the overall ontology content	1. Accuracy and appropriateness of ontology content	0.97	Consistent
	2. Ontology overview	0.95	Consistent
Consistency average	0.96	Consistent	
Total	0.97	Consistent	

The results of the evaluation can be used in class design, relationships between classes, and properties of classes within the ontology for information retrieval about ethnic groups in Chiang Mai, making the developed ontology more suitable and consistent with the query requirements.

C. Conclusions

The structural classification resulting from this research is based on the principle of main classes and subclasses and by stratification based on the knowledge found in the source material. Ontology of ethnic groups covers many dimensions and reflects the content of ethnic groups in Chiang Mai Province of Thailand. The classification of ethnic groups in Thailand is detailed in many aspects which grouped the population according to the cultural and ethnic group. This is classified by using the criteria of the original topographic location and other similar factors, such as social characteristics, customs, history, etc. The structure is concluded three groups: (1) cultural and ethnic similarities according to the classification criteria; (2) identification of ethnic groups or groups; the culture is more detailed than the first two levels and (3) livelihoods of knowledge classification and knowledge structure of ethnic groups in Thailand focuses on data extraction. Named ethnic groups of Thailand as the main constituent groups with similar and related topics. This research apart from others is the effort to categorize details under each main class and subclasses. For example, in Class 7, subsistence, the class of dress care has four subclasses, i.e., Shirt, Pants, Accessories, Foot. This research organizes classes and subclasses of knowledge margins and creates a knowledge structure that delves into the content of various researches. Details are given hierarchically from subclasses to different properties and it will be useful in the future, although this ethnic knowledge structure is for an ontology developed to support semantic web for searching capabilities and recommendation system [21], [22]. Also can be applied to data extraction in other ways, such as for a large number of ethnic sources, for example, semantic web construction. Therefore, ethnic classifications in Thailand can be combined with and used to expand the assigned classification notation. To categorize ethnic group outcomes appropriate to an automated retrieval system that provides access to the content of information resources rather than lists, the researchers also saw that the methods used in the study could be applied to improve knowledge classification.

IV. DISCUSSIONS

The ontology design for information retrieval about ethnic groups in Chiang Mai is developed to define the classification structure of knowledge subjects arising from the classification structure based on the source of knowledge and ethnic and cultural experts. This is in accordance with the principle of grouping as well as sub-components of ethnic knowledge, which is comprehensive and reflects the content of ethnic groups of Chiang Mai. It is also in line, where there is a detailed grouping of the ethnic structure of Thailand with a hierarchical structure analysis that includes the original geographic location and other similar factors, such as social characteristics, customs, history, etc. [23] These include structures that can be divided into three levels: (1) geography; (2) cultural and ethnic similarity according to classification criteria; and (3) ethnic

identification, group, or culture with details. When cultural grouping is conducted in accordance with the process for grouping and retrieval of the body of knowledge, which consists of a body of knowledge derived from wisdom and culture, such as religion, art, and culture, as well as important historical sites, it can also be applied to the body of knowledge derived from other fields [24].

Eventually, the researcher has synthesized a guideline derived from the conceptual process of studying knowledge about ethnic groups in Chiang Mai Province, which contains the semantic ontology of knowledge about ethnic groups in Chiang Mai as a model that can be applied as a source of information. Furthermore, the researcher has applied SPARQL language to retrieve information rather than the relational database system and using SQL language in the original pattern, which will assist in obtaining more information in ethnic areas according to the ideas [25], [26].

V. RECOMMENDATIONS

1) Increasing the class's attributes to support ethnic group data collection in other Northern provinces can expand the scope of learning and data storage even more.

2) An ontology may be used to develop a semantic search program by providing search methods or alternatives that allow users to make better use of information resources.

REFERENCES

- [1] T. H. Eriksen, *Ethnicity and nationalism: Anthropological perspectives*. Pluto press, 1993.
- [2] R. Jenkins and K. D. Haggerty, "Rethinking ethnicity: arguments & explorations," *Canadian Journal of Sociology*, vol. 24, no. 2, p. 130, 1999.
- [3] R. William, *Keyword: A Vocabulary of Culture and Society*. New York: Oxford University Press, 1983.
- [4] Committee on Children, Youth, Women, Elderly, Disabled, Ethnic Groups and LGBT People House of Representatives, Thailand, "Report on the results of the study on the condition of problems and guidelines for the promotion and protection of ethnic groups in Thailand", 2020. <https://dl.parliament.go.th/handle/lirt/572116>.
- [5] S. Srisantisuk, "Principles of qualitative research with ethnic communities," *Journal of Language and Culture*, vol. 15, no. 2, pp. 4-13, 1996.
- [6] A. Cohen, *Introduction: The lesson of ethnicity*. In A. Cohen (Ed.). *Urban ethnicity*. London: Tavistock, 1974.
- [7] P. Leepreecha, "Paradigms of Studies on Ethnicity," *Journal of Mekong Societies*, vol. 10 no. 3, pp. 219-242, 2014.
- [8] S. Jiranathanaporn, O. Chinakhrapong, and U. Singnoi, *Language Attitudes of Tai Ethnic Groups Towards Their Own Language in Thai Lower Northern Region*. Faculty of Humanities, Naresuan University: Phitsanulok, 2008.
- [9] J. Gao and I. Onkam, "Way of life of Hmong Ethnic Group : The case study of Ban Mae Sa Mai, Pongyang Sub-district, Maerim District, Chiangmai Province," *Liberal Arts Review*, vol. 16, no. 1, pp. 27-44, 2021.
- [10] T. R. Gruber, "A translation approach to portable ontology specifications," *Knowledge Acquisition*, vol. 5, no. 2, pp. 199-220, 1993. <https://doi.org/10.1006/knac.1993.1008>.
- [11] K. Kumar, *Theory of Classification*. New Delhi: Vani Educational Books, 1985.
- [12] V. Broughton, *Essential Thesaurus Construction*. London: Facet Publishing, 2004.
- [13] J. Chaikhambung and K. Tuamsuk, "Development of Semantic Ontology of Knowledge on Ethnic Groups," *TLA Research Journal*, vol. 10, no. 2, pp. 1-15, 2017.
- [14] D. Siharad, "The Semantic Knowledge Base Searching System for Promoting Cultural and Traditional of Mong Tribe, Bankeknoi, Kaokor District, Phetchabun Province using WordPress and Ontology," *Research Journal Rajamangala University of Technology Thanyaburi*, vol. 19, no. 2, pp. 144-155, 2020. DOI: 10.14456/rj-rmutt.2020.25.
- [15] M. Uschold and M. King, "Towards a methodology for building ontologies," Paper presented at the Workshop on Basic Ontological Issues in Knowledge Sharing, held in conjunction with IJCAI-95. New York, 1995.
- [16] N. F. Noy, & D. L. McGuinness, "Ontology development 101: A guide to creating your first ontology," *Stanford Medical Informatics Technical Report*, 2001. SMI-2001-0880. <http://citeseer.ist.psu.edu/viewdoc/download;jsessionid=BCD0804A95E679C04930558DFFBCB8F4?doi=10.1.1.136.5085&rep=rep1&type=pdf>.
- [17] M. A. Musen, "Use of a domain model to drive an interactive knowledge-editing tool," *International Journal of Man-Machine Studies*, Vol. 26, pp. 105-121, 1987.
- [18] L. Obrst, B. Ashpole, W. Ceusters, M. Mani, S. Ray, and B. Smith, *The Evaluation of Ontologies*, Springer, New York, 2006.
- [19] P. Pasunon, "Reliability of Questionnaire in Quantitative Research," *Parichart Journal*, vol. 27 no. 1, pp. 144-163, 2014.
- [20] P. Tuntavanitch and P. Jindasri, "The Real Meaning of IOC," *Journal of Educational Measurement Mahasarakham University*, vol. 24 no. 2, pp. 3-12, 2018. [In Thai].
- [21] K. Puritat, P. Julrode, P. Ariya, S. Sangamuang, and K. Intawong, "Book Recommendation for Library Automation Use in School Libraries by Multi Features of Support Vector Machine," *International Journal of Advanced Computer Science and Applications*, vol. 12 no. 4, pp. 190-196, 2021.
- [22] B. Stark, C. Knahl, M. Aydin, and K. Elish, "A Literature Review on Medicine Recommender System," *International Journal of Advanced Computer Science and Applications*, Vol. 10, No. 8, pp. 6-13, 2019.
- [23] J. Chaikhambung Digital, "Knowledge Base about Ethnic Groups in Thailand," *Journal of Information Science*, vol. 39, no. 4, pp. 46-58, 2021. doi:10.14456/jiskku.2021.21.
- [24] W. Sunkanaporn, "Cultural capital of Sanpatong district study for guidelines with Creative Economy thinking," *Veridian E-Journal, Silpakorn University*, vol. 9, no. 3, pp. 815-829, 2016.
- [25] P. Suwannaphachana and N. Sampao-Ngern, "Information System Concept and Development of Musical Instruments Documentation of Ethnic Groups in Thailand," *Rangsit Music Journal*, vol. 15, no. 2, pp. 84-98, 2020.
- [26] S. Middleton, D. D. Roure, and N. Shadbolt, *Ontology-Based Recommender Systems*, 2009. DOI:10.1007/978-3-540-92673-3_35.

CoSiT: An Agent-based Tool for Training and Awareness to Fight the Covid-19 Spread

Henri-Joël Azemena¹

and Franck-Anael K. Mbiaya²

Institut Francophone International (IFI)
Vietnam National University in Hanoi
Hanoi, Vietnam

Selain K. Kasereka³

University of Kinshasa

Mathematics and Computer Science Dpt
ABIL Research Center
Kinshasa, Democratic Republic of the Congo

Ho Tuong Vinh⁴

Institut Francophone International (IFI)

Vietnam National University in Hanoi
Hanoi, Vietnam
Sorbonne University, IRD
UMMISCO F-93143, Bondy, France

Abstract—Since the beginning of 2020 and following the recommendation of the Emergency Committee, the WHO (World Health Organization) Director General declared that the Covid-19 outbreak constitutes a Public Health Emergency of International Concern. Given the urgency of this outbreak, the international community is mobilizing to find ways to significantly accelerate the development of interventions. These interventions include raising awareness of ethical solutions such as wearing a face mask and respecting social distancing. Unfortunately, these solutions have been criticized and the number of infections and deaths by Covid-19 has only increased because of the lack of respect for these gestures on the one hand, and because of the lack of awareness and training tools on the spread of this disease through simulation packages on the other. To give importance to the respect of these measures, the WHO is going to try to propose to his member states, training and sensitization campaigns on coronavirus through simulation packages, so that the right decisions are taken in time to save lives. Thus, a rigorous analysis of this problem has enabled us to identify three directions for reflection. First, how to propose an IT tool based on these constraints in order to generalize training and awareness for all? Secondly, how to model and simulate these prescribed measures in our current reality? Thirdly, how to make it playful, interactive, and participative so that it is flexible according to the user's needs? To address these questions, this paper proposes an interactive Agent-Based Model (ABM) describing a pedagogical (training and educational) tool that can help understanding the spread of Covid-19 and then show the impact of the barrier measures recommended by the WHO. The tool implemented is quite simple to use and can help make appropriate and timely decisions to limit the spread of Covid-19 in the population.

Keywords—Multi-agent system; covid-19; CoSiT; modeling-simulation; barrier measures; complex systems

I. INTRODUCTION

To sensitize everyone in the fight against the spread of the new virus through the respect of non-pharmaceutical measures while waiting for a pharmaceutical solution to be set up, the WHO in a report entitled "SituationReport-156" [1], recommends through tabletop exercises and textual presentations to its member states, the implementation of educational training and awareness-raising campaigns through seminars and symposiums on the coronavirus (Covid-19). For this purpose it will put at their disposal, different packages of textual simulation, to form and sensitize in the fight against the Covid-19, with the help of textual plans and presentations with slides [2]. At the WHO, for that matter, the Department of Health Security and Preparedness has set up the various table top exercise programs

named SimEx (Simulation Exercise) Covid-19 [3] as part of the coronavirus training (Covid-10), which it defines in its 2017 Simulation Exercise Manual [4], as an exercise that uses progressive scenarios, with series of scripted messages to allow participants to consider, the impact of a potential public health emergency on existing plans, procedures and capabilities: in these words that "A TTX (Table Top Exercise) simulates an emergency situation in an informal stress-free environment". Although these plans (non-pharmaceutical measures), in a textual format, are easy to manipulate by individual stakeholders, there are no accessible tools and pedagogical means to train and sensitize all stakeholders on the importance of respecting these measures, as these actors may have different interpretations of these measures and the protocol set up, in an environment where they are geographically distributed and distant from each other, and these training course are only held in the organization's offices around the world, and are purely professional, which considerably restricts listening, and limits training and awareness.

Taking into account the above mentioned observations, and with the increase in contamination, the need for training and sensitization, especially of political decision-makers and populations who are not always able to understand the merits of these measures, is becoming increasingly necessary and important, so that they can make early decisions on the adoption of these measures to save lives. This solution could also be very useful to avoid any misinterpretation of what these textual response plans mean. It is therefore essential to propose an educational tool that can simulate the current reality with all its aspects (particularly social) to understand, control and monitor this disease throughout its life cycle.

The aim of this paper is to contribute to the engineering of coordination and decision making, in a multi-agent universe, and this in the fields of epidemiology, while providing a global approach that takes into account without confusing them and by articulating them, the essential aspects of crisis management: ethical measures (social distancing and wearing of protective masks) and social behavior.

To achieve this, we used the Simple Reflex Agent model to simulate the propagation of the pandemic and to visualize the impact of barrier measures. We then specified and formalized this approach with the UML and AML languages, and documented it with the ODD (Overview, Design concepts and Details) protocol. Then, we proposed a pedagogical architecture, centered on interactive and participative agents, to allow

users to play themselves on the existing parameters, according to the context in which they are, and to visualize the results of the simulation in an interface provided for this purpose.

The implementation and simulation of the system was done on the GAMA (GIS and Agent-Based Modelling Architecture) modeling and simulation platform. To validate the obtained model, we defined and simulated several real-life scenarios which revealed results similar to what is observed today.

This paper is organized as follows: in the second section, we propose a review of the literature on infectious diseases, then on the mathematical and computer models existing in the fight against the spread of these diseases, and finally on the educational tools that can play the role of training support in the current context. In the third section, we propose a description and formalization of the agent model we propose as a solution, after which we document it using the ODD protocol. Section four concerns the implementation and experimentation as well as the validation tests through the defined scenarios. The fifth section concerns the general conclusion and outlook.

II. KEY CONCEPTS

A. Complex Systems

A system is complex when it is made up of a large number of differentiated autonomous components that interact with each other in a non-trivial way. This system is also characterized by the emergence at the global level of new properties, not observable at the level of components system and by a global operating dynamic difficult to predict from the observation of the constituents and their elementary interactions [5].

B. Modeling - Simulation

Modeling – simulation, first of all, consists of the designing of a model. It is a way of making explicit the complexity of a system to better understand its functioning and to make good decisions [5].

C. Model

A model is a mathematical, or graphic and computerized representation of the objects and the relations between them in a confined zone of the real world. A model can also be viewed as a simplified representation of a complex reality. To be useful, models must be adapted to their objects and be conveniently studied and validated [6].

D. The New Coronavirus

The new Coronavirus named Covid-19 is caused by the SARS-CoV-2 virus, which is spread through close contact with an infected person when small liquid particles are expelled through the mouth or nose of an infected person or when people are in direct or close contact with an infected person. Transmission can also occur in specific settings, particularly in crowded, poorly ventilated indoor spaces where one or more infected persons spend long periods with others. People with the virus can leave infectious droplets when they touch objects or surfaces, such as tables, door knobs and railings. We can then become infected with the virus if we touch these contaminated surfaces before washing our hands [7].

E. Measures to Control the Spread of Covid-19

To limit the risk of contracting Covid-19, the WHO recommends that everyone follows certain basic precautions such as [7]:

- Follow local recommendations.
- Keep at least one meter away from others.
- Wear a mask, in public places.
- Avoid touching surfaces, especially in public places.
- Wash your hands regularly with soap and water or with a hydroalcoholic solution.
- Cough and sneeze into your elbow or a tissue.

In the following, the system that will be modeled will take into account only two of these measures: the wearing of the mask, and the respect of the distancing.

III. RELATED WORKS

Several solutions in the field of infectious disease control through mathematical modeling have been well established. Among these solutions, we can mention the one proposed by Kermack and McKendrick in the paper entitled “A contribution to the mathematical theory of epidemics” [8]. The aim was to understand the evolution of the epidemic in large populations of constant size. The application of this mathematical modeling technique was motivated by the need for more accurate predictions of the spread of infections at the population level. This has contributed to a better understanding of the mechanisms of spread to help develop optimal control strategies through public health interventions. In [9], the authors address the problem through a representation in the form of compartments of the various stages of infection. We find several of these compartment models in the literature [10], [11], [12], among which we can cite the SI, SIR, and SEIR models.

The work of Kieczkowski & Grenfell [13], presents a new approach based on an increased interest in modeling the interactions between people in a network with a mixture of local and global interactions, by proposing a stochastic model called Mean-field, to demonstrate that even in the presence of a high level of local correlation their model can succeed. To achieve this, they referred to the work of Watts & Strogatz, [14], in which they analyzed some properties of mesh networks, and showed that they behave like a network model, even for a relatively small mesh parameter.

Another similar model was analyzed by Boccaro & Cheong, [15], where individuals were allowed to change places on a two-dimensional network. Thus, they proved that when the interactions between the agents are over a long-range, it causes a very fast spread of the epidemic in the population. In the work of Kieczkowski [13], the authors studied the effects of local spatial correlations of a temporal epidemic spread as a function of the increasing proportion of global contacts in a cellular automaton (CA) model. They deduce that even in the presence of high local correlations, the model (Mean field types equations) can be quite suitable if the contact rate is treated as a free parameter. They conclude that the contact rate reflects not only a microscopic and epidemiological situation,

but also a complex social structure, including short and long term contacts following a hierarchical structure of the society. Among the works that are based on this small-world network principle, we can mention [13], [14].

While these approaches (compartmental and stochastic) rely on mathematical models and representations to propose solutions in the field of epidemiology, the Agent-Based approach is relatively new and more powerful, more realistic in simulating the spread of diseases and predicting the impacts in the population and especially regarding the effectiveness of interventions. According to [16], this model is classified as a solution to model complex social interactions in a real world.

In the same perspective, in [17] authors present an Agent-Based approach for modeling dynamics of contagious disease spread. The aim here was to overcome the limitations of different approaches, such as cellular automata and classical epidemic models. In this paper the authors also allow the modeling of interactions between individuals, which facilitates the study of specific spatial aspects of the spread of epidemics and to address the stochastic nature of the epidemic process. In [18] authors present a tool, EpiSimdemics which is different from the other systems and allows to simulate the propagation of contagious diseases. According to this work, all of these simulators have been widely evaluated and used in dozens of large-scale public health studies.

Among the computer tools used in the fight against Covid-19, the literature informs us that several tools are already available for this purpose, among which: The most powerful computer in the world Fugaku [19], that works particularly at the molecular level, and at the macroscopic level. In addition, the MODSIR19 project [20] developed within the framework of research for the fight against Covid-19, allowing to model the various factors which influence an epidemic, and to visualize the effects on a graph, according to the R0 factor. It also allows to better predict the evolution of the pandemic, to simulate the number of hospitalizations, the needs in resuscitation beds, and the effects of confinement and de-confinement, and is also for pedagogical purposes. Learn to fight: “Good practices when treating patients”, on the other hand, is a digital training simulator for the management of patients with the symptoms of Covid-19 [21]. Another powerful tool is the COMOKIT which is a GAMA model on the evaluation and comparisons of policy responses to the Covid-19 [22] pandemic. Its goal is to help policymakers and researchers answer questions such as: Does closing schools decrease peak transmission? What is the impact of wearing masks on the dynamics of the epidemic? How long should a lockdown ideally last?

However, with the increase in the number of cases from day to day, several public health organizations and mainly the WHO have found it necessary to train and sensitize people on coronavirus through various training and sensitization packages through so-called tabletop exercises (TTX) [2]. Although this training is necessary to sensitize and train decision-makers and individuals to curb the spread of the virus. The means and tools of the training set up by the WHO remain a hindrance, and a limit as to the objectives to be reached, for several reasons. Firstly, these simulations are done on paper and through presentations, there are no specialized software tools for this. Secondly, it is restricted to the members of the organization

and takes place only in its premises around the world, which reduces the target to be reached. Third, it is targeted and concerns only one category of people. Moreover, the actors being geographically distributed, each of them can have a different interpretation of these measures, and more seriously, the disease changes phase each time and new measures must be adopted each time. Thus, proposing a computer simulation tool for educational purposes to train and raise awareness on the measures prescribed by the WHO becomes an urgent task.

Our work will consist in conducting an in-depth study on the impact of these measures in the fight against the virus, by looking at the training through simulations proposed by the WHO.

IV. PROPOSED MODEL

A. Analysis and Design

To answer the questions raised by the literature, we propose a solution to create an educational, simple, interactive, participative and generalist computer tool that can help in the fight against infectious diseases. This tool named CoSiT (Covid-19 Simulation Tools) is based on the GAMA (GIS and Agent-based Modelling Architecture) modeling and simulation platform and follows a set of principles and requirements as follows :

- It is first and foremost an educational tool for training and raising awareness on the importance of respecting barrier measures in the fight against the spread of Covid-19.
- It is also and above all an interactive and participative tool.
- CoSiT is based on the so-called non-pharmaceutical measures prescribed as part of the fight against Covid-19, to produce simulations of our daily lives and to visualize the results obtained in an interface provided for this purpose.
- CoSiT is based on a detailed and realistic representation of the impact of barrier measures in controlling the spread of Covid-19 in the environment of our choice.
- CoSiT is generic, flexible and applicable to any case study.
- CoSiT is open and modular enough to support interdisciplinary cooperation.
- CoSiT provides easy access to small-scale training, experimentation and sensitization, making it easy to explore its parameters.

To do so, we followed the following process as shown in Fig. 1.

Fig. 2 gives us an overview of the structure of the model to be implemented in the form of a UML class diagram.

In Fig. 3 we can see the AGR representation with AML of our model.

The design of the simulation environment is done upstream of the simulation according to the plan of the place where we

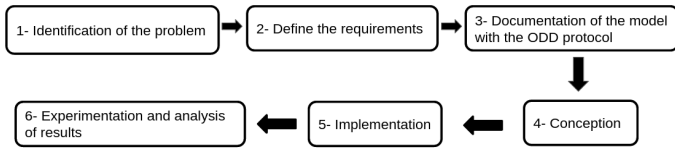


Fig. 1. Solution Implementation Process.

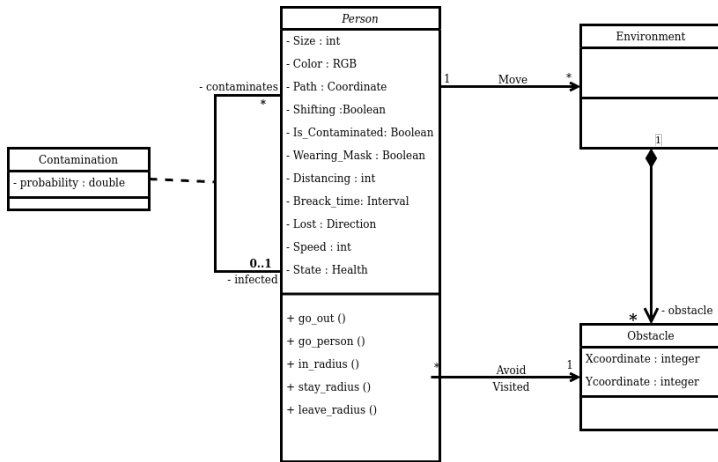


Fig. 2. Overview of the Model Structure in the Form of a UML Class Diagram.

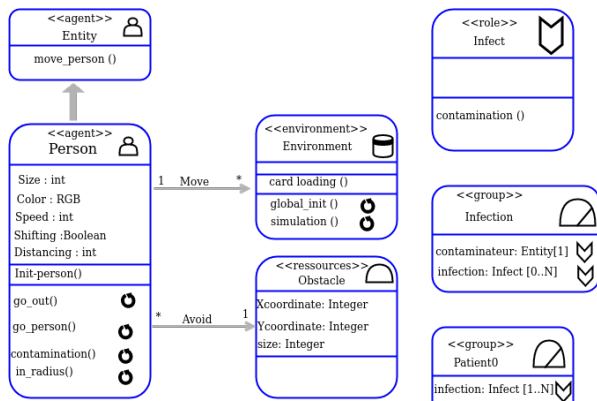


Fig. 3. AGR Representation with AML of the Model.

want to define a scenario, to do this, we have defined some basic rules.

Fig. 4 shows the design of the simulation environment. It is after this step that the file can be exported in CVS (Comma Separated Values) format and imported into our model as a simulation environment.

B. Model Description using ODD Protocol

To describe the model that we propose as a solution, we have used as a tool, the ODD protocol [23], [24].

1) Overview :

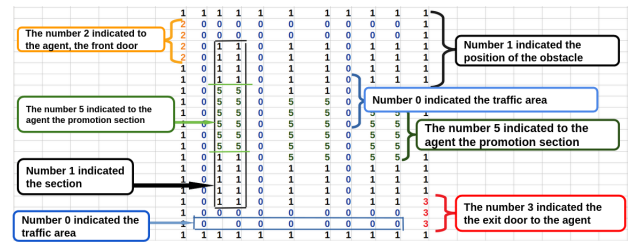


Fig. 4. Design of the Simulation Environment using Libre Office Calc Spreadsheet.

- **Purpose:** The objective of the model is to explore, in a low-scale real environment of our choice, the impact of barrier measures in the fight against Covid-19.

- **Entities, state variables, and scale:** The model is composed of a single variable, the human agent, which represents the different people in the considered area with their characteristics and epidemiological status. Each agent is localized in space by its coordinates, and can recognize objects in the environment.

It should be noted that the environment is composed of a set of obstacles which are the objects of the living world, and of agents which are people. It corresponds to a cell of 70m x 70m that can be parameterized.

As for the temporal resolution, the simulation is done by a succession of iterations for which the time step is fixed at one second. This time step is defined in such a way that the displacement distance during an iteration of an agent does not exceed the dimension of a cell. The simulated duration is not defined by default, because it depends on the type of environment and the number of initial agents. This duration corresponds to a day of work and activities.

The simulation is divided into four phases, which are distinguished by the agents' behaviors:

- A "Life without constraint" phase, which includes two types of agents: "infected and susceptible". A phase of "Life with a constraint of wearing face mask", during which agents are forced to wear the mask. A phase of "Life with constraint, respect of social distancing", during which they must respect a certain distance from each other. And a phase of "Life with a constraint of facial mask-wearing, and respect of social distancing", which combines the two previously mentioned.
- Several other variables are also defined as parameters of the model: the number of people who can intervene throughout the simulation, the probability of contamination within a population, the measure of social distancing, the simulation environment. The model gives the user the possibility to act on the behavior of the agents before and during the simulation through the activation and deactivation of these barrier measures.

2) Design Elements:

- **Basic Principles:** The aim is to show, through modeling and computer simulation, the importance of barrier measures in the fight against Covid-19. The aim is to provide an educational tool that can be used as a training and awareness support.
- **Emergence:** There is a phenomenon of spatial spread of disease that is conditioned by the movements and behaviors of human agents. **Perception:** Agents can perceive other agents in their vicinity, as well as objects in the world they are in.
- **Interaction:** The only interactions present in the model are the interactions between human agents.
- **Stochasticity:** The model contains some stochasticity in both the initialization and the dynamics. The position of the agents in the space is random on one of the cells. The number of initially sick agents is also chosen randomly. During the simulation, when a new agent is created, its status is chosen randomly according to a probability. Moreover, an agent moves a more or less constant distance but in a randomly chosen direction according to its objectives.
- **Observation:** The main display of the simulator is an environment containing the different types of agents, as well as the obstacles. It is updated at each time step, allowing to visualize the dynamics of the disease propagation. During the simulation, we can observe the evolution of the number of contamination with the help of a curve representing these values as a function of time, and also in textual form for the non-professionals of the domain.
- **Adaptation:** the individual behavior of each agent is a process of adaptation at each time step, it adapts to evolve within its environment and to reach its objectives.
- **Objectives:** the objective of the agents is to move according to the established rules. These objectives are not fixed but depend on the parameters and the scenario we want to simulate.

3) Details:

- **Initialization:** During this phase, we have to define the basic parameters of the simulation such as: importing the simulation environment, creating and initializing the agents, setting the parameters of the behavior of these agents.
- **Input Data:** The main input data is in CSV format previously provided by the user.

V. IMPLEMENTATION

The aim is to develop a tool capable of simulating the propagation of the Covid-19 in a public environment such as supermarkets, bars, or restaurants, and then to display the results obtained in a clear and accessible way for everyone. The solution implemented here is a simple reflex agent-based model, documented by the ODD protocol, implemented, modeled and simulated using GAMA Platform [25]. Its interface has different parts and offers two solutions:

the CoSiT1 solution which is an interactive and customizable training environment and the CoSiT2 solution, which is more generalist, and uses the parameters of CoSiT1 to offer on a single screen, all possible results.

The Gama modeling and simulation platform is the one with which we implemented this solution. Fig. 5 gives us a descriptive overview of this solution.

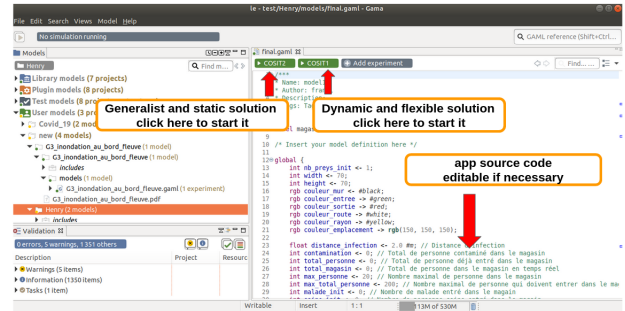


Fig. 5. Gama Modeling and Simulation Platform Uses

The CoSiT1 interface The main requirements implemented in this part are summarized in Fig. 6.

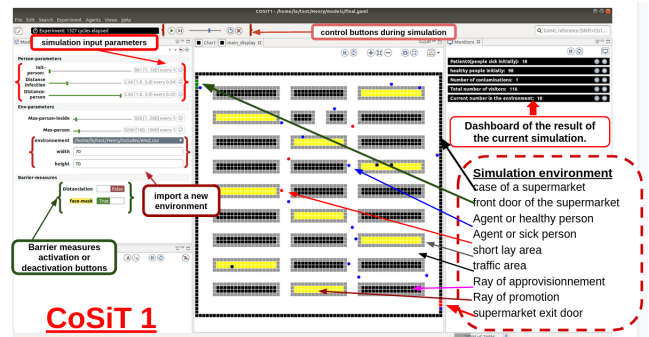


Fig. 6. CoSiT1 Simulation Interface.

The CoSiT2 interface The main requirements implemented in this part are summarized in Fig. 7.

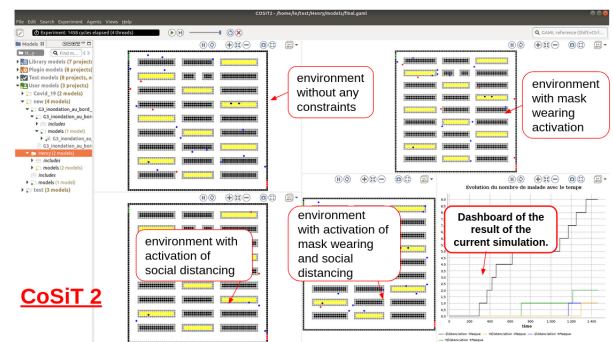


Fig. 7. CoSiT2 Simulation Interface.

VI. NUMERICAL SIMULATION AND EXPERIMENTATION

In this section, the simulations performed are presented. Table I describes the parameters used and the estimated baseline values.

TABLE I. PARAMETER VALUES AND THEIR MEANINGS

Parameters	Estimated baseline values
Distance infection	[0 – 2.0] meters
Maximum persons inside the supermarket	50
Maximum visitor per day	500
Distanciation value	[0 – 4.0] meters
Respect of wearing face mask	Yes/No
Respect for distancing	Yes/No
Probability of infection	0.05
Probability of wearing a face mask	[0.5 – 1.0]
Probability of distancing respect	[0.5 – 1.0]

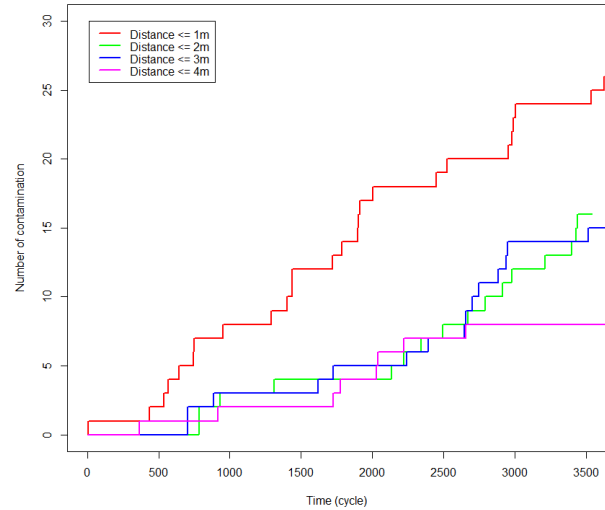


Fig. 9. Impact of Social Distancing.

A. Experimentation 1: Influence of Wearing a Mask on the Spread of the Virus in a Supermarket

There is scientific debate about their use, one study showed the ability of surgical masks to prevent the exhalation of respiratory viruses. Therefore, the use of masks by the population could reduce peak contamination.

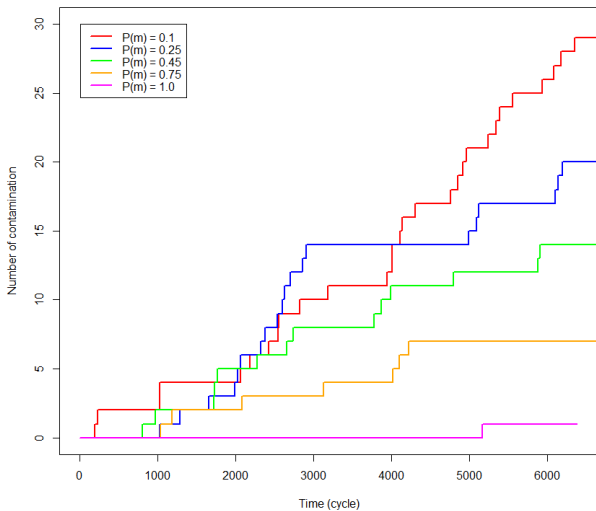


Fig. 8. Several Probability of Wearing Masks are Considered (0.1, 0.25, 0.45, 0.75 and 1) and the Social Distancing is not Respected.

B. Experimentation 2: Influence of Social Distancing on the Spread of Covid-19 in a Supermarket

Like the wearing of masks, maintaining a certain distance has been recommended. The positive effects of such actions are visible on the number of contaminations, depending on whether one practices it or not.

C. Experimentation 3: Influence of Mask Wearing and Respect of Social Distancing on the Spread of Covid-19 in the Environment

The main objective of this experiment is to find the best protocol that can have an optimal impact on the spread of the pandemic, reducing the spread factor R0. To do this, we decided to simulate a scenario in which the two previous barrier measures are found under the same conditions.

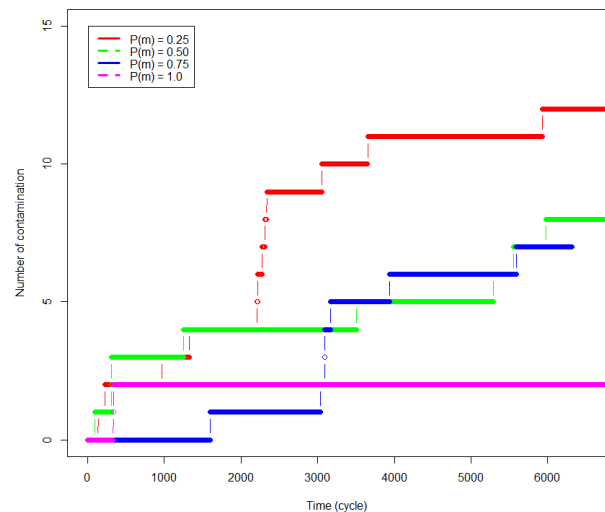


Fig. 10. Impact of Wearing Face-Mask and Respect of Social Distancing. Several Probability of Wearing mask are Considered while the Social Distancing Considered is 2 Meters

As shown in Fig. 10, we start this exploration with the simplest possible scenario, i.e. a free spread of the disease with a percentage of 25% as the probability of wearing a face

mask, and 2 meters as the distance measure to be respected.

D. Experimentation 4: Consideration of Promotion Area in the Supermarket Environment

This experimentation attempts to display the dynamics of the pandemic in a supermarket that contains promotion areas.

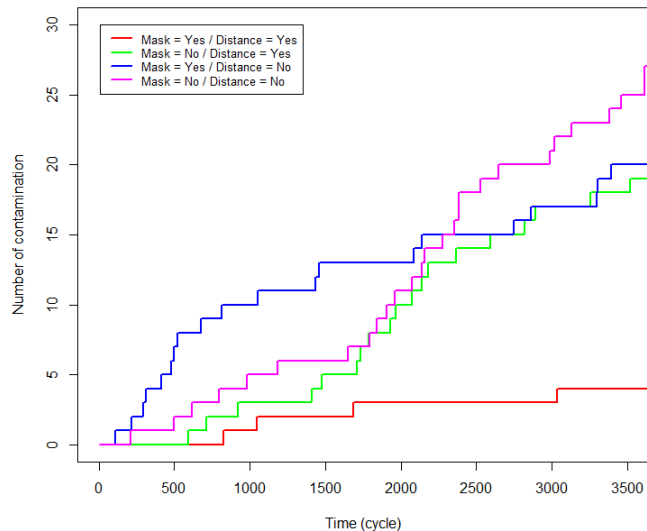


Fig. 11. Impact of Wearing Face-Mask (Yes/No) and Respect of Social Distancing (Yes/No) in the Environment with Promotion Area.

In Fig. 11, we consider a percentage of 25% as the probability of wearing a face mask, and 2 meters as the distance measure to be respected.

VII. DISCUSSION OF THE RESULTS

In Fig. 8 it can be seen that the use of masks does indeed reduce the peak of contamination. Therefore, recommending the use of face masks would avoid overloading hospitals and intensive care units as much as possible, and would contribute to slowing down the speed of spread of the virus while reducing the R_0 factor. The greatest change was achieved with a face mask probability of 0.75 and above, which avoided the sudden increase in cases that were still noticeable with a face mask probability of 0.5.

As presented in Fig. 9 the social distancing would act on the extent of the propagation. It also shows us that the smaller the radius of propagation of the virus (e.g. 1 meter), the fewer contaminations there are. For large distances, the results show that it is not always obvious to adopt such behavior in society, which justifies the high epidemiological peak when the distance increases. If social distancing also appears to be one of the best ways to reduce the spread of the virus and to relieve the health centers, it raises several questions about the right distance to adopt in order not to be contaminated. As in the case of wearing a mask, the simulations were run several times with a distancing measure varying from 1 to 5 meters.

Based on the results described in Fig. 10, we can compare the two different measures. It seems that these two policies taken individually correlate with the behavior of the individuals according to the environment where they are. On the other hand, these two measures taken together allow us to observe an antagonistic reaction (when the mask does not work, the distancing protects and vice versa, and when both work the protection is of high quality).

The presence of promotion areas has an impact on the spread of the disease as shown in Fig. 11. It appears that even if the supermarket contains promotional areas, the application of the two barrier measures is recommended to avoid the spread of the disease.

VIII. CONCLUSION AND PERSPECTIVES

Based on the results obtained in this paper, we confirm that the objectives assigned at the beginning of this work have been successfully achieved. Results clearly show that the adherence to the WHO prescribed barrier measures influences the spread of the virus and is a means of controlling Covid-19, which supports the hypothesis of this research. Public health experts also claim to be already aware of this solution. However, it is not clear what the average distance would be in the general case, and how long it would take to change masks. These factors would therefore deserve to be examined more systematically. The main advantage of CoSiT over the WHO TTX tabletop simulation schemes is that it is user-centered, educational, interactive, participatory, general-purpose, and flexible, with a quick learning curve.

However, making this tool available through a web portal so that it can be accessed and used by all in contexts of their choice, remains a challenge because the GAMA technology we used does not yet allow it.

Therefore, we recommend that technologies for deploying simulation models in the Cloud (online) be explored more systematically to facilitate mass remote training and awareness in real-time when an epidemiological crisis occurs. This would allow everyone to be aware in time of the need to adopt certain measures and would also help policymakers and political actors in making timely decisions to save lives. This solution will also help public health organizations in their training and awareness campaigns in the fight against infectious diseases.

AVAILABILITY OF MATERIALS

For materials request, please find material documentations and source code using Gama Platform by clicking [HERE](#). A video of the implemented tool is available on the following [LINK](#).

REFERENCES

- [1] WHO, *Coronavirus disease (COVID-19) Situation Report – 156*. World Health Organization, 24 June 2020.
- [2] W.H.O, “Country and technical guidance - coronavirus disease (Covid-19),” June 2020. [Online]. Available: <https://www.who.int/emergencies/diseases/novel-coronavirus-2019/technical-guidance>
- [3] WHO, “Coronavirus disease (covid-19) training: Simulation exercise,” 2020. [Online]. Available: <https://www.who.int/emergencies/diseases/novel-coronavirus-2019/training/simulation-exercise>

- [4] WHO, *Manuel OMS d'exercices de simulation*. World Health Organization, Février 2017.
- [5] S. K. Kasereka, "Towards hybrid stochastic modeling and simulation of complex systems in multi-scale environments with case studies on the spread of tuberculosis in democratic republic of the congo," Ph.D. dissertation, UNISA, 2020.
- [6] S. Kasereka, N. Kasoro, and A. P. Chokki, "A hybrid model for modeling the spread of epidemics: Theory and simulation," in *2014 4th International Symposium ISKO-Maghreb: Concepts and Tools for Knowledge Management (ISKO-Maghreb)*. IEEE, 2014, pp. 1–7.
- [7] OMS, "Questions-réponses : Comment se transmet la covid-19 ?" 9 juillet 2020. [Online]. Available: <https://www.who.int/fr/news-room/q-a-detail/coronavirus-disease-covid-19-how-is-it-transmitted>
- [8] W. O. Kermack and A. G. McKendrick, "A contribution to the mathematical theory of epidemics," *Proceedings of the royal society of London. Series A, Containing papers of a mathematical and physical character*, vol. 115, no. 772, pp. 700–721, 1927.
- [9] F. Brauer, C. Castillo-Chavez, and C. Castillo-Chavez, *Mathematical models in population biology and epidemiology*. Springer, 2012, vol. 2.
- [10] A. Chokki, S. Kasereka, N. Kasoro *et al.*, "Un modèle centré agents interactifs pour simuler la propagation de la grippe aviaire," *Annales de la Faculté des Sciences de l'Université de Kinshasa*, vol. 1, pp. 59–68, 2014.
- [11] H. W. Hethcote, "The mathematics of infectious diseases," *SIAM Rev.*, vol. 42, no. 4, pp. 599–653, 2000. [Online]. Available: <https://doi.org/10.1137/S0036144500371907>
- [12] A. Ndong, S. Kasereka, S. Bisuta, K. Kyamakya, E. Doungmo, and R. M. Ngoie, "Analysis, modeling and optimal control of covid-19 outbreak with three forms of infection in the Democratic Republic of the Congo," *Results in Physics*, vol. 24, p. 104096, 2021.
- [13] A. Kleczkowski and B. T. Grenfell, "Mean-field-type equations for spread of epidemics: The 'small world' mode!" *Physica A: Statistical Mechanics and Its Applications*, vol. 274, no. 1, pp. 355–360, 1999.
- [14] D. J. Watts and S. H. Strogatz, "Collective dynamics of 'small-world' networks," *nature*, vol. 393, no. 6684, pp. 440–442, 1998.
- [15] N. Boccara and K. Cheong, "Critical behaviour of a probabilistic automata network sis model for the spread of an infectious disease in a population of moving individuals," *Journal of Physics A: Mathematical and General*, vol. 26, no. 15, p. 3707, 1993.
- [16] E. Stattner and N. Vidot, "Social network analysis in epidemiology: Current trends and perspectives," in *2011 Fifth International Conference on Research Challenges in Information Science*. IEEE, 2011, pp. 1–11.
- [17] L. Perez and S. Dragicevic, "An agent-based approach for modeling dynamics of contagious disease spread," *International journal of health geographics*, vol. 8, no. 1, pp. 1–17, 2009.
- [18] K. R. Bisset, X. Feng, M. Marathe, and S. Yardi, "Modeling interaction between individuals, social networks and public policy to support public health epidemiology," in *Proceedings of the 2009 Winter Simulation Conference (WSC)*. IEEE, 2009, pp. 2020–2031.
- [19] V. Cimino, "Fujitsu présente le 415-pflops : l'ordinateur le plus puissant du monde," Publié le 24 juin 2020 à 07h58 - Mis à jour le 24 juin 2020 à 08h15. [Online]. Available: <https://siecledigital.fr/2020/06/24/fujitsu-presente-le-415-pflops-lordinateur-le-plus-puissant-du-monde/>
- [20] P.-E. Moreau, "MODSIR19 : Un outil de simulation de l'épidémie covid19," 2020. [Online]. Available: <https://www.loria.fr/fr/modsir19-un-outil-de-simulation-de-lepidemie-covid19/>
- [21] SimforHealth., "La formation comme outil de lutte contre le coronavirus." 28 avril 2020. [Online]. Available: <https://simforhealth.fr/1er-simulateur-numerique-de-prise-en-charge-de-patients-covid-19/>
- [22] B. Gaudou, Q. H. Nghi, D. Philippon, A. Brugière, K. Chapuis, P. Taillandier, P. Larmande, and A. Drogoul, "Comokit: A modeling kit to understand, analyze, and compare the impacts of mitigation policies against the covid-19 epidemic at the scale of a city," *Front. Public Health*, 24 September 2020, 2020. [Online]. Available: <https://www.frontiersin.org/articles/10.3389/fpubh.2020.563247/full>
- [23] V. Grimm, G. Polhill, and J. Touza, "Documenting social simulation models: the odd protocol as a standard," in *Simulating social complexity*. Springer, 2017, pp. 349–365.
- [24] V. Grimm, U. Berger, D. L. DeAngelis, J. G. Polhill, J. Giske, and S. F. Railsback, "The odd protocol: a review and first update," *Ecological modelling*, vol. 221, no. 23, pp. 2760–2768, 2010.
- [25] A. Drogoul, E. Amouroux, P. Caillou, B. Gaudou, A. Grignard, N. Marilleau, P. Taillandier, M. Vavasseur, D.-A. Vo, and J.-D. Zucker, "Gama: A spatially explicit, multi-level, agent-based modeling and simulation platform," in *International Conference on Practical Applications of Agents and Multi-Agent Systems*. Springer, 2013, pp. 271–274.

Parallel Hough Transform based on Object Dual and Pymp Library

Abdoulaye SERE
ER-SIC, LAMDI
Université Nazi BONI,
RECIF, <https://recifaso.org>
Burkina Faso

Moïse OUEDRAOGO
ER-SIC, LAMDI
Université Nazi BONI,
RECIF, <https://recifaso.org>
Burkina Faso

Armand Kodjo ATIAMPO
UREN
Université Virtuelle de Côte d'Ivoire
Côte d'Ivoire

Abstract—Geometric shape detection in an image is a classical problem that leads to many applications, in cartography to highlight roads in a noisy image, in medical imaging to localize disease in a region and in agronomy to fight against weeds with pesticides. The Hough Transform method contributes effectively to the recognition of digital objects, as straight lines, circles and arbitrary objects. This paper deals with the theoretical comparisons of object dual based on the definition of Standard Hough Transform. It also focuses on parallelism of Hough Transform. A generic pseudo-code algorithm, using the Openmp library for the parallel computing of object dual is proposed in order to improve the execution time. In simulation, a triangular mesh superimposed on the image is implemented with the pymp library in python, in considering threads as inputs to read the image and to update the accumulator. The parallel computing presents reduction of the execution time accordingly to the rate of lit pixels in each virtual object and the number of threads. In perspectives, it will contribute to strengthen the development of a toolkit for the Hough Transform method.

Keywords—Hough transform; parallel computing; pattern recognition

I. INTRODUCTION

Digital object recognition in an image is a classical problem that arises many applications in cartography to highlight noisy roads, in medical imaging for disease detection, in agronomy for weed detection and in cyber-security, as Facial Recognition using deep learning through convolutive neural network application. That supposes the definition of a model for digital objects and establishment of its adequate recognition method. In this sense, Bresenham's line in [18], Reveilles in [9], Andres in [10] have established several digital models, particularly for analytical straight lines. Parallel algorithms such as parallelization Bresenham Line and circle in [19] have been introduced to improve the execution time to draw digital object.

The Hough Transform method has been initially introduced by Paul Hough in [3] in 1962 and applied to the detection of straight lines in an image : It transforms a point in an image space to a straight line in a parameter space. It transposes the problem of straight line detection in the image space to an intersection of straight lines in the parameter space. But this method is limited in the detection of vertical straight lines.

Another variant of the Hough transform method named the standard Hough Transform, associates continuous points in an image space to sine curves in a parameter space. It allows to overcome the problems of vertical straight line recognition

that occurs in the case of the classical Hough Transform, which transforms a continuous point in the image space to a straight line in the parameter space.

Forward, the Hough Transform method has been extended to the detection of others shapes such as circles, ellipses. Duda and others in [4] have also proposed the recognition of arbitrary shapes in an image.

In 1985, Henri Maître in [1] has also proposed a survey on the Hough Transform method with an unified definition of Hough transform. Several works have studied the application of Hough Transform, for instance to mouth recognition in [11] and to action detection in [12].

Moreover, extensions of Hough transform for straight line recognition have been proposed by scientists. For instance, in 2006 Martine Dexet in [2], [6] introduced a new method based on the initial definition of Hough Transform, computing the Hough transform of continuous points in a square. Then, the dual of a square is a set of continuous straight lines in the parameter space.

By analogy to the works of Dexet in [2], SERE and others in [5] extends the standard Hough transform, to define the dual of a square and the dual of a triangle. Others extensions followed these works in [5] with the dual of a rectangle in [14], the dual of an hexagon in [16] and the dual of an octagon in [15]. All these works will lead to build a toolkit for the Hough Transform methods.

The serial execution of Hough transform consists of the serial execution of each real pixel or each virtual cell defined by the mesh generation, layed on an image.

Many works have carried out improvements of Hough transform to reduce the execution time. Acceleration of Hough transform has been studied by Jořth and others in [21] to allows real time line detection.

Parallelization of the Hough Transform method is also an alternative in order to improve the execution time. For instance, SERE and others in [7] have demonstrated the application of Hough Transform with the map-reduce algorithm for straight line recognition. These works have been extended by Mateus Coelho and others in [8] to deal with circle recognition.

Through recent innovations precisely in deep learning on Convolutive Neural Network, scientists have worked to combine the Hough Transform method with Convolutive Neural

Network to improve algorithms working in object detection, as studied by Spratling in [20].

In Traffic Management on roads, various techniques of Hough Transform have been proposed in Detection of Traffic Saturation, Traffic Light and Traffic Sign. For instance, SERE and others in [16] have introduced an application of the Hough Transform method in Traffic Saturation using GPS.

Our motivation is the study of parallel processing for the dual of geometry shapes related to squares, triangles, rectangles, hexagons and octagons with pypm library in python, in considering a set of threads as input parameters to compute different duals and to update the accumulator data in order to reduce the execution time.

Here, the parallel execution is outside the framework map-reduce in [7]. It takes into account previous works in a serial execution on :

- improvements of standard Hough transform in [13],
- straight line recognition in a rectangular grid in [14],
- straight line recognition in a triangular grid in [22]

But it considers the parallel execution of object dual for any grid to shorten the execution time.

This paper is organized as follows : the Section II recalls the definitions of geometric shape duals and analytical straight lines. The Section III focuses on parallelization of object dual. Experimental results in Section IV use the pypm library to implement parallelism in python on real images.

II. PRELIMINARIES

As previously introduced in Section I, Standard Hough Transform (SHT) associates a point in the image space to a sine curve in the parameter space, to achieve straight line recognition, as defined by :

Definition 1: (Standard Hough Transform)

The dual $S(x,y)$ of the point (x,y) in a two dimensional space where $(x, y) \in R^2$, is the Standard Hough Transform defined by the set of points :

$$\{(\theta, r) \in [0, \pi] \times [-\sqrt{l^2 + h^2}, \sqrt{l^2 + h^2}] / r = x \cos \theta + y \sin \theta\} \quad (1)$$

Duality is described as establishment of the relation between a digital object in the image space and the set of standard Hough transform of its internal points in the parameter space. For instance, let O be a digital object such as $O = \cup_{i=1}^n P_i$ where $P_i \in O$. P_i could be a discrete point or a set of discrete points. The dual of O is the union of the dual of each element ($P_i \in O$), accordingly to the standard Hough transform of P_i in definition 1.

That means formally :

$$Dual(O) = \cup_{i=1}^n dual(P_i) \quad (2)$$

The relation 2 has been specialized precisely to obtain the definitions for the dual of geometric shapes, such as rectangles,

triangles, as defined by SERE and others in [5], [13], [15] as follows :

Definition 2: (Rectangle dual) the dual of a square (or a rectangle) is the area localized between the curves corresponding to the duals of its two internal diagonal segments in the parameter space.

Definition 3: (Triangle dual) the dual of a triangle is the area localized between the curves corresponding to the duals of its two adjacent sides in the parameter space.

An octagon is the union of four internal rectangles. While a hexagon is the union of three internal rectangles. Definition 2 leads to establish hexagon dual and octagon dual as follows :

Definition 4: (Hexagon dual) the dual of an hexagon is the area localized between between the curves corresponding to the duals of its three internal diagonal segments in the parameter space.

Definition 5: (Octagon dual) the dual of an octagon is the area localized between the curves corresponding to the duals of its four internal diagonal segments in the parameter space.

The dual contributes to analytical straight line recognition, particularly those proposed by Reveilles in [9] related to standard analytical straight line and extended by Andres in [10] to have the supercover model.

Definition 6: analytical digital straight line ([9], [10]) with parameters (a,b,μ) and thickness w is defined by the set of integer points (x,y) verifying : $\mu \leq ax + by < \mu + w$, $(a,b,\mu,w) \in Z^4$, $pgcd(a,b) = 1$.

Thus, Analytical digital straight line is then :

- thin, if $w < \max(|a|, |b|)$
- naive, if $w = \max(|a|, |b|)$
- thick, if $w > (|a| + |b|)$
- standard, if $w = (|a| + |b|)$

Parallel computing of object dual will be described in Section III and applied to analytical straight line recognition in Section IV.

III. METHOD DESCRIPTION

This section is focusing on parallel computing of object dual, previously defined in Section II. It also proposes pseudo-algorithms using openmp library to compute object dual in the parallel context.

As an object dual is defined previously by the relation :

$$Dual(O) = \cup_{i=1}^n dual(P_i) \quad (3)$$

Where O is extracted from an image and $P_i \in O$. Then, parallel computing of Dual (O) consists firstly of splitting an object to several components and secondly to apply parallel computing to each elementary components P_i . Threads will assume easily these elementary tasks. Let n and v be respectively the number of components in an initial object O and

the number of threads. Each thread will compute normally almost $\lfloor \frac{n}{v} \rfloor$ elementary components. That means if the number of threads is superior to the number of elementary components, some threads will not be launched.

Moreover, instead of parallel computing for the dual of all the components P_i , a constraint is introduced by the rate of lit components in O : If an object O has the rate of lit components, superior to the rate α , the dual of this object will be computed in the accumulator data.

Let O_l be a subset of O , constituted only of lit components. Suppose that lc is the number of lit components. We have $lc = \text{card}(O_l)$ and $\alpha \leq \lfloor \frac{lc}{n} \rfloor$. Then, the dual(O) will be approximately the dual(O_l).

Moreover, suppose that $\alpha = \lfloor \frac{m}{n} \rfloor$. We constitute the subsets of O_l that contain exactly m elements of O_l , denoted $P(O_l)$. There are C_{lc}^m subsets (as a combinaison) in O_l that verify the constraint $\alpha = \lfloor \frac{m}{n} \rfloor$. As $O_m \in P(O_l)$. Now, the dual(O) also becomes approximately the dual(O_m).

Finally :

$$Dual(O_m) = \cup_{i=1}^n dual(P_i) \quad (4)$$

Where O_m is extracted from O_l (O_l is a subset of O) and parallelization will concern with the $dual(P_i)$, where $P_i \in O_m$.

Let us explain the dual of an object with more details through different algorithms in the following sections.

A. Therorical Comparisons of Computing Object Dual

Definitions 2, 3, 4, 5 extend Standard Hough Transform in two ways :

- the first one is to achieve object detection in virtual grid based on geometry shapes in computing its duals in the accumulator : digital objects pass through this virtual grid. Thus, parallel computing is applied to elementary shapes issued by this virtual grid in order to improve the execution time.
- the second one is to analyze the internal structure of points inside these duals in the accumulator data to highlight properties or characteristics for square, rectangle, triangle, hexagon, octagon recognition in the image. The future works will analyzed in details the internal structure of these dual.

Let us focus on the first case. Computing the dual of an hexagon and the dual of an octagon, could take more time than the dual of a square or the dual of a triangle. Because the number of internal diagonal segments in an hexagon or an octagon, building the area between different segment dual is important. For instance, according to SERE and others in [15], the dual of an hexagon and the dual of an octagon depend respectively on the dual of four internal segments and the dual of three internal segments. The dual of internal segments in objects can be realized through threads computing simultaneously the dual of each segment.

Our purpose is to use the dual of geometric objects in the parallel context to improve the execution time of Hough transform.

Hough Transform uses two spaces, namely an image space and a parameter space (or accumulator data). Proposed parallel Hough Transform takes into account these two spaces : that means the parallel reading of data in the image space and the parallel updating of the accumulator data

B. Analysis of Parallel Algorithm to Read the Data in the Image Space

Mesh generation establishes a virtual grid, superimposed on an image to bring out internal elementary virtual objects. For instance, An elementary object could be a rectangle, a triangle, an hexagon or an octagon. Fig. 1 presents an example of a virtual grid with triangles, created by Ouedraogo and others in [22], an extension of the method proposed by Cheick and others in [14] to generate rectangles, where the triangles are its components.

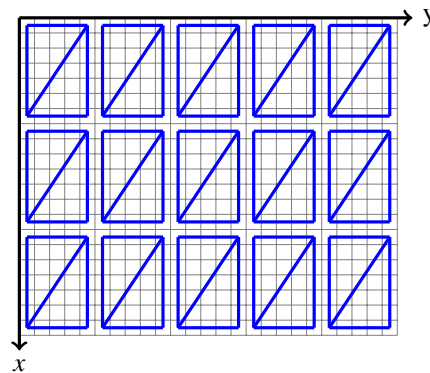


Fig. 1. An Example of the Triangular Mesh, Used by Ouedraogo and Others in [22] to Compute the Dual of a Triangle

Consider an image with (w x h) pixels. Algorithm 1 presents a generic serial execution. It uses a virtual mesh to perform an image, where each elementary object is referenced by the references Image(i, j). For instance, it takes particularly the dual of rectangles into account, as defined by SERE and others in [5] (see in preliminaries) where dual(Object x) corresponds precisely to dual(Rectangle x).

In this way, generalization is done by substitution of an object by any geometric shape .

Algorithm 1: Computing the Dual of Objects

Result: the dual of objects
 image: Matrix ;
 ob:Object ;
 i, j : Integer ;
 Image=pretreated(load(URL)) ;
for (i=1; i ≤ w; i++) **do**
 for (j=1; j ≤ h; j++) **do**
 ob=(Object) extract(Image(i, j));
 if light(ob) **then**
 | dual(ob);
 end
end
end

Let α and β be parameters corresponding to the number of threads to read data in the initial image. Data parallelism

is introduced in algorithm 1 by OPENMP primitives as ” # pragma omp parallel for” to define the parallel section as illustrated precisely in algorithm 2.

Algorithm 2: Data Parallelism with Openmp Primitives in a Pseudo-Code Algorithm

```

Result: the dual of objects
image: Matrix ;
ob:Object ;
i, j : Integer ;
Image=pretreated(load(URL)) ;
omp_set_num_threads( $\alpha$ ) ;
# pragma omp parallel for ;
for (i=1; i  $\leq$  w; i++) do
|   omp_set_num_threads( $\beta$ ) ;
|   # pragma omp parallel for ;
|   for (j=1; j  $\leq$  h; j++) do
|   |   ob=(Object) extract(Image(i, j));
|   |   if light(ob) then
|   |   |   dual(Ob);
|   |   end
|   end
end

```

In both the algorithm 1 and the algorithm 2, there are different functions :

- the function load(String URL) loads an image, according to its URL;
- the function pretreated (Matrix m) uses operators of binarization and filtering on the image ;
- the function extract(Matrix m) allows to get an elementary object generated by the grid superimposed on the image;
- The function light(Object x) consists of verifying if or not all the pixels in the object ob respect certain constraints to make it eligible for computing its dual ;
- the function dual(Object x) executes effectively the dual of the object ob, in application of the standard Hough Transform to an object. It updates the accumulator data, discussed forward in details in section III-C.

On the other hand, Fig. 2 presents a graph to modelize threads created by algorithm 2 with $\alpha=3$ and $\beta=3$, following the Fork/Join model.

Let us study this model of graph in Fig. 2. Suppose that $I=\{1,2,\dots,w-1,w\}$ and $J=\{1,2,\dots,h-1,h\}$. We have obviously $i \in I$ and $j \in J$ where i, j are the counters of two loops :

- At the first level of loop with the counter i , the number of threads being α , each thread t_k manages at average $\lceil \frac{w}{\alpha} \rceil$ iterations with different value $i \in I$. $\lceil \frac{w}{\alpha} \rceil$ is an integer value and $k \in \{1,2,\dots,\alpha-1,\alpha\}$. If $\alpha > w$, there will be some $k \in \{1,2,\dots,\alpha-1,\alpha\}$ -I, corresponding to the threads t_k that will never be created. But thread creation depends on availability of resources such as microprocessor and memory. That means even if $\alpha \leq w$, threads will be created according to availability of resources. The future works will

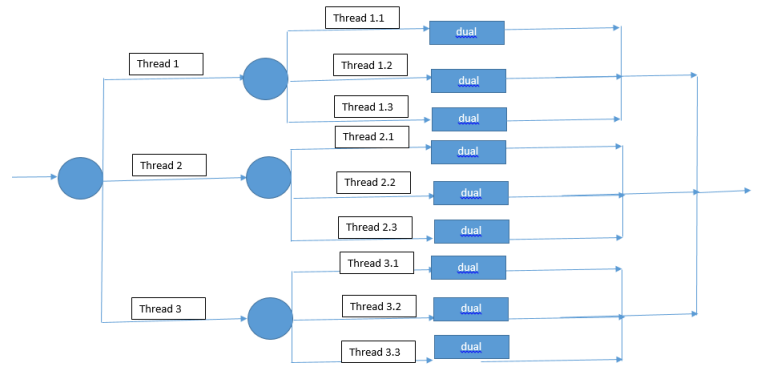


Fig. 2. Threads Created by Openmp Primitives with $\alpha=3$ and $\beta=3$, Accordingly to Algorithm 2

study predictions of availability of resources to manage threads that could even be used in thread management in operating system and in security to detect malicious software, using additional resources.

- At the second loop with the counter $j \in J$, each thread with a new iteration on $i \in I$, creates β threads to manage some iterations on $j \in J$. For instance, the thread with the iteration $i=1$, creates $\beta=3$ threads to manage together all the iterations on $j \in J$. Among β threads, in the same manner as the first level, each thread will compute $\lceil \frac{h}{\beta} \rceil$ iterations. As a conclusion, in considering an initial image I with its size height x width : The number of pixels is then determined by (height x width), to be submitted and shared for analysis by all the threads.

image, corresponding to the size width. While the second loop is associated to the column of the image, corresponding to the size height . Finally, $\alpha \times \beta$ threads work together on the same image and each thread will process approximately $\lceil \frac{w}{\alpha} \rceil \times \lceil \frac{h}{\beta} \rceil$ pixels.

The function dual(Object x) updates the accumulator and is studied in more details in section III-C.

C. Analysis of Parallel Algorithms to Update the Accumulator Data

This section focuses on data processing in the accumulator : it concerns precisely computation of dual(Object), as mentioned previously in calling, in algorithm 1. The number of threads used to update the accumulator is defined by the parameters γ, θ , as described in details in algorithm 3. Consider a accumulator with the size (wacc x lacc).

By analogy previously to section III-B related to the proposed algorithms, in algorithm 3, the number of γ threads is created, just before beginning the first loop with the counter m . These threads share iterations on a table that contains the number of lacc cells.

Algorithms 2 and 3 are generic : they can be specialized and adapted to any grid with its specific geometric shape, through computing object dual. For instance, the main specialized algorithm 6 in appendix is based on a triangular grid, implemented in Section IV.

Algorithm 3: dualObject(m, n : integer)

```

Result: the accumulator accc
acc: Matrix;
m, n : Integer ;
omp_set_num_threads( $\gamma$ ) ;
# pragma omp parallel for ;
for (m=1; m  $\leq$  lacc; m++) do
    omp_set_num_threads( $\theta$ ) ;
    # pragma omp parallel for ;
    for (n=1; n  $\leq$  wacc; n++) do
        if verify(m, n) then
            | acc[m][n]=acc[m][n]+1;
        end
    end
end
return acc;
    
```

IV. SIMULATION AND DISCUSSIONS

Simulation considers the case study of a triangular mesh superimposed on an image. It follows and extends the initial works on the Hough Transform method, applied to triangular shapes in a serial execution, introduced by Ouedraogo and others in [22], similar to compute the dual of rectangles proposed by Traore and others in [14], also in a serial execution.

At the present time, computers have several microprocessors as Dual Core, Quad Core, i5, i7, i9 and super calculators with a shared memory that allows and increases performance to execute multiple threads.

In both the serial execution and the parallel execution, simulation uses a computer with the following characteristics :

- Processor : Intel(R) Core(TM) i5 CPU M 480@2.67GHz 2.67GHz
- Memory usable : 4,00 Go
- operating system : Kali Linux

Different tests have been realized on the initial images in figures 3 and 4. Illustrations take into account parameters as the threshold to indicate the number of vote in the accumulator, the rate of pixels in each triangle represented by the value α , the height and the base of the triangle and the number of threads.

The previous generic algorithms 2 and 3 have been detailed and specialized by the main algorithm 6 calling algorithms 4, 5 and 7, all in appendix for recognition in a triangular mesh. Implementations of parallelization have been realized in python, using opencv and pypm available in [17] to bring openmp-like functionality to python.

A. The Case of the Parameters (Threshold =100, the Number of Threads =2, The Height of the Triangle =4 Pixels, The Base of the Triangle=4 Pixels)

An analysis of the execution time for the parallel case and the serial case in varying the value α , has been summarized in the Tables I and II. It reveals effectively that the parallel



Fig. 3. A Building Image



Fig. 4. A Road Image

computing of object dual is obviously better than the serial case.

TABLE I. THE EXECUTION TIME (IN SECOND) IN THE SERIAL CASE AND THE PARALLEL CASE FOR THE BUILDING IMAGE WITH THE PARAMETERS (THRESHOLD =100, THE NUMBER OF THREADS =2, THE HEIGHT OF THE TRIANGLE =4 PIXELS, THE BASE OF THE TRIANGLE=4 PIXELS)

α	Number of detected lines	Serial case	Parallel case	Time difference
0.1	370	8.7	6.5	1.8
0.15	243	7.8	5.6	2.2
0.2	243	5.6	5.6	0
0.25	62	6.5	4.6	1.9
0.3	62	6.5	6.5	0
0.35	6	4.5	3.5	1
0.4	6	4.5	3.5	1
0.45	2	3	2.5	0.5
0.5	2	3	2.5	0.5
0.55	0	2.4	2.1	0.3

TABLE II. THE EXECUTION TIME (IN SECOND) IN THE SERIAL CASE AND THE PARALLEL CASE FOR THE ROAD IMAGE WITH THE PARAMETERS (THRESHOLD =100, THE NUMBER OF THREADS =2, THE HEIGHT OF THE TRIANGLE =4 PIXELS, THE BASE OF THE TRIANGLE=4 PIXELS)

α	Number of detected lines	Serial case	Parallel case	Time difference
0.1	236	5	4	1
0.15	169	4.8	3.85	0.95
0.2	169	4.8	3.85	0.95
0.25	37	4.1	3.4	0.7
0.3	37	4.1	3.4	0.7
0.35	3	3.3	2.7	0.6
0.4	3	3.3	2.7	0.6
0.45	0	2.2	2.1	0.1

Difference between the processing time in the serial case and the parallel case, also appears in the Fig. 6 and 8, where the curve of the serial case is more up on the curve of the parallel case with the small values of α .

The Fig. 5 and 7 show decreasing the number of straight lines for increasing values of α .

Moreover, the surface of each triangle of the grid is determined by $(\text{height} \times \text{base})/2$: that means $\frac{(4 \times 4)}{2} = 8$ pixels.

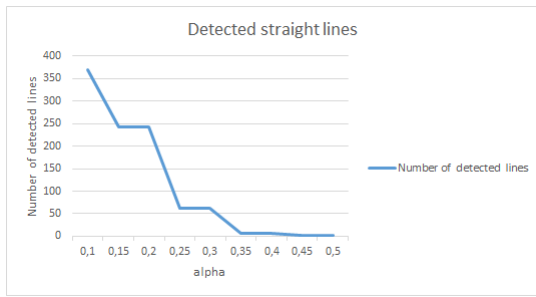


Fig. 5. The Number of Detected Lines in the Building Image Related to the Table I, Accordingly to the Values α



Fig. 6. The Curves of the Execution Time for the Building Image Related to the Table I

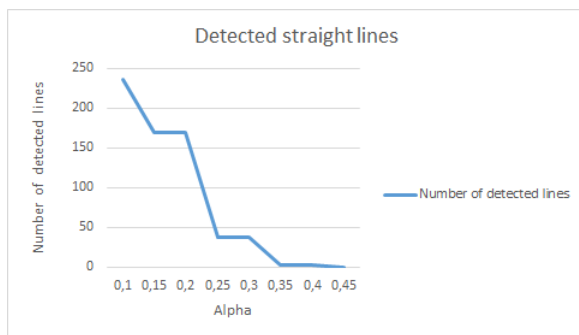


Fig. 7. The Number of Detected Lines in the Road Image Related to the Table II, Accordingly to the Values α

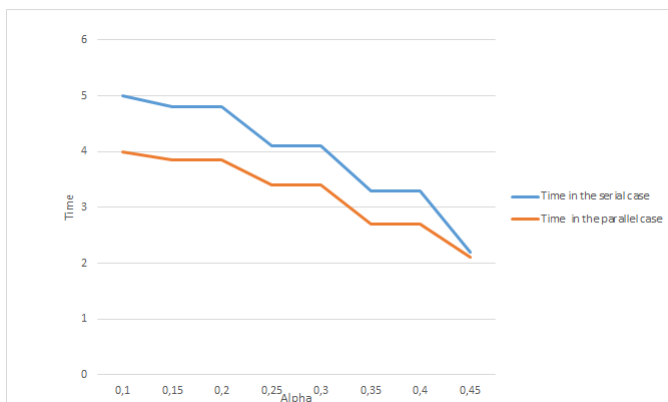


Fig. 8. The Curves of the Execution Time for the Road Image Related to the Table II

An image has $(w \times h)$ pixels, divided into $\lceil \frac{(w \cdot h)}{8} \rceil$ triangles.

Valid triangles have the number of internal lit pixels, superior to $\lceil 8 \cdot \alpha \rceil$: they will be considered for computing dual. For instance, with $\alpha=0.5$, it appears at least $(8 \cdot \alpha)=4$ lit pixels for each triangle, to be valid.

Thus, if the number of valid triangles is the value nv , then the loose triangles will be $(\lceil \frac{(w \cdot h)}{8} \rceil - nv)$ in computing dual. That leads to loss approximately $((\lceil \frac{(w \cdot h)}{8} \rceil - nv) \cdot 8)$ pixels (for all the image), representing a possibility to reduce the execution time.

If the value α is increasing, then the number of pixels $(8 \times \alpha)$ to be considered for triangle validation will be reduced: that reduces effectively the number of straight lines to be detected and the execution time for any case (serial case and parallel case). In more details, with the value α increasing, the surface to be respected in each valid triangle will become small, but included more triangles that are engaged in the process: more straight lines passes through a reduced number of aligned triangles. More aligned triangles indicate reduced corresponding straight lines that pass through them, accordingly to the value of the threshold applied to the accumulator.

B. The Case of the Parameters ($\alpha = 0.1$, The Number of Threads =2, The Height of the Triangle =4 Pixels, The Base of the Triangle=4 Pixels)

With a fixed $\alpha = 0.1$, in varying the threshold, the Tables III and IV show respectively the execution time for the building image and for the road image: it presents naturally reduction in the number of detected lines and the execution time. Because the number of cells, having the maximum vote is reduced and the time taken to read the accumulator data is short for the serial case and for the parallel case.

TABLE III. THE EXECUTION TIME (IN SECOND) IN THE SERIAL CASE AND THE PARALLEL CASE FOR THE BUILDING IMAGE WITH THE PARAMETERS ($\alpha = 0.1$, THE NUMBER OF THREADS =2, THE HEIGHT OF THE TRIANGLE =4 PIXELS, THE BASE OF THE TRIANGLE=4 PIXELS)

Threshold	Number of detected lines	Serial case	Parallel case
100	370	8.7	6.5
125	53	7.6	5.6
150	13	7.6	5.4
175	7	7.6	5.3
200	5	7.4	5.3
225	2	7.8	5.3
250	1	7.4	5.4
275	0	7.7	5.4

TABLE IV. THE EXECUTION TIME (IN SECOND) IN THE SERIAL CASE AND THE PARALLEL CASE FOR THE TOAD IMAGE WITH THE PARAMETERS ($\alpha = 0.1$, THE NUMBER OF THREADS =2, THE HEIGHT OF THE TRIANGLE =4 PIXELS, THE BASE OF THE TRIANGLE=4 PIXELS)

Threshold	Number of detected lines	Serial case	Parallel case
100	236	5	4
125	24	4.83	3.8
150	6	4.8	3.7
175	1	4.7	3.7
200	0	4.7	3.7

C. The Case of the Parameters (Threshold =100, Number of Threads =2, The Height of the Triangle =8, The Base of the Triangle=8)

Tables V and VI illustrate the case of a large triangle with the parameters (height = 8 pixels, base =8 pixels).

TABLE V. THE EXECUTION TIME (IN SECOND) IN THE SERIAL CASE AND THE PARALLEL CASE FOR THE BUILDING IMAGE WITH THE PARAMETERS (THRESHOLD =100, NUMBER OF THREADS =2, THE HEIGHT OF THE TRIANGLE =8, THE BASE OF THE TRIANGLE=8)

α	Number of detected lines	Serial case	Parallel case	Time Difference
0.1	140	7	5.3	1.7
0.15	79	6.7	4.8	1.9
0.2	57	6.2	4.5	1.7
0.25	19	5.3	4	1.3
0.3	5	4.1	3.2	0.9
0.35	3	3.1	2.5	0.6
0.4	3	2.4	2	0.4
0.45	3	1.9	1.8	0.1
0.5	3	1.8	1.7	0.1
0.55	3	1.8	1.7	0.1
0.6	3	1.8	1.7	0.1
0.65	3	1.8	1.7	0.1
0.7	3	1.8	1.7	0.1
0.75	3	1.8	1.7	0.1

TABLE VI. THE EXECUTION TIME (IN SECOND) IN THE SERIAL CASE AND THE PARALLEL CASE FOR THE TOAD IMAGE WITH THE PARAMETERS (THRESHOLD =100, NUMBER OF THREADS =2, THE HEIGHT OF THE TRIANGLE =8, THE BASE OF THE TRIANGLE=8)

α	Number of detected lines	Serial case	Parallel case	Time Difference
0.1	97	4.5	3.6	0.9
0.15	55	4.3	3.5	0.8
0.2	29	4.1	3.2	0.9
0.25	8	3.6	3	0.6
0.3	0	2.9	2.6	0.2

As a conclusion, for any case of triangle, the difference between the parallel execution time and the serial one will be more large, in favour to the parallel case that has a short reduced time with the small values of α .

D. Straight Line Recognition in Real Images

This section is focusing on the application of parallel Hough Transform to real images.

1) *Straight Line Recognition in the Building Image with a Triangle 4 x 4*: For the building image, the accumulator data and the results of straight line recognition are respectively illustrated in Fig. 9 in Fig. 10.

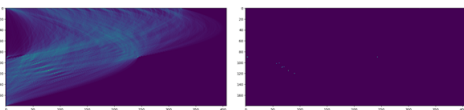


Fig. 9. The Accumulator Data after Application of the Parallel Computing: On the Left Image, The Sinusoid Curves and on the Right the Maximum Votes Superior to the Threshold =150

2) *Straight Line Recognition in the Road Image with a Triangle 4 x 4*: For the road image, the accumulator data and the straight line detection also appear respectively in Fig. 11 and 12, in considering the parameters (thread=2, threshold=100, $\alpha=0.3$).

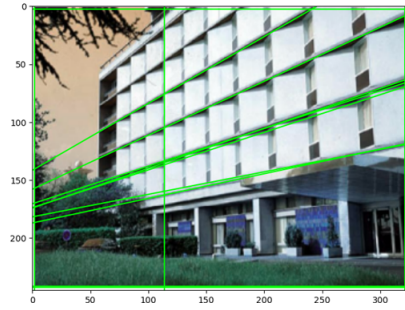


Fig. 10. Straight Line Recognition in the Building Image with the Parameters (Threads =2, Threshold = 150, $\alpha=0.1$)

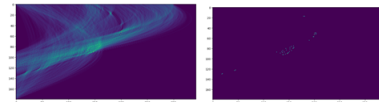


Fig. 11. The Accumulator Data after Application of the Parallel Computing: On the Left Image, The Sinusoid Curves; On the Right Image the Maximum Votes is Superior to the Threshold =100

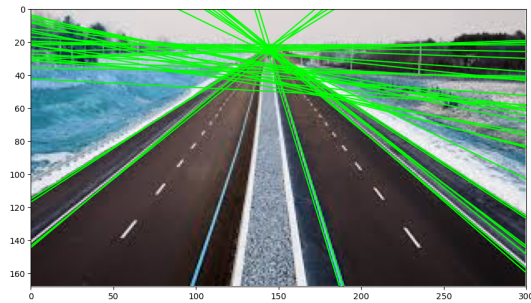


Fig. 12. Straight Line Recognition in the Road Image with the Parameters (Threads =2, Threshold = 100, $\alpha=0.3$)

V. CONCLUSION AND PERSPECTIVES

A new parallel Hough method has been proposed effectively to compute the dual of objects based on the standard Hough transform, through algorithms using openmp library to create threads. An image is analyzed with a meshing technique and different threads, computing the dual of virtual generated objects for updating the accumulator data.

Experimental results have been realized with the pypm library in python for parallelization and reveal reduction on the execution time in parallel execution than in the serial one. As outputs, the detection of straight lines is effectively realized in a building image and a road image. But optimizations of the proposed algorithms to improve more the execution time in the parallel case and comparisons with similar parallel methods still remain to do .

In perspectives, the study of parallelism will focus on straight line recognition in a rectangular grid, in an hexagonal grid or in an octagonal grid.

The future works will also analyze in detail, the internal structure of object dual to determine recognition for rectangles, triangles, hexagons and octagons in the image.

All these works will contribute forward to strengthen the building of a toolkit for the Hough Transform method, being integrated to a software for image processing, to bring out extensions for new functionalities, as a plug-in or a library for programming languages.

REFERENCES

- [1] H. Maitre, *A review on Hough Transform*, Traitement du signal, 1985, volume 2, number 4, pages 305-317,
- [2] M.Dexet, *Architecture d'un modeleur géométrique à base topologique d'objets discrets et méthodes de reconstruction en dimensions 2 et 3*, Université de Poitiers (France) Thèse en informatique et applications, 2006, decembre
- [3] P.-V.-C. Hough, *Method and means for recognizing complex patterns*, In United States Patent, 1962 volume 3069654, 47-64,
- [4] R.O. Duda and P.E. Hart, *Use of the hough transform to detect lines and curves in pictures*, Communications of the ACM, 1972,15(1),11-15
- [5] A. Sere, O. Sie and E. Andres, *Extended Standard Hough Transform for analytical line recognition*, 6th International Conference on Sciences of Electronics, Technologies of Information and Telecommunications (SETIT), Sousse, Tunisia, 2012, pp. 412-422, doi: 10.1109/SETIT.2012.6481950.
- [6] M Dexet and E. Andres, *A generalized preimage for the digital analytical hyperplane recognition*, Discrete Applied Mathematics, 2009, volume 157, Issue 3, pages 476-489,
- [7] Abdoulaye SERE, Dario COLAZZO, Oumarou SIE, *A Hough Transform Based On a Map-Reduce Algorithm*, International Journal of Engineering Research and Application ISSN : 2248-9622, Vol. 6, Issue 8 (part 2)
- [8] Mateus Coelho, Dylan Sugimoto, Gabriel Melo, Vitor Curtis and Juliana Bezerra *A MapReduce based Approach for Circle Detection*, In Proceedings of the 14th International Conference on Software Technologies - Volume 1: ICISOFT, 454-459, 2019 , Prague, Czech Republic
- [9] J.P.Reveillès, *Combinatorial pieces in digital lines and planes*. In proceeding SPIE 2573, Vision Geometry volume IV, issue 23, (1995)
- [10] E.Andres , *Discrete linear objects in dimension n : the standard model*. In Graphical Models, volume 65, issue 1-3, pages 92-111(2003).
- [11] Angella Yao, Juergen Gall, Luc Van Goo, *A Hough Transform-Based Voting Framework for Action Recognition*, IEEE Conference on computerVision and Pattern Recognition (CVPR 10), (2010).
- [12] Gabriel Fanelli, Juergen Gall, Luc Van Goo, *Hough Transform-based Mouth Localization for Audio-Visual Speech Recognition*, British Machine Vision Conference, September (2009).
- [13] Séré A., Ouedraogo T. F., Zerbo B.; *An improvement of the standard Hough transform method based on geometric shapes*, Future of Information and communication conference (FICC), 2018, 5-6
- [14] Cheick Amed Diloma Gabriel TRAORE, Abdoulaye SERE, *Straight Line Detection with the Hough Transform Method based on a Rectangular Grid*, Fifth International Conference on Information and Communication Technology for Competitive Strategies (ICTCS-2020)
- [15] Abdoulaye SERE, Yaya TRAORE, Frederic T OUEDRAOGO, *Towards New Analytical Straight Line Definitions and Detection with the Hough Transform Method*, International Journal of Engineering Trends and Technology 62.2 (2018): 66-73.
- [16] Abdoulaye SERE, Cheick Amed Diloma Gabriel TRAORE, Yaya TRAORE, Oumarou SIE, *Towards Traffic Saturation Detection Based on the Hough Transform Method*. In: Proceedings of the Future Technologies Conference (FTC) 2020, Volume 2. FTC 2020. Advances in Intelligent Systems and Computing, vol 1289. Springer, Cham.
- [17] Awani Kendurkar, Mohith J. A *Comparative Analysis of Parallelisation Using OpenMP and Pympp for Image Convolution* . International Research Journal of Engineering and Technology (IRJET) ISSN: 2395 0056 Volume : 08 Issue: 09, Sep 2021 www.irjet.net p ISSN: 2395 0072
- [18] Jack E Bresenham, *Algorithm for computer control of a digital plotter*, IBM Systems Journal, ACM.
- [19] Wright William E., *Rendering, Parallelization of Bresenham's Line and Circle Algorithms*, IEEE Computer Society Press, <https://doi.org/10.1109/38.59038>
- [20] M. W. Spratling, *A neural implementation of the Hough transform and the advantages of explaining away*, Image and Vision Computing, doi: 10.1016/j.imavis.2016.05.001
- [21] Jošth R., Dubská M., Herout A., Havel J. (2011) *Real-Time Line Detection Using Accelerated High-Resolution Hough Transform*. In: Heyden A., Kahl F. (eds) Image Analysis. SCIA 2011. Lecture Notes in Computer Science, vol 6688. Springer, Berlin, Heidelberg
- [22] Ouedraogo, M., Sere, A., Some, B.M.J., Traore, C.A.G.D, *Straight-Line Recognition Using a Triangular Grid*. In: Arai, K. (eds) Advances in Information and Communication. FICC 2022. Lecture Notes in Networks and Systems, vol 438. Springer, Cham.

APPENDIX

Algorithm 4: Building a triangular grid

Function *meshing2*(*Nl, Nc, h, b*: integers): table of integers
Variables: *tab*: table of 6 integers
Output: *tab*[1] (*tab*[3]): base (height) of the triangle of our meshing ;
tab[0]: number of parts of length *tab*[3] on the line ;
tab[2]: number of parts of length *tab*[1] on the column ;
tab[4]: the remainder of the Euclidean division of *Nl* by *h* ;
tab[5]: the remainder of the Euclidean division of *Nc* by *b* ;
begin
tab[1] ← *b* ;
tab[3] ← *h* ;
tab[0] ← *int*[*Nl*/*h*] ;
tab[2] ← *int*[*Nc*/*b*] ;
tab[4] ← *Nl* mod *h* ;
tab[5] ← *Nc* mod *b* ;
return *tab* ;

Algorithm 5: Rate of lit pixels

Function *count*(*img_pymp* : image, *A, B, C* : 3 tables of two integers containing the coordinates of the vertices of the triangle) : real
Variables: *k, l* : integers;
D : table of two integers
begin
k ← 0 ;
l ← 0 ;
D ← *A* ;
if *B*[1] ≥ *A*[1] and *C*[0] ≥ *A*[0] **then**
 for *x* between *A*[0] and *C*[0] **do**
 $DE \leftarrow \frac{|x - C[0]| \times |A[1] - B[1]|}{|A[0] - C[0]|}$;
 *y*₀ ← *A*[1] + *round*(*DE*) ;
 for *y* between *A*[1] and *y*₀ **do**
 if *img_pymp*[*x, y*] ≠ 0 **then**
 k ← *k* + 1 ;
 else
 l ← *l* + 1 ;
if *B*[1] ≤ *A*[1] and *C*[0] ≤ *A*[0] **then**
 for *x* between *C*[0] and *A*[0] **do**
 $DE \leftarrow \frac{|x - C[0]| \times |A[1] - B[1]|}{|A[0] - C[0]|}$;
 *y*₀ ← *A*[1] - *E*[*DE*] ;
 for *y* between *y*₀ and *A*[1] **do**
 if *img_pymp*[*x, y*] ≠ 0 **then**
 k ← *k* + 1 ;
 else
 l ← *l* + 1 ;
return $\frac{k}{k+l}$;

Algorithm 6: Recognition of discrete lines

Pre-condition: 0 < α < 1, 0 < threshold
Data: α
Variables: *tab* : table of 6 integers ;
A, B, C : tables of two integers ; *accum_row, accum_column, irho, Ni, Nc* : integers ;
accum : matrix of dimensions "accum_row × accum_column" ;
threshold, α, dtheta, rho, theta, DE : real ;
Begin
% import of pymp library
import pymp ;
% image reading
=cv2.imread("image.jpg") ;
=pretraited image ;
% the dimensions of the image ;
Nl ← number of rows of image ; *Nc* ← number of columns of image ;
% create a pymp type matrix
Nl, Nc) ;
% α : the rate of lit pixels from which the triangle is selected ;
α = 0.8 ;
% threshold : the minimum number of votes ;
threshold ← 150 ;
% the dimensions of the virtual triangles to be entered manually ;
h ← 4 ; *b* ← 4 ;
% the dimensions of the matrix "accum_pymp"
accum_row ← 180 ; *accum_column* ← *E*(√(*Nc*² + *Nl*²)) ;
dtheta = π/180 ;
% creation of the pymp type accumulator matrix
accum = pymp.shared.array(*Ntheta, Nrho*) ;
accum_scutl = pymp.shared.array(*Ntheta, Nrho*) ;
tab ← *meshing*(*Nl, Nc, h, b*) ;
H = *Nl* - *tab*[4] ; *L* = *Nc* - *tab*[5] ;
% assign the pixel values of the pre-processed image to the matrix of type pymp
for *x* in range(*Nl*) **do**
 for *y* in range(*Nc*) **do**
 [*x, y*] ← *img*[*x, y*]
% walk through all the triangles of the grid without taking into account any residues and updating the accumulator
%
pymp.config.nested=False ;
% the maximum number of threads allowed
pymp.config.thread_limit = 4 ;
with pymp.parallel(2) **as** *p* :
 for *x* in *tab*[3] and *Nl* with a step of *tab*[3]+1 **do**
 for *y* between *tab*[1] and *Nc* with a step of *tab*[1]+1 **do**
 A[0] = *x* - *tab*[3] ; *A*[1] = *y* - *tab*[1] ; *B*[0] = *x* - *tab*[3] ; *B*[1] = *y* ; *C*[0] = *x* ;
 C[1] = *y* - *tab*[1] ; *D* = *A* ;
 if *B*[1] > *A*[1] and *C*[0] > *A*[0] **then**
 if *count*(*img_pymp, A, B, C*) ≥ α **then**
 for *z* between *A*[0] and *C*[0] **do**
 $DE \leftarrow \frac{|x - C[0]| \times |A[1] - B[1]|}{|A[0] - C[0]|}$;
 *y*₀ ← *A*[1] + *round*(*DE*) ;
 for *t* between *A*[1] and *y*₀ **do**
 Acc_update() ;
 A[0] = *x* ; *A*[1] = *y* ; *B*[0] = *x* - *tab*[3] ; *B*[1] = *y* ; *C*[0] = *x* ; *C*[1] = *y* - *tab*[1] ; *D* = *A* ;
 if *B*[1] < *A*[1] and *C*[0] < *A*[0] **then**
 if *count*(*img_pymp, A, B, C*) ≥ α **then**
 for *z* between *C*[0] and *A*[0] **do**
 $DE \leftarrow \frac{|x - C[0]| \times |A[1] - B[1]|}{|A[0] - C[0]|}$;
 *y*₀ ← *A*[1] - *E*[*DE*] ;
 for *t* between *E*[*y*₀] and *A*[1] **do**
 Acc_update() ;
 if *tab*[4] ≠ 0 **then**
 for *z* between *H* and *Nl* **do**
 for *t* between 0 and *Nc* **do**
 Acc_update() ;
 if *tab*[5] ≠ 0 **then**
 for *z* between 0 and *Nl* **do**
 for *t* between *L* and *Nc* **do**
 Acc_update() ;
Search for maxima in the accumulator ;
Line drawing ;
End

Algorithm 7: Accumulator update

```
Procedure Acc_update(): void
  % Updating the accumulator
  if img_pymp[z,t]  $\neq$  0 then
    for itheta in p.range(accum_row) do
      theta  $\leftarrow$  itheta  $\times$  dtheta;
      rho  $\leftarrow$  t  $\times$  cos(theta) + z  $\times$  sin(theta);
      irho  $\leftarrow$  int(rho);
      if irho > 0 and irho < accum_column then
        accum[itheta][irho]  $\leftarrow$ 
          accum[itheta][irho] + 1
```

Prototyping a Mobile Application for Children with Dyscalculia in Primary Education using Augmented Reality

Misael Lazo-Amado¹, Leoncio Cueva-Ruiz², Laberiano Andrade-Arenas³
Facultad de Ciencias e Ingeniería
Universidad de Ciencias y Humanidades^{1,2,3}

Abstract—Dyscalculia is a disorder of difficulty in understanding, understanding of numbers and mathematical operations in such a way that the child has a greater stress by not solving the exercises proposed by the teacher, leading to the objective of the research in making an innovation plan dedicated to the mobile prototype with augmented reality for children with dyscalculia in primary education. Design Thinking was used as a methodology that allows us to know the needs of users and implement new solutions to their problems, so that the project team makes decisions to choose the best idea proposed, likewise this idea must be applied to a model or design, for this the Miro application was used for the mobile prototype, for the 3D design TinkerCad was used for educational games and finally the App Augmented Class application that was responsible for the visualization of augmented reality. The results were obtained through interviews with parents, indicating that the mobile prototype with augmented reality is a great contribution of impact and should be applied for children, finally this prototype is validated by five experts who mentioned that the final prototype has 86% acceptance. The conclusion of this research is to make an innovation model to solve the problems of dyscalculia, improving understanding and comprehension in mathematics.

Keywords—App augmented class; design thinking; dyscalculia; miro app; TinkerCad

I. INTRODUCTION

Dyscalculia is a disorder that demonstrates learning difficulties in understanding, learning and performing subjects involving mathematical numbers, and also affects reading and writing, as well as attention deficits and visual problems [1]. Dyscalculia exists in every 5-8% of children in schools worldwide with symptoms of this disorder [2], in schools in India, between 13% and 14% of school-aged children are reported to have these learning disabilities. In such a way that covid-19 also influences the process of this disorder in school children when virtual classes are established, students do not have a monitor to guide them in their educational process, and children with symptoms of dyscalculia tend to be easily distracted [3].

In Latin America there are learning difficulties in children in such a way that the teaching of mathematics has a low performance of 49.9% to 70.3% and in this way the schools do not provide a good quality of teaching in their schools, considering a serious problem for dyscalculia to indicate the low preparation in education regarding mathematics is why children do not have highly trained teachers to provide good teaching [4]. In Brazil, which considers that dyscalculia

impairs school performance and achievement in mathematical operations [5], it also considers that out of every 304 schoolchildren aged 7-12 years of both sexes are assessed and 22 children are diagnosed with dyscalculia [6].

The majority of children with dyscalculia in Peru have difficulties in their academic development, thus indicating that students have teachers who are not trained to meet the needs of children [7]. In the Covid-19 pandemic, because they are not prepared to establish virtual classes, they do not have enough materials to carry out their activities, which is a big problem for many students, especially in rural areas of Peru, where they have problems in mathematics [8][9]. This is why the level of stress in children with dyscalculia can greatly affect their concentration to perform their activities [10].

These problems have been identified in the world, and we can see the need for a strategic plan to solve the problems related to dyscalculia, so that students with these disorders can improve their understanding and comprehension of subjects, strengthening their attention span. Proposing this solution for children with dyscalculia is affecting education in Peru as it requires the support of parents or teachers for its use. It also makes serious learning more affectionate as the child feels more confident to improve these learning problems.

The aim of the project is to develop a prototype of a mobile application for children with dyscalculia in primary education using augmented reality. Cognitive games or therapies will be made to solve mathematical problems with certain learning levels, in order to capture the attention of children with dyscalculia. The structure of the following: in Section II the literature review is explained, in Section III the methodology to be developed, in Section IV the results of our work, in Section V the discussions, in Section VI the conclusions and finally in Section VII the future work.

II. LITERATURE REVIEW

Augmented reality in mobile applications for the treatment of dyscalculia or strengthening skills in education meets the expectations to improve learning. So they implement augmented reality to help students with dyscalculia to perform their activities in the subject of arithmetic, fulfilling learning in addition, subtraction, multiplication and division [11]. They also carry out an evaluation of children with dyscalculia and how it interacts with augmented reality since it indicates that the use of these technologies such as augmented reality draws the attention of students and facilitates the understanding

of mathematical activities [12]. The educational plan to use augmented reality has many advantages that will help teachers to understand the problems of children with dyscalculia also involves the dedication and patience it takes this process since they claim in their research that 92% of students interacting with augmented reality, improves their ability to understand [13].

Similarly, augmented reality in mobile applications can be more effective as people have a mobile phone in their homes giving them the opportunity to transmit education from the mobile application using augmented reality, as well as children with problems are treated with the help of their parents or loved ones without the need to have a specialist for these problems [14]. That is why this research makes a mobile prototype with augmented reality, giving a simulation of learning for children with learning disabilities, fulfilling the objective of helping them to perform their activities of their subjects in their respective classrooms [15]. For this reason, they indicate that the mobile application is very effective in attracting the attention of the child with dyscalculia, making it easier for them to concentrate during the treatment process, accompanied by educational games to increase the effectiveness of the treatment [16]. In this way this research in Arequipa, Peru uses this method of creating educational video games with 3D animations in their respective implemented in a mobile application giving in conclusion that these tools are very good to improve the education of the country [17].

There are tools for the implementation of augmented reality in mobile applications, in which programmers use Unity Game for the development of games with the purpose of optimising visual and auditory learning, by using this application children with learning disabilities can improve their reading and mathematics [18]. Similarly it is understood in this research that has problems with attention and comprehension in their primary level students as they have low performance in their chemical activities, with the help of augmented reality helps them to understand easily also 87.90% students in Indonesia validate their improvement [19]. The analysis of augmented reality applications for dyscalculia or any problem that involves education, meets its objective of supporting their treatment or improvement in their learning, which is why they also use tools such as surveys where they indicate how valuable these innovative solutions are in education [20].

The mobile application with augmented reality indicated by the authors in this literature review, in dyscalculia as well as in education. They show the importance that are tools that they use to improve their understanding and attention in children, in such a way that applying these innovative methods can solve problems in education, science, research, business, security among others. By finding problems in education and investigating solutions in different researchers, it is proposed that in our research we propose to improve the understanding of children with dyscalculia in primary education in Peru with the help of augmented reality.

III. METHODOLOGY

For the use of the meta-logic we use the Design Thinking that is in charge of realising creative solutions for the user, which is divided into 5 stages (Empathise, Define, Ideate, Pro-

tototype and Test), these stages have tools for their development that are explained in detail in this section.

A. Design Thinking

It is a very pleasant methodology with the aim of solving the problems of the users using innovative ideas with the use of technologies to improve the expectation of those involved [21], It is a methodology that can be carried out in a short time and it is also necessary to have the approval of the final product and possible improvements [22]. It is a methodology of great interest to improve or create new products to improve the user's lifestyle using strategies and a variety of solutions, it is highly recommended by designers dedicated to innovation [23], the steps to be followed are shown in Fig. 1.

1) *Empathise*: This is the first stage of the Design Thinking methodology that fulfils its objective of finding user needs and it is necessary to use information gathering techniques to identify them [24]. This is why the best way to carry out this stage is to use tools such as surveys or interviews to get an in-depth understanding of people's relevant needs [25].

2) *Define*: This is the second stage of the methodology, which is responsible for organising or aggregating the data from the first stage in order to identify or understand the most important user problems. To do this, it is necessary to use techniques to group and prioritise these problems [26].

3) *Ideate*: This is the third stage, which has the main function of producing a greater number of ideas or solutions that respond to the problems of the second stage, it is necessary that the design or innovation team has a clear idea of the problems in order to assign impactful solutions for the users [27].

4) *Prototype*: This is the fourth stage which is in charge of making a prototype, mock-up or design according to the impacting idea of the third stage. The prototype will serve to show the user the solution to their problem that fits their needs, for this it is necessary to use prototyping applications or as well as using physical mock-up [28].

5) *Testing*: This is the last stage of the methodology that fulfils the main objective of validating that the user is completely satisfied with the prototype that is the design of the solution to their problems as well as helping us to provide new improved versions of the proposed solution, it is necessary to use tools that interact with the end users [29].

B. Tools for Mobile Prototype Design with Augmental Reality

In this part it is necessary to know the tools to implement the design of the mobile application and the augmented reality model, as well as to visualise in detail the interaction of the applications that are in charge of fulfilling the objective as shown in Fig. 2.

1) *Miro APP*: It is a collaborative platform that its main function is teamwork in real time, is widely used for project management, has a number of free templates for efficiency and understanding of the meetings among them are mind maps, whiteboards, charts, flowcharts, wireframe web and mobile [30].

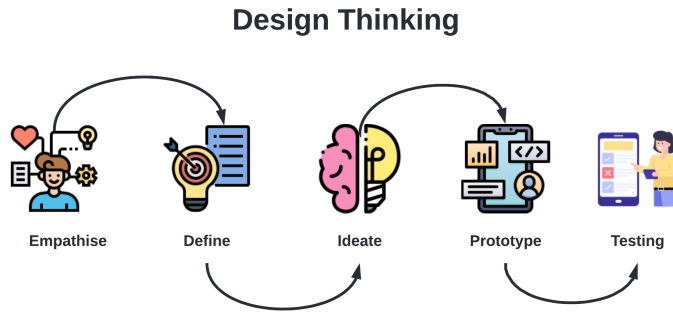


Fig. 1. Methodology Design Thinking.

2) *Tinkercad*: It is an application that takes care of real 3D modelling or design for free and online. It is built precisely for any user with no experience or with experience in design allowing you to create complex models [31]. It has a variety of features so that your 3D modeller can visualise using augmented reality as well as use programming for arduino circuits, import and export files, among others [32]. Tinkercad can be used in any browser as the main basic requirement for the use of the user is to have a mobile device, tablet, computer or laptop [33].

3) *App Augmented Class*: This application can be found in the play store for free and allows you to visualise projects with augmented reality, for which it is not necessary to have basic technical knowledge and its use is simple and intuitive. App Augmented Class has its own designs to learn about augmented reality and also add your own 3D designs [34].

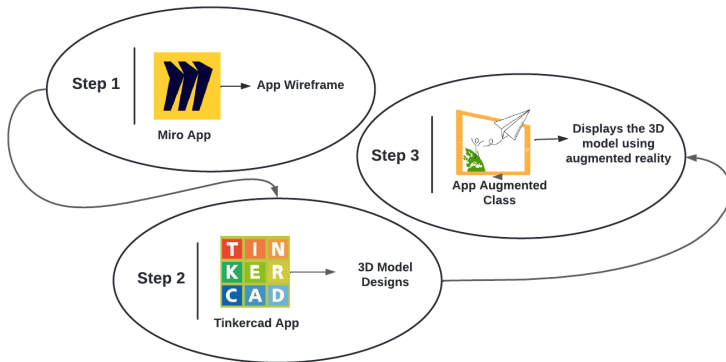


Fig. 2. Application Design Steps and Augmented Reality Modeling.

IV. RESULTS

This section of the results shows how to develop the phases of the Design Thinking methodology that will allow us to know the problems of users and provide the solution in the short term, as well as using the proposed tools to implement mobile design with augmented reality, on the other hand will have the validation of experts who ensure the efficiency and impact that has the mobile design with augmented reality and finally will share the advantages, disadvantages and comparisons that our methodology has.

A. Results of Empathise

To understand the results of the first phase of the methodology it is necessary to identify the six questions proposed (Q1 to Q6) by the project team that are addressed to the parents, in order to find out their children's problems in mathematics as shown in Table I.

TABLE I. QUESTIONS

Questions	
ID	Questions
Q1	What grade is the child in?
Q2	Sex ?
Q3	In which district of Lima is the child located
Q4	Does the child have difficulties in understanding and comprehension?
Q5	Does the child experience stress when not solving the problems proposed by the teacher?
Q6	Does the child have difficulty recognising numbers?

B. Results of Define

In the results of the second phase of the methodology which is in charge of verifying the answers of the questionnaire (R1 to R6) of the parents, there are a total of 70 answers for analysis as shown in Table II.

TABLE II. PARENTS' RESPONSE TO THEIR CHILDREN

Answers	
ID	Answers
R1	First Grade Primary 35.7%, Second Grade Primary 15.7%, Third Grade Primary 8.6%, Fourth Grade Primary 17.1%, Fifth Grade Primary 14.3%, Sixth Grade Primary 8.6%
R2	Male 68.6% Female 31.4%
R3	Los Olivos 28.6%, San Martín de Porres 18.6%, Carabayllo 14.3%, Lima 12.9%, Independencia 11.4%, Comas 14.3%
R4	Yes 74.3% , No 25.7%
R5	Yes 70% , No 30%
R6	Yes 71.4% , No 28.6%

a) *R1*: The first response which refers to the 70 respondents in which parents indicate that their children were questioned in the first grade of primary school has 35.7%, second grade of primary school has 15.7%, third grade of primary school has 8.6%, fourth grade of primary school has 17.1%, fifth grade of primary school has 14.3% and sixth grade of primary school has 8.6%.

b) *R2*: The responses to the second question indicate that male students 68.6% and female students 31.4% were correctly answered.

c) *R3*: The answers to the third question indicate the districts of Peru-Lima that have been surveyed, indicating that in Puente Piedra 8.6%, Los Olivos 27.1%, Carabayllo 28.6%, San Martín de Porres 15.7%, Comas 17.1%, Rimac 2.9%.

d) *R4*: The answers to the fourth question indicate that children have greater difficulty in understanding and comprehension, with 74.3% of respondents saying this is the case and 25.7% saying it is not.

e) *R5*: The answer to the fifth question indicates that 70% of the respondents have more stress when they do not solve the problems proposed by the teacher and 30% have a solid education without stress.

f) R6: The answer to the fifth question indicates that 71.4% of respondents have difficulty with number recognition and 28.6% do not have this problem.

C. Results of Ideate

For the results of the third phase of the methodology, plans or solutions are developed for the problems found in the surveys in Fig.3 shows the graph where the innovation developers make their score to decide which of the ideas show the greatest impact for the user, likewise the idea with the highest score is: Develop a mobile application with augmented reality.

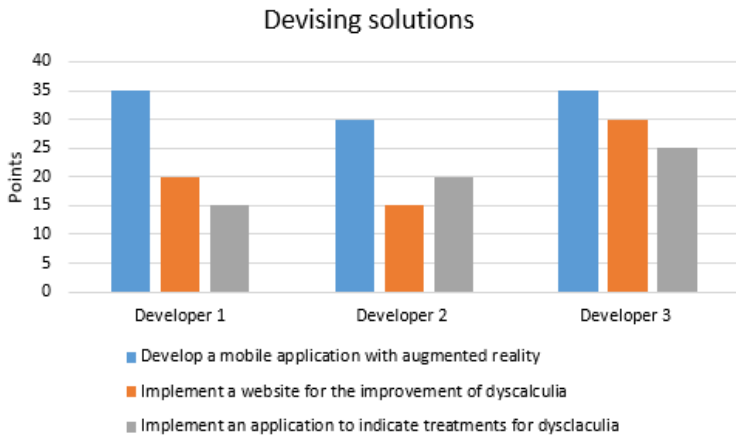


Fig. 3. Results of Idear.

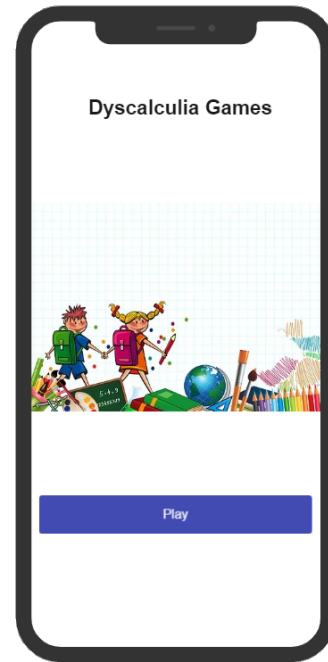


Fig. 4. Start of the Mobile Application.

D. Results of Prototyping

For the results of the prototype that was made with the tools indicated in Fig. 2, it will show the main functions that the mobile application with augmented reality will have, therefore in Fig.4 it will start with the welcome to the application to start the educational game with augmented reality where the user with dyscalculia problems must press the play button to advance with the following steps.

The second prototype refers to the selection of the child's level as shown in Fig. 5, click on the child's primary school grade and then look for the child's age, and we will continue with the next step.

Fig. 6 shows the first game to be developed for the first grade of primary school where the child can learn thanks to augmented reality with a dynamic design for better understanding and comprehension. In this way, it will have stars that indicate how the first game is developing, which tries to complete the sequence of numbers and finally the child can indicate whether he/she likes or dislikes the game.

Fig. 7 shows the addition in augmented reality so that the child can select the correct answer. The aim is not to guess the result, but to allow the child to mentally develop the sum or to have the support of the teacher to supervise the child's understanding of the exercise.

Similarly, Fig. 8 shows the same dynamics of the second game, the difference is that it shows the subtraction with augmented reality.

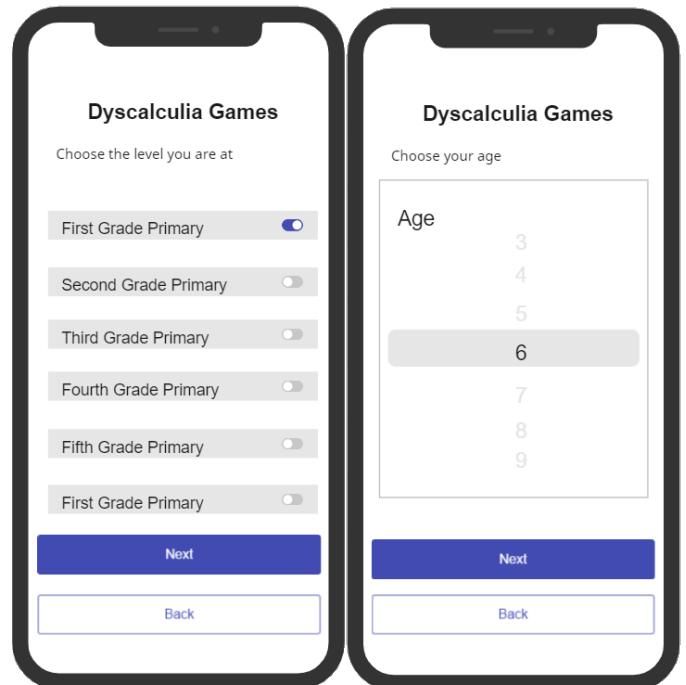


Fig. 5. Level and Age Selection.

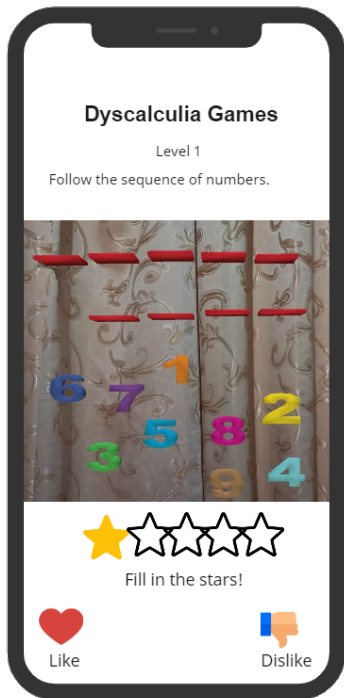


Fig. 6. First Game of the Mobile Application with Augmented Reality.

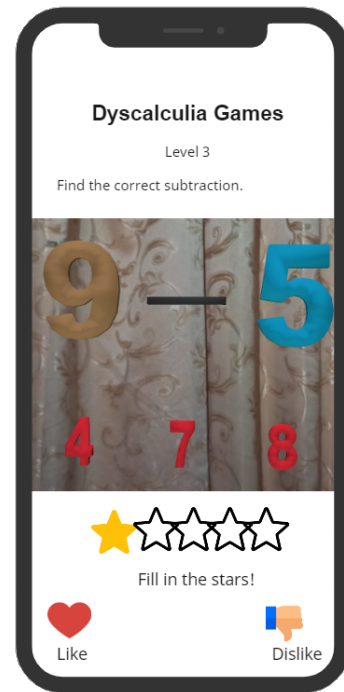


Fig. 8. Third Game of the Mobile Application with Augmented Reality.

Finally, Fig. 9 shows the game that will try to display the figures in such a way that you must identify or select the total number of figures for each row.

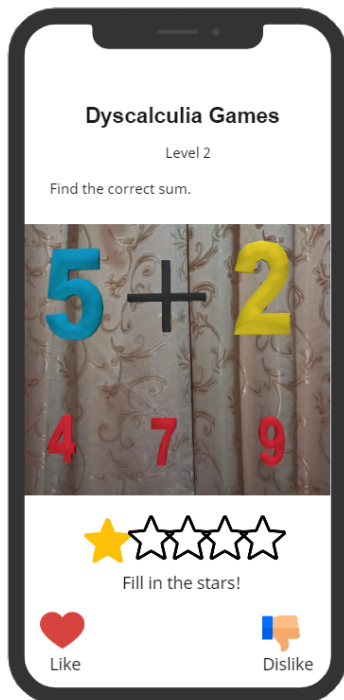


Fig. 7. Second Game of the Mobile Application with Augmented Reality.

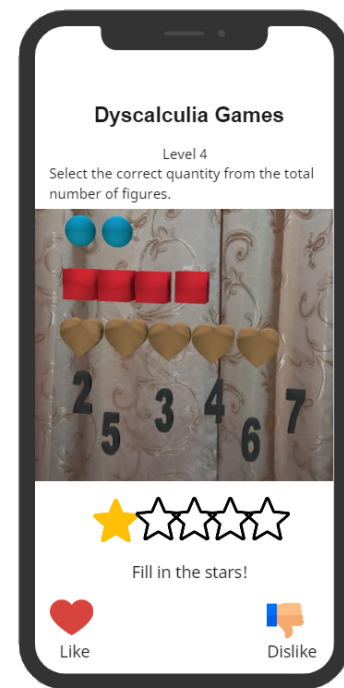


Fig. 9. Fourth Game of the Mobile Application with Augmented Reality.

E. Results of Testing

To develop this last stage of the Design Thinking methodology it is necessary to carry out a survey to validate that our prototype with augmented reality is correct for the user, in such a way that Table III identifies the five questions (Q1 and Q5) that will be sent to the users for their corresponding analysis.

TABLE III. TESTING QUESTIONS

Questions for parents about the augmented reality prototype	
ID	Questions
Q1	Does the prototype meet the goal of comprehension and understanding?
Q2	Do you think that by developing this design you can improve your child's dyscalculia?
Q3	Do you think this mobile application will have a great impact on society?
Q4	Do you think that the mobile application with augmented reality should be used with the teacher or parents for better understanding or doubt?
Q5	Do you recommend the use of the augmented reality mobile application to schools and health centres for the treatment of dyscalculia?

According to the questionnaire that was carried out, 70 parents indicate their answers for each question as shown in Fig. 10, in the first question indicates that 79% say that the prototype meets the objective of comprehension and understanding and 21% say it does not. In the second question, it indicates that developing the application with augmented reality will improve the dyscalculia of their children, 83% and 17% say no. In the third question, 77% of the respondents say that the mobile application will have a great impact on society and 23% say no. In the fourth question, it indicates that 89% of the respondents say that the mobile application will have a great impact on society and 23% say no. In the fourth question, 89% indicated that the mobile application with augmented reality should be used by the teacher or guardian to check the development of their child and 11% that it should not. In the last question, parents indicated that the mobile application with augmented reality should be implemented in schools and health centres for the treatment of dyscalculia, with 84% stating this and 16% stating that it should not.

and Integration) must be taken into account, which will serve to define that the prototype has the security and acceptance by the experts.

For this it is necessary to consider that to score these criteria you must have a representative level: Low, Moderate and High. In the low level it will have as a result in the 0% to 49% shows the little interest and the low acceptance by the prototype. In the moderate level it will have the result of 50% to 79% that indicates that the prototype must obtain some improvements for its acceptance and finally the high level will have the 80% to 100%, as a result it will indicate that the prototype is considered a good project of innovation and accepted by the expert, as well as it shows in the Table IV.

TABLE IV. LEVEL OF ACCEPTANCE

Level		
Under	Moderate	High
0% - 49%	50% - 79%	80% - 100%

To find the total level of acceptance it is necessary to perform an equation, so that the criteria (Functionality, Usability, Coherence and Integration) are added up and divided by the number of criteria, so that the level of acceptance (Low, Moderate and High) is obtained.

Once the levels of acceptance are understood, the scoring of each expert should be done in such a way that each criterion is scored from 0% to 100%, and finally the total sum for each criterion and the level of acceptance of the prototype is displayed, as shown in Table V.

TABLE V. SCORING BY EXPERTS

Question about the prototype with augmented reality						
Experts	Functionality	Usability	Consistency	Integration	Total	Level
Expert 1	82%	95%	79%	80%	84%	High
Expert 2	83%	93%	86%	92%	89%	High
Expert 3	87%	85%	81%	87%	85%	High
Expert 4	89%	91%	88%	83%	88%	High
Expert 5	82%	86%	83%	91%	86%	High

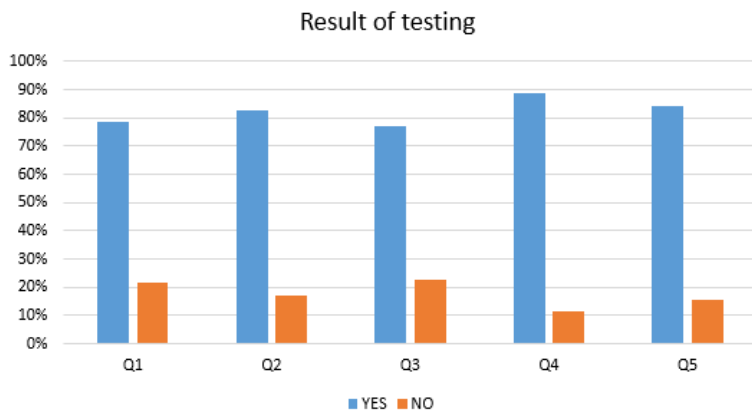


Fig. 10. Application Design Steps and Augmented Reality Modeling.

F. Expert Validation of the Prototype

To verify these validation results, which must be verified by 5 experts, the 4 criteria (Functionality, Usability, Consistency

In such a way Fig. 11 shows the validation by experts who have the high level of acceptance, indicating that the final prototype is a good innovation project, in detail it is shown that expert 1 shows the high level with 84%, expert 2 shows the high level with 89%, expert 3 shows the high level with 85%, expert 4 shows the high level with 88% and expert 5 shows the high level with 86%. As total average of all validations by all experts counts 86%.

G. About the Methodology

1) *Advantages:* The advantages of the Design Thinking methodology help us to know the needs of the users in order to solve their problems, using technology. Likewise, working in a group is effective to get to know different points of view in such a way that we reach the same objective of satisfying the client. Creativity and innovation are the main characteristics of this methodology, which involves research and analysis to come up with new ideas to contribute to society.

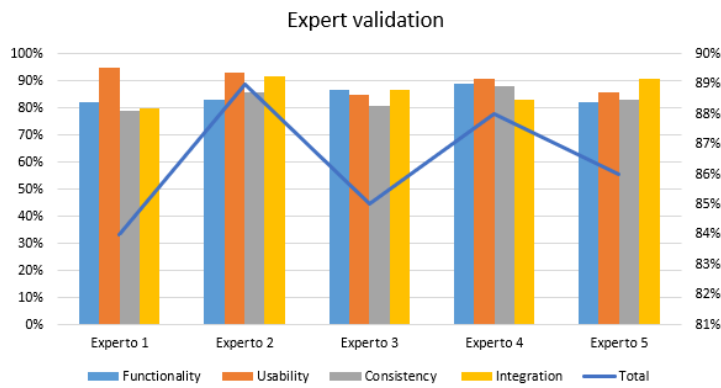


Fig. 11. Expert Validation.

2) *Disadvantages:* The main disadvantage of the Design Thinking methodology is the prototyping that it involves as a final solution and not in its development, so that this methodology can be grouped with other types of methodology dedicated to the development of the application in order to carry out a complete project.

3) *Comparison:* The Design Thinking methodology gives us the facility to use innovation and creativity to reach the needs of people, compared to other methodologies that are only responsible for the development and implementation with more complex phases [35],[36], this methodology is dedicated to the contribution to society and its ease of understanding is totally simple.

V. DISCUSSIONS

In the research work that proposes to make a mobile prototype with augmented reality for dyscalculia, it turns out to be a very effective plan for the treatment of the student in such a way that there is a variety of similarities in different works that have the same objective of improving the treatment and quality in their teachings for children with problems in their understanding of mathematical operations, this coincides with the author [13],[37] which is in charge of developing augmented reality to improve children's comprehension skills in such a way that they become familiar with technology, and it is also discussed that their work makes a great contribution to society, implying that by using these technologies they can help solve different problems. On the other hand, augmented reality should be visualised by a device in such a way that the author [14], affirms the ease of having a mobile device and that when using it with augmented reality it is more effective since there are millions of users with a mobile phone in their homes, it is in this way that together the two points of view of different authors can be similar in my project giving the assurance that the development will generate a great impact on education. to know or understand the needs of users is necessary to establish multiple solutions to their problems so that the author [20], the methodology of the methodology matches our strategy, indicating that tools such as interviews and surveys are a fundamental part of the analysis with respect to the mobile application with augmented reality.

VI. CONCLUSIONS

The mobile prototype with augmented reality that is carried out in this project, proposes the improvement and treatment of dyscalculia in children in primary education, precisely a variety of problems identified by the surveys, indicating the problems that children have with their learning and the difficulty in performing their mathematical operations, for this dynamic games are made with augmented reality giving ease of understanding and comprehension. The Design Thinking methodology was a fundamental part to know the needs of the parents and the decision making by the team for the analysis of the problem, giving an infinity of ideas for the search of its solution. The prototype will not only be dedicated to education, but can also be easily integrated into health centres and clinics, in such a way that its contribution with the use of technology will be effective for the adequate treatment of children with dyscalculia. The main limitation of our project is the development of the mobile application with augmented reality, since our methodology does not focus on development, it is only used for design and prototyping.

VII. FUTURE WORK

For future work, it is suggested that this prototype with augmented reality be developed with the methodology focused on implementation or also be able to develop virtual reality technology with artificial intelligence for greater experience with the technology. In such a way that the development meets the objective of improving and treating dyscalculia in children, it is suggested that the work should be done in conjunction with specialists who have knowledge about dyscalculia for a better understanding of these learning disorders.

ACKNOWLEDGMENT

This work was sponsored by the University of Sciences and Humanities and the research direction. Thank for the unconditional support.

REFERENCES

- [1] C. Luoni, M. Scorza, S. Stefanelli, B. Fagiolini, and C. Termine, "A neuropsychological profile of developmental dyscalculia: The role of comorbidity," *Journal of Learning Disabilities*, p. 00222194221102925, 2022.
- [2] F. Ashraf and N. Najam, "An epidemiological study of prevalence and comorbidity of non-clinical dyslexia, dysgraphia and dyscalculia symptoms in public and private schools of pakistan," *Pakistan Journal of Medical Sciences*, vol. 36, no. 7, p. 1659, 2020.
- [3] M. Barr and A. Copeland-Stewart, "Playing video games during the covid-19 pandemic and effects on players' well-being," *Games and Culture*, vol. 17, no. 1, pp. 122–139, 2022.
- [4] B. V. Dorneles, "Mathematical learning and its difficulties in latin-american countries," in *International handbook of mathematical learning difficulties*. Springer, 2019, pp. 201–212.
- [5] A. A. S. Martins, G. M. Paiva, C. G. R. Matosinho, E. M. Coser, P. A. d. S. Fonseca, V. G. Haase, and M. R. S. Carvalho, "Working memory and arithmetic impairments in children with fmr1 premutation and gray zone alleles," *Dementia & Neuropsychologia*, vol. 16, pp. 105–114, 2022.
- [6] F. H. Santos, F. S. Ribeiro, A. L. Dias-Piovezana, C. Primi, A. Dowker, and M. von Aster, "Discerning developmental dyscalculia and neurodevelopmental models of numerical cognition in a disadvantaged educational context," *Brain Sciences*, vol. 12, no. 5, p. 653, 2022.
- [7] Á. Salvatierra Melgar, W. A. Quispe-Cutipa, I. Reyes-Blácido, L. S. Rodríguez-Baca, M. F. Guevara-Duarez, and M. A. Alarcón-Díaz, "Cognitive reflections in children with adhd and proposals to promote logical thinking," 2021.

- [8] J. Castro-Bedriñana, D. Chirinos-Peinado, and G. Castro-Chirinos, "Emergency remote education satisfaction during covid-19 at a public university in central andes, peru with low resources and little online teaching experience," *Educational Sciences: Theory & Practice*, vol. 22, no. 1, pp. 46–61, 2022.
- [9] N. F. G. Gutiérrez, E. G. R. Arellano, J. M. Vergaray, F. d. S. T. Caceres, M. J. L. Cuadros, and E. R. Navarro, "Teaching experiences in urban and rural areas of peru in covid-19 context," *Journal of Positive School Psychology*, vol. 6, no. 2, pp. 62–70, 2022.
- [10] Á. Salvatierra Melgar, W. A. Quispe-Cutipa, I. Reyes-Blácido, L. S. Rodríguez-Baca, M. F. Guevara-Duarez, and M. A. Alarcón-Díaz, "Cognitive reflections in children with adhd and proposals to promote logical thinking," 2021.
- [11] K. Miundy, H. B. Zaman, A. Nordin, and K. H. Ng, "Early intervention through identification of learners with dyscalculia as initial analysis to design an assistive learning application," in *International Visual Informatics Conference*. Springer, 2019, pp. 110–122.
- [12] —, "Screening test on dyscalculia learners to develop a suitable augmented reality (ar) assistive learning application," *Malaysian Journal of Computer Science*, pp. 92–107, 2019.
- [13] R. Kariyawasam, M. Nadeeshani, T. Hamid, I. Subasinghe, and P. Ratnayake, "A gamified approach for screening and intervention of dyslexia, dysgraphia and dyscalculia," in *2019 International Conference on Advancements in Computing (ICAC)*. IEEE, 2019, pp. 156–161.
- [14] T. Debnath, "Investigating the effectiveness of an augmented reality game to enhance the mathematics learning experience of dyscalculic," 2021.
- [15] Z. Bhatti, N. Shabbir, M. Arshad, and M. Shaikh, "Virtual reality based android application for special children," *Journal of Information Systems and Digital Technologies*, vol. 3, no. 2, pp. 76–83, 2021.
- [16] Z. Turan and G. Atila, "Augmented reality technology in science education for students with specific learning difficulties: Its effect on students' learning and views," *Research in Science & Technological Education*, vol. 39, no. 4, pp. 506–524, 2021.
- [17] E. Castro-Gutierrez, "Voluminis: Mobile application for learning mathematics in geometry with augmented reality and gamification," in *Human-Computer Interaction: 6th Iberomeric Workshop, HCI-Collab 2020, Arequipa, Peru, September 16–18, 2020, Proceedings*, vol. 1334. Springer Nature, 2021, p. 295.
- [18] I. Ahmad, A. J. Mohamad, F. F. Roszali, and N. Sarudin, "Dyslexiar: Augmented reality game based learning on reading, spelling and numbers for dyslexia user's," in *Computational Science and Technology*. Springer, 2021, pp. 259–269.
- [19] I. J. Fitriyah, A. Setiawan, M. F. Marsuki, and E. Hamimi, "Development of augmented reality teaching materials of chemical bonding," in *AIP Conference Proceedings*, vol. 2330, no. 1. AIP Publishing LLC, 2021, p. 020043.
- [20] B. Y. Yenioglu, F. Ergulec, and S. Yenioglu, "Augmented reality for learning in special education: a systematic literature review," *Interactive Learning Environments*, pp. 1–17, 2021.
- [21] G. Wang, "Digital reframing: The design thinking of redesigning traditional products into innovative digital products," *Journal of Product Innovation Management*, vol. 39, no. 1, pp. 95–118, 2022.
- [22] R. Kijima, M. Yang-Yoshihara, and M. S. Maekawa, "Using design thinking to cultivate the next generation of female steam thinkers," *International Journal of STEM Education*, vol. 8, no. 1, pp. 1–15, 2021.
- [23] R. Parizi, M. Prestes, S. Marczak, and T. Conte, "How has design thinking being used and integrated into software development activities? a systematic mapping," *Journal of Systems and Software*, p. 111217, 2022.
- [24] K. Jaskyte and J. Liedtka, "Design thinking for innovation: Practices and intermediate outcomes," *Nonprofit Management and Leadership*, vol. 32, no. 4, pp. 555–575, 2022.
- [25] C. Anton, A. E. Micu, and E. Rusu, "Introducing the living lab approach in the coastal area of constanta (romania) by using design thinking," *Inventions*, vol. 7, no. 1, p. 19, 2022.
- [26] C. T. A. Pham, S. Magistretti, and C. Dell'Era, "The role of design thinking in big data innovations," *Innovation*, vol. 24, no. 2, pp. 290–314, 2022.
- [27] L. Vendraminelli, L. Macchion, A. Nosella, and A. Vinelli, "Design thinking: strategy for digital transformation," *Journal of Business Strategy*, 2022.
- [28] J. Vrana and R. Singh, "Nde 4.0—a design thinking perspective," *Journal of nondestructive evaluation*, vol. 40, no. 1, pp. 1–24, 2021.
- [29] M.-J. Tsai and C.-Y. Wang, "Assessing young students' design thinking disposition and its relationship with computer programming self-efficacy," *Journal of Educational Computing Research*, vol. 59, no. 3, pp. 410–428, 2021.
- [30] H. L. Bradwell, G. E. A. Noury, K. J. Edwards, R. Winnington, S. Thill, and R. B. Jones, "Design recommendations for socially assistive robots for health and social care based on a large scale analysis of stakeholder positions: Social robot design recommendations," *Health Policy and Technology*, vol. 10, no. 3, p. 100544, 2021.
- [31] E. A. Juanda and F. Khairullah, "Tinkercad application software to optimize teaching and learning process in electronics and microprocessors subject," in *6th UPI International Conference on TVET 2020 (TVET 2020)*. Atlantis Press, 2021, pp. 124–128.
- [32] S. Tsolakis, T. Theofanellis, and E. Voulgari, "Introducing steam through tinkercad and arduino," in *Handbook of Research on Integrating ICTs in STEAM Education*. IGI Global, 2022, pp. 239–264.
- [33] M. S. Sanadi, P. S. Satpute, and M. N. Mestri, "Simulation of drainage cleaning robotics system using solid work tinkercad software," *Asian Journal For Convergence In Technology (AJCT) ISSN-2350-1146*, vol. 7, no. 1, pp. 17–19, 2021.
- [34] M. L. Amado, L. C. Ruiz, and L. Andrade-Arenas, "Prototype of an augmented reality application for cognitive improvement in children with autism using the desingscrum methodology," *Advances in Science, Technology and Engineering Systems*, vol. 6, no. 1, pp. 587–596, 2021.
- [35] R. Arias-Marreros, K. Nalvarte-Dionisio, and L. Andrade-Arenas, "Design of a mobile application for the learning of people with down syndrome through interactive games," *International Journal of Advanced Computer Science and Applications*, vol. 11, 2020.
- [36] F. Andrade-Chaico and L. Andrade-Arenas, "Projections on insecurity, unemployment and poverty and their consequences in lima's district san juan de lurigancho in the next 10 years," 2019.
- [37] A. Carrion-Silva, C. Diaz-Nunez, and L. Andrade-Arenas, "Admission exam web application prototype for blind people at the university of sciences and humanities," *International Journal of Advanced Computer Science and Applications*, vol. 11, 2020.

Adaptive Lane Keeping Assist for an Autonomous Vehicle based on Steering Fuzzy-PID Control in ROS

Hoang Tran Ngoc, Luyl-Da Quach
Software Engineering Department
FPT University Can Tho city, Vietnam

Abstract—An autonomous vehicle is a vehicle that can run autonomously using a control. There are two modern autonomous assistant systems that are proposed in this research. First, we introduce a real-time approach to detect lanes of the streets. Based on a series of multi-step image processing through input data from the camera, the vehicle's steering angle is estimated for lane keeping. Second, the steering control system ensures that autonomous vehicles can operate stably, and smoothly, and adapt to various road conditions. The steering controller consists of a PID controller and fuzzy logic control strategy to adjust the controller parameters. The simulation experiments by Gazebo simulator of the Robot Operating System (ROS) not only indicate that the vehicle can keep the lane safely, but also demonstrate that the proposed steering angle controller is more stable and adaptive than the conventional PID controller.

Keywords—Autonomous vehicles; automated steering; lane detection; fuzzy PID control; ROS, Gazebo

I. INTRODUCTION

Every year nearly 1.25 million people die in traffic accidents. Therefore, safety is the most important criterion when driving on the road. Traffic accidents are caused by human errors up to 90% according to National Highway Traffic Safety Administration (NHTSA) statistics [1]. In recent five years, autonomous vehicles, and many advanced driver assistance systems (ADAS) have been developed to help drivers to drive safely. It attracts great attention not only in academia but also in automotive industries such as Google, Tesla, BMW, and Hyundai. In there, lane boundary detection and steering control systems play a key role in autonomous vehicles (AVs).

To detect the lanes as well as the steering angle, common sensors are used such as radar, light imaging detection and ranging (LIDAR), laser sensors, and even global positioning systems (GPS) [2-5]. However, sensors with high accuracy of distance measurement are very expensive. Therefore, numerous studies have been developing vision-based systems using camera sensors for lane detection [6-7] in recent years. These studies indicate that the lane detection process has major challenges such as lighting and background clutter.

Along with the studies of determining steering angle based on lane detection via vision, approaches to improve the stability and accuracy of the steering angle controller are also interesting in several studies around the world. For example, a basic steering control algorithm based on a PID controller was proposed in [8]. Moreover, to address a repeated problem of steering control, a robust PID controller is designed in

[9]. Another approach was nested conventional PI and PID controllers to improve the accuracy of the steering angle controllers [10-15]. However, the damping effect of the conventional PID controller is not good enough to keep the vehicle running smoothly for lane tracking. Therefore, to develop the autonomous system without mentioned problems, we have two main goals: estimating the steering angle and designing the steering controller with high stability.

In this research, the steering angle is estimated through a sequence of image processing steps and computer vision approaches. The image will be filtered, determined the region of interest (ROI), and finally extracted the line segments using the simplified Hough Transform technique. After obtaining the estimated steering angle, this paper proposed a method to optimize the performance of the steering control system. The idea is to use the fuzzy logic control strategy to tune the parameters of the PID controller. The fuzzy controller adjusts the parameters of the PID based on the steering angle error and previous information. The effectiveness of the two proposed systems is verified by the robot simulation results in the Gazebo environment.

The structure of this research paper is organized as follows. First, in Section 2, the vehicle steering model is introduced. In Section 3, lane detection and steering angle estimation are presented. The proposed steering control system using a Fuzzy-PID controller is analyzed and designed in Section 4. Then, the simulation results and analysis of the corresponding system are compared in Section 5. Finally, the conclusions in Section 6 will summarize the content of this research.

II. VEHICLE DYNAMIC MODEL

The vehicle dynamics and vehicle steering behavior are considered in the 2D bicycle model [16]. The linear vehicle steering model is described as follows:

$$\begin{bmatrix} \dot{y} \\ \dot{\beta} \\ \dot{\psi} \\ \dot{\dot{\psi}} \end{bmatrix} = \begin{bmatrix} 0 & V & V & 0 \\ 0 & -\frac{D_r+D_f}{MV} & 0 & \frac{D_r L_r - D_f L_f}{MV^2} \\ 0 & 0 & 0 & 1 \\ 0 & \frac{D_r L_r - D_f L_f}{L_z} & 0 & \frac{D_r L_r^2 - D_f L_f^2}{L_z V} \end{bmatrix} \begin{bmatrix} y \\ \beta \\ \psi \\ \dot{\psi} \end{bmatrix} + \begin{bmatrix} 0 \\ \frac{D_f}{MV} \\ 0 \\ \frac{D_f L_f}{L_z} \end{bmatrix} \delta \quad (1)$$

where y , β , ψ , $\dot{\psi}$, V , L_z , M , L_f and L_r are vehicle position, side slip angle, yaw angle, yaw rate, vehicle speed, vehicle inertia, vehicle mass, and the center of gravity distance from front tires, and rear tires. The lateral forces with

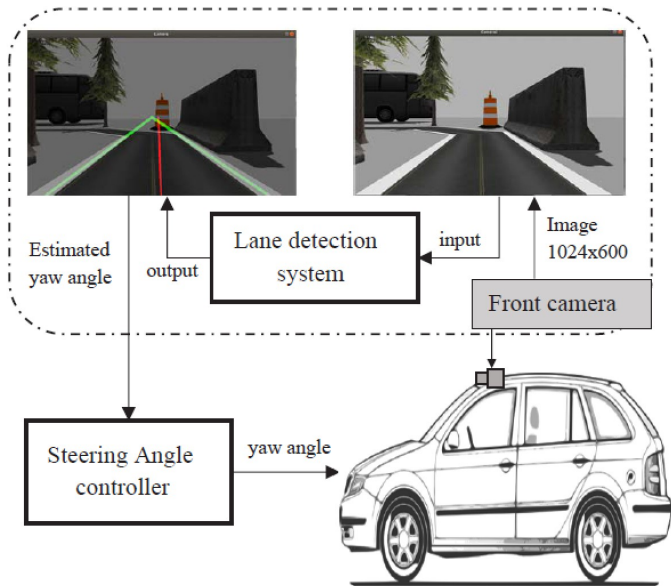


Fig. 1. Block Diagram of the Proposed System.

linearized cornering stiffness of the front, and rear wheel (D_f and D_r) are shown in (2) below:

$$\begin{cases} F_{yf} = D_f \alpha_f = D_f \left(\delta - \beta - \frac{L_f \dot{\psi}}{V} \right) \\ F_{yr} = D_r \alpha_r = D_r \left(-\beta + \frac{L_r \dot{\psi}}{V} \right) \end{cases} \quad (2)$$

where α_f , α_r , and δ are front, rear tire slip angle, and steering angle from the forward direction of the vehicle.

The proposed system and variables of the vehicle model are presented in Fig. 1 and Fig. 2. In this research, the yaw angle is estimated from the lane detection system and used as the steering angle to control the robot model in the Gazebo simulator environment. In the real system, the front wheel steering angle (δ) will be converted from a yaw angle (ψ).

A. Lane Detection Algorithm

To control the proposed autonomous vehicle to keep the lane accurately, we used algorithms [17] and adapted them to match our system by using the following steps: First, to detect the white lanes, we isolate all the white areas on the image. To do this, we converted the color space of the image from RGB (Red/Green/Blue) to the HSV (Hue/Saturation/Value) and created the mask image for a range of white colors. Second step, we extracted edges in the white mask by using the Canny edge detector [18-19]. This algorithm is developed by John F. Canny that can detect edges and reduce the number of erroneous edges detected in mask images. In the third step, we need to detect a few white edge areas that are no lane lines. The extraction of an Isolate Region of Interest (IROI) is performed in this step. We cropped the detected edges in the top half of the image. Fourth step, line segment detection is applied. We extracted the coordinates of the lane lines from white pixels by using the Hough Transform technique [20]. The Hough Transform is a common algorithm, used in image processing to find features such as lines, circles, and ellipses.

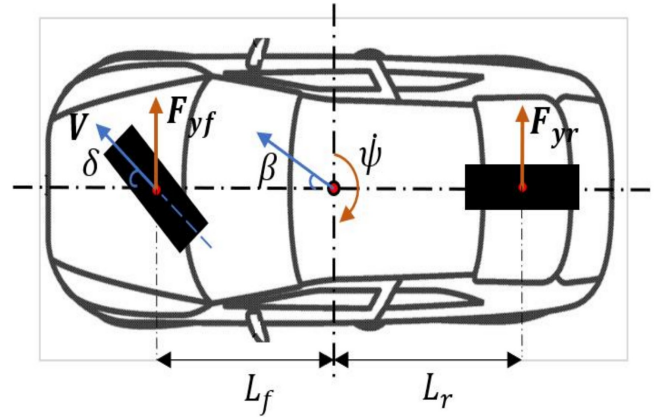


Fig. 2. Block Diagram of the Proposed System.

We applied it to detect straight lines from pixels that seem to line up.

The Hough Transform is the transformation from points to curves, which converts the Cartesian coordinate system of the image to the polar coordinate Hough space as (3):

$$\rho = x \cos(\theta) + y \sin(\theta), \quad \theta \in [-\pi \quad \pi] \quad (3)$$

where (x, y) is the pixel coordinates; (θ, ρ) is the polar coordinates; ρ the distance of the straight line from the coordinate origin; θ is the minimum angle of the straight line in the normal direction with the positive direction of the x-axis. Points on the same line satisfy the (3) with a set of (θ, ρ) constants. Fig. 3 shows the basic principle of the Hough Transform. From this basic principle, line segments are determined.

III. LANE DETECTION AND STEERING ANGLE ESTIMATION

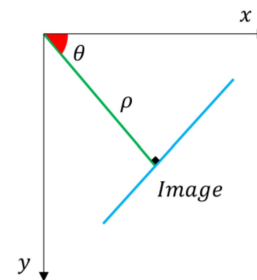


Fig. 3. Basic Principle of Hough Transform.

The final step is to combine line segments into two-lane lines. We classified small line segments into two groups by their slope. All the line segments of the left lane line have an upward slope (θ range from 15° to 85°), whereas all line segments of the right lane line have a downward slope (θ range from -15° to -85°). We then averaged the slope and the intersection point to detect the left and right lanes. Fig. 4 shows the lane detection stages and results of our system in the Gazebo simulation environment.

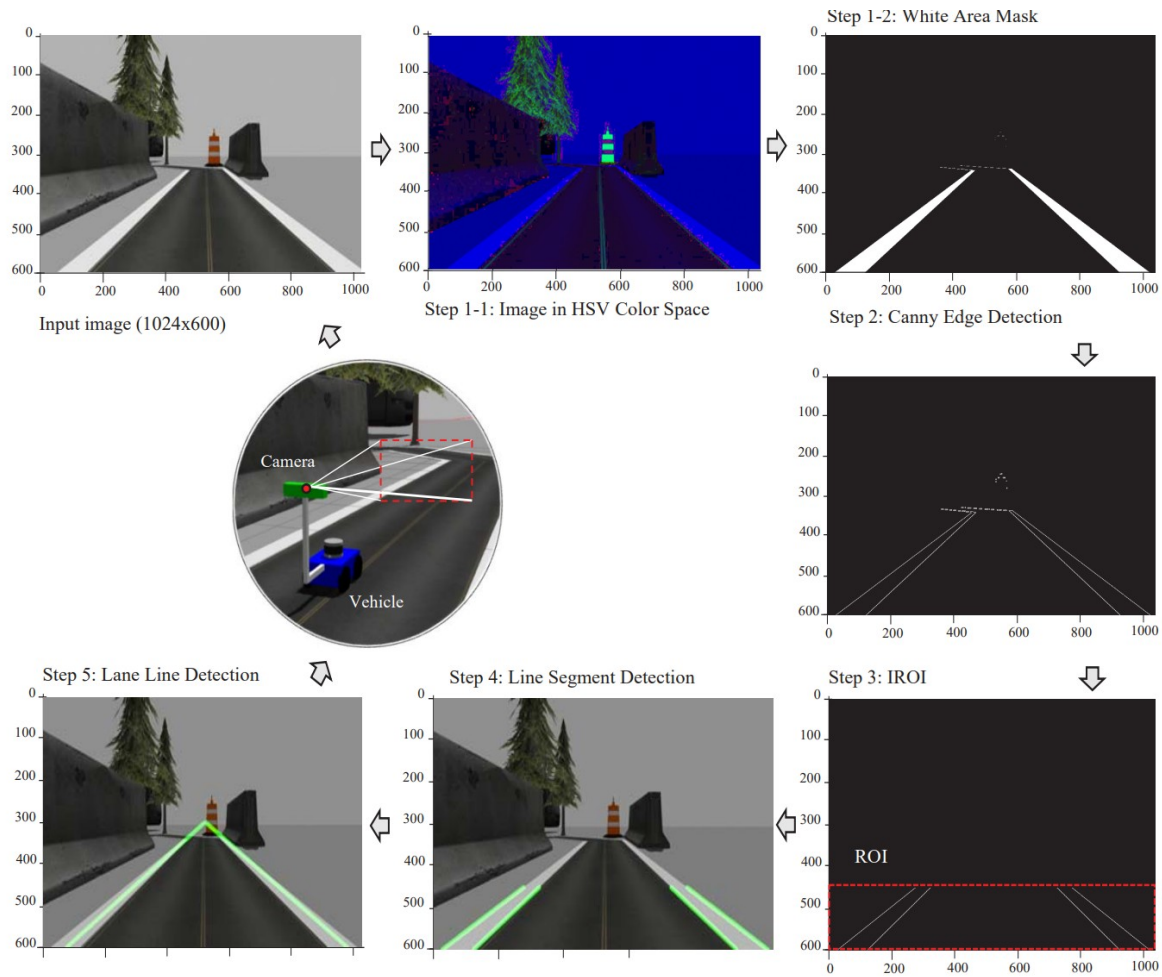


Fig. 4. Lane Detection Steps and Results of our System.

A. Steering Angle Estimation

After using the lane detection algorithm, we have the coordinates of two lanes. We need to estimate the steering angle to steer the car so that it keeps in the middle of the two lanes. We have two cases where the vehicle drifts to the left side or the right side of the road, and the vehicle is already in the middle of the lane. From the coordinates of the two lanes, the steering angle will be determined according to the following (4):

$$\hat{\psi} = \tan\left(\frac{x_{offset}}{\frac{H_i}{2}}\right) \quad (4)$$

$$\hat{\psi} = \begin{cases} \tan\left(\frac{\left(\frac{x_{1(R)} - x_{1(L)}}{2} + x_{1(L)}\right) - \frac{W_i}{2}}{H_i/2}\right), & \text{if } \begin{cases} < 0, \text{ right side.} \\ > 0, \text{ left side.} \end{cases} \\ 0, & \text{vehicle on center,} \end{cases}$$

where $\hat{\psi}$ is the yaw angle estimated for use as the steering control angle in the Gazebo simulator; x_{offset} is the distance from the vehicle's center to the line between the two detected lanes; $(x_{1,2(L)}, y_{1,2(L)})$ and $(x_{1,2(R)}, y_{1,2(R)})$ are the start points and endpoints of the left lane and the right lane; W_i and H_i are width and height of the image input (unit: pixel).

Fig. 5 shows the sample coordinates of the system on the right side (a) and the left side (b).

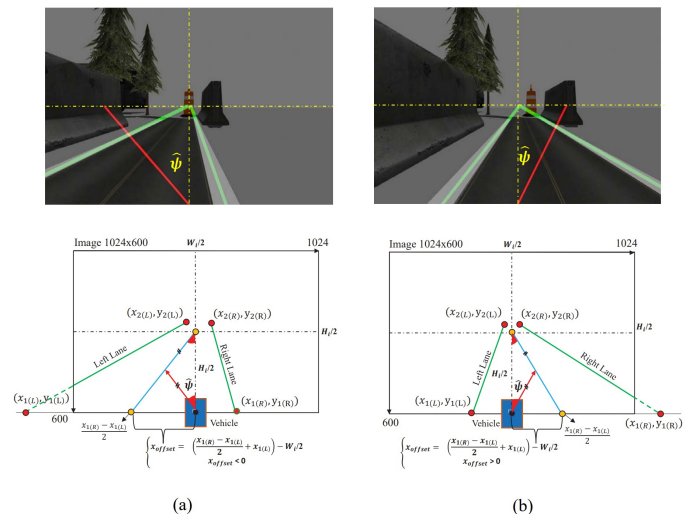


Fig. 5. Sample Coordinates of the System on the Right Side (a) and the Left Side (b).

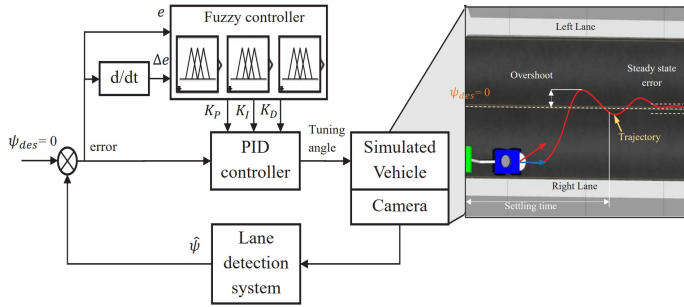


Fig. 6. Fuzzy PID Control Algorithm Structure Diagram for our Vehicle Autonomous System.

TABLE I. FUZZY CONTROL RULES

K_p		Δe				
		N	NM	Z	PM	P
e	N	V_h	H	H	M_e	M_e
	NM	V_h	H	H	M_e	L_o
	Z	H	H	M_e	M_e	L_o
	PM	H	H	M_e	M_e	L_o
	P	H	H	M_e	M_e	L_o
K_i		Δe				
		N	NM	Z	PM	P
e	N	Z_e	Z_e	M_e	M_e	M_e
	NM	Z_e	M_e	H	M_e	M_e
	Z	M_e	H	H	M_e	M_e
	PM	H	H	H	M_e	Z_e
	P	H	H	M_e	Z_e	Z_e
K_d		Δe				
		N	NM	Z	PM	P
e	N	L_oL	M_e	M_e	Z_e	Z_e
	NM	M_e	M_e	Z_e	Z_e	H
	Z	M_e	Z_e	Z_e	M_e	H
	PM	Z_e	Z_e	M_e	M_e	V_h
	P	Z_e	H	H	V_h	V_h

IV. STEERING CONTROL SYSTEM

The steering control system controls the vehicle to keep the center of the lane. To achieve this, the desired steering angle (ψ_{des}) must be controlled at 0. However, the damping effect of ordinary PI and PID controllers is not good enough to keep the vehicle running smoothly and stably, so a fuzzy PID controller is proposed to tune the PID parameters for further improvement. Fig. 6 shows the fuzzy PID control algorithm structure diagram for our vehicle autonomous system. A mathematical equation for controlling the steering angle of a typical PID controller is expressed in (5).

$$\psi_{Tuning}(t) = K_p e(t) + K_i \int_0^t e(t) + K_d \frac{de}{dt} \quad (5)$$

where $K_{p,i,d}$ are the proportional gain, integral gain, and derivative gain; ψ_{Tuning} is the tuning steering angle; e is the angle error between the estimated steering angle ($\hat{\psi}$) and the desired steering angle ($\psi_{des} = 0$).

The fuzzy logic controller is designed with two input signals the error and the derivative of the error, while the three outputs are K_p, K_i , and K_d . The range of e , and Δe are limited as $-45, 45$ and $-10, 10$, respectively. The fuzzy rule base is shown in Table I. The membership functions are N (Negative); NM (Negative medium); Z (Zero); PM (Positive medium); P (Positive) for error input, and Z_e (Zero); L_o (Low);

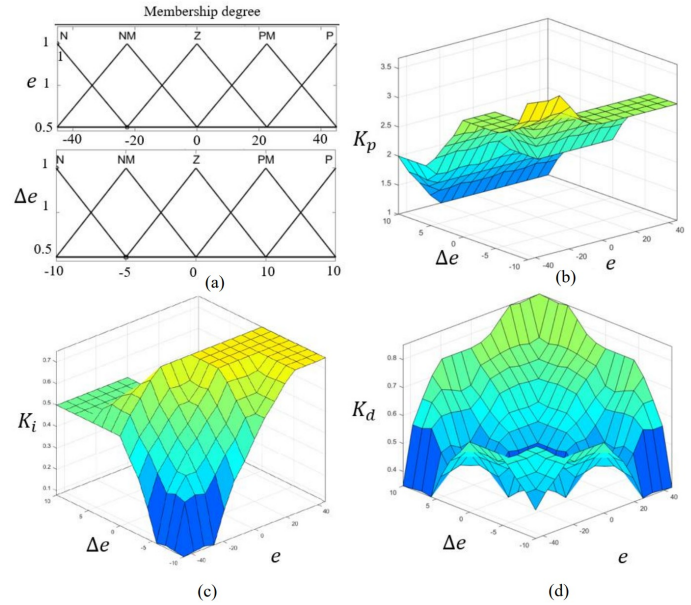


Fig. 7. Fuzzy Logic. (a) Membership Function of e and Δe . (b), (c) and (d) View of the Fuzzy Rule-Base of K_p, K_i , and K_d .

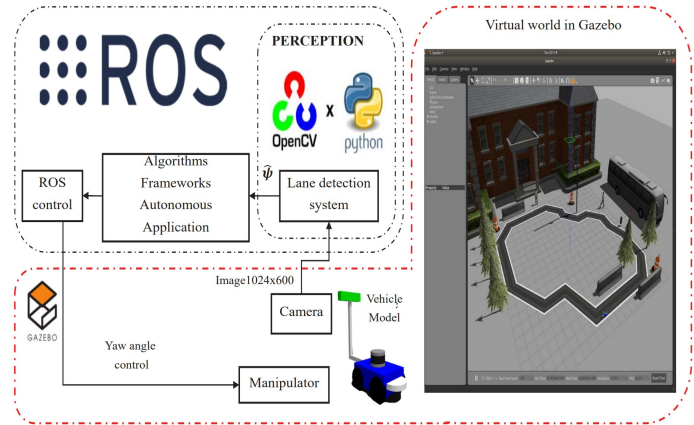


Fig. 8. Architecture of Simulation System.

M_e (Medium); H (High); V_h (Very high) for parameters output. The Segeno model is applied to the fuzzy logic structure to obtain the best value for PID parameters.

By using the Scikit-Fuzzy library for the Python computing language, the steering angle controller was tuned based on the designed rule, so that the best dynamic response of the vehicle is achieved with the smallest overshoot and steady-state error when comparing centerline lane keeping. Fig. 7(a) shows the membership function and Fig. 7(b)-(d) the rule base of the fuzzy logic controller.

The simulation results of vehicle operation in the Gazebo environment are provided later to demonstrate the effectiveness of the two proposed systems.

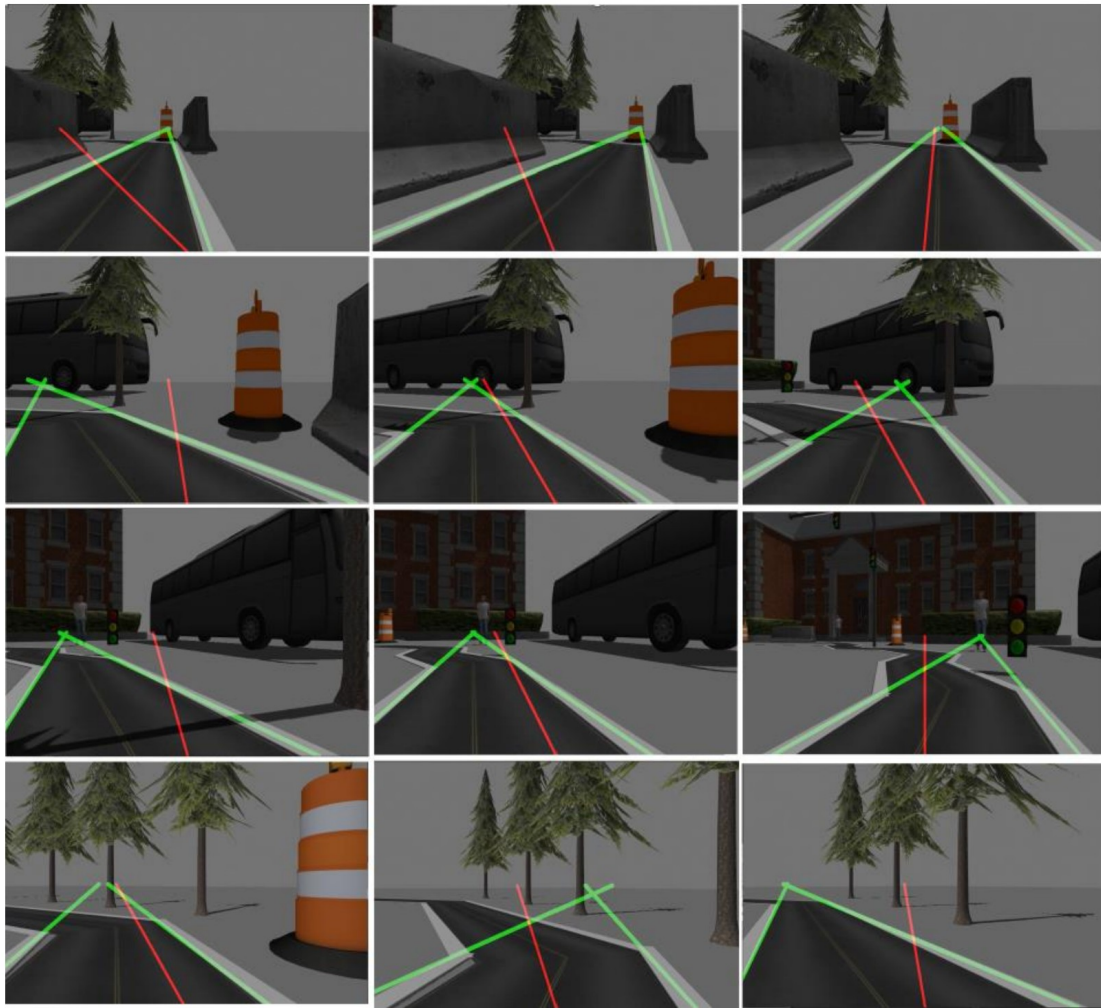


Fig. 9. Results of our Lane Detection System in the Virtual World.

V. SIMULATION AND RESULTS

The virtual world is designed by using the software Gazebo/ROS. Fig. 8 shows the vehicle model, Gazebo environment, and the software used to apply the two proposed algorithms. We have performed two kinds of experiments to verify our lane detection algorithm and our steering control algorithm with the operating system Ubuntu 18.04.4, and CPU: Intel i7 3.4 GHz, GPU: Nvidia GTX 1650-4GB, RAM 16 GB. Our algorithm is implemented in Python language using the open source OpenCV and rospy library. The camera is simulated from the actual parameters of the WGE100 camera. The image size is 1024×600; the image was recorded at 30 frames per second. We tested that the lane detection algorithm is applied according to [17].

The lane detection results are like previous approaches. In the virtual world, the image data obtained with two-lane detection results are correct, as shown in Fig. 9. We also achieve good results for the estimated yaw angle when applying the steering angle estimation algorithm in Section 3.

We also verify the performance of the proposed steering angle controller by reading the odometry information of

vehicle autonomous over ROS including trajectory and yaw angle. Fig. 10 and Fig. 11 show the lane-keeping performance of the PID steering controller, and the fuzzy-PID steering controller under low-speed, and high-speed conditions. It is easy to see that the proposed method can minimize the desired angle error and reduce the damping effects better than another method. Table II shows the performance comparison of the PID controller and fuzzy-PID controller. The overshoot of the fuzzy-PID controller is less than 5%, however, with the conventional controller, it is 25% more than 5 times. Therefore, we concluded that the proposed assist system obtains higher accuracy of lane-keeping performance and better stability.

VI. CONCLUSION

In this research, we develop a lane-keeping assist for an autonomous vehicle. The algorithm is based on a sequence of image processing, filtering, determination ROI, line segments detection, and steering angle estimation to detect lanes in the virtual world. All lanes are detected in still images at a high rate of 30Hz. Then, the steering controller with the fuzzy-PID algorithm is also proposed to reduce the steering angle error and minimize the damping effects. In the future, the algorithms

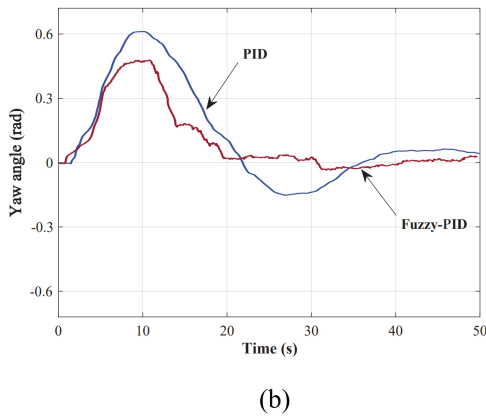
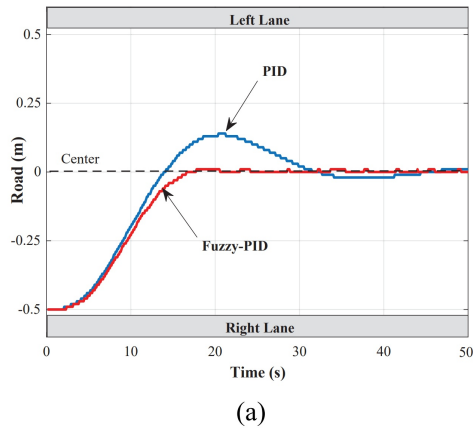


Fig. 10. Performance Comparison of the PID Steering Controller and Fuzzy-PID Steering Controller at Low Speed (2m/s). (a) The Vehicle's Trajectory on the Road, and (b) the Yaw Angle of the Vehicle.

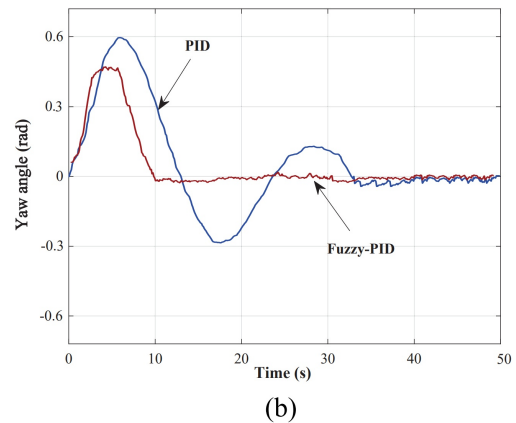
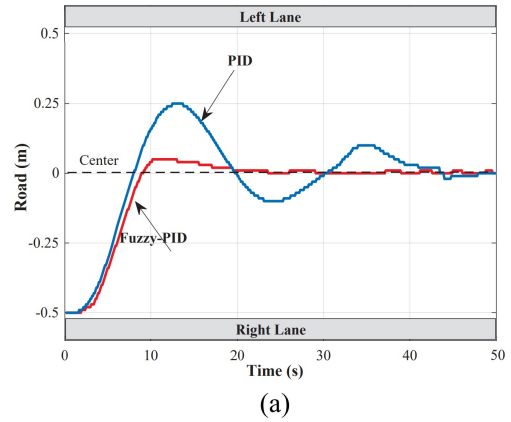


Fig. 11. Performance Comparison of the PID Steering Controller and Fuzzy-PID Steering Controller at High Speed (4m/s). (a) The Vehicle's Trajectory on the Road, and (b) the Yaw Angle of the Vehicle.

will be tested and evaluated on real systems. In addition, deep learning algorithms will also be studied and applied.

TABLE II. OVERSHOOT AND SETTLING TIME OF THE PERFORMANCE COMPARISON

	Overshoot (%)		Settling time (s)	
	Low speed	High speed	Low speed	High speed
PID	25%	51%	28s	43s
Fuzzy-PID	1%	5%	12s	15s

REFERENCES

- [1] R. Ramani, *Vehicle Dynamics and Control*, Springer, 2012.
- [2] Y. Matsushi, and J. Mijura, *On-line Road Boundary Modeling with Multiple Sensory Features Flexible Road Model and Particle Filter*, *Robotic and Autonomous Systems*, vol. 59, pp. 274-284, 2011.
- [3] Y. Kang, C. Roh, S. B.Suh, and B. Song *A Lidar-Based DecisionMaking Method for Road Boundary Detection Using Multiple Kalman Filters*, *IEEE Transactions on Industrial Electronics*, pp. 4360 – 4368, 2012.
- [4] H. Fahmy, G. Baumann, M. AbdelGhany, and H. Mostafa.: *V2V-Based Vehicle Risk Assessment and Control for Lane-Keeping and Collision Avoidance*, in *IEEE International Conference on Microelectronics (ICM 2017)*, Beirut, Lebanon, pp. 61-65, 2017.
- [5] J. Huang, P. K. Choudhury, S. Yin and L. Zhu, *Real-Time Road Curb and Lane Detection for Autonomous Driving Using LiDAR Point Clouds*, in *IEEE Access*, vol. 9, pp. 144940-144951, 2021
- [6] Pallavi V. Ingale and Prof. K. S. Bhagat.: *Comparative Study of Lane Detection Techniques*, in *International Journal on Recent and Innovation Trends in Computing and Communication*, vol. 4, no. 5, 2016.
- [7] Ammu M Kumar and Philomina Simon.: *Review of Lane Detection and Tracking Algorithms in Advanced Driver Assistance System*, in *International Journal of Computer Science & Information Technology (IJCSIT)*, vol. 7, no. 4, 2015.
- [8] A. Broggi, P. Medici, P. Zani, A. Coati, and M. Panciroli.: *Autonomous vehicles control in the VisLab intercontinental autonomous challenge*, *Annual Reviews in Control*, vol. 36, no. 1, pp. 161–171, 2012.
- [9] J. Ackermann, J. Guldner, W. Sienel, R. Steinhauser, and V. I. Utkin.: *Linear and Nonlinear Controller Design for Robust Automatic Steering*, *IEEE Transactions on Control Systems*, vol. 3, no. 1, 1995.
- [10] R. Marino, S. Scalzi, and M. Netto.: *Nested PID Steering Control for Lane Keeping in Autonomous Vehicles*, *Control Engineering Practice*, vol. 19, no. 12, pp. 1459– 1467, 2011.
- [11] W. Farag and Z. Saleh, *Tuning of PID track followers for autonomous driving*, 2018 *Int. Conf. Innov. Intell. Informatics, Comput. Technol. 3ICT 2018*, pp. 1–7, 2018.
- [12] S. Surendharan, J. Jennifer Ranjani *Environment conscious automated vehicle navigation system using PID controller*, *Indian J, Sci, Technol*, 2016.
- [13] C.K. Chandni, V.V. Sajith Variyar, K. Guruvayurappan, *Vision based closed loop PID controller design and implementation for autonomous car*, In *Proceedings of the 2017 International Conference on Advances in Computing, Communications and Informatics (ICACCI)*, Udupi, India, pp. 1928–1933, 2017.
- [14] A. Simorgh, A. Marashian, and A. Razminia, *Adaptive PID Control Design for Longitudinal Velocity Control of Autonomous Vehicles*, *Proc. - 2019 6th Int. Conf. Control. Instrum. Autom. ICCIA 2019*, pp. 1–6, 2019.
- [15] V. Robila, L. Paulino, M. Rao, I. Li, M. Zhu, and W. Wang, *Design and Implementation of PID-Based Steering Control for 1/10-Scale*

- Autonomous Vehicle*, 2021 IEEE 12th Annual Ubiquitous Computing, Electronics & Mobile Communication Conference (UEMCON), pp. 0758-0762, 2021.
- [16] M. E. Abed, M. Aly, H. H. Ammar, and R. Shalaby.: *Steering Control for Autonomous Vehicles Using PID Control with Gradient Descent Tuning and Behavioral Cloning*, 2020 2nd (NILES), pp. 583-587, 2020.
- [17] Sharma, A., Kumar, M., Gupta, R.K., Kumar, R.: *Lane Detection using Python* - Anmol Sharma, Maneesh Kumar, Rajesh Kumar – IJIRMP, vol. 9, 2021.
- [18] Sekehravani, E.A., Babulak, E., Masoodi, M.: *Implementing Canny Edge Detection Algorithm for Noisy Image*. Bull. Electr. Eng. Inform, vol. 9, no. 4, pp. 1404–1410, 2020.
- [19] P. Subhasri, S. Santhoshkumar and A. Sumath, *Edge Filtering through Recursive Application using Canny Edge Detector algorithm on small sub-blocks in an Image*, 2020 International Conference on Smart Electronics and Communication (ICOSEC), pp. 563-566, 2020.
- [20] Messom C. H., Sen Gupta G. and Demidenko S.N.: *Hough Transform Run Length Encoding for Real-Time Image Processing*, IEEE Trans. Instrum. Meas., vol. 56, no. 3, pp. 962-967, 2007.

Money Laundering Detection using Machine Learning and Deep Learning

Johrha Alotibi¹, Badriah Almutanni², Tahani Alsubait³, Hosam Alhakami⁴, Abdullah Baz⁵
College of Computers and Information Systems,
Umm Al-Qura University, Makkah, Saudi Arabia^{1,2,3,4,5}

Abstract—In recent years, money laundering activities have shown rapid progress and have indeed become the main concern for governments and financial institutions all over the world. As per recent statistics, \$800 billion to \$2 trillion is the estimated value of money laundered annually, in which \$5 billion of the total is obtained from cryptocurrency money laundering. As per the financial action task force (FATF), the criminals may trade illegally obtained fiat money for the cryptocurrency. Accordingly, detecting and preventing illegal transactions becomes a serious threat to governments and it has been indeed challenging. To combat money laundering, especially in cryptocurrency, effective techniques for detecting suspicious transactions must be developed since the current preventive efforts are outdated. In fact, deep learning and machine learning techniques may provide novel methods to detect suspect currency movements. This study investigates the applicability of deep learning and machine learning techniques for anti-money laundering in cryptocurrency. The techniques employed in this study are Deep Neural Network (DNN), random forest (RF), K-Nearest Neighbors(KNN), and Naive Bayes (NB) with the bitcoin elliptic dataset. It was observed that the DNN and random forest classifier have achieved the highest accuracy rate with promising findings in decreasing the false positives as compared to the other classifiers. In particular, the random forest classifier outperforms DNN and achieves an F1-score of 0.99%.

Keywords—Anti-money laundering; machine learning; supervised learning; cryptocurrency

I. INTRODUCTION

Money laundering is one of the most concerning threats to the stability and progress of the global economy [1]. Such activity is defined as the use of money acquired from illegal activities by hiding the identity of the person and making that money appear legal [2]. Money laundering can also be described as the method of cleaning suspicious money, which represents money collected from illicit or criminal activities, such as illegal gambling, tax evasion, and drug trafficking [3] [4]. Moreover, Integration, layering, and placement are the three primary phases of money laundering. In the placement phase, money is obtained through illicit activities and presented to the system. In the second phase, which is the layers, the source of the funds is hidden through distributing the funds by different intermediaries. In the final phase, the illicit money is transmitted to the criminal [5] [4] [6].

In recent years, money laundering has become more common in news headlines and other forms of media. It has been a fundamentally global problem with social ramifications and economic severe since the mid-1980s [7]. Thus, governments strive to reduce illegal transactions that impact capital [8].

Furthermore, governments around the globe have recommendations and issued regulations for anti-money laundering [3] and are expanding them involving cryptocurrencies [9].

Money laundering has obtained particular attention with the appearance of cryptocurrencies. Bieler illustrates assessed that money laundering earnings are between \$ 800 billion to \$2 trillion worldwide [10]. About \$5 billion of the total is obtained from cryptocurrency money laundering [11].

Because of the anonymity of cryptocurrencies, Campbell-Verduyn [12] discusses that combat money laundering efforts currently require to be improved, because it does not detect money laundering in cryptocurrencies such as Bitcoin, Ethereum, Ripple, and Litecoin. Traditional systems were used by financial institutions specifically on cryptocurrency exchanges, to detect illegal transactions. The results of these traditional systems indicated high low detection rates and high false-positive rates. This means that traditional systems are ineffective at detecting errors and are prone to bias [13]. Traditional systems in financial institutions must be improved and developed in order to detect suspicious transactions [14]. Accordingly, machine learning approaches began being utilized to detect suspicious transactions in 2004 [15]. Thus, studies in recent years have illustrated that the results of using deep learning and machine learning techniques in combating money laundering are indeed promising [16]. Based on machine learning techniques, an anti-money laundering monitoring system is employed at a financial institution in [17] and evaluated using real-life data and feedback from specialized experts. In view of the same, we aim to apply the KNN, NB, RF, and DNN algorithms to the Elliptic Bitcoin dataset to recede the effect of financial crimes on governments and the financial sector. The evaluation models' performance depends on recall, F1-score, and precision, RUC to detect money laundering activities and fraud in cryptocurrency. In addition, it compares the findings with related studies in the same field.

This study is organized as follows. The second section II provides information around the reviews of relevant literature for the study, the reviewed literature covers three major concepts. The third section III presents the research methodology and the deep learning and machine learning techniques used to achieve the results. The fourth section IV presents the details of the data and the preprocessing of the data. The fifth section V presents the final results obtained from the models and compares the previous studies with our results. The final section VI, concludes with a summary of the evaluation of the results obtained and describes the study's limitations and future work.

II. LITERATURE REVIEW

In this section, existing literature related to using of machine learning and deep learning techniques for anti-fraud and money laundering activities in cryptocurrency is reviewed. In fact, cryptocurrencies pose a serious threat to anti-money laundering efforts. In addition, lawbreakers attempt to exploit cryptocurrencies to provide illegal services. As a result, governments such as FATF have developed advanced techniques for anti-money laundering [18]. In view of the same, various techniques and strategies have been widely studied in literature to investigate multiple activities in cryptocurrency data. Essentially, machine learning (ML) and deep learning (DL) are eminent techniques that are capable of investigating vast amounts of data to discover the patterns of illegal financial behavior that have gone undetected [19].

Canhoto [18] and Weber et al. [20], [21] stated that deep learning and machine learning beats the traditional methods of anti-money laundering. Particularly, Weber et al. [21] highlighted the significance of ML regulations and provided the Elliptic dataset for detecting illegal Bitcoin transactions. Different machine learning techniques were used to evaluate the Elliptic dataset, including logistic regression (LR), multilayer perceptrons (MLP), random forest (RF), and graph convolutional networks (GCNs). It was observed that RF technique achieved the high results with a precision, recall-store and F1-score of 0.95, 0.67, and 0.788, respectively. To classify and detect suspicious currency on the Bitcoin network, Lee et al. [22] implemented the artificial neural network (ANN) and RF algorithms. The illegal and legal Bitcoin data were collected from various websites such as Blockchain Explorer and Silk Road. The F1-scores showed that the RF algorithm achieved a high rate of 0.98, while the ANN algorithm achieved a lower rate of 0.89. In the same regard, a novel method for predicting illegal currencies in the Bitcoin currency is proposed by Alarab et al. [23] using a graph convolutional neural network (GCN). The MLP and GCN were combined to enhance the model's performance for which a 0.974 of accuracy was achieved under the proposed method. However, The same author [24] used RF, Extra Trees, Gradient Boosting, XGBoost, LR, and MLP, where RF outperformed with a rate of 0.82. Along similar lines, Ostapowicz and Zbikowski [25] implemented different algorithms on the Ethereum network to identify fraudulent accounts based on supervised learning approach. The accounts were classified and analyzed as "not fraudulen" or "fraudulent" using SVM, XGBoost, and RF. It was observed that the RF algorithm achieved the best results with a detection precision of 85.71. In another study, eight different supervised machine learning techniques were presented and analyzed by Bhowmik et al. [26] to investigate illegal transactions on the blockchain network. These include Naive Bayes (NB), LR, MLP, SVM, RF, Ada Boost, etc. The results of the comparison study found that among the five algorithms, SVM, RF, and NB algorithms obtained the best results with an accuracy of 97%. In view of the same, Monamo et al. [27] also employed an unsupervised learning method based on trimmed k-means and a k-means in order to track down illegal behavior and detect fraudulent activity on the Bitcoin transactions. To classify these transactions, Monamo et al. [28] applied clustering algorithms and machine learning techniques in which several assumptions were imposed to categorize transactions into illegal and legal categories. In addition, different Bitcoin fraud activities were

illustrated from both global and local perspectives by using kd-trees and trimmed k-means. To further investigate these two methods, three classification algorithms were used including the maximum likelihood-based, random forests, and boosted binary regression. Based on the obtained results, it was found that the random forest outperformed the other two classification models. Related to the detection and classification of suspected Bitcoin network addresses, several studies have been reported in literature based on different approaches and techniques [13], [29]–[31]. In fact, the unsupervised models for detecting money laundering activities were found to be inadequate for the Bitcoin network as per Lorenz et al. [13]. Therefore, they have developed supervised learning models to identify illegal money laundering activities in the network. In their study, a rule-based technique was employed that showed low detection rates and high false-positive rates. By Lin et al. [29], suspected Bitcoin network addresses transactions were detected and classified by adding the distribution data of transactions, detailed transaction summaries, and time series as new statistics. The model performance was improved and the variance in data was increased. In this study, various machine learning techniques, including LR, SVM, AdaBoost, XGBoost, and LightGBM were implemented. However, LightGBM achieves the best results as compared to the other techniques. A novel method based on a cascade of classifiers and entity characterization to assail bitcoin anonymity was proposed by Zola et al. [30]. In this study, three different algorithms, including the gradient boosting, random forest, and Adaboost, were used to identify illicit transactions on the Bitcoin blockchain network. The inter-entity transactions (organizations or people with multiple accounts) were also investigated, and the classification performance was improved by utilizing 34 features. Bartoletti et al. [31] used data mining and machine learning-based approaches to detect Ponzi schemes related to the Bitcoin addresses. In their study, three machine learning algorithms were provided for evaluation including the Bayes network, random forest, and RIPPER. As a result, the random forest has been proven to detect 96% of addresses. However, it is worth mentioning that the proposed approach was tested against Ponzi schemes.

Kumar et al. [32] classified a 10000-transaction dataset to identify money laundering activities using Naive Bayes algorithms. The obtained results showed that the proposed model achieved 81% accuracies. In another study, the light gradient boosting machine (LGBM) is proposed by Aziz et al. [33] to detect fraudulent transactions. The MLP, RF, and KNN were compared with the LGBM approach for the identification and classification of fraudulent Ethereum datasets. Relative to the other techniques, the LGBM algorithm has achieved the highest accuracy of 99.03.

Based on the above discussion related to existing literature, it is evident that machine learning algorithms play a vital role in the detection of suspicious transactions in money laundering activities. However, it is worth mentioning that there are still several problems and challenges associated with the detection process that require further improvements. In addition, it seems that there exist very few studies on using deep learning approaches to detect money laundering activities. In view of the same, this paper mainly aims at using deep learning methods with machine learning to detect such suspicious activities in Cryptocurrency.

III. METHODOLOGY

The money laundering transaction detection model includes five main stages i.e. data understanding, data preprocessing, data splitting, model training, model testing, and model evaluation. Fig. 1 illustrates the methodological framework of the study. Several ML and DL algorithms are employed in this chapter for transaction classification e.g. NB, RF Classifier, KNN Classifier, and DNN.

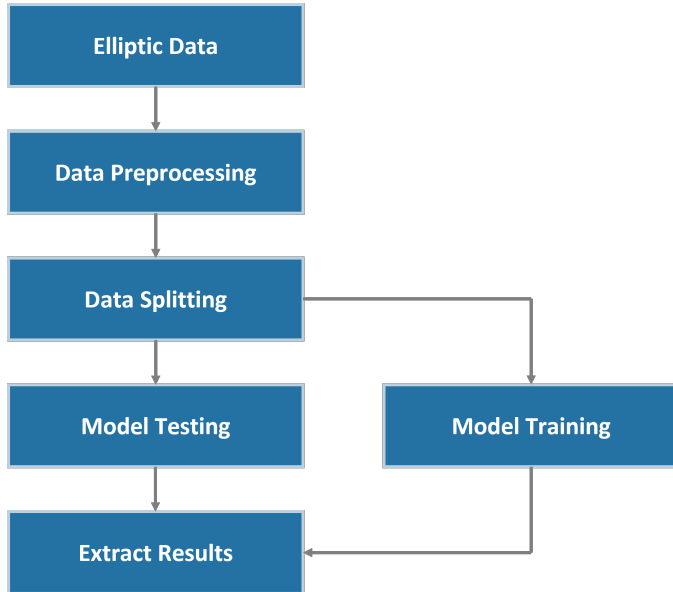


Fig. 1. Methodology.

A. KNN

This approach is considered as a simple instance-based learning algorithm in which the new case/instance is compared with all existing instances and then classified based on a similarity measure. Accordingly, a class is assigned for the new instance based on the nearest available instance. The idea of the instance-based KNN method was first presented by [34]. The measure used is the Minkowski distance.

- Minkowski distance represents the distance between a couple of points in a normalized vector space, and it is defined as following:

$$d(x, y) = \left(\sum_{i=0}^{n-1} |x_i - y_i|^p \right)^{\frac{1}{p}} \quad (1)$$

B. RF

Single trees are highly sensitive to training data and might become unstable in certain cases. To overcome this issue, the ensemble strategy is introduced to determine the class label for each data point by enhancing a collection of aggregating and modeling their predictions. On the other hand, decision trees become very popular in data mining due to their simplicity, flexibility, and interpretability especially in handling various data feature types. A RF is represented by a group of regression or classification trees [35]. These groups perform efficiently in case of individual members are not identical.

C. NB

Gaussian Naive Bayes, which uses the Bayes' theorem, is common to the Naive Bayes (NB) algorithms. The Bayesian theorem represents the possibility that an event will happen if you have prior information about a condition associated with the specified event. The method is intended to deal with continuous attributes that are associated with each category and are distributed using a Gaussian distribution. The main advantage of the Naive Bayes is to effectively train in supervised learning, and are used for practical classification problems. A main disadvantage of the Naive Bayes is that the attributes are presumed to be independent, which is nearly impossible to achieve. With Naive Bayes it is considered that all features are independent given the value of a class, this is indicated as conditional independence. There are two categories in this study, illegal transactions = 0 and legal transactions = 1. The Equation 2 shows the likelihood that sample x belongs to a category c

$$P(c|x) = \frac{p(x|c) * p(c)}{P(x)} \quad (2)$$

D. DNN

DL is a form of ML technique that does not require the construction of feature representation to learn the hierarchical data representation. Instead, it merely uses the training data to automatically learn such representation [36]. This method is based on DNN, which is made up of essential elements including perceptrons, convolutions, and nonlinear activation functions. These elements are structured as layers and trained to understand different complex concepts based on the available raw data. These layers might construct from only a few to over a thousand layers [37]. Lower network layers are typically associated with the low-level features (for example, edges and corners). On the other hand, the higher layers are associated with high-level important features [38].

E. Evaluation Metrics

We use evaluation metrics to evaluate the performance of the model in DL and ML. The evaluation metrics employed for implementing the algorithms are F1-Score, Recall, Precision, and ROC curve. These metrics are commonly applied when dealing with imbalanced datasets, as in the data set used in this study.

Precision refers to the measurement of correct positive predictions in the positive class. The mathematical equation 3 illustrates the concept of precision as follows:

$$Precision = \frac{TruePositive}{TruePositive + FalsePositive} \quad (3)$$

Recall indicates the number of actual positive data the model was able to correctly predict. The mathematical equation 4 illustrates the concept of recall as follows:

$$Recall = \frac{TruePositive}{TruePositive + FalseNegative} \quad (4)$$

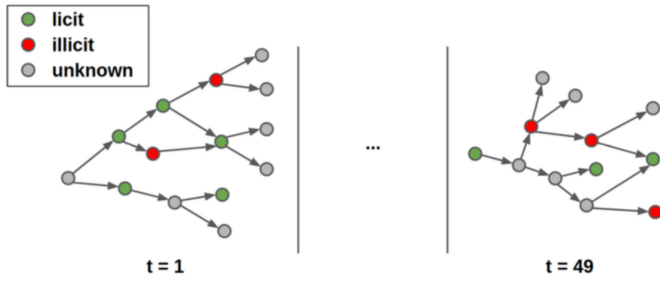


Fig. 2. Structure of the Dataset [39].

F1-score is calculated by the precision and recall value. The mathematical equation 5 illustrates the concept of F1-score as follows:

$$F1 - score = 2 * \frac{Precision * Recall}{Precision + Recall} \quad (5)$$

ROC Curve is a graph that measures the performance of a binary classifier across all classification thresholds. The mathematical equations 6 and 7 illustrates the concept of the ROC curve as follows:

$$FPR = \frac{FP}{FP + TN} \quad (6)$$

$$TPR = \frac{TP}{TP + FN} \quad (7)$$

- where FPR stands for False Positive Rate
- where TRP stands for True Positive Rate

IV. EXPERIMENTS

In this section, a brief overview of the data set used for this study and preprocessing of the data.

A. Dataset

In this study, the Ellipse dataset¹ created by Weber et al. [21] is employed to detect the cryptocurrency activities. Elliptic is a cryptocurrency monitoring company aimed to protect cryptocurrencies from illegal activity, and it has the largest publicly available dataset for transactions in cryptocurrencies. The dataset contains 49 graphs of BTC transactions obtained at different periods of time. Each graph illustrates a directed acyclic graph (DAG), which means that each edge describes a single directional flow, and there are no loops in the graph. The graph begins from a single transaction and expands to include all the following related transactions, containing two weeks of transaction data created during such period as shown in Fig. 2. As shown in Fig. 2, the BTC transactions are represented in the graph network by nodes (with 203,769 nodes). On the other hand, the flow of BTC are represented by edges (with 234,355 edges). The nodes are classified into illegal, legal, and

¹Available At: <https://www.kaggle.com/datasets/ellipticco/elliptic-data-set>

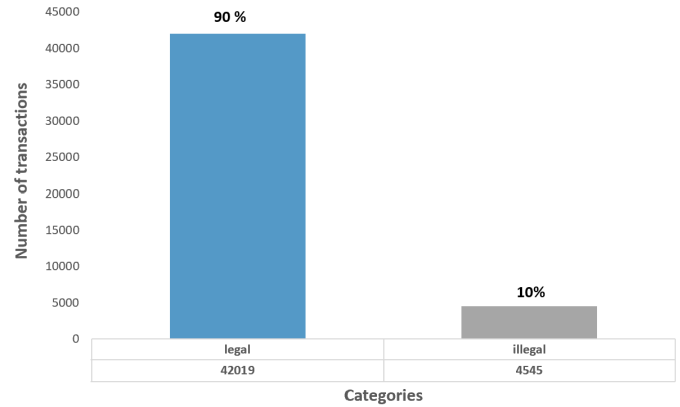


Fig. 3. Distribution of the Transactions.

unknown categories. The unknown labels are not considered in this study due to the following reasons:

- The techniques used in this study are based on supervised learning, which requires the ground truth for each data point. Accordingly, supervised learning cannot be used when transactions have unknown labels.
- The number of unknown labels (with 157205 transactions) requires highly efficient hardware resources to train and test models. Unfortunately, such resources are currently not available for the author.

Fig. 3 illustrates the distribution of the elliptic dataset after removing the unknown transactions.

It can be observed that about 10% of the transactions (4,545 samples) are classified as illegal, while 90% (42,019 samples) are classified as legal transactions. Essentially, the legitimate category contains legitimate services, exchanges, and wallet providers, while the illegal category contains scams, Ponzi schemes, terrorist organizations, ransomware, etc. In fact, there exist 166 features associated with each transaction to specify whether they are legal or illegal. Due to the intellectual property rights, the elliptic company has not revealed the nature of the features.

B. Preprocessing of Data

As the model performance can be affected by irrelevant features, it is indeed necessary to detect and select the important features. Particularly, there are 166 features associated with each transaction in the elliptic dataset. Due to intellectual property rights, the elliptic company has not disclosed the details and nature of the features. The class distribution of the dataset is provided in Table I.

TABLE I. CLASS DISTRIBUTION OF ELLIPTIC DATASET

Label	Number of Samples
Unknown	157,205
legal transactions	42,019
illegal transaction	4,545

It can be observed from Table I that the dataset is unbalanced and contains 157,205 samples with unknown labels.

To handle this issue, these unknown samples are eliminated in the first step of data preprocessing. Accordingly, only the samples with legal label (42,019 samples) and illegal label (4,545 samples) are kept for further steps. Fig. 3 illustrates the distribution of categories after removing the unknown samples. In fact, the dataset contains 166 features which is indeed a large number of features and may consequently lead to overfitting and computational problems. Essentially, the classification techniques require the most relevant features only, which have a high correlation to the class label. In view of the same, a correlation matrix is employed in this study to show the relationship between the features. Accordingly, all features with a correlation greater than 0.90 are eliminated except for the class label. It is worth mentioning that such samples have almost the same effect on the dependent features, and the performance of the model will be significantly affected if no one of them is removed. Based on that, 77 features out of 166 are dropped. However, the number of the remaining features is still large, which is 89 features. Therefore, a preprocessing step has been further implemented to select the most important features based on feature selection techniques through the scikit-learn package. Consequently, the best 53 features have been selected. After choosing the suitable features, we utilize the StandardScaler from scikit-learn for normalizing all features with a standard deviation of 1 and an average value of 0; the purpose is to eliminate bias in classification results.

C. Training and Testing

In this subsection, the model training and testing for transaction classification are discussed. Consequently, the transactions in Elliptic dataset will be classified into legal and illegal transactions. Particularly, the techniques employed in this study are based on supervised learning, which cannot be used when transactions have unknown labels. Therefore, such labels are omitted and not included in the training and testing phases as previously discussed. Essentially, the training set is utilized for model training and hyperparameter tuning. On the other hand, the testing set is utilized to evaluate the performance of the trained model. In the Elliptic dataset, there exist 46,564 transactions which includes both legal and illegal transactions. The dataset was divided into two parts (70% for training and 30% for testing). This is equivalent for 32,594 transactions for training and 13,969 transactions for testing including both legal and illegal transactions. The main purpose here is to check and evaluate how the trained model will perform under new transaction data. In fact, a random seed of 42 was determined for splitting the data, which ensures that the data split does not change each time the program is implemented. The data split task was implemented in python through test-train-split from the sklearn library. It is worth noting that two crucial problem associated with machine learning (ML) methods are consequently eliminated under the utilized approach. The first problem is the under-fitting, which is the inability of a ML model to remember the correlations. The second one is the over-fitting, which occurs when a ML algorithm memorizes the patterns.

D. Choice of Algorithms and Hyperparameters

In existing literature, several ML algorithms are used and employed for transaction classification of the elliptic dataset

[13], [21], [23], [24], in which the RF algorithm was found to achieve promising results. In [32], [33], NB and KNN algorithms were also used to classify the suspicious transactions and achieved satisfactory results although they were implemented on different data. Based on that, NB, RF, and KNN algorithms are selected in this study in order to achieve high results. On the other hand, DNN techniques are also tested and used in the experiments of this work. It is worth mentioning that DNN techniques have not yet explored and applied on the Elliptic dataset in existing literature. Table II summarizes the hyperparameters utilized in the selected algorithms.

TABLE II. SELECTED ALGORITHM AND HYPERPARAMETERS

Algorithm	Hyperparameters	Description
RF	N-estimatorsint(default=100)	Number of trees
	Max-depth (default=None)	Maximum depth of the tree
	Min_samples_split(default=2)	Minimum of samples
KNN	N-neighbors = 3	Number of neighbors
	weights(default=uniform)	Uniform weights
	Algorithm (default=auto)	Calculate the nearest neighbors
NB	Var-smoothing (default=1e-9)	Portion of the largest variance
DNN	Epoch=10	Total number of iterations
	Optimizer=adam	Adam is an optimization algorithm
	Layer=2	Architecture of the model

In fact, different values are selected during the experiments for hyperparameters of the four models. However, the obtained results were generally unsatisfactory. The results are further improved by choosing the values presented in Table II.

E. Experimental Setup

In this work, the experiments are performed on Core(TM) i7-1065G7 CPU @ 1.30GHz 1.50 GHz based processor, windows 11 with 16.0 GB of RAM. Anaconda environment have been downloaded. In addition, Python 3.7.1 is used as it has a large number of models and libraries available for classification. Some examples of the libraries used in this work include pandas, numpy, seaborn, and matplotlib. The implemented metrics and techniques are obtained by scikit-learn. Tensorflow 2.3.1 and Keras version 2.4.3 are also utilized.

V. RESULTS AND DISCUSSION

The study explores how DL and ML can be used for anti-money laundering using cryptocurrency. This is achieved by using different most common algorithms, including DNN, RF, KNN, and NB, to classify the bitcoin elliptic dataset. discusses the findings obtained in terms of F1 score, recall, precision, and ROC curve and compares our results with previous studies.

A. Results

The machine learning technique has outperformed DNN in classifying legal and illegal transactions. The RF has shown its ability to classify well with an F1 score, precision, ROC curve, and recall of 0.99, the reason for the RF achieving a proper value is the ability to handle an unbalanced dataset. The DNN came in second, which performed an F1 score of 0.98, followed by the KNN with an F1 score of 0.97. When it comes to the NB model, the value is low compared to the RF, KNN, and DNN, it achieved 0.90 in ROC curve and 0.99 in precision. However, the F1-score and recall are only 0.74

and 0.59, respectively. Table III illustrates F1 scores, precision, recall, and ROC curve for each model, using a bold font to highlight the highest value. The RF model has the highest overall value, with an F1 score, precision, recall, and ROC curve. The NB model had the lowest value.

TABLE III. COMPARISON OF THE RESULTS OF THE FOUR MODELS

Models	Measures			
	ROC curve	F1-score	Precision	Recall
NB	0.90	0.74	0.99	0.59
RF	0.99	0.99	0.99	0.99
KNN	0.92	0.97	0.97	0.98
DNN	0.97	0.98	0.98	0.98

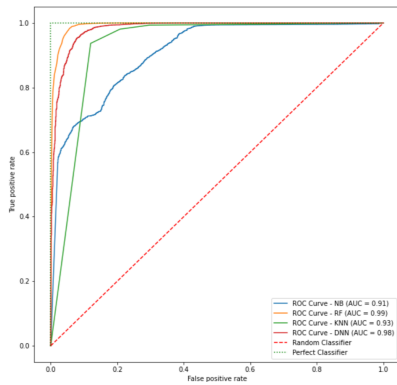


Fig. 4. Comparison of the Results of the Four Models with AUROC Curve

Based on Fig. 4 for the AUROC value for NB, KNN, RF, and DNN, it is shown that the AUC of RF is better than the other three classifiers as it scored in training (1.00) and testing 0.99 while the other models achieved less than 1.00 in training and testing models, but AUROC value in NB model is 0.91, these are the lowest values out of the three models.

B. Discussion and Comparison with Related Works

In comparison to previous studies’ results, some studies used DL and ML for the purpose of detecting money laundering in cryptocurrency. Table IV compares the findings of the four previous studies with F1-scores, in [13] which achieved a high value with an f1-score of 0.83 in the RF model, while [23] achieved a value of 0.77% and in [21] achieved a value of 0.78%. Our model outperforms studies by achieving the highest total F1 score of 0.99, as shown in Table IV.

TABLE IV. COMPARISON WITH RELATED WORKS

Ref.	Method	Dataset	Evaluation
Weber et al. [21]	RF - LR - GCNs - MLP	Elliptic dataset	(RF) F1 score =0.78%
Alarab et al. [23]	GCN		(GCN) F1 score =0.77%
Alarab et al. [24]	RF - ExtraTrees - GB - XGBoost - LR -MLP		(RF) F1 score = 0.82%
Lorenz et al. [13]	RF - XGBoost - LR		(RF) F1 score = 0.83%
Current study	NB-RF -KNN-DNN		(RF) F1 score = 0.99%

VI. CONCLUSION

Money laundering represents a serious threat to governments all over the world and it has been indeed challenging. Various ML and DL techniques have been employed in literature to detect illegal transactions. However, there is still a serious need to further explore and develop suitable algorithms for detecting money-laundering activities, which was the main purpose of the study. Essentially, this research aims to determine the appropriate DL and ML algorithms for detecting money laundering using Elliptic BTC Dataset. To achieve this objective, the results of four algorithms are extensively analyzed and compared. These algorithms include three ML algorithms (RF, KNN, NB), and one DL (DNN). In addition, four key evaluation metrics were used to quantify the performance. These metrics include the precision, recall, F1-score, and ROC curve. the ML technique (RF) proved to be better at classifying fraudulent activities than DL. It was observed from the obtained results that the RF algorithm achieved the best results as compared to other algorithms. It results in 0.99 of the average F1 score. In fact, this technique outperformed the classification due to its ability in handling an unbalanced data set. On the other hand, DNN technique achieved an average F1-score of 0.98 and was placed in the second position followed by the KNN algorithm with an average of 0.97. However, the F1-score for the NB model was found to be 0.74, which is the lowest value as compared to the other three models.

VII. LIMITATIONS AND FUTURE WORK

In fact, the classification model in this study was trained on approximately 46546 bitcoin transactions. However, the dataset contains unlabeled data. To handle this situation, it is more appropriate to use a semi-supervised learning model. However, the unlabeled data will require more CPU power, and therefore, cloud computing services such as Amazon Web Services (AWS) could be used. As the considered model indicates an adequate performance of the algorithms, it would be interesting to conduct the experiment once again with a different data set to prove the validity of the obtained results.

REFERENCES

- [1] U. W. Chohan, “The fatf in the global financial architecture: challenges and implications,” 2019.
- [2] W. Firmansyah and H. T. Atmadja, “Juridical analysis awareness of profession advocacy to financial transaction reports and analysis centre (ppatk) during prevent and eradicate money laundering crime,” *Journal of Multidisciplinary Academic*, vol. 5, no. 4, pp. 308–314, 2021.
- [3] R. Soltani, U. T. Nguyen, Y. Yang, M. Faghani, A. Yagoub, and A. An, “A new algorithm for money laundering detection based on structural similarity,” in *2016 IEEE 7th Annual Ubiquitous Computing, Electronics & Mobile Communication Conference (UEMCON)*. IEEE, 2016, pp. 1–7.
- [4] A. Salehi, M. Ghazanfari, and M. Fathian, “Data mining techniques for anti money laundering,” *International Journal of Applied Engineering Research*, vol. 12, no. 20, pp. 10 084–10 094, 2017.
- [5] C. Alexandre and J. Balsa, “A multiagent based approach to money laundering detection and prevention.” in *ICAART (1)*, 2015, pp. 230–235.
- [6] D. Savage, Q. Wang, X. Zhang, P. Chou, and X. Yu, “Detection of money laundering groups: Supervised learning on small networks,” in *Workshops at the Thirty-First AAAI Conference on artificial intelligence*, 2017.

- [7] G. Sobreira Leite, A. Bessa Albuquerque, and P. Rogerio Pinheiro, "Application of technological solutions in the fight against money laundering—a systematic literature review," *Applied Sciences*, vol. 9, no. 22, p. 4800, 2019.
- [8] S. N. F. S. M. Nazri, S. Zolkafail, and N. Omar, "Mitigating financial leakages through effective money laundering investigation," *Managerial Auditing Journal*, 2019.
- [9] "Financial Crimes Enforcement Network. 2019. Application of FinCEN's Regulations to Certain Business Models Involving Convertible Virtual Currencies — FinCEN.gov, howpublished = <https://www.fincen.gov/resources/statutes-regulations/guidance/application-fincens-regulations-certain-business-models>."
- [10] S. A. Bieler, "Peeking into the house of cards: Money laundering, luxury real estate, and the necessity of data verification for the corporate transparency act's beneficial ownership registry," *Fordham J. Corp. & Fin. L.*, vol. 27, p. 193, 2022.
- [11] S. Butler, "Criminal use of cryptocurrencies: a great new threat or is cash still king?" *Journal of Cyber Policy*, vol. 4, no. 3, pp. 326–345, 2019.
- [12] M. Campbell-Verduyn, "Bitcoin, crypto-coins, and global anti-money laundering governance," *Crime, Law and Social Change*, vol. 69, no. 2, pp. 283–305, 2018.
- [13] J. Lorenz, M. I. Silva, D. Aparício, J. T. Ascensão, and P. Bizarro, "Machine learning methods to detect money laundering in the bitcoin blockchain in the presence of label scarcity," in *Proceedings of the First ACM International Conference on AI in Finance*, 2020, pp. 1–8.
- [14] D. S. Demetis, "Fighting money laundering with technology: A case study of bank x in the uk," *Decision Support Systems*, vol. 105, pp. 96–107, 2018.
- [15] J. McPherson, K.-L. Ma, P. Krystosk, T. Bartoletti, and M. Christensen, "Portvis: a tool for port-based detection of security events," in *Proceedings of the 2004 ACM workshop on Visualization and data mining for computer security*, 2004, pp. 73–81.
- [16] Z. Chen, L. D. Van Khoa, E. N. Teoh, A. Nazir, E. K. Karuppiah, and K. S. Lam, "Machine learning techniques for anti-money laundering (aml) solutions in suspicious transaction detection: a review," *Knowledge and Information Systems*, vol. 57, no. 2, pp. 245–285, 2018.
- [17] P. Tertychnyi, M. Godgildieva, M. Dumas, and M. Ollikainen, "Time-aware and interpretable predictive monitoring system for anti-money laundering," *Machine Learning with Applications*, vol. 8, p. 100306, 2022.
- [18] A. I. Canhoto, "Leveraging machine learning in the global fight against money laundering and terrorism financing: An affordances perspective," *Journal of business research*, vol. 131, pp. 441–452, 2021.
- [19] C. Yan, C. Zhang, Z. Lu, Z. Wang, Y. Liu, and B. Liu, "Blockchain abnormal behavior awareness methods: a survey," *Cybersecurity*, vol. 5, no. 1, pp. 1–27, 2022.
- [20] M. Weber, J. Chen, T. Suzumura, A. Pareja, T. Ma, H. Kanezashi, T. Kaler, C. E. Leiserson, and T. B. Schardl, "Scalable graph learning for anti-money laundering: A first look," *arXiv preprint arXiv:1812.00076*, 2018.
- [21] M. Weber, G. Domeniconi, J. Chen, D. K. I. Weidele, C. Bellei, T. Robinson, and C. E. Leiserson, "Anti-money laundering in bitcoin: Experimenting with graph convolutional networks for financial forensics," *arXiv preprint arXiv:1908.02591*, 2019.
- [22] C. Lee, S. Maharjan, K. Ko, and J. W.-K. Hong, "Toward detecting illegal transactions on bitcoin using machine-learning methods," in *International Conference on Blockchain and Trustworthy Systems*. Springer, 2019, pp. 520–533.
- [23] I. Alarab, S. Prakoonwit, and M. I. Nacer, "Competence of graph convolutional networks for anti-money laundering in bitcoin blockchain," in *Proceedings of the 2020 5th International Conference on Machine Learning Technologies*, 2020, pp. 23–27.
- [24] I. Alarab and S. Prakoonwit, "Effect of data resampling on feature importance in imbalanced blockchain data: Comparison studies of resampling techniques," *Data Science and Management*, 2022.
- [25] M. Ostapowicz and K. Żbikowski, "Detecting fraudulent accounts on blockchain: a supervised approach," in *International Conference on Web Information Systems Engineering*. Springer, 2020, pp. 18–31.
- [26] M. Bhowmik, T. S. S. Chandana, and B. Rudra, "Comparative study of machine learning algorithms for fraud detection in blockchain," in *2021 5th International Conference on Computing Methodologies and Communication (ICCMC)*. IEEE, 2021, pp. 539–541.
- [27] P. Monamo, V. Marivate, and B. Twala, "Unsupervised learning for robust bitcoin fraud detection," in *2016 Information Security for South Africa (ISSA)*. IEEE, 2016, pp. 129–134.
- [28] P. M. Monamo, V. Marivate, and B. Twala, "A multifaceted approach to bitcoin fraud detection: Global and local outliers," in *2016 15th IEEE International Conference on Machine Learning and Applications (ICMLA)*. IEEE, 2016, pp. 188–194.
- [29] Y.-J. Lin, P.-W. Wu, C.-H. Hsu, I.-P. Tu, and S.-w. Liao, "An evaluation of bitcoin address classification based on transaction history summarization," in *2019 IEEE International Conference on Blockchain and Cryptocurrency (ICBC)*. IEEE, 2019, pp. 302–310.
- [30] F. Zola, M. Eguimendia, J. L. Bruse, and R. O. Urrutia, "Cascading machine learning to attack bitcoin anonymity," in *2019 IEEE International Conference on Blockchain (Blockchain)*. IEEE, 2019, pp. 10–17.
- [31] M. Bartoletti, B. Pes, and S. Serusi, "Data mining for detecting bitcoin ponzi schemes," in *2018 Crypto Valley Conference on Blockchain Technology (CVCBT)*. IEEE, 2018, pp. 75–84.
- [32] A. Kumar, S. Das, and V. Tyagi, "Anti money laundering detection using naïve bayes classifier," in *2020 IEEE International Conference on Computing, Power and Communication Technologies (GUCON)*. IEEE, 2020, pp. 568–572.
- [33] R. M. Aziz, M. F. Baluch, S. Patel, and A. H. Ganie, "Lgbm: a machine learning approach for ethereum fraud detection," *International Journal of Information Technology*, pp. 1–11, 2022.
- [34] D. W. Aha, D. Kibler, and M. K. Albert, "Instance-based learning algorithms," *Machine learning*, vol. 6, no. 1, pp. 37–66, 1991.
- [35] L. Breiman, "Random forests," *Machine learning*, vol. 45, no. 1, pp. 5–32, 2001.
- [36] I. Goodfellow, Y. Bengio, and A. Courville, *Deep learning*. MIT press, 2016.
- [37] K. He, X. Zhang, S. Ren, and J. Sun, "Deep residual learning for image recognition," in *Proceedings of the IEEE conference on computer vision and pattern recognition*, 2016, pp. 770–778.
- [38] M. D. Zeiler and R. Fergus, "Visualizing and understanding convolutional networks," in *European conference on computer vision*. Springer, 2014, pp. 818–833.
- [39] Bellei, "The elliptic data set: opening up machine learning on the blockchain." <https://medium.com/elliptic/the-elliptic-data-st-opening-up-machine-learning-on-the-blockchain-e0a343d99a14>. 2010 (accessed Apr 29, 2022).

Multi-Channel Speech Enhancement using a Minimum Variance Distortionless Response Beamformer based on Graph Convolutional Network

Nguyen Huu Binh, Duong Van Hai, Bui Tien Dat, Hoang Ngoc Chau and Nguyen Quoc Cuong*
School of Electrical and Electronic Engineering, Hanoi University of Science and Technology
Hanoi, Vietnam

*Corresponding author

Abstract—The Minimum Variance Distortionless Response (MVDR) beamforming algorithm is frequently utilized to extract speech and noise from noisy signals captured from multiple microphones. A frequency-time mask should be employed to compute the Power Spectral Density (PSD) matrices of the noise and the speech signal of interest to obtain the optimal weights for the beamformer. Deep Neural Networks (DNNs) are widely used for estimating time-frequency masks. This paper adopts a novel method using Graph Convolutional Networks (GCNs) to learn spatial correlations among the different channels. GCNs are integrated into the embedding space of a U-Net architecture to estimate a Complex Ideal Ratio Mask (cIRM). We use the cIRM in an MVDR beamformer to further improve the enhancement system. We simulate room acoustics data to experiment extensively with our approach using different types of the microphone array. Results indicate the superiority of our approach when compared to current state-of-the-art methods. The metrics obtained by the proposed method are significantly improved, except the Scale-Invariant Source-to-Distortion Ratio (SI-SDR) score. The Perceptual Evaluation of Speech Quality (PESQ) score shows a noticeable improvement over the baseline models (i.e., 2.207 vs. 2.104 and 2.076). Our implementation of the proposed method can be found in the following link: <https://github.com/3i-hust-asr/gnn-mvdr-final>.

Keywords—Multi-channel speech enhancement; graph convolutional networks; minimum variance distortionless response beamformer; complex ideal ratio mask

I. INTRODUCTION

Speech enhancement is a subject studied and applied in many applications, e.g., automatic speech recognition, teleconference, or aided hearing [1-4]. There are two algorithm categories of speech enhancement: single-channel algorithms (using a single microphone) [5-8] and multi-channel algorithms (using multi microphones) [9], [10]. The performance of multi-channel algorithms is generally better than that of single-channel algorithms because they use not only statistical information related to signals but also more spatial information [11].

Speech enhancement using microphone array beamforming is a type of multi-channel approach. The basis of these techniques is to enhance signals from desired directions (signals of interest) and attenuate signals from uninterested directions (noise signals). One of the beamforming algorithms used in speech enhancement is the MVDR beamforming [12-14]. There are two conventional approaches to determine MVDR filter weights for noise reduction and/or dereverberation.

The first approach is to estimate the characteristic vector of Acoustic Transfer Functions (ATF) from the speech source to the microphone array based on a priori assumptions such as the position of the desired signal source, the microphone array's configuration, and room acoustics. In a real environment, the performance of this approach is reduced since the effect of multi-paths [15], [16].

The second approach does not involve any such a priori assumptions. Instead of using an ATF vector, a Relative Transfer Function (RTF) vector is estimated based on data collected from the microphone array. The (RTF) vector is defined as the (ATF) vector normalized to a reference microphone of the microphone array. The (RTF) vector estimate is calculated from (PSD) matrices of noise and desired signal. A time-frequency mask is used to estimate the matrices. There are some techniques to create the mask [17], [18].

Recently DNNs have been widely used for speech-related task for better robustness and performance [10], [19-23]. GCNs are considered a generalization of Convolutional Neural Networks (CNNs) [24]. In [23], the GCNs are used to learn spatial features and incorporate them with a U-net to estimate a cIRM. The cIRM is used directly to estimate clean speech based on spectral information obtained from multi-channel. Some experiments in [23] show that speech enhancement using GCNs and U-Net has results that outperform the prior state-of-the-art approach.

This paper adopted the idea of using GCNs and U-Net architecture of [23] for a speech enhancement system with two contributions. Firstly, instead of using the number of nodes of GCNs in [23] as the number of microphones, we increase the node number of GCNs. It helps GCNs learn spatial features more precisely. Therefore a cIRM can be better estimated by incorporating GCNs in the U-Net architecture. Secondly, we use an MVDR beamformer based on the obtained cIRM to estimate the clean speech rather than the attention layer as in [23].

These works are implemented and tested on the dataset provided from ConferencingSpeech2021 Challenge [25]. The results demonstrate that the combination between MVDR beamforming and GCNs improves the performance of the speech enhancement system. The metrics obtained by the proposed method are significantly improved, except for the SI-SDR score. The PESQ score shows a noticeable improvement over the baseline models (i.e., 2.207 vs. 2.104 and 2.076).

The rest of the paper is organized as follows. In Section II, a brief basis of speech enhancement, MVDR beamformer, GCNs, as well as evaluation metrics is described. In Section III, we review some related works. In Section IV, the proposed speech enhancement approach is detailed. In Section V, we explain some experimental setups and analyze the results of the proposed approach. Finally, the conclusions are presented in Section VI.

II. PRELIMINARY

A. Speech Enhancement

The noisy speech signal can be represented in the Short-Time Fourier Transform (STFT) domain:

$$X(t, f) = S(t, f) + N(t, f) \quad (1)$$

where $X(t, f)$ represents the complex-valued time-frequency (t, f) bin of noisy speech, $S(t, f)$ denotes the reverberated signal received at the microphone and $N(t, f)$ indicates the interference noise at time frame t and frequency bin f with $t = 0, \dots, T-1$ and $f = 0, \dots, F-1$. T and F are the number of frames and frequency bins, respectively. The neural beamformer here focuses on the task of suppressing noise. The objective is to remove the interference noise $N(t, f)$ and retrieve the speech signal $S(t, f)$.

Deep learning-based speech enhancement approaches are usually designed in a supervised manner. Based on how to obtain the target, the applied techniques can be classified into *mapping-based* or *masking-based* methods. In *mapping-based* approaches, the goal is to approximate a non-linear function from the noisy speech into the desired speech through a learning process. Meanwhile, the most popular methods recently used are *masking-based*, where the target is masks computed between desired and noisy speech.

The masking-based approaches try to approximate a non-linear function from an observed noisy speech spectrum $X(t, f)$ to a Time-Frequency ($T - F$) mask $M(t, f)$ through the learning/training process. The commonly used masks in recent researches include: binary-based mask [17] and ratio-based mask [18].

The binary-based mask usually indicates the Ideal Binary Mask (IBM). Each entry of the $T - F$ mask is set to 1 when the local Signal-to-Noise Ratio (SNR) is greater than a pre-defined threshold value R (indicates that speech is dominated over noise), or 0 if otherwise (indicates that noise is dominated over speech). In particular,

$$M_{\text{IBM}}(t, f) = \begin{cases} 1, & \text{if } \text{SNR}(t, f) > R. \\ 0, & \text{otherwise.} \end{cases} \quad (2)$$

here $\text{SNR}(t, f)$ indicates the SNR at the frame index t and the frequency bin f within the $T - F$ mask.

Typical ratio-based mask commonly refers to Ideal Ratio Mask (IRM), where each entry of the $T - F$ mask is set by the soft ratio of the reverberated speech over the observed noisy signal, that is:

$$M_{\text{IRM}}(t, f) = \frac{|S(t, f)|^\alpha}{|S(t, f)|^\alpha + |N(t, f)|^\alpha} \quad (3)$$

here $|S(t, f)|$ indicates the magnitudes of reverberated speech, $|N(t, f)|$ denotes the noise in the $T - F$ domain, and α is a factor over the magnitudes, which is to scale the value of each entry of the mask or change the dynamic ranges of the features. From Eq. 2 and 3, we could deduce that IRM-based methods could provide an enhanced signal with less distortion, while it may possibly lead to much computation [26].

Williamson et al. [27] further improved this approach, called cIRM. The complex ratio mask (CRM), demonstrated to be more effective than the ideal ratio mask (IRM) [28-30]. Given the complex spectrum of noisy speech, $X(t, f)$, we get the spectrum of reverberated speech, $S(t, f)$, that is:

$$S(t, f) = X(t, f) \odot M_{\text{cIRM}}(t, f) \quad (4)$$

where \odot is the element-wise multiplication. Note that, $X(t, f)$, $S(t, f)$ and $M_{\text{cIRM}}(t, f)$ are complex-valued matrices.

Given the observed input noisy signals $X(t, f)$ from the $T - F$ domain and the target mask $M(t, f)$, the deep neural networks are optimized by the Mask Approximation (MA) objective function, which minimizes the Mean Squared Error (MSE) loss between the estimated and the target mask. On the other hand, recently, more approaches have been starting to employ Signal Approximation (SA) objective functions [31-33]. This objective aims to minimize the MSE loss between the estimated and the target reverberated speech spectrum. Besides, another approach minimizes MSE between the estimated reverberated signal and the target one in the time-domain by additionally applying inverse STFT. Furthermore, the conclusions in [31], [34] show that mixing the objectives (i.e., MA and SA) could lead to further improvement in both the magnitude and the spectral domains.

B. MVDR Beamformer

The separated speech can be obtained as

$$\hat{S}_{\text{MVDR}}(t, f) = \mathbf{h}^{\text{H}}(f)X(t, f) \quad (5)$$

here $\mathbf{h}(f) \in \mathbb{C}^M$ denotes the weights of MVDR beamformer at frequency index f , M denotes the number of channels and $(\cdot)^{\text{H}}$ indicates Hermitian operation. The main target of the MVDR beamformer is to suppress the interference noise while keeping the desired signal undistorted as much as possible, that is:

$$\begin{aligned} \mathbf{h}(f) &= \underset{\mathbf{h}}{\text{argmin}} \mathbf{h}^{\text{H}}(f)\Phi_N(f)\mathbf{h}(f) \\ \text{s.t. } &\mathbf{h}^{\text{H}}(f)\mathbf{v}(f) = 1 \end{aligned} \quad (6)$$

Here $\Phi_N(f)$ is the PSD matrix of the noise, and $\mathbf{v}(f) \in \mathbb{C}^M$ represents the steering vector to the target source.

Different approaches could be adopted to find the optimal weights of the MVDR beamformer. To reduce the computation in the beamforming block, we employ the MVDR solution of Souden et al. [12]:

$$\mathbf{h} = \frac{(\Phi_N(f))^{-1}\Phi_S(f)}{\text{trace}((\Phi_N(f))^{-1}\Phi_S(f))} \mathbf{u} \quad (7)$$

where $\Phi_S(f) \in \mathbb{C}^{M \times M}$ is the PSD matrix of speech, $\Phi_N(f) \in \mathbb{C}^{M \times M}$ indicates the PSD matrix for noise. $\mathbf{u} \in \mathbb{R}^M$ is a one-hot vector representing a reference microphone.

Two masks, $M_S(t, f)$ and $M_N(t, f)$, will be used to estimate the desired PSD matrices:

$$\Phi_S(f) = \sum_{t=1}^T (X(t, f) \odot M_S(t, f))(X(t, f) \odot M_S(t, f))^H \quad (8)$$

$$\Phi_N(f) = \sum_{t=1}^T (X(t, f) \odot M_N(t, f))(X(t, f) \odot M_N(t, f))^H \quad (9)$$

where \odot is the element-wise multiplication.

C. Evaluation Metrics

The standard metric to measure the performance of Automatic Speech Recognition (ASR) systems is Word Error Rate (WER). However, other objective metrics are also employed to evaluate the performance of the front-end techniques, such as denoising. The typical metrics include Short-Time Objective Intelligibility (STOI) [35], Extended Short-Time Objective Intelligibility (ESTOI) [36], SI-SDR [37], and PESQ [38]. It is worth looking at [39] for more detailed definitions and explanations of the objective metrics.

D. Graph Neural Networks

1) *Definition:* Graph Neural Network (GNN) [24] is a new type of deep neural network designed to work with graph data. Graphs provide a much more flexible way to process and aggregate information. GNN allows for generalizing DNN operations to graph-structured processing [40], [41]. By aggregating information from neighboring nodes, GNN models encode structural-relational information into the representation, which then is applied in a wide range of tasks, including biochemical structure discovery [42], [43], computer vision [44], and recommendation systems [45].

A specific variance of GNN is the convolutional GNN (so-called GCN) which is similar to CNN [46] with the basis of shared weights through training. There are two approaches for building GCN, Spectral GCN and Spatial GCN [47-49]. Spectral GCN, infrequently used nowadays, is based on the Eigen-decomposition of graph Laplacian. Spatial GCN defines convolution operations that work directly on a graph through the nodes and edges and aggregate spatial information between neighboring nodes and edges. Therefore, Spatial GCN is less computational and complex and can generalize better than spectral GCN. Recently, new convolutional GNN structures [47] have drastically leveraged the performance of GNN by employing various techniques, including normalization [46], attention [50], and activation [51].

2) *Graph Convolutional Network:* Given a graph $\mathcal{G} = (\mathcal{V}, \mathcal{E})$, where \mathcal{V} represents the set of nodes v_i of the graph and \mathcal{E} represents the edges of the graph between two nodes (v_i, v_j) . The GCN applies non-linear transformation on the input $\mathcal{X} \in \mathbb{R}^{|\mathcal{V}| \times N}$, where $|\mathcal{V}|$ is the number of nodes and N is node feature size. In particular, GCN can be mathematically represented as follows:

$$\mathcal{H}^{(l)} = g(\mathcal{D}^{-1/2} \mathcal{A} \mathcal{D}^{-1/2} \mathcal{H}^{(l-1)} \mathcal{W}^{(l-1)}) \quad (10)$$

where $\mathcal{D} \in \mathbb{R}^{|\mathcal{V}| \times |\mathcal{V}|}$ is the diagonal matrix, $\mathcal{A} \in \mathbb{R}^{|\mathcal{V}| \times |\mathcal{V}|}$ is the adjacency matrix, $\mathcal{H}^{(l)} \in \mathbb{R}^{|\mathcal{V}| \times K}$ is the l^{th} GCN layer with K hidden features, $\mathcal{H}^{(0)} = \mathcal{X}$, $\mathcal{W}^{(l-1)}$ is the trainable parameters at the $l-1^{th}$ layer, and g is a non-linear activation function.

III. RELATED WORK

A. LSTM-Based Speech Enhancement

For the recognition of sequence-based data, context information is essential. Certain straightforward approaches for processing context-dependent data have been adopted, such as concatenating several consecutive features to construct long-context input features [52]. Moreover, Recurrent Neural Networks (RNNs), especially the Long Short-Term Memories (LSTMs), have been experimented with to be able to capture the information of the long sequence [53-56].

ConferencingSpeech 2021 Challenge¹ [25] adopted LSTM to suppress noise in distorted input signal. In particular, the multi-channel noisy speech is converted into frequency-domain by STFT transformation.

The STFT features were stacked with ‘‘cosIPD’’ features [57], a smoother version of Inter-channel Phase Difference (IPD), to obtain the input features, and then used to train the model. A 3-layer real-valued LSTM is used to capture the temporal information of input features. The output of the LSTM model is treated as the cIRM then a real-valued fully connection layer is added to map the output into real and imaginary components of the mask, respectively.

The cIRM mask was multiplied with the first microphone channel of STFT features of noisy speech to filter out the noise. The model was trained with SA objective functions, minimizing MSE between the estimated reverberant signal and the target signal in time-domain. Code and samples can be found in this repository².

B. GCN-Based Speech Enhancement

Recently proposed solutions are introduced to tackle the problem of speech enhancement by employing DNN models with spatial post-filtering techniques such as the filter-and-sum beamformer [23], [58-60]. Tzirakis et al. [23] proposed a novel approach by treating each audio channel (microphone) as a node of a graph structure.

The well-known U-Net architecture was incorporated to learn representations for the inputs, especially in speech improvement problems [61], [62]. GCN was used in the embedding space of a U-Net architecture to learn spatial correlations between the different nodes (or channels/microphones).

This approach utilizes both real and imaginary parts of the complex features in the STFT domain. Complex spectrograms from each channel are fed into the encoder part of the architecture. The higher level features obtained after the Encoder part are used to construct the multi-channel GCN. After that, the Decoder produces the estimated cIRM for a reference microphone with the same dimension as the input. Finally, cIRM for noisy STFT features is computed, which is used to estimate the desired clean speech.

¹<https://tea-lab.qq.com/conferencingspeech-2021/>

²<https://github.com/ConferencingSpeech/ConferencingSpeech2021>

IV. PROPOSED MULTI-CHANNEL PROCESSING METHOD

A. Proposed System

This paper proposes a novel pipeline for multi-channel speech enhancement tasks by incorporating GNN with a neural MVDR beamformer. GNN is successfully applied in a wide range of tasks with structural data, including computer vision [44] and speech processing [23]. At the same time, MVDR demonstrates its superior performance over the Filter-and-Sum technique [63]. However, to the best of our knowledge, no prior work focuses on integrating both these techniques to tackle the speech enhancement problem.

The overall proposed model is schematically depicted as Fig. 1. The whole pipeline consists of three main processes:

- 1) Signal transformation includes signal conversion from the time domain to the STFT domain (STFT block) and signal inversion from the STFT domain back to the time domain (iSTFT block);
- 2) Mask estimation for both clean speech and noise (Mask Estimator block);
- 3) Applying MVDR for noise suppression (MVDR block). However, only the parameters in the Mask Estimator block are trainable (details illustrated in Algorithm 1).

The two signal transformation blocks are trivial, while the mask estimation and the MVDR blocks are more advanced and described below.

1) *Mask Estimator Block*: Firstly, we employ the well-known U-Net architecture for mask estimation blocks. The u-Net model has been shown very successfully in many computer vision tasks and used in some recent approaches in speech processing [64]. In addition, U-Net architecture comprises an encoder/decoder part with an embedding layer. The encoder/decoder parts in U-Net are set to be cascaded CNN layers, while the GCN is used as a core embedding layer. We adopt this idea from the currently published approach of [23].

Secondly, our proposed U-Net model is unique and different from [23] because we use other graph construction methods for the embedding layer. In [23], the input channels, denotes as M , is preserved as GCN nodes, so that, GCN has only M nodes ($M = \{2, 4\}$ as reported in [23]). With such a few nodes, we realize that GCN's ability to capture spatial information is restricted.

From that deduction, we propose a novel graph construction method such that GCN's nodes are now set equal to the number of channels (kernels) of the last CNN layer in the encoder part of U-Net. In detail, suppose that the STFT features with the shape of $(M \times T \times 2F)$ dimensional feeds to the encoder. The latter then represents with the dimension of $(H \times T' \times F')$, where H is the number of kernels of the last CNN layer in the encoder, while T' , F' are the reduced size of T and F after all layers of CNN in the encoder, respectively. As a result, the number of nodes in GCN is H , allowing us to choose an appropriate number of nodes during the training process. For more detail about the graph construction process, see Section IV-C.

Finally, outputs of the mask estimation process are two masks for clean speech and noise, denote as $mask_speech$ and $mask_noise$ in Fig. 1, respectively.

2) *MVDR Beamformer*: We utilize a neural MVDR beamformer as posterior filtering to leverage the enhancement performance. The MVDR uses these aforementioned estimated masks from the previous step to compute beamforming weights on-the-fly. The detailed computation is introduced in section II-B. The process of MVDR beamformer is integrated with mask estimation and trained as a unified model so that, making the enhancement system more robust.

B. System Procedure

The overall procedure of this approach in Fig. 1 is shown in Algorithm 1.

First, the multi-channel speech signals are transformed into the time-frequency domain with STFT transformation. The components of the complex STFT features are stacked together to create a new feature with a two-channel of size $(T \times F \times 2)$, where T denotes the number of frames, and F indicates the number of frequency bins, in total.

Considering M channels, the input features will have the shape of $(M \times 2 \times T \times F)$ dimensional, in which each entry is a real value. After that, these STFT input features are fed to the Encoder of Mask Estimator, which produces more complex and high-level representations. The feature is reshaped into $(M \times T \times 2F)$ dimensional to fit the requirement of our proposed method. The Encoder then produces representations with the dimension of $(H \times T' \times F')$, where H is a number of filters of the last CNN layer in the encoder. At the same time, T' and F' are the reduced size of T and F after the entire layers of CNN in the encoder, respectively. Next, the GCN is used as a core embedding layer between the encoder and decoder parts. The representations produced from the Encoder are utilized in constructing a graph with H nodes, which captures the spatial information by aggregating the information of its nodes and edges. The GCN construction process is described in detail in Section IV-C.

The output of GCN layers is forwarded through the decoder part, which converts the hidden features to the original dimension. The decoder outputs could be treated as two cIRM masks for clean and noisy speech, then used to compute the PSD matrices and MVDR weights. Estimated STFT features of reverberant speech \hat{S} are computed by applying MVDR processing as in Section II-B. Finally, the inverse STFT transformation is applied to obtain the estimated reverberant speech in the time domain.

C. Graph Construction

We adopt a recently published approach that captures multi-channel signal information with graph structure [23]. The graph structure is first constructed using the hidden feature representations obtained after the Encoder. We construct an undirected graph, $\mathcal{G} = (\mathcal{V}, \mathcal{E})$, where \mathcal{V} represents the set of nodes v_i of the graph. For example, with hidden features of shape $(H \times T' \times F')$ from the previous step, a graph with H nodes with a feature size is $N = T'F'$ will be constructed by flattening function. \mathcal{E} represents the edges of the graph

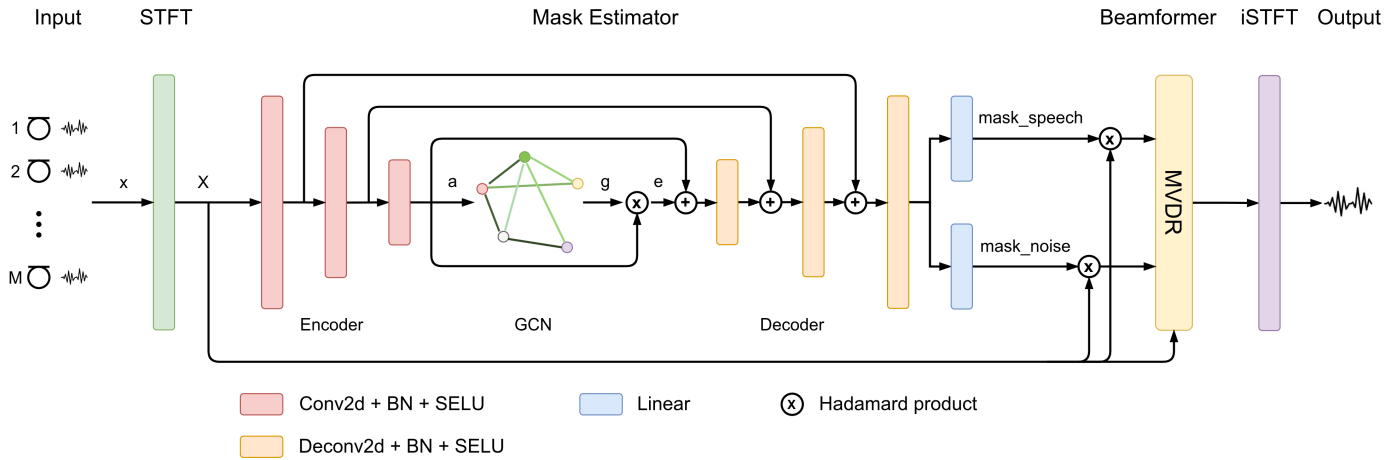


Fig. 1. Proposed MVDR System using GNN-Based U-Net Architecture as mask Estimator. The Estimated Masks are then used to Compute the Beamformer Weights and Applied to a Noisy Signal to Provide the Enhanced Signal.

between two nodes (v_i, v_j) . Then, an adjacency matrix of the graph, $\mathcal{A} \in \mathbb{R}^{H \times H}$, is computed.

We also employ a learnable adjacency matrix, where each entry of \mathcal{A} is treated as a weighted obtaining from edge $(v_i, v_j) \in \mathcal{E}$. Intuitively, each entry represents a similarity between two nodes in the graph. In our approach, the learnable weights, $w_{ij}, \{i, j \in \mathcal{V}\}$, of the adjacency matrix \mathcal{A} are optimized during the training process. For two nodes v_i and v_j , their representations will be concatenated, $\mathbf{f}_{v_i}, \mathbf{f}_{v_j} \in \mathbb{R}^N$ as $[\mathbf{f}_{v_i} \parallel \mathbf{f}_{v_j}]$ and then passed through a non-linear layer $F([\mathbf{f}_{v_i} \parallel \mathbf{f}_{v_j}])$. The node degree matrix \mathcal{D} is a diagonal matrix, where $\mathcal{D}_{ii} = \sum_j \mathcal{A}_{ij}$.

The graph constructed \mathcal{G} provides an efficient way to capture the structured information from its nodes (e.g., microphones). We use the GCN to produce high-level abstraction for the hidden node representations by learning aggregated features for each node w.r.t its neighbors. The mathematical detail of the GCN layer can be seen in Section II-D2.

D. Loss Functions

In the training process of the proposed network, we adopt loss computations in different forms. We use a loss function with magnitude features and raw signals in the time domain. More specifically, these losses are:

$$\mathcal{L}_{mag} = \left\| |\hat{S}| - |S| \right\|_1 \quad (11)$$

$$\mathcal{L}_{raw} = \left\| \hat{s} - s \right\|_1 \quad (12)$$

$$\mathcal{L} = \mathcal{L}_{mag} + \mathcal{L}_{raw} \quad (13)$$

where $\|\cdot\|_1$ indicates the L1 norm, $|S|$ indicates the magnitude spectrogram of the complex spectrogram S , s indicates reverberant signal, and $\hat{\cdot}$ sign indicates the corresponding predicted entities.

V. EXPERIMENTAL EVALUATION

A. Dataset

With some missing information about the dataset configurations and the authors did not publish the implementation of their proposed model in [23], we decided to utilize the dataset provided from ConferencingSpeech 2021 Challenge [25]. The simulation set was provided for all participants to develop the enhancement systems and estimate the objective scores. To focus on the development of algorithms, the authors designed the challenge with the *close* training condition. In other words, only the provided list of open-source clean speech and noise datasets could be used in the training process.

1) *Training Set*: Clean training speech set signals are chosen from three open source speech databases: AISHELL-1³ [65], AISHELL-3⁴ [66], and Librispeech [67]. The speech utterances with SNR higher than 15 dB are selected for training. The total duration of the clean training example is around 550 hours. The noise set is selected from MUSAN [68] and AudioSet [69]. The total duration is around 120 hours.

The imaging method is used to simulate Room Impulse Response (RIR) for three types of microphone arrays: (i) a linear microphone array with uniformly distributed 8 microphones, (ii) a circular microphone array, and (iii) a linear microphone array with non-uniformly distributed 8 microphones. The room size ranged from $3 \times 3 \times 3 \text{ m}^3$ to $8 \times 8 \times 3 \text{ m}^3$, and provided RIR set contains more than 2500 rooms.

The microphone array is randomly placed in the room with a height ranging from 1.0 to 1.5 m. The sound source, including speech and noise, comes from any possible position in the room with a height ranging from 1.2 to 1.9 m. The angle between two sources is wider than 20° . The distance between the source and microphone array are ranged from 0.5 to 5.0 m. The total number of RIR is more than 10000 for each microphone array. The simulated SNR ranges from 0 to 30 dB, and the duration of each clip is 6 seconds.

³<https://www.openslr.org/33/>

⁴<http://www.openslr.org/93/>

Algorithm 1 Summary the Process of the Proposed Model for Multi-Channel Speech Enhancement

Require: M -channel noisy speech $x \in \mathbb{R}^{M \times L}$ in time domain; reference microphone vector \mathbf{u} .

Ensure: Enhanced speech $\hat{s} \in \mathbb{R}^L$ in time domain.

```

1:  $X = STFT(x)$  ▷  $X \in \mathbb{R}^{M \times 2 \times T \times F}$ 
2:  $X = reshape(X, [M, T, 2 * F])$  ▷  $X \in \mathbb{R}^{M \times T \times 2F}$ 
3:  $skips = []$ 
4:  $a = copy(X)$  ▷  $a \in \mathbb{R}^{M \times T \times 2F}$ 
5: for  $enc\_layer$  in  $Encoder$  do ▷ UNet Encoder
6:    $a = enc\_layer(a)$ 
7:    $skips.append(a)$ 
8: end for
9:  $\mathcal{A} = construct\_adj(a)$  ▷  $a \in \mathbb{R}^{H \times T' \times F'}$ ,  $\mathcal{A} \in \mathbb{R}^{H \times H}$ , see Section IV-C
10:  $g = GCN(\mathcal{A}, a)$  ▷  $g \in \mathbb{R}^{H \times T' \times F'}$ , Applying GCN, see Equation 10
11:  $e = a \otimes g$  ▷  $e \in \mathbb{R}^{H \times T' \times F'}$ ,  $\otimes$  Hadamard product
12: for  $dec\_layer$  in  $Decoder$  do ▷ UNet Decoder
13:    $skip = skips.pop(-1)$ 
14:    $e = e + skip$ 
15:    $e = dec\_layer(e)$ 
16: end for
17:  $mask\_speech = linear\_speech(e)$  ▷  $e \in \mathbb{R}^{M \times T \times 2F}$ ,  $mask\_speech \in \mathbb{R}^{M \times T \times 2F}$ 
18:  $mask\_noise = linear\_noise(e)$  ▷  $e \in \mathbb{R}^{M \times T \times 2F}$ ,  $mask\_noise \in \mathbb{R}^{M \times T \times 2F}$ 
19:  $\Phi_S = get\_psd\_matrix(mask\_speech, X)$  ▷  $\Phi_S \in \mathbb{C}^{F \times M \times M}$ , see Equation 8
20:  $\Phi_N = get\_psd\_matrix(mask\_noise, X)$  ▷  $\Phi_N \in \mathbb{C}^{F \times M \times M}$ , see Equation 9
21:  $\mathbf{h} = get\_mvdr\_weights(\Phi_S, \Phi_N, \mathbf{u})$  ▷  $\mathbf{h} \in \mathbb{C}^{F \times M}$ , see Equations 7
22:  $\hat{S} = \mathbf{h}^H X$  ▷  $\hat{S} \in \mathbb{R}^{T \times F \times 2}$ , Applying MVDR, see Equation 5
23:  $\hat{s} = iSTFT(\hat{S})$  ▷ Enhanced speech  $\hat{s} \in \mathbb{R}^L$ 

```

2) *Development Set*: The development set is categorized into three parts: Simulation clips, Semi-real recordings, and Real recordings. In this experiment, we only experiment with simulated audio with a single microphone array scenario (there also exists another task using multiple microphone arrays). 1588 clips are simulated for three types of the microphone array. 1624 clean speech selected from AISHELL-1, AISHELL-3, and 800 noise clips selected from MUSAN are used to simulate these sets. The simulated SNR ranges from 0 to 30 dB, and the duration of clips is 6 seconds.

B. Experimental Setup

For a convenient comparison with other approaches, we set up the training configurations as follows. The AdamW [70] optimization algorithm is adopted to optimize the proposed models with a fixed learning rate of 10^{-4} and a mini-batch of size 16. The number of microphones in the experiments is set to $M = 8$. The complex features are the STFT computed with a window of length 1024, the window's type is set to Hanning, and an overlap size of 512.

Our proposed model (MVDR-GCN) uses the optimized configuration. Each block in the Encoder (Decoder) part of U-net architecture comprises one CNN layer, followed by batch normalization and a SELU activation function. Each Encoder block's kernels of CNN layers are set to $\{64, 128, 128, 128, 32\}$, respectively. The blocks in the Decoder have the same configurations as the Encoder but in reverse order. All the kernel sizes of CNN layers are 3×3 , and the stride is 2×2 , with no padding.

For the embedding layer of U-Net, GCN, a bottle-neck layer is used with the hidden size of 64, then two GCN layers are integrated with hidden units as same as the dimension of the bottle-neck layer. In order to generate two masks for speech and noise, after the Decoder part, two Linear layers are added with an input size equal to the hidden size of the last CNN layer in the Decoder, while the output size is set to the same as feature size of STFT features.

The LSTM-based baseline model (Section III-A) is set up as same as the model in [25]. The model is composed of three layers of RNN with 512 hidden units. The input features are

TABLE I. DETAILED ENHANCEMENT RESULTS OF BASELINES AND OUR PROPOSED SYSTEM ON THE DEVELOPMENT SIMULATION SET

MA	Model	PESQ	STOI	E-STOI	SI-SDR
Linear	Noisy	1.551	0.807	0.716	4.673
	Baseline (LSTM)	2.091	0.867	0.779	13.065
	Baseline (GNN)	2.088	0.853	0.772	12.001
	Proposed System (MVDR-GCN)	2.101	0.861	0.773	10.996
Circular	Noisy	1.558	0.807	0.716	4.633
	Baseline (LSTM)	2.129	0.872	0.782	13.118
	Baseline (GNN)	2.077	0.852	0.771	12.007
	Proposed System (MVDR-GCN)	2.260	0.886	0.804	12.270
Non-uniform	Noisy	1.543	0.804	0.712	4.536
	Baseline (LSTM)	2.091	0.867	0.777	13.042
	Baseline (GNN)	2.061	0.851	0.768	11.769
	Proposed System (MVDR-GCN)	2.261	0.889	0.806	12.333

TABLE II. OVERALL RESULT OF BASELINES AND OUR PROPOSED SYSTEM ON THE DEVELOPMENT SIMULATION SET

Model	PESQ	STOI	E-STOI	SI-SDR
Noisy	1.551	0.806	0.715	4.614
Baseline (LSTM)	2.104	0.869	0.758	13.075
Baseline (GNN)	2.076	0.852	0.770	11.926
Proposed System (MVDR-GCN)	2.207	0.879	0.794	11.866

STFT stacking up with cosine of IPD features.

The GNN-based baseline model (Section III-B) has the same configurations as our proposed system, which includes input STFT features and parameters of layers in Encoder/Decoder blocks, except that number of kernels in each CNN layer, are slightly different from our proposed model ($\{64, 128, 256, 128, 32\}$). Note that this is the optimized configuration in [23].

Finally, a noisy scenario is obtained by directly computing the metrics with noisy data, simulated with SNR ranging from 0 to 10, and scaling from 0.2 to 0.9.

C. Enhancement Results and Evaluation

Our proposed approach's results are compared with Tzirakis et al. [23], a novel GCN-based multi-channel enhancement model. The detailed enhancement results are presented in Table I.

For overall comparison, the result of scenarios is averaged and reported as in Table II. Combining the MVDR algorithm showed an improvement in scores. The metrics obtained by the MVDR method are significantly improved, as expected, except for the SI-SDR score. The PESQ score achieved by the MVDR system shows a noticeable improvement over the baseline or GCN-based model (i.e., PESQ 2.207 vs. 2.104 and 2.076).

However, in the linear array scenario, our proposed system obtains worse scores than others, except for the PESQ metric, because of the distribution of the microphone in arrays. In circular and non-uniform scenarios, the position of microphones is various to capture more spatial information. The masks are more accurately estimated, and the model can achieve decent overall metrics. Conversely, the microphones are placed equidistant for the linear array, the information may be symmetric, and the mask estimator model may receive less information than others and get worse scores.

VI. CONCLUSION

In this approach, we propose a new method of using a graph neural network to exploit the spatial correlations among the different channels in the speech enhancement task. We use the U-Net architecture with the encoder, which tries to produce higher-level representations for each channel. After that, the GCN is constructed using these hidden features. GCN is used to learn spatial features by propagating and aggregating information in the graph. Then the features are fed to the decoder to reconstruct into the original forms of each channel. By integrating the GCN-based U-Net into the MVDR system, the experimental results validate our approach's effectiveness when compared with recent state-of-the-art approaches.

ACKNOWLEDGMENT

This research is funded by the Hanoi University of Science and Technology under grant number T2021-PC-003.

REFERENCES

- [1] M. R. Bai, J.-G. Ih, and J. Benesty, *Acoustic array systems: theory, implementation, and application*. John Wiley & Sons, 2013.
- [2] K. Tan, X. Zhang, and D. Wang, "Real-time speech enhancement using an efficient convolutional recurrent network for dual-microphone mobile phones in close-talk scenarios," in *ICASSP 2019-2019 IEEE International Conference on Acoustics, Speech and Signal Processing (ICASSP)*. IEEE, 2019, pp. 5751–5755.
- [3] S. A. Nossier, M. Rizk, N. D. Moussa, and S. el Shehaby, "Enhanced smart hearing aid using deep neural networks," *Alexandria Engineering Journal*, vol. 58, no. 2, pp. 539–550, 2019.
- [4] C. R. Kumar and M. P. Chitra, "Implementation of modified wiener filtering in frequency domain in speech enhancement," *International Journal of Advanced Computer Science and Applications*, vol. 13, no. 2, 2022. [Online]. Available: <http://dx.doi.org/10.14569/IJACSA.2022.0130251>
- [5] Y. Li and S. Kang, "Deep neural network-based linear predictive parameter estimations for speech enhancement," *IET Signal Processing*, vol. 11, no. 4, pp. 469–476, 2017.
- [6] B. M. Mahmmod, S. H. Abdulhussian, S. A. R. Al-Haddad, W. A. Jassim *et al.*, "Low-distortion mmse speech enhancement estimator based on laplacian prior," *IEEE Access*, vol. 5, pp. 9866–9881, 2017.
- [7] B. M. Mahmmod, T. Baker, F. Al-Obeidat, S. H. Abdulhussain, W. A. Jassim *et al.*, "Speech enhancement algorithm based on super-gaussian modeling and orthogonal polynomials," *IEEE Access*, vol. 7, pp. 103 485–103 504, 2019.
- [8] N. Jamal, N. Fuad, and M. Shaabani, "A hybrid approach for single channel speech enhancement using deep neural network and harmonic regeneration noise reduction," *International Journal of Advanced Computer Science and Applications*, vol. 11, no. 10, 2020. [Online]. Available: <http://dx.doi.org/10.14569/IJACSA.2020.0111033>
- [9] J. Benesty, J. Chen, and Y. Huang, *Microphone array signal processing*. Springer Science & Business Media, 2008, vol. 1.
- [10] S. Chakrabarty and E. A. Habets, "Time-frequency masking based online multi-channel speech enhancement with convolutional recurrent neural networks," *IEEE Journal of Selected Topics in Signal Processing*, vol. 13, no. 4, pp. 787–799, 2019.
- [11] S. Gannot, E. Vincent, S. Markovich-Golan, and A. Ozerov, "A consolidated perspective on multimicrophone speech enhancement and source separation," *IEEE/ACM Transactions on Audio, Speech, and Language Processing*, vol. 25, no. 4, pp. 692–730, 2017.
- [12] M. Souden, J. Benesty, and S. Affes, "On optimal frequency-domain multichannel linear filtering for noise reduction," *IEEE Transactions on audio, speech, and language processing*, vol. 18, no. 2, pp. 260–276, 2009.
- [13] R. Ali, T. Van Waterschoot, and M. Moonen, "Integration of a priori and estimated constraints into an mvdr beamformer for speech enhancement," *IEEE/ACM Transactions on Audio, Speech, and Language Processing*, vol. 27, no. 12, pp. 2288–2300, 2019.
- [14] J. Malek, Z. Koldovský, and M. Bohac, "Block-online multi-channel speech enhancement using deep neural network-supported relative transfer function estimates," *IET Signal Processing*, vol. 14, no. 3, pp. 124–133, 2020.
- [15] J. Benesty, M. M. Sondhi, Y. Huang *et al.*, *Springer handbook of speech processing*. Springer, 2008, vol. 1.
- [16] L. Pfeifenberger, M. Zöhrer, and F. Pernkopf, "Eigenvector-based speech mask estimation for multi-channel speech enhancement," *IEEE/ACM Transactions on Audio, Speech, and Language Processing*, vol. 27, no. 12, pp. 2162–2172, 2019.
- [17] D. Wang, "On ideal binary mask as the computational goal of auditory scene analysis," in *Speech separation by humans and machines*. Springer, 2005, pp. 181–197.
- [18] S. Srinivasan, N. Roman, and D. Wang, "Binary and ratio time-frequency masks for robust speech recognition," *Speech Communication*, vol. 48, no. 11, pp. 1486–1501, 2006.
- [19] A. A. Alnuaim, M. Zakariah, A. Alhadlaq, C. Shashidhar, W. A. Hatamleh, H. Tarazi, P. K. Shukla, and R. Ratna, "Human-computer interaction with detection of speaker emotions using convolution neural networks," *Computational Intelligence and Neuroscience*, vol. 2022, 2022. [Online]. Available: <https://doi.org/10.1155/2022/6005446>
- [20] D. Wang and J. Chen, "Supervised speech separation based on deep learning: An overview," *IEEE/ACM Transactions on Audio, Speech, and Language Processing*, vol. 26, no. 10, pp. 1702–1726, 2018.
- [21] T. Higuchi, K. Kinoshita, N. Ito, S. Karita, and T. Nakatani, "Frame-by-frame closed-form update for mask-based adaptive mvdr beamforming," in *2018 IEEE International Conference on Acoustics, Speech and Signal Processing (ICASSP)*. IEEE, 2018, pp. 531–535.
- [22] B. Tolooshams, R. Giri, A. H. Song, U. Isik, and A. Krishnaswamy, "Channel-attention dense u-net for multichannel speech enhancement," in *ICASSP 2020-2020 IEEE International Conference on Acoustics, Speech and Signal Processing (ICASSP)*. IEEE, 2020, pp. 836–840.
- [23] P. Tzirakis, A. Kumar, and J. Donley, "Multi-channel speech enhancement using graph neural networks," in *ICASSP 2021-2021 IEEE International Conference on Acoustics, Speech and Signal Processing (ICASSP)*. IEEE, 2021, pp. 3415–3419.
- [24] M. M. Bronstein, J. Bruna, Y. LeCun, A. Szlam, and P. Vandergheynst, "Geometric deep learning: going beyond euclidean data," *IEEE Signal Processing Magazine*, vol. 34, no. 4, pp. 18–42, 2017.
- [25] W. Rao, Y. Fu, Y. Hu, X. Xu, Y. Jv, J. Han, Z. Jiang, L. Xie, Y. Wang, S. Watanabe *et al.*, "Interspeech 2021 conferencingspeech challenge: Towards far-field multi-channel speech enhancement for video conferencing," *arXiv preprint arXiv:2104.00960*, 2021.
- [26] E. M. Grais, G. Roma, A. J. Simpson, and M. Plumbley, "Combining mask estimates for single channel audio source separation using deep neural networks," *Interspeech2016 Proceedings*, 2016.
- [27] D. S. Williamson and D. Wang, "Time-frequency masking in the complex domain for speech dereverberation and denoising," *IEEE/ACM transactions on audio, speech, and language processing*, vol. 25, no. 7, pp. 1492–1501, 2017.
- [28] Y. Xu, C. Weng, L. Hui, J. Liu, M. Yu, D. Su, and D. Yu, "Joint Training of Complex Ratio Mask Based Beamformer and Acoustic Model for Noise Robust Asr," in *ICASSP 2019 - 2019 IEEE International Conference on Acoustics, Speech and Signal Processing (ICASSP)*, May 2019, pp. 6745–6749, iSSN: 2379-190X.
- [29] D. S. Williamson, Y. Wang, and D. Wang, "Complex Ratio Masking for Monaural Speech Separation," *IEEE/ACM Transactions on Audio, Speech, and Language Processing*, vol. 24, no. 3, pp. 483–492, Mar. 2016, conference Name: IEEE/ACM Transactions on Audio, Speech, and Language Processing.
- [30] D. S. Williamson and D. Wang, "Time-Frequency Masking in the Complex Domain for Speech Dereverberation and Denoising," *IEEE/ACM Transactions on Audio, Speech, and Language Processing*, vol. 25, no. 7, pp. 1492–1501, Jul. 2017, conference Name: IEEE/ACM Transactions on Audio, Speech, and Language Processing.
- [31] F. Weninger, J. R. Hershey, J. Le Roux, and B. Schuller, "Discriminatively trained recurrent neural networks for single-channel speech separation," in *2014 IEEE Global Conference on Signal and Information Processing (GlobalSIP)*. IEEE, 2014, pp. 577–581.
- [32] P.-S. Huang, M. Kim, M. Hasegawa-Johnson, and P. Smaragdis, "Deep learning for monaural speech separation," in *2014 IEEE International Conference on Acoustics, Speech and Signal Processing (ICASSP)*. IEEE, 2014, pp. 1562–1566.
- [33] P.-S. Huang, M. Kim, M. Hasegawa-Johnson, and P. Smaragdis, "Joint optimization of masks and deep recurrent neural networks for monaural source separation," *IEEE/ACM Transactions on Audio, Speech, and Language Processing*, vol. 23, no. 12, pp. 2136–2147, 2015.
- [34] Y. Wang and D. Wang, "A deep neural network for time-domain signal reconstruction," in *2015 IEEE International Conference on Acoustics, Speech and Signal Processing (ICASSP)*. IEEE, 2015, pp. 4390–4394.
- [35] S. R. Quackenbush, T. P. Barnwell, and M. A. Clements, *Objective measures of speech quality*. Prentice-Hall, 1988.
- [36] C. H. Taal, R. C. Hendriks, R. Heusdens, and J. Jensen, "An algorithm

- for intelligibility prediction of time–frequency weighted noisy speech,” *IEEE Transactions on Audio, Speech, and Language Processing*, vol. 19, no. 7, pp. 2125–2136, 2011.
- [37] E. Vincent, R. Gribonval, and C. Févotte, “Performance measurement in blind audio source separation,” *IEEE transactions on audio, speech, and language processing*, vol. 14, no. 4, pp. 1462–1469, 2006.
- [38] A. W. Rix, J. G. Beerends, M. P. Hollier, and A. P. Hekstra, “Perceptual evaluation of speech quality (pesq)-a new method for speech quality assessment of telephone networks and codecs,” in *2001 IEEE international conference on acoustics, speech, and signal processing. Proceedings (Cat. No. 01CH37221)*, vol. 2. IEEE, 2001, pp. 749–752.
- [39] Y. Hu and P. C. Loizou, “Evaluation of objective quality measures for speech enhancement,” *IEEE Transactions on audio, speech, and language processing*, vol. 16, no. 1, pp. 229–238, 2007.
- [40] M. Zhang, Z. Cui, M. Neumann, and Y. Chen, “An end-to-end deep learning architecture for graph classification,” in *Thirty-Second AAAI Conference on Artificial Intelligence*, 2018.
- [41] Z. Zhang, P. Cui, and W. Zhu, “Deep learning on graphs: A survey,” *IEEE Transactions on Knowledge and Data Engineering*, 2020.
- [42] J. Gilmer, S. S. Schoenholz, P. F. Riley, O. Vinyals, and G. E. Dahl, “Neural message passing for quantum chemistry,” in *International conference on machine learning*. PMLR, 2017, pp. 1263–1272.
- [43] F. Wan, L. Hong, A. Xiao, T. Jiang, and J. Zeng, “Neodti: neural integration of neighbor information from a heterogeneous network for discovering new drug–target interactions,” *Bioinformatics*, vol. 35, no. 1, pp. 104–111, 2019.
- [44] M. Kampffmeyer, Y. Chen, X. Liang, H. Wang, Y. Zhang, and E. P. Xing, “Rethinking knowledge graph propagation for zero-shot learning,” in *Proceedings of the IEEE/CVF Conference on Computer Vision and Pattern Recognition*, 2019, pp. 11 487–11 496.
- [45] R. Ying, R. He, K. Chen, P. Eksombatchai, W. L. Hamilton, and J. Leskovec, “Graph convolutional neural networks for web-scale recommender systems,” in *Proceedings of the 24th ACM SIGKDD International Conference on Knowledge Discovery & Data Mining*, 2018, pp. 974–983.
- [46] T. N. Kipf and M. Welling, “Semi-supervised classification with graph convolutional networks,” *arXiv preprint arXiv:1609.02907*, 2016.
- [47] Z. Wu, S. Pan, F. Chen, G. Long, C. Zhang, and S. Y. Philip, “A comprehensive survey on graph neural networks,” *IEEE transactions on neural networks and learning systems*, vol. 32, no. 1, pp. 4–24, 2020.
- [48] M. Balcilar, G. Renton, P. Héroux, B. Gauzere, S. Adam, and P. Honeine, “Bridging the gap between spectral and spatial domains in graph neural networks,” *arXiv preprint arXiv:2003.11702*, 2020.
- [49] A. Senthilkumar, M. Gupte, and S. S, “Dynamic spatial-temporal graph model for disease prediction,” *International Journal of Advanced Computer Science and Applications*, vol. 13, no. 6, 2022. [Online]. Available: <http://dx.doi.org/10.14569/IJACSA.2022.01306112>
- [50] P. Veličković, G. Cucurull, A. Casanova, A. Romero, P. Lio, and Y. Bengio, “Graph attention networks,” *arXiv preprint arXiv:1710.10903*, 2017.
- [51] F. Wu, A. Souza, T. Zhang, C. Fifty, T. Yu, and K. Weinberger, “Simplifying graph convolutional networks,” in *International conference on machine learning*. PMLR, 2019, pp. 6861–6871.
- [52] Y. Xu, J. Du, L.-R. Dai, and C.-H. Lee, “An experimental study on speech enhancement based on deep neural networks,” *IEEE Signal processing letters*, vol. 21, no. 1, pp. 65–68, 2013.
- [53] M. Wöllmer, B. Schuller, F. Eyben, and G. Rigoll, “Combining long short-term memory and dynamic bayesian networks for incremental emotion-sensitive artificial listening,” *IEEE Journal of selected topics in signal processing*, vol. 4, no. 5, pp. 867–881, 2010.
- [54] A. Graves, “Generating sequences with recurrent neural networks,” *arXiv preprint arXiv:1308.0850*, 2013.
- [55] S. Gupta, R. S. Shukla, R. K. Shukla, and R. Verma, “Deep learning bidirectional lstm based detection of prolongation and repetition in stuttered speech using weighted mfcc,” *International Journal of Advanced Computer Science and Applications*, vol. 11, no. 9, 2020. [Online]. Available: <http://dx.doi.org/10.14569/IJACSA.2020.0110941>
- [56] M. A. A. Al-Rababah, A. Al-Marghilani, and A. A. Hamarshi, “Automatic detection technique for speech recognition based on neural networks inter-disciplinary,” *International Journal of Advanced Computer Science and Applications*, vol. 9, no. 3, 2018. [Online]. Available: <http://dx.doi.org/10.14569/IJACSA.2018.090326>
- [57] C. Deng, H. Song, Y. Zhang, Y. Sha, and X. Li, “Dnn-based mask estimation integrating spectral and spatial features for robust beamforming,” in *ICASSP 2020-2020 IEEE International Conference on Acoustics, Speech and Signal Processing (ICASSP)*. IEEE, 2020, pp. 4647–4651.
- [58] X. Xiao, S. Zhao, D. L. Jones, E. S. Chng, and H. Li, “On time-frequency mask estimation for MVDR beamforming with application in robust speech recognition,” in *2017 IEEE International Conference on Acoustics, Speech and Signal Processing (ICASSP)*, Mar. 2017, pp. 3246–3250, iSSN: 2379-190X.
- [59] T. Nakatani, N. Ito, T. Higuchi, S. Araki, and K. Kinoshita, “Integrating DNN-based and spatial clustering-based mask estimation for robust MVDR beamforming,” in *2017 IEEE International Conference on Acoustics, Speech and Signal Processing (ICASSP)*, Mar. 2017, pp. 286–290, iSSN: 2379-190X.
- [60] T. Higuchi, N. Ito, T. Yoshioka, and T. Nakatani, “Robust MVDR beamforming using time-frequency masks for online/offline ASR in noise,” in *2016 IEEE International Conference on Acoustics, Speech and Signal Processing (ICASSP)*, Mar. 2016, pp. 5210–5214, iSSN: 2379-190X.
- [61] R. Giri, U. Isik, and A. Krishnaswamy, “Attention Wave-U-Net for Speech Enhancement,” in *2019 IEEE Workshop on Applications of Signal Processing to Audio and Acoustics (WASPAA)*, Oct. 2019, pp. 249–253, iSSN: 1947-1629.
- [62] C. Macartney and T. Weyde, “Improved Speech Enhancement with the Wave-U-Net,” Nov. 2018, arXiv:1811.11307.
- [63] T. Ochiai, S. Watanabe, T. Hori, J. R. Hershey, and X. Xiao, “Unified architecture for multichannel end-to-end speech recognition with neural beamforming,” *IEEE Journal of Selected Topics in Signal Processing*, vol. 11, no. 8, pp. 1274–1288, 2017.
- [64] A. Defossez, G. Synnaeve, and Y. Adi, “Real time speech enhancement in the waveform domain,” *arXiv preprint arXiv:2006.12847*, 2020.
- [65] H. Bu, J. Du, X. Na, B. Wu, and H. Zheng, “Aishell-1: An open-source mandarin speech corpus and a speech recognition baseline,” in *2017 20th Conference of the Oriental Chapter of the International Coordinating Committee on Speech Databases and Speech I/O Systems and Assessment (O-COCOSDA)*. IEEE, 2017, pp. 1–5.
- [66] Y. Shi, H. Bu, X. Xu, S. Zhang, and M. Li, “Aishell-3: A multi-speaker mandarin tts corpus and the baselines,” *arXiv preprint arXiv:2010.11567*, 2020.
- [67] V. Panayotov, G. Chen, D. Povey, and S. Khudanpur, “Librispeech: an asr corpus based on public domain audio books,” in *2015 IEEE international conference on acoustics, speech and signal processing (ICASSP)*. IEEE, 2015, pp. 5206–5210.
- [68] D. Snyder, G. Chen, and D. Povey, “Musan: A music, speech, and noise corpus,” *arXiv preprint arXiv:1510.08484*, 2015.
- [69] J. F. Gemmeke, D. P. Ellis, D. Freedman, A. Jansen, W. Lawrence, R. C. Moore, M. Plakal, and M. Ritter, “Audio set: An ontology and human-labeled dataset for audio events,” in *2017 IEEE International Conference on Acoustics, Speech and Signal Processing (ICASSP)*. IEEE, 2017, pp. 776–780.
- [70] I. Loshchilov and F. Hutter, “Decoupled weight decay regularization,” *arXiv preprint arXiv:1711.05101*, 2017.

Impact of Input Data Structure on Convolutional Neural Network Energy Prediction Model

Imen Toumia

National School of Computer Sciences
University of Manouba
Manouba, Tunisia

Ahlem Ben Hassine

College of Computer Science and Engineering
University of Jeddah
Jeddah, Saudi Arabia

Abstract—Energy demand continues to increase with no prospect of slowing down in the future. This increase is caused by several sociological and economical factors such as population growth, urbanization and technological developments. In view of this growth, it becomes crucial to predict energy consumption for a more accurate management and optimization. Nevertheless, consumption estimation is a complex task due to consumer behaviour fluctuation and weather alterations. Several efforts were proposed in the literature. Almost, all of them focused on improving the prediction model to increase the accuracy of the results. They use the LSTM (*Long-Short Term Memory*) model to reflect the temporal dependencies between historical data despite its spatial and temporal complexities. The main contribution in this paper is a novel and simple Convolutional Neural Network energy prediction model based on input data structure enhancement. The main idea is to adjust the structure of the input data instead of using a more complicated deep learning model for better performance. The proposed model was implemented, tested using real data and compared to existing ones. The obtained results showed that the proposed data structure has a great influence on the model performance measurement.

Keywords—Deep learning; convolutional neural network; energy consumption; energy prediction

I. INTRODUCTION

The demand for energy increases with population size and economic growth and also depends on the consumers' behavior and their deployed appliances. Faced with this growth, consumption prediction is a crucial task that enables efficient and optimized energy management. Several techniques have been developed to predict demand for the next hours, days, weeks, months and even years. Most of them are based on historical data [1] and use Machine Learning or Deep learning models such as Artificial Neural Networks (ANN) [2], Support Vector Machine (SVM) [3], Convolutional Neural Network with Long- Short Term Memory (CNN-LSTM) [4], etc.

Deep Learning (DL) is an advanced Machine Learning approach that has been widely applied in many fields and has shown great performance for many problems such as image processing [5], [6], computer vision [7], [8], natural language processing [9], [10] and time series prediction [11], [12]. Also, the DL approaches have provided good accuracy for energy systems such as solar irradiance forecasting [13], [14] and wind speed prediction [15], [16]. Recently, DL approaches have been widely applied to predict the quantity of energy to be consumed. In most of the time, the consumed energy data are presented in time series. Energy consumption forecasting is

therefore a multivariate time series forecasting problem. LSTM is a Recurrent Neural Network (RNN) specification that is characterized by the capacity to control the flow of separate information [17] and mainly to detect temporal dependencies between data [18]. These advantages make LSTM effective for short-term or near-real-time forecasting. Consequently LSTM has been widely used for energy consumption prediction.

All these efforts focused on enhancing the ML/DL existing models for a better accuracy regardless of the complexity of the resulting one. However none of them dealt with adjusting the input data to attain same and even better performance. The main contribution of this paper is to propose a new DL based model that shows the impact of the input data structure on the prediction results.

The remaining of the paper is structured as follows: the next section describes the various existing researches that deal with energy consumption prediction using CNN and LSTM. Section III defines the CNN model and explains the proposed one. Section IV discusses the experimental evaluation and the conclusion is presented in Section V.

II. RELATED WORKS

During the last two decades, several researchers have contributed to the solving of energy consumption prediction problems, resulting in a wide range of studies. These studies can be divided into two categories: those that use static methods, while others apply physical methods. Among static methods, Machine Learning techniques have been widely applied for predicting energy consumption. In [19], authors applied to the Support Vector Machine (SVM) while in [20], authors proposed Artificial Neural Networks (ANN) based solutions. ANN based models were also applied to different datasets in order to analyze them and select the relevant ones. However, recent trends are oriented towards applying Deep Learning models as Recurrent Neural Network (RNN), Convolutional Neural Network (CNN), LSTM, etc.

In [21], the authors presented two approaches based on LSTM for energy load prevention, and tested them on both data steps of one hour and one minute. The first approach uses the standard LSTM while the second one uses the Sequence to Sequence architecture. In [22], the authors applied CNN to predict the energy load per hour within a smart grid. Their aim is to demonstrate the effectiveness of their proposed CNN compared to other convolutional models. Another CNN model for energy load prediction was discussed in [23]. The authors

proposed the use of a set of historical input loads on which they applied convolutions. The obtained results were passed to a fully connected layer that produced the final output. Experimental tests showed that the results of their proposed model are similar to ANN, but outperforms those of Support Vector Regression model. As for [24], the objective was to solve the problem of load profile uncertainty for predicting household energy consumption. To do this, the authors proposed a model based on RNN where they grouped the load profiles in an input pool. The results showed that this model performs better than the classical RNN, Support Vector Regression and Auto Regressive Integrated Moving Average in terms of RMSE. The authors of [25] provided a Recurrent Inception Convolution Neural Network RICNN to solve the problems of existing RNN methods for daily energy load prediction. The proposed model combines RNN and one-dimensional CNN (1-D CNN). The obtained results proved the efficiency of the proposed model compared to benchmarked multi-layer perceptron, RNN and 1-D CNN.

In the context of a short-term prediction for residential energy consumption, an LSTM model has been proposed in [26]. This model is called Quantile LSTM (Q-LSTM) whose objective is to predict the probabilistic residential load with LSTM in quantile term. The results showed the efficiency of the proposed method compared to traditional ones in terms of averaging quantile score. As for the prediction of future energy demand, the authors in [27] defined and tested two types of approaches, the first one based on CNN and the second one based on neural networks and two optimization algorithms, the Genetic Algorithm (NNGA) and the Particle Swarm Optimization algorithm (NNPSO). The authors in [28] proposed a model based on feed forward back propagation neural network named FFBPNN. The proposed model involves four layers which are data collection layer, preprocessing layer, prediction layer and evaluation layer. The last layer provides the performance measures MAE, MAPE and RMSE. In 2021, in [29], authors presented a multi-seasonal short-term memory network LSTM-MSNet for time series forecasting with multiple seasonal models. The evaluation of the LSTM-MSNet model shows that this model has the best execution time and accuracy compared to existing ones. A new hybrid model for energy consumption prediction named DB-NET was presented in [30]. The proposed model combines the dilated CNN (DCNN) and bidirectional LSTM (BiLSTM). Experimental tests proved the efficiency of the DB-Net model.

In [4], the authors proposed a CNN-LSTM model combining both CNN and LSTM. This model extracts (1) spatial features using the CNN layer which allows feature extraction between multiple variables and (2) temporal features using LSTM which models irregular temporal information. Although this latter yielded to a good prediction performance, an improved EECP-CBL version has been presented in [31]. The experimental results of EECP-CBL proved that it is more efficient in predicting energy consumption than the CNN-LSTM model and other existing ones. The authors of [32] presented a new hybrid M-BDLSTM method combining CNN with the multi-layer bidirectional long-term memory method. Recently, in 2021, the authors of [33] proposed a meta-heuristic based on LSTM and Butterfly Optimization Algorithm (BOA) for the prediction of energy consumption. Butterfly Optimization Algorithm was used to discover the dynamic time series. This

model showed a lower error rate on the IHEPC dataset [34] compared to existing one. In 2022, [35] they proposed a hybrid model combining CNN and echo state network allowing both power generation and consumption forecasting. In this model, CNN performed the extraction of features from historical data while the echo state network ensured the learning of temporal features. The experimental results of this model on the IHEPC dataset showed a good performance in terms of RMSE, MSE, NRMSE, and MAE.

All these efforts contributed to improve the efficiency of energy prediction models. Their main goal focus on updating and enhancing previous ML/DL models for a better performance. They proceeded by combining several Machine Learning and Deep Learning techniques or/and adding optimization algorithms to increase the results accuracy. Nevertheless and despite the effectiveness of these models, we believe that it is possible to improve the prediction performance by using a less complex Convolutional model and different input data structures. The idea is to focus on finding the optimal data structure for the input data that may improve the results of prediction without resorting to sophisticated, complex and time/space consuming ML/DL models.

III. PROPOSED CNN MODEL

An accurate prediction model for energy consumption is essential to simulate an energy management system between consumers and suppliers in order to optimize the energy use and to minimize its waste. However, the estimation process is a complex task due to the influence of several environmental factors and to the users' behavior.

Traditional network-based techniques are the main models to predict future energy consumption [36]. These models are based on the short-term memory for considering dependencies between the input data. Other models involve the LSTM network for integrating historical context. Nonetheless, these solutions would increase the time and space complexities of the estimation process.

In this article, we focused on simplifying the temporal and spatial complexity of existing models. Therefore, the principal contribution of our research is to reflect temporal dependencies between historical data without using the LSTM model. For this purpose, we tried to turn our investigation towards the input data rather than the deployed models. Hence, we thought of *i*) adjusting the input structure representation to emerge the time-series relationship between the historical data, *ii*) applying a simple CNN-based model to predict the future energy consumption with higher accuracy. We choose the CNN model presented in [37] and [38] for its promising results in both electricity consumption prediction [37] and load forecasting [38].

A. Input Data Proposed Structures

Since the meteorological seasons divide the year into four periods (Spring, Summer, Autumn and Winter) more or less equal, their duration varies from 89 to 93 days. Hence the energy consumption varies according to the weather characteristics of each season; For example in summer the temperature is high and therefore the need to use air conditioners increases. In addition, the climate of one season has a great impact on

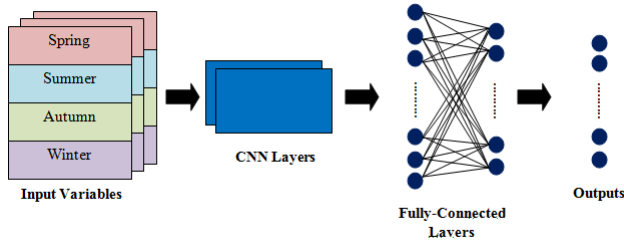


Fig. 1. Overview Architecture of Proposed Model using the Serial Matrix.

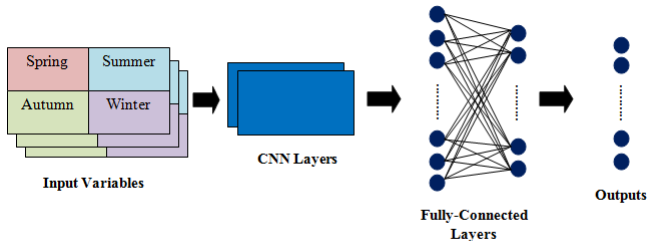


Fig. 2. Overview Architecture of Proposed Model using the Cycle Matrix.

the climate of the following ones. Generally, a too cold winter is usually followed by a too hot summer.

All existing researches manipulates the historical information of the energy consumption in a sequential form. No physical link between same season of different years, despite their intrinsic logical one. Most efforts rely on the LSTM model to take into consideration the logical relationships among consumption data. Our idea is to find a simpler way to reflect the logical link between the same season through several years. Therefore, we thought about improving the structure input data instead of investigating on the underlying prediction model. So the main idea of this paper is to present the data in a 3-dimensional matrix to be able to (1) maintain the different states of the same season over several years and (2) model the temporal dependencies between the different seasons.

In this paper, we will employ two different data structures for the input data. For the first data structure, we will use a matrix that indicates the four seasons of a year in a series manner. In this case the height of this matrix is the number of days in a year, its width is the number of features and its depth represents the number of years in the dataset. Fig. 1 shows the overall architecture of the proposed model using the first matrix form.

For the second proposed data structure, the data are organized in a cycle, i.e. in the same row we include the data of two consecutive seasons (Spring and Summer followed by Autumn and Winter). In this matrix the number of rows is half the number of days in a year, the width is twice the number of variables and the depth is the number of years in the dataset. The architecture of the model using this matrix is given by the Fig. 2.

The input of our model is the 3-D matrix on which two CNN layers are applied to extract the input variables which

are transmitted to the two fully connected layers to generate the prediction of future energy consumption.

B. CNN-based Model

In our model we used convolutional 3D Layers, Pooling 3D Layers and fully connected Layers. In detail, we used two convolutional layers with a filter number equal to 64 and a kernel size (3,3,2). These two layers are followed by two max-pooling layers with a kernel size of (3,2,1). The max-pooling layer allows reducing the network computational cost as it selects only the most important features. Then flatten layer is applied to flatten the feature vector. Finally, two fully connected layers are used to adjust the result by providing the estimated energy consumption. The architecture and configuration of the proposed model are detailed in Table I.

TABLE I. ARCHITECTURE OF THE PROPOSED MODEL

Layer Type	Kernel size	Filter size	Parameters
Convolution3D	(3,3,2)	64	832
MaxPooling3D	-	-	0
Convolution3D	(3,2,1)	64	24640
MaxPooling3D	-	-	256
Flatten	-	-	0
Fully connected(128)	-	-	221312
Dropout	-	-	0
Fully connected(364)	-	-	45440

IV. EXPERIMENTAL EVALUATION

In this section, first, we will describe the used dataset. Then, we will exhibit the obtained experimental results expressed in terms of performance measures, including MSE (Mean square error), RMSE (Root MSE), MAE (Mean Absolute error), MAPE (Mean Absolute Percentage Error) and the CPU time (training and testing times). Finally, we will compare the obtained results with existing energy prediction models in the literature.

A. Dataset Description

To evaluate the proposed model and compare its performance with the models described in [4] and [31], we have applied our model to the same dataset used by aforementioned ones. The IHEPC dataset [34] available at UCI (University of California, Irvine) Machine Learning Repository. The data of this dataset are collected from a house located in Sceaux in France over five years from December 2006 to November 2010. This set contains 2,075,259 measurements with 25979 missing values equivalent to 1.25% of the total amount of data. The missing data have been processed in the pre-processing phase.

IHEPC contains nine variables e.i., day, month, year, hour, minute, global active power, global reactive power, voltage and global intensity. In addition to three variables collected from the energy consumption sensors which are sub metering 1, sub metering 2 and sub metering 3. Table II presents all these variables and their meanings as defined in the literature [39].

TABLE II. THE FEATURES OF THE IHEPC DATASET

Variable	Description
Day	A value from 1 to 31
Month	A value from 1 to 12
Year	A value from 2006 to 2010
Hour	A value from 0 to 23
Minute	A value from 1 to 60
Global active power	The household global minute-averaged active power (in kilowatt)
Global reactive power	The household global minute-averaged reactive power(in kilowatt)
Voltage	The minute-averaged voltage (in Volt)
Global intensity	The household global minute-averaged current intensity (in Ampere)
Sub metering 1	This variable corresponds to the kitchen, containing mainly a dishwasher, an oven and a microwave, hot plates being not electric, but gas powered (in watt-hour of active energy)
Sub metering 2	This variable corresponds to the laundry room, containing a washing machine, a tumble-drier, a refrigerator and a light (in watt-hour of active energy)
Sub metering 3	This variable corresponds to an electric water heater, and an air conditioner (in watt-hour of active energy)

B. Evaluation Metrics

Energy consumption prediction is a time-series data problem. Several metrics are used to evaluate the performance of a prediction model. These metrics are based on analyzing the correlation and error between the actual values and the estimated ones. These performance metrics are detailed in [40]. For the proposed model, we used the same metrics as given in [4] and [31] to be able to perform a fair comparison on the same scale, i.e. MSE, RMSE, MAE and MAPE.

- 1) *Mean Square Error*: MSE is used to measure the average difference between the actual and estimated values as shown in the equation 1.

$$MSE = \frac{1}{N} \sum_1^N (a - p)^2 \quad (1)$$

- 2) *Root Mean Square Error*: RMSE is the most widely used one for evaluating current forecasts. It allows finding the difference between the current values and the predicted ones(equation 2).

$$RMSE = \sqrt{\frac{1}{N} \sum_1^N (a - p)^2} \quad (2)$$

- 3) *Mean Absolute Error*: MAE measures the mean distance between the actual and predicted values as given in the equation 3.

$$MAE = \frac{1}{N} \sum_1^N |(a - p)| \quad (3)$$

- 4) *Mean Absolute Percentage Error*: MAPE expresses the percentage accuracy of the prediction as stated in the equation 4.

$$MAPE = \frac{1}{N} \sum_1^N |(a - p)| * 100\% \quad (4)$$

with, a and p represent the actual and predicted values, while N is the total number of records.

C. Performance Comparison

From the IHEPC set, we created a daily dataset for the period between March 2007 and February 2010. From this set we have created the two different proposed structures of matrix. For the first one, the matrix in series, we associate the model called *New Model-1* and for the second matrix structure, the model named *New Model-2*. To evaluate these two models, we performed three different experiments. For the first experiment, we considered the first and second years for the training set and the second and third years for the testing set. For the second experiment and in order to avoid duplicating the use of the second year for both training and testing sets, we used the first two years for the training set and we kept only the third year for the testing set. For the last experiment, the first year only is used for the training set and the other two years for the testing set. The two models were implemented with the tensorflow and keras libraries of Python and trained in 100 epochs with Adam optimization. The obtained experimental results were compared with the results given by LSTM, CNN-LSTM [4] and EECP-CBL [31] in terms of the four previously described performance metrics, i.e. equations 1, 2, 3 and 4.

TABLE III. MODEL-1: PERFORMANCE OF THE EXPERIMENTAL METHODS

Model	MSE	RMSE	MAE	MAPE	Training time (s)	Prediction time(s)
LSTM	0.241	0.491	0.413	38.72	106.06	2.97
CNN-LSTM	0.104	0.322	0.191	31.38	42.35	1.91
EEPC-CBL	0.065	0.225	0.191	19.15	61.36	0.71
Exp. 1	0.017	0.131	0.022	2.29	6.01	0.18
Exp. 2	0.023	0.154	0.008	0.841	6.18	0.179
Exp. 3	0.017	0.131	0.018	1.844	5.87	0.19

1) Model-1 Evaluation Results:

a) *Experiment 1*: In this experiment we selected the first and second years for the training set and the second and third years for the testing set. The performance measures of the proposed model and of the LSTM, CNN-LSTM and EECP-CBL models are presented in Table III. Thus, Fig. 3 and 4 present a comparison of the MSE, RMSE, MAE and MAPE values of our model with existing models. We conclude that the proposed model achieves best results compared to the other models. The MSE value of our approach (0.017) is improved by more than 50% compared to the EECP-CBL model (0.65). Meanwhile, the LSTM and CNN-LSTM models achieve very high MSE values of 0.104 and 0.241 respectively. For the RMSE and MAE measures, the proposed model obtains respectively 0.131 and 0.022 which are the best results compared to the other models. The MAPE value of the proposed model is equal to 2.297 and that of LSTM, CNN-LSTM and EECP-CBL is respectively 38.72, 31.83 and 19.15, we note that this value is improved by about 80% compared to the last model.

Table III and Fig. 5 compare the training and prediction time of the proposed model with the LSTM, CNN-LSTM and EECP-CBL models. The training time of the proposed model is equal to 6.014 seconds while the LSTM, CNN-LSTM and EECP-CBL models require 106.06, 42.35 and 61.36 seconds respectively to train. We can see that the gap in training time is very large between our model and the other models.

In Machine Learning, the most important thing is not the

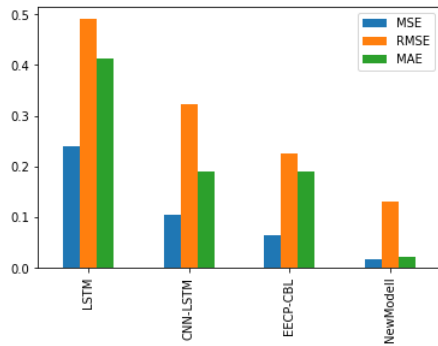


Fig. 3. New Model-1-Experiment-1 vs. LSTM/CNN-LSTM/EEPC-CBL in Terms of MSE, RMSE and MAE.

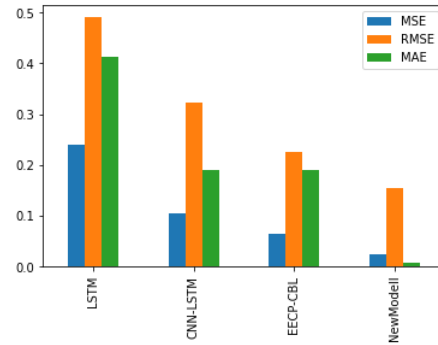


Fig. 6. New Model-1-Experiment-2 vs. LSTM/CNN-LSTM/EEPC-CBL in Terms of MSE, RMSE and MAE.

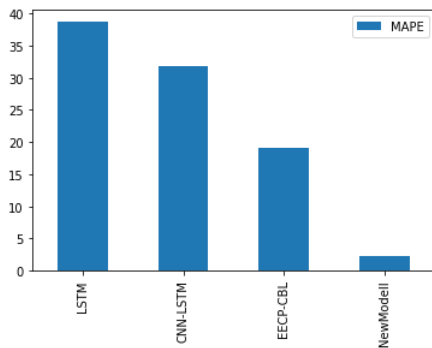


Fig. 4. New Model-1-Experiment-1 vs. LSTM/CNN-LSTM/EEPC-CBL in Terms of MAPE.

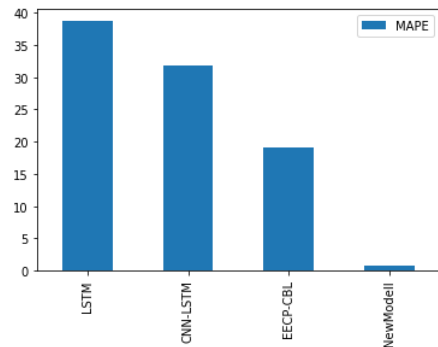


Fig. 7. New Model-1-Experiment-2 vs. LSTM/CNN-LSTM/EEPC-CBL in Terms of MAPE.

training time, but the prediction time because a model is trained only once while it is used for prediction several times. For our model, the prediction time is reduced from 0.71 seconds for EECP-CBL to 0.18 seconds. However, this time is high for the LSTM (2.97 seconds) and CNN-LSTM (1.91 seconds) models. Consequently, the proposed model required the best training and prediction times to estimate future energy consumption.

b) Experiment 2: For the second experiment, the training set is formed by the first and second years while the third year is used for the testing set. Table III and Fig. 6 and 7 show that for this experiment our model reaches the best values of MSE, RMSE, MAE and MAPE which are respectively 0.023,

0.154, 0.008 and 0.841.

Moreover, referring to Table III, we observed that the proposed model was trained for 5.69 seconds and required 0.175 seconds for prediction. From Fig. 8 we can see that our model has spent the shortest time for training and for predicting.

c) Experiment 3: By modifying the training set (one year) and the test set (2 years), the results of the proposed model remain better than the existing models in terms of performance measures (Fig. 9 and 10) with the values 0.017, 0.131, 0.018 and 1.844 of MSE, RMSE, MAE and MAPE,

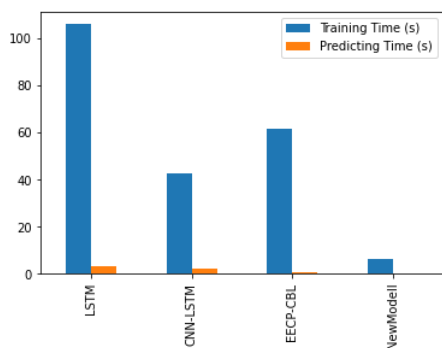


Fig. 5. New Model-1-Experiment-1 vs. LSTM/CNN-LSTM/EEPC-CBL in Terms of Training Time and Prediction Time.

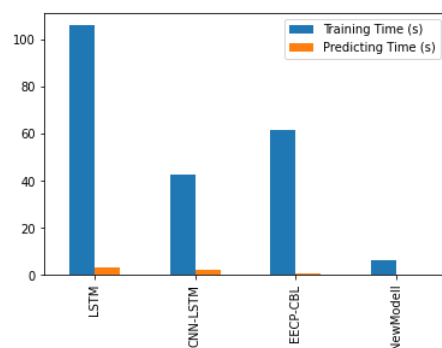


Fig. 8. New Model-1-Experiment-2 vs. LSTM/CNN-LSTM/EEPC-CBL in Terms of Training Time and Prediction Time.

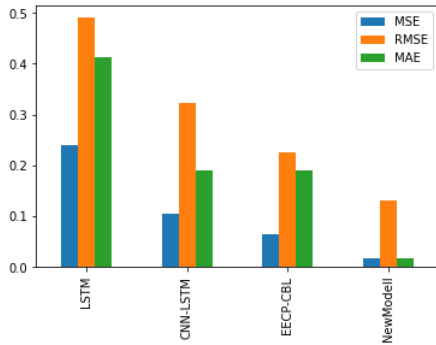


Fig. 9. New Model-1-Experiment-3 vs. LSTM/CNN-LSTM/EEPC-CBL in Terms of MSE, RMSE and MAE.

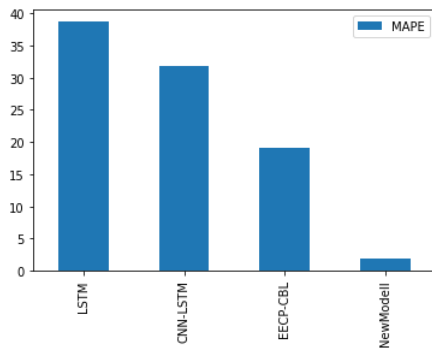


Fig. 10. New Model-1-Experiment-3 vs. LSTM/CNN-LSTM/EEPC-CBL in Terms of MAPE.

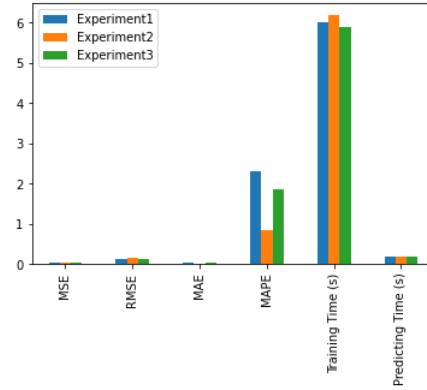


Fig. 12. Summary of New Model-1 Results.

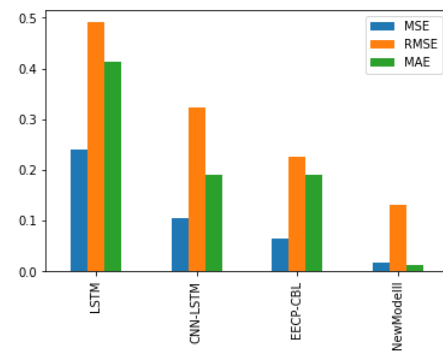


Fig. 13. New Model-2-Experiment-1 vs. LSTM/CNN-LSTM/EEPC-CBL in Terms of MSE, RMSE and MAE.

respectively (Table III).

Also, we deduce from Table III and Fig. 11 that the proposed model has the shortest prediction training time.

d) *Model-1 Experiments' Comparison:* Fig. 12 compares the results of the three experiments to evaluate the proposed model. We see that the MSE and RMSE values of experiments 1 and 3 are similar while the MAE and MAPE values are slightly different. On the other hand, the values of the performance measures of experiment 3 are slightly different from those of the other experiments. Additionally, the training and prediction times of the three experiments are too close together. We conclude that our model achieves the best

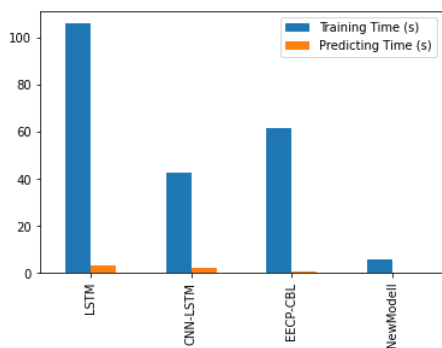


Fig. 11. New Model-1-Experiment-3 vs. LSTM/CNN-LSTM/EEPC-CBL in Terms of Training Time and Prediction Time.

performance measures and the shortest training and prediction times, regardless of the choice of training and testing sets.

TABLE IV. MODEL-2: PERFORMANCE OF THE EXPERIMENTAL METHODS

Model	MSE	RMSE	MAE	MAPE	Training time (s)	Prediction time(s)
LSTM	0.241	0.491	0.413	38.72	106.06	2.97
CNN-LSTM	0.104	0.322	0.191	31.38	42.35	1.91
EEPC-CBL	0.065	0.225	0.191	19.15	61.36	0.71
Exp. 1	0.017	0.131	0.013	1.386	5.22	0.17
Exp. 2	0.023	0.154	0.008	0.841	5.69	0.17
Exp. 3	0.017	0.131	0.0122	2.552	4.81	0.16

2) *Model-2 Evaluation Results:*

a) *Experiment 1:* The second proposed model also achieved the best values of the performance measures MSE, RMSE, MAE and MAPE comparing to the LSTM, CNN-LSTM and EEPC-CBL models as shown in Fig. 13 and 14. All values are detailed in Table IV.

Similar to the previous experiments, Table IV and Fig. 15 show that our model spends the shortest time for training and for predicting.

b) *Experiment 2:* From Table IV, we can observe that the value of MSE is improved by more than 25% compared to the EEPC-CBL model and the values of RMSE, MAE and MAPE are approved by almost 20% compared to the EEPC-CBL model. Fig. 16 and 17 demonstrate that our model

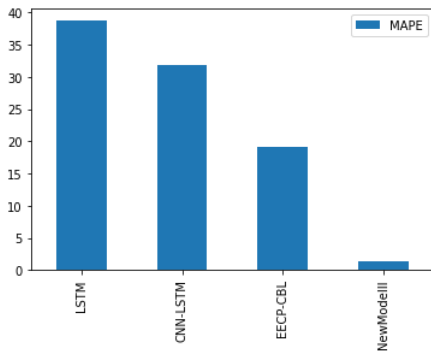


Fig. 14. New Model-2-Experiment-1 vs. LSTM/CNN-LSTM/EEPC-CBL in Terms of MAPE.

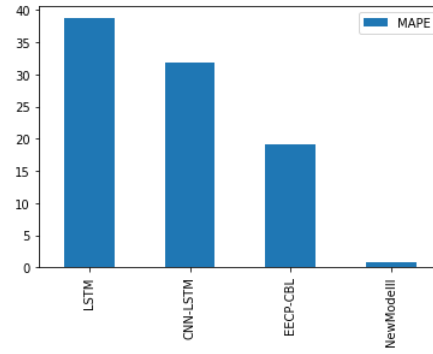


Fig. 17. New Model-2-Experiment-2 vs. LSTM/CNN-LSTM/EEPC-CBL in Terms of MAPE.

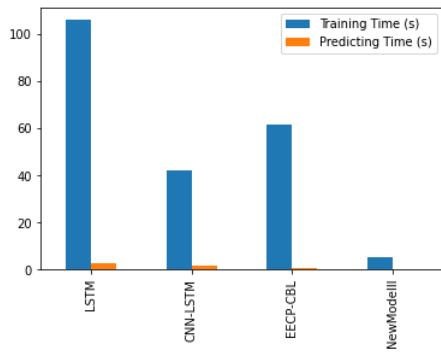


Fig. 15. New Model-2-Experiment-1 vs. LSTM/CNN-LSTM/EEPC-CBL in Terms of Training Time and Prediction Time.

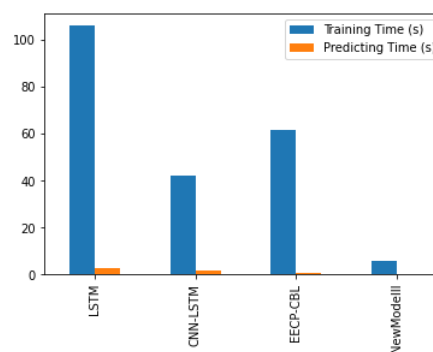


Fig. 18. New Model-2-Experiment-2 vs. LSTM/CNN-LSTM/EEPC-CBL in Terms of Training Time and Prediction Time.

achieves the best accuracy performance compared to other models.

Referring to Table IV and Fig. 18, our model achieves the shortest training and prediction time.

c) *Experiment 3:* Finally, the evaluation results of Experiment 3 are presented in Table IV. For the values of MSE, RMSE, MAE and MAPE, our model reaches better values than the improved EEPC-CBL model. Fig. 19 and 20 show that our model has the best performance measures.

In terms of training time and prediction, our approach gives better results as shown in Table IV and Fig. 21.

d) *Model-2 Experiments' Comparison:* Fig. 22 presents a synthesis of the results obtained by the second model proposed in the three experiments. We can see that the values of MSE, RMSE and MAE are almost equal with a slight difference between the values obtained by the second experiment and the two other experiments. We also notice that the value of MAPE differs slightly from one experiment to another with the best value being obtained for two years of training and one year of testing. In terms of training and prediction time, the three experiments reach very close duration. Consequently, we conclude that our model achieves the best performance for all experiments. To conclude, for the two proposed models we

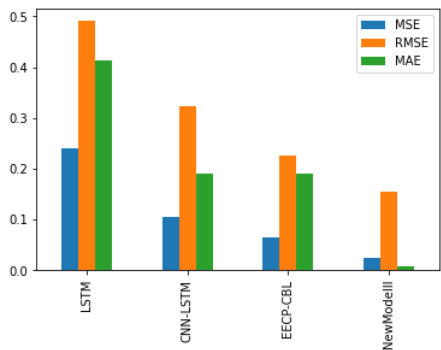


Fig. 16. New Model-2-Experiment-2 vs. LSTM/CNN-LSTM/EEPC-CBL in Terms of MSE, RMSE and MAE.

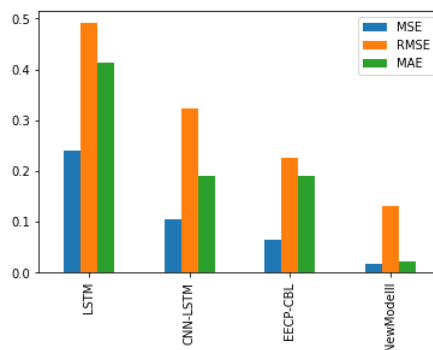


Fig. 19. New Model-2-Experiment-3 vs. LSTM/CNN-LSTM/EEPC-CBL in Terms of MSE, RMSE and MAE.

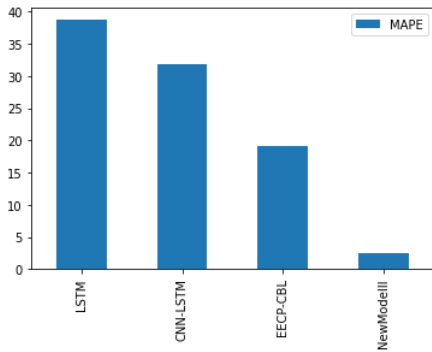


Fig. 20. New Model-2-Experiment-3 vs. LSTM/CNN-LSTM/EEPC-CBL in Terms of MAPE.

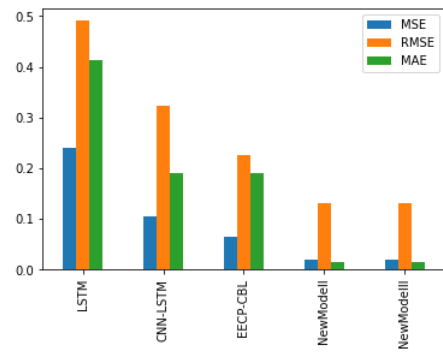


Fig. 23. Average of Model-1 and Model-2 vs. LSTM/CNN-LSTM/EEPC-CBL in Terms of MSE, RMSE and MAE.

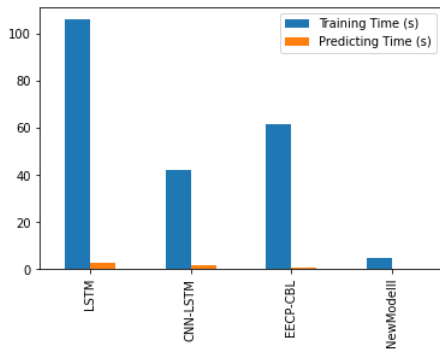


Fig. 21. New Model-2-Experiment-3 vs. LSTM/CNN-LSTM/EEPC-CBL in Terms of Training Time and Prediction Time.

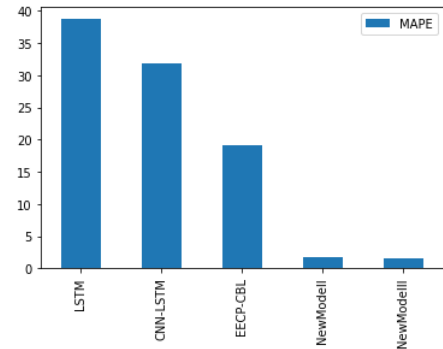


Fig. 24. Average of Model-1 and Model-2 vs. LSTM/CNN-LSTM/EEPC-CBL in Terms of MAPE.

calculated the average of the results obtained and compared them to those of the LSTM, CNN-LSTM and EEPC-CBL models. The comparison of the MSE, RMSE, MAE and MAPE measurements is presented in Fig. 23 and 24. While Fig. 25 shows the comparison of all models in terms of training time and prediction time.

We observe that for the two proposed models reach the best values of MSE, RMSE, MAE and MAPE compared to the existing models LSTM, CNN-LSTM and EEPC-CBL which proves the effectiveness of our model in terms of accuracy performance. Moreover, we studied the learning and

prediction time of the proposed models in both models. The learning time of our models is equal to 70% of the best time obtained by the CNN-LSTM model. Moreover, our approach requires only 39% of the time required by the EEPC-CBL model.

Therefore, we conclude that the results obtained from the new models significantly outperform the other models in terms of predictive efficiency. In addition, our models improve the training time, but most importantly, they deemphasize the prediction time. Therefore, the proposed models enhance energy consumption prediction results on the daily dataset derived

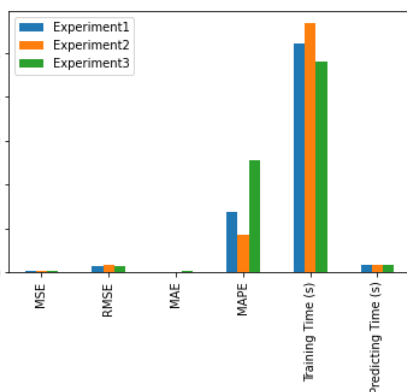


Fig. 22. Summary of New Model-2 Results.

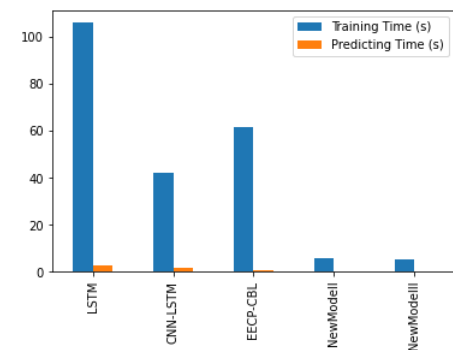


Fig. 25. Average of Model-1 and Model-2 vs. LSTM/CNN-LSTM/EEPC-CBL in Terms of Training Time and Prediction Time.

from IHEPC in terms of performance measures MSE, RMSE, MAE and MAPE and in terms of training and prediction time.

V. CONCLUSION

Since the demand for energy is growing more and more following the demographic and technological development, it has become imperative to manage and optimize the use of energy between consumers and suppliers. For an efficient energy management system, it is necessary to predict the future demand of users in energy which is a difficult target due to several factors. Various techniques based ML/DL for predicting energy consumption were proposed in the literature. However, most of them combine several models to be able to reflect temporal and logical dependencies between data. The focus of most researchers is how to make their models able to deal with these relationships by integrating recurrent mechanism. Nevertheless, the resulting models are often costly in terms of time and space. In this paper, we proposed a new research direction that deals with improving the structure of the input data rather than emphasizing on upgrading the model itself. The proposed model for energy consumption prediction is a simple 3-dimensional CNN that uses a new structure based matrices for the input data that physically reflects its logical dependencies. The experimental evaluation with the existing models LSTM, CNN-LSTM and EECF-CBL showed that our model outperforms existing ones in terms of MSE, RMSE, MAE, MAPE and required time for training/testing.

In a future work, we will integrate this model into the intelligent A-RESS system proposed in [41].

REFERENCES

- [1] H. R. Khosravani, M. D. M. Castilla, M. Berenguel, A. E. Ruano and P. M. Ferreira, "A comparison of energy consumption prediction models based on neural networks of a bioclimatic building," *Energies*, vol 9, pp. 57, 2016.
- [2] Ne. Fumo, M. A. R. Biswas. "Regression analysis for prediction of residential energy consumption," *Renewable and Sustainable Energy Reviews*, vol 47, pp. 332-343, 2015.
- [3] I. Ullah, R. Ahmad and D. Kim, "A prediction mechanism of energy consumption in residential buildings using hidden Markov model," *Energies*, vol 11, pp. 358 2018.
- [4] T. Y. Kim and S. B. Cho, "Predicting residential energy consumption using CNN-LSTM neural networks," *Energy*, vol. 182, pp. 72-81, September 2019.
- [5] H. Kaiming, Z. Xiangyu, R. Shaoqing and S. Jian, "Deep Residual Learning for Image Recognition," *IEEE Conference on Computer Vision and Pattern Recognition (CVPR)*, pp. 770-778, 2016.
- [6] MSajjad, M. Nasir, F. U. Min Ullah, K. Muhammad, A. K. Sangaiah and S. W. Baik, "Raspberry Pi assisted facial expression recognition framework for smart security in law-enforcement services," *Information Sciences*, vol 479, pp. 416-431, 2019.
- [7] S. Khan, K. Muhammad, S. Mumtaz, S. W. Baik and V. H. C. de Albuquerque, "Energy-Efficient Deep CNN for Smoke Detection in Foggy IoT Environment," *IEEE Internet of Things Journal*, vol 6, no. 6, pp. 9237-9245, December 2019.
- [8] M. Khan, K. Salman, P. Vasile, M. Irfan and V. H. C. de Albuquerque, "Edge Intelligence-Assisted Smoke Detection in Foggy Surveillance Environments," *IEEE Transactions on Industrial Informatics*, vol. 16, no. 2, pp. 1067-1075, February 2020.
- [9] N. Majumder, S. Poria, A. Gelbukh and E. Cambria, "Deep learning-based document modeling for personality detection from text," *IEEE Intelligent Systems*, vol. 32, no. 2, pp. 74-79, March-April 2017.
- [10] D. W. Otter, J. R. Medina and J. K. Kalita, "A Survey of the Usages of Deep Learning for Natural Language Processing," *IEEE Transactions on Neural Networks and Learning Systems*, vol. 32, no. 2, pp. 604-624, February 2021.
- [11] P. Jiang, C. Chen and X. Liu, "Time series prediction for evolutions of complex systems: A deep learning approach," *IEEE International Conference on Control and Robotics Engineering (ICCRE)*, pp. 1-6 2016.
- [12] Y. Hua, Z. Zhao, R. Li, X. Chen, Z. Liu and H. Zhang, "Deep Learning with Long Short-Term Memory for Time Series Prediction," *IEEE Communications Magazine*, vol. 57, no. 6, pp. 114-119, June 2019.
- [13] A. Alzahrani, P. Shamsi, M. Ferdowsi and C. Dagli, "Solar irradiance forecasting using deep recurrent neural networks," *IEEE 6th International Conference on Renewable Energy Research and Applications (ICRERA)*, pp. 988-994, 2017.
- [14] H. Lee and B. -T. Lee, "Bayesian Deep Learning-based Confidence-aware Solar Irradiance Forecasting System," *International Conference on Information and Communication Technology Convergence (ICTC)*, pp. 1233-1238, 2018.
- [15] M. Khodayar, J. Wang and M. Manthouri, "Interval Deep Generative Neural Network for Wind Speed Forecasting," *IEEE Transactions on Smart Grid*, vol. 10, no. 4, pp. 3974-3989, July 2019.
- [16] M. Khodayar and J. Wang, "Spatio-Temporal Graph Deep Neural Network for Short-Term Wind Speed Forecasting," *IEEE Transactions on Sustainable Energy*, vol. 10, no. 2, pp. 670-681, April 2019.
- [17] J. Chen, G. Q. Zeng, W. Zhou, W. Du and K. D. Lu, "Wind speed forecasting using nonlinear learning ensemble of deep learning time series prediction and extremal optimization," *Energy Conversion and Management*, vol. 165, no. 1, pp. 681-695, June 2018,.
- [18] A. T. Eseye, J. Zhang and D. Zheng, "Short-term photovoltaic solar power forecasting using a hybrid Wavelet-PSO-SVM model based on SCADA and Meteorological information," *Renewable Energy*, vol. 118, pp. 357-367, April 2018.
- [19] Bo-Juen Chen, Ming-Wei Chang and Chih-Jen lin, "Load forecasting using support vector Machines: a study on EUNITE competition 2001," *IEEE Transactions on Power Systems*, vol. 19, no. 4, pp. 1821-1830, November 2004.
- [20] S. L. Wong, K. K. W. Wan and T. N. T. Lam, "Artificial neural networks for energy analysis of office buildings with daylighting," *Applied Energy*, vol. 87, no. 2, pp. 551-557, February 2010.
- [21] D. L. Marino, K. Amarasinghe and M. Manic, "Building energy load forecasting using Deep Neural Networks," *IECON 2016 - 42nd Annual Conference of the IEEE Industrial Electronics Society*, pp. 7046-7051, 2016.
- [22] X. Dong, L. Qian and L. Huang, "A CNN based bagging learning approach to short-term load forecasting in smart grid," *IEEE Smart-World, Ubiquitous Intelligence & Computing, Advanced & Trusted Computed, Scalable Computing & Communications, Cloud & Big Data Computing, Internet of People and Smart City Innovation (Smart-World/SCALCOM/UIC/ATC/CBDCOM/IOP/SCI)*, pp. 1-6, 2017.
- [23] K. Amarasinghe, D. L. Marino and M. Manic, "Deep neural networks for energy load forecasting," *IEEE 26th International Symposium on Industrial Electronics (ISIE)*, pp. 1483-1488, 2017.
- [24] H. Shi, M. Xu and R. Li, "Deep Learning for Household Load Forecasting—A Novel Pooling Deep RNN," in *IEEE Transactions on Smart Grid*, vol. 9, no. 5, pp. 5271-5280, September 2018
- [25] J. Kim, J. Moon, E. Hwang and P. Kang, "Recurrent inception convolution neural network for multi short-term load forecasting," *Energy and Buildings*, vol. 194, pp. 328-341, July 2019.
- [26] D. Gan, Y. Wang, N. Zhang and W. Zhu, "Enhancing short-term probabilistic residential load forecasting with quantile long-short-term memory," *The Journal of Engineering*, vol 2017, no. 14, pp. 2622-2627, May 2017.
- [27] K. Muralitharan, R. Sakthivel and R. Vishnuvarthan, "Neural network based optimization approach for energy demand prediction in smart grid," *Neurocomputing*, vol. 273, pp. 199-208, January 2018.
- [28] M. Fayaz, H. Shah, A. M. Ascere, W. K. Mashwani and A. S. Shah, "A framework for prediction of household energy consumption using feed forward back propagation neural network," *Technologies*, vol. 7, no. 2, pp. 30, 2019.
- [29] K. Bandara, C. Bergmeir and H. Hewamalage, "LSTM-MSNet: Leveraging Forecasts on Sets of Related Time Series With Multiple Seasonal Patterns," *IEEE Transactions on Neural Networks and Learning Systems*, vol. 32, no. 4, pp. 1586-1599, April 2021.

- [30] N. Khan, I. Ul Haq, S. U. Khan, S. Rho, M. Y. Lee and S. W. Baik, "DB-Net: A novel dilated CNN based multi-step forecasting model for power consumption in integrated local energy systems," *International Journal of Electrical Power and Energy Systems*, vol. 133, pp. 107023, December 2021.
- [31] T. Le, M. T. Vo, B. Vo, E. Hwang, S. Rho and S. W. Baik, "Improving Electric Energy Consumption Prediction Using CNN and Bi-LSTM," *Applied Sciences*, vol. 9, no. 20, 2019.
- [32] F. U. M. Ullah, A. Ullah, I. U. Haq, S. Rho and S. W. Baik, "Short-Term Prediction of Residential Power Energy Consumption via CNN and Multi-Layer Bi-Directional LSTM Networks," *IEEE Access*, vol. 8, pp. 123369-123380, 2020.
- [33] S. K. Hora, R. Poongodan, R. P. de Prado, M. Wozniak and P. B. Divakarachari, "Long Short-Term Memory Network-Based Metaheuristic for Effective Electric Energy Consumption Prediction," *Applied sciences*, vol. 11, no. 23, pp.11263, 2021.
- [34] G. Hebrail and A. Berard, "Individual Household Electric Power Consumption Data Set," <https://archive.ics.uci.edu/ml/datasets/individual+household+electric+power+consumption/>, last accessed 2022/02/15
- [35] Z. A. Khan, T. Hussain and S. W. Baik, "Boosting energy harvesting via deep learning-based renewable power generation prediction," *Journal of King Saud University - Science*, vol. 34, no. 3, pp. 101815, April 2022.
- [36] F. Kaytez, M. C. Taplamacioglu, E. Cam and F. Hardalac, "Forecasting electricity consumption: A comparison of regression analysis, neural networks and least squares support vector machines," *International Journal of Electrical Power & Energy Systems*, vol. 67, pp. 431-438, May 2015.
- [37] S. Khan, N. Javaid, A. Chand, A. B. M. Khan, F. Rashid and I. U. Afridi, "Electricity Load Forecasting for Each Day of Week Using Deep CNN," *Workshops of the International Conference on Advanced Information Networking and Applications, WAINA 2019: Web, Artificial Intelligence and Network Applications*, pp. 1107-1119, 2019.
- [38] A. Syeda, N. Javaid, T. Islam, W. Z. Khan, M. Y. Aalsalem and H. Sajjad, "An efficient CNN and KNN data analytics for electricity load forecasting in the smart grid," *Workshops of the International Conference on Advanced Information Networking and Applications, WAINA 2019: Web, Artificial Intelligence and Network Applications*, pp. 592-603, 2019.
- [39] J. Y. Kim and S. B. Cho, "Electric energy consumption prediction by deep learning with state explainable autoencoder," *Energies*, vol. 12, no. 4, pp. 739, 2019.
- [40] T. Hussain, F. U. M. Ullah, K. Muhammad, S. Rho, A. Ullah, E. Hwang, J. Moon and S. W. Baik, "Smart and intelligent energy monitoring systems: A comprehensive literature survey and future research guidelines," *International Journal of Energy Research*, vol. 45, no. 3, pp. 3590-3614, 2021.
- [41] I. Toumia and A. Ben Hassine, "A-RESS new dynamic and smart system for renewable energy sharing problem," *PeerJ Computer Science*, vol. 7, pp. 610, 2021.

Decode and Forward Coding Scheme for Cooperative Relay NOMA System with Cylindrical Array Transmitter

Samuel Tweneboah-Koduah¹

Department of Computer and Electrical Engineering
University of Energy and Natural Resources
Sunyani, Ghana

Emmanuel Ampoma Affum²

Department of Telecommunication Engineering
University of Science and Technology
Kumasi, Ghana

Kingsford Sarkodie Obeng Kwakye³

Department of Telecommunication Engineering
University of Science and Technology
Kumasi, Ghana

Owusu Agyeman Antwi⁴

Department of Telecommunications Engineering
Ghana Communication Technology University
Accra, Ghana

Abstract—The Non-Orthogonal Multiple Access (NOMA) technique has enormous potential for wireless communications in the fifth generation (5G) and beyond. Researchers have recently become interested in the combination of NOMA and cooperative relay. Even though geometric-based stochastic channel models (GBSM) have been found to provide better, practical, and realistic channel properties of massive multiple-input multiple-output (mMIMO) systems, the assessment of Cooperative Relay NOMA (CR-NOMA) with mMIMO system is largely based on correlated-based stochastic channel model (CBSM). We believe that this is a result of computational difficulties. Again, not many discussions have been done in academia about how well CR-NOMA systems perform when large antenna transmitters with the GBSM channel model are used. As a result, it is critical to investigate the mMIMO CR-NOMA system with the GBSM channel model that takes into account channel parameters such as path loss, delay profile, and tilt angle. Moreover, the coexistence of large antenna transmitters and coding methods requires additional research. In this research, we propose a two-stage, three-dimension (3D) GBSM mMIMO channel model from the 3GPP, in which the transmitter is modelled as a cylindrical array (CA) to investigate the efficiency of CR-NOMA. By defining antenna elements placement vectors using the actual dimensions of the antenna array and incorporating them into the three-dimension (3D) channel model, we were able to increase the analytical tractability of the 3D GBSM. Bit-error rates, achievable rates, and outage probabilities (OP) are investigated utilizing the decode-and-forward (DF) coding method: the results are compared with that of a system using the CBSM channel model. Despite the computational difficulties of the proposed GBSM system, there is no difference in performance between CBSM and GBSM.

Keywords—CR-NOMA; 3D GBSM; DF coding scheme; Cylindrical Array (CA); cooperative relay

I. INTRODUCTION

One of the major hurdles for future wireless communication systems is to facilitate large data traffic whilst maintaining reasonable communication latency [1]–[3]. This is due to the development of information and communication applications and a rapidly expanding user base. It also requires concurrent

access to various network resources from anywhere and at any time while maintaining a good quality of service.

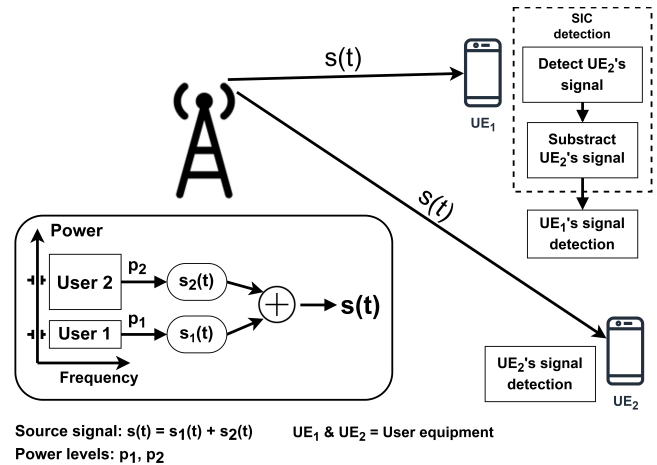


Fig. 1. NOMA System Architecture for Downlink Communication.

In a cellular system where the channel conditions vary for various users due to the near-far effect, Nonorthogonal multiple access (NOMA) provides performance improvement regarding the trade-off between the system's capacity and user fairness [4]–[7]. Fig. 1 Figure 1 illustrates the NOMA system architecture for downlink (DL) communication. According to the NOMA concept in the power domain, users share the same resource block such as frequency, code or time. The users, however, are assigned different power levels per the channel conditions. Users with a poor channel are given more power than those with a good channel state. The data signal of various users in the NOMA system is added together by using superposition coding into a single data signal that is transmitted to all users within the network. This will be seen in later sections of this work. At the destination, the users employ successive interference cancellations to mitigate interference and recover individual data signals. NOMA, which has been

incorporated into the new 5G standard, is a promising method that is anticipated to meet the requirements and also deliver a greater spectrum efficiency [6], [7].

Given the incredibly high number of IoT devices enabled by 5G (such as Smart Cities or Autonomous Vehicles), this trait is important in situations where the spectrum is limited. Users who are nearer the transmitter utilize lower transmit powers, but users who are farther away need greater transmit powers. As a result, NOMA employs these attributes to distinguish between signals since transmissions from various users who share the same spectrum have varying received power levels. Naturally, in addition to the near-far issue, fading and power regulation are other elements that cause variances in the received power levels of users. These characteristics are also taken into consideration by the NOMA receiver. When using NOMA, a user receiving the superposition broadcast with its signal delivered at a lower power level decodes the stronger signal components of other users and then cancels them out. This allows for a considerable spectral efficiency increase over standard orthogonal multiple access [8]. Some of the major technologies that enable 5G communications to achieve the initial targets in terms of throughput, spectrum efficiency, and network capacity are massive multiple-input, multiple output (mMIMO), millimeter-wave (mmWave) Communications, Cooperative relay NOMA (CR-NOMA), and so on [9], [10].

The advantage of mmWave, which uses carrier frequencies of about 60 GHz, is that it has a substantially larger channel coherence bandwidth but also has significantly higher path loss. Additionally, the relatively short wavelength of mmWave makes it easier to deploy mMIMO since it allows for smaller antennas and closer spacing between mMIMO antenna components (typically 3 to 4 wavelengths for the signals in adjacent antennas to be uncorrelated).

Recent works have seen the integration of NOMA and different transmission techniques, such as mMIMO, mmWave, block transmission techniques, and cooperative-relay communication. This is to achieve better system performance. Cooperation among network users is crucial in wireless communication since it reduces fading effect, increases capacity, and broadens the coverage area. Cooperative communication occurs when a node works with the source to forward data to the destination as indicated in Fig. 2 and 3. Two types of cooperation, namely cooperation among NOMA users and cooperation via specialized relays, can be employed to create cooperative diversity in the NOMA system. By utilizing idle users to relay data to other users, the previous method is used to increase the data rate and data dependability for the weak users. The latter is used to serve cell edge NOMA customers effectively within a network and to increase wireless network coverage [11].

II. LITERATURE REVIEW

1) *Channel Models for 5G Massive MIMO*: A channel model is a mathematical depiction of the impacts of a communication channel used to transmit wireless communications. The channel model can reflect the signal's power loss as it passes via the wireless link. There are two types of channel models that are typically used to evaluate the performance of 5G wireless communication systems: correlation-based

stochastic models (CBSMs) and geometry-based stochastic models (GBSMs) [12].

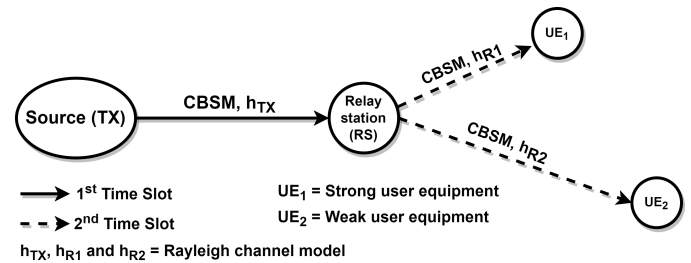


Fig. 2. Downlink cooperative-Relay NOMA Network with CBSM Channel Model.

Table I gives further details of these channel models and their applications. The former is less accurate and is mostly used to study the theoretical performance of MIMO systems. The exactitude of a true MIMO system, on the other hand, is limited, and simulating wireless channels with the nonstationary phenomenon and wavefront effects is difficult [12], [13]. GBSM, on the other hand, has more processing complexity, but it can accurately represent actual channel characteristics and is ideally adapted for mMIMO channel estimation [12].

For performance improvements and evaluation, GBSM combines channel features such as angle of arrivals, delay profile, tilt angle, path-loss, and so on into the channel models [12], [14]–[16].

2) *CR-NOMA with CBSM Channel Model*: As explained previously, the effectiveness of CR-NOMA has been thoroughly investigated using a variety of network coding methods. However, the vast majority of CR-NOMA performance assessments are only based on CBSM, which is mainly used for theoretical MIMO channel analyses. Cooperation among devices in a network has been studied in numerous literature, where some network nodes act as a relay to other devices by using network coding strategies. The network coding strategies improve system performance and allow the far or network edge users to improve their quality of services. For instance, [17] investigated network coding techniques such as amplify-and-forward and decode-and-forward. One of the most well-known relaying protocols is Decode-and-forward (DF). In this protocol, a relay decodes the message from a source and resends the decoded symbols to a destination. DF MIMO relay systems' transmission strategy and performance analyses have been done in [18]. Additionally, the compress-and-forward (CF) and compute-and-forward (CpF) techniques have been examined in [19], [20] and [21]–[24], respectively. The above coding schemes were used to analyze resource allocation optimization in [25]–[30].

CR-NOMA using MIMO as well as mMIMO have been investigated in [31], [32] to increase system spectral efficiency and lessen difficulties in acquiring channel state information (CSI). The applicability of relay to mMIMO NOMA has been researched by the authors of [32]. However, CBSM was the foundation of the analyses with mMIMO cooperative relay NOMA. According to [12], the authors' circular array at the transmitter (TX) can not be considered as a typical antenna array arrangement for mMIMO systems.

TABLE I. COMPARISON OF MIMO CHANNEL MODELS [12], [15]

Specifications	GBSM	CBSM
Suitable environments	<ul style="list-style-type: none">• Scatters are stochastically distributed between link ends.• Realistic analysis of physical propagation environment.	<ul style="list-style-type: none">• Describes channel characteristic by correlation matrices instead of propagation parameters.
Benefits	<ul style="list-style-type: none">• Suitable for simulation of geometric path using numerous random parameters.• High degree of random parameters yields high accuracy.• Suitable for adaptive antenna application.	<ul style="list-style-type: none">• Serves as a better calibration (channel) mode.• Suitable for link-level simulation.• Better calibration model.• Suitable for evaluating theoretical performance of MIMO system due to low complexity.
Limitation	<ul style="list-style-type: none">• High complexity due to high degree of parameter randomness.	<ul style="list-style-type: none">• Simple and computational efficient.• Inaccurate for realistic MIMO system analysis.• Not suitable for system-level simulation due to over simplification of channel model.
Features	<ul style="list-style-type: none">• Distinctive random variables of multiple subpath of a cluster path.• Correlation properties depend on spatial characteristics and antenna array configuration.	<ul style="list-style-type: none">• Correlation properties depend of channel matrices depends on Doppler and spatial filtering.• Describes channel characteristic by correlation matrices instead of propagation parameters.
Classification	<ul style="list-style-type: none">• 2D Models (Parabolic and Elliptical)• 3D Models (Ellipsoid, 5G channel and Twin-cluster)• Saleh-Valenzuela model	<ul style="list-style-type: none">• I.I.D. Rayleigh fading channel• Rician channel model• Kronecker model• Mutual coupling model (Weichselberge model and Virtual channel representation)
Application	<ul style="list-style-type: none">• 5G, vehicle-to-vehicle (V2V) communication, high-speed train (HDT) communication, unmanned aerial vehicle (UAV) communication, etc.	<ul style="list-style-type: none">• Low frequency, low speed applications.

A. Motivation

According to research, CBSM [23], [33]–[36] is the only focus of the approaches and analyses utilized to enhance CR-NOMA system performance. Due to nonstationary phenomena and spherical effects, CBSM is used for theoretical study and has lower accuracy for real-world mMIMO systems [12], [37]. Table I provides a comparative study of CBSM and GBSM that clearly outlines the drawbacks of the CBSM channel model. GBSM on other hand provides accurate and realistic channel characteristics for the mMIMO system. In this regard, the authors in [31] have, as far as we can determine, used GBSM to examine CR-NOMA performance based on the Saleh-Valenzuela channel model. The authors considered the channel for beamforming analysis without network coding strategies. Again, a user relay rather than a specialized relay station was the focus of their investigation. The purpose of this study is to fill in the gap in the literature on CR-NOMA related to the adoption of the 3GPP's 3D GBSM channel model with large antenna transmitters like cylindrical antenna array (CA), as well as its implications for wireless communications. To meet future demands of wireless communication technologies

the paper addresses the following research challenges: 1) What are the effects of large antenna transmitters such as CA on the performance of mMIMO CR-NOMA systems when the communication links from the transmitter to users are modeled as 3D GBSM channel model? 2) How will mMIMO CR-NOMA performance be impacted by the combination of large antenna transmitters, 3D GBSM channel models, and coding schemes on outage probability, achievable rate, and bit-error rate (BER)?

B. Contribution

By taking into account a two-stage downlink network model system with a dedicated relay, we can address the challenges above. We use 3GPP and WINNER+ models, which adhere to the GBSM strategy, see [38], [39] for more information [14], [40]. Therefore, according to [41], defining propagation paths in azimuth does not enhance performance. By combining a space-time signal with scanning acceleration, CA may be utilized to lessen clutter and enables concentrated beams in any horizontal direction [14]. By defining the antenna element placement vector using its physical structure and

including it in the three-dimension (3D) channel model, we were able to minimize the computing complexity of the 3D GBSM. To improve the functionality of the mMIMO CR-NOMA system, the RS employs a DF coding scheme to obtain results regarding achievable rate, outage probability, and bit-error rate through simulation. The main contribution this work are:

- i. We determine the placement vector of the antenna element based on the physical structure of the antenna array to reduce the computational complexity of the model.
- ii. We analyze a two-stage downlink mMIMO CR-NOMA system and offer a new 3D GBSM channel model when the transmitter is modelled as CA.
- iii. We use DF coding scheme with the 3D channel model to improve on the performance of the mMIMO CR-NOMA system.
- iv. For the two-stage CR-NOMA system's performance study, we report the outage probability, achievable rate and bit-error assessment. We compare these results with similar existing work that uses CBSM.
- v. Results are shown to demonstrate the potential benefits of the joint contribution of large antenna transmitters and coding schemes using 3D GBSM model with mMIMO CR-NOMA to future communications systems in terms of achievable rate, outage probability, and bit-error rate (BER).

The paper is structured as follows. Section II gives the literature of prior work where the communication channel in the system is modeled as CBSM. It also establishes the motivation and contribution of the work. The proposed system model of the mMIMO CR-NOMA network and the proposed 3D GBSM model when the transmitter is cylindrical array (CA) is present in Section III. Sections IV and V contain the system's performance analysis, as well as numerical findings. Section VI concludes the paper, and state future works using 3D GBSM in NOMA and 5G systems.

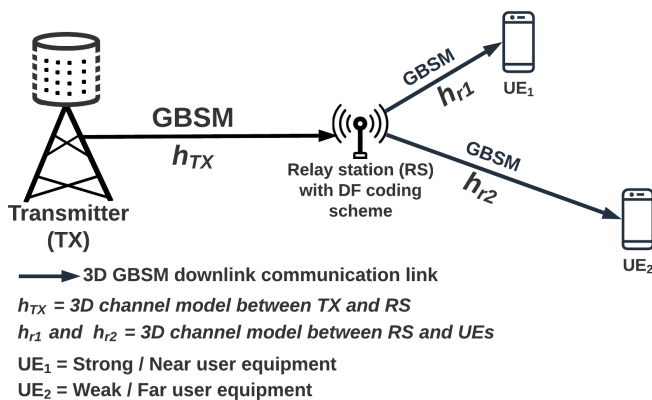


Fig. 3. Proposed Model of the Downlink Cooperative Relay NOMA Network with mMIMO.

III. SYSTEM MODEL

As shown in Fig. 3, this section considers a two-stage downlink (DL) communication system in which the transmitter

(TX) transfers messages to user equipment (UE) via a dedicated relay. The TX has a large-scale antenna array such as CA for high spectral-efficient massive access, whereas the UEs and relay station (RS) each have a single antenna. Unlike the CR-NOMA model in Fig. 2, where the channel connecting the TX, RS, and UEs is modelled with CBSM, the proposed model substitutes the CBSM channel with a 3D GBSM, as illustrated in Fig. 3. The strong user equipment (UE_1) in the proposed system shown in Fig. 3 is located near to the RS, whereas the weak user equipment (UE_2) is located further away from the RS. We employ a fixed power allocations, and assign α_1 to UE_1 , and α_2 to UE_2 according to NOMA principles where $\alpha_1 < \alpha_2$. TX combines the signal of the two UEs into one according to superposition principles. The combined signal (\mathbf{x}) of two is given by

$$\mathbf{x} = \sum_{i=1}^2 \sqrt{\alpha_i} s_i \quad (1)$$

where i^{th} user transmit power allocation and the source signal are α_i and s_i respectively. Noticeably $\sum_{i=1}^2 \alpha_i \leq P_s$, where P_s is the total transmit power at TX. We assume that TX uses a pilot signal to estimate the downlink (DL) channel. Additionally, we take advantage of channel reciprocity using the traditional time division duplex mode [42]. The system uses two-time slots to transmit the combined signal to the user. During the first, the received signal (y) at the relay with DL data transmission is given by

$$y = \mathbf{H}\mathbf{x} + n \quad (2)$$

where \mathbf{x} is an $N_t \times 1$ data signal from (1), \mathbf{H} is the channel matrix generated in (11) and n is the additive Gaussian white noise with zero mean and variance, σ^2 .

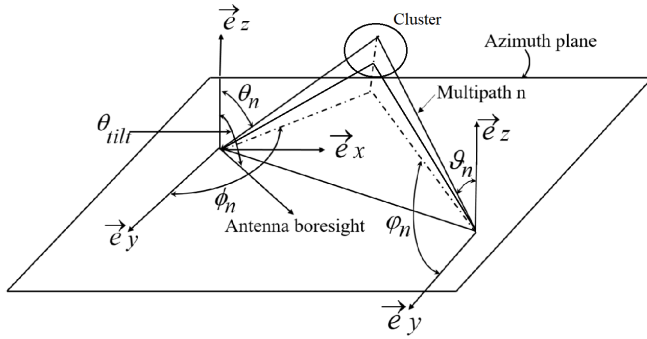
A. Proposed 3D GBSM Models

We assess the GBSM-based 3GPP standard and offer a 3D channel model in which the TX antenna is treated as a CA. The main parameters of significance in the 3D channel model are the delay spread (DS), angle of arrival (AoA), azimuth of departure (AoD), the elevation angle of arrival, and elevation angle of departure [12], [43], [44].

Additionally, the proposed 3GPP standard allows for dynamic adaptation of the antenna's downtilt angles and the elevation angle of the boresight into the channel. According to [40], this offers several benefits for 3D beamforming, which can significantly boost system performance. Fig. 4 illustrates the 3D channel model, where the key parameters have been listed.

The effective channel between s^{th} TX antenna port with M subpath and u^{th} UE antenna port can be expressed as stated in [14], [39] as

$$[\mathbf{H}_{s,u}^{3D}] = \sqrt{\frac{P_n \sigma_{SF}}{M}} \sum_{n=1}^N \alpha_n \begin{bmatrix} \sqrt{G_{TX}^{3D}(\phi_n^{AoD}, \theta_n^{AoD}, \theta_{tilt})} \\ \times \sqrt{G_{RS}^{3D}(\varphi_n^{AoA}, \vartheta_n^{AoA})} \\ \times [a_{RX}(\varphi_n^{AoA}, \vartheta_n^{AoA})]_u \\ \times [a_{TX}(\phi_n^{AoD}, \theta_n^{AoD})]_s \end{bmatrix} \quad (3)$$



θ_{tilt} = Elevation angle of the boresight
 θ_n, ϑ_n = Elevation AoD & AoA of the n^{th} path respectively
 ϕ_n, φ_n = Azimuth AoD & AoA of the n^{th} path respectively

Fig. 4. 3D Channel Model.

where α_n is the complex random amplitude of the n^{th} path. $s = 1, \dots, N_{TX}$, $u = 1, \dots, N_{RS}$, $(\phi_n^{AoD}, \theta_n^{AoD})$ are the azimuth and elevation angles-of-departure (AoD) respectively. $(a_{RX}(\varphi_n^{AoA}, \vartheta_n^{AoD}))$ and $(a_{TX}(\phi_n^{AoD}, \theta_n^{AoD}))$ are the antenna array response of transmitter and receiver antenna respectively. The azimuth and elevation AoA of the n^{th} path respectively $(\varphi_n^{AoA}, \vartheta_n^{AoD})$, and θ_{tilt} are the downtilt angles of the antenna. The gain of the antenna array at the TX is $(\varphi_n^{AoA}, \vartheta_n^{AoA})$, and θ_{tilt} .

$$G_{TX}^{3D}(\varphi_n^{AoD}, \theta_n^{AoD}, \theta_{tilt}) \approx G_{TX,H}(\varphi_n^{AoD}) G_{TX,V}(\theta_n, \theta_{tilt}) \quad (4)$$

where the G_{TX}^{3D} and G_{TX}^{3D} are given by the method in [14] and [45].

$$G_{TX,H}(\varphi^{AoD}) = -12 \left(\frac{\varphi^{AoD}}{\varphi_{3dB}} \right)^2 \quad (5)$$

and

$$G_{TX,V}(\theta^{AoD}, \theta_{tilt}) = -12 \left(\frac{\theta^{AoD} - \theta_{tilt}}{\theta_{3dB}} \right)^2 \quad (6)$$

where φ^{AoD} is the azimuth angle between the user and the boresight of the array in the horizontal domain, θ^{AoD} is the elevation angle between the user and the boresight of the array in the vertical domain, φ_{3dB} and θ_{3dB} are the half-power beamwidth in horizontal and vertical domains, respectively. Equation (5) and (6) provide accurate 3D antenna radiation pattern in both the horizontal and vertical planes respectively.

We consider CA at the TX serving a single antenna RS and UEs with half duplex connection in this model. The path between TX and RS has a single bounce cluster giving us N number of paths. Using CA structure in Fig. 5, we consider the array dimension radius given by $\rho = 4\lambda/l$, where $l = 4\lambda$. If $d_z = 4\lambda/M$ is the wavelength distance in meters between the first and second antenna elements in the z direction, then $4\lambda(m-1)/M$ wavelengths may be used to estimate the placement of the third and fourth antenna components; where $m = 1, \dots, M$ is the number of antenna elements on a ring in the z -axis. λ is the wavelength in meters. The angular position

of the n^{th} element of the m^{th} of the CA on the x - y plane is

$$\varphi_s = 2\pi(n-1)/N \quad (7)$$

Consequently, the location vector of the elements can be expressed as

$$v_t \cdot x_s = \cos(\phi - \varphi_s) \sin \theta \quad (8)$$

Furthermore, the array response of s^{th} transmit antenna port of the CA is given by

$$[a_{TX}(\phi_n^{AoD}, \theta_n^{AoD})]_s = \exp \left(ik\rho \frac{4\lambda(m-1)}{M} \times \cos(\phi_n - \varphi_s) \sin \theta_n^{AoD} \right) \quad (9)$$

Similarly, the response of the u^{th} UE antenna port with regards to the 3D channel model is

$$[a_{RX}(\varphi_n^{AoA}, \vartheta_n^{AoA})]_u = \exp(ik(u-1)d_r \sin \varphi \sin \vartheta) \quad (10)$$

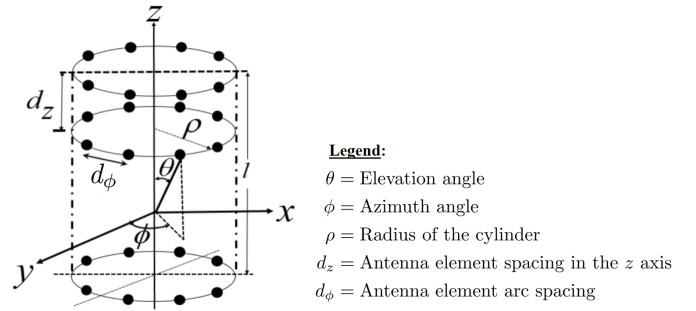


Fig. 5. Cylindrical Array Geometric Structure.

The final 3D GBSM channel model [33], [46], [47] of the communication link in the proposed system in Fig. 3 between a single antenna receiving port u^{th} and a CA transmitter antenna port s^{th} [14] is

$$H_{s,u}^{CA} = \sqrt{\frac{P_n \sigma_{SF}}{M}} \times \sum_{n=1}^N \alpha_n \left[\begin{array}{l} \sqrt{G_{TX}^{3D}(\varphi_n^{AoD}, \theta_n^{AoD}, \theta_{tilt})} \\ \times \exp \left(ik\rho \frac{4\lambda(m-1)}{M} \right. \\ \left. \times \cos(\phi_n - \varphi_s) \sin \theta_n \right) \\ \times \sqrt{G_{RX}^{3D}(\varphi_n^{AoA}, \vartheta_n^{AoA})} \\ \left. \times \exp(ik(u-1)d_r \sin \varphi \sin \vartheta) \right] \quad (11)$$

IV. SYSTEM ANALYSIS

A. Transmission between TX and RS

We presented a 3D GBSM mMIMO CR-NOMA system model [46], [48] with large antenna transmitters such as CA, as shown in Fig. 3 The system model takes into consideration two fundamental presumptions. First of all, TX and UEs cannot directly communicate with one another. Second, in a half-duplex communication mode, users are outfitted with a single antenna. There are two phases to the communication between TX and UEs. During the first step, the TX sends a superposition of two unique signals (\mathbf{x}) to the relay, which

relays it to all UEs after decoding. The received signal (y_{RS}) at the relay is

$$y_{RS} = \sqrt{\alpha_R} \mathbf{h}_{S,R} \mathbf{x} + \eta_R \quad (12)$$

where η_R is the additive white Gaussian noise (AWGN) with unit variance, $\mathbf{h}_{S,R}$ is the proposed 3D GBSM channel coefficient between the TX and RS presented in (11). The distance-dependent path loss, denoted by the expression α_R , depends on the distance between TX and RS and the path loss exponent. The use of the NOMA scheme necessitates that the power coefficients must be placed in the order $\alpha_1 < \alpha_2$, which corresponds to the channel gains.

B. Transmission between RS and UE

1) *Application of DF Coding Scheme:* The TX sends a superimposed signal to the relay during the first time slot in accordance with NOMA concepts. The achievable rates ($R_{x_1}^{RS}$ and $R_{x_2}^{RS}$) for the relay to decode x_1 and x_2 are given [49] by

$$R_{x_1}^{RS} = \text{Blog}_2 \left(1 + \frac{\alpha_1 \gamma |\mathbf{h}_{S,R}|^2}{\alpha_2 \gamma |\mathbf{h}_{S,R}|^2 + 1} \right) \quad (13)$$

and

$$R_{x_2}^{RS} = \text{Blog}_2 \left(1 + \alpha_2 \gamma |\mathbf{h}_{S,R}|^2 \right) \quad (14)$$

where α_1 and α_2 are power allocation associated with x_1 and x_2 respectively.

Given that, the relay can decode the signal from the TX of the two NOMA users, the observable signal (y_k^{DF}) at UE₁ and UE₂ in the second slot may be stated as

$$y_k^{DF} = \mathbf{h}_{R,k} \sqrt{\beta_k} \mathbf{x} + \eta_k \quad (15)$$

where $k = 1, 2$ of users and $\beta_k > 0$ is the power allocation coefficient of the k^{th} user, where $\beta_1 + \beta_2 = 1$.

Following the principle of NOMA scheme, the decoding order at the relay is $x_1 \rightarrow x_2$. The relay first detects x_1 by treating x_2 as noise. It then removes x_1 from the y_{RS} in (12) to detect x_2 . By employing successive interference cancellation (SIC), the signal-to-interference ratio (SINR) ($\gamma_{1,2}^{DF}$) at UE₁ to detect x_2 is given [49] by

$$\gamma_{1,2}^{DF} = \frac{\beta_2 \gamma |\mathbf{h}_{R,1}|^2}{\beta_1 \gamma |\mathbf{h}_{R,1}|^2 + 1} \quad (16)$$

The SINR ($\gamma_{R,1}^{DF}$) for UE₁ to detect its own signal is given by

$$\gamma_{R,1}^{DF} = \beta_1 \gamma |\mathbf{h}_{R,1}|^2 \quad (17)$$

Similarly, the SINR ($\gamma_{R,2}^{DF}$) at UE₂ is given [49] by

$$\gamma_{R,2}^{DF} = \frac{\beta_2 \gamma |\mathbf{h}_{R,2}|^2}{\beta_1 \gamma |\mathbf{h}_{R,2}|^2 + 1} \quad (18)$$

C. Achievable Rates Analysis

The system's maximum achievable rate in the channel is when the BER goes to zero. The achievable rates of UEs may be determined based on the SINR values when the CSI is unknown at the transmitter with independent equi-powered transmissions. With regards to DF coding scheme, the achievable rates at the destination nodes from (16)–(18) are given by

$$\begin{aligned} R_{UE_1}^{DF} &= \min[R_{x_1}^{RS}, \text{Blog}_2(1 + \gamma_{R,1}^{DF})] \quad \text{and} \\ R_{UE_2}^{DF} &= \min[R_{x_2}^{RS}, \text{Blog}_2(1 + \gamma_{R,2}^{DF})] \end{aligned} \quad (19)$$

The relay transmits the decoded signals to all UEs during the second time slot.

D. Outage Probabilities Analysis

To estimate the possibility of an outage event occurring in a data stream where the achievable data rate is lower than the encoded data rate [20], [50], we investigate the outage probability when the UE₁ is capable of detecting x_2 and x_1 . The outage probability (P_1) of UE₁ in relation to the threshold signal-to-noise ratio (SNR) for CR-NOMA users UE₁, UE₂ (denoting Ω_1 , Ω_2 , respectively) may be characterized as follows based on the preceding definition:

$$\begin{aligned} P_1 &= [1 - P_r(\xi_{RS} \geq \xi'_{\Omega_2}, \xi_{RS} \geq \xi'_{\Omega_1})] \\ &\times [1 - P_r(\xi_{1,2}^{DF} \geq \xi'_{\Omega_2}, \xi_1^{DF} \geq \xi'_{\Omega_1})] \end{aligned} \quad (20)$$

where $\xi'_{\Omega_1} = 2^{2\bar{\mathcal{R}}_1} - 1$ and $\xi'_{\Omega_2} = 2^{2\bar{\mathcal{R}}_2} - 1$ are the decoding threshold with $\bar{\mathcal{R}}_1$ and $\bar{\mathcal{R}}_2$ being the target rate of UE₁ and UE₂ respectively. ξ_{RS} is the SINR between TX and RS, ξ_{RS} is the decoding threshold of the direct transmission to the RS. ξ_1^{DF} and ξ_2^{DF} are the SINR defined at (17) and (18). Similarly, the outage probability (P_2) of UE₂ can be expressed as

$$P_2 = P_r(\xi_{RS} < \xi'_{\Omega_2}, \xi_2^{DF} < \xi'_{\Omega_2}) \quad (21)$$

E. Bit-Error Rates Analysis

We provide the bit-error analysis for the proposed CR-NOMA system in accordance with the recommendations in the [51]. According to [51], the average percentage error ($P_e^{UE_1}$) of the UE₁ under the assumption that its symbols are successfully and mistakenly recognized by using SIC processing is

$$\begin{aligned} P_e^{UE_1} &= \frac{1}{2} \left(1 - \sqrt{\frac{\gamma_{B_1}}{2 + \gamma_{B_1}}} \right) \\ &+ \frac{1}{8} \left[\sqrt{\frac{\gamma_{B_2}}{2 + \gamma_{B_2}}} - \sqrt{\frac{\gamma_{B_3}}{2 + \gamma_{B_3}}} \right] \\ &+ \frac{1}{8} \left[\sqrt{\frac{\gamma_{B_4}}{2 + \gamma_{B_4}}} - \sqrt{\frac{\gamma_{B_5}}{2 + \gamma_{B_5}}} \right] \end{aligned} \quad (22)$$

where, for various constellation points of x_1 and x_2 , the SNRs are provided by with signal energies (ε_1 , ε_2).

$$\begin{aligned} \gamma_{B_1} &= \frac{\varepsilon_1}{N_0} E \left[|\mathbf{h}_{R,1}|^2 \right] \\ \gamma_{B_2} &= \frac{(\sqrt{2\varepsilon_2} + \sqrt{\varepsilon_1})^2}{N_0} E \left[|\mathbf{h}_{R,1}|^2 \right] \\ \gamma_{B_3} &= \frac{(\sqrt{2\varepsilon_2} - \sqrt{\varepsilon_1})^2}{N_0} E \left[|\mathbf{h}_{R,1}|^2 \right] \end{aligned} \quad (23)$$

and

$$\begin{aligned}\gamma_{B_4} &= \frac{(2\sqrt{2\varepsilon_2} + \sqrt{\varepsilon_1})^2}{N_0} E \left[|\mathbf{h}_{R,1}|^2 \right] \\ \gamma_{B_5} &= \frac{(2\sqrt{2\varepsilon_2} - \sqrt{\varepsilon_1})^2}{N_0} E \left[|\mathbf{h}_{R,1}|^2 \right]\end{aligned}\quad (24)$$

Equation (24) reflects the circumstance in which UE₁ is unable to detect its signals properly, whereas (23) describes the circumstance in which the signals are successfully detected. Comparably, the UE₂'s overall average BER ($P_e^{UE_2}$) performance from citation [51] is

$$P_e^{UE_2} = \frac{1}{4} \left[\left(1 - \sqrt{\frac{\gamma_{A_1}}{2 + \gamma_{A_1}}} \right) + \left(1 - \sqrt{\frac{\gamma_{A_2}}{2 + \gamma_{A_2}}} \right) \right] \quad (25)$$

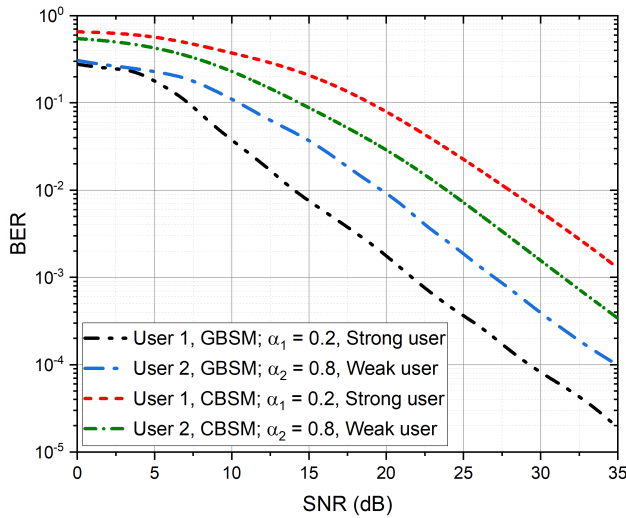


Fig. 6. BER of DF Schemes of the Proposed 3D Channel Model with CA.

where γ_{A_1} and γ_{A_2} are the SNRs of different signal constellation points expressed as

$$\begin{aligned}\gamma_{A_1} &= \frac{(\sqrt{2\varepsilon_2} + \sqrt{\varepsilon_1})^2}{N_0} E \left[|\mathbf{h}_{R,2}|^2 \right], \\ \gamma_{A_2} &= \frac{(\sqrt{2\varepsilon_2} - \sqrt{\varepsilon_1})^2}{N_0} E \left[|\mathbf{h}_{R,2}|^2 \right]\end{aligned}\quad (26)$$

V. NUMERICAL RESULTS AND DISCUSSION

In this section, we validate the proposed 3D channel model for mMIMO CR-NOMA applications using simulation and numerical assessment. By setting the AoA cluster to 0.7 and the AoA offset standard deviations to ($\sigma_{\Delta_\phi}, \sigma_{\Delta_\theta}$) at 2.6 GHz carrier frequency, we are able to analyze the proposed 3D GBSM models. Adjacent antenna elements on the z axis are separated by $l = 4\lambda$ and are situated at a maximum radius of $\rho = 2\pi/l$ from the cylinder centre with respect to the x, y plane. There were two circular arrays in the azimuth domain, each with $N_t = 4$ elements, making up the $2 \times N_t$ number of elements of the CA. Summary of other simulation parameters is listed in Table II

For the TX antenna topology, we calculated the channel coefficient based on the channel realization between the s th

TABLE II. 3D GBSM CR-NOMA MMIMO SIMULATION PARAMETERS

Parameter	Value
Frequency	2.6 GHz
θ_{tilt}	95°
θ_{3dB}	15°
ϕ_{3dB}	70°
Number of clusters	1
Number of users	2
Path-loss exponent	4
Environment	Urban Macrocell
Fixed power allocation	$\alpha_1 = 0.3, \alpha_2 = 0.7$

transmit antenna port and uth receive antenna port. $\theta_{tilt} = 95^\circ$, $\theta_{3dB} = 15^\circ$ and $\phi_{3dB} = 70^\circ$ were taken into consideration to validate the proposed model for the 3D channel modeling from the TX to UEs through RS in Fig. 3. Furthermore, the 3GPP-specified Laplacian distributions are used to describe the power of the azimuth spectrum reaching the RS, multipath components for each AoA, and the multipath delay related to each AoD. We examined the DF in conjunction with the 3D GBSM channel. The outage probability (OP), achievable rate and BER are calculated for the DF coding scheme of Fig. 2 and compared with the outcomes of a system using theoretical channel models such as CBSM throughout.

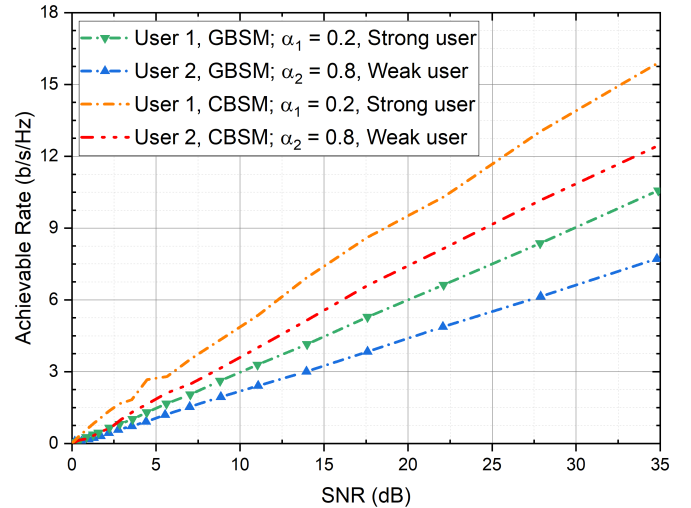


Fig. 7. Achievable Rates of DF of the Proposed 3D Channel Model with CA.

A. BER Performance

The channel coefficients between both the transmitter and the relay have been produced using (11), respectively, for BER performance evaluation. Using (22) and (25), respectively, the BER of UE₁ and UE₂ was calculated. The BER for different SNR values in dB for the proposed 3D GBSM channel model of CA uses 68 antenna components is shown in Figs. 6.

In Fig. 6, the performance of UE₁ is better than that of UE₂, which is owing to the fact that UE₁ is closer to the RS and has a good channel condition than that of UE₂. It should be noted that 3D GBSM models have high computational complexity with unpredictability parameters which could affect

TABLE III. COMPARISON OF OP AND BER WITH PRIOR WORKS AT SNR OF 20 dB

Ref	Antenna Type	No. of Users	BER	OP
Proposed	Multiple antenna TX, single antenna RS and UE	2	$10^{-2.85}$	$10^{-2.50}$
[20]	Single antenna TX, RS and UE	2	$10^{-2.10}$	$10^{-1.50}$
[52]	Single antenna TX, RS and UE	2	-	$10^{-0.80}$
[53]	Single antenna TX, RS and UE	1	$10^{-2.70}$	-
[54]	Single antenna TX, RS and UE	2	$10^{-4.96}$	-
[55]	Multiple antenna TX, single antenna RS and UE	1	-	$10^{-2.45}$
[56]	Multiple antenna TX, UE, single antenna RS	1	-	$10^{-0.28}$

the performance of the system. However, our results on the BER using DF coding strategy at 20 dB are comparable to prior works done in the literature that employs the CBSM channel models (Table III). This may be due to the use of the antenna element placement vector, which we defined based on the physical structure of the antenna as described in Fig. 5. Table III compares the proposed system’s outage probability and BER performance to previous research studies that employ the CBSM channel model which confirms the results of Fig. 6. Except for [52], which contains M relays, all other references including the proposed system employ a single relay device.

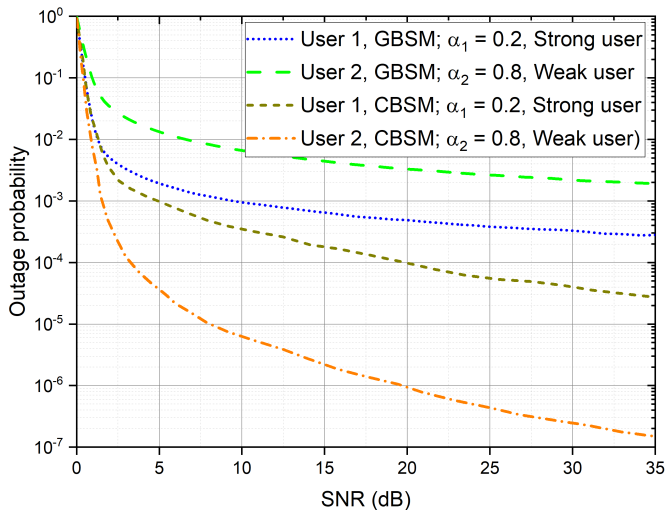


Fig. 8. Comparison of OP of Two Users using DF Scheme of the Proposed Channel Models with CA.

In contrast to GBSM, which has high computational complexity, a high proportion of random propagation, and channel parameters like path-loss, delay profile, tilt angle, angle of arrival, angle of departure, etc. that reflect realistic and practical mMIMO systems, CBSM is primarily used for link-level simulation and to analyze the theoretical performance of mMIMO systems. Consequently, CBSM performance is

superior to GBSM as indicated in Table III and the figures above.

B. Achievable Rate and Outage Probability Performances

Equation (19) calculates the achievable rates of DF for the achievable rate analysis. In Fig. 7, the achievable rate of using DF coding scheme shows considerable improvement as compared with the results of CBSM. We demonstrate the outage performance of the proposed system as a function of transmit SNR in Fig. 8 by using 3D GBSM channel model with CA in (11). The performance differences between two users, UE₁ and UE₂, extends over the entire SNR range. The system outage performance may be significantly improved by changing the transmitter array configuration, increasing the TX’s antenna capacity, and maintaining a single antenna at the relay node. Furthermore, it reveals that UE₂ has a worse outage than UE₁. This is expected since further from the RS than UE₁, and therefore, it has poor channel condition.

Again, the system uses less transmit power at the relay for RS–UEs links to process the second-hop signal, which decreases the performance of the hop’s outage. Fig. 8 gives the outage probability of the two users using the 3D GBSM channel and the DF relay coding strategy. It can be demonstrated that the OP of the DF coding scheme performs better with the 3D GBSM channel model.

VI. CONCLUSION AND FUTURE WORK

We provided a 3D GBSM channel model between TX–RS and TX–UEs in this study. We investigated a two-stage mMIMO CR-NOMA downlink system with a 3D GBSM channel model, where the transmitter is represented by CA. We defined the antenna placement vector based on the physical structure of the antenna design to reduce the computational complexity of the channel. For improved channel performance, the proposed 3D GBSM channel model uses a DF network coding scheme. For the two-stage system, we calculated the probability of an outage, the achievable rate, and the BER. In terms of outage probability, attainable rate, and other crucial network performance parameters, integrating NOMA with cooperative relay transmission mechanism guarantees a notable boost to the performance of the 5G networks. The outage probability of cooperative relay integrated NOMA over a 3D GBSM channel is explored in this work. Lastly, despite the fact that the proposed 3D GBSM channel model has a greater computational cost in terms of complexity, the results show that the differences in performance between CBSM and GBSM channel models are marginal. The marginal performance of CBSM over the GBSM model is due to the channel model’s lower computing complexity and less random channel parameters, which makes it suitable for theoretical analysis of mMIMO systems. The research may be expanded to include millimetre-wave CR-NOMA with multiple antennas at the TX, RS, and UE. The influence of spatial correlation of antenna array arrangement on 3D GBSM performance in CR-NOMA system may be explored for certain applications such as high-speed train communication, unmanned aerial vehicle, the vast internet of things, and so on.

ACKNOWLEDGMENT

The authors are grateful to Ghana National Petroleum Corporation Foundation and Center for RFIC and System Technology, School of Communication and Information Engineering, University of Electronic Science and Technology of China for their contribution.

REFERENCES

- [1] M. W. Akhtar, S. A. Hassan, R. Ghaffar, H. Jung, S. Garg, and M. S. Hossain, "The shift to 6g communications: vision and requirements," *Human-centric Computing and Information Sciences*, vol. 10, no. 1, pp. 1–27, 2020.
- [2] I. Rosaline, A. Kumar, P. Upadhyay, and A. H. Murshed, "Four element mimo antenna systems with decoupling lines for high-speed 5g wireless data communication," *International Journal of Antennas and Propagation*, vol. 2022, 2022.
- [3] A. Al-Ansi, A. M. Al-Ansi, A. Muthanna, I. A. Elgendy, and A. Koucheryavy, "Survey on intelligence edge computing in 6g: Characteristics, challenges, potential use cases, and market drivers," *Future Internet*, vol. 13, no. 5, p. 118, 2021.
- [4] O. Omarov, G. Naurzybayev, S. Arzykulov, M. S. Hashmi, and A. M. Eltawil, "Capacity analysis of wireless powered cooperative noma networks over generalized fading," in *2021 IEEE Wireless Communications and Networking Conference (WCNC)*. IEEE, 2021, pp. 1–6.
- [5] A. Al Amin and S. Y. Shin, "Capacity analysis of cooperative noma-mimo based full-duplex relaying for 6g," *IEEE Wireless Communications Letters*, vol. 10, no. 7, pp. 1395–1399, 2021.
- [6] I. Budhiraja, N. Kumar, S. Tyagi, S. Tanwar, Z. Han, D. Y. Suh, and M. J. Piran, "A systematic review on noma variants for 5g and beyond," *IEEE Access*, 2021.
- [7] S. R. Islam, M. Zeng, O. A. Dobre, and K.-S. Kwak, "Resource allocation for downlink noma systems: Key techniques and open issues," *IEEE Wireless Communications*, vol. 25, no. 2, pp. 40–47, 2018.
- [8] A. Akbar, S. Jangsher, and F. A. Bhatti, "Noma and 5g emerging technologies: A survey on issues and solution techniques," *Computer Networks*, vol. 190, p. 107950, 2021.
- [9] L. Han, R. Liu, Z. Wang, X. Yue, and J. S. Thompson, "Millimeter-wave mimo-noma-based positioning system for internet-of-things applications," *IEEE Internet of Things Journal*, vol. 7, no. 11, pp. 11 068–11 077, 2020.
- [10] E. J. Oughton, W. Lehr, K. Katsaros, I. Selinis, D. Bublely, and J. Kusuma, "Revisiting wireless internet connectivity: 5g vs wi-fi 6," *Telecommunications Policy*, vol. 45, no. 5, p. 102127, 2021.
- [11] R. Shankar, "Examination of a non-orthogonal multiple access scheme for next generation wireless networks," *The Journal of Defense Modeling and Simulation*, vol. 19, no. 3, pp. 453–465, 2022.
- [12] K. Zheng, S. Ou, and X. Yin, "Massive mimo channel models: A survey," *International Journal of Antennas and Propagation*, vol. 2014, 2014.
- [13] P. Zhang, J. Chen, X. Yang, N. Ma, and Z. Zhang, "Recent research on massive mimo propagation channels: A survey," *IEEE Communications Magazine*, vol. 56, no. 12, pp. 22–29, 2018.
- [14] A. E. Ampoma, G. Wen, Y. Huang, K. O. Gyasi, P. I. Tebe, and K. Ntiemoah-Sarpong, "Spatial correlation models of large-scale antenna topologies using maximum power of offset distribution and its application," *IEEE Access*, vol. 6, pp. 36 295–36 304, 2018.
- [15] K. Zheng, L. Zhao, J. Mei, B. Shao, W. Xiang, and L. Hanzo, "Survey of large-scale mimo systems," *IEEE Communications Surveys & Tutorials*, vol. 17, no. 3, pp. 1738–1760, 2015.
- [16] D. He, B. Ai, K. Guan, L. Wang, Z. Zhong, and T. Kürner, "The design and applications of high-performance ray-tracing simulation platform for 5g and beyond wireless communications: A tutorial," *IEEE Communications Surveys & Tutorials*, vol. 21, no. 1, pp. 10–27, 2018.
- [17] S. Joshi and M. S. Bhakta, "Power efficient multi-relay cooperative diversity in wireless network using hybrid relaying protocol," in *Future of Information and Communication Conference*. Springer, 2020, pp. 60–78.
- [18] M. B. Uddin, M. F. Kader, and S. Y. Shin, "Cooperative relaying using mimo noma," in *2018 4th international conference on wireless and telematics (ICWT)*. IEEE, 2018, pp. 1–6.
- [19] M. Liaqat, K. A. Noordin, T. A. Latef, and K. Dimiyati, "Power-domain non orthogonal multiple access (pd-noma) in cooperative networks: an overview," *Wireless Networks*, vol. 26, no. 1, pp. 181–203, 2020.
- [20] K. Ntiemoah-Sarpong, Z. Huang, G. Wen, and A. E. Ampoma, "Performance of non-orthogonal multiple access: analysis using compute-and-forward cooperative relaying in 5g networks," *IET Communications*, vol. 14, no. 17, pp. 3058–3064, 2020.
- [21] M. Zeng, W. Hao, O. A. Dobre, and Z. Ding, "Cooperative noma: State of the art, key techniques, and open challenges," *IEEE Network*, vol. 34, no. 5, pp. 205–211, 2020.
- [22] V. Goutham and V. Harigovindan, "Full-duplex cooperative relaying with noma for the performance enhancement of underwater acoustic sensor networks," *Engineering Science and Technology, an International Journal*, 2021.
- [23] J. Sushma, M. N. Gayathri, S. Srivani, V. N. Nayak, and K. K. Gurralla, "Performance analysis and power allocation for multi relay wireless cooperative noma networks with diversity combining strategies," in *2020 IEEE International Students' Conference on Electrical, Electronics and Computer Science (SCEECS)*. IEEE, 2020, pp. 1–6.
- [24] G. Li, D. Mishra, Y. Hu, Y. Huang, and H. Jiang, "Adaptive relay selection strategies for cooperative noma networks with user and relay cooperation," *IEEE Transactions on Vehicular Technology*, vol. 69, no. 10, pp. 11 728–11 742, 2020.
- [25] Z. Zhang and Z. Si, "Performance evaluation and optimization of cooperative noma over rayleigh fading channels," in *2020 IEEE International Conference on Communications Workshops (ICC Workshops)*. IEEE, 2020, pp. 1–6.
- [26] H. Wang, R. Shi, K. Tang, J. Dong, and S. Liao, "Performance analysis and optimization of a cooperative transmission protocol in noma-assisted cognitive radio networks with discrete energy harvesting," *Entropy*, vol. 23, no. 6, p. 785, 2021.
- [27] G. Alnwaimi, H. Boujemaa, and K. Arshad, "Throughput optimization of cooperative non orthogonal multiple access," *Telecommunication Systems*, vol. 76, no. 3, pp. 359–370, 2021.
- [28] K. Reshma and A. Babu, "Cooperative noma system with incremental relaying and energy harvesting: Performance analysis and optimization," *Transactions on Emerging Telecommunications Technologies*, vol. 31, no. 9, p. e4075, 2020.
- [29] A. Nazari, M. R. Javan, and S. S. Hosseini, "Resource allocation in power domain noma-based cooperative multicell networks," *IET Commun.*, vol. 14, no. 7, pp. 1162–1168, 2020.
- [30] A. Rezaei, P. Azmi, N. M. Yamchi, M. R. Javan, and H. Yanikomeroğlu, "Robust resource allocation for cooperative miso-noma-based heterogeneous networks," *IEEE Transactions on Communications*, vol. 69, no. 6, pp. 3864–3878, 2021.
- [31] J. Kaur and M. L. Singh, "User assisted cooperative relaying in beamspace massive mimo noma based systems for millimeter wave communications," *China Communications*, vol. 16, no. 6, pp. 103–113, 2019.
- [32] X. Chen, R. Jia, and D. W. K. Ng, "The application of relay to massive non-orthogonal multiple access," *IEEE Transactions on Communications*, vol. 66, no. 11, pp. 5168–5180, 2018.
- [33] T. Zhou, Y. Yang, L. Liu, C. Tao, and Y. Liang, "A dynamic 3-d wideband gbsm for cooperative massive mimo channels in intelligent high-speed railway communication systems," *IEEE Transactions on Wireless Communications*, 2020.
- [34] G. Li and D. Mishra, "Cooperative noma networks: User cooperation or relay cooperation?" in *ICC 2020-2020 IEEE International Conference on Communications (ICC)*. IEEE, 2020, pp. 1–6.
- [35] R. R. Kurup, S. Mahin, M. Sandhyana, V. Priyanka, A. Babu *et al.*, "Outage performance of cooperative noma system in log-normal fading channels," in *2020 IEEE International Conference on Electronics, Computing and Communication Technologies (CONECT)*. IEEE, 2020, pp. 1–6.
- [36] M. Aldababsa and O. Kucur, "Outage and ergodic sum-rate performance of cooperative mimo-noma with imperfect csi and sic," *International Journal of Communication Systems*, vol. 33, no. 11, p. e4405, 2020.

- [37] A. L. Imoize, A. E. Ibhaze, A. A. Atayero, and K. Kavitha, "Standard propagation channel models for mimo communication systems," *Wireless Communications and Mobile Computing*, vol. 2021, 2021.
- [38] T. Zugno, M. Polese, N. Patriciello, B. Bojović, S. Lagen, and M. Zorzi, "Implementation of a spatial channel model for ns-3," in *Proceedings of the 2020 Workshop on ns-3*, 2020, pp. 49–56.
- [39] Q.-U.-A. Nadeem, A. Kammoun, M. Debbah, and M.-S. Alouini, "Spatial correlation characterization of a uniform circular array in 3d mimo systems," in *2016 IEEE 17th International Workshop on Signal Processing Advances in Wireless Communications (SPAWC)*, 2016, pp. 1–6.
- [40] A. Kammoun, M. Debbah, M.-S. Alouini *et al.*, "3d massive mimo systems: Modeling and performance analysis," *IEEE Transactions on wireless communications*, vol. 14, no. 12, pp. 6926–6939, 2015.
- [41] L. Bai, Z. Huang, Y. Li, and X. Cheng, "A 3d cluster-based channel model for 5g and beyond vehicle-to-vehicle massive mimo channels," *IEEE Transactions on Vehicular Technology*, vol. 70, no. 9, pp. 8401–8414, 2021.
- [42] E. Björnson, J. Hoydis, M. Kountouris, and M. Debbah, "Massive mimo systems with non-ideal hardware: Energy efficiency, estimation, and capacity limits," *IEEE Transactions on information theory*, vol. 60, no. 11, pp. 7112–7139, 2014.
- [43] K. Guan, D. He, B. Ai, Y. Chen, C. Han, B. Peng, Z. Zhong, and T. Kuerner, "Channel characterization and capacity analysis for thz communication enabled smart rail mobility," *IEEE Transactions on Vehicular Technology*, vol. 70, no. 5, pp. 4065–4080, 2021.
- [44] K. Guan, B. Ai, D. He, F. Zhu, H. Yi, J. Dou, and Z. Zhong, "Channel sounding and ray tracing for thz channel characterization," in *2020 13th UK-Europe-China Workshop on Millimetre-Waves and Terahertz Technologies (UCMMT)*. IEEE, 2020, pp. 1–3.
- [45] J. Meredith, "Study on channel model for frequency spectrum above 6 ghz," *3GPP TR 38.900, Jun. Tech. Rep.*, 2016.
- [46] Y. Zheng, L. Yu, R. Yang, and C.-X. Wang, "A general 3d non-stationary massive mimo gbsm for 6g communication systems," in *2021 IEEE Wireless Communications and Networking Conference (WCNC)*. IEEE, 2021, pp. 1–6.
- [47] W. Zeng, Y. He, B. Li, and S. Wang, "3d multiple-antenna channel modeling and propagation characteristics analysis for mobile internet of things," *Sensors*, vol. 21, no. 3, p. 989, 2021.
- [48] Y. Xie, B. Li, X. Zuo, M. Yang, and Z. Yan, "A 3d geometry-based stochastic model for 5g massive mimo channels," in *2015 11th International Conference on Heterogeneous Networking for Quality, Reliability, Security and Robustness (QSHINE)*. IEEE, 2015, pp. 216–222.
- [49] Z. Wang, Z. Peng, Y. Pei, and H. Wang, "Performance analysis of cooperative noma systems with incremental relaying," *Wireless Communications and Mobile Computing*, vol. 2020, 2020.
- [50] Z. Zhang, P. Dong, X. Tan, Y. Li, and K. Xiong, "Outage performance of wireless powered decode-and-forward relaying networks in rician fading," *Entropy*, vol. 24, no. 6, p. 763, 2022.
- [51] F. Kara and H. Kaya, "Ber performances of downlink and uplink noma in the presence of sic errors over fading channels," *IET Communications*, vol. 12, no. 15, pp. 1834–1844, 2018.
- [52] Z. Yang, Z. Ding, Y. Wu, and P. Fan, "Novel relay selection strategies for cooperative noma," *IEEE Transactions on Vehicular Technology*, vol. 66, no. 11, pp. 10 114–10 123, 2017.
- [53] X. Wu and L.-L. Xie, "On the optimal compressions in the compress-and-forward relay schemes," *IEEE Transactions on Information Theory*, vol. 59, no. 5, pp. 2613–2628, 2013.
- [54] Q. Li, M. Wen, E. Basar, H. V. Poor, and F. Chen, "Spatial modulation-aided cooperative noma: Performance analysis and comparative study," *IEEE Journal of Selected Topics in Signal Processing*, vol. 13, no. 3, pp. 715–728, 2019.
- [55] T. M. Hoang, B. C. Nguyen, X. N. Tran, and L. T. Dung, "Outage probability and ergodic capacity of user clustering and beamforming mimo-noma relay system with imperfect csi over nakagami- m fading channels," *IEEE Systems Journal*, pp. 1–12, 2020.
- [56] C.-B. Le, D.-T. Do, and M. Voznak, "Wireless-powered cooperative mimo noma networks: Design and performance improvement for cell-edge users," *Electronics*, vol. 8, no. 3, p. 328, 2019.

A Decision Concept to Support House Hunting

Tanjim Mahmud¹
Department of Computer
Science and Engineering
Rangamati Science and
Technology University, Bangladesh

Dilshad Islam²
Department of Physical and
Mathematical Sciences
Chattogram Veterinary and Animal
Sciences University, Bangladesh

Manoara Begum³
Department of Computer
Science and Engineering
Port City International
University, Bangladesh

Sudhakar Das⁴
Department of Computer
Science and Engineering
Rangamati Science and
Technology University, Bangladesh

Lily Dey⁵
Department of Computer
Science and Engineering
University of Chittagong, Bangladesh

Koushick Barua⁶
Department of Computer
Science and Engineering
Rangamati Science and
Technology University, Bangladesh

Abstract—House hunting, or the act of seeking for a place to live, is one of the most significant responsibilities for many families around the world. There are numerous criteria/factors that must be evaluated and investigated. These traits can be both statistically and qualitatively quantified and expressed. There is also a hierarchical link between the elements. Furthermore, objectively/quantitatively assessing qualitative characteristics is difficult, resulting in data inconsistency and, as a result, uncertainty. As a result, ambiguity must be dealt with using the necessary processes; otherwise, the decision to live in a particular property would be incorrect. To compare criteria, the Analytic Hierarchy Process (AHP) is employed, evidential reasoning is used to evaluate houses based on each criterion, and TOPSIS is used to rank house sites for selection. It was necessary to analyze qualitative and quantitative elements, as well as economic and social features of these residences, in order to arrive at the final order of houses, which was not an easy process. As a result, the authors developed a decision support model to aid decision makers in the management of activities related to finding a suitable dwelling. This study describes the development of a decision support system (DSS) capable of providing an overall judgment on the location of a house to live in while taking into account both qualitative and quantitative factors.

Keywords—AHP; multiple criteria decision Making (MCDM); uncertainty; evidential reasoning

I. INTRODUCTION

Chittagong is a lovely town with a business district that looks out over the port. Because of its tranquil and secure environment, Chittagong attracts a large number of families. However, house seeking is a tedious activity in Chittagong and around the world. It's difficult to find the right neighborhood to reside in without first conducting extensive research into the city's many communities. For a home buyer or renter, selecting the most amazing house is a multi-step procedure. It necessitates the measurement and evaluation of a large number of criteria at the same time. Because several of these criteria are linked, they frequently collide, with one improvement usually resulting to a decrease in another [1]. Furthermore, because house features are quantifiable and qualitatively expressed, decision-makers must consider both quantitative and subjective data [2]. House hunting in Bangladesh is a terrible since various real estate businesses employ static ways to find houses

in databases [1], such as the typical search methodology as shown in Fig. 1. This is a time-consuming procedure that yields no relevant results. As a result, potential homeowners may still miss out on their desired property.

In real life, MCDM issues are fairly common. One of the issues is house hunting. Many concepts have been proposed to address the home hunting dilemma but no model provides proper ranking or human level accuracy due to some limitation. Analytical Hierarchical Process technique can handle both quantitative and qualitative information [1, 2]. A multiple criteria decision model with a hierarchical structure is provided for the house-buying process, in which both quantitative and qualitative information is represented in a combined manner [3, 4]. After that, the AHP [5] approach is used to fully investigate the house hunting problem. As a result, the paper discusses the design, development, and implementation of a Decision Support System [6] that can accurately find a suitable house in a short amount of time at a low cost but this paper could not address the uncertainty.

Research [7] contains a lot of evidence. Using a belief structure to characterize an assessment as a distribution is advised for house seeking with 16 criteria and 5 alternatives. Four alternative evaluation grades were used to calculate the degree of belief: excellent, good, average, and bad. The ER approach was used to compute the cumulative degree of trust for a hierarchy's top level attribute based on its bottom level

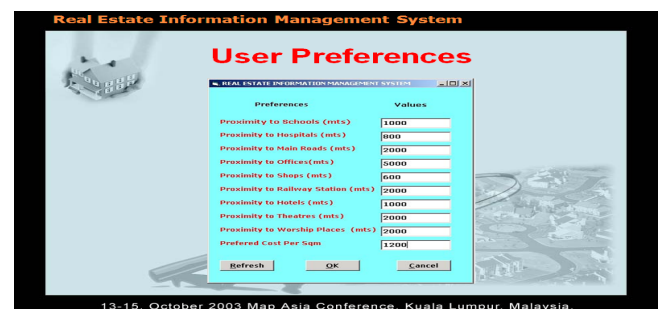


Fig. 1. Scenario in Bangladesh.

attribute. After that, the utility function was used to rank the various options. Many authors have solved various problems using AHP. The AHP technique was presented by Lakshmanan [8] for the condition ranking of reinforced concrete bridges. Rashidi et al. [9] developed a decision-making system for steel bridge asset management that meets acceptable safety, functionality, and sustainability criteria. Mahmoud et al. [10] demonstrated how to conduct a genuine bridge evaluation, which includes visual examination and data collection in order to provide an accurate estimate of the bridge's restoration and road network priority. As a result, a Bridge Overall Need Indicator was developed, which assigns a rating to bridges depending on their condition and priority for maintenance. For the selected bridges and their rehabilitation priority ranking, the Approach for Order Preference by Similarity to an Ideal Solution (TOPSIS) [11] technique is also used as a multi-criteria analysis tool. The Euclidian distances between each option from the ideal and anti-ideal alternative are determined when the ideal and anti-ideal alternatives have been found. Finally, the relative closeness (RC) of the bridges is shown, with the bridge with the lowest RC obtaining the highest repair priority. Paper [12] experiments with *Temnothorax albipennis* ant colonies in order to select the best one, compare and contrast huge and tiny colonies. The ant [13] colony house-hunting challenge has been approached from a distributed computing standpoint [14]. Where two different types of algorithms are shown.

There has never been a study that combined the AHP, TOPSIS, and evidential reasoning to develop a house priority ranking that has been shown to be more precise and accurate than previous methods. In this approach, a new concept for selecting outstanding houses is suggested. The goal hierarchy [15] structure is developed in three stages with the help of interactive groups [16]. Real estate professionals, economic specialists, and users make up four different types of decision makers. Each expert developed criteria based on their knowledge and experience. The Analytic Hierarchy Process (AHP) method is used to compute Saaty's scale criteria weights [17, 18]. Depending on whether the criterion is qualitative or quantitative; it is assigned an interval rating. These ratings are also used to rate the houses within each category. Each group developed a set of common evaluations based on feedback from all of the participants. The evidential reasoning approach is used to determine the house assessments based on each criterion. The aggregated belief judgment matrix is used to determine the final house evaluations. Furthermore, the Technique for Order Preference by Similarity to an Ideal Solution (TOPSIS) [17] technique is utilized to rank the shortlisted houses based on a multi-criteria analysis. The Euclidian distances between each option from the ideal and anti-ideal alternative are determined when the ideal and anti-ideal alternatives have been found. Finally, the relative closeness (RC) is displayed, with the option with the lowest RC being chosen first. The proposed solution is based on a multi-criteria analysis, which would improve decision-making quality in the home site selection process.

The study is broken into five sections. Sections II, III and IV covers the theoretical basis of multi-criteria procedures like AHP, TOPSIS, and evidential reasoning, followed by a discussion of the suggested model. Section V states the proposed concept. In Section VI, the obtained results are

provided, and throughout the discussion and the obtained results are compared to those of previous studies. This section also examines the new proposed model's advantages and disadvantages.

II. AHP FOR HOUSE HUNTING

In Bangladesh and around the world, the home hunting problem (HHP) is a big concern [2]. It takes into account both qualitative and quantitative criteria, such as closeness to hospitals, major roads, educational institutions, shops, offices, recreation centers, and police precincts. Multiple criterion's decision-making (MCDM) is a technique for determining the "best" home for a customer by balancing a number of aspects. The majority of these factors are linked in some way. Furthermore, as one criterion improves, it is common for many others to improve as well. Using language traits, DMs can make subjective assessments more easily. However, merging these two sorts of indicators, one quantitative and the other linguistic, can be difficult, which could generate issues when evaluating solutions. As a result, any MCDA method must be capable of aggregating these two types of measures consistently and reliably, resulting in a ranking of all decision options [19]. We gave some of the house searchers the same list of criteria they used for the house hunting problem [2] and asked them to choose the factors they consider when purchasing a property. We found that 80% of house hunters failed to meet the following criteria: pleasant neighborhood, proximity to stores, proximity to bus and rail stations, proximity to recreation center, police precincts, property insurance, and population density [2]. Qualitative and quantitative parameters such as proximity to a main road, a hospital, an office, a school, and cost per square foot [1] impact house hunting.

The nine comparisons in Fig. 2 were combined into a matrix. We have a 9 by 9 matrix because we have 9(nine) comparisons. We just need to fill up the upper triangular matrix because the diagonal components of the matrix are always 1. The following two rules [1, 20] are used to fill the upper triangular matrix:

1. Utilize the true judgment value if the judgment value is on the left side of one.
2. Utilize the reciprocal value if the judgment value is on the right side of 1. utilize the reciprocal values of the top

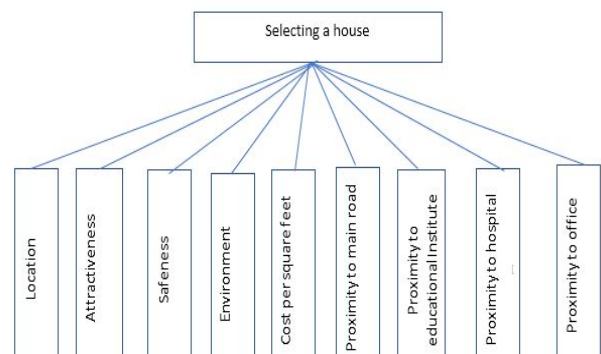


Fig. 2. Structure of Problem.

TABLE I. COMPARISON MATRIX OF CRITERIA

Criteria	Location	Attractiveness	Safeness	Environment	Prox. edu. org.	Prox. hospital	Prox. main roads	Prox. office	Cost per sq. ft
Location	1	2	1/3	1/4	1/5	1/6	4	1/5	1/2
Environment	4	3	1/4	1	4	1/3	7	1/3	1/2
Safeness	3	2	1	4	5	2	3	2	2
Prox. edu. org.	5	6	1/5	1/4	1	1/8	9	5	2
Prox. hospital	6	4	1/2	3	8	1	8	1/7	1/5
Prox. main roads	1/4	1/2	1/3	1/7	1/9	1/8	1	5	2
Prox. office	5	4	1/2	3	1/5	7	1/5	1	1/2
Cost per sq. ft	2	4	1/2	2	1/2	5	1/2	2	1

diagonal [1] to fill the lower triangular matrix. If a_{ij} is a row i and column j element in the matrix, the bottom diagonal is filled using eq. (1):

$$a_{ij} = \frac{1}{a_{ji}} \quad (1)$$

Users define their preferences for one criterion over another is illustrated in Table I, in the form of a comparison matrix. The comparison matrix's entries, which range from 1 to 9, represent the degree to which one criterion is preferred over another. For example, the 9 in the "Proximity to education institution" row against "Proximity to main roads" column indicates that "Proximity to education institution" is preferred over "Proximity to main road".

A. Criteria Weights

It is important to normalize the prior comparison matrix in Table I, in order to evaluate and assign relative weights to each condition. Normalization is performed by dividing each table value by the total column value, as shown in eq. (2).

$$Z_{ij} = A_{ij} / \sum_{i=0}^n A_{ij} \quad (2)$$

The sum of all elements in a column in the normalized primary Eigen vector displayed in Table II is 1. Because it is normalized, the total of all elements in a column is 1.

The priority vector is then calculated by averaging each row in Table I and setting the overall priority vector to 1.

TABLE II. CRITERIA WEIGHTS

Location	0.05
Attractiveness	0.04
Safeness	0.17
Environment	0.10
Prox. edu. org.	0.15
Prox. hospital	0.16
Prox. mainroad	0.08
Prox. office	0.14
Cost per sq.ft	0.12

The priority vector represents the relative weights of the items we've compared. 5% for location, 4% for attractiveness, 17% for safety, 10% for the environment, 15% for proximity to education, 16% for proximity to hospital, 8% for proximity to main road, 14% for proximity to office, and 12% for cost per square foot. The most important selection criterion for a property buyer is safety, which is followed by the other elements. More than their rating is required in this scenario. The relative weight, in reality, is a ratio scale that can be divided among them. Customers value safety 3.4 (=17/5) times more than location and 2.1 (=17/8) times more than accessibility to a major route, for example.

III. EVIDENTIAL REASONING

The evidential reasoning algorithm lies at the heart of the ER approach. This method was created using an evaluation analysis model [1, 21] and the Dempster-Shafer theory's evidence combination rule [22, 23], which is well-suited to dealing with incomplete uncertainty [24]. The ER method models an assessment as a distribution using a belief framework. It differs from prior Multi Criteria Decision Making (MCDM) modeling systems in that it reaches a result using evidence-based reasoning [15]. This method has the advantage of being able to deal with the uncertainties that arise in MCDM situations when dealing with quantitative and qualitative data [1, 2].

A. Assessment

The ER algorithm has strategies for dealing with such ignorance, as will be demonstrated. It's also important to distribute the degree of confidence throughout evaluation classes for some quantitative input data. If the hospital is within 1 kilometer of the residence, it is considered great, average if it is within 1.5 kilometers, ordinary if it is within 2 kilometers, and horrible if it is within 3 kilometers. However, when a hospital is only 1.3 kilometers away, it can be both beneficial and dangerous. It is crucial, however, that we recognize the distinction between exceptional and regular belief. This phenomena can be calculated using the method provided below [1, 23].

$$\beta_{n,i} = \frac{h_{n+1} - h}{h_{n+1,i} - h_{n,i}}, \beta_{n+1,i} = 1 - \beta_{n,i} \text{ if } h_{n,i} \leq h \leq h_{n+1,i} \quad (3)$$

As a result, equation (3) can be used to evaluate the distribution of degree of belief within 1.3 km of the hospital's

position from the residence, obtaining the following results: (Excellent, 0.4), (Good, 0.6), (Average, 0), (Bad,0).

B. Weight Normalization

Determining the value of the traits is crucial since each characteristic serves a specific purpose in the decision-making process. At level , there are eight sub attributes in the “Facilities” category, including proximity to educational institutions, major roads, hospitals, shops, offices, bus and railway stations, police precincts, and recreation centers. When evaluating their parent characteristic “Facilities”, it’s critical to determine which of the eight features is the most important. This can be accomplished using a variety of weight normalization approaches, including Eigenvector, AHP, and Pairwise comparison [1, 24].

$$\omega_i = \frac{y_i}{\sum_{i=1}^j y_i}; i = 1 \dots \dots \dots j \quad (4)$$

$$\sum_{i=1}^L \omega_i = 1 \quad (5)$$

Equation (4) is used to estimate the significance of an attribute (w_i). This has been designed by dividing the significance of an element (y_i) by the $\sum_{i=1}^j Y_i$ summation of significance of all the elements. Equation (5) is to see if the sum of the importance of all the qualities was one or if they were normalized.

C. Basic Probability Assignment

Not resembles to Dempster-Shafer [25] evidence theory finding degrees of belief in the attribute evaluation grades must be converted into fundamental probability masses using equation (6). The fundamental probability mass represents the precise belief provided to an attribute’s n-th evaluation grade. It also demonstrates how strong the evidence is in support of the attribute’s n-th evaluation grade(H_n) [23].

$$m_{n,i} = m_i(H_n) = w_i \beta_{n,i}(a_i), \quad n = 1, \dots, N; i = 1, \dots, L \quad (6)$$

After the i-th attribute has been examined, the residual probability mass unassigned to any given grade can be calculated using the equation below.

$$m_{H,i} = m_i(H) = 1 - \sum_{n=1}^N m_{n,i} = 1 - w \sum_{n=1}^N \beta_{n,i}(a_i), i = 1, \dots, L \quad (7)$$

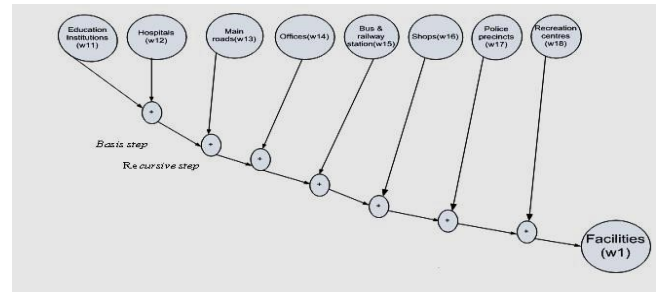


Fig. 3. Recursive Assessment.

D. Kernel of ER Approach

The ER approach calculates the cumulative degree of confidence at the top level attribute of a hierarchy using the hierarchy’s bottom level features, also known as fundamental attributes. An excellent information synthesizing/aggregation process achieves this. A recursive ER algorithm is used to aggregate fundamental attributes, which can be stated as $A(S) = \{(H_n, \beta_n), n = 1, \dots, N\}$ evaluating the cumulative degree of confidence of the top level attribute in a hierarchy. In this recursive ER algorithm, all the basic attributes are aggregated recursively in the following manner as shown in Fig. 3.

$$M_1 = \begin{bmatrix} m_{11} & m_{21} & m_{31} & m_{41} & m_{H1} \\ m_{12} & m_{22} & m_{32} & m_{42} & m_{H2} \\ m_{13} & m_{23} & m_{33} & m_{43} & m_{H3} \\ m_{14} & m_{24} & m_{34} & m_{44} & m_{H4} \\ \dots & \dots & \dots & \dots & \dots \\ \dots & \dots & \dots & \dots & \dots \\ \dots & \dots & \dots & \dots & \dots \\ m_{18} & m_{28} & m_{38} & m_{48} & m_{H8} \end{bmatrix}$$

From matrix M_1 , it can be seen that each sub-attribute is associated with five basic probability assignment (bpa), where four first four bpa ($m_{11}, m_{21}, m_{31}, m_{41}$ are associated with four evaluation grades (H_1, H_2, H_3, H_4) and final bpa i.e. is showing the remaining probability mass unassigned to any individual grades after the assessments on sub-attribute have been considered. The aggregation is carried out in a recursive way. This aggregation can be achieved by using the following equation(8) , which will yield combined bpa (such as $m_{1I(2)}, \dots, m_{4I(2)}$) as shown in the first row of the second matrix [1, 23].

$$m_{1I(2)} = K_{I(2)}(m_{11}m_{12} + m_{H1}m_{12} + m_{H2}m_{11}) \quad (8)$$

Similarly $m_{2I(2)}, m_{3I(2)}, m_{4I(2)}$ can be calculated.

Where $K_{I(2)}$ is a normalization factor used to resolve the conflict and this can be calculated using the equation (9) [1, 23].

$$K_{I(i+1)} = \left[1 - \sum_{n=1}^N \sum_{t=1, t \neq n}^N m_{n,(i)} m_{t,i+1} \right], i = 1, \dots, L - 1 \dots \quad (9)$$

Equation (9) represents the more generalized version of equation (7) [1, 23].

$$\{H_n\} : m_{n,(i+1)} = K_{I(i+1)} [m_{n,T(i)} m_{n,i+1} + m_{n,(i)} m_{H,i+1} + m_{H,T(i)} m_{n,i+1}] \quad (10)$$

$$m_{H,I(i)} = \overline{m_{H,I(i)}} + \tilde{m}_{H,I(i)} \quad n = 1, \dots, \dots, N \quad (11)$$

$$\{H\} : \tilde{m}_{H,I(i+1)} = K_{I(i+1)} [\tilde{m}_{H,I(i)} \tilde{m}_{H,i+1} + \tilde{m}_{H,T(i)} \tilde{m}_{H,i+1} + \tilde{m}_{H,(i)} \tilde{m}_{H,i+1}] \quad (12)$$

$$\{H\} : \bar{m}_{H,I(i+1)} = K_{I(i+1)} [\bar{m}_{H,I(i)} \bar{m}_{H,i+1}] \quad (13)$$

The combined degree of belief is calculated using equation 14 based on the final combined basic probability assignment, which in this case is “facilities”.

$$M_2 = \begin{bmatrix} m_{1/(2)} & m_{2/(2)} & m_{3/(2)} & m_{4/(2)} & m_{HI/(2)} \\ m_{13} & m_{23} & m_{33} & m_{43} & m_{H3} \\ m_{14} & m_{24} & m_{34} & m_{44} & m_{H4} \\ m_{15} & m_{25} & m_{35} & m_{45} & m_{H5} \\ \dots & \dots & \dots & \dots & \dots \\ \dots & \dots & \dots & \dots & \dots \\ m_{18} & m_{28} & m_{38} & m_{48} & m_{H8} \end{bmatrix}$$

$$\{H_n\} : \beta_n = \frac{m_{n,I(L)}}{1 - \bar{m}_{H,I(L)}}, n = 1, \dots, \dots, N \quad (14)$$

$$H : \beta_H = \frac{\tilde{m}_{H,I(L)}}{1 - \bar{m}_{H,I(L)}}, \text{ Where } m_{n,I(1)} = m_{n,1} (n = 1, \dots, N) \quad (15)$$

β_n and β_H represent the belief degrees of the aggregated assessment, to which the general factor (such as “facilities”) is assessed to the grade H_n and H, respectively. The combined assessment can be denoted by $S(y(a)) = \{(H_n, \beta_n(a_i)), n = 1, \dots, N\}$. It has been proved that $\sum_{n=1}^N \beta_n + \beta_H = 1$. As shown in Table II, the recursive ER technique runs over each piece of evidence one by one. The belief decision matrix was created by combining all of your beliefs using equation (16) [2, 23].

$$\beta_j = \frac{\mu \times \left[\prod_{k=1}^L \left((\omega_k \beta_{jk} + 1 - \omega_k \sum_{j=1}^N \beta_{jk}) \right) - \prod_{k=1}^L (1 - \omega_k \sum_{j=1}^N \beta_{jk}) \right]}{1 - \mu \times \left[\prod_{k=1}^L (1 - \omega_k) \right]} \quad (16)$$

IV. THE TOPSIS METHOD

TOPSIS is a method for rating preferences based on how near they are to the ideal solution, not as A Belief Rule Base (BRB) [26, 27] it is a conceptual modeling structure that facilitates the capturing of ambiguous information TOPSIS is a helpful and practical non-linear decision-making method for real problems [11]. In accordance this theory, ideal alternative is the one that is closest to the positive ideal option rather than

negative one [11]. The positive ideal choice increases benefits while decreasing costs, whereas the other one(negative) increases costs while decreasing benefits. Hence the positive ideal option contains all conceivable ideal criteria values, rest one contains all attainable worst criterion values [11]. Each criteria is expected to increase or decrease over time. If each criterion has a monotonic ascending (or falling) efficient mechanism, the positive ideal option with the best assessment criteria and the rest one with the lowest criteria values may be determined [28]. To find the distance between positive and negative ideal decision Euclidean distances is being used. Best order of possibilities is determined by comparing Euclidean distances.

V. THE PROPOSED DECISION CONCEPT

Vagueness predominates in real-life decisions due to insecurity, inaccessible, and ambiguous information such as fuzziness, imprecision, incompleteness, and ignorance [28]. Rather than being made by a single decision maker, the bulk of decisions are made by a group of decision makers. As a result, the focus of this research is on decision-making under uncertainty and the use of multiple decision-makers in groups to solve a belief multi-criteria decision-making problem. The decision concept was created to describe decision makers’ judgments in ambiguous decision situations [29]. The decision concept was developed and is used to describe decision makers’ judgments in unclear choice circumstances. Because of the aforementioned setting, the AHP-evidential reasoning-TOPSIS approach is employed to develop the choice concept for the group multi criteria decision making problem using 13 phases [29].

Phase 1: Addressing the issue and bringing together the required expertise and parties. Organizing them into groups and deciding on a study subject.

Phase 2: The second part involves locating and mapping old pedestrian bridges.

Phase 3: Establish a goal hierarchical system by establishing the core goal and then dividing up it into objectives, criterion, and choices at the bottom level.

Phase 4: Using the AHP approach, create a comparison matrix for every group.

Phase 5: The priority vector and highest eigenvalue of each matrices are obtained once each group has defined its criterion weights.

Phase 6: Using the consistency ratio to determine the reliability of comparison matrices.

Phase 7: Create a belief choice matrix for every group and assign weights to the decision-makers’ groupings.

Phase 8: Create a belief choice matrix that includes all of your beliefs.

Phase 9: Normalize the group belief choice matrix once it has been aggregated.

Phase 10: Specify the A+ and A- characters, which represent positive and negative ideal alternatives.

Phase 11: Using the Euclidean distance, , calculate the distance(E_i^+ and E_i^-) between the existent options and the positive and negative ideal alternatives.

Phase 12: Use the following method to determine the degree of resemblance to the ideal alternative.

Phase 13: Prioritize the options using RCi.

VI. RESULTS AND ANALYSIS

A numerical representation of the suggested decision notion is included in this section in Table V. The AHP method is used to calculate the criteria weights. The distance between each choice and the positive-ideal and negative-ideal alternatives is determined using the multi-criteria TOPSIS technique, which scores the options. Each criterion has a minimum and maximum value, allowing benefit and cost criteria to be distinguished. Houses are given a priority rating as a result of the proposed method. The ranking results are then presented to the final decision maker, who is now better equipped to make decisions concerning the next steps in the home selection process. We looked at the ER strategy and how to put it into practice in the previous section. As a result, we'll look at the results of applying the proposed idea to dwelling quality in Chittagong in this part. As shown in Fig. 1, house quality can be divided into two categories: objective and subjective qualities, with each attribute weighted. Positive and negative ideal alternatives are found form Table III.

As a result, the residential site with the shortest relative closeness receives the lowest score. Table III shows the priority ranking of housing locations with RC = 0.81 and 0.05, Devpahar is ranked first, whereas Jamal Khan is ranked last. These studies were compared to a proposed decision concept based on the AHP-evidential reasoning-TOPSIS methodology, in which collected data is run through the AHP, TOPSIS, and AHP-TOPSIS, and the results are compared to a proposed decision concept based on the AHP-evidential reasoning-TOPSIS methodology. The results are presented in the Table IV From the given outcomes, it is obvious that the combination of the two multi-criteria methods gain more precise ranking, but still not quite similar as obtained by the proposed approach. Table V shows belief determination matrix created using the alternate assessments of all groups.

(E – Excellent, G – Good, A – Average, B – Bad)

$A^+ = \{ \{ E(0.4), G(0.0), A(0.3), B(0.1) \}; \{ E(0.4), G(0.2), A(0.1), B(0.1) \}; \{ E(0.3), G(0.2), A(0.3), B(0.1) \}; \{ E(0.4), G(0.0), A(0.1), B(0.1) \}; \{ E(0.3), G(0.2), A(0.3), B(0.1) \}; \{ E(0.4), G(0.4), A(0.1), B(0.0) \}; \{ E(0.4), G(0.2), A(0.3), B(0.1) \}; \{ E(0.4), G(0.3), A(0.3), B(0.0) \}; \{ E(0.4), G(0.1), A(0.3), B(0.1) \}; \{ E(0.4), G(0.4), A(0.1), B(0.1) \}; \{ E(0.4), G(0.2), A(0.1), B(0.1) \}; \{ E(0.4), G(0.1), A(0.3), B(0.1) \}; \{ E(0.4), G(0.4), A(0.0), B(0.0) \}; \{ E(0.3), G(0.2), A(0.3), B(0.1) \}; \{ E(0.4), G(0.2), A(0.1), B(0.1) \} \}$

$A^- = \{ \{ E(0.4), G(0.1), A(0.3), B(0.1) \}; \{ E(0.4), G(0.1), A(0.1), B(0.3) \}; \{ E(0.3), G(0.2), A(0.3), B(0.2) \}; \{ E(0.4), G(0.0), A(0.2), B(0.1) \}; \{ E(0.3), G(0.2), A(0.3), B(0.0) \}; \{ E(0.4), G(0.4), A(0.0), B(0.0) \}; \{ E(0.4), G(0.1), A(0.3), B(0.1) \}; \{ E(0.4), G(0.3), A(0.0), B(0.0) \}; \{ E(0.4), G(0.0), A(0.3), B(0.1) \}; \{ E(0.3), G(0.4), A(0.1), B(0.1) \}; \{ E(0.4), G(0.2), A(0.0), B(0.1) \}; \{ E(0.3), G(0.3), A(0.3), B(0.1) \}; \{ E(0.3), G(0.1), A(0.3), B(0.1) \}; \{ E(0.5), G(0.1), A(0.3), B(0.0) \}; \{ E(0.3), G(0.2), A(0.3), B(0.1) \} \}$

TABLE III. THE DISTANCES BETWEEN ALTERNATIVES AND THE IDEAL AND ANTI-IDEAL, AS WELL AS PROXIMITY COEFFICIENTS

Alternative	khulsi	Devpahar	Jamal Khan	Suganda	Chandgoan
E_i^+	0.15	0.11	0.4	0.30	0.40
E_i^-	0.10	0.05	0.5	0.40	0.45
Relative Closeness(RC)	0.72	0.81	0.05	0.20	0.10
Ranking	2	1	5	3	4

TABLE IV. THE PROPOSED CONCEPT IS CONTRASTED TO THE FINDINGS OF OTHER STUDIES

Methodology	Ranking
AHP	Khulsi > Jamal khan > Suganda > DevPahar > Chandgoan
TOPSIS	Khulsi > DevPahar > Suganda > Jamal khan > Chandgoan
AHP + TOPSIS	Khulsi > Suganda > Jamal khan > DevPahar > Chandgoan
Evedential Reasoning	Khulsi > Jamal khan > Suganda > Dev Pahar > Chandgoan
AHP + Evidential Reasoning TOPSIS	DevPahar > Khulsi > Suganda > Chandgoan > Jamal Khan

TABLE V. A BELIEF DETERMINATION MATRIX WAS CREATED USING THE ALTERNATE ASSESSMENTS OF ALL GROUPS

Alt	khulsi	Devpahar	Jamal Khan	Suganda	Chandgoan
Location	E(0.4), G(0.2), A(0.3), B(0.1)	E(0.8), G(0.2), A(0.8), B(0.2)	E(0.4), G(0.4), A(0.1), B(0.1)	E(0.4), G(0.2), A(0.8), B(0.1)	E(0.4), G(0.8), A(0.8), B(0.0)
Attractiveness	E(0.5), G(0.4), A(0.0), B(0.1)	E(0.4), G(0.2), A(0.8), B(0.1)	E(0.4), G(0.4), A(0.1), B(0.1)	E(0.4), G(0.2), A(0.8), B(0.1)	E(0.4), G(0.8), A(0.8), B(0.0)
Safety	E(0.4), G(0.4), A(0.1), B(0.1)	E(0.8), G(0.2), A(0.8), B(0.1)	E(0.4), G(0.4), A(0.1), B(0.1)	E(0.8), G(0.2), A(0.8), B(0.1)	E(0.4), G(0.8), A(0.8), B(0.0)
Environment	E(0.4), G(0.5), A(0.0), B(0.1)	E(0.2), G(0.2), A(0.8), B(0.1)	E(0.4), G(0.4), A(0.1), B(0.1)	E(0.5), G(0.2), A(0.8), B(0.0)	E(0.4), G(0.8), A(0.8), B(0.0)
Nice neighborhood	E(0.4), G(0.2), A(0.8), B(0.1)	E(0.4), G(0.2), A(0.8), B(0.0)	E(0.4), G(0.8), A(0.1), B(0.1)	E(0.4), G(0.2), A(0.8), B(0.0)	E(0.4), G(0.8), A(0.8), B(0.0)
Prox. to edu org	E(0.4), G(0.8), A(0.8), B(0.0)	E(0.4), G(0.2), A(0.8), B(0.1)	E(0.4), G(0.2), A(0.1), B(0.1)	E(0.4), G(0.2), A(0.8), B(0.1)	E(0.8), G(0.2), A(0.8), B(0.1)
Prox. to hospital	E(0.4), G(0.2), A(0.8), B(0.1)	E(0.2), G(0.2), A(0.8), B(0.1)	E(0.8), G(0.4), A(0.1), B(0.1)	E(0.4), G(0.2), A(0.8), B(0.0)	E(0.4), G(0.2), A(0.8), B(0.0)
Prox. to shops	E(0.4), G(0.1), A(0.8), B(0.1)	E(0.8), G(0.2), A(0.8), B(0.1)	E(0.4), G(0.4), A(0.1), B(0.1)	E(0.4), G(0.0), A(0.8), B(0.1)	E(0.4), G(0.8), A(0.8), B(0.0)
Prox. to office	E(0.4), G(0.2), A(0.8), B(0.1)	E(0.5), G(0.2), A(0.8), B(0.0)	E(0.8), G(0.4), A(0.1), B(0.1)	E(0.4), G(0.2), A(0.8), B(0.1)	E(0.4), G(0.8), A(0.8), B(0.0)
Prox. to bus and rail station	E(0.4), G(0.1), A(0.8), B(0.1)	E(0.4), G(0.2), A(0.8), B(0.1)	E(0.4), G(0.4), A(0.1), B(0.0)	E(0.1), G(0.2), A(0.8), B(0.1)	E(0.8), G(0.8), A(0.8), B(0.1)
Prox. to recreation centers	E(0.4), G(0.0), A(0.8), B(0.1)	E(0.4), G(0.2), A(0.8), B(0.1)	E(0.4), G(0.4), A(0.0), B(0.1)	E(0.8), G(0.2), A(0.8), B(0.1)	E(0.4), G(0.8), A(0.8), B(0.1)
Prox. to main road	E(0.4), G(0.0), A(0.8), B(0.1)	E(0.4), G(0.1), A(0.8), B(0.1)	E(0.4), G(0.0), A(0.1), B(0.1)	E(0.8), G(0.2), A(0.8), B(0.1)	E(0.8), G(0.8), A(0.8), B(0.1)
Police precincts	E(0.4), G(0.0), A(0.8), B(0.1)	E(0.4), G(0.2), A(0.2), B(0.1)	E(0.4), G(0.0), A(0.1), B(0.1)	E(0.4), G(0.2), A(0.8), B(0.1)	E(0.4), G(0.8), A(0.8), B(0.0)
Property insurance	E(0.4), G(0.2), A(0.8), B(0.1)	E(0.4), G(0.2), A(0.1), B(0.1)	E(0.4), G(0.4), A(0.1), B(0.1)	E(0.1), G(0.2), A(0.8), B(0.1)	E(0.8), G(0.8), A(0.8), B(0.1)
Population density	E(0.4), G(0.1), A(0.8), B(0.1)	E(0.4), G(0.2), A(0.8), B(0.1)	E(0.4), G(0.2), A(0.1), B(0.1)	E(0.4), G(0.1), A(0.8), B(0.1)	E(0.4), G(0.8), A(0.8), B(0.0)
Cost per sq. ft	E(0.4), G(0.1), A(0.8), B(0.1)	E(0.8), G(0.2), A(0.8), B(0.1)	E(0.4), G(0.4), A(0.1), B(0.1)	E(0.4), G(0.2), A(0.2), B(0.1)	E(0.8), G(0.8), A(0.8), B(0.1)

VII. CONCLUSION

The AHP-evidential reasoning-TOPSIS approach was used to handle multiple criteria house hunting challenges with unclear, incomplete, imprecise, and/or missing information. It is fair to argue that our proposed notion is a mathematically accurate technique for measuring housing quality since it uses

a belief structure to characterize a judgment as a distribution. In several aspects, this technique varies from previous Multi Criteria Decision Making systems. As a result, because the attribute can be ordered or numbered at random, the AHP-evidential reasoning-TOPSIS technique can accommodate new attributes without having to redo the previous assessment. As a result, the order in which the essential qualities are collected has no bearing on the final findings. In contrast to Saaty's AHP technique, any number of additional homes can be analyzed without triggering a "rank reversal problem". The proposed decision paradigm's merits include the correctness and assurance of the achieved outcomes. Using a mix of multi-criteria approaches, more specific findings can be determined. The concept is simple to put into practice and may be applied to any decision-making problem.

VIII. FUTURE WORKS

In a future study an expert system [30, 31] will be implemented into the suggested decision concept to reduce human involvement because stakeholders and experts must be involved throughout the process.

REFERENCES

- [1] T. Mahmud, J. Sikder, and S. R. Naher, "Decision support system for house hunting: A case study in chittagong," in *Proceedings of the Future Technologies Conference*. Springer, 2020, pp. 676–688.
- [2] T. Mahmud and M. S. Hossain, "An evidential reasoning-based decision support system to support house hunting," *International Journal of Computer Applications*, vol. 57, no. 21, pp. 51–58, 2012.
- [3] T. L. Saaty, "Fundamentals of the analytic network process—multiple networks with benefits, costs, opportunities and risks," *journal of systems science and systems engineering*, vol. 13, no. 3, pp. 348–379, 2004.
- [4] —, "Relative measurement and its generalization in decision making why pairwise comparisons are central in mathematics for the measurement of intangible factors the analytic hierarchy/network process," *RACSAM-Revista de la Real Academia de Ciencias Exactas, Físicas y Naturales. Serie A. Matematicas*, vol. 102, no. 2, pp. 251–318, 2008.
- [5] S. Cao, "Development potential evaluation for land resources of forest tourism based on fuzzy ahp method," *Mathematical Problems in Engineering*, vol. 2022, 2022.
- [6] A. Gupta, D. Basu, R. Ghantasala, S. Qiu, and U. Gadiraju, "To trust or not to trust: How a conversational interface affects trust in a decision support system," in *Proceedings of the ACM Web Conference 2022*, 2022, pp. 3531–3540.
- [7] J. Malczewski and M. Jelokhani-Niaraki, "An ontology-based multicriteria spatial decision support system: a case study of house selection," *Geo-spatial Information Science*, vol. 15, no. 3, pp. 177–185, 2012.
- [8] S. Sasmal, K. Ramanjaneyulu, and N. Lakshmanan, "Priority ranking towards condition assessment of existing reinforced concrete bridges," *Structure and Infrastructure Engineering*, vol. 3, no. 1, pp. 75–89, 2007.
- [9] M. Rashidi, M. Ghodrat, B. Samali, B. Kendall, and C. Zhang, "Remedial modelling of steel bridges through application of analytical hierarchy process (ahp)," *Applied Sciences*, vol. 7, no. 2, p. 168, 2017.
- [10] D. M. M. Mansour, I. M. Moustafa, A. H. Khalil, and H. A. Mahdi, "An assessment model for identifying maintenance priorities strategy for bridges," *Ain Shams Engineering Journal*, vol. 10, no. 4, pp. 695–704, 2019.
- [11] G.-N. Zhu, J. Hu, and H. Ren, "A fuzzy rough number-based ahp-topsis for design concept evaluation under uncertain environments," *Applied Soft Computing*, vol. 91, p. 106228, 2020.
- [12] N. R. Franks, A. Dornhaus, C. S. Best, and E. L. Jones, "Decision making by small and large house-hunting ant colonies: one size fits all," *Animal behaviour*, vol. 72, no. 3, pp. 611–616, 2006.
- [13] T. O. Richardson, C. Mullon, J. A. Marshall, N. R. Franks, and T. Schlegel, "The influence of the few: a stable 'oligarchy' controls information flow in house-hunting ants," *Proceedings of the Royal Society B: Biological Sciences*, vol. 285, no. 1872, p. 20172726, 2018.
- [14] M. Ghaffari, C. Musco, T. Radeva, and N. Lynch, "Distributed house-hunting in ant colonies," in *Proceedings of the 2015 ACM Symposium on Principles of Distributed Computing*, 2015, pp. 57–66.
- [15] S. Fraiman, "Hgtv's house hunters and the right to coziness," *Canadian Theatre Review*, vol. 191, pp. 20–24, 2022.
- [16] C. Ng, "Evidential reasoning-based fuzzy ahp approach for the evaluation of design alternatives' environmental performances," *Applied Soft Computing*, vol. 46, pp. 381–397, 2016.
- [17] V. Del Giudice, P. De Paola, P. Nijkamp, F. Pagliara, and F. Torrieri, "A dss for real estate location choice," *A DSS for Real Estate Location Choice*, pp. 1000–1018, 2010.
- [18] M. Rymarzak and E. Siemińska, "Factors affecting the location of real estate," *Journal of Corporate Real Estate*, 2012.
- [19] F. Antoniou and G. N. Aretoulis, "Comparative analysis of multi-criteria decision making methods in choosing contract type for highway construction in greece," *International journal of management and decision making*, vol. 17, no. 1, pp. 1–28, 2018.
- [20] J. Jablonsky et al., "Analytic hierarchy process as a ranking tool for decision making units," *International Journal of Management and Decision Making*, vol. 14, no. 3, pp. 251–263, 2015.
- [21] S.-C. Ngan, "Evidential reasoning approach for multiple-criteria decision making: A simulation-based formulation," *Expert Systems with Applications*, vol. 42, no. 9, pp. 4381–4396, 2015.
- [22] A. K. Thiam, "An evidential reasoning approach to land degradation evaluation: Dempster-shafer theory of evidence," *Transactions in GIS*, vol. 9, no. 4, pp. 507–520, 2005.
- [23] Y.-M. Wang, J.-B. Yang, and D.-L. Xu, "Environmental impact assessment using the evidential reasoning approach," *European Journal of Operational Research*, vol. 174, no. 3, pp. 1885–1913, 2006.
- [24] T. L. Saaty and M. Sagir, "Extending the measurement of tangibles to intangibles," *International Journal of Information Technology & Decision Making*, vol. 8, no. 01, pp. 7–27, 2009.
- [25] L. L. Li, Z. G. Li, M. Wu, and C. T. Zhao, "Decision-making based on dempster-shafer evidence theory and its application in the product design," in *Applied Mechanics and Materials*, vol. 44. Trans Tech Publ, 2011, pp. 2724–2727.
- [26] M. M. Islam, T. Mahmud, and M. S. Hossain, "Belief-rule-based intelligent decision system to select hospital location," *Indonesian Journal of Electrical Engineering and Computer Science*, vol. 1, no. 3, pp. 607–618, 2016.
- [27] J. Sikder, M. Shafiul, S. R. Naher, M. M. Mia, and T. Mahmud, "Belief-rule-based decision support system for evaluating of job offers," *International Journal of Computer Applications*, vol. 975, p. 8887, 2015.
- [28] I. Yuniwati, "Correlation test application of supplier's ranking using topsis and ahp-topsis method," *Cauchy*, vol. 4, no. 2, pp. 65–73, 2016.
- [29] K. Rogulj, J. Kilić Pamuković, and N. Jajac, "A decision concept to the historic pedestrian bridges recovery planning," *Applied Sciences*, vol. 11, no. 3, p. 969, 2021.
- [30] T. Mahmud, J. Sikder, U. Salma, S. R. Naher, J. Fardoush, N. Sharmen, and S. Tripura, "An optimal learning model for training expert system to detect uterine cancer," *Procedia Computer Science*, vol. 184, pp. 356–363, 2021.
- [31] M. J. A. Patwary, S. Akter, and T. Mahmud, "An expert system to detect uterine cancer under uncertainty," *IOSR Journal of Computer Engineering (IOSR-JCE)*, e-ISSN, pp. 2278–0661, 2014.

A Drone System with an Object Identification Algorithm for Tracking Dengue Disease

Diego Moran-Landa¹, Maria del Rosario Damian²,
Pedro Miguel Portillo Mendoza³, Carlos Sotomayor-Beltran⁴
Facultad de Ingeniería
Universidad Tecnológica del Perú
Lima, Peru

Abstract—In recent decades, it has been shown that epidemiological surveillance is one of the most valuable tool that public health has, since it allows us to have an overview of the population general health, thus allowing to anticipate outbreaks of epidemics by helping in timely interventions. Currently there is an increase in cases of dengue disease in several regions of Peru. Therefore, to control this outbreak and to help population centers and human settlements that are far from the city this work puts forward a drone system with an object recognition algorithm. Drones are very efficient in terms of surveillance, allowing easy access to places that are difficult for humans. In this way, drones can carry out the field work that is required in epidemiological surveillance, carrying out photography or video work in real time, and thus identifying infectious foci of diverse diseases. In this work, an object detection algorithm that uses convolutional neural networks and a stable detection model is designed, this allows the detection of water reservoirs that are possible infectious sources of dengue. In addition the efficiency of the algorithm is evaluated through the statistical curves of precision and sensitivity that result of the training of the neural network. To validate the efficiency obtained, the model was applied to test images related to dengue, achieving an efficiency of 99.2%.

Keywords—Epidemiological surveillance; drones, neural networks; recognition algorithms

I. INTRODUCTION

Currently there is an increase in dengue cases in several areas of Peru, and for this does not exist a rapid surveillance system to detect areas where there is possibly dengue. At the moment Peru carries out traditional surveillance of going from house to house to carry out the detections of cases of dengue, through blood tests, filling out symptom files, etc.

The large increase in dengue cases in Peru occurs because the epidemiological focus of dengue is not being taken into account as before the pandemic, given that during the pandemic health personnel have focused mainly on COVID-19 leaving aside this disease that has afflicted Peru for approximately 30 years. Therefore, the most affected are the population centers and human settlements that have roads or accesses far from the city and with narrow main roads. Faced with this, there are various solutions through prevention campaigns against dengue, but in terms of the use of algorithms for the detection of dengue, they are very unusual and at the same time efficient.

Currently, the National Center for Epidemiology, Disease Prevention and Control (CDC - MINSa), shows in its epidemiological bulletin that there is currently a considerable increase in dengue cases in several regions of our country. Therefore,

there is a way to support the surveillance carried out by the prevention system, using drones, since these devices can carry out aerial surveillance in areas of difficult access that detect dengue infectious foci.

II. RELATED WORKS

Regarding the technology of drones currently used, in [1] they provide in their article a complete review of current and future drones applied in medicine. For example, in 2013, drones were used in the aftermath of Typhoon Haiyon in the Philippines to assess initial storm damage and prioritize relief efforts. Another example mentions a study conducted in southern Italy, they used drones equipped with high-resolution photogrammetry software to accurately access and predict cancer risk from high-level copper concentrations in agricultural areas. And like other studies mentioned in the article, it highlights the advantage of using the drone as an aerial surveillance tool to assess biological risk areas and natural disaster areas. In addition, in [2], they carried out a project in which the design and construction of a drone with optimal characteristics to carry out photogrammetric plans to later be used in telecommunication networks, such as work in fiber optic networks, is proposed, because these they are found in places of difficult access such as high forests and steep mountains, for the design of both the chassis and the electronic part, easily accessible materials were used, which helps to design the drone according to the calculations made to take advantage of its resources and dimensions, since they were evaluated with commercial devices.

Regarding the drones used in epidemiological surveillance, in [3] the “IRIS PX4” drone was used as an identifier of violations of social distancing rules for an intelligent surveillance system against COVID-19, which the device uses two cameras, a frontal one for the detection of obstacles and another ventral one for the detection of people, in addition that it has an integrated GPS that locates the area observed by the drone. On the other hand, in [4] drones were used to transport blood samples, medicines, supplies in cases of disasters such as humanitarian aid and even as a portable laboratory. To carry out these tasks, Quadcopter drones (4 rotors, 20km range, 36km/h speed and with a maximum payload of 2kg) were used, most of DJI brands, for example, the DJI Phantom 4 Pro drone. It is mentioned that the models of medical drones made by the Zipline company, which are fixed-wing drones capable of flying at a speed of 128km/h with a range of 160km (round trip) while carrying a payload of 1.75 kg, are efficient

in terms of transporting medicines, laboratory samples, blood donations, etc. Also in [5], drones are used to review assigned areas infected with malaria, which are sent by GPS to only capture images within the assigned geographic space, in this way they compare the progress of malaria in that area with respect to previous years such as the of 2013 and 2014.

In reference to its application in image and video acquisition, a study was carried out in [6] that aims to produce accurate geospatial 3D data by acquiring images captured by the drone or unmanned aerial vehicle. For this reason, an image of an area of the Najran University campus in Saudi Arabia was captured using a DJI Mavic Pro Platinum drone. Similarly in [7], they mention that the use of unmanned aerial vehicles (UAV) provides the option of collecting detailed spatial information in real-time at a relatively low cost and thus avoids limitations associated with satellite data (such as cloud pollution, low resolution, bad camera angle and shooting time for taking pictures). Therefore, in their inspection of breeding habitats through drone surveillance, they used a low-cost Phantom 4 Pro DJI model drone, which integrates a 20-megapixel camera with a focal length of 35 mm and a theoretical resolution of 1 cm, which has a battery for a flight of 12 to 15 minutes, which allowed them to take photos of 15 to 20 houses per day.

Regarding the use of convolutional neural networks, in [8] they propose an efficient surveillance based on radiofrequency to detect and classify drones, for which they used the RF-UAVNet network, said network is characterized by having grouped convolutional layers because reduce the size of the network and the computational cost, these were tested in drones of the Phantom and Bebop brands. In addition, in [9], they propose to identify weapons through surveillance applications based on Convolutional Neural Networks (CNNs) and Convolutional Long-Short-Term Memory (ConvLSTM). Simulation tests are performed on the data set using Python 3.5, Tensor Flow and Keras, which will be captured by wireless sensors distributed in networks for military applications.

Since the system has object detection and recognition techniques in the algorithm, in [10] they designed a deep YOLO-v3 model to detect small objects. The project consists of training the YOLO-v3 model previously trained with drone images, 106 convolution layers with several feature maps were designed to learn the small objects of the drones. The proposed deep YOLO-v3 revealed 99.99% accuracy because it used multi-scale predictions and backbone classifiers to better classify them. Likewise, in [11] they propose to use the YOLOv4 program to differentiate drones from birds through images captured by a digital camera which will have a visible sensor that has a resolution between 96 dpi and 300 dpi, the images will be captured in different environments and with different illumination. Similarly, in [12] they perform a vehicle detection using deep learning in UAV, which is proposed to record videos using the DJI drone, where the results show that the use of HSV for transformation data can enrich the set of samples. Thus, improving the detection accuracy, likewise, the SSD model can act on multiple feature layers, and its detection effect is better.

Finally, in relation to the current situation of dengue, in [13] studies related to coinfections of Dengue and COVID-19 were found. Most of the studies were case reports with

a detailed description of clinical and co-infection features. Common symptoms were fever, dyspnea, headache, and cough. The cases were found in Brazil, Indonesia, India, France, Argentina, Pakistan, Thailand, among others. Because both diseases are present in several places, the study is necessary to verify the differences between both infections. On the other hand, in [14], he presents two cases of patients with dengue and coronavirus coinfection, due to severe acute respiratory syndrome. This research found that severe dengue infection is common in young adults, while coronavirus disease is generally asymptomatic. They also comment that, in older people, the severity of this disease will depend on their comorbidities or the infectious serotype, but contagion by coronavirus is consistently more serious.

In this work, it is proposed to carry out a drone system with an algorithm that detects and recognizes pools of water that are possible foci of dengue. To check its efficiency, a database that contains images of objects that store water will be used.

III. METHODOLOGY

For the development of the methodology, the efficiency of the design of the detection algorithm for epidemiological surveillance of dengue will be evaluated using drones, for which the research will be developed based on the following strategy shown in Fig. 1; a database, which will have images of the objects to be detected, the selection of a suitable drone, the software, which will carry out the programming, and the model of the algorithm that will be used for the detection and recognition of objects.

Therefore, for its procedure, as shown in Fig. 2, the drone will perform an acquisition of images and/or videos of the area for its evaluation, the use of a database containing images of objects that store water, in addition to the model of the object detection and recognition algorithm, which is one of the applications of convolutional neural networks. All this will be programmed in software that the computer will have, which will process the images to identify the pools of water in the photos or videos that the drone captured. In this way, the possible transmitting sources of dengue will be detected.

A. Database

To carry out this procedure, there will be a database of the objects to be detected, for example: buckets, pots, bottles, tires, tubs and vases.

B. Dron Selection

To select a suitable drone for the field of epidemiology, you must be able to take good resolution images and/or video in places or areas of difficult access that are affected by some type of disease. Therefore, the following technical specifications will be analyzed as indicated in Fig. 3, to select a suitable drone for this field.

Considering the main points necessary for the selection of an optimal drone in the investigation, they are the following: the camera must have a maximum of 12MP, because the smaller the image size, the shorter the processing time; Regarding the operating range, a range of [4 – 10] km of maximum transmission distance will be chosen. As a last point,

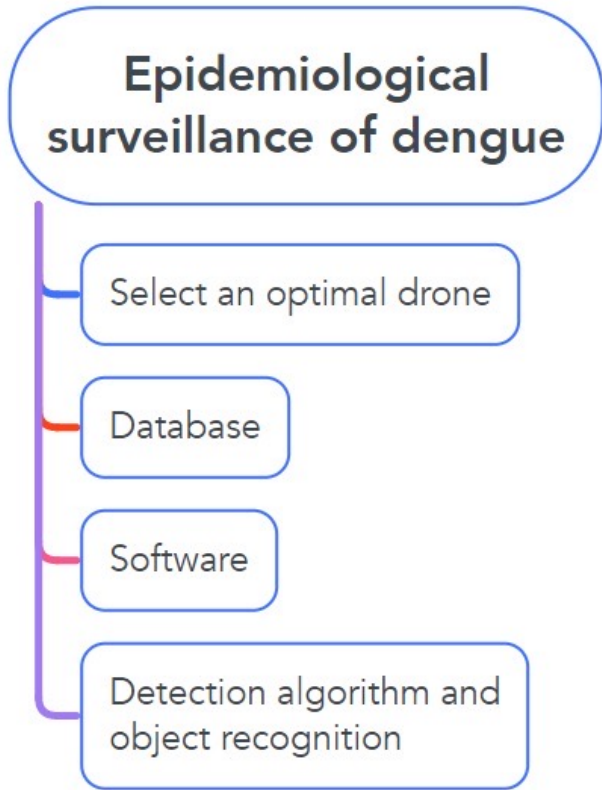


Fig. 1. Diagram of the Strategy of Research.

cost and accessibility will be taken into account, since most drones are acquired by import, therefore, the search for brands available for our country was carried out, obtaining DJI drones as a result.

Taking into account the importance of a drone with an affordable cost, as well as the criteria of the main technical specifications of the drone, DJI MINI 2 is chosen as the first option, since it has a maximum operating range of 10km, in comparison to the DJI MAVIC Mini drone, as a second option, which has only 4km.

C. Software

Since the object detection algorithm needs software that contains libraries on neural networks for its training, it is decided to choose the free software “Google Collaborate”, which is compatible with the Yolo algorithm, and its environment is developed using the language of Python programming. Its environment is very friendly to users, it does not require configuration, it gives free access to GPUs for fast code execution.

D. Detection Algorithm

In the case of the algorithm required for object detection, some main detection techniques were found: SORT, YOLO and SDD.

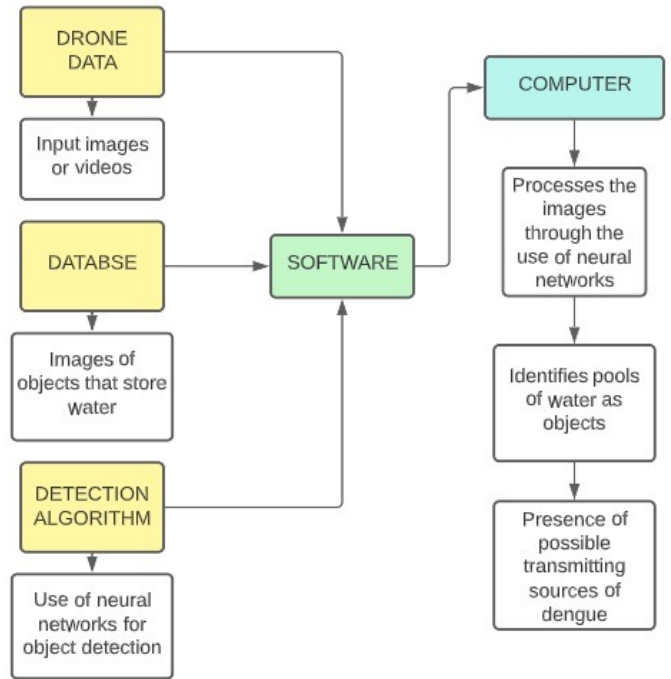


Fig. 2. Diagram of the Design of the System.

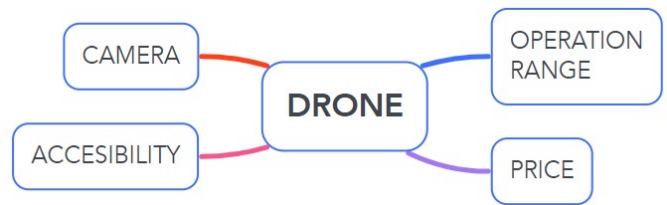


Fig. 3. Characteristics Considered to Select the Drone.

In the case of YOLO, compared to other detection techniques, it makes predictions with a single network evaluation through the use of CNN. In addition to having continuous updates or versions to improve its efficiency in terms of detection in both images and videos in real time. For this reason, the Yolo algorithm will be applied in its version 3 “Yolov3”, due to its stability and precision for object detection, as shown in Fig. 4, the Yolov3 algorithm in the Google Colab environment.

This algorithm requires “labels” of the images found in the database, which will be obtained through “Makesense”, a tool to label photos and thus organize the images into classes, as shown in Fig. 5, an example of classifying images of the “buckets” type.

In addition, Makesense allows you to export the labels in a “.txt” file for the operation of the YOLO algorithm. This will allow pre-training of the neural network for image classification.

YOLOv3 ALGORITHM FOR OBJECT DETECTION AND RECOGNITION

```
[ ] 1 !git clone https://github.com/ultralytics/yolov3 # clone
    2 %cd yolov3
    3 %pip install -qr requirements.txt # install
    4
    5 import torch
    6 from yolov3 import utils
    7 display = utils.notebook_init() # checks
```

Fig. 4. Algorithm YOLOv3.

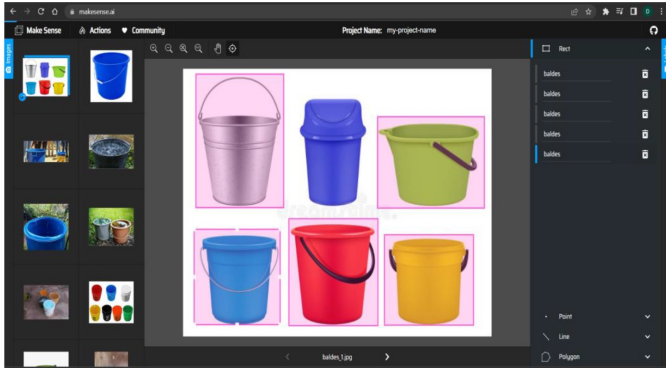


Fig. 5. Images Classification using Makesense.

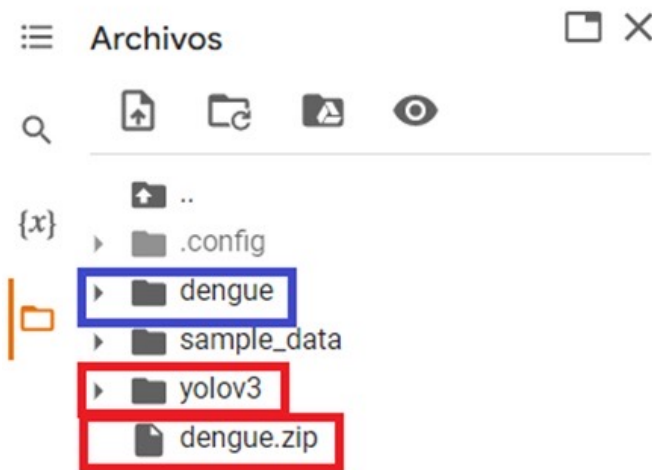


Fig. 6. Adding YOLOv3 Folder to the Database dengue.zip.

E. Programming

Given that at this stage the necessary elements are already available to carry out the recognition of dengue, the programming part will be developed, which will carry out the identification of the possible infectious foci of said disease.

As a first step, the database will be added in .zip format to extract it in the section and in turn compile the “Add Yolov3 algorithm” cell, as shown in Fig. 6 in the Files section, the yolov3 folder and the dengue.zip database highlighted in red.

```
# YOLOv3

train: ../dengue/images/train
val: ../dengue/images/val

# Classes
nc: 6 # number of classes
names: ['buckets', 'bottle', 'vases', 'pots', 'tire', 'tubs'] # class names
```

Fig. 7. File dengue.yaml for Training and Network Validation.

```
TRAINING OF THE CONVOLUTIONAL NEURAL NETWORK THROUGH YOLO

[ ] 1 !python train.py --img 640 --batch 16 --epochs 100 --data dengue.yaml --weights yolov3.pt --cache
```

Fig. 8. Training Expression for the Neural Network with 100 Epochs.

```
TRAINING OF THE CONVOLUTIONAL NEURAL NETWORK THROUGH YOLO

[ ] 1 !python train.py --img 640 --batch 16 --epochs 20 --data dengue.yaml --weights yolov3.pt --cache

VALIDATION OF TRAINING USING IMAGES OR VIDEO FOR OBJECT DETECTION

[ ] 1 # python detect.py --source 0 # webcam
    2 # img.jpg # image
    3 # vid.mp4 # video
    4 # path/ # directory
    5 # path/*.jpg # glob
    6 # "https://youtu.be/g1q1k3k9qc" # YouTube
    7 # "rtsp://example.com/media.mp4" # RTSP, RTP, HTTP stream

VALIDATION CODE

[ ] 1 !python detect.py --weights yolov3.pt --img 640 --conf 0.25 --source data/images

EXAMPLE

[ ] 1 # !python detect.py --weights 'PLACE TRAINING WEIGHTS' --img 700 --conf 0.25 --source 'PLACE IMAGE OR VIDEO'
    2 # !python detect.py --weights /content/yolov3/runs/train/exp6/weights/last.pt --img 700 --conf 0.25 --source ../Imagen_1.jpg
```

Fig. 9. Training Expression using an Image or Video.

As a second step, the “.yaml” file is created, in which the classes and locations of the images that will be trained and validated by the neural network are declared. As can be seen in Fig. 7, the training variables “train” and “val”, followed by the classes associated with the objects to be detected in the images.

As a third step, the convolutional neural network training command will be executed, which is made up of the size of the image, the number of epochs, the data and the weights provided by the yolov3 algorithm, as can be seen in Fig. 8.

Finally, Fig. 9 presents the command for the validation of the Yolo algorithm through an image or video, for the detection of water pools, using the weights of the trained network.

IV. RESULTS AND DISCUSSION

Regarding the technical characteristics that a drone must have to adapt an epidemiological surveillance system, the drone selected in the methodology is evaluated, the DJI MINI 2 drone, which offers greater stability despite being very light (250gr), it has an acceptable wind resistance (29 – 38 km/h), however in [4] it mentions a study that used the DJI Phantom 4 Pro drone for epidemiological surveillance of malaria in the Peruvian Amazon, identifying breeding sites through multispectral images captured by the drone, said drone has an autonomy greater than 30 minutes, in the same way in [7] they used the same drone to capture images in an endemic city of Tapachula in Mexico. Likewise, in [6] the use of the DJI Mavic Pro Platinum drone is mentioned to obtain images of a test area, which has a flight time of 30 minutes, considered



Fig. 10. Drone DJI MINI 2 and its Remote Control.

very high, it also has GPS, a 12.35 MP camera, among other features. Taking into account the mentioned specifications, both studies considered autonomy or flight time as the main characteristic. In Fig. 10, the DJI MINI 2 drone is shown.

Regarding the development of the database, in [7] a database acquired by the drone of a total of 2579 images of various house roofs was used to identify *Aedes Aegypti* breeding sites, divided into 10 categories. On the other hand, in [15] they use Microsoft's COCO data set, which contains a base of 330,000 images, divided into 91 categories that can be freely used by any user. Instead, [11] mentions the use of a database of 3,000 images, including 1,000 of birds, 1,000 of helicopter-type drones, and 1,000 of multi-rotor drones. Therefore, it is recommended to use a greater number of possible images to carry out an optimal detection. Since a total of 86 images were used in the investigation for six classes or types of objects, which are buckets, bottles, vases, pots, tires and tubs.

With respect to the simulation, images containing the objects to be detected were used, for example buckets, tubs, bottles, pots, vases, tires, etc., which were extracted from the internet. Similarly in [7], for the detection of dengue it is recommended to identify these objects.

From the training carried out in Fig. 11, it is visualized that 60 images were used for the validation of the training, the different classes used, the number of labels of each class, the "P" value of total precision and of each class, the value "R" for recall (Sensitivity) total and of each class and the Accuracy value "mAP" total and of each class. Similarly, in [11] and [12], the use of these variables is highlighted to evaluate the accuracy and sensitivity of the proposed model. Furthermore, in [11], they obtained a 90% accuracy "P" to identify drones and birds in test images. On the other hand, the proposed model has an accuracy value "P" of 98.6% to identify water reservoirs.

Fig. 12 shows the graphs of the curves F1, P, R and PR that indicate the combination of P and R in a single measure, the quality of prediction, the quantity that can be identified and the performance of the predictive model, respectively.

Of the curves, the most important is the P-R curve that generally indicates the efficiency of the Yolov3 model applied to the detection of dengue, whose value is 99.2%, this indicates that the use of the algorithm for the detection of dengue is efficient. and that the simulation helps in part to validate its

```
100 epochs completed in 0.232 hours.
Optimizer stripped from runs/train/exp/weights/last.pt, 123.6MB
Optimizer stripped from runs/train/exp/weights/best.pt, 123.6MB

Validating runs/train/exp/weights/best.pt...
Fusing layers...
Model Summary: 261 layers, 61524355 parameters, 0 gradients, 154.6 GFLOPs

```

Class	Images	Labels	P	R	mAP@.5	mAP@.5:95	100% 2/2	[00:01:00:00, 1.391t/s]
all	60	118	0.986	0.979	0.992	0.842		
balde	60	39	0.985	0.923	0.993	0.874		
botella	60	14	1	0.949	0.995	0.885		
florero	60	17	0.992	1	0.995	0.813		
maceta	60	22	0.997	1	0.995	0.85		
llanta	60	19	0.942	1	0.98	0.828		
tina	60	7	1	1	0.995	0.881		

```
Results saved to runs/train/exp
```

Fig. 11. Training Results using 100 Epochs.

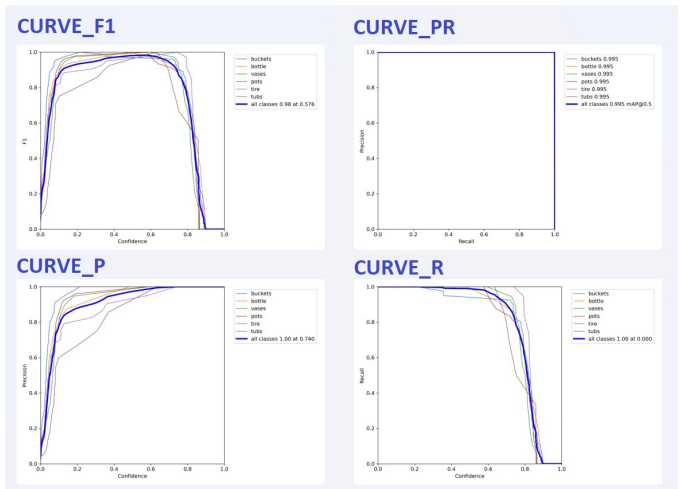


Fig. 12. Curves F1, P, R and PR from de Neural Network.

efficiency.

In Fig. 13 it can be seen that each class is detected in reference to the image of the database, in addition to showing a number between 0 and 1, which means the value of precision that it has when recognizing the object, said value will be higher if the number of epochs increases.

The design of the detection algorithm proposed for dengue surveillance using drones allowed the recognition of objects or containers that store water to identify the infectious foci of the disease through the precision and sensitivity value which are the result of training the neural network. In addition, through test images, which contain figures of buckets, bottles, vases, pots, tires and tubs, it was possible to identify these objects with a total efficiency value of 99.2%. This design is an important contribution, since, in terms of disease surveillance in the country, this type of technology is not available, due to the fact that there is little research regarding drones dedicated to epidemiological surveillance.

The information on the technical specifications of the drones is important for their selection in cases of epidemiological surveillance, since, according to the authors, they consider the MP of the camera for the images, the flight time or its autonomy, and the cost of the device. Therefore, taking into account these considerations, it is concluded that the DJI MINI 2 drone is optimal to perform the image acquisitions required for the development of the proposed detection algorithm.



Fig. 13. Validation of the Neural Network with the Test Images.

V. CONCLUSIONS

The test simulation was optimal for the evaluation of the detection algorithm, using some input images to detect the pools of water that are possible infectious foci of the disease. Resulting in the value of 99.2% total efficiency of the detection algorithm.

The design of the detection algorithm uses the Yolov3 model, since it is more stable, but the following versions such as Yolov4 and Yolov5 could be used to improve its efficiency, precision and sensitivity. As for drones, the recommendations for their selection vary according to the field, since most of these devices cover the military field, agriculture, archeology, medicine, home deliveries, etc.

Regarding the simulation of the evaluation of the algorithm, it is recommended to use software that runs without the need for an internet connection, for example, Octave, Visual Studio, among others, that have libraries applied to the detection and recognition of objects.

REFERENCES

- [1] J. Rosser, V. Vignesh, B. Terwilliger and B. Parker, "Surgical and Medical Applications of Drones: A Comprehensive Review", *JSLs : Journal of the Society of Laparoendoscopic Surgeons*, vol. 22, no. 3, pp. e2018.00018, 2018
- [2] Y. Apaza Canqui and c. Mamani Rojas, "Implementación de un drone para estudios de sitios de enlaces de fibra óptica", *Repositorio.umsa.bo*, 2022
- [3] P. Somaldo, F. Ferdiansyah, G. Jati and W. Jatmiko, "Developing Smart COVID-19 Social Distancing Surveillance Drone using YOLO Implemented in Robot Operating System simulation environment", 2020 IEEE 8th R10 Humanitarian Technology Conference (R10-HTC), 2020
- [4] M. Poljak and A. Šterbenc, "Use of drones in clinical microbiology and infectious diseases: current status, challenges and barriers", *Clinical Microbiology and Infection*, vol. 26, no. 4, pp. 425-430, 2020
- [5] W. Kaewwae and A. Bhumiratana, "Landscape Ecology and Epidemiology of Malaria Associated with Rubber Plantations in Thailand: Integrated Approaches to Malaria Ecotoping", *Interdisciplinary Perspectives on Infectious Diseases*, vol. 2015, pp. 1-17, 2015
- [6] I. Elkhachy, "Accuracy Assessment of Low-Cost Unmanned Aerial Vehicle (UAV) Photogrammetry", *Alexandria Engineering Journal*, vol. 60, no. 6, pp. 5579-5590, 2021
- [7] K. Valdez-Delgado, D. Moo-Llanes, R. Danis-Lozano, L. Cisneros-Vázquez, A. Flores-Suarez, G. Ponce-García, C. Medina-De la Garza, E. Díaz-González and I. Fernández-Salas, "Field Effectiveness of Drones to Identify Potential *Aedes aegypti* Breeding Sites in Household Environments from Tapachula, a Dengue-Endemic City in Southern Mexico", *Insects*, vol. 12, no. 8, p. 663, 2021
- [8] T. Huynh-The, Q. Pham, T. Nguyen, D. Benevides Da Costa and D. Kim, "RF-UAVNet: High-Performance Convolutional Network for RF-Based Drone Surveillance Systems", 2022
- [9] N. F. Soliman, E. A. Alabdulkreem, A. D. Algarni, G. M. El Banby, F. E. Abd El-Samie and A. Sedik, "Efficient Deep Learning Modalities for Object Detection from Infrared Images", *Computers, Materials & Continua*, vol. 72, no. 2, pp. 2545-2563, 2022
- [10] K. Madasamy, V. Shanmuganathan, V. Kandasamy, M. Lee and M. Thangadurai, "OSDDY: embedded system-based object surveillance detection system with small drone using deep YOLO", *EURASIP Journal on Image and Video Processing*, vol. 2021, no. 1, 2021
- [11] F. Samadzadegan, F. Dadrass Javan, F. Ashtari Mahini and M. Gholamshahi, "Detection and Recognition of Drones Based on a Deep Convolutional Neural Network Using Visible Imagery", *Aerospace*, vol. 9, no. 1, p. 31, 2022

- [12] X. Wang, "Vehicle Image Detection Method Using Deep Learning in UAV Video", *Computational Intelligence and Neuroscience*, vol. 2022, pp. 1-10, 2022
- [13] T. Tsheten, A. Clements, D. Gray, R. Adhikary and K. Wangdi, "Clinical features and outcomes of COVID-19 and dengue co-infection: a systematic review", *BMC Infectious Diseases*, vol. 21, no. 1, 2021
- [14] O. Agudelo Rojas, M. Tello-Cajiao and F. Rosso, "Challenges of dengue and coronavirus disease 2019 coinfection: two case reports", *Journal of Medical Case Reports*, vol. 15, no. 1, 2021
- [15] D. Moreira Ramos, "Aplicación de un modelo de reconocimiento de objetos utilizando yolo (You only look once)", *Universidad Estatal Peninsula de Santa Eelena*, vol. 16, 2022

Analysis of the Intuitive Teleoperated System of the TxRob Multimodal Robot

Jeyson Carpio A.^{*,1}, Samuel Luque C.^{*,2},
Juan Chambi C.^{*,3}, Jesús Talavera S.^{*,4}
Universidad Nacional de San Agustín
de Arequipa, Perú*

Abstract—Natural disasters such as earthquakes, avalanches, landslides, among others, leave in their path people who may be trapped in the rubble, which are hardly found by rescue agents, so a reliable system in the operation of an exploration and rescue robot is essential. This paper aims to evaluate the systems proposed for the operation of the TxRob exploration robot. The teleoperated control systems that were developed for the manipulation of the robot are: a multimodal system feedback with information through different sensors, and a GUI control system using joystick buttons. These systems were analyzed using subjective metrics such as NASA-TLX, Scale Utility System (SUS) and Microsoft Reaction Cards, which provide interesting data when evaluating the performance of an interface, as well as the workload, user satisfaction and usability; these aspects are used to conclude which system is the most intuitive when performing rescue operations in case of a disaster, among others. 15 operators were evaluated to validate this system; the age range of the operators was between 20 and 43 years old and 20% of them had previously used VR headsets. Priority is given to the most immersive, easy to use and the most efficient system to perform the task of handling the robot.

Keywords—Multimodal interface; immersive teleoperation; exploration robot; gyroscope and subjective measurements

I. INTRODUCTION

In Peru there is a constant interaction between the Nazca and South American plates that generate natural disasters such as earthquakes, which put the population at risk of possible trapping due to landslides. According to the “Instituto Geofísico del Perú” (IGP), a total of 811 earthquakes were reported in 2020, 834 earthquakes in 2021 and approximately 581 earthquakes so far in 2022. The average of these earthquakes is of magnitude greater or equal to 4.5 ML (Richter scale), and also that the average number of earthquakes that occur per month is greater or equal to 58 earthquakes [1]; on average there are at least 2 earthquakes per day which is a constant risk to the Peruvian population. In the event that an earthquake has a greater magnitude, it would result in trapped people, uninhabitable houses or houses on the verge of collapse, at any time generating greater difficulty for the various rescue groups such as firefighters or members of the police who are also exposed to these dangers. Because of these problems, several robots are currently used for exploration and rescue, which reduce the exposure of the rescue agents, but do not reduce the mental load of the operators when making decisions [2].

For a successful operation there must be trust between the operator and the robotic partner, the cobots are designed

with the purpose that the robot can support the various tasks of the operator, for them the human-robot interaction (HRI) is paramount. HRI covers the various fields such as design, understanding and evaluation of robotic systems, which involve humans and robots interacting through communication [3], [4]. The trust with a cobot can decrease drastically if it provides constant wrong information in risky situations, therefore a good robotic system that increases the trust with cobots is necessary [5].

For a robotic system in rescue operations to be classified as good, it should not miss proprioceptive sensors, nor should it miss good image processing, otherwise it would decrease the usability of search and rescue (SAR) robots and the performance of the operators by increasing the work performed using minimal information from the sensors. SAR robots should also have modular sensors and modular payloads increasing the usability of the robots and robot feedback can create more levels of competence [6]. The need for robotic interventions in hazardous environments is high, due to the presence of dust, fire, pressurized water or radioactivity; for that reason, robotic platforms must be reliable and user interfaces appropriate due to the complexity of the environment, for them the use of different inputs such as visual user interfaces help a better understanding of the environment for the operator [7], [8].

This paper presents an analysis of the user interface developed for the operation of the TxRob robot using subjective metrics such as NASA-TLX, SUS and Microsoft Reaction Cards [9]. It is believed that a developed bidirectional multimodal feedback system will help to decrease the operator’s workload, resulting in less stress and better teleoperation. The TxRob robot was presented by our team in a previous article [10]; this robot has the advantages of being low cost, its compact size allows it to enter into confined spaces for the search of possible people trapped in the rubble, it also has a sensor feedback system, in addition to a graphical interface that generates a greater immersion in his teleoperation.

The distribution of information in this document is divided as follows: In Section II the works related to this research are presented, the methodology is developed in Section III, the description of the proposed multimodal interface and the interfaces used for comparison are described in Section IV, the description of the experimentation used in this paper is presented in Section V, the results and discussions obtained are presented in Section VI, and the conclusions of this research are found in Section VII.

II. RELATED WORK

According to [11], the combination of different tools such as stereo vision, haptic feedback and auditory feedback increases the manipulation performance of a robotic system. For this, the multiple information that we can provide to the operator would generate a more immersive system for the teleoperation of a robot. For that reason, the use of multi-modal interfaces generates a higher performance in robotic teleoperation. In [12] they propose a method to organize the presentation of information and a set of visual assistance to facilitate the visual communication of data in teleoperation control panels, seeking to make them understandable and not generating a greater workload to the operator to understand the different information of the system where their interface combined immersive visualization, three-dimensional mixed reality and visual assistance.

With a gyroscope it is possible to know, maintain or change the orientation in space of an object; a gyroscope provides angular velocity readings usually in $^{\circ}/s$ on the x, y and z axes to determine the rotational speed of the object on which it is located; in addition, the use of the gyroscope in immersive virtual reality systems can be seen in [13] where making use of the gyroscope of a mobile device the manipulation of objects in a virtual environment is achieved, in [14] where to obtain continuous visual effects a gyroscope was incorporated, being very helpful for the detection of the direction of vision of a person in a virtual environment and in [15] where the gyroscope is used to estimate the posture of an operator to integrate the virtual environment with the real environment.

In [16], they use a haptic interface for robotic control in which immersive interaction with the person being rescued significantly improves task performance compared to other control systems; and visual feedback further increases user performance metrics. In [17], they evaluate different multi-modal interfaces to find the system with the most intuitive and least operator workload; using visual interfaces, GUI interfaces and NUI interfaces. It is shown that a multimodal interface helps considerably in an intuitive teleoperation improving robotic efficiency. In [18] they present a new haptic mediator interface for teleoperative mobile robotic platforms that have a variety of manipulators and functions; employing identical bilateral master-slave teleoperation of robotic manipulators is achieved by representing them in virtual reality and allowing the operator to interact with them using a multipoint haptic device. As a result, the operator can perform a wide range of control functions and achieve functionality similar to that of conventional teleoperation schemes using a single haptic interface.

In [19], they measure the effects of working with autonomous robots on perceived workload and work performance, measuring both objective and subjective tests such as NASA-TLX, with the results of the study showing the viability of applying fully autonomous mobile robots to improve the productivity of the human-robot team while prioritizing physical safety and reasonable increases in mental workload.

In [20], they present an HMI which they developed to be able to control virtual forearm prostheses for extended periods of time. By calculating the physical performance for the given tasks, they develop an algorithm that adapts to the mental states

of a user, thus improving its usability. According to the NASA-TLX evaluation, a better physical performance was improved.

III. METHODOLOGY

This document explains the two systems that will be analyzed for the manipulation of the TxRob robot. The control system for the movement of the robot is done by the joystick control which has functions that will be detailed later. For the vision system we present two interfaces:

- Traditional Interface: Uses a display screen that shows in real time the graphical interface developed for the TxRob.
- VR interface: Uses virtual reality (VR) glasses for visualization of the developed graphical interface and a gyroscope system for feedback, see Fig. 1.

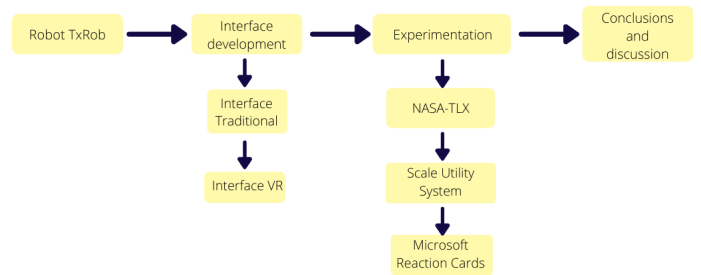


Fig. 1. Methodology Performed.

In addition, the evaluation procedure to be applied to the operators in the teleoperation of a simulated rescue is explained. The objective is to find an immersive and intuitive multimodal interface for the operator, understanding all the information obtained by the proximity and gas sensors, the images from the cameras and the microphone of the TxRob robot. To determine which of the proposed interfaces is better for the user, both interfaces are tested to 15 operators, which are evaluated by subjective metric tests that help to obtain the value of the workload generated by each interface in the immersive teleoperation; the usability as well as the utility of the system and the satisfaction of the operator when manipulating the proposed systems.

IV. PROPOSED MULTIMODAL INTERFACES

Fig. 2, shows the distribution of the two developed interfaces. The traditional interface is the HMI interface that performs the motion control of the TxRob robot by means of a joystick control and the vision is given by a graphical interface displayed on a screen. On the other hand, the VR interface performs the same motion control as the previous interface but the vision is provided by VR glasses and a feedback system generated by a gyroscope and a two-axis turret for the camera.

A. TxRob Control Interface

The motion control of the TxRob was previously developed by means of a joystick control as shown in Fig. 3(a), in this work we have optimized the motion control by increasing the

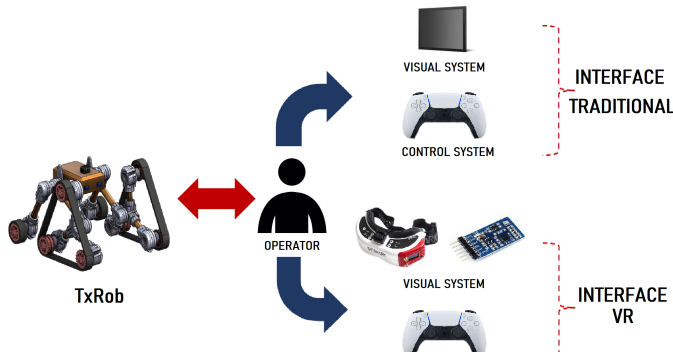


Fig. 2. Visuals and Control Interfaces.

control of a turret where the cameras are located. The turret was implemented in order to obtain the video in real time and to be able to manipulate it in two axes to cover the largest possible space of vision for the operator in the occlusion points without the need to move the TxRob. In this way, images of the upper part of the TxRob robot were obtained.

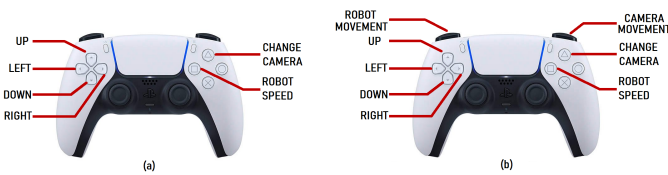


Fig. 3. Button Assignments. (a) First Configuration. (b) Last Configuration.

In the section (a), the change of cameras is controlled by pressing the triangle button; to choose the speed of movement of the robot the square button must be pressed and then by means of the two direction buttons (Up and Down) we regulate the speed of the TxRob. In section (b), to choose the robot movement control, press the L1 key (Robot Movement) and control by means of the four direction buttons (Up, Down, Left and Right); to choose the turret movement control, press the R1 key (Camera Movement) and control by means of the four direction buttons. The rest of the functions of the first configuration were maintained.

B. Traditional Teleoperation Multimodal Interface

In most teleoperated robot vision systems, the interfaces presented consist of cameras and a screen where the video can be observed in real time. In the previous work [10], a control system was realized by means of a screen, which shows the developed interface. This interface shows the images captured from the cameras in addition to the values sampled by the various sensors incorporated.

In Fig. 4, the previously presented interface is improved, in this new interface the collected images are shown on the left side together with the developed motion detection system. The upper right side shows the real-time measured values of the gas sensors (CO_2 , O_2 , NO_X) and the lower part shows an anti-shock system, which indicates the proximity of different objects around the TxRob.



Fig. 4. Improved Teleoperation Interface.

C. Proposed Multimodal Teleoperation Interface

This developed system works by means of specular imitation, that is to say that all the movement made by the operator in the X and Y axis detected by the gyroscope of the VR lenses, will be replicated in the camera turret. This turret consists of two servomotors, each servomotor manages to control the movement in each respective axis, see Fig. 5.

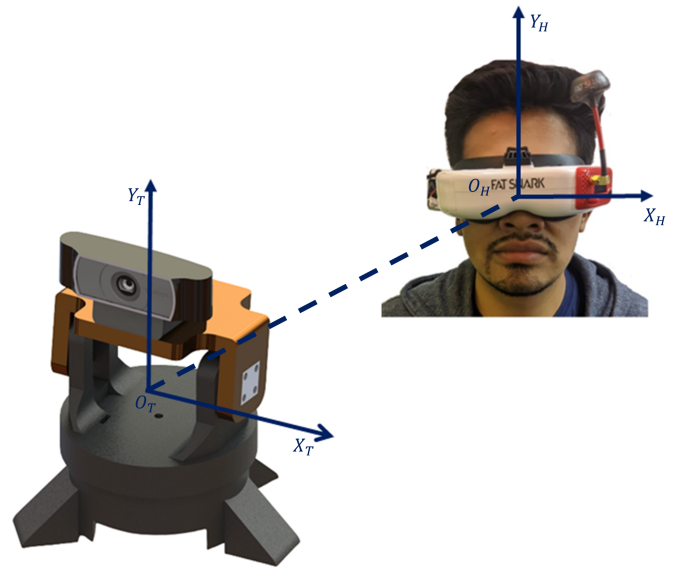


Fig. 5. Coordinates System.

When using VR lenses, the visual interface developed can become overloaded for the operator due to the FPV resolution that this system uses and at the same time the viewing space is reduced, our priority is to have an immersive and intuitive multimodal interface for the user. According to the literature reviewed, the overwhelming amount of data in teleoperation tends to confuse the user, decreasing the effectiveness of the task. For them, a more intuitive interface was developed for this system as shown in Fig. 6.

The interface proposed for the VR glasses is a first-person-view (FPV) interface, this format makes the proposed interface

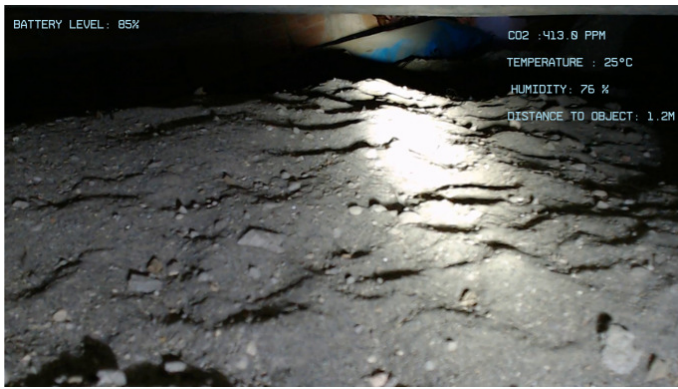


Fig. 6. Display Shown to the User.

more immersive and the immersion is complete; to avoid saturating the operator's view we prioritized the real-time image of the cameras and in the corners we displayed the data from the different sensors of the robot that will help the teleoperation.

V. EXPERIMENTATION

In order to confirm that the VR system with gyroscope feedback can achieve a high performance, it was evaluated by taking measurements in two stages: the first stage consists of the gyroscope attached to the VR device, the measurements recorded in the three axes for 20 seconds; the second stage consists of the measurement of the gyroscope attached to the camera, the movement of the motors are regulated with encoders after receiving the signal from the first gyroscope. In order to compare these two proposed multimodal systems, a debris entrapment rescue environment was simulated. A mirror environment was created for each multimodal interface. The proposed circuit is in the shape of an "S" for the traditional interface and for the proposed interface it is in the shape of an "inverse S" so that the experience is equal in both. This teleoperation test of the TxRob was performed on 15 operators, who ranged in age from 20 to 43 years old and 20% indicated that they had experience in handling VR systems. Each operator must manipulate the two multimodal systems to find the person trapped in the rubble, for this purpose they were given 5 minutes of tests so that they could familiarize themselves with the interfaces to be evaluated. At the time of the real tests, the time it takes to perform the search with each interface is measured, the time increases due to the presence of debris in the test scenario. At the end of the test, each operator performs the three subjective metric tests: NASA-TLX, SUS and Microsoft Reaction Cards; these data are used to obtain the values and scores of both multimodal systems.

VI. RESULTS AND DISCUSSION

A. Gyroscope Measurements

Fig. 7 shows each of the gyroscope axes with the VR lenses on the operator; where the operator moved his head for 20 seconds, making a total of 500 samples taken for each axis of the gyroscope. These measurements correspond to the angular velocity of motion recorded during the experimental phase. Fig. 8 shows each of the gyro axes with the turret camera

on the TxRob .Where the motors simultaneously triggered the movement of the camera according to the data recorded by the gyroscope attached to the VR device.

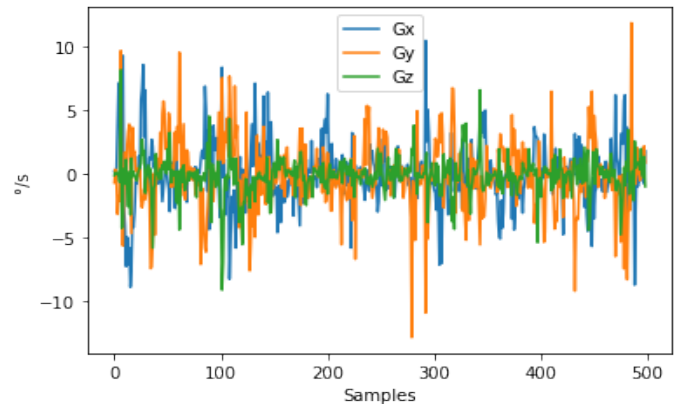


Fig. 7. 3-Axis Plot for the First Gyroscope.

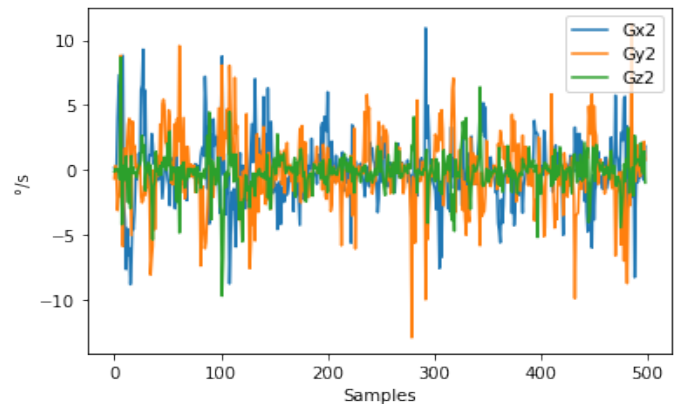


Fig. 8. 3-Axis Plot for the Second Gyroscope.

A comparison was also made between the measurements of both gyroscope divided on each axis defined as Gx, Gy and Gz. Data obtained from both the X-axis lens and turret camera gyroscopes are shown in Fig. 9, while Y-axis data are shown in Fig. 10 and Z-axis data are shown in Fig. 11. On average, a 4.13% variation is found due to the configuration of the motors driven by the encoders.

B. Subjective Measurements

The following values were obtained from Fig. 12, where an improvement in time per task performed with the new proposed multimodal interface is noticeable. We consider this improvement to be relevant because in human rescue operations, time is the most important element. As long as an operation is performed in the shortest time, the possibility of saving more people increases considerably.

The overall workload per operator evaluated was reduced when using the multimodal VR interface. The traditional interface showed an average of 60.66 of overall workload appreciated in performing the experiment as opposed to the VR interface which showed 50.56 of overall workload presented. It

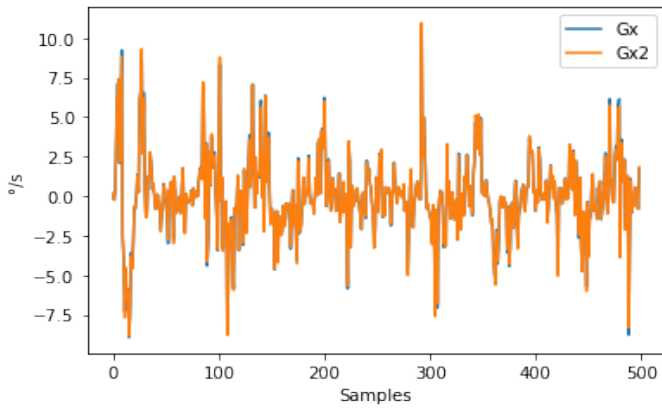


Fig. 9. Comparative Graph between Gx of Both Gyroscopes.

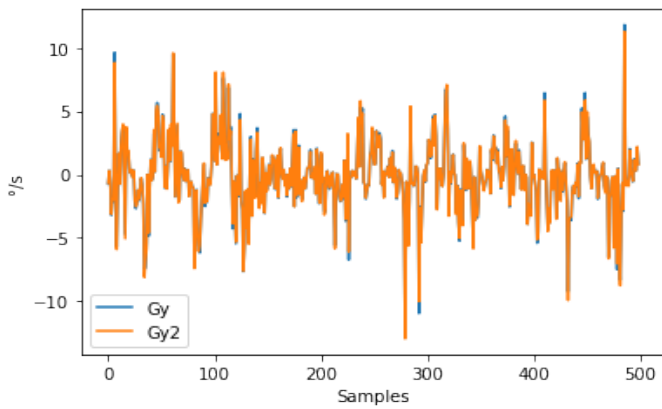


Fig. 10. Comparative Graph between Gy of Both Gyroscopes.

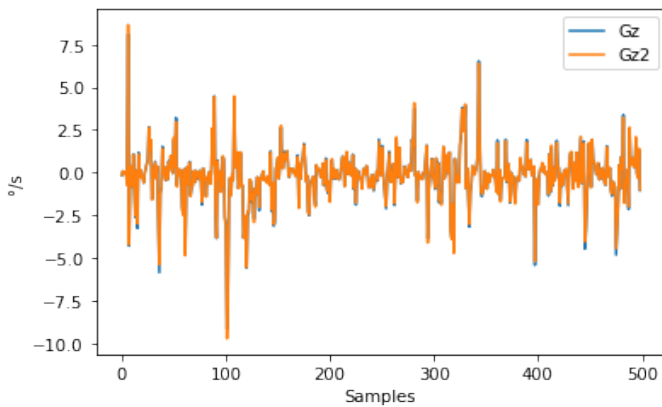


Fig. 11. Comparative Graph between Gz of Both Gyroscopes.

was also noted that the overall workload was higher for people with no experience in manipulating teleoperated systems and older people. This reduced workload helps make teleoperation more intuitive and easier for operators to manipulate. In Fig. 13 the blue bar is the first interface evaluated and the orange bar is the VR interface.

In Fig. 14 we present the dimensions evaluated by the NASA-TLX subjective method such as mental demand, phys-

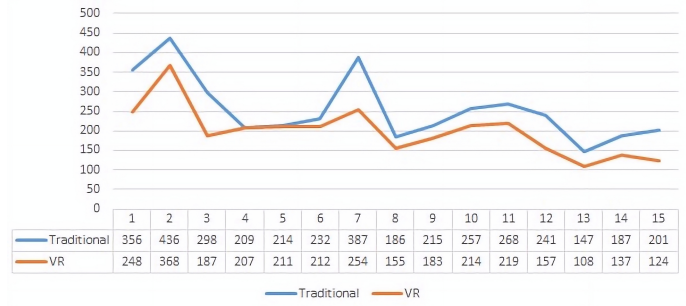


Fig. 12. Time Taken in the Corresponding Tests.

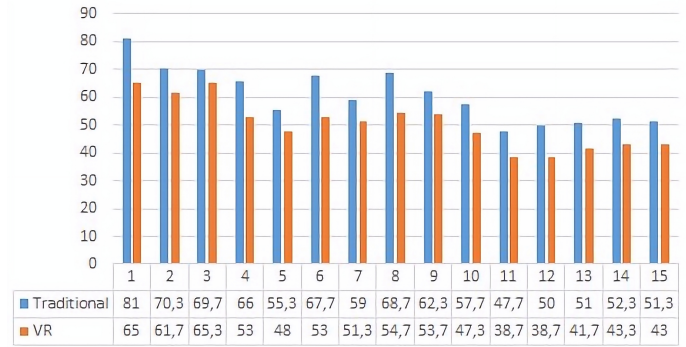


Fig. 13. General Workload - NASA TLX.

ical demand, temporal demand, effort, performance and level of frustration that may occur in the task. We have taken the average of the 15 operators to evaluate each dimension independently. According to the results obtained, the physical demands are lower because both systems are teleoperated and do not require physical labor. The mental demand is higher because the systems require most of the senses of people to manipulate both interfaces. When comparing the results of both interfaces, a reduction is observed when using the VR interface, in some dimensions this difference is more noticeable, such as the effort and frustration presented by the operators.

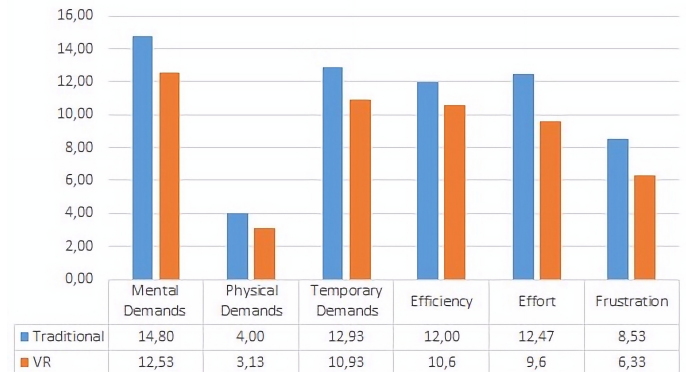


Fig. 14. Average Dimensions - NASA TLX.

The operators were also evaluated with the SUS metric, which will help us to see the usability of the systems, for

the first interface an average of 85.33 was obtained, which indicates that the interface has a wide usability in the tasks of the experiments carried out. In addition, the second interface obtained an average of 95.66, a much more favorable result; in Fig. 15 you can see the scores obtained by each operator, it can be seen that most of them are above 80 points in the traditional interface and above 90 points in the VR interface.

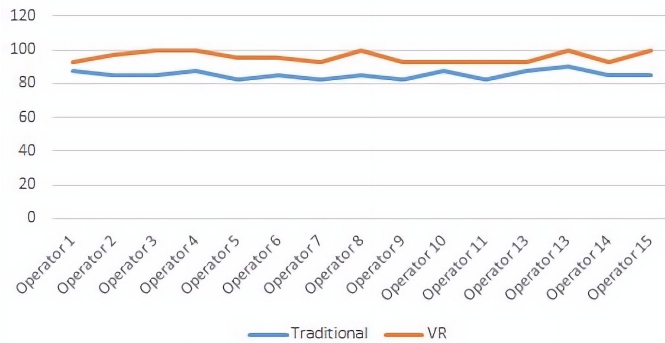


Fig. 15. SUS Results.

Microsoft’s product reaction cards are, in essence, a list of 118 words that are used to describe a product or a completed good. The list includes positive words such as ‘Useful’, ‘Comfortable’ and ‘Innovative’, along with negative words, such as ‘Stressful’, ‘Complex’ and ‘Dull’. The test consists of asking the robot operators to choose words from the list that they would use to describe the robot and, for each one, asking them why they chose that particular word. In these tests each of the 15 operators were limited to choosing 5 words that they felt best qualified the traditional system with joysticks to control the robot (light blue color), while on the other hand, in orange color are the results of the proposed system, see Fig. 16; only the cards with scores were considered, the rest of the words were ignored.

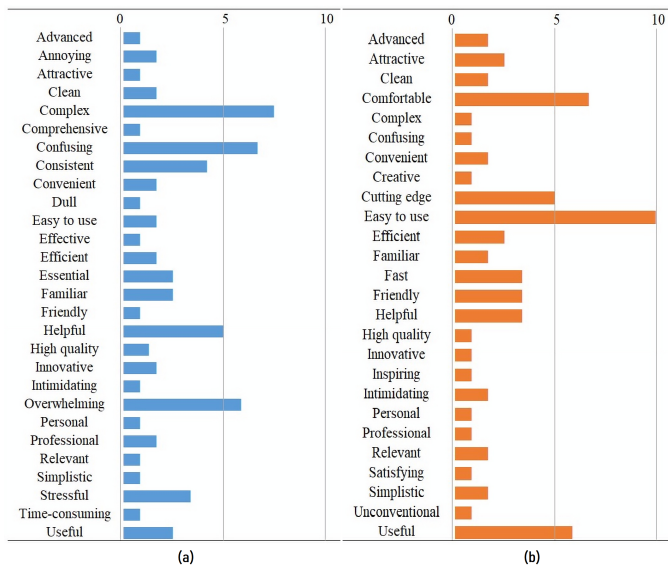


Fig. 16. Results of Microsoft Reaction Cards: (a) Traditional System. (b) VR System.

It can be seen in Fig. 16 that the words that were most chosen by the users were: “Complex”, “Confusing”, “Overwhelming”, “Helpful” and “Consistent”. Although some of the words are positive, it is clear that most of the operators feel that the traditional system with joysticks is not as comfortable to use, unlike the proposed system which in its absence most of the words selected were positive, of which the most chosen were: “Easy to use”, “Comfortable”, “Useful”, “Cutting edge”, “Fast”, “Friendly” and “Helpful”. This information shows that the proposed system is the one preferred by the operators who carried out the TxRob robot handling tests.

VII. CONCLUSION

In this paper an evaluation of the multimodal interface developed for the operation of the TxRob robot was performed. The teleoperated control systems that were developed for the manipulation of the robot are: multimodal system fed back information through the different sensors and a GUI control system using joystick buttons. These interfaces were analyzed using subjective metrics such as NASA-TLX, Scale Utility System (SUS) and Microsoft Reaction Cards, which provided us with data such as workload, experiences such as user satisfaction and usability of each system in order to designate the most intuitive when performing rescue operations in case of a disaster. The results of the NASA-TLX tests showed that the multimodal system with gyroscope feedback for camera control is the best because it greatly reduces stress generation when manipulating robots. In the SUS tests, the proposed system obtained an average score of 95 points, demonstrating that it is a better interface than the joystick control system, which only obtained an average score of 85 points. Finally, the Microsoft Reaction Cards tests showed that the majority of operators chose the proposed interface as more comfortable and easier to use, unlike the majority of words chosen to qualify the traditional joystick system.

ACKNOWLEDGMENT

The authors would like to thank Universidad Nacional de San Agustín de Arequipa.

REFERENCES

- [1] Geophysical Institute of Peru, 2022, Reported Earthquakes.
- [2] R. R. Murphy, “Human-robot interaction in rescue robotics,” in IEEE Transactions on Systems, Man, and Cybernetics, Part C (Applications and Reviews), vol. 34, no. 2, pp. 138-153, May 2004, doi: 10.1109/TSMCC.2004.826267.
- [3] Garrett M. Clayton. Mechatronics for humanitarian explosive ordnance disposal in cambodia. ASME Mechanical Engineering, 140:S4–S10, 2018. <http://dx.doi.org/10.14569/IJACSA.2022.01307104>.
- [4] Deborah R. Billings, Kristin E. Schaefer, Jessie Y.C. Chen, and Peter A. Hancock. 2012. Human-robot interaction: developing trust in robots. In Proceedings of the seventh annual ACM/IEEE international conference on Human-Robot Interaction (HRI '12). Association for Computing Machinery, New York, NY, USA, 109–110. <https://doi.org/10.1145/2157689.2157709>.
- [5] P. Robinette, A. M. Howard and A. R. Wagner, “Effect of Robot Performance on Human–Robot Trust in Time-Critical Situations,” in IEEE Transactions on Human-Machine Systems, vol. 47, no. 4, pp. 425-436, Aug. 2017, doi: 10.1109/THMS.2017.2648849.
- [6] J. Casper and R. R. Murphy, “Human-robot interactions during the robot-assisted urban search and rescue response at the World Trade Center,” in IEEE Transactions on Systems, Man, and Cybernetics, Part B (Cybernetics), vol. 33, no. 3, pp. 367-385, June 2003, doi: 10.1109/TSMCB.2003.811794.

- [7] Angulo, A.M.; Pinto, L.P.; Espinoza, E.S.; Vidal, Y.S.; Colquehuanca, E.S. Assisted Operation of a Robotic Arm Based on Stereo Vision for Positioning Near an Explosive Device. *Robotics* 2022, 11, 100. <https://doi.org/10.3390/robotics11050100>.
- [8] J. Carff, M. Johnson, EM El-Sheikh y JE Pratt, "Human-robot team navigation in visually complex environments", *Proc. Internacional IEEE/RSJ. Conf. Intel. Sistema de robots*, pp. 3043-3050, octubre de 2009.
- [9] Brooke, John. (1995). SUS: A quick and dirty usability scale. *Usability Eval. Ind.* 189.
- [10] Rafael Verano M, Jose Caceres S, Abel Arenas H, Andres Montoya A, Joseph Guevara M, Jarelh Galdos B and Jesus Talavera S, "Desarrollo de un robot explorador teleoperado de bajo costo (TXRob)" *International Journal of Advanced Computer Science and Applications (IJACSA)*, 13(7), 2022. <http://dx.doi.org/10.14569/IJACSA.2022.01307104>.
- [11] E. Triantafyllidis, C. Mcgreavy, J. Gu and Z. Li, "Study of Multimodal Interfaces and the Improvements on Teleoperation," in *IEEE Access*, vol. 8, pp. 78213-78227, 2020, doi: 10.1109/ACCESS.2020.2990080.
- [12] S. Livatino et al., "Intuitive Robot Teleoperation Through Multi-Sensor Informed Mixed Reality Visual Aids," in *IEEE Access*, vol. 9, pp. 25795-25808, 2021, doi: 10.1109/ACCESS.2021.3057808.
- [13] Hudak, M., Korecko, S., Sobota, B., Balluch, T., & Grib, J. (2018). Walking Pad and Gyroscope-Based Object Manipulation for Virtual Reality CAVE. 2018 IEEE 18th International Symposium on Computational Intelligence and Informatics (CINTI). doi:10.1109/cinti.2018.8928223.
- [14] Shanmin, C., Tao, N., & Ke, W. (2011). Motion Control of Virtual Human Based on Optical Motion Capture in Immersive Virtual Maintenance System. 2011 International Conference on Virtual Reality and Visualization. doi:10.1109/icvrv.2011.24.
- [15] Fang, D., Xu, H., Yang, X., & Bian, M. (2019). An Augmented Reality-Based Method for Remote Collaborative Real-Time Assistance: from a System Perspective. *Mobile Networks and Applications*. doi:10.1007/s11036-019-01244-4.
- [16] M. Aggravi, A. A. S. Elsherif, P. R. Giordano and C. Pacchierotti, "Haptic-Enabled Decentralized Control of a Heterogeneous Human-Robot Team for Search and Rescue in Partially-Known Environments," in *IEEE Robotics and Automation Letters*, vol. 6, no. 3, pp. 4843-4850, July 2021, doi: 10.1109/LRA.2021.3067859.
- [17] Goyzueta, Denilson V., Joseph Guevara M., Andrés Montoya A., Erasmo Sulla E., Yuri Lester S., Pari L., and Elvis Supo C. 2022. "Analysis of a User Interface Based on Multimodal Interaction to Control a Robotic Arm for EOD Applications" *Electronics* 11, no. 11: 1690. <https://doi.org/10.3390/electronics11111690>
- [18] Q. -Z. Ang, B. Horan and S. Nahavandi, "Multipoint Haptic Mediator Interface for Robotic Teleoperation," in *IEEE Systems Journal*, vol. 9, no. 1, pp. 86-97, March 2015, doi: 10.1109/JSYST.2013.2283955.
- [19] Y. Chen, C. Yang, Y. Gu and B. Hu, "Influence of Mobile Robots on Human Safety Perception and System Productivity in Wholesale and Retail Trade Environments: A Pilot Study," in *IEEE Transactions on Human-Machine Systems*, vol. 52, no. 4, pp. 624-635, Aug. 2022, doi: 10.1109/THMS.2021.3134553.
- [20] I. M. Rezazadeh, M. Firoozabadi, H. Hu and S. M. R. H. Golpayegani, "Co-Adaptive and Affective Human-Machine Interface for Improving Training Performances of Virtual Myoelectric Forearm Prosthesis," in *IEEE Transactions on Affective Computing*, vol. 3, no. 3, pp. 285-297, July-September 2012, doi: 10.1109/T-AFFC.2012.3.

Exploring Power Advantage of Binary Search: An Experimental Study

Muhammad Al-Hashimi¹, Naif Aljabri²
Department of Computer Science
King Abdulaziz University, Jeddah, Saudi Arabia

Abstract—As exascale systems come online, more ways are needed to keep them within reasonable power budgets. This study aims to help uncover power advantages in algorithms likely ubiquitous in high-performance workloads such as searching. This study explored the power efficiency of binary search and its ternary variant, comparing consumption under different scenarios and workloads. Accurate modern on-chip integrated voltage regulators were used to get reliable power measurements. Results showed the binary version of the algorithm, which runs slower but relies on a barrel-shifter circuit, to be more power efficient in all studied scenarios offering an attractive time-power tradeoff. The cumulative savings were significant and will likely be valuable where the search may be a substantial fraction of workloads, especially massive ones.

Keywords—Binary search; ternary search; time-power tradeoff; exascale computing; barrel shifter

I. INTRODUCTION

The fastest supercomputers in the world today are capable of solving problems at the petascale level, i.e., 10^{15} floating point operations/second (flops). Complex simulations of more realistic models are becoming less feasible on current petascale supercomputers. These workloads need exascale (10^{18}) machines. The main obstacle to exascale was the projected power consumption [1]–[4]. If petascale-era technology had been scaled, it would have consumed absurd amounts of power in the order of gigawatts. The US Defense Advanced Research Projects Agency (DARPA) specified that the peak power consumption should be below 20 megawatts (MW), which led [4] to conclude that substantial advances in hardware, software, and algorithms were needed to meet that requirement. Some experts [5], [6] had predicted that a complete exascale system would enter service by 2020. The first one that also meets the DARPA provision arrived in 2022 [7]. The Frontier supercomputer (Oak Ridge National Lab, USA) made its official debut on the 2022 Top500 list as the first supercomputer to exceed 1.0 exaflops [8], [9]. Engineers project reaching 1.5 exaflops peak at 29 MW (19.33 MW/exaflop) [10].

The previous studies on power and energy reduction focused on architecture, chip technology, algorithm optimization, and management. This study aims to explore the inherent power advantages in algorithms, i.e., those stemming from the method. It pays particular attention to the power (the time rate), which once was an obstacle in the path to exascale and likely will continue to be a significant concern. The work relies on direct measurement and observations at the micro-architectural level. It encourages rethinking time optimization, which has long been a classic interest in computing, as it may sometimes interfere with the power concerns of systems where

saving power may be of primary interest. With those concerns in mind, [11] examined the power efficiency of mergesort against that of quicksort, the standard general-purpose sorting algorithm. Their results showed that the power consumption of the mergesort was significantly better than an optimized quicksort when it exploited the barrel shifter, a digital binary shift circuit, to do the partitioning phase. The barrel shifter is a simple, power-efficient component in modern processors utilized to perform powers (exponent) of two divisions and multiplications in one clock cycle. The quicksort ran faster on average, as expected. Hence switching sorting methods did involve a time-power tradeoff.

The preceding encouraged a look into more algorithms that rely on the shifter hardware to see if similar power trends hold elsewhere. Accordingly, binary search should perhaps have a power advantage against a ternary version since it divides search lists by two, which could utilize the power-efficient barrel shifter. This study attempts to investigate and quantify that advantage. Binary search is a log-efficient procedure for unordered querying an array of ordered keys based on an implicit optimal binary tree [12, see S. 6.2], which is very useful for multiple random queries. It is a significant part of various general workloads [13]. Conceptually, it looks for a key value X in a sorted list as follows:

```
if ( X == middle element )
    X is found
else if ( X < middle element )
    search 1st half of list using the same method
else
    search 2nd half of list using the same method
```

A ternary search algorithm works as outlined next:

```
if ( X == middle1 element )
    X is found
if ( X == middle2 element )
    X is found
else if ( X < middle1 element )
    search 1st third of list using the same method
else if ( X > middle2 element )
    search 3rd third of list using the same method
else
    search 2nd third of list using the same method
```

The rest of the paper is organized as follows: Section II reviews related work in chronological order. Section III describes the experiments. In Section IV, findings are presented and discussed. Finally, concluding remarks and suggestions for further research are in Section V.

II. RELATED WORK

The research in [14]–[16] introduced a new energy management component and used it to select the best energy-saving sorting algorithm on mobile platforms. The energy management component selects the best algorithm dynamically. The results show good energy saving and encourage more investigation.

The author in [17] presented a new methodology to estimate power consumption for parallel computation in a multicolor environment. They also prove that the total power consumption for the computation is not equal to the sum of each core individually. The results show that their measurement accuracy was 95%. In [18], the author enhanced the performance and energy consumption for a parallel program running on the Intel Core i7-2600 processor by increasing the data locality. They increased energy efficiency by more than six times.

The author in [19] presented a methodology to predict the energy consumption for algorithms using the algorithm atomic operations analysis. They use it to evaluate the energy consumption for the classical bubble sort algorithm. Their prediction methodology accuracy was more than 95%. The author in [20] used the scheduler control information to estimate the needed number of cores to execute the waiting program threads. Their results show some power savings. The author in [21] developed a power-efficient algorithm based on mathematical modeling for sorting on a mesh-connected network that utilized an optical pyramid layout (on chips equipped with optics capabilities). They showed a reduction in energy consumption due to data movement based on energy modeling vs. time. There was no direct assessment of power. The author in [22] presented a new methodology to save power in mobile platforms using Intel Core i5 processor by running different workloads on a limited number of cores. They reduce the power consumption by 40%.

In [23], the author presented a methodology to save power consumption in multicore environments by reducing the thread idle time. They applied it to the concurrent execution of ILU-PACK (an *LU* decomposition software). The results showed that they achieved good savings in power. In [24], the author presented a new method to save energy by adopting an energy-efficient I/O management approach in supercomputers. They examined three radically different I/O schemes, including time partitioning, dedicated cores, and dedicated nodes. They also characterized how different configurations of the application and the system can impact performance and energy consumption. Reference [25] translated the CPU dissipated power into tokens to select the best power-saving technique. The dissipated power was predicted at cycle level and basic block level. They enhanced the energy consumption by 11%.

The authors in [26] and [27] observed power efficiency characteristics of the barrel shifter circuit in the context of digital signal processing where powers of two divisions and multiplications are dominant.

The author in [28] investigated power and energy consumption of mergesort against that of quicksort running on the Intel Xeon E5-2640 (Sandy Bridge). That study had two drawbacks. First, it eliminated some, but not enough, side activities that could contribute to the readings. Second, it relied on an older

part that did not support fine power control or detailed internal instrumentation, including crucial cache activity information. Nevertheless, their results identified a statistically significant power advantage for basic mergesort. The author in [29], [30] developed a methodology for evaluating power and energy consumption on the NVIDIA Tesla K40c GPU and used it to compare GPU-optimized bitonic mergesort and quicksort. Their results showed that the mergesort outperformed quicksort in power consumption. The bitonic mergesort was further analyzed in [31] for power and energy consumption on the NVIDIA platform. They identified the factors that caused the mergesort to have a power advantage (in a follow-up study, [32] showed that varying the block size on the GPU further improved the power performance of the mergesort).

In [11], the author developed a rigorous experimental procedure to eliminate sources that could taint measurements based on a CPU with improved power instrumentation. They showed natural mergesort to have a clear power advantage against a highly optimized 3-way quicksort. A meta-analytical comparison of the energy consumption of mergesort and quicksort was conducted in [33] based on an extensive literature review that included [11]. The study concluded that there was no significant difference in energy needs. Results in [11] had earlier agreed on energy but found the mergesort to consume less power based on direct measurement, stressing a concern when two systems go through the same energy budget at different rates. It is the basis of time-power tradeoffs. In some applications, the time rate, i.e., power, is perhaps more consequential.

III. EXPERIMENTAL DESIGN AND PROCEDURES

Realistic measurement of the power consumption of a program running on a CPU is not easy. In a modern run environment, a program runs on a CPU with many other pieces of code that share the CPU and other resources. Programs run on many CPU cores under OS control. Therefore environmental factors, which confound measurement that may credibly be attributed to the experiment's code, had to be eliminated. Some challenges are not unlike those faced when profiling program run time or studying the time behavior of an algorithm. In addition, empirical assessment of power characteristics presents extra challenges. Ambient and CPU-generated heat act as thermal noise that can distort measurements. A modern CPU actively manages power, adjusting its cooling fan speeds, internal voltages, and frequencies to maintain health and keep power consumption in check, which changes power performance unpredictably. In this study, the authors strove to eliminate as many external factors and sources of power consumption as needed to ensure proper, consistent readings that serve the purpose of the study. The classic generic iterative versions of the binary and ternary search algorithms, hereafter referred to as BS and TS, respectively, were used. Finally, timing data was collected as an experimental control to verify programming and expected complexity behavior.

The following describes the experimental environment, the tools used to profile power, the executables that code the algorithms, and the datasets and related test procedures.

TABLE I. SPECIFICATIONS OF THE TEST BED WORKSTATION

Processor	Intel Xeon E5-2680 v3 (Haswell-EP) 12 Cores (24 Logical) TDP Limit = 120 W
Cache Memory	L1/core: 32 KB Instruction, 32 KB Data L2/core = 256 KB L3 Shared = 30 MB
OS	Linux Ubuntu 16.04 LTS 64-bit
Physical Memory (RAM)	8.00 GB

A. The Environment

The test bed machine was a FUJITSU HPC workstation kept under consistent server-room conditions to control ambient thermal effects. Specifications are listed in TABLE I. The experiments ran with the power supply fan ON. The processor environment is an HPC-grade Intel Xeon CPU that appears in machines such as the SGI ICE X supercluster, which ranked 40 in the 2015 Top500 list.

The following settings were applied to the CPU and the OS to eliminate thermal noise and other factors that could contaminate the power readings:

- Disabled hyper-threading (architectural optimization).
- Disabled power management options (architectural optimization).
- Disabled the CPU fan to eliminate effects of cooling (an external fan was used between runs to bring the CPU back to a consistent initial thermal state).
- Closed unnecessary OS services and processes to run the OS with minimum resources.
- Moved the necessary OS processes and services to cores 2 and above to dedicate core 0 for the experiments.
- Left core 1 idle to reduce thermal interference from the other cores.

B. The Profiler

The Linux *perf* tool was used to profile the CPU. The profiler, part of the Linux kernel, provides a wealth of information about the CPU, including power and energy consumption. It largely depends on the RAPL (running average power limiting) interface, which, in turn, depends on the quality of CPU state control and probe components embedded in the processor. The HPC-grade 2600v3 Haswell-series, including the part used in this work, featured [34]: 1) a shift from an indirect model-based reporting to actual measurement based on fully integrated voltage regulators (FIVR), and 2) the addition of per core voltage regulators that control the frequency and power states of cores individually. Previous generations relied on one mainboard regulator to infer detailed information. A 2018 study found that RAPL closely matched plug power readings in the Haswell architecture [35]. As a result, the profiler can provide reliable, higher-resolution instrumentation on the Xeon 2680v3. The tool was configured to obtain an average of 300 runs and used the following command for each one.

```
perf stat -e power/energy-pkg ./algorithm
```

```
Disassembly of section .text:
00000000004005b6 <binarySearch(int*, int, int)>:
_Z12binarySearchPiii():
0.31  push    %rbp
      mov   %rsp,%rbp
      mov   %rdi,-0x18(%rbp)
      mov   %esi,-0x1c(%rbp)
      mov   %edx,-0x20(%rbp)
0.31  movl   $0x0,-0xc(%rbp)
      mov   -0x1c(%rbp),%eax
      sub   $0x1,%eax
      mov   %eax,-0x8(%rbp)
2.83  le:   mov   -0xc(%rbp),%eax
1.26  cmp   -0x8(%rbp),%eax
      jg   8b
      mov   -0xc(%rbp),%edx
1.89  mov   -0x8(%rbp),%eax
1.26  add   %edx,%eax
      mov   %eax,%edx
0.94  shr   $0x1f,%edx
1.57  add   %edx,%eax
1.57  sar   %eax
1.26  mov   %eax,-0x4(%rbp)
13.84 mov   -0x4(%rbp),%eax
3.14  cltq
3.14  lea   0x0(,%rax,4),%rdx
      mov   -0x18(%rbp),%rax
4.40  add   %rdx,%rax
24.84 mov   (%rax),%eax
      cmp   -0x20(%rbp),%eax
10.69 jne   5a
3.46  mov   -0x4(%rbp),%eax
      jnp  90
0.31  5a:   mov   -0x4(%rbp),%eax
      cltq
      lea   0x0(,%rax,4),%rdx
4.09  mov   -0x18(%rbp),%rax
```

Fig. 1. Barrel Shifter Instructions SAR and SHR in Disassembled BS Code.

TABLE II. DATASETS AND RUN SCENARIOS

Dataset Size	Number Datasets	Number Runs	Total Runs	
Set 1	48,000	20	300	20×300 = 6000
Set 2	64,000	20	300	20×300 = 6000
Set 3	512,000	20	300	20×300 = 6000
Set 4	8,000,000	20	300	20×300 = 6000

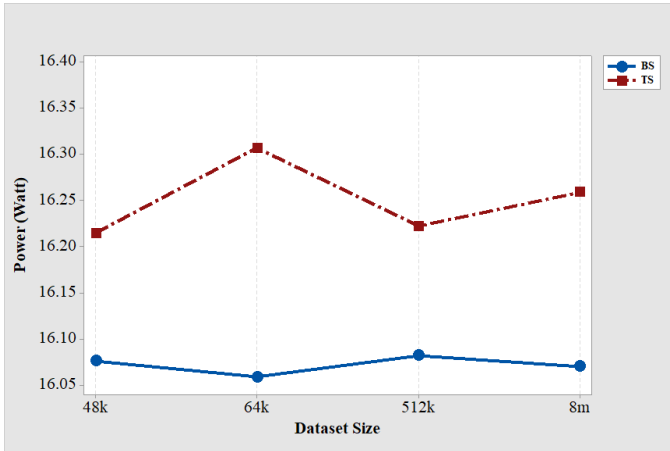
C. The Executable Files

The search code was generated using the GCC 64-bit compiler in release mode. All optimization options in the compiler were disabled to avoid those that replace bare code with parts optimized for specific architectural features. Optimizations do not serve the purpose of the experiments. They may result in readings that reflect the machine or the compiler more than the algorithms in principle. The authors consider bare code a fair rendition of the algorithm on machines from the same instruction set architectural (ISA) style. Turning off power features in an otherwise power-efficient CPU also fits that concern. Finally, disassembled code from the BS executable was examined to confirm that it utilized the shifter circuit instructions to halve the sizes of search lists (Fig. 1).

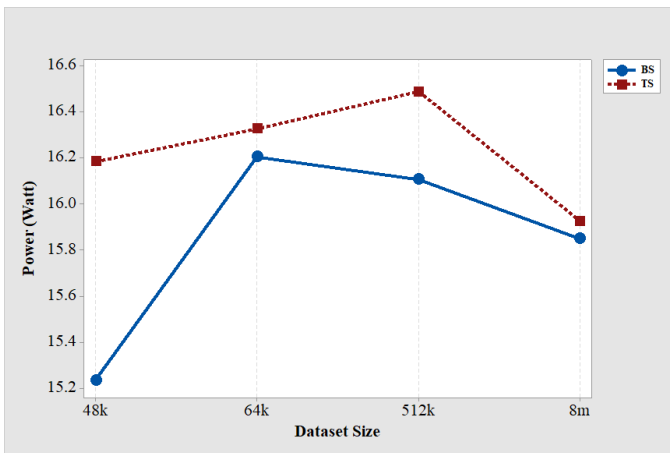
TABLE IV shows the average power consumption for various dataset sizes under the different run scenarios for each search algorithm. The averages were calculated from 290 runs/list (after discarding the first ten of 300) for 20 different lists. So each power value in the table represents 5800 runs. Fig. 2 show these findings comparatively.

TABLE III. NUMBER OF ITERATIONS FOR SIMILAR-ITERATIONS AND SINGLE-ELEMENT SEARCH SCENARIOS

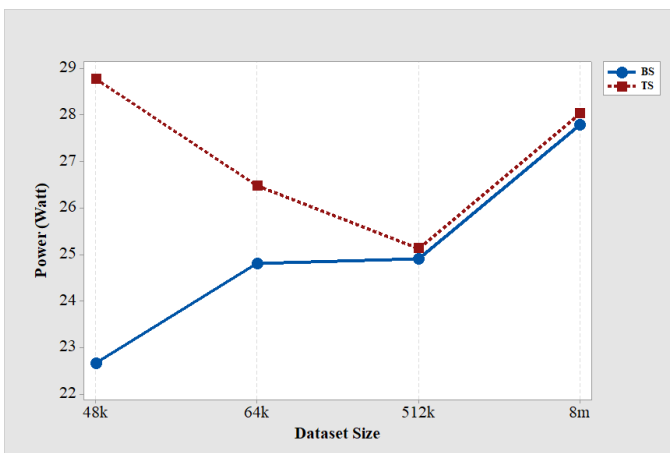
Dataset Size	Similar-Iterations		Single-Element	
	BS	TS	BS	TS
48k	9	9	14	9
64k	9	9	16	9
512k	11	11	19	11
8M	15	15	23	15



(a) Similar-Iterations



(b) Single-Element



(c) All-Elements

Fig. 2. Average Power Consumption in Watts for Search Scenarios.

D. The Datasets

Lists of unique random integers, sorted in ascending order, were generated in four size sets, each comprising 20 different lists. Each dataset ran 300 times for a total number of 24,000 runs. The first ten runs/dataset were discarded to avoid effects from the initial thermal state of the CPU. See TABLE II for a summary of the datasets and run scenarios.

The authors chose 300 after running test trials and found that averages tended to start converging after 230 runs. Dataset sizes were chosen based on cache miss data from [11], where they used the same CPU. Some experimentation with different sizes confirmed that power readings for datasets located in the same cache level were reasonably similar. So sizes were based on crossing L1, L2, and L3 cache boundaries. Sizes of sets 1 and 2 represent lists in L1 and L2, respectively, and those of sets 3 and 4 represent small and large lists in the L3 cache, taking care not to cross over to DRAM. The DRAM was excluded for two reasons. First, to maintain comparable readings since the on-chip SRAM-based cache levels likely share the same physical characteristics, hence the power profile. Second, to better discern effects from algorithmic operations that the off-chip DRAM access may further drown. Data movement along communication links is a known prominent contributor to power consumption, so the decision works for the authors' approach to emphasizing the algorithm.

IV. RESULTS AND DISCUSSION

To avoid unpredictable effects from the best and worst cases on averages and to gain better insights, the experiments ran in three controlled search scenarios:

- 1) **Similar-iterations search:** The scenario picks an element near the middle of the randomly-generated list, then calculates the iterations needed to find this element. Each algorithm needs a different number of iterations to find it. The smallest is selected to set both to run iterations equal to that number. For example, if BS needed nine iterations and TS needed eleven, both are set to run nine iterations. It represents the minimum run cost to find the key. It also quantifies the power cost of searches/finds that take the same amount of iterating, which may be a fair basis to compare the algorithms. TABLE III shows the number of iterations used for this scenario.
- 2) **Single-element search:** Again, set the two algorithms to search for an element near the middle of the list. Here each algorithm runs all the needed iterations to find it. This scenario quantifies the full cost of a find that can compare with the first scenario. The number of iterations for this scenario is in TABLE III.

TABLE IV. AVERAGE POWER IN WATTS (COLUMN $\Delta\%$ SHOWS PERCENT INCREASE FROM BS TO TS)

Dataset Size	Similar Iterations			Single Element			All Elements		
	BS	TS	$\Delta\%$	BS	TS	$\Delta\%$	BS	TS	$\Delta\%$
48k	16.08	16.21	0.81	15.23	16.18	6.24	22.65	28.77	27.02
64k	16.06	16.31	1.56	16.20	16.33	0.80	24.80	26.48	6.77
512k	16.08	16.22	0.87	16.11	16.49	2.36	24.90	25.13	0.92
8M	16.07	16.26	1.18	15.85	15.92	0.44	27.78	28.03	0.90

- 3) **All-element search:** This scenario sets each algorithm to search for all the elements in the dataset in each run. For example, if the dataset size is 100, the algorithm searches for element 1, then 2, until 100. Some element locations are the worst for the algorithms, while others are the best. The power consumption of all searches is measured to avoid the impact of the element's location on the power consumption and averaged to find the average power consumption for all the positions for each algorithm.

The results show that BS was consistently more power efficient, with slim margins in the similar-iterations and single-element search scenarios (datapoint 64k-single-element appears anomalous). Power savings, however, were substantial in the all-elements case. The savings seem to depend on the cache level. They seem to diminish as the computation spills to the next cache level and then stabilize at around 1% in L3.

Before discussing the results, readers are minded that both algorithms are incredibly fast, with TS holding a slight runtime edge. They go quickly through keys to reach either a found or not found outcome. The run times are comparable since both belong to the logarithmic efficiency class (TS in base 3, hence its edge). Therefore, it is perhaps unsurprising to see close power readings in the similar-iterations and single-element search scenarios. They both depict an isolated query. Notably, BS still manages to hold a consistent edge in power consumption. In the similar-iterations case, had BS taken as few iterations as TS, it would have consumed less power, i.e., it had a lower power cost of iterating. The all-elements search scenario paints a more realistic picture of what to expect as a cumulative effect likely to be experienced during an extended period. It is where those seemingly minor differences observed in the other two scenarios come into play.

Furthermore, cache memory interferes with the run time performance of the binary search (likewise the TLB, if DRAM is involved) [13]. With large subarrays, binary search is prone to generating indices to elements in distant memory. The effects of weaker locality increase as datasets grow in size. Power consumption should follow a similar trend. Power overheads due to cache miss rise as more physical circuits are engaged to satisfy the misses. Interactions with cache memory generally may explain the decline in power savings as the effects from misses increase. Therefore, limiting list sizes was conducive to the aims of the experiments. The L1 cache is expected to yield the most realistic view of power from the algorithmic operations since it suffers the least from the power overheads of misses.

Little differences in power consumption may not look promising when viewed from a single application standpoint. In a large-scale system, however, the cumulative effect should be significant, especially for a computation likely a good frac-

tion of the general workload for extended times like searching. The savings may be substantial, which may be more valuable for a power-sensitive system like an exascale supercomputer. Moreover, those savings were really due to the algorithm. BS calls for an inherently inexpensive operation on a binary computer, which reflects in simple power-efficient hardware, not the other way around. If not mindful, it may be tempting to pick the ternary version to speed up runs, especially since the cost of implementation is negligible.

The findings seem to support the idea that some algorithms have a power (not energy necessarily) advantage over those that need to work harder, i.e., expend energy at a higher rate, to achieve the same results. The inherent power efficiency of an operation reflects in the hardware, as is the case with the division by two on a binary device. One may expect an algorithm that relies on that operation to be more power efficient. This observation should be interesting where power savings are more significant than some runtime gains, such as those offered by TS. Eventually, interactions with microarchitectural features, such as those underlying the memory, may erode those savings in the real world. However, the savings can add up system-wide in pervasive computations. Thus a massive exascale system may be in a better position to benefit from the cumulative savings. Mobile systems should also benefit from power-focused optimizations since they relate to the critical concern of how quickly a battery drains. A power-efficient *workload* helps a smaller (lighter) battery go a long way.

V. CONCLUSIONS

This work experimentally explored the power efficiency of two variants of binary search: the classic binary decision (BS) and the faster-running ternary decision version (TS), both in the same time efficiency class. The authors tuned the experimental environment to focus on the search code while eliminating other run environment factors. Under the experimental conditions, the results showed that BS outperformed TS in power consumption under different search scenarios. The BS could take advantage of the more efficient shift hardware. The findings seem to corroborate the authors' initial suspicions about BS, which stemmed from work reported in [11]. The savings in BS were likely inconsequential for individual searches, but the cumulative effects may be significant.

The study has been an early attempt to establish the binary decision version of binary search as a preferred alternative for exascale applications. It quantified a power advantage and exposed a potentially interesting tradeoff with time, especially from a workload-wide view. Further investigation with different scenarios and environments may be needed to argue that the reported findings stem from the method (algorithmic) rather than the run environment, i.e., a binary decision is inherently efficient in terms of power consumption on any binary computer. Future investigations in other processor environments

would be interesting, for example, later core processors or GPUs whose importance in HPC continues to grow. Higher resolution instrumentation and better reporting tools should provide deeper insights. Such studies may uncover trends independent of architecture. Eliminating other microarchitectural interferences help further amplify behaviors due to the algorithm. For example, basic binary search is quite branchy, so it may be helpful to turn off branch prediction. Other algorithms that rely on the binary shift hardware may be worth exploring. Finally, this work focused on average power. It may be interesting to observe peak power, which should be of interest from a system-wide workload in a massive supercomputer viewpoint.

ACKNOWLEDGMENT

This work was funded by King Abdulaziz University, under grant No. (1-611/1433 HiCi). The authors, therefore, acknowledge technical and financial support of KAU.

REFERENCES

- [1] K. Bergman, S. Borkar, D. Campbell, W. Carlson *et al.*, "Exascale computing study: Technology challenges in achieving exascale systems Peter Kogge, editor & study lead," DARPA Information Processing Techniques Office, Exascale Working Group Report, September 2008.
- [2] S. Ashby, P. Beckman, J. Chen, P. Colella *et al.*, "The opportunities and challenges of exascale computing," US Department of Energy Office of Science, Summary Report of the Advanced Scientific Computing Advisory Committee (ASCAC) Subcommittee, Fall 2010.
- [3] O. Villa, D. R. Johnson, M. O'Connor, E. Bolotin, D. Nellans, J. Luitjens, N. Sakharnykh, P. Wang, P. Micikevicius, A. Scudiero *et al.*, "Scaling the power wall: a path to exascale," in *Proceedings of the International Conference for High Performance Computing, Networking, Storage and Analysis*. IEEE Press, 2014, pp. 830–841.
- [4] D. A. Reed and J. Dongarra, "Exascale computing and big data," *Communications of the ACM*, vol. 58, no. 7, pp. 56–68, 2015.
- [5] P. Beckman, "On the road to exascale," *Scientific Computing World*, no. 116, pp. 26–28, 2011.
- [6] J. Hsu, "When will we have an exascale supercomputer?" *IEEE spectrum*, vol. 52, no. 1, pp. 13–16, 2015.
- [7] D. Schneider, "The exascale era is upon us," *IEEE spectrum*, vol. 110, no. 1, pp. 34–35, 2022.
- [8] T. Trader, "Top500: Exascale is officially here with debut of frontier," *HPCwire*, 2022. [Online]. Available: <https://www.hpcwire.com/?p=142590>
- [9] C. Q. Choi, "Beneath the hood of the first exascale computer," *IEEE spectrum*, vol. 59, no. 8, pp. 8–9, 2022.
- [10] T. Trader, "US closes in on exascale: Frontier installation is underway," *HPCwire*, 2021. [Online]. Available: <https://www.hpcwire.com/?p=125875>
- [11] N. Aljabri, M. Al-Hashimi, M. Saleh, and O. Abulnaja, "Investigating power efficiency of mergesort," *The Journal of Supercomputing*, vol. 75, pp. 6277–6302, 2019.
- [12] D. E. Knuth, *The art of computer programming*, 2nd ed. Addison-Wesley, April 1988 (36th printing), vol. 3 (Sorting and Searching).
- [13] P.-V. Khuong and P. Morin, "Array layouts for comparison-based searching," *ACM Journal of Experimental Algorithmics*, vol. 22, no. 1, pp. 1.3:1–1.3:39, may 2017.
- [14] C. Bunse, H. Höpfner, S. Roychoudhury, and E. Mansour, "Energy efficient data sorting using standard sorting algorithms," in *International Conference on Software and Data Technologies*. Springer, 2009, pp. 247–260.
- [15] C. Bunse, H. Höpfner, E. Mansour, and S. Roychoudhury, "Exploring the energy consumption of data sorting algorithms in embedded and mobile environments," in *Mobile Data Management: Systems, Services and Middleware, 2009. MDM'09. Tenth International Conference on*. IEEE, 2009, pp. 600–607.
- [16] C. Bunse, H. Höpfner, S. Roychoudhury, and E. Mansour, "Choosing the "best" sorting algorithm for optimal energy consumption," in *ICSOFT (2)*, 2009, pp. 199–206.
- [17] R. Basmadjian and H. de Meer, "Evaluating and modeling power consumption of multi-core processors," in *Proceedings of the 3rd International Conference on Future Energy Systems: Where Energy, Computing and Communication Meet*. ACM, 2012, p. 12.
- [18] A. Al Hasib, P. G. Kjeldsberg, and L. Natvig, "Performance and energy efficiency analysis of data reuse transformation methodology on multicore processor," in *European Conference on Parallel Processing*. Springer, 2012, pp. 337–346.
- [19] Y. Yuechuan, Z. Guosun, D. Chunling, and W. Wei, "Analysis method of energy for c source program and its application," in *Green Computing and Communications (GreenCom), 2013 IEEE and Internet of Things (iThings/CPSCoM), IEEE International Conference on and IEEE Cyber, Physical and Social Computing*. IEEE, 2013, pp. 1397–1402.
- [20] T. Kodaka, A. Takeda, S. Sasaki, A. Yokosawa, T. Kizu, T. Tokuyoshi, H. Xu, T. Sano, H. Usui, J. Tanabe *et al.*, "A near-future prediction method for low power consumption on a many-core processor," in *Proceedings of the Conference on Design, Automation and Test in Europe*. EDA Consortium, 2013, pp. 1058–1059.
- [21] P. Poon and Q. F. Stout, "Time-power tradeoffs for sorting on a mesh-connected computer with optical connections," in *Parallel and Distributed Processing Symposium Workshops & PhD Forum (IPDPSW), 2013 IEEE 27th International*. IEEE, 2013, pp. 611–619.
- [22] F. Hamady, A. Kayssi, A. Chehab, and M. Mansour, "Evaluation of low-power computing when operating on subsets of multicore processors," *Journal of Signal Processing Systems*, vol. 70, no. 2, pp. 193–208, 2013.
- [23] J. I. Aliaga, M. Barreda, M. F. Dolz, A. F. Martín, R. Mayo, and E. S. Quintana-Ortí, "Assessing the impact of the cpu power-saving modes on the task-parallel solution of sparse linear systems," *Cluster computing*, vol. 17, no. 4, pp. 1335–1348, 2014.
- [24] O. Yildiz, M. Dorier, S. Ibrahim, and G. Antoniu, "A performance and energy analysis of i/o management approaches for exascale systems," in *Proceedings of the sixth international workshop on Data intensive distributed computing*. ACM, 2014, pp. 35–40.
- [25] J. M. Cebrián, D. Sánchez, J. L. Aragón, and S. Kaxiras, "Managing power constraints in a single-core scenario through power tokens," *The Journal of Supercomputing*, vol. 68, no. 1, pp. 414–442, 2014.
- [26] S. K. Mitra and A. R. Chowdhury, "Optimized logarithmic barrel shifter in reversible logic synthesis," in *VLSI Design (VLSID), 2015 28th International Conference on*. IEEE, 2015, pp. 441–446.
- [27] M. M. Kamble and S. P. Ugale, "FPGA implementation and analysis of different multiplication algorithm," *International Journal of Computer Applications*, vol. 149, no. 2, pp. 33–36, 2016.
- [28] M. Al-Hashimi, M. Saleh, O. Abulnaja, and N. Aljabri, "On the power characteristics of mergesort: an empirical study," in *Advanced Control Circuits Systems (ACCS) Systems & 2017 Intl Conf on New Paradigms in Electronics & Information Technology (PEIT), 2017 Intl Conf on*. IEEE, 2017, pp. 172–178.
- [29] M. A. Al-Hashimi, O. A. Abulnaja, M. E. Saleh, and M. J. Ikram, "Evaluating power and energy efficiency of bitonic mergesort on graphics processing unit," *IEEE Access*, vol. 5, pp. 16429–16440, 2017.
- [30] M. J. Ikram, O. A. Abulnaja, M. E. Saleh, and M. A. Al-Hashimi, "Measuring power and energy consumption of programs running on kepler GPUs," in *Advanced Control Circuits Systems (ACCS) Systems & 2017 Intl Conf on New Paradigms in Electronics & Information Technology (PEIT), 2017 Intl Conf on*. IEEE, 2017, pp. 18–25.
- [31] O. A. Abulnaja, M. J. Ikram, M. A. Al-Hashimi, and M. E. Saleh, "Analyzing power and energy efficiency of bitonic mergesort based on performance evaluation," *IEEE Access*, vol. 6, pp. 42757–42774, 2018.
- [32] M. J. Ikram, M. E. Saleh, M. A. Al-Hashimi, and O. A. Abulnaja, "Investigating the effect of varying block size on power and energy consumption of GPU kernels," *The Journal of Supercomputing*, vol. 78, pp. 14919–14939, 2022.
- [33] G. Dlamini, F. Jolha, Z. Kholmatova, and G. Succi, "Meta-analytical comparison of energy consumed by two sorting algorithms," *Information Sciences*, vol. 582, pp. 767–777, 2022.

- [34] D. Hackenberg, R. Schöne, T. Ilsche, D. Molka, J. Schuchart, and R. Geyer, "An energy efficiency feature survey of the intel haswell processor," in *2015 IEEE International Parallel and Distributed Processing Symposium Workshop*, 2015, pp. 896–904.
- [35] K. N. Khan, M. Hirki, T. Niemi, J. K. Nurminen, and Z. Ou, "Rapl in action: Experiences in using rapl for power measurements," *ACM Trans. Model. Perform. Eval. Comput. Syst.*, vol. 3, no. 2, pp. 9:1–9:26, 2018.

CertOracle: Enabling Long-term Self-Sovereign Certificates with Blockchain Oracles

Shaoxi Zou, Fa Jin, Yongdong Wu*
Jinan University, Guangzhou, China
*Corresponding author

Abstract—Identity certificate is an endorsement of identity attributes from an authority issuer, and plays a critical role in many digital applications such as electronic banking. However, the existing certificate schemes have two weaknesses: (1) a certificate is valid only for a short period due to expiry of the issuer's private key, and (2) privacy leaks because all the attributes have to be disclosed in the attribute verification process. To overcome the weaknesses, this paper proposes a blockchain-based certificate scheme called CertOracle. Specifically, CertOracle allows a traditional certificate owner to encrypt the off-chain certificate attributes with fully homomorphic encryption algorithms. Then, the uploading protocol in CertOracle enables to post the encrypted off-chain attributes into the blockchain via a blockchain oracle in an authenticated way, i.e., the off-chain attributes and on-chain encrypted attributes are consistent. Finally, the attribute verification protocol in CertOracle enables anyone to verify any set of on-chain attributes under the control of the attribute owner. As the on-chain certificate attributes are immutable forever, a traditional short-term certificate is transformed into a long-term one. Besides, the owner of the on-chain certificate attributes can arbitrarily select his/her attributes to meet the requirements of target applications, i.e., the on-chain certificate has the self-sovereign merit. Moreover, the proposed scheme is implemented with fully homomorphic encryption and secure two-party computation algorithms, and its experiments show that it is viable in terms of computation time and communication overhead.

Keywords—Digital certificate; blockchain oracle; fully homomorphic encryption; secure two-party computation

I. INTRODUCTION

As an important way to identify persons or other objects, an identity certificate is a set of electronic credentials that are used to verify the certificate owner's identity. It can be an electronic ID card, an electronic graduation certificate, a health certificate, or other identity certificate issued by a Certificate Authority(CA) such as a government, university, hospital, etc. Since most digital identity schemes use digital certificates to uniquely identify people on the Internet, this will lead to the frequent use of digital certificates in daily lives.

Most existing digital certificate schemes are based on public-key cryptography. During the issuance of a certificate, the CA's private key will be used to sign on the attributes of the certificate. However, according to the specification of NIST, the private key of CA should be updated within three years [1], otherwise the security of certificate scheme may be compromised. Usually, the period of a private source-authentication key, such as signing key, is the same as the period of associated public key. Therefore, once the key of CA is refreshed, the verification on previously issued digital

certificates (e.g., electronic ID card or electronic graduation certificate) may fail, and hence cause inconvenience or security vulnerability. Therefore, it's necessary to extend the life cycle of these digital certificates and verify identity attributes even if the CA's private key has expired.

Usually, digital identity certificates contain multiple user attributes, including user's private information. When users want to use certain services supported by verifiers, they have to present a part of attributes in their certificates. However, if the identity certificate is presented straightforwardly, all the attributes in the certificate will also be exposed. This is a coarse-grained representation that does not satisfy the principle of least leakage. Meanwhile, someone can't verify the certificate's authenticity when only some attributes of the certificate are displayed. Therefore, it is necessary to propose a method to perform fine-grained verification of attributes in certificate.

To solve the above problems of expiry of CA's private key and privacy leakage of user's attributes, Self-Sovereign Identity(SSI) [2] solutions are proposed to enable the owners to control their attributes with decentralized technologies [3] such as blockchain or distributed ledger. Presently, there are many mature decentralized identity schemes, such as Hyperledger *Indy* and *Civic* built on consortium blockchains and *ION* built on public blockchains. However, these proposed solutions mostly rely on on-chain issuers. It is difficult for them to tackle the off-chain certificates, i.e., the traditional digital identity certificates.

Since the blockchain is characterized by decentralization, immutability and openness, the on-chain certificate lifetime will be extended to long-term. Nonetheless, since the information on the blockchain is public and traceable, storing digital certificates on the blockchain in plaintext can lead to privacy leakage. Therefore, the attributes of on-chain certificates should be encrypted. To ensure the encrypted traditional certificates are uploaded into a blockchain authentically, blockchain oracle can be played as a middleware role in building a bridge between off-chain and on-chain.

This paper presents CertOracle, a management scheme for long-term and fine-grained certificates by transforming an off-chain traditional digital certificate into an on-chain certificate. Technically, CertOracle enables users to encrypt their digital certificates by themselves and ensures that the encrypted identity certificate is uploaded into the blockchain in an authentic way via a blockchain oracle. The on-chain encrypted attributes can be arbitrarily selected for verification under the control of the attribute owner. CertOracle ensures that on-chain certificate attributes are fine-grained verifiable and

long-term. Additionally, CertOracle is implemented with fully homomorphic encryption and secure two-party computation algorithms, and the experiments demonstrate that CertOracle is practical.

The remainder of this paper is organized as follows. Section II shows recent work. Section III introduces the preliminaries. Section IV describes the system model, security model, and the protocol details of CertOracle. Section V analyzes CertOracle. Section VI elaborates the CertOracle implementation and evaluates CertOracle with abundant experiments. Finally, Section VII draws conclusions.

II. RELATED WORK

To feed blockchain with encrypted certificates, blockchain oracles need to verify the correctness of the encrypted certificate. According to recent research, the implementation of blockchain oracles could be divided into three categories [4]: TLS-based scheme, Enclave-based scheme, and Voting-based scheme.

TLS-based schemes are conducted to construct a protocol based on Transport Layers Security (TLS), such as TLS-N [5], DECO [6], etc. TLS is a protocol instrumented to guarantee message integrity and server authentication through the exchange of certificates during TLS-handshake. TLS-N, as a practical and decentralized blockchain oracle, enhances the audibility and reliability of web content based on the TLS. However, the scheme is less deployable, which requires some improvements to TLS. Therefore, DECO proposes a three-party protocol based on modifications of TLS client, which minimizes the modification requirements of the TLS protocol and enhances compatibility. CanDID [7] uses TLS-based oracles to fetch identity information securely from outside systems. However, the oracles are not viable for protecting the digital identity certificates issued by traditional identity systems.

Enclave-based oracle is constructed with Trusted Execution Environment (TEE), such as Intel Software Guard Extensions (Intel SGX) and TrustZone. Using the technology of Intel SGX, Town Crier [8] can encrypt and decrypt data requests from smart contracts and external data from data sources, securely managing sensitive information. But Town Crier highly depends on the trusted execution environment and may be vulnerable to side-channel attack [9].

Voting-based schemes, such as Augur, Oraclize [10], Chainlink [11] and Augur [12], motivate oracles to vote for data honestly through monetary rewards and penalties. Oraclize provides proof for the data it fetches, ensuring that the original data source is real and untampered. But its centralized model cannot guarantee that the service will always be available. ChainLink is a decentralized oracle solution on Ethereum. By querying multiple sources, ChainLink can avoid dependency of a single oracle. Augur is a prediction market platform oracle built on Ethereum. It allows users to vote on information from the outside world based on their tokens. Therefore, the prediction accuracy is limited by the scale of the platform, and the uneven distribution of tokens affects the credibility of results. Apart from that, voting-based schemes do not provide authenticity of the data and are not suitable when data is not publicly available, especially digital certificates.

III. PRELIMINARIES

A. Digital Certificate

Digital certificate such as X.509 [13] is an electronic document issued by CA. Since the user's digital identity certificate is issued by a trusted center, it can be used to prove personal attributes such as age, gender, and country. To produce a certificate, the attributes will be compressed using a one-way hash algorithm such as 256-bit Secure Hash Algorithms (SHA256) [14] first. Then a CA adopts a digital signature algorithm such as ECDSA and its private key to sign on the hash value. As a result, anyone can verify the signature with the CA's public key.

Taking the hash algorithm SHA256 and digital signature algorithm RSA as examples, CA chooses randomly two large prime numbers p and q , and computes $N = pq$ and $\phi = (p - 1)(q - 1)$ first. Secondly, it chooses a random integer e ($1 < e < \phi$), so that $\gcd(e, \phi) = 1$, and computes d ($1 < d < \phi$), so that $ed \equiv 1 \pmod{\phi}$. Then CA owns public key (N, e) and private key d . Thirdly, to generate hash value of certificate content M with l bits, CA adds a bit "1" at the end of the message, then add k "0", and finally, fills in 64 bits representing the length of the message. k is the smallest non-negative integer that satisfies:

$$l + 1 + k + 64 = 0 \pmod{512}$$

The padded message is divided into several message blocks M_0, M_1, \dots, M_n in unit of 512 bits, and the M_i is encoded using big-endian and represented as $W_i^0, W_i^1, \dots, W_i^{15}$. Then CA construct W_i tables for every block according to $W_i^0, W_i^1, \dots, W_i^{15}$. Then, for $t = 16 \dots 64$,

$$W^t = \sigma_1(W^{t-2}) + W^{t-7} + \sigma_0(W^{t-15}) + W^{t-16}$$

After initializing $A \dots H$, CA runs 64 rounds of compression function with W_i table for every block, denoted as $A_{64} \dots H_{64} = Com(A \dots H, W_i)$, where $Com(\cdot)$ is the hash operation of one block. The $A_{64} \dots H_{64}$ will be assigned to $A \dots H$ for compressing the next message block. After performing $Com(\cdot)$ on every block sequentially, CA gets the hash value h .

Finally, CA computes $\sigma = h^d \pmod{N}$ (Hereafter, we omit the padding processing in the digital signature algorithm for the sake of simplicity) and obtains σ as signature. To verify the signature, any entity can compute $h = \sigma^e \pmod{N}$ and calculate h' using SHA256 with certificate to be verified. If the value of $h = h'$, it means that the certificate has not been tampered with and is indeed issued by the CA.

B. Secure Multi-Party Computation

Secure multi-party computation (SMPC) protocol [15], is a cryptographic primitive that allows several participants to jointly calculate some functions and outputs correct results without revealing the original input data of the participants. It is suitable for distributed networks like blockchain because it deals with security and trust issues in a distributed environment.

As the simplest one in SMPC, a two-party computation (2PC) ensures that two non-trusted parties attempt to securely evaluate a function. Technically, it specifies a random

process that maps pairs of inputs to pairs of outputs, i.e., $f : \{0, 1\}^* \times \{0, 1\}^* \rightarrow \{0, 1\}^* \times \{0, 1\}^*$, where each party has one private input and one output. For example, Goldreich-Micali-Wigderson (GMW) [16] protocol is a secret-shared-based 2PC scheme and can evaluate NOT, XOR and AND. For instance, for an XOR gate with input values $x = \{x_i\}$ and $y = \{y_i\}$ and output value $z = \{z_i\}$, two parties can compute their shares of the output value as $z_i = x_i \oplus y_i$ locally, where \oplus is eXclusive OR (XOR). The evaluation of AND gate can be achieved using multiplication triples [17]. Multiplication triples are random shares $\{a_i, b_i, c_i\}$, $i \in \{1, 2\}$ with $(c_1 \oplus c_2) = (a_1 \oplus a_2) \wedge (b_1 \oplus b_2)$. They can be generated using 1-out-of-4 oblivious transfer protocol in the offline set-up phase which precedes the online phase. During online phase, the parties can use these multiplication triples to mask the input shares of the AND gate. Both parties exchange $u_i = x_i \oplus a_i$ and $v_i = y_i \oplus b_i$, and compute $u = u_1 \oplus u_2$ and $v = v_1 \oplus v_2$. Then the output can be computed as

$$z_1 = (u \wedge v) \oplus (b_1 \wedge u) \oplus (a_1 \wedge v) \oplus c_1 \quad (1)$$

and

$$z_2 = (b_2 \wedge u) \oplus (a_2 \wedge v) \oplus c_2 \quad (2)$$

for each party from their private input x and y .

C. Fully Homomorphic Encryption

A Fully homomorphic encryption(FHE) scheme allows homomorphic evaluation of ciphertext addition and multiplication an arbitrary amount of times without decrypting the ciphertext or revealing the secret key [18]. That is to say, for any messages x and y , and a constant α ,

$$\text{FHE}(\alpha x + y) = \text{FHE}(\alpha) \cdot \text{FHE}(x) + \text{FHE}(y) \quad (3)$$

for a fully homomorphic encryption algorithm $\text{FHE}(\cdot)$.

TFHE(Torus-FHE) [20] is the third generation of FHE based on the hardness of Learning with Errors(LWE) problem and its ring variant(Ring LWE). Running over the real Torus $\mathbb{T} = \mathbb{R} \bmod 1$, TFHE can fix the message space as a discrete subset $\mathcal{M} \subseteq \mathbb{T}$. A message $\mu \in \mathcal{M}$ can be encrypted by computing

$$b = s \cdot a + \mu + e \quad (4)$$

where $s \in \{0, 1\}^n$ is the secret key, $a \in \mathbb{T}^n$ is uniformly random and e is sampled from an error distribution over \mathbb{T} . Then, the ciphertext is a pair $c = (b, a) \in \mathbb{T}^{n+1}$. In order to decrypt, phase φ_s is introduced to compute

$$\varphi_s(c) = b - a \cdot s \quad (5)$$

After rounding $\varphi_s(c)$ to the nearest point in \mathcal{M} , message μ can be obtained.

TFHE can transform an arbitrary function into a boolean circuit, then uses bit-wise homomorphic evaluation on ciphertext c_1, c_2 as each gate's input. For example, the AND gate in TFHE is done by evaluating $c = \text{BootsAND}(c_1, c_2, bk)$, in which bk is a key used for bootstrapping. Other operations are also supported with similar gate operations, such as NOT, NAND, OR, XOR, etc. Since TFHE can evaluate arbitrary boolean circuits, it is very suitable for functions that can be represented by several logical operations.

IV. THE PRESENT SCHEME CERTORACLE

CertOracle aims to feed the blockchain-based system with encrypted identify attributes so as to provide long-term self-sovereign identity. That is to say, the on-chain encrypted attributes can be used for fine-grained verification, ensuring that the attribute holder can have complete autonomy over their personal identity attributes for a long time. Thus, the scheme shall achieve the following goals:

- **Privacy:** The user's attributes in certificate are protected during the on-chaining process and on the chain.
- **Unforgeability:** The user's encrypted on-chain certificate attributes are verifiable as the traditional certificates and cannot be forged when uploading.
- **Fine-grained verification:** The on-chain attributes of certificates can be verified in a fine-grained way securely.

The parameters of CertOracle are shown in Table I.

TABLE I. NOTATIONS

Variable	Definition
$Attr_i$: The i -th attribute
V_i	: The i -th attribute set V
h_i	: The i -th bit of hash value h
X'	: The FHE encryption of a message X
\hat{X}	: The obfuscated value of a message X
$\{X_i\}$: Vector $X = \{X_0, X_1, \dots, X_{ X -1}\}$
$cert$: Identity certificate
σ	: Signature of a certificate

A. System Model

As shown in Fig. 1, the blockchain-based identity system supports the management and control of users' identities. When a user has a digital identity certificate generated by an off-chain CA, he/she can upload the digital identity certificate to the system through blockchain oracle of CertOracle. To ensure users' self-sovereign of the on-chain certificates, CertOracle permits users to encrypt private information of digital certificates by themselves. Technically, oracle verifies the encrypted certificate, in order to confirm that the on-chain certificate is produced authentically. Then any verifier can check the selected attributes in a trusted and privacy-preserving way.

With reference to Fig. 1, CertOracle includes four components as follows.

- **User:** A user owns a certificate which can be represented as $cert = (ID, \mathcal{M}, \sigma)$, where ID is an identifier of the user, \mathcal{M} is the attributes of certificate and σ is signature generated by CA. \mathcal{M} can be seen as an array of $\{Attr_i, V_i\}$, where V_i is the value of the attribute $Attr_i$, and signature $\sigma = \text{sign}(\text{hash}(\mathcal{M}))$ for attributes in the certificate with hash algorithm $\text{hash}(\cdot)$ and signing algorithm $\text{sign}(\cdot)$. The user has a pair of self-generated FHE keys (pk_U, sk_U) , and can cooperate with the oracle to prove his encrypted attributes in the certificate.

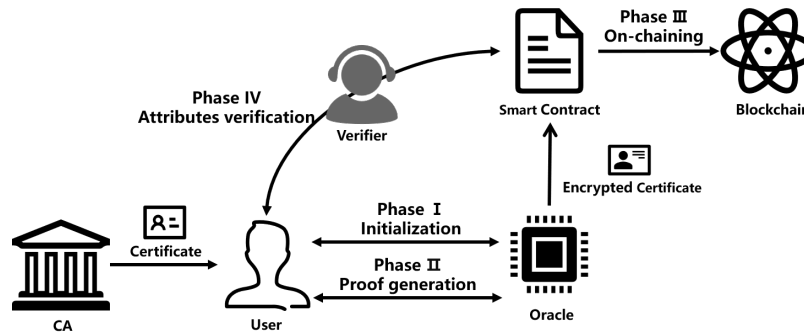


Fig. 1. The System Model of CertOracle.

- Oracle: Oracle has the trusted public keys of the CAs so as to verify the signatures of the certificates. In addition, by cooperating with users, oracle will prove/disapprove the encrypted certificate submitted from the user.
- Smart Contract: It can upload the encrypted attributes of certificates after attributes verification. Meanwhile, It can fetch any set of on-chain attributes and provide them to the verifier to check user's claims.
- Verifier: When a user likes to prove his attributes to a verifier, a verifier can validate on-chain encrypted attributes by interacting with the user and smart contract.

B. Security Model

With reference to Fig. 1, there are 5 components or participants. CA is assumed to be honest and trusted by all. However, CA's private key may be updated irregularly, resulting in a decrease in the credibility of the old digital certificate. Therefore, only when the CA's private key is valid, the digital certificate issued by the CA is credible, otherwise the verification of the previously issued digital certificate will be considered to be unreliable. The security assumptions of the other components are as follows:

- Oracle is semi-honest. It honestly follows the protocol of CertOracle and will not be corrupted by users, but is curious about the personal attributes of the certificate.
- User is untrustworthy. A malicious user wants to 1) upload a forged digital certificate to blockchain through oracle; 2) deceive the verifier with fake attributes in order to obtain unauthorized services. In addition, the ciphertexts sent to the user are assumed to be well-formed. This assumption can be met with padding such as OAEP (Optimal Asymmetric Encryption Padding).
- Smart contract, as a part of the blockchain system, is trusted and can provide reliable services.
- Verifier is semi-honest. He follows the protocol to verify some attributes of the users but attempts to obtain user's attributes that do not need to be verified

C. CertOracle Protocol

In Fig. 1, CertOracle comprises of four phases. 1) *Initialization* (Phase I) configures the parameters in CertOracle; 2) *Proof generation* (Phase II) validates the authenticity of the encrypted certificate; 3) *On-chaining* (Phase III) uploads the verified attributes in the certificate; 4) *Attribute verification* (Phase IV) checks the on-chain encryption of the user attributes. In this protocol, assume that the size of hash value is $(n_1 + 1)$. Without loss of generality, assume every attribute is binary, and the number of attributes is $(n_2 + 1)$.

1) *Phase I (Initialization)*: In the initialization stage, a user firstly sends a request to establish a connection with the oracle, and runs FHE key generation function to get public/private key pair (pk_U, sk_U) . The user keeps the private key sk_U during the proof generation and verification process for the encrypted attributes, and publishes the public key pk_U to oracle. Then the user encrypts some private attributes $\{Attr_i, V_i\}$ in *cert* bit by bit using pk_U , and publishes other attributes of certificate, such as Version, Certificate Serial Number, Algorithm Identifier, and Validity Period in Certificate Information in the certificate format like X.509. In this paper, the public attributes are omitted, unless otherwise stated. Denote the ciphertexts $V'_0, V'_1, \dots, V'_{n_2}$. Denote the encrypted certificate $cert' = (ID, \{Attr_0, V'_0\}, \dots, \{Attr_{n_2}, V'_{n_2}\}, \sigma)$. The user constructs *ProofRequest* as

$$(op, ID, \{Attr_0, V'_0\}, \dots, \{Attr_{n_2}, V'_{n_2}\}, pk_U, \sigma)$$

and sends *ProofRequest* to the oracle. In *ProofRequest*, *op* is the operations on each attribute $\{Attr_j, V'_j\}$, such as Insert, Update and Delete operation on attributes.

After receiving *ProofRequest*, the oracle will verify the signature σ against the encryption of attributes. To this end, the oracle calculates the hash value of the ciphertext and runs the signature verification function with the public key of CA. If the verification result is positive and the certificate is not on the blockchain, the oracle starts to run the following phases.

2) *Phase II (Proof Generation)*: For any digital certificate generated from the hash-then-sign algorithm, the proof process of CertOracle can be divided into two solutions. If the user cannot keep connected with the oracle during proof generation, non-interactive proof protocol can be used; otherwise, interactive proof protocol is recommended

Non-interactive proof protocol: As shown in Fig. 2, if user can not stay online during proof generation, the ora-

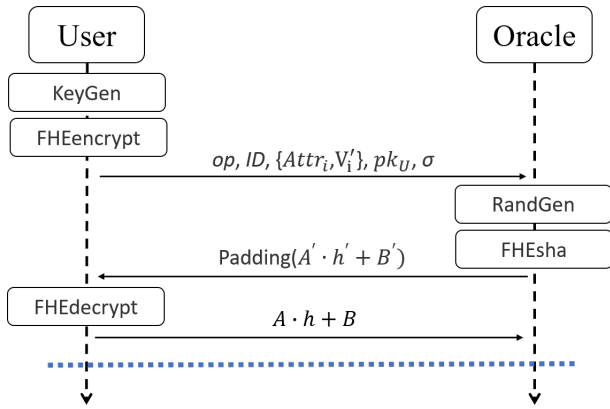


Fig. 2. The Non-Interactive Proof Protocol in CertOracle.

cle utilizes properties of fully homomorphic encryption to realize the proof process. Specifically, the oracle holds the $cert' = (ID, \{Attr_i, V'_0\}, \dots, \{Attr_{n_2}, V'_{n_2}\}, \sigma)$. It uses pk_U to encrypt each attribute $\{Attr_i, V_i\}$ bit by bit.

To calculate the hash value of the fully homomorphic encryption of the certificate attributes, the oracle will run algorithm FHEsha whose input is the encryption of messages and whose output is the fully homomorphic encryption of hash of the messages¹. That is to say, the oracle gets the encrypted hash

$$h' = \{h'_0, h'_1, \dots, h'_{n_1}\} = \text{FHEsha}(V'_1, V'_2, \dots, V'_{n_2}) \quad (6)$$

where V'_i is an FHE encryption of the i^{th} -bit message V_i , and h'_i is an FHE encryption of the i^{th} -bit of the hash value $h = \text{hash}(V_0, V_1, \dots, V_{n_2})$.

Moreover, the oracle generates two random arrays $A = \{a_0, a_1, \dots, a_{n_1}\}$, and $B = \{b_0, b_1, \dots, b_{n_1}\}$, and encrypts A and B to $A' = \{a'_0, a'_1, \dots, a'_{n_1}\}$ and $B' = \{b'_0, b'_1, \dots, b'_{n_1}\}$ using user's public key pk_U respectively, for all $i = 0, 1, \dots, n_1$,

$$a'_i = \text{FHEncrypt}(a_i) \quad \text{and} \quad b'_i = \text{FHEncrypt}(b_i) \quad (7)$$

and obfuscates h' as²

$$\hat{h}'_i = a'_i \cdot h'_i + b'_i. \quad (8)$$

Oracle can pack³ $\{\hat{h}'_i\}$ into \hat{h}' and pad the ciphertext by⁴

$$BLOB = \text{FHEncrypt}(2^k) \cdot \hat{h}' + \hat{h}', \quad (9)$$

in which k is the number of bits of \hat{h}' , and obtains a blob equivalent to $\hat{h}' || \hat{h}'$.

¹A hash function of plaintext can be translated into the encryption of the hash function of FHE ciphertext with google transpiler. Please refer to <https://research.google/pubs/pub50428/>

² $\{h'_i\}$ can be obfuscated in batch for quick process in Eq.8. Similar for $\{V'_i\}$ in Eq.12 and $\{\Delta'_i\}$ in Eq.15.

³Multiple LWE ciphertexts can be packeted into a ciphertext.

⁴Assume that the value of \hat{h} is less than half of the FHE domain. Similar for \hat{V} in Eq.13 and $\hat{\Delta}$ in Eq.16

Afterwards, the oracle sends $BLOB$ to the user for decrypting. The user uses his sk_U to decrypt the $BLOB$ by

$$blob = \text{FHEdecrypt}(BLOB) \quad (10)$$

and determines that the $blob$ conformed to the format of $\hat{h} || \hat{h}$. If the format is correct, the user returns \hat{h} . The oracle can recover

$$h_i = (\hat{h}_i - b_i) / a_i \quad (11)$$

and the hash value $h = \{h_0, h_1, \dots, h_{n_1}\}$ for proving the authenticity of the encryption $\{V'_i\}$ of the certificate attributes.

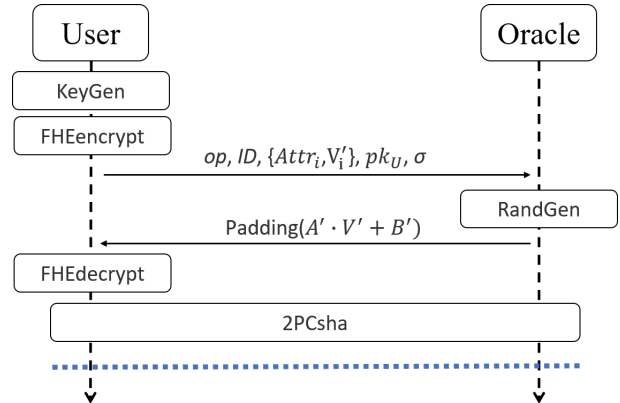


Fig. 3. The Interactive Proof in CertOracle.

Interactive proof protocol: as shown in Fig. 3, the oracle will interactive with the user using secure two-party computation based on secret sharing. The oracle holds the $cert' = (ID, \{Attr_0, V'_0\}, \dots, \{Attr_{n_2}, V'_{n_2}\}, \sigma)$. Similar to the non-interactive solution, the oracle generates two random arrays $A = \{a_0, a_1, \dots, a_{n_2}\}$, $B = \{b_0, b_1, \dots, b_{n_2}\}$, and encrypts them to $A' = \{a'_0, a'_1, \dots, a'_{n_2}\}$, $B' = \{b'_0, b'_1, \dots, b'_{n_2}\}$ using pk_U as Eq.7. The oracle obfuscates the encrypted attribute V' as

$$\hat{V}'_i = a'_i \cdot V'_i + b'_i \quad (12)$$

After obfuscating, the oracle can pack $\{\hat{V}'_i\}$ into \hat{V}' and send the padded ciphertext

$$BLOB = \text{FHEncrypt}(2^k) \cdot \hat{V}' + \hat{V}', \quad (13)$$

in which k is the number of bits of \hat{V}' , to the user. The user uses sk_U to decrypt $BLOB$ according to Eq.10 and determines that the $blob$ is equivalent to $\hat{V}' || \hat{V}'$, that is, equivalent to $\{\hat{V}'_i\} || \{\hat{V}'_i\}$.

To calculate the digest value of the encrypted certificate, the oracle and user jointly run 2PCsha based on boolean sharing. According to Subsection III-B, the user provides $\{\hat{V}'_i\}$ and the oracle provides $A = \{a_0, a_1, \dots, a_{n_2}\}$ and $B = \{b_0, b_1, \dots, b_{n_2}\}$ to complete the 2PCsha protocol.

$$\{h_0, \dots, h_{n_1}\} = 2\text{PCsha}\left(\frac{\hat{V}'_0 - b_0}{a_0}, \dots, \frac{\hat{V}'_{n_2} - b_{n_2}}{a_{n_2}}\right) \quad (14)$$

In the 2PCsha scheme, the deobfuscation circuit will securely produce $V_i = (\hat{V}_i - b_i) / a_i$ in the internal wires of the boolean circuit, and then perform the hash circuit to output the hash value h for attribute proof.

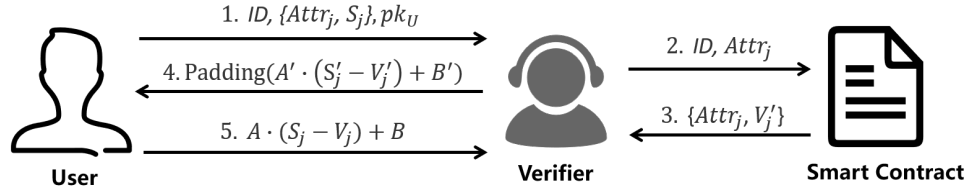


Fig. 4. The Workflow of Attribute Verification.

3) *Phase III (On-Chaining)*: After recovering the hash value h , the oracle can check the authenticity of the certificate signature with the signature verification algorithm. If and only if the recovered hash h matches the signature, the oracle determines that $\{Attr_0, V_0'\}, \{Attr_1, V_1'\}, \dots, \{Attr_{n_2}, V_{n_2}'\}$ in *ProofRequest* are authentic and then uploads the encrypted certificate to the blockchain.

After oracle generates the proof of the encrypted certificate, smart contract checks if the user has certificate attributes on the blockchain. If not, it creates a DID (Distributed IDENTITY) for the user. If the user already exists, the smart contract verifies whether the user has permission to perform the specified operation through *op* such as Insert, updates or deletes the corresponding attributes in the blockchain.

4) *Phase IV (Attribute Verification)*: As the certificate attributes are encrypted and stored in the blockchain, anyone can query and verify user's attributes publicly without compromising the privacy of the attribute owner. Furthermore, in order to meet the requirement of self-sovereign identity, querying and verifying need the assistance of the owner as shown in Fig. 4.

Technically, when the verifier needs to check whether the value of the attribute $Attr_j$ is S_j , $j = 0, 1, \dots, n_3$, $n_3 \leq n_2$, it will encrypt S_j to S_j' using the user's public key pk_U . After that, the verifier generates two random arrays $A = \{a_0, a_1, \dots, a_{n_3}\}$ and $B = \{b_0, b_1, \dots, b_{n_3}\}$, and retrieves the encryption V_j' of the attribute $Attr_j$ from the blockchain. To securely authenticate the user, the verifier computes

$$\hat{\Delta}'_i = \Delta'_i \cdot a'_i + b'_i \quad (15)$$

where a'_i, b'_i are ciphertext of a_i, b_i according to Eq.7 and Δ'_i represents i^{th} -bit of $S'_j - V'_j$. Then the verifier packs $\{\hat{\Delta}'_i\}$ into $\hat{\Delta}'$ and sends padded blob

$$BLOB = FHEncrypt(2^k) \cdot \hat{\Delta}' + \hat{\Delta}', \quad (16)$$

in which k is the number of bits of $\hat{\Delta}'$, to the user.

After the user decrypts $BLOB$ with private key sk_U , confirms that the decryption result conforms to the structure of $\hat{\Delta} || \hat{\Delta}$, and returns the obfuscated plaintext $\hat{\Delta}$ to the verifier, the verifier deobfuscates $\hat{\Delta}_i$ as

$$\Delta_i = (\hat{\Delta}_i - b_i) / a_i. \quad (17)$$

The verifier confirms the selected attributes of the user if and only if all the Δ_i are 0 (The decision policies may depend on the applications).

V. ANALYSIS OF CERTORACLE

As trust in identity certificates is transferred to the blockchain, the life cycle of these certificates can be extended to be the same as the lifetime of the blockchain. So these certificates become long-term certificates. This section discusses how CertOracle meets the goals to enable long-term self-sovereign certificates.

A. Privacy

In our protocol, the attributes of the certificate are encrypted bit by bit using TFHE. The attributes of on-chain certificates are protected to guarantee user's self-sovereign over his identity. When CertOracle is running, oracle is semi-honest. It wants to know the plaintext of encrypted attributes in *ProofRequest*. Since oracle just gets pk_U , it cannot learn the plaintext V_i from $\{Attr_i, V_i'\}$. Meanwhile, oracle can't know the plaintext of $V_1', V_2', \dots, V_{n_2}'$ through *hash* because of the non-reversibility of hash function.

In the non-interactive solution, the security is based on TFHE. There are many bit-wise operations in hash function. With the public key pk_U , the oracle of CertOracle can encrypt the attributes of certificate bit by bit so that it can calculate the hash value of the ciphertext message by itself. In the interactive solution, the security of the scheme is based on the GMW protocol. During 2PCsha, \hat{V}_i, A , and B are shared between oracle and user using boolean sharing. Thus, they look like uniformly distributed random data and this prevents the leakage of the data. A semi-honest adversary corrupting at most one of the participants can just observe secret shares of other's inputs. Meanwhile, the oracle can't learn the internal states of the circuit.

Moreover, we pad the output of Eq. 8, Eq. 12 and Eq. 15, that is, repeat the plaintext before encrypting it. By letting the decryptor check whether the decryption result meets a specific format, our system is resistant to potential fault injection attacks [19] from oracles and verifier.

B. Unforgeability

Before users encrypt their certificates, malicious users may forge attributes by modifying the critical payload $\{Attr_i, V_i'\}$ into another attribute's ciphertext $\{Attr_i, \tilde{V}_i'\}$. However, because of the collision resistance of hash function, it is impossible to find a \tilde{V}_i' replacing the true data V_i' to get the same hash. In the non-interactive solution, malicious users may submit forged *ProofRequest* but return true h when oracle sends h' back to decrypt after FHEsha. This may result in fake attributes being successfully verified. However, CertOracle obfuscates the h' by multiplying and adding a random number. It is

hard for malicious users to find out the relationship between obfuscated data and real data, and then forge data to pass verification. In the interactive solution, malicious users may submit forged *ProofRequest* but provide true data in the process 2PCsha. But they can't achieve because of obfuscation. In conclusion, CertOracle can effectively prevent forged certificates from being uploaded.

C. Fine-Grained Verification

User can upload multiple certificates to the blockchain and aggregate the attributes of certificates. When a user needs to use some attributes from different certificates to meet the requirement of a target application, he can construct a claim about the attributes based on the on-chain certificate. The on-chain attributes are encrypted and the verification process requires user's assistance which prevents all attributes from being exposed. Meanwhile, CertOracle ensures that the user attribute can be verified in a fine-grained manner, thereby ensuring the principle of least leakage. In addition, when a verifier checks the users' attributes $\{Attr_i, V'_i\}$, he obfuscates the attributes to be verified. Since the malicious user does not know the random array A, B , they cannot forge \hat{V} to pass verification. However, verifiers may utilize deobfuscation to learn attributes that do not need to be verified. This can be mitigated by limiting the number of interactions between the verifier and the same user.

VI. IMPLEMENTATION

The scheme is implemented and tested with an AMD Ryzen 7 4800U CPU with 1.8 GHz and 4 GB RAM, running Ubuntu 20.04 LTS. The implementation adopts TFHE library and ABY [21]. Although the scheme is suitable for all secure hash algorithms, SHA256 is used as an example in the implementation. In the experiments, the attribute value is an integer, and one user may have certificates from different CAs. As shown in Fig. 5, when a user clicks "Upload Certificate" button, the certificate will be uploaded to the chain via CertOracle. When a user clicks "Create Claim" button, an attribute verification process will be activated and the off-chain certificates can be uploaded through Oracle and shown in *CertificateList*. Thus, the user can select an on-chain certificate and create a claim according to the service's requirement.

A. TFHE Setting

In CertOracle, we encrypt the certificate bit by bit using TFHE library. In the TFHE library, it needs at least one FFT processor to run the library. We choose FFTW3, which claims to be the fastest free FFT processor available, as the component. Meanwhile, the library provides two types of keys: cloud key and secret key. The cloud key is essentially a bootstrapping key used for cloud to perform homomorphic operations as well as encrypt constants, whereas the secret key is for encrypting the initial message and decrypting. Although addition and multiplication are not directly provided in TFHE library, we can utilize logical operations to build addition and multiplication of arbitrary bits.

In the TFHE library, the parameters are only implemented for 80-bit and 128-bit of security. Both these parameters are estimated using LWE estimator so that they can resist known

attacks integrated in LWE estimator, such as primal attack and dual-lattice attack. As cryptographers recommend at least 128-bit security in practice [22], we use the 128-bit security version of parameter set in the implementation. However, the TFHE library does not yet support ciphertext packing. Therefore we ignore the realization of padding in the experiment. Instead, the user directly decrypt the output of Eq. 8, Eq. 12 and Eq. 15 using FHEdecrypt.

B. Basic Bitwise Operators

In the SHA256, there are many additional operations in the algorithm. The efficiency of CertOracle will be mainly limited by three basic operators: adder, multiplier and obfuscator.

1) *Bitwise Addition*: Addition between two integers can be implemented using two XOR gates, a AND gate and a MUX gate. The adder is based on the simple logic equations

$$S = X \oplus Y \oplus V'_{in} \quad (18)$$

and

$$V'_{out} = MUX_{(X \oplus Y)}(V'_{in}, X \cdot Y) \quad (19)$$

where X and Y are binary, V'_{in} is a bit that is carried in from the one less significant bit, and V'_{out} is a bit that is to be carried to the next significant digit. In $MUX_{(X \oplus Y)}(V'_{in}, X \cdot Y)$, the gate outputs V'_{in} if $X \oplus Y = 1$ and outputs $X \cdot Y$ otherwise. As the addition in our protocol is 16-bit addition or 32-bit addition, a 16-bit addition costs about 1.33s.

2) *Bitwise Multiplication*: It can be implemented using a combination of adder and multiplexer. The multiplexer, worked as $MUX_{B[i]}(0, A)$ with A and B are 16-bit, outputs 0 if i -th bit of B is equal to 1 and outputs A otherwise. With the multiplexer worked on 16-bit, it will run 16 times and then perform addition every time. In short, the 16-bit multiplier includes 16 multiplexers and $16 \cdot 16$ adders and takes about 11.457s on average which is expensive in time consumption.

3) *Bitwise Obfuscation*: With the bitwise adder and multiplier, we can evaluate the process of obfuscation. In both proof solutions, we need to obfuscate the data to be decrypted by users to prevent users from cheating. According to the number of obfuscated data, the oracle generates A, B . After the oracle selects the bytes to obfuscate, the data multiply and add different random numbers to get the same amount of obfuscated data. When deobfuscating, the oracle performs one subtraction and division to recover the original data. In the experiments, the obfuscation protocol takes about 127.939s to randomly obfuscate 10 bytes.

C. Non-Interactive Proof Protocol

The non-interactive solution relies on TFHE library using parameters with security level of 128-bit. Since the additions modulo 2^{32} in SHA256 need many gates, it is time-consuming for the oracle to perform a complete SHA256. To improve the efficiency of the protocol, a user may perform some steps of SHA256, including message padding, dividing, and W table construction. The user creates the W table for each block, and then sends the W tables to the oracle. The oracle only needs to perform the compression function.

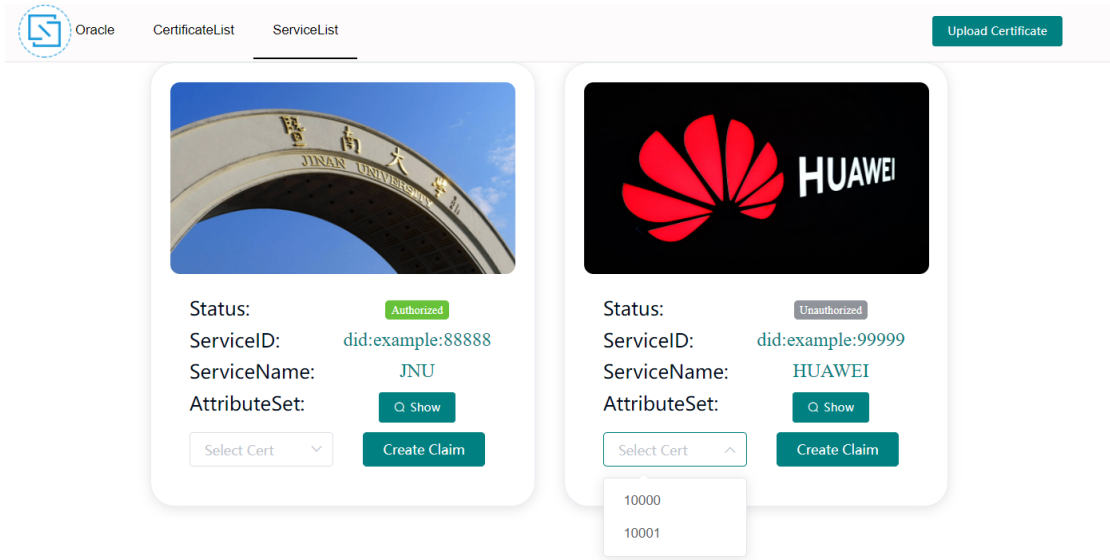


Fig. 5. The User-Interface of CertOracle.

The protocol is evaluated from two aspects. On the user side, we evaluate the function of key generation, procedure of partial SHA256(Message padding, Message dividing, and W table construction), encryption of 32 bits, and decryption of 16 bits. First, cloud key and secret key are generated in KeyGen. Secondly, PartialSHA256(64bytes) is to perform partial SHA256 calculation on 64bytes message and generate two blocks message. Thirdly, the time of certificate encryption is the time of multiple Enc(32bits) and the Dec(16bits) is a part of FHEdecrypt. On the oracle side, the result of running FHEsha with 64bytes and 128bytes messages are investigated. For instance, FHEsha256(64Bytes) is a homomorphic compression function for 64 bytes messages.

In the Table II for the evaluation results, the computation time of FHEsha in Table III doesn't include the time of obfuscation. Meanwhile, since the time spent in FHEsha is relatively large, the time on the user side is almost negligible. In all, the total time of the solution is the sum of FHEsha time plus obfuscation time.

TABLE II. EVALUATION OF NON-INTERACTIVE PROOF

Procedure	Time	Size
KeyGen	682.1ms	108.4MB / 108.4MB
PartialSHA256(64bytes)	0.041ms	2048bits
Enc(32bits)	0.42ms	0.077MB
Dec(16bits)	0.06ms	16bits
FHEsha(64bytes)	1834s	4.953MB
FHEsha(128bytes)	3668s	4.953MB

D. Interactive Proof Protocol

ABY is a framework for efficient mixed-protocol secure two-party computation in the interactive solution. It combines secure computation schemes based on arithmetic sharing, boolean sharing, and Yao sharing. The boolean sharings are used to evaluate functions represented as boolean circuits using the GMW protocol. Though ABY allows developers to manually specify which part of a function should be computed in

which sharing to achieve the best overall efficiency, we use the boolean sharing part of ABY to test the present protocol. This framework, using the semi-honest adversary model, works like a virtual machine that abstracts secure computation protocols. Thus, the implementation of CertOracle constructs 2PCsha using GMW protocol [16] in the ABY.

Using an XOR-based secret sharing scheme to share a variable, the boolean sharing can perform the evaluation on NOT, XOR, AND, and others. While XOR gate and NOT gate can be evaluated locally, AND gate is evaluated using a precomputed boolean multiplication triple which reduces the impact of the latency during the online time. Next, we introduce the evaluation of the interactive solution in a local area network(LAN) environment.

In the ABY framework, the OT (Oblivious Transfer) extension protocol uses few base-OTs to quickly compute a large number of OTs so as to generate multiplication triples. As the base-OTs are performed once when the connection between the client and the server is established, their computation time is omitted in the total time. As a result, the average run-time is 377.595s and the communication overhead is 49,964 bytes.

The main part of 2PCsha comprises setup phase and online phase. The setup phase includes the pre-computation of some nonces generation for one-time pad operation and the multiplication triples for the AND gates. The run-time and communication overhead depend on the AND depth of the circuit, that is the number of messages. The online phase takes place after the setup phase is done and the inputs to the circuit are supplied by both parties. During online phase, two independent 2-bit messages have to be transmitted per layer of AND gates. This interaction in online phase causes a performance bottleneck, especially in high latency networks. Meanwhile, the ABY framework implements load balancing for the setup phase. As a consequence, the computation and communication cost are equally distributed among the two parties.

TABLE III. RUN-TIME AND COMMUNICATION OVERHEAD OF INTERACTIVE PROOF

Message Size	Time[ms]			Communication[bytes]		
	Setup phase	Online phase	Total	Setup phase	Online phase	Total
64	262.579	3,507.48	3,770.07	6,607,027	113,993	6,721,020
128	380.033	4,991.22	5,371.27	10,774,766	185,713	10,960,479
196	435.822	6,505.23	6,941.07	14,948,640	257,417	15,206,057

In the circuit of 2PCsha, the oracle and user will jointly perform subtraction and division to deobfuscate data provided by the user. Then both get the intermediate wires and run the SHA256 circuit. On average, the run-time and communication overhead in 2PCsha for different message sizes are shown in Table III. And each part is also divided into the setup phase and the online phase to display separately. Clearly, the interactive solution has better performance than non-interactive solution.

VII. CONCLUSION

This paper presents CertOracle, a management scheme that provides long-term and self-sovereign certificate to solve the problem of traditional certificate expiration and privacy leakage. Specifically, CertOracle allows users to encrypt the private data of the digital certificate by themselves, ensuring that the encrypted certificate is uploaded to blockchain authentically via oracle. Therefore, the blockchain-based identity system can achieve privacy, unforgeability and fine-grained verification. Meanwhile, the uploading method of the certificate can be selected according to the latency of the network between the oracle and the user. The implementation and experiments of CertOracle show that both non-interactive proof and interactive proof protocols can satisfy the requirements of the long-term and self-sovereign certificates.

ACKNOWLEDGMENT

This work was in part supported by Guangdong KeyR&D Plan2020 (No. 2020B0101090002), National Natural Science Foundation of China (Grant No. 61932011), Guangdong Basic and Applied Basic Research Foundation (Grant No. 2019B1515120010), Guangdong Key Laboratory of Data Security and Privacy Preserving (Grant No. 2017B030301004), National KeyR&D Plan2020 (No. 2020YFB1005600), National Joint Engineering Research Center of Network Security Detection and Protection Technology(Grant Nos. 2016B010124009), Guangdong Provincial Special Funds for Applied Technology Research and Development and Transformation of Important Scientific and Technological Achieve (2017B010124002).

REFERENCES

- [1] Barker E, Dang Q. Nist special publication 800-57 part 1, revision 4[J]. NIST, Tech. Rep, 2016, 16.
- [2] Christopher Allen. The Path to Self-Sovereign Identity [EB/OL]. <http://www.coindesk.com/pah-self-sovereign-identity>, 2018-08-19/2022-05-17
- [3] Manu Sporny, Dave Longley and David Chadwick. Verifiable Credentials Data Model 1.0, 19 Nov 2019. [Online]. Available: <https://www.w3.org/TR/verifiable-claims-data-model/>. [Accessed: 27 Apr 2020]
- [4] Heiss J, Eberhardt J, Tai S. From oracles to trustworthy data on-chaining systems[C]//2019 IEEE International Conference on Blockchain (Blockchain). IEEE, 2019: 496-503.
- [5] Signing E U C. TLS-N: Non-repudiation over TLS Enabling Ubiquitous Content Signing[J].
- [6] Zhang F, Maram D, Malvai H, et al. DECO: Liberating web data using decentralized oracles for TLS[C]//Proceedings of the 2020 ACM SIGSAC Conference on Computer and Communications Security. 2020: 1919-1938.
- [7] D. Maram et al., "CanDID: Can-Do Decentralized Identity with Legacy Compatibility, Sybil-Resistance, and Accountability," 2021 IEEE Symposium on Security and Privacy (SP), 2021, pp. 1348-1366, doi: 10.1109/SP40001.2021.00038.
- [8] Zhang F, Cecchetti E, Croman K, et al. Town crier: An authenticated data feed for smart contracts[C]//Proceedings of the 2016 ACM SIGSAC conference on computer and communications security. 2016: 270-282.
- [9] Lerman L, Bontempi G, Markowitch O. Power analysis attack: an approach based on machine learning[J]. International Journal of Applied Cryptography, 2014, 3(2): 97-115.
- [10] Oraclize: Understanding oracles. <https://blog.oraclize.it/understanding-oracles99055c9c9f7b>, accessed 23 Sep 2017.
- [11] Breidenbach L, Cachin C, Chan B, et al. Chainlink 2.0: Next steps in the evolution of decentralized oracle networks[J]. 2021.
- [12] Peterson J, Krug J. Augur: a decentralized, open-source platform for prediction markets[J]. arXiv preprint arXiv:1501.01042, 2015, 507.
- [13] Delignat-Lavaud A, Fournet C, Kohlweiss M, et al. Cinderella: Turning shabby X. 509 certificates into elegant anonymous credentials with the magic of verifiable computation[C]//2016 IEEE Symposium on Security and Privacy (SP). IEEE, 2016: 235-254.
- [14] Pittalia P P. A comparative study of hash algorithms in cryptography[J]. International Journal of Computer Science and Mobile Computing, 2019, 8(6): 147-152.
- [15] Lindell Y, Riva B. Cut-and-choose Yao-based secure computation in the online/offline and batch settings[C]//Annual Cryptology Conference. Springer, Berlin, Heidelberg, 2014: 476-494.
- [16] Schneider T, Zohner M. GMW vs. Yao? Efficient secure two-party computation with low depth circuits[C]//International Conference on Financial Cryptography and Data Security. Springer, Berlin, Heidelberg, 2013: 275-292.
- [17] Pullonen P. Actively secure two-party computation: Efficient beaver triple generation[J]. Instructor, 2013.
- [18] Boura C, Gama N, Georgieva M, et al. Chimera: Combining ring-lwe-based fully homomorphic encryption schemes[J]. Journal of Mathematical Cryptology, 2020, 14(1): 316-338.
- [19] Chillotti I, Gama N, Goubin L. Attacking FHE-based applications by software fault injections[J]. Cryptology ePrint Archive, 2016.
- [20] Chillotti I, Gama N, Georgieva M, et al. TFHE: fast fully homomorphic encryption over the torus[J]. Journal of Cryptology, 2020, 33(1): 34-91.
- [21] Demmler D, Schneider T, Zohner M. ABY-A framework for efficient mixed-protocol secure two-party computation[C]//NDSS. 2015.
- [22] Lenstra A K. Key length. Contribution to the handbook of information security[J]. 2004.

Evaluation of Online Machine Learning Algorithms for Electricity Theft Detection in Smart Grids

Ashraf Alkhresheh
Computer Science Department
Tafila Technical University
Tafila, Jordan

Mutaz A. B. Al-Tarawneh
Computer Engineering Department
Mutah University
Karak, Jordan

Mohammad Alnawayseh
MIS Department
The University of Jordan
Amman, Jordan

Abstract—Electricity theft-induced power loss is a pressing issue in both traditional and smart grid environments. In smart grids, smart meters can be used to track power consumption behaviour and detect any suspicious activity. However, smart meter readings can be compromised by deploying intrusion tactics or launching cyber attacks. In this regard, machine learning models can be used to assess the daily consumption patterns of customers and detect potential electricity theft incidents. Whilst existing research efforts have extensively focused on batch learning algorithms, this paper investigates the use of online machine learning algorithms for electricity theft detection in smart grid environments, based on a recently proposed dataset. Several algorithms including Naive Bayes, K-nearest Neighbours, K-nearest Neighbours with self-adjusting memory, Hoeffding Tree, Extremely Fast Decision Tree, Adaptive Random Forest and Leveraging Bagging are considered. These algorithms are evaluated using an online machine learning platform considering both binary and multi-class theft detection scenarios. Evaluation metrics include prediction accuracy, precision, recall, F-1 score and kappa statistic. Evaluation results demonstrate the ability of the Leveraging Bagging algorithm with an Adaptive Random Forest base classifier to surpass all other algorithms in terms of all the considered metrics, for both binary and multi-class theft detection. Hence, it can be considered as a viable option for electricity theft detection in smart grid environments.

Keywords—Smart grid; power loss; electricity theft; online machine learning

I. INTRODUCTION

Utilizing energy resources effectively and efficiently is a crucial part of every nation's social and economic growth due to the high cost of energy acquisition and the scarcity of energy resources [1]. Future energy monitoring may now be used to its fullest potential thanks to the smart grid. The smart grid system can be characterized as a whole electrical network made up of the power system infrastructure, computers to control and monitor energy usage, and a sophisticated monitoring system that keeps track of the behavior and usage patterns of all system users [2]. Today, one of the most obvious problems affecting both traditional power grids and smart grids is electric power loss. Countries experience different levels of electricity losses. For instance, 6%, 10%, 16%, and 18% of each country's total energy production was lost in the USA, Russia, Brazil, and India, correspondingly [1]. In the transmission and distribution of electricity, there are two different categories of losses: technical and nontechnical. Energy losses in the machinery required for power transmission and distribution are referred to as technical losses. Power theft, fraud on the part of

utility employees, and irregular billing practices all contribute to non-technical losses (NTL) [3]. The NTL is estimated to cost utilities around the world US\$96 billion annually [4]. Power providers, engineers, and academics are working to reduce NTL in a number of creative and effective ways due to the significant economic loss [5]. One of the most effective strategies to prevent energy theft is the use of smart meter-based Energy Internet (EI) [6]. Such a technique may be used to remotely track consumption data from customers, record any suspicious activity, and quickly send the data to the utility. Despite their many benefits, smart meters are impractical for countries experiencing severe economic difficulties due to the significant costs associated with their deployment and maintenance. Before these tools are extensively deployed, it is also necessary to adequately manage the expanding cyber dangers. It is difficult to secure the information flow of the EI because of the unique characteristics of advanced metering infrastructure (AMI). By deploying intrusion tactics, the unauthorized users can alter data from smart meters. Because of this, power thefts on the EI are distinct from those that occurred on the traditional grid and were primarily the result of physically avoiding or extinguishing the mechanical [3]. The energy usage patterns of consumers may be automatically tracked by machine learning (ML) algorithms. When examining the data from smart meters, it may help to identify power thieves with greater accuracy. In other words, Machine learning technologies, such as decision trees, random forests, support vector machines, neural networks, and others, can be used to create classification models in order to assess the daily electricity usage habits of customers [7], [8]. Typically, machine learning algorithms can be applied in either offline or online scheme. In the offline (i.e. batch) learning, a dataset of electricity consumption patterns is assumed to be available offline. Thereafter, a classification model is trained and evaluated to classify users as either malicious or benign based on their consumption patterns [9], [10]. The developed model can then be deployed in a real environment to make online predictions. On the other hand, the online (a.k.a incremental) learning scheme relies on the fact that smart meters reading arrive as a continuous stream of data. Hence, a classification model needs to be incrementally constructed by examining one instance at a time. Apparently, the batch learning scheme assumes that the whole dataset is stored in memory while building a machine learning model. However, it is well recognized that the batch learning approach has a number of drawbacks. First, the training phase could take a very long time and use up a significant portion of computer resources. Second, the amount of the training dataset has an

impact on the trained model's performance. Third, after the model is trained, it cannot acquire new experience from new input instances since in a offline (i.e., batch) learning scheme, the training data are assumed to be static and unchanging over time. To put it another way, it is necessary to build a new model whenever the statistical characteristics of the model's input change (i.e., a concept drift is encountered). Online classification algorithms are advantageous over off-line (i.e. batch) classification algorithms for a number of reasons, especially given that the smart meter readings in smart grids provide a constant stream of data. First off, algorithms for online classification are built to handle infinite amounts of data and gradually pick up new information. While creating projections as necessary, they are continuously updated. Second, real-time applications that conventional (i.e. batch) learning algorithms cannot handle can be addressed by online data stream classification systems. Online classification is thus viewed as a viable technique for classifying electricity consumption patterns in smart grid systems because user behavior may change over time in an unanticipated way. Numerous techniques have been put forth for the classification of data streams [11]–[13]. To the best of the authors' knowledge, no study has ever been done on how well these algorithms perform in detecting electricity theft in smart grids, despite the fact that some of them have been studied in various fields [14]–[21]. In addition, previous research efforts have tackled electricity theft detection using batch learning algorithms [9], [22]–[25]. Hence, the contribution of this paper is threefold. First, implementing online machine learning models for electricity theft detection, based on a recent specialized dataset. Second, performing an extensive set of experiments under both binary and multi-class theft detection scenarios. Third, identifying the most viable online machine learning model for theft detection in smart grids, considering a representative set of performance metrics.

The rest of this paper is organized as follows. Section II provides background information on the considered algorithms. Section III explains the research tools and evaluation methodology. Evaluation results are shown in Section IV. Finally, Section V concludes and summarizes this paper.

II. BACKGROUND

Models from static datasets have traditionally been created using ML techniques. The need for models that can handle enormous data streams is, nevertheless, expanding. This means that additional data samples might appear at any time, and it is unsuitable to store them in a static dataset.

On the one hand, learning from continuous and evolving data streams necessitates the development of the ML model and continual stream upgrades. Additionally, it is crucial to combat concept drift, in which the statistical characteristics of the evolving data change with time [26], [27]. The resultant ML model must also be immediately updated for smart grid environments, needing algorithms with appropriate levels of accuracy subject to constrained memory and processing capacity.

A. Bayes Learning Algorithms

The Naive Bayes (NB) algorithm is used in this category. The NB method uses Bayesian prediction on the presumption

that each input feature included within an input instance is independent. An NB model predicts every incoming data sample's class with a high degree of certainty. The NB algorithm is distinguished by its simplicity and minimal processing demands [12].

B. Lazy Learning Algorithms

The k-Nearest Neighbors classifier (kNN) and the self-adjusting memory combined with the kNN classifier (SAM-kNN) [28], [29] are two well-known lazy learning algorithms that are taken into consideration in this work. In online learning environments, the kNN algorithm relies on maintaining track of a window with a fixed number of recently encountered input data samples. The kNN algorithm looks within the recently stored window and, using a predetermined distance metric, determines the closest neighbors whenever a new input data sample is observed. The current input sample's class label is then allocated appropriately. The SAM-kNN, on the other hand, is an improvement over the standard KNN. A self-adjusting memory (SAM) model creates an ensemble of classification models for either current or prior concepts in SAM-KNN. Depending on the needs of the present concept, several models can be used. A short-term (STM) and long-term (LTM) memory are built specifically by the SAM model. The STM is built to represent the current concept, whereas the LTM is used to represent earlier concepts. A cleaning procedure is utilized to regulate the STM's size and keep the LTM and the STM consistent.

C. Tree-based Learning Algorithms

Online machine learning applications frequently employ tree-based methods. The Hoeffding Tree (HT) [30] and the Extremely Fast Decision Tree (EFDT) from [31] are the two main tree-based algorithms employed in this work. The HT method is a decision tree induction method that, under the premise that the distribution that yields the entering data samples is constant and does not evolve over time, may learn gradually and whenever from immense online data streams. It is based on the observation that choosing the best splitting attribute may frequently be done with only a limited quantity of input samples. This statement is supported theoretically by the Hoeffding bound, which counts the number of input instances needed to estimate a particular set of statistics with a given precision. The HT technique is potentially more enticing than other incremental (i.e., online) tree-based algorithms because it provides high performance guarantees. It can be demonstrated that the outcome of an HT model is asymptotically identical to that of a batch-based learner employing infinitely many input data samples by depending on the Hoeffding bound. Additionally, the EFDT classification algorithm incrementally constructs a tree. Once it is certain that a split is useful, it looks for picking and deploying that split. Later, it reviews that split choice and replaces it if it becomes clear that a more advantageous split is there. If the distribution that generates the input instances is stable, the EFDT can quickly pick up on static distributions and finally learn the asymptotic offline tree.

D. Ensemble Learning Algorithms

Two ensemble learning methodologies are assessed in this article including Leveraging Bagging LB [32] and Adaptive

Random Forest ARF [33]. Leveraging bagging is an enhanced online bagging algorithm. In this regard, online bagging mimics conventional offline Bagging to cope with incremental learning. For offline bagging scheme, N samples are taken from an N sized training dataset with replacement creating N separate datasets for M classifiers to be trained on. Since there is no training dataset but only a stream of samples in online learning environments, drawing input samples with replacement is not an easy task. The online bagging simulates the batch based training process by training each base estimator on each incoming instance over k times, where k is drawn from the binomial distribution. Given that the input stream may be considered endless and that the binomial distribution approaches a Poisson $\lambda = 1$ distribution with infinite samples, the work in [34] has found that the procedure used by the on-line bagging algorithms is a good "drawing with replacement". The LB algorithm makes an effort to enhance classification outcomes when assuming an infinite input data stream by modifying Poisson distribution's parameters produced from the binomial distribution. The LB technique causes the λ value of the Poisson distribution to change from 1 to 6. The new value of λ would broaden the input space's diversity by giving the input data samples a variety of weights. In order to achieve even greater improvement, the LB approach uses output detecting codes. Each bit in the n -bit long binary code used to encode the detection codes for each class label corresponds to a particular one of the n classifiers. Every classifier is trained on its corresponding bit while a new input instance is being looked at. This helps the LB algorithm reduce linked errors to a certain extent.

The standard batch based random forest technique has been modified for the online learning scope by the ARF algorithm. A weighted voting method is used in ARF to decide how to categorize each incoming data instance after many decision trees have been built. The classification choice is prioritized and the voting procedure is weighted more heavily in favor of the decision tree that performs the best in terms of Kappa or the accuracy statistic.

III. RESEARCH TOOLS AND METHODOLOGY

A. Dataset

This work is based on the Theft Detection Dataset (TDD2022) proposed in [3]. The dataset was gathered using the Open Energy Data Initiative (OEDI) platform which is a consolidated repository for high-value energy research datasets collected from the Programs, Offices, and National Laboratories of the United States Department of Energy [35]. The information in TDD2022 stems from various domains such as private industrial parties, laboratories, institutions, etc. The dataset is composed energy consumption data for 16 different consumer types. It encloses several energy consumption measurements for distinct customer types during a one-year period. Those measurements are recorded on hourly basis during the day. This data was then used to implement a theft generator for six different types of electricity theft. Each instance in the dataset contains 11 meter readings, consumer type, and a class label as either normal consumption or one of the six theft types. Tables I, II, III and IV illustrate the dataset general statistics, feature types, customer types and instances distribution on classes, respectively.

TABLE I. GENERAL STATISTICS

Item	values
Number of instances	560640
Number of categorical features	1
Number of numerical features	10
Customer types	16
Instances per customer type	35040
Number of classes	7

TABLE II. CUSTOMER TYPES

Type	Integer code
Full service restaurant	1
Hospital	2
Large hotel	3
Large office	4
Medium office	5
Medrise apartment	6
Primary school	7
Outpatient	8
Warehouse	9
Secondary school	10
Small hotel	11
Small office	12
Stand-alone retail	13
Strip mall	14
Supermarket	15
Quic service restaurant	16

TABLE III. FEATURE TYPES

Name	Type
Electricity-Facility (KW/Hr)	Numeric
Fans-Electricity (KW/Hr)	Numeric
Cooling-Electricity (KW/Hr)	Numeric
Heating-Electricity (KW/Hr)	Numeric
Interior lights-Electricity (KW/Hr)	Numeric
Interior equipment-Electricity (KW/Hr)	Numeric
Gas-Facility (KW/Hr)	Numeric
Heating-Gas (KW/Hr)	Numeric
Interior equipment-Gas (KW/Hr)	Numeric
Water systems-Gas (KW/Hr)	Numeric
Consumer Type (KW/Hr)	Categorical

TABLE IV. INSTANCES DISTRIBUTION

Class name	Total number of instances
Normal	331824
Theft-1	51083
Theft-2	22958
Theft-3	44349
Theft-4	41460
Theft-5	33553
Theft-6	35413

The first theft type consists of a pronounced reduction of electricity consumption during the day. Such reduction is attained by multiplying the consumption by a uniformly distributed random number in the interval[0.1,0.8]. For the second theft type, electricity consumption is randomly dropped to zero throughout an arbitrary period. In addition, the third theft type resembles the first type except the fact that each hourly consumption is multiplied by a random number. Moreover, a random portion of the mean consumption is generated for the fourth theft type. Furthermore, the fifth type of theft reports the mean consumption. Finally, the sixth theft type reverses the order of the consumption values.

B. Evaluation Methodology

This section outlines the key procedures used to assess the effectiveness of the online machine learning (i.e., classification) algorithms on the TDD2022 dataset. The evaluation process using the scikit-multiflow evaluation platform [36] is shown in Fig. 1. Every online classification algorithm goes through this review process. As seen, the dataset is initially loaded as an input stream and then sent to the classification algorithm after that algorithm's initialization for online testing, incremental learning, and evaluation.

The prequential or the interleaved test then train method is used in this study to assess the classification algorithms. As each incoming input sample (i.e. instance) serves two purposes and is analyzed sequentially in order of arrival before becoming instantly inaccessible, the prequential assessment approach was created specifically for online learning environments. In prequential evaluation, each observed input instance is first employed to test the classification model (i.e. to generate a prediction), and then the same input instance is used to train that classification model. Each tested model's performance is continuously updated after each encountered instance and its capacity to handle unobserved cases is continuously monitored in real-time. As a result, a classification model that has been instantiated is constantly tested and the metrics that go with it are updated for input instances that it has not yet encountered. A number of commonly used performance metrics including accuracy, precision, recall, F-1 score and the kappa statistic derived from online learning models are used to quantify the performance of the classification algorithms. These measures are defined as follows:

- **Classification accuracy:** is the proportion of correctly classified input instances.

$$Accuracy = \frac{TN + TP}{TP + FP + FN + TN} \times 100\% \quad (1)$$

where, respectively, TP, TN, FP, and FN stand for true positive, true negative, false positive, and false negative. TP is the total number of cases that were successfully identified as positive (i.e., theft). The number of successfully identified negative (i.e., normal) events is referred to as TN. FP is the total number of positive samples that are mistakenly labeled as negative ones. The total number of negative occurrences that are mistakenly labeled as positive occurrences is known as FN.

- **Precision:** determines the proportion of predictions for the positive class that are in fact members of the

positive class.

$$Precision = \frac{TP}{TP + FP} \quad (2)$$

- **Recall:** calculates the proportion of correctly predicted classes that are positive out of all occurrences that are positive in the observed stream.

$$Recall = \frac{TP}{TP + FN} \quad (3)$$

- **F-score:** is the precision and recall harmonic mean.

$$F - score = \frac{2 \times Precision \times Recall}{Precision + Recall} \quad (4)$$

- **Kappa statistic (κ):** is a reliable classification accuracy metric that takes the likelihood of agreement by chance into account. It indicates the superiority over the majority class classifier, which assume that all

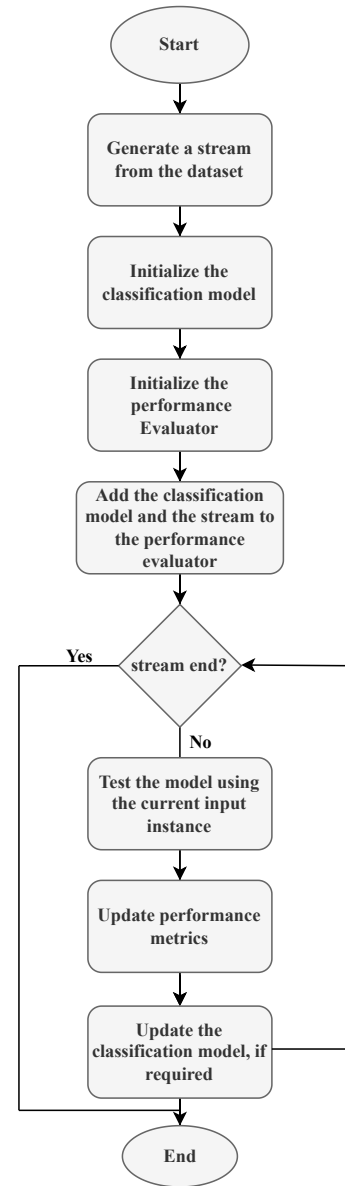


Fig. 1. Evaluation Flowchart.

incoming cases will fall within the majority class [37]. In particular for data streams with unbalanced class distribution, it is crucial in assessing classification accuracy.

$$\kappa = \frac{p_0 - p_c}{1 - p_c} \quad (5)$$

where p_0 denotes the classifier's predictive accuracy and p_c denotes the likelihood that a random classifier will produce an accurate prediction [38]. The classification procedure is always correct if $\kappa = 1$.

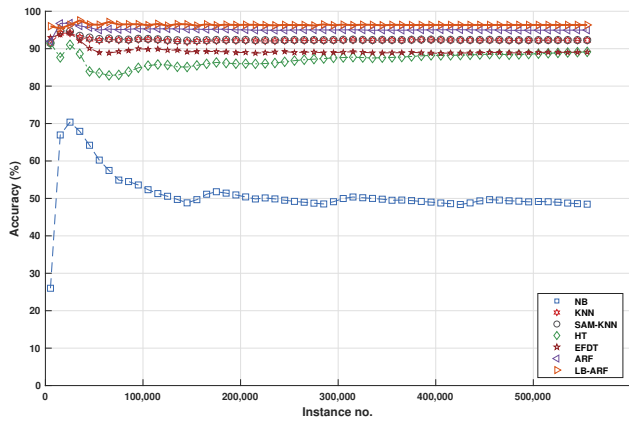
IV. RESULTS AND ANALYSIS

This section shows the predictive performance of the considered online machine learning algorithm on a data stream generated from the TDD2022 dataset. The considered algorithms were tested under both binary and multi-class classification settings. In binary classification, each instance in the TDD2022 dataset is labelled as either normal or theft instance regardless of the theft type. For the multi-class classification, the consumption instances retain their original labelling (i.e., normal, Theft-1, Theft-2, Theft-3, Theft-4, Theft-5 or Theft-6). Fig. 2(a), 2(b), 2(c), 2(d) and 2(e) depict the running mean prediction accuracy, precision, recall, F-1 score and kappa statistics of the considered learning algorithms under binary classification settings. They considered algorithms were pre-trained on the first 5000 samples and then prequentially evaluated and trained on the remaining part of the consumption stream. As shown, the KNN, SAM-KNN, ARF and LB-ARF algorithms have steadily maintained high mean values of accuracy, precision, F-1 score and kappa statistic, as compared to the NB, HT and EFDT algorithms. In addition, the NB, HT and EFDT algorithms demonstrate fluctuating performance during the first 100,000 instances. On the other hand, the NB, ARF and LB-ARF have maintained higher mean recall values, when compared to the other algorithms. However, the NB algorithm exhibits fluctuating behaviour during the 200,000 instances. Furthermore, the relatively high kappa values of the ARF and LB-ARF algorithms indicate reasonable reliability of their predictive performance. In other words, they are able to incrementally learn the statistical characteristics of the incoming normal and theft instances adapt reliably to unseen instances. Overall, the LB-ARF algorithms outperforms the other algorithm under all the considered performance metrics. Fig. 3(a), 3(b), 3(c), 3(d) and 3(e) depict the running mean prediction accuracy, precision, recall, F-1 score and kappa statistics of the considered learning algorithms under multi-class classification settings. On the one hand, Fig. 3(a) depicts that the KNN, SAM-KNN, ARF and LB-ARF have achieved relatively acceptable accuracy levels ($\geq 80\%$), as compared to the other algorithms, taking into account the complexity of multi-class classification as compared to the binary one. On the other hand, Fig. 3(b), 3(c) and 3(d) demonstrate the ability of the LB-ARF algorithm to maintain acceptable precision, recall and F-1 score, when compared to the other algorithms. Similar to the case of binary classification, the relatively high kappa value of the LB-ARF demonstrate its superior performance reliability over other algorithms. Fig. 4(a), 4(b), 4(c), 4(d) and 4(e) compare the predictive performance of the considered algorithms on binary and multi-class theft detection settings. In general, the predictive performance of all

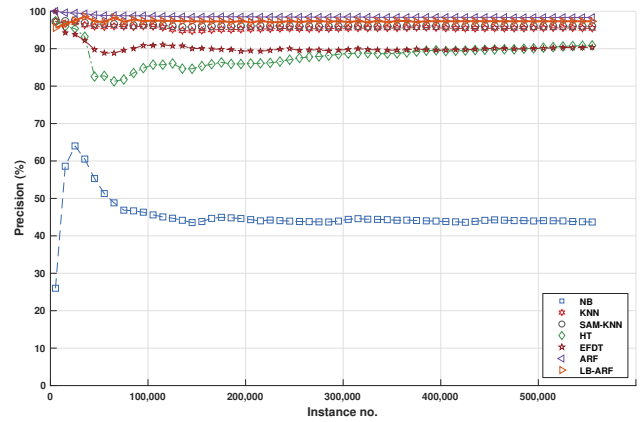
algorithms in binary classification is higher as compared to that of multi-class classification. Unlike other algorithms, the LB-ARF algorithm has maintained comparable performance levels under all metrics for both binary and multi-class classification. It is worth noting that the tree-based algorithms exhibit higher performance drop when moving from binary to multi-class classification, as compared to the other categories.

In summary, the LB-ARF (i.e., Leveraging Bagging algorithm with an Adaptive Random Forest base classifier) demonstrates consistent competence to perform theft detection under both binary and multi-class classification scenarios. This algorithm keeps a collection of n ARF base classifiers, where n in the used evaluation platform is set by default to 10 [36]. In order to classify an incoming instance, each classifier will make a prediction (i.e., a vote), and the ultimate classification result is produced by combining the individual forecasts. The Condorcet's jury theorem has a theoretical demonstration, assuming two criteria are satisfied, that the error rate of a particular ensemble tends to zero in the limit [39]–[41]. First, Individual base classifiers must outperform random guessing. This requirement is attained as the ARF algorithm achieves relatively high predictive performance that is better than random guessing as shown in Fig. 2, 3 and 4. Typically, the accuracy of a random classifier (i.e., random guess) is equal to $1/k$ where k is the total number of classes. In this work, the total number of classes is equal to 2 in case of binary classification and 7 in case of multi-class classification.

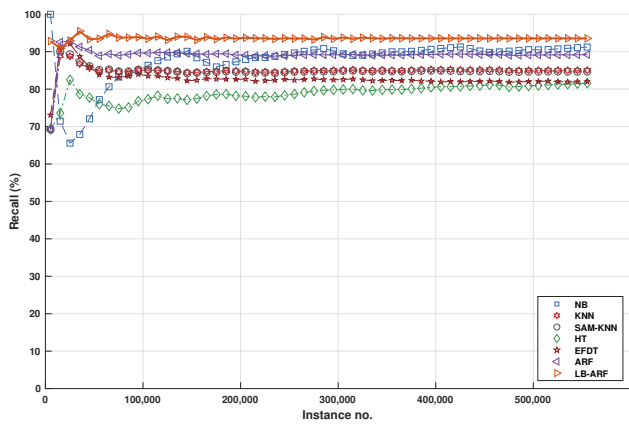
Second, each classification model must be diverse; that is, it must not generate correlated errors. For the LB-ARF method, online bagging is used by the LB algorithm to train its associated base classification models. In this context, an online re-sampling is carried out as each incoming classification case is noticed by showing that instance to every model k *sim* Poisson (λ) times and updating every model in accordance. The value of k is treated as the incoming instance's weight. In order to increase online re-sampling, the λ value of the Poisson distribution is typically set to 6 in the LB algorithm. The LB ensemble algorithm is making the incoming instances weights more random with such a value of λ . As a result, it increases the diversity of the input space by giving each incoming instance a new range of weights. The LB technique further improves bagging performance by applying output codes to add randomization to the ensemble's output. As seen in Section II-D, Each prospective class label is given an n -bit binary string, where n is the total number of base classifiers in the ensemble. Each base classifier learns a single bit from the binary string. The LB algorithm utilized random output codes instead of deterministic ones, in contrast to typical ensemble approaches. To put it another way, employing output codes enables each classifier in the LB ensemble to predict a separate function, whereas the base classifiers in the traditional approaches predict the same function [32]. This would reduce the impact of correlations among base classifiers and, as a result, improve the ensemble's diversity [42], [43]. The ensemble thus partially satisfies the second criteria of the Condorcet's jury theorem by adding randomization to both the input and the output of the ensemble's base classifiers. Additionally, the LB method employs the ADWIN method to handle concept drift, employing ADWIN instance per classifier in the ensemble [28]. The poorest classifier is reset whenever a concept drift is found. As a result, the LB algorithm con-



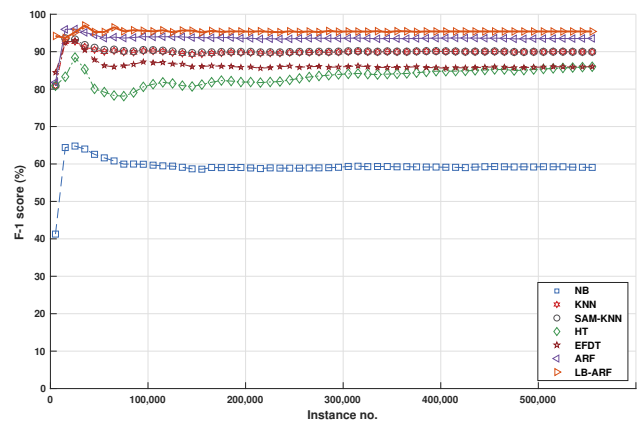
(a) Accuracy



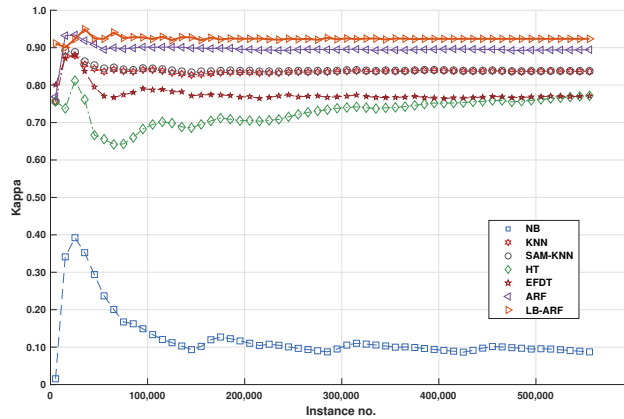
(b) Precision



(c) Recall



(d) F-1 score

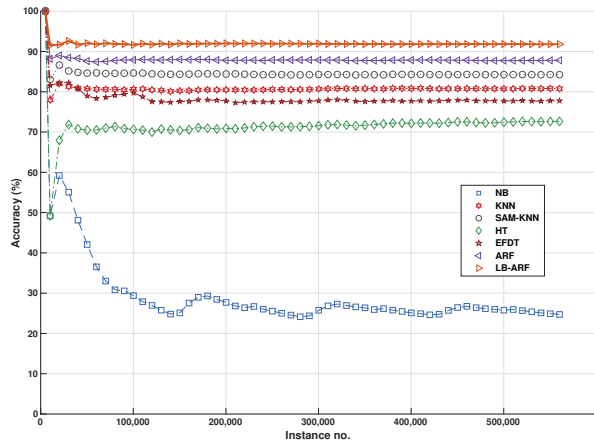


(e) Kappa

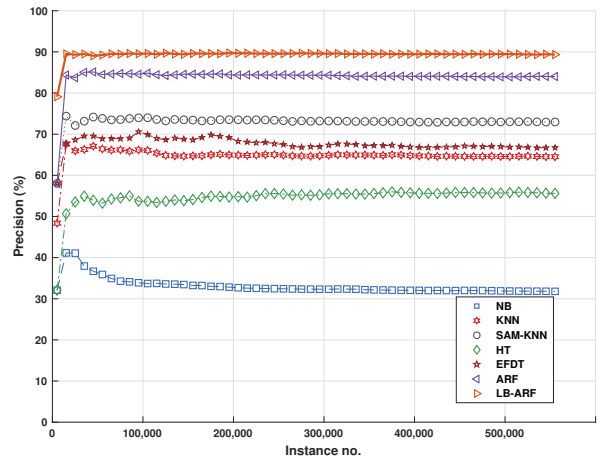
Fig. 2. Performance Results - Binary Classification

tinuously assesses the effectiveness of its learning procedure and follows the current distribution of class labels within the incoming classification examples. The classification errors caused by any given classifier would typically be offset by the LB-ARF's diversity among its basic classifiers. This can be observed in Fig. 2, 3 and 4 wherein an LB ensemble of ARF classifiers always achieve higher predictive performance

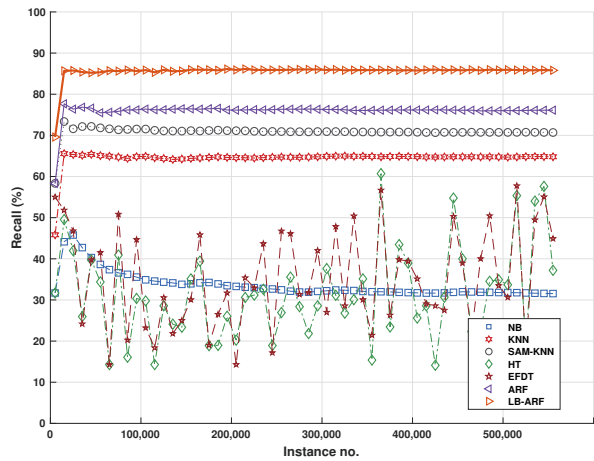
than a single ARF instance. Overall, the LB-ARF algorithm has demonstrated its ability to sustain an audible performance under all taken into account performance metrics. This makes it a viable option for online theft detection (i.e. classification) in real-world smart grids.



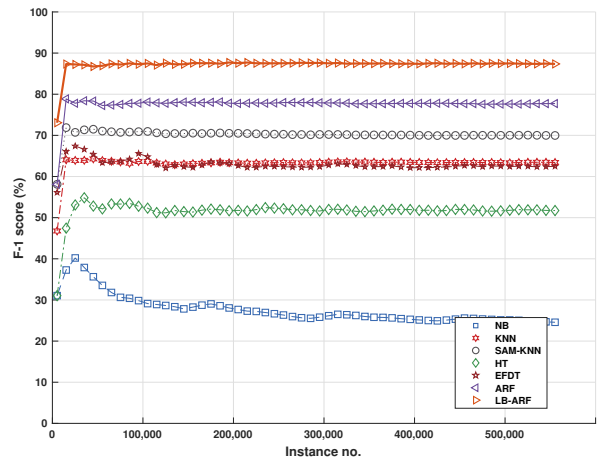
(a) Accuracy



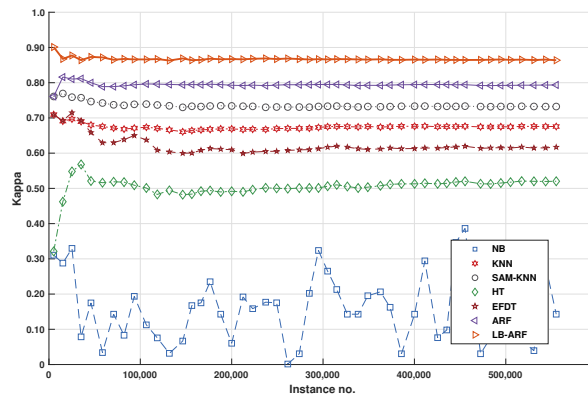
(b) Precision



(c) Recall



(d) F-1 score



(e) Kappa

Fig. 3. Performance Results - Multi-Class Classification

V. CONCLUSION

Power loss brought on by electricity theft is a critical issue in both traditional and smart grid settings. Smart meters can be used in smart grids to monitor power usage patterns and spot any questionable activities. However, using hacking techniques

or cyber attacks can undermine smart meter readings. In this sense, machine learning algorithms can be employed to evaluate client daily consumption patterns and identify probable instances of electricity theft. This work studied the application of online machine learning algorithms for electricity theft detection in smart grid systems, based on a recently

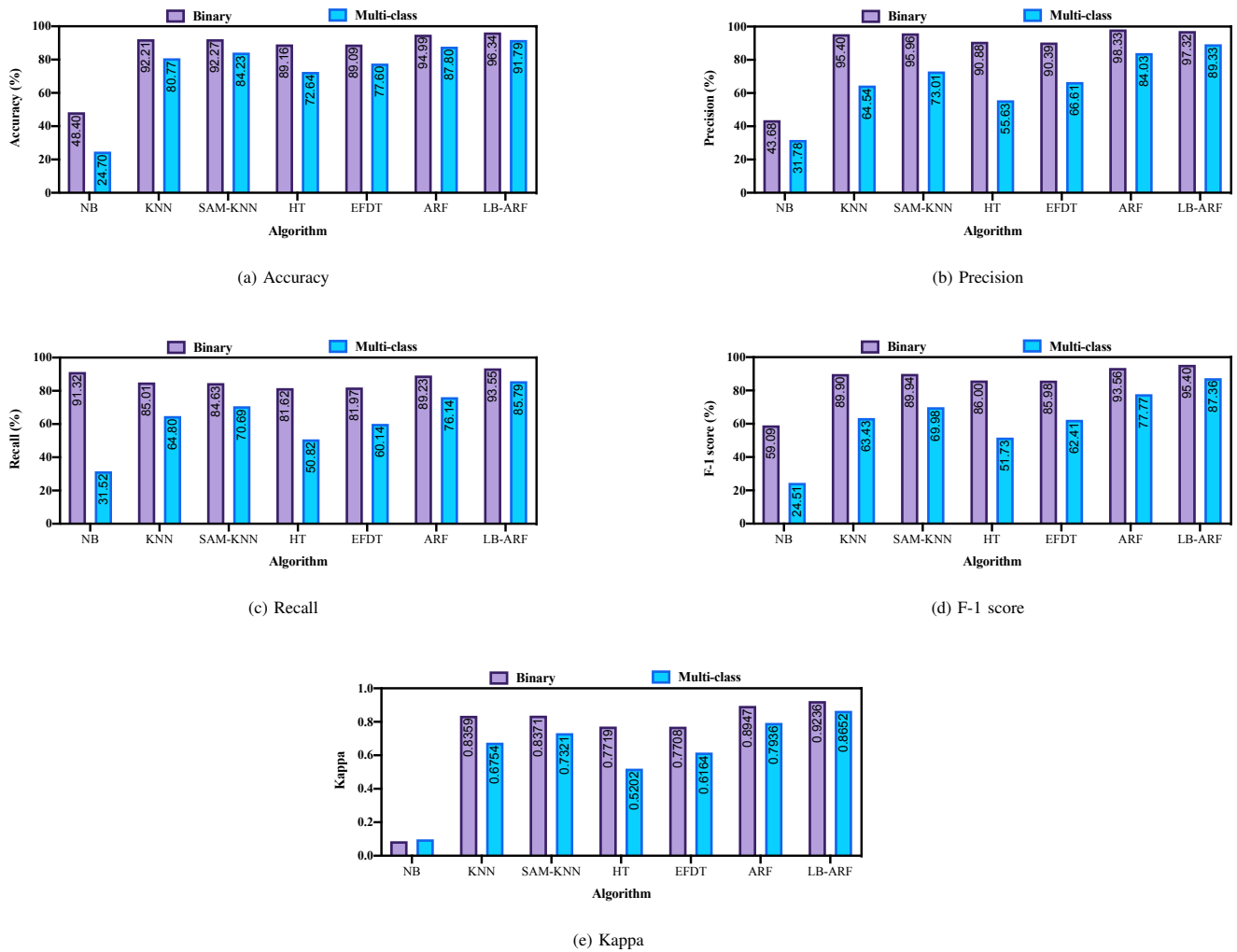


Fig. 4. Performance Comparison - Binary vs. Multi-Class

proposed theft detection dataset. Evaluation results showed that leveraging bagging with an adaptive random forest base estimator surpassed its online machine learning counterparts in both binary and multi-class theft detection. Hence, it can be viewed as a promising online learning model for electricity theft detection in smart grids.

REFERENCES

- [1] M. N. Hasan, R. N. Toma, A.-A. Nahid, M. M. M. Islam, and J.-M. Kim, "Electricity theft detection in smart grid systems: A cnn-lstm based approach," *Energies*, vol. 12, no. 17, 2019. [Online]. Available: <https://www.mdpi.com/1996-1073/12/17/3310>
- [2] M. Adil, N. Javaid, U. Qasim, I. Ullah, M. Shafiq, and J.-G. Choi, "Lstm and bat-based rusboost approach for electricity theft detection," *Applied Sciences*, vol. 10, no. 12, 2020. [Online]. Available: <https://www.mdpi.com/2076-3417/10/12/4378>
- [3] S. Zidi, A. Mihoub, S. Mian Qaisar, M. Krichen, and Q. Abu Al-Haija, "Theft detection dataset for benchmarking and machine learning based classification in a smart grid environment," *Journal of King Saud University - Computer and Information Sciences*, 2022. [Online]. Available: <https://www.sciencedirect.com/science/article/pii/S1319157822001562>
- [4] S. Hussain, M. W. Mustafa, T. A. Jumani, S. K. Baloch, H. Alotaibi, I. Khan, and A. Khan, "A novel feature engineered-catboost-based supervised machine learning framework for electricity theft detection," *Energy Reports*, vol. 7, pp. 4425–4436, 2021. [Online]. Available: <https://www.sciencedirect.com/science/article/pii/S2352484721004716>
- [5] L. G. Arango, E. Decache, B. D. Bonatto, H. Arango, and E. O. Pamplona, "Study of electricity theft impact on the economy of a regulated electricity company," *Journal of Control, Automation and Electrical Systems*, vol. 28, no. 4, pp. 567–575, Aug 2017. [Online]. Available: <https://doi.org/10.1007/s40313-017-0325-z>
- [6] K. Zheng, Q. Chen, Y. Wang, C. Kang, and Q. Xia, "A novel combined data-driven approach for electricity theft detection," *IEEE Transactions on Industrial Informatics*, vol. 15, no. 3, pp. 1809–1819, 2019.
- [7] S. S. S. R. Depuru, L. Wang, V. Devabhaktuni, and P. Nelapati, "A hybrid neural network model and encoding technique for enhanced classification of energy consumption data," in *2011 IEEE Power and Energy Society General Meeting*, 2011, pp. 1–8.
- [8] A. Jindal, A. Dua, K. Kaur, M. Singh, N. Kumar, and S. Mishra, "Decision tree and svm-based data analytics for theft detection in smart grid," *IEEE Transactions on Industrial Informatics*, vol. 12, no. 3, pp. 1005–1016, 2016.
- [9] L. J. Lepolesa, S. Achari, and L. Cheng, "Electricity theft detection in smart grids based on deep neural network," *IEEE Access*, vol. 10, pp. 39 638–39 655, 2022.
- [10] A. Ullah, N. Javaid, M. Asif, M. U. Javed, and A. S. Yahaya, "Alexnet, adaboost and artificial bee colony based hybrid model for electricity theft detection in smart grids," *IEEE Access*, vol. 10, pp. 18 681–18 694, 2022.
- [11] A. Gepperth and B. Hammer, "Incremental learning algorithms and applications," in *European Symposium on Artificial Neural Networks (ESANN)*, Bruges, Belgium, 2016. [Online]. Available: <https://hal.archives-ouvertes.fr/hal-01418129>

- [12] Q. Yang, Y. Gu, and D. Wu, "Survey of incremental learning," in *2019 Chinese Control And Decision Conference (CCDC)*, 2019, pp. 399–404.
- [13] K. K. Wankhade, S. S. Dongre, and K. C. Jondhale, "Data stream classification: a review," *Iran Journal of Computer Science*, vol. 3, no. 4, pp. 239–260, Dec 2020. [Online]. Available: <https://doi.org/10.1007/s42044-020-00061-3>
- [14] U. Adhikari, T. H. Morris, and S. Pan, "Applying hoeffding adaptive trees for real-time cyber-power event and intrusion classification," *IEEE Transactions on Smart Grid*, vol. 9, no. 5, pp. 4049–4060, 2018.
- [15] Z. E. Mrabet, D. F. Selvaraj, and P. Ranganathan, "Adaptive hoeffding tree with transfer learning for streaming synchrophasor data sets," in *2019 IEEE International Conference on Big Data*, 2019, pp. 5697–5704.
- [16] C. Nixon, M. Sedky, and M. Hassan, "Practical application of machine learning based online intrusion detection to internet of things networks," in *2019 IEEE Global Conference on Internet of Things (GCIoT)*, 2019, pp. 1–5.
- [17] V. G. Turrissi da Costa, E. J. Santana, J. F. Lopes, and S. Barbon, "Evaluating the four-way performance trade-off for stream classification," in *Green, Pervasive, and Cloud Computing*. Cham: Springer International Publishing, 2019, pp. 3–17.
- [18] J. Fernandes Lopes, E. J. Santana, V. G. Turrissi da Costa, B. Bogaz Zarpelão, and S. Barbon Junior, "Evaluating the four-way performance trade-off for data stream classification in edge computing," *IEEE Transactions on Network and Service Management*, vol. 17, no. 2, pp. 1013–1025, 2020.
- [19] M. Al-Tarawneh, "Data stream classification algorithms for workload orchestration in vehicular edge computing: A comparative evaluation," *International Journal of Fuzzy Logic and Intelligent Systems*, vol. 21, no. 2, pp. 101–122, 2021.
- [20] M. Rahouti, M. Ayyash, S. K. Jagatheesaperumal, and D. Oliveira, "Incremental learning implementations and vision for cyber risk detection in iot," *IEEE Internet of Things Magazine*, vol. 4, no. 3, pp. 114–119, 2021.
- [21] M. A. B. Al-Tarawneh and S. E. Alnawayseh, "Performance assessment of context-aware online learning for task offloading in vehicular edge computing systems," *International Journal of Advanced Computer Science and Applications*, vol. 12, no. 4, 2021. [Online]. Available: <http://dx.doi.org/10.14569/IJACSA.2021.0120439>
- [22] D. Gu, Y. Gao, K. Chen, S. Junhao, Y. Li, and Y. Cao, "Electricity theft detection in ami with low false positive rate based on deep learning and evolutionary algorithm," *IEEE Transactions on Power Systems*, pp. 1–1, 2022.
- [23] A. Arif, T. A. Alghamdi, Z. A. Khan, and N. Javaid, "Towards efficient energy utilization using big data analytics in smart cities for electricity theft detection," *Big Data Research*, vol. 27, p. 100285, 2022. [Online]. Available: <https://www.sciencedirect.com/science/article/pii/S2214579621001027>
- [24] F. Shehzad, N. Javaid, S. Aslam, and M. Umar Javed, "Electricity theft detection using big data and genetic algorithm in electric power systems," *Electric Power Systems Research*, vol. 209, p. 107975, 2022. [Online]. Available: <https://www.sciencedirect.com/science/article/pii/S037877962200205X>
- [25] M. Ezeddin, A. Albaseer, M. Abdallah, S. Bayhan, M. Qaraqe, and S. Al-Kuwari, "Efficient deep learning based detector for electricity theft generation system attacks in smart grid," in *2022 3rd International Conference on Smart Grid and Renewable Energy (SGRE)*, 2022, pp. 1–6.
- [26] G. I. Webb, R. Hyde, H. Cao, H. L. Nguyen, and F. Petitjean, "Characterizing concept drift," *Data Mining and Knowledge Discovery*, vol. 30, no. 4, pp. 964–994, Jul 2016. [Online]. Available: <https://doi.org/10.1007/s10618-015-0448-4>
- [27] J. Demšar and Z. Bosnić, "Detecting concept drift in data streams using model explanation," *Expert Systems with Applications*, vol. 92, pp. 546 – 559, 2018. [Online]. Available: <http://www.sciencedirect.com/science/article/pii/S0957417417306772>
- [28] A. Bifet and R. Gavaldà, "Learning from time-changing data with adaptive windowing," in *Proceedings of the Seventh SIAM International Conference on Data Mining*. SIAM, 2007, pp. 443–448. [Online]. Available: <https://doi.org/10.1137/1.9781611972771.42>
- [29] V. Losing, B. Hammer, and H. Wersing, "Knn classifier with self adjusting memory for heterogeneous concept drift," in *2016 IEEE 16th International Conference on Data Mining (ICDM)*, 2016, pp. 291–300.
- [30] G. Hulten, L. Spencer, and P. Domingos, "Mining time-changing data streams," in *Proceedings of the Seventh ACM SIGKDD International Conference on Knowledge Discovery and Data Mining*, ser. KDD '01. New York, NY, USA: Association for Computing Machinery, 2001, p. 97–106. [Online]. Available: <https://doi.org/10.1145/502512.502529>
- [31] C. Manapragada, G. I. Webb, and M. Salehi, "Extremely fast decision tree," in *Proceedings of the 24th ACM SIGKDD International Conference on Knowledge Discovery and Data Mining*, ser. KDD '18. New York, NY, USA: Association for Computing Machinery, 2018, p. 1953–1962. [Online]. Available: <https://doi.org/10.1145/3219819.3220005>
- [32] A. Bifet, G. Holmes, and B. Pfahringer, "Leveraging bagging for evolving data streams," in *Machine Learning and Knowledge Discovery in Databases*, J. L. Balcázar, F. Bonchi, A. Gionis, and M. Sebag, Eds. Berlin, Heidelberg: Springer Berlin Heidelberg, 2010, pp. 135–150.
- [33] H. M. Gomes, A. Bifet, J. Read, J. P. Barddal, F. Enembreck, B. Pfahringer, G. Holmes, and T. Abdesslem, "Adaptive random forests for evolving data stream classification," *Machine Learning*, vol. 106, no. 9, pp. 1469–1495, Oct 2017. [Online]. Available: <https://doi.org/10.1007/s10994-017-5642-8>
- [34] N. C. Oza, "Online bagging and boosting," in *2005 IEEE International Conference on Systems, Man and Cybernetics*, 2005, pp. 2340–2345.
- [35] J. B. Leite and J. R. S. Mantovani, "Detecting and locating non-technical losses in modern distribution networks," *IEEE Transactions on Smart Grid*, vol. 9, no. 2, pp. 1023–1032, 2018.
- [36] J. Montiel, J. Read, A. Bifet, and T. Abdesslem, "Scikit-multiflow: A multi-output streaming framework," *Journal of Machine Learning Research*, vol. 19, no. 72, pp. 1–5, 2018. [Online]. Available: <http://jmlr.org/papers/v19/18-251.html>
- [37] T. Vasiloudis, F. Beligianni, and G. De Francisci Morales, "Boostvht: Boosting distributed streaming decision trees," in *Proceedings of the 2017 ACM on Conference on Information and Knowledge Management*, ser. CIKM '17. New York, NY, USA: Association for Computing Machinery, 2017, p. 899–908. [Online]. Available: <https://doi.org/10.1145/3132847.3132974>
- [38] A. Bifet, G. de Francisci Morales, J. Read, G. Holmes, and B. Pfahringer, "Efficient online evaluation of big data stream classifiers," in *Proceedings of the 21th ACM SIGKDD International Conference on Knowledge Discovery and Data Mining*, ser. KDD '15. New York, NY, USA: Association for Computing Machinery, 2015, p. 59–68. [Online]. Available: <https://doi.org/10.1145/2783258.2783372>
- [39] L. K. Hansen and P. Salamon, "Neural network ensembles," *IEEE Transactions on Pattern Analysis and Machine Intelligence*, vol. 12, no. 10, pp. 993–1001, 1990.
- [40] K. K. Ladha, "Condorcet's jury theorem in light of de finetti's theorem," *Social Choice and Welfare*, vol. 10, no. 1, pp. 69–85, Jan 1993. [Online]. Available: <https://doi.org/10.1007/BF00187434>
- [41] J. N. van Rijn, G. Holmes, B. Pfahringer, and J. Vanschoren, "The online performance estimation framework: heterogeneous ensemble learning for data streams," *Machine Learning*, vol. 107, no. 1, pp. 149–176, Jan 2018. [Online]. Available: <https://doi.org/10.1007/s10994-017-5686-9>
- [42] Y. Lv, S. Peng, Y. Yuan, C. Wang, P. Yin, J. Liu, and C. Wang, "A classifier using online bagging ensemble method for big data stream learning," *Tsinghua Science and Technology*, vol. 24, no. 4, pp. 379–388, 2019.
- [43] M. Kolárik, M. Sarnovský, and J. Paralič, "Diversity in ensemble model for classification of data streams with concept drift," in *2021 IEEE 19th World Symposium on Applied Machine Intelligence and Informatics (SAMII)*, 2021, pp. 355–360.

Artificial Intelligence for Automated Plant Species Identification: A Review

Khaoula Labrighli¹, Chouaib Moujahdi², Jalal El Oualidi³
Department of Botany & Plant Ecology,
Scientific Institute of Rabat,
Mohammed V University in Rabat,
Morocco^{1,2,3}

Laila Rhazi⁴
Laboratory of Botany, Mycology & Environment,
Research Center of Plant and Microbial Biotechnology,
Biodiversity & Environment. Faculty of Sciences,
Mohammed V University in Rabat, Morocco⁴

Abstract—Plants are very important for life on Earth. There is a wide variety of plant species and their number increases each year. The plants identification using conventional keys is complex, takes time and it is frustrating for non-experts because of the use of specific botanical terms/techniques. This creates a difficult obstacle to overcome for novices interested in acquiring knowledge about species, which is very important to develop any environmental study, like climate change anticipation models for example. Today, there is an increasing interest in automating the species identification process. The availability and omnipresence of relevant technologies, such as digital cameras, mobile devices, pattern recognition and artificial intelligence techniques in general, have allowed the idea of automated species identification to become a reality. In this paper, we present a review of automated plant identification over all significant available studies in literature. The main result of this synthesis is that the performance of advanced deep learning models, despite the presence of several challenges, is becoming close to the most advanced human expertise.

Keywords—Plants identification; species; artificial intelligence; machine learning; deep learning

I. INTRODUCTION

Species diversity of vascular plants is relatively important on the scale of global biodiversity. There are no less than 390000 distinct species known around the world. This number is very approximate, insofar as there is at least an equivalent number of taxa cited in the literature but in fact only falling under simple synonymies. This clearly shows the difficulty that exists in the determination and taxonomy of plants. Species identification is the essential step to properly identify biodiversity and better act in terms of conservation.

Among techniques used in biosystematics to diagnose discriminant characters, that allow us to differentiate taxa and draw practical keys of determination, absolutely herbariums remain an indispensable tool for the botanist daily work. Indeed, research in botanical taxonomy cannot be considered without the presence alongside us of a rich herbarium with collections of references and specimen's types that provide basic information very important for systematic research.

In general, botanists use various methods that involve memory and observation. They may have implicit knowledge of morphology and variability of species, as a result of experience and learning. Other elements may also be involved in the identification process and especially in the wild field, for example, botanists must take into account abiotic factors,

edaphic characters, climate and seasonal change that influence the morphology, appearance and distribution of species. These elements also provide useful information for identification. In addition to morphology, taxonomists can use a range of characters or taxonomic arguments including anatomy, palynology, chromosomes, biochemistry and molecular systematics to estimate the actual evolution of the species, to define it and to place it in its correct taxonomic rank.

In practice, each species has its own evolutionary history marked by genetic, ecological or morphological changes. There are several differences between species in morphology, ecology, reproductive system, interfertility, pollination, disease resistance, genes and many other traits. Systematics comes to find the product of this evolutionary history. To do this, taxonomists base themselves, in addition to morphology, on a set of characters or taxonomic arguments, in particular: odor, chromosomes, anatomy, molecular and biochemistry, to estimate the real evolution of species, grouping them into entities called taxa, to also give them scientific names according to the international code of botanical nomenclature and classify them, according to precise determination keys, in their correct taxonomic ranks starting with Kingdom then Phylum, Class, Order, Family, Gender and finally Species (Fig. 1).

In addition, there is the constraint in term of the specialized training required by the discipline and in particular the language of botany and its works (Flores, checklists, synopsis, monograph, etc.). That is why despite its importance, plant taxonomy remains a barely known and available notion to the majority of biologists. Indeed, defining taxa is a very complex task requiring a serious biosystem study based on the confrontation of several techniques.

This demanding situation by scientific, material and human needs push botanists to think about the idea where plants can be an object perfectly adapted to an automatic recognition system, able to make decisions about the belonging of a presented plant to any of the learned species [1][2]. In fact, accelerating the identification process and making possible for everyone is highly suggested, especially if we consider the continuous loss of plant biodiversity day after day. More than sixteen years ago, authors of [3] have argued that the developments of artificial intelligence and digital image processing would make automatic species identification from digital images real in the near future. Today, artificial intelligence, omnipresent mobile technologies and the emergence of smart phones make it possible to propel technological applications and make the

idea of automatic species identification close to reality.

In this paper, we will categorize and present the different proposed approaches for automated plant identification, then we will discuss and answer questions like: how far can automated systems be from human expertise? Can they completely take the place of botanists and provide accurate results even for difficult groups that require more than just image observation? What is the best methodology currently and how can it be optimized? Are there still other alternatives?

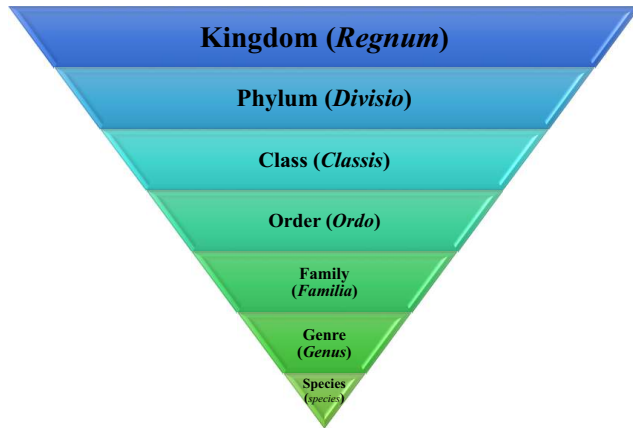


Fig. 1. The Seven Main Taxonomic Ranks Recognized by the International Code of Botanical Nomenclature (ICBN). Names in Italic are Latin Names.

It should be noted here that for our search strategy of papers that deal with the automated plant identification issue using AI, we have searched the Web of Science database to find relevant articles and books up to April 2022. The systematic search of the published literature was conducted using several keywords related generally to AI and plant identification.

The rest of the paper is organized as follows. In Section II, we will review automated plant identification categories / approaches. Our discussion is provided in Section III. Finally, we conclude the paper in Section IV.

II. LITERATURE REVIEW

The term of Artificial Intelligence (AI) was proposed and used for the first time by the late American programming expert John McCarthy in 1956, and it meant the ability to perform intelligent tasks by machines, especially tasks that mimic human intelligence.

Now that artificial intelligence techniques have developed and its uses have expanded, the definition of artificial intelligence can be developed as making computer system able of performing tasks that normally require simulating human intelligence, such as visual perception, pattern recognition, speech recognition, decision-making and translation between languages.

The use of artificial intelligence techniques has expanded in the last decade very significantly, and this is due to many reasons, the most important of which are: the power of modern computers (i.e., evolution of hardware) and their very large capabilities, which made the possibility of implementing very complex algorithms, that were not previously able to solve.

We cannot ignore as well the spread of sensors connected to the web service that transfer huge quantity of data in a fast way. These sensors are also a huge source of data that are very necessary to improve the functioning of the AI techniques.

We can divide the artificial intelligence according to the amount of intelligence that the machine has reached into three categories:

- **Artificial Narrow Intelligence:** It means that computers perform one specific task with high efficiency and high repetition capacity that exceeds the ability of humans to accomplish, but at the same time it has not yet reached the level of human intelligence. Indeed, all that we see now of applications and devices are of this type.
- **Artificial General Intelligence:** It means that machines reach a level of intelligence that simulates human intelligence. It is possible that we will see its first “complete” applications during the few coming years, and absolutely the reason for not reaching this level yet is that we still do not know the details of many aspects of the human brain.
- **Artificial Super Intelligence:** It means that machine intelligence surpasses the human intelligence. It is absolutely not clear when humanity can reach that, but we can hear already scientists today warn of and fear that machines will control humans with this level of intelligence.

In this paper, we are talking exactly about the “Artificial General Intelligence” techniques. We can distinguish here two main categories: 1) Machine Learning (ML) techniques and Deep Learning (DL) techniques. To be simple, we can say that the main difference between Machine Learning and Deep Learning is that ML models get progressively better, and they always need human intervention to give them an outline of how they learn from the data, while deep learning models learn itself, without relying on human intervention. For example, if a ML algorithm is taught to open a gate when it hears the word “open”, the algorithm will respond only when it hears that word. If the model receives data such as “*I am unable to enter*” then Machine Learning techniques will not respond, however Deep Learning algorithms can infer that the meaning is the same, and then respond and open the door.

Technically speaking, in the context of automated plant identification (Fig. 2), generally all proposed AI techniques or systems use *plant images* as an input and the output, after several processing operations (i.e., feature extraction + classification), will be of course the identification result of the entered plant (i.e., the species or any other taxonomic rank). For all systems, we can consider two stages, the *training* stage where the system will learn about all available plants, then the *identification* stage where the system will be able to give answers about entered plants. In the next two subsections, We will give more details about the difference between Machine Learning and Deep Learning techniques and we will present all significant approaches proposed in literature for each category.

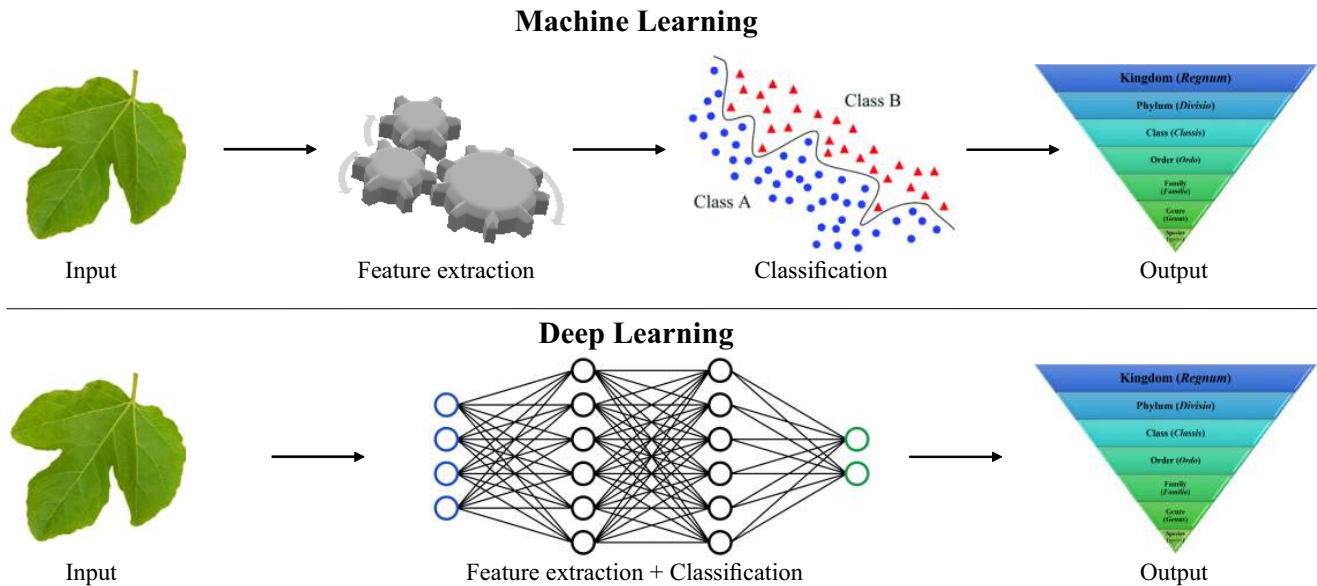


Fig. 2. The Main Modules of Machine Learning and Deep Learning Techniques.

A. Machine Learning Techniques

Speaking about automated plant identification using ML techniques (Fig. 3), we can say that during the *training* stage, all Machine Learning techniques apply, on the input images of all learned plant species, several classical feature extraction techniques, like PCA [4], to create plant *templates* (most of the time are “numerical vectors”) that will be stored in the system database. Then, during *identification* stage, users can submit any test plant image to the system, this last will apply the same feature extraction technique of the training stage then will match the query template with all stored templates in the system database, matching can take place using some classical classifier like SVM [5]. It should be noted that the majority of proposed ML techniques in literature add a pre-processing step on input images before applying the feature techniques to enhance data quality (i.e., to remove noisy information and keep the most useful data for learning and identification). In the next paragraphs of this sub-section, we will present the most significant works of this category according to an ascending chronological order.

In the context of the first edition of the PlantCLEF challenge, authors of [6] have used a dataset containing almost 5436 images belonging to 71 species of the French Mediterranean region. The dataset images are subdivided into three categories: scans, pseudo-scans and digital photos. Authors of this study focused on the identification of tree species from leaf images, with the aim of associating the correct tree species to each test image. The best results were obtained on scans and pseudo-scans, with accuracy equals to 53.8% and 68.5% respectively, while identification using digital images has not exceeded 52%.

As a continuation of the 2011 PlantCLEF challenge, the number of plant species in [7] has been increased from 71 to 126 and so the number of data has reached 11572 images subdivided always into three categories: scans, pseudo-scans

and photos. The scores are globally lower than those obtained during the 2011 campaign, of which the best for scans, pseudo-scans and photos are successively: 58%, 51% and 45%. During the same year, a technique that use the fuzzy local binary pattern and fuzzy color histogram as extracted features and a probabilistic neural network (PNN) for classification task has been proposed in [8]. A dataset of 2448 leaf images, obtained from medicinal plants in Indonesian forests, has been used for the experimentation. Authors have achieved a classification accuracy of 74.5%.

During the third edition of the PlantCLEF challenge, [9] moved towards the use of organ images for the identification of tree and grass species and not only their leaves. The number of used species in this challenge edition is about 250 with a total of 26077 photos belonging to two categories: SheetAsBackground (i.e., photos of leaves taken in front of a uniform background) and NaturalBackground (i.e., natural photographs in the wild). The results obtained are slightly higher than those obtained during the 2012 challenge, and as expected the results for NaturalBackground are significantly lower than for SheetAsBackground due absolutely to the noisy backgrounds. In the same year, the authors of [10] have proposed an approach that uses the fractal dimensional features of leaf shape and vein patterns for the feature extraction step. A KNN classifier [11] is used for comparison. Authors achieved an identification accuracy of 87.1%. Using the same Flavia dataset, but this time with only 930 images belonging to 31 species, [12] have obtained an accuracy of 97.6%, using a neuro-fuzzy classifier (NFC) with a 44 element texture vector and a 3-element shape vector. [13] achieved almost a similar accuracy of [12] using only the shape features frequencies of 1865 leaves taken from the Flavia dataset. The features are extracted using the Fourier transform followed by a traditional dimensionality reduction technique like Principal Component Analysis (i.e., PCA) technique for example. Then the selected features are submitted to test several classification models:

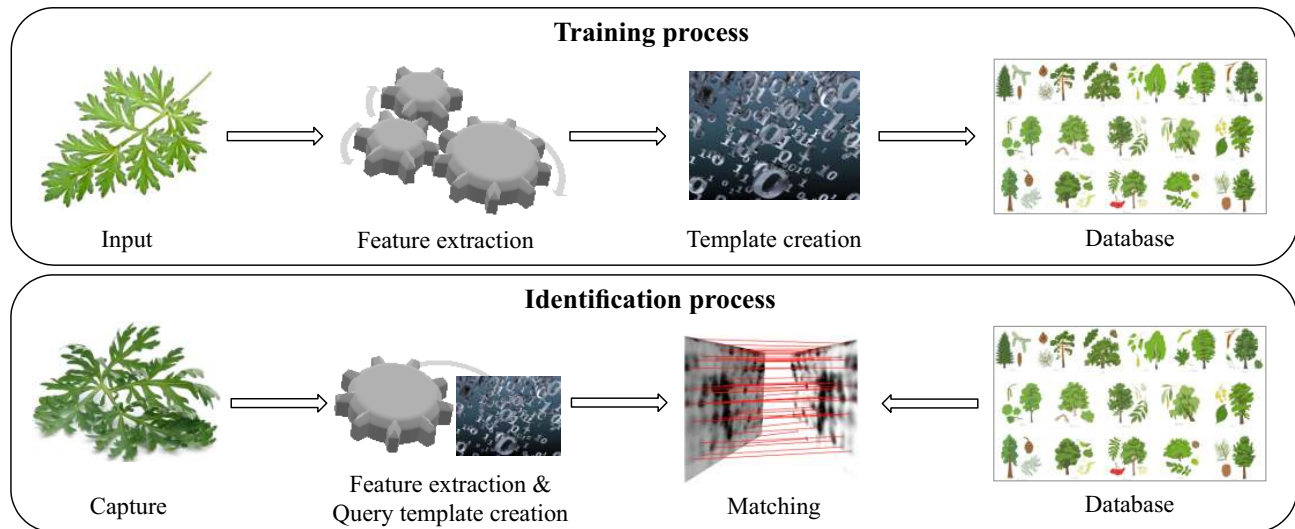


Fig. 3. The Main Steps of Machine Learning Techniques.

Pattern Net (feedforward neural network), Random forest, Rotation forest, Bayes Network, Model trees, Naive Bayes and C4.5 decision tree. The highest accuracy was achieved using the Pattern Net model with the vectors in the PCA space. Always during 2015, [14] developed an algorithm based on 817 leaf images of 14 tree species. This algorithm uses an artificial neural network (ANN) with backpropagation. An input vector of morphological features and Fourier descriptors (FDs), was fed into the ANN, resulting in a classification accuracy of 96% for their own dataset. To verify its effectiveness, they tested their algorithm on the Flavia and ICL datasets and achieved an accuracy of 36% for the both databases. For the fourth edition of the PlantCLEF challenge [15], the task of species identification has focused on observation and not on images, which means that the same person takes several photos of detailed views of different organs during the same day using the same camera under the same lighting conditions of the same plant. The constructed dataset for this challenge contains 113205 images of 1000 species. Experiments have showed that systems that combine different views of the same plant observation have proved a higher accuracy compared to those that use single images, up to 66.7%.

The authors of [16] have created two datasets with the same species: a clean one and a noisy one. They used the histogram of curvature on scale (HCoS) and local binary pattern variance (LBVP) algorithms to extract contour and texture features. Authors have claimed that the accuracy levels of the two datasets are very close, and they conclude that images taken directly without preprocessing can produce satisfactory results. [17] authors were the first team that uses images of old herbarium specimens of 26 tree species to classify them into categories. Using the support vector machine (SVM) after preprocessing, normalization and character extraction, they obtained an accuracy of 73.23% using a test set (I) that contains 24 species, and an accuracy of 84.88% using a test set (II) containing 17 species.

In [18], authors have used a set of leaf images of 24 different medicinal plant species collected from Mauritius. They extracted several features of each leaf such as: length, width, perimeter, color, number of vertices and shell area. A number of classifiers such as: KNN, naive bayes, SVM, neural networks and random forest were tested, of which the random forest classifier achieved the highest accuracy of 90.1%. [19] have focused on three Ficus species with similar leaf shapes. They used two classification models: an artificial neural network (ANN) and a support vector machine (SVM). Based on the morphological characteristics of the leaves, both models achieved the same accuracy of 83.3%.

The authors of [20] have lunched their experiments on 1125 leaf images of 15 Swedish species. Pre-processing was done using Gaussian filtering mechanism, then color and texture features were extracted and finally the classification was executed using a multi-class support vector machine. They obtained an accuracy of 93.26%. Finally, the team of [21] have used the ICL dataset to test a method that performs classification by automatically extracting shape features. The classification is then performed using a back propagation neural network. This experiment has achieved an accuracy of 96% for the test images and 99% for the training image.

Table I provides a comparison of all studies based on Machine Learning techniques. We will discuss the results of this comparison in Section III.

B. Deep Learning Techniques

We can say that the concept of Deep Learning is a discipline of Machine Learning which in turn is a discipline of Artificial Intelligence. The Deep Learning is the field concerned with the study of Artificial Neural Networks (i.e., ANN) that simulate neural networks in the human brain. As we know, the basic processing unit in the human brain is the neuron, and the artificial neuron in the DL techniques

TABLE I. SUMMARY OF STUDIES BASED ON MACHINE LEARNING TECHNIQUES

	Features	Dataset	Accuracy (%)
Goeau et al. (2011) [6]	Shape	5436 images (71 species)	52 53.3 68.5
Goeau et al. (2012) [7]	Shape	11572 images (126 species)	45 51 58
Herdiyeni and Wahyuni (2012) [8]	Texture, color	2448 images (51 species)	74,5
Goeau et al. (2013) [9]	Shape, color, texture	26077 images (250 species)	60.7 39.3
Du et al. (2013) [10]	Shape, curvature, veins	2422 images (30 species)	87,1
Chaki et al. (2015) [12]	Shape, texture	930 images (31 species)	97,6
Siravenha and Carvalho (2015) [13]	Shape	1865 images (32 species)	97,5
Aakif and Khan (2015) [14]	Shape	817 images (14 species)	96
Go"eau et al. (2015) [15]	Shape, texture, color	113205 images (1000 species)	66.7
C.-Rojas and M.-Montero (2016) [16]	Curvature, texture	2345 images (184 species)	87.2
Unger and Merhof (2016) [17]	Shape, veins	260 images (26 species)	73.23 84.88
Begue et al. (2017) [18]	Shape, color, shell area	720 images (24 species)	90.1
Kho et al. (2017) [19]	Shape	54 images (3 species)	83.3
Kaur and Kaur (2019) [20]	Texture, color	1125 images (15 species)	93.26
Amlekar and Gaikwad (2019) [21]	Shape	No details are available!	96

corresponds to it. An assembly of artificial neurons is known as an Artificial Neural Network. The discipline of Deep Learning emerged as an extension and development of Machine Learning when traditional ML algorithms were unable to perform some complex tasks (e.g., learning from large datasets such as different sound waves and high resolution images dimensions).

Generally, as shown in Fig. 4, DL techniques consist of a multi-layer structure where the layer on the left end is the input layer, the layer on the right is the output layer, and in the middle are several hidden layers responsible for processing. Each layer consists of some *neurons*, *weights* and *activation functions*. Indeed, unlike the traditional Machine Learning algorithms that require a lot of human intervention to adjust and improve, the deep learning algorithms requires a lower level of human intervention in optimizing the algorithm's results, because they learns and improve from their mistakes on their own thanks to their special architectures. However, these last make DL techniques require a lot of time and high computing power to learn from huge data set to build a viable model.

Speaking about automated plant identification using DL techniques (Fig. 4), we can say that during the *training* stage, unlike ML methods, the set of images of all species will be used as inputs in a recursive way to train the system. In fact, the weights will be adjusted until an optimal model is built for identification. Then, during identification stage, users can submit any test plant image to the trained model that will extracts features and perform the matching to give an identification result.

Depending on the network architecture, we can define several categories of DL methods, like: Multi-Layer Perceptron (i.e., MLP), Recurrent Neural Networks (i.e., RNN) and Convolutional Neural Networks (i.e., CNN). For example, MLP networks are *fully connected layers* where each neuron in a layer often communicates with all the neurons in the layers that precede it. For RNN networks, they are suitable for ap-

plications that must take into account the relationship between data and the temporal context, such as speech recognition for example. RNN networks solve this problem by remembering what has been learned from previous inputs, so that the past state can be learned and used with the current input. For CNN networks, they mostly deal with two-dimensional matrices, which are most time likely images. We can say that in the context of automated plant identification, CNN are is the most used category of DL techniques.

In the context of the fifth edition of the PlantCLEF challenge [22], it was the first time where participants introduced the use of the deep learning techniques, plant identification task was based on the use of a dataset that contains 113205 images representing plant organs and whole plants as well, covering 1000 woody and herbaceous species. 94 groups of participants have tried to use CNNs and only eight of them have submitted successfully their models. The highest classification accuracy was 72.4%. Always during 2016, in order to provide information on weeds for the good management of agricultural fields, [23] have trained and tested a convolutional neural network using a database that contains 10,413 images of 22 weed species. These images were taken from six datasets that present variations in terms of lighting, resolution and soil type. The developed CNN has provided an accuracy of 86.2%. In other work, [24] proposed to use the CNN for plant identification based on the morphological characters of the leaf veins of three legume species. After segmentation of the veins and extraction of the central spot to eliminate all possible influences of leaf shape, two scenarios (S1 and S2) were studied. In the first one only one image per sample was provided to train the CNN model, while in the second one three resized images (100%, 80% and 60%) were used as input to the CNN. They obtained almost similar average accuracy: 92.6% for S1 and 96.9% for S2.

The PlantCLEF challenge of 2017 [25], was organized on a dataset that contains 10000 plant species and 1.1 million

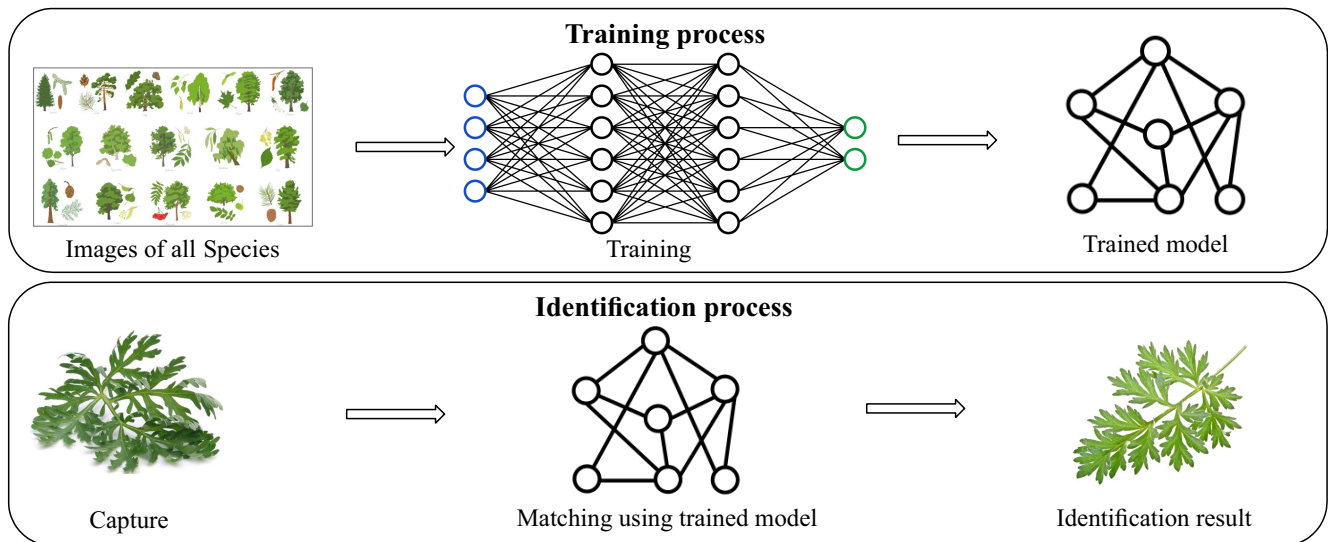


Fig. 4. The Main Steps of Deep Learning Techniques.

image in total. This was the first evaluation at this scale in the world where the test data to be analyzed was a large sample of raw query images. This dataset is divided into two sub-datasets: 1) the first one is huge and built using noisy web crawlers collected via the web; 2) the second one is smaller than the first sub-dataset and built using reliable training package verified by experts. The results obtained are almost similar, with systems using the reliable training set achieving almost 84% and systems processing a noisy training set exceeding 80%. While the systems that use both datasets achieved astonishing results of up to 92%. During the same year, [26] developed a plant identification system based on a Convolutional Neural Network called *LeafNet*. To evaluate it, they used three datasets: LeafSnap [27], Flavia [28] and Foliage [29]. On the LeafSnap dataset they obtained an accuracy of 86.3% for the top-1 and 97.8% for the top-5. Using the Flavia dataset, they obtained an accuracy of 97.9% for the top-1 and 99.99% for the top-5. Finally, for the Foliage dataset they obtained an accuracy of 95.8% for the top-1 and 99.6% for the top-5. Based on leaf features, [30] have used a Convolutional Neural Network to identify the most relevant features for a correct classification. They used two datasets: D1 and D2 with the same species, except that in the first one the images represent leaf shape as a classification feature, while in the second one venation and divergence between different venation orders are considered as selected features. They have obtained an accuracy of 98.1% for D1 and 99.5% for D2. In other work, [31] have proposed a 26-layer ResNet model for plant identification in a natural scene. They have used the BJFU100 dataset where images are taken using mobile phone cameras. It contains 10000 images of 100 plant species. The proposed model has achieved an accuracy of 91.78%. Always during 2017, [32] were the first team that has tested the classification of plant species using a large number of herbarium leaves and a Convolutional Neural Network. They have used five datasets: two of them (i.e., Herbarium255 and Herbarium1K) contain images of herbarium sheet images of leaves token from iDigBio; two others (i.e., CRLeaves and PlantCLEF 2015) contain images of leaves taken by a digital

camera; and the last one is the ImageNet database [33] which is used to train the CNN model. They have conducted a series of experiments to evaluate the effectiveness of herbarium leaves alone for plant species identification and to see if the combination with plant photos in the wild field is relevant in terms of accuracy. The best results are obtained when combination is considered. For example, the top1 accuracy of the H1K herbarium sheets is 72.6% and the accuracy of the H1K sheets combined with ImageNet is 79.6%.

Same team [34] has tested several Deep Learning models to identify plant species using herbarium leaves. The identification task in this work take place not only at the species level, but also at other taxonomic levels such as genus and family. They used the Herbaria1K dataset and ImageNet (for pre-training of the Deep Learning model). The tested architectures are the Flat Classification Model (FCM), the Multi-Task Classification Model (MCM) and the Hierarchical Classification Model (TaxonNet). They obtained in general almost similar results using the different architectures. For FCM, they obtained 63.02% for the species; 70.51% for the genus and 75.55% for the family. For MCM the results are 64.32%, 75.95% and 88.17% for species, genus and family respectively. TaxonNet showed an accuracy of 62.39% for species, 76.23% for genus and 86.92% for family. The family classification was still the best of the three which is evident since the number of classes will be less in this scenario of test. In the same year, [35] have used a deep Convolutional Neural Network consisting of 19 layers in combination with linear SVM for plant classification using the database of the PlantCLEF 2015 edition that contains images of different plant organs. They obtained better results, up to 90.20%, compared with other models that use the same database.

In addition to plant identification using images, Convolutional Neural Network models have also been developed to identify and diagnose plant pathologies. In this context, [36] has developed a CNN model to detect plant diseases using images of diseased and healthy leaves. The author has used an open database of 87848 images of 25 species containing

in a set of 58 combination classes (Plants, Diseases). He obtained an accuracy of 99.53%. [37] have tested several pre-trained Convolutional Neural Network architectures using the PlantVillage dataset [38] for plant disease identification. The tested architectures are: AlexNet [39], DenseNet-169 [40], Inception v3 [41], ResNet-34 [42], SqueezeNet-1.1 [43] and VGG13 [44]. The results obtained are globally high with an accuracy of up to 99.76%.

In the same context, [45] have developed a plant pathology identification model based on a Deep Convolutional Neural Network composed of 9 layers. Authors have used an open database contains 39 combination classes (Healthy Plant / Diseased Plant). The proposed model was trained using 55636 images and tested using 1950 images. Data augmentation methods [46] such as image flipping, rotation to scale, etc., were used. An accuracy of 96.46% was obtained. The result obtained shows that the use of augmentation methods can improve the performance of CNN models. To identify large-scale plants in a natural environment, [47] have tested a five-layer deep Residual Neural Network using a database that contains 185 classes of leaf images taken from the Columbia University, the University of Maryland and the Smithsonian Institution. They achieved an accuracy of 93.09%. In the 2019 edition of the PlantCLEF challenge, [48] have extended the challenge to flora in data-poor countries such as the Amazon rainforest. The results obtained illustrate the difficulty of species identification using a single image. The top accuracy of human experts ranges from 15.4% to 67.5%. However, the best automated system achieves an accuracy of 32% which can be explained by the fact that there is generally much diversity in tropical regions and by other reasons that we will discuss in the Section III. Always during 2019, [49] have carried out a series of experiments that compare five Convolutional Neural Network models, one of which was developed individually and the remaining four are transfer learning models. Four publicly available plant datasets were used for experimentations: Flavia, Swedish Leaf [50], UCI Leaf [51] and PlantVillage. The obtained results show that the transfer learning approaches perform better than the developed model for all datasets. For example, using the UCI Leaf dataset, the end-to-end model accuracy is 76.15%, while it reached up to 90.56% in a transfer learning model.

To answer this question: “among the images of plant leaves and flowers, what kind of perspectives contain more characteristic information and allow a high accuracy of identification?”, the study of [52] was conducted. They developed an image capture system to create observations of flowering plants. Each observation contains images of whole plants, front and side views of flowers, top and back views of leaves. The collected data set includes 101 species that are morphologically similar. They have used a Convolutional Neural Network to perform experiments. They obtained top-1 accuracies ranging from 77% (whole plant) to 97% (when merging all features). Flowers achieved the highest accuracy of 88%. The fusion between flowers and leaves gives an accuracy of 96%. In other work during 2019, [53] have studied automated plant classification at the genus and family level. They have tested a CNN model using a dataset that contains 1000 images of representative species of the Western European flora belonging to 516 genera and 124 families. The classification accuracy of the trained species increased from 82.2% at the species level

to 85.9% and 88.4% at the genus and family level. While the accuracy decreases considerably to 38.3% and 38.7% at genus and family level for untrained species.

We can say that the 2020 edition of PlantCLEF challenge [54] is entirely different from all previous editions. It is based on a large collection of over 60000 herbarium sheets of 1000 species from the Guiana Shield region of South America. A valuable asset of this collection is that many herbarium sheets are accompanied by a few photos of the same specimen in the field. For the test set, they used field images from different sources, including Pl@ntNet and Encyclopedia of Life. The metrics used for the evaluation of the task are classification accuracy and Mean Reciprocal Ranking (MRR) which is calculated according to the following equation:

$$MRR = \frac{1}{|Q|} \sum_{i=1}^{|Q|} \frac{1}{Rank_i} \quad (1)$$

where $|Q|$ is the total number of specie occurrences in the test set.

Authors of [54] claimed that the highest accuracy is MRR= 0.18 for ITCR PlantNet Run 10, followed by MRR= 0.17 for ITCR PlantNet Run 9. Always during 2020, [55] have organized a sub-competition hosted on the Kaggle platform to encourage the development of an automated species identification algorithm using herbarium leaves. 22 teams have participated with 254 models for species identification of Melastomataceae. They have used a large collection of photographed herbarium specimens for experiments (46469 specimens representing 683 species). Four models out of 254 obtained the highest accuracies exceeding 88% of correct identification.

For the 2021 edition of PlantCLEF challenge [56], we can say that the training dataset is based on the same visual data used during the previous challenge of 2020. Indeed, the 2021 task was particularly challenging, focusing on species rarely photographed in the field in the northern tropical Amazon. PlantCLEF 2021 introduces also new data related to five “traits” covering exhaustively all the 1000 species of the challenge. Traits are very valuable information that can potentially help to improve prediction models. Indeed, it can be assumed that species which share the same traits also share to some extent common visual appearances. The five most exhaustive traits (“plant growth form”, “habitat”, “plant life form”, “trophic guild” and “woodiness”) were verified and completed by experts of the Guyanese flora, so that each of the 1000 species have a value for each trait. The main evaluation measure for the challenge was the MRR.

Finally, to build an reliable system, the authors of [57] have proposed an efficient method of behavioral similarity developed through three models based on deep learning. To train their models, they have used the MalayaKew dataset that includes 44 classes of plant species and the FLavia dataset that contains 32 plant species. The results obtained for all the proposed models using the two datasets are respectively 99.67% and 99.81%.

Table II provides a comparison of all studies based on Deep Learning techniques. We will discuss the results of this comparison in Section III.

TABLE II. SUMMARY OF STUDIES BASED ON DEEP LEARNING TECHNIQUES

	Dataset	Accuracy (%)
Dyrmann et al. (2016) [23]	10413 images (22 species)	86.2
Goeau et al. (2016) [22]	113205 images (1000 species)	72.4
Grinblat et al. (2016) [24]	15 images (3 species)	92.6 96.9
Barré et al. (2017) [26]	LeafSnap (7719 images of 185 species)	86.3
	Flavia (60 images of 32 species)	97.9
	Foliage (120 images of 60 species)	95.8
Goeau et al. (2017) [25]	1.1 million images of 10000 species	92
Lee et al. (2017) [30]	MalayaKew (2816 images of 44 classes)	98.1
		99.5
Sun et al. (2017) [31]	10000 (100 species)	91.78
C.-Rojas et al. (2017) [32]	Herbier255 (11071 images of 255 species)	79.6
	Herbier1K (253733 images of 1204 species)	
C.-Rojas et al. (2018) [34]	Herbier1K, ImageNet (1 Million arbitrary hand-annotated images)	63.2
		64.32
		62.39
		70.51
		75.95
		76.23
		75.55
88.17		
86.92		
Zhu et al. (2018) [35]	113205 (1000 species)	90.2
Ferentinos (2018) [36]	87848 (25 species)	99.53
Brahimi et al. (2018) [37]	PlantVillage (54323 images of 14 species)	99.76
G. and J. (2019) [45]	55636 images of 13 species	96.46
Bodhwani et al. (2019) [47]	27000 images of 185 leaf classes	93.09
Goeau et al. (2019) [48]	434251 images of 10000 species	32
Kaya et al. (2019) [49]	Flavia, PlantVillage	90.56
	UCI Leaf (443 images of 40 species)	
	Swedish Leaf (1125 images of 15 species)	
Rzanny et al. (2019) [52]	9090 images of 100 observations (no data about species)	97.1
Seeland et al. (2019) [53]	500000 images of 1000 species	82.2 for specie
		85.9 for genus
		88.4 for family
Joly et al. (2020) [54]	60000 images (1000 herbarium species)	MRR = 0.18
Ambrose et al. (2020) [55]	46469 images of 683 species	≥ 88
Goeau et al. (2021) [56]	60000 images of 1000 species	MRR = 0.18
		MRR = 0.158
KBeikmohammadi et al. (2022) [57]	MalayaKew (2816 images of 44 classes)	99.67
	Flavia (60 images of 32 species)	99.81

III. DISCUSSION AND FUTURE DIRECTION

It should be noted that while several results are discussed separately here, they are interrelated in many ways. Therefore, this discussion tends to overlap in some parts.

Before discussing any of the results of Section II, we can immediately draw these six observations: 1) Most of results do not give a clear and sure view on the indicators that can improve the accuracy of plant identification. 2) There is no better approach for automated plant identification (with a priority of DL techniques compared to ML approaches); and the current available identification systems are not yet mature enough for a large-scale deployment. 3) There are no common protocols of test, no common performance indicators or metrics and no common databases used and shared between all proposed approaches, which make any comparison of results not fair or even wrong. 4) No information are given about the taxonomy of each family / genus / specie which is very important to specify the degree of resemblance between

classes (i.e., intra- and inter- subject variations) that gives as well an idea of the complexity of any identification task. 5) Recent automated plant identification systems might be in the way to surpass the ability of the human expert botanists. 6) Most of proposed systems are developed by computer science experts and only very few of botanists.

For our first observation, we believe that the clearest results that we can get are:

- **Image type and identification accuracy:** We can say that the systems analyzed during the first edition of PlantCLET challenge [6] have provided good classification scores, especially using scans and pseudo-scans categories, while using digital photos performance has been degraded. Thus, the evidence conclusion here is that the images type influences the identification accuracy. The same observation can be drawn from the results of the 2012 edition [7], even that the difficulty of the challenge has increased and that the

technological progress made by the participants has not compensated for the increased difficulty.

- **Feature extraction and identification accuracy:** We can say that for Machine Learning techniques, the improvement and the fusion of several methods of feature extraction / selection can improve identification accuracy. For example, the improvement of classification accuracy in [8] was due to the effective fusion between the FLBP and the FCH methods. The same result can be confirmed in [9] where most of approaches focused on the extraction of shape, texture and color. In the same context, [18] added more characters to be extracted such as length, width, perimeter, number of vertices, and hull area to get better results.
- **Image view and identification accuracy:** Always for Machine Learning techniques, we believe that observing different plant organs, using different views of the same plant specie, which is a current practice of botanists, can improve the identification accuracy. This is slightly confirmed in [15] where systems that combine different views of the same plant observation showed higher accuracy compared to systems that use single images.
- **Image pre-processing and identification accuracy:** We believe that adding a pre-processing of images before feature extraction can improve performance. This can be confirmed in the experiments of [16] and [17] who obtained good scores even if the used herbarium images were old, thanks to the added pre-processing step.
- **CNNs and identification accuracy:** Without any doubt, performance of automated plant identification systems has started to increase concretely since the 2016 PlantCLEF challenge [22]. Knowing that the database used during this edition is the same one used in the previous edition, the proposed systems gave higher scores in 2016. These systems were based on Convolutional Neural Networks. This definitely confirms the supremacy of Deep Learning approaches over the Machine Learning methods previously adopted for plant identification. In addition, all CNNs systems can use a huge database with a very high number of images. These last can be noisy, collected via the web, taken by digital cameras or cell phones and do not undergo any pre-processing step.
- **Taxonomic levels and identification accuracy:** The idea of moving to the classification at higher taxonomic levels has also given good performance whether in the experiment of [34] or that of [53]. The main idea to note here is that the higher the taxonomic level, the more relevant the classification accuracy becomes.
- **Species diversity and identification accuracy:** The remarkable decrease in the results of the 2019 challenge [48] dedicated to regions lacking data. This can be explained by the fact that there is generally much more diversity in tropical regions compared to temperate regions, already studied in the previous challenges, for the same reference areas. In addition, tropical plants in high forests are much less accessible to

humans who have much more difficulty in improving their knowledge of these ecosystems. The decline in results is continuing despite attempts to improve data in 2020 [54] and 2021 [56] challenges, the tasks were particularly difficult, focusing on rarely photographed species in the field from data deficient regions (while CNNs require huge number of images per class for the training step).

For our second observation, as we have said before, performance of automated plant identification systems has started to be increased with the first uses of Deep Learning techniques in the 2016 PlantCLEF challenge [22], which means already that DL techniques have proven a superiority compared to ML techniques. However, we believe that all current available identification systems are not yet mature enough for a large-scale deployment.

For the third observation, we believe that, before giving any judgment about the best approach or the good practices to follow to improve accuracy of automated plant systems, the community of research of this field must establish a common evaluation protocol to make researchers able to compare their results. In this context, we think that even the basic metrics of evaluation, like the ROC curve and the Error Equal Rate (ERR), are not used by all proposed technique of literature. In addition, we believe as well that a common database must be built to make the use of the common evaluation protocol fair and correct as well. The best example in this context to be followed is the Fingerprint Verification Competition (FVC) [58]. This is an international competition that has been organized by academic laboratories to evaluate fingerprint verification algorithms developed by both academics and industry. Several databases (i.e., FVC2000, FVC2002, FVC2004 and FVC2006), which are acquired with various types of sensors while increasing difficulty, were provided to the participants to allow them to test and compare their techniques according to a predefined test protocol². The proposed protocol / databases are used until now by all researchers in fingerprinting field. We believe that the same strategy must be adopted for automated plant identification.

For our fourth observation, we can say that the majority of works in literature do not give any information about the taxonomy of each family / genus / specie in the used dataset, such information is very important for any identification system to define the degree of resemblance between classes and therefore define the difficulty of the database. All that confirm again the need to build common databases of test while taking in consideration the complexity of identification that is related to the chosen plant for every database.

For the fifth observation, we think that the current automated plant identification systems might be in the way to surpass the ability of the human expert botanists. This can be confirmed especially in the results of the 2019 PlantCLEF challenge [48] and in Fig. 5 taken from the same challenge. We can notice also that the results of automated systems improves well in the Top 5 scenario compared to human experts, which means that if we are looking for a tools to minimize the list of candidate plants during a classic systematic identification (top

¹<https://www.imageclef.org/PlantCLEF2019>

²<https://biolab.csr.unibo.it/fvcongoing/UI/Form/Home.aspx>

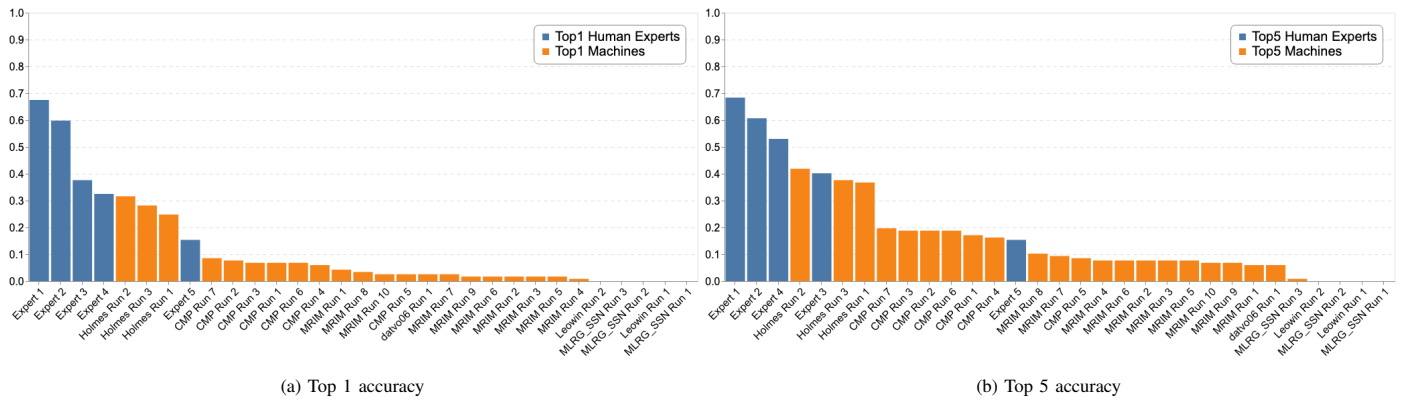


Fig. 5. Results of Automated Plant Identification Systems vs the Human Experts (Taken from [1]).

10 or top 20 list for example), absolutely automated systems can be this very useful / fast tool.

For our last observation, we have noticed that the majority of proposed systems are developed by computer science experts and only very few of botanists which is absolutely not a good practice to build successfully a robust automated system. This prove why all works of literature have a huge lake of taxonomic information about tested plant species. We believe that All teams of work on this challenge must contain computer scientist and botanist to optimize the design and results of automated plant identification systems.

IV. CONCLUSION AND PERSPECTIVE

In this paper, we present a review of automated plant species identification issue over all significant available studies in literature. The main result of this synthesis is that the performance of advanced deep learning models is becoming close to the most advanced human expertise. However, we have to mention that several fundamental challenges are remaining to be solved to achieve the design of an efficient system. This is exactly the objective of our future works. First, we have a plan to propose an efficient evolution protocol to be used with any plant identification system. Second, we will publish several databases (with different level of difficulty) for tests while giving all needed taxonomic information, including a national database of Moroccan toxic plants species. Third, we will test our first identification system (as a personalized architecture of Convolutional Neural Network) using the Moroccan toxic plants database since the complexity of this last will be low because the degree of similarity is weak due to the high diversity of families / genus of Moroccan toxic plants. Finally, we will perform and optimize our system using harder databases with high degree of similarity.

REFERENCES

- [1] P. Bonnet, A. Joly, H. Goëau, J. Champ, C. Vignau, J.-F. Molino, D. Barthélémy, and N. Boujemaa, "Plant identification: man vs. machine," *Multimedia Tools and Applications*, vol. 75, no. 3, pp. 1647–1665, jun 2015.
- [2] J. Wäldchen, M. Rzanny, M. Seeland, and P. Mäder, "Automated plant species identification—trends and future directions," *PLOS Computational Biology*, vol. 14, no. 4, p. e1005993, apr 2018.
- [3] K. Gaston and M. O'Neill, "Automated species identification: Why not?" *Philosophical transactions of the Royal Society of London. Series B, Biological sciences*, vol. 359, pp. 655–67, 2004.
- [4] A. Mackiewicz and W. Ratajczak, "Principal components analysis (pca)," *Computers & Geosciences*, vol. 19, pp. 303–342, 1993.
- [5] C. Burges, "A tutorial on support vector machines for pattern recognition," *Data Mining and Knowledge Discovery*, vol. 2, pp. 121–167, 2004.
- [6] H. Goëau, P. Bonnet, A. Joly, N. Boujemaa, D. Barthélémy, J.-F. Molino, P. Birnbaum, E. Mouysset, and M. Picard, "The clef 2011 plant images classification task," vol. 1177, 01 2011.
- [7] H. Goëau, A. Joly, P. Bonnet, V. Bakic, D. Barthélémy, N. Boujemaa, and J.-F. Molino, "The imageclef 2012 plant identification task," vol. 1178, 10 2012, pp. 23–28.
- [8] Y. Herdiyeni and N. K. S. Wahyuni, "Mobile application for indonesian medicinal plants identification using fuzzy local binary pattern and fuzzy color histogram," in *2012 International Conference on Advanced Computer Science and Information Systems (ICACSIS)*, 2012, pp. 301–306.
- [9] H. Goëau, A. Joly, P. Bonnet, V. Bakic, D. Barthélémy, N. Boujemaa, and J.-F. Molino, "The imageclef plant identification task 2013," in *Proceedings of the 2nd ACM International Workshop on Multimedia Analysis for Ecological Data*. New York, NY, USA: Association for Computing Machinery, 2013, p. 23–28.
- [10] J.-X. Du, C.-M. Zhai, and Q.-P. Wang, "Recognition of plant leaf image based on fractal dimension features," *Neurocomputing*, vol. 116, pp. 150–156, 2013, advanced Theory and Methodology in Intelligent Computing.
- [11] G. Biau and L. Devroye, "The nearest neighbor distance," in *Lectures on the Nearest Neighbor Method*. Springer International Publishing, 2015, pp. 13–23.
- [12] J. Chaki, R. Parekh, and S. Bhattacharya, "Plant leaf recognition using texture and shape features with neural classifiers," *Pattern Recognition Letters*, vol. 58, no. C, p. 61–68, 2015.
- [13] A. C. Q. Siravenha and S. R. Carvalho, "Exploring the use of leaf shape frequencies for plant classification," in *2015 28th SIBGRAPI Conference on Graphics, Patterns and Images*, 2015, pp. 297–304.
- [14] A. Aakif and M. F. Khan, "Automatic classification of plants based on their leaves," *Biosystems Engineering*, vol. 139, pp. 66–75, 2015.
- [15] H. Goëau, P. Bonnet, and A. Joly, "LifeCLEF Plant Identification Task 2015," in *CLEF: Conference and Labs of the Evaluation Forum*, ser. Working Notes of CLEF 2015 - Conference and Labs of the Evaluation forum, vol. CEUR Workshop Proceedings, no. 1391, Toulouse, France, Sep. 2015.
- [16] J. Carranza-Rojas and E. Mata-Montero, "Combining leaf shape and texture for costa rican plant species identification," *CLEI electronic journal*, vol. 19, pp. 7:1–7:29, 04 2016.
- [17] J. Unger and D. Merhof, "Computer vision applied to herbarium specimens of german trees: Testing the future utility of the millions of herbarium specimen images for automated identification," *BMC Evolutionary Biology*, vol. 16, 12 2016.

- [18] A. Begue, V. Kowlessur, U. Singh, F. Mahomoodally, and S. Pudaruth, "Automatic recognition of medicinal plants using machine learning techniques," *International Journal of Advanced Computer Science and Applications*, vol. 8, no. 4, 2017.
- [19] S. J. Kho, S. Manickam, S. Malek, M. Mosleh, and S. K. Dhillon, "Automated plant identification using artificial neural network and support vector machine," *Frontiers in Life Science*, vol. 10, no. 1, pp. 98–107, 2017.
- [20] S. Kaur and P. Kaur, "Plant species identification based on plant leaf using computer vision and machine learning techniques," *Journal of Multimedia Information System*, vol. 6, pp. 49–60, 06 2019.
- [21] M. M. Amlekar and A. T. Gaikwad, "Plant classification using image processing and neural network," in *Data Management, Analytics and Innovation*, V. E. Balas, N. Sharma, and A. Chakrabarti, Eds. Singapore: Springer Singapore, 2019, pp. 375–384.
- [22] H. Goëau, P. Bonnet, and A. Joly, "Plant Identification in an Open-world (LifeCLEF 2016)," in *CLEF: Conference and Labs of the Evaluation Forum*, vol. CEUR Workshop Proceedings, no. 1609, Évora, Portugal, Sep. 2016, pp. 428–439.
- [23] M. Dyrmann, H. Karstoft, and H. S. Midtby, "Plant species classification using deep convolutional neural network," *Biosystems Engineering*, vol. 151, pp. 72–80, 2016. [Online]. Available: <https://www.sciencedirect.com/science/article/pii/S1537511016301465>
- [24] G. L. Grinblat, L. C. Uzal, M. G. Larese, and P. M. Granitto, "Deep learning for plant identification using vein morphological patterns," *Computers and Electronics in Agriculture*, vol. 127, pp. 418–424, 2016.
- [25] H. Goëau, P. Bonnet, and A. Joly, "Plant identification based on noisy web data: the amazing performance of deep learning (LifeCLEF 2017)," in *CLEF: Conference and Labs of the Evaluation Forum*, vol. CEUR Workshop Proceedings, no. 1866, Dublin, Ireland, Sep. 2017.
- [26] P. Barré, B. C. Stöver, K. F. Müller, and V. Steinhage, "Leafnet: A computer vision system for automatic plant species identification," *Ecological Informatics*, vol. 40, pp. 50–56, 2017.
- [27] N. Kumar, P. N. Belhumeur, A. Biswas, D. W. Jacobs, W. J. Kress, I. Lopez, and J. V. B. Soares, "Leafsnap: A computer vision system for automatic plant species identification," in *The 12th European Conference on Computer Vision (ECCV)*, October 2012.
- [28] S. G. Wu, F. S. Bao, E. Y. Xu, Y.-X. Wang, Y.-F. Chang, and Q.-L. Xiang, "A leaf recognition algorithm for plant classification using probabilistic neural network," in *2007 IEEE International Symposium on Signal Processing and Information Technology*. IEEE, dec 2007.
- [29] P. Beardsley and G. Chaurasia, "Editable parametric dense foliage from 3d capture," in *2017 IEEE International Conference on Computer Vision (ICCV)*. IEEE, oct 2017.
- [30] S. H. Lee, C. S. Chan, S. J. Mayo, and P. Remagnino, "How deep learning extracts and learns leaf features for plant classification," *Pattern Recognition*, vol. 71, pp. 1–13, 2017.
- [31] Y. Sun, Y. Liu, G. Wang, and H. Zhang, "Deep learning for plant identification in natural environment," *Computational Intelligence and Neuroscience*, vol. 2017, pp. 1–6, 05 2017.
- [32] J. Carranza-Rojas, H. Goëau, P. Bonnet, E. Mata-Montero, and A. Joly, "Going deeper in the automated identification of herbarium specimens," *BMC Evolutionary Biology*, vol. 17, 2017.
- [33] J. Deng, W. Dong, R. Socher, L.-J. Li, K. Li, and L. Fei-Fei, "ImageNet: A large-scale hierarchical image database," in *2009 IEEE Conference on Computer Vision and Pattern Recognition*. IEEE, jun 2009.
- [34] J. Carranza-Rojas, A. Joly, H. Goëau, E. Mata-Montero, and P. Bonnet, "Automated identification of herbarium specimens at different taxonomic levels," in *Multimedia Tools and Applications for Environmental & Biodiversity Informatics*. Springer International Publishing, 2018, pp. 151–167.
- [35] H. Zhu, Q. Liu, Y. Qi, X. Huang, F. Jiang, and S. Zhang, "Plant identification based on very deep convolutional neural networks," *Multimedia Tools and Applications*, vol. 77, 2018.
- [36] K. P. Ferentinos, "Deep learning models for plant disease detection and diagnosis," *Computers and Electronics in Agriculture*, vol. 145, pp. 311–318, 2018.
- [37] M. Brahimi, M. Arsenovic, S. Laraba, S. Sladojevic, K. Boukhalfa, and A. Moussaoui, *Deep Learning for Plant Diseases: Detection and Saliency Map Visualisation*. Cham: Springer International Publishing, 2018, pp. 93–117.
- [38] D. P. Hughes and M. Salath'e, "An open access repository of images on plant health to enable the development of mobile disease diagnostics through machine learning and crowdsourcing," *CoRR*, vol. abs/1511.08060, 2015. [Online]. Available: <http://arxiv.org/abs/1511.08060>
- [39] A. Krizhevsky, I. Sutskever, and G. E. Hinton, "ImageNet classification with deep convolutional neural networks," *Communications of the ACM*, vol. 60, no. 6, pp. 84–90, may 2017.
- [40] G. Huang, Z. Liu, L. van der Maaten, and K. Q. Weinberger, "Densely connected convolutional networks," 2016. [Online]. Available: <https://arxiv.org/abs/1608.06993>
- [41] C. Szegedy, W. Liu, Y. Jia, P. Sermanet, S. Reed, D. Anguelov, D. Erhan, V. Vanhoucke, and A. Rabinovich, "Going deeper with convolutions," in *2015 IEEE Conference on Computer Vision and Pattern Recognition (CVPR)*, 2015, pp. 1–9.
- [42] K. He, X. Zhang, S. Ren, and J. Sun, "Deep residual learning for image recognition," in *2016 IEEE Conference on Computer Vision and Pattern Recognition (CVPR)*, 2016, pp. 770–778.
- [43] F. N. Iandola, S. Han, M. W. Moskewicz, K. Ashraf, W. J. Dally, and K. Keutzer, "Squeezenet: Alexnet-level accuracy with 50x fewer parameters and 0.5mb model size," 2016. [Online]. Available: <https://arxiv.org/abs/1602.07360>
- [44] K. Simonyan and A. Zisserman, "Very deep convolutional networks for large-scale image recognition," 2014. [Online]. Available: <https://arxiv.org/abs/1409.1556>
- [45] G. Geetharamani and J. Arun Pandian, "Identification of plant leaf diseases using a nine-layer deep convolutional neural network," *Computers and Electrical Engineering*, vol. 76, pp. 323–338, 2019.
- [46] C. Shorten and T. M. Khoshgoftaar, "A survey on image data augmentation for deep learning," *Journal of Big Data*, vol. 6, no. 1, jul 2019.
- [47] V. Bodhwani, D. Acharyya, and U. Bodhwani, "Deep residual networks for plant identification," *Procedia Computer Science*, vol. 152, pp. 186–194, 2019.
- [48] H. Goëau, P. Bonnet, and A. Joly, "Overview of LifeCLEF Plant Identification Task 2019: diving into Data Deficient Tropical Countries," in *CLEF 2019 Working Notes - Conference and Labs of the Evaluation Forum*, ser. CEUR Workshop Proceedings, vol. 2380. Lugano, Switzerland: Linda Cappellato and Nicola Ferro and David E. Losada and Henning Müller, Sep. 2019.
- [49] A. Kaya, A. S. Keceli, C. Catal, H. Y. Yalic, H. Temucin, and B. Tekinerdogan, "Analysis of transfer learning for deep neural network based plant classification models," *Computers and Electronics in Agriculture*, vol. 158, pp. 20–29, 2019.
- [50] O. Söderkvist, "Computer vision classification of leaves from swedish trees," 2001.
- [51] P. F. B. Silva, A. R. S. Marçal, and R. M. A. da Silva, "Evaluation of features for leaf discrimination," in *Lecture Notes in Computer Science*. Springer Berlin Heidelberg, 2013, pp. 197–204.
- [52] M. Rzanny, P. Mäder, A. Deggelmann, C. Minqian, and J. Wäldchen, "Flowers, leaves or both? how to obtain suitable images for automated plant identification," *Plant Methods*, pp. 15–77, 2019.
- [53] M. Seeland, M. Rzanny, D. Boho, J. Wäldchen, and P. Mäder, "Image-based classification of plant genus and family for trained and untrained plant species," *BMC Bioinformatics*, vol. 20, no. 1, jan 2019.
- [54] A. Joly, H. Goëau, S. Kahl, B. Deneu, M. Servajean, E. Cole, L. Picek, R. R. de Castañeda, I. Bolon, A. Durso, T. Lorieul, C. Botella, H. Glotin, J. Champ, I. Eggel, W.-P. Vellinga, P. Bonnet, and H. Müller, "Overview of LifeCLEF 2020: A system-oriented evaluation of automated species identification and species distribution prediction," in *Lecture Notes in Computer Science*. Springer International Publishing, 2020, pp. 342–363.
- [55] D. P. Little, M. Tulig, K. C. Tan, Y. Liu, S. Belongie, C. Kaeser-Chen, F. A. Michelangeli, K. Panesar, R. Guha, and B. A. Ambrose, "An algorithm competition for automatic species identification from herbarium specimens," *Applications in Plant Sciences*, vol. 8, no. 6, jun 2020.
- [56] H. Goëau, P. Bonnet, and A. Joly, "Overview of plantclef 2021: cross-domain plant identification," in *Proceedings of the Working Notes of CLEF 2021 - Conference and Labs of the Evaluation Forum, Bucharest*,

- Romania, September 21st - to - 24th, 2021, ser. CEUR Workshop Proceedings, G. Faggioli, N. Ferro, A. Joly, M. Maistro, and F. Piroi, Eds., vol. 2936. CEUR-WS.org, 2021, pp. 1422–1436.
- [57] A. Beikmohammadi, K. Faez, and A. Motallebi, “Swp-leafnet: A novel multistage approach for plant leaf identification based on deep cnn,” *Expert Systems with Applications*, vol. 202, p. 117470, 2022.
- [58] R. Cappelli, D. Maio, D. Maltoni, J. Wayman, and A. Jain, “Performance evaluation of fingerprint verification systems,” *IEEE Transactions on Pattern Analysis and Machine Intelligence*, vol. 28, no. 1, pp. 3–18, jan 2006.

Arduino for Developing Problem-Solving and Computing Competencies in Children

Cristian Vidal-Silva^{1*}
Ingeniería en Desarrollo de Videojuegos
y Realidad Virtual
Facultad de Ingeniería, Universidad de Talca
Talca, Chile

Claudia Jiménez-Quintana²
Ingeniería Civil Informática
Escuela de Ingeniería y Negocios
Universidad Viña del Mar
Viña del Mar, Chile

Erika Madariaga-García³
Escuela de Ingeniería
Facultad de Ingeniería y Negocios
Universidad de Las Américas
Santiago, Chile

Abstract—Fostering children’s problem-solving and computational programming competencies is crucial at the current time. Like in other in-developing nations, children grew up with technology in Chile. Developing programming and problem-solving competencies in children seems a reachable task using high-level block-based programming languages. However, programming and electronics competencies often emerge at higher educational levels. This article presents that using Arduino can enhance the development of programming and problem-solving competencies in children and encourages them to think in new ways. This article uses TinkerCAD, an online emulator of Arduino, to teach fundamental electronic circuits and computer programming components. Using TinkerCAD effectively addresses various computing and electrical difficulties, such as turning on and off a group of lights and reading sensors to respond to the acquired values. This article seeks to develop problem-solving and computer programming competencies in primary school students, given the significance of both competencies, the open nature of Arduino, and the applicability of TinkerCAD, which permits using a block-based programming language. Children that took part in the trial saw an increase in their academic performance on average, which is a critical concomitant finding. The essential drawbacks of this project were the children’s lack of knowledge of electronics and programming principles and the need to use a computer with an internet connection.

Keywords—Arduino; competencies; programming; problem-solving; children

I. INTRODUCTION

The ability to use other skills to achieve objectives and solve complex and specified problems are traits of problem-solving competency [1]. It refers to the skills students need to acquire to discover efficient, sophisticated, and worthwhile solutions to issues in the interest of long-term learning. Informally, a computing method with clear boundaries, known as an algorithm, accepts an input value or set of values and produces an output value or set of values. An algorithm is a series of precise, constrained, and obvious procedures for attaining a particular goal or objective [2]. Because programs created in programming languages reflect algorithms, algorithms are the foundation of programming [3]. So, programming is the process of giving a computer a set of instructions it needs to follow to do a certain job. As Knuth [4] proposes, programming can be a fun endeavor like writing poetry or music. Similarly, Vidal

et al. [5] stress the need to acquire logical and computational abilities for problem analysis and solution delivery in both computer-based and real-world settings. Getting young people to think logically and algorithmically is one of the goals of the education systems in several European and South American countries [6].

High-level abstraction, main-focus skills, and algorithmic reasoning are necessary for developing programming skills in textual programming languages [6]. Contrarily, students who use textual programming languages usually spend more time understanding and adhering to syntactic conventions than comprehending, learning, mastering algorithmic abilities, and resolving issues. One strategy is to use the block-structured programming language Scratch [7], which is kid-friendly, to develop algorithmic skills. Come up with electrical computer solutions. Due to the programming requirements and the necessity to be wary about compromised physical components in the final execution of the electrical circuit, a reducible risk by employing simulators, it seems to be a challenging operation. As an open-source electronics platform built on simple hardware and software, Arduino intends to increase accessibility for interactive computing-electronic applications [8]. Aside from the warning about working with physical electronics, the essential parts of Arduino’s programming approach for kids are the syntax, and semantic instructions of the C/C++ programming language [9].

TinkerCAD circuits [10], [11] seem to be intended to address issues with Arduino-based computing-electronic systems in terms of design and programming: When combined with Arduino-compatible electrical components, TinkerCAD, a block-structured programming language, may be used to build computer solutions.

The simplicity with which computing-electronic devices can be built and programmed using TinkerCAD platforms seems to be a feasible goal. Similar to that, the primary objective of this article is to respond to the following research question: Can people use Arduino to educate youngsters to enhance their problem-solving and programming skills? This article provides proof by outlining the positive results of a TinkerCAD and Arduino workshop for children of a primary school in Valparaiso, Chile. This paper presents TinkerCAD and highlights the results obtained to persuade students and instructors to use TinkerCAD in developing algorithmic and problem-solving abilities.

* Corresponding author

In today's connected and computerized environment, programming and creating computing-electronic systems are challenging tasks [12], [13]. As Vidal et al. [10] highlight, developing children's programming and electronic abilities should be a stimulating challenge for their interest and motivation in computer and electronic systems. You may construct algorithmic and computing-electronic conditions, for example, to turn on a light using resistance or without it while properly understanding physical and scientific principles.

This article may be summed up as follows: In Section II, the TinkerCAD platform, Arduino, and an example of its block-structured programming language are introduced. The participants and setting of the workshop "Programming and Electronics for Everyone" conducted in Valparaiso, Chile, are explained in Section III. One of the experiments made by students is shown in Section IV. The academic performance enhancements of the workshop participants are highlighted in Section V. Section VI describes related work. Section VII presents conclusions of this work. Section VIII presents the main findings and suggests research directions.

II. TINKERCAD CIRCUITS AND ARDUINO

To create computing-electronic solutions using Arduino, TinkerCAD is a free, user-friendly web platform [14] for 3D design, electronics, and scripting [15], [10]. To enable students to combine computers and electronics in low-cost, open-hardware settings easily, Arduino was established in Italy in 2005 [16]. As Peace [17] argued, a vast selection of inexpensive hardware and software compatible with Arduino is available on the market. Liquid Crystal Displays (LCDs), sensors, and integrated web development platforms like TinkerCAD are available. TinkerCAD-based solutions are facilitated and supported by TinkerCAD. TinkerCAD considers a design area for the solution's hardware parts, a classification of the many more hardware parts, and a coding area for the software. Fig. 1a shows a straightforward example of how to turn on a led by connecting it to a 9-volt battery, which is analogous to the electrical "Hello World" program [6]. Fig. 1b, on the other hand, illustrates an unsuccessful operation for the same purpose without using a resistor.

Fig. 2a shows a hardware design created in TinkerCAD to turn on a red LED. It is similar to Fig. 1, except the Arduino is in charge of the positive and ground signals. This method may be modified to cyclically turn on the light for t_1 seconds and then turn it off for t_2 seconds by adding code. Creating Arduino solutions requires extensive programming abilities because of the new syntax and semantics of the related C/C++ programming language. Like Scratch, TinkerCAD supports programming solutions utilizing block-structured languages [18]. Fig. 2a and 2b presents the color-coded division of blocks: output (blue), input (purple), notation (gray), control (yellow), mathematics (green), and variables (rose). That figure additionally shows the block-structured code for turning on and off the LED for times t_1 and t_2 along with the variables declaration section.

Fig. 2b shows a semaphore simulator that is an extension of Fig. 2a. This figure also presents the associated block-structure code for the semaphore functioning. Fig. 2b does not use variables to define the light-time of each LED: the green

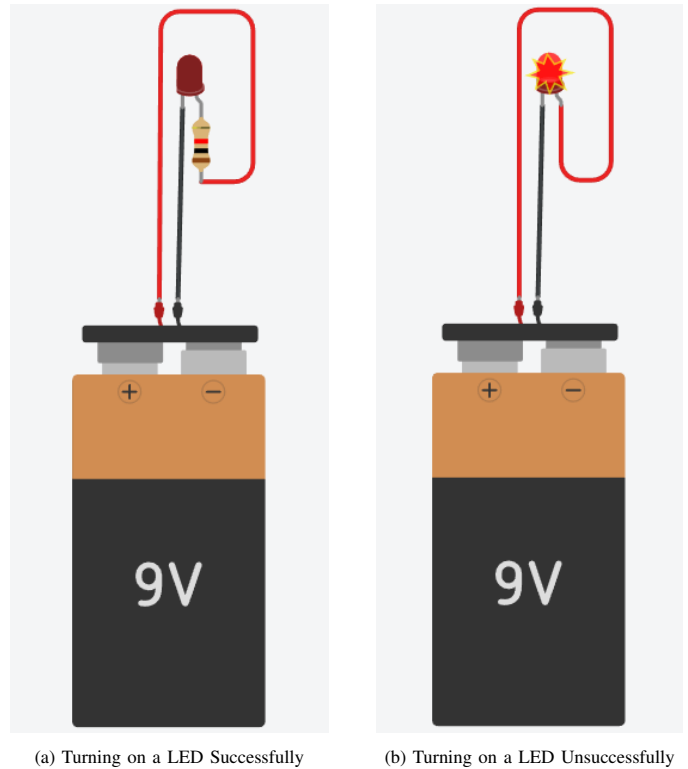


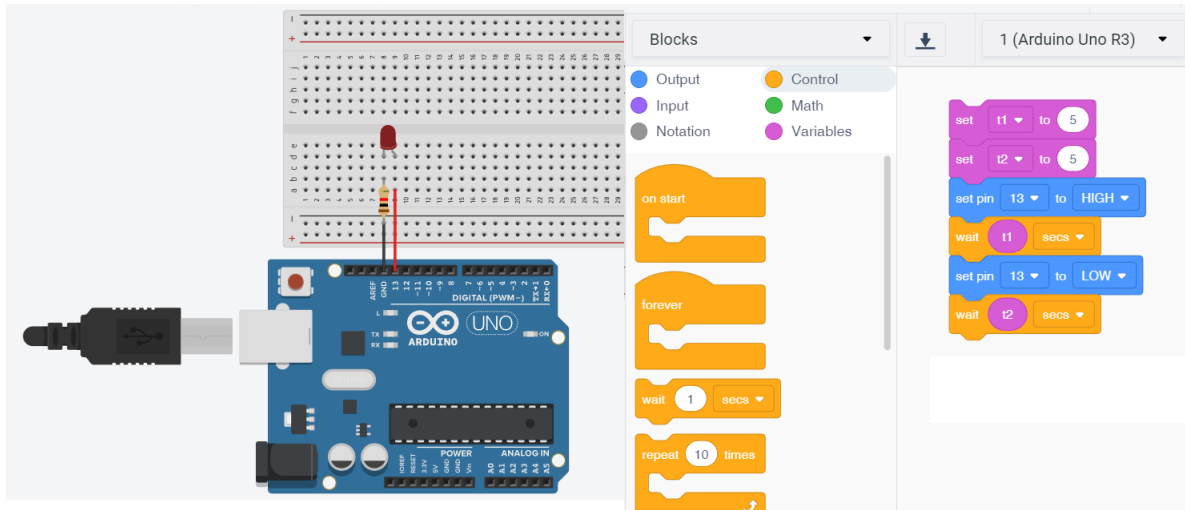
Fig. 1. Flipping a Led Both Successfully and Unsuccessfully with an Arduino.

LED will be turned on for 5 seconds (pin 2), the yellow LED for 3 seconds (pin 3), and the LED red for 5 seconds (pin 4), respectively.

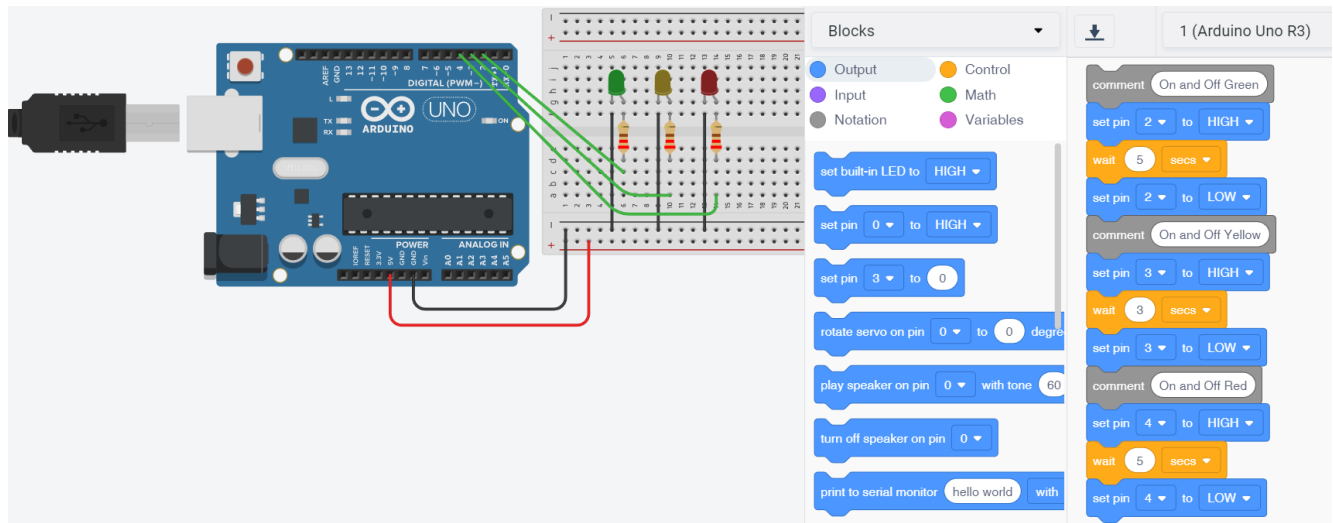
Another amazing feature of TinkerCAD is the ability to produce Arduino C/C++ code from a block-structured code solution. TinkerCAD is a great online tool for researching Arduino-based computing and electronics solutions.

III. WORKSHOP ON PROGRAMMING AND ELECTRONICS FOR EVERYONE

A project called "Future Education" links universities, basic colleges, and schools in Chile's Valparaiso region to provide seminars in various subject areas at participating higher education institutions [19]. "Future Education" develops activities that include students in experiments and debates with academics and researchers from various subjects using a rigorous and active approach. To help nine primary school students from four different schools and cities in the Valparaiso region develop their programming and computing-electronic skills, "Programming and Electronics for Everyone" was included in the 2020 edition of "Future Education". Specifically, there were two schools with three students (schools A and B), one school with two students (school C), and one school with one student (school D). The 5-session program, titled "Programming and Electronics for Everyone", had a start date of October and a finish date of mid-November 2020. The first two days of the training covered the fundamentals of Arduino and TinkerCAD programming environment. After that, students went over basic sensor tools and response ideas as the



(a) Turn On and Off a Red LED in TinkerCAD.



(b) Simulate a Semaphore in TinkerCAD.

Fig. 2. Turn On and Off a Red LED and Simulate a Semaphore in TinkerCAD.

course progressed with intermediate Arduino and Tinkercad (3 sessions). The course ended with a final presentation to share the results with the community. Students who took part in the session had no knowledge of programming and much fewer electronics and associated physical principles. Their prior academic record at those institutions was above average (6.0 on a scale of 1.0 to 7.0). Consequently, the workshop's objectives appear a touch too ambitious. Participants were nonetheless encouraged to participate physically and primarily for the live results while utilizing the Arduino simulation in TinkerCAD. The first two workshop sessions taught students about the Arduino inputs and outputs (structure). Authors experimented using a real battery and Arduino to turn on and off a light (Fig. 1 and 2a), and implementing a semaphore (Fig. 2b). The Arduino loop cycle, in which this code is continually executed, was grasped by the students. Students studied more about conditional structures, variables, and sensors in the next three sessions.

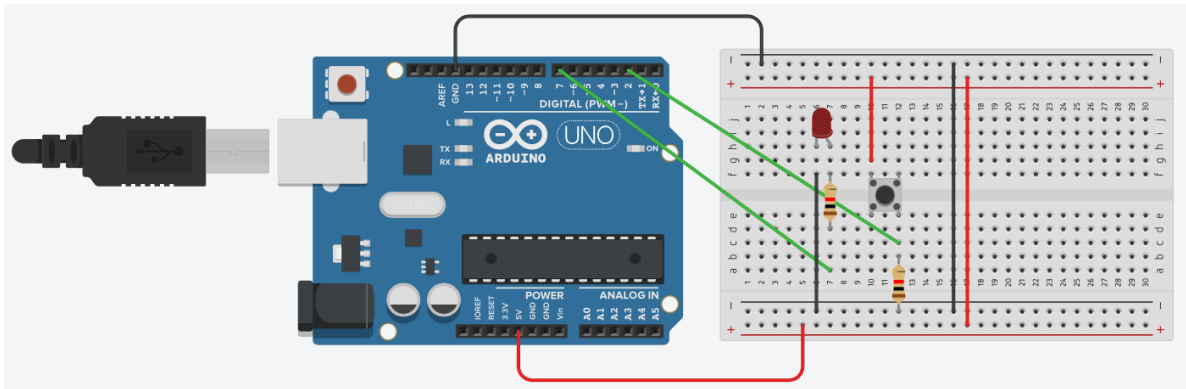
This project proved that by using Arduino, people could effectively educate and develop students' programming and problem-solving skills. This page displays the primary school test scores from various Chilean primary schools, a nation that is still growing. These findings may inspire other institutions and countries to do comparative research to enhance and develop these skills in elementary school children. The researchers of this project want to conduct a more extended experiment with younger primary school pupils to help them develop their programming and problem-solving skills.

IV. SUCCULENT STUDENT EXPERIMENTS

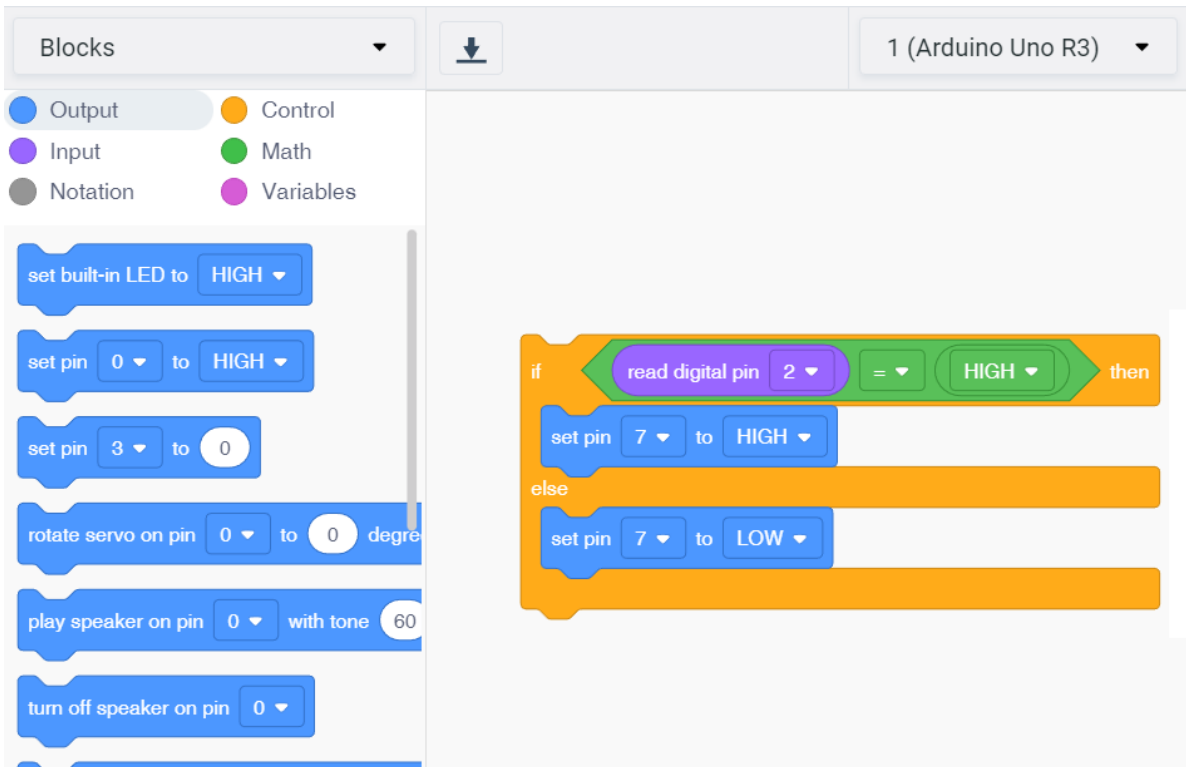
Students were considerably more enthusiastic about studying electronics using Arduino after learning about using TinkerCAD to build circuits and its block-structured programming environment. A TinkerCAD method to turn on a red led when pushing a button and turn it off in another situation is shown in Fig. 3.

The circuit is shown in part a of this solution, and part b shows the block-structured code. Students go through the key concepts of the Arduino loop cycle once again to determine whether or not the button is pushed to turn on and off the red LED accordingly. Students were, therefore, able to distinguish between input and output signals. In the fourth lesson, students received examples of how variables are used in human life (for example, to record a friend's phone number) and on the Arduino (e.g., to know what the previous button pressed was for a circuit with a set of buttons). Students also knew about a few distinctions between digital and analog signals using sensors. In this lesson, the authors created a TinkerCAD solution with the primary objective of turning on the red light when the temperature exceeds a particular value (Fig. 4

illustrates the circuit and the block-structured code). The block-structured code defines the maximum temperature using the MaxTemp variable (35 Celsius). In another instance, the red led is switched on and off when the read temperature, using a mathematical calculation, exceeds that maximum value. This TinkerCAD exercise was completed by seven students, while the remaining two were assisted. Thus, all pupils could understand how their first sensor system worked. As a motivation for using an ultrasonic sensor to calculate the distance of an object concerning the sensor position and turn on a led concerning the current distance of that object, the authors went over the main steps of the previous TinkerCAD temperature systems in the final session of the workshop. There are three variables for the detected value (distance), the lowest distance

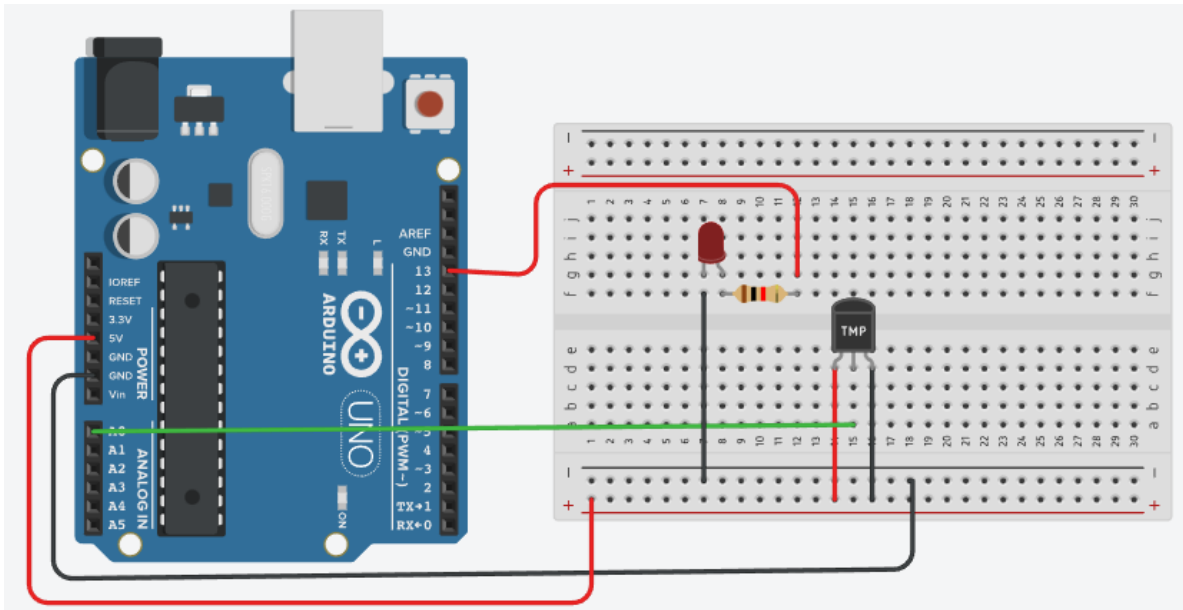


(a) TinkerCAD Circuit Solution for Turning on the Led when a Button is Pressed.

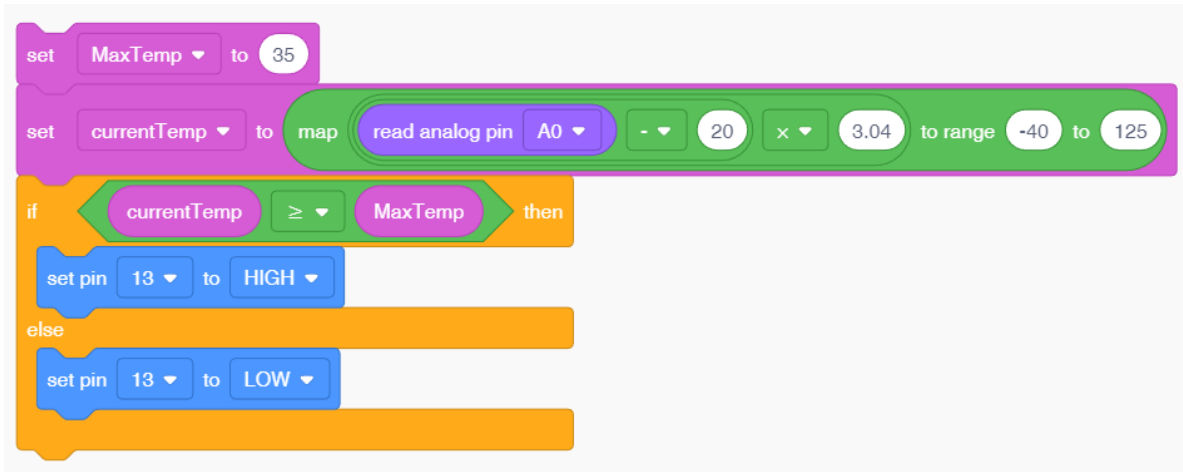


(b) TinkerCAD Code Solution for Turning on the Led when a Button is Pressed.

Fig. 3. TinkerCAD Solution for Turning on the Led when a Button is Pressed.



(a) TinkerCAD Circuit for Reading a Temperature Sensor and Activating a Light.



(b) TinkerCAD Block-Structured Code for Reading a Temperature Sensor and Activating a Light when the Temperature Rises over a Certain Threshold, Called MaxTemp.

Fig. 4. Using TinkerCAD for Reading a Temperature Sensor and Activating a Light when the Temperature Rises over a Certain Threshold, Called MaxTemp.

allowed (minDistance), and the maximum distance allowed (maxDistance) in the block-structured code. The authors are grateful for the circuit's red, yellow, and green-led instances that can be turned on individually. If the distance is less than the minimum distance, the red led turns on; if it is between the minimum and maximum distance, the yellow led turns on; and if it is more than the maximum distance, the green led turns on. Some of the experimental findings that students obtained during the last three workshop sessions are summarized in Fig. 3 and 4.

V. ACADEMIC PROGRESS

According to their primary school records, students who participated in the workshop demonstrated improved academic performance from their prior academic performance, particularly in the math and science classes. The authors understand

that these pupils might significantly benefit from courses where developing algorithmic thinking and problem-solving skills is relevant. The following lines provide further information about such upgrades.

A. Improved Math Test Results

The primary academic gains made by pupils in the math class are shown in Table I. Authors may acknowledge that pupils improved their scores by 9.21% on average. All of the pupils also scored close to their post-test records. Because algorithmic and problem-solving skills are closely related to logical and mathematical reasoning, these results are expected to rise.

TABLE I. MATH COURSE ACADEMIC RESULT - CHILEAN SCORE RECORDS FROM 1.0 TO 7.0

# Students	School	Academic Performance		
		Previous record	Post record	Improvement
3	School A	5.8	6.3	8.62%
3	School B	5.6	6.1	8.92%
2	School C	5.7	6.2	8.77%
1	School D	5.5	6.1	10.53

TABLE II. SCIENCE COURSE ACADEMIC RESULT: CHILEAN SCORE RECORDS FROM 1.0 TO 7.0

# Students	School	Academic Performance		
		Previous record	Post record	Improvement
3	School A	6.0	6.4	6.66%
3	School B	6.1	6.4	4.92%
2	School C	5.8	6.2	6.90%
1	School D	5.9	6.3	6.78

B. An improvement in science test results

The primary academic gains made by pupils in the science class are shown in Table II. Authors may acknowledge that pupils improved their scores by, on average, 6.32%. Regarding the arithmetic course, every student received a post-record score close to the maximum. Authors could say that algorithmic and problem-solving skills help students improve in science, even though this improvement is not as significant as in math.

VI. RELATED WORK

Research about developing programming and problem-solving competencies in university students and children exists. Lineros et al. [20] present positive experiences developing electronic and computing architecture competencies using Arduino. Vidal et al. [21] highlight experiments in the same academic experience at the Viña del Mar University. The work of Vidal et al. [10] shows positive experiences with school children in Viña del Mar, Chile, using Scratch and Arduino to develop programming and electronic competencies. Tupac et al. [22] describe positive experiences and results using Arduino in a first programming course with university students in Huancayo, Perú. Tupac et al. [23] highlight results and academic performance regarding previous experiences in Huancayo, Perú, even more during the pandemic time applying online education.

Regarding programming competencies in university students, Ortega et al. [24] and Vidal et al. [25] remark on the usefulness of Python for developing multiprogramming and web development competencies, respectively, not necessarily for computer science students. Likewise, Vidal et al. [26] describe the positive results and experience developing multiprogramming and programming competencies applying Python in two majors with the different primary focus, computer engineering, and business administration. Even though those works are not related to Arduino, they also demonstrate confidence in applying high-level programming languages to develop programming and problem-solving competencies.

VII. CONCLUSIONS

This project proved that by using Arduino, people could effectively educate and develop students' programming and

problem-solving skills. This page displays the primary school test scores from various Chilean primary schools, a nation that is still growing. These findings may inspire other institutions and governments to do comparative research to enhance and develop these skills in elementary school children. The people doing this research want to do a more extended experiment with younger kids in primary school to help them learn how to code and solve problems.

TinkerCAD's online functionality goes hand in hand with the global education trend. For example, the universities of the authors of this work are currently offering programs applying partially or fully to that system. Hence, TinkerCAD can be part of those programs for developing programming, circuit design, and problem-solving competencies.

VIII. FUTURE WORK

This research invites us to investigate the usefulness of Arduino and TinkerCAD for first-year primary school and first-year university students to develop programming, circuit design, and problem-solving competencies. That is a current project in the universities of the authors. They expect to publish the obtained results.

The authors will also investigate Arduino and TinkerCAD's impact on developing programming, circuit design, and problem-solving competencies in kindergarten children. The block-based programming language seems attractive, and appreciating results after coding seems useful for learning purposes. Nowadays, children are born in a computer and information world that invite them to use and learn about technology.

The block-based language of TinkerCAD for developing programming, electronics, and problem-solving competencies also motivates researchers to apply tools in videogame development, such as Unity [27] and Unreal Engine [28]. Videogames attract children, teens, and adults; their development can motivate them to develop programming and problem-solving competencies.

The main issue of this work was the requirement for internet connection and computer availability, although it seems an irrelevant problem nowadays.

ACKNOWLEDGMENT

The authors would like to thank the positive experience developing programming and electronics competencies in primary school children. Educating children represents a marvelous task overall for university professors. After that, the authors want to continue applying this teaching-learning experience in their Chilean cities, specifically in Viña del Mar, Santiago, and Talca.

REFERENCES

- [1] I. Levchyk, H. Chaikovska, O. Yankovych, I. Kuzma, and T. Rozhko-Pavlyshyn, "Formation of sustainable development competencies in primary school children," *Journal of Education Culture and Society*, vol. 12, no. 2, pp. 341–360, 2021.
- [2] R. K. Hill, "What an algorithm is," *Philosophy & Technology*, vol. 29, no. 1, pp. 35–59, 2016.

- [3] G. K. Wong and S. Jiang, "Computational thinking education for children: Algorithmic thinking and debugging," in *2018 IEEE International Conference on Teaching, Assessment, and Learning for Engineering (TALE)*. IEEE, 2018, pp. 328–334.
- [4] D. E. Knuth, *Art of computer programming, volume 2: Seminumerical algorithms*. Addison-Wesley Professional, 2014.
- [5] C. L. Vidal, C. Cabezas, J. H. Parra, and L. P. López, "Experiencias prácticas con el uso del lenguaje de programación scratch para desarrollar el pensamiento algorítmico de estudiantes en Chile," *Formación universitaria*, vol. 8, no. 4, pp. 23–32, 2015.
- [6] M. Tupac-Yupanqui, C. V. Silva, L. Pavesi-Farriol, A. S. Ortiz, J. Cárdenas-Cobo, and F. Pereira, "Exploiting arduino features to develop programming competencies," *IEEE Access*, vol. 10, pp. 20 602–20 615, 2022. [Online]. Available: <https://doi.org/10.1109/ACCESS.2022.3150101>
- [7] J. Maloney, M. Resnick, N. Rusk, B. Silverman, and E. Eastmond, "The scratch programming language and environment," *ACM Trans. Comput. Educ.*, vol. 10, no. 4, nov 2010. [Online]. Available: <https://doi.org/10.1145/1868358.1868363>
- [8] M. Banzi and M. Shiloh, *Getting started with Arduino*. Maker Media, Inc., 2022.
- [9] F. Corno, L. De Russis, and J. P. Sáenz, "Computational notebooks to support developers in prototyping IoT systems," *International Journal of Human-Computer Studies*, vol. 165, p. 102850, 2022. [Online]. Available: <https://www.sciencedirect.com/science/article/pii/S1071581922000684>
- [10] C. V. Silva, J. Serrano-Malebran, and F. Pereira, "Scratch and arduino for effectively developing programming and computing-electronic competences in primary school children," in *38th International Conference of the Chilean Computer Science Society, SCCC 2019, Concepcion, Chile, November 4-9, 2019*. IEEE, 2019, pp. 1–7. [Online]. Available: <https://doi.org/10.1109/SCCC49216.2019.8966401>
- [11] J. Kang and S. Temkin, "Integration of web-based arduino/circuits simulator in enhancing future engineering student projects," in *AIAA SCITECH 2022 Forum*, 01 2022, p. 1352.
- [12] K. M. Noga and B. Palczynska, "The simulation laboratory platform based on multisim for electronic engineering education," in *2018 International Conference on Signals and Electronic Systems (ICSES)*. IEEE, 2018, pp. 269–274.
- [13] D. E. Bolanakis, "A survey of research in microcontroller education," *IEEE Revista Iberoamericana de Tecnologías del Aprendizaje*, vol. 14, no. 2, pp. 50–57, 2019.
- [14] Autodesk, "Autodesk Tinkercad," <https://www.tinkercad.com/>, September 2022.
- [15] D. Luchaninov, R. Bazhenov, V. Sabirova, M. Mamyrova, and A. Zholdosheva, "Online training of students of applied physics in the field of circuitry," in *Journal of Physics: Conference Series*, vol. 1889, no. 2. IOP Publishing, 2021, p. 022030.
- [16] A. Garrigós, D. Marroquí, J. M. Blanes, R. Gutiérrez, I. Blanquer, and M. Cantó, "Designing arduino electronic shields: Experiences from secondary and university courses," in *2017 IEEE Global Engineering Education Conference (EDUCON)*, 2017, pp. 934–937.
- [17] J. M. Pearce, "Economic savings for scientific free and open source technology: A review," *HardwareX*, vol. 8, p. e00139, 2020.
- [18] O. O. Campbell and H. I. Atagana, "Impact of a scratch programming intervention on student engagement in a nigerian polytechnic first-year class: verdict from the observers," *Heliyon*, vol. 8, no. 3, p. e09191, 2022. [Online]. Available: <https://www.sciencedirect.com/science/article/pii/S2405844022004790>
- [19] Fundación Educación Futuro, "Educación Futuro," <https://academiadialogo.cl/educacion-futuro/>, September 2022.
- [20] M. Lineros, B. Bastías, F. Muñoz, K. Aravena, M. Figueroa, L. Rodríguez, B. Villegas, F. Hinojosa, B. Gutiérrez, A. Guerra *et al.*, "Electronics for everybody: Student practical experiences using arduino," in *2018 37th International Conference of the Chilean Computer Science Society (SCCC)*. IEEE, 2018, pp. 1–8.
- [21] C. Vidal-Silva, M. I. Lineros, G. E. Uribe, and C. J. Olmos, "Electrónica para todos con el uso de arduino: Experiencias positivas en la implementación de soluciones hardware-software," *Información tecnológica*, vol. 30, no. 6, pp. 377–386, 2019.
- [22] M. Tupac-Yupanqui, C. L. Vidal-Silva, A. Sánchez-Ortiz, and F. Pereira, "Experiencias y beneficios del uso de arduino en un curso de programación de primer año," *Formación universitaria*, vol. 14, no. 6, pp. 87–96, 2021.
- [23] M. Tupac-Yupanqui, C. Vidal-Silva, L. Pavesi-Farriol, A. S. Ortiz, J. Cardenas-Cobo, and F. Pereira, "Exploiting arduino features to develop programming competencies," *IEEE Access*, vol. 10, pp. 20 602–20 615, 2022.
- [24] F. Ortega, B. General, B. Vega, C. Vidal, C. Jiménez, and J. M. Rubio, "Teaching-learning multi-tasks programming using python," *Journal of Management Information and Decision Sciences*, vol. 24, pp. 1–7, 2021.
- [25] C. L. Vidal-Silva, A. Sánchez-Ortiz, J. Serrano, and J. M. Rubio, "Experiencia académica en desarrollo rápido de sistemas de información web con python y django," *Formación universitaria*, vol. 14, no. 5, pp. 85–94, 2021.
- [26] C. Vidal-Silva, N. Barriga, F. Ortega-Cordero, J. González-López, C. Jiménez-Quintana, C. Pezoa-Fuentes, and I. Veas-González, "Developing computing competencies without restrictions," *IEEE Access*, 2022.
- [27] U. Technologies, "THE FUTURE IS YOURS - The world's leading platform for real-time content creation," <https://unity.com/>, 2022, [Online; accessed 22-October-2022].
- [28] E. Games, "The world's most open and advanced real-time 3D creation tool," <https://www.unrealengine.com/>, 2022, [Online; accessed 22-October-2022].

An Integrated Hardware Prototype for Monitoring Gas Leaks, Fires, and Remote Control via Mobile Application

Md. Ashiqur Rahman, Humayra Ahmed, Md. Mamun Hossain
Computer Science and Engineering
Bangladesh University of Business
and Technology
Dhaka, Bangladesh

Abstract—Liquefied petroleum gas (LPG) is used in a wide range of applications such as home and industrial appliances, vehicles, and refrigerators. However, leakage of gas can have a dangerous and toxic effect on humans and other living organisms. In this paper, an IoT based system is employed for this purpose to monitor gas leakage, detect flames, and alert users. The MQ-5 gas sensor was used to understand the concentration level of a closed volume of gas, while the infrared flame sensor was used to detect the spread of fire in this study. The proposed system has the capacity to detect fire and gas leaks as well as take additional action to lower gas concentration by air ventilation with exhausted fan and put out fires with fire extinguisher. The suggested approach will contribute to increasing safety, lowering the mortality toll, and minimizing harm to the environment. Overall system is implemented with IOT cloud-based remote controls to prevent gas leakage by using android application in response to individual feedback or feed-forward commands. The controller used here is Arduino Uno Rev3 SMD. This study provides design approaches to both software and hardware.

Keywords—Gas leakage; infrared flame detection; IoT; android; arduino UNO

I. INTRODUCTION

When natural gas or another gaseous product escapes from a pipeline or cylinders into an area where it is not supposed to is referred to as gas leakage. These gasses are usually colorless and some are odorless, so there is no way to know if there has been a gas leakage in the environment. It may result in life threatening explosions if these leakage can not be detected [1]. Gas leaks have been a common occurrence in recent years, owing to a combination of poor equipment maintenance and a lack of public knowledge [2]. Therefore, a gas leakage detection system is needed to be introduced to detect gas leakages from domestic or industrial gas pipes or cylinders. It is essential to prevent loss of lives and properties. With the help of Wireless Sensor Networks (WSN), Radio Frequency Identification (RFID), and cloud computing, IoT device communication has become more practical than it once was[3].IoT is a system of web-enabled devices that use sensors to gather data from their environment, process it, and transmit it over the network [4]. Everything is becoming more connected to the internet, which is causing the Internet of Things to grow exponentially [5].

Nowadays a great number of people around the world are using smartphones. So it will be greatly convenient if we can

use smartphones as a surveillance device in order to detect gas leakage. Therefore, we have developed a gas leakage detection system accompanied by an android application. However, this system does not only detect the gas leakage but also it can take actions against the explosions that might happen due to leakage.

Currently, the gas leak detection system is a widely used mechanism. These function nicely and substantially reduce damage. If they adopt additional safety measures in addition to looking for gas leaks, they may be more effective. Existing gas leak detection systems can find leaks, sound audible alarms, and text or contact users to alert them to a leak. However, there is no safety precaution, which means that if there is no user, any accident could occur. Our recommended system, however, has safeguards. For instance, the user can promptly take action by utilizing their Android mobile phone in the event of a gas leak, such as cutting off the gas and power supply to lessen the likelihood of an accident. Using our developed app on their phone, they can remotely operate the entire system.

Our system's main goal is to create a gas leakage detection system and take the required actions to avoid disasters caused by gas leakage. The entire system is powered by Arduino. When a gas leak, smoke, or flame is detected, the proper procedures can be performed to notify the users. The entire system can be controlled from remote location by designing an Android app using cloud database. In addition, an automatic fire extinguishing mechanism has been incorporated to provide more reliability to the system's user.

This paper presents the latest IoT and app based intelligent system and provides a substantial new research direction. Some significant contributions of this paper are outlined as follows:

- **Smart Management:** A smart system is developed using edge cutting technology to monitor and control the gas leakage and fire break out.
- **Remote Controlling:** A mobile application is developed to control the system remotely.
- **Smart Decision Making:** A decision tree algorithm is developed based on the data to help the user making intelligent decision.
- **System Integration:** This system's components and integration are both cost-effective and dependable.

The rest of the paper is segmented as follows. Section II discusses about related works. Section III provides a detailed description of the hardware that we have used to build our proposed system. Section IV provides a detailed description of our proposed system. Section V presented the whole scenarios of implementation of our proposed system and Section VI, provides a detailed view whether our system works properly or not. Section VII shows performance evaluation of our system with the existing system and Section VIII gives a detailed view of how security is provided in our IoT system. Section IX concludes the paper.

II. RELATED WORKS

Srivastava et al. [6] presented a home automation system for consumer safety in . The suggested system automatically cuts off the gas supply whenever a gas leak is identified. Customers can also keep track of their gas consumption and bring refills before the gas runs out by using the system. They did not employ LPG cylinders in practice due to budgetary and timing constraints. They used a water container and lighters to demonstrate gas leaking in the test case experiment. In [7], Keshamoni et al. built an IOT based system for monitoring gas levels, booking new cylinders, and detecting gas leaks to avoid mishaps. The device reduces gas accidents by informing users of leaks and pre-alerting them to schedule a replacement cylinder. They just alert the users that there is a leakage happening in the system but no remote controlling or monitoring is not implemented there. In [8], Varma et al. presented an IoT based system for detecting harmful gasses. The system notifies customers through personal call, SMS, and email when a gas leak is detected by the gas sensor. The system uses relays to turn off the main power supply when the gas concentration is likely to reach the Lower Explosion Limit (LEL). However if relays fail to perform, there is no alternate way to cut down the main power supply which may lead to a great accident. In [9], Siddika et al. build a microcontroller-based system for monitoring LPG gas leaks and warning users using an Arduino and a MQ-135 sensor. The device activates and sounds an alarm by buzzing the buzzer when the gas sensor detects a gas leak. It also sends a message labeled "GAS LEAKAGE" to a predefined mobile number through the GSM module. They didn't provide any sort of automatic safety system in place.

In [10], Tamizharasan et al. proposed an IoT-based automated system for monitoring gas density in LPG cylinders. The gas sensor delivers information to the micro controller, which activates the buzzer when a gas leak is detected. They employed a load sensor to measure the weight of the LPG cylinder in this arrangement. When this weight drops to a dangerously low level, the system alerts the user and instantly orders a replacement cylinder by contacting the registered gas booking number. They just monitor the gas density level but they do not detect the leakage occurred in the cylinder. In [11], Tharad et al. proposed a method for detecting LPG leakage using an Arduino-based microcontroller. MQ2 gas sensors, an Arduino microprocessor, a GSM module, an LCD display, a temperature and humidity module, as well as a buzzer were all employed in the system. The gas concentration in the surrounding area will be displayed on the LCD display, and a buzzer will sound when leakage is found. With the aid of a stepper motor, the power source is turned off. But, if the stepper motor fails to perform its action there is no such other

option in it which can protect from destruction. Dmitry et al. [12] developed an architecture using Wavelength Modulation Spectroscopy instrument to identify the presence of gas and estimate the gas concentration. The output is sent via Bluetooth protocol to the developed application running on a LG G2 D802. The application was developed to access the HITRAN database in real-time. But there isn't any automatic action put in it that can be crucial if a user doesn't receive the notification or take the action. Rahul et al. [13] implemented a system to detect the liquefied petroleum gas (LPG). The system used the high sensitivity sensors to detect the gas leakage as early as possible. They did not include in their system such as cut off power supply, alert system, flame detection, etc.

Anindya et al. [14] presented a new approach for detection of domestic cooking gas leakage. During the experiment the humidity and temperature maintained in a fixed value. Different concentration of LPG has been tested under coated and uncoated conditions. Then the concentration was analyzed for different situations. However, this system doesn't do anything in response to the presence of gas in the surroundings. Noor et al. [15] proposed a gas leakage detection system using two Internet of Things (IOT) platforms. In this system, MQ-2 gas sensor is used to detect the gas leakage. Then the sensor sends the signal to microcontroller and after that microcontroller sends it to an external device such as cell phone. Blynk IoT application is used to alert the concerned person using alarm and Thingspeak IoT cloud is used to record and visualize the data. To monitor LPG leakage, Malviya et al. [16] presented an LPG gas leakage detection and indication system. This setup uses a gas sensor to detect LPG gas leaks and simultaneously sounds an alarm. After the gas leakage equals or exceeds the predetermined threshold, it also uses a Wi-Fi module to send a message to mobile phones. But they didn't provide any suggestion how to control the leakage using mobile phone or any other device.

In order to facilitate user engagement with the suggested system, QI Sarhan et al. [17] employed an Arduino Uno microcontroller in conjunction with a number of suitable sensors, actuators, and GSM as a wireless communication channel. Users may be alerted to events like fire, gas leaks, and home invasions via SMS messages, emails with attachments, etc. In this research, MR Habib et al. [18] suggested an automatic fire alarm system with an extinguishing device that is based on Arduino for fire protection. Smoke detector and temperature sensor support the flame sensor in the proposed system, which is explained together with a thermal model of a dwelling. They didn't use the cloud server and automated decision making approach in their system.

III. SYSTEM HARDWARE

1) Arduino UNO (Fig. 1):

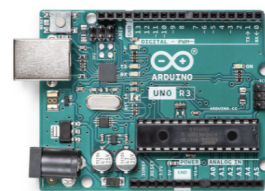


Fig. 1. Arduino UNO.

Features:

- Operating voltage : 5V
- Input voltage range : 6v to 20V
- Input/Output pins : 14
- Analog i/p pins : 6
- DC Current for each input/output pin : 40 mA
- DC Current for 3.3V Pin : 50 mA

2) Gas sensor(MQ-5) (Fig. 2):



Fig. 2. Gas Sensor (MQ-5).

Features:

- Good sensitivity to harmful gasses in a wide range.
- Long life and low cost.
- Possesses high sensitivity to ammonia, benzene, sulfide gases.
- Simple drive circuit.

3) Sim module (Sim 800L) (Fig. 3):



Fig. 3. Sim Module.

Features:

- Works between the voltage range 3.4V to 4.4V and it works in low power mode.
- Operates in 2 mode: Sleep Mode, Ideal Mode.
- Consumption of power is less than 2 mA in Sleep Mode and less than 7 mA in Ideal Mode.
- Supports micro SIM card.
- Searches its corresponding network.
- Helps to send and receive call and SMS.
- Indicates different states by using LED such as: first blinking(no network coverage or searching), slow blinking (logged in), not blinking (power problem).

4) Infrared Flame Detection Sensor (Fig. 4):

Features:

- The sensor can detect fires with wavelengths ranging from 760 to 1100 nm.
- It can detect a lighter flame from 80cm, the larger the flame the farther the sensing distance.

5) ESP Module (ESP 8266) (Fig. 5):

Features:

- Integrated with TCP/IP protocol stack.
- Built in temperature sensor.
- Power consumption - 70 mA.
- Voltage range - 3V to 3.6 V.
- We need to program our device and communicate with the ESP8266 chip by converting USB signals to serial.

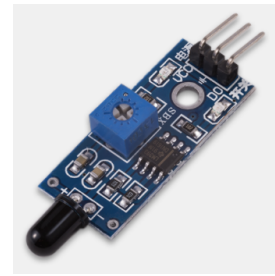


Fig. 4. Infrared Flame Detection Sensor.

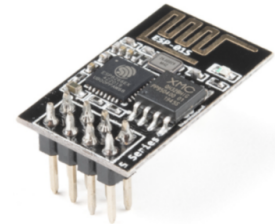


Fig. 5. ESP Module.

IV. PROPOSED METHODOLOGY

Arduino UNO micro controller is the main component of our proposed system. It works as the brain of our system. As it is a low cost device, and easily programmable, we use it as the integrator of our system. It is connected with every other component shown in Fig. 7.

A. System Architecture

The product consists of an outer wooden casing in the shape of a box to carry the Arduino controller, LCD Display, GSM Module, MQ-5 gas sensor, ESP Wi-Fi module, a Buzzer, servo motor and exhaust fan. The gas sensor is placed right above the mouth of the cylinder and the pipeline. Fig. 6 shows the overall architecture of our system.

A servo motor is placed in such a way that whenever there is a signal, it will close the pipe to stop the flow of gas and with help of ESP Wi-Fi module it can stop electricity supply also. Arduino acts as the brain of control. GSM module, ESP Wi-Fi module, LCD display all are connected to Arduino controllers. An LCD display is connected which always shows how much gas is present in the air. There is a Buzzer and two exhaust fans in our system which will be helpful in case of emergency. The GSM module is connected to the Arduino UNO to send alert messages.

B. Operational Principle

- **Collecting Data from Sensor:** The sensors we have used in our system are MQ-5 gas sensor and fire sensor.

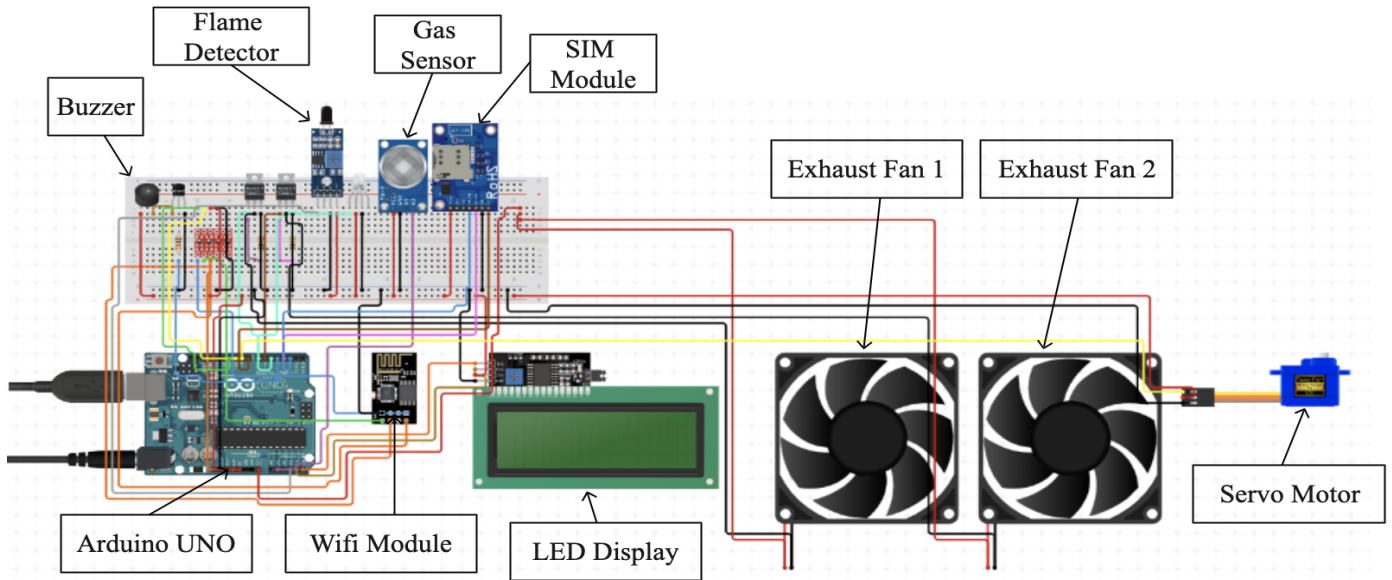


Fig. 6. System Architecture.

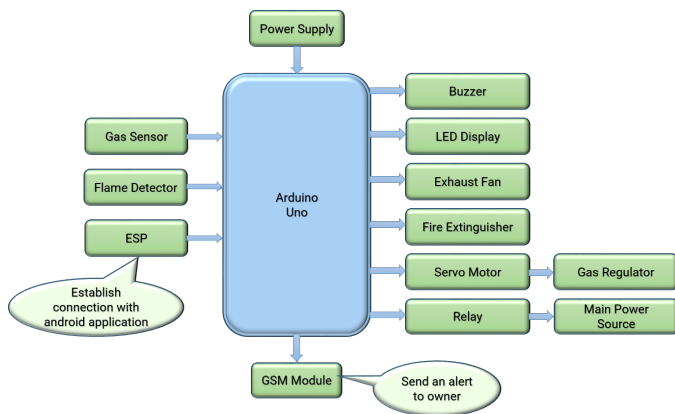


Fig. 7. Block Diagram of the Proposed System.

MQ-5 gas sensor is used to detect whether gas leakage occurs or not. It can also detect toxic gasses like ammonia gas, sulfide, benzene series steam and also trace the smoke and other gasses. The primary material of the MQ-5 gas sensor is SnO₂. It possesses very low conductivity in clean air. When the gas leakage occurs, the gas concentration in that place gets higher. So when it comes into contact with SnO₂ its conductivity changes. Its conductivity rises along with the level of the gas in the air. This is how the MQ-5 gas sensor works and produces a corresponding output voltage from which we can understand the level of gas in the air.

The fire breakout is detected using an infrared flame sensor. Flame detectors that use infrared (IR) or wide-band infrared (greater than 1.1 m) sense and analyze the infrared spectral band to locate predetermined patterns emitted by hot gases.

All of these sensors are connected with the Arduino

UNO board and data from the sensors has been displayed on the LCD monitor. If the gas leakage occurs in the system, an alarm or buzzer rings to alert everyone within the house. And an alert message is sent to the user's phone using GSM module shown in Fig. 8.

- **Sending Data to Cloud Server:**

All of the data that is collected from the sensor has been sent to the cloud server using the Wi-Fi module that is associated with the Arduino UNO server. For cloud service, we have used the Firebase database. The Firebase saves the data as parent child combination pair. The cloud server is basically used for remote controlling of our system.

- **Data Extraction and Mobile Application Development:**

All of these data that is stored in the cloud has been collected and sent to the mobile application that we have been built using the MIT app inventor. By using this application, the user can control the system from anywhere. The sensor data is visible to the user through the application interface.

- **Remote Controlling:**

A decision tree algorithm is applied in the data that is collected from the cloud server and a suggestion is visible in the interface of the mobile application. Then the user can easily take the decision of turning the gas regulator off or turning on the exhaust fan or cutting off the electric supply or turn on the fire extinguisher depending on the situation. When the user gives command in the mobile application, it immediately sends the signal to the cloud database and from that the signal is executed in the Arduino UNO board. This is how remote controlling is done in our system using mobile application.

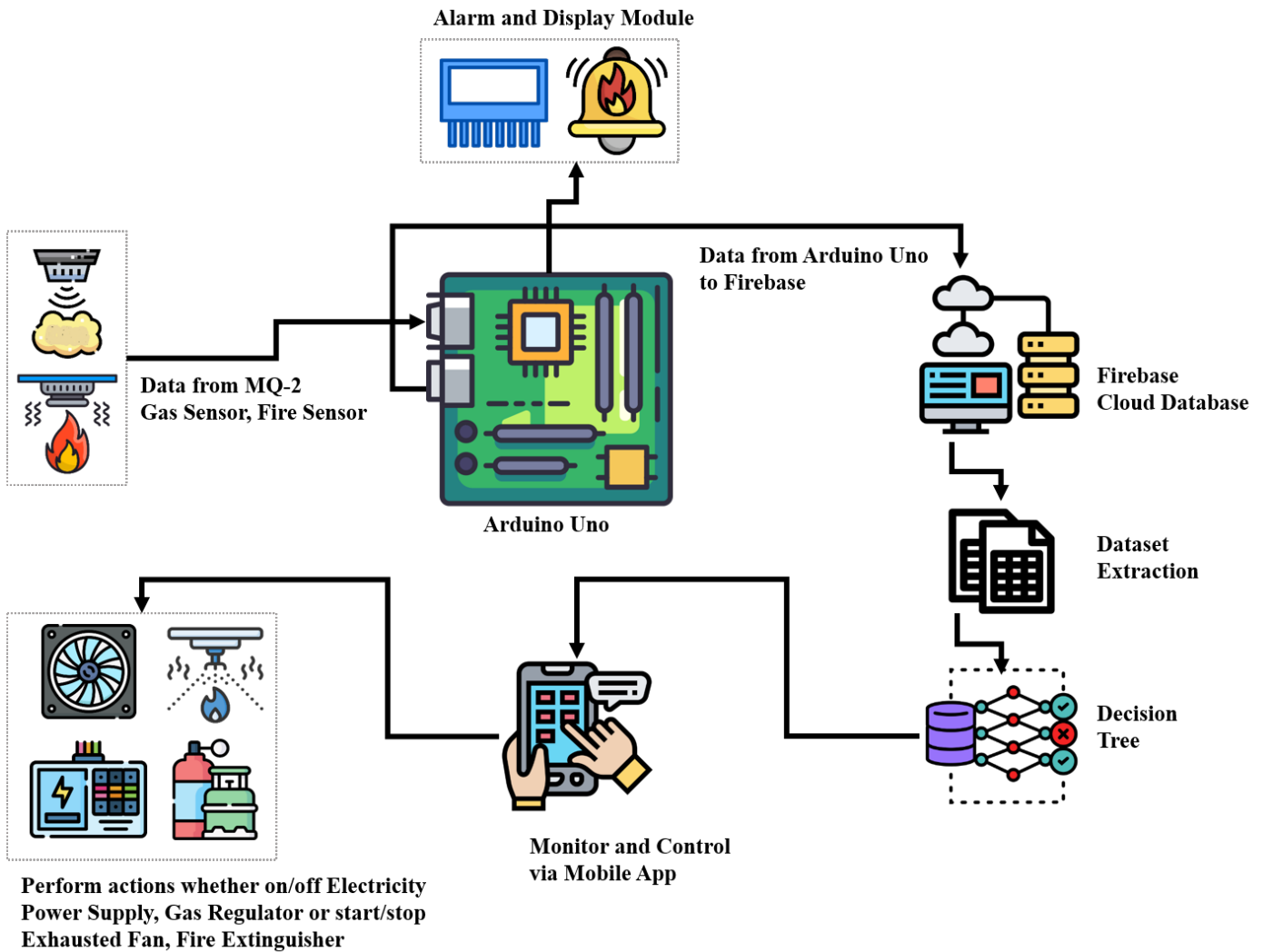


Fig. 8. Operational Flow of Detecting Gas Leakage.

V. IMPLEMENTATION

A. System Implementation

The below Fig. 9 represents our whole system implementation. Before implementing the overall system, we have tested every single component. In place of exhaust fans and fire extinguisher, we have used LED bulbs to minimize our implementation cost and simplification. To monetize the power supply, we have used a single LED bulb. Arduino UNO is connected with every single component of the system and acts as a brain of our system.

B. Android Mobile App Implementation

Here we have developed an android app which helps to control our leakage system from a remote distance. The user may turn the gas and electricity off and exhaust fan on in case of found leakage through apps. Fig. 10 the interface of our android app. We have implemented the decision tree algorithm 1 in the mobile application to provide suggestion about taking action to control the gas leakage.

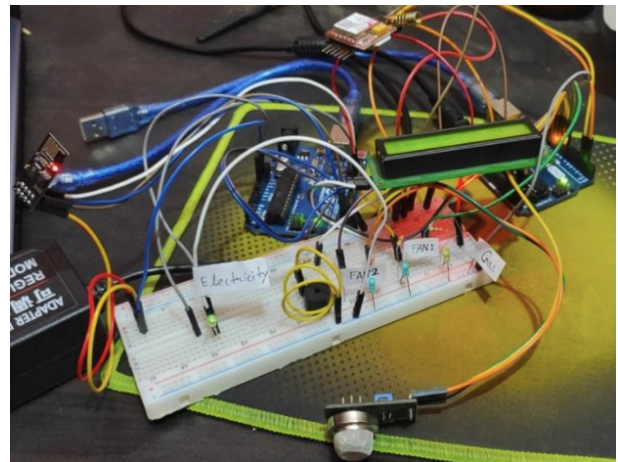


Fig. 9. System Implementation.

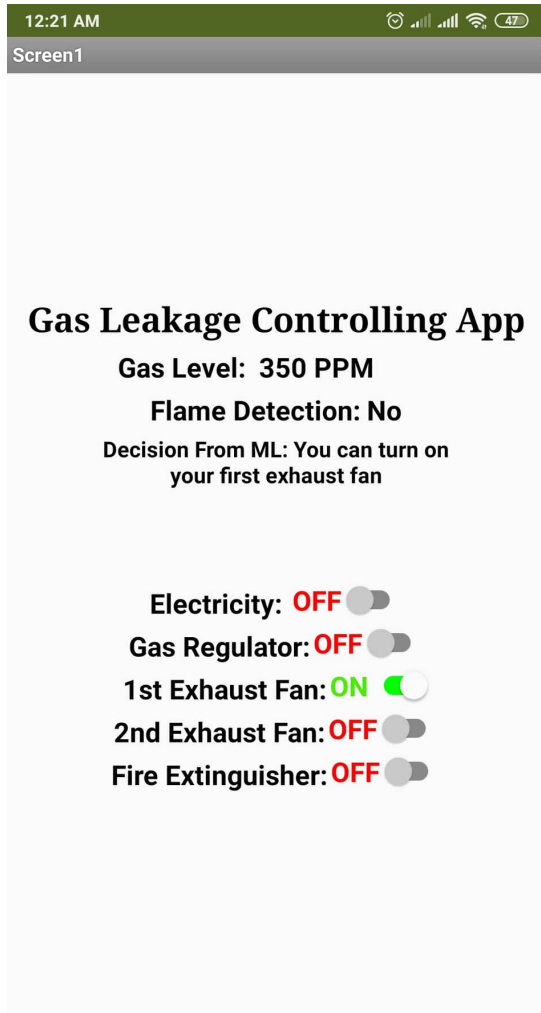


Fig. 10. Mobile Application Interface.

VI. TEST AND RESULTS

This system has been examined by taking a small amount of LPG gas near to the sensor. The MQ-5 gas sensor detects the LPG gas and then it sends a signal to the micro controller. The sensor detects gas leakage once the system is launched, if there is no gas leakage, it displays “Gas Level Normal” on the display which is shown in Fig. 11.

When gas is leaked and it crosses its limit which we set (300ppm) a signal from the micro controller goes to the display and shows “Leakage Found” which is shown in Fig. 12. Simultaneously the buzzer rings.

Then the sensor data goes to the cloud and gives a notification or alert message “Leakage Found on your kitchen” to the owner’s phone to let him know about the incident shown in Fig. 13.

After getting from leakage found message, we can stop the gas and power supply by the help of our android app. When the owner stays at home and wants to be sure of his safety, he can turn off the gas supply with his mobile through this

Algorithm 1: Decision Tree for Gas Leakage Controlling

1. Enter the gas level
2. Enter the flame status
3. **if** $gaslevel \geq 300 \ \&\& \ gaslevel \leq 3000$ **then**
 - if** $flamestatus == true$ **then**
 - suggestion = 1st Exhaust Fan on & Buzzer on & Fire Extinguisher on
 - else**
 - suggestion=1st Exhaust Fan on & Buzzer on
4. **else if** $gaslevel > 3000 \ \&\& \ gaslevel \leq 7000$ **then**
 - if** $flamestatus == true$ **then**
 - suggestion = 2nd Exhaust Fan on & Gas Regulator Off & Fire Extinguisher on
 - else**
 - suggestion=2nd Exhaust Fan on & Gas Regulator Off
5. **else if** $gaslevel > 7000 \ \&\& \ gaslevel \leq 10000$ **then**
 - if** $flamestatus == true$ **then**
 - suggestion = Power Supply off & Fire Extinguisher on
 - else**
 - suggestion=Power Supply off
6. **else**
 - suggestion = Gas Level Normal

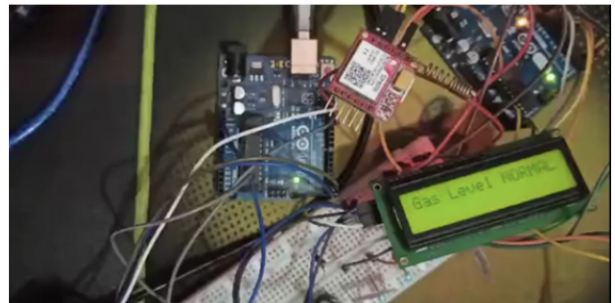


Fig. 11. Show Gas Level Normal.



Fig. 12. Leakage Found Message Display.

application. And if he stays outside the home, then he can turn off both the gas supply and power supply with the help of this application. If the flame detector sensor detects the flame then it will immediately sends message to the user and the user then

TABLE I. DIFFERENCE WITH OTHER EXISTING SYSTEMS

Features	[6]	[7]	[8]	[9]	[10]	[12]	[13]	[14]	[15]	Proposed System
Detection of gas leakage	Y	N	Y	N	Y	Y	Y	Y	Y	Y
Detection of fire	Y	N	N	Y	N	Y	N	N	N	Y
Detection of harmful gases	N	N	Y	N	N	N	N	N	N	Y
Alert by Alarm	Y	N	Y	Y	N	N	N	N	Y	Y
Alert by SMS	N	Y	Y	N	N	N	N	N	N	Y
Alert by Personal Call	N	N	Y	N	N	N	N	N	N	N
Controlling exhaust fan	N	N	N	N	N	N	Y	N	N	Y
Controlling power supply	N	N	N	N	N	N	N	N	N	Y
Controlling gas regulator	N	N	N	N	N	N	N	N	N	Y
Controlling fire extinguisher	N	N	N	N	N	N	N	N	N	Y
Message shown in LCD display	N	N	N	Y	Y	N	N	N	N	Y



precautions or actions to avoid severe accidental cases happen due to gas leakage which is absent in the existing systems.

VIII. SECURITY

The majority of internet technologies and networking protocols have been created exclusively for unrestrained items, which has presented significant security concerns when integrating IoT objects into the standard Internet [19]. We must ensure security in order for the various sensors attached to our system and the data saved in the cloud database to function properly. The security measures put in place in our system to keep it secure are listed below.

- **Providing Authentication and Password:** For our smartphone application that we designed to allow remote operation of our IoT system, we have enabled authentication and strong passwords. It aids in protecting our system from brute-force attacks.
- **Monetizing and Updating System:** We have a frequent update option installed in our system and regularly monitor to detect the vulnerabilities of our system.
- **Ensuring Security of Data:** Our data is stored in the Firebase database. To protect the data, we have used their built-in authorization mechanism. In order to safeguard the data from manipulation or tampering from other sources, we have additionally deployed rule-based permission of the Firebase database for data retrieval. This makes our data secure when retrieving.



Fig. 13. Alert Message about Leakage of Gas.

using the mobile app can turn on the fire extinguisher.

VII. EVALUATION

We have evaluated our system with other existing systems in respect to the feature that they have introduced in their system. The Table I shows the difference between our proposed system and existing system.

Here, Y represents ‘Yes’ and N represents ‘No’.

Comparing the proposed system to the other systems it can be clearly seen that from Table I, the proposed system incorporated more features in comparing with the other system. It can not only detect the gas leakage but also take necessary

IX. CONCLUSION

In this research, we proposed a gas leakage detection approach for home safety reasons to reduce the accidental cases occur owing to gas leakage and a flame detection system is provided to manage the fire outbreak. To remotely operate the entire system, we also developed an android application. Additionally, it accomplishes some important properties that the current approaches do not. A more potent gas sensor, such as MEMS, can be used to increase system effectiveness. If a Philips micro controller is utilized, the micro controller’s efficiency and memory can be improved. To generate intelligent decisions, advanced machine learning algorithms might be introduced.

ACKNOWLEDGMENTS

We would like to acknowledge the support of the Bangladesh University of Business and Technology and IoT lab for their suggestion and resource sharing.

REFERENCES

- [1] S. Shrestha, V. K. Anne, and R. Chaitanya, "Iot based smart gas management system," in *2019 3rd International Conference on Trends in Electronics and Informatics (ICOEI)*. IEEE, 2019, pp. 550–555.
- [2] E. J. Leavline, D. A. A. G. Singh, B. Abinaya, and H. Deepika, "Lpg gas leakage detection and alert system," *International Journal of Electronics Engineering Research*, vol. 9, no. 7, pp. 1095–1097, 2017.
- [3] M. A. Razzaq, S. H. Gill, M. A. Qureshi, and S. Ullah, "Security issues in the internet of things (iot): A comprehensive study," *International Journal of Advanced Computer Science and Applications*, vol. 8, no. 6, 2017.
- [4] M. Humayun, "Role of emerging iot big data and cloud computing for real time application," *International Journal of Advanced Computer Science and Applications*, vol. 11, no. 4, 2020.
- [5] J. Ali, T. Ali, S. Musa, and A. Zahrani, "Towards secure iot communication with smart contracts in a blockchain infrastructure," *International Journal of Advanced Computer Science and Applications*, vol. 9, no. 10, 2018. [Online]. Available: <http://dx.doi.org/10.14569/IJACSA.2018.091070>
- [6] A. K. Srivastava, S. Thakur, A. Kumar, and A. Raj, "Iot based lpg cylinder monitoring system," in *2019 IEEE International Symposium on Smart Electronic Systems (iSES)(Formerly iNiS)*. IEEE, 2019, pp. 268–271.
- [7] K. Keshamoni and S. Hemanth, "Smart gas level monitoring, booking & gas leakage detector over iot," in *2017 IEEE 7th International Advance Computing Conference (IACC)*. IEEE, 2017, pp. 330–332.
- [8] A. Varma, S. Prabhakar, and K. Jayavel, "Gas leakage detection and smart alerting and prediction using iot," in *2017 2nd International Conference on Computing and Communications Technologies (ICCT)*. IEEE, 2017, pp. 327–333.
- [9] A. Siddika and I. Hossain, "Lpg gas leakage monitoring and alert system using arduino," *International Journal of Science and Research (IJSR)*, vol. 7, no. 42, pp. 1734–1737, 2018.
- [10] V. Tamizharasan, T. Ravichandran, M. Sowndariya, R. Sandeep, and K. Saravanavel, "Gas level detection and automatic booking using iot," in *2019 5th International Conference on Advanced Computing & Communication Systems (ICACCS)*. IEEE, 2019, pp. 922–925.
- [11] H. Tharad and A. Pandey, "Arduino based gas leakage detecting system."
- [12] D. Duda, P. Martín-Mateos, B. Jerez, M. Ruiz-Llata, and P. Acedo, "Optical gas sensor based on an android application for real-time, reconfigurable spectroscopic data analysis," in *SENSORS, 2014 IEEE*. IEEE, 2014, pp. 1054–1056.
- [13] R. Kurzekar, H. Arora, and R. Shrestha, "Embedded hardware prototype for gas detection and monitoring system in android mobile platform," in *2017 IEEE International Symposium on Nanoelectronic and Information Systems (iNIS)*. IEEE, 2017, pp. 6–10.
- [14] A. Nag, A. I. Zia, X. Li, S. C. Mukhopadhyay, and J. Kosel, "Novel sensing approach for lpg leakage detection: Part i—operating mechanism and preliminary results," *IEEE Sensors journal*, vol. 16, no. 4, pp. 996–1003, 2015.
- [15] N. K. Jumaa, Y. M. Abdulkhaleq, M. A. Nadhim, and T. A. Abbas, "Iot based gas leakage detection and alarming system using blynk platforms," 2022.
- [16] S. Malviya, S. D. Pande, P. P. Kalaskar, and A. Hingane, "Lpg gas leakage detector system using iot," *International Journal of Scientific Research and Engineering Development*, vol. 2, no. 6, 2019.
- [17] Q. I. Sarhan, "Arduino based smart home warning system," in *2020 IEEE 6th International Conference on Control Science and Systems Engineering (ICCSSE)*. IEEE, 2020, pp. 201–206.
- [18] M. R. Habib, N. Khan, K. Ahmed, M. R. Kiran, A. Asif, M. I. Bhuiyan, and O. Farrok, "Quick fire sensing model and extinguishing by using an arduino based fire protection device," in *2019 5th International Conference on Advances in Electrical Engineering (ICAEE)*. IEEE, 2019, pp. 435–439.
- [19] H. A. Abdul-Ghani, D. Konstantas, and M. Mahyoub, "A comprehensive iot attacks survey based on a building-blocked reference model," *International Journal of Advanced Computer Science and Applications*, vol. 9, no. 3, 2018.

Performance Evaluation of Raspberry Pi as an IoT Edge Signal Processing Device for a Real-Time Flash Flood Forecasting System

Aslinda Hassan¹, Haniza Nahar², Wahidah Md Shah³, Azlianor Abd-Aziz⁴, Sarah Afifah Sahiran⁵, Nazrulazhar Bahaman⁶, Mohd Riduan Ahmad⁷, Isredza Rahmi A. Hamid⁸, and Muhammad Abu Bakar Sidik⁹
Fakulti Teknologi Maklumat dan Komunikasi (FTMK), Universiti Teknikal Malaysia Melaka (UTeM),
Jalan Hang Tuah Jaya, 76100 Durian Tunggal, Melaka, Malaysia^{1,2,3,4,5,6}
Fakulti Kejuruteraan Elektronik dan Kejuruteraan Komputer (FKEKK), Universiti Teknikal Malaysia Melaka (UTeM),
Jalan Hang Tuah Jaya, 76100 Durian Tunggal, Melaka, Malaysia⁷
Fakulti Sains Komputer Dan Teknologi Maklumat, Universiti Tun Hussein Onn (UTHM),
86400 Parit Raja, Batu Pahat Johor, Malaysia⁸
Department of Electrical Engineering, Faculty of Engineering, Universitas Sriwijaya (UNSRI), Palembang, Indonesia⁹

Abstract—The Raspberry Pi has evolved in recent years into a popular, low-cost, tiny computer for a wide range of IoT applications. Raspberry Pi is not only successful for data collection but also for data processing, including data storage and analysis. Thus, this study investigates the capability of Raspberry Pi as an edge processing device for capturing lightning strike signals in predicting flash flood locations. An electric and magnetic sensor (EMS) is connected to a Raspberry Pi in the experiment setup. The Raspberry Pi is then used to process digitised lightning signals. From the experiment, Raspberry Pi's performance is measured using the performance metrics: central processing unit (CPU) usage and temperature. The results revealed that the Raspberry Pi could handle the real-time collection and processing of lightning signals from the EMSs without affecting the hardware capability.

Keywords—Raspberry Pi; IoT; edge; performance

I. INTRODUCTION

The Internet of Things (IoT) is changing how we live, work, travel and do business. It is also the cornerstone of a modern industrial revolution known as Industry 4.0 and the key to the digital transformation of businesses, communities, and society. An IoT ecosystem comprises web-enabled intelligent devices that use embedded systems, such as processors, sensors, and communication hardware. These intelligent devices collect, transmit and act on data they acquire from their environments. The devices then share the sensor data they acquire by connecting to an IoT gateway or other edge device, where the data is either transferred to the cloud for analysis or locally analysed. According to Priceonomics.com, the number of connected devices is projected to rise from 8.7 billion in 2012 to 50 billion in 2020 [1]. Huawei predicts that 100 billion connected devices will be used in every business and living area by 2025 [2]. Consequently, the data generated by the IoT is projected to reach 4.4 zettabytes by 2020 from just 0.1 zettabytes in 2013 [1].

The value of IoT goes further than data collection and real-time monitoring. Companies can gradually see the need to upload vast amounts of data to the cloud and support flexible resource management and visualised operations. They will also

strive to process their data using machine learning and predictive analytics in order to introduce better technologies that will bring them success. Previously, placing all computational tasks on the cloud has proved to be an efficient way to process data since the power of cloud computing outperforms the capacity of the IoT. However, over the past few years, the significant increase of data generated by smart devices has put a strain on bandwidth utilisation [3].

Furthermore, digital traffic jams are almost anticipated, with the world estimated to generate up to 4.4 zettabytes of data by 2020. There is also the "last mile" bottleneck problem. Essentially, the last mile defines the final networking segment, which connects an organisation's local network to the Internet. Since all network traffic destined for a particular organisation is channelled through that connection, it can be a bottleneck in networking throughput [4].

Due to the miniaturisation of processing and storage technology, current IoT devices have become more potent in collecting, storing, and processing data. This scenario has opened opportunities for organisations to optimise their networks and relocate more processing functions closer to where data is collected at the edge of the network. Gartner defines *edge computing* as a "part of a distributed computing topology where information processing is located close to the edge, where things and people produce or consume that information" [5]. In essence, edge computing brings computation and data storage closer to the smart devices rather than depending on a central location that might be thousands of kilometres away. Edge computing allows the data from the IoT devices to be analysed before being sent to the data centre. The main objective of edge computing is to prevent data, especially real-time data, from suffering latency issues that can affect the performance of an application [6].

Recent years have seen the development of Raspberry Pi as a popular, low-cost, tiny computer for several IoT applications. Raspberry Pi, referred to as a Single Board Computer (SBC), can run a complete operating system and has sufficient peripherals like memory, central processing unit (CPU), and power to initiate execution without additional hardware. In the present

TABLE I. TABLE OF ABBREVIATIONS

Abbreviation	Meaning
CAPPI	Constant Altitude Plan Position Indicator
CG	Cloud-to-Ground
CPU	Central Processing Unit
EMS	Electric and Magnetic Sensor
GPS	Global Positioning System
IoT	Internet of Things
LF	Low Frequency
LPDDR	Low-Power Double Data Rate
NBE	Narrow Bipolar Event
PaaS	Platform as a Service
RAM	Random Access Memory
RPi	Raspberry Pi
SDRAM	Synchronous Dynamic Random-Access Memory
SBC	Single Board Computer
VLF	Very Low Frequency

society, Raspberry Pi is not only an essential data-gathering device, but it can also analyse and store data in a server-like fashion.

In this study, Raspberry Pi devices are used as one of the components in the proposed architecture to illustrate its viability as an edge computing device and to evaluate its performance in terms of CPU system-wide utilisation and temperature. In this study, we believe Raspberry Pi devices may function as data processing edge devices, given their current CPU, memory, and storage capacity. If Raspberry Pi devices merely function as data collectors without additional processing and transfer all data to the cloud, then a significant amount of computer power is squandered. Consequently, in this study, our aim is not only to cut data transfer time by using Raspberry Pi's local processing capacity but also efficiently uses the otherwise underused distributed computing power. This study's contribution is to reveal the viability and potential of edge computing by doing hands-on experiments and analysing the performance in terms of CPU usage and temperature.

The rest of the paper is organised as follows. An overview of the Raspberry Pi as an edge device and similar studies on Raspberry Pi's performance as an edge device is discussed in Section II. Section III presents this study's background works. The experiment setup for the performance evaluation is presented in Section IV. Section V reports and discusses the results of the experimental evaluation. We conclude the paper in Section VI.

II. RELATED WORKS

On March 14, 2018, the Raspberry Pi Foundation introduced the Raspberry Pi 3 Model B+ as an upgrade to its predecessor [7]. It is also known as a Single Board Computer (SBC) with a Linux-based operating system, and a micro SD card is often required for boot file system storage. General Purpose Input-Output (GPIO) connectors are meant to control a vast array of electrical components in addition to being a small, low-cost computer programmatically[7]. In addition to its usage in education, it has become a popular edge processing device for other IoT applications.

The research articles in [8], [9], [10], [11] are examples of the existing literature on edge computing research utilising Raspberry Pi. The authors of [8] have created a lightweight edge computing-based distributed system that uses

Raspberry Pi to directly handle the raw picture data from each camera. Consequently, the identified emotions may be easily communicated to the end user. In this study, the optimised and bespoke algorithms in the edge devices increase data processing speed, reduce network bandwidth requirements, and enhance application performance. The authors of [9] propose an automated service and resource discovery technique to effectively deploy nano services on local IoT nodes. Using a scenario involving remote healthcare monitoring, the authors offer a Raspberry Pi platform prototype implementation of the suggested method.

Several works in [12], [13], [14], [15], [16], [17] are related to performance evaluation on Raspberry Pi as edge devices. A study in [12] comparing data processing in various network setups and data stream speeds has been done in semantic data enrichment. It implemented a tiered IoT-Edge-Cloud system employing automotive sensor data at the IoT layer, Raspberry Pi at the edge layer, and Node-Red server at the cloud level in real architecture. The outcome demonstrates that data processing at the edge layer has enhanced efficiency, memory utilisation, and round-trip time.

Deep learning-based voice recognition applications have been studied in [13] to compare the performance and efficiency of Raspberry Pi with Nvidia Jetson Nano edge devices. Even if the Nvidia Jetson Nano is superior to Raspberry Pi, the word error rate for real-time inference on the Raspberry Pi CPU slightly degrades. The word error rate on the edge layer is generally more significant than the server inference, although it is not too far behind.

The objective of [14] is to conduct a comparative and experimental investigation of the performance of five distinct Raspberry Pi models (RPi Zero W, RPi Zero 2 W, RPi 3B, RPi 3B+, and RPi 4B) under a variety of situations and configurations. In conclusion, RPi 4B is significantly surpassed by competitors. In the meanwhile, the performance of the RPi Zero 2 W, RPi 3B, and RPi 3B+ is comparable, and the RPi Zero W is suggested for applications with minimal CPU and RAM capacity.

In [16], the authors demonstrate how to implement a cloud Platform as a Service (PaaS) architecture on a Raspberry Pi cluster. The main goal of the implementation is to make the cluster a suitable platform for more complex data gathering and analysis applications placed at the edge of a cloud. The findings show that while this is technically feasible, there are still some performance issues due to a relatively weak CPU, a limited network bandwidth, and problems with the file system.

Unlike the previous studies, this study aims to present the robustness and feasibility of Raspberry Pi as an edge-processing device for real-time data.

III. BACKGROUND

A. Proposed Architecture

In this paper, we are motivated to develop a real-time flash flood forecasting system utilising Raspberry Pi as an IoT edge processing device. The proposed system uses a new technique to forecast the flash flood-affected locations using the following parameters:

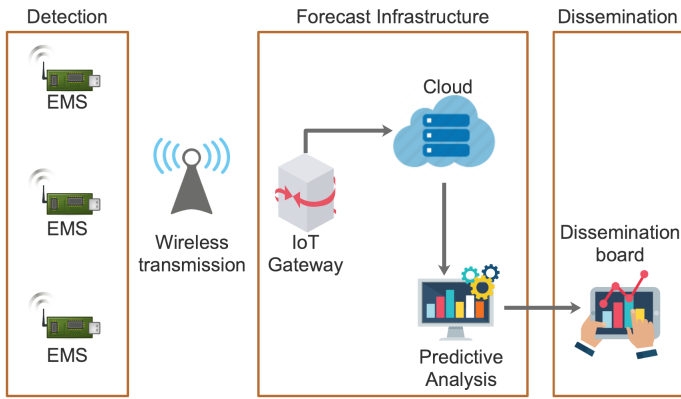


Fig. 1. The Proposed System Architecture.

- 1) Negative narrow bipolar event (-NBE) electric and magnetic fields signal.
- 2) Positive cloud-to-ground flash (+CG) electric and magnetic fields signal.
- 3) Cloud top height data [18]
- 4) Constant Altitude Plan Position Indicator (CAPPI) data [18]
- 5) Wind speed
- 6) Wind direction

Briefly, the -NBE and +CG lightning signals are collected and located by several lightning sensors in real-time [19]. Our research group at Universiti Teknikal Malaysia Melaka (UTeM) built these homemade sensors from scratch. These sensors have been working since 2015, tested, and calibrated [20][21]. The signal coverage for a single sensor is within a 300 km radius. Together with the rest of the parameters, real-time tracking can be done for any storms in Malaysia that can lead to flash floods. Specifically, cloud top height and CAPPI data are used to monitor rainfall and lightning flash rate intensity. The wind speed and direction are used to predict where a particular storm is heading and at what rate. By monitoring the occurrences of +CG and -NBEs produced by a storm in real-time, together with cloud top height and CAPPI rainfall rate, the proposed system will be able to forecast the rainfall intensity and rate for the next 1-3 hours period. Facilitated by wind speed and direction, the system can forecast the location where the downpour would impact most significant. Additional details for real-time forecasting of flash floods using the above technique are given in [19], [20], [21].

Fig. 1 illustrates the architecture of the proposed Flash Flood Early Warning System. Fig. 1 provides a general view of the proposed system that includes the three components. The three components are detection, forecast architecture and dissemination. The first component falls under the detection category, which contains the lightning sensors. The lightning sensor is called *Electric and Magnetic Field Sensor (EMS)*. The main purpose of this sensor is to detect and locate lightning signals, particularly +CG and -NBE, within a 300 km radius. The signal is a combination waveform of electric and magnetic fields that are used to identify different types of lightning signals [19][21]. As shown in Fig. 2, there are five major components (or subsystems) in EMS system:

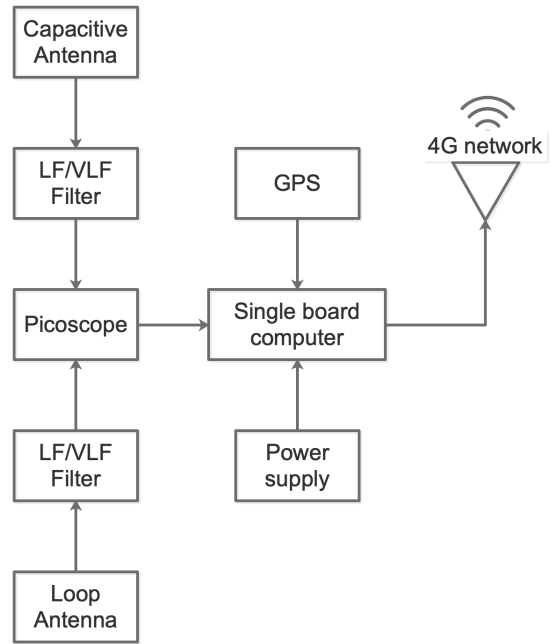


Fig. 2. Five Major Components or Subsystems of Electric and Magnetic Fields Sensor (EMS).

- 1) Antenna part with capacitive antenna to detect Electric field and two loop antennas to detect orthogonal components of magnetic field [20].
- 2) Filter circuits designed for detection of electric and magnetic fields at low frequency/very low frequency (LF/VLF) bands (or below than 1 MHz) [20].
- 3) Digitizer to digitize the captured analog lightning signals. Currently we are using the PicoScope and it is reliable.
- 4) A single board computer is used convert the digitized lightning signals to the coordinates of the lightning strikes and stream the EMS data in real time back to Forecasting Infrastructure via 4G network (or any available network infrastructure). Currently, the conversion and real time data streaming are implemented using Raspberry Pi platform.
- 5) Power supply from solar power, batteries, and power bank.

The focus of this paper is to evaluate the performance of the detection component, specifically the single board computer, in analysing and converting the digitised lightning signals to coordinates of the lightning strikes.

IV. EXPERIMENT ENVIRONMENT

As previously mentioned, this study aimed to evaluate the performance of the single board computer in the EMS system of the detection component (refer to Fig. 2). Fig. 3 presents the flowchart for the EMS system processes. As shown in Fig. 3, the antennas in the EMS will capture the lightning signals whenever the lightning event occurs [20][21]. The analogue signals are then digitised using the PicoScope. Next, the digitised lightning signals using a custom-written Python program that synchronises the signals with the Global Positioning System (GPS) clock and produces the coordinates

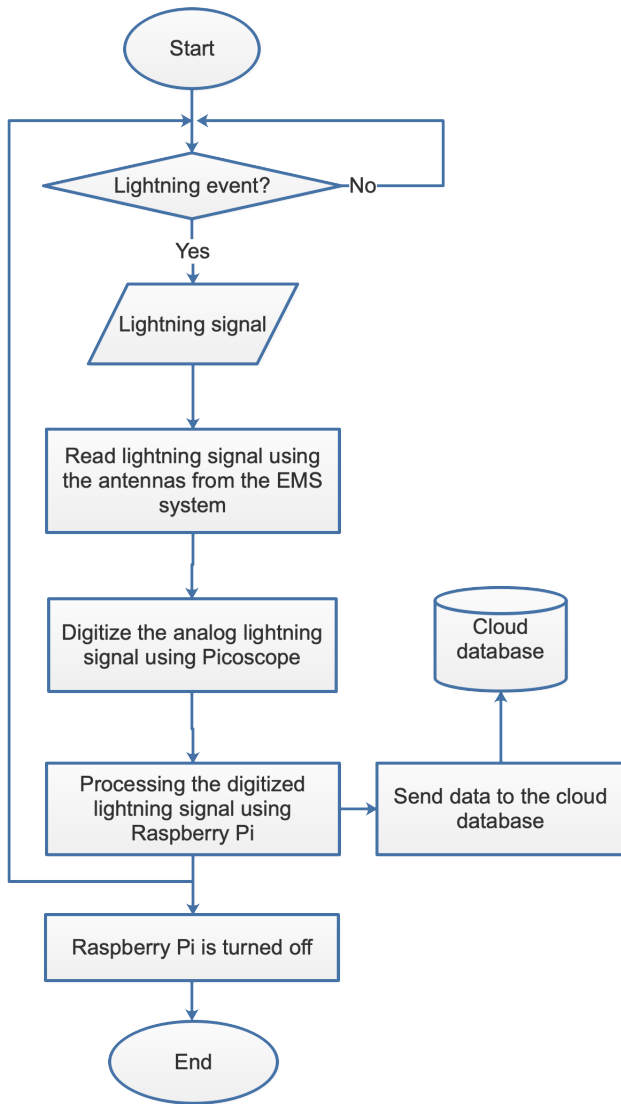


Fig. 3. The Flowchart for the EMS System.

of the lightning strikes [20][21]. Subsequently, the resulting coordinates are sent to the cloud database via IoT Gateway using any available wireless transmission (refer to Fig. 1).

A. Experiment Setup

In our experiment, as shown in Fig. 4, the components were integrated around the Raspberry Pi 3 as the main computer. The integration is done by connecting the EMS to the Raspberry Pi with the specification listed below in Table II. Fig. 3 shows that the digitised lightning signal is being fed into the Raspberry Pi to be processed by the custom-written Python program (refer to Algorithm 1) and produce the lightning strike locations. The resulting lightning strike locations are sent to the cloud database via an IoT gateway.

In the experiment, the process of converting the lightning signals into the lightning strike locations is repeated for 50 iterations in one cycle. The cycle is then repeated five times for statistical validity. However, in the actual scenario, the

Algorithm 1 Signal Processing Program for the Digitised Lightning Signals

```

for each sequence until 100 do
    SET current time
    print sequence attempt
    INIT empty arrays: az, az2, d, ftype, pola, timeLDloc, ranges,
    typeflash, polar
    result ← CPU Temperature
    if ranges array is empty then
        print NO FLASHES WITHIN SELECTED RANGE
    else
        INIT empty arrays: flash, flashS
        for each element of typeflash array do
            if element of typeflash array is empty then
                if element of polar array is empty then
                    flash array ← 1
                    flashS array ← 'CG+'
                else
                    flash array ← 2
                    flashS array ← 'CG-'
                end if
            else
                if element of polar array is empty then
                    flash array ← 3
                    flashS array ← 'IC+'
                else
                    flash array ← 4
                    flashS array ← 'IC-'
                end if
            end if
        end for
        CALL math.radians(2.3139) RETURNING latitude radians
        INTO lat1
        CALL math.radians(102.3185) RETURNING longitude radi-
        ans INTO lon1
        INIT empty arrays: lat2, lon2, rangedeg
        for each element of ranges array do
            CALL math.radians(element of rangedeg
            array/40075.01*360)
            return value radians INTO rangedeg array
        end for
        for each element of ranges array do
            dlon2 ← math.asin(math.sin(lat1) ×
            math.cos(element of rangedeg array)
            +
            math.cos(lat1) × math.sin(element of rangedeg array) ×
            math.cos(element of az2 array))
            a ← math.sin(element of az2 array) ×
            math.sin(element of rangedeg array) × math.cos(lat1)
            b ← math.cos(element of rangedeg array)
            -
            math.sin(lat1) × math.sin(dlon2)
            dlat2 ← lon1 + math.atan2(a, b)
            CALL math.degrees(dlat2) RETURNING value degrees
            INTO lat2 array
            CALL math.degrees(dlon2) RETURNING value degrees
            INTO lon2 array
        end for
    end if
end for
    
```

process in Fig. 3 only happens during a lightning storm. The main goal of this experiment is to observe the Raspberry Pi's performance if the lightning signal processing in Fig. 3 is executed repeatedly by measuring the Raspberry Pi's CPU

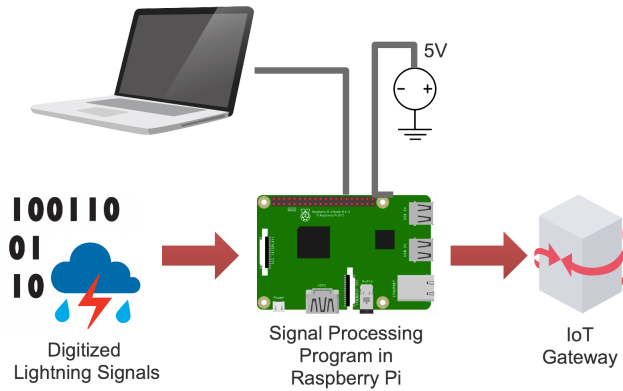


Fig. 4. The Experiment Setup.

TABLE II. HARDWARE SPECIFICATION FOR RASPBERRY PI

Hardware Specification	Raspberry Pi 3B+
CPU	ARMv8 Cortex-A5, 1.4GHz
CPU Cores	4
Memory	1GB LPDDR2 SDRAM
Integrated Wi-Fi	2.4GHz and 5GHz IEEE 802.11.b/g/n/ac wireless LAN

usage and temperature.

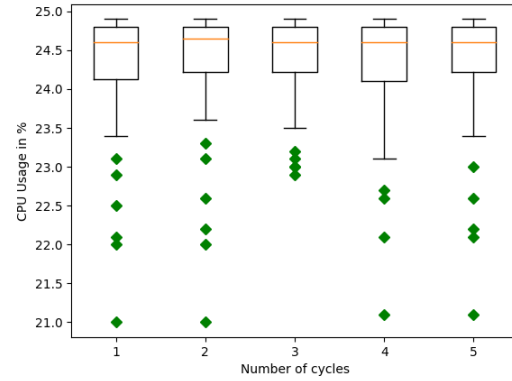
In each iteration, the CPU usage and the Raspberry Pi's temperature are measured using Python cross-platform library for retrieving information on running processes and system utilisation called psutil[22] library. In the experiment, the "cpu_percent()" function from the psutil library is used to measure the Raspberry Pi's system-wide CPU utilisation [22]. Another function called "CPUtemperature()" is used to monitor the Raspberry Pi's current temperature. This function is called from an application programming interface library for Raspberry Pi devices' general-purpose input/output (GPIO) devices [23]. In essence, the CPUtemperature function returns the Raspberry Pi's current temperature in degrees Celcius.

V. RESULTS AND DISCUSSION

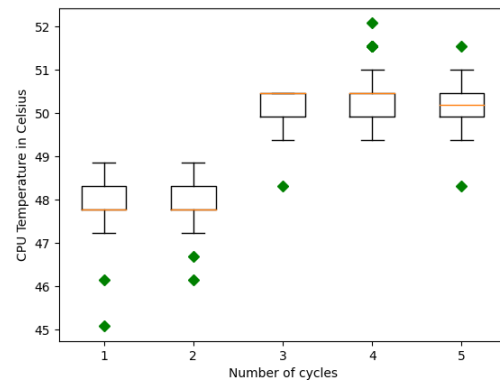
This section presents the performance evaluation results on the Raspberry Pi for digitised lightning signal processing. As mentioned in the previous section, the processing is repeated in 50 iterations in each cycle. Box plots in Fig. 5 show the statistic of the CPU usage and temperature measured in the experiment. For each data set, the first and third quartiles are represented by a box, with the median indicated in the box's centre. Whiskers, the lines extending from the box's edges, display the minimum and highest CPU utilisation and temperature.

Figs. 5a and 5b show the boxplots for the Raspberry Pi's system-wide CPU utilisation percentage and the Celcius's CPU temperature, respectively. In Fig. 5a, the interquartile range for Raspberry Pi's CPU usage is consistently between 23% and 25%, with a median of approximately 24.6% for each cycle. Each of the box plots for the CPU usage in Fig. 5a skews toward the value of 25%, which indicates that the processing of the lightning signals uses only 25% of the Raspberry Pi's CPU.

Fig. 5b shows the Raspberry Pi's CPU temperature distribution. The box plots in Fig. 5b demonstrate an increase in



(a) CPU Usage



(b) Temperature

Fig. 5. The Raspberry Pi CPU Usage and Temperature Distributions.

the CPU temperature from 47 degrees Celcius to a maximum of 51 degrees Celcius. The median for cycles 1 and 2 is approximately 48 degrees Celcius with an increment to 50 degrees Celcius for cycles 3, 4 and 5. According to the Raspberry Pi official documentation [24], the Raspberry Pi is constructed with commercial-grade chips that are qualified for varied temperature ranges to keep prices down; the manufacturers indicate the USB and Ethernet controller of the Pi 3+ (Microchip LAN7515) as being qualified from 0°C to 70°C. The operating temperature range for the SoC (System on Chip - the integrated circuit that performs the Pi's processing, a Broadcom BCM2837B0) is -40 to 85 degrees Celsius [24], [25], [26]. Based on the official specification [24], the current workload in the experiment that is subjected to the Raspberry Pi is not enough to spike the temperature to a level that can damage the hardware.

Figs. 6 and 7 shows the distribution for system-wide CPU utilisation and temperature for each cycle in the experiment. Figs. 6 show that the system-wide CPU utilisation is consistently at a maximum of 25% in each cycle, whereas Figs. 7 show an increment in the CPU temperature from Cycle 1 until Cycle 5. The distributions of CPU utilisation and temperature for 50 iterations in each cycle shown in Figs. 6 and 7 are consistent with the boxplot statistical distribution shown in

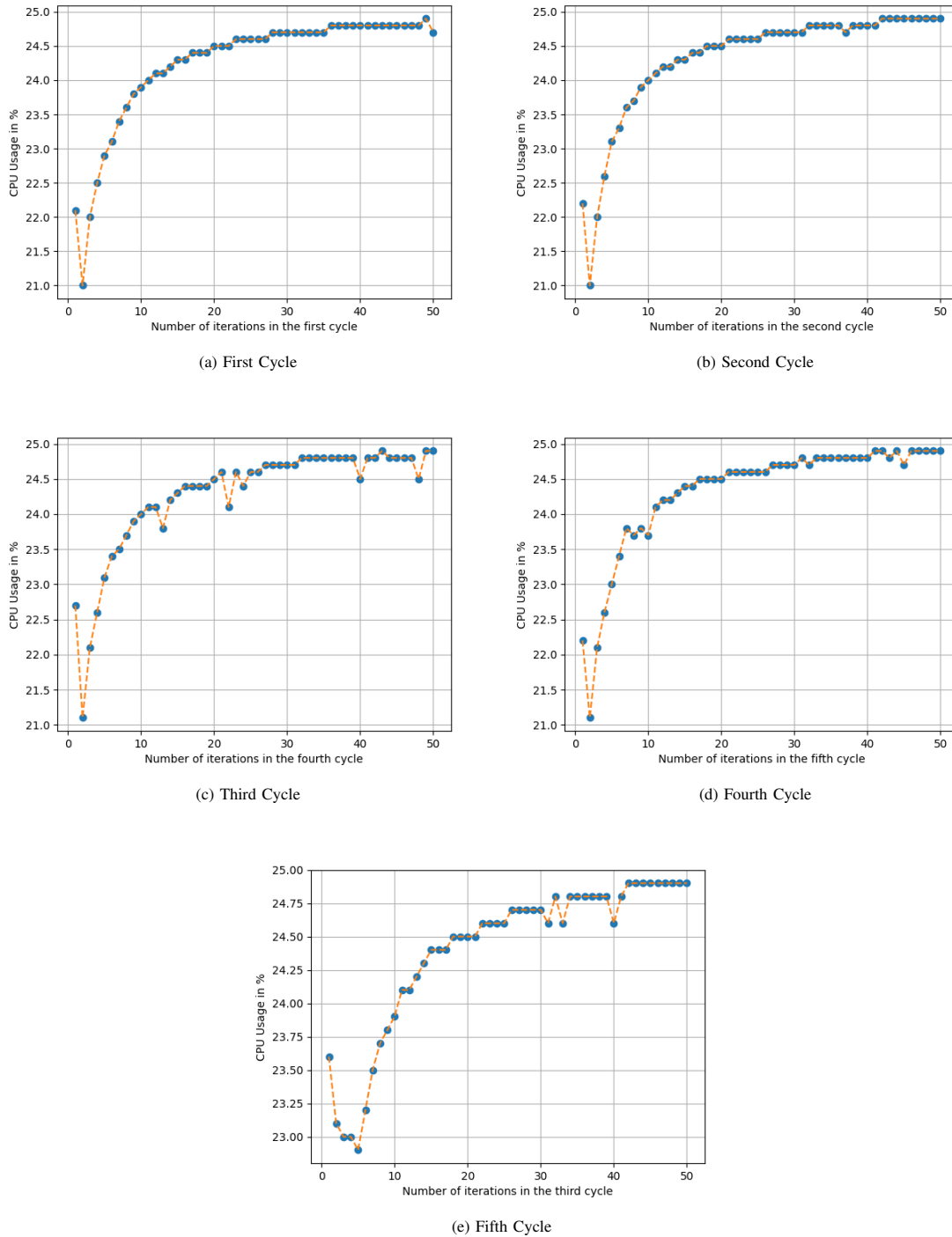


Fig. 6. The Raspberry Pi System-Wide CPU Utilisation for Five Cycles.

Figs. 5.

As mentioned in the previous section, the experiment conducted in this study involved the processing of converting lightning signals to lightning strike locations are run for fifty iterations throughout a single cycle where the cycle is repeated five times. Based on the workload introduced to Raspberry Pi in this experiment and the results obtained (Refer to Figs. 5

- 7), it can be ascertained that the Raspberry Pi can function as an IoT edge processing device. Figs. 5 - 6 demonstrate that Raspberry Pi maintains only 25% system-wide CPU utilisation with a maximum temperature of 51 degrees Celcius. As stated in the preceding section, the Raspberry Pi will not be subjected to a persistent heavy workload in a practical scenario since the collection and conversion processes are done during a

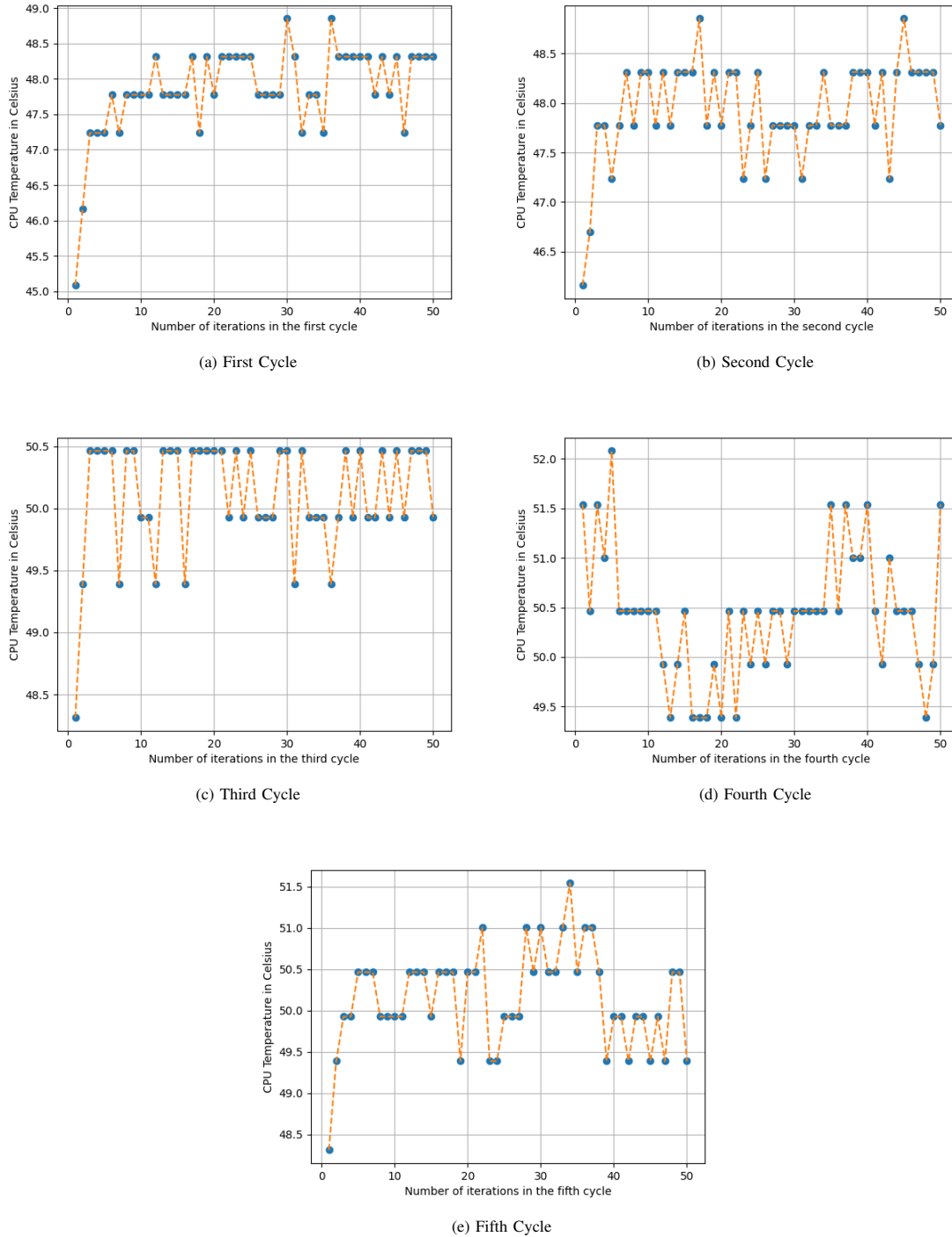


Fig. 7. The Raspberry Pi CPU Temperature for Five Cycles.

thunderstorm only.

VI. CONCLUSION

This research analysed the CPU utilisation and temperature of Raspberry Pi as an edge device that processes lightning strike signals to anticipate the location of flash floods. The experiment aimed to transmit continuous digital signals for

processing to Raspberry Pi. The data indicate that the CPU is only utilised to a maximum of 25%, with a maximum temperature of 51 degrees Celsius. In a real-world scenario, data collection and processing are only performed during a thunderstorm. Therefore, these findings demonstrate Raspberry Pi's capability to handle a persistently substantial workload. As less processing is needed in a real scenario because the

processing occurs only when a thunderstorm strikes, the results prove the Raspberry Pi's capability to process real-time signals.

Currently, this study only focuses on the performance evaluation of Raspberry Pi as an edge processing device in the proposed architecture. The proposed architecture will be implemented and evaluated in a real scenario for future work.

ACKNOWLEDGEMENTS

Authors are grateful to Universiti Teknikal Malaysia Melaka for the financial support through Collaborative Reserch Grant (CRG) S01707 and Short Term Grant (PJP/2020/FTMK/PP/S01764).

REFERENCES

- [1] Priceonomics Data Studio, "The IoT Data Explosion: How Big Is the IoT Data Market?" 2019. [Online]. Available: <https://priceonomics.com/the-iot-data-explosion-how-big-is-the-iot-data/>
- [2] Huawei.com, "Internet of Things Sensing Our Way into the Future," p. 1, 2017. [Online]. Available: <https://www.huawei.com/en/industry-insights/technology/digital-transformation/iot> <http://www.huawei.com/en/industry-insights/digital-transformation/iot>
- [3] Cbinsights.com, "What Is Edge Computing? — CB Insights Research," 2020. [Online]. Available: <https://www.cbinsights.com/research/what-is-edge-computing/>
- [4] K. Gyarmathy, "The Benefits and Potential of Edge Computing," 2019. [Online]. Available: <https://www.vxchnge.com/blog/the-5-best-benefits-of-edge-computing>
- [5] Gartner, "Information Technology (IT) Glossary - Essential Information Technology (IT) Terms & Definitions — Gartner," n.d. [Online]. Available: <https://www.gartner.com/en/information-technology/glossary/edge-computing>
- [6] K. Shaw, "What is edge computing and why it matters — Network World," 2019. [Online]. Available: <https://www.networkworld.com/article/3224893/what-is-edge-computing-and-how-it-s-changing-the-network.html>
- [7] "Buy a Raspberry Pi 3 Model B+ – Raspberry Pi," n.d. [Online]. Available: <https://www.raspberrypi.com/products/raspberry-pi-3-model-b-plus/>
- [8] J. Yang, T. Qian, F. Zhang, and S. U. Khan, "Real-Time Facial Expression Recognition Based on Edge Computing," *IEEE Access*, vol. 9, pp. 76 178–76 190, 2021.
- [9] J. Islam, T. Kumar, I. Kovacevic, and E. Harjula, "Resource-aware Dynamic Service Deployment for Local IoT Edge Computing: Healthcare Use Case," *IEEE Access*, 2021.
- [10] T. Gizinski and X. Cao, "Design, Implementation and Performance of an Edge Computing Prototype Using Raspberry Pis," in *2022 IEEE 12th Annual Computing and Communication Workshop and Conference, CCWC 2022*. Institute of Electrical and Electronics Engineers Inc., 2022, pp. 592–601.
- [11] C. Hegde, Z. Jiang, P. B. Suresha, J. Zelko, S. Seyedi, M. A. Smith, D. W. Wright, R. Kamaleswaran, M. A. Reyna, and G. D. Clifford, "AutoTriage - An open source edge computing Raspberry Pi-based clinical screening system," *medRxiv*, pp. 1–13, April 2020.
- [12] F. Xhafa, B. Kilic, and P. Krause, "Evaluation of IoT stream processing at edge computing layer for semantic data enrichment," *Future Generation Computer Systems*, vol. 105, pp. 730–736, April 2020.
- [13] S. Gondi and V. Pratap, "Performance evaluation of offline speech recognition on edge devices," *Electronics (Switzerland)*, vol. 10, no. 21, p. 2697, Nov 2021.
- [14] E. Gamess and S. Hernandez, "Performance Evaluation of Different Raspberry Pi Models for a Broad Spectrum of Interests," *International Journal of Advanced Computer Science and Applications*, vol. 13, no. 2, pp. 819–829, Aug 2022.
- [15] T. J. Freeborn, "Performance evaluation of raspberry Pi platform for bioimpedance analysis using least squares optimization," *Personal and Ubiquitous Computing*, vol. 23, no. 2, pp. 279–285, Feb 2019.
- [16] A. Komninos, I. Simou, N. Gkorgkolis, and J. Garofalakis, "Performance of raspberry pi microclusters for edge machine learning in tourism," *Network (Mbps)*, vol. 100, no. 100, p. 100, 2019.
- [17] L. Miori, J. Sanin, and S. Helmer, "A platform for edge computing based on raspberry pi clusters," in *British International Conference on Databases*. Springer, 2017, pp. 153–159.
- [18] "MetMalaysia: Radar Semenanjung," n.d. [Online]. Available: <http://www.met.gov.my/pencerapan/radar/radarsemenanjung>
- [19] M. R. Ahmad, M. R. Esa, V. Cooray, Z. A. Baharudin, and P. Het-tiarachchi, "Latitude dependence of narrow bipolar pulse emissions," *Journal of Atmospheric and Solar-Terrestrial Physics*, 2015.
- [20] D. Periannan, M. R. Ahmad, M. H. M. Sabri, M. R. M. Esa, S. A. Mohammad, G. Lu, and S. B. York, "Environmental study of tropical hailstorm and its relationship with negative narrow bipolar event and positive ground flashes," *Ekoloji*, 2019.
- [21] M. H. Sabri, M. R. Ahmad, M. R. Esa, D. Periannan, G. Lu, H. Zhang, V. Cooray, E. Williams, M. Z. Aziz, Z. Abdul-Malek, A. A. Alkahtani, and M. Z. Kadir, "Initial electric field changes of lightning flashes in tropical thunderstorms and their relationship to the lightning initiation mechanism," *Atmospheric Research*, 2019.
- [22] PSUtil, "psutil documentation — psutil 5.8.1 documentation," 2021. [Online]. Available: <https://psutil.readthedocs.io/en/latest/>
- [23] B. Nuttall and D. Jones, "gpiozero — GPIO Zero 1.6.2 Documentation," 2021. [Online]. Available: <https://gpiozero.readthedocs.io/en/stable/>
- [24] R. pi Foundation, "Raspberry Pi Documentation," p. 1, 2014. [Online]. Available: <https://www.raspberrypi.com/documentation/>
- [25] H. Leadbeater and L. Walsh, "Prototyping on a pi," Brainboxes, Tech. Rep., 2020. [Online]. Available: <https://offer.brainboxes.com/prototyping-on-a-pi>
- [26] Brainboxes Buff, "BB-440 Industrial Edge Controller powered by Raspberry Pi," 2020. [Online]. Available: <https://www.rs-online.com/designspark/how-does-raspberry-pi-deal-with-overheating>

Decentralized Payment Aggregator: Hyperledger Fabric

Md.AI-Amin¹

Faculty
Department of Computer Science
Faculty of Science And Technology
American International
University-Bangladesh

Khondoker Shahrina²

Department of Computer Science
Faculty of Science And Technology
American International
University-Bangladesh

Rubyet Hossain³

Department of Computer Science
Faculty of Science And Technology
American International
University-Bangladesh

Debashish Sarker⁴

Department of Computer Science
Faculty of Science And Technology
American International
University-Bangladesh

Sumya Sultana Meem⁵

Department of Computer Science
Faculty of Science And Technology
American International
University-Bangladesh

Abstract—Blockchain has become a great trend and very popular in the present era. There are two types of Blockchain technology, centralized and decentralized. In this research, the main concern is about the decentralized payment gateway, which is a trustworthy architecture and does not depend on third parties. For recording the transaction, decentralized payment systems use distributed ledger. Previously, Bitcoin and Ethereum payment systems were used to verify the consistency of the ledger of blockchain and also the transaction data along with the sender-receiver address and transaction value, but as all the payment system is public, so the transaction mode is also public. However, here the main concern is privacy and security. Because anyone can easily access the network, the attacker can also attack the network and the identity and transaction records and the address of the user identity, which is a privacy challenge. This research incorporates the Hyperledger Fabric, which is private, to overcome this challenge. Moreover, no one can access it from outside of the network. The transaction cost is low and the timing is fast during transactions. Considering the above scenario, this research proposes a decentralized payment system architecture using Hyperledger Fabric.

Keywords—Blockchain; decentralized; hyperledger fabric; bitcoin; payment system

I. INTRODUCTION

In the present world, transactions have become one of the communication mediums. So it is imperative to ensure that the transaction should be safe and secure. Because of the many uses of distributed ledger technology, some companies have built their version of Blockchain systems to meet their requirements, resulting in the in-house creation of many blockchain solutions using multiple systems and architectures. Such projects use various technologies and consensus methods tailored to specific applications and use cases. Because of the vast number of initiatives, development has become increasingly fragmented, with no or little compatibility across various blockchain protocols [1]. In the earlier, third-party interference was the only medium for transactions. However, it was proven to be very insecure. The increasing number of

online platforms has raised the necessity of payment systems. Payment gateways enabled online platforms to integrate multiple payment methods at once, often leading to more sales and engagement to the online platform. In short, many payment gateways are available, including international and local ones. Currently, they are built on a centralized system and use several strategies to minimize the cost of each transaction. They often tend to save up the money received from customers and hold the money for several days to earn revenue from the saved money. This method causes the merchants not to be able to receive money immediately but reduces the cost of the transferred money. Hyperledger Fabric, a distributed ledger platform, solves the problem of reducing third-party dependencies and removes double spending issues. It is a successful innovation that ensures money is spent only once. Decentralized systems are a platform where they can interact with other parties without involving the third party or any intermediaries. Hyperledger Fabric is a decentralized permissioned blockchain infrastructure and the fastest open source permissioned blockchain [24]. It is challenging to hack because it uses mathematical computation. Chaincode is the primary smart contract in the Hyperledger Fabric. Chaincode is executed by the peer nodes of a Fabric network, accessing the ledger data and endorsing transactions. Mainly the architecture of Hyperledger Fabric provides flexibility and a high degree of resilience in implementation and design. The flexibility of design achieves privacy, scalability, and other essential attributes. Blockchain service is the central part of the Fabric. Hyperledger Fabric chain code allows any programming language but commonly used Go language, JavaScript and Java, but appropriate modules should be installed [2]. This paper aims to construct a decentralized payment gateway that allows unlimited payments of any amount, is more secure, low cost in transactions, gives the best performance, and the main thing that Hyperledger Fabric ensures is the system's security. The problems of a centralized payment gateway can be understood from the above discussion and how decentralized payment gateways can solve them. In the Asian subcontinent, there is no

service to address the issues of a centralized payment gateway. To address this issue, this work presents a gateway to improve the payment service.

A. Research Goal

1) *Research Objective:* This research aims to construct a decentralized payment system that will solve the loopholes that come with the centralized payment system.

2) *Significance of Research:* Currently, centralized payment systems are using several strategies to lessen the cost of transactions and earn revenue from pending transactions. A decentralized payment system can eliminate this issue and make the process more secure and efficient. This research is taking place to improve the payment service by introducing a decentralized payment system.

3) *Research Question:* The main purpose of conducting this research can be expressed as below:

- 1) What are the problems of centralized payment systems?
- 2) Will decentralized payment systems eliminate or lessen the existing problems?
- 3) How will people be benefited from a decentralized payment system?
- 4) What will be the challenges of introducing a decentralized payment system?

II. RELATED WORKS

Decentralized cryptocurrencies like as Bitcoin [3], Hyperledger Fabric [4], Zcash [5] and Ethereum [6] have been a trending issue, and blockchain technology, received increasing attention. Currently, the blockchain plays a significant role also in financial sector [7]. In previous before blockchain invention, many authors proposed different protocols and solutions to make the transaction procedure secure and easy way. Such as, The authors of [8] presented is a payment mechanism for peer-to-peer (P2P) commercial transactions. It facilitates electronic currency transactions between purchasers and vendors. In this arrangement, financial companies become collaborators in their clients' Internet-based e-commerce transactions [23]. The uniqueness of the proposed approach is the restriction of the finance sector' engagement to supplementary services and support but in that circumstance there were some drawbacks regarding the security. Blockchain invention by S.Nakamoto [9] brought also progress in the financial sector where A peer-to-peer formed of electronic currency which would enable internet payments to be transmitted through one party to another, bypassing banking institutions. The main concern of the solution was to remove double-spending issue [10]. All the transactions are hashed into a chain which is hash-based proof-of-work of that network and after establishing record cannot be modified without repeating the proof-of-work. It provides the main security issue. In article [11] the authors describes a distributed payment method which is based in payment tokens that uses Blockchain technology to safeguard consumers from data theft caused by illegal use of their payment card information owing to payment system inefficiency. Furthermore, the privacy and security of the system is consolidated by a permissioned Blockchain consortium. Using blockchain technology, the authors [12] create a centralized payment

counter money transfer mechanism. Blockchain technology inherent decentralization, distributed verification, transparency on transmission, as well as other features, the method not only recognizes that transaction records can also increases payment security, and completely protects client privacy. It eliminates the issues of money usage security and danger created by inappropriate teller operation in the standard counter cash withdrawal method. In [13] the authors proposed a method called Fastpay where the authors combined the concepts of blockchain technology and IoT [14]. FastPay, which ensures the security of quick payments in blockchain-powered edge and IoT systems. FastPay is based upon the smart contract concept, which is implemented by several well-known blockchain platforms, including Ethereum [15]. The system ensures quick payments by requiring consumers and guarantors to produce transaction proofs before payment is done. With these evidence, consumers and guarantors will face harsh fines if they attempt double-spending scams [25]. A payment takes 9 seconds to confirm. The authors [16] approach a system that supports late payments using our novel idea known as latent-transactions. This study also incorporates the tools for making effective off-chain contracts between the entities engaged in a transactions. As a result, one may profit from a service before paying for it. Furthermore, the system provides a service expansion mechanism by offering a catalog to which any Blockchain user can register and one may offer services with flexible pricing based on the context such as need, activity at execution time, etc. The authors proposed an algorithm using blockchain concept. The algorithm will enable users to operate on blockchain networks using cryptocurrencies. It differs significantly from the current system in that customers would be able to exchange without the assistance of third parties, and merchants will also be eased with their transaction. This form of transaction will be highly convenient for both buyers and sellers. Consumers and suppliers may both have this whole transaction time, date and all the things they engaged with while the transaction has been taken place [17].

III. BACKGROUND STUDY

A. Blockchain

Blockchain service contains P2P Protocol, Distributed Ledger and Consensus Manager, these three major components. P2P Protocol provides capabilities like flow control and bidirectional streaming as it uses Google RPC [18]. It works along with existing internet system [9].

Distributed ledger calculates a crypto hash after each block, transmits minimal delta of changes of out of sync peers and minimize the size of data efficiently to manage the world state and blockchain. It uses a special database environment called RocksDB [19] to preserve the dataset. Other large files are not stored on the ledger but their hashes can be stored on the ledger. There are two types of transaction Hyperledger supports: code-deploying and code-invoking. Code-deploying transactions are to install, update or remove a Chaincode. On the other hand, code-invoking transactions are to execute a Chaincode function through API call. Consensus Manager accepts transactions and decides the way to organize and the time to execute a transaction depending on algorithm. If a transaction is successfully executed, it causes the ledger to be changed. Hyperledger has implementation of PBFT (Practical

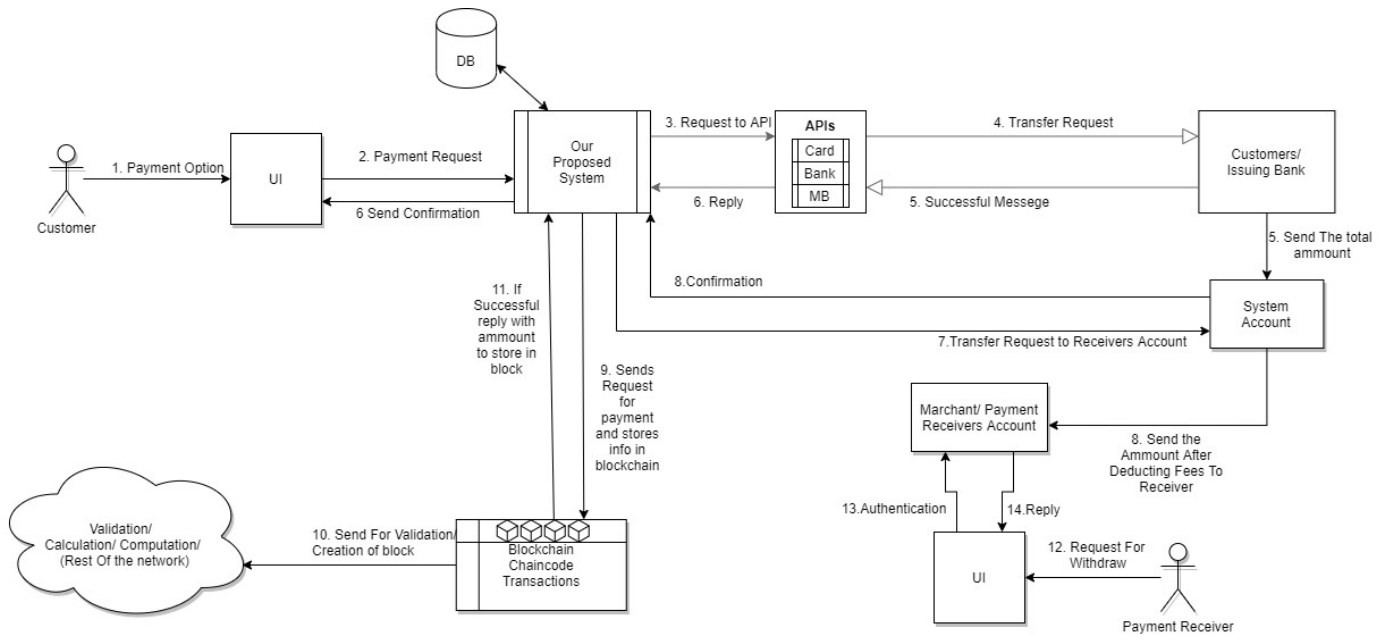


Fig. 1. Architecture of Proposed System.

Byzantine Fault Tolerance) which ensures advanced scalability and fault tolerance.

B. Hyperledger Fabric

Now a days blockchain technology is the most emerging technology and it can be implemented in many different ways. Research is going on this field and researcher create different types of DLT(distributed ledger technology) for different purposes and construction [26]. In present moment three of the most popular DLT's are "Ethereum"² [6], "R3 Corda"³ (Corda) [20], "Hyperledger Fabric"⁴ (Fabric) [6]. These DLT's have different visions of the application of blockchain in different fields. Ethereum is the independent and it is a less and public approval DLT. On the other hand, Hyperledger Fabric and Corda DLT are allowed. Corda focuses on the financial services industry; Fabric focuses on developing a modular and extensible architecture that can be used in various industries, with a focus on banking and healthcare services, the supply chain. Hyperledger takes a unique method to the traditional blockchain model, in part by manipulating the admission of participants to its base. In other words, Hyperledger is an authorized shared ledger. Hyperledger records computational cycles, reduces scales and meets the multitude of case requirements. Hyperledger is based on the expectation that there will be many blockchain networks, with each network registration serving a different purpose. Although there is a single popular instance of a common network, it is not necessary for a network registry to rely on another network for its basic functionality. Despite this network independence, Hyperledger still needs an addressing system that allows transactions in one registry to identify and use appropriate transactions and chain code in other registers.

C. Chaincode

Chaincode service hosts the Chaincode using Docker which yields a lightweight and secure system for Chaincode execution. Secured Docker Registry of Hyperledger images and Chaincode containing custom images are enabled by Secure Registry Services. Alike invocation of webservice or database call, Chaincode transactions are configured while deploying the Chaincode and they are time bounded [27]. The ledger will not update if a transaction runs out of time. After reaching consensus for a block, the database is committed with the changes and number of world state block increments. If peers fail to reach consensus, the update is discarded and database no not change.

IV. PROPOSED SYSTEM MODULES

As discussed earlier, the proposed system designed a payment gateway that will allow Sender to pay directly to the receiver using a decentralized network. The proposed have designed the system in a manner that if any organization or individual wants to receive payment they can integrate our API to their website and Immediately start getting payment. Unlike other centralized payment gateways it doesn't delays the payment. The system will autonomously handle all the account creating process, transactions, building blocks, Committing to the blockchain and retrieving data from the blockchain [29].

A. Architectural Infrastructure

The proposed system has used the linux foundations Hyperledger Fabric [28] as a framework for this project. The whole architecture is designed according to that. Hyperledger Fabric's architecture allows us to create a private network for all the organizations. All the automation part will be handled by the Chaincode. This is the smart contract of Hyperledger Fabric. There will be a central database which will keep the

data while the whole process ends, but to make sure the safety and privacy our system doesn't give access to the database to anyone only accessed by the system itself and also data can't be manipulated because only big data is kept here, and all the information about this is referred to the blocks of blockchain.

Fig. 1 shows how the whole system works from taking the sender/customer sends the money and the receiver receives their payment. The first step is the customer uses the user interface to send money that uses our API to communicate with out automated system. Customer sends the payment request by using their preferred method. Full details about this is discussed in the next modules section.

When the system gets request from the UI then it immediately forwards to the respective bank or card processors. It handles the communication with the bank verifies all the information. If everything is verified and ok then at the same time bank transfers the whole amount to our systems bank and a notification of confirmation to this system.

After the system gets successful transfer notification from the bank, at the same time it sends confirmation to the customer that the payment is complete. At this time our system sends requests to commit this change of asset from customer through different type of payment methods to our bank account. This data flow will be discussed in the net section.

While the first phase is complete it is ready to send the money to the receiver. Receivers will have a fixed account to receive money that he gives while registering. It checks if enough balance is available to be transferred to the receivers account or not. If not, then it waits for some times before transferring. Meanwhile it collects all the money from the all types of payment methods and transfers it to the systems main bank account. Then when there is enough money, Our system makes another request to systems bank to send the rest of amount after deducting the fees from the whole amount to the receivers account.

Bank sends the amount to the receivers account and at the same time gives confirmation to our system. This whole time all the information was kept safe in our system and when these two confirmations are received by our system, it sends the whole request to add them to the blockchain. Then it gets verified and also confirmation is sent back to our system after the transitions is added to the block. This whole verification process is also described later in the modules section.

At the same time there can be more than one transaction from more than one customer. And also, this system is designed to accept all the transactions for all the registered company. For example, two customers from "XYZ" Company is paying online. Both of the transaction will happen individually and as different transaction but it doesn't mean that will create individual blocks. There can be more than one transaction in the block. But using the hashes and timestamp of the block it can easily be found each individual transaction.

Organizations can register with valid information to integrate and use our service and that will also happen using our UI and that information are also saved in to blockchain so that no one can temper those data. The whole operation will run autonomously once the system is up in the network. Here is the Short Pseudocode the of whole operation is provided.

Algorithm 1 Payment Operation for a Customer

```
1: Output: Transfer money from senders account to re-
2:   ceivers account and store the transaction information
3:  $m \leftarrow$  Payment Method (Card, Bank, etc.)
4:  $r \leftarrow$  The Receiver
5:  $a \leftarrow$  The Amount To Be Transacted
6: if  $m$  is card then
7:   Check Card Validity
8:   Attempt to perform money transfer to system account
9:   Set status received from card API
10: else if  $m$  is bank then
11:   Get redirection URL from bank API
12:   Redirect to URL with System account number and
13:   amount
14:   Bank API listens to response from the bank
15: end if
16: if successful transaction then
17:   Generate token
18:   Update Ledger
19:   Calculate charge from set of rules
20:   Attempt money transfer (deducting charge) from system
21:   account to  $r$ 
22: if successful transaction then
23:   Update token
24:   Update Ledger
25:   Broadcast Ledger
26:   Return to origin website with status true and token
27: else
28:   Broadcast Ledger
29:   Return to origin website with status partial
30: end if
31: else
32:   Return to origin website with status false
33: end if
```

B. Data Flow:

As in this proposed system have used hyperledger Fabric as our framework while designing the whole architecture we are following the convention and rules of hyperledger Fabric. In our system two transactions will be committed against each payment or money sending.

The first one is the asset transfer from customer or the sender to our bank. In the figure, this first step is represented by Org 1 and Org 2. There are multiple users in Org 1. They represent the payment methods. Our system will get an API response from them when any transfer is done then it will take those information and commit them to the blockchain.

In the 2nd part the system will request a transfer, from our bank to the receivers bank. This asset transfer part is represented using Org 2 and Org 3. Also there are different uses in the Org 3. They represent a company or event. If a company wants to receive the money the endorsement are handled by the p2 and p3 peers. And if events want to receive money then P2 and P4 is the endorsers because there might be different permissions set to different type of peers.

So, the transaction flow for both of the committing steps are like this:

The transaction request is generated from application and

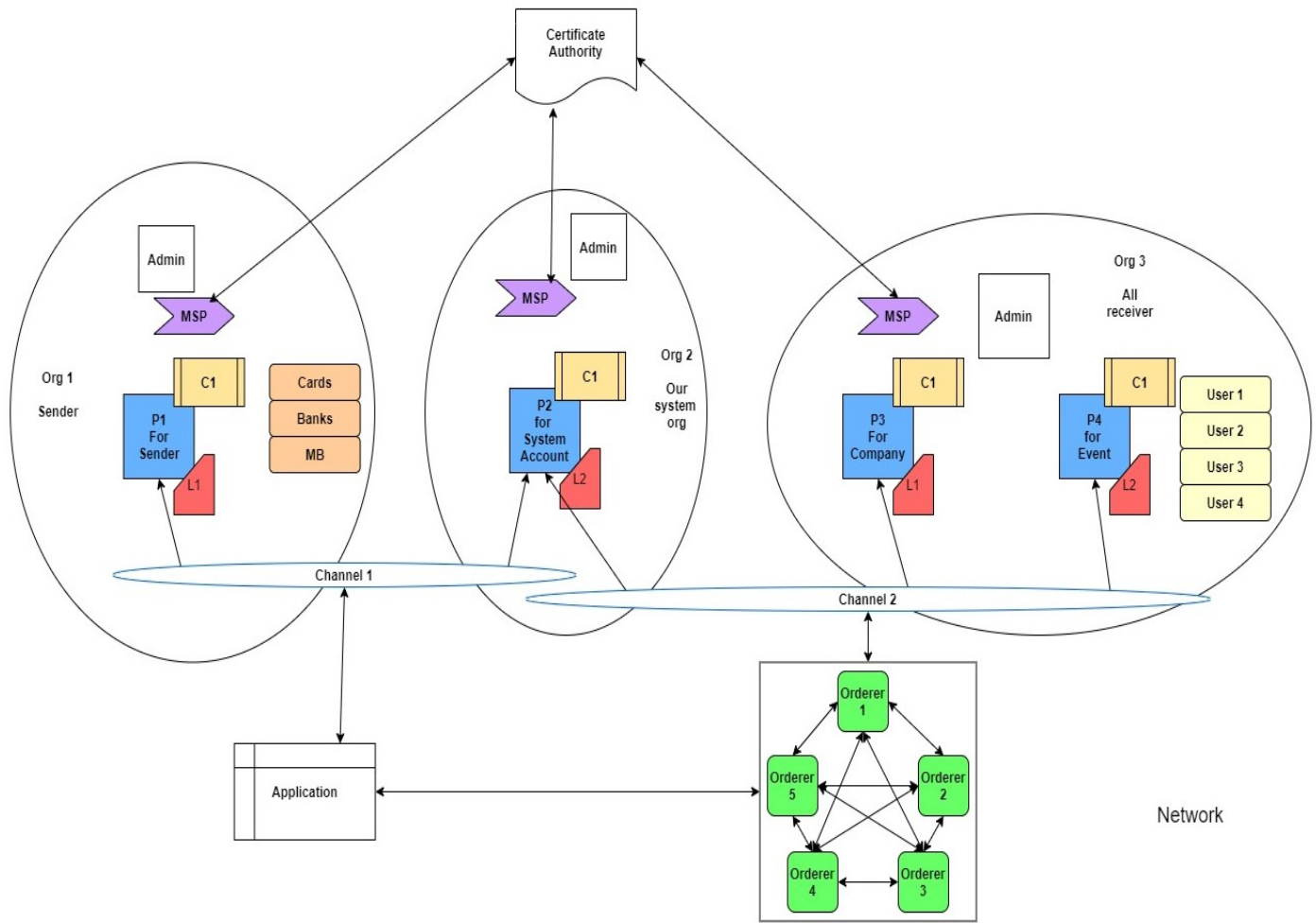


Fig. 2. Data Flow and Committing Procedure into Blockchain.

this application leveraging a supported SDK utilizes one of each Organizations peers to generate transaction proposal. This transaction proposal is send to the peer and these peers are registered through certificate authority. But the responsibilities of the peers are defined by the MSP. That means which transaction is belong to which peer and this peers endorsing and committing permissions are defined by MSP. In each peer there is also a ledger where all the transactions are stored. When the transaction is transfer to the peer, the peer executes the chaincode and validates the transaction but this transaction is not stored in the ledger yet. Only a validate proposal with valid sign is generated and this proposal is verified by the application. If both signed proposal from both peer is matched then it sends this updated proposal to the orderer node.

Meanwhile as there are multiple orderer nodes available, the RAFT consensus protocol is used to choose which orderer will commit the next block. Also, as there are multiple nodes so if one node is down rest of the nodes can build the block.

These orderer node at a time can accept multiple transaction from various application and check the validity of these nodes and generate a block. These blocks are sent to the endorsing peer again to check all those transactions which are endorsed using endorsing peers. If any transactions are

remaining in any block which is not endorsed before then this block will consider as invalid block. Otherwise the block will be considered as valid block and add in the ledger of every peer of the network. A pictorial presentation of the scenario is given in Fig. 2.

- 1) Balance transfer request is generated from the application and it's broadcast through channel 1 to peer1 or p1 which is the peer of org1 and peer2 or p2 which is the peer of org2.
Note: Every peer is registered or generate an authorized signature through certificate authority and the responsibility of each peer is defined by MSP.
- 2) This peer actually performs four things 1st one is that the if transaction proposal is well formed or not 2nd one is this proposal is new or has been submitted at past. 3rd one is if the signature is valid. 4th one is that the submitter is fully authorized to perform this specific transaction.
- 3) This p1 and p2 endorsing peer uses the transaction request as argument to invoke the chaincode.
- 4) The chaincode is then executed against the current state database to produce transaction results including a response value, read set, and write set but not update

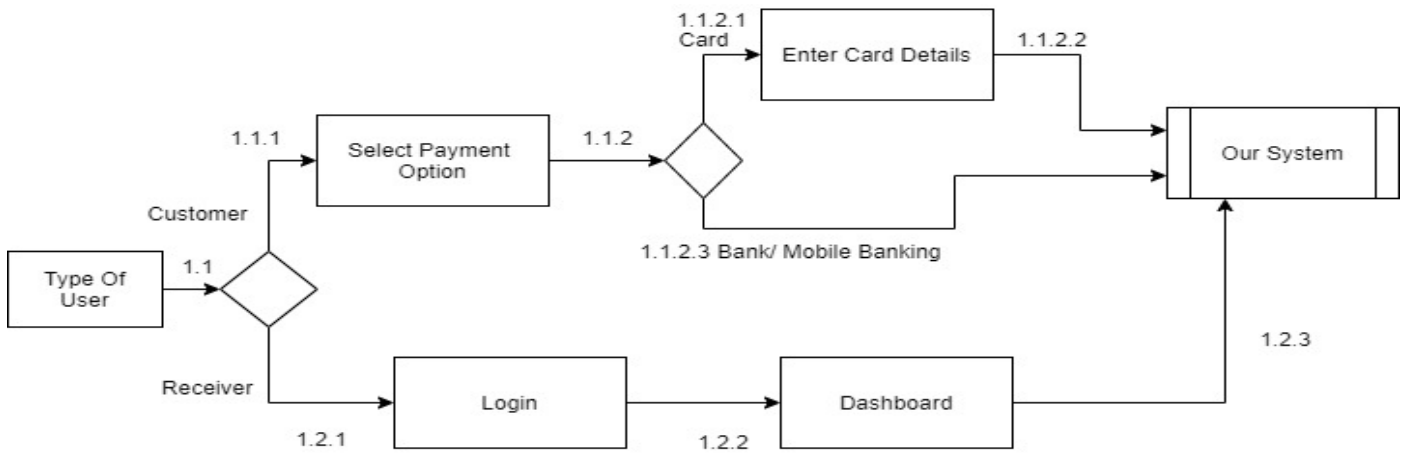


Fig. 3. Data Flow of User Interface Module(Part-1).

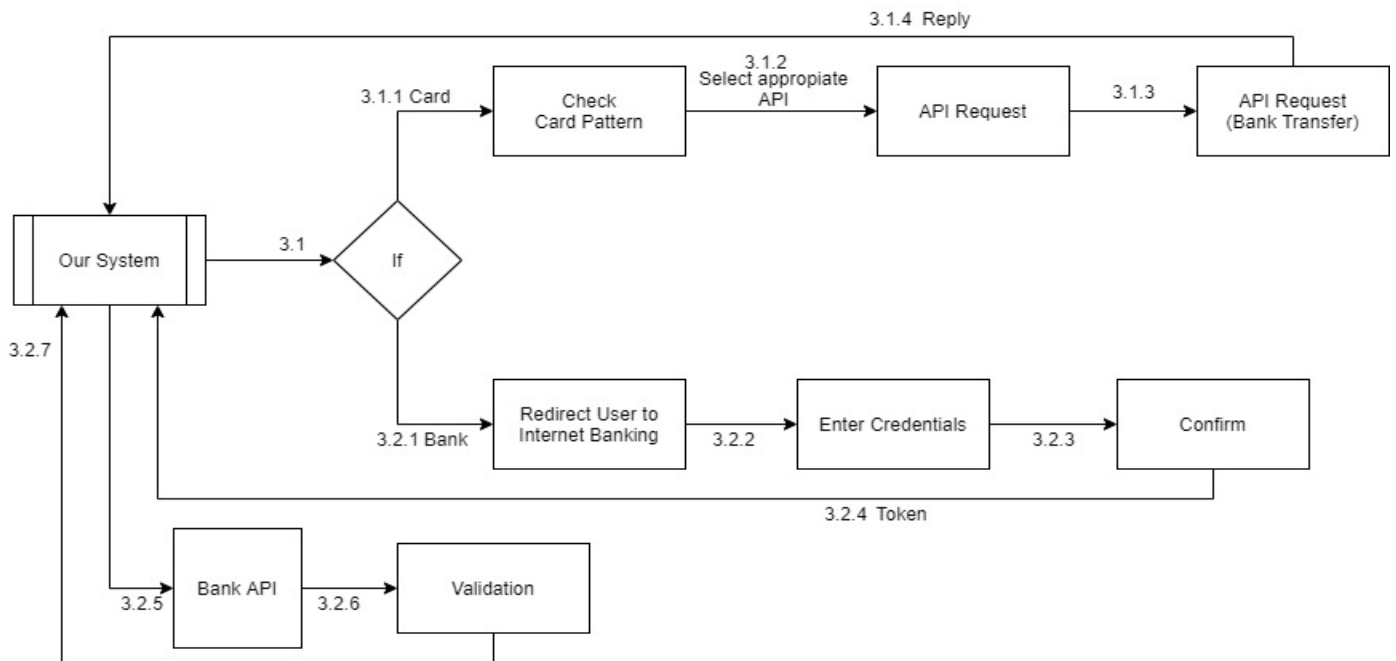


Fig. 4. Data Flow of User Interface Module(Part-2).

- the ledger.
- 5) The set of these values, along with the endorsing peer's signature is passed back as a "proposal response" to the application.
 - 6) The application verifies the endorsing peer signatures and compares the proposal responses to determine if the proposal responses are the same.
 - 7) Then the application sends it to the orderer nodes and in this step the application choose a leader orderer node and remains as follower.
 - 8) After receiving the proposal response the orderer node make a block.
 - 9) After creating the block the orderer node then transfer it to all the peers that means p1(org1), p2(org2) and p3, p4(org3) through a global channel.
 - 10) Then these endorsing peers check the signature and

the channel ID and if match then commit the block is valid and finally add it in every peers ledger.

C. Modules:

All the operations in the main architecture, We have separated into 3 different modules. These are,

- User Interface Module
- Bank API Module
- Blockchain Module

1) *User Interface Module:* This module uses our UI to do all the interaction. Customer uses this to select payment method and pay to the receiver. On the other hand, Receiver or the organization can login to their account to see all the

history and other information in their dashboard. The data flow is shown in Fig. 3.

If customer wants to pay, it redirects to the payment option. There are multiple options, for simplicity we are representing bank/mobile banking option and direct card option here. If user selects card option then they put their card details. They can choose to save the details for further use. We use our system to also store the card info to the blockchain if needed. Then the card details is send to system to communicate with the card API. Else if customer choose to pay direct through bank then it requests to out system and it forwards the customer to the internet/mobile banking site for further steps.

From the receiver side, organizations can register to use our service and after successful registration, they can use our interface to login to their account and see their dashboard. In there, all their information is stored and all the histories and all the transactions are displayed.

2) *Bank API Module*: Whether the customer chooses the card or bank our system requests to the proper API to communicate with the bank. The data flow is shown in Fig. 4.

When the customer chooses the Card option it checks the card pattern and requests to the proper API, Like if pattern is for VISA then it sends request to VISA API, which completes all the processing with the bank and transfers the money to our bank and sends success reply to our system.

If the customer chooses bank, then our system redirects it to the internet banking site or mobile banking site and there they give their credential and follow the steps to transfer money to our system's bank account. When successful, it returns a token. Our system takes that token and verifies with the bank API and if all goes right then the transaction gets completed.

3) *Blockchain Module*: This module validates and adds data to the block and adds the block to the blockchain [?]. As Hyperledger Fabric is used, their system is also being used as the architecture of this module. The data flow is shown in Fig. 5.

- 1) Initiate to complete the transfer request to Our System (SDK)
- 2) The SDK sends a transaction proposal to the Peers for the endorsement
- 3) The proposals are sent to the peers to execute solve and validate.
- 4) The Peers endorses, performs Chaincode / Smart Contract execution at this point, before endorsing the transaction proposal.
- 5) After Success it returns to the peers.
- 6) Then they sign the transaction proposal and returns it to the SDK. (SDk Checks for the validation by comparing to the proposal with the response).
- 7) If the proposal and Response matches SDK sends request to the Orderer for ordering service.
- 8) Executes and creates new block.
- 9) After ordering the transactions, forming block, it broadcasts the block to the Peers
- 10) The Peers notifies the SDK — the block is committed in the Blockchain for the data also the Peer performs transactions validation and block commitment at this point, before notifying the SDK.

- 11) The SDK sends a response to the customer and receiver — the block is committed in the Blockchain for the transfer.

This is how the full cycle is done. This gateway uses the decentralized network of Hyperledger Fabric and all the process happens synchronously any autonomously. The system is designed in such a way that no central authority is needed for the operation. And no one can even change any data as there is no control or access over the system. The system only gives read-only data as a query result and only writes data when chaincode is executed, validated and added to the blockchain.

V. CHALLENGES

During the time of research, we faced some challenges. We have established the architecture of the network and its working procedure in this research paper. However, we could not implement the network in a physical device due to time constraints and a lack of proper documentation on the chosen technology. Research should be carried on by implementing the network in a physical device for a better understanding of the network [22]. Due to the nature of the blockchain network, the transactions' validation process takes longer than in a centralized system, leading to a slow completion time for any transaction. Nevertheless, it provides a more secure environment than a centralized system. It is a trade-off between time and security. Blockchain network does not recommend storing large data, as extensive data makes the network vulnerable. As a result, centralized data storage was necessary for extensive data.

VI. CONCLUSION

In this research, a payment system based on decentralized ledger technology is proposed to keep transactions more secure and allow merchants to receive payment as soon as a transaction is verified. Saving time on receiving the payments and security was the primary concern in this research. We focused on the security and reliability part by using Hyperledger Fabric. A blockchain-based decentralized network gives each user high security and an immutable ledger. Furthermore, private network like Hyperledger Fabric allows reliability by keeping sensitive data private. Current progress indicates the foundation towards building a decentralized payment gateway. This fundamental architecture will help to build a more secure and fast payment gateway and will be able to overcome the shortage of traditional methods.

VII. FUTURE WORK

In future, this research can be used to build an actual working gateway and storage system independent from any centralized storage by making the data structure more efficient. Some improvements and more efficient data management can be made in the future. Error handling, such as when the customer successfully sends money to the system account, but our system fails to transfer money to the desired merchant account, is not shown in the research. Future research can work on how the errors should be handled.

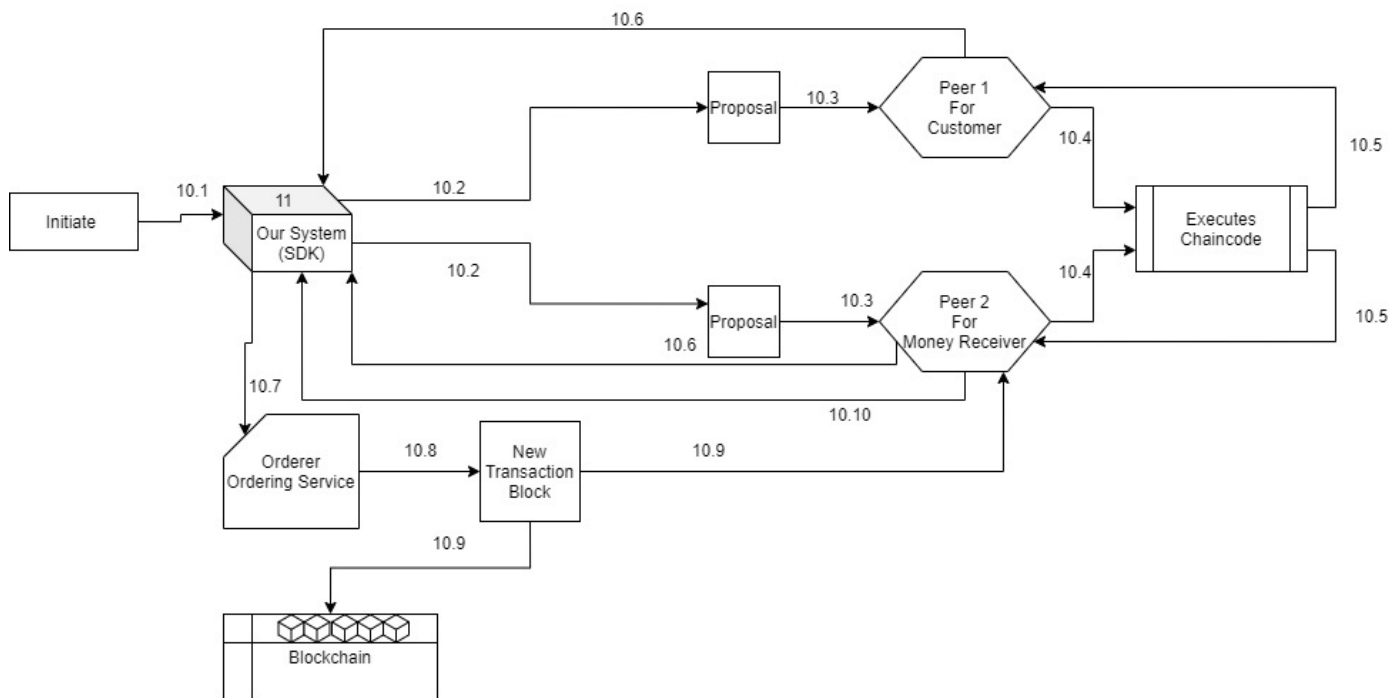


Fig. 5. Data Flow of Blockchain Module.

REFERENCES

- [1] Jin, H., Dai, X., & Xiao, J. (2018, July). Towards a novel architecture for enabling interoperability amongst multiple blockchains. In 2018 IEEE 38th International Conference on Distributed Computing Systems (ICDCS) (pp. 1203-1211). IEEE.
- [2] Androulaki, E., Barger, A., Bortnikov, V., Cachin, C., Christidis, K., De Caro, A., Enyeart, D., Ferris, C., Laventman, G., Manevich, Y. and Muralidharan, S., 2018, April. Hyperledger Fabric: a distributed operating system for permissioned blockchains. In Proceedings of the thirteenth EuroSys conference (pp. 1-15).
- [3] Nakamoto, S. (2009). Bitcoin: A peer-to-peer electronic cash system Bitcoin: A Peer-to-Peer Electronic Cash System. Bitcoin. org. Disponible en <https://bitcoin.org/en/bitcoin-paper>.
- [4] Aggarwal, S., & Kumar, N. (2021). Hyperledger. In Advances in Computers (Vol. 121, pp. 323-343). Elsevier.
- [5] Hopwood, D., Bowe, S., Hornby, T., & Wilcox, N. (2016). Zcash protocol specification. GitHub: San Francisco, CA, USA, 1.
- [6] Vujičić, D., Jagodić, D., & Randić, S. (2018, March). Blockchain technology, bitcoin, and Ethereum: A brief overview. In 2018 17th international symposium infotech-jahorina (infotech) (pp. 1-6). IEEE.
- [7] Cermeño, J. S. (2016). Blockchain in financial services: Regulatory landscape and future challenges for its commercial application. BBVA Research Paper, 16, 20.
- [8] Palaka, D., Daras, P., Petridis, K., & Strintzis, M. G. (2004). A Novel Peer-to-Peer Payment System. ICETE (1), 245-250.
- [9] Nakamoto, S. (2008). Bitcoin: A peer-to-peer electronic cash system. Decentralized Business Review, 21260.
- [10] Chohan, U. W. (2021). The double spending problem and cryptocurrencies. Available at SSRN 3090174.
- [11] Zouina, M., & Outtai, B. (2019, April). Towards a distributed token based payment system using blockchain technology. In 2019 International Conference on Advanced Communication Technologies and Networking (CommNet) (pp. 1-10). IEEE.
- [12] Shen, B., & Wang, X. (2021, December). Design of treasury centralized payment counter cash withdrawal system based on blockchain Technology. In ICMLCA 2021; 2nd International Conference on Machine Learning and Computer Application (pp. 1-5). VDE.
- [13] Hao, Z., Ji, R., & Li, Q. (2018, October). FastPay: a secure fast payment method for edge-IoT platforms using blockchain. In 2018 IEEE/ACM Symposium on Edge Computing (SEC) (pp. 410-415). IEEE.
- [14] Madakam, S., Lake, V., Lake, V., & Lake, V. (2015). Internet of Things (IoT): A literature review. Journal of Computer and Communications, 3(05), 164.
- [15] Wood, G. (2014). Ethereum: A secure decentralised generalised transaction ledger. Ethereum project yellow paper, 151(2014), 1-32.
- [16] Popa, A. B., Stan, I. M., & Rughiniş, R. (2018, September). Instant payment and latent transactions on the Ethereum Blockchain. In 2018 17th RoEduNet Conference: Networking in Education and Research (RoEduNet) (pp. 1-4). IEEE.
- [17] Ahamed, S., Siddika, M., Islam, S., Anika, S., Anjum, A., & Biswas, M. (2021). Bps: Blockchain based decentralized secure and versatile light payment system. Asian Journal of Research in Computer Science, 12-20.
- [18] Ahamed, S., Siddika, M., Islam, S., Anika, S., Anjum, A., & Biswas, M. (2021). Bps: Blockchain based decentralized secure and versatile light payment system. Asian Journal of Research in Computer Science, 12-20.
- [19] Cao, Z., Dong, S., Vemuri, S., & Du, D. H. (2020). Characterizing, Modeling, and Benchmarking RocksDBKey-Value Workloads at Facebook. In 18th USENIX Conference on File and Storage Technologies (FAST 20) (pp. 209-223).
- [20] Mohanty, D. (2019). R3 Corda for Architects and Developers: With Case Studies in Finance, Insurance, Healthcare, Travel, Telecom, and Agriculture. Apress.
- [21] Transaction flow." <https://hyperledger-fabric.readthedocs.io/en/release-2.0/txflow.html>.
- [22] Rajawat, Anand Singh, et al. "Blockchain-based model for expanding IoT device data security." Advances in Applications of Data-Driven Computing. Springer, Singapore, 2021. 61-71.
- [23] Hong, Weiyin, and Kevin Zhu. "Migrating to internet-based e-commerce: Factors affecting e-commerce adoption and migration at the firm level." Information & management 43.2 (2006): 204-221.
- [24] Cachin, Christian. "Architecture of the hyperledger blockchain fabric." Workshop on distributed cryptocurrencies and consensus ledgers. Vol. 310. No. 4. 2016.

- [25] Chohan, Usman W. "The double spending problem and cryptocurrencies." Available at SSRN 3090174 (2021).
- [26] Sunyaev, Ali. "Distributed ledger technology." *Internet Computing*. Springer, Cham, 2020. 265-299.
- [27] Foschini, Luca, et al. "HyperLedger fabric blockchain: chaincode performance analysis." *ICC 2020-2020 IEEE International Conference on Communications (ICC)*. IEEE, 2020.
- [28] Dhillon, Vikram, David Metcalf, and Max Hooper. "The hyperledger project." *Blockchain enabled applications*. Apress, Berkeley, CA, 2017. 139-149.
- [29] Elghaish, Faris, Sepehr Abrishami, and M. Reza Hosseini. "Integrated project delivery with blockchain: An automated financial system." *Automation in construction* 114 (2020): 103182.

Efficient HPC and Energy-Aware Proactive Dynamic VM Consolidation in Cloud Computing

Rukshanda Kamran

Faculty of Computer Science and
Information Technology,
University Malaysia Sarawak

94300 Kota Samarahan Sarawak, Malaysia

Ali A. El-Moursy

Computer Engineering Department,
University of Sharjah
Sharjah, UAE

Amany Abdelsamea

Computers and Systems Department,
Electronics Research Institute
Giza, Egypt

Abstract—The adoption of High-Performance Computing (HPC) applications has gained an extensive interest in the Cloud computing. Current cloud vendors utilize separate management tools for HPC and non-HPC applications, missing out on the consolidation benefits of virtualization. Non-HPC applications executed in the cloud may interfere with resource-hungry HPC applications, which is a key performance challenge. Furthermore, correlations between application major performance indicators, such as response time and throughput, with resource capacities reveal that conventional placement strategies are impacting virtual machine efficiency, resulting in poor resource optimization, increased operating expenses, and longer wait times. Since applications often underutilized the hardware, smart execution of HPC and Non-HPC applications on the same node can boost system and energy efficiency. This research incorporates proactive dynamic VM consolidation to enhance the resource usage and performance while maintaining energy efficiency. The proposed algorithm generates a workload-aware fine-grained classification by employing machine learning techniques to generate complementary profiles that alleviate cross-application interference by intelligently co-locating non-HPC and HPC applications. The research used CloudSim to simulate real HPC workloads. The results verified that the proposed algorithm outperforms all heuristic methods with respect to the metrics in key areas.

Keywords—Cloud computing; HPC (High-Performance Computing); virtual machine consolidation; placement; optimization

I. INTRODUCTION

Cloud computing [1] provides organizations with an affordable, high-performance computing [2] infrastructure. HPC programs have a repetitive and predictable nature and based on the characteristics of the data that is utilized as input, their resource consumption patterns (CPU and memory, I/O, and network) are predictable. Strategies can be developed to increase queue throughput and resource utilization while reducing performance impacts on applications. HPC applications' performance can be adversely affected by virtualized layers, heterogeneous hardware, HPC-agnostic schedulers such as MOAB [3] or Load Leveler [4], and resource sharing policies. Currently, cloud providers for HPC either offer specialized clouds with dedicated nodes, lacking the consolidation advantages of virtualization, or cloud scheduling that is HPC-agnostic, resulting in inadequate performance. Although modern systems have enormous compute power per node, HPC applications seldom use all of the resources assigned to them. Other applications, such as non-HPC applications, can make use of this feature by utilizing underutilized resources.

Separate technologies have been used to manage the resources and applications on dedicated systems for HPC and Non-HPC applications. This isolation has become an increasing burden, and hence there is an increased demand for the adoption of a standardized shared platform. Execution of both HPC/Non-HPC applications on the same cluster boosts the system efficiency, allowing programs to take advantage of all the available hardware resources. However, even with these advantages, there is still a hindrance in using the full potential of sharing the resources. It is vital that the researcher must devise a method of bridging the gap between dedicated infrastructures and standardized shared platforms by balancing the trade-off between resource utilization, performance, and energy usage, by choosing a suitable VM to physical machine placement methods, with the intention of exploring the best physical machine (PM) that can be used to host the virtual machines. Workload heterogeneity has become norm in cloud computing [5]. Workload characterization is critical since it can group various resource-intensive workloads based on their defining qualities. Classifying workloads that have common consumption patterns can enhance resource management, which improves system performance while maintaining Quality of Service. Clustering techniques are frequently used to cluster workloads in the cloud data center to reduce energy usage and SLA violations for resource allocation.

In terms of VM placement strategies, there are two types: reactive and proactive/predictive strategies. Reactive strategies enhance the initial VM after the system reaches a certain undesired state. While proactive/predictive strategies attempt to enhance VM placement results by projecting future workloads or resource demands using prediction techniques. Identifying proper co-allocated combinations of applications that can be run on the common platform guarantees optimum utilization of resources [6]. The optimum utilization of active resources will allow the reduction of the number of operating servers, which will lead to saving energy spent on computation [7]. Hence, the total energy consumed by a data center will be reduced and optimum utilization of hardware will maintain the performance of applications. Most of the earlier well-established research refers to VM consolidation as a key approach for data centers to save energy and achieve a balance between utilization and SLA violations. The goal behind this strategy is to carefully consolidate VMs or workloads onto a smaller number of PMs and then convert the unused (idle) PMs into a power-saving state or shut them down when they are no longer needed.

Available literature indicates that there have been only a few attempts that proposed automatic workload clustering, virtual machine placement and VM consolidation techniques [8] to eliminate or at least reduce the impact of energy [9], performance [10], and interference [11] in co-located HPC and Non-HPC applications. Moreover, the HPC application characteristics of the strongly coupled processes that perform constant interprocess communication and synchronizations have also rarely been studied.

This study aims to combine and execute both HPC and non-HPC applications on cloud resources using a smart and innovative technique which can balance the trade-off between energy, performance, and resource utilization [12]. The researchers have proposed proactive dynamic VM consolidation for co-scheduling of HPC and non-HPC applications that is based on utilization predictions and an application's profile employing machine learning techniques. Our approach looks for applications that work well together and can be deployed on the same hardware, and the execution profiles for these applications do not compete with each other. This will allow for more efficient usage of the hardware. As part of the VM consolidation process, the proposed approach to VM consolidation also examines the application's resource usage requirements across multiple dimensions, such as the CPU, RAM, and the network. By co-locating suitable virtual machines on hosts during consolidation, resource contention and virtualization overhead can be reduced on application performance without losing the benefits of VM consolidation. Thus, the major contributions to this study can be stated as follows:

- 1) Introduces and implements HPC and energy-aware, efficient proactive dynamic virtual machine (VM) consolidation technique in cloud datacenter that makes cloud schedulers as well as VM placement HPC-aware.
- 2) Attempt to make VM consolidation application-centric while considering the requirements of the applications' resource utilization (i.e., CPU, memory, and bandwidth). The paper explores automatic clustering of workload and virtual machines using k-mean cluster technique. It also aims to explore smart VM placement strategies to intelligently schedule HPC and non-HPC applications on a single pool of resources to increase utilization of resources and overcome the performance issues caused by resource contention.
- 3) Explicitly examines the real-world HPC workload in order to demonstrate the reliability of our numerical analysis in terms of how well our proposed approach is suited to both HPC and non-HPC applications.

This paper is structured as follows: Section II presents the background and motivation for the study. Section III presents the related work to gain knowledge of contemporary research and discusses the importance of the proposed algorithm. while Section IV demonstrates the proposed energy-efficient HPC aware proactive dynamic VM consolidation (EAMDOBP). Section V introduces the evaluation methodology. Section VI discusses the simulation results and analysis. Lastly, the conclusion and future work is discussed in Section VII.

II. BACKGROUND AND MOTIVATION

One of the primary goals of modern datacenter architecture is to cut down on energy usage. Data center energy demands are expected to rise to 752 TWh in 2030. This means that data centers consume 2.13% of total global electricity demand [13]. The inefficient utilization of hardware resources is the root cause of high energy consumption. Idling servers might use 60% of their maximum power [14]. Clustering of workload [15] and Virtual machine consolidation are the most effective and crucial approach for optimizing resource consumption and improve energy efficiency in cloud datacenters. VM consolidation can be implemented in two ways, static and dynamic. Fig. 1(a) is static consolidation. When a job arrives, the size and location of virtual machines on physical machines (VMs) are explicitly pre-determined, and the placement does not change during execution. Static VM placement resembles the N-dimensional bin-packing issue where the bins symbolize physical machines (PM). The items for packing represent the VMs and the size of the bin depends on the volume, types and nature of resources. Static VM consolidation is better suited for small jobs spanning a few hours, where PMs resources for various kinds of VMs can be defined explicitly [16]. Simple heuristics or historical VM demand patterns are the basis of energy minimization. However, during low-demand resource periods, an increase in the cost of application providers is likely to occur. Similarly, the available resources may be insufficient in high utilization periods [17].

On the other hand Fig. 1(b) shows dynamic VM consolidation. To improve the effectiveness of a placement, dynamic VM consolidation allows relocation during execution. Mostly virtual machine workloads are bursty in nature, dynamic VM consolidation is highly beneficial in a cloud computing environment, assuming that monitoring is in place to prevent any violations of Service-Level Agreements (SLAs). Accordingly, dynamic VM consolidation conserves energy and enhances the consumption of resources by using the minimum resources necessary to meet the workload requirements. Consequently, if the workload requirement decreases, unused servers are shut down or kept in low-power mode. Similarly, as consumption grows, additional servers are brought online.

The VM migration and VM placement are considered as the backbone of the VM consolidation technique. The problems like scalability of resources, heterogeneity, migration cost, and unpredictable workloads cause that the VM consolidation process becomes very challenging. The virtual machines (VMs) placement to physical machines (known as VM-Placement) can significantly impact performance. It is very important to choose an appropriate host to enhance power efficiency, better use of resources and support for QoS to attain Resiliency in the Cloud [34].

Clustering is an unsupervised learning strategy for subdividing a big group into multiple smaller groups. As a result, it may be used to find patterns in massive datasets. In current research, the advantages of this group building technique of clustering have been applied to locate groupings in the jobs (incoming request). The ability to locate groupings within jobs based on the number of resources consumed is helpful since this methodology allows to find groupings within jobs.

Cross application interference can occur when different

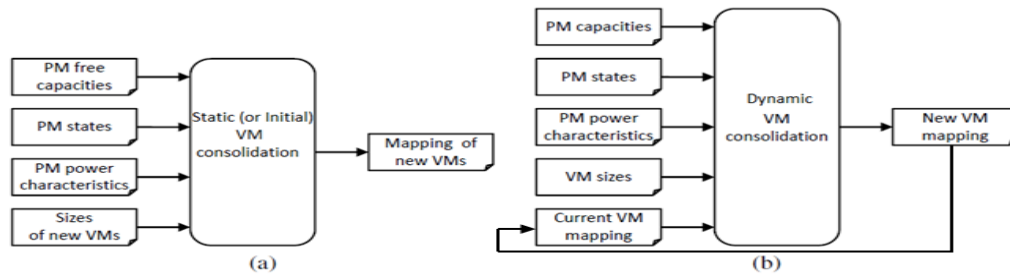


Fig. 1. Inputs and Outputs of (a) Static VM Consolidation and (b) Dynamic VM Consolidation.

cloud workload compete for shared resources, resulting in considerable performance degradation and, results in increase Service Level Agreement violations. Despite this, state-of-the-art VM scheduling still relies heavily on resource capacity, employing heuristics like bin-packing and ignoring the cross application interference overhead. To the best of our knowledge, only a few studies were made for VM scheduling algorithms that consider the tightly connected processes that perform frequent inter-process communication and synchronizations. Improved resource efficiency, cost savings, and, ultimately, broader acceptance of high-performance computing in clouds can be achieved by the strategic placement of virtual machines and the execution of HPC and non-HPC workloads in cloud environments.

Hence, this study focused on a multi-objective challenge that seeks to explore automatic online workload clustering using machine learning, smart VM consolidation and placement strategies to intelligently schedule or provision HPC and non-HPC applications on cloud resources to overcome the aforementioned gap and issues of rigorous consolidation.

III. RELATED WORK

Primarily due to the enhanced efficiency, a significant number of heuristic algorithms have already been suggested for handling VM consolidation challenges in recent years. Among them, Mosa et al. [18] suggest the solution to virtual machine placement that dynamically reallocates virtual machines depending on their actual request for the individual VMs. The suggested approach evaluates various resource categories (particularly CPU and memory) to minimize under and over-utilization in cloud-based data centers. The conducted experiments highlighted the significance of incorporating a variety of resource types. Finally, they concluded for dynamic VM placement, the genetic algorithm outperforms the Best-Fit algorithm. However, the paper neither takes into account the HPC workload nor discusses the issues of cross-application interference. Kraemer et al. [19] developed a job migration mechanism for transferring jobs from the cloud environment to the high-performance computing environment. The primary goal is to reduce the amount of response time violations associated with cloud jobs while not interfering with the execution of HPC jobs.

V. Antonenko [20] developed a strategy for migrating jobs from the cloud environment to the high-performance computing environment. The major objective is to reduce cloud job response time violations without conflicting HPC

task execution. The author's study discusses the suggested job scheduling methods using the SimGrid simulator in various execution scenarios, and recorded findings revealed no reaction time violations. However, the authors did not incorporate support for parallel jobs and did not run experiments with higher rates of incoming cloud jobs.

Alves et al. [11] describes the Interference-aware Virtual Machine Placement Issue (IVMPP) in small-scale High-Performance Computing (HPC) applications executing in Clouds. When applications run on a common physical machine, cross-interference is likely to happen, which harms the application's performance. This problem is very common in HPC that is executed in clouds. The iterated local search framework is proposed as a new solution to prevent the Interference-aware Virtual Machine Placement Problem (IVMP) from happening in HPC applications in clouds. In this study, they limited the interference that happens to HPC applications when sharing common physical machines. The results indicated that the proposed method limited interference by more than 40% in contrast to the most commonly applied heuristics to address the issue. However, the energy and the effect of consolidation are not taken into consideration.

A. Souza [12] proposed a hybrid resource management system for both DI (Data-Intensive) workload systems and HPC systems that will allow combining both of them on the same platform. The most significant feature between HPC systems and DI (Data-Intensive) systems is the fixed set of resources allocated completely to an application in HPC systems. Contrary to the DI (Data-Intensive) systems, in which allocation of resources and control are dependent on application needs. It also describes the design of a hybrid framework which helps for dual-level scheduling of DI jobs on the HPC infrastructure. The core benefit of this hybrid system is that it relies on real-time resource utilization monitoring that could successfully co-schedule high-performance computing (HPC) and data-intensive workloads. It can easily be adapted and extended to different types of workloads. For HPC and DI workloads, the architecture is based on the resource managers Slurm and Mesos. In a particular cluster, the hybrid architecture raises resource consumption by 20%, allowing it to meet all the constraints for HPC jobs, with a 12% reduction in queue makespan. Nevertheless, the paper does not explore ways to reduce the interference and co-location effects on energy as well as resource utilization.

Gupta et al. [21] presented scheduler for cloud platforms that is HPC-aware and incorporates topological needs for

HPC applications. Their scheduler uses benchmarking data to classify the application's network requirements and how resource sharing affects performance. Using three apps and NAS benchmarks, their scheduler outperformed the HPC-agnostic scheduler. Despite all the benefits, Gupta et al. [21] ignored SLA and energy breaches in their study. Furthermore, the trade-off among optimal HPC performance and ideal resource usage is primarily discussed in terms of throughput. Static VM consolidation techniques and Off-line applications profiling were used for classification. Hence, it is necessary to investigate the trade-off in terms of other dimensions as well. As part of earlier research, the researchers investigated CloudSim's default VM placement technique for energy consumption in contrast to the VM placement technique proposed by Gupta, which uses Multi-Dimensional Online Bin Packing (MDOBP). Fig. 2 illustrates that MDOBP uses more energy than CloudSim's default VM placement technique. The findings show an increase in energy consumption due to the possible restrictions of static VM placement. The findings of this experiment served as the foundation for the current research.

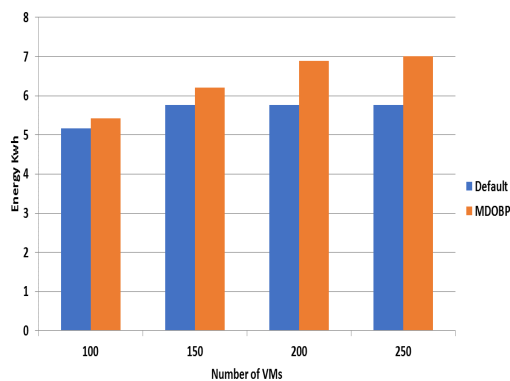


Fig. 2. Energy Comparison of Default vs MDOBP.

Cluster analysis is critical for detecting workloads with similar resource usage patterns. Several approaches for clustering workloads using K-Means have been proposed. Di, Sheng et al. [22] characterize a one-month Google cluster trace by CPU and memory utilization using the Forgy approach for centroid initialization. A merge ratio threshold is used to calculate the optimal number of clusters. Moreno et al. [23] employ K-Means clustering to group workloads based on user behavior and task characteristics. The number of clusters is obtained by comparing the variability of all items within a cluster to a threshold value.

In a previous project [24], the authors studied and implemented the Hybrid Local Regression Host Overload Detection algorithm (HLRHOD). An innovative energy efficient VM consolidation method that uses hybrid factors for host overload detection in cloud datacenters. We concluded that using hybrid factors (CPU, Memory, Bandwidth) can provide a more accurate indication of host utilization and outperform the techniques based on single factors. Thus, using the HLRHOD, the server in operation can be optimally minimized and, hence

helps in the reduction of energy utilization. Nevertheless, the paper does not explore ways to reduce the interference and co-location effects of the HPC and non-HPC applications on resource utilization as well as energy.

In this study, Gupta et al. [21] heuristics for initial VM placement for high-performance computing (HPC) applications were followed and expanded. Additionally, this study expands VM consolidation work [24] by making VM consolidation application-centric while simultaneously taking into account the requirements of the application's resource consumption (i.e., CPU, memory, and bandwidth). We also explore smart VM consolidation and placement strategies to intelligently schedule or provision HPC and non-HPC applications on cloud resources to increase utilization of resources and overcome the aforementioned issues of consolidation. Furthermore, automatic and dynamic classification of the application workload using k-mean is implemented.

IV. ENERGY-AWARE MULTI-DIMENSIONAL ONLINE BIN PACKING (EAMDOBP)

HPC applications are often constructed to operate in a homogenous as well as dedicated environment to eliminate unwanted interference by apps that are located concurrently. This is due to the fact that the performance of high-performance computing applications are significantly dependent on the slowest node. In contrast, cloud infrastructure is changing from homogeneous to heterogeneous. Heterogeneity dramatically lowers performance in parallel applications, especially in repetitive and bulk concurrent workloads. VM scheduling for HPC is challenging because of the trade-off between better HPC performance and improved resource consumption. A technique for intelligently optimizing the placement and execution of virtual machines (VMs) for HPC and non-HPC applications can improve resource usage, improve energy efficiency, and hence promote HPC cloud acceptance.

Sharing resources typically causes critical interference. Contention of shared resources has poor impact on applications performance. Caches are small stores of temporary memory. Cache memory has an impact on the program execution because its access time is less than the access time of the other memories. It is the fastest component in the memory hierarchy and approaches the speed of CPU components. They can degrade system performance if they become too large. System performance is a decreasing function of the cache miss rate, the cache access time, and the number of processor cycles taken to service a miss. They also can consume memory that other applications might need, negatively impacting application performance. Cache, memory, I/O channels, and network access are all shared resources, but cache are one of the most significant applications performance degradation factors [25]. It is advantageous to have cache-intensive applications; endure more LLC misses per second; co-located with applications that use little or no cache on the same node. Cache-sensitivity awareness assists in the avoidance of interference.

Most of the studies reviewed recently, a static classification of the behavior of different workloads/applications is created to examine their studies in order to find solutions for interference scheduling issues in cloud environments. EAMDOBP algorithm presents an automatic workload clustering using machine

learning techniques. The EAMDOBP classifier initially cluster the workload based on memory utilization and workload length then VMs are grouped based on their processing capacity. Afterwards the individual cloudlets in each cluster is scheduled to the appropriate VM in the VM groups. The flowchart in Fig. 3 depicts the execution flow of the proposed algorithm EAMDOBP, which is detailed in the following subsections.

A. Clustering of Workload and VM

A workload can be defined as a certain amount of work operated inside the data center while consuming specific limited resources. In the current context, cloud computing data centers are defined as computer resource pools that can bear variable workloads whether long scientific jobs (HPC) or transactional operations (non-HPC). Normally, workloads are different in heterogeneous environments because of the placement constraints they have and the number of resources they consume [26]. In fact, the amount of resources a job consume is defined as job resource requirements, while the type and characteristics of resources are defined as job placement constraints. Therefore, these main elements must be addressed for intelligent and efficient scheduling. The proposed EAMDOBP initially classifies incoming requests according to job characteristics. This classification further is used to make crucial scheduling decisions, such as scheduling jobs from various clusters based on the amount of resources they consume.

1) Clustering Jobs using K-Means and Silhouette Method:

The EAMDOBP classifier divides workload into specified classes by using the k-means algorithm [35] and the silhouette approach [36]. K in k-means algorithm denotes the quantity of pre-defined clusters that must be produced during the process. It is a centroid-based technique, with each cluster having its own centroid. The algorithm's main goal is to minimize the sum of distances between data points and their respective clusters. As input, the EAMDOBP classifier takes memory utilization and its length from METACENTRUM-02.swf logs of the parallel workload archive, separates it into $k = 4$ clusters, and then continues the procedure until the centroids don't change. The technique for creating job clusters using the K-Means clustering algorithm is summarized in Algorithm-1. Once the clustering process is completed, the average memory utilization for each cluster is calculated.

Algorithm 1 Basic K-Means Algorithm

- 1: Select k points as initial centroid
 - 2: **repeat**
 - 3: Form k clusters by assigning each point to its closest centroid
 - 4: Re-compute the centroid of each cluster
 - 5: **until** the centroids don't change
-

Clusters presented in Table I are obtained applying k-means algorithm in cloudSim on the first 250 logs from METACENTRUM-02.swf logs of the parallel workload archive [27]. K-means algorithm clusters data into four clusters. From the cluster centroid analysis, four different types of workloads can be outlined. These have been labeled as "IntenseHPC", "ConcurrentHPC", "DiscreteHPC", and non-HPC.

Table II displays the input (memory use and length) classified into each cluster using k-means algorithm. The number of objects by cluster represents the total number of objects per cluster. Within-cluster variance is the sum of squared distance between the average point (centroid) and every point of the cluster. The smaller the within-cluster variance value the better is the clustering. The average distance between observations and the cluster centroid is a measure of observation diversity within each cluster. A cluster with a smaller average distance is generally more compact than one with a bigger average distance. Clusters with higher values show more variation in the observations within the cluster. A larger maximum value of maximum distance to centroid, especially when compared to the average distance, suggests a cluster observation that is located further away from the cluster centroid.

Furthermore, silhouette score is utilized to determine the quality of clusters formed by using K-means clustering algorithms. The silhouette approach analyzes the quality of clustering by determining how well each point fits into its cluster. Using Eq. 1, the silhouette score is calculated for each cluster data (i.e. memory utilization and its length). where (a) is mean intra-cluster distance and (b) is the mean nearest-cluster distance. Fig. 4 depicts the mean silhouette score of each cluster. When the silhouette score equals 1, it means that the clusters are very dense and well separated. When the silhouette score equals 0, it means that clusters are overlapping. If the score is less than 0, this indicates that the data could be incorrect.

$$SilhouetteScore = (b - a) / \max(a, b). \quad (1)$$

Subsequent workload clustering, the processing capability of each virtual machine is determined based on its MIPS, size, bandwidth, and RAM. The virtual machines are then grouped into four clusters Extreme High (EHVMs), High (HVMs), Medium (MVMs) and Low (LVMs), using the modified K-means clustering algorithm. Afterwards, all cloudlet clusters are mapped to Virtual Machine (VM) clusters. The cloudlet with the high memory consumption is assigned to high processing capability. For example, IntenseHPC applications are assigned to Extreme High (EHVMs). Fig. 5 shows the simulation time with kmeans and without kmeans. As depicted in the Fig. 5 the simulation time has shown improved result.

B. Virtual Machine Placement

EAMDOBP selects the PM that will host the VM based on the VM's class. The EAMDOBP begins the process with the target that IntenseHPC applications VMs can be assigned to the same host and rack as much as possible to reduce cross-interference for HPC/ Non-HPC applications. When applications share a physical machine, cross-interference can occur, negatively impacting their performance. EAMDOBP VM request contains the application's cluster name, as well as any existing parameters, unlike traditional VM requests. Based on the VM provisioning request, VM and cloudlets are generated depending on the Application type, capacity (number of CPU, RAM, and bandwidth), and instance type. VMs are allocated to a host and the cloudlet is allocated to VM. The algorithm then calculates the current host and rack free capacity, which is the number of extra VMs of the

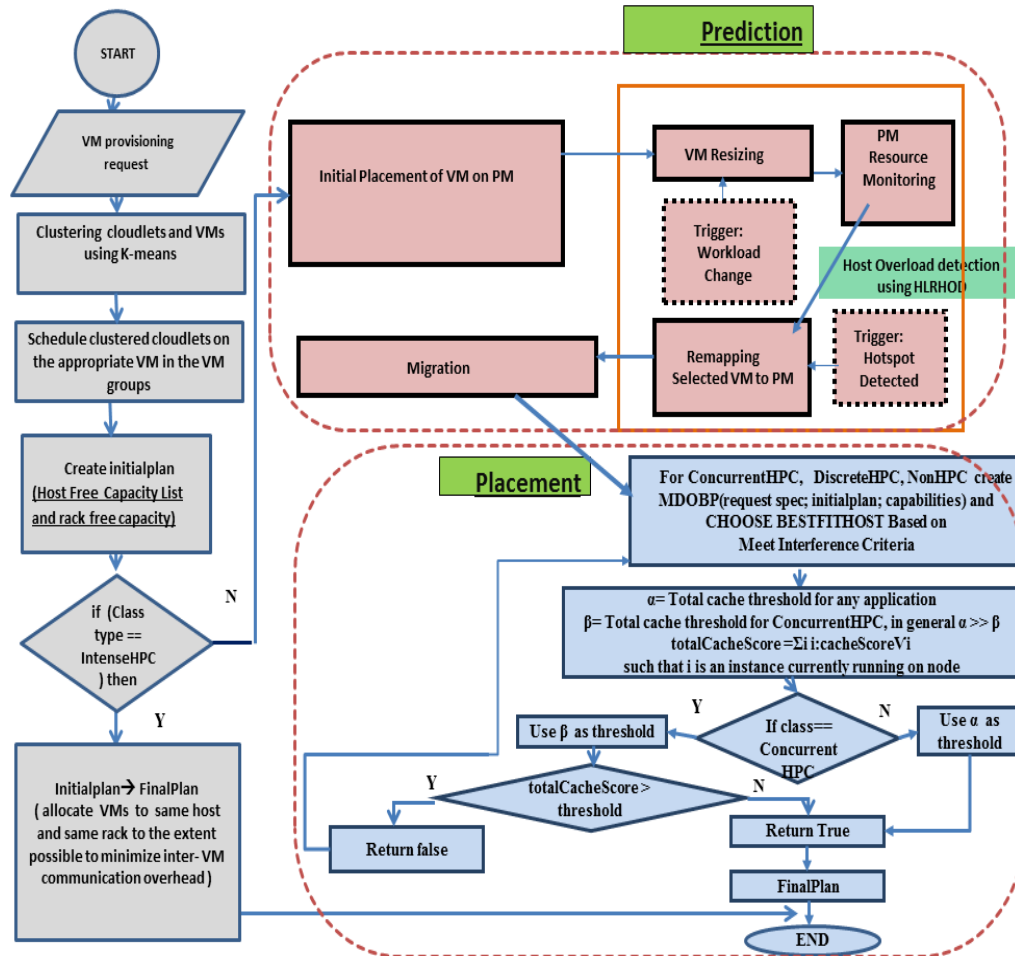


Fig. 3. Energy-Aware Multi-Dimensional Online Bin Packing (EAMDOBP).

TABLE I. POPULATION AND DESCRIPTION OF CLUSTERS RESULTING FROM CLUSTERING FIRST 250 DATA OF METACENTRUM-02.SWF LOGS OF THE PARALLEL WORKLOAD ARCHIVE

Cluster	Population	Memory usage	Clustering description
IntenseHPC (Cluster-4)	2	26749856.000	This cluster shows high memory consumption
DiscreteHPC (Cluster-3)	15	326042.000	This cluster shows moderate memory consumption
ConcurrentHPC (Cluster-1)	17	4732608.750	This cluster shows memory consumption is lower then DiscreteHPC.
non-HPC (Cluster-2)	215	86285.953	This cluster shows low memory consumption

TABLE II. K-MEAN CLUSTERS RESULT

Cluster	1	2	3	4
Number of objects by cluster	17	215	15	2
Sum of weights	17	215	15	2
Within-cluster variance	-0.223	-0.582	1.472	-0.667
Minimum distance to centroid	1.397	-0.540	-0.870	0.013
Average distance to centroid	0.276	-0.711	1.296	-0.860
Maximum distance to centroid	-0.384	0.713	0.906	-1.234

requested specification which can be deployed on a specific host and rack. To assure that IntenseHPC is only run on dedicated nodes, it sets all hosts with a active VM to zero,

if the required VM category is IntenseHPC. The scheduler then prepares a initial plan, which is a list of hosts sorted by rackCapacity and hostCapacity for hosts in the same rack, if

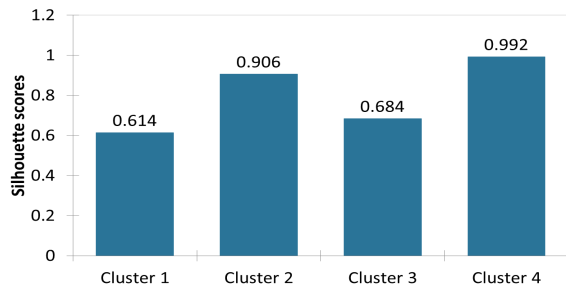


Fig. 4. Mean Silhouette Score of Clusters.

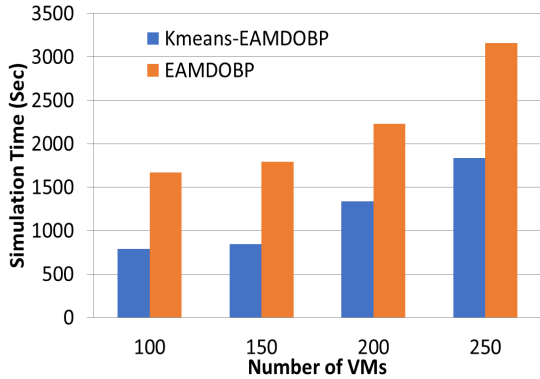


Fig. 5. Simulation Time with Kmeans and Without Kmeans

the required VM cluster is IntenseHPC or DiscreteHPC. The idea is to keep as many VMs on the same host and rack as possible to avoid inter or cross-VM communication overhead for these application types. This initialPlan is used for VM provisioning in IntenseHPC, whereas for the other classes (DiscreteHPC, ConcurrentHPC, and NonHPC), the method does multi-dimensional online bin packing to group VMs with variety of attributes on the same host.

C. Virtual Machine Consolidation

Since changing workloads modify VM resource utilization over time, initial VM placement should be complemented by a regular VM consolidation procedure. Status is examined for every scheduled interval by using the EAMDOBP proactive dynamic consolidation technique. Notably, the detection of host overload/underload is the initial stage in virtual machine consolidation whose main target is energy reduction. The default underload detection algorithm is applied every scheduled interval, and underutilized hosts are deactivated after moving all VM to other active PM. Afterward, Hybrid Local Regression Host Overload Detection algorithm (HLRHOD) [24] is applied to detect the overloaded hosts. VM is chosen from the overloaded hosts to migrate to available hosts. HLRHOD calculates host utilization based on hybrid factors by utilizing a metric which measures the combined CPU-network-memory load of physical and virtual servers. Following the calculation of host utilization, the program employs local regression. The basic concept behind the process of local regression is that it involves fitting simple models to confined subsets of data in order to construct a curve that approximates the original data. To identify whether the host is overloaded or underloaded,

HLRHOD estimates the host utilization based on a hybrid factor. VM consolidation requires two more phases after the overloaded hosts are identified. The first phase is to identify the virtual machines (VMs) that will be migrated from the overloaded hosts to other hosts (known as VM migration), and the second phase is to replace the VMs that were selected for migration on new hosts (known as VM placement).

D. Virtual Machine Placement

Multi-dimensional online bin packing (MDOBP) algorithm is used for VM placement and it allows VMs with diverse characteristics to be placed on the same host to reduce energy and enhances the consumption of resources. MDOBP treats hosts as bins, and virtual machines as objects that must be packed into the bins. A host is represented as a d-dimensional vector, which is referred to as the host's vector of capacities. Each dimension indicates the host's capacity corresponding to a specific resource, such as CPU utilization, memory utilization, or disk bandwidth. Similarly, each virtual machine is represented by a vector of requirements. The aim is to place all of the VMs on as few hosts as appropriate, while ensuring that, across all dimensions, the total demand of VMs placed on a host does not exceed the capacity of the host.

Additionally, each job is assigned a cache score from (0-30) The cache score represents the amount of pressure being placed on the both memory controller subsystem as well as shared cache. The chosen host is furthermore verified for compliance with the interference requirements i.e estimated demand for contested resources from the physical hosts. If the sum of cache scores for the requested VM and all other VMs running on the host exceeds a certain threshold α (Total cache threshold for any application), the request will be denied. which needs to be determined through experimental analysis. A different threshold β (Total cache threshold for DiscreteHPC) is used when a requested virtual machine (VM) or one or more virtual machines operating on that host are of the class DiscreteHPC, because applications of this type can tolerate less interference compared to IntenseHPC. When the cache threshold β is too high, the efficiency is decreased as cache-intensive applications on the same node are aggressively packaged. Furthermore, very low thresholds lead to an excessive waste of certain CPU cores if very small cache scores do not exist. A record of interference indices is saved to examine interference between the applications that face a big performance penalty when being executed on the same host. Having this information is beneficial in avoiding co-locations, which are detrimental to the performance of high-performance computing (HPC) applications. Following that, a FinalPlan is established, which contains a list of hosts on which the virtual machines should be provisioned. After each repetition, a log is also created, which can be used to track energy consumption and quality of service.

V. EVALUATION METHODOLOGY

A. Experimental Setup

As it is very challenging to conduct repeatable large-scale experiments on a real infrastructure [28], simulations are recommended to show the improvement of our suggested algorithms. The CloudSim toolkit facilitates the modeling of

cloud system resources from both a system and a behavior perspectives specifically virtual machines, data centers, and resource management policies. It incorporates common application delivery techniques that can be extended quickly and with minimal effort. Therefore, the experiments were conducted with the CloudSim 3.0 simulation toolkit [29] using four VM types and two PM types. Cloudsim is extended with energy-aware simulations, originally not present in the core framework [29].

Furthermore, while implementing our scheduling and migration techniques the researchers identified multiple limitations in the CloudSim 3.0, that need to be addressed. They include that CloudSim is designed and implemented for the cloud, and primarily operates for tasks involving just one processor while HPC machines require quite a huge number of processors. In this research work, the researchers extended CloudSim 3.0 to provision the simulation of HPC in the cloud. Hence, the key change performed to enhance the execution of multi-core jobs to simulate HPC in a cloud thus the PowerDatacenter class that empowers simulation of power-aware data centers in the cloud environment.

In order to efficiently map jobs to virtual machines (VM), a predetermined number of virtual machines (of various types) will be constructed at the beginning of the simulation, and jobs (cloudlets) will be submitted to the DatacenterBrokerEAMDOBP broker. The cloudlets class is also modified, in addition to existing parameters, it includes the application class and name for VM provisioning. Furthermore, for cache-awareness, used a uniform distribution random number generator by giving a cache value from 0 to 30 to each job.

Further, DatacenterBroker class was also extended to DatacenterBrokerEAMDOBP, with two additional features: i) it allocates a cloudlet to VM after determining the characteristics of both VM and Cloudlets, to assign lengthy cloudlets (jobs) to the more efficient VMs so that the VM is not idle in a data center and the cloudlet execution time will be reduced. This does not only results in the efficient and improved utilization of the system but also helps to overcome the drawbacks of the default cloudSim 3.0 DatacenterBroker policy. ii) Furthermore, cache-awareness is also added to DatacenterBrokerEAMDOBP policy to efficiently address the issue of cross-interference. The cross-interference problem arises at a high scale when high-performance applications are executed in clouds. The proportion of additional time spent by one program when it runs simultaneously with another is known as the slowdown of that application. Thus the accurate forecasting of the slowdown due to interference in each application has many advantages: for example, it can help to enhance efficient shared resource utilization to avoid unreasonable application slowdowns from consolidation. DatacenterBrokerEAMDOBP policy will allocate cloudlets to VM that do not surpass the criteria of interference. Similar approach as Gupta [21], the interference is calculated based on following criteria: The sum of cache value of the VM requested does not exceed a threshold for any VM running on a host. The value of the threshold value is set to 60 after careful and thorough experimentation. If the threshold is set to a large value, it will decrease efficiency as a result of aggressive cache-intense applications packaged on the same node. On the other hand, too small value of threshold will result in an unreasonable waste of certain CPU cores if few applications are having insignificant

cache values. Interference indices maintained to record and save interference between applications that experience high-performance penalties when hosts are shared. While DatacenterBrokerEAMDOBP policy assigns suitable cloudlet(job) to VM, the knowledge of recorded interference indices is used to prevent co-locations of HPC/non-HPC applications that consumed more resources.

Furthermore, the default CloudSim VmAllocationPolicySimple class extended to PowerVmAllocationPolicyMigrationEAMDOBP which manages a user request encompasses multiple types of VM. Two methods findHostForVm (for initial VM allocation) and optimizeAllocation (for VM consolidation) in the PowerVmAllocationPolicyMigrationEAMDOBP class carries out proposed Energy-aware multi-dimensional online bin packing scheduling. When HLRHOD [24] detects a host overload, certain VMs will be chosen to be migrated from the overloaded host to other hosts.

Furthermore, the researchers compare the proposed Energy-Aware Multi-Dimensional Online Bin Packing (EAMDOBP) algorithm against the following algorithms from the literature:

- The Power-Aware-Best-Fit Decreasing algorithm (PABFD) algorithm [28].
- The Modified- Worst-Fit Decreasing algorithm (MWFD) algorithm [30].

B. Power Model

The CPU, disk storage, memory, and cooling systems utilize the majority of the power in cloud data centers [28]. Establishing exact analytical models for modern multicore CPUs is a difficult research problem due to the complex power model of modern multicore CPUs. Hence, we employ real data on power rate obtained from the results of the SPECpower benchmark [28] as an alternative to the use of an analytical model of a host's power consumption. The host overload is evaluated on a regular basis according to the scheduling interval, which is set at 300 seconds. The host types are: HP ProLiant ML110 G4 (Intel Xeon 3040, 2 cores 1860 MHz, 4 GB), and HP ProLiant ML110G5 (Intel Xeon 3075, 2 cores 2660 MHz, 4 GB). The power consumption features of the chosen hosts are presented in Table III.

C. Performance metrics

To conduct in-depth analysis of the suggested algorithm and to evaluate and contrast the algorithm's performance, several number of experiments were carried out and examined in the current research using the following metrics:

Simulation Time (ST): It is defined as the amount of time spent conducting an experiment in seconds, commonly known as the makespan. Based on the number of applications that were processed, the total time required to generate the simulation was calculated. The simulation time (MakeSpan) is used to determine the efficiency of the algorithm.

Throughput: In computing, it is the quantity of work that a computer or a system of computers is able to perform in a given period of time. Increasing throughput is an ongoing challenge that IT managers, researchers, and scientists must

TABLE III. POWER CONSUMED BY THE CHOSEN HOSTS AT VARIOUS LOAD LEVELS IN WATTS [28]

SERVER	0%	10%	20%	30%	40%	50%	60%	70%	80%	90%	100%
HP PROLIANT G4	86	89.4	92.6	96	99.5	102	106	108	112	114	117
HP PROLIANT G5	93.7	97	101	105	110	116	121	125	129	133	135

meet and exceed. The throughput of a system is used to evaluate its overall performance.

Efficient Resource Utilization (ERU): It is used determine how much CPU, memory and network bandwidth are needed for HPC and non-HPC workloads deployed in cloud-based data centers

Power Usage Effectiveness (PUE): The Power Usage Effectiveness (PUE) is used as indices for measurement of datacenter performance. PUE is considered the most used datacenter metric. The PUE is calculated using Eq. 2, where P_{CS} is the cooling power, and P_C is the computing power of the host. This calculation is iterated over each host.

$$PUE = \frac{P_{CS} + P_C}{P_C} \quad (2)$$

Table IV shows the PUE values based on several experiments which were performed in a small datacenter [31]. Low PUE indicates higher efficiency as a significant amount of the power has been consumed by computing power [32].

TABLE IV. PUE EFFICIENCY VALUES [31]

PUE	Level of efficiency
3.0	Very inefficient
2.5	Inefficiency
2.0	Average
1.5	Efficient
1.2	very Efficient
1.1	Standard

The number of VM migrations: For dynamic VM consolidation, when the overloaded or under-loaded hosts are detected, the VMs are then chosen to move. Reducing the VM migration time is the most significant obstacle in the migration step and the default method to achieve that is by reducing the total number of VM migrations.

Energy and SLA Violations (ESV): There is an adverse relation between the energy consumed by physical hosts and SLAV because energy can be frequently reduced by allowing more SLA violations. The objective of the host management framework is to decrease both energy consumption and service level agreement violations. Thus, a mixed metric denoted by Energy and SLA Violations (ESV) is proposed in [28] and is shown in Eq. 3. For the ESV metric lower is better.

$$ESV = E \times SLAV \quad (3)$$

D. Workloads

The workload contains several months of accounting records from the national grid of the Czech Republic, called Metacentrum. This grid is composed of 14 clusters (called nodes), each with several multiprocessor machines, for a total of 806 processors [27]. The workload data contains CPU and memory usage [33]. Standard workload format (SWF) includes the log. METACENTRUM-2013-1.swf. is used while relying on accounting data collected by the scheduler. three utilization models rebuilt to examine the CPU and RAM, and calculate the BW, respectively, from the workload and send it to the cloudlets.

VI. SIMULATION RESULTS AND ANALYSIS

Memory utilization, workload length and number of VMs are crucial parameters that are used to configure the algorithms implemented besides the performance metrics presented in Section V

A. Sensitivity Analysis

The effect of changing the number of VMs on the performance of the proposed algorithms in terms of metrics is provided in Section 5.3.

1) Number of VMs:

Our sensitivity analysis is based on changing the number of virtual machines while fixing the number of hosts to 800 and scheduling interval to 300 sec. The effect of varying the number of VMs using Metacentrum workload traces on the energy consumption and other system and performance metrics for different algorithms are examined.

Algorithms comparison are performed on (CPU, RAM, and Network) traces using Metacentrum HPC workload. Measurement of simulation time is one of the most critical indicators for measuring performance in a dynamic system. Observe in Fig. 6(a), EAMDOBP algorithm reduces the execution times better than the other algorithms. This proves that application awareness results in fewer contentions for resources as only the most compatible VMs are consolidated. The new EAMDOBP algorithm results in the lowest simulation time compared to PABFD and MWFD regardless of the number of VM. The simulation time is the highest in the case of PABFD when the number of VM is high. Besides, the simulation time is always less in the case of MWFD when compared to PABFD.

The HPC framework involves the co-scheduling of tasks with the same nature to make some synchronous development. In the present virtualized environment, all VMs progress independently of each other, so that the need that all VMs of the same HPC function must be arranged together using EAMDOBP algorithm. Results are shown in Fig. 6(b) indicate

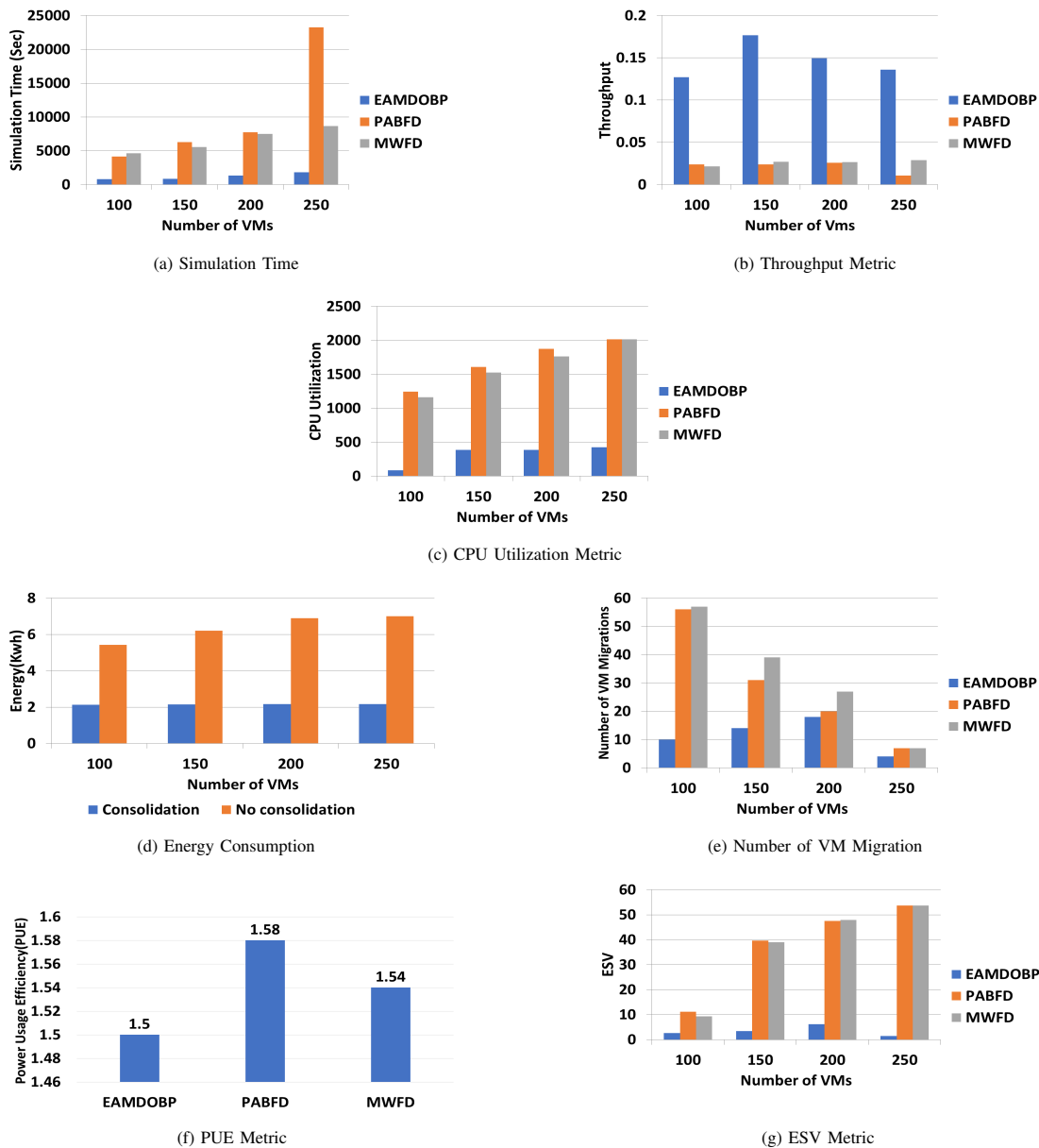


Fig. 6. Algorithms Comparison for Metacentrum HPC workload, where the various metrics are depicted in log-scale

that the throughput levels are the highest when the EAMDOBP algorithm is used. While throughput levels are almost equal when using PABFD and MWFD algorithms.

It is important to address the issue of machine utilization or “busy” time that is commonly used to evaluate throughput effectiveness. It is often only moderately correlated with a hardware measure such as utilization. The prediction method of the resource utilization based on HLRHOD is used, Fig. 6(c) indicates better CPU utilization. The use of HLRHOD prediction technique improves CPU utilization as well as increase the effectiveness of HPC-application execution

B. Algorithms Comparative Analysis

The EAMDOBP beforehand has the expertise to forecast the best node for VM allocation without venturing with the

energy consumption. While the energy and interference-aware co-location of the VMs is used for all the workload allocations to the VMs running on the system nodes. The need for rising VM migrations is therefore low and it helps to reduce energy depletion. The same is shown through Fig. 6(d) and (e). The graph in Fig. 6(d) indicates how energy usage increases with the increase in the number of VM when no consolidation is allowed. Significantly, energy consumption is fixed regardless of the increase in the number of VMs when consolidation is allowed, meaning that the VMs are allowed to migrate to run on fewer physical servers. Thus, VM consolidation helps reduce energy consumption. As observed in Fig. 6(e) VM migrations are the lowest when using the EAMDOBP algorithm compared to PABFD and MWFD. VM migration is the highest when using MWFD. Each host’s cooling and

processing power, as well as its power utilization efficiency (PUE), are measured after each migration, and the impacts are averaged. Results depicted in Fig. 6(f) indicate that PUE is the lowest in the case of EAMDOBP compared to PABFD and MWFD. It is worth mentioning that low PUE indicates better efficiency. This is because a considerable part of the power is consumed by computing power. However, PUE is the highest in the case of PABFD. Results revealed in Fig. 6(g) indicate that ESV is the lowest when using the EAMDOBP algorithms compared to PABFD and MWFD. ESV levels increase significantly with the increase in the number of VM when using PABFD and MWFD algorithms.

VII. CONCLUSION

Cloud computing has become a popular solution for the exponential growth in the demand for high-performance computing. Huge data centers use a considerable amount of energy, which leads to an increase in operating costs. Therefore, virtual machine consolidation is a perfect solution as it allows VM live migration to run on fewer physical servers to save energy consumption. Many studies have tried to investigate the currently available cloud service architectures for running HPC applications in the most effective approach. The major obstacles are cross-application interference, energy concerns, and guaranteeing SLAs in different metrics, e.g. response time (web application) vs. execution time (HPC application). However, for a successful VM consolidation host overload detection is necessary to predict if a physical server will be overloaded with VMs. This paper proposes new algorithm named Energy-Aware Multi-Dimensional Online Bin Packing (EAMDOBP) algorithm that will provide better results. Specifically, In comparison to PABFD and MWFD, experiments reveal that the Energy Aware Multi-Dimensional Online Bin Packing (EAMDOBP) has improved CPU, RAM, and bandwidth consumption by a relative improvement of 77%, 84%, and 70%, respectively. The Energy Aware Multi-Dimensional Online Bin Packing (EAMDOBP), according to experiments, improves CPU usage, lowers PUE, and rationalizes energy consumption. Additionally, EAMDOBP achieves faster throughput, less VM migration, and lower ESV when compared to PABFD and MWFD. According to the results analysis, the EAMDOBP algorithm outperforms PABFD and MWFD in terms of all the parameters employed. In current paper the researcher has focused on bridging the HPC-cloud gap by enhancing application performance and resource and energy efficiency however, there are two important limitations in this study that could be addressed in future investigations. First, the only information provided by current performance analysis tools is the application's performance. They don't go into depth about the additional tasks that could have used up other parameters such the network and I/O. Also, the work should be extended to be run on a real cloud system not simulation. In future, we plan to run our algorithm on a real cloud system; also we will consider other factors such as I/O which can affect performance of VMs. We can apply other machine learning techniques such as Naive Bayesian classifiers for classification of VMs.

ACKNOWLEDGMENT

This research was supported in part by the the cloud computing center of excellence grant number 5220, Science

and Technology Development Fund (STDF), Egypt, and in part by the Distributed and Networked Systems Research Group Operating Grant number 150410, University of Sharjah, UAE.

REFERENCES

- [1] P. Mell, T. Grance *et al.*, The nist definition of cloud computing (2011).
- [2] V. Mauch, M. Kunze and M. Hillenbrand, High performance cloud computing, *Future Generation Computer Systems* **29**(6) (2013) 1408–1416.
- [3] H. Moab, Suite, URL: adaptivecomputing.com/products/hpc-products/maob-hpc-basic-edition/basic-edition-solution-architecture (2019).
- [4] S. Kannan, M. Roberts, P. Mayes, D. Brelsford and J. F. Skovira, Workload management with loadleveler, *IBM Redbooks* **2**(2) (2001) p. 58.
- [5] D. A. Menasce and V. A. Almeida, *Capacity Planning for Web Performance: metrics, models, and methods* (Prentice-Hall, Inc, 1998)
- [6] M. Gienger, High performance computing in the cloud: A survey on performance and usability, in *Sustained Simulation Performance 2015*, (Springer, 2015) pp. 29–40.
- [7] A. Shehabi, S. Smith, D. Sartor, R. Brown, M. Herrlin, J. Koomey, E. Masanet, N. Horner, Azevedo and W. Lintner, United states data center energy usage report, tech. rep., Lawrence Berkeley National Lab.(LBNL), Berkeley, CA (United States) (2016).
- [8] A. A. El-Moursy, A. Abelsamea, R. Kamran and M. Saad, Multi-dimensional regression host utilization algorithm (mdrhu) for host overload detection in cloud computing, *Journal of Cloud Computing* **8**(1) (2019) 1–17.
- [9] Z. Li, X. Yu, L. Yu, S. Guo and V. Chang, Energy-efficient and quality-aware vm consolidation method, *Future Generation Computer Systems* **102** (2020) 789–809.
- [10] H. Jin, H. Qin, S. Wu and X. Guo, Ccap: a cache contention-aware virtual machine placement approach for hpc cloud, *International Journal of Parallel Programming* **43**(3) (2015) 403–420.
- [11] M. M. Alves, L. Teylo, Y. Frota and Drummond, An interference-aware virtual machine placement strategy for high performance computing applications in clouds (2018) 94–100.
- [12] A. Souza, M. Rezaei, E. Laure and J. Tordsson, Hybrid resource management for hpc and data intensive workloads, *19th IEEE/ACM International Symposium on Cluster, Cloud and Grid Computing, CC-Grid 2019, May 14-17, 2019, Larnaca, Cyprus* (2019) 399–409.
- [13] M. Koot and F. Wijnhoven, Usage impact on data center electricity needs: A system dynamic forecasting model, *Applied Energy* **291** (2021) p. 116798.
- [14] L. A. Barroso and U. Hözl, The case for energy-proportional computing, *Computer* **40**(12) (2007) 33–37.
- [15] A. Shahidinejad, M. Ghobaei-Arani and M. Masdari, Resource provisioning using workload clustering in cloud computing environment: a hybrid approach, *Cluster Computing* **24**(1) (2021) 319–342.
- [16] Y.-C. Shim, Performance evaluation of static vm consolidation algorithms for cloud-based data centers considering inter-vm performance interference, *International Journal of Applied Engineering Research* **11**(24) (2016) 11794–11802.
- [17] Q. Zheng, R. Li, X. Li, N. Shah, J. Zhang, F. Tian, K.-M. Chao and J. Li, Virtual machine consolidated placement based on multi-objective biogeography-based optimization, *Future Generation Computer Systems* **54** (2016) 95–122.
- [18] A. Mosa and R. Sakellariou, Dynamic virtual machine placement considering cpu and memory resource requirements, *2019 IEEE 12th International Conference on Cloud Computing (CLOUD)* (2019) 196–198.
- [19] A. Kraemer, C. Maziero, O. Richard and D. Trystram, Reducing the number of response time service level objective violations by a cloud-hpc convergence scheduler, *Concurrency and Computation: Practice and Experience* **30**(12) (2018) p. e4352.
- [20] V. Antonenko, A. Chupakhin, I. Petrov and R. Smeliansky, Improving resource usage in hpc clouds (2019).

- [21] A. Gupta, L. V. Kale, D. Milojevic, P. Faraboschi and S. M. Balle, Hpc-aware vm placement in infrastructure clouds, *2013 IEEE International Conference on Cloud Engineering (IC2E)* (2013) 11–20.
- [22] S. Di, D. Kondo and F. Cappello, Characterizing cloud applications on a google data center, in *2013 42nd International Conference on Parallel Processing*, IEEE2013, pp. 468–473.
- [23] I. S. Moreno, P. Garraghan, P. Townend and J. Xu, Analysis, modeling and simulation of workload patterns in a large-scale utility cloud, *IEEE Transactions on Cloud Computing* **2**(2) (2014) 208–221.
- [24] A. Abdelsamea, A. A. El-Moursy, E. E. Hemayed and H. Eldeeb, Virtual machine consolidation enhancement using hybrid regression algorithms, *Egyptian Informatics Journal* **18** (2017) p. 161–170.
- [25] S. Zhuravlev, J. C. Saez, S. Blagodurov, A. Fedorova and M. Prieto, Survey of scheduling techniques for addressing shared resources in multicore processors, *ACM Computing Surveys (CSUR)* **45**(1) (2012) 1–28.
- [26] S. Li, L. Wang, W. Wang, Y. Yu and B. Li, George: Learning to place long-lived containers in large clusters with operation constraints, in *Proceedings of the ACM Symposium on Cloud Computing*, 2021, pp. 258–272.
- [27] "The metacentrum hpc workload", Cs.huji.ac.il, 2022. [Online]. Available: <http://www.cs.huji.ac.il/labs/parallel/metacentrum>. [Accessed: 22-Sep- 2022]
- [28] A. Beloglazov and R. Buyya, Optimal online deterministic algorithms and adaptive heuristics for energy and performance efficient dynamic consolidation of virtual machines in cloud data centers, *Concurrency and Computation: Practice and Experience* **24**(13) (2012) 1397–1420.
- [29] R. N. Calheiros, R. Ranjan, A. Beloglazov, B. De Rose and Rajkumar, Cloudsim a toolkit for modeling and simulation of cloud computing environments and evaluation of resource provisioning algorithms, *Software Practice and experience* **41**(1) (2011) 23–50.
- [30] M. R. Chowdhury, M. R. Mahmud and R. M. Rahman, Implementation and performance analysis of various vm placement strategies in cloudsim, *Journal of Cloud Computing* **4**(1) (2015) p. 20.
- [31] M. Uddin, A. Shah, R. Alsaqour and J. Memon, Measuring efficiency of tier level data centers to implement green energy efficient datacenters, *Middle-East Journal of Scientific Research* **15**(2) (2013) 200–207.
- [32] M. J. Usman, A. S. Ismail, G. Abdul-Salaam, H. Chizari, O. Kaiwartya, A. Y. Gital, M. Abdullahi, A. Aliyu and S. I. Dishing, Energy-efficient nature-inspired techniques in cloud computing datacenters, *Telecommunication Systems* **71**(2) (2019) 275–302.
- [33] "Parallel Workloads Archive", Cs.huji.ac.il, 2022. [Online]. Available: <http://www.cs.huji.ac.il/labs/parallel/workload>. [Accessed: 22-Sep- 2022]
- [34] Chinnasamy, P and Vinothini, B and Praveena, V and Subaira, AS and Sujitha, B Ben: Providing Resilience on Cloud Computing, in *2021 International Conference on Computer Communication and Informatics (ICCCI)*, IEEE 2021, pp. 1–4.
- [35] Hartigan, J. A., and M. A. Wong: Algorithm AS 136: A K-Means Clustering Algorithm. *Journal of the Royal Statistical Society. Series C (Applied Statistics)*, 1979, pp"100–08" .
- [36] P. J. Rousseeuw, Silhouettes: a graphical aid to the interpretation and validation of cluster analysis, *Journal of computational and applied mathematics*, Elsevier, 1987 .

Triple SVM Integrated with Enhanced Random Region Segmentation for Classification of Lung Tumors

Sukruth Gowda M A

Dept. of Computer Science and Engineering
School of Engineering
Presidency University
Bengaluru, India

A Jayachandran

Dept. of Computer Science and Engineering
School of Engineering
Presidency University
Bengaluru, India

Abstract—The rapid growth of Computer vision and Machine Learning applications, especially in Health care systems, assures a secure, innovative lifestyle for society. The implication of these technologies in the early diagnosis of lung tumors helps in lung cancer detection and promises the survival rate of patients. The existing general diagnosis method of lung radiotherapy, i.e., Computed Tomography imaging (CT), doesn't spot exactly affected parts during injuries on lung malignancy. Herein, we propose a computer vision-based diagnostic method empowered with machine learning algorithms to detect lung tumors. The primary objective of the proposed method is to develop an efficient segmentation method to enhance the classification accuracy of lung tumors by implementing a Triple Support Vector Machine (SVM) for the classification of data samples into normal, malignant, or benign, Random Region Segmentation (RSS) for image segmentation and SIFT and GLCM algorithms are applied for feature extraction technique. The model is trained considering the dataset IQ - OTH or NCCD with 300 epochs, with an accuracy of 96.5% achieved under 200 cluster formations.

Keywords—Benign; computed tomography; malignant; lung cancer; radiation; triple support vector machine

I. INTRODUCTION

According to WHO results nearly 10 million death occurred due to cancer. Among 10 million cancer types, about 2.21 million cases are of lung cancer. The most common cancer deaths of 2020 were of lung cancer as per WHO. The deadliest pandemic Covid19 has also affected the Lungs very badly. Hence under these circumstances, it is vital to predict and thereby prevent any onset of cancer in the human body. Early detection of cancer can considerably reduce the mortality rate[1]. In general, cancer is observed with the presence of growth of cells (nodules) in the lungs and if it can spread to the remaining cells of the body is called to be as malignant. The nodules are termed benign if the cells restrain from spreading yet are harmful to the specific organ alone. The development in technology can be utilized in a scalable manner to detect and diagnose the disease [2] [3] [4].

When cells in the lungs grow uncontrollably, lung cancer develops into a tumor and this can cause respiratory problems and spread to other sections of the body. Lung cancer is caused mostly by smoking and drinking alcohol [5]. Around 80% of the people who are observed with lung cancer are habituated to drinking and smoking. People who have the habit

of smoking in past are the ones getting lung cancer mostly and only a few of them are never smoked. Lung cancer is mainly caused by the factors such as radiation, smoking from nearby people, living in a polluted environment and other related factors in cases of people who don't smoke [6] [7] [8]. In addition, there is a greater chance of the possibility of spreading into the lungs if any other place of the body is affected with cancer. As an overall result, the detection of cancer and predicting the probability of survival requires timely help in case of malignancy in the early stages. The chance of survival for the detection and progress of treatment at the early stages of cancer is higher when compared to severe stages (Borel 1997). Hence, the proposed research develops a system that detects cancer-free people, and the cancer portions which are benign and do not spread to other portions of the body. The proposed research also determines the malignancy in cancer regions which can spread to further parts of the body to diagnose early and provide appropriate treatment. For diagnosis of lung cancers, a variety of imaging has been used including sputum cytology, CT, chest x-ray, and magnetic resonance imaging (MRI) (<http://colah.github.io/posts/>). The tumors can be classified as benign or malignant types of cancer and the prognosis of the identified tumor is carried out by an expert like a doctor who can look over the individuals based on the causes. During detection, the number of false positives is reduced significantly which will have a severe impact on the patient's mental or financial well-being.

Manual detection of lung cancer is a very tedious task. To aid in detection, several machine learning approaches to aid in early diagnosis. The input to such approaches can be MRI, CT scan, and X-ray of the affected organ. These inputs are being fed to detect whether the organ is benign, malignant, or normal. Several types of research have already been conducted in the underlying area using different algorithms and techniques. A considerable amount of studies on image processing applications [1] [9] in lung cancer detection paves way for data processing easier for Machine learning classification. With the advent of image segmentation for separating cancerous nodules, the task of detecting the type of cancer and stages of cancer has become quite simpler. In region growth segmentation, watershed segmentation provides an effective result in CT image processing of lung cancer. The SVM and neural networks play a key role in the identification

of the type of cancer in the lungs.

The crucial issues are developing a system for automatically identifying lung illness and accurately segmenting the precise region. Additionally, the heterogeneity of the tumor makes segmentation a difficult task [10]. Due to the low feature of photographs, it is difficult to notice impacted areas that are small in size [11]. The aforementioned problems serves as a motivation for effective lung tumor identification using RRS segmentation and supervised machine learning algorithm namely triple SVM.

The contributions of this research are summarized as follows:

- 1) The median and Wiener filters are used to preprocess the input images. The reason to choose median filter is that it preserves the sharp edges and Wiener filter removes the additive noise.
- 2) Subsequently, the precise segmentation is done by using RRS followed by SIFT and GLCM that are used to perform the feature extraction. The features from SIFT is invariant to light and viewpoints and GLCM is used to extract texture features.
- 3) Further, the triple SVM is used to perform an effective classification of lung tumor based on its comprehensible margin of dissociation.

The paper's organization of the paper is given as follows: Section II describes the image processing concept of region growth segmentation of lung tumors and later Section III has the methodology of a proposed model of segmentation. Section IV describes the experimental set up which includes the dataset description and model building. Section V concludes the final research output.

II. LITERATURE SURVEY

A boosted deep CNN concept for lung tumor classification was introduced by Rani *et al.* [12] For segmentation purposes, the Advance Target Map Superpixel-based Region was suggested. The tumor region was then quantified using the nanoimaging theory. Image recognition was possible using the idea of boosted deep convolutional neural networks, which provides 97.3% accuracy. The current methodology demonstrated the stated efficacy which proved to greatly increase the execution of the recommended technique. Moreover, the data was handled quickly with deep learning.

Xie *et al.* [13] presented a method for epidermal growth factor receptor (EGFR) prediction with the lung cancer-based alterations. The system employs CNN with the layers counts upto 6 to learn the characteristics of the image deeper, and the process is followed by a Support Vector Machine (SVM) classifier for prediction. Yu's system was evaluated on two kinds of datasets, for which Dataset 1 attains an accuracy score of 76.16% and Dataset2 attains accuracy score of 67.55% respectively. Typical machine learning algorithms are performing inferior to the deep learning models by utilizing the learning obtained through the hierarchical data and deep-layered nature (chaudhary, & Sukhraj Singh 2012). Moreover, the data is being handled quickly with deep learning.

The approaches followed in Kareem *et al.* [14] preserve the fundamental structure of the data while using approaches

similar to autoencoder and the approaches also uncover the analysis information via the deep learning approach. When it comes to picture categorization, CNN is the most preferred option and to categorize pictures efficiently, the process of convolution and the traditional process of the neural network is combined effectively in the design of the CNN model.

Lung cancer detection process using the deep learning algorithm has been examined for efficacy by the author da Silva *et al.* 2021 through the database named Lung Image Database Consortium (LIDC). The findings of the research demonstrated that the potential evaluation performance of models with deep learning possesses a better accuracy value of about 79.40%. The authors wanted to examine if the deeper layers network schemes might be used to diagnose lung cancer and if there were any more efficient techniques to reduce the downsample impact. Using the same dataset, they are evaluated in comparison with the techniques of Stacked Denoising Auto Encoder (SDAE) and the model of Deep Belief Networks (DBNs). On using DBN and SDAE, the models possess the accuracy value of 81.19% and 79.29%, respectively. The findings of the study showed that deeply layered network algorithms and automatic learning image features have a numerous amount of potential in the field of medical imaging.

A deep neural network model with the help of reinforcement learning has been developed for the early-stage detection of lung cancer by the authors of Ali *et al.* (The IQ-OTHNCCD lung cancer dataset Published: 19-10-2020, Version 1, DOI:10.17632/bhmdr45bh2.1 Contributor:hamdalla alyasriy.) And the performance has achieved the accuracy of 99.1% and 64.44% for training and testing respectively for the employed model on LIDC/IDRI subsets of data.

Another technique was suggested by (The IQ- OTH-NCCD lung cancer dataset Published: 19-10- 2020, Version 1, DOI:10.17632/bhmdr45bh2.1 Contributor:hamdalla alyasriy), in which the authors built a CAD system based on a CNN network with multi-view and multi-scale nature for lung nodule categorization. On the datasets of ELCAP and LIDC/IDRI, the system obtained the values of 92.3% and 90.3% accuracy for detection, respectively. According to the aforementioned research work, CNN performance might be enhanced in many cases to improve accuracy performance and also aids in the detection process of early diagnosis of the lung cancer disease with minimal error [15].

Humayun *et al.* [16] presented the transfer learning (TL) with Convolutional Neural Network (CNN) to classify the lung disease. This work comprised three stages: Initially data augmentation was accomplished followed by pretrained CNN which was used to ensure the classification. Further, the localization was completed, once the classification was done. There are three TL methods such as VGG 16, VGG 19, and Xception that were used with fine-tuning hyperparameters to generate the network for training and testing process. The developed TL with CNN achieved higher accuracy in training and low accuracy in testing process.

Kareem *et al.* [14] developed the lung cancer detection using SVM classifier. In this work, the preprocessing techniques of bit plane slicing, Gaussian filtering, erosion technique and outlining operation were used to enhance the CT images. Subsequently, the Otsu's thresholding was used to separate the

nodules followed by SVM that was used to perform the classification. This work mainly concentrated on the preprocessing approach for classifying the lung cancer.

The following are some of the issues with the most recent ways to classifying lung diseases: In classification, it is necessary for testing accuracy to exceed training accuracy [16]. Because training uses the same input data for analysis while testing uses a different input data for categorization. When segmentation is inadequate, classification performance suffers [14]. As a result, developing an efficient segmentation and classification is necessary to improve the classification of lung tumors.

III. PROPOSED METHOD

The primary objective of the work is to detect and classify lung cancer using image processing and machine learning techniques. In this research, the RRS based segmentation is proposed for separating the tumor portions from the input image. The SIFT and GLCM extracts optimal features from the segmented image. In that, the SIFT features are invariant light viewpoints whereas GLCM extracts statistical texture descriptors. Further, the triple SVM is used to perform the classification based on extracted features. The methodology can be outlined as shown in Fig. 1.

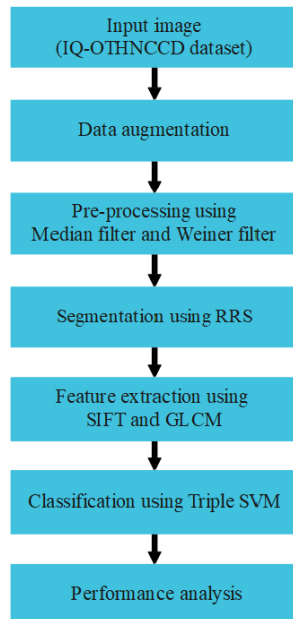


Fig. 1. Architecture of the Proposed Methodology.

Six stages of the proposed methodology have shown in Fig. 1. The procedure of the proposed method begins with collecting the input image data, then the image is augmented, which helps modify the input image to be ready for processing. Using ensembling filters like Weiner and median, the clarity of the vision is enhanced. RRS algorithm is applied to the resultant image, and after the segmentation, we adopt hybrid feature extraction techniques like SIFT and GLCM. The SVM is trained to classify the image into benign or malignant depending on the features. The obtained results are compared with existing techniques in the last phase. The detailed explanation is done in the following sections:

A. Dataset Description

The data for lung cancer has been collected at Iraq- Oncology Teaching Hospital or National Center for Cancer Diseases (IQ-OTH or NCCD) (The IQ- OTH-NCCD lung cancer dataset Published: 19-10-2020, Version 1,DOI:10.17632/bhmdr45bh2.1 Contributor:hamdalla alyas-riy). The data collected constitutes three different stages of lung cancer CT scans of patients along with scans of healthy patients over 3 months. For the categories of benign, normal, and malignant groups of lung cancer, 110 patients are providing 1190 CT scans. By analyzing the images of lung cancer, the proposed model can be trained to detect cancer that can spread (malignant) or which cannot spread (benign) or it is a healthy tissue (normal) with the help of this dataset. Among the total data, 55 cases are normal, 40 cases are malignant and 15 cases are benign. The dataset is in DICOM format. The task is to classify the segmented lung nodules into benign, normal, or malignant [17].

B. Data Preprocessing and Morphological Features

The original CT scan images are preprocessed to remove noise to improve the image quality. Before performing the preprocessing, the data augmentation techniques such as cropping, flipping, rotation, translation, contrast, color augmentation are used to increase the number of inputs to meet the real-world requirements in classification. This is achieved by using an image processing technique called filtering. Two types of filters are used in this project to understand the underlying clarity. Fig. 2 and Fig. 3 represent the image after application of median filter and Weiner filter respectively. In the process of lung nodule segmentation, morphology [18][19] is one of the prominent techniques, especially when it comes to handling the cases of tumors that are attached to regions that are not on target for example paranchymal wall or the diaphragm (juxtapleural) or vessels (juxtavasular). The representation of 0's and 1's as a matrix for a binary view of images on which 1's are called the neighbors.

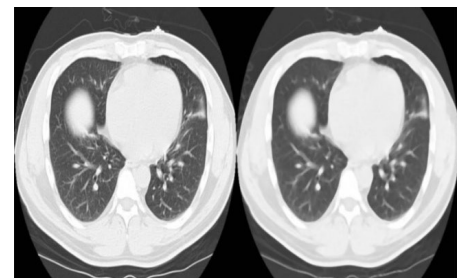


Fig. 2. Original Image and Median Filtered Image.

According to a comparison of the detected region with the corresponding pixel on the input image with respect to neighbor pixels of the output image as equals the value of every pixel. In the process of dilation for the given image pixels are added at the boundaries of the object, whereas it's the reverse process in erosion where in which the pixels are removed. The removed or added amount of pixels has been determining the shape and size of the element structure. Neighboring pixels

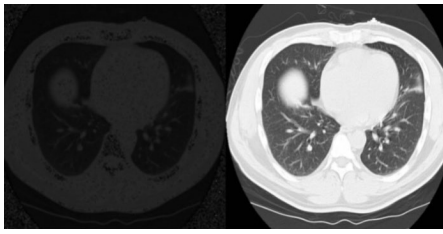


Fig. 3. Original Image and Weiner Filtered Image.

in the input image and the determined pixel through applying rules of morphological operations for the output image. Fig. 4 represents the identification of tumors by using morphological operations.

Cancerous nodules are recognized from the image segmentation in the upcoming stage of analysis and it is being depicted in Fig. 5 as left and right lungs. By using the proposed approach, the extraction of lungs from the images is done with the help of the region growing segmentation approach. The output of the nodule segmentation for one of the lung CT scans is shown in Fig. 6.

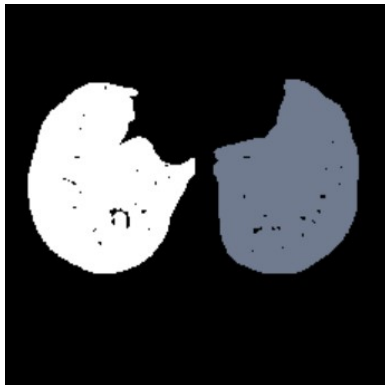


Fig. 5. Left and Right Lung Segmentation.



Fig. 6. Segmentation of Cancer Nodules.

Fig. 6 illustrate the segmentation output of the entire dataset. Fig. 7 shows the original CT scan images and Fig. 8 shows the segmented output using region growth algorithm.

C. Segmentation

Image segmentation [6] [2] [3] is the process to partition the image into multiple segments used to locate objects and boundaries. The region growth segmentation examines the neighboring pixels to determine whether it is to be added to the region or not. This is continued until no more regions can be added. The region is grown iteratively by considering all the neighboring pixels to the region.

The difference between the region means and pixel intensity is used as the similarity measure. A certain threshold value is set for the image. The region growth commences from the dark region of the image taken for segmentation. From Fig. 6 one can see that the cancerous nodules are segmented from the original image. Hence this segmentation helps in understanding the shape and size of the cancer nodules. Therefore, by using region growth segmentation, the tumor cells are identified. The following equations depict the operation of region growth segmentation. For every pixel in a region, the neighboring pixels are compared and if the difference is less than the threshold, then the neighboring pixel is added to the region.

Segmenting the image R into n non-empty subsets ($R_1, R_2, R_3, \dots, R_n$) in this segmentation. The following conditions given in equation (1) and (2) are required to be met during the segmentation.

- $R_i, i = 1, 2, \dots, n$ is digitally connected that is the regions has the contiguous lattice points.

$$U_{i=1}^n R_i = R \text{ --- } > (1)$$

$$R_i \cap R_j = \phi, i \neq j \text{ --- } > (2)$$

Where, ϕ defines the null set. Equation (1) defines the segmentation is complete i.e., each pixel must be in the desired region whereas the equation (2) states that the points in a region is connected in the predefined sense. The RRS gives the capability to segment an image into any number of objects, where is the user-specified arbitrary number of objects. Also treats the image as a graph, with the pixels acting as its nodes or vertices. Hence, the proposed RRS is used to segment lung tumor from the input image.

The main goal is to calculate the similarity of images in different regions

D. Feature Extraction

After performing the RRS based segmentation, the segmented lung tumor (SI) is given as input to the feature extraction. Image feature extraction is the most important stage in any classification problem.

SIFT determines the local features of an image. These are often termed as key points and constitute of scale and rotation

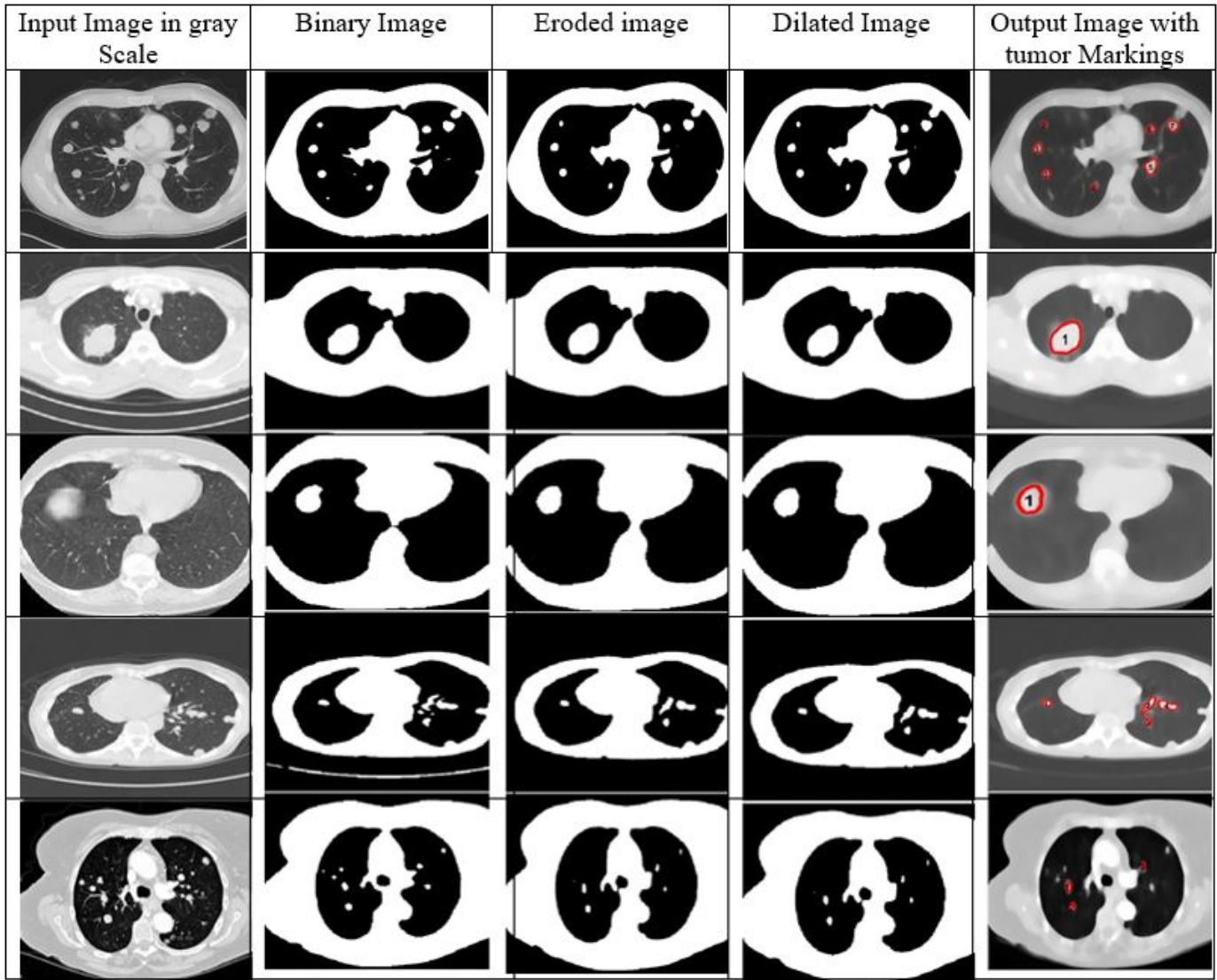


Fig. 4. (a) Represents the Input Image in Gray Scale Format. (b) Represents the Binary Image of the given Input Image. (c) Represents the Image after Applying Erosion Operation. (d) Represents the Image after Applying Dilation Operation. (e) Represents the Output Image along with the Tumor Markings.

invariant. The advantage of using SIFT is that it is independent of the size and orientation of an image. Gaussian blur is used to compute the scale of an image. The idea is to find out the local maxima and local minima for the images and then remove the low contrast key points. Finding the keypoint descriptor is the final stage for SIFT and it computes the orientation and magnitude of a descriptor which are expressed in equation (3) and (4), respectively. According to the local image gradient directions, the keypoints are allocated orientations.

$$m(x, y) = \sqrt{(Diff_x)^2 + (Diff_y)^2} \text{ --- } > (3)$$

$$\theta(x, y) = \tan^{-1} \frac{Diff_x}{Diff_y} \text{ --- } > (4)$$

where, x and y are the dimensions of segmented lung tumor image (SI) ; $Diff_x$ and $Diff_y$ are pixel differences; The

calculations of magnitude and direction are performed for an each pixel in an adjacent region around the keypoint at the Gaussian-blurred image.

GLCM (Grey Level Co-occurrence Matrix (Mohanaiah et al. 2013) determines the spatial relationship of image pixels. This calculates how often the pixel pairs and spatial relationships occur in an image. The statistical measures are obtained from the GLCM matrix. The most common measures obtained are contrasted (local variation in the matrix), correlation (joint probability of the pixel pairs), energy (sum of squared elements), homogeneity (closeness of the distribution) and entropy. Hence, this GLCM provides the statistical texture descriptors for the segmented lung tumor image (SI). Further, the features from both the SIFT and GLCM are concatenated together as shown in equation (5).

$$F_{ca} = \{m, \theta, GLCM\} \text{ --- } > (5)$$

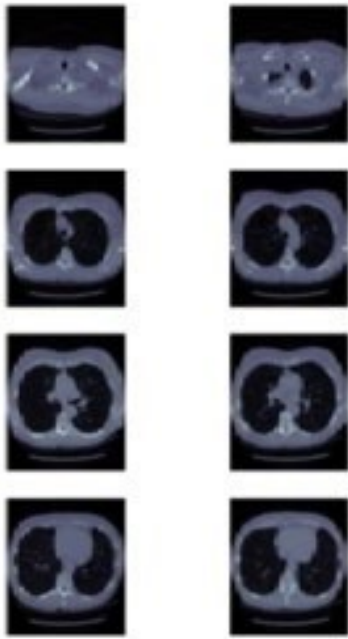


Fig. 7. Original CT Images.

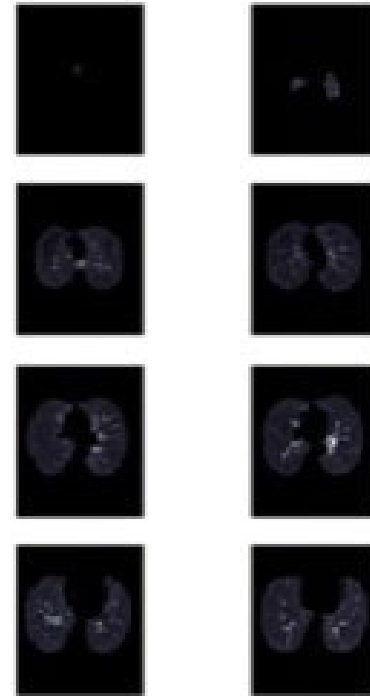


Fig. 8. Segmented Output.

The concatenated features are given to the Triple SVM to perform the classification.

E. Triple Support Vector Machine Classification

Initially, the features from the SIFT and GLCM are taken as input to the triple SVM to perform the classification. SVM is a supervised machine learning algorithm that uses a hyperplane to classify the data. The task is to find out a best-fitting hyperplane that segregates data based on the given input features and the process is termed a marginal classifier. The SVM has proved to achieve good performance in the data which has no prior knowledge from the related study. The basic idea is to map the input data (i.e., concatenated features of SIFT and GLCM (FFFFFF)) onto a higher dimensional feature space and determine the separate margin between the classes in the feature space. SVM is built using a kernel function that has the best fitting hyperplane [7] [20]. In the current work, Triple SVM is used for multi-class classification, which helps in preventing the loss of information where class data is considered against each of the other classes. Further, Triple SVM achieves better performances in the IQ-OTH or NCCD dataset, because it minimizes the inter-class and maximize the intra-class. The linear classifier is depends on the linear discriminant function

$$f(F_{ea})$$

which is expressed in equation (6).

$$f(F_{ea}) = w^T F_{ea} + b - - - - > (6)$$

Where, w is the weight vector and b is the bias value.

Building the model involves classifying the images into normal, benign, or malignant cases. The classification algorithm named SVM has been employed as the technique to be carried for the current phase [14] [21] [22]. The dataset is split into train and test sets. The classification is achieved by optimal separating hyperplane. The data after feature extraction is fed to the SVM kernel function as input. The model is built using a polynomial SVM kernel.

IV. RESULTS AND DISCUSSION

The proposed system is implemented using Google Co-lab software (<http://colab.github.io/posts/>). The model is trained for 100 iterations and achieved an accuracy of 96.5%. The f1-score for normal, Benign and Malignant cases are 0.92, 1 and 0.93, respectively. It is likely to achieve validation accuracy of over 99% when the number of iterations is increased by 300 epochs. Table I and Fig. 9 shows the classification report and accuracy plot of triple-SVM, respectively.

TABLE I. CLASSIFICATION REPORT

	Precision	Recall	f1-Score	Support
Normal Cases	1.00	0.86	0.92	7
Benign Cases	1.00	1.00	1.00	7
Malignant Cases	0.88	1.00	0.93	7
Accuracy			0.965	21
Macro Avg	0.96	0.95	0.95	21
Weighted Avg	0.96	0.95	0.95	21

Algorithm 1 Region Random Segmentation Algorithm

- Step 1:** The lung CT is uploaded as the input image.
- Step 2:** The coordinate of the lung(left and right) is specified.
- Step 3:** Contrast enhancement is done so that the lung region can be easily extracted.
- Step 4:** The threshold value is considered as a 20% gray threshold of the entire image.
- Step 5:** The seed value to be selected for both lungs and a point value which is the neighboring pixel is considered.
- Step 6:** The point value is verified against seed value and threshold value and repeatedly moved across the pixel till it reaches edges.
- Step 7:** A graph represented with edges and vertices is extracted from the resultant lung image on which edges are the relationship between pixels and vertices are the image pixels.
- Step 8:** To do nodule localization and for the lung region representation two seed points are user defined.
- Step 9:** Differences in intensity between the pixels which are unlabelled are being computed by utilizing the euclidean method distance as the seed point.
- Step 10:** Gaussian weight computation and normalization of resultant value.
- Step 11:** Gaussian weighting function used by seeded pixels of lung region and the reached nodule by the probability of walking across each pixel by computation two probabilities with the help of 2 predefined pixels.
- Step 12:** The maximum probability ($p_n > p_l$) pixel will be selected as nodule pixel and label that pixel from the vector of probabilities.
- Step 13:** Nodule representation as the region is separately considered as nodule label pixels to segment.

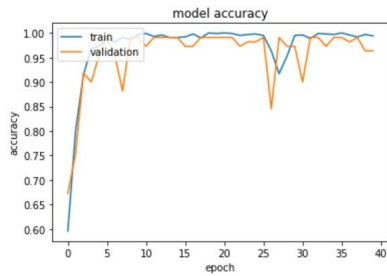


Fig. 9. Accuracy Plot of Triple-SVM Model (300 Epochs).

For classification, 80% of the data is used for training, while the remaining 20% of the data is used for testing. The correlation matrix for the classification accuracy is shown in below Fig. 10.

Table II displays the study of the proposed RRS and triple SVM model's results in relation to the suggested segmentation methodology, variation with various feature extraction methods, and region-based segmentation. Utilizing triple SVMs, the suggested RRS together with selected features from SIFT and GLCM provided higher accuracy of 96.5%. However, when the background has a comparable texture, the segmentation using standard region growth is compromised. Next, little modifications to the input data have an impact on the classification performed using decision trees.

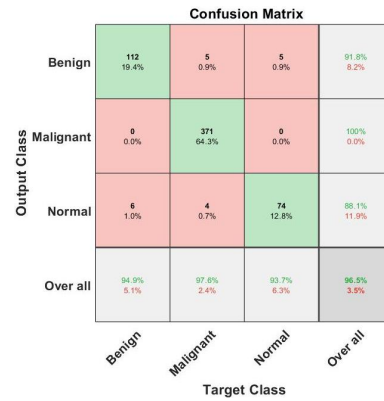


Fig. 10. Correlation Matrix.

TABLE II. RESULT ANALYSIS

Methods	Result Obtained
Particle Swarm Optimization, Genetic Algorithm, SVM	Accuracy : 89.50%
K-NN Classification using Genetic Algorithm	Accuracy : 90%
Artificial Neural Network Approach	Accuracy : 90%
Region Growing Approach with GLCM and Decision Trees	Specificity : 68% Sensitivity : 70% Accuracy : 69%
Region Growing Approach with GLCM and Triple SVM classifier	Specificity : 90% Sensitivity : 93% Accuracy : 89%
Region Growing Approach with SIFT, GLCM and Decision Trees	Specificity : 85% Sensitivity : 84% Accuracy : 93%
Region Growing Approach with SIFT, GLCM and Triple SVM classifier	Specificity : 91% Sensitivity : 87% Accuracy : 96.5%
Proposed Segmentation RR algorithm with SIFT, GLCM and Triple SVM classifier	Specificity : 94% Sensitivity : 89%

The comparative analysis of RRS with Triple SVM with existing researches such as TL-VGG 16 (Humayun *et al.* [16]), TL-VGG 19, TL-Xception and SVM (Kareem *et al.* [14]) are shown in the Table III. From the Table III, it is concluded that the RRS with Triple SVM achieves better results than the TL-VGG 16 (Humayun *et al.* 2022), TL-VGG 19, TL-Xception and SVM. But, the proposed RRS is used to perform precise segmentation of lung tumor portions which leads to improve the classification using triple SVM. The capacity of handling higher dimensional spaces of triple SVM is used to increase the classification accuracy.

TABLE III. COMPARATIVE ANALYSIS

Methods	Accuracy
TL-VGG 16[16]	83.39 %
TL-VGG 19 [16]	80.97 %
TL-Xception[16]	89.68 %
SVM [14]	89.88 %
RRS with Triple SVM	96.5 %

Table III shows the comparative analysis of various methods. RRS with Triple SVM has been compared to previous researches such as, TL-VGG 16, TL-VGG 19 and TL-Xception [16], and SVM [14]. This comparison is given in Table III. According to Table III, the RRS with Triple SVM outperforms the existing TL-VGG 16, TL-VGG 19, TL-Xception and SVM in terms of accuracy (96.5%). Also, the exact segmentation of lung tumor sections were carried out using the proposed RRS which enhances the classification using triple SVM. Triple SVM's ability to handle greater dimensional spaces is employed to improve classification accuracy.

From the overall analysis, the classification is improved by the precise segmentation of lung tumor sections which is carried out utilizing the proposed RRS. To increase classification accuracy, Triple SVM is used because of its capacity for handling higher dimensional spaces. The recommended RRS and a few SIFT and GLCM features combined with triple SVMs produced a greater accuracy of 96.5%. Further, the proposed RRS with Triple SVM was evaluated with existing models such as TL-VGG 16, TL-VGG 19, TL-Xception and SVM in terms of accuracy. From that study, it clearly shows that proposed RRS with Triple SVM has achieved higher accuracy of 96.5%.

V. CONCLUSION

A lung cancer detection and classification model is built using an effective segmentation and triple SVM classifier. The CT scan images are preprocessed and segmented to obtain the cancerous nodules in the lungs. The features are extracted using SIFT and GLCM. The input is then fed to triple SVM classifier with SIFT and GLCM extracted features. The classification accuracy of lung tumor is enhanced based on precise segmentation achieved by RRS. The triple SVM is trained for 300 epochs initially and achieved an accuracy of 96.5% with 200 clusters. If the cluster size is increased to 500, then the model achieves more accuracy. The technique can be enhanced by using multiple algorithm comparisons as well as incorporating deep learning algorithms into this dataset. The proposed methodology can also be implemented using different lung cancer datasets to study the efficiency of the proposed methodology. The prediction accuracy of the proposed model can be varied according to the number of epochs, clusters, and varying preprocessing feature extraction used in building the SVM model. However, the proposed RRS with triple SVM doesn't predict the size of affected portion and classify the supplementary abnormality of tumor. Therefore, the future work involves identifying the volume of the lung and classifying it with any other abnormality and also identifying the thoracic tumor.

REFERENCES

- [1] N. S. Nadkarni and S. Borkar, "Detection of lung cancer in ct images using image processing," pp. 863–866, 2019.
- [2] R. S. Kabade and M. Gaikwad, "Segmentation of brain tumour and its area calculation in brain mr images using k-mean clustering and fuzzy c-mean algorithm," *Int. J. Comput. Sci. Eng. Technol.*, vol. 4, no. 05, pp. 524–531, 2013.
- [3] B. A. Skourt, A. El Hassani, and A. Majda, "Lung ct image segmentation using deep neural networks," *Procedia Computer Science*, vol. 127, pp. 109–113, 2018.
- [4] B. Pellini and A. A. Chaudhuri, "Circulating tumor dna minimal residual disease detection of non-small-cell lung cancer treated with curative intent," *Journal of Clinical Oncology*, vol. 40, no. 6, pp. 567–575, 2022.
- [5] P. Mohanaiah, P. Sathyanarayana, and L. GuruKumar, "Image texture feature extraction using glcm approach," *International journal of scientific and research publications*, vol. 3, no. 5, pp. 1–5, 2013.
- [6] U. Kamal, A. M. Rafi, R. Hoque, J. Wu, M. Hasan *et al.*, "Lung cancer tumor region segmentation using recurrent 3d-denseunet," pp. 36–47, 2020.
- [7] P. Sangamithraa and S. Govindaraju, "Lung tumour detection and classification using ek-mean clustering," pp. 2201–2206, 2016.
- [8] M. P. Arakeri *et al.*, "Real time multi-object tracking based on faster rcnn and improved deep appearance metric," *International Journal of Advanced Computer Science and Applications*, vol. 12, no. 12, 2021.
- [9] P. R. Katre and A. Thakare, "Detection of lung cancer stages using image processing and data classification techniques," pp. 402–404, 2017.
- [10] S. P. Sankar and D. E. George, "Regression neural network segmentation approach with lidc-idri for lung lesion," *Journal of Ambient Intelligence and Humanized Computing*, vol. 12, no. 5, pp. 5571–5580, 2021.
- [11] P. Nanglia, S. Kumar, A. N. Mahajan, P. Singh, and D. Rathee, "A hybrid algorithm for lung cancer classification using svm and neural networks," *ICT Express*, vol. 7, no. 3, pp. 335–341, 2021.
- [12] K. V. Rani and S. J. Jawhar, "Superpixel with nanoscale imaging and boosted deep convolutional neural network concept for lung tumor classification," *International Journal of Imaging Systems and Technology*, vol. 30, no. 4, pp. 899–915, 2020.
- [13] Y. Xie, W.-Y. Meng, R.-Z. Li, Y.-W. Wang, X. Qian, C. Chan, Z.-F. Yu, X.-X. Fan, H.-D. Pan, C. Xie *et al.*, "Early lung cancer diagnostic biomarker discovery by machine learning methods," *Translational oncology*, vol. 14, no. 1, p. 100907, 2021.
- [14] H. F. Kareem, M. S. Al-Huseiny, F. Y. Mohsen, and K. Al-Yasriy, "Evaluation of svm performance in the detection of lung cancer in marked ct scan dataset," *Indonesian Journal of Electrical Engineering and Computer Science*, vol. 21, no. 3, p. 1731, 2021.
- [15] J. Yang, B. Wu, L. Li, P. Cao, and O. Zaiane, "Msd-unet: A multi-scale deeply supervised 3d u-net for automatic segmentation of lung tumor in ct," *Computerized Medical Imaging and Graphics*, vol. 92, p. 101957, 2021.
- [16] M. Humayun, R. Sujatha, S. N. Almuayqil, and N. Jhanjhi, "A transfer learning approach with a convolutional neural network for the classification of lung carcinoma," vol. 10, no. 6, p. 1058, 2022.
- [17] H. Alyasriy, "The iq-othnccd lung cancer dataset," 2020.
- [18] A. Chaudhary and S. S. Singh, "Lung cancer detection on ct images by using image processing," pp. 142–146, 2012.
- [19] S. HARIPRASAD, H. Gururaj *et al.*, "Artifact removal techniques for lung ct images in lung cancer detection?" *International Journal of Data Informatics and Intelligent Computing*, vol. 1, no. 1, pp. 21–29, 2022.
- [20] H. Hu, Q. Li, Y. Zhao, and Y. Zhang, "Parallel deep learning algorithms with hybrid attention mechanism for image segmentation of lung tumors," *IEEE Transactions on Industrial Informatics*, vol. 17, no. 4, pp. 2880–2889, 2020.
- [21] K. Sun and D. Yang, "Human health big data evaluation based on fpga processor and big data decision algorithm," *Microprocessors and Microsystems*, vol. 81, p. 103793, 2021.
- [22] A. Naik and D. R. Edla, "Lung tumor classification using cnn-and glcm-based features," in *ICT Systems and Sustainability*. Springer, 2021, pp. 157–163.

Optimized Automatic Course Timetabling Service Architecture for Integration with Vendor Management Systems

Marwah M. Alansari

Department of IT, College of Computing and Informatics
Saudi Electronic University,
Riyadh, Saudi Arabia

Abstract—Generating university course timetables is a complex problem, especially in large environments such as institutions. Currently, some universities in Saudi Arabia manually generate timetables for classes because they use Vendor Management Systems (VMS) for registration and management. Manually generating course timetables is time-consuming and laborious for the academic staff. Although various methods have been proposed to generate timetables, they address specific environments or systems that can be extended to or work as separate components of the university management system. In this paper, we propose a service-based system with a decentralized architecture that can fully automate the process of course timetable generation and can be easily integrated into VMS. The proposed service-based system employs a genetic algorithm to optimize the process of scheduling courses and generating timetables. The system was implemented using JAVA RESTful web services, and the algorithm was tested by generating various course timetables with various constraints. The results showed that the proposed decentralized architecture is applicable to and can be fully integrated with any VMS. Furthermore, the use of genetic algorithm set up to 200 generations and iterate 1000 times produces acceptable timetables without violating any of the defined constraints.

Keywords—Courses timetable generation; genetic algorithm; course scheduling; service-based system; service-oriented architecture; optimization; web services

I. INTRODUCTION

Some universities in Saudi Arabia use vendor management systems (VMS) such as Banner [1] to enroll and manage students. The main architecture of a VMS constitutes a database management system deployed on the server side and a web portal for accessing the system from the client side. However, a VMS implements only common generic requirements related to registration and management processes. Therefore, such systems can only function for general use cases, such as publishing, presenting, and manipulating student timetables. Currently, university vendor management software cannot consider specific requirements related to course management at universities. Examples of these requirements include the registration and timetable generation processes, which typically comprise many essential periodic tasks that have been performed manually thus far. Although extensive studies by artificial intelligence (AI) communities and operational research have focused on performing timetable generation through various algorithms [2] [3], VMS developers have not considered applying automatic algorithms to their systems for handling specific tasks. Extending and implementing specific

tasks lengthens the development process and makes it costlier. Although such systems are being continuously developed, it is still costly to implement the specific cases and scenarios required by universities to automatically generate complete course timetables. Therefore, most universities prefer using VMS to perform general tasks and manually perform specific tasks.

Universities are encouraged to apply digital transformation and use AI solutions to reduce repetitive processes and move toward their complete automation. We discovered that generating course timetables is one of the repetitive, costly, and time-consuming tasks. Generally, generating university course timetables is considered complex and categorized as an NP-hard problem. This means that they entail exponential growth in search time and effort, wherein the problem factors such as the number of courses or students increases in size [4]. Therefore, we must pursue heuristic approaches that can handle different numbers of constraints, both hard and soft, that can vary from one institution to another. Thus, the objective of this study was to fully automate the process of preparing and allowing students to register on a timetable. This process is performed by generating the term timetable using heuristic approaches, which are elucidated in this study.

We encountered another characteristic of the generic architecture of VMS: they have a centralized architecture that primarily depends on a centralized database management system. By contrast, universities comprise several colleges, each of which comprises several departments. Therefore, a centralized architecture can result in various performance and availability problems, and the staff is unable to automate or enhance the registration process effectively. This research motivation is to improve and fully automate the registration process by overcoming the following two essential challenges:

- 1) Creating a service-based system that can be deployed in the form of decentralized architecture.
- 2) Designing and implementing an algorithm to generate course timetables effectively.

The structure of the paper is as follows. Section II includes a brief background of service-oriented architecture (SOA) and genetic algorithms (GAs). Section III covers related research on auto-generating university timetables. Section IV presents description of the problem. Section V contains an explanation of the proposed solution and introduces the design of the

proposed service-based automatic timetable generation architecture. Section VI presents the proposed GA design. Section VII describes the implementation of the architecture and the proposed GA. Section VIII discusses the results, figures, and findings, and Section IX presents our suggestions for future research directions and conclusions.

II. BACKGROUND

SOA is a design paradigm employed to support distributed business applications, whereas a GA is an evolutionary algorithm that can be applied to solve optimization problems. In this section, we present a brief background of both SOA and GAs and the methods applied in our research.

A. Service-based System

The concept of SOA is applied to engineering business processes within large distributed systems. It ensures that a system has various characteristics, such as being interoperable, service-based, loosely coupled, usable, and fault-tolerant [5]. In an SOA, services are considered self-contained logical functionalities and designed through web services [6]. Furthermore, the backgrounds of the services can be encapsulated in different programming languages, wherein the service client only uses the description for the service without any knowledge of its implementation. There are two types of web service implementations: simple object access protocol (SOAP) and representational state transfer (REST). Another feature of the SOA is that it can provide an enterprise service bus (ESB), which is an infrastructure that enables high interoperability between deployed distributed services. ESBs are managed through business processes. The final feature of SOAs addressed in this section is loose coupling. SOAs enable delivering a service-based system with a reduced number of dependencies [5] [6]. It is important to remember that a single service can offer various capabilities grouped together if they relate to a functional context established by the service [6].

In an SOA, a distributed system is designed and built based on a basic software engineering concept: the theory of concerns. The strategic goals associated with service-oriented computing services indicate their purpose and capabilities through a service contract [6] that emphasizes the positioning of services as enterprise resources within agnostic functional contexts. Numerous design considerations have been proposed to ensure that individual service capabilities are appropriately defined based on an agnostic service context utilities are appropriately defined in relation to an agnostic service context [5].

The two common implementations of services are REST and SOAP. The REST service is required to identify resources that include one or more representations, either expected or provided, an address to uniquely locate the resource, a set of HTTP methods exposed at the interface-level metadata included in headers for requirements such as security tokens or caching information, and a REST-based service interaction. Standard HTTP methods are used in conjunction with HTTP response codes to establish a communication framework based on a uniform contract that can invoke service capabilities and communicate success, failure, and error conditions [6]. Resources that represent a resource in JavaScript object notation

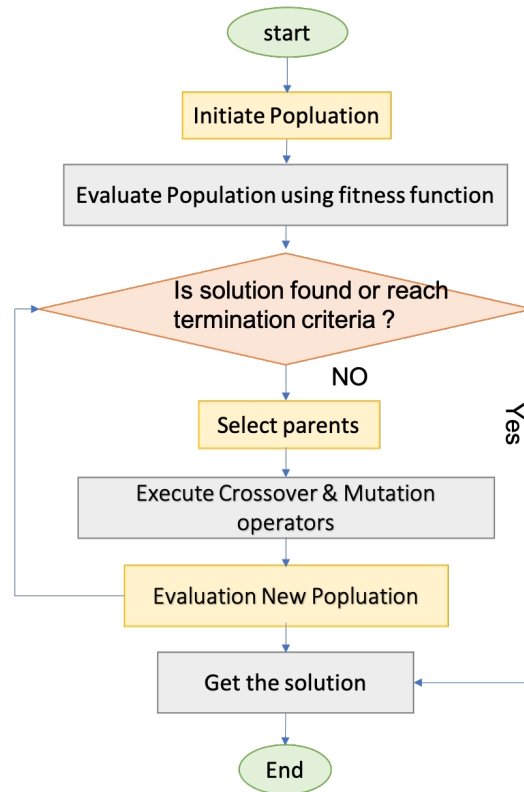


Fig. 1. General Steps of a Genetic Algorithm [7].

(JSON) can be considered as an alternative. In JSON, data are described in the name-value format [6].

The specific method of encoding data “on the wire” and passing them among services is captured in SOAP services. In a SOAP service, both service requests and responses are encoded into XML documents [6]. SOAP-based web services rely heavily on the web services description language, which provides a method of expressing the service contract as a collection of operations with corresponding request/response messages [6].

B. Genetic Algorithm

GAs are evolutionary algorithms proposed by Holland in 1975 and recommended for solving optimization problems by Goldberg in 1975, who later suggested in 1989 that they can be used for solving optimization problems [7]. GAs are based on the Darwinian principle of the survival of the fittest among animals exposed to predators and environmental threats. The fittest entities are those that can adapt to evolving conditions, and their offspring inherit their characteristics and learn their skills, resulting in the creation of the best possible future generations. Furthermore, genetic mutations occur randomly among members of the same species, and some of these alterations may enhance the long-term stability of the superior individuals and their evolutionary offspring [8]. of the parent population that comprises surviving individuals (chromosomes) from previous generations and their offspring. The offspring, which represent new solutions, are generated through genetic operators such as crossover and mutation.

Parents that are selected to produce a new generation are those whose probability of selection is proportional to their fitness values. The higher the fitness value, the better the chance of surviving and reproducing [7] [8]. The algorithm begins with randomly generated initial population solutions, and the generated population gradually improves over time. It uses special criteria to select optimal individuals, who are then used to produce offspring. Offspring are generated using crossover and mutation operators [7] [8]. Fig. 1 shows the steps of a GA.

III. RELATED WORK

The generation of university timetables is a well-studied problem in literature. It is considered a complex NP-hard problem owing to the complexity of the university environment. In this section, we describe some algorithms proposed in various studies to address the problem of generating university timetables.

A new version of the simulated annealing algorithm to address the problem of examination timetabling was proposed in [9]. The algorithm employs an acceptance criterion to move a selected exam and assess the moves by evaluating their acceptance through a temperature bin. The algorithm comprises 10 temperature bins to evaluate the number of evaluations uniformly. It uses the crystalized concept, which is assigned to the selected exam, and does not record any future acceptance moves in the temperature bins. It employs saturation degree-based heuristics combined with conflict-based statistics to eliminate the looping effect during initialization [9].

The authors of [10] proposed using particle swarm optimization (PSO) for generating university timetables. Unlike GAs, PSO simulates social behaviors to evaluate solutions. The evaluation is performed by determining the positioning and velocity of each particle by using the fitness value of the selected particle. The algorithm uses an initial step to assign time slots to the exam, whereas the remaining steps are used to assign rooms to time slots and solve exam timetabling problems at universities.

A modified event-grouping algorithm for finding the best solution by ordering events into groups was developed in [11], wherein events and conflicts are presented on an undirected graph. It should be noted that the execution time of the event-grouping algorithm increases when the number of groups increases [11].

The author in [12] proposed using an AI expert system to automatically generate a scheduling system for the course timetable problem. The auto-generated scheduling system was developed such that no conflict could occur among all the input facts, and features were provided to customize the timetable as required. The rule is executed based on the priority and ranking of the constraints. No specific information regarding the designed rule used in the expert system or definitions of hard and soft constraints were provided.

The author in [13], proposed reformulating an existing integer programming model. It employed the XML for high school timetabling (XHSTT) format to formulate a mathematical model of the problem. The authors developed a model for the problem and a set of models to formulate the constraints and operative functions to avoid clashes. The computational

experiments also showed that the integer programming models resulting from the proposed formulation solved most of the instances in the XHSTT model more effectively. However, this algorithm cannot be generalized to other university models [13].

In [14], there is a suggestion to a hybrid method based on the improved parallel genetic algorithm and local search (IPGALS) to solve the course timetabling problem. The local search (LS) approach proposed in this work supports GA. The distance to feasibility (DF) criterion is applied to measure the hard constraints and ensure that they are never violated. The results showed that using DF improved performance for finding a feasible solution. A parallel approach is used to handle a higher number of constraints. The LS and elitism operators were implemented after applying the crossover and mutation operators. Therefore, the major limitation of IPGALS is that it cannot ensure the generation of a feasible timetable for large groups [14].

The author in [15] proposed applying two methods to solve the room-optimization problem in timetable generation [15]. The first method involves two-stage integer linear programming (ILP), which applies lexicographic optimization. The objective is to maximize the number of students seated and then apply it to optimize room allocation. The ILP is suitable for smaller domains; however, the computation time increases for larger domains. A greedy algorithm was proposed to enhance the first approach. The lecturer is assigned to a room based on the computation of the cost function. The objective is to maximize the number of allocated students. Cost function identification enhances the performance of the greedy algorithm [15].

Guo et al. proposed a new algorithm based on the greedy method combined with a GA to solve the course timetabling problem, wherein the greedy algorithm is applied to generate the initial population [16].

In [4], a design and implementation of timetable generation based on GA were proposed using different combinations of selection algorithms and mutation types. The system uses tournament and roulette wheel selections to evaluate two cases and determine the selection technique that provides a better solution. Furthermore, the study also applied a mutation error to determine if it can retrieve a better solution faster. A similar approach was proposed in [17], wherein a GA model was applied to automatically arrange a university timetable and further study the effect of changing the crossover and mutation rates. Their simulation results showed a crossover rate of 0.70, and no hard constraints appeared in the timetable, but the authors did not mention the effect of changing the mutation rate [17].

In [18], a hybrid genetic hill-climbing algorithm with an embedded elitist mechanism was used to solve the lecturer course timetable problem. Hill-climbing optimization was implemented in the mutation phase to enable an LS. Hill-climbing optimization offers fast convergence and the capability to avoid local optima. The algorithm requires a longer time because hill-climbing optimization is frequently used. However, it does not achieve a fitness value of one, which indicates no conflict. It reaches when the population size reaches 80, but the execution time increases significantly [18].

A pragmatic algorithm implementation is presented in [19] to solve the university course timetabling problem. The algorithm was implemented as a web application deployed on the Azure cloud. The system was based on the manual assignment of courses to time slots and rooms. The objective was to engineer a timetable system programmatically as a web-based system [19]. A man-machine interaction system based on modeling the problem. The proposed algorithm uses column-generation heuristics to collect generated timetable columns by employing the relaxed integer programming method. The modeling timetable works for a reasonable number of instances; however, it may face computational complexity at a larger scale [20].

The authors in [21] presented a greedy algorithm combined with a genetic fusion algorithm to efficiently solve the course timetabling problem. It can obtain the local optimal solution using the greedy algorithm, which is efficient for generating the initial population used in GAs. A greedy algorithm includes an adaptive heuristic search combined with an evolutionary search algorithm. The approach was implemented on simulated data with a small population of approximately 20. Therefore, its effectiveness on a larger population must be evaluated and the fitness values must be compared [21].

Automatic timetable generation using GA with dynamic chromosomes was implemented in [22]. The algorithm suggests using a nonfixed chromosome size, which is adjusted according to the number of courses in the department. The algorithm implements the roulette wheel algorithm to select chromosomes. It uses harder and softer constraints to solve the room-allocated-to-time-slot problem. The performance results and implementation process of the algorithm showed that it was ineffective [22].

A hybrid genetic-based discrete PSO algorithm with two LS algorithms, LS and tabu search, was used in [23]. The objective was to enhance the performance for search solutions. The concept of PSO is based on a swarm of birds (particles) that search for food in an open space. Without any prior knowledge of the space, the birds spread and begin their search in a random space, and the position of all particles corresponds to the candidate solution for an optimization problem. Therefore, all particles are assigned a fitness function, which is determined according to the corresponding problem. Even if each particle moves to a new location in the search space, it maintains the optimal local information. Furthermore, each particle maintains its own information, shares information with the other particles, and maintains the best global information. Subsequently, each particle updates its velocity and position to correspond to the optimal local and global information, moves forward to the optimal value, and seeks the optimal solution. Tabu search is used to improve the solution quality after the LS operation is completed. the GA operation is applied (crossover and mutation) to enhance the global search. However, the execution time of the algorithm increases when a complex timetable model is introduced. This algorithm can be used for the room allocation problem [23].

IV. THE DESCRIPTION OF THE PROBLEM

The process of generating course timetables is classified as repetitive or periodic. However, we discovered that the

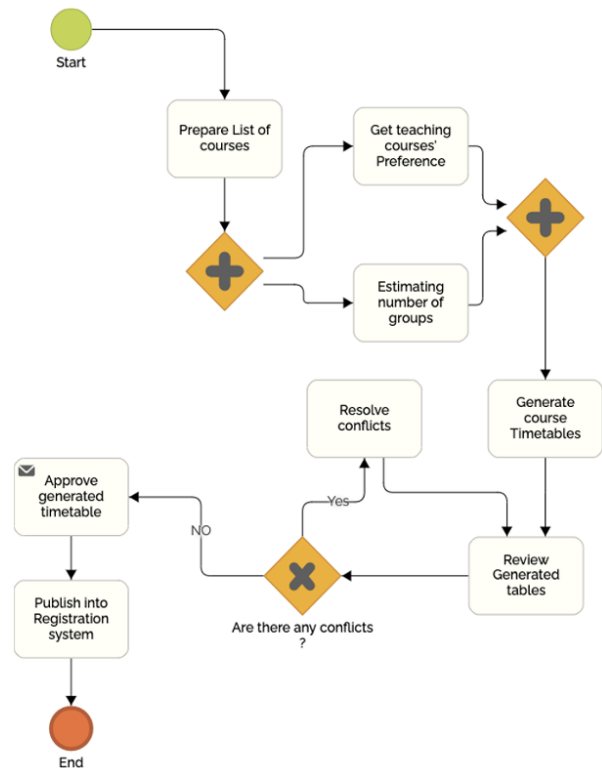


Fig. 2. The Business Process for Generating Course Timetables.

academic departments in some universities in our region still manually generate course timetables. The entire procedure depends on humans playing the primary role in creating and maintaining such timetables.

Fig. 2 shows the framework of business process modeling used to capture the common activities for producing course timetables. The process starts when the staff in a department prepare a list of courses to be taught in the next term. This is followed by collecting course preferences from teaching staff and estimating the number of students who will register for a course. Professors must also be assigned to their selected courses. After the preparation process, timetables are manually generated using spreadsheet software. This process is time-consuming because it requires several review cycles to ensure that timetables do not include any conflicts among groups of students, as shown in Fig. 2. Following the timetable generation step, the faculty administration approves the created course timetables and publishes them on a university course management system with a centralized software architecture.

The student course registration procedures also employ manual processes. It is the students' responsibility to create their entire timetable using the university registration system. At the beginning of each term, students should follow the curriculum plan published by the department after the selected courses are approved by their academic advisers. The student searches for targeted courses and selects a suitable teaching group based on their preferred time slots. If any conflict occurs in time slots, the student keeps changing the teaching groups until a conflict-free timetable is created. We noticed that manually creating and maintaining course timetables re-

sults in serious issues. One such issue is the occurrence of time-slot conflicts among courses, which affects the student registration process. Another problem is the increased number of groups in courses that contain a small number of students, because students have complete freedom to select their desired group at a suitable time slot. Hence, we have observed a misdistribution of student problems, which appears after the registration process is completed. This leads to insufficient resource allocation. After examining these common issues over several years, we conclude that manually generating timetables is time-consuming, laborious, and complex. The process creates stress among staff and students and thus needs to be addressed. Universities use VMS, wherein it is difficult and expensive to include automatic features. Thus, a system that includes optimization methods for timetable generation is required, which can be easily integrated with the registration management system.

V. PROPOSED SOLUTION

This study aimed to solve the problems mentioned in the previous section by developing a service-based system comprising components responsible for publishing and generating timetables. The service-based approach is characterized by a decentralized architecture that is scalable and sufficient for the architecture used by universities. The system interacts with a university management system only to request data and publish the student and staff timetables it generates. The interaction is achieved through messages/requests and responses using RESTful web services. The data are transmitted in the JSON format. Therefore, the proposed service-based system works as a standalone feature that can be used by university departments. Each department has its own deployed service-based component to generate a timetable. In the next section, we explain service-based architecture in more detail. Furthermore, the proposed solution includes the design of a suitable algorithm for automatically generating timetables. Our objective was to eliminate the number of manual activities performed by the staff. Therefore, we designed a heuristic GA to create a departmental timetable that considers a set of hard and soft constraints. A detailed explanation of the proposed GA is presented in Section VI.

A. The Architecture of the System

Fig. 3 shows the main components of the automatic service-based system used to generate timetables. The system comprises five main components: a data notification center, notification service, data communication center, data communication service, and faculty autogen timetable service.

- 1) **Data Notification Center:** This component is responsible for broadcasting a scheduled and timed notification to all active notification services. It also receives replies and notification messages from notification services when the timetable generation processes are completed.
- 2) **Data Communication Center:** This is the communication channel between the university management system and the communication service. The communication center is responsible for filtering the requests

for data from the communication services and transforming them into query passed as a message to the university management system.

- 3) **Notification Service:** This is an active component deployed in each university academic department. It is responsible for sending and receiving notification messages from the data notification center.
- 4) **Data Communication Service:** This component filters student and academic staff data and generates a timetable data format to send and receive data from the data communication center.
- 5) **Faculty Autogen Timetable Service:** This is the primary component responsible for automatically generating course timetables based on a set of requirements. It includes a GA to create an optimized timetable. The following Section provides a detailed explanation of this component.

B. The Architecture of the Faculty Autogen Timetable Service

The component responsible for automatically generating an optimized course timetable comprises various elements, as shown in Fig. 3. The service consists of two components: a **data filtering service** and **timetable generator**. The **data filtering service** handles received and sent data and is composed of three separate entities: course description filtering, department student filtering, and assigning student and faculty timetables.

- 1) *Course Description Filtering:* This entity is used to store the program course plan. The department can add courses, course details, and any updates regarding the program plan. The courses and plans are stored as JSON files.
- 2) *Department Students Filtering:* All the student data required to generate a timetable is received from the university management system database through the data communication service and filtered in this component. Filtering is required to determine the courses that students are expected to register for in the next term. Additionally, the component generates groups of students expected to opt for a course in the next term.
- 3) *Assigning Students and Faculty Timetable:* This component is responsible for assigning each student and academic staff member a timetable after the general timetable generated by the timetable generator component is approved.

The second component of the faculty autogen timetable service is a **timetable generator**. This is an essential service that creates an optimized course timetable. As shown in Fig. 4, this service comprises the following five entities:

- 1) *Department Criteria and Hard and Soft Constraints Configuration:* This entity configures the algorithm parameters, as well as the hard and soft constraints used in the customized scheduling algorithm.
- 2) *Customized Scheduling Algorithm:* This entity is the core of the timetable generator. It includes the implementation of the GA used to generate the expected timetable for the specific teaching plan of a department. Section VI describes the design of the GA in detail.

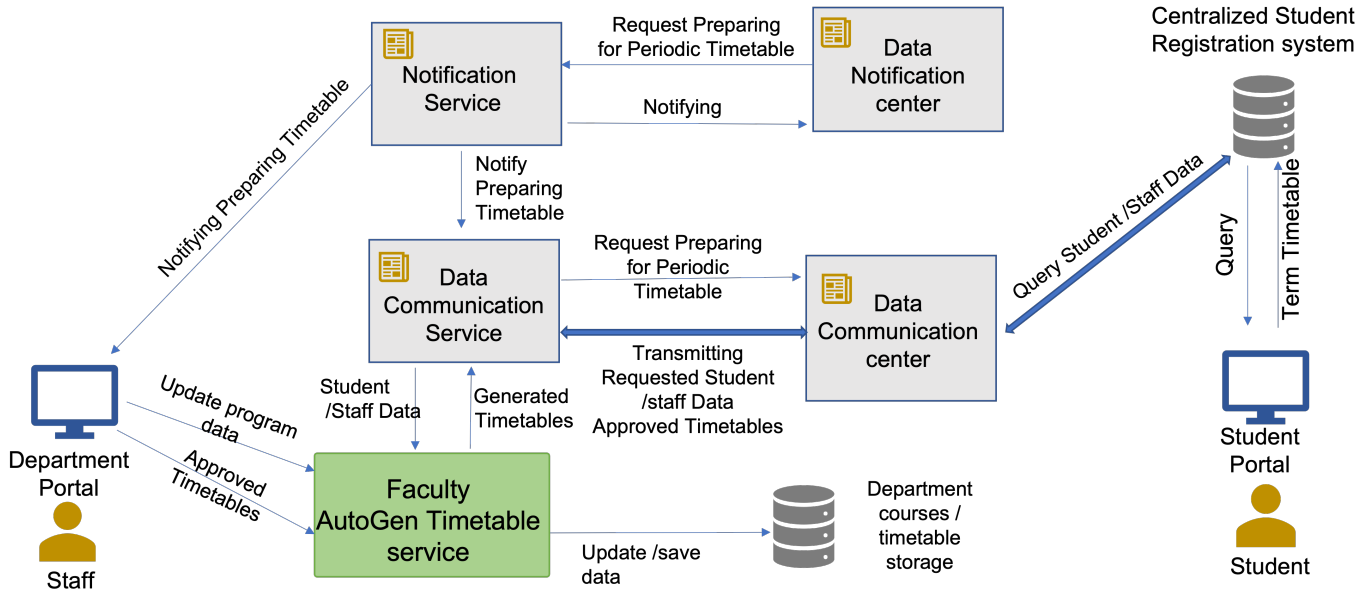


Fig. 3. The Architecture of the Service-Based System for Auto-Generating Course Timetables

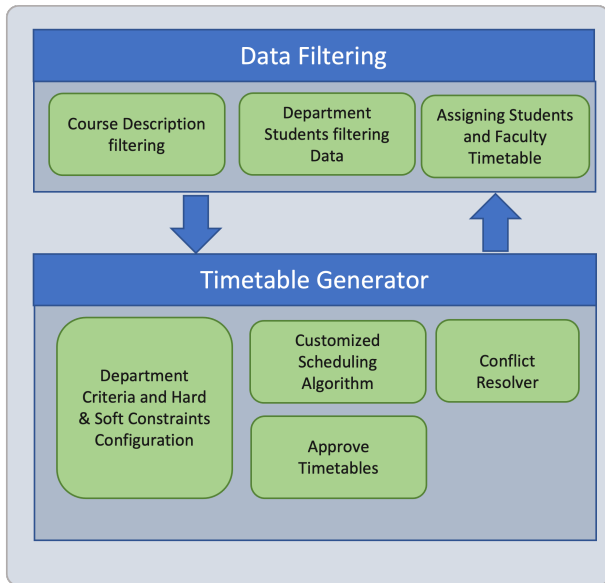


Fig. 4. The Architecture of the Faculty AutoGen Timetable Service

- 3) *Conflict Resolver*: This component runs if the timetable generator is suitable for the department but contains several soft constraints that are violated. It allows for manual resolution of timetable conflicts.
- 4) *Timetable Approval*: This component obtains approvals of the generated timetables and divides them into sub-timetables based on the level to which they can be suitably applied.

VI. GENETIC ALGORITHM DESIGN

This section explains the design and implementation of the GA in detail. Before presenting the designed algorithm, it is

necessary to mathematically model the operating environment. Furthermore, we are required to extract the possible hard and soft constraints required for optimization.

A. The Courses Timetable Mathematical Model

We mathematically modeled the courses timetable problem based on the common requirements and environments of our universities as follows :

A teaching program of a department was divided into levels. These levels comprised a set of courses. During the autumn term, all odd levels are taught, whereas during the spring term, even levels are taught. For simplicity, the summer term or special cases were not included. These levels are denoted as $L = \{l_1, l_2, l_3, \dots, l_n\}$.

Any level l_i includes several courses $C = \{c_1, c_2, c_3, \dots, c_m\}$, and student groups $G = \{g_1, g_2, g_3, \dots, g_k\}$. Additionally, there should be no more than three groups per level. Any course c_i has one or more and no more than three sessions per week. Therefore, the sessions are denoted as $S = \{S_1, S_2, \dots, S_l\}$. Moreover, two types of sessions were defined, theoretical and practical, based on course type and number of teaching hours. Any course c_i is associated with teaching professor tp_i . The teaching professor tp_i who was selected from $TP = \{tp_1, tp_2, \dots, tp_k\}$.

The environment model can be summarized as follows:

- 1) Any teaching program comprises a set of levels as follows:

$$L = \{l_1, l_2, l_3, \dots, l_n\} \quad (1)$$

- 2) Any level l_i has several courses and groups of students and is associated with a teaching professor as

follows:

$$\begin{aligned} C &= \{c_1, c_2, c_3, \dots, c_m\} \\ G &= \{g_1, g_2, g_3, \dots, g_k\} \\ TP &= \{tp_1, tp_2, \dots, tp_r\} \end{aligned} \quad (2)$$

3) Any course c_i has one or more sessions as follows

$$\begin{aligned} S &= \{S_1, S_2, \dots, S_l\} : l \leq 3 \\ s_i &= \textit{Theoretical} \textit{ or } s_i = \textit{Practical} \end{aligned} \quad (3)$$

We want to emphasize that the algorithm proposed in this study does not consider the allocation of lecture rooms. This will constitute a further step in the system in the future, or will be handled as a separate problem. The existing timetable algorithms discussed in Section III consider room allocation to be an essential part of the course timetable allocation algorithm. However, in our case, room allocation always occurs after a suitable timetable is generated. Furthermore, our algorithm contains some factors related to building management, for which course timetables with courses and time slots assigned must be generated first.

B. The Hard Constraints

To create a suitable timetable, we defined a set of hard constraints that must be satisfied and a set of soft constraints that should not be violated. We denoted the set of hard constraints as H . The teaching professors and groups of students are defined as follows:

- 1) A teaching professor, tp_i must not teach two different courses in the same time slot on the same day.
- 2) A group of students g_i must not be assigned two different courses at the same time slot on the same day.
- 3) A group of students must not have two sessions of the same course on the same day. This condition has also been applied to the teaching professors assigned to the course.
- 4) Teaching professor tp_i who is an assistant professors or above, should have at least one day off.
- 5) Group of students g_i must not have more than six hours of theoretical lectures per day.

C. The Soft Constraints

A finite set of soft constraints S , which incur a small weighted plenty value when violated, is defined.

- 1) Teaching Professor tp_i might prefer to start the day in the morning or afternoon, according to their conditions.
- 2) Any practical session $s_i \in P$ for a course c_i can be started in the late morning time slot.
- 3) A group of students g_i should not have a gap longer than two hours between lectures.

D. Objective Function

The optimization problem is to maximize the assignment of all available classes to the sets of defined time events, sections, and teaching professors to assign the maximum number of



Fig. 5. Class Representation.

courses possible from the preferred list. It can be expressed as:

$$f(x) = \textit{Maximize} \sum_{i=1} \textit{Classes}_i \quad (4)$$

The following are the defined decision variables:

- 1) $v_1 = \textit{event day}$
- 2) $v_2 = \textit{event time slot}$

E. The Algorithm Design

A GA must contain chromosomes. To encode chromosomes with a course timetable, a set of classes must be generated. Using the mathematical model, specific courses and sessions at each level are defined as described in Section VI-A, and a set of targeted classes is formulated and denoted as $\textit{Classes}$ as follows:

$$\textit{Classes} = \{\textit{class}_1, \textit{class}_2, \textit{class}_3, \dots, \textit{class}_m\} \quad (5)$$

Fig. 5 shows the class representation and its formulation. As shown in the figure, any \textit{class}_i is assigned a teaching professor TP_i , a group of students g_i , a type that can be theoretical or practical, and a duration d_i . Additionally, \textit{class}_i such as course name and number. The class type, duration, and other details are combined into class information \textit{Cinfo}_i as shown in Fig. 5. Moreover, these classes must be allocated to a particular time event. A time event includes assigning one of the five working days and a time slot, $ts = \{t_{start}, t_{end}\}$.

The algorithm starts with an initialization stage, where in objective is to determine the number of student groups and generate the classes possible, including sessions. Furthermore, the initialization step entails assigning teaching staff to the classes. The selection of teaching staff is based on the ranking obtained from the preference table. Based on this knowledge, a vector class that comprises all classes that can be taught for all programs at all levels is generated, as shown in Fig. 5 .

The GA must allocate the day and time slots for each class in the vector class without violating the hard constraints and no or minimum violation of the soft constraints. After formulating the real class timetable model, the chromosome and genes used in the algorithm must be formulated, as explained in the following section.

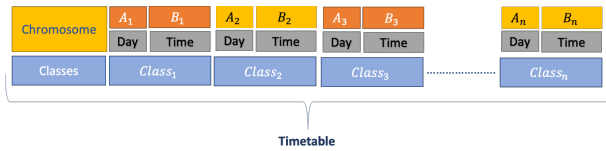


Fig. 6. The Chromosome Representation.

F. The Chromosome Representation

As shown in Fig. 6, a timetable comprises a set of classes and a chromosome. The chromosome contains a vector consisting of genes. There are two types of genes. The first, denoted as A_i , contains a numerical integer that represents the day of a week. The second, denoted as B_i , is a collection of two numerical values representing the time slot. The time slot represents the start and finish times of a class. Chromosome length is twice the class vector length, which is calculated as follows:

$$chromosome_{length} = \sum_{i=0}^n Class_i * 2 \quad (6)$$

G. The Fitness Function

It is important to include a fitness function in the GA because it is used to measure the accuracy of a specific solution. In our case, a good solution should have a fitness value of one, which indicates that the generated timetable does not violate either the hard or soft constraints. Thus, the fitness value is computed as follows:

$$fitness = \frac{1}{(\sum_{i=1}^n \omega_i V_{hard} + \sum_{j=1}^m \sigma_j V_{soft}) + 1} \quad (7)$$

Both V_{hard} and V_{soft} represent the violations of hard and soft constraints, respectively, occurring in the solution. ω and σ denote the penalty weights associated with the hard and soft constraint violations, respectively. Any violation of the hard constraints is assigned a larger weight, whereas that of the soft constraints is assigned a lower weight.

H. Parent Selection and Genetic Operations

Crossover and mutation are the two basic operators of GAs. We used a uniform crossover and uniform mutation, as shown in Fig. 7 and 8, respectively. The crossover operation continues throughout the population and employs the parent selection process, which is based on the tournament selection technique [7] [24]. After parents with effective fitness values are selected, crossover is performed on them. Half of the genes from each parent are randomly selected to generate new offspring. Fig. 7 shows an example of a crossover operation, wherein genes are randomly selected from chromosome parents 1 and 2. In this example, the first gene, which represents the day for class 1, is obtained from parent 2, whereas the time slot is obtained from the time-slot gene of parent 1. We want to emphasize that the class ordering is similar for both parents. Thus, we ensured that no conflicts occurred. If the chromosome does not go through crossover, it will be inserted directly into the new population.

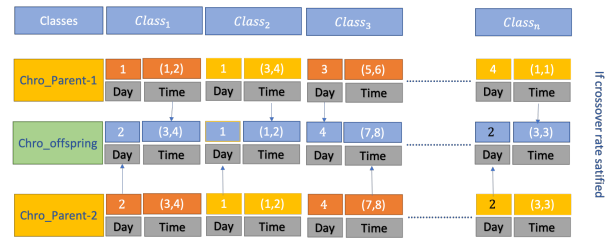


Fig. 7. Representation of the Crossover Operation.

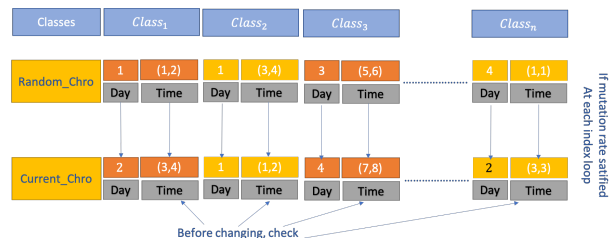


Fig. 8. Representation of the Mutation Operation.

The elitism method was applied to ensure that the best solution from the old population was not lost and the GA was optimized between class duration when the time slots are changed. If the chromosome does not undergo crossover, it is inserted directly into the new population. This method allows individual chromosomes with the best fitness values to be kept unaltered and moved to the next generation. However, we retained only a small number of elite chromosomes compared with the population size and controlled the value using the elite window size.

For the mutation operation, we used the value of mutation rate. When satisfied, a chromosome that allocates the days and effective time slots for the intended classes. The gene values of the chromosome selected for alteration were then replaced with the values generated by the random chromosome. Fig. 8 an example of replacing the gene values of the chromosome selected for mutation with those of a randomly generated chromosome.

VII. IMPLEMENTATION AND EXPERIMENTS

The designed GA was implemented as an application programming interface (API) written in JAVA programming language. The API can be integrated into services that can be easily integrated into any university management system. The course, staff, and student data were included in a JSON file, which enables easy transmission to and from the university management system. All system components were implemented as RESTful web services when deployed on a docker container. They include the faculty autogen timetable service, data communication service, notification service, data notification center, and data communication center. However, a more challenging problem is the implementation of a customized scheduling algorithm, which depends on the GA implementation, as explained in Section VI. Therefore, this component was constructed as a standalone JAVA program for testing and experimentation, as explained in the following section. After the experiments, the program was transferred

TABLE I. THE EXPERIMENTS' CONFIGURATION

Tests	Timetable Parameters				Algorithm Parameters					Tests #
	Courses #	Level #	staff #	Groups	Population Size	Crossover Rate	Mutation Rate	Elite #	Elite Size	
Experiment 1	21	4	19	one group at each level	100,150,300,500	0.7	0.01	2	10	19
Experiment 2	21	4	19	varied groups (2,2,2,1)	100,150,300,500	0.7	0.01	2	10	19
Experiment 3	21	4	19	one group at each level	100,150,300,500	0.5	0.1	2	10	18
Experiment 4	21	4	19	varied groups (2,2,2,1)	100,150,300,500	0.5	0.1	2	10	18

Tests	Constraints		Run
	Hard	Soft	
All Experiments	5	3,2,0	15

Algorithm 1 Random Course Section Generation

Require: CoursesInfoList, ExpectedStudentList, LevelsList
Ensure: CourseInfo with Generated Sections

```

for level in Level List do
    Extract all expected students in the level associated with
    their expected courses to take
    for course in CourseLevelList do
        Count Number of Students
        if TotalStudent ≤ MaxCapacity then
            Generate only one section
        else if TotalStudent > MaxCapacity then
            Sections = TotalStudents/SectionCapacity
            for section in Sections do
                Pick Random Students from Expected Course
                List
                Add Picked Student Random in Section List
                Update Students Info with course and section
            end for
        end if
    end for
end if
end for

```

Algorithm 2 Assign Teaching Professors

Require: Teaching Prof. List, TP Preference List, CoursesInfo List
Ensure: CourseInfo Assigned TP

```

Sort TP list based on Rank and Experience
Order Preference Ranked List
for TPi in TP List do
    Courses ← FindChoicesinCourseInfoList
    for choicei in TP Preference List do
        if Check Courses with choicei is not assigned then
            Assign TP to Course with its sections
            Update teaching hours
        end if
    end for
    if TP remaining teaching hours ≠ 0 then
        randomly picked unassigned course with sections
        and assigned it TPi
    end if
end for

```

Algorithm 3 Timetable Generation using GA

Require: ClassesList
Ensure: Timetable

Initiate Population by:
 Generate Classes
 Initialize Chromosome for each Individual
for Individual in Individuals **do**
 for Class_i in Class List **do**
 Generate Random Time Slot and Day
 Assign Generated Chromosome to Individual
 end for
end for
 Evaluate Randomly generated population
while Termination Condition in not met **do**
 Call Crossover Population ▷ See Fig. 7 explaining used
 crossover operation
 Call Mutation Population ▷ See Fig. 8 explaining used
 mutation operation
 Call Evaluate Population ▷ by calculating fitness values
 using Equation 7
end while

into a module included in timetable generator APIs. The following subsection explains the experimental environment and configuration.

A. The Experiment Environment

A MacBook Pro laptop with a 2.8 GHz Quad-core Intel Core i7 processor and 16 GB RAM was used. During the testing process, all ineffective processes were terminated. A tool was integrated within the API to measure the execution time of the algorithm and record the time required to obtain a solution. Furthermore, the algorithm was configured to enforce termination if it reached 1,000 generations without finding a solution.

B. The Configuration for Experiments

The objective of the experiment was to determine the ideal settings for the algorithm parameters (population size, crossover rate, and mutation rate) that are suitable for creating a course timetable without violating either hard or soft constraints. Furthermore, we wanted to assess the impact on the algorithm performance when the number of student groups increased. Therefore, we focus on the following two special impacts:

- 1) Factors that might affect the algorithm if the number of soft and hard constraints increases.
- 2) The extent to which an increased number of student groups might affect the execution time of the algorithm.

The experiment was divided into four sub-experiments: Experiments 1, 2, 3, and 4, each of which comprised 12 tests. Each test assumed a population configuration and tested few constraints. For example, in Test 1, Experiment 1 assumed a population size of 100 and tested eight constraints (five hard and three soft), whereas in Test 2, Experiment 1 assumed a population size of 100 and tested six constraints (five hard and two soft). The same process was followed for all the tests in each experiment. Each test was performed 15 times to ensure the accuracy. Experiment 1 assessed the execution time and average of conflicts when the mutation and crossover rates were fixed at 0.01 and 0.7, respectively, with respect to the changes in population size and the numbers of soft and hard constraints. We selected population sizes of 100, 150, 300, and 500; 3, 2, and 0 soft constraints; and five hard constraints. The experimental configurations are listed in Table I.

Experiments 1 and 2 aimed to measure the execution times and average conflicts when the mutation and crossover rates were set at 0.01 and 0.7, respectively. Both experiments included four tests, each of which was used to examine the effects of different population sizes and configurations of the number of soft constraints. Each test was performed 10 times. The difference between Experiments 1 and 2 was the number of students groups: Experiment 1 was performed with each level containing only one student group, whereas Experiment 2 was performed using various numbers of student groups, where the three levels contained two student groups. Experiments 3 and 4 followed a similar strategy as the first two experiments, but the mutation and crossover parameters were changed to 0.1 and 0.5, respectively. The objective was to determine the effect on the execution time and average conflicts when this conflict rate was used and the population size was changed. In the final two experiments, we focused on the effect on execution time and conflict rate if the number of courses was increased from 21 to 30 (a major effect on the increasing number of courses). Both experiments were performed using two population sizes, 100 and 200, and changing the number of soft constraints.

VIII. RESULTS AND DISCUSSION

After conducting the experiments described in Section VII, we measured the average execution time and the average number of conflicts with either hard or soft constraints. The results of all four experiments are shown in Fig. 9 and Fig. 10. Fig. 9 contains four subfigures that show the average execution times in milliseconds for all experiments, whereas Fig. 10 contains four subfigures that show the average numbers of constraint conflicts that occurred in the experiments.

Fig. 9a and Fig. 9b show the average execution times of Experiments 1 and 2, respectively, indicating that the average overall execution time of Experiment 1 was lower than that of Experiment 2. Both experiments were performed using crossover and the mutation rates of 0.7 and 0.01, respectively. The main difference in Experiments 1 and 2 was the number of student groups. In Experiment 1, each level contained only one

student group for each teaching course, whereas in Experiment 2, the number of student groups in each course varied. Hence, the algorithm required a longer execution time to obtain a solution. Additionally, an increase in the number of hard and soft constraints affected the execution time.

Fig. 9a shows the effect of increasing the population size and number of tested hard and soft constraints on the execution time. In Case A, the execution time resulted from testing five hard and three soft constraints; in Case B, it resulted from testing five hard and two soft constraints; and in Case C, it resulted from testing only five hard constraints.

For sub-figures Fig. 9b - 9d, we observed that the execution time for the path in Case C1 was lower than those for both Cases A1 and B1. The execution time for Case A1 path was the longest, whereas that for Case B1 was between those of the others. Looking deeply in Fig. 9b, the execution times were longer in the paths shown in these figures because the number of student groups and crossover and mutation rates were changed. Currently, we have determined that the algorithm execution time is affected by an increase in the number of tested constraints. However, if five hard constraints are considered to not have been violated, the average algorithm execution time can be maintained below 30 ms in all sub-figures. In Fig. 9c and Fig. 9d, execution time for the Case C paths was less than 100 ms, owing to the alterations in the algorithm parameters.

We observed that the execution time was affected when the population and the number of tested constraints were increased. Regarding the execution paths of Cases A1-A4 shown in Fig. 9a - 9d the execution time increases dramatically when the population exceeded 300. Thus, we conclude that if the population is set at 500, the algorithm would not obtain effective results in terms of time execution. In fact, it will take approximately 1,000 ms, as shown in Fig. 9a and close to 4,500 ms if the number of student groups is increased, as shown in Fig. 9b. These results would not be affected if the crossover and mutation rates were changed; the execution time for a population of 500 could be above 3,000 ms for a single student group in each course, as shown in Fig. 9c, and can reach over 12,000 ms for various numbers of student groups, as shown in Fig. 9d.

Therefore, it can be determined that the algorithm can generate the best results if the population size is set between 100 and 150 with single or varied number of student groups. This result can be maintained even if both the crossover and mutation rates are changed. Furthermore, the algorithm can produce effective results if a lower number of constraints is maintained, close to five. Furthermore, we assume that the algorithm can generate a reasonable solution if the number of constraints is set to six. However, if the number of constraints is set to eight or more, the algorithm can execute within a reasonable time if the population rate is maintained between 100 and 150, which will reduce the search time.

The conflict rates shown in Fig. 10 for each course are lower than those for the various numbers of student groups assigned to each course. The average number of conflicts shown in Fig. 10a is lower than those in the other figures. We observed that, if the population size was set to 100, the algorithm generated a solution without violating any of the

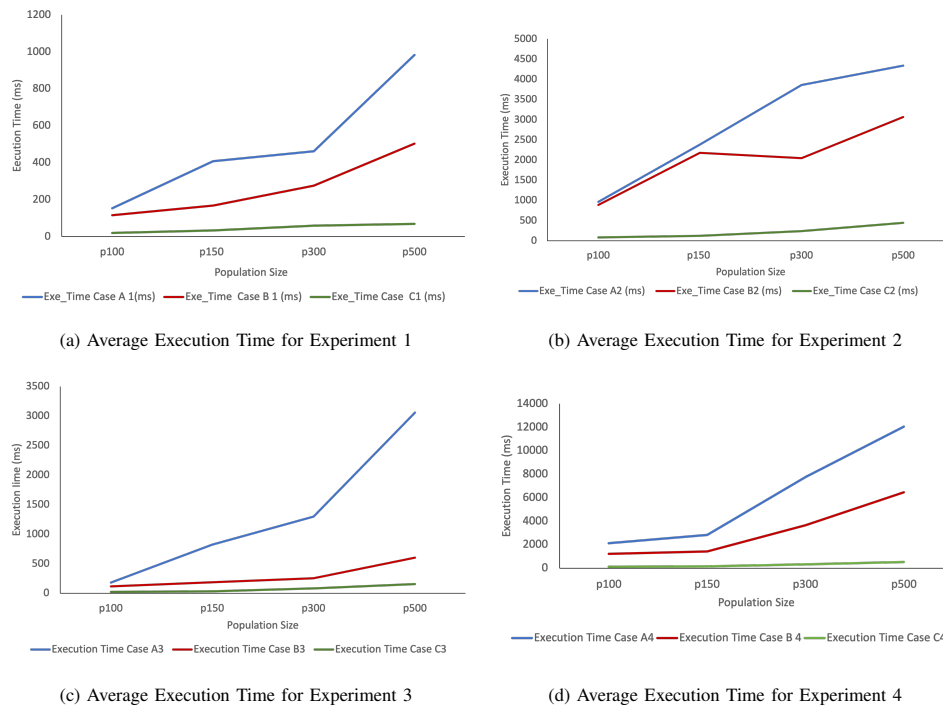


Fig. 9. The Average Execution Time in Milliseconds for All Performed Experiments Experiment 1, Experiment 2, Experiment 3 and Experiment 4

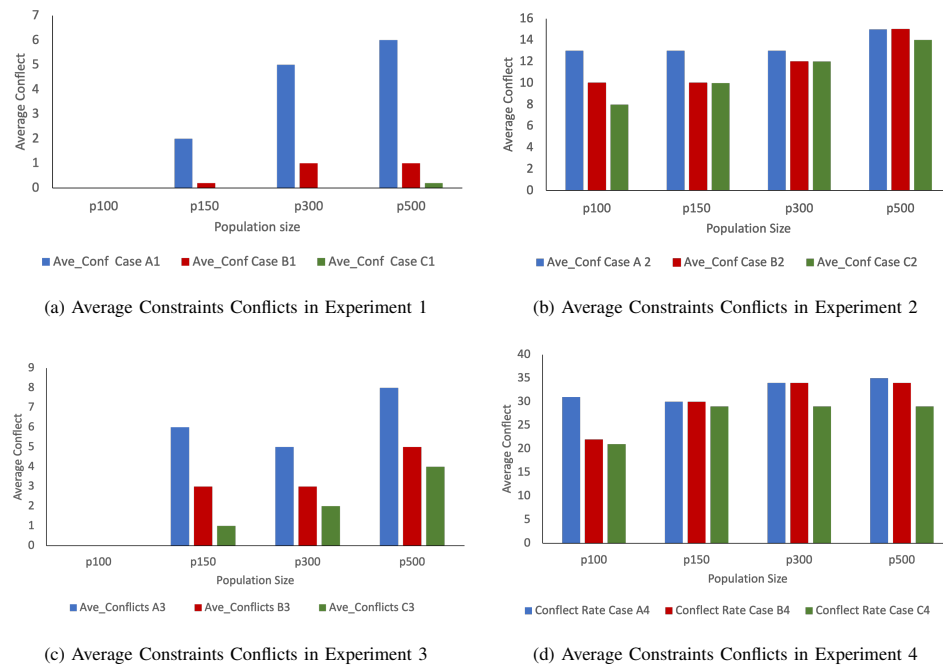


Fig. 10. Averages of Hard / Soft Constraint Conflicts in All Experiments Performed

eight tested constraints. Furthermore, relatively lower number of conflicts can occur if the number of violations is between zero and two. This could have occurred if the population size was 150

and there were six to eight tested constraints. We observed that if the number of tested constraints was five,

there would be no conflicts. A similar result was obtained by setting the population sizes to 300 and 500. We observed that conflicts appeared six or more constraints were applied, and the number of conflicts were higher than those when the population size was set to 150. Thus, we can conclude that the algorithm can produce effective results if the population size is

set to 100, even if the numbers of courses and staff increase. Furthermore, the algorithm would obtain a reasonable result when the population size was set at 150.

The conflict rate results shown in Fig. 10b were used to test the violating number of student groups using similar settings for crossover and mutation rates, as shown in Fig. 10a. We observed that the conflict rate appeared for all quantities of tested constraints. For example, while examining the conflict rate for a population size of 100, the average number of conflicts for testing five constraints was close to eight. If the number of tested constraints was between 6 and 8, the conflict rate was between 10 and 14. Nevertheless, when the population was set at 150, the conflict rate was higher than when it is set at 100. Similar results were obtained when the number of tested constraints was five and above. As shown in Fig. 10b, if the population size is set at 300 and 500, the conflict rate for all the tested constraints is between 12 and 16. Therefore, for a situation wherein various numbers of student groups are tested, a good result can be obtained if the number of tested constraints is maintained at five or lower for a population size of 100. However, the algorithm must be improved to handle various situations more effectively by partitioning the search for each level. However, this requires further investigation and will be addressed in a future study.

The final test involved changing the crossover and mutation rates, as shown in Fig. 10a and 10c. By comparing the results shown in Fig. 10a and 10c it can be observed that there the conflict rates did not differ if the population size was set at 100 in both situations. However, the conflict rate shown in Fig. 10c is higher than that in Fig. 10a.

To summarize our findings:

- 1) The effective population size that will lead the algorithm to produce results without any violation of the constraints and with minimum execution time is 100, and the crossover and mutation rates are set at 0.7 and 0.01, respectively. This occurs even if both the courses and the number of teaching staff are increased at each level. However, we aim to make the algorithm work with more constraints, especially user-defined constraints. This requires further improvement, which will be the subject of future study.
- 2) We also discovered that if the number of student groups is increased at each level, the execution time and conflict rates increase significantly. To handle more student groups at each program level, we will develop a partitioning process for inclusion within the proposed algorithm, which will be executed only if more groups need to be allocated. However, this also requires further investigation.

IX. CONCLUSION

In this study, we looked at the problem for manual generation for courses timetable at universities that uses Vendor Management System (VMS) as centralized system for course registration. To solve the problem, we proposed a decentralized automatic course-timetable-generation service architecture uses Genetic algorithm as a core for generating courses timetable. The system can easily be integrated into university

management systems. The architecture comprises several components: a data notification center, data communication center, notification service, and faculty autogen timetable service. The faculty autogen timetable service comprises several components, of which an essential component is customized timetable generation, which implements using Genetic Algorithm. The proposed decentralized software architecture in the paper can handle scalability issues introduced by integrating architecture with universities VMS. In addition, to make automatic generation a customized course model was used as implemented component. The customized course model includes a set of defined common hard and soft constraints.

However, the objective was to customize the constraint definitions based on the requirements of each department. The purpose of the GA is to allocate the courses that the student groups have signed up for to teaching staff in feasible time slots. During the initialization step, the class population was generated based on the number of student groups that had signed for it, and the teaching staff were randomly allocated based on their rankings. The objective was to allocate these classes to events. The algorithm was tested through a number of experiments to determine the suitable parameters for generating feasible solutions. The algorithm generated a feasible solution with a fitness value of 1 when the population number was set to 100, and the crossover and mutation rates were set to 0.7 and 0.01, respectively. Furthermore, we observed that if the number of student groups increased with no increase in the number of teaching staff, the conflict rate increased. Therefore, to improve the algorithm, we must analyze cases wherein the number of students groups taking a course is increased, which will be the subject of a future study. If a timetable is selected and the number of conflicts is constrained, the auto-generation component has a conflict resolution algorithm that either manually fixes the department staff conflicts or suggests enhancement by omitting soft constraints that can be violated.

A future direction for this study is to propose a parallel GA to enhance the component and handle a higher number of student groups taking the same course. We will also investigate the possibility of building customized hard and soft constraints to add more flexibility in generating course timetables. This requires a method to define a domain-specific language to build constraints and automatically transform them into executable constraints.

REFERENCES

- [1] Ellucian. (2021, 11) Ellucian student banner. [Online]. Available: <https://www.ellucian.com/solutions/ellucian-banner>
- [2] E. A. Abdelhalim and G. A. El Khayat, "A utilization-based genetic algorithm for solving the university timetabling problem (uga)," *Alexandria Engineering Journal*, vol. 55, no. 2, pp. 1395–1409, 2016.
- [3] P. Guo, J.-x. Chen, and L. Zhu, "The design and implementation of timetable system based on genetic algorithm," in *2011 International Conference on Mechatronic Science, Electric Engineering and Computer (MEC)*. IEEE, 2011, pp. 1497–1500.
- [4] H. M. Mousa and A. B. El-Sisi, "Design and implementation of course timetabling system based on genetic algorithm," in *2013 8th International Conference on Computer Engineering Systems (ICCES)*, November 2013, pp. 167–171.
- [5] T. Erl, *Service-Oriented Architecture : Analysis and Design for Services and Microservices*, ser. The Pearson Service Technology Series from Thomas Erl, 2, Ed. Pearson Education, 2016.

- [6] N. Josuttis, *SOA in Practice: The Art of Distributed System Design*, ser. Software engineering. O'Reilly Media Inc., 2007.
- [7] S. Sivanandam and S. Deepa, *Introduction to Genetic Algorithm*. Springer-Verlag Berlin Heidelberg, 2008.
- [8] F. Buontempo, *Genetic Algorithms and Machine Learning for Programmers: Create AI Models and Evolve Solutions*, ser. Pragmatic programmers. Pragmatic Bookshelf, 2019.
- [9] N. Leite, F. Melício, and A. C. Rosa, "A fast simulated annealing algorithm for the examination timetabling problem," *Expert Systems with Applications*, vol. 122, pp. 137–151, 2019.
- [10] A. Ahmad and F. Shaari, "Solving university/polytechnics exam timetable problem using particle swarm optimization," in *Proceedings of the 10th International Conference on Ubiquitous Information Management and Communication*, ser. IMCOM '16, January 2016.
- [11] V. S. Kravev, R. S. Kraveva, and S. Kumar, "A modified event grouping based algorithm for the university course timetabling problem," *International Journal on Advanced Science, Engineering and Information Technology*, vol. 9, no. 1, pp. 229–235, 2019.
- [12] N. I. Ilham, E. H. M. Saat, N. H. A. Rahman, F. Y. A. Rahman, and N. Kasuan, "Auto-generate scheduling system based on expert system," in *2017 7th IEEE International Conference on Control System, Computing and Engineering (ICCSCE)*, November 2017, pp. 6–10.
- [13] G. H. Fonseca, H. G. Santos, E. G. Carrano, and T. J. Stidsen, "Integer programming techniques for educational timetabling," *European Journal of Operational Research*, vol. 262, no. 1, pp. 28–39, 2017.
- [14] A. Rezaeipanah, S. Sechin Matoori, and G. Ahmadi, "A hybrid algorithm for the university course timetabling problem using the improved parallel genetic algorithm and local search," *Applied Intelligence*, vol. 51, January 2021.
- [15] A. Lemos, F. S. Melo, P. T. Monteiro, and I. Lynce, "Room usage optimization in timetabling: A case study at universidade de lisboa," *Operations Research Perspectives*, vol. 6, p. 100092, 2019.
- [16] P. Guo, J.-x. Chen, and L. Zhu, "The design and implementation of timetable system based on genetic algorithm," in *2011 International Conference on Mechatronic Science, Electric Engineering and Computer (MEC)*, August 2011, pp. 1497–1500.
- [17] P. Khonggamnerd and S. Innet, "On improvement of effectiveness in automatic university timetabling arrangement with applied genetic algorithm," in *2009 Fourth International Conference on Computer Sciences and Convergence Information Technology*, November 2009, pp. 1266–1270.
- [18] M. Yusoff and N. Roslan, "Evaluation of genetic algorithm and hybrid genetic algorithm-hill climbing with elitist for lecturer university timetabling problem," in *Advances in Swarm Intelligence*, Y. Tan, Y. Shi, and B. Niu, Eds. Cham: Springer International Publishing, 2019, pp. 363–373.
- [19] R. Ferdiana, N. Ridwan, and N. F. Hidayat, "A pragmatic algorithm approach to develop course timetable web application based on cloud technology," in *2017 7th International Annual Engineering Seminar (InAES)*, August 2017, pp. 1–5.
- [20] H. Komaki, S. Shimazaki, K. Sakakibara, and T. Matsumoto, "Interactive optimization techniques based on a column generation model for timetabling problems of university makeup courses," in *2015 IEEE 8th International Workshop on Computational Intelligence and Applications (IWCI)*, November 2015, pp. 127–130.
- [21] K. Wang, W. Shang, M. Liu, W. Lin, and H. Fu, "A greedy and genetic fusion algorithm for solving course timetabling problem," in *2018 IEEE/ACIS 17th International Conference on Computer and Information Science (ICIS)*, June 2018, pp. 344–349.
- [22] G. Alnowaini and A. A. Aljomai, "Genetic algorithm for solving university course timetabling problem using dynamic chromosomes," in *2021 International Conference of Technology, Science and Administration (ICTSA)*, March 2021, pp. 1–6.
- [23] T. Unprasertporn and D. Lohpetch, "An outperforming hybrid discrete particle swarm optimization for solving the timetabling problem," in *2020 12th International Conference on Knowledge and Smart Technology (KST)*, 2020, pp. 18–23.
- [24] H. A. L. Omid Bozorg-Haddad, Mohammad Solgi, *Meta-heuristic and Evolutionary Algorithms for Engineering Optimization*. Wiley, 2017.

Cryptocurrency Price Prediction using Forecasting and Sentiment Analysis

Shaimaa Alghamdi¹, Sara Alqethami², Tahani Alsubait³, Hosam Alhakami⁴

College of Computers and Information Systems, Umm Al-Qura University, Makkah, Saudi Arabia^{1,2,3,4}

Abstract—In recent years, many investors have used cryptocurrencies, prompting specialists to find out the factors that affect cryptocurrencies' prices. Therefore, one of the most popular methods that have been used to predict cryptocurrency prices is sentiment analysis. It is a widespread technique utilized by many researchers on social media platforms, particularly on Twitter. Thus, to determine the relationship between investors' sentiment and the volatility of cryptocurrency prices, this study forecasts the cryptocurrency prices using the Long-Term-Short-Memory (LSTM) deep learning algorithm. In addition, Twitter users' sentiments using Support Vector Machine (SVM) and Naive Bayes (NB) machine learning approaches are analyzed. As a result, in the classification of the bitcoin (BTC) and Ethereum (ETH) datasets of investors' sentiments into (Positive, Negative, and Neutral), the SVM algorithm outperformed the NB algorithm with an accuracy of 93.95% and 95.59%, respectively. Furthermore, the forecasting regression model achieves an error rate of 0.2545 for MAE, 0.2528 for MSE, and 0.5028 for RMSE.

Keywords—Sentiment analysis; cryptocurrencies; forecasting; bitcoin; ethereum

I. INTRODUCTION

Recently, the prices of financial assets have been dynamically changing, which means it changes asynchronously as new information becomes available [1]. Therefore, the future prediction of finance growth in stocks, shares, and digital currency flow data is difficult for speculators and investors; these cryptocurrencies have skyrocketing and sudden fall characteristics, which means they have high price volatility over time [2].

In addition, cryptocurrencies are an alternative medium of exchange consisting of numerous decentralized crypto coin types. The essence of each crypto coin is in its cryptographic foundation. Secure peer-to-peer transactions are enabled through cryptography in this secure and decentralized exchange network based on blockchain technology [3]. Since its inception in 2009 [4], BTC has become a digital commodity of interest as some believe the crypto coins' worth is comparable to that of traditional fiat currency [5]. Unlike our usual currencies, cryptocurrencies are free from regulatory norms and do not have a central governing authority [6]. Therefore, the cryptocurrency market is investor-driven. Thus, it can be said to be affected by socially constructed opinions, and future expectations of the cryptocurrency holders and future investors [7].

Many currency users share stock price recommendations via electronic platforms. According to Abualigah et al. [8], Twitter is one of the essential sources of users' opinions on various topics. Thus, individuals can express their opinions and share alternative viewpoints on any topic. As a result, it is

necessary to use modern technologies and advanced artificial intelligence methods to analyse Twitter users' opinions.

The research contributions are as follows: (i) Apply machine learning (ML) algorithms to analyse the cryptocurrency users' sentiments, (ii) Apply deep learning (DL) models to forecast the cryptocurrencies' prices, (iii) Analyse the correlation between cryptocurrency users' sentiments and price volatility in the cryptocurrency market, and (iv) Evaluate the performance of the proposed method and compare the results with those of state-of-the-art algorithms and previous studies in the same field.

This paper is structured as follows: Section II provides a literature review of the previous studies on cryptocurrency price forecasting and sentiments analysis. Section III illustrates the overall structure of the research model and the methods utilized to achieve the results. Section IV contains the collected datasets and the pre-processing techniques. Section V presents the experimental results in tables and figures and compares the results with other previous studies. In the final Section VI, we provide a conclusion, limitations, and future work.

II. LITERATURE REVIEW

Cryptocurrencies are a form of alternative currency comprised of various types of decentralized crypto [9]. These cryptocurrencies exhibit rapid growth and rapid downturn characteristics, implying a high degree of price volatility over time [10]. Many studies focused on predicting the "Price" of cryptocurrency by using various techniques such as the Autoregressive Integrated Moving Average (ARIMA) time-series model [11]. They aim to predict the prices using daily, weekly, and monthly time series. On the other hand, several recent studies have analyzed the sentiments of cryptocurrency users using ML [12] and DL models [5]. Additionally, These studies examined whether public sentiment measured by social media datasets are related to or predictive of cryptocurrency values. In particular, it is possible to predict the volatility of cryptocurrencies price by analyzing public sentiment on Twitter and determining the relationship between the sentiments expressed by investors on Twitter.

Accordingly, Rahman et al. [12] presented ML models based on the Twitter dataset. The researchers aim to find an association between user sentiment and BTC price. However, they use a variety of algorithms, such as Support Vector Regression, Decision Tree Regression DTR, and Linear Regression LR. As a result of the experiment, there is a discernible relationship between sentiment on Twitter and price change, based on the highest accuracy obtained from the decision tree algorithm compared with other algorithms is 75%. Similarly,

Sattarov et al. [13] examined the extent to which BTC prices are influenced by investors' sentiments using a ML model. Twitter and the BTC price datasets were collected over a 60-day period, from March 12 to May 12. Additionally, the researchers used the Random Forest RF algorithm to determine a correlation between cryptocurrency users' opinions and feelings and price variation. The implemented model achieves 62.48% accuracy and a minimum error of 21.84%.

In another study conducted by Mittal et al. [14], The interrelationships between BTC price and Twitter and Google search were identified using the BTC price, tweets, and Google search patterns. According to the investigation, there is a correlation between BTC pricing, Twitter, and Google search behaviors. In addition, the authors apply Linear regression LR, polynomial regression PG, Recurrent Neural networks, and LSTM based analysis of different datasets collected from 9 April 2014 to 07 January 2019. The polynomial regression method outperforms the other techniques by achieving an accuracy of 77.01% and 66.66% of Tweet Volume and Google trends, respectively. Thus, the findings show a significant association between Google Trends and Tweet volume data and the price of BTC, but no significant correlation with tweet sentiments.

Other studies applying sentiment analysis technology to cryptocurrency trading had similar results. For example, Pant et al. [5] developed a novel DL algorithm by combining the BTC sentiment score and historical price. Their objective is to establish a link between user emotions and BTC price volatility using the Recurrent Neural Network RNN model. The datasets chosen covered the same time period, from January 1 to December 31, 2015, in order to investigate the correlation between them. According to the experiment results, the distinction between positive and negative tweets is 81.39 percent accurate. The same proposed model achieves a 77.62 percent accuracy in predicting BTC prices. Moreover, Pathak and Kakkar [15] present DL trained model using LSTM networks. They intend to forecast the overall price trend by analyzing BTC and Twitter data spanning 450 hours. Their study established a link between Twitter users' sentiments and the BTC trading currency's pricing, as the relationship between them was 77.89% accurate.

Furthermore, Aggarwal et al. [16] utilized a symmetric-deep learning approach with value parameters to assess the impact of BTC price prediction on socioeconomic indicators. In particular, they investigated the effect of Gold price and investors' sentiments on the price of BTC by using DL models such as Convolutional Neural Network (CNN), LSTM, and Gated Recurrent Unit (GRU). To enhance the results, they used a variety of datasets from January 15, 2017, to May 12, 2017. Researchers have noticed the significant effect between Twitter users' sentiments and BTC price volatility as the posting of tweets containing positive feelings leads to an increase in the price of BTC. And vice versa. In another study conducted by [17], DL models based on the StockTwits platform and cryptocurrencies datasets are utilized. The authors applied efficient language modeling tools such as recursive neural networks (RNNs) using datasets from March 2013 to May 2018. The findings show a significant association between speculators' posts and cryptocurrency volatility prices.

Most studies used either deep neural network models such

as LSTM or conventional ML models such as RF to forecast cryptocurrency price volatility. Additionally, they employ various preprocessing strategies when developing a cryptocurrency models. However, only a few studies conducted a comparative analysis of DL to identify an optimal preprocessing strategy. These studies were conducted over various timeframes, making them relatively old in this rapidly evolving cryptocurrency market. Thus, additional research is required on forecasting cryptocurrency prices and analyzing investor sentiments using DL approaches, as the literature has not been extensively exploited. Therefore, new studies must be conducted to ensure that these results remain valid in 2022 and to discover new patterns.

III. METHODOLOGY

This section explains the proposed cryptocurrency forecasting model using DL and ML. The sentiments analysis model pre-processes the tweets, calculates the sentiment score using ML algorithms, and classifies them into (Positive, Negative, and Neutral). In contrast, the forecasting model uses the historical price dataset and works on predicting the next three months using the DL algorithm. The methodology of the classification and regression models used to forecast the prices and find the correlation between investors' sentiments and cryptocurrency historical price is presented in Fig. 1.

A. Sentiment Analysis Model

This step aims to apply the primary goal of the research, which is sentimental characteristics tweets measurements such as polarity and subjectivity. The TextBlob3 Python library was utilized to process the Twitter dataset by providing the natural-language processing NLP features [18]. This strategy classifies the polarity of the tweet into positive, neutral, and negative groups as '1', '0', and '-1'. Table I presents the sentiments divided process into three groups (positive, negative, and neutral) depending on the tweets' polarity.

TABLE I. POLARITY CLASSIFICATION

Value of Polarity	Sentiment
>0	Positive
0	Neutral
<0	Negative

The sentiments analysis model of cryptocurrency users was utilized using supervised ML approaches, including SVM, and NB chose these approaches for modeling because it is faster and more lightweight in the classification processes.

1) *Support Vector Machine (SVM)*: is a supervised ML algorithm utilized for classification and regression purposes. Both linear and nonlinear classification is executed by SVM. It is created the line between two classes. That means all points in the same part has the same category. Moreover, It can be more than two lines to separate the categories. The vectors near the hyperplane are the support vectors. In addition, to solve classification problems, there are four kernel functions (linear, polynomial, radial-based, and sigmoid) [19]. The advantages of the SVM algorithm are the better classification accuracy and the best analysis performance if the input data is correctly labeled before the process [20].

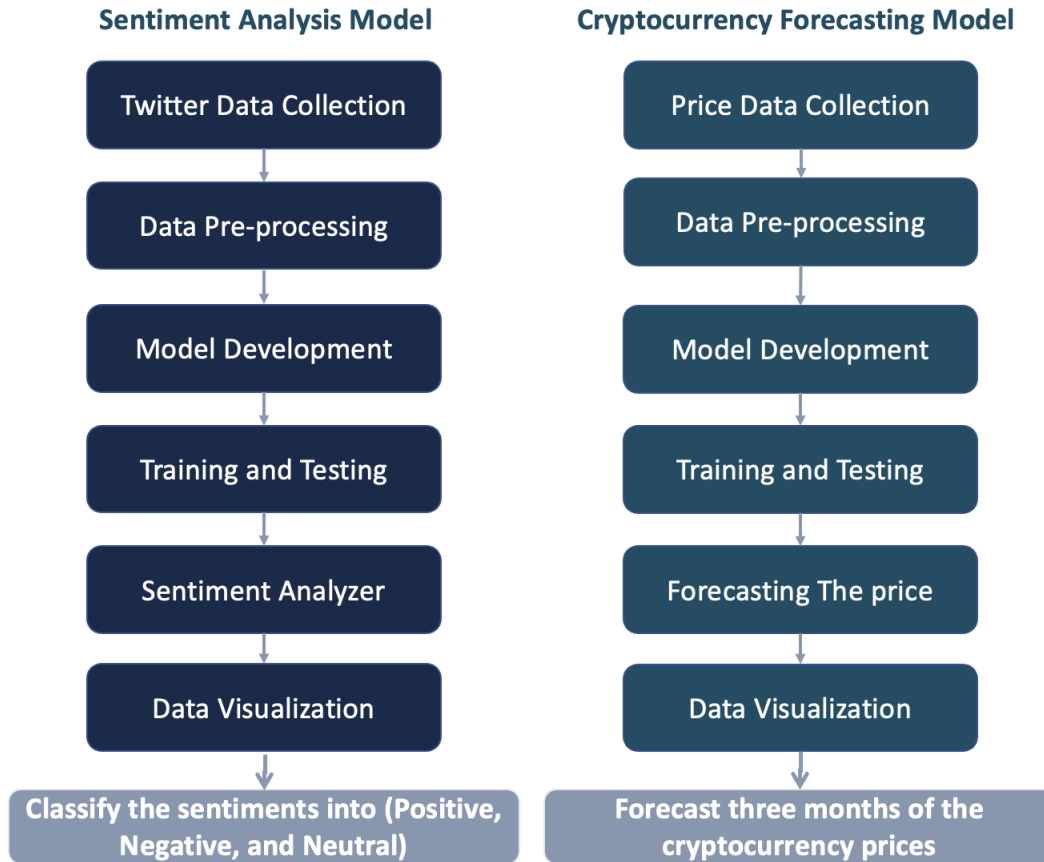


Fig. 1. Forecasting Model Structure.

2) *Naive Bayes (NB)*: is a generative learning algorithm that solves text classification and sentiment analysis ML models based on Bayes' theorem. All features assumed as independent thought give the class value [21]. The term "Naive" directs to data points that are unrelated to one another. The advantages of the NB algorithm, multinomial classifier NB is commonly utilized in text categorization cases, and capable to build, use, train, and ignoring useless variables [22]. The (1) presents in the mathematical equation of NB.

$$P(c|x) = \frac{P(x|c)p(c)}{P(x)} \quad (1)$$

Where:

- $P(c | x)$ is the probability posterior of the given class value.
- $P(c)$ is a prior probability of class.
- $P(x)$ is a prior probability of value.
- $P(x | c)$ is the probability of value given class.

B. Cryptocurrency Forecasting Model

LSTMs were chosen for modeling the cryptocurrency forecasting model since it is an ideal algorithm for time series forecasting and works well with historical data by storing

memory. Furthermore, it solves complex problems that earlier recurrent network algorithms have never been able to solve. Therefore, Table II presents the hyperparameter, the values that control the learning process for the LSTM model.

TABLE II. HYPERPARAMETER VALUES

Activation Function	Sigmoid
Epochs	150
Hidden layers	One hidden layer
Batch size	256
Optimizer	Adam
Learning rate	0.00050

1) *Long-Term-Short-Memory (LSTM)*: is a form of RNN with extra elements for memorizing sequential input. The cell state, which transmits information across the sequence chain, is a crucial component of LSTM. It serves as the network's memory. Because information can be withdrawn or added via gates, the cell state can truly hold only the necessary information in the sequence. During training, the gates learn what information is important to keep or forget. As a result, information from previous stages now influences later stages in the sequence [23].

C. Evaluation Metrics

There is a need to evaluate the performance of the models involved.

- **Regression**

In the regression model, the accuracy of forecasts can only be determined by considering how well a model performs on new data that were not used when fitting the model. Scale-dependent errors are commonly used, such as Mean Absolute Error (MAE), Mean Squared Error (MSE), and Root Mean Squared Error (RMSE) [24] as follows:

Mean Absolute Error (MAE): calculated the average of the original and forecasted values [24]. This is expressed in mathematical terms as (2):

$$MAE = \frac{1}{n} \sum_{n=1}^{t=1} |e_t| \quad (2)$$

Mean Squared Error (MSE): calculated the square average of the difference between original and forecasted values [24]. This is expressed in mathematical terms as (3):

$$MSE = \frac{1}{n} \sum_{n=1}^{t=1} e_t^2 \quad (3)$$

Root Mean Squared Error (RMSE): The forecast errors standard deviation. That means the residuals measurement of far points from the regression line data [24]. This is expressed in mathematical terms as (4):

$$RMSE = \sqrt{\frac{1}{n} \sum_{n=1}^{t=1} e_t^2} \quad (4)$$

Where:

- n is the sample's forecast total number.
- e is the real value of the sample.
- t is the forecasting value of the sample.

- **Classification**

On the other hand, the evaluation metrics used for classification models the performance of the algorithms are Accuracy, Precision, Recall, and F1-Score [25] as follows.

Precision The positive quantification, which are True Positives (TP) and False Positives (FP) number of predictions [25]. This is expressed in mathematical terms as (5):

$$Precision = \frac{TP}{TP + FP} \quad (5)$$

Recall The number of positive class predictions made from all positive cases in the dataset that can be counted. And when there is a large cost related to False Negatives (FN) [25]. This is expressed in mathematical terms as (6):

$$Recall = \frac{TP}{TP + FN} \quad (6)$$

F1-Score Precision and Recall have a harmonic mean [26]. This is expressed in mathematical terms as (7):

$$F1 - Score = \frac{2 * Precision * Recall}{Precision + Recall} \quad (7)$$

Accuracy The intuitive performance measure, which is the observed the correctly forecasted ratio to the total observations [26]. This is expressed in mathematical terms as (8):

$$Accuracy = \frac{(TP + TN)}{TP + TN + FP + FN} \quad (8)$$

IV. EXPERIMENTS

This section illustrates the selected dataset in this research and the pre-processing steps.

A. Dataset

According to Coinmarketcup [27], there are 10111 various types of cryptocurrencies in circulation, such as BTC, ETH, Binance (BNB), and Cardano (ADA). Furthermore, BTC is still the prevalent cryptocurrency that has been widely used since its creation. Then ETH followed it as the top cryptocurrency compared to other currencies. Thus, this study focuses on the two most-traded currencies: BTC and ETH.

- **Twitter Dataset**

An open-source Python library known as Tweepy [28] is used to access the Twitter API and extract the Twitter dataset. Therefore, tweets were collected using three hashtags and three keywords for two cryptocurrency types: The BTC cryptocurrency collection process used keywords "Bitcoin", "BTC", and "BTCUSD" along with their respective hashtags ["#Bitcoin", "#BTC", "#BTCUSD"]. And, the ETH cryptocurrency collection process used keywords "Ethereum", "ETH", and "Etherum" along with their respective hashtags ["#Ethereum", "#ETH", "#Etherum"]. Furthermore, the period we focus on is five months, and assigned to extract (2000 tweets) every seven days for 150 days, between January 1, 2022, and May 9, 2022. The final dataset was around 37,998 for BTC cryptocurrency tweets and around 37,997 for ETH cryptocurrency and separately saved in a CSV file. Hence, the dataset for all tweets with different cryptocurrencies is around 75,995 posted in the English language.

- **Cryptocurrency Dataset**

The dataset of the two currencies was collected from CoinMarketCap [27], the world's most-referenced price-tracking website for crypto assets in the rapidly increasing cryptocurrency market [10]. The BTC dataset starts from September 17, 2014, to March 31, 2022. On the other hand, the ETH dataset starts from November 9, 2017, to March 31, 2022. However, in this research, the 1-minute interval trading exchange data rate in USD is focused on. In addition, the two datasets consist of the Date, Opening, Closing, Low, Adj Close, and Volume of transactions which increase over time. Additionally, the BTC and ETH datasets are saved in CSV files separately.

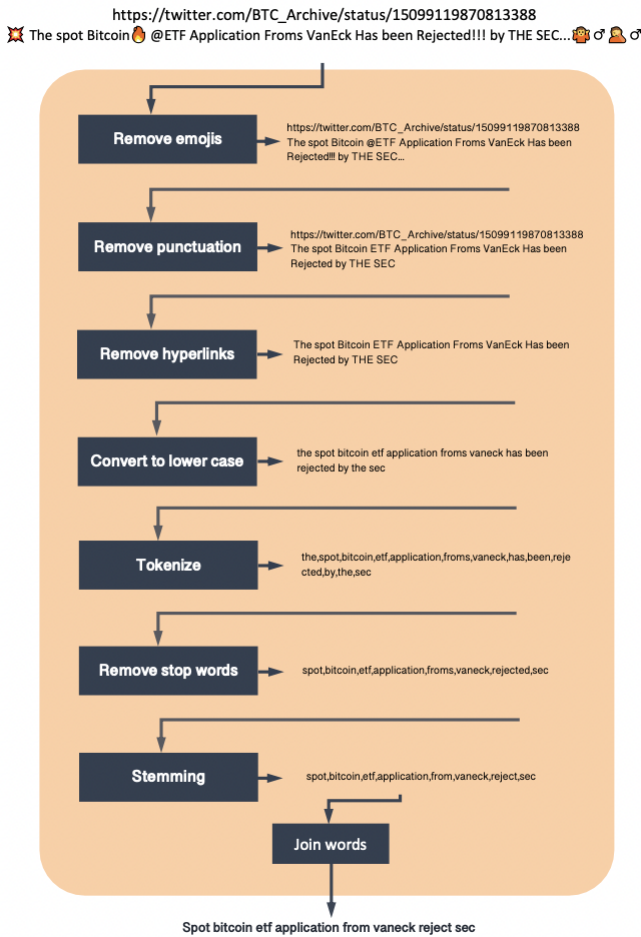


Fig. 2. The Pre-Processing of the “Cleaned” Function over BTC Sample Tweet Text.

B. Data Pre-Processing

Pre-processing the data is an important step in enhancing the model’s predictive accuracy and getting better results. The pre-processing techniques were applied in the Twitter and cryptocurrency datasets.

- Twitter Dataset Pre-Processing**
 The pre-processing data phase contains multiple procedures that remove parts of tweets that may excessively or unnecessarily impact the sentiment score. To achieve the goal, Python’s String methods and the library Natural Language Toolkit (NLTK) was utilized [29]. NLTK library allowed the text to process for classification, tokenization, stemming, tagging, parsing, and semantic reasoning. Fig. 2 presented the pre-processing steps applied in the BTC dataset with a tweet example. In addition, ETH follows the same pre-processing steps. As a result, the total number of tweets decreases from 37,998 to 17,608 on the BTC dataset and 37,997 to 17,373 on the ETH dataset.
- Cryptocurrency Dataset Pre-Processing**
 In the stage of pre-processing, as given in Table III, seven features were selected out of eight to forecast the

cryptocurrencies’ prices. The cryptocurrency dataset is updated daily. Therefore, trades where the date value is from September 17, 2014, to March 31, 2022, for BTC and November 9, 2017, to March 31, 2022, for ETH are considered. In addition, according to the collected dataset period, the Close column is modified in the Adj Close column. Thus, the Close column were removed and depending on the Adj Close column as the final result of the latest trade recorded day.

TABLE III. FEATURES SELECTION

Features	Definition
Date	recorded time of the price
Open	Opening trade (Open price on recorded day)
High	Opening trade (Open price on recorded day)
Low	Lowest trade (Least price on recorded day)
Adj Close	Adj Close price on recorded day
Volume	Volume of transactions

C. Experimental Environment

The experimental environment is Google Colaboratory [30], known as “Colab”, a suitable Python environment for ML and data analysis purposes. It provided free accessibility to GPU computing resources. Among the used tools and technologies in the experimental environment are statistical libraries used are NumPy [31] and Pandas [32]. Furthermore, the experiment is conducted on a MacBookPro laptop with 8 GB RAM, an M1 chip, and Macintosh 12.0.1 operating system. In addition, Open-source Neural Network libraries TensorFlow [33] and Keras [34] were implemented to cryptocurrencies’ future price prediction model.

V. RESULTS AND DISCUSSION

This section presents the results of the sentiments analysis model and the cryptocurrency forecasting model, implemented using BTC and ETH cryptocurrency datasets.

A. Result of Sentiment Analysis Model

To better understand the public opinion towards cryptocurrencies and find the relationship with the price volatility. The sentiment is classified into three groups. Fig. 3 presents the distribution of BTC and ETH users’ sentiments: (A) shows the bar graph of the BTC result. The tweets expressed an observed positive opinion that might have happened because most of the tweets contained sentences that did not express negative or neutral emotions. In addition, the rest are due to the BTC currency having a large number of transactions compared with the other cryptocurrencies. On the other hand, (B) presents the bar graph of the ETH result. The tweets expressed an observed neutral opinion towards ETH currency.

Moreover, Table IV presents the macro average of the employed SVM and NB methods to classify the BTC sentiments. While Table V presents the macro average of the employed SVM and NB methods to classify the ETH sentiments. The SVM method outperforms the NB by achieving an accuracy of 93.95% and 95.59%, respectively.

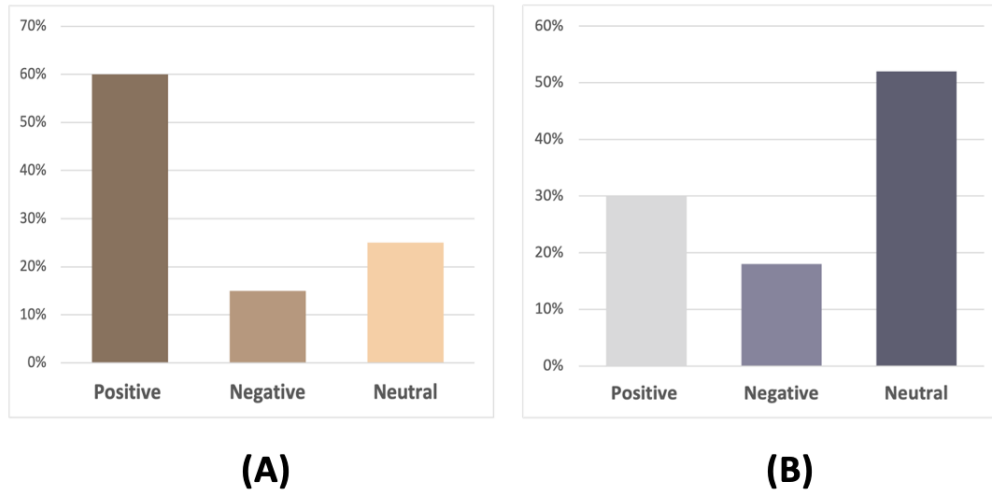


Fig. 3. Distribution of BTC and ETH Sentiments.

TABLE IV. COMPARISON BETWEEN SVM AND NB METHODS ON BTC DATASET

Models	Accuracy	Precision	Recall	F1-score
SVM	93.95%	0.90	0.94	0.91
NB	80.56%	0.67	0.84	0.69

TABLE V. COMPARISON BETWEEN SVM AND NB METHODS ON ETH DATASET

Models	Accuracy	Precision	Recall	F1-score
SVM	95.59%	0.91	0.95	0.93
NB	83.74%	0.69	0.88	0.72

B. Result of Cryptocurrency Forecasting Model

The results of the LSTM regression model for the BTC and ETH cryptocurrencies are presented in Fig. 4 and 6. Fig. 4 presented the BTC model, trained and tested from September 17, 2014, to March 31, 2022, to forecast the three following months (April, May, and June). As a result, BTC prices fall in the predicted months, as shown in Fig. 5. On the other hand, Fig. 6 presented the ETH model, trained and tested from November 9, 2017, to March 31, 2022, to forecast the three following months (April, May, and June). As a result, ETH prices fall in the predicted months, as shown in Fig. 7.

The MAE, RMSE, and MAPE are used to evaluate the performance of regression models. Table VI summarizes the results of training and testing errors. We observed that the BTC forecasting model outperformed the ETH model in terms of MAE, MSE, and RMSE, whereas the LSTM model's error in ETH is worse due to the smaller dataset size. It is noted that the small resample of time series data may get the worst result on MAE, MSE, and RMSE tests.

Fig. 8 and 9 introduced the study of the correlation between cryptocurrency users' opinions and price volatility in the cryptocurrency market from January 1, 2022, and May 9, 2022. Fig. 8 illustrates the relationship between BTC volatility prices and BTC users' sentiments. As well, Fig. 9 shows the

TABLE VI. PERFORMANCE OF LSTM REGRESSION MODELS WITH DIFFERENT CRYPTOCURRENCIES FOR PREDICTING THE DAILY CLOSING PRICE

Cryptocurrency type	MAE	MSE	RMSE
Bitcoin (BTC)	0.2545	0.2528	0.5028
Ethereum (ETH)	0.3838	0.4677	0.6839

relationship between ETH volatility prices and ETH users' opinions. We observe that the correlation in the BTC is close compared with ETH, which means when the BTC investors have a positive sentiment, the price of BTC cryptocurrency will be increased. Vice versa, when they have a negative emotion toward the BTC cryptocurrency, the price will be decreased. On the other hand, the ETH prices and users' sentiments do not have a relationship. Therefore, we may conclude that emotion is not always related to investor satisfaction.

C. Comparing with Related Works

Several researchers used various ML [12], [13] and DL [15], [5] techniques to analyze the cryptocurrency users' sentiments. As a result, Table VII compared the result of the current study with the previous studies which used the same dataset in different periods and techniques. In addition, They aim to analyze the sentiments of cryptocurrency users. The SVM appears to be a more appropriate method of classifying the sentiments depending on the accuracy result. To the researchers' knowledge, the reason for the superiority of this study's results is the followed pre-processing techniques that were used to clean the Twitter dataset [13], [15]. In addition, the classification of cryptocurrency sentiments is divided into negative and positive, and neutral, unlike the classification process used in other studies [5], [12], they excluded the presence of normal feelings for cryptocurrency users.

On the other hand, ML and DL techniques were applied to forecast cryptocurrency prices. Table VIII presents the error rate result of two cryptocurrencies compared to Alahmari et al. [11]. The current research outperforms another study and achieves good results for BTC and ETH cryptocurrencies. To



Fig. 4. LSTM Forecasting Model for Three Months for BTC Cryptocurrency Price.



Fig. 5. Forecasting (April, May, and June) Months of BTC Cryptocurrency Price.

TABLE VII. COMPARISON WITH RELATED WORK STUDIES ON SENTIMENT ANALYSIS

Study	Period	Methods	Accuracy
Pant et al. [5]	Jan 2015, to Dec 2015	RNN	81.39%
Rahman et al. [12]	Mar 2018, to Mar 2018	DTR	75%
Sattarov et al. [13]	Mar 2019, to May 2019	RF	62.48%
Pathak & Kakkar [15]	March 2019	LSTM	77.89%
This study	Jan 2022, to May 2022	SVM	95%

TABLE VIII. COMPARISON WITH RELATED WORK STUDIES ON FORECASTING

Study	Model	Crypto Type					
		BTC			ETH		
		MAE	MSE	RMSE	MAE	MSE	RMSE
Alahmari et al. [11]	ARIMA	313.8	294.5	542.7	12.9	410.1	20.3
This Study	LSTM	0.254	0.25	0.50	0.38	0.46	0.68

the researchers' knowledge, the reason for the superiority of this study's results is the volume of historical data and the time-series DL model applied in the experiment. It is noted that the small resample of time series data may get the worst result on MAE, MSE, and RMSE tests.

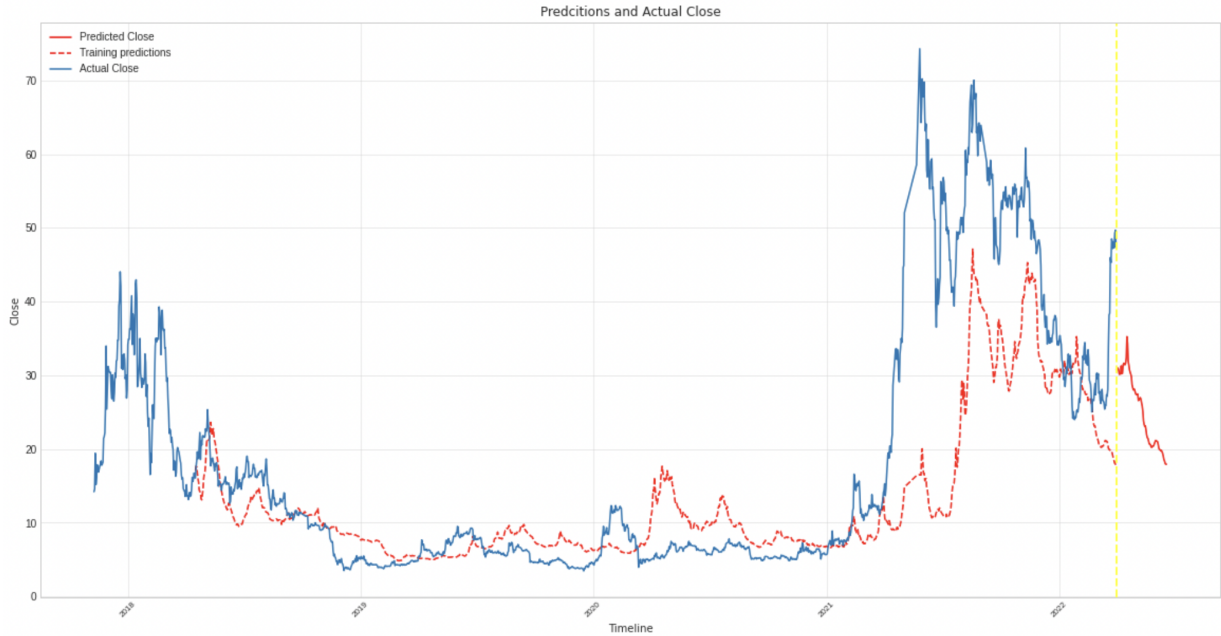


Fig. 6. LSTM Forecasting Model for Three Months for ETH Cryptocurrency Price.

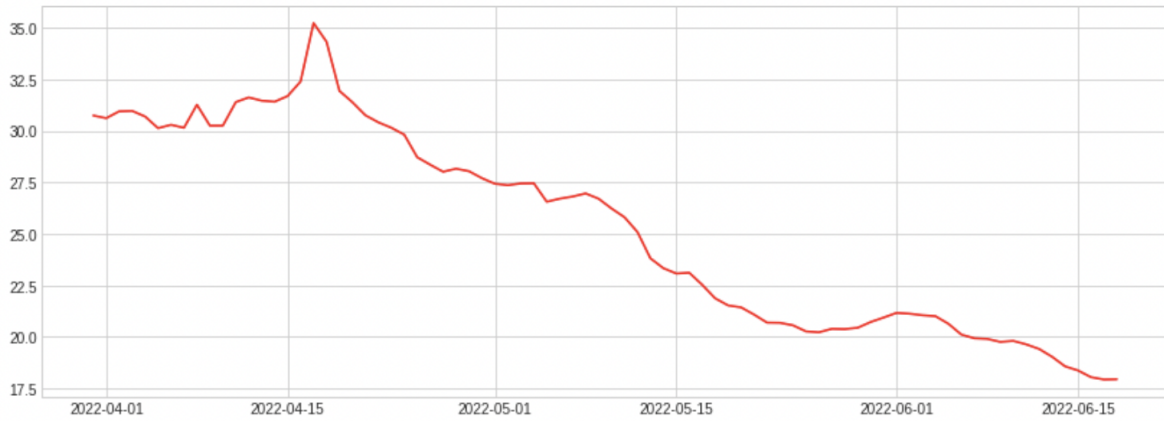


Fig. 7. Forecasting (April, May, and June) Monthes of ETH Cryptocurrency Price.

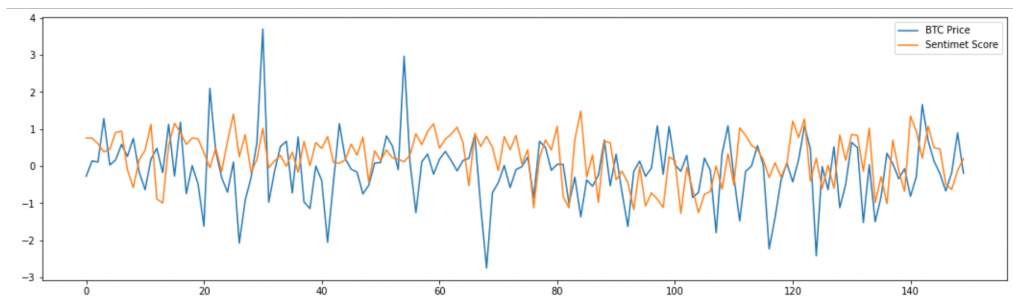


Fig. 8. Correlation between BTC Users' Opinions and Price Volatility.

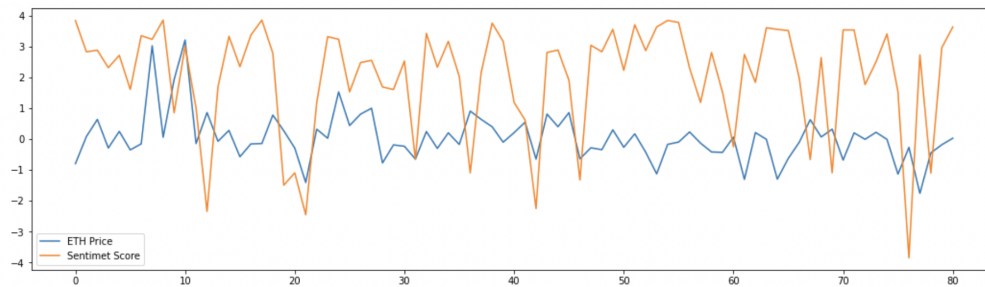


Fig. 9. Correlation between ETH Users' Opinions and Price Volatility.

VI. CONCLUSION AND FUTURE WORK

Experiments were conducted using two datasets about two cryptocurrencies, BTC and ETH, to study the relationship between traders' sentiment and the price of cryptocurrencies. To study the impact of the proposed method and confirm its superiority, we analyzed Twitter users' sentiments about these cryptocurrencies and classified their polarity (positive, negative, and neutral) using ML classification algorithms. The SVM classification method outperformed NB with 93.95% and 95.59% accuracy, respectively. In addition, the expected price for the next three months for the two selected currencies has been forecast using the LSTM model; the BTC prediction model outperformed the ETH model with an error rate of 0.2545 for MAE, 0.2528 for MSE, and 0.5028 for RMSE, whereas the LSTM model's error in ETH is worse due to the smaller dataset size. It is noted that the small resample of time series data may get the worst result. Furthermore, the relationship between cryptocurrency volatility prices and its users' sentiments was studied to achieve the research aims. We observe that the correlation in the BTC is close compared with ETH, which means when the BTC investors have a positive sentiment, the price of BTC cryptocurrency will be increased and vice versa. On the other hand, the ETH prices and users' sentiments do not have an observed relationship. Therefore, we may conclude that cryptocurrency price volatility is not always related to investor satisfaction.

Due to a lack of resources and time, the datasets and the selected cryptocurrency types restrictions were imposed to keep the research relevant. The Twitter data set utilized to train and test the sentiment analysis model was limited to five months because of computational power limitations. Although the prices of cryptocurrency are impacted by investors' sentiments worldwide, the Twitter dataset focuses on tweets written in the English language only. On the other hand, this study focuses on forecasting the prices of the two most-traded currencies: BTC and ETH, although thousands of different cryptocurrencies are in circulation. It will be necessary to cover other factors that may impact the cryptocurrency market instead of focusing on the investors' sentiments in future works. Furthermore, conducting experiments using more than two types of the most popular cryptocurrencies and improving the pre-processing steps to study the correlation between cryptocurrency price volatility, news events, and investors' sentiments on different social media platforms that might directly relate to cryptocurrency prices. Additionally, to further study cryptocurrencies' price forecasting, we intend to examine more time-series methods; one of them is ARIMA, a statistical

analysis model widely used to predict future trends through the time-series dataset.

REFERENCES

- [1] Y. Hua, "Bitcoin price prediction using arima and lstm," in *E3S Web of Conferences*, vol. 218. EDP Sciences, 2020, p. 01050.
- [2] C.-H. Wu, C.-C. Lu, Y.-F. Ma, and R.-S. Lu, "A new forecasting framework for bitcoin price with lstm," in *2018 IEEE International Conference on Data Mining Workshops (ICDMW)*. IEEE, 2018, pp. 168–175.
- [3] F. Fang, C. Ventre, M. Basios, L. Kanthan, L. Li, D. Martinez-Regoband, and F. Wu, "Cryptocurrency trading: a comprehensive survey," *arXiv preprint arXiv:2003.11352*, 2020.
- [4] S. Nakamoto, "Bitcoin: A peer-to-peer electronic cash system," *Decentralized Business Review*, p. 21260, 2008.
- [5] D. R. Pant, P. Neupane, A. Poudel, A. K. Pokhrel, and B. K. Lama, "Recurrent neural network based bitcoin price prediction by twitter sentiment analysis," in *2018 IEEE 3rd International Conference on Computing, Communication and Security (ICCCS)*. IEEE, 2018, pp. 128–132.
- [6] X. F. Liu, X.-J. Jiang, S.-H. Liu, and C. K. Tse, "Knowledge discovery in cryptocurrency transactions: A survey," *IEEE Access*, vol. 9, pp. 37 229–37 254, 2021.
- [7] P. Kayal and P. Rohilla, "Bitcoin in the economics and finance literature: a survey," *SN Business & Economics*, vol. 1, no. 7, pp. 1–21, 2021.
- [8] L. Abualgah, N. K. Kareem, M. Omari, M. A. Elaziz, and A. H. Gandomi, "Survey on twitter sentiment analysis: Architecture, classifications, and challenges," in *Deep Learning Approaches for Spoken and Natural Language Processing*. Springer, 2021, pp. 1–18.
- [9] A. Jain, S. Tripathi, H. D. Dwivedi, and P. Saxena, "Forecasting price of cryptocurrencies using tweets sentiment analysis," in *2018 eleventh international conference on contemporary computing (IC3)*. IEEE, 2018, pp. 1–7.
- [10] A. M. Khedr, I. Arif, M. El-Bannany, S. M. Alhashmi, and M. Sreedharan, "Cryptocurrency price prediction using traditional statistical and machine-learning techniques: A survey," *Intelligent Systems in Accounting, Finance and Management*, vol. 28, no. 1, pp. 3–34, 2021.
- [11] S. A. Alahmari, "Using machine learning arima to predict the price of cryptocurrencies," *The ISC International Journal of Information Security*, vol. 11, no. 3, pp. 139–144, 2019.
- [12] S. Rahman, J. N. Hemel, S. J. A. Anta, and H. Al Muhee, "Sentiment analysis using r: an approach to correlate bitcoin price fluctuations with change in user sentiments," Ph.D. dissertation, BRAC University, 2018.
- [13] O. Sattarov, H. S. Jeon, R. Oh, and J. D. Lee, "Forecasting bitcoin price fluctuation by twitter sentiment analysis," in *2020 International Conference on Information Science and Communications Technologies (ICISCT)*. IEEE, 2020, pp. 1–4.
- [14] A. Mittal, V. Dhiman, A. Singh, and C. Prakash, "Short-term bitcoin price fluctuation prediction using social media and web search data," in *2019 Twelfth International Conference on Contemporary Computing (IC3)*. IEEE, 2019, pp. 1–6.

- [15] S. Pathak and A. Kakkar, "Cryptocurrency price prediction based on historical data and social media sentiment analysis," in *Innovations in Computer Science and Engineering*. Springer, 2020, pp. 47–55.
- [16] A. Aggarwal, I. Gupta, N. Garg, and A. Goel, "Deep learning approach to determine the impact of socio economic factors on bitcoin price prediction," in *2019 Twelfth International Conference on Contemporary Computing (IC3)*. IEEE, 2019, pp. 1–5.
- [17] S. Nasekin and C. Y.-H. Chen, "Deep learning-based cryptocurrency sentiment construction," *Digital Finance*, vol. 2, no. 1, pp. 39–67, 2020.
- [18] Textblob.io, "Natural Language Textblob," <https://textblob.readthedocs.io/en/dev/>, [Online; accessed May 2022].
- [19] Y. Al Amrani, M. Lazaar, and K. E. El Kadiri, "Random forest and support vector machine based hybrid approach to sentiment analysis," *Procedia Computer Science*, vol. 127, pp. 511–520, 2018.
- [20] I. Ahmad, M. Basher, M. J. Iqbal, and A. Rahim, "Performance comparison of support vector machine, random forest, and extreme learning machine for intrusion detection," *IEEE access*, vol. 6, pp. 33 789–33 795, 2018.
- [21] K.-F. Selander, "Anomaly detection using lstm n. networks and naive bayes classifiers in multi-variate time-series data from a bolt tightening tool," 2021.
- [22] D. Berrar, "Bayes' theorem and naive bayes classifier," *Encyclopedia of Bioinformatics and Computational Biology: ABC of Bioinformatics*, vol. 403, 2018.
- [23] H. Abrishami, C. Han, X. Zhou, M. Campbell, and R. Czosek, "Supervised ecg interval segmentation using lstm neural network," in *Proceedings of the International Conference on Bioinformatics & Computational Biology (BIOCOMP)*. The Steering Committee of The World Congress in Computer Science, Computer ..., 2018, pp. 71–77.
- [24] J. Qi, J. Du, S. M. Siniscalchi, X. Ma, and C.-H. Lee, "On mean absolute error for deep neural network based vector-to-vector regression," *IEEE Signal Processing Letters*, vol. 27, pp. 1485–1489, 2020.
- [25] P. Flach and M. Kull, "Precision-recall-gain curves: Pr analysis done right," *Advances in neural information processing systems*, vol. 28, 2015.
- [26] K.-F. Selander, "Anomaly detection using lstm n. networks and naive bayes classifiers in multi-variate time-series data from a bolt tightening tool," 2021.
- [27] CoinMarketCap.com, "Top Cryptocurrency Spot Exchanges," Available online: <https://coinmarketcap.com/rankings/exchanges/>, [Online; accessed May 2022].
- [28] Tweepy.org, "An easy to use python library for accessing the twitter api," Available online: <https://www.tweepy.org/>, 2018, [Online; accessed March 2022].
- [29] Nltk.org, "Natural Language Toolkit," Available online: <https://www.nltk.org>, [Online; accessed May 2022].
- [30] G. Colaboratory.com, "Google colaboratory coding environment," <https://colab.research.google.com/>, [Online; accessed March 2022].
- [31] Textblob.io, "NumPy: A guide to NumPy," <https://numpy.org/>, [Online; accessed March 2022].
- [32] Pandas.org, "Pandas: A guide to pandas," <https://pandas.pydata.org/>, [Online; accessed March 2022].
- [33] Tensorflow.org, "Tensorflow machine learning," <https://www.tensorflow.org/>, [Online; accessed March 2022].
- [34] keras.io, "Keras machine learning," <https://keras.io/>, [Online; accessed March 2022].

The Multi-Objective Design of Laminated Structure with Non-Dominated Sorting Genetic Algorithm

Huiyao Zhang
Jiangsu Key Construction of IoT
Application Technology
Wuxi Taihu University
Wuxi, CHINA

Yuxiao Wang
College of Textiles
Donghua University
Shanghai CHINA

Fangmeng Zeng
College of Textile Science and Engineering
Zhejiang Sci-Tech University
Hangzhou, CHINA

Abstract—Non-dominated sorting genetic algorithm has shown excellent advantages in solving complicated optimization problems with discrete variables in a variety of domains. In this paper, we implement a multi-objective genetic algorithm to guide the design of the laminated structure with two objectives: minimizing the mass and maximizing the strength of a specified structure simultaneously, classical lamination theory and failure theory are adopted to compute the strength of a laminate. The simulation results have shown that a non-dominated genetic algorithm has great advantages in the design of laminated composite material. Experiment results also suggest that optimal run times are from 16 to 32 for the design of glass-epoxy laminate with non-dominated sorting genetic algorithm. We also observed that two stages involve the optimization process in which the number of individuals in the first frontier first increases, and then decreases. These simulation results are helpful to decide the proper run times of genetic algorithms for glass-epoxy design and reduce computation costs.

Keywords—Non-dominated sorting genetic algorithm; optimization; failure theory; laminated composite material; classical lamination theory

I. INTRODUCTION

Non-dominated sorting genetic algorithm (NSGA-II) provides [1], [2], [3] a collection of techniques to maintain multiple solutions in the mating pool and has shown excellent performance in domains [4], [5], [1], [6], [7], [8], [9], [10], [11], [12], [13]. Slowik and Kwasnicka [9] present the family of evolutionary algorithms for real-life application, such as genetic algorithms, genetic programming, differential evolution, and evolution strategies. Lu [10] et al. adopt NSGA for neural architecture search and has demonstrated the ability in finding competitive neural architecture with less computational resources. Kou [11] et al. propose a two-stage multiobjective feature-selection method for bankruptcy prediction of small and medium-sized enterprises.

The design of a laminate in nature is a tricky optimization problem involving several discrete variables and additional constraints. The traditional wisdom [14], [15], [16], [17], [18], [19], [20], [21], [22] suggests using an evolutionary algorithm to solve this problem with a single objective function, appending additional constraints to the objective function as punishment items, in which the coefficient of each punishment is a random number with a range from 0 to 1. Adams [23] et al. use a genetic algorithm approach by locally reducing a thick laminate to generate and evaluate valid globally blended

designs for composite panel structure optimization. Cho and Rowlands [24] implement a genetic algorithm to minimize tensile stress concentrations in a perforated laminated structure, obtaining more than one favorable stacking sequence with different fiber orientations. An [25] et al. present the two-objective design of composite laminates: minimizing cost and maximizing fundamental frequency and frequency gaps.

Although the non-dominated sorting genetic algorithm has demonstrated great efficiency in fields, there is rare literature on the application of NSGA-II for the design of a laminated structure. In this work, we implement this algorithm to guide the design of laminated composite material with multiple constraints. The experiment results have shown that NSGA offers great advantages in assisting the design of a laminate, where it provides a set of solutions. As far as we know, this is the first time to adopt a non-dominated sorting genetic algorithm for laminate design.

The rest of this work is organized as follows: Section II reviews the non-dominated genetic algorithm; Section III gives a brief introduction to laminate and covers the strength calculation process; in Section IV, we formulate the objective functions; in Section V, we present the experiment; finally, we analyze the simulation result and give the conclusion.

II. NON-DOMINATED SORTING GENETIC ALGORITHM AND LAMINATE REPRESENTATION

Non-dominated sorting genetic algorithm is an evolutionary algorithm that maintains solutions in the mating pool. The solutions are in the same frontier if none of them dominate each other, and NSGA-II can reserve frontiers in the population. NSGA-II outperforms other multiobjective algorithms in three aspects: 1) $O(MN^2)$ computational cost, where M is the number of objectives and N is the population size; 2) without specifying sharing parameters; 3) new selection operator which combines parents and children and selects individuals from the combination. Fig. 2 shows the process of NSGA-II in which the non-dominated sorting technique reduces the sorting time complexity from $O(MN^3)$ to $O(MN^2)$. The crowding distance sorting trick ranks the individual according to the values of the individual's objective function. We propose to adopt these techniques to guide the design of a laminate.

Fig. 1 shows individuals in the mating pool with two objective functions, f_1 and f_2 . In this figure, the cuboid is to measure the distance of individuals in the same frontier instead

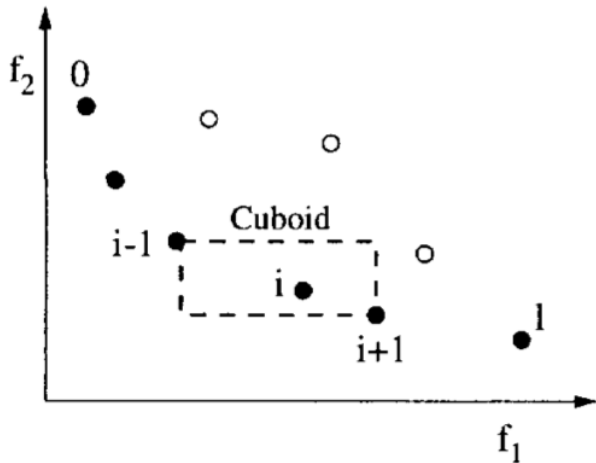


Fig. 1. Frontiers in the Population in which Individuals Marked with the same Color belong to One Frontier [26].

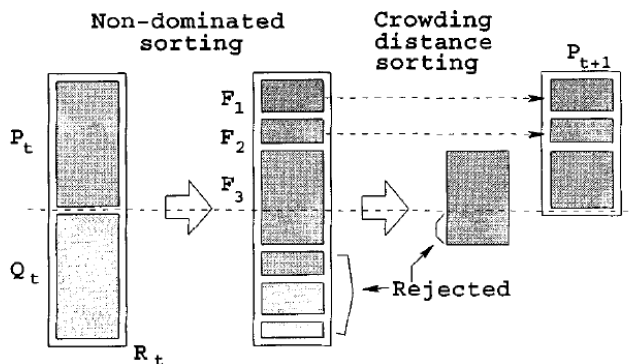


Fig. 2. NSGA-II Procedure[27].

of using sharing function. This technique can also measure the distance of laminates because the distance calculation only requires the value of objective functions. And a sequence of integers is able to represent the structure of a laminate. So we can evaluate the objective function according to the integer representation of a laminate.

III. A LAMINATE AND THE STRENGTH PREDICTION

As shown in Fig. 3, a laminate sequence of lamina binding together along the thickness direction, and lamina is a special composite material whose properties are determined by several variables: ply angle, ply thickness, and material properties. In this paper, to decide the strength of a laminate, it is necessary to know how to compute the strength of a single lamina.

A lamina's strength is highly related to the stress and strain within it. For a lamina under load, it is straightforward to calculate the stress and strain in a lamina by using of three-dimensional stress and strain model, as shown in

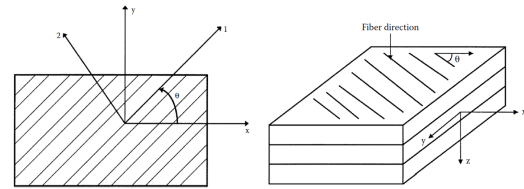


Fig. 3. A Lamina and the Structure of a Laminate.

$$\begin{bmatrix} \sigma_1 \\ \sigma_2 \\ \tau_{12} \end{bmatrix} = \begin{bmatrix} Q_{11} & Q_{12} & 0 \\ Q_{12} & Q_{22} & 0 \\ 0 & 0 & Q_{66} \end{bmatrix} \begin{bmatrix} \varepsilon_1 \\ \varepsilon_2 \\ \gamma_{12} \end{bmatrix}. \quad (1)$$

In this equation, $Q_{11}, Q_{12}, Q_{22}, Q_{66}$ are engineering constants, $\sigma_1, \sigma_2, \tau_{12}, \varepsilon_1, \varepsilon_2, \gamma_{12}$ are stress and strain along different directions.

Then failure theories can predict the strength of a lamina according to obtained stress and strain. Various failure theories have been proposed to compute the strength of lamina, and each has its advantage and disadvantages. Here we adopt the two most widely adopted criteria to calculate the strength: Tsai-Wu [28], [29] failure theory and Maximum stress [30], [31] failure theory.

The Tsai-Wu failure theory can compute the strength ratio of a laminate with the following equation. The strength ratio is an indicator of a material's strength under load.

$$H_1\sigma_1 + H_2\sigma_2 + H_6\tau_{12} + H_{11}\sigma_1^2 + H_{22}\sigma_2^2 + H_{66}\tau_{12}^2 + 2H_{12}\sigma_1\sigma_2 < 1 \quad (2)$$

In this equation, $H_1, H_2, H_6, H_{11}, H_{22}, H_{66}$ are coefficients related to five engineering constants $\sigma_1^T, \sigma_2^T, \sigma_1^C, \sigma_2^C, \tau_{12}$. The relation among them are as follows:

0
90
90
0
90

Fig. 4. Cross-Ply Laminate.

$$\begin{aligned}
 H_1 &= \frac{1}{(\sigma_1^T)_{ult}} - \frac{1}{(\sigma_1^C)_{ult}}, \\
 H_{11} &= \frac{1}{(\sigma_1^T)_{ult} (\sigma_1^C)_{ult}}, \\
 H_2 &= \frac{1}{(\sigma_2^T)_{ult}} - \frac{1}{(\sigma_2^C)_{ult}}, \\
 H_{22} &= \frac{1}{(\sigma_2^T)_{ult} (\sigma_2^C)_{ult}}, \\
 H_{66} &= \frac{1}{(\tau_{12})_{ult}^2}, \\
 H_{12} &= -\frac{1}{2} \sqrt{\frac{1}{(\sigma_1^T)_{ult} (\sigma_1^C)_{ult} (\sigma_2^T)_{ult} (\sigma_2^C)_{ult}}}.
 \end{aligned} \tag{3}$$

The five engineering constants are as follows: $(\sigma_1^T)_{ult}$ ultimate longitudinal tensile strength(in direction 1); $(\sigma_1^C)_{ult}$ ultimate longitudinal compressive strength; $(\sigma_2^T)_{ult}$ ultimate transverse tensile strength; $(\sigma_2^C)_{ult}$ ultimate transverse compressive strength; and $(\tau_{12})_{ult}$ and ultimate in-plane shear strength.

A laminate consists of laminae with a specified sequence, in which the ply angle, thickness, and composite material of one lamina could be different from another; Therefore, the strength computation of a laminate is more complicate than the strength prediction of a lamina. Classical lamination theory [32] is an analytical tool to compute the stress and strain for every lamina in a laminate. For a laminate, the relation between stress and strain is formulated as

$$\begin{bmatrix} \sigma_x \\ \sigma_y \\ \tau_{xy} \end{bmatrix} = \begin{bmatrix} \bar{Q}_{11} & \bar{Q}_{12} & \bar{Q}_{16} \\ \bar{Q}_{12} & \bar{Q}_{22} & \bar{Q}_{26} \\ \bar{Q}_{16} & \bar{Q}_{26} & \bar{Q}_{66} \end{bmatrix} \begin{bmatrix} \varepsilon_x \\ \varepsilon_y \\ \gamma_{xy} \end{bmatrix}. \tag{4}$$

In this equation, $\sigma_x, \sigma_y, \tau_{xy}$ and $\varepsilon_x, \varepsilon_y, \gamma_{xy}$ are stress and strain in global coordinate. And we can compute $\bar{Q}_{11}, \bar{Q}_{12}, \bar{Q}_{16}, \bar{Q}_{22}, \bar{Q}_{26}, \bar{Q}_{66}$ with the following equations.

$$\begin{aligned}
 \bar{Q}_{11} &= Q_{11} \cos^4 \theta + 2(Q_{12} + 2Q_{66}) \sin^2 \theta \cos^2 \theta + Q_{22} \sin^4 \theta \\
 \bar{Q}_{12} &= (Q_{11} + Q_{22} - 4Q_{66}) \sin^2 \theta \cos^2 \theta + Q_{12} (\cos^4 \theta + \sin^2 \theta) \\
 \bar{Q}_{22} &= Q_{11} \sin^4 \theta + 2(Q_{12} + 2Q_{66}) \sin^2 \theta \cos^2 \theta + Q_{22} \cos^4 \theta \\
 \bar{Q}_{16} &= (Q_{11} - Q_{12} - 2Q_{66}) \cos^3 \theta \sin \theta - (Q_{22} - Q_{12} - 2Q_{66}) \sin^3 \theta \cos \theta \\
 \bar{Q}_{26} &= (Q_{11} - Q_{12} - 2Q_{66}) \cos \theta \sin^3 \theta - (Q_{22} - Q_{12} - 2Q_{66}) \cos^3 \theta \sin \theta \\
 \bar{Q}_{66} &= (Q_{11} + Q_{22} - 2Q_{12} - 2Q_{66}) \sin^2 \theta \cos^2 \theta + Q_{66} (\sin^4 \theta + \cos^4 \theta)
 \end{aligned} \tag{5}$$

The mid-plane strains and curvature of laminate global

coordinates are obtained with the following equation:

$$\begin{bmatrix} N_x \\ N_y \\ N_{xy} \end{bmatrix} = \begin{bmatrix} A_{11} & A_{12} & A_{16} \\ A_{12} & A_{22} & A_{26} \\ A_{16} & A_{26} & A_{66} \end{bmatrix} \begin{bmatrix} \varepsilon_x^0 \\ \varepsilon_y^0 \\ \gamma_{xy}^0 \end{bmatrix} + \begin{bmatrix} B_{11} & B_{12} & B_{16} \\ B_{11} & B_{12} & B_{16} \\ B_{16} & B_{26} & B_{66} \end{bmatrix} \begin{bmatrix} k_x \\ k_y \\ k_{xy} \end{bmatrix}. \tag{6}$$

We can use Equation 7 to calculate every entry in matrix A, B, and D.

$$\begin{aligned}
 A_{ij} &= \sum_{k=1}^n (\bar{Q}_{ij})_k (h_k - h_{k-1}) i = 1, 2, 6, j = 1, 2, 6 \\
 B_{ij} &= \frac{1}{2} \sum_{k=1}^n (\bar{Q}_{ij})_k (h_k^2 - h_{k-1}^2) i = 1, 2, 6, j = 1, 2, 6 \\
 D_{ij} &= \frac{1}{3} \sum_{k=1}^n (\bar{Q}_{ij})_k (h_k^3 - h_{k-1}^3) i = 1, 2, 6, j = 1, 2, 6
 \end{aligned} \tag{7}$$

In Equation 7, h_k is the local coordinate of every lamina. With these equations, we can obtain the strength ratio of a lamina.

In this work, the experiment material is a laminate with 0 and 90 ply orientation, also known as cross-ply laminate, as shown in Fig. 4.

IV. PROBLEM FORMULATION

Our problem is to design cross-ply laminate whose strength ratio should be greater than two. So the ply orientation is 0 and 90. So the search problem can be reformulated as follows:

- (1) design variable: $\{\theta_k, n\} \theta_k \in \{0, 90\}$;
- (2) objective: maximization of strength ratio and minimization of mass
- (3) constraint: strength ratio should be greater than two.

V. SIMULATION RESULTS AND DISCUSSION

This section presents the experiment. Glass/epoxy is the experiment material and its properties are shown in Table I. The dimension of a lamina is $1000 \times 1000 \times 0.165 \text{ mm}^3$, and the load applied to the laminate is 2MPa. There are two objectives in this experiment: maximization of the strength ratio and minimization of the mass.

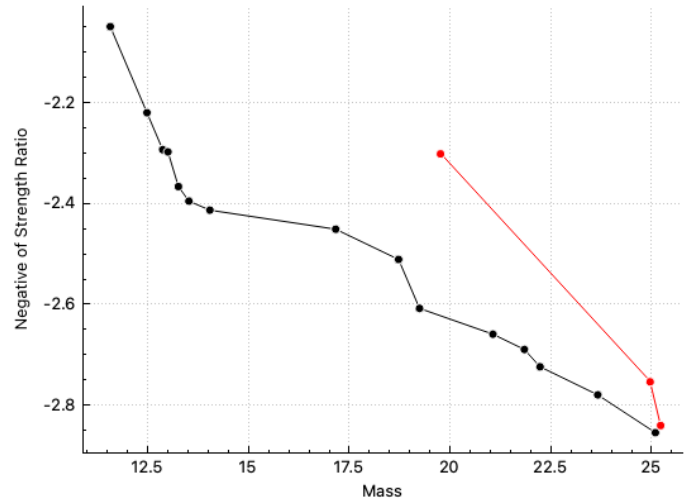
The Fig. 5 displays individuals in the mating pool during the NSGA-II process. In this figure, the x-axis is the mass, and the y-axis is the negative strength ratio because NSGA-II can only deal with minimization problems. Each individual corresponds to one feasible solution which represents the sequence of a laminate. In this figure, individuals are marked with a different color if they belong to a different frontier, then connect individuals in the same frontier, and there are two frontiers: the black and red frontiers. In the same frontier, no individual dominates the rest. For our problem, no individual is better than the other both in mass and strength ratio. This figure demonstrated that NSGA-II could maintain multiple solutions in the mating pool with one-time simulation.

TABLE I. GLASS/EPOXY PROPERTIES

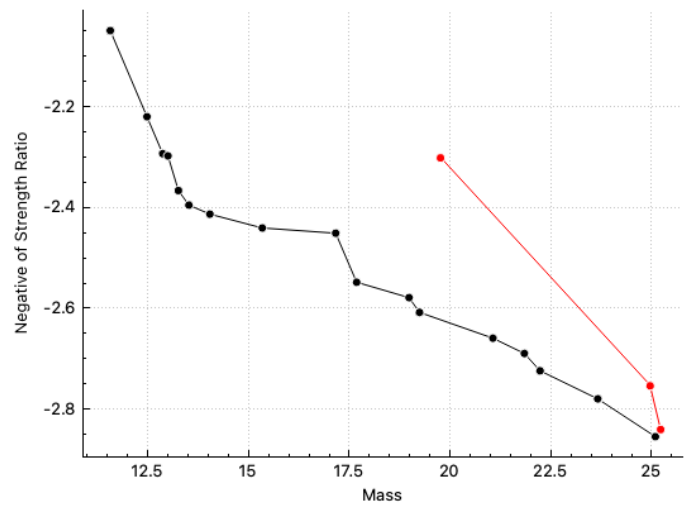
Property	Symbol	Unit	Glass/Epoxy
Longitudinal elastic modulus	E_1	GPa	38.6
Traverse elastic modulus	E_2	GPa	8.27
Major Poisson's ratio	ν_{12}		0.26
Shear modulus	G_{12}	GPa	4.14
Ultimate longitudinal tensile strength	$(\sigma_1^T)_{ult}$	MPa	1062
Ultimate longitudinal compressive strength	$(\sigma_1^C)_{ult}$	MPa	610
Ultimate transverse tensile strength	$(\sigma_2^T)_{ult}$	MPa	31
Ultimate transverse compressive strength	$(\sigma_2^C)_{ult}$	MPa	118
Ultimate in-plane shear strength	$(\tau_{12})_{ult}$	MPa	72
Density	ρ	g/cm^3	1.903

It also clearly shows that the whole NSGA-II process is consist of two stages: 1) in the first stage, the number of individuals in the first frontier keeps increasing. At the beginning of this process, there are only 10 individuals in the first frontier, and the number of individuals comes to a peak when the generation is 24th. 2) In the second stage, the number of individuals in the first frontier begins to decrease. As shown in Fig. 5(e), (f), (g), and (h), the number of individuals in the first frontier is less than the number in the previous figure.

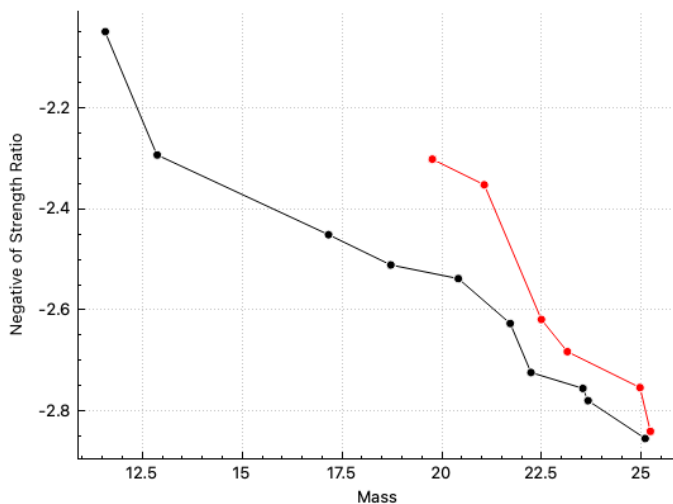
In this experiment, a set of feasible solutions is obtained using NSGA-II, which satisfies different strength requirements. In Javidrad [33] et al. work, only one feasible solution is found after one simulation with a hybrid PSO-SA algorithm, and therefore it is necessary to run this algorithm many times according to different constraints. Using non-dominated sorting genetic algorithms to optimize the design of laminates could reduce simulations times and improve efficiency.



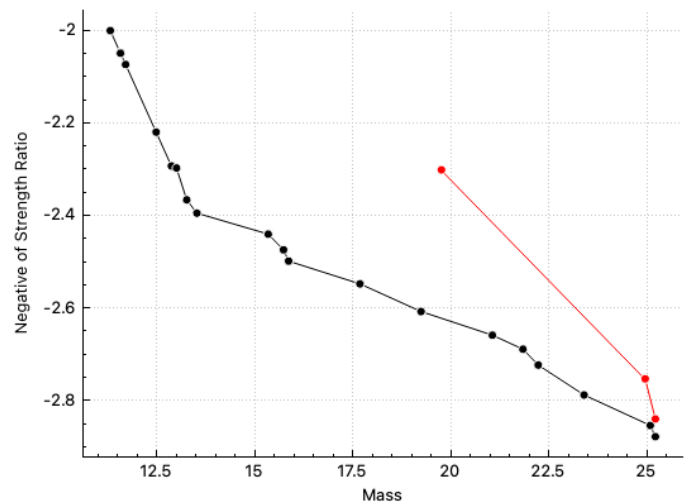
(b) The 8th Generation



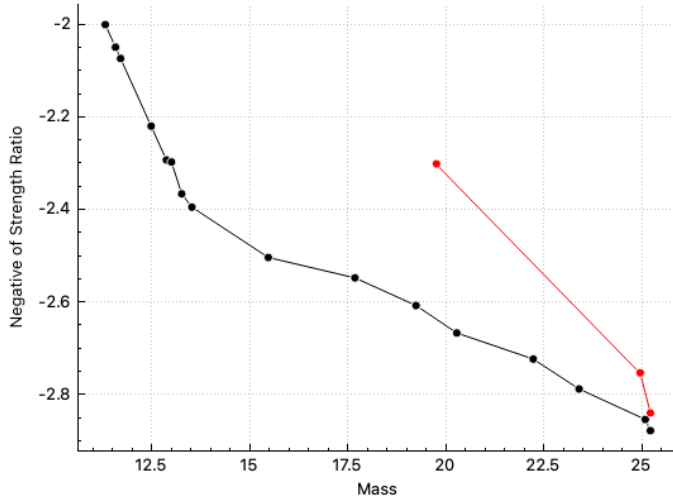
(c) The 16th Generation



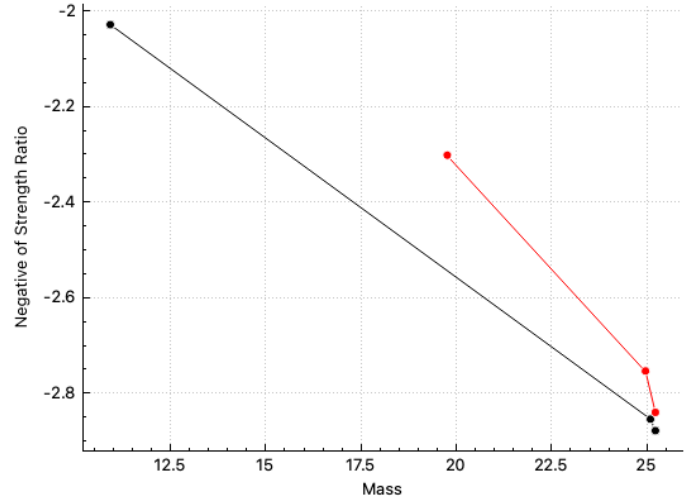
(a) The First Generation.



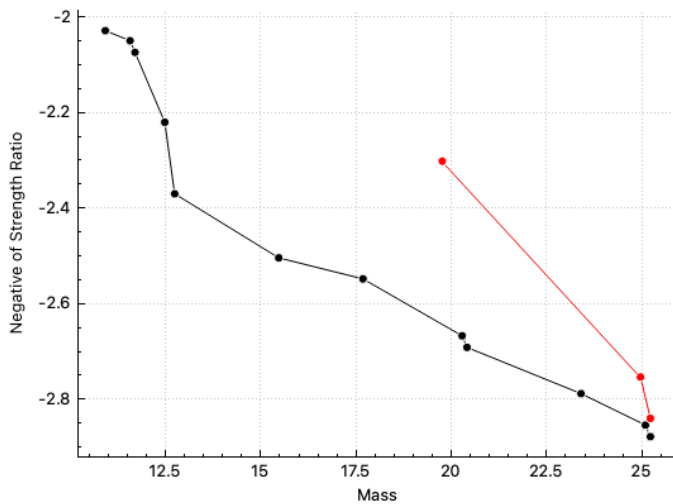
(d) The 24th Generation



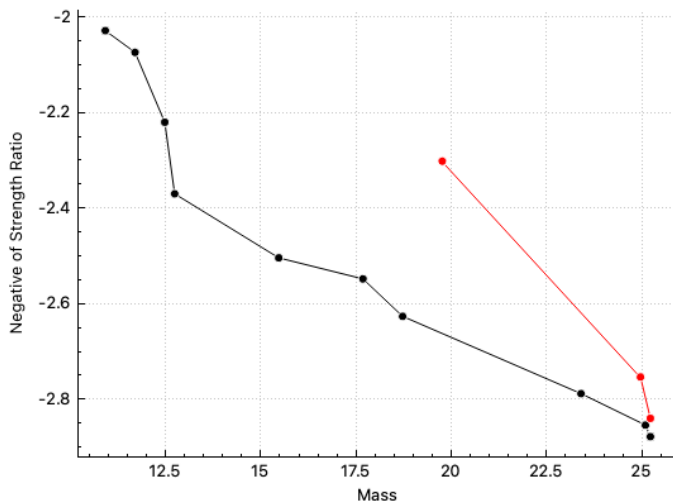
(e) The 32th Generation



(h) The 50th Generation



(f) The 40th Generation



(g) The 47th Generation

Fig. 5. The Variation of Individuals' Number in each Frontier in the Population as the NSGA-II Proceeds.

VI. CONCLUSION

In this work, we implement the non-dominated sorting genetic algorithm to guide the design of the laminated composite structure with two objectives: minimizing the mass and maximizing the strength ratio simultaneously. The experiment results have demonstrated that NSGA-II is an efficient algorithm to obtain multiple solutions in the first frontier. In our experiment, this algorithm obtains 19 individuals in the mating pool where each individual represent a feasible solution for solving the design problem. No solution dominates others in these individuals.

This simulation also demonstrated that the optimal run times for NSGA-II are from 16 to 32 for the design of glass/epoxy laminates. We also observe that the NSGA-II optimization process is consist of two stages: in the first stage, the number of individuals keeps increasing; however, during the second stage, the number in the first frontier keeps decreasing. The number of individuals in the first frontier comes to a peak if the run times of NSGA-II are from 16 to 32, which would significantly reduce computation cost and obtain an optimal result.

ACKNOWLEDGMENT

The work has partly been supported by China Scholarship Council(CSC) under grant no. 201806630112

REFERENCES

- [1] T. C. Bora, V. C. Mariani, and L. dos Santos Coelho, "Multi-objective optimization of the environmental-economic dispatch with reinforcement learning based on non-dominated sorting genetic algorithm," *Applied Thermal Engineering*, vol. 146, pp. 688–700, 2019.
- [2] U. Lee, S. Park, and I. Lee, "Robust design optimization (rdo) of thermoelectric generator system using non-dominated sorting genetic algorithm ii (nsga-ii)," *Energy*, vol. 196, p. 117090, 2020.

- [3] J.-H. Yi, S. Deb, J. Dong, A. H. Alavi, and G.-G. Wang, "An improved nsga-iii algorithm with adaptive mutation operator for big data optimization problems," *Future Generation Computer Systems*, vol. 88, pp. 571–585, 2018.
- [4] H. Li and Q. Zhang, "Multiobjective optimization problems with complicated pareto sets, moea/d and nsga-ii," *IEEE transactions on evolutionary computation*, vol. 13, no. 2, pp. 284–302, 2008.
- [5] A. A. Ahmadi, M. Arabbeiki, H. M. Ali, M. Goodarzi, and M. R. Safaei, "Configuration and optimization of a minichannel using water–alumina nanofluid by non-dominated sorting genetic algorithm and response surface method," *Nanomaterials*, vol. 10, no. 5, p. 901, 2020.
- [6] B. Milosevic and M. Begovic, "Nondominated sorting genetic algorithm for optimal phasor measurement placement," *IEEE Transactions on Power Systems*, vol. 18, no. 1, pp. 69–75, 2003.
- [7] Y. Wang, Y. Shen, X. Zhang, G. Cui, and J. Sun, "An improved non-dominated sorting genetic algorithm-ii (nsga-ii) applied to the design of dna codewords," *Mathematics and Computers in Simulation*, vol. 151, pp. 131–139, 2018.
- [8] Y. Zhou, W. Zhang, J. Kang, X. Zhang, and X. Wang, "A problem-specific non-dominated sorting genetic algorithm for supervised feature selection," *Information Sciences*, vol. 547, pp. 841–859, 2021.
- [9] A. Slowik and H. Kwasnicka, "Evolutionary algorithms and their applications to engineering problems," *Neural Computing and Applications*, vol. 32, no. 16, pp. 12363–12379, 2020.
- [10] Z. Lu, I. Whalen, V. Boddeti, Y. Dhebar, K. Deb, E. Goodman, and W. Banzhaf, "Nsga-net: neural architecture search using multi-objective genetic algorithm," in *Proceedings of the genetic and evolutionary computation conference*, 2019, pp. 419–427.
- [11] G. Kou, Y. Xu, Y. Peng, F. Shen, Y. Chen, K. Chang, and S. Kou, "Bankruptcy prediction for smes using transactional data and two-stage multiobjective feature selection," *Decision Support Systems*, vol. 140, p. 113429, 2021.
- [12] P. Murugan, S. Kannan, and S. Baskar, "Nsga-ii algorithm for multi-objective generation expansion planning problem," *Electric power systems research*, vol. 79, no. 4, pp. 622–628, 2009.
- [13] E. G. Bekele and J. W. Nicklow, "Multi-objective automatic calibration of swat using nsga-ii," *Journal of Hydrology*, vol. 341, no. 3–4, pp. 165–176, 2007.
- [14] S. Shrivastava, P. Mohite, T. Yadav, and A. Malagaudanavar, "Multi-objective multi-laminate design and optimization of a carbon fibre composite wing torsion box using evolutionary algorithm," *Composite Structures*, vol. 185, pp. 132–147, 2018.
- [15] G. Soremekun, Z. Gürdal, C. Kassapoglou, and D. Toni, "Stacking sequence blending of multiple composite laminates using genetic algorithms," *Composite structures*, vol. 56, no. 1, pp. 53–62, 2002.
- [16] B. Liu, R. T. Haftka, M. A. Akgün, and A. Todoroki, "Permutation genetic algorithm for stacking sequence design of composite laminates," *Computer methods in applied mechanics and engineering*, vol. 186, no. 2–4, pp. 357–372, 2000.
- [17] H. Ghiasi, K. Fayazbakhsh, D. Pasini, and L. Lessard, "Optimum stacking sequence design of composite materials part ii: Variable stiffness design," *Composite structures*, vol. 93, no. 1, pp. 1–13, 2010.
- [18] E. Daneshkhan, R. J. Nedoushan, D. Shahgholian, and N. Sina, "Cost-effective method of optimization of stacking sequences in the cylindrical composite shells using genetic algorithm," *European Journal of Computational Mechanics*, pp. 115–138, 2020.
- [19] S. Nikbakt, S. Kamarian, and M. Shakeri, "A review on optimization of composite structures part i: Laminated composites," *Composite Structures*, vol. 195, pp. 158–185, 2018.
- [20] R. Wei, G. Pan, J. Jiang, K. Shen, and D. Lyu, "An efficient approach for stacking sequence optimization of symmetrical laminated composite cylindrical shells based on a genetic algorithm," *Thin-Walled Structures*, vol. 142, pp. 160–170, 2019.
- [21] M. Jafari, H. Moussavian, and M. H. B. Chaleshtari, "Optimum design of perforated orthotropic and laminated composite plates under in-plane loading by genetic algorithm," *Structural and Multidisciplinary Optimization*, vol. 57, no. 1, pp. 341–357, 2018.
- [22] K. Li, X. Liu, Y. Jin, H. Qi, X. Liu, and S. Xu, "Structural strength and laminate optimization of composite connecting bracket in manned spacecraft using a genetic algorithm," *Applied Composite Materials*, vol. 26, no. 2, pp. 591–604, 2019.
- [23] D. B. Adams, L. T. Watson, Z. Gürdal, and C. M. Anderson-Cook, "Genetic algorithm optimization and blending of composite laminates by locally reducing laminate thickness," *Advances in Engineering Software*, vol. 35, no. 1, pp. 35–43, 2004.
- [24] H. Cho and R. Rowlands, "Reducing tensile stress concentration in perforated hybrid laminate by genetic algorithm," *Composites Science and Technology*, vol. 67, no. 13, pp. 2877–2883, 2007.
- [25] H. An, S. Chen, and H. Huang, "Multi-objective optimal design of hybrid composite laminates for minimum cost and maximum fundamental frequency and frequency gaps," *Composite Structures*, vol. 209, pp. 268–276, 2019.
- [26] K. Deb, S. Agrawal, A. Pratap, and T. Meyarivan, "A fast elitist non-dominated sorting genetic algorithm for multi-objective optimization: Nsga-ii," in *International conference on parallel problem solving from nature*. Springer, 2000, pp. 849–858.
- [27] K. Deb, A. Pratap, S. Agarwal, and T. Meyarivan, "A fast and elitist multiobjective genetic algorithm: Nsga-ii," *IEEE transactions on evolutionary computation*, vol. 6, no. 2, pp. 182–197, 2002.
- [28] B. Dejak, A. Mlotkowski, and M. Romanowicz, "Strength estimation of different designs of ceramic inlays and onlays in molars based on the tsai-wu failure criterion," *The Journal of prosthetic dentistry*, vol. 98, no. 2, pp. 89–100, 2007.
- [29] X. Chen, X. Sun, P. Chen, B. Wang, J. Gu, W. Wang, Y. Chai, and Y. Zhao, "Rationalized improvement of tsai-wu failure criterion considering different failure modes of composite materials," *Composite Structures*, vol. 256, p. 113120, 2021.
- [30] L. Zhao, T. Qin, J. Zhang, and R. A. Shenoi, "Modified maximum stress failure criterion for composite π joints," *Journal of composite materials*, vol. 47, no. 23, pp. 2995–3008, 2013.
- [31] Y. Lou, J. W. Yoon, H. Huh, Q. Chao, and J.-H. Song, "Correlation of the maximum shear stress with micro-mechanisms of ductile fracture for metals with high strength-to-weight ratio," *International Journal of Mechanical Sciences*, vol. 146, pp. 583–601, 2018.
- [32] C. W. Bert, "Classical lamination theory," in *Manual on Experimental Methods for Mechanical Testing of Composites*. Springer, 1989, pp. 11–16.
- [33] F. Javidrad, M. Nazari, and H. Javidrad, "Optimum stacking sequence design of laminates using a hybrid pso-sa method," *Composite Structures*, vol. 185, pp. 607–618, 2018.

From Monolith to Microservices: A Semi-Automated Approach for Legacy to Modern Architecture Transition using Static Analysis

Mohd Hafeez Osman¹, Cheikh Saadbouh², Khaironi Yatim Sharif³, Novia Admodisastro⁴ and Muhammad Hadri Basri⁵

Faculty of Computer Science and Information Technology

University Putra Malaysia

43400 Serdang, Malaysia^{1,2,3,4}

Malaysian Administrative Modernisation and Management Planning Unit

Prime Minister Department, Malaysia⁵

Abstract—Modern system architecture may increase the maintainability of the system and promote the sustainability of the system. Nowadays, more and more organizations are looking towards microservice due to its positive impact on the business which can be translated into delivering quality products to the market faster than ever before. On top of that, native support of DevOps is also desirable. However, transforming legacy system architecture to modern architecture is challenging. As manual modernization is inefficient due to its time-intensive and the significant amount of effort required, the software architect is looking for an automated or semi-automated approach for easy and smooth transformation. Hence, this work proposed a semi-automated approach to transform legacy architecture to modern system architecture based on static analysis techniques. This bottom-up approach utilized legacy source code to adhere to the modern architecture framework. We studied the manual transformation pattern for architectural conversion and explore the possibility of providing transformation rules and guidelines. A task-based experiment was conducted to evaluate the correctness and efficiency of the approach. Two open-source projects were selected and several software architects participated in an architectural transformation task as well as in the survey. We found that the new approach promotes an efficient migration process and produces correct software artifacts with minimum errors rates.

Keywords—Static analysis; software architecture; software modernisation; microservices

I. INTRODUCTION

Monolithic architecture is a typical cohesive paradigm for the construction of a software system. In this perspective, Monolithic means that it's all composed in one piece. Monolithic technology is developed to be self-contained; program components are strongly interconnected instead of decoupled, as is the case with modular software programs. Each element and its related accessories must be available in a tightly linked design for the software to be functional.

Microservices are a type of architecture of systems in which a huge and complex system is designed as a series of lightweight services (i.e. loosely coupled). Every module serves a common business purpose and provides a simple, excellently defined endpoint to connect with all other resources.

Modern architecture such as microservices is introduced to increase the maintainability of a system. However, the transition from monolith to modern architecture is challenging as the manual migration process is inefficient due to its Time intensive and the significant amount of effort required. Researches [1] [2] [3] [4] have confirmed that the manual migration process is complex and lacks automated (or semi-automated) tools supported. Nowadays, more and more organizations are looking towards microservice due to its positive impact on the business which can be translated into delivering quality products to the market faster than ever before. On top of that native support of DevOps is also desirable.

The study aims at providing a semi-automated platform to guide software architects in transforming legacy architecture to modern system architecture. Furthermore, we aimed to fulfil the research gaps in software modernization by developing a semi-automated tool that may increase the efficiency of the software modernization process which may satisfy the need of software companies that are looking forward to such a tool to minimize the resources of the software modernization and deliver more value to their prospects. Thus, we perceive that providing a practical solution is crucial. The refactoring rules should be formulated based on the practitioner's and experts' practice. Hence, the refactoring rules are extracted from the refactoring practice that was discussed by the microservices experts from online discussion forums. Several possibilities on (semi-)automating the refactoring task in modernising legacy systems to microservices are investigated.

The main contributions of this study are the following: (i) Refactoring rules to transform legacy to microservices; (ii) Legacy to microservices refactoring framework and metamodel and (iii) Semi-automated legacy to microservices tool.

The remainder of this paper is structured as follow: Section II discusses the related research. Section III explains the research methodology while Section IV describes the correctness and efficiency evaluation. Section V discusses our findings and Section VI presents the conclusions and future work.

II. RELATED WORK

This section discusses the transformation of the monolith to microservices architecture from the perspective of techniques

that were used such as model-driven, static analysis, dynamic analysis. We also discuss the other works that are related.

A. Model-Driven

There are several work that used model-driven technique in migrating monolith to microservices, such as [1], [4], [10], [23] and [24]. We detail some of these works in this paper.

Fritzsch et al. [1] has presented 10 refactoring methods in scientific literature to migrate monolithic systems into microservice. The methods are subdivided into four classes. The result has shown that most of these techniques shall only apply under several situations. The limitations have been identified such as input data size and the need for an implementation tool.

Kamimura et al. [4] discussed the efforts to distinguish candidates from monolithic systems to microservices, i.e. endpoints or sometimes called webservice resources which could be turned into coherent, work-alone smaller services. This is a long and complicated manual endeavor that involves the review of several aspects of information engineering and always relies heavily on the professional performer's knowledge and expertise. To solve this issue, they established a method that distinguishes microservice applicants from the codebase using the SARF technology clustering algorithm with the given application classes and information's to be able to generate microservice candidates. The approach also captures the candidates derived to demonstrate the connection between the candidates being extracted with the whole system.

B. Static Analysis

Several works have used static analysis as the main technique for the monolith to microservices migration. The work includes [5], [6], [2], [3] and [11]. We discuss some of this work in more detail.

Mazlami et al. [2] focus on the failure of automated support instruments and formal models in the area of software migration. They proposed a formal extraction model as a form of an algorithm suggestion to identify the microservices candidates as a web application prototype. They applied their proposed algorithm to 21 open-source projects (developed using different programming languages, e.g Java, C++, Python) and showed that the generated microservice can decrease the size of the development team to half.

Gysel et al. [5] introduced Service Cutter, a service decomposition based on 16 coupling criteria distilled from the literature and industry experience. Service Cutter offers a service extractor framework that implements graph aggregating algorithms along with includes ranking based on scoring beginning from building blocks and structured documents such as domain model with its use-cases.

Li et al. [3] proposed a semi-automatic decomposition approach that used data flow to extract services from the legacy monolith that relates to business logic. The decomposition has been specified into three stages: (i) define the use case along with business logic is assessed as a baseline of specifications; (ii) comprehensive DFD over various rates and its process-datastore are constructed through the business logic based on functional requirements; (iii) developed an

algorithm to instantly bind the DFD to an undependable DFD. A comparative analysis that focused on relevant cohesion metrics and coupling metrics showed that a data flow-driven methodology is ideal in providing fair, repeatable, and readable microservice applicants. However, two (2) major limitations have been identified: (i) the dataflow method largely relies on the precise DFDs at all levels, and (ii) secondly do not put into consideration the non-functional requirements (NFR) of the microservices.

Levcovits et al. [6] outlined a strategy for describing and distinguishing microservices on a monolithic enterprise application. The assessment indicated that their methodology may recognize successful microservice candidates on a 750 KLOC financial system in which decreased the size of the code base modules and took full advantage of the architecture of microservices, such as the independent development and deployment of services and technological freedom. However, in certain situations, extra effort would be necessary to move mutual subsystems to a collection of microservices.

C. Dynamic Analysis

This subsection discussed the related work that uses dynamic analysis and also the combination of dynamic and static analysis.

Mayer and Weinreich [14] proposed an approach to constantly extracting services from a legacy software system based on REST microservices. Their approach relies on static and dynamic data collection, gathering input at runtime execution, and merging static and dynamic analysis. This customizable analysis technique captures runtime information to one dimension, allowing an analysis of the architectural design transformation over a longer period. Evaluated the proposed technique of a system, by establishing an empirical test that included several communicating services. The findings demonstrated the feasibility of the process of collecting and aggregating data.

Carrasco et al. [12] have discussed nine (9) potential mistakes in terms of specific bad smells. Such mistakes can be noticed and fixed along the way while transitioning to the new architectural style. As an illustration of a common mistake, when team members are separated across layers, for example, a front-end, code business Logic, and operation department, basic changes can require resources and time between the members of the team in authorizing the required action. From that point of view, a team member may propose a change on which level of the application they possess direct exposure to which can be limited by dividing responsibilities within specific services only. This work offers a strong foundation for relevant insights on the effective transition of monolithic architecture to the new architectural style.

ToLambda is a tool created by Kaplunovich [13] that dynamically allows the generation of system base code, turning the existing systems into healthier architectures, and continually improving. The tool converts existing java code into Nodejs code and changing the code structure to more modular using a microservices architecture. No experiment has been conducted to evaluate the correctness of the conversion and the architectural change.

D. Other Related Work

There are several works that related such as [7], [8], [9], [15], [16], [17], [18], [19], [20], [21] and [22]. We discuss some of these works in more detail.

Ahmadvand and Ibrahim [8] introduced a scientific method for breaking up monolithic applications into microservice applicants, aimed at an optimal level in safety and scalability as a quality attribute. Using this methodology, requirements engineers should carefully compare security and scalability criteria. This initiates design decisions at the requirement engineering activity and thereby extends the vision of the software architect's point of view regarding the system to be.

Meanwhile, Ren et al. [9] introduced a program-based research approach for moving the traditional monolith code to cloud applications. They suggested merging dynamic and static analysis of the binary code to derive the properties of the existing monolith program. The reactive tracing has been used to trace the functionality of the application, the user input data, the called methods and the accessed database information, and the rate of the method invocation throughout tracing. The experimental findings indicated that the new approach was successfully addressed the re-designing issue of the legacy system.

Tyszberowicz [15] proposed a systemic and rational approach to identify Microservices based on requirements in use and functional breakdown of those specifications. This method offered highly cohesive and tight decomposition coupled. The evaluation was conducted by implementing the approach on three different systems.

Meanwhile, Jin et al. [16] suggested a feature-oriented microservice retrieval approach to automatically create microservices candidates through a monolithic legacy system. Execution traces are used to facilitate the classification of features. Compared to the conventional approaches (which use static analysis), traces of execution can better represent software functionalities.

III. METHODOLOGY

This section provides the study design and methodology of every stage and ethical considerations, in order to develop a supporting tool that can assist software architects while modernizing applications. The methodology of this study consists of the following four stages.

A. Stage 1 - Framework Development

At this stage, we develop the overall architecture of the framework that consists of several components that define the framework which will define the rules of software modernization. The relationship between the framework components will be depicted and describe briefly. Each component of the framework will follow the single responsibility principle so that components reuse is easy for further enhancement. The overall framework processes will be summarized in short and consist of an algorithm written in pseudo-code. Furthermore, the refactoring rules that will be applied on the web layer will be listed in detail as a table along with the UML class diagram that depicts how rules work.

B. Stage 2 - Tool Design and Development

For this first step, we will concentrate on developing our framework and the overall architecture to better understand the system elements, and we will use UML diagrams and IntelliJ as an integrated development environment platform to implements these design architectures. The tool would include features that allow users to import the legacy application to our current tool, then be able to re-architect the legacy applications using basic drag-and-drop features and automatically refactor rules to modernize the legacy features on the web layer and create compatible cloud artifacts.

C. Stage 3 - Evaluating Correctness and Efficiency of the Tool

We will conduct an experiment that is favorable in software engineering research to enable us to verify the proposed tool's correctness and efficiency. We will use 2 open source projects in this experimental research as a laboratory for this study. In this case, for a broader view of the problem anatomy, 2 open-source projects were both built-in java with distinct requirements. Selections will be made for the two open-source initiatives and further information will be given. In addition, with our latest proposed tool, we are also preparing to conduct an expert assessment and the participants will first be told of the general purpose of the analysis and asked to perform software migration using the semi-automated built tool and manual migration, then metrics will be guided by the outcomes of migration to compare both the manual and semi-automated solution. In addition, a structured questionnaire will be used to invite the participants selected for the research to participate in the survey and to share their views on the effectiveness of the process in the industry.

D. Stage 4 - Findings and Conclusion

Results from stage three (Experiment and expert assessment of the correctness and efficiency of the tool) will be addressed in this segment to see how the outcome fits the targets based on our established tool and eventually, conclusions will be drawn and potential work progress will be explored next.

E. Framework Architecture

Fig. 1 illustrates the framework components and how they interact to achieve a common goal which is modernizing legacy java application that is built on top of spring framework. A brief explanation of the Fig. 1 is as follows:

- **Legacy Code Container** is responsible for holding the legacy code and passing it to the filter component to be filtered.
- **Filter** is responsible for filtering incoming legacy codebase on the web Layer where controllers are located. Once controllers are identified they will be passed to the Refactoring component to be refactored.
- **Refactoring** is responsible for modernized legacy code to a new modern way it consists of four sub-components which are:
 - *Refactoring Rules* contains all the rules which will be applied to the legacy code

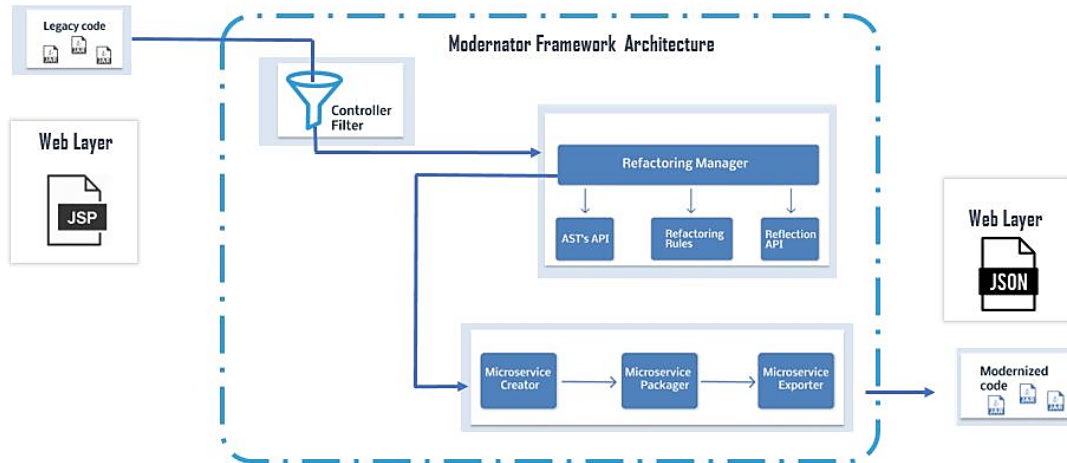


Fig. 1. Modernator Framework.

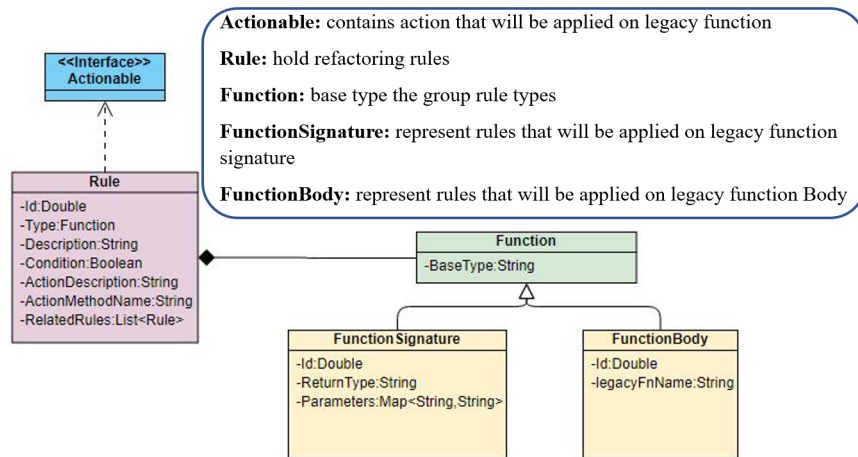


Fig. 2. Refactoring Rules Metamodel.

- *Refactoring Manager* process and takes care of the refactoring processes.
- *AST's API* contains needed API to understand the structure of the legacy code.
- *Reflection API* contains needed API to call rules that will be applied at runtime.
- **Microservices Creator** is responsible for taking refactored code and organize it and auto-generate the new microservices.
- **Microservices Packager** is responsible for taking newly created service and package it as a Docker image or jar/war.
- **Microservices Exporter** is responsible for exporting ready service to the user.

F. Framework Refactoring Rules Metamodel

Fig. 2 illustrates the metamodel of refactoring rules that are used in the framework. This figure shows that each rule

is associated with a function. Either it is associated with a function signature or a function body. Each rule should have an Id, Type, Description, Condition, Action Description, Action Method Name and Related Rules.

G. Framework Refactoring Rules Table

The below table contains all the rules that will be applied to a legacy code. The rules are categorized into two types as follow:

- **Function Signature** rules that will be applied on the legacy function signature which is either on the function parameter or function return type.
- **Function Body** is rules which will be applied in the body of the legacy function.

The main target of this work is designing and developing a tool that can modernize java applications. The legacy application will be used as input to the tool. The refactoring task will be performed at the controller's level in the web layer.

TABLE I. SET OF REFACTORING RULES

Rule ID	Rule-Condition	Related Rules	Before Refactoring	After Refactoring
Rule Type: Function Signature				
R1	Applied when : ModelMap object is presented as function parameter	R [2, 3, 4, 5, 6, 7, 8, 9, 10]	<i>String FunX (ModelMap map)</i>	<i>String FunX ()</i> {}
R11	Applied when: ModelAndView object is presented as function parameter	R [12 – 36]	String FunX(ModelAndView MAV){}	String FunX(){}
R37	Applied when: ConcurrentModel object is presented as function parameter		String FunX(ConcurrentModel CM){}	String FunX(){}
R38	Applied when: ExtendedModelMap object is presented as function parameter		String FunX(ExtendedModelMap EMM){}	String FunX(){}
R39	Applied when: RedirectView object is presented as function parameter		String FunX(RedirectView rv){}	String FunX(){}
Rule Type: Function Signature				
R40	Applied when: Map object is presented as function parameter		String FunX(Map m){}	String FunX(){}
R2	Applied when: addAttribute function is called	R1	String FunX(ModelMap map) map.addAttribute(“msg”,“hello”)	String FunX(ModelMap map) ArrayList<String,String>data = new ArrayList<>(); data.add(“msg”,“hello”)
R3	Applied when: ModelMap function is called	R1	ModelMap md = new ModelMap (attributeName, attributeValue);	ArrayList<String,String>md = new ArrayList<>(); md.add (attributeName, attributeValue)
R4	Applied when: ModelMap function is called	R1	ModelMap md = new ModelMap(attributeValue);# attributeValue is of type Object	ArrayList<String,String>md = new ArrayList<>(); md.add(attributeValue)
R5	Applied when: addAttribute function is called	R1	addAttribute(attributeValue); # attributeValue is of type Object	ArrayList<String,String>md = new ArrayList<>(); md.add(attributeValue)

R6	Applied when: addAllAttributes function is called	R1	addAllAttributes(attributeValues); # attributeValue is of type Collection<?>	ArrayList <String,String>md = new ArrayList<>(); md. add(attributeValues)
R7	Applied when: addAllAttributes function is called	R1	addAllAttributes(attributes); # attributes is of type Map<String,?>	ArrayList<String,String>md = new ArrayList<>(); md.add(attributes)
R8	Applied when: mergeAttributes function is called	R1	mergeAttributes(attributes); # attributes is of type Map<String,?>	ArrayList<String,String>md = new ArrayList<>(); md.add(attributes)
R9	Applied when: containsAttribute function is called	R1	containsAttribute(attribute); # attribute is of type String	# deleted
R10	Applied when: getAttribute function is called	R1	getAttribute(attribute); # attribute is of type String	# deleted
R12	Applied when: ModelAndView function is called	R11	ModelAndView mav = new ModelAndView()	# look for mav references move its data then delete it
R13	Applied when: ModelAndView function is called	R11	ModelAndView mav = new ModelAndView(viewName)	# look for mav references move its data then delete it
R14	Applied when: ModelAndView function is called	R11	ModelAndView mav = new ModelAndView(view)	# look for mav references move its data then delete it
R15	Applied when: ModelAndView function is called	R11	ModelAndView mav = new ModelAndView (viewName,Model) #model is type of Map<String,?>	HashMap<String,?>model = new HashMap<>(); Model.putAll(Model);
R16	Applied when: ModelAndView function is called	R11	ModelAndView mav = new ModelAndView (viewName,status) #model is type of HttpStatus	HttpStatus hs = status ;
R17	Applied when: ModelAndView function is called	R11	ModelAndView mav = new ModelAndView (viewName,model,status) #model is type of HttpStatus	HashMap<String,?>model = new HashMap<>(); Model.putAll(Model); HttpStatus hs = status ;
R18	Applied when: ModelAndView function is called	R11	ModelAndView mav = new ModelAndView (modelName,ModelObject) #ModelObject is of type Object	HashMap<String,Object>model=new HashMap<>(); Model.put(ModelName, ModelObject);
R19	Applied when: setViewName function is called	R11	setViewName(viewname)	# delete
R20	Applied when: getViewName function is called	R11	getViewName()	# delete
R21	Applied when: setView function is called	R11	setView(view)	# delete
R22	Applied when: getView function is called	R11	getView()	# delete
R23	Applied when: hasView function is called	R11	hasView()	# delete

R24	Applied when: isReference function is called	R11	isReference()	# delete
R25	Applied when: getModelInternal function is called	R11	getModelInternal()	# delete
R26	Applied when: getModelMap function is called	R11	getModelMap() #return Model (need review)	# delete
R27	Applied when: getModel function is called	R11	getModel() #return Model (need review)	# delete
R28	Applied when: setStatus function is called	R11	setStatus(status)	# HttpStatus hs = status ;
R29	Applied when: getStatus function is called	R11	getStatus()	# delete
R30	Applied when: addObject function is called	R11	addObject(attributeName, attributeValue)	HashMap <String,Object>model = new HashMap<>(); Model.put(attributeName, attributeValue);
R31	Applied when: addAllObjects function is called	R11	addAllObjects(modelMap) # attribute-Value is of type Map<String,?>	HashMap<String,?>model = new HashMap<>(); Model.putAll(modelMap);
R32	Applied when: clear function is called	R11	clear()	# delete
R33	Applied when: isEmpty function is called	R11	isEmpty()	# delete
R34	Applied when: wasCleared function is called	R11	wasCleared()	# delete
R35	Applied when: toString function is called	R11	toString()	# delete
R36	Applied when: formatView function is called	R11	formatView()	# delete

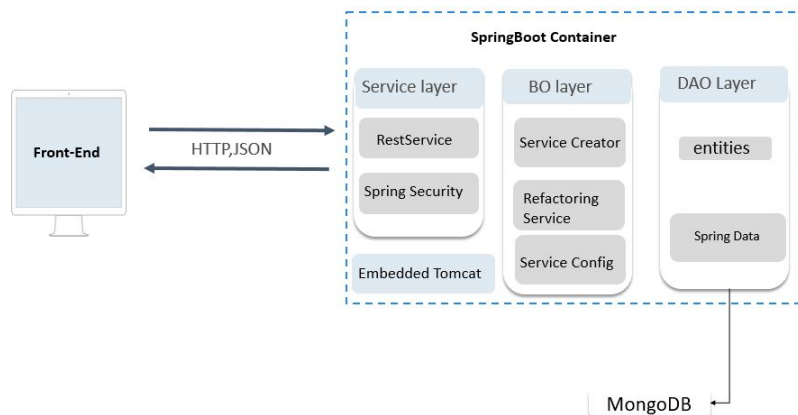


Fig. 3. Tool's Backend Architecture.

The refactoring task will be based on a set of rules (as shown in Table I) predefined by the tool to modernize the legacy application. Right after the refactoring, the tool can package the new application into a container which enables it to be cloud compatible, and in the final stage, the software architect will be able to download the newly modernized application.

The main target of this work is designing and developing a tool that can modernize java applications. The legacy application will be used as input to the tool. The refactoring task will be performed at the controller's level in the web layer. The refactoring task will be based on a set of rules (as shown in Table I) predefined by the tool to modernize the legacy application. Right after the refactoring, the tool can package the new application into a container which enables it to be cloud compatible, and in the final stage, the software architect will be able to download the newly modernized application. The proposed tool has been divided into two separate architectures: front-end architecture which represents the tool views and the Back-End architecture which represents the backbone of the developed tool and its functionalities. The front-end architecture is being developed using the Angular framework and comprises four (4) main modules:

- App Module: represent the starting point of the application such as index.html.
- Core Module: contains singleton components and services such as toolbar components.
- Feature Module: provides a feature that the application offers such as file upload.
- Shared Module: contains highly reusable components and services such as services that communicate with the back-end.

The core components (as illustrated in Fig. 3) of the back-end architecture are the following:

- Service Layer: handle incoming requests and security mechanisms such as authorization and authentication.
- Business Layer: concerned with service creation, refactoring, and packaging.
- Data access object layer: persist data into database.

IV. CORRECTNESS AND EFFICIENCY EVALUATION

In this study, we have conducted a survey to conduct an initial evaluation of the proposed semi-automated approach. The subsequent questions are formulated based on the research problem:

- Q1: Does the semi-automated approach promote efficiency in transforming legacy architecture into modern system architecture?
- Q2: How is the correctness of the generated system using a semi-automated approach?

A. Evaluation Setting

Since this work is an initial work of microservice modernisation, we conducted an initial expert evaluation to evaluate the effectiveness and the correctness of our approach. We

selected three (3) experts to evaluate our approach (based on our developed tool). All of the selected experts have at least five years of experience and have a software engineering background. The evaluation setting is the following:

- Step 1: The experts were asked to manually modernise a simple architecture module of software to microservice architecture.
- Step 2: The experts were introduced to the tool and allowed to use the tool.
- Step 3: The experts were asked to modernise a simple architecture module of software to microservice architecture by using the semi-automated tool.
- Step 4: The experts were required to answer several questions regarding the tool's correctness and efficiency in performing the modernisation task.

B. Results

As mentioned above, we aim at evaluating the correctness and the effectiveness of our approach (by using the semi-automated tool) in performing modernisation tasks. The result is based on the experts' answers to our survey.

1) *Correctness*: After performing all the required steps, we asked the experts about the error found (on average) when they use the manual approach and the error found after performing the modernisation task using our approach. In terms of the manual approach, one (1) expert mentioned that the 0 errors were found and the other two (2) experts stated that 1 – 5 errors were found in the manual approach. On the other hand, when we asked the experts on the correctness of our approach, all experts mentioned that (on average) they found 1 – 5 errors after they used our approach. From this result, we can summarize that the manual approach still produces better accuracy than using our approach. However, the result shows that the difference is not far (as illustrated in Fig. 4).

2) *Efficiency*: To evaluate the efficiency of our approach based on the semi-automated tool, after performing all the steps in Section IV, the experts were required to answer on the time to complete the tasks. By using a manual approach, all experts mentioned that they need to spend more than 4 hours to complete the microservice modernisation task. In contrast, by using the semi-automated approach, the experts stated that the modernisation task will be faster. One (1) expert mentioned that it takes 1-2 hours, one (1) expert mentioned that it takes 2-3 hours and another expert stated that it will take 3-4 hours. With this, we can summarize that by using our semi-automated approach, the modernisation task will be faster to complete compared to the manual approach (as illustrated in Fig. 5).

V. DISCUSSION

This chapter discusses the implications of the practical and theoretical implications of the study as well as a list of the limitation of this approach.

A. Practical Implications

To better understand the practical implication of this study will compare it to previous studies from an enterprise's point of

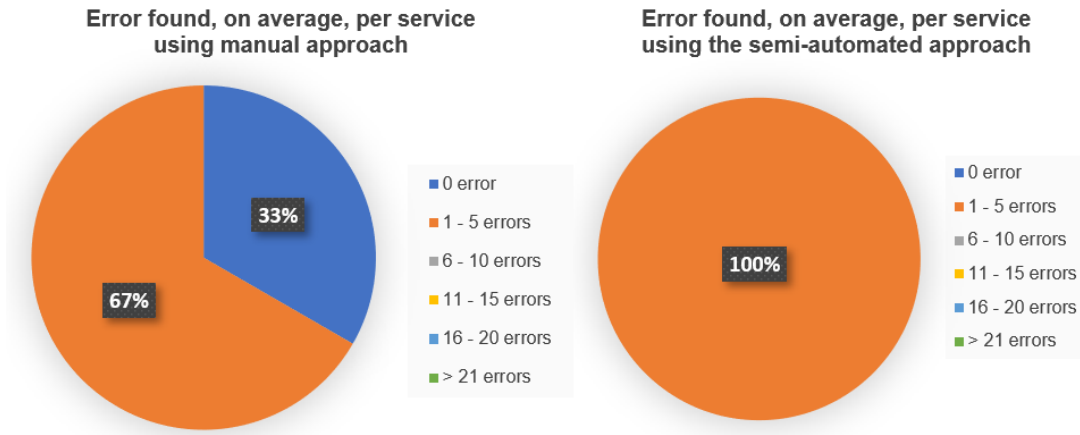


Fig. 4. Evaluation on the Tool's Correctness.

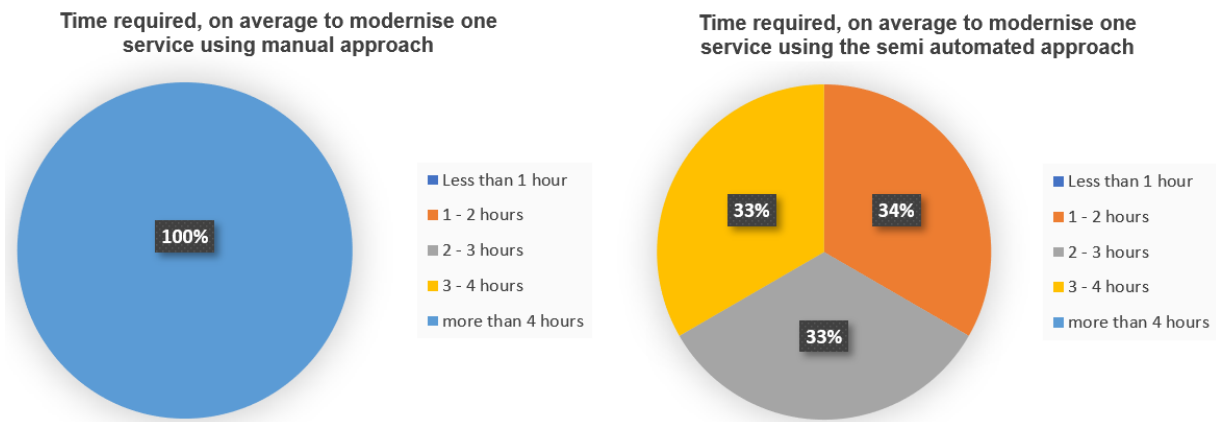


Fig. 5. Evaluation on the Tool's Efficiency.

view. Service cutter is a tool that assists in software transition from monolith to microservice by taking monolith domain model as input and suggested new decomposed domain model as microservices. On the other hand, our approach, Modernator is a tool that has been proposed and developed by this study which takes as an input monolith application (spring MVC) and does refactoring on the web layer, and produces microservice (spring boot) as an output.

We believe as organizations are looking to ease the transition from monolith to microservice while reducing the number of resources allocated to the transition in this case Modernator will have a positive impact on their transition as it produces production source code that can be alerted if needed comparing to service cutter that will produce domain model that needs to be implemented from scratch. However, Modernator will be useful only in the spring framework environment but since spring framework is widely used by enterprises as the backbone of their information systems that give Modernator a high rate to be widely used as well.

B. Theoretical Implications

This study has introduced a list of refactoring rules that can be used to refactor legacy spring MVC controllers that in nature returns JSP pages to modern spring boot controllers

that return data in JSON format that is compatible with modern architecture such as microservice.

The construction of the rules has been made by following spring framework documentation and by identifying spring MVC legacy classes and mapping them to spring boot classes. The proposed rules can be divided into two type function signature which focuses of refactoring legacy function signature and function boy that find legacy function calls. We were able to construct around 40 rules, however; these rules do not include all possible cases there might be other legacy classes that we did not discover in this study.

C. Limitation

Since this work is an initial work for this study, we see a lot of possibility to improve this work based on the following limitations:

- Lack of boarder Evaluation.
- Support limited to java and more specifically application built with spring framework.
- Did not test all proposed refactoring rules.
- Refactoring focused only on Web Layer.
- Did not propose all possible refactoring rules.

VI. CONCLUSION AND FUTURE WORK

The motivation behind this study is to fulfill the need of the industry to have a semi-automated approach for easy and smoothly transforming legacy system architecture to modern architecture. As the manual transition is inefficient due to its time-intensive and the significant amount of effort required. Therefore, this research proposed to develop a semi-automated tool to provide transformation rules and guidelines. An Expert Evaluation was conducted to evaluate the correctness and the efficiency of the approach. Lastly, this research has proved that the new approach promotes an efficient migration process and produces correct software to some extent.

For future work, we plan to conduct a Broader Evaluation of the proposed refactoring rules to further validated their correctness as well as constructing new rules for refactoring other layers such as the business layer and data access object layer.

REFERENCES

- [1] Fritsch J, Bogner J, Zimmermann A, Wagner S. From monolith to microservices: A classification of refactoring approaches. In International Workshop on Software Engineering Aspects of Continuous Development and New Paradigms of Software Production and Deployment 2018 Mar 5 (pp. 128-141). Springer, Cham.
- [2] Mazlami G, Cito J, Leitner P. Extraction of microservices from monolithic software architectures. In 2017 IEEE International Conference on Web Services (ICWS) 2017 Jun 25 (pp. 524-531). IEEE.
- [3] Li S, Zhang H, Jia Z, Li Z, Zhang C, Li J, Gao Q, Ge J, and Shan Z, "A dataflow-driven approach to identifying microservices from monolithic applications," *J. Syst. Softw.*, vol. 157, p. 110380, Nov. 2019, doi: 10.1016/j.jss.2019.07.008.
- [4] Kamimura M, Yano K, Hatano T, Matsuo A. Extracting candidates of microservices from monolithic application code. In 2018 25th Asia-Pacific Software Engineering Conference (APSEC) 2018 Dec 4 (pp. 571-580). IEEE.
- [5] Gysel M, Kölbener L, Giersche W, Zimmermann O. Service cutter: A systematic approach to service decomposition. In European Conference on Service-Oriented and Cloud Computing 2016 Sep 5 (pp. 185-200). Springer, Cham.
- [6] Levcovitz A, Terra R, Valente MT. Towards a technique for extracting microservices from monolithic enterprise systems. arXiv preprint arXiv:1605.03175. 2016 May 10.
- [7] Knoche H, Hasselbring W. Using microservices for legacy software modernization. *IEEE Software*. 2018 May 4;35(3):44-9.
- [8] Ahmadvand M, Ibrahim A. Requirements reconciliation for scalable and secure microservice (de) composition. In 2016 IEEE 24th International Requirements Engineering Conference Workshops (REW) 2016 Sep 12 (pp. 68-73). IEEE.
- [9] Ren Z, Wang W, Wu G, Gao C, Chen W, Wei J, Huang T. Migrating web applications from monolithic structure to microservices architecture. In Proceedings of the Tenth Asia-Pacific Symposium on Internetware 2018 Sep 16 (pp. 1-10).
- [10] Abdullah M, Iqbal W, Erradi A. Unsupervised learning approach for web application auto-decomposition into microservices. *Journal of Systems and Software*. 2019 May 1;151:243-57.
- [11] Shimoda A, Sunada T. Priority order determination method for extracting services stepwise from monolithic system. In 2018 7th International Congress on Advanced Applied Informatics (IIAI-AAI) 2018 Jul 8 (pp. 805-810). IEEE.
- [12] Carrasco A, Bladel BV, Demeyer S. Migrating towards microservices: migration and architecture smells. In Proceedings of the 2nd International Workshop on Refactoring 2018 Sep 4 (pp. 1-6).
- [13] Kaplunovich A. ToLambda—Automatic Path to Serverless Architectures. In 2019 IEEE/ACM 3rd International Workshop on Refactoring (IWorR) 2019 May 28 (pp. 1-8). IEEE.
- [14] Mayer B, Weinreich R. An approach to extract the architecture of microservice-based software systems. In 2018 IEEE Symposium on Service-oriented System Engineering (SOSE) 2018 Mar 26 (pp. 21-30). IEEE.
- [15] Tyszberowicz S, Heinrich R, Liu B, Liu Z. Identifying microservices using functional decomposition. In International Symposium on Dependable Software Engineering: Theories, Tools, and Applications 2018 Sep 4 (pp. 50-65). Springer, Cham.
- [16] Jin W, Liu T, Zheng Q, Cui D, Cai Y. Functionality-oriented microservice extraction based on execution trace clustering. In 2018 IEEE International Conference on Web Services (ICWS) 2018 Jul 2 (pp. 211-218). IEEE.
- [17] Balalaie A, Heydarnoori A, Jamshidi P. Migrating to cloud-native architectures using microservices: an experience report. In European Conference on Service-Oriented and Cloud Computing 2015 Sep 15 (pp. 201-215). Springer, Cham.
- [18] Gouigoux JP, Tamzalit D. "Functional-First" Recommendations for Beneficial Microservices Migration and Integration Lessons Learned from an Industrial Experience. In 2019 IEEE International Conference on Software Architecture Companion (ICSA-C) 2019 Mar 25 (pp. 182-186). IEEE.
- [19] Mazzara M, Dragoni N, Bucchiarone A, Giaretta A, Larsen ST, Dustdar S. Microservices: Migration of a mission critical system. *IEEE Transactions on Services Computing*. 2018 Dec 21.
- [20] De Alwis AA, Barros A, Fidge C, Polyvyany A. Discovering microservices in enterprise systems using a business object containment heuristic. In OTM Confederated International Conferences "On the Move to Meaningful Internet Systems" 2018 Oct 22 (pp. 60-79). Springer, Cham.
- [21] Eski S, Buzluca F. An automatic extraction approach: Transition to microservices architecture from monolithic application. In Proceedings of the 19th International Conference on Agile Software Development: Companion 2018 May 21 (pp. 1-6).
- [22] Sayara A, Towhid MS, Hossain MS. A probabilistic approach for obtaining an optimized number of services using weighted matrix and multidimensional scaling. In 2017 20th International Conference of Computer and Information Technology (ICCIT) 2017 Dec 22 (pp. 1-6). IEEE.
- [23] Baresi L, Garriga M, De Renzis A. Microservices identification through interface analysis. In European Conference on Service-Oriented and Cloud Computing 2017 Sep 27 (pp. 19-33). Springer, Cham.
- [24] Escobar D, Cárdenas D, Amarillo R, Castro E, Garcés K, Parra C, Casallas R. Towards the understanding and evolution of monolithic applications as microservices. In 2016 XLII Latin American Computing Conference (CLEI) 2016 Oct 10 (pp. 1-11). IEEE.

SDN Architecture for Smart Homes Security with Machine Learning and Deep Learning

Wesam Abdulrhman Alonazi¹, Hedi HAMDI²

Department of Computer Science, College of Computer and Information Sciences, Jouf University, Aljouf, KSA^{1,2}

Nesrine A. Azim³

Department of Information Systems & Technology, Faculty of Graduate Studies for Statistical Research
Cairo University, Cairo, Egypt³

A. A. Abd El-Aziz⁴

Department of Information Systems
College of Computer and Information Sciences
Jouf University, Aljouf, KSA⁴
Department of Information Systems & Technology
Faculty of Graduate Studies for Statistical Research
Cairo University
Cairo, Egypt⁴

Abstract—In recent decades, Intelligent home systems are popular because they improve comfort and quality of life. A growing number of homes are becoming "smarter" by incorporating Internet of Things (IoT) technology to improve comfort, energy efficiency, and safety. Increases in resource-constrained IoT devices heighten security threats and vulnerabilities connected with them. Using SDN and virtualization, the IoT's size and adaptability can be managed at a lower cost than ever before. Using these intelligent security solutions, we can achieve real-time detection and automation for attack detection and prevention using artificial intelligence. Consequently, a large variety of solutions utilizing machine learning and deep learning have been developed to mitigate attacks on the IoT. Thus, the goal of this work is to use machine learning and deep learning to defend smart homes with SDN-based. We have designed smart home environments using Software-Defined Networking and Mininet that provide Instant Virtual networks for IoT in smart homes. Two datasets were used in this work: the first SDN dataset, which we acquired from smart homes by launching real attacks and creating normal traffic, and the second IoTID20 dataset, which is publicly available online. On both datasets, conducted ML and DL experiments. The best accuracy on SDN Dataset was 99.9% using Xgboost classifier, and on IoTID20 was 98.9% LSTM in binary classification, and ANN 85.7% on multiclass.

Keywords—SDN; smart home; security; machine learning; deep learning

I. INTRODUCTION

The Internet of Things (IoT) paradigm attracted a lot of attention from the scientific and business communities throughout the last decade [1]. Basically, such a technique is responsible for transferring massive data over a large network without the need for human intervention. The environment of the IoT consists of a huge number of smart devices that communicate with one another for sending and collecting massive sensing data, including wearables devices, sensors, actuators, mobile phones, smart home devices, etc. In 2021, the total number of installed smart devices in the world was 35.82 billion devices, while the total number of smart devices might increase to 75.44 billion by 2025 [2]. An environment will

change the way we work, communicate, and interact with one another.

At the same trend, IoT devices in the Smart Home provide some facilities, such as monitoring temperature, air condition, humidity, gas leakage, and fire. The IoT devices furthermore can be used in smart Refrigerators to automatically check the available or missing foods and to automatically lock and open doors. The mentioned facilities are just some of many that can be provided by the IoT devices in the smart home environment. Therefore, the Internet of Things (IoT) is the core of Smart Homes that provides electronic, sensor, software, and network connectivity within a home. Smart home technology has revolutionized human life by allowing access to information and services from anywhere and at any time [3]. On the other hand, some limitations existed in the Smart Home environment because of using IoT devices. The IoT devices have limited resources and are vulnerable to various attacks, so much research has been investigated to lessen such attacks by taking into account the limited resources of the IoT devices. Machine and deep learning have been utilized to protect against various cyber-attacks in the Smart Home environment, such as distributed denial of service (DDoS) attacks, eavesdropping, Man in the middle attacks (MiTM), and many others. Furthermore, Software-Defined Networking (SDN) is a technique used for enhancing security in the Smart Home domain.

Large-scale IoT networks in smart homes provide new issues in areas including device management, data storage, transmission infrastructure, computation, and privacy protection due it has different connectivity methods, transmission protocols, architecture, and applications that make it a security and privacy challenge so have been extensively researched to improve it. Various types of attacks come from different resources due to the lack of security mechanisms in the architecture of smart homes such as attacks on application layer-based, attack network layer-based, attack perception layer-based, and attack on middleware layer.

Machine learning algorithms are support vector machine (SVM), Random Forest (RF), and XGboost. For deep learning algorithms, we use Artificial neural networks (ANN), Long

short-term memory (LSTM), and Convolutional neural networks (ConvNet/CNN). The main contributions of this work are as follows:

- We built a suitable framework that integrates machine learning or deep learning with SDN, which makes the framework able to detect and prevent various type of attacks like DDoS, Man-in-the-middle, Jamming, and SQL injection.
- Designed a smart home system to provide security at a low cost based on minicomputer Raspberry Pi and Zodiac-Fx OpenFlow Switch.
- The effectiveness of the proposed technique was verified utilizing a recent publicly available dataset.
- We selected an appropriate SDN controller that was compatible with our needs and implemented simulation for the proposed system and tested the result.

The remainder of this paper is formulated as follows. Section II reviews related works. Section III is the proposed methodology. Section IV presents the discussion of the experiment results. Finally, Section V presents a conclusion of our work and highlights our future research directions.

II. RELATED WORK

In [4], X. Huang et al. have proposed a Deep Reinforcement Learning paradigm, which combines two algorithms; Deep Learning and Reinforcement Learning which is based on learning by the concept of trial and error. This paradigm is proposed to be applied in SDN-based IoT networks to control the data overflow. This paradigm consists of three components, the environment, the SDN-enabled network, and the agent, which is the central controller of the network where Deep Reinforcement Learning is applied. The third component is the customer, who provides feedback regularly, where the agent responds immediately and controls the flow of the data accordingly to meet the customer's satisfaction. Their experimentation shows that this paradigm significantly enhanced the Quality of Experience of users compared to previously proposed studies. The simulated network topology was built using OMNET++, which is consisted of 65 nodes and 108 links, and the resulting confidence interval was 95%.

Another work conducted by G. Stampa et al.[5], also utilized the same concept of applying Deep Reinforcement Learning, but for the sake of optimizing the traffic routing, by learning on the go the normal and abnormal behavior of the flow of the network and keeping reconfiguring the network settings accordingly. For simulating the network topology, OMNET++ was used, and as stated by the authors, the results indicate a better user experience within SDN-based IoT networks in terms of network performance optimization.

In [6], T. Tang et al. have proposed a deep learning approach for SDN-based IoT networks to work as flow-based anomaly detection. Their proposed approach utilized the Deep Learning Network in Open Flow Controllers as the central network controller, where they applied it to a dataset called NSL-KDD. They worked on features selection and extraction, where they selected only six out of forty-one features, namely:

Duration, Protocol-type, Src-bytes, Dst-bytes, Count, and Srv-count. After that, they trained and tested the controller against common networking attacks. For the performance analysis, they used the following evaluation metrics: precision: 83, Recall: 75, and F1 score: 74, where the learning rate was set to 0.0001. for the accuracy, it was 75%, while the loss was 20%, compared to previously implemented algorithms such as Naïve bias, Random Forest, multi-layer perception, and support vector machine.

In [7], M. Ahmed et al. have proposed a mitigating DDoS attacks approach in SDN-based IoT networks, using machine learning algorithms such as Support Vector Machine, Gaussian Mixture Model, and Artificial neural networks. These algorithms are applied to the central controller of the network. The dataset used was a real dataset captured from the traces of a real network, where it contained 80,000 TCP connections, and these connections are split into three classes, 87% for HTTP, 6% for FTP, and 7% for attacks. The features of the data set are only three, which are being selected for training and testing the model that will classify the traffic of the network as either benign or malicious. The three features are the Total number of packets, Connection Duration Time, and the ratio of source and destination bytes. To prove the feasibility of their proposed approach, simulations were conducted by creating a prototype that utilizes the Dirichlet process mixture model for two web protocols, HTTP and FTP.

In [8], A. Al-Zahrani and M. Alenazi have proposed a machine learning-based Intrusion Detection system for SDN-based IoT networks. In their experimentations, they used the dataset NSL-KDD, and they selected only five features out of 41 features, namely: Duration, protocol type, Src-byte, Srv-count, Dst-host-same-src-port-rate. For the machine learning algorithms, they utilized the classical and advanced tree-based algorithms such as decision tree, random forest, and XGBoost, where they applied these algorithms at the OpenFlow switches to analyze the network traffic against network attacks such as Denial of service attacks, User to Root attacks, Remote to Local attacks, and probe attacks. The used dataset was split for training and testing, where the number of samples was 125.973 for training and 22.554 for testing. The results gave an accuracy of 95.95%, which indicates a high classification rate.

In [9], Q. Niyqz et al. have proposed a DDoS Detection System in IoT-based Software Defined Networks (SDN) using a stacked autoencoder as the deep learning algorithm used to build a classification model to analyze the network traffic against DDoS attacks. The dataset contains regular internet traffic with DDoS attacks in the protocols TCP, UDP, and ICMP. For performance analysis, all evaluation metrics were measures such as precision, recall, f1 score, and accuracy, where the last gave a value of 95%, indicating a high rate of classification that is suitable to be used in real networking environments. Moreover, an average computational time was computed where the training time took 524s, while the classification time took 0.0835s.

In [10], S. Sen et al. have proposed a DDoS detection system for SDN-based IoT networks using a Machine learning approach in the central controller of the network. For the experimentations, they applied a virtual SDN environment by

using the Adaboost decision stump to train the model on a dataset that contains private networking data. Their experimentation gave an accuracy value of 93%, with a low false-positive rate.

In [11], Y. Qin et al. have proposed an anomaly detection scheme based on machine learning algorithms to be applied in IoT-based SDN networks. An ensemble deep learning algorithm was used combining Convolutional Neural Network and Recurrent Neural Network, where this ensemble algorithm is used to deeply learn the main features of the traffic being analyzed against malicious attacks. The proposed method was implemented using Graphic Process Unit enabling a Tensor-Flow as the main controller of the SDN-based network. The experimentation was conducted on three datasets, namely: CTU-13, CSIC, and Sim_data. For performance analysis, evaluation metrics were computed, such as accuracy, recall, and F1-score, where the accuracy given was 99.86%.

In [12], S. Mohammed et al. have proposed a DDoS Detection system based on machine learning in an SDN-based IoT network to protect such networks from such threatening attacks. The machine-learning algorithm used is Naïve Bayes, and the data set was NSL-KDD. Precision, Recall, and F1 score were calculated for performance evaluation measurements.

In [13], S. Dey et al. have proposed an anomaly detection system based on machine learning to be also applied in the OpenFlow controller of the SDN-based IoT networks. The machine-learning algorithm that was used is the Random Forest Classifier, which was applied to NSL-KDD dataset that contained 41 features. These features were processed for features selection and extraction using automatic tools such as Info Gain, Gain Ration, and CFS Subset Evaluator. The resulting accuracy is 82%.

In [14], J. Wu et al. have proposed a network link congestion prediction methodology for predicting whether the links are congested or not in SDN-based networks. The proposed methodology used machine learning to learn the information that features network congestion. During their implementation, they simulated a network topology that consists of 12 hosts and 13 switches, using a Mininet Simulator, and produced 559929 records of data being recorded from this simulated network and saved as the dataset to be preprocessed and learned to be used later for congestion classification. For the learning process, four algorithms were used, SVM, MLP, KNN, and IDCNN, where the last one gave the highest accuracy of 98.3%.

In [15], T. Tang et al. have proposed an Intrusion Detection System based on Machine learning for SDN-based networks to classify the flow of data in the network into legitimate and anomaly to check against many types of attacks such as DoS, R2L, U2R, and Prob. They used the dataset NSL_KDD and two learning algorithms, namely: Gated Recurrent neural network and a Fully connected deep neural network. For performance analysis, they got 90% for GRNN. In addition, they evaluated the performance of their intrusion detection model over their simulated network in terms of resource utilization, throughput, and latency.

In [16], B. Susilo and R. F. Sari have proposed an Intrusion Detection Mechanism using Machine and Deep learning in SDN-based IoT networks, where their proposed methodology consists of three tiers, namely: Data plane that is responsible for the packet flow in a network, Control Plane that is responsible for network configuration and management, and Application plane that is responsible for the end-user applications. For implementation, they used three virtual machines: Kali Linux VM, Minimet VM, and Metasploitable VM, all installed on a Windows OS. For controlling the dataflows to classify and detect anomalies and network attacks, the Random Forest algorithm was used as a machine learning algorithm, and the Convolutional Neural network as a deep learning algorithm; both algorithms were applied to two datasets, BoT-IoT to be used for classifying Botnet Attacks, and CIC-IDS-2018 for classifying Intrusion attacks. Experimentations gave accuracy values of 90% for Bot-IoT and 99.95% for IDS-2018 when using CNN.

In [17], M. M. Raikar et al. have proposed a data traffic classification using supervised machine learning algorithms in SDN-based IoT networks, such as Support Vector Machine, Nearest Centroid, Gaussian Naïve Bayes (NB) over a dataset containing traces from a real network. The experimentation results gave accuracy values of 92.3% for SVM, 91.02% for nearest centroid, and 96.79% for NB.

In [18], Y. Handa and A. Mudanna have proposed an intrusion detecting model using deep learning to be applied in SDN-based IoT networks. As the network is split into three tiers, the data layer, controller layer, and application layer, the proposed model will be applied in the data layer of the network to check the data flow and classify it and filter it against anomalies and malicious attacks such as DoS attack, Probe Attack, User to root attacks (U2R), and Remote to Local attacks (R2L). For deep learning, Convolutional Neural Network was used first to do the feature extraction and then to do the learning and classification. The dataset used was called KDD 99, and the learned features were six; Duration, Protocol-Type, Src_bytes, Dst_bytes, Count, and Srv_Count, where the data being examined in these features are learned to classify the data in packets flow into normal or malicious and hence detect intrusion attacks in SDN based networks.

The authors in [32] suggest a deep learning classifier-based SDN-based intrusion detection system for the Internet of Things. The suggested study is carried out in a simulated setting, with test accuracy of IDSIoT-SDL compared using a number of different matrices. From previous studies, gaps in IoT security solutions are costly and occur during a realistic attack environment. So, it is of the utmost need to develop low-cost solutions that can detect and prevent cyber-attacks in simulation environments that are carried out against or through IoT devices in real attacks.

III. MATERIAL AND METHODS

A secure, adaptable architecture is proposed in this section for intelligent homes and is based on where monitoring network traffic. SDN architecture is examined from a security standpoint in this study. The proposed intelligent system for detecting attacks based on machine learning deep learning and utilizing SDN for security purposes SDN will be the suitable

technique for implementing SDN-based smart homes architecture. The proposed smart system uses the recent technique to classify network traffic and prevents attacks.

The proposed system consists of software or hardware that monitors traffic in real-time to detect and prevent security breaches as shown in Fig. 1. The system architecture consists of three layers: the First Layer sensor or data flow layer, the Second is the OpenFlow layer, and the third is the SDN controller. In our system, the Raspberry Pi will be used as a gateway for connecting sensors that use different protocols to the Internet via Wi-Fi, Ethernet, or Zigbee, Bluetooth, and cellular communications via protocol translation. OpenFlow switch called Zodiac-OpenFlow FX's it represents the second layer to forward data and control IoT device: There are four physical ports on Zodiac-OpenFlow FX's switch: port 4 for connecting the controller to the switch, and ports 1 to 3 for connecting switches with each other [19]. The controller in the system will be Raspberry Pi installed inside it ubuntu OS with Ryu controller. Data processing and forwarding are both under the control of the controllers.

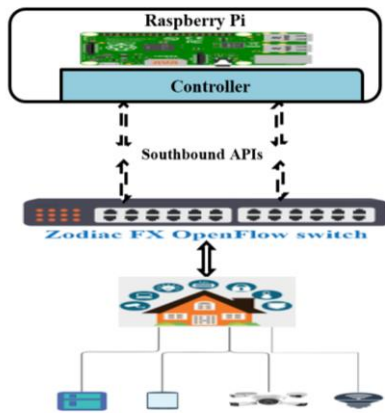


Fig. 1. Proposed System.

A. SDN Controller

SDN controller was used as middleware or as framework for our system. There are a lot of type of controllers such as ONOS, Open Daylight Controller, Ryu. In our study, we have used Ryu for high traffic and network agility, so the Ryu controller is the best choice in our study. APIs and well-defined software components were incorporated into Ryu. Python was used as the coding language of choice for the Ryu game controller. We suggested installing Ryu on Raspberry Pi 4, which will minimize the cost. A decision is made by the controller about how each flow is forwarded. The data plane's flow table stores the decision, which can be made either reactively to newly discovered flows or proactively in the flow table. The controller function as the following:

- Data collection by Information snooper based on statics features for each type of attack this snooper is a python script.
- Send a request to open for the switch to start collecting the static feature from data table entry via southbound API.

- Extract some features related to attacks like MITM DDoS attacks.
- Select the critical feature for attacks that were predefined previously, like packet size, number of hops, etc.
- Automatically call the Machine learning or deep learning classifier to identify if traffic is abnormal; if yes, add a flag to the header in the data flow entry to take any action to block the host and drop the packet.

B. Proposed System Simulation

The simulation and experimentation will be described in the following part. It is possible to prototype and conduct research quickly and easily with Ryu Controller's python-based fork of Ryu Controller, thanks to the language's ease of learning and short development cycle. We created a virtual network using the Mininet OpenFlow network to test our machine learning algorithm shown in Fig. 2.

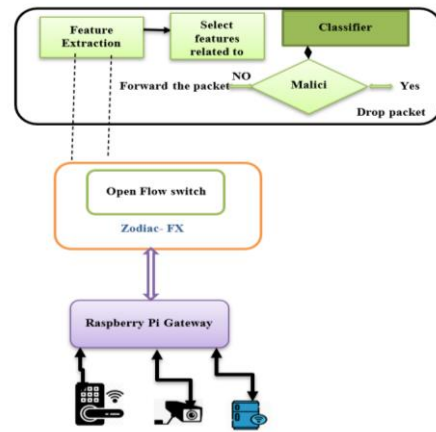


Fig. 2. System Scenario.

C. Mininet OpenFlow Emulator

Mininet is a network emulation tool used to create a network of virtual hosts, links, and switches. To facilitate software-defined networking and bespoke routing, the Linux distribution provides Networking software for Mininet hosts. Tir switches support OpenFlow [20]. Our study used this simulator to test the proposed system and its effectiveness in providing a secure environment for the Internet of Things devices that make up intelligent homes. This system can detect cyber-attacks with high accuracy and prevent them in real-time. We have created 20 virtual hosts representing the IoT devices in smart homes and 20 OpenFlow switches, as shown in Fig. 3.

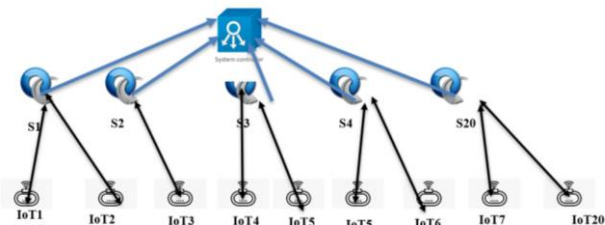


Fig. 3. Mininet Topology.

1) *Triggering attack*: Smurf attacks are distributed denial-of-service attacks in which huge numbers of Internet Control Message Protocol packets with the target victim's faked source IP are broadcast to a computer network using an IP broadcast address." In our experiment, we have triggered this type of attack for purpose traffic generation and collection. Parallelism is applied in traffic generation via the usage of the threading module, which allows several threads to execute at the same time. To produce faked IP addresses for non-existent nodes that are then used to flood targets, the `rand` function of the `Random` module is utilized, as is the `random` module. 0-255 is the range of the first, second, third, and fourth octets. It is also possible to utilize the `OS` module to allow. To specify the target IP address, port, and even the SYN TCP flag for the destination port. `Hping` tool has been used to generate this type of attack.

2) *Ryu controller*: Ryu is an open-source controller Python-based. Ryu can support a wide range of protocols. Ryu provides a well-defined API for software components. Network management and control apps may be quickly developed by developers [21]. RYU controller has been installed on a VMware machine that contains ubuntu OS. SDN is the system's brain to manage open flow switches and hosts. This controller works by sending a flow stats req message to the OpenFlow switch and asking the controller to send a flow stat to reply message back. Requests for data from the Ryu controller module are made every five seconds, which was considered the best time frame for detecting assaults early enough to safeguard the controller. There is a "Flow Removed" message that the switch sends the controller when a flow entry is deleted, either because of a hard timeout or because of a period of inactivity. Only if the "OFPPF SEND FLOW REM" flag is set in the Flow Mod message will the "Flow Removed" message be delivered. FlowMod messages from the controller may also remove flow entries, resulting in the "Flow Removed" message. It is possible that "Flow Removed" is caused by a timeout, which may be either an idle timeout, which occurs when there are no matching packets for some time or a hard timeout, which occurs when there is a predetermined amount of time remaining.

D. Data Processing and Models

1) *Dataset collection*: We have used two datasets; the first one is called the SDN dataset. It has been collected by training real attack on the SDN environment, and the second one it's available publicly on the internet for research purposes.

For SDN dataset, the data was captured using the Wireshark app as (pcap). This monitored all ports and captured the incoming and outgoing data in all ports with different protocols. The Wireshark program (pcap) captured the data by listening to all ports and capturing the incoming and outgoing data in multiple protocols. Protocols, flow duration flags, byte count per Second, and the source and destination IP port numbers. Python controller module accepts the flow monitor's data and extracts it into a format that the trained model can use for prediction. Then we utilize entropy (statistics features) to estimate the distribution of these variables and train the model

using normal and atypical traffic data for smurf or DDoS assault.

In this work, we have collected by triggering attacks and normal traffic. The Attack was performed on the Mininet host that represents Internet of things devices. The Attack is implemented using the `Hping` tool and "pingall" command and Normal traffic is collected by ping command between each device. Then data is collected as a CSV file on the SDN controller (RYU) that enables the socket to listen on all ports on the Open flow switch that is included on Mininet topology as shown in Fig. 8. The process iterated till we reached the required size of data. the data size reached above 250 MB that size is enough to train the model. The Normal traffic collection process shown in Fig. 4 and the attack traffic shown in Fig. 5.

For IoTID20 Dataset, we have used the IoTID20 dataset, collected by Imtiaz [22]. This dataset was collected using the SKT NGU and EZVIZ Wi-Fi cameras, which are smart home devices. The dataset contains 86 features; after pre-processing the features have been reduced to 80 features. We performed pre-processing; First, we removed all nulls and invalid values, then we labelled and scaled the data using a stander scaler, label encoder, and a data splitting using K-fold to 10 groups to combat overfitting in the second experiment splitting data by ratio of 25 %for testing and 75 for training.

2) *Data Pre-processing*: Data pre-processing is the process of transforming unstructured data into a form that can be read, accessed, and analyzed. The raw data cannot be used in data mining; therefore, this is a critical step. Check the data quality before using machine learning or other methods. The primary purpose of data pre-processing is quality control.

```
iot5 Downloading index.html from iot1
iot5 Downloading test.zip from iot1
generating ICMP traffic between iot16 and iot15 and TCP/UDP traffic between iot16 and iot1
iot16 Downloading index.html from iot1
iot16 Downloading test.zip from iot1
generating ICMP traffic between iot3 and h14 and TCP/UDP traffic between iot3 and iot1
iot3 Downloading index.html from iot1
iot3 Downloading test.zip from iot1
-----
Iteration n 3 ...
-----
generating ICMP traffic between iot9 and iot12 and TCP/UDP traffic between iot9 and iot1
iot9 Downloading index.html from iot1
iot9 Downloading test.zip from iot1
generating ICMP traffic between iot17 and iot7 and TCP/UDP traffic between iot17 and iot1
iot17 Downloading index.html from iot1
iot17 Downloading test.zip from iot1
generating ICMP traffic between iot18 and iot4 and TCP/UDP traffic between iot18 and iot1
```

Fig. 4. Normal Traffic Collection in Mininet.

```
26 updates can be applied immediately.
0 of these updates are standard security updates.
to see these additional updates run: apt list --upgradable

our Hardware Enablement Stack (HWE) is supported until April 2025.
last login: Mon Apr  4 13:12:06 2022 from 192.168.43.1
awfik@ubuntu:~$ cd Desktop/
awfik@ubuntu:~/Desktop$ cd sd
bash: cd: sd: No such file or directory
awfik@ubuntu:~/Desktop$ cd mysdn/
awfik@ubuntu:~/Desktop/mysdn$ cd sdn
awfik@ubuntu:~/Desktop/mysdn/sdn$ cd controller/
awfik@ubuntu:~/Desktop/mysdn/sdn/controller$ ls
Attack_traffic.py      mydata1.csv           pycache              test.csv
CP.py                 mydata.csv            SVM.py               Xgboost2_controller.py
CP.py                 Normal_traffic.py     switch.py
awfik@ubuntu:~/Desktop/mysdn/sdn/controller$ ryu-manager Attack_traffic.py
loading app Attack_traffic.py
instantiating app ryu.controller.ofp_handler
instantiating app ryu.controller.ofp_handler of OFPHandler
```

Fig. 5. Attack Traffic Collection in Mininet.

The following are ways to evaluate the level of quality to ensure that the data entered is accurate.

- Checking for completeness: determining whether the data has been captured.
- To ensure that all the data is maintained in the same location, one must ensure that all information is consistent.

3) *Data normalization*: Normalization is generally required when we are dealing with attributes on different scales because, if it is not done, it may lead to a dilution in the effectiveness of an important equally important attribute on a lower scale because of another attribute having values on a larger scale. Normalization is generally required when we are dealing with attributes on different scales. When there are several attributes, but those attributes have values that are measured on different scales, this can result in inadequate data models when executing data mining activities. Therefore, they must be normalized so that all the properties may be measured on the same scale.

4) *Feature extraction*: The goal of feature extraction is to cut down on the total number of features in a dataset by generating new features based on the ones that are already there and skipping the original features. After being trimmed down, this new collection of features ought to be capable of summarizing most of the information that was included in the initial set of features. By combining the components of the original set in this way, it is possible to generate a condensed version of the original features.

5) *Feature selection*: The act of selecting the features that will most significantly contribute to the prediction variable or output that you are interested in can be done either automatically or manually and is referred to as "feature selection." Feature selection reduces the amount of predictive model input variables. Reducing the amount of input variables can minimize modelling costs and increase model performance. Statistical-based feature selection approaches evaluate each input variable's relationship to the target variable and select those with the strongest association. The choice of statistical measures depends on the input and output data types.

6) *Machine learning models*: The project model's primary goal in the IoT-smart homes-based collection is to detect whether a traffic flow is normal or abnormal based on learning from an existing labelled data. The flow-based detection module needs a model that can distinguish an attack from a regular flow to work.

7) *Xgboost*: Extreme Gradient Boosting (Xgboost) Learning techniques are used to transform weak models into strong estimators that function sequentially as circular iterations [23]. As in neural networks, each one seeks to rectify a mistake in its preceding model in order to minimize the loss function. There are several ways to increase your model's performance, but Gradient Boosting is one that focuses on fitting the new predictor to fit on the pseudo-residuals (errors) of its predecessor, rather than modifying the weights for each

wrong classification at each iteration. In order to attain the best possible accuracy, ensemble machine learning uses a variety of ML models. An ensemble machine learning methodology for classification, regression, and ranking problems, XGBOOST is a current ensemble machine learning method. Fast and efficient implementation of Gradient boosting structure to identify the best tree models. On August 1st, 2016, Tianqi Chen and Carlos Guestrin launched the project. Uses Gradient Boosting to discover the best and most accurate tree model, emphasizing computation speed. Parallelization, Cache Optimization, Distributed Computing, and processing a vast dataset are all supported by XGBoost.

We have used this algorithm in our study. After training the model, we tested the pre-trained model's performance on actual attacks on IoT devices in an intelligent home virtual environment using the Mininet with SDN controller. The captured data from the OpenFlow switch passes through this classifier to identify if traffic is benign or malicious. If the traffic is malicious, add a flag to the packet in SDN to take any action and send a request to open the flow switch to drop it, as shown in Fig. 6.

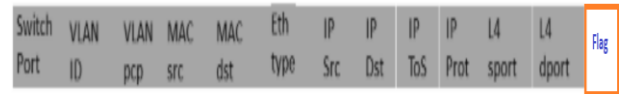


Fig. 6. Packet with Flag.

8) *Support Vector Machines (SVM)*: SVM is a set of supervised learning techniques applied for classification or regression. SVM classifier has been adopted in our model for intelligent home security. A key objective of the SVM technique is to find the optimum decision boundary or line that can divide n-dimensional space into classes [24], allowing us to classify new data points quickly. A hyperplane denotes the border of optimal decision-making inside a problem domain. To create the hyperplane, the SVM uses the most extreme points/vectors in the dataset. So-called "support vectors" refer to these extreme circumstances, and the process is known as a Support Vector Machine.

9) *Random Forest (RF)*: It is commonly utilized in Classification and Regression issues as a supervised Machine Learning Algorithm. It creates decision trees on various samples and uses their majority vote to classify and average the data[25, 26]. The Random Forest Algorithm's ability to handle data sets with continuous variables, such as regression, and categorical variables, such as classification, is critical. When it comes to categorization challenges, it does a better job.

10) *ANN classifier*: Computerized Brains ANN is a computer system component that attempts to simulate the human brain by personifying the nervous system. Many neurons link to one other. Every node or neuron in an artificial neural network follows the same paradigm for receiving information. An artificial neural network (ANN) consists of input neurons, weights, biases, hidden layers, activation functions, and an output layer that can be fed-forward or back-propagated.

11) *Long short-term memory*: Schmid Huber and Hoch Reiter proposed the LSTM deep learning algorithm in 1997 as a variant of the RNN network. It's made to store previously entered data. Classification and forecasting of time series are both possible applications most frequently used on Sequential data, such as speech recognition, translation, and picture captioning, which are well-suited to LSTM. LSTM is a good choice for applications related to the period. It types a back-propagation neural network. Forget, input, and output are the three gates of the LSTM [27].

The input gate picks the appropriate value from input samples to adjust the cell's memory and input. For three gates, the Sigmoid function is employed as a combining function that returns a value between 0 and 1. Calculated values are given additional weight by the Tanh or Relue functions. Sigmoid is a forget gate that decides whether new information should be stored in the cell state or discarded. Sigmoid input gate layers pick Tanh and Relue to update next. The next concealed state that should be remembered when the output gate is closed is selected. The concealed state decides what data should be preserved for the following phase and the hidden state is used for predictions.

We will use two layers of LSTM with 200-500 neurons and various optimizers, such as Adam, Rmsprob, Nadam, -SGD, loss sparse categorical cross-entropy, Activation Relu, and Activation Relu. Dropout = 0.2 or 0.5, 6 Dense layers with varying values, SoftMax for towing and four classes.

12) *Convolutional neural network*: ConvNet/CNN) is a deep learning system that can feed an image or numerical data and apply a filter, adding adjusted weights and minimizing biases to various objects in the picture and be able to discern one from the other. This approach requires less pre-processing than previous classification methods. Rather than relying on hand-engineered or traditional technique filters, CNN may be trained to learn these filter characteristics over time. The arrangement of the Visual Cortex served as inspiration for the design of the CNN architecture, which is similar to the neuronal connection pattern found in the human brain [28]. A visual field area known as the Receptive Field is where neurons respond to visual input. The whole visual field is covered by a group of such fields that overlap. Neurons in convolutional neural networks are geometric functions that calculate the weighted sums of numerous inputs, output and initiation values. The first layer of CNN commonly detects essential visual characteristics. Data is then passed from one layer to the next, allowing for increasingly complex features each time. The layers of CNN can recognize more complex characteristics, such as faces, objects etc.

IV. EXPERIMENTAL RESULTS

In this experiment, four machine learning algorithms have been used KNN, Xgboost, SVM, and random forest. Each classifier is trained to classify the IoT traffic as either normal or abnormal. The binary classification shows excellent results in detecting the attack in passive mode and real-time mode, the result is shown in Table I.

TABLE I. PERFORMANCE METRICS IN MACHINE LEARNING

Classifier	Accuracy	Confusion Matrix
SVM	99.8	[[6860 1] [0 217712]]
RF	99.9	[[6861 0] [1 217711]]
XGBOOST	99.9	[[6861 0] [0 217712]]
KNN	99.7	[[6861 2] [0 217703]]

1) *Artificial Neural Network (ANN)*: Artificial neural network model consists of three layers with 100 neurons for each layer, input shape 78, and RELU Activation function. And sigmoid for binary classification. The same architecture has been used on multi-classification but with differences in last layer SoftMax for five classes. The model was trained with 200 epochs by the Adam optimizer. the obtained accuracy reached 98.9 for binary classification and 83.2 % for multi-classification as shown in Fig. 7 and Fig. 8. Confusion matrix of ANN binary classification shown in Fig. 9.

In the LSTM model the architecture consists of two layers with 200 neurons for first one and 50 neurons for second. The next layers are dropout with 0.2, four dense layers with activation Relu, and the last layer is softmax for two classes. The model trained on binary classes and multiclass with five classes on different optimizers. The best result was obtained for the binary classes with an Adam optimizer, 200 epochs, and batch size 3000. The performance of the two models for LSTM shown in Fig. 10 and Fig. 11. The accuracy reached to 99% on binary classification and 84.7% for multiclassification. Confusion matrix of LSTM with multi classification shown in Fig. 12.

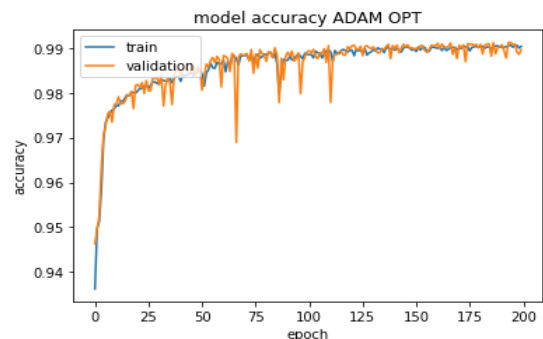


Fig. 7. Accuracy ANN Model with Binary Classification.

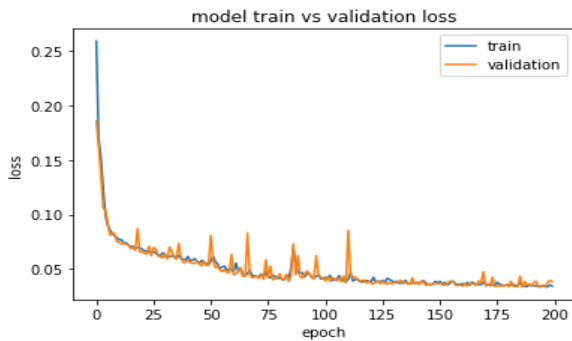


Fig. 8. Loss for Train vs Validation with Binary Classification.

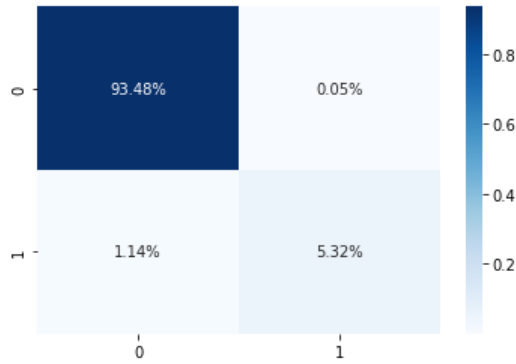


Fig. 9. Confusion Matrix for ANN Model with Binary Classification.

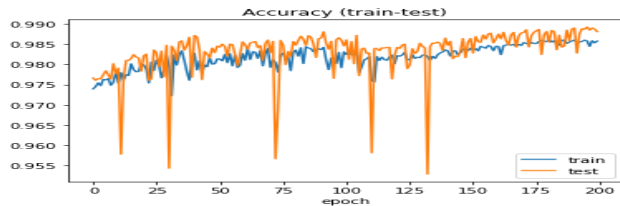


Fig. 10. Accuracy on Two Classes with Adam Optimizer.

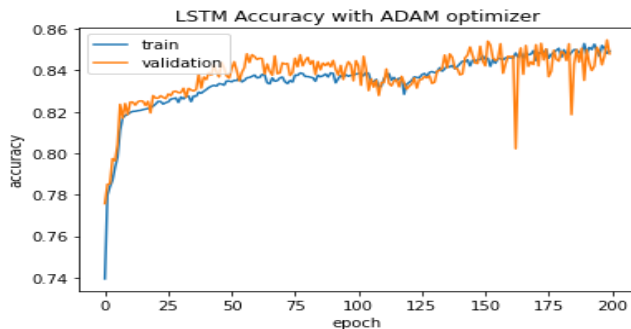


Fig. 11. Loss for Train vs Validation with Multi Classification.

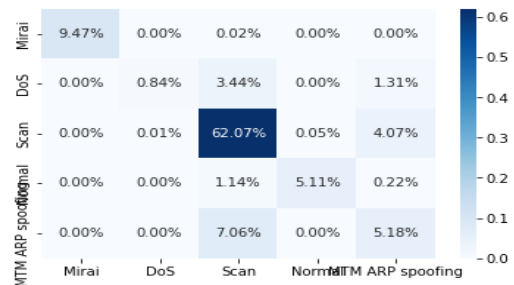


Fig. 12. Confusion Metric for LSTM Model with Multi Classification.

V. DISCUSSION

After running an experiment, we triggered attacks for data collection purposes and trained three Machine Learning algorithms on the training set. In the Software-Defined Networking (SDN) environment we have made simple attacks to test the machine learning models in real-time. The second section shows the result deep learning experiment. The evaluation of the two experiments on two datasets is shown below. The result shows an excellent performance to detect the attack on IoT devices on smart homes that have been simulated on SDN and open virtual open flow switches and (Hosts) that represent IoT devices. Five machine learning classifiers have been used; the highest obtained accuracy achieved by Xgboost classifier. In the second experiment on IoTID20. Several experiments have been conducted using machine learning and deep learning:

- On binary classification two classes normal and attack.
- Multiclassification for five classes ("Mira, Dos, Scan cat, Normal, MTM ARP Spoofing").
- Binary classification with 5-k fold cross-validation and 10-k fold cross-validation.
- Multiclassification with 5-k fold cross validation and 10-k fold cross-validation.

The result shows the superiority of deep learning in detecting electric attacks, Internet of things devices in smart homes as shown in Table II and Table III. The output has been evaluated using accuracy, precision, f1-score, Sensitivity, and Specificity. Two models have been implemented for each neural network. The evaluation on stander data splitting using traditional method 70% and 30 % is shown in Table IV. The second experiment conducted by splitting date to 10-k fold groups the result was better than 5-k fold groups is shown in Table IV. According to the results of our model compared to the results of previous studies shown in Table III, the proposed model achieved high accuracy results and it is recommended to apply it to actual discovery in IoT environments.

TABLE II. PERFORMANCE METRICS USING 70-30% SPLITTING

Model	Accuracy	Sensitivity	Specificity	F-Score Class0	F-Score Class1	F-Score Class2	F-Score Class3	F-Score Class4
ANN 2classes	98.9	84.9	99.9	0.99	0.91	-	-	-
ANN 5classes	83.2	85	99.2	0.99	0.25	.88	.76	.52
LSTM 2classes	98.9	83.3	99.8	0.99	0.90	-	-	-
LSTM 5classes	83.3	100	99.9	1.00	0.27	0.89	0.78	0.51
CNN2classes	98.6	86.8	99.5	0.99	0.90	-	-	-
CNN5classes	85.7	100	99.9	1.00	0.29	.90	.77	.53
SVM 2classes	96.5	83.4	99	.99	86	-	-	-
SVM5 classes	79.2	80	99	.99	0.26	.87	.75	.49
Xgboost 2classes	97.2	83	99.8	.99	.92	-	-	-
Xgboost 5classes	81.3	82	99	98	.27	.88	.76	.50
RF 2classes	96	83.4	99	.99	88	-	-	-
RF5classes	80.1	82	98	.98	.26	.85	77	.51
KNN2classes	97	84.4	99	.99	89	-	-	-
KNN5classes	77.5	92	80	.98	.24	.85	.73	.38

TABLE III. PERFORMANCE A COMPARISON OF MODEL WITH OTHER ML & DL MODELS FOR BINARY AND MULTI CLASSIFICATION

Ref	Algorithm	Accuracy in binary class %	Algorithm	Accuracy in multi class %	Dataset used
[29]	Xgboost	98.89	Xgboost	93.48	IoTID20
[30]	DT	94.22	ANN	96	Bot-IoT and the IoTID20
[31]	LR	91	ANN	96	IoTID20
[32]	autoencoder models	94.70	autoencoder	95.20	NSL-KDD, IoTID20
[33]	DCNN	99.84	DCNN	98.12	IoTID20
Our model	Xgboost	99.9	LSTM	98.9	IoTID20 and SDN dataset collected

TABLE IV. K-FOLD SPLITTING DATA TO 10 GROUPS

Model	Accuracy	Sensitivity	Specificity	F-Score Class0	F-Score Class1	F-Score Class2	F-Score Class3	F-Score Class4
ANN 2classes	97.3	84.9	99.8	0.97	0.92	-	-	-
ANN 5classes	83.2	85	99.2	0.99	0.25	.88	.76	.52
LSTM 2classes	98.9	83.3	99.8	0.99	0.90	-	-	-
LSTM 5classes	83.3	100	99.9	1.00	0.27	0.89	0.78	0.51
CNN2classes	98.6	86.8	99.5	0.99	0.90	-	-	-
CNN5classes	85.7	100	99.9	1.00	0.29	.90	.77	.53
SVM 2classes	96.5	83.4	99	.99	86	-	-	-
SVM5 classes	79.2	80	99	.99	0.26	.87	.75	.49
Xgboost 2classes	97.2	83	99.8	.99	.92	-	-	-
Xgboost 5classes	81.3	82	99	98	.27	.88	.76	.50
RF 2classes	96	83.4	99	.99	88	-	-	-
RF5classes	80.1	82	98	.98	.26	.85	77	.51
KNN2classes	97	84.4	99	.99	89	-	-	-

VI. CONCLUSION

There is a rapid expansion of the Internet of Things (IoT) into previously unimagined areas and domains. In addition to factories, agriculture, cities, and transportation are included in this. In recent years, the Internet of Things (IoT) has grown in popularity as a growing number of applications and devices, such as medical devices, home sensors, wireless sensors, and other closely linked IoT gadgets, have been implemented. IoT security is sometimes overlooked since it takes time to fully assess a device's vulnerabilities. Widespread use and quick adoption of such technologies raises security concerns. Cyberattacks affect resource availability, causing financial and material damage. As a result, fresh strategies are needed to increase not only IoT's security against cyberattacks, but also their identification and mitigation from IoT networks. Smart-home security IoT is a big concern due to lack of computing power and device heterogeneity. IoT devices can't handle computationally intensive and latency-sensitive security tasks due to their low processing power. Our research aimed to defend smart home-based Internet of Things devices from hacking. It is of the utmost need to develop low-cost solutions that can detect and prevent cyber-attacks that are carried out against or through IoT devices. We thus proposed in this work a smart system to guard against attacks on smart homes utilizing Software-Defined Networking, Machine learning, and Deep learning at a cheap cost to prevent threats on devices from both the inside and the outside.

We have implemented the classification process of the IoT traffic in a simulation environment using Ryu SDN controller and Mininet for detection attacks on traffic using Machine learning classifiers; SVM, KNN, RF, Xgboost, we collected data by triggered real attacks on IoT devices and generated normal traffic also, then we have trained the models and test them on testbeds environment (SDN). The result showed the ability to identify the normal and abnormal traffic with accuracy reached 99.9 %. Then we introduced deep learning as proof of concept to detect the attack in a smart home environment, IoTID20 dataset has been used for training the deep learning models, ANN, LSTM, and CNN. The turning process was conducted on the binary classification to classify their traffic as normal or abnormal, and multi-classification to identify the attack type on IoT. The highest achieved accuracy for binary classification was 98.9 % using long short-term memory (LSTM), 85.7 % on multiclass using Convolutional Neural Network (CNN). Other deep learning classifiers can be investigated for use in the improvement of future work. The suggested model's simulation results can be put to the test in a live setting with both heavy attack and typical traffic.

ACKNOWLEDGMENT

The authors would like to thank the Deanship of Graduate Studies at Jouf University for funding and supporting this research through the initiative of DGS, Graduate Students Research Support (GSR) at Jouf University, Saudi Arabia.

REFERENCES

- [1] G. Eason, B. Noble, and I. N. Sneddon, "On certain integrals of Lipschitz-Hankel type involving products of Bessel functions," *Phil. Trans. Roy. Soc. London*, vol. A247, pp. 529–551, April 1955.
- [2] G. Spanos, K. M. Giannoutakis, K. Votis and D. Tzovaras, "Combining statistical and machine learning techniques in IoT anomaly detection for smart homes," in *Proc. IEEE 24th International Workshop on Computer Aided Modeling and Design of Communication Links and Networks (CAMAD)*, pp. 1–6, 2019.
- [3] S. Al-Sarawi, M. Anbar, R. Abdullah and A. B. Al Hawari, "Internet of things market analysis forecasts, 2020--2030," in *Proc. Fourth World Conference on smart trends in systems, security and sustainability (WorldS4)*, pp. 449–453, 2020.
- [4] X. Huang, T. Yuan, G. Qiao and Y. Ren, "Deep Reinforcement Learning for Multimedia Traffic Control in Software Defined Networking," *IEEE Network*, pp. 35 - 41, 2018.
- [5] S. Mahindrakar and R. K. Biradar, "Internet of things: Smart home automation system using raspberry Pi," *Int. J. Sci. Res.*, vol. 6, no. 1, pp. 901–905, 2017.
- [6] X. Huang, T. Yuan, G. Qiao and Y. Ren, "Deep reinforcement learning for multimedia traffic control in software defined networking," *IEEE Network*, vol. 32, no. 6, pp. 35–41, 2018.
- [7] G. Stampa, M. Arias, D. Sanchez-Charles, V. Munte-Mulero and A. Cabellos, "A Deep-reinforcement learning approach for software-defined networking routing optimization," *arXiv preprint arXiv:1709.07080*, 2017.
- [8] T. A. Tang, L. Mhamdi, D. McLernon, S. A. R. Zaidi and M. Ghogho, "Deep learning approach for network intrusion detection in software defined networking," in *Proc. International Conference on Wireless Networks and Mobile Communications (WINCOM)*, pp. 258–263, 2016.
- [9] M. E. Ahmed, H. Kim and M. Park, "Mitigating DNS query-based DDoS attacks with machine learning on software-defined networking," in *Proc. MILCOM, IEEE Military Communications Conference (MILCOM)*, pp. 11–16, 2017.
- [10] R. H. Jensen, Y. Strengers, J. Kjeldskov, L. Nicholls and M. B. Skov, "Designing the desirable smart home: a study of household experiences and energy consumption impacts," in *Proc. CHI Conference on Human Factors in Computing Systems*, 2018.
- [11] Q. Niyaz, W. Sun and A. Y. Javaid, "A Deep learning based DDoS detection system in software-defined networking (SDN)," *ICST Transactions on Security and Safety*, vol. 4, no. 12, pp. 153515, 2017.
- [12] S. Sen, K. D. Gupta and Md. Manjurul Ahsan, "Leveraging machine learning approach to setup software-defined network (SDN) controller rules during DDOS attack," in *Proc. of International Joint Conference on Computational Intelligence*, pp. 49–60, 2020.
- [13] Y. Qin, J. Wei and W. Yang, "Deep learning based anomaly detection scheme in software-defined networking," in *Proc. 20th Asia-Pacific Network Operations and Management Symposium (APNOMS)*, pp. 1–4, 2019.
- [14] S. S. Mohammed, R. Hussain, O. Senko, B. Bimaganbetov, J. Y. Lee et al., "A new machine learning-based collaborative DDOS mitigation mechanism in software-defined network," in *Proc. 14th International Conference on Wireless and Mobile Computing, Networking and Communications (WiMob)*, pp. 1–8, 2018.
- [15] S. K. Dey, Md. M. Rahman and Md. R. Uddin, "Detection of flow based anomaly in openflow controller: machine learning approach in software defined networking," in *Proc. 4th International Conference on Electrical Engineering and Information & Communication Technology (iCEEICT)*, pp. 416–421, 2018.
- [16] J. Wu, Y. Peng, M. Song, M. Cui and L. Zhang, "Link congestion prediction using machine learning for software-defined-network data plane," in *Proc. International Conference on Computer, Information and Telecommunication Systems (CITS)*, pp. 1–5, 2019.
- [17] T. A. Tang, L. Mhamdi, D. McLernon, S. A. R. Zaidi, M. Ghogho and F. el Moussa, "DeepIDS: Deep learning approach for intrusion detection in software defined networking," *Electronics (Basel)*, vol. 9, no. 9, pp. 1533, 2020.
- [18] B. Susilo and R. F. Sari, "intrusion detection in software defined network using deep learning approach," in *Proc. IEEE 11th Annual Computing and Communication Workshop and Conference (CCWC)*, pp. 0807–0812, 2021.

- [19] A. O. Alzahrani and M. J. F. Alenazi, "Designing a network intrusion detection system based on machine learning for software defined networks," *Future Internet*, vol. 13, no. 5, pp. 111, 2021.
- [20] Q. Niyaz, W. Sun and A. Y. Javaid, "A deep learning based ddos detection system in software-defined networking (SDN)," *arXiv preprint arXiv:1611.07400*, 2016.
- [21] I. Mansour, "Towards effective live cloud migration on public cloud IaaS," Ph.D. dissertation, Bournemouth University, 2018.
- [22] S. Y. Wang, "Comparison of SDN openflow network simulator and emulators: EstiNet vs. Mininet," in *Proc. IEEE Symposium on Computers and Communications*, 2014.
- [23] S. Asadollahi, B. Goswami and M. Sameer, "Ryu controller's scalability experiment on software defined networks," in *Proc. IEEE International Conference on Current Trends in Advanced Computing, ICCTAC*, pp. 1–5, 2018.
- [24] I. Ullah and Q. H. Mahmoud, "A scheme for generating a dataset for anomalous activity detection in IOT networks," *Lecture Notes in Computer Science*, vol. 12109 LNAI, pp. 508–520, 2020.
- [25] T. Chen and T. He, *xgboost: eXtreme Gradient Boosting*, 2022, 2004. [Online]. Available: <https://cran.r-project.org/web/packages/xgboost/vignettes/xgboost.pdf>.
- [26] L. Auria and R. A. Moro, "Support vector machines (SVM) as a technique for solvency analysis," *SSRN Electronic Journal*, vol. 1, no. 1, pp. 1-18, 2008.
- [27] J. Frausto-Solís, L. J. Hernández-González, J. J. González-Barbosa, J. Paulo Sánchez-Hernández, E. Román-Rangel et al., "Convolutional neural network–component transformation (CNN–CT) for confirmed covid-19 cases," *Mathematical and Computational Applications*, vol. 26, no. 2, pp. 29, 2021.
- [28] Wani, A., & Khaliq, R. (2021). SDN-based intrusion detection system for IoT using deep learning classifier (IDSIoT-SDL). *CAAI Transactions on Intelligence Technology*, 6(3), 281-290.
- [29] Bajpai, S., & Sharma, K. (2022). A Framework for Intrusion Detection Models for IoT Networks using Deep Learning.
- [30] Albulayhi, K., Smadi, A. A., Sheldon, F. T., & Abercrombie, R. K. (2021). IoT Intrusion Detection Taxonomy, Reference Architecture, and Analyses. *Sensors*, 21(19), 6432.
- [31] Song, Y., Hyun, S., & Cheong, Y. G. (2021). Analysis of autoencoders for network intrusion detection. *Sensors*, 21(13), 4294.
- [32] Ullah, S., Ahmad, J., Khan, M. A., Alkhamash, E. H., Hadjouni, M., G, Y., Hyun, S., & Cheong, Y. G. (2021). Analysis of autoencoders for network intrusion detection. *Sensors*, 21(13), 4294.
- [33] hadi, Y. Y., ... & Pitropakis, N. (2022). A New Intrusion Detection System for the Internet of Things via Deep Convolutional Neural Network and Feature Engineering. *Sensors*, 22(10), 3607.

Skin Melanoma Classification from Dermoscopy Images using ANU-Net Technique

Vankayalapati Radhika, Dr. B. Sai Chandana

School of Computer Science Engineering, VIT-AP University, Amaravati, Andhra Pradesh, India

Abstract—Cells in any area of the body might develop cancer when they begin to grow uncontrollably. Other body regions may become affected by it. Skin cancer known as melanoma develops when melanocytes, or cells that create melanin, the pigment that gives skin its appearance of color, start to develop out of control. Melanoma is deadly because, if not caught early and addressed, it has a high propensity to spread to other regions of the body. Analyzing digital dermoscopy images, create a unique approach to categorizing melanocytic tumors as malignant or benign. Every single newly formed mole has a unique shape and colour compared to the pre-existing moles and given few more issues to classify the melanoma. To overcome all of these issues, this paper uses deep learning techniques. In this paper, a four-step system for classifying melanoma is described. The first stage is pre-processing, followed by the removal of hair from dermoscopic images using a Laplacian-based algorithm and then removing noise from the images using a Median filter. The second method is feature extraction from pre-processed images. Extracting features including texture, shape, and color using the Principal Component Analysis (PCA) technique. Thirdly, the LeNet-5 approach is utilized to locate the lesion location and segment the skin lesion. Fourth, the ANU-Net technique is used to categorize the lesion as cancerous (melanoma) or non-cancerous (non-melanoma). Evaluated based on performance parameters such as precision, sensitivity, accuracy, and specificity. Results are compared to those of current systems and show higher accuracy.

Keywords—Melanoma; LeNet-5; ANU-Net; dermoscopy images; benign; classification

I. INTRODUCTION

Melanoma is a prevalent form of malignant that develops in the epidermal layer of the skin from abnormal cells caused by exposure to UV light. In an area with intense sunlight, one in five Americans (US) is at risk of developing skin cancer. Melanoma is the nineteenth most prevalent malignancy overall among all forms of skin cancer, with around 3.0 million new cases reported in 2018 [1]. In the US alone in 2019, melanoma claimed the lives of 2,490 females and 4,740 males on average. In 2020, there will likely be 1.0 million new cases of melanoma, according to projections. 2020 is expected to see an estimated 6,850 additional cases of melanoma deaths in the US alone, with 2,240 females and 4,610 males [2]. Skin cancer is currently diagnosed using a variety of imaging methods, including dermoscopic images, magnetic resonance imaging, optical coherence tomography, and confocal scanning laser microscopy. Dermatologists examine those images visually, which is frequently a laborious and time-consuming operation.

Melanoma is the worst type of cancer among skin cancers, and its prevalence is rising quickly globally. Early detection is crucial since skin cancer can be treated with a straightforward excision. Most of the time, the visual analysis could be inappropriate and result in a false identification because the different skin lesions (non-melanoma and melanoma) are similar to one another [3-5]. A non-invasive skin imaging procedure called dermoscopy enables a magnified view of the skin's surface and subdermal processes. By aiding in the early detection of MM, dermoscopy images have significantly increased the survival rate of patients. While still the undisputed top standard, expert human diagnoses are nevertheless prone to bias.

The number of skin cancer diagnoses is increasing in past years. Melanoma and benign skin cancer are the two main varieties. Melanoma is one of the worst forms of skin cancer and is a major cause of death in young people each year [6, 7]. The severity and symptoms of skin disorders vary; for instance, a nevus is a normal skin lesion caused by the growth of pigment-producing cells also known as melanocytes, but melanoma is a severe form of skin cancer that can arise from a benign lesion [8].

The same nevus cells that produce pigment can give rise to melanoma. Melanoma is a fast-evolving disease that is responsible for a high death rate among the global population, according to research in both the medical and analytical fields [9-11]. With the early-stage discovery, the skin lesion can be treated. If melanoma is detected early, the survival percentage will be higher and it will be treatable. However, the manual diagnosing process necessitates dermatology specialists with appropriate training. An experienced dermatologist is very expensive and takes a lot of time. The most important phase in these systems is feature extraction, where several features can be utilized to check the pigmentation, shape, or evolution of skin lesions or to distinguish melanomas from benign lesions [12]. These features include asymmetry, border irregularity, and color. Dermoscopy technology offers a further improvement in diagnosis. Applying the dermoscopy approach to the skin will allow you to highlight locations by taking illuminated, magnified images of the skin lesion without making any incisions. Additionally, if the skin surface reflection is eliminated, the visual impact of the deeper skin layer can be enhanced. However, due to a variety of problems, classifying melanoma dermoscopy images is a challenging task [13]. In this paper, proposed four steps to classify the melanoma. They are pre-processing, feature extraction, segmentation, and classification. Initially, utilize a Laplacian-based algorithm to remove hair from dermoscopic images

during the pre-processing stage, and then a Median filter to eliminate noise to segment the dermoscopic images. The principal component analysis method is used for feature extraction to extract features including texture, shape, and color. After feature extraction completed, the skin lesion is segmented using the LeNet-5 technique to identify the lesion region, and the classification process is then carried out. Using the ANU-Net approach, categorize the lesion into benign (non-melanoma) and malignant (melanoma) during the classification stage. The key contribution of this paper is:

- This paper uses deep learning techniques for classifying melanoma into malignant and benign by using dermoscopic images. First, do pre-processing to remove hairs on images to get better segmentation and also remove noise on images.
- A PCA method using for feature extraction process to obtain the features such as shape, color, and texture of the image.
- Then utilizing LeNet-5 technique for segment the skin lesion area in dermoscopic images and after that classify the skin lesion into non-melanoma or melanoma using ANU-Net technique. Here collect dermoscopic images from ISIC 2020 dataset.

This paper is structured as follows. The related research on deep learning-based melanoma classification is covered in Section II. The proposed methodology and its components are covered in detail in Section III. The experimental strategy is described in Section IV. The study is reviewed in Section V along with suggestions for additional research.

II. LITERATURE SURVEY

A literature review is presented and discussed in this paper to offer a speculative background about melanoma skin cancer classification. Hosny et al. [14] suggested a classification method based on DCNN. There are three primary steps in the suggested procedure. In the beginning, the ROI is segmented in the input color skin images during preprocessing. Second, translation transformations and rotation are used to enhance the segmented ROI images. Third, various deep convolutional neural network (DCNN) designs are used, including GoogleNet, Alex-net, and ResNet101. To better suit the task of classifying lesions, the final three layers are removed and replaced with fresh ones. DermIS & DermQuest, MED-NODE, and ISIC 2017 are three separate datasets that were used to assess the performance of the suggested technique.

To detect and categorize dangerous skin lesions (melanoma type), Ponomaryov et al. [15] introduced a computer-aided detection (CAD) system that combines handcrafted features from the medical algorithm Asymmetry Borders-Colors-Dermatoscopic Structures (ABCD) rule with DL features using Mutual Information (MI) measurements. Pre-processing, extraction of features, feature fusion, and categorization are the steps in a CAD system that may be distilled into a single phrase. To identify the Region of Interest (ROI), a lesion image is improved, segmented, and filtered during the preprocessing stage. The feature extraction method is then carried out. Shape, color, and texture are examples of

handcrafted features that are utilized to represent the ABCD rule. DL features are obtained using a CNN framework that has been pre-trained on ILSVRC ImageNet. Utilizing MI denotes a fusion rule, the most crucial data from both kinds of characteristics are gathered. Finally, numerous techniques are used during the classification process, including Relevant Vector Machines (RVMs), Linear Regression (LR), and Support Vector Machines (SVMs). The public dataset from ISIC 2018 was used to evaluate the developed system.

An excellent and efficient melanoma detection approach was presented by Masood et al. [16]. Three steps make up the suggested approach: 1) image preprocessing, 2) use of a Faster-RCNN for skin cancer localization, and 3) application of an SVM for the categorization of customized skin cancer regions into malignant and benign classes. The suggested technique's effectiveness is assessed utilizing data from the benchmark ISIC-2016 dataset, which was made available by the ISBI Challenge 2016. This dataset is diverse in terms of differences in color, luminescence, melanoma size, and texture, as well as the noise presence, blurring, small blood vessels, and hairs, among other things. Additionally, they validated the technique across multiple datasets using the ISIC-2017 dataset to demonstrate its effectiveness in practical settings.

The Automated Skin-Melanoma Detection (ASMD) system with Melanoma-Index (MI) was presented by Tang et al. [17] as being unique and original. The system includes binary classification, entropy, and energy feature mining, image pre-processing, Bi-Dimensional Empirical Mode Decomposition (BEMD), and image texture improvement. The system's design was influenced by feature ranking, and the quality of the system was evaluated using Student's t-test and other statistical techniques. Using benchmark databases, the proposed ASMD was applied to 600 DD malignant and 600 benign images.

Four steps are included in the Kumar et al. [18] proposed system for melanoma identification and categorization: pre-processing, which includes dermoscopic images being resized, and noise and hair being eliminated; image segmentation, which involves locating the site of the lesion; extraction of feature, which involves obtaining features from the segmented lesion and then categorization; and classifying the lesion as benign or malignant. To produce skin lesions, a modified GrabCut algorithm is used. Using machine learning techniques like ANN, k-NN, SVM, and logistic regression, segmented lesions are categorized, and their performance is assessed in terms of specificity, accuracy, and sensitivity.

Rahman et al. [19] introduced an automated approach for pixel-based seed-segmented images with multilevel and fusion characteristics downsizing for the recognition and detection of skin lesions. The suggested approach entails four crucial steps: Implemented methods include: (a) mean-based function feeding input to bottom-hat and top-hat filters that were later fused for contrast increasing; (b) graph-cut method-based lesion segmentation and seed region growing and fusing both segmented lesions through pixel-based fusion; (c) simple concatenation and multilevel feature extraction; The method's effectiveness is tested in two independent experiments.

From the literature survey, some of common problems are noticed. They are, every single newly generated mole differs from the pre-existing moles in terms of shape and colour. The mole's outline or outer covering is uneven, largely asymmetrical, and appears gritty. It states that around half of the moles present do not match the other half of the moles. Accurately determining the importance of a specific feature is challenging. For effective medical image diagnosis, a collection of more sophisticated deep-learning architectures should be used. To overcome these issues this paper used effective recent proposed methodologies to classify the melanoma clearly.

III. PROPOSED METHODOLOGY

The most dangerous type of skin cancer, melanoma is on the rise all over the world. Melanoma incidence has increased globally during the past ten years. The proposed methodology has four steps: Pre-processing, Feature Extraction, Segmentation, and Classification. And every step is evaluated below. Initially, pre-processing for removing hair from the dermoscopic images using the Laplacian-based algorithm, and then removing noise from the images using the Median filter. In addition, feature extraction from pre-processed images using the Principal Component Analysis (PCA) approach for extracting the characteristics like texture, shape, and color. Furthermore, the segmentation process for identifying the lesion area and segmenting skin lesion using the LeNet-5

technique, and then, classification; here categorizing lesion as benign and malignant using the ANU-Net method. It is classified into benign (non-melanoma) and malignant (melanoma).

The complete performance of the melanoma classification process is displayed in Fig. 1.

A. Pre-processing

In pre-processing step, remove the hair from input images and then denoise the images for better segmentation of melanoma. Initially, remove the hair from dermoscopic input images because some melanoma is significantly or partially obscured by body hairs using Laplacian-based algorithm to every image. A sharpening filter based on the Laplace operator is applied to the image is made grayscale. Then the original input image is separate from the filtered image. It employs a 3x3 Wiener filter adaptive noise removal to eliminate any potential noise. After hair removal done, here remove noise from dermoscopic images.

Such noise is removed from dermoscopic images using the median filter, which uses a weighted average sum of the nearest pixels. The median filter performs well in terms of maintaining an image's edges. After hair removal, images are given to a median filter to eliminate noise. Fig. 2 illustrates the effectiveness of the noise and hair removal processes during the pre-processing stage.

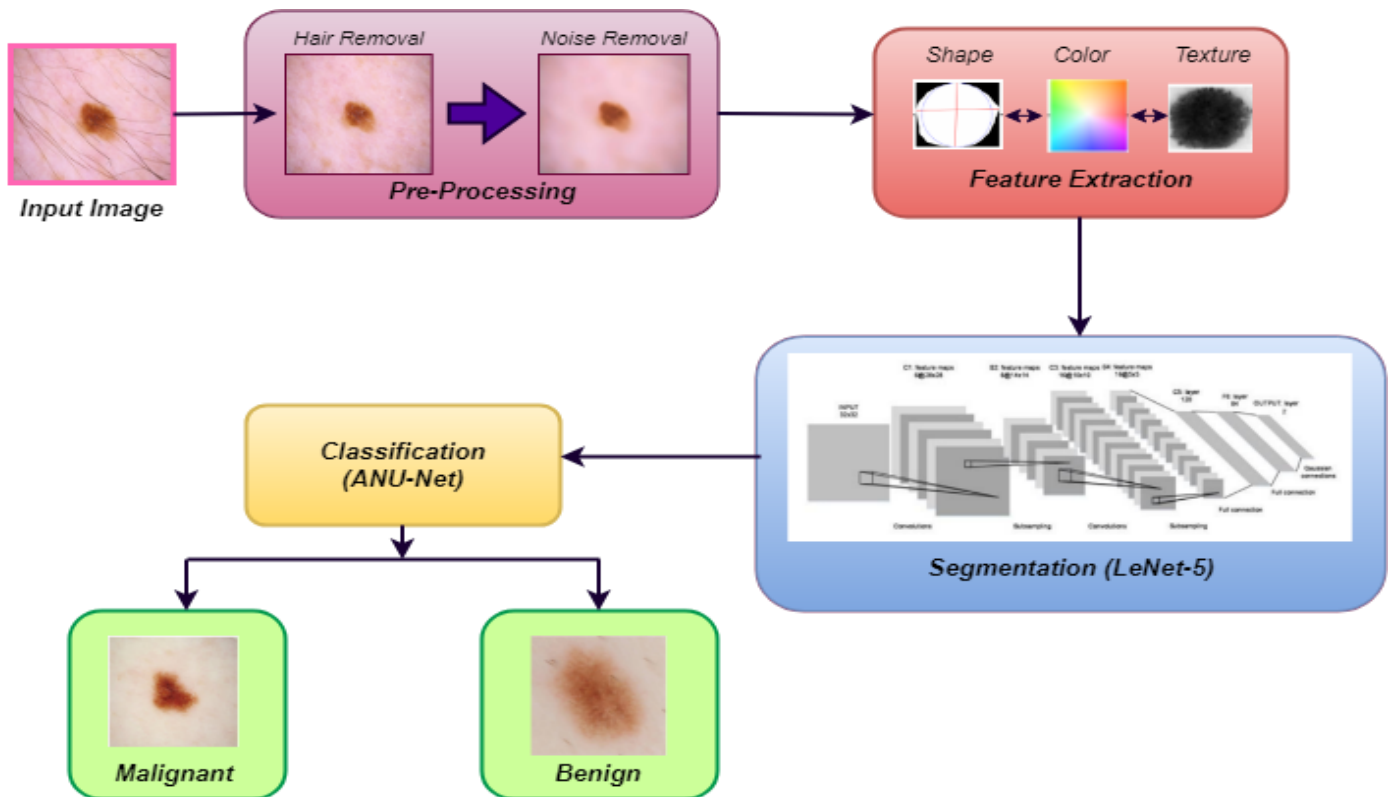


Fig. 1. The Proposed Architecture for Melanoma Classification.



Fig. 2. Process of Hair Remove and Noise Removal in Pre-processing Step.

B. Feature Extraction

After pre-processing, the characteristics that would be useful in features of the images are extracted using feature extraction techniques. For better prediction of melanoma from dermoscopic images, features like shape, color, and texture should be extracted. In this step, the features were extracted by using Principal Component Analysis (PCA). The obtaining of features is a significant phase in the model construction process. A system can be built using a variety of features, including color, shape, and texture, as well as SURF (speeded-up robust features). The PCA method is utilized to increase explainable while simultaneously reducing the loss of details to reduce the dimension of the dataset being used. The goal of PCA, a mathematical approach that uses a principal component examination, is to reduce the dataset dimension. An orthogonal linear transformation is another name for the process of transforming data into a new coordinate system. With the aid of linear combinations, the native features show new features. The traits with increasing variance are appropriate for dispatching. Accordingly, the PCA method converts the n vectors x_1, x_2, \dots, x_n from the d -dimensional space to the n vectors x_1, x_2, \dots, x_n in a new d -dimensional space.

$$x'i = \sum k = 1d'ak, iek, d' \leq d, \quad (1)$$

Where, d' is a space with n dimensions, n vectors, and ek eigenvectors that are the greatest eigenvectors for ak , i are the projections of the original vector $x'i$ and scatter matrix S on the eigenvector ek .

In PCA, Single Value Decay (SVD) is typically established on the input data matrix. Based on the optimization algorithm, a PCA technique may be developed. During the optimization process, the data reconstruction error and variance maximization of the projected input data can be examined.

$\overline{W}_i \in S^n, i = 1, 2, 3, \dots, o, o < n$ information variance can be estimated in the orthonormal direction with a constrained amount of options using PCA to determine the orthonormal

direction O in a given space. Without losing any data in the resulting structure of dimension $d \in S^n$, the input vector is translated into O -dimensional space. In the input data, which consists of vector d , the O -Dimension is projected using \overline{W} , where the inner product $(d^T \overline{W}_i)$ is obtained and the misplaced outcome dimension is obtained. Since PCA calculates unit directions, the information can be anticipated into the input vector. Where $Y = d^T \overline{W}_i$, it has a large variance and is signified by greater variance. It will be written as:

$$\sigma_{PCA}(W) = \sigma[y^2] = d^T C \overline{W}_i = \frac{W^T C W}{\|W\|^2} \quad (2)$$

where $\overline{W} = W / \|W\|$

Apply the estimation in the linear square estimation after reconstructing the input data, or \hat{d} .

$$\hat{d}_t = \sum_{i=1}^o g_{i(t) \overline{W}_i} \quad (3)$$

With the use of data reconstruction, the error can be recreated and identified by comparing the differences between the original and corrected data.

$$e = d - \hat{d}_t = \sum_{i=O+1}^n a_i \overline{W}_i \quad (4)$$

To predict this issue, implement a novel method for dimension restricting and increasing the entertainment of PCA following in overall presentation development. Based on PCA, the reconstruction error can be reduced. When extending k -dimensional data to subspace, calculations are visible.

$$\begin{aligned} \text{PCA reconstruction} \\ = PC \text{ scores. Eigenvectors } T + \text{Mean} \end{aligned}$$

Based on the proposed technique, a maximum likelihood-based model may be used to map the underlying space into the data space.

$$x = \varepsilon + \mu + \int \Lambda \quad (5)$$

In a linear transformation, the variable $(p * 1)$ is designated as the variable, x is denoted as the high-dimensional factor and is also defined as $(p \times O)$, f is $(O \times 1)$, $\Lambda \rightarrow x$, $\mu(p \times 1)$ is defined as the mean vector, and ε is defined as Gaussian random error, the $\mu(p \times 1)$ denoted as the input signal vector of noise. The feasible result's input vector is represented by

$$p(\varepsilon; \sigma^2) = \left(2\pi\sigma^2\right)^{-\frac{p}{2}} \exp\left(\frac{-1}{2} \varepsilon' \varepsilon\right) \quad (6)$$

It will increase by the conditional probability of

$$p\left(\frac{x}{f}; \Lambda, \mu, \sigma^2\right) = \left(2\pi\sigma^2\right)^{-\frac{P}{2}} \exp\left(-\frac{1}{2}\|x - \mu - f\Lambda\|^2\right) \quad (7)$$

The dataset of the absolute distribution of a specific space is delivered by such a model without changing any errors or data that were not distributed for the specified probabilistic limit. The PCA model's primary goal can be achieved by fully revealing unknown parameters like Λ and μ , maximum noise variance σ^2 -based likelihood observations.

$$L\left(\Lambda, \mu, \sigma^2 \mid x\right) \\ (2\pi)^{-\frac{np}{2}} |\Sigma|^{-\frac{n}{2}} \exp\left[-\frac{1}{2} \sum_{i=1}^n (x_i - \mu)' \Sigma^{-1} (x_i - \mu)\right] \\ \left(x_i - \mu\right)' \Sigma^{-1} (x_i - \mu) \quad (8)$$

Another way to express maximum likelihood observation is in $tr\left(\Sigma^{-1}S\right)$ where S is a possible expression,

$$S = \frac{1}{n} \sum_{i=1}^n (x_i - \hat{\mu})(x_i - \hat{\mu})' \quad (9)$$

The maximum log-likelihood can be expressed using the equation below.

$$L\left(\Lambda, \mu, \sigma^2 \mid x\right) = -\frac{np}{2} \log(2\pi) - \frac{n}{2} \log |\Sigma| - \frac{n}{2} tr\left[\Sigma^{-1}S\right] \quad (10)$$

Based on PCA's data reconstruction, Λ and σ^2 the error can be minimized while still producing a superior answer. The highest possible possibility of σ^2 .

$$\hat{\sigma}^2_{ML} = \sum_{j=m+1}^p \lambda_j \times \frac{1}{p-m} \quad (11)$$

Effective parameters are reduced in the feature reconstruction process by applying the maximum likelihood model, which is based on the above-mentioned model's decreased error and increased production in feature extraction based on PCA. The PCA method giving significant results as expected and extract the feature of melanoma or benign dermoscopic images well. The major benefit of PCA for index generation over traditional techniques is that it does not assign arbitrary and subjective weights to various indicators. The results of a multivariate statistical analysis of a few chosen indicators are used to determine the weights allocation in PCA for the construction of the index. The principal component analysis method extracted the features such as shape, color, and texture very well. And this method work better to feature extraction without any issues.

C. Segmentation

Following feature extraction, the image segmentation procedure separates the scene into the background and foreground. After extracted the features from dermoscopic images, at next step need to segment the issue part from images. Because segmentation of issue part is more important to predict that if it's melanoma or not. In this research, the segmentation process was carried out using LeNet-5 technique. When the background and foreground colors of an image are highly similar, the LeNet-5 method is used. Because the other technique's results are unsuccessful. Below is a description of the LeNet-5 method.

Using this segmentation network, the effective deep skin lesions are divided into groups. Many other CNN types can be used for segmentation depending on the objectives of the application, and the melanoma was segmented using a LeNet-5 pre-trained network. An input layer, two pooling levels, one fully connected layer, two convolutional layers, and an output layer made up a total of seven layers in LeNet-5 [21]. Table I displays the precise design of the LeNet-5. LeNet-5's weighted layers are constructed using the idea of removing convolution layer blocks by utilizing shortcut connections. The "bottleneck" blocks, which are the fundamental construction blocks, follow two design principles: The same amount of filters are used to create the same output feature size. The convolution layers down-sample at a rate of two strides per layer. Batch normalization is carried out both before and after each convolution and before the rectified linear unit (ReLU) is activated.

An identity shortcut is used when the input and output dimensions are identical. The projection shortcut utilising 1x1 convolutions is used to match the dimensions when the dimensions are enhanced. The segment of the skin lesion region is transmitted to the classification and RPN networks from the last convolutional layer. In the LeNet-5 segmentation network, only the 49 convolutional layers are utilized; fully connected and average pooling layers are not. Because only the segmentation network, not the final classification is required by the RPN and classification network.

These region proposals are used by the final segmentation network to classify objects. In the RPN, anchor boxes with various scales and aspect ratios are first formed across each pixel of the feature map. Usually, nine anchor boxes with aspect ratios of 1:1, 1:2, and 2:1 and scales of 128, 256, and 512 are used. RPN forecasts the likelihood that a backdrop or item will appear in an anchor box. The necessary object proposals are forwarded to the following stage as a list of filtered anchor boxes. To convert the final anticipated region proposals from the anchor boxes, apply Eq. (12) and (13). Equation illustrates the scale-invariant translation between the center coordinates (12). The height and width are translated into log space using equation (13).

$$V_x = \frac{x_p - x_a}{w_a}, V_y = \frac{y_p - y_a}{h_a} \quad (12)$$

$$V_w = \log\left(\frac{w_p}{w_a}\right), V_h = \log\left(\frac{h_p}{h_a}\right) \quad (13)$$

TABLE I. LeNET-5 SEGMENTATION NETWORK

Layers	Name of the Layers	Input size	Output size	Pooled area	Convolution kernel size	Step size
Input	Input layer	32*32	28*28		5*5	1
Layer1	Convolutional layers	6@28*28	6@14*14	2*2		2
Layer 2	Pooled layers	6@14*14	16@10*10		5*5	1
Layer 3	Convolutional layers	16@10*10	16@5*5	2*2		2
Layer 4	Pooled layers	16@5*5	120@1*1		5*5	1
Layer 5	Fully connected layer	1*120	1*84			
Layer 6	Fully connected layer	1*84	1*7			
Output	Output layer	1*7				

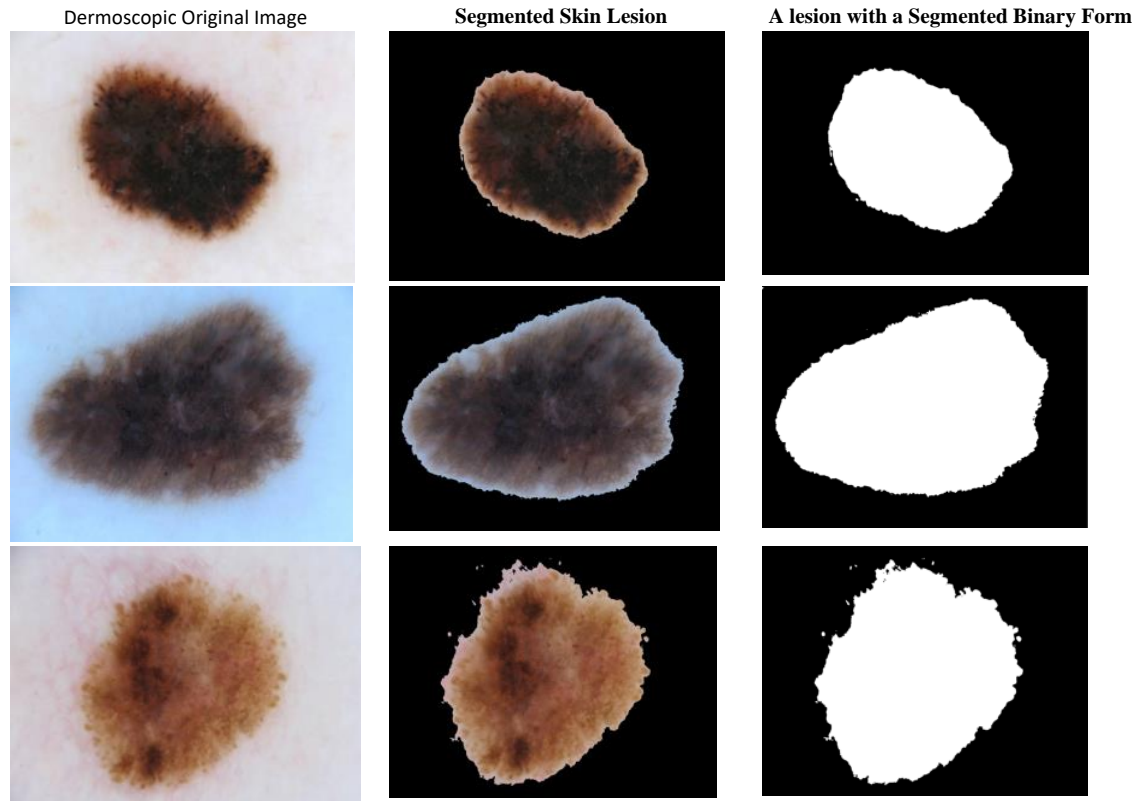


Fig. 3. Sample Segmentation Performance using the LeNet-5 Technique.

Where the bounding box regression vectors are represented by V_x , V_y , V_w , and V_h , and coordinates for the height, width, and center in x and y are depicted by h , w , and x , y . Additionally, x_a , x_p are the corresponding centers of the anchor and proposal box. The convolutional layers and fully connected layers of LeNet-5 technique are utilized in segmentation step to segment the melanoma issue part in dermoscopic images based on extracted features. The LeNet-5 method segments the skin lesion area accurately.

Some of the sample processes of segmentation of skin lesion performance are shown in above Fig. 3. It shows the segmented skin lesion area from dermoscopic images and also given the binary form of segmented skin lesion area using segmented technique LeNet-5.

D. Classification of Benign and Malignant

In the classification step, classify the segmented skin lesion into malignant or benign using the ANU-Net technique. It uses the skin lesion from segmented images for classifying whether the issue part is melanoma or not. Images with closely matched foreground and background colors are used with the ANU-Net technique. The ANU-Net technique is described below.

Develop an integrated network called Attention U-Net++ for medical image classification. Using nested U-Net architecture, which takes it from DenseNet, a series of U-Nets with different depths are integrated. In contrast to U-Net, which used nested convolutional blocks and constructed dense skip links between the decoder and encoder at various levels, the nested Framework makes use of convolutional blocks that are layered within each other [20]. Every nested convolutional

block in layered U-Nets employs numerous convolution layers to gather semantic data. The concatenation layer can integrate semantic data from different levels since each layer in the block is connected via connections. The following are some benefits of the new nested design:

- Layered architecture may avoid the time-consuming procedure of choosing deep and shallow features by assessing the value of features at various depths on its own.
- Only an encoder must be trained because the feature extractor is shared by all of the U-Nets in a nested arrangement.
- Since different decoder paths independently restore distinct layers of features, they can collect hierarchical decoded masks from a variety of levels in tiered architecture.

1) *Attention Gate (AG)*: Attention Gate employs the PASSR net's model and includes an effective AG into nested architecture.

The AG feature selection Phase is described as follows:

$$F = \sigma_1[(W_f^T \times f + b_f) + (W_g^T \times g + b_g)] \quad (14)$$

$$\alpha = \sigma_2(W_\theta^T \times F + b_\theta) \quad (15)$$

$$\text{output} = f \times \alpha \quad (16)$$

The effective function of the Attention Gate allows it to classify the task-related target region more effectively while suppressing the task-unrelated target region. In research, Attention Gate is used to enhance the capability of semantic data propagation across skip links in the creatively recommended network.

2) *Attention-based nested U-Net*: The ANU-Net is a network that is integrated for classifying medical images and is based on the Attention mechanism and Nested U-Net architecture. In the ANU-Net, which utilizes nested U-Net as its main network architecture. Then, additional helpful hierarchical characteristics can be retrieved. The encoder sends the context data it has gathered to the appropriate layers' decoder via the wide skip connections.

For each convolutional block, the decoder receives two equivalent image features when there are multiple dense skip connections: The preliminary feature maps are produced by earlier Attention Gates with residual connections at the same depth, while the final feature map is produced by a deeper block deconvolution procedure. The decoder reconstructs features starting at the bottom and adding up all received feature maps.

The extracted feature map from ANU-Net may be expressed as follows: Let $X_{i,j}$ indicate the outcome of the convolutional block, while the feature depth is denoted as i and the convolution block's sequence as j .

$$X_{i,j} = \begin{cases} \Phi[X_{i-1,j}] & , j=0 \\ \Phi[\sum_{k=0}^{j-1} \text{Ag}(X_{i,k}), \text{Up}(X_{i+1,j-1})] & , j>0 \end{cases} \quad (17)$$

$\text{Up}(X_{i+1,j-1})$ and $\text{Ag}(X_{i,k})$ the attention gate and mean up-sampling selection accordingly, $\sum_{k=0}^{j-1} \text{Ag}(X_{i,k})$ indicate that concatenate the outcome of the AG from node $X_{i,k=0}$ to $X_{i,k=j-1}$ in the i^{th} layer.

After the concatenation operation, the decoder's convolution blocks will only employ the encoder's chosen same-scale feature maps rather than all of the feature maps that were acquired via dense skip connections. This layer's output from the j previous blocks acts as an input, while the second layer's up-sampling function of block X1 provides additional input. The network transfer of features gathered by the encoder is one of two significant ANU-Net innovations. Furthermore, Attention Gate is used in the decoder path between layered blocks that are recovered at different layers and can be connected with a specific choice. As a result, ANU-Net accuracy ought to be raised. The proposed classification technique works well and classify the dermoscopic image as malignant or benign. The ANU-Net techniques improved the time complicity of classification and given better classification accuracy.

IV. RESULTS AND DISCUSSION

This section's compares the approach to "state-of-the-art" techniques by categorizing melanoma using the dataset's analysis and technique for extracting features from skin lesions. Given are the assessment findings based on experimental data in the following subsections to evaluate methodology.

A. Dataset Description

There are 33,126 dermoscopic images of benign and malignant skin lesions in the ISIC-2020 dataset, with a high percentage of benign lesions. Only 584 of the 33,126 skin lesion images were classified as malignant melanoma. The primary factor that led to the selection of this dataset above others was the fact that the skin lesions are discernible and are not masked by any artifacts. Furthermore, the skin lesions' micro-features are distinct and easy to see. The efficiency of feature extraction is improved by this. The dataset sample images are seen in Fig. 4.

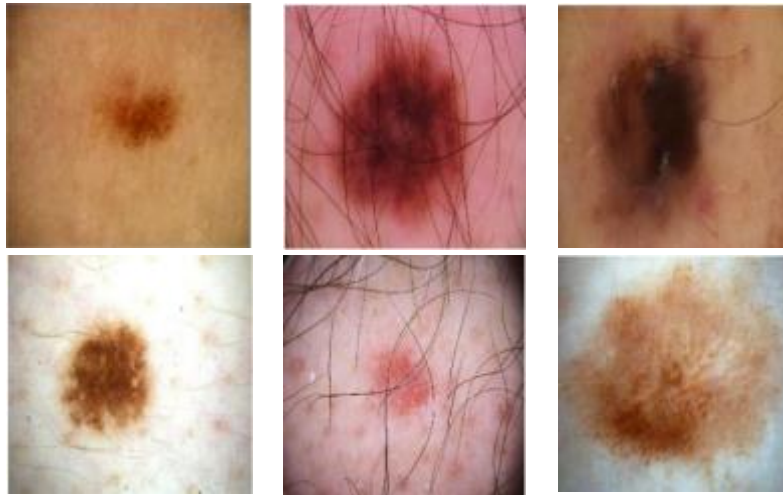


Fig. 4. Shows Various Images of Skin Lesions in the Dataset.

Original Picture	After-Hair Removal Image	After Noise Removal Image	Segmented Images	Classification of Melanoma
				Melanoma Affected
				Non-Melanoma
				Melanoma Affected
				Melanoma Affected

Fig. 5. The Experimental Outputs: (a) Original Image, (b) After Hair Removal Image, (c) After Noise Removal Image, (d) Segmented Images, (e) Classification of Melanoma.

B. Quantitative Metrics

The performance of the proposed method for classifying the skin lesion into malignant or benign is to give a better result. Here, first, are given an input dermoscopic image from ISIC 2020 dataset. For a better segmentation process, remove the hair from input dermoscopic images and then the noise from this input image in pre-processing step. Segment the skin lesion portion from the dermoscopic image using LeNet-5 technique. It determines the skin lesion's malignant (melanoma) or benign (benign) status using this segmented image (non-melanoma) utilizing the classification technique ANU-Net. The experiment performed well and produced superior results. The findings of the experiment are displayed in Fig. 5.

C. Evaluation Metrics

In terms of performance measures, looked at the proposed method's Accuracy (A), Precision (P), F1-score (F), and Recall (R). These metrics indicate:

Accuracy

The percentage of samples that were correctly identified relative to all samples is known as accuracy. In general, a classifier performs better the higher accuracy. Eq. (18) illustrates the meaning of accuracy.

$$Accuracy = \frac{TP+TN}{TP+FN+FP+TN} \quad (18)$$

Sensitivity

Sensitivity, also known as recall, measures how well a classifier can identify positive samples by representing the percentage of all positive samples that are predicted. Eq. (19) defines sensitivity.

$$Sensitivity = \frac{TP}{TP+FN} \quad (19)$$

Specificity

Specificity measures the classifier's capacity to identify negative samples by representing the percentage of all negative samples that are successfully classified. Eq. (20) illustrates the definition of specificity.

$$Specificity = \frac{TN}{TN+FP} \quad (20)$$

Precision

Precision is defined as the ratio of precisely anticipated positive occurrences to all anticipated positive observations. Precision is the capacity to do the following things:

$$Precision = \frac{TP}{TP+FP} \quad (21)$$

D. Performance Evaluation

In experimental performance, the proposed technique has the highest classification accuracy compared with other existing techniques. Table II shows the results for DenseNet-121, ResNet-50, Inceptionv3, and the proposed ANU-Net on the ISIC 2020 dataset in terms of accuracy, specificity, sensitivity, and Precision. Based on the results, the proposed methodology has higher classification accuracy values than

other existing approaches. It is consistent with the experimental findings for the melanoma classification into two types, malignant and benign. By using the proposed ANU-Net classification technique, the time complexity is reduced, effective training is performed, and the overall performance of the classification is improved compared with other existing techniques.

Here, for comparison three other existing methods are chosen to compare with the proposed technique. Compared with other techniques, the proposed methodology gives high accuracy values for classification. In Table II, the classification accuracy achieved 98.78% utilizing the proposed methodology ANU-Net technique compared with other techniques DenseNet-121 has 93.65%, ResNet-50 has 96.96%, and Inceptionsv3 has 97.17%. The proposed methodology provide effective outcomes and the classification accuracy is higher than others. Additionally, when compared to other existing methodologies, DenseNet-121 has the lowest accuracy rate at 93.65%. This accuracy comparison model is shown in Fig. 6.

In Table II, the sensitivity metric achieved 98.39% using the proposed method ANU-Net technique compared with other techniques DenseNet-121 has 95.83%, ResNet-50 has 96.53%, and Inceptionsv3 has 96.32%. This sensitivity comparison model is shown in Fig. 7.

TABLE II. THE PERFORMANCE OF CLASSIFICATION TECHNIQUE

Models	Accuracy	Sensitivity	Specificity	Precision
DenseNet-121	93.65	95.83	93.48	96.13
ResNet-50	96.96	96.53	96.53	95.32
Inceptionv3	97.17	96.32	96.46	97.74
Proposed (ANU-Net)	98.78	98.39	97.98	98.12

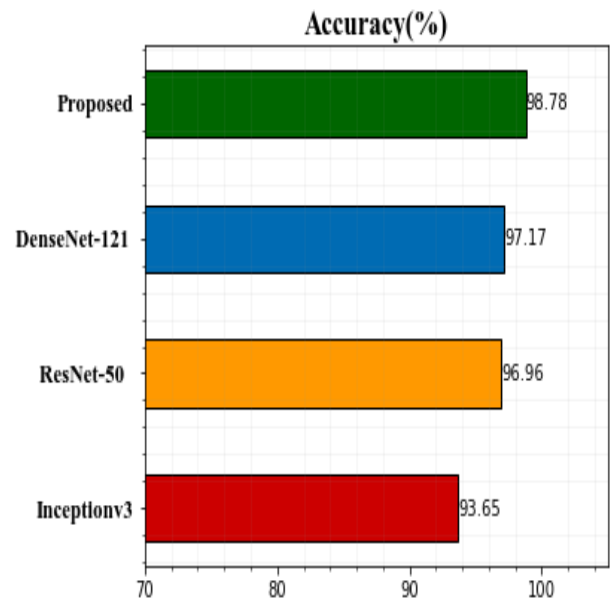


Fig. 6. Analysis of Accuracy based on different Techniques.

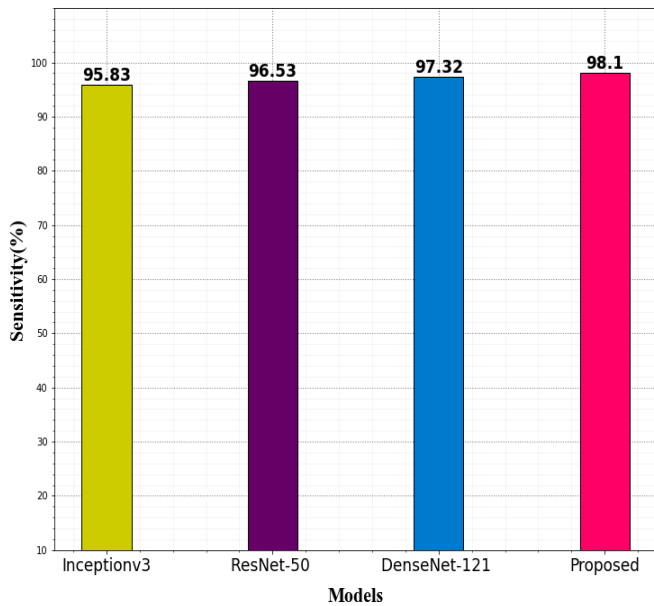


Fig. 7. Analysis of Sensitivity based on different Techniques.

The specificity metric achieved 97.98% using the proposed method ANU-Net technique compared with other techniques DenseNet-121 has 93.48%, ResNet-50 has 96.53%, and Inceptionsv3 has 96.46%. This sensitivity comparison model is shown in Fig. 8.

The precision metric achieved 98.12% using the proposed method ANU-Net technique compared with other techniques DenseNet-121 has 96.13%, ResNet-50 has 95.32%, and Inceptionsv3 has 97.74%. This sensitivity comparison model is shown in Fig. 9.

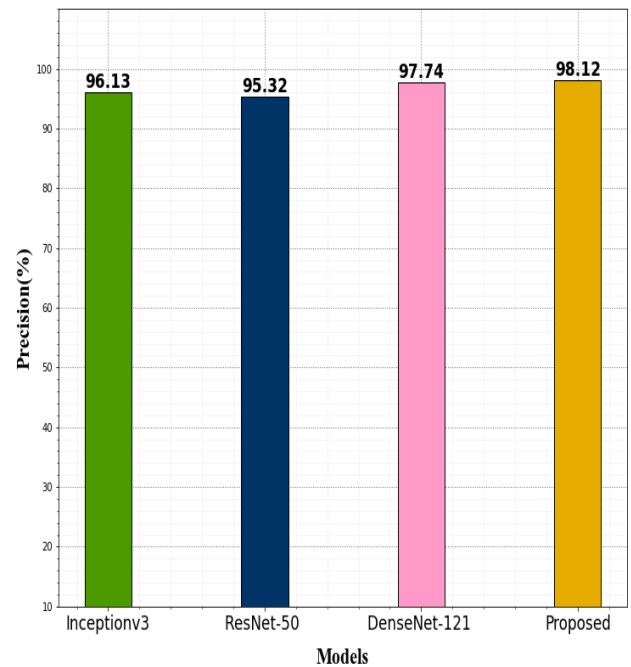


Fig. 9. Analysis of Precision based on different Techniques.

The analysis made by the different classification techniques is illustrated in the above figures. Compared with InceptionV3, ResNet-50, and DenseNet-121, the sensitivity value of ANU-Net is high and accurate the values are very clear and deep as shown in Fig. 7. And the same time also gives a better specificity percentage compared with other techniques as shown in Fig. 8. And also Fig. 9 shows the recall comparison of the ANU-Net technique.

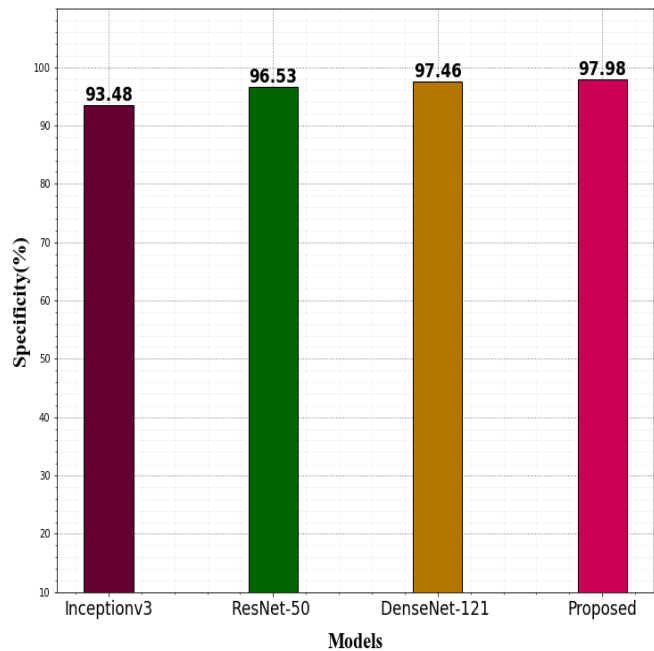


Fig. 8. Analysis of Specificity based on different Techniques.

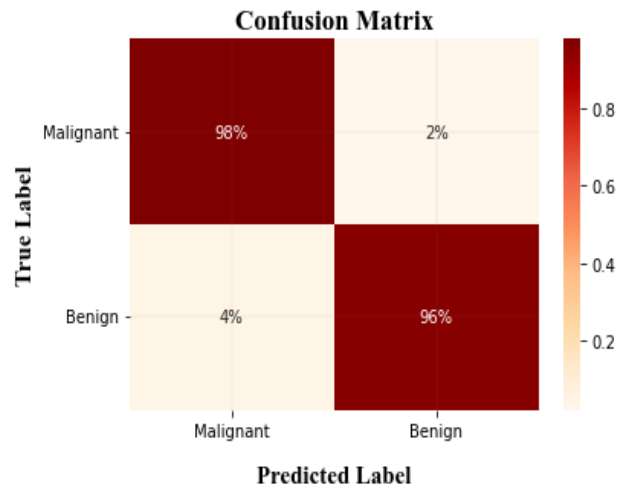


Fig. 10. Confusion Matrix of ANU-Net for Classification.

The confusion matrix is the most common tool for evaluating classification errors. Developed the confusion matrix for the ANU-Net proposed model based on the confusion matrix explanations offered. The graphic illustrates that the ANU-Net model can correctly categorize the two melanoma states (Malignant and Benign), with melanoma having a high ratio to malignant images and melanoma having

the lowest ratio to benign images. This indicates the classification of the two statuses has been completed appropriately. Fig. 10 presents the retrieved confusion matrix for the classification cross-validation test.

V. CONCLUSION AND FUTURE WORKS

Melanoma is the worst type of cancer among skin cancers, and its prevalence is rising globally. Early detection is crucial since skin cancer can be treated with a straightforward excision. But the mole's outline or outer covering is uneven, largely asymmetrical, and appears gritty. It states that around half of the moles present do not match the other half of the moles. To overcome all of this issues, proposed an effective methodology in this work. In this paper, the proposed system for melanoma classification involves four steps: Initially, pre-processing, removing hair from the dermoscopic images using a Laplacian-based algorithm, and then removing noise from the images using a Median filter. In addition, feature extraction from pre-processed images. Using the principal component analysis approach for extracting the characteristics like texture, shape, and color. These features for help to segment the skin lesion accurately from dermoscopic images. Furthermore, the segmentation process for identifying the lesion area and segmenting skin lesion using the LeNet-5 technique, and then, classification; categorizing lesion as benign (non-melanoma) and malignant (melanoma) using the ANU-Net method from the segmented skin lesion. It is classified into benign and malignant. The proposed technique solve these challenges in melanoma classification and given higher classification accuracy compared to other existing approaches. Therefore, based on the experimental findings, the ANU-Net method's accuracy for the ISIC2020 dataset is 98.78%. Since the ANU-Net model has the maximum level of accuracy, it can be effectively employed as a classifier to distinguish between malignant and benign skin lesions. It was established that the proposed model's categorization output was more accurate than that of the approaches under comparison. In the future, will work on new optimization techniques for better classification accuracy.

REFERENCES

- [1] Balasubramaniam, V. (2021). Artificial intelligence algorithm with SVM classification using dermoscopic images for melanoma diagnosis. *Journal of Artificial Intelligence and Capsule Networks*, 3(1), 34-42.
- [2] Rehman, A., Khan, M. A., Mehmood, Z., Saba, T., Sardaraz, M., & Rashid, M. (2020). Microscopic melanoma detection and classification: A framework of pixel-based fusion and multilevel features reduction. *Microscopy research and technique*, 83(4), 410-423.
- [3] Raza, R., Zulfiqar, F., Tariq, S., Anwar, G. B., Sargano, A. B., & Habib, Z. (2021). Melanoma classification from dermoscopy images using ensemble of convolutional neural networks. *Mathematics*, 10(1), 26.
- [4] Damian, F. A., Moldovanu, S., Dey, N., Ashour, A. S., & Moraru, L. (2020). Feature selection of non-dermoscopic skin lesion images for nevus and melanoma classification. *Computation*, 8(2), 41.
- [5] Thomas, S. M., Lefevre, J. G., Baxter, G., & Hamilton, N. A. (2021). Interpretable deep learning systems for multi-class segmentation and classification of non-melanoma skin cancer. *Medical Image Analysis*, 68, 101915.
- [6] Almaraz-Damian, J. A., Ponomaryov, V., Sadovnychiy, S., & Castillejos-Fernandez, H. (2020). Melanoma and nevus skin lesion classification using handcraft and deep learning feature fusion via mutual information measures. *Entropy*, 22(4), 484.
- [7] Maron, R. C., Utikal, J. S., Hekler, A., Hauschild, A., Sattler, E., Sondermann, W., ... & Brinker, T. J. (2020). Artificial intelligence and its effect on dermatologists' accuracy in dermoscopic melanoma image classification: web-based survey study. *Journal of medical Internet research*, 22(9), e18091.
- [8] Pereira, P. M., Fonseca-Pinto, R., Paiva, R. P., Assuncao, P. A., Tavora, L. M., Thomaz, L. A., & Faria, S. M. (2020). Skin lesion classification enhancement using border-line features—The melanoma vs nevus problem. *Biomedical Signal Processing and Control*, 57, 101765.
- [9] Roslin, S. E. (2020). Classification of melanoma from Dermoscopic data using machine learning techniques. *Multimedia tools and applications*, 79(5), 3713-3728.
- [10] Dutta, A., Hasan, K., & Ahmad, M. (2021). Skin lesion classification using convolutional neural network for melanoma recognition. In *Proceedings of International Joint Conference on Advances in Computational Intelligence* (pp. 55-66). Springer, Singapore.
- [11] Cheong, K. H., Tang, K. J. W., Zhao, X., Koh, J. E. W., Faust, O., Gururajan, R., ... & Acharya, U. R. (2021). An automated skin melanoma detection system with melanoma-index based on entropy features. *Biocybernetics and Biomedical Engineering*, 41(3), 997-1012.
- [12] Cao, X., Pan, J. S., Wang, Z., Sun, Z., ul Haq, A., Deng, W., & Yang, S. (2021). Application of generated mask method based on Mask R-CNN in classification and detection of melanoma. *Computer Methods and Programs in Biomedicine*, 207, 106174.
- [13] Gulati, S., & Bhogal, R. K. (2020). Classification of melanoma from dermoscopic images using machine learning. In *Smart intelligent computing and applications* (pp. 345-354). Springer, Singapore.
- [14] Hosny, K. M., Kassem, M. A., & Foad, M. M. (2020). Skin melanoma classification using ROI and data augmentation with deep convolutional neural networks. *Multimedia Tools and Applications*, 79(33), 24029-24055.
- [15] Almaraz-Damian, J. A., Ponomaryov, V., Sadovnychiy, S., & Castillejos-Fernandez, H. (2020). Melanoma and nevus skin lesion classification using handcraft and deep learning feature fusion via mutual information measures. *Entropy*, 22(4), 484.
- [16] Nawaz, M., Masood, M., Javed, A., Iqbal, J., Nazir, T., Mehmood, A., & Ashraf, R. (2021). Melanoma localization and classification through faster region-based convolutional neural network and SVM. *Multimedia Tools and Applications*, 80(19), 28953-28974.
- [17] Cheong, K. H., Tang, K. J. W., Zhao, X., Koh, J. E. W., Faust, O., Gururajan, R., ... & Acharya, U. R. (2021). An automated skin melanoma detection system with melanoma-index based on entropy features. *Biocybernetics and Biomedical Engineering*, 41(3), 997-1012.
- [18] Saxena, V. S., Johri, P., & Kumar, A. (2021). AI-Enabled Support System for Melanoma Detection and Classification. *International Journal of Reliable and Quality E-Healthcare (IJRQEH)*, 10(4), 58-75.
- [19] Rehman, A., Khan, M. A., Mehmood, Z., Saba, T., Sardaraz, M., & Rashid, M. (2020). Microscopic melanoma detection and classification: A framework of pixel-based fusion and multilevel features reduction. *Microscopy research and technique*, 83(4), 410-423.
- [20] Li, C., Tan, Y., Chen, W., Luo, X., He, Y., Gao, Y., & Li, F. (2020). ANU-Net: Attention-based Nested U-Net to exploit full resolution features for medical image segmentation. *Computers & Graphics*, 90, 11-20.
- [21] Fan, Y., Rui, X., Poslad, S., Zhang, G., Yu, T., Xu, X., & Song, X. (2020). A better way to monitor haze through image based upon the adjusted LeNet-5 CNN model. *Signal, Image and Video Processing*, 14(3), 455-463.

Method for Determination of Tealeaf Plucking Date with Cumulative Air Temperature: CAT and Photosynthetically Active Radiation: PAR

Kohei Arai¹

Information Science Dept.
Saga University, Saga City, Japan

Yoshiko Hokazono²

Oita Prefectural Agriculture, Forestry and Fisheries
Research Center, Bungo-Ohno City, Oita, Japan

Abstract—Method for determination of tealeaf plucking date with cumulative air temperature and Photosynthetically Active Radiation: PAR which is provided by the remote sensing satellites: Terra/MODIS and Aqua/MODIS is proposed. Also, a confirmation of thermal environment at the intensive study tea farm areas with Landsat-9 TIR (Thermal Infrared) image is conducted. Through a regressive analysis between the harvested tealeaf quality and the cumulative air temperature and PAR at the intensive study areas, it is found that there is a highly reliable relation between both. Also, an importance of air temperature environment at the sites is confirmed with Landsat-9 TIR image.

Keywords—Plucking date; elapsed days after sprouting; cumulative air temperature; Landsat-9 TIR; theanine; regressive analysis

I. INTRODUCTION

It is obvious that nitrogen rich tealeaves taste good while fiber rich tealeaves taste bad. Theanine: 2-Amino-4-(ethyl carbamoyl) butyric acid that is highly correlated to nitrogen contents in new tealeaves are changed to catechin [1],[2],[3] due to sun light. In accordance with sunlight, new tealeaves growth up so that there is a most appropriate time for harvest to maximize harvest amount and taste of new tealeaves simultaneously. On the other hand, fiber content indicates the age of the tealeaf in concern. Fiber content is getting large in accordance with the age and old tealeaf is getting harder. Therefore, young tealeaf is much tasty rather than the old taleaf.

Depending on the elapsed days after sprouting, tealeaf quality (theanine content) is decreased. On the other hand, tealeaf yield is increased with increasing of the days after sprouting. Therefore, there is most appropriate plucking date and is very important. Usually, it is determined by the Normalized Difference Vegetation Index: NDVI derived from handheld NDVI cameras, drone mounted NDVI cameras, and visible to Near Infrared: NIR radiometer onboard satellites because NIR reflection and NDVI depend on tealeaf quality and yield. It, however, does not work so well in terms of poor regression accuracy (r^2 value: determination coefficient) and there is a species dependency. Moreover, it takes time consumable works for finding appropriate tealeaves for determination from the acquired camera images [4].

Although the previous method for determination of most appropriate plucking date using the elapsed days after sprouting is effective in some extent, reliability of the method is not good

enough. The method proposed here for determination of most appropriate plucking date is using the cumulative air temperature together with Photosynthetically Active Radiation: PAR derived from Terra and Aqua satellites at the tea farm areas. PAR represents much more directly connected with the tealeaf quality (theanine content) than the other factors, air temperature, sunshine duration time a day. This approach is totally new and is expected to improve reliability of the method. Experiments with the proposed method are conducted and confirmed its reliability with the thermal environment at the areas with Landsat-9 TIR image (thermal environment). Plucking date determination with PAR and cumulative air temperature is the first attempt, brand new approach.

In the following section, the research background is described followed by the proposed method. Then, the experimental method together with experimental results are described. After that, concluding remarks and some discussions are also described.

II. RELATED RESEARCH WORKS

There are some related research works to the determination of the most appropriate plucking date determination for harvesting the best quality of tealeaves, theanine content rich tealeaves. This section describes such those research works from a methodology point of view.

A method for estimation of grow index of tealeaves based on Bi-directional Reflectance Distribution Function: BRDF measurements with ground-based network cameras is proposed [5]. Wireless sensor network for tea estate monitoring in complementally usage with Earth observation satellite imagery data based on Geographic Information System: GIS is also proposed and validated through a plenty of experiments [6]. A method for estimation of total nitrogen and fiber contents in tealeaves with ground-based network cameras is, on the other hand, proposed [7].

Monte Carlo Ray Tracing: MCRT simulation for BRDF and grow index of tealeaves estimation is conducted with the ground truth data [8] together with fractal model-based tea tree and tealeaves model for estimation of well opened tealeaf ratio which is useful to determine tealeaf harvesting timing of plucking date [9]. Grow index can be measured with green meter of instruments. Using this, growing processes are monitored.

Meanwhile, a method for tealeaves quality, theanine content estimation through measurements of degree of polarization, Leaf Area Index: LAI, photosynthesis available radiance (PAR) and normalized difference vegetation index (NDVI) for characterization of tealeaves is proposed [10]. On the other hand, optimum band, and band combinations for retrieving total nitrogen, which is closely related to the theanine content, water, fiber, etc. in tealeaves through remote sensing based on regressive analysis is discussed [11].

Appropriate tealeaf harvest timing (plucking date) determination based on NIR images of tealeaves is attempted [12] together with appropriate harvest timing determination referring fiber content in tealeaves derived from ground based NIR camera images [13].

Method for vigor diagnosis of tea trees based on nitrogen content in tealeaves relating to NDVI is proposed [14]. In the meantime, cadastral and tea production management system with wireless sensor network, GIS, based system and IoT technology is created [15].

BRDF model for new tealeaves and tealeaves monitoring with network cameras is well reported [16] together with BRDF model for new tealeaves on old tealeaves and new tealeaves monitoring through BRDF measurement with web cameras [17].

Estimation method for total nitrogen and fiber contents in tealeaves as well as grow index of tealeaves and tea estate monitoring with network cameras is proposed [18]. Meanwhile, multi-layer observation for agricultural (tea and rice) field monitoring is overviewed [19]. Furthermore, Tealeaf plucking workloads and environmental studies is conducted [20].

III. RESEARCH BACKGROUND

Accelerating market-in product creation is desired so that strengthening production area power to win the competition between production areas. Also, special crop is focused. Meantime, further expansion of strategic items is required together with enhancement of safe and secure product supply system and promotion of environment-friendly agriculture, forestry, and fisheries. Further acceleration of structural reform for realization of smart agriculture, forestry, and fisheries. Also, labor saving and efficiency improvement of work.

With the conversion of tea gardens to adultery, the development of base tea factories is underway, and it is important to secure a stable supply of actual demand and profitability commensurate with investment.

The management scale of the contracted tea plantation exceeds 40 ha per corporation, and it is an issue to achieve both work efficiency and proper management at the production site.

Therefore, it is important to establish management technology for the second tea season, when working conditions are strict, and improve quality. The following items are, therefore, major concern,

- 1) Clarification of criteria for determining the appropriate time for plucking.
- 2) Development of technology for extending the optimum plucking period.

- 3) Introduction of physical control technology.

For that, it is developed a diagnostic imaging technology that is supposed to be installed in a field management system and improve labor productivity through advanced use of the system. Development of ichiban-cha¹ (first plucking tealeaves of a year) sprouting day specific technology by image diagnosis is needed which results in the following steps are needed.

Sprouting date identification → Growth diagnosis → Optimal plucking time → Appropriate prediction management

After sprouting (after plucking), the growth of each tea season is diagnosed from the accumulated temperature. Thus, the following items are getting much important,

- 1) The first tea sprouting day is the reference date for the start of tea growth.
- 2) In the annual management system until winter dormancy.
- 3) An important element of growth diagnosis.

In the past, experienced people made judgments based on their own perspective.

To realize the following economic effects by introducing new technology for tea producers, profit improvement by quality improvement for second plucking tealeaves in particular, improvement of labor productivity is needed.

IV. PROPOSED METHOD

Although the previous method for determination of most appropriate plucking date using the elapsed days after sprouting is effective in some extent, accuracy and reliability of the method are not good enough. Another attempt for determination of most appropriate plucking date using the cumulative air temperature which is obtained from the meteorological agency in Japan and PAR derived from Terra and Aqua satellite at the tea farm areas is proposed here together with a confirmation of its validity with the thermal environment at the areas with Landsat-9 TIR image. Plucking date determination with PAR is the first attempt, brand new approach together with the cumulative air temperature.

A component with a wavelength of 400 to 700 nm (effective photosynthesis wavelength range) used for photosynthesis of green leafy plants. Normally, the light that passes through clouds and the atmosphere from the sun and reaches the surface of the earth has a wavelength range of 300 to 4,000 nm, of which the energy ratio of the wavelength range of photosynthetically active radiation is about 45%. Some of the light that hits the leaves is not absorbed but is reflected on or inside the leaves or passes through the leaves. Since the photosynthetic pigment absorbs the red and blue wavelength regions of the photosynthetically active radiation well, the reflected light contains a large amount of the green wavelength region. That is why the leaves look green. Photosynthetically active radiation is measured in units of energy (W/m²) or mol/m²/s as the photosynthetic effective wavelength region photosynthetic flux density (photosynthetic effective photon flux density). In tea cultivation, around 88 nights, counting from the beginning of spring, is the time to pick the shoots that contain plenty of nutrients stored during the winter. The climate

¹Tea is called "Cha" in Japanese.

differs depending on the production area, so there are various times when new tea is picked. In warm Kagoshima, early April, in Shizuoka, mid-April, and in Kyoto, etc., new tea picking often starts from late April to early May. Therefore, plucking date determination using cumulative days after Lichen: the first day of spring is meaningful but not so accurate. Meanwhile, PAR is directly present a required light energy from the sun. Therefore, it is expected that much accurate plucking date determination can be done with PAR rather than cumulative date from the Lichen.

In order to investigate a relation between nitrogen content in the harvested tealeaf and cumulative air temperature, regressive analysis is conducted together with a relation between NDF: fiber content in the harvested tealeaf. Cumulative air temperature can be gathered from the meteorological agency of Japan. Also, Landsat-9 TIR image can be gotten through EO browser site provided by European Space Agency: ESA². On the other hand, PAR data can be downloaded from the NASA Earth Data Search site³. It is MODIS/Terra and MODIS/Aqua Photosynthetically Active Radiation Daily/3-Hour L3 Global 5km SIN Grid V006 data.

V. EXPERIMENT

A. Intensive Study Area

The intensive study area is situated at Oita Prefectural Agriculture, Forestry and Fisheries Research Center, Bungo Ohno in Oita Prefecture, Japan (32.99 N, 131.59 E). The institute is established by Oita prefectural local government for promoting agriculture, forestry and fisheries as well as training and guidance of farmers and fishermen. Fig. 1 shows the location of the intensive study area. There is experimental tea farming area in which several species of tea trees (Okumidori, Fushun, Sayama-Kaori, Meiryoku, and Yabukita) are planted.

The tea tree "Okumidori", which is the basis of sencha, is a breed made by crossing "Yabukita", "Yabukita" and "Shizuoka Zairai No. 16", and it reaches its season after "Yabukita". It is characterized by its mild taste and low bitterness. It is also attracting attention as tencha (a raw material for tencha and matcha) and gyokuro. Okumidori tea tree has a large number of buds, so you can expect a large yield.

In "Fushun", which has a slightly upright tree, if the spacing between plants is 60 cm and the row spacing is changed from the customary 50 cm to 25 or 60 cm, the annual yield of fresh leaves will decrease. In the case of Fushun, when the row spacing is 50 cm, the annual fresh leaf yield decreases when the plant spacing is increased from the conventional 60 cm to 75 cm and the planting density is reduced to 80% of the conventional planting density (1481 plants/10a).

"Sayamakaori" is characterized by its strong aroma. The leaves are firmer and have a better shape than Yabukita tea. Because it contains a lot of catechins, which are tannins, the tea has a strong and astringent taste.

The plucking period of "Meiryoku" is the same as or slightly earlier than that of "Yabukita", and the tree is vigorous

and grows vigorously. Four or five years after planting, the total yield of first and second tea leaves is relatively high. The quality is the same as or slightly better than that of Yabukita. It is suitable because it is rather strong.

One of the characteristics of "Yabukita" is its strong cold resistance. It is resistant to red wilt, blue wilt, and frost damage. It is also characterized by good rooting and is highly adaptable to various soils. Another strength in terms of growth is that the roots and shoots are uniform and grow quickly, making it easy to replant. For this reason, it is highly rated by farmers as an easy-to-grow variety.

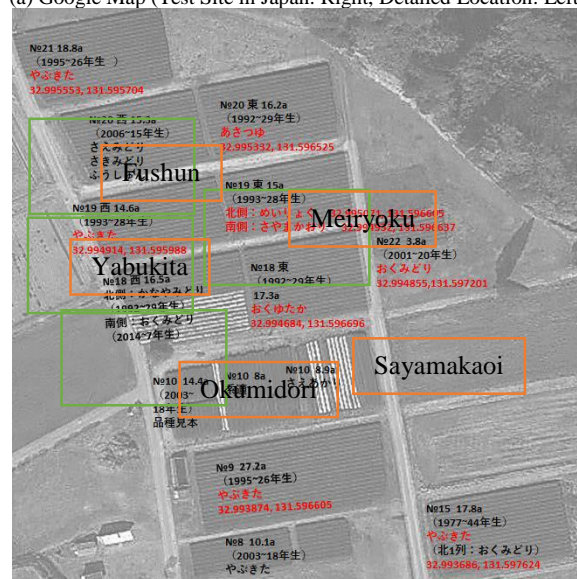
B. Estimation of Most Appropriate Plucking Date

The most appropriate plucking date is defined as the date on when the nitrogen content in a harvested tealeaf is getting maximum and Neutral Detergent Fiber: NDF of fiber content in a harvested tealeaf is much lower. Nitrogen content is proportional to Theanine of Amino Acid which is highly correlated to the taste of tea. On the other hand, fiber content is negatively proportional to the age of tealeaf (obviously, young tealeaf is much better quality).

If harvest day is delayed, then Theanine changes to catechin (taste not so good) and fiber content is getting large. Therefore, it is important to determine the most appropriate plucking date. Through a monitor the nitrogen content and fiber content, then the most appropriate plucking date can be determined. In the proposed method, cumulative air temperature after the sprouting is used.



(a) Google Map (Test Site in Japan: Right, Detailed Location: Left).

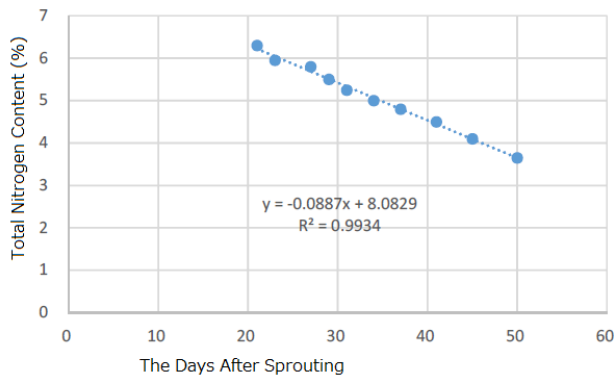


(b) Detailed Location of the Test Site for Five Species of Tealeaves.

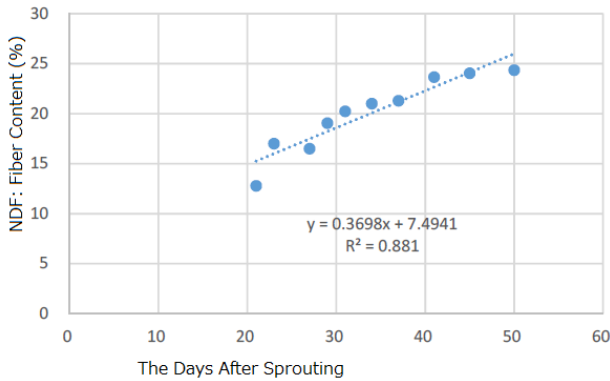
Fig. 1. Intensive Study Area of Bungo Ohno, Oita, Japan.

² <https://apps.sentinel-hub.com/eo-browser/>

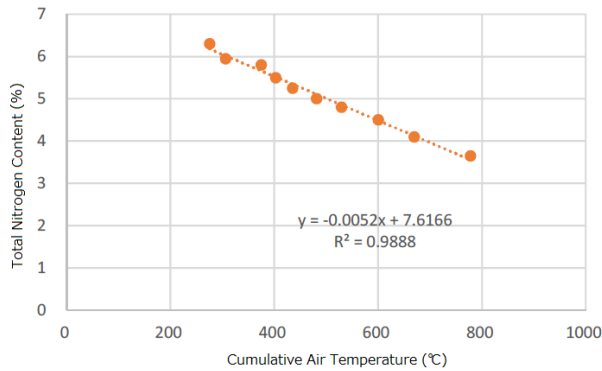
³ [https://search.earthdata.nasa.gov/search/granules?p=C1420474189-LPDAAC_ECS&pg\[0\]\[v\]=f&pg\[0\]\[gsk\]=-start_date&q=C1420474189-LPDAAC_ECS&sb\[0\]=130.85156%2C32.56312%2C131.48438%2C33.19624&tl=1652665964!3!!&lat=30.758713867830966&long=105.046875&zoom=3](https://search.earthdata.nasa.gov/search/granules?p=C1420474189-LPDAAC_ECS&pg[0][v]=f&pg[0][gsk]=-start_date&q=C1420474189-LPDAAC_ECS&sb[0]=130.85156%2C32.56312%2C131.48438%2C33.19624&tl=1652665964!3!!&lat=30.758713867830966&long=105.046875&zoom=3)



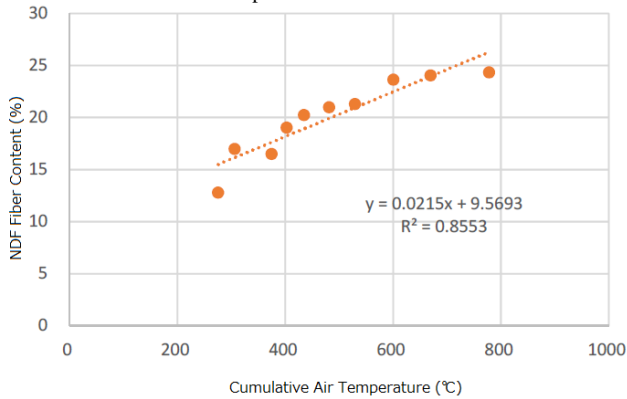
(a) Relations between Total Nitrogen Content and the Days after the Sprouting.



(b) Relations between NDF: Fiber Content and the Days after the Sprouting.



(c) Relations between Total Nitrogen Content and the Cumulative Air Temperature at the Site.



(d) Relations between Fiber Content and the Cumulative Air Temperature at the Site.

Fig. 2. Relations between Total Nitrogen Content and NDF: Fiber Content and the Days after the Sprouting as well as the Cumulative Air Temperature.

Fig.2 (a), (b) shows relations between (1) total nitrogen content and the days after the sprouting as well as (2) fiber content and the days after the sprouting. Fig.2 (c), (d) shows relations between (3) total nitrogen content and the cumulative air temperature as well as (4) fiber content and the cumulative air temperature at the fields.

C. Relation among Cumulative Air Temperature, Solar Irradiance and PAR

In these cases, cumulative air temperature and irradiance as well as PAR after the Vernal Equinox Day is shown in Fig. 3. In Fig. 3, PAR data is downloaded through the NASA Earth Data Search site. A screenshot of the site as searching the intensive study area is shown in Fig. 4.

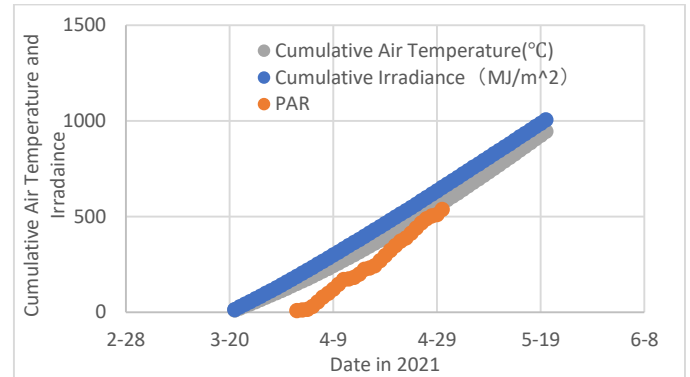


Fig. 3. Relation among Cumulative Air Temperature and Irradiance as Well as PAR after the Vernal Equinox Day.

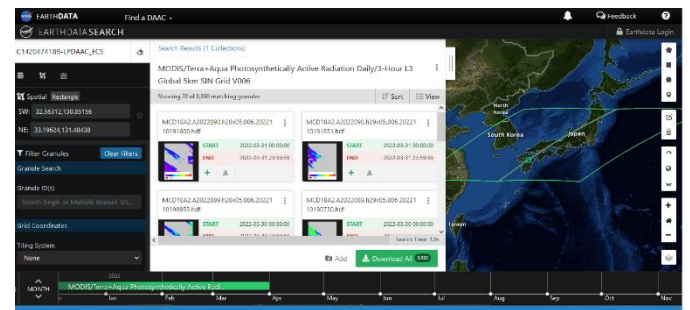


Fig. 4. NASA Earth Data Search Site.

D. Confirmation of Uniformity of Air Temperature at the Sites

It is found that the most appropriate plucking date can be determined with cumulative air temperature. The next thing it would be better to do is confirmation of uniformity of air temperature at the sites because the temperature environment in the sites is not uniform. In order to check the uniformity, Landsat-9 TIR image which is acquired on 19 April 2021 is used. Fig. 5 shows the intensive study site of tea farm areas and thermal infrared image which is taken by Landsat-9 satellite and, false color composite image which is acquired by Landsat-9 satellite.

Table I shows the specification of Landsat-9 of TIR-1 and 2. Thermal environment can be evaluated with Landsat-9/TIR-2 of band 11 data with 100 m of spatial resolution. As a result, it is found that the temperature environment in the sites is uniform enough with 232.88 (Mean) and 1.97 (Standard Deviation).

VI. CONCLUSION

A method for estimation of most appropriate tealeaf plucking date is proposed. The method uses cumulative air temperature, Photosynthetically Active Radiation: PAR, and thermal environment. These are gathered from the remote sensing satellite data. Through a regressive analysis between the harvested tealeaf quality and the cumulative air temperature at the intensive study areas, it is found that there is a highly reliable relation between both. Thus, the tealeaves quality of theanine content can be monitored and also the plucking date can be determined maximizing the theanine content in tealeaves.

VII. FUTURE RESEARCH WORKS

Next thing it would be better to do is estimation of most appropriate harvest date with deep learning which can be applied to these estimations.

ACKNOWLEDGMENT

The authors would like to thank to Professor Dr. Hiroshi Okumura and Professor Dr. Osamu Fukuda for their valuable discussions.

REFERENCES

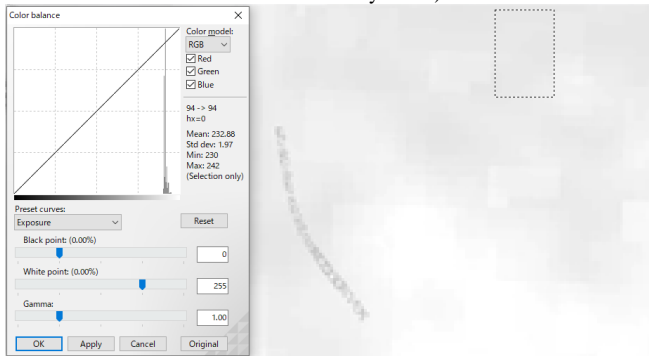
- [1] Greivenkamp, John E., Field Guide to Geometrical Optics. SPIE Field Guides vol. FG01. SPIE. ISBN 0-8194-5294-7, 2004.
- [2] Seto R H, Nakamura, F, Nanjo, Y, Hara, Bioscience, Biotechnology, and Biochemistry, Vol.61 issue9 1434-1439 1997.
- [3] Sano M, Suzuki M ,Miyase T, Yoshino K, Maeda-Yamamoto, M.,J.Agric.Food Chem., 47 (5), 1906-1910 1999.
- [4] Kohei Arai, Yoshiko Hokazono, Method for Most Appropriate Plucking Date Determination based on the Elapsed Days after Sprouting with NIR Reflection from Sentinel-2 Data, International Journal of Advanced Computer Science and Applications, Vol. 12, No. 4, 22-29, 2021
- [5] Kohei Arai, Method for estimation of grow index of tealeaves based on Bi-Directional reflectance function: BRDF measurements with ground-based network cameras, International Journal of Applied Science, 2, 2, 52-62, 2011.
- [6] Kohei Arai, Wireless sensor network for tea estate monitoring in complementally usage with Earth observation satellite imagery data based on Geographic Information System (GIS), International Journal of Ubiquitous Computing, 1, 2, 12-21, 2011.
- [7] Kohei Arai, Method for estimation of total nitrogen and fiber contents in tealeaves with ground-based network cameras, International Journal of Applied Science, 2, 2, 21-30, 2011.
- [8] Kohei Arai, Monte Carlo ray tracing simulation for bi-directional reflectance distribution function and grow index of tealeaves estimation, International Journal of Research and Reviews on Computer Science, 2, 6, 1313-1318, 2011.
- [9] Kohei Arai, Fractal model-based tea tree and tealeaves model for estimation of well opened tealeaf ratio which is useful to determine tealeaf harvesting timing, International Journal of Research and Review on Computer Science, 3, 3, 1628-1632, 2012.
- [10] Kohei Arai, Method for tealeaves quality estimation through measurements of degree of polarization, leaf area index, photosynthesis available radiance and normalized difference vegetation index for characterization of tealeaves, International Journal of Advanced Research in Artificial Intelligence, 2, 11, 17-24, 2013.
- [11] Kohei Arai, Optimum band and band combination for retrieving total nitrogen, water, and fiber in tealeaves through remote sensing based on regressive analysis, International Journal of Advanced Research in Artificial Intelligence, 3, 3, 20-24, 2014.
- [12] Kohei Arai, Yoshihiko Sasaki, Shihomi Kasuya, Hideto Matsuura, Appropriate tealeaf harvest timing determination based on NIR images of



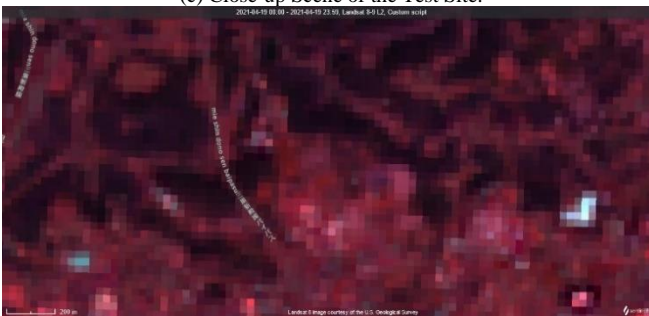
(a) Google Map of the Intensive Study Sites of Tea Farm Areas.



(b) Landsat-9/L2: Brightness Temperature Image (Orange Rectangle Shows the Intensive Study Areas).



(c) Close-up Scene of the Test Site.



(d) False Color Composite Image of Landsat-9/L1.

Fig. 5. Intensive Study Site of Tea Farm Areas and Thermal Infrared Image Which is Taken by Landsat-9 Satellite and, False Color Composite Image Which is Acquired by Landsat-9 Satellite which is Acquired on 19 April 2021.

TABLE I. SPECIFICATION OF LANDSAT-9 OF TIR-1 AND 2

Band No.	Thermal No.	Wavelength Region	Spatial Resolution
Band 10	TIR 1	10.60–11.19	100m
Band 11	TIR 2	11.50–12.51	100m

- tealeaves, International Journal of Information Technology and Computer Science, 7, 7, 1-7, 2015.
- [13] Kohei Arai, Yoshihiko Sasaki, Shihomi Kasuya, Hideo Matsura, Appropriate harvest timing determination referring fiber content in tealeaves derived from ground based NIR camera images, International Journal of Advanced Research on Artificial Intelligence, 4, 8, 26-33, 2015.
- [14] Kohei Arai, Method for Vigor Diagnosis of Tea Trees Based on Nitrogen Content in Tealeaves Relating to NDVI, International Journal of Advanced Research on Artificial Intelligence, 5, 10, 24-30, 2016.
- [15] Kohei Arai, Cadastral and Tea Production Management System with Wireless Sensor Network, GIS, Based System and IoT Technology, International Journal of Advanced Computer Science and Applications, 9, 1, 38-42, 2018.
- [16] Kohei Arai, Lili, Long --BRDF model for new tealeaves and tealeaves monitoring with network cameras, Saga University Faculty of Science and Engineering Bulletin, 38, 1, 23-28, 2009.
- [17] Kohei Arai and Long Lili, BRDF model for new tealeaves on old tealeaves and new tealeaves monitoring through B RDF measurement with web cameras, Abstract of the 50th COSPAR(Committee on Space Research/ICSU) Congress, A3.1-0008-08 ,992, Montreal, Canada, July, 2008.
- [18] Kohei Arai, Estimation method for total nitrogen and fiber contents in tealeaves as well as grow index of tealeaves and tea estate monitoring with network cameras, Proceedings of the IEEE Computer Society, Information Technology in Next Generation, ITNG, 595-600, 2009.
- [19] Kohei Arai, Multi-Layer Observation for Agricultural (Tea and Rice) Field Monitoring, Proceedings of the Seminar at Bogor Agriculture University, Keynote Speech, 2016.
- [20] R N Sen, A K Ganguli, G G Ray, A De, D Chakrabarti, Tea-leaf plucking-workloads and environmental studies, ergonomics, 1983 Sep;26(9):887-93. doi: 10.1080/00140138308963416.

AUTHORS' PROFILE

Kohei Arai, He received BS, MS and PhD degrees in 1972, 1974 and 1982, respectively. He was with The Institute for Industrial Science and Technology of the University of Tokyo from April 1974 to December 1978 also was with National Space Development Agency of Japan from January, 1979 to March, 1990. During from 1985 to 1987, he was with Canada Centre for Remote Sensing as a Post Doctoral Fellow of National Science and Engineering Research Council of Canada. He moved to Saga University as a Professor in Department of Information Science on April 1990. He was a councilor for the Aeronautics and Space related to the Technology Committee of the Ministry of Science and Technology during from 1998 to 2000. He was a councilor of Saga University for 2002 and 2003. He also was an executive councilor for the Remote Sensing Society of Japan for 2003 to 2005. He is a Science Council of Japan Special Member since 2012. He is an Adjunct Professor of University of Arizona, USA since 1998. He also is Vice Chairman of the Science Commission "A" of ICSU/COSPAR since 2008 then he is now award committee member of ICSU/COSPAR. He wrote 55 books and published 620 journal papers as well as 450 conference papers. He received 66 of awards including ICSU/COSPAR Vikram Sarabhai Medal in 2016, and Science award of Ministry of Mister of Education of Japan in 2015. He is now Editor-in-Chief of IJACSA and IJISA. <http://teagis.ip.is.saga-u.ac.jp/index.html>.

Remote Monitoring Solution for Cardiovascular Diseases based on Internet of Things and PLX-DAQ Add-in

Jeanne Roux NGO BILONG¹, Yao Gaspard Magnificat BOSSOU²
Adam Ismael Paco SIE³, Gervais MENDY⁴, Cheikhane SEYED⁵

Laboratory LIRT, Polytechnic Superior School, University Cheikh Anta DIOP (UCAD), Dakar, SENEGAL^{1,4,5}
Institut Supérieur de Management, Dakar, SENEGAL²
University of Ouagadougou, Burkina Faso³

Abstract—Access to health remains a real problem in Africa especially for the follow up of patients with chronic diseases. Many cases of heart attack deaths are still recorded before victims can access treatment. This is due to several factors, namely the insufficient number of cardiologists, the inaccessibility of hospitals with adequate infrastructure, the carelessness and ignorance of people about their health. In response to these limitations, internet of Things, thanks to its remarkable technological contribution, allow to follow from afar and easily patient's condition. In this paper, we offer a ubiquitous surveillance solution distance from patients with cardiovascular disease in order to minimize or eliminate the risk of heart attacks. The proposed solution is based on a micro-service architecture and consists of two essential parts that are data acquisition and data transfer. It will allow the patient to access their physical data and submit them in real time to the doctor through a dedicated medical application. The doctor will then be able to analyse the data obtained and return a prescription to the patient in case of abnormality. We used the microcontroller Arduino esp8066, the heart Rate Monitor AD8232 ECG (electrocardiogram) to measure the electrical activity of the heart that can be traced as an ECG, a pulse-eater, a photoresistor LDR and an potentiometer to regulate and modify the current flow in the circuit. We also used add-in PLX-DAQ for data acquisition and Jira software for data transfer to the doctor. Our solution is inexpensive and allows people not yet suffering from cardiovascular disease to prevent it.

Keywords—Cardiovascular diseases; microcontroller arduino; esp8086; AD8232; Plx-DAQ; IoT; ECG

I. INTRODUCTION

According to the World Health Organization, cardiovascular diseases are a group of troubles affecting the heart and blood vessels, with the most common being heart attacks and strokes. These diseases are and expected to remain the leading cause of death with a mortality rate of 31% worldwide [1] [2]. By 2030, almost 23.3 million people will die from cardiovascular disease (mainly heart disease and cerebrovascular accident) [3].

The cardiovascular morbidity and mortality burden is increasing worldwide, reaching even younger subjects in both developing and developed countries. The work of Kantako et al. reveals that, on a sample of 666 hospitalized patients, 301

were suffering from cardiovascular diseases. Considering Table I below, these authors show that cardiovascular diseases can reach subjects as soon as 15 years old [4].

The Kantako et al. studies proposed Table II, to show that cardiac insufficiency was the most frequent reason for hospitalization with 41.9% of cardiovascular diseases.

To prevent most cardiovascular diseases, behavioral risk factors such as smoking, unhealthy diet, obesity, physical inactivity, alcoholism and many others must be strategically addressed. Lifestyle change and physical effort would be one of the World Health Organization's recommendations for the prevention of cardiovascular disease [1]. Unfortunately, the precarious living conditions of populations in developing countries do not allow for easy prevention of cardiovascular diseases. Studies have shown that the symptoms of a heart attack, even a severe one, do not appear until two hours after the event. Hence the need to monitor cardiac activity and therefore to have an appropriate and low-cost sensor solution to prevent cardiovascular disease.

Usually, people with cardiovascular disease live at home and go to the doctor when they feel sick. This is because the disease manifests itself when it is at a very advanced stage, and the damage is irreversible. Most of these patients die before receiving any treatment [5]. It becomes urgent to adapt to the current sociological changes, incorporating the digital revolution that improves the way patients interact with health institutions [6]. Patients of all ages will be able to be monitored without the need to travel.

TABLE I. DISTRIBUTION OF CARDIOVASCULAR MORTALITY BY AGE GROUP [4]

Age Range	Numbers		Number	Specific mortality
	Deaths	Percentage		
[15 – 29]	3	17.65	38	7.89%
[30 – 44]	4	23.52	54	7.40%
[45 – 59]	3	17.65	87	3.44%
[60 – 74]	4	23.52	83	4.76%
75 et plus]	3	15.65	39	7.69%
Total	17	100	301	31.18%

TABLE II. REPARTITION OF PATIENTS WITH RISK FACTORS [4]

Reason of hospitalization	Numbers	Percentage
Hypertensive flare-up	96	31.9
Chest Pain	6	2.0
Heart insufficiency	126	41.9
Rhythm trouble	13	4.3
Stroke	58	19.3
Other	2	0.7
Total	301	100.0

Using Internet of Things technologies, the physical condition of patients can be monitored in a customary way and in real time wherever they are. The acquired data can be sent to remote doctors at low cost [7] [8]. These technologies can also be used to prevent these diseases.

The aim of this paper is to propose a solution that will allow subjects from 15 years old, to be followed by a doctor at a distance if they already have a cardiovascular disease, or to follow their physiological parameters to prevent any cardiovascular pathology.

In this work, the technologies of the Internet of Things are used to realize a solution dedicated to the recovery of certain physiological parameters of the person, in particular the heart rate and the number of pulsations. The data collected via a data acquisition software will be transmitted to the doctor via a dedicated platform.

The rest of this paper will proceed as follows. Related work will be discussed in Section II and Section III will illustrate the system under three aspects namely: the architecture of the proposed system, data acquisition, data transmission. In Section IV we will present the results and a discussion with a presentation of a prototype of the proposed system. Section V presents the conclusions and perspectives.

II. RELATED WORK

All related work on smart health systems integrating the internet of Things unanimously demonstrate the efficiency and time savings in patient care. The internet of Things has become an important technology for health monitoring systems. In professional medical centers, ECG data collection is done using twelve electrodes due to their good performance in short-term calibration. Unfortunately, these devices are not laptops and patients are often forced to visit medical centers for regular checks-up. Which could be tedious and very expensive for patients [9].

Tamana Shawn et al. designed a system to frequently monitor the electrocardiogram signal collected from the patient's body using the wearable sensors and the data is stored in the database of data that can be viewed by authorized personnel [7]. This solution has been implemented so that seniors can receive accurate care without having to make frequent trips to hospitals. When a malformation is detected, an automatic email is sent to users and doctors to analyse the critical condition of patients and provide emergency health assistance.

Hasan et al. proposed an ECG monitoring system that consists of an AD8382 ECG sensor to read patient data, an Arduino Uno, an ESP8266 Wi-Fi module, and the Blynk IoT app. The proposed ECG allows the physician to monitor the patient remotely via the Blynk IoT app installed on the patient's smartphone. The monitoring process can be performed anytime and anywhere without the need to physically come to the hospital [10].

Deli and AL. proposed a platform for disease prediction cardiovascular. This platform uses an IRI compatible ECG telemetry system that acquires the signal ECG, processes it and alerts the doctor in case of emergency. Their contribution incorporates a monitoring system based on lot for ECG signal analysis. The statistical characteristics of the raw ECG signal are calculated. They have analysed the ECG signal using the QRS detection algorithm of Pan lampkins to obtain the dynamic characteristics of the ECG signal to capture the characteristics of heart rate variability. The statistical characteristics and dynamics are then applied to the classification process to classify cardiac arrhythmias. This solution allows users to check their heart condition by acquiring the ECG signal, even when they are at home. The size of the system is reduced, and requires less maintenance and operational costs [11].

A wearable health monitoring system combined with the Internet of Things (IoT) is a promising alternative to conventional health systems according to author Wu and colleagues. They proposed a small, flexible, and wearable real-time electrocardiograph (ECG) monitoring system embedded on a T-shirt. This system uses a biopotential analogy front-end chip (AFE), AD8232, to collect ECG data from subjects. The collected ECG data is transmitted via Bluetooth low energy (BLE) to an end device for real-time display. Their solution incorporates a PC graphical user interface (GUI) and smartphone application designed for real-time viewing. The power consumption of the proposed portable ECG monitoring system can be as low as 5.2 mW. Their portable system is Powered by a 240 mAh rechargeable battery and can operate for over 110 hours continuously. To extend the battery life, a flexible solar energy sensor is also integrated into this system [12].

Mishra et al. proposed and implemented a smart healthcare application using an IoT system. They used an AD8232 heart rate sensor interfaced with Arduino UNO and connected to the Cloud. Their system uses an ESP8266 wireless LAN module for data transfer [13].

Xu has proposed an Internet of Things-assisted electrocardiogram (ECG) monitoring framework with secure data transmission. The proposed solution aims to contribute to the continuous monitoring of cardiovascular health. The author analysed the ECG signal intensity for automatic classification. For the implementation of the solution, he used ECG sensors, Arduino microcontroller, Android phones, Bluetooth and a cloud server. The work also proposed Lightweight Secure IoT (LS-IoT) and Lightweight Access Control (LAC) for secure data transmission [14]. The authors do not specify the security levels of the cloud that stores the data collected by the proposed system.

Chao LI and al. monitor multiple parameters that may not be limited to single parameters physiological. These non-physiological parameters are considered because they provide information contextual services. This can facilitate remote analysis or support for contextual services. Their solution involves a ubiquitous system that can send patients' physical signs to remote medical applications in real time. Compared to single parameter monitoring systems, multi-parameter systems can provide more accurate and richer information to remote experts [5]. The solution proposed by Chao does not provide follow-up for subjects already suffering from cardiovascular disease. The doctor cannot plan the follow-up with the patients.

The work presented in this literature review, although very interesting and edifying, has some limitations. Some authors have worked on heart activity monitoring using the Internet of Things. For this purpose, they used in most cases the unique AD8232 sensor for heart rate monitoring and the Arduino microcontroller. These solutions allow patients to be followed by their respective doctors in real time via a dedicated platform. Other work has focused on multi-parameter monitoring systems. The results of these approaches offered more accuracy and help to make the best decisions on the condition of the subjects. On the other hand, the proposed works do not specify the level of security of the cloud in which the data acquired via sensors are stored. The proposed solutions are dedicated either to subjects in senior age or suffering from a cardiovascular disease.

The literature also reveals that cardiovascular diseases affect a layer of young people from the age of 15 years and that the mortality rate is higher for the age intervals of [15-29], [30-44] and [75-plus] See Table I of this paper. The mortality rate from cardiovascular disease is expected to increase by 2030 according to the WHO. This paper proposes a real-time monitoring (multi-parameter) and management system for patients of all ages with cardiovascular disease. In order to prevent the explosion of the mortality rate due to cardiovascular diseases, the proposed monitoring system will also allow people not yet affected by cardiovascular disease to monitor their activity and participate in the reduction of the mortality rate of cardiovascular diseases. The proposed monitoring system is designed at very low cost and the acquired data is stored on a platform based on the plans made by the physician.

III. INTERNET OF THINGS (IOT) BASED HEART ACTIVITY MONITORING SYSTEM ARCHITECTURE

Detecting a heart attack encompasses several purposes. It is above all a question of making an appropriate diagnosis, so that the patient who suffers a heart attack receives treatment as soon as possible. The monitoring of cardiac activity from the ECG module makes it possible to prevent a heart attack, but also to guide subjects to improve their lifestyle to safeguard their health. To monitor the patient's cardiac activity, our solution uses heart rate sensors and the pulse sensor.

A. Proposed System Architecture

Our architecture (Fig. 1) includes two essential phases, which are data acquisition, and data transfer. This architecture

is designed on the general model of IoT applications composed of the detection layer, the transport layer and the application layer. Fig. 1 shows the architecture of the Internet of Things-based remote heart activity monitoring system for heart disease patients.

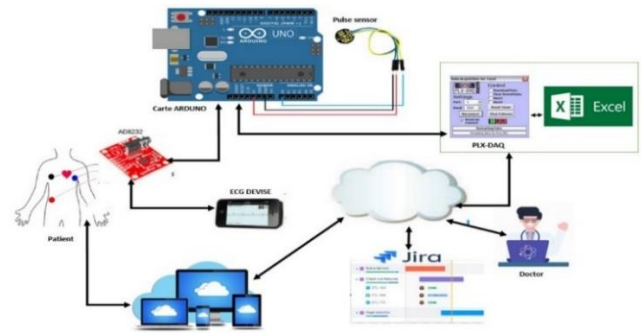


Fig. 1. System Architecture.

1) *Components of the architecture:* The proposed architecture is composed of sensors (AD8232 module, pulse sensor, potentiometer, LDR photoresistor), an Arduino board, PLX-DAQ, the ECG signal display screen and the Jira platform.

a) *AD8232 ECG sensor:* The AD8232 ECG module shown in Fig. 2 separates nine connections from the IC commonly referred to as "pins" to connect wires or header pins. It is used to determine the heart rate (heart rate or HR).

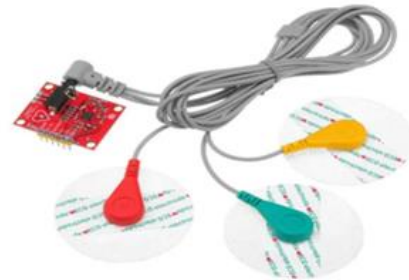


Fig. 2. AD8232 ECG.

As shown in Fig. 3, we have connected five of the nine pins of the ECG module to the Arduino Uno microcontroller. The five pins are labeled GND, 3.3v, OUTPUT, LO- and LO+. This connection collects signals from the human body which can be displayed on the screen as an ECG signal via the Arduino IDE.

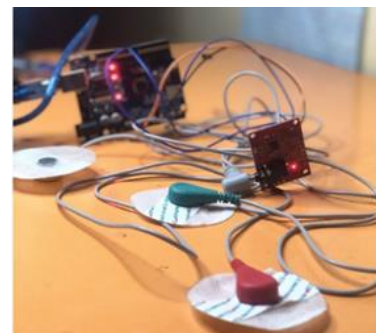


Fig. 3. Connected the Pins of the ECG Module to the Arduino.

b) *Electrocardiography ECG:* Electrocardiography (ECG) is the analysis of the electrical activity of the heart over a period. It is used to determine the heart rate, the regularity of the heartbeats, the size and position of the cavities, the existence of a possible heart attack.

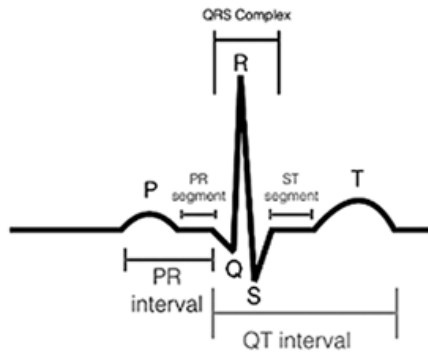


Fig. 4. ECG Signal.

The normal ECG signal is shown in Fig. 4. The ECG signal contains five characteristic peaks and valleys called P, Q, R, S, and T. The intervals of the ECG signal are the PR interval, the QT interval, and the QRS [15]. Fig. 4 illustrates a normal ECG signal

c) *Pulse sensor:* It is connected directly on the Arduino board using the Signal VCC and GND pins. The operating voltage of this sensor is +5V or +3.3V. Once the sensor is connected to the Arduino board, the code entered in the Arduino IDE and uploaded back to the board will activate the pulse sensor.

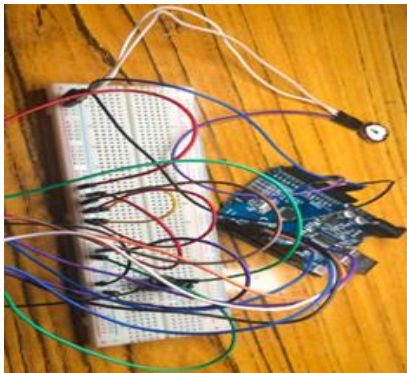


Fig. 5. Prototype Connection of the Pulse Sensor.

Fig. 5 shows a prototype connection of the pulse sensor that we have made.

d) *Arduino Uno:* The Arduino Uno in Fig. 6 is a board based on the 16 MHz ATmega328P microchip. It has 14 digital I/O pins, six analog pins, and an ICSP In-Circuit Serial Programming header. It can supply up to 5 V to the components that connect to it. The Arduino Uno board is relatively large and has the disadvantage of using a USB connector to interface with computers [16].

2) *Functioning of the architecture:* When the patient connects to the AD8232 ECG sensor and pulse sensor, the signals are picked up by the Arduino board and displayed on

the screen as a curve. Thanks to the PLX-DAQ software, a macro that only runs on Excel, the data is retrieved and stored on an Excel sheet. The patient can then save them and transfer them to the doctor via the Jira platform. The doctor receives the results, analyzes and provides feedback on the results to the patient. The patient sends his results according to the planning made by the doctor in the Jira platform.



Fig. 6. Arduino Uno.

B. Data Acquisition with PLX-DAQ

The data acquisition part is mainly composed of sensors worn by the patients or connected to them, as shown by the architecture of the proposed system illustrated in Fig. 1. These sensors will collect the signals and transmit them to the microcontroller. The parameters to be monitored in this solution are the heart rate and the pulsation.

Data management plans typically include sections on data collection, data storage and backup, data security, data retention, data sharing and reuse [17]. It is in the sense that we used the add in PLX-DAQ confer Fig. 7, for Microsoft Excel in order to acquire up to 26 channels of data from any microcontroller. Easy spreadsheet analysis of data collected in real time will be done.

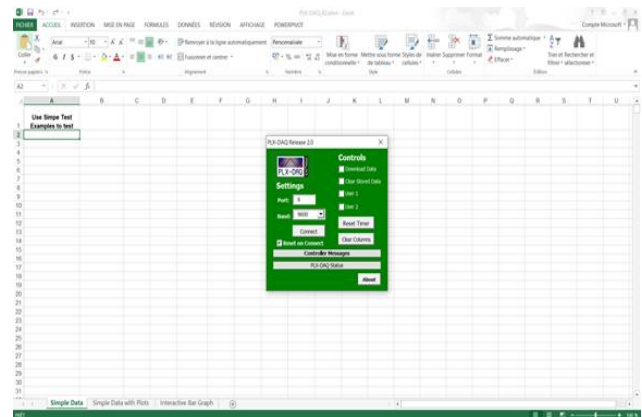


Fig. 7. PLX-DAQ.

C. Transmission of Data Collected from the Patient to the Doctor

After collecting the data from PLX-DAQ, the patient will send it to his doctor via the Jira platform so that it can be analyzed. Indeed, the dedicated Jira platform will make work fluid and facilitate exchanges between the patient and the doctor through a single interface.

IV. USE CASE DIAGRAM SYSTEM

To properly express the needs of this backend and to identify the functionalities of each actor, we used the UML (Unified Modeling Language) formalism of use cases. These were developed by Ivar Jacobson long before the appearance of UML. Nevertheless, they have been integrated into this modeling language to represent the functionalities of the system from the user's point of view.

As shown in Fig. 8, these use cases allow us to structure and articulate the interactions between the actors.

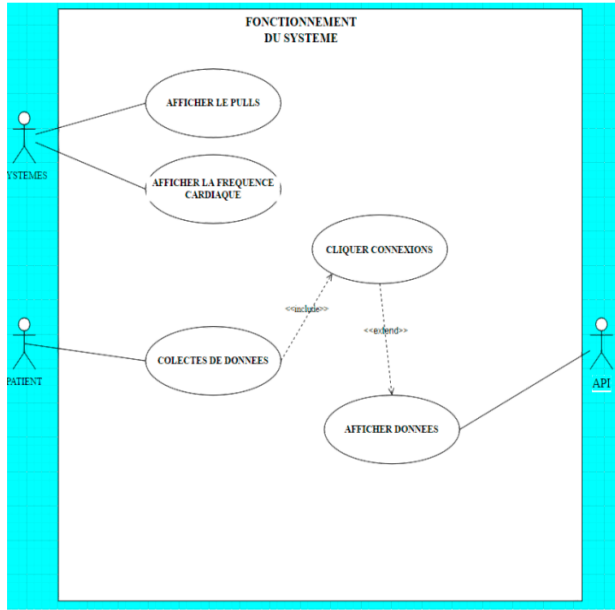


Fig. 8. The use Case of System.

We illustrate below the description of the two main use cases.

A. Description of the use Case to Display it Heart Rate

The Table III shows the description of the use case to display it heart rate.

TABLE III. DESCRIPTION OF THE USE CASE TO DISPLAY IT HEART RATE

Title	Show Data
Actor	Patient, System, API
Purpose	Display the patient's heart rate
Preconditions	Have a card and install Arduino IDE and the LFCSP box, having a computer, having AD8232 or Pulse sensor sensors,
Nominal scenario	<ol style="list-style-type: none"> 1 - The patient places the sensor on him and connects to Arduino 2 - The patient executes the code already uploaded on the Arduino environment 3 - The system will display the frequency heart on an electrogram
Alternate Scenario	<ol style="list-style-type: none"> 1-The sensor is not properly connected to the patient 2-Server unavailable 3-Error in entering the code

B. Description of the Data Collection use Case

The Table IV shows the description of the use case of data collection.

TABLE IV. DESCRIPTION OF THE DATA COLLECTION USE CASE

Title	Collect data
Actor	Patient, Micro-service
Purpose	Collect patient data
Preconditions	Have a card and install Arduino IDE and the LFCSP box, having a computer, having AD8232 or Pulse sensor sensors,
Nominal scenario	<ol style="list-style-type: none"> 1 – The patient connects to PLX-DAQ 2 – The patient presses connect 3 – PLX-DAQ automatically displays the data collected 4-The patient saves the results file
Alternate Scenario	1-The data is not displayed because the sensors are incorrectly connected

V. RESULTS AND DISCUSSION

As mentioned above, the implementation of our solution involves two main processes which are the acquisition of the ECG signal and that of the pulse, then the transfer of data.

The ECG signal is detected using the prototype implementation shown in Fig. 9. The AD8232 ECG sensor is connected to the Arduino microprocessor.

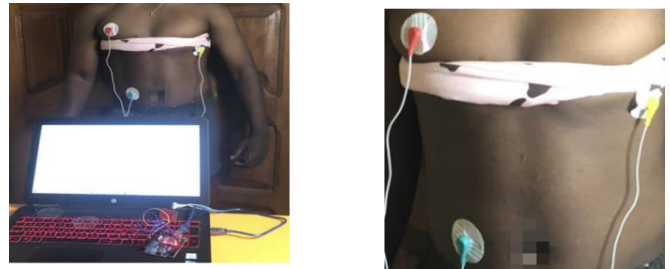


Fig. 9. The AD8232 ECG Sensor.

With the use of the serial port, the system obtains the analog values after uploading the code to the Arduino board. The sensors are connected to a 24-year-old young man. The sensors will retrieve the data and transmit it via the microcontroller once the system is activated. The following Fig. 10 show the codes that will allow communication between different peripherals, the collection and display of information from the AD8232 ECG sensor and the pulse sensor.

The code in Fig. 10 specifically shows the connection of the AD8232 ECG and Pulse sensors. It also considers the connection between the Arduino IDE and PLX-DAQ for data acquisition. This code allows to generate the ECG signal as shown in Fig. 11.

The code in Fig. 12 only relates to the activation of the pulse sensor. It will allow the led connected to Pin 13 to turn on and off each heartbeat.

```

ECG
int AD8232 = A0;
int PulseSensor = A1;

void setup() {
  // initialize the serial communication:
  Serial.begin(9600);
  pinMode(10, INPUT);
  pinMode(11, INPUT);
  Serial.println(F("CLEARDATA"));
  Serial.println(F("LABEL, Temps, FAP, FCR"));
}

void loop() {

  int ValeurMesuree = analogRead(AD8232);
  delay(4);
  int FCR = analogRead(PulseSensor);
  Serial.print ("DATA, TIME,");
  Serial.print (ValeurMesuree);
  Serial.print (F(", "));
  Serial.println(FCR);
  delay(250);
}
    
```

Fig. 10. Uploading the Code to the Arduino.

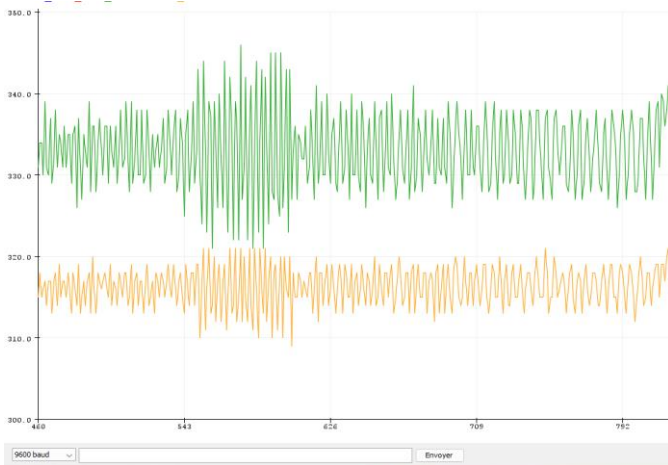


Fig. 11. The Electrocardiogram in Green and its Derivative in Orange.

```

pulse_sensor
//code copied from arduino.cc
int pulsePin = A0;
int blinkPin = 13;

// Volatile Variables,
volatile int BPM;
volatile int Signal;
volatile int IBI = 600;
volatile boolean Pulse = false;
volatile boolean QS = false;

static boolean serialVisual = true;

volatile int rate[10];
volatile unsigned long sampleCounter = 0;
volatile unsigned long lastBeatTime = 0;
volatile int P = 512;
volatile int T = 512;
volatile int thresh = 525;
volatile int amp = 100;
volatile boolean firstBeat = true;
volatile boolean secondBeat = false;

void setup()
{
  pinMode(blinkPin, OUTPUT);
  Serial.begin(115200);
  interruptSetup();
}
    
```

Fig. 12. The Codes to Activate the Pulse Sensor.

It should be noted that the normal heart rate of an adult at rest varies between 70 and 250 beats per minute. In children aged 7 to 15, it is between 70 and 115 beats per minute. Fig. 13 and 14 display the pulse sensor results (Fig. 13) and the Pulse plot results (Fig. 14), respectively.

COM7

15:20:16.246	->	MS?? Heart-Beat Found BPM: 54
15:20:16.900	->	Heart-Beat Found BPM: 56
15:20:18.771	->	Heart-Beat Found BPM: 52
15:20:33.208	->	Heart-Beat Found BPM: 73
15:20:36.700	->	Heart-Beat Found BPM: 163
15:20:37.073	->	Heart-Beat Found BPM: 163
15:20:37.305	->	Heart-Beat Found BPM: 168
15:20:37.864	->	Heart-Beat Found BPM: 161
15:20:38.143	->	Heart-Beat Found BPM: 163
15:20:38.421	->	Heart-Beat Found BPM: 169
15:20:38.748	->	Heart-Beat Found BPM: 169
15:20:39.029	->	Heart-Beat Found BPM: 175
15:20:39.263	->	Heart-Beat Found BPM: 181
15:20:39.870	->	Heart-Beat Found BPM: 170
15:20:43.036	->	Heart-Beat Found BPM: 205
15:20:43.270	->	Heart-Beat Found BPM: 208
15:20:43.550	->	Heart-Beat Found BPM: 207
15:20:43.878	->	Heart-Beat Found BPM: 205
15:20:44.205	->	Heart-Beat Found BPM: 204
15:20:44.439	->	Heart-Beat Found BPM: 207
15:20:44.718	->	Heart-Beat Found BPM: 210

Fig. 13. The Pulse Sensor Results.

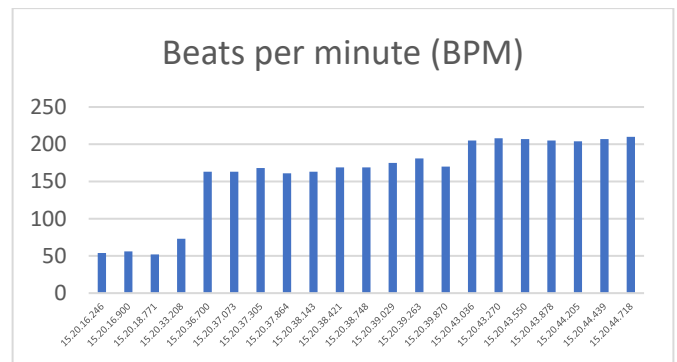


Fig. 14. The Pulse Sensor Results.

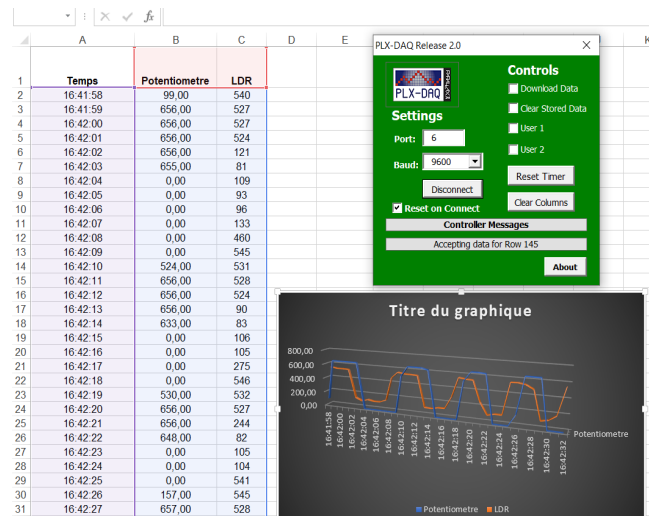


Fig. 15. Potentiometer and LDR of the Subject.

Electrical components such as the potentiometer and the LDR have been connected to the proposed system. Their data can be retrieved using data acquisition software. PLX-DAQ. La Fig. 15 shows the acquisition of the data emitted from the IDE on Arduino using the PLX-DAQ.

VI. CONCLUSION

The damage caused by cardiovascular diseases remains spectacular. These diseases are the first cause of death in the world and reach all age groups from the 15 years old. The urgent need to minimize the mortality rate caused by these diseases consists in using the Internet of Things, in order to connect the physical world to the virtual world.

This paper proposes a cardiac activity monitoring system based on the Internet of Things and integrating the PLX-DAQ add-on module. For the design and implementation of the system, low-cost equipment's have been used. They are a computer, sensors (pulse, ECG AD8232), electrical components (potentiometer and LDR), the Arduino microcontroller for the recovery and display of information on the heart rate as well as the pulse of the subject, the JIRA software which allowed to establish the connection to facilitate the exchange of data between the actors of the system, the PLX-DAQ for the collection of these data. The results of the analysis of the data collected via the Arduino board allow the user to follow his health status and monitor his performance. In addition, the subject no longer needs to travel to health centers to be monitored. This represents a saving of time and money. The Jira platform allows the physician to plan the submission periods of the data acquired via PLX-DAQ.

In perspective, the solution will be improved by integrating more sensors to collect physiological data (temperature, blood sugar, etc.) from the subject. For emergency management, the aim will be to integrate environmental parameters to facilitate patient location in case of emergency. The security of the transferred data and the handling of the connected object will be addressed.

ACKNOWLEDGMENT

I would like to give thanks to all people who supported in this work. Particularly to Mouhamadou Mansour SY, Mohamed SY TOUMBA, Jacques-David NGUEMA, Alioune SY and all my family members.

REFERENCES

- [1] Mondiale de la Santé, O. (2020). Lignes directrices de l'OMS sur l'activité physique et la sédentarité: en un coup d'oeil J. Clerk Maxwell, A Treatise on Electricity and Magnetism, 3rd ed., vol. 2. Oxford: Clarendon, 1892, pp.68–73.
- [2] Organisation Mondiale De La Sante. OMS | À propos des maladies cardiovasculaires [En ligne]. WHO. 2015 [cité 06/02/2015]. Disponible sur: http://www.who.int/cardiovascular_diseases/about_cvd/fr/
- [3] Quedraogo, P. V., Savadogo, A. A., Samadoulougou, S., Millogo, A., & Héma, A. (2019). Clinical Studies/ Mortality among Patients Admitted for Acute Stroke in Sourô Sanou Teaching Hospital of Bobo-Dioulasso; Burkina FASO. ", 38(2), 22.
- [4] Kantako, K., Mariko, S., Traoré, B., Sidibé, S., Dara, C., Kassambara, Y., ... & Diall, I. B. (2022). Morbidité et Mortalité Cardiovasculaires à l'Hôpital de Tombouctou: Morbidité et Mortalité Cardiovasculaires à l'Hôpital de Tombouctou. HEALTH SCIENCES AND DISEASE, 23(1).
- [5] Li, C., Hu, X. et Zhang, L. (2017). Le système de surveillance des maladies cardiaques basé sur l'IdO pour les services de santé omniprésents. Procedia informatique, 112, 2328-2334.
- [6] Aguerrebere, Pablo & Pacanowski, Toni & Medina, Eva. (2021). Online Reputation Management in Canadian Hospitals. ZER - Revista de Estudios de Comunicación. 26. 13-33. 10.1387/zer.22667.
- [7] Shawown, T., Hasan, I., Mim, MMR et Hossain, MS (2019, mai). Système de surveillance ECG portable basé sur l'IoT pour les soins de santé intelligents. En 2019, 1st International Conference on Advances in Science, Engineering and Robotics Technology (ICASERT) (pp. 1-5). IEEE.
- [8] Ranjana, S., Hegde, R., & Divya, CD (2021, novembre). Système de surveillance des patients en temps réel utilisant BLYNK. En 2021 Conférence internationale IEEE sur l'informatique distribuée, VLSI, circuits électriques et robotique (DISCOVER) (pp. 327-331). IEEE.
- [9] Umer, M., Sadiq, S., Karamti, H., Karamti, W., Majeed, R., & Nappi, M. (2022). IoT Based Smart Monitoring of Patients' with Acute Heart Failure. Sensors, 22(7), 2431.
- [10] Hasan, D., & Ismaeel, A. (2020). Designing ECG monitoring healthcare system based on internet of things blynk application. Journal of applied science and technology trends, 1(3), 106-111.
- [11] Devi, R. L., & Kalaivani, V. (2020). Machine learning and IoT-based cardiac arrhythmia diagnosis using statistical and dynamic features of ECG. The journal of supercomputing, 76(9), 6533-6544.
- [12] Wu, T., Redouté, J. M., & Yuce, M. (2019). A wearable, low-power, real-time ECG monitor for smart t-shirt and IoT healthcare applications. In Advances in body area networks I (pp. 165-173). Springer, Cham.
- [13] Mishra, A., Chakraborty, B., Das, D., & Bose, P. (2018). AD8232 based smart healthcare system using internet of things (IoT). Int. J. Eng. Res. Technol.(IJERT), 7(4), 13-16.
- [14] Xu, G. (2020). IoT-assisted ECG monitoring framework with secure data transmission for health care applications. IEEE Access, 8, 74586-74594.
- [15] Jain SK, Bhaumik B (2017) An energy efficient ECG signal processor detecting cardiovascular dis- eases on smartphone. IEEE Trans Biomed Circuits Syst 11(2):314–323.
- [16] Bedi, H. S., Raju, D. V., Nandyala, M. R. C., Kumar, P. S., & Varma, M. R. (2022). Design of Gesture-Based Hand Gloves Using Arduino UNO: A Grace to Abled Mankind. Digital Forensics and Internet of Things: Impact and Challenges, 37-43.
- [17] Hagen, M., L., Kuonen, D., Sacco, F. (2022), Littératie des données : plébiscite du Conseil national, Rev Med Suisse, 8, no. 787, 1284–1284.

Anomaly Detection in Video Surveillance using SlowFast Resnet-50

Mahasweta Joshi¹

Computer Engineering Department
CSPIT, CHARUSAT University, Changa, India

Jitendra Chaudhari²

Electronics and Communication Department
CSPIT, CHARUSAT University, Changa, India

Abstract—Surveillance systems are widely used in malls, colleges, schools, shopping centers, airports, etc. This could be due to the increasing crime rate in daily life. It is a very tedious task to monitor and detect abnormal activities 24x7 from the surveillance system. So the detection of abnormal events from videos is a hugely demanding area of research. In this paper, the proposed framework is used for deep learning concepts. Here SlowFast Resnet50 has been used to extract and process the features. After that, the deep neural network has been applied to generate a class using the Softmax function. The proposed framework has been applied to the UCF-Crime dataset using Graphics Processing Unit (GPU). It includes 1900 videos with 13 classes. Our proposed algorithm is evaluated by accuracy. Our proposed algorithm works better than the existing algorithm. It achieves 47.8% more accuracy than state of art method and also achieves good accuracy compared to other approaches used for detecting abnormal activity on the UCF-Crime dataset.

Keywords—Accuracy; GPU (Graphics Processing Unit); SlowFast Resnet50; Softmax; UCF-Crime dataset

I. INTRODUCTION

Abnormal activity detection is a very monotonous process for monitoring and identifying the abnormal events. In daily life, the use of surveillance cameras is increasing due to the huge crime rate. It may happen for somebody activity is suspicious activity while for others it is not. So to choose an appropriate framework for identifying suspicious activity plays a very significant role [1]. Recently surveillance system uses deep learning models to identify abnormal activities. Deep learning is very popular and one of the classes of machine learning. It is popular because of its ability to perform well on unstructured data. Deep learning uses and implements deep learning neural networks. It has good computing capability. It also provides good flexibility when it has to process a large number of features. These features have been taken from unstructured data. The Deep learning models have several layers and it passes the data through these layers. Each layer extracts the features progressively from unstructured data. These features have been passed to the next layer of the network. Low-level features have been extracted from initial layers and succeeding layers combines the features. It creates a complete form of feature representation. It addresses a variety of challenges that occur in a conventional surveillance system. It gives better performance with deep neural networks [2]. The literature study [2, 3, 4, 5, 6] summarizes the following point that inspire to use of deep learning in the surveillance systems.

- Anomaly events are irregular and unknown.
- Due to this one class of anomaly may differ from the other class of anomaly.
- The scalability of the data also plays a vital role in increasing the complexities of a system.
- Because the chances of misclassification of anomalies is too costly than the normal instances, the classes are imbalanced.
- Diversity in types of abnormalities.

II. RELATED WORK

Abnormal activity detection can be performed in two kinds of categories. The first one is an individual activity video and the second one is a crowd activity video. Sonkar et al. [7] represent the deep learning system which provides control over the crowd. This will help to avoid suspicious activities. CNN model has been used to analyze crowd behavior. With CNN model KNN- K Nearest Neighbour is also used to calculate the position difference between two consecutive frames of an object. The motion has been analyzed using three attributes: Speed, Direction and angle. Using the thresholding technique, the event is classified. This may vary based on the application. Chaudhary et al. [8] proposed framework, in which five different features are extracted. The features are Speed, Centroid, Direction, Movement and Dimensions. After extracting features, rule based classification has been performed. This algorithm is capable of handling multiple activities which are abnormal activities. It performs successfully and gives an accuracy up to 90%. Kaminski et al. [9] proposed an unsupervised method for detecting abnormality from videos. UMN dataset has been used. They have used motion descriptors for classification, Particle filter algorithm is used. This algorithm does not require any predefined samples. The results obtained are highly efficient compared to other existing algorithms. Landi et al. [10] explored the need for spatiotemporal tubes instead of the whole frame from the surveillance video. The experimental results show that the network trained with these features gives much better performance than the ordinary way. This method is robust against different localization errors. Dubey et al. [11] focuses on minimizing false rate in abnormal activity detection.

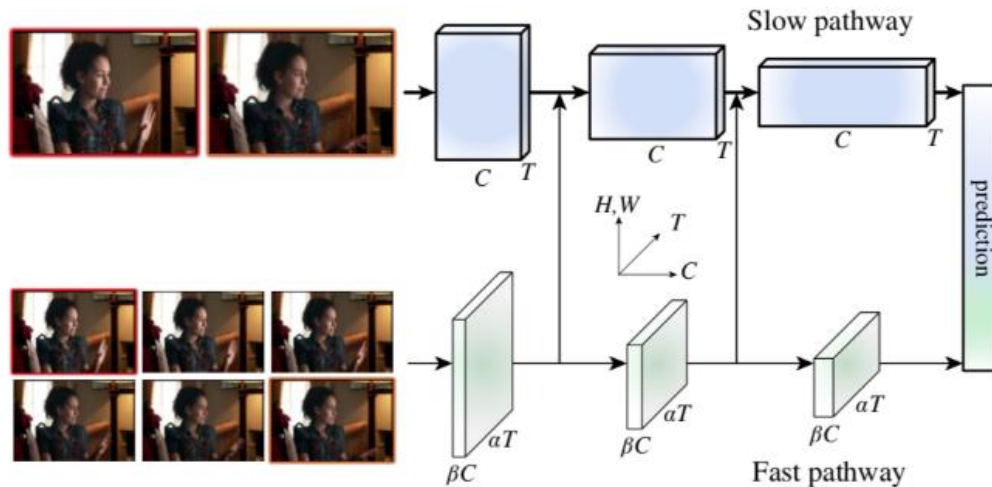


Fig. 1. Illustration of the SlowFast Network with Parameters [15].

3D Resnet has been used to extract spatio-temporal features. These features are used for deep neural networks and greatened scores. Multiple Instance Learning is used to classify the activities. The algorithm gives the best performance in the UCF-Crime dataset. Sargano et al. [12] present a novel method using CNN and a combination of SVM and KNN. In terms of accuracy, the proposed algorithm gives better performance than the existing methods. Sultani et al. [13] proposed a ranking method to classify the activities from the bag of videos. For better localization, sparsity and smoothness have been used. The results of experiments show that the proposed algorithm performs significantly higher than the other baseline algorithms.

III. SLOWFAST RESNET – 50

Generally, with videos, the frames consist of two part: static area in frames and Dynamic area in frames. The static area cannot be changed or slowly changed though the frame has been changed while in a dynamic area, it has changed the object, background and other things. For example, during a meeting, two persons doing handshaking is dynamic and fast but the background and other objects are static. Here in this paper, SlowFast CNN [14] has been introduced for capturing abnormality. Here slow pathway is designed to capture static information from video with low frame rates and slow refreshing speed. Another pathway is the fast pathway where all dynamic information is captured with high frame rates and fast refreshing speed. The formal pathway is very light weighted. Both pathway are merged by lateral connections. SlowFast network uses the Resnet model in both pathways and runs 3D convolution operations on it. The slow pathway uses a large strides. The stride means the number of frames skipped per second. In general, it is set to 16. Approximately allowing two sampled frames per second. The fast pathway uses too smaller a stride typically eight. This allows 15 frames per second.

Fig. 1 shows the illustration of the network with parameters. The parameters used in networks are as follows [15]:

- S = Spatial.
- T = Temporal.
- C = Channel size.
- α = Speed ratio (Frame skipping rate).
- β = Channel ratio.

Both the SlowFast network uses the 3D Resnet model. It captures several frames from videos and applies 3D convolution operation on them. The Slow Pathway uses a large stride, here it is 16. The Fast Pathway uses small size stride, here it uses two. As shown in Fig. 1, data from the Fast pathway faded to the Slow pathway via lateral connections. This connection allows the Slow pathway to be aware of the result of the Fast pathway. Data transformation should require as the shape of the data is different. This can be done by applying Time-strided convolution. In this, it performs 3D convolution of 5x12 kernel. Global average pooling has been one at the end of each pathway. It reduced its dimensionality of it. Now it concatenates the result of both pathways and inserts it into a fully connected classification layer [15].

IV. PROPOSED METHOD

Fig. 2 shows the flow of the proposed algorithm. The proposed algorithm has been classified as abnormal and normal activity. Here UCF – Crime data set has been used. It is a very large dataset and it contains 1900 videos. It includes videos of normal and abnormal activities. There are 13 abnormal activities in this dataset [13]. This algorithm has been implemented with the SlowFast Resnet50 model. Resnet is a residual network that implemented identity mapping. Because of it, Resnet is able to solve vanishing gradient problem. So in the proposed algorithm Resnet has been used. This model is pre trained model. The steps of the algorithm have been mentioned below:

- 1) Take a surveillance video S for processing.
- 2) Initialize the value of the number of frames and the number of the segment.

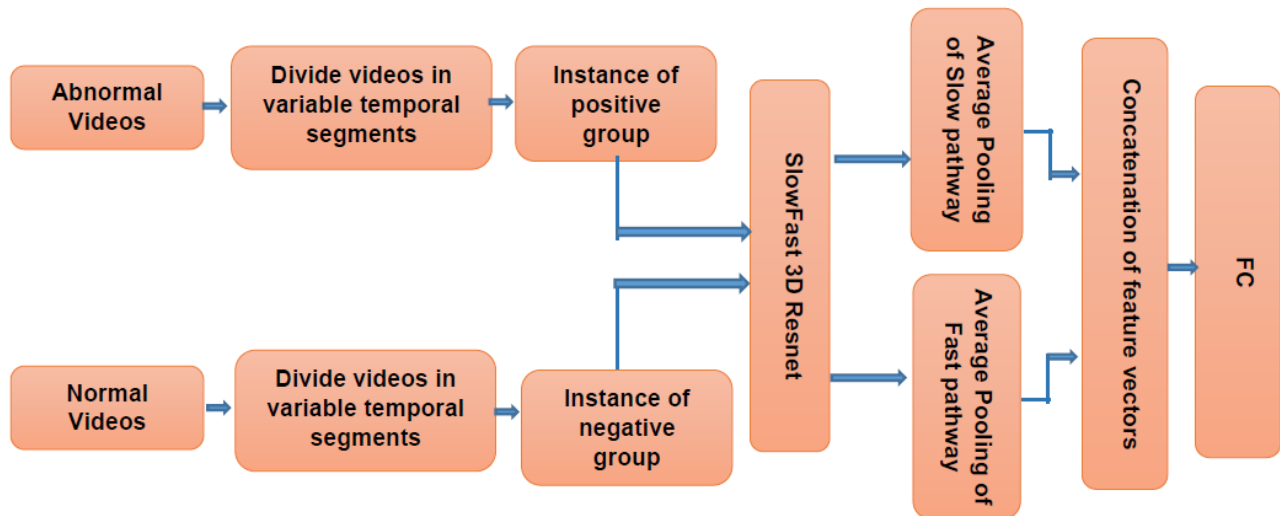


Fig. 2. Proposed Algorithm: Abnormal Activity Detection using SlowFast Resnet50 (AADSFR50).

3) Evenly divide Normal and abnormal videos into variable segments using the below formula.

$$clip = \frac{Total_frame_video}{I_frame * I_segment} \quad (1)$$

Where Total_frame_video is a total number of frames of the video, I_frame is the initial value of the number of frames and I_segment is the initial value of the segment.

4) The instance of normal and abnormal video groups has been given to SlowFast Resnet pre-trained models.

5) Data from the fast pathway is going to feed into the slow pathway network using the lateral connection.

6) Using average pooling, slow pathway feature vector has been generated.

7) Using average pooling, fast pathway feature vector has been generated.

8) Two feature vectors have been fused by performing concatenation.

9) A fused feature vector has been given to a fully connected classifier layer where the Softmax function is used to classify the activity.

V. IMPLEMENTATION RESULTS AND DISCUSSION

UCF-Crime dataset has been used to evaluate the AADSFR50 – proposed algorithm. This dataset is widely used to research abnormal activity detection. It contains 1900 videos and 13 classes. The classes are Abuse, Arrest, Arson, Assault, Accident, Burglary, Explosion, Fighting, Robbery, Shooting, Stealing, Shoplifting, and Vandalism [13]. Google colab has been used to implement this algorithm. It provides NVIDIA Tesla K80.

Table I shows the comparison of different existing algorithms and our proposed algorithm (AADSFR50). Here as a measuring parameter Accuracy has been used. As observed

from Table I, our proposed algorithm works better than the existing algorithm.

Fig. 3 describes the pictorial information of a comparative study of existing algorithms and our proposed algorithm AADSFR50. Here the evaluation parameter taken is accuracy. Fig. 3 shows that our proposed method works better than existing algorithms. It achieves 47.8% increase in accuracy compared to state of the art method. Other approaches also have been considered. In that case also our proposed method (AADSFR50) achieves better accuracy.

Fig. 4 shows the sample of the output video that has been generated after implementing AADSFR50. Fig. 4(a) shows the true positive case where abnormal video was detected as abnormal. Fig. 4(b) shows the true negative case where normal video was detected as normal. Fig. 4(c) shows the false positive case where abnormal video was detected as normal. Fig. 4(d) shows the false negative case where normal video was detected as abnormal.

TABLE I. COMPARISON OF DIFFERENT EXISTING ALGORITHMS AND OUR PROPOSED ALGORITHM (AADSFR50)

Sr. No	Algorithm	Accuracy (%)
1	C3D[16]	23
2	TCNN[17]	28.4
3	3D Resnet 34[18]	27.2
4	3D ConvNets[19]	45
5	Semi- supervised GAN[20]	40.9
6	VGG-16[21]	72.66
7	VGG-19[21]	71.66
8	FlowNet[22]	71.33
9	Our proposed Algorithm (AADSFR50)	75

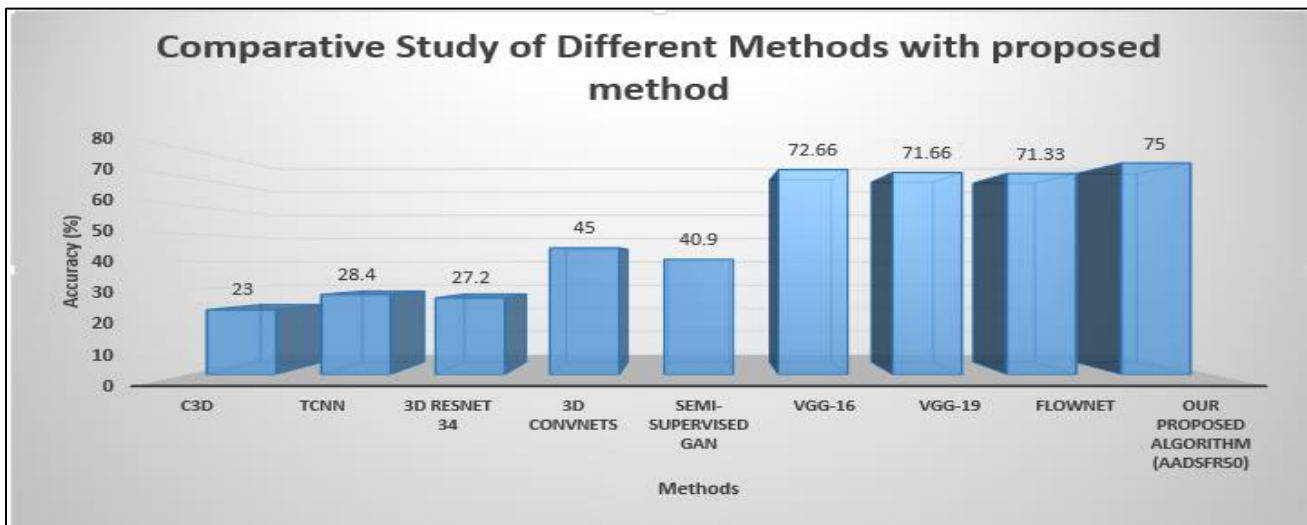


Fig. 3. Comparative Study of Different Methods with our Proposed Method (AADSFR50).



Fig. 4. Implementation Results of our Proposed Method (AADSFR50) - (a) Sample of Abnormal Video Detected as Abnormal (b) Sample of Normal Video Detected as Normal (c) Sample of Abnormal Video Detected as Normal (d) Sample of Normal Video Detected as Abnormal.

VI. CONCLUSION

Well known task has been found among researchers to detect abnormal activity from surveillance videos. Much progress has been achieved on this task but still, it is an open and interesting task for the researcher. Here in this paper, UCF crime dataset has been taken which contains challenging videos for the classification of abnormal and normal activities. SlowFast Resnet 50 has been used to perform the feature extraction. The fast pathway is used to analyze the static content and the Slow pathway is used to analyze the dynamic content of videos. Good accuracy has been achieved with the AADSF50 method compared to state of art method and other existing approaches. For state of art method 47.8% accuracy increases and with other approaches 2.34% – 52% accuracy is increased. Still, there is the scope for applying a more optimized model such as Deeper Resnet to achieve more accurate results.

REFERENCES

- [1] Divya Thakur, Rajdeep Kaur, An Optimized CNN based Real World Anomaly Detection in Surveillance Videos, International Journal of Innovative Technology and Exploring Engineering (IJITEE) , vol. 8, pp.465-473, 2019.
- [2] Guansong Pang, Chunhua Shen, Longbing Cao, Anton Van Den Hengel, Deep Learning for Anomaly Detection: A Review, ACM Computing Surveys, vol. 1, pp.1-36, 2020.
- [3] Leman Akoglu, Hanghang Tong, and Danai Koutra, Graph based anomaly detection and description: a survey, Data Mining and Knowledge Discovery, vol. 29, pp. 626–688, 2015.
- [4] Azzedine Boukerche, Lining Zheng, and Omar Alfandi, Outlier Detection: Methods, Models and Classifications, ACM Computing Surveys, vol. 53, pp. 1-37, 2021.
- [5] Varun Chandola, Arindam Banerjee, and Vipin Kumar, Anomaly detection: A survey, ACM Computing Surveys, vol. 41, pp. 1-72, 2009.
- [6] Dr. Joy Iong Zong Chen, Dr. S. Smys, Social Multimedia Security and Suspicious Activity Detection in SDN using Hybrid Deep Learning Technique, Journal of Information Technology and Digital World, vol. 2, pp.108-115, 2020.
- [7] Riddhi Sonkar, Sadhana Rathod, Renuka Jadhav, Deepali Patil, Crowd abnormal behaviour detection using deep learning, in Proc. of International Conference on Automation, Computing and Communication, pp. 1-5, 2020.
- [8] Sarita Chaudhary, Mohd Aamir Khan, Charul Bhatnagar, Multiple Anomalous Activity Detection in Videos, in Proc. of 6th International Conference on Smart Computing and Communications, pp. 336-345, 2017.
- [9] Laukasz Kaminski, Pawel Gardzinski, Krzysztof Kowalok, Slawomir Mackowiak, Unsupervised Abnormal Crowd Activity Detection in Surveillance Systems, in Proc. of 23rd International Conference on Systems, Signals and Image Processing, pp. 1-4, 2016.
- [10] Federico Landi, Cees G. M. Snoek, Rita Cucchiara, Anomaly Locality in Video Surveillance, arXiv preprint arXiv: 1901.10364, pp. 1-5 , 2019.
- [11] Shikha Dubey, Abhijeet Boragule, Moongu Jeon, 3D ResNet with Ranking Loss Function for Abnormal Activity Detection in Videos, in Proc. of International Conference on Control, Automation and Information Sciences, pp. 1-7, 2019.
- [12] Allah Bux Sargano, Xiaofeng Wang, Plamen Angelov, Zulfiqar Habib, Human Action Recognition using Transfer Learning with Deep Representations, IEEE, in Proc. of International Joint Conference on Neural Networks, pp. 463-469, 2017.
- [13] Waqas Sultani, Chen Chen, Mubarak Shah, Real-world Anomaly Detection in Surveillance Videos, Cornell University Library, arXiv:1801.04264, pp. 1-10, 2018.
- [14] Christoph Feichtenhofer, Haoqi Fan, Jitendra Malik, Kaiming He, SlowFast Networks for Video Recognition, arXiv:1812.03982v3, pp. 1-10, 2019.
- [15] The towardsdatascience website, Available: <https://towardsdatascience.com/slowfast-explained-dual-mode-cnn-for-video-understanding>, 2018.
- [16] Tran, D., Bourdev, L., Fergus, R., Torresani, L., Paluri, M., Learning Spatiotemporal Features with 3D Convolutional Networks, in Proc. of the IEEE International Conference on Computer Vision (ICCV), pp. 1-16, 2015.
- [17] Hou, R.; Chen, C.; Shah, M., Tube Convolutional Neural Network (T-CNN) for Action Detection in Videos, in Proc. Of the IEEE International Conference on Computer Vision (ICCV), pp. 5823–5832, 2017.
- [18] Hara, K., Kataoka, H., Satoh, Y., Learning Spatio-Temporal Features with 3D Residual Networks for Action Recognition, in Proc. of the IEEE International Conference on Computer Vision Workshop (ICCV), pp. 3154–3160, 2017.
- [19] Ramna Maqsood, Usama Ijaz Bajwa, Gulsha Saleem, Rana Hammad Raza, Anomaly Recognition from Surveillance Videos using 3D Convolution Neural Network, Multimedia Tools and Applications, vol. 80, pp. 18693-18716, 2021.
- [20] Juan Montenegro and Yeojin Chung, Semi-supervised generative adversarial networks for anomaly detection, Innovative Economic Symposium 2021 – New Trends in Business and Corporate Finance in COVID-19 Era , vol. 132, pp. 1-8, 2022.
- [21] Simonyan, K.; Zisserman, A., Very deep convolutional networks for large-scale image recognition, arXiv:1409.1556.61., pp. 1-14, 2014.
- [22] Ilg, E. Mayer, N., Saikia T., Keuper M., Dosovitskiy A., Brox, T., FlowNet 2.0: Evolution of optical flow estimation with deep networks, in Proc. of the IEEE Conference on Computer Vision and Pattern Recognition, pp. 2462–2470, 2017.

Address Pattern Recognition Flash Translation Layer for Quadruple-level cell NAND-based Smart Devices

Se Jin Kwon¹

Department of AI Software
Kangwon National University, Samcheok, South Korea

Abstract—The price of the solid-state drives has become a major factor in the development of flash memory technology. Major semiconductor companies are developing quadruple-level cell NAND-based SSDs for smart devices. Unfortunately, SSDs composed of quadruple-level cell (QLC) flash memory may suffer from low performance. In addition, few studies on internal page buffering mechanisms have been conducted. As a solution to these problems, an address pattern recognition flash translation layer (APR-FTL) is proposed in this study. APR-FTL gathers the data in a page unit and separates random data from sequential data. Furthermore, APR-FTL proposes address mapping algorithm which is compatible to the page buffering algorithm. Experimental results show that APR-FTL generates a lower number of write and erase operations compared to previous FTL algorithms.

Keywords—Memory management; nonvolatile memory; smart devices

I. INTRODUCTION

Price has become an important factor in the development of flash memory system, as many semiconductor manufacturing companies are competing for dominance in the smart device market [1]. Some semiconductor companies have recently turned their attention to developing QLC flash memories for smart devices as a means of providing large capacity at a low price [2]. As a result, instead of applying high-performing single-level cell (SLC) or multi-level cell (MLC) technology to smart devices, major semiconductor companies are developing QLC flash memory for smart devices. However, implementing QLC flash memories on smart devices may drastically diminish device performance and durability and even generate inconsistent response times, as smart devices must generate frequent updates from temporary files and metadata [3].

Furthermore, smart devices may execute unnecessary write operations on QLC-based SSDs because of the large page size of QLC flash memory. Although the page size of SLC or MLC flash memory is only four to eight times larger than the data sector of the file system [4], the page size of QLC flash memory is predicted to be 64 to 512 sectors. Because of the large page size of QLC flash memory, there is a considerable chance that the file system may frequently command a page re-access in the flash memory. However, the number of partial programming (NOP) requirements within a page is limited to only one to avoid program-disturbing errors [5]. Therefore, QLC flash memory tends to use an internal register or page buffer to gather data in a page unit.

Well-optimized flash translation layers (FTLs) are based on SLC/MLC/TLC flash memory [6], and therefore they do not give considerable attention to their own page buffering mechanisms (PBMs). This is an issue that has yet to be fully researched. In this study, the implementation of an address pattern recognition flash translation layer is proposed. APR-FTL gathers the data sectors and rearranges them into the page size of the QLC flash memory, instead of writing data on the flash memory immediately. Furthermore, APR-FTL proposes address mapping algorithm which is compatible to the page buffering algorithm. The efficient data collection of APR-FTL provides improved performance and consistent response despite the use of low-performing QLC flash memories.

II. RELATED WORKS

Previous PBMs can be classified into fine- and coarse-level PBMs. A fine-level PBM [7] gathers data sectors without a logical address boundary. However, this method reveals every corresponding physical sector number in DRAM. Therefore, it requires approximately 8 GB per 1 TB of flash memory. By contrast, a coarse-level PBM [8][9] gathers data using the same logical page number (LPN). Fig. 1 shows an example of a coarse-level PBM. Here, the extensive data from the write command are broken down into a unit of file system data sectors. A logical sector number (LSN) and its corresponding data are shown as (LSN, data). For simplicity, the size of a block is assumed to be four pages, where each page consists of only four sectors. Because they all belong to LPN 0, (0, A), (1, B), and (2, C) belong to a single page ($= 0/4, = 1/4, = 2/4$). However, when (16, D) occurs, the data within the page buffer are sealed as a page and written to flash memory because (16, D) belongs to LPN 4 ($= 16/4$). Finally, the page buffer is flushed, and data “D” are written to the emptied page buffer. Similarly, other data are gathered as a page unit. The coarse-level PBM generates six subpages, as shown in Fig. 1, although the file system issues only nine data sectors. If each page is filled with data, the coarse-level PBM generates only three pages. In Fig. 1, it is assumed that a page consists of only four subpages. However, we should note that the page size of QLC flash memory ranges from 64 to 512 sectors. There is a considerable chance that the space utilization of a QLC-NAND SSD will decrease drastically because of the frequent occurrence of subpages.

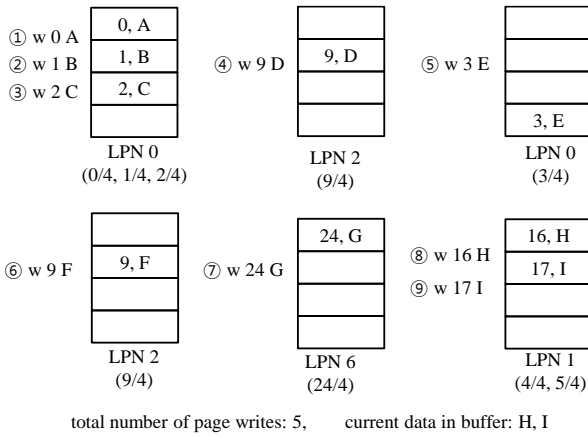


Fig. 1. Coarse-level Page Buffering Mechanism.

III. ADDRESS PATTERN RECOGNITION FLASH TRANSLATION LAYER

A. Address Pattern Recognition Algorithm

Address pattern recognition algorithm (APRA) modifies previous adaptation layer [10] and provides compatible address mapping algorithm according to the experiments in Section III.B. In other words, the address pattern recognition FTL is composed of address pattern recognition algorithm and address mapping algorithm.

The QLC flash memory cannot access to a page for an additional write operation because of the restricted NOP. Therefore, the QLC flash memory requires an efficient PBM. Unfortunately, the coarse-level PBM generates five page write operations, as previously explained in Section II. We should note that the QLC flash memory consists of 8 to 16 sectors per page. Because the amount of random data tends to fill the space of only one to four sectors, it is likely that the scenario will frequently occur. As a solution for the unnecessary write operations, the address pattern recognition algorithm (APRA) has been proposed [10].

APRA is shown as Algorithm I. The main objective of APRA is to segregate the random data from the sequential data and to allow the address mapping algorithm in FTL to separately manage them [10]. When the file system issues a write command along with the LSN, APRA first checks whether (LSN, data) is sequential to the sequential buffer (Algorithm 1 line 1). If (LSN, data) is sequential to the sequential page buffer, it is considered as the sequential data, and therefore it is inserted into the sequential page buffer (Algorithm 1 line 2). On the other hand, if the incoming data's LSN already exists in the page buffers (Algorithm 1 line 3), APRA consider (LSN, data) as an update, and therefore it is inserted into the random page buffer (Algorithm 1 line 4). Finally (LSN, data) is included in the undefined buffer if (LSN, data) is not sequential pattern nor an update.

ALGORITHM I: Address Pattern Recognition

Input: logical sector number (*LSN*), data (*data*)

Procedure: write_page_buffer (*LSN*, *data*)

1: **if** (*LSN*, *data*) is sequential **then**

2: data_insert(*sequential_buffer*, *LSN*, *data*);
 3: **else if** (*LSN*, *data*) is update **then**
 4: data_insert(*random_buffer*, *LSN*, *data*);
 5: **else**
 6: data_insert(*undefined_buffer*, *LSN*, *data*);
 13 **end if**

Input: page buffer (*PB*), *LSN*, *data*

Procedure: data_insert (*PB*, *LSN*, *data*)

14: **if** *PB* is full **then**
 15: Write *PB* to flash memory;
 16: Flush *PB*;
 17: Insert (*LSN*, *data*) into *PB*;
 18: **else**
 19: Insert (*LSN*, *data*) to *PB*;
 20: **end if**

B. Address Mapping Algorithm

The page buffering layer reorganizes the data sectors at the page unit, and the address mapping layer determines the physical address of the data to be written onto the flash memory. To evaluate the performance of the PBM and APRA, previous log-block algorithms were implemented in the address mapping layer.

Log blocks are temporary buffers for physical blocks. Of previous address mapping algorithms, log-block algorithms are well known to be the most optimized FTL algorithms with respect to their DRAM requirements and performance. Previous log-block algorithms made use of variations in the associativity between the blocks and log blocks, which can be classified into block-level associativity, full associativity, and superblock-level associativity. In this study, address mapping algorithms based on block-level associativity, full associativity, and superblock-level associativity are referred to as BAST, FAST, and SAST, respectively.

IV. PERFORMANCE EVALUATION

A. Experimental Setup

For this study's experiment, an FTL simulator was developed, and trace-driven simulations were conducted. The traces were retrieved from smartphones running various multimedia services and applications. The developed FTL simulator consisted of two layers: a page buffering layer and an address mapping layer. The previous PBM and APRA were implemented in the page buffering layer, and the number of pages generated by both algorithms were then monitored. It is also assumed that each page and block consist of 64 sectors and 256 pages, respectively, and that the performances of the read, write, and erase operations are 100 μ s, 1,500 μ s, and 6 ms, respectively. Furthermore, ARPA-FTL is analyzed by implementing block-level, full, superblock-level associative address mapping algorithms.

B. Performance Analysis

After PBM and APRA generates the data in the unit of a page, the address mapping layer determines the physical address within the flash memory. Fig. 2 shows the number of write and erase operations executed on BAST, FAST, and SAST. In the case of Trace A, the PBM generated approximately 1,575,200, 1,571,900, and 1,569,800 write and 358, 347, and 321 erase operations in BAST, FAST, and SAST, respectively. By contrast, APRA-FTL it executed approximately 1,546,700, 1,547,300, and 1,543,900 write and 271, 269, and 261 erase operations in BAST, FAST, and SAST,

respectively. Similarly, APRA-FTL executed fewer write and erase operations in the overall traces, as shown in Fig. 2.

As previously indicated, the number of pages transferred from the page buffering layer considerably affects the number of write and erase operations. A close observation reveals that APRA-FTL avoids numerous operations in the address mapping layer because it collects small-sized random data at the page unit. We should note that the number of write operations executed on the flash memory is higher than that of the pages themselves.

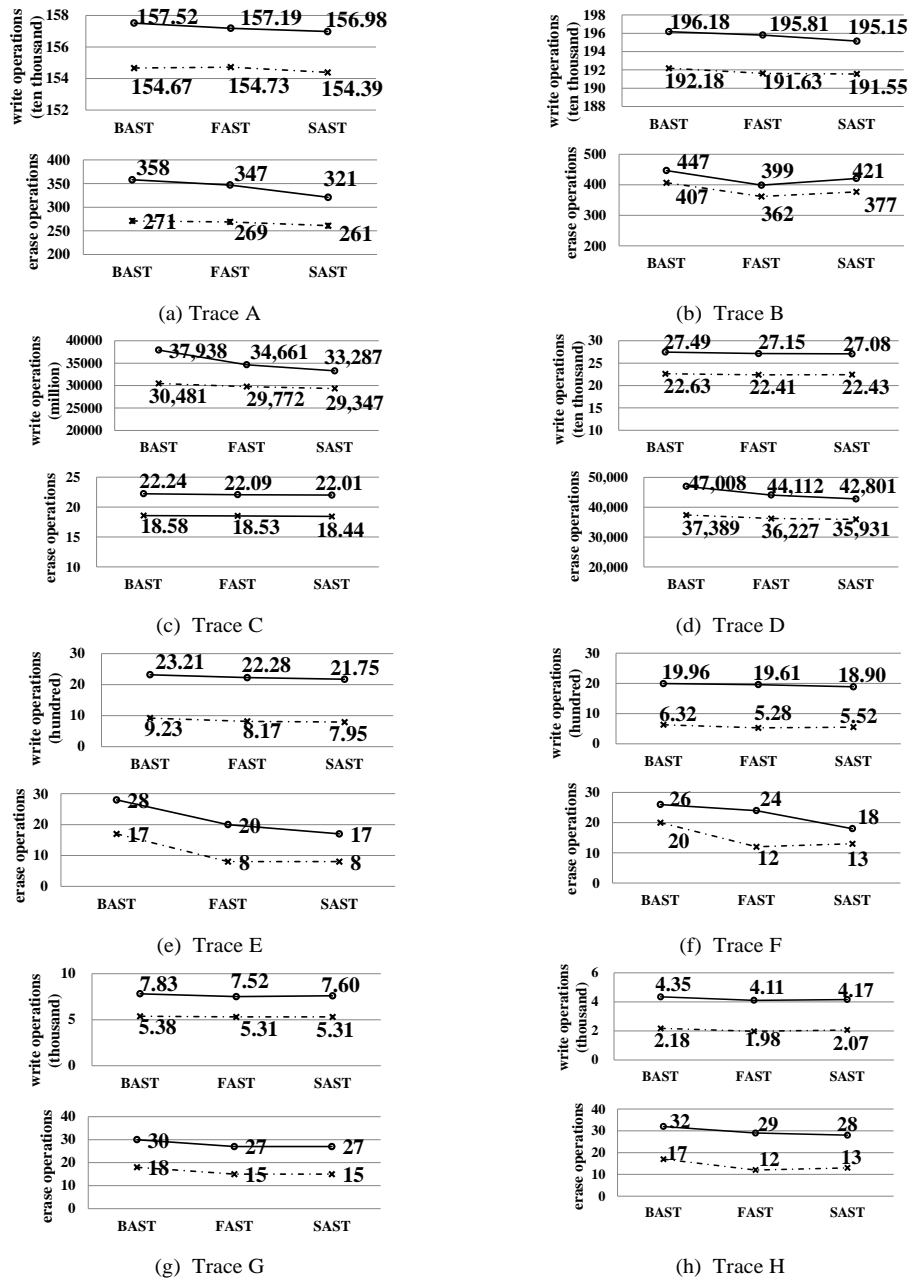


Fig. 2. Number of Write and Erase Operations.

The cause of the deviation between the number of pages and write operations might be of interest, as the page buffering layer issues a write operation to the address mapping layer whenever it gathers the data into a page unit. This is because the address mapping layer executes additional write operations internally to copy the data from an old to a new block. When a block is determined to be erased in the address mapping layer, BAST, FAST, and SAST copy the valid data from the old block to a new block and then execute an erase operation on the old data block. Therefore, the number of additional write operations for copying the data is considerably influenced by the number of erase operations. Because APRA-FTL reduces the number of erase operations by gathering random data and avoiding unnecessary write commands, it reduces the overall number of write operations as well.

V. CONCLUSION

Major semiconductor companies are using QLC flash memory in smart devices to lower the prices of smart devices. Unfortunately, previous page buffering algorithms do not segregate random data, thus generating many unnecessary write commands in the QLC flash memory. This results in a drastic performance degradation in smart devices. Furthermore, there has not been any experiment that considers the compatibility between page buffering algorithm and address mapping algorithm. As a solution, an APRA-FTL was proposed in this study. The APRA-FTL may require additional DRAM or the use of an internal buffer. However, we showed that it accurately identifies random data and thus considerably reduces the number of write operations. From experiments conducted in this study, APRA-FTL reduced the overall number of operations. In a future study, APRA-FTL will be implemented in various wear-leveling algorithms, and additional

experiments will be conducted on the durability and power-off recovery of smart devices.

REFERENCES

- [1] MICRON Electronics, "Cache Programming Operations," MICRON Electronics Technical Notes, 2022.
- [2] S. Kumar, P. K. Singh, S. Gupta, "A Survey of Erase Operation in NAND Flash Memory," 2022 1st International Conference on Informatics (ICI), Noida, India, 2022, pp. 186-190.
- [3] Z. Du et al., "A Novel Program Suspend Scheme for Improving the Reliability of 3D NAND Flash Memory," IEEE Journal of the Electron Devices Society, vol. 10, pp. 98-103, 2022.
- [4] Y. Luo, M. Lin, Y. Pan and Z. Xu, "Dual Locality-Based Flash Translation Layer for NAND Flash-Based Consumer Electronics," IEEE Transactions on Consumer Electronics, vol. 68, no. 3, pp. 281-290, 2022.
- [5] W. Zhou et al., "Temporal Correlation Detection Based on 3D NAND Flash In-Memory Computing," IEEE Electron Device Letters, vol. 43, no. 6, pp. 874-877, 2022.
- [6] H. Chen, Y. Dang, H. Wang, X. Xu, J. Zhang and Y. Huang, "Process Optimization and Yield Improvement for Erase Failure in Embedded Flash Memory," 2022 China Semiconductor Technology International Conference (CSTIC), 2022, pp. 1-3.
- [7] P. Jin, C. Yang, X. Wang, L. Yue and D. Zhang, "SAL-Hashing: A Self-Adaptive Linear Hashing Index for SSDs," IEEE Transactions on Knowledge and Data Engineering, vol. 32, no. 3, pp. 519-532, 2020.
- [8] R. Mativenga, J.-Y. Paik, J. Lee, T. S. Chung, and Y. Kim, "RFTL: Improving performance of selective caching-based page-level FTL through replication," Cluster Comput., vol. 22, no. 1, pp. 1-17, 2019.
- [9] D. Lee, D. Hong, W. Choi and J. Kim, "MQSim-E: An Enterprise SSD Simulator," IEEE Computer Architecture Letters, vol. 21, no. 1, pp. 13-16, 2022.
- [10] S. J. Kwon, "An Adaptation Layer for Hardware Restrictions of Quadruple-Level Cell Flash Memories" International Journal of Advanced Computer Science and Applications (IJACSA), vol. 13, no. 8, 2022.

Hybrid Deep Learning Signature based Correlation Filter for Vehicle Tracking in Presence of Clutters and Occlusion

Shobha B.S, Deepu.R

Department of Computer Science and Engineering
ATME College of Engineering, Mysore, Mysore, India

Abstract—This vehicle tracking is an important task of smart traffic management. Tracking is very challenging in presence of occlusions, clutters, variation in real world lighting, scene conditions and camera vantage. Joint distribution of vehicle movement, clutter and occlusions introduces larger errors in particle tracking based approaches. This work proposes a hybrid tracker by adapting kernel and particle-based filter with aggregation signature and fusing the results of both to get the accurate estimation of target vehicle in video frames. Aggregation signature of object to be tracked is constructed using a probabilistic distribution function of lighting variation, clutters and occlusions with deep learning model in frequency domain. The work also proposed a fuzzy adaptive background modeling and subtraction algorithm to remove the backgrounds and clutters affecting the tracking performance. This hybrid tracker improves the tracking accuracy even in presence of larger disturbances in the environment. The proposed solution is able to track the objects with 3% higher precision compared to existing works even in presence of clutters.

Keywords—Smart traffic management; background subtraction; vehicle detection; aggregation signature; hybrid tracker

I. INTRODUCTION

The Video surveillance based smart traffic management is the cost-effective solution for traffic monitoring and control. With the convergence of image processing and artificial intelligence, various traffic related applications like vehicle classification, congestion detection, accident detection, over-speeding detection, tracking vehicles etc. can be realized for smart traffic management. Vehicle tracing is an important application in smart traffic management for various traffic violation detections and criminal forensics.

Traditional vehicle tracking algorithms predict the vehicle location in consecutive frames based on its position in the previous frames. Some of the well-known tracking algorithms in this category are Kalman filter [1], mean shift [2], particle filter [3] and tracking learning detection [4]. Many methods have been proposed extending these approaches. Edge feature-based extension to Kalman filter [5], SIFT based extension to mean shift filter [6], integrated mean shift with particle filter [7] and long-term TLC combining detection and tracking [8] are some of the works extending traditional tracking algorithms. The traditional algorithms and its extension have many challenges in tracking due to clutters, occlusion, speed

of vehicle and lighting conditions [9]. In presence of these challenges, target vehicle localization becomes erroneous. The five important challenges considered in this work are lighting variations, object occlusion, fast movement, shape deformation and false positive. These challenges result in failure to detect and track the vehicles. Occlusion makes object detection difficult both in current frame and for updating future images. Fast movement introduces blurred effect in video frames. Clutters and occlusion jointly introduce either partial or complete deformation of the target object. False positives are introduced due to presence of multiple similar objects [10].

Based on functionality, the existing tracking methods can be divided into two classes: background modeling and foreground modeling [11]. Background modeling-based approaches uses the first frame or few initial frames to build a background model, and then compare the current frame with the background model to detect moving foreground objects, and finally review the background model. Most of the backgrounds modeling methods are supported on Bayesian filtering, Kalman and particle filters. Background modeling approaches suffer from illumination changes and dynamic background. Detailed survey on vehicle detection, recognition and tracking is provided [12]. Foreground modeling approach uses vehicle shape properties to track the vehicle. Various features like local binary pattern (LBP), histogram, Scale invariant feature transform (SIFT) etc. are used for vehicle detection but in presence of occlusions, vehicle shape distortions create higher false positives in vehicle tracking. Thus the proposed solution addresses the problem of tracking in presence of lighting variations, object occlusion, fast movement, shape deformation and false positive which affects the precision of tracking the vehicles.

In our proposed work we combine the best of both background and foreground modeling for effective vehicle tracking. The proposed solution preprocesses the video using background modeling that is adaptive to eliminate the effect of shadows, illuminations and clutters in the foreground. A novel hybrid tracker combining particle filtering with aggregation signature-based object detection is proposed for accurate tracing of object in presence of clutters and occlusion. The proposed aggregation signature is a deep learning feature of probability distribution of object in presence of clutter and occlusions in the frequency domain. The regions in the image are scored combining the results of particle filters and

aggregation signature tracking and the target vehicle is localized in the higher scored region. Following are the important contributions of this work.

- 1) Adaptive background modeling to eliminate shadows, illuminations and clutters.
- 2) A novel deep learning aggregation signature feature for occlusion and clutter distributed target object in frequency domain applying Quaternion Discrete Cosine Transform (QDCT) in frequency domain.
- 3) An integrated hybrid tracker combining particle filter with deep learning-based aggregation signature feature.

II. LITERATURE SURVEY

The existing deep learning models for tracking of objects are detailed and the issues are presented in this section.

Many deep learning models have been proposed for tracking of vehicles. These deep learning models are used separately or in combination with particle filter for tracking the vehicles. Zhang et al. [14] proposed a method to track vehicles using recurrent convolutional neural network. Recurrent network trained with reinforcement learning predicts the future locations in the next frames. Learning is done based on continuous inter frame correlation. The approach does not consider the presence of occlusions in learning process. Shobha B S et al. [13] proposed a traffic adaptive multiple vehicle classification using deep learning which tries to address the problem of vehicle categorisation in presence of clutters and occlusion. Multiple online trackers are fused for vehicle tracking by Leang et al. [15]. Set of trackers are combined in different stages of tracking. But in presence of occlusions, the localization error is amplified. Chen et al. [16] addressed the problem of occlusions in tracking but their approach was template based and computational complexity was very high. Hua et al. [17] used deep learning to localize the patches of interest. But the accuracy of localization decreases with decrease in the visibility of patch. Speed was prediction based on localization of patches. But with error in localization patches, the speed prediction also becomes erroneous. A two-stage model to track vehicles is proposed by Liu et al. [18]. In the first stage, recurrent convolutional neural network is adapted to detect object and in the second stage, Kalman filtering is done to track vehicles. In presence of clutters and occlusions, first stage fails and due to this tracking also fails. Integrated YOLOv3 with ORB tracking is used for localization of vehicles by Song et al. [19]. Feature points needed for ORB cannot be extracted in presence of occlusions and thus this approach fails in presence of occlusions. Xu et al. [20] used faster RCNN to detect objects. Features collected from target object were classified by RCNN to detect object. But the overhead is very high in this approach and in presence of large variances in features due to occlusion, the detection fails. A particle-based filtering based on motion of particles is proposed by Fang et al. [21] to track vehicles. But the model needs to be trained for all poses of vehicle. A fully convolutional region-based detector was used to track vehicles by Dai et al. [22]. The method is faster compared to R-CNN

but it is not resilient to even a small shape distortion. A correlation filter using the activations from convolutional layer of CNN was proposed Danelljan et al. [23]. Though method was able to detect vehicles better than hand crafted features, it is very sensitive to occlusions. Ma et al. [24] model the hierarchy of convolutional layers as a pyramid representation of image and use these multiple levels of abstraction for visual tracking. The correlation between the filters at each layer and the visual appearance is adaptively learnt and the response of each layer to detect the target is analysed. The features from the detected layer are then used for object localization. In presence of occlusions, the detection layer response is varying and thus training becomes cumbersome. Various filters extending linear correlation filter for object tracking have been proposed. Works by Bolme et al. [27], Henriques et al. (2015) and Wang et al. [30] are some of the noteworthy extensions. Bolme et al. [27] extended the linear filter with sum of square error filtering. Though this extension made the approach robust against lighting, scale, pose and non-rigid transformations, the filter performance degrades in presence of clutters and occlusions. A dual correlation filter extending the linear correlation filter was proposed by Henriques et al. [26] for tracking the vehicles. The computational complexity increases exponentially with increase in the number of objects in the frames and the approach is not resilient to occlusions and clutters. A discriminant correlation filter (DCF) was proposed by Wang et al. [25]. It is an end to end light weight network architecture using Siamese network and back propagation trained to provide a heat map of object location in the frames. In presence of occlusion, the false positive is higher in this approach. Yang et al. [28] proposed a detection-based tracking framework using YOLO deep learning model. A light weight feature extraction for object using YOLO is combined along with filter template matching to localize the object. In presence of occlusions, the features have higher spatial difference compared to the region to be tracked in this method. This reduces the accuracy of tracking.

III. HYBRID TRACKER

The architecture of the proposed hybrid technique to track vehicles is given in Fig.1 Background is subtracted from the current frames using a fuzzy adaptive background model. The target vehicle to be tracked is selected by marking a rectangular bounding region. Aggregation signature is learnt for the target vehicle. Kernel correlation filter (KCF) and Particle correlation filter (PCF) are adapted to use the aggregation signature and provide the response. The response of the KCF and PCF filter are fused with weighted Newton fusion function to get the predicted position of the target vehicle in any frame. The details of each of the process are detailed in following subsections.

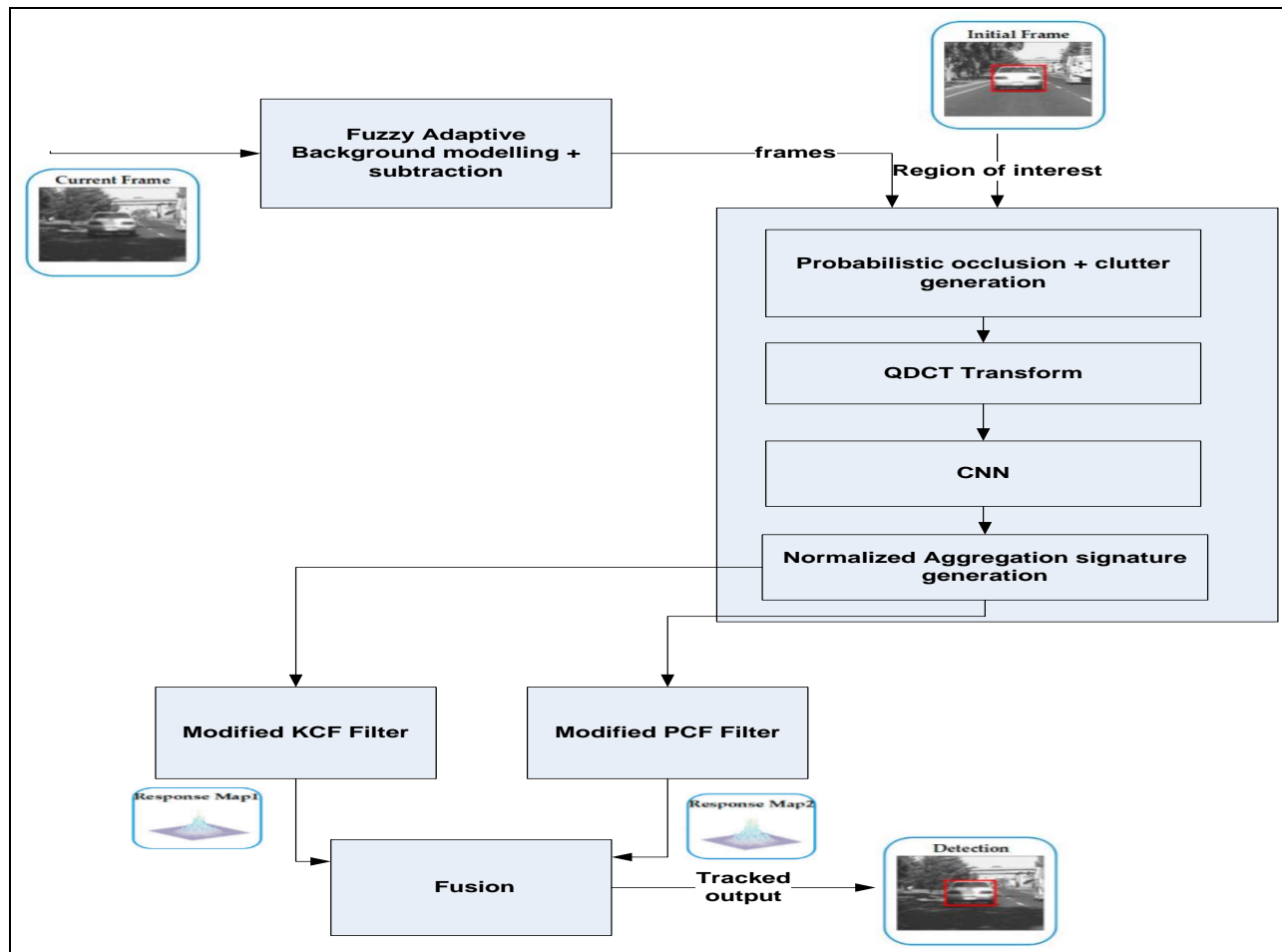


Fig. 1. Hybrid Tracking Architecture.

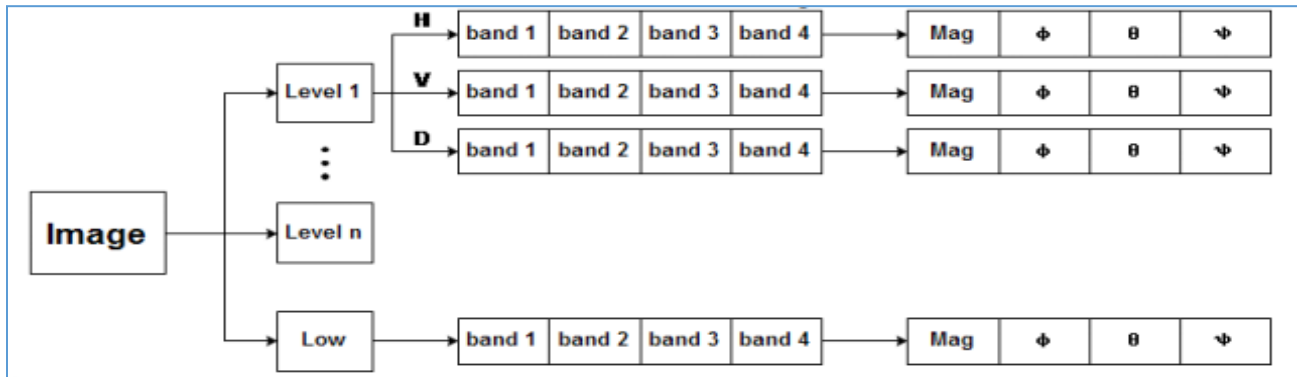


Fig. 2. QDCT Coefficients.

A. Fuzzy Adaptive Background Modelling

A fuzzy adaptive background model is constructed from few initial frames and it is updated on every successive frames. The background for every frame is subtracted from this model. The model is designed to eliminate the impact of shadows, illuminations and clutters in the foreground. The initial model is constructed based on first k frames as

$$p_k(x) = \tilde{p}_{k-1}(x) + \frac{1}{G_k \sqrt{2\pi\sigma^2}} \exp\left(\frac{-1}{2} \left(\frac{x - x_k}{\sigma}\right)^2\right)$$

where

$$\tilde{p}_k(x) = \frac{p_k(x)}{\sum_0^N p_k(x)} \quad (1)$$

Where, x_k is the pixel value observed at the k^{th} frame. The value of \tilde{p}_k is calculated for N frames. The parameter G_k is the learning rate whose value varies from 0 to 1. This value is adapted based on minimization of energy value between the current background and previous background. The energy (U) of a background is calculated in spatial and temporal level as

$$U = \sum_i E_T(i) + \sum_i E_S(i) \quad (2)$$

Where $E_T(i)$ is the temporal energy of a pixel i and $E_S(i)$ is the spatial energy of a pixel i .

$$E_S(i) = \sum_{j \in N_i} Sim(i, j) \quad (3)$$

Where N_i is the eight pixel neighborhood of i and Sim is the similarity function between pixel i and j .

$$Sim(i, j) = \begin{cases} 1, & \text{if } |intensity_t(i) - intensity_t(j)| < D \\ -1, & \text{otherwise} \end{cases} \quad (4)$$

The temporal energy of pixel i is calculated as

$$E_t(i) = \sum_{j \in N_i} TSim(i, j) \quad (5)$$

$$TSim(i, j) = \begin{cases} 1, & \text{if } |intensity_{t+1}(i) - intensity_t(j)| < D \\ -1, & \text{otherwise} \end{cases}$$

Every time before selecting the best value of G_k , the best value from 0 to 1 is selected which leads to a small difference to U .

B. Aggregation Signature

Most of existing trackers fail to localize the target vehicle in presence of occlusions. In this work an aggregation signature for target vehicle is created accommodating the clutter. Aggregation signature of image patch is formed from a set of probable noise occluded image patches using frequency domain deep learning model. On the image patch of the target vehicle, occlusion patches of various probabilistic distributions are added. QDCT is applied to the Noised image patches of target vehicles to get the low and high frequency components. QDCT for an image $f(x, y)$ is calculated as.

$$(x, y) = A_n^q f(x, y) + \sum_{s=1}^n [D_{s,1}^q f(x, y) + D_{s,2}^q f(x, y) + D_{s,3}^q f(x, y)] \quad (6)$$

Where $A_n^q f(x, y)$ and $D_{s,1}^q f(x, y)$ are low frequency and high frequency band of the image respectively.

A low frequency part and n groups of high frequency parts are obtained after QDCT is applied on the image.

The frequency of the coefficients are as shown in Fig.2.

To reduce the dimension of the coefficients, average fusion is done on low frequency sub bands. Fusing of High frequency sub bands based on maximum value of energy of coefficients. Fusing the low frequency bands is carried by average of the coefficients pair wise between the Low frequency coefficients of two patch images. Selecting the maximum value of coefficient between the pair wise high frequency sub band is the fusion rule for fusing the high frequency sub bands.

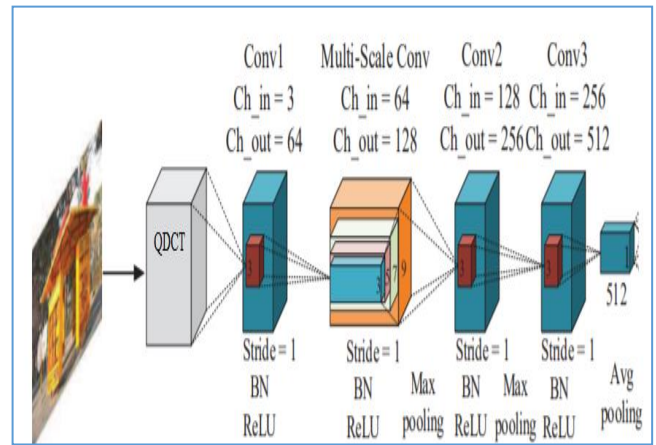


Fig. 3. Deep Learning Features Extraction.

The QDCT coefficients are given as input to a frequency domain convolutional neural network shown in Fig.3. The coefficients pass through a sequence of ReLU and max pooling layer and a final average pooling layer to provide an output of 1×512 dimension feature vector. The CNN configuration used for feature extraction is given in Table I. An aggregation signature is constructed from the feature vectors belonging to same image patch as below:

- A unit random vector of dimension d ($d < 512$) is generated $\{r_0, r_1, \dots, r_d\}$. A Gaussian function with mean 0 and variance 1 is used to sample each element. The d vector is put together into a matrix D of dimension $512 \times d$. This is generated on time at time of collecting the video as input for tracking.
- An inner product between the feature vectors v and the matrix D is done to get vector $u = D^T v$.
- For every vector u , following transformation function tf is applied produce the transformed feature vector \bar{u}
- $tf(u) = \begin{cases} 1 & r \cdot u \geq 0 \\ 0 & r \cdot u < 0 \end{cases}$
- $\bar{u} = \{tf_{r_1}(u), tf_{r_2}(u), \dots, tf_{r_d}(u)\}$

The feature vectors belonging to same image patch is now represented as bit stream of length d called as aggregation signature of the target image patch.

The benefits of converting the features of same patch to binary bit stream of aggregation signature have two benefits of: compressed form and reduced time complexity for matching the aggregation distance between aggregation signatures. The value of d can be selected by making a compromise between the matching time and accuracy of matching. The time complexity for construction of aggregation signature is $O(n \times 512 * d)$ where n is the number of feature vectors.

TABLE I. CNN CONFIGURATION FOR FEATURE EXTRACTION

Layer	Input	Filter	Stride	Padding	Out
MaxPool	32×32×128	2×2	2	0	16×16×128
Conv2	16×16×128	3×3	1	1	16×16×256
MaxPool	16×16×256	2×2	2	0	8×8×256
Conv3	8×8×256	3×3	1	1	8×8×512
AvgPool	8×8×512	8×8	1	0	1×1×512
FC	512×1	-	-	-	2×1

C. Hybrid Tracking

The hybrid trackers performs vehicle tracking by fusing the results of modified KCF filter and modified PCF filter. Though KCF filter [24] is known for its effectiveness and robustness, it cannot handle the appearance variations caused due to occlusions. This is because it does not make decisions based on tracking result but utilizes the maximum response in the output response graph to localize the target and update the template. Occlusion results in tracking deviation in KCF. The modified KCF filter adds a re-detection module to the standard KCF filter. The re-detection is activated by calculating the average peak correlation energy (AC) as in [28] and comparing it historical mean.

$$AC = \frac{|F_{max} - F_{min}|^2}{mean(\sum_{w,h}(F_{w,h} - F_{min})^2)} \quad (7)$$

Target re-detection is initiated when the AC is greater than historical mean. Re-detection is done by combining sliding window and template matching procedure. Template matching is done by calculating the hamming distance between the aggregation signature between the target and the candidate regions. Template matching on entire area of image takes significant amount of time, to avoid the probable area for matching is selected using Gray model GM (1,1) approach proposed in [29]. For each of the candidate regions identified by GM(1,1), template matching with aggregation signature is done with sliding window approach to get the hamming distance matching scores for each of the candidate regions as.

$$R1 = \{ \langle C_1, h_{s1} \rangle, \langle C_2, h_{s2} \rangle, \dots, \langle C_n, h_{sn} \rangle \} \quad (8)$$

Particle filters apply Monte Carlo simulation for visual tracking [30]. A particle filter can be effective only if it can capture all the variations in state space. But this introduces a higher computation overhead. Many approaches [31-34] have been proposed to increase the capability of particle filters. But these models don't accommodate the appearance variations introduced due to occlusions. A correlation particle filter model is proposed in [35] which solves the problem of occlusions using a mixture and correlation filter. We modify the correlation particle filter algorithm proposed in [35] at the step 5 by removing the prediction step.

Algorithm 1: The proposed correlation particle filter tracking algorithm.

```

Input : Image Sequences and Initialization.
Output: Tracking Results  $s_t \forall t$ .
1 for each frame do
2   Generate particles using the transition model
    $p(s_t | s_{t-1})$  and re-sample them.
3   Shift particles with a mixture correlation filter
    $s_t^i \rightarrow S_{mcf}(s_t^i)$ .
4   Update particle importance weights
5   Predict target object state
6 end
    
```

Fig. 4. Correlation PCF [35].

Instead of step 5 of correlation PCF shown in Fig.4, we calculate the hamming distance scores for the results achieved in step 4 between aggregation signature of target and particle regions and return the result. The modified algorithm is given below.

Algorithm: Modified PCF

```

Input: frame ,agg_sig
Output: Candidate regions
1. Collect the current frame
2. Generate particles using the transition model
 $p(s_t | s_{t-1})$  and resample them
3. Shift particles with a KCF correlation filter
 $s_t^i \rightarrow S_{mcf}(s_t^i)$ 
4.  $R2 = \{ \}$ 
5. for each particle region r
6.  $R2 = \{ R2, (r, Hamming(r, agg\_sig)) \}$ 
7. end
8. return
    
```

From the results of modified KCF (R1) and modified PCF(R2), the final target is found by fusion. Fusion is done by selecting the region with least hamming distance score in R1 and R2 and calculating the overlap of these regions. The overlap provides the target region. KCF filter is through the procedure of re-detection. The entire process flow of hybrid tracker is given in Fig. 5.

TABLE II. COMPARISON FOR DIFFERENT DISTURBANCES

Parameters/Solutions	KCF tracker	Parallel correlation filter	Combined detector-tracker	MUSTER	Proposed hybrid filter
Illumination					
variation					
Precision	0.548	0.846	0.907	0.862	0.961
SR	41.4	81	84	86	97
Background					
clutter					
Precision	0.366	0.748	0.83	0.87	0.962
SR	45.22	76	82.12	89.6	91.23
Occlusions					
Precision	0.635	0.743	0.855	0.881	0.97
SR	40.54	75	82.12	89.1	91.96

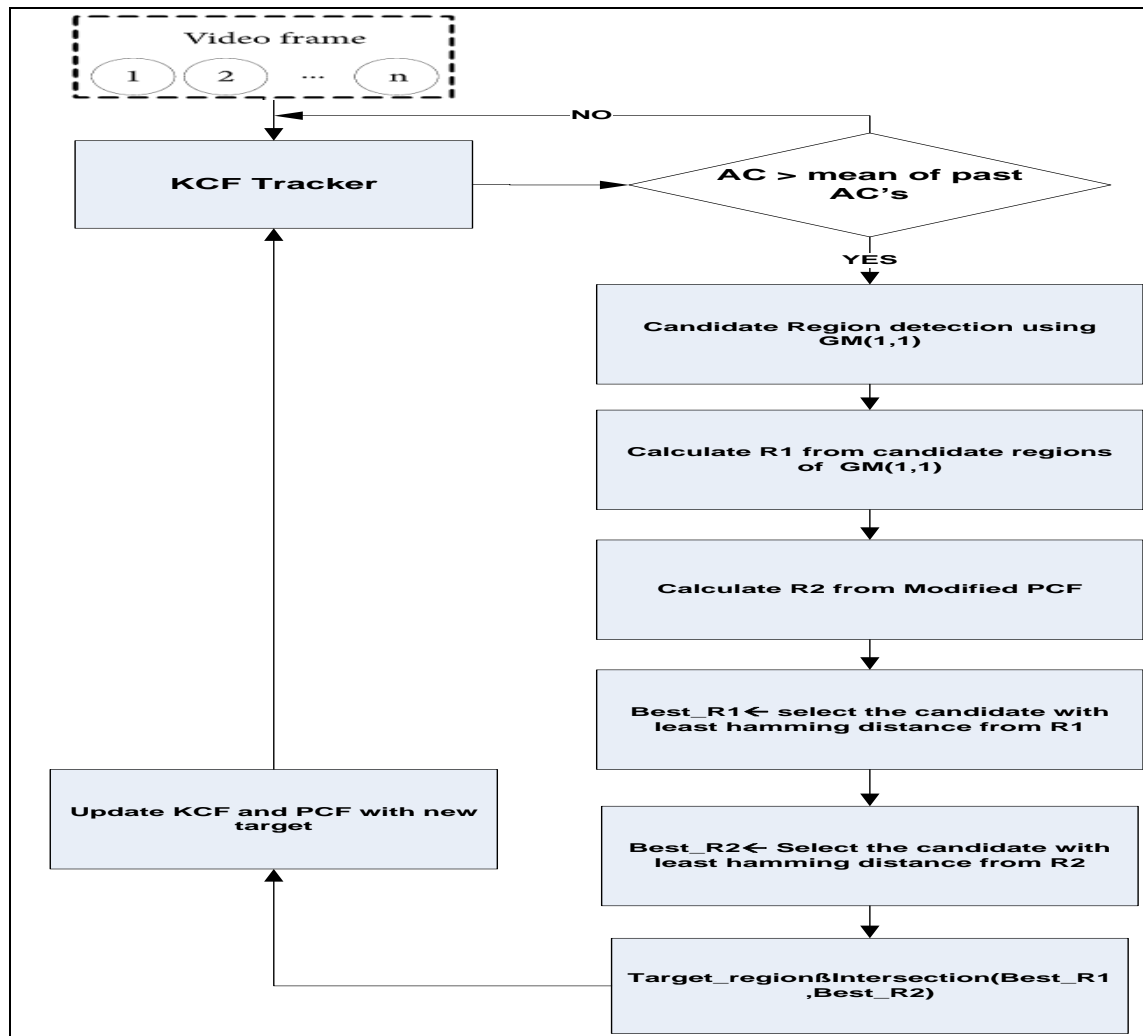


Fig. 5. HybridTracker Process Flow.

IV. RESULTS

The performance of the proposed hybrid tracker is tested against 10 videos from OTB 100 dataset [27]. OTB dataset is the visual tracking benchmark widely used for testing the performance of object tracking algorithms. The dataset has 100 video sequences in different categories of objects, humans, vehicles etc. The video sequences have wide distribution of clutter, illumination variations and occlusions. The samples for testing are selected with presence of background clutter, illumination variation and occlusions. The performance is compared against vehicle tracking algorithms of KCF tracker [24], Parallel correlation filter [37], combined detector-tracker [26] and Multistore Tracker (MUSTER) [36]. The performance is measured in terms of precision and success rate. Precision is calculated in terms of central location error (CLE). It is calculated as the Euclidean distance with respect to the central location of tracked objects and manually labelled ground truth. Precision is computed as

$$Precision = \frac{\prod_{N} CLE < Th}{N} \quad (9)$$

Where N is the total number of frames and the Th value is set as 20 in the experiment as tracking performance evaluated for every 20 frames. Keeping a higher value, may lose the minor changes and reducing to lower value, increases computational complexity. So an optimum value of 20 was selected trial and error in the experimental setup.

Success rate is computed as

$$SR = \frac{area(R_t \cap R_{gt})}{area(R_t \cup R_{gt})} \quad (10)$$

R_t is the bounding box object tracked and R_{gt} is the bounding box corresponding to the ground truth. The performance is also compared in terms of two parameters of success rate and precision for varied degrees of occlusions/clutters.

The average precision and success rate for videos are measured for various disturbances and the result is given in Table II. Both precision and success rate is higher compared to all the existing works. Comparison of precision and success rate across different solutions is shown in Fig.6 and Fig.7 respectively.

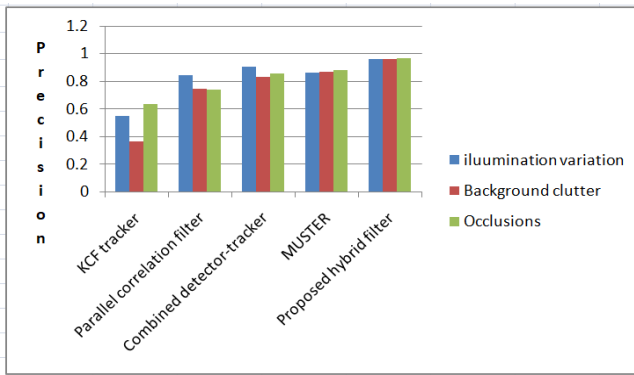


Fig. 6. Comparison of Precision Across Solutions.

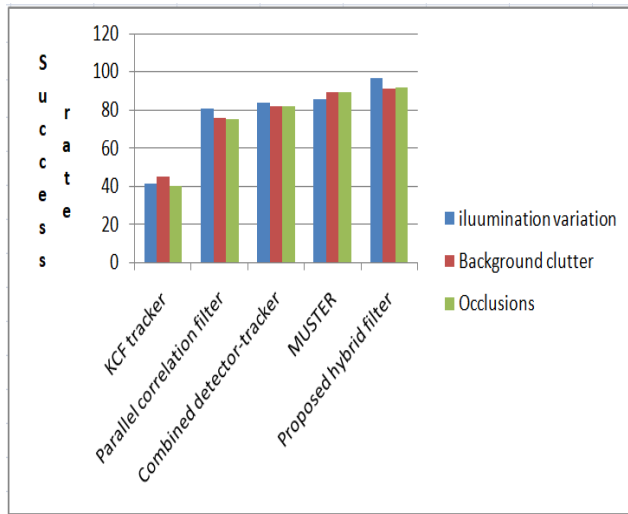


Fig. 7. Comparison of Success Rate Across Solutions.

The precision and success rate has increased in proposed solution due to use of hybrid trackers which combines the best of modified KCF and modified PCF. Also the influence of lighting variations, clutters, occlusion have been reduced due to use of novel background modeling with adaptive gain in the proposed solution.

The precision is measured for different error thresholds and the result is given in Fig. 8.

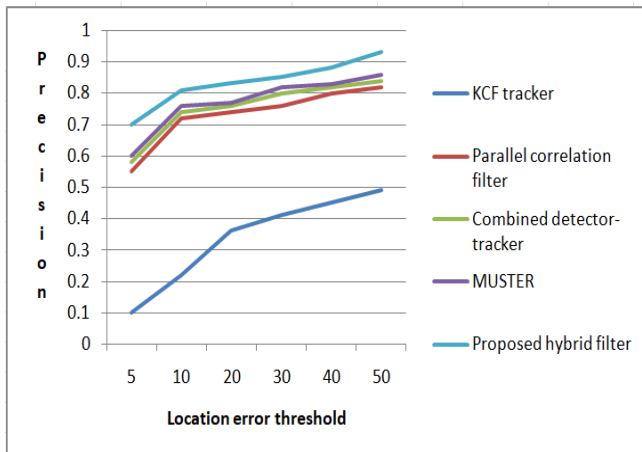


Fig. 8. Precision vs Location Error Threshold.

As location error threshold increases, the precision increases. Proposed hybrid tracker achieves highest precision among all other solutions even when location error threshold increases. Even if 50% of object is visible, the proposed solution is able to localize the vehicle accurately due to use of aggregation signature rather than exact matching. Aggregation signature is constructed with consideration for different probabilities of occlusions in the proposed solution and this helps to achieve better localization.

The success rate is measured for different overlap threshold and the result is given in Fig. 9.

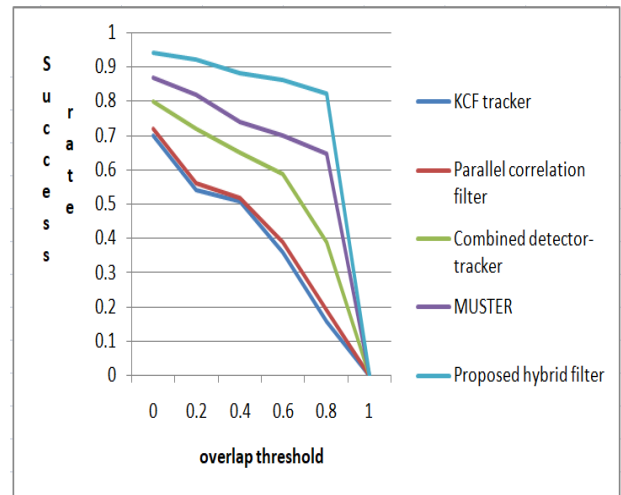


Fig. 9. Success Rate vs Overlap Threshold.

Even in presence of higher percentage of overlap, the proposed tracker is able to localize the object with higher success rate due to use of aggregation signature which already accommodates overlaps.

Video with a synthetic shape in varied percentage of occlusion is created. The performance of precision and success rate is measured with this synthetic data and the result is given in Fig.10 and Fig. 11.

Even in presence of 50% occlusion, the proposed hybrid tracker is able to achieve success rate of 0.82 and precision of 84%.

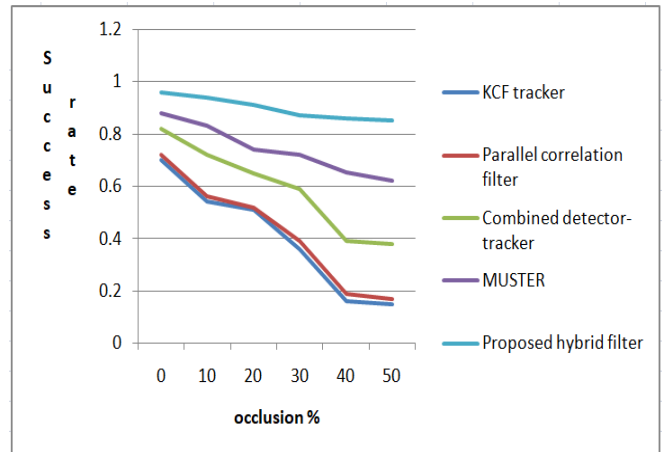


Fig. 10. Success Rate vs Occlusion %.

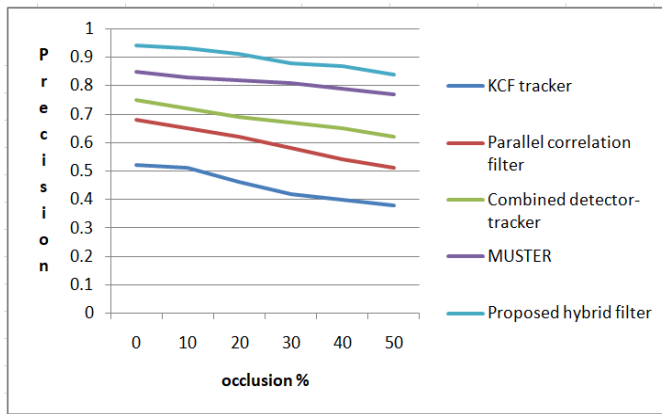


Fig. 11. Precision vs Occlusion %.

The success rate decreases as the occlusion percentage increases, but the success rate is higher in proposed solution compared to other solutions. The average success rate in proposed solution is at least 3% higher compared to others. Usage of aggregation signature-based matching within the KCF and PCF has increased the success rate in the proposed solution. The average precision in the proposed solution is at least 3% higher compared to other solutions/ Use of deep learning features with operating on image in frequency domain has increased the precision in the proposed solution.

A. Discussion

Through performance results, the proposed tracker is found to effectively localize the target vehicle even in presence of various degrees of occlusion and overlap. Localization accuracy has improved due to use of aggregation signature in the proposed solution. The aggregation signature is constructed considering different probabilities of occlusions and it is binary signature. Matching is realized using hamming distance. Due to this, vehicle localization accuracy has increased. Most of the existing works used in comparison used deep learning features and comparison of the features to localize the object. But in presence of occlusion, the distance match crossed the threshold and they failed to localize the object. Due to error in localization, their tracking performance too reduced. Tracking performance improved in proposed solution due to two reasons: (i) avoidance of unnecessary background objects through adaptive gain background subtraction and(ii) hybrid tracker to localize combining both kernel and particle filtering. This helped to localize object even in presence of higher overlap.

V. CONCLUSION

A hybrid tracking technique combining deep learning-based aggregation signature features with modified KCF & PCF is proposed in this work. Aggregation signature of target vehicle is created in frequency domain using QDCT and dimension reduced using deep learning. The proposed solution is able to achieve about 82% success rate and 86% precision in target even at 50% occlusion rate. In addition, the solution performs well against disturbances of occlusion, clutter and illumination variations. Improving the solution to work for even higher occlusion rate and various lighting conditions is in scope of future work.

REFERENCES

- [1] Yin, S. (2019). Estimation of rotor position in brushless direct current motor by memory attenuated extended Kalman filter, *European Journal of Electrical Engineering*, 21(1): 35-42.
- [2] Ha, D.B., Zhu, G.X., Zhao, G.Z. (2010). Vehicle tracking method based on corner feature and mean-shift. *Computer Engineering*, 36(06): 196-197.
- [3] Cao, X., Gao, C., Lan, J., Yuan, Y., Yan, P. (2014). Ego motion guided particle filter for vehicle tracking in airborne videos. *Neurocomputing*, 124: 168-177.
- [4] Oh, J., Min, J., Choi, E. (2010). Development of a vehicle image-tracking system based on a long-distance detection algorithm. *Canadian Journal of Civil Engineering*, 37(11).
- [5] Choi, I.H., Pak, J.M., Ahn, C.K., Mo, Y.H., Lim, M.T., Song, M.K. (2015). New preceding vehicle tracking algorithm based on optimal unbiased finite memory filter. *Measurement*, 73: 262-274.
- [6] Li, Z., He, S., Hashem, M. (2015). Robust object tracking via multi-feature adaptive fusion based on stability: contrast analysis. *The Visual Computer*, 31(10): 1319-1337.
- [7] Wu, S.Y., Liao, G.S., Yang, Z.W., Li, C.C. (2010). Improved track-before-detect algorithm based on particle filter. *Control and Decision*, 25(12): 1843-1847.
- [8] Kalal, Z., Mikolajczyk, K., Matas, J. (2011). Tracking-learning-detection. *IEEE Transactions on Pattern Analysis and Machine Intelligence*, 34(7): 1409-1422.
- [9] Wang, Y. (2020). Moving vehicle detection and tracking based on video sequences. *Traitement du Signal*, Vol. 37, No. 2, pp. 325-331B. Abidi, A. Jilbab, and E. H. Mohamed, "An energy efficiency routing protocol for wireless body area networks," *J. Med. Eng. Technol.*, vol. 42, no. 4, pp. 290-297, 2018.
- [10] Shrestha, Sandesh. (2019). Vehicle Tracking Using Video Surveillance. 10.5772/intechopen.89405.
- [11] Xu, Yong & Dong, Jixiang & Zhang, Bob & Xu, Daoyun. (2016). Background modeling methods in video analysis: A review and comparative evaluation. *CAAI Transactions on Intelligence Technology*.
- [12] Shobha B S and R. Deepu, "A Review on Video Based Vehicle Detection, Recognition and Tracking," 2018 3rd International Conference on Computational Systems and Information Technology for Sustainable Solutions (CSITSS), 2018, pp. 183-186, doi: 10.1109/CSITSS.2018.8768743.
- [13] Shobha B. S and Deepu. R, "Traffic Adaptive Deep Learning based Fine Grained Vehicle Categorization in Cluttered Traffic Videos" *International Journal of Advanced Computer Science and Applications (IJACSA)*, 12(9), 2021. <http://dx.doi.org/10.14569/IJACSA.2021.0120911>.
- [14] D. Zhang, H. Maei, X. Wang, and Y.-F. Wang. Deep reinforcement learning for visual object tracking in videos. *arXiv preprint arXiv:1701.08936*, 2017.
- [15] I. Leang, S. Herbin, B. Girard, et al., On-line fusion of trackers for single-object tracking [J]. *Pattern Recognition* 74, 459-473 (2018).
- [16] Z. Chen, X. You, B. Zhong, et al., Dynamically modulated mask sparse tracking [J]. *IEEE transactions on cybernetics* 47(11), 3706-3718 (2016).
- [17] Hua S , Kapoor M, Anastasiu D C. Vehicle Tracking and Speed Estimation from Traffic Videos[C]// 2018 IEEE/CVF Conference on Computer Vision and Pattern Recognition Workshops (CVPRW). IEEE, 2018: 153-160.
- [18] Liu S , Wang S , Shi W , et al. Vehicle tracking by detection in UAV aerial video[J]. *SCIENCE CHINA Information Sciences*, 2019, 62(2): 24101.
- [19] H.S. Song, Y. Li, J. Yang, Vehicle object tracking method based on highway scenario [J]. *Computer Systems & Applications* 28(6), 82-88 (2019).
- [20] Xu Y , Wang J. A unified neural network for object detection, multiple object tracking and vehicle re-identification[J]. *arXiv preprint arXiv:1907.03465*, 2019.

- [21] Fang Y , Wang C , Yao W , et al. On-road vehicle tracking using part-based particle Filter[J]. IEEE Transactions on Intelligent Transportation Systems, 2019:1-15.
- [22] Dai J, Li Y, He K, et al. R-fcn: Object detection via region-based fully convolutional networks[C]//Advances in neural information processing systems. 2016: 379-387.
- [23] Danelljan M, Hager G, Shahbaz Khan F, et al. Convolutional features for correlation filter based visual tracking[C]//Proceedings of the IEEE International Conference on Computer Vision Workshops. 2015: 58-66.
- [24] Ma C, Huang J B, Yang X, et al. Hierarchical convolutional features for visual tracking[C]//Proceedings of the IEEE international conference on computer vision. 2015: 3074-308.
- [25] Wang Q, Gao J, Xing J, et al. Dcfnet: Discriminant correlation filters network for visual tracking[J]. arXiv preprint arXiv:1704.04057, 2017.
- [26] J.F. Henriques, R. Caseiro, P. Martins, et al., High-speed tracking with kernelized correlation filters[J]. IEEE Transactions on Pattern Analysis and Machine Intelligence 37(3), 583–596 (2015).
- [27] D. S. Bolme, J. R. Beveridge, B. A. Draper and Y. M. Lui, Visual object tracking using adaptive correlation filters, 2010 IEEE Computer Society Conference on Computer Vision and Pattern Recognition, San Francisco, CA, 2010, pp. 2544-2550.
- [28] Yang, B., Tang, M., Chen, S. et al. A vehicle tracking algorithm combining detector and tracker. J Image Video Proc. 2020, 17 (2020).
- [29] <https://paperswithcode.com/dataset/otb>.
- [30] M. Wang, Y. Liu, Z. Huang. Large Margin Object Tracking with Circulant Feature Maps, IEEE Conference on Computer Vision and Pattern Recognition(CVPR), 2017,1:4800-4808.
- [31] Q. Yu, J. Lyu, L. Jiang, and L. Li, "Traffic anomaly detection algorithm for wireless sensor networks based on improved exploitation of the GM(1,1) model," International Journal of Distributed Sensor Networks, vol. 12, no. 7, 2016.
- [32] M. Isard, A. Blake, Condensation - conditional density propagation for visual tracking, International Journal of Computer Vision 29 (1) (1998) 5–28.
- [33] C. Yang, R. Duraiswami, L. Davis, Fast multiple object tracking via a hierarchical particle filter, in: Proceedings of the IEEE International Conference on Computer Vision, 2005.
- [34] Z. Khan, T. Balch, F. Dellaert, A rao-blackwellized particle filter for eigentracking, in: Proceedings of IEEE Conference on Computer Vision and Pattern Recognition, 2004.
- [35] S. K. Zhou, R. Chellappa, B. Moghaddam, Visual tracking and recognition using appearance-adaptive models in particle filters, IEEE Transactions on Image Processing 11 (1) (2004) 1491–1506. 3.
- [36] A. Doucet, N. De Freitas, N. Gordon, Sequential monte carlo methods in practice, in: Springer-Verlag, New York, 2001.
- [37] T. Zhang, S. Liu, C. Xu, B. Liu and M. Yang, "Correlation Particle Filter for Visual Tracking," in IEEE Transactions on Image Processing, vol. 27, no. 6, pp. 2676-2687, June 2018.

Improving Slope Stability in Open Cast Mines via Machine Learning based IoT Framework

Sameer Kumar Das¹, Subhendu Kumar Pani², Abhaya Kumar Samal³, Sasmita Padhy⁴, Sachikanta Dash⁵, Singam Jayanthu⁶

Dept. of Comp. Science and Engineering, Biju Patnaik University of Technology, Odisha, India¹
Principal Krupajal Computer Academy Bhubaneswar, India²

Dept. of Comp. Science and Engineering, Academy of Technology, Bhubaneswar, India³

School of Computing Science and Engineering, VIT Bhopal University, Bhopal, India⁴

Dept. of Comp. Science and Engineering, GIET University, Gunupur, India⁵

Department of Mining Engineering, National Institute of Technology, Rourkela, India⁶

Abstract—Slope stability has been a matter of concern for most geologists, mainly due to the fact that unstable slopes cause a greater number of accidents, which in turn reduces efficiency of mining operations. In order to reduce the probability of these slope instabilities, methods like tension crack mapping, inclinometer measurements, time domain reflectometry, borehole extensometers, piezometer, radar systems and image processing systems are deployed. These systems work efficiently for single site slope failures, but as the number of mining sites increase, dependency of one site slope failure on nearby sites also increases. Current systems are not able to capture this data, due to which the probability of accidents at open cast mines increases. In order to reduce this probability, a high efficiency internet of things (IoT) based continuous slope monitoring and control system is designed. This system assists in improving the efficiency of real-time slope monitoring via usage of a sensor array consisting of radar, reflectometer, inclinometer, piezometer and borehole extensometer. All these measurements are given to a high efficiency machine learning classifier which uses data mining, and based on its output suitable actions are taken to reduce accidents during mining. This information is dissipated to nearby mining sites in order to inform them about any inconsistencies which might occur due to the slope changes on the current site. Results were simulated using High REsolution Slope Stability Simulator (HIRESSS), and an efficiency improvement of 6% is achieved for slope analysis in open cast mines, while probability of accident reduction is increased by 35% when compared to traditional non-IoT based approach.

Keywords—Opencast; mining; slope; IoT; stability; machine learning; data mining

I. INTRODUCTION

In order to design a highly efficient slope analysis model parameters like apparent dip of cutting slopes, joint dip, angle between slope aspect & joint aspect, friction angle of joint plane, cohesion of joint, joint persistence, height of slope, weight of sliding blocks, uplift force due to water pressure of joints, force due to water pressure in tension crack, etc. must be recorded and analyzed [1]. These parameters require a large variety of sensors, which must be connected in tandem in order to evaluate these values with highest possible efficiency. Depending upon these parameters, different slope stability factors are evaluated, and based on the value of these factors,

approximations are done on the stability of slope on the given opencast mining site [2]. For instance, in order to evaluate factor of safety (FoS), measurements of resting moments and disturbing moments are done, and the following equation is evaluated,

$$FoS = \frac{M_R}{M_D} \quad (1)$$

$$MR = c * \phi * R2 \quad (2)$$

$$MD = Aregion * \partial * x \quad (3)$$

Where, 'c' is a constant, ϕ is the angle of measurement, 'R' is radius of measurement,

A region is area of region, ∂ is weight of soil, and 'x' is distance between start point and center of slope, M_R is resting moment, M_D is disturbing moment. A high value of 'FoS' indicates that the surface has high resting moment, and low disturbing moment, which indicates that the surface is slope stable and can be used for mining operations with high efficiency. Similar measurements including shear resistance of force acting on slice, shear resistance offered by soil, etc. are also used to evaluate FoS values for opencast soil surfaces. Depending upon these values, short-term stability and long-term stability values are evaluated. Short term stability conditions include, stability of slope immediately after construction, which consists of undrained conditions and is evaluated using undrained parameters. Here, change in pore water pressure is totally dependent upon stress change. While long term stability analysis uses effective weight of soil and here changes in pore water pressure is independent of stress changes [3].

More precisely, despite the fact that this study has significantly advanced our understanding of slope stability, it is still limited by the following drawbacks of the aforementioned techniques, which prevent it from being fully resolved:

- The simulations are inaccurate. The slope stability, for instance, can be reflected by the limit equilibrium approach, but the non-uniformity of the stress distribution and the impact of deformation are not taken into consideration. Therefore, this technique cannot

accurately reflect the slope's actual level of safety and dependability.

- The safety factor's limitations are ambiguous and undefined. A slope with $FS > 1.20$ is generally considered safe. However, in actual engineering there have been slopes that failed with $FS > 1.2$.
- These techniques are influenced by human subjectivity.

Throughout the course of an opencast mining operation, slope stability analysis is a crucial part of the process. A terrible social, economic, as well as a major safety catastrophe might result from a failure of slope in the vicinity of a mine being operated. The fundamental failure scenarios are extremely complex & diversified. These failure processes heavily rely on the regional geology, which is rather particular to a particular area of the rock mass. The process of developing slopes is wholly based on the field experience in recent years as well. A better strategy may be created by planning slopes safely.

The major aim of this work is to do numerical modelling for increasing the efficiency of slopes through the simulator with diverse rock qualities and slope diameters. Utilizing HIRESSS, numerical modelling is done to determine the safety factor. Every slope has different characteristics, and each step's safety factor is determined. To determine how the factor of safety alters when the bench parameters vary, these numbers are connected with them. Here our objective is to understand the different types of slope failures and the concepts of Safety.

Based on this analysis, a large number systems have been proposed over the past several years [4]. Each of these systems has its own advantages and limitations.

In the outline of this paper, the next section reviews the systems and evaluates best practices that must be used in order to improve the performance of slope stability in opencast mining conditions. This is followed by the section on the design of the proposed model, which is inspired by cutting edge IoT devices, and their interconnections for improved slope stability using a novel data mining approach. Next to this, the result analysis and comparison of the proposed model is done in order to evaluate the performance and performance gaps in existing system. Finally, this text concludes with some interesting observations about the proposed model and suggests methods to improve the same.

II. LITERATURE REVIEW

Slope stability analysis for open cast mines is a multidomain signal processing task, wherein data from different sensors must be captured such that slopes are analyzed with high accuracy. In order to perform this task, various signal processing models are described, for instance, the work in [5] proposes a model that uses Spatio-Temporal Kriging Interpolation for improving slope stability. The model is able to perform highly accurate analysis on both open cast and open pit mines, due to efficient utilization of data interpolation. Similar models can be observed from [6, 7, 8], where Neural Networks, Gaussian processes, and 3D non-linear finite difference analysis are used. These models can be used for high performance applications like highway corridor slope analysis [9] for improving road stability.

Simpler methods like strength reduction [10], and variational calculus [11], can be used for analysing stability of slope analysis for open cast mines, National Highway (NH) development [12], and perched water conditions [13] with high efficiency. Slope stability can also be analyzed for specialized geographies like 3D geometries [14, 15], and methods like Technique for Order Preference by Similarity to Ideal Solution (TOPSIS) [16] can be used. These techniques can be extended by referring to different algorithmic models as suggested in [17], wherein Limit equilibrium method, artificial neural network, Vector sum method, Numerical simulation method and Limit analysis method are described. These methods utilize slope height & angle factors [18] while designing slope analysis models, and can be used for specialized applications like Stone Column- Supported Embankments [19]. The performance of these models can be improved via use of deep learning models as described in [20], wherein hybrid stacking ensemble method is used, which is based on finite element analysis and field data. The model is able to achieve high accuracy of slope analysis, and thereby adapt to varying structural scenarios. Various specialized methods for slope analysis can be observed from [21, 22, 23, 24, 25, 26], wherein volumetric behavior of rock salt, electromagnetic radiation mechanism of rock fracturing, uniaxial compressive strength of sandstone, influence of bedding structure, spectral induced polarization, bender element models, and pre-flawed sandstones are studied. These models assist in evaluation of slopes in open cast mines that are located near stone beds, thereby improving their scalability.

Artificial neural networks (ANN) have been applied successfully in slope stability problems (Feng, et. al 2018) [27], however they do have certain drawbacks. The restrictions are detailed below:

- Contrary to other statistical models, ANN models do not reveal the relative relevance of the individual parameters, which is a significant drawback (Samui, P. 2019) [28].
- Since the knowledge learned during training is implicitly stored in ANNs, it can be exceedingly challenging to interpret the network's general structure in a way that makes sense (Baghbani, et.al (2022)[29] has been proposed in their review. This gave rise to the phrase "black box," which many researchers use to describe the behaviour of ANNs.
- Additionally, ANN has certain intrinsic flaws such as sluggish convergence, poor generalisation, finding local minimums, and over-fitting issues.

The author's primary contribution is to provide an output utilizing several classifiers employing IoT devices and a simulator. Its result is used to determine the best course of action to decrease mining accidents. This information is shared with surrounding mining operations in order to alert them to any discrepancies that might arise as a result of the site's current slope variations. The HIgh REsolution Slope Stability Simulator (HIRESSS) was used to model the outcomes, and then it was compared to a conventional, non-IoT based technique.

Models for analysis of submerged pools [30], use of random field Gaussian methods [31], blocky structure systems [32], near-surface rock strength slope analysis [33], and reinforcement learning models [34-37] are also used for high efficiency slope analysis. It can be observed that most of these models do not define sensor placement analysis, due to which their efficiency is limited. In order to improve this efficiency, the proposed model combines various sensing elements, and defines positions for these elements in order to improve stability of slope analysis in open cast mines. The proposed model along with its analysis and comparative evaluation can be observed in the next sections.

III. PROPOSED MACHINE LEARNING MODEL FOR IMPROVING SLOPE STABILITY ANALYSIS USING IOT

In order to improve the efficiency of slope stability analysis in open cast mines, it is mandatory that various conditions like above water table, drained, partly drained, water table 10m above toe, and water table 16m above toe must be analyzed. The significance and primary goal of this work is to put the aforementioned categorization model into practice for predicting the stability state of a soil slope.

- A weak zone in the soil profile is used to perform slope stability, which is a prevalent sort of coal mine failure in many nations.
- Practically significant numerical challenges are addressed for the simulation and investigation of the issue.
- The stability of the mine's slopes is determined by the inclination, shear strength, and water conditions in the weak zone.

The results of these conditions are given to the proposed model in order to reduce their probability of occurrence. Various IoT sensors are placed onsite in order to sense presence of these conditions, and efficient steps are taken to reduce their effect. To improve the efficiency of slope stability analysis, the following process is used, and based on the results of this process action plans are executed for improving the condition of open cast mines.

- Inputs to the model
 - Number of iterations (N_i).
 - Number of solutions (N_s).
 - Maximum number of sensors in the system (S_{max}) (radar, reflectometer, inclinometer, piezometer, borehole extensometer, etc.).
 - Learning rate (L_r).
 - Minimum advisable slope stability (SL_{min}).
 - Maximum advisable slope stability (SL_{max}).
- Outputs of the model
 - Estimated slope (SL_{es}).
- Process of execution

- For each iteration in 1 to N_i
 - For each solution in to N_s
 - If the solution is marked as 'not to be changed', then skip it and go to the next solution.
 - Else, generate a new solution using the following process,
 - Select a random number of sensors from the list of available sensors = $Sense_{sel}$

$$Sense_{sel} = (1, S_{max}) \quad (4)$$
 - For the selected sensors, perform random placement on the mining site, so that different sensor readings can be obtained.
 - Using these sensors, measure the slope stability from each sensor using equations 5, 6, 7, 8 and 9.

$$SS_{rader} = \frac{(ABS(H_{measured} - H_{actual}) + ABS(D_{measured} - D_{actual}))}{2 \cdot (\text{MAX}(H_{measured}, H_{actual}) + \text{MAX}(D_{measured}, D_{actual}))} \quad (5)$$

$$SS_{ref} = \frac{ABS(R_{measured} - R_{actual})}{\text{MAX}(R_{measured}, R_{actual})} \quad (6)$$

$$SS_{inc} = \frac{ABS(I_{measured} - I_{actual})}{\text{MAX}(I_{measured}, I_{actual})} \quad (7)$$

$$SS_{piez} = \frac{ABS(P_{measured} - P_{actual})}{\text{MAX}(P_{measured}, P_{actual})} \quad (8)$$

$$SS_{bh} = \frac{ABS(D_{measured} - D_{actual})}{\text{MAX}(D_{measured}, D_{actual})} \quad (9)$$

Where, SS_{ra} , SS_{ref} , SS_{inc} , SS_{piez} , and SS_{bh} are slope stability values for radar, reflectometer, inclinometer, piezoelectric sensor and borehole extensometer, while H, D, R, I, and P are measured height, distance, reflectance, inclination, and soil pressure respectively.

- Based on the number of selected sensors, the value of fitness is estimated using equation 10.

$$F_i = \frac{\sum_{i=1}^{Sense_{sel}} SS_i}{Sense_{sel}} \quad (10)$$

- If the value of F_i satisfies the constraints of equation 11, then use it for processing, else generate a new solution.

$$F_i > SL_{min} \text{ and } F_i < SL_{max} \quad (11)$$

- After generation of all solutions, evaluate the fitness threshold using equation 12, wherein learning rate and other parameters are also utilized.

$$F_{th} = \sum_{i=1}^{N_s} F_i * \frac{L_r}{N_s} \quad (12)$$

- Mark all solutions as 'to be changed', where fitness is less than the threshold, while mark all other solutions as 'not to be changed'.
- At the end of last iteration, the following Table I is formed, which indicates information about each

solution, its stability, number of sensors used, and their placements.

- Select the solution with maximum fitness value, use the sensors and place them in given locations as decided by the algorithm.

Once the sensor placement is complete, then evaluate slope for the given open cast mine, and communicate this value to other locations. Generate ‘R’ random locations for deployment, and gather slope data from all these locations using the given machine learning model. Once the data is collected, then use a mode operation for find slope analysis.

$$S_{final} = MODE(|S_i|R_{i=1}) \quad (13)$$

Based on this evaluation, accuracy of slope stability, precision, recall, and fMeasure values are estimated. This estimation is done on various sites across different open cast mines, and the results are tabulated in the next section. These results are also compared with some of the reviewed models that perform highly efficient slope stability analysis in the same open cast mines.

IV. RESULT AND ANALYSIS

Performance evaluation of the proposed model required in depth analysis and simulations for different open cast sites. In order to perform this task, 20 different open cast mines were simulated on the High Resolution Slope Stability Simulator (HIRESSS) software, and 100 different locations were evaluated for estimation of slope stability analysis. Based on these simulation settings, accuracy of slope stability analysis (ASL) was evaluated using the following equation,

$$A_{SL} = \frac{S_c}{S_T} \quad (14)$$

Where, S_c and S_T are number of sites where slopes were correctly identified, and total number of evaluated sites respectively. We have implemented the methodologies used in [5] and [20] in our simulator and compared them with our proposed work. These results are tabulated in Table I to V, wherein accuracy of the proposed model is compared with other reference models as in Table I.

Based on this analysis it can be observed that the proposed model is 5% more effective than [5], and 6% more effective than [20] under different open mining sites. Using similar simulation settings, recall of slope stability analysis (P_{SL}) was evaluated using the following equation,

$$P_{SL} = \frac{S_{Cl}}{S_T} \quad (15)$$

Where, S_{Cl} and S_T are number of sites where slopes were correctly identified but had lower slope values when compared with actual and total number of evaluated sites respectively. These results are tabulated in Table II, wherein Precision of the proposed model is compared with other reference models.

Based on this analysis it can be observed that the proposed model is 6% more effective than [5], and 5% more effective than [20] under different open mining sites. Using similar simulation settings, recall of slope stability analysis (RSL) was evaluated using the following equation,

$$R_{SL} = \frac{S_{CC}}{S_T} \quad (16)$$

TABLE I. ACCURACY OF SLOPE STABILITY ANALYSIS FOR DIFFERENT SITES

Number of site locations	A_{SL} [5]	A_{SL} [20]	A_{SL} Proposed
2000	0.72	0.76	0.81
3000	0.74	0.77	0.83
4000	0.77	0.79	0.84
5000	0.78	0.80	0.85
6000	0.79	0.81	0.86
7000	0.80	0.81	0.87
8000	0.81	0.82	0.88
9000	0.81	0.83	0.89
10000	0.82	0.84	0.90
11000	0.83	0.86	0.91
12000	0.84	0.87	0.92
13000	0.85	0.88	0.94
14000	0.87	0.89	0.95
15000	0.88	0.90	0.96
16000	0.89	0.91	0.97
17000	0.90	0.92	0.97
18000	0.91	0.93	0.98
19000	0.93	0.93	0.98
20000	0.94	0.94	0.99

TABLE II. THE PRECISION OF SLOPE STABILITY ANALYSIS FOR DIFFERENT SITES

Number of site locations	P_{SL} [5]	P_{SL} [20]	P_{SL} Proposed
2000	0.68	0.72	0.77
3000	0.70	0.73	0.78
4000	0.73	0.75	0.80
5000	0.74	0.76	0.81
6000	0.75	0.76	0.81
7000	0.76	0.77	0.82
8000	0.76	0.78	0.83
9000	0.77	0.79	0.85
10000	0.78	0.80	0.86
11000	0.79	0.81	0.87
12000	0.80	0.82	0.88
13000	0.81	0.83	0.89
14000	0.82	0.84	0.90
15000	0.83	0.86	0.91
16000	0.84	0.87	0.92
17000	0.86	0.87	0.92
18000	0.87	0.88	0.93
19000	0.88	0.89	0.93
20000	0.89	0.89	0.94

TABLE III. RECALL OF SLOPE STABILITY ANALYSIS FOR DIFFERENT SITES

Number of site locations	R_{SL} [5]	R_{SL} [20]	R_{SL} Proposed
2000	0.72	0.76	0.81
3000	0.74	0.77	0.83
4000	0.77	0.79	0.84
5000	0.78	0.80	0.85
6000	0.79	0.81	0.86
7000	0.80	0.81	0.87
8000	0.81	0.82	0.88
9000	0.81	0.83	0.89
10000	0.82	0.84	0.90
11000	0.83	0.86	0.91
12000	0.84	0.87	0.92
13000	0.85	0.88	0.94
14000	0.87	0.89	0.95
15000	0.88	0.90	0.96
16000	0.89	0.91	0.97
17000	0.90	0.92	0.97
18000	0.91	0.93	0.98
19000	0.93	0.93	0.98
20000	0.94	0.94	0.99

Where, S_{cc} and S_r are number of sites where slopes were correctly identified but had higher slope values when compared with actual, and total number of evaluated sites respectively. These results are tabulated in Table III, wherein Recall of the proposed model is compared with other reference models.

Based on this analysis it can be observed that the proposed model is 5% more effective than [5], and 4% more effective than [20] under different open mining sites. Using similar simulation settings, fMeasure of slope stability analysis (F_{SL}) was evaluated using the following equation,

$$F_{SL} = 2 * P_{SL} * \frac{R_{SL}}{R_{SL} + R_{SL}} \quad (17)$$

These results are tabulated in Table IV, wherein FMeasure of the proposed model is compared with other reference models.

Based on this analysis it can be observed that the proposed model is 5% more effective than [5], and [20] under different open mining sites. Similarly, analysis of probability of accidents (P) on each site was estimated using equation 18, and results were tabulated using Table V, where a major difference in accident reduction probability can be observed.

$$P_{Acc} = \frac{Accidents\ Occoured}{Total\ Accident\ Scenarios} \quad (18)$$

From this analysis, it can be observed that the proposed model is able to reduce number of accidents by over 35% when compared with reviewed models. This can also be observed from Fig. 5.

TABLE IV. FMEASURE OF SLOPE STABILITY ANALYSIS FOR DIFFERENT SITES

Number of site locations	F_{SL} [5]	F_{SL} [20]	F_{SL} Proposed
2000	0.70	0.74	0.79
3000	0.72	0.75	0.80
4000	0.75	0.77	0.82
5000	0.76	0.78	0.83
6000	0.77	0.78	0.84
7000	0.77	0.79	0.85
8000	0.78	0.80	0.86
9000	0.79	0.81	0.87
10000	0.80	0.82	0.88
11000	0.81	0.83	0.89
12000	0.82	0.84	0.90
13000	0.83	0.86	0.91
14000	0.84	0.87	0.92
15000	0.85	0.88	0.93
16000	0.87	0.89	0.94
17000	0.88	0.90	0.95
18000	0.89	0.90	0.95
19000	0.90	0.91	0.96
20000	0.91	0.91	0.96

TABLE V. ACCIDENT PROBABILITY FOR DIFFERENT SITES

Number of site locations	P_{Acc} [5]	P_{Acc} [20]	P_{Acc} Proposed
2000	0.56	0.59	0.37
3000	0.58	0.60	0.38
4000	0.60	0.61	0.39
5000	0.61	0.62	0.40
6000	0.61	0.63	0.40
7000	0.62	0.64	0.41
8000	0.63	0.64	0.41
9000	0.64	0.65	0.42
10000	0.64	0.66	0.42
11000	0.65	0.67	0.43
12000	0.66	0.68	0.43
13000	0.67	0.68	0.44
14000	0.68	0.69	0.44
15000	0.68	0.70	0.45
16000	0.69	0.71	0.46
17000	0.70	0.72	0.46
18000	0.71	0.72	0.47
19000	0.72	0.73	0.47
20000	0.73	0.73	0.48

A. Simulation Results

As per our proposed work different statistical measure has been performed. A comparison study has been performed as shown in table from Table I to Table V by taking different site locations. The simulation results of the above mentioned analysis have been shown in Fig. 1 to Fig. 5. It has been found that our proposed work is comparatively showing good result in different analytical aspects.

This reduction assists in making it useful for safe and highly accurate slope estimations. The estimated slopes can be used for taking suitable actions for estimation of open cast mine accidents, and avoiding them with high efficiency.

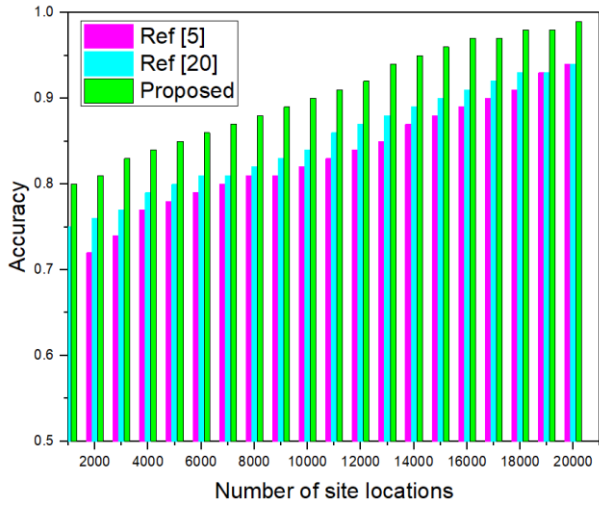


Fig. 1. Accuracy of Slope Stability Analysis for Different Sites.

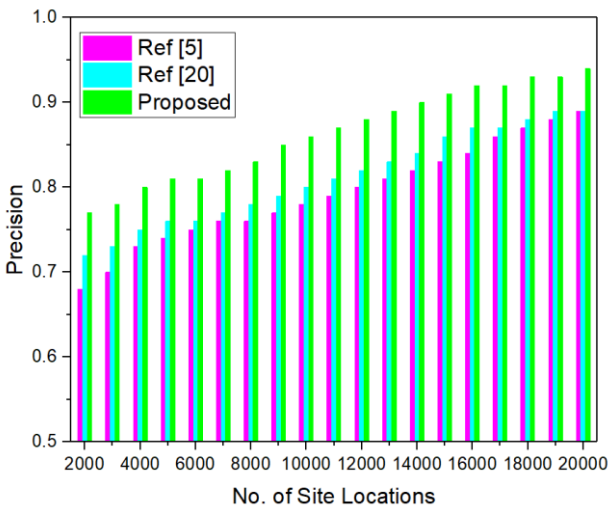


Fig. 2. Precision of Slope Stability Analysis for Different Sites.

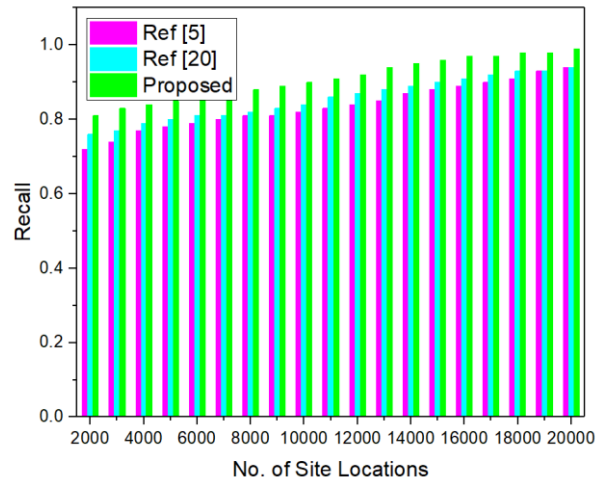


Fig. 3. Recall of Slope Stability Analysis for Different Sites.

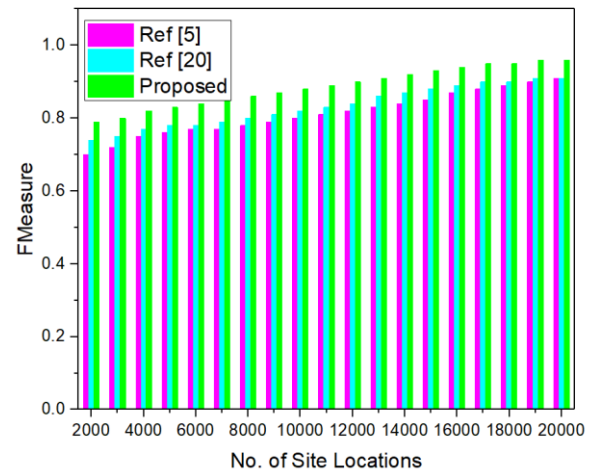


Fig. 4. FMeasure of Slope Stability Analysis for Different Sites.

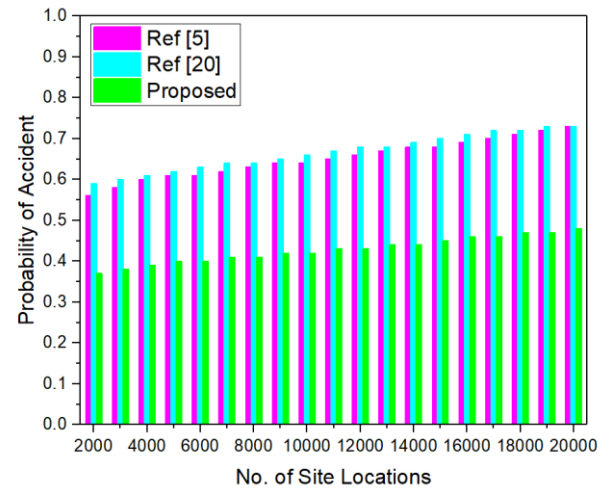


Fig. 5. Accident Probability for Different Sites.

V. CONCLUSION AND FUTURE SCOPE

Based on the extensive result analysis, it can be observed that the proposed model is capable of improving the accuracy of slope stability analysis by 6% when compared with state-of-the-art models, while similar results are obtained for precision, recall, and F-measure values. Due to this, the number of accidents at these mines is drastically reduced, which enforces better safety measures, and thereby assists in reducing cost of mining operations. All these parameters are improved due to proper sensor placement, and improvement of stability analysis models by the machine learning model. Stochastic placement of sensors, and randomized inference of models positions from these placements further assists in identification of new placement spots on the site, thereby improving site coverage and utility. In future, researchers can improve this performance via use of deep learning models, wherein more number of sensors can be integrated in order to improve stability of slope analysis.

REFERENCES

- [1] S. Li, L. Wu, X. Bian, C. Song, P. Li and Z. Han, "Statistically Analysis for the Stability of Various Protection Modes of Expansive Soil Cutting Slope," 2019 International Conference on Virtual Reality and Intelligent Systems (ICVRIS), 2019, pp. 320-323, doi: 10.1109/ICVRIS.2019.00084.
- [2] Y. Yang, H. Xu, Y. He and Z. Yin, "Stability Analysis of Earth-rock Dam Slopes based on Big Data Fuzzy Ant Colony Clustering," 2019 IEEE 3rd Information Technology, Networking, Electronic and Automation Control Conference (ITNEC), 2019, pp. 2153-2156, doi:10.1109/ITNEC.2019.8729524.
- [3] H. Zhi-Fang, "Analysis on the Impact of Expansive Soil Slope Stability by Rainfall Infiltration," 2018 International Conference on Engineering Simulation and Intelligent Control (ESAIC), 2018, pp. 26-30, doi: 10.1109/ESAIC.2018.00014.
- [4] Y. Lin, K. Zhou and J. Li, "Prediction of Slope Stability Using Four Supervised Learning Methods," in IEEE Access, vol. 6, pp. 31169-31179, 2018, doi: 10.1109/ACCESS.2018.2843787.
- [5] Acharya, B., Sarkar, K., Singh, A.K. et al. Preliminary slope stability analysis and discontinuities driven susceptibility zonation along a crucial highway corridor in higher Himalaya, India. J. Mt. Sci. 17, 801–823 (2020). <https://doi.org/10.1007/s11629-019-5524>.
- [6] N. Gunasekaran, N. M. Thoiyab, P. Muruganatham, G. Rajchakit and B. Unyong, "Novel Results on Global Robust Stability Analysis for Dynamical Delayed Neural Networks Under Parameter Uncertainties," in IEEE Access, vol. 8, pp. 178108-178116, 2020, doi: 10.1109/ACCESS.2020.3016743.
- [7] B. Hu, G. Su, J. Jiang, J. Sheng and J. Li, "Uncertain Prediction for Slope Displacement Time-Series Using Gaussian Process Machine Learning," in IEEE Access, vol. 7, pp. 27535-27546, 2019, doi: 10.1109/ACCESS.2019.2894807.
- [8] B. Hu, J. Li, J. Sheng and Z. Ye, "Crack Cause in the High Slope of Chinese Ancient Copper Mine Relics: A Three-Dimensional Non-Linear Finite Difference Analysis," in IEEE Access, vol. 8, pp. 13987-13997, 2020, doi: 10.1109/ACCESS.2020.2965593.
- [9] 6H. Xiao, Z. Zhang, L. Chen and Q. He, "An Improved Spatio-Temporal Kriging Interpolation Algorithm and Its Application in Slope," in IEEE Access, vol. 8, pp. 90718-90729, 2020, doi: 10.1109/ACCESS.2020.2994050.
- [10] Liu, F. Stability Analysis of Geotechnical Slope Based on Strength Reduction Method. Geotech Geol Eng 38, 3653–3665(2020). <https://doi.org/10.1007/s10706-020-01243-3>.
- [11] Belandria, N., Úcar, R., León, F.M. et al. Stability analysis of slopes with planar failure using variational calculus and numerical methods. Front. Struct. Civ. Eng. 14, 1262–1273 (2020). <https://doi.org/10.1007/s11709-020-0657-9>.
- [12] Kumar, A., Sharma, R.K. & Mehta, B.S. Slope stability analysis and mitigation measures for selected landslide sites along NH-205 in Himachal Pradesh, India. J Earth Syst Sci 129, 135 (2020). <https://doi.org/10.1007/s12040-020-01396-y>.
- [13] Tang, D., Jiang, Z., Yuan, T. et al. Stability Analysis of Soil Slope Subjected to Perched Water Condition. KSCE J Civ Eng 24, 2581–2590 (2020). <https://doi.org/10.1007/s12205-020-1728-0>.
- [14] Yu, G., Xie, M., Liang, J. et al. A GIS- based 3D slope stability analysis method based on the assumed normal stress on the slip surface. Sci Rep 10, 4442 (2020). <https://doi.org/10.1038/s41598-020-61301-x>.
- [15] Bunn, M., Leshchinsky, B., & Olsen, M. J. Geologic Trends in shear strength properties inferred through three- dimensional back analysis of landslide inventories. Journal of Geophysical Research: Earth Surface, 125, 2020. <https://doi.org/10.1029/2019JF005461>.
- [16] Wenqiang Chen, Yufei Zhao, Lipeng Liu, Xiaogang Wang, "A New Evaluation Method for Slope Stability Based on TOPSIS and MCS", Advances in Civil Engineering, vol. 2020, Article ID 1209470, 10 pages, 2020. <https://doi.org/10.1155/2020/1209470>.
- [17] Ullah, Sami & Khan, Muhibullah & Rehman, Gohar. A Brief Review Of The Slope Stability Analysis Methods, Geological Behavior. 4. 73-77. 10.26480/gbr.02.2020.73.77.
- [18] Shiferaw, H.M. Study on the influence of slope height and angle on the factor of safety and shape of failure of slopes based on strength reduction method of analysis. Beni- Suef Univ J Basic Appl Sci 10, 31 (2021). <https://doi.org/10.1186/s43088-021-00115-w>.
- [19] Dar, L.A., Shah, M.Y. Deep-Seated Slope Stability Analysis and Development of Simplistic FOS Evaluation Models for Stone Column-Supported Embankments. Transp. Infrastruct. Geotech. 8, 203–227 (2021). <https://doi.org/10.1007/s40515-020-00134-7>.
- [20] Kardani, Navid & Zhou, Annan & Nazem, Majidreza & Shen, Shui-Long Improved prediction of slope stability using a hybrid stacking ensemble method based on finite element analysis and field data. Journal of Rock Mechanics and Geotechnical Engineering, 2020 13.10.1016/j.jrmge.2020.05.011.
- [21] Azabou, Mejda & Rouabhi, Ahmed & Blanco-Martín, Laura. Effect of insoluble materials on the volumetric behavior of rock salt. Journal of Rock Mechanics and Geotechnical Engineering. 13, 2020. 10.1016/j.jrmge.2020.06.007.
- [22] Padhy, S., Dash, S., Routray, S., Ahmad, S., Nazeer, J., & Alam, A. (2022). IoT-Based Hybrid Ensemble Machine Learning Model for Efficient Diabetes Mellitus Prediction. Computational Intelligence and Neuroscience, 2022.
- [23] Padhy, S., Dash, S., Malla, P. P., Routray, S., & Qi, Y. (2021, November). An Energy Efficient Node Localization Algorithm for Wireless Sensor Network. In 2021 IEEE 2nd International Conference on Applied Electromagnetics, Signal Processing, & Communication (AESPC) (pp. 1-5). IEEE.
- [24] Lin, Peng & Pengcheng, Wei & Wang, Cheng & Kang, Shengzu & Wang, Xin. Effect of rock mechanical properties on electromagnetic radiation mechanism of rock fracturing. Journal of Rock Mechanics and Geotechnical Engineering, 2021, 10.1016/j.jrmge.2021.01.001.
- [25] Zhang, Jinyuan & Shen, Yanjun & Yang, Gengshe & Zhang, Huan & Wang, Yongzhi & Xin, Hou & Sun, Qiang & Li, Guoyu. Inconsistency of changes in uniaxial compressive strength and P-wave velocity of sandstone after temperature treatments. Journal of Rock Mechanics and Geotechnical Engineering. 13,2020, 10.1016/j.jrmge.2020.05.008.
- [26] Li, Xiaying & Lei, Xinglin & Li, Qi & Chen, Dianguo. Influence of bedding structure on stress-induced elastic wave anisotropy in tight sandstones. Journal of Rock Mechanics and Geotechnical Engineering. 13. 98-113, 2021, 10.1016/j.jrmge.2020.06.003.
- [27] Bate, Bate & Cao, Junnan & Zhang, Chi & Hao, Na & Wang, Song, Journal Pre-proof Monitoring lime and cement improvement using spectral induced polarization and bender element techniques Monitoring lime and cement improvement using spectral induced polarization and bender element techniques. Journal of Rock Mechanics and Geotechnical Engineering. 13, 2020, 10.1016/j.jrmge.2020.06.005.
- [28] Ke Zhang, Xianghua Liu, Yulong Chen, Heming Cheng, Quantitative description of infrared radiation characteristics of preflawed sandstone during fracturing process, Journal of Rock Mechanics and Geotechnical

- Engineering, Volume 13, Issue 1, 2021, Pages 131-142, ISSN 1674-7755, <https://doi.org/10.1016/j.jrmge.2020.05.003>.
- [29] Feng, X., Li, S., Yuan, C., Zeng, P., & Sun, Y. (2018). Prediction of slope stability using naive Bayes classifier. *KSCE Journal of Civil Engineering*, 22(3), 941-950.
- [30] Samui, P. (2019, September). Application of artificial intelligence in ge-engineering. In *International Conference on Inforatmion technology in Geo-Engineering* (pp. 30-44). Springer, Cham.
- [31] Baghbani, A., Choudhury, T., Costa, S., & Reiner, J. (2022). Application of artificial intelligence in geotechnical engineering: A state-of-the-art review. *Earth-Science Reviews*, 228, 103991.
- [32] Wang, W, Griffiths, DV. Analysis of the critical pool level of partially submerged slopes. *Int J Numer Anal Methods Geomech.* 2020; 44: 405–417. <https://doi.or g/10.1002/nag.3022>.
- [33] Zhu, B, Hiraishi, T, Pei, H, Yang, Q. Efficient reliability analysis of slopes integrating the random field method and a Gaussian process regression-based surrogate model. *Int J Numer Anal Methods Geomech.* 2021; 45: 478– 501. <https://doi.or g/10.1002/nag.3169>.
- [34] Jia, C, Huang, Q, Wang, G. Stability analysis of blocky structure system using discontinuity layout optimization. *Int J Numer Methods Eng.* 2020; 121: 5766– 5783. <https://doi.org/ 10.1002/nme.6523>.
- [35] Panda, R., Dash, S., Padhy, S., & Das, R. K. (2023). Diabetes Mellitus Prediction Through Interactive Machine Learning Approaches. In *Next Generation of Internet of Things* (pp. 143-152). Springer, Singapore.
- [36] Townsend, K. F., Gallen, S. F., & Clark, M. K. (2020). Quantifying near-surface rock strength on a regional scale from hillslope stability models. *Journal of Geophysical Research: Earth Surface*, 125, e2020JF005665. <https://doi.org/10.1029/202 0JF005665>.
- [37] Wei Chen, Dongbai Li, Ting Ma, Helin Fu, Yanpeng Du, "Stability Analysis of a Slope considering Two Reinforcement Processes", *Geofluids*, vol. 2020, Article ID 8828747, 13 pages, 2020. <https://doi.org/10.1155/2020/8828747>.

Cross-Event User Reaction Prediction on a Social Network Platform

Pramod Bide¹

Department of Computer Engineering
Sardar Patel Institute of Technology
Mumbai, Maharashtra, India 400058

Sudhir Dhage²

Department of Computer Engineering
Sardar Patel Institute of Technology
Mumbai, Maharashtra, India 400058

Abstract—Social network surges with multiple tweets with mixture of multiple emotions by many users when events like rape, robbery, war and murder, we use this user data to analyze user emotions between cross-events and try to predict user reactions for the next possible such event. Cross-events are a series of events that belong under the same umbrella of topics and are related to the events occurring prior to it. The proposed system solve this problem using collaborative filtering using Topical and Social context. The Text Rank Algorithm is an unsupervised algorithm used for keyword extraction. Count Vectorizer is used on preprocessed text to get the frequency of words throughout the text which is used as training data to get a probability of emotion using a logistic regression model. We incorporated social context along with topical context to account for homophily and used the Low-rank matrix factorization method for user-topic prediction. The model as an output gives a total of 8 emotions which include Shame, Disgust, Anger, Fear, Sadness, Neutral, Surprise and Joy. Finally, the model is able to predict emotions with an accuracy of 95% considering cross events.

Keywords—Twitter; cross events; collaborative filtering; logistic regression; social and topical context

I. INTRODUCTION

With the advancement in technology, global news can quickly spread across the globe in a very small amount of time. Popular news spreads quickly through the internet like wildfire and all the people across the world try putting forth their opinion on social media. Social media has given rise to a platform where people can express their views on a particular topic. It has led to a formation of a community where like minded people group together. One of the most popular social media platforms to voice opinions is twitter where opinions about various global news are shared. There are over 330 million active users on twitter monthly and 145 million active users on twitter daily. There have been 1.3 billion twitter accounts created ever since twitter was launched in 2006. Thus, twitter's popularity and purpose can be a platform where a person's subjective feeling about a particular news is found in what a person tweets about it. It is a reflection of emotions a person feels towards the news and can be therefore equated. Twitter data has been used for multiple analysis because it acts as a dataset which tells us about the user. It has been used for applications like emotion detection [8], opinion tracking [9] and so on. However in our research work we have focused on a completely different domain of exploration that is to predict how a user will react to various events or sub events based on his historical tweets. Through our model we can identify the emotion a user will show if any

futuristic or hypothetical event is provided to a model. This kind of user reaction prediction can have a wide application in various domains. The government can use the data to predict the overall response on policies or it can also be used by companies to predict what a user reaction can be when a new product is launched in the market [10] [16] [17]. Additionally it can be used to model recommendations of new products [11]. To achieve this goal, we model the user-topic opinion prediction problem as a collaborative filtering task and present the topical context and social context incorporated matrix factorization method (TcScMF) framework, which includes social context and topical context as regularisation constraints. This paradigm is quite broad, and it may easily be applied to various social network setups or expanded to include other requirements. A real-world data set is gathered from Twitter, and labelled positive/negative user-topic opinions are obtained for evaluation by assessing sentiment in the observed tweets with a credible tool. We compare the proposed framework to state-of-the-art collaborative filtering methods in the trials. The experimental results show that using the TcScMF framework with social and topical context improves prediction accuracy.

A key point in our methodology is that we make use of ingenious ways to gather meaningful and clean data from twitter. One major problem that we faced while improving the accuracy of the model was sparseness of the user topic matrix. It was indeed very difficult to identify topics where the set of users are closely related to each other and have reacted to similar topics. We solve this problem by improving our data collection methodology where we first focus on identifying closely related users followed by filtering out common topics where they have reacted. This allowed us to improve the accuracy of our model by twice its original value.

Other than this, we were also keen on finalizing the ideal metric to compare users and topics in order to incorporate social and topical context. We experimented with different vector similarity measures like Cosine Similarity, Soft Cosine Similarity, Jaccard Similarity and Spearman's Rank Correlation Coefficient and we concluded that the choice of the similarity function is closely related to the type of dataset that we are working with. In our case we proceed with cosine similarity considering the size of our dataset as well as the results reflected by our model.

Last but not the least, we also expand the range of emotions that we are working with. Most data analysing techniques usually classify the given data in a binary fashion. But we incorporate a range of emotions and make sure that our model

works with this range at every stage including the loss function and the accuracy measure step. This allows our model to be robust in nature and accommodate a diverse dataset and reflect the same in the results produced.

The structure of the remaining paper is as follows. Section II is the literature survey that we undertook before working on this. It identifies the current research work and gaps in them. In Section III we talk about our method of identifying the dataset and what the dataset looks like. In Section IV we have described our model in detail. In Section V we talk about results and in Section VI what we conclude from the research work. In Section VII, we talk about the references.

II. LITERATURE SURVEY

Nicolas Esquivel et al. [1] presents a CLSTM-NN to forecast the existence of crime events across Baltimore. Matrixes of previous criminal occurrences, in particular, are utilised as input to forecast the existence of at least single event that happens. The dataset was acquired from the Open Baltimore portal's Public Safety domain. The model performed better, with an accuracy of 0.86 utilising sequences of matrices of events that occurred over the course of seven days. The results suggest that model can learn past geographical patterns and forecast the presence of crimes in the future. The spatio-temporal resolution of forecasts is hampered by poor performance for a small percentage of crime episodes.

Yizhou Xu et al. [2] proposed to model which would predict alarm events that are due, using similar alarm patterns in flood alarm sequences. It begins by arranging the alert patterns in order of resemblance to the current alert in descending order. A Bayesian approximation is used to calculate the probabilities and confidence levels for all projected alert events. When nuisance alerts were received, they were ignored and produced no anomalies.

A method that takes into consideration the behaviours and characteristics of the user, to identify and accurately predict hot events is given by Xichan Nie, et al. [3] The similar topics on twitter are collected and segregated using semantic similarity, all this is done after applying natural language processing on the keywords extracted from these tweets. Then a relationship between the users is derived. The user information proved to be useful and gave better results on experimentation. When compared to previous models, the suggested method enhanced prediction precision by 27%, 23.5 percent accuracy, as well as 20 percent recall rate, indicating that the model efficiently anticipated hot events. Other similar methods also work on identifying "social hotspots" such as Krishna et al. [23] and Xiao et al. [19].

Alberto Rossi, et al. [4] develops an attention mechanism as well as a LSTM network - RNN method for modelling taxi driver performance and storing the semantics of famous attractions in order to anticipate a cab's next destination using spatial location from LBSNs. The datasets used were taxi paths datasets. The results show that LSTM lowers the EDS in Porto and Manhattan by 10.5 percent and 18 percent, respectively, compared to MMLP. The suggested model, like most deep-learning algorithms, lacks explainability. Because travel utility features such as journey distance, cost, and time are not accessible at the time of the prediction, the approach cannot

use them. Owing to the length limit, it may be difficult to create a precise estimation that will identify catastrophic occurrences using tweets, which may lack appropriate context and be difficult to discriminate due to word ambiguity. Song, Guizhe and Huang, Degen [5] designed a model named SentiBERT-BiLSTM-CNN which detects diaster using Tweets. To generate sentimental contextual embeddings from a Tweet the proposed pipeline uses SentiBERT, for feature extraction they used a 1D convolutional layer. The suggested model outperforms the competition in the F1 score, making it a viable model for Tweets-based diaster prediction. The CNN model gave a precision of 0.8064, BiLSTM gave 0.8571 while SentiBERT-BiLSTM-CNN gave a precision of 0.9305 making it the best model. Because specific keywords may occur in both catastrophe and non-disaster Tweets, the model's recommended accuracy can be considerably improved. However, it is difficult to successfully employ the words as additional information to help enhance the detection accuracy.

Gan, Mingxin and Xiao, Kejun [6] concluded that prior studies had failed to account for the sequential characteristics of users' click behaviour, hence the focus was on overcoming such restrictions. R-RNN is a model for understanding a user's interest from his general click history, according to the study. The Amazon Dataset was used to conduct the study. Few of the previous models are all outperformed by the recommended model, thanks to the newly introduced click behaviour patterns and the R-RNN for CTR prediction design's adopted RNN, which gathers user stats from the most recent click sequences.

Song et al. [7] suggested a semi-online Computational Offloading Model. Reinforcement learning is used to investigate user behaviour in a sophisticated action space in order to catch unknown environment information. The research proposes a dynamic edge computing simulation environment to show that user behaviour has a significant impact on system utilisation. According to their research, the mean size of offloading activities accomplished is roughly ten thousand. Large-scale Computation offloading projects could not be resolved using these strategies. This paradigm offloads compute chores based on changing contexts, although it is made up of MEC systems loosely.

A variety of media is used by different authors; C.Fu et al. [13] use micro blog user features, while Z.Zhang et al. [15] apply a situational analysis method on data from multimedia social networks. Other approach's such as M.Nyugen et al.'s hybrid generative model [12] and Chen et al.'s ensemble methodology [14] seek to combine multiple techniques to give a better result.

Through their work in [18] N Zhang et al. proposed a novel user behavior prediction model which uses automatic annotation. The model uses a combination of the Discontinuous Solving Order Sequence Mining (DVSM) behavior recognition model coupled with the LSTM based behavior prediction model. Factorization machines are applied to predict user behavior in the work of Y Wang et al. [20].

In their paper[22], Hao. et al. perform analysis on huge multi-data source of comprehensive quality. They analyse the user behavior acquisition and simulation prediction framework construction method which relies on user perception.

Hui Zhang et al.'s research[21] proposes a solution for user

prediction that concerns the single user - multiple terminal use-case. They perform weight correction that is based on adapted feedback, which is used to create a Markov model. This model can predict the user's future service states. A corresponding heavy tailed model is used to predict the duration of the service as well. Their work further integrates preference of service with the attributes of the terminal. This establishes a matching metric of services and terminal. This enables the proposal of terminal service model for recommending the best service terminal to each user.

III. DATASET

The dataset was collected by scrapping twitter data. The data collected by us have many users who might have tweeted over multiple different topics. We used sns scrape a python package to scrape data because of it increased limits. There were multiple major events identified and under every major events many sub events were considered. For example Covid-19 was the major event and the sub events under it were lockdown, vaccination and so on. The methodology we decided to use was to identify the top most 100 influential users which solved our problem of overlapping users. After that we scrapped only their tweets from their profile about our list of subtopics. The dataset thus formed had over 10,00,000 tweets across all sub events.

IV. PROPOSED METHODOLOGY

A. Keywords Extraction

A keyword extraction models goal is to automatically find a group of phrases in a tweet that best characterise the content. TextRank algorithm has been used for Keywords extraction from tweets. This algorithm is fully unsupervised.

Non-printable characters (if any) are removed from the raw input tweet before it is converted to lower case. The tokenization of the processed input text is performed using Natural Language Toolkit (NLTK) library methods. To allow the words to be lemmatized based on their Part-of-speech (POS) tags, Natural Language toolkit is used to Part-of-speech (POS) tag the input tweet. Lemmatization is used to normalise the tokenized text (mostly nouns and adjectives). Different grammatical equivalents of a word are replaced by a single fundamental lemma in lemmatization. The lemmatized text is then Part-of-speech (POS) labelled. Later on, the tags are utilised for filtering.

Any word from the lemmatized text that is not a noun, adjective, or a foreign word is regarded a stop word in this context. This is predicated on the premise that keywords are often nouns, adjectives, or gerunds. Punctuations are also included to the list of stopwords. Even after we eliminate the stop words, there may still be some exceedingly frequent nouns, adjectives, or gerunds that are poor candidates for being keywords. An external file containing a list of stopwords is loaded, and each word is added to the preceding stopwords to form the final list stopwords-plus, which is then turned into a set. Stopwords-plus are all stop words and possible phrase-delimiters combined. The contents of this collection are used to divide the lemmatized text into n-gram phrases later on. However, we simply eliminate the stop words and operate with a bag-of-words method. The stop words are then removed from

the lemmatized text. Only unique words from the processed text are stored in a set.

TextRank is a graph-based approach, which necessitates the creation of a graph. Each word in the dictionary will act as a graph vertex. The phrases in the vertices will be indicated by their index in the list. The edge connections between all vertices are stored in the weighted edge matrix. A graph is made with undirected, heavy edges. The weight of the connecting edge between the word vertex represented by index a and the word vertex represented by b is stored in weighted edge[a][b]. When weighted edge[a][b] is 0, it signifies that there is no edge or relationship between the words represented by index a and b. If the words co-occur inside a window of a defined window size in the processed text, there is a relationship between them and hence between a and b, which represents them. For each link detected between the same words in various regions of the text, we raise the value of the weighted edge[a][b] by $(1/(\text{distance between positions of words now represented by a and b}))$. The covered co-occurrences list which contains of a list of pairs of absolute positions in processed text of words whose co-occurrence at that location has already been checked, is managed in such a way that the same two words located in the same positions in processed text are not counted repeatedly while sliding the window one text unit at a time. All vertices start with a score of one. Because self-connections are ignored, weighted edge [a][b] are 0 initially. The total number of undirected edges associated with the vertex represented by p are stored in $x[p]$.

The formula for scoring a vertex represented by a is as follows:

$$s[a] = (1 - r) + r[\sum(j)((we[a][b]/x[b]) * s[b])] \quad (1)$$

In the Eq. (1), r is the damping factor and b is one of the vertices that has a relationship to a. 'we' represents weighted edge. The score is updated repeatedly until convergence is reached.

Using stopwords as delimiters, lemmatized text is partitioned into phrases. These phrases are also potential possibilities for keyphrase extraction. Then a list of unique phrases is created and removing single-word key-candidates in favour of multi-word alternatives. Candidate-key phrases are scored and a list of key phrases is compiled by listing untokenized variants of tokenized words. Phrases are graded by summing the scores of their constituents i.e. words or text-units that were ranked by the graph algorithm. Keys are ranked based on their computed scores.

B. Emotion Detection

For setting up the emotion detection domain of our proposed solution, we leveraged neattext python library. A data set having more than 34 thousand tweets and its corresponding emotion was used for this. Firstly, all the username and tags were removed from each individual tweet and after that removal of stopwords took place. After this step all the stopwords like 'an', 'be', 'some', 'for', 'do', 'its', 'of', 'as', etc. are removed from the tweets for optimising the emotion prediction, reducing the computation time and resources.

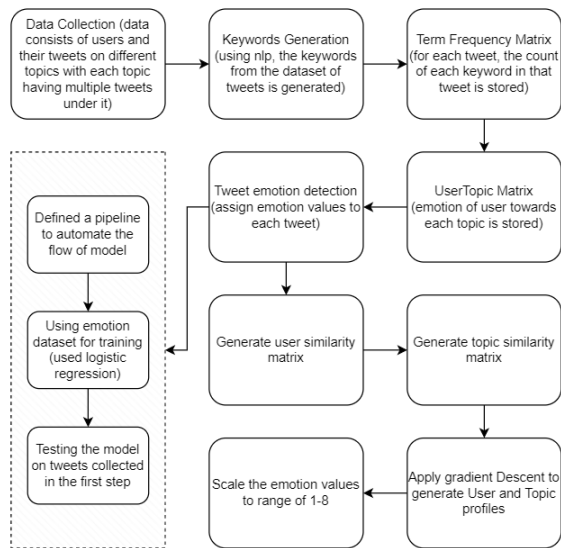


Fig. 1. Social and Topical Context System Framework.

The algorithm was trained using a dataset of 34762 tweets that included their moods. The data set is separated into training and test sets after usernames, tags, and stopwords are removed, and the model is trained on this data. Count Vectorizer is a tool that converts a text into a vector depending on the count of each word in the text. Logistic Regression is a machine learning classification algorithm which is applied to train the model precisely and predict the probability of an emotion. Finally, the web scraped twitter data set is passed to the model and emotion of each tweet is predicted.

C. Social and Topical Context System Framework

In the above Fig. 1, the basic flow of the execution of the model is given, starting from data collection to getting the results from the trained model. The initial step is the data collection, in which data about different twitter users and the tweets of specific topics they have tweeted on, is gathered. The next step is the processing of the tweets to generate the keywords file, which is done using nlp(natural language processing) which has been described above. Then the term frequency matrix is generated following which the UserTopic matrix is generated. Emotion detection model is applied on the collected tweets, the process of which is given in detail in the 'Emotion Detection' section. After completing these steps, we then generate the similarity matrices for users and tweets and after training the model, we then scale the emotion values which we get in the result in the range of 1-8.

D. Model Outline

The main purpose of the model is to analyse the users in a given set and predict their reactions on related events. It has been historically proven that the views of any user is influenced by the closest networks of users with similar interests as the user in question along with the similarity of the actual topic to other topics the user has already reacted upon. Although this system should be enough to deduce the reaction of a

user in any two non-related events as well, we found that solely relying on user similarity or topic similarity yielded poor results as compared to using both of them. The most effective use of the above mentioned strategy is in the case of multi-phase events which are closely related to each other. At the same time, the similarity measures used to calculate the similarity of different users and different topics also plays a key role in the preparation of the model. Inline with our previous approach, we experimented with different similarity measures, some of which are Cosine Similarity, Manhattan Distance, Jaccard Similarity, Euclidian Distance and we found that the choice of the similarity function is closely related to the type of dataset we are working with. In our original scenario where we were dealing with sparse data, we found that Cosine Similarity was very effective however, implementing the same for dense matrices proved to be computationally expensive and in such scenarios, a simple Euclidian calculation was far easier.

E. Data Scarcity Problem and our Solution

In a quest to find similar users who reacted on similar topics, we found that such datasets are very difficult to acquire and in most cases, the data itself appeared to be biased as we would end up reading multiple accounts of the same user. Eliminating the above problem left us with a very scarce user-topic matrix where only a couple of users might have reacted on the same topic and vice versa. In order to make the user-topic matrix denser, we come up with a unique solution which is explained as follows; We first divide the user-topic matrix into different sections, essentially following a divide and conquer strategy. In the smaller subsections of the matrix, we make sure that multiple users have tweeted or reacted on the same topic and similarly, a single user has tweeted on multiple topics in the same sub-section. We found experimentally, that such local optimizations eventually lead to global patterns, and helps us develop a more robust model.

F. Social and Topical Context Mode Framework

We follow the below mentioned algorithm which incorporates our unique approach to solve the data scarcity problem and gives an outline of the model pipeline which is explained in detail later in the paper. Table I indicates all the parameters used in designing the Social Context and Topical Context Mode Framework (ScTcMF).

G. Example

Let say we have 4 users, User A, User B, User C and User D. We'll consider the main topic Covid and use the tweets by the users on the sub topics - 1st Dose, Omicron, Booster Dose and Lockdown.

User A (Newsweek) tweeted "Kate Middleton shares COVID vaccine photo, "hugely grateful" after 1st dose" on the sub topic 1st Dose and the emotion for the tweet was predicted to be Joy. User A tweeted "The highly mutated and contagious Omicron variant has driven the country to record the most cases in a day that any country has reported." on the sub topic Omicron and the emotion for the tweet was predicted to be Joy. User A tweeted "People struggling to get booster dose appointments could leave millions of Americans vulnerable as Omicron spreads." and the emotion for the tweet was

TABLE I. IMPORTANT PARAMETERS IN OUR MODEL

Sr. no.	Parameter	Description
1	α	Balances the error function between front terms and the social context normalisation terms
2	β	Controls the topical context's regularisation requirement
3	λ_0	Controls the reach of regularization
4	λ_1	Controls the reach of regularization
5	A	User-Topic Opinion Matrix
6	E	Latent Representation of User
7	G	Latent Representation of Topic
8	$\ \cdot\ _F$	Frobenius norm of a matrix
9	P	Indicator Matrix
10	\odot	Hadamard product
11	$Q(v,w)$	Weighted number representing the similarity of two social friends' past opinions
12	$F(v)$	Set of social friends of $u(v)$
13	$Tr(\cdot)$	Matrix Trace
14	$Diag_Q$	Diagonal Matrix
15	L_Q	Laplacian Matrix

Algorithm 1 Social and Topical Context Model Framework (ScTCMF)

- 1) Collect data for different kinds of events and identify sub-events of each of the events.
- 2) Identify the most active users from each of the sub-events and collect their twitter data.
- 3) Use the keywords extraction pipeline to extract important words from each and every tweet. This is further used for emotion detection.
- 4) Use the emotion detection pipeline to understand the text of the tweets and extract meaningful emotions in a range of 1-8.
- 5) Use TF-IDF to calculate the frequencies of each word of each tweet across multiple tweets of the same sub-event.
- 6) Initialize hyper-parameters like social and topical regularization factors and learning rate.
- 7) Calculate user and topic similarity using Laplace reductions and the original frequency matrix calculated previously. While doing so, choose an appropriate similarity function.
- 8) Perform stochastic gradient descent to estimate the user-topic matrix thereby predicting the user's reaction to unknown events.
- 9) Compare the result with the original matrix to retrieve the accuracy of the model. Different deviations can be used to calculate the accuracy in different scenarios.

predicted to be Disgust. User A tweeted “Xi’an residents can’t leave homes, purchasing food difficult as COVID lockdown continues” on the sub topic Lockdown and the emotion for the tweet was predicted to be Sadness.

User B (bsindia) tweeted “TOP HEADLINES — PM @narendramodi receives his 1st #Covid19vaccine dose at AIIMS; @TheOfficialSBI reduces #homeloan rates to 6.7% ; European #stocks rebound as bond markets stabilise and more...” on the sub topic 1st Dose and the emotion for the tweet was predicted to be Joy. User B tweeted “Amid surging COVID-19 cases, the Delhi Disaster Management Authority has decided to impose a weekend curfew in the national capital.” on the sub topic Omicron and the emotion for the tweet was predicted to be Anger. User B tweeted “A Delhi-based doctor said that a booster dose of Cov vaccine is a must as the protection cover of two doses declines over three to six months” on the sub topic Booster Dose and the emotion for the tweet was predicted to be Sadness. User B tweeted “#Mumbai Mayor Kishori Pednekar on Tuesday said if the daily COVID-19 cases here cross the 20,000-mark, a #lockdown will be imposed in the city as per the Union government’s rules.” on the sub topic Lockdown and the emotion for the tweet was predicted to be Anger.

User C (ChannelNewsAsia) tweeted “Duchess of Cambridge ‘hugely grateful’ for 1st vaccine dose” on the sub topic 1st Dose and the emotion for the tweet was predicted to be Joy. User C tweeted “Commentary: With Omicron threat, will returning to offices and schools bring new anxieties?” on the sub topic Omicron and the emotion for the tweet was predicted to be Joy. User C tweeted “Australia to shorten COVID-19 booster dose intervals from January” on the sub topic Booster Dose and the emotion for the tweet was predicted to be Joy. User C tweeted “Amid Omicron surge, UK PM Johnson resists another lockdown” on the sub topic Lockdown and the emotion for the tweet was predicted to be Neutral.

User D (TheQuint) tweeted “#Live — Around 90 percent adult population #vaccinated With #1stDose.” on the sub topic 1st Dose and the emotion for the tweet was predicted to be Sadness. User D tweeted “#Podcast — Given the explosive growth of #COVID cases in India, are we underplaying the threat of #Omicron and its potential impact on our fragile health care system? We discuss with @MenonBioPhysics and @RajeevJayadevan. Tune in!” on the sub topic Omicron and the emotion for the tweet was predicted to be Fear. User D tweeted “#BharatBiotech on 20 Dec, sought approval from the #DCGI for the conduction of phase-3 trials for its intranasal vaccine (BBV154), which is to be used as a booster dose.” on the sub topic Booster Dose and the emotion for the tweet was predicted to be Fear. User D tweeted “#LIVE — ‘We will have to impose #lockdown in #Mumbai if daily #COVID cases cross the 20,000-mark,’ said Mayor Kishori Pednekar.” on the sub topic Lockdown and the emotion for the tweet was predicted to be Anger.

Now we’ll take a different sub topic say “Social Distancing” and we’ll see the tweets and its emotions predicted by our model for the above users. The model predicts that User A will tweet “Many health experts are now calling on the South Korean government to reimpose social distancing measures.” on the given sub topic Social distancing and the emotion predicted by the model for the tweet was found

to be Sadness. The model predicts that User B will tweet “#Britain’s economic growth slowed more than expected in July as concern about the spread of the delta variant of #Covid-19 overshadowed the government’s decision to end most social distancing rules” on the given sub topic Social distancing and the emotion predicted by the model for the tweet was found to be Fear. The model predicts that User C will tweet “France plans tighter social distancing rules, booster ramp-up to fight COVID-19 wave” on the given sub topic Social distancing and the emotion predicted by the model for the tweet was found to be Sadness. The model predicts that User D will tweet “Amid videos of crowds flouting social distancing norms in #SarojiniNagar market surfaced, the Delhi High Court on 24 December rapped the New Delhi Municipal Council and Delhi Police for allowing illegal vendors to operate from there.” on the given sub topic Social distancing and the emotion predicted by the model for the tweet was found to be Fear.

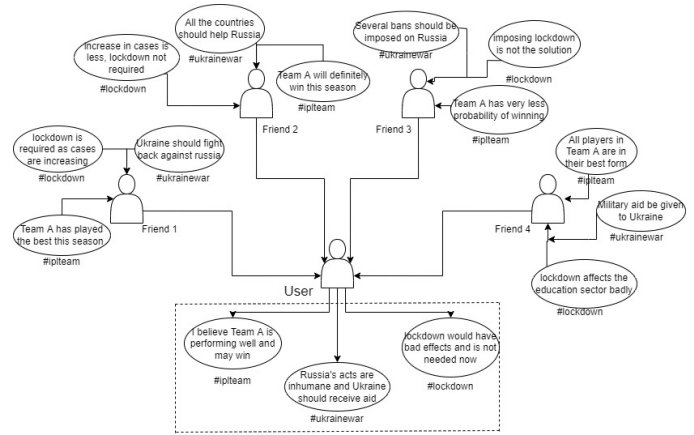


Fig. 2. Opinion Prediction.

H. User Topic Matrix

For user topic view prediction, a low rank matrix factorization algorithm was applied. The user-topic prediction model incorporates social and topical context mathematically. Matrix Factorization is commonly used in cutting-edge Collaborative filtering works.

In our scenario, because the user topic opinions in Twitter data is so less, the matrix A is highly scattered. Based on the assumptions that only a few factors impact the opinions, a more concise but accurate depiction is provided and goal to replicate the matrix by a multiplication of low rank factors.

$$A \approx EG^T \quad (2)$$

In Eq. (2), $E \in \mathbb{R}^p$ and $G \in \mathbb{R}^q$ where $p = a * c$ where $q = b * c$ with $c \ll \min(a,b)$ the row vector $E(k, :)$, $1 \leq k \leq a$ and $G(o, :)$, $1 \leq o \leq b$ are the existing depictions of user e_k and topic g_o . Here R denotes Real numbers, E is the Latent Representation of user and G represents the Latent representation of Topic. By minimising the following aim, the matrix factorization technique approximates the matrix A given in Eq. (3):

$$\min_{E,G} \|A - EG^R\|_F^2 \quad (3)$$

In order to simulate the labelled viewpoints i.e. opinions we make use of matrix P $\in \mathbb{R}^r$ where $r = a*b$. If e_k provided his view for g_o then we will consider the value at k,o index in the matrix P to be 1 and equal to 0 otherwise. Normalisation terms have been added to avoid overfitting. λ_0 and λ_1 are the control parameters. The basic low rank factorisation model is as follows illustrated by Eq. (4):

$$\min_{E,G} \|P \odot (A - EG^R)\|_F^2 + \lambda_0 \|E\|_F^2 + \lambda_1 \|G\|_F^2 \quad (4)$$

Fig. 2 illustrates the opinion prediction for user under influence. As shown, the user has four friends with different opinions on three different topics and based on the opinions the user’s opinion on these topics is impacted. Considering the topic “#Ukrainevar” the user’s friends have shown support to Ukraine in their tweets and also few tweets with support to Russia. The opinion of the user for this topic is also seen to be in favour of Ukraine. Thus the tweet of the user shows a similar emotion to that of the majority of his followers or tweets of people he/she sees.

I. Implementing Social Context

Homophily is a phenomenon that occurs in social networks. Forming a following connection on any social media platform typically suggests that the follower and the buddy have similar interests, and hence have more comparable perspectives on the same issue. Both users friends and followers are considered to be his social buddies. To establish the social context, we convert the directed network to undirected network. The Twitter users’ social environment may thus be represented as an undirected weighted network with a symmetric adjacency matrix Q. Social friends are more likely to have similar viewpoints on issues than non social friends. Based on the above premise, we evaluate previous opinion similarity across social friends to represent user viewpoint variety and suggest a normalisation constraint as shown below,

$$\frac{1}{2} \sum_{v=1}^a \sum_{w \in F(v)} Q(v,w) \|E(v, :) - E(w, :)\|_F^2 \quad (5)$$

In Eq. (5), F(v) indicates a group of social acquaintances and Q(v,w) is the weighted number representing the similarity of two social friends’ past opinions. Large value of Q(v,w) indicates that divergence will be less and vice versa.

Matrix form of the above equation,

$$\begin{aligned}
 X &= \frac{1}{2} \sum_{v=1}^a \sum_{w \in F(v)} Q(v, w) \|E(v, :) - E(w, :)\|_F^2 \\
 &= \frac{1}{2} \sum_{v=1}^a \sum_{w \in F(v)} \sum_{x=1}^c Q(v, w) (E(v, x) - E(w, x))^2 \\
 &= \sum_{v=1}^a \sum_{w \in F(v)} \sum_{x=1}^c Q(v, w) [E^2(i, k) - E(v, x)E(w, x)] \\
 &= \sum_{x=1}^c E^T(:, x) (Diag_Q - Q) E(:, x) \\
 &= Tr(E^R L_Q E)
 \end{aligned} \tag{6}$$

In Eq. (6), $Diag_Q$ is the diagonal matrix, L_Q is the laplacian matrix and Tr denotes the trace of the matrix. The resulting Matrix Factorisation model which involves social context is as follows illustrated by Eq. (7),

$$\begin{aligned}
 \min_{E, G} \|P \odot (A - EG^O)\|_F^2 + \lambda_0 \|E\|_F^2 + \\
 \lambda_1 \|G\|_F^2 + \alpha Tr(E^O L_Q E)
 \end{aligned} \tag{7}$$

The regularisation parameter balances the reconstruction error between the social context regularisation term and the front terms, $\alpha \geq 0$. The User Opinion Similarity (UOS) is calculated by the given formula in Eq. (8),

$$UOS(e_v, e_w) = \frac{\sum_{x=1}^b A_{i_x} \cdot A_{j_x}}{\sqrt{\sum_{x=1}^b A_{v_x}^2} \sqrt{\sum_{x=1}^b A_{w_x}^2}} \tag{8}$$

A mapping is used to constrain the range of User Opinion Similarity between [0,1] where $UOS(e_v, e_w) = (UOS(e_v, e_w) + 1)/2$ is given by Eq. (9),

$$Q(v, w) = \begin{cases} UOS(e_v, e_w), & \text{if } e_w \in F(e_v) \\ 0, & \text{otherwise} \end{cases} \tag{9}$$

J. Implementing Topical Context

The topical context interpretation model is that consumers will supply more similar opinions to two topics that are more related in content.

$$\frac{1}{2} \sum_{v=1}^b \sum_{w=1}^b R(v, w) \|G(v, :) - G(w, :)\|_F^2 \tag{10}$$

In Eq. (10), $G(v, w)$ represents the similarity index between the topics r_v and r_w . Greater value of $R(v, w)$ infers that the topics r_v and r_w are very similar to each other having more similar opinions of users. On the other hand, low value of $R(v, w)$ infers that the topic representations $G(v, :)$ and $G(w, :)$ have large distance between them. As per the topical context derivations mentioned earlier, we can obtain the matrix equivalent of the above equation as follows in Eq. (11):

$$\begin{aligned}
 Z &= \frac{1}{2} \sum_{v=1}^b \sum_{w=1}^b R(v, w) \|G(v, :) - G(w, :)\|_F^2 \\
 &= \sum_{x=1}^d G^R(:, x) (Diag_R - R) G(:, x) \\
 &= Tr(G^R L_R G)
 \end{aligned} \tag{11}$$

Likewise, $Diag_R$ is a diagonal matrix and L_R is the laplacian matrix. The model with topical context regularization is given below in Eq. (12),

$$\begin{aligned}
 \min_{E, G} \|P \odot (A - EG^R)\|_F^2 + \lambda_0 \|E\|_F^2 + \\
 \lambda_1 \|G\|_F^2 + \beta Tr(G^R L_R G)
 \end{aligned} \tag{12}$$

Here, A regularisation parameter $\beta \geq 0$ is used to adjust the regularisation requirement of topical context. After analyzing many approaches for measuring similarity using topic distribution, we chose Cosine Similarity due to its efficacy and simplicity. By using the unique terms showing up in the tweets collection as features upon removing stop words and the term frequency as a feature value, a cosine similarity between term frequency vectors could have been used to quantify the content based resemblances between similar topics. A term frequency vector f_{v_i} could be formed for each topic t_i by taking the unique terms making an appearance in the tweets gathering as features after removing stop words and the term frequency as a feature value. The similarity values in this definition vary from 0 to 1 since the word frequency cannot be negative. As a result, Topic Content Similarity was assigned (TCS).

$$TCS(r_v, r_w) = \frac{\sum_{x=1}^B f_{v_{v_x}} \cdot f_{v_{w_x}}}{\sqrt{\sum_{x=1}^B f_{v_{v_x}}^2} \sqrt{\sum_{x=1}^B f_{v_{w_x}}^2}} \tag{13}$$

In Eq. (13), f_{v_v} and f_{v_w} denote the term frequency vectors of r_v and r_w respectively, and B is the number of features in the vectors. Finally the element $R(v, w)$ can be shown as follows in Eq. (14):

$$R(v, w) = \begin{cases} TCS(r_v, r_w), & \text{if } v \neq w \\ 0, & \text{otherwise} \end{cases} \tag{14}$$

K. Framework with Topical and Social Context

We created and comprehended functions for social context and topical context, and then used them to describe regularisation restrictions. In this part, we develop a shared framework that incorporates both social and topical background.

This framework is used to minimize the objective function

given below in Eq. (16):

$$\begin{aligned}
 f(E, G) = & \|P \odot (A - EG^R)\|_F^2 + \lambda_0 \|E\|_F^2 + \lambda_1 \|G\|_F^2 \\
 & + \frac{\alpha}{2} \sum_{v=1}^a \sum_{w \in F(v)} Q(v, w) \|E(v, :) - E(w, :)\|_F^2 \\
 & + \frac{\beta}{2} \sum_{v=1}^a \sum_{w=1}^b R(v, w) \|G(v, :) - G(w, :)\|_F^2
 \end{aligned} \tag{15}$$

$$\begin{aligned}
 f(E, G) = & \|P \odot (A - EG^R)\|_F^2 + \lambda_0 \|E\|_F^2 + \lambda_1 \|G\|_F^2 \\
 & + \alpha \text{Tr}(E^R L_Q E) + \beta \text{Tr}(G^R L_R G)
 \end{aligned} \tag{16}$$

where $\alpha \geq 0$ and $\beta \geq 0$ are the social and topical normalisation parameter that can be changed to impact the findings in different ways. $\alpha=0$ and $\beta > 0$ infers that the framework discusses just the topical context. On the other hand $\alpha > 0$ and $\beta = 0$ infers that the framework discusses just the social context. When $\alpha = 0$ and $\beta = 0$ the method reverts to the simplest matrix factorization. In the proposed method it is suggested to keep $\alpha > 0$ and $\beta > 0$.

For proper training and simplicity purpose we implement gradient descent to find the local maxima/minima and solve the objective function, thus updating E_{r+1} and G_{r+1} . The formula for which are given in Eq. (17) and Eq. (18),

$$E_{r+1} = E_r - \gamma \nabla_E f(E_r, G_r) \tag{17}$$

$$G_{r+1} = G_r - \gamma \nabla_G f(E_r, G_r) \tag{18}$$

Here the step size is γ , $\nabla_E f(E_r, G_r)$ and $\nabla_G f(E_r, G_r)$ are gradients in step $r+1$ which are termed as partial derivatives to E and G,

$$\begin{aligned}
 \nabla_E f(E_r, G_r) = & -2(P \odot A_r)G_r + 2P \odot (E_r G_r^R)G_r \\
 & + 2\lambda_0 E_r + 2\alpha L_Q E_r
 \end{aligned} \tag{19}$$

$$\begin{aligned}
 \nabla_G f(E_r, G_r) = & -2(P \odot A_r)^R E_r + 2(P \odot (E_r G_r^R))^R E_r \\
 & + 2\lambda_1 G_r + 2\beta L_R G_r
 \end{aligned} \tag{20}$$

V. EXPERIMENTAL RESULTS

Our proposed model compares non zero values of the original matrix with a value of the model predicted matrix. We have considered a total of 8 emotions which include Shame, Disgust, Anger, Fear, Sadness, Neutral, Surprise and Joy and they were numbered from 1-8.

When there was no deviation i.e. we tried for an exact match of emotions we get an accuracy of 65%. If we allow the prediction model to have a deviation of +1 or -1 from the original emotion, we get an accuracy of 84%. If we allow

the prediction model to have a deviation of +2 or -2 from the original emotion, we get an accuracy of 95%.

We must note that +1 or -1 deviation should also be acceptable since many a times shame can be misjudged as disgust and vice versa. The model generated the best results when the gradient descent steps were fixed at 100. In both the original matrix factorization and the regularisation terms, the regularisation parameters are set to balance the reconstruction error. As a result, α and β are critical in deciding how much the framework approach can benefit from the social and topical environment's regularisation limits.

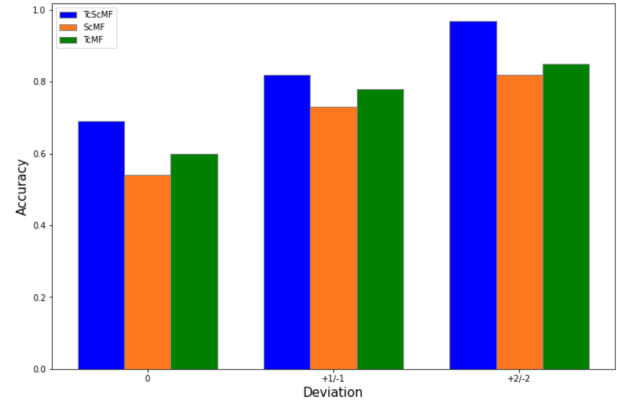


Fig. 3. Accuracy Comparison.

Fig. 3 gives a brief description of the accuracy of the model with different toleration levels. In order to calculate the accuracy of the model we first obtain a matrix that contains known values. This is because it is not necessary that every user in our original dataset or test set has reacted to every different tweet in the dataset. Hence to eliminate verifying against known data we first take a subset of the original dataset and maintain only known values in the matrix. The format of the matrix is constructed in a manner that each row represents unique users in the dataset and the columns represent unique topics. Hence each cell represents the opinions of a user on a given topic. Since our scale of emotions ranges from 1-8 we replace the value of cells with unknown values with 0. Our model is able to predict the reaction of every user on every topic, hence it returns a populated user and topic matrix whose product results in a matrix that is similar to the original user topic matrix. Once we obtain the predictions of the model, we iterate over each user and consecutively each topic and then compare the predicted value with the original value. Note that this is done only for cells whose value is not 0 in the original user topic matrix. Next we define a tolerance level which ranges from 0 to 2. This means that if a user had a reaction of 1 in the original matrix and if the model predicted 2, then we will consider this as a correct prediction only if the tolerance level is 1 or 2. This is because we assume that a tolerance level of 1 allows a deviation of 1 from the original value. Let's consider an example where we have users A and B and topics X and Y. Now user A has only reacted to topic X with an emotion of 2 and user B has reacted to topic Y with an emotion of 7. The original matrix in this case will look as follows: $\{ \{2, 0\}, \{0, 7\} \}$. Now let's assume that after passing our data through the model we obtain a predicted matrix which

looks like this: $[\{3, 1\}, \{6, 7\}]$. Now while calculating the accuracy of the model we will iterate over user A and B and in a nested for loop iterate over topics X and Y. We will first encounter the first cell (0, 0). We will consider this value since the user A had reacted to topic X in the original scenario. Now if the tolerance level is 0, the predicted and original value will have a difference of 1 which does not fall within our tolerance level/deviation allowed. Hence we will not consider this as a correct prediction. Next we will ignore cells (0, 1) and (1, 0) since their values are not known (0) in the original dataset. Moving onto cell (1, 1), we will consider this value as a correct prediction since the difference between the predicted value and original value is 0 and they are an exact match. Hence in this scenario, out of 2 known values our model was able to predict 1 value properly as per our tolerance level and hence the accuracy turns out to be $\frac{1}{2} * 100$ which is 50%.

Fig. 3 displays the Accuracy comparison of the methods ScMF, TcMF and the ScTcMF incorporated by us. The results prove that ScTcMF: Framework with Topical and Social Context is the most efficient method. While testing our model, The values of λ_0 and λ_1 in the matrix factorization method was set to 1 and the values of α was set to 10 and that of β was set to 0.01. The Learning Rate was considered to be 0.01 and Number of Steps was set to 100. The Hyper parameters were tweaked so that we could get better accuracy.

VI. CONCLUSION

Our objective while writing this paper was to create a model and a framework that utilizes previous user reactions given a series of cross events to achieve user topic opinion prediction for future events. This was a novel idea because there are solutions that are used in predicting user emotion, but none of them explored this across cross events, which had its own set of challenges. We had to go through multiple iterations of data collection to get the right dataset which included multiple users that have tweeted on multiple topics. In this approach, we searched users on the basis of their activity across all the tweets and the top 100 among them were used as the dataset. This was crucial as a sparse matrix used for the low-rank factorization method would have resulted in poor model accuracy. Using this data, the keywords were extracted and the emotion was detected on a scale of 1 to 8 using the ScTcMF method. Finally, the results demonstrated that both social context and topical context can help improve the performance of the user-topic opinion prediction and by incorporating them we were able to get the model to the desired accuracy.

REFERENCES

- [1] Nicol áas Esquivel, Orietta Nicolis, Billy Peralta e Jorge Mateu. "Spatio-Temporal Prediction of Baltimore Crime Events Using CLSTM Neural Networks". Em: IEEE Access 8 (2020), pp. 209101–209112. DOI: 10.1109/ACCESS.2020.3036715.
- [2] Yizhou Xu, Jiandong Wang e Yan Yu. "Alarm Event Prediction From Historical Alarm Flood Sequences Based on Bayesian Estimators". Em: IEEE Transactions on Automation Science and Engineering 17.2 (2020), pp. 1070–1075. DOI: 10.1109/TASE.2019.2935629.
- [3] Xichan Nie, Wanshan Zhang, Yang Zhang e Dunhui Yu. "Method to Predict Bursty Hot Events on Twitter Based on User Relationship Network". Em: IEEE Access 8 (2020), pp. 44031–44040. DOI: 10.1109/ACCESS.2020.2977424.
- [4] Alberto Rossi, Gianni Barlacchi, Monica Bianchini e Bruno Lepri. "Modelling Taxi Drivers' Behaviour for the Next Destination Prediction". Em: IEEE Transactions on Intelligent Transportation Systems 21.7 (2020), pp. 2980–2989. DOI: 10.1109/TITS.2019.2922002.
- [5] Guizhe Song e Degen Huang. "A Sentiment-Aware Con-textual Model for Real-Time Disaster Prediction Using Twitter Data". Em: Future Internet 13.7 (2021). ISSN: 1999-5903. DOI: 10.3390/fi13070163. URL: <https://www.mdpi.com/1999-5903/13/7/163>.
- [6] Mingxin Gan e Kejun Xiao. "R-RNN: Extracting User Recent Behavior Sequence for Click-Through Rate Prediction". Em: IEEE Access 7 (2019), pp. 111767–111777. DOI: 10.1109/ACCESS.2019.2927717.
- [7] Shinan Song, Zhiyi Fang, Zhanyang Zhang, Chin-Ling Chen e Hongyu Sun. "Semi-Online Computational Offloading by Dueling Deep-Q Network for User Behavior Prediction". Em: IEEE Access 8 (2020), pp. 118192–118204. DOI: 10.1109/ACCESS.2020.3004861.
- [8] B. Pang and L. Lee, "Sentiment Analysis and Opinion Mining," Foundations and Trends in Information Retrieval, vol. 1, pp. 1-135, 2008.
- [9] X. An, R. A. Ganguly, Y. Fang, B. S. Scyphers, M. A. Hunter, and G. J. Dy. Tracking Climate Change Opinions from Twitter Data. In KDD'14: Workshop on Data Science for Social Good, 2014.
- [10] Lynn R. Kahle (1997, June). The real-time response survey in new product research: it's about time. Journal of Consumer Marketing, Vol 14, Issue 3, pp.234 – 248
- [11] Z. Su, Z. Lin, J. Ai and H. Li, "Rating Prediction in Recommender Systems Based on User Behavior Probability and Complex Network Modeling," in IEEE Access, vol. 9, pp. 30739-30749, 2021, doi: 10.1109/ACCESS.2021.3060016.
- [12] M. Nguyen and Y. Cho, "A Hybrid Generative Model for Online User Behavior Prediction," in IEEE Access, vol. 8, pp. 3761-3771, 2020, doi: 10.1109/ACCESS.2019.2962539.
- [13] C. Fu et al., "Forwarding Behavior Prediction Based on Microblog User Features," in IEEE Access, vol. 8, pp. 95170-95187, 2020, doi: 10.1109/ACCESS.2020.2995411.
- [14] L. Chen and H. Deng, "Predicting User Retweeting Behavior in Social Networks With a Novel Ensemble Learning Approach," in IEEE Access, vol. 8, pp. 148250-148263, 2020, doi: 10.1109/ACCESS.2020.3015397.
- [15] Z. Zhang, R. Sun, X. Wang and C. Zhao, "A Situational Analytic Method for User Behavior Pattern in Multimedia Social Networks," in IEEE Transactions on Big Data, vol. 5, no. 4, pp. 520-528, 1 Dec. 2019, doi: 10.1109/TBDDATA.2017.2657623.
- [16] G. Zhao, X. Qian and X. Xie, "User-Service Rating Prediction by Exploring Social Users' Rating Behaviors," in IEEE Transactions on Multimedia, vol. 18, no. 3, pp. 496-506, March 2016, doi: 10.1109/TMM.2016.2515362.
- [17] Q. Yanfang and L. Chen, "Research on E-commerce user churn prediction based on logistic regression," 2017 IEEE 2nd Information Technology, Networking, Electronic and Automation Control Conference (ITNEC), 2017, pp. 87-91, doi: 10.1109/ITNEC.2017.8284914.
- [18] N. Zhang, Y. Yan, X. Zhu and J. Wang, "A novel user behavior prediction model based on automatic annotated behavior recognition in smart home systems," in China Communications, doi: 10.23919/JCC.2022.00.005.
- [19] Y. Xiao, J. Li, Y. Zhu and Q. Li, "User Behavior Prediction of Social Hotspots Based on Multimessage Interaction and Neural Network," in IEEE Transactions on Computational Social Systems, vol. 7, no. 2, pp. 536-545, April 2020, doi: 10.1109/TCSS.2020.2969484.
- [20] Y. Wang, W. Shang and Z. Li, "The application of factorization machines in user behavior prediction," 2016 IEEE/ACIS 15th International Conference on Computer and Information Science (ICIS), 2016, pp. 1-4, doi: 10.1109/ICIS.2016.7550927.
- [21] H. Zhang and J. Chen, "A Novel User Behavior Prediction and Optimization Algorithm for Single-User Multi-terminal Scenario" 2016 9th International Symposium on Computational Intelligence and Design (ISCID), 2016, pp. 144-147, doi: 10.1109/ISCID.2016.2042.
- [22] C. Hao and Y. Zhou, "Design and Implementation of User Behavior Acquisition and Simulation Prediction Framework for Mobile Intelligent Terminal Based on User Perception," 2020 IEEE Conference on Telecommunications, Optics and Computer Science (TOCS), 2020, pp. 125-128, doi: 10.1109/TOCS50858.2020.9339698.

- [23] B. Ravi Krishna, P. Akhila, S. Sowjanya and B. Keerthana, "Prediction of Hot Topic in Social Media Based on User Participation Behavior in Social Hotspots," 2021 5th International Conference on Electronics, Communication and Aerospace Technology (ICECA), 2021, pp. 1545-1548, doi: 10.1109/ICECA52323.2021.9676120.